Initial Reports of the Deep Sea Drilling Project

Volume LXXXV

Los Angeles, California to Honolulu, Hawaii
March—April 1982

NATIONAL SCIENCE FOUNDATION
National Ocean Sediment Coring Program

NSFSP—85

October 1985

READEX FICHE best copy available

85

Drilling locations

Leg	Location	Sites
Phase 1 1968–1970		
1	North Atlantic	1–7
2	North Atlantic	8–12
3	South Atlantic	13–22
4	Central Atlantic	23–31
5	North Pacific	32–43
6	North Pacific	44–60
7	Central Pacific	61–67
8	Central Pacific	68–75
9	Central Pacific	76–84
Phase 2 1970–1972		
10	Gulf of Mexico	85–97
11	North Atlantic	98–108
Re-entry trials		109–110
12	North Atlantic	111–119
13	Mediterranean	120–134
14	Central Atlantic	135–144
15	Caribbean	146–154
16	Central Pacific	155–163
17	Central Pacific	164–171
18	North Pacific	172–182
19	North Pacific	183–193
20	North Pacific	194–202
21	Coral Sea	203–210
22	Indian Ocean	211–218
23	Arabian Sea	219–230
24	Indian Ocean	231–238
25	Indian Ocean	239–249
Phase 3 1972–1975		
26	Indian Ocean	250–258
27	Indian Ocean	259–263
28	Antarctic	264–274
29	Tasman Sea	275–284
30	South Pacific	285–289
31	North Pacific	290–302
32	North Pacific	303–313
33	North Pacific	314–318
34	South Pacific	319–321
35	South Pacific	322–325
36	South Atlantic	326–331
37	North Atlantic	332–335
38	Arctic	336–352
39	Atlantic	353–359
40	South Atlantic	360–365
41	South Atlantic	366–370
42A	Mediterranean	371–378
42B	Black Sea	379–381
43	North Atlantic	382–387
44	North Atlantic	388–392
44A	North Atlantic	393–394
IPOD I 1975–present		
45	North Atlantic	395–396
46	North Atlantic	396A–396B
47	North Atlantic	397–398
48	North Atlantic	399–406
49	North Atlantic	407–414
50	North Atlantic	415–416
51A	North Atlantic	417–417A
51B	North Atlantic	417B–417D
52	North Atlantic	417D–418A
53	North Atlantic	418A–418B
54	Central Pacific	419–429
55	North Pacific	430–433
56	North Pacific	434–437
57	North Pacific	438–441
58	North Pacific	442–446
59	North Pacific	447–451
60	North Pacific	452–461
61	Central Pacific	462
62	North Pacific	463–466
63	North Pacific	467–473
64	Gulf of California	474–481
65	Gulf of California	482–485
66	Central Pacific	486–493
67	Central Pacific	494–500
68	Central Pacific	502–503
69	Central Pacific	504–505, 501
70	Central Pacific	506–510, 504B
71	South Atlantic	511–514
72	South Atlantic	515–518
73	South Atlantic	519–524
74	South Atlantic	525–529
75	South Atlantic	530–532
76	North Atlantic	533–534
77	Caribbean	535–540
78	North Atlantic	541–543, 395A, B
79	North Atlantic	544–547
80	North Atlantic	548–551
81	North Atlantic	552–555
82	North Atlantic	556–564
83	Central Pacific	504B
84	Central Pacific	565–570
85	Central Pacific	571–575

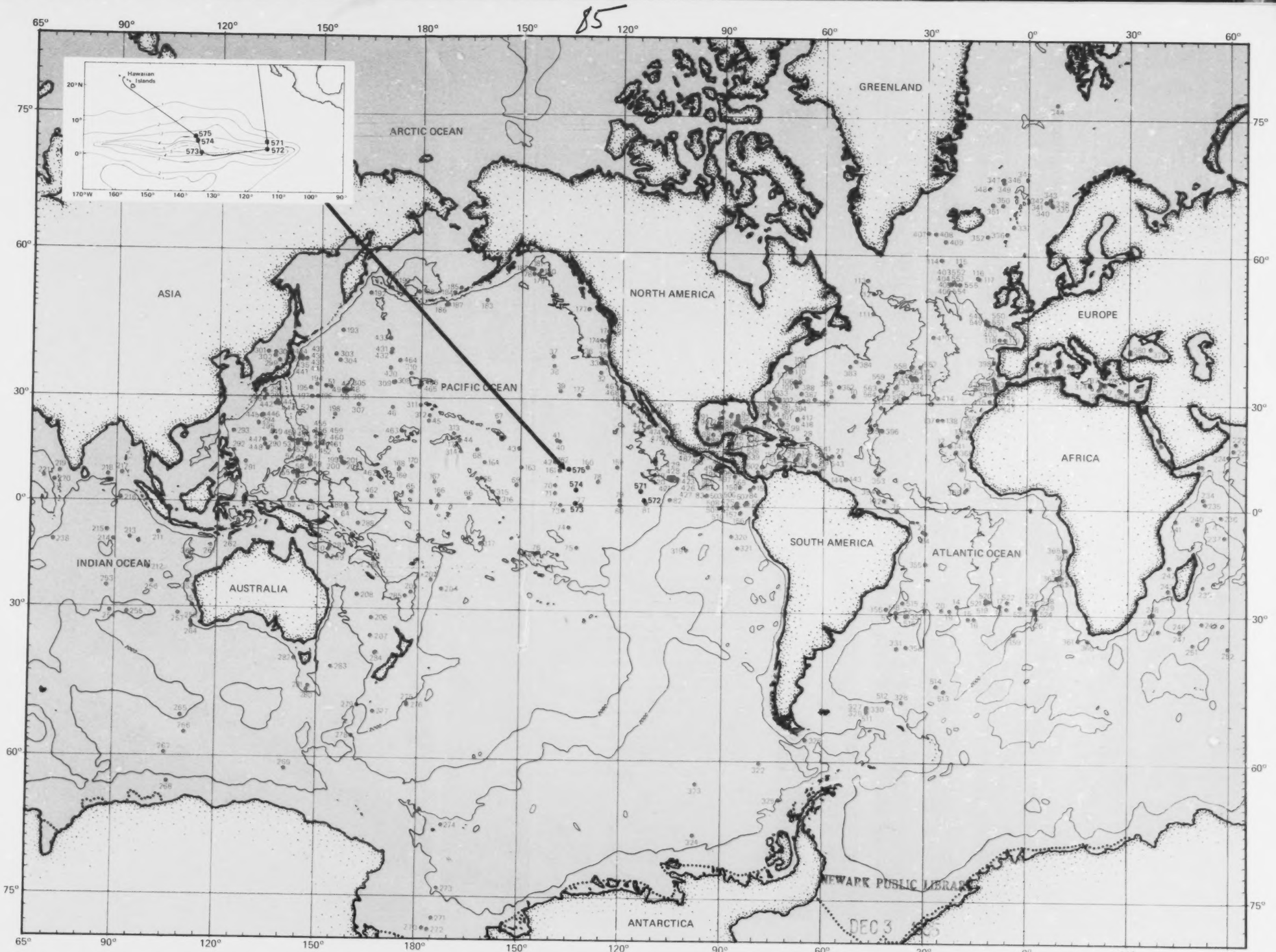

DEEP SEA DRILLING PROJECT

NEWARK PUBLIC LIBRARY
DEC 3

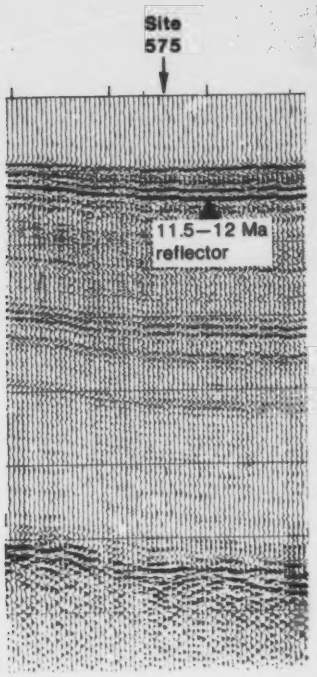

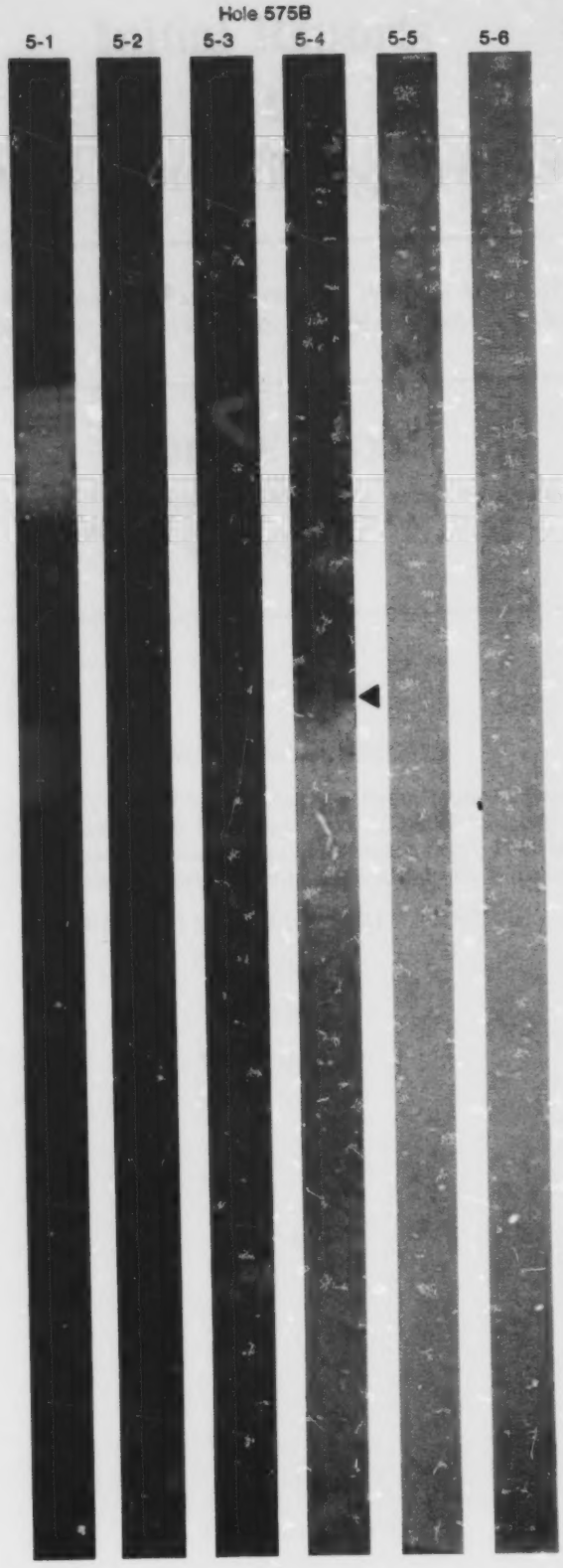

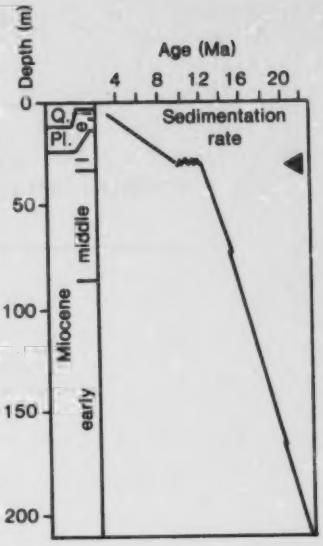

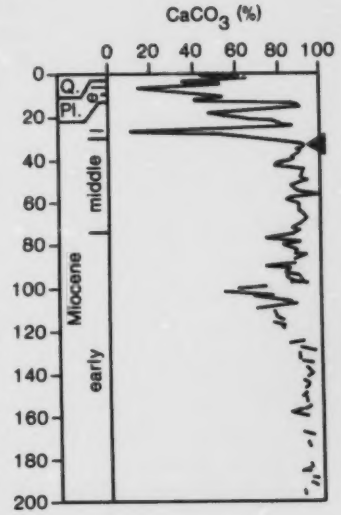

Equatorial Pacific sediments can be considered an indicator of global paleoenvironmental change. An increase in the production of North Atlantic Deep Water results in an increase in the production of Antarctic Bottom Water, which results in a major change in the style of pelagic sedimentation (carbonate, silica) in the equatorial Pacific. The change is reflected in the seismic record, core lithology, sedimentation rate, and sediment calcium carbonate content at Site 575.

Initial Reports of the Deep Sea Drilling Project

A Project Planned by and Carried Out With the Advice of the
JOINT OCEANOGRAPHIC INSTITUTIONS FOR DEEP EARTH SAMPLING (JOIDES)

VOLUME LXXXV

covering Leg 85 of the cruises of the Drilling Vessel *Glomar Challenger*
Los Angeles, California, to Honolulu, Hawaii
March–April 1982

PARTICIPATING SCIENTISTS

Larry Mayer, Fritz Theyer, John A. Barron, Dean A. Dunn, Tim Handyside, Scott Hills, Ian Jarvis, Catherine A. Nigrini, Nicklas C. Pisias, Annick Pujos, Tsunemasa Saito, Paul Stout, Ellen Thomas, Norbert Weinreich, and Roy H. Wilkens

SHIPBOARD SCIENCE REPRESENTATIVE

Ellen Thomas

EDITOR

Marian G. Bailey

Prepared for the
NATIONAL SCIENCE FOUNDATION
National Ocean Sediment Coring Program
Under Contract C-482
By the
UNIVERSITY OF CALIFORNIA
Scripps Institution of Oceanography
Prime Contractor for the Project

This material is based upon research supported by the National Science Foundation under Contract No. C-482.

Any opinions, findings, and conclusions or recommendations expressed in this publication are those of the author(s) and do not necessarily reflect the views of the National Science Foundation.

It is recommended that reference to the whole or to part of this volume be made in one of the following forms, as appropriate:

Mayer, L., Theyer, F., et al., 19__. *Init. Repts. DSDP*, 85: Washington (U.S. Govt. Printing Office).

Miller, K. G., and Thomas, E., 19__. Late Eocene to Oligocene benthic foraminiferal isotopic record, Site 574, equatorial Pacific. *In* Mayer, L., Theyer, F., et al., *Init. Repts. DSDP*, 85: Washington (U.S. Govt. Printing Office), ___-___.

Effective Publication Dates of DSDP *Initial Reports*

According to the International Code of Zoological Nomenclature, the date of publication of a work and of a contained name or statement affecting nomenclature is the date on which the publication was mailed to subscribers, placed on sale, or when the whole edition is distributed free of charge, mailed to institutions and individuals to whom free copies are distributed. The mailing date, *not the printed date*, is the correct one.

Mailing dates of the more recent *Initial Reports of the Deep Sea Drilling Project* are as follows:

Volume 76—November, 1983
Volume 77—September, 1984
Volume 78A,B—August, 1984
Volume 79—November, 1984
Volume 80—March, 1985
Volume 81—January, 1985

Printed October 1985

Library of Congress Catalog Card Number 74—603338

For sale by the Superintendent of Documents, U.S. Government Printing Office
Washington, D.C. 20402

Stock Number 038-000-00558-8

Foreword

The world's first major oceanographic expedition took place between 1872 and 1876. This expedition, aboard the H.M.S. *Challenger* covering nearly 70,000 nautical miles and gathering oceanographic data from 362 stations, expanded our knowledge of the ocean and provided a solid foundation for future studies in marine geology. A century later, another vessel also named *Challenger* continued to expand our knowledge of the world's ocean and helped revolutionize our concepts of how the seafloor and the continents form and change. The drilling vessel *Glomar Challenger* sailed the same waters as its historic counterpart, seeking answers to new questions concerning the history of our planet and the life it supports. The continued advancement of knowledge about the fundamental processes and dynamics of the earth is leading to a greater understanding of our planet and more intelligent use of its resources.

Since 1968, the Deep Sea Drilling Project (DSDP) has been supported by the National Science Foundation, primarily through a contract with the University of California which, in turn, subcontracted to Global Marine Incorporated for the services of the D/V *Glomar Challenger*.

Through contracts with Joint Oceanographic Institutions, Inc. (JOI, Inc.), the National Science Foundation supported the scientific advisory structure for the project and funded predrilling geophysical site surveys. Scientific planning was conducted under the auspices of the Joint Oceanographic Institutions for Deep Earth Sampling (JOIDES). The JOIDES advisory group consisted of over 250 members who made up 24 committees, panels, and working groups. The members were distinguished scientists from academic institutions, government agencies, and private industry all over the world.

In 1975, the International Phase of Ocean Drilling (IPOD) began. The IPOD member nations, Federal Republic of Germany, Japan, United Kingdom, Soviet Union, and France, partially supported the project. Each member nation actively participated in the scientific planning of the project through membership in JOIDES. Scientists from these countries also took part in the field work aboard the D/V *Glomar Challenger* and postcruise scientific studies.

The first ocean coring operations for the Deep Sea Drilling Project began on August 11, 1968. During the ensuing years of drilling operations in the Atlantic, Pacific, and Indian oceans, the Gulf of Mexico, Caribbean Sea, Mediterranean Sea, and Antarctic waters, the scientific objectives that had been proposed were successfully accomplished. Primarily, the age of the ocean basins and their processes of development were determined. The validity of the hypothesis of seafloor spreading was firmly demonstrated and its dynamics studied. Emphasis was placed on broad reconnaissance and testing the involvement of mid-oceanic ridge systems in the development of the ocean basin. Later legs of the *Challenger's* voyages concentrated on the nature of the oceanic crust, the sedimentary history of the passive ocean margins, sediment dynamics along active ocean margins, and other areas of interest. The accumulated results of this project have led to major new interpretations of the pattern of sedimentation and the physical and chemical characteristics of the ancient oceans.

Technological advances have provided new tools which in turn have opened new dimensions of scientific discovery. The introduction of the Hydraulic Piston Corer in 1979 permitted virtually undisturbed cores of soft sediment layers to be obtained. This technological advance has greatly enhanced the ability of scientists to study ancient ocean environments, as recorded by sediment characteristics and flora and fauna preserved in these deposits.

A second major advance has been the use of the hole after drilling. The project routinely logged holes and performed geophysical and geochemical studies before, during, and after drilling. Long-term downhole geophysical seismic monitoring devices have been implanted successfully in DSDP holes. These new listening devices and geophysical studies have provided valuable information about the origin and nature of the dynamic processes of plate tectonics.

These reports contain the results of the initial studies of the recovered core material and the associated geophysical information. All the world's people benefit either directly or indirectly from this fundamental research. Knowledge about past and present conditions and processes are the foundations for future predictions and developments. Both short- and long-term benefits are obtained by advances in drilling technology and instrumentation. Information is being obtained about the origin and geographic distribution of natural resources. Just as the H.M.S. *Challenger* had a profound impact on scientific thought for over a century, this second *Challenger* expedition has given a greater understanding of the oceans and the processes that form and shape the earth.

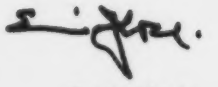

Erich Bloch,
Director

Washington, D.C.

Preface

Recognizing the need in the oceanographic community for scientific planning of a program to obtain deep sedimentary cores from the ocean bottoms, four of the major oceanographic institutions that had strong interests and programs in the fields of marine geology and geophysics formed, in May 1964, the Joint Oceanographic Institutions for Deep Earth Sampling (JOIDES). This group, Lamont-Doherty Geological Observatory; Rosenstiel School of Marine and Atmospheric Science, University of Miami; the Scripps Institution of Oceanography, University of California at San Diego; and the Woods Hole Oceanographic Institution, expressed an interest in undertaking scientific planning and guidance of the sedimentary drilling program. It was the purpose of this group to foster programs to investigate the sediments and rocks beneath the deep oceans by drilling and coring. The membership of this original group was later enlarged in 1968 when the University of Washington became a member, and again in 1975 when University of Hawaii Institute of Geophysics, the Oregon State University School of Oceanography, the University of Rhode Island Graduate School of Oceanography, and Texas A&M University Department of Oceanography became members. In accordance with international agreements, institutions of participating nations became members of JOIDES. Thus, during 1974 to 1976, the Bundesanstalt für Geowissenschaften und Rohstoffe of the Federal Republic of Germany, the Centre National pour l'Exploitation des Océans of France, the Natural Environment Research Council of the United Kingdom, the University of Tokyo of Japan, and Academy of Sciences of the USSR became JOIDES members.

Through discussions sponsored by the JOIDES organization, with support from the National Science Foundation, Columbia University's Lamont-Doherty Geological Observatory operated a drilling program in the summer of 1965, on the Blake Plateau region off Jacksonville, Florida.

With this success in hand, planning began for a more extensive deep sea effort. This resulted in the award of a contract by the National Science Foundation to the Scripps Institution of Oceanography, University of California at San Diego for an eighteen-month drilling program in the Atlantic and Pacific oceans, termed the Deep Sea Drilling Project (DSDP). Operations at sea began in August 1968, using the now-famous drilling vessel, the *Glomar Challenger*.

The goal of the Deep Sea Drilling Project is to gather scientific information that will help determine the age and processes of development of the ocean basins. The primary strategy is to drill deep holes into the ocean floor, relying largely on technology developed by the petroleum industry.

Through the efforts of the principal organizations and of the panel members, who were drawn from a large cross section of leading earth scientists and associates, a scientific program was developed.

Cores recovered from deep beneath the ocean floor provide reference material for a multitude of studies in fields such as biostratigraphy, physical stratigraphy, and paleomagnetism that afford a new scope for investigating the physical and chemical aspects of sediment provenance, transportation, deposition, and diagenesis. In-hole measurements, as feasible, provide petrophysical data to permit inference of lithology of intervals from which no cores were recovered.

A report, describing the core materials and information obtained both at sea and in laboratories onshore, is published after the completion of each cruise. These reports are a cooperative effort of shipboard and shore-based scientists and are intended primarily to be a compilation of results which, it is hoped, will be the starting point for many future new and exciting research programs. Preliminary interpretations of the data and observations taken at sea are also included.

Core materials and data collected on each cruise will be made available to qualified scientists through the Curator of the Deep Sea Drilling Project, following a Sample Distribution Policy (p.xvii) approved by the National Science Foundation.

The advent of *Glomar Challenger*, with its deep-water drilling capability, is exceedingly timely. It has come when geophysical investigation of the oceans has matured through 20 to 30 years of vigorous growth to the point where we have some knowledge about much of the formerly unknown oceanic areas of our planet. About one million miles of traverses have been made which tell us much about the global pattern of gravity, magnetic and thermal anomalies, and about the composition, thickness, and stratigraphy of the sedimentary cover of the deep sea and continental margin. The coverage with such data has enabled the site selection panels to pick choice locations for drilling. The knowledge gained from each hole can be extended into the surrounding area. Detailed geophysical surveys were made for most of the selected locations prior to drilling.

The earth sciences have recently matured from an empirical status to one in which substantial theories and hypotheses about major tectonic processes are flourishing. Theories about the origin of magnetic fields and magnetic reversals, about ocean floor spreading and continental drift, and about the thermal history of our planet have led to specific predictions that could be tested best by an enlightened program of sampling of deep sea and continental margin sediments and underlying rocks.

In October 1975, the International Phase of Ocean Drilling (IPOD) began. This international interest, and the true participation of both the scientists and governments of a number of nations, are eloquent testimony to the importance of the work being done by the Deep Sea Drilling Project.

The members of JOIDES and DSDP and the scientists from all interested organizations and nations who have served on the various advisory panels are proud to have been of service and believe that the information and core materials that have been obtained will be of value to students of earth sciences and to all humanity for many years to come.

Deep Sea Drilling Project

MEMBER ORGANIZATIONS OF THE JOINT OCEANOGRAPHIC INSTITUTIONS FOR DEEP EARTH SAMPLING (JOIDES):[1]

Bundesanstalt für Geowissenschaften und Rohstoffe, Federal Republic of Germany

University of California at San Diego, Scripps Institution of Oceanography

Centre National pour l'Exploitation des Océans, Paris

Columbia University, Lamont-Doherty Geological Observatory

University of Hawaii, Hawaii Institute of Geophysics

University of Miami, Rosenstiel School of Marine and Atmospheric Science

Natural Environment Research Council, London

Oregon State University, School of Oceanography

University of Rhode Island, Graduate School of Oceanography

Texas A&M University, Department of Oceanography

University of Tokyo, Ocean Research Institute

University of Washington, Department of Oceanography

U.S.S.R. Academy of Sciences[2]

Woods Hole Oceanographic Institution

[1] Includes member organizations during time of cruise.
[2] This institution and its committees and panel members were noncontributing members of JOIDES at time of cruise.

OPERATING INSTITUTION:

Scripps Institution of Oceanography
University of California at San Diego
La Jolla, California
W. A. Nierenberg, Director

DEEP SEA DRILLING PROJECT

Dr. M. N. A. Peterson
Principal Investigator
Project Manager

Mr. Robert S. Bower
Assistant Project Manager for Administration and Contracts

[1]Dr. Yves Lancelot
Chief Scientist

Mr. Ed Dean
Finance Administrator

Ms. Sue Strain
Personnel Officer

Participants aboard GLOMAR CHALLENGER for Leg Eighty-five

Dr. Larry Mayer
Co-Chief Scientist
School of Oceanography
University of Rhode Island
Kingston, Rhode Island 02881

Dr. Fritz Theyer
Co-Chief Scientist
Hawaii Institute of Geophysics
University of Hawaii
Honolulu, Hawaii 96822

Dr. John A. Barron
Paleontologist (diatoms)
Branch of Paleontology and Stratigraphy
U.S. Geological Survey
Menlo Park, California 94025

Dr. Dean A. Dunn
Sedimentologist
Graduate School of Oceanography
University of Rhode Island
Narragansett, Rhode Island 02882

Dr. Tim Handyside
Organic Geochemist
Department of Geology
The University
Newcastle-upon-Tyne NE1 7RU
United Kingdom

Mr. Scott Hills
Sedimentologist
Graduate Department
Scripps Institution of Oceanography
La Jolla, California 92093

Dr. Ian Jarvis
Sedimentologist
Department of Geology
City of London Polytechnic
London E1-2NG, United Kingdom

Dr. Catherine A. Nigrini
Paleontologist (radiolarians)
510 Papyrus Drive
La Habra Heights, California 90631

Dr. Nicklas G. Pisias
Sedimentologist
School of Oceanography
Oregon State University
Corvallis, Oregon 97331

Dr. Annick Pujos
Paleontologist (nannofossils)
Département de Géologie et Océanographie
Université de Bordeaux I
33405 Talence, France

Dr. Tsunemasa Saito
Paleontologist (foraminifers)
Department of Geology
Yamagata University
Faculty of Science
Yamagata 990, Japan

Mr. Paul Stout
Sedimentologist
Graduate Department
Scripps Institution of Oceanography
La Jolla, California 92093

Dr. Ellen Thomas
Paleontologist (foraminifers)/Staff
Science Representative
Deep Sea Drilling Project
Scripps Institution of Oceanography
La Jolla, California 92093

Dr. Norbert Weinreich
Paleomagnetist
Institut für Geophysik
Ruhr-Universität Bochum
D-4630 Bochum
Federal Republic of Germany

Dr. Roy H. Wilkens
Physical Properties Specialist
Department of Earth and
Planetary Sciences
Massachusetts Institute of Technology
Cambridge, Massachusetts 02139

Mr. Stan Serocki
Cruise Operations Manager
Deep Sea Drilling Project
Scripps Institution of Oceanography
La Jolla, California 92093

Captain Loyd E. Dill
Master of the Drilling Vessel
Global Marine, Inc.
San Diego, California 92111

Mr. A. C. Wheeler, Jr.
Drilling Superintendent
Global Marine, Inc.
San Diego, California 92111

Mr. Burnette W. Hamlin
Laboratory Officer
Deep Sea Drilling Project
Scripps Institution of Oceanography
La Jolla, California 92093

Mr. David Allard
Curatorial Representative
Deep Sea Drilling Project
Scripps Institute of Oceanography
La Jolla, California 92093

Mr. Kenneth A. Thompson
Chemist
Deep Sea Drilling Project
Scripps Institution of Oceanography
La Jolla, California 92093

Mr. Paul L. Laughlin
Electronics Technician
Deep Sea Drilling Project
Scripps Institution of Oceanography
La Jolla, California 92093

Mr. Craig Dootson
Marine Technician
Deep Sea Drilling Project
Scripps Institution of Oceanography
La Jolla, California 92093

Mr. Craig M. Hallman
Marine Technician
Deep Sea Drilling Project
Scripps Institution of Oceanography
La Jolla, California 92093

Mr. David L. Ripley
Marine Technician
Deep Sea Drilling Project
Scripps Institution of Oceanography
La Jolla, California 92093

Mr. Leonard Lopez
Marine Technician
Deep Sea Drilling Project
Scripps Institution of Oceanography
La Jolla, California 92093

Ms. Marguerite Schears
Marine Technician/Storekeeper
Deep Sea Drilling Project
Scripps Institution of Oceanography
La Jolla, California 92093

Mr. Victor S. Sotelo
Photographer
Deep Sea Drilling Project
Scripps Institution of Oceanography
La Jolla, California 92093

Ms. Joanne R. Collins
Yeoperson
Deep Sea Drilling Project
Scripps Institution of Oceanography
La Jolla, California 92093

Deep Sea Drilling Project Publication Staff

Publications Manager
Jan H. Blakeslee

Editors
Marian G. Bailey
Susan Orlofsky
Katie L. Turner
Elizabeth Whalen

Production Manager
Raymond F. Silk

Production Assistants
Elaine Bruer
Madeleine A. Mahnken

Production Coordinators
Carolina Bertling
Mary A. Young

Art-Photo Supervisor
Virginia L. Roman

Illustrators
Aileen Bobryk (this volume)
Vicki Cypherd
Kathleen Sanderson
Alice N. Thompson

JOIDES Advisory Groups[1]

Executive Committee

Dr. D. James Baker, Jr.
University of Washington

Prof. Dr. Friedrich Bender
Bundesanstalt für Geowissenschaften und Rohstoffe

Dr. G. Ross Heath
Oregon State University

Dr. Charles E. Helsley
Hawaii Institute of Geophysics

Sir Peter Kent, F.R.S.
Natural Environment Research Council

Dr. John A. Knauss
University of Rhode Island

Dr. Noriyuki Nasu
University of Tokyo

Dr. William A. Nierenberg, Chairman
Scripps Institution of Oceanography

Dr. M. N. A. Peterson (ex-officio)
Scripps Institution of Oceanography

M. Gerard Piketty
Centre National pour l'Exploitation des Océans

Dr. Barry Raleigh
Lamont-Doherty Geological Observatory

Prof. Robert D. Reid
Texas A&M University

Dr. Alexander V. Sidorenko
U.S.S.R. Academy of Sciences

Dr. John Steele
Woods Hole Oceanographic Institution

Dr. Edward L. Winterer (ex-officio Planning Committee Representative)
Scripps Institution of Oceanography

Dr. Warren Wisby
Rosenstiel School of Marine and Atmospheric Science

Planning Committee

Dr. Jean Aubouin
Université Pierre et Marie Curie

Dr. Helmut Beiersdorf
Bundesanstalt für Geowissenschaften und Rohstoffe

Dr. William R. Bryant
Texas A&M University

Dr. Joe R. Cann
University of Newcastle-upon-Tyne

Dr. John B. Corliss
Oregon State University

Dr. Joe S. Creager
University of Washington

Mr. John I. Ewing
Woods Hole Oceanographic Institution

Dr. Dennis E. Hayes
Lamont-Doherty Geological Observatory

Dr. Jose Honnorez
Rosenstiel School of Marine and Atmospheric Science

Dr. James P. Kennett
University of Rhode Island

Dr. Kazuo Kobayashi
University of Tokyo

Dr. Yves Lancelot (ex-officio)
Scripps Institution of Oceanography

Dr. Ralph Moberly
Hawaii Institute of Geophysics

Dr. Lev Nikitin
U.S.S.R. Academy of Sciences

Dr. E. L. Winterer, Chairman
Scripps Institution of Oceanography

Advisory Panel on Sedimentary Petrology and Physical Properties

Dr. Richard Bennett
National Oceanic and Atmospheric Administration

Dr. John W. Handin
Texas A&M University

Dr. George deVries Klein, Acting Chairman
University of Illinois, Urbana

Dr. Leland Kraft
McClelland Engineers, Inc.

Dr. I. Nick McCave
University of East Anglia

Dr. Frédéric Mélières
Université Pierre et Marie Curie

Dr. Ralph Moberly (ex-officio)
Hawaii Institute of Geophysics

Dr. Orrin H. Pilkey
Duke University

Dr. Peter Rothe
Universität Mannheim

Dr. Matthew Salisbury (ex-officio)
Scripps Institution of Oceanography

Dr. Peter Timofeev
U.S.S.R. Academy of Sciences

[1] Membership at time of cruise.

Advisory Panel on Organic Geochemistry

Dr. Earl W. Baker
Florida Atlantic University

Dr. Simon C. Brassel
The University of Bristol

Dr. John B. Corliss (ex-officio)
Oregon State University

Dr. William T. Coulbourn (ex-officio)
Scripps Institution of Oceanography

Dr. Gordon Erdman
Phillips Petroleum Company

Dr. Eric Galimov
U.S.S.R. Academy of Sciences

Dr. John M. Hunt
Woods Hole Oceanographic Institution

Dr. Keith Kvenvolden
U.S. Geological Survey

Dr. Philip A. Meyers
University of Michigan

Dr. Bernd R. Simoneit, Chairman
Oregon State University

Dr. Colin P. Summerhayes
Exxon Production Research Company

Dr. Bernard Tissot
Institut Français du Pétrole

Dr. Dietrich Welte
Lehrstuhl für Geologie, Geochemie und Lagerstätten des Erdöls und der Kohle

Advisory Panel on Information Handling

Dr. Daniel E. Appleman, Chairman
Smithsonian Institution

Dr. Joe S. Creager (ex-officio)
University of Washington

Dr. John C. Hathaway
U.S. Geological Survey

Dr. Alfred Loeblich, Jr.
University of California, Los Angeles

Dr. Michael S. Loughridge
National Oceanic and Atmospheric Administration

Dr. Marthe Melguen
Centre Océanologique de Bretagne (BNDO)

Mrs. Judit Nowak
Bundesanstalt für Geowissenschaften und Rohstoffe

Mr. Peter Woodbury (ex-officio)
Scripps Institution of Oceanography

Industrial Liaison Panel

Mr. R. L. Adams
Conoco Inc.

Prof. Nikolai P. Budnikov
Ministry of Geology of the U.S.S.R.

Mr. Melvin J. Hill
Gulf Oil Exploration and Production Company

Dr. Ing. Guenter Peterson
Gewerkschaft Walter

Mr. W. A. Roberts, Chairman
Energy Concepts, Inc.

Dr. Gilbert Rutman
Société Nationale des Pétroles d'Aquitaine

Mr. G. Williams
United Kingdom Offshore Operators Association, Ltd.

Advisory Panel on Ocean Crust

Dr. Roger N. Anderson
Lamont-Doherty Geological Observatory

Dr. Henri Bougault
Centre Océanologique de Bretagne (CNEXO)

Dr. John B. Corliss (ex-officio)
Oregon State University

Prof. Dr. Rolf Emmermann
Universität Karlsruhe

Dr. Paul J. Fox, Chairman
University of Rhode Island

Dr. Paul Johnson
University of Washington

Dr. Ralph Moberly (ex-officio)
Hawaii Institute of Geophysics

Dr. James Natland (ex-officio)
Scripps Institution of Oceanography

Dr. Minoru Ozima
University of Tokyo

Dr. Paul Robinson
Dalhousie University

Dr. Hans Schouten
Woods Hole Oceanographic Institution

Dr. Ralph Stephen
Woods Hole Oceanographic Institution

Dr. John Tarney
University of Leicester

Dr. Andrei A. Tsvetkov
U.S.S.R. Academy of Sciences

Advisory Panel on Ocean Margin (Active)

Dr. Peter F. Barker
University of Birmingham

Dr. Jean-Paul Cadet
Université d'Orléans

Dr. Darrel Cowan
University of Washington

Dr. Joe S. Creager (ex-officio)
University of Washington

Dr. Yury I. Dmitriev
U.S.S.R. Academy of Sciences

Dr. Dennis E. Hayes (ex-officio)
Lamont-Doherty Geological Observatory

Dr. Donald M. Hussong, Chairman
Hawaii Institute of Geophysics

Dr. Daniel Karig
Cornell University

Dr. John W. Ladd
Lamont-Doherty Geological Observatory

Dr. Kazuaki Nakamura
University of Tokyo

Dr. James Natland (ex-officio)
Scripps Institution of Oceanography

Dr. Roland von Huene
U.S. Geological Survey

Dr. Hansjust Walther
Bundesanstalt für Geowissenschaften und Rohstoffe

Advisory Panel on Ocean Margin (Passive)

Dr. Mikhail E. Artemiev
U.S.S.R. Academy of Sciencies

Dr. Arnold H. Bouma
Gulf Science and Technology Company

Dr. William R. Bryant (ex-officio)
Texas A&M University

Dr. Karl Hinz
Bundesanstalt für Geowissenschaften und Rohstoffe

Dr. Hideo Kagami
University of Tokyo

Dr. Charlotte Keene
Geological Survey of Canada

Dr. Yves Lancelot (ex-officio)
Scripps Institution of Oceanography

Dr. Lucien Montadert
Institut Français du Pétrole

Dr. David G. Roberts, Chairman
British Petroleum Co., Ltd.

Dr. William B. F. Ryan
Lamont-Doherty Geological Observatory

Dr. Sigmund Snelson
Shell Oil Company

Dr. Jørn Thiede
Universitetet i Oslo

Dr. Brian E. Tucholke
Woods Hole Oceanographic Institution

Dr. Peter R. Vail
Exxon Production Research Company

Dr. Jan E. van Hinte
Vrije Universiteit

Dr. Edward L. Winterer (ex-officio)
Scripps Institution of Oceanography

Advisory Panel on Pollution Prevention and Safety

Dr. Nikolai I. Beliy
Ministry of Gas Industry, U.S.S.R.

Dr. Rustum Jean Byramjee
Compagnie Français des Pétroles

Dr. George Claypool
U.S. Geological Survey

Mr. Brian E. Davies
Sohio Petroleum Company

Dr. Louis E. Garrison, Chairman
U.S. Geological Survey

Dr. Arthur E. Green
Exxon Production Research Company

Prof. A. J. Horn
Atherton, California

Dr. Ernst Hotz
Deminex, Essen, Federal Republic of Germany

Dr. Yves Lancelot (ex-officio)
Scripps Institution of Oceanography

Dr. David B. MacKenzie
Marathon Oil Company

Dr. Geoffrey D. Taylor
British Petroleum Company, Ltd.

Dr. Edward L. Winterer (ex-officio)
Scripps Institution of Oceanography

Advisory Panel on Inorganic Geochemistry

Dr. Joe R. Cann (ex-officio)
University of Newcastle-upon-Tyne

Dr. Henry Elderfield
University of Leeds

Dr. Michael Hoffert
Université Louis Pasteur

Dr. Miriam Kastner, Acting Chairman
Scripps Institution of Oceanography

Dr. Margaret Leinen
University of Rhode Island

Dr. Igor D. Ryabchikov
U.S.S.R. Academy of Sciences

Dr. Sam Savin
Case Western Reserve University

Dr. Fred L. Sayles
Woods Hole Oceanographic Institution

Dr. Karl-Heinz Wedepohl
Universität Göttingen

Stratigraphic Correlations Panel

Dr. Ivan Basov
U.S.S.R. Academy of Sciences

Dr. Lloyd H. Burckle
Lamont-Doherty Geological Observatory

Dr. William Coulbourn (ex-officio)
Scripps Institution of Oceanography

Dr. Joe S. Creager (ex-officio)
University of Washington

Dr. D. Graham Jenkins
The Open University, Buckinghamshire

Prof. Dr. Erlend Martini
Universität Frankfurt

Dr. Catherine Nigrini
La Habra Heights, California

Dr. Richard Poore, Chairman
U.S. Geological Survey

Dr. John B. Saunders
Naturhistorisches Museum, Basel

Downhole Measurements Panel

Dr. Heinz Beckmann
Technische Universität Clausthal

Mr. Robert E. Boyce (ex-officio)
Scripps Institution of Oceanography

Dr. William R. Bryant (ex-officio)
Texas A&M University

Dr. Nikolas I. Christensen
University of Washington

Dr. Timothy J. G. Francis
Natural Environment Research Council

Dr. Roy Hyndman
Department of Energy, Mines and Resources, British Columbia

Mr. Alfred H. Jageler
Amoco Production Research Company

Dr. Hajimu Kinoshita
Chiba University

Dr. Mark Mathews
Los Alamos National Laboratory

Dr. Yury Neprochnov
U.S.S.R. Academy of Sciences

Dr. Lev Nikitin (ex-officio)
U.S.S.R. Academy of Sciences

Dr. Vincent Renard
Centre National pour l'Exploitation des Océans

Dr. Richard P. Von Herzen, Chairman
Woods Hole Oceanographic Institution

Advisory Panel on Ocean Paleoenvironment

Dr. Helmut Beiersdorf (ex-officio)
Bundesanstalt für Geowissenschaften und Rohstoffe

Dr. Hervé Chamley
Université des Sciences et Techniques de Lille

Dr. Robert G. Douglas, Chairman
University of Southern California

Dr. Dieter Fütterer
Universität Kiel

Dr. Robert E. Garrison
University of California, Santa Cruz

Dr. James D. Hays
Lamont-Doherty Geological Observatory

Dr. James P. Kennett (ex-officio)
University of Rhode Island

Dr. Robert B. Kidd
Natural Environment Research Council

Dr. Yves Lancelot (ex-officio)
Scripps Institution of Oceanography

Dr. Seymour O. Schlanger
Northwestern University

Dr. Yokichi Takayanagi
Tohoku University

Dr. Fritz Theyer
Hawaii Institute of Geophysics

Dr. Peter P. Timofeev
U.S.S.R. Academy of Sciences

Advisory Panel on Site Surveying

Dr. Helmut Beiersdorf (ex-officio)
Bundesanstalt für Geowissenschaften und Rohstoffe

Dr. LeRoy M. Dorman
Scripps Institution of Oceanography

Dr. Dennis Hayes (ex-officio)
Lamont-Doherty Geological Observatory

Dr. E. John W. Jones, Chairman
University College, London

Dr. Shozaburo Nagumo
University of Tokyo

Dr. Philip Rabinowitz (ex-officio)
Lamont-Doherty Geological Observatory

Dr. Vincent Renard
Centre National pour l'Exploitation des Océans

Dr. Matthew Salisbury (ex-officio)
Scripps Institution of Oceanography

Dr. Alexander A. Schreider
U.S.S.R. Academy of Sciences

Dr. Wilfried Weigel
Universität Hamburg

SAMPLE DISTRIBUTION POLICY*

Distribution of Ocean Drilling Program and of Deep Sea Drilling Project samples is undertaken in order to (1) provide support to shipboard scientists in achieving the scientific objectives of their cruise, and support shorebased investigators who are preparing contributions to DSDP and ODP reports; (2) provide individual investigators with materials to conduct detailed studies beyond the scope of ODP reports; (3) provide paleontological reference centers with samples for reference and comparison purposes; and (4) provide educators with samples for teaching purposes.

Funding for sample-related activities must be secured by the investigator independently of requesting the samples.

The Ocean Drilling Program Curator is responsible for distributing samples and for preserving and conserving core material. The Curator, who may accept advice from chairmen of the appropriate JOIDES advisory panels, is responsible for enforcing the provisions of this sample distribution policy. He is responsible for maintaining a record of all samples that have been distributed, both onboard ship and subsequently from the repositories, indicating the recipients and the nature of investigations proposed. This information is available to interested investigators on request.

Every sample distributed from the ship or from a repository is labeled with a standard identifier, which includes leg number, hole number, core and section numbers, and interval within the section from which the sample was removed. It is imperative that this standard identifier be associated with all data reported in the literature, and that residues of the sample remain labeled throughout their lives, so that later workers can relate the data to the cores.

Distribution of sample materials is made directly from the repositories (Lamont-Doherty Geological Observatory, Scripps Institution of Oceanography, or Texas A&M University) by the Curator or his designated representative.

1. *Distribution of Samples for Research Leading to Contributions to ODP Reports*

Any investigator who wishes to contribute to the reports of a scheduled cruise may write to the Curator, Ocean Drilling Program, Texas A&M University, College Station, Texas 77843-3469, U.S.A., in order to request samples from that cruise. Requests for a specific cruise must be received by the Curator at least TWO MONTHS in advance of the departure of that cruise, in order to allow time for the review of the request in conjunction with other requests, so that a suitable shipboard sampling program can be assembled. The request should include a statement of the nature of the proposed research, size and approximate number of samples required to complete the study, and any particular sampling technique or equipment which may be required. Requests will be reviewed by the staff representative and co-chief scientists of the cruise and by the Curator. Approval/disapproval will be based upon the scientific requirements of the cruise as determined by the appropriate JOIDES advisory panel(s). The scope of a request must be such that samples can be processed, that proposed research can be completed, and that the paper can be written in time for submission to the relevant ODP cruise report.

Except for rare, specific instances involving ephemeral properties, the total volume of samples removed during a cruise-related sampling program will not exceed one-quarter of the volume of core recovered, and no interval will be depleted. One-half of all recovered materials will be retained in the archives in as pristine a condition as is practicable. Investigators requesting shipboard samples of igneous materials may receive a maximum of 100 igneous samples per cruise.

Because many sample requests are received for shipboard work and because the time of the shipboard party is at a premium, co-chief scientists are strongly urged to limit shipboard sampling to the minimum necessary to accomplish the cruise objectives. Shorebased investigators whose requests for cruise-related samples are approved should expect that they will receive the samples after the cores are returned to the repository, and should schedule research activities accordingly.

Co-chief scientists may invite investigators who are not cruise participants to perform special studies of selected core samples in direct support of shipboard activities. If this occurs, the names and addresses of these investigators and details of all samples loaned or distributed to them must be forwarded to the Curator, via the ODP Staff Representative to that cruise, immediately after the cruise. These investigators are expected to contribute to the cruise reports as though they had been cruise participants. All requirements of the Sample Distribution Policy apply.

Any publication of results other than in ODP reports within twelve (12) months of completion of the

*Revised October 1984

cruise must be approved and authored by the whole shipboard party and, where appropriate, shorebased investigators. After twelve months, individual investigators may submit related papers for open publication provided they have already submitted their contributions to ODP reports. Investigations which are not completed in time for inclusion in ODP reports for a specific cruise may be published in a later edition of ODP reports; however, they may not appear in another journal until the ODP report for which they were intended has been published.

2. *Distribution of Samples for Research Leading to Publication Outside of the DSDP and ODP Reports*

   A. Researchers who wish to use samples for studies beyond the scope of the DSDP or ODP reports should obtain sample request forms from the Curator, Ocean Drilling Program, Texas A&M University, College Station, Texas 77843-3469, U.S.A. Requestors are required to specify the quantities and intervals of core required, to make a clear statement of the nature of the proposed research, to state the time which will be required to complete the work and to submit results for publication, and to specify funding status and the availability of equipment and space for the research.

   Additionally, if the requestor has received samples from ODP or from DSDP previously, he/she will be required to account for the disposition of those samples by citing published works, six (6) copies of which must be sent to the Curator. If no report has been published, this requirement can be fulfilled by sending a brief (two or three page) report of the status of the research. Unused and residual samples should be returned and data should be sent to the Curator if the project has terminated. Paleontological materials may be returned either to the Curator at ODP or to one of the designated paleontological reference centers. If material is returned to a reference center, notify the Curator when it is sent.

   Requests for samples from researchers in industrial laboratories will be honored in the same manner as those from academic organizations. Industrial investigators have the same obligations as other investigators to publish all results promptly in the open literature and to provide the Curator with copies of all reports published and of all data acquired in their research.

   In order to ensure that all requests for highly desirable but limited samples can be considered together, approval of requests and distribution of samples will be delayed until twelve (12) months after completion of the cruise or two (2) months after official publication of the core descriptions, whichever occurs earlier. The only exceptions to this policy will be made for specific requests involving ephemeral properties. Requests for samples may be based on core descriptions published in ODP reports produced by the shipboard party, copies of which are on file at various institutions throughout the world. Copies of original core logs and data are kept on open file at ODP, and at the repositories at Lamont-Doherty Geological Observatory and at Scripps Institution of Oceanography.

   B. Most investigations can be accomplished handily with sample volumes of 10 ml or less. Investigators must provide explicit justification of requests for larger sample sizes or for frequent intervals within a core. Requests which exceed reasonable size or frequency limits will require explicit justifications and more time to process, and are unlikely to be granted in their entirety.

   Requests for samples from thin layers, from stratigraphically important boundaries, from sections which are badly depleted or in unusually high demand may be delayed in order to coordinate requests from several investigators or while the Curator seeks advice from the community. Investigators who submit such requests may expect to receive suggestions for alternative sampling programs or that they join a research consortium which will share the samples. In any event, such exceptional requests will require more time for processing than will more routine requests.

   Investigators who wish to study ephemeral properties may request a waiver of the waiting period; however, such requests will be referred automatically to the relevant co-chiefs. If approved, the investigator will join the shorebased contributors to the shipboard science effort, and will incur the obligations thereof (see section 1).

   C. Samples will not be provided until the requestor assures the Curator that funding for the proposed research is available or unnecessary. If a sample request is dependent in any way upon proposed funding, the Curator is prepared to provide the proposed funding organization with information on the availability (or potential availability) of suitable samples.

D. Investigators who receive samples incur the following obligations:

(1) To publish significant results promptly; however, no contribution may be submitted for publication prior to twelve (12) months following the termination of the relevant leg unless it is approved and authored by the entire shipboard party.

(2) To acknowledge in all publications that the samples were supplied through the assistance of the international Ocean Drilling Program and others as appropriate.

(3) To submit six (6) copies of reprints of all published works to the Curator, Ocean Drilling Program, Texas A&M University, College Station, Texas 77843-3469, U.S.A. These reprints will be distributed to the repositories, to the ship, to the National Science Foundation, and to the Curator's reprint file.

(4) To submit all final analytical data obtained from the samples to Data Base Manager, Ocean Drilling Program, Texas A&M University, College Station, Texas 77843-3469, U.S.A. Please consult recent issues of the JOIDES Journal or call (409-845-2673) for information on acceptable data formats. Investigators should be aware that they may have other data obligations under NSF's Ocean Science Data Policy or under relevant policies of other funding agencies which require submission of data to national data centers.

(5) To return all unused or residual samples, in good condition and with a detailed explanation of any processing they may have experienced, upon termination of the proposed research. In particular, all thin sections and smear slides manufactured onboard the vessel or in the repositories are to be returned to the Curator. Paleontological materials may be returned either to the Curator at ODP or to one of the designated paleontological reference centers.

Failure to honor these obligations will prejudice future applications for samples.

E. Cores are available for examination by interested parties at the repositories. Investigators are welcome to visit the repositories in order to inspect cores and to specify sample locations when that is required for their research; however, time and space in the workrooms are limited, so advance appointments are required. Occasionally, the space may be fully booked several weeks in advance, so investigators are urged to call for appointments well ahead in order to avoid disappointment. Only the Curator or his delegate may actually remove samples from the cores.

F. A reference library of thin sections, smear slides, and archive photographs is maintained in the repositories for the use of visting investigators. All thin sections and smear slides produced onboard the ship or in the repositories belong to this library.

3. *Distribution of Samples to Paleontological Reference Centers*

As a separate and special category of repository activity, selected samples are being distributed to paleontological reference centers, where the prepared material may be studied by visitors. As of this writing (mid-1984), Foraminifera and Calcareous Nannofossils can be viewed; Radiolaria and Diatoms will be prepared in the future. The present centers are Scripps Institution of Oceanography, California (W. R. Riedel, tel. 619-452-4386); Basel Natural History Museum, Switzerland (J. B. Saunders, tel. 061-25.82.82); and New Zealand Geological Survey, Lower Hutt, New Zealand (A. R. Edwards, tel. 699.059). Future centers are likely to include Texas A&M University, College Station, Texas (S. Gartner, tel. 409-845-8479); Smithsonian Institution, Washington, D.C.; Lamont-Doherty Geological Observatory, Palisades, New York; and an as yet undesignated center in Japan.

Further details concerning the paleontological reference centers are reported periodically in the JOIDES Journal.

4. *Distribution of Samples for Educational Purposes*

Samples may be available in limited quantities to college-level educators for teaching purposes. Interested educators should request application forms from the Curator, Ocean Drilling Program, Texas A&M University, College Station, Texas 77843-3469, U.S.A. Requestors are required to specify preferred sample size and location, to make a very clear statement of the nature of the coursework in which the samples will be used, to explain how the core samples will be prepared and how they will be used in the classroom, to explain in detail why they cannot use similar materials derived from outcrops or dredge hauls (it is NOT acceptable to argue that it requires less effort for the requestor to obtain samples from ODP than to assemble them from other sources), and to certify that funds are available to prepare the materials for classroom use. In general, only samples of materials which are abundant in the collection and which are in little demand for research purposes should be requested for educational purposes. The Curator will not ap-

prove requests for materials which are limited in supply or for which demand (real or potential) is great, including most paleontological materials.

5. *Distribution of Data*

The Deep Sea Drilling Project and the Ocean Drilling Program routinely capture much of the data generated onboard ship and published in Program reports. Additionally, data supplied by investigators who have received samples are incorporated into the data bases, so data sets which are larger than can be published are available to investigators. Magnetics, downhole logging, seismic reflection, bathymetric data, and other data collected by the drilling vessel become available for distribution to investigators at the same time as core samples.

At least through mid-1986, DSDP data will continue to be distributed by the Data Base Manager, Deep Sea Drilling Project, A-031, University of California, San Diego, California 92093, U.S.A. A charge will be made to recover expenses in excess of $50.00 incurred in filling individual requests. If required, estimates of charges can be furnished before the work is performed. As DSDP phases down, DSDP data will be available primarily from the National Geophysical Data Center, Boulder, Colorado.

Requests for ODP data should be addressed to the Data Base Manager, Ocean Drilling Program, Texas A&M University, College Station, Texas 77843-3469, U.S.A. Many varieties of DSDP data will be included in ODP data bases. Information on sources of DSDP data will be available from the ODP Data Base Manager.

CONTENTS

Chapter — Page

ACKNOWLEDGMENTS 1

PART I: INTRODUCTION AND SITE REPORTS

1. INTRODUCTION: BACKGROUND AND EXPLANATORY NOTES, DEEP SEA DRILLING PROJECT LEG 85, CENTRAL EQUATORIAL PACIFIC 5
Shipboard Scientific Party

2. SITE 571 23
Shipboard Scientific Party

3. SITE 572 33
Shipboard Scientific Party

4. SITE 573 137
Shipboard Scientific Party

5. SITE 574 225
Shipboard Scientific Party

6. SITE 575 331
Shipboard Scientific Party

PART II: PALEONTOLOGY AND BIOSTRATIGRAPHY

7. NEOGENE AND QUATERNARY DINOFLAGELLATE BIOSTRATIGRAPHY OF THE EASTERN EQUATORIAL PACIFIC: DEEP SEA DRILLING PROJECT LEG 85 ... 407
I. Jarvis and B. A. Tocher

8. LATE EOCENE TO HOLOCENE DIATOM BIOSTRATIGRAPHY OF THE EQUATORIAL PACIFIC OCEAN, DEEP SEA DRILLING PROJECT LEG 85 413
J. A. Barron

9. A HIGH RESOLUTION LATE MIOCENE-PLIOCENE DIATOM BIOSTRATIGRAPHY FOR THE EASTERN EQUATORIAL PACIFIC 457
J. G. Baldauf

10. TROPICAL PACIFIC SILICOFLAGELLATE ZONATION AND PALEOTEMPERATURE TRENDS OF THE LATE CENOZOIC 477
D. Bukry

Chapter — Page

11. QUATERNARY RADIOLARIANS FROM THE EQUATORIAL PACIFIC, DEEP SEA DRILLING PROJECT LEG 85 499
M. Labracherie

12. RADIOLARIAN BIOSTRATIGRAPHY IN THE CENTRAL EQUATORIAL PACIFIC, DEEP SEA DRILLING PROJECT LEG 85 ... 511
C. A. Nigrini

13. NANNOFOSSILS FROM QUATERNARY DEPOSITS IN THE HIGH-PRODUCTIVITY AREA OF THE CENTRAL EQUATORIAL PACIFIC, DEEP SEA DRILLING PROJECT LEG 85 553
A. Pujos

14. CENOZOIC NANNOFOSSILS, CENTRAL EQUATORIAL PACIFIC, DEEP SEA DRILLING PROJECT LEG 85 581
A. Pujos

15. CALCAREOUS NANNOFOSSIL BIOSTRATIGRAPHY, DEEP SEA DRILLING PROJECT LEG 85, EASTERN EQUATORIAL PACIFIC 609
S. Gartner and J. Chow

16. PLANKTONIC FORAMINIFERAL BIOSTRATIGRAPHY OF EASTERN EQUATORIAL PACIFIC SEDIMENTS, DEEP SEA DRILLING PROJECT LEG 85 621
T. Saito

17. LATE EOCENE TO RECENT DEEP-SEA BENTHIC FORAMINIFERS FROM THE CENTRAL EQUATORIAL PACIFIC OCEAN 655
E. Thomas

18. STRATIGRAPHIC RESOLUTION OF LEG 85 DRILL SITES: AN INITIAL ANALYSIS... 695
N. G. Pisias, J. A. Barron, C. A. Nigrini, and D. A. Dunn

PART III: ISOTOPIC AND CARBONATE STRATIGRAPHY

19. HIGH RESOLUTION CARBONATE RECORDS FROM THE HYDRAULIC PISTON CORED SECTION OF SITE 572 711
N. G. Pisias and W. L. Prell

Chapter Page

20. PLIOCENE STABLE ISOTOPE AND CARBONATE STRATIGRAPHY (HOLES 572C AND 573A): PALEOCEANOGRAPHIC DATA BEARING ON THE QUESTION OF PLIOCENE GLACIATION 723
W. L. Prell

21. STABLE ISOTOPE AND CALCIUM CARBONATE RECORDS FROM HYDRAULIC PISTON CORED HOLE 574A: HIGH-RESOLUTION RECORDS FROM THE MIDDLE MIOCENE 735
N. G. Pisias, N. J. Shackleton, and M. A. Hall

22. OXYGEN AND CARBON ISOTOPE RECORD FOR THE EARLY AND MIDDLE MIOCENE IN THE CENTRAL EQUATORIAL PACIFIC (LEG 85) AND PALEOCEANOGRAPHIC IMPLICATIONS 749
E. Vincent and J. S. Killingley

23. LATE EOCENE TO OLIGOCENE BENTHIC FORAMINIFERAL ISOTOPIC RECORD, SITE 574, EQUATORIAL PACIFIC 771
K. G. Miller and E. Thomas

PART IV: GEOCHEMISTRY

24. GEOCHEMISTRY AND ORIGIN OF EOCENE-OLIGOCENE METALLIFEROUS SEDIMENTS FROM THE CENTRAL EQUATORIAL PACIFIC: DEEP SEA DRILLING PROJECT SITES 573 AND 574... 781
I. Jarvis

25. INTERSTITIAL WATER CHEMISTRY AND DIAGENESIS OF BIOGENIC SEDIMENTS FROM THE EASTERN EQUATORIAL PACIFIC, DEEP SEA DRILLING PROJECT LEG 85 805
P. M. Stout

26. COMPOSITION AND SOURCES OF PUMICES IN LEG 85 CORES..... 821
H. Sigurdsson and A. N. Davis

PART V: GEOPHYSICS

27. SEABEAM BATHYMETRIC AND WATERGUN SEISMIC REFLECTION SURVEYS IN THE EQUATORIAL PACIFIC..... 825
T. H. Shipley, E. L. Winterer, M. Goud, S. J. Hills, C. V. Metzler, C. K. Paull, and J. T. Shay

28. PHYSICAL PROPERTIES OF EQUATORIAL PACIFIC SEDIMENTS 839
R. H. Wilkens and T. Handyside

Chapter Page

29. PALEOMAGNETISM OF DEEP SEA DRILLING PROJECT LEG 85 SEDIMENTS: NEOGENE MAGNETOSTRATIGRAPHY AND TECTONIC HISTORY OF THE CENTRAL EQUATORIAL PACIFIC 849
N. Weinreich and F. Theyer

PART VI: PALEOCEANOGRAPHY AND SYNTHESES

30. SYNTHESIS OF BIOSTRATIGRAPHY, CENTRAL EQUATORIAL PACIFIC, DEEP SEA DRILLING PROJECT LEG 85: REFINEMENT OF OLIGOCENE TO QUATERNARY BIOCHRONOLOGY 905
J. A. Barron, C. A. Nigrini, A. Pujos, T. Saito, F. Theyer, E. Thomas, and N. Weinreich

31. DIATOM PALEOCEANOGRAPHY AND PALEOCLIMATOLOGY OF THE CENTRAL AND EASTERN EQUATORIAL PACIFIC BETWEEN 18 AND 6.2 MA 935
J. A. Barron

32. SEISMIC MODELING AND PALEOCEANOGRAPHY AT DEEP SEA DRILLING PROJECT SITE 574..... 947
L. A. Mayer, T. H. Shipley, F. Theyer, R. H. Wilkens, and E. L. Winterer

33. THE EQUATORIAL PACIFIC HIGH-PRODUCTIVITY BELT: ELEMENTS FOR A SYNTHESIS OF DEEP SEA DRILLING PROJECT LEG 85 RESULTS..... 971
F. Theyer, L. A. Mayer, J. A. Barron, and E. Thomas

APPENDIX. SEDIMENT PHYSICAL PROPERTIES, LEG 85 987

BACK POCKET FOLDOUTS

CHAPTER 17: APPENDIX A: COUNTS OF BENTHIC FORAMINIFER SPECIMENS FOR ALL SAMPLES STUDIED, SITES 573, 574, AND 575.

CHAPTER 17: APPENDIX A: (CONTINUED).

CHAPTER 17: APPENDIX A: (CONTINUED).

CHAPTER 22: FIGURE 6. ISOTOPE STRATIGRAPHY AND BIOSTRATIGRAPHY AT SITES 216 (TROPICAL INDIAN OCEAN), 575 (CENTRAL EQUATORIAL PACIFIC), AND 289 (WEST EQUATORIAL PACIFIC).

ACKNOWLEDGMENTS

We thank the U.S. National Science Foundation and agencies in the Federal Republic of Germany, France, Japan, the United Kingdom, and the U.S.S.R. for support of the Deep Sea Drilling Project. Our special thanks go to Captain Dill and the crew and technical staff of the *Glomar Challenger* Leg 85 for their competent work. Leg 85 marked the end of an era with the retirement of Captain Dill. We are sure we speak for all those who have sailed with him when we express our gratitude for all that he has done for the drilling program. We also extend our thanks to R. G. Douglas, J. D. Hays, and the JOIDES Ocean Paleoenvironment Panel, whose efforts made Leg 85 possible.

The preparation of this volume benefited greatly from the organizational abilities of Jan Blakeslee and Carol Bertling, and from the editing by Marian Bailey.

The following people reviewed chapters in this volume; their contributions are gratefully acknowledged.

W. Abbott
J. Baldauf
P. Baker
J. Barron
C. Barton
C. Blome
E. Boltovskoy
D. Bukry
L. Burckle
D. Cronan
N. Christensen
W. Curry
R. Embley
A. Fleet
J. Gardner
R. Garrison
D. Goldberg
R. Harland
S. Jenkins
L. Keigwin
G. Keller
M. Leinen
G. Lombari
A. McIntyre
E. Martini
G. Mountain
J. Natland
C. Nigrini
H. Okada
J. Resig
W. Riedel
K. Romine
C. Schreiber
N. Shackleton
W. Showers
J. Steinmetz
T. Takayama
L. Tauxe
R. Thunell
J. Varekamp
E. Vincent
S. Williams

PART I: INTRODUCTION AND SITE REPORTS

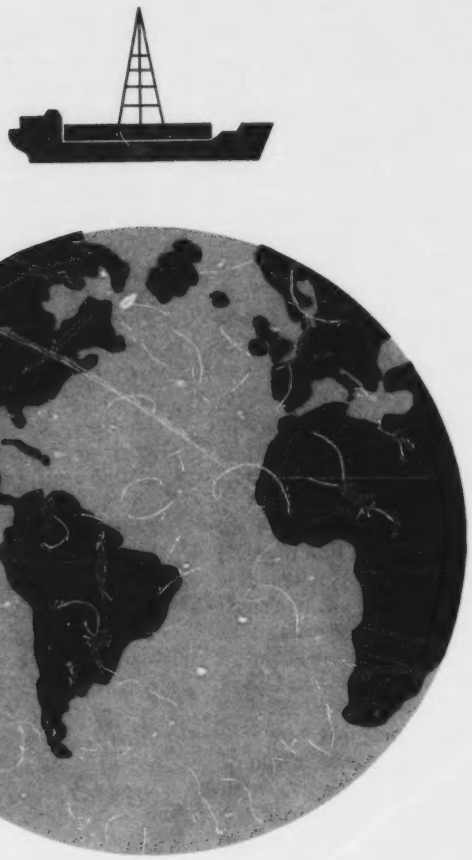

1. INTRODUCTION: BACKGROUND AND EXPLANATORY NOTES, DEEP SEA DRILLING PROJECT LEG 85, CENTRAL EQUATORIAL PACIFIC[1]

Shipboard Scientific Party[2]

BACKGROUND

Since the inception of the Deep Sea Drilling Project (DSDP), the central equatorial Pacific has been a primary target for oceanic drilling. Four DSDP legs have drilled in this region (Legs 5, 8, 9, and 16; Fig. 1), and the materials and data recovered by this drilling, as well as by numerous other programs, have been instrumental in establishing global Tertiary tropical biostratigraphy and chronology, in shaping our understanding of past oceanographic events, and in the development of tectonic models for the Pacific Plate. Beginning with such pioneering investigations as Arrhenius (1952), Bramlette (1961), Riedel and Funnell (1964), Hays et al. (1969), Hays et al. (1972), Berger (1973), and Winterer (1973), hosts of studies have demonstrated that Tertiary equatorial sediments are sensitive recorders of the interplay between tectonism, oceanic circulation patterns, biological productivity, dissolution, and diagenesis. Foremost among this research is the synthesis of the Cenozoic history of the equatorial Pacific by van Andel et al. (1975), which is largely based on DSDP results. Despite this wealth of information, the conduct of fine-scale research in sediments beyond the reach of conventional piston coring has been hampered by drilling disturbance. The disturbance is especially troublesome in the unconsolidated sediments in the upper 100 to 300 m of the sediments, which often comprise much of the Neogene.

When DSDP developed the hydraulic piston corer (HPC), it became possible to recover fairly undisturbed samples from the upper 100 to 300 m and thus to carry out high resolution stratigraphic studies. DSDP Leg 85 was designed to take advantage of this capability. A modified HPC (the VLHPC—variable length hydraulic piston corer) and rotary coring were to be used to recover complete, undisturbed equatorial Pacific sections. The biostratigraphy, magnetostratigraphy, and seismic, carbonate, and stable isotope stratigraphy of these sections were to be studied to develop a better understanding of the paleoceanographic and paleoclimatic history of the region.

The JOIDES Ocean Paleoenvironment Panel selected five drill sites that would best address the Leg 85 objectives within the constraints of available ship time. Two sites (571 and 572) are in the eastern Pacific, and the three others (573, 574, and 575) form a north–south line that lies at approximately 133°W across the equatorial high productivity zone (Fig. 1). The operational plan was to piston core each site twice (to ensure the recovery of a complete section) and then to use rotary coring to drill to basement through the stiffer sediments below the reach of the VLHPC. The drilling at all five sites was expected to result in the recovery of "reference" sections for the study of foraminifers, nannofossils, radiolarians, diatoms, and other fossils. Except at Sites 571 and 572, where basement age was known to be Miocene (Site 572 repeats Site 81, Leg 9), the basement age at all the sites was expected to be latest Eocene. Therefore, we hoped to recover complete or nearly complete records of the Eocene–Oligocene transition.

A secondary objective was to make a detailed examination of the relationships between paleoceanographic changes and the acoustic and physical properties of the sediments. Understanding these relationships could substantially increase the ability to use seismic stratigraphy as a paleoceanographic tool. Because such studies must be made in undisturbed sediments, however, they have been restricted in the past to the penetration depth of standard piston cores (10 to 20 m; Mayer, 1979a, b; Embley and Johnson, 1980). During Leg 85, the VLHPC would allow us to extend this research to sub-bottom depths of about 200 m and thus to evaluate variations in the factors that control acoustic properties as far back as the early to middle Miocene.

Another secondary objective was to conduct an *in situ* heat flow and pore water experiment to study pore water advection in a region of unusually low heat flow (Site 571).

THE VARIABLE LENGTH HYDRAULIC PISTON CORER

In December 1978 the Deep Sea Drilling Project deployed the first hydraulically actuated wireline piston corer (HPC). This coring system, which is described in Prell, Gardner, et al. (1982), operates on a hydraulic piston principle. Fluid pumped through the drill pipe acti-

[1] Mayer, L., Theyer, F., et al., *Init. Repts. DSDP*, 85: Washington (U.S. Govt. Printing Office).

[2] Larry Mayer (Co-Chief Scientist), Dalhousie University, Halifax, Nova Scotia, Canada; Fritz Theyer (Co-Chief Scientist), Hawaii Institute of Geophysics, University of Hawaii, Honolulu, Hawaii (present address: University of Southern California, Los Angeles, California); John A. Barron, U.S. Geological Survey, Menlo Park, California; Dean A. Dunn, University of Rhode Island, Narragansett, Rhode Island (present address: University of Southern Mississippi, Hattiesburg, Mississippi); Tim Handyside, The University, Newcastle upon Tyne, United Kingdom; Scott Hills, Scripps Institution of Oceanography, La Jolla, California; Ian Jarvis, City of London Polytechnic, London, United Kingdom (present address: Kingston Polytechnic, Kingston-upon-Thames, United Kingdom); Catherine A. Nigrini, La Habra Heights, California; Nicklas G. Pisias, Oregon State University, Corvallis, Oregon; Annick Pujos, Université de Bordeaux, Talence, France; Tsunemasa Saito, Yamagata University, Yamagata, Japan; Paul Stout, Scripps Institution of Oceanography, La Jolla, California; Ellen Thomas, Scripps Institution of Oceanography, La Jolla, California (present address: Lamont-Doherty Geological Observatory, Columbia University, Palisades, New York); Norbert Weinreich, Institut für Geophysik, Ruhr Universität Bochum, Bochum, Federal Republic of Germany; and Roy H. Wilkens, Massachusetts Institute of Technology, Cambridge, Massachusetts.

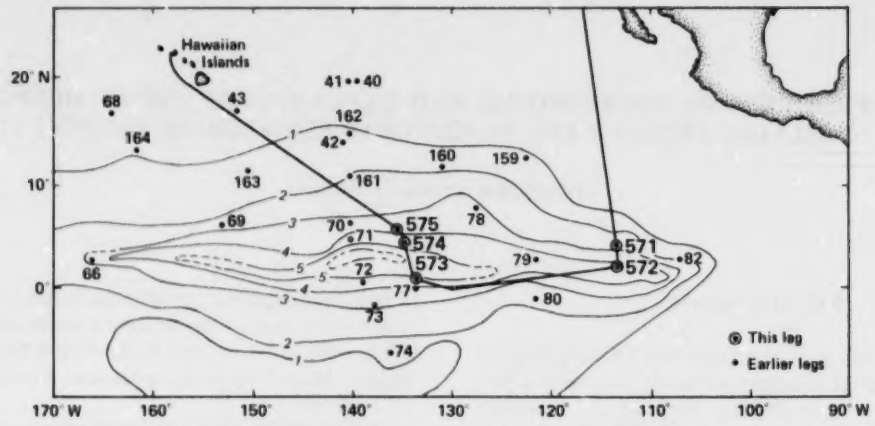

Figure 1. Cruise track and site locations of Leg 85 in relation to acoustic sediment thickness (contours in tenths of seconds of two-way traveltime) and previous DSDP drill sites (Legs 5, 8, 9, 16). Acoustic stratigraphy from Ewing et al. (1968).

vates a piston-driven core barrel, which is ejected through the core bit into the sediment at the rate of approximately 60 m/s. Because of this extremely high penetration rate, the motion of the core barrel is decoupled from the motion of the drill string. After each coring operation, the core barrel assembly is retrieved by wireline, as in a conventional coring operation. The drill bit is then "washed down" to the next coring point, where the piston coring procedure is repeated.

Since Leg 80 (May 1981), the improved coring system referred to as the variable length hydraulic piston corer has been in use (Fig. 2). The VLHPC is capable of recovering cores up to 9.5 m in length, whereas the HPC could recover cores of only 4.5 m. On Legs 80 to 86, recovery with the VLHPC has averaged more than 93%, with some holes achieving 100%.

The VLHPC recovers core in a standard (6.6 cm inner diameter) butyrate core liner. The drill bit used is a special 11.5 in. outer diameter roller cone drill bit with a 3.62 in. core throat. Coring must be discontinued when the sediments become too indurated. On Leg 85 the factor that limited the use of the VLHPC was not the shear strength of the sediment, however. The maximum shear encountered was 700 g cm^{-2}, and the HPC has successfully penetrated sediment with a shear strength of 1200 g cm^{-2}. On Leg 85 drilling in many holes terminated because of the loss of the lower core barrel assembly as a result of the excessive force (overpull) necessary to remove the core barrel from the sediment. When overpull exceeded about 15 to 25 tons, the quick release on the core barrel failed, leaving the lower barrel in the mud. This meant abandoning the hole, although not tripping the pipe, for continued coring.

The intervals of excessive overpull (Fig. 3), although often deeper than about 150 m, showed no obvious correlation with age, depth, lithology, or shear strength. This intriguing and bothersome distribution made coring difficult to plan. When we encountered excessive overpull with the 9.5 m core barrel, we switched to the 5 m barrel, but even the shorter barrel was subject to excessive forces, and several of them were lost.

HEAT FLOW EXPERIMENTS

The use of heat flow probes in drill holes has been described by Erickson et al. (1975); von Rad, Ryan, et al. (1979); and Uyeda et al. (1982). Leg 85, however, was the first leg to use the heat flow tool in conjunction with the VLHPC (at Site 571). Unfortunately, the tool did not seat properly. The landing subassembly in the heat flow assembly landed on top of the piston corer seal sleeve, allowing seawater to bypass the seals and contaminate the heat flow and pore water measurements. By the time the problem was corrected we had time for only one more run, and the data were lost as a result of electronic problems. At Site 573 we attempted another heat flow measurement. This time the sandline parted while the sampler was being retrieved. The instrument was not damaged, and the pore water data obtained were valid, but the heat flow data were questionable.

BIOSTRATIGRAPHIC TIME SCALE

The Leg 85 biostratigraphic time scale (Fig. 4) incorporates the planktonic foraminiferal zones of Blow (1969), the calcareous nannofossil zones of Bukry (1975) with notation after Okada and Bukry (1980), the radiolarian zones of Nigrini (1971) and Riedel and Sanfilippo (1978), and the diatom zones of Burckle (1972) and Barron (in press and this volume). Calibration of microfossil datum levels to paleomagnetic stratigraphy follows Saito et al. (1975), Burckle (1972, 1978), Theyer et al. (1978), Haq et al. (1980), Vincent (1981), Poore et al. (1984), Berggren et al. (in press), and Theyer (unpubl. data). The absolute ages and the sequence of anomalies in the paleomagnetic time scale follow Berggren et al. (in press), and epoch and subepoch boundaries are after Van Couvering and Berggren (1977), Berggren (1983), and Berggren et al. (in press). Cross correlation of microfossil zones and subzones was adjusted slightly after study of Sites 572 to 575.

For an updated version of the time scale incorporating more information from shore-based research, see Barron et al. (this volume).

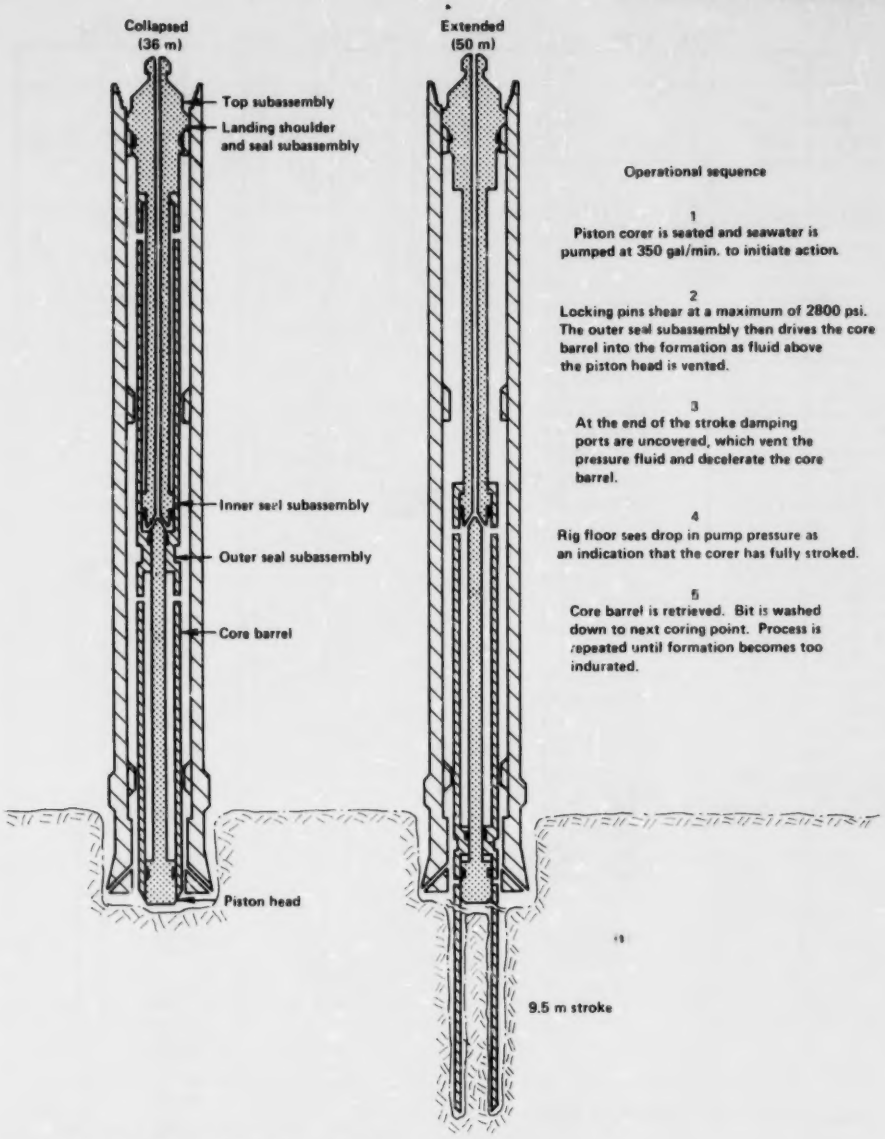
Collapsed
(36 m)
Extended
(50 m)
Top subassembly
Landing shoulder
and seal subassembly
Inner seal subassembly
Outer seal subassembly
Core barrel
Piston head
9.5 m stroke
Operational sequence
1
Piston corer is seated and seawater is pumped at 350 gal/min. to initiate action.
2
Locking pins shear at a maximum of 2800 psi. The outer seal subassembly then drives the core barrel into the formation as fluid above the piston head is vented.
3
At the end of the stroke damping ports are uncovered, which vent the pressure fluid and decelerate the core barrel.
4
Rig floor sees drop in pump pressure as an indication that the corer has fully stroked.
5
Core barrel is retrieved. Bit is washed down to next coring point. Process is repeated until formation becomes too indurated.

Figure 2. Variable length hydraulic piston corer.

In this volume, the use of Ma follows that advocated by Berggren et al. (1976).

SEDIMENT ACCUMULATION RATES

Sedimentation rates for all sites occupied on Leg 85 were calculated by using the biodatums listed in Table 1. Almost all of the datums have been correlated directly to the magnetic reversal stratigraphy (see Table 1 for references).

Sedimentation rate curves were constructed for each site by plotting the estimated age range for each core-catcher sample versus sub-bottom depth. The sedimentation rate curve was taken as the fewest number of straight-line segments that passed through all age range estimates. In each site chapter only the sedimentation rate curves are shown (not the data); however, each curve except that for Site 571 was defined from at least 30 data points.

Mean mass accumulation rates were calculated within the intervals of constant sedimentation rates. The accumulation rates for the total sediment, as well as the calcium carbonate and carbonate-free fraction, were calculated by using the mean bulk density and calcium carbonate values calculated for each interval.

CLASSIFICATION OF SEDIMENTS

The sediments are classified according to the types and proportions of their components. Component proportions are determined from smear slide observations and expressed as percentages. The terms used for (and definitions of) relative abundances are trace amounts (less than 1%), rare (1 to 5%), common (5 to 25%),

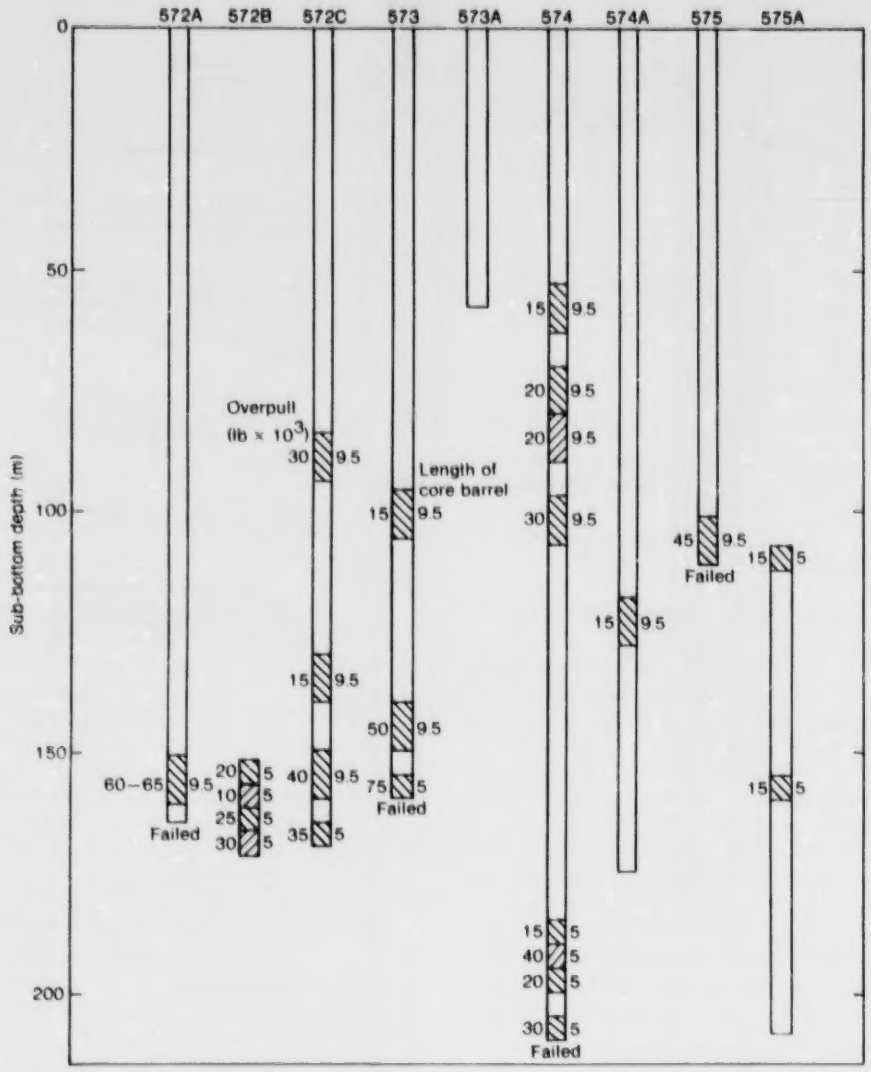

Figure 3. Intervals of excessive overpull.

abundant (25 to 75%), and dominant (greater than 75%). The percentages are estimates of areal abundances in the smear slides and may differ from the more accurate laboratory analyses of grain size, carbonate content, and mineralogy. Experience has shown that distinctive minor components can be estimated accurately (±1 to 2%) but that an accuracy of ±10% is all that can be expected for major constituents. Carbonate content is especially difficult to estimate in smear slides, as is the amount of clay-sized material present. Since Leg 85 examined pelagic sediments from the equatorial region almost exclusively, we used a classification scheme intended to emphasize recognizable differences in biogenic components (Fig. 5).

Descriptive Data

Figure 5 shows the categories into which the sediments are classified. If an individual component (calcareous nannofossils, foraminifers, radiolarians, diatoms, or pelagic nonbiogenic material) makes up more than 10% of the sediment, that component is included in the formal name of the sediment. If several components are present in amounts greater than 10%, they are listed in order from most to least abundant, up to a maximum of four names. For example, a sediment composed of 15% radiolarians, 25% foraminifers, and 55% nannofossils would be called a radiolarian foraminiferal nannofossil ooze. If a combination of either siliceous or calcareous components makes up more than 10% of a sediment, but no single component itself constitutes 10%, the modifier calcareous or siliceous is used in the name. For example, a sediment composed of 7% radiolarians, 6% diatoms, and 87% nannofossils is called a siliceous nannofossil ooze. The modifier calcareous is also used if more than 10% of the sediment consists of unrecognizable carbonate components.

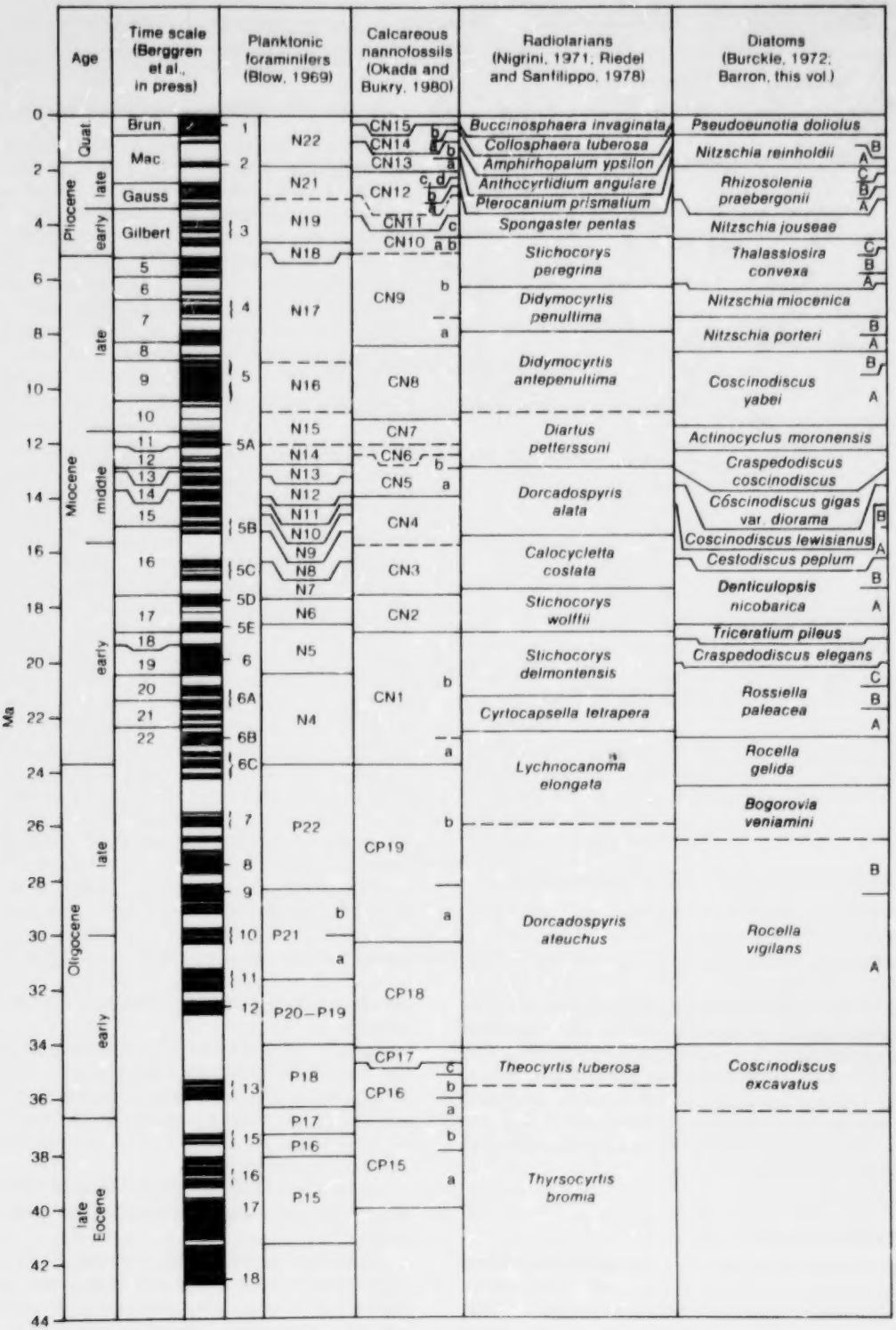

Figure 4. Biostratigraphic time scale adopted for DSDP Leg 85.

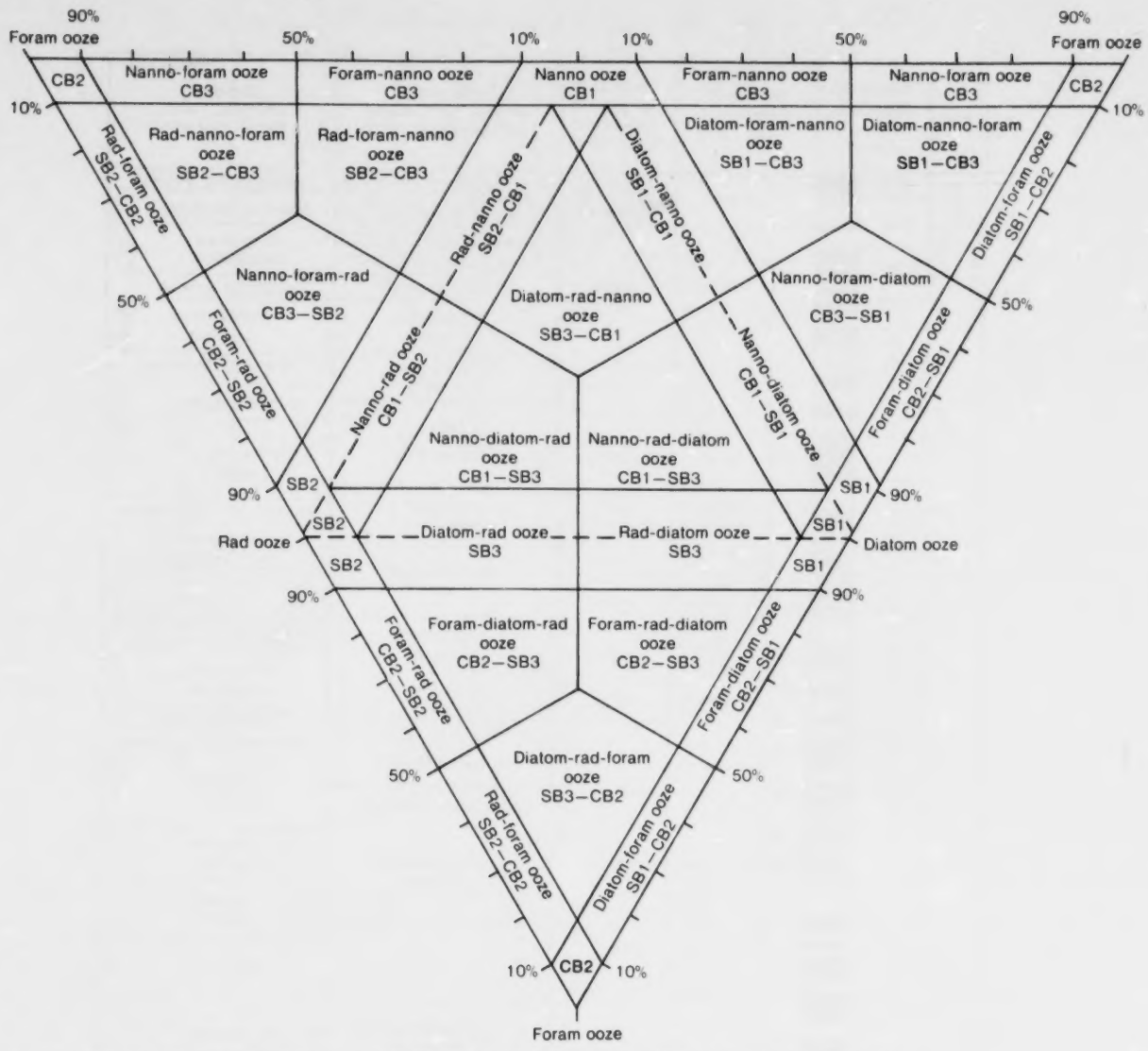

Figure 5. Sediment classification categories used in DSDP Leg 85. For an explanation of the codes, see Figure 10.

Grain-size boundaries between sand–silt and silt–clay are those described by Wentworth (1922). The grain-size estimates are probably accurate within 20 to 30%. The size of many of the nannofossils is about 4 μm, which defines the silt/clay boundary. Breakage of larger grains (foraminifers and radiolarians) during smear slide preparation probably accounts for the limited reliability of the grain-size estimates.

Induration of Sediments

Determinations of induration are highly subjective, but field geologists have successfully made such distinctions for years. Our criteria are described below. The criteria for calcareous (50% carbonate) sediments are those of Gealy et al. (1971). The criteria for other sediments are based on subjective estimates of behavior in core-cutting.

Calcareous sediments. Oozes have little strength and are readily deformed under the finger or the broad blade of a spatula. Chalks, which are partly indurated oozes, are friable and readily scratched with a fingernail or the edge of a spatula blade. Limestones are cemented and resistant to scratching.

Siliceous sediments. Oozes are as above. Cherts are impossible to scratch and must be cut with a diamond saw.

Other sediments. If the material is soft enough for the core to be split with a wire cutter, only the sediment name is used (e.g., silty clay, sand). If the core has to be sawn, the suffix "stone" is added (e.g., claystone, sandstone).

CLASSIFICATION OF IGNEOUS ROCKS

The few sections of igneous rock recovered were classified by visual inspection only. No thin sections were studied on board ship.

SHIPBOARD PALEOMAGNETIC STUDIES

The paleomagnetism of samples selected from all holes was measured on board. The sampling intervals, normally 30 to 50 cm, were adjusted according to drilling disturbance and the intensities encountered (few or no samples were taken in intervals with intensities in the range of the noise level of the magnetometer). The untreated natural remanent magnetization (NRM_0) was measured with a Digico spinner magnetometer and calibrated against a shipboard standard. The calibration was checked at least once per hour, and intensity drift was found to be insignificant. The magnetometer was driven at 2^7 or 2^8 spins (depending upon the intensity), and the noise level of the instrument was on the order of 10^{-8} G.

An absolute azimuthal Kuster orientation device was used on the VLHPC to orient the core liner photographically with respect to magnetic north. Although it was difficult to read the photographic orientation slides (as a result of pre-trip flash failure and blurring), about 57% of the records contain reasonable data. Unfortunately, onshore paleomagnetic work showed that there are systematic downcore variations in the measured declinations, and these variations make it very difficult to correlate declination with azimuthal orientation. As an example, Figure 6 shows the variation of the declination data down Cores 4 and 5 of Hole 573. Whereas the marked (x) 180° declination offsets are produced by reversals of the geomagnetic field, clockwise, as well as anticlockwise, variable rotations of different magnitude are clearly shown by the declination data. In Core 4 the gradient decreases with depth, and in Core 5 it almost stops at the lower part, being very high in the upper part. These are only a few of the possible kinds of rotation. The variations are expressions of relative motion between sediment, core liner, and possibly even the VLHPC barrel itself. Thus, if the Kuster system is usable at all, it most likely orients only the uppermost part of a twisted core, and a correction must be derived for the lower part. The device records the barrel's azimuthal orientation only once, just prior to coring, which is an unsatisfactory solution, given the multiple possibilities of the torsioning of the sediments during the coring itself. Systematic studies of these gear-induced rotations are necessary to obtain an idea of their magnitude and direction.

INORGANIC GEOCHEMISTRY

Samples were processed for the analysis of interstitial waters in the manner described by Gieskes (1973, 1974). Samples were refrigerated immediately after recovery until squeezing, which was done at room temperature. Samples from Hole 572, however, were taken after the core had reached thermal equilibrium with room temperature (approximately 10 hr.). Reactions during such extended storage at room temperature greatly reduce the reliability of the data from Hole 572.

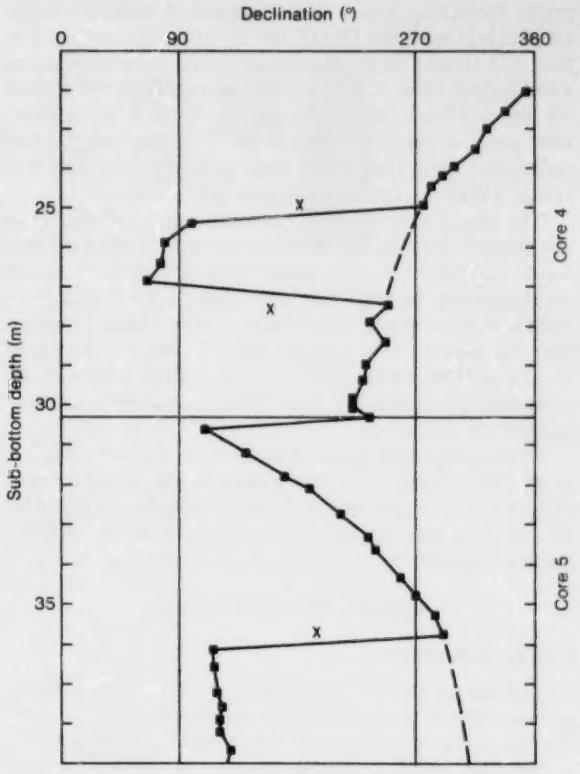

Figure 6. Downcore rotation (x) of paleomagnetic declination data produced by VLHPC coring. Hole 573.

Standard "Karbonat Bombe" shipboard techniques (as described by Müller and Gastner, 1971, and Dunn, 1980) were followed.

MEASUREMENT OF PHYSICAL PROPERTIES

Detailed measurements of physical properties were carried out at all sites. The experiments included the use of the gamma ray attenuation and porosity evaluator (GRAPE; Boyce, 1976a) to determine the saturated bulk density; the gravimetric determination of wet-bulk density and water content (Boyce, 1976a); and the measurement of sonic velocity (Boyce, 1976b), thermal conductivity (Von Herzen and Maxwell, 1959), electrical conductivity (Manheim and Waterman, 1974), and shear strength (Boyce, 1976b). The sampling interval was usually once per section (1.5 m) for all parameters, except for shear strength, which was measured once per core (9.5 or 5 m) at Sites 574 and 575. The sampling interval was generally halved in duplicate HPC sections where the first section had produced undisturbed sediments. In all cases, cores were allowed to reach thermal equilibrium before any physical properties were measured.

Thermal conductivity data were reduced from analog records at Site 572. At Site 573 and thereafter the Woods Hole Oceanographic Institution (WHOI) digital multi-

probe measuring system was employed. A well-documented problem with the DSDP needle probe system used at Site 572 results in measurement values that are somewhat higher than those generally accepted for the area. At Site 573 both the DSDP and the WHOI instruments were used. A correction factor for the DSDP probes was calculated from these data and applied to the Site 572 results (Wilkens and Handyside, this volume).

The electrical conductivity measurements suffered from occasional shifts in the baseline values of indicated seawater conductivity. The shifts were not critical to the measurement, because the formation factor is a ratio of sediment-to-seawater resistivities. Thus, absolute values may be slightly less precise than hoped for, but they should still be within 10% of true values, which is acceptable in a parameter that varies over orders of magnitude for sediments.

Gravimetric and sonic velocity data were dependable at all sites. There was some scatter in the upper reaches of Site 572, possibly as the result of sampling technique. All the data were standardized quickly, however, and the results from all the sites are generally consistent.

VISUAL DESCRIPTIONS

Coring Deformation

The use of the VLHPC greatly reduced the amount of disturbance in cores of soft sediments. Nevertheless, the following four types of disturbance were found:

Wash-in. Wash-in occurs at the top (about 1 m) of many cores and results from hole cave-in and bit motion. It is easy to recognize and does not represent a serious problem.

Liner collapse. The liners shattered occasionally, usually when we cored sediment with zones of alternating induration. Liner collapse causes severe disturbance, but it was infrequent on this leg.

Flow-in. Flow-in looks the same as it does in a standard piston core (Fig. 7). It occurs in the middle of cores and is usually bounded by sharp contacts with undisturbed sediment. The origin of flow-in is not understood, but it may be related to the lack of a breakaway piston in the VLHPC, the extreme vacuum generated by the pull-out process when the sediment does not completely fill the liner, and drill string motion.

O-rings. O-rings placed outside the liner often end up in the middle of the core. When the core is split, the splitting device drags the rings through the sediment. The problem is not serious, but it is annoying.

Mechanical disturbance in rotary-drilled sections is the result of the coring technique, which uses a large (25 cm diameter) bit with a small (6 cm diameter) opening for the core samples. The following disturbance categories were used:

Slightly deformed. Bedding contacts are slightly bent.

Moderately deformed. Bedding contacts have undergone extreme bowing, and firm sediment is fractured.

Very deformed. Bedding is extremely disturbed or homogenized, and some sections show diapir-like structures and other fluidization phenomena.

Soupy. Sediment is saturated with water and has lost all aspects of bedding.

Breccia. Indurated sediment has been broken into angular fragments by the drilling process.

The categories above are designated in the core description forms (Fig. 8) by the symbols shown in the "Drilling Disturbance" column. In rotary-drilled sections, firm sediment may also be broken into "drill biscuits" that are enclosed in a breccia or soup. These sections are not automatically designated as very deformed; they are evaluated according to the degree of displacement shown by the undeformed biscuits.

Downhole contamination occurs when sediment falls, is dragged, or is washed to a lower stratigraphic interval and then cored. This material is generally recognized by its soupy character, contrasting color, and the younger fossils it contains. Where downhole contaminants are recognized, they are marked on the core descriptions.

Sedimentary Structures

In cores of oozes (and even some indurated sediments), it may be extremely difficult to distinguish between natural structures and structures created by the coring process. Identifiable megascopic sedimentary structures include graded bedding, cross bedding, bioturbation, microfaulting, and lamination. Where it is reasonably certain that these features are not the product of coring disturbance, they are logged graphically (with the symbols shown in Fig. 9) in the "Sedimentary Structures" column of the core description form.

Bioturbation, which often includes undeformed and identifiable burrow types, is a prominent feature of many cores recovered on Leg 85. Where ichnogenera have been identified they are included in the core descriptions. The most important ichnogenera found are Planolites, Zoophycos, and Chondrites.

Color

The colors of the rocks were determined with a Munsell or Geological Society of America Rock-Color Chart immediately after the cores were split and while they were still wet.

Graphic Lithology

The graphic column on the core description form is based on the lithologies, which are represented by a single pattern or a grouping of two or more symbols (Fig. 10). The symbols in a grouping correspond to end-members of sedimentary constituents, such as clay or nannofossil ooze. The symbol for the clastic or authigenic components appears on the right side of the column, and the symbol for the biogenic constituents appears on the left side. The abundance of a component approximately equals the percentage of the width of the graphic column its symbol occupies. Since graphic lithologies represent average compositions derived from smear slides they do not, however, always reflect the detailed alternation of sediment types. Major lithologic boundaries are shown, but gradational contacts, small-scale cyclicity, and ooze–chalk alternations are represented schematically.

Because of the difference in length-to-width ratio between the actual core and the graphic lithology column it is not possible to reproduce structures as they appear

Figure 7. Flow-in in a VLHPC core (Section 2). Note the sharp contacts between disturbed and undisturbed sediments. Hole 572A, Core 13, 109.9 to 119.1 m sub-bottom.

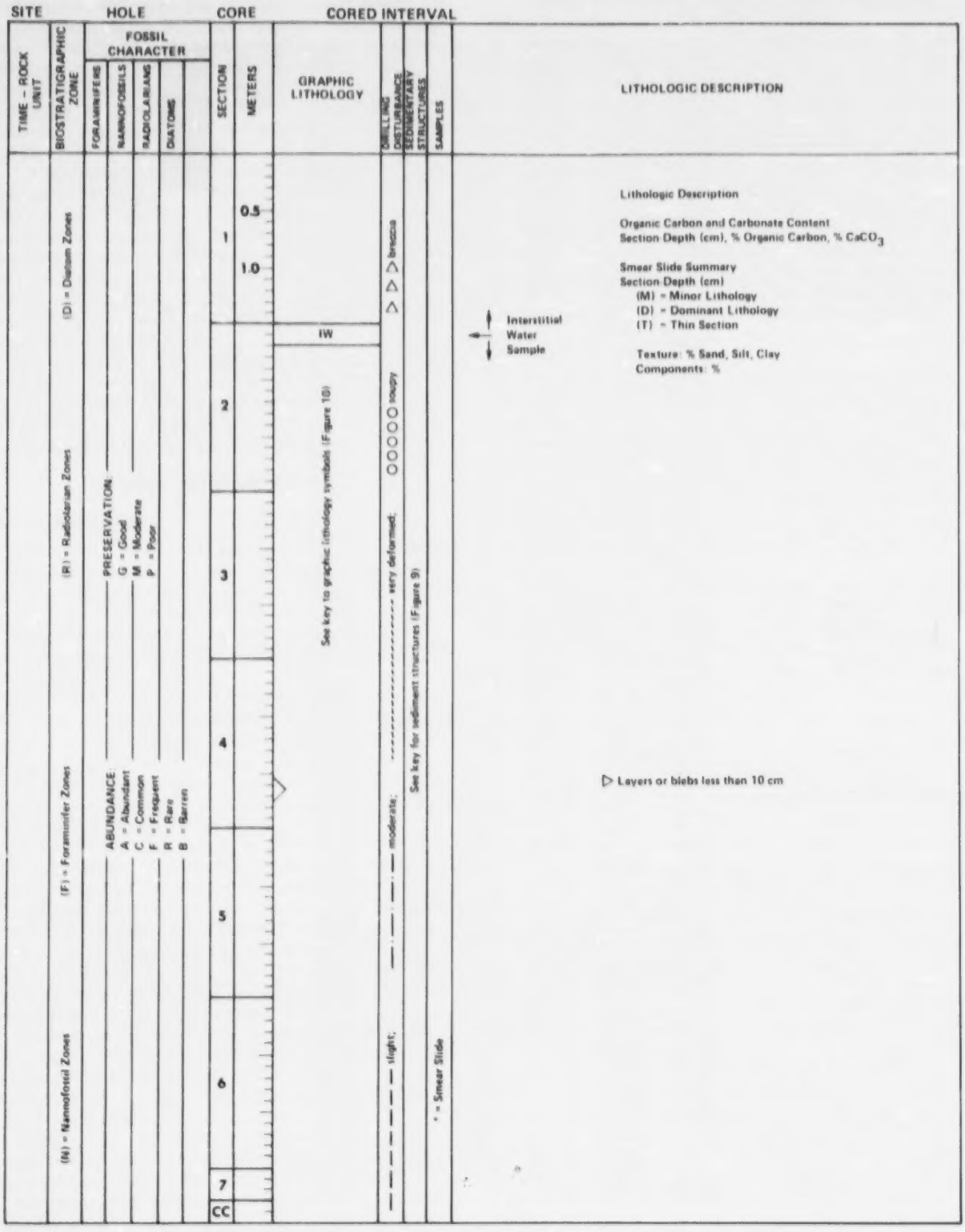

Figure 8. Sample core description form.

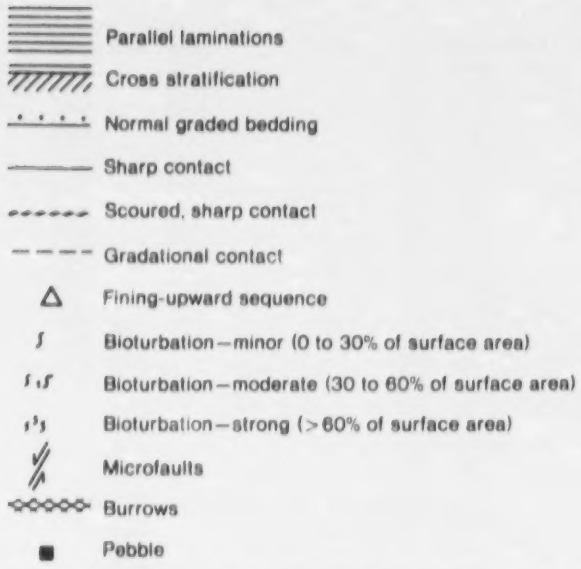

Figure 9. Symbols used in the "sedimentary structures" column of the core description form.

in the core: in the graphic representation they are highly flattened or distorted. The same is true for rock fragments or pebbles in the core. The locations of pebbles are shown by solid squares, and the depth of small patches of ash or other lithologically different components is given by a triangular inset of the appropriate lithologic symbol on the right side of the column (Figs. 8 and 10). Prominent beds thinner than 10 cm are exaggerated in thickness in the lithologic column; less prominent intervals are given in the inset. Voids of less than 10 cm are not shown.

Smear slide compositions and carbonate content (% $CaCO_3$) determined on board are listed below the core description. The locations of the samples used to make these determinations and the codes used to specify sample type are identified in the column headed "Samples" (Fig. 8). Locations and intervals of interstitial water (IW) samples are shown in the lithology column.

Igneous Rocks

All igneous rocks were split into working and archive halves with a rock saw. Descriptions are based on visual inspection only (no thin sections were made on board). Each piece is accurately drawn in the "Graphic Representation" column of the core description forms. Two closely spaced horizontal lines indicate the location of the styrofoam spacers taped between the pieces inside the liner. Each piece is numbered sequentially from the top of the section. Spacers are only placed between pieces that do not fit together.

HANDLING OF CORES

A core is normally cut into 1.5 m sections, sealed, labeled, and then brought into the shipboard core laboratory for processing. Continuous wet-bulk density determinations are made with the GRAPE before the plastic liner is split. Before the liners are split the cores are left on the rack for several hours for thermal equilibration.

The cores are then split longitudinally into working and archive halves. Samples are taken from the working half, including those used for the determination of sonic velocity (by the Hamilton Frame method), wet-bulk density (by a static GRAPE technique), water content (by gravimetric analysis), calcium-carbonate content (Karbonat Bombe), geochemistry, and paleontology.

Smear slides (or thin sections for lithified sedimentary and igneous rocks) are usually prepared from each major lithology, and slides of most minor lithologies are prepared and examined microscopically. The archive half is then described and photographed: physical disturbances, color, texture, structures, and the composition of the various lithologies are noted on standard core description forms. All raw data are routinely microfilmed, and some are digitized for computer retrieval.

After the cores are sampled and described, they are kept in cold storage on board the *Glomar Challenger* until they are transferred to the DSDP repository. Sediment sections removed for the study of organic geochemistry are frozen immediately on board and kept frozen. As of this writing (April 1983), all Leg 85 cores are at the DSDP West Coast Repository (Scripps Institution of Oceanography).

NUMBERING OF SITES, HOLES, CORES, AND SAMPLES

DSDP drill sites are numbered consecutively from the first site drilled by *Glomar Challenger* in 1968. Site numbers are slightly different from hole numbers. A site number refers to one or more holes drilled while the ship is positioned over one acoustic beacon; these holes can be located within a radius as great as 900 m from the beacon. Several holes may be drilled at a single site by pulling the drill pipe above the seafloor (above one hole), moving the ship 100 m or more from the previous hole, and then drilling another hole.

The first (or only) hole drilled at a site takes the site number. A letter suffix distinguishes each additional hole at the same site. Thus, the first hole takes only the site number, the second takes the site number with suffix A, the third takes the site number with suffix B, and so forth. It is important, for sampling purposes, to distinguish between the holes drilled at a site, because the sediments or rocks at a given depth in different holes usually come from different positions in the stratigraphic column. Correlations between cores drilled on Leg 85 are given in Figure 11.

The cored interval is measured in meters below the seafloor. The depth interval of an individual core spans from the depth below seafloor at which the coring began to the depth at which coring ended. The nominal coring interval is 9.5 m long during rotary drilling and for the VLHPC's long barrel. It is 5 m for the VLHPC's short barrel. In practice, these coring intervals may be shorter or slightly longer. For example, when we encountered excessive overpull at Site 575, we rerigged the 5 m VLHPC barrel and washed 5 m, pulling up the corer 2 m between each core. In this way the corer traveled

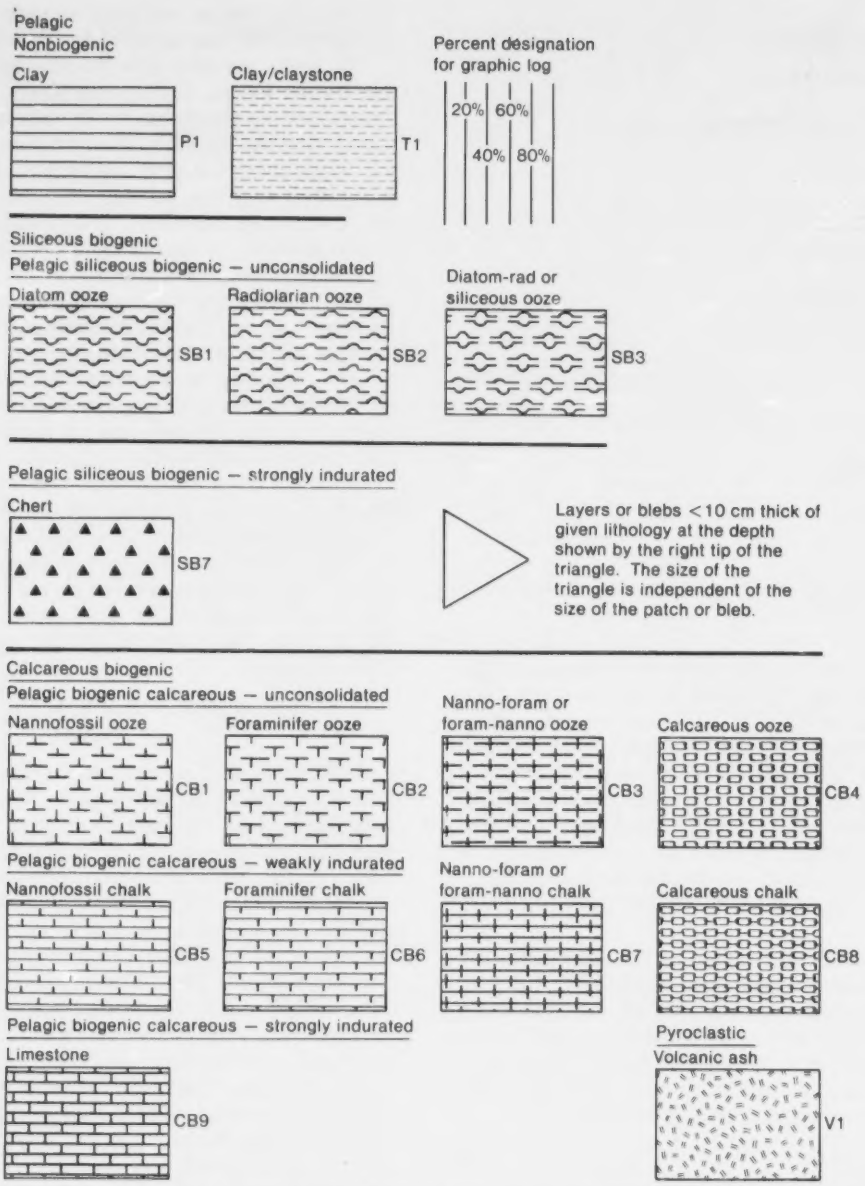

Figure 10. Symbols used in the "graphic lithology" column of the core description form. Acronyms are pattern numbers.

through 2 m of wash and 3 m of previously uncored material, collecting, in essence, a 3 m core.

Cored intervals are not necessarily adjacent to each other, but may be separated by drilled intervals. In soft sediment the drill string can be "washed ahead": that is, the core barrel is in place, but does not recover sediment. This is achieved by pumping water down the pipe at high pressure, which washes the sediment out of the way of the bit, up the space between the drill pipe and the wall of the hole. During this procedure fragments of resistant layers may be caught in the core barrel, so the cored interval may be greater than 9.5 m.

When full, a core normally recovers 9.28 m of sediment or rock in a plastic liner with a 6.6 cm inner diameter. In addition, there is about 0.2 m of sediment or rock (no plastic liner) in the core catcher. With the short barrel of the VLHPC, about 4.75 m are collected in the liner when it is full, and about 0.2 m is collected in the core catcher. The core catcher is a device at the bottom of the core barrel that prevents the cored sample from sliding out when the barrel is being retrieved from the hole.

Each core is cut into 1.5 m long sections, which are numbered serially from the top of the core (Fig. 12).

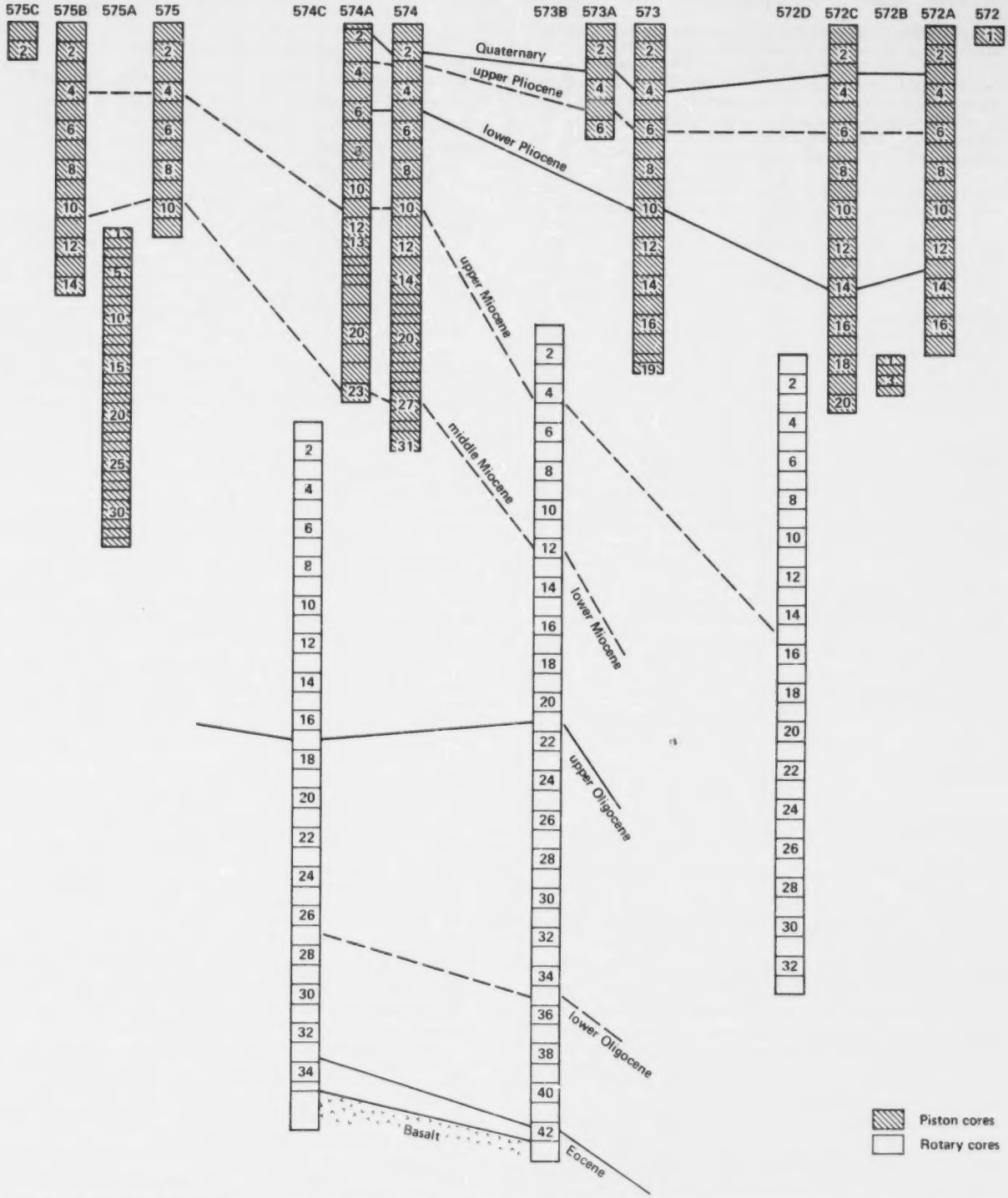

Figure 11. Correlations between the cores recovered on DSDP Leg 85. Solid lines indicate boundaries between time units (e.g., Miocene/Pliocene); dashed lines indicate boundaries between subdivisions of time units (e.g., middle/lower Miocene). Note that the deepest sediments cored in Hole 572D are basal middle Miocene.

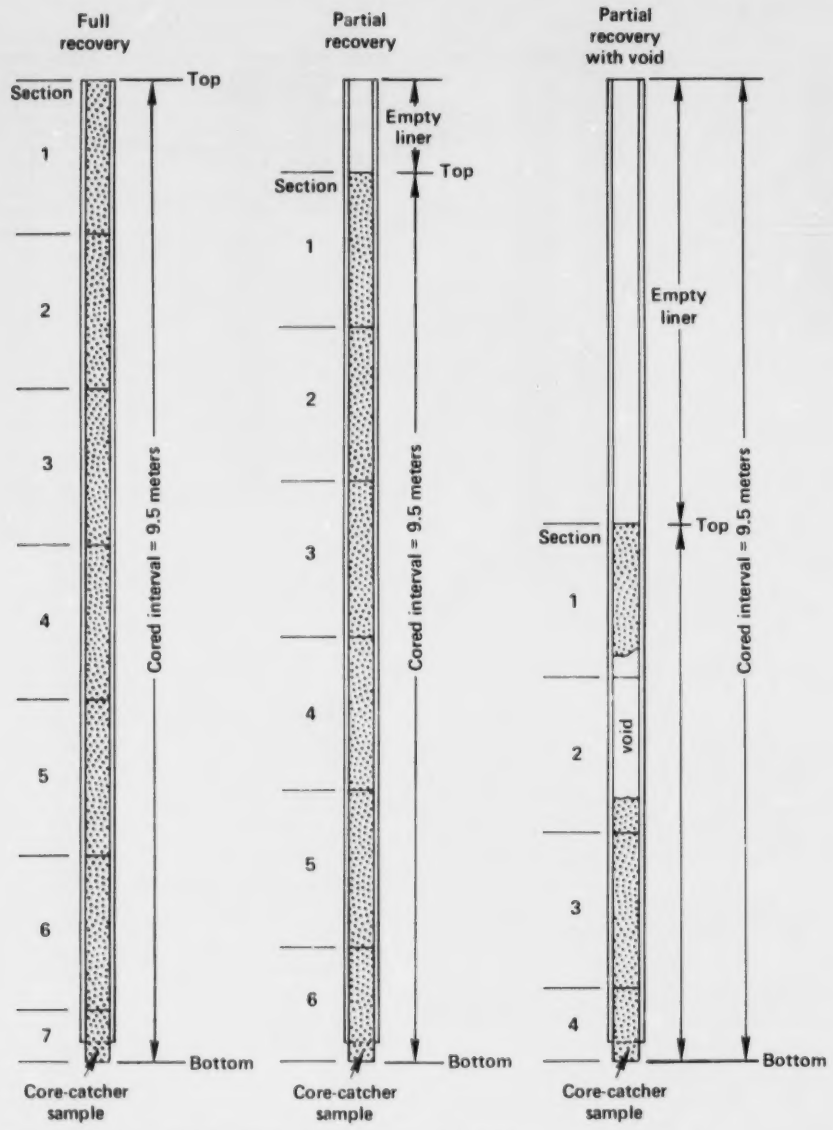

Figure 12. Conventions for cutting and labeling core sections.

When recovery is full, the sections are numbered from 1 through 7 for rotary drilled and long-barrel VLHPC cores, 1 through 4 for short-barrel VLHPC cores. In each case last section is shorter than 1.5 m. The core-catcher sample is placed below the last section when the core is described and labeled core catcher (CC); it is treated as a separate section.

In the case of partial recovery, the original stratigraphic position of the sediment in the cored interval is unknown. If the recovered rocks and sediments are contiguous, the top of this material becomes the top of the cored interval. Section numbering is serial, begins at the top with Section 1 (Fig. 12), and ends when the recovered sediment is accommodated. For example, 4 m of sediment are divided into three sections—two upper sections 1.5 m long and one lower section 1 m long. If the sediment is determined to be discontinuous by the shipboard scientists, sections are divided and numbered serially, but gaps are labeled voids (as in Fig. 12). In igneous sections, voids are marked with spacers.

Cores taken from a hole are numbered serially from the top of the hole downward. The assignment of core numbers and associated depths in meters below the seafloor is usually straightforward, although problems may arise if an interval is cored twice.

Samples are designated by centimeter distances from the top of each section to the top and bottom of the sample in the section. A complete sample number consists of leg-site-hole-core-section, interval in centimeters. For instance, Sample 85-574C-12-3, 12–14 cm is taken 12–14 cm from the top of Section 3 of Core 12, from the fourth hole drilled at Site 574 during Leg 85. A

sample from the core catcher of this core is designated 85-574C-12,CC.

OBTAINING SAMPLES

Investigators who want to obtain samples should refer to the DSDP–NSF Sample Distribution Policy (see the front matter for this volume). Requests must be as specific as possible and include site, core, section, interval within a section, and volume of samples required.

REFERENCES

Arrhenius, G. O., 1952. Sediment cores from the east Pacific. *Rep. Swed. Deep Sea Exped., 1947–1948*, 5(3):189–201.

Barron, J. A., Keller, G., Dunn, D. A., Kennett, J. P., Lombari, G., Burckle, L. H., and Vincent, E., in press. A multiple microfossil biochronology for the Miocene. *In* Kennett, J. P. (Ed.), *Cenozoic Paleoceanography Synthesis (CENOP)*, Mem. Geol. Soc. Am.

Berger, W. H., 1973. Cenozoic sedimentation in the eastern tropical Pacific. *Geol. Soc. Am. Bull.*, 84:1941–1954.

Berggren, W. A., 1983. Correlation of Atlantic, Mediterranean and Indo-Pacific Neogene stratigraphies: geochronology and chronostratigraphy. *IGCP Project 114: International Workshop on Pacific Neogene Biostratigraphy* (Osaka and Kobe, Japan), November 24–29, 1981.

Berggren, W. A., Benson, R. H., Haq, B. U., Riedel, W. R., Sanfilippo, A., et al., 1976. The El Cuervo section (Andalusia, Spain): micropaleontologic anatomy of an early late Miocene lower bathyal deposit. *Mar. Micropaleontol.*, 1:195–247.

Berggren, W. A., Kent, D. V., and Flynn, J. J., in press. Paleogene geochronology and chronostratigraphy. *In* Snelling, N. J. (Ed.), *Geochronology and the Geological Record*, Spec. Pap. Geol. Soc. London.

Blow, W. H., 1969. Late middle Eocene to Recent planktonic foraminiferal biostratigraphy. *In* Brönniman, P., and Renz, H. H. (Eds.), *Proc. First Internat. Conf. Planktonic Microfossils*: Leiden (Brill), pp. 199–422.

Boyce, R. E., 1976a. Definitions and laboratory techniques of compressional sound velocity parameters and wet-water content, wet-bulk density, and porosity parameters by gravimetric and gamma ray attenuation techniques. *In* Schlanger, S. O., Jackson, E. D., et al., *Init. Repts. DSDP*, 33: Washington (U.S. Govt. Printing Office), 931–958.

_____, 1976b. Deep Sea Drilling Project procedures for shear strength measurement of clayey sediment using modified Wykeham Farrance Laboratory vane apparatus. *In* Barker, P. F., Dalziel, I. W. D., et al., *Init. Repts. DSDP*, 36: Washington (U.S. Govt. Printing Office), 1059–1068.

Bramlette, M. N., 1961. Pelagic sediments. *Oceanography*: Washington, D.C. (Am. Assoc. Adv. Sci.), pp. 345–366.

Bukry, D., 1975. Coccolith and silicoflagellate stratigraphy, northwestern Pacific Ocean, Deep Sea Drilling Project, Leg 32. *In* Larson, R. L., Moberly, R., et al., *Init. Repts. DSDP*, 32: Washington (U.S. Govt. Printing Office), 677–701.

Burckle, L. H., 1972. Late Cenozoic planktonic diatom zones from the eastern equatorial Pacific. *Nova Hedwigia Beih.*, 39:217–246.

_____, 1977. Pliocene and Pleistocene diatom datum levels for the equatorial Pacific. *Quat. Res.*, 7:330–340.

_____, 1978. Early Miocene to Pliocene datum levels for the equatorial Pacific. *Proc. Second Working Group Mtg., IGCP Proj. 114, Biostratigraphic Datum Planes of the Pacific Neogene* (Bandung, Indonesia), pp. 25–44.

Burckle, L. W., Hammond, S. R., and Seyb, S. M., 1978. A stratigraphically important new diatom from the Pleistocene of the North Pacific. *Pac. Sci.*, 32:209–214.

Burckle, L. W., and Trainer, J., 1979. Middle and late Pliocene datum levels from the central Pacific. *Micropaleontology*, 25:281–293.

Casey, R. E., and Reynolds, R. A., 1980. Late Neogene radiolarian biostratigraphy related to magnetostratigraphy and paleoceanography with suggested cosmopolitan radiolarian datums. *Spec. Publ. Cushman Found. Foraminiferal Res.*, 19:287–300.

Dunn, D. A., 1980. Revised techniques for quantitative calcium carbonate analysis using the "Karbonate Bombe," and comparisons to other quantitative analysis methods. *J. Sediment. Petrol.*, 50: 631–637.

Embley, R. W., and Johnson, D. A., 1980. Acoustic stratigraphy and biostratigraphy of Neogene carbonate horizons in the north equatorial Pacific. *J. Geophys. Res.*, 85(B10):5423–5437.

Erickson, A. J., Von Herzen, R. P., Sclater, J. G., Girdler, R. W., Marshall, B. W., and Hyndman, R., 1975. Geothermal measurements in deep-sea drill holes. *J. Geophys. Res.*, 80:2515–2528.

Ewing, J., Ewing, M., Aitkeu, T., and Ludwig, W. J., 1968. North Pacific sediment layers measured by seismic profiling. *Am. Geophys. Union Monogr.*, 12:147–186.

Gartner, S., 1973. Absolute chronology of the late Neogene calcareous nannofossil succession in the equatorial Pacific. *Geol. Soc. Am. Bull.*, 84:2021–2034.

Gealy, E. L., Winterer, E. L., and Moberly, R., 1971. Methods, conventions and general observations. *In* Winterer, E. L., Riedel, W. R., et al., *Init. Repts. DSDP*, 7, Pt. 2: Washington (U.S. Govt. Printing Office), 9–26.

Gieskes, J. M., 1973. Interstitial water studies, Leg 15—alkalinity, pH, Mg, Ca, Si, PO_4. *In* Heezen, B. C., MacGregor, I. D., et al., *Init. Repts. DSDP*, 20: Washington (U.S. Govt. Printing Office), 813–829.

_____, 1974. Interstitial water studies, Leg 25. *In* Simpson, E. S. W., Schlich, R., et al., *Init. Repts. DSDP*, 25: Washington (U.S. Govt. Printing Office), 361–394.

Haq, B. U., Worsley, T. R., Burckle, L. H., Douglas, R. G., Keigwin, L. D., Jr., Opdyke, N. D., Savin, S. M., Sommer, M. A., II, Vincent, E., and Woodruff, F., 1980. Late Miocene marine carbon-isotope shift and synchroneity of some phytoplanktonic biostratigraphic events. *Geology*, 8:427–431.

Hays, J. D., 1970. Stratigraphy and evolutionary trends of Radiolaria in North Pacific deep-sea sediments. *Mem. Geol. Soc. Am.*, 126: 185–218.

Hays, J. D., Cook, H. E., III, Jenkins, D. G., Cook, F. M., Fuller, J. T., and Shipboard Scientific Party, 1972. An interpretation of the geologic history of the eastern equatorial Pacific from the drilling results of *Glomar Challenger*, Leg 9. *In* Hays, J. D., et al., *Init. Repts. DSDP*, 9: Washington (U.S. Govt. Printing Office), 909–931.

Hays, J. D., Saito, T., Opdyke, N. D., and Burckle, L. H., 1969. Pliocene–Pleistocene sediments of the equatorial Pacific: their paleomagnetic, biostratigraphic and climatic record. *Geol. Soc. Am. Bull.*, 80:1481–1514.

Henry, K. W., and Opdyke, N. D., 1970. Paleomagnetism of specimens from Leg 3 of the Deep Sea Drilling Project. *In* Maxwell, A. E., Von Herzen, R., et al., *Init. Repts. DSDP*, 3: Washington (U.S. Govt. Printing Office), 667–696.

Johnson, D. A., and Knoll, A. H., 1974. Absolute ages of Quaternary radiolarian datum levels in the equatorial Pacific. *Quat. Res.*, 5: 99–110.

Manheim, F. T., and Waterman, L. S., 1974. Diffusimetry (diffusion coefficient estimation) on sediment cores by resistivity probe. *In* von der Borch, C. C., Sclater, J. G., et al., *Init. Repts. DSDP*, 22: Washington (U.S. Govt. Printing Office), 633-670.

Mayer, L. A., 1979a. The origin of fine scale acoustic stratigraphy in deep-sea carbonates. *J. Geophys. Res.*, 84(B11):6177–6184.

_____, 1979b. Deep-sea carbonates: acoustic, physical and stratigraphic properties. *J. Sediment. Petrol.*, 49(3):819–836.

Müller, G., and Gastner, M., 1971. The "Karbonat-Bombe," a simple device for the determination of the carbonate content in sediments, soils, and other materials. *Neues Jahrb. Mineral. Monatsh.*, 10: 466–469.

Nigrini, C., 1971. Radiolarian zones in the Quaternary of the equatorial Pacific Ocean. *In* Funnell, B. M., and Riedel, W. R. (Eds.), *The Micropaleontology of the Oceans*: Cambridge (Cambridge Univ. Press), pp. 443–461.

Okada, H., and Bukry, D., 1980. Supplementary modification and introduction of code numbers to the low-latitude coccolith biostratigraphic zonation (Bukry, 1973; 1975), *Mar. Micropaleontol.*, 5: 321–325.

Poore, R. Z., Tauxe, L., Percival, S. F., Jr., LaBrecque, J. L., Wright, R., Petersen, N. P., Smith, C. C., Tucker, P., and Hsü, K. J., 1984. Late Cretaceous–Cenozoic magnetostratigraphic and biostratigraphic correlations for the South Atlantic Ocean, Deep Sea Drilling Project Leg 73. *In* Hsü, K. J., LaBrecque, J. L., et al., *In-*

it. Repts. DSDP, 73: Washington (U.S. Govt. Printing Office), 645–656.

Prell, W. L., Gardner, J. V., et al., 1982. *Init. Repts. DSDP*, 68: Washington (U.S. Govt. Printing Office).

Riedel, W. R., and Funnell, B. M., 1964. Tertiary sediment cores and microfossils from the Pacific Ocean floor. *Q. J. Geol. Soc. London*, 120:305–368.

Riedel, W. R., and Sanfilippo, A., 1978. Stratigraphy and evolution of tropical Cenozoic radiolarians. *Micropaleontology*, 23:61–96.

Ryan, W. B. F., Cita, M. B., Dreyfuss, R. M., et al., 1974. A paleomagnetic assignment of Neogene stage boundaries and the development of synchronous datum planes between the Mediterranean, the Pacific and Indian oceans in order to investigate the response of the world oceans to the Mediterranean Salinity Crisis. *Riv. Ital. Paleontol.*, 80:631–688.

Saito, T., Burckle, L. H., and Hays, J. D., 1975. Late Miocene to Pleistocene biostratigraphy of equatorial Pacific sediments. *In* Saito, T., and Burckle, L. H. (Eds.), *Late Neogene Epoch Boundaries*: New York (Micropaleontology Press), pp. 226–244.

Theyer, F., Mato, C. Y., and Hammond, B. R., 1978. Paleomagnetic and geochronologic calibration of latest Oligocene to Pliocene radiolarian events, equatorial Pacific. *Mar. Micropaleontol.*, 3: 377–395.

Thierstein, H. R., Geitzenauer, K., Molfino, B., et al., 1977. Global synchroneity of late Quaternary coccolith datums: validation by oxygen isotopes. *Geology*, 5:400–404.

Thompson, P. R., 1976. Planktonic foraminiferal dissolution and the progress towards a Pleistocene equatorial Pacific transfer function. *J. Foraminiferal Res.*, 6:208–277.

Uyeda, S., and Horai, K., 1982. Heat flow measurements on Deep Sea Drilling Project Leg 60. *In* Hussong, D. M., Uyeda, S., et al., *Init. Repts. DSDP*, 60: Washington (U.S. Govt. Printing Office), 789–800.

van Andel, T. H., Heath, G. R., and Moore, T. C., Jr., 1975. Cenozoic history and paleoceanography of the central equatorial Pacific. *Mem. Geol. Soc. Am. 143*.

Van Couvering, J. A., and Berggren, W. A., 1977. Biostratigraphic basis of the Neogene time scale. *In* Kaufmann, E. G., and Hazel, J. E. (Eds.), *Concepts and Methods in Biostratigraphy*: Stroudsburg, PA (Dowden, Hutchinson, Ross), pp. 283–306.

Vincent, E. S., 1981. Neogene stratigraphy of Hess Rise (central North Pacific) and paleoceanographic implications. *In* Thiede, J., Vallier, T. L., et al., *Init. Repts. DSDP*, 62: Washington (U.S. Govt. Printing Office), 571–606.

Von Herzen, R. P., and Maxwell, A. E., 1959. The measurement of thermal conductivity of deep-sea sediments by a needle probe method. *J. Geophys. Res.*, 64:1557–1563.

von Rad, U., Ryan, W. B. F., et al., 1979. *Init. Repts. DSDP*, 47, Pt. 1: Washington (U.S. Govt. Printing Office).

Wentworth, C. K., 1922. A scale of grade and class terms of clastic sediments. *J. Geol.*, 30:377–392.

Winterer, E. L., 1973. Sedimentary facies and plate tectonics of the equatorial Pacific. *Am. Assoc. Pet. Geol. Bull.*, 57:265–282.

Date of Initial Receipt: 29 April 1983
Date of Acceptance: 1 July 1983

Table 1. Biodatums used to calculate accumulation rates for Leg 85 sites.

Fossil group[a]	Datum[b]	Age (Ma)[c]	References
F	T *Globigerina pseudofoliata*	0.2	Saito et al. (1975)
R	B *Buccinosphaera invaginata*	0.3	Johnson and Knoll (1974)
R	T *Stylatractus universus*	0.44	Hays
N	T *Pseudoemiliania lacunosa*	0.47	Thierstein et al. (1977)
F	T *Globorotalia tosaensis*	0.6	Thompson (1976)
D	T *Nitzschia reinholdii*	0.65	Burckle (1977)
D	T *Rhizosolenia matuyamai*	0.93	Burckle et al. (1978)
D	B *Rhizosolenia matuyamai*	1.0	Burckle et al. (1978)
R	T *Anthocyrtidium angulare*	1.1	Johnson and Knoll (1974)
R	T *Lamprocyrtis neoheteroporos*	1.15	Johnson and Knoll (1974)
F	T *Pulleniatina finalis*	1.3	Saito et al. (1975)
R	B *Theocorythium trachelium*	1.35	Johnson and Knoll (1974)
R	T *Pterocanium prismatium*	1.5	Theyer et al. (1978)
D	T *Rhizosolenia praebergonii robusta*	1.55	Burckle (1977)
F	T *Globigerinoides fistulosus*	1.6	Saito et al. (1975)
F	T *Globigerinoides obliquus*	1.7	Saito et al. (1975)
D	B *Pseudoeunotia doliolus*	1.8	Burckle (1977)
F	B *Globorotalia truncatulinoides*	1.9	Saito et al. (1975)
R	T *Lamprocyclas heteroporos*	2.0	Hays (1970)
D	T *Thalassiosira convexa*	2.1	Burckle and Trainer (1979)
R	T *Stichocorys peregrina*	2.4	Theyer et al. (1978)
D	T *Nitzschia jouseae*	2.6	Burckle and Trainer (1979)
F	T *Globoquadrina altispira*	2.9	Hays et al. (1969)
D	B *Rhizosolenia praebergonii*	3.0	Burckle and Trainer (1979)
F	T *Sphaeroidinellopsis seminulina*	3.05	Saito et al. (1975), Hays et al. (1969)
F	B *Globorotalia tosaensis*	3.2	Hays et al. (1969)
R	T *Spongaster pentas*	3.4	Theyer et al. (1978)
F	T *Globorotalia margaritae*	3.4	Saito et al. (1975), Hays et al. (1969)
D	B *Thalassiosira convexa convexa*	3.6	Burckle and Trainer (1979)
R	B *Spongaster tetras*	3.6	Theyer et al. (1978)
R	T *Didymocyrtis penultima*	3.69	Theyer et al. (1978)
F	T *Globigerina nepenthes*	3.85	Saito et al. (1975), Hays et al. (1969)

Table 1. (Continued).

Fossil group[a]	Datum[b]	Age (Ma)[c]	References
D	B *Acteromphalus elegans*	3.9	Burckle (1978)
R	B *Lamprocyclas heteroporos*	4.3	Casey and Reynolds (1980)
R	B *Spongaster pentas*	4.3	Theyer et al. (1978)
D	T *Nitzschia cylindrica*	4.35	Burckle (pers. comm., 1983)
D	B *Nitzschia jouseae*	4.5	Burckle (1978)
N	B *Ceratolithus rugosus*	4.75	Burckle (1978)
R	B *Pterocanium prismatium*	4.8	Theyer et al. (1978)
F	B *Sphaeroidinella dehiscens*	5.0	Saito et al. (1975)
R	T *Acrobotrys tritubus*	5.0	Theyer et al. (1978)
D	T *Thalassiosira miocenica*	5.05	Burckle (1978)
F	B *Globorotalia tumida*	5.2	Saito et al. (1975)
F	T *Globoquadrina dehiscens*	5.4	Saito et al. (1975)
D	T *Asterolampra acutiloba*	5.4	Burckle (1978)
N	B *Ceratolithus acutus*	5.65	Gartner (1973)
D	T *Nitzschia miocenica*	5.7	Burckle (1978)
D	T *Thalassiosira praeconvexa*	5.9	Burckle (1978)
F	B *Globorotalia margaritae*	6.0	Saito et al. (1975)
D	B *Thalassiosira convexa* var. *aspinosa*	6.15	Burckle (1978)
D	B *Thalassiosira miocenica*	6.15	Burckle (1978)
F	B *Pulleniatina primalis*	6.2	Saito et al. (1975)
D	B *Thalassiosira praeconvexa*	6.4	Burckle (1978)
R	B *Stichocorys peregrina*	6.4	Theyer et al. (1978)
R	B *Solenosphaera omnitubus*	6.6	Theyer et al. (1978)
D	B *Nitzschia miocenica*	7.4	Burckle (1978)
D	T *Rossiella paleacea*	7.5	Burckle (1978)
N	B *Discoaster quinqueramus*	7.6	Gartner (1973)
D	T *Thalassiosira burckliana*	7.9	Burckle (1978)
R	B *Didymocyrtis penultima*	8.2	Theyer et al. (1978)
R	T *Diartus hughesi*	8.2	Theyer et al. (1978)
D	T *Coscinodiscus yabei*	8.6	Burckle (1978)
D	B *Thalassiosira burckliana*	9.2	Burckle (1978)
R	T *Diartus petterssoni*	9.7	Theyer et al. (1978)
F	B *Neogloboquadrina acostaensis*	10.8	Ryan et al. (1974)
N	T *Discoaster hamatus*	11.1	Burckle (1978)
D	B *Coscinodiscus vetustissimus javanica*	11.1	Burckle (1978)
R	B *Acrobotrys tritubus*	11.2	Theyer et al. (1978)
D	T *Actinocyclus ellipticus moronensis*	11.4	Burckle (1978)
R	B *Didymocyrtis antepenultima*	11.5	Theyer et al. (1978)
R	B *Diartus hughesi*	11.5	Theyer et al. (1978)
R	T *Stichocorys wolffii*	11.6	Theyer et al. (1978)
R	T *Cyrtocapsella cornuta*	11.8	Theyer et al. (1978)
R	T *Dorcadospyris alata*	11.8	Theyer et al. (1978)
F	T *Turborotalia mayeri*	12.0	Ryan et al. (1974)
D	T *Coscinodiscus tuberculatus*	12.0	Burckle (1978)
D	T *Denticula punctata hustedtii*	12.2	Burckle (1978)
R	B *Diartus petterssoni*	12.3	Theyer et al. (1978)
D	T *Craspedodiscus coscinodiscus*	12.3	Burckle (1978)
R	T *Cyrtocapsella tetrapera*	12.5	Theyer et al. (1978)
F	B *Globigerina nepenthes*	12.7	Ryan et al. (1974)
D	B *Hemidiscus cuneiformis*	12.7	Burckle (1978)
D	T *Denticulopsis nicobarica*	13.1	Burckle (1978)
D	T *Coscinodiscus lewisianus*	13.8	Burckle (1978)
R	B *Didymocyrtis laticonus*	13.8	Theyer et al. (1978)
R	B *Lithopera neotera*	14.2	Theyer et al. (1978)
D	T *Cestodiscus peplum*	14.3	Burckle (1978)
D	B *Coscinodiscus tuberculatus*	14.4	Burckle (1978)
R	T *Calocycletta virginis*	14.8	Theyer et al. (1978)
D	T *Annellus californicus*	15.0	Burckle (1978)
R	T *Calocycletta costata*	15.4	Theyer et al. (1978)
R	B *Dorcadospyris alata*	15.7	Theyer et al. (1978)
R	T *Dorcadospyris dentata*	15.8	Theyer et al. (1978)
R	T *Didymocyrtis prismatica*	15.8	Barron et al. (in press)
R	T *Lychnocanoma elongata*	15.9	Barron et al. (in press)
D	T *Thalassiosira fraga*	16.2	Barron et al. (in press)
R	B *Calocycletta costata*	16.8	Theyer et al. (1978)
R	B *Dorcadospyris dentata*	17.1	Theyer et al. (1978)
D	B *Denticulopsis nicobarica*	18.0	Barron et al. (in press)
R	B *Stichocorys wolffii*	18.9	Barron et al. (in press)
R	T *Dorcadospyris ateuchus*	19.7	Theyer et al. (1978)
D	T *Bogorovia veniamini*	19.9	Burckle (pers. comm., 1982)
R	B *Cyclampterium leptetrum*	20.0	Theyer et al. (1978)
R	B *Didymocyrtis violina*	20.2	Theyer et al. (1978)
R	B *Stichocorys delmontensis*	21.1	Barron et al. (in press)

Table 1. (Continued).

Fossil group[a]	Datum[b]	Age (Ma)[c]	References
R	T *Theocyrtis annosa*	21.3	Theyer et al. (1978)
R	B *Calocycletta virginis*	21.4	Theyer et al. (1978)
N	T *Triquetrorhabdulus carinatus*	21.8	Theyer (unpubl. data)
R	B *Cyrtocapsella cornuta*	22.2	Barron et al. (in press)
R	T *Cyrtocapsella tetrapera*	22.2	Barron et al. (in press)
R	T *Dorcadospyris papilio*	22.6	Barron et al. (in press)
R	T *Artophormis gracilis*	22.6	Barron et al. (in press)
N	B *Discoaster druggi*	22.8	Theyer (unpubl. data)
N	T *Sphenolithus ciperoensis*	23.7	Poore et al. (1984)
F	B *Globigerapsis kugleri*	23.7	Poore et al. (1984)
R	B *Dorcadospyris praeforcipata*	25.7	Theyer (unpubl. data)
R	B *Lychnocanoma elongata*	25.9	Theyer et al. (1978)
N	T *Sphenolithus distentus*	26.7	Theyer (unpubl. data)
F	T *Globorotalia opima*	28.3	Poore et al. (1984)
N	B *Sphenolithus ciperoensis*	30.2	Poore et al. (1984)
N	T *Sphenolithus pseudoradians*	31.0	Poore et al. (1984)
R	B *Dorcadospyris papilio*	31.6	Theyer (unpubl. data)
N	B *Sphenolithus distentus*	34.1	Poore et al. (1984)
R	B *Dorcadospyris ateuchus*	34.4	Theyer (unpubl. data)
N	T *Reticulofenestra hillae*	34.7	Poore et al. (1984)
N	T *Reticulofenestra umbilica*	34.7	Poore et al. (1984)
N	T *Cyclococcolithina formosa*	35.1	Poore et al. (1984)
R	B *Artophormis gracilis*	36.3	Theyer (unpubl. data)
F	T *Turborotalia cerroazulensis*	36.3	Poore et al. (1984)
N	T *Discoaster barbadiensis*	36.8	Poore et al. (1984)
N	T *Discoaster saipanensis*	36.8	Poore et al. (1984)

[a] F = foraminifers, R = radiolarians, N = nannofossils, D = diatoms.
[b] T = top of range, B = bottom of range.
[c] Ages follow an interim (unpublished) time scale of Berggren et al., widely circulated in 1983. This time scale is similar to a revised scale now in press (Berggren, in press), except that in the later version Anomaly 5 is correlated with Chron 11 instead of Chron 9. See Barron et al. (this volume) for the updated time scale.

2. SITE 571[1]

Shipboard Scientific Party[2]

HOLE 571

Date occupied: 19 March 1982

Date departed: 21 March 1982

Time on hole: 50 hr., 2 min.

Position: 03°59.84′N,114°08.53′W

Water depth (sea level; corrected m, echo-sounding): 3962

Water depth (rig floor; corrected m, echo-sounding): 3972

Bottom felt (m, drill pipe): 3969.5

Penetration (m): 199.5

Number of cores: 1

Total length of cored section (m): 7.11

Total core recovered (m): 7.11

Core recovery (%): 100

Oldest sediment cored:
Depth sub-bottom (m): 7.11
Nature: Light yellow brown foraminifer nannofossil ooze
Age: Pleistocene
Measured velocity (km/s): 1.55

Basement: Not reached

Principal results: Technical difficulties (see Operations) made it impossible to achieve the primary objectives of Site 571, which were to make downhole heat-flow measurements and to sample pore water to maximum hydraulic piston corer (HPC) penetration depth. A first interpretation of the heat-flow measurements suggests that the heat-flow/pore-water probe sampled and measured seawater instead of sub-bottom sediments. This idea is corroborated by initial chemical analyses of the water collected by the probe.

Technical difficulties also delayed operations to the point where only one HPC core, the mudline core, was recovered. Core 1 is 7.11 m long, and it is entirely composed of calcareous to siliceous-calcareous oozes of Quaternary age. It contains (in broad order of abundance) calcareous nannofossils, planktonic foraminifers, radiolarians, diatoms, benthic foraminifers, and silicoflagellates, all of which are generally well preserved. In addition, minor nonbiogenous components occur, and evidence of bioturbation is widespread. Calcium carbonate analyses indicate cyclic variations between about 60 and 90% and allow initial correlation with known Pleistocene carbonate events. Gamma-ray attenuation porosity evaluator (GRAPE) density fluctuations, as well as nannofossil abundance cycles, appear to match the carbonate results. The relationship of these variations to color alternations (dark brown and light brown) in the sediments is, at present, unclear. The sediments are estimated to have accumulated at an average rate of 16 m/m.y. (or 1.0 gm/cm^2/1000 yr.). By extrapolation, the age of the core-catcher sediment is about 0.46 Ma. Paleomagnetic results indicate stable remanent magnetization, of normal direction, acquired at a site-compatible paleolatitude. The physical properties fall within the range of published results for similar pelagic sediments.

BACKGROUND AND OBJECTIVES

Recent studies (Crowe, 1981; Von Herzen et al., 1979) have shown that parts of the equatorial Pacific seafloor are characterized by unusually low heat flow and nonlinear temperature gradients (down to 10 m depth). Low heat flow and nonlinear gradients have been interpreted as being indicative of the loss of heat by hydrothermal circulation. This circulation may be occurring through basement outcrops and/or the sediments. Drilling at Site 571 was proposed by the Hydrogeology Working Group with support from the JOIDES Ocean Crust and Inorganic Geochemistry Panels. The site was intended to serve as the locus of detailed heat-flow and geochemical measurements aimed at examining the advection of pore waters through the sediment in this region. Such measurements would permit the testing of convection models and have important implications for the physics of Layer 2, geochemical mass balances, and seabed waste disposal.

Because of the extremely tight schedule for Leg 85, the JOIDES Planning Committee approved only a curtailed program for Site 571. The directive from the Planning Committee called for a total of 48 hr. (including surveys and pipe run-in and trip) on site. Our first priority was to collect six or seven temperature measurements downsection. If time permitted we also planned to spot core (with the HPC) the intervals at which the temperature measurements were made.

The site selection was based on a detailed seismic and geothermal survey conducted by the R/V *Knorr* (KN-73-4) and a Seabeam survey conducted by the German vessel *Sonne*. The *Knorr* survey (Crowe, 1981) revealed that in addition to exhibiting nonlinear heat-flow gradients, the heat-flow values in the region around Site 571 changed by a factor of two, from a high in the east to a low in the west (Fig. 1). Crowe (1981) correlated this east-west heat-flow transition with a change from rough to smooth basement topography. Site 571, just west of this transition (the low-heat-flow side), is at a spot that showed a high inferred surficial temperature gradient (Fig. 2). Seismic profiles revealed a gently undulating

---

[1] Mayer, L., Theyer, F., et al., *Init. Repts. DSDP*, 85: Washington (U.S. Govt. Printing Office).

[2] Larry Mayer (Co-Chief Scientist), Dalhousie University, Halifax, Nova Scotia, Canada; Fritz Theyer (Co-Chief Scientist), Hawaii Institute of Geophysics, University of Hawaii, Honolulu, Hawaii (present address: University of Southern California, Los Angeles, California); John A. Barron, U.S. Geological Survey, Menlo Park, California; Dean A. Dunn, University of Rhode Island, Narragansett, Rhode Island (present address: University of Southern Mississippi, Hattiesburg, Mississippi); Tim Handyside, The University, Newcastle upon Tyne, United Kingdom; Scott Hills, Scripps Institution of Oceanography, La Jolla, California; Ian Jarvis, City of London Polytechnic, London, United Kingdom (present address: Kingston Polytechnic, Kingston-upon-Thames, United Kingdom); Catherine A. Nigrini, La Habra Heights, California; Nicklas G. Pisias, Oregon State University, Corvallis, Oregon; Annick Pujos, Université de Bordeaux, Talence, France; Tsunemasa Saito, Yamagata University, Yamagata, Japan; Paul Stout, Scripps Institution of Oceanography, La Jolla, California; Ellen Thomas, Scripps Institution of Oceanography, La Jolla, California (present address: Lamont-Doherty Geological Observatory, Columbia University, Palisades, New York); Norbert Weinreich, Institut für Geophysik, Ruhr Universität Bochum, Bochum, Federal Republic of Germany; and Roy H. Wilkens, Massachusetts Institute of Technology, Cambridge, Massachusetts.

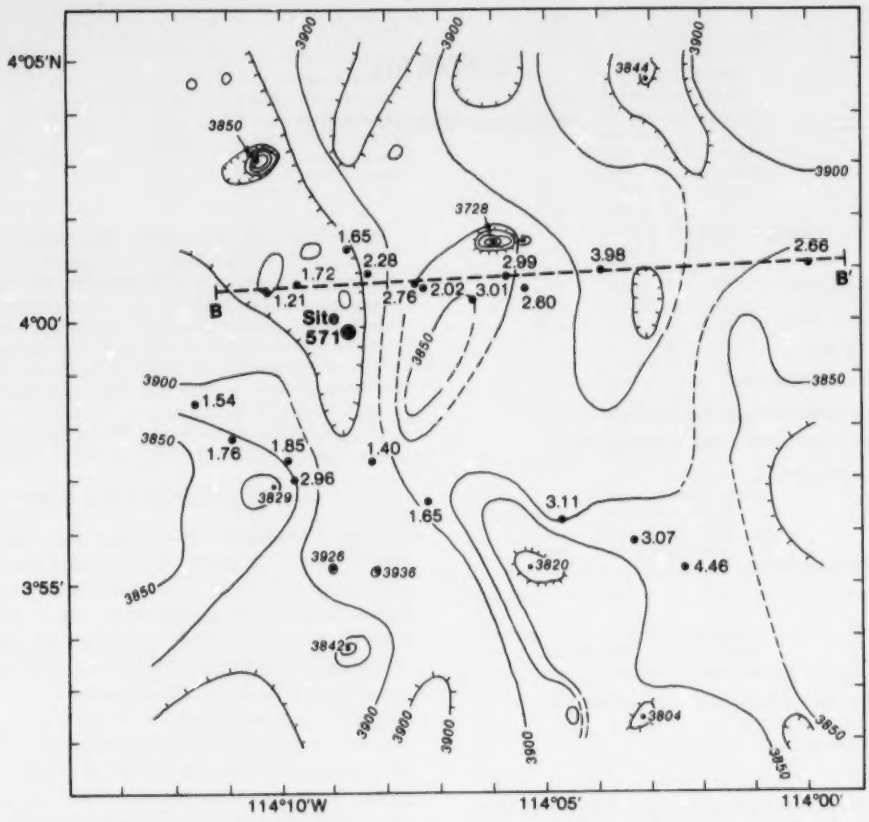

Figure 1. Bathymetry and heat-flow stations near Site 571. Heat-flow values in heat-flow units (HFU), bathymetry in m (after Crowe, 1981).

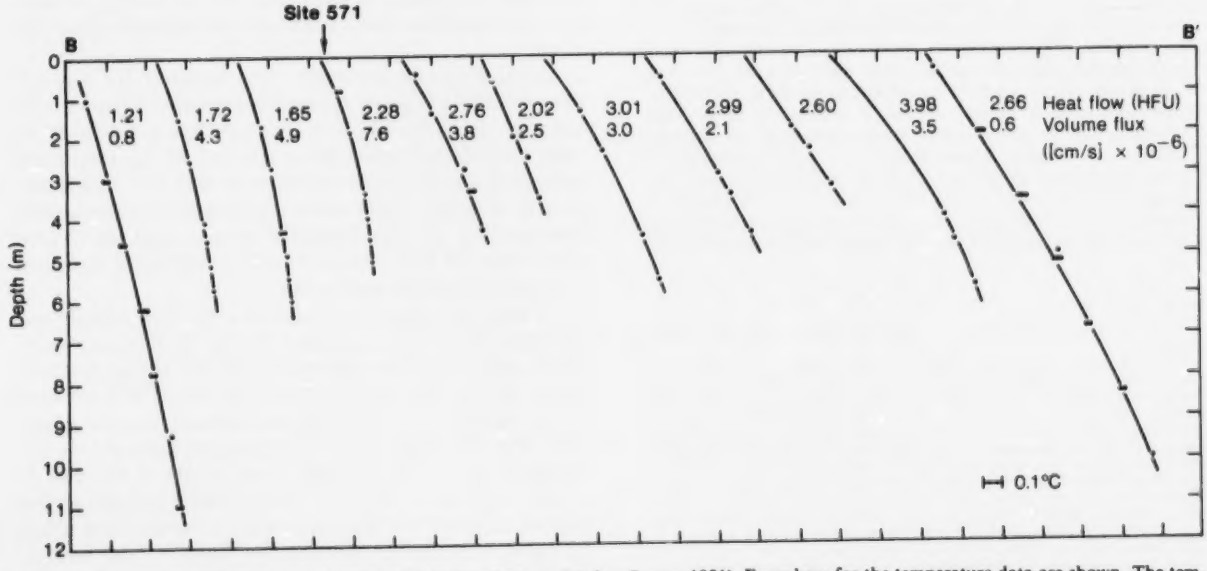

Figure 2. Temperature gradients (°C) along Profile B–B′ of Figure 1 (after Crowe, 1981). Error bars for the temperature data are shown. The temperature profiles are staggered to prevent overlap.

acoustic basement with an occasional basement peak. We were careful to select a site away from basement highs; the D/V *Challenger's* seismic profiler showed 0.34 s of sediment conformably overlying basement at the drill site (Fig. 3). Interpolation of isochron patterns (Herron, 1972; Sclater et al., 1980) indicated the crust at Site 571 to be approximately 15 m.y. old.

The bathymetry generated by the *Sonne* Seabeam system proved to be accurate and extremely useful in determining the ship's position relative to the desired drill site. The regional bathymetry is characterized by lineated troughs and highs with relief of approximately 100 m. This lineation runs northwest–southeast, roughly parallel to the trend of the ridge crest. The drill site (selected for its high inferred surficial temperature gradient) lies near the base of an elongated trough (Fig. 1).

OPERATIONS

The D/V *Glomar Challenger* was scheduled to depart San Pedro, Calif. on 8 March 1982. Difficulty in loading approximately 6000 m of new drill string, however, delayed our departure until 0200Z on 11 March. We arrived in the vicinity of Site 571 at 0600Z on 19 March. While we were under way, continuous seismic profiles (air gun and 3.5 kHz), bathymetric, and magnetic data were collected.

When we were able to locate the ship's position relative to the Seabeam bathymetry collected by the *Sonne* (at approximately 0630Z), we began our presite survey. We first traveled on course 212°, aiming for a spot 2 n. mi. west of the proposed drill site. We then turned east and surveyed a line going directly over the proposed drill site and continuing 2 n. mi. beyond. At the end of this line we proceeded to a point approximately 1 mi. south of the proposed site and turned north, dropping the beacon at 0838Z on 19 March 1982. We continued surveying for 2 n. mi. north of the site and then pulled the geophysical gear and returned to the site. A strong easterly current was present during the survey. We launched the beacon at a position chosen on the basis of bathymetry and dead reckoning that proved to be a few hundred meters south of the preselected site location. The final location for the drill site is 03°59.84′N, 114°08.53′W, slightly south and west of the planned position, but certainly well within the zone of low heat flow and strong nonlinear gradients.

We began to run in the drill pipe at 1025Z in sea state 4 and with a substantial swell. Because of the difficulty of making up new pipe and the sea state, over 16 hr. elapsed between the initial run-in and the first HPC. We took this first core (7.11 m of upper Pleistocene material) to establish mudline depth. The drill string length and precision depth recorder (PDR) depth agreed within 2.5 m.

The rest of the program at Site 571 called for making a series of temperature measurements and, if time permitted, spot piston coring. This was the first time the temperature probe had been used with the HPC, and operation in this mode was far from routine. The first station where heat-flow measurements were to be made (and interstitial water was to be sampled) was 47.5 m sub-bottom (see Table 1). The sediment at this depth was a little too soft to bear enough of the weight of the drill string for the bumper subassembly to function properly, so the drill string was lowered 5 m as the temperature measurement was being made to put more of the drill string's weight on the sediment. (If the sediment does not bear some of the weight of the drill string, the bumper subs remain fully extended, and the end of the drill string is subject to the full force of the ship's mo-

Table 1. Heat-flow measurement, Site 571.

Station	Date (Mar. 1982)	Local time (hr.)	Depth from drill floor (m)	Sub-bottom depth (m)	Measured quantity
1	19	2010	3976.6–4017.0	47.5–52.5	Pore-water sample, temperature
2a	19	2330	4017.0–4036.0	66.5	Temperature
2b	19	2340	4036.0–4055.0	85.5	Temperature
3	20	0230	4055.0–4074.0	104.5–107.5	Pore-water sample, temperature
4	20	1000	4074.0–4121.5	152.0	Temperature
5	20	1300	4121.5–4131.0	161.5	Pore-water sample, temperature
6	20	1600	4131.0–4169.0	199.5	Temperature

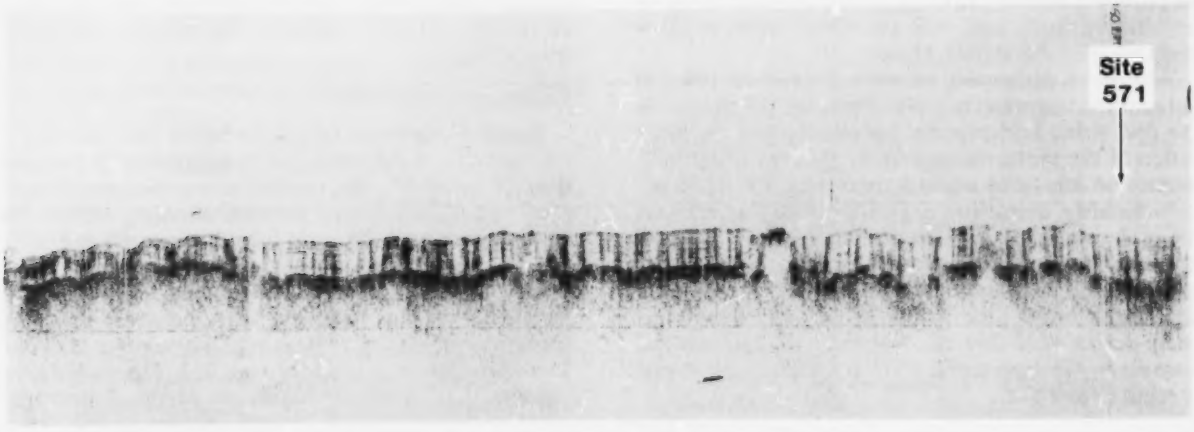

Figure 3. Seismic reflection profile during approach to Site 571. Profile is from *Challenger* air gun records.

tion [substantial at Site 571]. This motion is acceptable for the operation of the HPC, which samples almost instantaneously, but it places tools like the temperature and interstitial water probes in great jeopardy, because these tools must remain extended for 30 to 40 min.)

Data from heat-flow (HF) Station 1 were processed as HF Stations 2a and b were being occupied (at 66.5 and 85.5 m). The results were ambiguous; we attributed the ambiguity to the excessive motion of the tool in the soft sediment. We washed down to HF Station 3, and as we attempted to retrieve the tool the bottom plug on the pressure case for the Kuster orientation tool backed off, causing the tool to separate from the sandline. We fished for the tool and recovered it undamaged 4 hr. later. During this time, analysis of the temperature and pore-water data led us to suspect that both measurements were contaminated by seawater. This meant a leak in the seals that were used to keep hydraulic pressure on the temperature and pore-water tool.

When the temperature tool is used in conjunction with a rotary drill bit, it is mechanically latched into position at the end of the drill string. With the HPC, there is no mechanical latching mechanism; instead, O-ring seals at the top of the tool and hydraulic pressure in the drill string are used to keep the tool extended beyond the bit. If the O-ring seals fail, the drill string cannot maintain pressure, the tool is not held firmly in place, and, most important, the seawater used to pressurize the drill string can run by the temperature and pore-water probes.

During operation at HF Station 4 the blow-out preventor (BOP) was closed so that the pressure in the drill string could be closely monitored. As suspected, the drill string could not maintain pressure, confirming that there was a leak in the system. After the tool was returned, the seals were changed, the top sub was tightened, and the tool was sent down for HF Station 5. To the frustration of all, the drill string could still not retain pressure. Close inspection of the tool revealed that a landing sub on the bottom of the tool was too wide to pass through the seal sleeves that the O-rings at the top of the tool were supposed to seat on. Thus, the bottom of the tool was stuck 20 m up from the end of the drill string, and pumped seawater was free to circulate around the probes. The guilty landing sub is used only in the rotary drilling mode, and so it was turned down to allow clearance past the sealing sleeve.

With great excitement we washed down to 199.5 m and sent the temperature probe down for HF Station 6. The drill string held pressure beautifully and the penetration of the probe was proven by the significant pull-out tension measured when the tool was first retrieved. Unfortunately, an electronic problem with the temperature probe prevented data from being collected. We were all greatly disappointed, but we were already 2 hr. over our allotted time, and any additional work would have required an offset (due to the induration of the sediments deeper than 200 m). Naturally we collected no more cores. We departed Site 571 at 1022Z on 21 March en route to Site 572.

LITHOSTRATIGRAPHY

Lithostratigraphic Subdivision

The sediment in the single core taken at Site 571 belongs to one lithologic unit, a cyclic unit of Quaternary siliceous calcareous ooze. The unit contains cycles of dark brown (10YR 3/3) to yellowish brown (10YR 5/4) siliceous foraminifer nannofossil ooze and yellowish brown (10YR 5/8) to dark yellowish brown (10YR 4/4) diatom nannofossil ooze, alternating with very pale brown (10YR 8/3) foraminifer nannofossil ooze. The contacts between the cyclic bands are usually gradational, and many show evidence of bioturbation.

The sediments are uniform in composition, with common (5 to 25%) to abundant (25 to 75%) sand-sized particles, common silt, and abundant clay. Calcareous nannofossils are abundant to dominant (greater than 75%), foraminifers are common to abundant, and diatoms and radiolarians are rare (1 to 5%) to common. The relative proportion of siliceous microfossils does not appear to influence the color of the sediment directly. Silicoflagellates, terrigenous clay, and volcanic glass occur sporadically in rare amounts. Color variations appear to be due to differential amounts (1 to 5%) of iron oxides.

Bioturbation

Bioturbation is common throughout the section. Burrow mottling consists of subhorizontal burrows with 1-cm oval to elliptical cross sections (Planolites). The mottling is most obvious at cycle boundaries, where sediment of contrasting color has been burrowed down below the contacts. Occasional 1-cm burrows with light-colored "reaction rims" (rind burrows) are visible in the darker units. Two open burrows occur in Section 4 at 7 and 112 cm.

Sedimentary Cycles

The dominant feature of this core is the cyclic change in color from darker brown siliceous calcareous oozes containing iron oxides to lighter-colored calcareous oozes. These color changes may be related to glacial–interglacial cycles of the last 400,000 to 500,000 yr.; however, the carbonate record (Fig. 4) shows that there is no clear correlation between carbonate fluctuations and cyclic color changes.

Carbonate Stratigraphy

Detailed shipboard carbonate bomb analyses at 20-cm intervals of the single 7.1-m core taken at this site show pronounced cyclic variations in carbonate percentages, with high-carbonate intervals exceeding about 90% and low-carbonate intervals lying between 60 and 80% (Fig. 4). These percentages are typical of sediment cores from the eastern equatorial Pacific, and we were able to correlate Site 571 with the standard Pleistocene carbonate event stratigraphy of Hays et al. (1969). Site 571 contains carbonate events B3 through B12 (Fig. 4), indicating that the uppermost 33,000 yr. of the record may

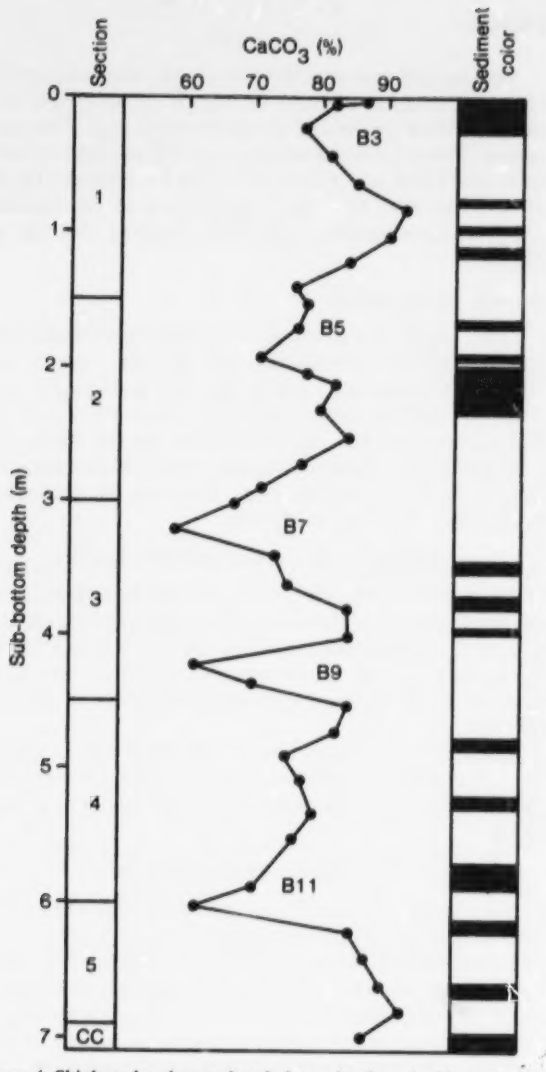

Figure 4. Shipboard carbonate bomb determinations for Site 571. Section numbers for Core 1 are in the left column. Shaded areas in the right column indicate darker brown layers (10YR 3/3). Carbonate minima (Hays et al., 1969) are labeled.

have been lost in the coring process. This inference is in agreement with the sediment accumulation rate calculations for Site 571.

BIOSTRATIGRAPHY

Summary

Planktonic foraminifers, calcareous nannofossils, diatoms, and radiolarians are all represented and well preserved in the sediments recovered at Site 571, although dissolution is marked at some levels. For details on preservation see the sections on the individual fossil groups. The benthic foraminifers are rare but well preserved.

The single core recovered is Quaternary in age, correlates with planktonic foraminiferal Zone N23 and the *Pseudoeunotica doliolus* diatom Zone, and spans three nannofossil and radiolarian zones. The age of the core-catcher radiolarian and nannofossil assemblages (respectively, the top of the "*Stylatractus universus*" and the *Pseudoemiliania lacunosa* zones) lies between 0.44 and 0.60 Ma. The other fossil assemblages do not contradict this age assignment.

Planktonic Foraminifers

The planktonic foraminifers are generally abundant and well preserved, although abundance and state of preservation vary somewhat in different parts of the cored sequence. Of the nine layers examined, faunas affected by marked dissolution occur in Sections 1 (140–144 cm) and 3 (41–43 cm). These faunas contain fewer species and lack many solution-susceptible species, such as *Globigerina rubescens* and *Globigerinoides ruber*.

On the basis of two extinction datum levels, *Globoquadrina pseudofoliata* and *Globorotalia tosaensis* (Thompson and Saito, 1974; Saito, 1977), the core is assigned to the Brunhes Chron of the geomagnetic time scale and the foraminiferal Zone N23 of Blow (1969). Since no noticeable change in faunal composition occurs, the sequence appears to be continuous. The extinction horizon of *G. pseudofoliata*, which is known to have an age of 0.22 Ma, lies between 119–120 cm and 131–132 cm of Section 2. *G. tosaensis* is conspicuously absent from recovered assemblages, so this datum was apparently not reached by this core; as a result, the base of the core is believed to be younger than 0.6 Ma.

Calcareous Nannofossils

Calcareous nannofossils were observed in 39 samples (some of which are shown in Fig. 5). Coccoliths are al-

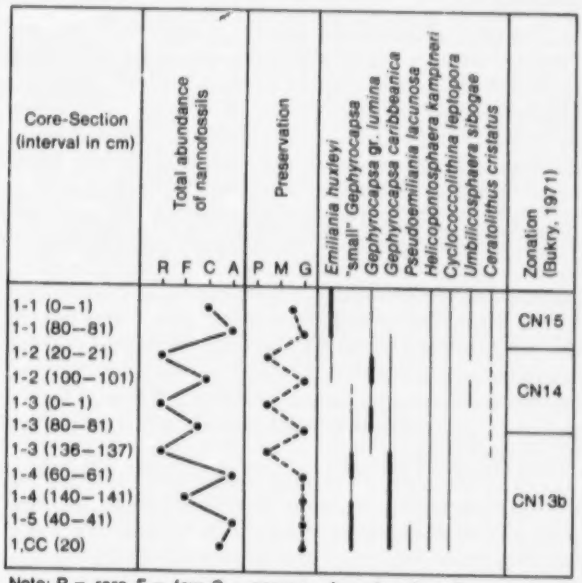

Note: R = rare, F = few, C = common, A = abundant; P = poor, M = moderate, G = good.

Figure 5. Occurrence of nannofossil species at Site 571.

ways present, and, in general, they are very abundant and well preserved. They are rare in some samples (Section 1, 40–41 cm; Section 3, 0–1 and 20–21 cm; Section 3, 120–121 and 137–138 cm) where there is evidence of dissolution.

From the top of the core to Section 2 (0–1 cm), the assemblage is dominated by very small coccoliths that can only tentatively be identified as *Emiliania huxleyi* (Zone CN15 of Bukry, 1971). They are associated with *Gephyrocapsa lumina, Helicopontosphaera kamptneri*, and *Cyclococcolithina leptopora*.

Between Section 2, 20–21 cm and Section 3, 120–121 cm, the small species are very rare. The nannoflora is mainly composed of large *Gephyrocapsa (G. lumina* and *G. caribbeanica)* and *C. leptopora. Ceratolithus cristatus* is always present. This assemblage is characteristic of the *C. cristatus* Subzone (CN14b) of the *G. oceanica* Zone. The base of this subzone has been dated by Bukry (1971) at 0.3 Ma.

From Section 3, 136–137 cm to Section 5, 0–1 cm, nannofossils are very abundant and are dominated by *G. caribbeanica* and *G. aperta*. The former species is represented by rather small coccoliths that differ slightly from the original description; the difference may be due to something special about the environment. This part of the core is correlated with the *G. caribbeanica* Subzone (CN13b).

The nannoflora of the core catcher is not very different from the younger assemblage. In addition, there are rare specimens of *Pseudoemiliania lacunosa*, the extinction of which is usually dated 0.42 to 0.45 Ma.

Very few specimens are reworked. In two samples (Section 3, 40–41 and 120–121 cm) there is a partially dissolved specimen of *Discoaster kugleri* (middle Miocene).

Radiolarians

The core contains common, well preserved and diverse Quaternary radiolarians. Samples from Sections 1 (136–137 cm) and 2 (136–137 cm) are in the *Buccinosphaera invaginata* Zone of Nigrini (1971), which is defined by the presence of *B. invaginata* and *Collosphaera tuberosa*. The absence of *B. invaginata* and the presence of *C. tuberosa* in Section 3 (143–145 cm) places that sample in the *Collosphaera tuberosa* Zone. The absence of *C. tuberosa* from Sections 4 (135–137 cm) and 5 (79–81 cm) places the remainder of the core in the *Amphirhopalum ypsilon* Zone. "*Stylatractus universus*", the top of which has been dated at 0.425 Ma, was found in the core-catcher sample but not in the Section 5 sample examined. Since Section 5 is 91 cm long and the core catcher is 20 cm long, an age of 0.425 Ma can be assigned to the sediment interval between 679 and 711 cm below the mudline.

The preservation of radiolarians is good throughout the core, although the fauna found in Section 4 is less robust than that found in other sections of the core. Samples from Sections 1 and 2 show particularly good preservation, with many delicate and elaborate forms present, as well as fragments of the diatom *Ethmodiscus rex*. Orosphaerid fragments are present in Section 5 (79–81 cm).

Diatoms

One sample was examined from the core catcher (9–10 cm). Common diatoms with good preservation were observed after processing in hydrochloric acid. The presence of *Pseudoeunotia doliolus* and the absence of *Nitzschia reinholdii* are indicative of the *Pseudoeunotia doliolus* Zone (0–0.65 Ma). The absence of multinodule forms of *Coscinodiscus nodulifer* supports that age assignment.

Benthic Foraminifers

One sample was examined from the core catcher (15–16 cm). Benthic foraminifers are rare: the sample contained 106 specimens, which were assigned to 32 taxa. Preservation is excellent. The fauna is diverse; *Epistominella, Gyroidinoides*, and *Nuttallides* are the most common genera (33 specimens in all). Only 13 specimens belong to rectilinear species (e.g., *Bolivina, Fursenkoina*). Agglutinants are extremely rare.

SEDIMENT ACCUMULATION RATES

Plotted in Figure 6 are the age range estimates for all the fossil groups in the core-catcher sample. The extinction of *G. pseudofoliata* occurs between 2.6 and 2.8 m. These data suggest an average sedimentation rate of 16 m/m.y. for the upper Pleistocene sediments of Site 571 (Fig. 6).

Mass accumulation rates for the total sediment and for the carbonate and noncarbonate fractions were estimated to be 1.0, 0.79, and 0.21 g/cm^2/1000 yr., respectively.

PHYSICAL PROPERTIES

The physical properties measured for this site included wet-bulk density, sonic velocity, formation factor, and thermal conductivity. Measurements were made at regular intervals within the HPC core except where the sediment was disturbed. A discussion of the data collection techniques, procedures, and pertinent references is presented in the Introduction (this vol.). The data for the single sediment core at this site are tabulated in Table 2. The values are in generally good agreement with the range of values published for deep-sea sediments. Scatter in the values may reflect variability that is expected in the uppermost sediments, which are only beginning to be affected by compaction.

PALEOMAGNETISM

Because of the Brunhes age of Core 1, only a few measurements were carried out. The measurements were made mainly to test the Kuster core orientation system and to obtain a general idea of the magnetic response of the sediments.

The natural remanent magnetization (NRM) intensity of the 14 samples measured varies from 2.4×10^{-6} to 7.4×10^{-6} G, with a mean value of 4.7×10^{-6} G. The directions are stable, with only a small amount of scatter. The mean value of the inclination is 9.8°, which corresponds to a dipole paleolatitude of 4.9°, which is in good agreement with the latitude of the site.

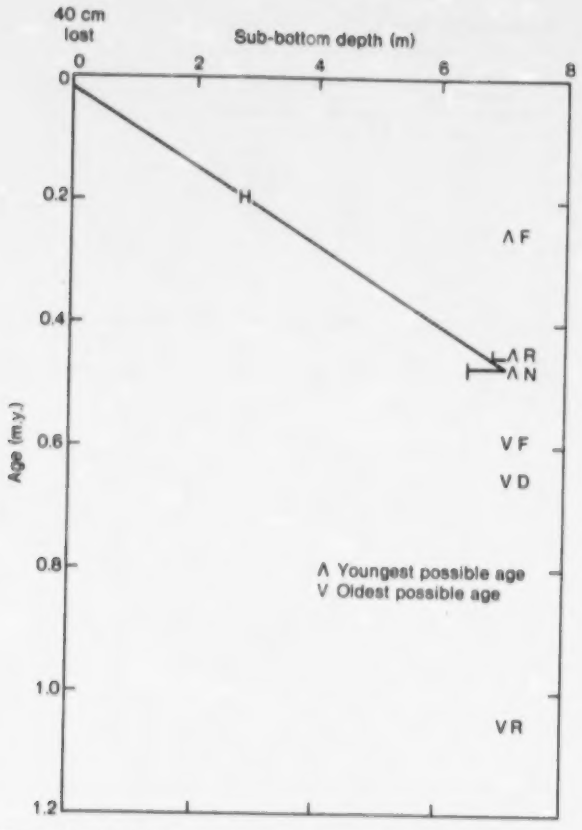

Figure 6. Sedimentation rate at Site 571 (16.0 m/m.y.). Age ranges are shown for foraminifers (F), radiolarians (R), calcareous nannofossils (N), and diatoms (D).

INTERSTITIAL-WATER CHEMISTRY

Very slight changes in concentration occur in the pore waters from these sediments with increasing depth (Fig. 7). The ranges of values for each constituent generally fall within experimental error. Alkalinity shows its largest increase in the uppermost meter of sediment. Since we apparently did not recover the top 40 cm of sediments, we cannot investigate potentially significant changes immediately below the sediment/water interface.

The *in situ* samples verified that the sampling device was malfunctioning. Salinity, pH, and alkalinity data indicate contamination by surface seawater.

SUMMARY AND CONCLUSIONS

As a result of technical difficulties, the activity at Site 571 failed to accomplish its primary goals, namely, to recover downhole heat-flow data, *in situ* pore-water samples, and correlative sediments from an area of unusually low heat flow in the central equatorial Pacific.

The 711 cm-long mudline core recovered yielded no scientific surprises: it contained predominantly calcareous Quaternary oozes with a 16 m/m.y. sedimentation rate and a mass accumulation rate of about 1.0 g/cm^2/1000 yr. The core is heavily bioturbated and characterized by distinct cyclic color changes (from dark to light brown), which is typical for this depositional depth in the high productivity equatorial belt of the Pacific. As expected, all major microfossil groups are abundantly represented, and, with some exceptions, they are well preserved. Calcareous nannofossils and planktonic foraminifers generally dominate, although radiolarians and diatoms never make up less than 1% of the fossil assemblage and usually more. The calcium carbonate content of the sediments varies cyclically, generally between 70 and 85%. These carbonate fluctuations are matched by variations in the abundance of the nannofossil flora and are also expressed in (GRAPE) downcore density cycles, low density corresponding to low carbonate content. The coherence of these data allows the identification of Pleistocene carbonate events B12 to B3 (Hays et al., 1969). The identification of these events is corroborated by the extrapolated age of the bottom of Core 1 (about 0.46 Ma) and the absence of the topmost 40 cm of sediment, which were lost during coring. The sediment's physical properties and geochemistry (as indicated by shipboard analysis) are also compatible with results published earlier for similar biogenous oozes. The magnetization of the sediments is stable, of normal direction, and of typical intensity; it was acquired at Site 571 latitude.

REFERENCES

Blow, W. H., 1969. Late middle Eocene to Recent planktonic foraminiferal biostratigraphy. *In* Brönnimann, P., and Renz, H. H. (Eds.), *Proc. First Internat. Conf. Planktonic Microfossils*: Leiden (Brill), 1:199–422.

Bukry, D., 1971. Cenozoic calcareous nannofossils from the Pacific Ocean. *Trans. San Diego Soc. Nat. Hist.*, 16:307–327.

Crowe, J., 1981. Mechanisms of heat transfer through the floor of the equatorial Pacific Ocean [Ph. D. dissert.]. Woods Hole Oceanographic Institution, Woods Hole.

Hays, J. D., Saito, T., Opdyke, N. D., and Burckle, L. H., 1969. Pliocene–Pleistocene sediments of the equatorial Pacific: their paleomagnetic, biostratigraphic and climatic record. *Geol. Soc. Am. Bull.*, 80:1481–1514.

Herron, E. M., 1972. Seafloor spreading and the Cenozoic history of the east-central Pacific. *Geol. Soc. Am. Bull.*, 83:1671–1692.

Nigrini, C., 1971. Radiolarian zones in the Quaternary of the equatorial Pacific Ocean. *In* Funnell, B. M., and Riedel, W. R. (Eds.), *The Micropaleontology of Oceans*: Cambridge (Cambridge Univ. Press), pp. 443–461.

Saito, T., 1977. Late Cenozoic planktonic foraminiferal datum levels: the present state of knowledge toward accomplishing pan-Pacific stratigraphic correlation. *Proc. First Internat. Cong. Pacific Neogene Stratigraphy* (Tokyo), pp. 61–80.

Sclater, J. G., Jaupart, C., and Galson, D. A., 1980. The heat flow through oceanic and continental crust and heat loss of the earth. *Rev. Geophys. Space Phys.*, 18:269–311.

Thompson, R. R., and Saito, T., 1977. Pacific Pleistocene sediments: planktonic foraminifera dissolution cycles and geochronology. *Geology*, 2:333–335.

Von Herzen, R. P., Crowe, J., and Green, K. E., 1979. Fluid convection in the eastern Pacific Ocean crust. *EOS Trans. Am. Geophys. Union*, 60:382.

Table 2. Site 571 physical properties summary. All data are for Core 1.

Section	Level (cm)	Wet-bulk density (g/cm^3)	Porosity (%)	Sonic velocity (km/s)	Thermal conductivity (mcal/cm·s·°C)	Formation factor	
						Vertical	Horizontal
1	116	1.38	75	1.55	2.53	1.63	1.57
2	59	1.30	75	1.54	2.43	1.33	1.29
3	52			1.47	2.53	1.22	1.19
4	41			1.55	2.76	1.67	1.62
5	36	1.52	71	1.54	2.77	1.58	1.57

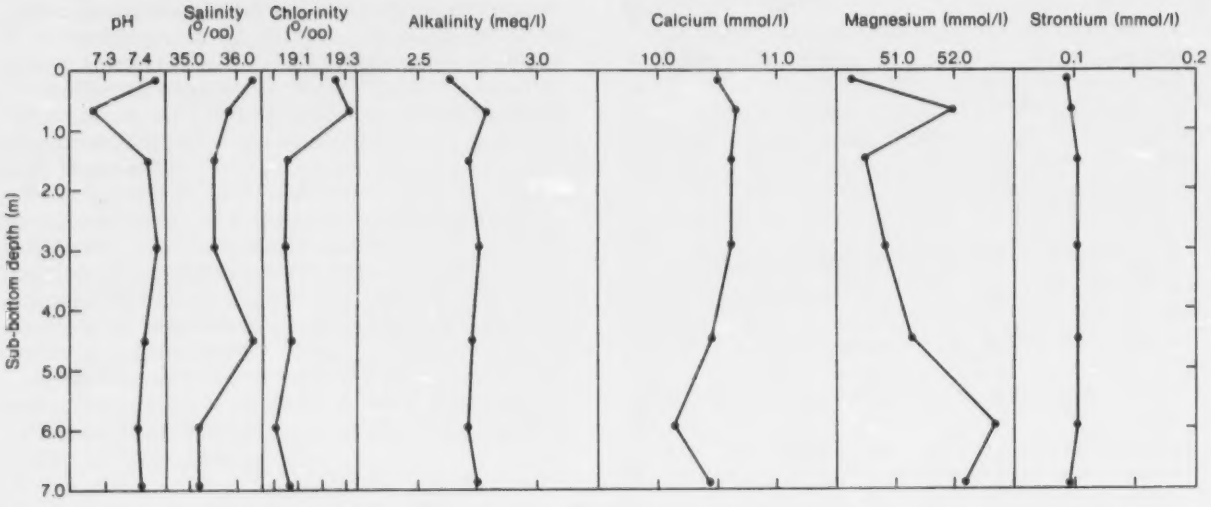

Figure 7. Interstitial-water geochemistry at Site 571.

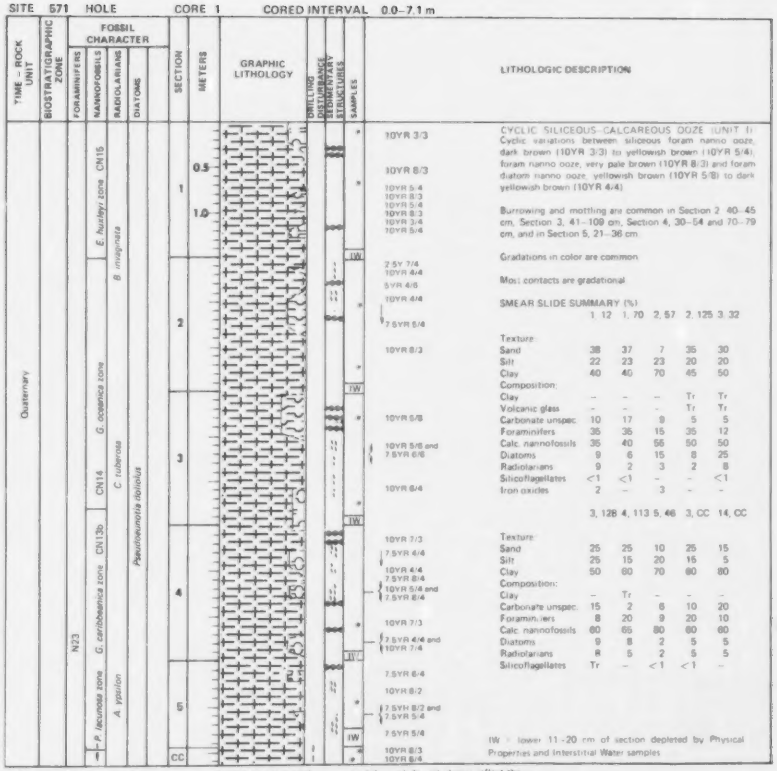
SITE 571 HOLE CORE 1 CORED INTERVAL 0.0–7.1 m
TIME – ROCK UNIT
BIOSTRATIGRAPHIC ZONE
FOSSIL CHARACTER
FORAMINIFERS
NANNOFOSSILS
RADIOLARIANS
DIATOMS
SECTION
METERS
GRAPHIC LITHOLOGY
DRILLING DISTURBANCE
SEDIMENTARY STRUCTURES
SAMPLES
LITHOLOGIC DESCRIPTION
Quaternary
N23
P. lacunosa zone
G. cariboensis zone
CN13b
CN14
G. oceanica zone
E. huxleyi zone
CN15
A. ypsilon
C. tuberosa
B. invaginata
Pseudoeunotia doliolus
10YR 3/3
10YR 8/3
10YR 5/4
10YR 8/3
10YR 5/4
10YR 8/3
10YR 3/4
10YR 5/4
2.5Y 7/4
10YR 4/4
5YR 4/6
10YR 4/4
7.5YR 5/4
10YR 8/3
10YR 5/8
10YR 5/8 and 7.5YR 6/6
10YR 6/4
10YR 7/3
7.5YR 4/4
10YR 4/4
7.5YR 8/4
10YR 5/8 and 7.5YR 8/4
10YR 7/3
7.5YR 4/4 and 10YR 7/4
7.5YR 6/4
10YR 8/2
7.5YR 8/2 and 7.5YR 5/4
7.5YR 5/4
10YR 8/3
10YR 8/4
IW
CYCLIC SILICEOUS-CALCAREOUS OOZE (UNIT I): Cyclic variations between siliceous foram nanno ooze, dark brown (10YR 3/3) to yellowish brown (10YR 5/4), foram nanno ooze, very pale brown (10YR 8/3) and foram diatom nanno ooze, yellowish brown (10YR 5/8) to dark yellowish brown (10YR 4/4).
Burrowing and mottling are common in Section 2, 40–45 cm, Section 3, 41–109 cm, Section 4, 30–54 and 70–79 cm, and in Section 5, 21–36 cm.
Gradations in color are common.
Most contacts are gradational.
SMEAR SLIDE SUMMARY (%)
1, 12 1, 70 2, 57 2, 125 3, 32
Texture:
Sand 38 37 7 35 30
Silt 22 23 23 20 20
Clay 40 40 70 45 50
Composition:
Clay – – – Tr Tr
Volcanic glass – – – Tr Tr
Carbonate unspec. 10 17 8 5 5
Foraminifers 35 35 15 35 12
Calc. nannofossils 35 40 55 50 50
Diatoms 9 6 15 8 25
Radiolarians 9 2 3 2 8
Silicoflagellates <1 <1 – – <1
Iron oxides 2 – 3 – –
3, 128 4, 113 5, 46 3, CC 14, CC
Texture:
Sand 25 25 10 25 15
Silt 25 15 20 15 5
Clay 50 60 70 60 80
Composition:
Clay – Tr – – –
Carbonate unspec. 15 2 6 10 20
Foramin.fers 8 20 9 20 10
Calc. nannofossils 60 65 80 60 60
Diatoms 9 8 2 5 5
Radiolarians R 5 2 5 5
Silicoflagellates Tr – <1 <1 –
IW = lower 11–20 cm of section depleted by Physical Properties and Interstitial Water samples

NOTE: Graphic lithologies represent average compositions derived from smear slides and do not always reflect the detailed alternation of sediment types. Major lithologic boundaries are shown but gradational contacts, small scale cyclicity and ooze-chalk alternations are represented schematically. Color changes approximate to lithologic changes.

Site 571 Core 1
CARBONATE BOMB

1, 2 cm = 86%	3, 22 cm = 58%
1, 21 cm = 77%	3, 42 cm = 73%
1, 41 cm = 81%	3, 62 cm = 75%
1, 61 cm = 85%	3, 82 cm = 84%
1, 81 cm = 92%	3, 102 cm = 84%
1, 101 cm = 90%	3, 122 cm = 61%
1, 121 cm = 84%	3, 135 cm = 70%
1, 139 cm = 76%	4, 2 cm = 84%
2, 3 cm = 78%	4, 23 cm = 82%
2, 21 cm = 76%	4, 38 cm = 75%
2, 42 cm = 71%	4, 58 cm = 77%
2, 61 cm = 82%	4, 82 cm = 79%
2, 82 cm = 80%	4, 102 cm = 76%
2, 102 cm = 84%	4, 138 cm = 70%
2, 122 cm = 77%	5, 2 cm = 61%
2, 138 cm = 71%	5, 22 cm = 84%
3, 2 cm = 67%	5, 41 cm = 87%

Information on core description sheets, for ALL sites, represents field notes taken aboard ship under time pressure. Some of this information has been refined in accord with post-cruise findings, but production schedules prohibit definitive correlation of these sheets with subsequent findings. Thus the reader should be alerted to the occasional ambiguity or discrepancy.

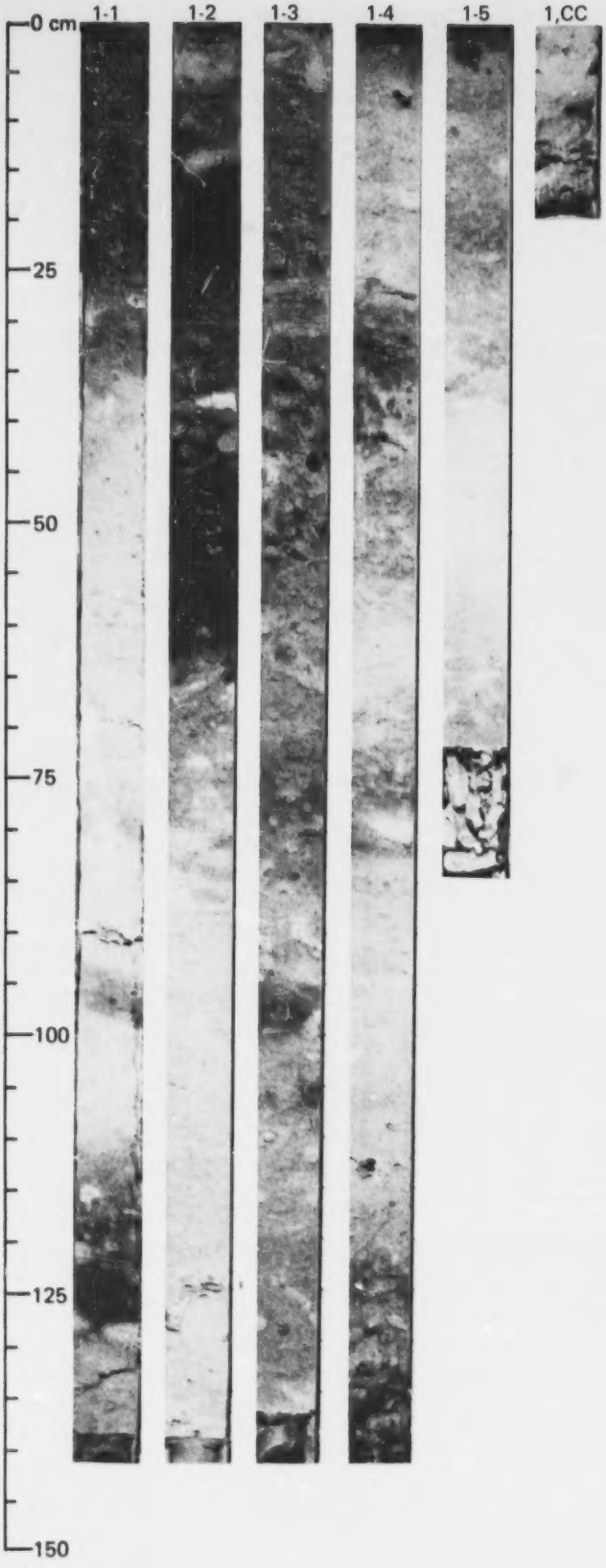
0 cm
1-1
1-2
1-3
1-4
1-5
1,CC
25
50
75
100
125
150

3. SITE 572[1]

Shipboard Scientific Party[2]

HOLES 572, 572A, 572B, 572C, 572D

Dates occupied: 572—22 March 1982
572A—22, 23 March 1982
572B, 572C—24 March 1982
572D—26 March 1982

Date departed Hole 572D: 28 March 1982

Time on site: 6.3 days

Position: 01°26.09′N, 113°50.52′W

Water depth (sea level; corrected m, echo-sounding): 3893

Water depth (rig floor; corrected m, echo-sounding): 3903

Bottom felt (m, drill pipe): 3903

Penetration (m): 572—19.9
572A—154.0
572B—18.10
572C—169.5
572D—320.0

Number of cores: 572—1
572A—17
572B—4
572C—20
572D—34

Total length of cored section (m): 572—19.0
572A—153.97
572B—18.10
572C—164.50
572D—320

Total core recovered (m): 572—9.25
572A—154.35
572B—19.95
572C—161.56
572D—258.87

Core recovery (%): 572—49
572A—100
572B—100
572C—95
572D—81

Oldest sediment cored (Hole 572D):
Depth sub-bottom (m): 464.5
Nature: Siliceous nannofossil chalk
Age: Basal middle Miocene
Measured velocity (km/s): 1.75

Basement (Hole 572D):
Depth sub-bottom (m): 479.5
Nature: Basalt

Principal results: Site 572 (1°26.1′N, 113°50.5′W), in 3900 m of water on the eastern edge of the equatorial high productivity zone, is located just a few miles south and west of DSDP Site 81. The site was selected to permit high resolution stratigraphies to be established and to further our understanding of Neogene paleoceanographic and climatic variations through the study of the site's thick Neogene section. The result of drilling five holes was the recovery of two continuous piston-cored sequences from the upper 170 m of the section and one nearly continuous rotary-drilled sequence from the bottom 310 m of the section. The oldest sediment recovered (from 464.5 m sub-bottom) was lower middle Miocene (about 15 Ma). A sediment/basalt contact was encountered at 479.5 m, and 43 cm of fine-grained basalt with glassy rind were recovered. The sediment section can be divided into two units (the first of which is subdivided into four subunits) as follows.

Unit I is cyclic siliceous calcareous ooze chalk. *Subunit IA* is (Quaternary) gray brown ooze and occurs from 0 to 2.35 m. More specifically, the sediment consists of brown and gray foraminiferal siliceous nannofossil oozes. *Subunit IB* is Quaternary to upper Pliocene varicolored ooze and occurs from 2.35 to 37.45 m. The sediment consists of purple, light gray, and yellow siliceous nannofossil oozes. *Subunit IC* is upper Pliocene to middle Miocene green varicolored ooze chalk and occurs from 37.45 to 458.75 m. The sediment consists of purple, light gray, yellow, and green siliceous nannofossil oozes that grade into siliceous nannofossil chalks. In the lower part of this subunit there are several diatom-rich layers and laminated chert horizons 3 to 4 cm thick. *Subunit ID* is lowermost middle Miocene yellow chalk and occurs from 458.75 to 464.5 m. The sediment consists of pale yellow to yellow green siliceous foraminiferal nannofossil chalk.

Unit II is middle Miocene metalliferous chalk. It consists of siliceous foraminiferal nannofossil chalk with common pyrite and iron oxides.

These units can be correlated with the Clipperton (our Subunits IA and IB), San Blas (our Subunit IC), and Line Islands (our Subunits ID and II) oceanic formations described on Leg 9.

Sedimentation rates are variable and, in some intervals, remarkably high:

Age of interval (Ma)	Average sedimentation rate (m/m.y.)
15.3–14.3	65
14.3–13.7	54
13.7–13.0	35
13.0–12.0	73
12.0–7.0	13
7.0–4.5	50
4.5–3.0	15
3.0–2.0	21
2.0–0.5	13

[1] Mayer, L., Theyer, F., et al., *Init. Repts. DSDP*, 85: Washington (U.S. Govt. Printing Office).

[2] Larry Mayer (Co-Chief Scientist), Dalhousie University, Halifax, Nova Scotia, Canada; Fritz Theyer (Co-Chief Scientist), Hawaii Institute of Geophysics, University of Hawaii, Honolulu, Hawaii (present address: University of Southern California, Los Angeles, California); John A. Barron, U.S. Geological Survey, Menlo Park, California; Dean A. Dunn, University of Rhode Island, Narragansett, Rhode Island (present address: University of Southern Mississippi, Hattiesburg, Mississippi); Tim Handyside, The University, Newcastle upon Tyne, United Kingdom; Scott Hills, Scripps Institution of Oceanography, La Jolla, California; Ian Jarvis, City of London Polytechnic, London, United Kingdom (present address: Kingston Polytechnic, Kingston-upon-Thames, United Kingdom); Catherine A. Nigrini, La Habra Heights, California; Nicklas G. Pisias, Oregon State University, Corvallis, Oregon; Annick Pujos, Université de Bordeaux, Talence, France; Tsunemasa Saito, Yamagata University, Yamagata, Japan; Paul Stout, Scripps Institution of Oceanography, La Jolla, California; Ellen Thomas, Scripps Institution of Oceanography, La Jolla, California (present address: Lamont-Doherty Geological Observatory, Columbia University, Palisades, New York); Norbert Weinreich, Institut für Geophysik, Ruhr Universität Bochum, Bochum, Federal Republic of Germany; and Roy H. Wilkens, Massachusetts Institute of Technology, Cambridge, Massachusetts.

Associated with the zones of high sedimentation rate are diatom assemblages that are indicative of upwelling, the enhanced dissolution of carbonate, decreased carbonate content, and increased porosity. The hydraulic piston corer (HPC) provided beautifully preserved cores, in many of which millimeter-scale laminations were visible. The usefulness of the HPC was limited by the ability of the tool to withstand pullout force—not the corer's ability to penetrate the sediment. Two HPC cores were lost when the quick disconnect parted upon pullout (pullout forces of greater than 2.5 tons were necessary). These problems were minor, however; recovery was excellent and sedimentation rates were high. The cores recovered at Site 572 are invaluable for the study of Neogene oceanography.

BACKGROUND AND OBJECTIVES

For Site 572, the JOIDES Ocean Paleoenvironmental Panel proposed drilling again at the location of Site 81 (Fig. 1), which was first drilled during DSDP Leg 9 (Hays et al., 1972). Site 81 was drilled mainly to determine the age of the lithosphere, and coring was incomplete. The hole was 409 m deep and terminated in basalt; fine-grained basalt, a baked interface, and thermally altered sediments were recovered in the bottom core. The estimated age of the basal sediments (15 Ma) was assumed to be representative of basement age at this spot, even though the basalt recovered was recognized as an intrusive flow.

Site 572 is located at 1°26.1′N, 113°50.5′W, in water 3903 m deep. The sediment is about 0.6 s thick and acoustically well stratified (Fig. 2). The site is on the northwestern border of a northwest-trending basement trough just south and west of Site 81.

The tectonic framework of the region of Sites 572 and 81 is poorly understood. In large measure the uncertainty is due to the difficulty of interpreting magnetic lineations at low latitudes (Herron, 1972). Further uncertainty stems from the possibility that a fossil ridge system thought to have become extinct about 11 m.y. ago (van Andel et al., 1975) once lay west of, and parallel to, the East Pacific Rise. The specific tectonic relationship between this hypothetical fossil ridge and the area of Site 572 is a matter of conjecture; however, if the ridge existed, the seafloor at Site 572 would presumably have participated in the motion of two separate plates. One motion—ceasing about 11 m.y. ago—of easterly direction would have been generated by the fossil ridge. The other, primarily of westerly direction but with a minor northerly rotation, is still active and is associated with the East Pacific Rise. Proceeding despite these uncertainties, van Andel et al. (1975) backtracked and rotated Site 81 to find its position 15 m.y. ago; they predict a paleoposition for the site of about 2°S and 103°W, with an initial water depth of about 3200 m. If those estimates are correct, the present position of the site (just north of the equator at a water depth of about 3900 m) suggests that the site's absolute motion is, in paleoceanographic terms, less important (it has remained in close proximity to the equator since its origin) than its bathymetric descent of about 700 m. The latter involves a gradual sinking into the reaches of the lysocline, which in the central equatorial Pacific lies between about 3700 and 4000 m (Berger, 1970). This descent should find its expression in noticeable changes in the preservation of calcareous microfossils that are independent of the deposition of biogenic silica.

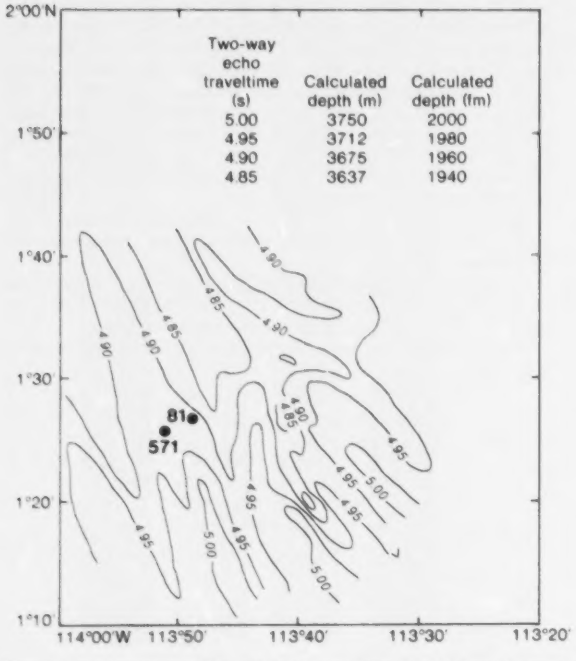

Figure 1. Bathymetry at Site 572. Data are from SCAN Leg 10 survey (Jan. 1970). In the calculation of depth, sound was assumed to travel at 1500 m/s or 800 fm/s.

The primary objective of the drilling at Site 572 was the recovery of a complete, undisturbed sedimentary section comprising approximately 15 m.y. of oceanographic and tectonic history at a location in the so-called equatorial "bulge." The latter is the depositional expression of a narrow belt of high planktonic productivity associated with the equatorial divergence. This narrow equatorial band has been a reliable marker of the equator during much of the Cenozoic, climatic and tectonic changes notwithstanding (van Andel et al., 1975).

OPERATIONS

The *Glomar Challenger* arrived in the vicinity of Site 572 at 0300Z on 22 March, 17 hr. after departing Site 571. During transit (we averaged 9 knots on a course of 172°), we collected continuous seismic profiles (air gun and 3.5 kHz) and bathymetric and magnetic data. Our plan was to find the position of DSDP Site 81, make a short survey of the area, and then drill where the sedimentary section appeared to be thickest. Unfortunately, the low latitude of the region (which meant that satellite fixes were infrequent) and overcast skies (which meant that star fixes were impossible) prevented an accurate determination of our position. When the first satellite fix came in (at 0230Z), we were about 12 n. mi. due west of Site 81, a position consistent with the presence of the strong (2-knot) westerly current that was with us throughout our stay at the site. We decided to aim for a position several miles south of Site 81 and to survey to the north. We attempted to find our location with respect to bathymetric data collected during a post-drilling site survey at Site 81 (SIO Expedition SCAN 10), but the data proved

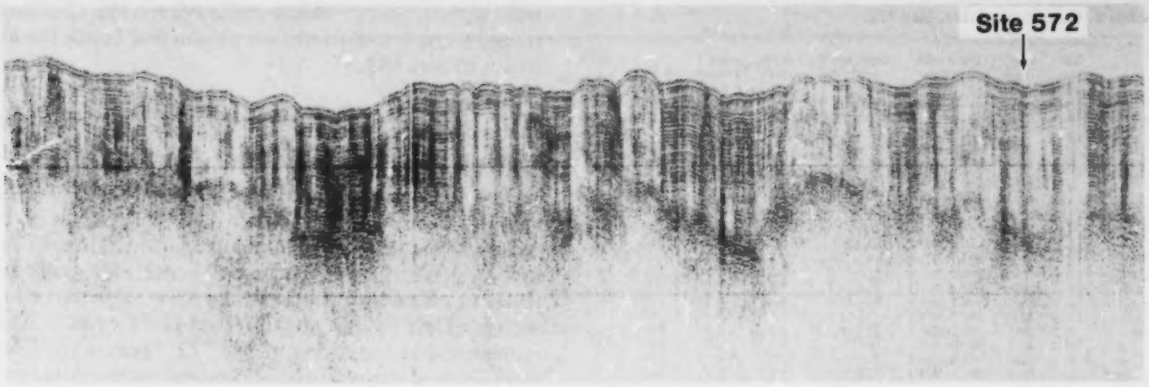

Figure 2. *Glomar Challenger* air gun seismic profile in the vicinity of Site 572 (5-s two-way traveltime).

to be too inaccurate to be useful. Of much greater help were depth-to-basement and isopach maps (also based on SCAN 10 data) that revealed a northwest-trending basement trough that was filled with more than 0.5 s of sediment. We followed this trough north until its closest approach to Site 81 and then dropped the beacon (at 0536Z on 22 March). We continued to acquire profiles for 2 n. mi. beyond the beacon drop; we then pulled the geophysical gear and returned to the site, now officially Site 572. The final location of Site 572 is 01°26.09′N, 113°50.52′W, approximately 0.4 n. mi. south and 1.5 n. mi. west of Site 81 (Fig. 1).

Drill pipe run-in began at 0745Z, with the first hydraulic piston core barrel on its way down at 1800Z. This first core barrel returned empty, and the drill string was lowered another 7 m. The next core overpenetrated, making the depth of the mudline impossible to determine. When our next core came back empty (because of a collapsed liner), we decided to pull up to the mudline and start Hole 572A. The mudline was established at 3903 m, in exact agreement with the depth estimated from the precision depth recorder (PDR).

We drilled Hole 572A to a sub-bottom depth of 154.1 m (17 cores; see Table 1). We used the 9.5-m variable-length HPC (VLHPC), and after each core was recovered we washed down the length of the previously recovered core. This maximized the chances of continuous recovery. We were disappointed to discover that 40% of the first 10 cores recovered were significantly disturbed. Most of the disturbance fell into the categories described in the Introduction (this vol.). To attempt to reduce disturbance the coring procedure was changed: pressure in the stand pipe was not bled off immediately after the corer shot off; instead, the pressure was allowed to bleed off through the HPC. Core quality improved, although the improvement was probably also due partly to the calmer seas and firmer sediments.

The coring at Hole 572A proceeded smoothly, with HPC stroking out completely and almost full recovery until Core 18, at 154.1 m sub-bottom, was reached. To retrieve Core 18 we had to generate 60,000 to 65,000 lb. of pullout force. When the end of the sandline arrived at the rig floor, we found that the ears on the quick disconnect had become deformed and that the quick disconnect had parted, leaving the core barrel behind in the hole. The problem was unexpected, because there had been no advance warning in the form of high pullout forces or poor recovery.

Because it would be difficult to fish for the lost core barrel, we decided to abandon the hole, wash down to 154 m in Hole 572B, and then continue to core with the 5-m HPC. We were able to collect four cores in this hole before limited penetration and more than 30,000 lb. of pullout force forced us to stop at 172.1 m sub-bottom.

We were supposed to double core this site, so we pulled back to the mudline, and at 1100Z on 24 March we once again began to collect 9.5-m hydraulic piston cores. As we drilled this hole (572C) we washed down 9.6 m after each core irrespective of core recovery. This policy resulted in the loss of some of the section (when the HPC returned with less than 9.6 m of sediment), but it enabled us to offset intercore gaps between the A and the C holes. At 96.5 m sub-bottom in Hole 572C, 30,000 lb. of pullout force became necessary, and we decided to switch to the 5-m core barrel. After three 5-m cores were retrieved with very low pullout force we returned to the 9.5-m core barrel, and we were able to take another six 9.5-m cores before pullout force once again became excessive.

At 160 m sub-bottom we again switched to the 5-m barrel, and we were able to penetrate another 8.5 m. After 168.5 m of nearly continuous coring, we pulled out of Hole 572C, tripped the drill string, and changed to a rotary drilling setup.

We began Hole 572D by washing down to 151 m sub-bottom and then rotary drilling with continuous coring. The average recovery from this hole was 81%. Drilling disturbance was fairly serious in the upper few cores, but it rapidly decreased as the sediment grew firmer. The sediments acquired at 360 m sub-bottom (Core 23, Section 6) could no longer be split with a wire and had to be cut with a rock saw instead. At 464.5 m sub-bottom we had not yet contacted basement, and we decided to wash to basement to establish the thickness of the section. We washed 15 m (through a part of the section previously cored at Site 81) and encountered basement at 479.5 m sub-bottom. After 1 hr. of drilling in basement, a 28-cm sample of basalt was returned to the deck. The drill string

Table 1. Coring summary, Site 572.

Core	Date (Mar. 1982)	Local time (hr.)	Depth from drill floor (m)	Depth below seafloor (m)	Length cored (m)	Length recovered (m)	Recovery (%)
Hole 572							
1	22	1250	3906.2–3915.5	0–9.5	9.5	9.25	100
2	22	1406	3915.5–3925.0	9.5–??	9.5	0	0
					19.0	9.25	49
Hole 572A							
1	22	1600	3903.0–3912.5	0.0–9.5	9.5	9.64	100+
2	22	1715	3912.5–3922.0	9.5–19.0	9.5	9.18	97
3	22	1840	3922.0–3931.6	19.0–28.6	9.6	9.66	100+
4	22	2010	3931.6–3939.3	28.6–36.3	7.7	7.7	100
5	22	2120	3939.3–3948.9	36.3–45.9	9.6	9.64	100
6	22	2235	3948.9–3958.2	45.9–55.2	9.3	9.31	100
7	23	0015	3958.2–3967.1	55.2–64.1	8.9	8.90	100
8	23	0155	3967.1–3975.3	64.1–72.3	8.2	8.22	100
9	23	0240	3975.3–3984.8	72.3–81.8	9.5	9.54	100+
10	23	0352	3984.8–3994.4	81.8–91.4	9.6	9.67	100+
11	23	0500	3994.4–4003.7	91.4–100.7	9.3	9.33	100+
12	23	0610	4003.7–4012.9	100.7–109.9	9.2	9.21	100+
13	23	0730	4012.9–4022.1	109.9–119.1	9.2	9.28	100+
14	23	0905	4022.1–4031.3	119.1–128.3	9.2	9.26	100+
15	23	1010	4031.3–4040.1	128.3–137.1	8.7	8.77	100+
16	23	1116	4040.1–4048.3	137.1–145.3	8.2	8.18	99
17	23	1240	4048.3–4057.1	145.3–154.1	8.8	8.86	100+
					154.00	154.35	100
Hole 572B							
1	23	1746	4057.0–4062.3	154.0–159.3	5.3	5.31	100
2	23	1920	4062.3–4067.2	159.3–164.2	4.9	4.93	100
3	23	2030	4067.2–4071.8	164.2–168.8	4.6	4.60	100
4	23	2210	4071.8–4075.1	168.8–172.1	3.3	3.38	100
					18.10	19.95	100
Hole 572C							
1	24	0255	3903.0–3913.1	0–10.1	10.1	9.57	95
2	24	0355	3913.1–3922.9	10.1–19.7	9.6	9.69	100+
3	24	0500	3922.9–3932.3	19.7–29.3	9.6	9.72	100+
4	24	0600	3932.3–3941.9	29.3–38.9	9.6	9.54	99
5	24	0700	3941.9–3951.5	38.9–48.5	9.6	9.62	100+
6	24	0805	3951.5–3961.1	48.5–58.1	9.6	9.65	100+
7	24	0911	3961.1–3970.7	58.1–67.7	9.6	9.80	100+
8	24	1014	3970.7–3980.3	67.7–77.3	9.6	9.64	100+
9	24	1120	3980.3–3989.9	77.3–86.9	9.6	9.42	98
10	24	1230	3989.9–3999.5	86.9–96.5	9.6	9.65	100+
11	24	1401	3999.5–4004.5	96.5–101.5	5.0	4.59	100+
12	24	1515	4004.5–4009.5	101.5–106.5	5.0	5.0	100
13	24	1630	4009.5–4014.5	106.5–111.5	5.0	5.06	100+
14	24	1850	4014.5–4024.1	111.5–121.1	9.6	9.48	83
15	24	1950	4024.1–4033.7	121.1–130.7	9.6	9.26	96
16	24	2105	4033.7–4043.3	130.7–140.3	9.6	9.38	98
17	24	2200	4043.3–4052.8	140.3–149.9	9.6	5.80	60
18	24	2305	4052.8–4062.4	149.9–159.5	9.6	9.30	97
19	25	0040	4062.4–4067.4	159.5–164.5	5.0	4.90	98
20	25	0156	4067.4–4071.4	164.5–168.5	5.0	4.0	80
					169.50	161.56	95
Hole 572D							
1	26	0138	4054.0–4063.5	151.0–160.5	9.5	5.30	56
2	26	0313	4063.5–4073.0	160.5–170.0	9.5	9.83	100+
3	26	0454	4073.0–4082.5	170.0–179.5	9.5	9.76	100+
4	26	0610	4082.5–4092.0	179.5–189.0	9.5	9.55	100+
5	26	0756	4092.0–4101.5	189.0–198.5	9.5	9.77	100+
6	26	0929	4101.5–4111.0	198.5–208.0	9.5	9.59	100+
7	26	1058	4111.0–4120.5	208.0–217.5	9.5	9.62	100+
8	26	1230	4120.5–4130.0	217.5–227.0	9.5	9.78	100+
9	26	1345	4130.0–4139.5	227.0–236.5	9.5	5.06	53
10	26	1500	4139.5–4149.0	236.5–246.0	9.5	9.60	100+
11	26	1620	4149.0–4158.5	246.0–255.5	9.5	9.73	100+
12	26	1747	4158.5–4168.0	255.5–265.0	9.5	6.33	67
13	26	1910	4168.0–4177.5	265.0–274.5	9.5	7.50	79
14	26	2045	4177.5–4187.0	274.5–284.0	9.5	7.46	79
15	26	2200	4187.0–4196.5	284.0–293.5	9.5	3.91	41
16	26	2330	4196.5–4206.0	293.5–303.0	9.5	9.50	100+
17	28	0050	4206.0–4215.5	303.0–312.5	9.5	3.43	36
18	28	0215	4215.5–4225.0	312.5–322.0	9.5	8.63	91
19	28	0345	4225.0–4234.5	322.0–331.5	9.5	3.76	40
20	28	0508	4234.5–4244.0	331.5–341.0	9.5	3.46	36
21	28	0642	4244.0–4253.5	341.0–350.5	9.5	7.63	80
22	28	0750	4253.5–4263.0	350.5–360.0	9.5	4.26	45
23	28	0925	4263.0–4272.5	360.0–369.5	9.5	9.46	96
24	28	1045	4272.5–4282.0	369.5–379.0	9.5	9.15	96
25	28	1200	4282.0–4291.5	379.0–388.5	9.5	9.73	100+
26	28	1320	4291.5–4301.0	388.5–398.0	9.5	8.65	90
27	28	1435	4301.0–4310.5	398.0–407.5	9.5	9.68	100+
28	28	1545	4310.5–4320.0	407.5–417.0	9.5	7.21	76
29	28	1715	4320.0–4329.5	417.0–426.5	9.5	7.04	74
30	28	1845	4329.5–4339.0	427.5–436.0	9.5	7.55	79
31	28	2000	4339.0–4348.5	436.0–445.5	9.5	8.50	89
32	28	2120	4348.5–4358.0	445.5–455.0	9.5	8.59	90
33	28	2210	4358.0–4367.5	455.0–464.5	9.5	9.79	100+
Wash to basement			4367.5–4382.5	464.5–479.5			
34	28	0830	4382.5–4392.0	479.5–489.0	9.5	0.28	3
					320.0	258.92	81

was tripped, and at 1630Z on 28 March the *Challenger* turned its bow toward the setting sun and began the long steam to Site 573.

LITHOSTRATIGRAPHY

Lithostratigraphic Subdivision

The lithology cored at Site 572 consists of two sedimentary units that overlie basalt. Unit I, the cyclic siliceous calcareous ooze chalk, consists of laminated, burrow-mottled siliceous calcareous oozes that grade into siliceous calcareous chalks in the lowermost part of the section. Unit II, the metalliferous chalk, was not well represented in the coring at Site 572, because the lowermost 15 m of the sedimentary section were washed away in order to reach basement in the time allotted to the drilling at this site. However, the metalliferous chalk unit was recovered during the drilling at Site 81. The lithostratigraphic subdivision of Site 572 is shown in Table 2.

Unit I: Cyclic Siliceous Calcareous Ooze Chalk (Quaternary to middle Miocene)

Unit I extends from the sediment/water interface to a depth (in Hole 572D) of 464.5 m. It consists of siliceous calcareous oozes to siliceous nannofossil oozes, which grade into siliceous nannofossil chalks. The transition between ooze and chalk takes place in the interval between 293.5 and 367.5 m sub-bottom.

There are cyclic variations in color throughout the section. The dominant color variations have been used to subdivide Unit I into four subunits: the gray brown, varicolored, green varicolored, and the yellow chalk subunits. This subdivision is based solely on color; the sediment's color does not appear to be directly related to texture or microfossil content.

Subunit IA: Gray Brown Ooze (Quaternary)

The gray brown subunit extends from the sediment/water interface to a depth of 2.35 m in Hole 572A. The unit is composed of alternating brown and gray sediment. The brown sediment consists of grayish brown (10YR 5/3), light brown (7.5YR 5/2 to 10YR 7/4), and yellow brown (2.5Y 8/2) foraminiferal diatom nannofossil ooze to foraminiferal siliceous nannofossil ooze. The gray sediment has the same composition but is dark gray (N3 to N6), greenish gray (5G 7/1 to 5Y 7/2), and light gray (2.5Y 7/1 to 5Y 7/1). The siliceous microfossil content of the sediment does not directly influence its color. Contacts between the brown and gray intervals are sharp to gradational. This cyclic alternation extends down to the first purple (5P 2/2 to 5RP 2/2) band in the sediment.

Sediments of the gray brown subunit are of uniform composition, with abundant (30 to 50%) clay-sized particles, abundant (30 to 40%) silt-sized particles, and common (10 to 30%) sand-sized particles. Calcareous nannofossils are abundant (25 to 75%), foraminifers are common (5 to 25%), radiolarians are rare (1 to 5%) to common (5 to 15%), and diatoms are common to abundant. Silicoflagellates, sponge spicules, and volcanic glass particles occur sporadically in rare (1 to 5%) amounts.

Table 2. Lithostratigraphy of Site 572.

Lithologic unit	Unit sub-bottom depth (m)	Unit depth (Hole-Core-Section, level in cm)
I (cyclic siliceous calcareous ooze chalk) A (gray brown ooze)	0–2.35	572-1-1, 1 to 572-1-1, 105 572A-1-1, 1 to 572A-1-2, 85 572C-1-1, 1 to 572C-1-1, 125
B (varicolored ooze)	2.35–37.45	572-1-1, 105 to 572-1,CC 572A-1-2, 85 to 572A-5-1, 98 572C-1-1, 125 to 572C-4-6, 65
C (green varicolored ooze)	37.45–458.75	572A-5-1, 98 to 572A-17,CC 572B-1-1, 1 to 572B-4,CC 572C-4-6, 65 to 572C-20,CC 572D-1-1, 1 to 572D-33-3, 75
D (yellow chalk)	458.75–464.50	572D-33-3, 75 to 572D-33-7, 54
II (metalliferous chalk)	464.50–?	572D-33,CC
III (basalt)	479.50–489.00	572D-34-1, 1 to 572D-34,CC

Subunit IB: Varicolored Ooze (Quaternary to upper Pliocene)

The varicolored subunit extends from 2.35 to 37.45 m. This subunit is defined as extending from the first band of purple ooze (5P 2/2 to 5RP 2/2) down to the appearance of pale green (10G 6/2 to 5G 7/1) ooze. The varicolored subunit is typified by the cyclic alternation of bands (5 to 25 cm in thickness) of purple, light gray, and yellow sediments. The purple bands are composed of pale purple (5P 2/2 to 5RP 2/2), dark gray (N3 to N6), and greenish gray (5G 7/1 to 5Y 7/1) sediments; the light gray bands are composed of bluish white (5B 9/1), white (N9), and light gray (N7 to N8) sediments; and the yellow bands consist of pale yellow (2.5Y 8/4), yellow green (2.5Y 7/2 to 5Y 7/2), and yellow gray (5Y 8/1) sediments. There is no apparent relationship between sediment color and microfossil composition; Subunit IB ranges from diatom nannofossil oozes and siliceous nannofossil oozes to foraminiferal radiolarian diatom nannofossil oozes.

The varicolored subunit sediments are composed of abundant to dominant (30 to 80%) clay-sized particles, common to abundant (5 to 40%) silt-sized particles, and common (10 to 30%) sand-sized particles. Calcareous nannofossils are abundant (40 to 80%), foraminifers are generally rare (1 to 10%), and radiolarians are rare to common (2 to 25%). Diatoms are generally abundant (20 to 40%), although they are less abundant (1 to 5%) in the siliceous nannofossil oozes. Occasional trace (1%) amounts of pyrite, silicoflagellates, and volcanic glass are found in the varicolored subunit.

Subunit IC: Green Varicolored Ooze Chalk (upper Pliocene to middle Miocene)

The green varicolored subunit extends from 37.45 to 458.75 m sub-bottom. It is defined as occurring from the first band of pale green (10G 6/2 to 5G 7/1) ooze down to the burrow-mottled laminated yellow (2.5Y 8/1 to 2.5Y 7/4) chalks. The green varicolored ooze contains alternating bands 5 to 25 cm thick of four different colors: (1) purple to pale purple (5P 2/2 to 5RP 2/2), dark gray (N3 to N6), greenish gray (5G 7/1 to 5Y 7/1), and pale blue (5PB 7/2); (2) bluish white (5B 9/1), white (N9), and light gray (N7 to N8); (3) pale yellow (2.5Y 8/4), yellow green (2.5Y 7/2 to 5Y 7/2), and yellow gray (5Y 8/1); and (4) pale green (5G 6/2 to 5GY 7/1), olive green (5GY 3/2), and blue green (5BG 7/2). At the top of this subunit, these colors are cyclic, the bands of light gray passing down into those of purple, green, and yellow. In some cores only the purple and light gray bands alternate, however.

The transition from ooze to chalk occurs in Subunit IC from 293.5 to 367.5 m sub-bottom (572D-16-1 to 572D-23-6). The transition starts in a core (572-16-1) that contains friable instead of plastic sediments, and it continues through an interval in which chalk alternates with ooze. Chalk becomes continuous in Section 572D-23-6; splitting of all deeper cores required the use of a rotary saw. Toward the base of the unit (572D-28-1 to 572D-33-3), the sediments become more uniformly green in color, and they contain burrow structures that are better preserved. In this interval there are discrete layers of bright green (5G 3/2 to 5BG 3/2) diatomites (e.g., 572D-29-1, 125 cm). Foraminifers are common (10 to 25%) only within this lowermost green chalk interval (572D-28-1 to 572D-33-3).

Middle Miocene chert fragments occur within and below the ooze chalk transition beds of Subunit IC (572D-18-1 to 572D-24-1). Separate 1-cm-diameter fragments of olive green (5Y 5/3) and light green (5GY 7/1) banded chert appear in the uppermost sediments of Sections 572D-18-1 and 572D-19-1, and a few small (0.5-cm-diameter) chert fragments were recovered from the top few centimeters of Section 572D-24-1. In the lower chalks of this subunit (572-30-1, 36–40 cm and 88–91 cm), we observed chert bands 3 to 4 cm thick of alternating dark and light gray.

The grain size of the green varicolored subunit is relatively constant, with abundant (50 to 75%) clay-sized particles, common to abundant (5 to 40%) silt-sized particles, and common to abundant (5 to 45%) sand-sized particles. The upper part of the unit is made up of diatom nannofossil to siliceous nannofossil oozes, with oc-

casional discrete layers of nannofossil diatom ooze. There are occasional traces (1%) of volcanic glass, pyrite, and zeolite. From 293.5 to 367.5 m sub-bottom the subunit consists of siliceous nannofossil and diatom nannofossil oozes, which grade into chalks of the same composition. Below 367.5 m the unit is composed of foraminiferal siliceous chalks and foraminiferal radiolarian diatom chalks.

Subunit ID: Yellow Chalk (middle Miocene)

The yellow chalk subunit extends from 458.75 m to 464.50 m sub-bottom. It is defined as extending from the first burrow-mottled laminated yellow chalk down to the first metalliferous chalk. Subunit ID is composed of pale yellow (2.5Y 8/4 to 2.5Y 7/4), yellow white (2.5Y 8/2 to 2.5Y 8/1), and pale yellowish green (10Y 8/1) siliceous foraminiferal nannofossil chalks. These sediments have abundant (35 to 60%) clay-sized particles, common to abundant (20 to 30%) silt-sized particles, and common to abundant (20 to 35%) sand-sized particles. The subunit contains rare (1 to 8%) radiolarians and diatoms, common (20 to 35%) foraminifers, and abundant (30 to 50%) nannofossils, plus abundant (15 to 40%) unspecified carbonate particles, which may be the result of carbonate recrystallization.

Unit II: Metalliferous Chalk (middle Miocene)

The lowermost sediment sample in Hole 572D (33,CC) contains siliceous foraminiferal nannofossil chalk, with common (5%) pyrite and iron oxides (10%). Although recovery is minimal, we believe that these sediments belong to the metalliferous chalk unit that was cored at Site 81. The metalliferous enrichment of this sediment may be associated with the hydrothermal activity that takes place at or near ridge crests. The drilling results at Site 81 lead us to assume that this unit extends from 572D-33,CC (464.5 m sub-bottom) to the sediment/basalt contact at 479.5 m.

Unit III: Basalt

We recovered 28 cm (9 pieces) of basalt from drilling Hole 572D from 479.50 to 489.00 m sub-bottom.

Bioturbation

Bioturbation is common to abundant throughout the sedimentary section. It occurs primarily as subhorizontal burrows with 1-cm circular to elliptical cross sections (Planolites). Burrow mottling is most obvious just below the subunit boundaries, where sediments of different color have mixed. Burrow fill with high pyrite content (up to 30%) occurs in the varicolored subunit. There are dark-colored pyrite-rich oval burrows in both the varicolored ooze and the green varicolored ooze–chalk subunits, and several elongate (3- to 5-cm-long), flattened pyrite rods were found within them. The best preserved burrows are found in the green varicolored chalk and the yellow chalk. The ichnogenera Planolites (Fig. 3), Zoophycos (Fig. 4), and Chondrites were identified in these subunits.

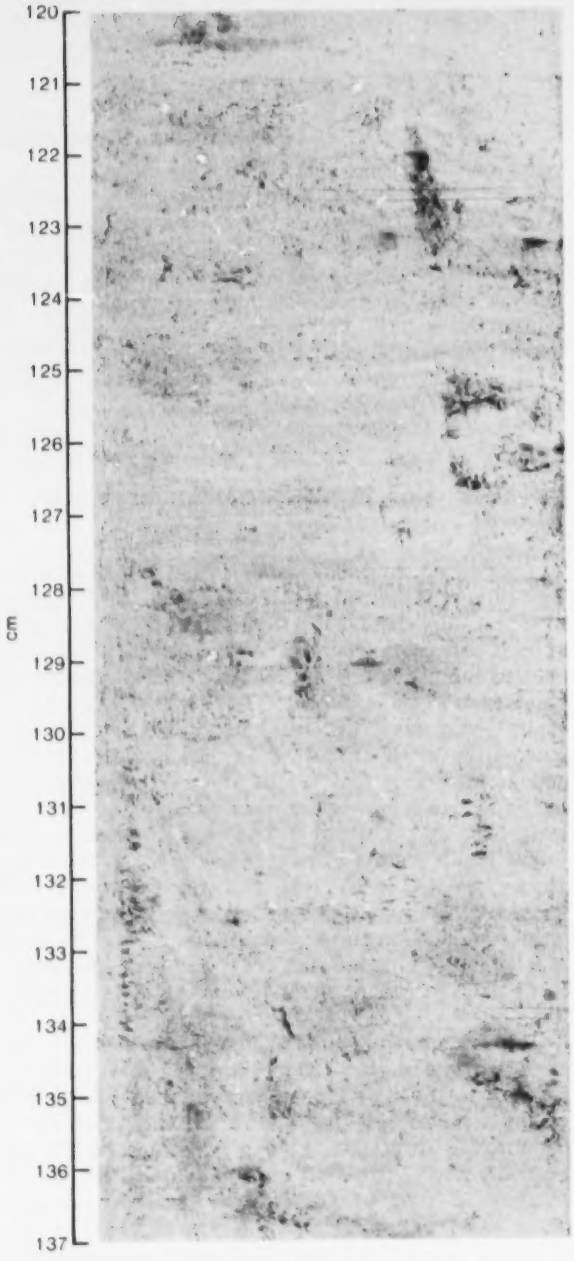

Figure 3. Burrow structures of the ichnogenus Planolites (from 572C-6-2; see 122 cm and 135 cm).

Sedimentary Cycles

The dominant feature of the Site 572 sediments is cyclicity of color. The color changes are not accompanied by changes in grain size or microfossil composition. The horizontal color boundaries may reflect chemical inhomogeneities produced by diagenesis. In some cores the

Figure 4. Burrow structures of the ichnogenus Zoophycos (from 572D-31-1; see 137 cm, 140 cm, and 142 cm).

alternation of millimeter-scale dark and light laminae is spectacular (Fig. 5).

Correlation with Site 81

Although the coring at Site 81 was not continuous, our color-based lithologic classification enabled us to correlate our lithostratigraphic units with the oceanic formations defined by Hays et al. (1972). The gray brown ooze (Subunit IA) corresponds to the cyclic unit in the Clipperton Oceanic Formation, and our varicolored subunit (IB) corresponds to the varicolored unit in the Clipperton Oceanic Formation. We found the transition from the varicolored ooze to the green varicolored ooze at 37.45 m instead of the 60 m predicted by Hays et al. (1972) from seismic correlations. Our green varicolored ooze–chalk (IC) corresponds to the predominantly green San Blas Oceanic Formation. Although the individual laminae in the green varicolored ooze chalk may be quite thin (Fig. 5), this sedimentary unit was described as massive bedding at Site 81, probably because the discrete green laminae were smeared into a homogeneous green sediment by rotary drilling. Our yellow chalk (Subunit ID) corresponds to the Line Islands Ocean Formation of Hays et al. (1972). Metal-rich mudstones immediately overlie the basalt/sediment contact at Site 81; our recovery of this sequence was incomplete.

Carbonate Stratigraphy

As shown by Figure 6, the sequence at Site 572 alternates between intervals of high carbonate content (80 to 90%) and low carbonate content (45 to 65%). The alternation is typical of sedimentary sequences from the eastern equatorial Pacific. Extreme carbonate minima (carbonate contents less than 45%) occur near the upper/lower Miocene boundary (265 to 315 m sub-bottom), a zone of extreme foraminiferal dissolution.

There are distinct changes in the sedimentation rate curve at depths of 70, 208, 272, and 360 m sub-bottom, all of which are correlated with pronounced carbonate minima. Further analysis would be necessary to determine whether the correlation is apparent or real, however, because other extreme carbonate minima (e.g., those at 162, 172, 290, 310 m) occur without corresponding changes in sedimentation rate. There are possible hiatuses in sedimentation rate at 382 and 420 m. Both depths are characterized by pronounced carbonate minima, so the hiatuses may be due to either carbonate dissolution or reduced accumulation rate. See Barron et al. (this vol.) for a more detailed discussion.

The data in Figure 6 (shipboard carbonate data taken at 1.5-m intervals) can be correlated with the equatorial Pacific carbonate event stratigraphy developed for the Pleistocene by Hays et al. (1969), for the Pliocene to late Miocene by Dunn and Moore (1981), and for the middle to early Miocene by Dunn (1982).

BIOSTRATIGRAPHY

A complete sequence of sediments from the upper Pleistocene through the lowermost middle Miocene was recovered at Site 572. The siliceous microfossils are consistently common to abundant throughout the sequence,

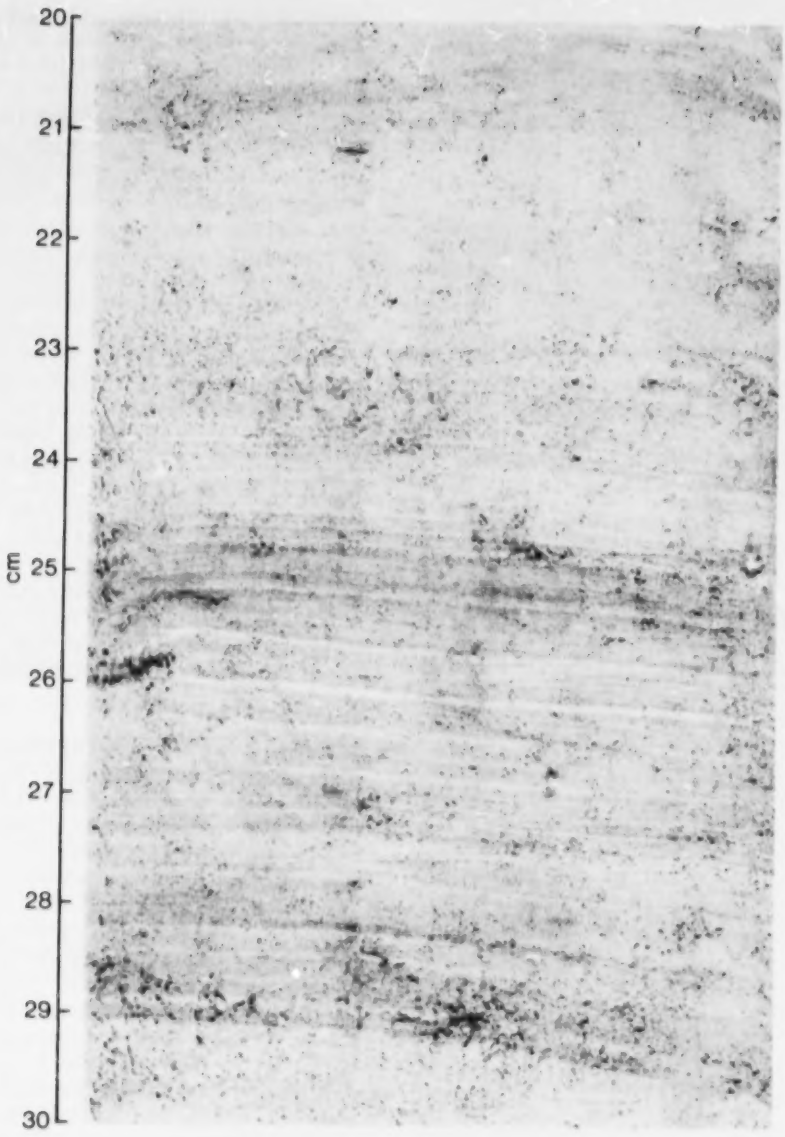

Figure 5. Millimeter-scale alternation of dark and light laminae at Site 572 (572C-6-3, 20–30 cm).

whereas the calcareous microfossils are abundant only in its upper part (Pliocene and Pleistocene). Calcareous fossils are rare in the middle part of the cored sequence (most of the upper Miocene) as the result of severe dissolution.

The succession of diatom and planktonic foraminifer datums in the Pliocene–Pleistocene sequence is identical to the succession of datums in paleomagnetically dated deep-sea sequences from the eastern equatorial Pacific (Burckle, 1972, 1978; Hays et al., 1972; Saito et al., 1975). The previously established dates for these datums provided good control for our time–rock subdivisions. The biostratigraphy at Site 572 is summarized in Figure 7. An updated version of this summary is presented in Barron et al. (this vol.).

The Pliocene/Pleistocene boundary is in Core 3 (28 m sub-bottom) in both Holes 572A and 572C. It is recognized by the extinction of planktonic foraminifer *Globigerinoides obliquus*, nannofossil *Discoaster brouweri*, and radiolarian *Pterocanium prismatium*. The Miocene/Pliocene boundary is in Cores 572A-13 and 572C-14. The first appearance level of *Globorotalia tumida* and the concomitant disappearance of *Globoquadrina dehiscens* mark the boundary, which is nearly coincident with the disappearance of the diatom *Thalassiosira miocenica*. The disappearance of *T. miocenica* marks the B/C Subzone boundary within the *Thalassiosira convexa* Zone.

In the European type area, the middle/upper Miocene boundary lies within the foraminiferal Zone N15

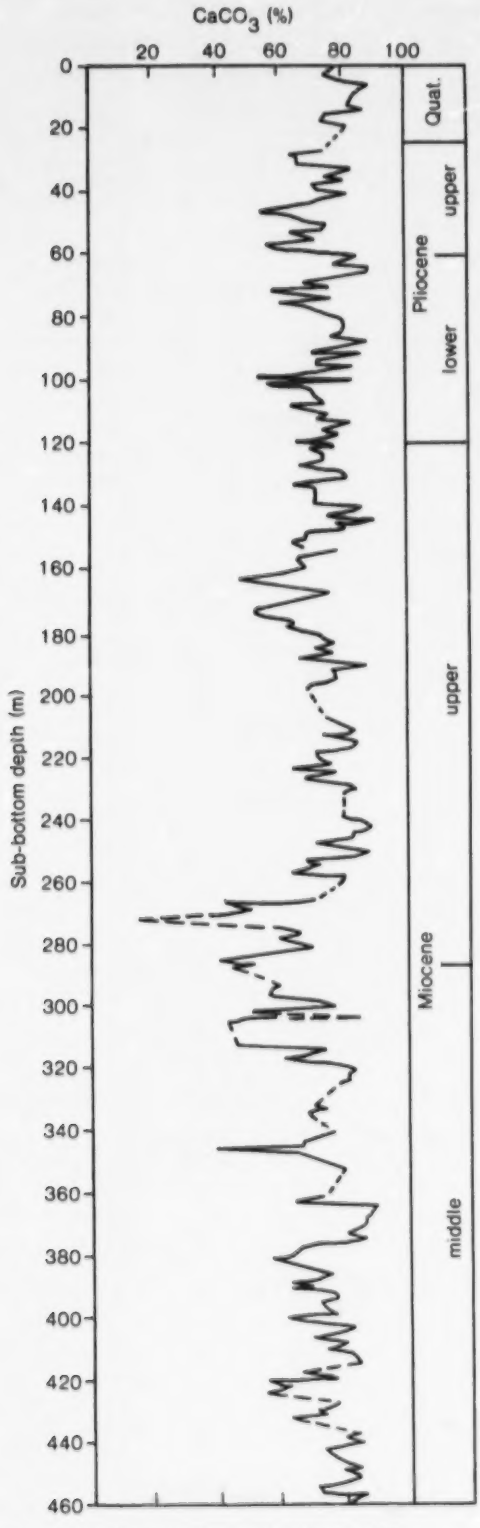

Figure 6. Shipboard carbonate data for Site 572.

and the nannofossil *Discoaster hamatus* Zone (Van Couvering and Berggren, 1977). In our time scale, this boundary has an age of approximately 11.1 Ma. The sediment accumulation rate curve for Site 572 indicates that a boundary of this age should occur in Core 572D-15. The oldest sediment recovered at this site contains nannofossils indicative of the *Sphenolithus heteromorphus* Zone, planktonic foraminifers belonging to Zone N9, radiolarians assignable to the *Dorcadospyris alata* Zone, and diatom floras diagnostic of the *Cestodiscus peplum* A Subzone. Thus, the oldest sediment at Site 572 is from the beginning of the middle Miocene; its age is estimated to be about 15 Ma.

The upwelling diatoms *Thalassionema nitzschioides* and *Thalassiothrix longissima* are a dominant element in the siliceous microfossil assemblages from Sections 572A-8,CC through 572D-7,CC (from 4.0 to 7.8 Ma) and from Sections 572D-11,CC through 572D-18,CC (from 10.0 to 12.2 Ma). These diatom-rich intervals correspond closely to intervals of low carbonate content (from 4.2 to 6.95 Ma) and to intervals where the calcareous microfossils are strongly affected by dissolution (from 6.95 to 13.0 Ma). The correlation between an abundance of upwelling diatoms and an increase in carbonate dissolution suggests that the same mechanism caused both phenomena. High sediment accumulation rates characterize two intervals of the Site 572 sedimentary column the upper middle section (68 to 208 m sub-bottom) and the lower section (272 to 480 m sub-bottom). Since there is no marked increase in calcareous microfossils or radiolarians in these intervals, the high sediment accumulation rates are most likely to be the result of high diatom productivity. See Theyer et al. (this vol.) for an updated discussion.

Planktonic Foraminifers

The analysis of the planktonic foraminifers permits the division of the cored sequence into an upper sequence (from Cores 1 through 17 in the A and C holes), which contains abundant and well preserved faunas, and a lower sequence, which yields moderately well preserved but impoverished assemblages. The impoverished assemblages consist of solution-resistant forms: robust globoquadrinids, globorotaliids, and cortex-covered sphaeroidinellids.

The downhole change from the upper rich to lower monotonous assemblages is sharp. In Hole 572C it occurs between Cores 17 and 18. Almost no planktonic species are present in Section 572C-17,CC. A well preserved and diverse assemblage is encountered toward the basement (Hole 572D, Cores 30 through 33), however.

To graphically illustrate the varying degrees of foraminifer dissolution, the 10-point foraminifer solution code of Berger and von Rad (1972) was calculated for each assemblage (Fig. 8; high solution code numbers correspond to higher solution). The plot shows two intervals of marked dissolution in the middle of the cored sequence (Hole 572D, Cores 2 to 8 and 11 to 18; 160 to 220 m and 250 to 320 m).

The upper carbonate-rich sequence at this site can be correlated with the paleomagnetically dated deep-sea se-

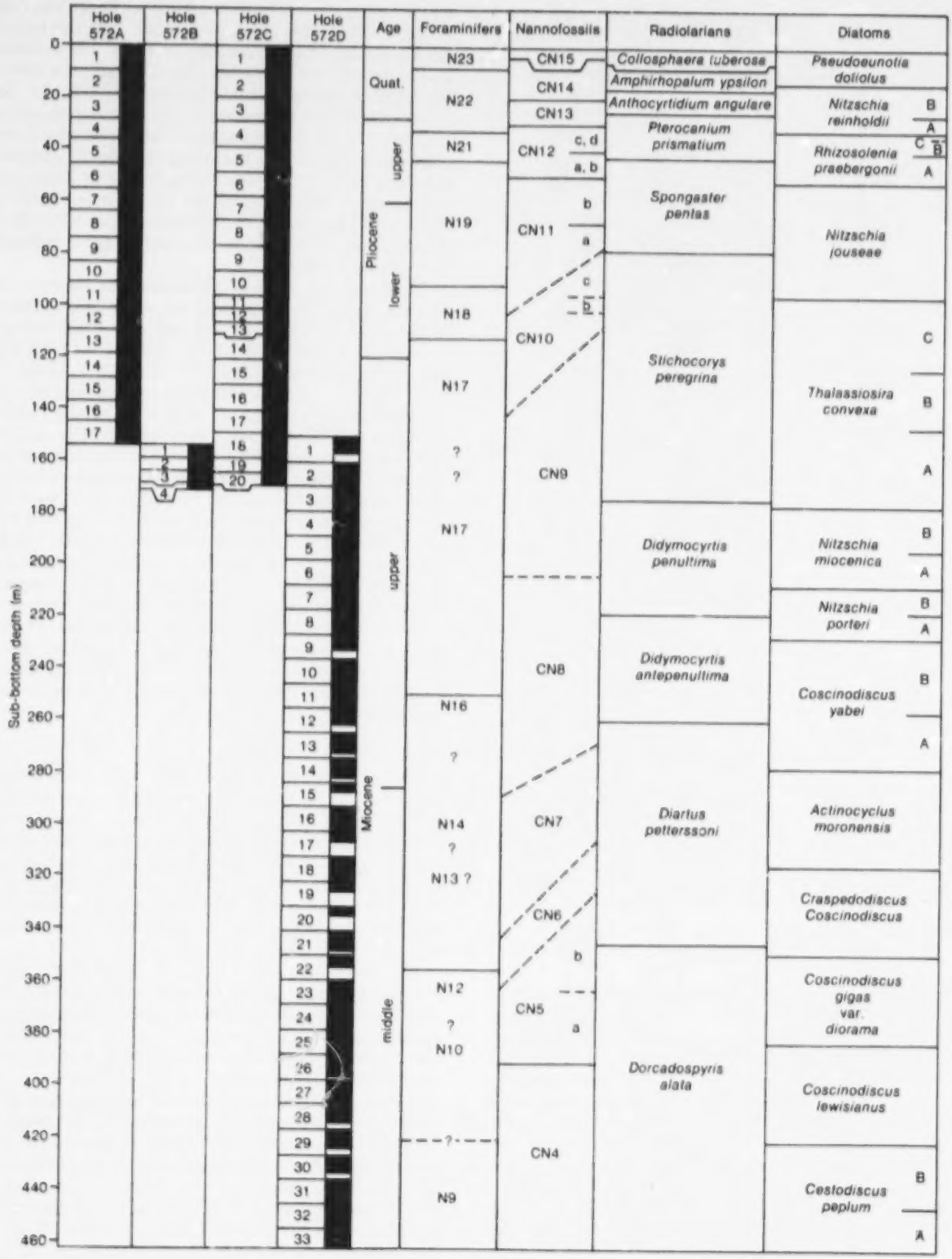

Figure 7. Summary of biostratigraphy at Site 572. Black portions of cores show recovery. Zonal boundaries are dashed when the position is uncertain or varies between the holes.

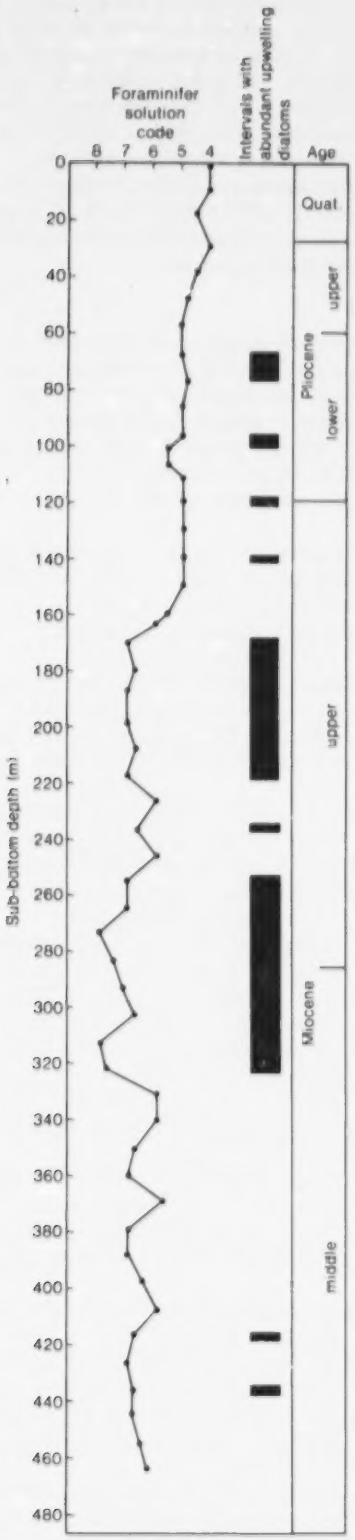

Figure 8. Foraminifer solution curve for Site 572; numbers after Berger and von Rad (1972).

quence from the eastern equatorial Pacific (Hays et al., 1969; Saito et al., 1975). Such a correlation places the base of the Quaternary between Sections 3,CC and 4,CC in both Holes 572A and 572C. The conspicuous presence of *Globoquadrina pseudofoliata* in Sample 572A-1-1, 2–5 cm indicates that no Holocene or uppermost Pleistocene sediments were recovered. The position of the Miocene/Pliocene boundary is based on the evolutionary appearance of *Globorotalia tumida*, which is accompanied by the extinction of *Globoquadrina dehiscens*; in Hole 572A these events occur between Sections 12,CC and 13,CC, and in Hole 572C they occur between Sections 13,CC and 14,CC.

Because of the effects of dissolution, the Miocene is difficult to divide into time-rock units. The successive appearance of all the zonally diagnostic species (Blow, 1969) in the downhole sequence, however, indicates that sedimentation was continuous at this site throughout the upper and middle Miocene.

The base of the sequence corresponds to lowermost middle Miocene, as evidenced by the rare occurrence of *Orbulina universa* in Section 572D-33,CC. In addition to *Orbulina*, this lowermost assemblage includes *Globorotalia peripheroronda* and *Globorotalia praemenardii* and is assigned to Zone N9, the lowest zone in the middle Miocene.

The Leg 9 paleontologists reported lower Miocene *Globigerinoides bisphericus* assemblages at the base of Hole 81 (Hays et al., 1972). Since *G. bisphericus* is an ancestor of *Orbulina universa*, the obvious implication is that the basal sediment at Site 81 is older than the basal sediment in Hole 572D by one foraminiferal zone. However, the zonal assignment of Leg 9 was based not on the presence of the zonal marker species but rather on the occurrence of *Hastigerinella bermudezi* (referred to as *Clavatorella bermudezi* in this report). *C. bermudezi* does occur at Site 572—in Core 32, where it is associated with a Zone N9 assemblage. Blow (1969) reported *H. bermudezi* to range from the uppermost part of Zone N8 through the lower part of Zone N10, so the basal sediment at Site 81 might be of Zone N8 age. Before the discovery of this species in the eastern equatorial Pacific by Leg 9 scientists, however, *C. bermudezi* was known only from the Caribbean region (Blow, 1965; Saito et al., 1976). The same Leg 9 report shows the range of *C. bermudezi* in a more continuously cored sequence at Site 77, about 960 km due west of both Sites 81 and 572 in the same general eastern equatorial Pacific region, to be restricted to the middle Miocene (in zones equivalent to N9 and N10). The basal sediment at Site 81 is interpreted here to be of Zone N9 age, in agreement with the findings at Site 572.

Nannofossils

Coccoliths are common to abundant in all samples from the five holes at this site. In some intervals dissolution is present, as indicated by the presence of slightly slashed shields and (in some species) missing central grids. The effects of dissolution are particularly pronounced in some samples from Holes 572A (Sections 1,CC to 4,CC), 572B (Sections 3,CC to 4,CC), and 572D (Sec-

tions 6,CC to 17,CC and 28,CC to 33,CC). The abundance and range of nannofossil species at Site 572 are shown in Figure 9.

In the Miocene–Pliocene interval, discoasters are generally present, although they are seldom abundant because of dissolution (which is particularly severe in 572A-7,CC; 572C-7,CC, -10,CC, -11,CC; 572D-2,CC, -11,CC). They disappear entirely in some sections (572A-8,CC to -13,CC and in -16,CC; 572-6,CC, -9,CC, -11,CC, and -20,CC; 572D-3,CC, to -7,CC, -12 to -21,CC, and in -25,CC). In Sections 572D-29,CC through -33,CC, the discoasters are partially dissolved and recalcified. Identification of *Discoaster* specimens was often difficult. Ceratoliths are rare at this site, with the exception of *Ceratolithus cristatus*.

In establishing the present nannofossil zonation, we made use of the stratigraphic chart of Bukry (1973), which includes some Pacific species. The five holes can easily be correlated with one another. Hole 572 consists of only one Pleistocene core. The well preserved nannofossils in this core are assigned to Zones CN15 and CN13. The dominant taxa present include *Emiliania huxleyi, Gephyrocapsa lumina, G. caribbeanica, Pseudoemiliania lacunosa*, and *Crenalithus doronicoides*. The same assemblages of Pleistocene nannofossils were found at the top of Holes 572A and 572C. The earliest Pleistocene assemblage (CN13a: in Sections 572A-3,CC and 572C-3,CC) is characterized by the presence of *Cyclococcolithina macintyrei*.

Pliocene floras are present in Holes 572A and 572C, with abundant nannofossils in the upper part of the Pliocene section. The discoasters characteristic of this period (*D. surculus, D. pentaradiatus, D. tamalis*, and the dominant *D. brouweri*) are rare. The lower part of the Pliocene sequence is distinguished in Hole 572C by a few *Sphenolithus neoabies* and *D. asymmetricus* (CN11b: in 572C-6,CC and -7,CC) and some very rare *Ceratolithus amplificus* (CN10b: in 572C-11-3, 0–1 cm).

The Miocene/Pliocene boundary occurs in Holes 572A and 572C in sediments that contain few diagnostic species. In both holes, however, this interval is characterized by common *D. quintanus*, which may be considered a marker for this period (Bukry and Bramlette, 1969)

In the lower part of the upper Miocene, the dominant species of *Discoaster* is *D. berggrenii*. In the eastern equatorial Pacific (Bukry, 1973), *D. berggrenii* appears in Zone CN8b, and it becomes most abundant in Zone CN9a. This species is abundant in Sections 572C-14,CC through -18,CC and in Sections 572D-8,CC through -14,CC. The distinction of Zone CN9 from CN8 depends on the criteria used. If the earliest period of maximum abundance of the marker species *D. berggrenii* is used to define the CN8/CN9 zonal boundary, the boundary lies in Hole 572D between Sections 14,CC and 15,CC. However, this boundary position is incompatible with the other taxa present. Therefore, the latest period of peak abundance of *D. berggrenii* is chosen to define the base of Zone CN9a. The earliest period of peak abundance is assigned to Zones CN7 to CN8. We propose the placement of a transition zone ("CN8/9") between the two peak abundance periods.

The upper/middle Miocene boundary cannot be placed with nannofossils, because it occurs (in Hole 572D) in sediments that contain moderately preserved placoliths and few discoasters. The oldest sediment at this site (Sections 572D-27,CC to -33,CC) yields abundant specimens of *Sphenolithus heteromorphus*, a species indicative of Zone CN4. The presence of some specimens of *Cyclicargolithus floridanus* and *Helicopontosphaera ampliaperta* from Core 31 to Section 572D-33,CC suggests that these samples lie near Zone CN3 (upper lower Miocene), although this zone was not reached.

Radiolarians

Radiolarians are common to abundant in the sediment recovered at this site. In some sections they are overwhelmed by an abundant upwelling diatom flora, but they constitute a diverse fauna nevertheless. The radiolarians are well preserved throughout the section, although the samples become more indurated as depth in Hole 572D increases, making prolonged cleaning necessary.

Hole 572 yielded a single core, the core-catcher sample from which can be placed in the *Amphirhopalum ypsilon* Zone. An additional core-catcher sample recovered during the second attempt to core Hole 572 belongs to the *Anthocyrtidium angulare* Zone.

The radiolarian zonation for the rest of the sediments recovered at this site is summarized in Figure 7 (the zonation is after Nigrini, 1971, and Riedel and Sanfilippo, 1978). The following features of the zonation warrant mention:

1. The boundary between the *Spongaster pentas* Zone and the *Stichocorys peregrina* Zone is marked primarily by the first occurrence of *Pterocanium prismatium*. The transition between *Spongaster berminghami* and *S. pentas* cannot be well documented because of the rarity of both species at the boundary level. *S. berminghami* occurs more frequently at lower levels in the cored sequence.

2. The *Stichocorys peregrina* Zone is unusually thick at this site because of the very high sediment accumulation rate in the area. The only known datum for radiolarians within the *S. peregrina* Zone is the latest occurrence of *Acrobotrys tritubus* at 5.0 Ma. However, the species is so rare at this site that its latest occurrence cannot be reliably determined.

3. In the *Didymocyrtis antepenultima* Zone neither the last occurrence of *Dictyocoryne ontongensis* nor the first occurrence of *Acrobotrys tritubus* could be determined because of the rarity of specimens of these species.

4. No species of *Dorcadospyris* were observed at Site 572, so it cannot be determined whether the *Calocycletta costata* Zone was penetrated. However, the last appearance of *Calocycletta virginis* in Section 572D-31,CC suggests that the hole bottomed very close to the *D. alata* (middle Miocene)/*C. costata* (early Miocene) zonal boundary.

5. Observable events within the *Dorcadospyris alata* Zone include: an abrupt transition from *Lithopera renzae* to *L. neotera* between 572D-22,CC and -23,CC; the first occurrence of *L. thornburgi* at 572D-25,CC; and the first occurrence of *Phormostichoartus corbula* at

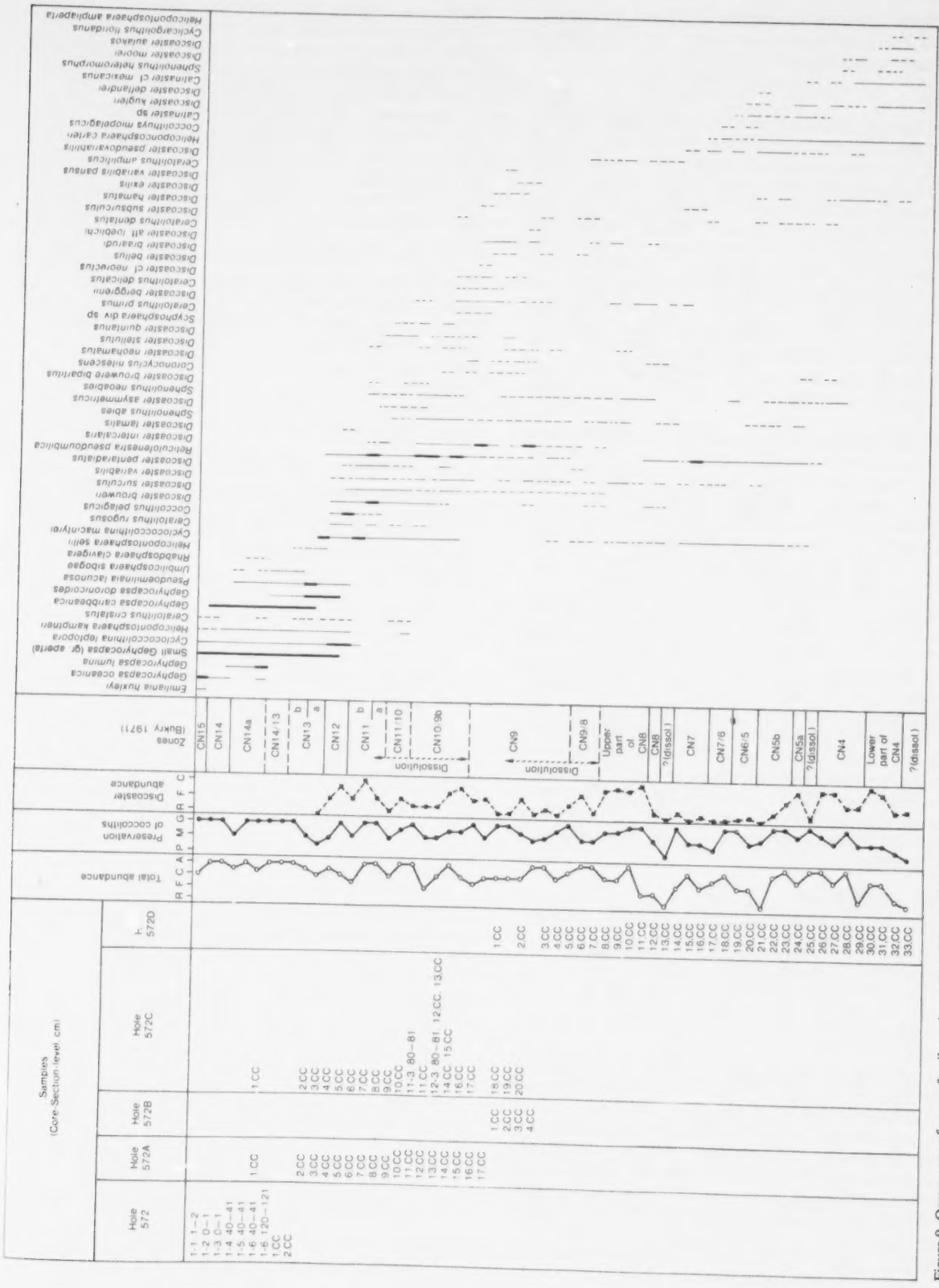

Figure 9. Occurrence of nannofossil species at Site 572; zonal boundaries are dashed when uncertain. R = rare; F = frequent; C = common; A = abundant; P = poor; M = moderate; G = good.

572D-28,CC. *Calocycletta tetrapera* is found throughout the zone, but is not accompanied by *C. cornuta*, which occurs only sporadically.

Diatoms

Diatoms are abundant to rare throughout the five holes drilled at Site 572. In general, preservation is good above 365 m sub-bottom (Section 572D-23,CC) and poor to moderate below that level. The sequence is complete from the late Quaternary *Pseudoeunotia doliolus* Zone through Subzone B of the early middle Miocene *Cestodiscus peplum* Zone. The sequence of diatom datums (Barron, this vol.) is essentially identical to that observed at eastern equatorial Pacific DSDP Hole 77B and Site 158 (Barron, 1981; Keller et al., 1982; Barron, unpubl. data). Most of the datums listed have been tied to paleomagnetic stratigraphy by Burckle (1972; 1978; pers. comm., 1982, to J. Barron), and the ages used have been adjusted to the Berggren (1983) paleomagnetic time scale.

High percentages of the upwelling diatoms *Thalassionema nitzschioides* and *Thalassiothrix longissima* dominate the intervals between 4.0 and 8.0 Ma (Sections 572A-8,CC through 572D-7,CC) and between about 10.0 and 12.2 Ma (Section 572D-11,CC through Section 572D-18,CC). Both of these intervals are characterized by high sediment accumulation rates (50 and 73 m/m.y., respectively) and presumably reflect periods of high siliceous productivity. Site 158 to the east contains coeval intervals dominated by *Thalassionema* and *Thalassiothrix* (Bukry and Foster, 1973) and high sediment accumulation rates (Keller et al., 1982). As at Site 158, calcium carbonate dissolution is severe during these intervals (see the section on planktonic foraminifers). It has been suggested that these intervals correspond to periods of expanded Antarctic glaciation (Keller et al., 1982), which may have increased both gyral circulation and the upwelling in the eastern equatorial Pacific. The enhanced production of Antarctic Bottom Water during these periods may have caused the calcium carbonate dissolution (Keller and Barron, 1983).

Benthic Foraminifers

Benthic foraminifers are present throughout the cores, although they are never abundant. They are well preserved except in the intervals from Sections 572-1,CC to 572A-5,CC and from Sections 572D-2,CC to -5,CC. The benthic foraminifers in the intervals from Sections 572C-6,CC to -8,CC and -10,CC to -12,CC are insufficient for study.

The diversity of the benthic foraminiferal fauna is generally high (about 50 to 60 species per 200 individuals), as is usually the case with deep-sea assemblages (Douglas and Woodruff, 1981). Rotaliid forms are much more numerous than rectilinear forms. Miliolids and agglutinated forms constitute less than 15% of the fauna in all samples, but they are present in most samples. The hyaline genera *Epistominella, Gyroidinoides*, and *Oridorsalis* (all known to be resistant to dissolution) are the most common, together with *Cibicidoides*. Other common constituents are *Globocassidulina subglobosa, Melonis (M. barleeanus* group), and *Pullenia*. Relative abundances fluctuate considerably. High abundances of *Epistominella, Nuttallides*, and (less obviously) *Gyroidinoides* and *Oridorsalis* are correlated with levels of high dissolution of planktonic foraminifers.

The faunas in the lower part of the cored interval (Section 572D-25,CC downward) are the most diverse. Several species are found in this interval only (e.g., *Heronallenia lingulata, Vulvulina spinosa, Favocassidulina subfavus*, and *Bolivina striatula*). The last of these species appears at other sites (573 to 575) in sediments dated between 15.5 and 18.7 Ma.

Sections 572C-15,CC and 572A-14,CC are characterized by a large relative abundance of *Uvigerina*. *Cibicidoides* is present in larger numbers than average at about the same level, and *Globocassidulina* shows a small peak. Above this level *Cibicidoides* is less common than in the lower part of the cored section. These changes in the benthic fauna occur in the upper part of planktonic foraminiferal Zone N17, just below the Miocene/Pliocene boundary, and they can be dated at about 5.5 Ma.

SEDIMENT ACCUMULATION RATES

The estimated sedimentation rates for Site 572 show considerable variation (Fig. 10, Table 3). The rates from about 12 to 15 Ma (middle Miocene) are relatively high, with an average sedimentation rate of about 60 m/m.y. Before 12 Ma the rate decreases to 13 m/m.y., and it re-

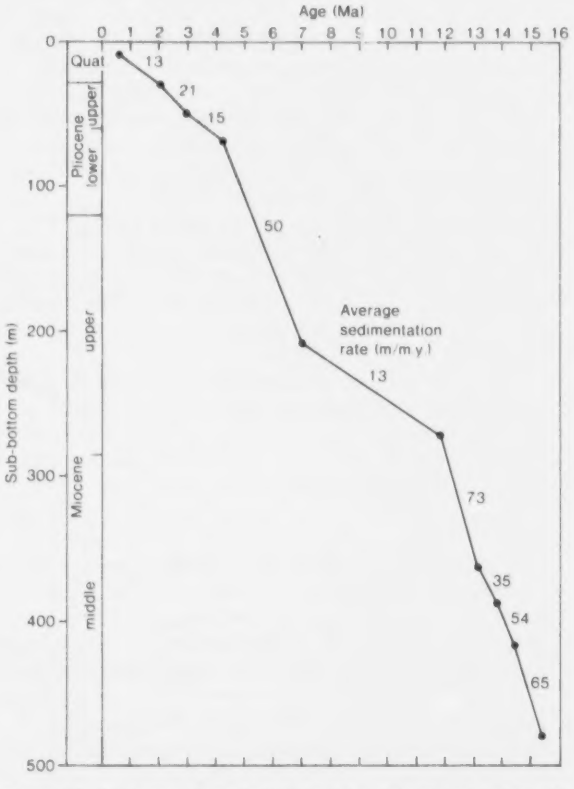

Figure 10. Age versus depth in hole based on biodatums at Site 572.

Table 3. Sedimentation rates and carbonate and noncarbonate mass accumulation rates at Site 572.

Sub-bottom depth (m)	Age (Ma)	Sedimentation rate (m/m.y.)	Mean dry bulk density (g/cm^3)	Mean $CaCO_3$ (%)	Mean mass accumulation rate ($[g/cm^2]/1000$ yr.)		
					Total	$CaCO_3$	Non $CaCO_3$
9.5	0.55	13	0.57	79	0.74	0.58	0.16
29.0	2.0	21	0.61	73	1.28	0.93	0.35
49.0	2.95	15.2	0.70	75	1.0	0.80	0.2
68.0	4.2	50.0	0.72	73	3.6	2.6	1.0
208.0	6.95	13	0.84	74	1.1	0.8	0.3
272.0	11.8	73	0.60	66	4.4	2.9	1.5
360.0	13.0	35	0.89	76	3.2	2.4	0.8
388.0	13.8	54	0.89	77	4.6	3.6	1.1
415.0	14.3	65	0.92	76	5.9	4.5	1.4
480.0	15.3						

mains low to about 7 Ma, when the sedimentation rate increases to about 50 m/m.y. This high rate persists into the early Pliocene until about 4.2 Ma, when the sedimentation rate decreases to about 15 m/m.y. The sedimentation rate in the early Pliocene may be as high as 70 m/m.y.; early Pliocene diatom zones are found in more than 20 m of section. A lower sedimentation rate of first 15 m/m.y. and then 21 m/m.y. is found in the upper Pliocene; the rate decreases to 13 m/m.y. during the Pleistocene. For further discussion and an update see Barron et al. (this vol.).

The proportion of sediment made up of calcium carbonate varies inversely with sedimentation rate; the relationship suggests that increased noncarbonate deposition dilutes the calcium carbonate (the amount of nonbiogenic material in the sediments recovered at Site 572 is low, so noncarbonate sediment is assumed to be dominated by biogenic silica). However, the mass accumulation rate data show that the accumulation of carbonate and noncarbonate sediments vary together (Table 3; Fig. 11). In the upper 100 m, noncarbonate accumulation rates decrease between times of high accumulation rates and succeeding periods of lower rates by a factor of five, as compared with a threefold decrease in calcium carbonate accumulation. Thus, the inverse relationship between sedimentation rate and calcium carbonate content reflects dilution and does not show the true nature of the changes in calcium carbonate sedimentation.

There are three intervals of relatively high accumulation of noncarbonate (siliceous) sediments at Site 572: 4 to 7, 12 to 13, and 14 to 15 Ma. The youngest interval, 4 to 7 Ma, coincides with the period when Site 572 (and Site 81) crossed the equator (Leinen, 1979); thus, the increase in the accumulation of silica and carbonate may be due to the maximum surface productivity at the equator. The interval from 12 to 13 Ma is about 1 Ma older than the peak in biogenic silica accumulation that Leinen (1979) found took place in the equatorial Pacific during

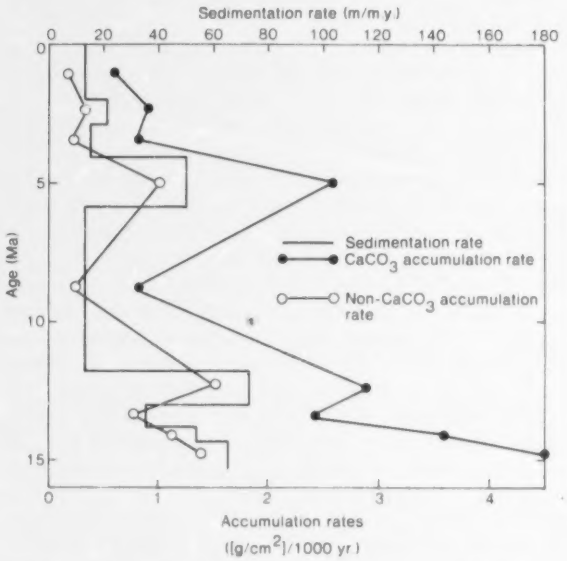

Figure 11. Sedimentation rate and average mass accumulation rates for carbonate and carbonate-free sediments at Site 572.

the Neogene. The age difference may reflect a difference between the time scale used in this report and that used by Leinen (1979). The oldest interval of high noncarbonate accumulation rate at Site 572, 14 to 15 Ma, is not visible as a peak in a curve of average equatorial Pacific silica accumulation, but a peak in silica accumulation exists at certain sites in the Pacific. The peak in carbonate accumulation rate at 14 to 15 Ma is consistent with the pattern of carbonate deposition defined by van Andel et al. (1975) for the equatorial Pacific. However, at this particular site the increased accumulation in the lower part of the section may be related to the proximity of the site to a spreading center.

Except in one interval, the relationship between the mass accumulation rates of carbonate and noncarbonate is nearly linear (Fig. 12). The exceptional interval is the peak in noncarbonate accumulation from 12 to 13 Ma. The increased accumulation of noncarbonate (presumably silica) during this interval may reflect the increased preservation of the silica, however. The general pattern of noncarbonate and carbonate accumulation suggests that the accumulation of both responds similarly to regional oceanographic change. See Theyer et al. (this vol.) for an updated discussion of mass accumulation rates.

PHYSICAL PROPERTIES

The physical properties measured for this site included wet-bulk density (ρ_b), sonic velocity (V_p), formation factor (F), thermal conductivity (K), and shear strength. In the VLHPC-cored section, measurements were made at regular intervals except where the sediment was disturbed. In the rotary-drilled sections, measurements were made only in selected, undisturbed parts of the core instead of at regular intervals. Data collection techniques are given together with pertinent references in the Introduction (this vol.).

The data for Site 572 are plotted versus depth in Figures 13 to 17. There is no profile of shear strength, because only occasional values were calculated. These values are 700, 222, 514, and 152 g/cm^2 for depths of 166.5, 206.80, 207.39, and 281.21 m, respectively.

Long depth intervals were almost totally unsampled at this site because of the effects of drilling disturbance. The absence of sampling accounts for the sparsity of data in some parts of the profiles (Figs. 13 to 17). The data for depths between 155 and 350 m should be interpreted with the knowledge that although this interval appeared to be undisturbed, it may have undergone some disaggregation and have been subject to the addition of water during drilling. However, in similar piston- and rotary-cored sections acquired in holes about 50 km apart in the Panama Basin (Leg 69), the data trends and maximum and minimum values were approximately the same; thus, data similar to those collected at Site 572 appear to be reliable. Below 350 m, in Hole 572D, the sediment was consolidated enough to preserve sections intact.

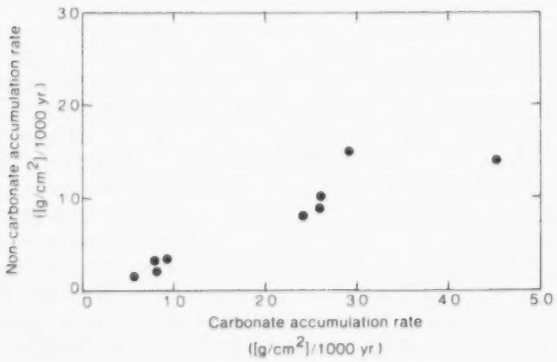

Figure 12. Carbonate versus carbonate-free mass accumulation rates at Site 572.

Within the VLHPC part of this section, sonic velocity (Fig. 13) is the most constant of the parameters measured, ranging between 1.52 and 1.56 km/s, with a slight gradient (0.2 per s) between 50 and 100 m. The uniformity of the sonic velocity data indicates that the variations in acoustic impedance are due almost entirely to the variations in wet-bulk density (Fig. 14), since impedance, Q, is the product of density (ρ_b) and velocity (V_p). The wet-bulk density (Fig. 14) varies between 1.2 and 1.6 g/cm^3, with a scatter of approximately 0.1 g/cm^3 locally. The wet-bulk density data and the carbonate-content data (Fig. 6) are similar, with high wet-bulk density corresponding to high carbonate content. The similarity of the curves is probably due to the high grain density of carbonate compared with that of biogenous silica and the fact that the calcareous nannofossils pack together more closely than the siliceous tests, which have a generally more open structure. Thus, lower grain densities correspond to higher porosities. It is interesting to note that the carbonate data support the density maximum at 140 m and the broad maximum at 240 m in the region of disturbed coring.

The porosity of the sediment decreases gradually with depth (Fig. 15) and complements the wet-bulk density profile (Fig. 14). From 0 to 180 m the values vary between 80 and 65%, from 200 to 340 m between 75 and 60%, and for the final 100 m of the hole between 70 and 55%.

The formation factor (Fig. 16) varies approximately between 1.2 and 2.0 for the first 160 m, 1.8 and 2.0 between 200 and 300 m, and between 1.8 and 2.5 for the last 50 m of the hole. Thermal conductivity (Fig. 17) increases gradually with depth, the initial values ranging between 2.4 and 3.0 (mcal/cm·s·°C) for the remainder of the section. The formation factor and thermal conductivity curves exhibit weak local minima at 100 m and maxima at 140 to 150 m. These features approximately correspond to a porosity maximum at 110 m and a porosity minimum at 140 to 150 m; the coincidence of the features illustrates the effect of water content on formation factor and thermal conductivity in soft sediments.

Toward the bottom of the section, where the recovered material has changed from ooze to chalk, all the parameters exhibit uniformity down to a depth of 400 m. At that depth all measurements indicate a change in the properties of the sediment. The decrease in porosity (from 60 to 55%) indicates compaction and lithification (i.e., an increase in grain-to-grain contact area). Compaction is also illustrated by the velocity increase from 1.6 to 1.8 km/s for the depths between 360 and 460 m.

PALEOMAGNETISM

The shipboard paleomagnetic analysis of Site 572 was complicated by the following factors:

1. Viscous components of magnetization appeared to be present in the samples from the Brunhes Normal Epoch. The problem was compounded by the possibility that chemical overprinting during sediment diagenesis had destroyed the primary magnetization.

2. The intensities of nearly all samples were low (below 1.0×10^{-6} G); 40% of the samples showed intensities of 1.0×10^{-8} G. The latter intensities required 2^8

spins and are in the range of the noise level of the onboard spinner magnetometer, precluding AF demagnetization experiments.

3. The absence of an azimuthal orientation of the HPC cores prevented us from orienting the different cores with respect to one another (see Introduction).

Because of these problems, no magnetostratigraphy was determined on board for this site (see Weinreich and Theyer, this vol.).

INTERSTITIAL-WATER CHEMISTRY

Shipboard pore-water analyses were conducted on two types of samples from Site 572: 20-cm lengths of the split core and 5-cm lengths of the whole core. The whole-core samples proved to be much more reliable.

Profiles of the variation of alkalinity and the concentration of calcium and magnesium with increasing depth show several trend reversals (Fig. 18). The reversals are probably related to diagenetic reactions and variations in the rate of sediment accumulation. Overall, calcium and magnesium decrease gradually to minimum values, then increase steadily toward the basement. Alkalinity displays an opposing trend—it gradually reaches a maximum value, then decreases toward the bottom of the hole.

The increase in strontium content with increasing depth suggests that calcite recrystallization has occurred. Concentrations steadily increase to a maximum near 350 m; they then abruptly decrease toward the base of the sedimentary section.

Samples from Hole 572 were allowed to sit at room temperature for up to 10 hr. before the interstitial water was analyzed. There is clear evidence that chemical reactions occurred during this waiting period. Evaporation is indicated by the higher chlorinity values for all samples from Hole 572. Values of pH are higher, and those of alkalinity and calcium are lower than in samples refrigerated immediately after the core arrived on deck. These differences in concentration are attributed to precipitation of calcium carbonate during storage at higher temperatures.

SUMMARY AND CONCLUSIONS

Site 572, which was located in 3900 m of water at the eastern edge of the equatorial high productivity zone, was drilled to acquire an expanded sequence of uppermost Miocene, Pliocene, and Pleistocene biogenous sediments. This site is just a few miles from DSDP Site 81, where the drilling (which was confined to one hole) recovered only the uppermost and lowermost few meters of the sediment section. Five holes were drilled at Site 572; the hydraulic piston coring used in the upper 170 m resulted in continuous recovery, and the rotary coring used in the bottom 310 m of the section resulted in nearly continuous recovery. A more detailed drilling summary follows.

In Hole 572, one HPC core was obtained in an unsuccessful attempt to establish the mudline.

In Hole 572A, 17 HPC cores were obtained. Total penetration was 154.1 m, and recovery was 99%. Coring stopped when the HPC was lost in the hole as the result of excessive pullout force (60,000 lb.).

In Hole 572B, four 5-m hydraulic piston cores were obtained. The coring began at the depth at which Hole 572A terminated (154.1 m) and ended at 172.1 m sub-bottom, where excessive pullout force forced an end to the coring. Total penetration was 18.1 m, with 100% recovery.

In Hole 572C, 20 HPC cores penetrated from the mudline to 168.5 m sub-bottom with 95% recovery. This hole, which represented the second coring of the upper part of the sedimentary section, was drilled to ensure continuous recovery.

In Hole 572D, 34 rotary cores were acquired. Drilling started at 151.0 m sub-bottom and penetrated 334.5 m, for a final sub-bottom depth of 485.5 m. Recovery at this hole was 81%; basement was encountered at 479.5 m sub-bottom, and Core 34 recovered 28 cm of basalt.

Lithology

The 479.5-m sedimentary section consists of laminated and burrow-mottled siliceous calcareous oozes to siliceous nannofossil oozes that grade to siliceous nannofossil chalks. The oozes and chalks have been assigned to a single lithologic unit. A second unit (metalliferous chalk) was defined as the result of the correlation of a small sample with the lithology defined for Site 81. Color varies cyclically throughout the sediment section, and the dominant colors were used to divide the first unit into four subunits. The subdivisions are lithologically arbitrary; sediment color does not appear to be directly related to texture or microfossil composition. The sedimentary units can, however, be recognized in all five holes, and they can be correlated with the oceanic formations defined for Site 81.

Lithologic Units

Unit I: Cyclic Siliceous Calcareous Ooze Chalk (0 to 464.50 m)

Subunit IA

Subunit IA consists of gray brown foraminiferal diatom nannofossil ooze to foraminiferal siliceous nannofossil ooze. It occurs from 0 to 2.35 m.

The average carbonate content of this subunit is 77%. The subunit corresponds to the cyclic unit of the Clipperton Oceanic Formation described by the scientists of DSDP Leg 9.

Subunit IB

Subunit IB consists of varicolored diatom nannofossil oozes to foraminiferal radiolarian nannofossil oozes and siliceous nannofossil oozes that are Quaternary to late Pliocene in age. It occurs from 2.35 to 37.45 m and contains purple, light gray, and yellow bands that are between 5 and 25 cm thick.

The average carbonate content of the subunit is 77%. Bioturbation is common; occasional burrow fillings have high pyrite content (30%) and elongate pyrite rods. This

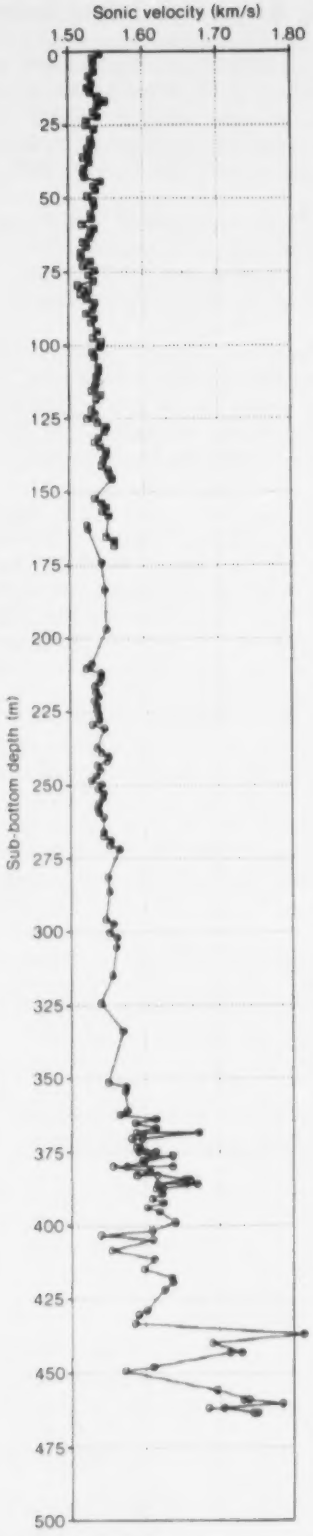

Figure 13. Sonic velocity plotted versus depth for Site 572. Profile is a composite of data from Holes 572C (squares, cored by HPC) and 572D (circles, rotary drilled).

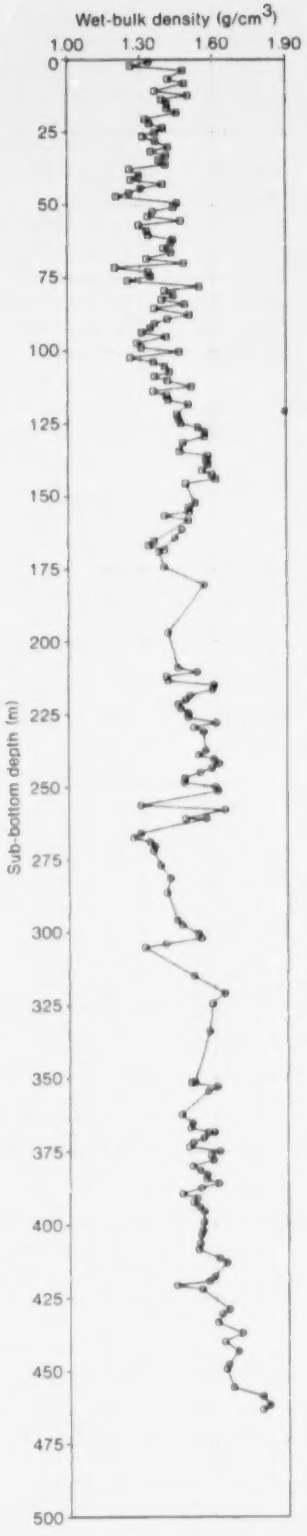

Figure 14. Wet-bulk density plotted versus depth for Site 572. Profile is a composite of data from Holes 572C (squares, cored by HPC) and 572D (circles, rotary drilled).

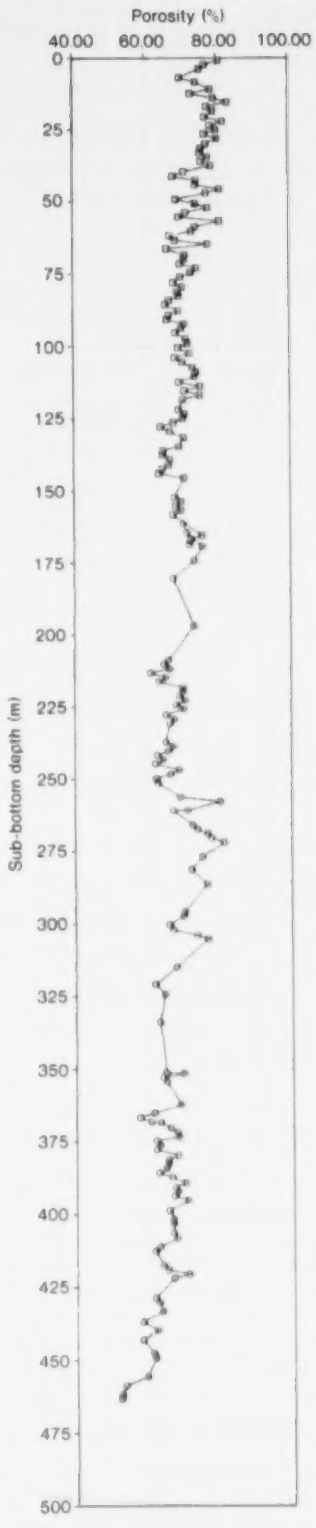

Figure 15. Porosity plotted versus depth for Site 572. Profile is a composite of data from Holes 572C (squares, cored by HPC) and 572D (circles, rotary drilled).

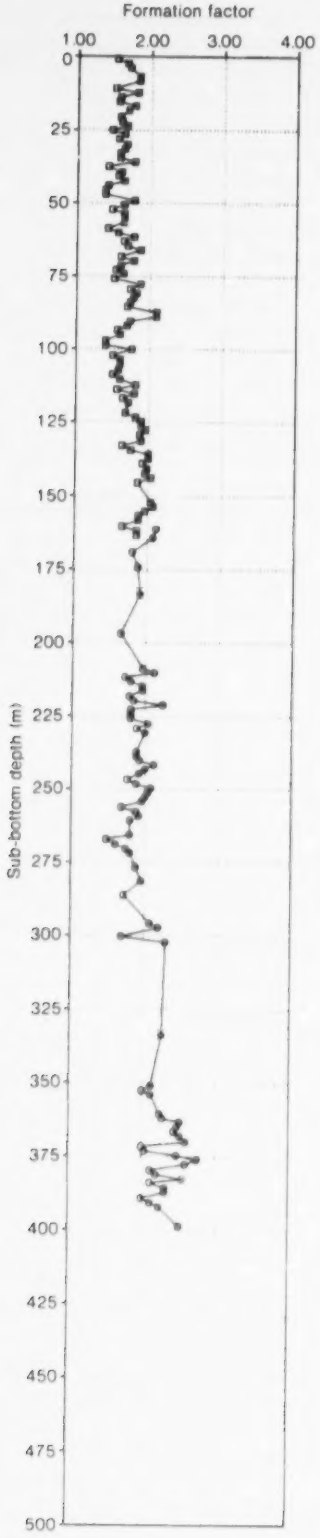

Figure 16. Formation factor (horizontal) plotted versus depth for Site 572. Profile is a composite of data from Holes 572C (squares, cored by HPC) and 572D (circles, rotary drilled).

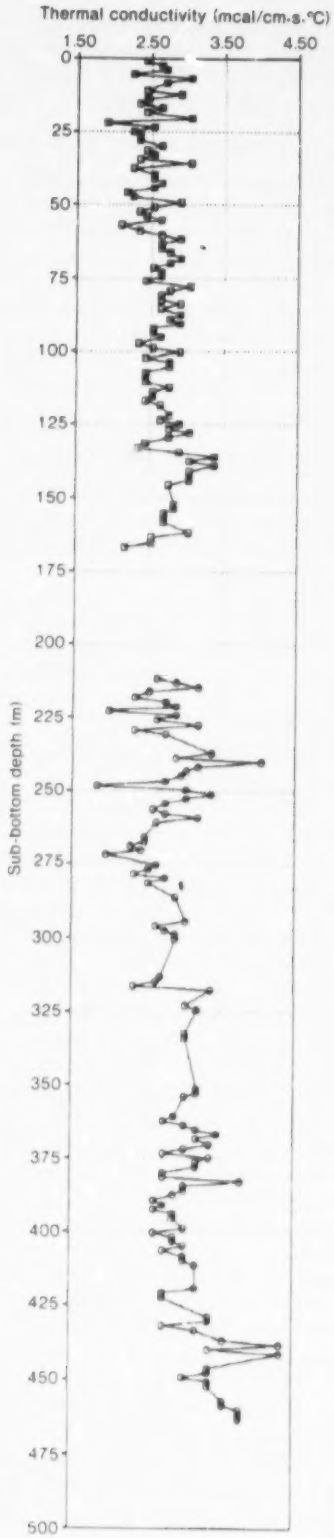

Figure 17. Thermal conductivity (uncorrected for temperature) plotted versus depth for Site 572. Profile is a composite of data from Holes 572C (squares, cored by HPC) and 572D (circles, rotary drilled).

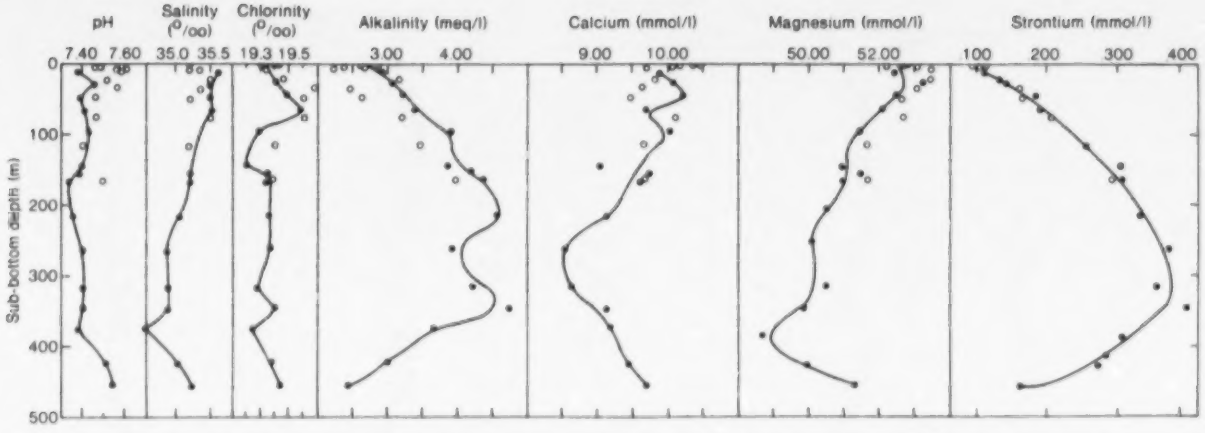

Figure 18. Interstitial-water chemistry, Site 572. Open circles are samples from Hole 572; solid circles are samples from all other holes.

subunit corresponds to the varicolored unit of the Clipperton Oceanic Formation described during DSDP Leg 9.

Subunit IC

Subunit IC consists of green varicolored ooze chalk that is late Pliocene to middle Miocene in age. It occurs from 37.45 to 458.75 m. The color varies between purple, light gray, yellow, and green; the variation is cyclic in the upper part of the subunit.

The chalk–ooze transition occurs within this subunit between 293.5 and 367.5 m. Within this interval there are alternating zones of stiff friable material and ooze. The material deeper than 367.5 m is consistently chalk and had to be split with a rock saw. There are well-preserved burrow structures in this unit, with excellent examples of the ichnogenera Chondrites, Planolites, and Zoophycos. From 37.45 to 293.5 m the unit consists of diatom nannofossil to siliceous nannofossil oozes, with an occasional discrete layer of nannofossil diatom ooze. From 293.5 to 367.5 m, siliceous nannofossil and diatom nannofossil oozes alternate with siliceous nannofossil and diatom nannofossil chalks; within this interval there are several small, green, banded chert fragments. Below 367.5 m, the subunit is composed of foraminiferal siliceous nannofossil chalk and foraminiferal radiolarian diatom nannofossil chalk. This lower part of the subunit, which is predominantly green in color, contains discrete layers of bright green diatomites and several laminated chert horizons 3 to 4 cm thick. The subunit has an average carbonate content of 72%; it corresponds to the San Blas Oceanic Formation described during DSDP Leg 9.

Subunit ID

Subunit ID consists of yellow chalk that is lowermost middle Miocene in age. It occurs from 458.5 to 464.5 m. The lowest sample is pale yellow and yellowish green siliceous foraminiferal nannofossil chalk. The burrow structures, which include Chondrites, Planolites, and Zoophycos, are well preserved.

Unit II: Metalliferous Chalk (464.5–? m)

The lowermost sample at Site 572 contains common pyrite (5%) and iron oxides (10%). We believe that the sedimentary unit to which the sample belongs overlies the basement, as it did at Site 81, and that the unit's lithology has probably been affected by interaction with hydrothermal fluids and basalt. The average carbonate content of this unit is 76%; Unit II and Subunit ID correspond to the Line Islands Oceanic Formation described by the scientists of DSDP Leg 9.

Carbonate Content

The entire sediment section is characterized by the cyclic alternation of intervals of high (80 to 90%) and low (45 to 65%) carbonate content. Many of these variations can be tied into previously established equatorial carbonate stratigraphies.

Biostratigraphy

At Site 572 a continuous sequence from the upper Pleistocene (0.22 Ma) through the lowermost middle Miocene (about 15 Ma) was sampled. Holocene and uppermost Pleistocene sediments were not recovered (they were probably lost in the coring process); the extinction of *Globoquadrina pseudofoliata* indicates that the youngest sediment cored is 0.22 Ma or older. The Pliocene/Pleistocene boundary is marked by the extinction of the foraminifers *Globigerinoides obliquus*, the nannofossil *Discoaster brouweri*, and the radiolarian *Pterocanium prismatium*. The first appearance of *Globorotalia tumida* and the disappearance *Globoquadrina dehiscens* mark the Miocene/Pliocene boundary. The oldest sediment recovered contains nannofossils of the *Sphenolithus heteromorphus* Zone, planktonic foraminifers of the N9 Zone, radiolarians that can be assigned to the *Dorcadospyris alata* Zone, and diatoms of the *Cestodiscus peplum* A Subzone. We have assigned an age of earliest middle Miocene (about 15 Ma) to this sediment.

All the major microfossil groups are represented at Site 572. Siliceous microfossils are common to abundant throughout the section. The abundance of calcareous microfossils depends on the degree of carbonate dissolution. Calcareous microfossils are abundant and well preserved throughout the Pliocene and Pleistocene. An abrupt change in preservation takes place at approximately 150 m sub-bottom (upper part of the upper Miocene, about 6 Ma). From that level down to the lowermost part of the section (435 m, middle Miocene), calcareous microfossils are represented by solution-resistant forms only, with particularly high dissolution indices at approximately 6.1 and 11 Ma. Well-preserved assemblages reappear in the deepest three cores in the section (436 to 464.5 m, middle Miocene, 14 to 15 Ma).

Radiolarians are well preserved throughout the section. Diatoms show good preservation above 365 m sub-bottom (13.3 Ma) but generally poor to moderate preservation below that level. High percentages of the upwelling diatoms *Thalassionema nitzschioides* and *Thalassiothrix longissima* dominate the intervals from 4.0 to 8.0 Ma (62 to 226 m) and 10.0 to 12.2 Ma (255 to 322 m). These intervals correspond to periods of high sedimentation rate, and they are characterized by severe carbonate dissolution.

Sedimentation Rate

The sedimentation rates at Site 572 are variable, and, in some intervals, remarkably high.

Shipboard physical property and carbonate analyses were used to calculate carbonate and noncarbonate mass accumulation rates. There is an inverse relationship between carbonate content and sedimentation rate; the inference is that carbonate was diluted during periods of high sedimentation rate. Comparisons of carbonate and noncarbonate accumulation rates reveal that when accumulation rates shift from low to high, the carbonate accumulation rate increases by a factor of three while the noncarbonate (biogenous silica) rate increases by a factor of five. The three intervals with a relatively high noncarbonate accumulation rate can be tentatively correlated with the passage of the site across the equator (4 to 7 Ma); an equatorial Pacific–wide interval of very high biogenic silica accumulation (12 to 13 Ma); and an interval characterized by a higher than usual silica accumulation rate (14 to 15 Ma) that affected more localized portions of the Pacific. A maximum carbonate accumulation rate at 14 to 15 Ma is consistent with previously established trends for the equatorial Pacific.

Although the initial analysis of the sedimentation rate curves suggests that sedimentation was continuous, the data may also be interpreted as indicative of three short hiatuses (at 120, 360, and 425 m sub-bottom). See Barron et al. (this vol.) and Theyer et al. (this vol.) for updated and more detailed discussions.

Paleomagnetism

Numerous paleomagnetic samples were taken on cores from all five holes at Site 572, but interpretation was virtually impossible because of the extremely low intensities measured. Compounding the problem of interpreting the low intensities was the apparent acquisition of viscous components of magnetization in samples from the Brunhes Normal Epoch and the overprinting of primary information by chemical alteration.

Interstitial-Water Chemistry

Calcium ion concentration and alkalinity show a roughly opposed trend overall, although they show a similar trend between 230 and 350 m sub-bottom. An increase in alkalinity at 140 to 220 m coincides with the occurrence of an H_2S odor, an increase in the abundance of pyrite, high sedimentation rates, and numerous diatom-rich layers. These observations suggest the rapid deposition of organic-carbon-rich material and the depletion of oxygenated interstitial water by microbial combustion.

Physical Properties

Thermal conductivity, electrical resistivity, and sonic velocity were measured on Site 572 cores. Samples were taken for the shipboard calculation of wet-bulk density, grain density, water content, and porosity. The values appear to be reliable except for those for the interval between 165 and 350 m—an interval too deep for the HPC and yet not indurated enough to be drilled without significant disturbance.

Sonic velocities are almost constant with increasing depth (ranging from 1.52 to 1.56 km/s) down to about 360 m; the variations in acoustic impedance are thus due primarily to the substantial variations in wet-bulk density (1.2 to 1.6 g/cm^3). Wet-bulk density variations correlate with changes in the sediment's percentage of calcium carbonate; the inference was drawn that the intervals characterized by high carbonate content (and high wet-bulk density) were dominated by dense, closely packed calcareous nannofossils and that the intervals characterized by low carbonate were dominated by less dense, loosely packed, biogenous silica. The variations in grain density support this interpretation. The formation factor and thermal conductivity curves show a maximum at 140 to 150 m sub-bottom that is correlated with a porosity minimum and a carbonate maximum. Deeper than about 400 m, all the physical properties except grain density exhibit an abrupt change. An increase in wet-bulk density and sonic velocity without a concurrent increase in grain density or carbonate content suggests that this part of the section is affected by diagenesis.

The seismic section at Site 572 is highly stratified throughout. The stratification is consistent with the presence of cyclic variations in wet-bulk density.

Site Migration and Subsidence History

The history of the migration and subsidence of Site 572 (and Site 81) is complicated by the possibility that a fossil ridge once ran between 5°N and the equator at about 115°W. The migration of the site depends on the existence and the time of extinction of this ridge crest; Site 572 may have participated in the motion of two successive plates (Cocos and Pacific). Uncertainties in the interpretation of the magnetic anomalies and topographic features of the area make it difficult to resolve whether the extinct ridge existed or not. In the following dis-

cussion we assume that the migration track calculated by van Andel et al. (1975) for Site 81 applies to Site 572 as well. Fortunately, these sites are relatively young, so the latitudinal errors that would result from miscalculating their paths are minimal.

The crust upon which Site 572 sits was generated approximately 16 Ma at about 2°30′S and a depth of 3200 m. The shallow initial depth and low latitude of the site explain the extremely high sedimentation and carbonate accumulation rates during the period between 16 and 14 Ma. The dominance of the accumulating sediment by the carbonate component indicates moderate productivity with diminished dissolution of carbonate. This high carbonate accumulation rate occurs in a period for which van Andel et al. (1975) reported a relatively low carbonate accumulation rate and a shallow CCD. The dissolution index for the oldest samples is moderate; it increases for sediments dated between 15 and 13.5 Ma, which were deposited as the site sank about 130 m. At about 13.5 Ma there was a small decrease in the accumulation rate of noncarbonate (biogenous silica), a decrease associated with a parallel but more pronounced decrease in the accumulation of carbonate. The decrease in the accumulation of carbonate is probably an effect of increased depth.

From approximately 13.0 to 11.8 Ma (3330 to 3430 m paleodepth, 1°53′S to 1°24′S paleolatitude), there is a large increase in the noncarbonate accumulation rate. This increase is associated with the presence of diatoms that are indicative of upwelling, a small increase in the carbonate accumulation rate, a decrease in carbonate content, and a high dissolution index. We interpret these factors to represent a time of very high productivity; the abundance of organic matter results in steep dissolution rate gradients and enhanced dissolution. The low carbonate content results from increased dissolution and dilution by biogenous silica.

From approximately 11.8 to 9 Ma, there is a sharp drop in both the carbonate and noncarbonate accumulation rates, as well as a decline in the abundance of upwelling diatoms. During this time period, the site sank from 3430 to 3680 m and migrated from 1°24′S to 0°21′S. Despite the deepening of the site and its proximity to the equator, there is evidence that carbonate dissolution decreased and that productivity also decreased.

Site 572 crossed the equator in the time period from 7 to 4 Ma (3678 to 3800 m paleodepth, 0°21′S to 0°24′N paleolatitude). The crossing is characterized by an increase in noncarbonate accumulation, with a proportional increase in carbonate accumulation. The resulting noncarbonate accumulation rate is significantly less than that of the period from 13.0 to 11.8 Ma, while the carbonate accumulation rate is equal to that for 13.0 to 11.8 Ma. The abundance of upwelling diatoms increases again, and there is a short interval (7 to 6.3 Ma) of elevated dissolution index, but for most of the interval the dissolution index is low and carbonate percentages are high (although slightly less than in the preceding period). Productivity has increased again, although not to the same degree as in the period from 13.0 to 11.8 Ma. The result is high carbonate and noncarbonate accumulation rates without the increased dissolution apparent between 13.0 and 11.8 Ma

From 4 Ma to the Pleistocene (3800 to 3900 m paleodepth, 0°24′N to 1°26′N paleolatitude), both carbonate and noncarbonate accumulation rates decrease, and as a result both carbonate preservation and content increase. We interpret these characteristics to be indicative of a period of relatively low productivity, slow accumulation, and enhanced carbonate preservation.

We have constructed a preliminary sedimentation model for Site 572 from a cursory evaluation of the accumulation rate curves and an examination of the site's depth and latitudinal migration. (See Theyer et al., this vol., for an update.) From 0 to 11.5 Ma and between 13 and 13.5 Ma, the carbonate and noncarbonate accumulation rates vary proportionally. During periods of low noncarbonate accumulation (low productivity), sedimentation rates are low, and the dilution and dissolution of carbonate material are also low; as a result, carbonate content is high. When productivity increases, sedimentation rates increase, and preservation and carbonate content decrease slightly. During two periods of time, however, the carbonate and noncarbonate accumulation rate curves vary disproportionately. From 11.8 to 13.0 Ma, the noncarbonate accumulation rate increases much more than the carbonate accumulation rate, with a concurrent large decrease in carbonate preservation. We interpret this to be the result of increased dilution by biogenous silica and enhanced dissolution from excess organic matter. From 13.0 to 15 Ma, the carbonate accumulation rate greatly exceeded the noncarbonate rate. This is attributed to the enhanced preservation of carbonate at the shallow depth of the site during that time.

A basic premise of this model is that the noncarbonate accumulation rate is a measure of productivity. This assumption is based on the presence of diatom species that are indicative of upwelling during times of high noncarbonate accumulation, the parallelism of the carbonate and noncarbonate accumulation rate curves, and the conclusion that the noncarbonate component is dominated by biogenous silica. Other mechanisms may be at work, but their determination and the investigation of their causes and relationships will have to await more detailed studies.

REFERENCES

Barron, J. A., 1981. Middle Miocene diatom biostratigraphy of equatorial Pacific DSDP Hole 77B. *Geosci. J.*, 2:137–144.

Berger, W. H., 1970. Planktonic Foraminifera: selective solution and the lysocline. *Mar. Geol.*, 8:111–138.

Berger, W. H., and von Rad, U., 1972. Cretaceous and Cenozoic sediments from the Atlantic Ocean. *In* Hayes, D. E., Pimm, A. C., et al., *Init. Repts. DSDP*, 14: Washington (U.S. Govt. Printing Office), 787–954.

Berggren, W. A., 1983. Correlation of Atlantic, Mediterranean, Indo-Pacific Neogene stratigraphies: geochronology and chronostratigraphy. *Proc. IGCP Project 114: International Workshop on Pacific Neogene Biostratigraphy* (Osaka and Kobe, Japan), November 24–29, 1981.

Blow, W. H., 1965. *Clavatorella*, a new genus of the Globorotaliidae. *Micropaleontology*, 11:365–368.

_____, 1969. Late middle Eocene to Recent planktonic foraminiferal biostratigraphy. *In* Brönniman, P., and Renz, H. H. (Eds.), *Proc. First Internat. Conf. Planktonic Microfossils*: Leiden (Brill) pp. 199–422.

Bukry, D., 1971. Cenozoic calcareous nannofossils from the Pacific Ocean. *Trans. San Diego Soc. Nat. Hist.*, 16:307–327.

_____, 1973. Coccolith stratigraphy, eastern equatorial Pacific, Leg 16, DSDP. *In* van Andel, T. H., Heath G. R., et al., *Init. Repts. DSDP*, 16: Washington (U.S. Govt. Printing Office), 965–1004.

Bukry, D., and Bramlette, M. N., 1969. Some new and stratigraphically useful calcareous nannofossils of the Cenozoic. *Tulane Stud. Geol. Paleontol.*, 7:131–142.

Bukry, D., and Foster, J. H., 1973. Silicoflagellate and diatom stratigraphy, Leg 16, DSDP. *In* van Andel, T. H., Heath, G. R., et al., *Init. Repts. DSDP*, 16: Washington (U.S. Govt. Printing Office), 815–871.

Burckle, L. H., 1972. Late Cenozoic planktonic diatom zones from the eastern equatorial Pacific. *Nova Hedwigia Beih.*, 39:217–246.

_____, 1978. Early Miocene to Pliocene datum levels for the equatorial Pacific. *Proc. Second Working Group Mtg., IGCP Proj. 114, Biostratigraphic Datum Planes of the Pacific Neogene* (Bandung, Indonesia), pp. 25–44.

Douglas, R., and Woodruff, F., 1981. Deep sea benthic foraminifera. *In* Emiliani, C. (Ed.), *The Sea* (Vol. 7): New York (Wiley Interscience), pp. 1233–1327.

Dunn, D. A., 1982. Miocene sediments of the equatorial Pacific Ocean: carbonate stratigraphy and dissolution history [Ph.D. dissert.]. Univ. Rhode Island, Narragansett.

Dunn, D. A., and Moore, T. C., Jr., 1981. Late Miocene-Pliocene (Magnetic Epoch 9-Gilbert Magnetic Epoch) calcium carbonate stratigraphy of the equatorial Pacific Ocean. *Geol. Soc. Am. Bull.*, 92:408–451.

Hays, J. D., Saito, T., Opdyke, N. D., and Burckle, L. H., 1969. Pliocene-Pleistocene sediments of the equatorial Pacific: their paleomagnetic, biostratigraphic and climatic record. *Geol. Soc. Am. Bull.*, 80:1481–1514.

Hays, J. D., et al., 1972. *Init. Repts. DSDP*, 9: Washington (U.S. Govt. Printing Office).

Herron, E. M., 1972. Seafloor spreading and the Cenozoic history of the east-central Pacific. *Geol. Soc. Am. Bull.*, 83:1671–1692.

Keller, G., and Barron, J. A., 1983. Paleoceanographic implications of Miocene deep sea hiatuses. *Geol. Soc. Am. Bull.*, 94:590–613.

Keller, G., Barron, J. A., and Burckle, L. H., 1982. North Pacific late Miocene correlations using microfossils, stable isotopes, percent $CaCO_3$, and magnetostratigraphy. *Mar. Micropaleontol.*, 7:327–357.

Leinen, M., 1979. Biogenic silica accumulation in the central equatorial Pacific and its implication for Cenozoic paleoceanography. *Geol. Soc. Am. Bull.*, 90:1310–1376.

Nigrini, C., 1971. Radiolarian zones in the Quaternary of the equatorial Pacific Ocean. *In* Funnell, B. M., Riedel, W. R. (Eds.), *The Micropaleontology of Oceans*: Cambridge (Cambridge Univ. Press), pp. 443–461.

Riedel, W. R., and Sanfilippo, A., 1978. Stratigraphy and evolution of tropical Cenozoic radiolarians. *Micropaleontology*, 23:61–96.

Saito, T., Burckle, L. H., and Hays, J. D., 1975. Late Miocene to Pleistocene biostratigraphy of equatorial Pacific sediments. *In* Saito, T., and Burckle, L. H. (Eds.), *Late Neogene Epoch Boundaries*: New York (Micropaleontology Press), pp. 226–244.

Saito, T., Thompson, P. R., and Berger, D., 1976. Skeletal ultramicrostructure of some elongate-chambered planktonic foraminifera and related species. *In* Takayanagi, Y., and Saito, T. (Eds.), *Progress in Micropaleontology*: New York (Micropaleontology Press), pp. 278–304.

van Andel, T. H., Heath, G. R., and Moore, T. C., Jr., 1975. Cenozoic history and paleoceanography of the central equatorial Pacific Ocean. *Geol. Soc. Am. Mem.*, 143.

Van Couvering, J. A., and Berggren, W. A., 1977. Biostratigraphical basis of the Neogene time scale. *In* Kauffman, E. G., and Hazel, J. E. (Eds.), *Concepts and Methods of Biostratigraphy*: Stroudsburg (Dowden, Hutchinson, Ross), pp. 283–306.

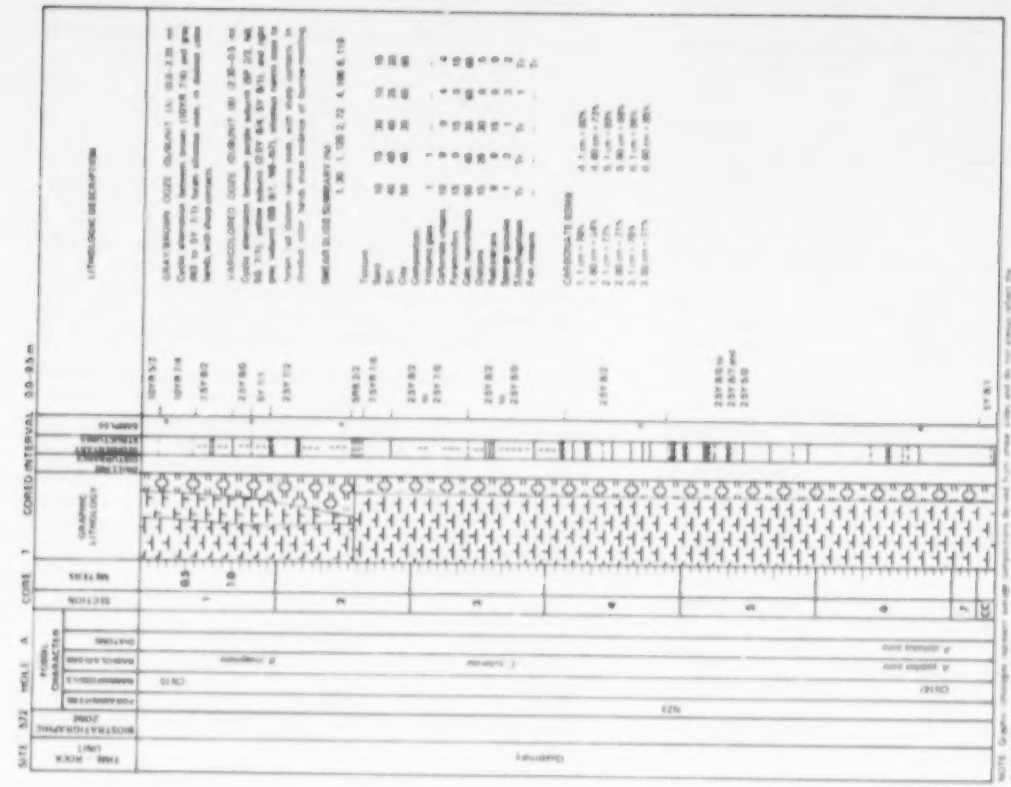

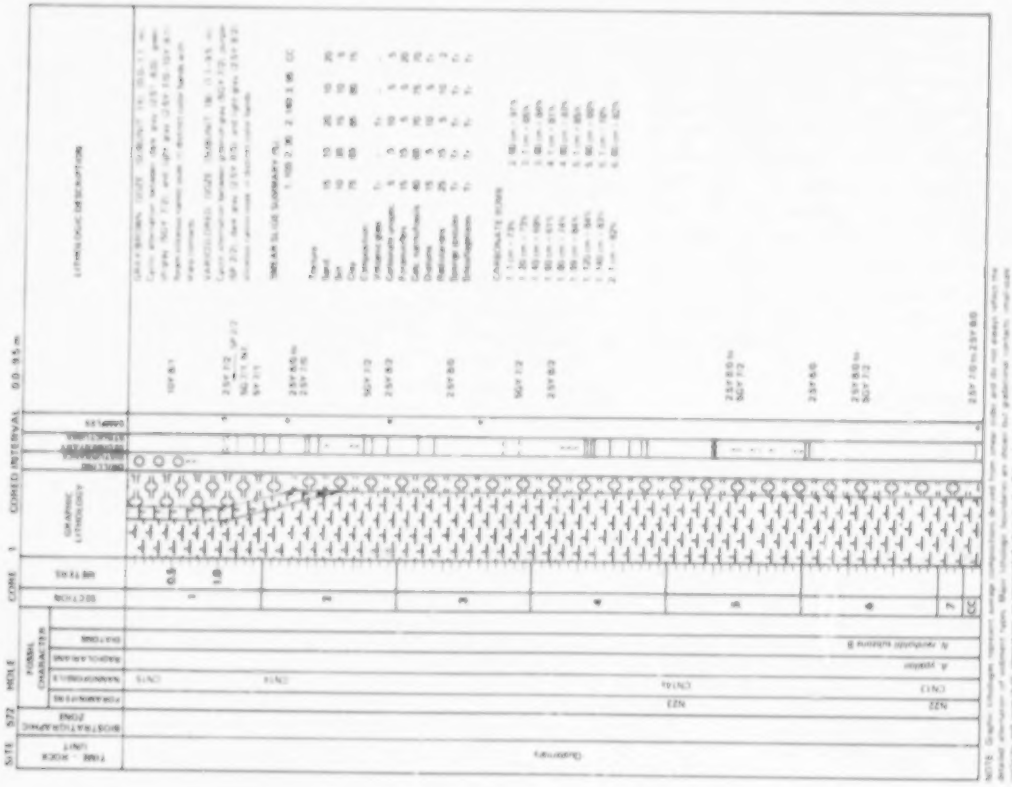

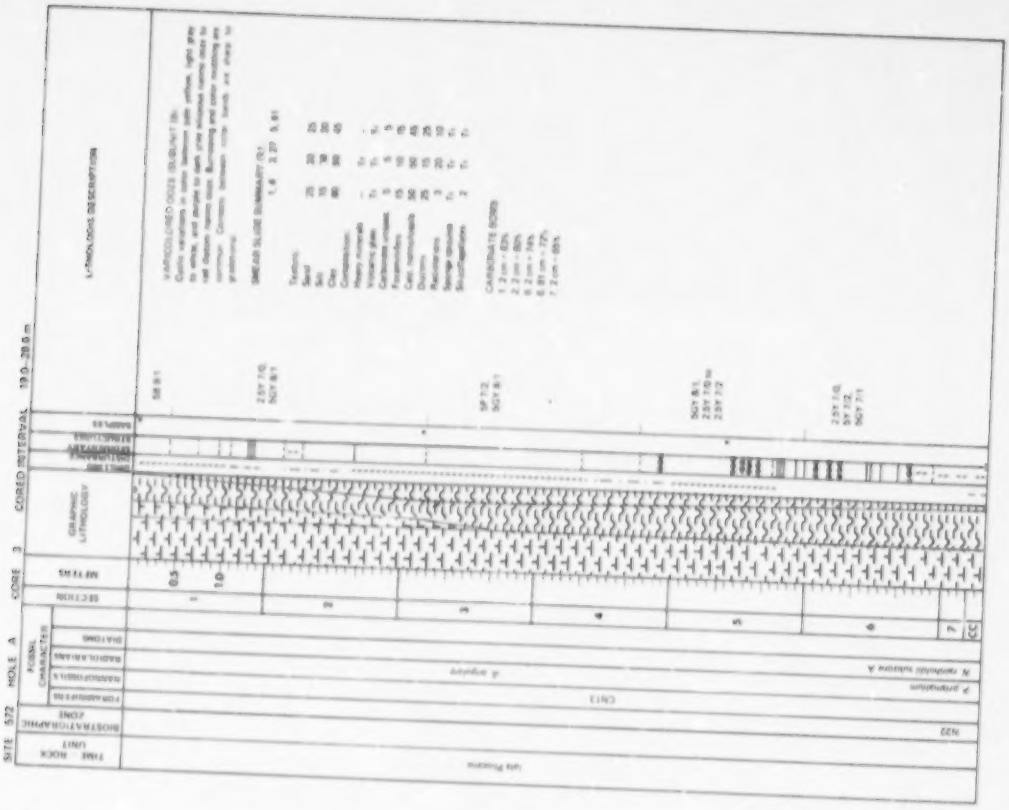

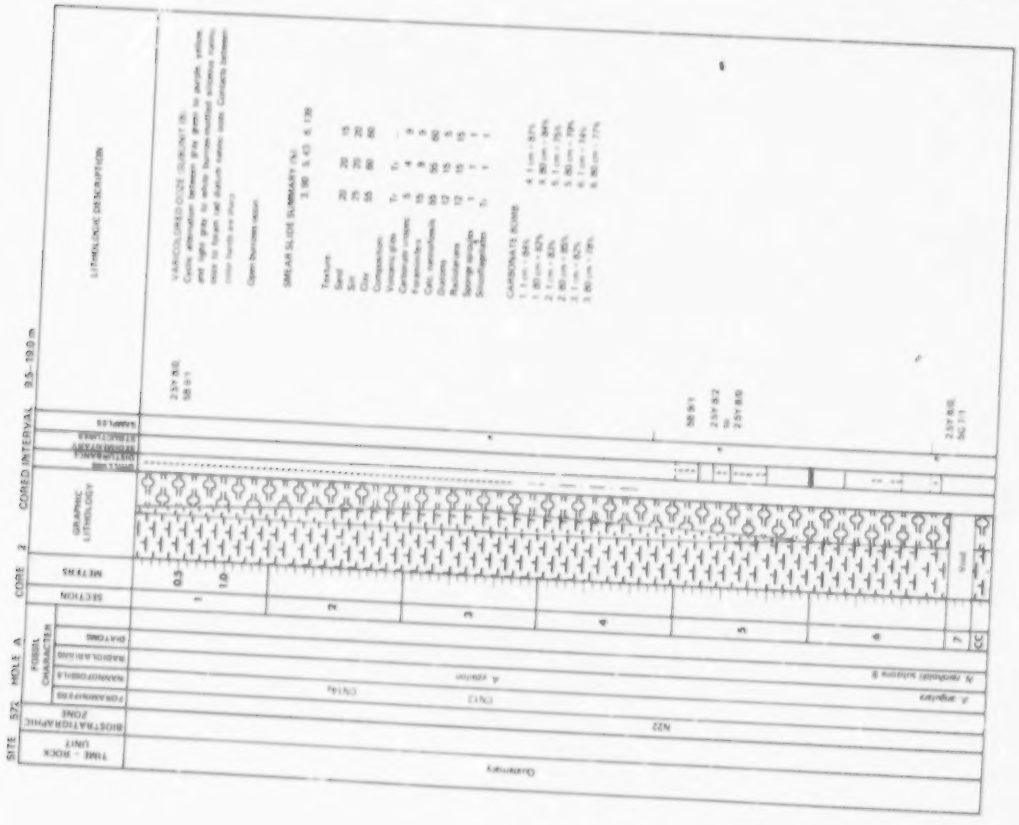

SITE 572 HOLE A CORE 4 CORED INTERVAL 28.6–36.3 m

TIME—ROCK UNIT	BIOSTRATIGRAPHIC ZONE	FOSSIL CHARACTER: FORAMINIFERS	FOSSIL CHARACTER: NANNOFOSSILS	FOSSIL CHARACTER: RADIOLARIANS	FOSSIL CHARACTER: DIATOMS	SECTION	METERS	GRAPHIC LITHOLOGY	DRILLING DISTURBANCE	SEDIMENTARY STRUCTURES	SAMPLES	LITHOLOGIC DESCRIPTION
late Pliocene	N21 / CN12		CN12		*P. praeatypicus*	1	0.5					5B 7/1
							1.0					N8
												5GY 8/1
						2						5Y 7/2
												5GY 7/1
												N7
						3						N3
												5GY 8/1
												N7
						4						5GY 7/1
												N3
												5Y 7/2
						5						5GY 7/1
												N7 to 5B 9/1
					R. praebergonii subzone B	CC						

VARICOLORED OOZE (SUBUNIT IB)

Cyclic color variations between white (N8), yellowish gray (5Y 7/2), gray green (5GY 7/1), and dark gray (N3) rad diatom nanno ooze. Burrowing and color mottling are common. Gradations in color between color bands are common. Laminations occur.

SMEAR SLIDE SUMMARY (%):

	1, 113	2, 7	4, 52
Texture:			
Sand	25	15	20
Silt	30	30	30
Clay	45	55	50
Composition:			
Volcanic glass	—	Tr	—
Pyrite	30	—	—
Carbonate unspec.	3	10	7
Foraminifers	10	10	8
Calc. nannofossils	40	40	40
Diatoms	15	25	25
Radiolarians	2	15	20
Sponge spicules	—	Tr	—
Silicoflagellates	—	Tr	Tr

CARBONATE BOMB:

1. 20 cm = 68%
1. 75 cm = 73%
2. 20 cm = 66%
2. 75 cm = 74%
3. 20 cm = 74%
3. 75 cm = 76%
4. 20 cm = 84%
4. 75 cm = 66%
5. 20 cm = 75%
5. 75 cm = 82%

SITE 572 HOLE A CORE 5 CORED INTERVAL 36.3–45.9 m

TIME—ROCK UNIT	BIOSTRATIGRAPHIC ZONE	FOSSIL CHARACTER: FORAMINIFERS	FOSSIL CHARACTER: NANNOFOSSILS	FOSSIL CHARACTER: RADIOLARIANS	FOSSIL CHARACTER: DIATOMS	SECTION	METERS	GRAPHIC LITHOLOGY	DRILLING DISTURBANCE	SEDIMENTARY STRUCTURES	SAMPLES	LITHOLOGIC DESCRIPTION
late Pliocene	N21 / CN12		CN12		*P. praeatypicus*	1	0.5					2.5Y 7/2
							1.0					N8
						2						5GY 7/1
												5Y 7/2
						3						N8
						4						2.5Y 7/2
						5						N8
						6						2.5Y 7/2 to 5GY 8/1
					S. ternata	7						
					R. praebergonii subzone A	CC						

VARICOLORED OOZE (SUBUNIT IB) (36.3–37.3 m):

Cyclic color variations between color bands: white (N8), yellowish gray (5Y 7/2), and gray green (5GY 7/1) rad diatom nanno ooze. Burrowing and color mottling are common. Gradations in color are common.

GREEN VARICOLORED OOZE (SUBUNIT IC) (37.3–45.9 m):

Cyclic color variations between green (10G 6/2), white (N8–5B 9/1), yellowish gray (5Y 7/20, and gray green (5GY 7/1) rad diatom nanno ooze. Gradations in color between color bands are common. Burrowing and color mottling are common. laminations also common.

SMEAR SLIDE SUMMARY (%):

	1, 98	3, 134	4, 103
Texture:			
Sand	15	10	25
Silt	5	30	25
Clay	80	60	50
Composition:			
Volcanic glass	Tr	—	Tr
Pyrite	Tr	—	—
Carbonate unspec.	12	15	8
Foraminifers	8	7	5
Calc. nannofossils	35	63	35
Diatoms	25	10	30
Radiolarians	20	5	20
Sponge spicules	Tr	Tr	—
Silicoflagellates	Tr	Tr	2

CARBONATE BOMB:

1. 1 cm = 79%
1. 80 cm = 73%
2. 1 cm = 71%
2. 80 cm = 73%
3. 1 cm = 72%
3. 80 cm = 85%
4. 1 cm = 82%
4. 80 cm = 78%
5. 1 cm = 73%
5. 80 cm = 82%
6. 1 cm = 70%
6. 80 cm = 67%
7. 1 cm = 60%

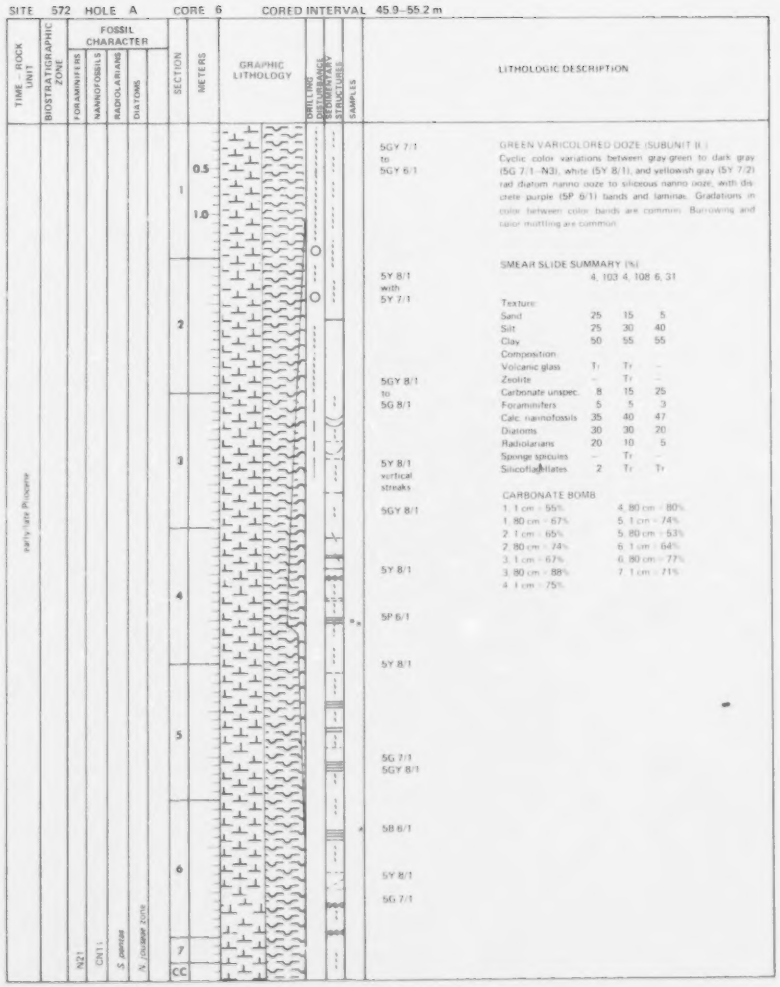
SITE 572 HOLE A CORE 6 CORED INTERVAL 45.9–55.2 m
TIME – ROCK UNIT
BIOSTRATIGRAPHIC ZONE
FOSSIL CHARACTER
FORAMINIFERS
NANNOFOSSILS
RADIOLARIANS
DIATOMS
SECTION
METERS
GRAPHIC LITHOLOGY
DRILLING DISTURBANCE
SEDIMENTARY STRUCTURES
SAMPLES
LITHOLOGIC DESCRIPTION
early late Pliocene
N21
CN11
S. peritas
N. jouseae zone
5GY 7/1 to 5GY 8/1
GREEN VARICOLORED OOZE (SUBUNIT II)
Cyclic color variations between gray green to dark gray (5G 7/1–N3), white (5Y 8/1), and yellowish gray (5Y 7/2) rad diatom nanno ooze to siliceous nanno ooze, with discrete purple (5P 6/1) bands and laminae. Gradations in color between color bands are common. Burrowing and color mottling are common.
SMEAR SLIDE SUMMARY (%)
4, 103 4, 108 6, 31
Texture:
Sand 25 15 5
Silt 25 30 40
Clay 50 55 55
Composition:
Volcanic glass Tr Tr –
Zeolite – Tr –
Carbonate unspec. 8 15 25
Foraminifers 5 5 3
Calc. nannofossils 35 40 47
Diatoms 30 30 20
Radiolarians 20 10 5
Sponge spicules – Tr –
Silicoflagellates 2 Tr Tr
CARBONATE BOMB
1. 1 cm = 55%
1. 80 cm = 67%
2. 1 cm = 65%
2. 80 cm = 74%
3. 1 cm = 67%
3. 80 cm = 88%
4. 1 cm = 75%
4. 80 cm = 80%
5. 1 cm = 74%
5. 80 cm = 53%
6. 1 cm = 64%
6. 80 cm = 77%
7. 1 cm = 71%
5Y 8/1 with 5Y 7/1
5GY 8/1 to 5G 8/1
5Y 8/1 vertical streaks
5GY 8/1
5Y 8/1
5P 6/1
5Y 8/1
5G 7/1 5GY 8/1
5B 6/1
5Y 8/1
5G 7/1

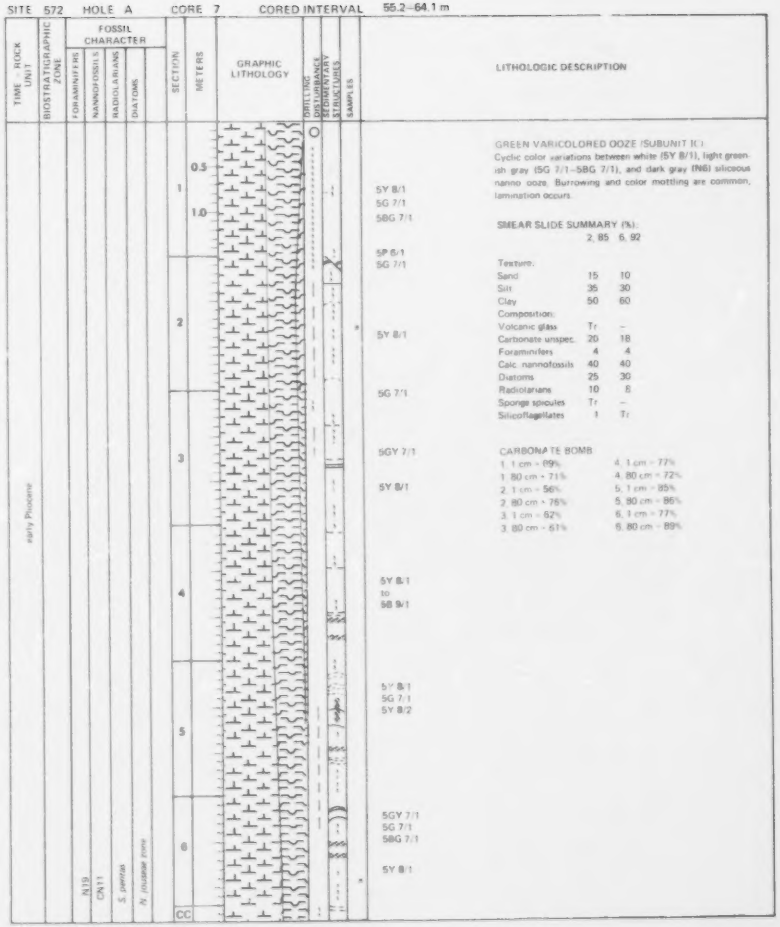
SITE 572 HOLE A CORE 7 CORED INTERVAL 55.2–64.1 m
TIME – ROCK UNIT
BIOSTRATIGRAPHIC ZONE
FOSSIL CHARACTER
FORAMINIFERS
NANNOFOSSILS
RADIOLARIANS
DIATOMS
SECTION
METERS
GRAPHIC LITHOLOGY
DRILLING DISTURBANCE
SEDIMENTARY STRUCTURES
SAMPLES
LITHOLOGIC DESCRIPTION
early Pliocene
N19
CN11
S. peritas
N. jouseae zone
GREEN VARICOLORED OOZE (SUBUNIT IC)
Cyclic color variations between white (5Y 8/1), light greenish gray (5G 7/1–5BG 7/1), and dark gray (N6) siliceous nanno ooze. Burrowing and color mottling are common, lamination occurs.
SMEAR SLIDE SUMMARY (%):
2, 85 6, 92
Texture:
Sand 15 10
Silt 35 30
Clay 50 60
Composition:
Volcanic glass Tr –
Carbonate unspec. 20 18
Foraminifers 4 4
Calc. nannofossils 40 40
Diatoms 25 30
Radiolarians 10 8
Sponge spicules Tr –
Silicoflagellates 1 Tr
CARBONATE BOMB
1. 1 cm = 89%
1. 80 cm = 71%
2. 1 cm = 56%
2. 80 cm = 76%
3. 1 cm = 62%
3. 80 cm = 61%
4. 1 cm = 77%
4. 80 cm = 72%
5. 1 cm = 85%
5. 80 cm = 86%
6. 1 cm = 77%
6. 80 cm = 89%
5Y 8/1
5G 7/1
5BG 7/1
5P 6/1
5G 7/1
5Y 8/1
5G 7/1
5GY 7/1
5Y 8/1
5Y 8/1 to 5B 9/1
5Y 8/1 5G 7/1 5Y 8/2
5GY 7/1 5G 7/1 5BG 7/1
5Y 8/1

SITE 572 HOLE A CORE 8 CORED INTERVAL 64.1–72.3 m

TIME – ROCK UNIT: early Pliocene

BIOSTRATIGRAPHIC ZONE: N19 / CN11 / *S. peregrina* / *N. inflata* zone

FOSSIL CHARACTER: FORAMINIFERS / NANNOFOSSILS / RADIOLARIANS / DIATOMS

SECTION: 1, 2, 3, 4, 5, 6, CC

METERS: 0.5, 1.0

GRAPHIC LITHOLOGY

DRILLING DISTURBANCE / SEDIMENTARY STRUCTURES / SAMPLES

LITHOLOGIC DESCRIPTION

5GY 7/1
5Y 8/1
5B 7/1
5Y 8/1
2.5Y 7/1
2.5Y 7/1
5Y 8/1,
5GY 8/1,
5B 8/1
5Y 8/1 to 5Y 8/2
5Y 8/2
5Y 8/2–5GY 8/1
5Y 8/1
5Y 8/2
5Y 8/1–N9, N7, 5Y 7/1
5Y 8/1 and 2.5Y 8/1
5Y 8/1–5Y 8/2
5Y 8/1

GREEN VARICOLORED OOZE (SUBUNIT II):
Cyclic color variations between white (5Y 8/1), light gray (N7), and greenish gray (5GY 8/1) diatom nanno ooze with discrete blue gray (5B 7/1) bands and laminae. Gradations in color between color bands are common. Burrowing and color mottling are common.

SMEAR SLIDE SUMMARY (%):

	4, 85
Texture:	
Sand	5
Silt	20
Clay	75
Composition:	
Pyrite	Tr
Carbonate unspec.	10
Foraminifers	5
Calc. nannofossils	40
Diatoms	40
Radiolarians	2
Sponge spicules	Tr
Silicoflagellates	Tr

CARBONATE BOMB:

1, 1 cm = 88%	4, 1 cm = 68%
1, 80 cm = 90%	4, 80 cm = 81%
2, 1 cm = 88%	5, 1 cm = 75%
2, 80 cm = 78%	5, 80 cm = 47%
3, 1 cm = 80%	6, 1 cm = 58%
3, 80 cm = 81%	

SITE 572 HOLE A CORE 9 CORED INTERVAL 72.3–81.8 m

TIME – ROCK UNIT: early Pliocene

BIOSTRATIGRAPHIC ZONE: N19 / CN11 / *S. peregrina* / *N. inflata* zone

FOSSIL CHARACTER: FORAMINIFERS / NANNOFOSSILS / RADIOLARIANS / DIATOMS

SECTION: 1, 2, 3, 4, 5, 6, 7, CC

METERS: 0.5, 1.0

GRAPHIC LITHOLOGY

DRILLING DISTURBANCE / SEDIMENTARY STRUCTURES / SAMPLES

LITHOLOGIC DESCRIPTION

5Y 8/1, N9, 5BG 7/1
5Y 8/1 and 5Y 6/2
5Y 6/2
5Y 8/1, 5Y 6/2, and 5BG 7/1
5Y 6/2
5Y 8/1–N9
5Y 8/1–N9
5Y 8/1, 5BG 7/1, N9

GREEN VARICOLORED OOZE (SUBUNIT II):
Cyclic color variations between white (N9, 5Y 8/1), pale yellow (5Y 6/2), and green (5BG 7/1) diatom nanno ooze to siliceous nanno ooze, with occasional purple (5RP 2/2) bands and laminae. Burrowing and color mottling are common.

SMEAR SLIDE SUMMARY (%):

	2, 143	4, 30	6, 81
Texture:			
Sand	45	45	10
Silt	15	15	10
Clay	40	40	80
Composition:			
Volcanic glass	Tr	Tr	Tr
Carbonate unspec.	9	5	3
Foraminifers	1	Tr	2
Calc. nannofossils	40	40	80
Diatoms	40	45	6
Radiolarians	5	5	6
Sponge spicules	4	4	2
Silicoflagellates	1	1	1
Fish remains	Tr	Tr	—

CARBONATE BOMB:

1, 1 cm = 72%	4, 80 cm = 83%
1, 80 cm = 76%	5, 1 cm = 74%
2, 1 cm = 77%	5, 80 cm = 79%
2, 80 cm = 72%	6, 1 cm = 80%
3, 1 cm = 50%	6, 80 cm = 85%
3, 80 cm = 70%	

SITE 572 HOLE A CORE 10 CORED INTERVAL 81.8–91.4 m

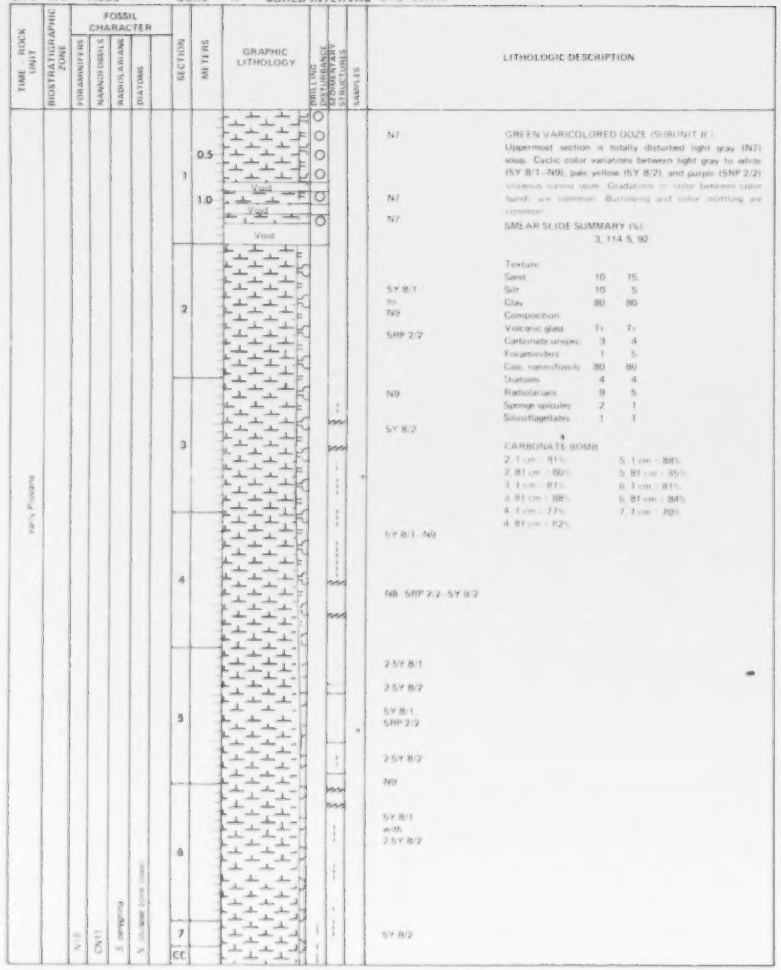

SITE 572 HOLE A CORE 11 CORED INTERVAL 91.4–100.7 m

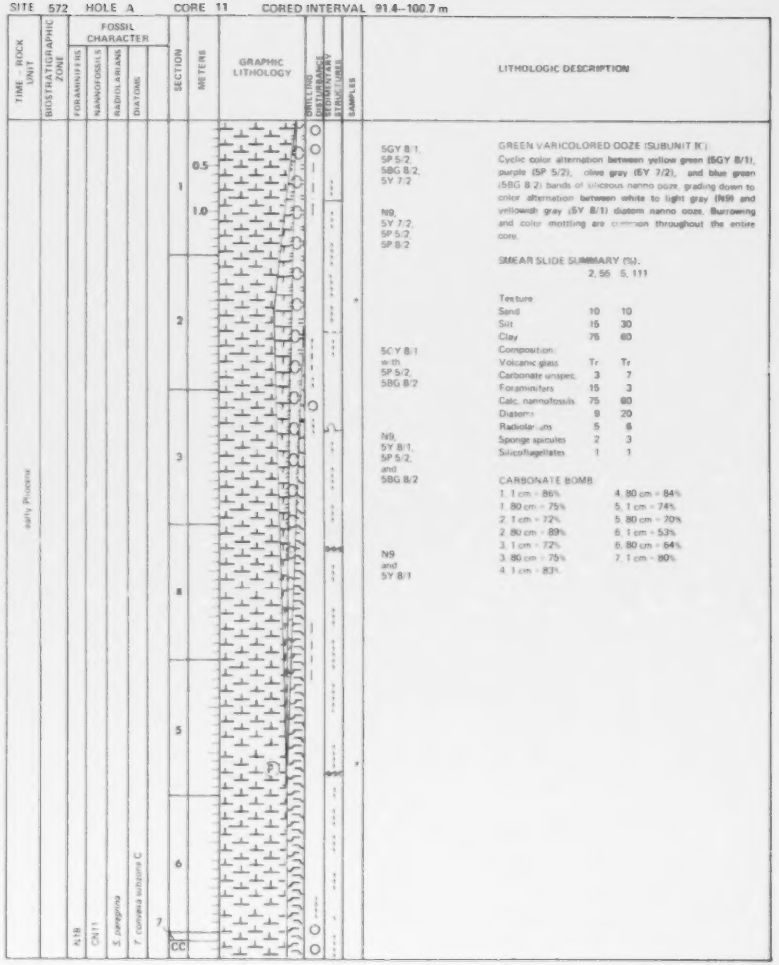
TIME – ROCK UNIT
BIOSTRATIGRAPHIC ZONE
FOSSIL CHARACTER
FORAMINIFERS
NANNOFOSSILS
RADIOLARIANS
DIATOMS
SECTION
METERS
GRAPHIC LITHOLOGY
DRILLING DISTURBANCE
SEDIMENTARY STRUCTURES
SAMPLES
LITHOLOGIC DESCRIPTION
early Pliocene
N18
CN11
S. peregrina
T. convexa subzone C
5GY 8/1, 5P 5/2, 5BG 8/2, 5Y 7/2
N9, 5Y 7/2, 5P 5/2, 5P 8/2
5CY 8/1 with 5P 5/2, 5BG 8/2
N9, 5Y 8/1, 5P 5/2, and 5BG 8/2
N9 and 5Y 8/1
GREEN VARICOLORED OOZE (SUBUNIT IC)
Cyclic color alternation between yellow green (5GY 8/1), purple (5P 5/2), olive gray (5Y 7/2), and blue green (5BG 8/2) bands of siliceous nanno ooze grading down to color alternation between white to light gray (N9) and yellowish gray (5Y 8/1) diatom nanno ooze. Burrowing and color mottling are common throughout the entire core.
SMEAR SLIDE SUMMARY (%):
2, 55 5, 111
Texture:
Sand 10 10
Silt 15 30
Clay 75 60
Composition:
Volcanic glass Tr Tr
Carbonate unspec. 3 7
Foraminifers 15 3
Calc. nannofossils 75 60
Diatoms 9 20
Radiolarians 5 6
Sponge spicules 2 3
Silicoflagellates 1 1
CARBONATE BOMB
1. 1 cm = 86%
1. 80 cm = 75%
2. 1 cm = 72%
2. 80 cm = 89%
3. 1 cm = 72%
3. 80 cm = 75%
4. 1 cm = 83%
4. 80 cm = 84%
5. 1 cm = 74%
5. 80 cm = 70%
6. 1 cm = 53%
6. 80 cm = 64%
7. 1 cm = 80%

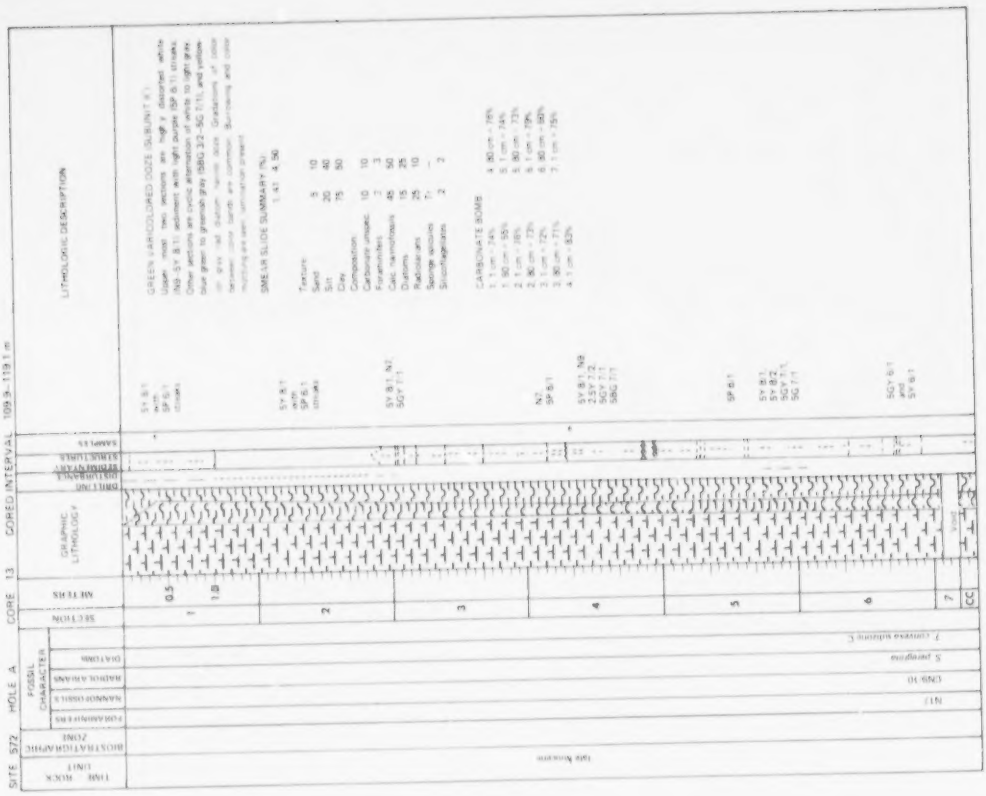

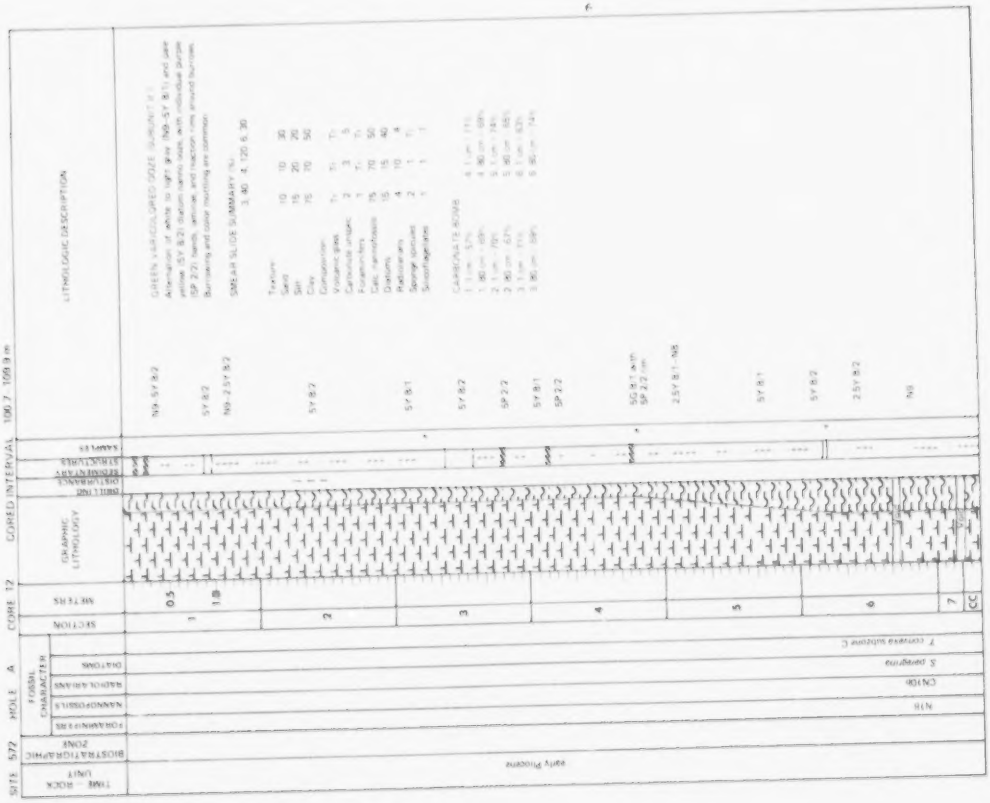

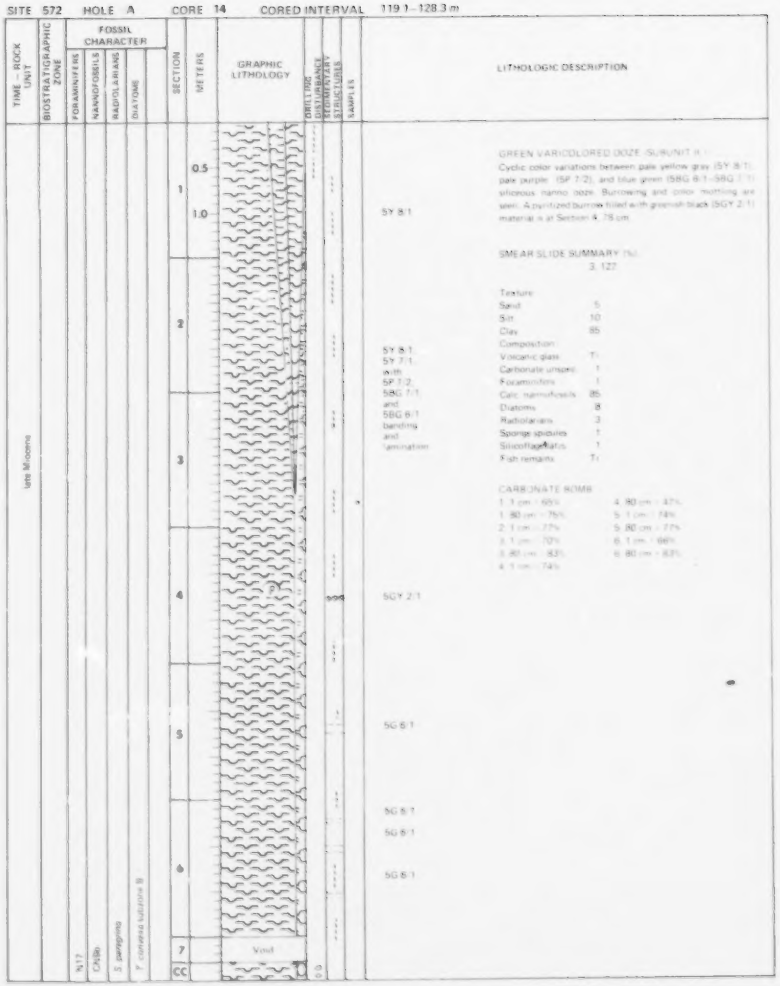
SITE 572 HOLE A CORE 14 CORED INTERVAL 119.1–128.3 m
TIME – ROCK UNIT
BIOSTRATIGRAPHIC ZONE
FOSSIL CHARACTER
FORAMINIFERS
NANNOFOSSILS
RADIOLARIANS
DIATOMS
SECTION
METERS
GRAPHIC LITHOLOGY
DRILLING DISTURBANCE
SEDIMENTARY STRUCTURES
SAMPLES
LITHOLOGIC DESCRIPTION
late Miocene
N17
CN9b
S. peregrina
T. convexa subzone B
Void
GREEN VARICOLORED OOZE (SUBUNIT II-)
Cyclic color variations between pale yellow gray (5Y 8/1), pale purple (5P 7/2), and blue green (5BG 8/1–5BG 7/1) siliceous nanno ooze. Burrowing and color mottling are seen. A pyritized burrow filled with greenish black (5GY 2/1) material is at Section 4, 75 cm.
5Y 8/1
5Y 8/1, 5Y 7/1, with 5P 7/2, 5BG 7/1 and 5BG 8/1 banding and lamination
5GY 2/1
5G 8/1
5G 8/1
5G 8/1
5G 8/1
SMEAR SLIDE SUMMARY (%)
3, 127
Texture:
Sand 5
Silt 10
Clay 85
Composition:
Volcanic glass Tr
Carbonate unspec. 1
Foraminifers 1
Calc. nannofossils 85
Diatoms 8
Radiolarians 3
Sponge spicules 1
Silicoflagellates 1
Fish remains Tr
CARBONATE BOMB
1, 3 cm = 65%
1, 80 cm = 75%
2, 1 cm = 77%
3, 1 cm = 70%
3, 80 cm = 83%
4, 1 cm = 74%
4, 80 cm = 47%
5, 1 cm = 74%
5, 80 cm = 77%
6, 1 cm = 66%
6, 80 cm = 83%

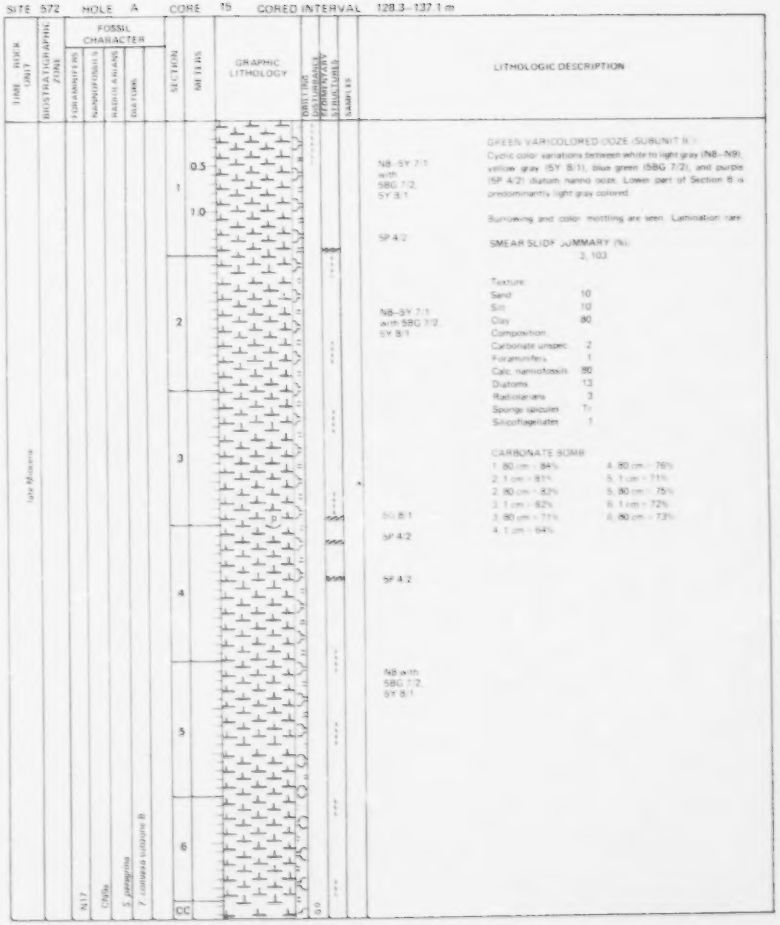
SITE 572 HOLE A CORE 15 CORED INTERVAL 128.3–137.1 m
TIME – ROCK UNIT
BIOSTRATIGRAPHIC ZONE
FOSSIL CHARACTER
FORAMINIFERS
NANNOFOSSILS
RADIOLARIANS
DIATOMS
SECTION
METERS
GRAPHIC LITHOLOGY
DRILLING DISTURBANCE
SEDIMENTARY STRUCTURES
SAMPLES
LITHOLOGIC DESCRIPTION
late Miocene
N17
CN9a
S. peregrina
T. convexa subzone B
GREEN VARICOLORED OOZE (SUBUNIT II-)
Cyclic color variations between white to light gray (N8–N9), yellow gray (5Y 8/1), blue green (5BG 7/2), and purple (5P 4/2) diatom nanno ooze. Lower part of Section 6 is predominantly light gray colored.
Burrowing and color mottling are seen. Lamination rare.
N8–5Y 7/1 with 5BG 7/2, 5Y 8/1
5P 4/2
N8–5Y 7/1 with 5BG 7/2, 5Y 8/1
5G 8/1
5P 4/2
5P 4/2
N8 with 5BG 7/2, 5Y 8/1
SMEAR SLIDE SUMMARY (%)
3, 103
Texture:
Sand 10
Silt 10
Clay 80
Composition:
Carbonate unspec. 2
Foraminifers 1
Calc. nannofossils 80
Diatoms 13
Radiolarians 3
Sponge spicules Tr
Silicoflagellates 1
CARBONATE BOMB
1, 80 cm = 84%
2, 1 cm = 81%
2, 80 cm = 82%
3, 1 cm = 82%
3, 80 cm = 71%
4, 1 cm = 64%
4, 80 cm = 76%
5, 1 cm = 71%
5, 80 cm = 75%
6, 1 cm = 72%
6, 80 cm = 73%

SITE 572

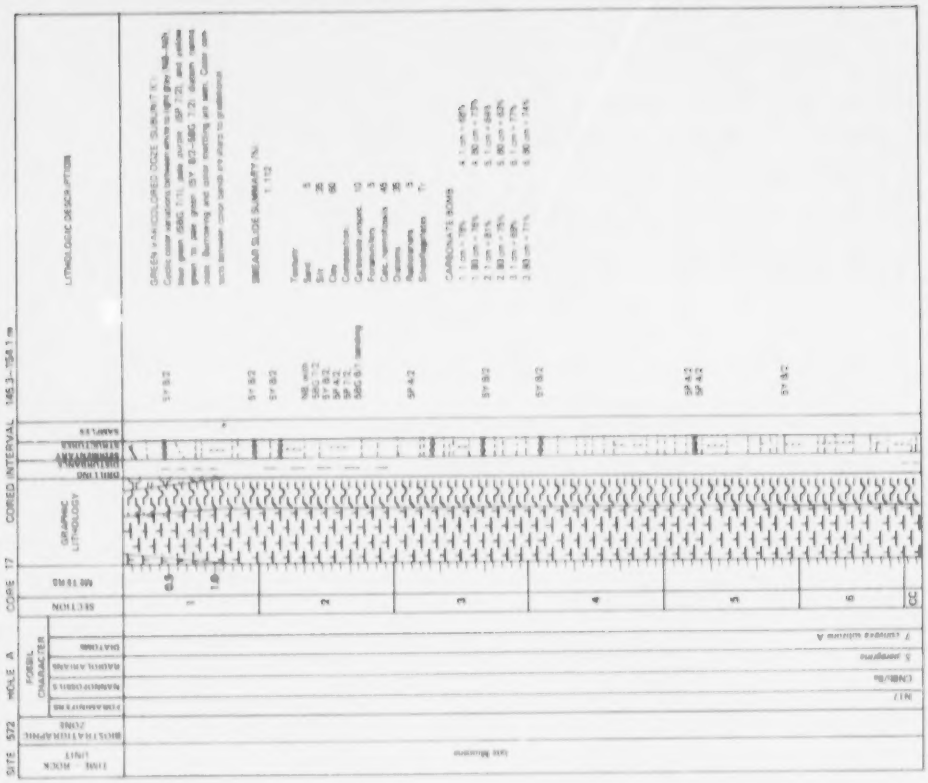

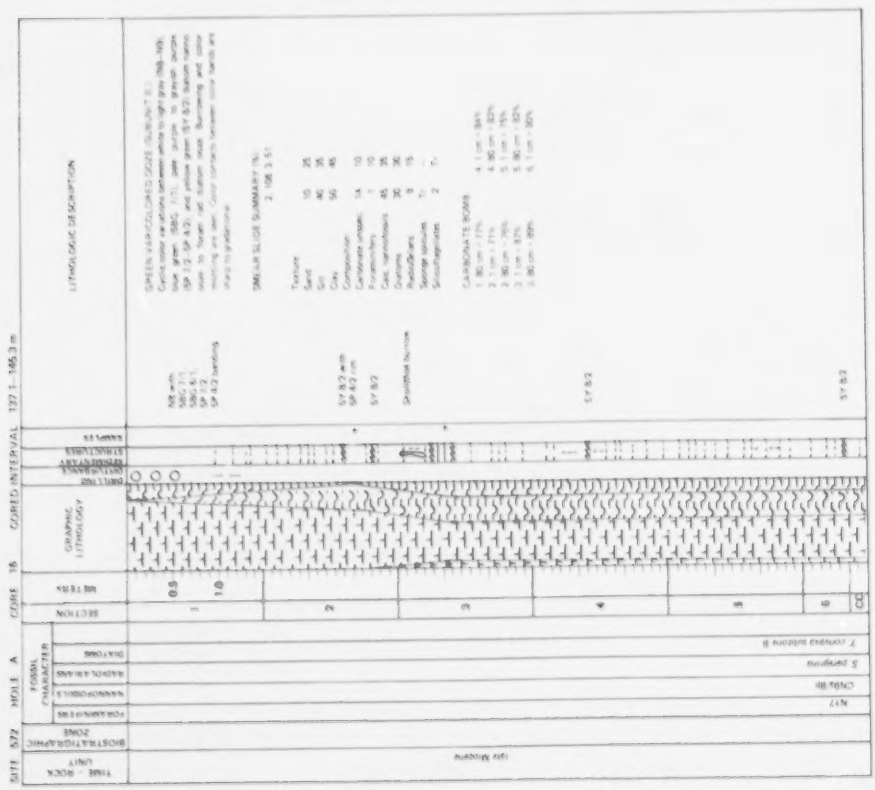

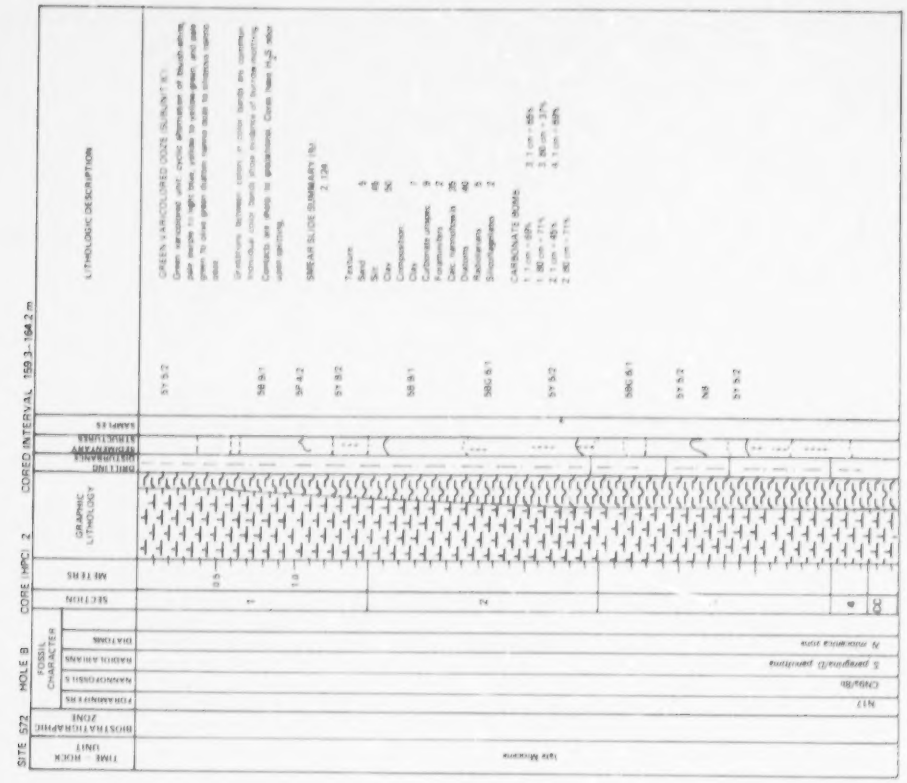

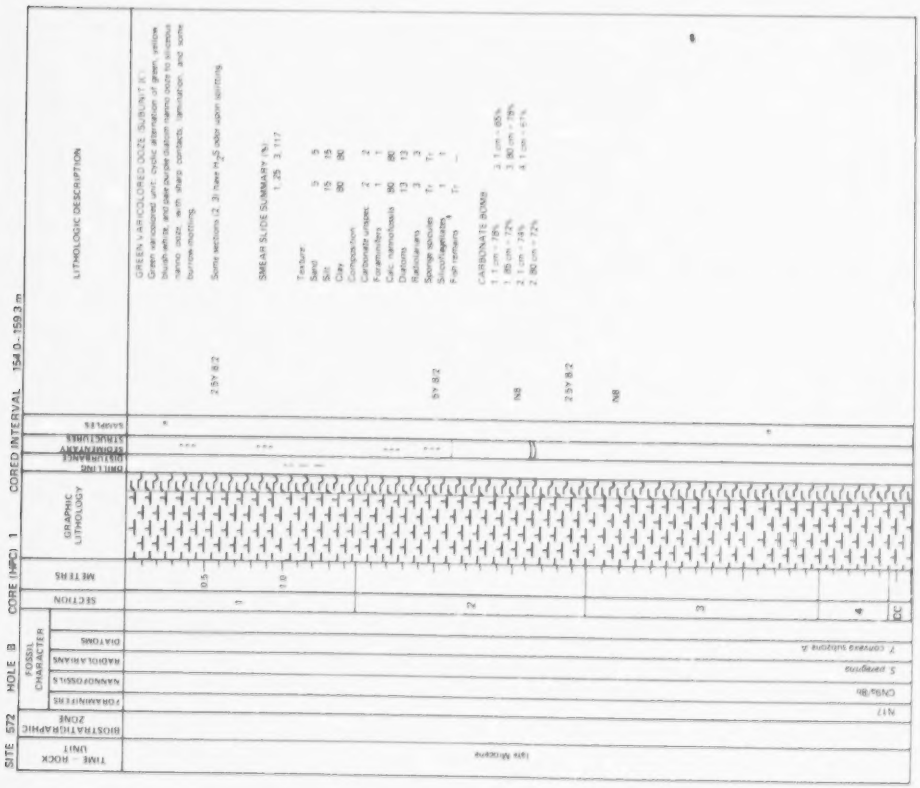

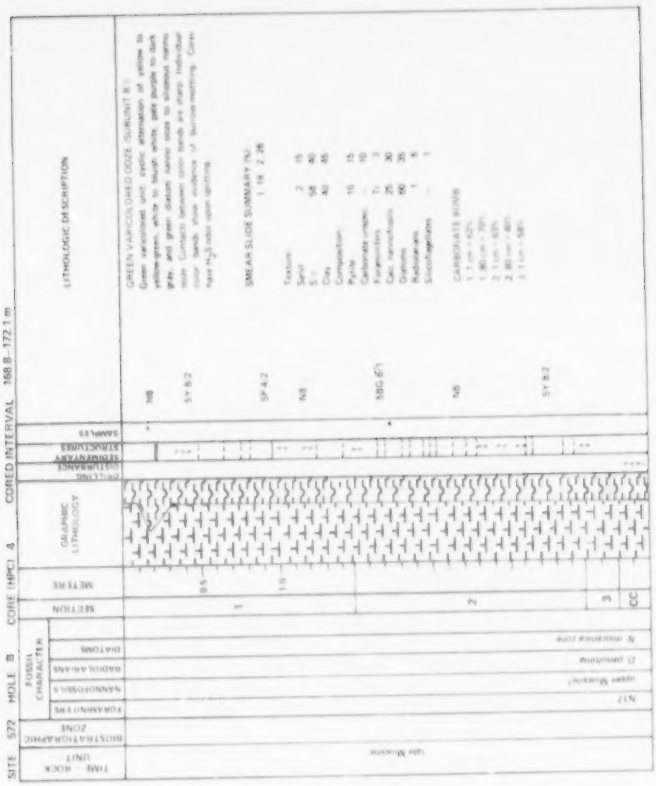

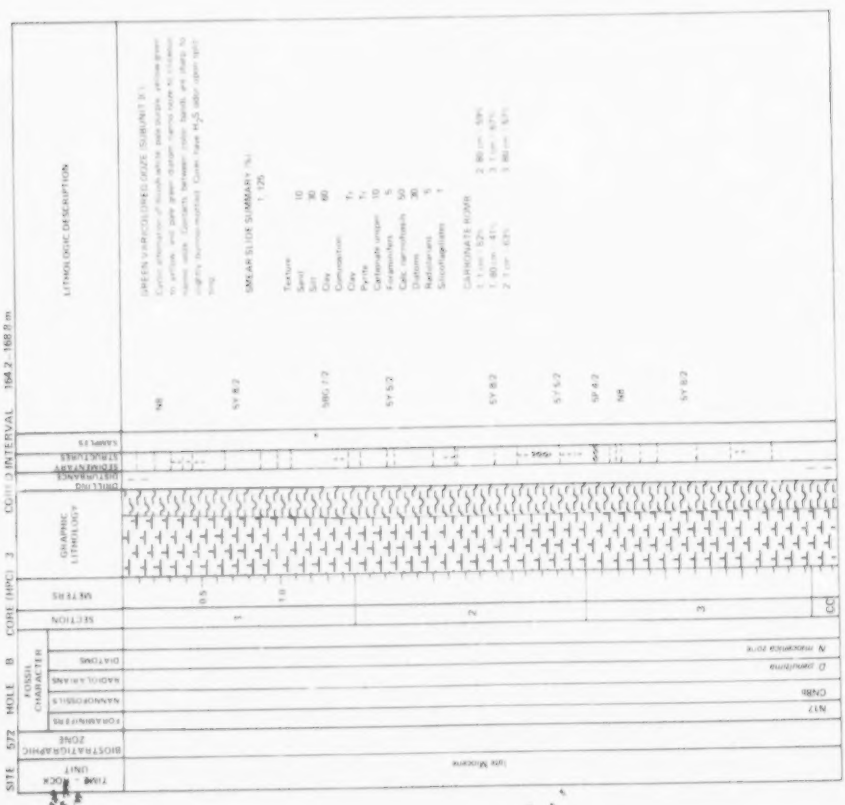

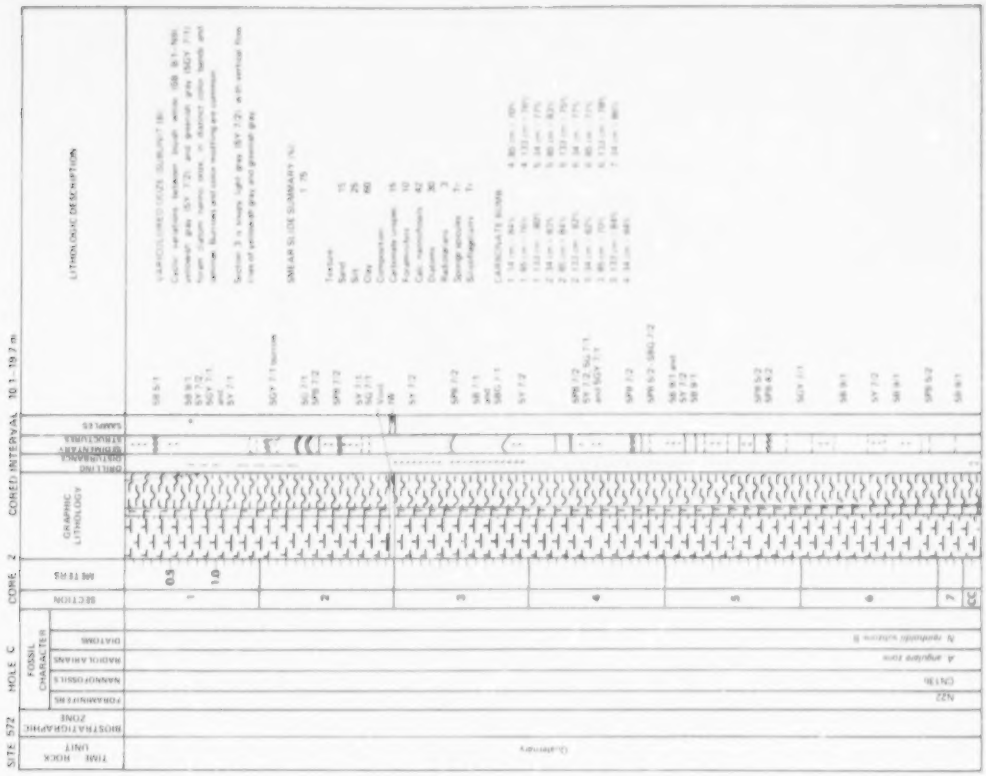

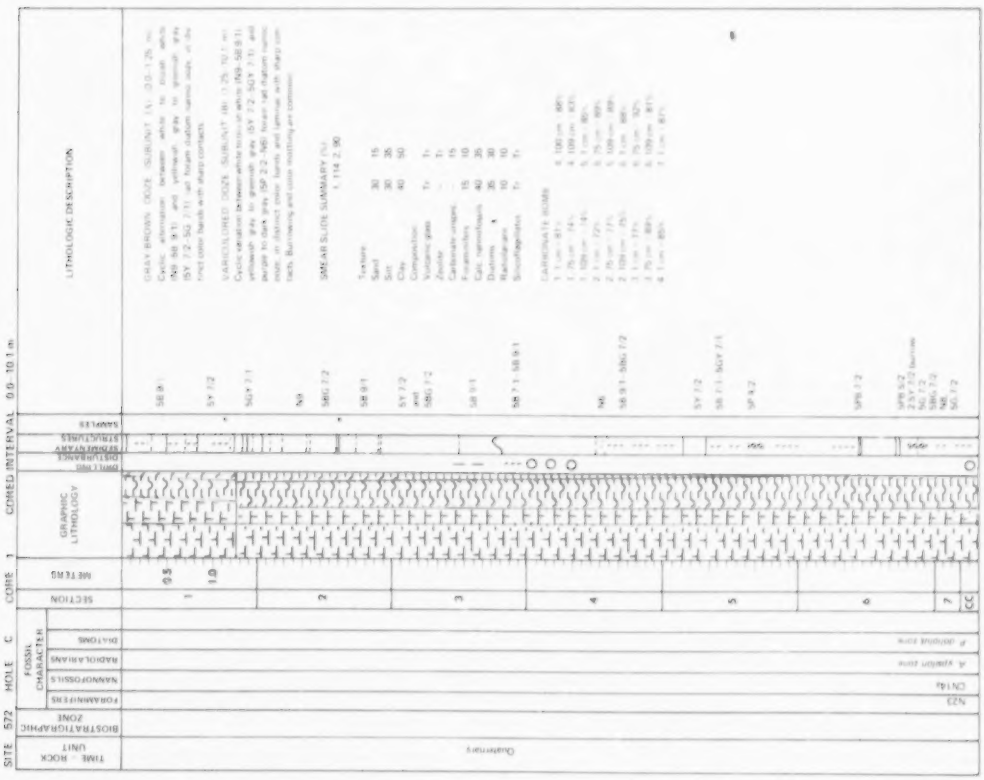

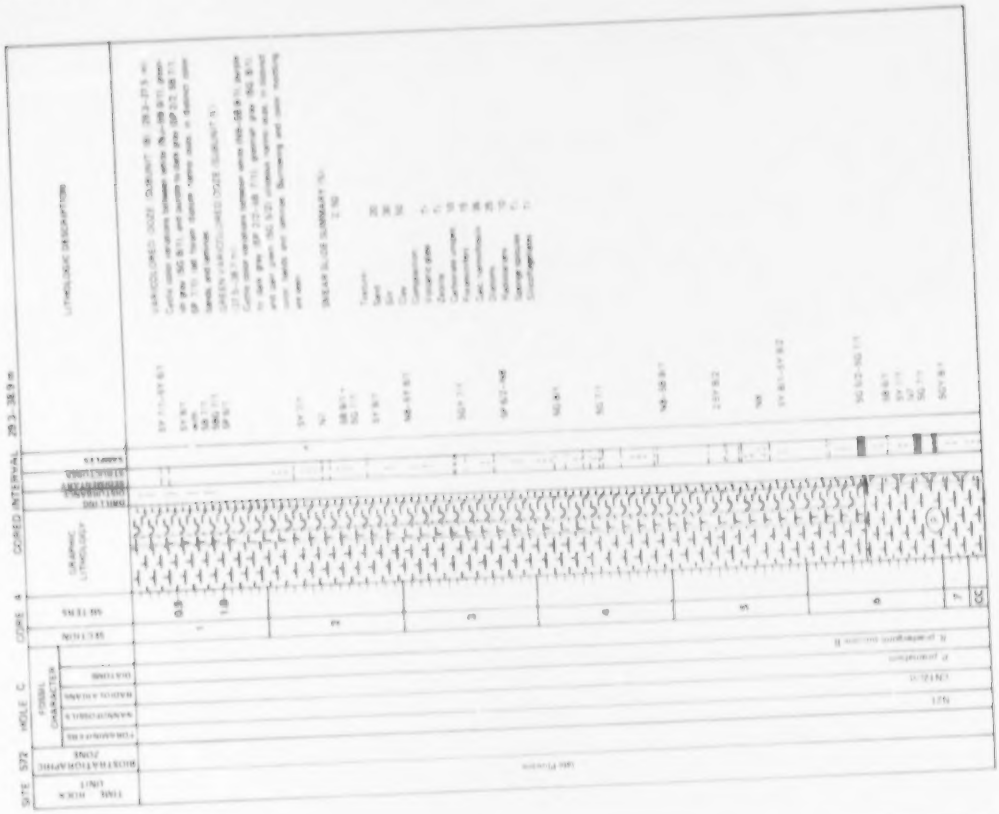

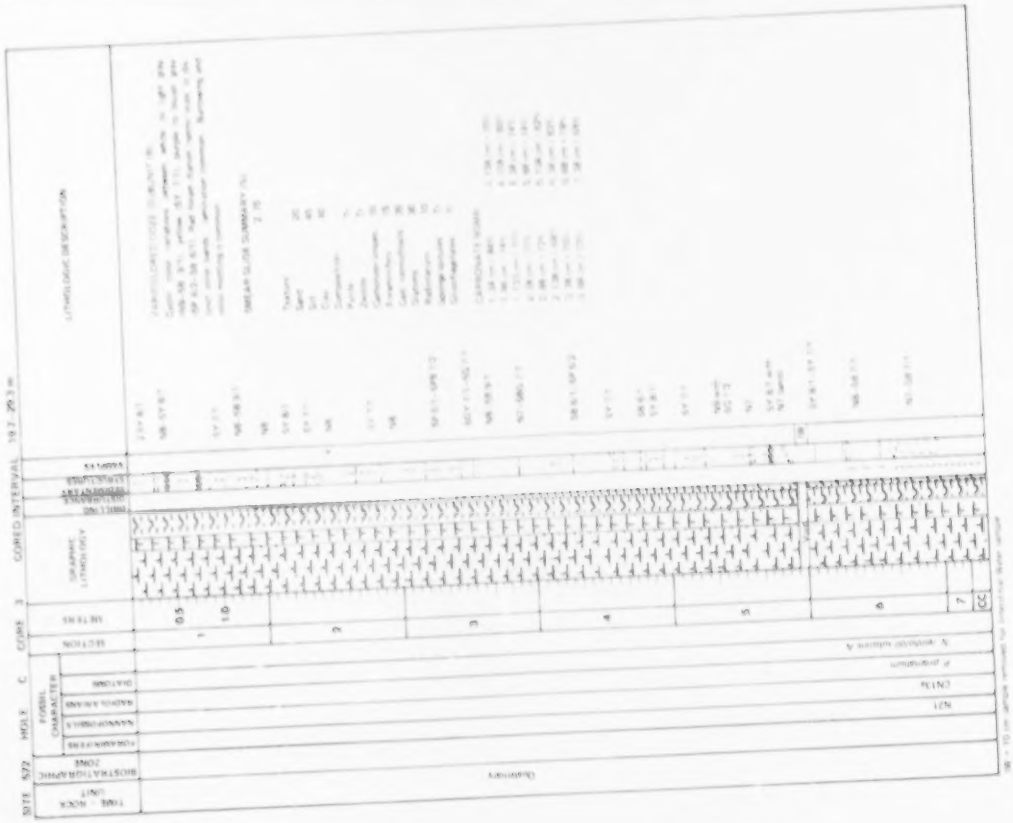

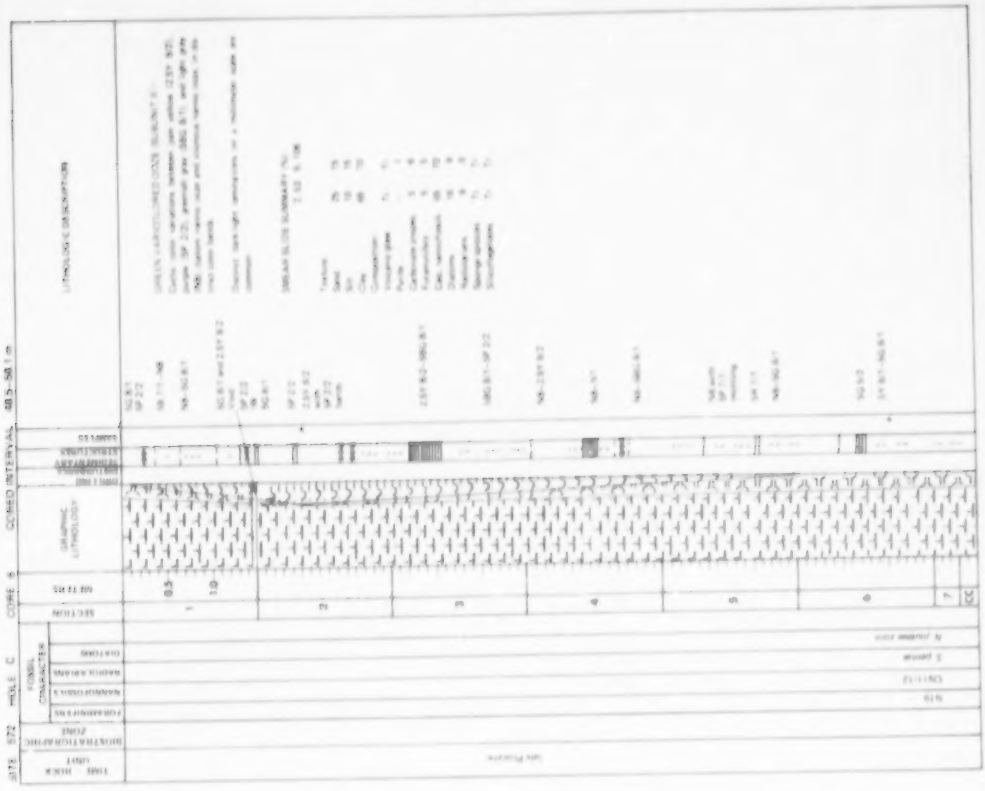

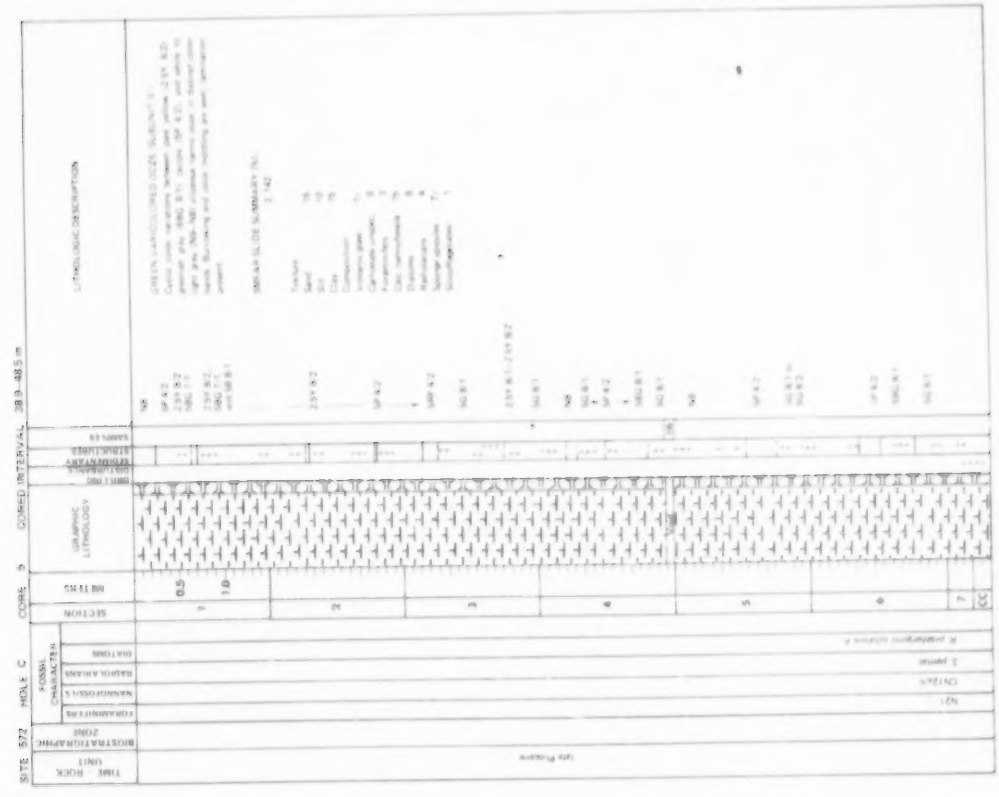

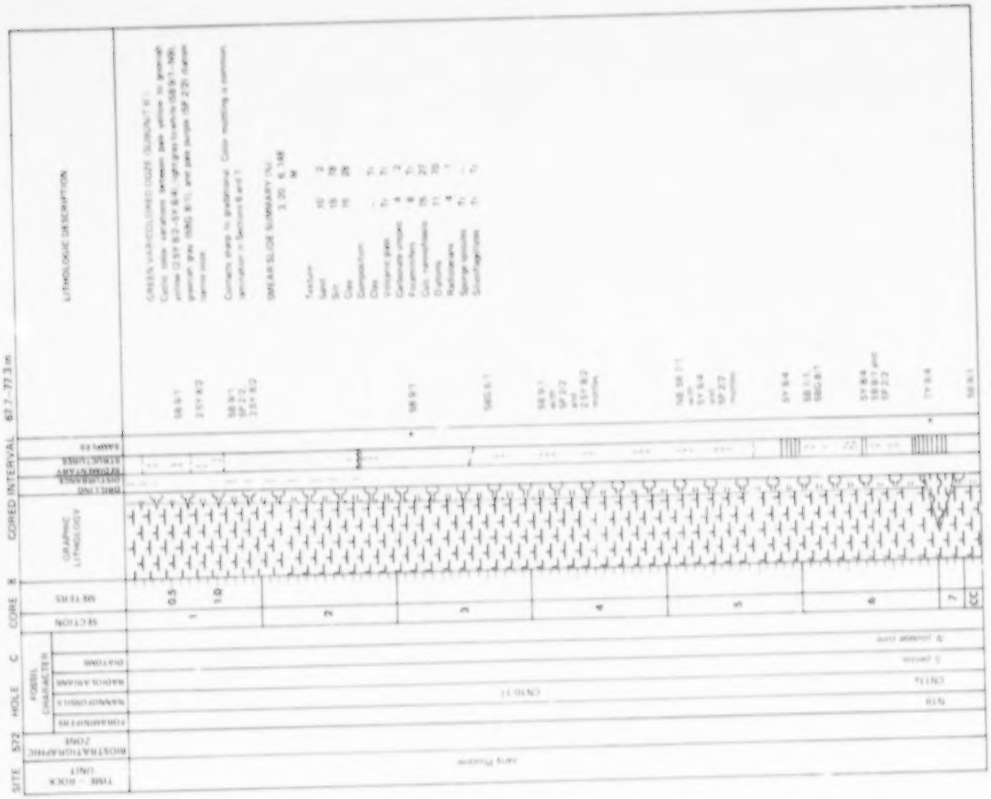

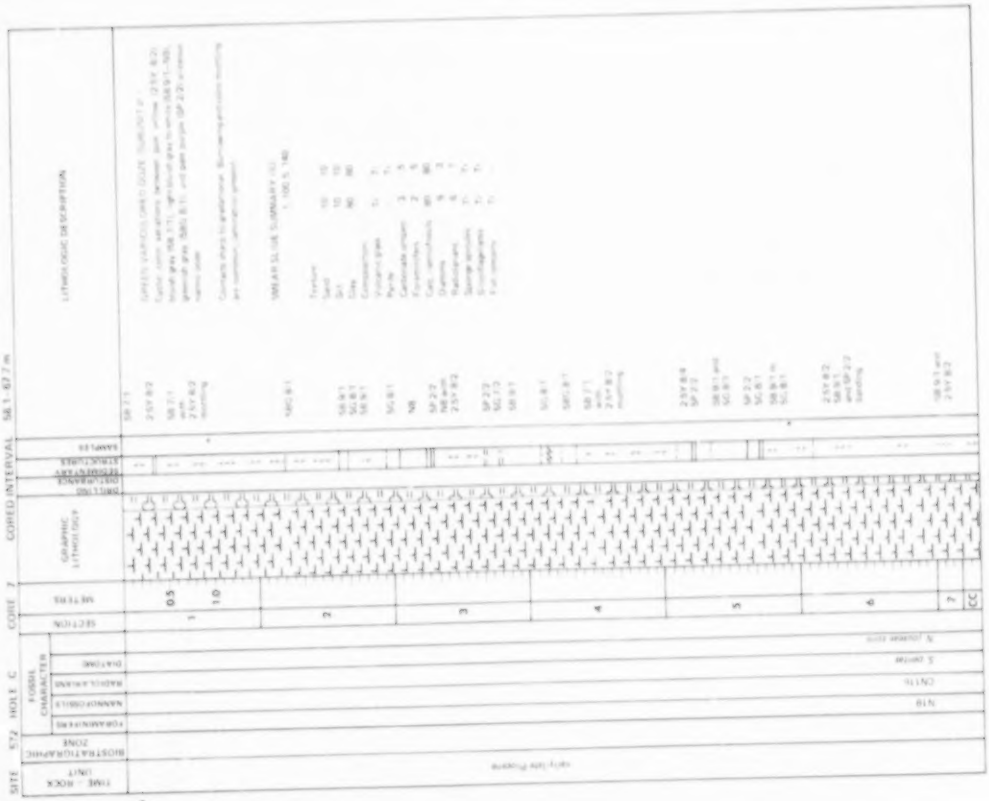

SITE 572 HOLE C CORE 9 CORED INTERVAL 77.3–86.9 m

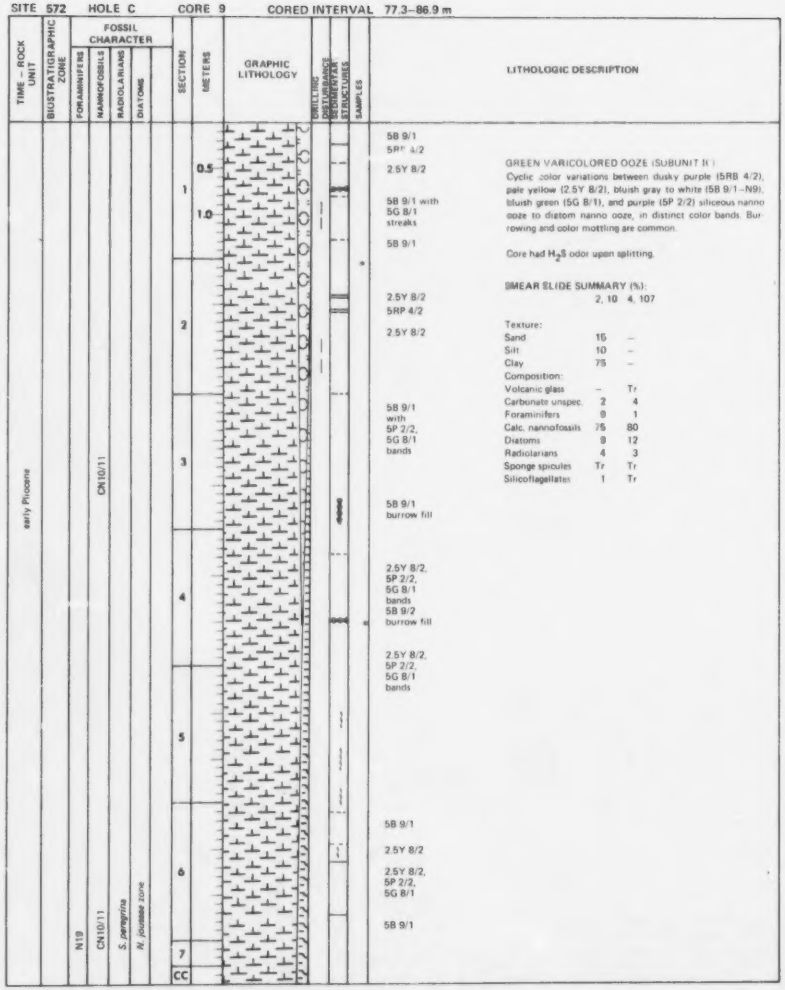

GREEN VARICOLORED OOZE (SUBUNIT IC)

Cyclic color variations between dusky purple (5RB 4/2), pale yellow (2.5Y 8/2), bluish gray to white (5B 9/1–N9), bluish green (5G 8/1), and purple (5P 2/2) siliceous nanno ooze to diatom nanno ooze, in distinct color bands. Burrowing and color mottling are common.

Core had H_2S odor upon splitting.

SMEAR SLIDE SUMMARY (%):

	2, 10	4, 107
Texture:		
Sand	15	–
Silt	10	–
Clay	75	–
Composition:		
Volcanic glass	–	Tr
Carbonate unspec.	2	4
Foraminifers	9	1
Calc. nannofossils	75	80
Diatoms	9	12
Radiolarians	4	3
Sponge spicules	Tr	Tr
Silicoflagellates	1	Tr

SITE 572 HOLE C CORE 10 CORED INTERVAL 86.9–96.5 m

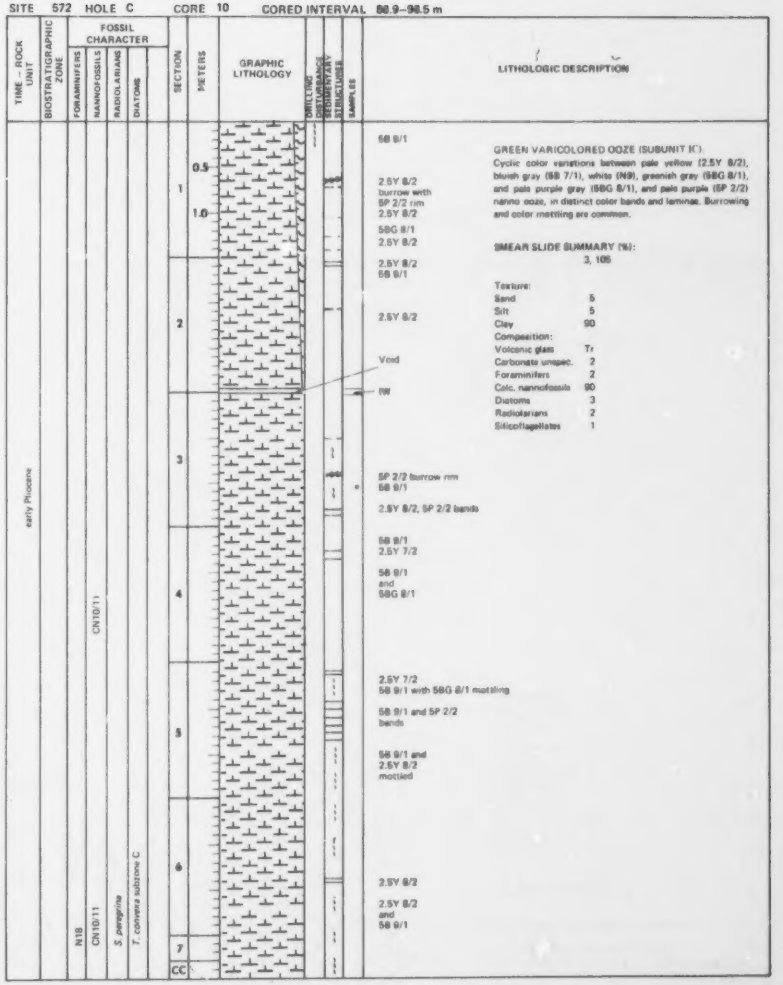

GREEN VARICOLORED OOZE (SUBUNIT IC)

Cyclic color variations between pale yellow (2.5Y 8/2), bluish gray (5B 7/1), white (N9), greenish gray (5BG 8/1), and pale purple gray (5BG 8/1), and pale purple (5P 2/2) nanno ooze, in distinct color bands and laminae. Burrowing and color mottling are common.

SMEAR SLIDE SUMMARY (%):

	3, 105
Texture:	
Sand	5
Silt	5
Clay	90
Composition:	
Volcanic glass	Tr
Carbonate unspec.	2
Foraminifers	2
Calc. nannofossils	90
Diatoms	3
Radiolarians	2
Silicoflagellates	1

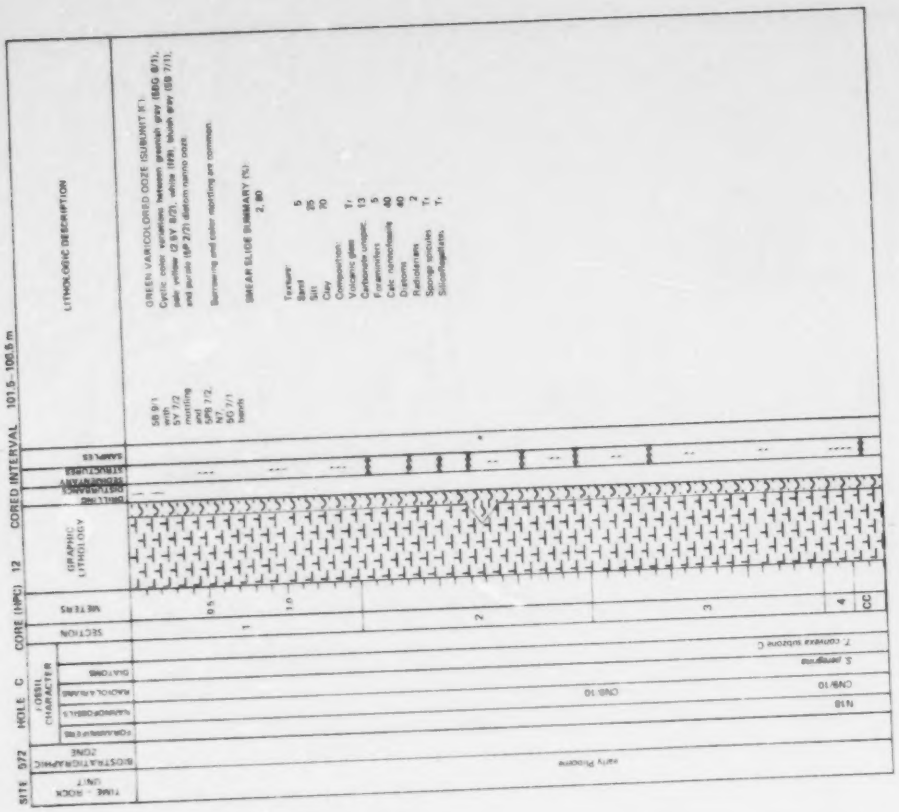

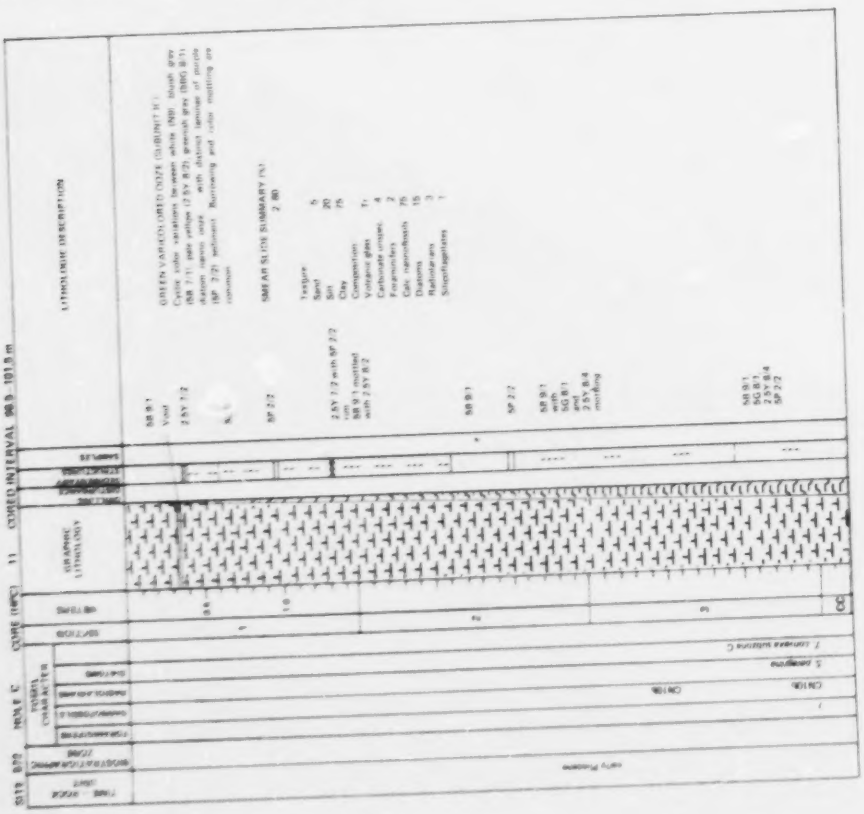

SITE 572 HOLE C CORE (HPC) 13 CORED INTERVAL 106.5–111.5 m

TIME – ROCK UNIT	BIOSTRATIGRAPHIC ZONE	FOSSIL CHARACTER: FORAMINIFERS	NANNOFOSSILS	RADIOLARIANS	DIATOMS	SECTION	METERS	GRAPHIC LITHOLOGY	DRILLING DISTURBANCE	SEDIMENTARY STRUCTURES	SAMPLES	LITHOLOGIC DESCRIPTION
early Pliocene	N18 / Chrb. / *S. peregrina* / *T. carinata* subzone C					1	0.5					5Y 7/1 with streaks of 5G 8/1, 5Y 8/1, 5P 8/1
							1.0					
						2						
						3						N9–5B 9/1 with bands of N7, 5P 8/2, 5BG 7/1, 5G 8/1
						4						
						CC						

GREEN VARICOLORED OOZE (SUBUNIT IC)

Cyclic color variations between pale yellow (2.5Y 8/2), greenish gray (5BG 8/1), white (5B 9/1–N9), bluish gray (5B 7/1), and purple (5P 2/2) diatom nanno ooze.

Upper two sections have severe vertical streaking of colored laminae within a dominantly white background.

SMEAR SLIDE SUMMARY (%):

	2, 87
Texture:	
Sand	10
Silt	40
Clay	50
Composition:	
Volcanic glass	Tr
Carbonate unspec.	11
Foraminifers	3
Calc. nannofossils	40
Diatoms	40
Radiolarians	6
Sponge spicules	Tr
Silicoflagellates	Tr

SITE 572 HOLE C CORE 14 CORED INTERVAL 111.5–121.1 m

TIME – ROCK UNIT	BIOSTRATIGRAPHIC ZONE	FOSSIL CHARACTER: FORAMINIFERS	NANNOFOSSILS	RADIOLARIANS	DIATOMS	SECTION	METERS	GRAPHIC LITHOLOGY	DRILLING DISTURBANCE	SEDIMENTARY STRUCTURES	SAMPLES	LITHOLOGIC DESCRIPTION
late Miocene	N17 top / Chrb. / *S. peregrina* / *T. carinata* subzone B					1	0.5					5Y 6/2–5Y 7/1
							1.0					5Y 8/1
						2						5GY 7/1
												5Y 8/1
						3						5Y 6/2
												N9
						4						5GY 7/1
												N9
						5						N9
												N9
						6						5Y 7/2
						CC						5P 6/2 N9 and 5P 8/2
												5Y 7/2 5GY 7/1 5GY 8/1–5Y 8/1
												N9
												N9
												5B 9/1
												5Y 7/2
												5B 9/1
												5GY 7/1 5P 6/2 5P 6/2
												N9
												5P 6/2
												5Y 8/2–8Y 7/1

GREEN VARICOLORED OOZE (SUBUNIT IC)

Cyclic color variations between white (N9–5Y 8/1), greenish gray (5GY 7/1), light gray (5Y 7/2), and pale purple (5P 8/3) diatom nanno ooze, in distinct color bands. Burrowing and color mottling are common. Laminations occurs.

SMEAR SLIDE SUMMARY (%):

	2, 77	4, 104
Texture:		
Sand	6	2
Silt	48	50
Clay	66	48
Composition:		
Volcanic glass	Tr	--
Pyrite	--	Tr
Zeolite	Tr	--
Carbonate unspec.	6	--
Foraminifers	2	Tr
Calc. nannofossils	46	40
Diatoms	40	60
Radiolarians	6	Tr
Silicoflagellates	Tr	--

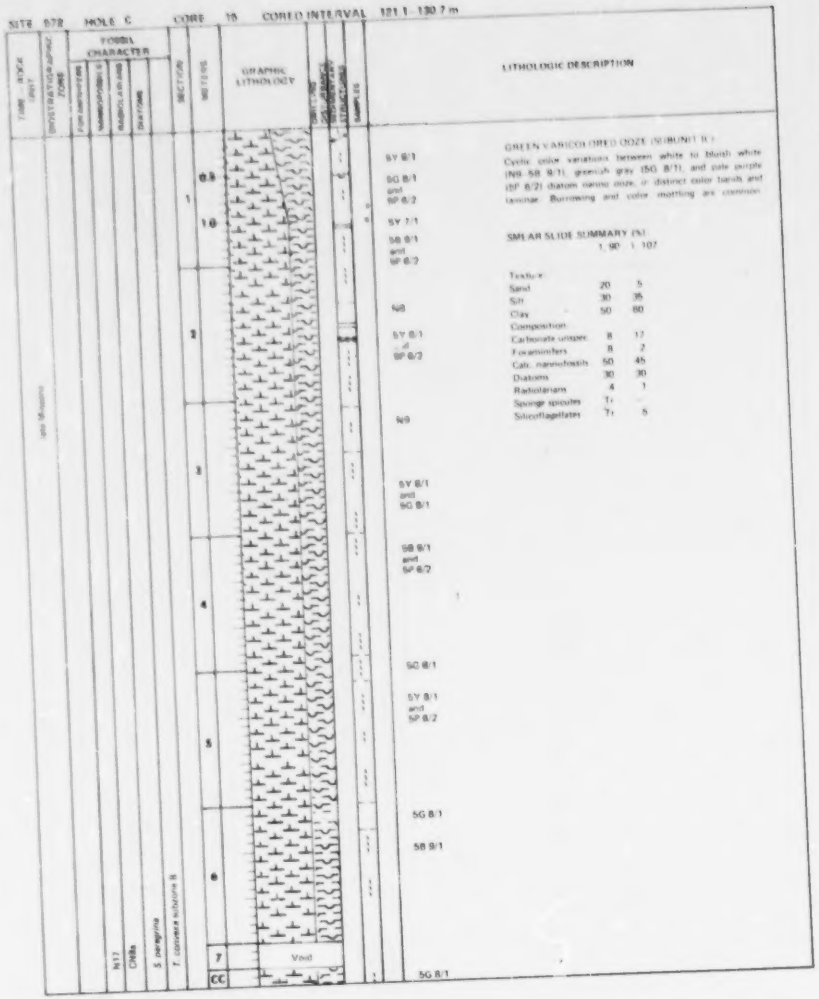
SITE 572 HOLE C CORE 15 CORED INTERVAL 121.1–130.7 m
TIME – ROCK UNIT
BIOSTRATIGRAPHIC ZONE
FOSSIL CHARACTER
FORAMINIFERS
NANNOFOSSILS
RADIOLARIANS
DIATOMS
SECTION
METERS
GRAPHIC LITHOLOGY
DRILLING DISTURBANCE
SEDIMENTARY STRUCTURES
SAMPLES
LITHOLOGIC DESCRIPTION
late Miocene
N17
CN8a/8b
S. peregrina
T. convexa subzone B
Void
5Y 8/1
5G 8/1 and 5P 8/2
5Y 7/1
5B 8/1 and 5P 8/2
5B
5Y 8/1 and 5P 8/2
N9
5Y 8/1 and 5G 8/1
5B 8/1 and 5P 8/2
5G 8/1
5Y 8/1 and 5P 8/2
5B 8/1
5G 8/1
GREEN VARICOLORED OOZE (SUBUNIT IC):
Cyclic color variations between white to bluish white (N9–5B 9/1), greenish gray (5G 8/1), and pale purple (5P 8/2) diatom nanno ooze, in distinct color bands and laminae. Burrowing and color mottling are common.
SMEAR SLIDE SUMMARY (%):
1, 90 1, 107
Texture:
Sand 20 5
Silt 30 35
Clay 50 60
Composition:
Carbonate unspec. 8 17
Foraminifers 8 2
Calc. nannofossils 50 45
Diatoms 30 30
Radiolarians 4 1
Sponge spicules Tr –
Silicoflagellates Tr 5

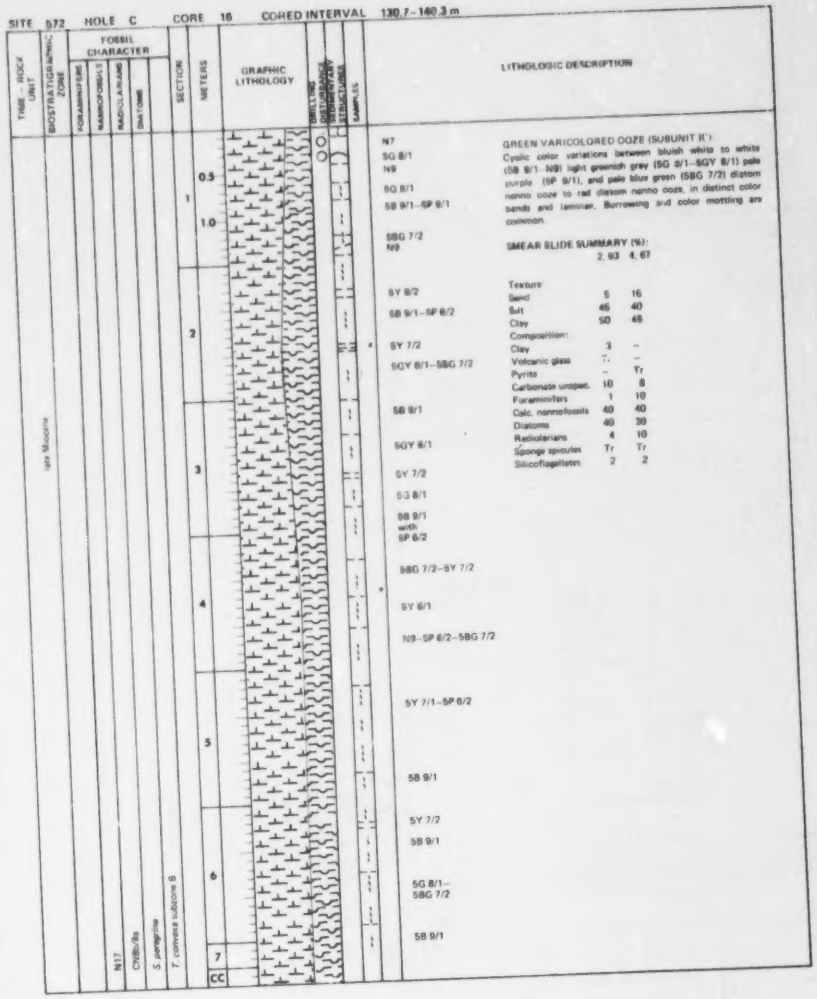
SITE 572 HOLE C CORE 16 CORED INTERVAL 130.7–140.3 m
TIME – ROCK UNIT
BIOSTRATIGRAPHIC ZONE
FOSSIL CHARACTER
FORAMINIFERS
NANNOFOSSILS
RADIOLARIANS
DIATOMS
SECTION
METERS
GRAPHIC LITHOLOGY
DRILLING DISTURBANCE
SEDIMENTARY STRUCTURES
SAMPLES
LITHOLOGIC DESCRIPTION
late Miocene
N17
CN8a/8b
S. peregrina
T. convexa subzone B
N7
5G 8/1
N9
5G 8/1
5B 9/1–5P 8/1
5BG 7/2
N9
5Y 8/2
5B 9/1–5P 8/2
5Y 7/2
5GY 8/1–5BG 7/2
5B 9/1
5GY 8/1
5Y 7/2
5G 8/1
5B 9/1 with 5P 8/2
5BG 7/2–5Y 7/2
5Y 8/1
N9–5P 8/2–5BG 7/2
5Y 7/1–5P 8/2
5B 9/1
5Y 7/2
5B 9/1
5G 8/1–5BG 7/2
5B 9/1
GREEN VARICOLORED OOZE (SUBUNIT IC):
Cyclic color variations between bluish white to white (5B 9/1–N9) light greenish grey (5G 8/1–5GY 8/1) pale purple (5P 9/1), and pale blue green (5BG 7/2) diatom nanno ooze to rad diatom nanno ooze, in distinct color bands and laminae. Burrowing and color mottling are common.
SMEAR SLIDE SUMMARY (%):
2, 93 4, 67
Texture:
Sand 5 15
Silt 45 40
Clay 50 45
Composition:
Clay 3 –
Volcanic glass Tr –
Pyrite – Tr
Carbonate unspec. 10 8
Foraminifers 1 10
Calc. nannofossils 40 40
Diatoms 40 30
Radiolarians 4 10
Sponge spicules Tr Tr
Silicoflagellates 2 2

SITE 572 HOLE C CORE 17 CORED INTERVAL 140.3–149.9 m

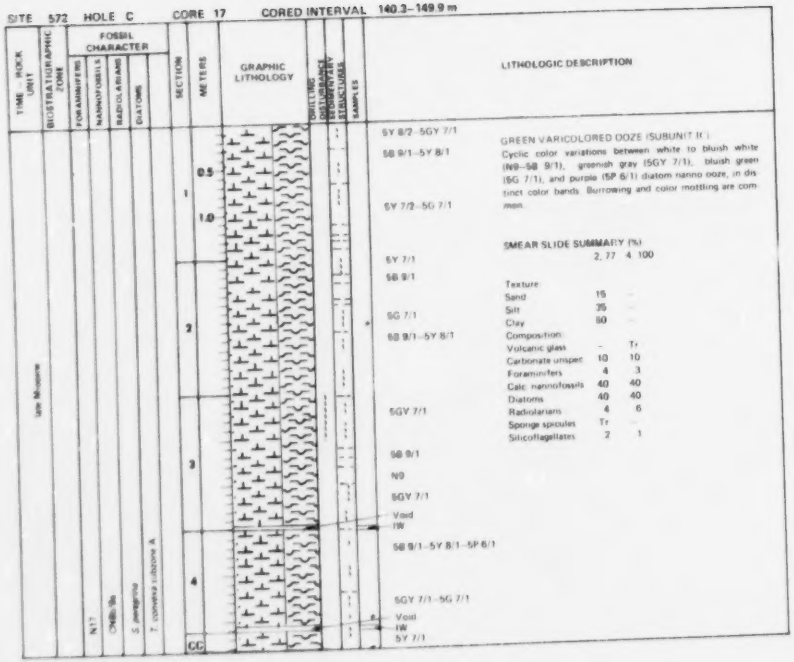

GREEN VARICOLORED OOZE (SUBUNIT IC)

Cyclic color variations between white to bluish white (N9–5B 9/1), greenish gray (5GY 7/1), bluish green (5G 7/1), and purple (5P 6/1) diatom nanno ooze, in distinct color bands. Burrowing and color mottling are common.

SMEAR SLIDE SUMMARY (%)

	2, 77	4, 100
Texture:		
Sand	15	–
Silt	75	–
Clay	50	–
Composition:		
Volcanic glass	–	Tr
Carbonate unspec.	10	10
Foraminifers	4	3
Calc. nannofossils	40	40
Diatoms	40	40
Radiolarians	4	6
Sponge spicules	Tr	–
Silicoflagellates	2	1

SITE 572 HOLE C CORE 18 CORED INTERVAL 149.9–159.5 m

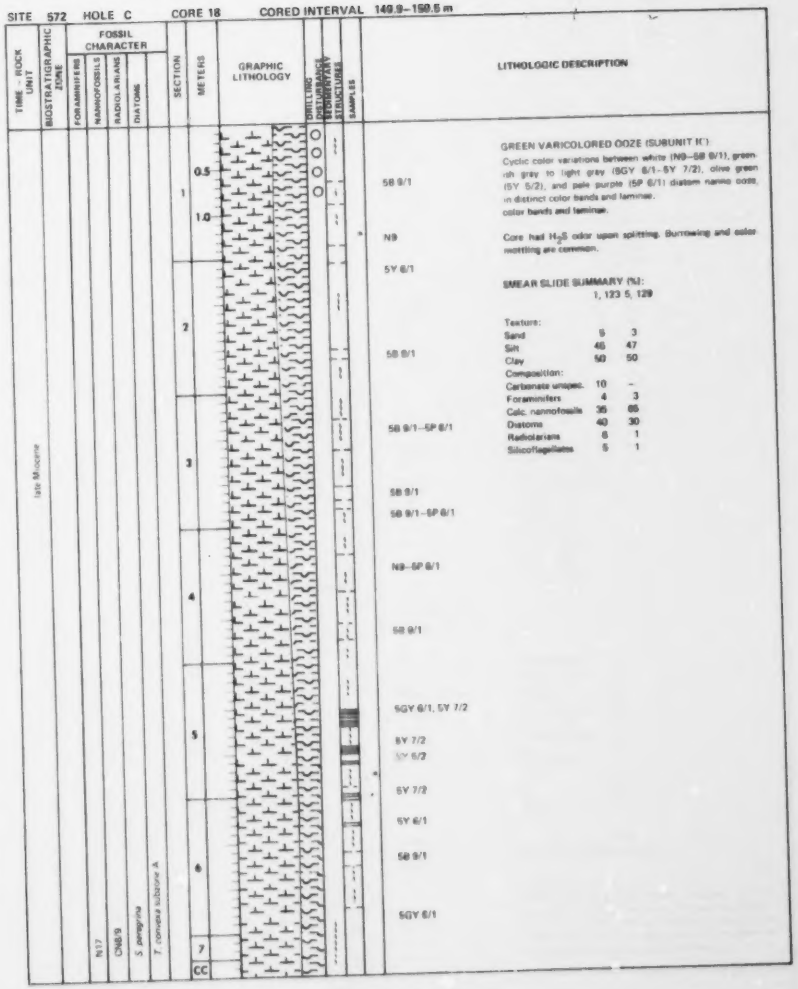

GREEN VARICOLORED OOZE (SUBUNIT IC)

Cyclic color variations between white (N9–5B 9/1), greenish gray to light gray (8GY 8/1–5Y 7/2), olive green (5Y 5/2), and pale purple (5P 6/1) diatom nanno ooze, in distinct color bands and laminae.

Core had H_2S odor upon splitting. Burrowing and color mottling are common.

SMEAR SLIDE SUMMARY (%):

	1, 123	5, 129
Texture:		
Sand	5	3
Silt	45	47
Clay	50	50
Composition:		
Carbonate unspec.	10	–
Foraminifers	4	3
Calc. nannofossils	35	65
Diatoms	40	30
Radiolarians	6	1
Silicoflagellates	5	1

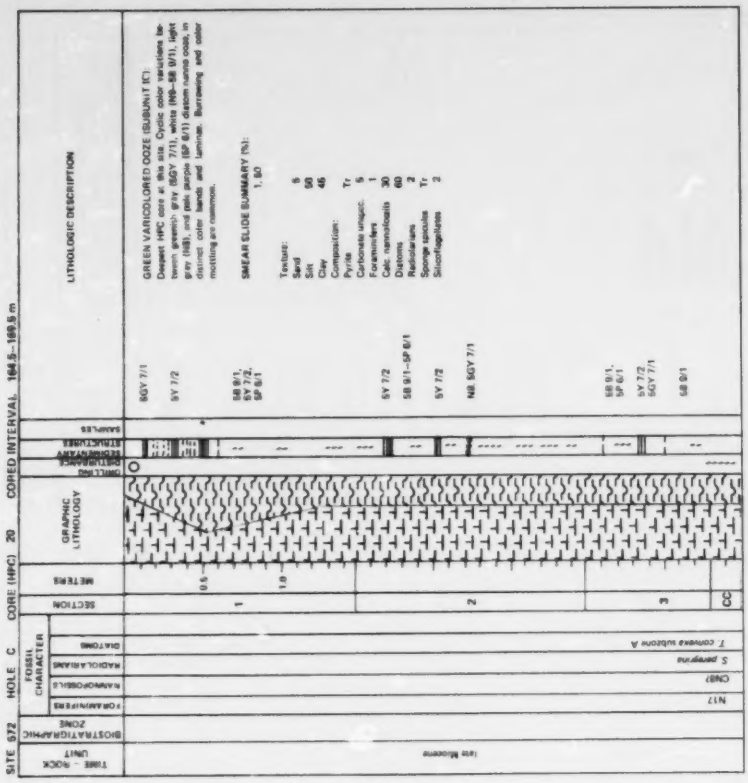
SITE 572
HOLE C
CORE (HPC) 20
CORED INTERVAL 164.5–169.5 m
LITHOLOGIC DESCRIPTION
GREEN VARICOLORED OOZE (SUBUNIT IC)
Deepest HPC core at this site. Cyclic color variations between greenish gray (5GY 7/1), white (N9—5B 9/1), light gray (N8), and pale purple (5P 6/1) diatom-nanno ooze, in distinct color bands and laminae. Burrowing and color mottling are common.
SMEAR SLIDE SUMMARY (%):
1, 80
Texture:
Sand 5
Silt 55
Clay 45
Composition:
Pyrite Tr
Carbonate unspec. 5
Foraminifers 1
Calc. nannofossils 30
Diastems 60
Radiolarians 2
Sponge spicules Tr
Siliceoflagellates 2
5GY 7/1
5Y 7/2
5B 8/1
5Y 8/1
5P 6/1
5Y 7/2
5B 8/1–5P 6/1
5Y 7/2
N8 5GY 7/1
5B 8/1
5P 6/1
5Y 7/2
5GY 7/1
5B 8/1
TIME – ROCK UNIT
BIOSTRATIGRAPHIC ZONE
FORAMINIFERS
NANNOFOSSILS
RADIOLARIANS
DIATOMS
FOSSIL CHARACTER
N17
CN8?
S. peregrina
T. convexa subzone A
SECTION
METERS
GRAPHIC LITHOLOGY
DRILLING DISTURB.
SED. STRUCTURES
SAMPLES

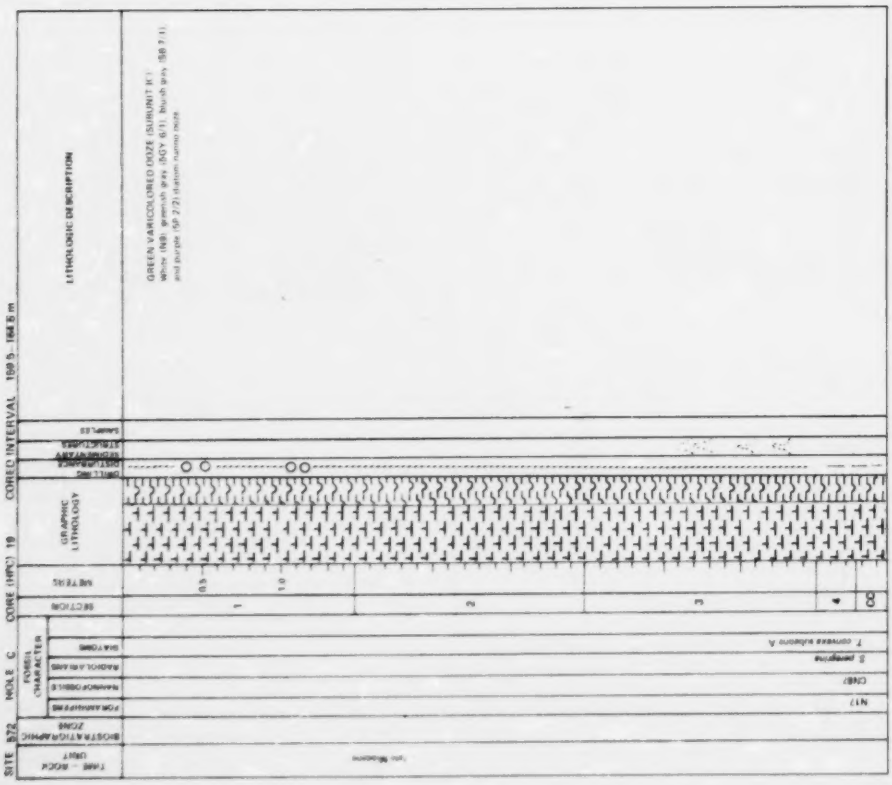
SITE 572
HOLE C
CORE (HPC) 19
CORED INTERVAL 159.5–164.5 m
LITHOLOGIC DESCRIPTION
GREEN VARICOLORED OOZE (SUBUNIT IC)
White (N9), greenish gray (5GY 6/1), bluish gray (5B 7/1), and purple (5P 7/2) diatom-nanno ooze
TIME – ROCK UNIT
BIOSTRATIGRAPHIC ZONE
FORAMINIFERS
NANNOFOSSILS
RADIOLARIANS
DIATOMS
FOSSIL CHARACTER
N17
CN8?
S. peregrina
T. convexa subzone A
SECTION
METERS
GRAPHIC LITHOLOGY
DRILLING DISTURB.
SED. STRUCTURES
SAMPLES

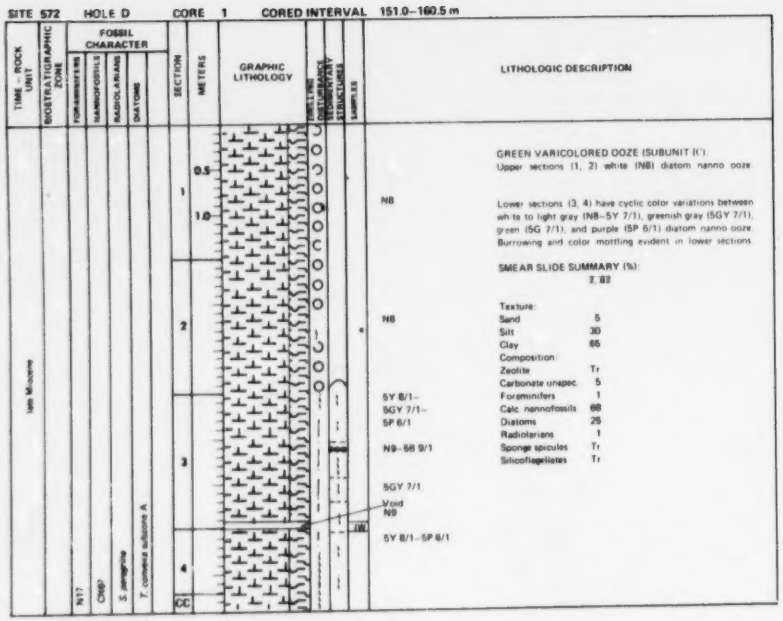
SITE 572 HOLE D CORE 1 CORED INTERVAL 151.0–160.5 m
TIME – ROCK UNIT
BIOSTRATIGRAPHIC ZONE
FOSSIL CHARACTER
FORAMINIFERS
NANNOFOSSILS
RADIOLARIANS
DIATOMS
SECTION
METERS
GRAPHIC LITHOLOGY
DRILLING DISTURBANCE
SECONDARY STRUCTURES
SAMPLES
LITHOLOGIC DESCRIPTION
late Miocene
N17
CN9
S. peregrina
T. convexa subzone A
0.5
1.0
CC
N8
N8
5Y 8/1–
5GY 7/1–
5P 6/1
N9–5B 9/1
5GY 7/1
Void
N9
5Y 8/1–5P 6/1
GREEN VARICOLORED OOZE (SUBUNIT IC):
Upper sections (1, 2) white (N8) diatom nanno ooze.
Lower sections (3, 4) have cyclic color variations between white to light gray (N8–5Y 7/1), greenish gray (5GY 7/1), green (5G 7/1), and purple (5P 6/1) diatom nanno ooze. Burrowing and color mottling evident in lower sections.
SMEAR SLIDE SUMMARY (%):
2, 82
Texture:
Sand 5
Silt 30
Clay 65
Composition:
Zeolite Tr
Carbonate unspec. 5
Foraminifers 1
Calc. nannofossils 68
Diatoms 25
Radiolarians 1
Sponge spicules Tr
Siliceoflagellates Tr

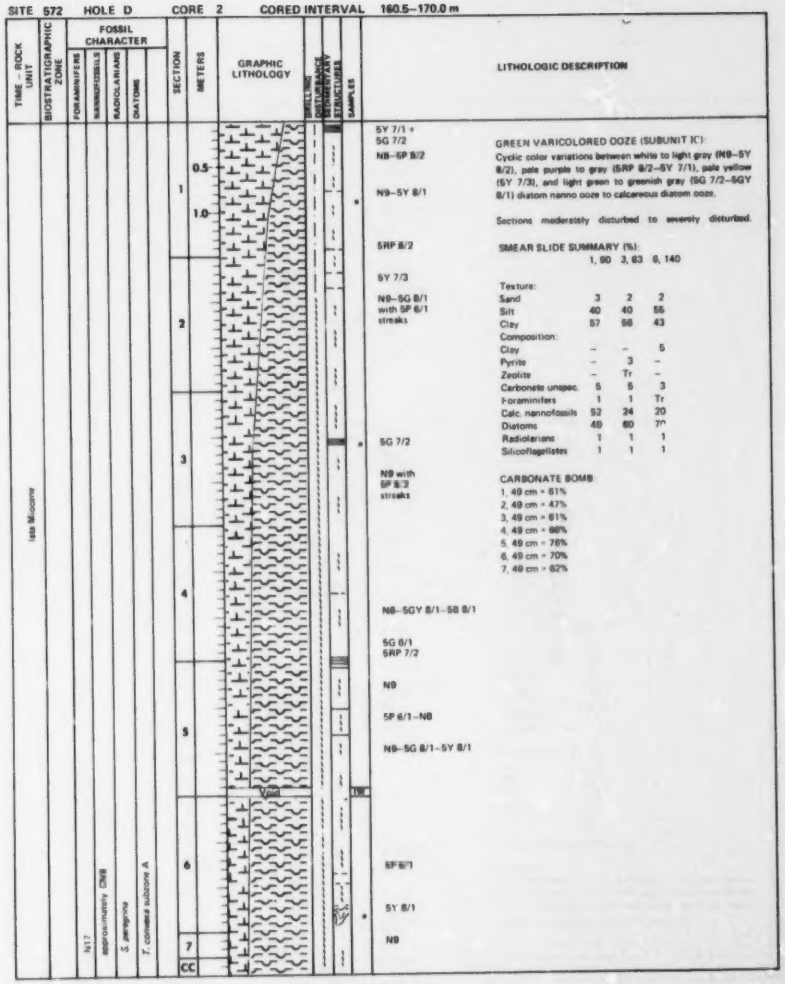
SITE 572 HOLE D CORE 2 CORED INTERVAL 160.5–170.0 m
TIME – ROCK UNIT
BIOSTRATIGRAPHIC ZONE
FOSSIL CHARACTER
FORAMINIFERS
NANNOFOSSILS
RADIOLARIANS
DIATOMS
SECTION
METERS
GRAPHIC LITHOLOGY
DRILLING DISTURBANCE
SECONDARY STRUCTURES
SAMPLES
LITHOLOGIC DESCRIPTION
late Miocene
N17
approximately CN9
S. peregrina
T. convexa subzone A
0.5
1.0
CC
5Y 7/1 + 5G 7/2
N8–5P 8/2
N9–5Y 8/1
5RP 8/2
5Y 7/3
N9–5G 8/1 with 5P 8/1 streaks
5G 7/2
N9 with 5P 8/2 streaks
N8–5GY 8/1–5B 8/1
5G 6/1 5RP 7/2
N9
5P 6/1–N8
N9–5G 8/1–5Y 8/1
Void
5P 8/1
5Y 8/1
N9
GREEN VARICOLORED OOZE (SUBUNIT IC):
Cyclic color variations between white to light gray (N9–5Y 8/2), pale purple to gray (5RP 8/2–5Y 7/1), pale yellow (5Y 7/3), and light green to greenish gray (5G 7/2–5GY 8/1) diatom nanno ooze to calcareous diatom ooze.
Sections moderately disturbed to severely disturbed.
SMEAR SLIDE SUMMARY (%):
1, 80 3, 83 6, 140
Texture:
Sand 3 2 2
Silt 40 40 55
Clay 57 58 43
Composition:
Clay – – 5
Pyrite – 3 –
Zeolite – Tr –
Carbonate unspec. 5 5 3
Foraminifers 1 1 Tr
Calc. nannofossils 52 24 20
Diatoms 40 60 77
Radiolarians 1 1 1
Siliceoflagellates 1 1 1
CARBONATE BOMB
1. 49 cm = 61%
2. 49 cm = 47%
3. 49 cm = 61%
4. 49 cm = 66%
5. 49 cm = 76%
6. 49 cm = 70%
7. 49 cm = 62%

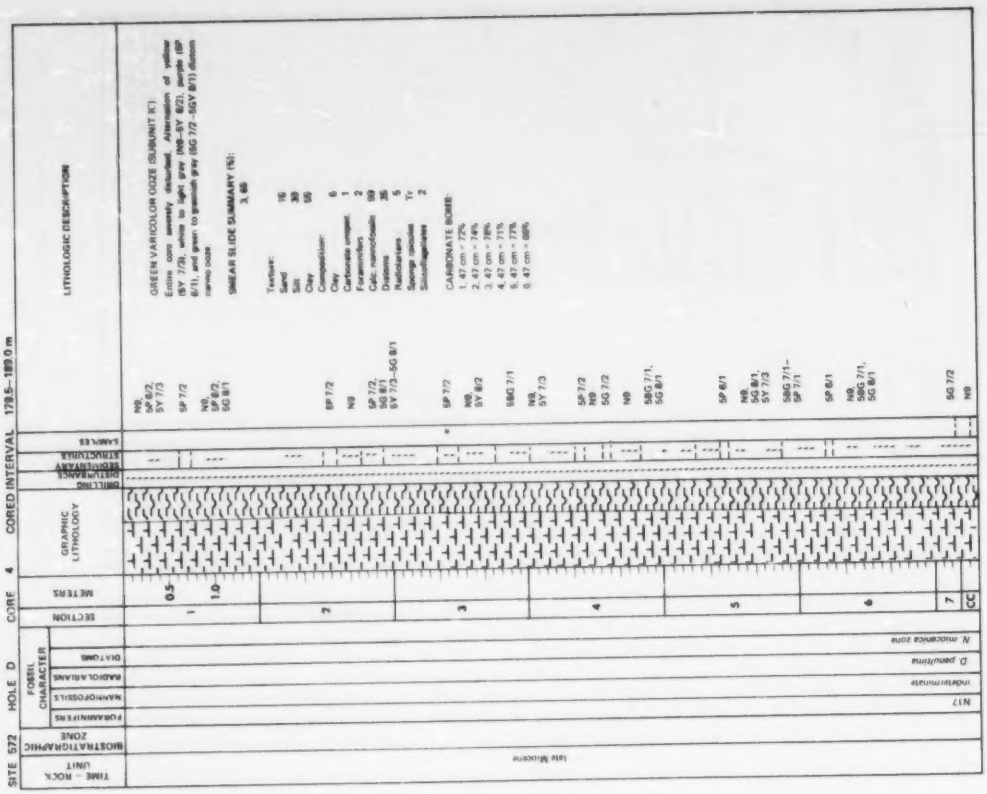

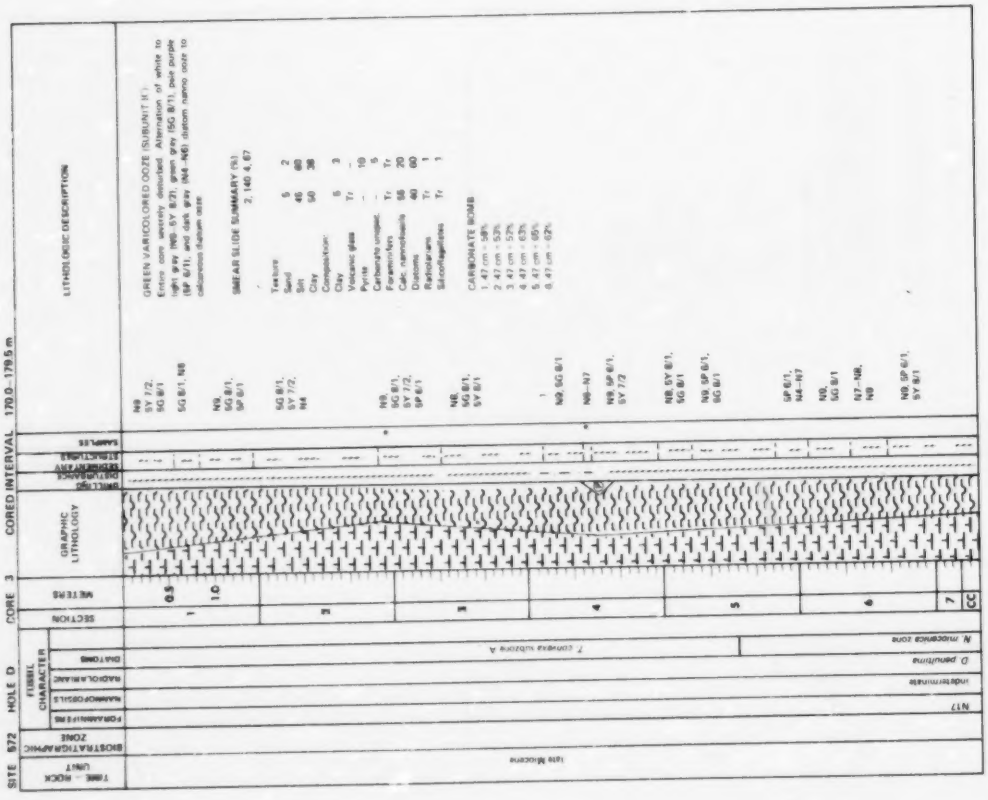

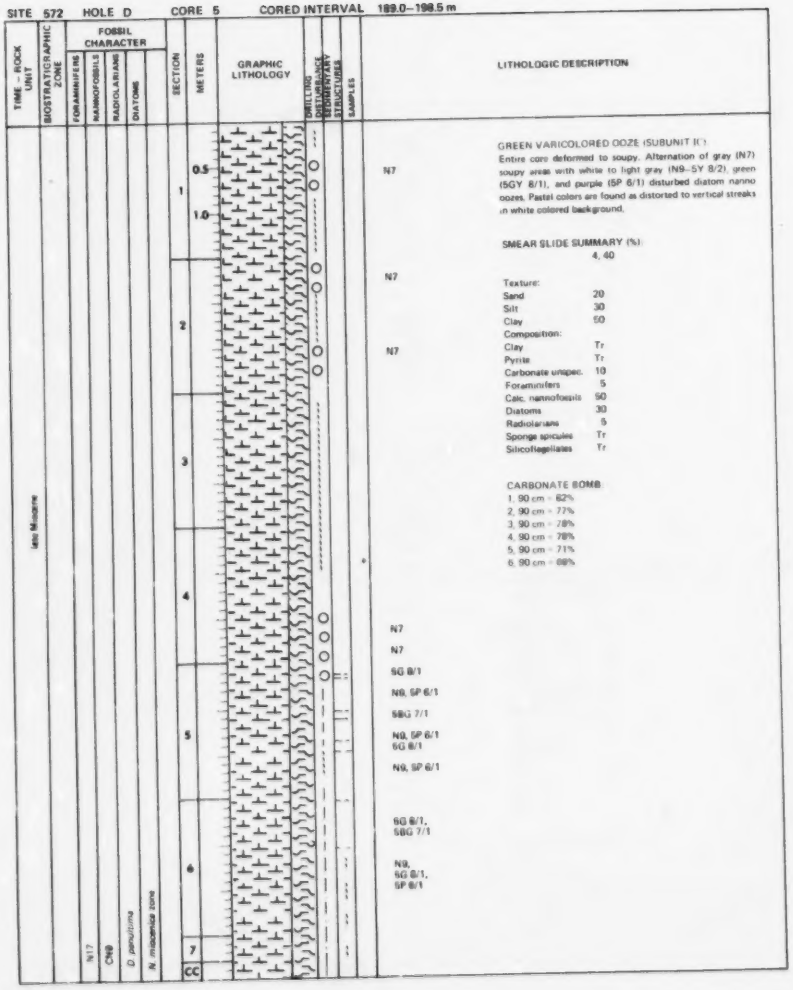
SITE 572 HOLE D CORE 5 CORED INTERVAL 189.0–198.5 m
TIME – ROCK UNIT
BIOSTRATIGRAPHIC ZONE
FOSSIL CHARACTER
FORAMINIFERS
NANNOFOSSILS
RADIOLARIANS
DIATOMS
SECTION
METERS
GRAPHIC LITHOLOGY
DRILLING DISTURBANCE
SEDIMENTARY STRUCTURES
SAMPLES
LITHOLOGIC DESCRIPTION
late Miocene
N17
CN9
D. penultima
N. miocenica zone
GREEN VARICOLORED OOZE (SUBUNIT IC)
Entire core deformed to soupy. Alternation of gray (N7) soupy areas with white to light gray (N9–5Y 8/2), green (5GY 8/1), and purple (5P 6/1) disturbed diatom nanno oozes. Pastel colors are found as distorted to vertical streaks in white colored background.
SMEAR SLIDE SUMMARY (%)
4, 40
Texture:
Sand 20
Silt 30
Clay 50
Composition:
Clay Tr
Pyrite Tr
Carbonate unspec. 10
Foraminifers 5
Calc. nannofossils 50
Diatoms 30
Radiolarians 5
Sponge spicules Tr
Silicoflagellates Tr
CARBONATE BOMB
1, 90 cm = 82%
2, 90 cm = 77%
3, 90 cm = 78%
4, 90 cm = 78%
5, 90 cm = 71%
6, 90 cm = 69%
N7
N7
N7
N7
N7
5G 8/1
N9, 5P 6/1
5BG 7/1
N9, 5P 6/1
5G 8/1
N9, 5P 6/1
5G 8/1,
5BG 7/1
N9,
5G 8/1,
5P 8/1

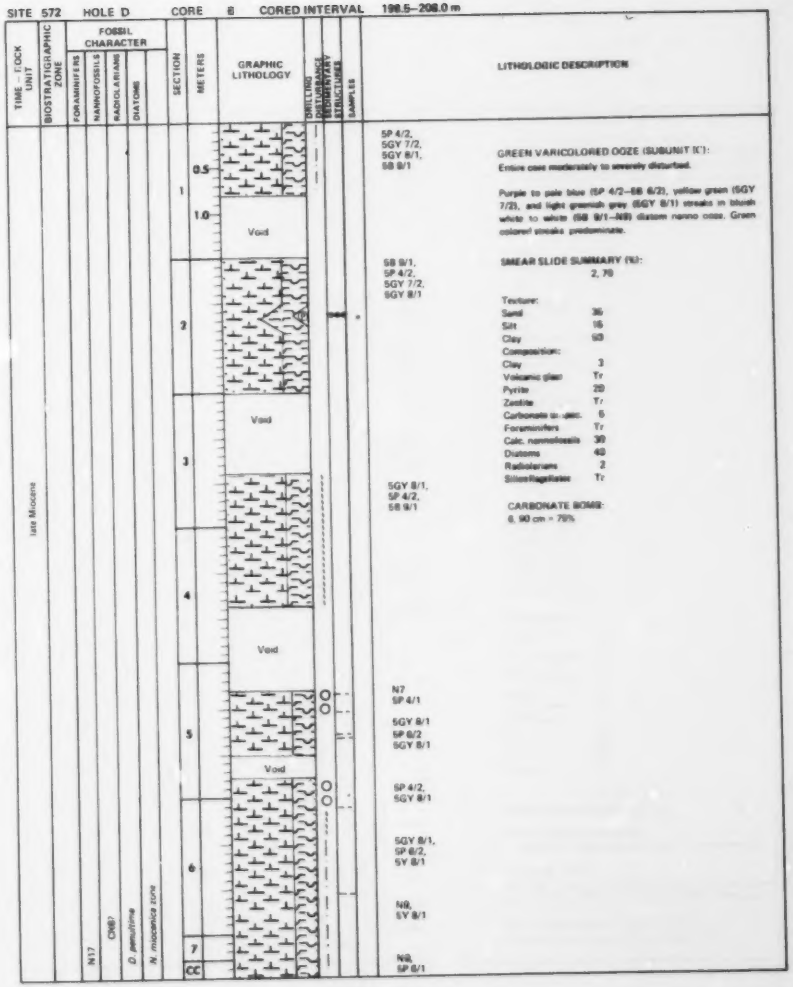
SITE 572 HOLE D CORE 6 CORED INTERVAL 198.5–208.0 m
TIME – ROCK UNIT
BIOSTRATIGRAPHIC ZONE
FOSSIL CHARACTER
FORAMINIFERS
NANNOFOSSILS
RADIOLARIANS
DIATOMS
SECTION
METERS
GRAPHIC LITHOLOGY
DRILLING DISTURBANCE
SEDIMENTARY STRUCTURES
SAMPLES
LITHOLOGIC DESCRIPTION
late Miocene
N17
CN9?
D. penultima
N. miocenica zone
Void
Void
Void
Void
5P 4/2,
5GY 7/2,
5GY 8/1,
5B 8/1
5B 8/1,
5P 4/2,
5GY 7/2,
5GY 8/1
5GY 8/1,
5P 4/2,
5B 8/1
N7,
5P 4/1
5GY 8/1
5P 6/2
5GY 8/1
5P 4/2,
5GY 8/1
5GY 8/1,
5P 6/2,
5Y 8/1
N9,
5Y 8/1
N9,
5P 8/1
GREEN VARICOLORED OOZE (SUBUNIT IC):
Entire core moderately to severely disturbed.
Purple to pale blue (5P 4/2–5B 6/2), yellow green (5GY 7/2), and light greenish gray (5GY 8/1) streaks in bluish white to white (5B 9/1–N9) diatom nanno ooze. Green colored streaks predominate.
SMEAR SLIDE SUMMARY (%):
2, 70
Texture:
Sand 35
Silt 15
Clay 50
Composition:
Clay 3
Volcanic glass Tr
Pyrite 20
Zeolite Tr
Carbonate unspec. 5
Foraminifers Tr
Calc. nannofossils 30
Diatoms 40
Radiolarians 2
Silicoflagellates Tr
CARBONATE BOMB:
6, 90 cm = 76%

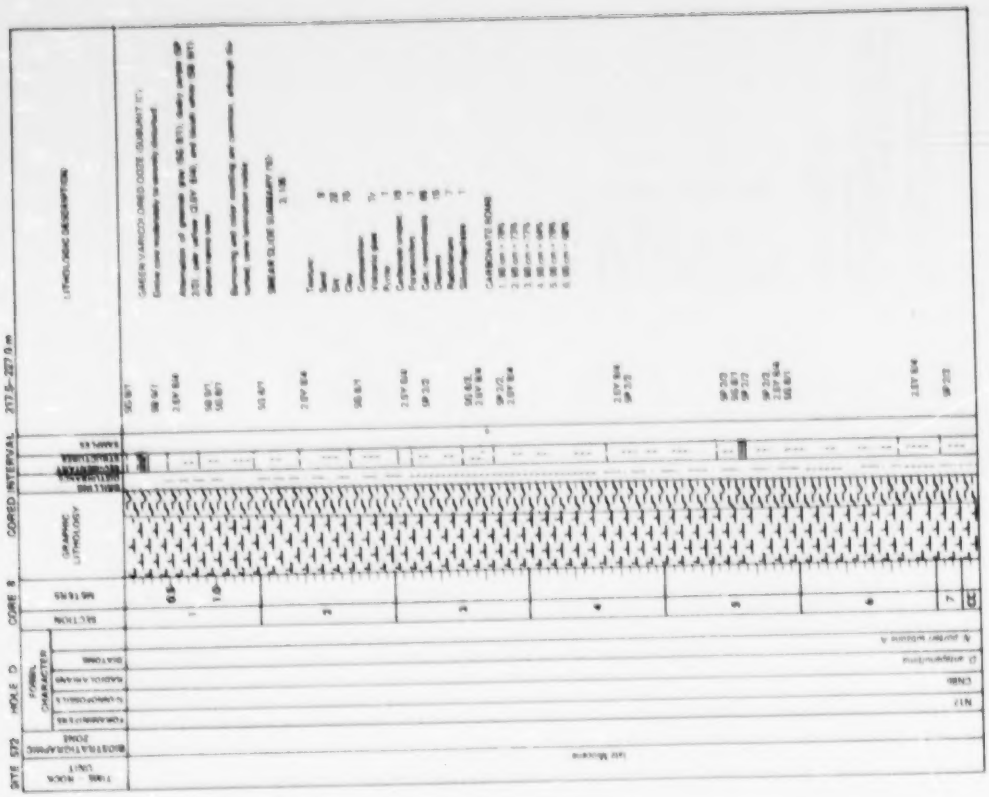

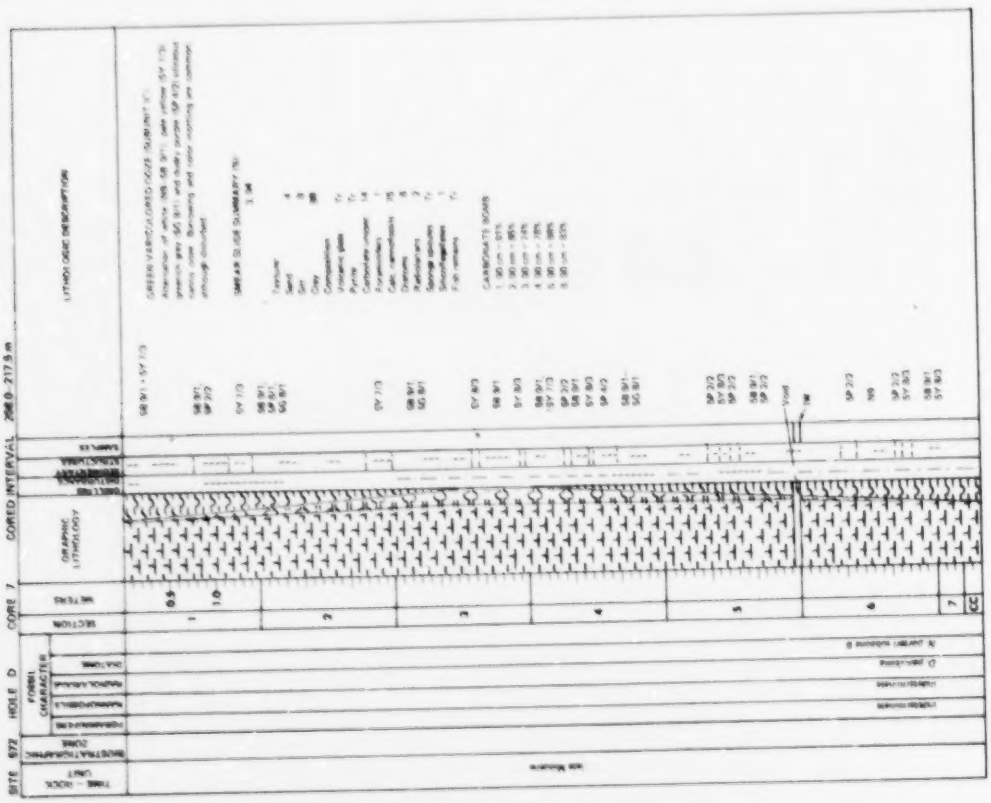

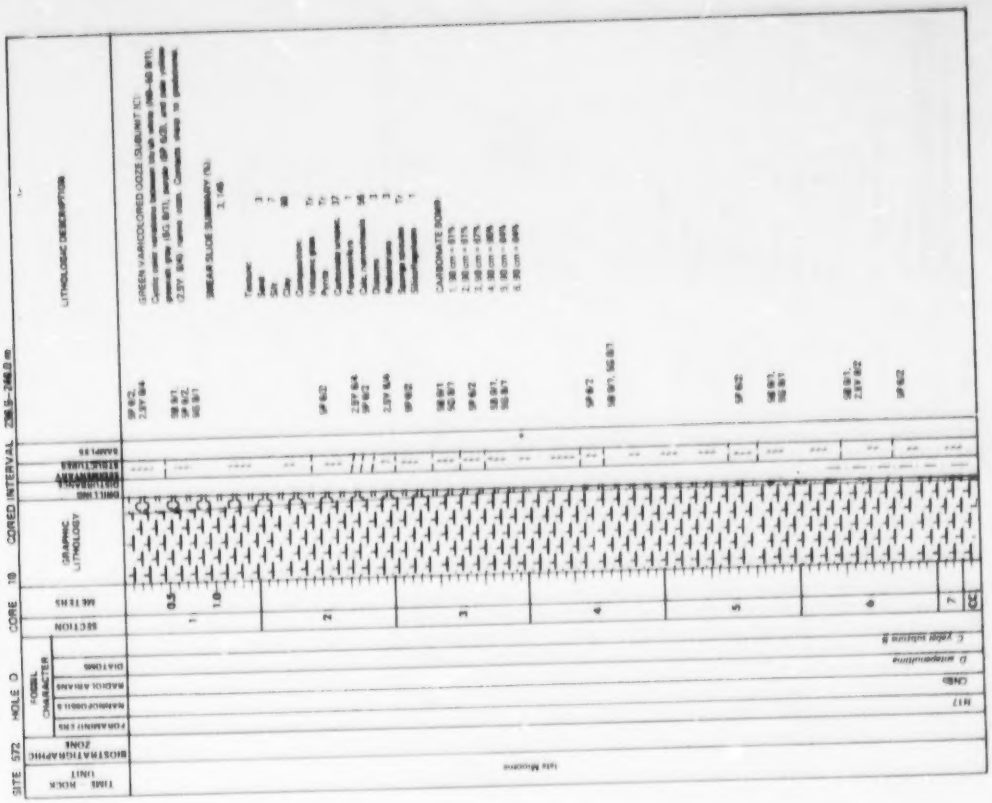

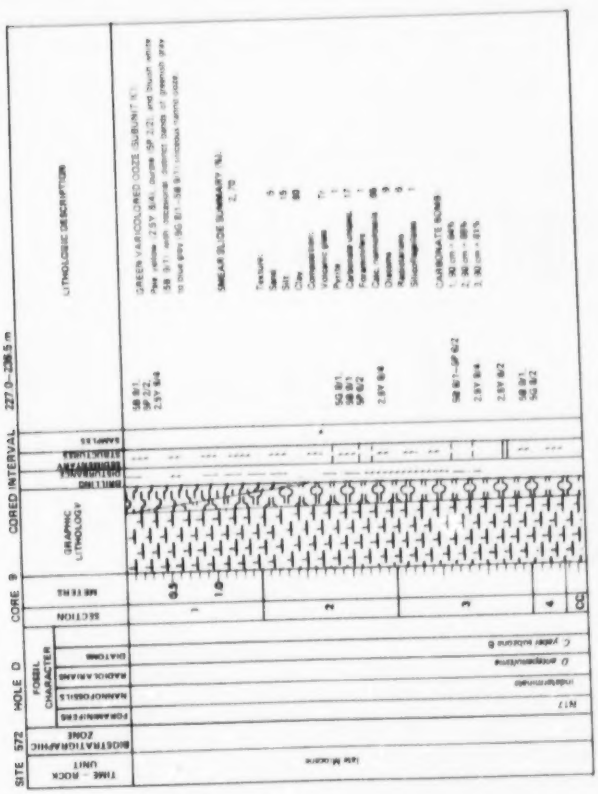

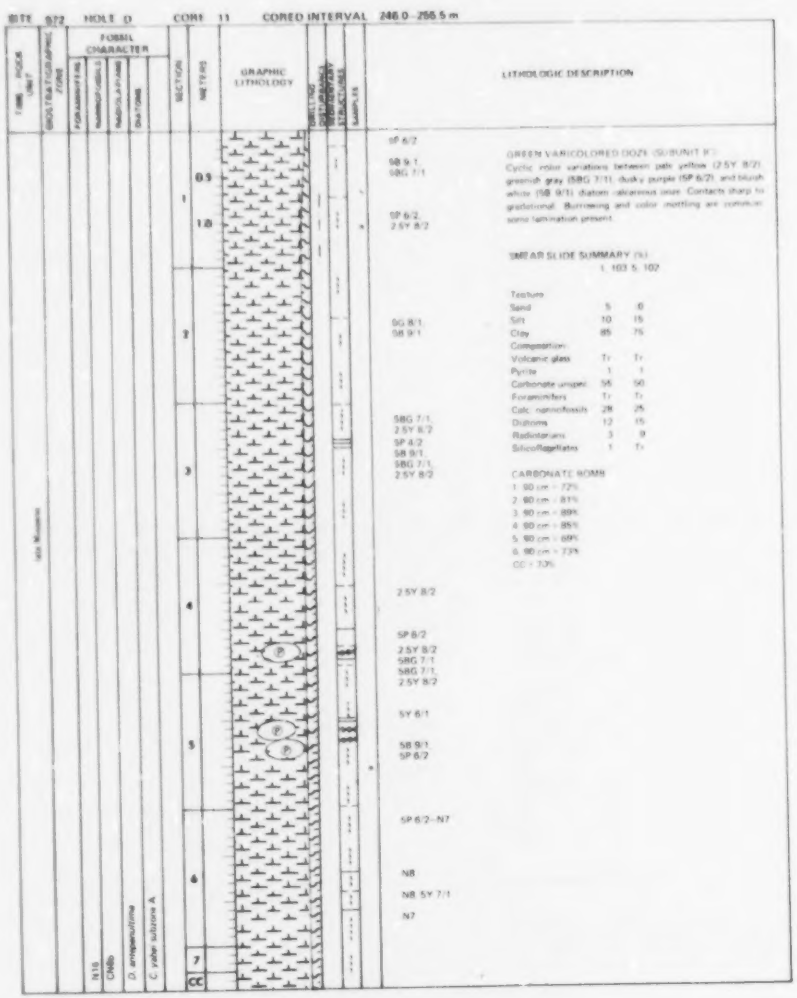
SITE 572 HOLE D CORE 11 CORED INTERVAL 246.0–255.5 m
TIME – ROCK UNIT
BIOSTRATIGRAPHIC ZONE
FOSSIL CHARACTER
FORAMINIFERS
NANNOFOSSILS
RADIOLARIANS
DIATOMS
SECTION
METERS
GRAPHIC LITHOLOGY
DRILLING DISTURBANCE
SEDIMENTARY STRUCTURES
SAMPLES
LITHOLOGIC DESCRIPTION
late Miocene
N16
CN8b
D. ampliconiscus
C. yabei subzone A
GREEN VARICOLORED OOZE (SUBUNIT IC)
Cyclic color variations between pale yellow (2.5Y 8/2), greenish gray (5BG 7/1), dusky purple (5P 6/2), and bluish white (5B 9/1) diatom calcareous ooze. Contacts sharp to gradational. Burrowing and color mottling are common; some lamination present.
SMEAR SLIDE SUMMARY (%)
1, 103 5, 102
Texture
Sand 5 0
Silt 10 15
Clay 85 75
Composition
Volcanic glass Tr Tr
Pyrite 1 1
Carbonate unspec 55 50
Foraminifers Tr Tr
Calc. nannofossils 28 25
Diatoms 12 15
Radiolarians 3 9
Silicoflagellates 1 Tr
CARBONATE BOMB
1. 90 cm = 72%
2. 90 cm = 81%
3. 90 cm = 89%
4. 90 cm = 85%
5. 90 cm = 69%
6. 90 cm = 73%
CC = 70%
5P 6/2
5B 9/1
5BG 7/1
5P 6/2
2.5Y 8/2
5G 8/1
5B 9/1
5BG 7/1
2.5Y 8/2
5P 8/2
5B 8/1
5BG 7/1
2.5Y 8/2
2.5Y 8/2
5P 8/2
2.5Y 8/2
5BG 7/1
5BG 7/1
2.5Y 8/2
5Y 6/1
5B 9/1
5P 6/2
5P 6/2–N7
N8
N8 5Y 7/1
N7

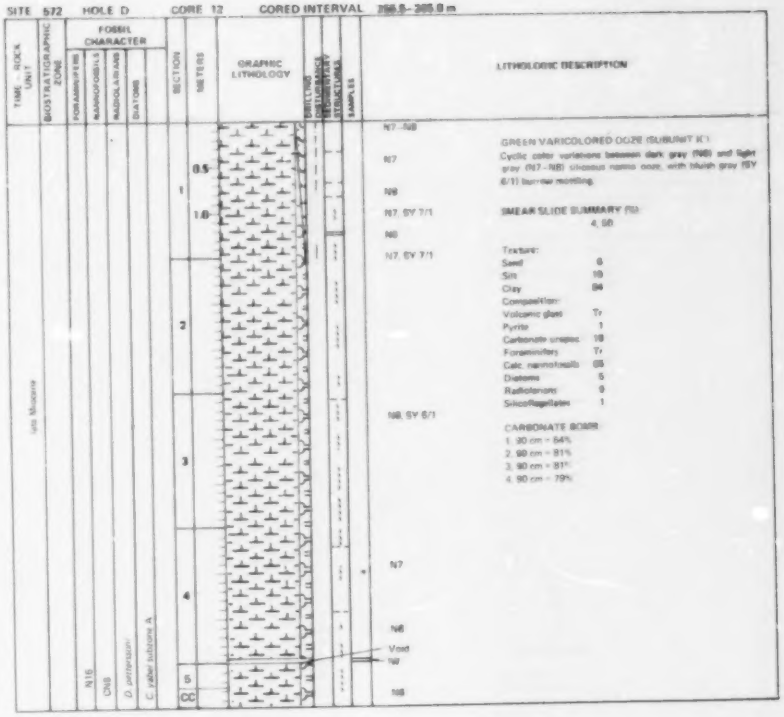
SITE 572 HOLE D CORE 12 CORED INTERVAL 255.5–265.0 m
TIME – ROCK UNIT
BIOSTRATIGRAPHIC ZONE
FOSSIL CHARACTER
FORAMINIFERS
NANNOFOSSILS
RADIOLARIANS
DIATOMS
SECTION
METERS
GRAPHIC LITHOLOGY
DRILLING DISTURBANCE
SEDIMENTARY STRUCTURES
SAMPLES
LITHOLOGIC DESCRIPTION
late Miocene
N16
CN8
D. ampliconi
C. yabei subzone A
GREEN VARICOLORED OOZE (SUBUNIT IC)
Cyclic color variations between dark gray (N3) and light gray (N7–N8) siliceous nannofossil ooze, with bluish gray (5Y 6/1) burrow mottling.
SMEAR SLIDE SUMMARY (%)
4, 95
Texture:
Sand 0
Silt 10
Clay 90
Composition:
Volcanic glass Tr
Pyrite 1
Carbonate unspec 10
Foraminifers Tr
Calc. nannofossils 85
Diatoms 5
Radiolarians 0
Silicoflagellates 1
CARBONATE BOMB
1. 90 cm = 64%
2. 90 cm = 81%
3. 90 cm = 81%
4. 90 cm = 79%
N7–N8
N7
N8
N7, 5Y 7/1
N8
N7, 5Y 7/1
N8, 5Y 6/1
N7
N8
Void
N8
N8

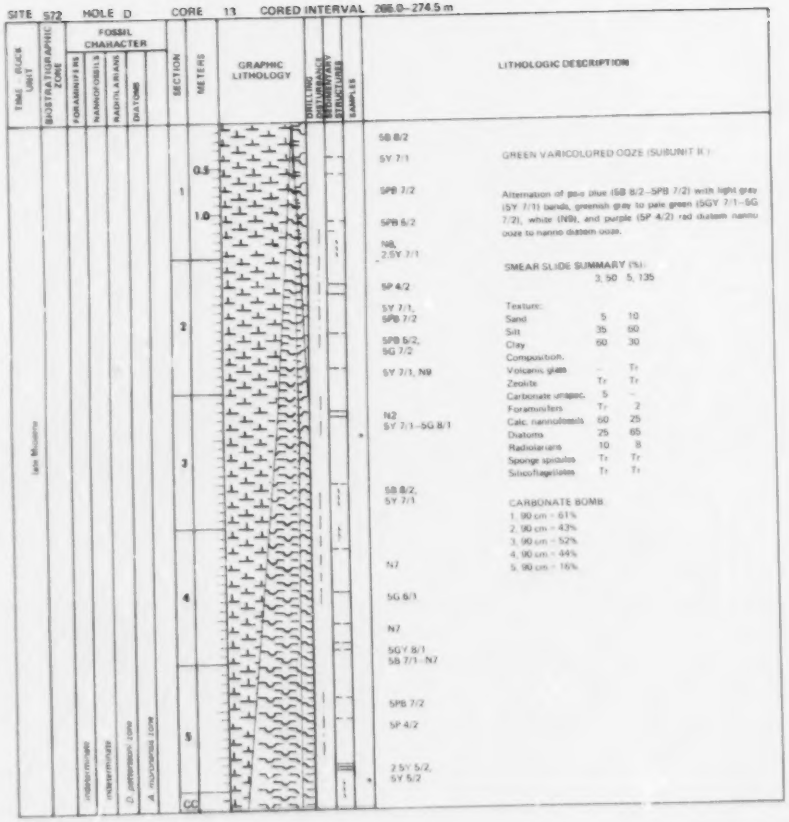
SITE 572 HOLE D CORE 13 CORED INTERVAL 265.0–274.5 m
TIME – ROCK UNIT
BIOSTRATIGRAPHIC ZONE
FOSSIL CHARACTER
FORAMINIFERS
NANNOFOSSILS
RADIOLARIANS
DIATOMS
SECTION
METERS
GRAPHIC LITHOLOGY
DRILLING DISTURBANCE
SECONDARY STRUCTURES
SAMPLES
LITHOLOGIC DESCRIPTION
late Miocene
indeterminate
CN7d?
D. petterssonii zone
A. moronensis zone
5B 8/2
5Y 7/1
5PB 7/2
5PB 6/2
N8, 2.5Y 7/1
5P 4/2
5Y 7/1, 5PB 7/2
5PB 6/2, 5G 7/2
5Y 7/1, N9
N2
5Y 7/1–5G 8/1
5B 8/2, 5Y 7/1
N7
5G 6/1
N7
5GY 8/1 5B 7/1–N7
5PB 7/2
5P 4/2
2.5Y 5/2, 5Y 5/2
GREEN VARICOLORED OOZE (SUBUNIT IC)
Alternation of pale blue (5B 8/2–5PB 7/2) with light gray (5Y 7/1) bands, greenish gray to pale green (5GY 7/1–5G 7/2), white (N9), and purple (5P 4/2) red diatom nannu ooze to nanno diatom ooze.
SMEAR SLIDE SUMMARY (%):
3, 50 5, 135
Texture:
Sand 5 10
Silt 35 60
Clay 60 30
Composition:
Volcanic glass – Tr
Zeolite Tr Tr
Carbonate unspec. 5 –
Foraminifers Tr 2
Calc. nannofossils 60 25
Diatoms 25 65
Radiolarians 10 8
Sponge spicules Tr Tr
Silicoflagellates Tr Tr
CARBONATE BOMB:
1. 90 cm = 61%
2. 90 cm = 43%
3. 90 cm = 52%
4. 90 cm = 44%
5. 90 cm = 16%

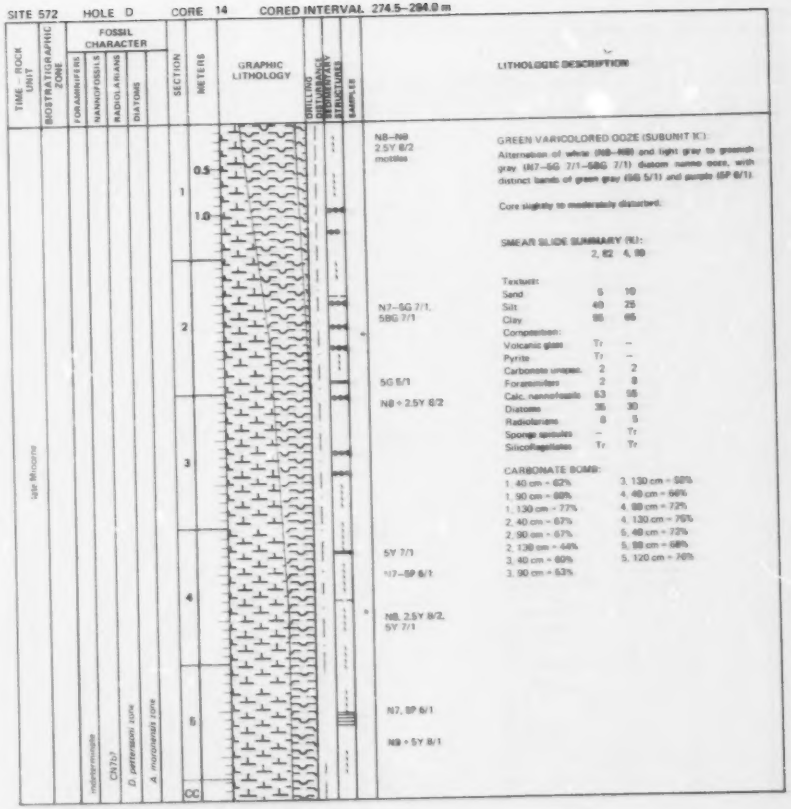
SITE 572 HOLE D CORE 14 CORED INTERVAL 274.5–284.0 m
TIME – ROCK UNIT
BIOSTRATIGRAPHIC ZONE
FOSSIL CHARACTER
FORAMINIFERS
NANNOFOSSILS
RADIOLARIANS
DIATOMS
SECTION
METERS
GRAPHIC LITHOLOGY
DRILLING DISTURBANCE
SECONDARY STRUCTURES
SAMPLES
LITHOLOGIC DESCRIPTION
late Miocene
indeterminate
CN7d?
D. petterssonii zone
A. moronensis zone
N8–N9 2.5Y 8/2 mottles
N7–5G 7/1, 5BG 7/1
5G 6/1
N8 + 2.5Y 8/2
5Y 7/1
N7–5P 6/1
N8, 2.5Y 8/2, 5Y 7/1
N7, 5P 6/1
N9 + 5Y 8/1
GREEN VARICOLORED OOZE (SUBUNIT IC)
Alternation of white (N8–N9) and light gray to greenish gray (N7–5G 7/1–5BG 7/1) diatom nanno ooze, with distinct bands of green gray (5G 5/1) and purple (5P 6/1).
Core slightly to moderately disturbed.
SMEAR SLIDE SUMMARY (%):
2, 62 4, 99
Texture:
Sand 5 10
Silt 40 25
Clay 55 65
Composition:
Volcanic glass Tr –
Pyrite Tr –
Carbonate unspec. 2 2
Foraminifers 2 8
Calc. nannofossils 53 55
Diatoms 35 30
Radiolarians 8 5
Sponge spicules – Tr
Silicoflagellates Tr Tr
CARBONATE BOMB:
1. 40 cm = 62%
1. 90 cm = 68%
1. 130 cm = 77%
2. 40 cm = 67%
2. 90 cm = 67%
2. 130 cm = 44%
3. 40 cm = 69%
3. 90 cm = 63%
3. 130 cm = 58%
4. 40 cm = 66%
4. 88 cm = 72%
4. 130 cm = 76%
5. 40 cm = 72%
5. 98 cm = 68%
5. 120 cm = 76%

SITE 572 HOLE D CORE 15 CORED INTERVAL 284.0–293.5 m

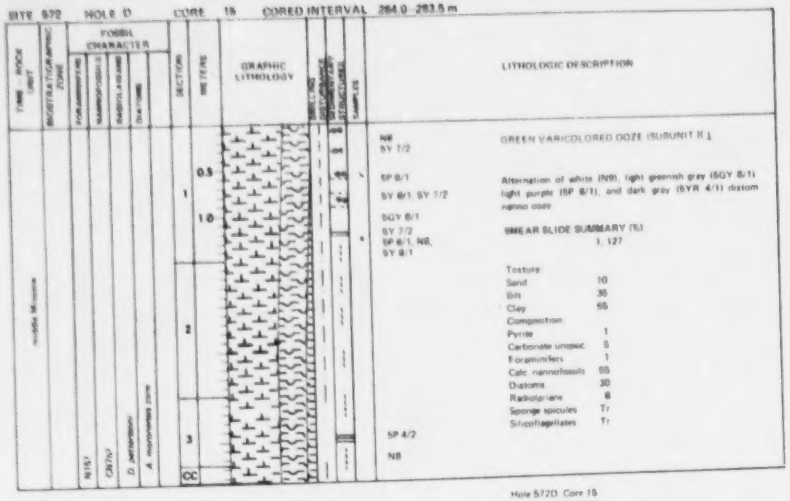

Hole 572D: Core 15
CARBONATE BOMB
1, 40 cm = 39%
1, 90 cm = 41%
1, 130 cm = 45%
2, 40 cm = 53%
2, 90 cm = 52%
2, 130 cm = 53%
3, 40 cm = 46%

SITE 572 HOLE D CORE 16 CORED INTERVAL 293.5–303.0 m

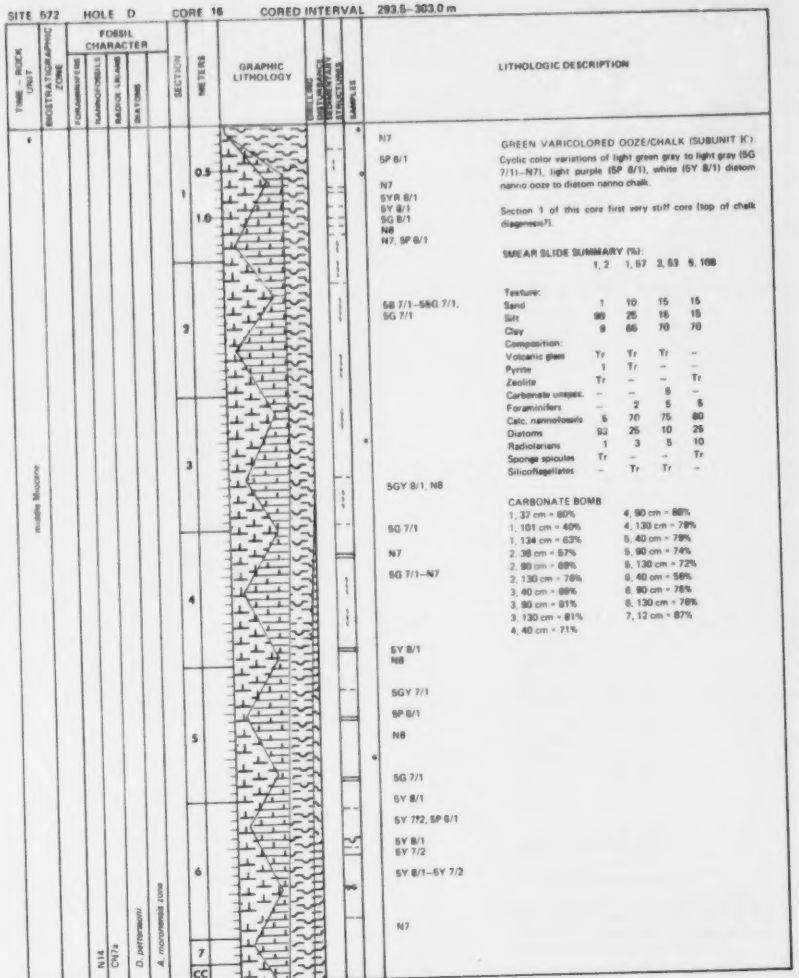

NOTE Graphic lithologies represent average compositions derived from smear slides and do not always reflect the detailed alternation of sediment types. Major lithologic boundaries are shown but gradational contacts, small-scale cyclicity and ooze-chalk alternations are represented schematically. Color changes approximate to lithologic changes.

SITE 572 HOLE D CORE 17 CORED INTERVAL 303.0–312.5 m

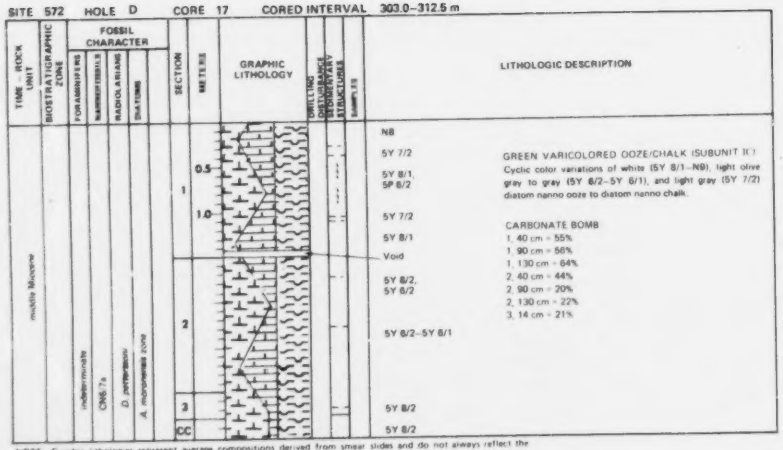

NOTE: Graphic lithologies represent average compositions derived from smear slides and do not always reflect the detailed alternation of sediment types. Major lithologic boundaries are shown but gradational contacts, small-scale cyclicity and ooze-chalk alternations are represented schematically. Color changes approximate to lithologic changes.

SITE 572 HOLE D CORE 18 CORED INTERVAL 312.5–322.0 m

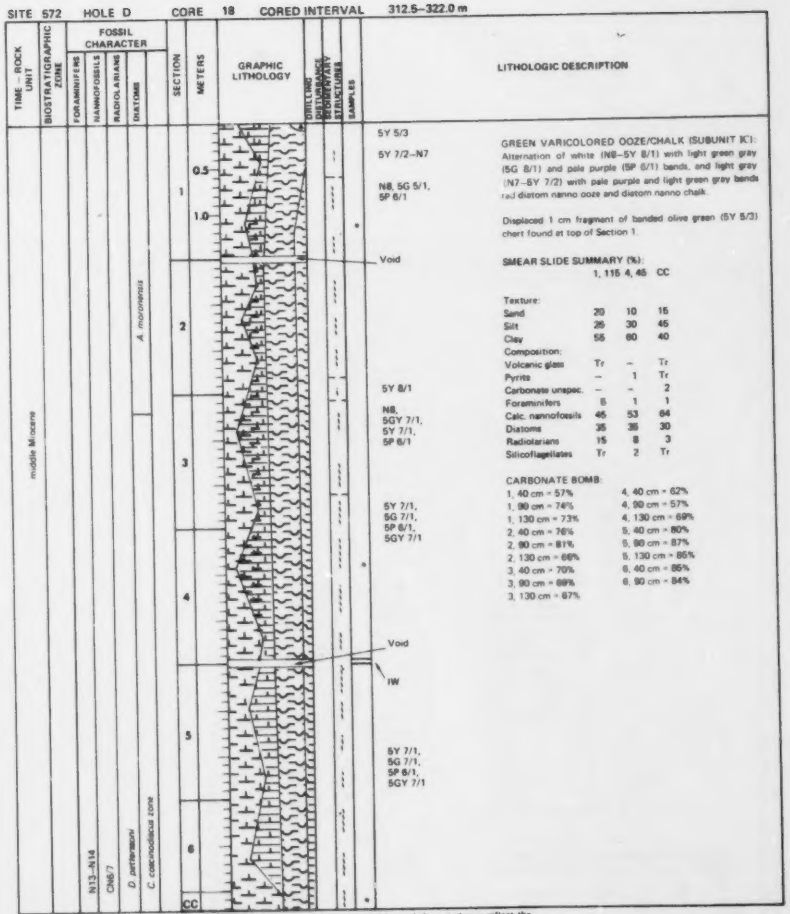

NOTE: Graphic lithologies represent average compositions derived from smear slides and do not always reflect the detailed alternation of sediment types. Major lithologic boundaries are shown but gradational contacts, small-scale cyclicity and ooze-chalk alternations are represented schematically. Color changes approximate to lithologic changes.

SITE 572 HOLE D CORE 19 CORED INTERVAL 322.0–331.5 m

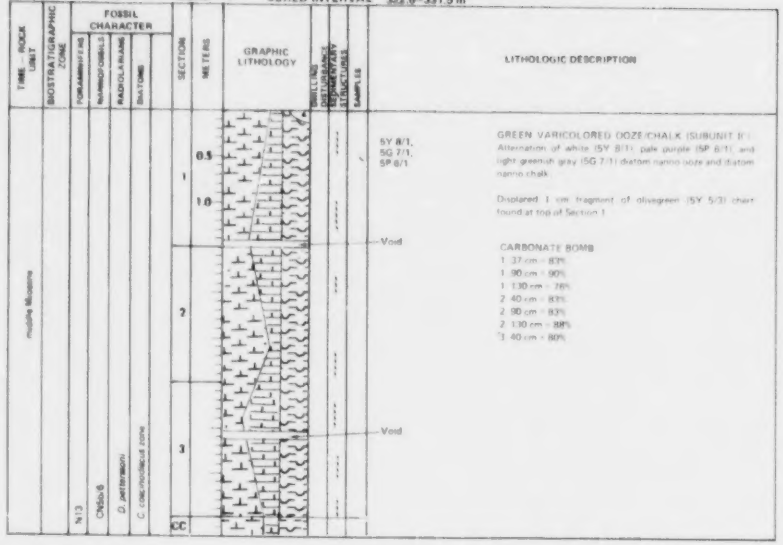

GREEN VARICOLORED OOZE/CHALK (SUBUNIT IC)

Alternation of white (5Y 8/1); pale purple (5P 6/1); and light greenish gray (5G 7/1) diatom nanno ooze and diatom nanno chalk.

Displaced 1 cm fragment of olivegreen (5Y 5/3) chert found at top of Section 1.

CARBONATE BOMB

1, 37 cm = 87%
1, 90 cm = 90%
1, 130 cm = 78%
2, 40 cm = 83%
2, 90 cm = 83%
2, 130 cm = 88%
3, 40 cm = 80%

SITE 572 HOLE D CORE 20 CORED INTERVAL 331.5–341.0 m

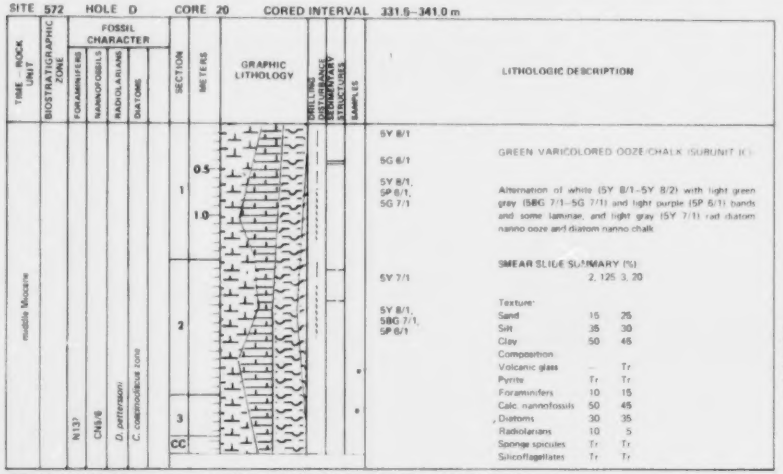

GREEN VARICOLORED OOZE/CHALK (SUBUNIT IC)

Alternation of white (5Y 8/1–5Y 8/2) with light green gray (5BG 7/1–5G 7/1) and light purple (5P 6/1) bands and some laminae, and light gray (5Y 7/1) rad diatom nanno ooze and diatom nanno chalk.

SMEAR SLIDE SUMMARY (%)

	2, 125	3, 20
Texture:		
Sand	15	25
Silt	35	30
Clay	50	45
Composition:		
Volcanic glass	—	Tr
Pyrite	Tr	Tr
Foraminifers	10	15
Calc. nannofossils	50	45
Diatoms	30	35
Radiolarians	10	5
Sponge spicules	Tr	Tr
Silicoflagellates	Tr	Tr

NOTE: Graphic lithologies represent average compositions derived from smear slides and do not always reflect the detailed alternation of sediment types. Major lithologic boundaries are shown but gradational contacts, small-scale cyclicity and ooze-chalk alternations are represented schematically. Color changes approximate to lithologic changes.

SITE 572 HOLE D CORE 21 CORED INTERVAL 341.0–350.5 m

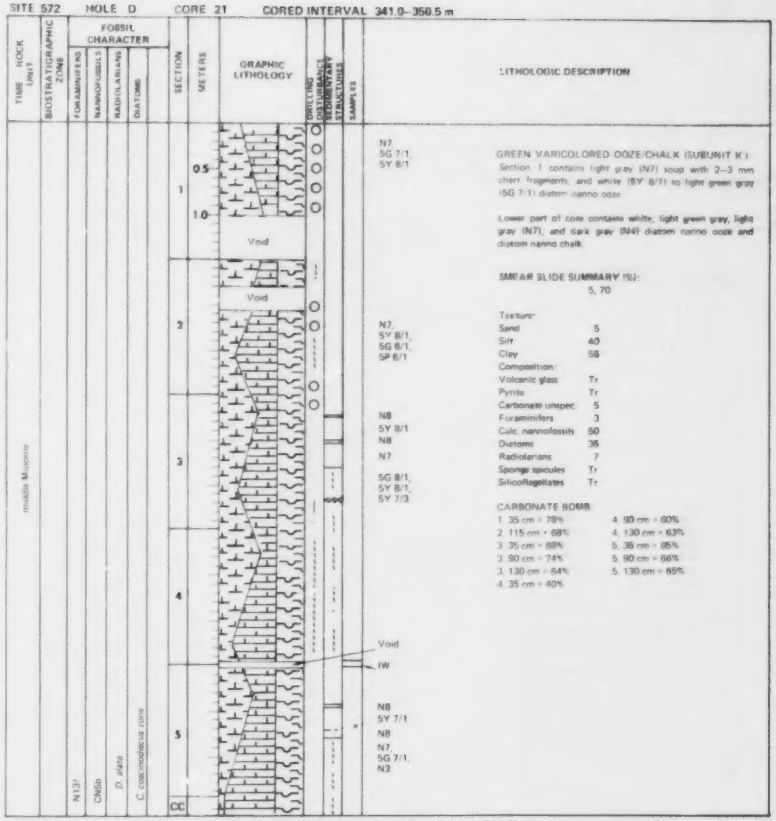

GREEN VARICOLORED OOZE/CHALK (SUBUNIT IC)

Section 1 contains light gray (N7) soup with 2–3 mm chert fragments, and white (5Y 8/1) to light green gray (5G 7/1) diatom nanno ooze.

Lower part of core contains white, light green gray, light gray (N7), and dark gray (N4) diatom nanno ooze and diatom nanno chalk.

SMEAR SLIDE SUMMARY (%):

	5, 70
Texture:	
Sand	5
Silt	40
Clay	55
Composition:	
Volcanic glass	Tr
Pyrite	Tr
Carbonate unspec.	5
Foraminifers	3
Calc. nannofossils	50
Diatoms	35
Radiolarians	7
Sponge spicules	Tr
Silicoflagellates	Tr

CARBONATE BOMB

1, 35 cm = 78%
2, 115 cm = 68%
3, 35 cm = 68%
3, 90 cm = 74%
3, 130 cm = 64%
4, 35 cm = 40%
4, 90 cm = 60%
4, 130 cm = 63%
5, 35 cm = 65%
5, 90 cm = 66%
5, 130 cm = 65%

NOTE: Graphic lithologies represent average compositions derived from smear slides and do not always reflect the detailed alternation of sediment types. Major lithologic boundaries are shown but gradational contacts, small-scale cyclicity and ooze-chalk alternations are represented schematically. Color changes approximate to lithologic changes.

Hole 572D, Core 20
CARBONATE BOMB

1, 40 cm = 72%
1, 92 cm = 79%
1, 130 cm = 74%
2, 40 cm = 76%
2, 92 cm = 86%
2, 130 cm = 76%
3, 30 cm = 70%

SITE 572 HOLE D CORE 22 CORED INTERVAL 350.5–360.0 m

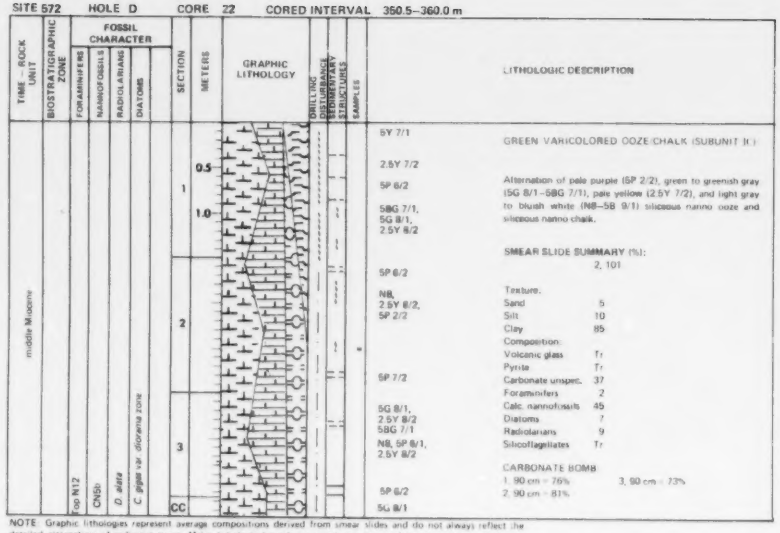

GREEN VARICOLORED OOZE/CHALK (SUBUNIT IC)

Alternation of pale purple (5P 2/2), green to greenish gray (5G 8/1–5BG 7/1), pale yellow (2.5Y 7/2), and light gray to bluish white (N8–5B 9/1) siliceous nanno ooze and siliceous nanno chalk.

SMEAR SLIDE SUMMARY (%):

	2, 101
Texture:	
Sand	5
Silt	10
Clay	85
Composition:	
Volcanic glass	Tr
Pyrite	Tr
Carbonate unspec.	37
Foraminifers	2
Calc. nannofossils	45
Diatoms	7
Radiolarians	9
Silicoflagellates	Tr

CARBONATE BOMB

1. 90 cm = 76%
2. 90 cm = 81%
3. 90 cm = 73%

NOTE Graphic lithologies represent average compositions derived from smear slides and do not always reflect the detailed alternation of sediment types. Major lithologic boundaries are shown but gradational contacts, small-scale cyclicity and ooze-chalk alternations are represented schematically. Color changes approximate to lithologic changes.

SITE 572 HOLE D CORE 23 CORED INTERVAL 360.0–369.5 m

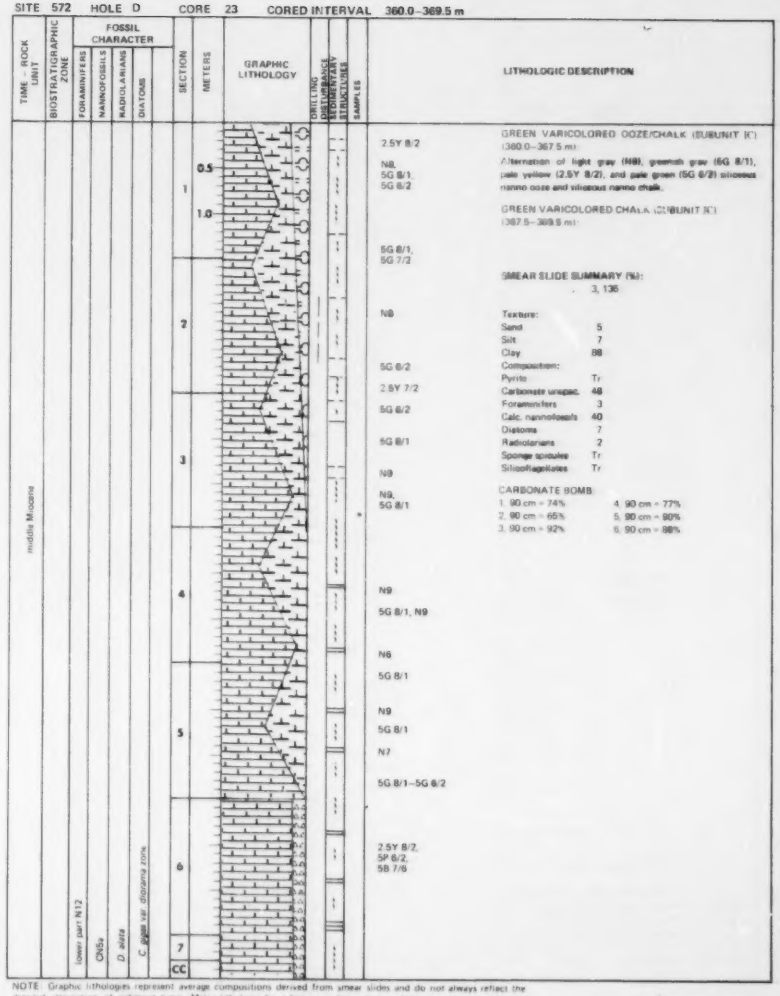

GREEN VARICOLORED OOZE/CHALK (SUBUNIT IC)
(360.0–367.5 m)

Alternation of light gray (N8), greenish gray (5G 8/1), pale yellow (2.5Y 8/2), and pale green (5G 8/2) siliceous nanno ooze and siliceous nanno chalk.

GREEN VARICOLORED CHALK (SUBUNIT IC)
(367.5–369.5 m)

SMEAR SLIDE SUMMARY (%):

	3, 136
Texture:	
Sand	5
Silt	7
Clay	88
Composition:	
Pyrite	Tr
Carbonate unspec.	48
Foraminifers	3
Calc. nannofossils	40
Diatoms	7
Radiolarians	2
Sponge spicules	Tr
Silicoflagellates	Tr

CARBONATE BOMB

1. 90 cm = 74%
2. 90 cm = 65%
3. 90 cm = 92%
4. 90 cm = 77%
5. 90 cm = 90%
6. 90 cm = 88%

NOTE Graphic lithologies represent average compositions derived from smear slides and do not always reflect the detailed alternation of sediment types. Major lithologic boundaries are shown but gradational contacts, small-scale cyclicity and ooze-chalk alternations are represented schematically. Color changes approximate to lithologic changes.

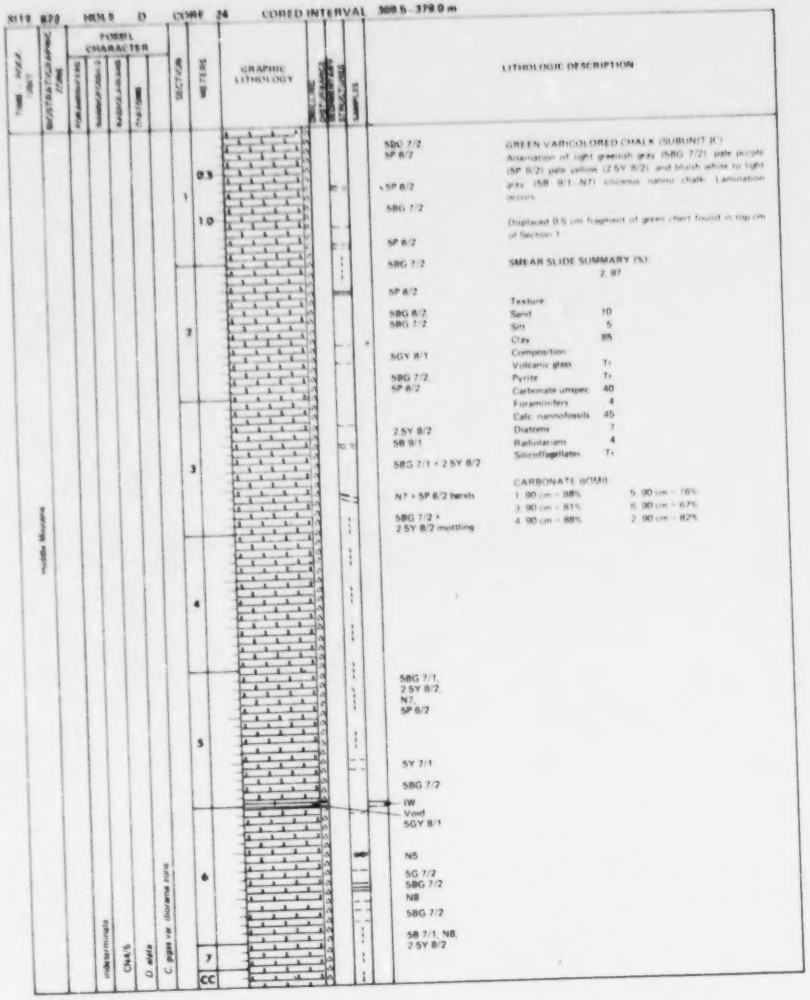
SITE 572 HOLE D CORE 24 CORED INTERVAL 369.5–379.0 m
FOSSIL CHARACTER
SECTION
METERS
GRAPHIC LITHOLOGY
LITHOLOGIC DESCRIPTION
GREEN VARICOLORED CHALK (SUBUNIT IC)
Alternation of light greenish gray (5BG 7/2), pale purple (5P 8/2), pale yellow (2.5Y 8/2), and bluish white to light gray (5B 9/1–N7) siliceous nanno chalk. Lamination occurs.
Displaced 0.5 cm fragment of green chert found in top cm of Section 1.
SMEAR SLIDE SUMMARY (%)
2, 97
Texture:
Sand 10
Silt 5
Clay 85
Composition:
Volcanic glass Tr
Pyrite Tr
Carbonate unspec 40
Foraminifers 4
Calc. nannofossils 45
Diatoms 7
Radiolarians 4
Silicoflagellates Tr
CARBONATE BOMB:
1, 90 cm = 88%
3, 90 cm = 81%
4, 90 cm = 88%
5, 90 cm = 76%
6, 90 cm = 67%
7, 90 cm = 82%
5BG 7/2
5P 8/2
5P 8/2
5BG 7/2
5P 8/2
5BG 7/2
5P 8/2
5BG 8/2
5BG 7/2
5GY 8/1
5BG 7/2, 5P 8/2
2.5Y 8/2
5B 9/1
5BG 7/1 + 2.5Y 8/2
N7 + 5P 6/2 bands
5BG 7/2 + 2.5Y 8/2 mottling
5BG 7/1, 2.5Y 8/2, N7, 5P 6/2
5Y 7/1
5BG 7/2
IW
Void
5GY 8/1
N5
5G 7/2
5BG 7/2
NB
5BG 7/2
5B 7/1, NB, 2.5Y 8/2
mixed Miocene
indeterminate
CN4/5
D. altis
C. gigas var. diomeda zone

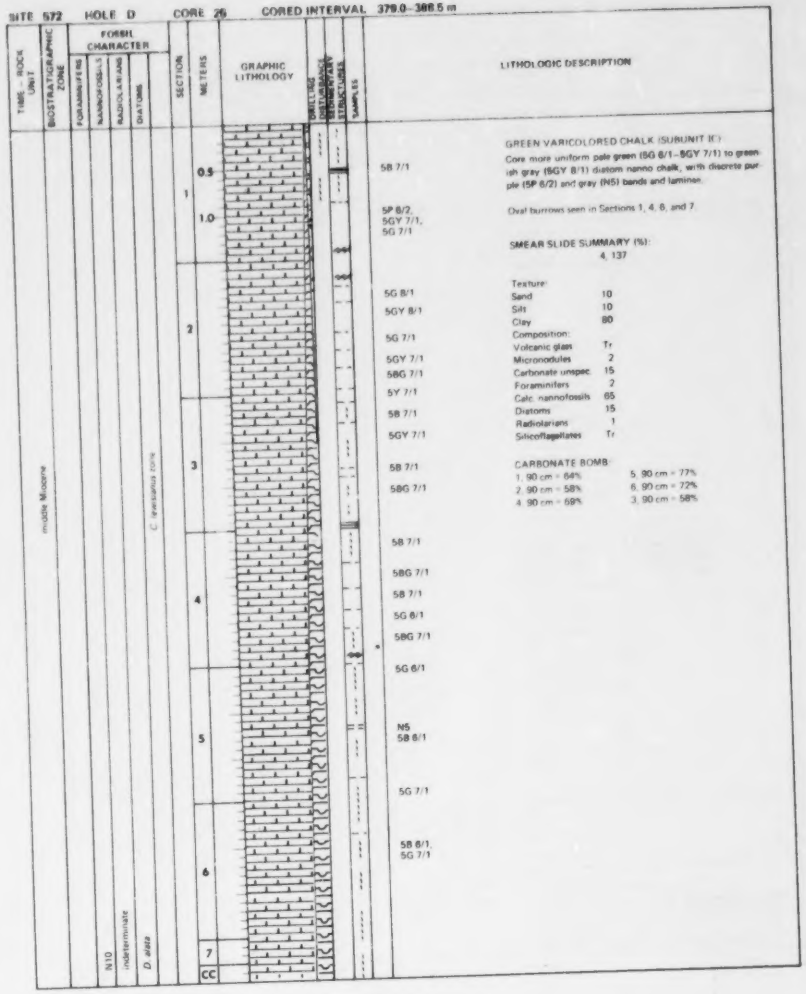
SITE 572 HOLE D CORE 25 CORED INTERVAL 379.0–388.5 m
TIME – ROCK UNIT
BIOSTRATIGRAPHIC ZONE
FOSSIL CHARACTER
FORAMINIFERS
NANNOFOSSILS
RADIOLARIANS
DIATOMS
SECTION
METERS
GRAPHIC LITHOLOGY
DRILLING DISTURBANCE
SEDIMENTARY STRUCTURES
SAMPLES
LITHOLOGIC DESCRIPTION
GREEN VARICOLORED CHALK (SUBUNIT IC)
Core more uniform pale green (5G 8/1–5GY 7/1) to greenish gray (5GY 8/1) diatom nanno chalk, with discrete purple (5P 6/2) and gray (N5) bands and laminae.
Oval burrows seen in Sections 1, 4, 6, and 7.
SMEAR SLIDE SUMMARY (%):
4, 137
Texture:
Sand 10
Silt 10
Clay 80
Composition:
Volcanic glass Tr
Micronodules 2
Carbonate unspec 15
Foraminifers 2
Calc. nannofossils 65
Diatoms 15
Radiolarians 1
Silicoflagellates Tr
CARBONATE BOMB:
1, 90 cm = 64%
2, 90 cm = 58%
4, 90 cm = 68%
5, 90 cm = 77%
6, 90 cm = 72%
3, 90 cm = 58%
5B 7/1
5P 8/2, 5GY 7/1, 5G 7/1
5G 8/1
5GY 8/1
5G 7/1
5GY 7/1
5BG 7/1
5Y 7/1
5B 7/1
5GY 7/1
5B 7/1
5BG 7/1
5B 7/1
5BG 7/1
5B 7/1
5G 8/1
5BG 7/1
5G 6/1
N5
5B 8/1
5G 7/1
5B 8/1, 5G 7/1
mixed Miocene
N10
indeterminate
D. altis
C. lewisianus zone

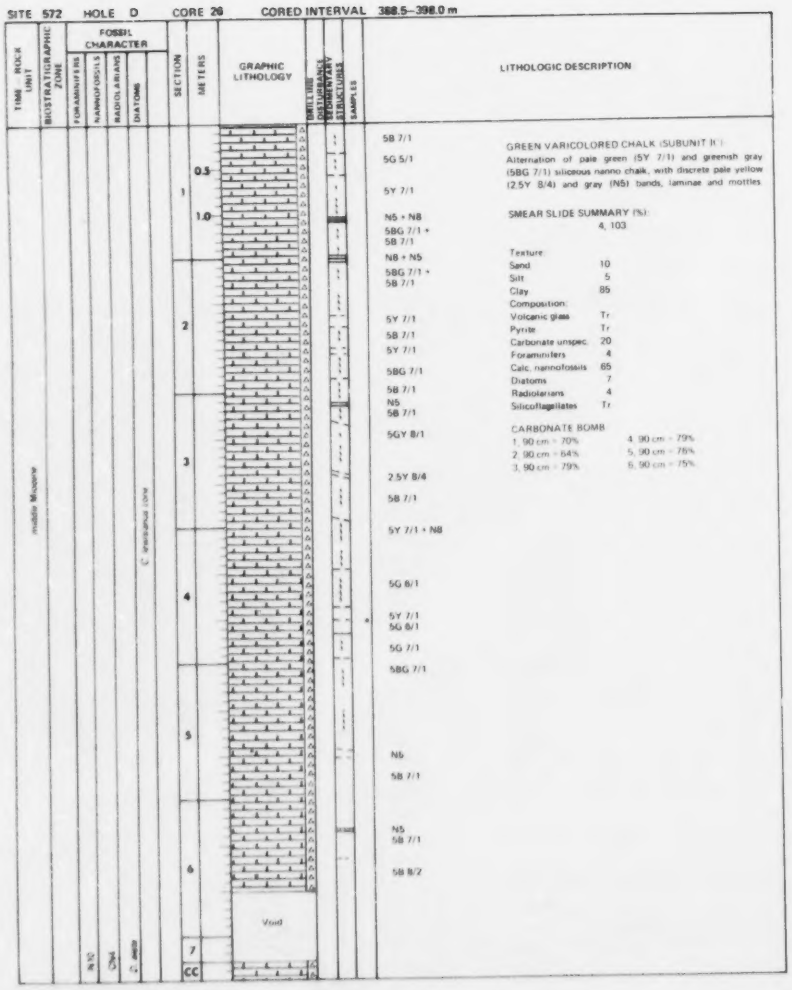
SITE 572 HOLE D CORE 26 CORED INTERVAL 388.5–398.0 m
TIME ROCK UNIT
BIOSTRATIGRAPHIC ZONE
FOSSIL CHARACTER
FORAMINIFERS
NANNOFOSSILS
RADIOLARIANS
DIATOMS
middle Miocene
N10
CN4
C. gracilipus zone
SECTION
METERS
GRAPHIC LITHOLOGY
DRILLING DISTURBANCE
SEDIMENTARY STRUCTURES
SAMPLES
Void
LITHOLOGIC DESCRIPTION
GREEN VARICOLORED CHALK (SUBUNIT IC):
Alternation of pale green (5Y 7/1) and greenish gray (5BG 7/1) siliceous nanno chalk, with discrete pale yellow (2.5Y 8/4) and gray (N5) bands, laminae and mottles
SMEAR SLIDE SUMMARY (%):
4, 103
Texture:
Sand 10
Silt 5
Clay 85
Composition:
Volcanic glass Tr
Pyrite Tr
Carbonate unspec. 20
Foraminifers 4
Calc. nannofossils 65
Diatoms 7
Radiolarians 4
Silicoflagellates Tr
CARBONATE BOMB
1. 90 cm = 70%
2. 90 cm = 64%
3. 90 cm = 79%
4. 90 cm = 79%
5. 90 cm = 76%
6. 90 cm = 75%

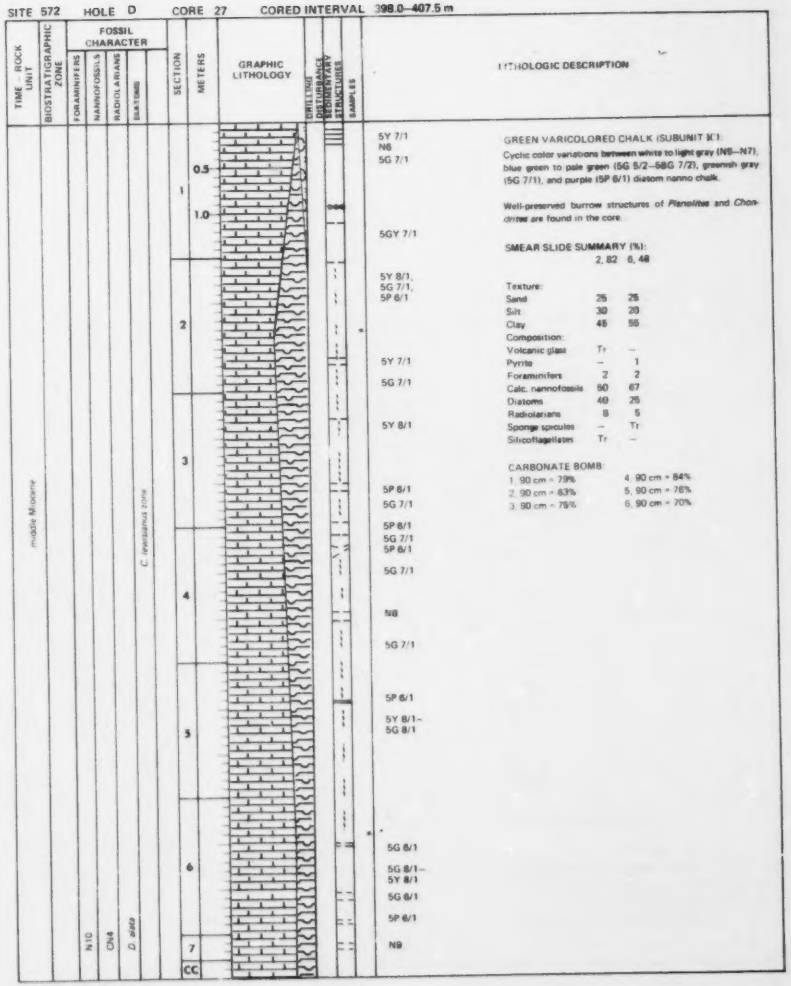
SITE 572 HOLE D CORE 27 CORED INTERVAL 398.0–407.5 m
TIME ROCK UNIT
BIOSTRATIGRAPHIC ZONE
FOSSIL CHARACTER
FORAMINIFERS
NANNOFOSSILS
RADIOLARIANS
DIATOMS
middle Miocene
N10
CN4
D. altispira
C. gracilipus zone
SECTION
METERS
GRAPHIC LITHOLOGY
DRILLING DISTURBANCE
SEDIMENTARY STRUCTURES
SAMPLES
LITHOLOGIC DESCRIPTION
GREEN VARICOLORED CHALK (SUBUNIT IC):
Cyclic color variations between white to light gray (N8–N7), blue green to pale green (5G 8/2–5BG 7/2), greenish gray (5G 7/1), and purple (5P 6/1) diatom nanno chalk.
Well-preserved burrow structures of Planolites and Chondrites are found in the core.
SMEAR SLIDE SUMMARY (%):
2, 82 6, 48
Texture:
Sand 25 25
Silt 30 28
Clay 45 56
Composition:
Volcanic glass Tr –
Pyrite – 1
Foraminifers 2 2
Calc. nannofossils 50 67
Diatoms 49 25
Radiolarians 8 5
Sponge spicules – Tr
Silicoflagellates Tr –
CARBONATE BOMB:
1. 90 cm = 79%
2. 90 cm = 63%
3. 90 cm = 76%
4. 90 cm = 84%
5. 90 cm = 76%
6. 90 cm = 70%

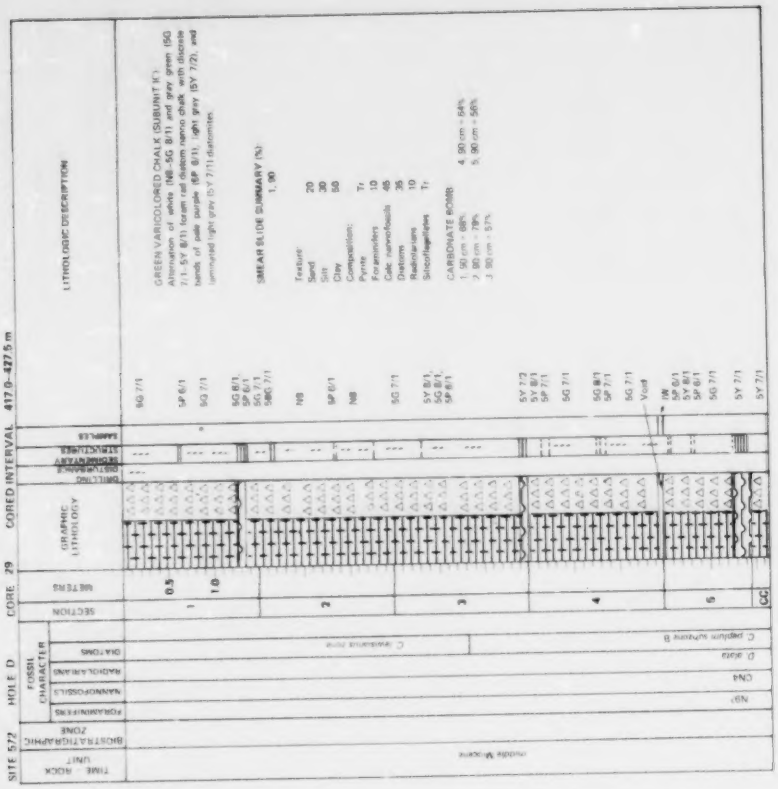

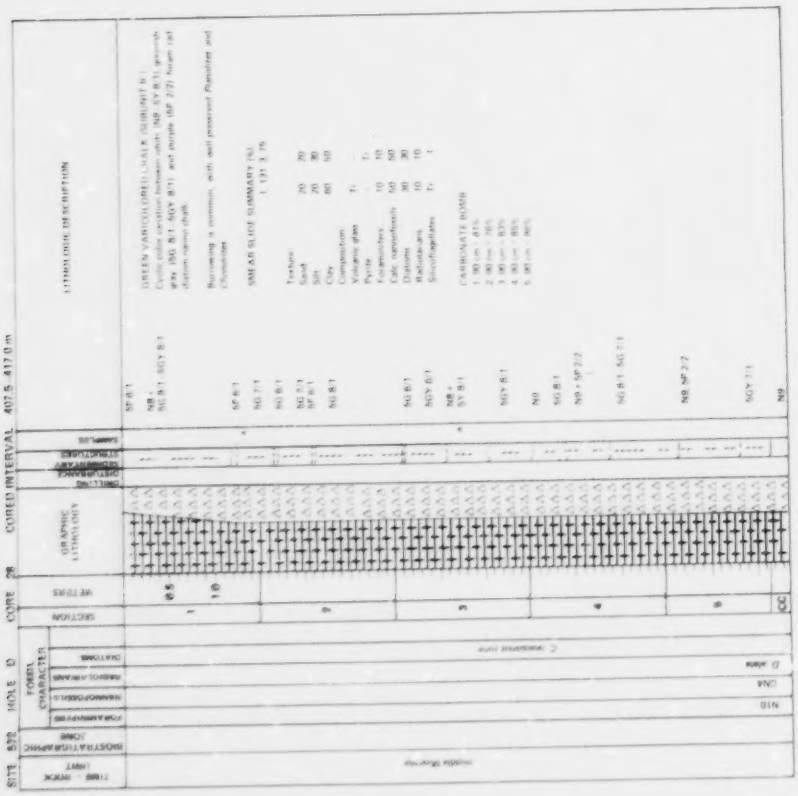

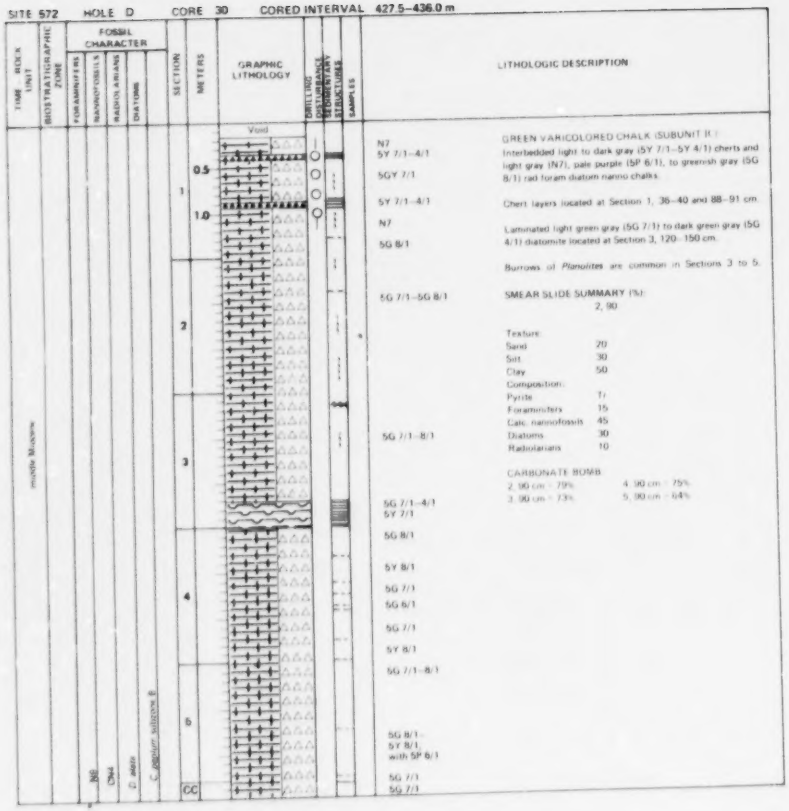
SITE 572 HOLE D CORE 30 CORED INTERVAL 427.5–436.0 m
TIME – ROCK UNIT
BIOSTRATIGRAPHIC ZONE
FOSSIL CHARACTER
FORAMINIFERS
NANNOFOSSILS
RADIOLARIANS
DIATOMS
SECTION
METERS
GRAPHIC LITHOLOGY
DRILLING DISTURBANCE
SEDIMENTARY STRUCTURES
SAMPLES
LITHOLOGIC DESCRIPTION
middle Miocene
Void
N7
5Y 7/1–4/1
5GY 7/1
5Y 7/1–4/1
N7
5G 8/1
5G 7/1–5G 8/1
5G 7/1–8/1
5G 7/1–4/1
5Y 7/1
5G 8/1
5Y 8/1
5G 7/1
5G 6/1
5G 7/1
5Y 8/1
5G 7/1–8/1
5G 8/1–
5Y 8/1;
with 5P 8/1
5G 7/1
5G 7/1
GREEN VARICOLORED CHALK (SUBUNIT IC):
Interbedded light to dark gray (5Y 7/1–5Y 4/1) cherts and light gray (N7), pale purple (5P 6/1), to greenish gray (5G 8/1) red foram diatom nanno chalks.
Chert layers located at Section 1, 36–40 and 88–91 cm.
Laminated light green gray (5G 7/1) to dark green gray (5G 4/1) diatomite located at Section 3, 120–150 cm.
Burrows of Planolites are common in Sections 3 to 5.
SMEAR SLIDE SUMMARY (%):
2, 90
Texture:
Sand 20
Silt 30
Clay 50
Composition:
Pyrite Tr
Foraminifers 15
Calc. nannofossils 45
Diatoms 30
Radiolarians 10
CARBONATE BOMB
2. 90 cm = 79%
3. 90 cm = 73%
4. 90 cm = 75%
5. 90 cm = 64%

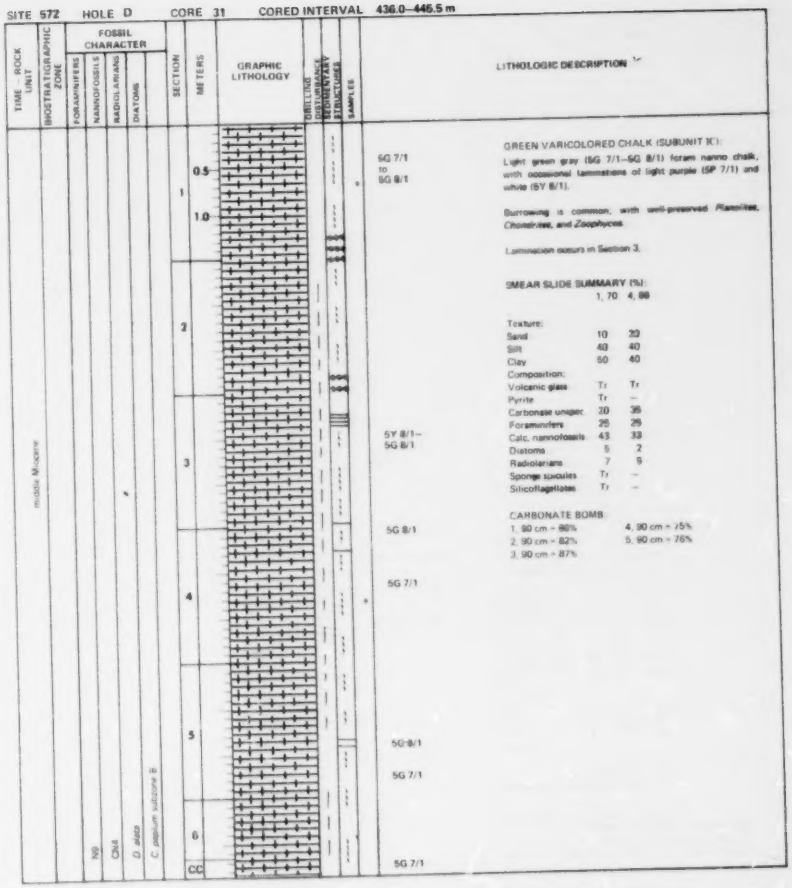
SITE 572 HOLE D CORE 31 CORED INTERVAL 436.0–446.5 m
TIME – ROCK UNIT
BIOSTRATIGRAPHIC ZONE
FOSSIL CHARACTER
FORAMINIFERS
NANNOFOSSILS
RADIOLARIANS
DIATOMS
SECTION
METERS
GRAPHIC LITHOLOGY
DRILLING DISTURBANCE
SEDIMENTARY STRUCTURES
SAMPLES
LITHOLOGIC DESCRIPTION
middle Miocene
5G 7/1
to
5G 8/1
5Y 8/1–
5G 8/1
5G 8/1
5G 7/1
5G 8/1
5G 7/1
5G 7/1
GREEN VARICOLORED CHALK (SUBUNIT IC):
Light green gray (5G 7/1–5G 8/1) foram nanno chalk, with occasional laminations of light purple (5P 7/1) and white (5Y 8/1).
Burrowing is common, with well-preserved Planolites, Chondrites, and Zoophycos.
Lamination occurs in Section 3.
SMEAR SLIDE SUMMARY (%):
1, 70 4, 88
Texture:
Sand 10 20
Silt 40 40
Clay 50 40
Composition:
Volcanic glass Tr Tr
Pyrite Tr –
Carbonate unspec. 20 35
Foraminifers 25 25
Calc. nannofossils 43 33
Diatoms 5 2
Radiolarians 7 5
Sponge spicules Tr –
Silicoflagellates Tr –
CARBONATE BOMB
1. 90 cm = 86%
2. 90 cm = 82%
3. 90 cm = 87%
4. 90 cm = 75%
5. 90 cm = 76%

SITE 572 HOLE D CORE 32 CORED INTERVAL 446.5–455.0 m

TIME – ROCK UNIT	BIOSTRATIGRAPHIC ZONE	FOSSIL CHARACTER: FORAMINIFERS	NANNOFOSSILS	RADIOLARIANS	DIATOMS	SECTION	METERS	GRAPHIC LITHOLOGY	DRILLING DISTURBANCE	SEDIMENTARY STRUCTURES	SAMPLES	LITHOLOGIC DESCRIPTION
middle Miocene	N9 / CN4 (lower part) / *D. altera* / *C. peplum* subzone A					1	0.5					5G 6/1
							1.0					5G 7/1–5G 8/1
						2						5G 6/1 / 5Y 8/1 / 5P 6/1 / 5Y 8/1–5G 8/1
						3						5Y 8/1–5G 8/1
						4						5P 6/2 / 5Y 8/1–5G 8/1 / 5P 6/1 / 5P 6/1 / 5G 7/1–8/1
						5						IW / Void / 5P 6/1 / 5G 7/1 / 5G 6/1
						6						5G 6/1–5Y 8/1 / 5P 6/1 / 5G 7/1–8/1
						CC						

GREEN VARICOLORED CHALK (SUBUNIT IC)

White (5Y 8/1) to light green gray (5G 8/1) foram nanno chalk, with discrete laminae of green gray (5G 6/1), pale purple (5P 6/1), and purple (5P 6/2).

Many parts have irregular and inclined laminations. Layers of pyrite particles 0.5–1.0 mm diameter found in Section 3, 3–8 and 85–86 cm.

Burrowing is common, with well-preserved *Planolites*, *Chondrites*, and *Zoophycos*.

SMEAR SLIDE SUMMARY (%)

	2, 63
Texture:	
Sand	30
Silt	30
Clay	40
Composition:	
Zeolite	Tr
Carbonate unspec.	25
Foraminifers	25
Calc. nannofossils	40
Diatoms	5
Radiolarians	5
Silicoflagellates	Tr

CARBONATE BOMB

1. 90 cm = 80%	4. 90 cm = 86%
2. 90 cm = 87%	5. 90 cm = 81%
3. 90 cm = 81%	6. 90 cm = 73%

SITE 572 HOLE D CORE 33 CORED INTERVAL 455.0–464.5 m

TIME – ROCK UNIT	BIOSTRATIGRAPHIC ZONE	FOSSIL CHARACTER: FORAMINIFERS	NANNOFOSSILS	RADIOLARIANS	DIATOMS	SECTION	METERS	GRAPHIC LITHOLOGY	DRILLING DISTURBANCE	SEDIMENTARY STRUCTURES	SAMPLES	LITHOLOGIC DESCRIPTION
middle Miocene	N9 / bottom CN4 / *D. altera* / *C. peplum* subzone B					1	0.5					5G 6/1
							1.0					5G 7/1 / 5G 6/1 / 5G 7/1 / 5G 6/1 / 5GY 7/1 / 5G 6/1 / 5G 7/1 / 5G 6/1 / 5G 7/1
						2						NB–5G 8/1 / 5G 7/1–5G 8/1
						3						10Y 8/1–5Y 8/1 / 10Y 8/1–10G 8/1
						4						2.5Y 8/2–2.5Y 8/4
						5						2.5Y 8/2–2.5Y 8/4
						6						2.5Y 7/4 / 2.5Y 7/4 / 2.5Y 8/2
						7						2.5Y 8/1
						CC						

GREEN VARICOLORED CHALK (SUBUNIT IC)
(455.0–458.8 m):

Alternation between light green gray (5G 7/1), green gray (5G 8/1), and white (N9) siliceous foram nanno chalk, in color bands with distinct contacts.

YELLOW CHALK (SUBUNIT ID) (458.8–464.5 m):

Alternation between yellow white (2.5Y 8/2), yellowish green (10Y 8/1), and white (5Y 8/1 to 2.5Y 8/1) foram nanno chalk. Burrowing is common, well-preserved *Zoophycos*, *Planolites*, and *Chondrites*.

SMEAR SLIDE SUMMARY (%):

	3, 106	5, 80	CC
Texture:			
Sand	30	20	35
Silt	30	20	30
Clay	40	60	35
Composition:			
Pyrite	–	–	5
Carbonate unspec.	25	38	15
Foraminifers	20	20	20
Calc. nannofossils	40	35	50
Diatoms	7	2	–
Radiolarians	8	5	Tr
Silicoflagellates	Tr	–	–
Fe-oxides	–	–	10

CARBONATE BOMB

1. 90 cm = 74%	4. 90 cm = 81%
2. 90 cm = 88%	5. 90 cm = 78%
3. 90 cm = 84%	6. 90 cm = 72%

86-572D-34-1 Depth 4785 - 4880 m

Nine pieces of fine grained basalt recovered. Total length of 28 cm. Piece 8 has glassy rind.

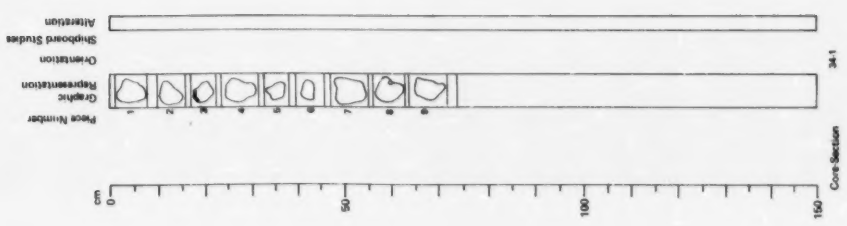

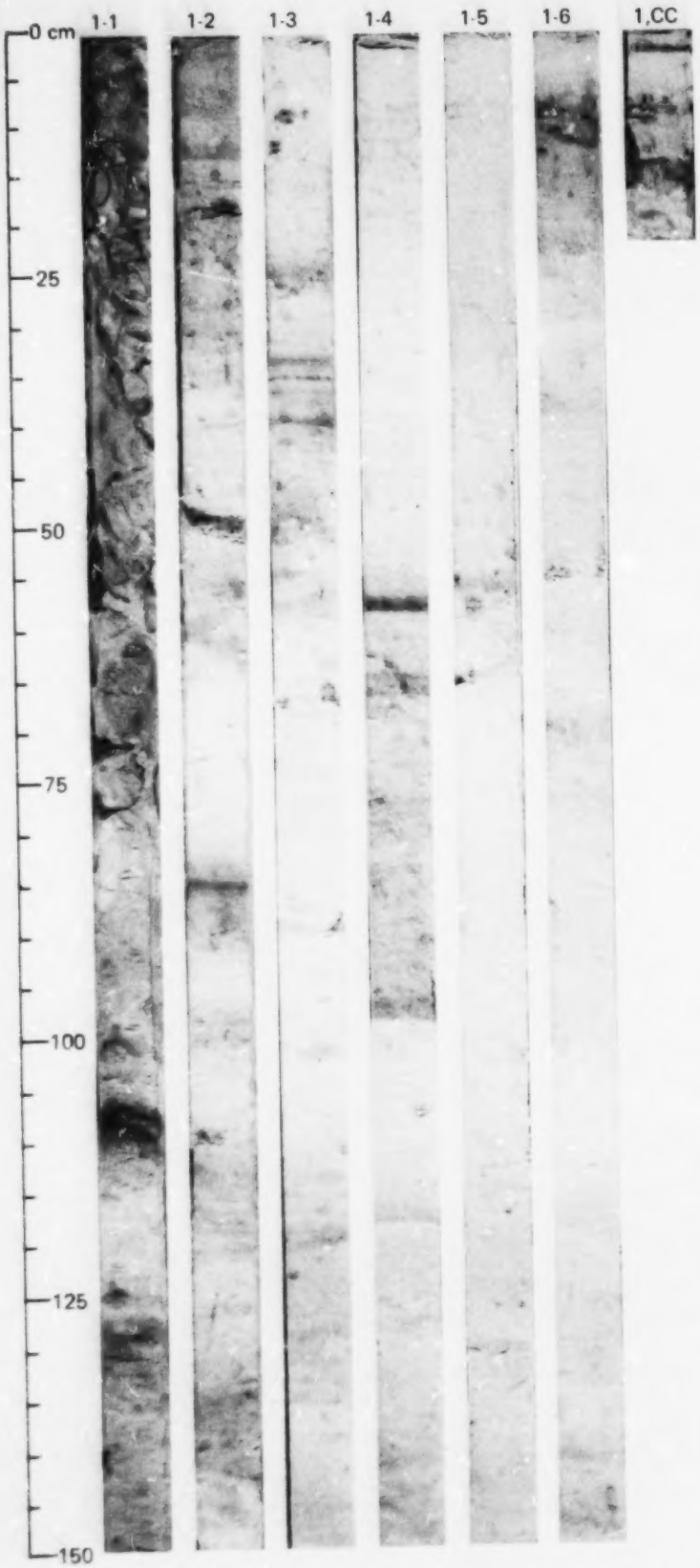
0 cm
1-1
1-2
1-3
1-4
1-5
1-6
1,CC
25
50
75
100
125
150

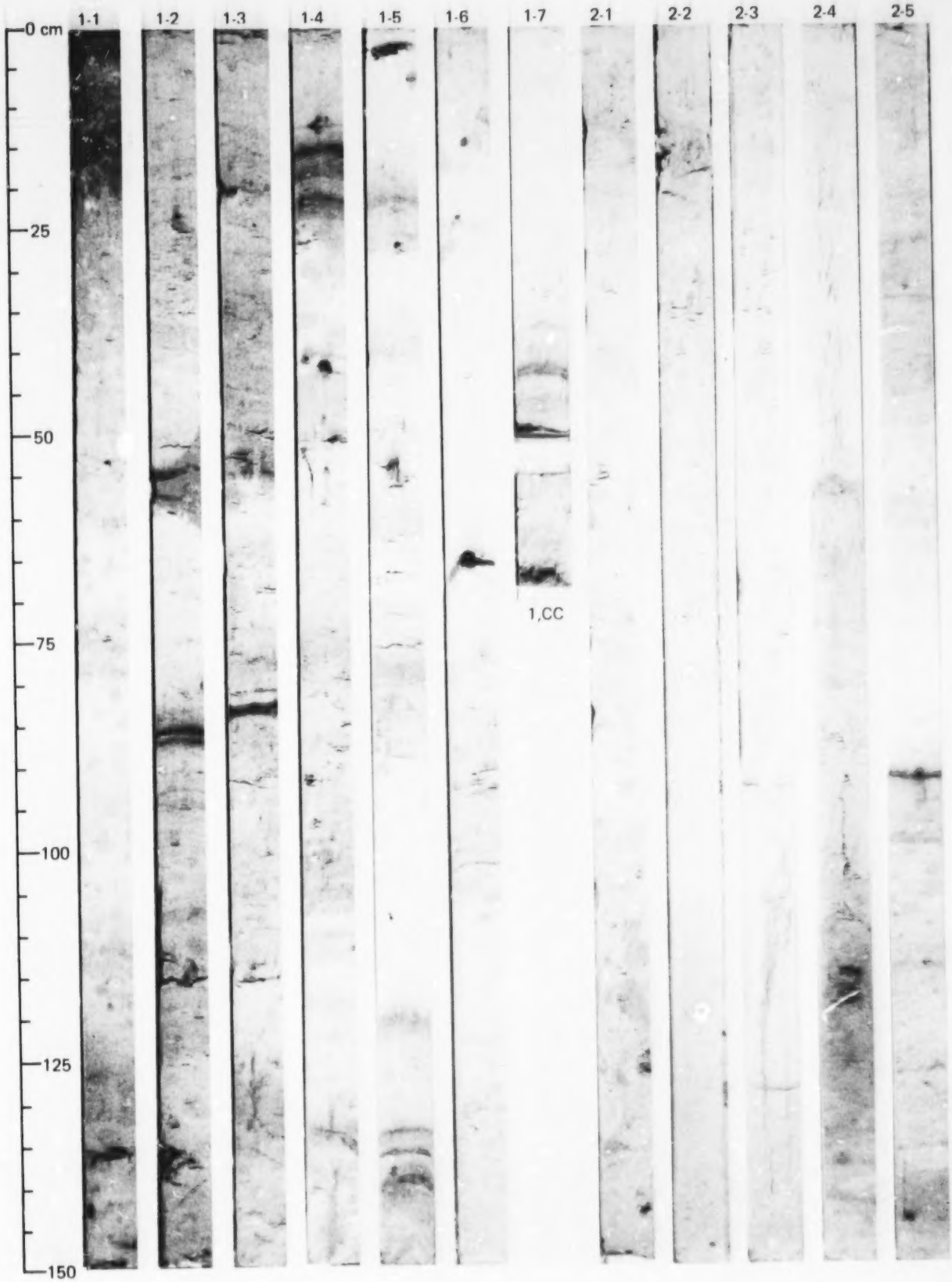
0 cm
25
50
75
100
125
150
1-1
1-2
1-3
1-4
1-5
1-6
1-7
1,CC
2-1
2-2
2-3
2-4
2-5

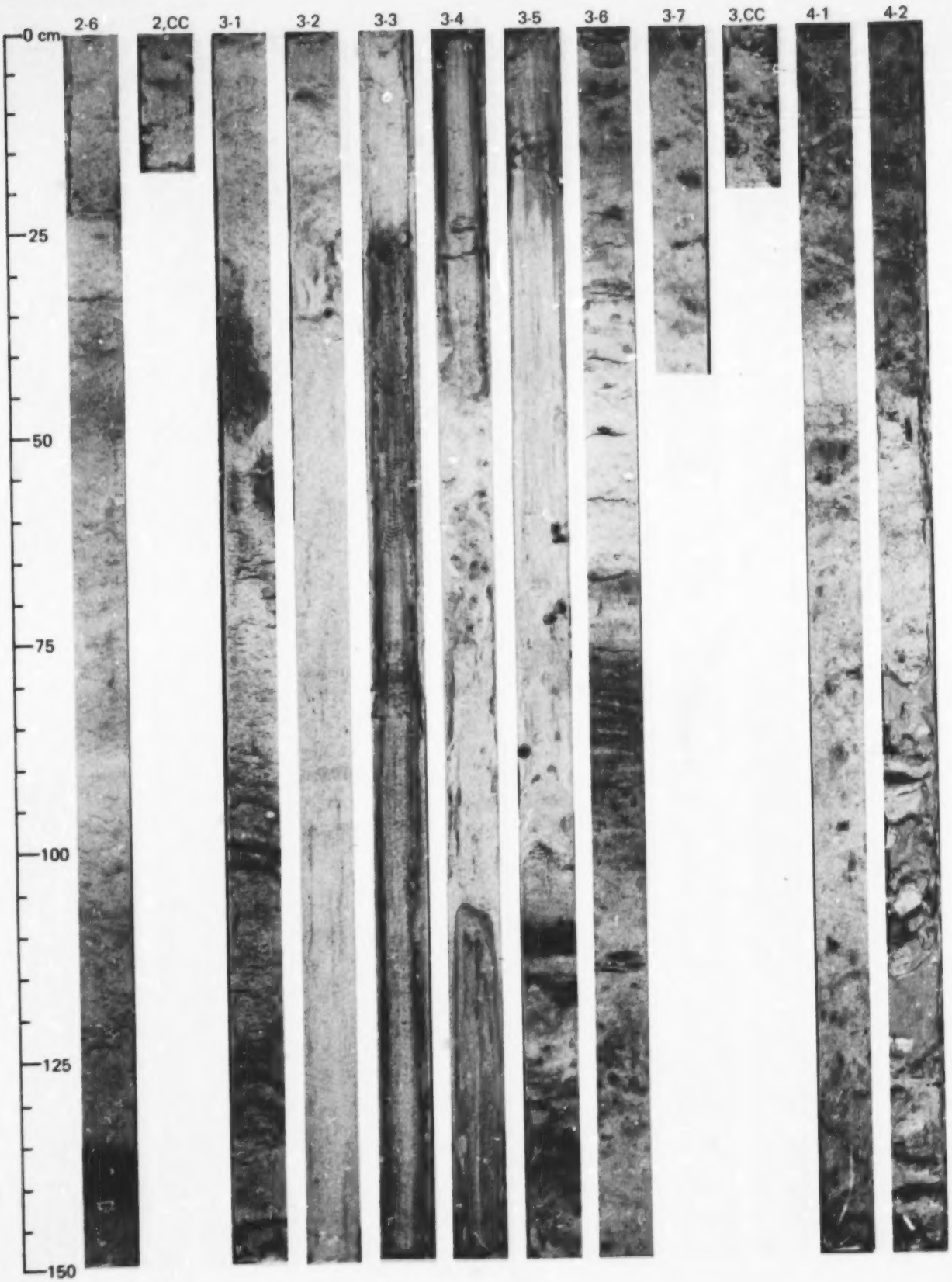
0 cm
25
50
75
100
125
150
2-6
2,CC
3-1
3-2
3-3
3-4
3-5
3-6
3-7
3,CC
4-1
4-2

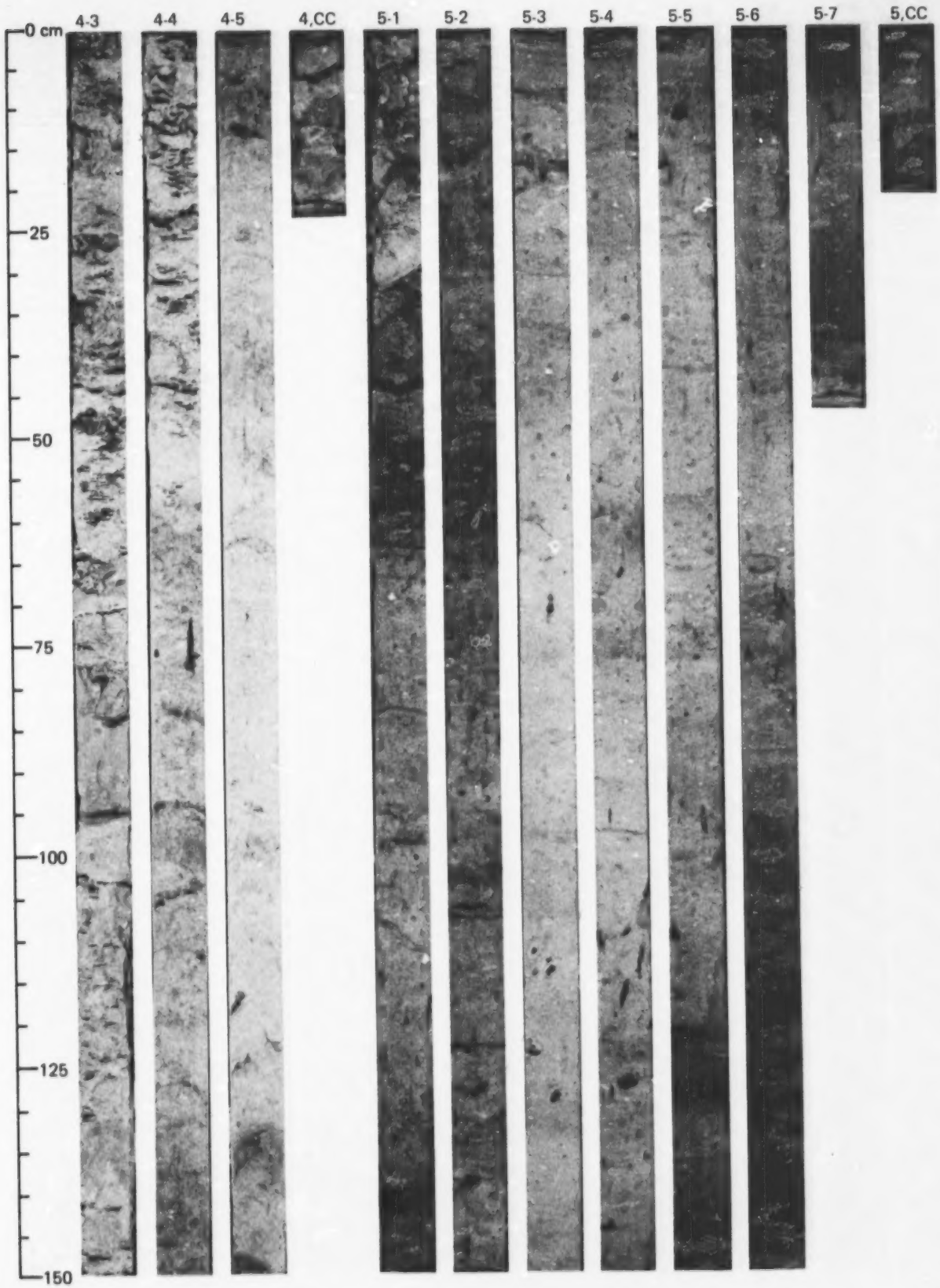
0 cm
25
50
75
100
125
150
4-3
4-4
4-5
4,CC
5-1
5-2
5-3
5-4
5-5
5-6
5-7
5,CC

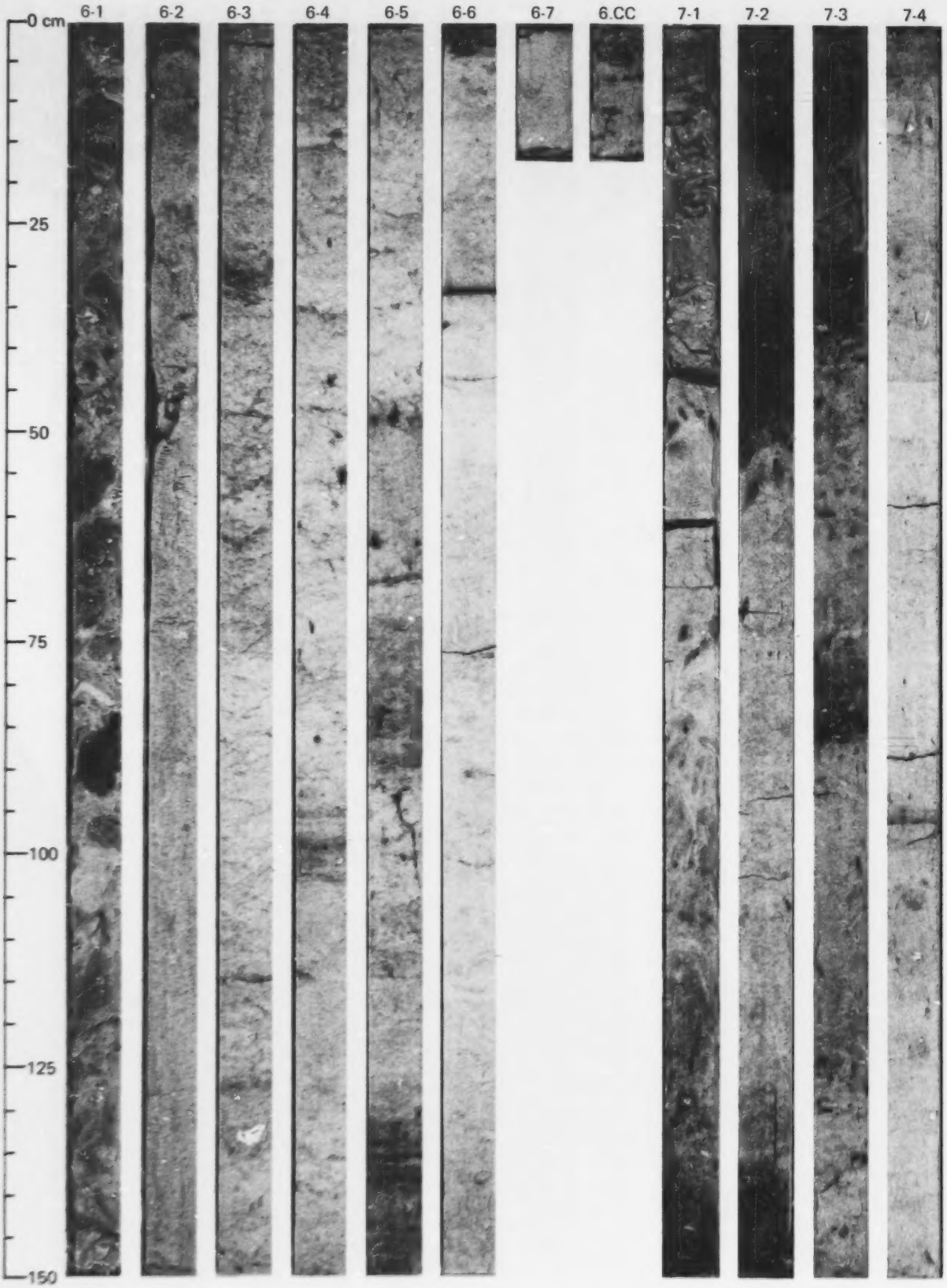
0 cm
25
50
75
100
125
150
6-1
6-2
6-3
6-4
6-5
6-6
6-7
6.CC
7-1
7-2
7-3
7-4

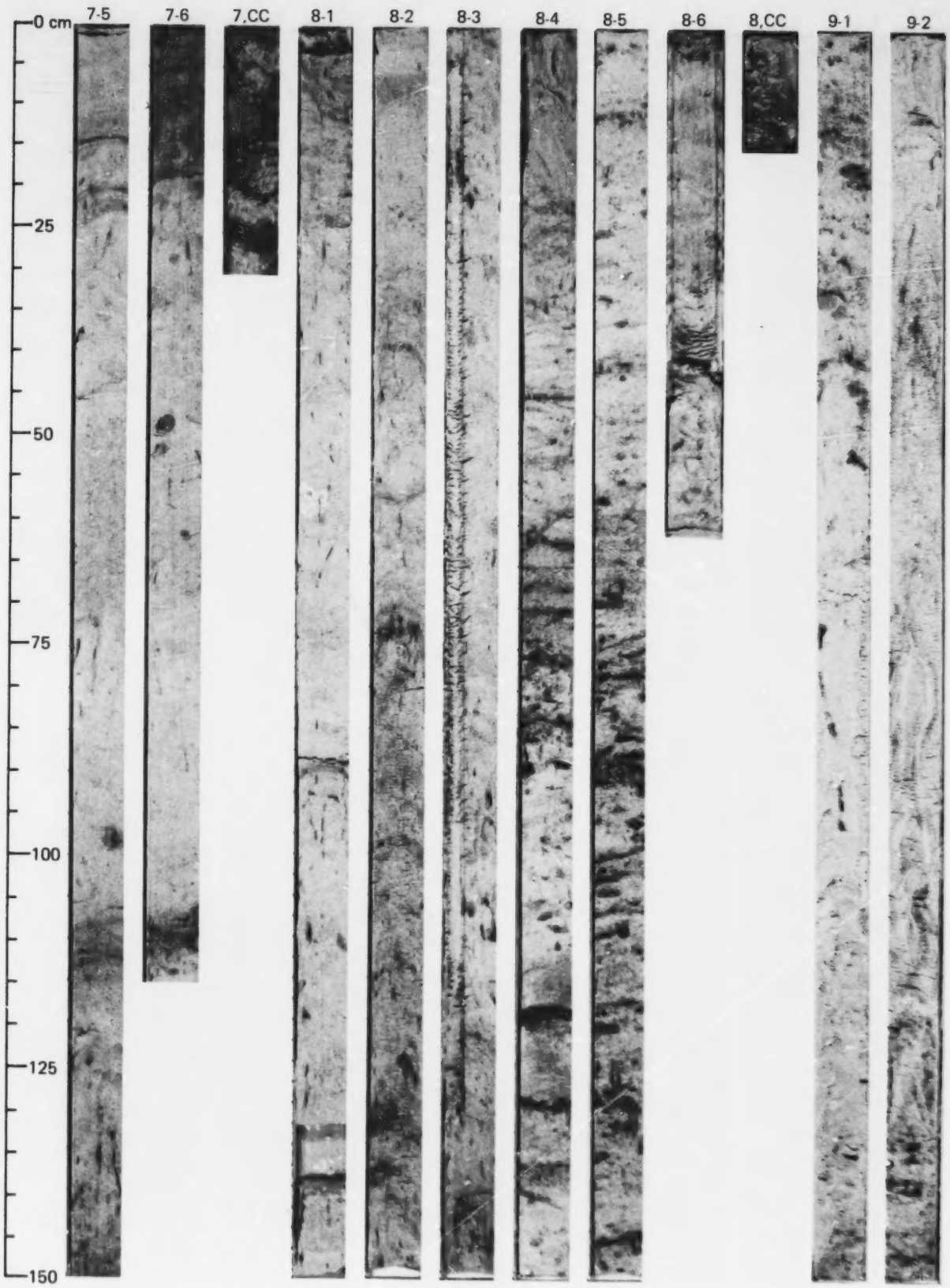
0 cm
25
50
75
100
125
150
7-5
7-6
7,CC
8-1
8-2
8-3
8-4
8-5
8-6
8,CC
9-1
9-2

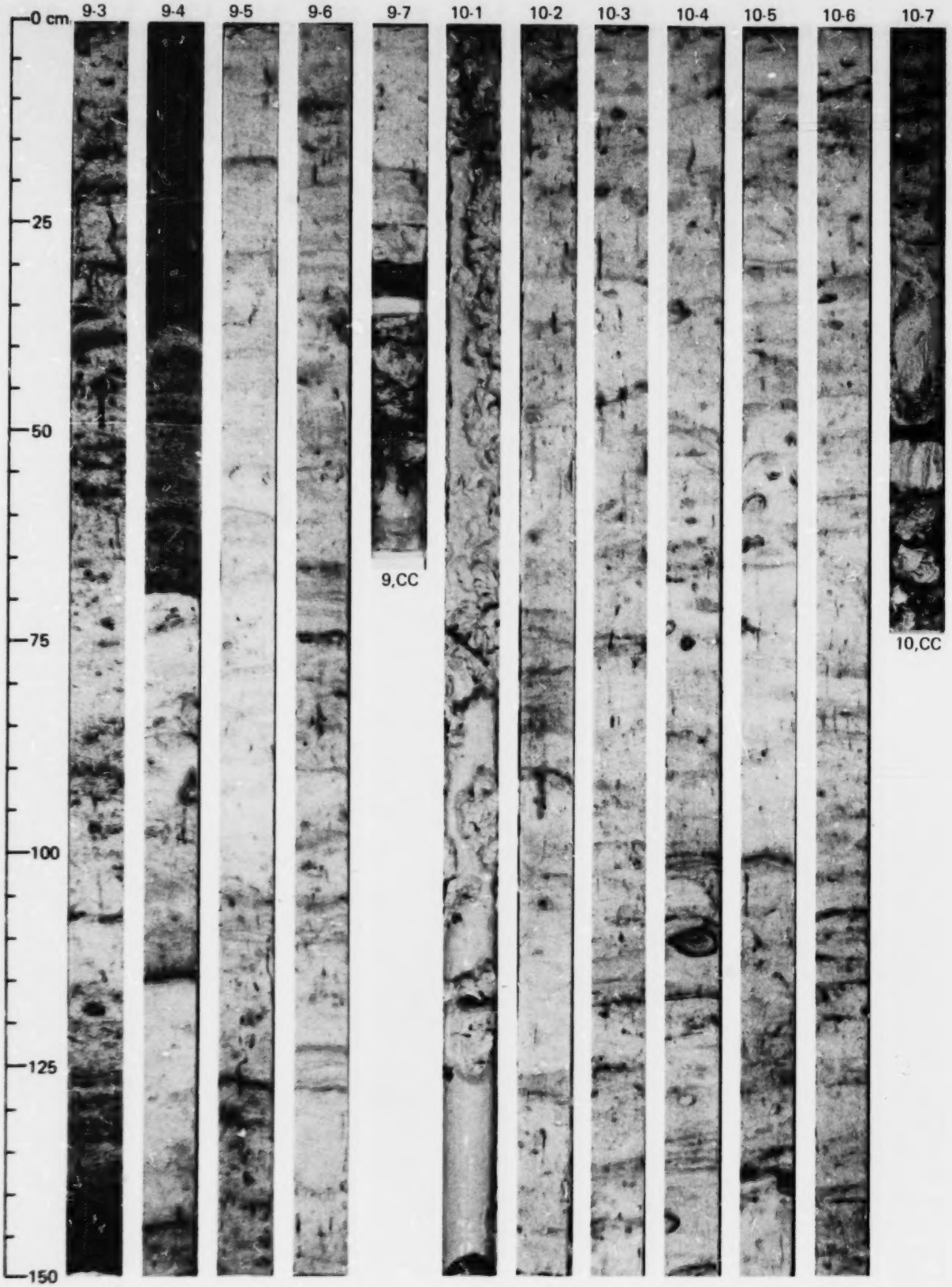
0 cm
25
50
75
100
125
150
9-3
9-4
9-5
9-6
9-7
9,CC
10-1
10-2
10-3
10-4
10-5
10-6
10-7
10,CC

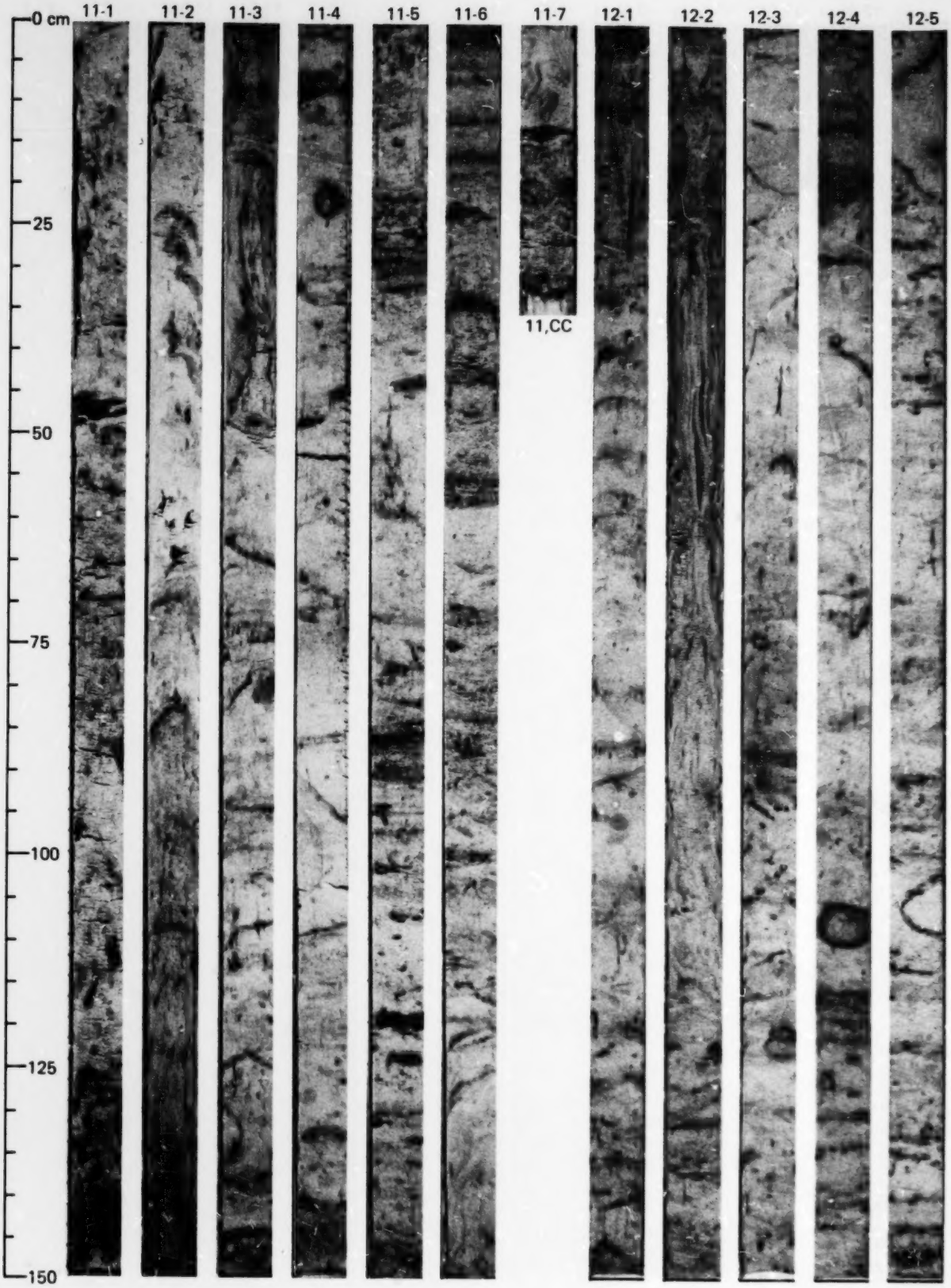
0 cm
25
50
75
100
125
150
11-1
11-2
11-3
11-4
11-5
11-6
11-7
11,CC
12-1
12-2
12-3
12-4
12-5

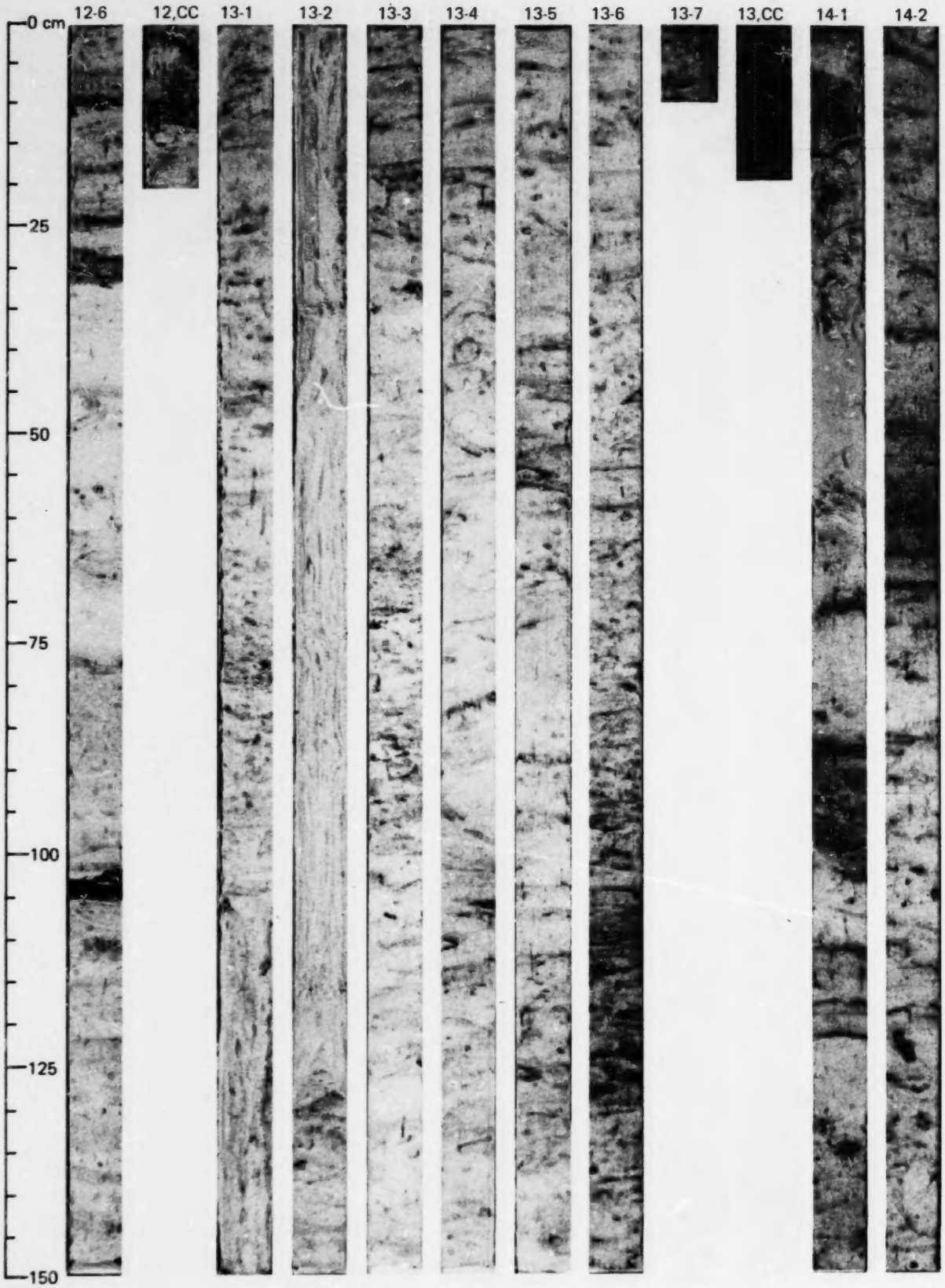
0 cm
25
50
75
100
125
150
12-6
12,CC
13-1
13-2
13-3
13-4
13-5
13-6
13-7
13,CC
14-1
14-2

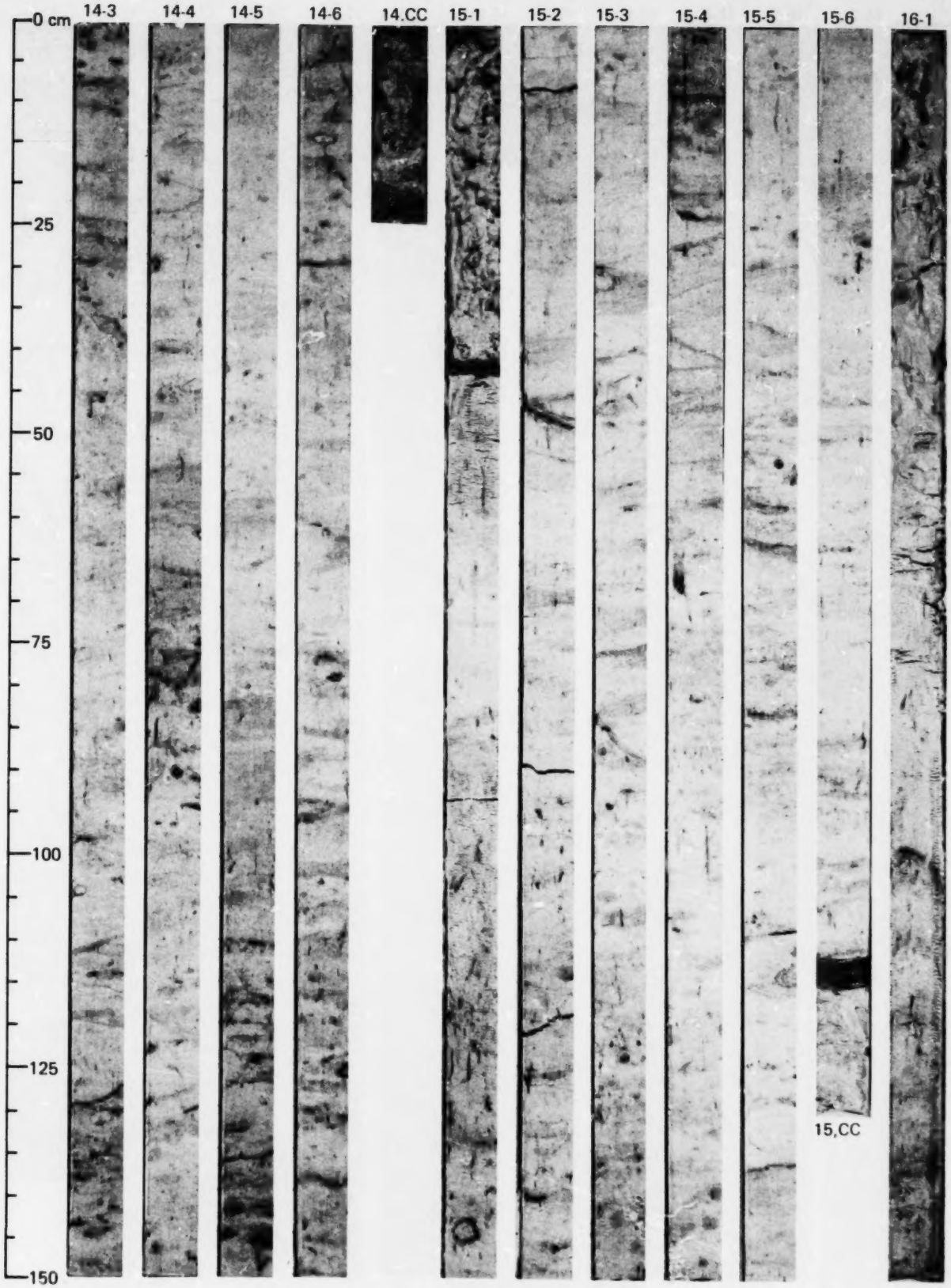
0 cm
14-3
14-4
14-5
14-6
14,CC
15-1
15-2
15-3
15-4
15-5
15-6
16-1
25
50
75
100
125
150
15,CC

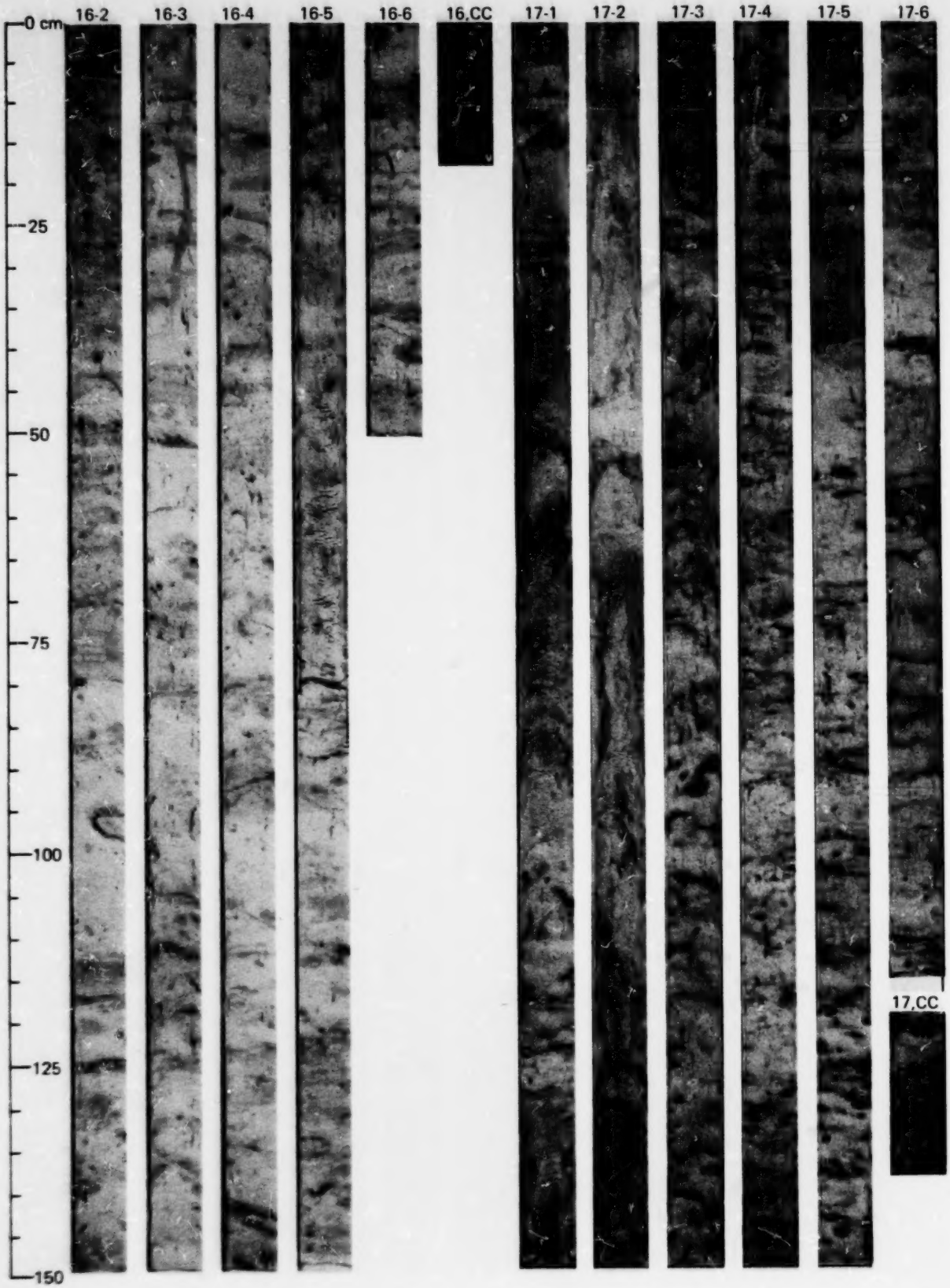
0 cm
25
50
75
100
125
150
16-2
16-3
16-4
16-5
16-6
16,CC
17-1
17-2
17-3
17-4
17-5
17-6
17,CC

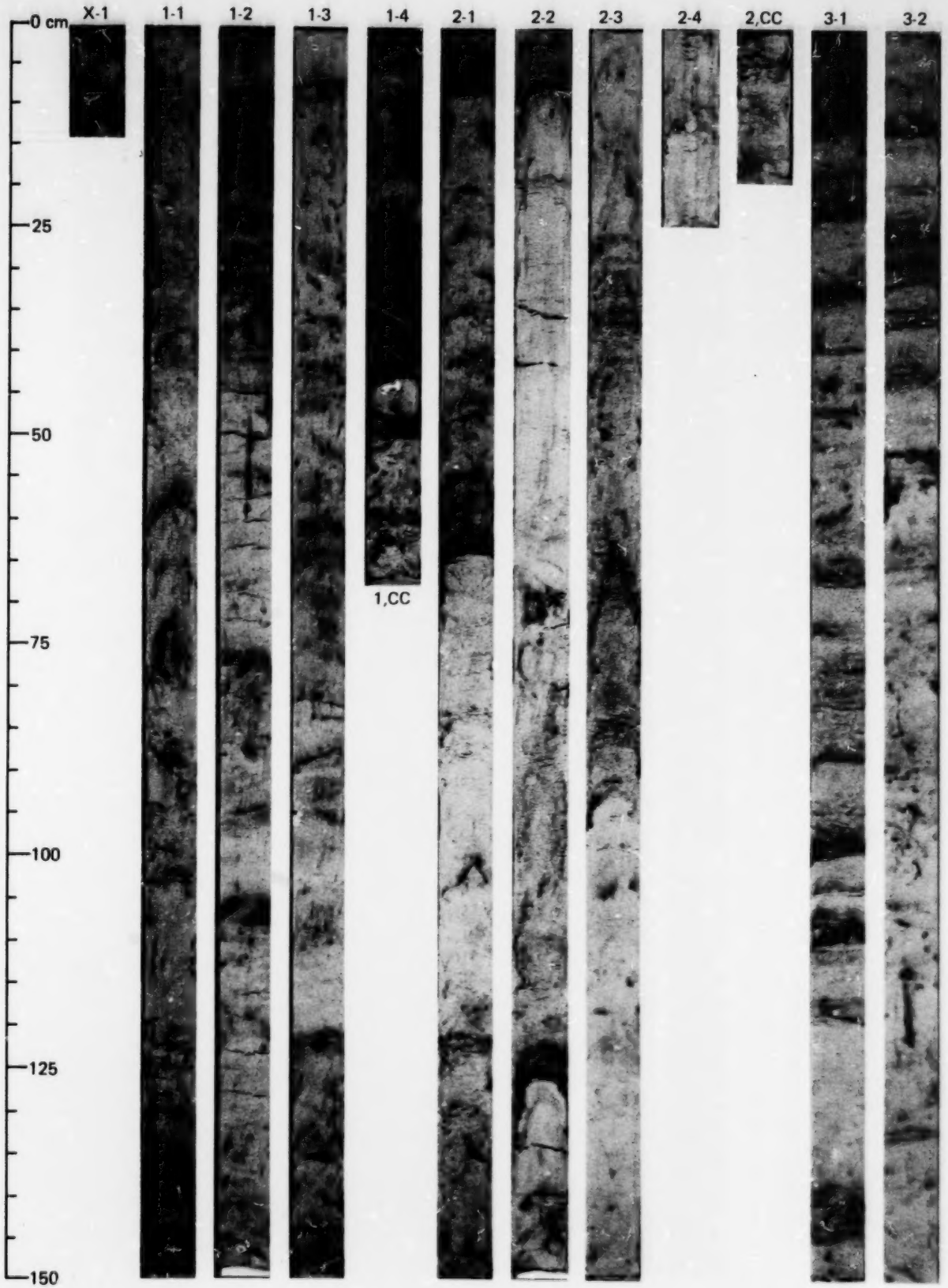
0 cm
25
50
75
100
125
150
X-1
1-1
1-2
1-3
1-4
1,CC
2-1
2-2
2-3
2-4
2,CC
3-1
3-2

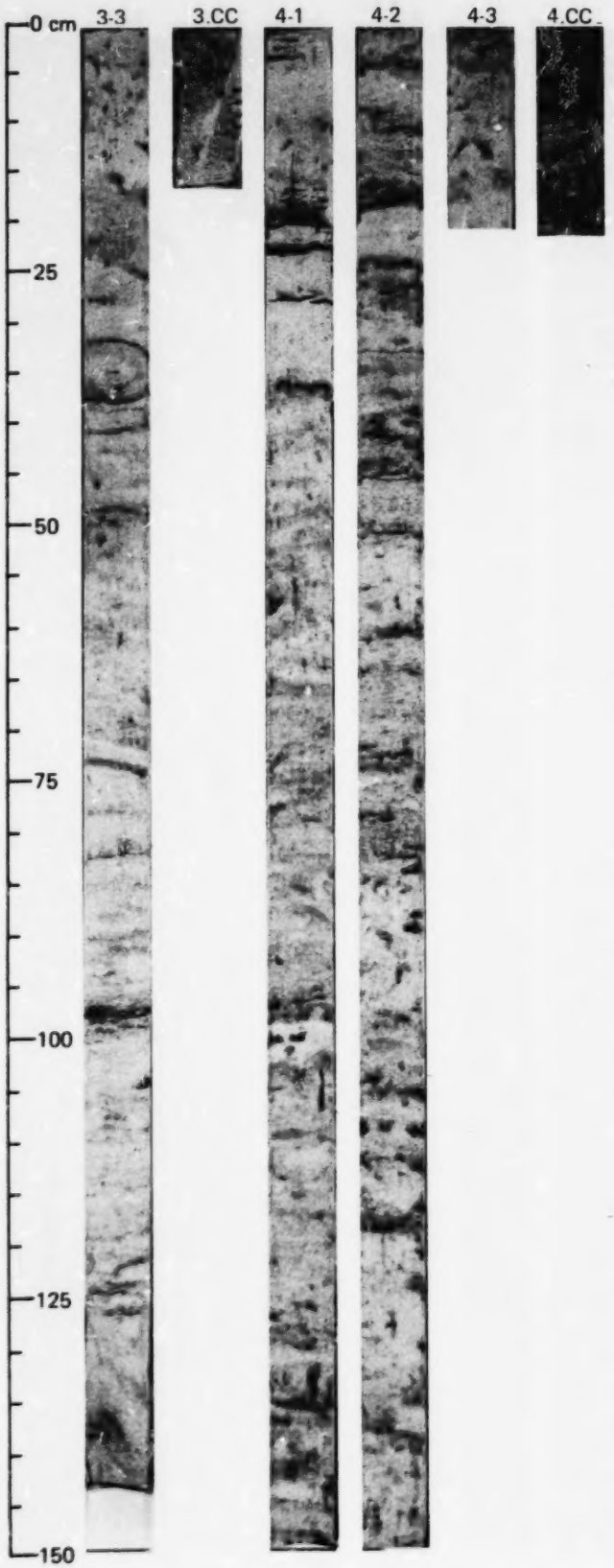
0 cm
3-3
3.CC
4-1
4-2
4-3
4.CC
25
50
75
100
125
150

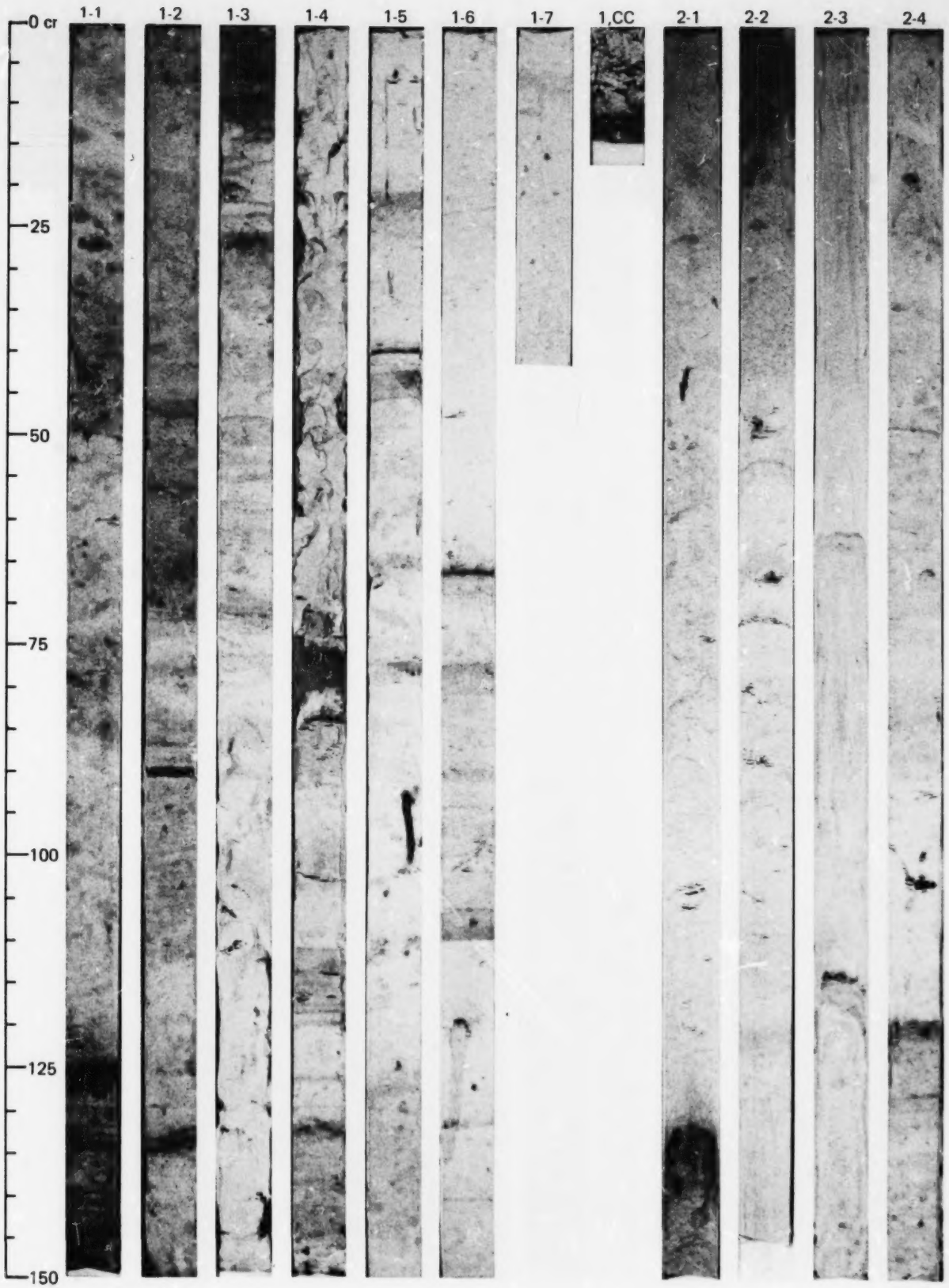
0 cr
25
50
75
100
125
150
1-1
1-2
1-3
1-4
1-5
1-6
1-7
1,CC
2-1
2-2
2-3
2-4

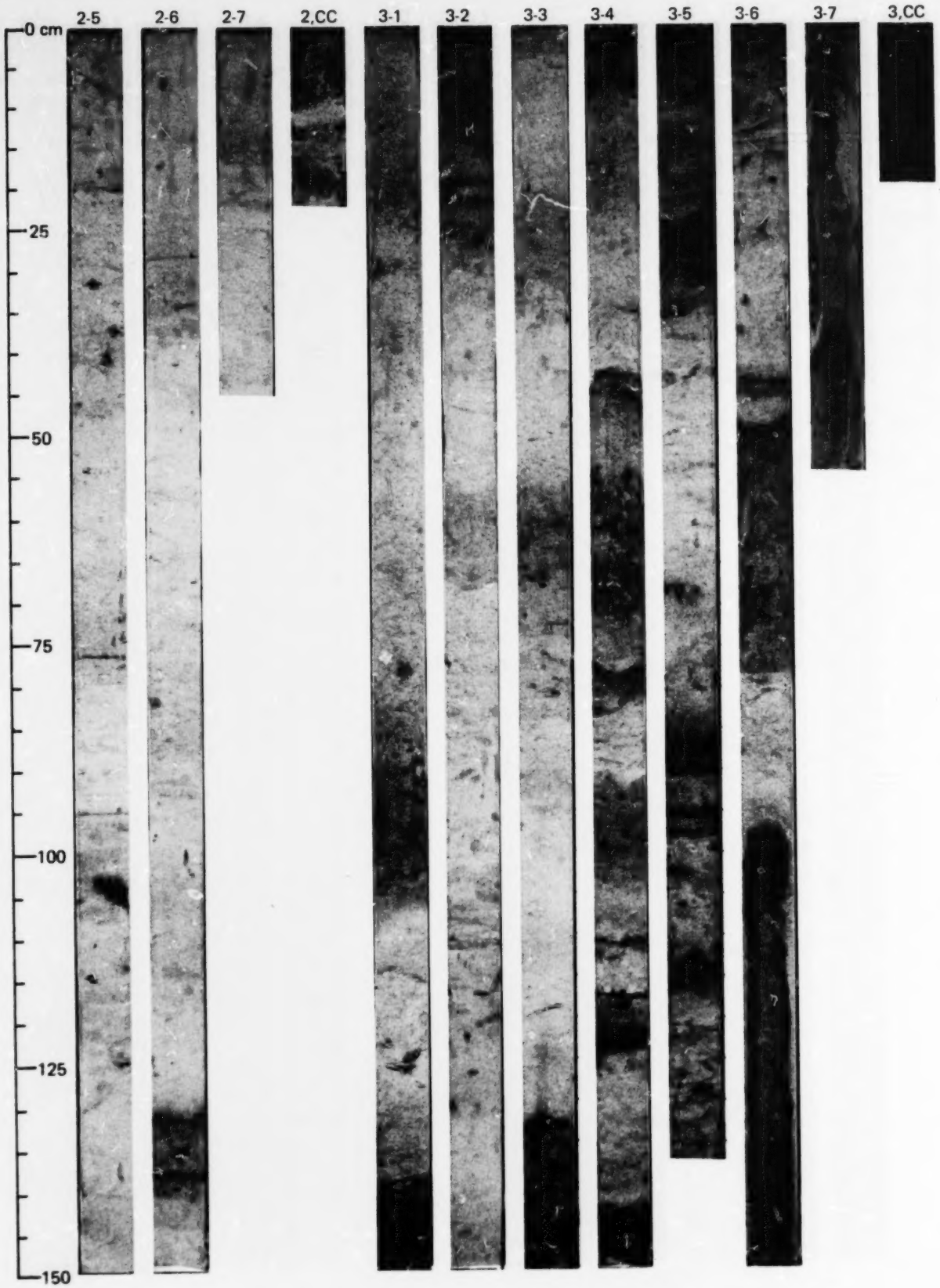
2-5
2-6
2-7
2,CC
3-1
3-2
3-3
3-4
3-5
3-6
3-7
3,CC
0 cm
25
50
75
100
125
150

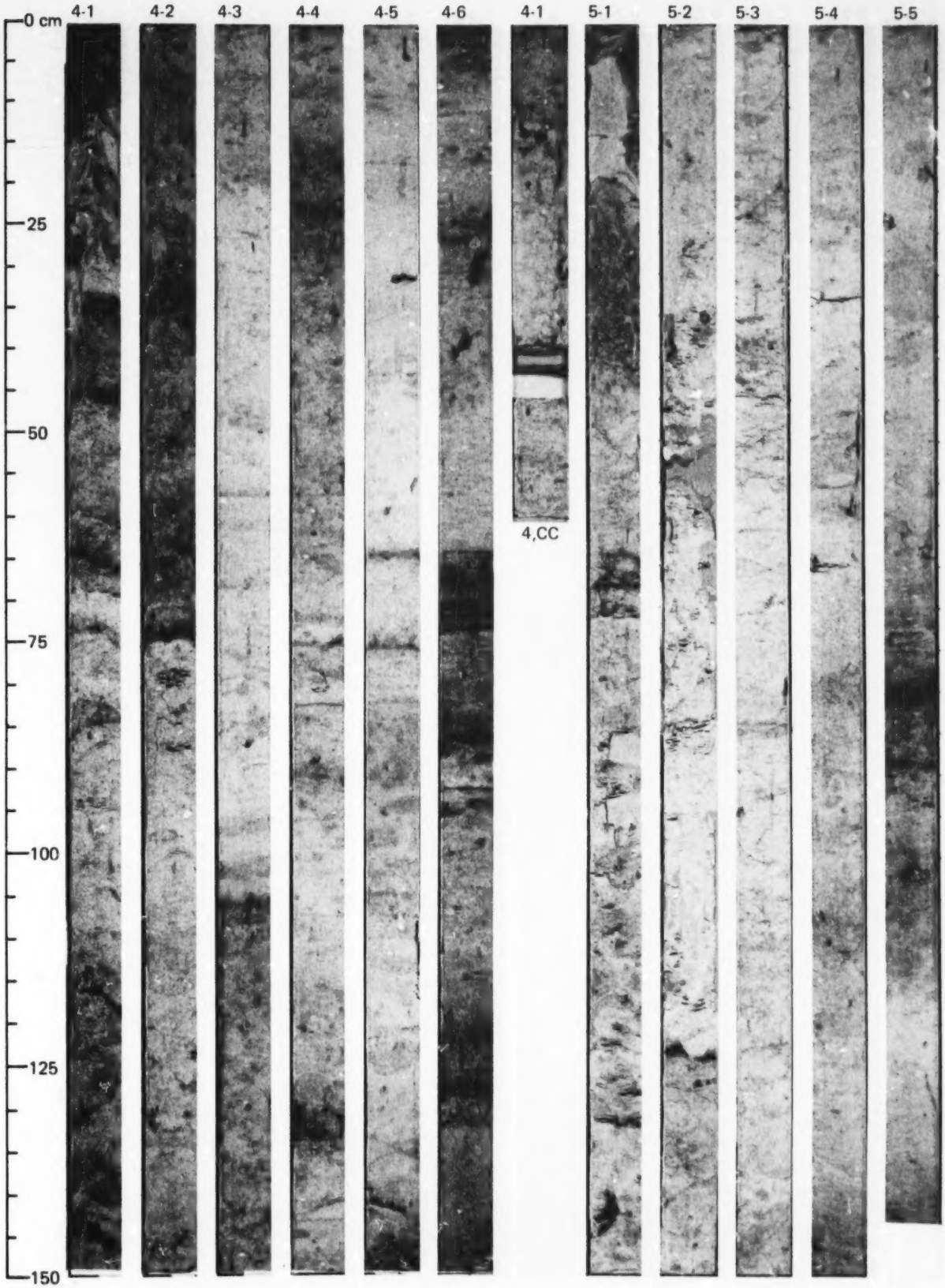
0 cm
25
50
75
100
125
150
4-1
4-2
4-3
4-4
4-5
4-6
4-1
4,CC
5-1
5-2
5-3
5-4
5-5

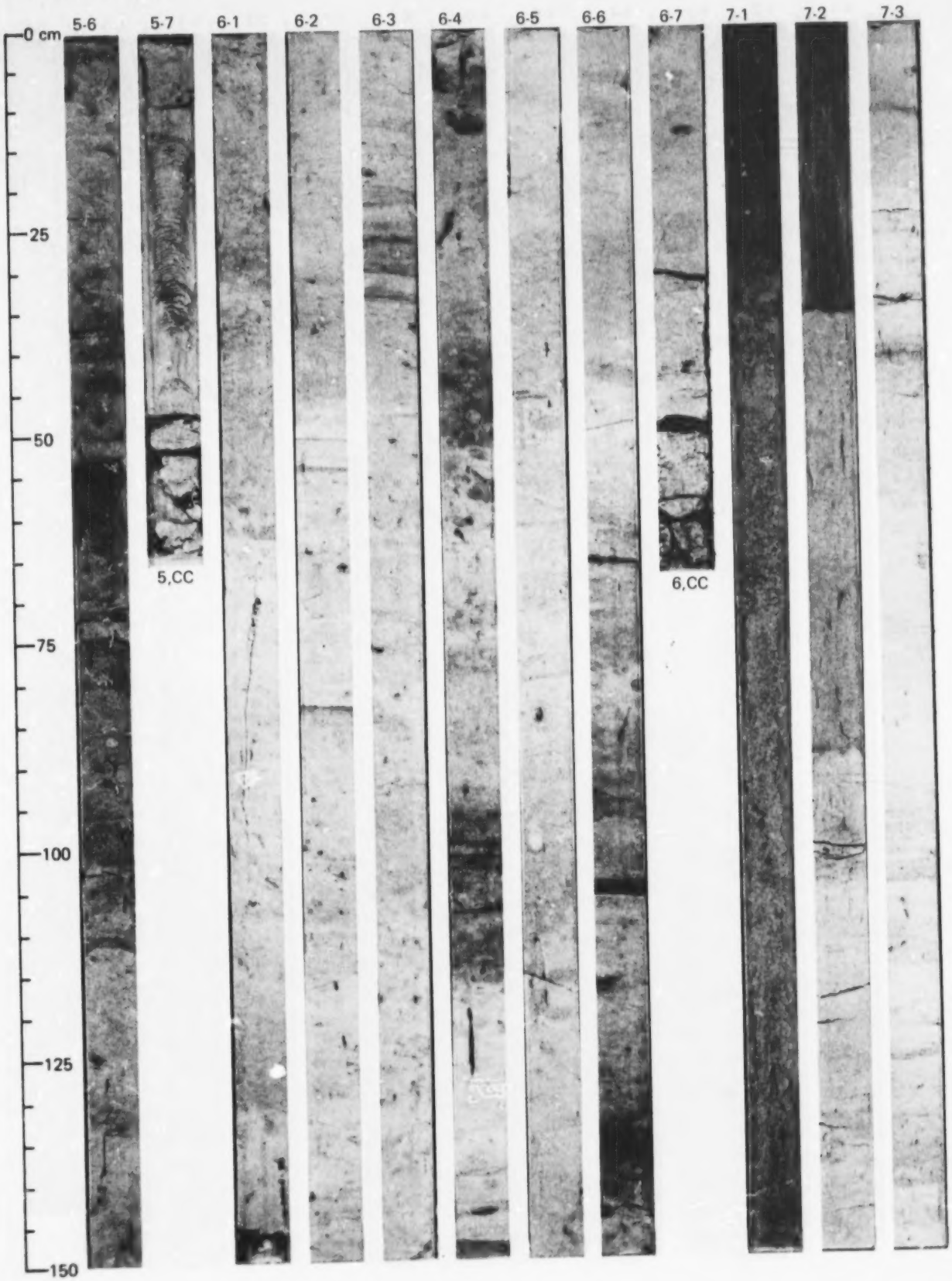
0 cm
25
50
75
100
125
150
5-6
5-7
5,CC
6-1
6-2
6-3
6-4
6-5
6-6
6-7
6,CC
7-1
7-2
7-3

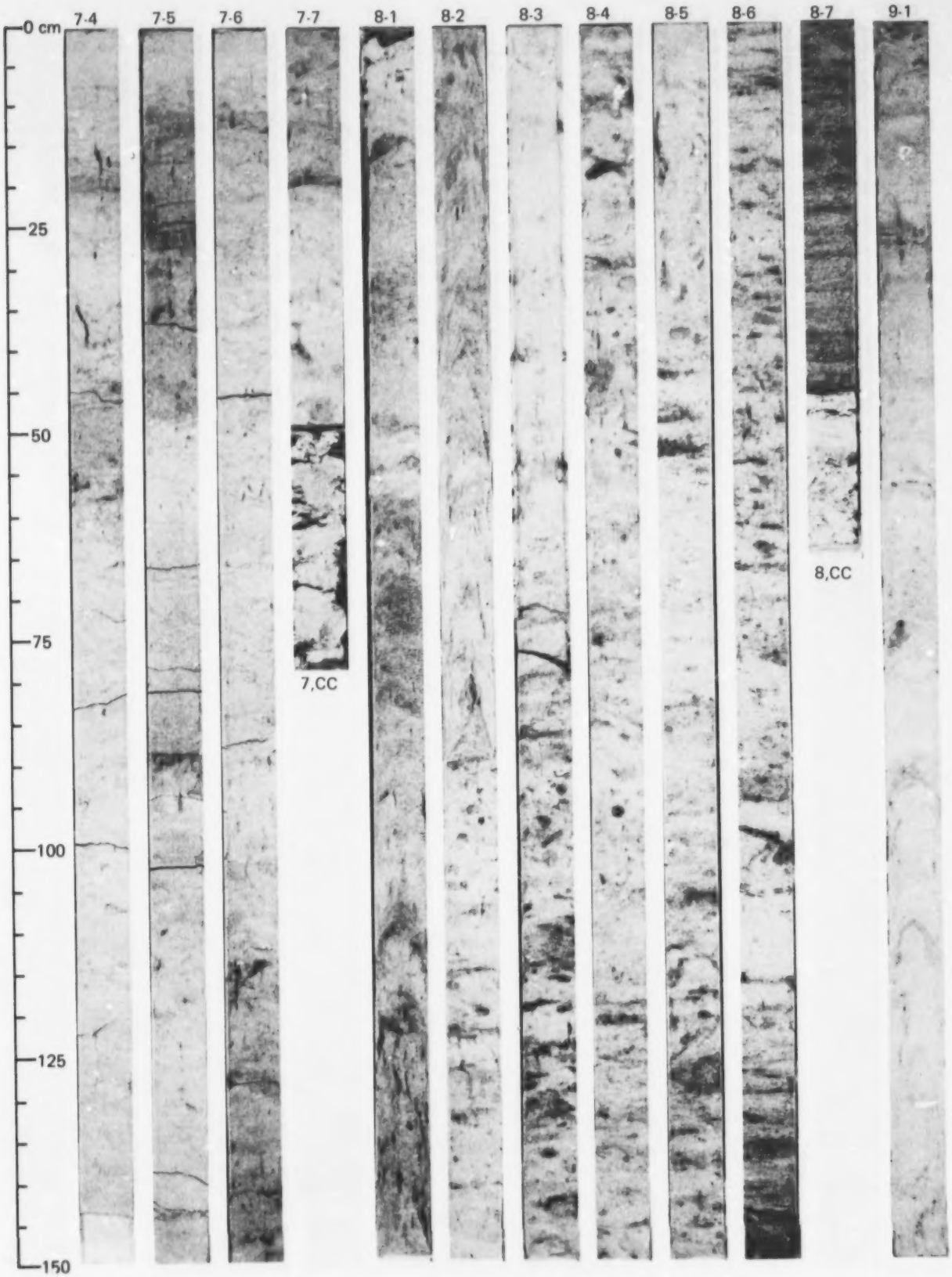
0 cm
25
50
75
100
125
150
7-4
7-5
7-6
7-7
7,CC
8-1
8-2
8-3
8-4
8-5
8-6
8-7
8,CC
9-1

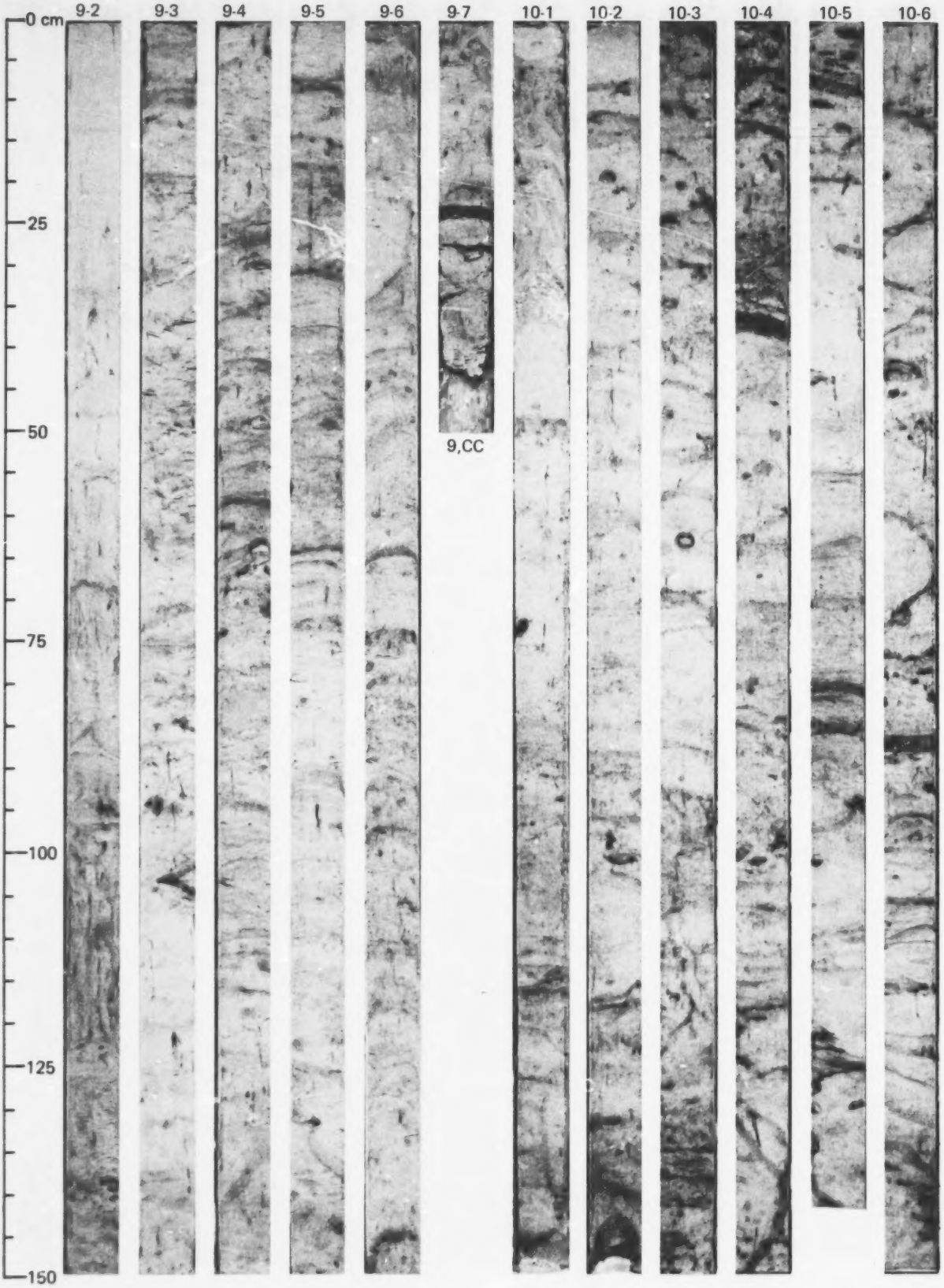
0 cm
25
50
75
100
125
150
9-2
9-3
9-4
9-5
9-6
9-7
9,CC
10-1
10-2
10-3
10-4
10-5
10-6

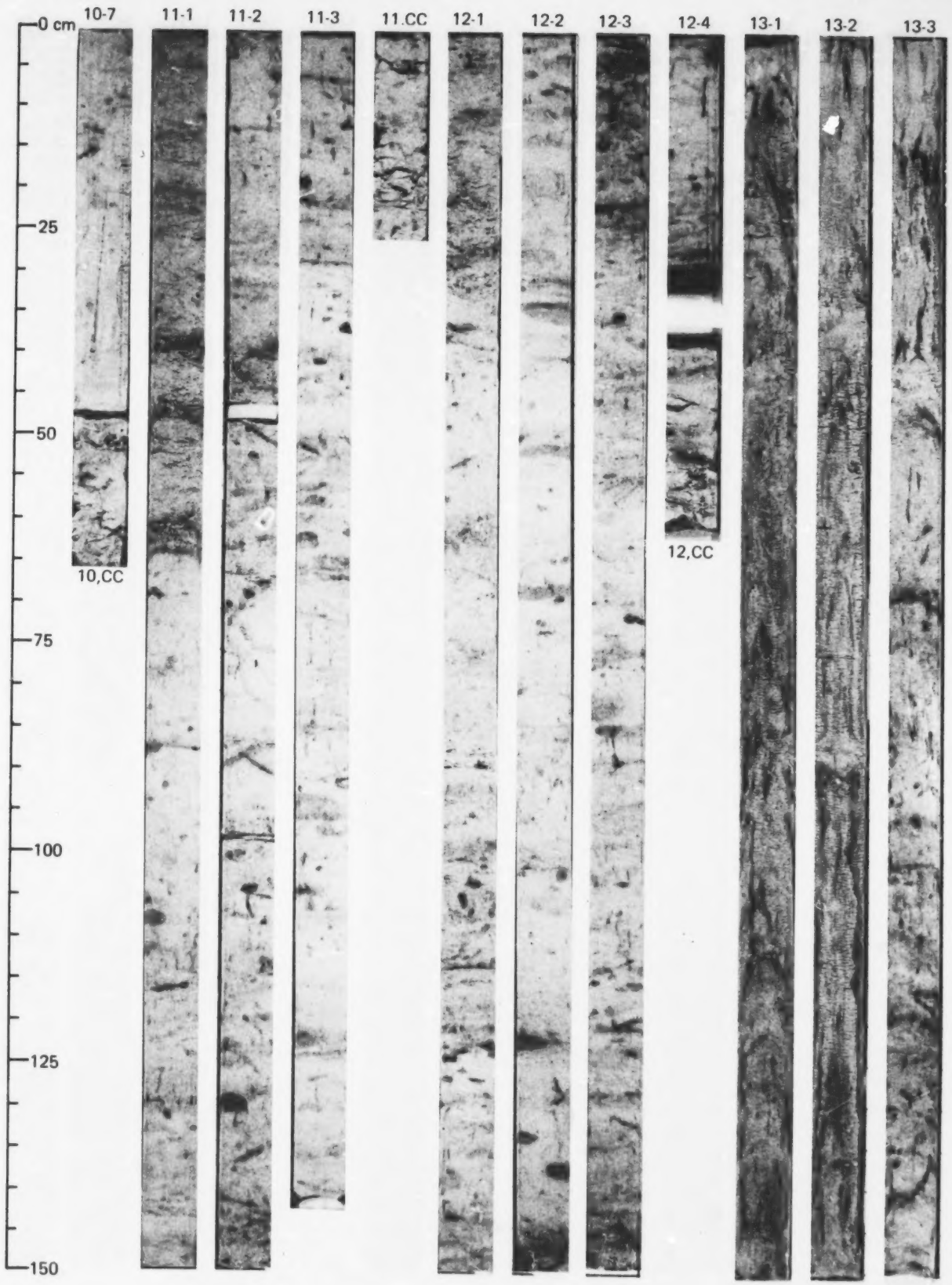
0 cm
25
50
75
100
125
150
10-7
10,CC
11-1
11-2
11-3
11,CC
12-1
12-2
12-3
12-4
12,CC
13-1
13-2
13-3

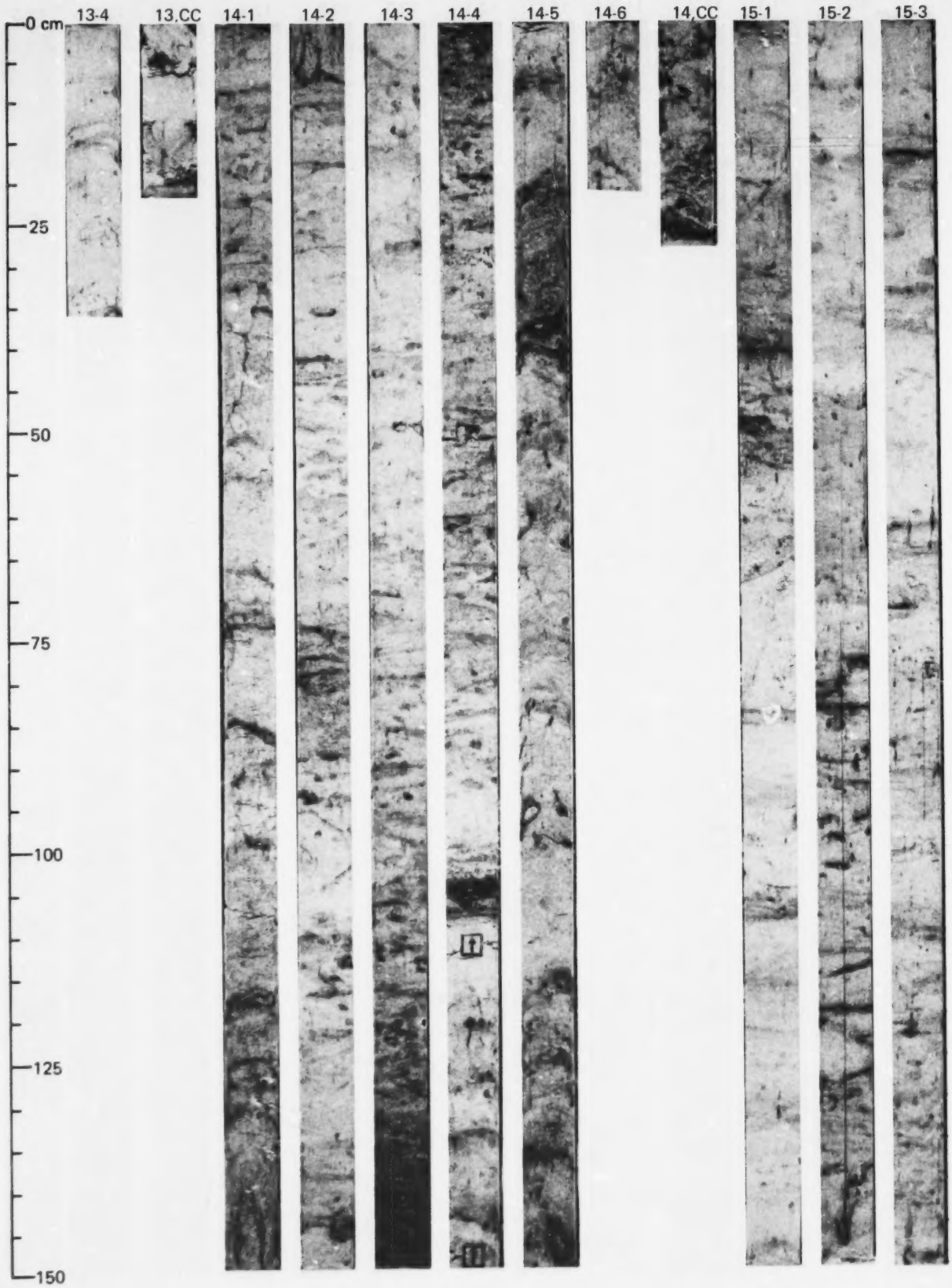
0 cm
25
50
75
100
125
150
13-4
13,CC
14-1
14-2
14-3
14-4
14-5
14-6
14,CC
15-1
15-2
15-3

0 cm
25
50
75
100
125
150
15-4
15-5
15-6
15,CC
16-1
16-2
16-3
16-4
16-5
16-6
16-7
16,CC

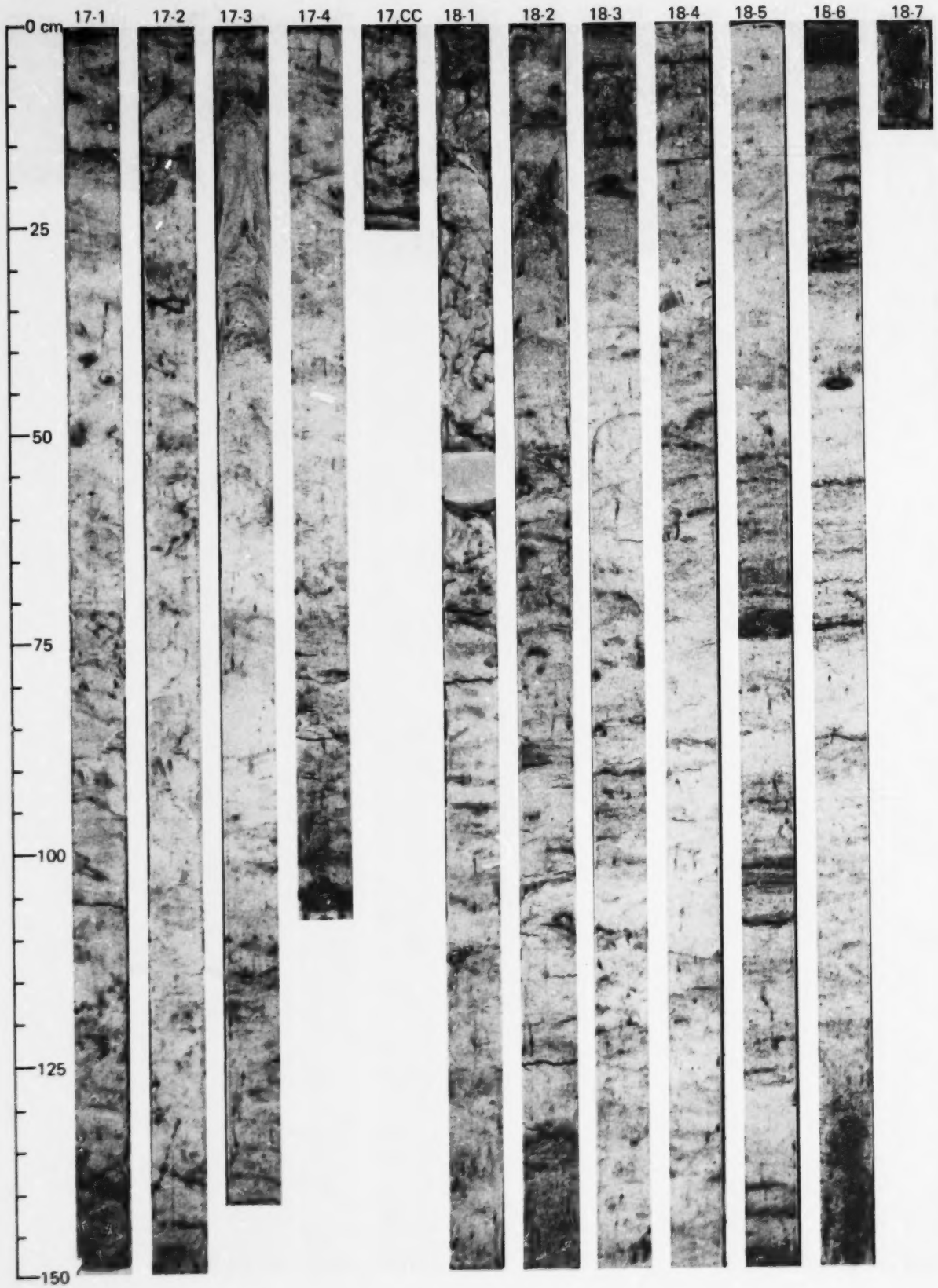
0 cm
25
50
75
100
125
150
17-1
17-2
17-3
17-4
17,CC
18-1
18-2
18-3
18-4
18-5
18-6
18-7

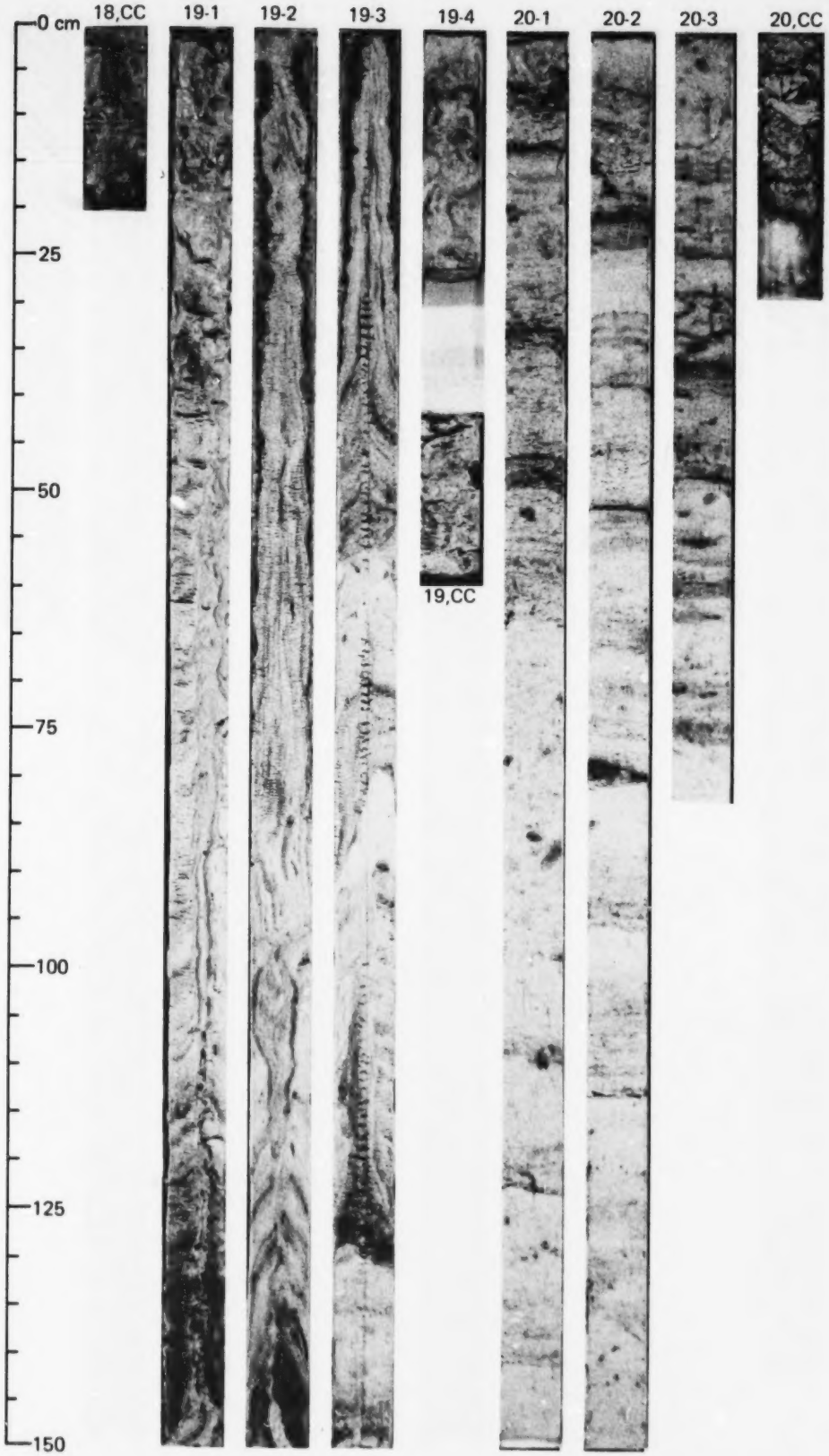
0 cm
18,CC
19-1
19-2
19-3
19-4
19,CC
20-1
20-2
20-3
20,CC
25
50
75
100
125
150

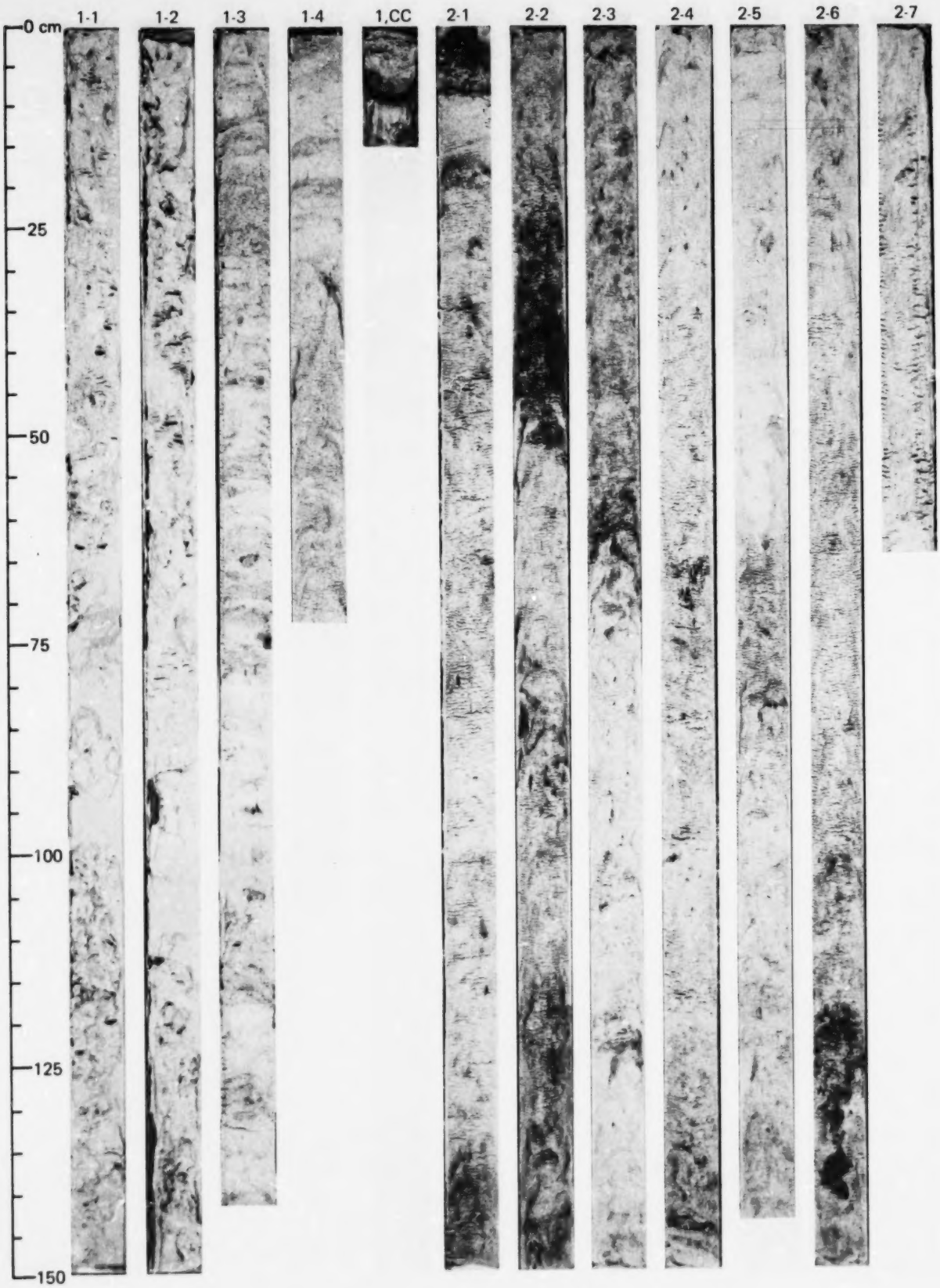
0 cm
25
50
75
100
125
150
1-1
1-2
1-3
1-4
1,CC
2-1
2-2
2-3
2-4
2-5
2-6
2-7

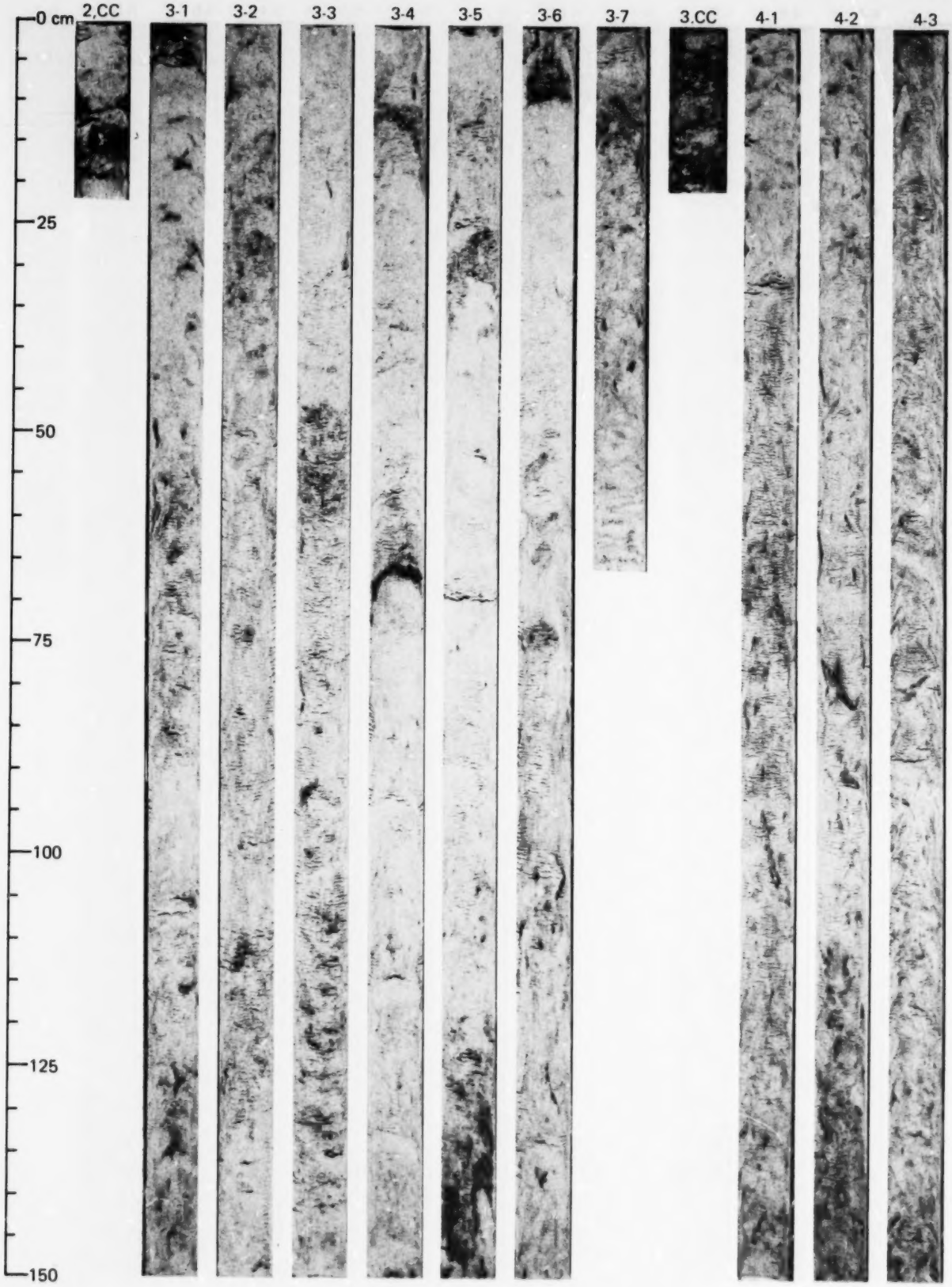
0 cm
2,CC
3-1
3-2
3-3
3-4
3-5
3-6
3-7
3,CC
4-1
4-2
4-3
25
50
75
100
125
150

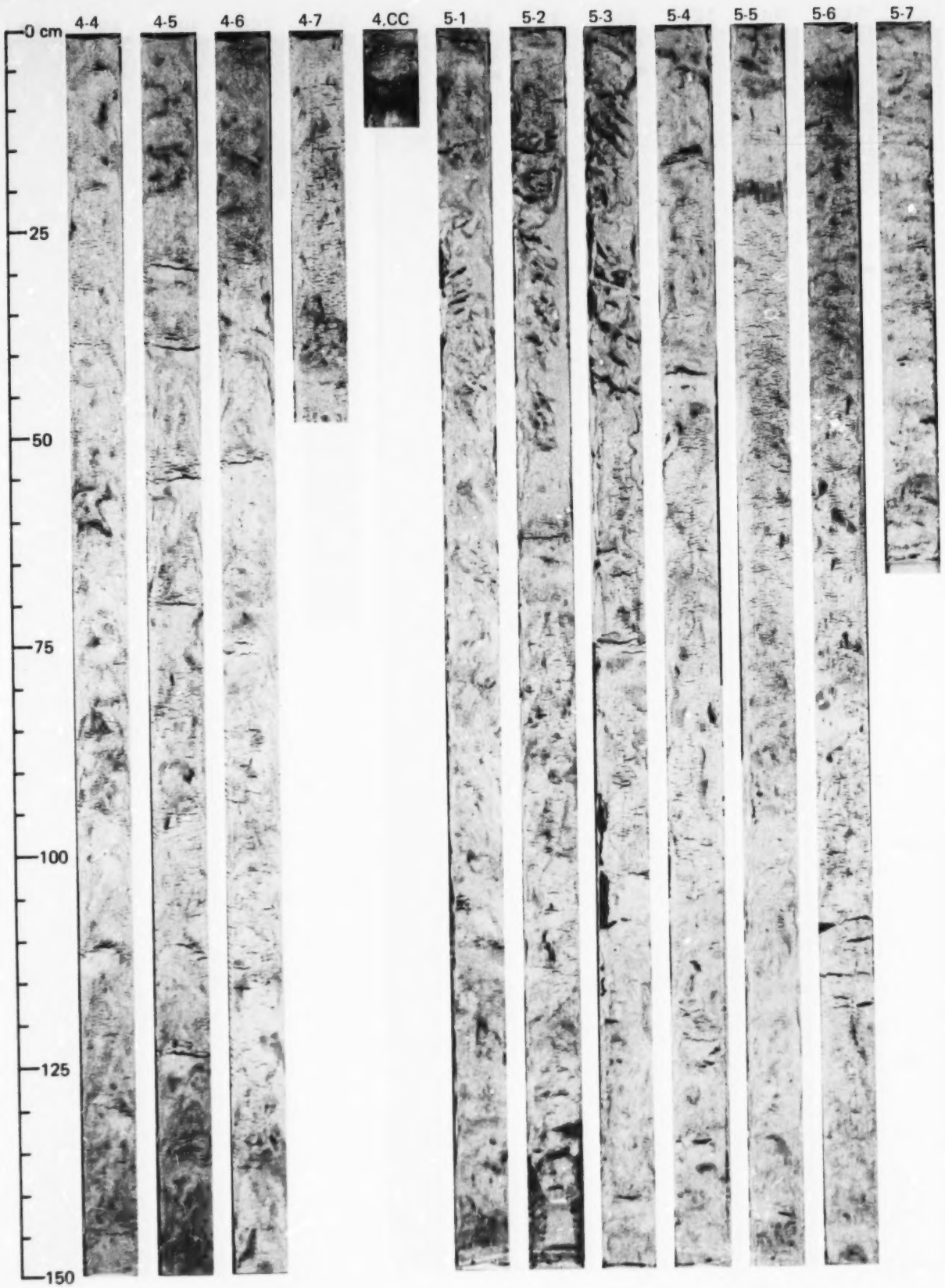
0 cm
25
50
75
100
125
150
4-4
4-5
4-6
4-7
4,CC
5-1
5-2
5-3
5-4
5-5
5-6
5-7

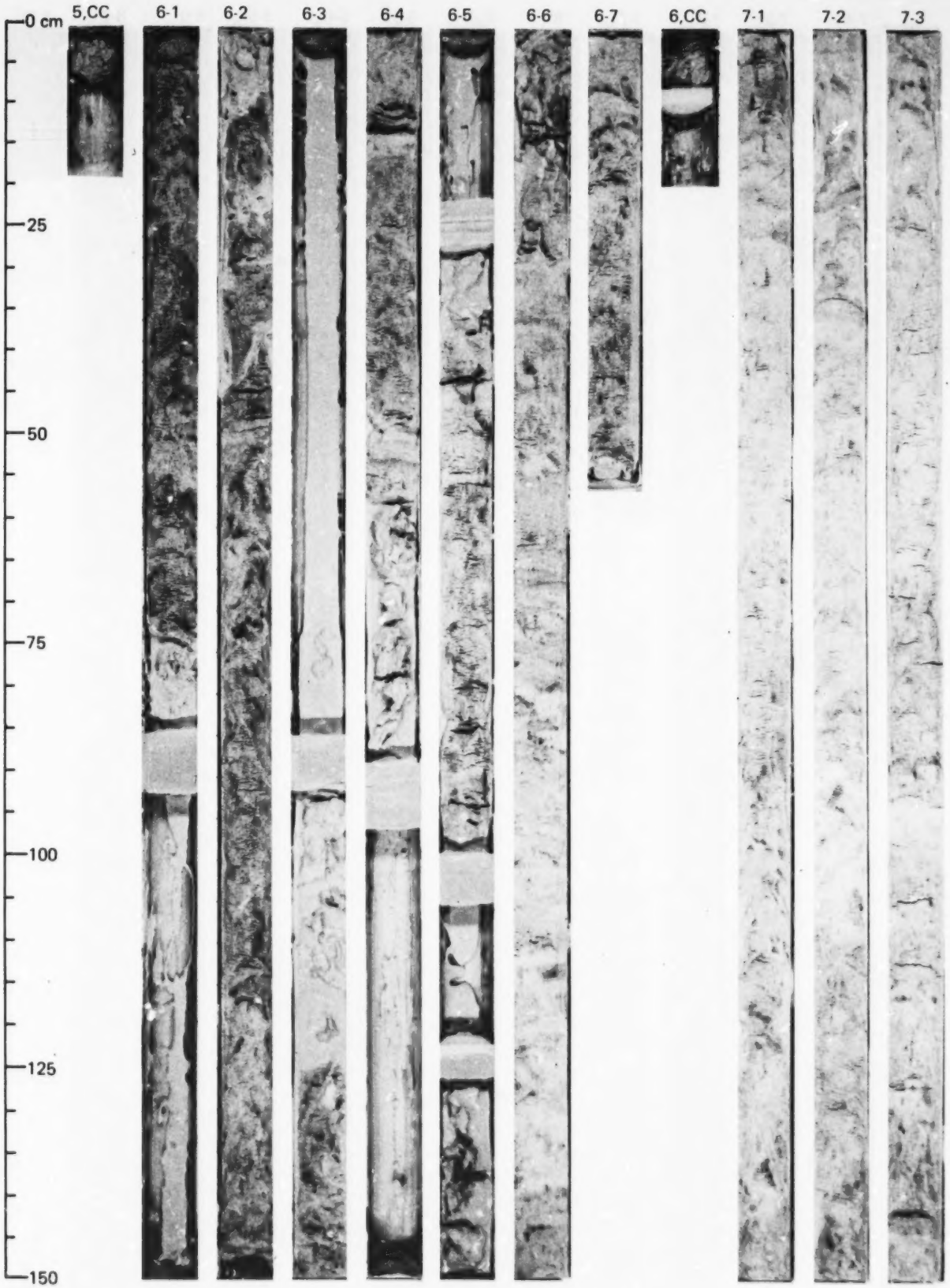
0 cm
25
50
75
100
125
150
5,CC
6-1
6-2
6-3
6-4
6-5
6-6
6-7
6,CC
7-1
7-2
7-3

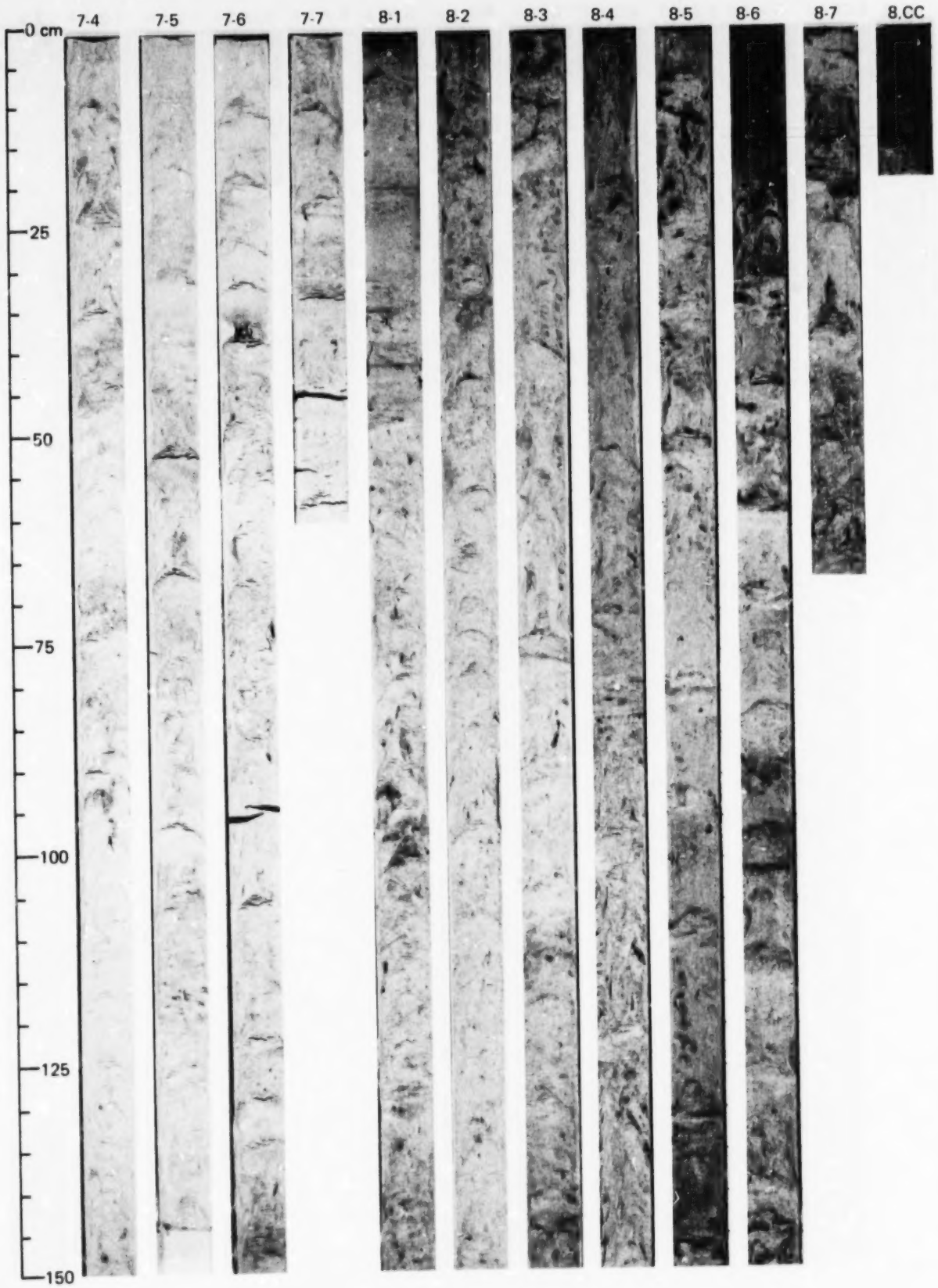
0 cm
25
50
75
100
125
150
7-4
7-5
7-6
7-7
8-1
8-2
8-3
8-4
8-5
8-6
8-7
8,CC

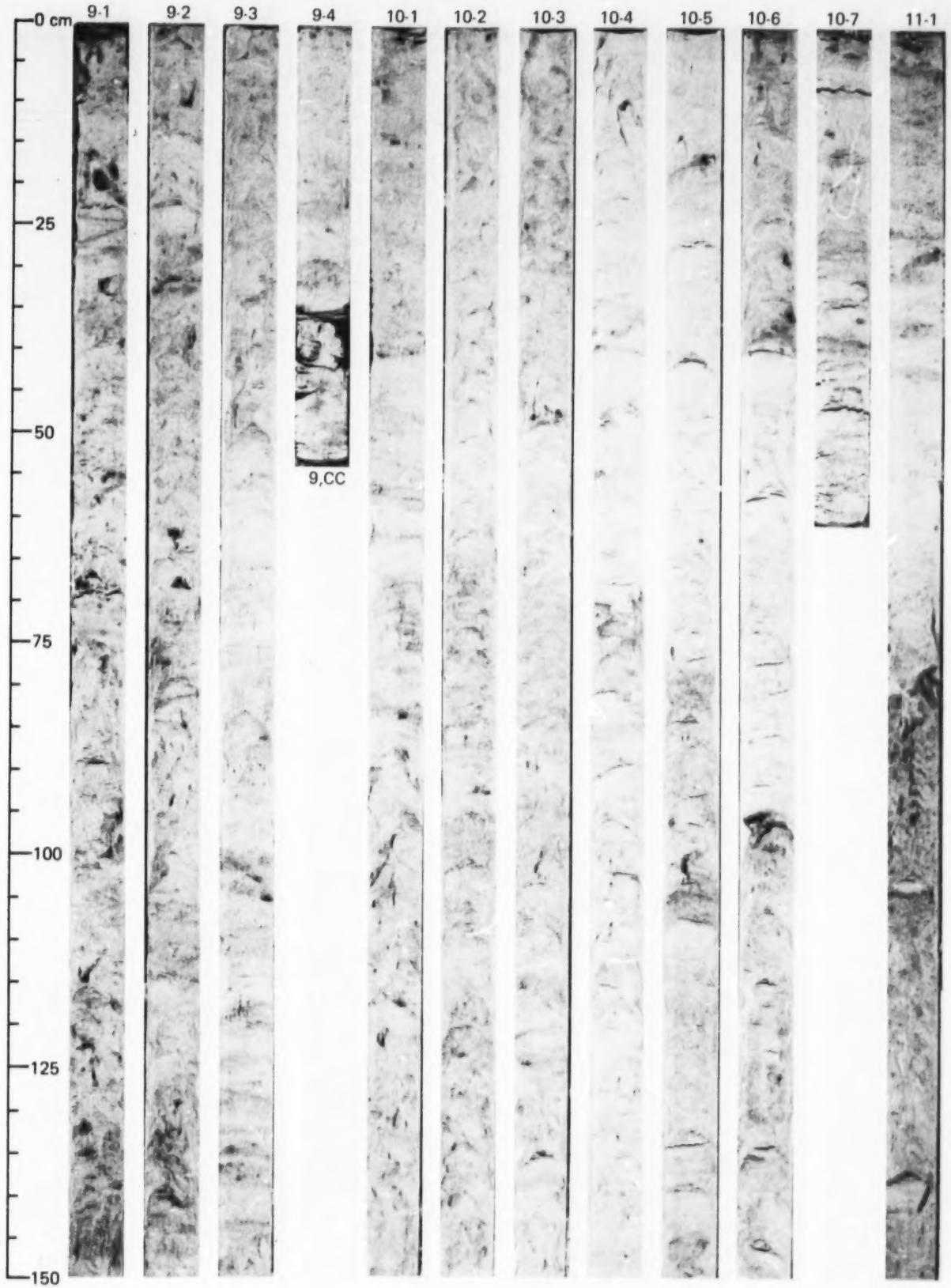
0 cm
25
50
75
100
125
150
9-1
9-2
9-3
9-4
9,CC
10-1
10-2
10-3
10-4
10-5
10-6
10-7
11-1

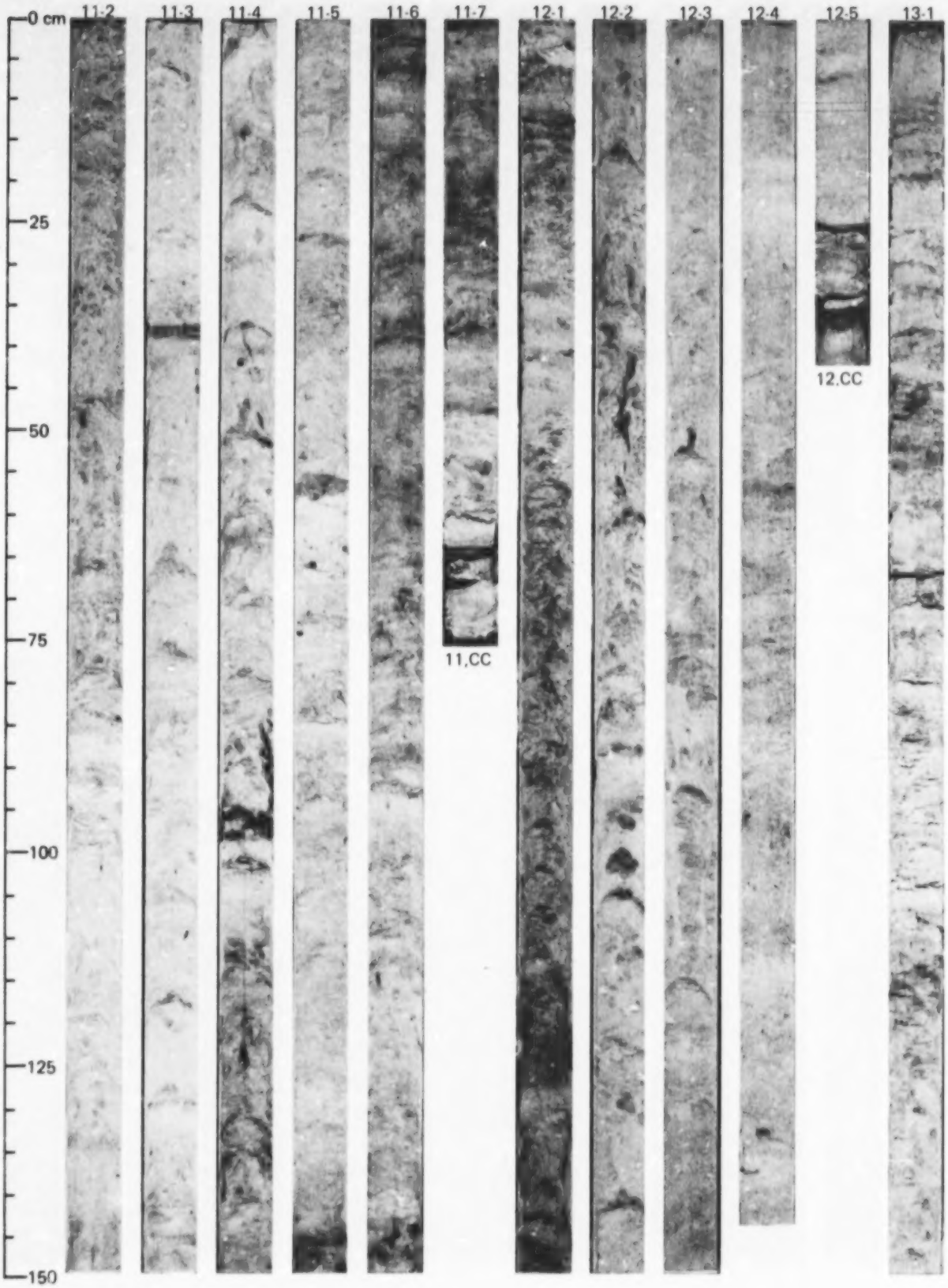
0 cm
25
50
75
100
125
150
11-2
11-3
11-4
11-5
11-6
11-7
11,CC
12-1
12-2
12-3
12-4
12-5
12,CC
13-1

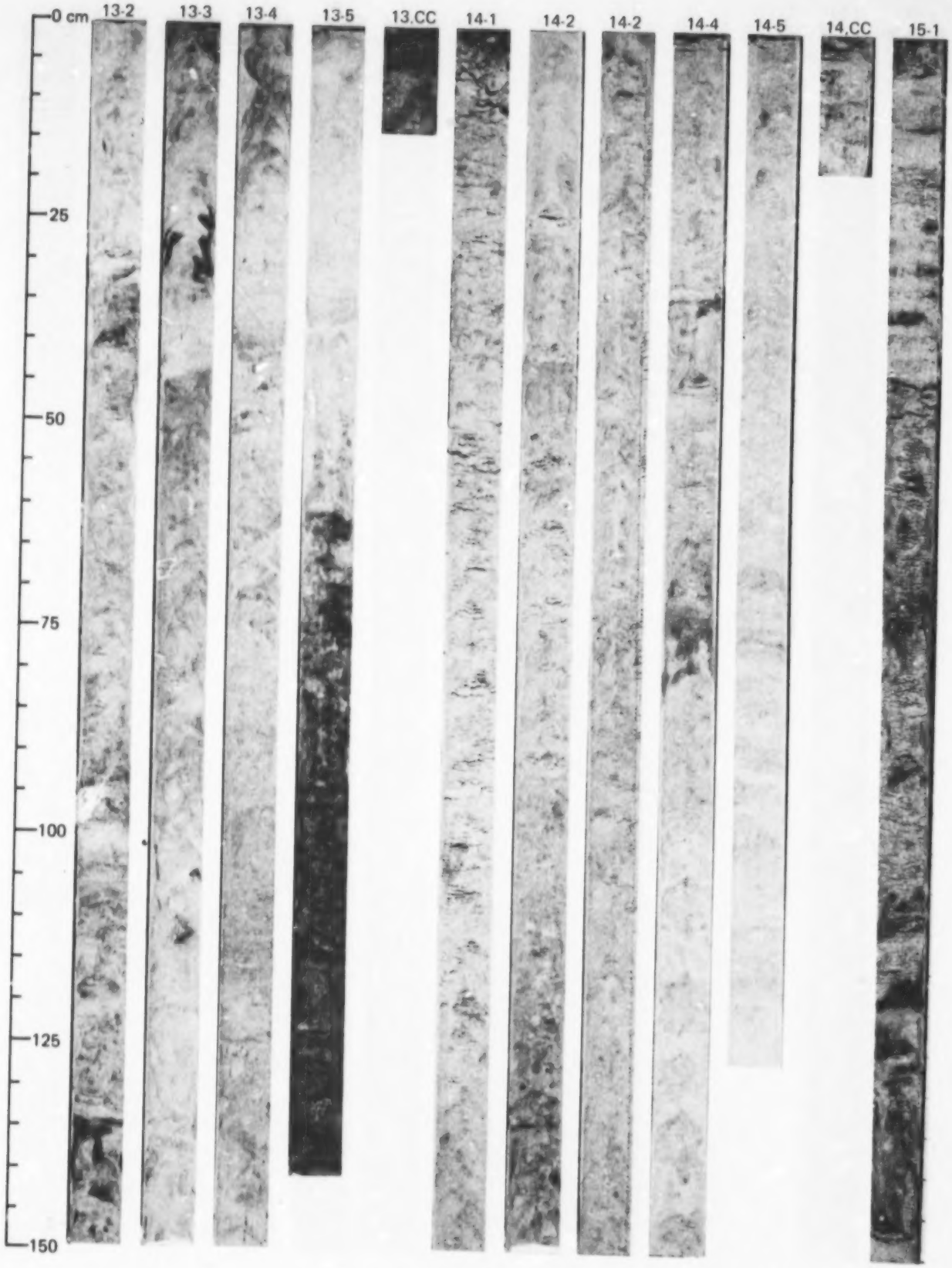
0 cm
13-2
13-3
13-4
13-5
13,CC
14-1
14-2
14-2
14-4
14-5
14,CC
15-1
25
50
75
100
125
150

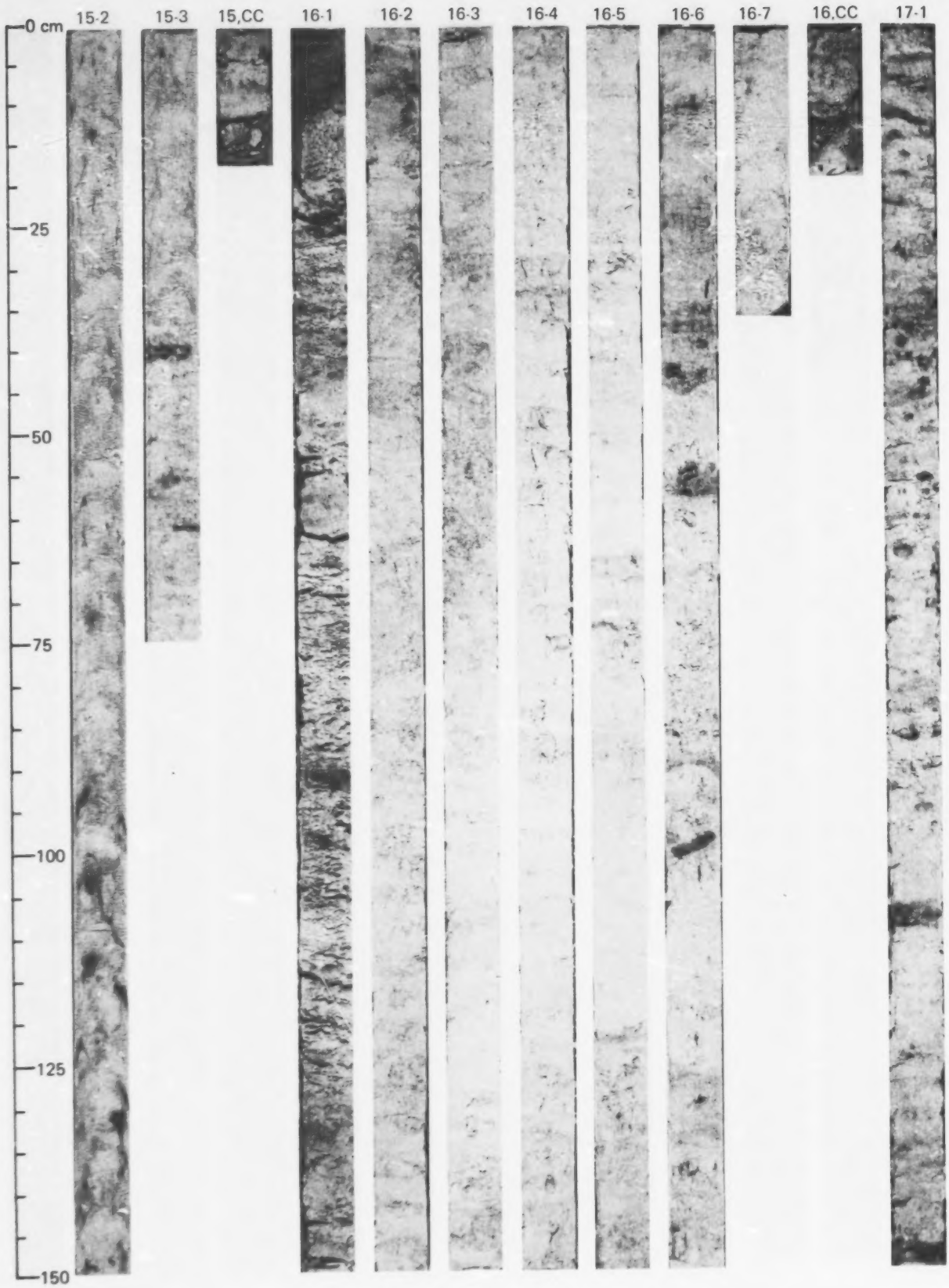
0 cm
25
50
75
100
125
150
15-2
15-3
15,CC
16-1
16-2
16-3
16-4
16-5
16-6
16-7
16,CC
17-1

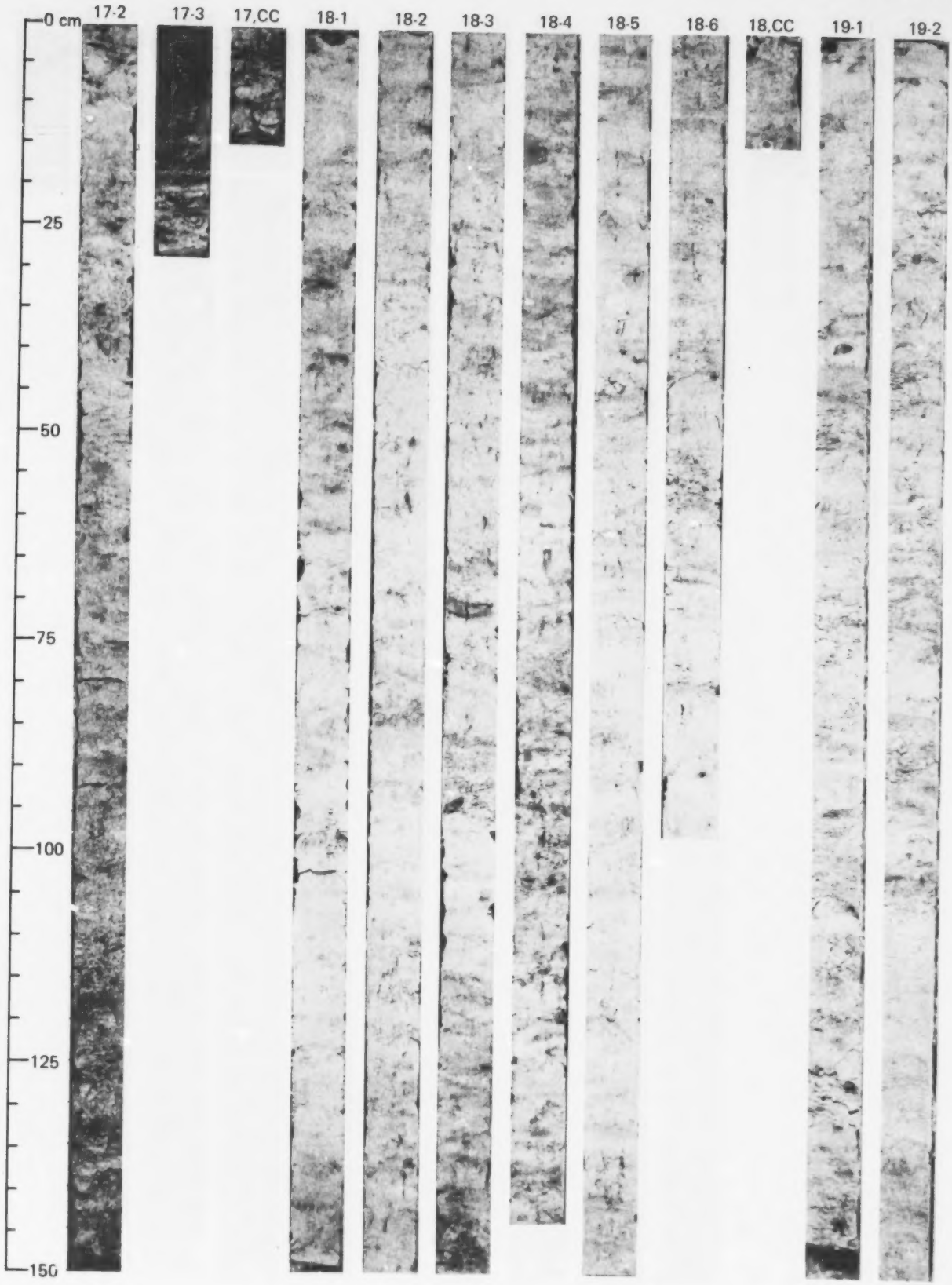
0 cm
17-2
17-3
17,CC
18-1
18-2
18-3
18-4
18-5
18-6
18,CC
19-1
19-2
25
50
75
100
125
150

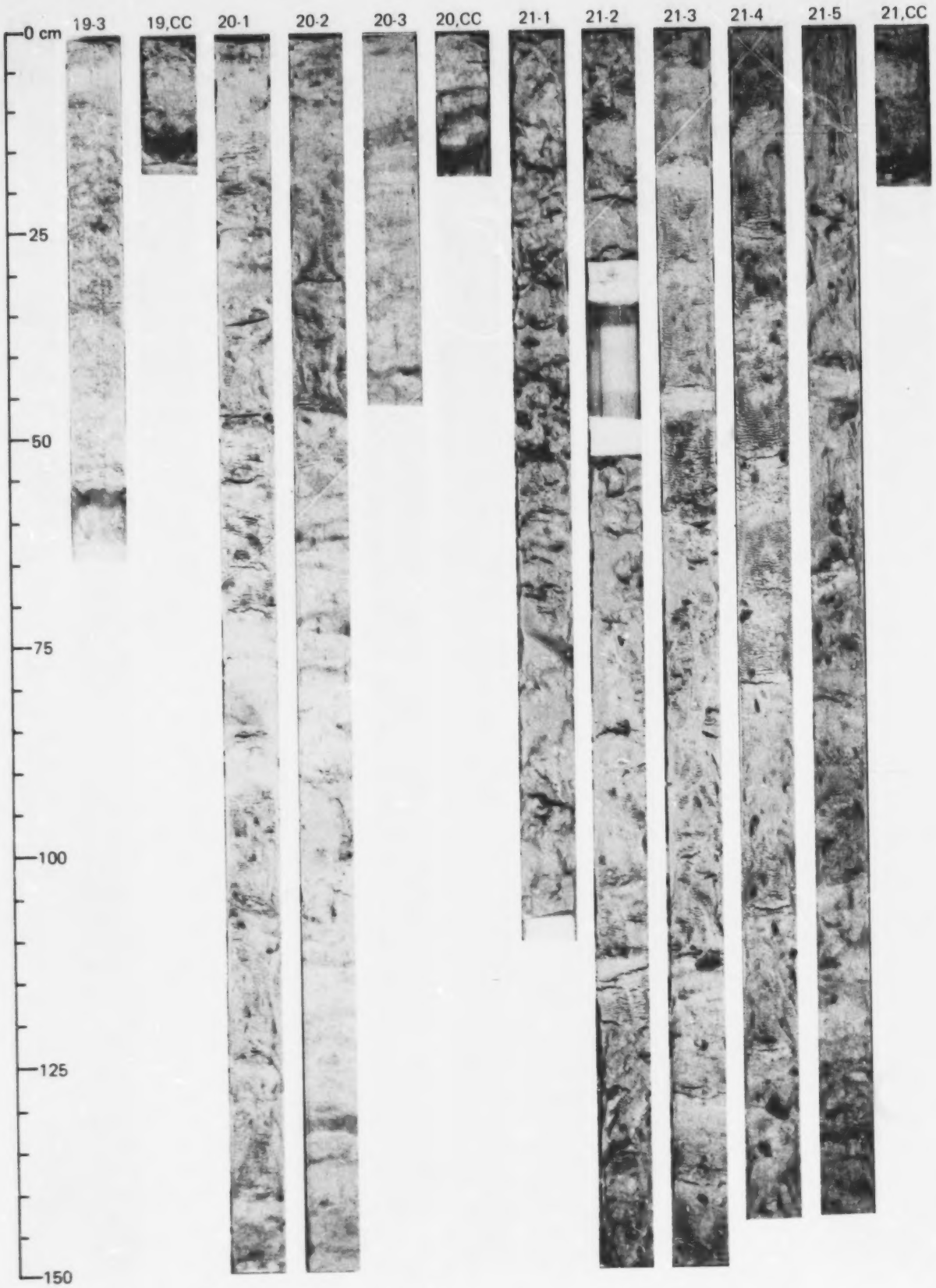
0 cm
25
50
75
100
125
150
19-3
19,CC
20-1
20-2
20-3
20,CC
21-1
21-2
21-3
21-4
21-5
21,CC

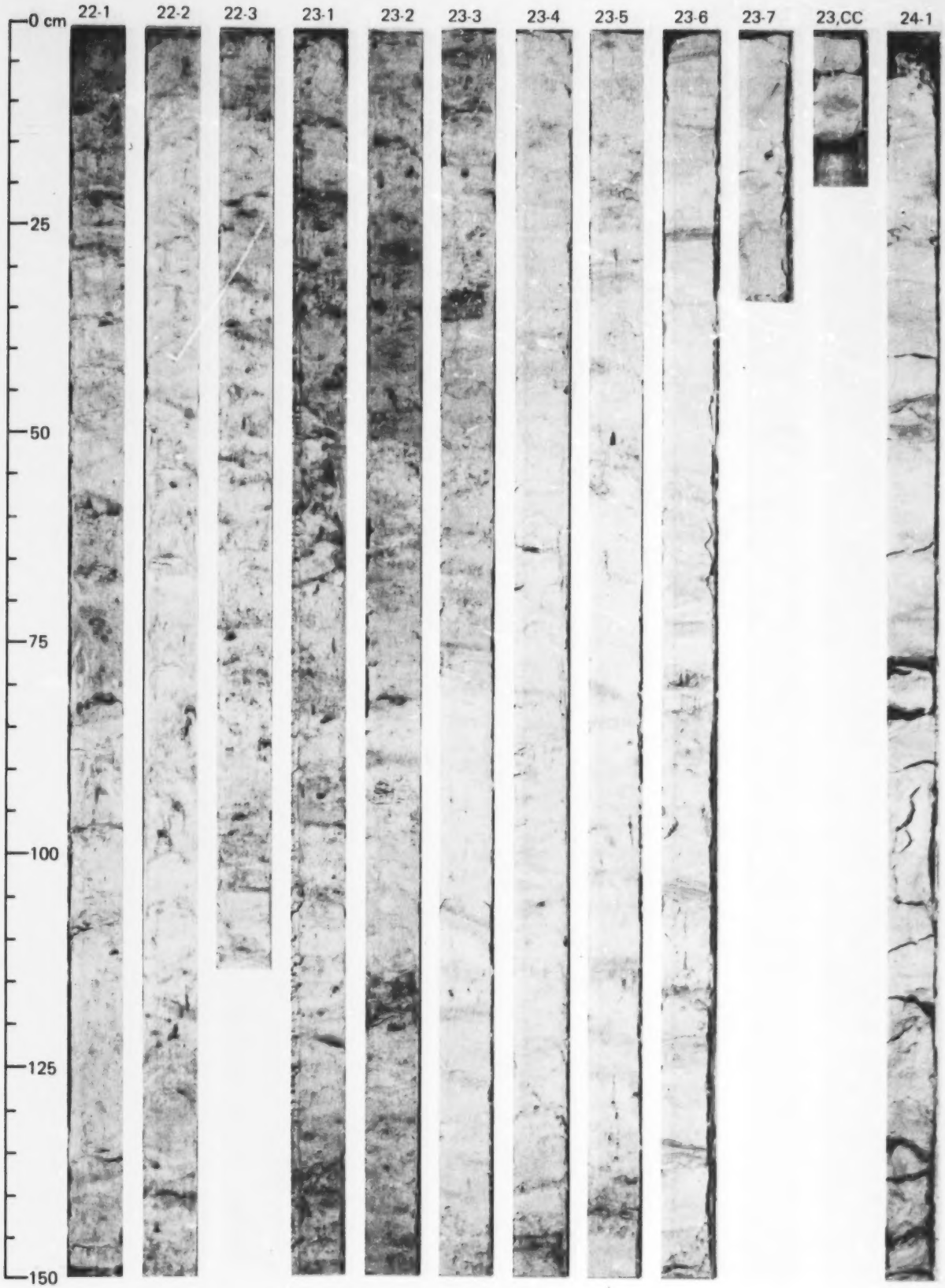
0 cm
25
50
75
100
125
150
22-1
22-2
22-3
23-1
23-2
23-3
23-4
23-5
23-6
23-7
23,CC
24-1

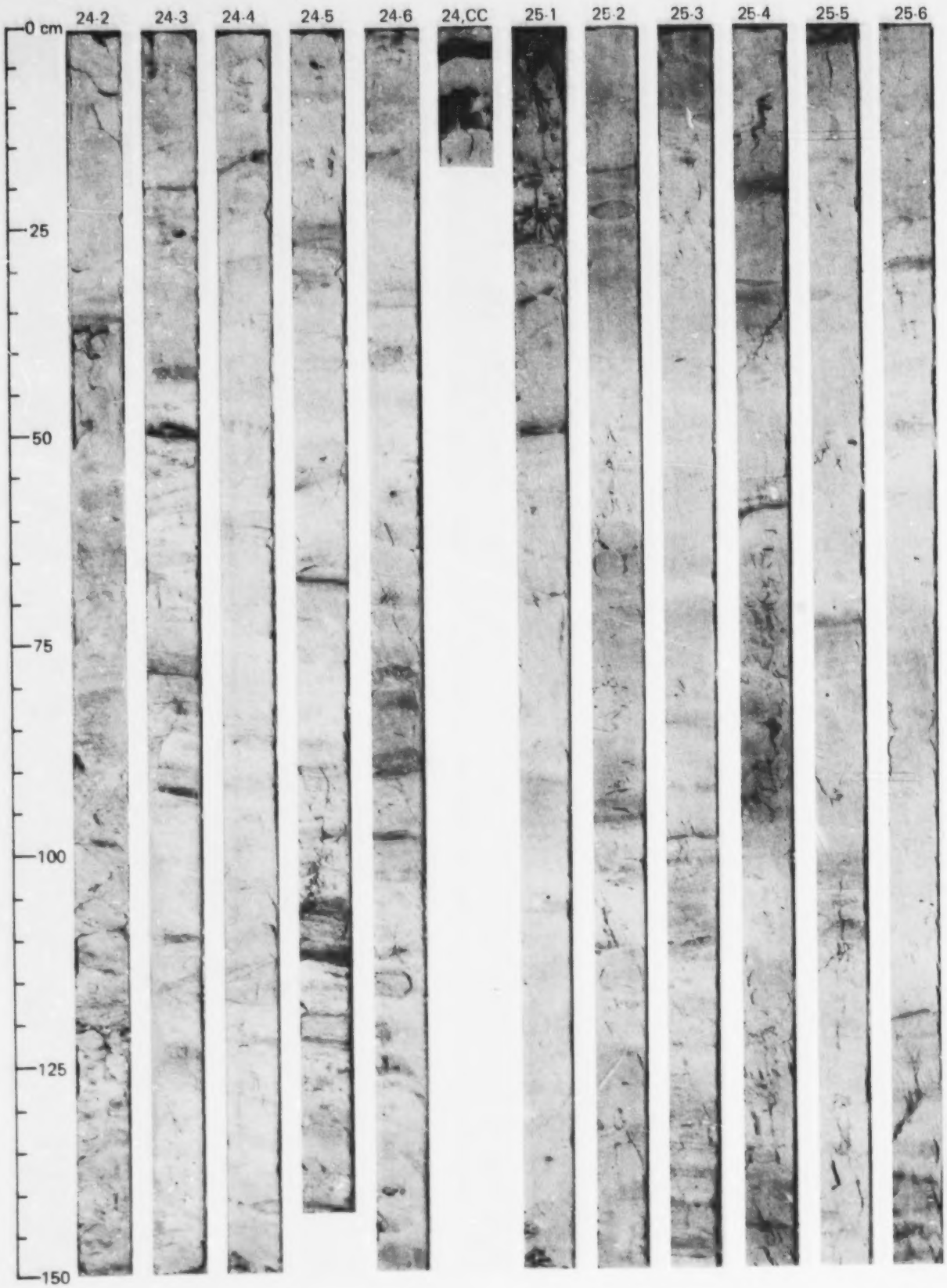
24-2
24-3
24-4
24-5
24-6
24,CC
25-1
25-2
25-3
25-4
25-5
25-6
0 cm
25
50
75
100
125
150

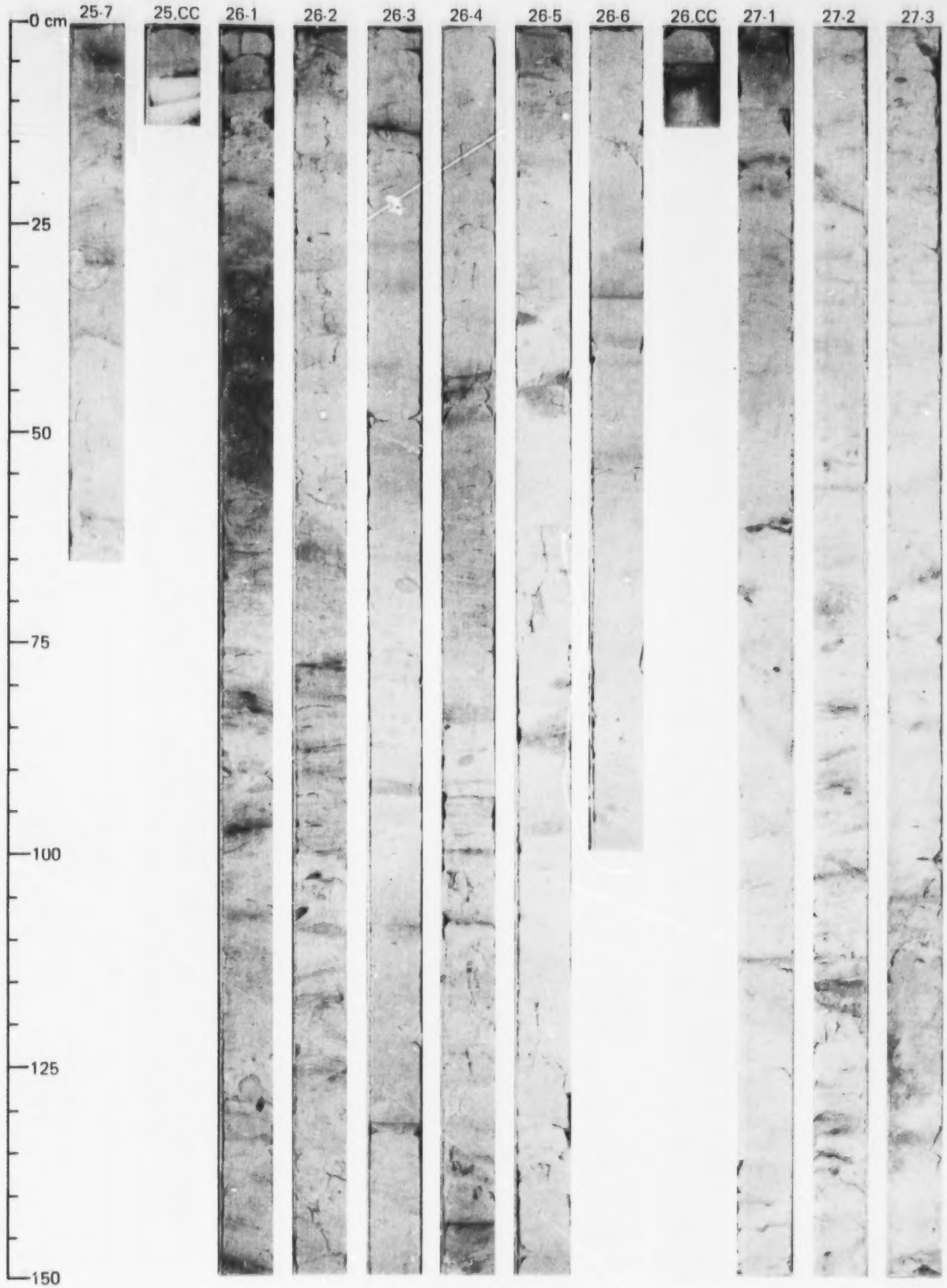
0 cm
25
50
75
100
125
150
25-7
25,CC
26-1
26-2
26-3
26-4
26-5
26-6
26,CC
27-1
27-2
27-3

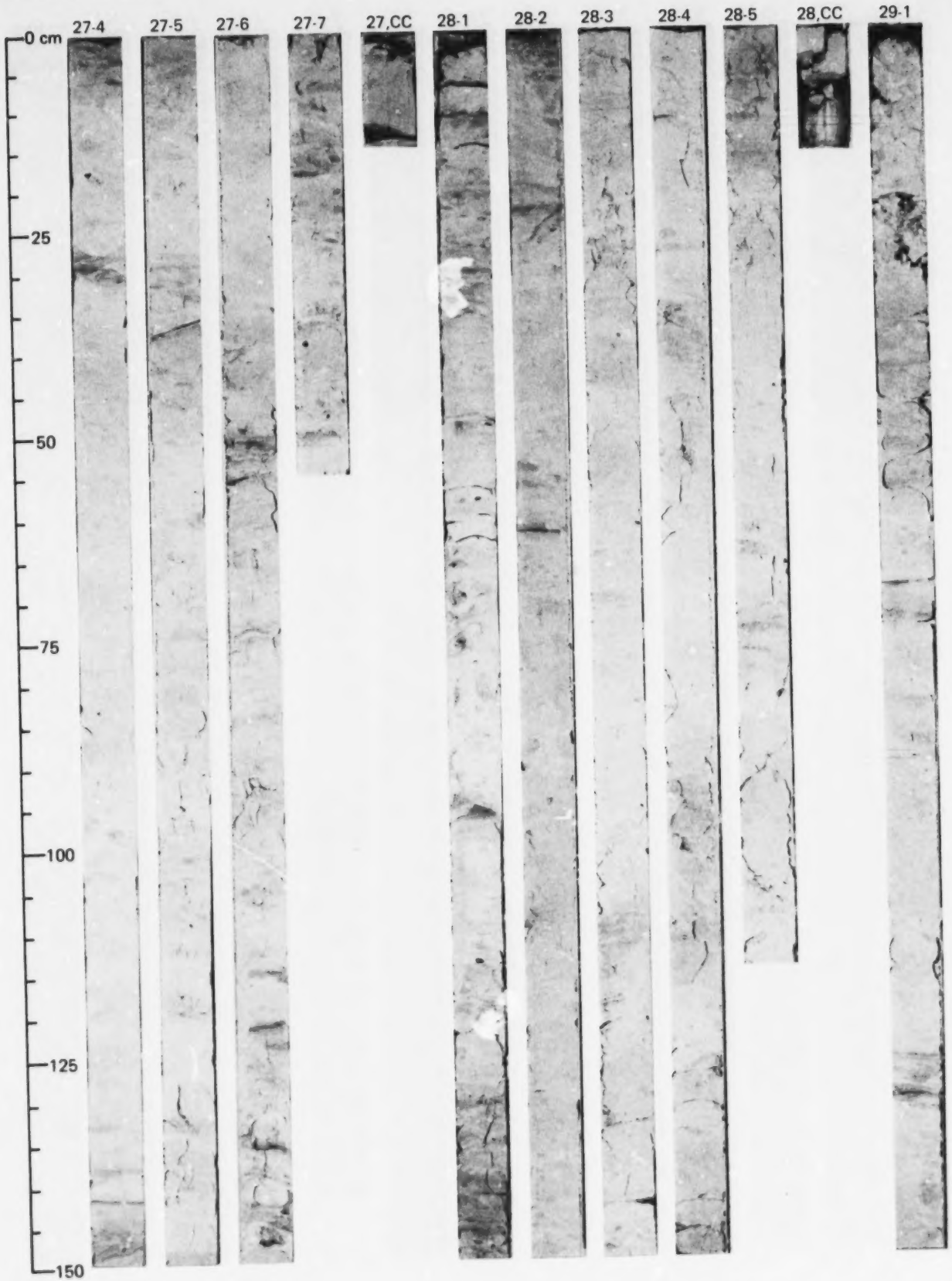
27-4
27-5
27-6
27-7
27,CC
28-1
28-2
28-3
28-4
28-5
28,CC
29-1
0 cm
25
50
75
100
125
150

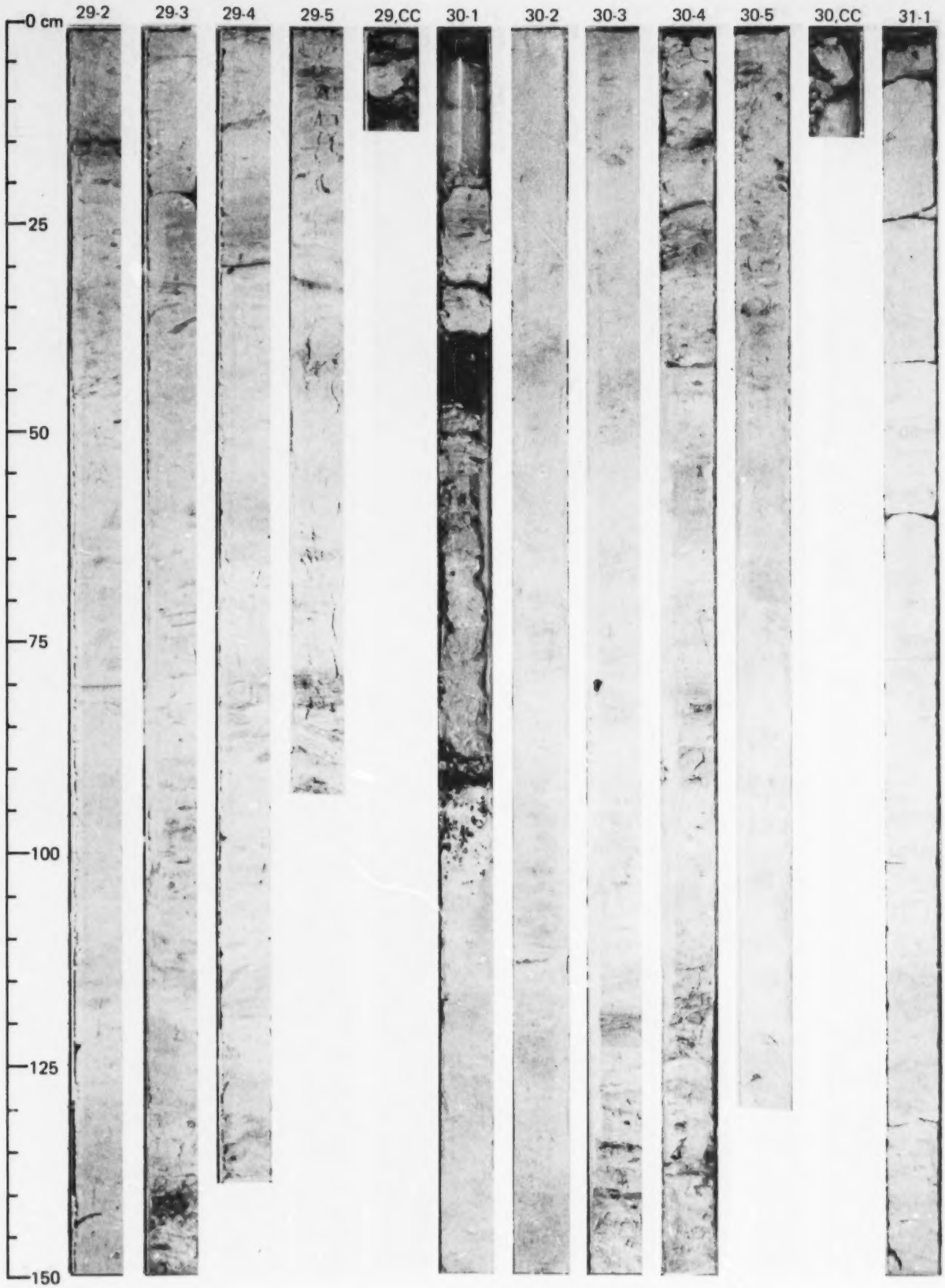
0 cm
25
50
75
100
125
150
29-2
29-3
29-4
29-5
29,CC
30-1
30-2
30-3
30-4
30-5
30,CC
31-1

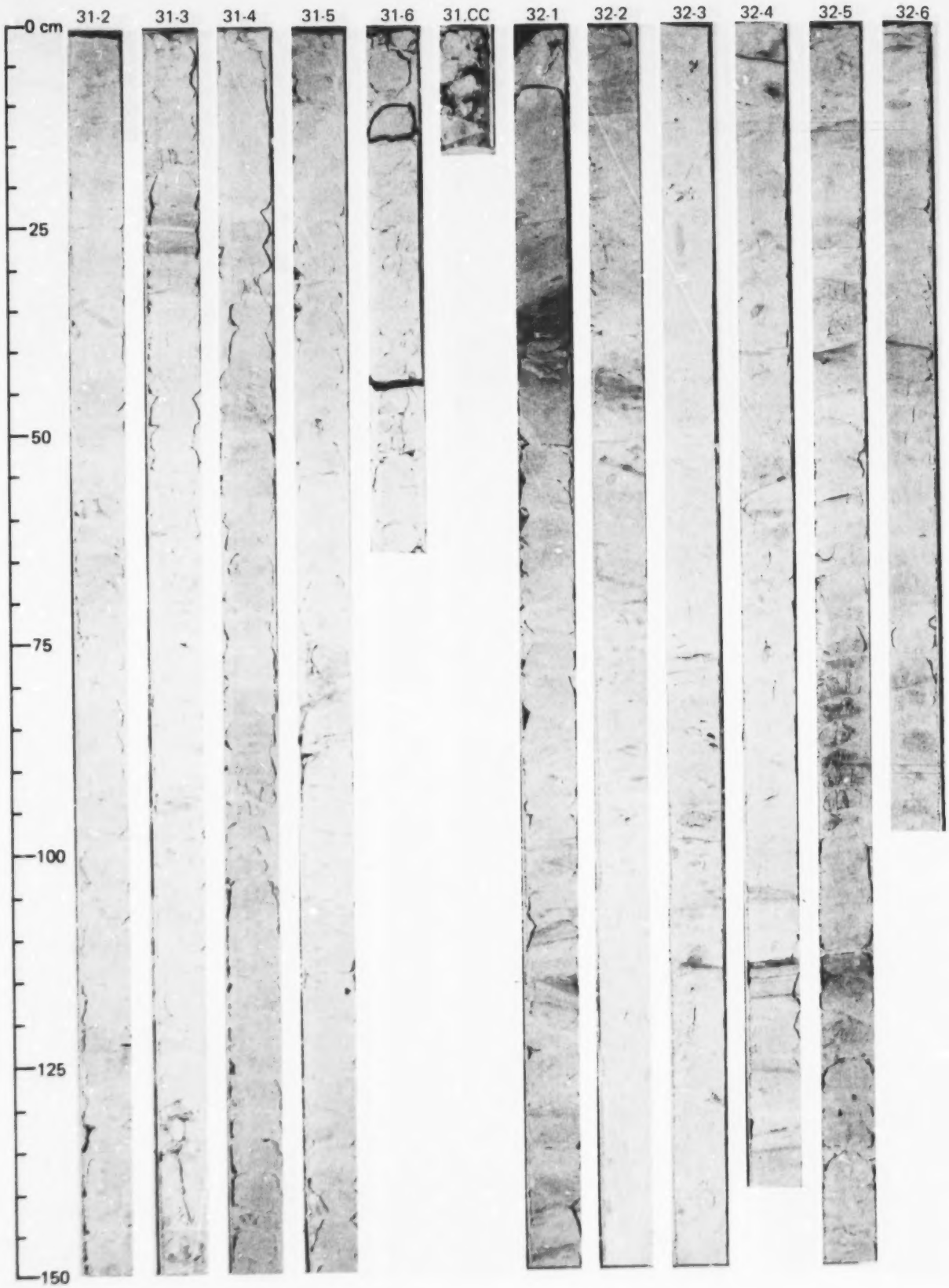
0 cm
25
50
75
100
125
150
31-2
31-3
31-4
31-5
31-6
31.CC
32-1
32-2
32-3
32-4
32-5
32-6

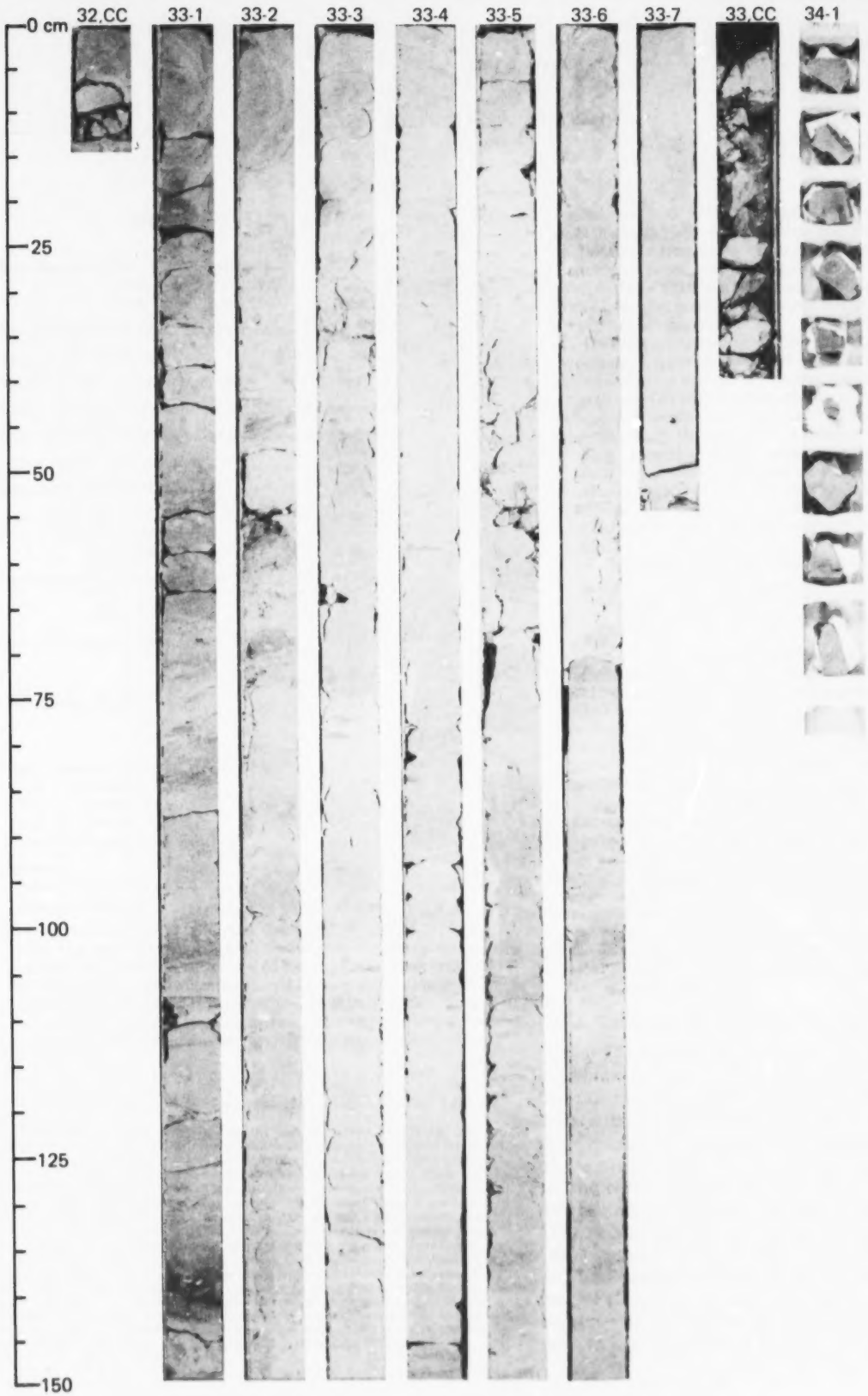
0 cm
32,CC
33-1
33-2
33-3
33-4
33-5
33-6
33-7
33,CC
34-1
25
50
75
100
125
150

Reprinted from Mayer, L., Theyer, F., et al., 1985
Initial Reports of the Deep Sea Drilling Project, Volume LXXXV, Washington (U. S. Government Printing Office)

4. SITE 573[1]

Shipboard Scientific Party[2]

HOLES 573, 573A, 573B

Dates occupied: 573—2 to 4 April 1982
573A—4 to 5 April 1982
573B—6 to 9 April 1982

Date departed Hole 573B: 9 April 1982

Time on site: 7.3 days

Position: 0°29.91′N; 133°18.57′W

Water depth (sea level; corrected m, echo-sounding): 4301

Water depth (rig floor; corrected m, echo-sounding): 4317

Bottom felt (m, drill pipe): 4311.5

Penetration (Hole 573B, m): 529

Number of cores: 573—19
573A—6
573B—43

Total length of cored section (m): 573—158.6
573A—53.2
573B—390.0

Total core recovered (m): 573—159.4
573A—53.5
573B—279.7

Core recovery (%): 573—100
573A—100
573B—71.6

Oldest sediment cored:
Depth sub-bottom (m): 528
Nature: Limestone
Age: late Eocene
Measured velocity (km/s): 1.74

Basement:
Depth sub-bottom (m): 529
Nature: Basalt

Principal results: Site 573 is located at 0°29.91′N, 133°18.57′W in 4300 m of eastern equatorial Pacific water over a basement trough covered by sediments that reach 0.68 s in thickness. The objective of drilling at the site, which was to obtain an expanded upper Eocene to Quaternary sedimentary section for high resolution stratigraphic and paleoceanographic studies, was met by drilling three holes. Hole 573 (hydraulic piston corer [HPC]) reached about 160 m sub-bottom; Hole 573A, a parallel HPC attempt, was abandoned at approximately 60 m sub-bottom; and Hole 573B (rotary drilling) was cored from about 140 to 529 m, with the recovery from its bottom of a baked sediment/basalt contact and about 1 m of basalt. As Hole 573B was being washed down to 140 m, the heat flow-pore water probe was deployed; it retrieved *in situ* pore water from 53 m sub-bottom.

The oldest sediment cored (Hole 573B, 528 m sub-bottom) was uppermost Eocene limestone. Four lithostratigraphic units were recognized in the sedimentary section. These units can be grouped so as to correlate with the three oceanic formations established for sediments at nearby Site 77 (DSDP Leg 9, Hays et al., 1972). In upsection order, the units are as follows:

1. An uppermost Eocene biogenic limestone (526.6 to 528.0 m).
2. A brown unit that contains metalliferous claystone and foraminiferal nannofossil chalk (520.5 to 526.6 m). This unit correlates with uppermost Eocene at its base, is virtually barren of fossils in its dark brown center, and correlates with lowermost Oligocene at its top.
3. Two units of siliceous calcareous oozes and chalks. These units make up the remaining part of the section (lower Oligocene to Pleistocene). The lower unit (calcareous chalk ooze) extends from 45.1 to 520.5 m, the upper unit (cyclic siliceous calcareous ooze) from 0 to 45.1 m.

Foraminifers, calcareous nannofossils, radiolarians, and diatoms are, with some exceptions, well represented in the cored sediments. Most Eocene to Quaternary biozonal and stratigraphic boundaries could be recognized and correlated. The Eocene/Oligocene boundary could not be located unequivocally, however. Either it falls within the barren midportion of the metalliferous unit or it coincides with a hiatus. Other brief hiatuses were found in the uppermost Oligocene and lower upper Miocene.

The sediment accumulation rates at Site 573 are relatively constant; they vary, in general, between 18 and 12 m/m.y. A peak of 30 m/m.y. occurs between 5.5 and 6 Ma, and a low of about 10 m/m.y. was recorded between 15 and 21 Ma. Some of the changes in rates of accumulation correlate with changes in lithology, physical properties, natural remanent magnetization (NRM) intensity, and interstitial-water geochemistry.

Except for the uncertainty associated with the Eocene/Oligocene boundary, the expanded, high resolution stratigraphic section recovered at Site 573 should enhance studies of the equatorial Pacific's Tertiary history.

BACKGROUND AND OBJECTIVES

Site 573 was proposed by the JOIDES Ocean Paleoenvironment Panel (OPP) as the southernmost drill site in a north–south transect of the equatorial high-productivity zone. The position of the site, just south of the axis of maximum sediment accumulation and just north of the equator, was chosen to duplicate the very popular section cored at DSDP Site 77, and to recover a detailed sedimentary record of the passage of this area from about 8°S, 39 Ma, into the equatorial high-productivity zone. Our operational objectives were to recover a complete and undisturbed section of Neogene sediments by using the HPC to core it twice and then to rotary drill and continuously core to basement. Our specific scientific objectives were to establish high-resolution bio-, magneto-,

[1] Mayer, L., Theyer, F., et al., *Init. Repts. DSDP*, 85: Washington (U.S. Govt. Printing Office).

[2] Larry Mayer (Co-Chief Scientist), Dalhousie University, Halifax, Nova Scotia, Canada; Fritz Theyer (Co-Chief Scientist), Hawaii Institute of Geophysics, University of Hawaii, Honolulu, Hawaii (present address: University of Southern California, Los Angeles, California); John A. Barron, U.S. Geological Survey, Menlo Park, California; Dean A. Dunn, University of Rhode Island, Narragansett, Rhode Island (present address: University of Southern Mississippi, Hattiesburg, Mississippi); Tim Handyside, The University, Newcastle upon Tyne, United Kingdom; Scott Hills, Scripps Institution of Oceanography, La Jolla, California; Ian Jarvis, City of London Polytechnic, London, United Kingdom (present address: Kingston Polytechnic, Kingston-upon-Thames, United Kingdom); Catherine A. Nigrini, La Habra Heights, California; Nicklas G. Pisias, Oregon State University, Corvallis, Oregon; Annick Pujos, Université de Bordeaux, Talence, France; Tsunemasa Saito, Yamagata University, Yamagata, Japan; Paul Stout, Scripps Institution of Oceanography, La Jolla, California; Ellen Thomas, Scripps Institution of Oceanography, La Jolla, California (present address: Lamont-Doherty Geological Observatory, Columbia University, Palisades, New York); Norbert Weinreich, Institut für Geophysik, Ruhr Universität Bochum, Bochum, Federal Republic of Germany; and Roy H. Wilkins, Massachusetts Institute of Technology, Cambridge, Massachusetts.

seismic, carbonate, and stable isotope stratigraphies to improve our understanding of the paleoceanography and paleoclimatology of the region.

The area in the vicinity of DSDP Sites 573 and 77 has been traversed by Scripps' R/V *Argo* and Lamont's R/V *Conrad* (C-10-05, 1966, and C-15-10, 1971). More recently, a detailed site survey was conducted by the R/V *Thomas Washington* (Ariadne I; see Shipley et al., this volume); the survey used a single-channel, digital, water and air gun seismic system and also acquired Seabeam bathymetry. The area surveyed is characterized by generally low relief; water depths range from 4200 to 4300 m (uncorrected) (Fig. 1). A thick (0.40 to 0.68 s), acoustically well stratified sediment section conformably fills a series of basement peaks and troughs trending north-northwest/south-southeast (Fig. 2). Basement relief is typically 80 to 100 m. In some of the basement troughs, the sediment fill is significantly thicker than over the surrounding basement highs (Fig. 2). There is a small, circular, 350-m basement high in the northeast corner of the survey area. This high has a surficial expression of about 200 m and is free of sediment at its surface. It was carefully avoided in the selection of Site 573.

Drilling at DSDP Site 77 resulted in the recovery of 481 m of predominantly siliceous calcareous and calcareous siliceous oozes. The average sedimentation rate was 13 m/m.y., with the rates increasing from the base to the top of the section. The bottom 18 m of the section consisted of dusky brown clay rich in iron and manganese that overlay a baked limestone/basalt contact. Basement age was estimated to be 36 Ma. Van Andel et al. (1975) calculated that the crust in this area was formed at 39 Ma, at a latitude of 7°47'S, and at a water depth of 2799 m.

After reviewing the site survey data, the OPP selected a spot approximately 6 n. mi. west of Site 77 for Site 573. The drill site was directly over a north-northwest/south-southeast lineated basement depression where the sediment section is extremely thick (0.62 s)—approximately 50 m thicker than the section at Site 77. A thick section was desired to maximize the possibility of recovering the Eocene/Oligocene boundary.

OPERATIONS

The *Glomar Challenger* arrived in the vicinity of Site 573 at 2300Z on 2 April after a 5.25-day steam from Site 572 (average speed: 9.4 knots). In transit we collected continuous seismic profiles (air gun and 3.5 kHz) and bathymetric and magnetic data. Our plan was to aim for DSDP Site 77 (0°28.9'N, 133°13.7'W) and then to head due west about 6 n. mi. to the basement trough selected by the OPP as the target site.

We entered the area covered by the Ariadne I site survey at 2305Z but found that the Seabeam bathymetry provided disagreed with the depths we were measuring. We could find no consistent offset or rotation that rectified the discrepancies between the two data sets; thus, we could not use the Seabeam bathymetry to find the proposed drilling site. Fortunately, we were able to determine our location relative to the air gun profiles collected during the Ariadne site survey, and at 0006Z on 3 April we crossed the proposed drill site. We continued 2 n. mi. beyond the site, turned right to 045° at 0020Z, and then turned south-southeast 8 min. later, following the trend of the basement trough to the proposed site. At 0043Z on 3 April we dropped the beacon. We then continued profiling for 2 n. mi. past the beacon. We pulled the geophysical gear and returned to the site to begin drilling operations (Table 1).

Drill pipe run-in began at 0200Z, with the first HPC core on deck at 1615Z. The mudline was established at the rig floor as 4311.5 m. Drilling at Hole 573 began with the 9.5-m variable-length HPC (VLHPC). We collected 17 9.5-m cores and two 5-m cores with nearly 100% recovery. Disturbance was minimal. Pullout force reached 14,000 lb. for Core 14 but was absent for Cores 15 and 16. Pullout force became significant again for Core 17 (50,000 lb.), and it proved to have deformed the

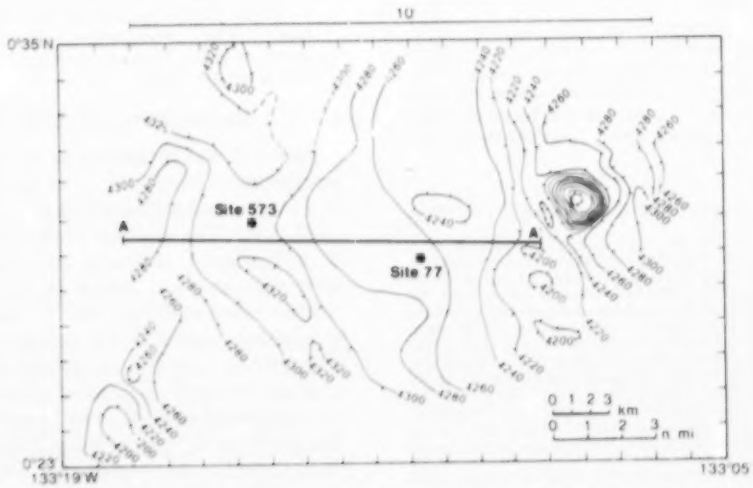

Figure 1. Bathymetry at Site 573. Profile A-A' is the seismic profile shown in Figure 2.

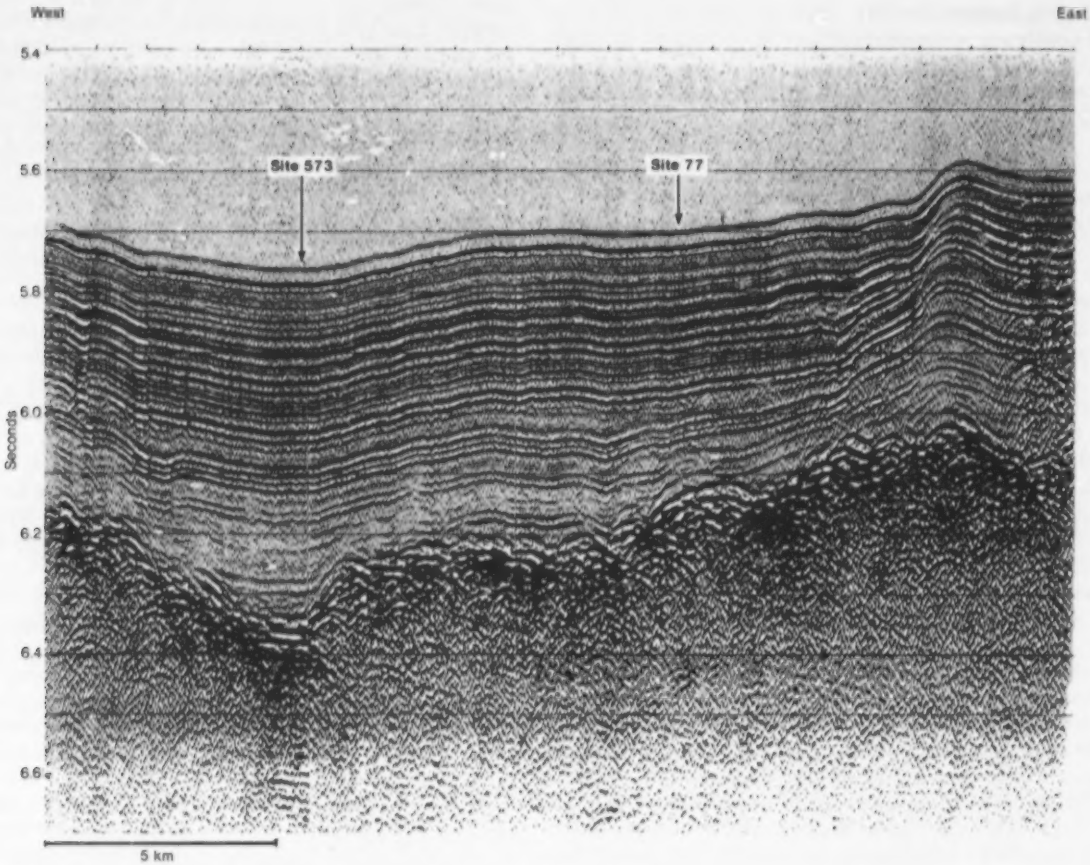

Figure 2. Seismic profile near Sites 573 and 77 (from Shipley et al., this volume).

ears of the quick disconnect when the equipment returned to the rig floor. We switched to the 5-m HPC and took two 5-m cores with no pullout force. We exerted 75,000 lb. of pullout force on the third 5-m core (Core 20), broke the quick disconnect, and lost the core in the bottom of the hole. We decided that it would be wise to terminate drilling, so we pulled back to the mudline and began to drill Hole 573A.

The drilling in Hole 573A began at 0200Z on 5 April with the depth of the HPC adjusted so as to minimize the loss of section due to intercore gaps. As we tried to retrieve the seventh core, the sandline parted, necessitating a drill string trip. To save time (we estimated that 12 hr. would be necessary to change sandlines, and continuing to drill with the second HPC and then changing to rotary drilling would involve two more pipe trips) and because recovery from the first HPC hole had been excellent, we decided to go directly to rotary drilling.

The sandline was changed and the drill pipe was run in and ready for rotary drilling by 1300Z on 6 April. We were to collect heat-flow measurements at this site, and we thought it most expedient to make them as we washed down to the starting point of Hole 573B (about 130 m sub-bottom). As the heat-flow probe was lowered down the pipe, a loop in the sandline (a result of the light weight of the tool) ran into a sheave; the wire parted, and the heat-flow probe and 1200 m of wire free fell down the pipe. A fishing tool retrieved the wire, and the slow task of hauling it in began. The heat-flow tool was finally retrieved at 0130Z on 7 April. The pore-water sampler in the heat-flow probe worked properly, but an analysis of the temperature data indicated that probe motion due to the inability of the sediment at 53 m sub-bottom (where the measurement was taken) to support the weight of the drill string had invalidated the heat-flow data.

Because of the large delays we had encountered, we decided to forgo further heat-flow measurements. We finally collected the first rotary-drilled core in Hole 573B from 138.5 m sub-bottom at 0430Z on 7 April. Rotary coring proceeded smoothly, although there was a significant amount of drilling disturbance in many of the upper few cores. The drilling rate and pumping pressure were lowered in an attempt to reduce the disturbance. The sediment in Core 20 became too stiff to cut with the wire splitter, and we switched to the rock saw. Coring proceeded smoothly to Core 43, which returned after 35 min. of drilling with a baked limestone/basalt contact and 1 m of basalt. Having reached basement (at 528 m sub-bottom), we ended Hole 573B (*total recovery* 72%) and tripped the pipe. We departed for Site 574 at 0800Z on 10 April.

Table 1. Coring summary, Site 573.

Core	Date (Apr. 1982)	Local time (hr.)	Depth from drill floor (m)	Depth below seafloor (m)	Length cored (m)	Length recovered (m)	Recovery (%)
Hole 573							
1	3	0815	4311.5–4313.5	0.0–2.0	2.0	2.0	100+
2	3	0940	4313.5–4323.0	2.0–11.5	9.5	9.42	100
3	3	1040	4323.0–4332.5	11.5–21.0	9.5	9.31	100
4	3	1211	4332.5–4342.0	21.0–30.5	9.5	9.56	100
5	3	1320	4342.0–4350.8	30.5–39.3	8.8	8.84	100
6	3	1440	4350.8–4359.5	39.3–48.0	8.7	8.71	100
7	3	1610	4359.5–4368.7	48.0–57.2	9.2	9.18	99
8	3	1720	4368.7–4378.2	57.2–66.7	9.5	9.69	100
9	3	1830	4378.2–4387.7	66.7–76.2	9.5	9.56	100
10	3	2000	4387.7–4397.2	76.2–85.7	9.5	9.66	100
11	3	2130	4397.2–4406.7	85.7–95.2	9.5	9.39	100
12	3	2255	4406.7–4415.5	95.2–104.0	8.8	9.04	100
13	4	0010	4415.5–4424.1	104.0–112.6	8.6	8.66	100
14	4	0123	4424.1–4433.6	112.6–122.1	9.5	9.50	100
15	4	0244	4433.6–4442.8	122.1–131.3	9.2	9.23	100
16	4	0401	4442.8–4451.6	131.3–140.1	8.8	8.87	100
17	4	0545	4451.6–4460.4	140.1–149.0	8.9	8.99	100
18	4	0750	4460.5–4465.5	149.0–154.0	5.0	4.63	93
19	4	0918	4465.5–4470.1	154.0–158.6	4.6	5.15	100
					158.60	159.39	100
Hole 573A							
1	4	1800	4316.0–4325.5	4.5–14.0	9.5	9.66	100+
2	4	1935	4325.5–4333.6	14.0–22.1	8.1	8.13	100+
3	4	2110	4333.6–4342.8	22.1–31.3	9.2	9.25	100+
4	4	2240	4342.8–4351.3	31.3–39.8	8.5	8.50	100
5	5	0005	4351.3–4360.7	39.8–49.2	9.4	9.41	100+
6	5	0800	4360.7–4369.2	49.2–57.7	8.5	8.55	100+
					53.20	53.52	100
Hole 537B							
			Heat flow to 4450.0				
1	6	2030	4450.0–4459.5	138.5–148.0	9.5	8.56	90
2	6	2230	4459.5–4469.0	148.0–157.5	9.5	9.64	100
3	7	0040	4469.0–4478.5	157.5–167.0	9.5	9.73	100
4	7	0140	4478.5–4488.0	167.0–176.5	9.5	9.63	100
5	7	0320	4488.0–4497.5	176.5–186.0	9.5	9.41	99
6	7	0455	4497.5–4507.0	186.0–195.5	9.5	9.70	100
7	7	0630	4507.0–4516.5	195.5–205.0	9.5	8.03	86
8	7	0805	4516.5–4526.0	205.0–214.5	9.5	9.79	100
9	7	0935	4526.0–4535.5	214.5–224.0	9.5	9.67	100
10	7	1120	4535.5–4545.0	224.0–233.5	9.5	8.84	93
11	7	1237	4545.0–4554.5	233.5–243.0	9.5	9.43	99
12	7	1353	4554.5–4564.0	243.0–252.5	9.5	7.25	76
13	7	1500	4564.0–4573.5	252.5–262.0	9.5	9.68	100
14	7	1620	4573.5–4583.0	262.0–271.5	9.5	9.62	100
15	7	1740	4583.0–4592.5	271.5–281.0	9.5	8.45	89
16	7	1907	4592.5–4602.0	281.0–290.5	9.5	7.80	100
17	7	2030	4602.0–4611.5	290.5–300.0	9.5	7.76	82
18	7	2147	4611.5–4621.0	300.0–309.5	9.5	4.64	49
19	7	2300	4621.0–4630.5	309.5–319.0	9.5	3.31	35
20	8	0038	4630.5–4640.0	319.0–328.5	9.5	9.32	98
21	8	0215	4640.0–4649.5	328.5–338.0	9.5	6.52	69
22	8	0347	4649.5–4659.0	338.0–347.5	9.5	6.05	64
23	8	0533	4659.0–4668.5	347.5–357.0	9.5	6.29	66
24	8	0700	4668.5–4678.0	357.0–366.5	9.5	5.28	56
25	8	0830	4678.0–4687.5	366.5–376.0	9.5	1.93	20
26	8	1008	4687.5–4697.0	376.0–385.5	9.5	7.76	82
27	8	1136	4697.0–4706.5	385.5–395.0	9.5	7.0	74
28	8	1330	4706.5–4716.0	395.0–404.5	9.5	4.91	52
29	8	1504	4716.0–4725.5	404.5–414.0	9.5	7.40	78
30	8	1622	4725.5–4735.0	414.0–423.5	9.5	6.40	67
31	8	1730	4735.0–4744.5	423.5–433.0	9.5	2.04	21
32	8	1910	4744.5–4754.0	433.0–442.5	9.5	4.04	43
33	8	2050	4754.0–4763.5	442.5–452.0	9.5	8.25	87
34	8	2220	4763.5–4773.0	452.0–461.5	9.5	2.48	26
35	8	2350	4773.0–4782.5	461.5–471.0	9.5	7.48	79
36	9	0130	4782.5–4792.0	471.0–480.5	9.5	5.36	56
37	9	0300	4792.0–4801.5	480.5–490.0	9.5	1.80	19
38	9	0436	4801.5–4811.0	490.0–499.5	9.5	4.48	47
39	9	0600	4811.0–4820.5	499.5–509.0	9.5	4.45	47
40	9	0730	4820.5–4825.5	509.0–514.0	5.0	2.06	41
41	9	0900	4825.5–4832.0	514.0–520.5	6.5	0.02	86
42	9	1035	4832.0–4839.5	520.5–528.0	7.5	6.44	86
43	9	1130	4839.5–4840.5	528.0–529.0	1.0	1.19	100
					390.0	279.69	71.6

LITHOSTRATIGRAPHY

Lithostratigraphic Subdivision

The lithostratigraphic succession at Site 573 consists of a variety of siliceous nannofossil oozes and pure nannofossil oozes, which pass down into chalks of similar composition. Metalliferous sediments and a pelagic limestone immediately overlie basalt at the base of the succession. Sediment composition is the primary criterion for dividing the section. We used color to subdivide the section. Color is not directly related to texture or microfossil content, but since texture and microfossil content display only a broad systematic variation, they are of limited lithostratigraphic use. The succession is divided into five units (Table 2): cyclic siliceous calcareous ooze, calcareous ooze chalk, metalliferous chalk claystone, pelagic limestone, and basalt. These units and their subunits can be correlated with the oceanic formations recognized at Site 77 by Hays et al. (1972).

Unit I: Cyclic Siliceous Calcareous Ooze (upper Pliocene to Quaternary)

The cyclic siliceous calcareous unit (0 to 45.1 m) is composed of 10- to 50-cm alternations of brown (10YR 5/2 to 6/2) and brownish white (10YR 8/2) to very pale brown (10YR 7/1 to 7/2) siliceous foraminiferal nannofossil oozes. The contacts between the beds are horizontal and sharp, although they are bioturbated. The burrow Planolites can be recognized in some of the darker beds.

The unit may be divided into three subunits. *Subunit IA* (0 to 6.6 m) is brown radiolarian foraminiferal diatom nannofossil ooze. *Subunit IB* (6.6 to 18.1 m) is light gray and consists of 50- to 90-cm beds of alternating white (N9 to 10YR 8/2) and very light greenish gray (5G 8/1 to 5GY 8.5/1) siliceous foraminiferal nannofossil ooze. *Subunit IC* (18.1 to 45.1 m) is brown radiolarian foraminiferal diatom nannofossil ooze. The color of the sediment is controlled by the presence of trace quantities of iron oxides, which color the oozes brown. The brown subunits contain a greater proportion of siliceous microfossils than the light gray subunit. The lower brown subunit is separated by a sharp planar contact from the underlying greenish gray calcareous ooze chalk unit.

Table 2. Lithostratigraphy of Site 573.

Lithologic unit	Unit sub-bottom depth (m)	Unit depth (Hole-Core-Section, level in cm)
I (cyclic siliceous calcareous ooze)		
A (brown ooze)	0–6.6	573-1-1, 1 to 573-2-4, 10 573A-1-1, 1 to 573A-1-3, 120
B (light gray ooze)	6.6–18.1	573-2-4, 10 to 573-3-5, 60 573A-1-3, 120 to 573A-2-4, 5
C (brown ooze)	18.1–45.1	573-3-5, 60 to 573-6-5, 1 573A-2-4, 5 to 573A-5-3, 145
II (calcareous ooze chalk)		
A (varicolored ooze)	45.1–160.2	573-6-5, 1 to 573-19,CC 573A-5-3, 145 to 573A-6,CC 573B-1-1, 1 to 573B-3-2, 125
B (gray ooze)	160.2–262.2	573B-3-2, 125 to 573B-14-1, 10
C (brown ooze)	262.2–290.6	573B-14-1, 10 to 573B-17-1, 5
D (white gray chalk)	290.6–520.5	573B-17-1, 5 to 573B-41-1, 3
III (metalliferous chalk claystone)		
A (brown chalk)	520.5–522.6	573B-42-1, 1 to 573B-42-2, 63
B (brown claystone)	522.6–526.6	573B-42-2, 63 to 573B-42-5, 6
IV (pelagic limestone)	526.6–528.0	573B-42-5, 6 to 573B-43-1, 1
V (basalt)	528.0–529.0	573B-43-1, 1

The sediments of the cylic siliceous calcareous ooze unit are generally abundant in clay-sized material (40 to 75%) and common to abundant in silt-sized (10 to 35%) and sand-sized (10 to 30%) material. In the light gray subunit (IB), the clay content reaches 85%, and the content of both silt and sand falls below 10%. Calcareous nannofossils are generally common to abundant (20 to 75%), but they are dominant (75 to 85%) in parts of the light gray unit. Foraminifers are common to abundant (5 to 30%), diatoms are rare to common (5 to 20%), and iron oxides occur as a rare component (<1 to 3%) in the brown beds. Clay minerals, volcanic glass, silicoflagellates, sponge spicules, and fish remains occur sporadically in trace amounts.

Unit II: Calcareous Ooze Chalk (lower Oligocene to upper Pliocene)

Unit I is underlain by a thick (45.1 to 520.0 m) succession of calcareous oozes and chalks that displays considerably less variation in siliceous microfossil content than the overlying sediment. Unit II may be divided into four subunits on the basis of color: varicolored ooze, gray ooze, brown ooze, and white gray chalk.

Subunit IIA: Varicolored Ooze (upper Miocene to upper Pliocene)

The varicolored ooze subunit (45.1 to 160.2 m) is characterized by shades of light green gray and purple. It consists of 10- to 50-cm beds of white (N9 to 5B 9/1) to light gray (N7 to N8) and light greenish gray (5G 6/1 to 8/1, 5GY 8/1) siliceous nannofossil oozes and radiolarian diatom nannofossil oozes, which pass down into similar beds of mottled light and dark purple (5PB 7/2, 5P 4/2 to 7/1). Thin beds and burrow fills (predominantly Planolites) of pale yellow gray (5Y 7/1 to 8/1) and greenish yellow (2.5Y 7/2) are common.

The contact with the overlying unit (Unit I) is marked by the appearance of green gray (5G 6/1 to 7/1) ooze. Purple bands do not occur until 50 m. The appearance of purple sediments coincides with the occurrence of H_2S in the cores, which continues down to the base of the varicolored subunit. Below 50 m, millimeter-scale purple bands are common in both the light and dark sediments, and the predominantly purple beds display numerous horizontal millimeter-thick laminations of dark purple (5P 2/2 to 4/2) sediment. Light green gray banding is visible occasionally.

At about 110 m the sediment becomes lighter in color (whites are dominant), and the purple coloration becomes less constrained by bedding, developing into diffusion-rings around burrows and forming sinuous discordant bands. Diatom nannofossil oozes and nannofossil oozes become more common downward. The sediments in the 10 to 20 cm at the base of the unit are characterized by the gradual disappearance of variegated pastel shades, purple banding, and H_2S.

In the varicolored subunit clay-sized material is abundant to dominant (50 to 95%), silt-sized material is rare to abundant (2 to 50%), and sand-sized material is rare to common (2 to 25%). Calcareous nannofossils are abundant to dominant (50 to 95%). Foraminifers represent 0 to 10%, diatoms 5 to 25%, and radiolarians 2 to 10% (rare to common) of the microfossil assemblage. Volcanic glass, pyrite, clay minerals, sponge spicules, and silicoflagellates occur in trace amounts throughout the subunit.

Subunit IIB: Gray Ooze (lower to upper Miocene)

The gray ooze subunit (160.2 to 262.2 m) is composed of white (N9 to 5B 9/1), very light gray (N8 to 8.5), and light greenish gray (5G 7/1 to 9/1, 5GY 7/1 to 9/1) beds 1 to 3 m thick that grade into each other over 10 to 20 cm. Pale purple (5P 9/1) horizons occur toward the top and light greenish gray horizons dominate toward the base of the subunit. Identifiable burrows are rare.

The top of the gray ooze subunit (160 to 200 m) is composed of radiolarian diatom nannofossil oozes and diatom nannofossil oozes, which are underlain by foraminiferal nannofossil oozes and nannofossil oozes (200 to 230 m) with occasional thin (<5 cm) beds of chalk. Below this portion of the subunit (i.e., from 230 to 262.2 m), beds of nannofossil chalk 3 to 5 cm thick alternate with beds of nannofossil ooze 20 cm thick. Radiolarians become common toward the base. Contacts between the lithologies are gradational.

The gray ooze subunit contains abundant to dominant (35 to 90%) clay-sized material, rare to abundant (2 to 70%) silt-sized material, and common (5 to 10%) sand-sized material. Foraminifers occur as trace constituents at the top of the subunit, but they rare to common (1 to 15%) in the underlying carbonate oozes and chalks. Conversely, diatoms are common (10 to 25%) at the top of the subunit, but they become rare (<1%) below. Calcareous nannofossils are uniformly abundant to dominant (60 to 85%), and radiolarians are rare to common (1 to 20%). Volcanic glass, pyrite, sponge spicules, and silicoflagellates occur as trace constituents. The base of the gray ooze subunit is marked by a sharp, planar contact with the light brown (10YR 8/2) sediment of the underlying subunit.

Subunit IIC: Brown Ooze (lower Miocene)

The brown ooze subunit (262.2 to 290.6 m) is composed of white (10YR 8/2) and very light brown (10YR 7/3 to 8/3) radiolarian nannofossil to nannofossil oozes and chalks. Beds are 1 to 3 m thick. They grade into each other over 10 to 20 cm and are composed of alternating bands of chalk (≈5 cm thick) and ooze (≈20 cm thick). Bioturbation is restricted to indeterminate burrow mottling within darker beds.

The subunit contains rare to common (2 to 20%) sand-sized material, common to abundant (20 to 48%) silt-sized material, and abundant (50 to 70%) clay-sized material. Calcareous nannofossils are abundant to dominant (70 to 98%), diatoms are absent to common (0 to 7%), and radiolarians are rare to common (<1 to 17%). The siliceous component decreases toward the base of the subunit. Clay minerals, volcanic glass, pyrite, foraminifers, sponge spicules, and silicoflagellates occur in trace (<1%) amounts. Occasional large (1 to 4 mm) fragments of pumice are present.

The base of the brown ooze subunit is marked by a sharp planar contact with pure white (N9) nannofossil oozes from the top of the underlying subunit.

Subunit IID: White Gray Chalk (lower Oligocene to lower Miocene)

Subunit IID (290.6 to 520.5 m) is composed primarily of brilliant white chalks (290.6 to 460 m), which are underlain by light gray chalks (460 to 520.5 m). The upper beds consist of alternating intervals of apparently unbedded white (N9) foraminiferal nannofossil and nannofossil oozes and chalks. Ooze–chalk alternations continue down to 320 m, below which chalks occur alone. Light gray (N7) banded horizons up to 10 cm thick occur at some levels. Burrows are rarely visible. The sediment is composed of abundant to dominant (40 to 90%) clay-sized material, common to abundant (5 to 50%) silt-sized material, and rare to common (1 to 20%) sand-sized components. Calcareous nannofossils are abundant to dominant (55 to 99%), and foraminifers are generally absent to common (0 to 20%). Radiolarians are rare (< 1 to 3%). Clay minerals, volcanic glass, sponge spicules, and pyrite occur in trace amounts. Diatoms are absent. Fragments of pumice up to 1 cm across occur throughout the sequence.

The light gray chalks are composed of white (N8.5 to 9), very light greenish gray (5GY 8.5 to 9/1), and very pale yellow to brown (5Y 8 to 9/1, 10YR 8 to 9/2) radiolarian diatom foraminiferal nannofossil chalks. These chalks are relatively uniform in composition; close examination shows that compositional variations should result in the exclusion of only one of the qualifiers from the formal lithological name of some horizons. Darker colors are concentrated in beds about 10 cm thick, some of which display indistinct banding. A diverse ichnofauna of Zoophycos, Planolites, and Chondrites is represented. The dominant lithology consists of abundant (30 to 55%) clay-sized particles, common to abundant (20 to 40%) silt-sized particles, and common to abundant (20 to 35%) sand-sized components. Calcareous nannofossils are abundant (40 to 70%), foraminifers and radiolarians are common (5 to 15%), diatoms are common to abundant (5 to 30%), and sponge spicules are rare (< 1%).

Scattered fragments of pumice and thin (< 1 cm) bands of volcanic ash are found in the gray chalks. At 492.1 m there is a graded band 10 cm thick of volcanic glass and ash that has a sharp, planar base and a finely laminated and cross-bedded top (Fig. 3). Ash becomes progressively less abundant in the overlying meter of chalk. This ash band is interpreted as a turbidite. Lower in the section (at 501.3 m) there is a bed 80 cm thick of very pale yellow (5Y 8/1) chalk containing common 0.1-mm to 1-cm angular fragments of volcanic glass. This bed does not display bedding but has a sharp bottom and top, indicating deposition by mass flow rather than current action.

The base of the white gray chalk subunit is marked by the first appearance of white (5Y 9/1 to N9) chalks above the light brown (10YR 8/3) chalks of the underlying metalliferous chalk claystone unit. The boundary

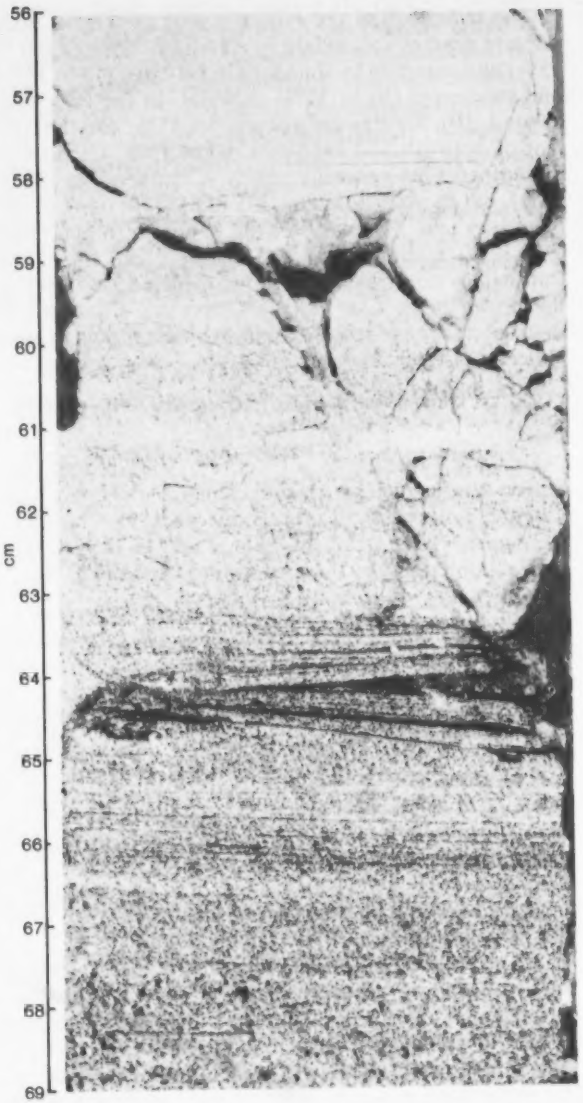

Figure 3. Lower Oligocene volcanic ash turbidite cored at 429.1 m in Site 573 (573B-38-2, 56–69 cm).

was not recovered, but it is sharp at Site 77 (Hays et al., 1972).

Unit III: Metalliferous Chalk Claystone (upper Eocene to lower Oligocene)

The sediment below 520.5 m becomes progressively darker brown as the result of the appearance of appreciable quantities of ferromanganese oxide. The sequence is divided into a brown chalk subunit at the top and a brown claystone subunit below.

Subunit IIIA: Brown Chalk (lower Oligocene)

The brown chalk subunit (520.5 to 522.6 m, lower Oligocene) consists of very pale brown (10YR 8/3) foraminiferal nannofossil chalk with abundant Zoophycos,

Planolites, and Chondrites. The chalk has abundant (65%) clay-sized particles, common (5%) silt-sized particles, and abundant (30%) sand-grade material. Calcareous nannofossils (55%) and foraminifers (30%) are abundant. Palagonite is rare (1%), and radiolarians and sponge spicules occur in trace amounts.

The brown chalk subunit passes down via a 10-cm intensely burrowed pale brown (10YR 6/3) bed into the brown claystone subunit.

Subunit IIIB: Brown Claystone (upper Eocene to lower Oligocene)

The brown claystone subunit (522.6 to 526.6 m, upper Eocene to lower Oligocene) consists of very dark brown (10YR 2/2) metalliferous claystone. There are strongly compressed Chondrites and white rind-burrows at the top and, to a lesser extent, at the base of the subunit. Clay is dominant (90%), with common silt-sized material and only a trace of sand-grade material. Smear slide examination indicates abundant (60%) clay minerals and ferromanganese oxides (36%), with rare feldspar (2%), carbonate (1%), and calcareous nannofossils (1%).

The claystone passes down via pale brown (10YR 6/2) chalks into the underlying limestone.

Unit IV: Pelagic Limestone (upper Eocene)

A strongly indurated very pale yellow (2.5Y 8/2) pelagic biogenic limestone (526.6 to 528.0 m) directly overlies basalt. Composed primarily of pelagic and benthic foraminifers and calcareous nannofossils, the limestone contains abundant millimeter-scale fragments of green basalt(?). Manganese oxide ("pyrolusite") dendrites are common.

Unit V: Basalt

The drilling at Site 573 resulted in the recovery of 119 cm (25 pieces) of basalt. The basalt was recovered from sub-bottom depths of 528.0 to 529.0 m.

Correlation with Site 77

Site 573 is in close proximity to Site 77. The units recognized by Hays et al. (1972) at Site 77 are similar to those at Site 573, which were established independently. Our cyclic siliceous calcareous unit (Unit I) corresponds to the cyclic unit of the Clipperton Oceanic Formation, and our varicolored ooze subunit (IIA) correlates with varicolored unit of the same formation. The gray ooze subunit defined here (IIB) corresponds to the gray unit of the Marquesas Oceanic Formation, and our brown ooze subunit (IIC) is equated with the upper brown unit defined by Hays et al. (1972). Our white gray chalk subunit (IID), however, corresponds to the basal three units of their Marquesas Formation. This difference in classification occurs primarily because we cannot distinguish the lower brown unit of the Marquesas Formation. The lower brown unit occurs at 408.1 to 426.6 m at Site 77 (Hays et al., 1972) and consists of very light brown (10YR 8/2) and white (N9) foraminiferal radiolarian chalks to nannofossil chalks. If we allow for the marginally thicker section at Site 573 (528 m compared with 481 m), the unit should occur at about 420 to 440 m. At Site 573 this interval is characterized by extremely poor recovery and great core disturbance, so the presence of the unit cannot be confirmed.

Our brown chalk subunit (IIIA), brown claystone subunit (IIIB), and pelagic limestone unit (IV) can be correlated with the Line Islands Formation of Hays et al. (1972) and Cook (1972). The thickness of this formation is 10.2 m at Site 77 and 8 m at Site 573. The difference may be attributed to the 9.5-m gap in the relevant part of the section at Site 573. It appears, therefore, that the extra 47 m of sediment at Site 573 are distributed throughout the section, except that the varicolored ooze subunit (IIA) is 15 m thicker at Site 77.

Carbonate Stratigraphy

Shipboard carbonate bomb analyses were done at 1.5-m intervals. The carbonate fluctuations show that the Site 573 carbonate record (Fig. 4) may be divided into two parts: an upper Miocene to Quaternary interval (0 to 180 m) with high-amplitude cyclic fluctuations between sediments of high and low carbonate content and a lower Oligocene to middle Miocene interval (180 to 520 m) with lower amplitude fluctuations and relatively constant carbonate values. In the high-amplitude section, the high-carbonate sediments have a carbonate content that ranges from 80 to 90%, and the low-carbonate sediments generally have a carbonate content that ranges from 60 to 70%, although certain minima have a carbonate content as low as 40%. The Oligocene to middle Miocene section has a rather uniform average carbonate content of about 90%, with fluctuations between 98 and 80%.

Distinct changes in the Site 573 sedimentation rate curve at 49, 104, 243 and 412 m all coincide with carbonate minima. The correlation may be fortuitous, because not all the sedimentation rate changes correspond to carbonate minima. A hiatus at 160 m occurs just above a carbonate minimum, so the hiatus may have been produced by carbonate dissolution. A second possible hiatus at 335 m does not appear to coincide with carbonate dissolution, although the carbonate curve at this level is difficult to interpret because the carbonate content of the upper Oligocene sediment at Site 573 is uniformly high.

The carbonate curves for Holes 573, 573A, and 573B (Fig. 4) can be correlated to the equatorial Pacific carbonate event stratigraphy of the Neogene as given by Dunn and Moore (1981) and Dunn (1982).

BIOSTRATIGRAPHY

Upper Eocene through Quaternary sediments were recovered at Site 573. Planktonic foraminifers, calcareous nannofossils, radiolarians, and diatoms are generally present and zonable throughout; thus, the site provides a reference section for the equatorial Pacific (Fig. 5). An updated version of the biostratigraphic summary is presented in Barron et al. (this volume). The precise position of the Eocene/Oligocene boundary is unknown; if sediments that correlate to this stratigraphic boundary were recovered in Hole 573B, they occur in the barren, metalliferous claystone unit from 526.6 to 522.6 m sub-

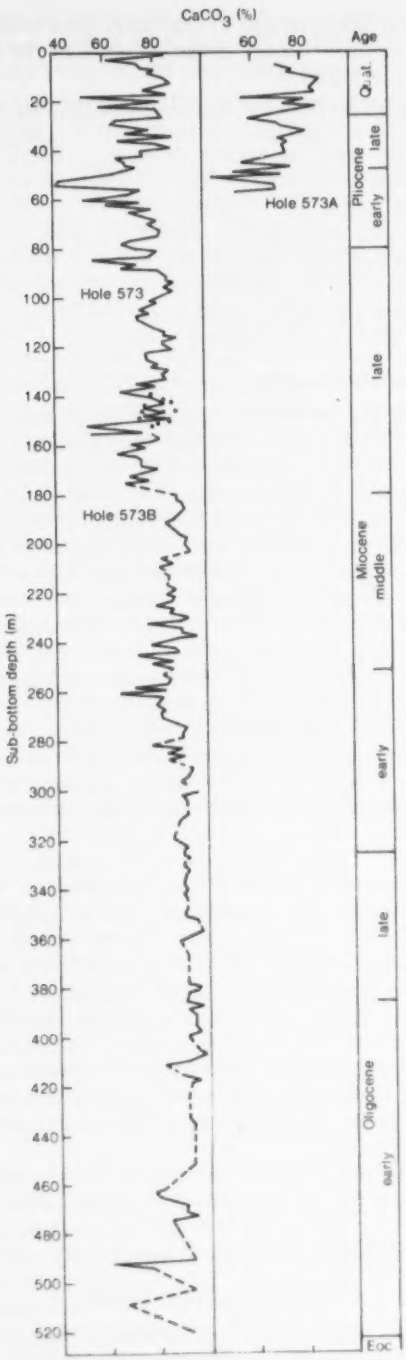

Figure 4. Shipboard carbonate data for Site 573; curves are for Holes 573 and 573B. In the depth interval where data from the holes overlap, the data for Hole 573B are shown as dots.

bottom (Core 573B-42, Sections 4 to 2). Planktonic and benthic foraminifers and calcareous nannofossils of latest Eocene and earliest Oligocene age bracket this barren 2-m interval. All four planktonic microfossil groups indicate that the lower/upper Oligocene boundary lies in Core 573B-27 (≈ 386 m). The planktonic foraminifers and radiolarians indicate that the Oligocene/Miocene boundary occurs in Core 573B-20 (≈ 326 m). The lower/middle Miocene boundary is near the base of Core 573B-12 (252 m), according to the radiolarians, diatoms, and calcareous nannofossils. Unfortunately, the *Orbulina* datum (planktonic foraminifers) could not be accurately determined. According to the diatoms and calcareous nannofossils, the middle/upper Miocene boundary occurs in the middle of Core 573B-5 (≈ 180 m). The planktonic foraminifers, calcareous nannofossils, and diatoms all place the Miocene/Pliocene boundary in Core 573-10 (≈ 80 m sub-bottom). The planktonic foraminifers indicate that the lower/upper Pliocene boundary lies in the lower parts of Cores 573-6 and 573A-5 (48 m). The Pliocene/Pleistocene boundary is placed in the upper part of Core 573-4 and the upper part of Core 573A-3 (at ≈ 25 m sub-bottom).

Hiatuses

Two hiatuses were recognized in the sediment section at Site 573, and three more were identified tentatively. Although the possibility that deposition across the Eocene/Oligocene boundary was continuous but slow cannot be ruled out entirely, biostratigraphic evidence suggests that there is a hiatus at the Eocene/Oligocene boundary (between Sections 2 and 3 of Core 573B-42). This hiatus would correspond to the absence of the lower part of planktonic foraminiferal Zone P18 and all of P17. A coeval hiatus is present at Site 289 on the Ontong–Java Plateau (Andrews et al., 1975) and over extensive areas of the Pacific (Kennett et al., 1975). Kennett et al. (1975) relate this hiatus to the onset of Antarctic glaciation in the early Oligocene and the intensification of bottom-water circulation.

A second hiatus or interval of greatly reduced sedimentation rate is present in the lower part of the upper Miocene (10.5 to 9.8 Ma). The first appearance datum of the diatom *Coscinodiscus yabei* var. *elliptica* (9.8 Ma) is immediately above a purple sedimentary unit 4.5 m thick in Core 573B-3 (573B-3-1, 71 cm). The last appearance of the diatom *Coscinodiscus vetustissimus* var. *javanicus* (10.7 Ma) appears to be immediately below the purple sedimentary unit, at 573B-3-4, 110 cm (Barron, this volume). This hiatus has also been reported at nearby Site 77 (Keller, 1981; Keller and Barron, 1983) and is extensive in the eastern equatorial Pacific.

One of the tentatively identified hiatuses occurs in the uppermost Oligocene (upper part of Core 573B-22 or the lower part of Core 573B-21), where the lower part of the *Lychnocanoma elongata* Zone (radiolarians) and the *Cyclococcolithus abisectus* Subzone (CN1a) of the *Triquetrorhabdulus carinatus* Zone (calcareous nannofossils) are absent. This hiatus has also been reported at nearby Site 77 by the Leg 9 scientists (Hays et al., 1972) and over extensive areas of the Pacific by Keller and Barron (1983).

Another possible hiatus or interval of decreased sediment accumulation occurs in the middle part of the lower Miocene (lower part of Core 573B-14 to Core 573B-16) (≈ 17.5 to 20.0 Ma). This hiatus corresponds to the two

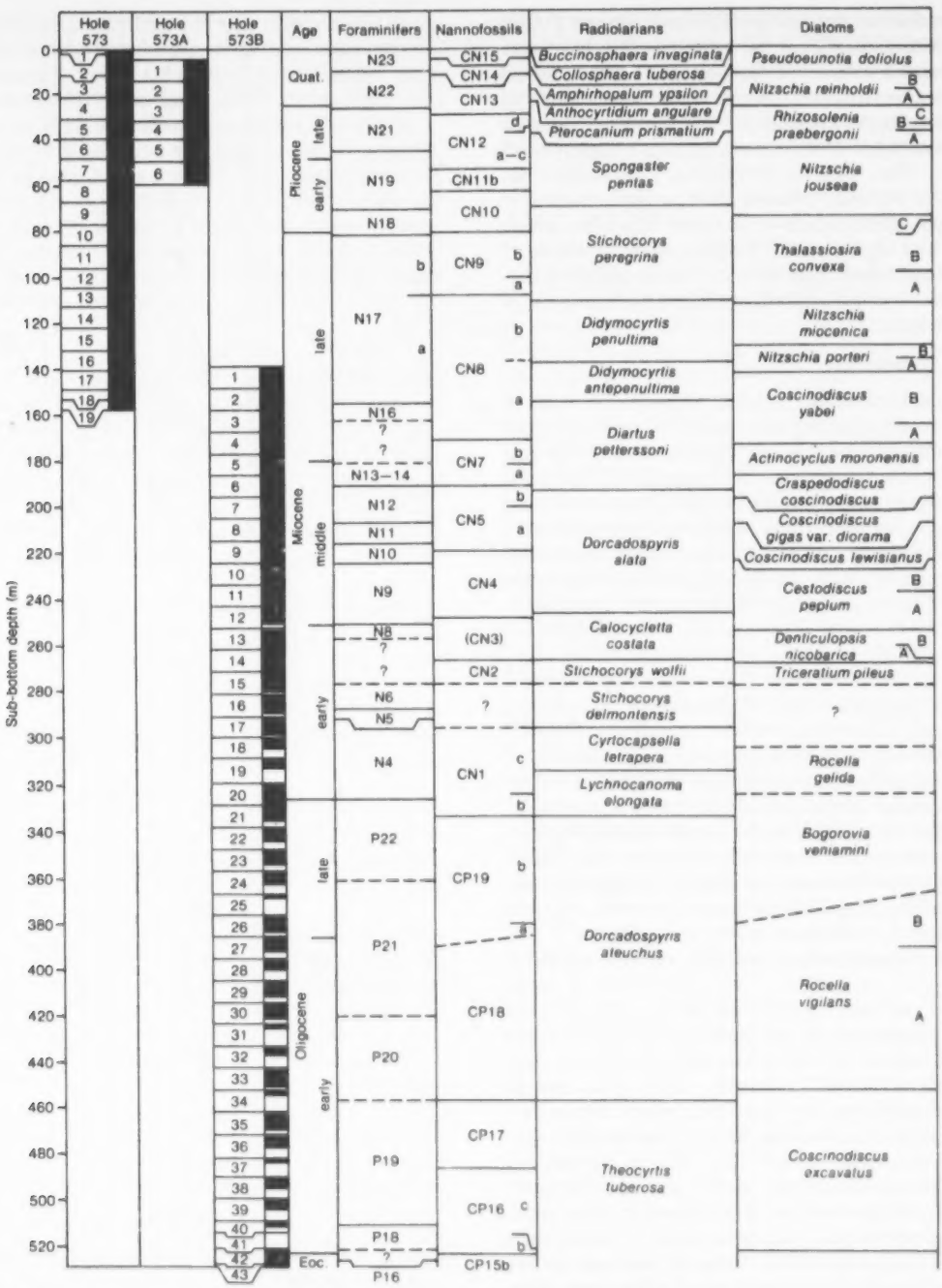

Figure 5. Summary of biostratigraphy at Site 573. Location of dashed boundaries is uncertain.

hiatuses reported by Keller (1981) in planktonic foraminiferal Zones N5 and N6 at nearby Site 77. More detailed study of these cores should reveal whether sedimentation rate is low or one or more hiatuses exist (see Barron et al., this volume).

Finally, a possible hiatus occurs in the middle part of the Pliocene (≈3.3 to 3.2 Ma, near the base of Section 573A-5-3), at a sharp break in lithology between gray sediment and overlying white sediment. Samples 573A-5-3, 129–140 cm and 573A-5-3, 144–145 cm bracket this lithologic boundary, and both lie between the first appearance datum of *Thalassiosira convexa* var. *convexa* (diatom) (3.6 Ma) and the first appearance datum of *Rhizosolenia praebergonii* (diatom) (3.0 Ma). The lower sample contains common *T. convexa*, whereas the upper sample contains very few *T. convexa*. According to the

quantitative diatom data of Burckle and Trainer (1979) from Core V28-179 (4°37.0′N, 139°36.0′W), the lower sample correlates with the lowermost part of the normal event of the Gauss paleomagnetic Epoch (≈3.35 Ma), and the upper sample correlates with the uppermost part of that normal event or with the overlying reversed event (≈3.2 to 3.1 Ma). This sharp lithologic break (or hiatus) correlates with the positive (0.4 per mil) excursion in the oxygen-isotope record in Core V28-179, which Shackleton and Opdyke (1977) equate with the onset of Northern Hemisphere glaciation. A more detailed discussion of these possible hiatuses is given in Barron et al. (this volume).

Planktonic Foraminifers

Site 573 yielded upper Eocene through Pleistocene planktonic foraminifers of varying abundance. None of the fossil assemblages exhibits maximum diversity because of the great water depth at the site, and all consist predominantly of such solution-resistant forms as keeled *Globorotalia, Globoquadrina, Sphaeroidinellopsis*, and *Catapsydrax*. However, all the species present show good preservation throughout the sequence. The abundance of foraminifers decreases markedly in two intervals—from 112 to 186 m and 252.5 to 366.5 m sub-bottom. These intervals approximately correspond to the N17 through N14 and N8 through P21 zones, respectively.

Because of dissolution (see the dissolution curve shown in Fig. 6), many interesting evolutionary series of planktonic foraminifers could not be studied. A number of prominent evolutionary series known to have undergone rapid development in the tropical latitudes were not recovered at this site. These series include *Globigerinoides triloba–Praeorbulina sicana–Orbulina universa, Globigerinita glutinata–Candeina praenitida–Candeina nitida*, and *Globigerinita* sp.–*Globigerinatella insueta*. The absence of these evolutionary series also precluded the establishment of many foraminiferal zonal boundaries (Fig. 5).

Well preserved upper Eocene planktonic foraminifers occur near the base of the sedimentary column just below the dark brown metalliferous layer. Although they are only moderately well preserved, a few specimens of such delicate spine-bearing species as *Hantkenina primitiva* and *Cribrohantkenina inflata bermudezi* were found (573B-42-4, 140–144 and 123–124 cm). Species belonging to the characteristic Eocene genera *Globigerinatheka* and *Globigerapsis* are also present in large numbers. Because of the joint occurrence of *C. inflata bermudezi* and *Globigerapsis mexicana* in the interval below the metalliferous layer, this interval is dated as Zone P16 (late Eocene). The presence of these varied forms of Eocene foraminifers at Site 573 is in marked contrast to the meager fauna reported from nearby Site 77, where only one species diagnostic of late Eocene age, *G. insolita*, was found.

The Eocene foraminifers decrease in number as the dark brown metalliferous layer is approached, and they are completely absent in that layer. Sample 573B-42-2, 48–50 cm, which was taken immediately above the metalliferous layer, contains rich benthic foraminifers dominated by calcareous forms, an assemblage that suggests the severe dissolution of planktonic species at this level. Forty cm above this sample there is an Oligocene planktonic assemblage indicative of the upper P18 Zone. These observations suggest the following: (1) the Eocene/Oligocene boundary is marked by a break in the foraminiferal sequence that encompasses at least the P17 and early P18 assemblages, which are absent, and (2) just before and immediately after the metalliferous layer was

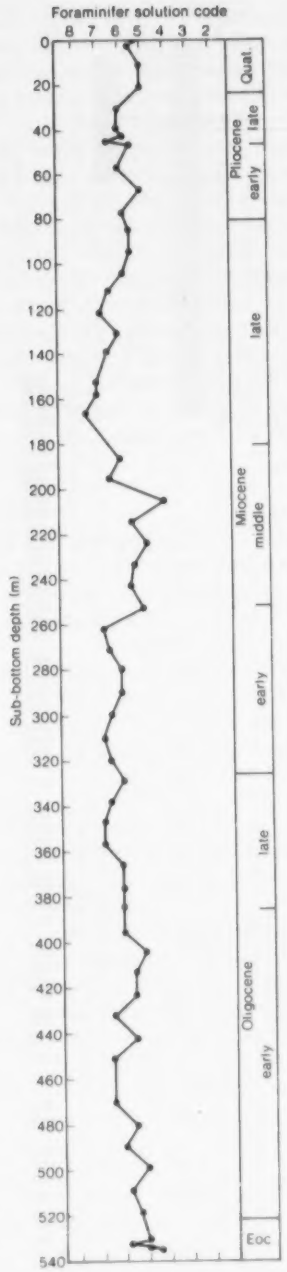

Figure 6. Foraminifer solution curve for Site 573; numbers after Berger and von Rad (1972).

deposited, the area near Site 573 was affected by the severe dissolution of foraminifers, calcareous nannoplankton, and some or most of the benthic foraminifers. Thus, the metalliferous layer was most likely to have been deposited during a period when dissolution was severe.

Debate over the position and age of the Oligocene/Miocene boundary has a long history; the position of the boundary has fluctuated from the top through the middle to the base of the *Globorotalia kugleri* Zone, and the age assigned the boundary has varied as much as 4 m.y. We use the base of the *Globorotalia kugleri* Zone to mark the boundary.

Nannofossils

At Site 573, all the zones and most of the subzones between the upper Pleistocene and the upper Eocene in Bukry's zonation (1971; 1973a, b) can be found. However, some marker species are lacking, and it becomes necessary to use secondary marker taxa. The lower part of Hole 573 (Core 573-17 through Section 573-19,CC) can be correlated with the first three core catchers of Hole 573B. Nannofossil species occurrences are shown in Figure 7.

In terms of abundance, the Pleistocene nannofossils alternate between abundant (Sample 573-1-1, 0–1 cm and Section 573-2,CC; and Sections 573A-1,CC and -2,CC) and rare (Sections 573-1,CC and -3,CC), and these variations may correspond to cool and warm periods.

The Pliocene nannofossils are better preserved in Hole 573 than in Hole 573A, where strong dissolution reduces the abundance of placoliths.

The upper Miocene placoliths are better preserved, but in the middle and lower Miocene and in the lower Oligocene sediments most of them are partly dissolved. In Hole 573B, Cores 15, 16, and 42,CC contain very few nannofossils, and cannot be dated.

Discoasters are abundant from the top of the Pliocene to the middle/upper Miocene boundary. Below the boundary the abundance of discoasters varies; they are rare in the lower Oligocene and Eocene. Discoasters are generally overgrown below the upper Miocene.

Reticulofenestra pseudoumbilica is abundant from Zone CN11 (Section 573-7,CC) through Zone CN5 (Section 573B-8,CC) but rare between Sections 573-9,CC and -18,CC and 573B-1,CC and -2,CC. This late Miocene reduction in the abundance of *R. pseudoumbilica* in Zones CN10a to CN8a is typical of the equatorial Pacific (Bukry, 1972).

In the upper part of lower Miocene, Zone CN3 does not contain *Helicopontosphaera ampliaperta* (Sections 573B-12,CC and -13,CC). The zone is identified by the presence of *Discoaster trinidadensis* and *Reticulofenestra gartneri* and by the absence of *Helicopontosphaera granulata* (Bukry, 1973a).

The lowest part of the Miocene, Zone CN1, contains very abundant *Triquetrorhabdulus carinatus*. *Orthorhabdus serratus* is present from Sections 573B-17,CC to -19,CC and characterizes the Subzone CN1c; the disappearance of this species downsection (in Section 573B-20,CC) marks the lower boundary of a short CN1b Subzone. No microfossils from Subzone CN1a were found.

Sphenolithus ciperoensis s.s. does not seem to be present in Zone CP19 at Site 573. The top of the Oligocene is marked by the last occurrences of *Dictyococcites scrippsae* and *D. bisectus* and the first occurrence of *T. carinatus*.

The separation of Zones CP18 and CP17 is based on the downsection change in dominance from *Sphenolithus distentus* to *S. predistentus*.

The lowest Oligocene zone (CP16) is represented mainly by its upper subzone (CP16c), which is characterized by the presence of *Reticulofenestra hillae* and rare specimens of *Coccolithus subdistichus* and *Pontosphaera vadosa* (Sections 573B-37,CC through -41,CC). As at Site 77 (Bukry, 1972), *Helicopontosphaera reticulata* is absent. *Cyclococcolithina formosa*, an indicator of Subzone CP16b, is abundant in Sample 573B-42-2, 50–51 cm. Subzone CP16a was not found at Site 573. Below some barren samples (573B-42-2, 60 cm through 573B-42-4, 50 cm), there is a sample (573B-42-4, 145 cm) with rare specimens of *Discoaster barbadiensis* and *D. saipanensis* and abundant specimens of *Cyclicargolithus reticulatus*, which characterize upper Eocene Subzone CP15b. As in other low-latitude sections, *Isthmolithus recurvus*, a marker of the uppermost Eocene, is absent (Bukry, 1973b).

Radiolarians

Radiolarians are common to abundant and well preserved in most of the sediment recovered at Site 573. However, in the lower Miocene and uppermost Oligocene sediments from Hole 573B they decrease in abundance and diversity, and many specimens are broken. Orosphaerid fragments and spyroid radiolarians are common in this interval; samples from 573B-15,CC to -17,CC are dominated by spyroids, primarily *?Tholospyris anthophora*. The oldest, moderately well preserved fauna is found in Section 573B-40,CC and belongs to the lower Oligocene (*Theocyrtis tuberosa* Zone); an impoverished fauna belonging to the same radiolarian zone occurs in Sample 573B-42-1, 0–1 cm. Radiolarians are absent entirely from Sample 573B-42-1, 149–150 cm.

The radiolarian zonation determined for the sediments recovered at this site is summarized in Figure 5. It should be pointed out that in this zonation, unlike that for Site 572, the lower limit of the radiolarian *Spongaster pentas* Zone coincides with the lower limit of the diatom *Nitzschia jouseae* Zone. The Site 573 zonation agrees with previously published reports (Burckle and Opdyke, 1977).

In some published reports (e.g., Riedel and Sanfilippo, 1978), the *Didymocyrtis antipenultima/Diartus petterssoni* zonal boundary is considered to be equivalent to the late/middle Miocene boundary. However, the base of the late Miocene is defined as the base of the Tortonian stratotype, and Van Couvering and Berggren (1977) report that the base of the Tortonian lies within planktonic foraminiferal Zone N15 and within the *Discoaster hamatus* Zone (NN9 of Martini; CN7 of Bukry). San-

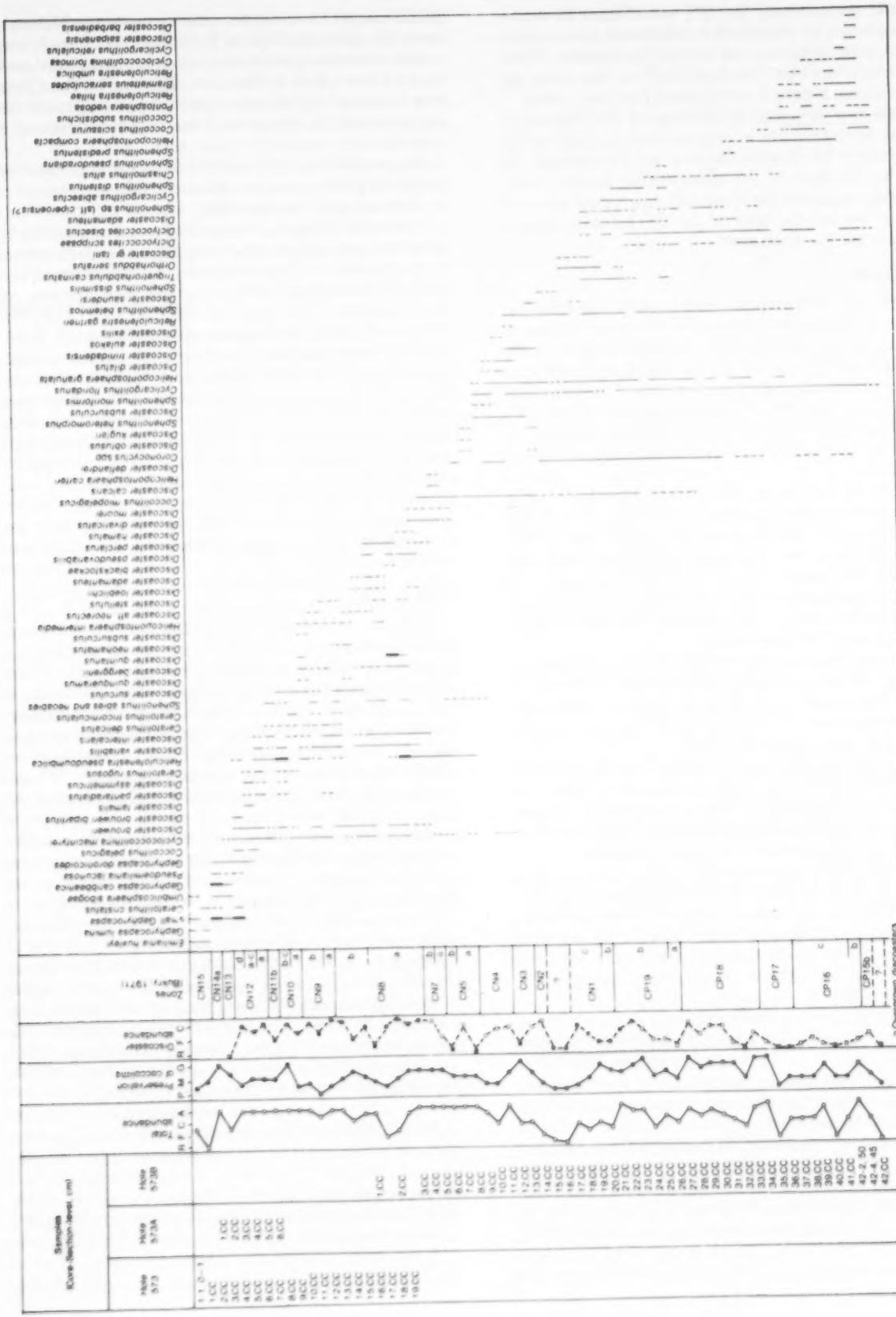

Figure 7. Occurrence of nannofossil species at Site 573; position of dashed zonal boundaries is uncertain.

filippo et al. have more recently (1981) placed the base of the *D. antepenultima* Zone within Zones NN10 and CN8 and, therefore, above the late/middle Miocene boundary. This latest correlation is consistent with our correlation for Site 573.

The shipboard examination of the Site 573 radiolarians could neither confirm nor deny the existence of the hiatuses suggested in the biostratigraphic summary.

Diatoms

Quaternary through lower Oligocene diatoms are present in the Site 573 sediment section. Above Core 573B-7 (upper middle Miocene), the diatoms are common to abundant, and preservation is generally good. Below Core 7 abundance and preservation vary from sample to sample, but abundance is generally smaller and preservation is generally worse. The diatoms decrease sharply in abundance and preservation as one moves downsection from Section 573B-14,CC to Sample 573B-15-1, 68–70 cm (≈ 17.5 Ma). Cores 573B-15 through 573B-22 contain only sparse, poorly preserved diatoms and are difficult to zone. Diatoms increase in abundance again in Core 573B-34 (top of the *Coscinodiscus excavatus* Zone), and they are common thereafter down to the base of the Oligocene section (Sample 573B-42-1, 0–1 cm).

The diatom datum sequence for the middle and upper Miocene is essentially identical to that obtained at Site 77 (Barron, 1981; Keller et al., 1982). The sequence for the middle Miocene through Quaternary is also very similar to that obtained at Site 572.

The first appearance datum of *Thalassiosira burckliana* has been identified precisely in Holes 573 and 573B. This datum occurs between the top and the base of the core-catcher sample for Core 573-18 (152.8 m), immediately above the top of a purple sediment layer. In Hole 573B this datum lies in Section 573B-3-1 between 71 and 81 cm (158.25 m), above a purple sediment layer. The inference is that the lithologies in Hole 573B are offset by about 5.5 m from those in Hole 573, those in the latter being shallower.

Benthic Foraminifers

Benthic foraminifers are present throughout the section. They are generally rare, although less so below Section 573B-33,CC. Diversity is high throughout (about 50 to 60 taxa per 200 counted specimens). There is no marked drop in diversity at the transition from ooze to chalk between 230 and 300 m, in contrast to observations by Douglas (1973) and Douglas and Woodruff (1981). Species that have been described as "least preservable" are present throughout the section (e.g., *Stilostomella* and *Pleurostomella* species).

The assemblage is similar to that found at Site 572. The main constituents of the Eocene through Quaternary faunas are *Nuttallides umbonifera* and species of *Pullenia, Cibicidoides, Gyroidinoides*, and *Oridorsalis*, and, above about 260 m, *Epistominella exigua* (i.e., from the beginning of the middle Miocene). The relative abundances of these constituents fluctuate, but overall the fauna is remarkably stable. Similar stability has been noted in benthic faunas in the Indian Ocean (Boltovskoy, 1978). *Stilostomella* and *Pleurostomella* are more abundant below Section 573B-9,CC than above. This change in abundance occurs in the early middle Miocene, at about the same time as important changes in faunas of the Ontong–Java Plateau (Woodruff and Douglas, 1981). At Site 573 the changes are much less striking (they do not constitute a faunal turnover), and they may occur slightly earlier (Thomas, this volume).

At the Eocene/Oligocene boundary there is a change in less common species. *Nuttallides truempyi*, the last occurrence of which marks the Eocene/Oligocene boundary (Miller et al., 1985), was found only in Sample 573B-42-4, 144–147 cm. *Alabamina dissonata* and *Osangularia mexicana* are present in the same sample. Just above the metalliferous sediments, *Stilostomella* and *Pleurostomella* decrease sharply in abundance. Peaks in the frequency of *Epistominella* occur from the middle Miocene upward.

The stratigraphic ranges of some rare species (e.g., *Favocassidulina favus, Bolivina striatula*, and *Bolivinopsis cubensis*) appear to be short; *B. striatula* occurs only between 15.5 and 18.7 Ma at Sites 573, 574, and 575. However, some of these species are found at different stratigraphic levels at Sites 572 and 573 (e.g., *Favocassidulina subfavus* occurs in planktonic foraminiferal Zone N9 at Site 572 and in Zone N17 at Site 573), so they cannot be used for biostratigraphy.

SEDIMENT ACCUMULATION RATES

Sedimentation rates (Fig. 8) were calculated for Site 573 from estimates of age ranges for all core-catcher

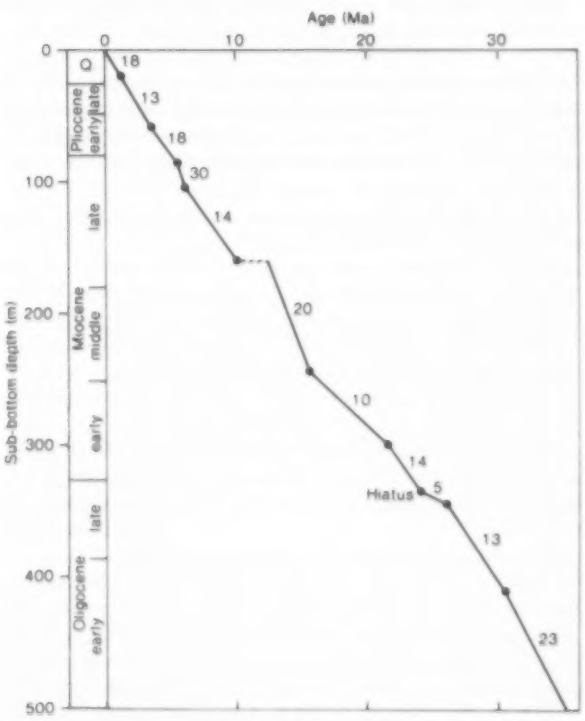

Figure 8. Age versus depth-in-hole based on biodatums at Site 573. Average sedimentation rate in m/m.y.

samples. In the upper 300 m we relied primarily on diatoms and radiolarians for age estimates. Sedimentation rates are relatively constant and hiatuses occur at 160 and 340 m sub-bottom. The hiatus at 340 m sub-bottom may be an interval of very low sedimentation rate and not a true hiatus. If so, the rate is at least a factor of 3 less than the sedimentation rates above and below.

The average sedimentation rate in the upper 85 m (0 to 5.5 Ma) is 16 m/m.y., with only small variations in this interval (Table 3). The maximum sedimentation rate observed at this site occurs between 85 and 104 m sub-bottom (30 m/m.y.). This maximum is separated from a secondary maximum (20 m/m.y., 160 to 243 m) by an interval of lower rate and the hiatus at 160 m. Below the secondary maximum, sedimentation rates are relatively constant at around 12 m/m.y. (with the exception of the hiatus at 340 m sub-bottom) until 100 m above basement, where sedimentation rates are high again (23 m/m.y.). For further discussion see Barron et al. (this volume).

The sedimentation rate changes at Site 573 correspond to changes in lithology. The hiatus at 160 m marks the boundary between the varicolored ooze of Subunit IIA and the upper gray ooze subunit (IIB). The silica-rich upper part of Subunit IIB (160 to 200 m sub-bottom) is an interval of high sedimentation rate (160 to 243 m), with the lower sedimentation rate interval between 243 and 300 m corresponding approximately to the brown ooze subunit (IIC, 260.2 to 290.6 m). The sedimentation rate increase at the base of the section and the hiatus at 340 m do not seem to correspond to changes in lithology.

Three factors that may have a bearing on the higher sedimentation rate observed 100 m above basement (and may operate independently or together) are (1) the proximity of the site to the ridge crest and the consequently good preservation of carbonate; (2) a regional peak in sediment accumulation during this time interval; and (3) the location of the site in a local basement depression in which sediment would accumulate more rapidly. Supporting evidence for the existence of the third factor is provided by the sedimentation rate calculated for the nearby Site 77, which averages around 10 m/m.y. for the entire Oligocene. In addition, the increase in accumulation rates occurs very close to the "sill" depth of the basement low occupied by Site 573.

Shipboard carbonate analysis and wet-bulk density measurements were used to calculate average mass accumulation rates for each time interval listed in Table 3 and plotted in Figure 9. One reason for calculating sediment mass accumulation rates is to remove the effect of compaction, which alters sedimentation rates, which are estimated as unit distance per unit time interval. Compaction was not as apparent at Site 573 as at Site 572, but it does have marked effects on sedimentation rate. For example, the interval between 25.9 and 31.3 Ma has a sedimentation rate equal to that of the interval between 1.3 and 3.5 Ma (12.6 versus 12.7 m/m.y.), but it has a mass accumulation rate greater by a factor of 2, a difference that is consistent with the higher density and greater compaction of the Oligocene chalk. The mass accumulation rate data show that the highest sedimentation rates occurred at the base of the section, the Oligocene interval being a time of generally high sediment accumulation rate. Only during the middle Miocene (11.3 to 15.5 Ma) and a very short interval in the upper Miocene did the accumulation rates exceed the Oligocene rates.

There is no correlation between carbonate content and sedimentation rate at Site 573 (Table 3, Fig. 10), although an inverse correlation could be found in the Site

Table 3. Sedimentation rates and carbonate and noncarbonate mass accumulation rates at Site 573.

Sub-bottom depth (m)	Age (m.y.)	Sedimentation rate (m/m.y.)	Mean dry bulk density (g/cm^3)	Mean $CaCO_3$ (%)	Mean mass accumulation rates (g/cm^2)/1000 yr.)		
					Total	$CaCO_3$	Non $CaCO_3$
0	0.1						
21	1.3	17.5	0.71	79	1.2	0.95	0.25
49	3.5	12.7	0.86	73	0.8	0.58	0.22
85	5.5	18.0	0.71	68	1.3	0.90	0.40
104	6.1	30.0	0.95	82	2.9	2.4	0.50
160	10.1	14.0	0.91	77	1.3	1.0	0.3
Hiatus							
160	11.3						
243	15.5	19.8	1.01	78	2.0	1.6	0.4
300	21.4	9.7	1.14	88	1.1	0.97	0.13
331	23.9	14.0	1.26	92	1.8	1.66	0.14
364	25.9	4.7					
412	31.3	12.6	1.28	92	1.6	1.50	0.10
510	35.5	23.1	1.26	89	2.9	2.58	0.31

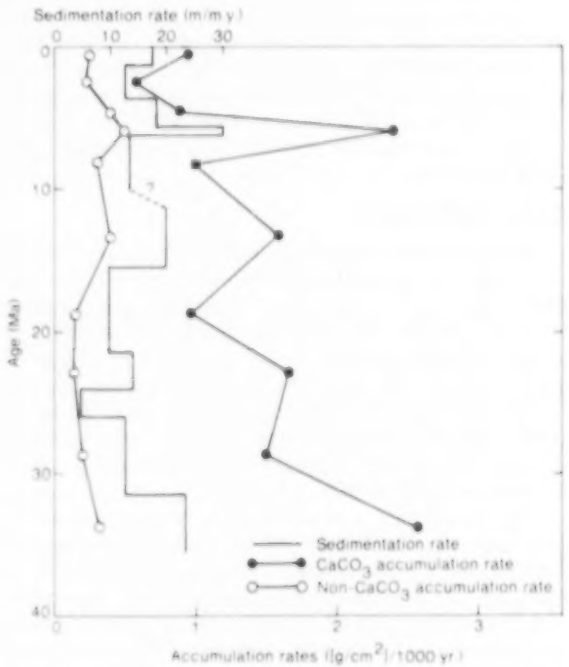

Figure 9. Sedimentation rates and average accumulation rates (g/cm²)/1000 yr.) for carbonate and carbonate-free sediments at Site 573.

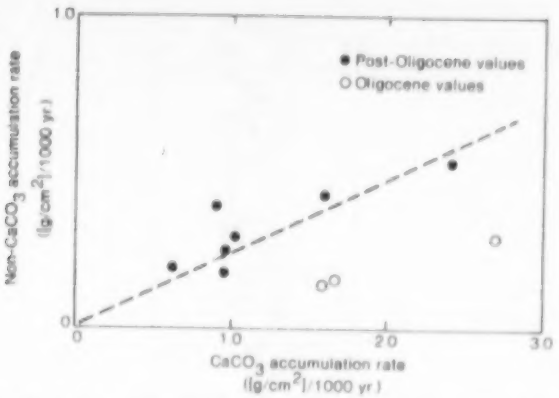

Figure 10. Carbonate versus carbonate-free accumulation rates at Site 573.

572 data. The absence of correlation reflects the relatively high carbonate contents observed at Site 573 and a different linear relationship between the mass accumulation rates of carbonate and noncarbonate sediments. (It is assumed that the noncarbonate fraction is dominated by biogenic silica.) At Site 572, the relationship between the carbonate and noncarbonate accumulation rates was linear and had a regression slope of 0.4 (noncarbonate rates = 0.5 carbonate rates; correlation coefficient $r = 0.95$). At Site 573 the regression slope is also linear (Fig. 10), but it is a factor of 2 less (slope 0.2, $r = 0.8$; the Oligocene intervals were not used in the calculations). Thus, at Site 573 increases in sedimentation rates are not accompanied by marked increases in noncarbonate mass accumulation rates, which would dilute the carbonate content. However, the linearity at both Sites 572 and 573 of the relationship between carbonate and noncarbonate sediment accumulation suggests that there are long-term controls on the deposition of these sediment components. In addition, the differences in the relationship between Oligocene and post-Oligocene times at Site 573 (Fig. 10) suggest that changes took place in these controls at the end of the Oligocene. Clearly, carbonate and siliceous sedimentation rates at this and other sites warrant more detailed study. See Theyer et al. (this volume) for an updated discussion.

PHYSICAL PROPERTIES

The physical properties measured for this site include wet-bulk density (ρ_b), sonic velocity (V_p), formation factor (F), thermal conductivity (K), and shear strength. Measurements were made at regular intervals in the HPC-cored sections except where the sediment was disturbed. In the rotary-cored sections, measurements were limited to selected, undisturbed parts of the core rather than at regular intervals. The Introduction (this volume) discusses the data collection techniques and procedures and gives pertinent references. A complete listing of numerical data is given in the Appendix (this volume).

Data from Site 573 are plotted versus depth in Figures 11 through 15. It is worth noting that where the piston- and rotary-cored intervals overlap (140 to 160 m) the measured values agree, suggesting that the effects of drilling disturbance can be minimized through careful sample selection. It is also noteworthy that the data from Holes 573 and 573A are virtually identical, indicating that the high-amplitude variations in the upper levels of the core are real excursions and not experimental noise.

Carbonate analyses discussed under Sediment Accumulation Rates indicate that the sediment silica/carbonate ratios at this site are rather uniform. This uniformity means that wet-bulk density is controlled by porosity; and, in fact, the plots of those properties are mirror images. Wet-bulk density (Fig. 11) gradually increases from values scattered around 1.4 g/cm³ near the top of the core to around 1.8 g/cm³ at 280 m. Porosity (Fig. 12) drops from 75% to less than 60% in the same interval. Below 280 m, both porosity and density show very little change in mean values until very near igneous basement.

Formation factor (Fig. 13) is a porosity-dependent property, and as such it also mirrors trends in the porosity–depth plot. F values of around 1.75 increase to near 3.00 at depths greater than 280 m. Sonic velocity values (Fig. 14) also increase in this interval, from near 1.5 km/s at the surface to 1.6 km/s at 280 m. Formation factor (Fig. 13) and thermal conductivity (Fig. 15) show similar maxima just above 100 m; both increase below 280 m. At this depth K increases from about 2.6 mcal/cm·s·°C to about 3.4 mcal/cm·s·°C.

Five shear strength measurements were made at this site. At depths of 42, 226, and 258 m the strengths were 245, 280, and 269 g/cm², respectively. At 287 m the value increases to 421 g/cm², and at 304 m, values of 464 and 718 g/cm² were recorded.

PALEOMAGNETISM

A shipboard survey of samples selected from Site 573 shows that the downhole intensities of untreated NRM (NRM_0) decrease rapidly (by a factor of at least 10) at the color change at about 45 m sub-bottom. It is hard to tell whether the change is caused by changes in the depositional environment or the chemical alteration of the sediments below the change; both factors can affect magnetic properties. In the upper parts of Holes 573 and 573A, polarity changes can be distinguished, but they are indicated only by a 180° change in the measured declination. The Matuyama/Gauss boundary can be identified (at a position in agreement with the biostratigraphy) in Holes 573 and 573A. In Hole 573 it falls between 34 and 37 m (Sections 573-5-3 to 573-5-5). In Hole 573A it occurs at 34 to 35 m (Section 573A 4-3). A mean sedimentation rate of 14 m/m.y. to 15 m/m.y. can be calculated for the upper 35 m of both holes by using these data.

With some reservations, we calculated a mean paleolatitude for Cores 573B-14 to -24, the only part of the section that permitted the calculation. The average NRM_0 inclination of −15.2° corresponds to a paleolatitude of about 7.7°S, in reasonably good agreement with generally accepted rates of plate motion. For an updated discussion see Weinreich and Theyer (this volume).

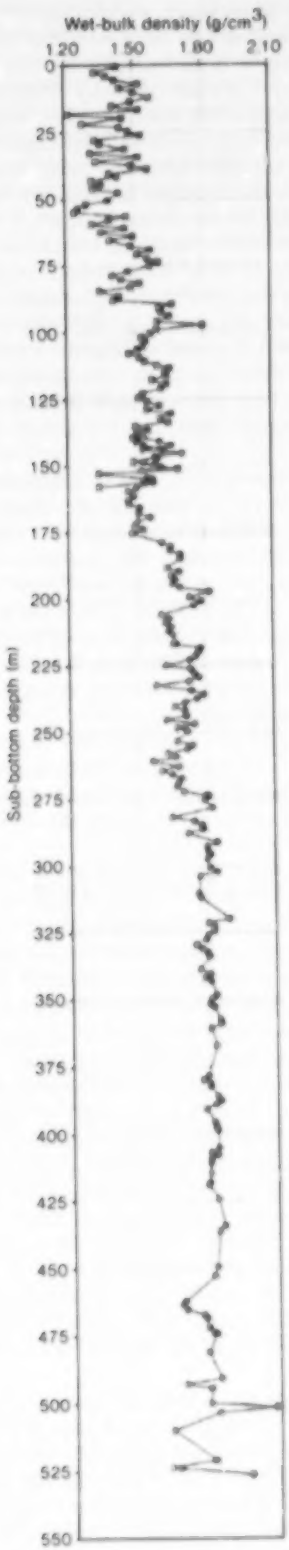

Figure 11. Wet-bulk density versus depth for Site 573.

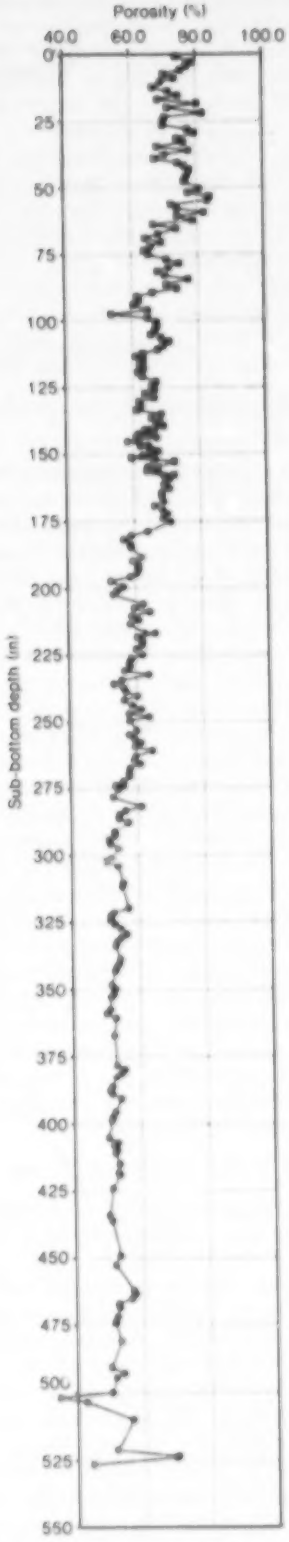

Figure 12. Porosity versus depth for Site 573.

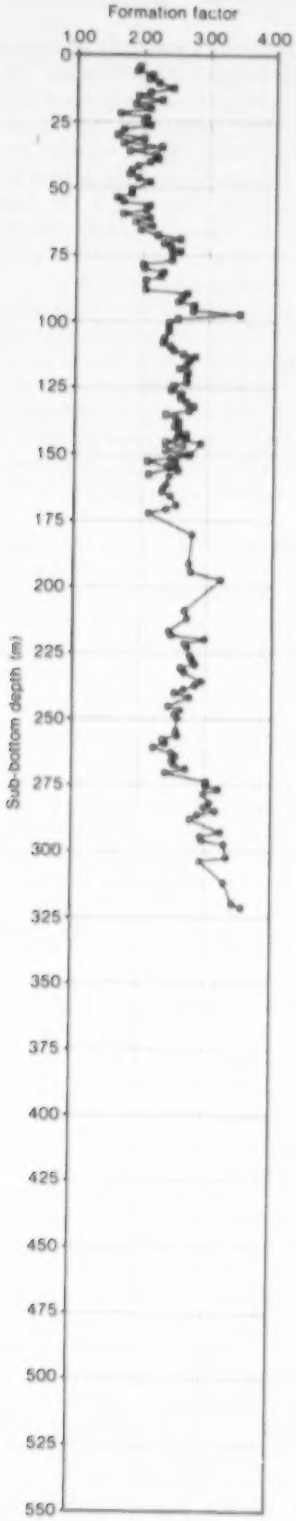

Figure 13. Formation factor (horizontal) versus depth for Site 573.

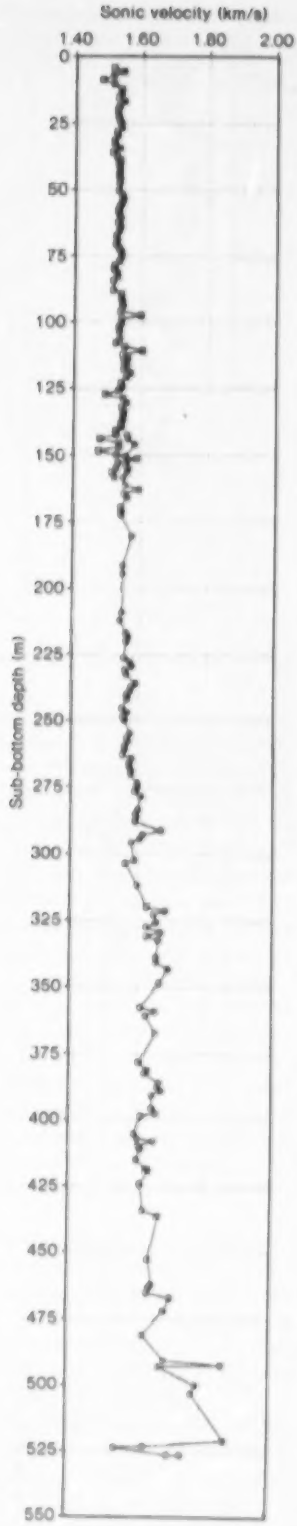

Figure 14. Sonic velocity versus depth for Site 573.

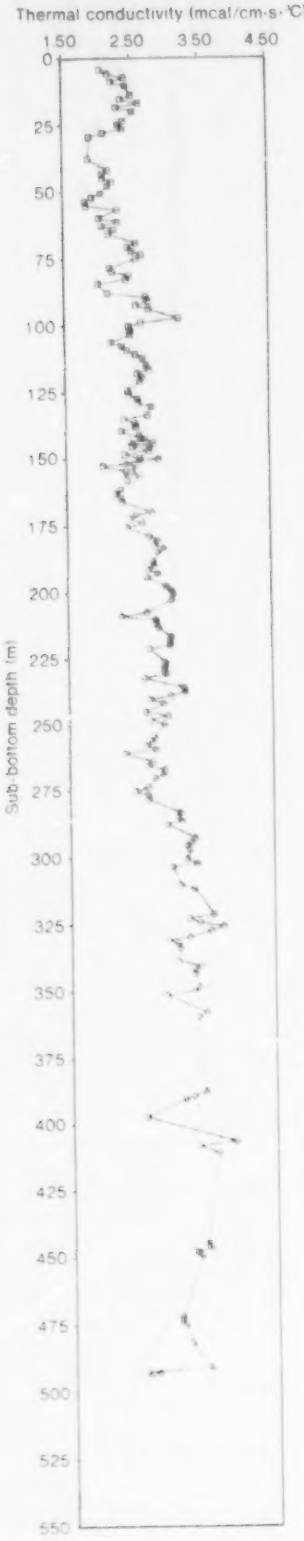

Figure 15. Thermal conductivity versus depth for Site 573.

INTERSTITIAL-WATER CHEMISTRY

Alkalinity and calcium gradually increase with increasing depth to maximum values between 250 and 300 m (Fig. 16). Both then decrease to lower levels near 360 m sub-bottom, increase again, and then show another decrease toward basement. The similarity in behavior of these chemical species is probably related to the chemistry of calcite solution. The profile for magnesium displays almost exactly opposite trends; values decrease to minimum concentrations between 150 and 250 m and then gradually increase downsection.

The strontium profile indicates that calcite recrystallization has occurred at relatively shallow depths. Values increase to a high level that remains roughly constant between depths of 140 and 210 m. The decrease below these depths may be related to downward diffusion and possibly authigenic mineral precipitation. Petrographic and mineralogic evidence suggest that celestite is present throughout the depth range from 280 to 400 m sub-bottom.

The data indicate that the *in situ* sampling device functioned properly. The high value for alkalinity relative to squeezed samples from similar depths makes contamination by surface seawater improbable. All values of chemical species measured, with the exception of salinity, were higher for the *in situ* samples than for the squeezed samples from similar depths.

SUMMARY AND CONCLUSIONS

Site 573 is located at 0°29.91′N, 133°18.57′W in 4301 m of eastern equatorial Pacific water over a basement trough covered by acoustically well stratified sediment that reaches 0.62 s in thickness. Site 77 (DSDP Leg 9), which is in the immediate vicinity (at 0°28.9′N, 133°13.7′W), was drilled on a basement flank with a 0.51 s-thick sediment cover of comparable stratification.

The primary objective of drilling the site was to obtain an expanded upper Eocene to Quaternary sedimentary section for high resolution stratigraphic and paleoceanographic studies. Three holes were drilled. Hole 573 (HPC) reached 158.6 m sub-bottom; Hole 573A, a parallel HPC attempt, was abandoned at 57.7 m sub-bottom; and Hole 573B (rotary) was cored from 138.5 to 529 m, terminating in basalt. We deployed the heat flow–pore water probe as we washed down to coring depth in Hole 573B (138.5 m) and retrieved *in situ* pore water from 53 m sub-bottom. In total, we spent 7.3 days on site and recovered 25 HPC and 43 rotary cores.

The oldest sediment recovered was uppermost Eocene limestone (Hole 573B, 528 m), below which we recovered 1.19 m of basalt that showed a baked sediment interface and glassy rinds. We divided the sedimentary section into four lithostratigraphic units and subdivided them on the basis of color. It proved to be possible to correlate our units with the three oceanic formations established for the sediments at Site 77. In upsection order, the lithostratigraphic subdivisions are as follows: an uppermost Eocene pelagic limestone (Unit IV) (528 to 526.6 m); metalliferous chalk claystone (Unit III) (526.6

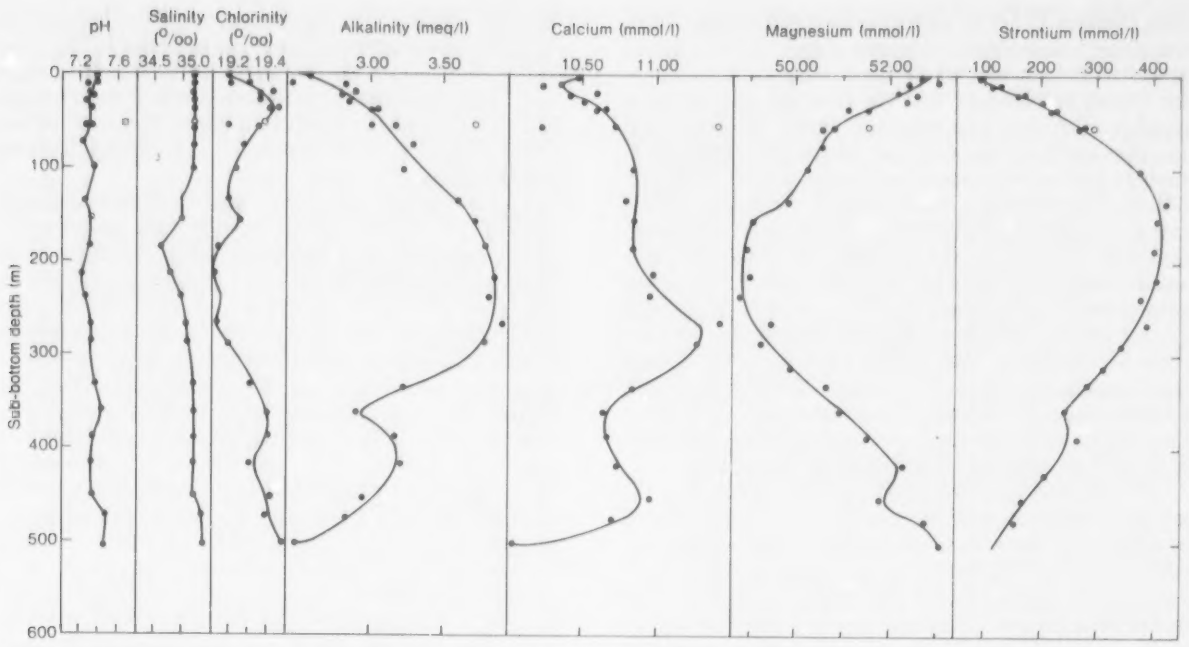

Figure 16. Interstitial-water chemistry, Site 573. Open circles are values for the *in situ* samples; solid circles are squeezed samples.

to 520.5 m), which correlates with the uppermost Eocene at its base, is virtually barren of fossils in its dark brown center, and contains lowermost Oligocene fossils at its top; a calcareous chalk ooze (Unit II) (520 to 45.1 m); and a cyclic siliceous calcareous ooze (45.1 to 0 m). Just above the brown Unit III there are turbidite layers that measure from centimeters to about 1 m in thickness and are composed of volcanic glass and ash intercalated with the pelagic sediments. The upper part of the section (0 to 180 m) is characterized by high-amplitude carbonate fluctuations; the lower part of the section (180 to 520 m) shows a relatively constant, high carbonate content with lower amplitude fluctuations.

Planktonic foraminifers, calcareous nannofossils, radiolarians, and diatoms are, with some exceptions, well represented in the cored sediments. They permit the recognition and correlation of nearly all of the Eocene to Quaternary biozonal and stratigraphic boundaries. For this reason it should be possible to use the cored sediments as a reference section for the equatorial Pacific, even though the Eocene/Oligocene boundary could not be located unequivocally. (The boundary either falls within the barren midportion of the metalliferous unit [528 to 524 m sub-bottom] or coincides with a hiatus.) The lower/upper Oligocene boundary falls in Core 573B-27 (≈ 386 m). The Oligocene/Miocene boundary occurs at about 326 m (in Core 573B-20); the lower/middle Miocene boundary is at 252 m (in Core 573B-12); the middle/upper Miocene boundary is at approximately 180 m (in Core 573B-5); and the top of the Miocene occurs at about 80 m sub-bottom (in Core 573-10). The Pliocene gives way to the Pleistocene at about 25 m sub-bottom (in Core 4 of Hole 573 and Core 3 of Hole 573A).

Biostratigraphic evidence suggests that there are at least two hiatuses in the cored sequence, although the intervals in question might also represent periods of drastically slower rates of accumulation. Most prominent among these potential hiatuses is the interval near the base of Hole 573B between foraminiferal Zones P16 (uppermost Eocene) and P18 (basal Oligocene) and nannofossil Subzones CP15b (Eocene) and CP16b (Oligocene). This interval contains the Eocene/Oligocene boundary as generally accepted. The absence of Zone P17 (foraminifers) can be explained either by postulating a hiatus or by assuming that the dark brown, barren metalliferous claystone in Core 573B-42 (520.5 to 528 m) represents the record of greatly slowed deposition in the latest Eocene and earliest Oligocene. It is also not inconceivable that the metalliferous layer is normal biogenous ooze from which all microfossils have been removed by solution. Another brief hiatus occurs in the lower upper Miocene. Correlative gaps were found in the record at nearby Site 77.

Benthic foraminifers occur throughout the section, although they are generally rare. The assemblages contain mainly long ranging, Eocene to Recent species that fluctuate in their relative abundances but are remarkably stable in terms of overall character. A few Eocene marker species were found in the upper Eocene sediments of Sample 573B-42-4, 144–147 cm.

The overall sediment accumulation rates at Site 573 are relatively constant, varying generally between 18 and 12 m/m.y. A peak of 30 m/m.y. occurs between 5.5 and 6.1 Ma, and a low of about 10 m/m.y. occurs between 15.5 and 21.4 Ma. In some instances, the accumulation rate changes correlate with breaks in the lithology and

with changes in NRM paleomagnetic intensities. Thus, the silica-rich sediments between about 160 and 200 m approximate an interval of rapid deposition, whereas the brown sedimentary unit between 260 and 300 m is roughly equivalent to a period of slower accumulation. In other parts of the record no relationship between lithology and rate of deposition seems to exist. Compaction at Site 573 has a marked effect on sedimentation rate estimates, as demonstrated by the mass accumulation rate calculations. For example, although the intervals between 25.9 and 31.3 Ma and 1.3 to 3.5 Ma show equal rates of sedimentation (about 13 m/m.y.), the Oligocene chalks—which are considerably denser—have a mass accumulation rate greater by a factor of 2 than the Pliocene–Pleistocene sediments. These estimates also show that the Oligocene interval at Site 573 was a time of generally high mass accumulation rate. See Theyer et al. (this volume) for an updated discussion.

The physical properties of the sediments at Site 573 are, by themselves, not very telling and are best reviewed in relation to the results from other sites. Noteworthy, nevertheless, is the constancy of grain density, which hovers near values of pure carbonate throughout most of the site's section. The grain density data thus suggest that the wet-bulk density of these sediments is controlled primarily by water content or porosity. Formation factor, another porosity-sensitive parameter, corroborates this idea.

The seismic section is characterized by the alternation of highly stratified and more transparent zones. The more acoustically stratified sections are correlated with high-amplitude, high-frequency fluctuations in saturated wet-bulk density (and calcium carbonate); the more transparent zones are correlated with intervals of lower amplitude, longer wavelength changes. Several distinct individual reflectors appear to correlate with major shifts in the wet-bulk density curve. See Mayer et al. (this volume) for more details.

Shipboard paleomagnetic results indicate that most of the samples analyzed are characterized by low NRM intensities. Except for the uppermost 50 m, a portion between 260 and 360 m, and the bottom 20 m of Hole 573B (where intensities on the order of 10^{-6} G and above were measured), the NRM_0 of most samples falls within, or barely above, the noise level of the shipboard magnetometer. Changes in intensity seem to coincide broadly with changes in lithology (color) and fluctuations in sedimentation rate. A preliminary Gauss to Matuyama magnetic stratigraphy can be recognized in the upper 50 m of Site 573, although it may be refined after the cores are demagnetized and oriented properly (see Weinreich and Theyer, this volume). A tentative paleolatitude calculation, based on the mean NRM_0 inclination of 22 specimens from Cores 573B-14 to -24, yields a paleolatitude of 7.7°S, somewhat farther north than that postulated for a comparable Oligocene–Miocene interval at Site 77.

Shipboard geochemical analysis of interstitial water suggests diagenetic activity within the sediments of the site. The trends in magnesium, calcium, and alkalinity concentration are nearly linear in the upper 100 m of the section; concavity in the curves below this level is significant (the magnesium trend is opposite to the other two). We interpret the concavity in the trends as being due to the production or consumption of these species and the more linear trends in the upper part of the section as the result of diffusional transport and exchange with seawater.

In conclusion, the tectonic and depositional history of Site 573 mirrors that of Site 77 (van Andel et al., 1975). Assuming that basement age at the site is about 39 Ma, these authors postulate an initial paleolatitude of nearly 8°S and a paleodepth of some 2800 m. The site's sediments should therefore record a descent into deeper, more corrosive waters near the lysocline and the northerly motion of the site into the equatorial belt. The metalliferous sediments and the presence of volcanic glass and/or ash turbidites in the upper Eocene to lowermost Oligocene sediments just above basement clearly indicate the proximity of the site to the ridge crest. The location of the site in a basement trough would cause such volcanic fragments and other mobile sediments from nearby highs to be trapped and explain why the section is thicker than that at Site 77, which is identical in age. During the subsequent Oligocene interval the site's water depth increased, but the sedimentary record remains relatively unchanged in terms of accumulation rate, which is almost uniformly high, and the solution of planktonic foraminifers, which increases very slowly and moderately until about 16 to 17 Ma (uppermost lower Miocene). The movement of the site into the equatorial high-productivity belt, which is dated as 1.5 Ma by van Andel et al., is hard to detect. It may be obscured by the increasing carbonate solution that would have accompanied the sinking of the site to its present depth of 4300 m; it is also possible, however, that the migration finds expression in the greater abundance and preservation of diatoms from the upper middle Miocene to Quaternary. Studies of the record of carbonate and silica accumulation, stratigraphy, and tectonic evolution will help to unravel details of the site's history.

REFERENCES

Andrews, J. E., Packham, G., et al., 1975. Site 289. *In* Andrews, J. E., Packham, G., et al., *Init. Repts. DSDP*, 30: Washington (U.S. Govt. Printing Office), 231–398.

Barron, J. A., 1981. Middle Miocene diatom biostratigraphy of equatorial Pacific DSDP Hole 77B. *Geosci. J.*, 2:137–144.

Berger, W. H., and von Rad, U., 1972. Cretaceous and Cenozoic sediments from the Atlantic Ocean. *In* Hayes, D. E., Pimm, A. C., et al., *Init. Repts. DSDP*, 14: Washington (U.S. Govt. Printing Office), 787–954.

Boltovskoy, E., 1978. Late Cenozoic benthonic foraminifera from the Ninety East Ridge (Indian Ocean). *Mar. Geol.*, 26:149–175.

Bukry, D., 1971. Cenozoic calcareous nannofossils from the Pacific Ocean. *Trans. San Diego Soc. Nat. Hist.*, 16:307–327.

_____, 1972. Coccolith stratigraphy, Leg 9, Deep Sea Drilling Project. *In* Hays, J. D., et al., *Init. Repts. DSDP*, 9: Washington (U.S. Govt. Printing Office), 817–832.

_____, 1973a. Low-latitude coccolith biostratigraphic zonation. *In* Edgar, N. T., Saunders, J. B., et al., *Init. Repts. DSDP*, 15: Washington (U.S. Govt. Printing Office), 685–703.

_____, 1973b. Coccolith stratigraphy, eastern equatorial Pacific, Leg 16, Deep Sea Drilling Project. *In* van Andel, T. H., Heath, G. R., et al., *Init. Repts. DSDP*, 16: Washington (U.S. Govt. Printing Office), 633–712.

Burckle, L. H., and Opdyke, N. D., 1977. Late Neogene diatom correlations in the circum-Pacific. *Proc. First Internat. Congr. Pacific Neogene Stratigraphy* (Tokyo, 1976), pp. 255–284.

Burckle, L. H., and Trainer, J., 1979. Middle and late Pliocene datum levels from the central Pacific. *Micropaleontology*, 25:281–293.

Cook, H. E., 1972. Stratigraphy and sedimentation. *In* Hays, J. D., et al., *Init. Repts. DSDP*, 9: Washington (U.S. Govt. Printing Office), 933–944.

Douglas, R. G., 1973. Benthonic foraminiferal biostratigraphy in the central North Pacific, Leg 17, Deep Sea Drilling Project. *In* Winterer, E. L., Ewing, J. I., et al., *Init. Repts. DSDP*, 17: Washington (U.S. Govt. Printing Office), 607–672.

Douglas, R., and Woodruff, F., 1981. Deep sea benthic foraminifera. *In* Emiliani, C. (Ed.), *The Sea* (Vol. 7): New York (Wiley Interscience), pp. 1233–1327.

Dunn, D. A., 1982. Miocene sediments of the equatorial Pacific Ocean: carbonate stratigraphy and dissolution history [Ph.D. dissert.]. Univ. Rhode Island, Narragansett.

Dunn, D. A., and Moore, T. C., Jr., 1981. Late Miocene–Pliocene (Magnetic Epoch 9–Gilbert Magnetic Epoch) calcium carbonate stratigraphy of the equatorial Pacific Ocean. *Geol. Soc. Am. Bull.*, 92:408–452.

Hays, J. D., et al., 1972. Site 77. *In* Hays, J. D., et al., *Init. Repts. DSDP*, 9: Washington (U.S. Govt. Printing Office), 43–208.

Keller, G., 1981. Miocene biochronology and paleoceanography of the North Pacific. *Mar. Micropaleontol.*, 6:535–551.

Keller, G., and Barron, J. A., 1983. Paleoceanographic implications of Miocene deep sea hiatuses. *Geol. Soc. Am. Bull.*, 94:590–613.

Keller, G., Barron, J. A., and Burckle, L. H., 1982. North Pacific late Miocene correlations using microfossils, stable isotopes, percent $CaCO_3$, and magnetostratigraphy. *Mar. Micropaleontol.*, 7:327–357.

Kennett, J. P., Houtz, R. E., Andrews, P. B., Edwards, A. R., Gostin, V. A., et al., 1975. Cenozoic paleoceanography in the southwest Pacific Ocean, Antarctic glaciation, and the development of the circum-Antarctic Current. *In* Kennett, J. P., Houtz, R. E., et al., *Init. Repts. DSDP*, 29: Washington (U.S. Govt. Printing Office), 1155–1169.

Miller, K. G., Curry, W. B., and Ostermann, D. R., 1985. Late Paleogene (Eocene to Oligocene) benthic foraminiferal oceanography of the Goban Spur region, Deep Sea Drilling Project Leg 80. *In* Graciansky, P. C. de, Poag, C. W., et al., *Init. Repts. DSDP*, 80, Pt. 1: Washington (U.S. Govt. Printing Office), 505–538.

Riedel, W. R., and Sanfilippo, A., 1978. Stratigraphy and evolution of tropical Cenozoic radiolarians. *Micropaleontology*, 23(1):61–96.

Sanfilippo, A., Westberg, M. J., and Riedel, W. R., 1981. Cenozoic radiolarians at Site 462, Deep Sea Drilling Project Leg 61, western tropical Pacific. *In* Larson, R. L., Schlanger, S. O., et al., *Init. Repts. DSDP*, 61: Washington (U.S. Govt. Printing Office), 495–505.

Shackleton, N. J., and Opdyke, N. D., 1977. Oxygen isotope and paleomagnetic evidence for early Northern Hemisphere glaciation. *Nature*, 270:216–219.

van Andel, T. H., Heath, G. R., and Moore, T. C., Jr., 1975. Cenozoic history and paleoceanography of the central equatorial Pacific Ocean. *Mem. Geol. Soc. Am. 143.*

Van Couvering, J. A., and Berggren, W. A., 1977. Biostratigraphy basis of the Neogene time scale. *In* Kauffman, E. G., and Hazel, J. E. (Eds.), *Concepts and Methods of Biostratigraphy:* Stroudsburg (Dowden, Hutchinson, Ross), pp. 283–306.

Woodruff, F., and Douglas, R. G., 1981. Response of deep-sea benthic foraminifera to Miocene paleoclimatic events. *Mar. Micropaleontol.*, 6:617–632.

SITE 573 HOLE CORE 1 CORED INTERVAL 0.0–2.0 m

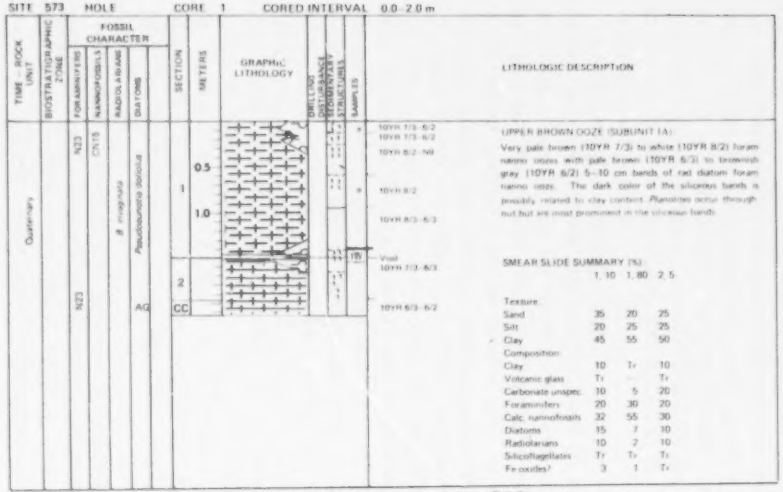

NOTE: Graphic lithologies represent average compositions derived from smear slides and do not always reflect the detailed alternation of sediment types. Major lithologic boundaries are shown but gradational contacts, small-scale cyclicity and ooze-chalk alternations are represented schematically. Color changes approximate to lithologic changes.

Hole 573, Core 1, CARBONATE BOMB: 1, 75 cm = 85%

SITE 573 HOLE CORE 2 CORED INTERVAL 2.0–11.5 m

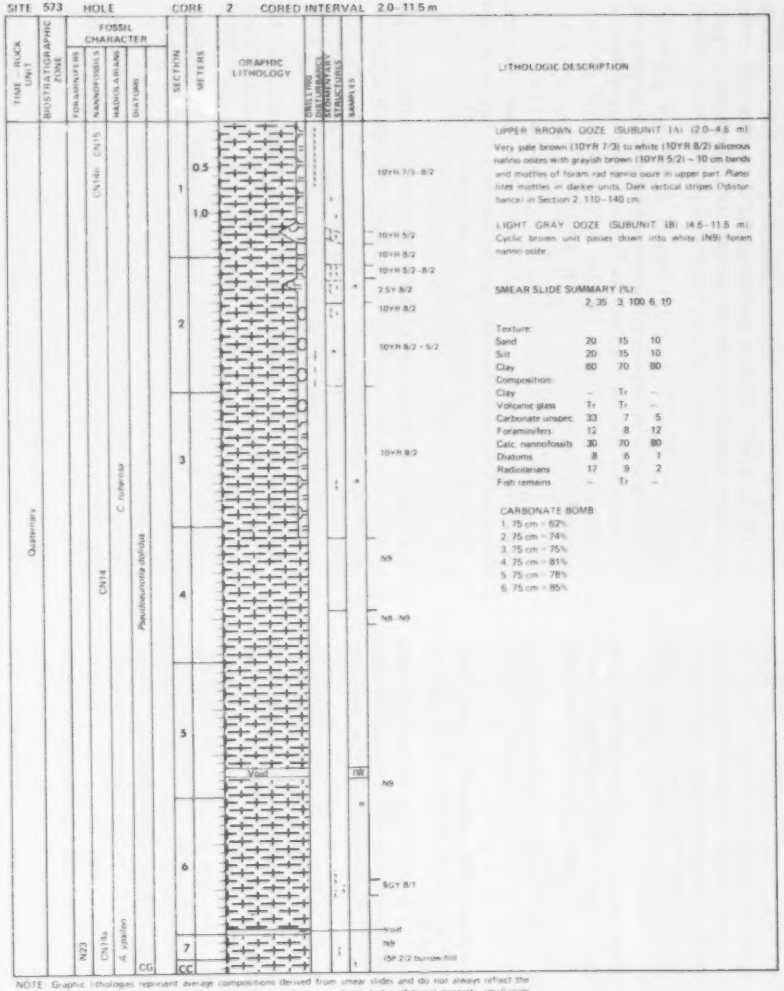

NOTE: Graphic lithologies represent average compositions derived from smear slides and do not always reflect the detailed alternation of sediment types. Major lithologic boundaries are shown but gradational contacts, small-scale cyclicity and ooze-chalk alternations are represented schematically. Color changes approximate to lithologic changes.

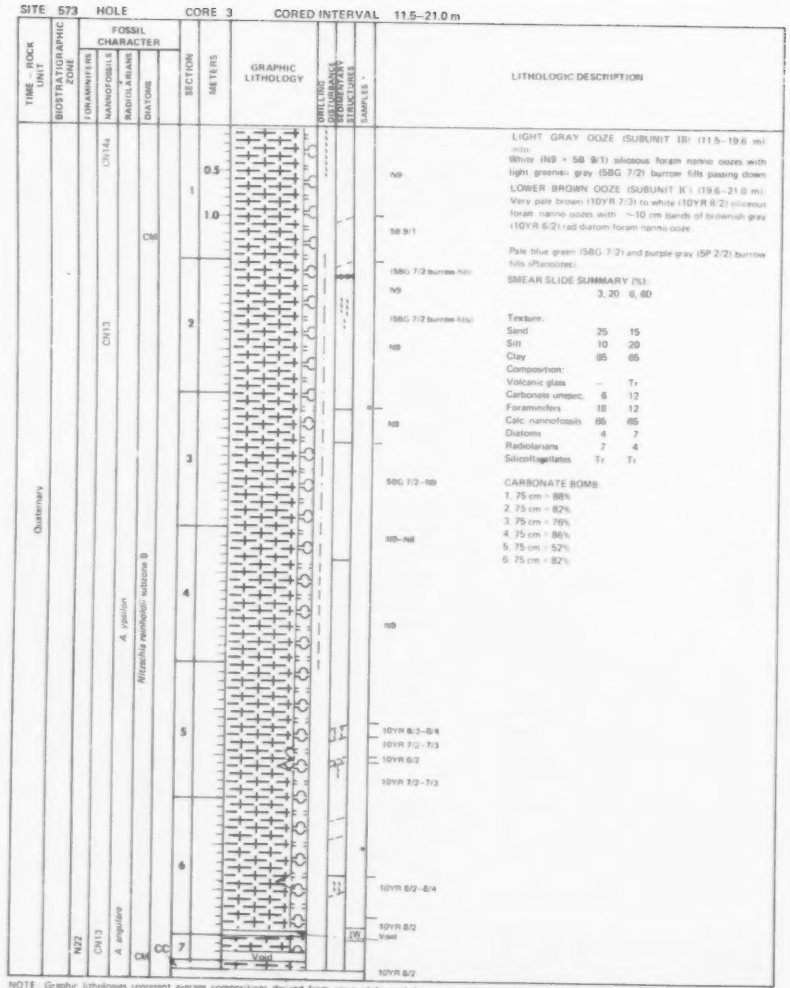

NOTE: Graphic lithologies represent average compositions derived from smear slides and do not always reflect the detailed alternation of sediment types. Major lithologic boundaries are shown but gradational contacts, small-scale cyclicity and ooze-chalk alternations are represented schematically. Color changes approximate to lithologic changes.

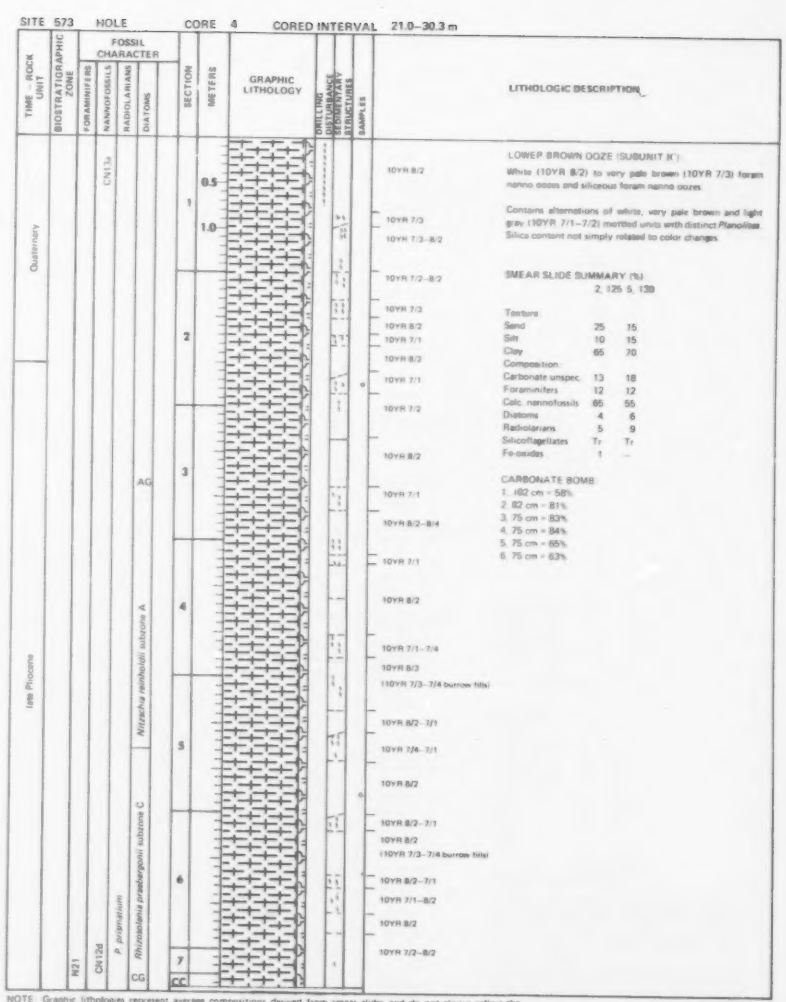

NOTE: Graphic lithologies represent average compositions derived from smear slides and do not always reflect the detailed alternation of sediment types. Major lithologic boundaries are shown but gradational contacts, small-scale cyclicity and ooze-chalk alternations are represented schematically. Color changes approximate to lithologic changes.

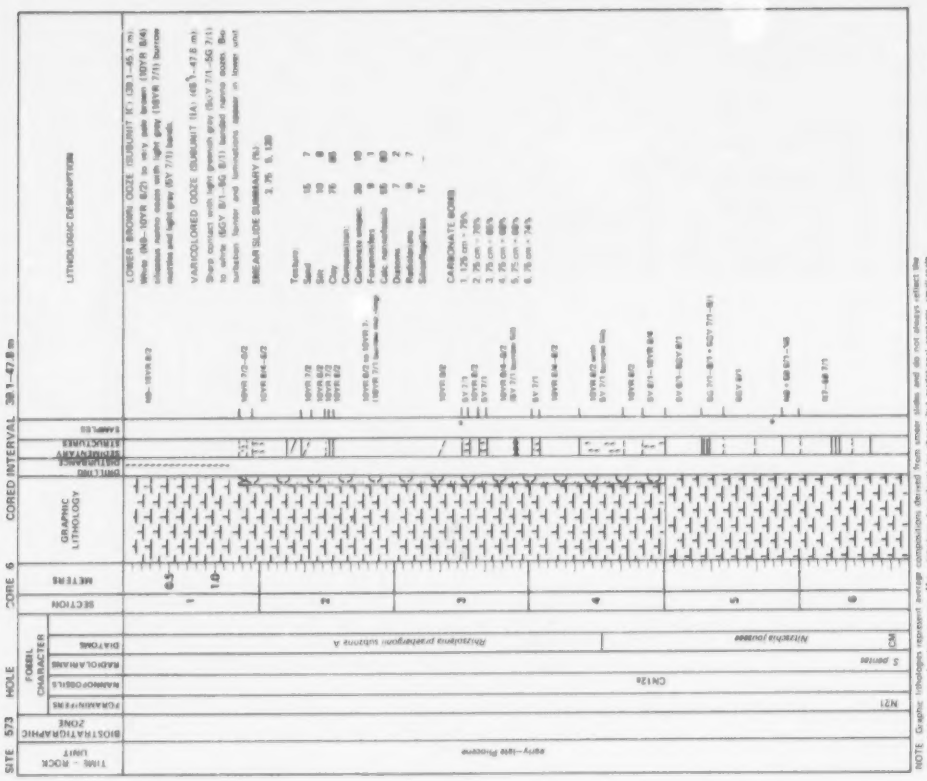

NOTE: Graphic lithologies represent average compositions derived from smear slides and do not always reflect the detailed alternation of sediment types. Major lithologic boundaries are shown but gradational contacts, small-scale cyclicity and color-shade alternations are represented schematically. Color changes approximate to lithologic changes.

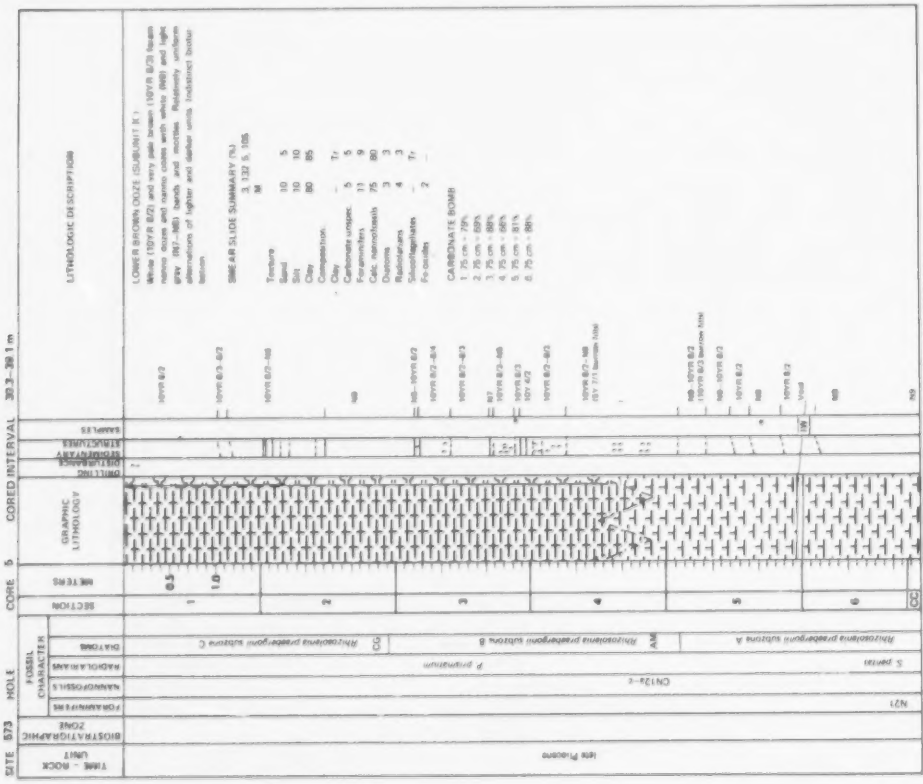

NOTE: Graphic lithologies represent average compositions derived from smear slides and do not always reflect the detailed alternation of sediment types. Major lithologic boundaries are shown but gradational contacts, small-scale cyclicity and color-shade alternations are represented schematically. Color changes approximate to lithologic changes.

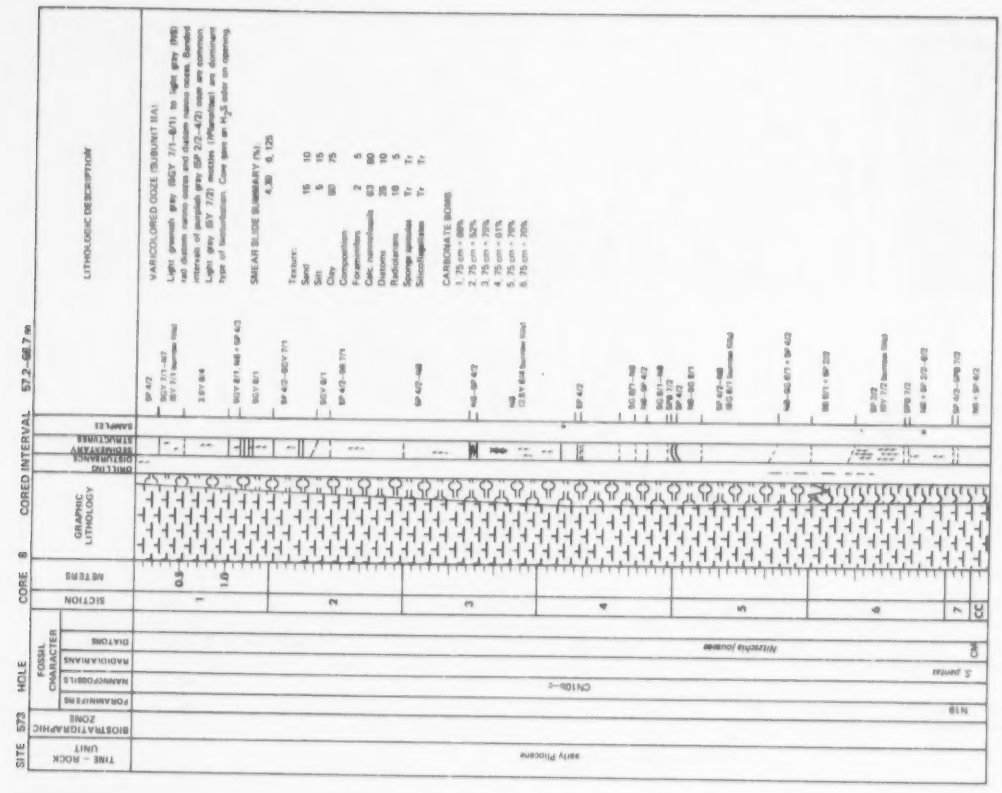

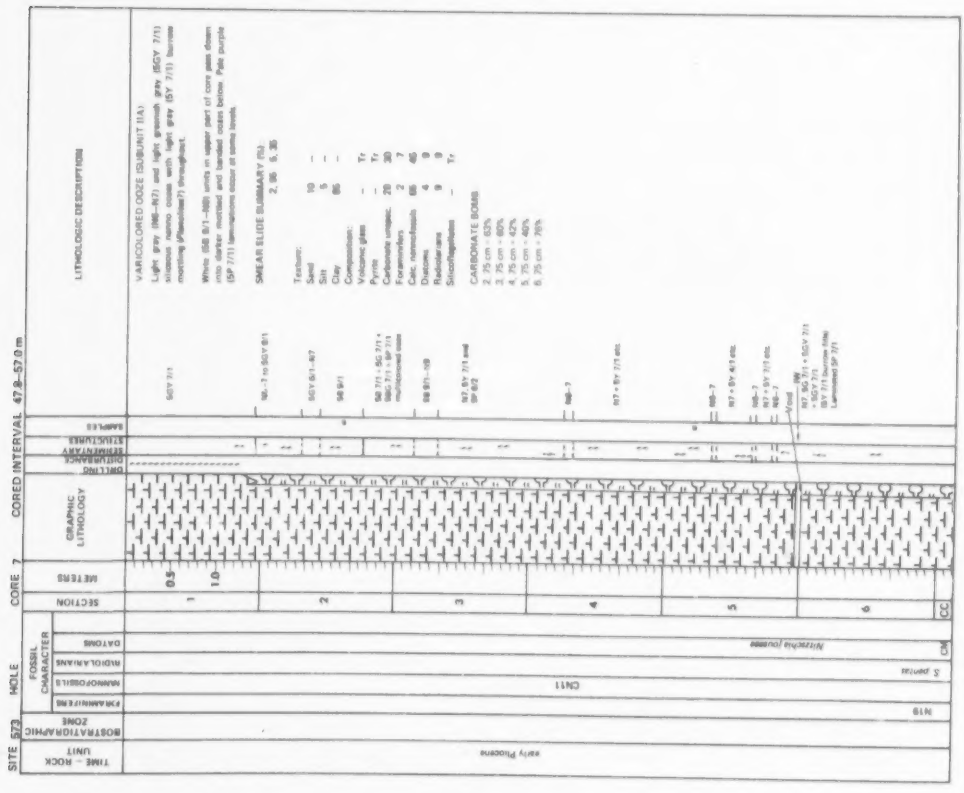

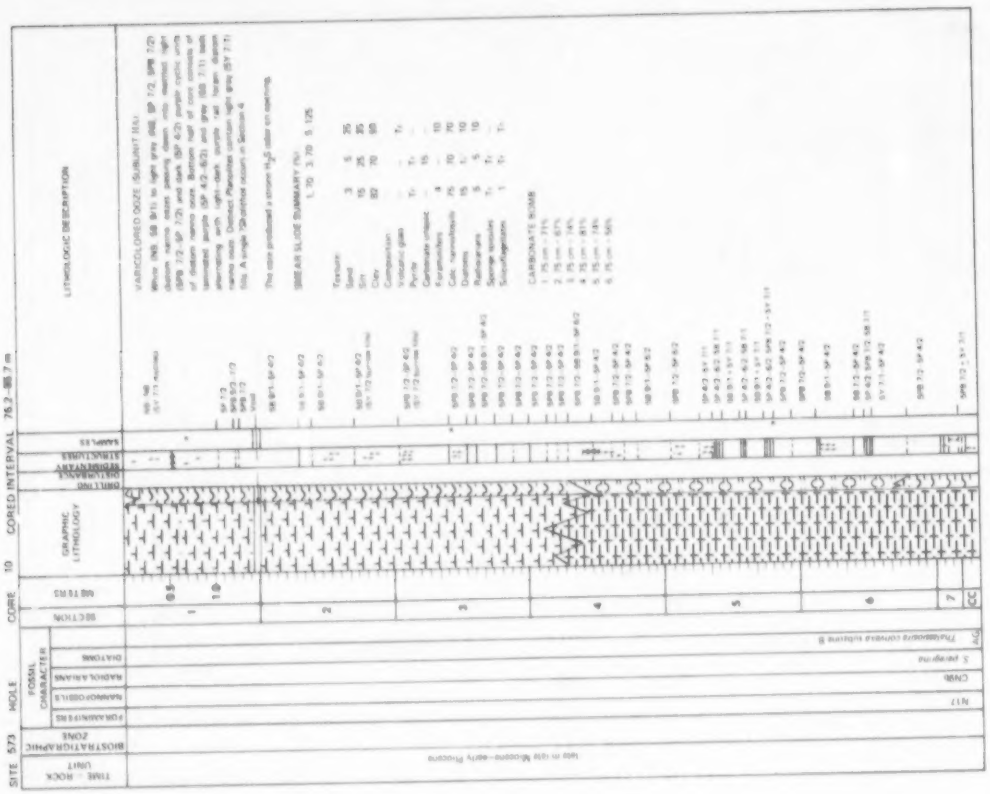

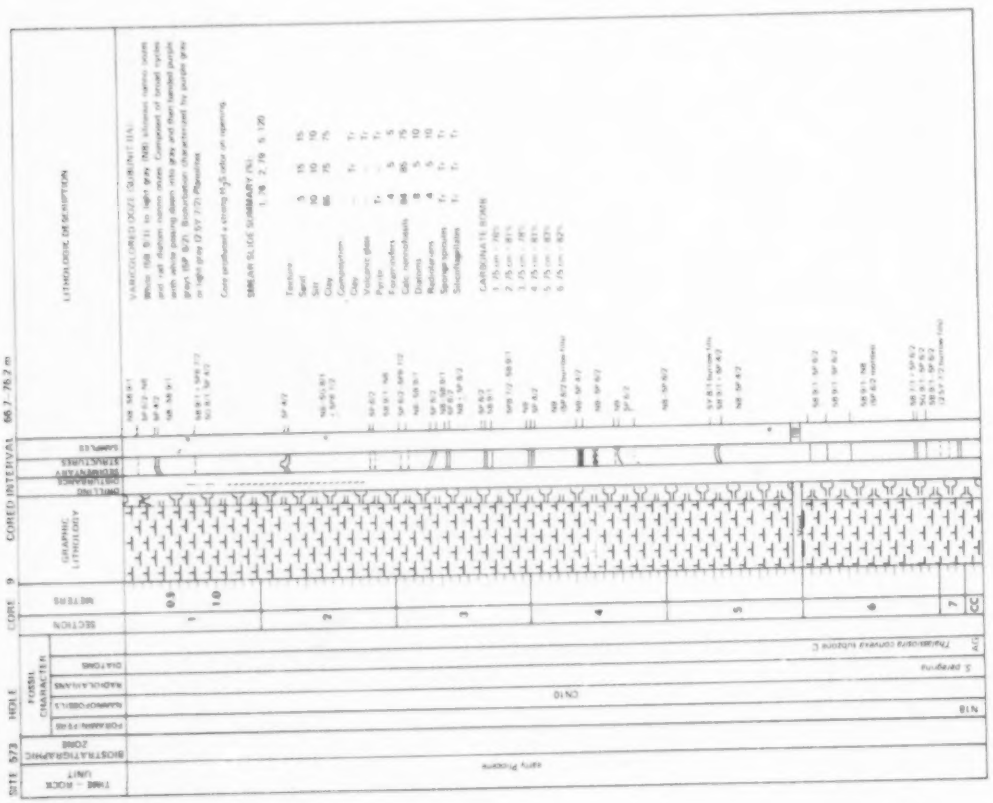

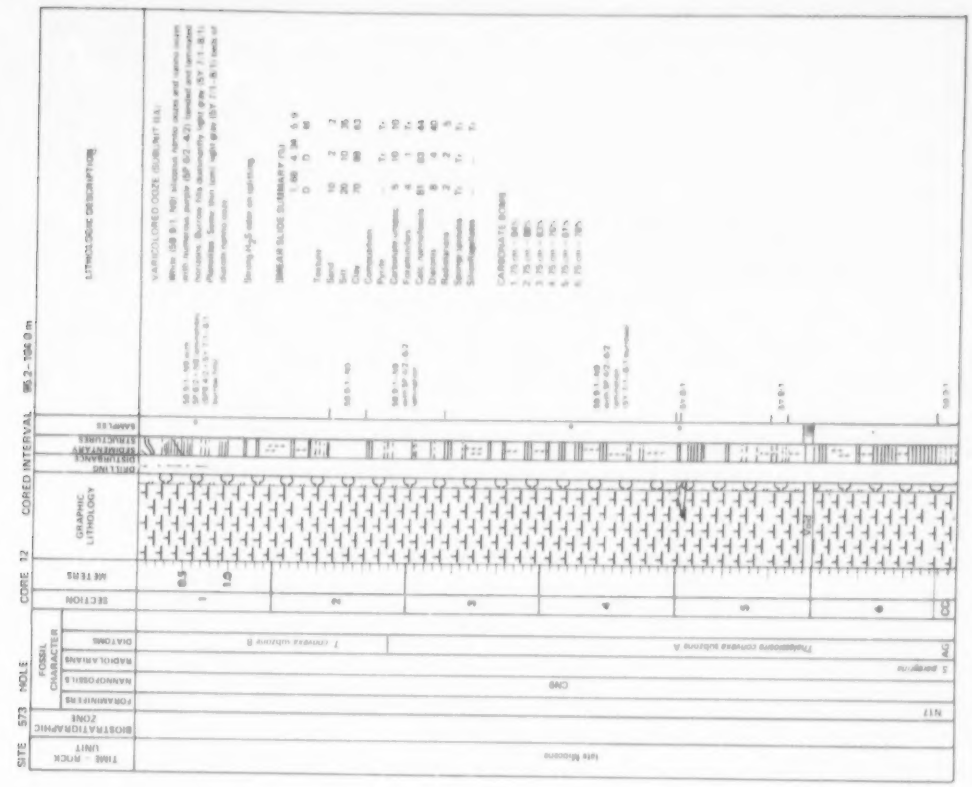

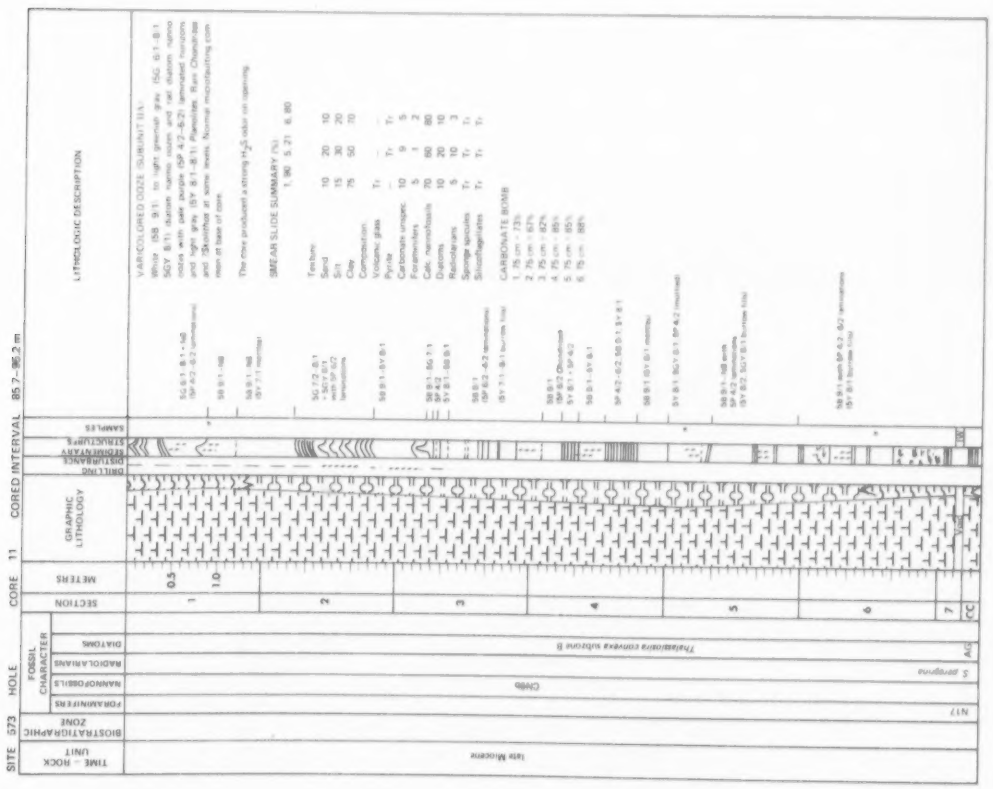

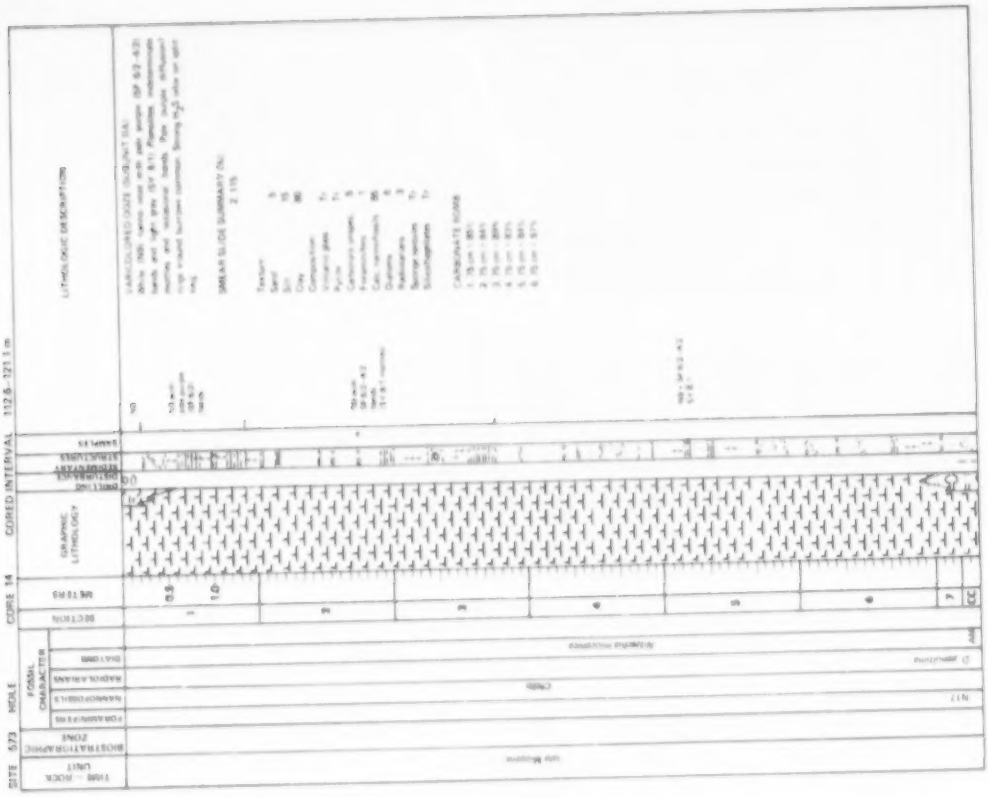

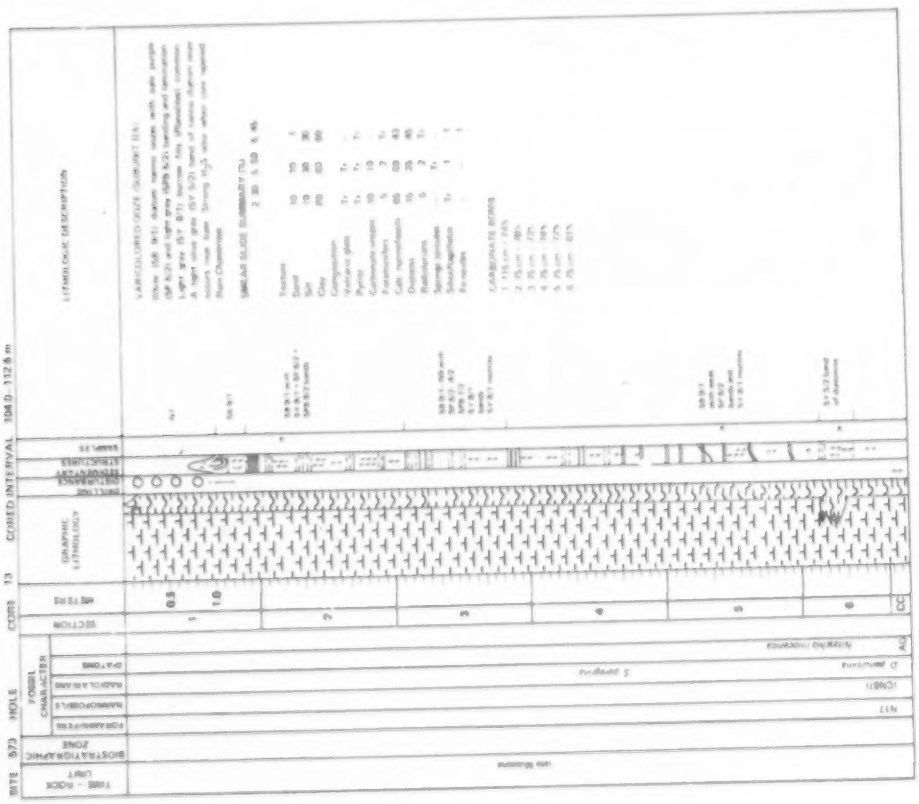

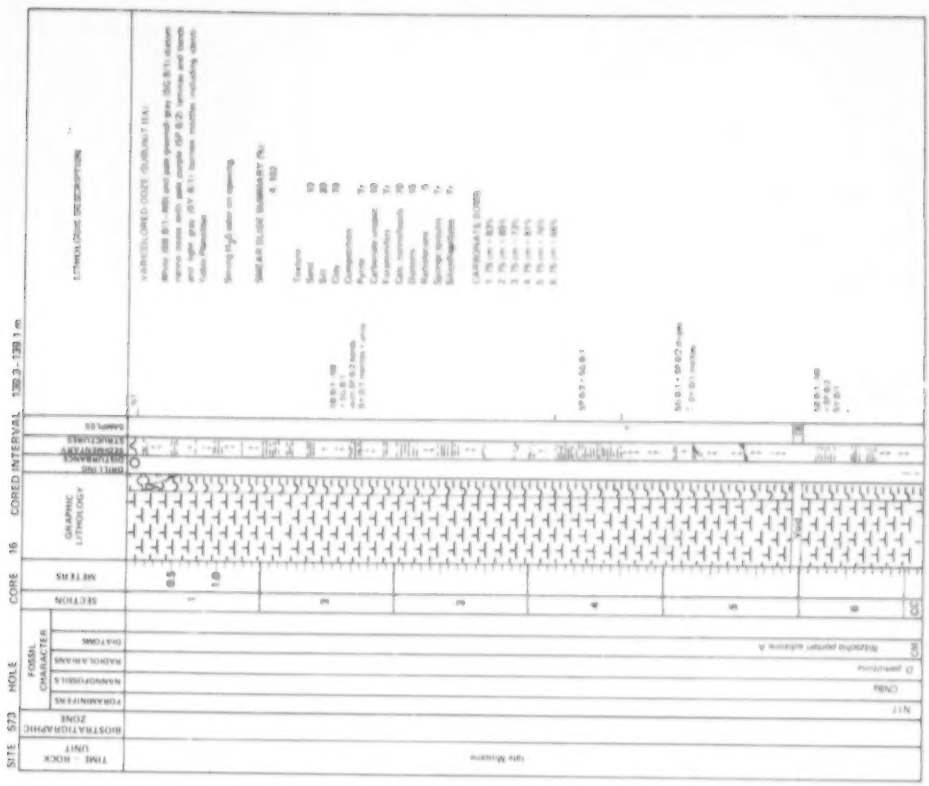

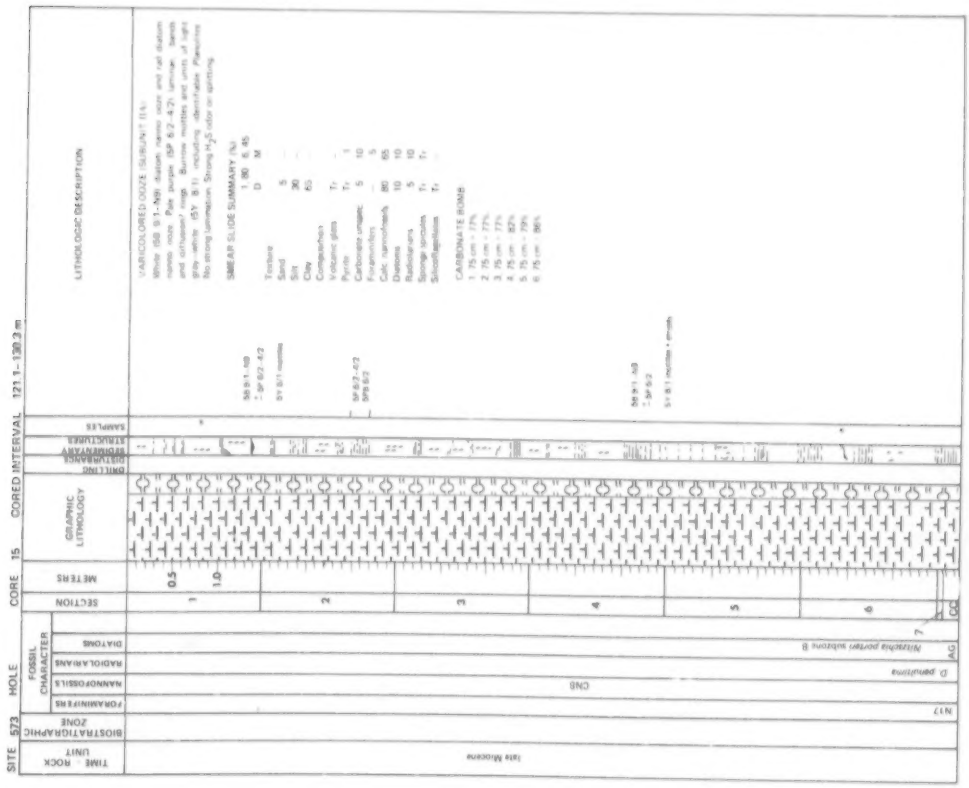

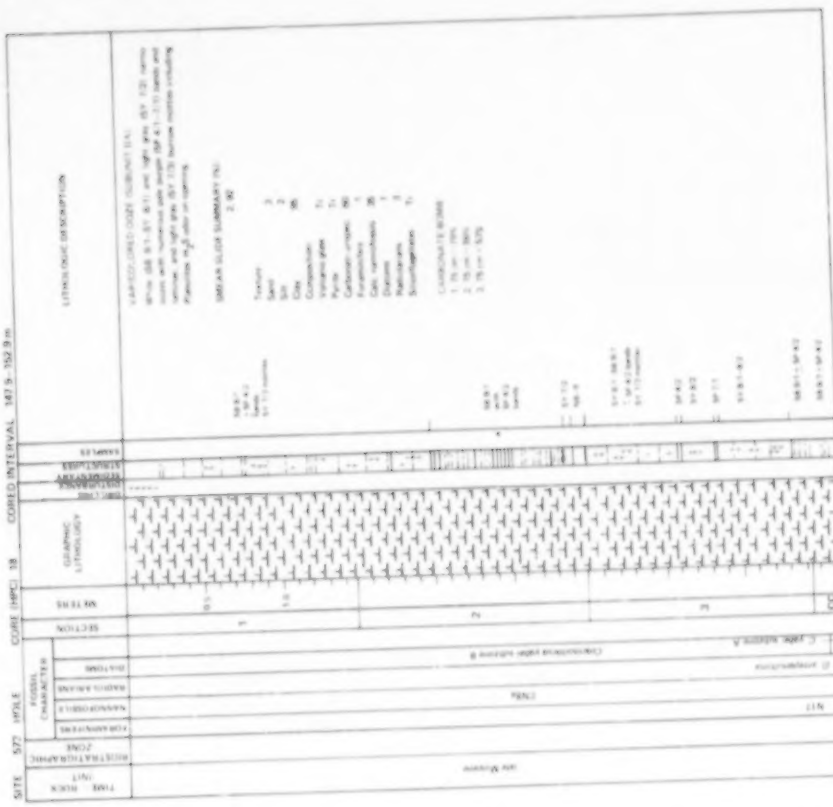

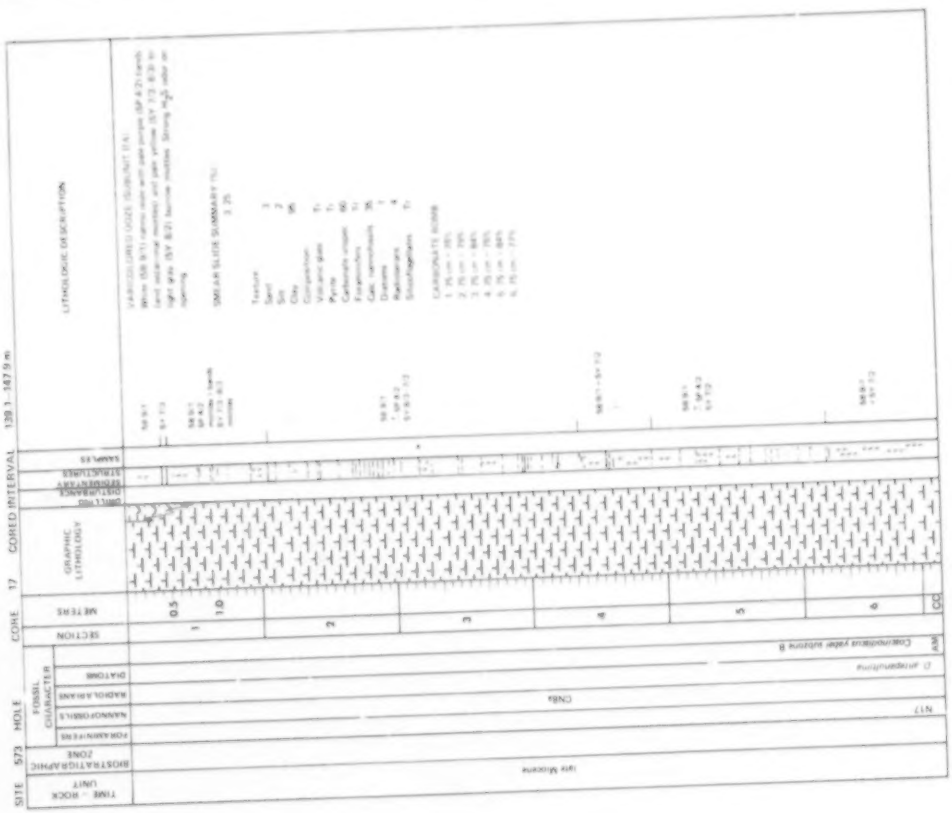

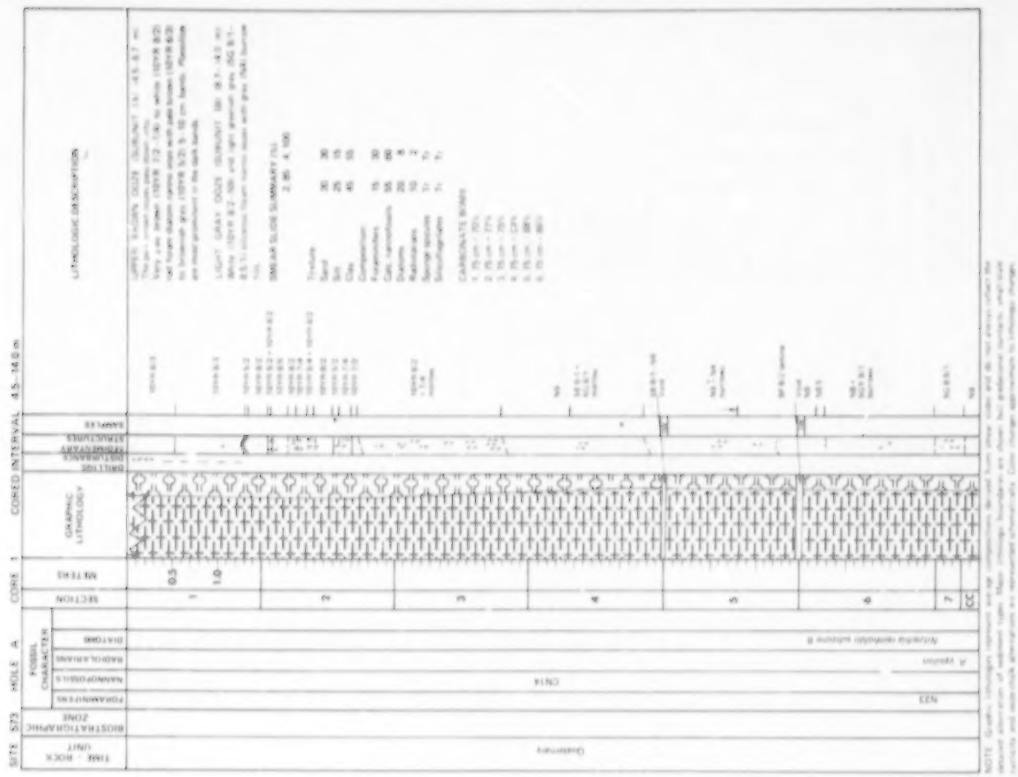

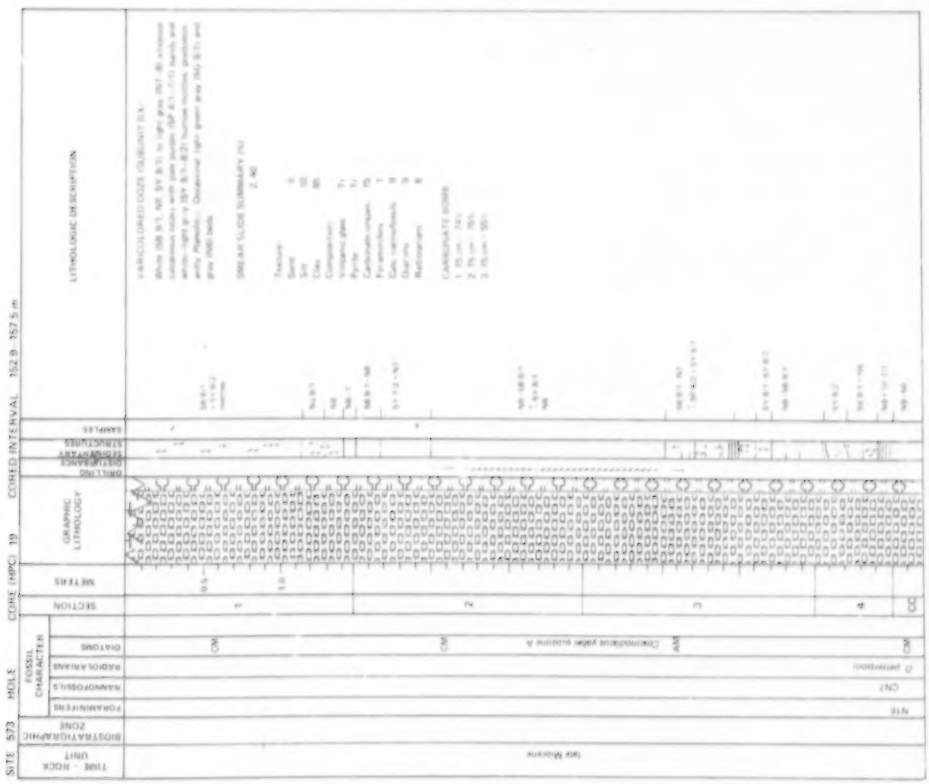

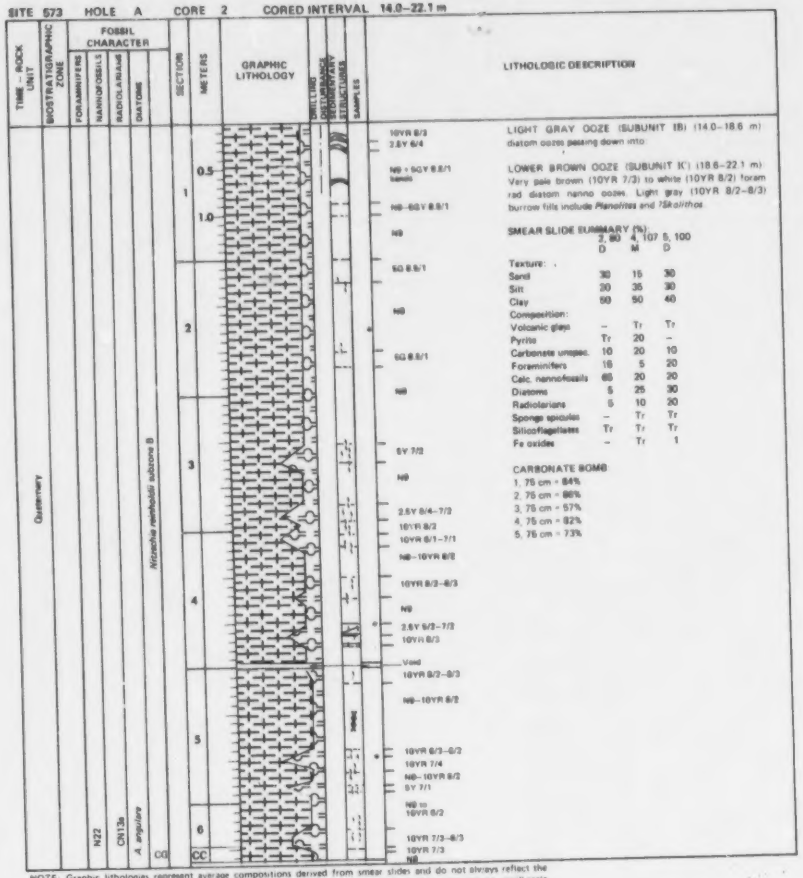

NOTE: Graphic lithologies represent average compositions derived from smear slides and do not always reflect the detailed alternation of sediment types. Major lithologic boundaries are shown but gradational contacts, small-scale cyclicity and ooze-chalk alternations are represented schematically. Color changes approximate to lithologic changes.

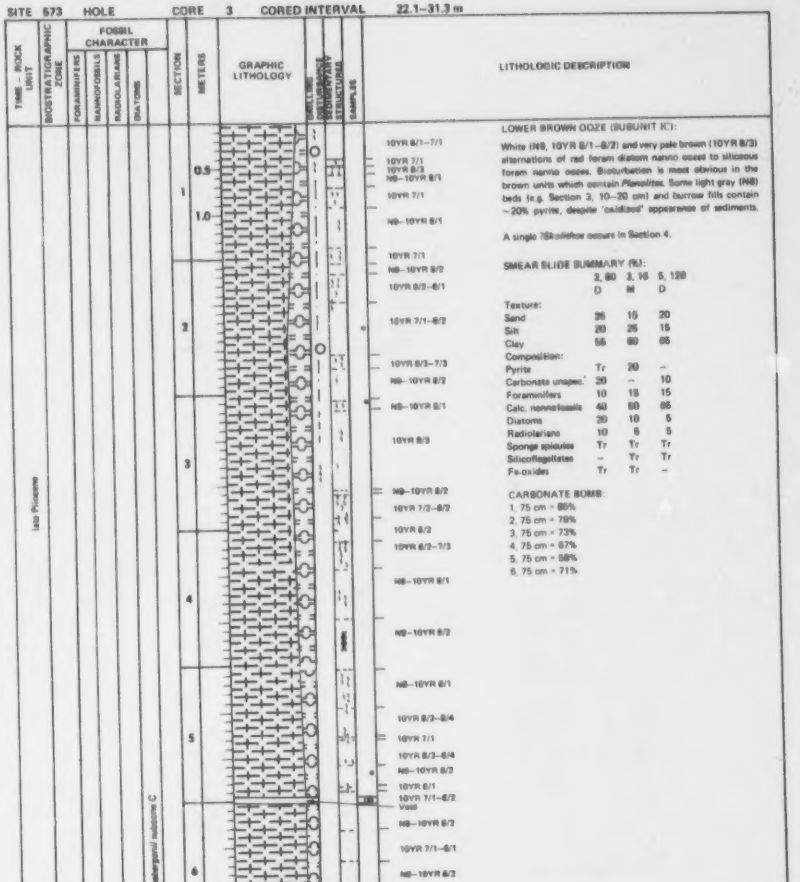

NOTE: Graphic lithologies represent average compositions derived from smear slides and do not always reflect the detailed alternation of sediment types. Major lithologic boundaries are shown but gradational contacts, small-scale cyclicity and ooze-chalk alternations are represented schematically. Color changes approximate to lithologic changes.

READER best copy available

SITE 573 HOLE A CORE 4 CORED INTERVAL 31.3–39.8 m

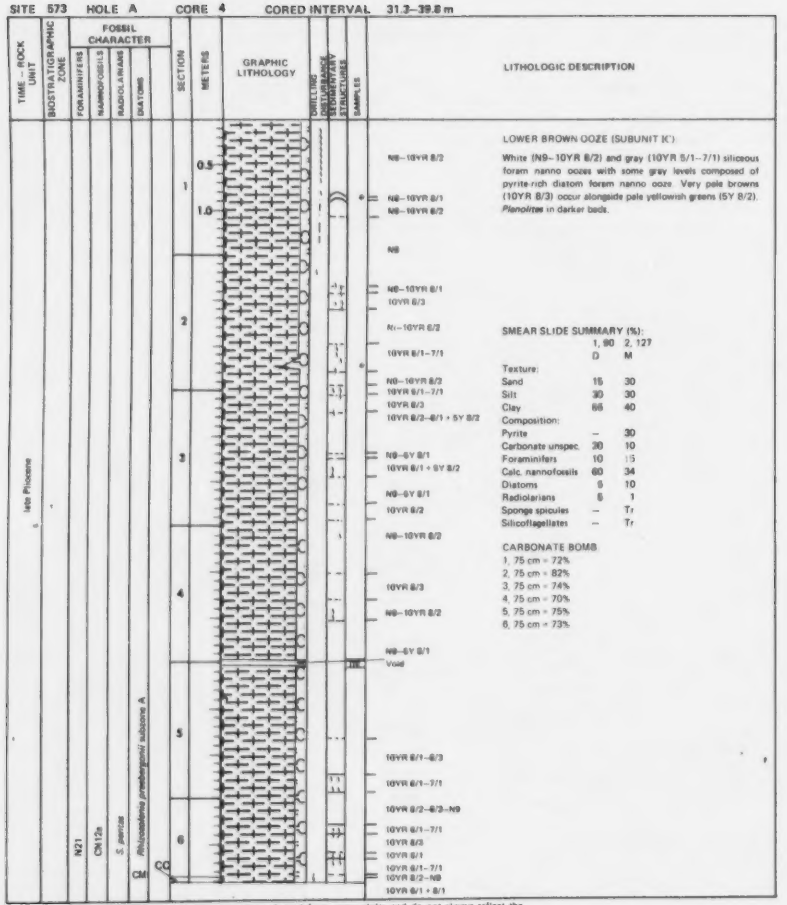

LOWER BROWN OOZE (SUBUNIT IC):

White (N9–10YR 8/2) and gray (10YR 5/1–7/1) siliceous foram nanno oozes with some gray levels composed of pyrite-rich diatom foram nanno ooze. Very pale browns (10YR 8/3) occur alongside pale yellowish greens (5Y 8/2). *Planolites* in darker beds.

SMEAR SLIDE SUMMARY (%):

	1, 90 D	2, 127 M
Texture:		
Sand	15	30
Silt	30	30
Clay	55	40
Composition:		
Pyrite	–	30
Carbonate unspec.	20	10
Foraminifers	10	15
Calc. nannofossils	60	34
Diatoms	5	10
Radiolarians	5	1
Sponge spicules	–	Tr
Silicoflagellates	–	Tr

CARBONATE BOMB:

1, 75 cm = 72%
2, 75 cm = 82%
3, 75 cm = 74%
4, 75 cm = 70%
5, 75 cm = 75%
6, 75 cm = 73%

NOTE: Graphic lithologies represent average compositions derived from smear slides and do not always reflect the detailed alternation of sediment types. Major lithologic boundaries are shown but gradational contacts, small-scale cyclicity and ooze-chalk alternations are represented schematically. Color changes approximate to lithologic changes.

SITE 573 HOLE A CORE 5 CORED INTERVAL 39.8–49.2 m

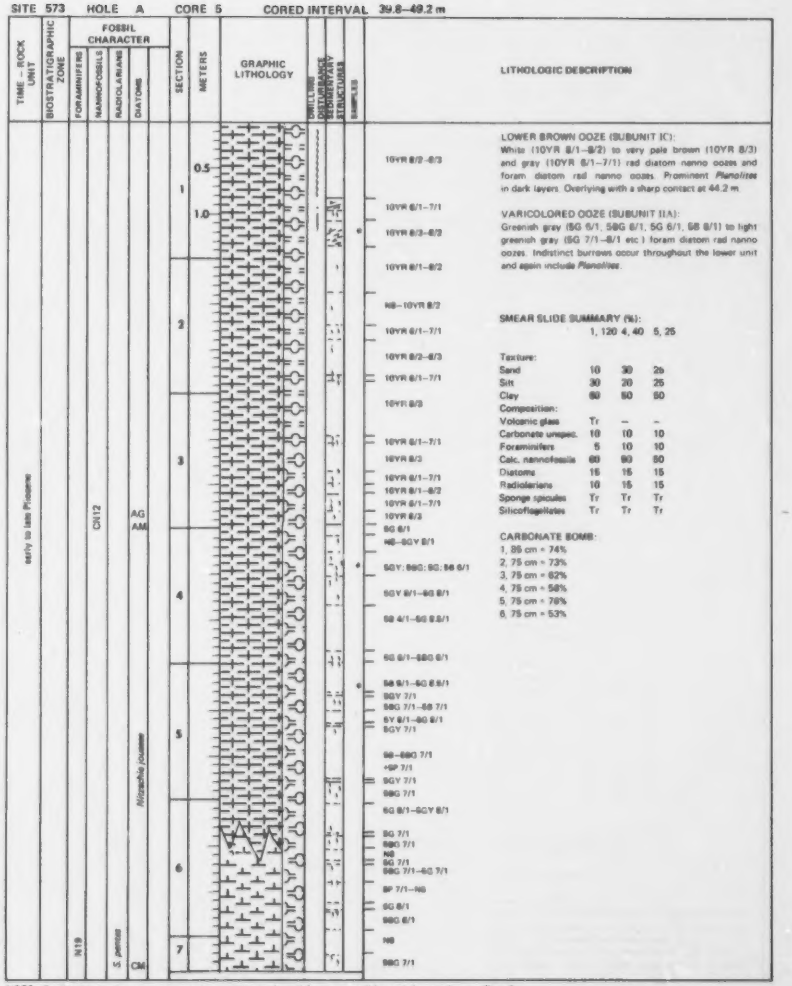

LOWER BROWN OOZE (SUBUNIT IC):

White (10YR 8/1–8/2) to very pale brown (10YR 8/3) and gray (10YR 6/1–7/1) rad diatom nanno oozes and foram diatom rad nanno oozes. Prominent *Planolites* in dark layers. Overlying with a sharp contact at 44.2 m.

VARICOLORED OOZE (SUBUNIT IIA):

Greenish gray (5G 6/1, 5BG 6/1, 5G 6/1, 5B 8/1) to light greenish gray (5G 7/1–8/1 etc.) foram diatom rad nanno oozes. Indistinct burrows occur throughout the lower unit and again include *Planolites*.

SMEAR SLIDE SUMMARY (%):

	1, 120	4, 40	5, 25
Texture:			
Sand	10	30	25
Silt	30	20	25
Clay	60	50	50
Composition:			
Volcanic glass	Tr	–	–
Carbonate unspec.	10	10	10
Foraminifers	5	10	10
Calc. nannofossils	60	50	50
Diatoms	15	15	15
Radiolarians	10	15	15
Sponge spicules	Tr	Tr	Tr
Silicoflagellates	Tr	Tr	Tr

CARBONATE BOMB:

1, 85 cm = 74%
2, 75 cm = 73%
3, 75 cm = 62%
4, 75 cm = 58%
5, 75 cm = 76%
6, 75 cm = 53%

NOTE: Graphic lithologies represent average compositions derived from smear slides and do not always reflect the detailed alternation of sediment types. Major lithologic boundaries are shown but gradational contacts, small-scale cyclicity and ooze-chalk alternations are represented schematically. Color changes approximate to lithologic changes.

SITE 573 HOLE A CORE 6 CORED INTERVAL 49.2–57.7 m

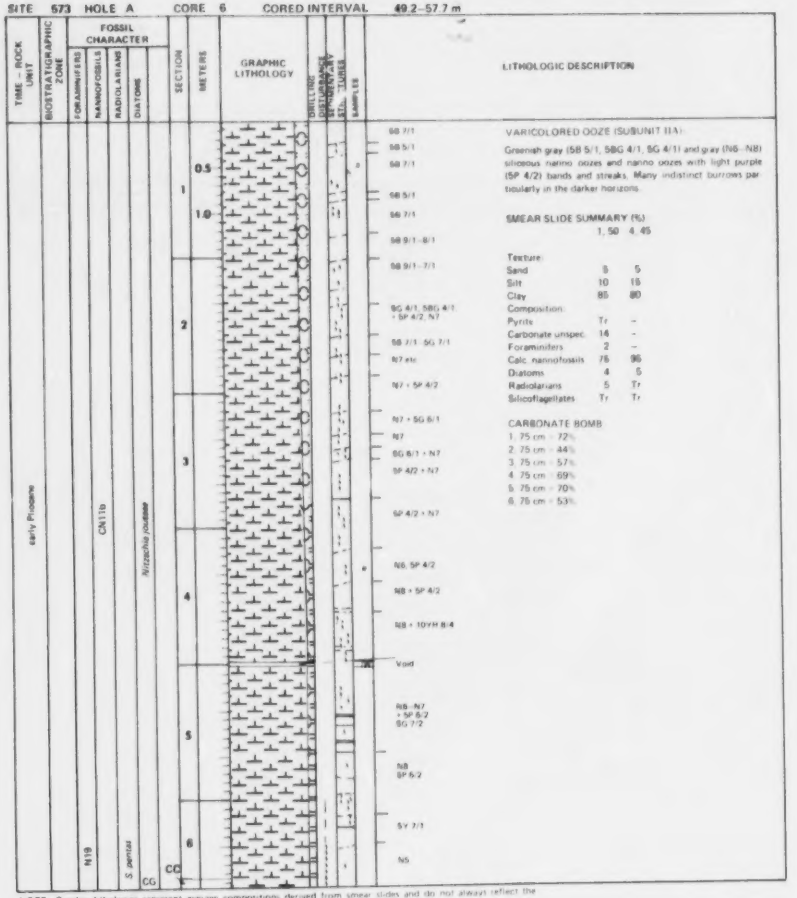

VARICOLORED OOZE (SUBUNIT IIA):

Greenish gray (5B 5/1, 5BG 4/1, 5G 4/1) and gray (N6–N8) siliceous nanno oozes and nanno oozes with light purple (5P 4/2) bands and streaks. Many indistinct burrows particularly in the darker horizons.

SMEAR SLIDE SUMMARY (%)

	1, 50	4, 45
Texture:		
Sand	5	5
Silt	10	15
Clay	85	80
Composition:		
Pyrite	Tr	–
Carbonate unspec.	14	–
Foraminifers	2	–
Calc. nannofossils	75	95
Diatoms	4	5
Radiolarians	5	Tr
Silicoflagellates	Tr	Tr

CARBONATE BOMB

1. 75 cm – 72%
2. 75 cm – 44%
3. 75 cm – 57%
4. 75 cm – 69%
5. 75 cm – 70%
6. 75 cm – 53%

NOTE: Graphic lithologies represent average compositions derived from smear slides and do not always reflect the detailed alternation of sediment types. Major lithologic boundaries are shown but gradational contacts, small-scale cyclicity and ooze-chalk alternations are represented schematically. Color changes approximate to lithologic changes.

SITE 573 HOLE B CORE 1 CORED INTERVAL 138.5–148.0 m

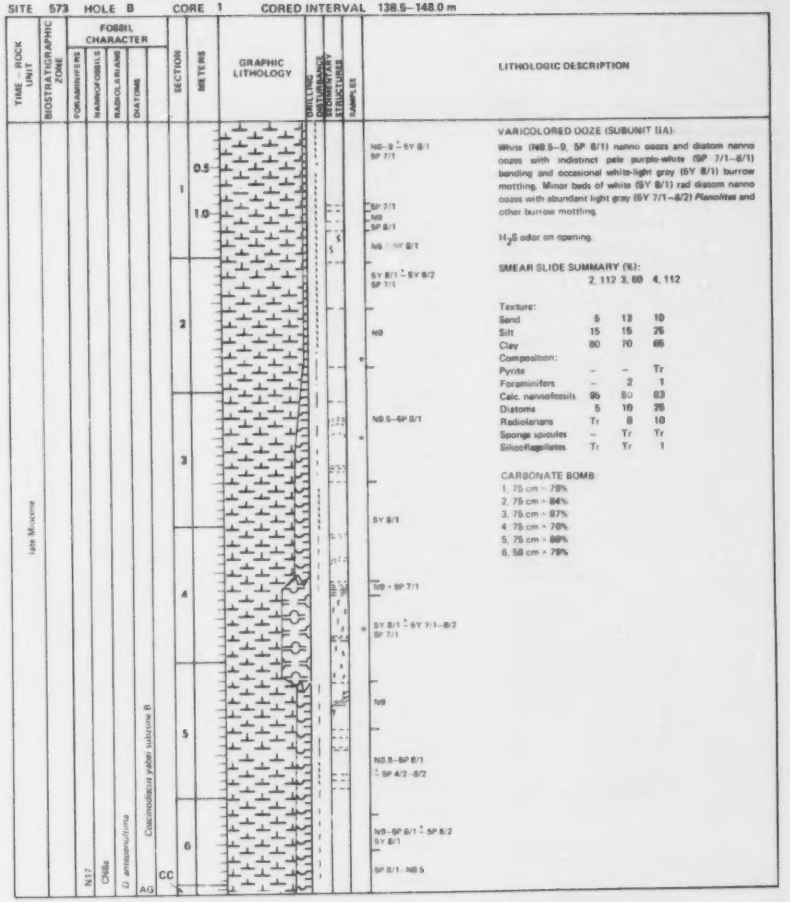

VARICOLORED OOZE (SUBUNIT IIA):

White (N8.5–9, 5P 8/1) nanno oozes and diatom nanno oozes with indistinct pale purple-white (5P 7/1–8/1) banding and occasional white-light gray (5Y 8/1) burrow mottling. Minor beds of white (5Y 8/1) rad diatom nanno oozes with abundant light gray (5Y 7/1–8/2) *Planolites* and other burrow mottling.

H_2S odor on opening.

SMEAR SLIDE SUMMARY (%):

	2, 112	3, 60	4, 112
Texture:			
Sand	5	13	10
Silt	15	15	25
Clay	80	70	65
Composition:			
Pyrite	–	–	Tr
Foraminifers	–	2	1
Calc. nannofossils	95	80	63
Diatoms	5	10	25
Radiolarians	Tr	8	10
Sponge spicules	–	Tr	Tr
Silicoflagellates	Tr	Tr	1

CARBONATE BOMB

1. 75 cm – 79%
2. 75 cm – 84%
3. 75 cm – 87%
4. 75 cm – 76%
5. 75 cm – 88%
6. 58 cm – 79%

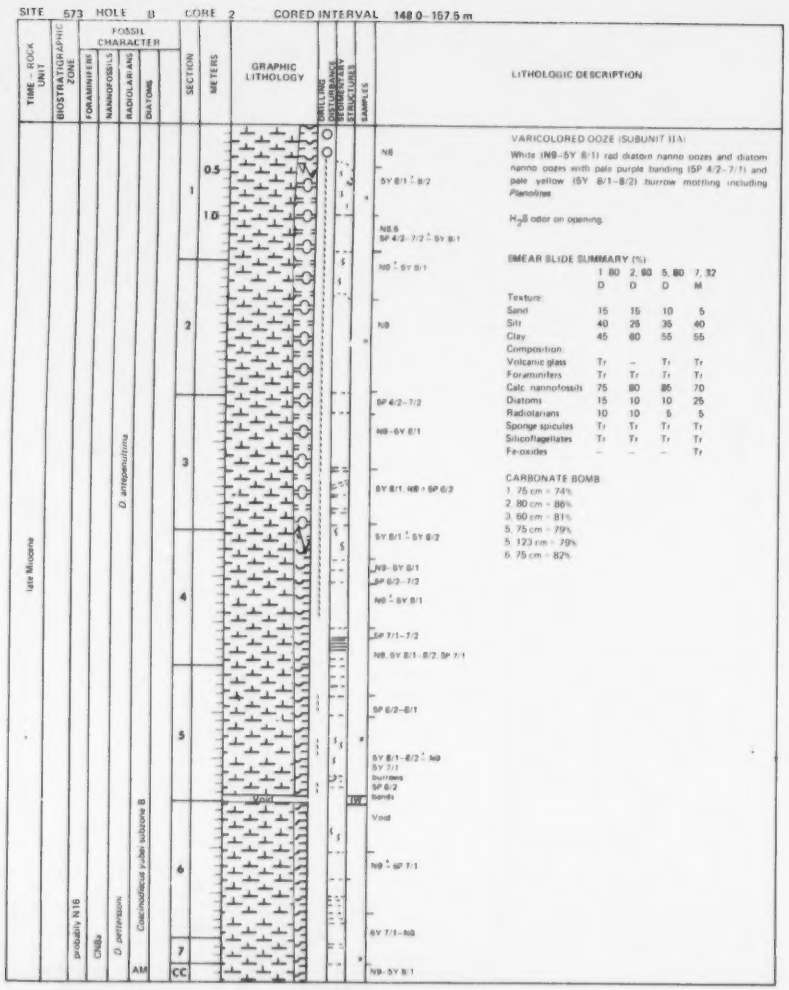
SITE 573 HOLE B CORE 2 CORED INTERVAL 148.0–157.5 m
TIME – ROCK UNIT
BIOSTRATIGRAPHIC ZONE
FOSSIL CHARACTER
FORAMINIFERS
NANNOFOSSILS
RADIOLARIANS
DIATOMS
SECTION
METERS
GRAPHIC LITHOLOGY
DRILLING DISTURBANCE
SEDIMENTARY STRUCTURES
SAMPLES
LITHOLOGIC DESCRIPTION
late Miocene
probably N16
CN8a
D. simonseni
Coscinodiscus yabei subzone B
AM
VARICOLORED OOZE (SUBUNIT IIA)
White (N9–5Y 8/1) rad diatom nanno oozes and diatom nanno oozes with pale purple banding (5P 4/2–7/1) and pale yellow (5Y 8/1–8/2) burrow mottling including Planolites
H2S odor on opening.
SMEAR SLIDE SUMMARY (%)
1, 80 D
2, 80 D
5, 80 D
7, 32 M
Texture:
Sand 15 15 10 5
Silt 40 28 35 40
Clay 45 60 55 55
Composition:
Volcanic glass Tr – Tr Tr
Foraminifers Tr Tr Tr Tr
Calc. nannofossils 75 80 85 70
Diatoms 15 10 10 25
Radiolarians 10 10 5 5
Sponge spicules Tr Tr Tr Tr
Silicoflagellates Tr Tr Tr Tr
Fe-oxides – – – Tr
CARBONATE BOMB
1. 75 cm = 74%
2. 80 cm = 86%
3. 60 cm = 81%
5. 75 cm = 79%
5. 123 cm = 79%
6. 75 cm = 82%
Void
CC

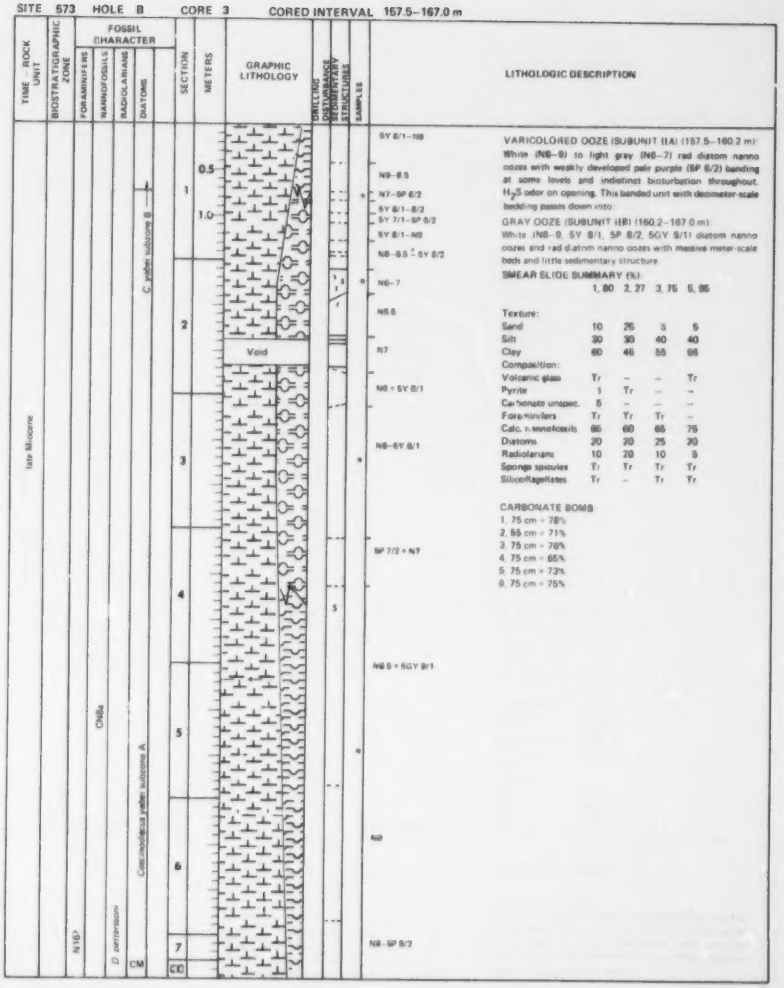
SITE 573 HOLE B CORE 3 CORED INTERVAL 157.5–167.0 m
TIME – ROCK UNIT
BIOSTRATIGRAPHIC ZONE
FOSSIL CHARACTER
FORAMINIFERS
NANNOFOSSILS
RADIOLARIANS
DIATOMS
SECTION
METERS
GRAPHIC LITHOLOGY
DRILLING DISTURBANCE
SEDIMENTARY STRUCTURES
SAMPLES
LITHOLOGIC DESCRIPTION
late Miocene
N18?
CN8a
D. simonseni
C. yabei subzone B
Coscinodiscus yabei subzone A
CM
VARICOLORED OOZE (SUBUNIT IIA) (157.5–160.2 m):
White (N6–9) to light gray (N6–7) rad diatom nanno oozes with weakly developed pale purple (5P 6/2) banding at some levels and indistinct bioturbation throughout. H2S odor on opening. This banded unit with decimeter-scale bedding passes down into:
GRAY OOZE (SUBUNIT IIB) (160.2–167.0 m):
White (N8–9, 5Y 8/1, 5P 8/2, 5GY 8/1) diatom nanno oozes and rad diatom nanno oozes with massive meter-scale beds and little sedimentary structure.
SMEAR SLIDE SUMMARY (%):
1, 80
2, 27
3, 75
6, 85
Texture:
Sand 10 25 5 5
Silt 30 30 40 40
Clay 60 45 55 55
Composition:
Volcanic glass Tr – – Tr
Pyrite 1 Tr – –
Carbonate unspec. 5 – – –
Foraminifers Tr Tr Tr –
Calc. nannofossils 65 60 65 75
Diatoms 20 20 25 20
Radiolarians 10 20 10 5
Sponge spicules Tr Tr Tr Tr
Silicoflagellates Tr – Tr Tr
CARBONATE BOMB
1. 75 cm = 78%
2. 55 cm = 71%
3. 75 cm = 76%
4. 75 cm = 65%
5. 75 cm = 73%
6. 75 cm = 75%
Void
CC

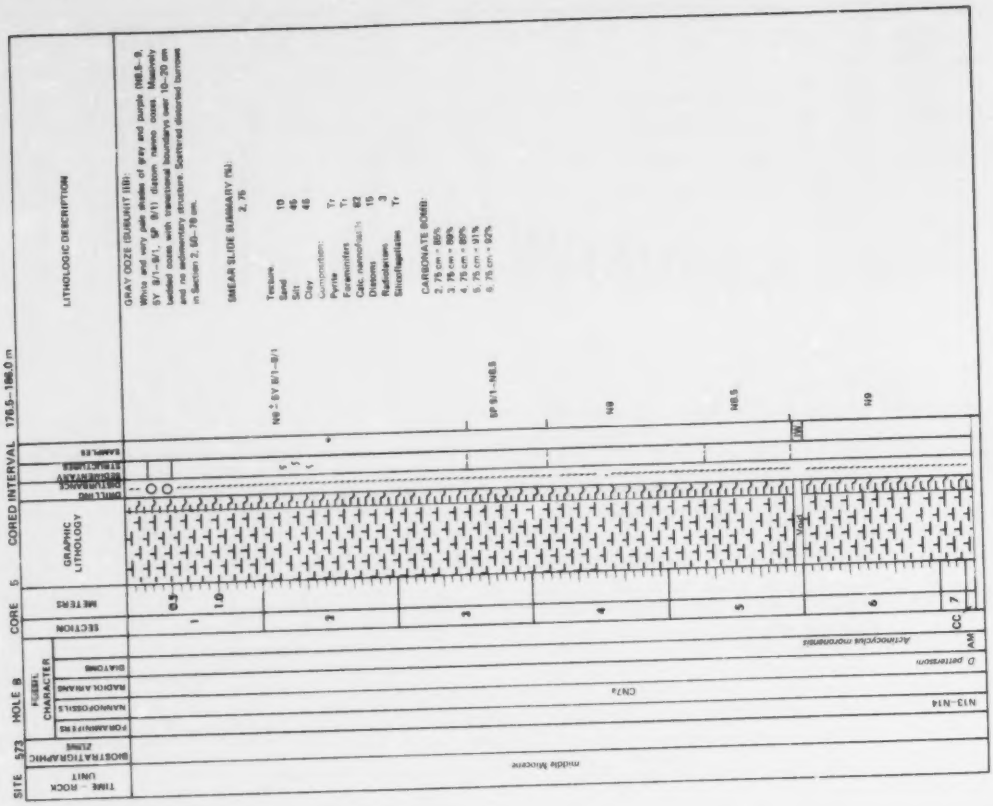
SITE 573
HOLE B
CORE 5
CORED INTERVAL 176.5–186.0 m
TIME – ROCK UNIT
middle Miocene
CN7a
N13–N14
D. petterssoni
Actinocyclus moronensis
CM
CC
LITHOLOGIC DESCRIPTION
GRAY OOZE (SUBUNIT IIB):
White and very pale shades of gray and purple (N8.5–9, 5Y 8/1–8/1, 5P 8/1) diatom nanno ooze. Massively bedded ooze with transitional boundaries over 10–20 cm and no sedimentary structure. Sometrd distorted burrows in Section 2, 68–78 cm.
SMEAR SLIDE SUMMARY (%):
2, 75
Texture
Sand 19
Silt 46
Clay 48
Composition:
Pyrite Tr
Foraminifers Tr
Calc. nannofossils 82
Diatoms 15
Radiolarians 3
Silicoflagellates Tr
CARBONATE BOMB:
2, 75 cm = 85%
3, 75 cm = 79%
4, 75 cm = 80%
5, 75 cm = 91%
6, 75 cm = 92%
N9
N8.5
5P 8/1–N8.5
5Y 8/1–8/1
N8 + 5Y 8/1–8/1

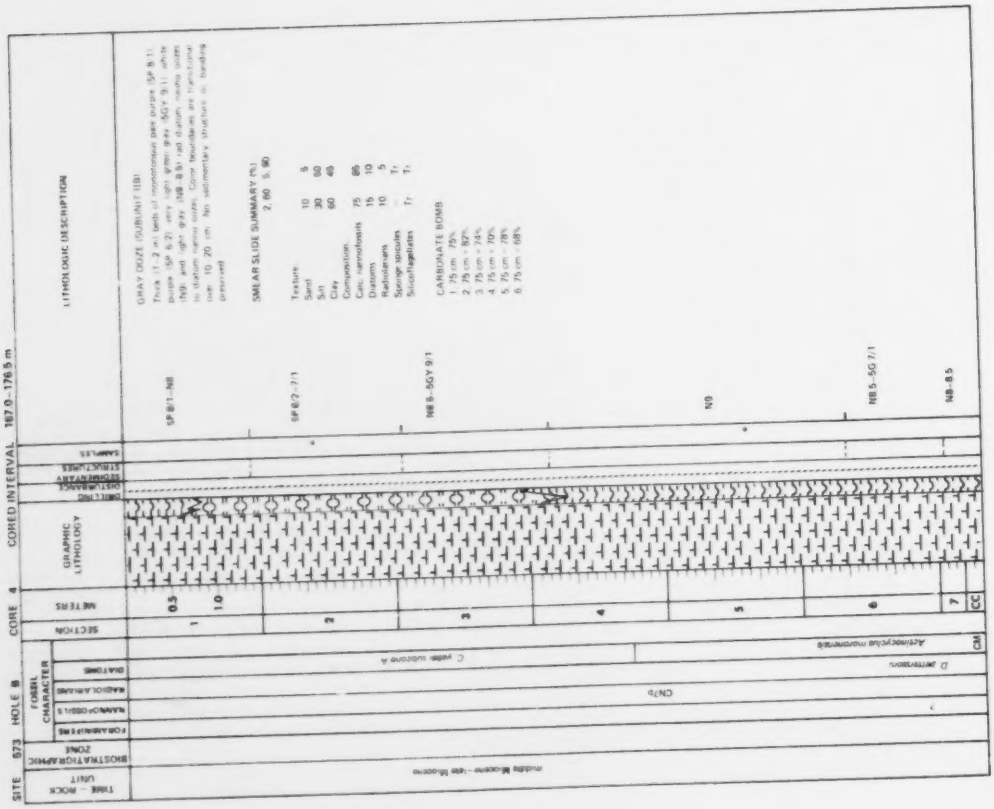
SITE 573
HOLE B
CORE 4
CORED INTERVAL 167.0–176.5 m
TIME – ROCK UNIT
middle Miocene – late Miocene
CN7b
D. petterssoni
C. peplum subsona s
Actinocyclus moronensis
CM
CC
LITHOLOGIC DESCRIPTION
GRAY OOZE (SUBUNIT IIB):
Thick (1–2 m) beds of monotonous pale purple (5P 8/1; purple (5P 6/2), very light gray (5Y 8/1), white (N9), and light gray (N8.5/5P 8/1) diatom nanno oozes to diatom nanno oozes. Core boundaries are transitional over 10–20 cm. No sedimentary structure or bedding preserved.
SMEAR SLIDE SUMMARY (%):
2, 80 5, 80
Texture
Sand 10 5
Silt 30 50
Clay 60 45
Composition
Calc. nannofossils 75 85
Diatoms 15 10
Radiolarians 10 5
Sponge spicules Tr Tr
Silicoflagellates Tr Tr
CARBONATE BOMB:
1, 75 cm = 75%
2, 75 cm = 82%
3, 75 cm = 74%
4, 75 cm = 70%
5, 75 cm = 78%
6, 75 cm = 68%
5P 8/1–N8
5P 6/2–7/1
N8.5–5G 9/1
N9
N8.5–5G 7/1
N8–8.5

SITE 573 HOLE B CORE 6 CORED INTERVAL 186.0–195.5 m

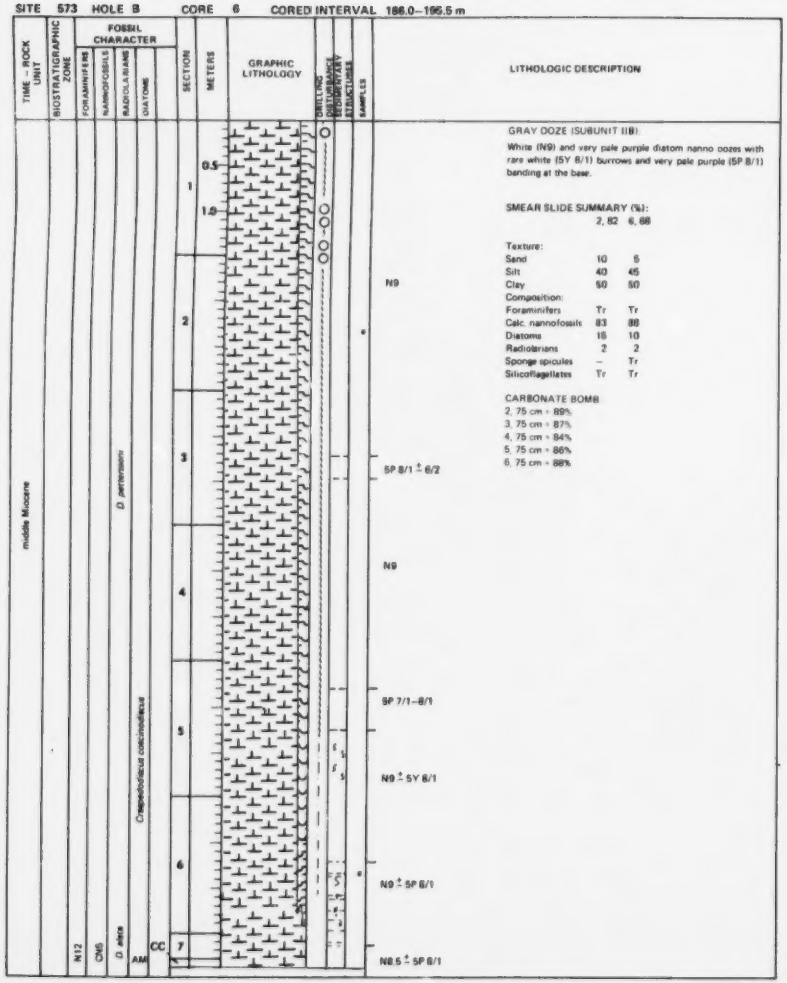

LITHOLOGIC DESCRIPTION

GRAY OOZE (SUBUNIT IIB):

White (N9) and very pale purple diatom nanno oozes with rare white (5Y 8/1) burrows and very pale purple (5P 8/1) banding at the base.

SMEAR SLIDE SUMMARY (%):

	2, 82	6, 68
Texture:		
Sand	10	5
Silt	40	45
Clay	50	50
Composition:		
Foraminifers	Tr	Tr
Calc. nannofossils	83	88
Diatoms	15	10
Radiolarians	2	2
Sponge spicules	–	Tr
Silicoflagellates	Tr	Tr

CARBONATE BOMB

2, 75 cm = 89%
3, 75 cm = 87%
4, 75 cm = 84%
5, 75 cm = 86%
6, 75 cm = 88%

SITE 573 HOLE B CORE 7 CORED INTERVAL 195.5–205.0 m

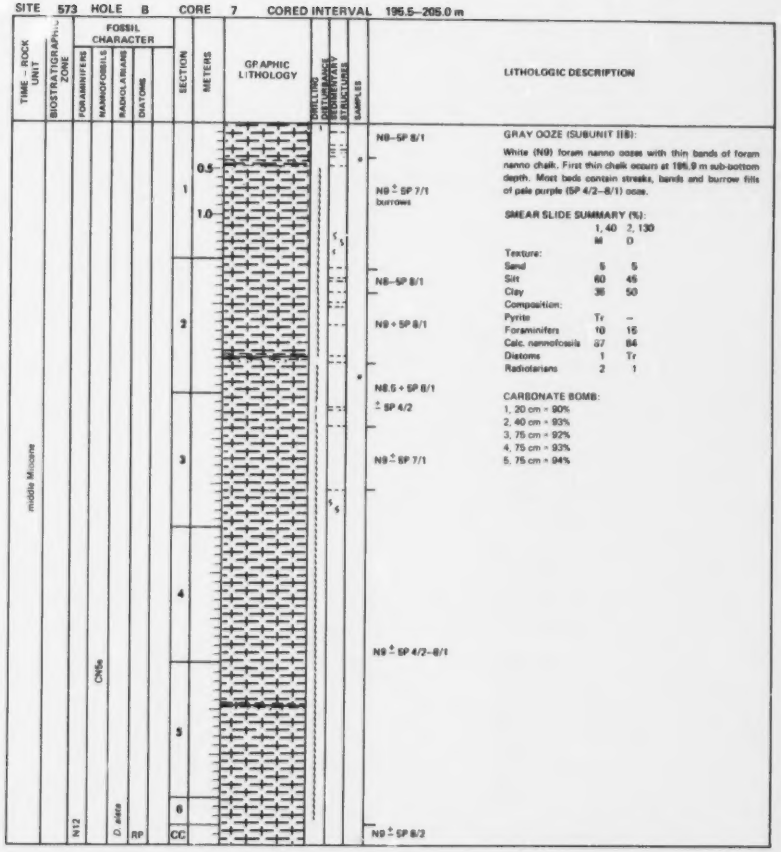

LITHOLOGIC DESCRIPTION

GRAY OOZE (SUBUNIT IIB):

White (N9) foram nanno oozes with thin bands of foram nanno chalk. First thin chalk occurs at 196.9 m sub-bottom depth. Most beds contain streaks, bands and burrow fills of pale purple (5P 4/2–8/1) ooze.

SMEAR SLIDE SUMMARY (%):

	1, 40 M	2, 130 D
Texture:		
Sand	5	5
Silt	60	45
Clay	35	50
Composition:		
Pyrite	Tr	–
Foraminifers	10	15
Calc. nannofossils	87	84
Diatoms	1	Tr
Radiolarians	2	1

CARBONATE BOMB:

1, 20 cm = 80%
2, 40 cm = 93%
3, 75 cm = 92%
4, 75 cm = 93%
5, 75 cm = 94%

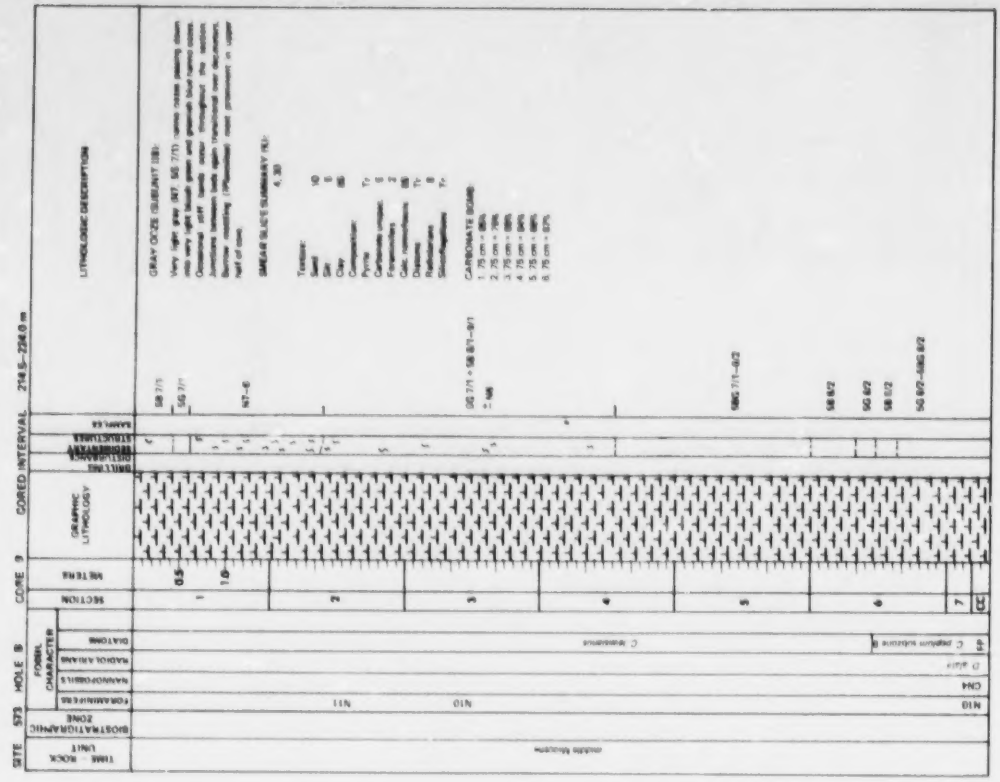

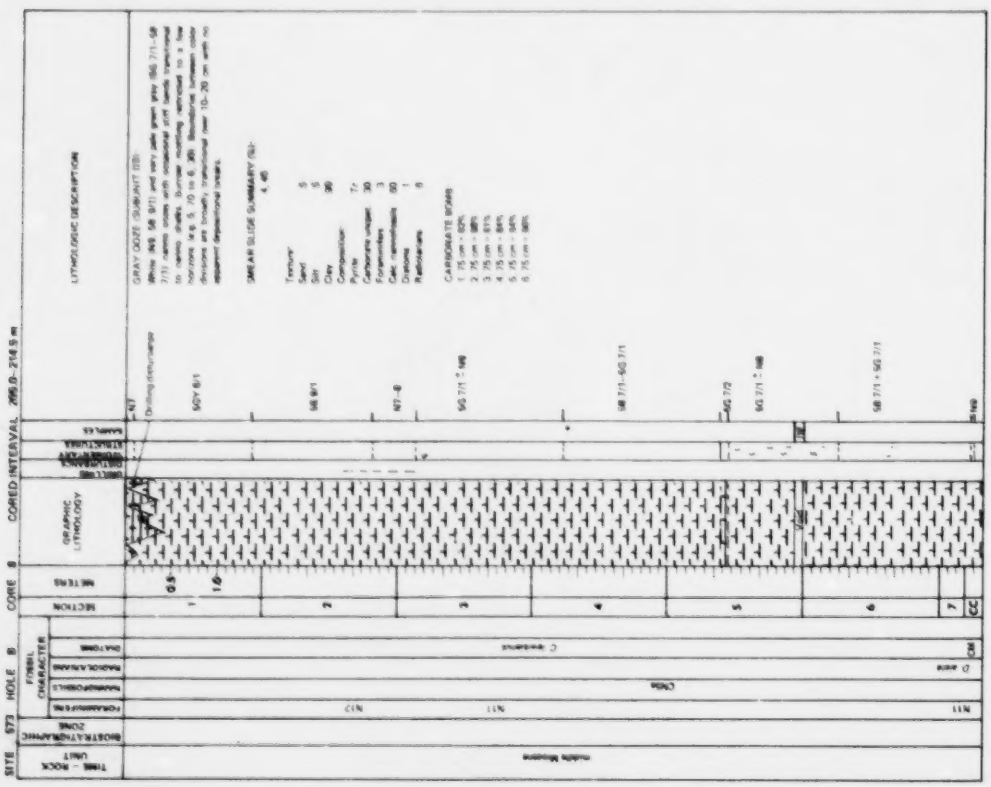

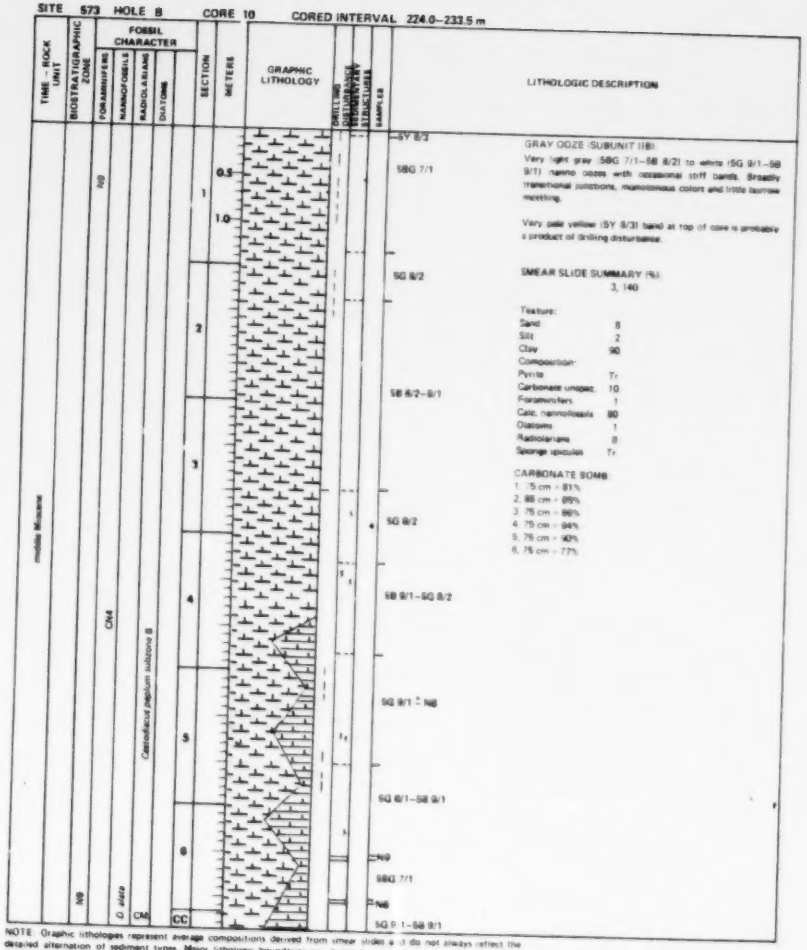

NOTE: Graphic lithologies represent average compositions derived from smear slides and do not always reflect the detailed alternation of sediment types. Major lithologic boundaries are shown but gradational contacts, small-scale cyclicity and ooze-chalk alternations are represented schematically. Color changes approximate to lithologic changes.

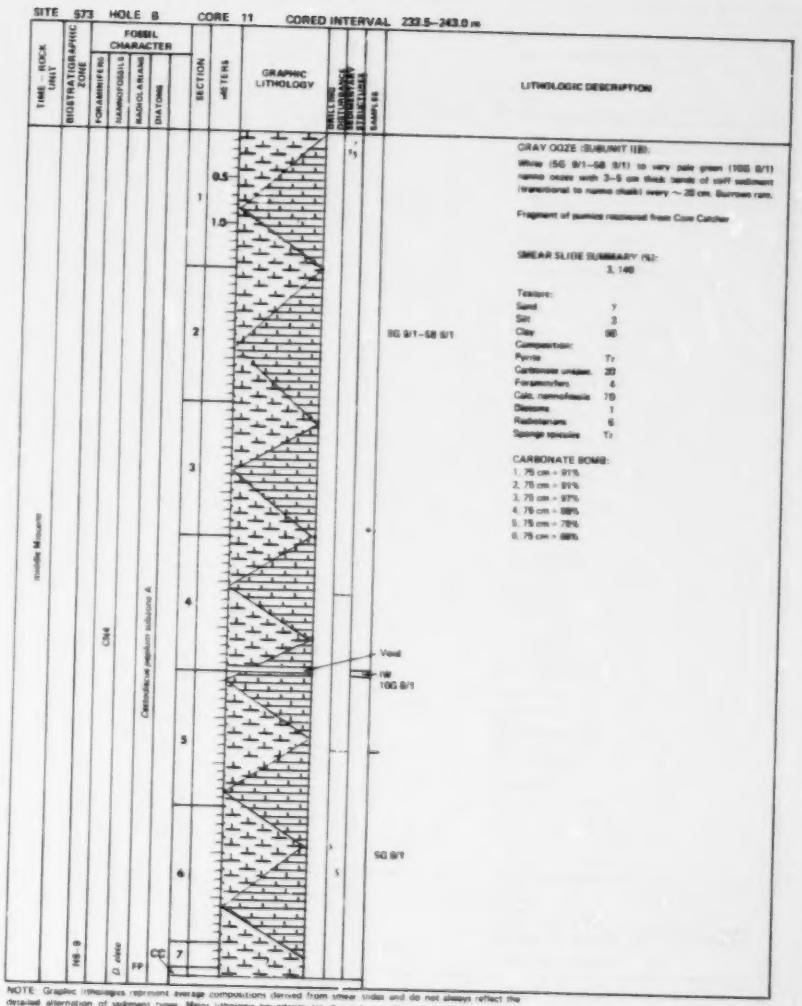

NOTE: Graphic lithologies represent average compositions derived from smear slides and do not always reflect the detailed alternation of sediment types. Major lithologic boundaries are shown but gradational contacts, small-scale cyclicity and ooze-chalk alternations are represented schematically. Color changes approximate to lithologic changes.

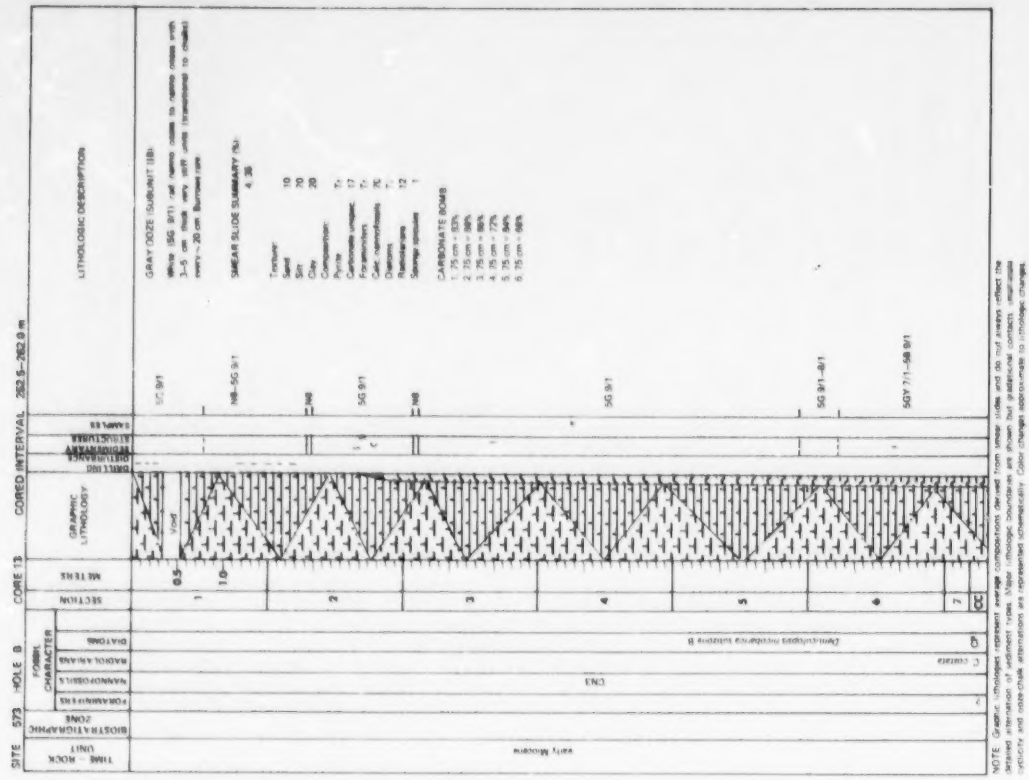

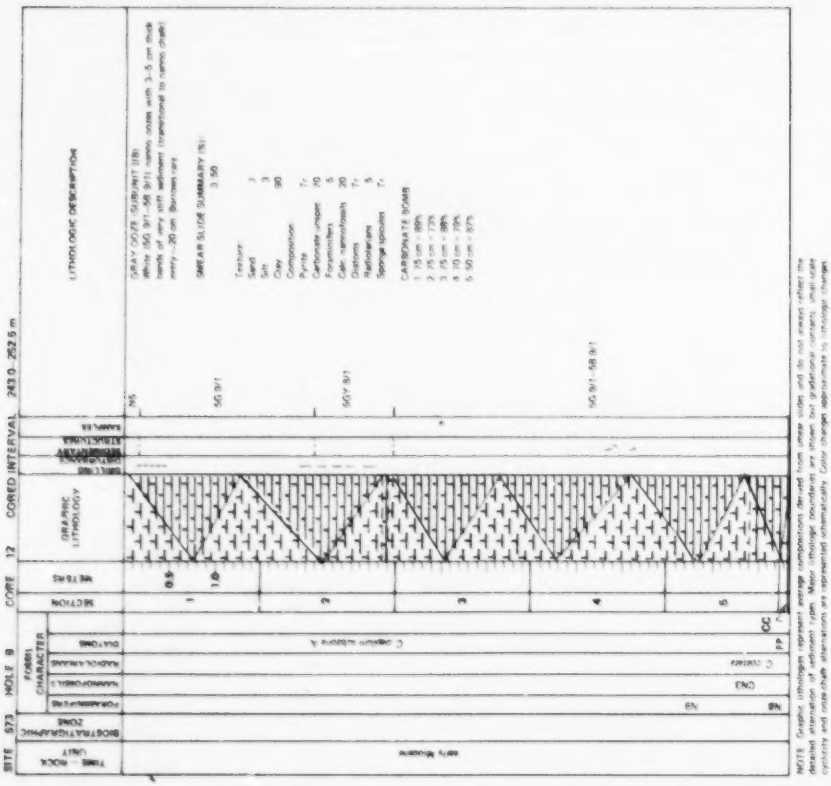

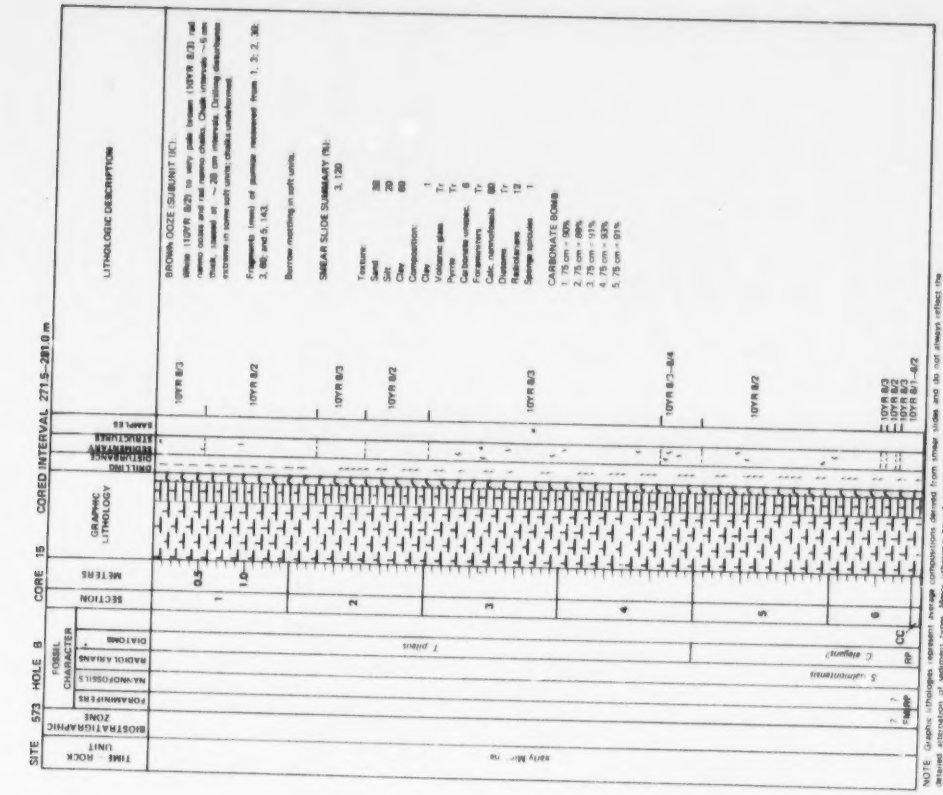
SITE 573 HOLE 8 CORE 15 CORED INTERVAL 271.5–281.0 m
TIME – ROCK UNIT
BIOSTRATIGRAPHIC ZONE
FORAMINIFERS
NANNOFOSSILS
RADIOLARIANS
DIATOMS
FOSSIL CHARACTER
SECTION
METERS
GRAPHIC LITHOLOGY
DRILLING DISTURBANCE
SEDIMENTARY STRUCTURES
SAMPLES
LITHOLOGIC DESCRIPTION
BROWN OOZE (SUBUNIT IIC)
SHEAR SLIDE SUMMARY (%):
3, 120
CARBONATE BOMB
NOTE: Graphic lithologies represent average compositions derived from shear slides and do not always reflect the detailed site-to-site variation of sediment types. Major lithologic boundaries are shown but gradational contacts, small-scale cyclicity and ooze-chalk alternations are represented schematically. Color changes approximate to lithologic changes.

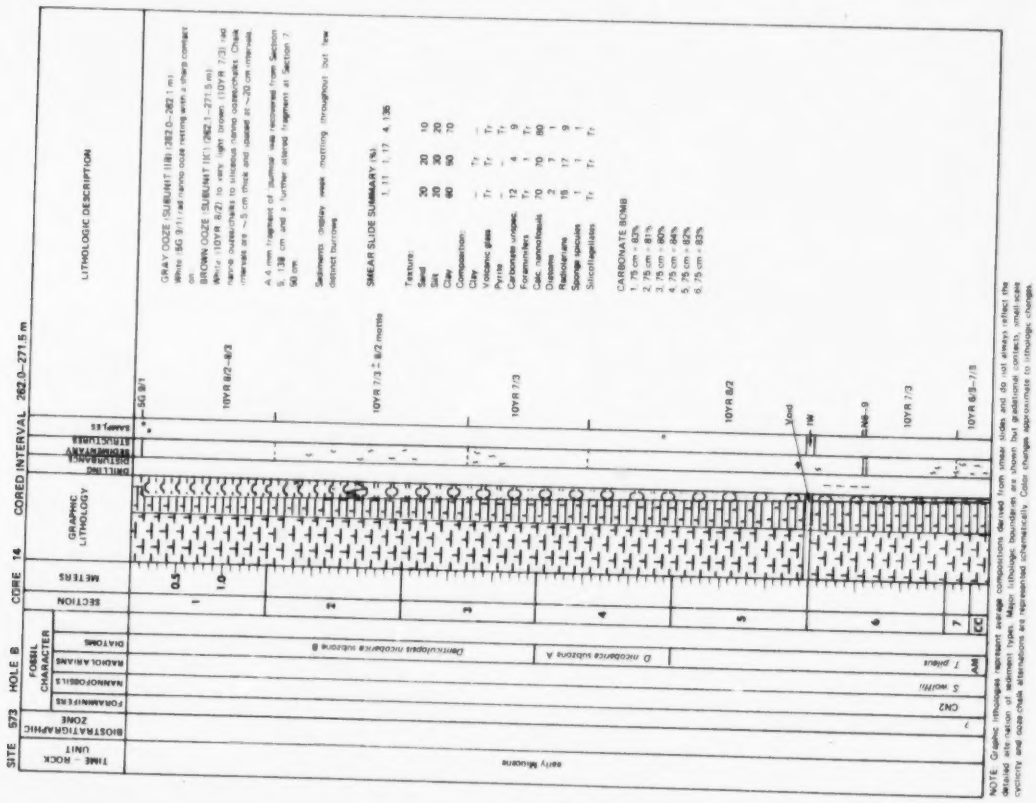
SITE 573 HOLE 8 CORE 14 CORED INTERVAL 262.0–271.5 m
TIME – ROCK UNIT
BIOSTRATIGRAPHIC ZONE
FORAMINIFERS
NANNOFOSSILS
RADIOLARIANS
DIATOMS
FOSSIL CHARACTER
SECTION
METERS
GRAPHIC LITHOLOGY
DRILLING DISTURBANCE
SEDIMENTARY STRUCTURES
SAMPLES
LITHOLOGIC DESCRIPTION
GRAY OOZE (SUBUNIT IIIB) (262.0–262.1 m)
BROWN OOZE (SUBUNIT IIC) (262.1–271.5 m)
SHEAR SLIDE SUMMARY (%):
1, 11 1, 17 4, 135
CARBONATE BOMB
NOTE: Graphic lithologies represent average compositions derived from shear slides and do not always reflect the detailed site-to-site variation of sediment types. Major lithologic boundaries are shown but gradational contacts, small-scale cyclicity and ooze-chalk alternations are represented schematically. Color changes approximate to lithologic changes.

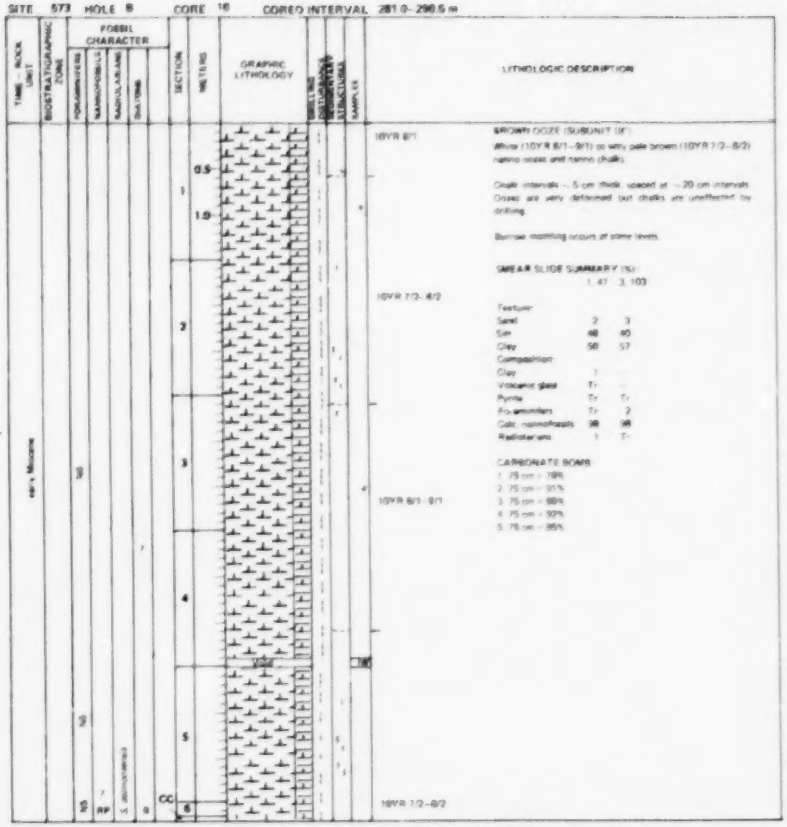
SITE 573 HOLE B CORE 16 CORED INTERVAL 281.0–290.5 m
TIME – ROCK UNIT
BIOSTRATIGRAPHIC ZONE
FOSSIL CHARACTER
FORAMINIFERS
NANNOFOSSILS
RADIOLARIANS
DIATOMS
SECTION
METERS
GRAPHIC LITHOLOGY
DRILLING DISTURBANCE
SEDIMENTARY STRUCTURES
SAMPLES
LITHOLOGIC DESCRIPTION
early Miocene
10YR 8/1
10YR 7/2–8/2
10YR 8/1–9/1
10YR 7/2–8/2
BROWN OOZE (SUBUNIT IIF)
White (10YR 8/1–9/1) to very pale brown (10YR 7/2–8/2) nanno ooze and nanno chalk.
Chalk intervals ~.5 cm thick spaced at ~ 20 cm intervals. Oozes are very deformed but chalks are unaffected by drilling.
Burrow mottling occurs at some levels.
SMEAR SLIDE SUMMARY (%)
1, 47 3, 103
Texture:
Sand 2 3
Silt 48 40
Clay 50 57
Composition:
Clay 1 –
Volcanic glass Tr –
Pyrite Tr Tr
Foraminifers Tr 2
Calc. nannofossils 98 98
Radiolarians 1 Tr
CARBONATE BOMB:
1. 75 cm = 78%
2. 75 cm = 91%
3. 75 cm = 88%
4. 75 cm = 93%
5. 75 cm = 85%
NOTE: Graphic lithologies represent average compositions derived from smear slides and do not always reflect the detailed alternation of sediment types. Major lithologic boundaries are shown but gradational contacts, small-scale cyclicity and ooze-chalk alternations are represented schematically. Color changes approximate to lithologic changes.

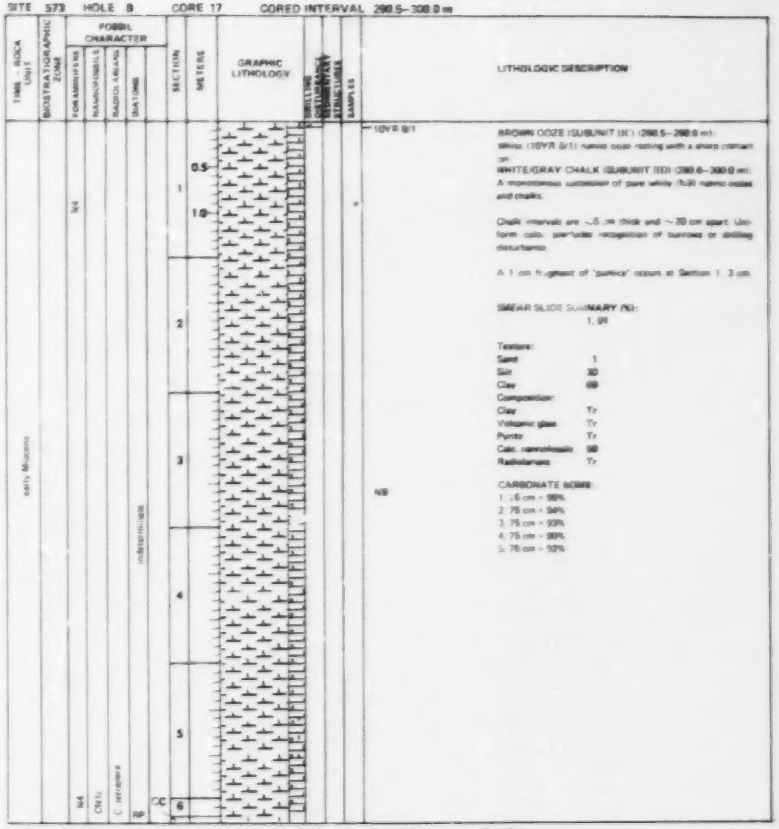
SITE 573 HOLE B CORE 17 CORED INTERVAL 290.5–300.0 m
TIME – ROCK UNIT
BIOSTRATIGRAPHIC ZONE
FOSSIL CHARACTER
FORAMINIFERS
NANNOFOSSILS
RADIOLARIANS
DIATOMS
SECTION
METERS
GRAPHIC LITHOLOGY
DRILLING DISTURBANCE
SEDIMENTARY STRUCTURES
SAMPLES
LITHOLOGIC DESCRIPTION
early Miocene
indeterminate
10YR 8/1
BROWN OOZE (SUBUNIT IIE) (290.5–290.6 m):
White (10YR 8/1) nanno ooze resting with a sharp contact on
WHITE/GRAY CHALK (SUBUNIT IIE) (290.6–300.0 m):
A monotonous succession of pure white (N9) nanno oozes and chalks.
Chalk intervals are ~.5 cm thick and ~ 20 cm apart. Uniform color, pervasive redigestion of burrows or drilling disturbance.
A 1 cm fragment of "pumice" occurs at Section 1, 3 cm.
SMEAR SLIDE SUMMARY (%):
1, 99
Texture:
Sand 1
Silt 30
Clay 69
Composition:
Clay Tr
Volcanic glass Tr
Pyrite Tr
Calc. nannofossils 99
Radiolarians Tr
CARBONATE BOMB:
1. .6 cm = 88%
2. 75 cm = 94%
3. 75 cm = 93%
4. 75 cm = 89%
5. 75 cm = 92%
N9
N4
CN1b
C. tetrapera
RP
CC
NOTE: Graphic lithologies represent average compositions derived from smear slides and do not always reflect the detailed alternation of sediment types. Major lithologic boundaries are shown but gradational contacts, small-scale cyclicity and ooze-chalk alternations are represented schematically. Color changes approximate to lithologic changes.

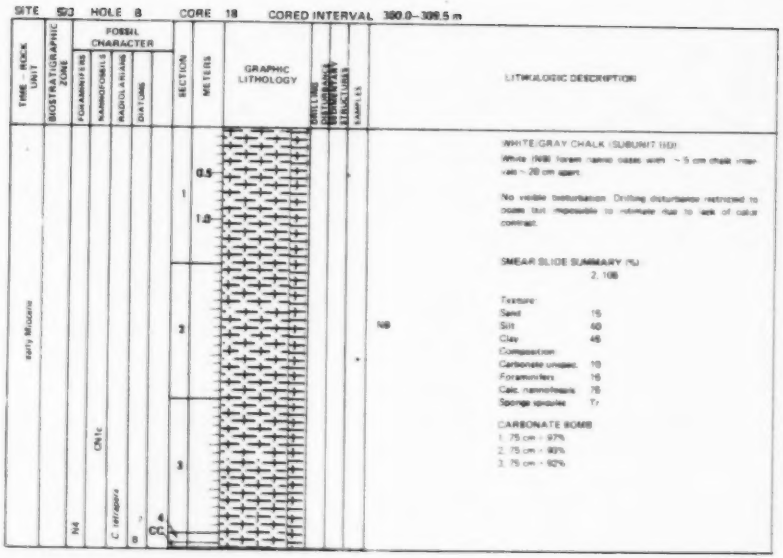

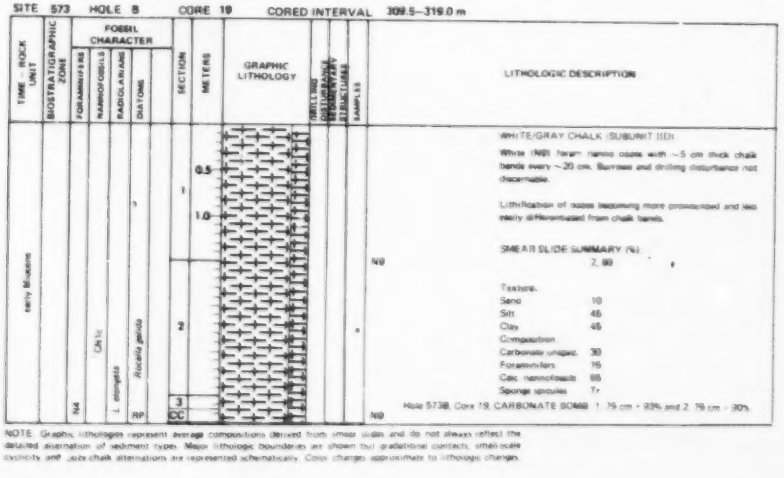

NOTE: Graphic lithologies represent average compositions derived from smear slides and do not always reflect the detailed alternation of sediment types. Major lithologic boundaries are shown but gradational contacts, small-scale cyclicity and ooze-chalk alternations are represented schematically. Color changes approximate to lithologic changes.

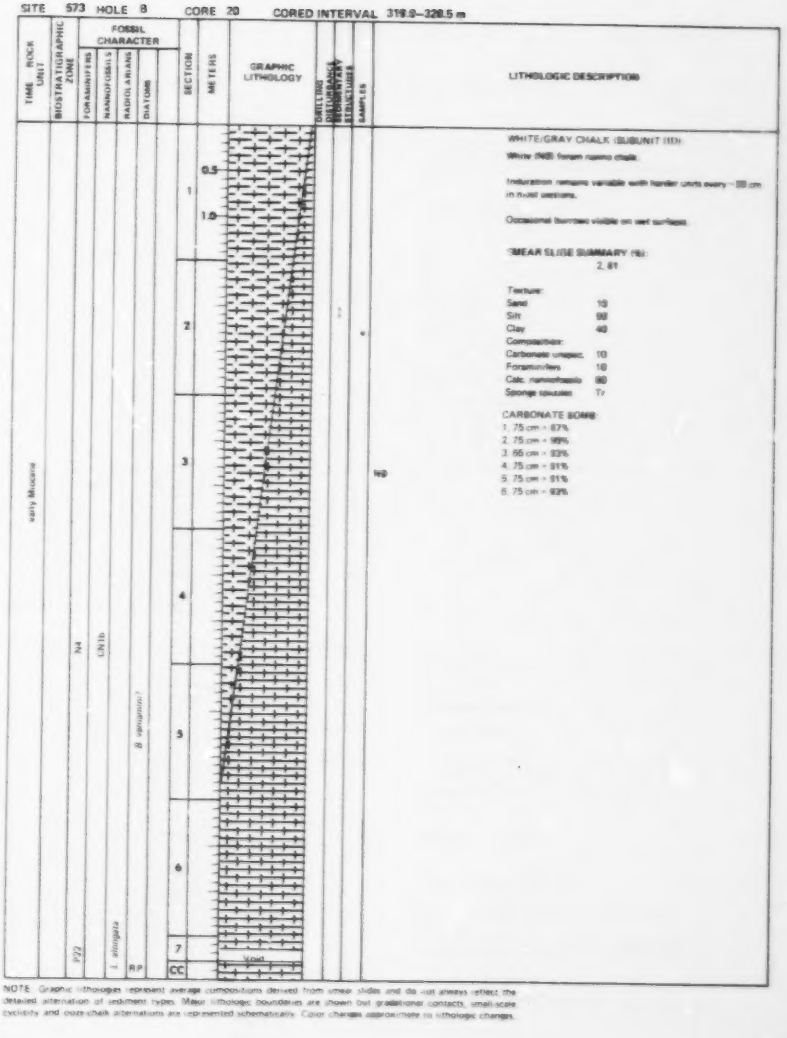

NOTE: Graphic lithologies represent average compositions derived from smear slides and do not always reflect the detailed alternation of sediment types. Major lithologic boundaries are shown but gradational contacts, small-scale cyclicity and ooze-chalk alternations are represented schematically. Color changes approximate to lithologic changes.

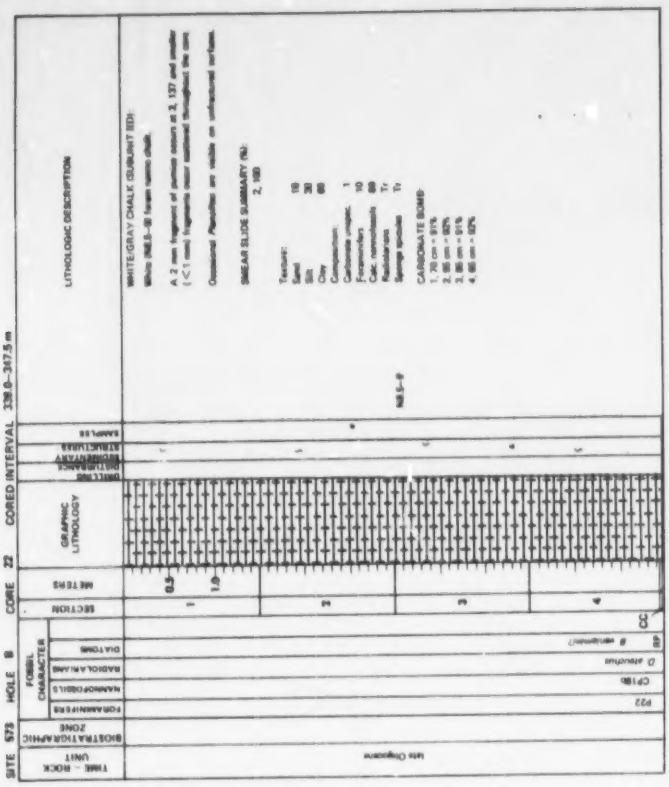

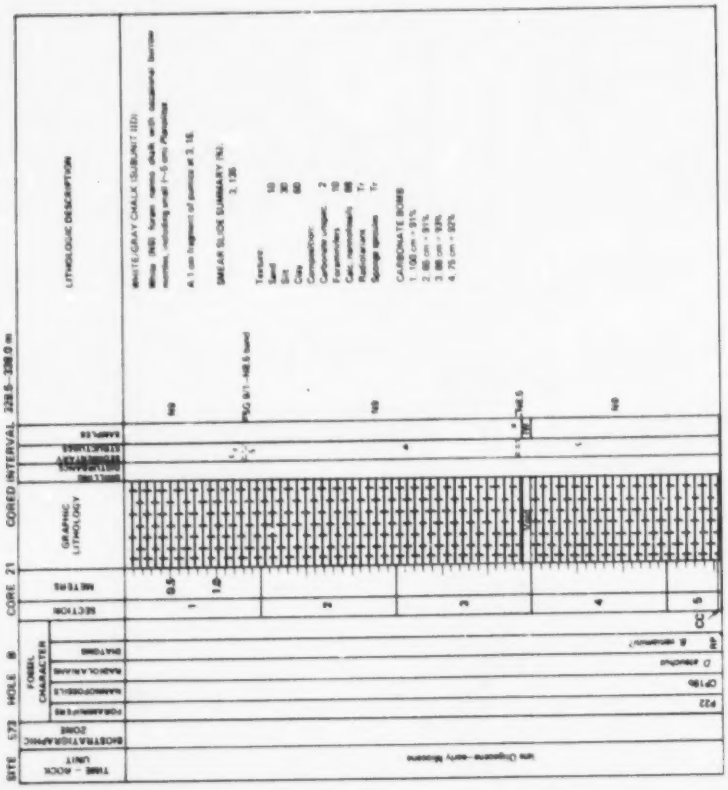

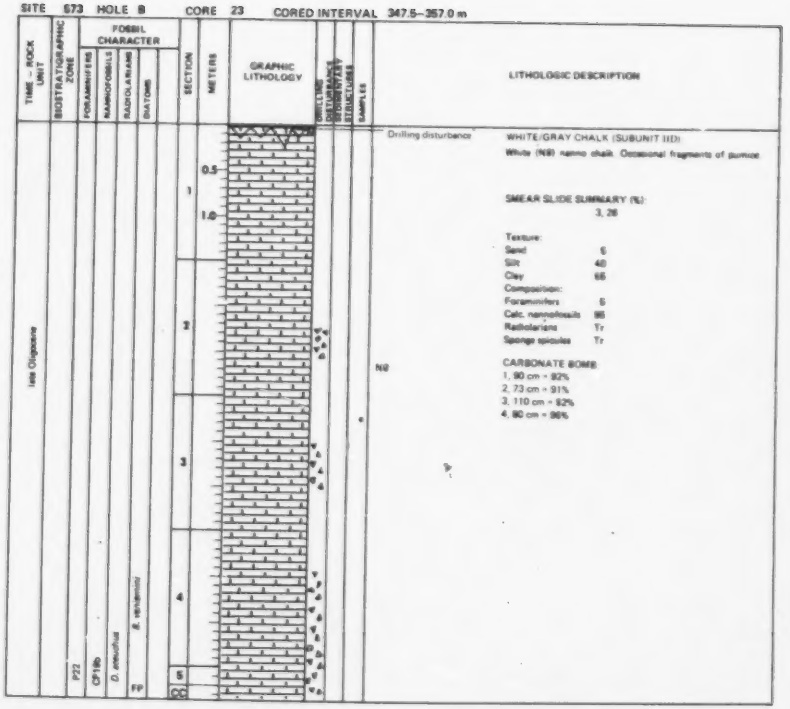

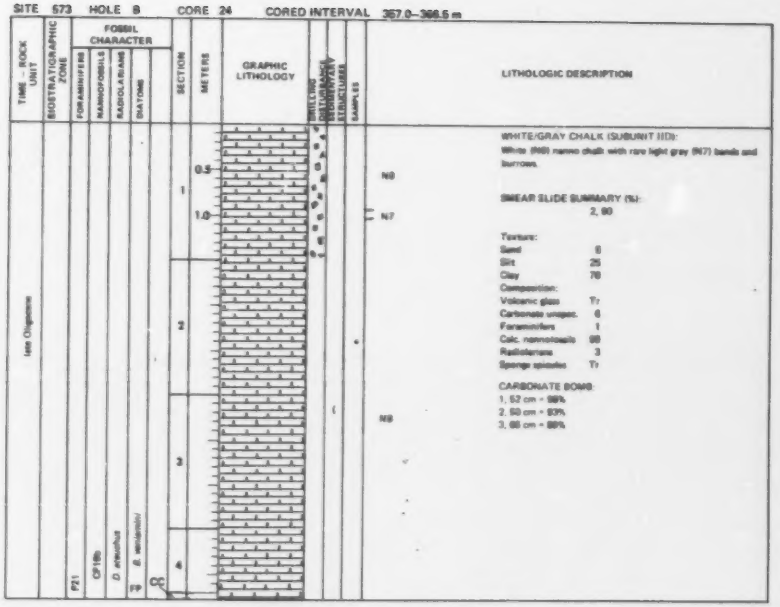

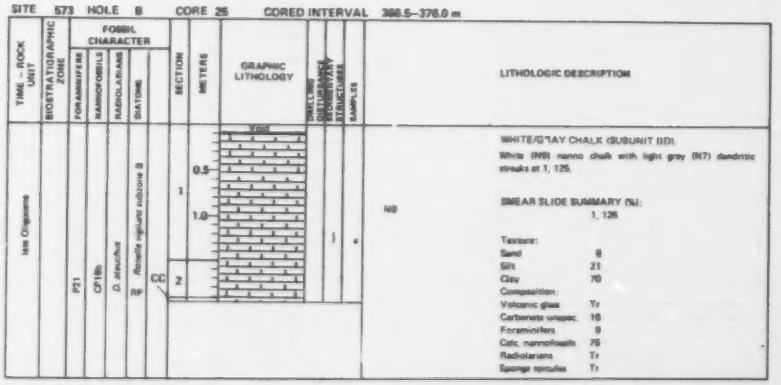

Hole 573B, Core 25, CARBONATE BOMB: 1, 71 cm = 92%

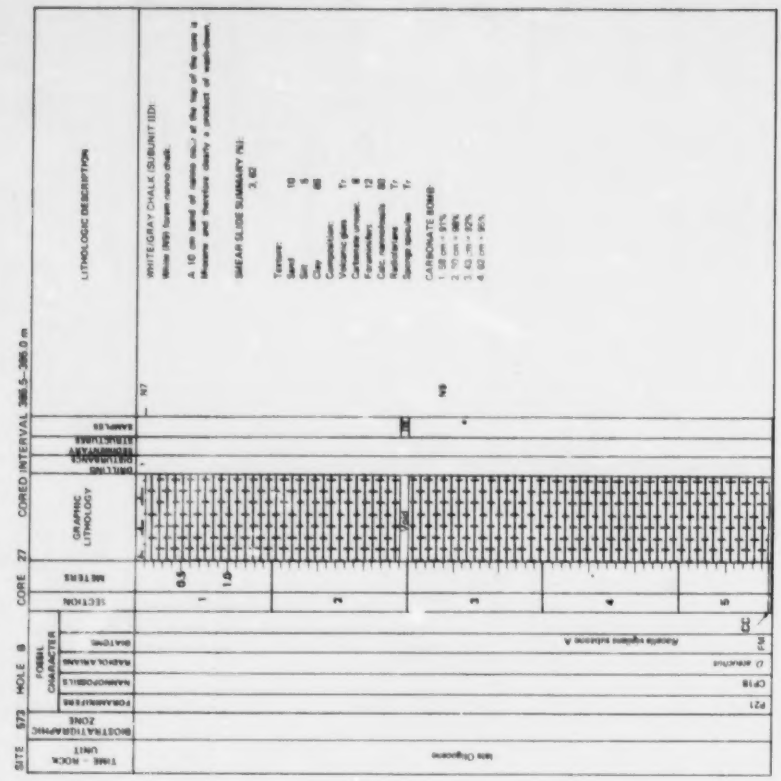

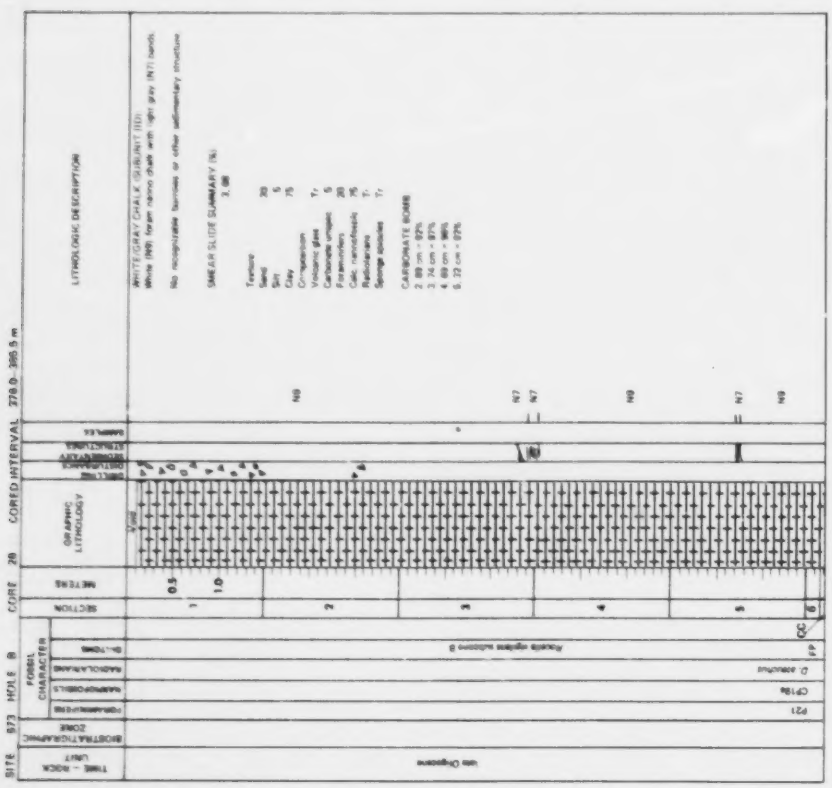

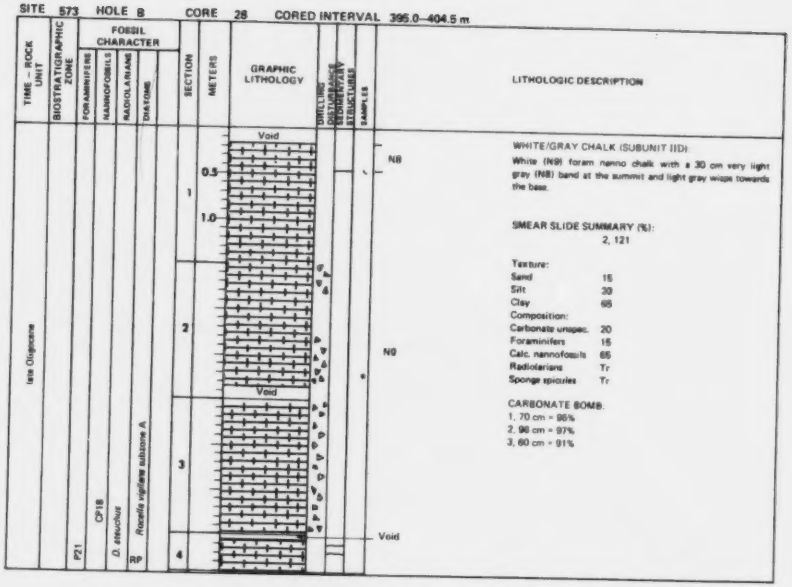
SITE 573 HOLE B CORE 28 CORED INTERVAL 395.0–404.5 m
TIME – ROCK UNIT
BIOSTRATIGRAPHIC ZONE
FOSSIL CHARACTER
FORAMINIFERS
NANNOFOSSILS
RADIOLARIANS
DIATOMS
SECTION
METERS
GRAPHIC LITHOLOGY
DRILLING DISTURBANCE
SED. STRUCTURES
SAMPLES
LITHOLOGIC DESCRIPTION
late Oligocene
P21
CP18
D. ansulus
RP
Rocella vigilans subzone A
Void
NB
N9
WHITE/GRAY CHALK (SUBUNIT IID):
White (N9) foram nanno chalk with a 30 cm very light gray (N8) band at the summit and light gray wisps towards the base.
SMEAR SLIDE SUMMARY (%):
2, 121
Texture:
Sand 15
Silt 30
Clay 65
Composition:
Carbonate unspec. 20
Foraminifers 15
Calc. nannofossils 65
Radiolarians Tr
Sponge spicules Tr
CARBONATE BOMB:
1, 70 cm = 86%
2, 96 cm = 97%
3, 60 cm = 91%

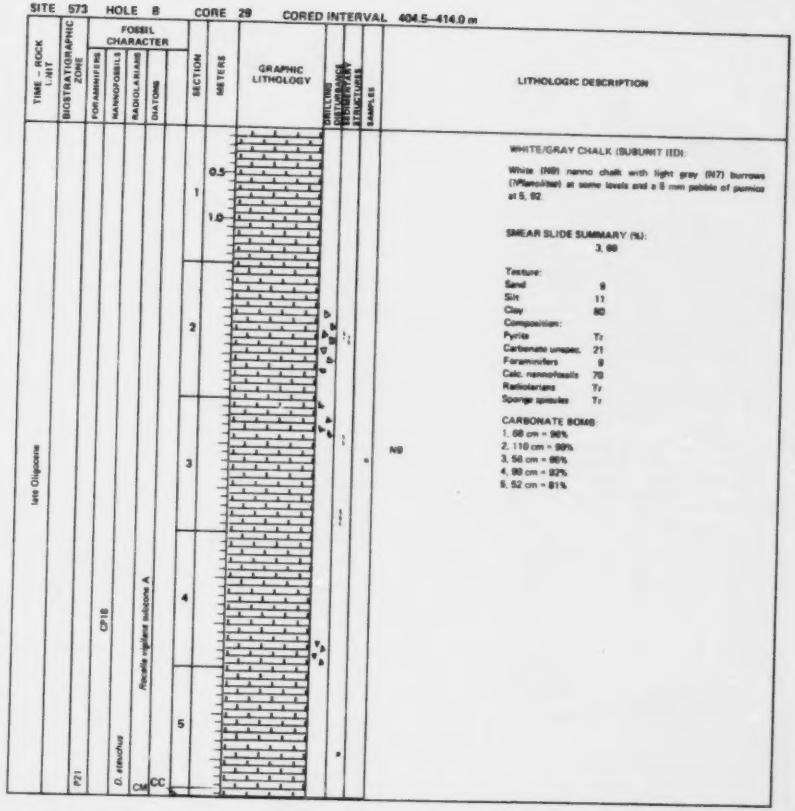
SITE 573 HOLE B CORE 29 CORED INTERVAL 404.5–414.0 m
TIME – ROCK UNIT
BIOSTRATIGRAPHIC ZONE
FOSSIL CHARACTER
FORAMINIFERS
NANNOFOSSILS
RADIOLARIANS
DIATOMS
SECTION
METERS
GRAPHIC LITHOLOGY
DRILLING DISTURBANCE
SED. STRUCTURES
SAMPLES
LITHOLOGIC DESCRIPTION
late Oligocene
P21
CP18
D. ansulus
Rocella vigilans subzone A
CC
N9
WHITE/GRAY CHALK (SUBUNIT IID):
White (N9) nanno chalk with light gray (N7) burrows (?Planolites) at some levels and a 5 mm pebble of pumice at 5, 92.
SMEAR SLIDE SUMMARY (%):
3, 69
Texture:
Sand 9
Silt 11
Clay 80
Composition:
Pyrite Tr
Carbonate unspec. 21
Foraminifers 9
Calc. nannofossils 70
Radiolarians Tr
Sponge spicules Tr
CARBONATE BOMB:
1, 68 cm = 96%
2, 110 cm = 99%
3, 56 cm = 96%
4, 80 cm = 92%
5, 52 cm = 91%

SITE 573 HOLE B CORE 30 CORED INTERVAL 414.0–423.5 m

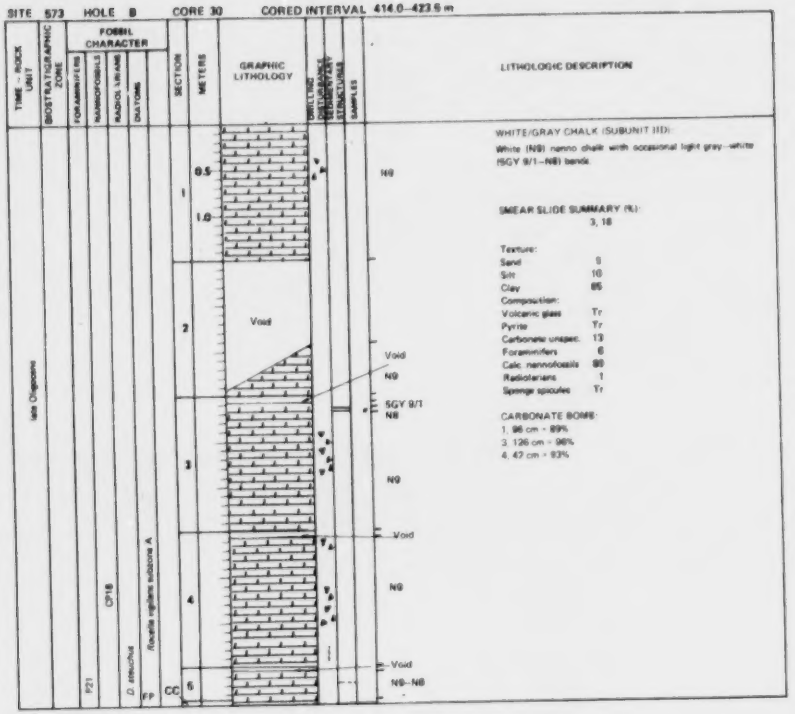

WHITE/GRAY CHALK (SUBUNIT IIB):

White (N9) nanno chalk with occasional light gray–white (5GY 9/1–N8) bands.

SMEAR SLIDE SUMMARY (%):

3, 18

Texture:	
Sand	5
Silt	10
Clay	85
Composition:	
Volcanic glass	Tr
Pyrite	Tr
Carbonate unspec.	13
Foraminifers	6
Calc. nannofossils	80
Radiolarians	1
Sponge spicules	Tr

CARBONATE BOMB:

1, 96 cm = 89%
3, 126 cm = 96%
4, 47 cm = 93%

SITE 573 HOLE B CORE 31 CORED INTERVAL 423.5–433.0 m

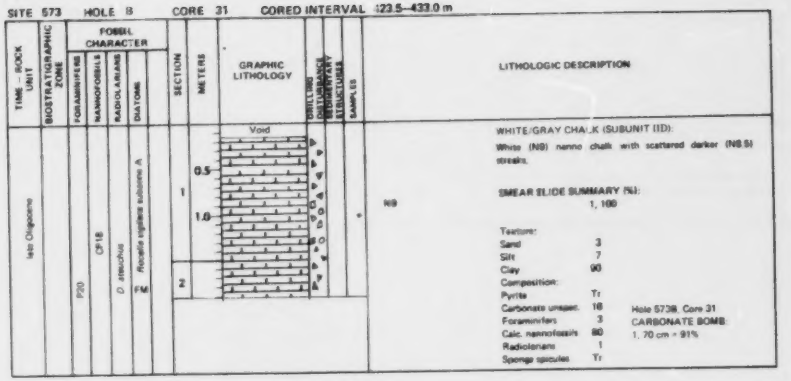

WHITE/GRAY CHALK (SUBUNIT IIB):

White (N9) nanno chalk with scattered darker (N8.5) streaks.

SMEAR SLIDE SUMMARY (%):

1, 100

Texture:	
Sand	3
Silt	7
Clay	90
Composition:	
Pyrite	Tr
Carbonate unspec.	10
Foraminifers	3
Calc. nannofossils	80
Radiolarians	1
Sponge spicules	Tr

Hole 573B, Core 31
CARBONATE BOMB:
1, 70 cm = 91%

SITE 573 HOLE B CORE 32 CORED INTERVAL 433.0–442.5 m

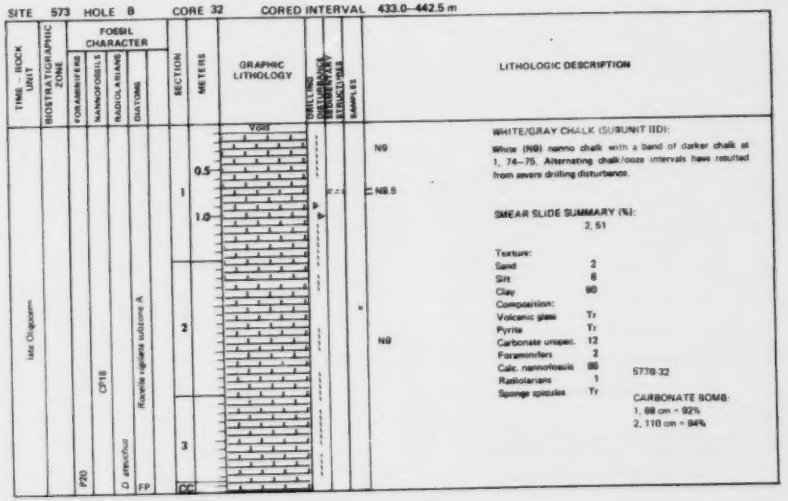

WHITE/GRAY CHALK (SUBUNIT IIB):

White (N9) nanno chalk with a band of darker chalk at 1, 74–75. Alternating chalk/ooze intervals have resulted from severe drilling disturbance.

SMEAR SLIDE SUMMARY (%):

2, 51

Texture:	
Sand	2
Silt	6
Clay	90
Composition:	
Volcanic glass	Tr
Pyrite	Tr
Carbonate unspec.	12
Foraminifers	2
Calc. nannofossils	85
Radiolarians	1
Sponge spicules	Tr

5738-32

CARBONATE BOMB:
1, 68 cm = 92%
2, 110 cm = 94%

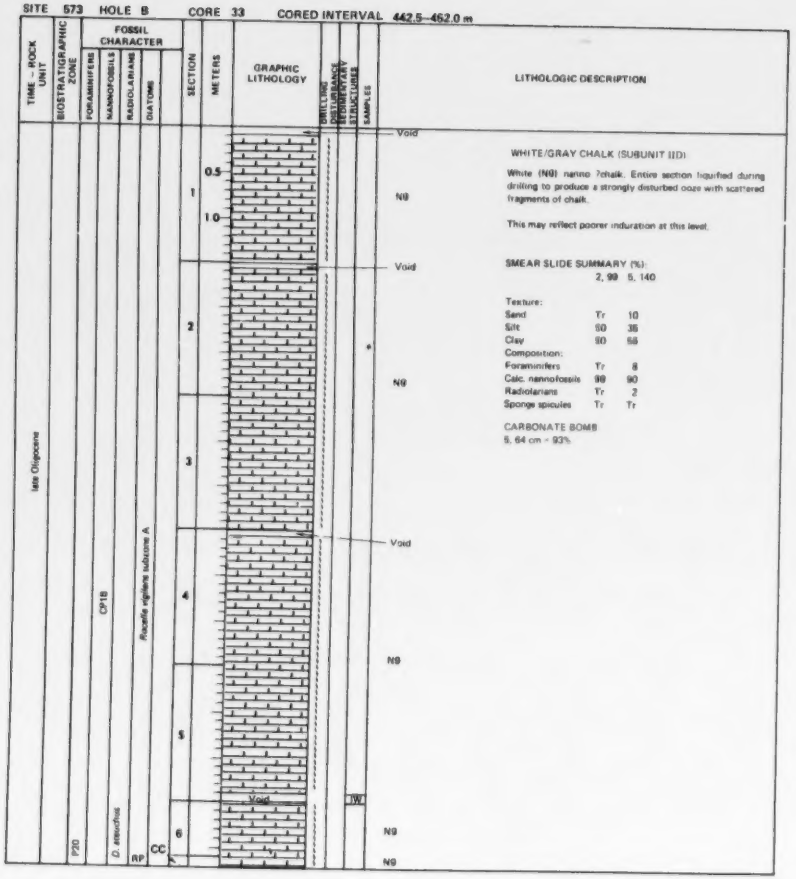
SITE 573 HOLE B CORE 33 CORED INTERVAL 442.5–452.0 m
TIME – ROCK UNIT
BIOSTRATIGRAPHIC ZONE
FOSSIL CHARACTER
FORAMINIFERS
NANNOFOSSILS
RADIOLARIANS
DIATOMS
SECTION
METERS
GRAPHIC LITHOLOGY
DRILLING DISTURBANCE
SEDIMENTARY STRUCTURES
SAMPLES
LITHOLOGIC DESCRIPTION
late Oligocene
P20
CP18
Rocella vigilans subzone A
D. ritscheii
RP
CC
Void
N9
WHITE/GRAY CHALK (SUBUNIT IID)
White (N9) nanno ?chalk. Entire section liquified during drilling to produce a strongly disturbed ooze with scattered fragments of chalk.
This may reflect poorer induration at this level.
SMEAR SLIDE SUMMARY (%):
2, 99 5, 140
Texture:
Sand Tr 10
Silt 90 35
Clay 90 55
Composition:
Foraminifers Tr 8
Calc. nannofossils 99 90
Radiolarians Tr 2
Sponge spicules Tr Tr
CARBONATE BOMB
5, 64 cm = 93%

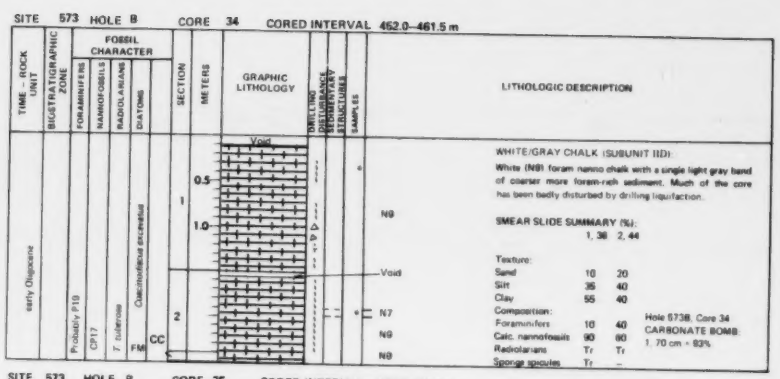
SITE 573 HOLE B CORE 34 CORED INTERVAL 452.0–461.5 m
TIME – ROCK UNIT
BIOSTRATIGRAPHIC ZONE
FOSSIL CHARACTER
FORAMINIFERS
NANNOFOSSILS
RADIOLARIANS
DIATOMS
SECTION
METERS
GRAPHIC LITHOLOGY
DRILLING DISTURBANCE
SEDIMENTARY STRUCTURES
SAMPLES
LITHOLOGIC DESCRIPTION
early Oligocene
Probably P19
CP17
T. rubiginosa
Craspedodiscus excavatus
Craspedodiscus elegans
FM
CC
Void
N9
N7
WHITE/GRAY CHALK (SUBUNIT IID)
White (N9) foram nanno chalk with a single light gray band of coarser more foram-rich sediment. Much of the core has been badly disturbed by drilling liquifaction.
SMEAR SLIDE SUMMARY (%):
1, 36 2, 44
Texture:
Sand 10 20
Silt 35 40
Clay 55 40
Composition:
Foraminifers 10 40
Calc. nannofossils 90 60
Radiolarians Tr Tr
Sponge spicules Tr –
Hole 573B, Core 34
CARBONATE BOMB:
1, 70 cm = 83%

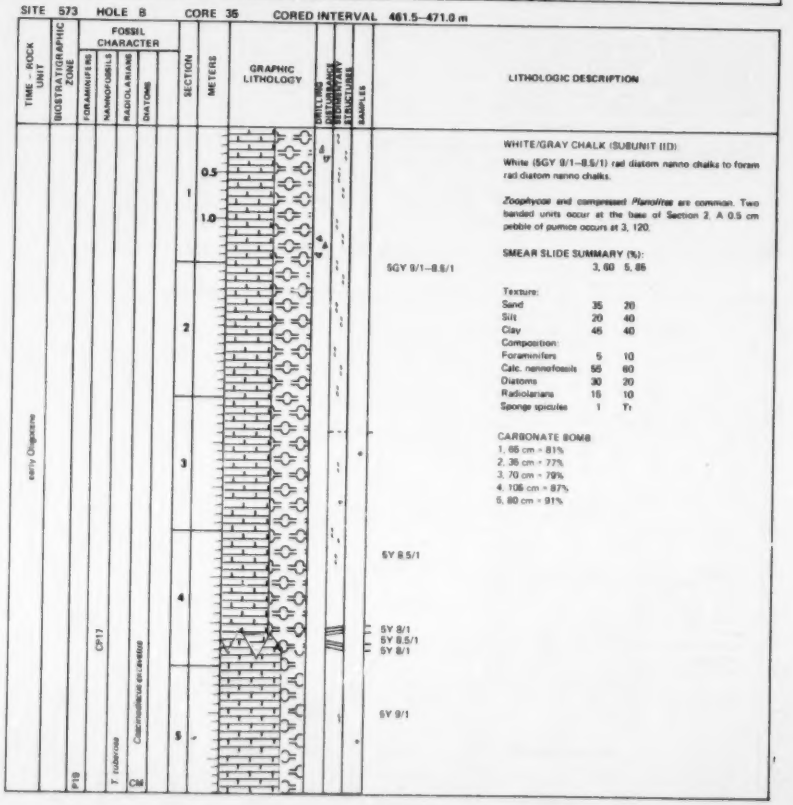
SITE 573 HOLE B CORE 35 CORED INTERVAL 461.5–471.0 m
TIME – ROCK UNIT
BIOSTRATIGRAPHIC ZONE
FOSSIL CHARACTER
FORAMINIFERS
NANNOFOSSILS
RADIOLARIANS
DIATOMS
SECTION
METERS
GRAPHIC LITHOLOGY
DRILLING DISTURBANCE
SEDIMENTARY STRUCTURES
SAMPLES
LITHOLOGIC DESCRIPTION
early Oligocene
P19
CP17
T. rubiginosa
Craspedodiscus elegans
CN6
5GY 9/1–8.5/1
5Y 8.5/1
5Y 8/1
5Y 8.5/1
5Y 8/1
5Y 9/1
WHITE/GRAY CHALK (SUBUNIT IID)
White (5GY 9/1–8.5/1) rad diatom nanno chalks to foram rad diatom nanno chalks.
Zoophycos and compressed Planolites are common. Two banded units occur at the base of Section 2. A 0.5 cm pebble of pumice occurs at 3, 120.
SMEAR SLIDE SUMMARY (%):
3, 60 5, 86
Texture:
Sand 35 20
Silt 20 40
Clay 45 40
Composition:
Foraminifers 5 10
Calc. nannofossils 55 60
Diatoms 30 20
Radiolarians 15 10
Sponge spicules 1 Tr
CARBONATE BOMB
1, 65 cm = 81%
2, 35 cm = 77%
3, 70 cm = 79%
4, 105 cm = 87%
5, 80 cm = 91%

SITE 573 HOLE B CORE 36 CORED INTERVAL 471.0–480.5 m

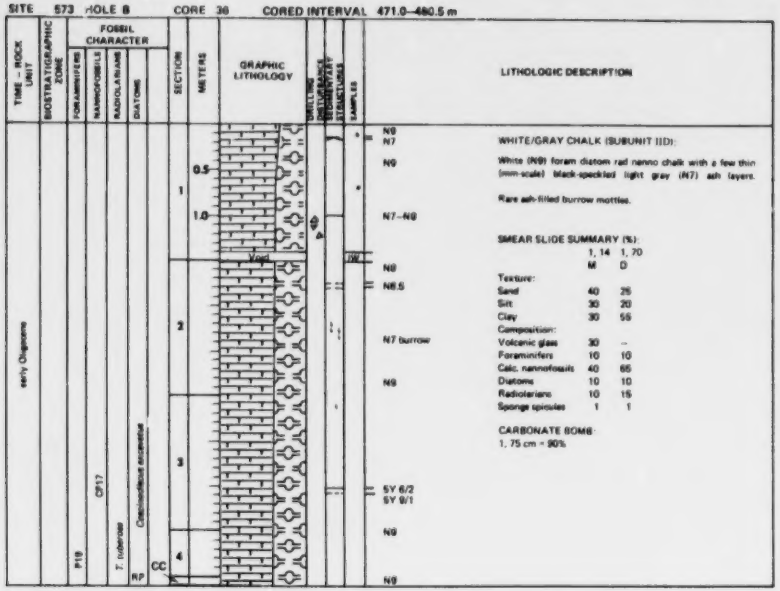

SITE 573 HOLE B CORE 37 CORED INTERVAL 480.5–490.0 m

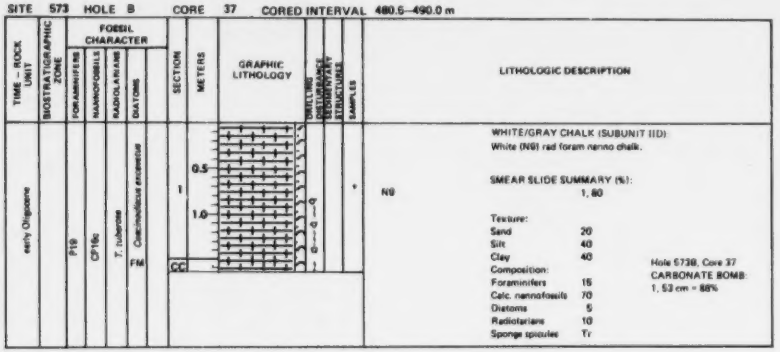

SITE 573 HOLE B CORE 38 CORED INTERVAL 490.0–499.5 m

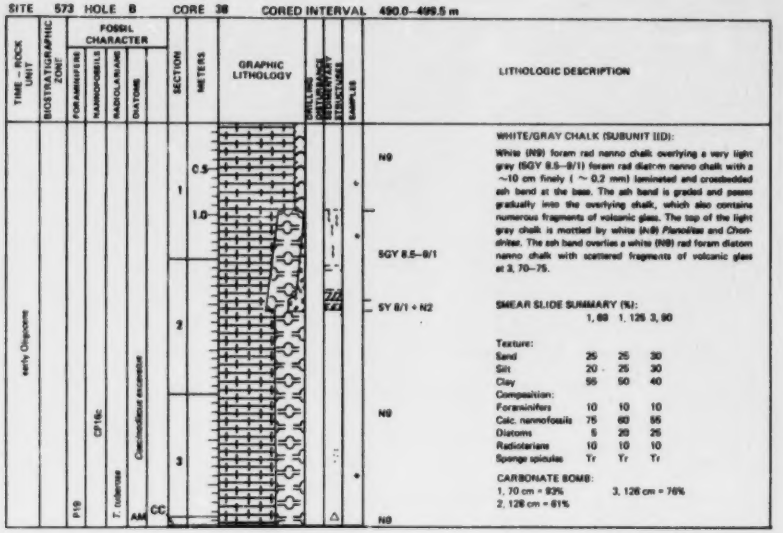
TIME – ROCK UNIT
BIOSTRATIGRAPHIC ZONE
FOSSIL CHARACTER
FORAMINIFERS
NANNOFOSSILS
RADIOLARIANS
DIATOMS
SECTION
METERS
GRAPHIC LITHOLOGY
DRILLING DISTURBANCE
SEDIMENTARY STRUCTURES
SAMPLES
LITHOLOGIC DESCRIPTION
early Oligocene
P19
CP16c
T. rubensae
Cavicondiscus excavatus
AM
CC
N9
5GY 8.5–9/1
5Y 8/1 + N2
N9
N9
WHITE/GRAY CHALK (SUBUNIT IID):
White (N9) foram rad nanno chalk overlying a very light gray (5GY 8.5–9/1) foram rad diatom nanno chalk with a ~10 cm finely (~ 0.2 mm) laminated and crossbedded ash bend at the base. The ash band is graded and passes gradually into the overlying chalk, which also contains numerous fragments of volcanic glass. The top of the light gray chalk is mottled by white (N9) *Planolites* and *Chondrites*. The ash band overlies a white (N9) rad foram diatom nanno chalk with scattered fragments of volcanic glass at 3, 70–75.
SMEAR SLIDE SUMMARY (%):
1, 60 1, 125 3, 90
Texture:
Sand 25 25 30
Silt 20 25 30
Clay 55 50 40
Composition:
Foraminifers 10 10 10
Calc. nannofossils 75 60 55
Diatoms 5 20 25
Radiolarians 10 10 10
Sponge spicules Tr Tr Tr
CARBONATE BOMB:
1, 70 cm = 93%
2, 126 cm = 81%
3, 126 cm = 76%

SITE 573 HOLE B CORE 39 CORED INTERVAL 499.5–509.0 m

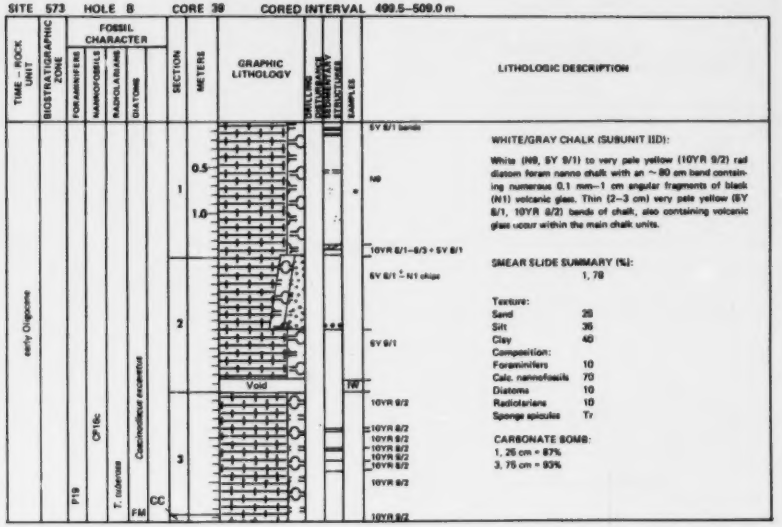

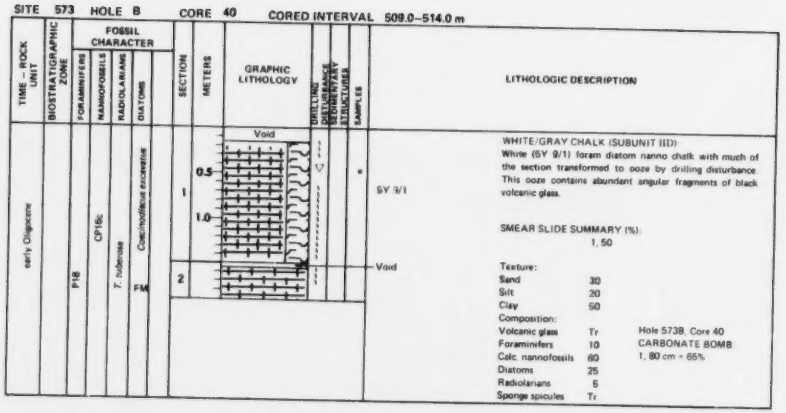
SITE 573 HOLE B CORE 40 CORED INTERVAL 509.0–514.0 m
TIME – ROCK UNIT
BIOSTRATIGRAPHIC ZONE
FOSSIL CHARACTER
FORAMINIFERS
NANNOFOSSILS
RADIOLARIANS
DIATOMS
SECTION
METERS
GRAPHIC LITHOLOGY
DRILLING DISTURBANCE
SEDIMENTARY STRUCTURES
SAMPLES
LITHOLOGIC DESCRIPTION
early Oligocene
P18
CP18c
T. tuberosa
Coccinodiscus excentricus
FM
Void
5Y 9/1
Void
WHITE/GRAY CHALK (SUBUNIT IIID)
White (5Y 9/1) foram diatom nanno chalk with much of the section transformed to ooze by drilling disturbance. This ooze contains abundant angular fragments of black volcanic glass.
SMEAR SLIDE SUMMARY (%):
1, 50
Texture:
Sand 30
Silt 20
Clay 50
Composition:
Volcanic glass Tr
Foraminifers 10
Calc. nannofossils 60
Diatoms 25
Radiolarians 5
Sponge spicules Tr
Hole 573B, Core 40
CARBONATE BOMB:
1, 80 cm = 65%

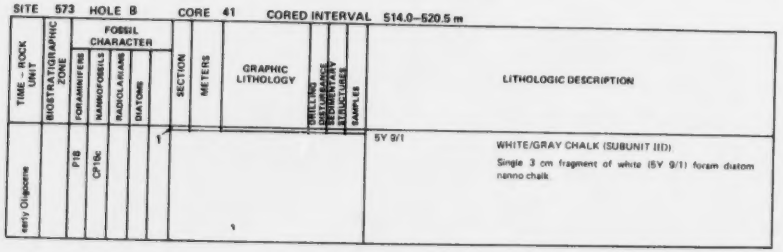
SITE 573 HOLE B CORE 41 CORED INTERVAL 514.0–520.5 m
TIME – ROCK UNIT
BIOSTRATIGRAPHIC ZONE
FOSSIL CHARACTER
FORAMINIFERS
NANNOFOSSILS
RADIOLARIANS
DIATOMS
SECTION
METERS
GRAPHIC LITHOLOGY
DRILLING DISTURBANCE
SEDIMENTARY STRUCTURES
SAMPLES
LITHOLOGIC DESCRIPTION
early Oligocene
P18
CP18c
5Y 9/1
WHITE/GRAY CHALK (SUBUNIT IID)
Single 3 cm fragment of white (5Y 9/1) foram diatom nanno chalk

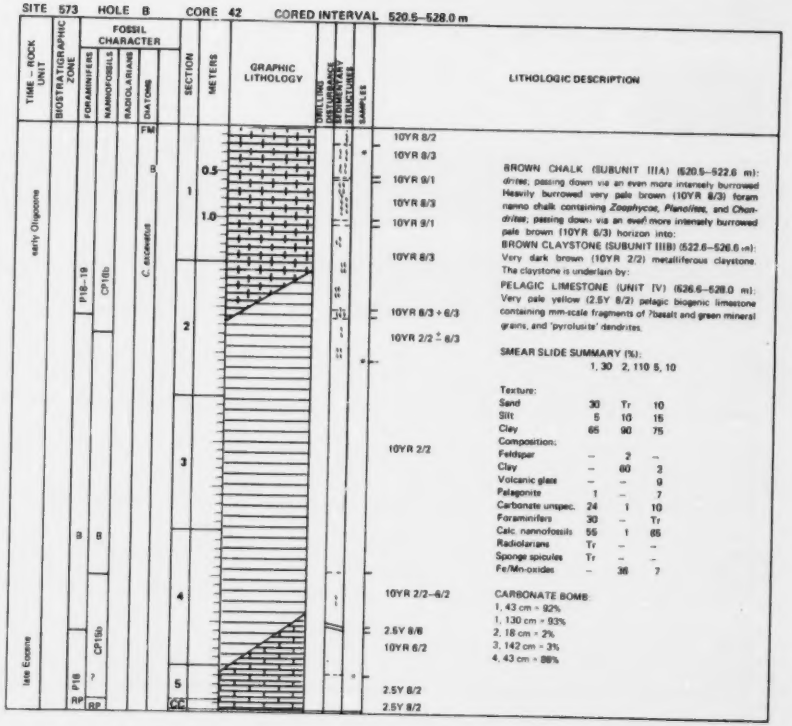
SITE 573 HOLE B CORE 42 CORED INTERVAL 520.5–528.0 m
TIME – ROCK UNIT
BIOSTRATIGRAPHIC ZONE
FOSSIL CHARACTER
FORAMINIFERS
NANNOFOSSILS
RADIOLARIANS
DIATOMS
SECTION
METERS
GRAPHIC LITHOLOGY
DRILLING DISTURBANCE
SEDIMENTARY STRUCTURES
SAMPLES
LITHOLOGIC DESCRIPTION
late Eocene
early Oligocene
P18
P18–19
CP15b
CP16b
C. stockwellii
FM
RP
CC
10YR 8/2
10YR 8/3
10YR 9/1
10YR 8/3
10YR 9/1
10YR 8/3
10YR 8/3 + 6/3
10YR 2/2 ± 6/3
10YR 2/2
10YR 2/2–4/2
2.5Y 8/6
10YR 6/2
2.5Y 8/2
2.5Y 8/2
BROWN CHALK (SUBUNIT IIIA) (520.5–522.6 m): drilled, passing down via an even more intensely burrowed Heavily burrowed very pale brown (10YR 8/3) foram nanno chalk containing Zoophycos, Planolites, and Chondrites, passing down via an even more intensely burrowed pale brown (10YR 6/3) horizon into:
BROWN CLAYSTONE (SUBUNIT IIIB) (522.6–526.6 m): Very dark brown (10YR 2/2) metalliferous claystone. The claystone is underlain by:
PELAGIC LIMESTONE (UNIT IV) (526.6–528.0 m): Very pale yellow (2.5Y 8/2) pelagic biogenic limestone containing mm-scale fragments of ?basalt and green mineral grains, and 'pyrolusite' dendrites.
SMEAR SLIDE SUMMARY (%):
1, 30 2, 110 5, 10
Texture:
Sand 30 Tr 10
Silt 5 10 15
Clay 65 90 75
Composition:
Feldspar – 2 –
Clay – 80 3
Volcanic glass – – 9
Pelagonite 1 – 7
Carbonate unspec. 24 1 10
Foraminifers 30 – Tr
Calc. nannofossils 55 1 65
Radiolarians Tr – –
Sponge spicules Tr – –
Fe/Mn-oxides – 38 7
CARBONATE BOMB:
1, 43 cm = 92%
1, 130 cm = 93%
2, 18 cm = 2%
3, 142 cm = 3%
4, 43 cm = 88%

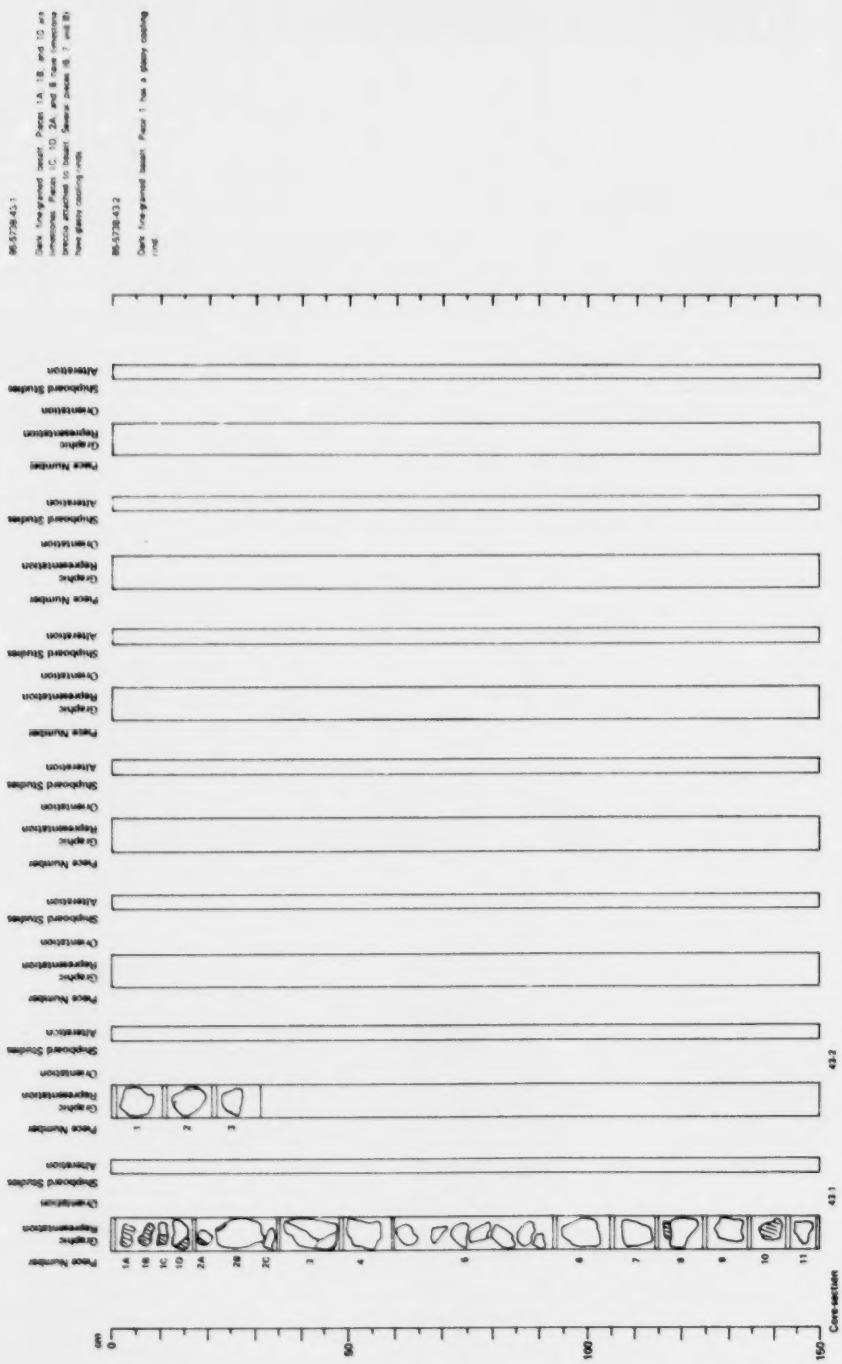
85-573E-43-1
Dark, fine-grained basalt. Pieces 1A, 1B, and 1C are interbrecciated. Pieces 1C, 1D, 2A, and 2B have limestone breccia attached to basalt. Several pieces (6, 7, and 8) have glassy cooling rinds.
85-573E-43-2
Dark, fine-grained basalt. Piece 1 has a glassy cooling rind.
Piece Number
Graphic Representation
Orientation
Sediment Studies
Alteration
1A
1B
1C
1D
2A
2B
2C
3
4
5
6
7
8
9
10
11
1
2
3
431
432
Core section
cm
0
50
100
150

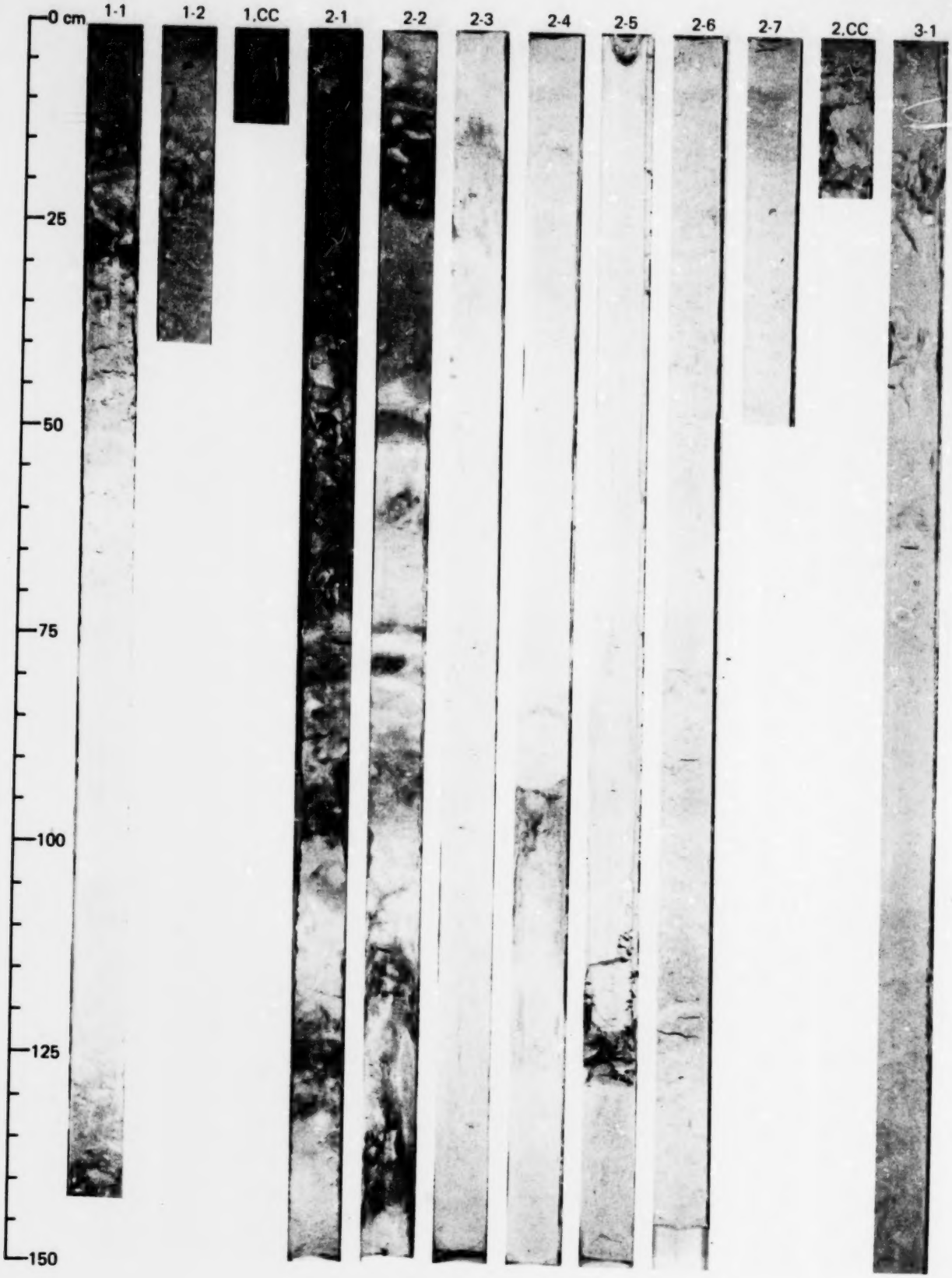
0 cm
1-1
1-2
1,CC
2-1
2-2
2-3
2-4
2-5
2-6
2-7
2,CC
3-1
25
50
75
100
125
150

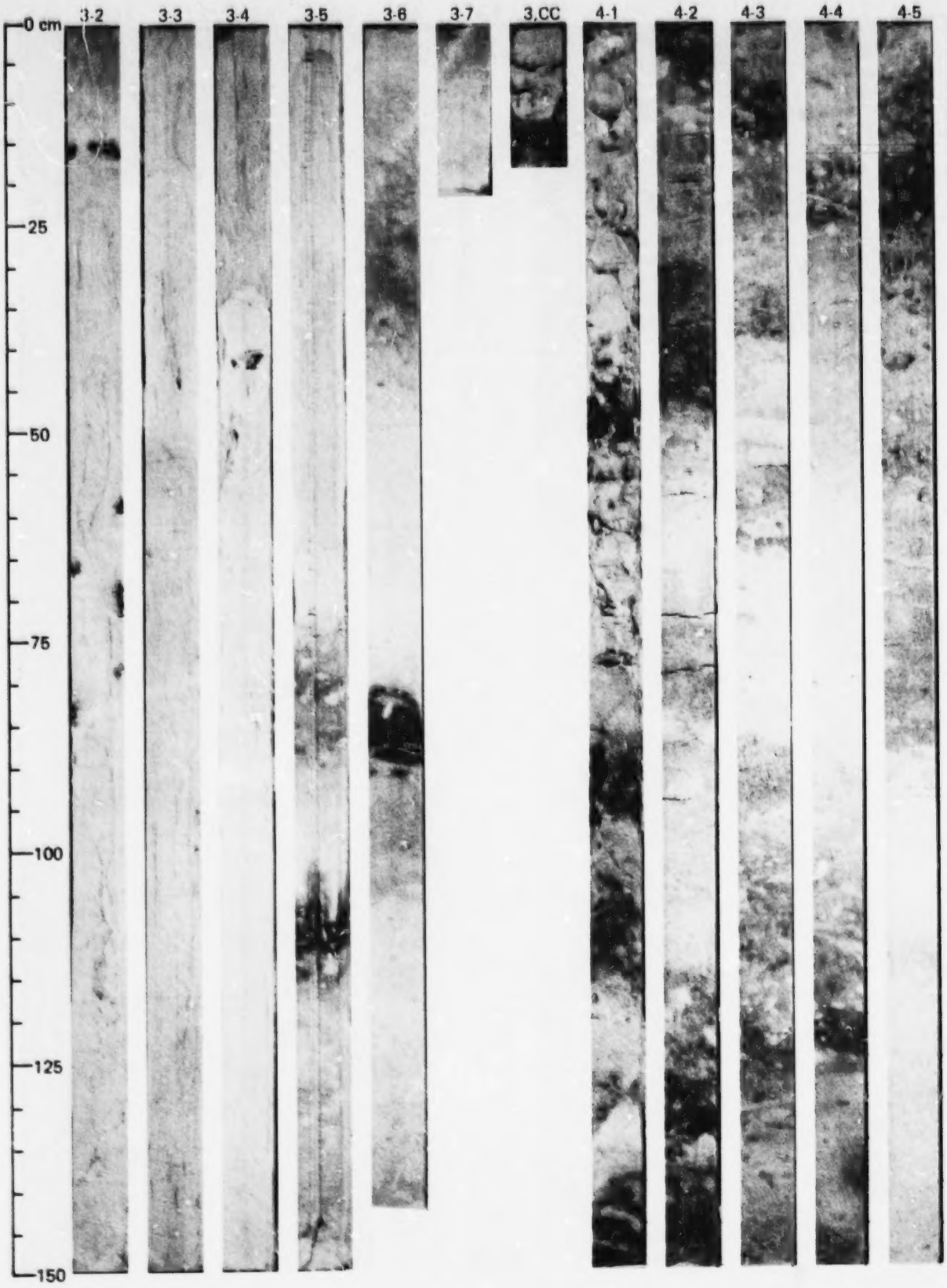
0 cm
25
50
75
100
125
150
3-2
3-3
3-4
3-5
3-6
3-7
3,CC
4-1
4-2
4-3
4-4
4-5

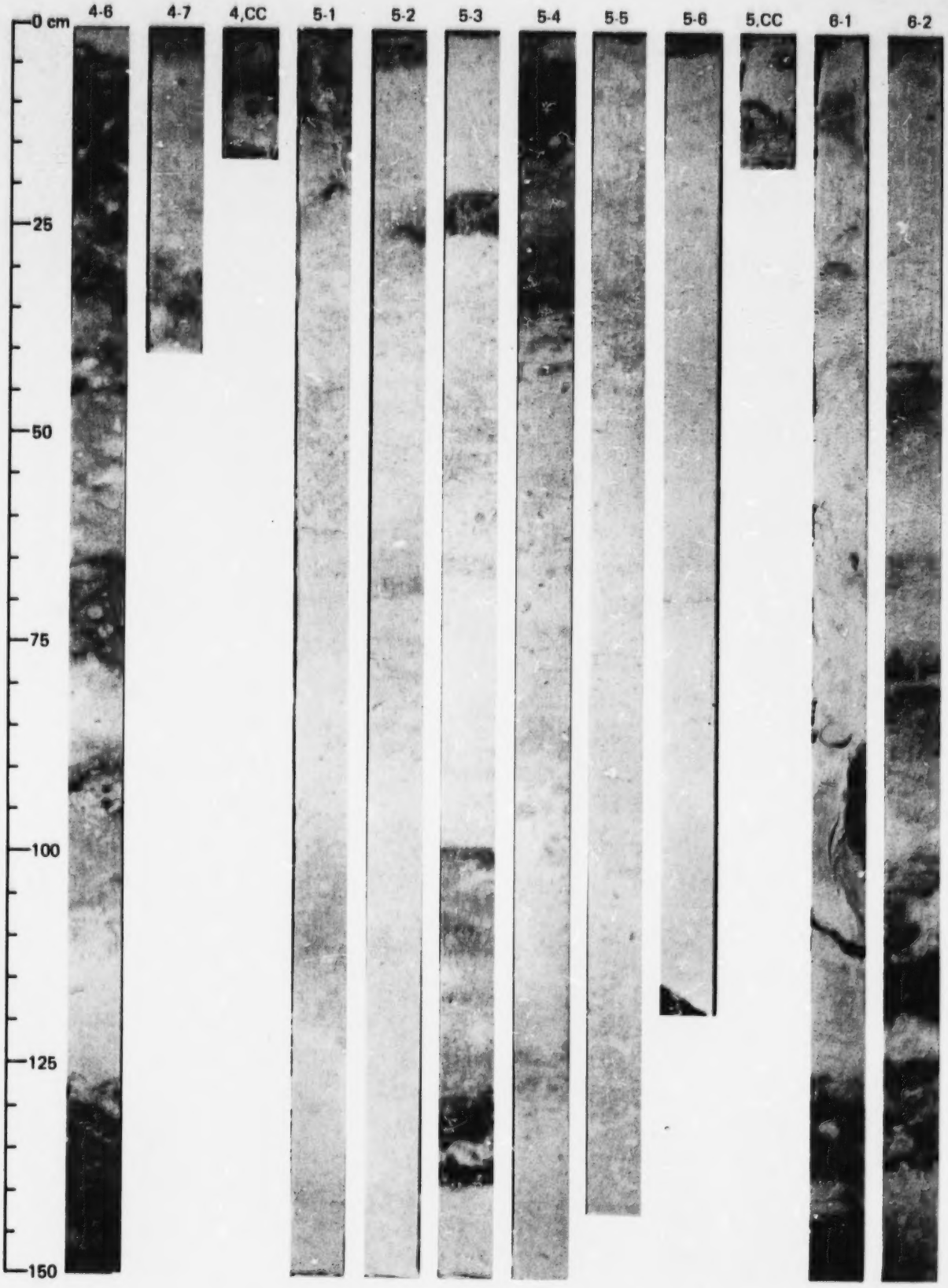
0 cm
25
50
75
100
125
150
4-6
4-7
4,CC
5-1
5-2
5-3
5-4
5-5
5-6
5,CC
6-1
6-2

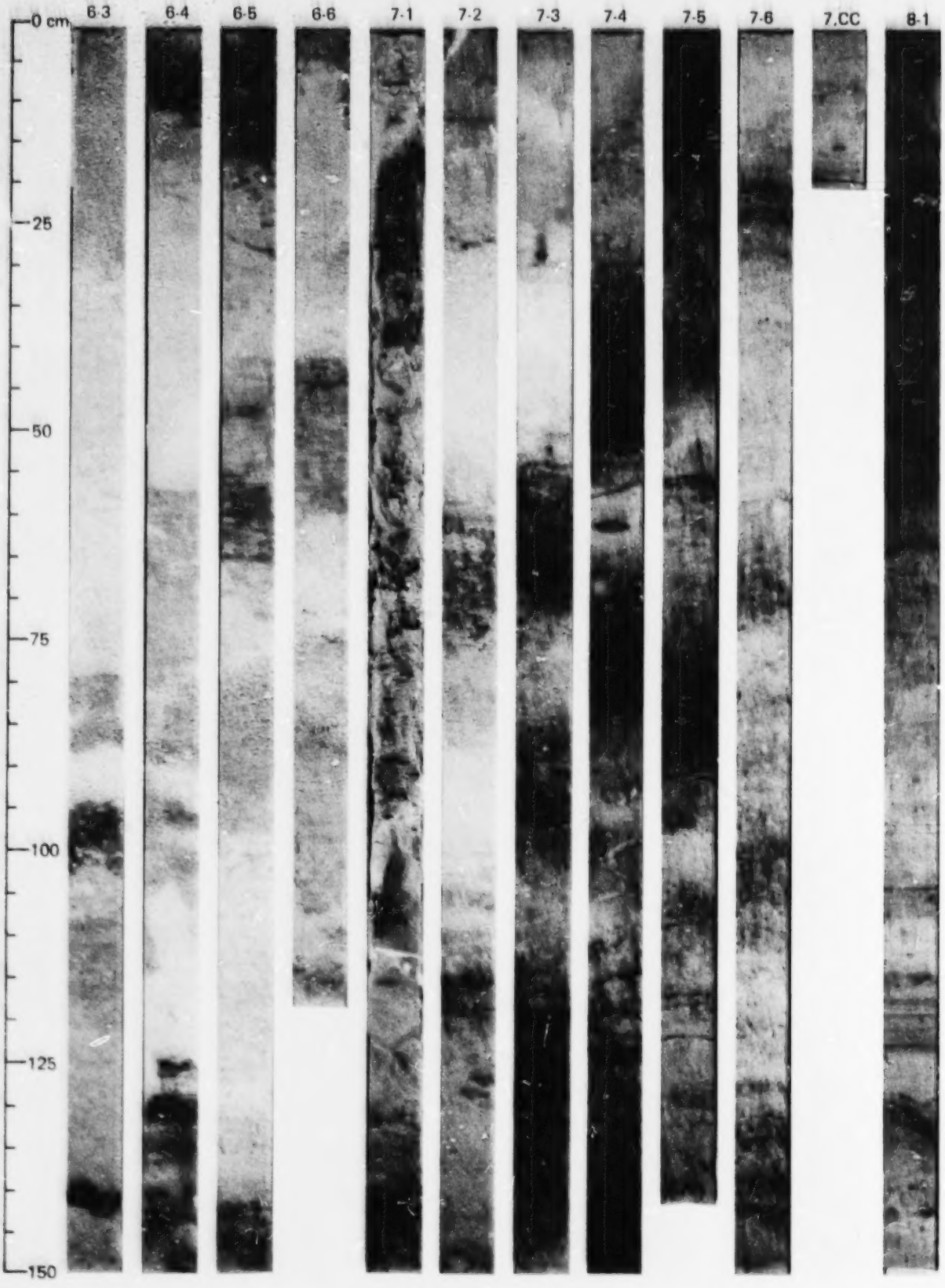
0 cm
25
50
75
100
125
150
6-3
6-4
6-5
6-6
7-1
7-2
7-3
7-4
7-5
7-6
7,CC
8-1

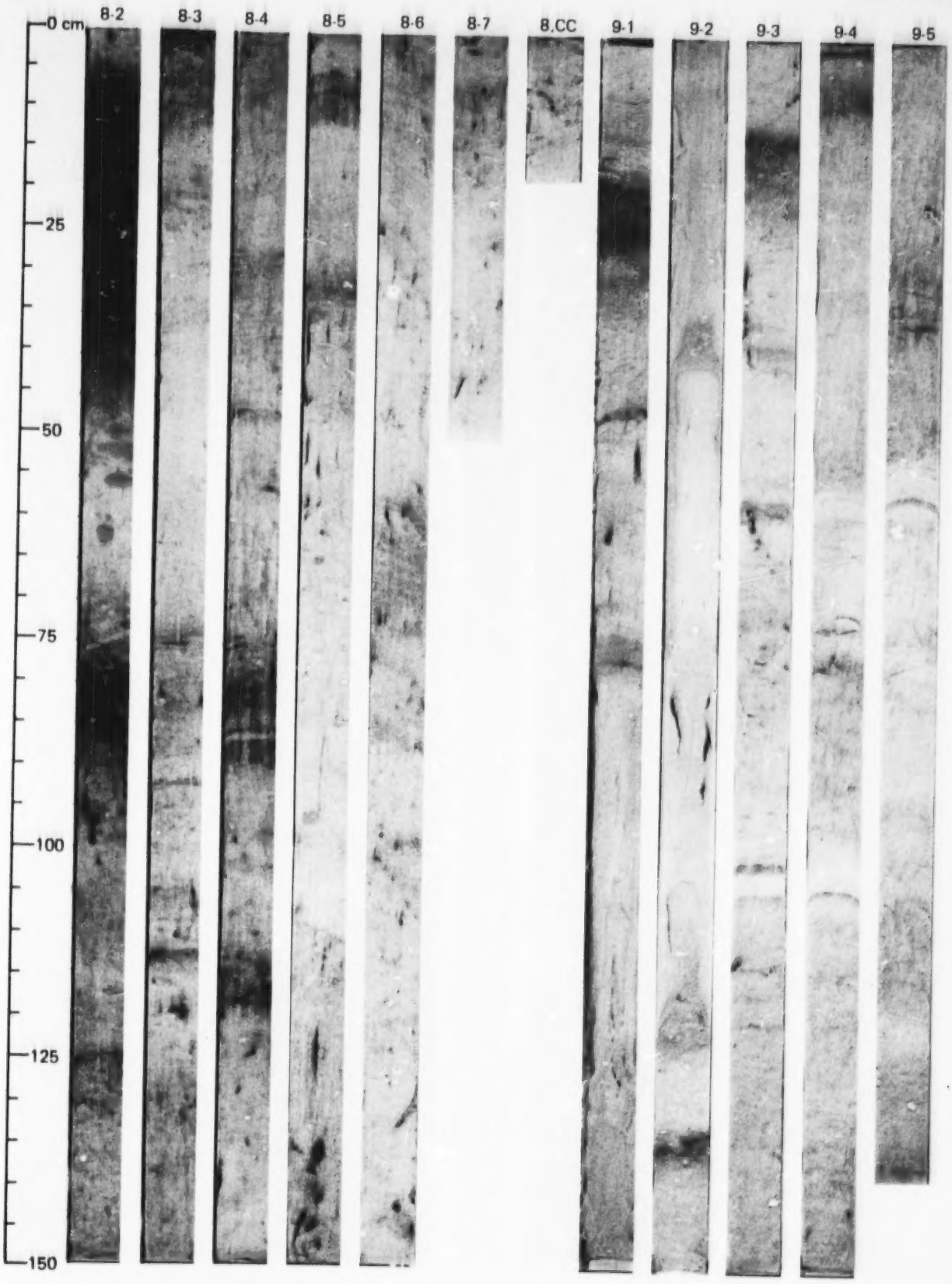
0 cm
25
50
75
100
125
150
8-2
8-3
8-4
8-5
8-6
8-7
8,CC
9-1
9-2
9-3
9-4
9-5

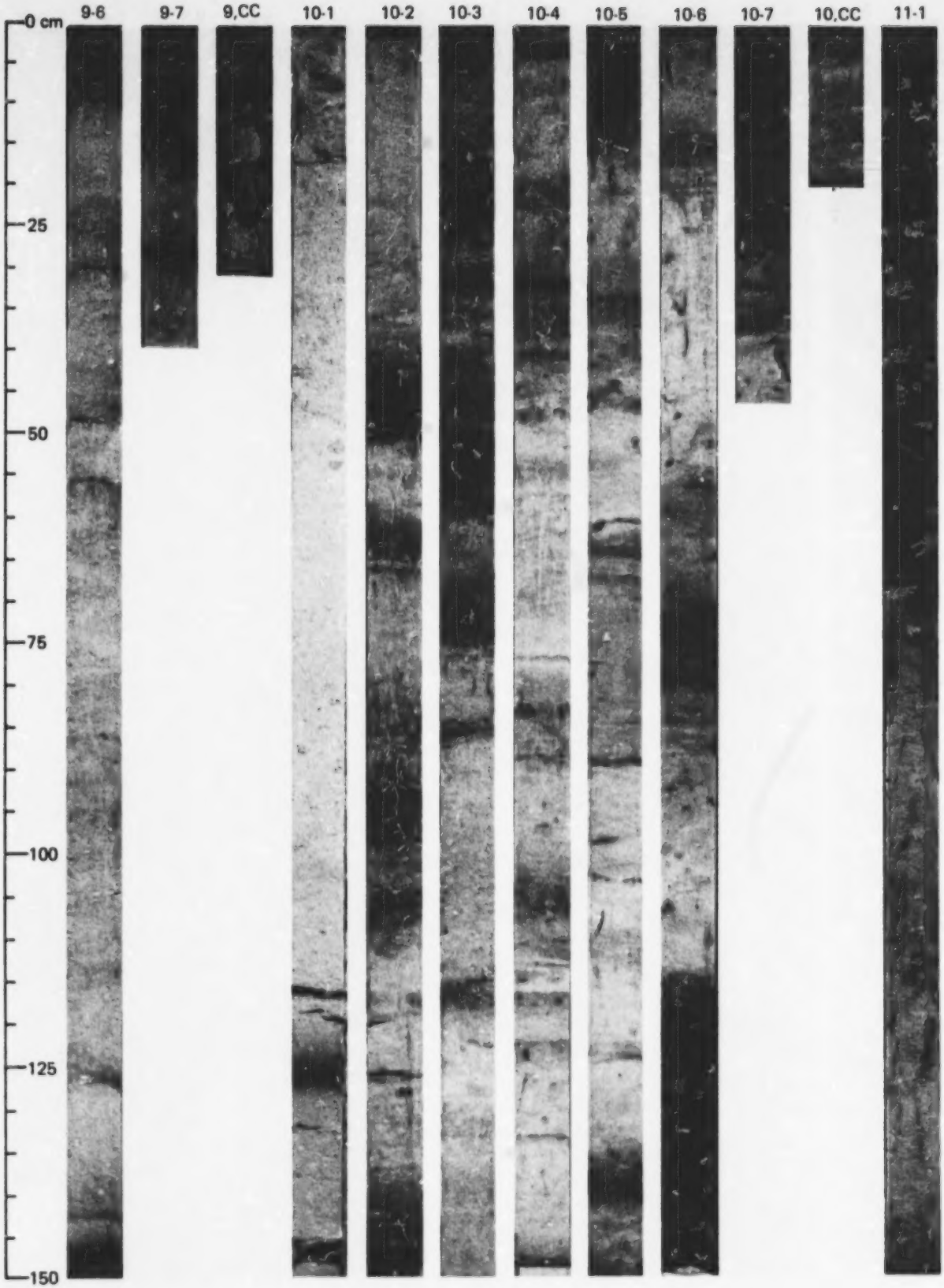
0 cm
25
50
75
100
125
150
9-6
9-7
9,CC
10-1
10-2
10-3
10-4
10-5
10-6
10-7
10,CC
11-1

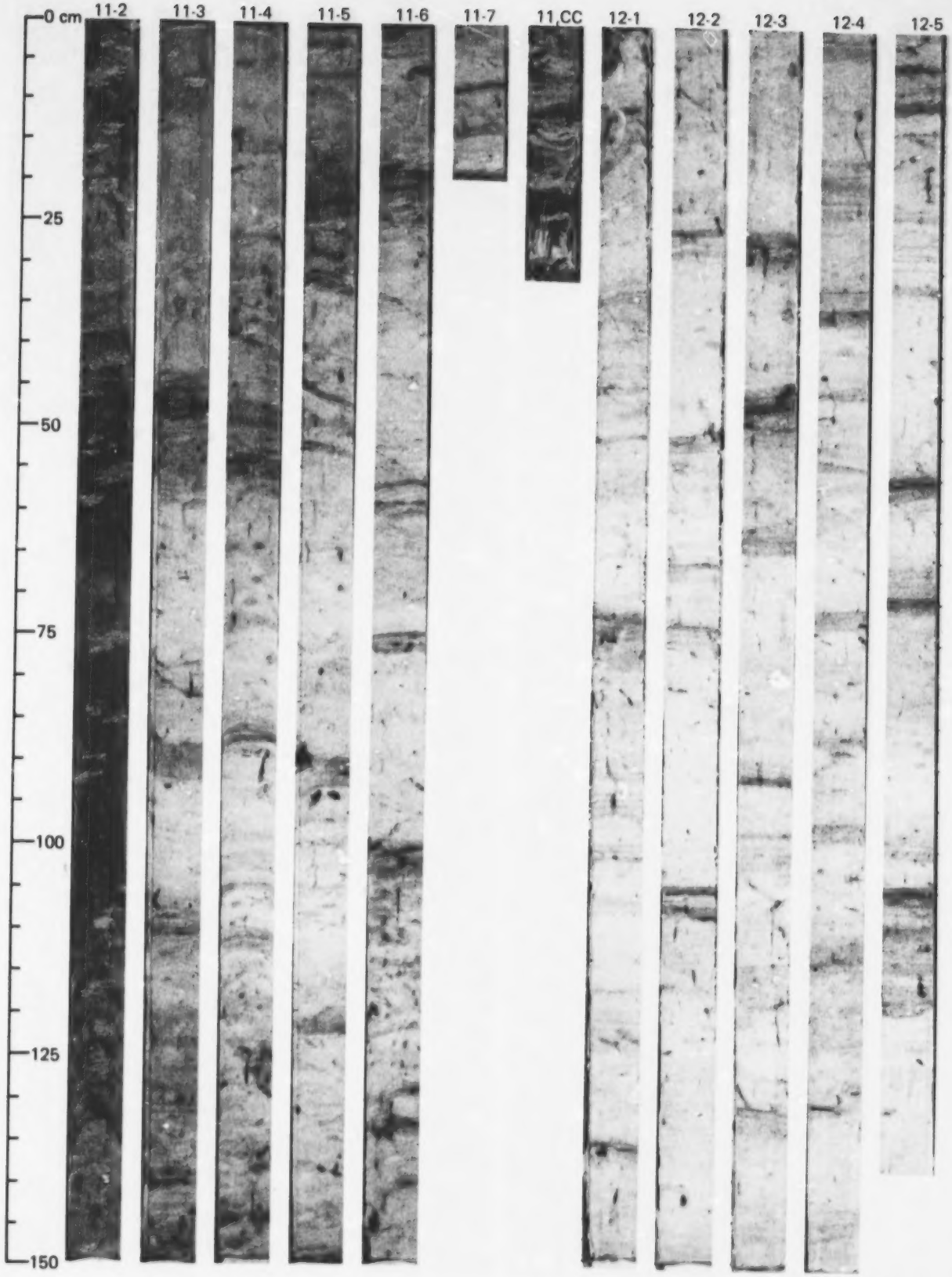
0 cm
11-2
11-3
11-4
11-5
11-6
11-7
11,CC
12-1
12-2
12-3
12-4
12-5
25
50
75
100
125
150

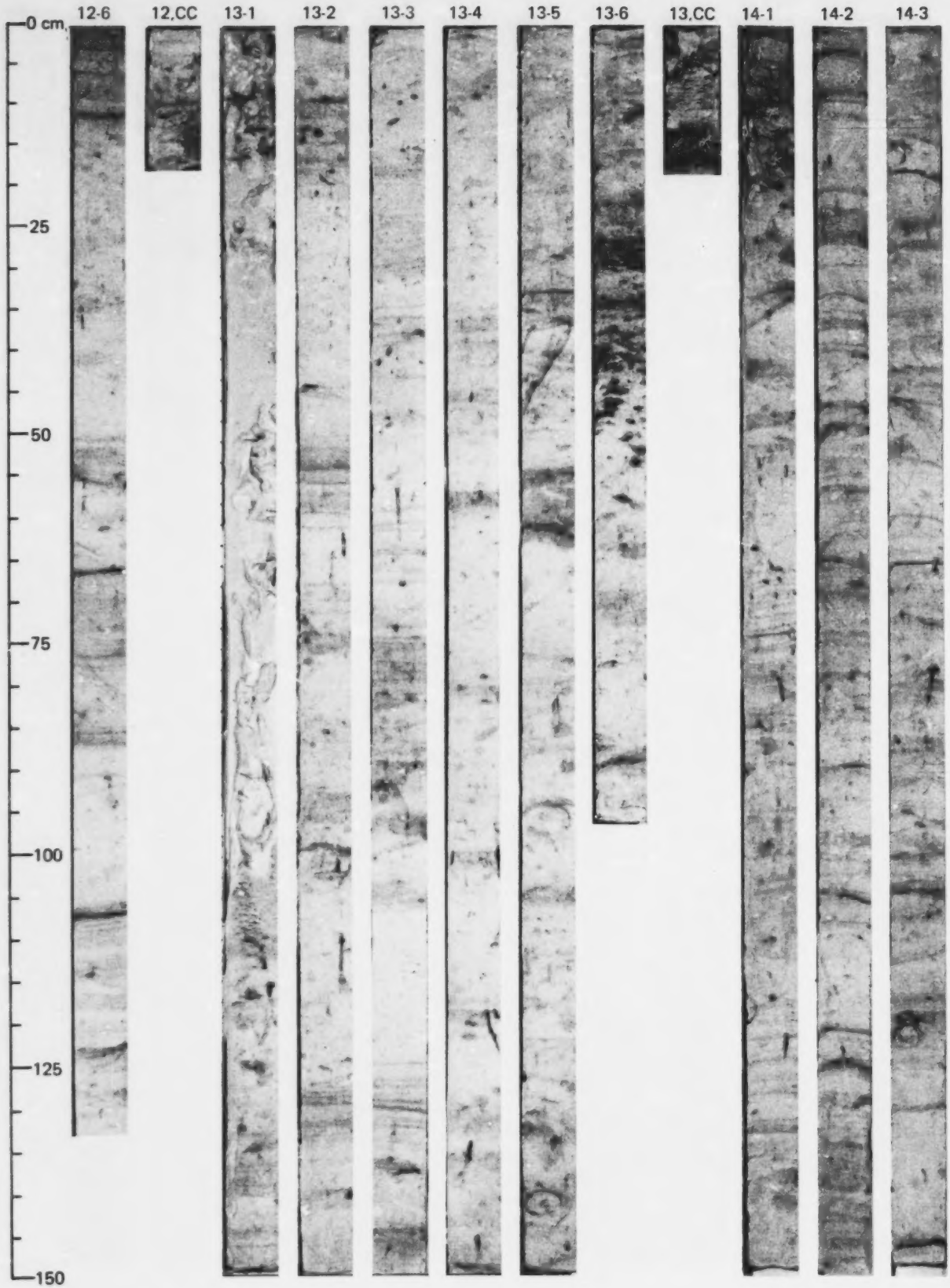
0 cm
25
50
75
100
125
150
12-6
12,CC
13-1
13-2
13-3
13-4
13-5
13-6
13,CC
14-1
14-2
14-3

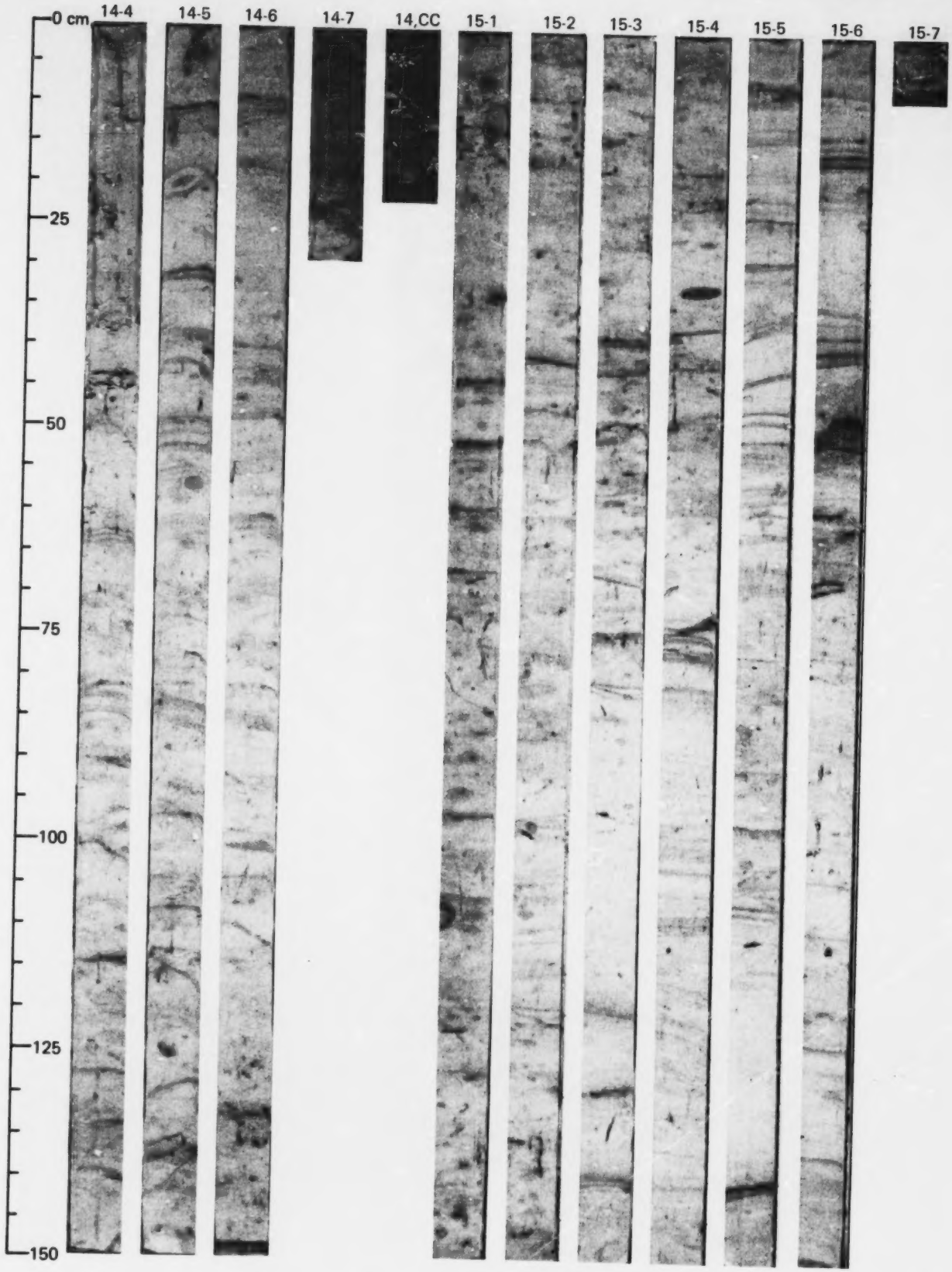
0 cm
14-4
14-5
14-6
14-7
14,CC
15-1
15-2
15-3
15-4
15-5
15-6
15-7
25
50
75
100
125
150

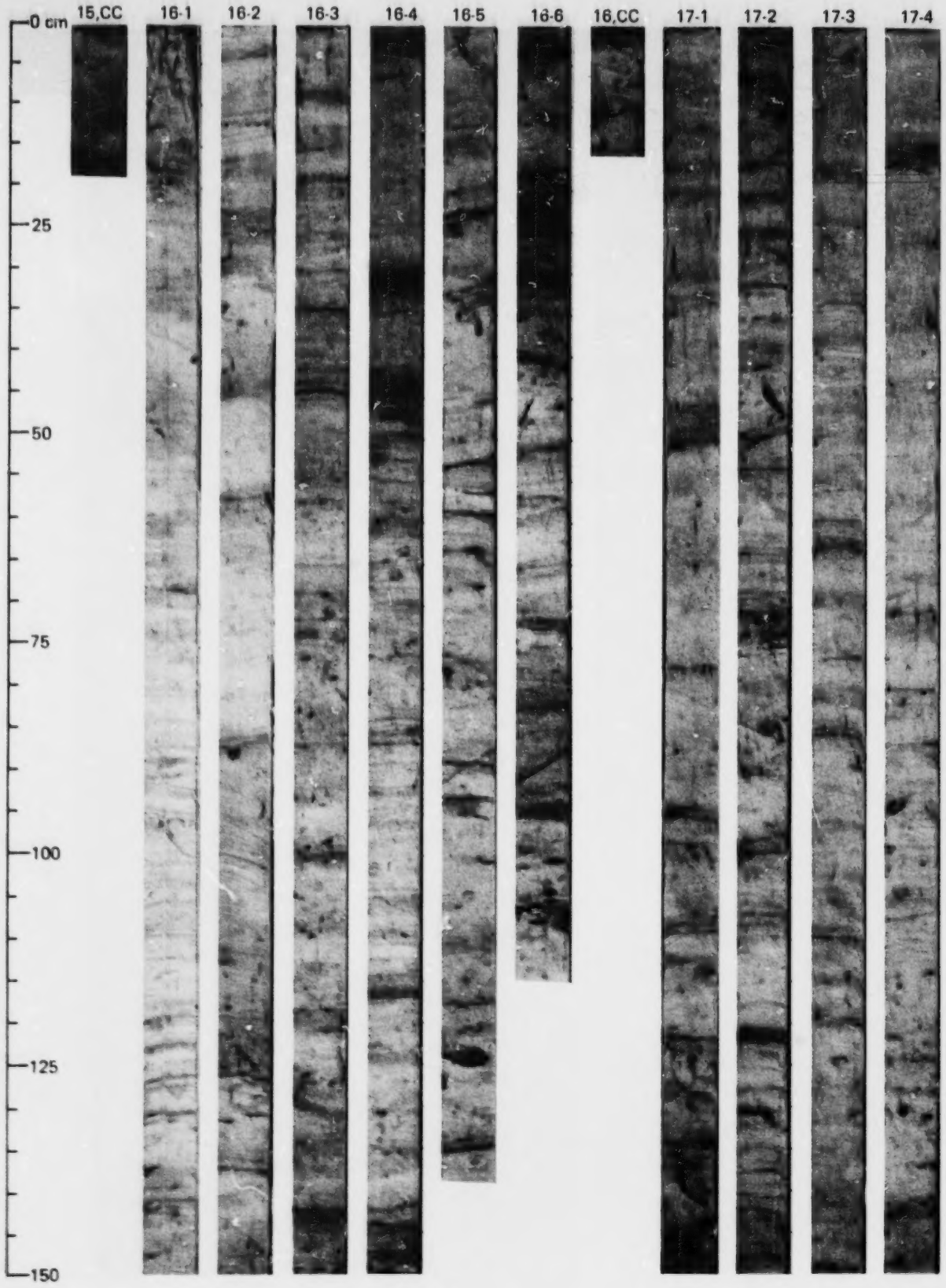
0 cm
15,CC
16-1
16-2
16-3
16-4
16-5
16-6
16,CC
17-1
17-2
17-3
17-4
25
50
75
100
125
150

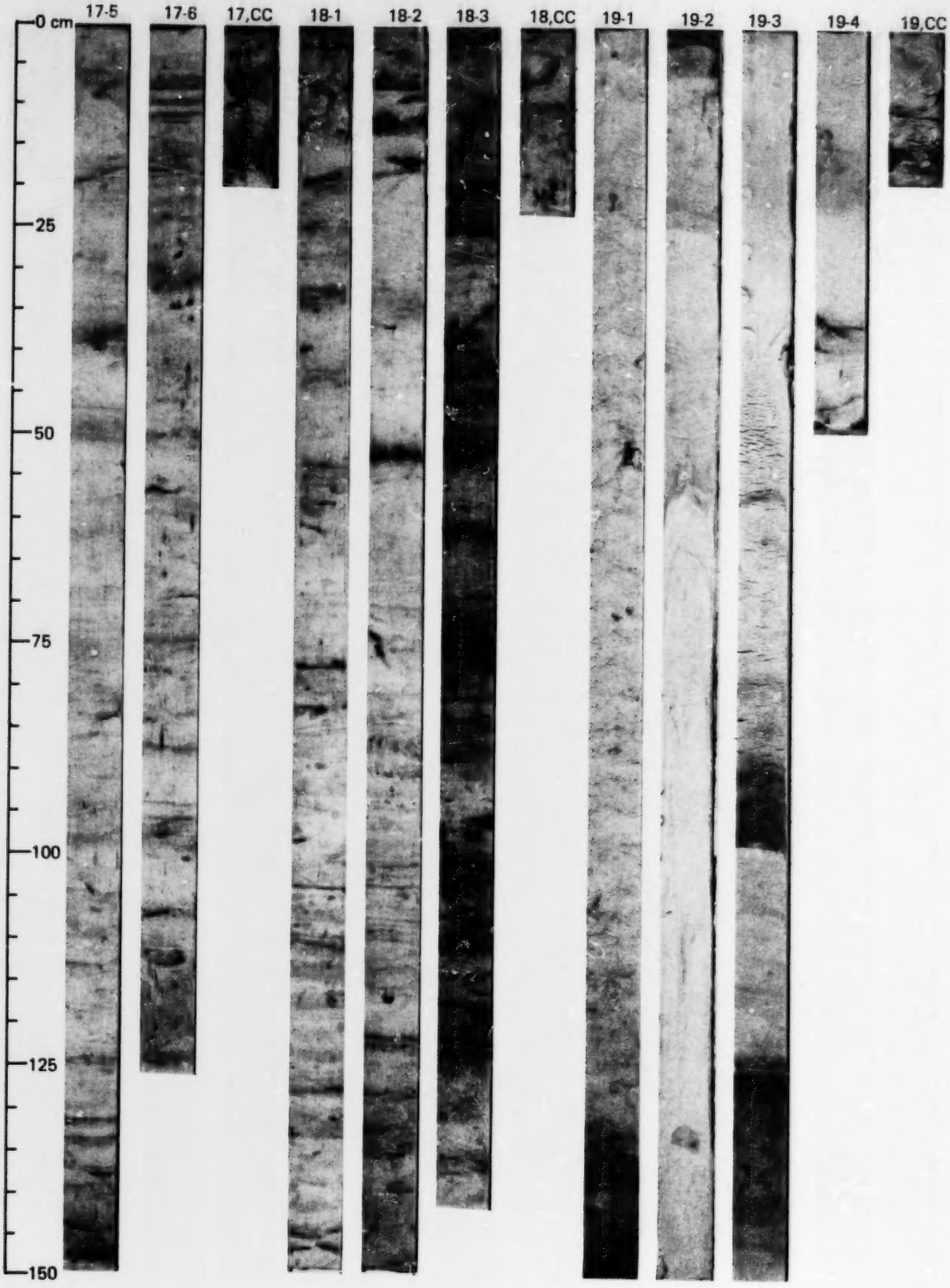
0 cm
25
50
75
100
125
150
17-5
17-6
17,CC
18-1
18-2
18-3
18,CC
19-1
19-2
19-3
19-4
19,CC

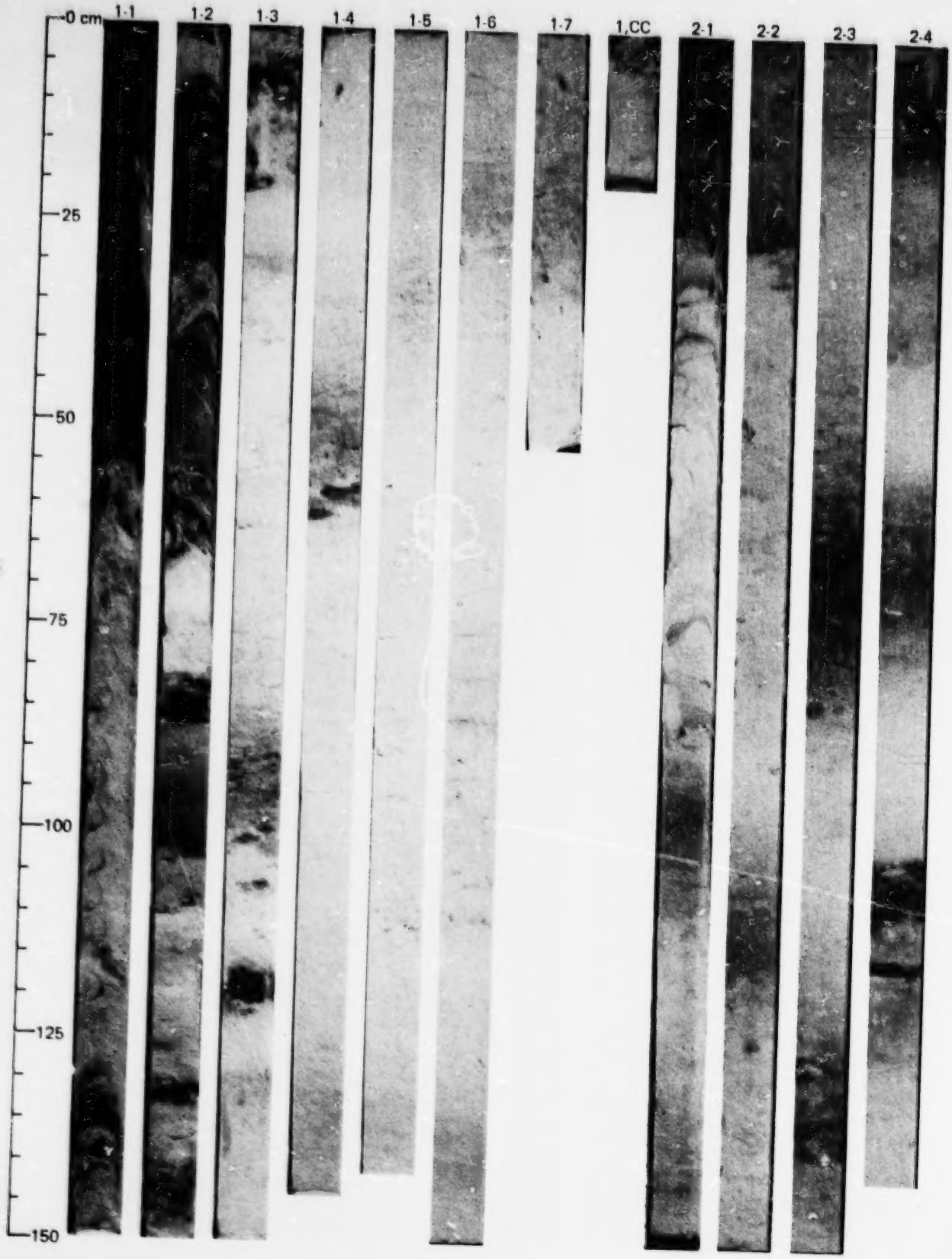
0 cm
1-1
1-2
1-3
1-4
1-5
1-6
1-7
1,CC
2-1
2-2
2-3
2-4
25
50
75
100
125
150

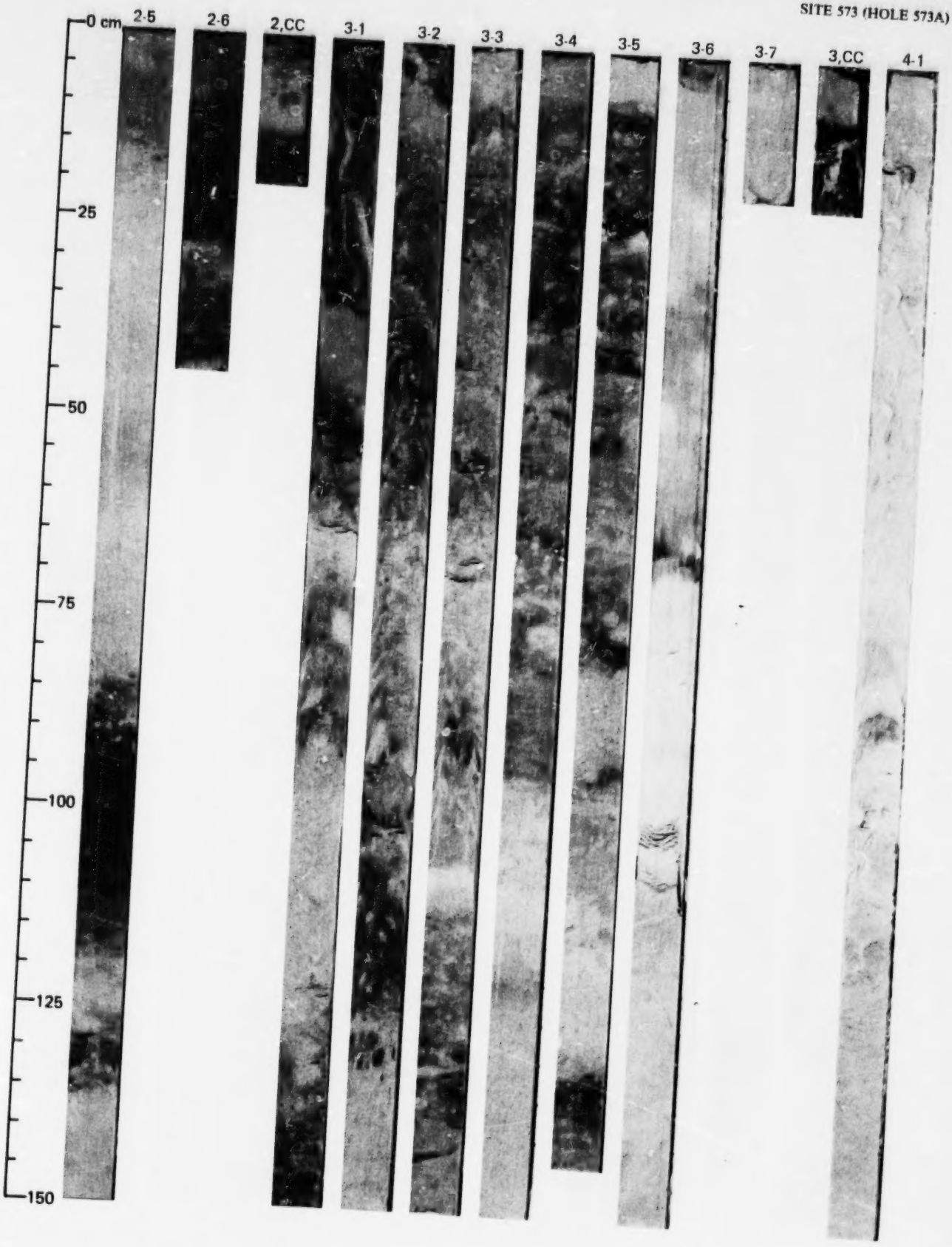
0 cm
25
50
75
100
125
150
2-5
2-6
2,CC
3-1
3-2
3-3
3-4
3-5
3-6
3-7
3,CC
4-1

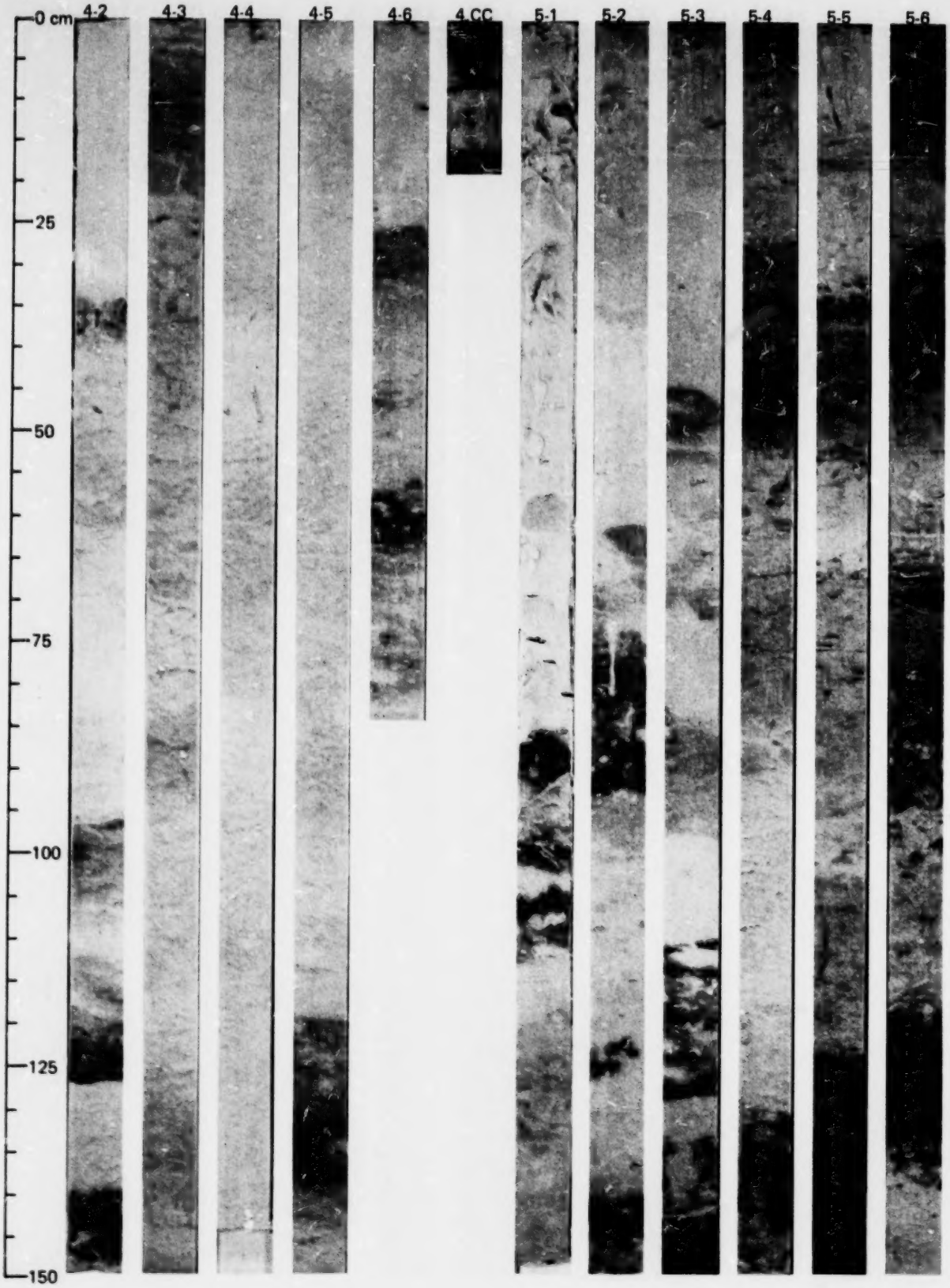
0 cm
25
50
75
100
125
150
4-2
4-3
4-4
4-5
4-6
4,CC
5-1
5-2
5-3
5-4
5-5
5-6

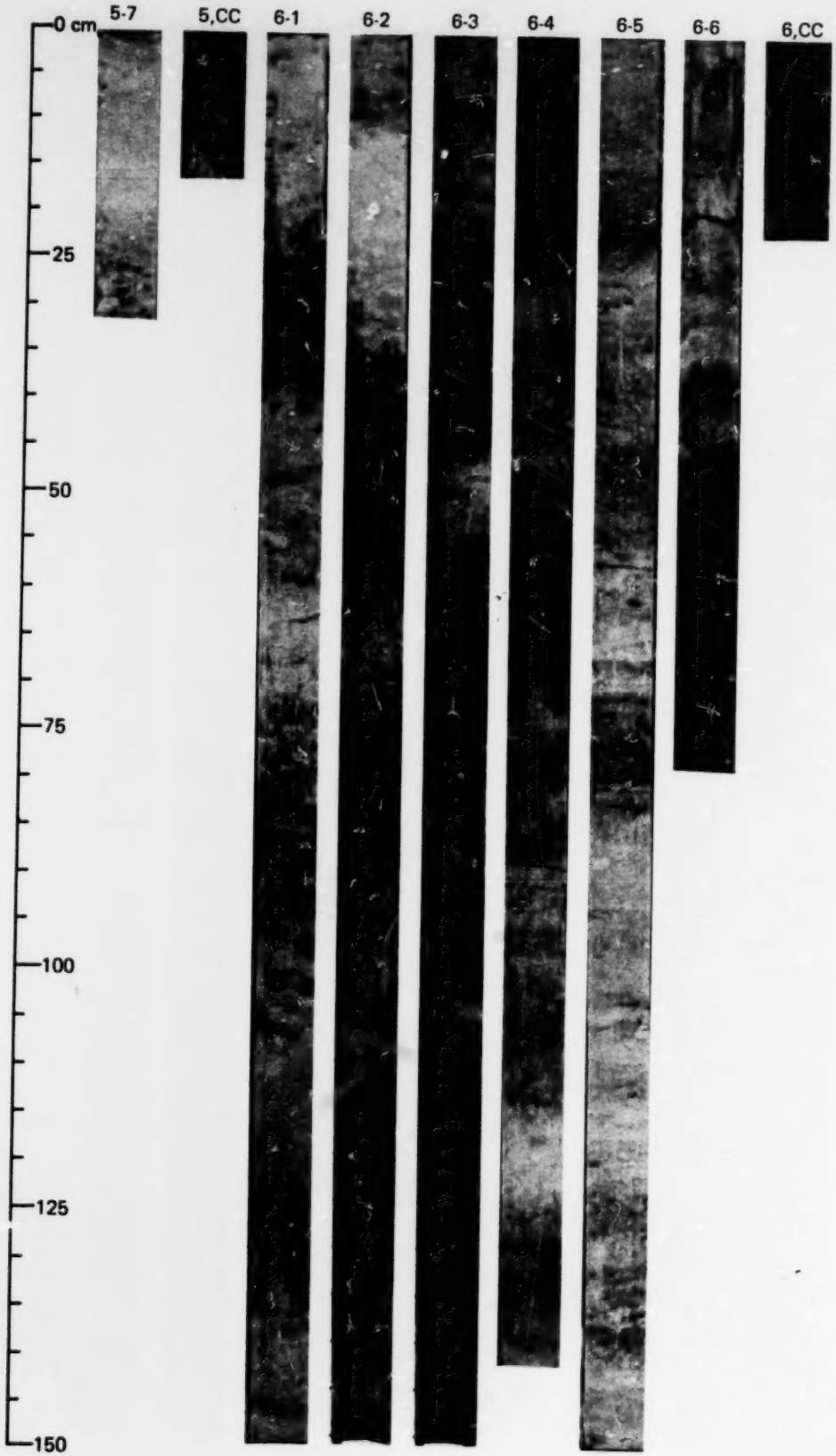
0 cm
5-7
5,CC
6-1
6-2
6-3
6-4
6-5
6-6
6,CC
25
50
75
100
125
150

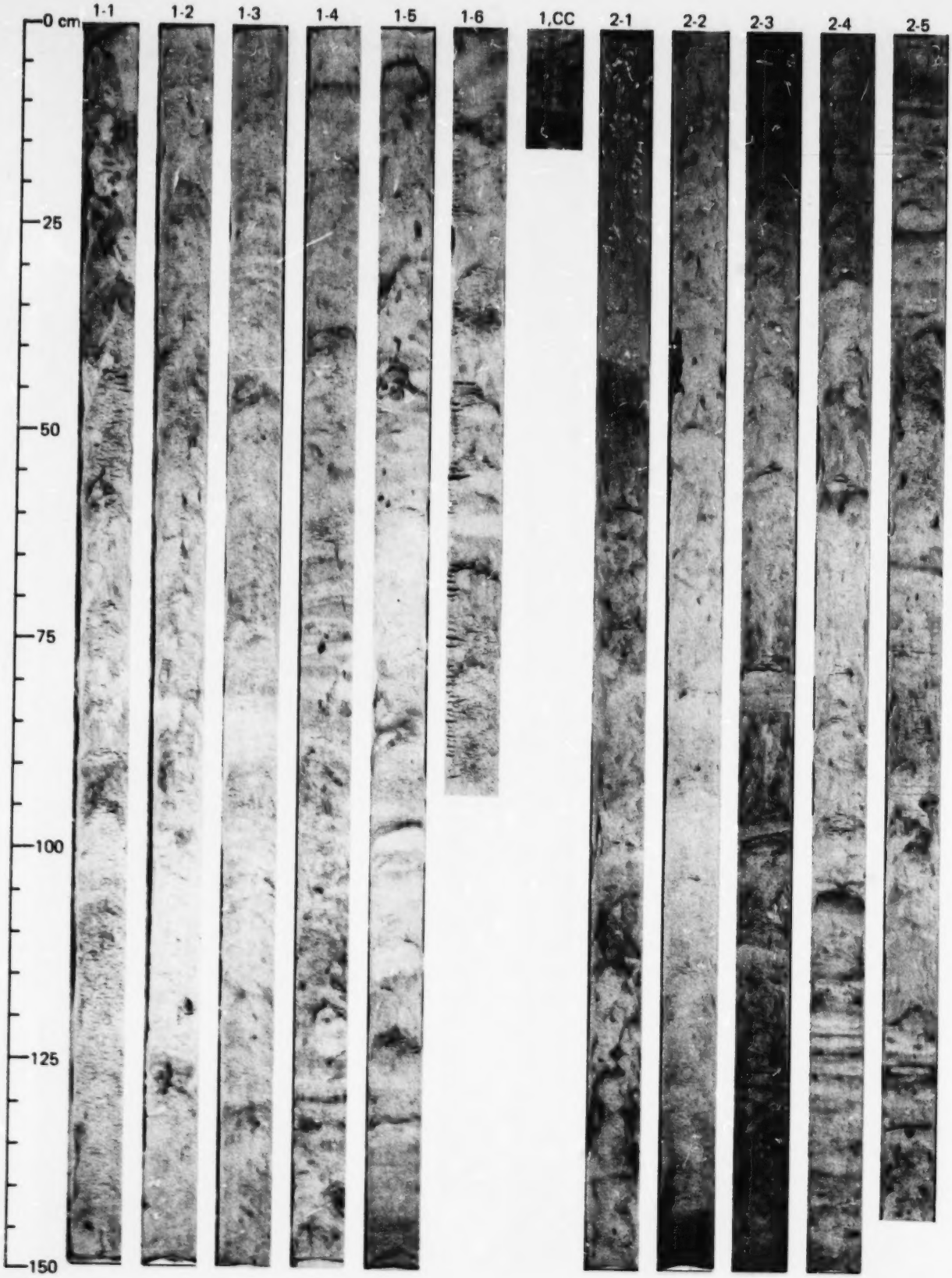
0 cm
25
50
75
100
125
150
1-1
1-2
1-3
1-4
1-5
1-6
1,CC
2-1
2-2
2-3
2-4
2-5

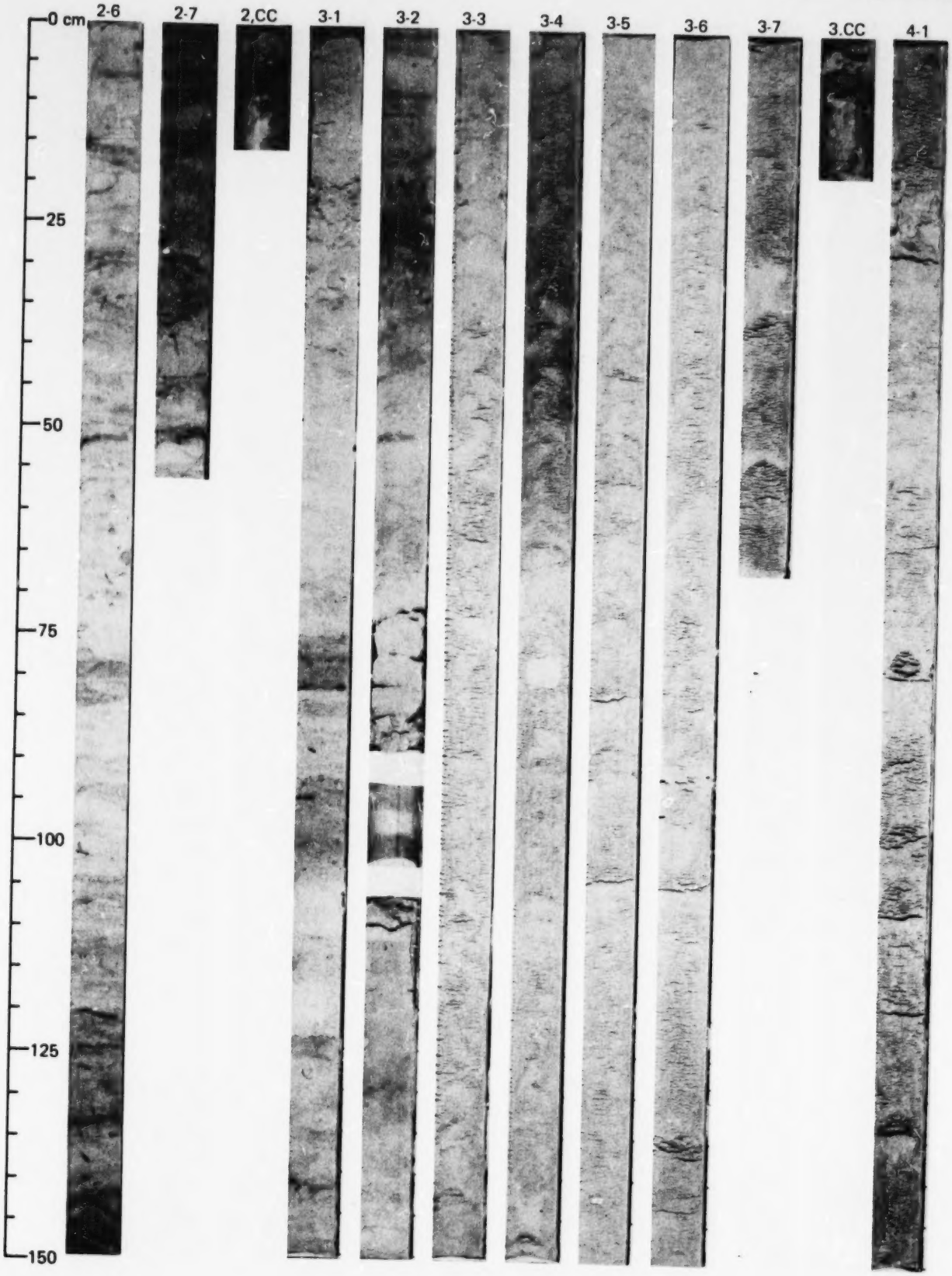
0 cm
2-6
2-7
2,CC
3-1
3-2
3-3
3-4
3-5
3-6
3-7
3,CC
4-1
25
50
75
100
125
150

SITE 573 (HOLE 573B)

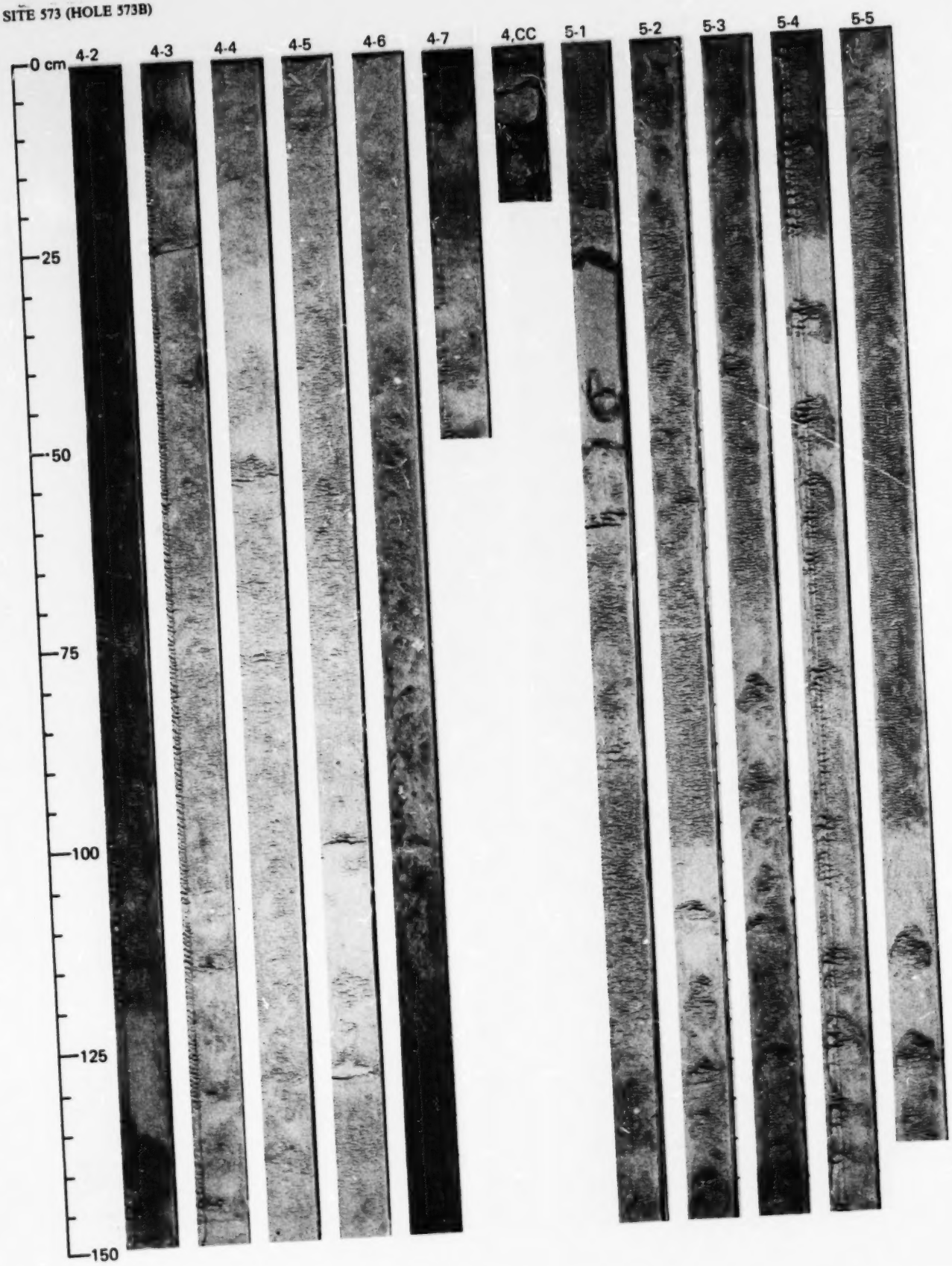

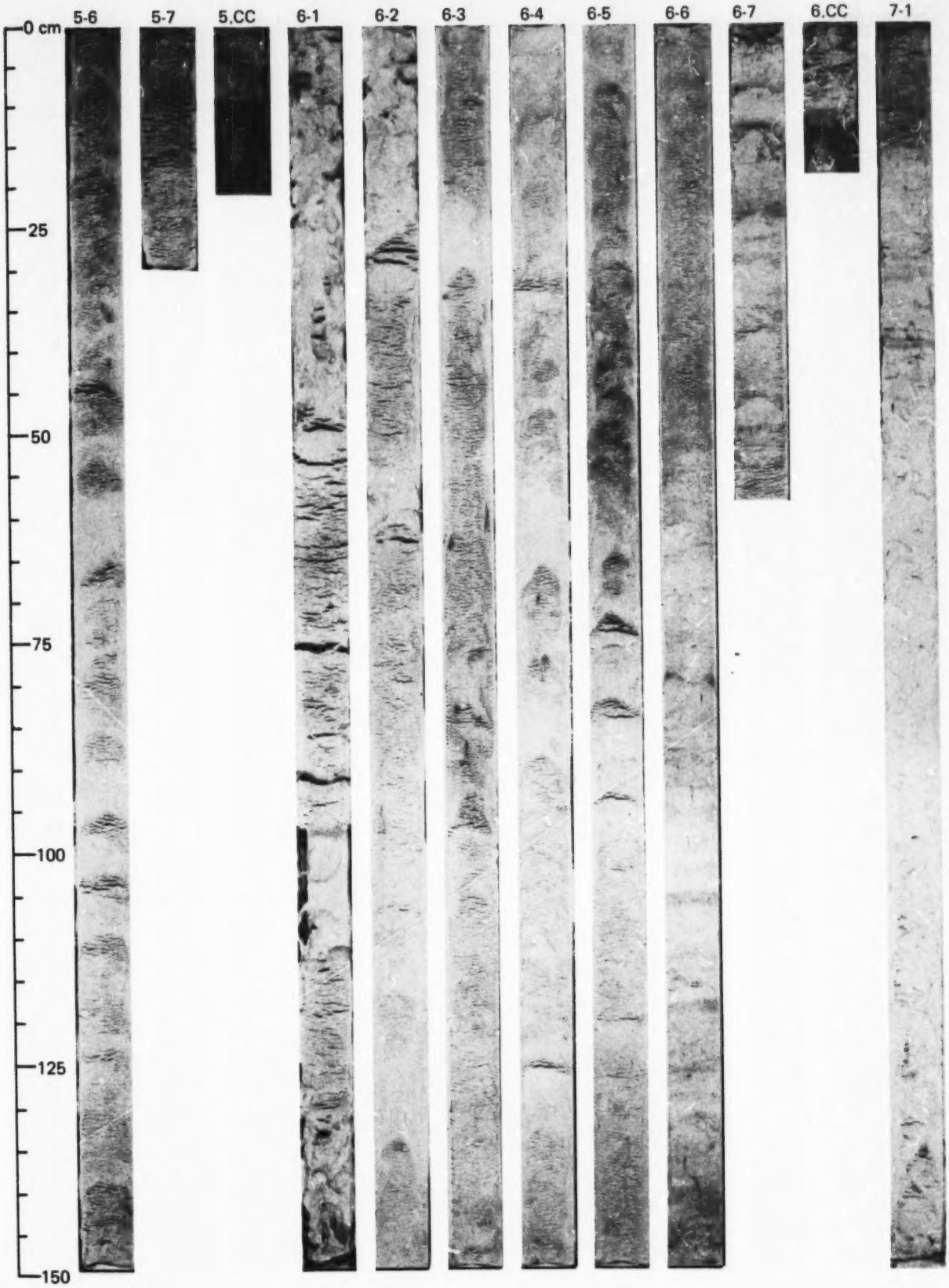
0 cm
25
50
75
100
125
150
5-6
5-7
5,CC
6-1
6-2
6-3
6-4
6-5
6-6
6-7
6,CC
7-1

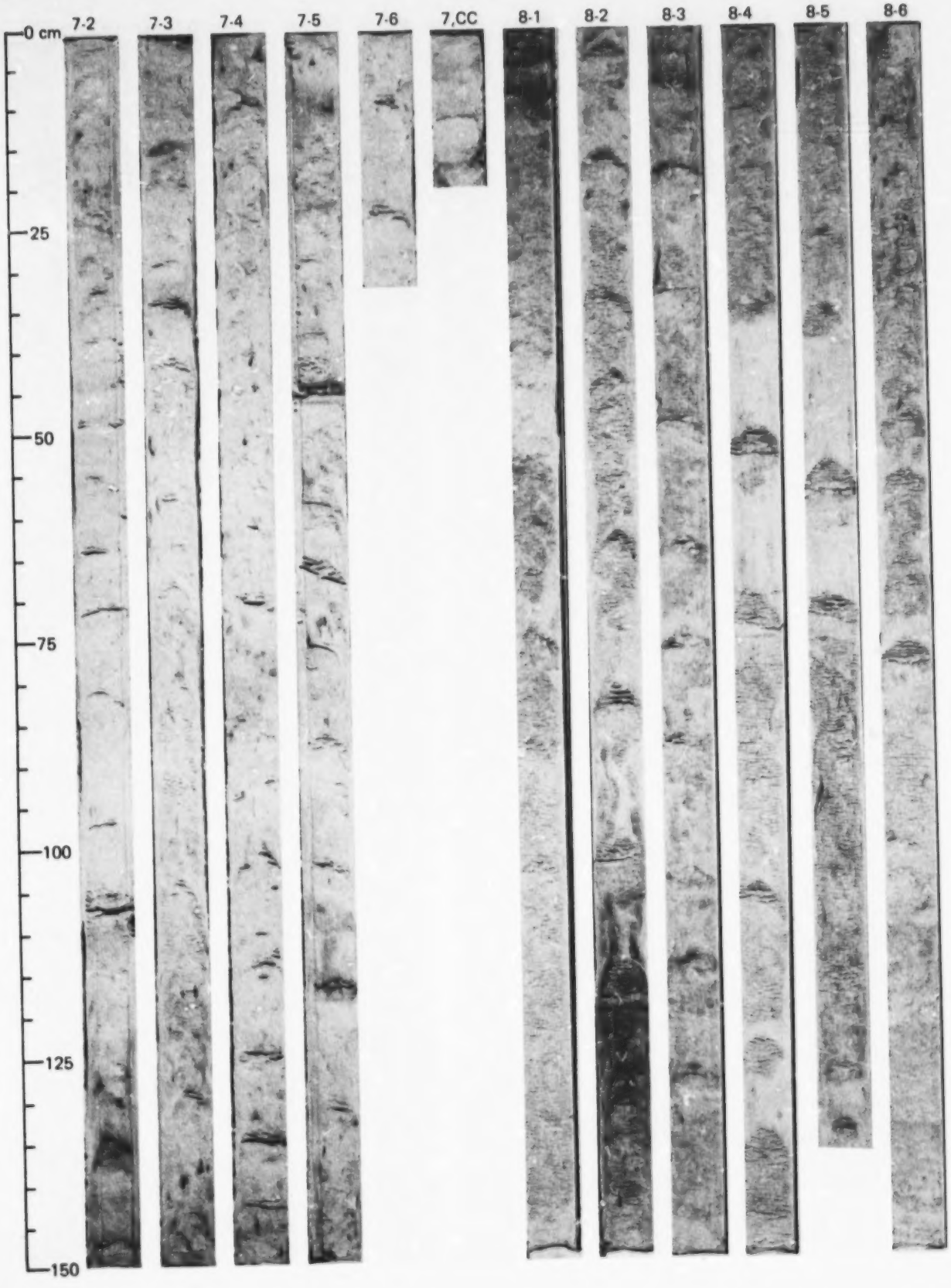
0 cm
25
50
75
100
125
150
7-2
7-3
7-4
7-5
7-6
7,CC
8-1
8-2
8-3
8-4
8-5
8-6

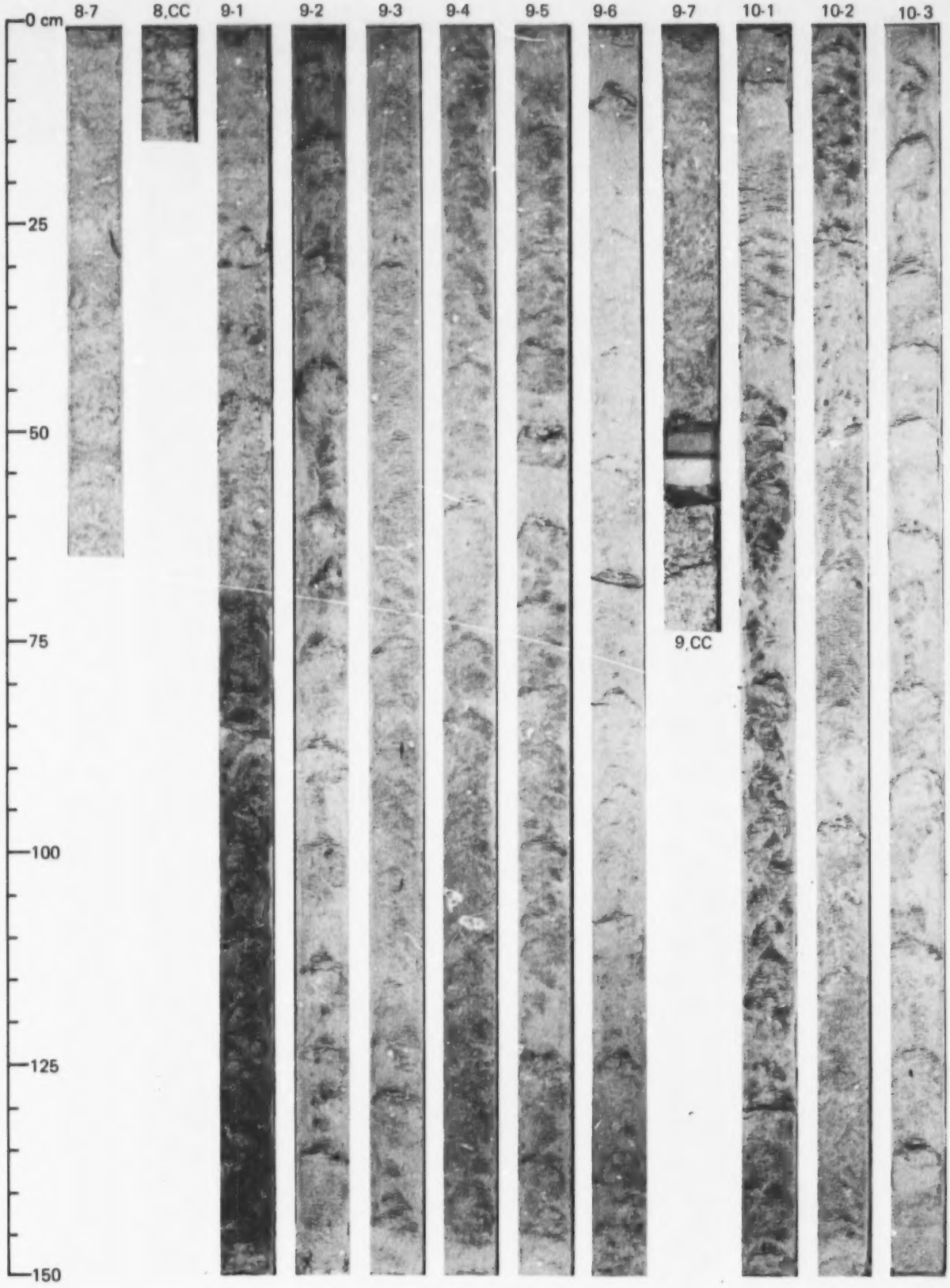
0 cm
25
50
75
100
125
150
8-7
8,CC
9-1
9-2
9-3
9-4
9-5
9-6
9-7
9,CC
10-1
10-2
10-3

0 cm
25
50
75
100
125
150
10-4
10-5
10-6
10,CC
11-1
11-2
11-3
11-4
11-5
11-6
11-7
11,CC

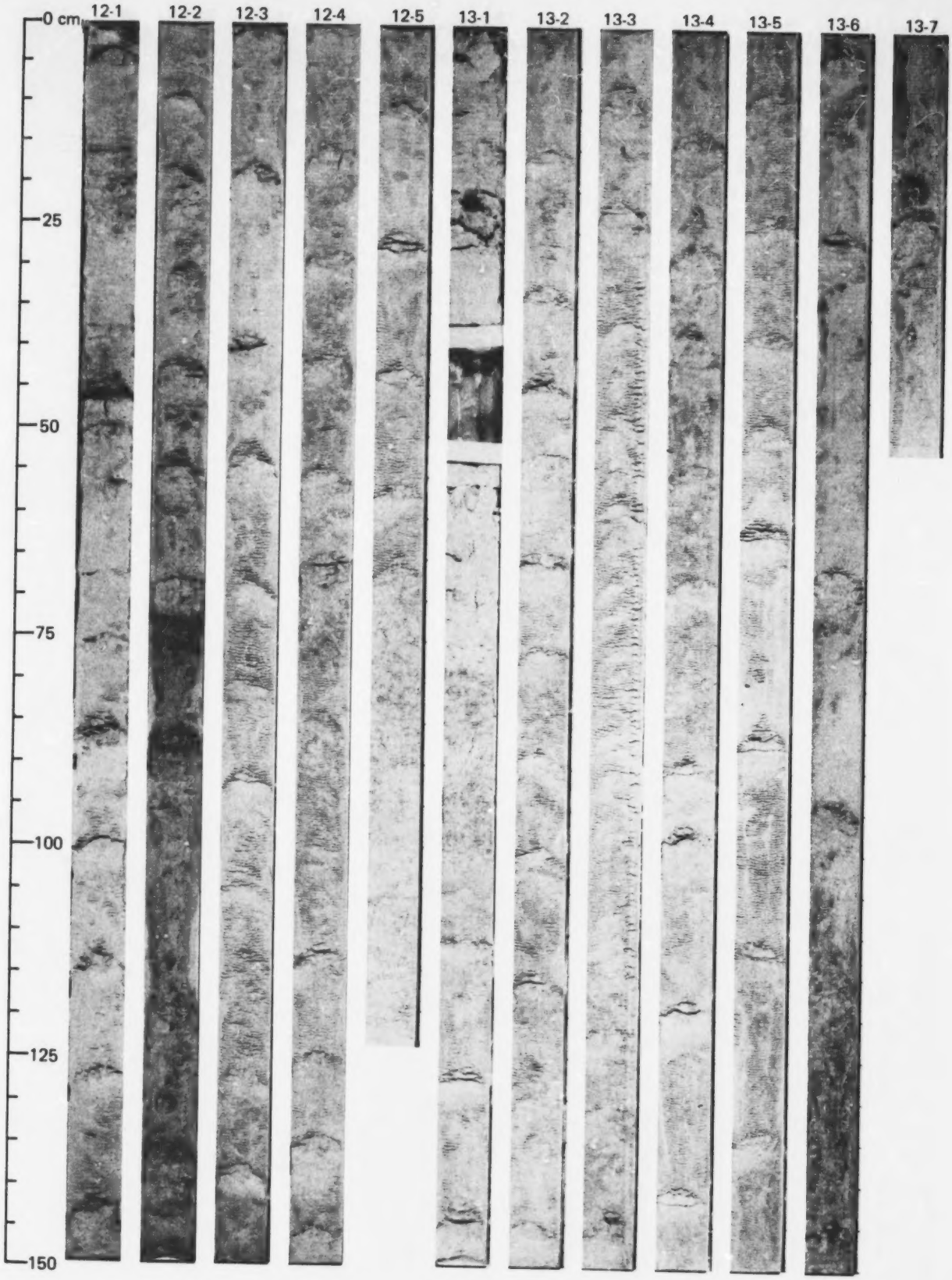
0 cm
12-1
12-2
12-3
12-4
12-5
13-1
13-2
13-3
13-4
13-5
13-6
13-7
25
50
75
100
125
150

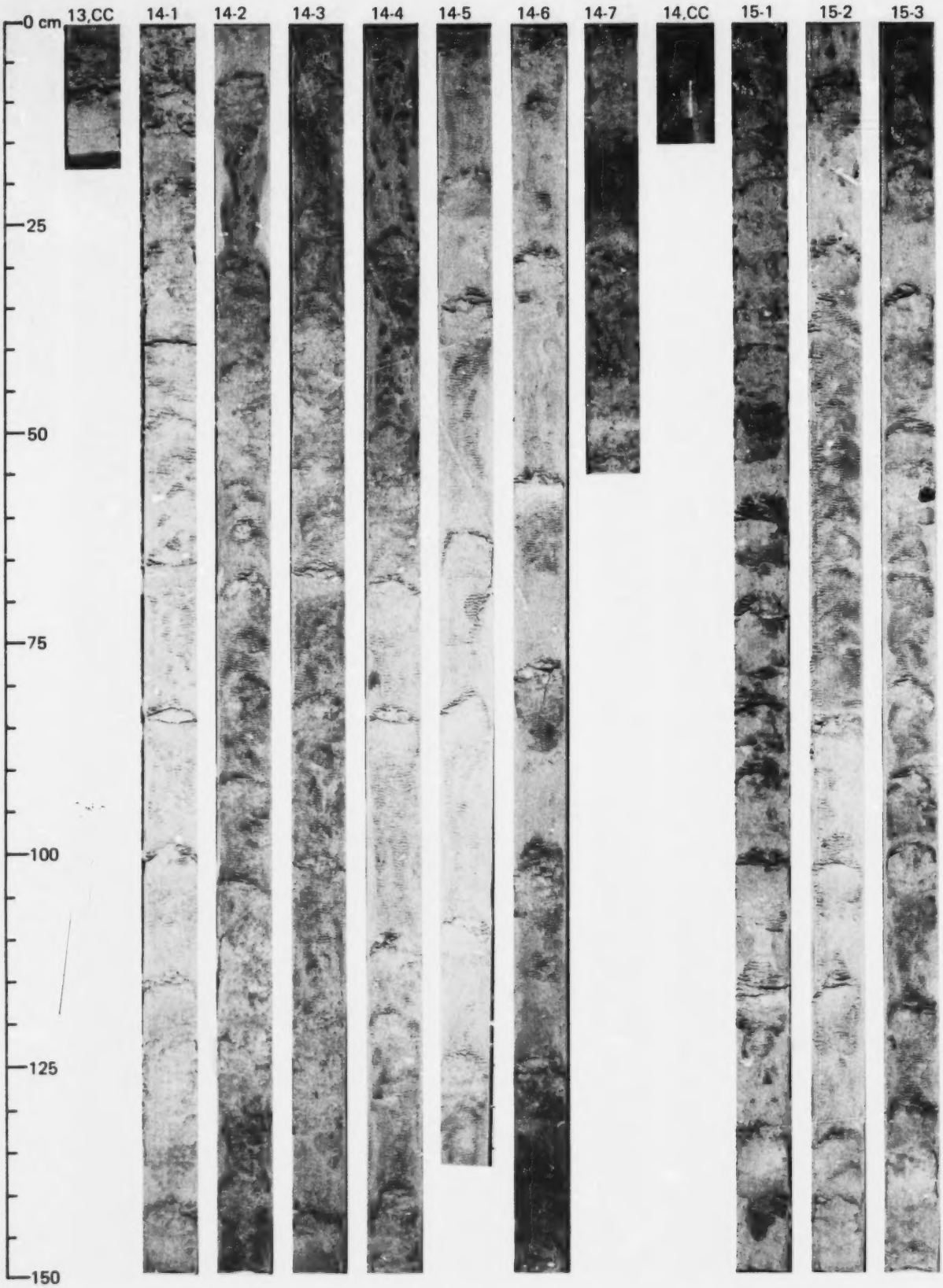
0 cm
25
50
75
100
125
150
13,CC
14-1
14-2
14-3
14-4
14-5
14-6
14-7
14,CC
15-1
15-2
15-3

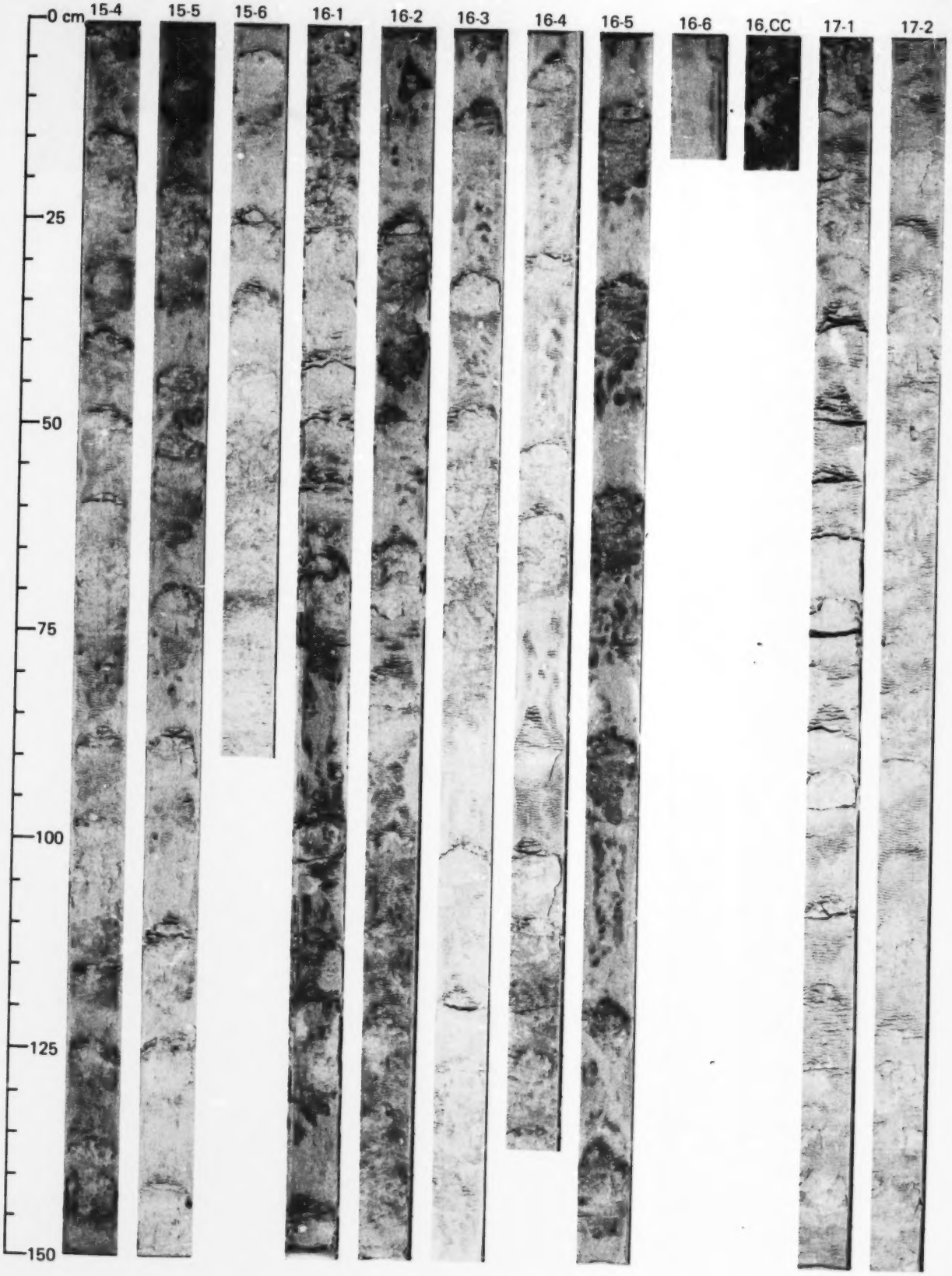
0 cm
15-4
15-5
15-6
16-1
16-2
16-3
16-4
16-5
16-6
16,CC
17-1
17-2
25
50
75
100
125
150

0 cm
17-3
17-4
17-5
17-6
17,CC
18-1
18-2
18-3
18-4
18,CC
19-1
19-2
19-3
25
50
75
100
125
150

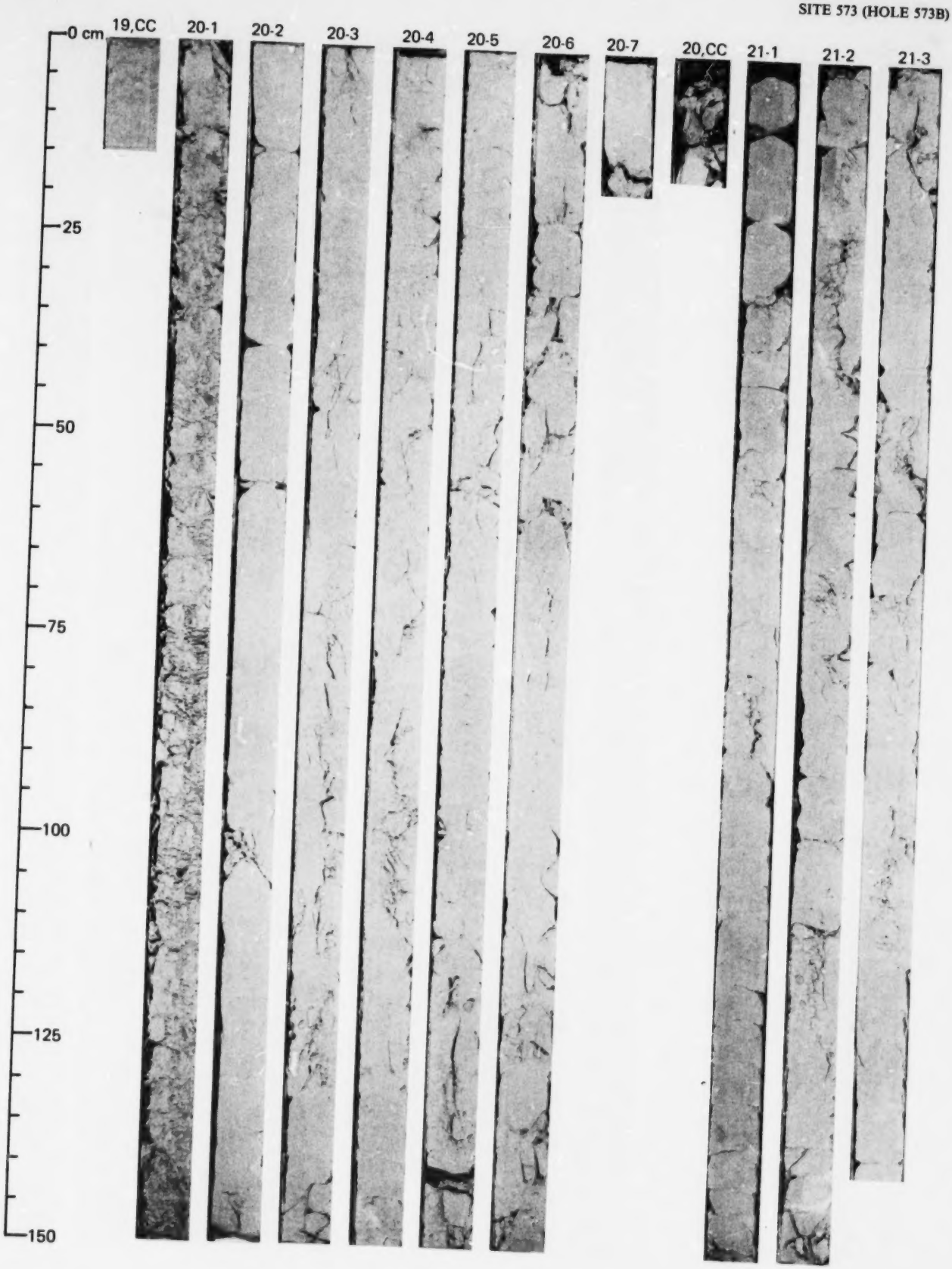
0 cm
19,CC
20-1
20-2
20-3
20-4
20-5
20-6
20-7
20,CC
21-1
21-2
21-3
25
50
75
100
125
150

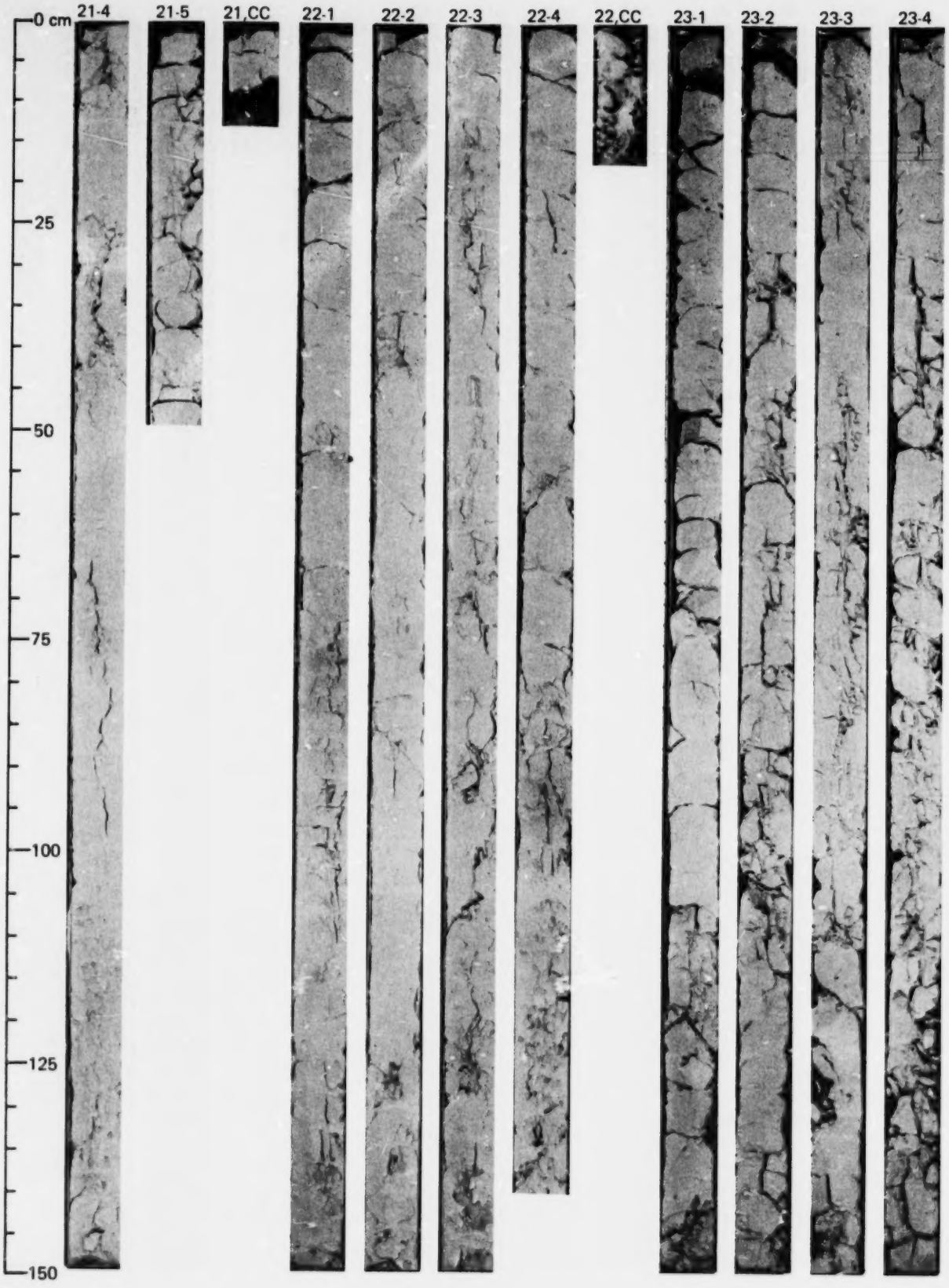
0 cm
25
50
75
100
125
150
21-4
21-5
21,CC
22-1
22-2
22-3
22-4
22,CC
23-1
23-2
23-3
23-4

0 cm
25
50
75
100
125
150
23-5
23,CC
24-1
24-2
24-3
24-4
24,CC
25-1
25-2
25,CC
26-1
26-2
26-3

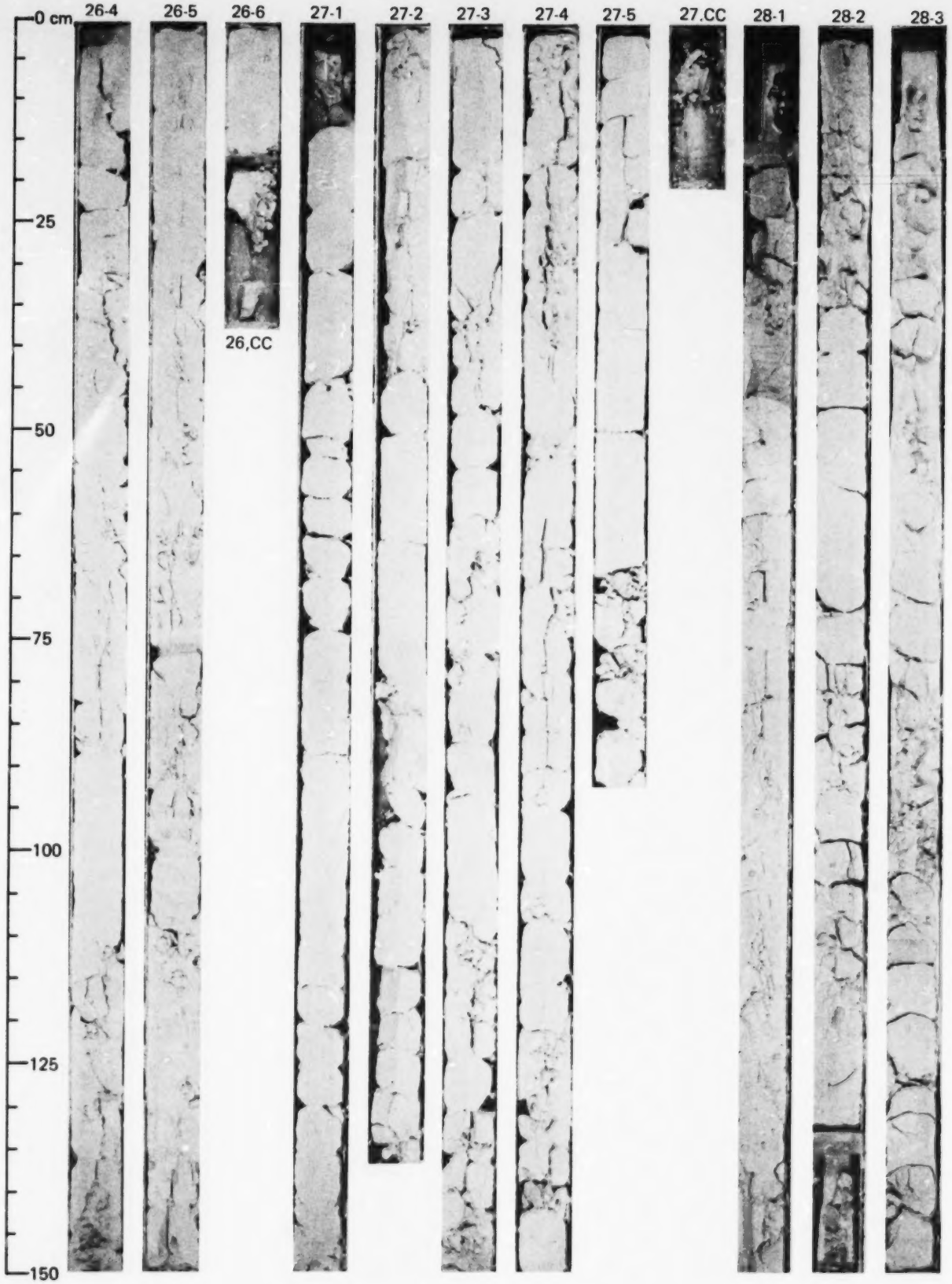
0 cm
25
50
75
100
125
150
26-4
26-5
26-6
26,CC
27-1
27-2
27-3
27-4
27-5
27,CC
28-1
28-2
28-3

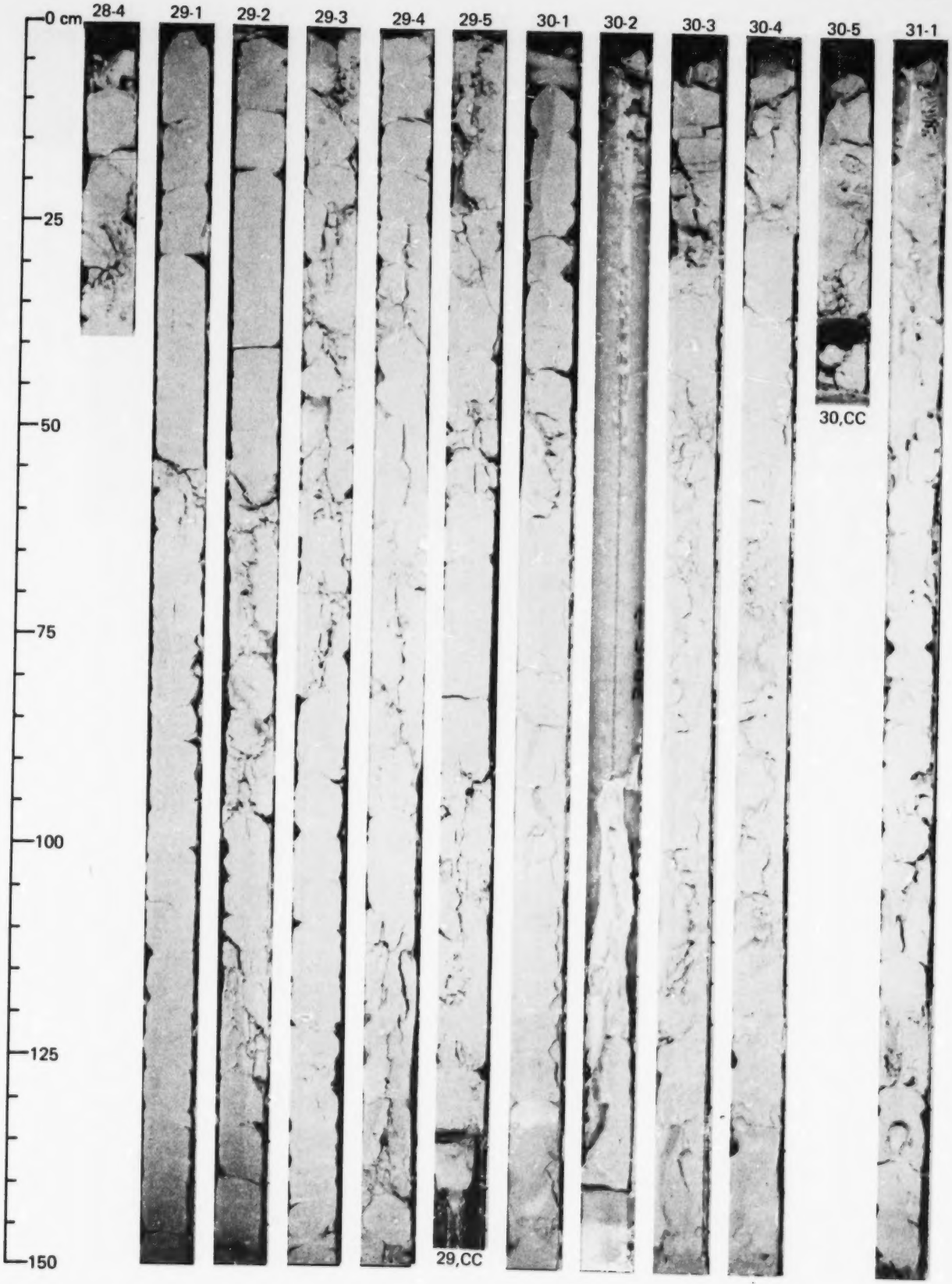
0 cm
25
50
75
100
125
150
28-4
29-1
29-2
29-3
29-4
29-5
30-1
30-2
30-3
30-4
30-5
31-1
30,CC
29,CC

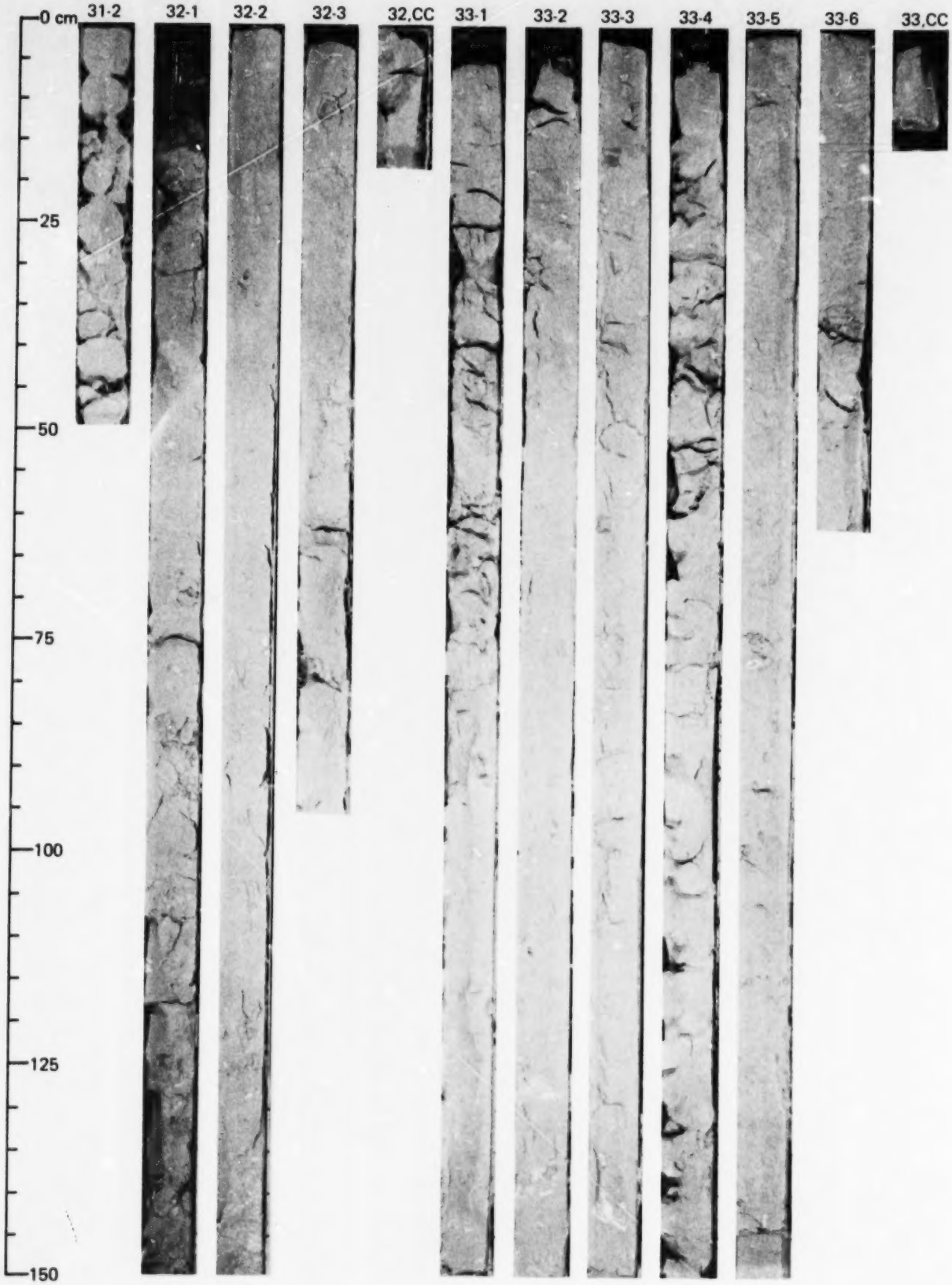
0 cm
31-2
32-1
32-2
32-3
32,CC
33-1
33-2
33-3
33-4
33-5
33-6
33,CC
25
50
75
100
125
150

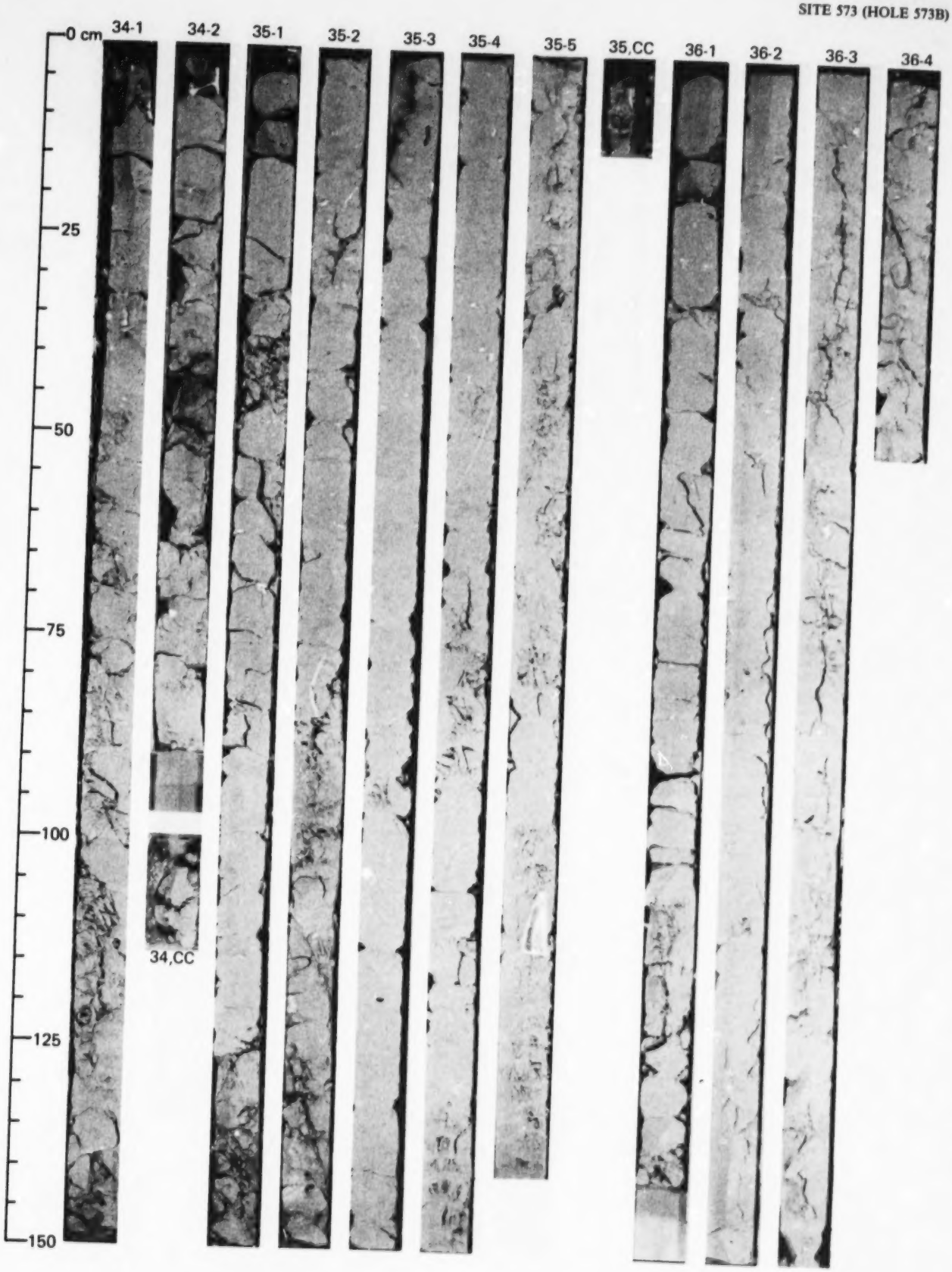
0 cm
34-1
34-2
35-1
35-2
35-3
35-4
35-5
35,CC
36-1
36-2
36-3
36-4
25
50
75
100
125
150
34,CC

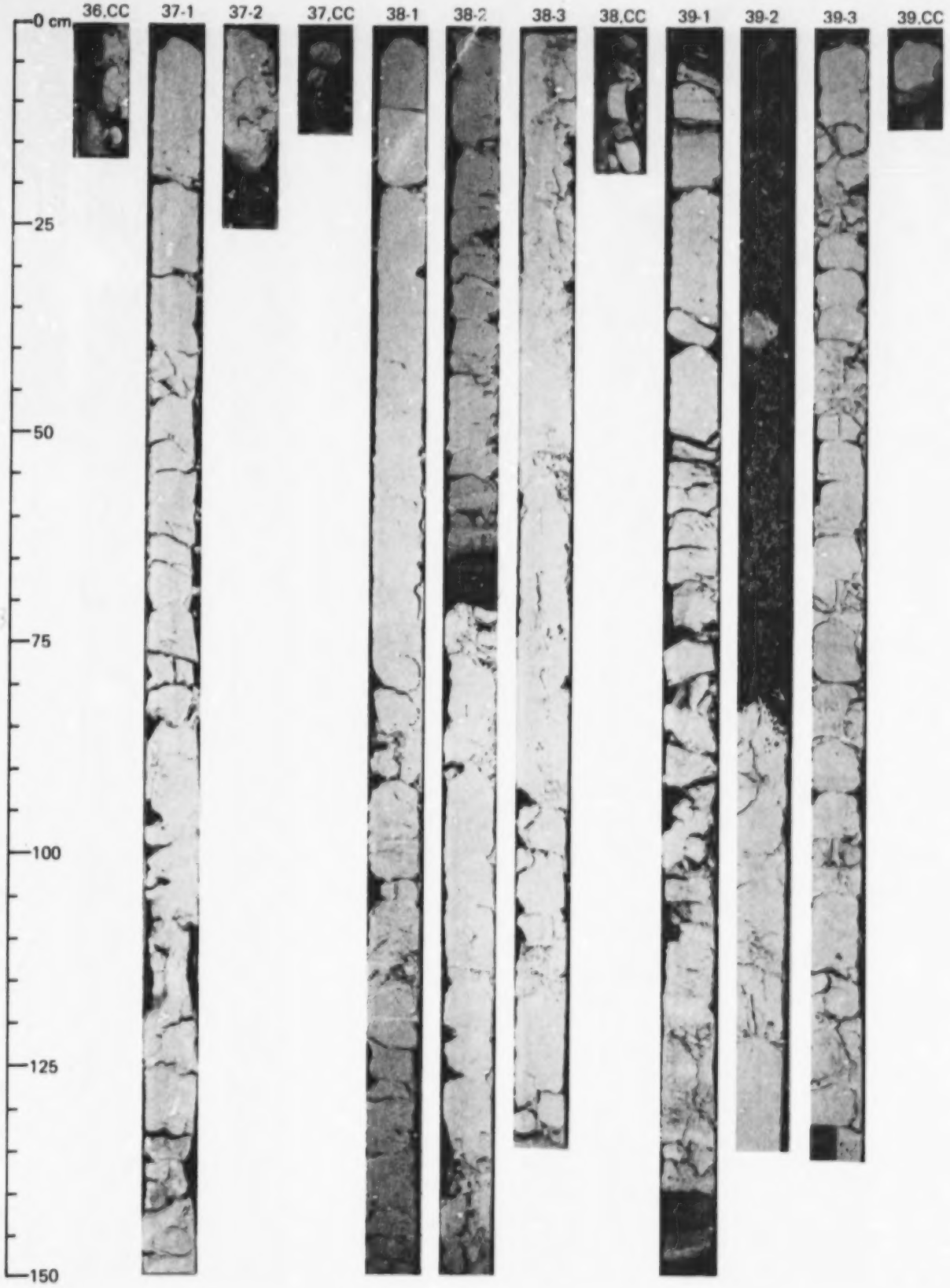
36,CC
37-1
37-2
37,CC
38-1
38-2
38-3
38,CC
39-1
39-2
39-3
39,CC
0 cm
25
50
75
100
125
150

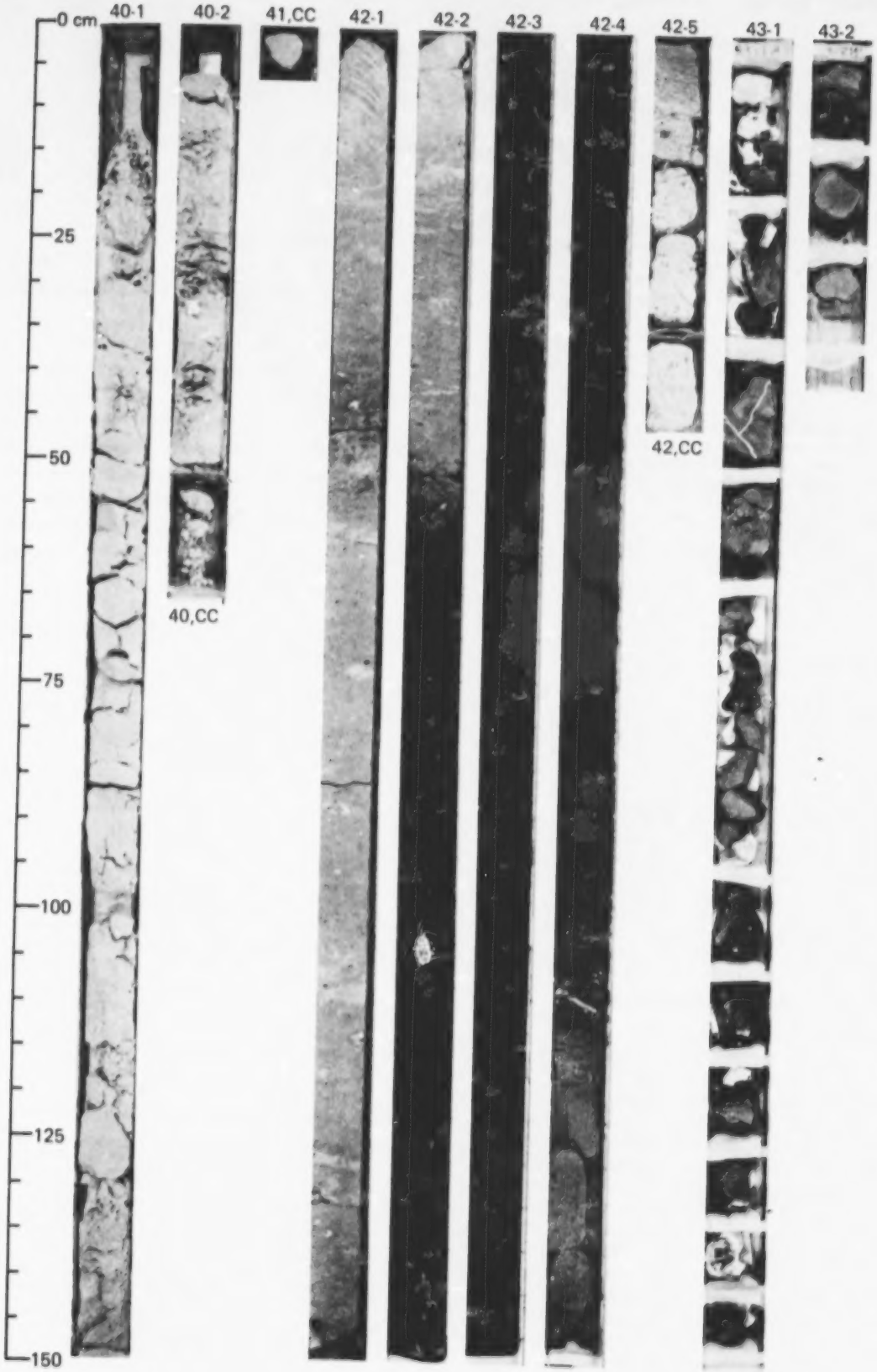
0 cm
25
50
75
100
125
150
40-1
40-2
40,CC
41,CC
42-1
42-2
42-3
42-4
42-5
42,CC
43-1
43-2

Reprinted from Mayer, L., Theyer, F., et al., 1985
Initial Reports of the Deep Sea Drilling Project, Volume LXXXV, Washington (U. S. Government Printing Office)

5. SITE 574[1]

Shipboard Scientific Party[2]

HOLES 574, 574A, 574B, 574C

Dates occupied: 574—11 to 13 April 1982
574A—13 to 14 April 1982
574B—15 to 16 April 1982
574C—17 to 19 April 1982

Date departed Hole 574C: 19 April 1982

Time on site: 8.9 days

Position: 04°12.52′N, 133°19.81′W

Water depth (sea level; corrected m, echo-sounding): 4561

Water depth (rig floor; corrected m, echo-sounding): 4571

Bottom felt (m, drill pipe): 4571

Penetration (Hole 574C, m): 532.5

Number of cores: 574—31
574A—23
574B—1
574C—37

Total length of cored section (m): 574—206.5
574A—180.2
574B—19.0
574C—338.0

Total core recovered (m): 574—208.93
574A—180.74
574B—9.45
574C—197.35

Core recovery (%): 574—101
574A—100
574B—50
574C—58

Oldest sediment cored:
Depth sub-bottom (m): 517.5
Nature: Metalliferous, siliceous chalk
Age: latest Eocene
Measured velocity (km/s): 1.8

Basement:
Depth sub-bottom (m): 520
Nature: Basalt

Principal results: Site 574 is located at 4°12.52′N, 133°19.81′W, in 4561 m of water, over an elongate basement trough covered by 0.57 s of flat, acoustically well stratified sediments. The site is just north of the crest of the sediment bulge in the equatorial high-productivity belt, and it is the second of a three-site latitudinal transect along 133°W. The site was drilled to provide detailed documentation of the area's migration across the equator and of Tertiary equatorial Pacific paleoceanography. To this end two holes were drilled with the hydraulic piston corer (HPC) to approximately the same depth (574, 0 to 206.5 m; 574A, 0 to 180.2 m), and two holes were rotary drilled (574B, 185 to 194.5 m; 574C, 194.5 to 525.5 m, i.e., to basement).

The oldest sediments in the sequence recovered are uppermost Eocene (520 m sub-bottom). Except for minor hiatuses, the sequence is continuous from this age through the Quaternary. The bottom cores contain about 60 cm of basalt, placing basement at 520 m sub-bottom. The sedimentary sequence is divided into a basal metalliferous calcareous unit (502.5 to 520.0 m), a calcareous ooze chalk unit in the middle (84.1 to 502.5 m), and a cyclic siliceous calcareous ooze unit at the top (0 to 84.1 m).

All major planktonic microfossils are represented, although the dissolution of the planktonic foraminifers limits their stratigraphic usefulness. Initial data from the foraminifers, diatoms, calcareous nannofossils, and radiolarians indicate that a remarkably complete uppermost Eocene to lowest Oligocene transition was collected near the bottom of Hole 574C (within the metalliferous calcareous sedimentary unit above basement).

The sediment accumulation rate is variable, ranging between 5 and 35 m/m.y.; it is low between 0 and 12 Ma, high between 12 and 23 Ma, and low again between 23 and 34 Ma. The mass accumulation rates are highest (about 3 g/cm^2 per 1000 yr.) in the lower Oligocene and at about 12.5 Ma, with a low of 0.28 g/cm^2 per 1000 yr. occurring between 0 and 5 Ma.

The records of calcium carbonate content and the sediment's physical properties show major fluctuations in the last 12 m.y. They are more uniform in the older part of the section. Natural remanent magnetization (NRM) intensity is broadly correlative to lithology; magnetization is strongest in the upper cyclic siliceous–calcareous unit and the basal metalliferous unit and extremely weak throughout most of the middle, calcareous unit. The analysis of inorganic geochemistry suggests the presence of a diffusional control in the section's upper 150 m and of diagenetic reactions in its lower portion.

BACKGROUND AND OBJECTIVES

The JOIDES Ocean Paleoenvironmental Panel considered Site 574 to have the second highest priority of the sites to be drilled in a latitudinal transect along 133°W across the equatorial high-productivity belt. Presently located 4° north of the equator (Fig. 1), and with a basement age of latest Eocene, the sedimentary section at Site 574 presumably recorded the site's migration from south of the equator into the high-productivity belt, and from there to its present position at the northern boundary of the belt. The operational objective was the same as at all Leg 85 sites: to recover a complete and undisturbed upper Eocene to Quaternary section by using the HPC to core the sediment section twice to the limit of penetration and to rotary drill from that level to basement.

Considerable survey data exist for the region as a result of cruises by Lamont-Doherty Geological Observa-

[1] Mayer, L., Theyer, F., et al., *Init. Repts. DSDP*, 85: Washington (U.S. Govt. Printing Office).

[2] Larry Mayer (Co-Chief Scientist), Dalhousie University, Halifax, Nova Scotia, Canada; Fritz Theyer (Co-Chief Scientist), Hawaii Institute of Geophysics, University of Hawaii, Honolulu, Hawaii (present address: University of Southern California, Los Angeles, California); John A. Barron, U.S. Geological Survey, Menlo Park, California; Dean A. Dunn, University of Rhode Island, Narragansett, Rhode Island (present address: University of Southern Mississippi, Hattiesburg, Mississippi); Tim Handyside, The University, Newcastle upon Tyne, United Kingdom; Scott Hills, Scripps Institution of Oceanography, La Jolla, California; Ian Jarvis, City of London Polytechnic, London, United Kingdom (present address: Kingston Polytechnic, Kingston-upon-Thames, United Kingdom); Catherine A. Nigrini, La Habra Heights, California; Nicklas G. Pisias, Oregon State University, Corvallis, Oregon; Annick Pujos, Université de Bordeaux, Talence, France; Tsunemasa Saito, Yamagata University, Yamagata, Japan; Paul Stout, Scripps Institution of Oceanography, La Jolla, California; Ellen Thomas, Scripps Institution of Oceanography, La Jolla, California (present address: Lamont-Doherty Geological Observatory, Columbia University, Palisades, New York); Norbert Weinreich, Institut für Geophysik, Ruhr Universität Bochum, Bochum, Federal Republic of Germany; and Roy H. Wilkens, Massachusetts Institute of Technology, Cambridge, Massachusetts.

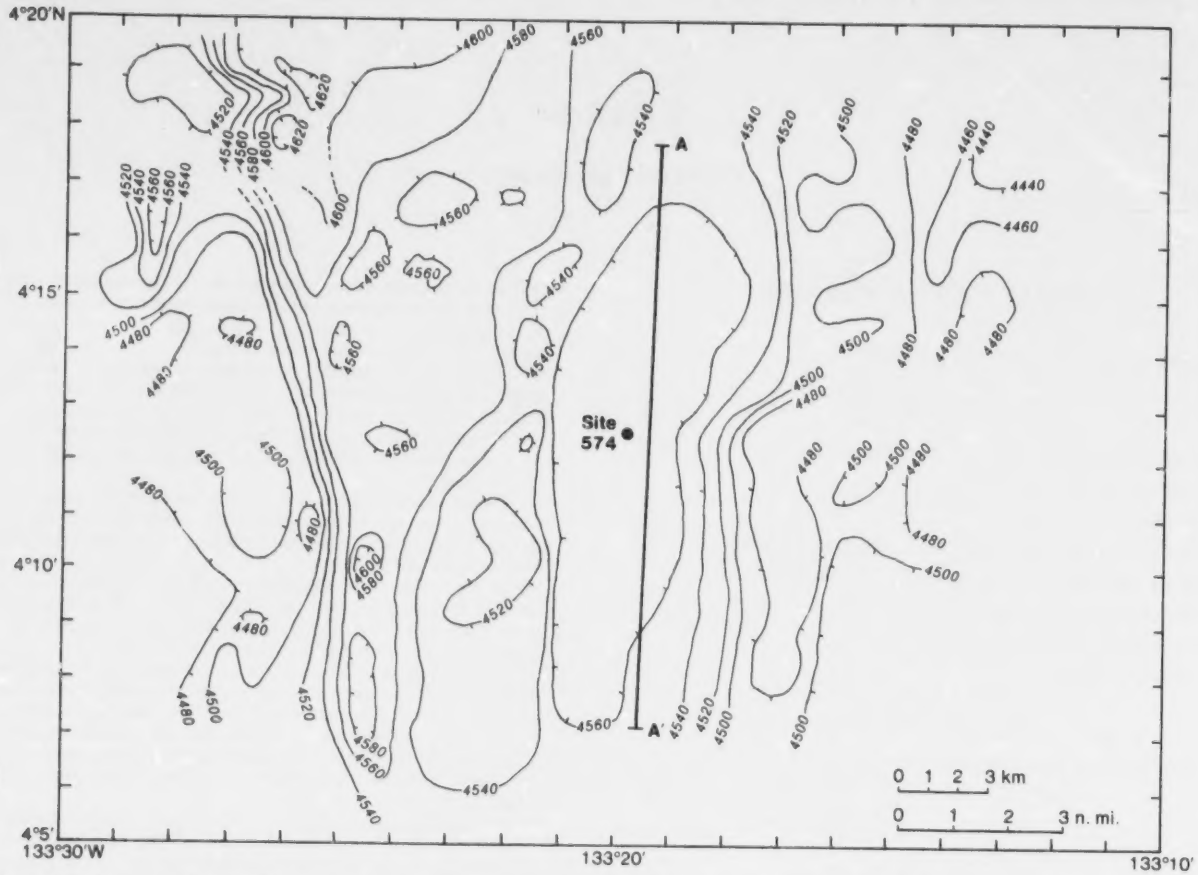

Figure 1. Bathymetry at Site 574 (20-m contour interval). Uncorrected water depth (velocity = 1.5 km/s) is 4553 m. Corrected water depth is 4561 m. Profile A–A′ is the seismic profile shown in Figure 2.

tory's R/V *Conrad* (*Conrad* 15-1, 1971; *Conrad* 20-11, 1977), the Scripps Institution of Oceanography RISE 3 cruise of January 1962, and a recent JOI site survey conducted by the Scripps R/V *Thomas Washington*. The site survey resulted in the acquisition of Seabeam bathymetry (Fig. 1) and single-channel, digitally recorded, water and air gun seismic profiles. In addition, *Challenger* collected air gun seismic profiles en route from Site 573 to 574. Site 574 is in a relatively wide, flat basin with a water depth of about 4560 m. The sediments are flat, acoustically well stratified, and about 0.57 s thick, and they overlie an equally flat depression in the basement (Fig. 2). This basin and its surrounding highs are part of a general pattern of troughs and highs trending virtually north–south.

The closest site previously drilled by DSDP is Site 71 (DSDP Leg 8) which, at 4°28.3′N and 140°19′W, is slightly north and considerably farther west than Site 574. At Site 71 uppermost Eocene to Quaternary sediments were recovered during continuous coring operations. The acoustic basement at Site 71 proved to be semi-indurated chalk and chert; the extrapolated lithospheric age of the region was 39 to 40 Ma.

OPERATIONS

The D/V *Glomar Challenger* arrived in the vicinity of Site 574 1 day after departing Site 573. We steamed on a course of 017° and averaged 9 knots in our 23-hr. transit. During this time we collected continuous seismic profiles (air gun and 3.5 kHz) as well as bathymetric and magnetic data. The valleys and ridges in the region trend north–northwest/south–southeast, so we aimed for a point about 3 n. mi. east of the proposed site so we would approach the site across the grain of the bathymetry. Our target was a broad (2 n. mi. wide) flat region in about 4550 m of water where approximately 0.6 s of sediment fills an elongate basement trough (Figs. 1 and 2).

We entered the area surveyed by the R/V *Thomas Washington* at around 0720Z on 11 April. We had difficulty matching the Seabeam bathymetry with the bathymetric data we were collecting until, after about 40 min. of steaming, we found we could match the general bathymetric trends by rotating the Seabeam chart several degrees and shifting it several minutes. Even with this offset only the relative bathymetric relationships matched up, not the absolute depth values. The depths indicated

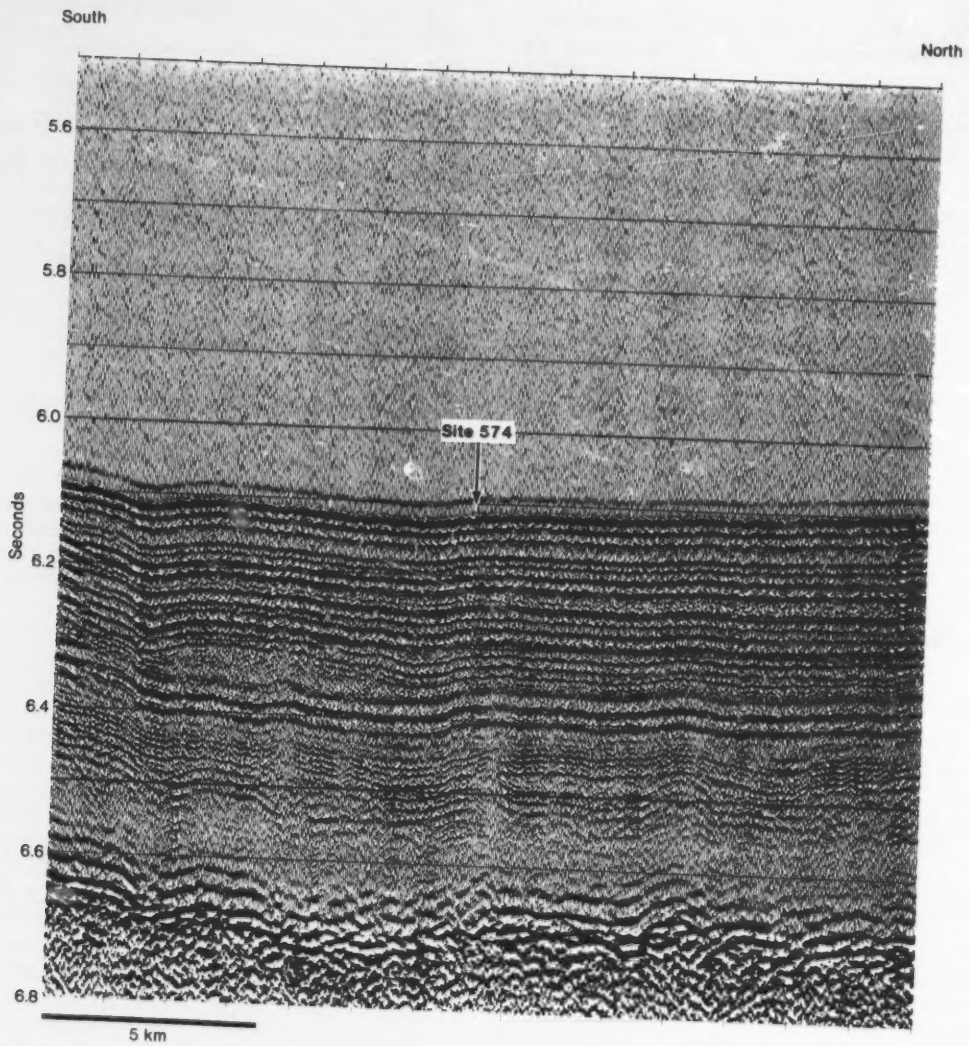

Figure 2. Seismic profile near Site 574 (from Shipley et al., this volume).

by the Seabeam bathymetry were consistently 10 to 30 m deeper than those we were measuring.

At 0755Z we began to travel along our westerly line, steaming 272° and aiming for our target position of 04° 12.5′N, 133°19.9′W. We quickly located ourselves relative to the bathymetry and the subsurface structure, and at 0810Z we crossed the proposed drill site. We continued several nautical miles past the site, turned to a point 1 n. mi. due north of it, and at 0852Z turned south on our final pass over the proposed site. At 0905Z, 11 April, we dropped the beacon and then continued 1 n. mi. south beyond the site to complete the presite survey. We pulled the geophysical gear and returned to the beacon, now officially Site 574.

Drill pipe run-in began at 1010Z on 11 April (Table 1). The first hydraulic piston core, which was on deck at 2115Z, established the mudline at 4571 m from the rig floor. The drilling in Hole 574 continued smoothly with the 9.5-m variable-length HPC. The pullout forces necessary for Cores 8 and 9 were 15,000 and 20,000 lb., respectively, but the pullout force for the next three cores was negligible. The pullout force for Core 13 was substantial again, however (more than 30,000 lb.), and the core had to be "washed over" to free it up. At this point we decided to switch to the 5-m HPC. Coring once again proceeded smoothly until Core 29, which required 10,000 lb. of pullout force. Cores 30 and 31 offered little resistance to pullout, but Core 32 stayed in the hole even after the exertion of 75,000 lb. of pullout force. This core, at 206.5 m sub-bottom, marked the end of the drilling in Hole 574. Recovery for the hole was close to 100%, and disturbance was minimal. The biggest problem from an operational standpoint was that many of the core liners shattered, a problem that seemed to occur during the coring of relatively hard intervals.

We began to drill Hole 574A with the 9.5-m variable-length HPC. Coring continued smoothly all the way to the bottom of the hole (at 180.2 m sub-bottom). We

Table 1. Coring summary, Site 574.

Core	Date (Apr. 1982)	Local time (hr.)	Depth from drill floor (m)	Depth below seafloor (m)	Length cored (m)	Length recovered (m)	Recovery (%)
Hole 574							
1	11	1315	4571.0–4575.5	0.0–4.5	4.5	4.55	100+
2	11	1415	4575.5–4585.0	4.5–14.0	9.5	9.64	100+
3	11	1540	4585.0–4594.5	14.0–23.5	9.5	9.56	100+
4	11	1653	4594.5–4604.0	23.5–33.0	9.5	9.69	100+
5	11	1805	4604.0–4613.5	33.0–42.5	9.5	9.62	100+
6	11	1925	4613.5–4623.0	42.5–52.0	9.5	9.57	100+
7	11	2095	4623.0–4632.0	52.0–61.0	9.0	8.99	99.8
8	11	2210	4632.0–4641.5	61.0–70.5	9.5	9.58	100+
9	11	2335	4641.5–4651.0	70.5–80.0	9.5	9.53	100+
10	12	0100	4651.0–4660.5	80.0–89.5	9.5	9.33	98+
11	12	0202	4660.5–4669.6	89.5–98.6	9.1	9.12	100+
12	12	0311	4669.6–4679.1	98.6–108.1	9.5	9.60	100+
13	12	0425	4679.1–4688.6	108.1–117.6	9.5	9.62	100+
14	12	0556	4688.6–4693.6	117.6–122.6	5.0	4.99	99.8
15	12	0712	4693.6–4698.6	122.6–127.6	5.0	5.62	100+
16	12	0815	4698.6–4703.6	127.6–132.6	5.0	5.03	100+
17	12	0935	4703.6–4708.6	132.6–137.6	5.0	5.00	100+
18	12	1044	4708.6–4713.6	137.6–142.6	5.0	4.66	93
19	12	1155	4713.6–4718.6	142.6–147.6	5.0	5.03	100+
20	12	1315	4718.6–4723.5	147.6–152.5	4.9	4.90	100
21	12	1435	4723.5–4728.5	152.5–157.5	5.0	5.05	100
22	12	1600	4728.5–4733.5	157.5–162.5	5.0	5.09	100+
23	12	1720	4733.5–4738.5	162.5–167.5	5.0	5.05	100+
24	12	1845	4738.5–4743.5	167.5–172.5	5.0	5.11	100+
25	12	2010	4743.5–4748.5	172.5–177.5	5.0	5.59	100+
26	12	2140	4748.5–4753.2	177.5–182.2	4.7	4.77	100+
27	12	2250	4753.2–4758.2	182.2–187.2	5.0	5.0	100
28	12	2350	4758.2–4763.2	187.2–192.2	5.0	5.16	100+
29	13	0100	4763.2–4767.2	192.2–197.2	5.0	5.06	100+
30	13	0230	4767.2–4772.2	197.2–202.2	5.0	5.05	100+
31	13	0345	4772.2–4776.5	202.2–206.5	4.3	4.38	100+
					206.50	208.93	101
Hole 574A							
1	13	0750	4577.2–4577.5	6.0–6.3	0.3	0.33	100
2	13	0900	4577.5–4586.7	6.3–15.5	9.2	9.22	100
3	13	1008	4586.7–4595.1	15.5–23.9	8.4	8.48	100
4	13	1116	4595.1–4604.3	23.9–33.1	9.2	9.29	100
5	13	1230	4604.3–4613.6	33.1–42.4	9.3	9.32	100
6	13	1338	4613.6–4623.1	42.4–51.9	9.5	9.58	100
7	13	1450	4623.1–4632.6	51.9–61.4	9.5	9.42	99
8	13	1550	4632.6–4641.6	61.4–70.4	9.0	9.08	100
9	13	1655	4641.6–4651.1	70.4–79.9	9.5	9.54	100
10	13	1804	4651.0–4660.4	79.9–89.2	9.3	9.31	100
11	13	1920	4660.4–4669.8	89.2–98.7	9.5	9.70	100
12	13	2025	4669.8–4679.4	98.7–108.2	9.5	9.54	100
13	13	2225	4679.4–4684.3	108.2–113.1	4.9	4.92	100
14	13	2335	4684.3–4689.3	113.1–118.1	5.0	5.02	100
15	14	0054	4689.3–4694.0	118.1–122.8	4.7	4.73	100
16	14	0144	4694.0–4699.0	122.8–127.8	5.0	4.30	86
17	14	0253	4699.0–4703.1	127.8–131.9	4.1	4.16	83
18	14	0410	4703.1–4712.6	131.9–141.4	9.5	9.59	100
19	14	0525	4712.6–4722.1	141.4–150.9	9.5	9.56	100
20	14	0635	4722.1–4731.1	150.9–159.9	9.0	9.09	100
21	14	0740	4731.1–4739.6	159.9–168.4	8.5	8.55	100
22	14	0850	4739.6–4749.1	168.4–177.9	9.5	9.71	100
23	14	0954	4749.1–4757.4	177.9–186.2	8.3	8.39	100
					180.2	180.74	100
Hole 574B							
1	15	1330	4756.0–4765.5	185.0–194.5	9.5	9.45	99
Hole 574C							
1	16	2051	4765.5–4775.0	194.5–204.0	9.5	7.75	82
2	16	2235	4775.0–4784.5	204.0–213.5	9.5	9.38	99
3	17	0005	4784.5–4794.0	213.5–223.0	9.5	5.33	56
4	17	0142	4794.0–4803.5	223.0–232.5	9.5	3.73	39
5	17	0310	4803.5–4813.0	232.5–242.0	9.5	6.34	67
6	17	0440	4813.0–4822.5	242.0–251.5	9.5	6.40	67
7	17	0650	4822.5–4832.0	251.5–261.0	9.5	9.63	100
8	17	0735	4832.0–4841.5	261.0–270.5	9.5	4.87	51
9	17	0949	4841.5–4851.0	270.5–280.0	9.5	4.05	43
10	17	1120	4851.0–4860.5	280.0–289.5	9.5	9.57	100
11	17	1300	4860.5–4870.0	289.5–299.0	9.5	4.50	47
12	17	1440	4870.0–4879.5	299.0–308.5	9.5	9.43	99
13	17	1615	4879.5–4889.0	308.5–318.0	9.5	6.50	68
14	17	1807	4889.0–4898.5	318.0–327.5	9.5	3.39	36
15	17	1945	4898.5–4908.0	327.5–337.0	9.5	9.37	99
16	17	2130	4908.0–4917.5	337.0–346.5	9.5	4.9	52
17	17	2310	4917.5–4927.0	346.5–356.0	9.5	7.54	78
18	18	0057	4927.0–4936.5	356.0–365.5	9.5	2.56	27
19	18	0230	4936.5–4946.0	365.5–375.0	9.5	2.74	29
20	18	0410	4946.0–4955.5	375.0–384.5	9.5	9.30	98
21	18	0549	4955.5–4965.0	384.5–394.0	9.4	6.23	66
22	18	0730	4965.0–4974.5	394.0–403.5	9.5	4.90	52
23	18	0908	4974.5–4984.0	403.5–413.0	9.5	8.88	93
24	18	1050	4984.0–4993.5	413.0–422.5	9.5	6.56	69

Table 1. (Continued).

Core	Date (Apr. 1982)	Local time (hr.)	Depth from drill floor (m)	Depth below seafloor (m)	Length cored (m)	Length recovered (m)	Recovery (%)
Hole 574C (Cont.)							
25	18	1245	4993.5–5003.0	422.5–432.0	9.5	2.09	22
26	18	1420	5003.0–5012.5	432.0–441.5	9.5	3.97	42
27	18	1617	5012.5–5022.0	441.5–451.0	9.5	5.46	57
28	18	1750	5022.0–5031.5	451.0–460.5	9.5	0.64	0.07
29	18	1940	5031.5–5041.0	460.5–470.0	9.5	4.83	50
30	18	2135	5041.0–5050.5	470.0–479.5	9.5	4.94	52
31	18	2315	5050.5–5060.0	479.5–489.0	9.5	3.75	39
32	19	0051	5060.0–5069.5	489.0–498.5	9.5	4.27	45
33	19	0230	5069.5–5079.0	498.5–508.0	9.5	7.57	80
34	19	0405	5079.0–5088.5	508.0–517.5	9.5	2.74	29
35	19	0554	5088.5–5091.0	517.5–520.0	2.5	2.82	100
36	19	0750	5091.0–5096.5	520.0–525.5	5.5	0.30	0.05
37	19	1010	5096.5–5103.5	525.5–532.5	7.0	0.30	0.04
					338.00	197.53	58

switched to the 5-m HPC for the depth interval in which substantial pullout force had been necessary in Hole 574 (100 to 121 m sub-bottom). We were then able to go back to the 9.5-m corer and continue to 180.2 m sub-bottom without difficulty. Our dwindling supply of coring assemblies prompted us to stop coring well short of the greatest depth reached in Hole 574 (which was 206.5 m). Recovery was once again near 100%, and disturbance was minimal. Occasional shattered liners continued to be the most severe problem.

We were to use the HPC to core to maximum penetration depth twice and then to drill to basement at each site, so we ended Hole 574A and began the pipe trip to switch to rotary drilling. The total time for the (two-way) pipe trip was 26 hr.; the interval was unusually long because of the need to retighten all joint connections in the new pipe. We washed to 185 m, and the first drilled core came on deck at 2130Z on 15 April. Unfortunately, the next wire run returned with the overshot and the top end of the coring assembly but no core barrel. There was no damage to the top assembly, but the core assembly appeared to have backed out of the threaded connection. The first fishing attempt brought the corer within 300 m of the rig floor, but the corer broke loose and went back down the pipe. Subsequent fishing attempts were foiled by liner in the top of the corer. Finally the liner jammed the corer in the pipe, and we were forced to abandon the hole (574B) and trip the pipe to recover the corer.

We completed the second round-trip pipe trip at this site, and the first core from Hole 574C (from 194.5 m sub-bottom) was brought on board at 0451Z, 17 April. The rotary coring continued smoothly; disturbance was serious in the softer sediment in the upper part of the section, and recovery was poor (58%). We used different drilling techniques to try to improve recovery, but nothing seemed to help. The source of the problem appeared to be the alternation between soft and hard sediment. The pumping pressure necessary to keep the hard material from plugging the bit washed away the soft material. The drilling in Hole 574C ended when 1 hr. of drilling at 525.5 m sub-bottom resulted in the recovery of 120 cm of basalt. The drill pipe was tripped, and the bottom-hole assembly was magnafluxed. At 0730Z, 20

April, we departed Site 574, running a brief seismic survey over the beacon.

LITHOSTRATIGRAPHY

Lithostratigraphic Subdivision

We divided the section at Site 574 into four lithologic units on the basis of composition: cyclic siliceous calcareous ooze, calcareous ooze chalk, metalliferous chalk, and basalt. The upper two units are subdivided on the basis of color (Table 2).

Unit I: Cyclic Siliceous Calcareous Ooze (middle Miocene to Quaternary)

Unit I (0 to 84.1 m) is characterized by cyclic changes in the relative abundance of siliceous and calcareous ooze. Biogenic silica constitutes 15 to 60% of the sediment; the remainder is predominantly calcareous material. The unit is subdivided into three subunits that are distinguished primarily by color: upper and lower brown ooze subunits are separated by an intervening green gray ooze subunit.

Subunit IA: Upper Brown Ooze (upper Miocene to Quaternary)

The upper brown ooze subunit (0 to 48.1 m) is composed of 5- to 100-cm intervals of alternating pale to very pale brown (10YR 7/2 to 7/4 to 10YR 8/2 to 8/4), brownish gray (10YR 6/2 to 6/4), and brown (10YR 5/3 to 5/4) to dark brown (10YR 3/2 and 4/3 to 4/4) siliceous nannofossil ooze to calcareous siliceous ooze. Sediment color does not appear to be related to variations in microfossil content. The subunit is usually highly burrow mottled (it includes recognizable Planolites burrows), and the contacts are sharp to gradational over 1 to 10 cm.

The sediments of this subunit are of variable grain size and microfossil content. Both clay- and silt-sized materials are rare to abundant (2 to 88% and 4 to 55%, respectively), and sand-sized material is common to abundant (8 to 75%). Calcareous nannofossils are rare to abundant (1 to 88%), foraminifers are rare to common (1 to 25%), diatoms are common to abundant (5 to 35%), and radiolarians are rare to abundant (1 to 64%). Other constituents that occur in trace to rare (1%) amounts are sponge spicules, silicoflagellates, clay, volcanic glass, and iron oxides.

Table 2. Lithostratigraphy, Site 574.

Lithologic unit	Sub-bottom depth (m)	Unit depth (Hole-Core-Section, level in cm)
I (cyclic siliceous calcareous ooze)		
A (upper brown ooze)	0–48.1	574-1-1,1 to 574-6-4,106 574A-1-1,1 to 574A-6-2,96
B (green gray ooze)	48.1–75.8	574-6-4,106 to 574-9-4,80 574A-6-2,96 to 574A-9-5,20
C (lower brown ooze)	75.8–84.1	574-9-4,80 to 574-10-3,108 574-A-9-5,20 to 574A-10-4,5
II (calcareous ooze chalk)		
A (green white ooze chalk)	84.1–470.2	574-10-3,108 to 574-31,CC 574A-10-4,5 to 574A-23,CC 574B-1-1,1 to 574B-1,CC 574C-1-1,1 to 574C-30-1,24
B (yellow white chalk)	470.2–502.5	574C-30-1,24 to 574C-33-3,100
III (metalliferous chalk)	502.5–520.0 m	574C-33-3,100 to 574C-35,CC
IV (basalt)	520.0–532.5 m	574C-36-1,1 to 574C-37-1,1

Subunit IB: Green Gray Ooze (upper Miocene)

The green gray ooze subunit (48.1 to 75.8 m) separates the upper and lower cyclic brown ooze subunits. Both the upper and lower contacts are sharply defined by a change in sediment color from brown to green. The subunit is composed of intergrading intervals 10 to 100 cm thick of white (N9) and green white (5G 8/1 to 9/1) to very pale green (5G 7/1 to 8/1) siliceous nannofossil ooze and pale green gray (5G 6/2 to 8/2) nannofossil siliceous ooze. Mottling is common but often subtle as the result of the poor contrast in sediment color. Planolites burrows are abundant.

The sediment varies in composition, although it is more uniform than in the adjacent subunits. Clay- and silt-sized materials are common to abundant (10 to 85% and 9 to 60%, respectively), and sand is common (10 to 30%). Calcareous nannofossils are common to abundant (5 to 70%), as are diatoms (8 to 40%) and radiolarians (6 to 50%); foraminifers are rare (0 to 5%). Trace amounts of sponge spicules, silicoflagellates, volcanic glass, and pyrite occur sporadically.

Subunit IC: Lower Brown Ooze (upper Miocene)

The lower brown ooze subunit (75.8 to 84.1 m) is similar in color and composition to Subunit IA. The base of the lower brown ooze is defined by the sharp change in sediment color from brown to the pastel greens, grays, and purples of the underlying calcareous ooze chalk unit. Planolites burrows are common.

The sediments of the subunit are composed of common to abundant clay- (5 to 85%) and silt-sized (5 to 60%) materials and common sand-sized material (5 to 35%). Calcareous nannofossils occur in trace to abundant amounts (up to 80%), diatoms are rare to abundant (3 to 47%), and radiolarians are common to abundant (5 to 50%); foraminifers are virtually absent. Sponge spicules and silicoflagellates consistently occur in amounts up to 1%; volcanic glass, pyrite, and iron oxides occur only sporadically in trace amounts (rarely in greater amounts).

Unit II: Calcareous Ooze Chalk (lower Oligocene to middle Miocene)

Unit II (84.1 to 502.5 m) is composed of calcareous ooze chalk. Siliceous microfossils are usually a common component (5 to 25%). Two subunits are defined on the basis of color: a green white ooze chalk (84.1 to 470.2 m) and a yellow white ooze chalk (470.2 to 502.5 m). The contact between the two subunits is a sharp color change.

Subunit IIA: Green White Ooze Chalk (upper Oligocene to middle Miocene)

The green white ooze chalk subunit (84.1 to 470.2 m) is composed of white (N9) and pale gray (N7 to 8) to green white (5G 5/1 to 9/1) nannofossil to siliceous nannofossil ooze chalk and very pale green gray (5G 7/1) nannofossil ooze chalk. Purple white (5P 8/1 to 9/1),

very pale purple (5P 7/1 to 7/2 and 5P 8/2 to 8/4), and purple gray (5P 4/2 to 6/2) sediments are common above 128 m. The darker purples generally occur as small-scale laminations and bands. The purple sediments occur occasionally between 128 and 315 m, and they are absent below.

The sediments of the green white ooze chalk subunit are much less variable than those of the overlying cyclic siliceous calcareous ooze unit. Sand-sized grains are generally rare to common (2 to 15%), silt-sized material is rare to abundant (1 to 60%), and clay-sized material is usually abundant (35 to 95%). Calcareous nannofossils are abundant (65 to 95%), whereas foraminifers are absent to common (0 to 10%, rarely 15%). Diatoms (0 to 15%, rarely to 30%) and radiolarians (1 to 20%, rarely to 40%) are rare to common. Siliceous microfossils rarely constitute more than 20% of the sediment, but they increase in abundance in the basal 20 m of the subunit. Sponge spicules, silicoflagellates, volcanic glass, pyrite, and iron oxides occur in trace amounts.

The transition from calcareous ooze to chalk occurs from 185 to 480 m, primarily within the green white ooze chalk subunit. The transition progresses from the alternation at about 185 m of very stiff ooze (which occurs in regularly occurring intervals 2 to 5 cm thick) and soft ooze (which occurs in intervals 5 to 130 cm thick) to the alternation at about 400 m of chalk (which occurs in intervals 3 to 20 cm thick) and firm ooze (which occurs in intervals 7 to 25 cm thick). Oozes are absent below 480 m, and there is some question as to whether the "ooze" in the lowest 70 m of the transition is actually the result of drilling disturbance.

Subunit IIB: Yellow White Chalk (lower to upper Oligocene)

The yellow white chalk subunit (470.2 to 502.5 m) is composed of uniform yellow white (10YR 8/2 to 9/2) siliceous nannofossil to nannofossil chalk. The siliceous microfossil content is higher than in the overlying green white ooze chalk. The base of Subunit IIB is defined by the first appearance of faintly banded pale brown chalk.

This subunit is composed of common sand- (10 to 15%) and silt-sized grains (5 to 35%) and abundant clay-sized material (60 to 85%). Calcareous nannofossils are abundant (82 to 85%), foraminifers are found in trace to common amounts (10%), diatoms are rare to common (3 to 10%), and radiolarians are found in trace to rare amounts (3%). The subunit appears to be composed entirely of biogenic material.

Unit III: Metalliferous Chalk (upper Eocene to lower Oligocene)

The metalliferous chalk unit (502.5 to 520.0 m) extends from the base of the calcareous ooze chalk unit to basement. The unit is composed of banded and/or highly mottled very pale yellow brown (10YR 8/2 to 8/3, 7/3), light yellowish brown (10YR 6/4 to 7/4), and yellow brown (10YR 5/4) metalliferous siliceous nannofossil chalks. Planolites, Chondrites, Zoophycos, and white halo (rind) burrows are abundant throughout the unit, forming a burrow community as described by Ekdale (1980).

The sediments of this unit are composed of abundant clay material (60 to 80%), common silt material (15 to 30%), and common sand-sized grains (5 to 10%, rarely absent). Calcareous nannofossils are abundant (67 to 98%), foraminifers are absent to rare (0 to 3%), diatoms are absent to common (0 to 15%), and radiolarians are found in trace to common abundances (< 1 to 15%). Of the nonbiogenic components, iron-manganese oxides are generally common (10%, rarely 2%) and pyrite is rare (3 to 5%, rarely trace amounts). Volcanic glass is ubiquitous in trace amounts, although it is more abundant on a macroscopic scale at the base of the unit.

Unit IV: Basalt

We recovered 120 cm (18 pieces) of basalt from Site 574 as we drilled from 520.0 to 532.5 m sub-bottom.

Carbonate Stratigraphy

The Site 574 samples analyzed for physical properties, which were taken at 1.5-m intervals, were also analyzed on board ship for carbonate content by the carbonate bomb method.

The carbonate record (Fig. 3) is similar to that for Site 573: both sites have a late Miocene to Quaternary interval with cyclic high-amplitude carbonate fluctuations and an Eocene to middle Miocene interval with relatively constant carbonate percentages with low-amplitude fluctuations. At Site 574 the interval with cyclic fluctuations extends from the sediment/water interface to 85 m sub-bottom, and the carbonate values range between 10 and 90%. The distinction between the high-carbonate and low-carbonate intervals is clear. Below the interval with cyclic fluctuations, the average carbonate percentage is a relatively constant 90%, with oscillations between 82 and 96%. An abrupt dissolution event occurs at 232 m, but it does not appear to coincide with any major change in lithology.

The change from the older, constant carbonate values to the younger high-amplitude carbonate cycles coincides with the change in lithology at 83.8 m from the calcareous ooze chalk (Unit II) to cyclic siliceous calcareous ooze (Unit I). The change from Unit III to Unit II is visible in the carbonate curve as a pronounced shift from carbonate values near 68% to values above 80%. There are also a number of distinct changes in the sedimentation rate curve for Site 574, and those at 33, 52, 62, and 98 m coincide with carbonate peaks in the high-amplitude cyclic interval. The carbonate data shown in Figure 3 also resemble the Neogene carbonate event stratigraphy of the equatorial Pacific (Dunn, 1981; Dunn and Moore, 1981).

BIOSTRATIGRAPHY

Sediments ranging in age from late Eocene to Quaternary were recovered at Site 574. Figure 4 summarizes the biostratigraphic zonation. An updated version of the biostratigraphic summary is presented in Barron et al. (this volume). The zonal sequence is complete except for the

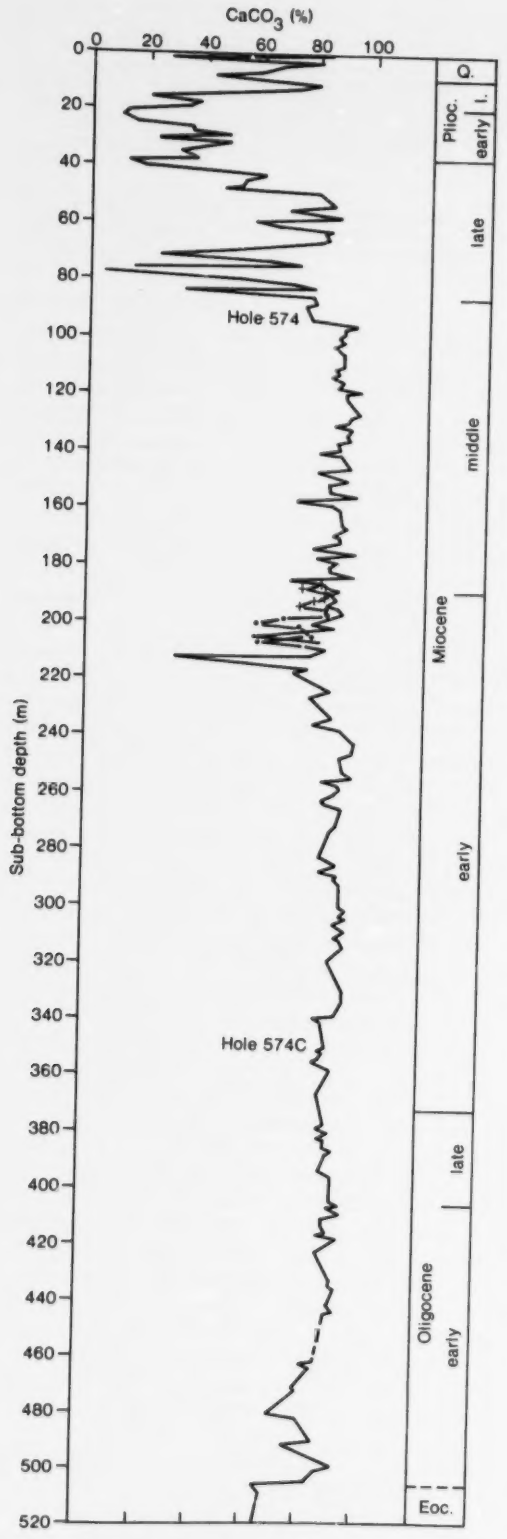

Figure 3. Shipboard carbonate data for Site 574. For interval from 185.0 to 206.5 m, solid line is for Hole 574, pluses mark line for Hole 574B, and dots mark line for Hole 574C.

apparent absence or compression of the lowermost Quaternary and uppermost Pliocene (between Sections 574-1,CC and 574-2,CC).

Siliceous microfossils range from common to abundant throughout most of the section, and preservation is good. There is a decline in diatom abundance and preservation in the upper Oligocene; the upper part of the lower Oligocene; and near the Eocene/Oligocene boundary (in Cores 574C-33 and -34). Core 574C-35 is barren of both diatoms and radiolarians.

The abundance of the calcareous microfossils fluctuates. The foraminifers provide good stratigraphic control only in the lower middle Miocene, the lower part of the lower Miocene, the upper Oligocene, and the 2.5-m interval immediately above the basalt. The nannofossils are usually common to abundant, but many samples contain a high proportion of reworked material.

The most remarkable sequence recovered at Site 574 is an apparently continuous sedimentary sequence across the Eocene/Oligocene boundary. However, the attempt to identify the precise level for the boundary brought to light an interesting problem. According to Hardenbol and Berggren (1978), the Eocene/Oligocene boundary lies at the top of the Priabonian and within the P17 foraminiferal zone at the extinction level of *Hantkenina primitiva* and *Globorotalia cerroazulensis*. The nannofossil zonation of Bukry (1971b) places the Eocene/Oligocene boundary between Zones CP15b and CP16a at the extinction of *Discoaster barbadiensis* and *D. saipanensis*. The radiolarian zonation of Riedel and Sanfilippo (1978) places the Eocene/Oligocene boundary at the evolutionary change from *Lithocyclia aristotelis* group to *L. angusta*, which is accompanied by the extinction of *Lophocyrtris*(?) *jacchia*, *Lynchnocanoma amphitrite*, and *Dictyoprora pirum* (*Theocampe pirum* in Riedel and Sanfilippo, 1978).[3] The Eocene/Oligocene boundary has not been well defined in the tropics for diatoms. For benthic foraminifers, Miller and Curry (1982), Miller et al. (1985), and Tjalsma and Lohmann (1982) have shown that the last occurrence of *Nuttallides truempyi* coincides with the Eocene/Oligocene boundary as defined by Atlantic Ocean planktonic foraminifers. Thus, these various criteria place the Eocene/Oligocene boundary at slightly different levels in Hole 574C, as noted below.

Eocene/Oligocene Boundary	Remarks
Planktonic foraminifers Between Section 574C-34,CC and Sample 574C-35-1, 126–128 cm (sub-bottom depths 510.74 and 518.77 m)	Extinction level of *Hantkenina primitiva* may be influenced by dissolution
Nannofossils Between Section 574C-33,CC and 574C-34-2, 93 cm (sub-bottom depths 506.03 and 508.94 m)	Identification of *Discoaster saipanensis* is hampered by overgrowths
Radiolarians Between Samples 574C-33-4, 49–51 cm and 574C-33-5, 57–59 cm (sub-bottom depths 503.5 and 505.08 m)	It is inherently difficult to find a boundary defined by the evolutionary transition between two forms that are rather rare (at this site, at least)

[3] However, see Radiolarians (this chapter).

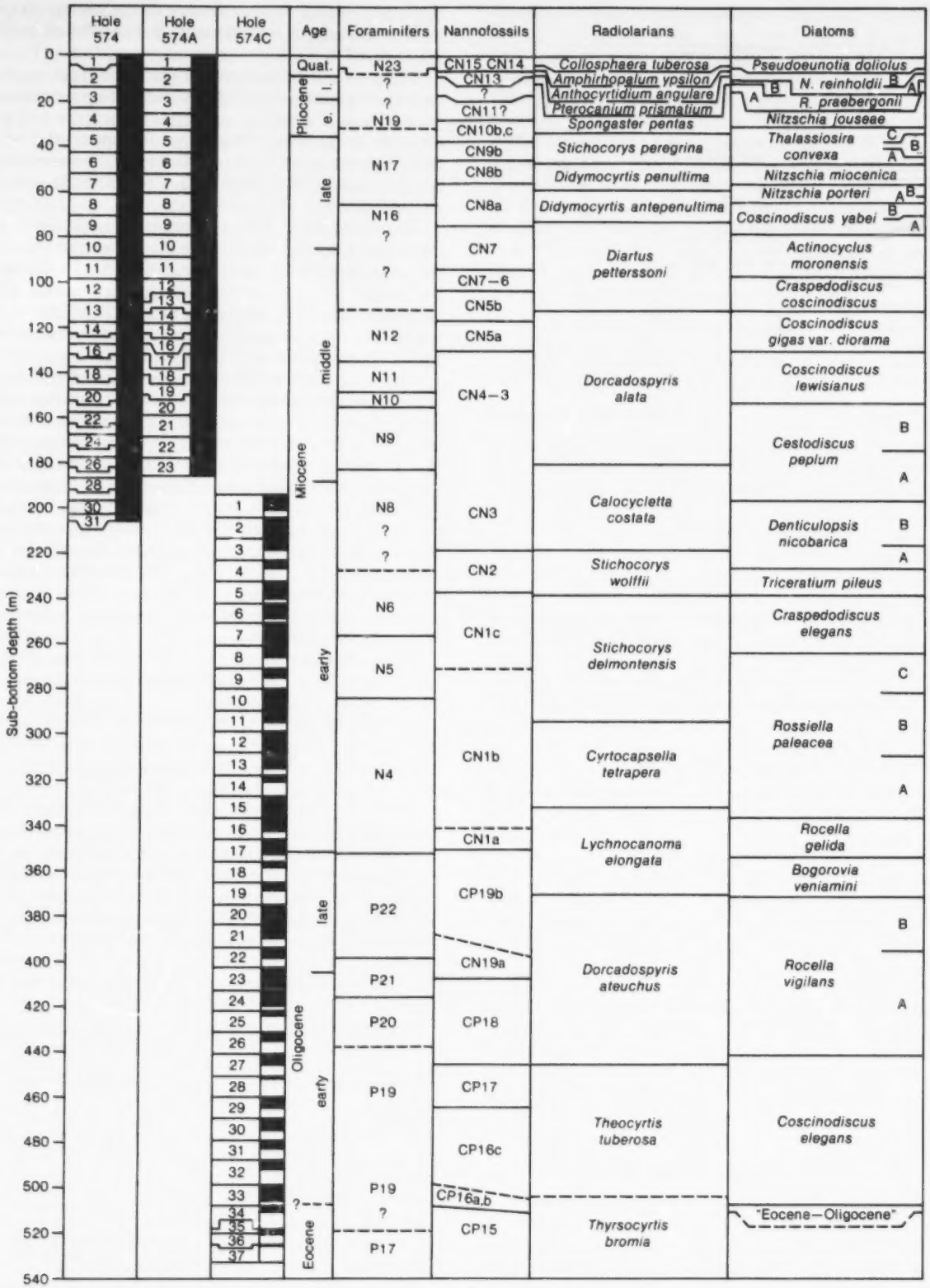

Figure 4. Summary of biostratigraphy at Site 574; position of dashed zonal boundaries is uncertain.

Eocene/Oligocene Boundary	Remarks
Benthic foraminifers	
Between Samples 574C-33-5, 90–92 cm and 574C-33-5, 141–143 cm (sub-bottom depths 505.41 and 505.92 m)	Boundary is placed at the last occurrence of *Nuttallides truempyi*
Diatoms	
Between Sections 574C-33,CC and 574-34,CC (sub-bottom depths 510.74 and 506.03 m)	Boundary is placed at the first appearance of *Coscinodiscus excavatus*

Planktonic Foraminifers

Upper Eocene through Pleistocene planktonic foraminifers are present in the recovered sequence. However, foraminiferal abundance fluctuates so markedly that these fossils provide good stratigraphic control in only three sections of the sequence (from 110 to 190 m, 230 to 440 m, and 517.5 m to the basement at 520 m sub-bottom). In the other intervals the assemblages are sparse, and zonal assignments can be made only by referring to other microfossil groups. The dissolution of planktonic foraminifers is shown in Figure 5.

At least three layers occur in the middle Miocene that contain exclusively reworked Oligocene planktonic foraminiferal faunas. One is approximately 9 m thick (from Sample 574A-17-3, 105–108 cm to Sample 574A-18-7, 27–29 cm); another is 6 m thick (from Sample 574A-21-2, 138–140 cm to Sample 574A-21,CC); and one is 4 m thick (from Sample 574A-22-3, 19–20 cm to Sample 574A-22-4, 141–144 cm). A similar layer is also present in the basal part of Core 574-22. The grain size of the sediments in these layers never exceeds 150 μm, and three species of Oligocene planktonic foraminifers (*Chiloguembelina cubensis, Cassigerinella chipolensis*, and *Globorotalia postcretacea*) make up almost 100% of the sand-sized sediment fraction (grains larger than 63 μm).

The sediment sequence recovered from the two HPC holes at this site yielded evidence of importance to two subjects in planktonic foraminiferal evolution. One is the well known, so-called *Globoratalia fohsi*-lineage. The evolution of *G. fohsi* was rapid in the tropical region during the middle Miocene; it progressed from the small nonkeeled *G. peripheroronda* through the medium-sized *G. praefohsi* to the robust and well keeled *G. fohsi robusta*. These species are zonal markers for Zones N9 through N12 and enable us to establish a precise global correlation. Another subject of stratigraphic significance is the position of the *Orbulina* datum. The first appearance of *Orbulina suturalis* after evolving from its immediate ancestor *Praeorbulina* occurs at the lower/middle Miocene boundary in the European type section and coincides with the foraminiferal zonal boundary between Zones N8 and N9 (Berggren and Van Couvering, 1974). In our section, this datum lies within Cores 574-27 and -26.

Moderately well preserved upper Eocene planktonic foraminiferal assemblages characterize both Sections 574C-35-1 and 574C-35-2. These assemblages, which are assigned to Zone P17, include rare specimens of *Hantkenina primitiva* and *Globorotalia cerroazulensis* but lack species belonging to the genera *Globigerinatheka* and

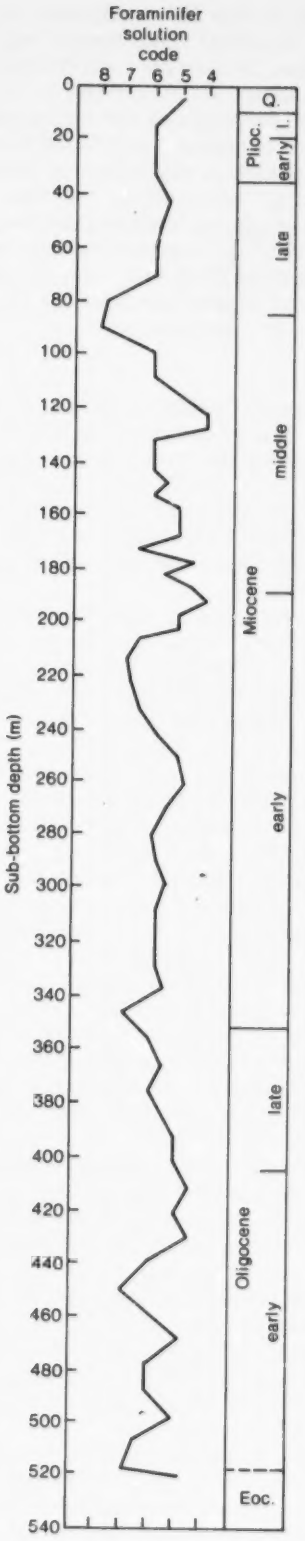

Figure 5. Foraminifer dissolution curve for Site 574; numbers after Berger and von Rad (1972).

Globigerapsis. At Site 573, the Eocene fauna assigned to Zone P16 contained many species belonging to the latter two genera. Because the sediments that contain the Eocene fauna at Site 574 are overlain by a siliceous nannofossil chalk that contains few foraminifers, the Eocene/Oligocene boundary was difficult to identify with foraminiferal evidence. The extinction level of both *H. primitiva* and *G. cerroazulensis* has been regarded as marking the boundary (Hardenbol and Berggren, 1978), and in Hole 574C this level lies between Section 574C-34,CC and Sample 574C-35-1, 126–128 cm. However, the disappearance of these age-diagnostic species may have been hastened by dissolution.

Nannofossils

Nannofossils are usually common to abundant at Site 574. Discoasters are often abundant, but they are rare in the samples where the placoliths are poorly preserved (Sections 574-2,CC, -3,CC, and -10,CC to -16,CC; and Sections 574C-25,CC to -34,CC). The discoasters are overgrown below Zone CN4 (between 574-17,CC and the bottom of the Hole 574C). Nannofossil species occurrence is shown in Figure 6.

Many samples contain a high proportion of reworked nannofossils. Specifically, these are reworked Miocene discoasters in Hole 574 from Sections 574-1,CC through -4,CC; reworked lower Miocene–upper Oligocene placoliths in Hole 574 (from Sections 574-17,CC through -19,CC and in Sections 574-22,CC and -27,CC) and in Hole 574C (Section 574C-1,CC); and reworked lower Oligocene nannofossils in Hole 574C (Sections 574C-3,CC through -9,CC). The upper middle Miocene and Oligocene samples do not show reworking.

Holes 574, 574A, and 574C contain nannofossils from the top of the Eocene to the Pleistocene. All the zones in Bukry's stratigraphy (1971b) are represented at this site.

The upper Pliocene nannofossils (Sections 574-3,CC and -4,CC) are too dissolved to allow the subzones in this period to be clearly differentiated. The problem recurs at the boundary between the middle and upper Miocene, where the main stratigraphic species are absent; the appearance of *Discoaster intercalaris* and *D. perclarus* places the bottom of Zone CN7–6 in Hole 574 between Sections 574-11,CC and -12,CC.

Zones CN4 and CN3 cannot be distinguished at Site 574. *Helicopontosphaera ampliaperta* is absent, and the ratio of long- to short-rayed discoasters (Bukry, 1973) cannot be used to place the boundary between the two zones because it can be used only in the uppermost part of Zone CN4 and the lowermost part of Zone CN3.

In the lowest Miocene (Zone CN1), *Cyclicargolithus abisectus* disappears between Sections 574C-15,CC and 574C-16,CC, and *Sphenolithus ciperoensis* disappears between Sections 574C-16,CC and 574C-17,CC: thus, Subzone CN1a is very short.

In the upper Oligocene sediments, small, stratigraphically useful sphenoliths could be distinguished, although the forms were difficult to identify (as has been the case elsewhere in the tropical latitudes; Bukry, 1971a) and occurred only sporadically.

The Eocene/Oligocene boundary occurs in the deepest sediments at Site 574. *Reticulofenestra samodurovi*, *Discoaster barbadiensis*, *D. saipanensis*, and *Cyclicargolithus reticulatus* characterize the upper Eocene Zone CP15b in Hole 574C (between Section 574C-35,CC and 574C-34-2, 93 cm). The lower Oligocene is represented in Section 574C-33,CC by Zone CP16 (Subzones a and b). Between 574C-34-2, 93 cm and Section 574C-33,CC, nannofossils are rare to common but often poorly preserved, and discoasters are overgrown: the age of these samples could not be determined definitively.

Radiolarians

Radiolarians are common and well preserved in most of the material recovered at Site 574. The fauna appears to be less abundant in Cores 574C-33 and -34, although the decline in abundance may result in part from the difficulty of processing the samples. Core 574C-35 is barren of radiolarians. Every radiolarian zone was recognizable down to the early Oligocene *Theocyrtis tuberosa* Zone (Fig. 4). The sequence in Hole 574A was similarly complete.

Hardenbol and Berggren (1978) show the boundary between the *T. tuberosa* and *Thyrsocyrtis bromia* zones to lie within the lower Oligocene (within P19). Goll (1972) also shows this zonal boundary to lie within the lower Oligocene. However, most of those working with radiolarians agree with Riedel and Sanfilippo (1978), who place the zonal boundary coincident with the Eocene/Oligocene boundary.

We place the *Theocyrtis tuberosa/Thyrsocyrtis bromia* zonal boundary for Site 574 tentatively between Samples 574C-33-4, 49–51 cm and 574C-33-5, 57–59 cm. The latter sample contains the last occurrence of *Lithocyclia aristotelis* and species of *Dictyoprora*. Section 574C-33,CC contains several species of *Dictyoprora*, *L. aristotelis*, and rare specimens of *Lophocyrtis* (?)*jacchia*. *T. bromia* was not observed, but Cores 574C-33 and -34 do contain several previously undescribed forms.

Diatoms

Diatoms are abundant to common, and preservation is generally good, from the Quaternary through the Miocene part of the section at Site 574. Below Core 574C-14 (327 m sub-bottom), abundance and preservation decline; abundance remains low and preservation remains poor through the upper Oligocene and upper part of the lower Oligocene (to Core 28, 460 m). Cores 574C-29 through -32 (lower Oligocene) contain abundant to common diatoms that are well to moderately well preserved. Preservation and abundance decrease downhole again in Cores 33 and 34, and Core 35, which is immediately above the basalt, is barren of diatoms.

The Quaternary through Oligocene section can readily be zoned (Fig. 4), although the upper Oligocene subzones could not be differentiated. The assemblages in Core 34 of Hole 574C lack *Coscinodiscus excavatus* and possess a general late Eocene character (*C. decrescens*, *Hemiaulus polycystinorum*, and *Melosira architecturalis*), although they lack the Eocene genera *Brightwellia* and *Rylandsia*.

The sequence of diatom datums is straightforward (Barron, this volume), and the Quaternary through middle Miocene sequence is comparable to that at Sites 572

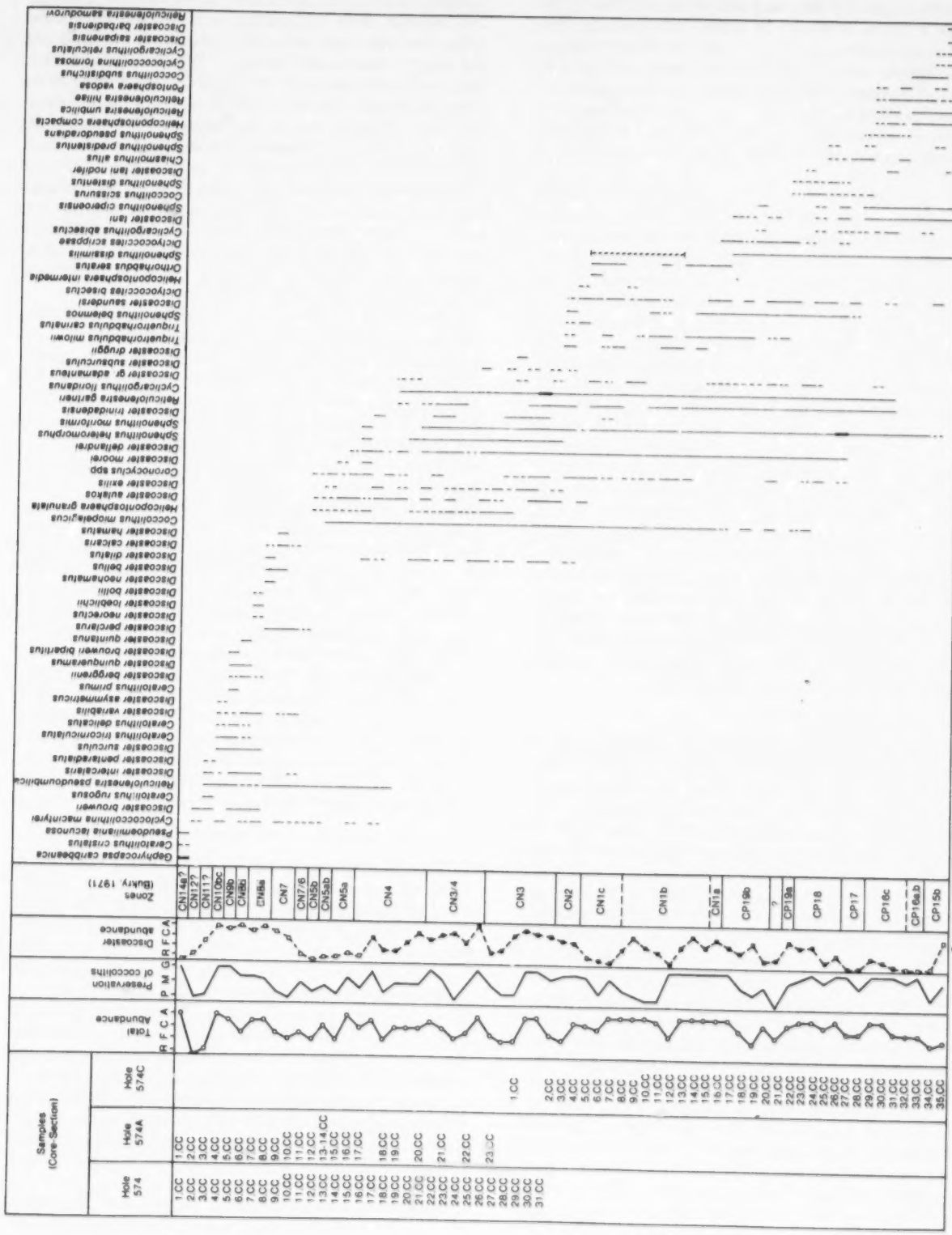

Figure 6. Occurrence of nannofossil species at Site 574; position of dashed zonal boundaries uncertain.

and 573. The diatoms suggest that part of the lower Pleistocene (≈0.8 to 1.5 Ma) may not be represented (there may be a hiatus or it may be greatly compressed). The fauna in the sample at 574-2-2, 130 cm, which contains *Pseudoeunotia doliolus* and *Nitzschia reinholdi* but lacks the silicoflagellate *Mesocena quadrangula*, suggests an age for the sample from 0.65 to 0.8 Ma. The sample at 574-2-3, 80 cm contains *Pseudoeunotia doliolus* and *Rhizosolenia praebergonii* var. *robusta* and is 1.8 to 1.55 m.y. old.

A lower upper Miocene hiatus at 70.5 m sub-bottom (base of Core 8 of both Holes 574 and 574A) is marked by the close stratigraphic proximity of the first appearance datum of *Coscinodiscus yabei* var. *elliptica* (9.8 Ma) (which occurs in Sample 574-9-1, 9–10 cm and in Core 574-9 above the core catcher) and the last appearance datum of *Coscinodiscus vetustissimus* var. *javanicus* (10.7 Ma) (which also occurs in Sample 574A-9-1, 9–10 cm and in Core 574-9 above the core catcher). Samples in the lower parts of Core 8 of both Holes 574 and 574A contain mixed assemblages of older (*C. temperei* var. *delicata, Denticulopsis hustedtii*, and *Actinocyclus ellipticus* var. *"oval"*) and younger (*Thalassiosira burckliana* and *Nitzschia cylindrica*) diatoms.

This hiatus occurs in an interval in which hiatuses in the eastern Pacific, including Site 77 (Barron, 1981a) and Site 573, are widespread (Keller and Barron, 1983). Hiatuses of this age are also present in the middle-latitude eastern North Pacific (Barron, 1981b), the central North Pacific (Keller, 1980), and the Southern Ocean (Ciesielski et al., 1982), and they have been related to the increased production of Antarctic Bottom Water associated with polar cooling. A more detailed discussion is presented in Barron et al. (this volume).

Benthic Foraminifers

Benthic foraminifers are extremely rare or absent in Samples 574-2,CC through -10,CC (i.e., in the Quaternary, Pliocene, and upper Miocene). They are generally rare in the rest of the cores. Preservation is variable; fragmentation is common in the lower 20 m of the cored interval. The diversity of the section is high (about 50 species per 200 specimens). Diversity does not decrease downhole, and it shows no apparent relation to lithology or dissolution (as indicated by the planktonic foraminifers).

The main constituents of the fauna are *Epistominella exigua* in the Miocene; *Nuttallides umbonifera* and species of *Pullenia, Gyroidinoides, Oridorsalis*, and *Cibicidoides* throughout the section; and species of *Stilostomella* and *Pleurostomella* from the lower Miocene downward. The relative abundance of the species fluctuates. The abundance of *Cibicidoides* species is relatively low from the upper Oligocene through the lower Miocene. The Oligocene species of *Cibicidoides* (e.g., *C. grimsdalei, C. laurisae, C. mexicanus*) are gradually replaced by a more modern assemblage which includes *C. kullenbergi* and *C. wuellerstorfi*) during the early Miocene. *Uvigerina graciliformis* peaks in abundance (it forms up to 30% of the assemblage in Section 574-10,CC) in samples that show extreme dissolution of planktonic foraminifers. *E. exigua* is known to be resistant to dissolution (e.g., Douglas and Woodruff, 1981), and it peaks in abundance in samples in which the planktonic foraminifers are strongly dissolved. Thus, the scarcity or absence of the species below the Oligocene/Miocene boundary is probably not the result of dissolution. Species of *Stilostomella* and *Pleurostomella* become more abundant from the lower Miocene downward. *Pleurostomella* is especially abundant in the lower Miocene. Again, the decrease in abundance in *Pleurostomella* and *Stilostomella* species in the lower middle Miocene is about coeval with or slightly earlier than important changes in benthic foraminifers on the Ontong-Java Plateau (Woodruff and Douglas, 1981). *Bolivina striatula* is present between 15.5 and 18.7 Ma. At Site 574 the changes from an Oligocene benthic fauna to a more modern association occur gradually (from the uppermost Oligocene through the lower Miocene).

The changes in the fauna at the Eocene/Oligocene boundary are not great. The abundance of the most common species (*Cibicidoides, Gyroidinoides, Oridorsalis, Globocassidulina*) remains relatively unchanged, in accordance with observations by Corliss (1981) and Miller et al. (1985). *Nuttallides truempyi* has its last occurrence in Sample 574C-33-5, 141–143 cm. Several other rare species have their last occurrence slightly later (e.g., *Alabamina dissonata* in Sample 574C-33-5, 71–73 cm; *Osangularia mexicana* in Sample 574C-33-5, 90–92 cm). *Gyroidinoides planulatus* has its last appearance in Sample 574C-34-1, 71–73 cm (before the last appearance of *N. truempyi*). *Cibicidoides laurisae* first occurs in Section 574C-32,CC. *O. mexicana* is, according to Douglas (1973), limited to the Eocene in the Pacific. *A. dissonata* was used as an Eocene marker species by Douglas (1973), Proto Decima and Bolli (1978), and Schnitker (1979). However, Miller and Curry (1982), Miller et al. (1985), and Tjalsma and Lohmann (1982) state that *N. truempyi* is the most reliable marker of the Eocene/Oligocene boundary. Thus, several events that have been described as occurring at the Eocene/Oligocene boundary occur in the benthic foraminiferal assemblages at Site 574, but they occur at slightly different levels.

SEDIMENT ACCUMULATION RATES

The age–depth curve for Site 574 is shown in Figure 7, which summarizes the sedimentation rate data in Table 3. The sedimentation rates through the Oligocene section of Site 574 average 12 m/m.y., with the rate beginning to increase at 22.9 Ma and reaching a high of 32 m/m.y. in the early Miocene (15 to 20 Ma). Across the early/middle Miocene boundary, there is a short interval (13.6 to 15.9 Ma) with a lower sedimentation rate; this interval is followed by the interval with the highest sedimentation rate observed at Site 574. This maximum rate lasts through most of the middle Miocene (12.4 to 13.6 Ma; Table 3). After the middle Miocene maximum, the rate decreases sharply, and except for a short interval of increased rate between 5 and 6.2 Ma, the rate remains low into the youngest sediments recovered. For further discussion see Barron et al. (this volume).

Mass accumulation rates at Site 574 were calculated by using the onboard physical properties measurements and from the sedimentation rates given in Table 3. Car-

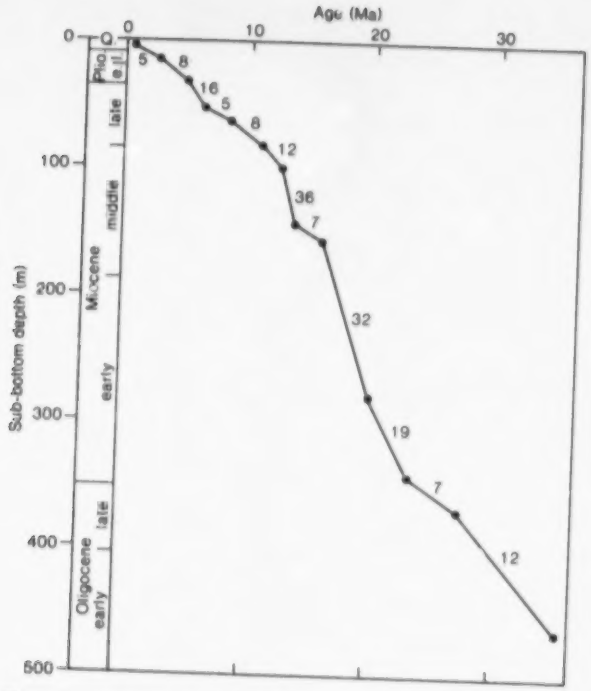

Figure 7. Age versus depth-in-hole based on biodatums at Site 574. Average sedimentation rates in m/m.y.

Table 3. Sedimentation rates, carbonate and noncarbonate mass accumulation rates at Site 574.

Sub-bottom depth (m)	Age (Ma)	Sedimentation rate (m/m.y.)	Mean dry bulk density (g/cm³)	Mean $CaCO_3$ (%)	Mean mass accumulation rate ([g/cm²]/1000 yr.)		
					Total	$CaCO_3$	Non $CaCO_3$
4	0.6	3.0	0.53	64	0.27	0.17	0.10
15	2.8	8.2	0.35	29	0.29	0.08	0.21
33	5.0	15.8	0.49	51	0.77	0.39	0.38
52	6.2	4.8	0.74	74	0.36	0.26	0.09
62	8.3	7.6	0.58	56	0.44	0.27	0.19
81	10.9	12.0	0.79	79	0.95	0.75	0.20
99	12.4	35.8	1.00	90	3.6	3.24	0.36
142	13.6	6.5	0.99	87	0.64	0.56	0.08
157	15.9	32.4	1.03	82	3.33	2.74	0.56
280	19.7	19.1	1.20	90	2.29	2.07	0.22
341	22.9	7.2	1.22	87	0.88	0.76	0.12
369	26.8	12.3	1.3	88	1.6	1.41	0.19
464	34.7						

bonate bomb analyses were used to calculate the mass accumulation rates for the carbonate and noncarbonate sediment fractions. See Theyer et al. (this volume) for further discussion.

Sedimentation rate and the mass accumulation rates are plotted versus time in Figure 8. There are two important differences between the pattern of sedimentation for Site 574 and the patterns for Sites 572 and 573: (1) there is a positive correlation between sedimentation rate and

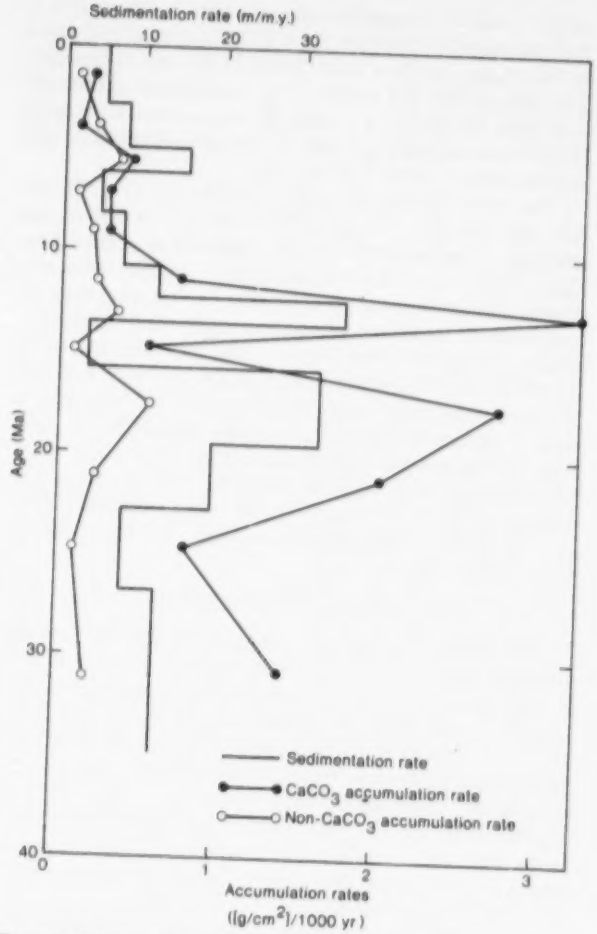

Figure 8. Sedimentation rate and average mass accumulation rates for carbonate and carbonate-free sediments at Site 574.

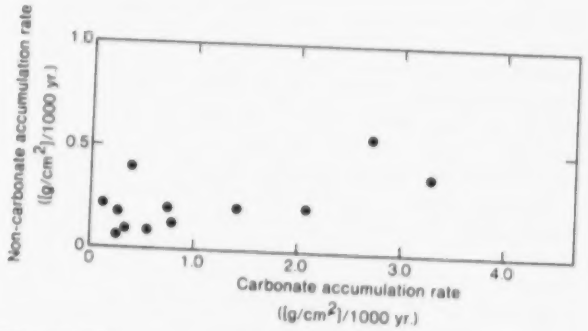

Figure 9. Carbonate versus carbonate-free mass accumulation rates at Site 574.

carbonate accumulation rate at Site 574, whereas the correlation is negative at Site 572 and essentially zero at Site 573; and (2) the relationship between carbonate and noncarbonate mass accumulation rate is not as clearly linear at Site 574 as at Sites 572 and 573 (Fig. 9). However, the data plotted in Figure 9 have a correlation coefficient

of 0.7, and the regression equation has a slope of 0.1, half the value for the data from Site 573 overall and equal to the value for data from Site 573 for the Oligocene. The data at Site 574 and the difference between that site and Sites 572 and 573 suggest that sediment accumulation is more strongly affected by the accumulation of carbonate than at Sites 572 and 573.

The sedimentation rate curve for Site 574 (Fig. 7), unlike that for Site 573, gives no clear indication of the presence of hiatuses. The hiatus suggested by diatom stratigraphy at about 10 Ma occurs within an interval of relatively low sedimentation rate, and the low rate may result in whole or in part from short intervals of nondeposition during this time period. The possible hiatus at 23 Ma at Site 573 occurs in an interval at Site 574 of low sedimentation rate; thus, this interval may represent a time of regional decrease in sediment accumulation. The zone of equatorial high productivity during the early Miocene was very narrow, and Site 573 is nearer the margin of the zone than Site 574, so a regional reduction in sediment accumulation might be expressed at Site 573 as a hiatus.

PHYSICAL PROPERTIES

The physical properties measured for this site include wet-bulk density (ρ_b), sonic velocity (V_p), formation factor (F), thermal conductivity (K), and shear strength. Measurements were made at regular intervals within the HPC-cored sections except where the sediment was disturbed. In the rotary-cored sections, measurements were limited to selected, undisturbed parts of the core rather than at regular intervals. The Introduction (this volume) discusses the data collection techniques and procedures and gives pertinent references. A complete listing of numerical data is given in the Appendix (this volume).

Figures 10 through 15 show the various physical properties plotted against depth. Wet-bulk density (Fig. 10) is highly variable near the top of the section (1.2 to 1.4 g/cm^3). At 90 m this range increases in mean value somewhat but is still variable. Just below 90 m there is a shift in densities to values around 1.6 g/cm^3. The data are less variable and remain at values near 1.6 g/cm^3 until a depth of around 220 m, where there is another fairly abrupt shift to values over 1.7 g/cm^3. Density remains between 1.7 and 1.8 g/cm^3 for about 200 m and then falls again at a layer of high-porosity material near basement.

Porosity (Fig. 11) shows many of the same trends as wet-bulk density and can be divided into a variable zone 90 m deep with porosities in excess of 80%; a less variable zone from 90 to 220 m with values near 60%; and a deep zone, in which porosity gradually decreases to a minimum at 440 m of about 45%. Below 440 m porosity increases as the result of an increase in the silica content of the lowermost sediments; the open structure of radiolarian tests tends to produce higher porosity values than the calcareous nannofossils, which pack more densely. Values of formation factor (Fig. 12) show the same trends, increasing from around 1.5 in the upper section to near 3.0 below 220 m. The induration of the sediments prohibited measurements of formation factor in the lowermost high-porosity zone.

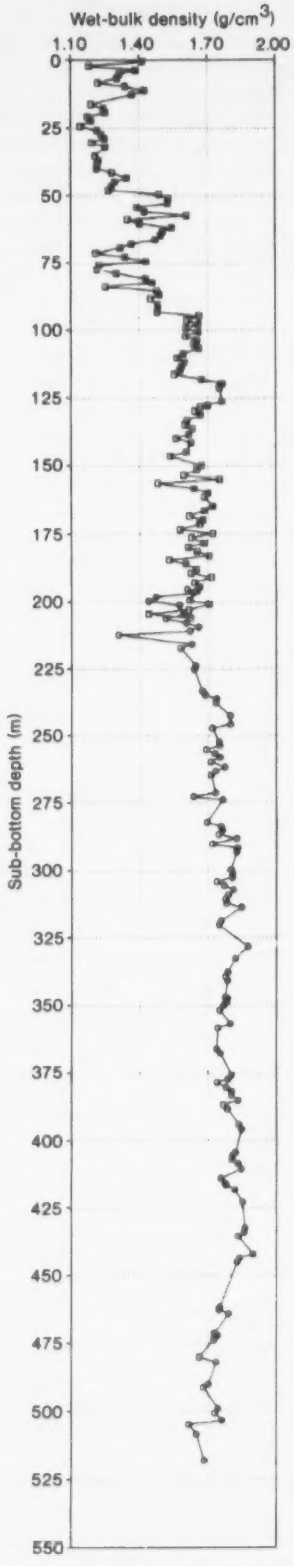

Figure 10. Wet-bulk density versus depth for Site 574.

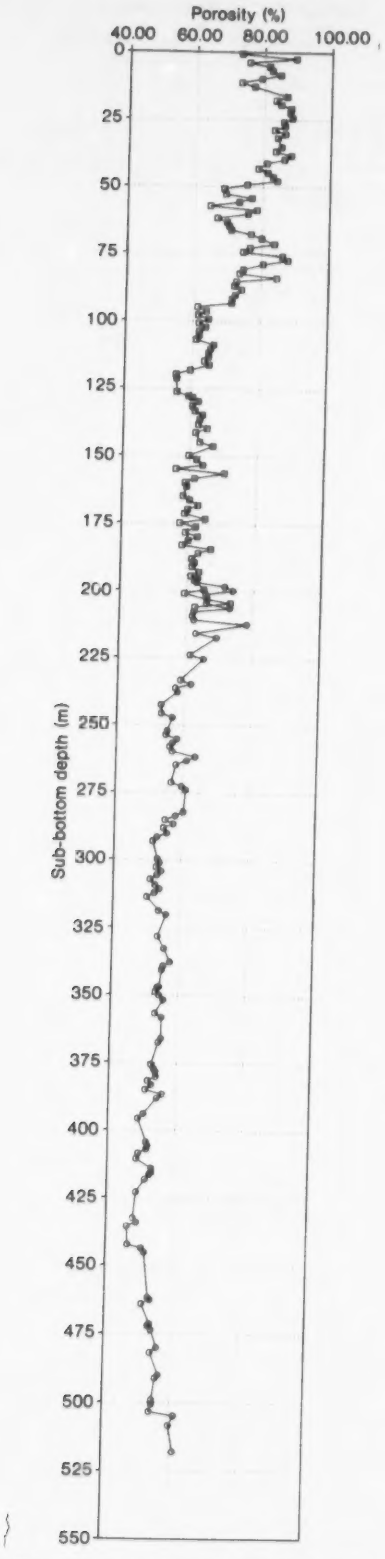

Figure 11. Porosity versus depth for Site 574.

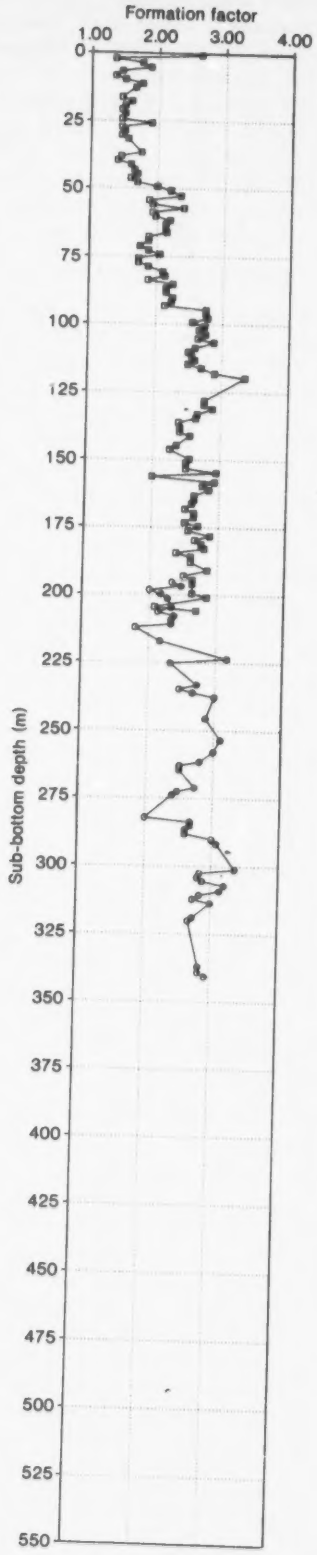

Figure 12. Formation factor (horizontal) versus depth for Site 574.

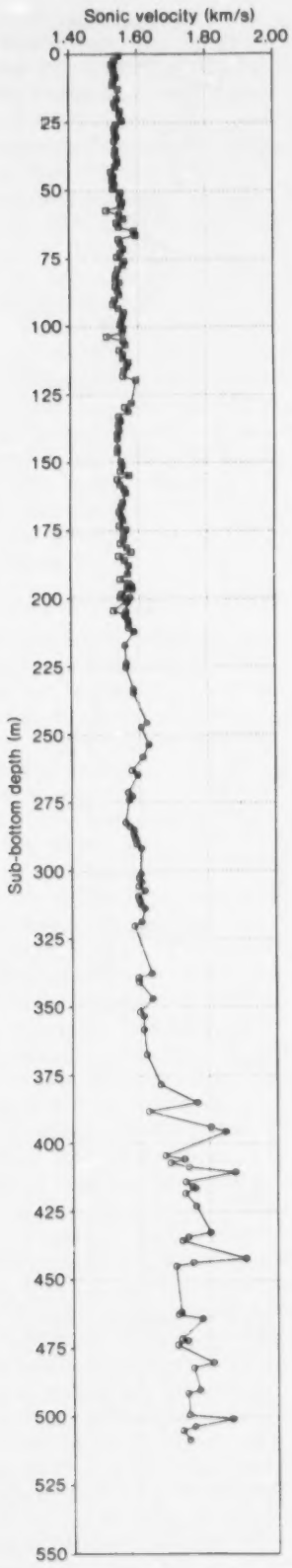

Figure 13. Sonic velocity versus depth for Site 574.

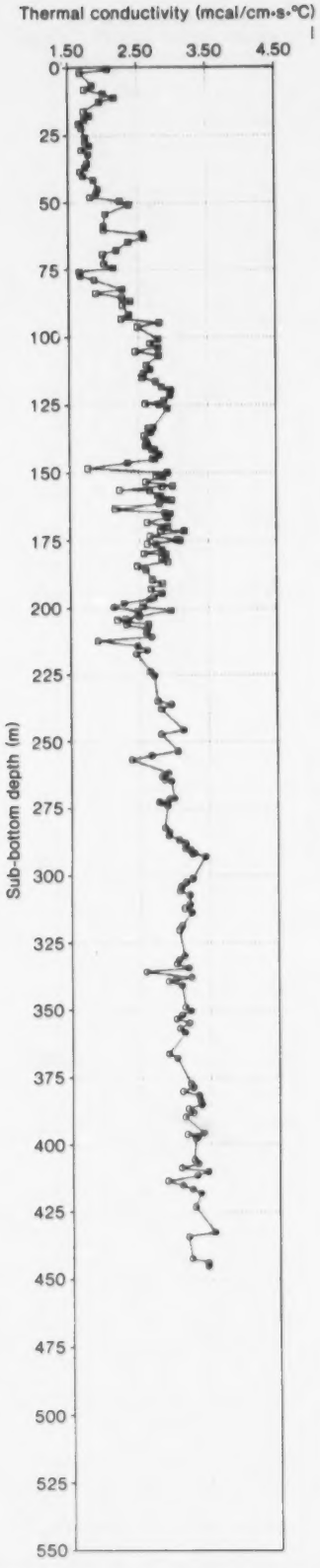

Figure 14. Thermal conductivity versus depth for Site 574.

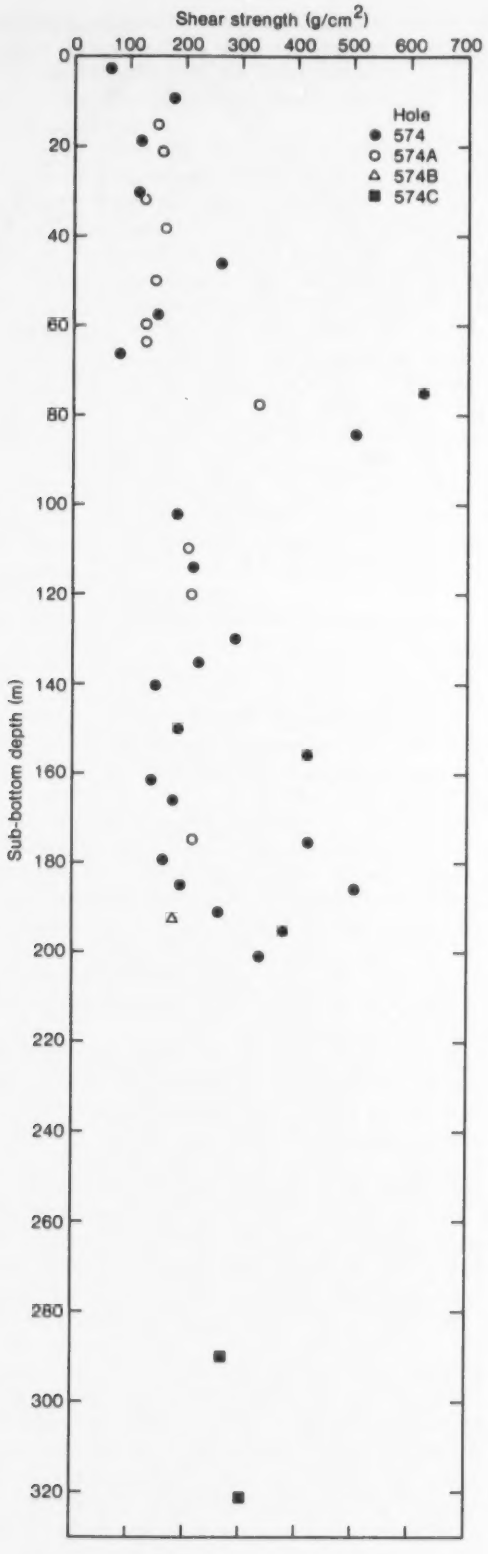

Figure 15. Shear strength versus depth for Site 574.

Thermal conductivity increases from values around 1.9 mcal/cm·s·°C to about 2.5 mcal/cm·s·°C in the interval between 50 and 90 m; values increase to about 3.4 mcal/cm·s·°C between 220 and 290 m (Fig. 14).

Shear strength (Fig. 15) is between 100 and 200 g/cm^2 at depths less than 70 m, exhibits several rather high values near 80 m, and then settles into the range from 200 to 300 g/cm^2 to a depth of 200 m. Two measurements near 300 m depth indicate a very small increase to values somewhat greater than 300 g/cm^2.

PALEOMAGNETISM

The magnetic properties of the upper 50 to 60 m of Holes 574 and 574A are reasonably good and permit polarity changes (as evidenced by 180° changes in the measured declination) to be distinguished. The untreated NRM_0 data, however, do not allow the identification of a specific reversal sequence. No AF demagnetization was carried out on board (see Weinreich and Theyer, this volume). The Kuster orientation device worked reasonably well and yielded readable slides in 80% of the cores.

At Site 573 the color of the sediment changed from brown to gray; this color change also occurred in Holes 574 and 574A. The change was again accompanied by a decrease by a factor of at least 10 in NRM_0 intensities. In general, Hole 574C shows very low intensities (about 1×10^{-7} G), although in the lower part (below 370 m), the variations in intensity are greater (sometimes up to 5.6×10^{-6} G). As in Hole 573B, the strongest intensity occurs in the dark brown sediment overlying the basalt; the values measured at Site 574 of 1.7×10^{-5} G are similar to the intensities of the metalliferous sediments of Hole 573B.

The variation of the NRM_0 intensities in the upper 60 to 80 m appears to be caused mainly by the variation of carbonate content. Between 80 and 200 m, however, the carbonate content is high and nearly constant, and NRM_0 intensities are low but variable. The variations in NRM_0 intensities in this part of the section may be due to changes in sedimentation rate. Low sedimentation rate appears to be accompanied by higher intensities, and high sedimentation rate seems to be accompanied by low intensities.

INTERSTITIAL-WATER CHEMISTRY

The profiles of magnesium and strontium and to a lesser extent calcium and alkalinity are roughly linear to sub-bottom depths of 150 to 175 m (Fig. 16). Calcium, strontium, and alkalinity gradually increase, whereas magnesium concentration steadily decreases. Reversals in these trends begin from 300 to 350 m sub-bottom and continue to the base of the section. Chlorinity shows a gradual steady increase and then abruptly decreases.

Large variations occur in the lowermost 150 m. Calcium and alkalinity show abrupt changes to very low values near 430 m sub-bottom. All profiles except pH and strontium contain abrupt concentration decreases in the deepest sample, but there is no evidence for contamination by surface seawater for the deeper samples. The fluctuations are probably related to diagenesis, which is influenced by differences in age, sediment accumulation rate, and sediment composition (especially in the metal-

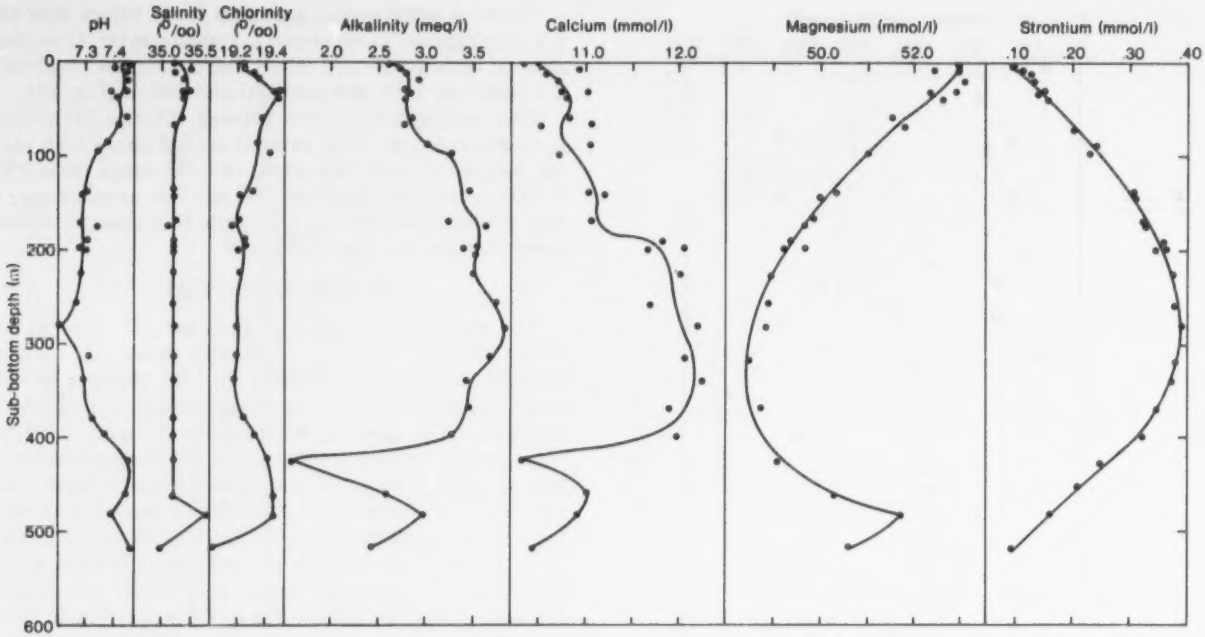

Figure 16. Interstitial-water geochemistry, Site 574.

liferous sediments that occur from 502 to 520 m sub-bottom).

Calcite recrystallization is indicated by the downhole increases in strontium; the values reach a maximum near 300 m sub-bottom. The overall profile is very smooth; it does not show the abrupt changes in the lower 150 m of section found for the other chemical species.

SUMMARY AND CONCLUSIONS

Site 574, located at 4°12.52′N, 133°19.81′W in 4550 m of water, is the second site in a three-site north–south transect across the equatorial high-productivity zone. The drill site, near the crest of the equatorial sediment bulge, was selected to provide a sedimentary record of the migration of this site across the equator as well as to permit recovery of the Eocene/Oligocene boundary. Three holes were drilled at Site 574. The coring may be summarized as follows.

In *Hole 574*, 32 hydraulic piston cores resulted in 206.5 m of penetration, and recovery was nearly 100%. In *Hole 574A*, 23 hydraulic piston cores were obtained. Penetration was 180.2 m, and recovery was nearly 100%. *Hole 574B* represented one rotary-drilled core recovered from 185 to 194.5 m sub-bottom. The corer was lost, and the pipe had to be tripped to recover it. In *Hole 574C*, 37 cores were recovered by rotary drilling from 194.5 to 525.5 m sub-bottom, where basalt was encountered. Recovery for this hole was 58%.

The sedimentary section at Site 574 was divided into three lithologic units on the basis of sediment composition. Unit I (0 to 84.1 m; upper Miocene to Quaternary) is cyclic siliceous calcareous ooze. It is characterized by cyclic variations in the relative abundance of siliceous and calcareous microfossils and thus ranges from siliceous nannofossil to calcareous siliceous ooze. The unit is subdivided into three subunits, primarily by color: an upper brown ooze subunit, a green gray ooze subunit, and a lower brown ooze subunit.

Unit II (84.1 to 502.5 m; lower Oligocene to upper Miocene) is calcareous ooze chalk. The components of this predominantly calcareous unit range from siliceous nannofossil to nannofossil ooze and chalk. Two subunits are recognized on the basis of color, a green white chalk subunit (83.8 to 470.2) and a yellow white chalk subunit (470.2 to 502.5 m). A gradual transition from ooze to chalk occurs in the green white subunit between about 185 and 480 m sub-bottom.

Unit III (502.5 to 520.0 m; upper Eocene to lower Oligocene) is metalliferous chalk. More specifically, it is a yellow brown siliceous nannofossil chalk with common iron–manganese oxides. This unit directly overlies basaltic basement.

The carbonate content curve for Site 574 is similar to that for Site 573. The upper (upper Miocene to Quaternary) 85 m of the section is characterized by high-amplitude, high-frequency fluctuations in carbonate content. The sediments deposited from the Eocene to the middle Miocene show high carbonate content with little variation.

All the major microfossil groups are represented at Site 574, and the section from the uppermost Eocene to the Quaternary is fairly complete. Siliceous microfossils are abundant and well preserved in most of the section. There is, however, a decline in diatom abundance and preservation in the upper Oligocene, the upper part of the lower Oligocene, and near the Eocene/Oligocene boundary. Planktonic foraminiferal abundances fluctuate and provide good stratigraphic control only in the lower mid-

dle Miocene. Calcareous nannofossils are common to abundant throughout the section. Both the foraminifers and the nannofossils indicate that there are at least three zones of reworked Oligocene microfossils in the middle Miocene sediments.

Several of the events recorded in the Site 574 sediments are of stratigraphic significance. The planktonic foraminifers reveal the *Globorotalia fohsi* lineage and the *Orbulina* datum. The transition from the uppermost Eocene to the lowermost Oligocene is remarkably complete. The transition occurs in the metalliferous unit (502.5 to 520.0 m) directly above basement; the criteria for each microfossil group differ, and the precise location of the boundary varies accordingly. The apparently continuous sequence offers an unusual opportunity to study the Eocene/Oligocene boundary. The Oligocene/Miocene boundary occurs in Core 574C-17 (≈350 m), and the Miocene/Pliocene boundary occurs in Core 574-5 at approximately 35 m sub-bottom. The diatom stratigraphy suggests hiatuses in the lower Pleistocene (≈0.8 to 1.5 Ma) and the lower upper Miocene (9.1 to 10.8 Ma), whereas the sedimentation rate curves indicate these to be times of decreased sedimentation.

The sedimentation rate at Site 574 is moderate; it averages 12 m/m.y. during the Oligocene and increases to 32 m/m.y. in the early Miocene (15 to 20 Ma). There is a short interval of low sedimentation rate (13.6 to 15.9 Ma), which is followed by a middle Miocene interval (12.4 to 13.6 Ma) with a relatively high (about 36 m/m.y.) rate. After the middle Miocene, the sedimentation rate decreases sharply (to about 12 m/m.y.), and except for a short interval of increased rate (about 16 m/m.y.) between 5 and 6.2 Ma, remains low into the youngest sediments recovered. The sedimentation rate and calcium carbonate curves for Site 574, unlike those for Sites 572 and 573, show positive correlation. Carbonate and noncarbonate mass accumulation rates continue to exhibit a linear relationship, but the regression has a much lower slope than at Sites 572 and 573. These data suggest that sediment accumulation is more strongly affected by the accumulation of carbonate than at the previous Leg 85 sites. (See also Theyer et al., this volume.)

Paleomagnetic studies at Site 574 were once again hampered by the extremely low NRM intensities that characterize much of the section, but the shipboard analyses produced interesting results nonetheless. Polarity reversals could be identified in lithologic Unit I (the cyclic calcareous siliceous ooze), where NRM intensities are an order of magnitude higher than in the rest of the section (except for the metalliferous sediments). In the part of section where NRM intensities are highest (about 0 to 80 m), the correlation between carbonate content and NRM intensity is extremely good, low carbonate content corresponding to high intensity. Below 80 m sub-bottom the carbonate content increases and shows little variation, and the NRM intensities decrease and appear to vary as a function of sedimentation rate (higher intensity is accompanied by lower sedimentation rate). The NRM intensities increase again in the metalliferous sediments at the base of the section.

Shipboard analyses of interstitial water reveal linear trends for alkalinity, calcium, and magnesium in the upper 150 m. Departures from linearity in this interval may be a function of changes in diffusion coefficients, which are suggested by variations in formation factor (see Physical Properties). Deeper in the section, variations in alkalinity, calcium, and magnesium are influenced by sedimentation rate, depth of burial, and compositional changes, and are probably indicative of diagenetic processes. High alkalinity values are associated with high sedimentation rate and sulfate reduction; low alkalinity occurs in intervals where calcium is at a minimum and there is an increase in the amount of chalk, indicating possible calcite precipitation. Most intriguing are the changes in the geochemical parameters associated with the metalliferous sediments at the base of the section (Jarvis, this volume).

Physical property measurements (wet-bulk density, sonic velocity, thermal conductivity, and formation factor) show an upper zone of large-amplitude variations (0 to 90 m), which is underlain by an interval of fairly consistent values (90 to 220 m), the mean of which is offset from that of the upper interval. Below about 220 m there is another major shift in mean values that appears to be associated with the beginning of chalk formation. In the lowermost part of Site 574 (420 to 510 m), unlike the previous sites, saturated wet-bulk and grain densities decrease (porosity increases). This unexpected result is associated with the abundance of siliceous microfossils in this interval.

The seismic section of Site 574 is characterized by numerous closely spaced reflectors that vary in strength and character. As in other Leg 85 sediments, variations in sonic velocity are minimal until about 380 m sub-bottom; thus, impedance contrasts above that depth are a function of changes in wet-bulk density only. The reflection pattern in the upper 0.1 s correlates extremely well with the density cycles in the upper 80 m of the section. Below this level several individual reflectors can be correlated with shifts in wet-bulk density, but the reflectors may also be interference composites. Acoustic basement correlates with a zone of rapid velocity and density excursions (deeper than about 400 m) and probably does not represent basalt (see Mayer et al., this volume).

By interpolating the migration tracks (van Andel et al., 1975) of nearby drill sites, a rough estimate of the paleodepths and latitudes of Site 574 can be made. The crust upon which Site 574 sits was generated 37 to 39 Ma at about 5°S and in water about 3000 m deep. The presence of a metalliferous chalk in contact with basalt is consistent with our present understanding of ridgecrest processes. Despite the shallow depth, the lower Oligocene sedimentation rate was fairly low, a result of the site's distance from the equator (the equatorial productivity zone was narrow during this time) and the generally decreased sedimentation rate (van Andel et al., 1975). The foraminiferal dissolution index during this interval is moderate to high. The deepening of the site with time is not apparent from the carbonate or noncarbonate mass accumulation rate curves. In fact, $CaCO_3$ content increases in the first few million years of the site's existence, probably as the result of the oceanwide tendency of carbonate to increase from the Eocene to the Oligocene.

Sonic velocity (Fig. 13) exhibits fairly uniform values throughout most of the core. Values are near 1.50 km/s at the top and generally increase with increasing depth to 1.60 km/s by a depth of 240 m. Below about 360 m the velocities increase and become more variable, an effect of the differing amount of lithification near the basement.

The Miocene part of the section is characterized by generally higher carbonate and noncarbonate mass accumulation rates and high, fairly constant carbonate values. The dissolution index is moderate and fairly stable. The carbonate and noncarbonate mass accumulation rates increase and decrease together, with carbonate accumulating faster than noncarbonate (unlike the carbonate at Site 572, which accumulates slower than noncarbonate). These data are indicative of moderate productivity that increases as the site migrates under the equatorial high-productivity zone.

At approximately 15.9 Ma there is a sharp drop in the carbonate and noncarbonate mass accumulation rates. The dissolution index does not increase steeply. Van Andel et al. (1975) show a distinct peak in sedimentation rates at this time, but our dates are based on a different time scale.

After this decrease there is a sharp increase in both the carbonate and noncarbonate mass accumulation rates that corresponds to the crossing of the equator (which took place from 13.6 to 12.4 Ma). Dissolution is moderate to low during this interval. After the equatorial crossing we see a sharp and then a slower but steady decrease in carbonate and noncarbonate accumulation rates with minor fluctuations. There are two periods (6.2 to 8.3 Ma and 10.9 to 12.4 Ma) in which the abundance of diatoms that are indicative of upwelling increases. At Site 572, the presence of these upwelling diatoms is associated with enhanced dissolution. At Site 574, however, it is associated with decreased dissolution of carbonate. The contrast is further evidence that, whereas sedimentation at Site 572 is characterized by extremely high productivity and biogenous silica, the sedimentation at Site 573 and 574 is characterized by lower productivity and is dominated by calcareous components.

REFERENCES

Barron, J. A., 1981a. Middle Miocene diatom biostratigraphy of equatorial Pacific DSDP Hole 77B. *Geosci. J.*, 2:231–398.

_____, 1981b. Late Cenozoic diatom biostratigraphy and paleoceanography of the middle-latitude eastern North Pacific, Deep Sea Drilling Project Leg 63. *In* Yeats, R. S., Haq, B. U., et al., *Init. Repts. DSDP*, 63: Washington (U.S. Govt. Printing Office), 507–538.

Berger, W. H., and von Rad, U., 1972. Cretaceous and Cenozoic sediments from the Atlantic Ocean. *In* Hayes, D. E., Pimm, A. C., et al., *Init. Repts. DSDP*, 14: Washington (U.S. Govt. Printing Office), 787–954.

Berggren, W. A., and Van Couvering, J. A., 1974. The late Neogene: biostratigraphy, geochronology and paleoclimatology of the last 15 m.y. in marine and continental sequences. *Palaeogeogr. Palaeoclimatol. Palaeoecol.*, 16:1–216.

Bukry, D., 1971a. Coccolith stratigraphy, Leg 8, Deep Sea Drilling Project. *In* Tracey, J. I., Jr., Sutton, G. H., et al., *Init. Repts. DSDP*, 8: Washington (U.S. Govt. Printing Office), 791–807.

_____, 1971b. Cenozoic calcareous nannofossils from the Pacific Ocean. *Trans. San Diego Soc. Nat. Hist.*, 16:307–327.

_____, 1973. Low-latitude coccolith biostratigraphic zonation. *In* Edgar, N. T., Saunders, J. B., et al., *Init. Repts. DSDP*, 15: Washington (U.S. Govt. Printing Office), 685–703.

Ciesielski, P. F., Ledbetter, M. T., and Ellwood, B. B., 1982. The development of Antarctic glaciation and the Neogene paleoenvironment of the Maurice Ewing Bank. *Mar. Geol.*, 46:1–52.

Corliss, B. H., 1981. Deep sea benthonic foraminiferal faunal turnover near the Eocene/Oligocene boundary. *Mar. Micropaleontol.*, 6:367–384.

Douglas, R. G., 1973. Benthonic foraminiferal biostratigraphy in the central North Pacific, Leg 17, Deep Sea Drilling Project. *In* Winterer, E. L., Ewing, J. I., et al., *Init. Repts. DSDP*, 17: Washington (U.S. Govt. Printing Office), 607–672.

Douglas, R., and Woodruff, F., 1981. Deep sea benthic Foraminifera. *In* Emiliani, C. (Ed.), *The Sea* (Vol. 7): New York (Wiley Interscience), 1233–1327.

Dunn, D. A., 1982. Miocene sediments of the equatorial Pacific Ocean: carbonate stratigraphy and dissolution history [Ph.D. dissert.]. Univ. Rhode Island, Narragansett.

Dunn, D. A., and Moore, T. C., Jr., 1981. Late Miocene–Pliocene (Magnetic Epoch 9–Gilbert Magnetic Epoch) calcium carbonate stratigraphy of the equatorial Pacific Ocean. *Geol. Soc. Am. Bull.*, 92:408–452.

Ekdale, A. A., 1980. Trace fossils in Deep Sea Drilling Project Leg 58 cores. *In* Klein, G. deV., Kobayashi, K., et al., *Init. Repts. DSDP*, 58: Washington (U.S. Govt. Printing Office), 601–605.

Goll, R. M., 1972. Section on Radiolaria for synthesis chapter, Leg 9. *In* Hays, J. D., et al., *Init. Repts. DSDP*, 9: Washington (U.S. Govt. Printing Office), 947–1058.

Hardenbol, J., and Berggren, W. A., 1978. A new Paleogene numerical time scale. *Stud. Geol. (Tulsa, Okla.)*, 6:213–214.

Keller, G., 1980. Middle to late Miocene planktonic foraminiferal datum levels and paleoceanography of the north and southeastern Pacific Ocean. *Mar. Micropaleontol.*, 5:249–281.

Keller, G., and Barron, J. A., 1983. Paleoceanographic implications of Miocene deep sea hiatuses. *Geol. Soc. Am. Bull.*, 94:590–613.

Miller, K. G., and Curry, W. B., 1982. Eocene to Oligocene benthic foraminiferal isotopic record in the Bay of Biscay. *Nature (London)*, 296:317–350.

Miller, K. G., Curry, W. B., and Ostermann, P. R., 1985. Late Paleogene (Eocene to Oligocene) benthic foraminiferal paleoceanography of the Goban Spur region, Deep Sea Drilling Project, Leg 80. *In* Graciansky, P. C. de, Poag, C. W., et al., *Init. Repts. DSDP*, 80, Pt. 1: Washington (U.S. Govt. Printing Office), 505–538.

Proto Decima, F., and Bolli, H. M., 1978. Southeast Atlantic DSDP Leg 40 Paleogene benthic foraminifers. *In* Bolli, H. M., Ryan, W. B. F., et al., *Init. Repts. DSDP*, 40: Washington (U.S. Govt. Printing Office), 783–809.

Riedel, W. R., and Sanfilippo, A., 1978. Stratigraphy and evolution of tropical Cenozoic radiolarians. *Micropaleontology*, 23:61–96.

Schnitker, D., 1979. Cenozoic deep water benthic foraminifers, Bay of Biscay. *In* Montadert, L., Roberts, D. G., et al., *Init. Repts. DSDP*, 48: Washington (U.S. Govt. Printing Office), 377–414.

Tjalsma, R. C., and Lohmann, G. P., 1982. Paleocene–Eocene bathyal and abyssal benthic Foraminifera from the Atlantic Ocean. *Micropaleontology*, Spec. Publ. 4.

van Andel, T. H., Heath, G. R., and Moore, T. C., Jr., 1975. Cenozoic history and paleoceanography of the central equatorial Pacific Ocean. *Mem. Geol. Soc. Am. 143.*

Woodruff, F., and Douglas, R. G., 1981. Response of deep sea benthic Foraminifera to Miocene paleoclimatic events. *Mar. Micropaleontol.*, 6:617–632.

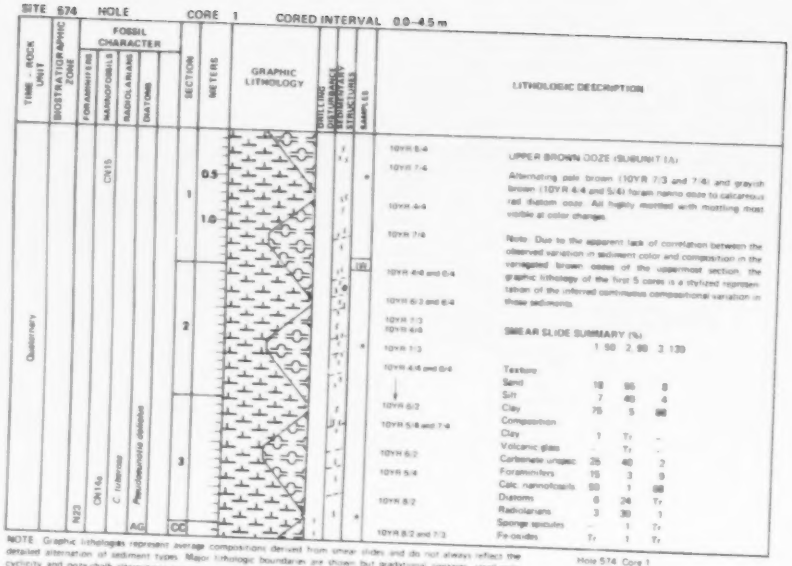
SITE 574 HOLE CORE 1 CORED INTERVAL 0.0–4.5 m
TIME – ROCK UNIT
BIOSTRATIGRAPHIC ZONE
FOSSIL CHARACTER
FORAMINIFERS
NANNOFOSSILS
RADIOLARIANS
DIATOMS
SECTION
METERS
GRAPHIC LITHOLOGY
DRILLING DISTURBANCE
BIOTURBANCY
STRUCTURES
SAMPLES
LITHOLOGIC DESCRIPTION
Quaternary
N23
CN15
C. tuberosa
Pseudoeunotia doliolus
A.C.
CC
UPPER BROWN OOZE (SUBUNIT 1A)
Alternating pale brown (10YR 7/3 and 7/4) and grayish brown (10YR 4/4 and 5/4) foram nanno ooze to calcareous rad diatom ooze. All highly mottled with mottling most visible at color changes.
Note: Due to the apparent lack of correlation between the observed variation in sediment color and composition in the variegated brown oozes of the uppermost section, the graphic lithology of the first 5 cores is a stylized representation of the inferred continuous compositional variation in these sediments.
SMEAR SLIDE SUMMARY (%)
1, 90 2, 80 3, 130
Texture
Sand 18 55 0
Silt 7 40 4
Clay 75 5 96
Composition
Clay 1 Tr –
Volcanic glass – Tr –
Carbonate unspec. 25 40 2
Foraminifers 15 3 9
Calc. nannofossils 50 1 68
Diatoms 6 24 Tr
Radiolarians 3 30 1
Sponge spicules – 1 Tr
Fe-oxides Tr 1 Tr
Hole 574 Core 1
CARBONATE BOMB
1, 64 cm = 84%
2, 75 cm = 28%
3, 74 cm = 80%

NOTE: Graphic lithologies represent average compositions derived from smear slides and do not always reflect the detailed alternation of sediment types. Major lithologic boundaries are shown but gradational contacts, small-scale cyclicity and ooze-chalk alternations are represented schematically. Color changes approximate to lithologic changes.

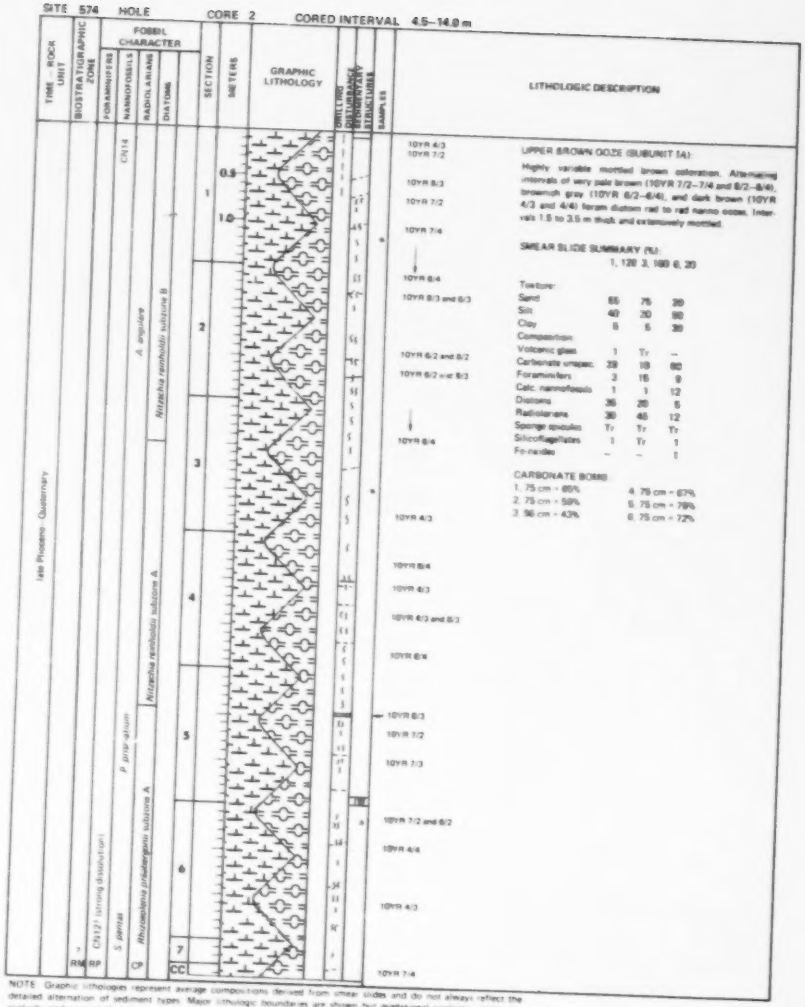

NOTE: Graphic lithologies represent average compositions derived from smear slides and do not always reflect the detailed alternation of sediment types. Major lithologic boundaries are shown but gradational contacts, small-scale cyclicity and ooze-chalk alternations are represented schematically. Color changes approximate to lithologic changes.

SITE 574 HOLE CORE 3 CORED INTERVAL 14.0–23.5 m

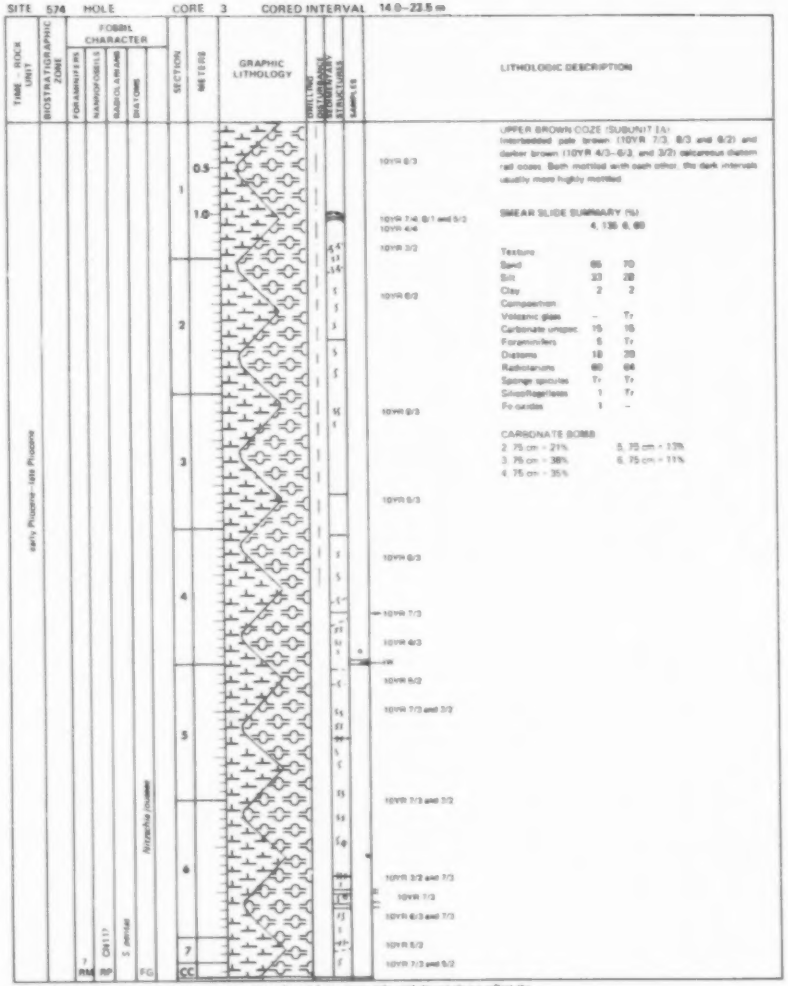

NOTE: Graphic lithologies represent average compositions derived from smear slides and do not always reflect the detailed alternation of sediment types. Major lithologic boundaries are shown but gradational contacts, small-scale cyclicity and ooze-chalk alternations are represented schematically. Color changes approximate to lithologic changes.

SITE 574 HOLE CORE 4 CORED INTERVAL 23.5–33.0 m

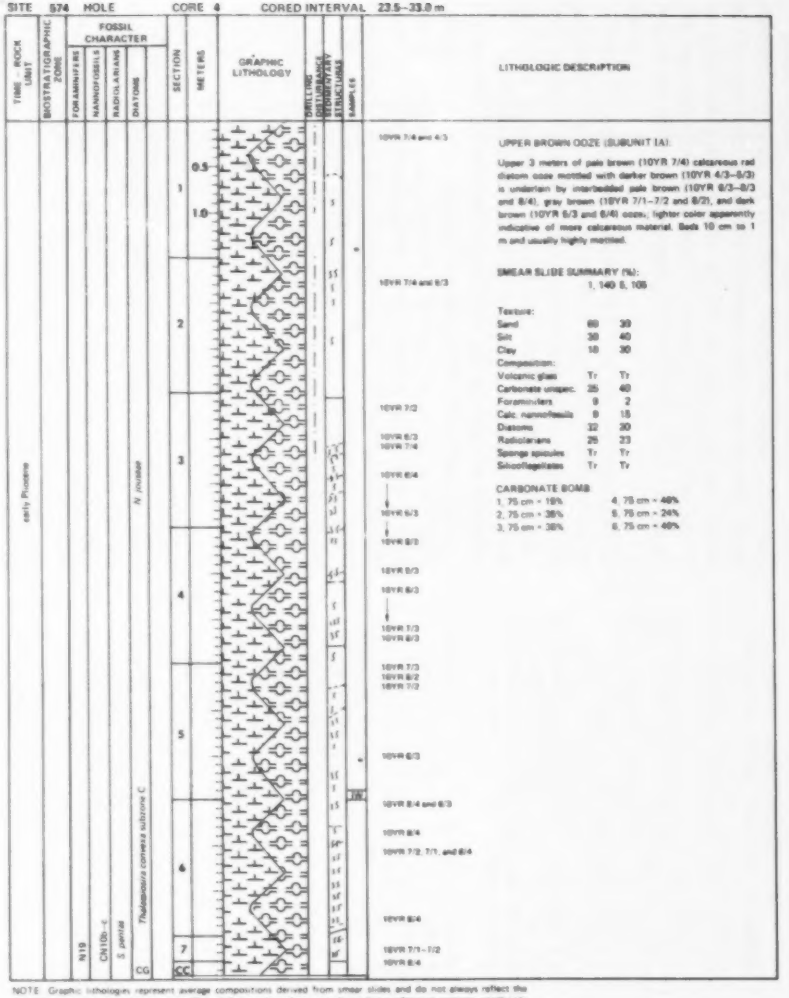
TIME – ROCK UNIT
BIOSTRATIGRAPHIC ZONE
FOSSIL CHARACTER
FORAMINIFERS
NANNOFOSSILS
RADIOLARIANS
DIATOMS
SECTION
METERS
GRAPHIC LITHOLOGY
DRILLING DISTURBANCE
SEDIMENTARY STRUCTURES
SAMPLES
LITHOLOGIC DESCRIPTION
early Pliocene
N19
CN10b–c
S. peritai
N. reinholdii
Thalassiosira convexa subzone C
UPPER BROWN OOZE (SUBUNIT 1A):
Upper 3 meters of pale brown (10YR 7/4) calcareous rad diatom ooze mottled with darker brown (10YR 4/3–6/3) is underlain by interbedded pale brown (10YR 6/3–8/3 and 8/4), gray brown (10YR 7/1–7/2 and 8/2), and dark brown (10YR 6/3 and 6/4) oozes; lighter color apparently indicative of more calcareous material. Beds 10 cm to 1 m and usually highly mottled.
SMEAR SLIDE SUMMARY (%):
1, 140 5, 105
Texture:
Sand 60 30
Silt 30 40
Clay 10 30
Composition:
Volcanic glass Tr Tr
Carbonate unspec. 35 40
Foraminifers 3 2
Calc. nannofossils 9 15
Diatoms 32 30
Radiolarians 25 23
Sponge spicules Tr Tr
Silicoflagellates Tr Tr
CARBONATE BOMB
1. 75 cm = 19%
2. 75 cm = 38%
3. 75 cm = 38%
4. 75 cm = 40%
5. 75 cm = 24%
6. 75 cm = 40%

NOTE: Graphic lithologies represent average compositions derived from smear slides and do not always reflect the detailed alternation of sediment types. Major lithologic boundaries are shown but gradational contacts, small-scale cyclicity and ooze-chalk alternations are represented schematically. Color changes approximate to lithologic changes.

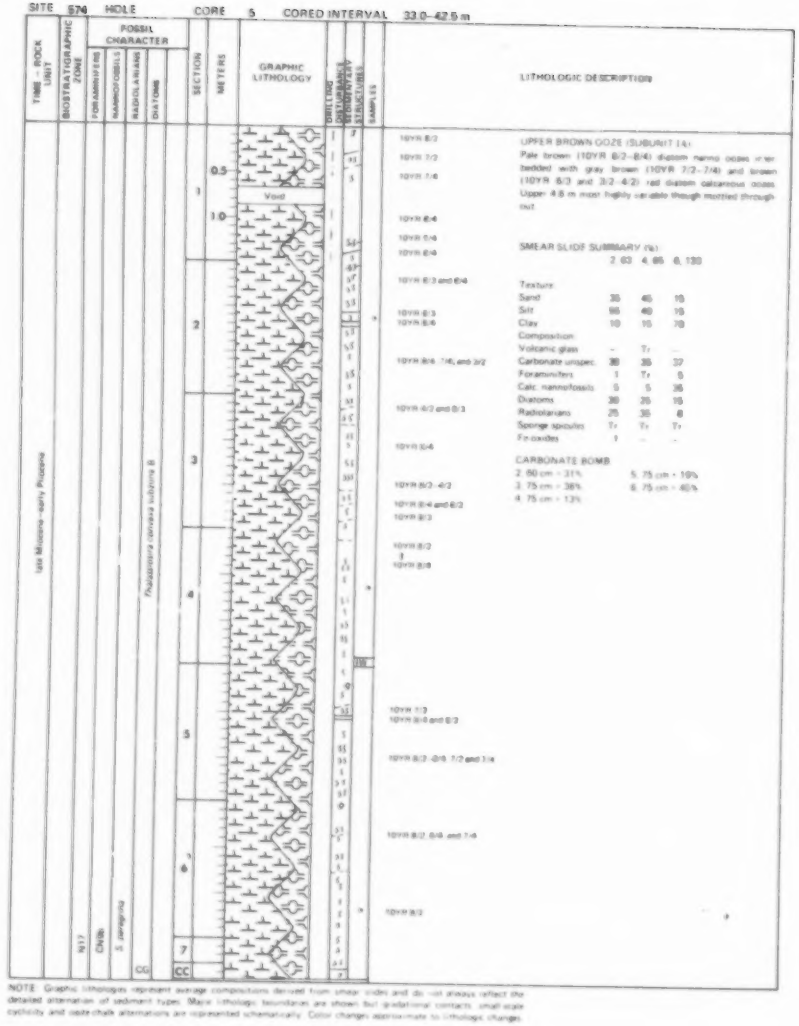
SITE 574 HOLE CORE 5 CORED INTERVAL 33.0–42.5 m
TIME – ROCK UNIT
BIOSTRATIGRAPHIC ZONE
FOSSIL CHARACTER
FORAMINIFERS
NANNOFOSSILS
RADIOLARIANS
DIATOMS
SECTION
METERS
GRAPHIC LITHOLOGY
DRILLING DISTURBANCE
SEDIMENTARY STRUCTURES
SAMPLES
LITHOLOGIC DESCRIPTION
late Miocene–early Pliocene
Void
Thalassiosira convexa subzone B
UPPER BROWN OOZE (SUBUNIT 1A):
Pale brown (10YR 8/2–8/4) diatom nanno ooze, inter-bedded with gray brown (10YR 7/2–7/4) and brown (10YR 6/3 and 3/2–4/2) red diatom calcareous oozes. Upper 4.8 m most highly variable though mottled throughout.
SMEAR SLIDE SUMMARY (%):
2, 63 4, 85 6, 130
Texture:
Sand 35 45 15
Silt 65 40 15
Clay 10 15 70
Composition:
Volcanic glass – Tr –
Carbonate unspec. 30 35 27
Foraminifers 1 Tr 5
Calc. nannofossils 5 5 35
Diatoms 30 25 15
Radiolarians 25 35 8
Sponge spicules Tr Tr Tr
Fe oxides 1 – –
CARBONATE BOMB
2. 60 cm = 31%
3. 75 cm = 38%
4. 75 cm = 13%
5. 75 cm = 19%
6. 75 cm = 46%

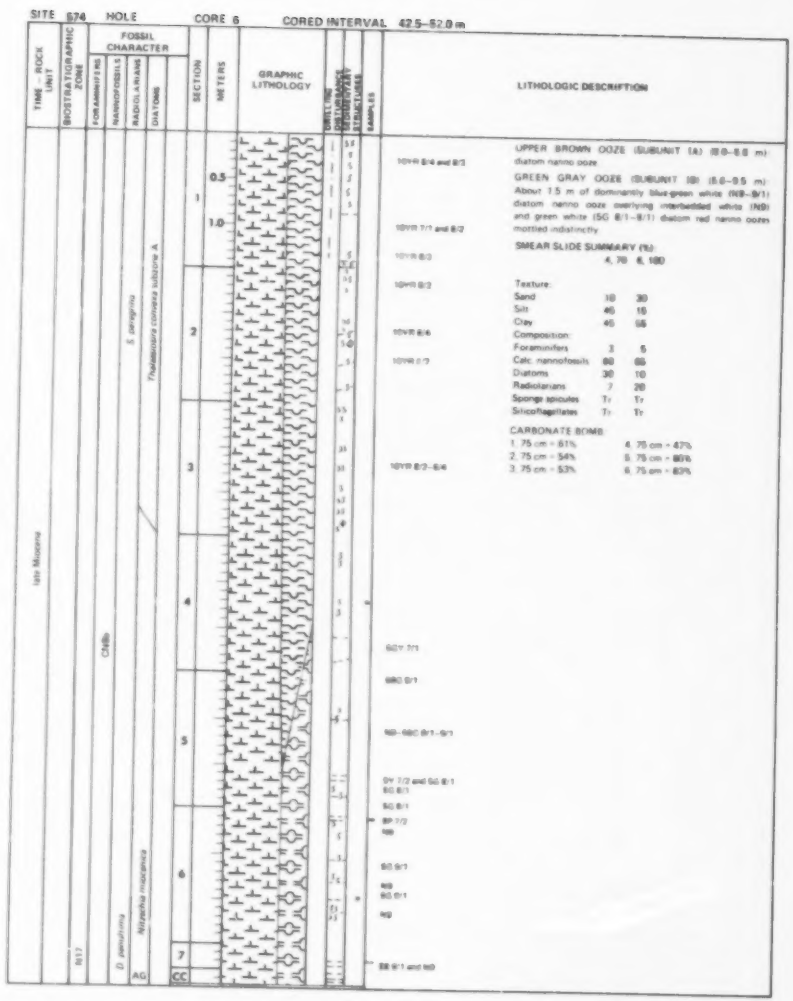

NOTE: Graphic lithologies represent average compositions derived from smear slides and do not always reflect the detailed alternation of sediment types. Major lithologic boundaries are shown but gradational contacts, small-scale turbidity and ooze/chalk alternations are represented schematically. Color changes approximate to lithologic changes.

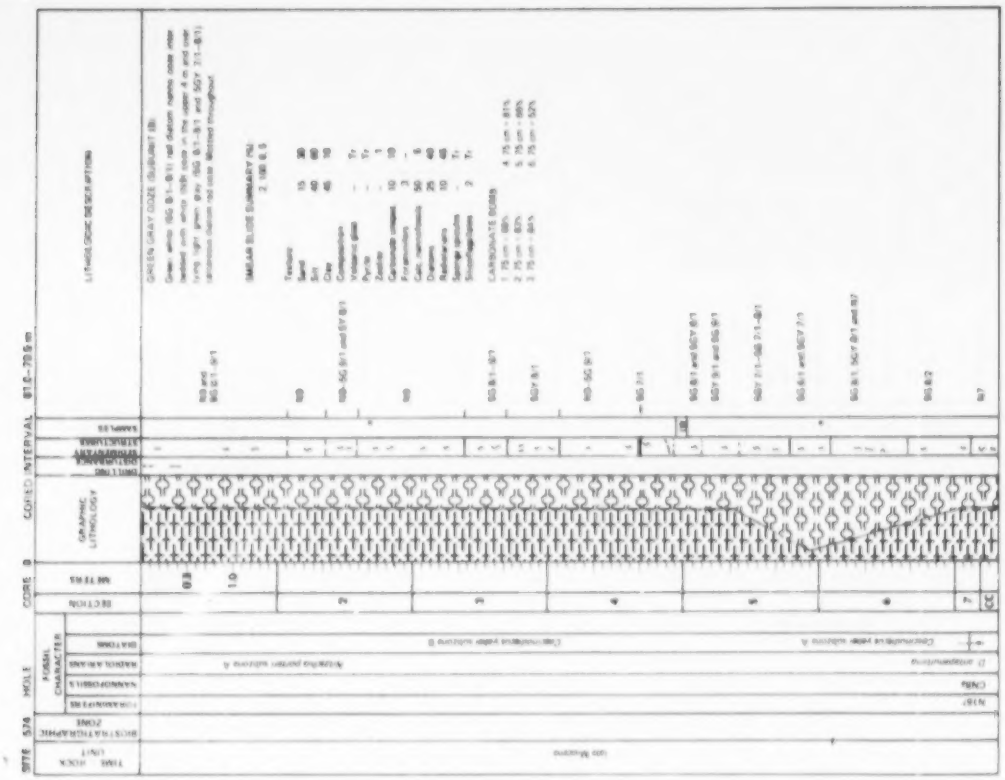

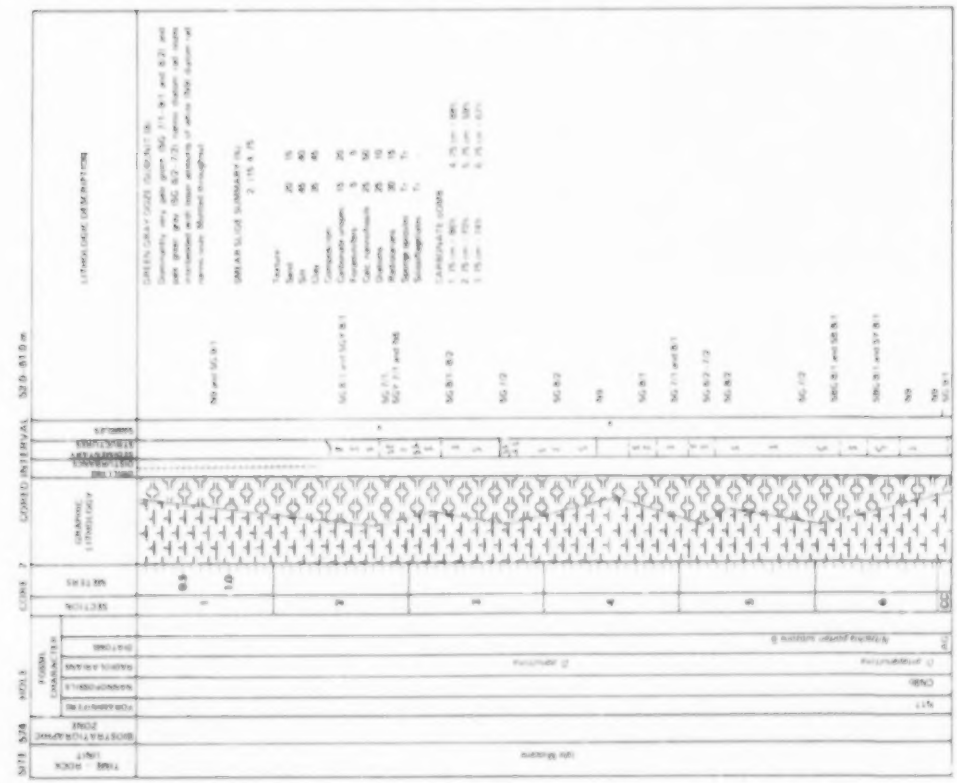

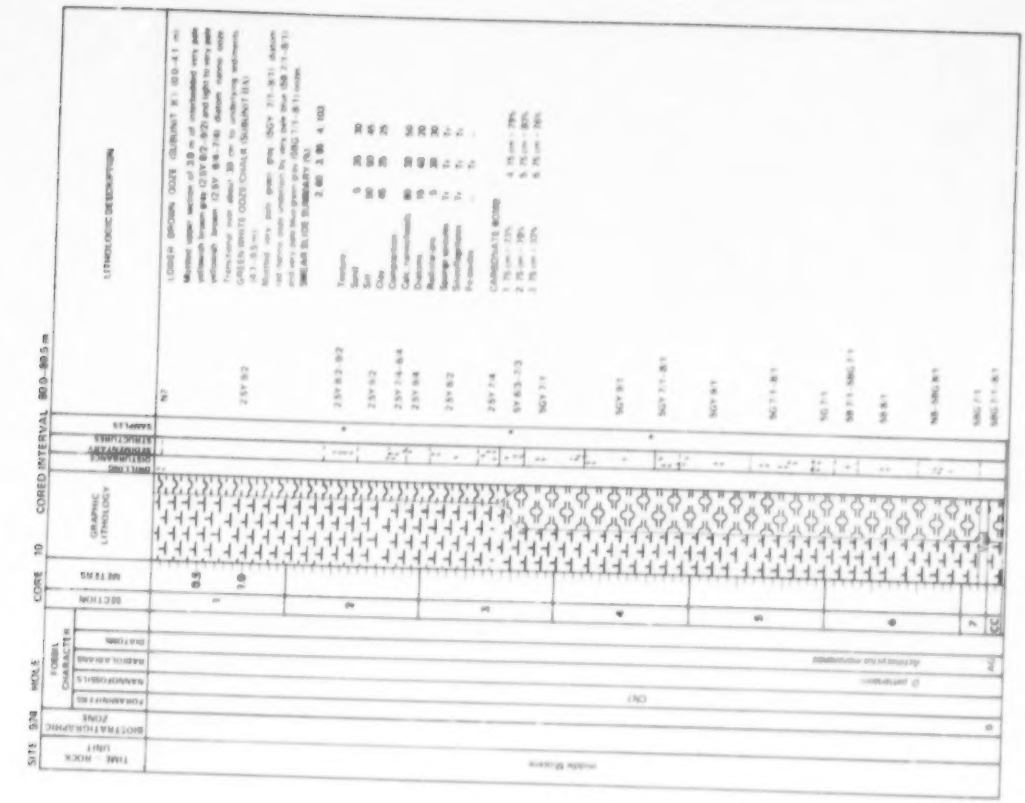

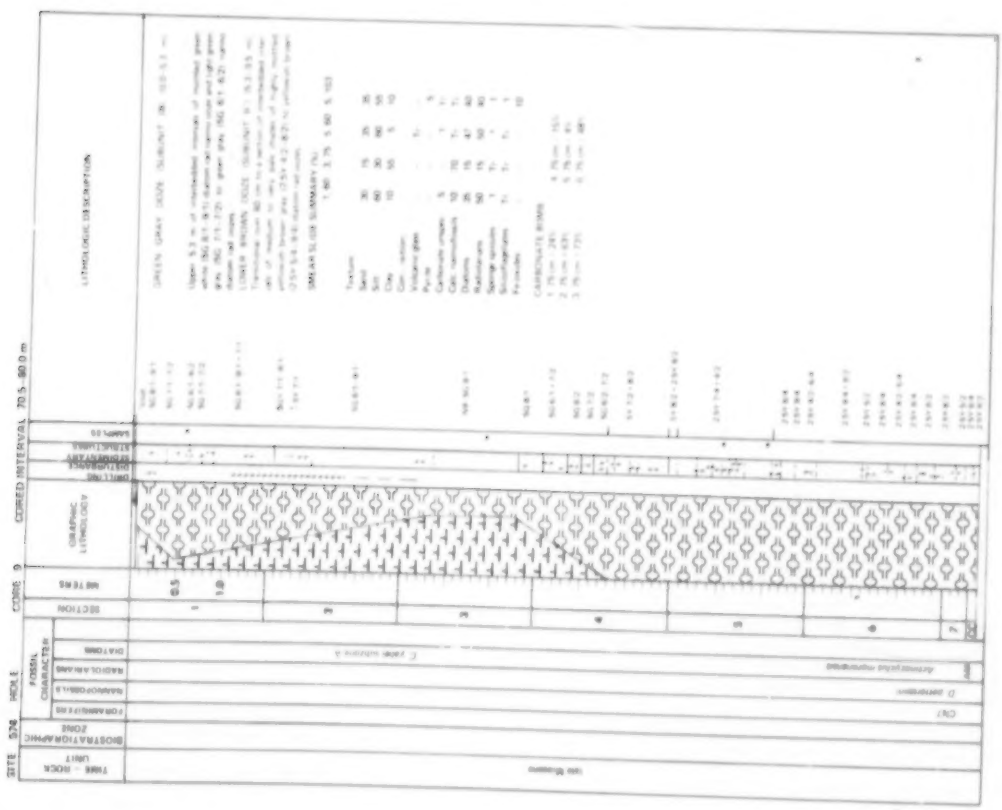

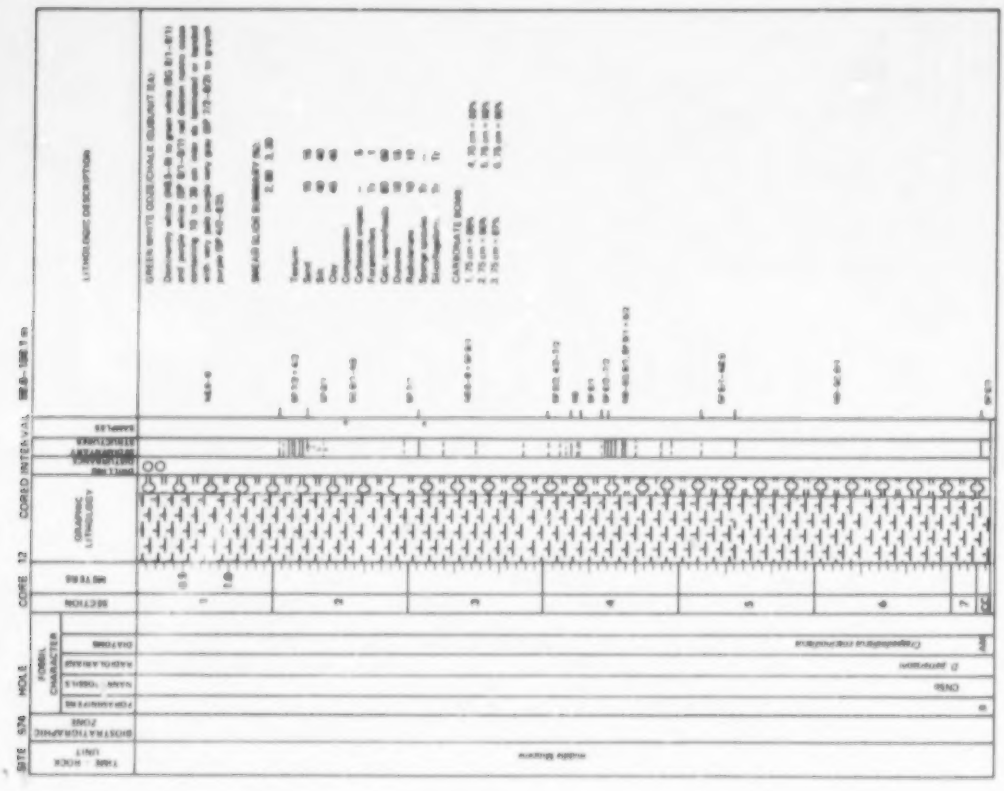

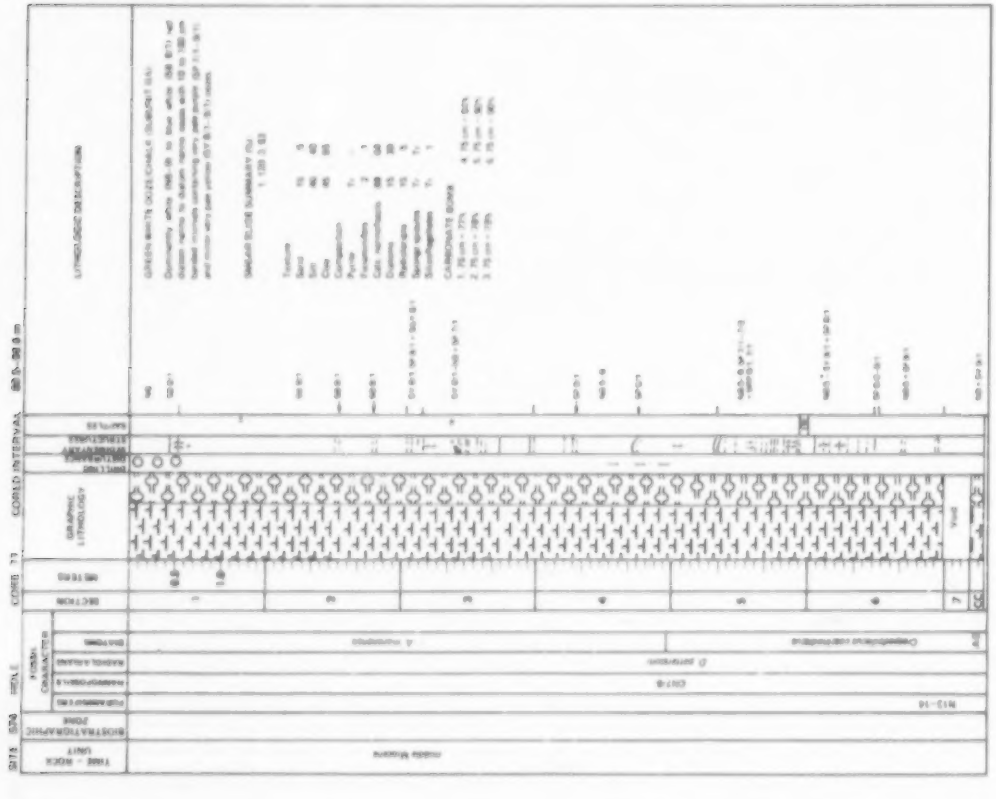

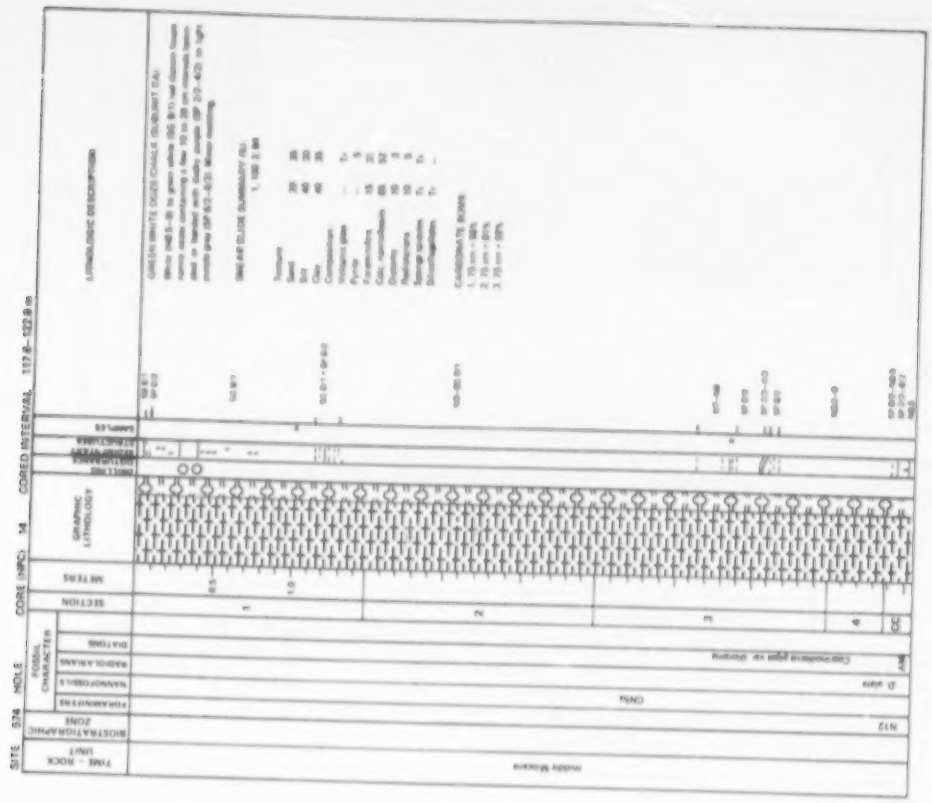

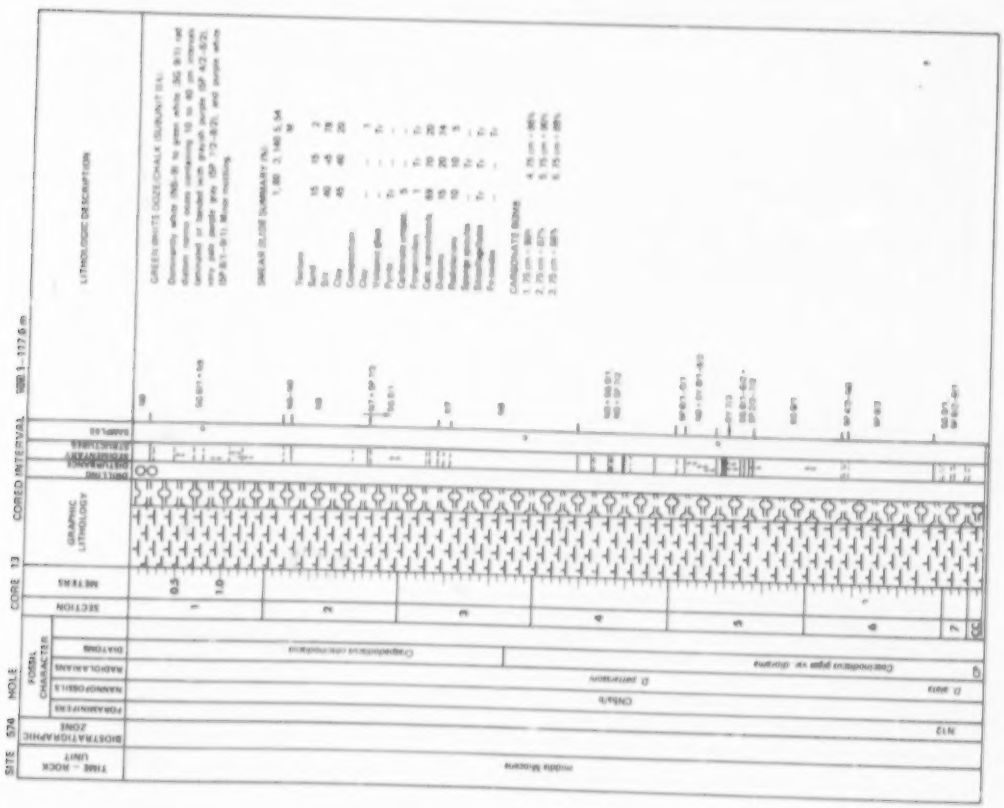

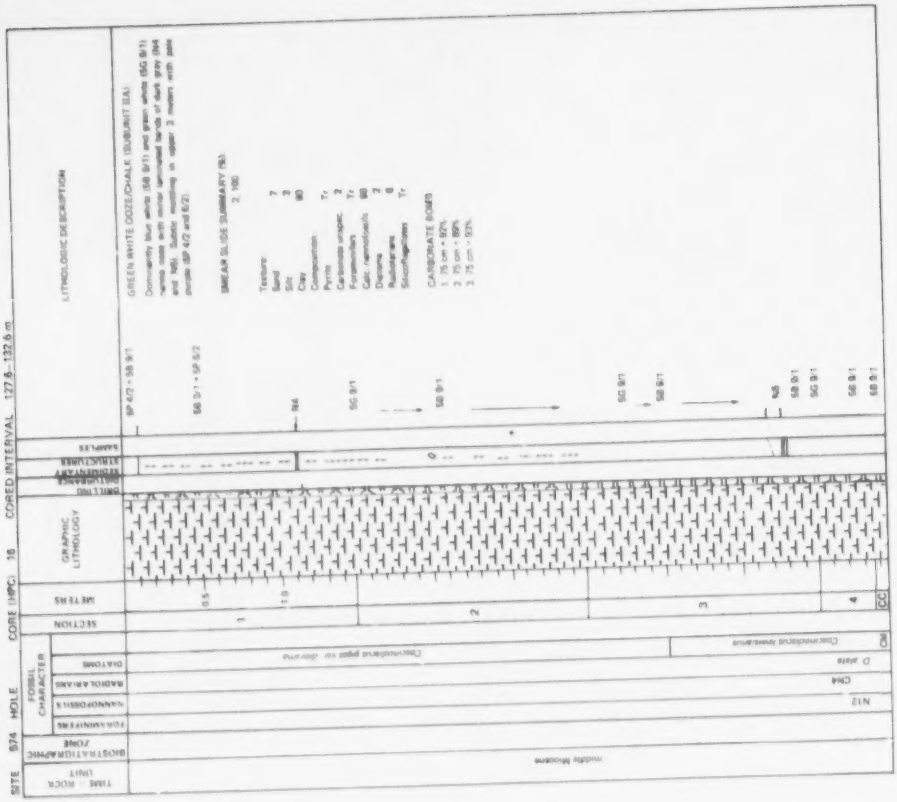

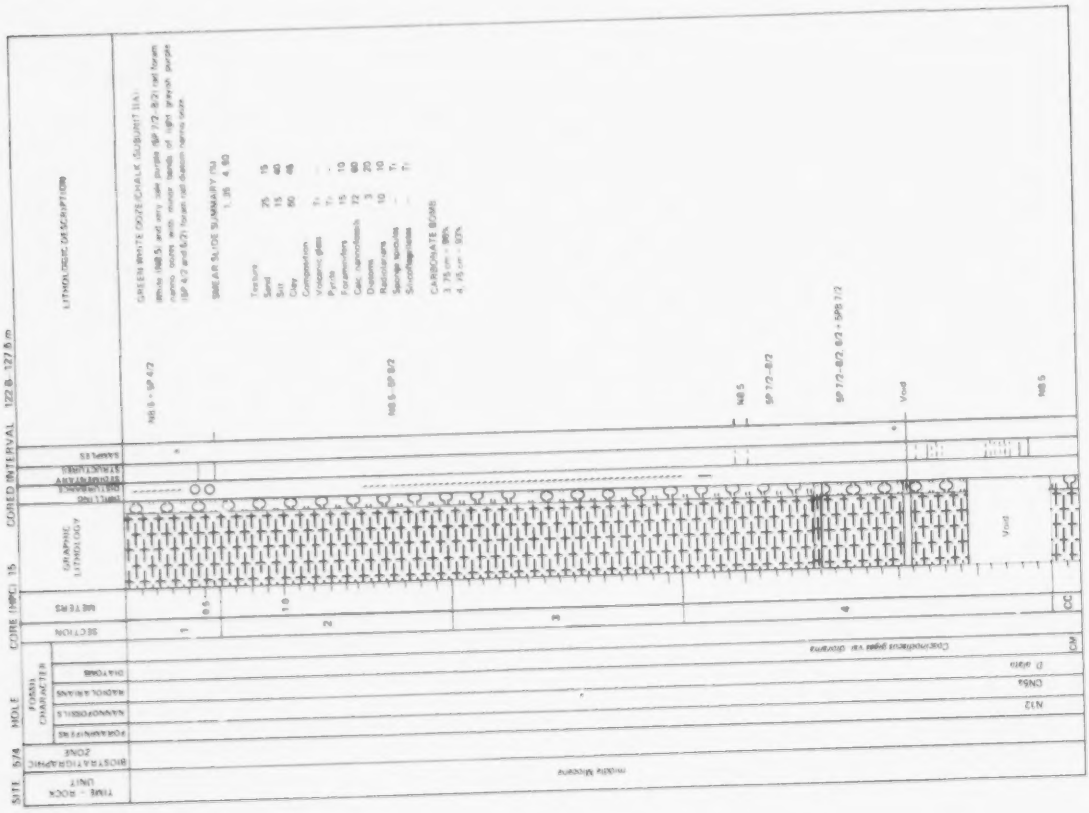

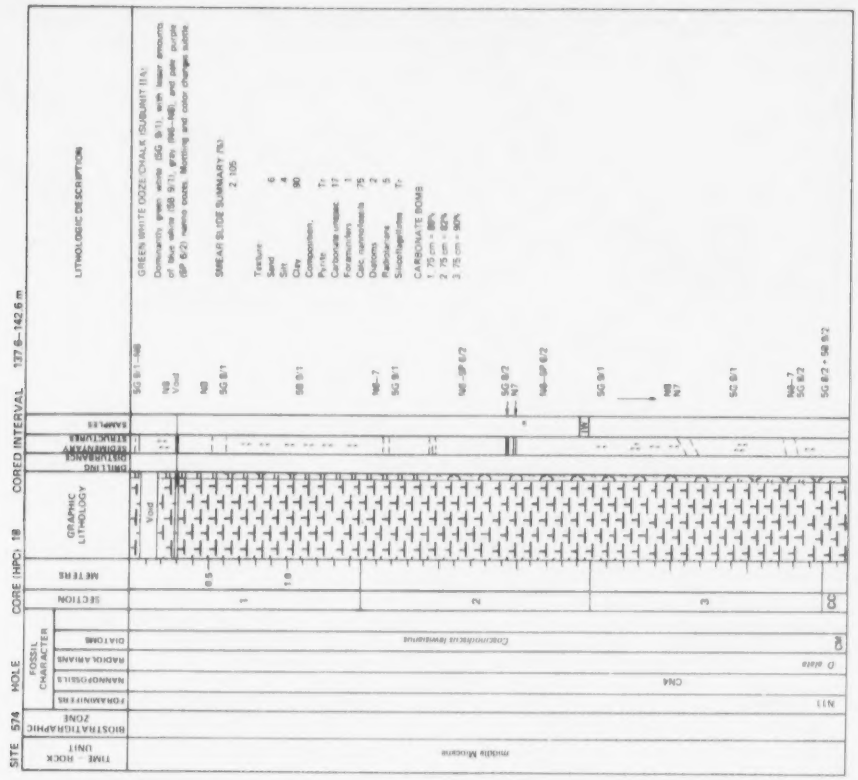
SITE 574
HOLE
CORE (HPC) 18
CORED INTERVAL 137.6–142.6 m
TIME – ROCK UNIT
middle Miocene
BIOSTRATIGRAPHIC ZONE
FORAMINIFERS
NANNOFOSSILS
CN4
D. altera
RADIOLARIANS
Cheirosiphonia frenguelliana
DIATOMS
FOSSIL CHARACTER
SECTION
METERS
GRAPHIC LITHOLOGY
DRILLING DISTURBANCE
SEDIMENTARY STRUCTURES
SAMPLES
LITHOLOGIC DESCRIPTION
GREEN WHITE OOZE/CHALK (SUBUNIT IIA)
SMEAR SLIDE SUMMARY (%)
2, 105
CARBONATE BOMB

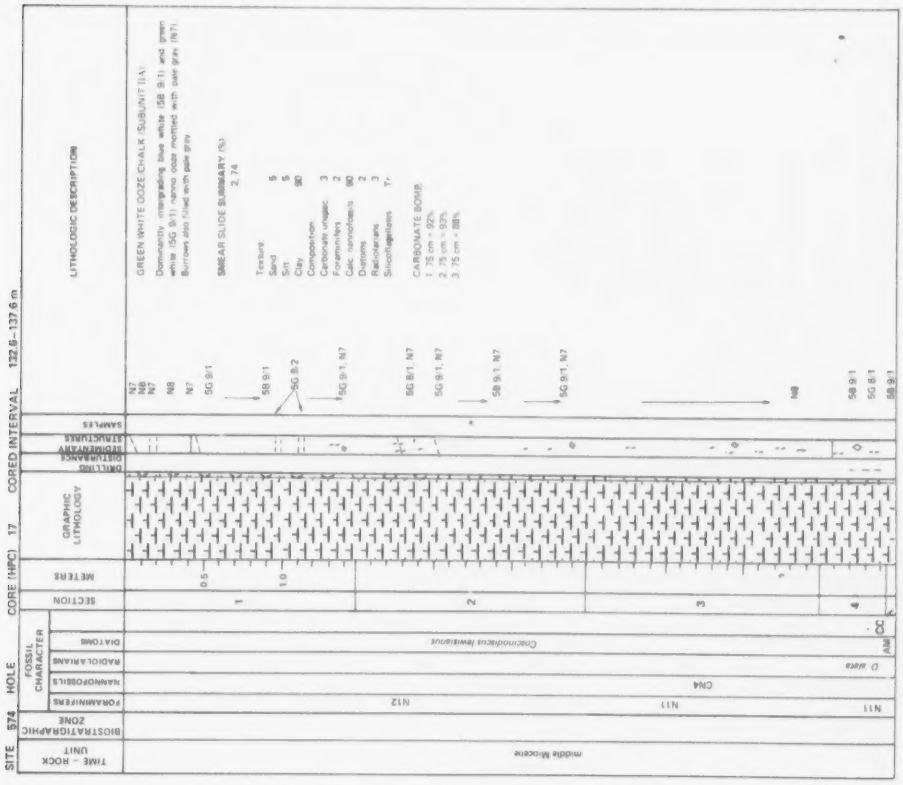
SITE 574
HOLE
CORE (HPC) 17
CORED INTERVAL 132.8–137.6 m
TIME – ROCK UNIT
middle Miocene
BIOSTRATIGRAPHIC ZONE
FORAMINIFERS
N11
N12
NANNOFOSSILS
CN4
D. altera
RADIOLARIANS
Cheirosiphonia frenguelliana
DIATOMS
FOSSIL CHARACTER
SECTION
METERS
GRAPHIC LITHOLOGY
DRILLING DISTURBANCE
SEDIMENTARY STRUCTURES
SAMPLES
LITHOLOGIC DESCRIPTION
GREEN WHITE OOZE/CHALK (SUBUNIT IIA)
SMEAR SLIDE SUMMARY (%)
2, 74
CARBONATE BOMB

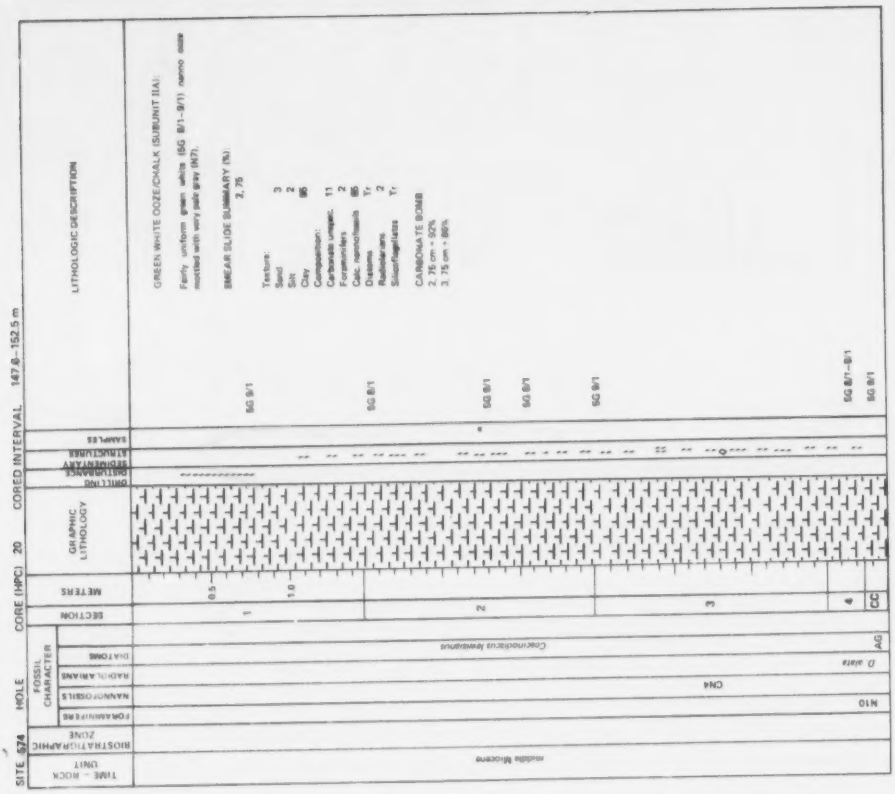
SITE 574 HOLE CORE (HPC) 20 CORED INTERVAL 147.6–152.5 m
TIME – ROCK UNIT
BIOSTRATIGRAPHIC ZONE
FOSSIL CHARACTER
FORAMINIFERS
NANNOFOSSILS
RADIOLARIANS
DIATOMS
SECTION
METERS
GRAPHIC LITHOLOGY
DRILLING DISTURBANCE
SEDIMENTARY STRUCTURES
SAMPLES
LITHOLOGIC DESCRIPTION
middle Miocene
N10
CN4
D. altaria
Coscinodiscus lewisianus
GREEN WHITE OOZE/CHALK (SUBUNIT IIA):
Fairly uniform green white (5G 8/1–8/1) nanno mare mottled with very pale gray (N7).
SMEAR SLIDE SUMMARY (%)
2, 75
Texture:
Sand 3
Silt 2
Clay 95
Composition:
Carbonate unspec. 11
Foraminifers 2
Calc. nannofossils 85
Diatoms Tr
Radiolarians 2
Siliceous fragments Tr
CARBONATE BOMB
2, 75 cm = 92%
3, 75 cm = 88%
5G 8/1
5G 8/1–8/1

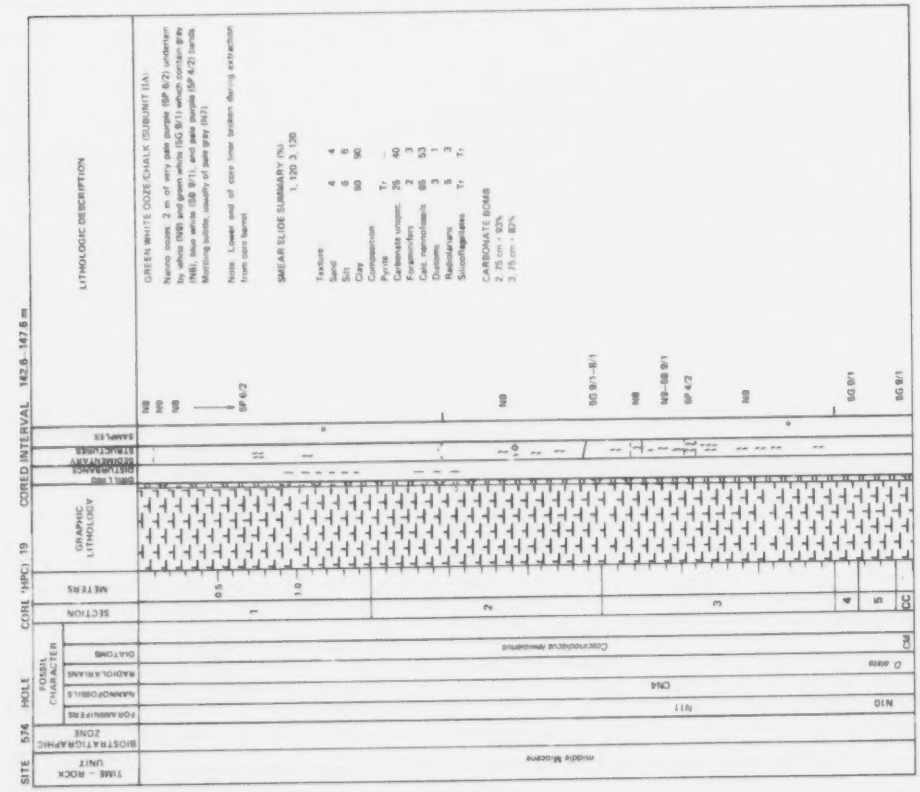
SITE 574 HOLE CORE (HPC) 19 CORED INTERVAL 142.6–147.6 m
TIME – ROCK UNIT
BIOSTRATIGRAPHIC ZONE
FOSSIL CHARACTER
FORAMINIFERS
NANNOFOSSILS
RADIOLARIANS
DIATOMS
SECTION
METERS
GRAPHIC LITHOLOGY
DRILLING DISTURBANCE
SEDIMENTARY STRUCTURES
SAMPLES
LITHOLOGIC DESCRIPTION
middle Miocene
N10
N11
CN4
D. altaria
Coscinodiscus lewisianus
GREEN WHITE OOZE/CHALK (SUBUNIT IIA):
Nanno ooze, 2 m of very pale purple (5P 6/2) underlain by white (N9) and green white (5G 8/1) which contain gray (N5), blue white (5B 8/1), and pale purple (5P 4/2) bands. Mottling burrow, caudry of pale gray (N7).
Note: Lower end of core liner broken during extraction from core barrel.
SMEAR SLIDE SUMMARY (%)
1, 120 3, 120
Texture
Sand 4 4
Silt 6 6
Clay 90 90
Composition
Pyrite Tr –
Carbonate unspec. 75 40
Foraminifers 2 3
Calc. nannofossils 68 53
Diatoms 3 1
Radiolarians 5 3
Siliceous fragments Tr Tr
CARBONATE BOMB
2, 75 cm = 93%
3, 75 cm = 82%
5P 6/2
N9
5G 8/1–8/1
5B 8/1
5G 8/1

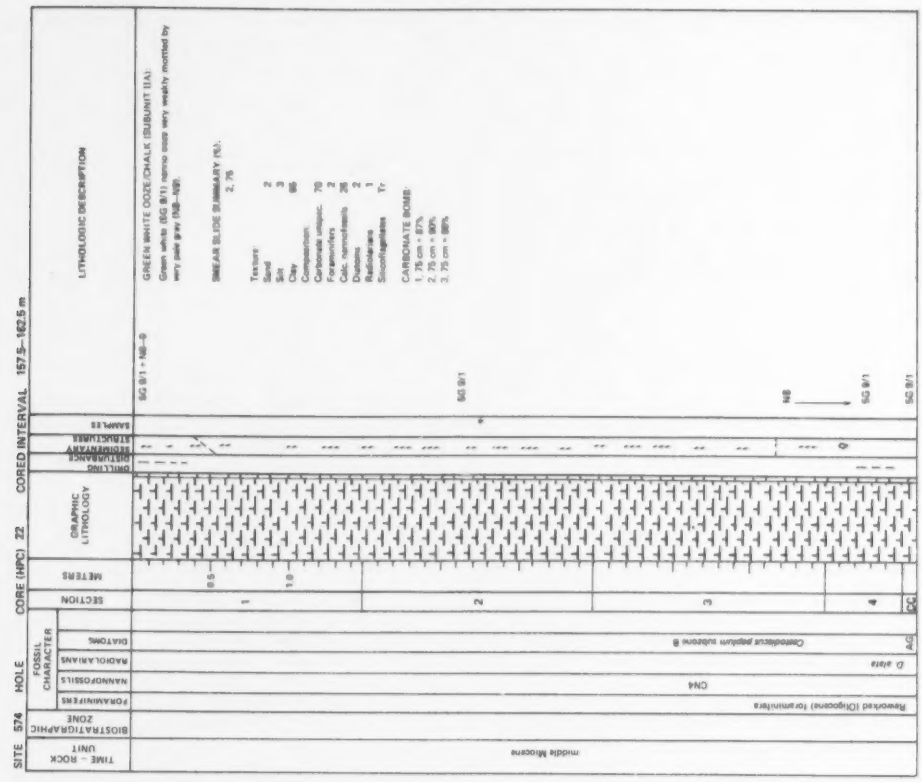
SITE 574
HOLE
CORE (HPC) 22
CORED INTERVAL 157.5–162.5 m
TIME – ROCK UNIT
middle Miocene
BIOSTRATIGRAPHIC ZONE
Reworked Oligocene) foraminifera
CN4
D. altiria
Catostelleus pelphim sustorne B
SG
FORAMINIFERS
NANNOFOSSILS
RADIOLARIANS
DIATOMS
FOSSIL CHARACTER
SECTION
METERS
GRAPHIC LITHOLOGY
DRILLING DISTURBANCE
SEDIMENTARY STRUCTURES
SAMPLES
LITHOLOGIC DESCRIPTION
SG 8/1 + N8–9
GREEN WHITE OOZE/CHALK (SUBUNIT IIA)
Green white (5G 8/1) nanno ooze very weakly mottled by very pale grey (N8–N9).
SMEAR SLIDE SUMMARY (%):
2, 75
Texture:
Sand 2
Silt 3
Clay 95
Composition:
Carbonate unspec. 70
Foraminifers 2
Calc nannofossils 26
Diatoms 2
Radiolarians 1
Sinicoflagellates Tr
CARBONATE BOMB:
1, 75 cm = 87%
2, 75 cm = 90%
3, 75 cm = 89%
SG 8/1
N8
SG 8/1
SG 8/1
1
2
3
4
CC

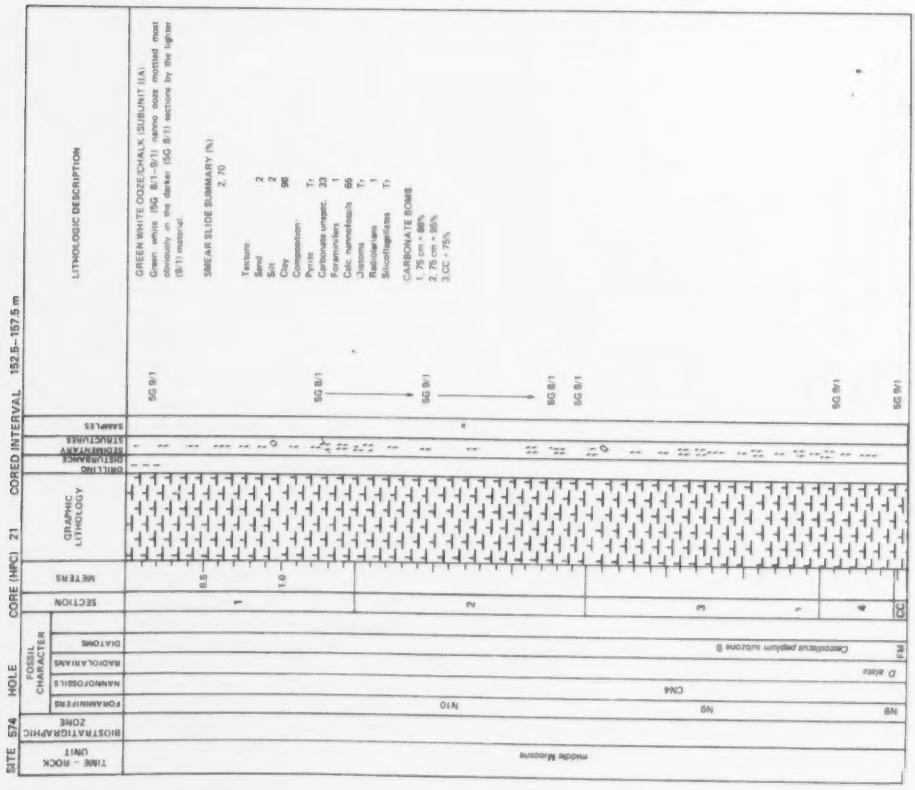
SITE 574
HOLE
CORE (HPC) 21
CORED INTERVAL 152.5–157.5 m
TIME – ROCK UNIT
middle Miocene
BIOSTRATIGRAPHIC ZONE
N8
N9
N10
CN4
D. altiria
Catostelleus pelphim sustorne B
FM
FORAMINIFERS
NANNOFOSSILS
RADIOLARIANS
DIATOMS
FOSSIL CHARACTER
SECTION
METERS
GRAPHIC LITHOLOGY
DRILLING DISTURBANCE
SEDIMENTARY STRUCTURES
SAMPLES
LITHOLOGIC DESCRIPTION
SG 8/1
GREEN WHITE OOZE/CHALK (SUBUNIT IIA)
Green white (5G 8/1–8/1) nanno ooze mottled most obviously in the darker (5G 8/1) sections by the lighter (8/1) material.
SMEAR SLIDE SUMMARY (%):
2, 70
Texture:
Sand 2
Silt 2
Clay 96
Composition:
Pyrite Tr
Carbonate unspec. 33
Foraminifers 1
Calc nannofossils 66
Diatoms Tr
Radiolarians 1
Sinicoflagellates Tr
CARBONATE BOMB
1, 75 cm = 88%
2, 75 cm = 86%
3, CC = 75%
SG 8/1
SG 8/1
SG 8/1
SG 8/1
SG 8/1
SG 8/1
1
2
3
4
CC

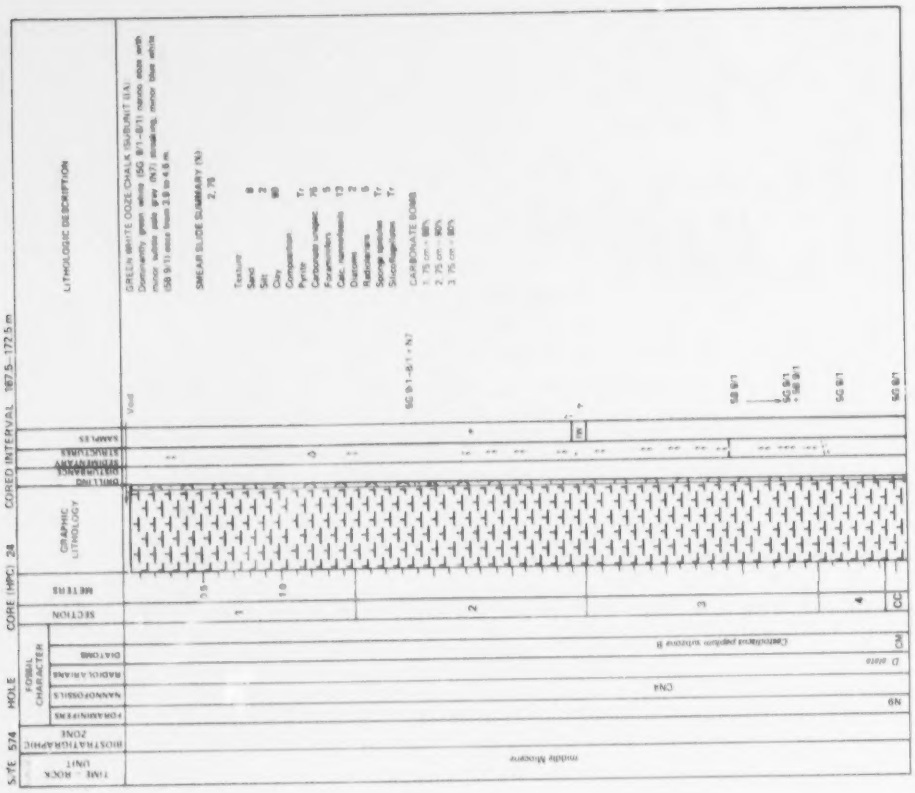

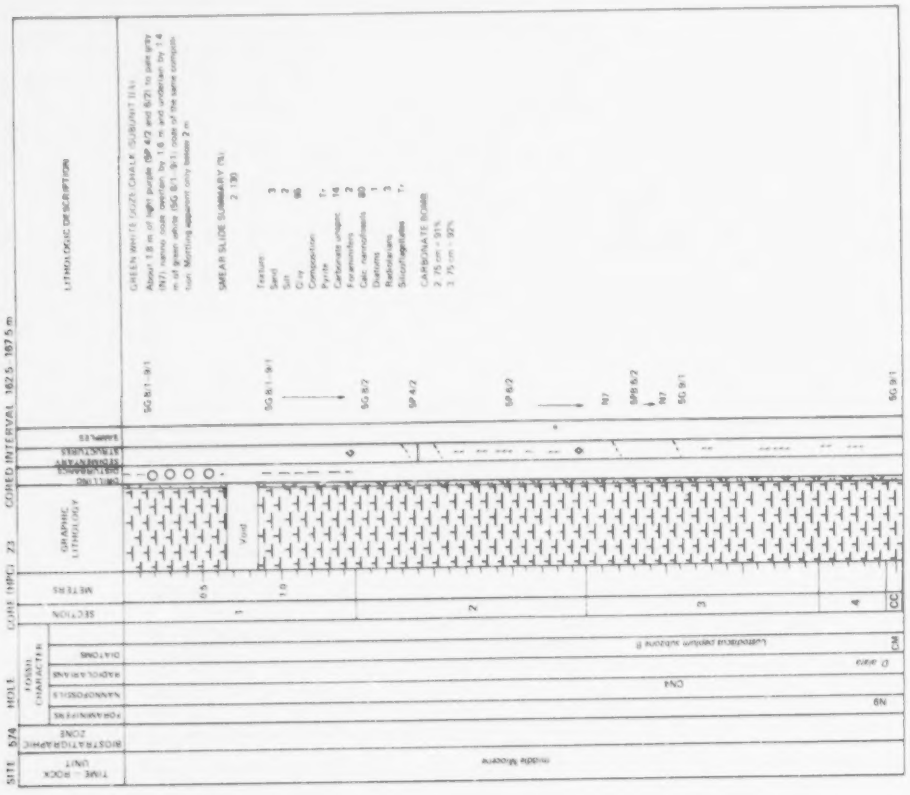

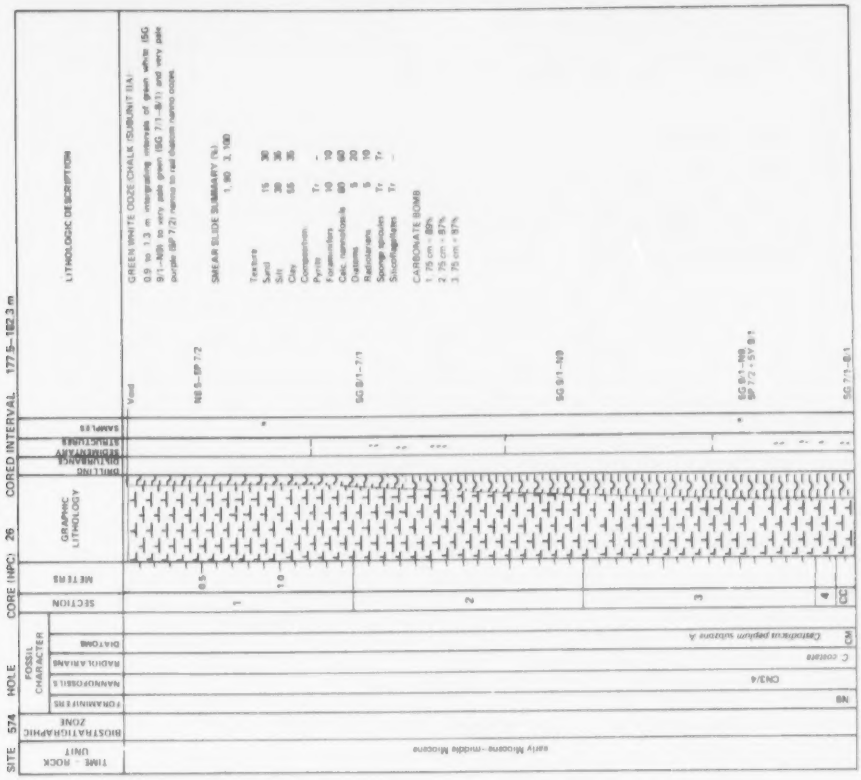
SITE 574 HOLE CORE (HPC) 26 CORED INTERVAL 177.5–182.3 m
TIME – ROCK UNIT
BIOSTRATIGRAPHIC ZONE
FOSSIL CHARACTER
FORAMINIFERS
NANNOFOSSILS
RADIOLARIANS
DIATOMS
SECTION
METERS
GRAPHIC LITHOLOGY
DRILLING DISTURBANCE
SEDIMENTARY STRUCTURES
SAMPLES
LITHOLOGIC DESCRIPTION
early Miocene–middle Miocene
NN
CN3/4
C. coalita
Cestodiscus peplum subzone A
CM
SECTION
METERS
GRAPHIC LITHOLOGY
SAMPLES
LITHOLOGIC DESCRIPTION
Void
GREEN WHITE OOZE CHALK (SUBUNIT IIA)
0.9 to 1.3 m intergrading intervals of green white (5G 8/1–N9) to very pale green (5G 7/1–8/1) and very pale purple (5P 7/2) nanno to rad diatom nanno oozes
SMEAR SLIDE SUMMARY (%)
1, 80 3, 100
Texture
Sand 15 30
Silt 30 35
Clay 55 35
Composition
Pyrite Tr –
Foraminifers 10 10
Calc. nannofossils 85 60
Diatoms 5 20
Radiolarians 5 10
Sponge spicules Tr Tr
Silicoflagellates Tr –
CARBONATE BOMB
1. 75 cm = 89%
2. 75 cm = 87%
3. 75 cm = 87%
5G 8/1–N9
N9
5G 8/1–7/1
5G 8/1–N9
5G 8/1–N9
5P 7/2–5Y 8/1
5G 7/1–8/1

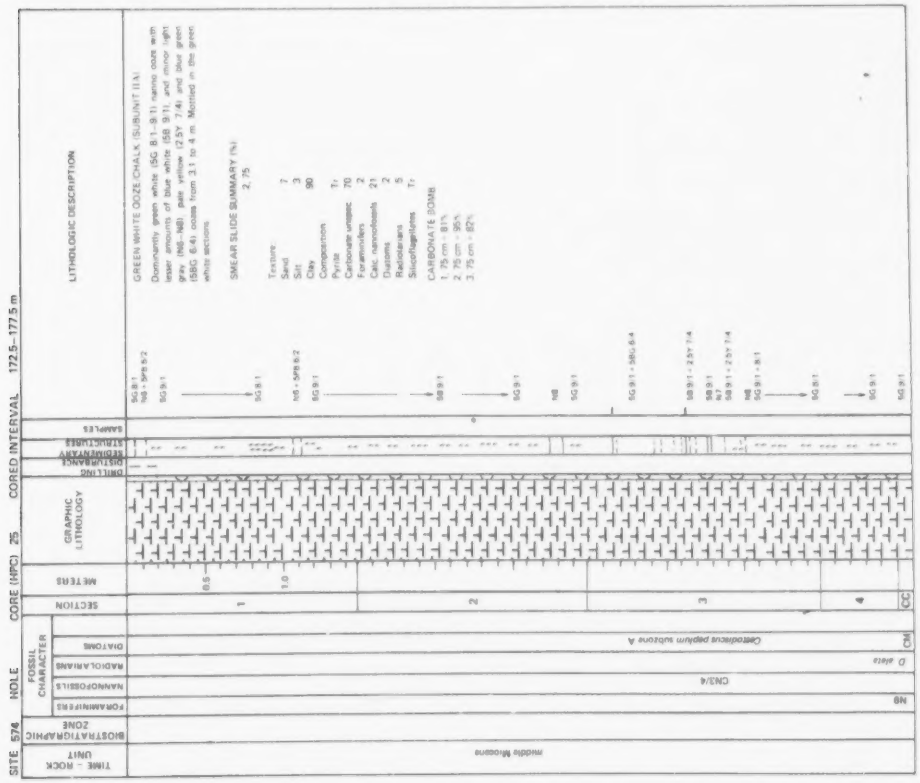
SITE 574 HOLE CORE (HPC) 25 CORED INTERVAL 172.5–177.5 m
TIME – ROCK UNIT
BIOSTRATIGRAPHIC ZONE
FOSSIL CHARACTER
FORAMINIFERS
NANNOFOSSILS
RADIOLARIANS
DIATOMS
SECTION
METERS
GRAPHIC LITHOLOGY
DRILLING DISTURBANCE
SEDIMENTARY STRUCTURES
SAMPLES
LITHOLOGIC DESCRIPTION
middle Miocene
NN
CN3/4
D. altaia
Cestodiscus peplum subzone A
CM
SECTION
METERS
GRAPHIC LITHOLOGY
SAMPLES
LITHOLOGIC DESCRIPTION
GREEN WHITE OOZE CHALK (SUBUNIT IIA)
Dominantly green white (5G 8/1–9/1) nanno ooze with lesser amounts of blue white (5B 9/1), and minor light gray (N5–N8), pale yellow (2.5Y 7/4) and blue green (5BG 6/4) oozes from 3.1 to 4 m. Mottled in the green white sections
SMEAR SLIDE SUMMARY (%)
2, 75
Texture
Sand 7
Silt 3
Clay 90
Composition
Pyrite Tr
Carbonate unspec 70
Foraminifers 2
Calc. nannofossils 21
Diatoms 2
Radiolarians 5
Silicoflagellates Tr
CARBONATE BOMB
1. 75 cm = 81%
2. 75 cm = 95%
3. 75 cm = 82%
5G 8/1
N5 – 5PB 8/2
5G 8/1
5G 8/1
N5 – 5PB 8/2
5G 8/1
5G 8/1
N8
5G 8/1
5G 8/1 – 5BG 6/4
5G 8/1 – 2.5Y 7/4
5B 8/1
5G 8/1 – 2.5Y 7/4
N8
5G 8/1 – 8/1
5G 8/1
5G 8/1
5G 8/1

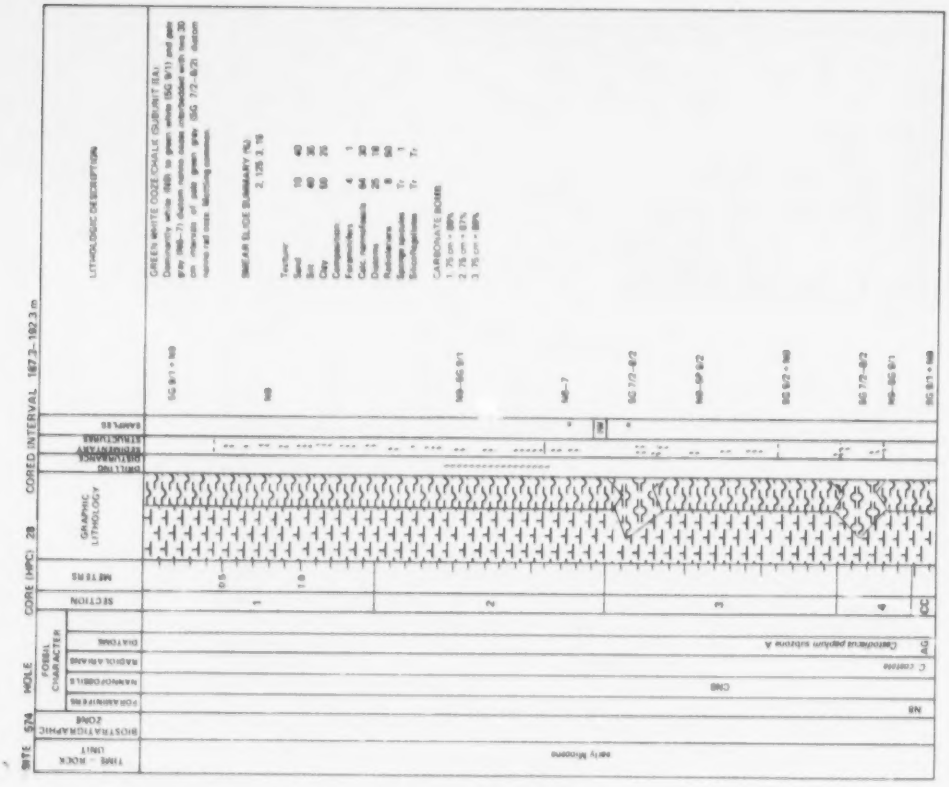

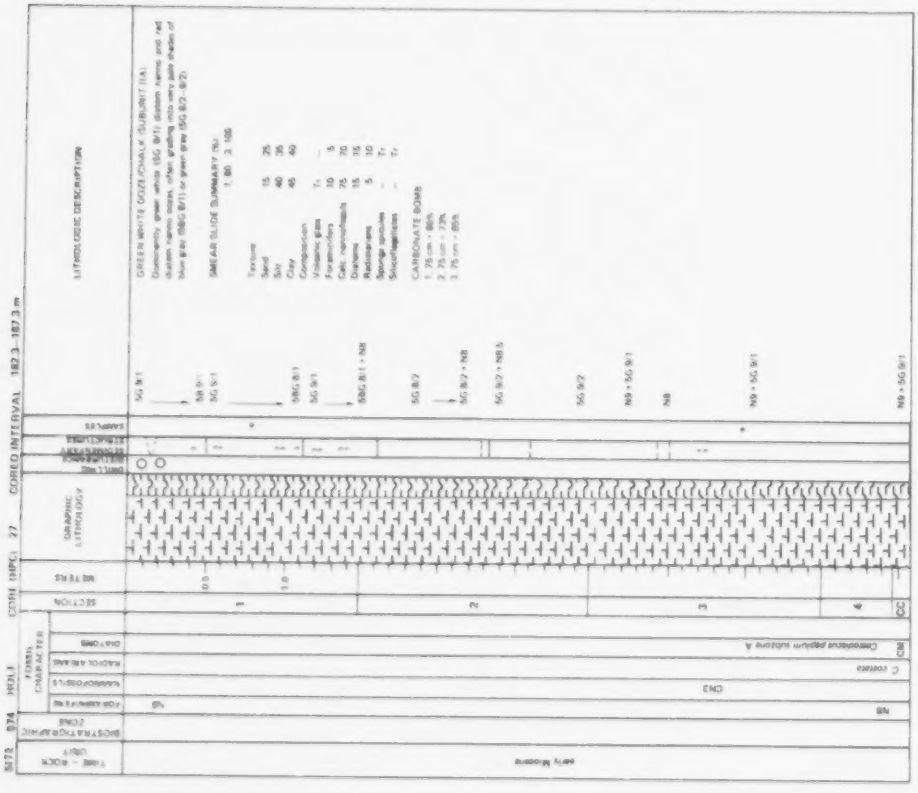

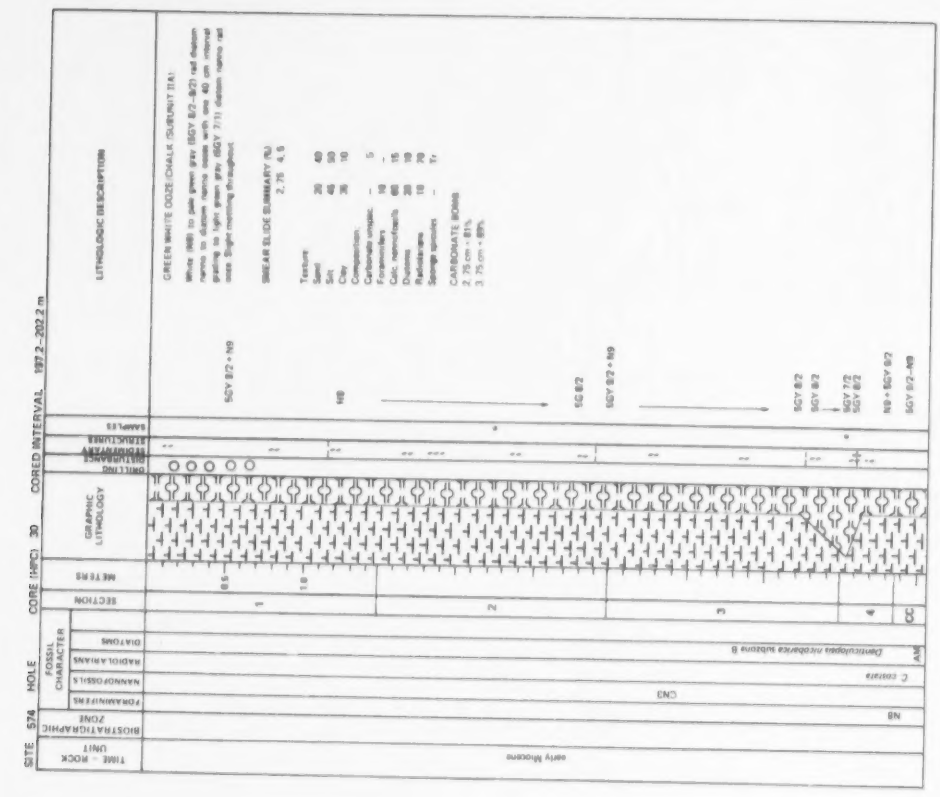
SITE 574
HOLE
CORE (HPC) 30
CORED INTERVAL 197.2–202.2 m
TIME – ROCK UNIT
early Miocene
BIOSTRATIGRAPHIC ZONE
NB
FORAMINIFERS
CN3
NANNOFOSSILS
C. coronata
RADIOLARIANS
Dictyocoptis nicobarica subzone B
DIATOMS
SECTION
1
2
3
4
CC
METERS
0.5
1.0
GRAPHIC LITHOLOGY
DRILLING DISTURBANCE
SEDIMENTARY STRUCTURES
SAMPLES
LITHOLOGIC DESCRIPTION
GREEN WHITE OOZE CHALK (SUBUNIT IIA)
SMEAR SLIDE SUMMARY (%)
2, 75 4, 5
Texture:
Sand 20 60
Silt 40 30
Clay 35 10
Composition:
Carbonate unspec. – 5
Foraminifers – 15
Calc. nannofossils 65 10
Diatoms 25 70
Radiolarians 10 –
Sponge spicules – Tr
CARBONATE BOMB
2, 75 cm = 81%
3, 75 cm = 85%
5GY 8/2 + N9
N9
5G 8/2
5GY 8/2 + N9
5GY 8/2
5GY 7/2
5GY 8/2
N9 + 5GY 8/2
5GY 8/2–N9

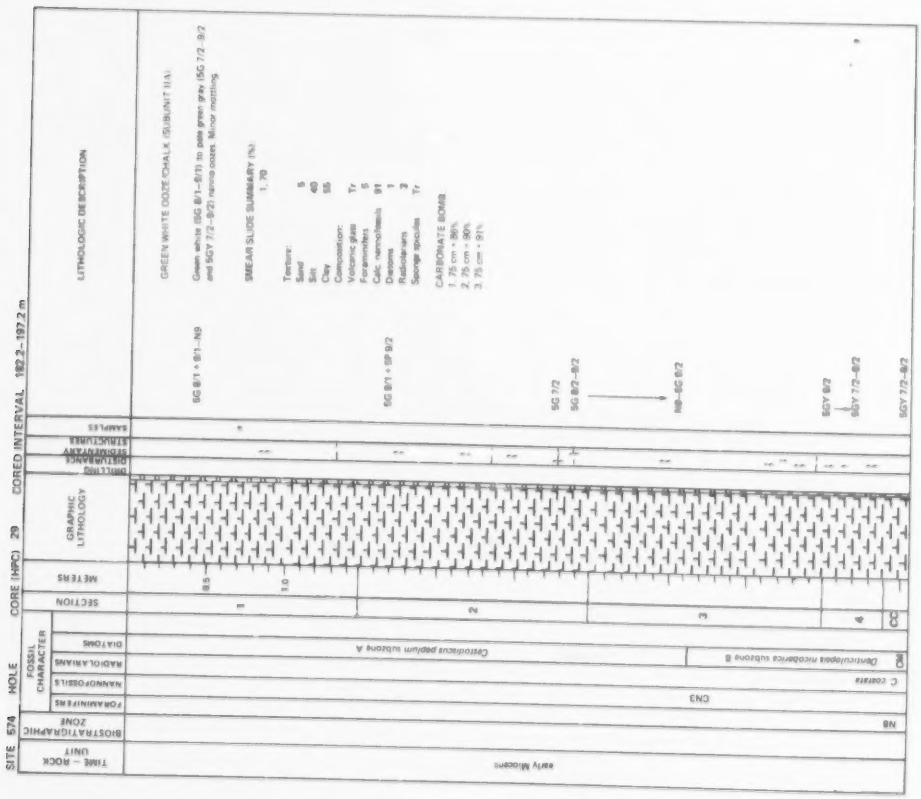
SITE 574
HOLE
CORE (HPC) 29
CORED INTERVAL 182.2–187.2 m
TIME – ROCK UNIT
early Miocene
BIOSTRATIGRAPHIC ZONE
NB
FORAMINIFERS
CN3
NANNOFOSSILS
C. coronata
RADIOLARIANS
Dictyocoptis nicobarica subzone B
Cestodiscus peplum subzone A
RP
DIATOMS
SECTION
1
2
3
4
CC
METERS
0.5
1.0
GRAPHIC LITHOLOGY
DRILLING DISTURBANCE
SEDIMENTARY STRUCTURES
SAMPLES
LITHOLOGIC DESCRIPTION
GREEN WHITE OOZE CHALK (SUBUNIT IIA)
Green white (5G 8/1–8/2) to pale green gray (5G 7/2–8/2 and 5GY 7/2–8/2) nanno oozes. Minor mottling
SMEAR SLIDE SUMMARY (%)
1, 70
Texture:
Sand 5
Silt 40
Clay 55
Composition:
Volcanic glass Tr
Foraminifers 5
Calc. nannofossils 91
Diatoms 1
Radiolarians 3
Sponge spicules Tr
CARBONATE BOMB
1, 75 cm = 96%
2, 75 cm = 90%
3, 75 cm = 91%
5G 8/1 + 8/1–N9
5G 8/1 + 8P 8/2
5G 7/2
5G 8/2–8/2
N9–5G 8/2
5GY 8/2
5GY 7/2–8/2
5GY 7/2–8/2

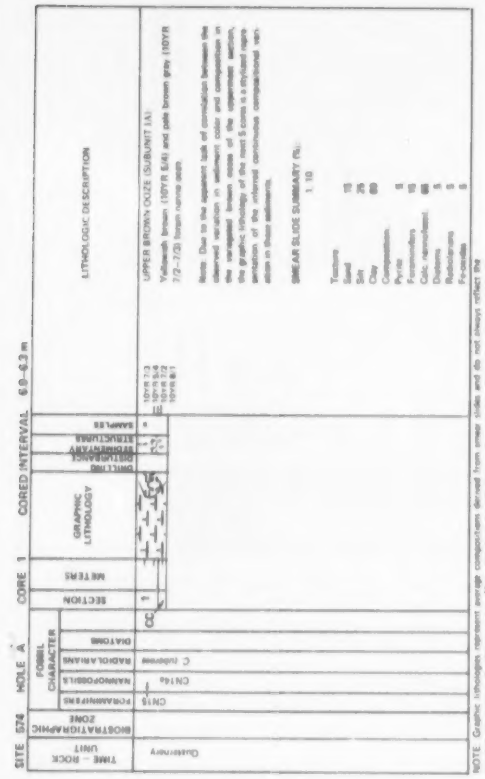
SITE 574
HOLE A
CORE 1
CORED INTERVAL 6.0–6.3 m
TIME – ROCK UNIT
Quaternary
BIOSTRATIGRAPHIC ZONE
CN15
FOSSIL CHARACTER
FORAMINIFERS
NANNOFOSSILS
CN15
CN14a
RADIOLARIANS
C. indosinai
DIATOMS
SECTION
CC
METERS
GRAPHIC LITHOLOGY
DRILLING DISTURBANCE
SEDIMENTARY STRUCTURES
SAMPLES
LITHOLOGIC DESCRIPTION
UPPER BROWN OOZE (SUBUNIT 1A)
10YR 7/3
10YR 5/4
10YR 7/2
10YR 6/1
Yellowish brown (10YR 5/4) and pale brown grey (10YR 7/2–7/3) foram nanno ooze
Note: Due to the apparent lack of correlation between the dominant lithology of the core catcher section in the interval between bottom of the grid and bottom of the graphic lithology of the next 5 cores is a stylized representation of the inferred continuous compositional variation in these sediments.
SMEAR SLIDE SUMMARY (%):
1, 10
Texture
Sand 15
Silt 25
Clay 60
Composition
Forams 5
Nannofossils 15
Calc. nannofossil 65
Diatoms 5
Radiolarians 5
Foraminifera 5
NOTE: Graphic lithologies represent average compositions derived from smear slides and do not always reflect the detailed alternation of sediment types. Major lithologic boundaries are shown but gradational contacts, small scale cyclicity and ooze-chalk alternations are represented schematically. Color changes approximate to lithologic changes.

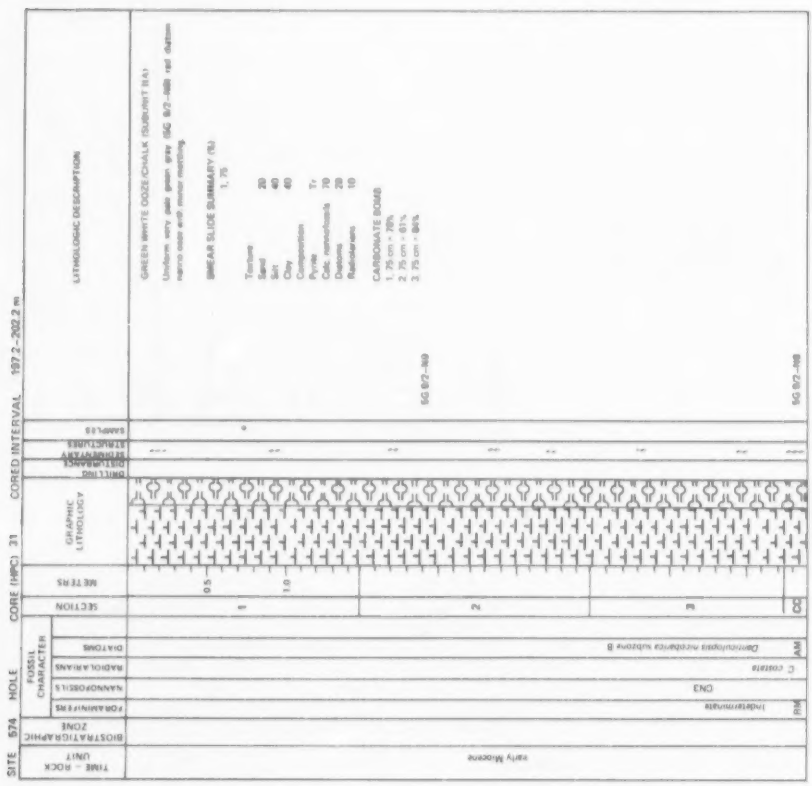
SITE 574
HOLE
CORE (HPC) 31
CORED INTERVAL 197.2–202.2 m
TIME – ROCK UNIT
early Miocene
BIOSTRATIGRAPHIC ZONE
FOSSIL CHARACTER
FORAMINIFERS
Globigerinoides
NANNOFOSSILS
CN2
RADIOLARIANS
C. costata
DIATOMS
Denticulopsis nicobarica–kolbeyi B
SECTION
METERS
GRAPHIC LITHOLOGY
DRILLING DISTURBANCE
SEDIMENTARY STRUCTURES
SAMPLES
LITHOLOGIC DESCRIPTION
GREEN WHITE OOZE/CHALK (SUBUNIT 3A)
Uniform very pale green grey (5G 8/2–N8) red clayton nanno ooze with minor mottling
SMEAR SLIDE SUMMARY (%):
1, 75
Texture
Sand 20
Silt 40
Clay 40
Composition
Pyrite Tr
Calc. nannofossils 70
Diatoms 20
Radiolarians 10
CARBONATE BOMB
1.75 cm = 78%
2.75 cm = 81%
3.75 cm = 84%
5G 8/2–N8
5G 8/2–N8

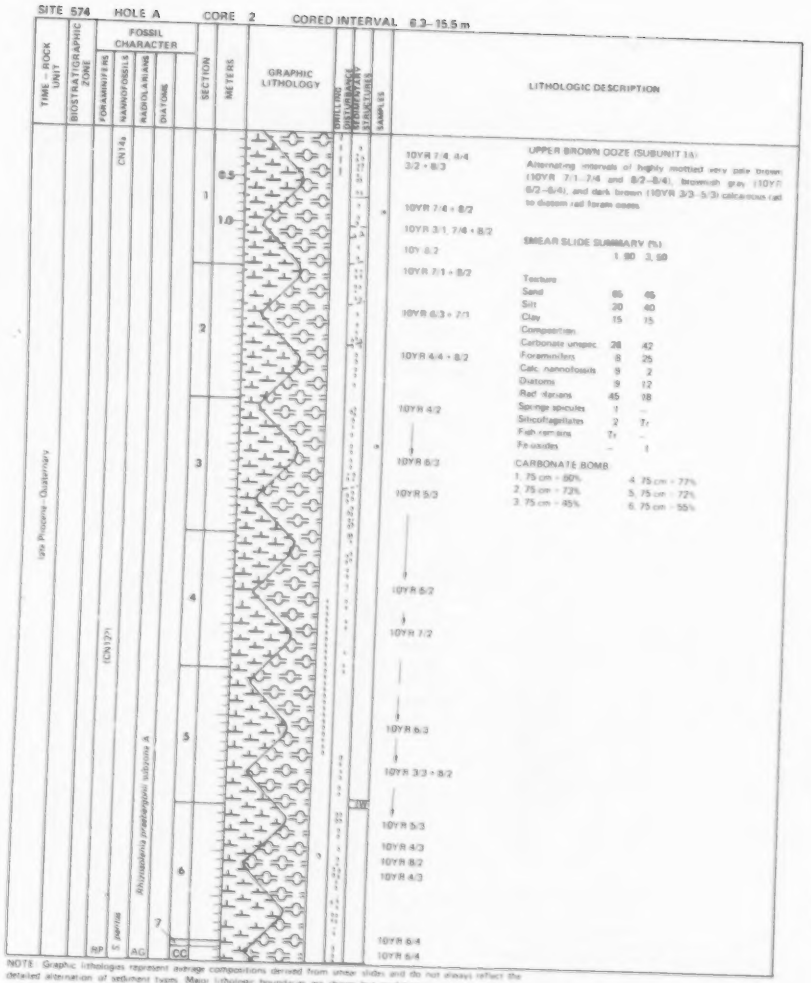

NOTE: Graphic lithologies represent average compositions derived from smear slides and do not always reflect the detailed alternation of sediment types. Major lithologic boundaries are shown but gradational contacts, small-scale cyclicity and ooze-chalk alternations are represented schematically. Color changes approximate to lithologic changes.

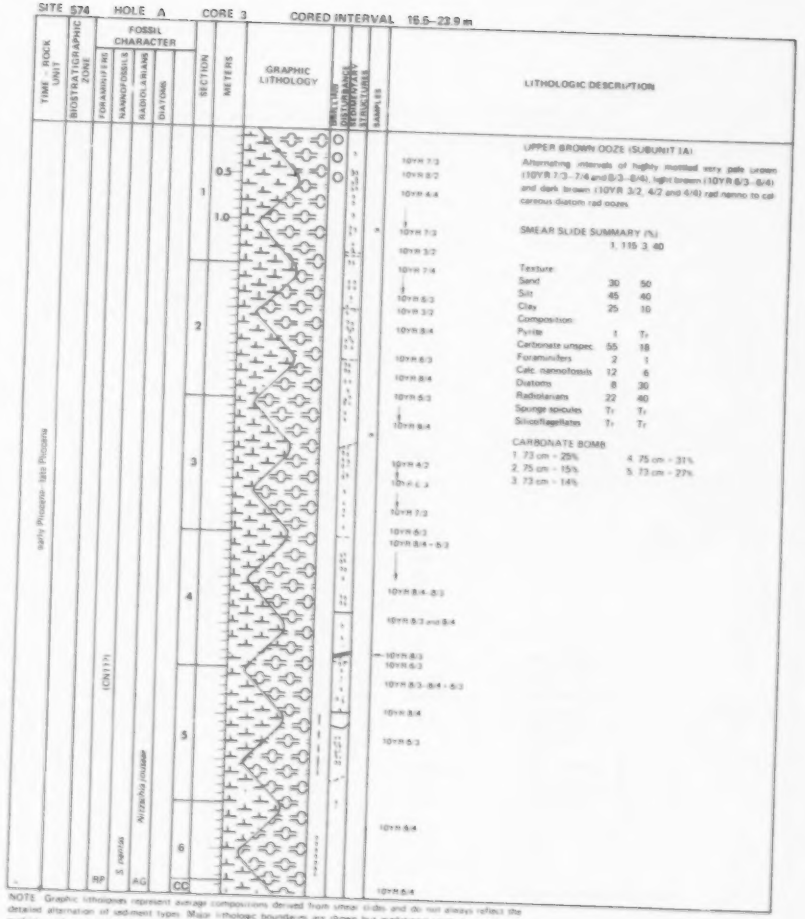

NOTE: Graphic lithologies represent average compositions derived from smear slides and do not always reflect the detailed alternation of sediment types. Major lithologic boundaries are shown but gradational contacts, small-scale cyclicity and ooze-chalk alternations are represented schematically. Color changes approximate to lithologic changes.

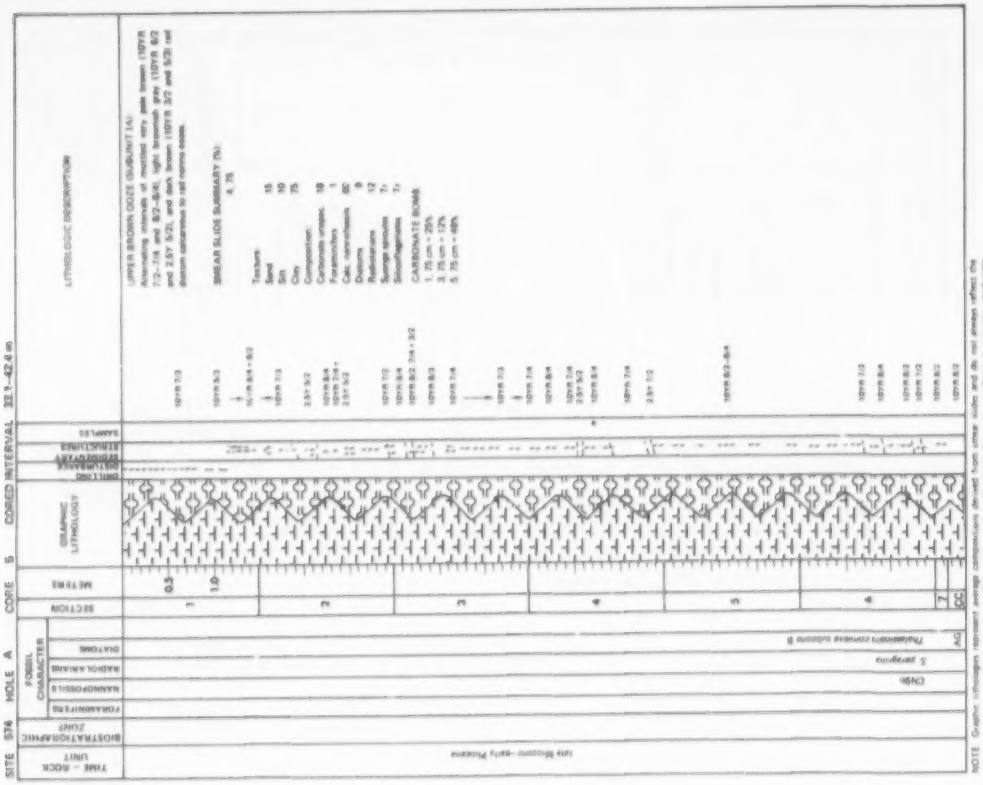

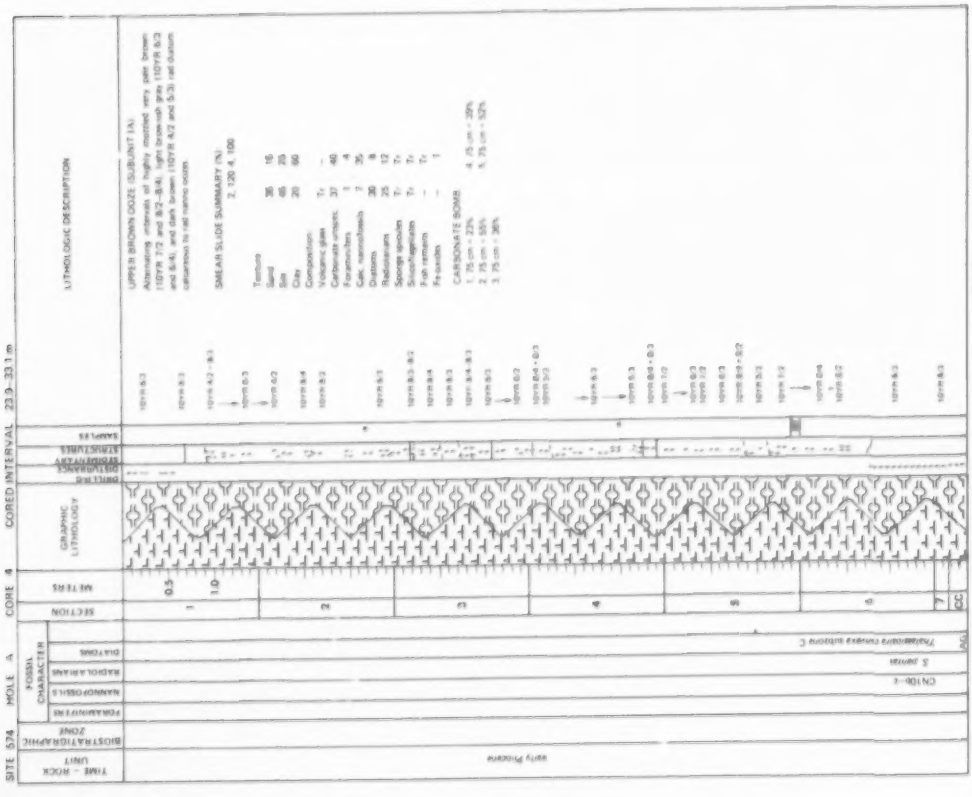

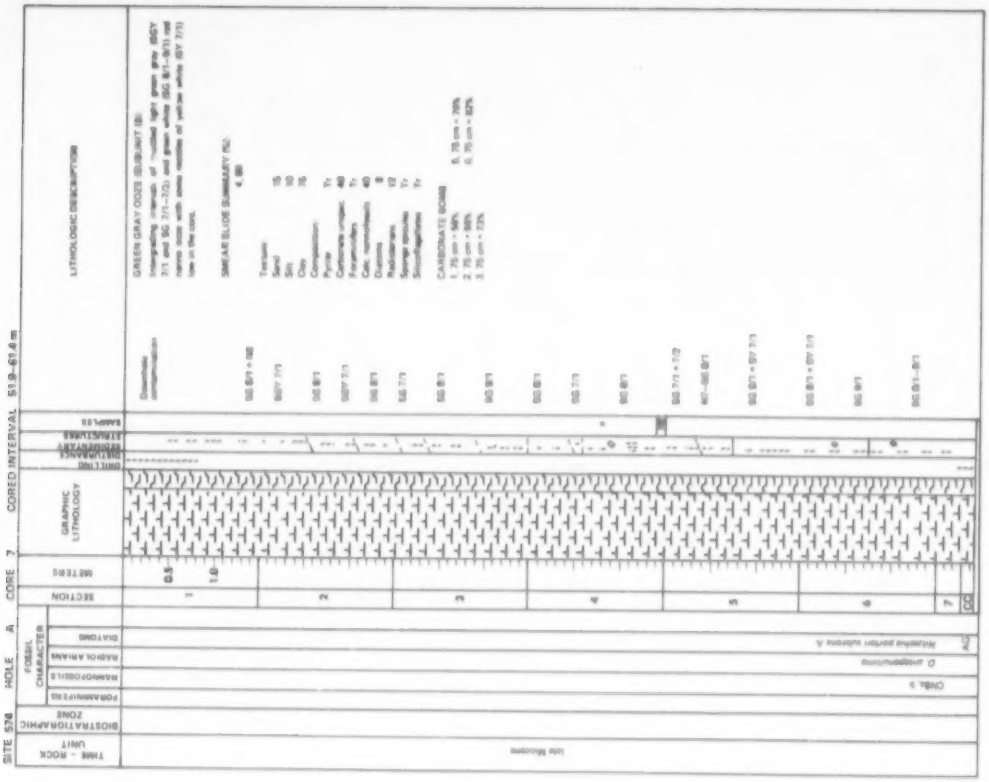

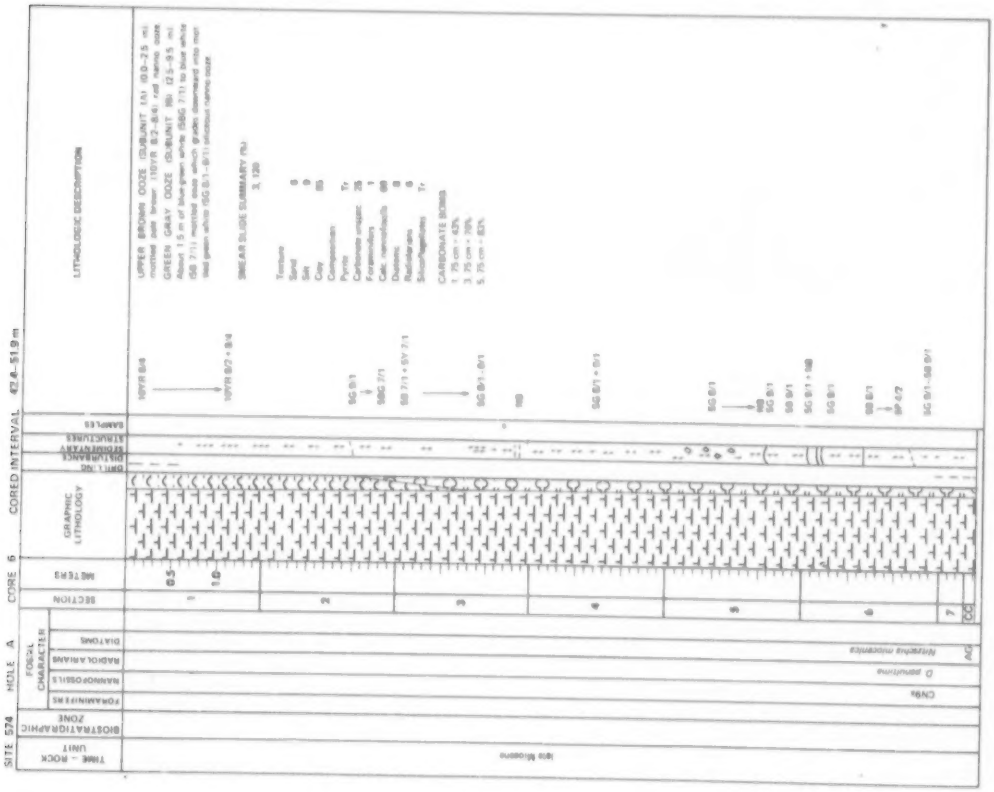

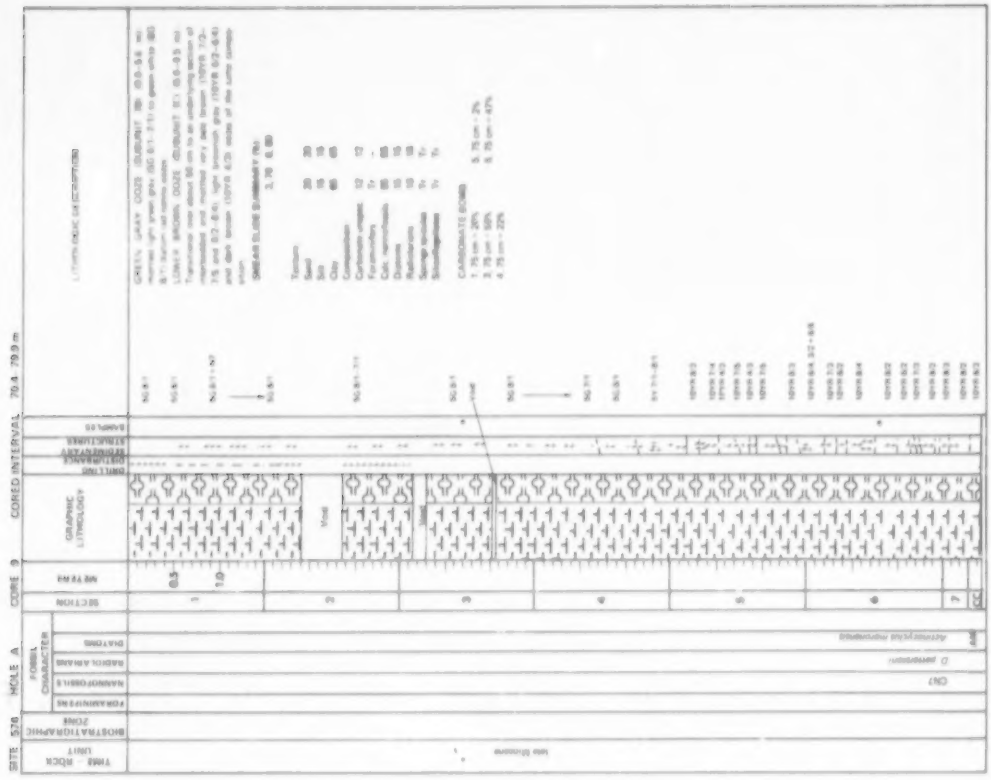

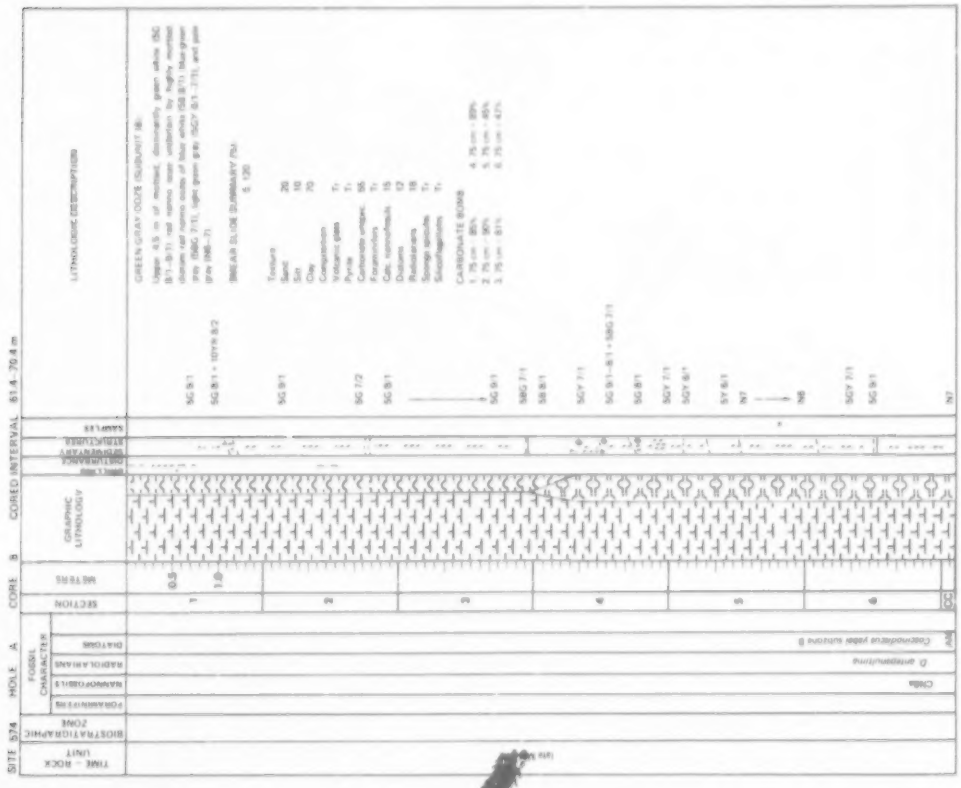

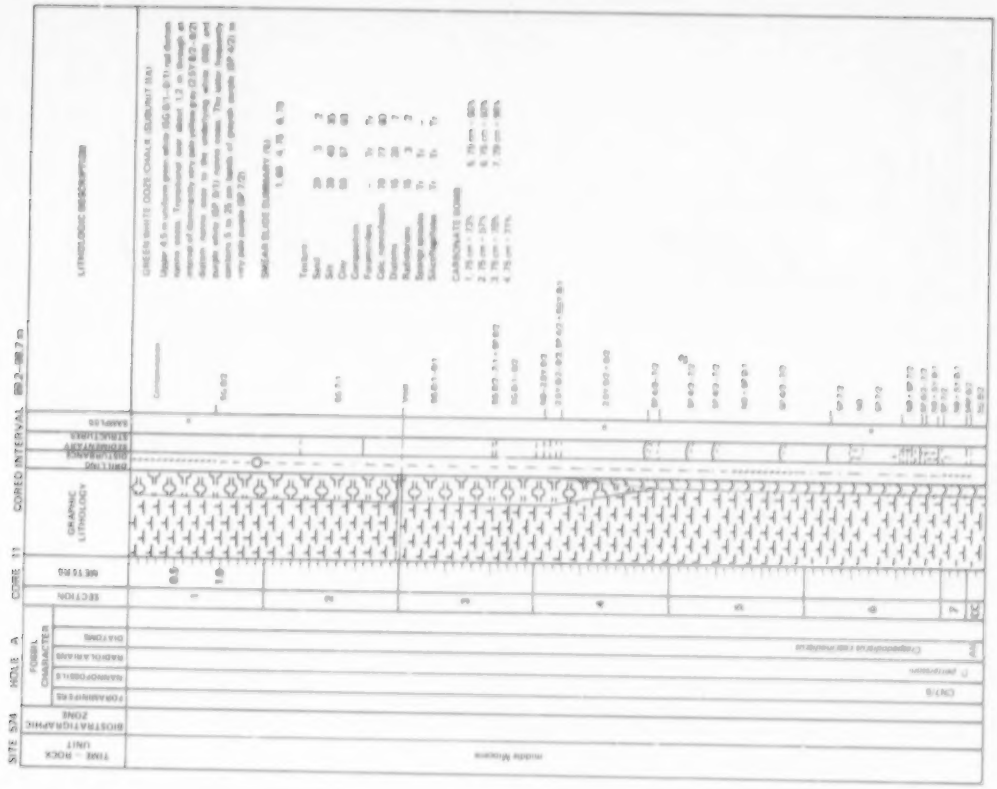

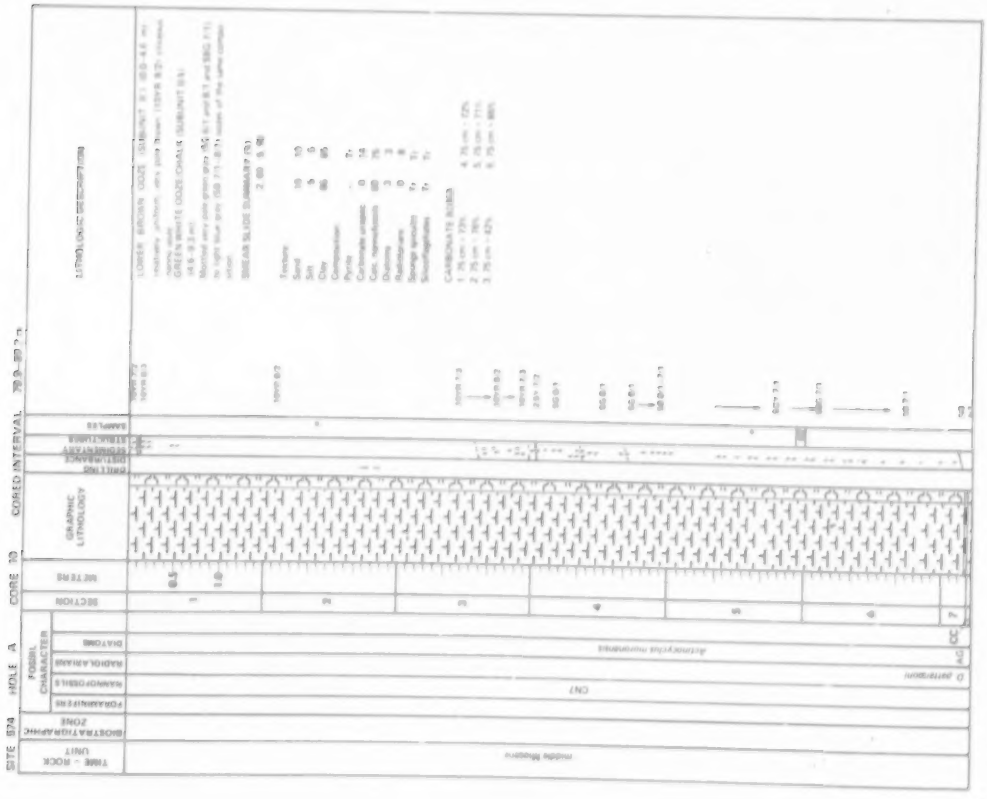

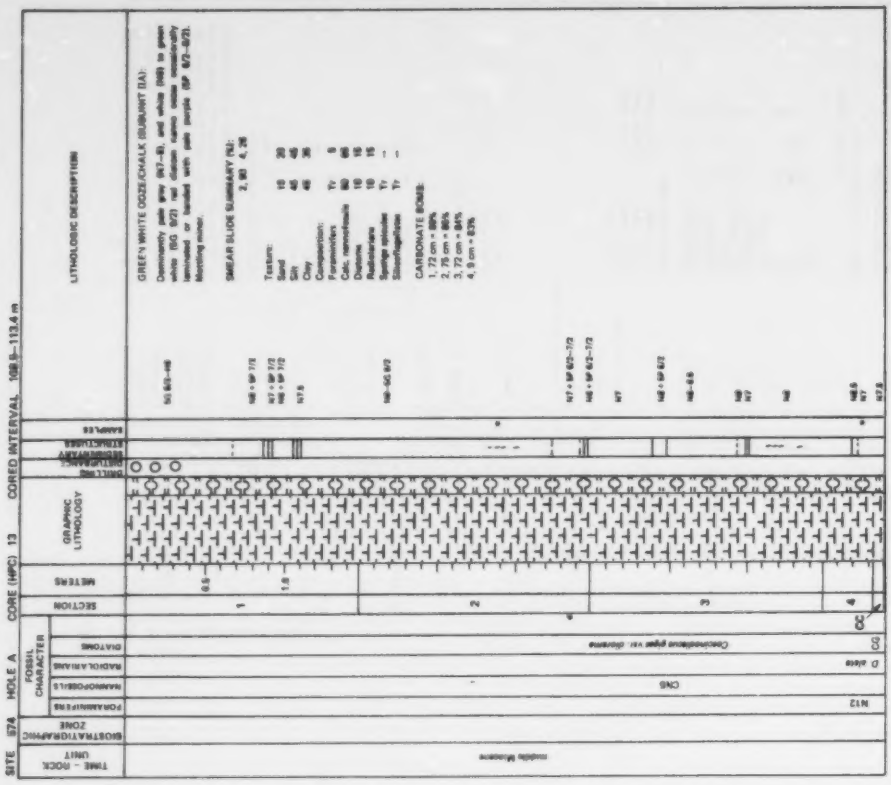

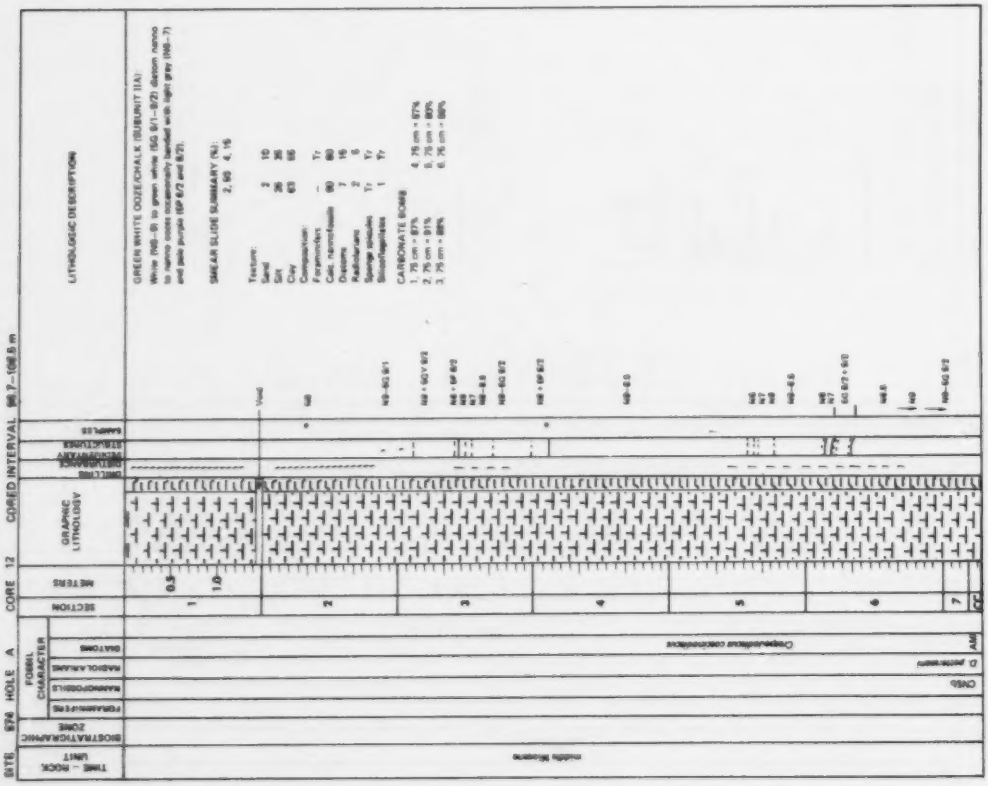

READEX FICHE
best copy available

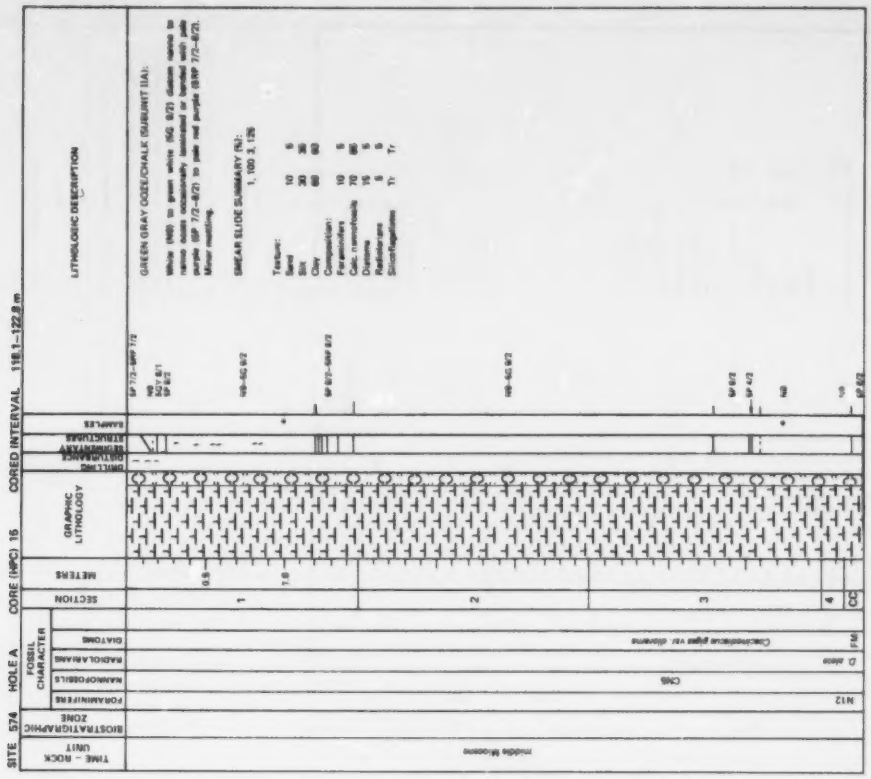

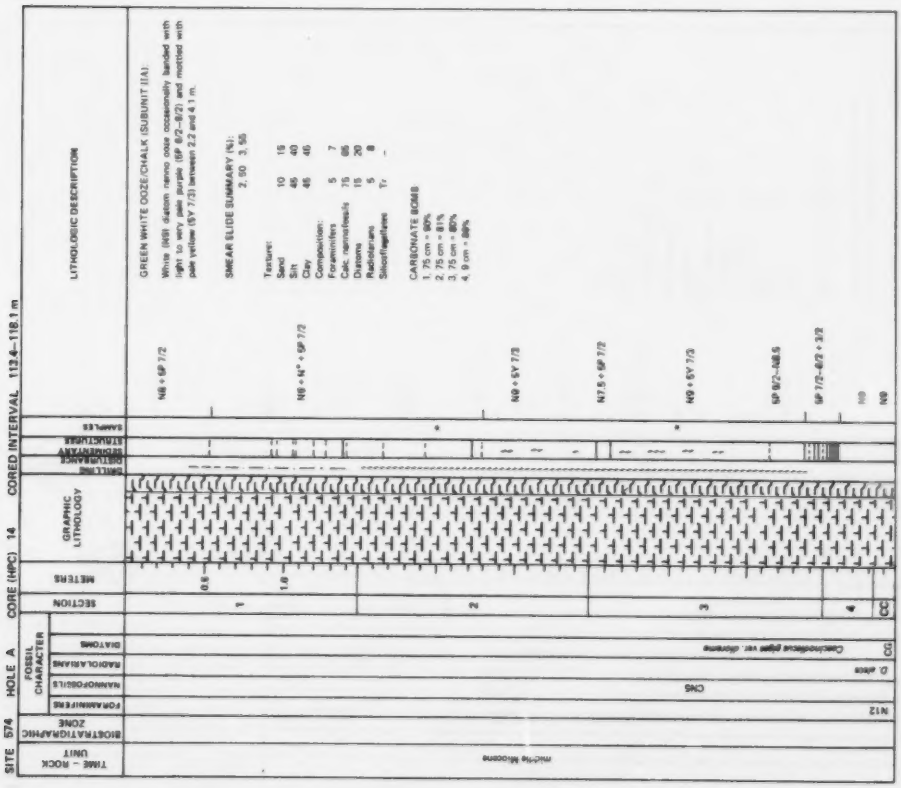

SITE 574 HOLE A CORE (HPC) 16 CORED INTERVAL 122.8–127.8 m

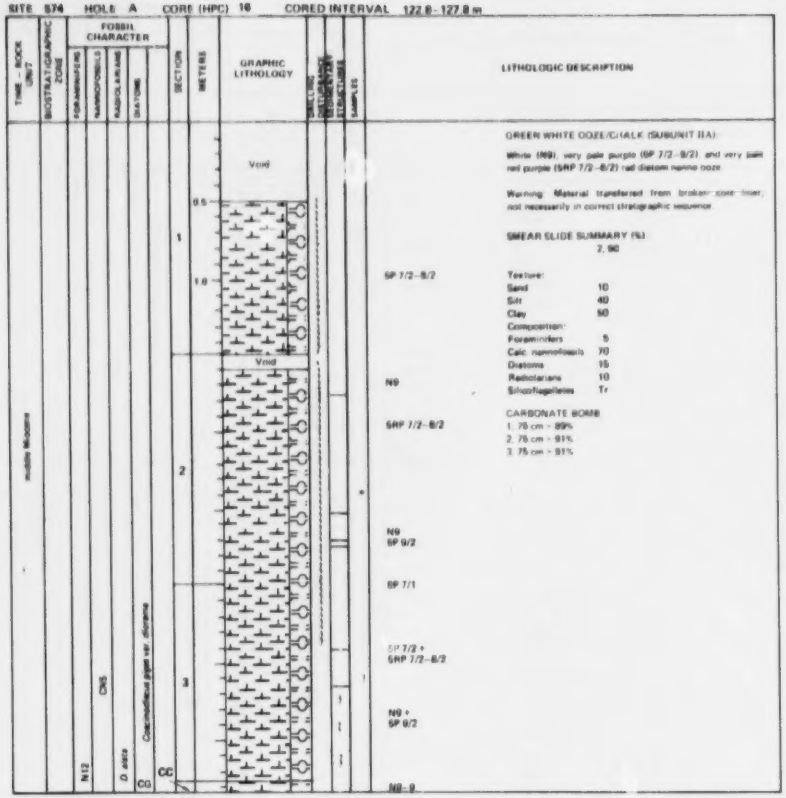

SITE 574 HOLE A CORE (HPC) 17 CORED INTERVAL 127.8–131.9 m

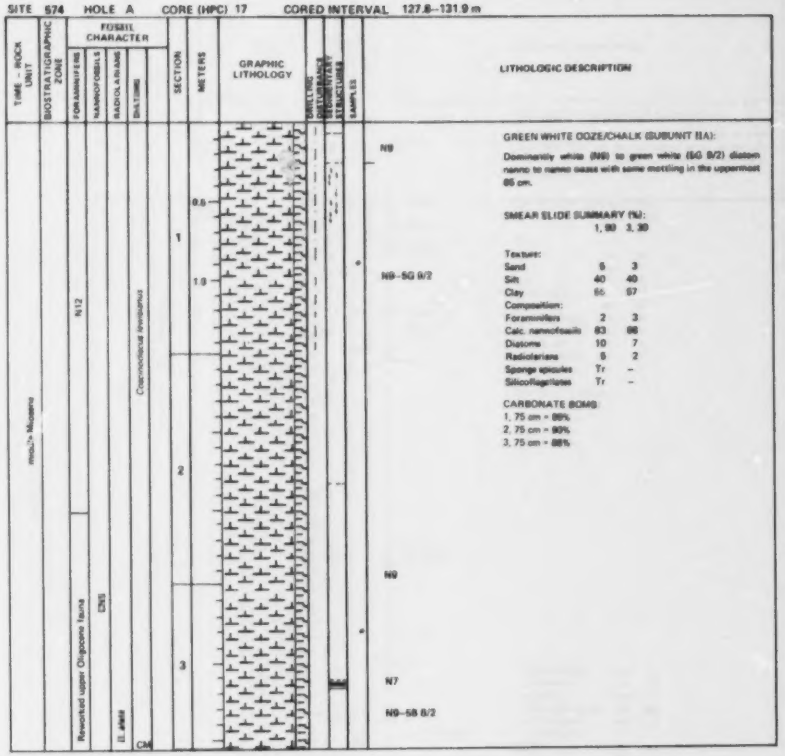

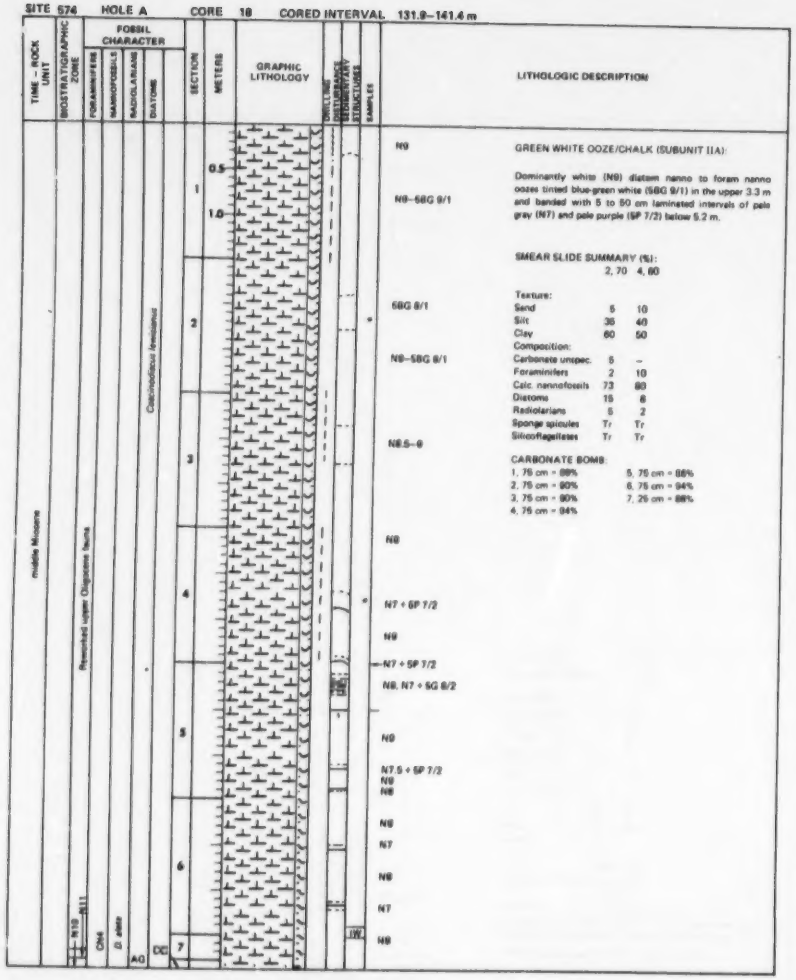
SITE 574 HOLE A CORE 18 CORED INTERVAL 131.9–141.4 m
TIME – ROCK UNIT
BIOSTRATIGRAPHIC ZONE
FOSSIL CHARACTER
FORAMINIFERS
NANNOFOSSILS
RADIOLARIANS
DIATOMS
SECTION
METERS
GRAPHIC LITHOLOGY
DRILLING DISTURBANCE
SEDIMENTARY STRUCTURES
SAMPLES
LITHOLOGIC DESCRIPTION
middle Miocene
Reworked upper Oligocene fauna
N10
N11
Chs
D. altus
A-C
Coscinodiscus lewisianus
CC
GREEN WHITE OOZE/CHALK (SUBUNIT IIA):
Dominantly white (N9) diatom nanno to foram nanno oozes tinted blue-green white (5BG 9/1) in the upper 3.3 m and banded with 5 to 50 cm laminated intervals of pale gray (N7) and pale purple (5P 7/2) below 5.2 m.
SMEAR SLIDE SUMMARY (%):
2, 70 4, 60
Texture:
Sand 5 10
Silt 35 40
Clay 60 50
Composition:
Carbonate unspec. 5 –
Foraminifers 2 10
Calc. nannofossils 73 80
Diatoms 15 6
Radiolarians 5 2
Sponge spicules Tr Tr
Silicoflagellates Tr Tr
CARBONATE BOMB:
1, 75 cm = 89%
2, 75 cm = 90%
3, 75 cm = 90%
4, 75 cm = 94%
5, 75 cm = 88%
6, 75 cm = 94%
7, 25 cm = 88%

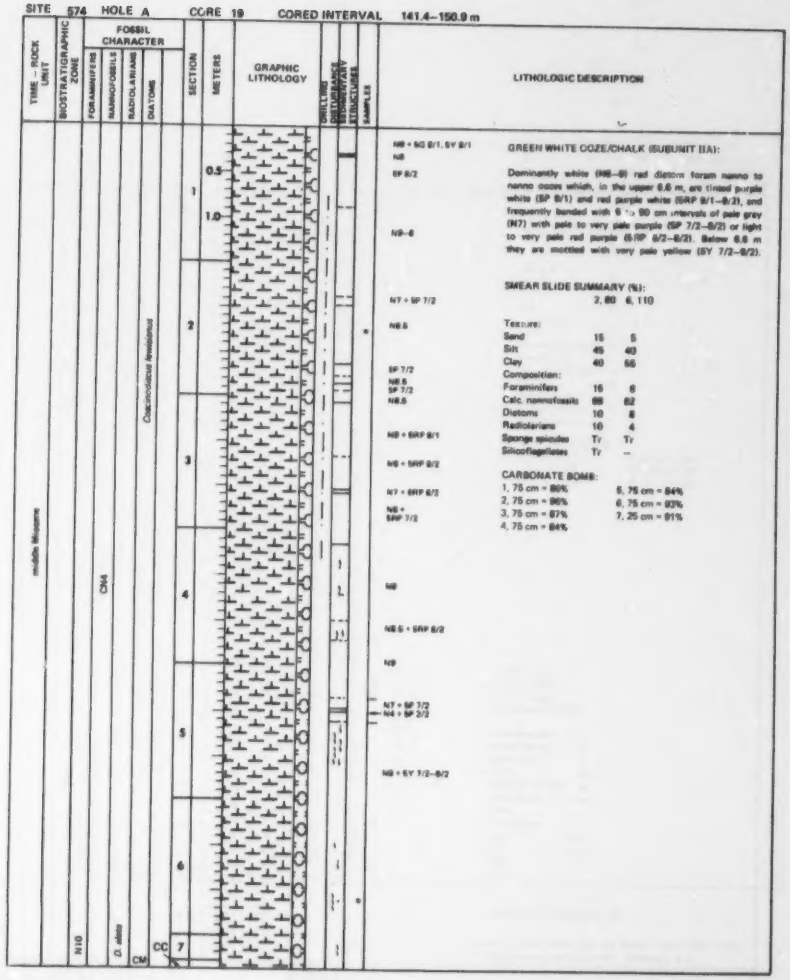
SITE 574 HOLE A CORE 19 CORED INTERVAL 141.4–150.9 m
TIME – ROCK UNIT
BIOSTRATIGRAPHIC ZONE
FOSSIL CHARACTER
FORAMINIFERS
NANNOFOSSILS
RADIOLARIANS
DIATOMS
SECTION
METERS
GRAPHIC LITHOLOGY
DRILLING DISTURBANCE
SEDIMENTARY STRUCTURES
SAMPLES
LITHOLOGIC DESCRIPTION
middle Miocene
Chs
N10
D. altus
CM
Coscinodiscus lewisianus
CC
GREEN WHITE OOZE/CHALK (SUBUNIT IIA):
Dominantly white (N8–9) red diatom foram nanno to nanno oozes which, in the upper 6.6 m, are tinted purple white (5P 8/1) and red purple white (5RP 8/1–8/2), and frequently banded with 5 to 50 cm intervals of pale gray (N7) with pale to very pale purple (5P 7/2–8/2) or light to very pale red purple (5RP 8/2–8/2). Below 6.6 m they are mottled with very pale yellow (5Y 7/2–8/2).
SMEAR SLIDE SUMMARY (%):
2, 80 6, 110
Texture:
Sand 15 5
Silt 45 40
Clay 40 55
Composition:
Foraminifers 15 6
Calc. nannofossils 69 82
Diatoms 10 8
Radiolarians 10 4
Sponge spicules Tr Tr
Silicoflagellates Tr –
CARBONATE BOMB:
1, 75 cm = 86%
2, 75 cm = 96%
3, 75 cm = 87%
4, 75 cm = 84%
5, 75 cm = 84%
6, 75 cm = 83%
7, 25 cm = 91%

SITE 574 HOLE A CORE 20 CORED INTERVAL 160.9–169.9 m

TIME — ROCK UNIT	BIOSTRATIGRAPHIC ZONE	FOSSIL CHARACTER: FORAMINIFERS	FOSSIL CHARACTER: NANNOFOSSILS	FOSSIL CHARACTER: RADIOLARIANS	FOSSIL CHARACTER: DIATOMS	SECTION	METERS	GRAPHIC LITHOLOGY	DRILLING DISTURBANCE	SED. STRUCTURES	SAMPLES	LITHOLOGIC DESCRIPTION
middle Miocene	CN4	N9	*D. altus*	*Cestodiscus peplum* subzone B	AG	1–7, CC	0.5, 1.0	VOID				N9 + 5G 8/2; N9; 5G 7/1; N9 + 5G 8/1–9/1; N9; N8.5 + 5P 9/2; N9 + 5G 9/1

GREEN WHITE OOZE/CHALK (SUBUNIT IIA):

Dominantly mottled white (N8–9) and green white (5G 8/1–9/1) nanno ooze, one 30 cm interval of mottled light green gray (5G 7/1) nanno diatom rad ooze.

SMEAR SLIDE SUMMARY (%):

	2, 85	4, 50
Texture:		
Sand	10	30
Silt	50	35
Clay	40	35
Composition:		
Pyrite	–	Tr
Foraminifers	10	–
Calc. nannofossils	80	30
Diatoms	5	30
Radiolarians	5	40
Sponge spicules	Tr	Tr
Silicoflagellates	–	Tr

CARBONATE BOMB:

1, 75 cm = 85%	5, 75 cm = 79%
3, 75 cm = 88%	7, 25 cm = 91%

SITE 574 HOLE A CORE 21 CORED INTERVAL 169.9–169.4 m

TIME — ROCK UNIT	BIOSTRATIGRAPHIC ZONE	FOSSIL CHARACTER: FORAMINIFERS	FOSSIL CHARACTER: NANNOFOSSILS	FOSSIL CHARACTER: RADIOLARIANS	FOSSIL CHARACTER: DIATOMS	SECTION	METERS	GRAPHIC LITHOLOGY	DRILLING DISTURBANCE	SED. STRUCTURES	SAMPLES	LITHOLOGIC DESCRIPTION
middle Miocene	Reworked upper Oligocene fauna	N9	CN4	*D. altus*	CM	1–6, CC	0.5, 1.0					N9; N9; N9; N8.5

GREEN WHITE OOZE/CHALK (SUBUNIT IIA):

Very uniform white (N8–N9) foram diatom nanno ooze.

SMEAR SLIDE SUMMARY (%):

	2, 70
Texture:	
Sand	5
Silt	45
Clay	50
Composition:	
Pyrite	Tr
Foraminifers	10
Calc. nannofossils	70
Diatoms	15
Radiolarians	5
Sponge spicules	Tr
Silicoflagellates	Tr

CARBONATE BOMB:

1, 75 cm = 89%
3, 75 cm = 90%
5, 75 cm = 87%

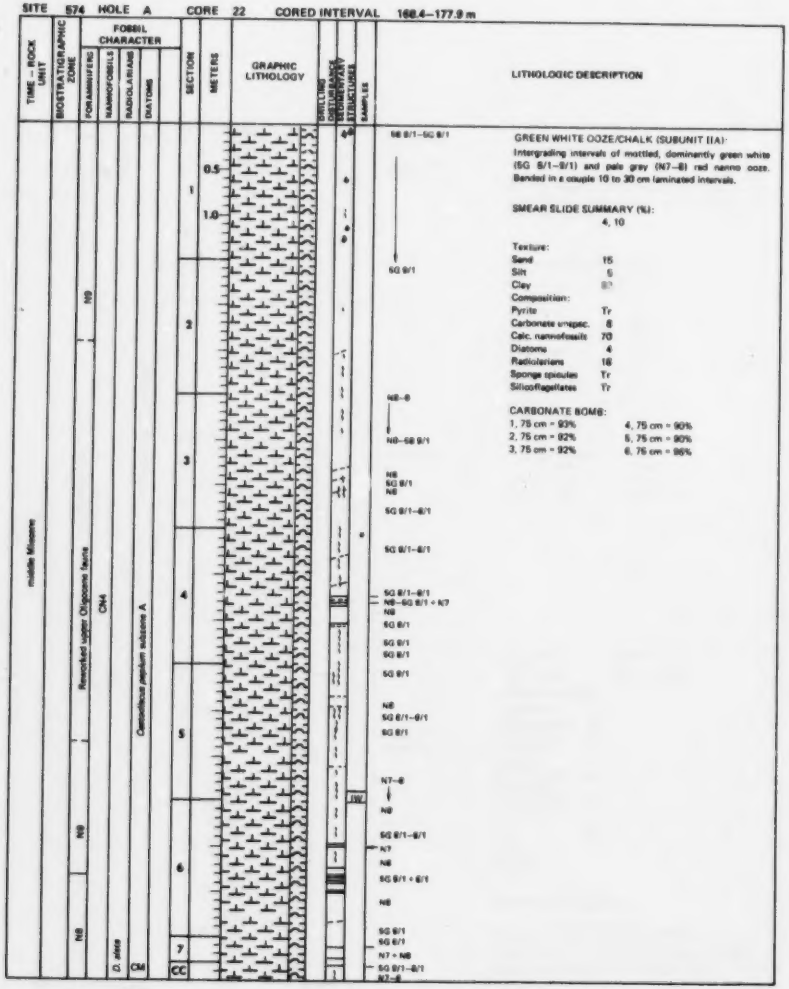
SITE 574 HOLE A CORE 22 CORED INTERVAL 168.4–177.9 m
TIME – ROCK UNIT
BIOSTRATIGRAPHIC ZONE
FOSSIL CHARACTER
FORAMINIFERS
NANNOFOSSILS
RADIOLARIANS
DIATOMS
SECTION
METERS
GRAPHIC LITHOLOGY
DRILLING DISTURBANCE
SEDIMENTARY STRUCTURES
SAMPLES
LITHOLOGIC DESCRIPTION
middle Miocene
Reworked upper Oligocene fauna
D. altus
Cestodiscus peplum subzone A
CM
GREEN WHITE OOZE/CHALK (SUBUNIT IIA):
Intergrading intervals of mottled, dominantly green white (5G 8/1–8/1) and pale gray (N7–8) red nanno ooze. Banded in a couple 10 to 30 cm laminated intervals.
SMEAR SLIDE SUMMARY (%):
4, 10
Texture:
Sand 15
Silt 5
Clay 80
Composition:
Pyrite Tr
Carbonate unspec. 8
Calc. nannofossils 70
Diatoms 4
Radiolarians 18
Sponge spicules Tr
Silicoflagellates Tr
CARBONATE BOMB:
1, 75 cm = 93%
2, 75 cm = 92%
3, 75 cm = 92%
4, 75 cm = 90%
5, 75 cm = 90%
6, 75 cm = 86%

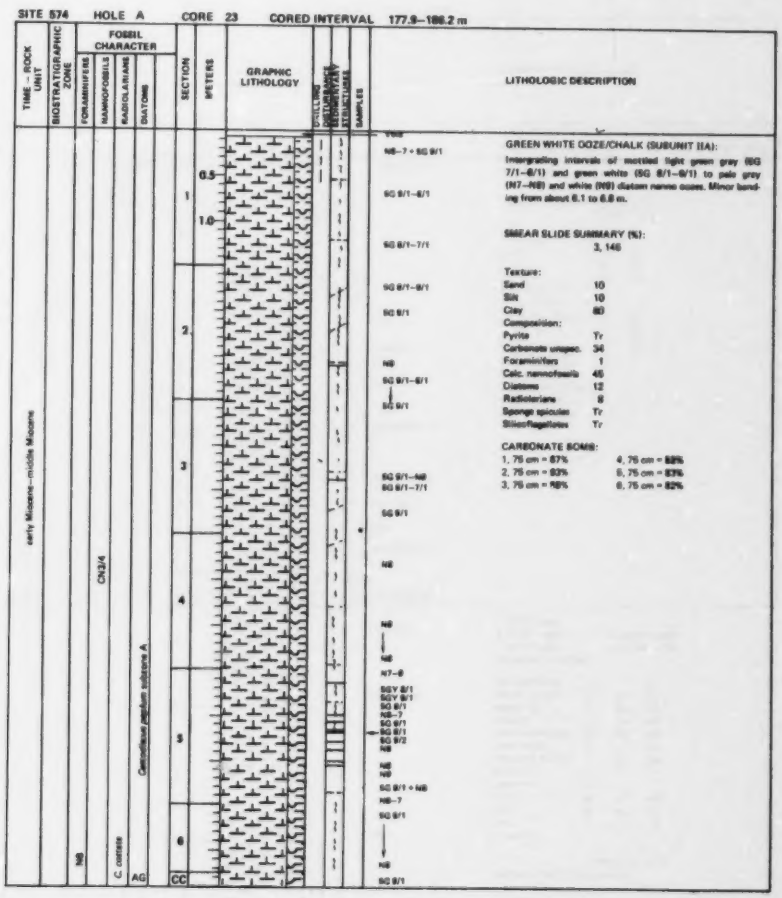
SITE 574 HOLE A CORE 23 CORED INTERVAL 177.9–186.2 m
TIME – ROCK UNIT
BIOSTRATIGRAPHIC ZONE
FOSSIL CHARACTER
FORAMINIFERS
NANNOFOSSILS
RADIOLARIANS
DIATOMS
SECTION
METERS
GRAPHIC LITHOLOGY
DRILLING DISTURBANCE
SEDIMENTARY STRUCTURES
SAMPLES
LITHOLOGIC DESCRIPTION
early Miocene–middle Miocene
CN3/4
C. cornuta
AG
Cestodiscus peplum subzone A
GREEN WHITE OOZE/CHALK (SUBUNIT IIA):
Intergrading intervals of mottled light green gray (5G 7/1–8/1) and green white (5G 8/1–9/1) to pale gray (N7–N8) and white (N9) diatom nanno oozes. Minor banding from about 6.1 to 6.8 m.
SMEAR SLIDE SUMMARY (%):
3, 146
Texture:
Sand 10
Silt 10
Clay 80
Composition:
Pyrite Tr
Carbonate unspec. 34
Foraminifers 1
Calc. nannofossils 46
Diatoms 12
Radiolarians 6
Sponge spicules Tr
Silicoflagellates Tr
CARBONATE BOMB:
1, 75 cm = 87%
2, 75 cm = 93%
3, 75 cm = 88%
4, 75 cm = 88%
5, 75 cm = 83%
6, 75 cm = 82%

SITE 574 HOLE B CORE 1 CORED INTERVAL 185.0–194.5 m

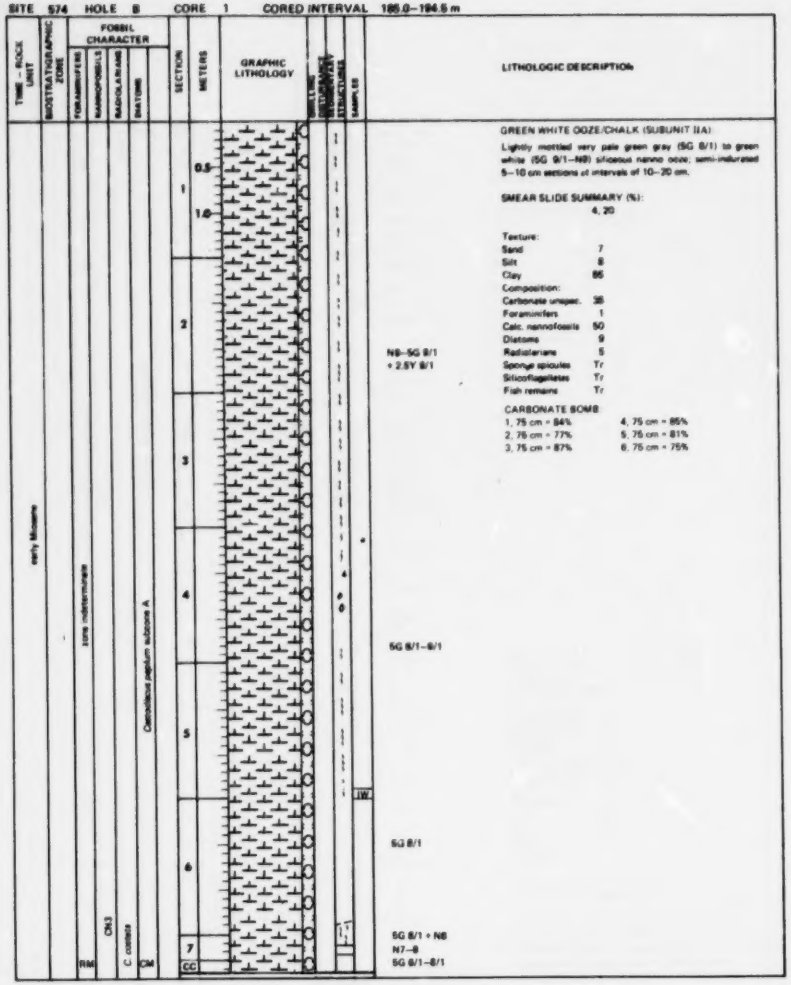

LITHOLOGIC DESCRIPTION

GREEN WHITE OOZE/CHALK (SUBUNIT IIA):

Lightly mottled very pale green gray (5G 8/1) to green white (5G 8/1–N8) siliceous nanno ooze; semi-indurated 5–10 cm sections at intervals of 10–20 cm.

SMEAR SLIDE SUMMARY (%):

	4, 20
Texture:	
Sand	7
Silt	8
Clay	85
Composition:	
Carbonate unspec.	35
Foraminifers	1
Calc. nannofossils	50
Diatoms	9
Radiolarians	5
Sponge spicules	Tr
Silicoflagellates	Tr
Fish remains	Tr

CARBONATE BOMB:

1, 75 cm = 94%	4, 75 cm = 85%
2, 75 cm = 77%	5, 75 cm = 81%
3, 75 cm = 87%	6, 75 cm = 75%

SITE 574 HOLE C CORE 1 CORED INTERVAL 194.5–204.0 m

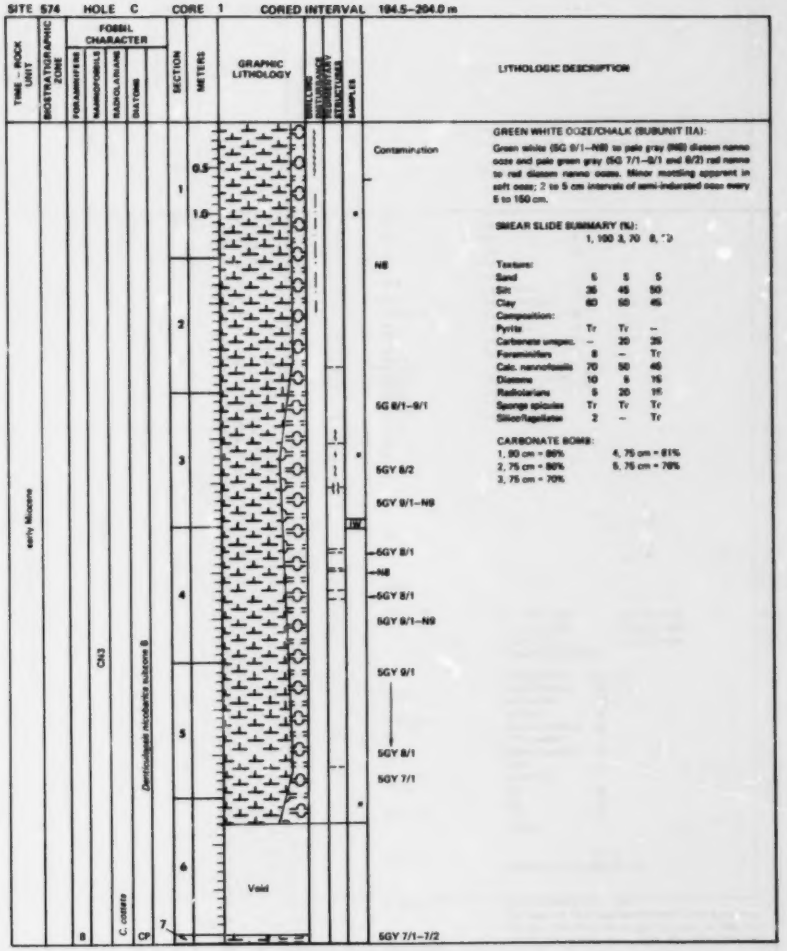

LITHOLOGIC DESCRIPTION

GREEN WHITE OOZE/CHALK (SUBUNIT IIA):

Green white (5G 8/1–N8) to pale gray (N8) diatom nanno ooze and pale green gray (5G 7/1–8/1 and 8/2) red nanno to red diatom nanno ooze. Minor mottling apparent in soft ooze; 2 to 5 cm intervals of semi-indurated ooze every 5 to 150 cm.

SMEAR SLIDE SUMMARY (%):

	1, 100	3, 70	6, 70
Texture:			
Sand	5	5	5
Silt	35	45	50
Clay	60	50	45
Composition:			
Pyrite	Tr	Tr	–
Carbonate unspec.	–	20	25
Foraminifers	5	–	Tr
Calc. nannofossils	70	50	45
Diatoms	10	5	15
Radiolarians	5	20	15
Sponge spicules	Tr	Tr	Tr
Silicoflagellates	2	–	Tr

CARBONATE BOMB:

1, 90 cm = 86%	4, 75 cm = 81%
2, 75 cm = 80%	5, 75 cm = 76%
3, 75 cm = 70%	

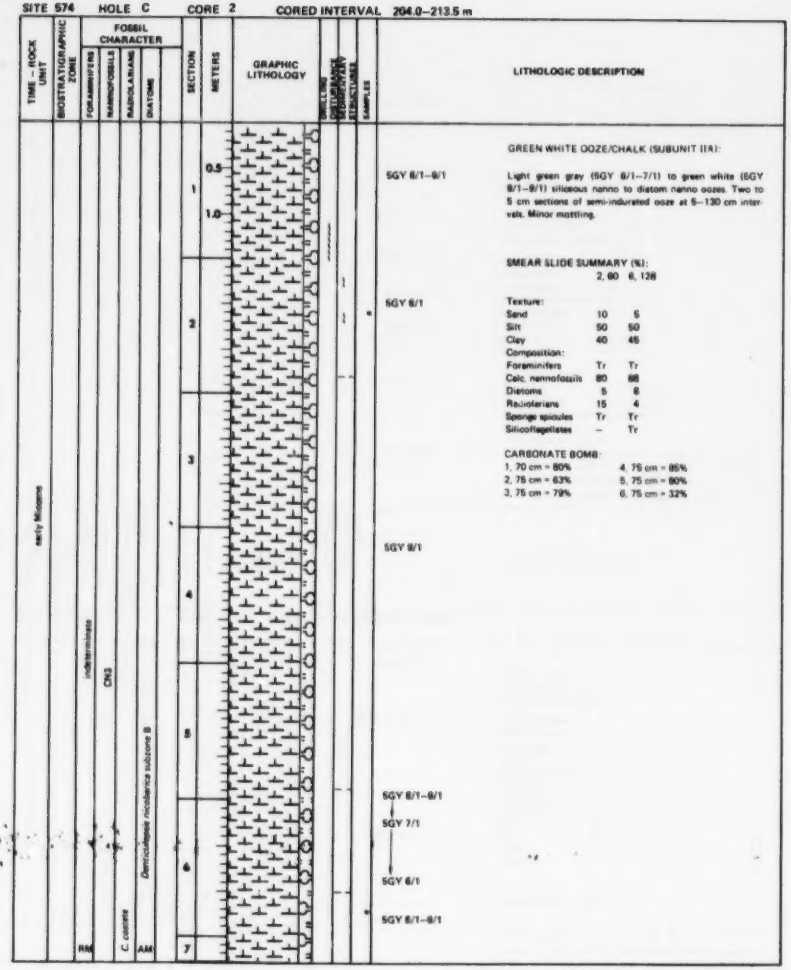
SITE 574 HOLE C CORE 2 CORED INTERVAL 204.0–213.5 m
TIME — ROCK UNIT
BIOSTRATIGRAPHIC ZONE
FOSSIL CHARACTER
FORAMINIFERS
NANNOFOSSILS
RADIOLARIANS
DIATOMS
SECTION
METERS
GRAPHIC LITHOLOGY
DRILLING DISTURBANCE
SED. STRUCTURES
SAMPLES
LITHOLOGIC DESCRIPTION
early Miocene
indeterminate
CN3
C. costata
Denticulopsis nicobarica subzone B
RM
AM
GREEN WHITE OOZE/CHALK (SUBUNIT IIA):
Light green gray (5GY 8/1–7/1) to green white (5GY 8/1–9/1) siliceous nanno to diatom nanno oozes. Two to 5 cm sections of semi-indurated ooze at 5–130 cm intervals. Minor mottling.
SMEAR SLIDE SUMMARY (%):
2, 60 6, 128
Texture:
Sand 10 5
Silt 50 50
Clay 40 45
Composition:
Foraminifers Tr Tr
Calc. nannofossils 60 68
Diatoms 5 6
Radiolarians 15 4
Sponge spicules Tr Tr
Silicoflagellates – Tr
CARBONATE BOMB:
1, 70 cm = 80%
2, 75 cm = 63%
3, 75 cm = 79%
4, 75 cm = 86%
5, 75 cm = 80%
6, 75 cm = 32%
5GY 8/1–9/1
5GY 8/1
5GY 9/1
5GY 8/1–9/1
5GY 7/1
5GY 6/1
5GY 8/1–9/1

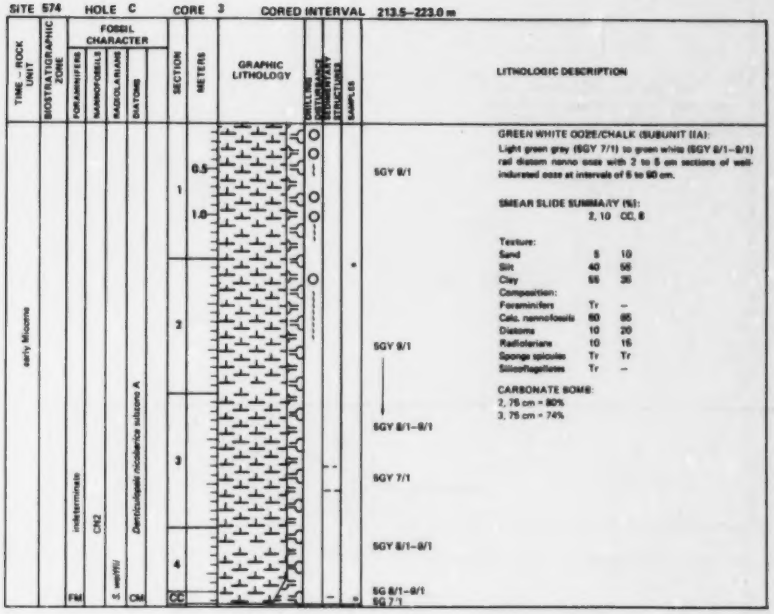
SITE 574 HOLE C CORE 3 CORED INTERVAL 213.5–223.0 m
TIME — ROCK UNIT
BIOSTRATIGRAPHIC ZONE
FOSSIL CHARACTER
FORAMINIFERS
NANNOFOSSILS
RADIOLARIANS
DIATOMS
SECTION
METERS
GRAPHIC LITHOLOGY
DRILLING DISTURBANCE
SED. STRUCTURES
SAMPLES
LITHOLOGIC DESCRIPTION
early Miocene
indeterminate
CN2
s. wolffii
Denticulopsis nicobarica subzone A
FM
CM
CC
GREEN WHITE OOZE/CHALK (SUBUNIT IIA):
Light green gray (5GY 7/1) to green white (5GY 8/1–9/1) rad diatom nanno ooze with 2 to 5 cm sections of well-indurated ooze at intervals of 6 to 60 cm.
SMEAR SLIDE SUMMARY (%):
2, 10 CC, 8
Texture:
Sand 5 10
Silt 40 55
Clay 55 35
Composition:
Foraminifers Tr –
Calc. nannofossils 60 65
Diatoms 10 20
Radiolarians 10 15
Sponge spicules Tr Tr
Silicoflagellates Tr –
CARBONATE BOMB:
2, 75 cm = 80%
3, 75 cm = 74%
5GY 9/1
5GY 9/1
5GY 8/1–9/1
5GY 7/1
5GY 8/1–9/1
5G 8/1–9/1
5G 7/1

SITE 574 HOLE C CORE 4 CORED INTERVAL 223.0–232.5 m

TIME – ROCK UNIT	BIOSTRATIGRAPHIC ZONE	FOSSIL CHARACTER: FORAMINIFERS	NANNOFOSSILS	RADIOLARIANS	DIATOMS	SECTION	METERS	GRAPHIC LITHOLOGY	DRILLING DISTURBANCE	SEDIMENTARY STRUCTURES	SAMPLES	LITHOLOGIC DESCRIPTION
early Miocene	NN5		CN2	*S. seminae*	*Triceratium pileus* AM	1	0.5					5GY 8/1–9/1
					D. kittonii subsp. *A*	2	1.0					
						3						5GY 8/1–9/1
						CC						5G 8/1–9/1

GREEN WHITE OOZE/CHALK (SUBUNIT IIA)

Uniform green white (5GY 8/1–9/1) siliceous nanno ooze with 2 to 5 cm sections of well-indurated ooze at intervals of 5 to 110 cm.

SMEAR SLIDE SUMMARY (%):

	2, 80
Texture:	
Sand	5
Silt	60
Clay	35
Composition:	
Carbonate unspec.	5
Foraminifers	Tr
Calc. nannofossils	85
Diatoms	3
Radiolarians	7
Sponge spicules	Tr
Silicoflagellates	Tr

CARBONATE BOMB:
1, 75 cm = 87%
2, 75 cm = 81%

SITE 574 HOLE C CORE 5 CORED INTERVAL 232.5–242.0 m

TIME – ROCK UNIT	BIOSTRATIGRAPHIC ZONE	FOSSIL CHARACTER: FORAMINIFERS	NANNOFOSSILS	RADIOLARIANS	DIATOMS	SECTION	METERS	GRAPHIC LITHOLOGY	DRILLING DISTURBANCE	SEDIMENTARY STRUCTURES	SAMPLES	LITHOLOGIC DESCRIPTION
early Miocene	NN5		CN1c	*S. delmontensis*	*Tr. pileus* CM *O. elegans*	1	0.5					N7 < 5G 8/2
						2	1.0					5G 7/2
												5G 8/2 + N7
												N7 + 5G 8/2
						3						5G 8/2 + N7
												N7
						4						5G 7/2–8/2
												N7
												N7–8 + 5G 8/2–9/2
						CC	5					N7 5G 9/2

GREEN WHITE OOZE/CHALK (SUBUNIT IIA)

Dominantly light gray (N7) siliceous nanno to nanno ooze occasionally mottled or banded with pale green gray (5G 7/2–8/2). Two to 5 cm sections of well-indurated ooze at intervals of 5 to 80 cm.

SMEAR SLIDE SUMMARY (%):

	1, 117	4, 37
Texture:		
Sand	2	5
Silt	55	30
Clay	43	65
Composition:		
Foraminifers	2	2
Calc. nannofossils	85	82
Diatoms	8	3
Radiolarians	5	3
Sponge spicules	–	Tr

CARBONATE BOMB
1, 75 cm = 88%
2, 75 cm = 82%
3, 75 cm = 89%
4, 75 cm = 92%

SITE 574 HOLE C CORE 6 CORED INTERVAL 242.0–251.5 m

TIME – ROCK UNIT	BIOSTRATIGRAPHIC ZONE	FOSSIL CHARACTER: FORAMINIFERS	NANNOFOSSILS	RADIOLARIANS	DIATOMS	SECTION	METERS	GRAPHIC LITHOLOGY	DRILLING DISTURBANCE	SEDIMENTARY STRUCTURES	SAMPLES	LITHOLOGIC DESCRIPTION
early Miocene	NN5		CN1c	*S. delmontensis*	*O. elegans* AG	1	0.5					N8–5G 9/1
							1.0					N8–7
												N8
												5G 8/1–8/1 + N8
												N8
						2						N7
												N9–5G 9/1
						3						5G 9/2–N8
												N8–9
						4						N7–8 + 5G 8/2–9/2
												N8 + 5Y 8/1
												N7
												N8 + 5G 9/2, 5P 8/2
						CC	5					N8
												N8
												N7.5

GREEN WHITE OOZE/CHALK (SUBUNIT IIA)

Light gray (N8–7) to white (N9–8) nanno ooze occasionally banded with pale green gray (5G 8/2–9/2) and green white (5G 8/1–8/1). In undisturbed intervals, 2 to 5 cm sections of well-indurated ooze every 5 to 30 cm.

SMEAR SLIDE SUMMARY (%):

	2, 80
Texture:	
Sand	3
Silt	30
Clay	67
Composition:	
Volcanic glass	Tr
Pyrite	Tr
Foraminifers	5
Calc. nannofossils	91
Diatoms	1
Radiolarians	3

CARBONATE BOMB:
1, 85 cm = 98%
3, 75 cm = 98%
4, 75 cm = 91%

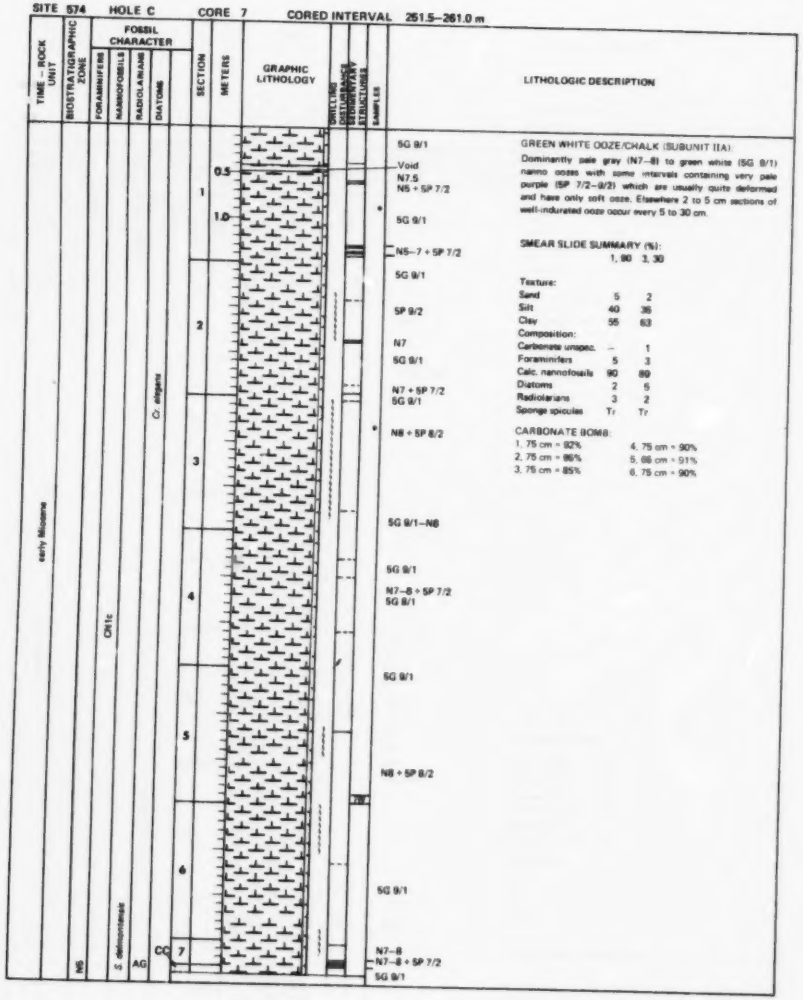
SITE 574 HOLE C CORE 7 CORED INTERVAL 251.5–261.0 m
TIME – ROCK UNIT
BIOSTRATIGRAPHIC ZONE
FOSSIL CHARACTER
FORAMINIFERS
NANNOFOSSILS
RADIOLARIANS
DIATOMS
SECTION
METERS
GRAPHIC LITHOLOGY
DRILLING DISTURBANCE
SEDIMENTARY STRUCTURES
SAMPLES
LITHOLOGIC DESCRIPTION
early Miocene
N5
CN1c
S. delmontensis
AG
Cr. elegans
CC
5G 9/1
Void
N7.5
N8 + 5P 7/2
5G 9/1
N5–7 + 5P 7/2
5G 9/1
5P 9/2
N7
5G 9/1
N7 + 5P 7/2
5G 9/1
N8 + 5P 8/2
5G 9/1–N8
5G 9/1
N7–8 + 5P 7/2
5G 8/1
5G 9/1
N8 + 5P 8/2
5G 9/1
N7–8
N7–8 + 5P 7/2
5G 9/1
GREEN WHITE OOZE/CHALK (SUBUNIT IIA)
Dominantly pale gray (N7–8) to green white (5G 8/1) nanno oozes with some intervals containing very pale purple (5P 7/2–8/2) which are usually quite deformed and have only soft ooze. Elsewhere 2 to 5 cm sections of well-indurated ooze occur every 5 to 30 cm.
SMEAR SLIDE SUMMARY (%):
1, 90 3, 30
Texture:
Sand 5 2
Silt 40 36
Clay 55 63
Composition:
Carbonate unspec. – 1
Foraminifers 5 3
Calc. nannofossils 90 89
Diatoms 2 5
Radiolarians 3 2
Sponge spicules Tr Tr
CARBONATE BOMB:
1, 75 cm = 92%
2, 75 cm = 86%
3, 75 cm = 85%
4, 75 cm = 90%
5, 68 cm = 91%
6, 75 cm = 90%

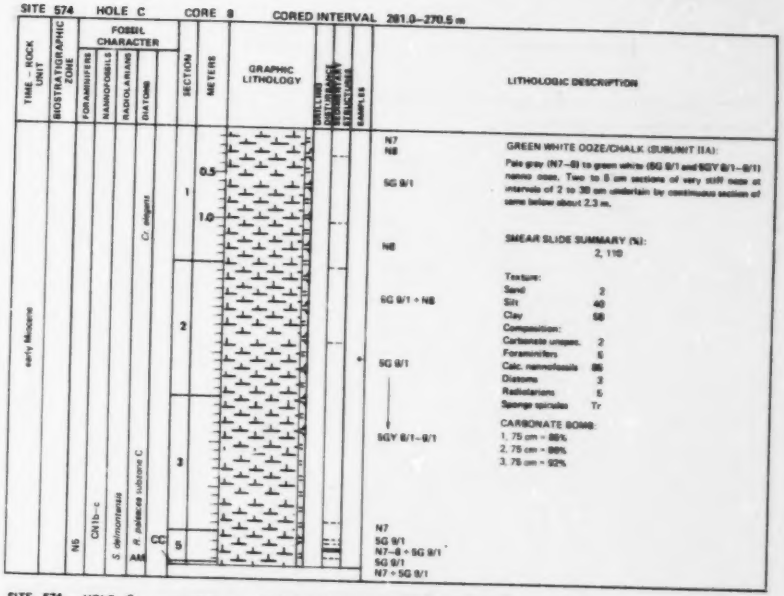
SITE 574 HOLE C CORE 8 CORED INTERVAL 261.0–270.5 m
TIME – ROCK UNIT
BIOSTRATIGRAPHIC ZONE
FOSSIL CHARACTER
FORAMINIFERS
NANNOFOSSILS
RADIOLARIANS
DIATOMS
SECTION
METERS
GRAPHIC LITHOLOGY
DRILLING DISTURBANCE
SEDIMENTARY STRUCTURES
SAMPLES
LITHOLOGIC DESCRIPTION
early Miocene
N5
CN1b–c
S. delmontensis
AM
R. pliocaes subzone C
Cr. elegans
CC
N7
N8
5G 9/1
N8
5G 9/1 + N8
5G 9/1
5GY 8/1–9/1
N7
5G 9/1
N7–8 + 5G 8/1
5G 8/1
N7 + 5G 8/1
GREEN WHITE OOZE/CHALK (SUBUNIT IIA)
Pale gray (N7–8) to green white (5G 8/1 and 5GY 8/1–8/1) nanno ooze. Two to 5 cm sections of very stiff ooze at intervals of 2 to 30 cm underlain by continuous section of same below about 2.3 m.
SMEAR SLIDE SUMMARY (%):
2, 110
Texture:
Sand 2
Silt 40
Clay 58
Composition:
Carbonate unspec. 2
Foraminifers 6
Calc. nannofossils 86
Diatoms 3
Radiolarians 5
Sponge spicules Tr
CARBONATE BOMB:
1, 75 cm = 88%
2, 75 cm = 88%
3, 75 cm = 92%

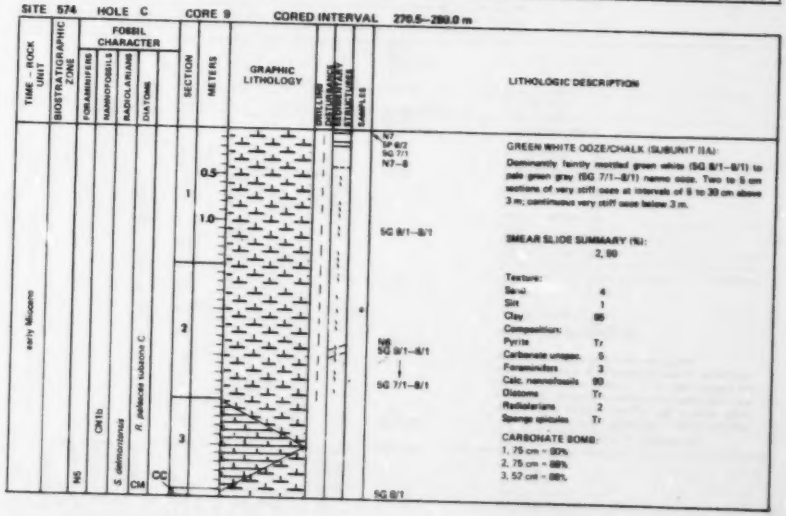
SITE 574 HOLE C CORE 9 CORED INTERVAL 270.5–280.0 m
TIME – ROCK UNIT
BIOSTRATIGRAPHIC ZONE
FOSSIL CHARACTER
FORAMINIFERS
NANNOFOSSILS
RADIOLARIANS
DIATOMS
SECTION
METERS
GRAPHIC LITHOLOGY
DRILLING DISTURBANCE
SEDIMENTARY STRUCTURES
SAMPLES
LITHOLOGIC DESCRIPTION
early Miocene
N5
CN1b
S. delmontensis
CM
R. pliocaes subzone C
CC
N7
5P 8/2
5G 7/1
N7–8
5G 8/1–8/1
5G 8/1–8/1
5G 7/1–8/1
5G 8/1
GREEN WHITE OOZE/CHALK (SUBUNIT IIA)
Dominantly faintly mottled green white (5G 8/1–8/1) to pale green gray (5G 7/1–8/1) nanno ooze. Two to 5 cm sections of very stiff ooze at intervals of 5 to 30 cm above 3 m; continuous very stiff ooze below 3 m.
SMEAR SLIDE SUMMARY (%):
2, 80
Texture:
Sand 4
Silt 1
Clay 95
Composition:
Pyrite Tr
Carbonate unspec. 5
Foraminifers 3
Calc. nannofossils 90
Diatoms Tr
Radiolarians 2
Sponge spicules Tr
CARBONATE BOMB:
1, 75 cm = 90%
2, 75 cm = 88%
3, 52 cm = 88%

SITE 574 HOLE C CORE 10 CORED INTERVAL 280.0–289.5 m

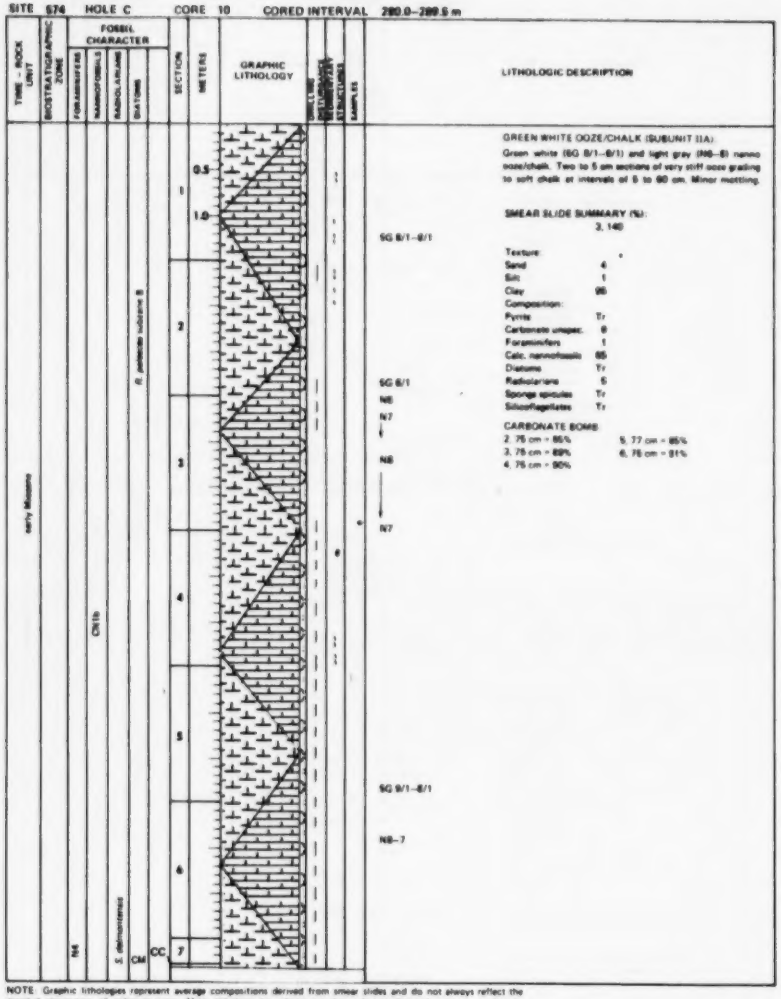

NOTE: Graphic lithologies represent average compositions derived from smear slides and do not always reflect the detailed alternation of sediment types. Major lithologic boundaries are shown but gradational contacts, small-scale cyclicity and ooze-chalk alternations are represented schematically. Color changes approximate to lithologic changes.

SITE 574 HOLE C CORE 11 CORED INTERVAL 289.5–299.0 m

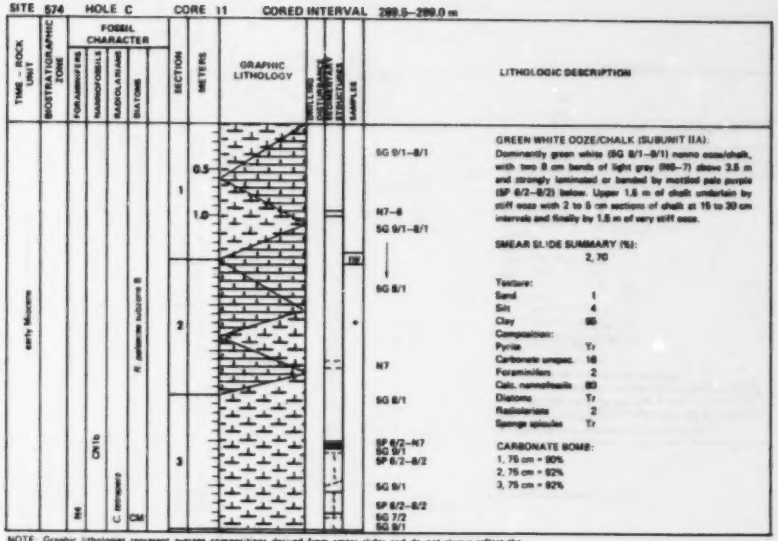

NOTE: Graphic lithologies represent average compositions derived from smear slides and do not always reflect the detailed alternation of sediment types. Major lithologic boundaries are shown but gradational contacts, small-scale cyclicity and ooze-chalk alternations are represented schematically. Color changes approximate to lithologic changes.

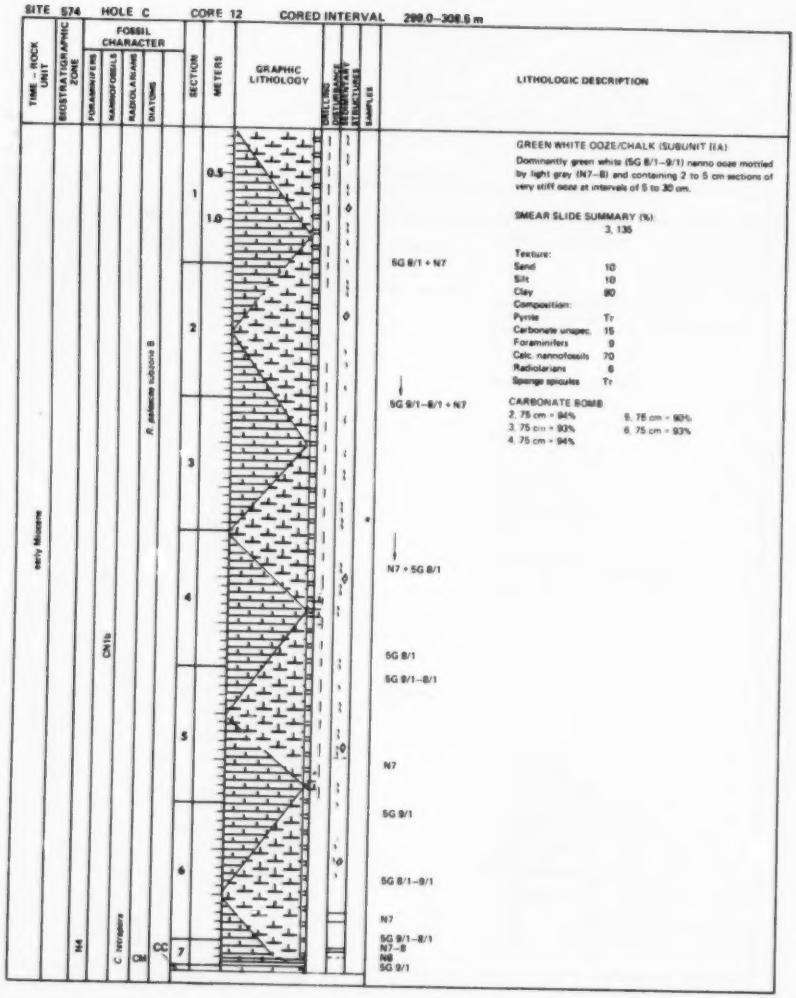
SITE 574 HOLE C CORE 12 CORED INTERVAL 298.0–308.5 m
TIME – ROCK UNIT
BIOSTRATIGRAPHIC ZONE
FOSSIL CHARACTER
FORAMINIFERS
NANNOFOSSILS
RADIOLARIANS
DIATOMS
SECTION
METERS
GRAPHIC LITHOLOGY
DRILLING DISTURBANCE
SEDIMENTARY STRUCTURES
SAMPLES
LITHOLOGIC DESCRIPTION
early Miocene
N4
CN1b
C. tetrapera
R. pliocenica subzone B
CM
CC
GREEN WHITE OOZE/CHALK (SUBUNIT IIA)
Dominantly green white (5G 8/1–9/1) nanno ooze mottled by light gray (N7–8) and containing 2 to 5 cm sections of very stiff ooze at intervals of 5 to 30 cm.
SMEAR SLIDE SUMMARY (%):
3, 135
Texture:
Sand 10
Silt 10
Clay 80
Composition:
Pyrite Tr
Carbonate unspec. 15
Foraminifers 5
Calc. nannofossils 70
Radiolarians 8
Sponge spicules Tr
CARBONATE BOMB
2, 75 cm = 94%
3, 75 cm = 93%
4, 75 cm = 94%
5, 75 cm = 90%
6, 75 cm = 93%
5G 8/1 + N7
5G 9/1–8/1 + N7
N7 + 5G 8/1
5G 8/1
5G 9/1–8/1
N7
5G 9/1
5G 8/1–9/1
N7
5G 9/1–8/1
N7–8
N8
5G 9/1

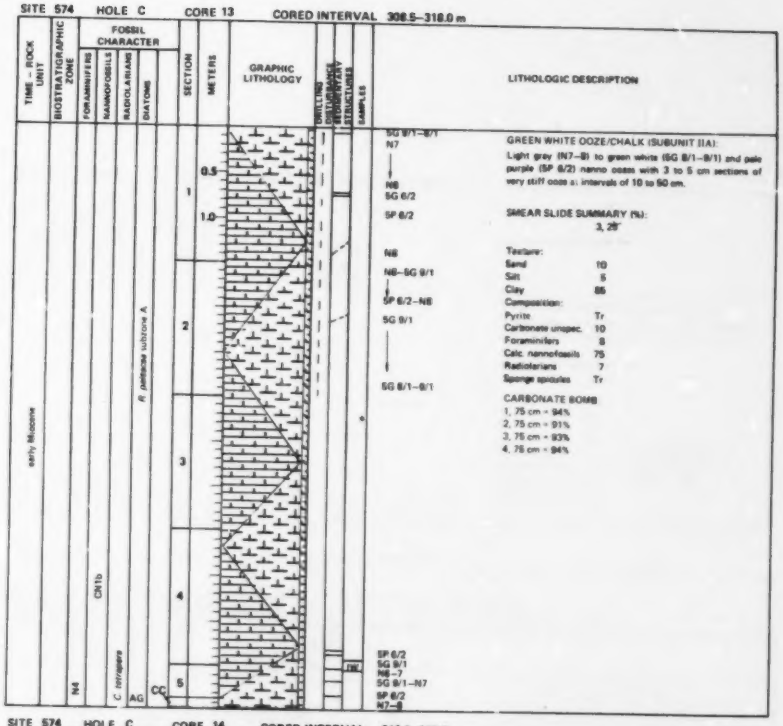
SITE 574 HOLE C CORE 13 CORED INTERVAL 308.5–318.0 m
TIME – ROCK UNIT
BIOSTRATIGRAPHIC ZONE
FOSSIL CHARACTER
FORAMINIFERS
NANNOFOSSILS
RADIOLARIANS
DIATOMS
SECTION
METERS
GRAPHIC LITHOLOGY
DRILLING DISTURBANCE
SEDIMENTARY STRUCTURES
SAMPLES
LITHOLOGIC DESCRIPTION
early Miocene
N4
CN1b
C. tetrapera
R. pliocenica subzone A
AG
CC
5G 9/1–8/1
N7
N8
5G 6/2
SP 6/2
N8
N8–5G 9/1
SP 6/2–N8
5G 9/1
5G 8/1–9/1
SP 6/2
5G 9/1
N8–7
5G 9/1–N7
SP 6/2
N7–8
GREEN WHITE OOZE/CHALK (SUBUNIT IIA)
Light gray (N7–8) to green white (5G 8/1–9/1) and pale purple (SP 6/2) nanno oozes with 3 to 5 cm sections of very stiff ooze at intervals of 10 to 50 cm.
SMEAR SLIDE SUMMARY (%):
3, 29
Texture:
Sand 10
Silt 5
Clay 85
Composition:
Pyrite Tr
Carbonate unspec. 10
Foraminifers 5
Calc. nannofossils 75
Radiolarians 7
Sponge spicules Tr
CARBONATE BOMB
1, 75 cm = 94%
2, 75 cm = 91%
3, 75 cm = 93%
4, 75 cm = 94%

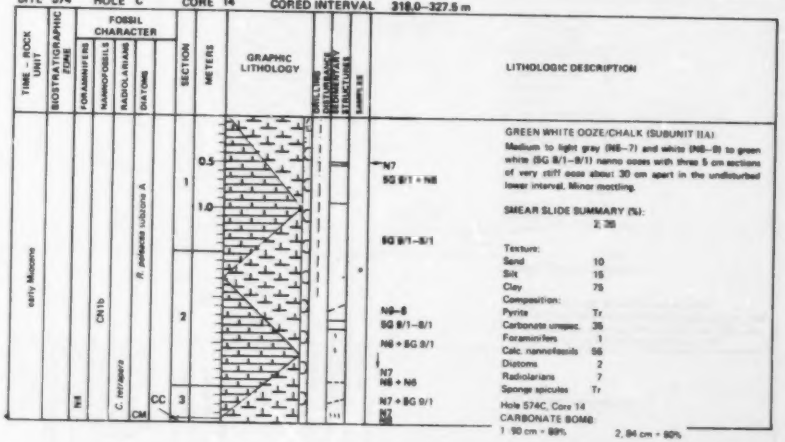
SITE 574 HOLE C CORE 14 CORED INTERVAL 318.0–327.5 m
TIME – ROCK UNIT
BIOSTRATIGRAPHIC ZONE
FOSSIL CHARACTER
FORAMINIFERS
NANNOFOSSILS
RADIOLARIANS
DIATOMS
SECTION
METERS
GRAPHIC LITHOLOGY
DRILLING DISTURBANCE
SEDIMENTARY STRUCTURES
SAMPLES
LITHOLOGIC DESCRIPTION
early Miocene
N4
CN1b
C. tetrapera
R. pliocenica subzone A
CM
CC
N7
5G 8/1 + N8
5G 8/1–8/1
N8–8
5G 8/1–8/1
N8 + 5G 8/1
N7
N8 + N8
N7 + 5G 8/1
N7
GREEN WHITE OOZE/CHALK (SUBUNIT IIA)
Medium to light gray (N6–7) and white (N8–8) to green white (5G 8/1–8/1) nanno oozes with three 5 cm sections of very stiff ooze about 30 cm apart in the undisturbed lower interval. Minor mottling.
SMEAR SLIDE SUMMARY (%):
2, 35
Texture:
Sand 10
Silt 15
Clay 75
Composition:
Pyrite Tr
Carbonate unspec. 35
Foraminifers 1
Calc. nannofossils 55
Diatoms 2
Radiolarians 7
Sponge spicules Tr
Hole 574C, Core 14
CARBONATE BOMB
1, 90 cm = 89%
2, 84 cm = 90%

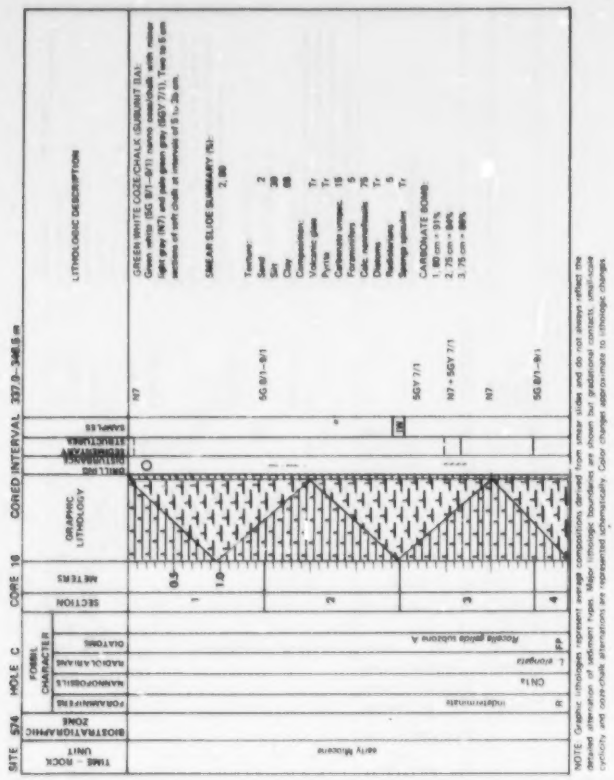

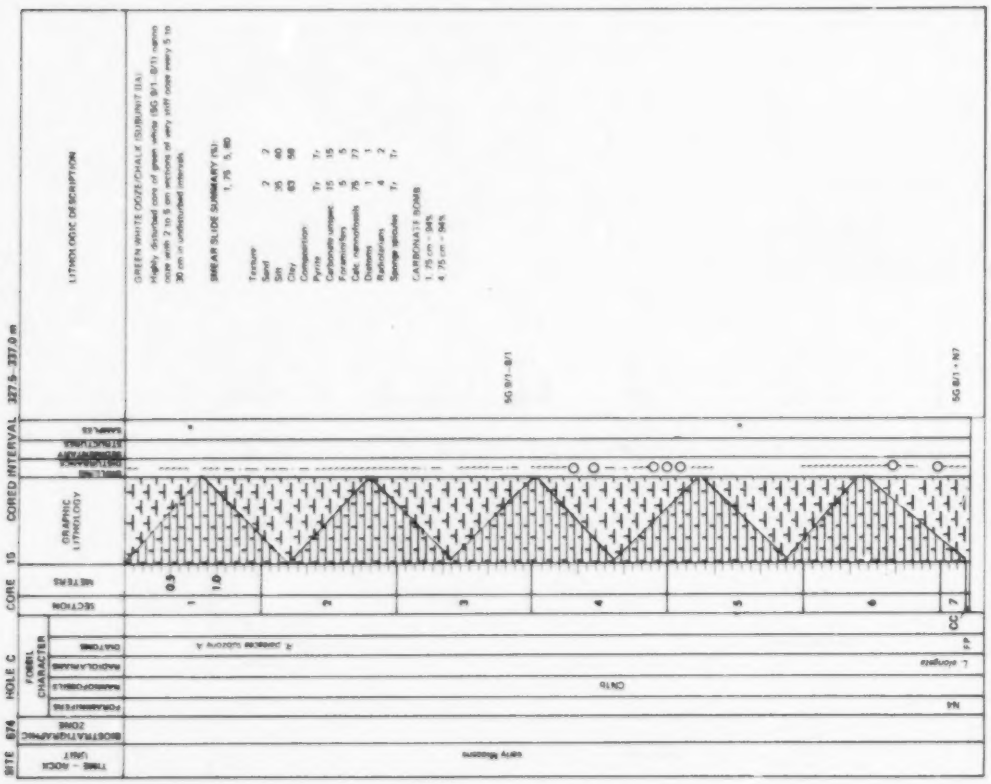

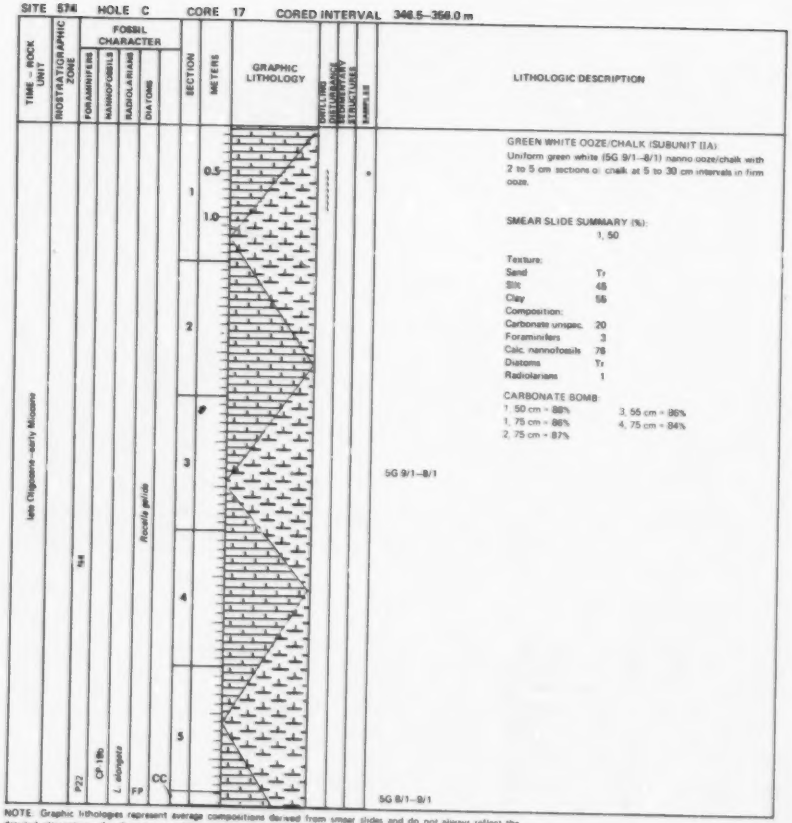

NOTE: Graphic lithologies represent average compositions derived from smear slides and do not always reflect the detailed alternation of sediment types. Major lithologic boundaries are shown but gradational contacts, small-scale cyclicity and ooze-chalk alternations are represented schematically. Color changes approximate to lithologic changes.

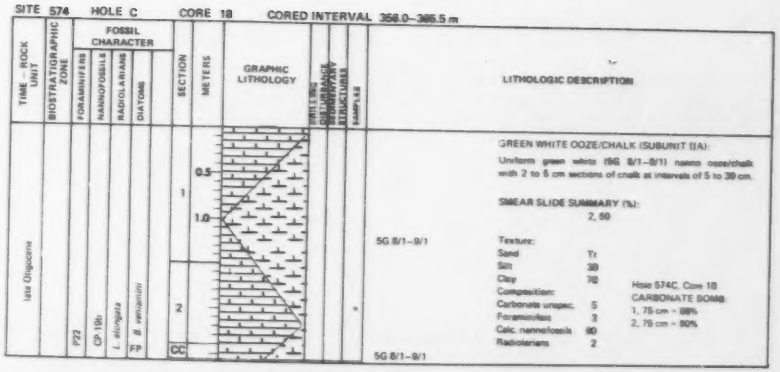

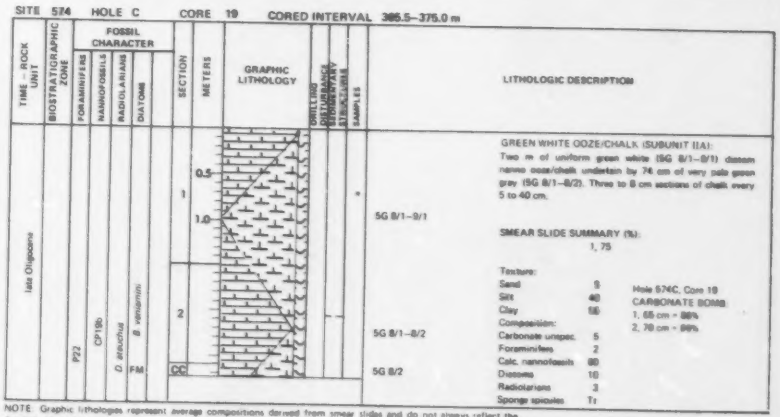

NOTE: Graphic lithologies represent average compositions derived from smear slides and do not always reflect the detailed alternation of sediment types. Major lithologic boundaries are shown but gradational contacts, small-scale cyclicity and ooze-chalk alternations are represented schematically. Color changes approximate to lithologic changes.

SITE 574 HOLE C CORE 20 CORED INTERVAL 375.0–384.5 m

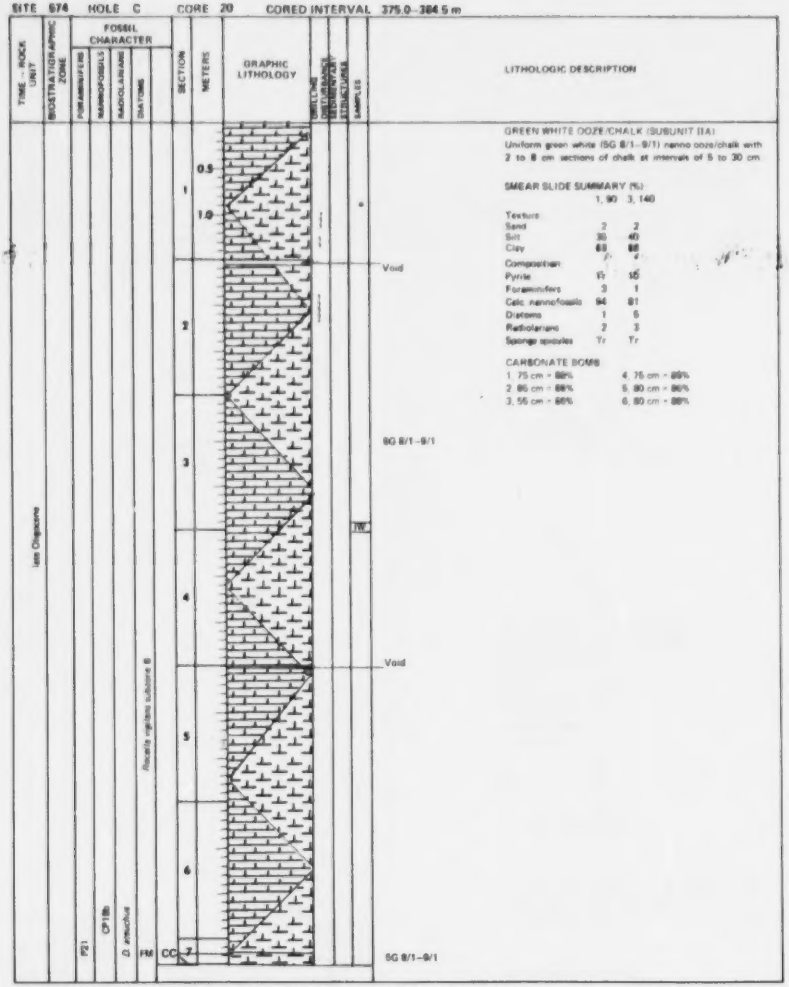

NOTE: Graphic lithologies represent average compositions derived from smear slides and do not always reflect the detailed alternation of sediment types. Major lithologic boundaries are shown but gradational contacts, small-scale cyclicity and ooze-chalk alternations are represented schematically. Color changes approximate to lithologic changes.

SITE 574 HOLE C CORE 21 CORED INTERVAL 384.5–394.0 m

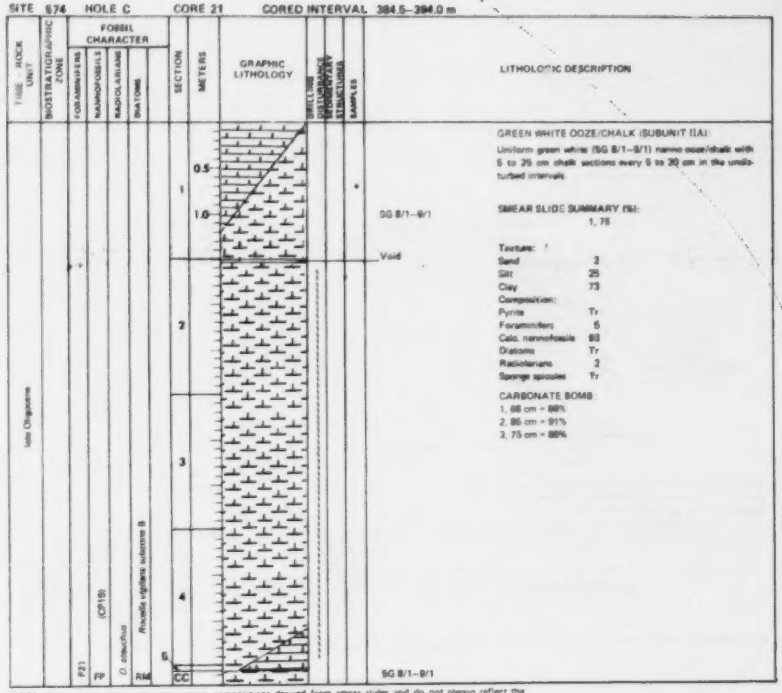

NOTE: Graphic lithologies represent average compositions derived from smear slides and do not always reflect the detailed alternation of sediment types. Major lithologic boundaries are shown but gradational contacts, small-scale cyclicity and ooze-chalk alternations are represented schematically. Color changes approximate to lithologic changes.

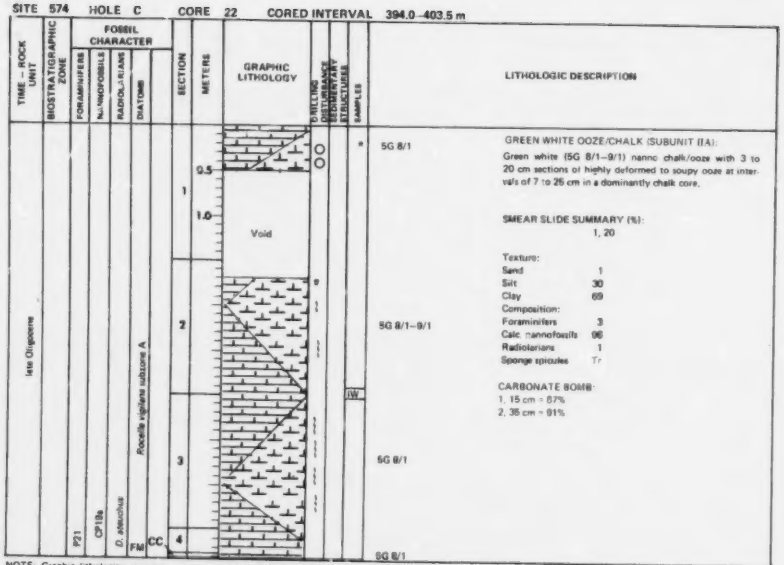

NOTE: Graphic lithologies represent average compositions derived from smear slides and do not always reflect the detailed alternation of sediment types. Major lithologic boundaries are shown but gradational contacts, small-scale cyclicity and ooze-chalk alternations are represented schematically. Color changes approximate to lithologic changes.

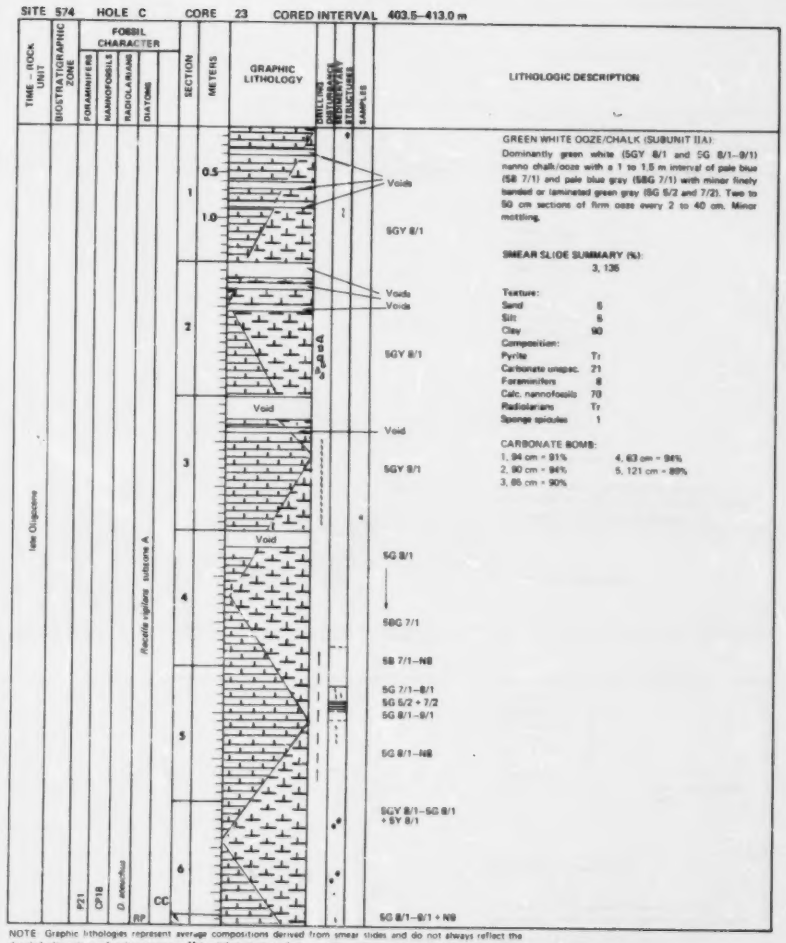

NOTE: Graphic lithologies represent average compositions derived from smear slides and do not always reflect the detailed alternation of sediment types. Major lithologic boundaries are shown but gradational contacts, small-scale cyclicity and ooze-chalk alternations are represented schematically. Color changes approximate to lithologic changes.

SITE 574 HOLE C CORE 24 CORED INTERVAL 413.0–422.5 m

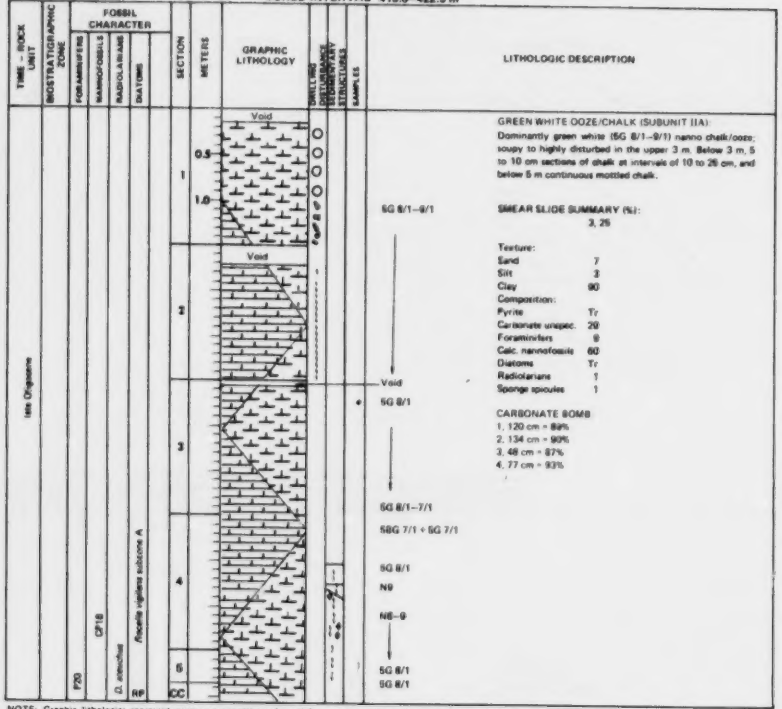

NOTE: Graphic lithologies represent average compositions derived from smear slides and do not always reflect the detailed alternation of sediment types. Major lithologic boundaries are shown but gradational contacts, small-scale cyclicity and ooze-chalk alternations are represented schematically. Color changes approximate to lithologic changes.

SITE 574 HOLE C CORE 25 CORED INTERVAL 422.5–432.0 m

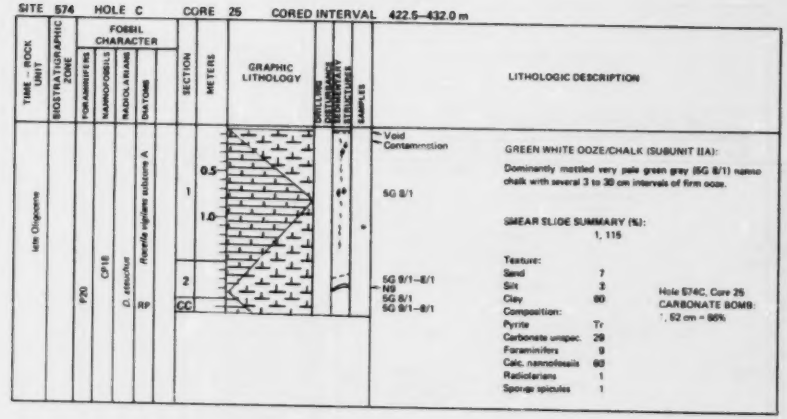

SITE 574 HOLE C CORE 26 CORED INTERVAL 432.0–441.5 m

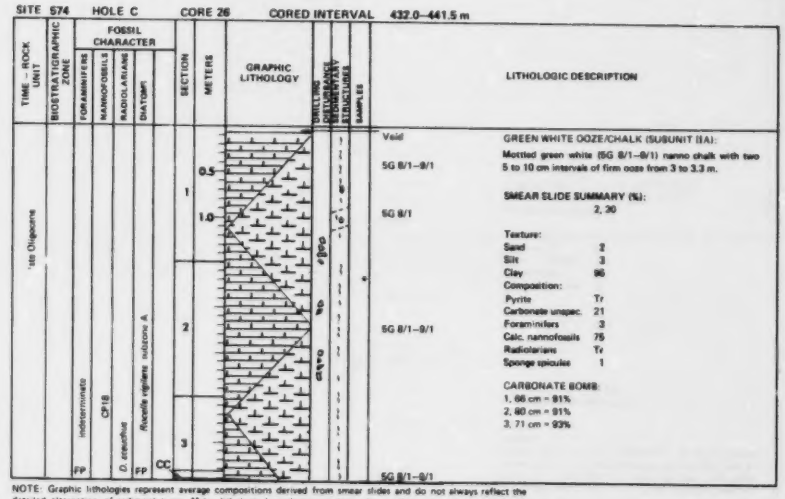

NOTE: Graphic lithologies represent average compositions derived from smear slides and do not always reflect the detailed alternation of sediment types. Major lithologic boundaries are shown but gradational contacts, small-scale cyclicity and ooze-chalk alternations are represented schematically. Color changes approximate to lithologic changes.

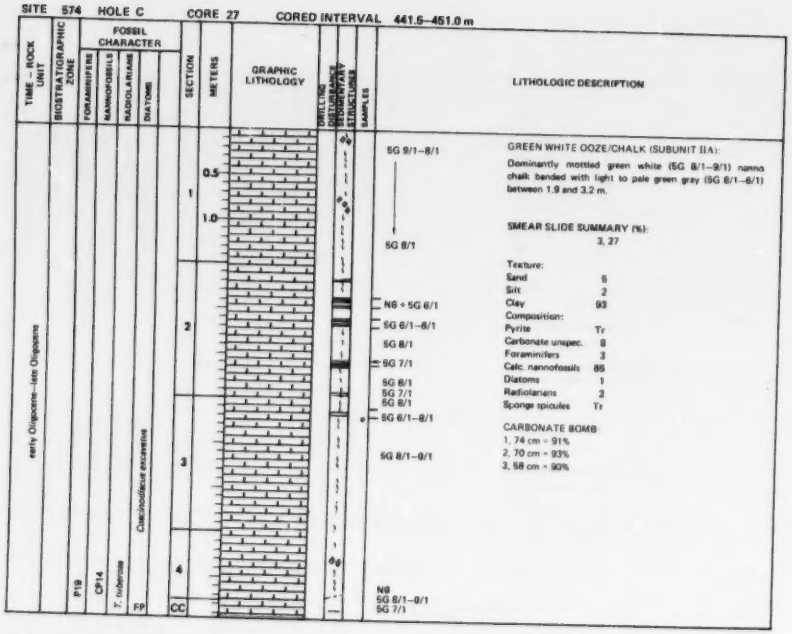

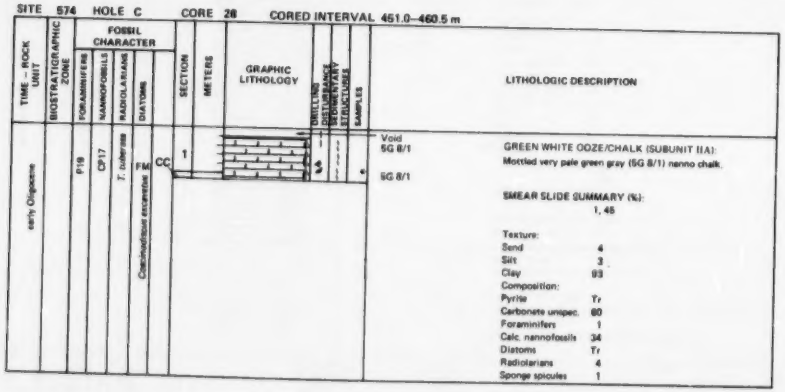

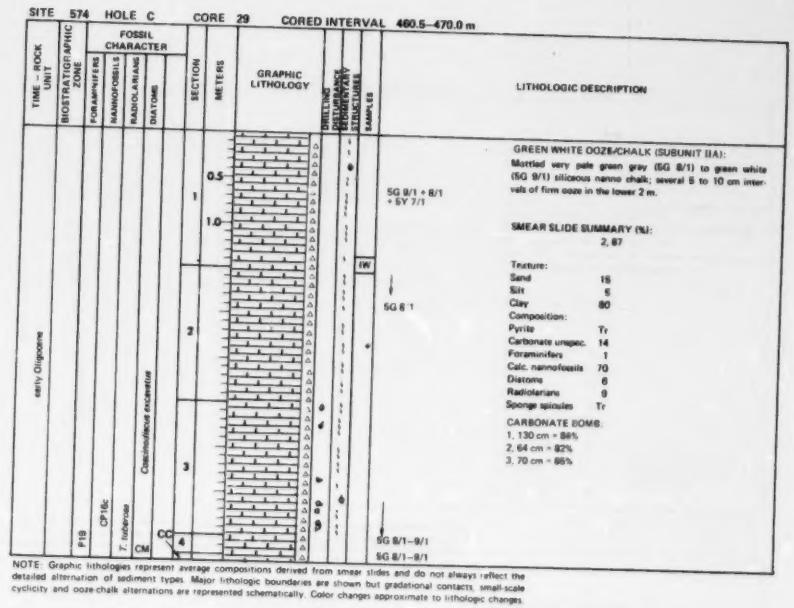

NOTE: Graphic lithologies represent average compositions derived from smear slides and do not always reflect the detailed alternation of sediment types. Major lithologic boundaries are shown but gradational contacts, small-scale cyclicity and ooze-chalk alternations are represented schematically. Color changes approximate to lithologic changes.

SITE 574 HOLE C CORE 30 CORED INTERVAL 470.0–479.5 m

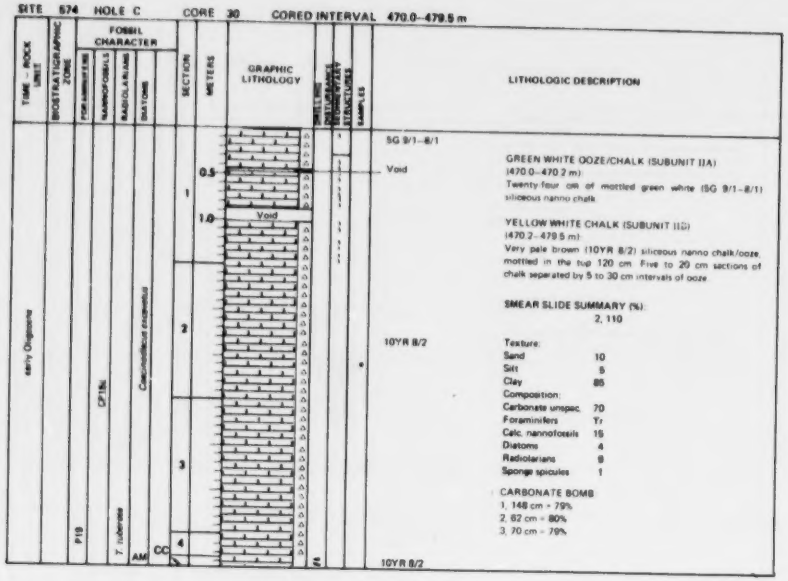

SITE 574 HOLE C CORE 31 CORED INTERVAL 479.5–489.0 m

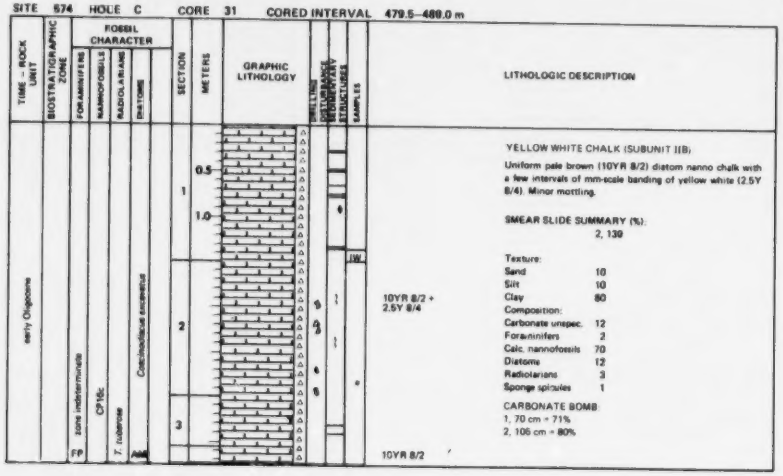

SITE 574 HOLE C CORE 32 CORED INTERVAL 489.0–498.5 m

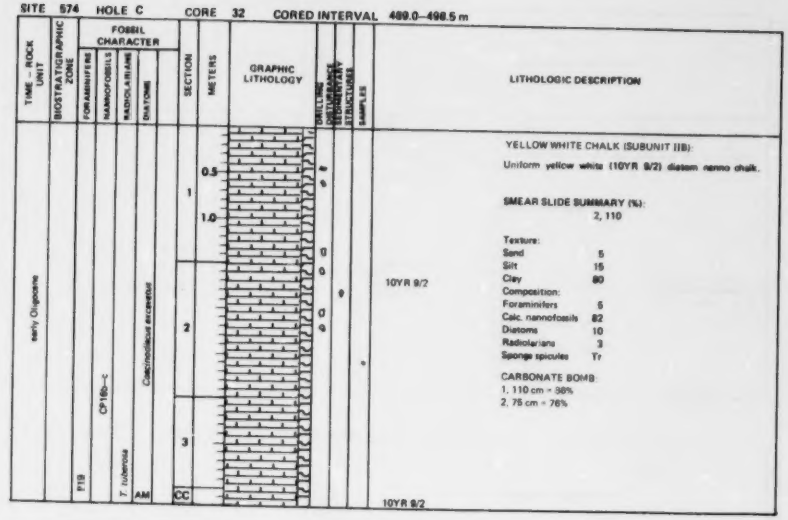

NOTE: Graphic lithologies represent average compositions derived from smear slides and do not always reflect the detailed alternation of sediment types. Major lithologic boundaries are shown but gradational contacts, small-scale cyclicity and ooze-chalk alternations are represented schematically. Color changes approximate to lithologic changes.

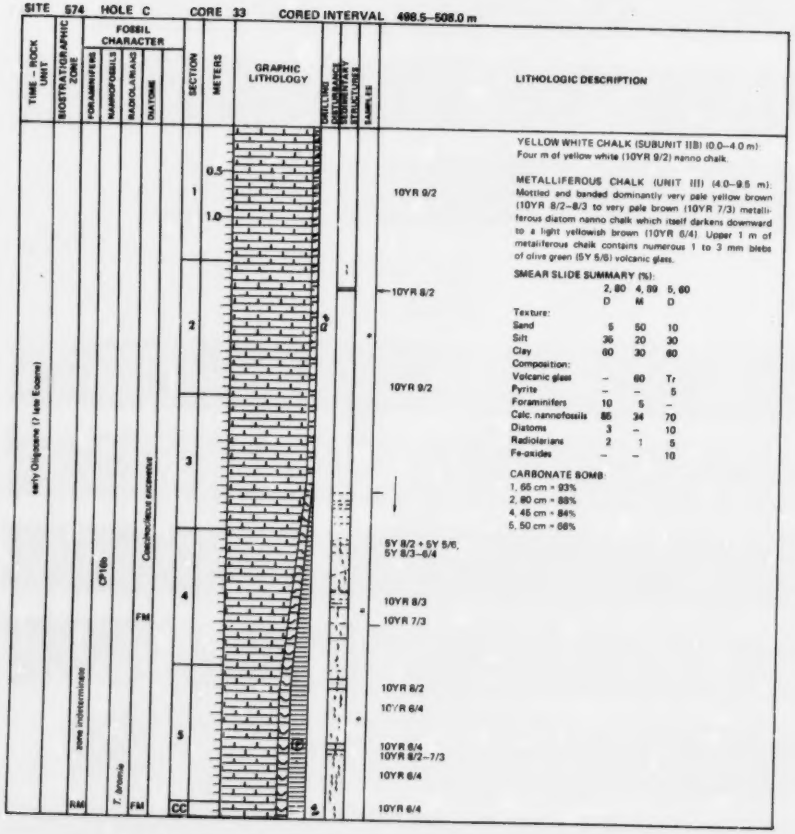
SITE 574 HOLE C CORE 33 CORED INTERVAL 498.5–508.0 m
TIME – ROCK UNIT
BIOSTRATIGRAPHIC ZONE
FOSSIL CHARACTER
FORAMINIFERS
NANHOFOSSILS
RADIOLARIANS
DIATOMS
SECTION
METERS
GRAPHIC LITHOLOGY
DRILLING DISTURBANCE
SEDIMENTARY STRUCTURES
SAMPLES
LITHOLOGIC DESCRIPTION
early Oligocene (? late Eocene)
zone indeterminate
CP16b
Cyclicargolithus floridanus
T. bromia
RM
FM
CC
10YR 9/2
10YR 8/2
10YR 9/2
5Y 8/2 + 5Y 5/6, 5Y 8/3–6/4
10YR 8/3
10YR 7/3
10YR 8/2
10YR 6/4
10YR 6/4
10YR 8/2–7/3
10YR 6/4
10YR 6/4
YELLOW WHITE CHALK (SUBUNIT IIB) (0.0–4.0 m):
Four m of yellow white (10YR 9/2) nanno chalk.
METALLIFEROUS CHALK (UNIT III) (4.0–9.5 m):
Mottled and banded dominantly very pale yellow brown (10YR 8/2–8/3 to very pale brown (10YR 7/3) metalliferous diatom nanno chalk which itself darkens downward to a light yellowish brown (10YR 6/4). Upper 1 m of metalliferous chalk contains numerous 1 to 3 mm blebs of olive green (5Y 5/6) volcanic glass.
SMEAR SLIDE SUMMARY (%):
2, 80 D
4, 89 M
5, 60 D
Texture:
Sand 5 50 10
Silt 35 20 30
Clay 60 30 60
Composition:
Volcanic glass – 60 Tr
Pyrite – – 5
Foraminifers 10 5 –
Calc. nannofossils 85 34 70
Diatoms 3 – 10
Radiolarians 2 1 5
Fe-oxides – – 10
CARBONATE BOMB:
1, 65 cm = 93%
2, 80 cm = 88%
4, 45 cm = 84%
5, 50 cm = 68%

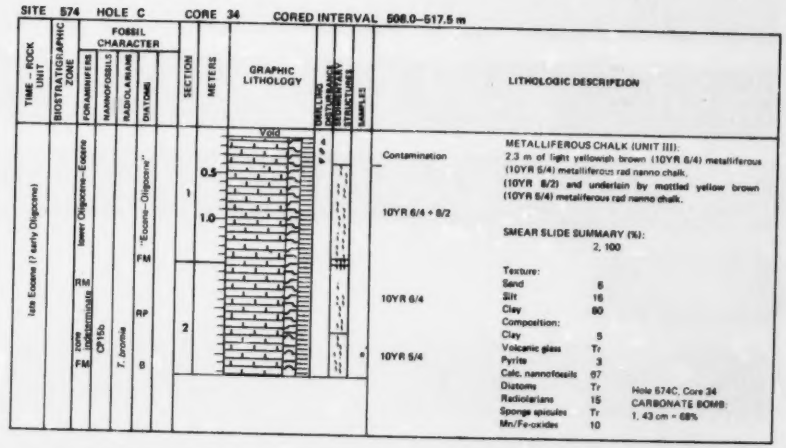
SITE 574 HOLE C CORE 34 CORED INTERVAL 508.0–517.5 m
TIME – ROCK UNIT
BIOSTRATIGRAPHIC ZONE
FOSSIL CHARACTER
FORAMINIFERS
NANNOFOSSILS
RADIOLARIANS
DIATOMS
SECTION
METERS
GRAPHIC LITHOLOGY
DRILLING DISTURBANCE
SEDIMENTARY STRUCTURES
SAMPLES
LITHOLOGIC DESCRIPTION
late Eocene (? early Oligocene)
lower Oligocene–Eocene
CP15b
RM
FM
T. bromia
"Eocene–Oligocene"
RP
B
Void
Contamination
10YR 6/4 + 8/2
10YR 6/4
10YR 5/4
METALLIFEROUS CHALK (UNIT III):
2.3 m of light yellowish brown (10YR 6/4) metalliferous (10YR 6/4) metalliferous rad nanno chalk.
(10YR 8/2) and underlain by mottled yellow brown (10YR 6/4) metalliferous rad nanno chalk.
SMEAR SLIDE SUMMARY (%):
2, 100
Texture:
Sand 5
Silt 15
Clay 80
Composition:
Clay 5
Volcanic glass Tr
Pyrite 3
Calc. nannofossils 97
Diatoms Tr
Radiolarians 15
Sponge spicules Tr
Mn/Fe-oxides 10
Hole 574C, Core 34
CARBONATE BOMB:
1, 43 cm = 68%

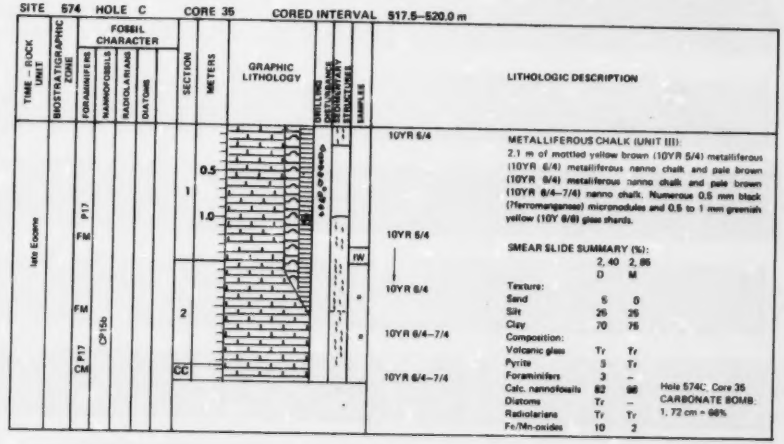
SITE 574 HOLE C CORE 35 CORED INTERVAL 517.5–520.0 m
TIME – ROCK UNIT
BIOSTRATIGRAPHIC ZONE
FOSSIL CHARACTER
FORAMINIFERS
NANNOFOSSILS
RADIOLARIANS
DIATOMS
SECTION
METERS
GRAPHIC LITHOLOGY
DRILLING DISTURBANCE
SEDIMENTARY STRUCTURES
SAMPLES
LITHOLOGIC DESCRIPTION
late Eocene
P17
CP15b
FM
CM
CC
IW
10YR 6/4
10YR 5/4
10YR 6/4
10YR 6/4–7/4
10YR 6/4–7/4
METALLIFEROUS CHALK (UNIT III):
2.1 m of mottled yellow brown (10YR 5/4) metalliferous (10YR 6/4) metalliferous nanno chalk and pale brown (10YR 6/4) metalliferous nanno chalk and pale brown (10YR 6/4–7/4) nanno chalk. Numerous 0.5 mm black (?ferromanganese) micronodules and 0.5 to 1 mm greenish yellow (10Y 8/8) glass shards.
SMEAR SLIDE SUMMARY (%):
2, 40 D
2, 85 M
Texture:
Sand 5 0
Silt 25 25
Clay 70 75
Composition:
Volcanic glass Tr Tr
Pyrite 5 Tr
Foraminifers 3 –
Calc. nannofossils 82 98
Diatoms Tr –
Radiolarians Tr Tr
Fe/Mn-oxides 10 2
Hole 574C, Core 35
CARBONATE BOMB:
1, 72 cm = 66%

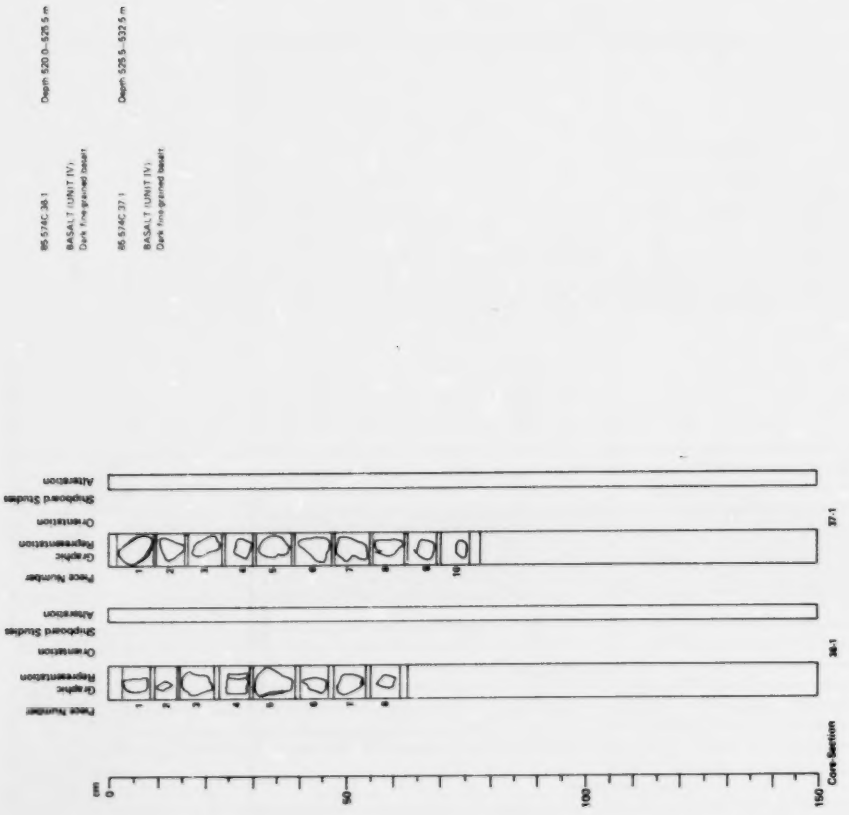
85-574C-36-1
Depth 520.0–525.5 m
BASALT (UNIT IV):
Dark fine-grained basalt
85-574C-37-1
Depth 525.5–532.5 m
BASALT (UNIT IV):
Dark fine-grained basalt
Piece Number
Graphic Representation
Orientation
Sheeted Dikes
Alteration
36-1
37-1
cm
0
50
100
150
Core Section

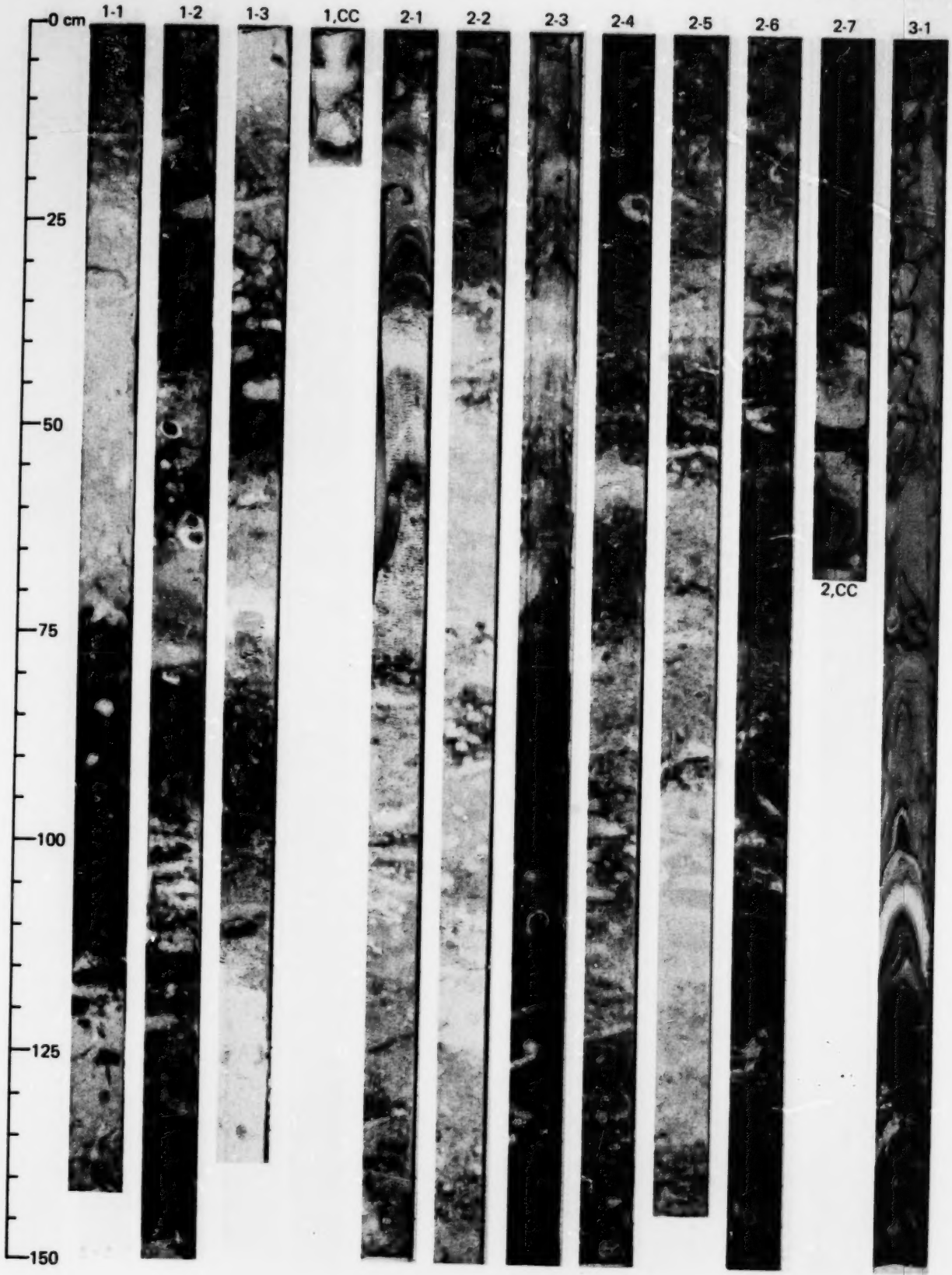
0 cm
25
50
75
100
125
150
1-1
1-2
1-3
1,CC
2-1
2-2
2-3
2-4
2-5
2-6
2-7
2,CC
3-1

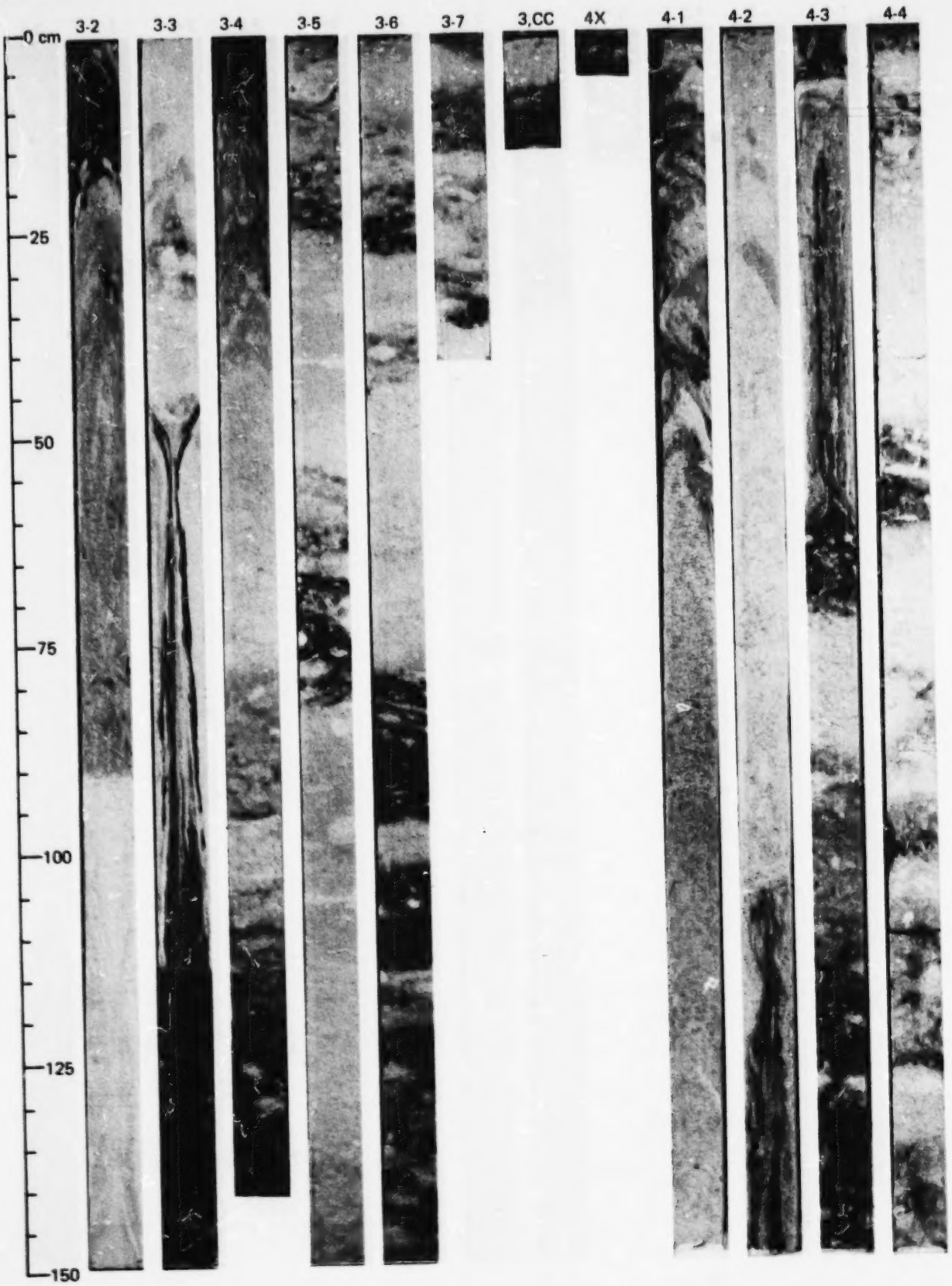
0 cm
25
50
75
100
125
150
3-2
3-3
3-4
3-5
3-6
3-7
3,CC
4X
4-1
4-2
4-3
4-4

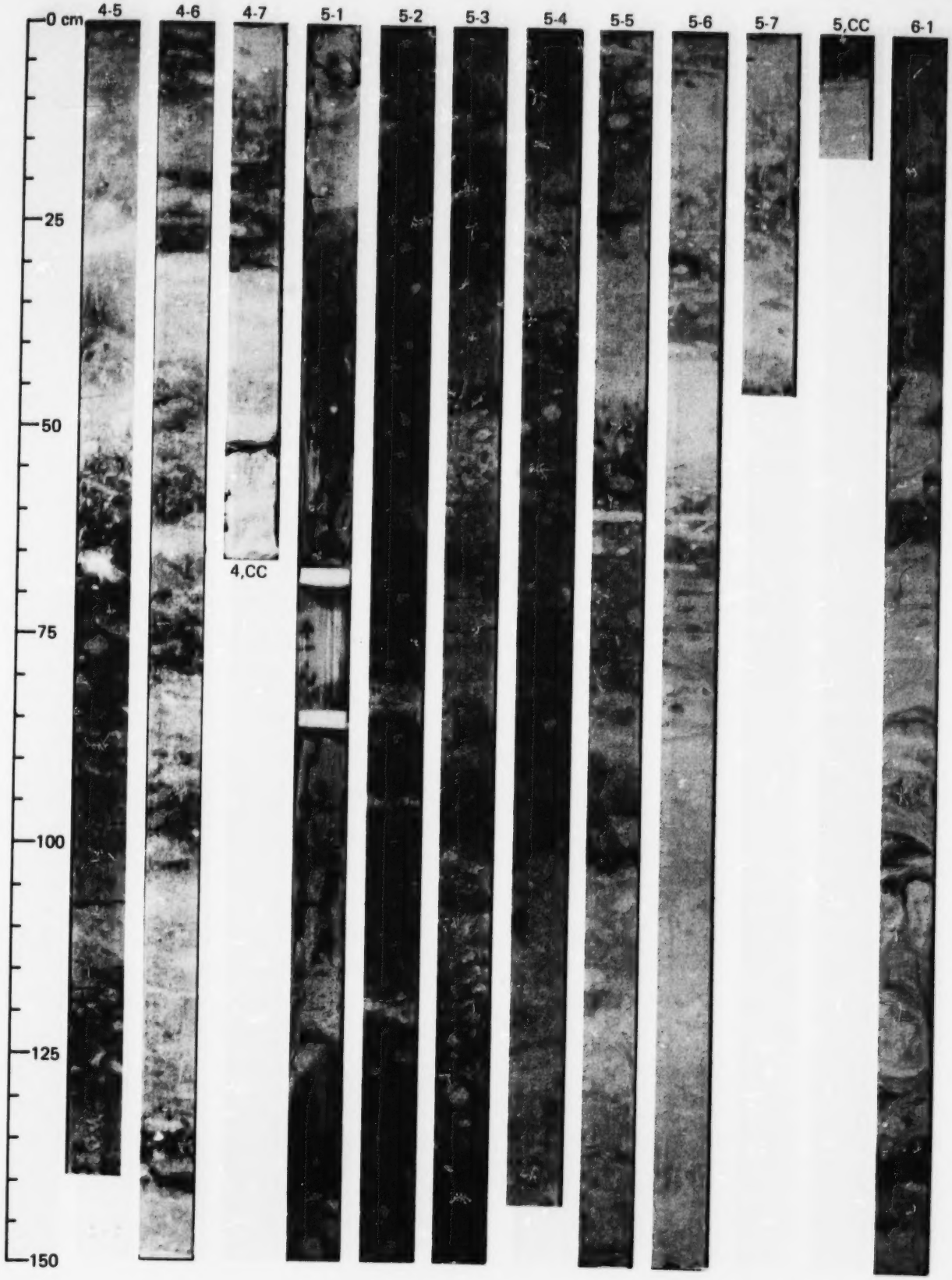
0 cm
25
50
75
100
125
150
4-5
4-6
4-7
4,CC
5-1
5-2
5-3
5-4
5-5
5-6
5-7
5,CC
6-1

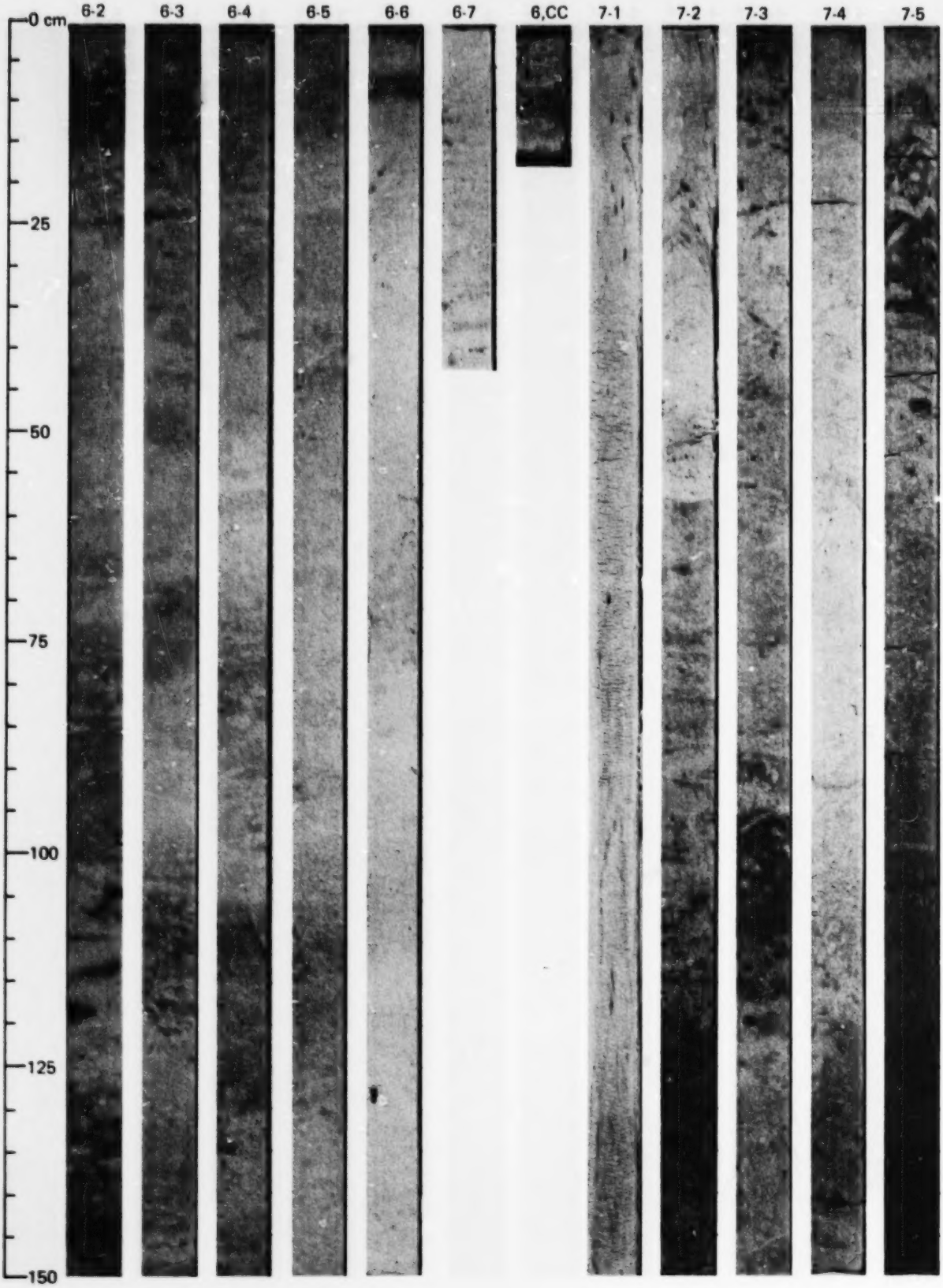
0 cm
25
50
75
100
125
150
6-2
6-3
6-4
6-5
6-6
6-7
6,CC
7-1
7-2
7-3
7-4
7-5

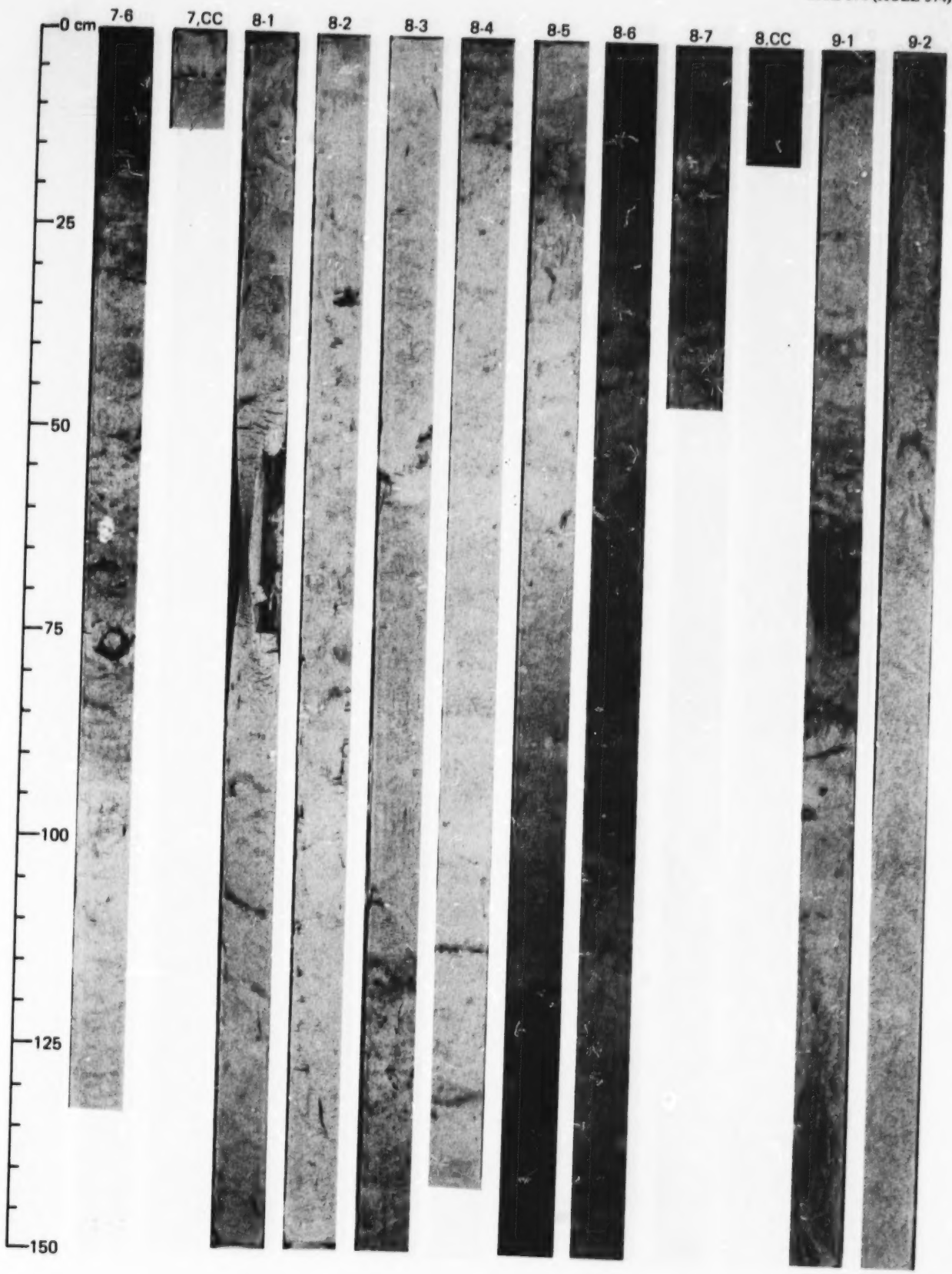
0 cm
25
50
75
100
125
150
7-6
7,CC
8-1
8-2
8-3
8-4
8-5
8-6
8-7
8,CC
9-1
9-2

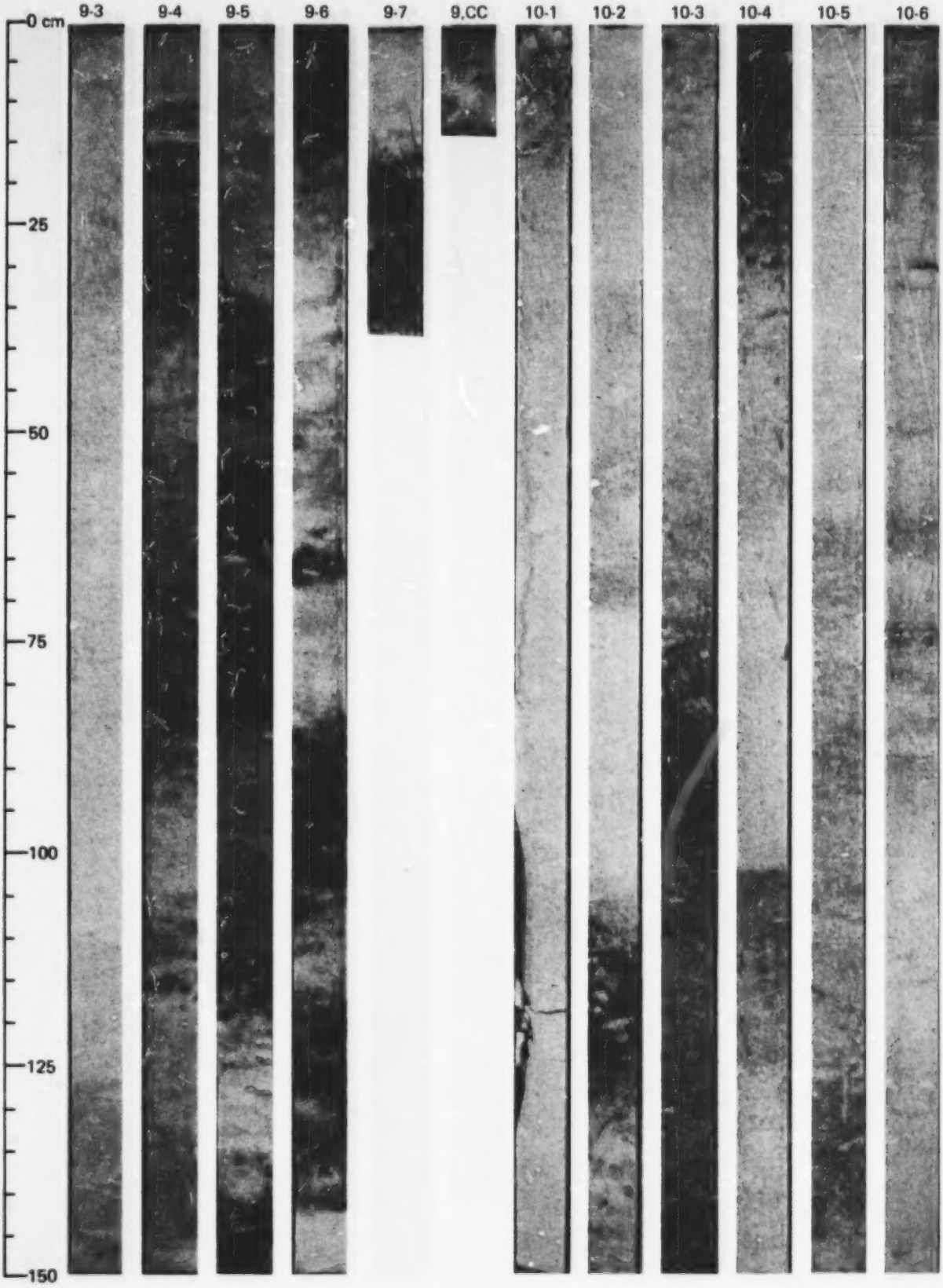
0 cm
25
50
75
100
125
150
9-3
9-4
9-5
9-6
9-7
9,CC
10-1
10-2
10-3
10-4
10-5
10-6

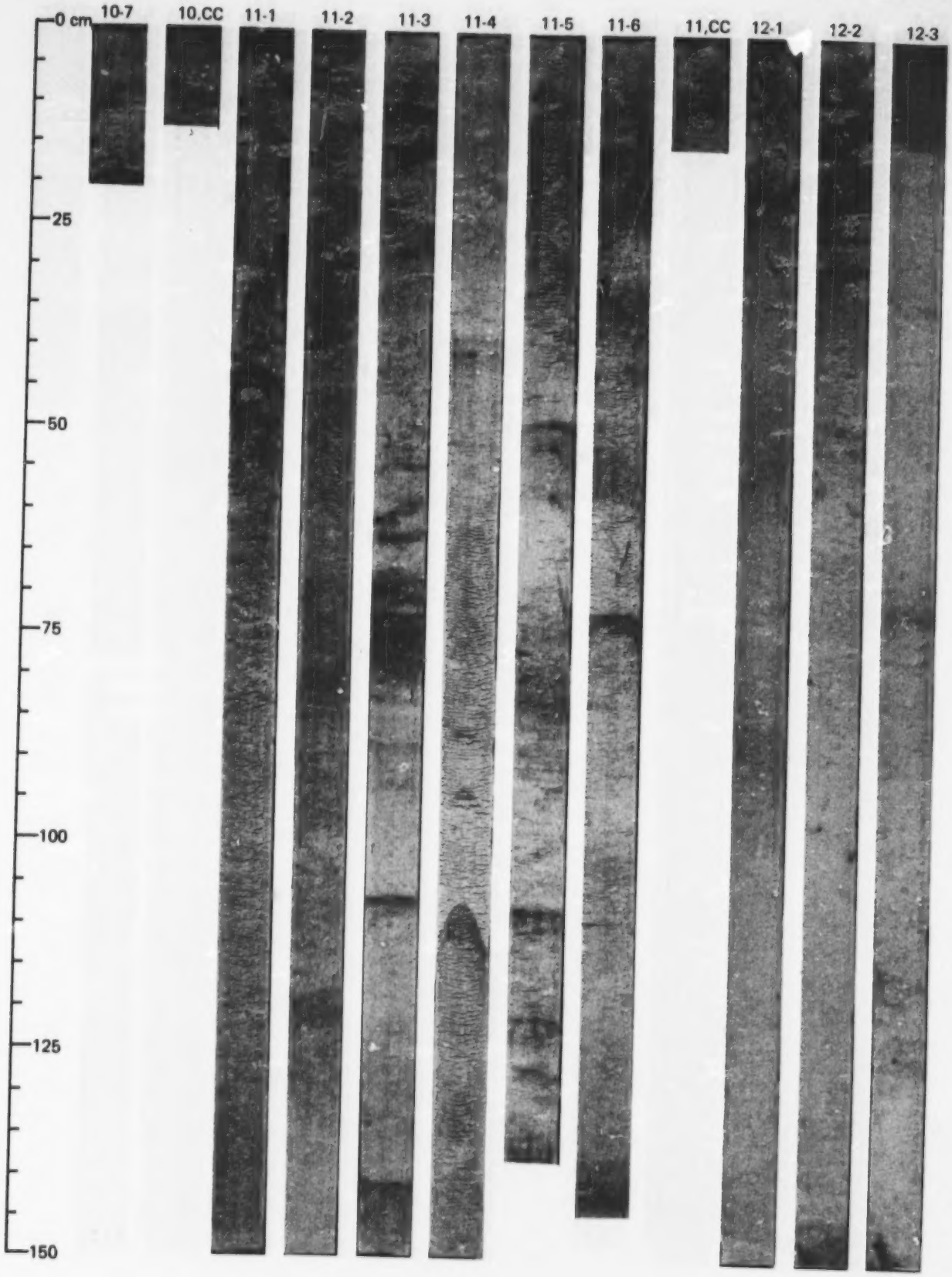
0 cm
10-7
10,CC
11-1
11-2
11-3
11-4
11-5
11-6
11,CC
12-1
12-2
12-3
25
50
75
100
125
150

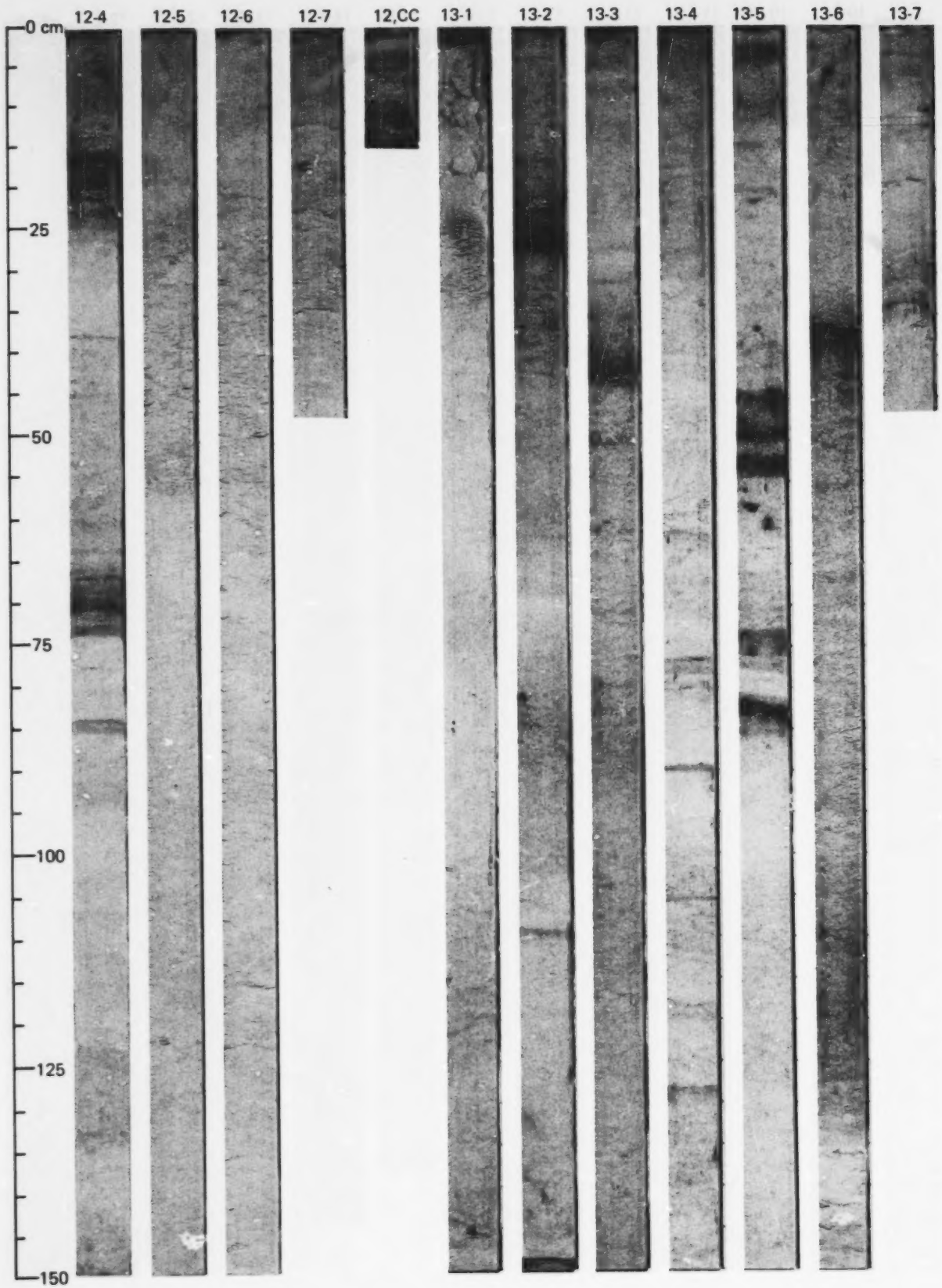
12-4
12-5
12-6
12-7
12,CC
13-1
13-2
13-3
13-4
13-5
13-6
13-7
0 cm
25
50
75
100
125
150

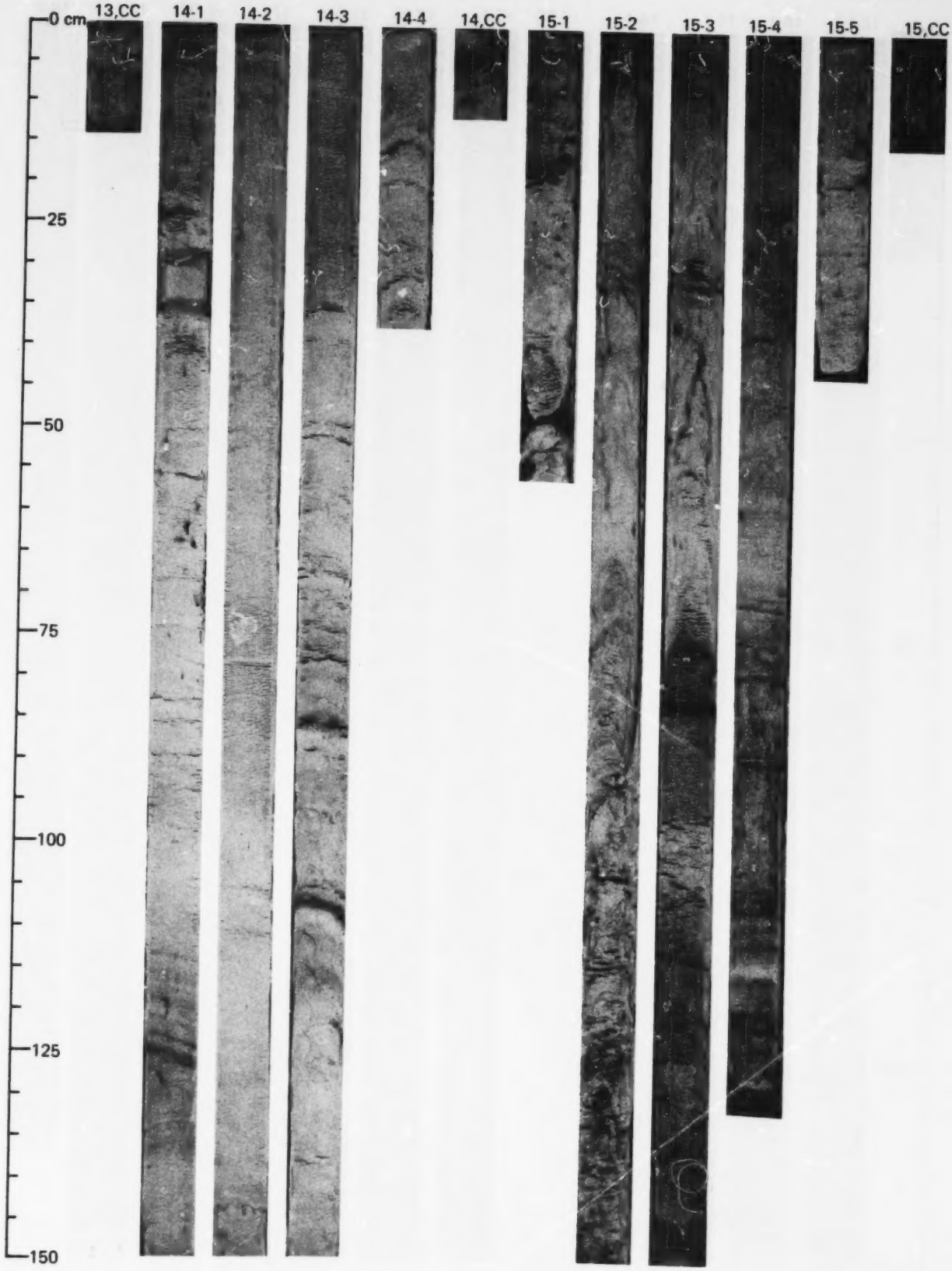
0 cm
13,CC
14-1
14-2
14-3
14-4
14,CC
15-1
15-2
15-3
15-4
15-5
15,CC
25
50
75
100
125
150

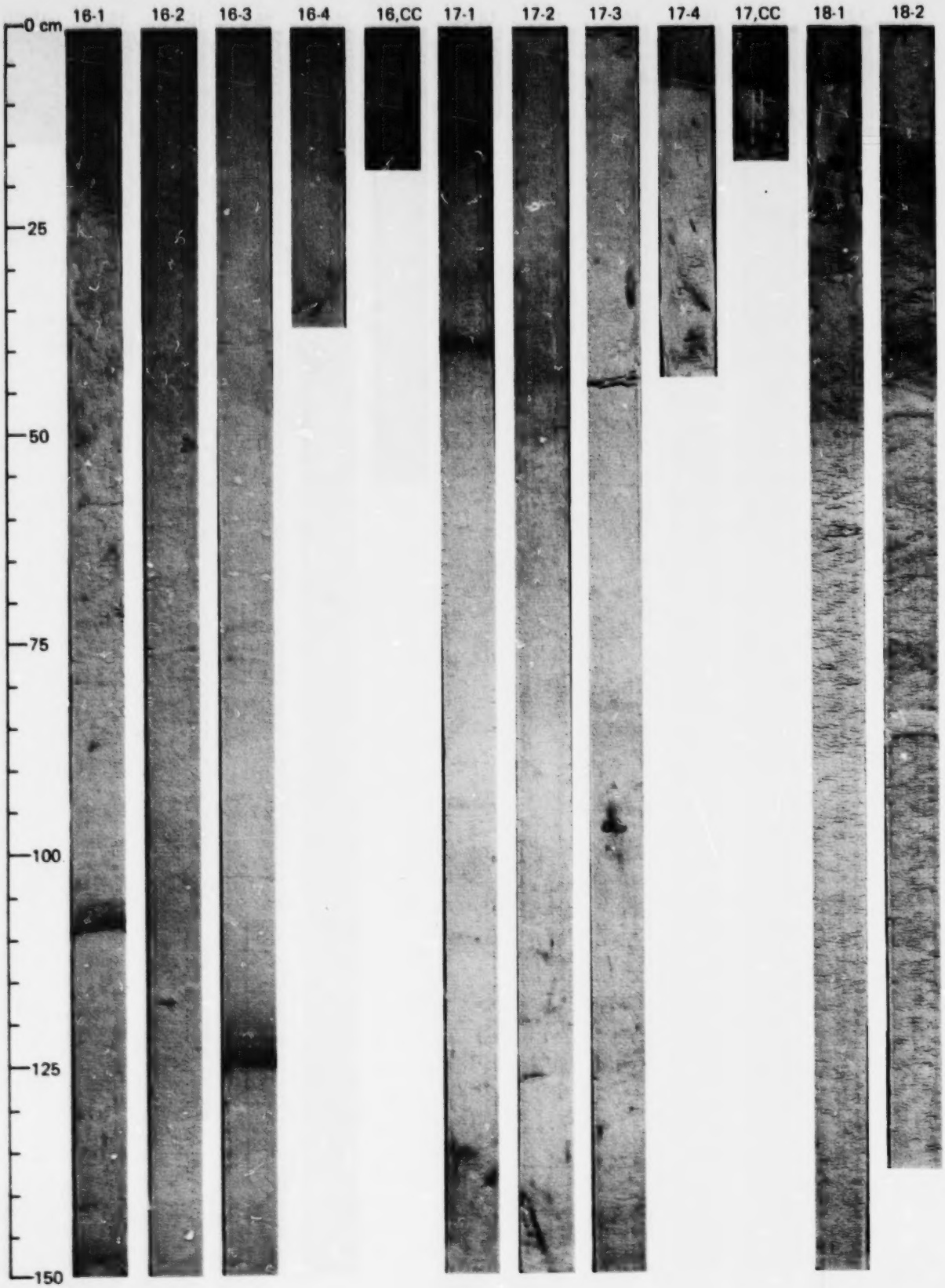
16-1
16-2
16-3
16-4
16,CC
17-1
17-2
17-3
17-4
17,CC
18-1
18-2
0 cm
25
50
75
100
125
150

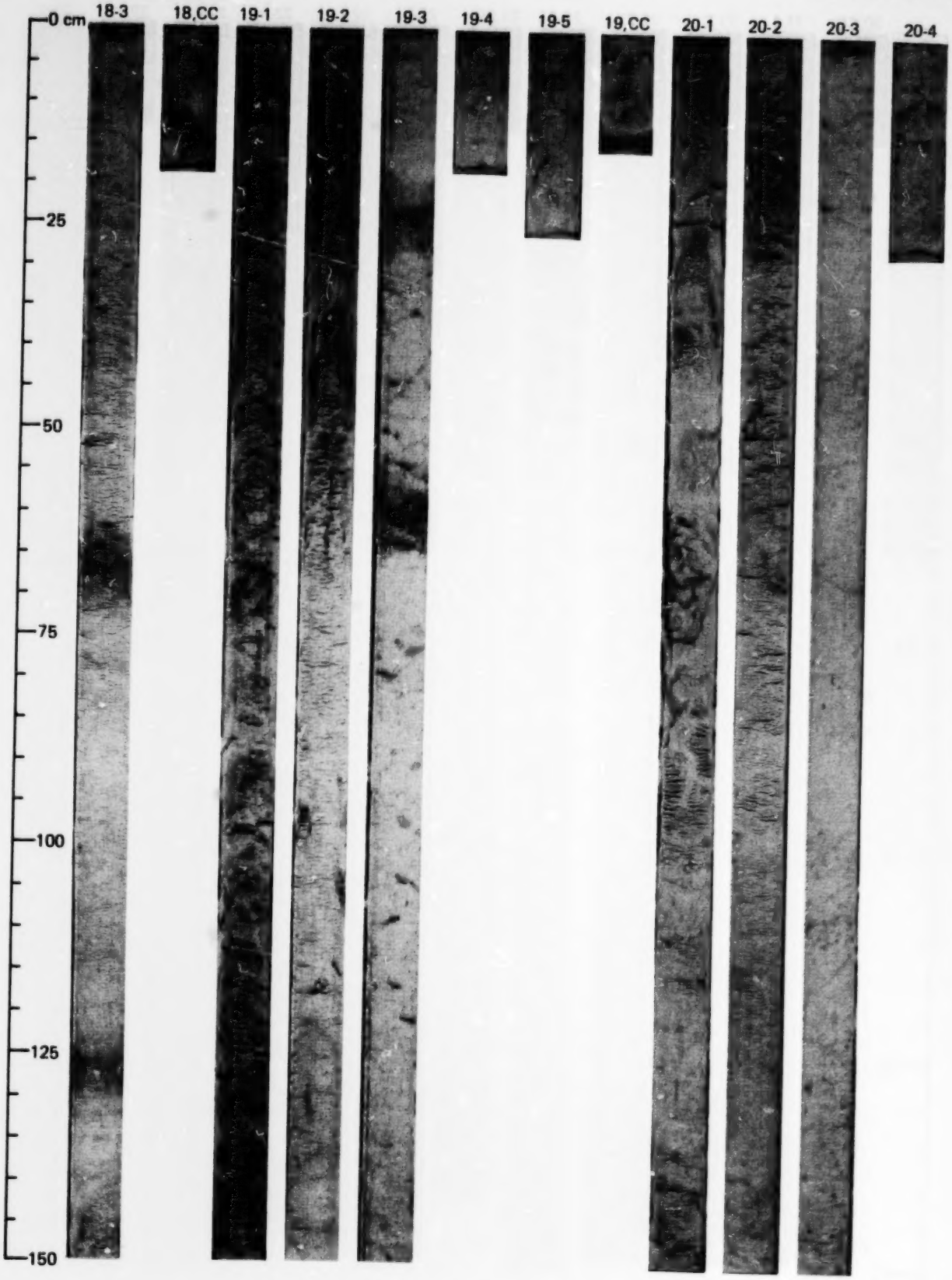
0 cm
25
50
75
100
125
150
18-3
18,CC
19-1
19-2
19-3
19-4
19-5
19,CC
20-1
20-2
20-3
20-4

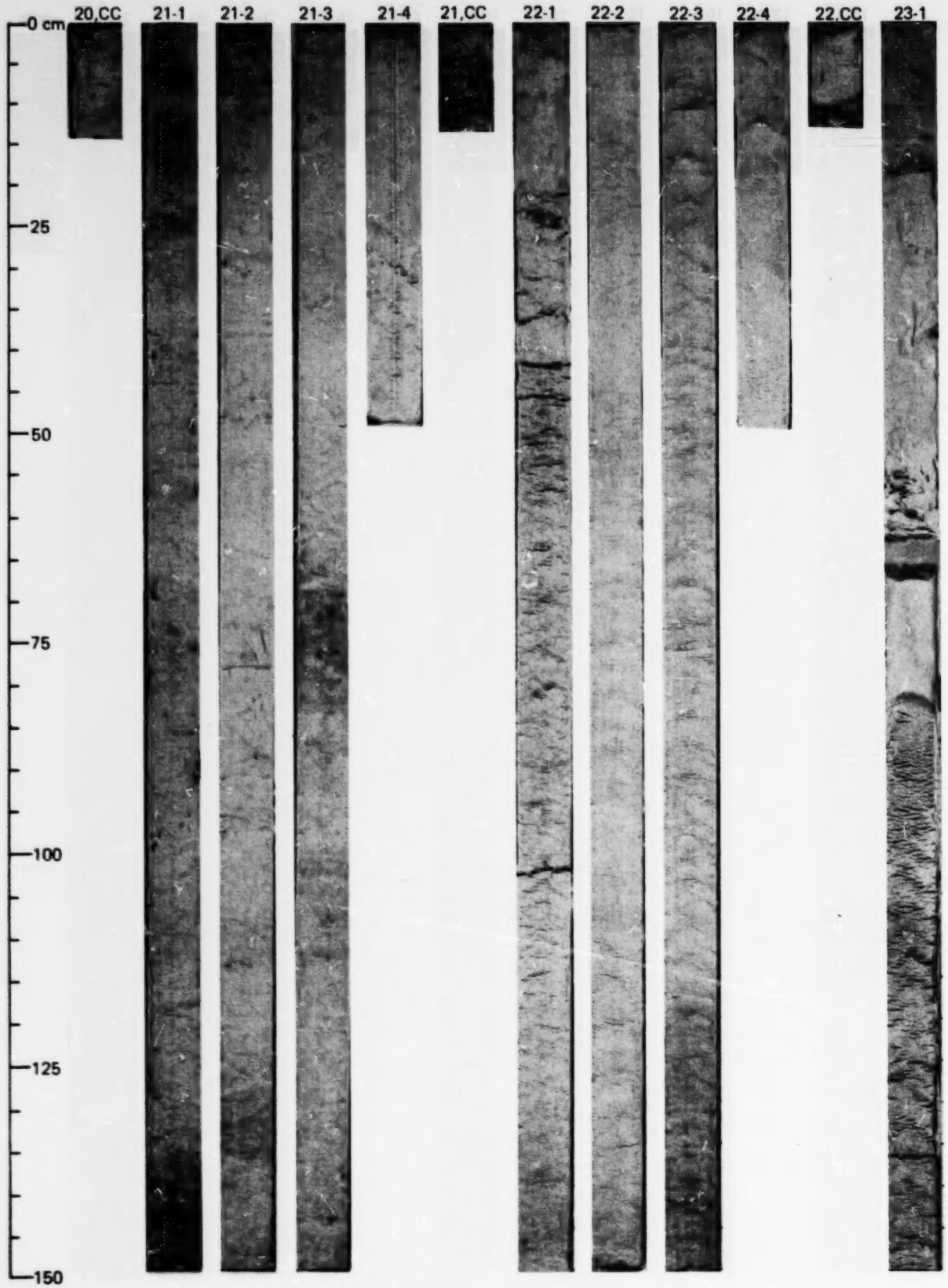
20,CC
21-1
21-2
21-3
21-4
21,CC
22-1
22-2
22-3
22-4
22,CC
23-1
0 cm
25
50
75
100
125
150

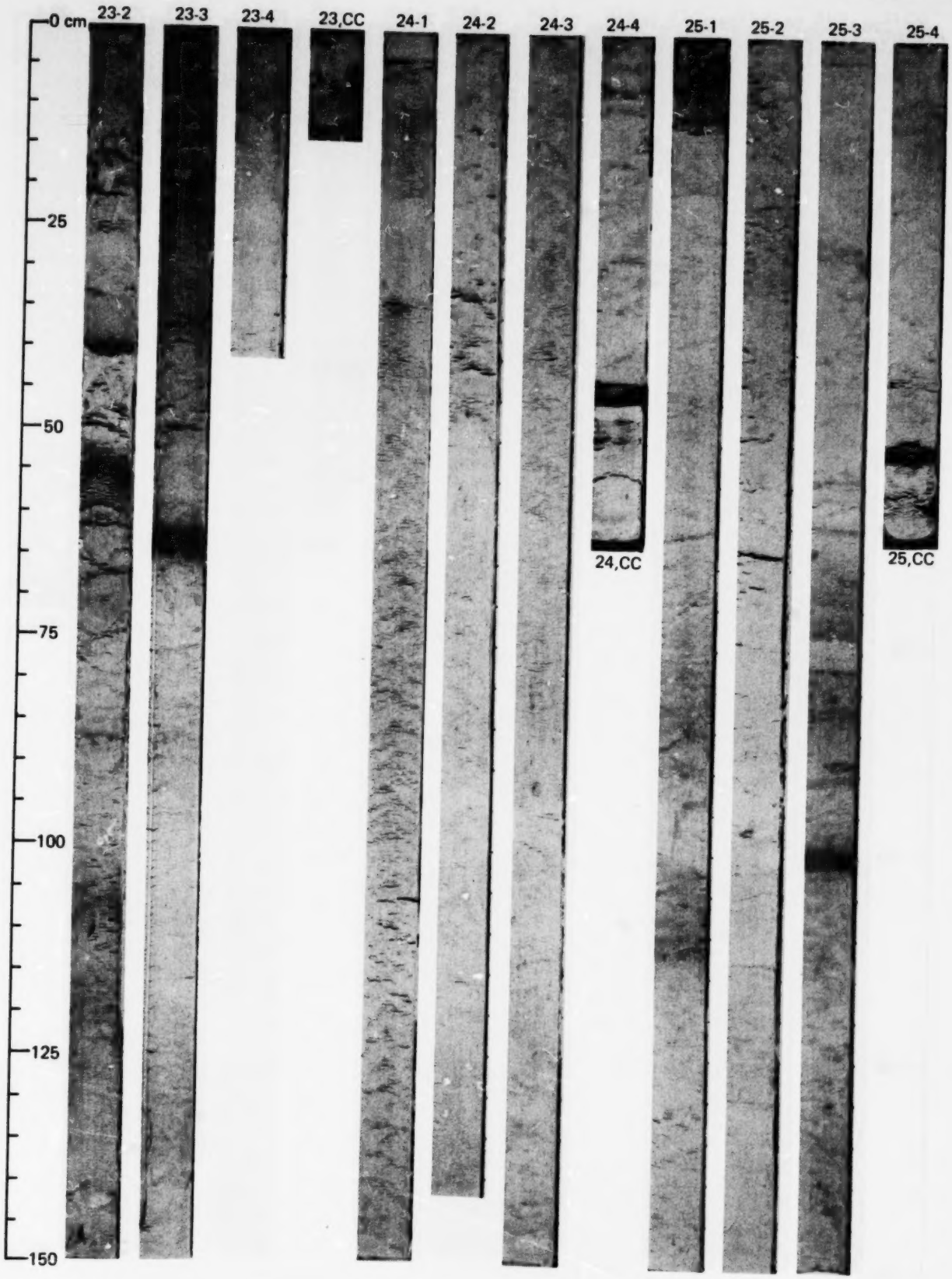
0 cm
25
50
75
100
125
150
23-2
23-3
23-4
23,CC
24-1
24-2
24-3
24-4
24,CC
25-1
25-2
25-3
25-4
25,CC

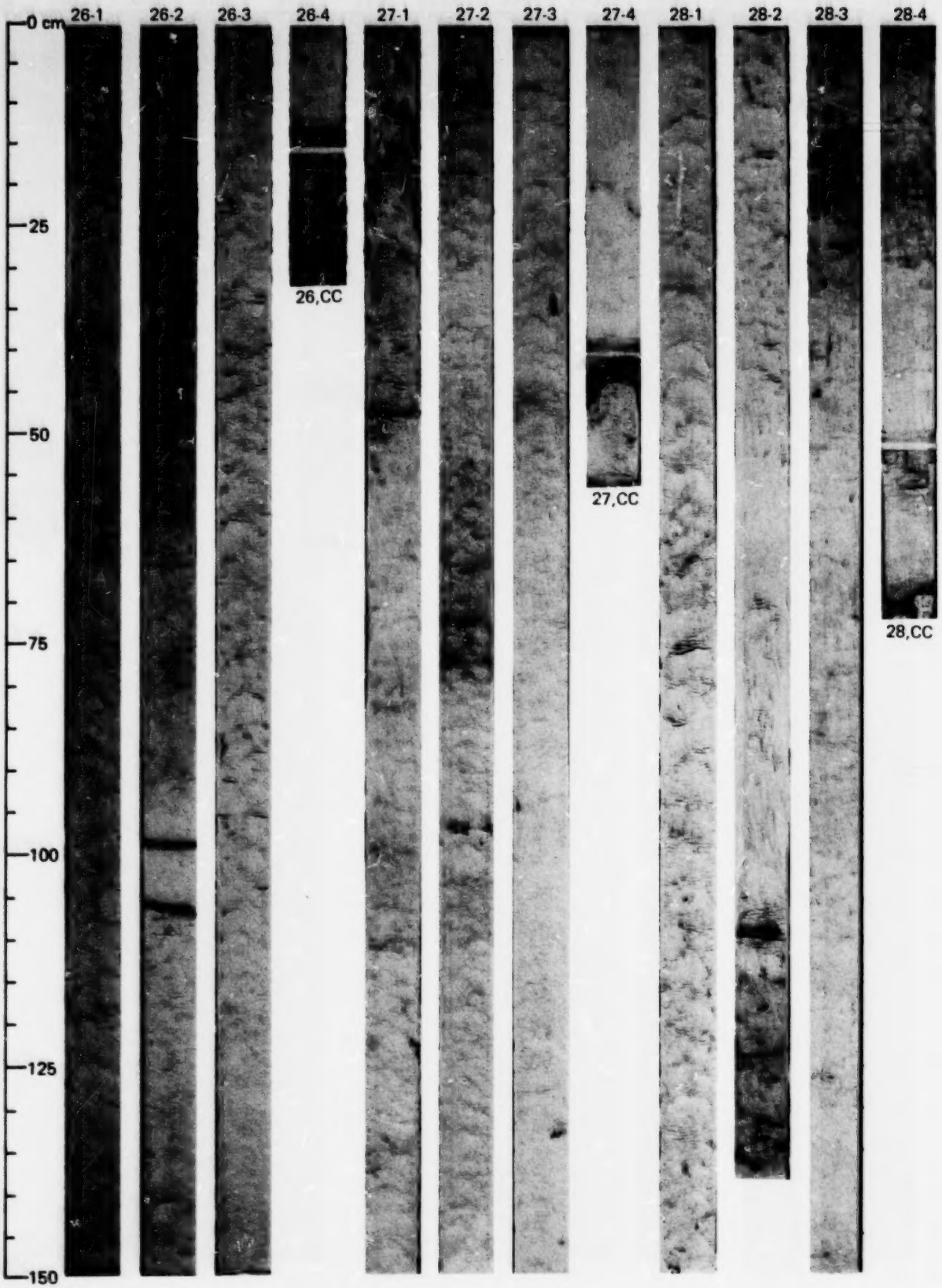
0 cm
25
50
75
100
125
150
26-1
26-2
26-3
26-4
26,CC
27-1
27-2
27-3
27-4
27,CC
28-1
28-2
28-3
28-4
28,CC

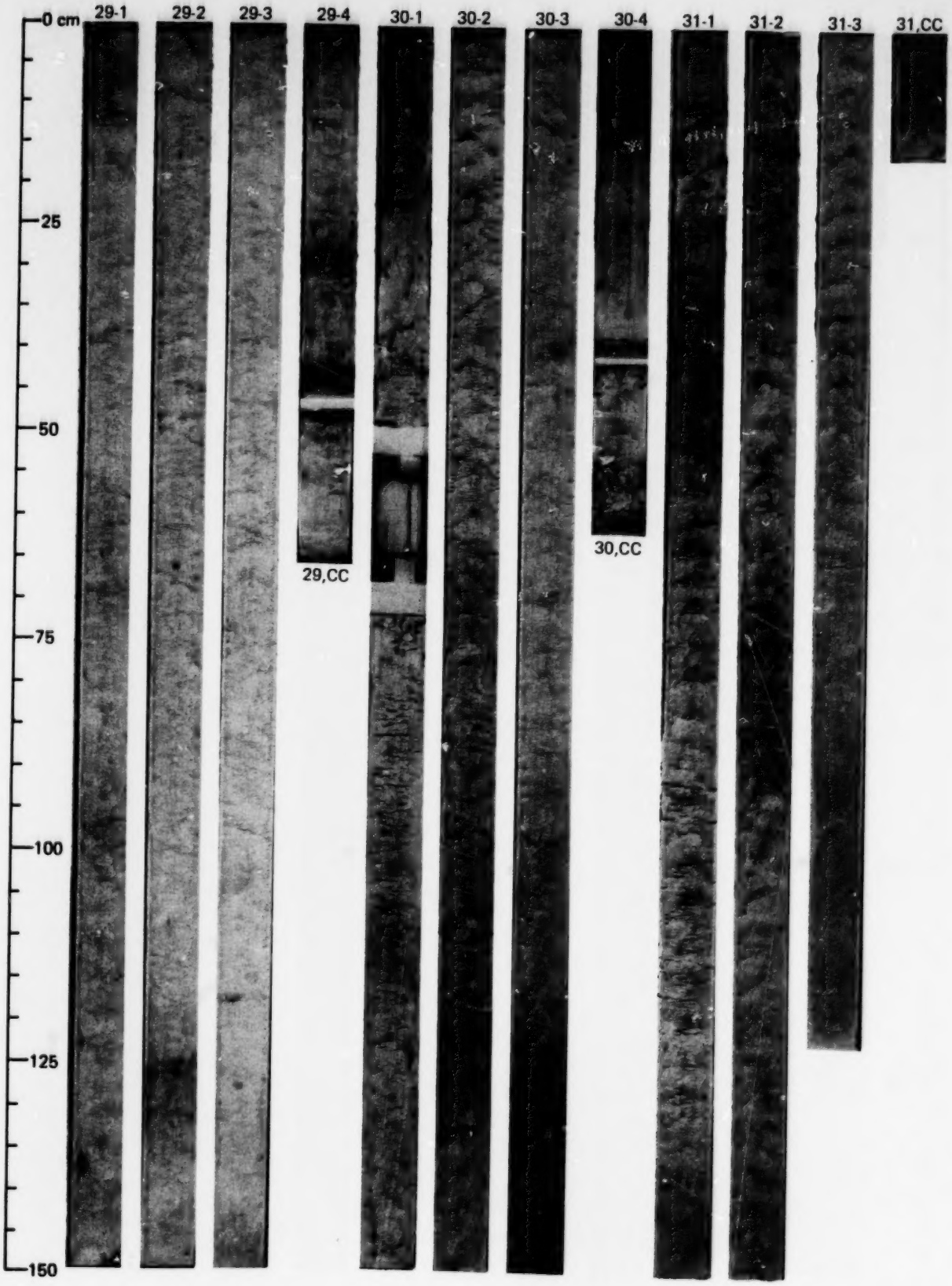
0 cm
25
50
75
100
125
150
29-1
29-2
29-3
29-4
29,CC
30-1
30-2
30-3
30-4
30,CC
31-1
31-2
31-3
31,CC

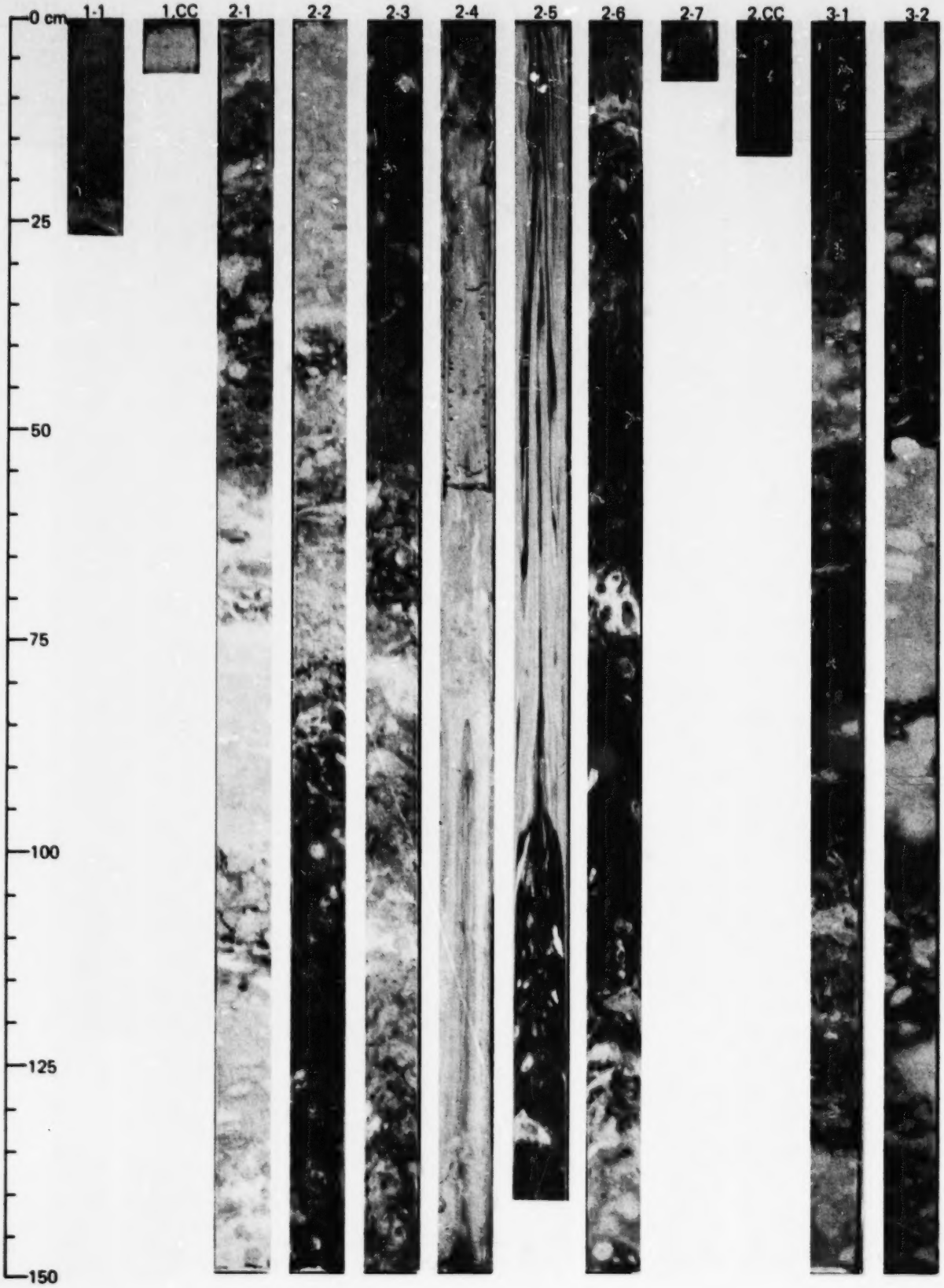
0 cm
1-1
1,CC
2-1
2-2
2-3
2-4
2-5
2-6
2-7
2,CC
3-1
3-2
25
50
75
100
125
150

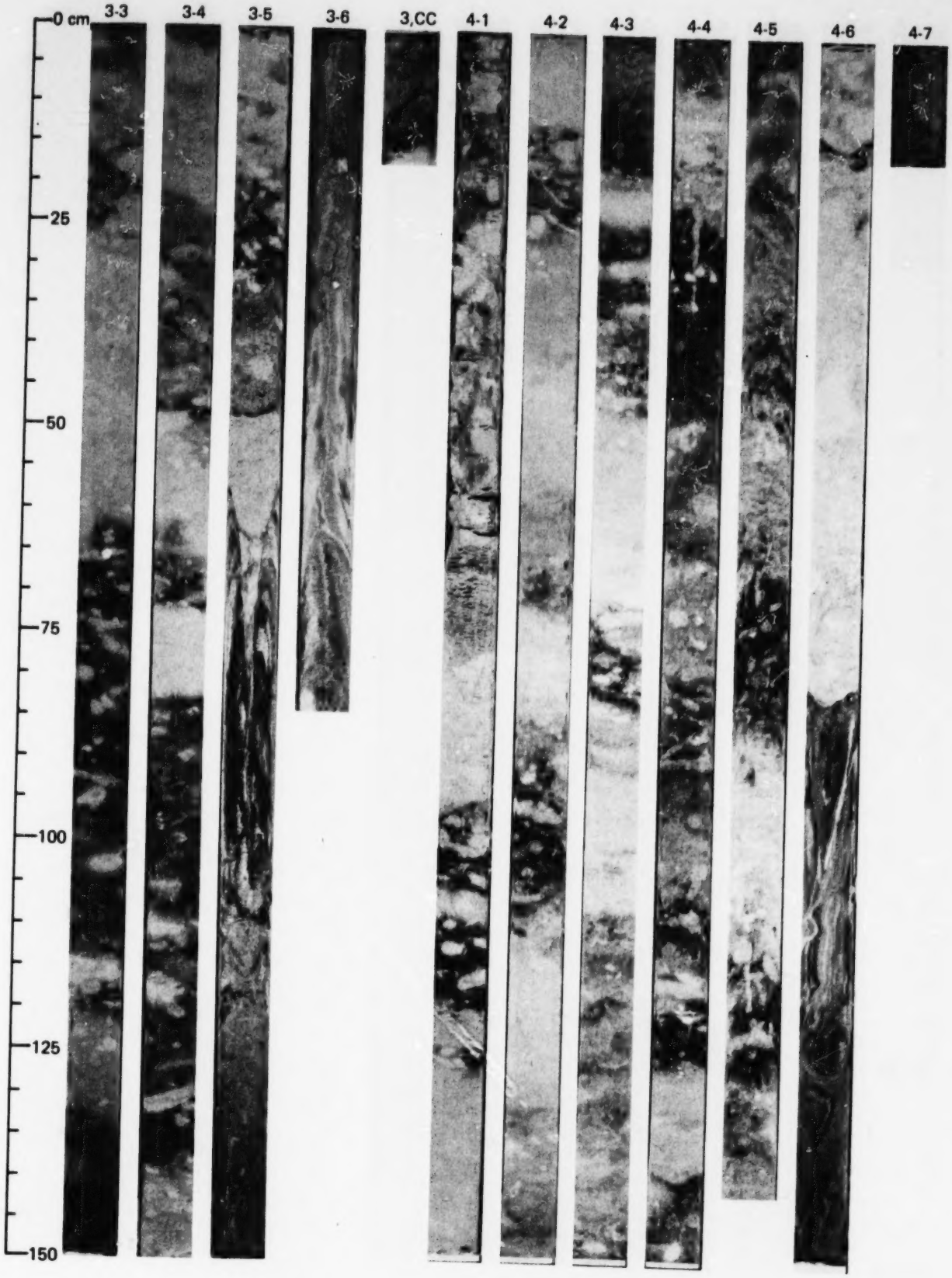
0 cm
25
50
75
100
125
150
3-3
3-4
3-5
3-6
3,CC
4-1
4-2
4-3
4-4
4-5
4-6
4-7

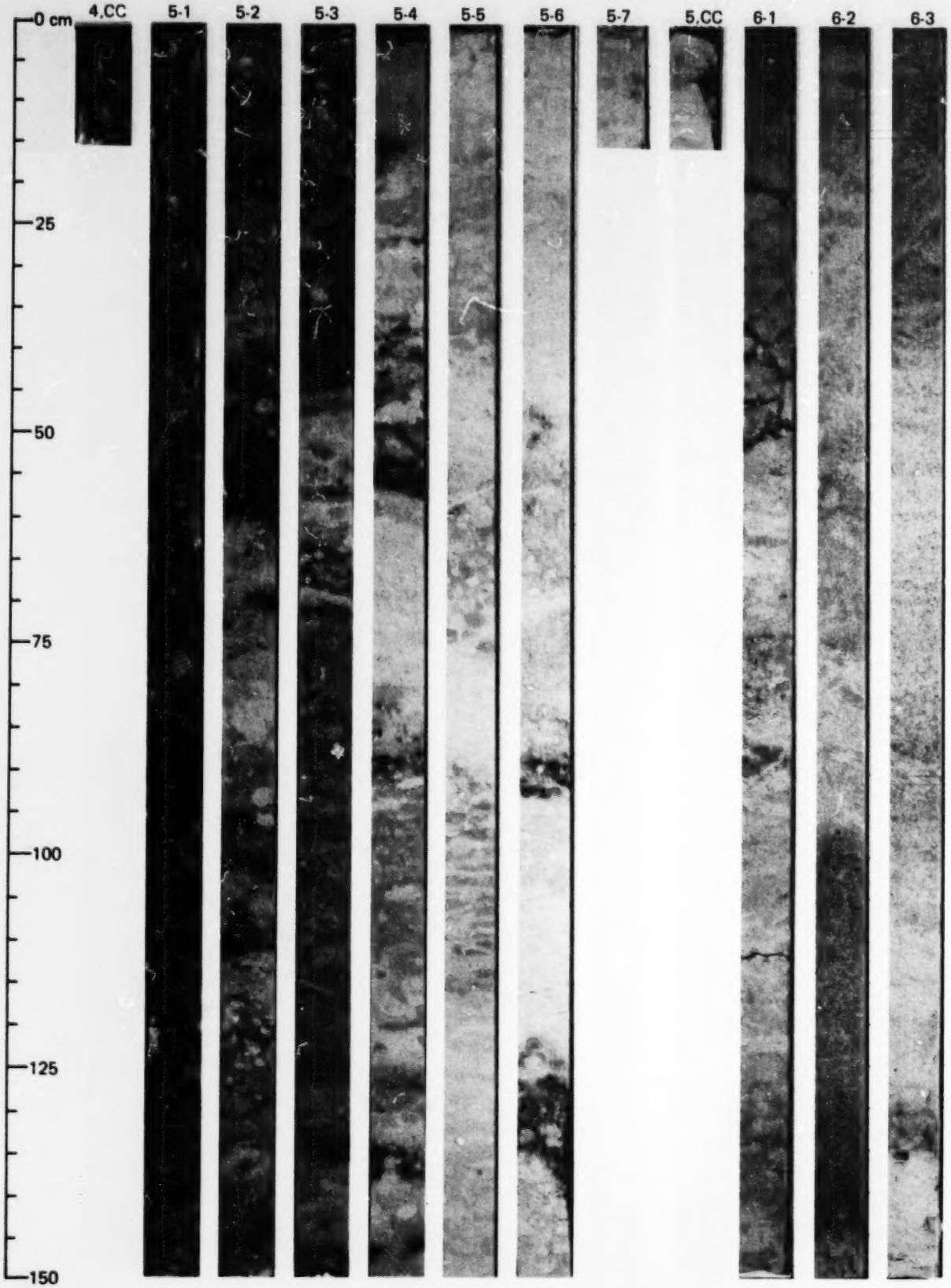
0 cm
25
50
75
100
125
150
4,CC
5-1
5-2
5-3
5-4
5-5
5-6
5-7
5,CC
6-1
6-2
6-3

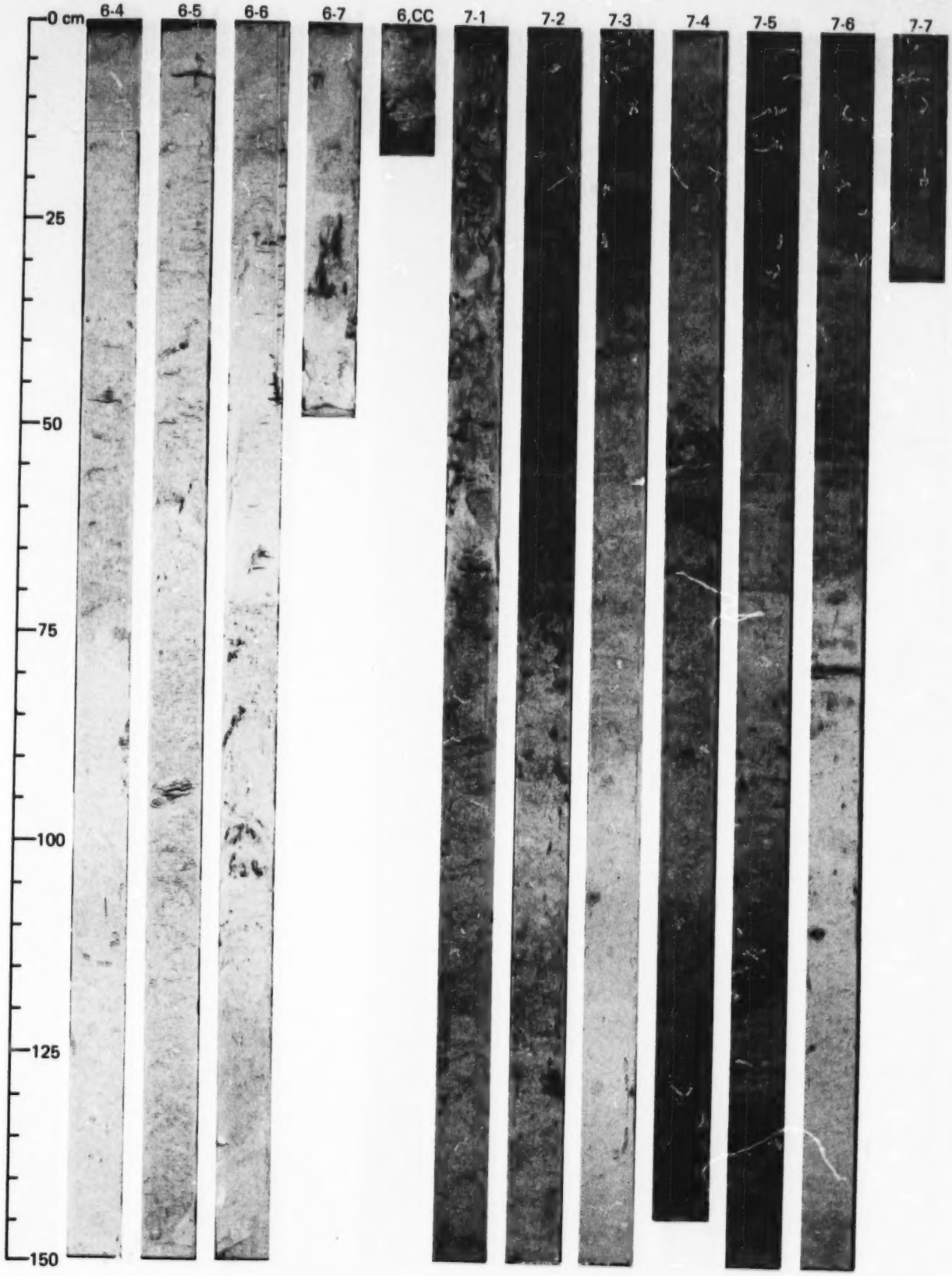
0 cm
6-4
6-5
6-6
6-7
6,CC
7-1
7-2
7-3
7-4
7-5
7-6
7-7
25
50
75
100
125
150

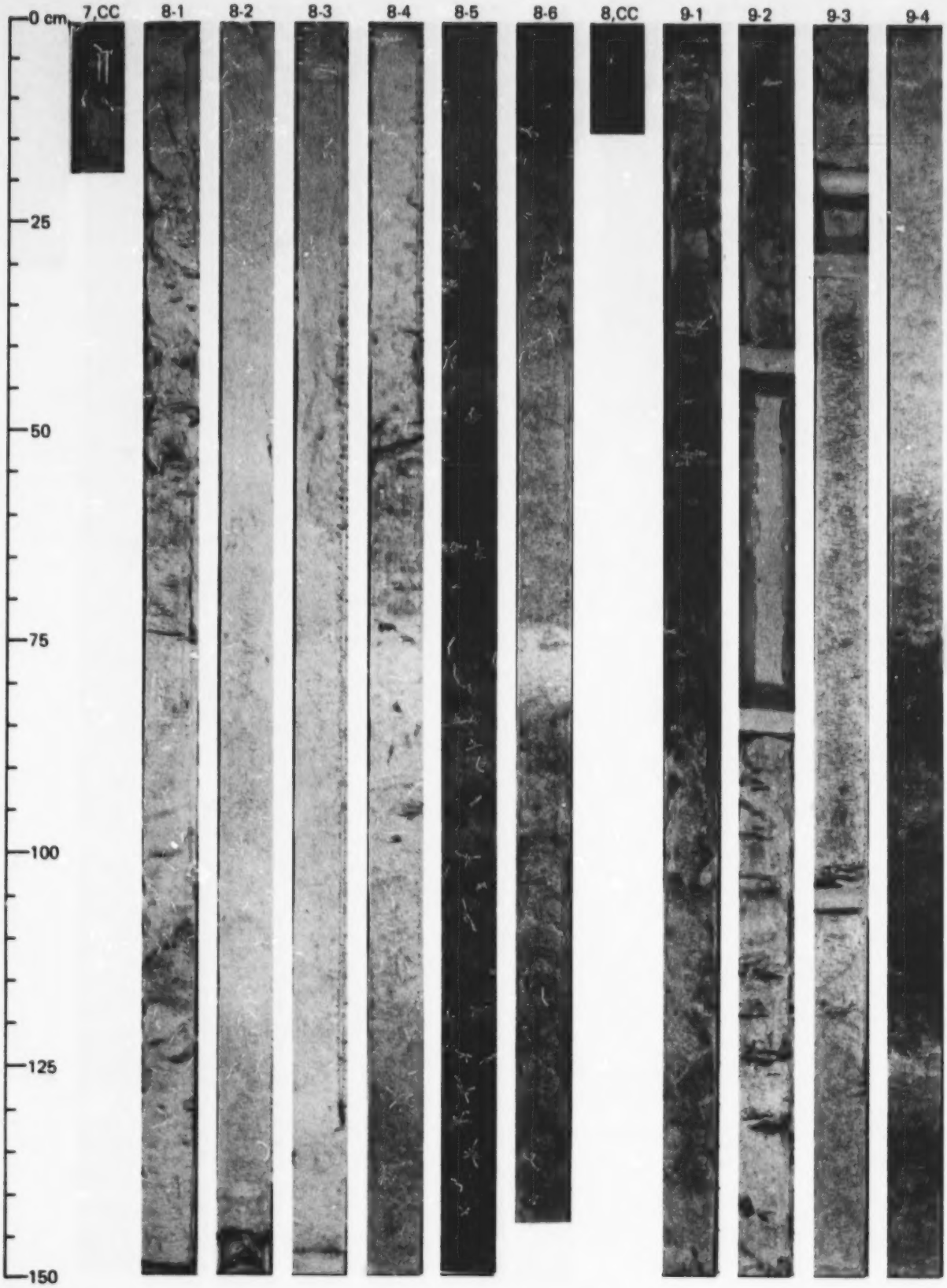
0 cm
25
50
75
100
125
150
7,CC
8-1
8-2
8-3
8-4
8-5
8-6
8,CC
9-1
9-2
9-3
9-4

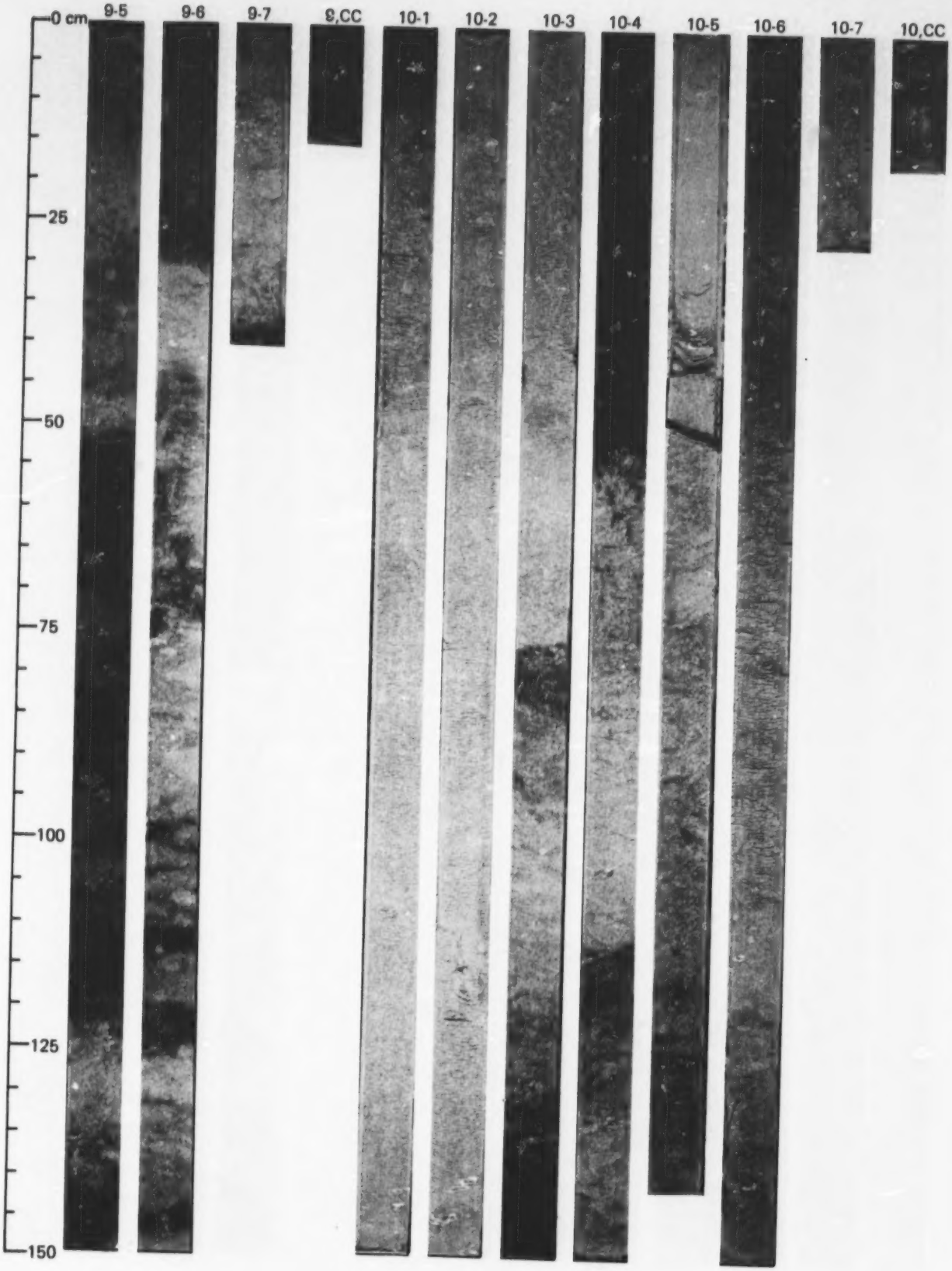
0 cm
9-5
9-6
9-7
8,CC
10-1
10-2
10-3
10-4
10-5
10-6
10-7
10,CC
25
50
75
100
125
150

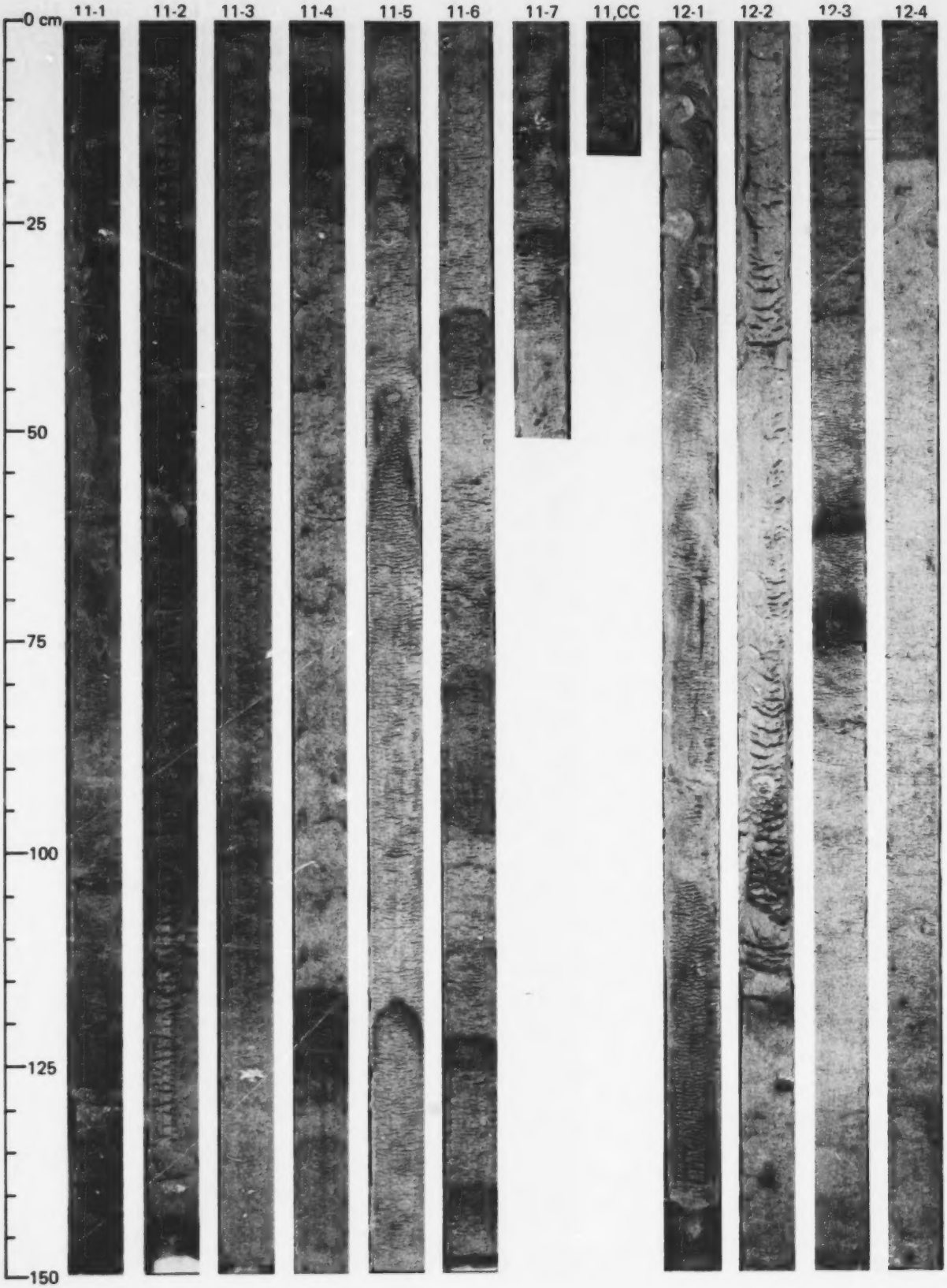
0 cm
25
50
75
100
125
150
11-1
11-2
11-3
11-4
11-5
11-6
11-7
11,CC
12-1
12-2
12-3
12-4

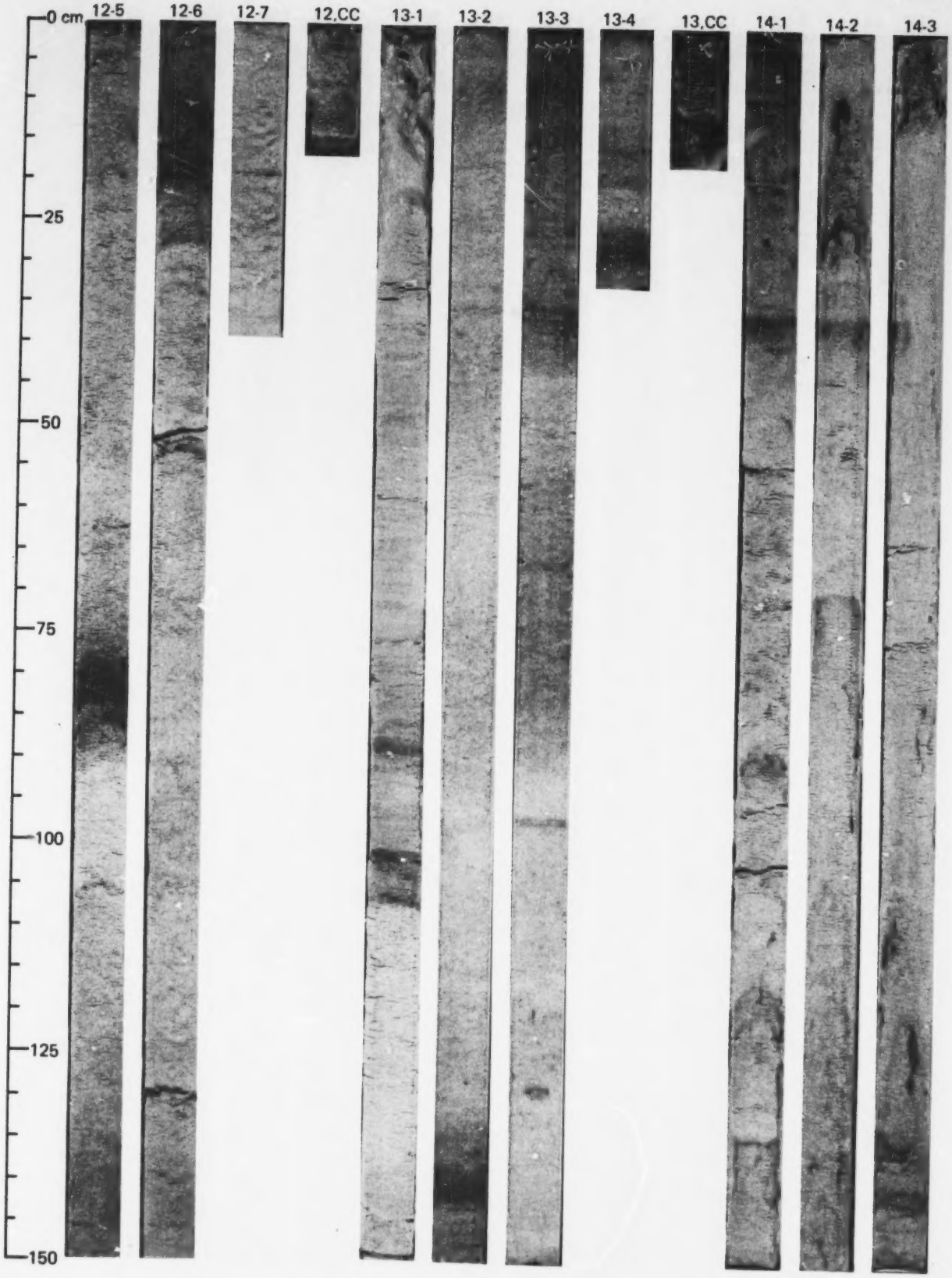
0 cm
12-5
12-6
12-7
12,CC
13-1
13-2
13-3
13-4
13,CC
14-1
14-2
14-3
25
50
75
100
125
150

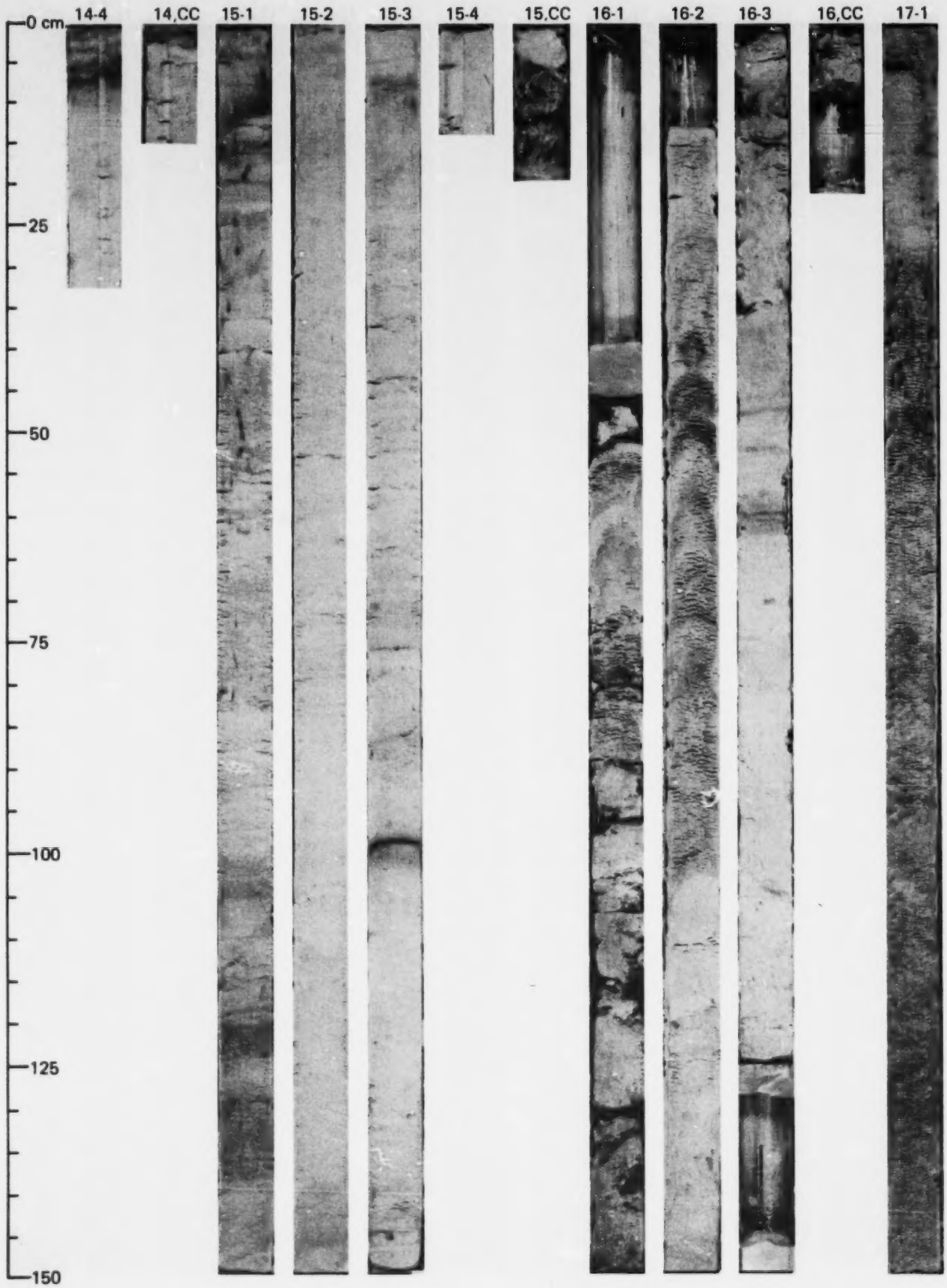
0 cm
25
50
75
100
125
150
14-4
14,CC
15-1
15-2
15-3
15-4
15,CC
16-1
16-2
16-3
16,CC
17-1

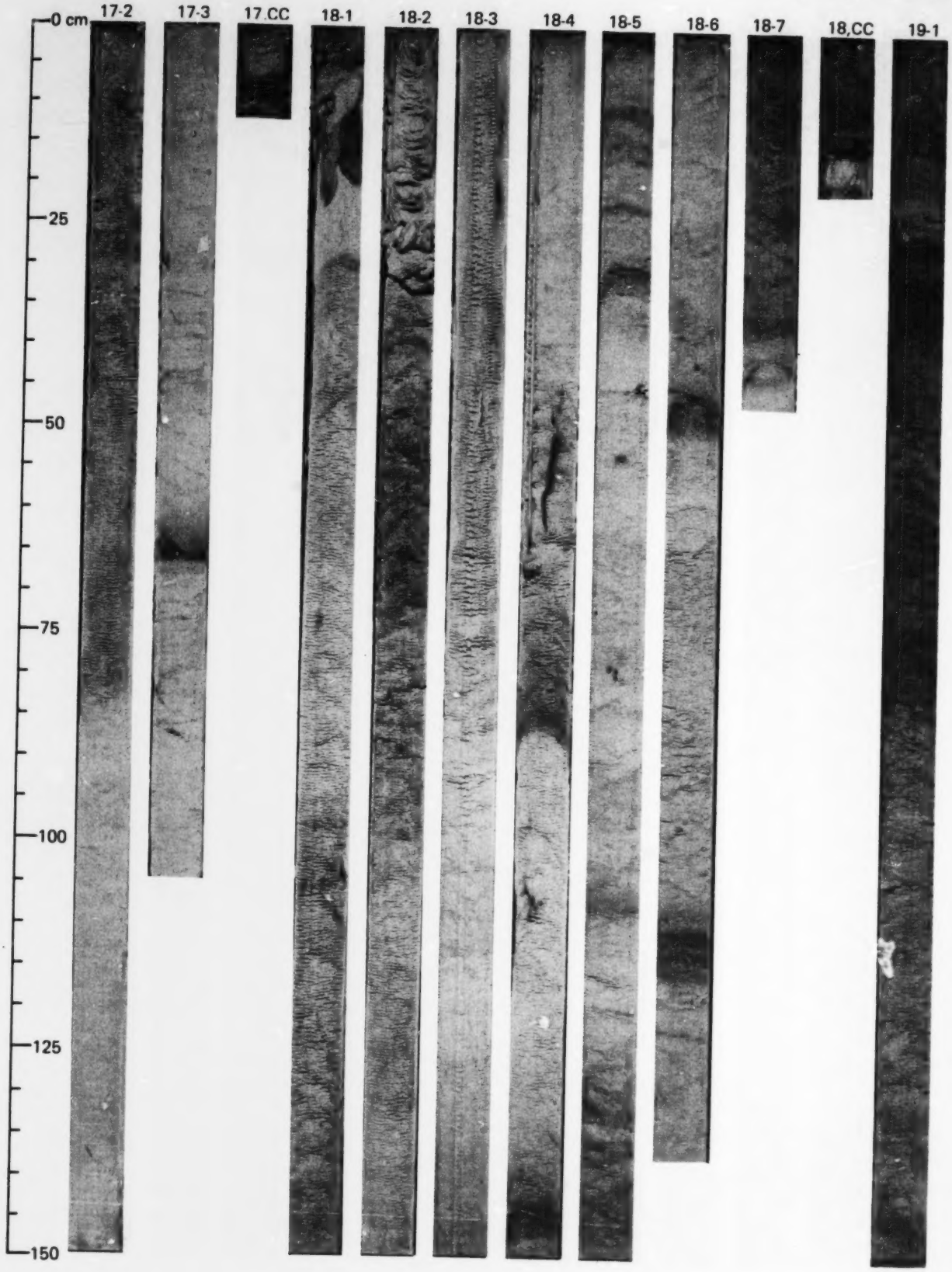
0 cm
17-2
17-3
17,CC
18-1
18-2
18-3
18-4
18-5
18-6
18-7
18,CC
19-1
25
50
75
100
125
150

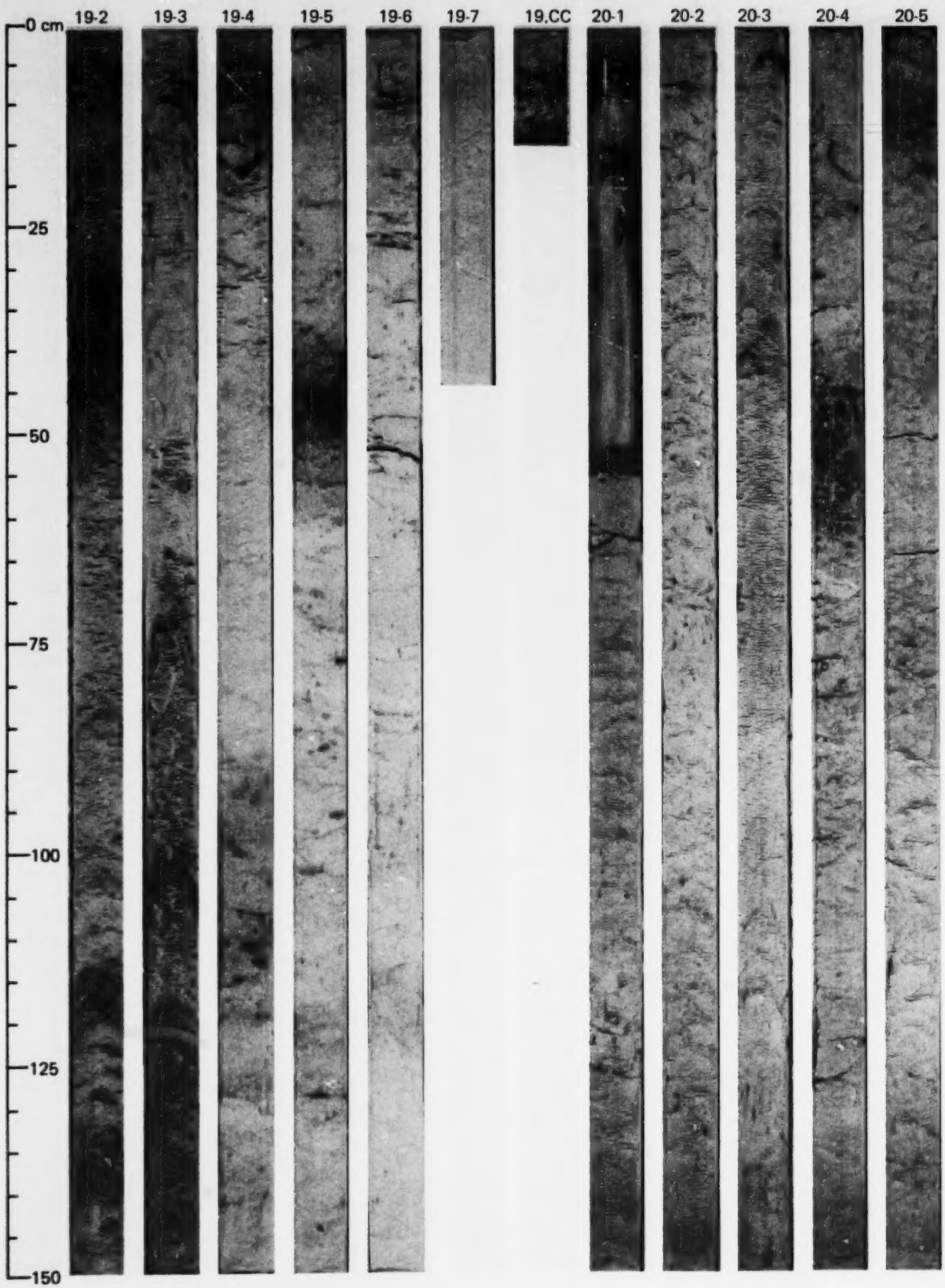
0 cm
25
50
75
100
125
150
19-2
19-3
19-4
19-5
19-6
19-7
19,CC
20-1
20-2
20-3
20-4
20-5

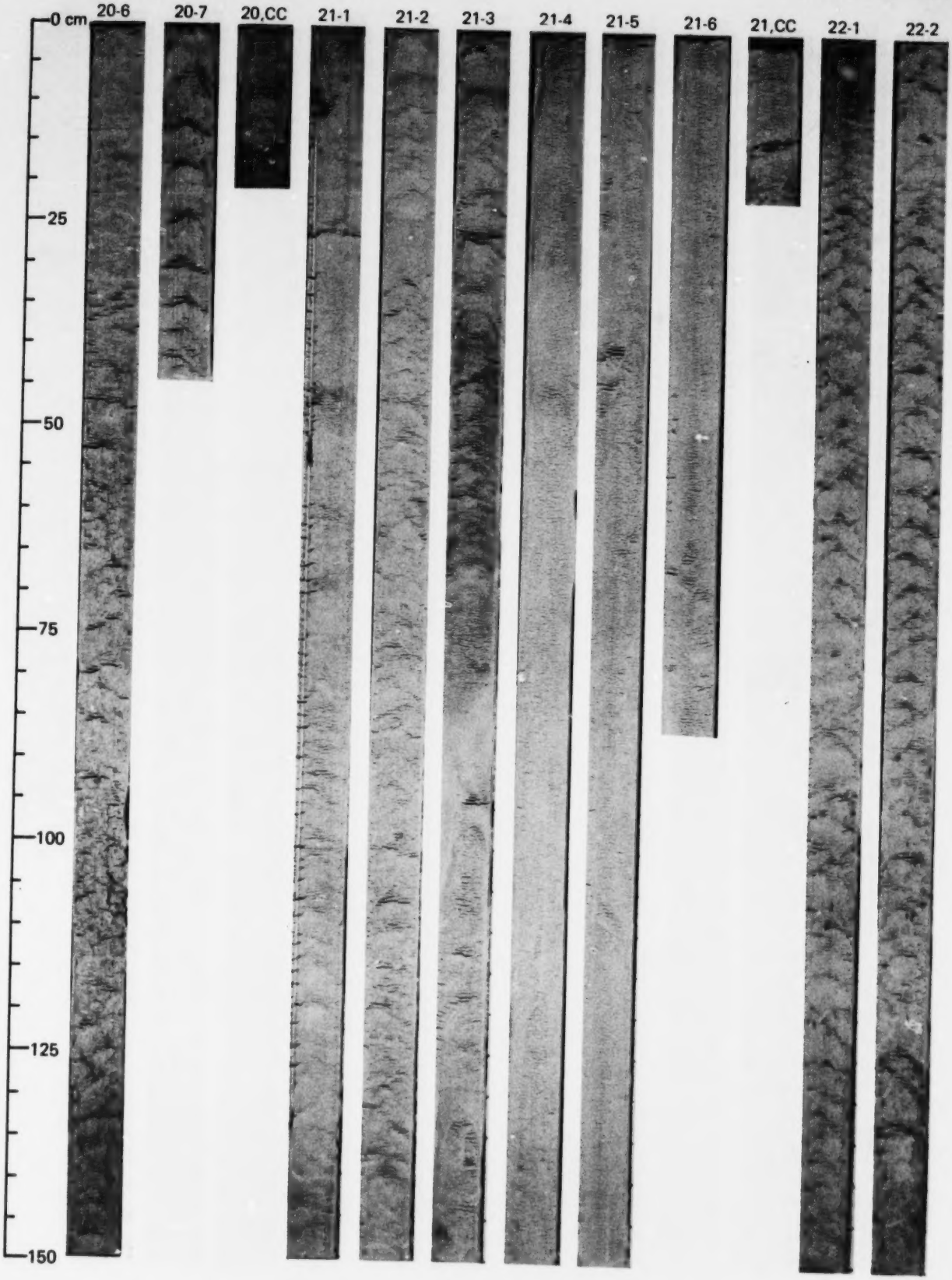
0 cm
20-6
20-7
20,CC
21-1
21-2
21-3
21-4
21-5
21-6
21,CC
22-1
22-2
25
50
75
100
125
150

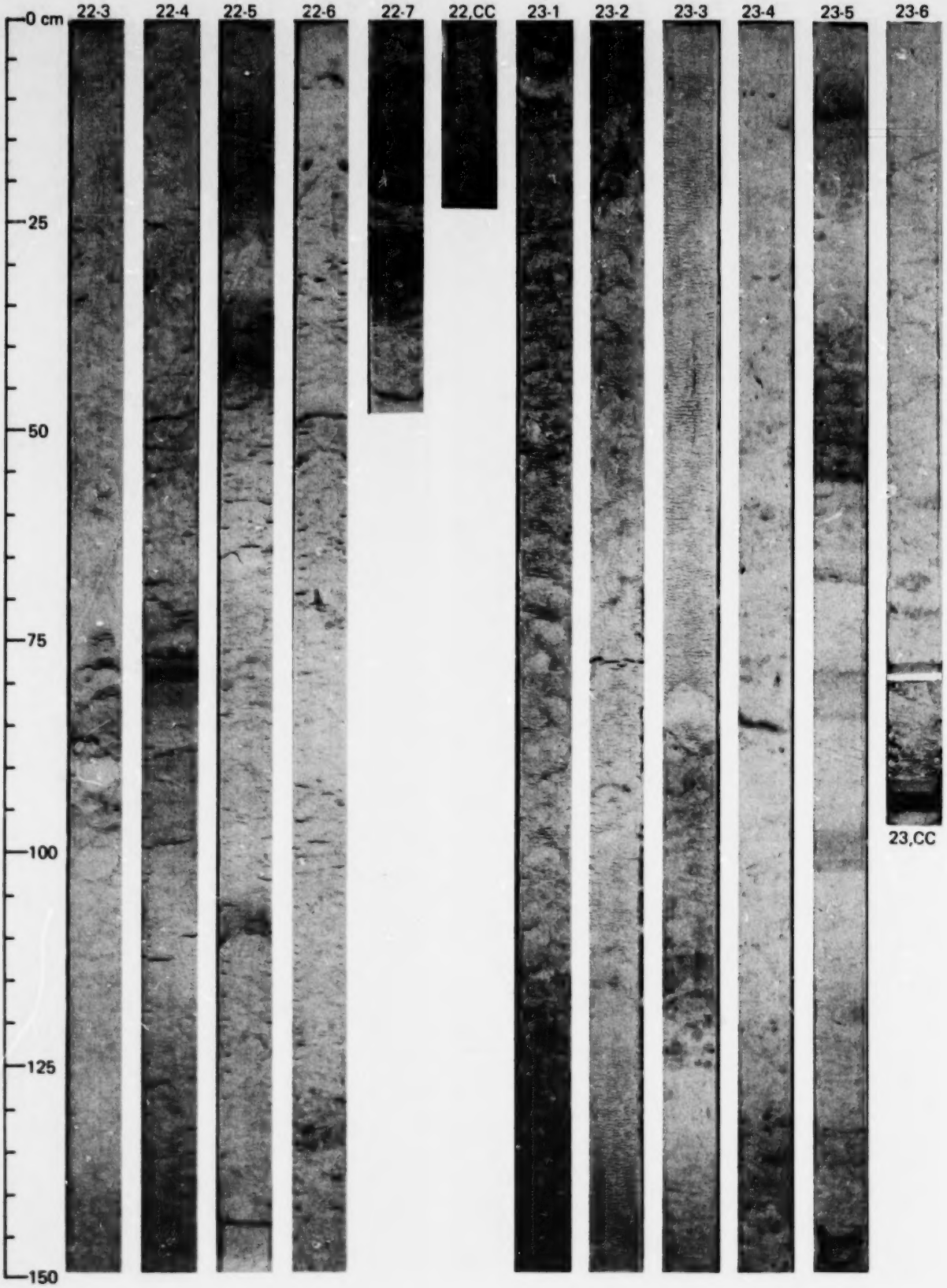
0 cm
25
50
75
100
125
150
22-3
22-4
22-5
22-6
22-7
22,CC
23-1
23-2
23-3
23-4
23-5
23-6
23,CC

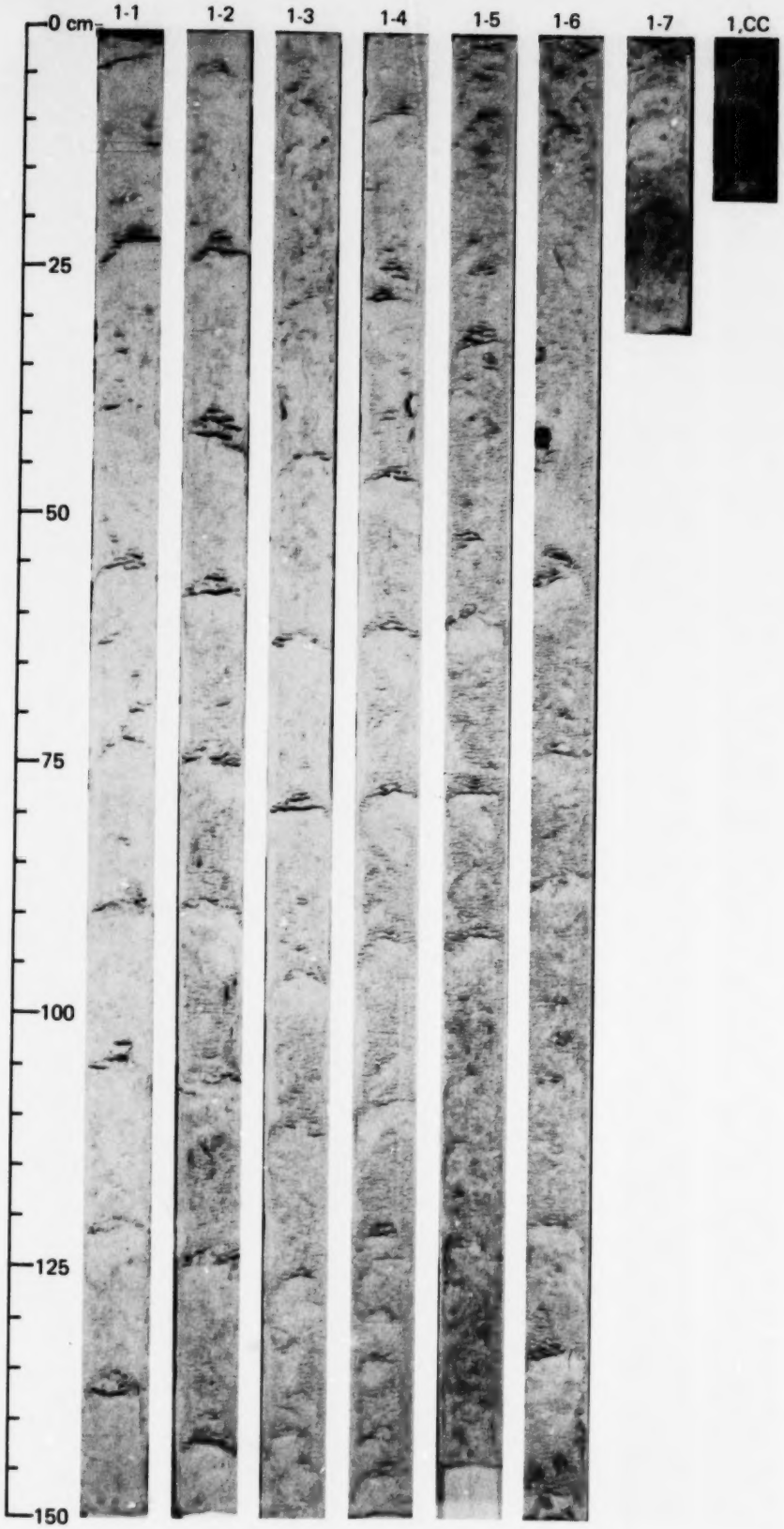
0 cm
1-1
1-2
1-3
1-4
1-5
1-6
1-7
1,CC
25
50
75
100
125
150

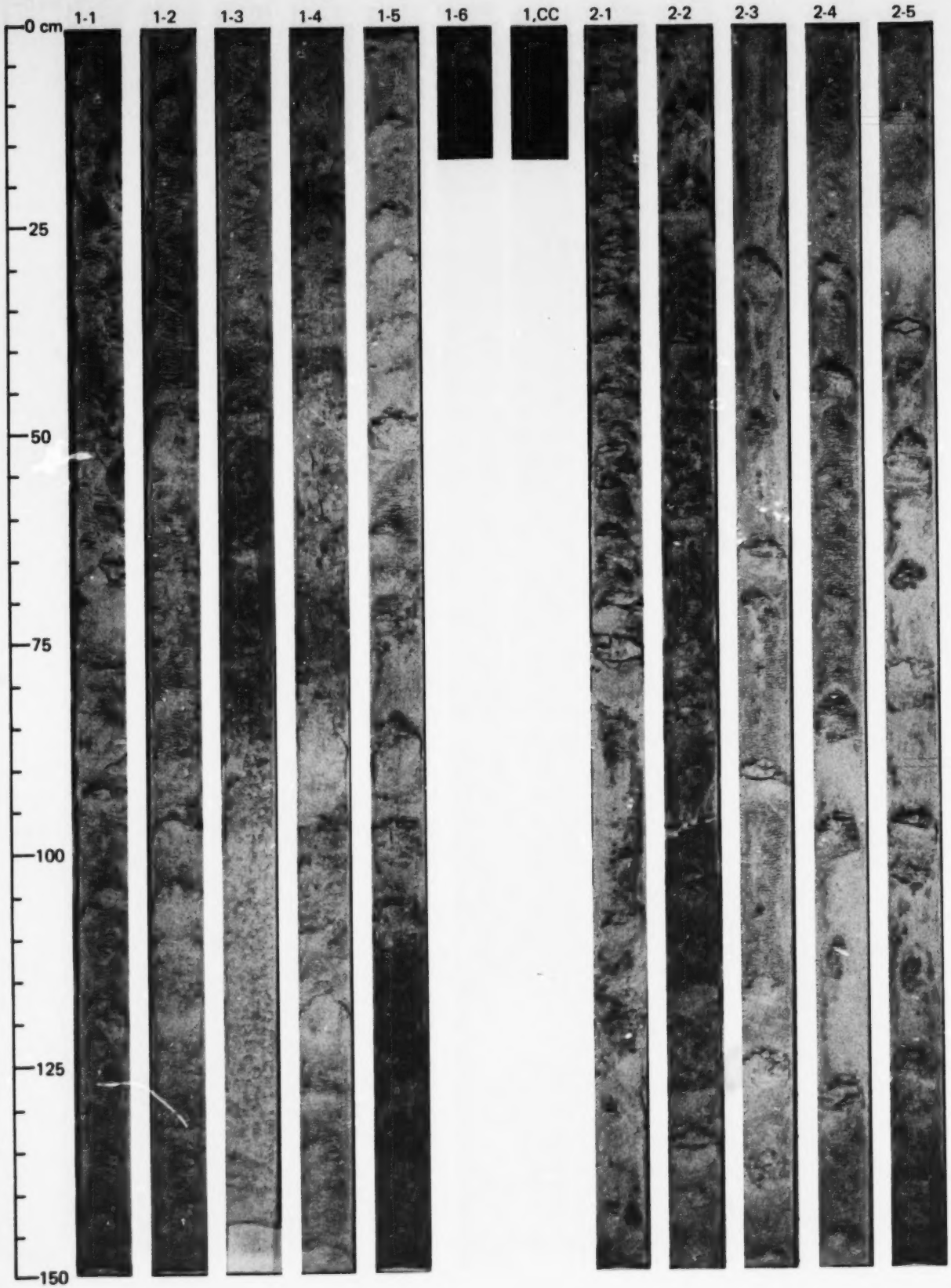
0 cm
25
50
75
100
125
150
1-1
1-2
1-3
1-4
1-5
1-6
1,CC
2-1
2-2
2-3
2-4
2-5

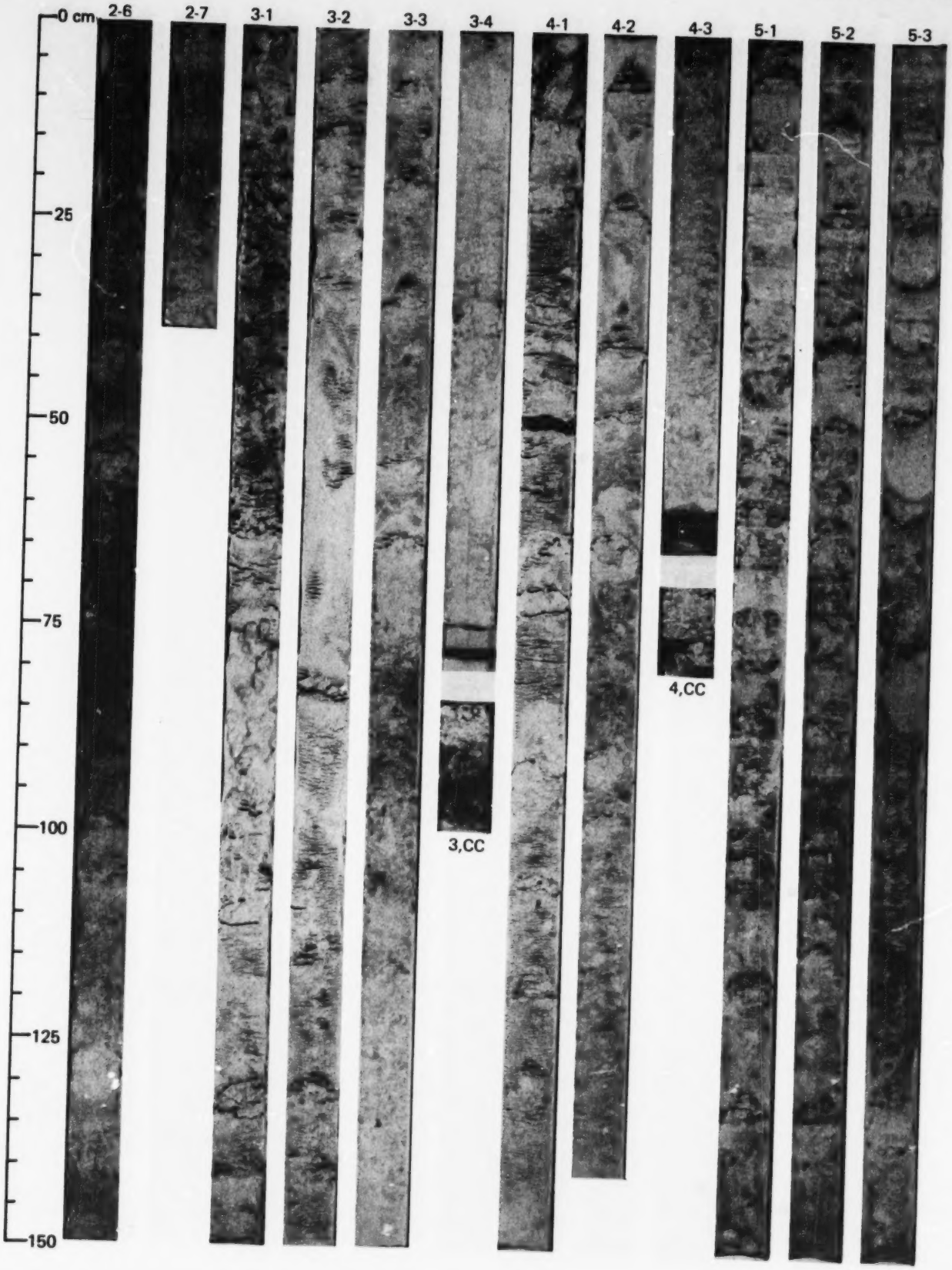
0 cm
25
50
75
100
125
150
2-6
2-7
3-1
3-2
3-3
3-4
3,CC
4-1
4-2
4-3
4,CC
5-1
5-2
5-3

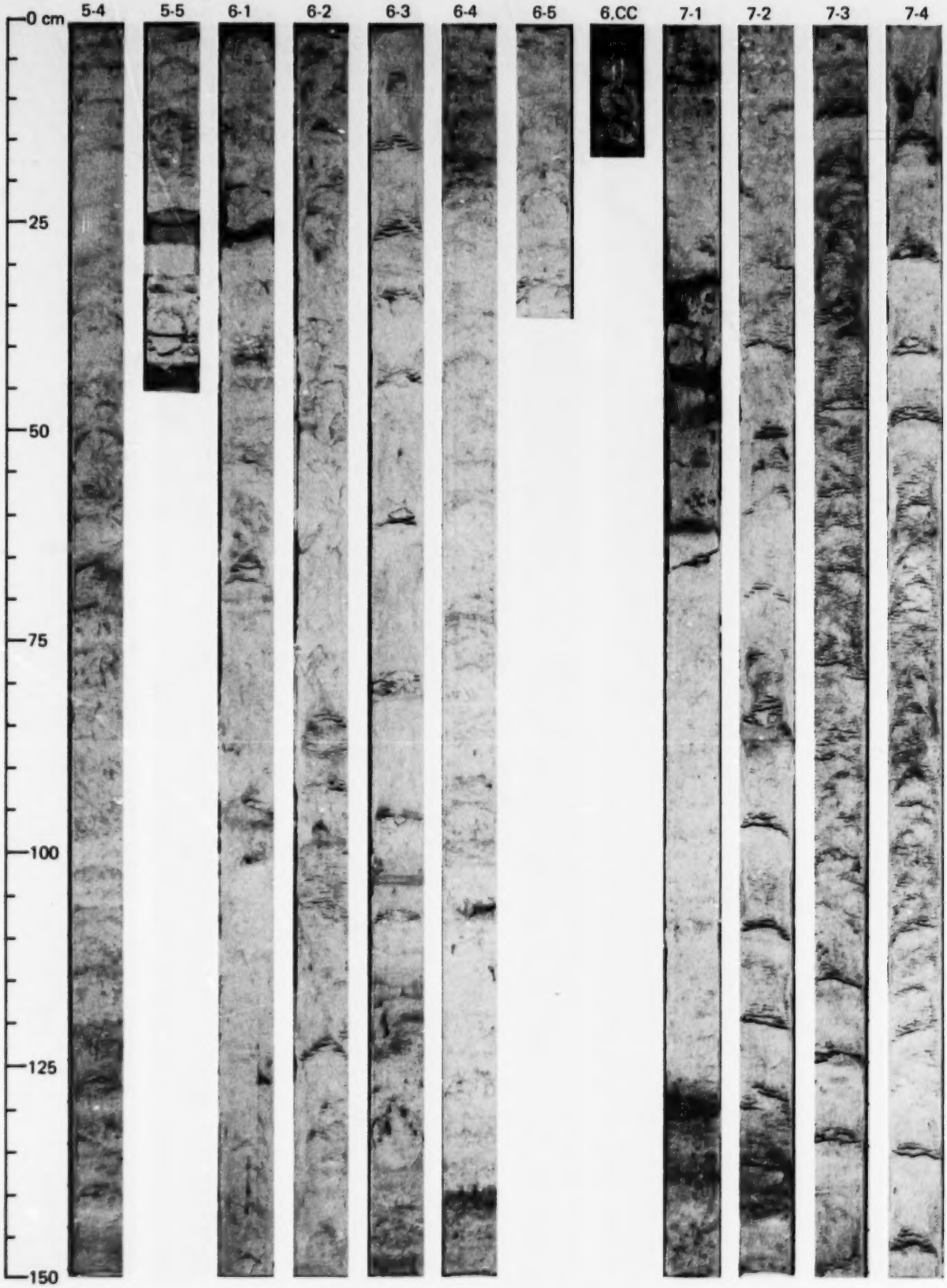
0 cm
25
50
75
100
125
150
5-4
5-5
6-1
6-2
6-3
6-4
6-5
6,CC
7-1
7-2
7-3
7-4

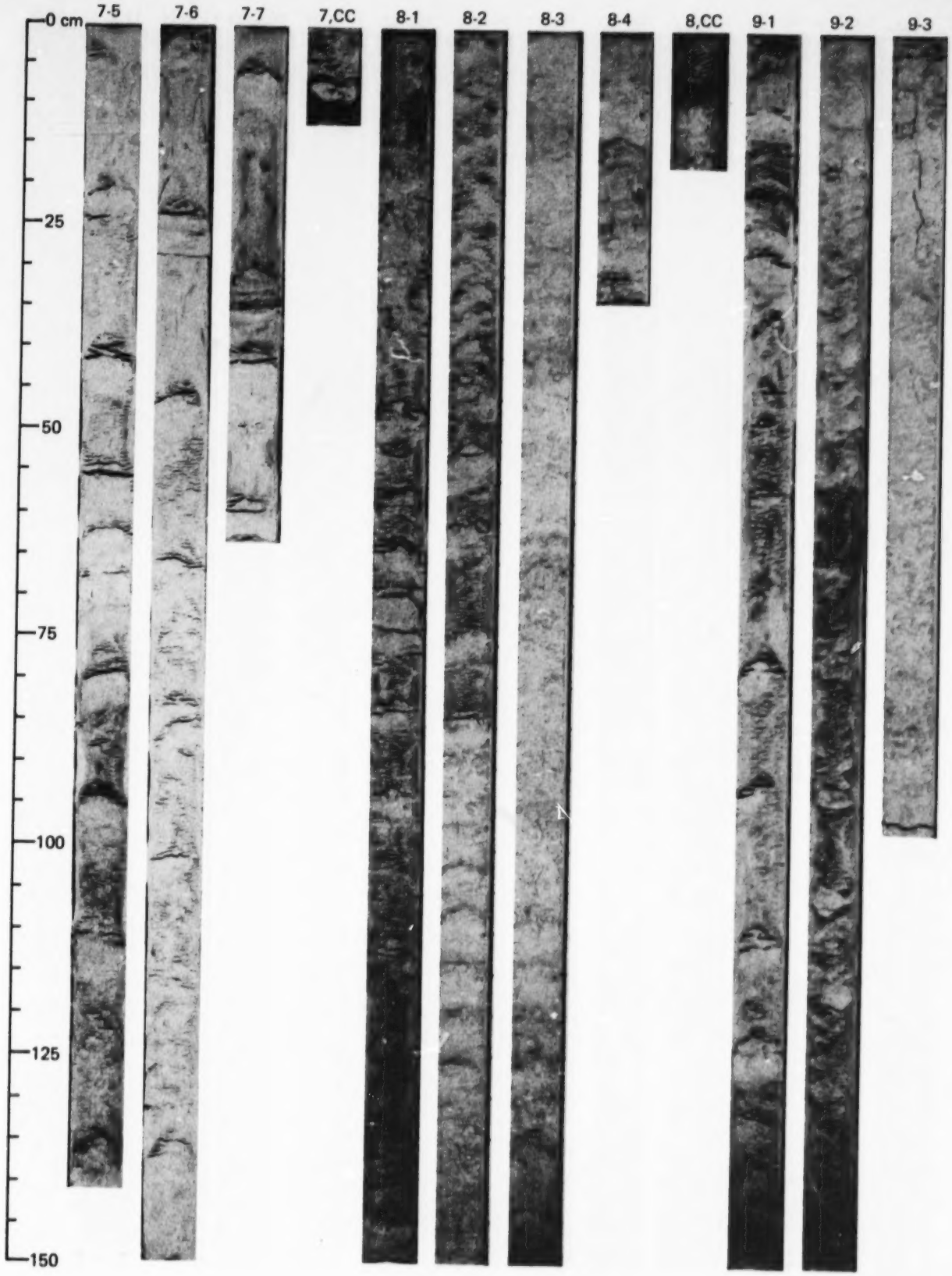
0 cm
25
50
75
100
125
150
7-5
7-6
7-7
7,CC
8-1
8-2
8-3
8-4
8,CC
9-1
9-2
9-3

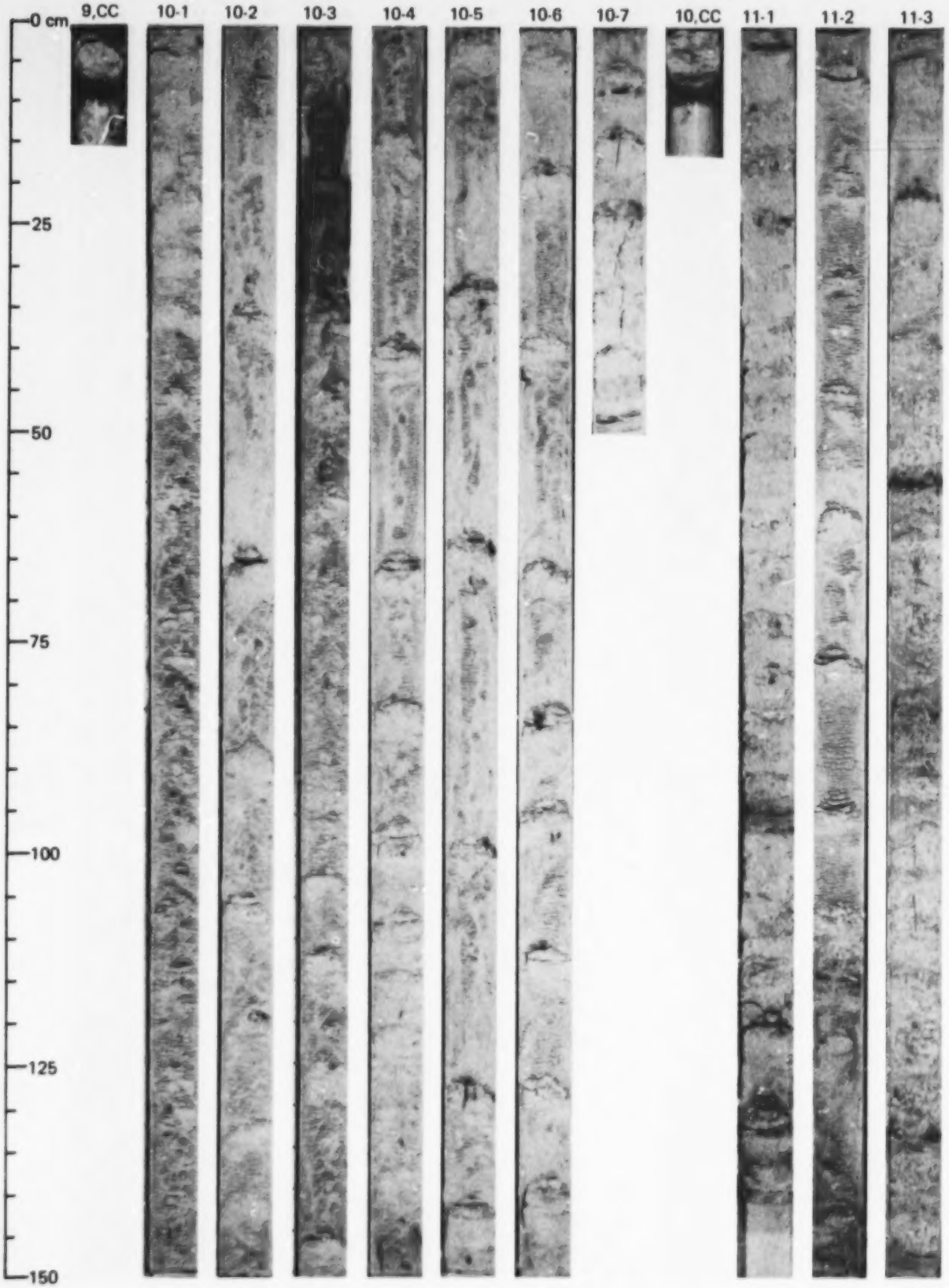
0 cm
25
50
75
100
125
150
9,CC
10-1
10-2
10-3
10-4
10-5
10-6
10-7
10,CC
11-1
11-2
11-3

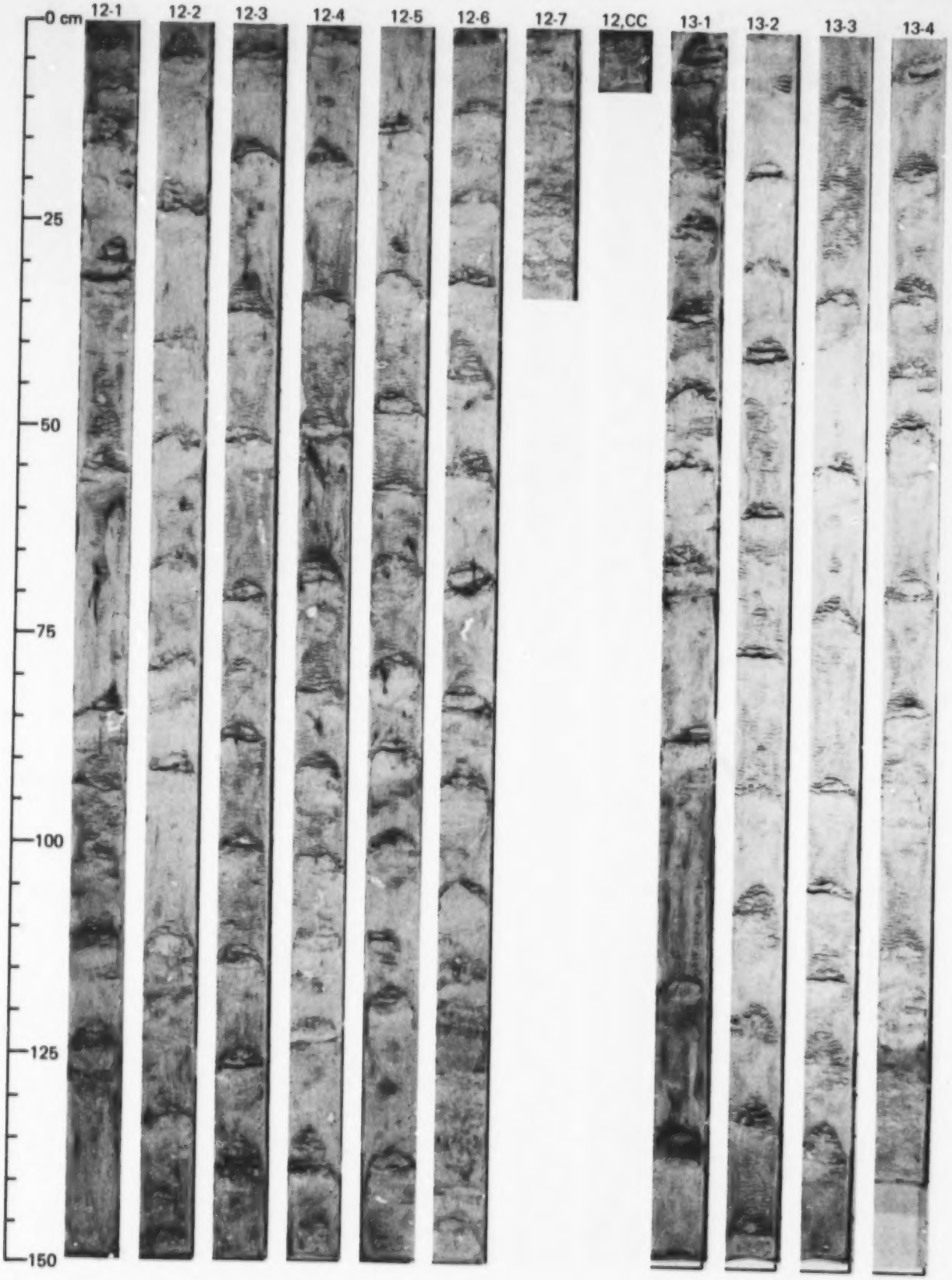
0 cm
12-1
12-2
12-3
12-4
12-5
12-6
12-7
12,CC
13-1
13-2
13-3
13-4
25
50
75
100
125
150

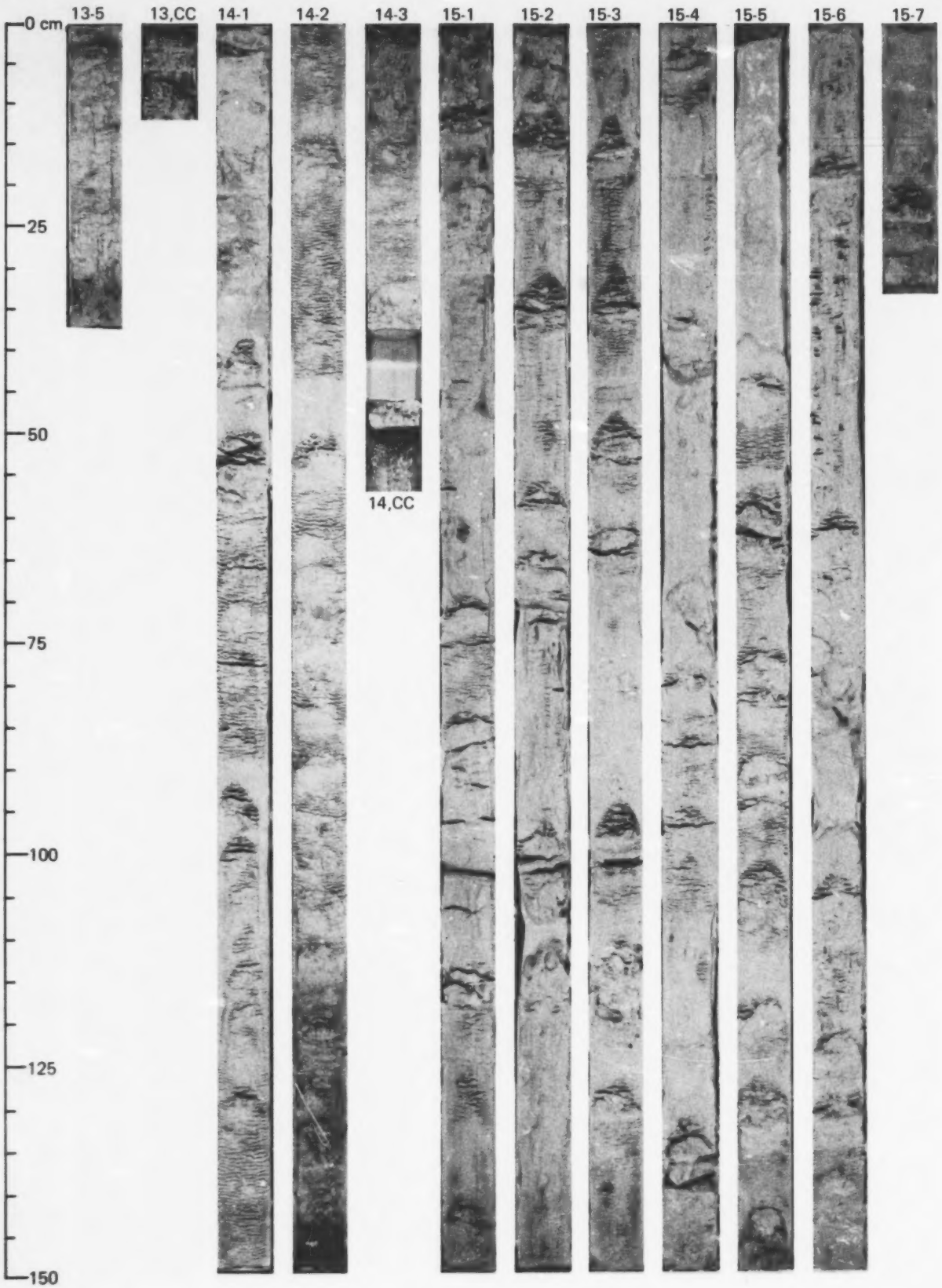
0 cm
25
50
75
100
125
150
13-5
13,CC
14-1
14-2
14-3
14,CC
15-1
15-2
15-3
15-4
15-5
15-6
15-7

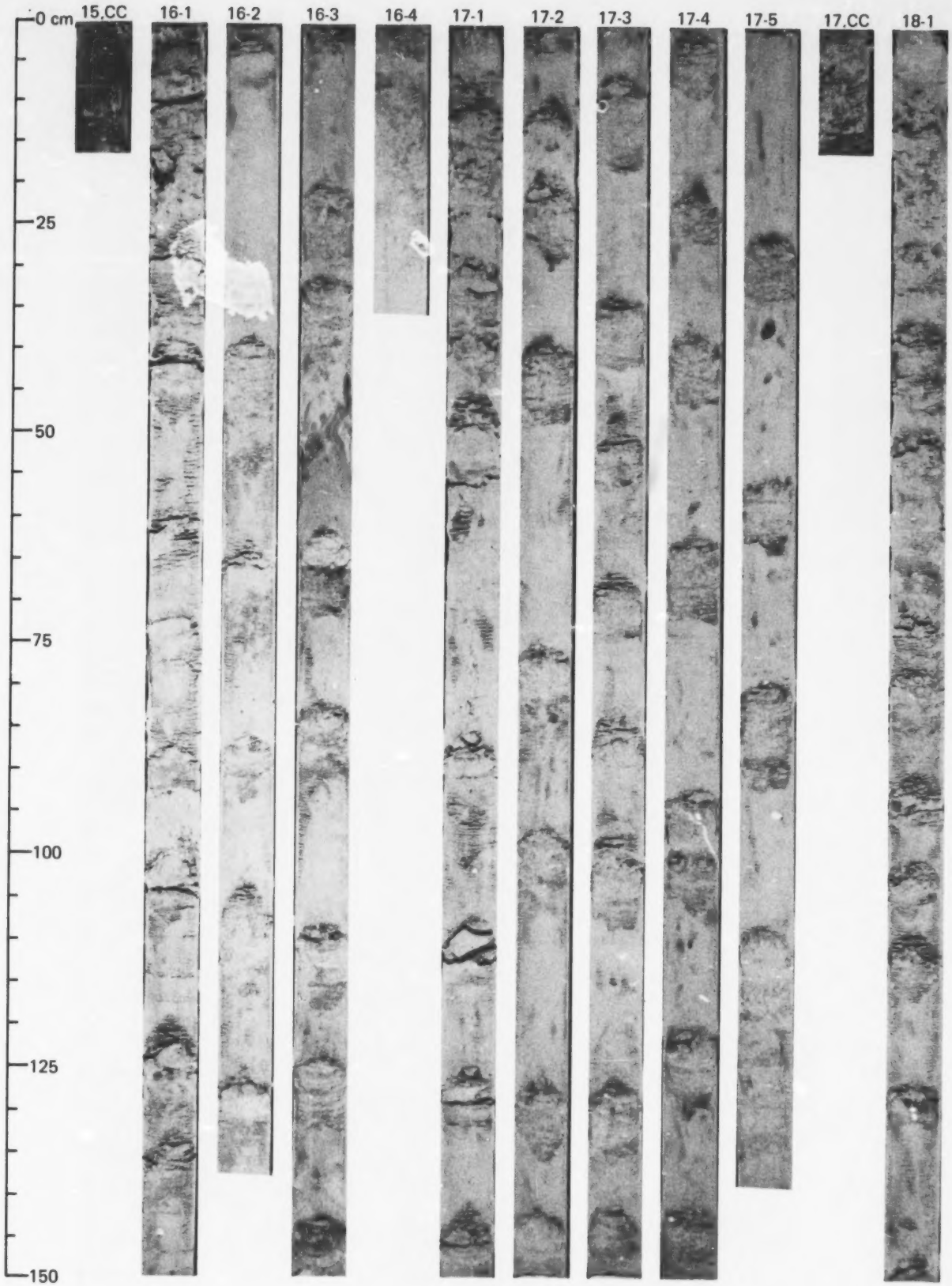
0 cm
15,CC
16-1
16-2
16-3
16-4
17-1
17-2
17-3
17-4
17-5
17,CC
18-1
25
50
75
100
125
150

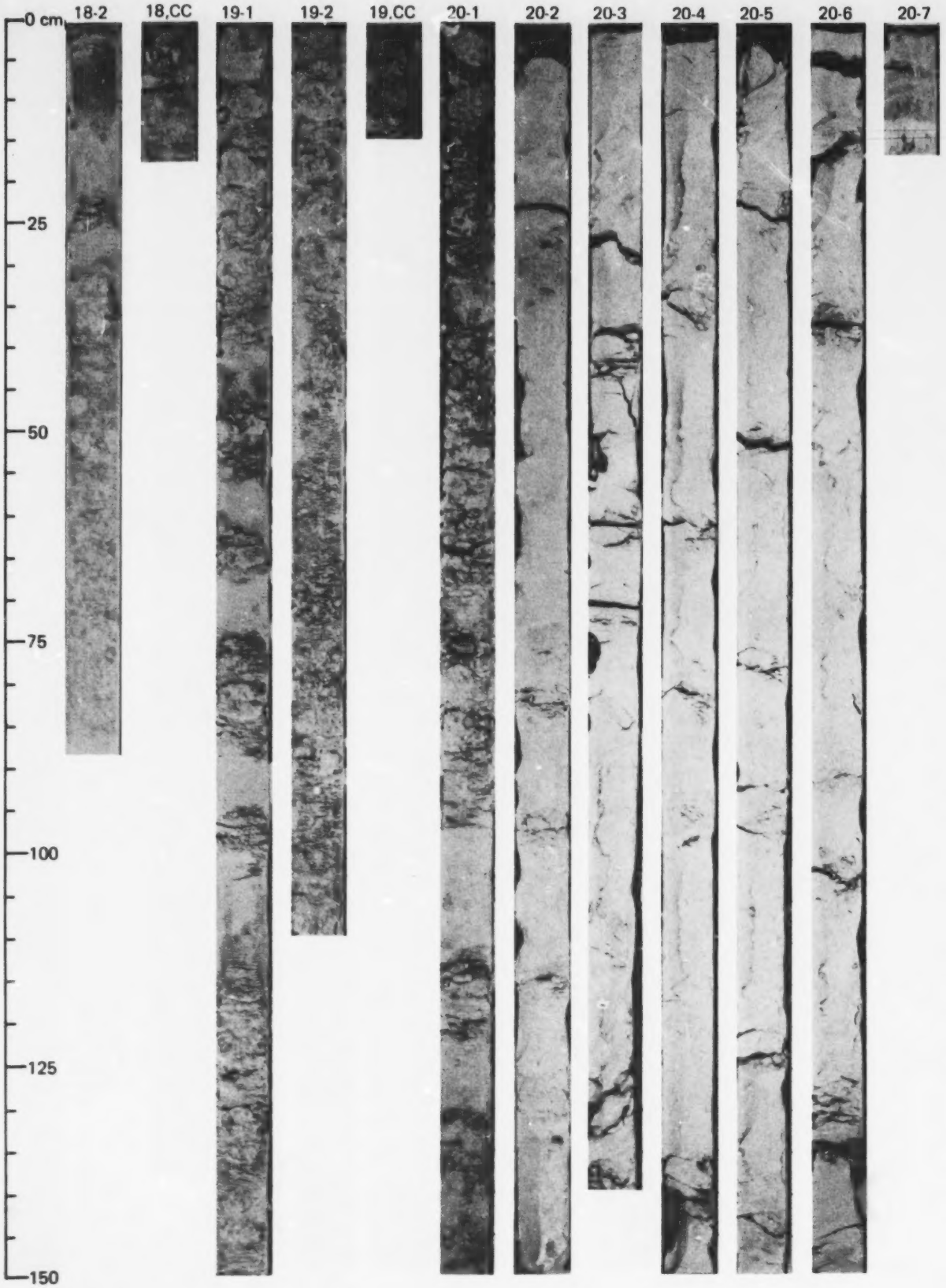
0 cm
25
50
75
100
125
150
18-2
18,CC
19-1
19-2
19,CC
20-1
20-2
20-3
20-4
20-5
20-6
20-7

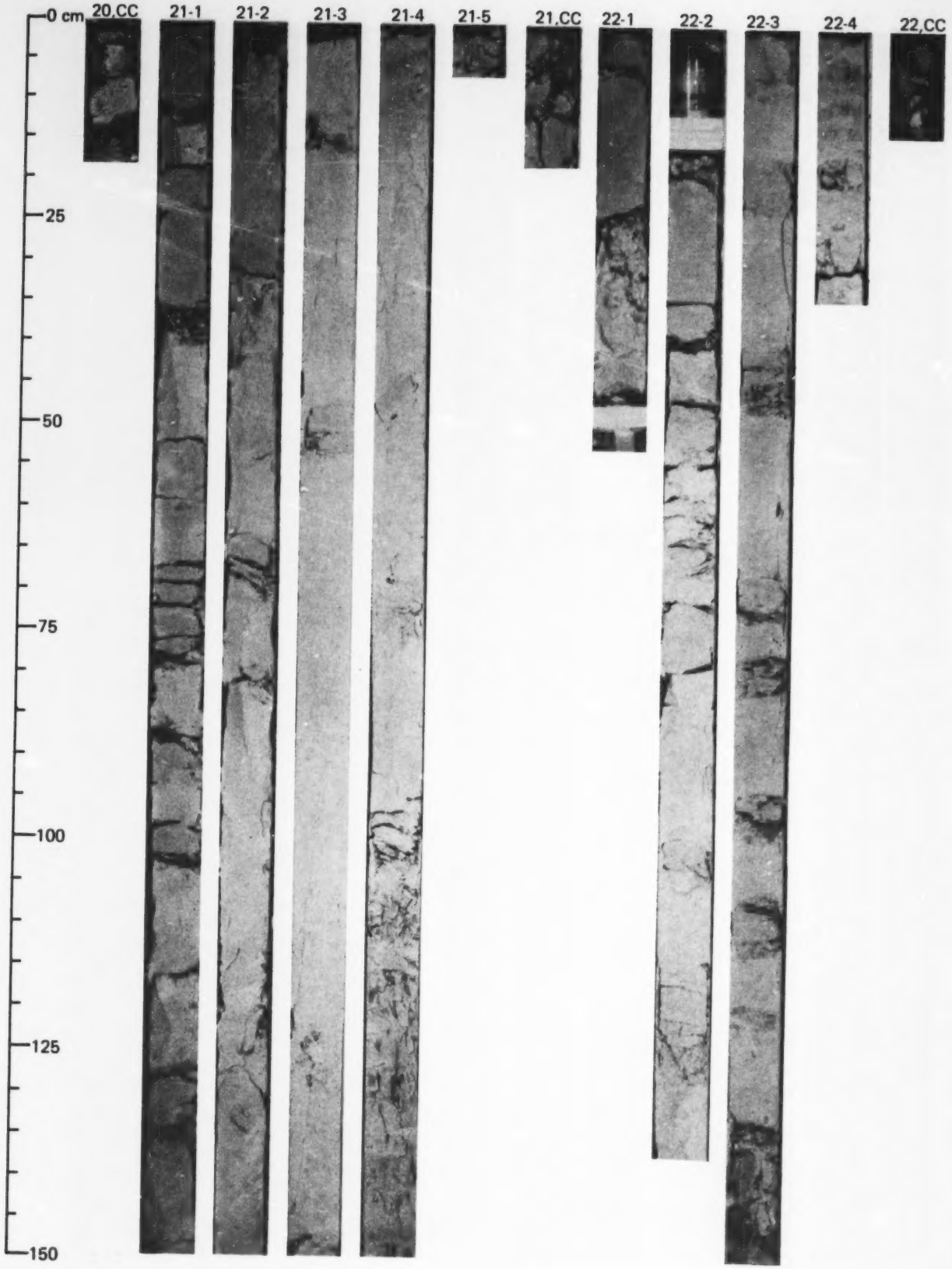
0 cm
20,CC
21-1
21-2
21-3
21-4
21-5
21,CC
22-1
22-2
22-3
22-4
22,CC
25
50
75
100
125
150

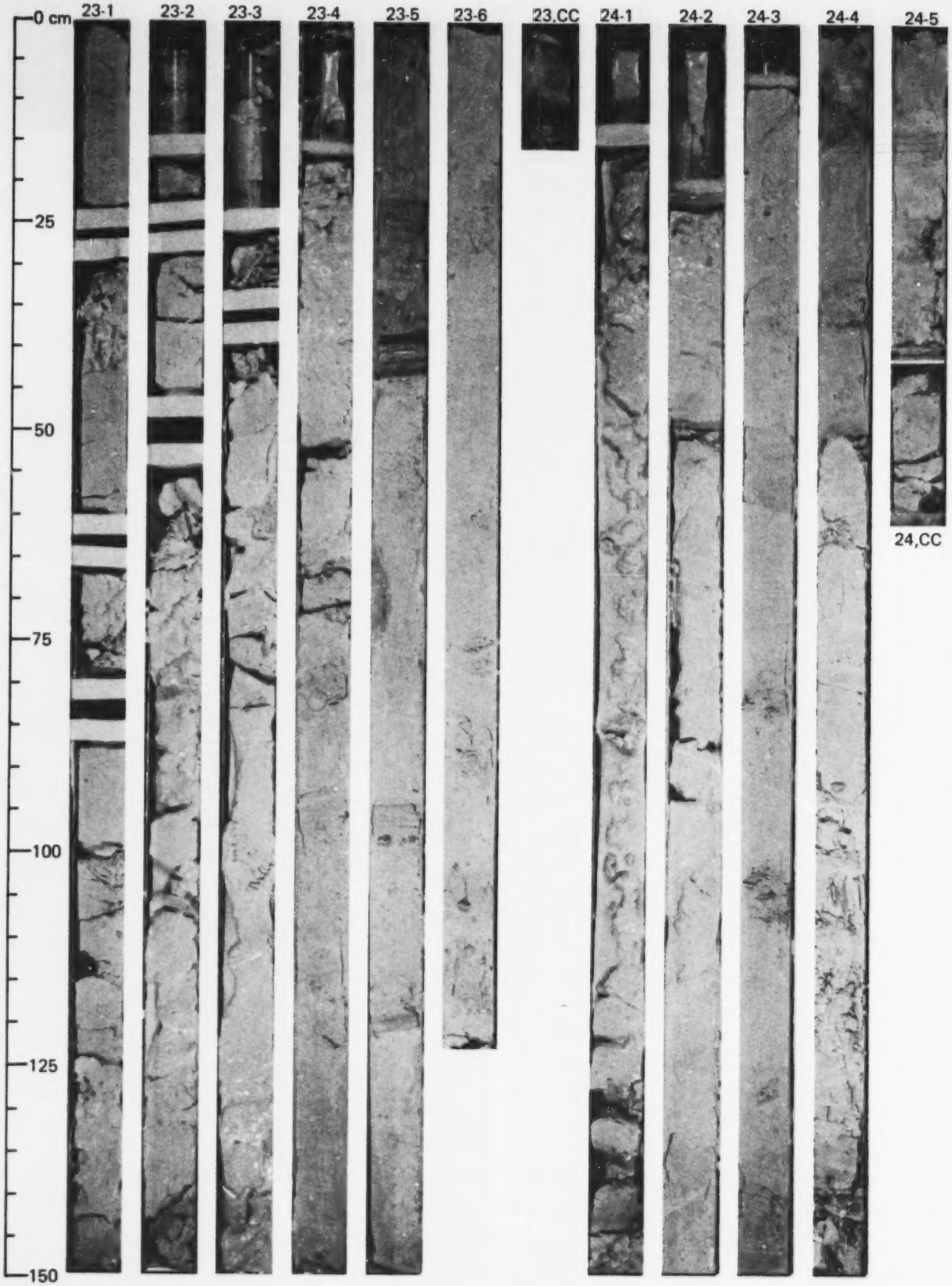
0 cm
25
50
75
100
125
150
23-1
23-2
23-3
23-4
23-5
23-6
23,CC
24-1
24-2
24-3
24-4
24-5
24,CC

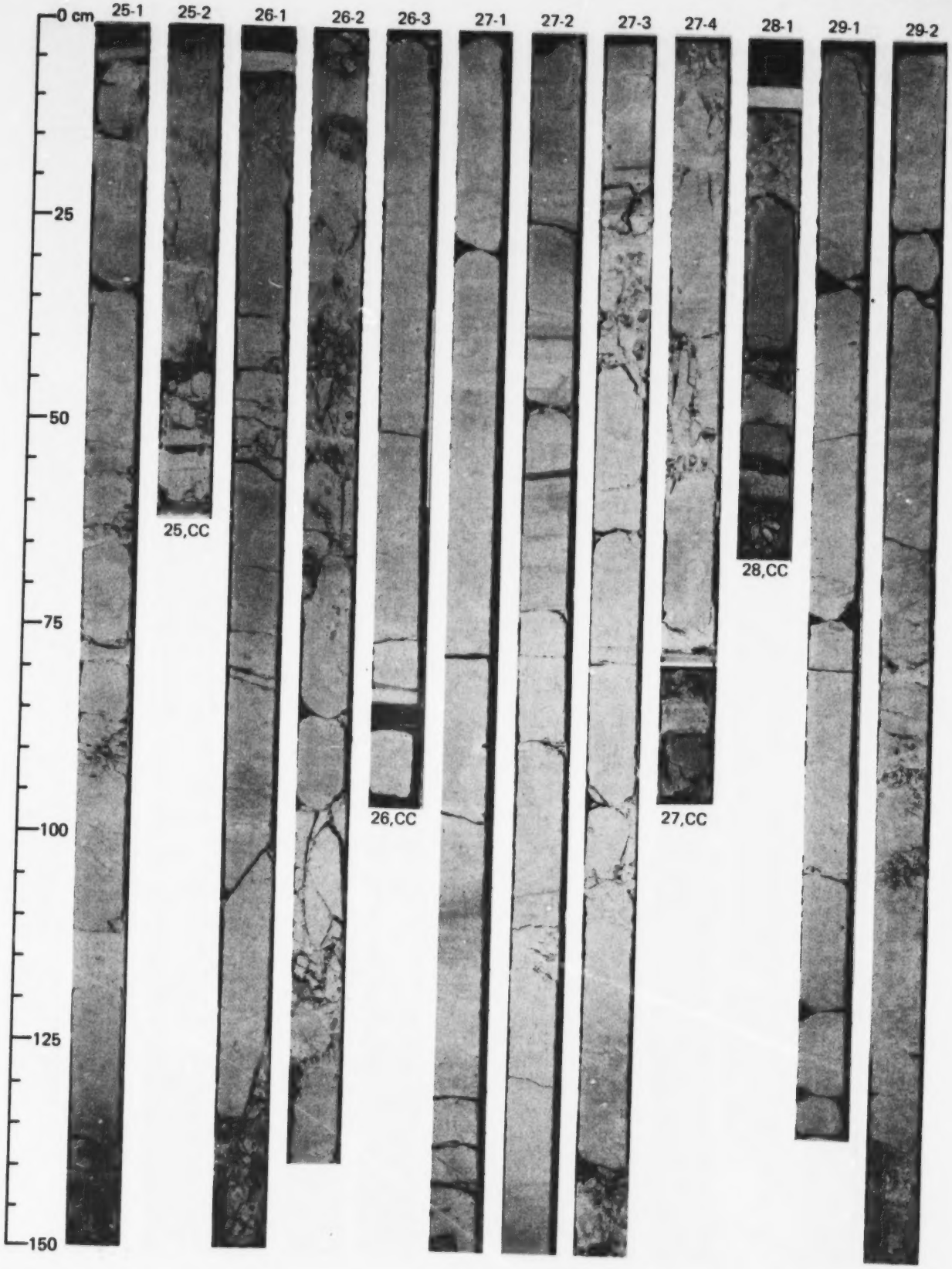
0 cm
25-1
25-2
26-1
26-2
26-3
27-1
27-2
27-3
27-4
28-1
29-1
29-2
25
50
75
100
125
150
25,CC
26,CC
27,CC
28,CC

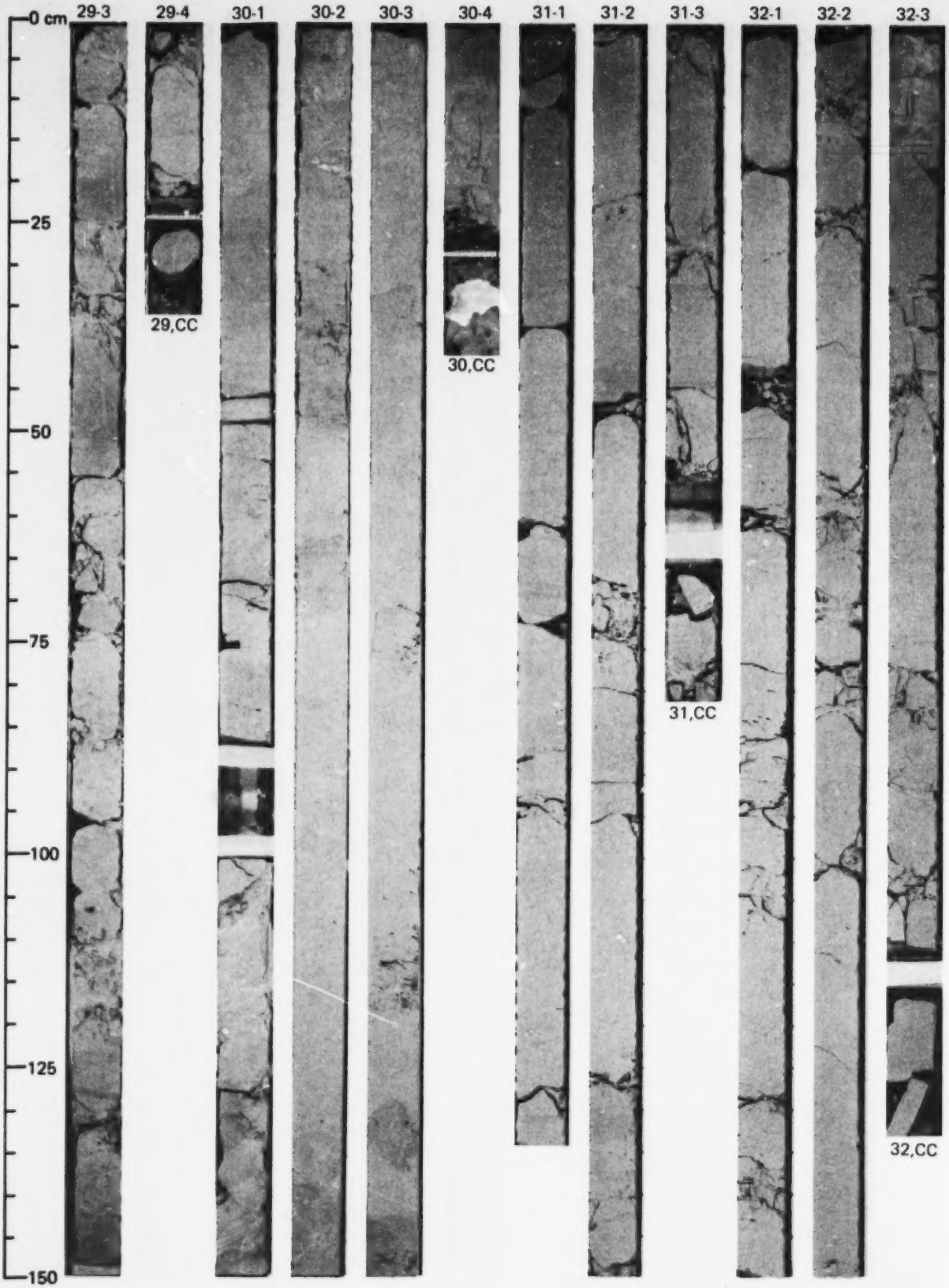
0 cm
25
50
75
100
125
150
29-3
29-4
29,CC
30-1
30-2
30-3
30-4
30,CC
31-1
31-2
31-3
31,CC
32-1
32-2
32-3
32,CC

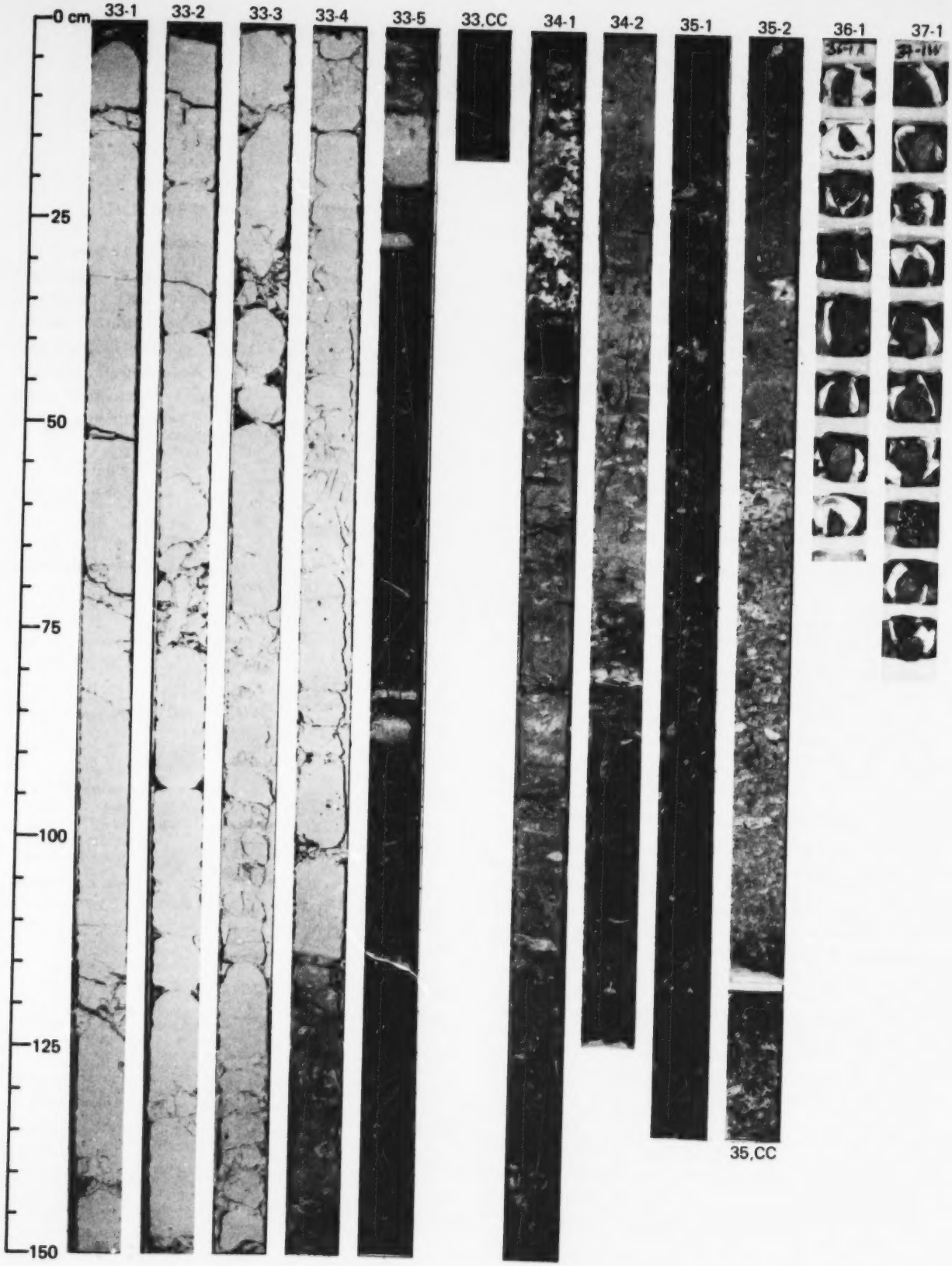
0 cm
25
50
75
100
125
150
33-1
33-2
33-3
33-4
33-5
33,CC
34-1
34-2
35-1
35-2
35,CC
36-1
37-1

6. SITE 575[1]

Shipboard Scientific Party[2]

HOLES 575, 575A, 575B, 575C

Date occupied: 20 April 1982

Date departed: 24 April 1982

Time on site: 3.9 days

Position: 05°51.00′N, 135°02.16′W

Water depth (sea level; corrected m, echo-sounding): 4536

Water depth (rig floor; corrected m, echo-sounding): 4552

Bottom felt (m, drill pipe): 4550

Penetration (m): 575—98.6
575A—208.4
575B—119.0
575C—15.8

Number of cores: 575—11
575A—33
575B—14
575C—2

Total length of cored section (m): 575—98.6
575A—114.6[3]
575B—115.7[3]
575C—15.8

Total core recovered (m): 575—99.35
575A—140.53[4]
575B—118.68[4]
575C—15.91

Core recovery (%): 575—100
575A—136[4]
575B—119[4]
575C—100

Oldest sediment cored:
Depth sub-bottom (m): 208.4
Nature: Nannofossil ooze
Age: earliest Miocene
Measured velocity (km/s): 1.6

Basement: Not reached

Principal results: Site 575 (05°51.00′N, 135°02.16′W), in water 4536 m deep, overlies acoustically well stratified sediments at least 0.57 s thick in a region where basement relief is minimal. Seismic records show evidence of considerable erosion throughout the region, and there is a seamount 1000 m high 10 km to the northeast. The operational objective of drilling this site, which was to recover a complete and undisturbed section of Eocene to Quaternary central Pacific sediments, was met only partially because of a lack of time. Hydraulic piston coring was used to drill four holes: 575 (0 to 98.6 m sub-bottom, 11 cores); 575A (93.8 to 208.4 m, 33 cores); 575B (3.3 to 119.0 m, 14 cores); and 575C (0 to 15.8 m, 2 cores).

A nearly complete and undisturbed section from lowest Miocene (22 Ma) to Pleistocene was recovered. The section was divided into a topmost cyclic siliceous calcareous ooze (0 to 32.3 m sub-bottom) and a lower calcareous ooze chalk (30 to 208.4 m sub-bottom). Centimeter-thick sandy to pebbly turbidite layers, containing mostly sand-sized foraminifers, basalts, and/or volcanic glass, were intercalated throughout the section.

With few exceptions, all major planktonic microfossils are well represented. They allow most early Miocene to Pleistocene biozonal boundaries to be recognized. The exceptions occur in the very compressed upper 30 m of the section, where the zones are difficult to distinguish.

The rates of sediment accumulation are variable but moderate (15.4 to 20 m/m.y.) in the older (12.5 to 22 Ma) part of the cored section and much lower (about 3.6 m/m.y.) and constant in the younger part (0 to 9 Ma). A hiatus, or perhaps a further compression of the depositional record, occupies the interval from 9 to 12.5 Ma.

The changes in natural remanent magnetization (NRM) intensity are correlated with changes in both sedimentation rate and lithology. The values are generally high (on the order of 10^{-6} G or above) in the upper unit (0 to 30 m) and in the brown subunits of the lower calcareous chalk unit. As at other sites, the physical properties are sensitive indicators of changes in lithology, particularly changes in carbonate content. Pore-water chemistry shows trends consistent with the findings at previous sites.

BACKGROUND AND OBJECTIVES

The JOIDES Ocean Paleoenvironment Panel proposed Site 575 as the northernmost in a three-site north–south transect at a latitude of approximately 133°W. Site 575 is on the northern flank of the equatorial high-productivity zone and just south of the Clipperton Fracture Zone. The sedimentary section recovered at Site 575 documents the migration of the site from about 3°S at 39 Ma, across the equatorial high-productivity zone, to its present location at about 5°50′N. Our operational objectives were to recover a complete and undisturbed section as deep as the hydraulic piston core (HPC) allowed, to repeat the hydraulic piston coring to ensure complete recovery, and, if time permitted, to rotary core the rest of the section to basement.

A detailed survey of the area around Site 575 was conducted for the Joint Oceanographic Institutions by the R/V *Thomas Washington* (Ariadne Leg I). Seabeam bathymetry, as well as digital, single-channel, water, and air gun data were collected. Additional seismic data were collected for the vicinity of Site 575 by Lamont's R/V *Conrad* (*Conrad* 15-1) in 1971. The region around Site

---

[1] Mayer, L., Theyer, F., et al., *Init. Repts. DSDP*, 85: Washington (U.S. Govt. Printing Office).

[2] Larry Mayer (Co-Chief Scientist), Dalhousie University, Halifax, Nova Scotia, Canada; Fritz Theyer (Co-Chief Scientist), Hawaii Institute of Geophysics, University of Hawaii, Honolulu, Hawaii (present address: University of Southern California, Los Angeles, California); John A. Barron, U.S. Geological Survey, Menlo Park, California; Dean A. Dunn, University of Rhode Island, Narragansett, Rhode Island (present address: University of Southern Mississippi, Hattiesburg, Mississippi); Tim Handyside, The University, Newcastle upon Tyne, United Kingdom; Scott Hills, Scripps Institution of Oceanography, La Jolla, California; Ian Jarvis, City of London Polytechnic, London, United Kingdom (present address: Kingston Polytechnic, Kingston-upon-Thames, United Kingdom); Catherine A. Nigrini, La Habra Heights, California; Nicklas G. Pisias, Oregon State University, Corvallis, Oregon; Annick Pujos, Université de Bordeaux, Talence, France; Tsunemasa Saito, Yamagata University, Yamagata, Japan; Paul Stout, Scripps Institution of Oceanography, La Jolla, California; Ellen Thomas, Scripps Institution of Oceanography, La Jolla, California (present address: Lamont-Doherty Geological Observatory, Columbia University, Palisades, New York); Norbert Weinreich, Institut für Geophysik, Ruhr Universität Bochum, Bochum, Federal Republic of Germany; and Roy H. Wilkens, Massachusetts Institute of Technology, Cambridge, Massachusetts.

[3] Not including overlap (see Operations).

[4] Including overlap (see Operations).

575 is characterized by moderate relief, with water depths ranging from 4500 m in the northeastern end of the survey area to approximately 4680 m in the western end (Fig. 1). Ten kilometers northeast of the site, a double-peaked seamount rises 1000 m above the regional mean seafloor depth.

The section is typically 0.5 to 0.6 s thick and seismically well stratified (Fig. 2). There is evidence of erosion throughout the area in both the low-frequency and 3.5-kHz records. Some of the erosion can be linked directly to the seamount (moating), but much of it seems to be regional in extent and may be related to the site's proximity to the Clipperton Fracture Zone. The spot selected for coring is one of the few places in the area that has retained the youngest part of the section (Fig. 2). This spot may be protected by the seamount from erosion by regional currents.

The ridges and valleys trend east-west in the eastern end of the area and north-northwest/south-southeast in the western end. The drill site is in a flat, elongated area that trends east-west and overlies a very slight basement depression. Sediment thickness is approximately 0.57 s to acoustic basement (Fig. 2); there is some seismic evidence that the acoustic basement is not basalt. Except for the seamount, basement relief is minimal, with a subdued north-northwest/south-southeast trend.

The closest previously drilled DSDP site is Site 70 (6°20.08′N, 140°21.72′W), which was drilled on Leg 8. Site 70, however, is north of the Clipperton Fracture Zone and is thus probably less like the section at Site 575 than the section at Site 71. At Site 71 (at 4°28.28′N, 140° 18.91′W), 558 m of uppermost Eocene to Quaternary calcareous and siliceous oozes and chalks were recovered. Acoustic basement at Site 71 proved to be indurated chalk and chert.

OPERATIONS

The D/V *Glomar Challenger* arrived in the vicinity of Site 575 at 0000Z on 21 April after completing the 150-mi. steam from Site 574 in 16.5 hr. In transit we collected continuous seismic profiles (air gun and 3.5 kHz), bathymetric, and magnetic data. Because the bathymetric features in the region of the proposed site run roughly northwest-southeast, we planned an approach that took us through a point northeast of the site and from there along a track at right angles to the orientation of

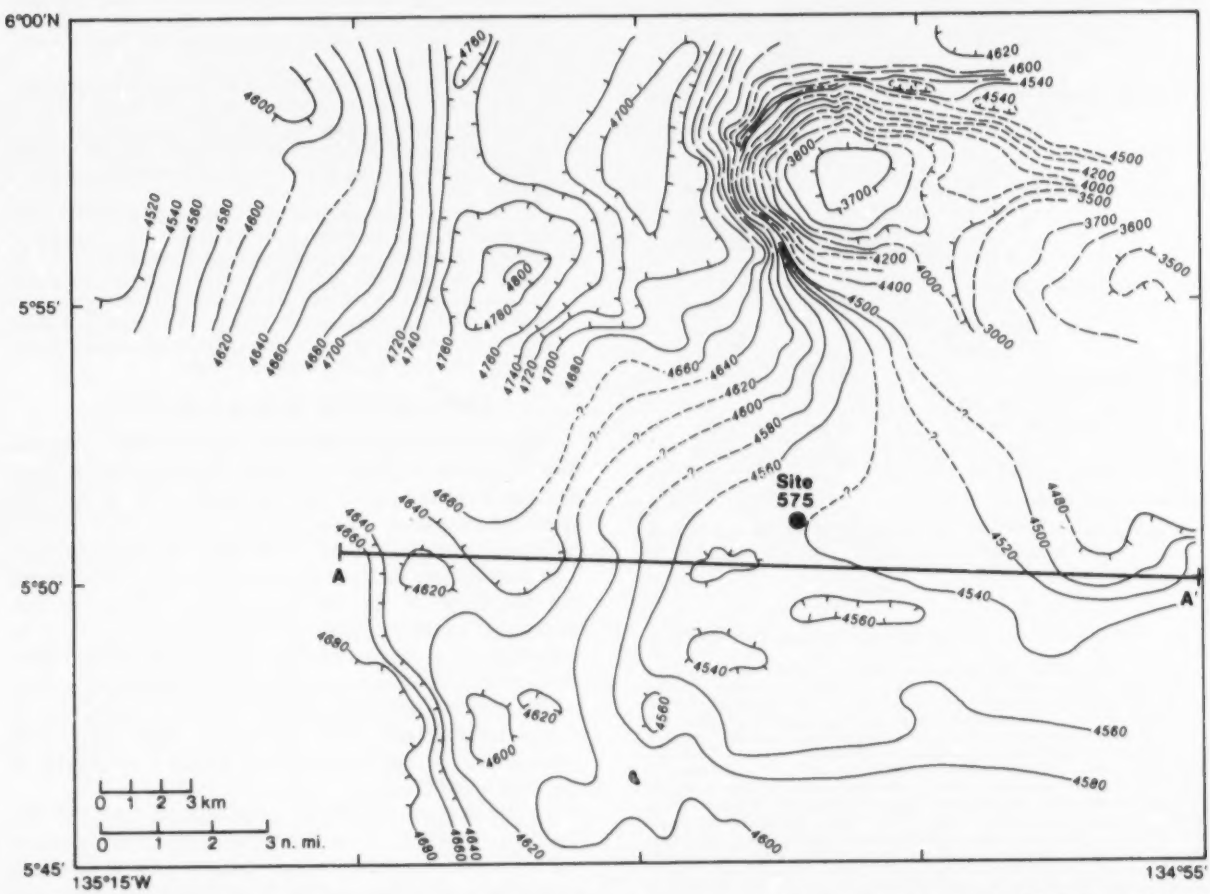

Figure 1. Bathymetry at Site 575 (20-m contour interval; 100-m contour interval for depths <4500 m). Uncorrected water depth (velocity = 1.5 km/s) of site is 4528 m. Corrected water depth is 4536 m. Profile A-A′ is the seismic profile shown in Figure 2.

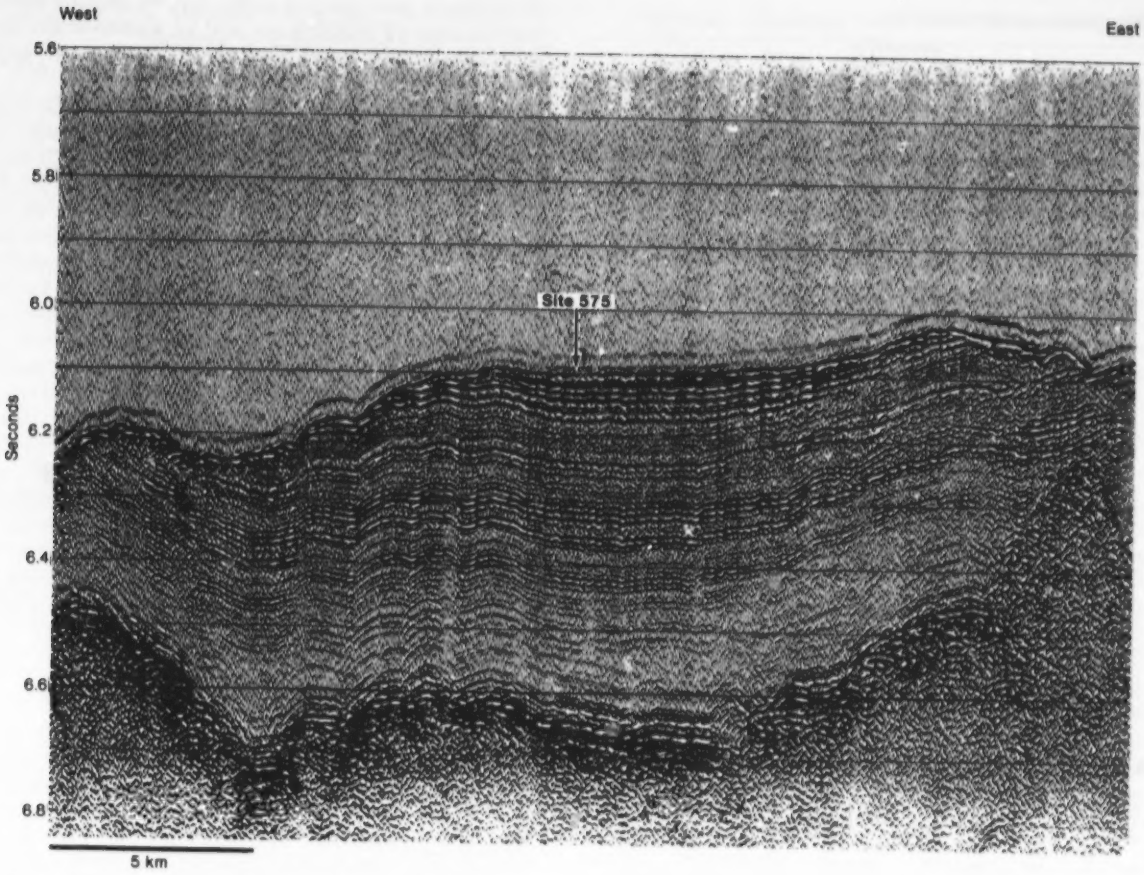

Figure 2. Seismic profile near Site 575 (see Shipley et al., this volume).

the bathymetry. Our target was a small flat region with a water depth of about 4550 m (uncorrected) and approximately 0.58 s of sediment overlying acoustic basement.

We entered the area covered by Seabeam bathymetry (from R/V *Thomas Washington*, Ariadne Leg I) at 0010Z on 21 April. As at Site 574, relative bathymetric relationships displayed on the Seabeam chart agreed with our findings, but the absolute depth values disagreed by 10 to 30 m. In general, the Seabeam depths were greater than those measured by the *Challenger's* echo sounder. Nonetheless, we had little difficulty in finding our location with respect to the bathymetry and the seismic section, and at 0104Z we crossed the proposed site. We continued past the site for approximately 1 n. mi., and at 0113Z we turned to return to the proposed site.

An unexpectedly strong current pushed us quite a bit north as we tried to return to the site, but since the flat area we wanted to drill extended to the north we dropped the beacon (at 0140Z, 21 April). We continued to survey for 1 n. mi. past the beacon.

The beacon was acquired quickly, and drill pipe run-in began at 0400Z on 21 April. In accordance with our primary directive, we rigged the 9.5-m variable-length HPC (VLHPC) and began coring. The first core established the mudline at 4550 m. We acquired 10 more 9.5-m hydraulic piston cores without difficulty. We exerted more that 40,000 lb. of pullout force on Core 12 (which was at 98.6 m sub-bottom), however, and the quick disconnect parted, leaving the core barrel in the mud.

We realized that we did not have enough time both to hydraulic piston core the upper section twice and to rotary drill to basement. Since a switch to rotary drilling would involve 24 hr. of pipe trip time, we decided not to try to rotary drill to basement but to re-rig the VLHPC with a 5-m barrel to see how deep we could get. To try to reduce the necessary pullout force we decided to wash 5 m after each core and then to pull up 2 m before shooting the next core. By coring in this manner the core barrel would travel through 2 m of wash and 3 m of previously uncored material. The resulting core is, in essence, only 3 m long, but the surface area of the corer exposed to undisturbed sediment is reduced.

We washed down to just above our deepest penetration in Hole 575 and began Hole 575A at 93.8 m sub-bottom. We collected five 3-m cores. The sediment seemed rather soft, so we tried a full 5-m core for Core 6, but we needed to exert 30,000 lb. of pullout force to retrieve the core barrel, so we went back to the 3-m method. We collected a total of 33 3-m cores and penetrated to a sub-bottom depth of 208.4 m (Table 1). The 1- to 2-m wash

Table 1. Coring summary, Site 575.

Core	Date (Apr. 1982)	Local time (hr.)	Depth from drill floor (m)	Depth below seafloor (m)	Length cored (m)	Length recovered (m)	Recovery (%)
Hole 575							
1	21	0502	4550.2-4557.5	0.0-7.3	7.3	7.36	100+
2	21	0625	4557.5-4567.0	7.3-16.8	9.5	9.66	100+
3	21	0735	4567.0-4576.5	16.8-26.3	9.5	9.70	100+
4	21	0830	4576.5-4585.2	26.3-35.0	8.7	8.72	100+
5	21	0945	4585.2-4594.7	35.0-44.5	9.5	9.60	100+
6	21	1043	4594.7-4604.0	44.5-54.0	9.3	9.53	100+
7	21	1143	4604.0-4613.5	54.0-63.5	9.3	9.62	100+
8	21	1311	4613.5-4623.0	63.5-73.0	9.5	9.56	100+
9	21	1420	4623.0-4630.2	73.0-80.2	7.2	7.22	100+
10	21	1530	4630.2-4639.1	80.2-89.1	8.9	8.91	100+
11	21	1640	4639.1-4648.6	89.1-98.6	9.5	9.47	99
					98.60	99.35	100
Hole 575A							
1	21	2108	4644.0-4649.1	93.8-98.9	5	5.11	100
2	21	2230	4647.4-4652.5	97.2-102.3	5	5.12	100
3	21	2330	4651.3-4655.3	101.1-105.3	5	4.25	85
4	22	0050	4655.4-4660.1	105.2-109.9	5	4.73	95
5	22	0150	4659.2-4664.3	109.0-114.1	5	5.06	100
6	22	0300	4664.3-4669.3	114.1-119.1	5	5.13	100
7	22	0400	4668.6-4673.5	118.4-123.3	5	4.90	98
8	22	0500	4673.3-4676.6	123.1-126.4	5	3.72	65
9	22	0610	4675.5-4678.4	125.4-128.2	5	2.92	58
10	22	0720	4677.5-4682.3	127.3-132.1	5	4.78	96
11	22	0820	4680.8-4685.9	130.6-135.7	5	5.05	100
12	22	0920	4685.3-4689.8	135.1-139.6	5	4.45	89
13	22	1030	4689.0-4693.1	138.8-142.9	5	4.11	82
14	22	1130	4692.1-4696.6	141.9-146.4	5	4.50	90
15	22	1305	4694.9-4699.3	146.7-149.1	5	4.36	87
16	22	1420	4698.2-4702.1	148.0-151.9	5	3.94	79
17	22	1530	4700.2-4703.9	150.0-153.7	5	3.74	75
18	22	1640	4702.7-4707.2	152.5-157.0	5	4.48	90
19	22	1750	4707.0-4711.0	156.8-160.8	5	3.96	79
20	22	1906	4711.0-4714.9	160.8-164.7	5	3.91	78
21	22	2025	4714.9-4718.9	164.7-168.7	5	4.00	80
22	22	2135	4718.3-4722.6	168.3-172.4	5	4.32	86
23	22	2245	4722.3-4725.2	172.1-175.0	5	3.91	78
24	23	0005	4724.4-4729.4	174.2-179.2	5	4.99	100
25	23	0059	4727.4-4732.2	177.2-182.0	5	4.83	97
26	23	0205	4730.3-4735.9	180.1-185.7	5	4.76	95
27	23	0310	4735.1-4738.6	184.9-188.4	5	3.56	71
28	23	0410	4737.4-4740.8	187.2-190.6	5	3.36	67
29	23	0510	4739.9-4743.9	189.7-193.7	5	4.05	81
30	23	0615	4563.8-4748.1	193.6-197.9	5	4.31	86
31	23	0715	4747.6-4752.0	197.4-201.8	5	4.41	88
32	23	0820	4751.5-4755.3	201.3-205.1	5	3.89	78
33	23	0920	4754.5-4758.6	204.3-208.4	5	4.06	81
					165.00	142.67	136
Hole 575B							
1	23	1230	4553.5-4563.0	3.3-12.8	9.5	9.60	100
2	23	1340	4562.2-4571.7	12.0-21.5	9.5	9.52	100
3	23	1450	4571.2-4579.9	21.0-29.7	9.5	8.70	92
4	23	1600	4579.7-4589.3	29.5-39.1	9.5	9.64	100
5	23	1715	4589.2-4598.5	39.0-48.3	9.5	9.30	98
6	23	1825	4598.2-4606.2	48.0-56.0	9.5	8.02	84
7	23	1935	4605.6-4614.9	55.4-64.7	9.5	9.37	99
8	23	2045	4614.9-4624.0	64.7-73.8	9.3	9.14	98
9	23	2200	4624.0-4631.6	73.8-81.4	9.5	7.61	80
10	23	2330	4631.6-4641.2	81.4-91.0	9.5	9.63	100
11	24	0038	4641.1-4649.8	90.9-99.6	9.5	8.69	91
12	24	0145	4649.8-4659.4	99.6-109.2	9.5	9.62	100
13	24	0305	4659.4-4664.3	109.2-114.1	5.0	4.90	98
14	24	0405	4664.3-4669.2	114.1-119.0	5.0	4.94	99
					123.80	118.68	119
Hole 575C							
1	24	0715	4549.2-4555.5	0.0-6.3	6.3	6.39	100
2	24	0850	4555.5-4565.0	6.3-15.8	9.5	9.52	100
					15.8	15.91	100

Note: All four holes were hydraulic piston cored. Lengths cored and recovered for Holes 575A and 575B include overlap (see Operations).

zone at the top of each core was of course badly disturbed, but the remaining 3 to 4 m were, in general, almost completely undisturbed. For reasons we do not yet understand, starting each core above the bottom of the hole appears to improve core quality. We probably could have gone deeper with the 3-m cores, but we decided not to, because time was running out and we wanted to get cores from overlapping depth intervals in at least the upper 100 m of the section.

At 1700Z on 23 April, we pulled back up to the mudline and started Hole 575B with the 9.5-m VLHPC. We decided to continue to shoot the core from 2 m above the bottom of the hole and proceeded to take 12 7.5-m cores, coring to a sub-bottom depth of 109.2 m. At that depth we switched to the 5-m HPC and took two full-length 5-m cores. Hole 575B ended at 119.0 m sub-bottom. When we pulled back out to the mudline we took two more 9.5-m cores (Hole 575C) to attempt to retrieve Plio–Pleistocene sediment that was undisturbed and therefore suitable for the study of the site's magnetostratigraphy. This attempt was successful: we recovered two undisturbed cores representing the interval from 0 to 15.8 m sub-bottom. Core 2 of Hole 575C came on deck at 1650Z on 24 April. We had agreed to begin pulling pipe at 1700Z, so this core was the last acquired on Leg 85. The pipe was pulled and the rig floor secured in a record time of 7.5 hr. At 2250Z on 24 April the *Glomar Challenger* turned toward the setting sun and got under way for an 8-day steam to Hawaii and the conclusion of Leg 85.

LITHOSTRATIGRAPHY

Lithostratigraphic Subdivision

We divided the sediments at Site 575 into two units: a cyclic siliceous calcareous ooze (Unit I) and a calcareous ooze chalk (Unit II). The division into units is based on sediment composition as determined from smear slide observation; a further division into subunits was based on color (Table 2). Thin turbidites of foraminiferal ooze occur throughout the succession.

Table 2. Lithostratigraphy of Site 575.

Unit	Unit sub-bottom depth (m)	Unit depth (Hole-Core-Section, level in cm)
I (cyclic siliceous calcareous ooze)		
A (mottled brown ooze)	0-14.1	575-1-1, 1 to 575-2-5, 75 575B-1-1, 1 to 575B-2-6, 45 575C-1-1, 1 to 575C-2-4, 150
B (brown white ooze)	14.1-25.7	575-2-5, 75 to 575-3-6, 140 575B-2-6, 45 to 575B-4-3, 150 575C-2-4, 150 to 575C-2,CC
C (gray brown ooze)	25.7-32.3	575-3-6, 140 to 575-4-4, 150 575B-4-3, 150 to 575B-5-4, 70
II (calcareous ooze chalk)		
A (pale brown ooze)	32.3-68.5	575-4-4, 150 to 575-8-4, 50 575B-5-4, 70 to 575B-10-2, 30
B (green ooze)	68.5-94.6	575-8-4, 50 to 575-11-4, 100 575A-1-1, 1 to 575A-1,CC 575B-10-2, 30 to 575B-14-2, 150
C (yellow brown ooze)	94.6-136.5	575-11-4, 100 to 575-11,CC 575A-2-2, 20 to 575A-12-1, 150 575B-14-2, 150 to 575B-14,CC
D (varicolored ooze chalk)	136.5-208.4	575A-12-1, 150 to 575A-33,CC

Note: Sub-bottom depths for Subunits IA to IIB are calculated from Hole 575 and for Subunits IIC to IID from Hole 575A only.

Unit I: Cyclic Siliceous Calcareous Ooze (upper Miocene to Pleistocene)

The sediments in Unit I (0 to 32.3 m) contain siliceous and calcareous microfossils, amorphous iron oxides, pyrite, and a relatively large amount of pelagic clay (up to 30%). The high clay content is consistent with the low sediment accumulation rate calculated for the upper 30 m of the site (Table 3). Bioturbation and sediment reworking are extensive, as evidenced by the presence of intense mottling of brownish color and mixtures of biogenic particles of different ages. The calcareous microfossils are intensely fragmented, and many are faint or barely visible under the microscope, characteristics suggestive of extensive dissolution. We divide the cyclic siliceous calcareous ooze unit into Subunits IA (mottled brown ooze), IB (brown and white ooze), and IC (gray brown ooze).

Subunit IA: Mottled Brown Ooze (upper Miocene to Quaternary)

The mottled brown ooze subunit (0 to 14.1 m) is heavily bioturbated, contains abundant burrows (Planolites common), and varies from brownish white (10YR 8/1 to 9/2) through dark grayish brown (10YR 6/2 to 3/2). The darker brown color probably results from the relative abundance of clays and iron oxides (up to 30%). The sediment ranges from clayey siliceous calcareous ooze to siliceous nannofossil and calcareous radiolarian diatom oozes. Microfossil composition varies widely. Nannofossils are rare to abundant (5 to 70%), foraminifers are absent to common (0 to 30%), and radiolarians and diatoms are common (5 to 20%). In terms of particle size, clay is abundant (40 to 75%) and silt and sand are common to abundant (silt, 25 to 40%; and sand, 5 to 40%). This subunit was 2 m thicker in Hole 575C than in Hole 575, probably because recovery in the Hole 575C mudline core was better. This subunit grades down into the brown white ooze.

Subunit IB: Brown and White Ooze (upper Miocene)

The brown white ooze subunit (14.1 to 25.7 m) ranges from very pale brown (10YR 7/3) to white (N9) radiolarian nannofossil to nannofossil oozes, and it contains very little pelagic clay (0 to 1%). Foraminifers are rare (trace to 5%), and nannofossils are common to dominant (14 to 92%). Biogenic silica may comprise up to 35% of the sediment, with radiolarians often more abundant than diatoms. The grain-size distribution is similar to that in the overlying (mottled brown ooze) subunit. This subunit grades down into the gray brown ooze.

Subunit IC: Gray Brown Ooze (upper Miocene)

The gray brown ooze (25.7 to 32.3 m) is a mottled light gray pale brown (2.5Y 7/2, 10YR 7/3) to dark brown (10YR 5/3 to 3/3) clayey radiolarian ooze. Both radiolarians and pelagic clay are abundant (radiolarians, 45%; pelagic clay, 40%), and calcite is common (10%). A layer of volcanic ash occurs at 29.5 m. There is a gradational contact between Subunit IC and the underlying (calcareous ooze chalk) unit.

Unit II: Calcareous Ooze Chalk (lower to upper Miocene)

The calcareous ooze chalk (32.3 to 208.4 m) comprises the remainder of the section drilled at Site 575. It consists of nannofossil oozes, with rare to common siliceous microfossils (0 to 20%) and foraminifers (0 to 20%). The sediments of Unit II contain rare to common sand (3 to 20%), rare to abundant silt (3 to 50%), and abundant to dominant pelagic clay (45 to 90%). Color was used to divide the unit into Subunits IIA (pale brown ooze), IIB (green ooze), IIC (yellow brown ooze), and IID (varicolored ooze chalk). The color changes do not seem to reflect major changes in sediment composition, although the more siliceous layers tend to be darker in color and display more prominent burrow mottling.

Subunit IIA: Pale Brown Ooze (middle to upper Miocene)

The pale brown ooze subunit (32.3 to 68.5 m) is characterized by its uniform very pale brown (10YR 8/3), brown white (10YR 8/1 to 8/2), to white (N9) color, and it is virtually devoid of burrow mottling. This subunit is composed of siliceous nannofossil to nannofossil oozes. In terms of particle size, clay is dominant (80 to 88%), sand is common (9 to 17%), and silt is rare to common (3 to 10%). Nannofossils are abundant (45 to 60%), and radiolarians, diatoms, and foraminifers are rare to common (radiolarians, 4 to 12%; diatoms, 1 to 6%; foraminifers, 2 to 6%). Subunit IIA rests with a very sharp contact on the underlying green subunit. The contact is a prominent color change from very pale brown (10YR 8/2) to light greenish gray (5G 8/1).

Subunit IIB: Green Ooze (lower to middle Miocene)

The green ooze subunit (68.5 to 94.6 m) consists of weakly mottled, greenish white (5G 9/1) to light greenish gray (5GY 7/1 to 8/1) siliceous nannofossil to nannofossil oozes that are similar in composition to those in the overlying subunit. Volcanic debris (particles about 3 mm in diameter) occurs in Cores 575-9 and 575-10, and a pebble of ignimbrite was found in Core 10. The green subunit grades down into the yellow brown subunit.

Subunit IIC: Yellow Brown Ooze (lower Miocene)

The yellow brown ooze subunit (94.6 to 136.5 m) contains yellowish white (2.5Y 8/1 to 8.2) to yellow (5Y 7/3), yellow brown (2.5Y 7/4, 10YR 6/4), and very pale brown (10YR 7/3 to 8.4) nannofossil to siliceous nannofossil ooze. The darker yellow brown (10YR 7/4) sediments tend to occur as discrete layers, and they are more bioturbated and richer in biogenic silica (up to 50%). In terms of particle size, sand in this subunit is common (5 to 20%), silt is common to abundant (5 to 50%), and clay is abundant (43 to 85%). Nannofossils are abundant to dominant (50 to 90%), radiolarians are common (3 to 20%), diatoms are rare to common (3 to 10%), and foraminifers are trace to common (>1 to 9%). Pyrite, iron oxides, and pelagic clay are also present in trace amounts. The yellow brown subunit grades down into the varicolored subunit.

Subunit IID: Varicolored Ooze Chalk (lower Miocene)

The varicolored ooze chalk subunit (136.5 to 208.4 m) is composed of yellow white (5Y 8/1), white (N9), pale purple (5P 7/2 to 8/2), gray (N6 to N7), and greenish gray (5G 8/1–9/1 to 5GY 7/1–8/1) foraminiferal nannofossil ooze, nannofossil ooze, and nannofossil chalk. The subunit is characterized by color banding and mottling, with streaks of the darker colors, particularly pale purple (5P 6/1 to 6/2). Between 158 and 178 m sub-bottom, the sediments are more uniform in color (brownish white to very pale brown and greenish white to greenish gray) and less banded and mottled. Sand-sized particles are rare to abundant (1 to 50%) in Subunit IID, silt is common to abundant (5 to 40%), and clay is common to dominant (20 to 90%). Nannofossils are common to dominant (30 to 93%), foraminifers are rare to abundant (2 to 50%), and radiolarians and diatoms occur in amounts from trace to common (radiolarians, < 1 to 7%; diatoms, < 1 to 7%). Iron oxides are rare to common (1 to 10%), and there are traces of pyrite. The content of biogenic silica decreases gradually from about 10% to 1–2% with increasing depth.

The section below 150 m is characterized by sporadic thin (5 cm or less) beds of chalk. The presence of undisturbed beds of chalk suggests that the chalk ooze variations at the other Leg 85 sites are primary features and not entirely drilling artifacts.

Foraminiferal Turbidites

Beds of foraminiferal sand and ooze are common throughout the succession cored at Site 575 (Fig. 3). These beds vary in thickness from a few millimeters to 45 cm and generally contain a darker colored layer of altered volcanic glass at the base. In general, the basal contacts of the foraminifer-rich turbidites are planar (possibly erosional). At some levels the volcanic glass includes welded aggregates (ignimbrite pebbles) and fragments of basalt up to 1 cm in diameter. Most beds display fining-upward sequences, with coarse foraminiferal and volcaniclastic sands at the base grading into fine-grained foraminiferal oozes above.

The foraminiferal assemblages in the turbidites are reworked and contain a benthic fauna that is older and inhabits shallower water than the fauna of the surrounding oozes (Thomas, this volume). These data suggest that the sands were deposited by turbidity currents originating from a topographic high in the immediate area. A seamount 1000 m high and 10 km to the northeast is a potential source region.

The turbidites in the upper part of the succession are generally poorly consolidated and highly porous; they contain more water than the more competent surrounding oozes. The foraminiferal sands toward the base of the cored succession, however, have undergone a high degree of dewatering and contrast with the surrounding oozes by being more indurated. The preferential induration of calcarenites in shallow-water carbonates is well known; it results from grain-size differences and higher permeability.

Carbonate Stratigraphy

Shipboard carbonate bomb analyses were made on sediment from Holes 575, 575A, and 575B at 1.5-m intervals (Fig. 4). The carbonate record for Site 575 is similar to the records for Site 573 and 574; the Pleistocene to upper Miocene section shows cyclic alternations between high-carbonate and low-carbonate intervals, and the lower to middle Miocene section shows relatively constant, high calcium carbonate values (80 to 95%). In the middle part of the lower Miocene, there is a shift from constant carbonate values of about 94% to relatively constant carbonate values of about 86%. This shift coincides with an increase in the proportion of siliceous microfossils.

The sedimentation rate curve for Site 575 reveals a hiatus (see Sediment Accumulation Rates) at a depth of 32 m. This hiatus coincides with an abrupt decrease in the carbonate content of the sediments from 92% (at 33 m) to 10% (at 27 m). Thus, the hiatus may be related to an increase in carbonate dissolution. This depth is also the level at which the sediments change from constant high carbonate values to cyclic high and low carbonate values. Analysis of Site 575 carbonate curves indicates that these data may be correlated with the Neogene carbonate event stratigraphy of the equatorial Pacific.

BIOSTRATIGRAPHY

The sediments recovered at Site 575 represent an almost complete sequence from the lower part of the lower Miocene through the upper Pleistocene (Fig. 5; see also Barron et al., this volume, for an updated version of this biostratigraphic summary). The preservation of the calcareous microfossils is good except in the upper 30 m of Holes 575, 575B, and 575C and in Sections 575A-3,CC, -4,CC and 575B-14,CC, where the planktonic foraminifers and nannofossils are strongly to moderately dissolved. The diatoms and radiolarians are well preserved throughout.

Two sequences can be distinguished. The lower sequence, which extends from the bottom of Hole 575A to the top of Core 4 in Holes 575 and 575B, has a high sedimentation rate (15 to 20 m/m.y.), and all early and middle Miocene zones can be found for each microfossil group studied. The lower/middle Miocene boundary occurs in Sections 575-9,CC and 575B-10,CC, and the middle/upper Miocene boundary lies in Core 4 in both Holes 575 and 575B.

Between Section 575-3,CC and the first section of Core 575-4, in the upper part of Subzone B of the *Coscinodiscus yabei* diatom Zone, there is a hiatus that seems to be comparable to hiatuses found at Sites 573 and 574. The upper sequence, which lies above this hiatus (above 30 m sub-bottom) and extends between the lower part of the upper Miocene and the upper Pleistocene, has a very low rate of sedimentation (3 m/m.y.). The diatom zonation suggests another possible hiatus between the lowermost Pleistocene and the uppermost Pliocene (in Sections 575-1-3 and -4). In both Holes 575 and 575B, there is

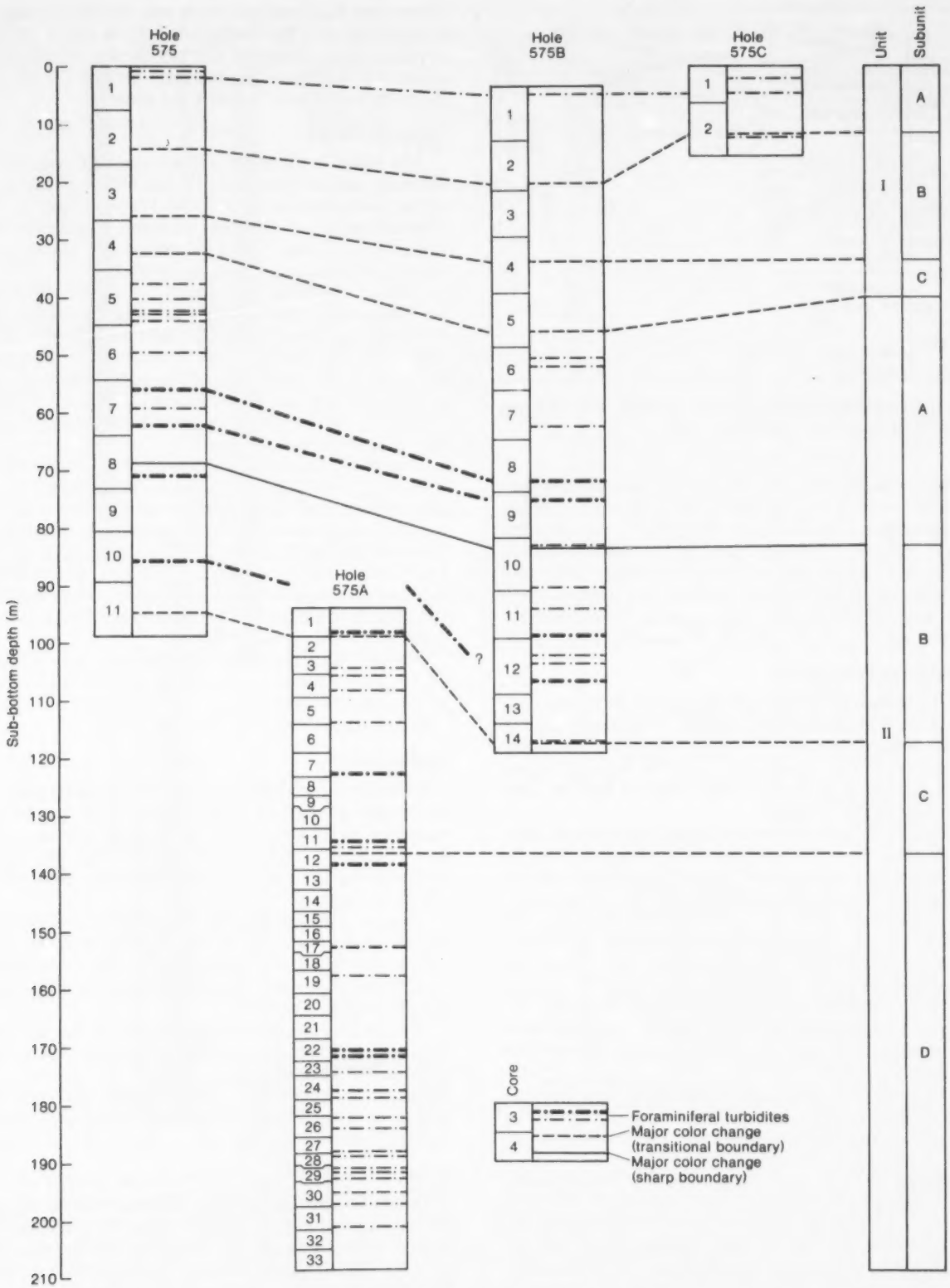

Figure 3. Hole-to-hole correlation of lithostratigraphic boundaries and foraminiferal turbidite layers at Site 575.

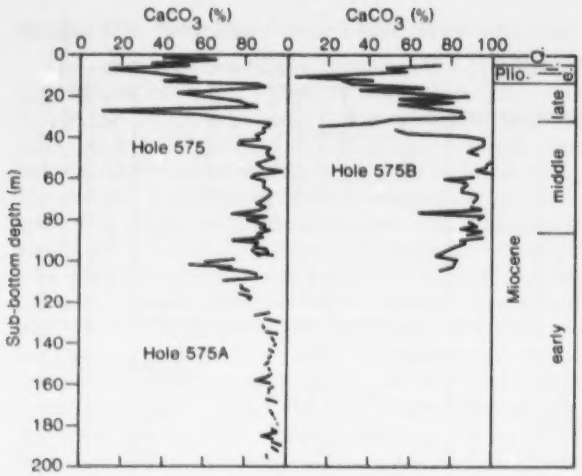

Figure 4. Carbonate content of sediments from Holes 575, 575A, and 575B (as indicated by shipboard analysis).

considerable reworking of radiolarians, diatoms, and nannofossils in Core 1, with lesser amounts in Cores 2 and 3.

Throughout the sequence, there are distinct turbidite layers containing reworked planktonic foraminifers from Zone N12 (for the uppermost layer) through P21 (for the lowest one). The benthic foraminifers in these layers also seem to be reworked; they inhabit shallower water depths than the *in situ* benthic foraminifers.

Planktonic Foraminifers

The sediments recovered from Site 575 yield abundant to common planktonic foraminifers. Preservation is good to moderate throughout the section except for the uppermost 25 m of the sequence (Cores 575-1 through -3) and a short interval in Cores 575A-3 and -4 and the age-equivalent Core 575B-14.

The rich foraminiferal assemblages recovered can readily be assigned to the standard zonal sequence (Fig. 5). The dissolution curve for planktonic foraminifers is shown in Figure 6. The evolution of *Orbulina* from *Praeorbulina*, which could be traced at Site 574, was also recovered at this site; the transition occurs in Cores 575-9 and 575B-10. The N7/N8 zonal boundary was difficult to recognize because of intense dissolution near the boundary. The interval from Zones N6 through N8 appears to be greatly condensed, although both the overlying zones (N9 through N12) and the underlying zones (N4 and N5) are very expanded.

Many discrete layers of foraminiferal sand that exhibit a distinct downward increase in grain size occur throughout the recovered sequence. The turbidite layers that occur in the uppermost part of the sequence (e.g., in Sample 575-1-4, 51–52 cm) contain a mixed assemblage indicative of Zones N12 through NN17. Those in the lower part of the sequence, on the other hand (e.g., Sample 575A-31-3, 70–71 cm), contain a Zone P21 assemblage. In general, the assemblages in a given turbidite layer are a few to several zones older than those in the *in situ* sediments, and the time lapse between the oldest reworked fossil and the *in situ* assemblage appears to decrease with increasing sub-bottom depth. If this trend continues downward through the uncored sequence at this site, the age of the basement for Site 575 and the turbidite source area is nearly the same.

Nannofossils

The nannofossils at Site 575 are generally common to abundant and well preserved. The placoliths are only moderately well preserved in Sections 575-2,CC and -3,CC. The discoasters and placoliths are highly dissolved in Sections 575-1,CC and 575A-3,CC and -4,CC. Nannofossil species occurrence is shown in Figure 7.

The top of Hole 575 (Section 575-1-1, ≈15 cm) is upper Pleistocene (Zone CN15), but strong dissolution prevents any age determination for Section 575-1,CC. Sections 575-2,CC through -4,CC correspond to the upper Miocene and the upper part of the middle Miocene. Because of the low rate of sedimentation, not all of Bukry's (1971) nannofossil zones could be found by examining the core-catcher samples.

Zones CN3 and CN4 (which occur from Sections 575-7,CC to 575A-5,CC) could not be separated with precision because *Helicopontosphaera ampliaperta* is absent at Site 575. *Sphenolithus heteromorphus* is common to abundant throughout Zone CN3–4 except in Section 575-7,CC, where it is absent. Section 575-7,CC also contains the first specimen of *Reticulofenestra pseudoumbilica* and the last specimen of *Cyclicargolithus floridanus*, so it can be placed in Zone CN4.

The oldest nannofossils at the site belong to Subzone CN1b. The presence of common specimens of *Cyclicargolithus abisectus* from Sections 575A-31,CC to -33,CC indicates the proximity of Subzone CN1a.

Radiolarians

Radiolarians in Holes 575 and 575A are common and well preserved, and the oldest among them may be assigned to the upper part of the *Cyrtocapsella tetrapera* Zone. Section 575A-33,CC marks the latest occurrence of *Theocyrtis annosa*. The zonal sequence observed is shown in Figure 5.

There is considerable reworking of Miocene and Oligocene species at the top of the cored sequence (in Core 575-1). Reworking is less common in Cores 575-2 and -3, although minor amounts of reworking occur throughout the recovered material.

The Quaternary and Pliocene zones in the top two cores of Site 575 are either missing or greatly compressed. From about 30 m downhole, all zones are present and apparently complete. Hole 575B contains the same sequence as Hole 575 and terminates in the *Calocycletta costata* Zone.

Diatoms

Diatoms are abundant to few, and preservation is good to moderate in the section cored at Site 575. The sequence is easy to zone from the late Quaternary *Pseudoeunotia doliolus* Zone (Sample 575-1-1, 51–52 cm) to the early Miocene Subzone A of the *Rossiella peleacea* Zone (Section 575C-33,CC) (Fig. 5).

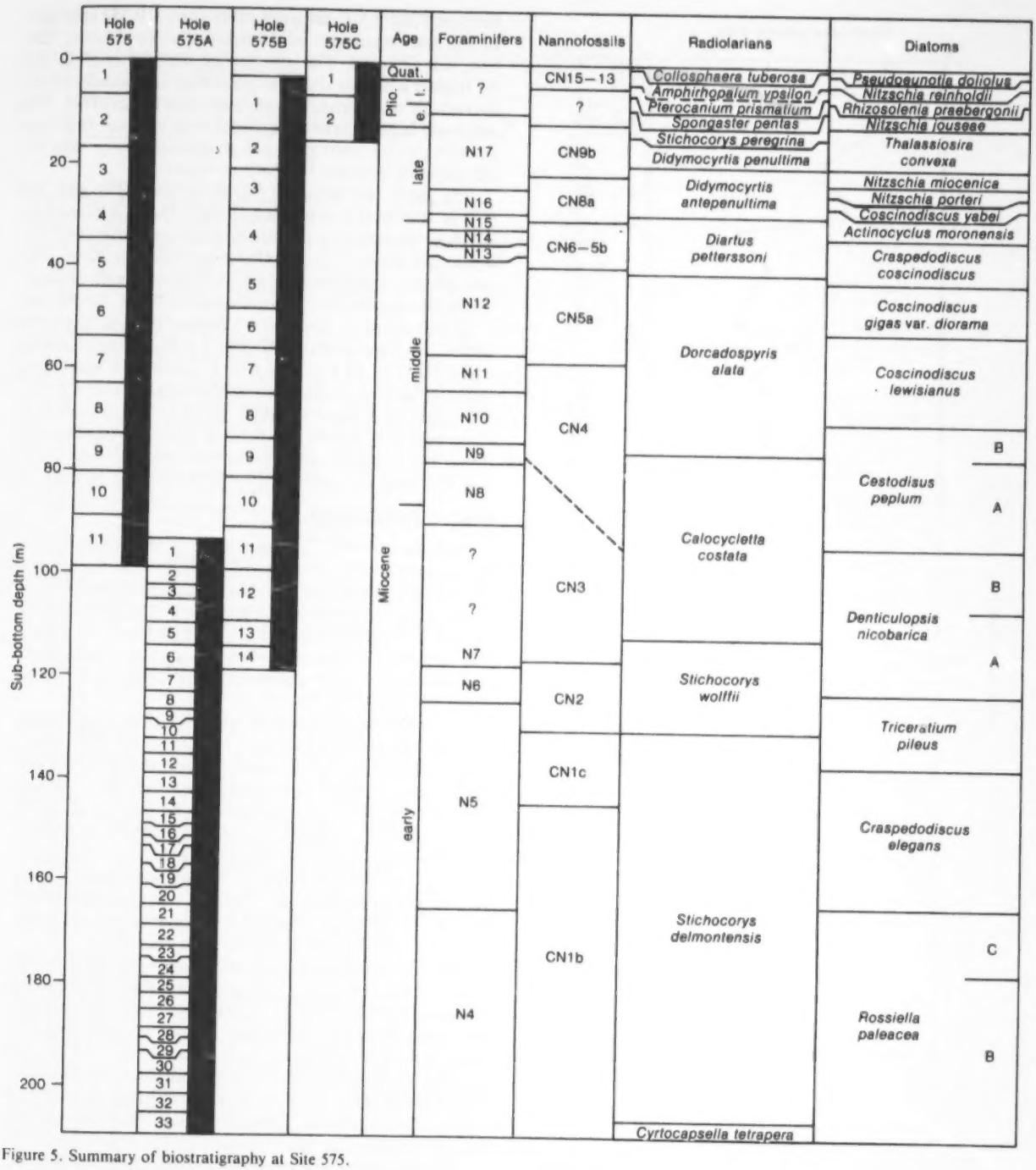

Figure 5. Summary of biostratigraphy at Site 575.

The uppermost part of the section (Cores 575-1 to -3) accumulated very slowly (≈ 3 m/m.y.), and further study will be necessary to locate the zonal and subzonal boundaries. Nevertheless, the diatoms suggest a hiatus or an even more greatly compressed section for the uppermost Pliocene to lowermost Quaternary: specimens of *Mesocena quadrangula* (a silicoflagellate that lived from 0.8 to 1.3 Ma) are common in Sample 575-1-3 (51–53 cm), and specimens of *Thalassiosira convexa* and *Rhizosolenia praebergonii* (which lived from 2.1 to 3.0 Ma) are present in Sample 575-1-4 (47–48 cm).

Core 575B-3 appears to be anomalously thick for the time interval it represents and may contain transported sediment from the nearby seamount. Section 575B-2,CC contains specimens of *Nitzschia miocenica* and is therefore less than 7.3 m.y. old, whereas the assemblages in

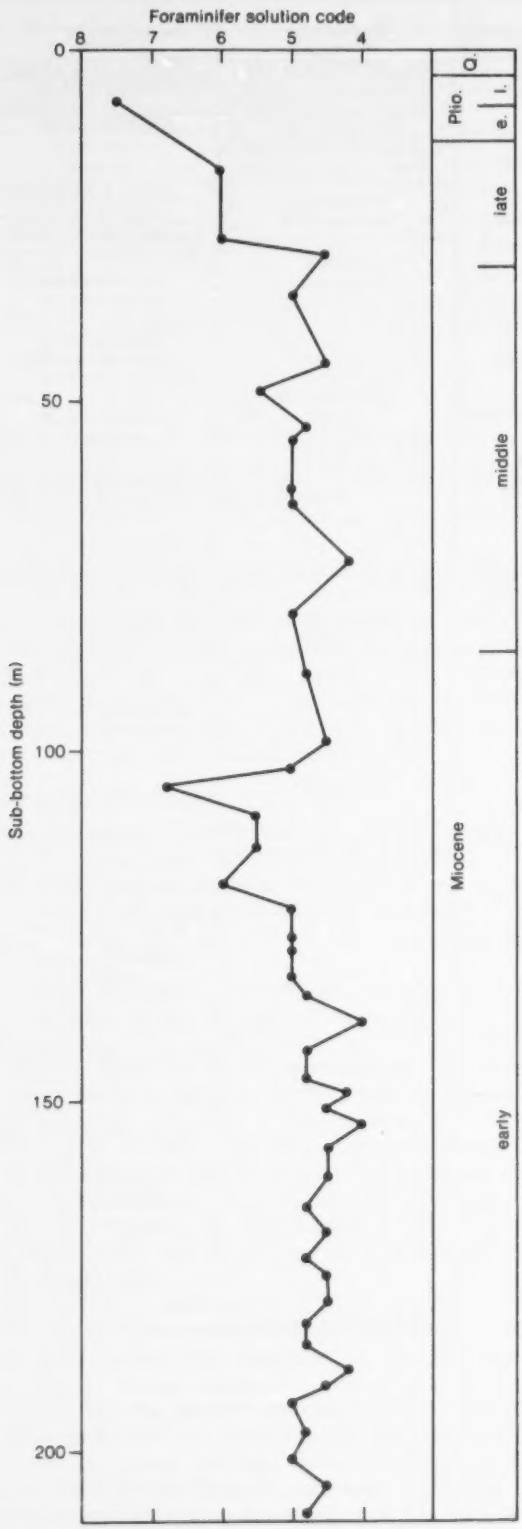

Figure 6. Foraminifer dissolution curve at Site 575 (solution code after Berger and von Rad, 1972).

Section 575B-3,CC are aged more than 8.0 Ma (the date of the last occurrence of *Thalassiosira burckliana*; Barron, this volume). The intervening samples contain latest middle Miocene diatoms, including *Coscinodiscus tuberculatus* and *Denticulopsis punctata* f. *hustedtii*. The relatively high sediment accumulation rate for this core (≈10 m/m.y.) contrasts with the much lower rate for this interval in Hole 575 (≈3 m/m.y.).

The early late Miocene hiatus at Sites 573 and 574 (9.8 to 10.5 Ma) is expanded at Site 575, as indicated by the close proximity of the first appearance datum of *Nitzschia cylindrica* s. ampl. (8.7 Ma) (Section 575-3,CC) and the last appearance datum of *Coscinodiscus vetustissimus* var. *javanica* (10.7 Ma) (Sample 575-4-1, 52–53 cm).

Comparison of the early Miocene diatom sequence within the *Triceratium pileus* and *Craspedodiscus elegans* zones (18.0 to 19.9 Ma) at Site 575 with the equivalent sequence at Site 71 (Barron, 1983) suggests that the Site 575 sequence is more complex. Keller (1981) argues for a short hiatus at 244 m sub-bottom (at the boundary between the *T. pileus* and *C. elegans* zones) at Site 71, so Site 575 may not contain this early Miocene hiatus.

Benthic Foraminifers

Benthic foraminifers are absent or extremely rare in Sections 575-1,CC through -3,CC and rare in the remainder of the section (except in the foraminiferal turbidites). Preservation is moderate to good and does not seem to be linked to the dissolution of planktonic foraminifers. The diversity of the assemblage is high (as many as 52 taxa in counts of 200 specimens), especially in the lower cores (Core 11 and below).

The main faunal constituents are *Epistominella exigua, Nuttallides umbonifera,* and species of *Gyroidinoides, Oridorsalis, Cibicidoides, Stilostomella,* and *Pleurostomella. Cibicidoides* species are much less common than at the other sites, especially below Section 575-8,CC (lower Miocene). Specimens of *Stilostomella* and *Pleurostomella* are most abundant below Section 575-10,CC (i.e., in the lower Miocene). *Uvigerina graciliformis* peaks in abundance in Section 575-4,CC, the first sample below the interval where benthic foraminifers are rare or absent as a result of dissolution, as at Site 574.

Site 575 differs from the other sites in that there are fewer specimens of the common genera (*Epistominella, Oridorsalis, Cibicidoides, Gyroidinoides*), especially in the lower Miocene. No single species or species group takes their place; many rare species are present instead (mainly species of miliolids, nodosariids, pleurostomellids, and agglutinants), with the result that diversity is high, as noted above. The ratio of rectilinear to rotaliid species is higher at Site 575 than at the other sites.

The lower few centimeters of some of the turbidites contain abundant benthic foraminifers. The assemblages in the turbidites are different from those in the normal sediments. Some species are found in both the turbidites and the other sediments, but the specimens of these species are larger in the turbidites. Large, thick-walled species (e.g., *Favocassidulina favus, F. subfavus, Globocassidulina subglobosa, Cibicidoides grimsdalei, Stilostomella abyssorum,* and *Oridorsalis umbonatus*) are well

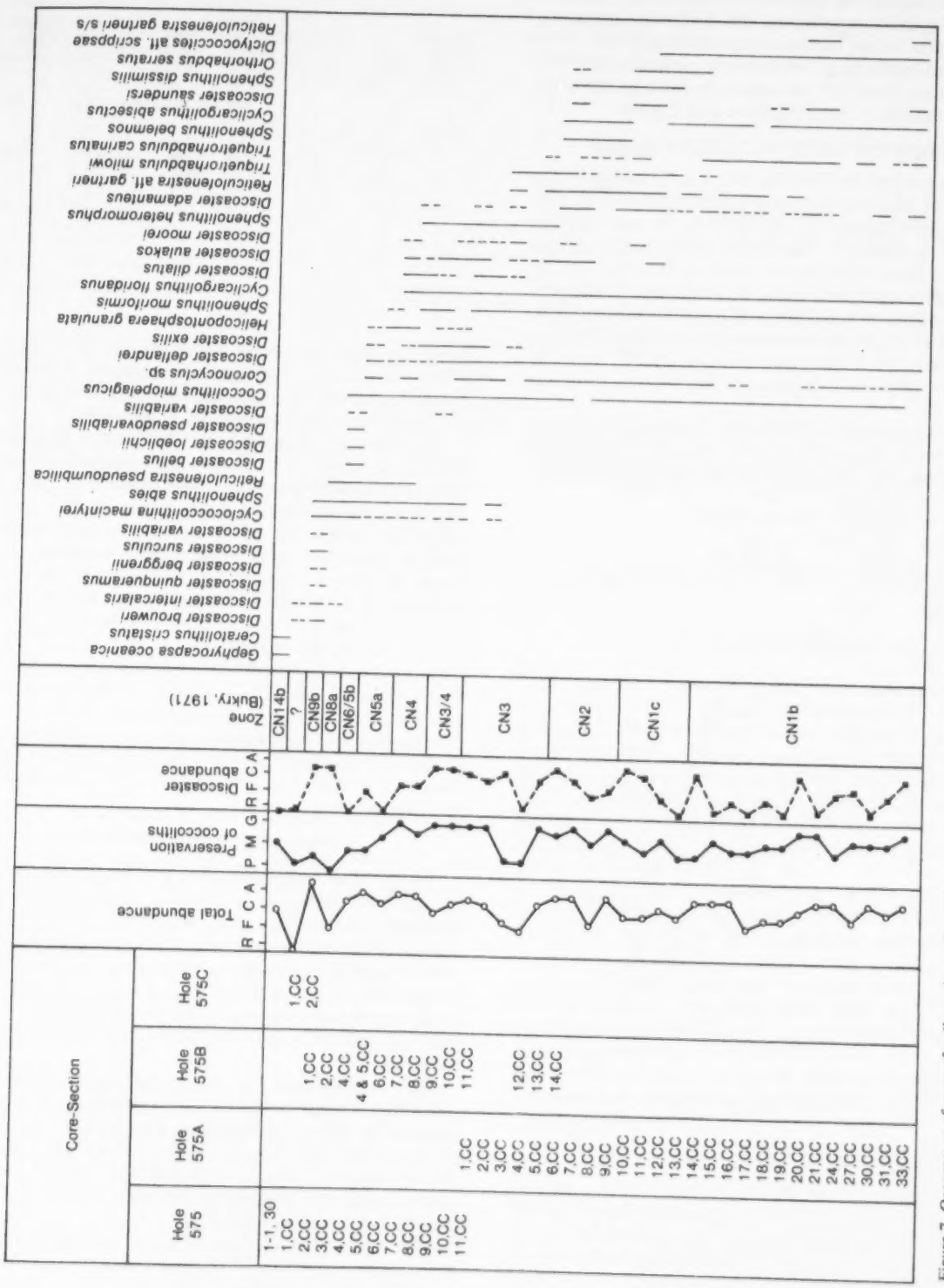

Figure 7. Occurrence of nannofossil species at Site 575.

represented in the turbidites. Some species in the turbidites are absent in the normal sediments (e.g., *Bulimina jarvisi, Eggerella propinqua,* and *Uvigerina spinulosa*; other species in the turbidites are extremely rare in the normal sediments (e.g., *Hanzawaia cushmani* and *Planulina renzi*). Some of the species present in the turbidites are typical of the Oligocene and Eocene.

SEDIMENT ACCUMULATION RATES

The age–depth plot for Site 575 (Fig. 8) indicates long intervals of relatively constant sedimentation rate. During the interval from 12.5 to 22.2 Ma the rates average 18.0 m/m.y. (Table 3). The slightly higher sedimentation rate at the base of the section (20.0 to 22.2 Ma) may reflect the proximity of the site to the equator during this time. This interval is followed by a hiatus that represents about 3.5 m.y. The interval above the hiatus (< 9 Ma) is characterized by a low sedimentation rate (3 m/m.y.). For a more detailed discussion see Barron et al. (this volume).

The extrapolated age of surface sediments from the data shown in Figure 8 is 1.6 Ma. This age is much older than the late Pleistocene age estimated for samples taken in the upper section of Core 1 of Site 575. Thus, as inferred from the biostratigraphic analysis, a hiatus or an interval of much lower sedimentation rate must occur in the late Pliocene or early Pleistocene.

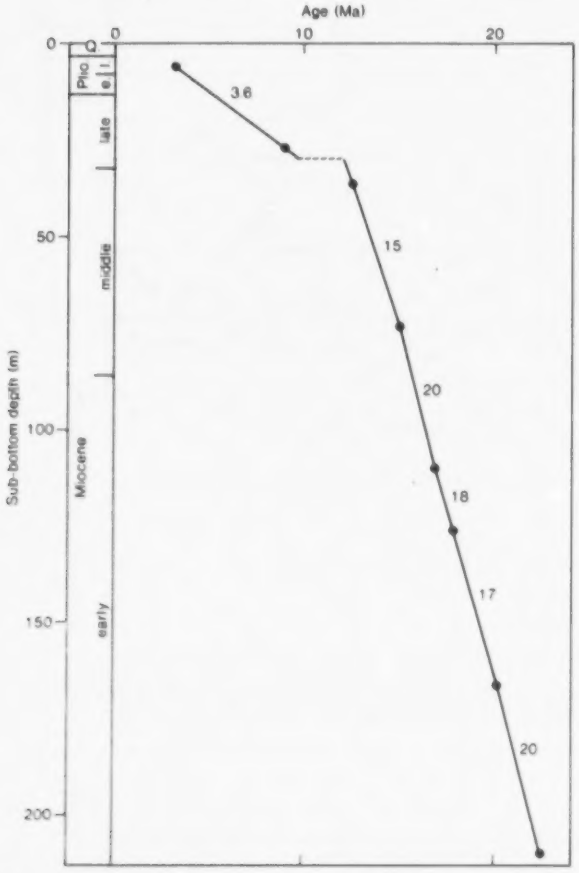

Figure 8. Age versus depth-in-hole based on biodatums at Site 575. Numbers on curve represent sedimentation rate in m/m.y.

Table 3. Sedimentation rates and carbonate and noncarbonate mass accumulation rates at Site 575.

Sub-bottom depth (m)	Age (Ma)	Sedimentation rate (m/m.y.)	Mean dry bulk density (g/cm³)	Mean $CaCO_3$ (%)	Mean mass accumulation rate ([g/cm²]/1000 yr.)		
					Total	$CaCO_3$	Non $CaCO_3$
6	3.2	3.6	0.60	56	0.21	0.12	0.09
27	9.0						
Hiatus							
36	12.5	15.4	0.99	88	1.52	1.34	0.18
73	14.9	19.5	0.91	83	1.77	1.47	0.30
110	16.8	17.8	0.92	80	1.64	1.31	0.33
126	17.7	17.4	1.10	91	1.91	1.74	0.17
166	20.0	20.0	1.08	94	2.20	2.07	0.13
210	22.2						

The mass accumulation rates for total sediment and for the carbonate and noncarbonate sediment fractions were calculated by using shipboard physical property and carbonate bomb analyses (Table 3; Fig. 9). The carbonate accumulation rate closely follows the total sediment mass accumulation rate, whereas the noncarbonate rate shows an inverse relationship. The noncarbonate accumulation rate is low in the highest sedimentation rate interval (between 20.0 and 22.2 Ma, or between 166 and 210 m). Above this interval (i.e., at 14.9 to 17.7 Ma, or 73 to 126 m), the noncarbonate rate increases to the maximum value for Site 575. In general, carbonate accumulation rates decrease with decreasing age. Thus, the relationship between noncarbonate and carbonate deposition at Site 575 is weakly negative (Fig. 10), unlike the relationships at Sites 572, 573, and 574 (see also Theyer et al., this volume).

PHYSICAL PROPERTIES

The physical properties measured for this site included wet-bulk density (ρ_b), porosity, sonic velocity (V_p), formation factor (F), and shear strength. Measurements were made at regular intervals except where the sediment was disturbed. A discussion of the data collection techniques, procedures, and pertinent references is presented in the introductory section before the individual site chapters. All numerical data are listed in the Appendix (this volume).

The data for Site 575 are plotted against depth and presented in Figures 11 to 16. The profile for formation factor (Fig. 14) is incomplete in the intervals from 30 to 60 m and 100 to 160 m and because of a malfunction in the conductivity meter. Overall, formation factor increases slightly with increasing depth, the range of values changing from 1.5–2.0 to 2.0–2.5.

The sonic velocity data (Fig. 13) increase from approximately 1.5 km/s at the top of the hole to 1.6 km/s at 200 m. The anomalously high velocities at depths of 38, 40, 42, 98, 118, 130, 160, and 180 m correspond to the depths of foraminiferal turbidites. The high sonic ve-

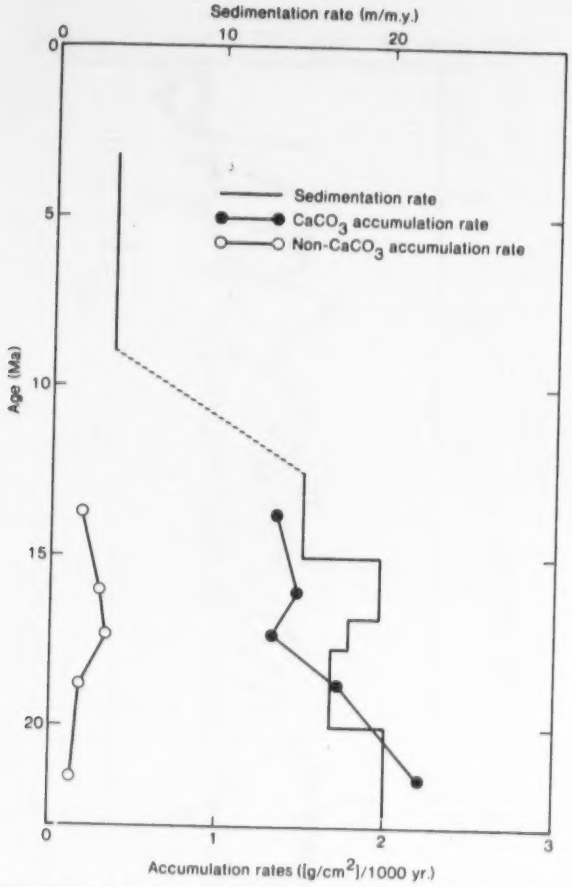

Figure 9. Sedimentation rate and average mass accumulation rates for carbonate and carbonate-free sediments at Site 575.

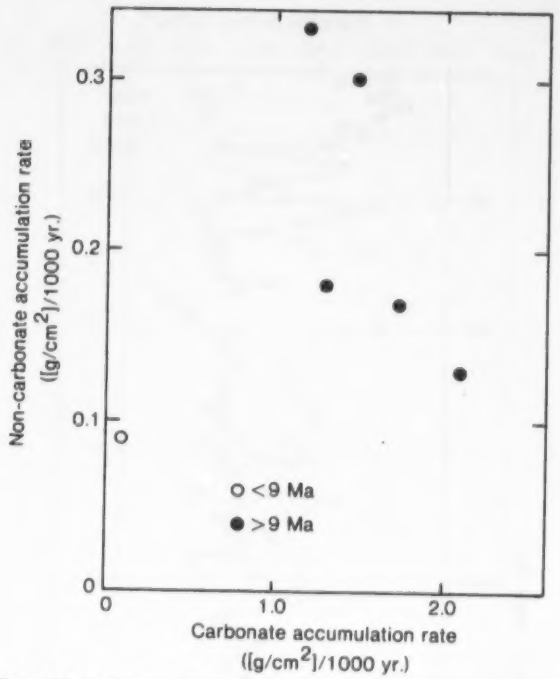

Figure 10. Carbonate versus carbonate-free mass accumulation rates at Site 575.

localities create contrasts in acoustic impedance that should appear as reflectors in the seismic survey.

The porosity and wet-bulk density data (Figs. 12 and 11) show similar but opposite trends (1.2 to 1.5 g/cm^3 and 85 to 65%) for the topmost 30 to 40 m. The interval from 40 to 130 m shows data scattered about comparatively constant mean values (1.6 g/cm^3 and 60%, respectively). Below (from 130 to 180 m), wet-bulk density generally increases (from 1.6 to 1.8 g/cm^3) and porosity generally decreases (from 65 to 55%). Below 180 m the values remain approximately constant (1.8 g/cm^3 and 55%, respectively).

Thermal conductivity increases from about 1.5 mcal/cm·s·°C at the surface to about 2.7 mcal/cm·s·°C at 25 m. It then remains generally stable until the bottom of the hole, with the exception of high values (up to 3.9 mcal/cm·s·°C) at about 175 m (Fig. 15).

A shear strength profile is presented in Figure 16. For the first 80 m, the values gradually increase from 100 to 400 g/cm^2. From 100 to 190 m the data show considerable scatter around an approximate mean value of 200 g/cm^2.

PALEOMAGNETISM

At Site 575 only a few polarity changes could be distinguished by 180° changes in the measured NRM_0 declinations. These apparent reversals are not accompanied by changes in the sign of the inclination. Conversely, sign changes in the inclination are not accompanied by a 180° rotation of the declination. Holes 575, 575A, 575C, and the top of Hole 575B (Cores 1 to 9) show reasonably strong NRM_0 magnetizations, with means varying from 2.4 to 3.7 $\times$ 10^{-6} G.

Hole 575C was cored because the first two cores in Holes 575 and 575B were badly disturbed. The sequence recovered from Hole 575C is complete and undisturbed down to a depth of 15.8 m below the seafloor, a depth that corresponds to an age of at least 5 m.y. The dark brown sediments recovered from Hole 575C show the strongest magnetization of the sediments recovered at this site, averaging 6.14 ($\pm$ 4.06) $\times$ 10^{-6} G. In general, the NRM intensities at this site seem to correlate better with changes in sedimentation rate than with changes in color of sediment.

INTERSTITIAL-WATER CHEMISTRY

The concentration of alkalinity, calcium, and strontium in the interstitial water increases gradually, and after an initial increase the concentration of magnesium decreases gradually (Fig. 17). The profiles for this site are difficult to interpret because we did not drill to basement, and the reactions at greater depths may be affect-

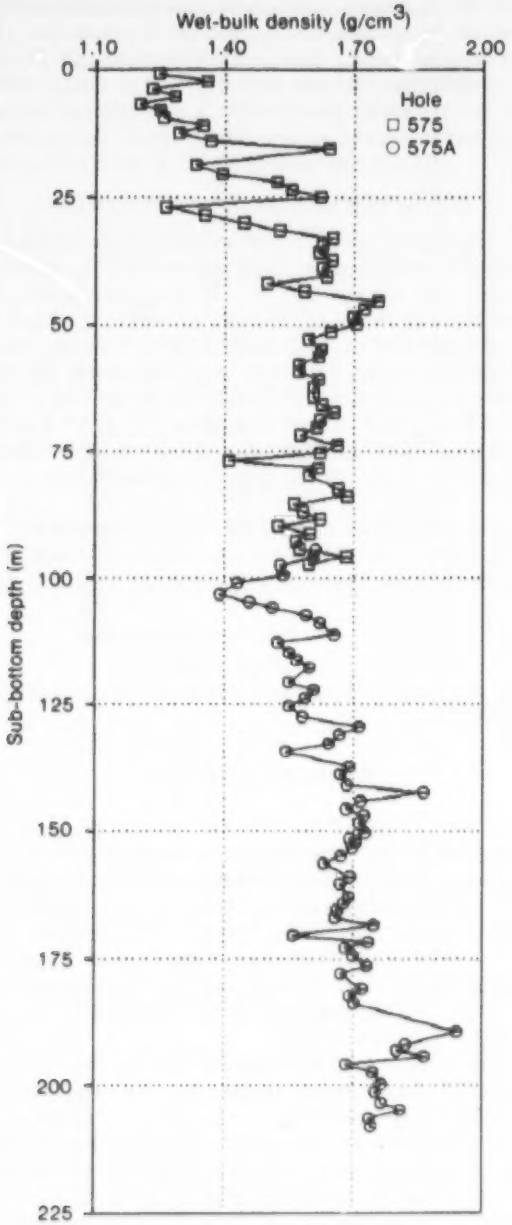

Figure 11. Wet-bulk density versus depth for Site 575.

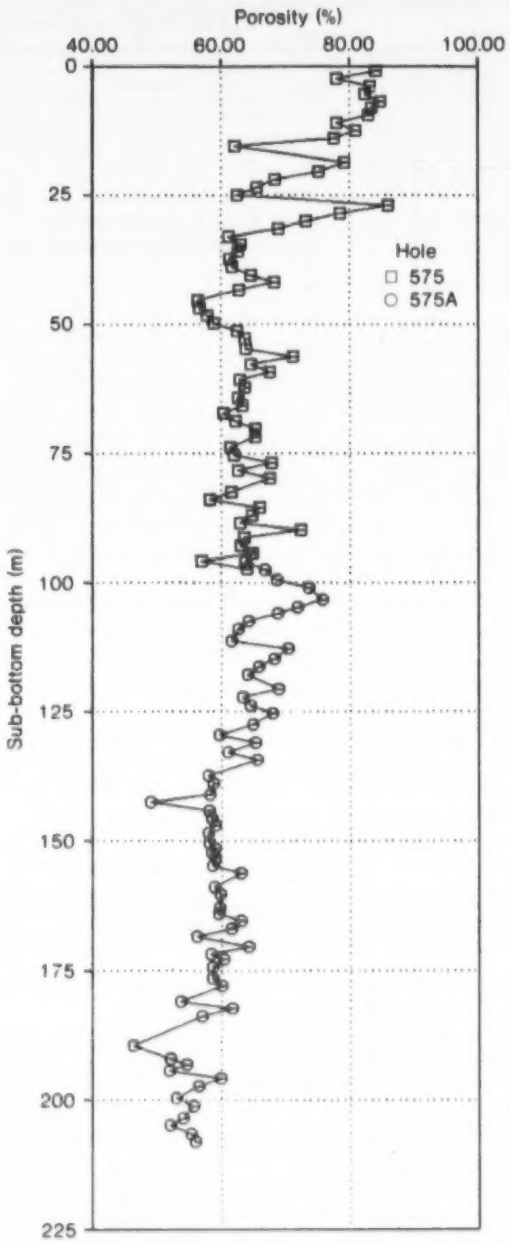

Figure 12. Porosity versus depth for Site 575.

ing the concentration gradients we observed. The abrupt increase in alkalinity near 180 m sub-bottom coincides with an increase in sediment accumulation rate. The concentration of magnesium and calcium may be influenced by the alteration of basaltic material. This would be indicated if the magnesium concentrations were to decrease and the calcium values were to increase down to basement.

The steady downhole increase in the concentration of strontium indicates calcite recrystallization. The shallow first occurrence of chalk (near 160 m) suggests that the increases in strontium are related to the diagenesis of calcite. However, the strontium profile may also be affected by reactions with volcanic material within the sediments or by the alteration of underlying basalt.

SUMMARY AND CONCLUSIONS

Located at almost 6°N and just south of the Clipperton Fracture Zone, Site 575 is the northernmost of three sites that were drilled in a north-south transect of the equatorial sedimentary bulge at approximately 133°W. Lack of time prevented us from drilling to basement. Nevertheless, the objectives of drilling the site, which were

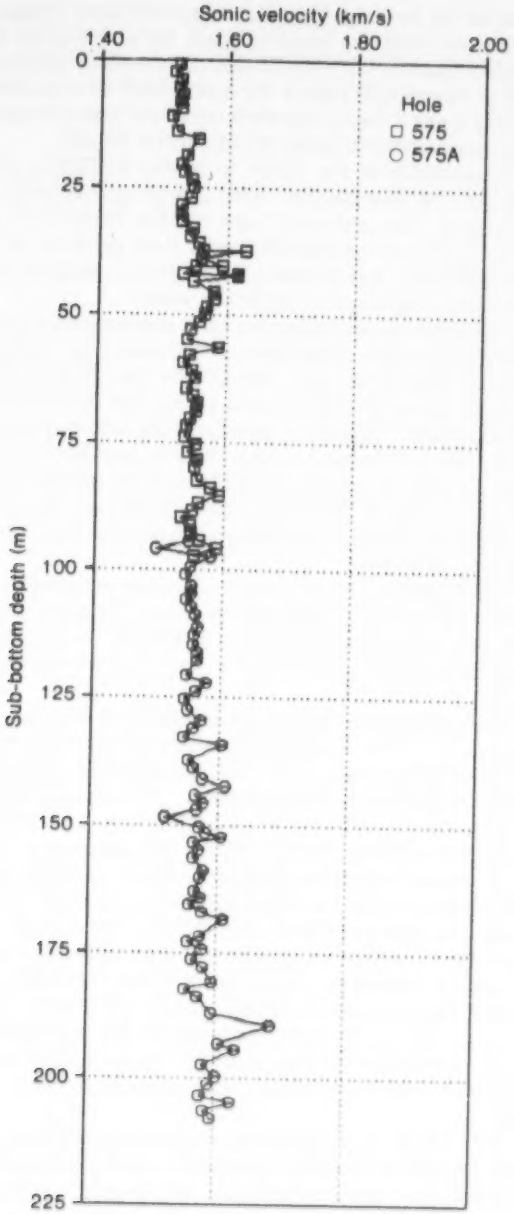

Figure 13. Sonic velocity (V_p) versus depth for Site 575.

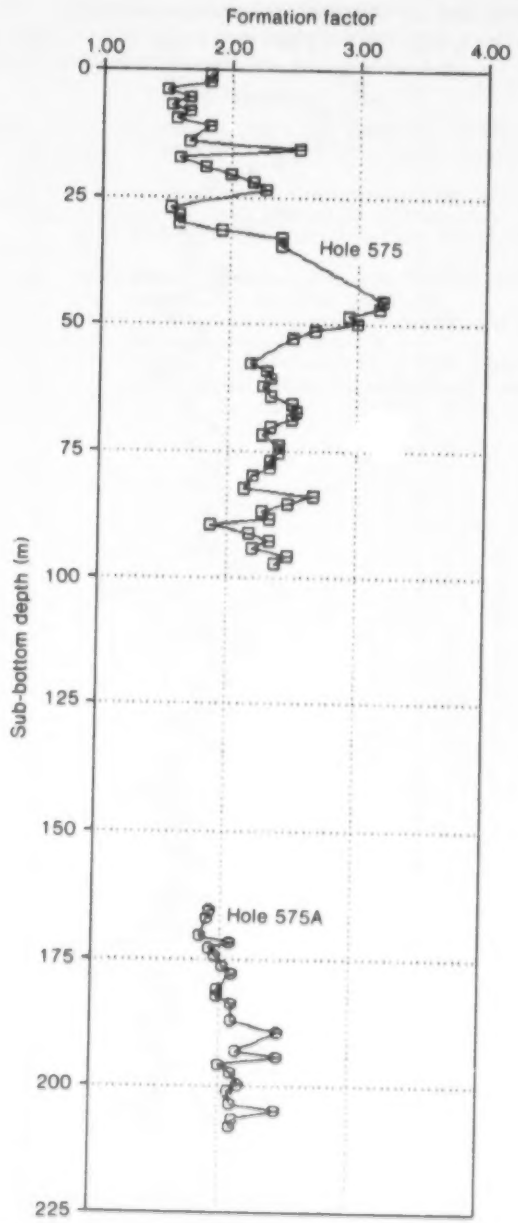

Figure 14. Formation factor (horizontal) versus depth for Site 575.

to study its paleoenvironment and stratigraphy, were met. Three HPC holes were drilled, which penetrated to a depth of 208.4 m sub-bottom and ended in lowermost Miocene sediment. In total, 374.47 m (the upper 120 m overlap) of sediment were recovered, most of it undisturbed. As expected, the nearly complete Neogene section bears out the tectonic depositional model most widely accepted for the equatorial Pacific high fertility belt (van Andel et al., 1975); the early to middle Miocene (12 to 22 Ma) sediments record a highly productive environment dominated by the equatorial belt, whereas the sediments deposited in the most recent 10 m.y. testify to the site's emergence from beneath this belt and its migration to the north.

Two sedimentary units express the lithostratigraphic makeup of the sequence: an upper Miocene to Quaternary cyclic siliceous calcareous ooze (Unit I, 0 to 32.3 m sub-bottom) and a lower to middle Miocene calcareous ooze chalk (Unit II, 32.3 to 208.4 m). Unit I is characterized by cyclic alternations in carbonate content, whereas Unit II has relatively high (94%), constant carbonate values down to the middle part of the lower Miocene, where there is a slight decrease in the mean carbonate content (to about 86%). Subunits based on color can be

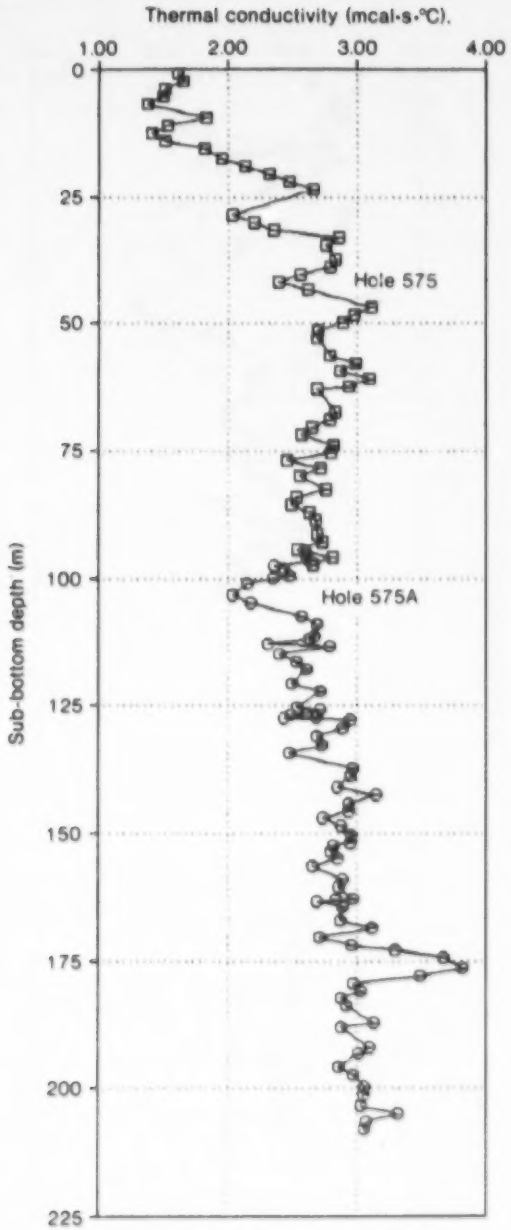

Figure 15. Thermal conductivity versus depth for Site 575.

distinguished in both units, and centimeter-thick sandy to pebbly turbidites are intercalated throughout them. The turbidites are composed primarily of allochthonous foraminifers and volcanic debris.

Except for a hiatus from 9.0 to 12.5 Ma, the sequence was complete from the lowest Miocene (22 Ma) to the upper Pleistocene. All major microfossils occur throughout, although the preservation of calcareous skeletons is poor to almost nil in the upper unit (cyclic siliceous calcareous ooze). The upper unit is characterized not only by calcareous dissolution, but also by microfossil reworking and extreme stratigraphic compression; as a result, some of the biozonal boundaries in these upper Neogene sediments could not be recognized. In contrast, the expanded sequence in Unit II and the excellent preservation of microfossils (except for a very brief interval about 17 Ma) make it one of the most complete lower Neogene sequences available from the equatorial Pacific.

Foraminifers in the sandy to pebbly turbidites indicate grading downsection, with coarser grains lower in the record. The planktonic and benthic foraminifers in these layers are considerably older than those in the *in situ* sediments, and the benthic foraminifers suggests that the layers originated in shallower water.

The sediment accumulation rates confirm the twofold lithostratigraphic subdivision. Moderate and variable rates of 14 to 20 m/m.y. characterize the siliceous nannofossil oozes of Unit II, and a very low but virtually constant rate of 3 m/m.y. generated the siliceous calcareous Unit I. The small fluctuations in rate in the lower unit are not necessarily correlated with the subunits; the maximum rate of 20 m/m.y. prevails between about 22 and 20 Ma. There is a prominent hiatus between about 9.0 and 12.5 Ma.

NRM intensity is correlated with both sedimentation rate and lithology as expressed by color. Consistently high values, on the order of 10^{-6} G or above, are typical of the sediments in Unit I and for most of the browner intervals in Unit II.

Physical properties show strong gradients over the topmost 30 to 40 m, followed by scatter about a constant mean in the subsequent 40 to 130 m sub-bottom; at 130 m a shift toward a new mean begins. In general, the changes in data closely reflect changes in lithology, particularly carbonate content. Sonic velocity (V_p) appears to have fluctuations of greater amplitude than at previous sites, although some of the fluctuations are the result of the turbidites interspersed in the column. The seismic section (the upper 200 m) consists of a zone of strong, closely spaced reflectors, which is underlain by a long interval with very weak, closely spaced reflections. As at most of the Leg 85 sites, the upper, seismically stratified zone correlates extremely well with the interval of large-amplitude, short-wavelength fluctuations in wet-bulk density.

The trends in inorganic pore-water geochemistry are comparable to those at the earlier sites, although the gradients are more compressed and possibly indicative of reactions deeper in the section. The evidence for a hiatus at 9.0 to 12.5 Ma is supported by the geochemical evidence.

In conclusion, the sedimentary column cored at Site 575 records a picture that is comparable to that of the other sites: first, deposition took place from about 22 to 12.5 Ma under the direct influence of the equatorial belt; and then (from 12.5 Ma to the present) the belt's influence waned as the underlying lithosphere migrated toward the northwest.

Finally, there is evidence of multiple episodes of erosion in the seismic records around the site, and this, the proximity of a prominent seamount, and the consistent appearance of brief turbidites (which contain basalt pebbles, volcanic glass, and allochthonous foraminifers) tell

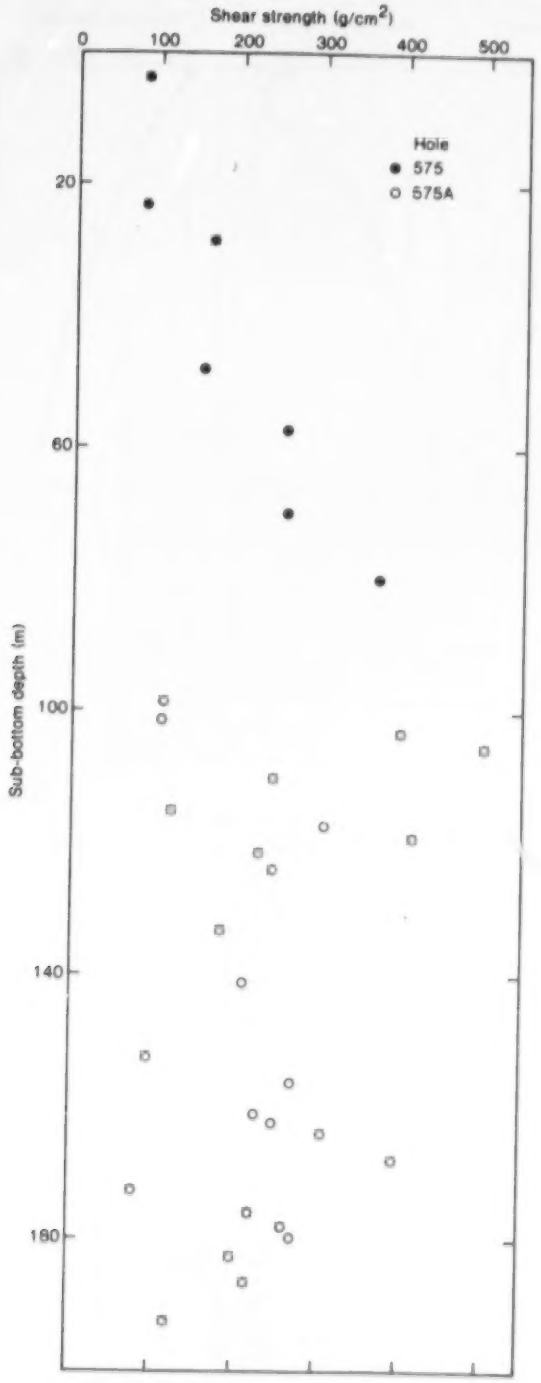

Figure 16. Shear strength versus depth for Site 575.

a story of discrete erosional, redepositional, and possibly volcanic events that punctuate the last 20 m.y. of the region's geological history.

REFERENCES

Barron, J. A., 1983. Latest Oligocene to early middle Miocene diatom biostratigraphy of the eastern tropical Pacific. *Mar. Micropaleontol.*, 7:487–515.

Berger, W. H., and von Rad, U., 1972. Cretaceous and Cenozoic sediments from the Atlantic Ocean. *In* Hayes, D. E., Pimm, A. C., et al., *Init Repts. DSDP*, 14: Washington (U.S. Govt. Printing Office), 787–954.

Bukry, D., 1971. Cenozoic calcareous nannofossils from the Pacific Ocean. *Trans. San Diego Soc. Nat. Hist.*, 16:307–327.

Keller, G., 1981. Miocene biochronology and paleoceanography of the North Pacific. *Mar. Micropaleontol.*, 6:535–551.

van Andel, T. H., Heath, G. R., and Moore, T. C., Jr., 1975. Cenozoic history and paleoceanography of the central equatorial Pacific Ocean. *Mem. Geol. Soc. Am. 143.*

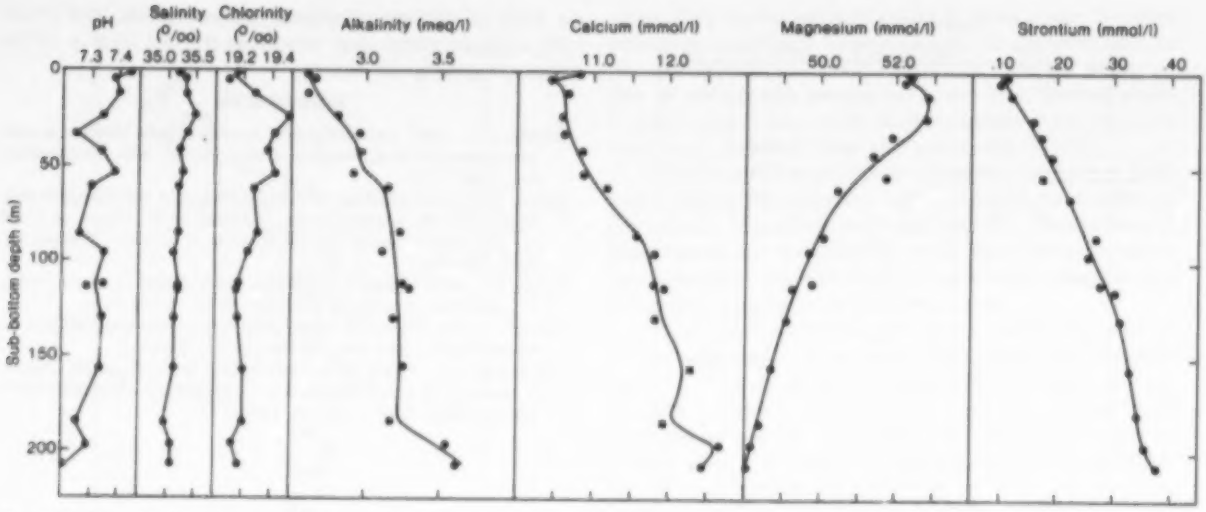

Figure 17. Interstitial-water chemistry, Site 575.

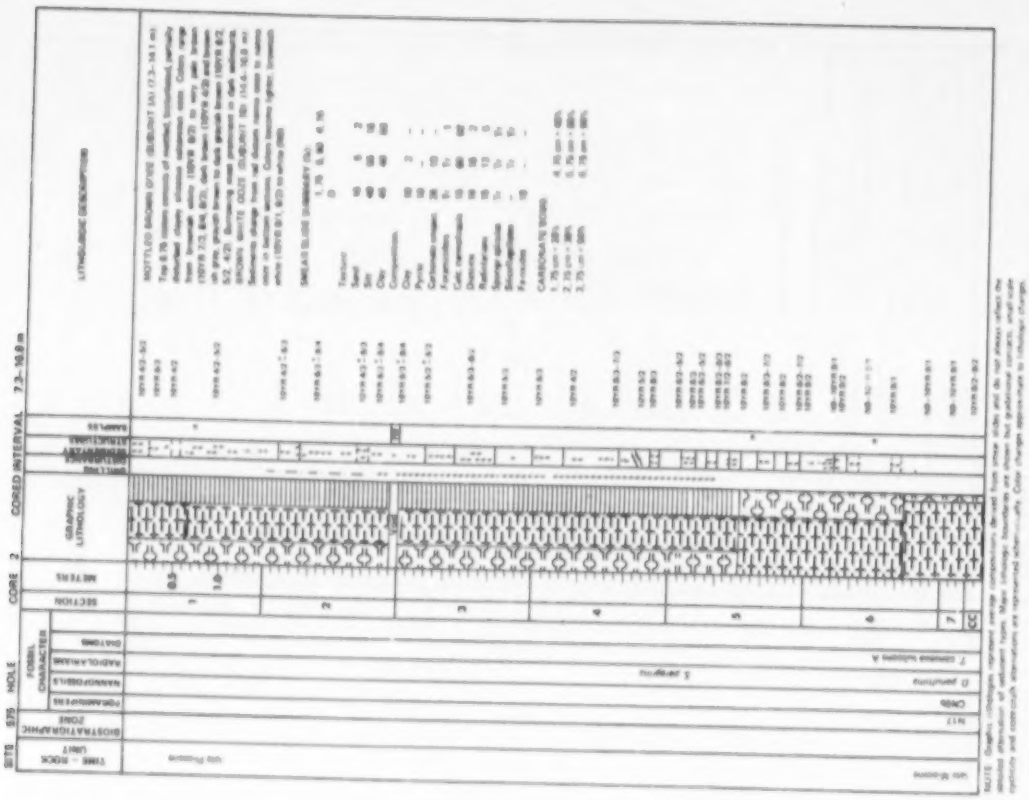

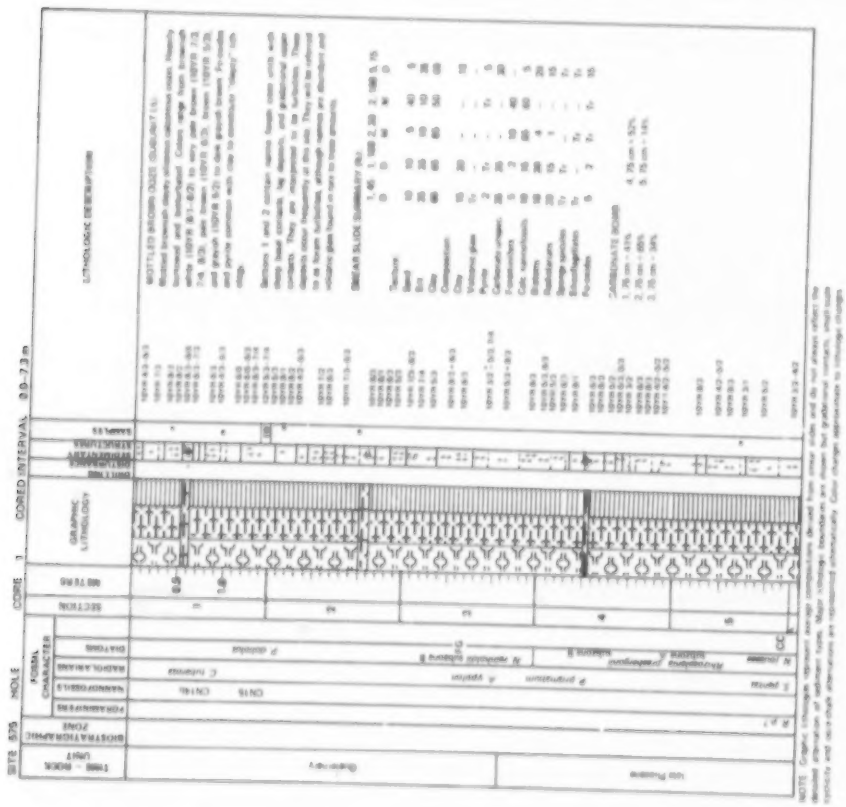

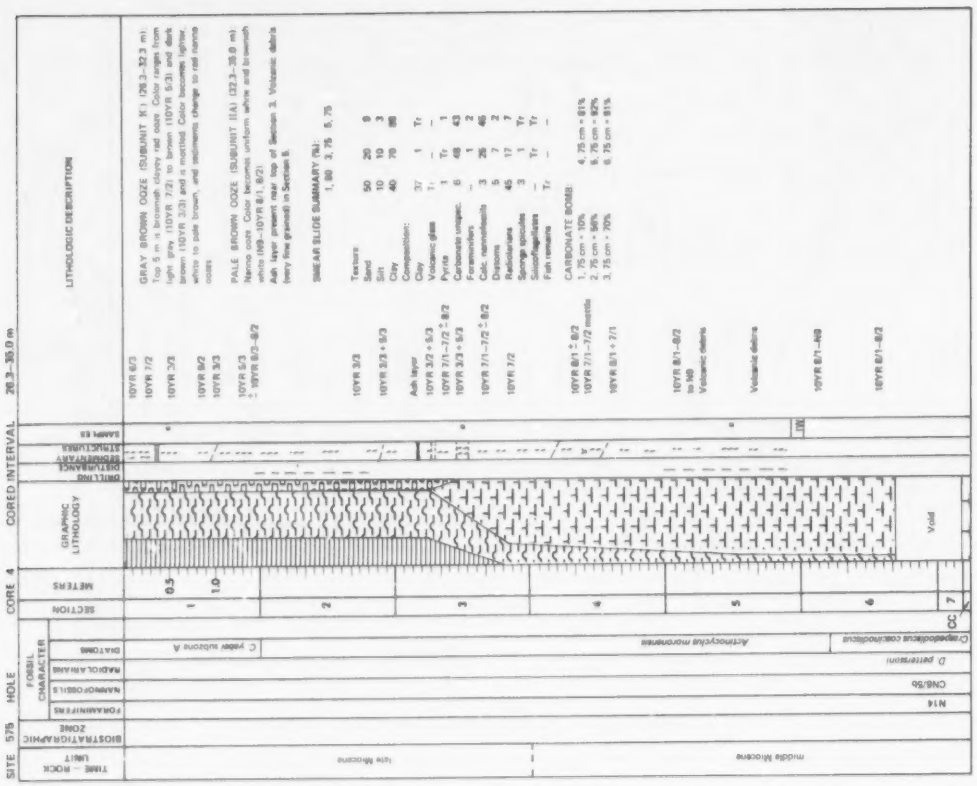

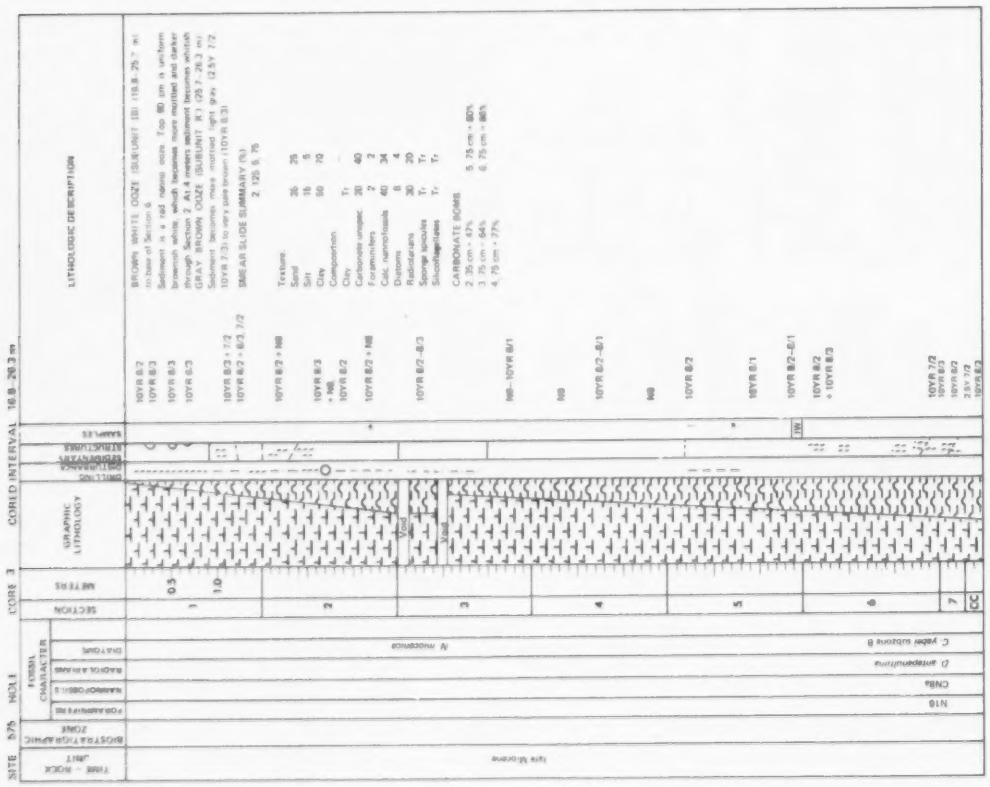

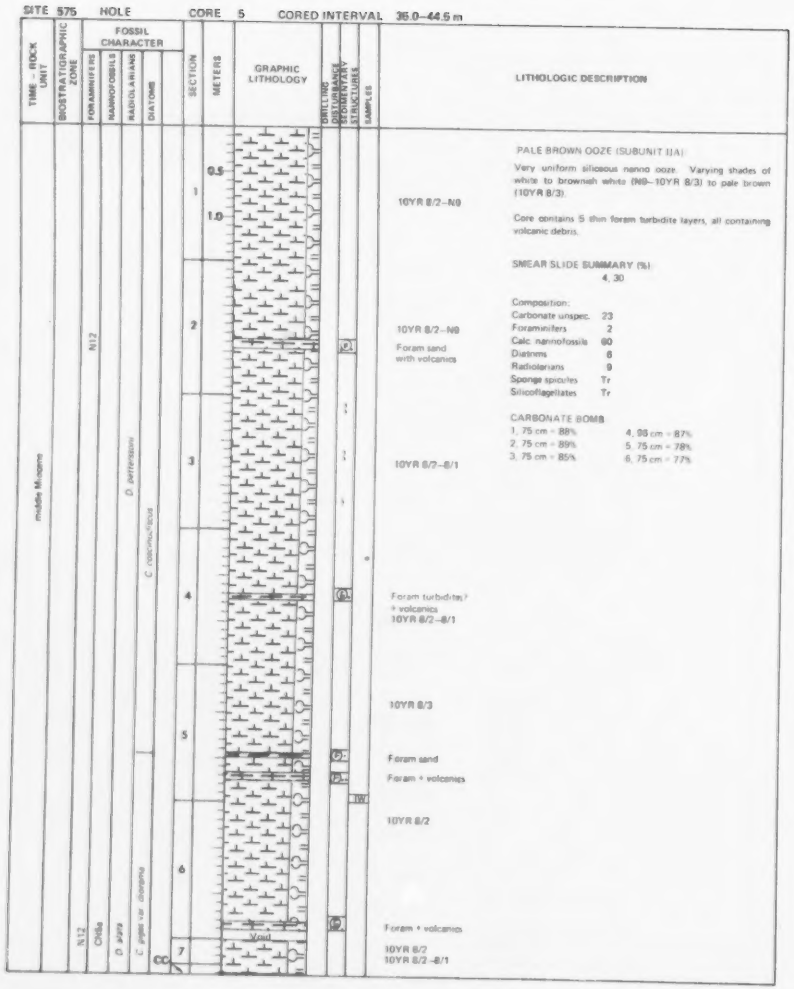
SITE 575 HOLE CORE 5 CORED INTERVAL 36.0–44.5 m
TIME – ROCK UNIT
BIOSTRATIGRAPHIC ZONE
FOSSIL CHARACTER
FORAMINIFERS
NANNOFOSSILS
RADIOLARIANS
DIATOMS
SECTION
METERS
GRAPHIC LITHOLOGY
DRILLING DISTURBANCE
SEDIMENTARY STRUCTURES
SAMPLES
LITHOLOGIC DESCRIPTION
middle Miocene
N12
CN8a
D. petterssonii
C. coronaCtiCus
D. altus
C. gigas var. diversus
PALE BROWN OOZE (SUBUNIT IIA)
Very uniform siliceous nanno ooze. Varying shades of white to brownish white (N9–10YR 8/3) to pale brown (10YR 8/3).
Core contains 5 thin foram turbidite layers, all containing volcanic debris.
SMEAR SLIDE SUMMARY (%)
4, 30
Composition:
Carbonate unspec. 23
Foraminifers 2
Calc. nannofossils 60
Diatoms 6
Radiolarians 9
Sponge spicules Tr
Silicoflagellates Tr
CARBONATE BOMB
1. 75 cm = 88%
2. 75 cm = 89%
3. 75 cm = 85%
4. 96 cm = 87%
5. 75 cm = 78%
6. 75 cm = 77%
10YR 8/2–N9
Foram sand with volcanics
10YR 8/2–8/1
Foram turbidite? + volcanics
10YR 8/3
Foram sand
Foram + volcanics
10YR 8/2
Void
Foram + volcanics
10YR 8/2
10YR 8/2–8/1

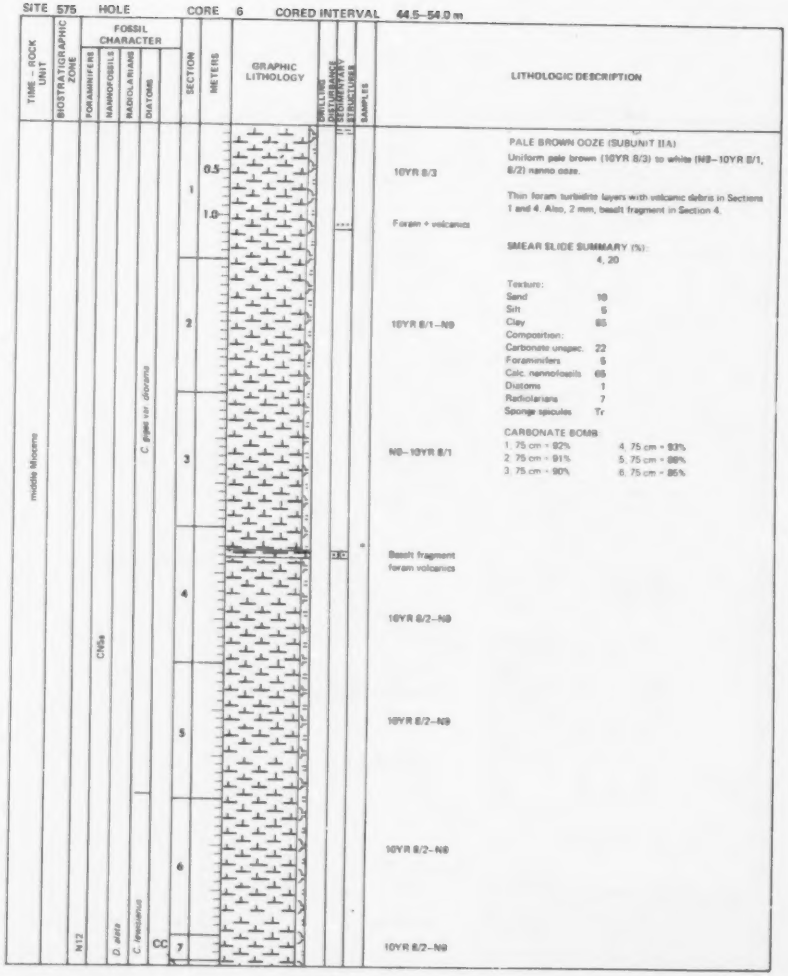
SITE 575 HOLE CORE 6 CORED INTERVAL 44.5–54.0 m
TIME – ROCK UNIT
BIOSTRATIGRAPHIC ZONE
FOSSIL CHARACTER
FORAMINIFERS
NANNOFOSSILS
RADIOLARIANS
DIATOMS
SECTION
METERS
GRAPHIC LITHOLOGY
DRILLING DISTURBANCE
SEDIMENTARY STRUCTURES
SAMPLES
LITHOLOGIC DESCRIPTION
middle Miocene
N12
CN8a
D. altus
C. gigas var. diversus
C. tricorniculatus
PALE BROWN OOZE (SUBUNIT IIA)
Uniform pale brown (10YR 8/3) to white (N9–10YR 8/1, 8/2) nanno ooze.
Thin foram turbidite layers with volcanic debris in Sections 1 and 4. Also, 2 mm, basalt fragment in Section 4.
SMEAR SLIDE SUMMARY (%)
4, 20
Texture:
Sand 10
Silt 5
Clay 85
Composition:
Carbonate unspec. 22
Foraminifers 5
Calc. nannofossils 65
Diatoms 1
Radiolarians 7
Sponge spicules Tr
CARBONATE BOMB
1. 75 cm = 92%
2. 75 cm = 91%
3. 75 cm = 90%
4. 75 cm = 93%
5. 75 cm = 88%
6. 75 cm = 86%
10YR 8/3
Foram + volcanics
10YR 8/1–N9
N9–10YR 8/1
Basalt fragment foram volcanics
10YR 8/2–N9
10YR 8/2–N9
10YR 8/2–N9
10YR 8/2–N9

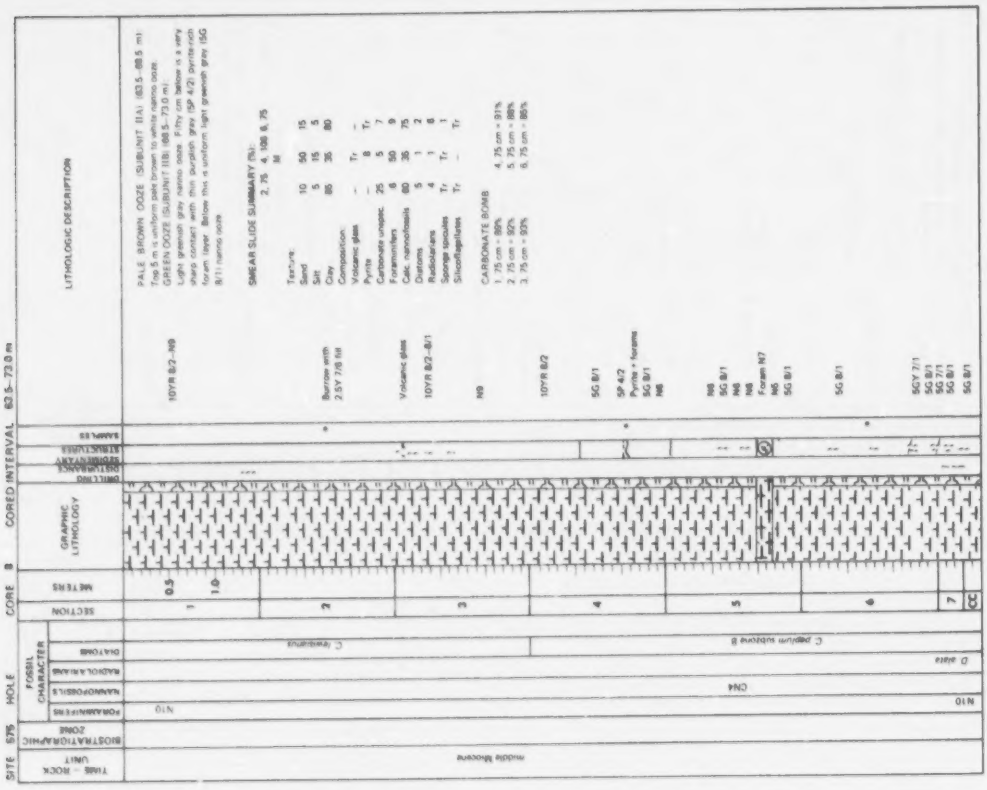

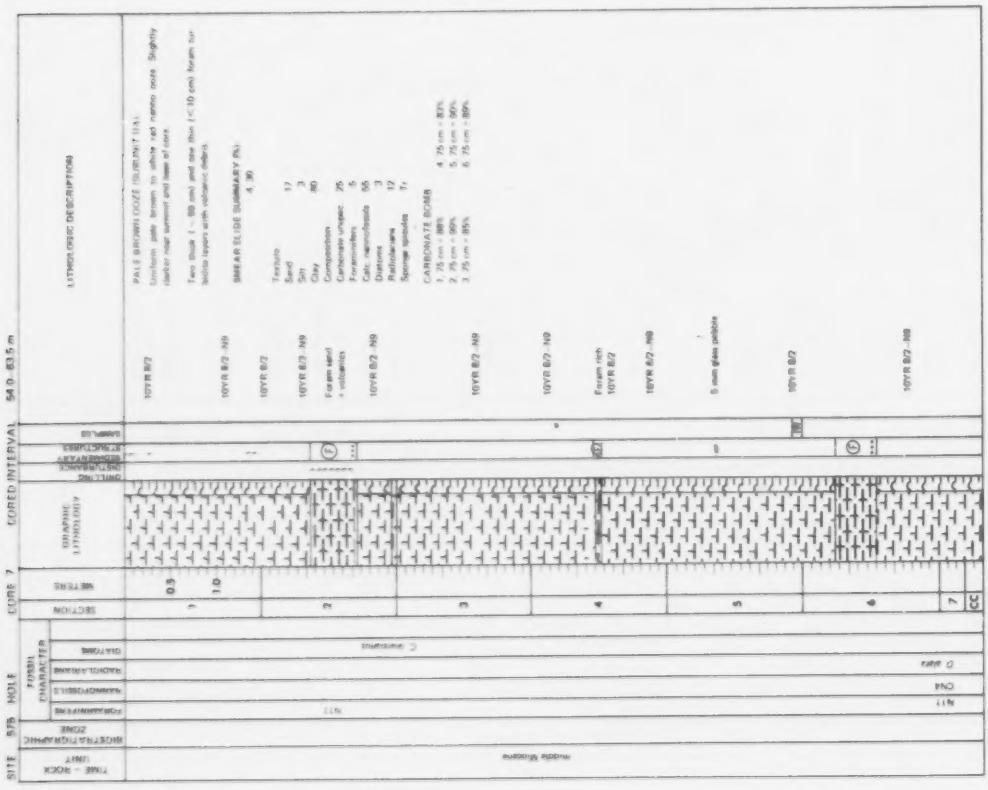

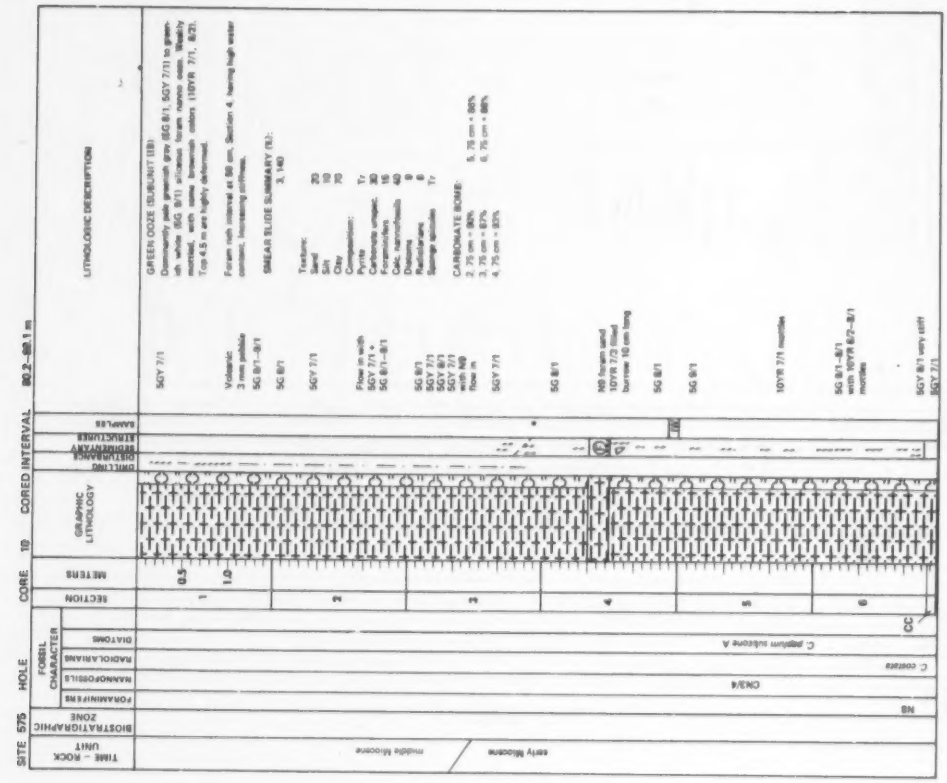
SITE 575
HOLE
CORE 10
CORED INTERVAL 80.2–89.1 m
TIME – ROCK UNIT
BIOSTRATIGRAPHIC ZONE
FOSSIL CHARACTER
FORAMINIFERS
NANNOFOSSILS
RADIOLARIANS
DIATOMS
SECTION
METERS
GRAPHIC LITHOLOGY
DRILLING DISTURBANCE
SEDIMENTARY STRUCTURES
SAMPLES
LITHOLOGIC DESCRIPTION
middle Miocene
early Miocene
CN3/4
C. coalitus
C. peplum subzone A
GREEN OOZE (SUBUNIT IIB)
Dominantly pale greenish gray (5G 8/1, 5GY 7/1) to greenish white (5G 8/1) siliceous foram nanno ooze. Weakly mottled, with some brownish colors (10YR 7/1, 8/2). Top 4.5 m are highly deformed.
Foram rich interval at 89 cm, Section 4, having high water content, increasing stiffness.
SMEAR SLIDE SUMMARY (%):
3, 140
Texture:
Sand 20
Silt 10
Clay 70
Composition:
Pyrite Tr
Carbonate unspec. 30
Foraminifers 15
Calc. nannofossils 40
Diatoms 5
Radiolarians 5
Sponge spicules Tr
CARBONATE BOMB:
2.75 cm = 80% 5.75 cm = 85%
3.75 cm = 87% 6.75 cm = 88%
4.75 cm = 85%
5GY 7/1
Volcanic 3 mm pebble
5G 8/1–8/1
5G 8/1
5GY 7/1
Flow in with 5GY 7/1 + 5G 8/1–8/1
5G 8/1
5GY 7/1
5GY 8/1
5GY 7/1 with N9
Flow in
5GY 7/1
5G 8/1
N9 frozen sand 10YR 7/3 mixed burrow 10 cm long
5G 8/1
5G 8/1
10YR 7/1 mottles
5G 8/1–8/1 with 10YR 8/2–8/1 mottles
5GY 8/1 very stiff 5GY 7/1

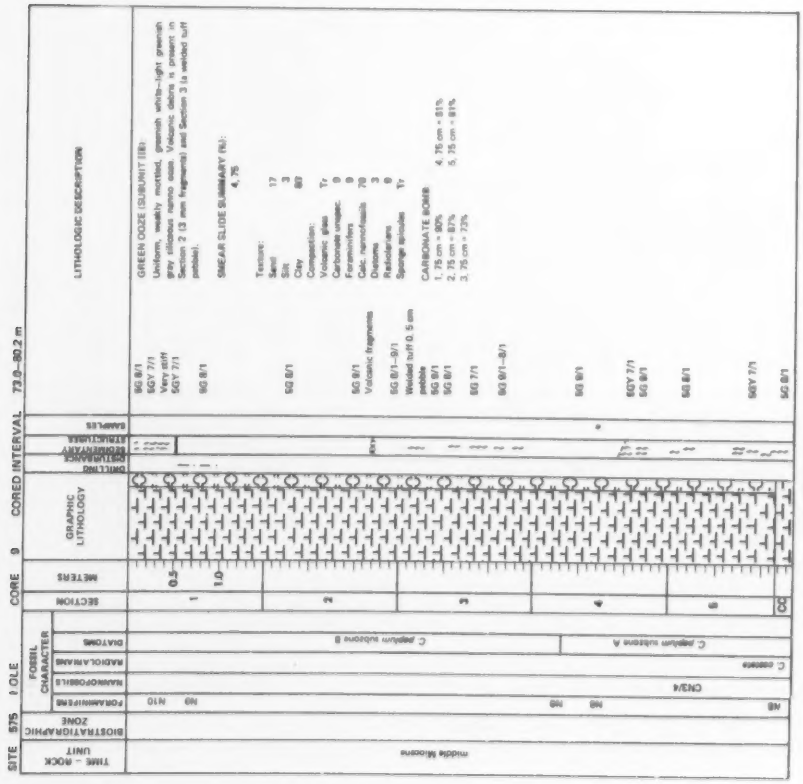
SITE 575
HOLE
CORE 9
CORED INTERVAL 73.0–80.2 m
TIME – ROCK UNIT
BIOSTRATIGRAPHIC ZONE
FOSSIL CHARACTER
FORAMINIFERS
NANNOFOSSILS
RADIOLARIANS
DIATOMS
SECTION
METERS
GRAPHIC LITHOLOGY
DRILLING DISTURBANCE
SEDIMENTARY STRUCTURES
SAMPLES
LITHOLOGIC DESCRIPTION
middle Miocene
CN3/4
C. coalitus
C. peplum subzone A
C. peplum subzone B
GREEN OOZE (SUBUNIT IIB)
Uniform, weakly mottled, greenish white–light greenish gray siliceous nanno ooze. Volcanic debris is present in Section 2 (3 mm fragments) and Section 3 (a welded tuff pebble).
SMEAR SLIDE SUMMARY (%):
4, 75
Texture:
Sand 17
Silt 3
Clay 80
Composition:
Volcanic glass Tr
Carbonate unspec. 0
Foraminifers 0
Calc. nannofossils 70
Diatoms 3
Radiolarians 0
Sponge spicules Tr
CARBONATE BOMB:
1.75 cm = 80% 4.75 cm = 81%
2.75 cm = 87% 5.75 cm = 81%
3.75 cm = 73%
5G 8/1
5GY 7/1
Very stiff
5GY 7/1
5G 8/1
Volcanic fragments
5G 8/1–8/1
Welded tuff 0.5 cm pebble
5G 8/1
5G 8/1
5G 7/1
5G 8/1–8/1
5G 8/1
5GY 7/1
5G 8/1
5G 8/1
5GY 7/1
5G 8/1

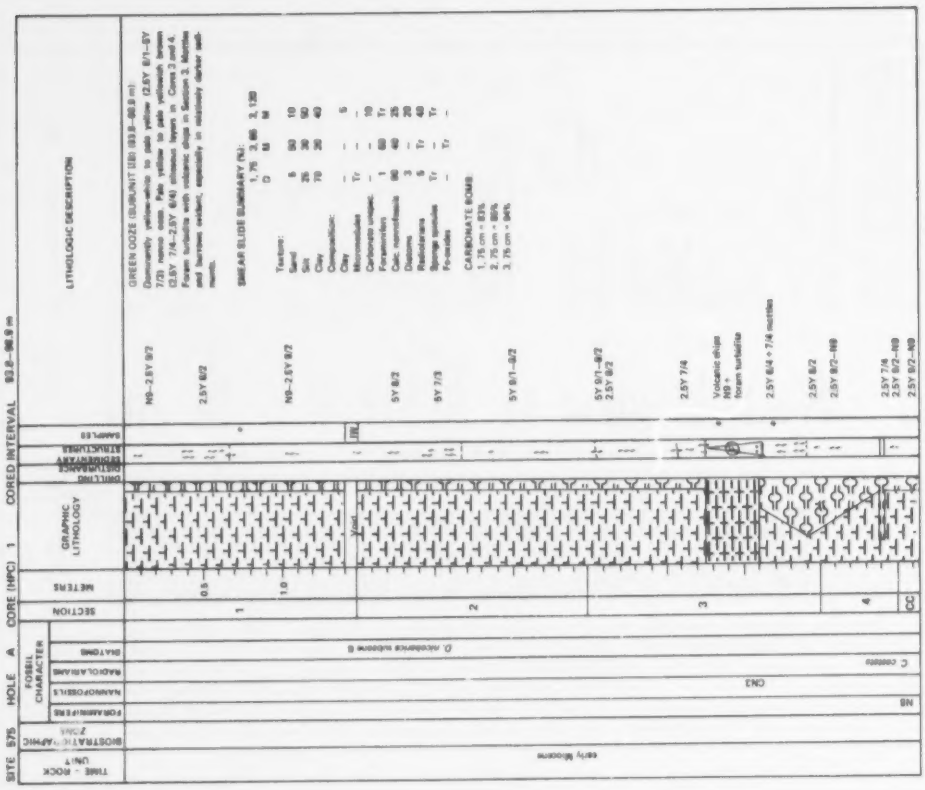

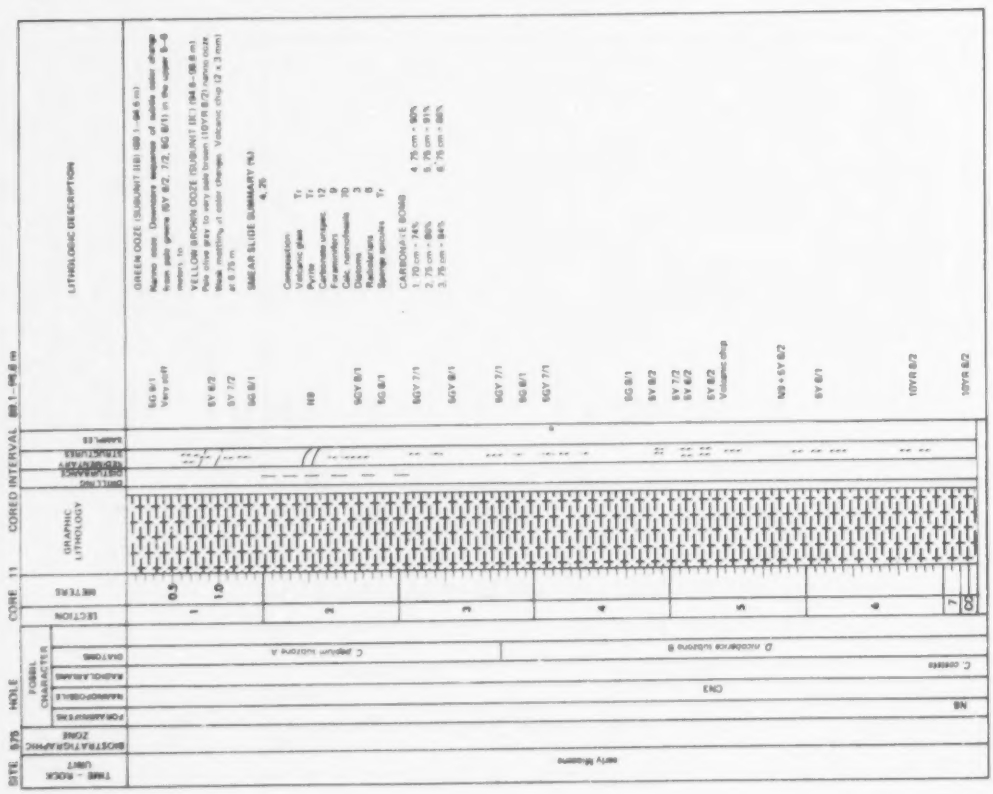

SITE 575 HOLE A CORE (HPC) 2 CORED INTERVAL 97.2–102.3 m

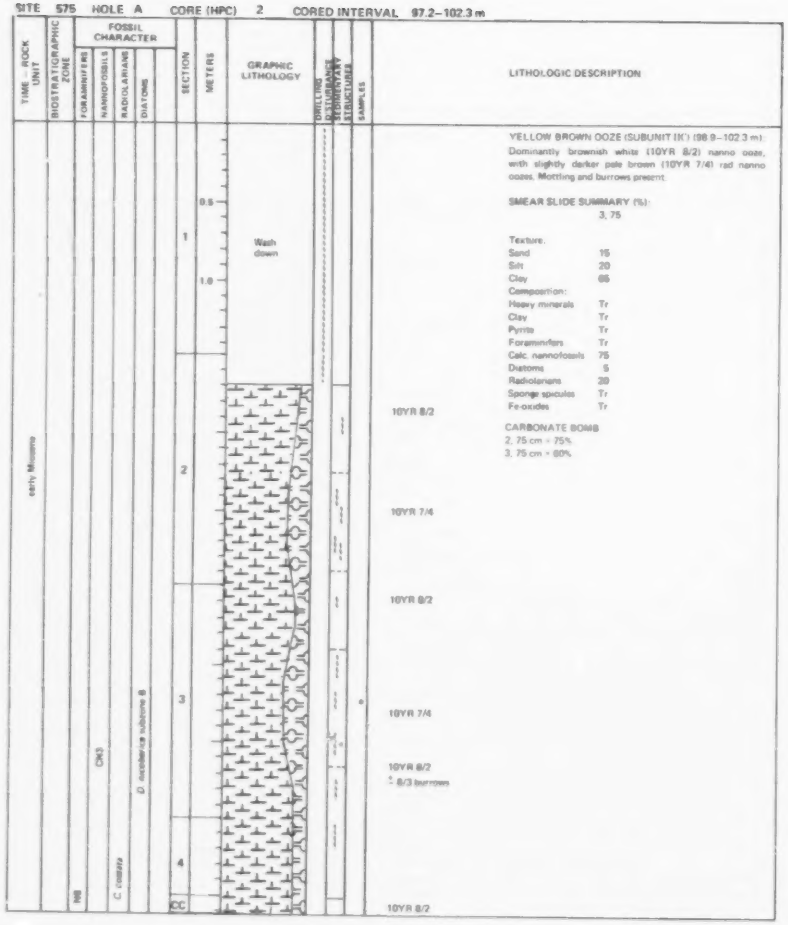

SITE 575 HOLE A CORE (HPC) 3 CORED INTERVAL 101.1–106.3 m

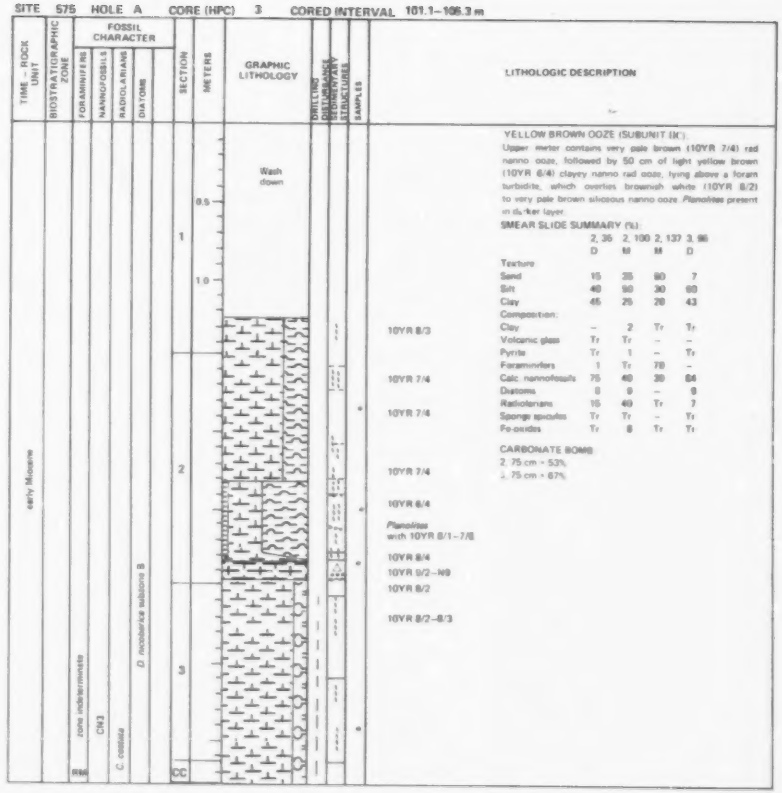

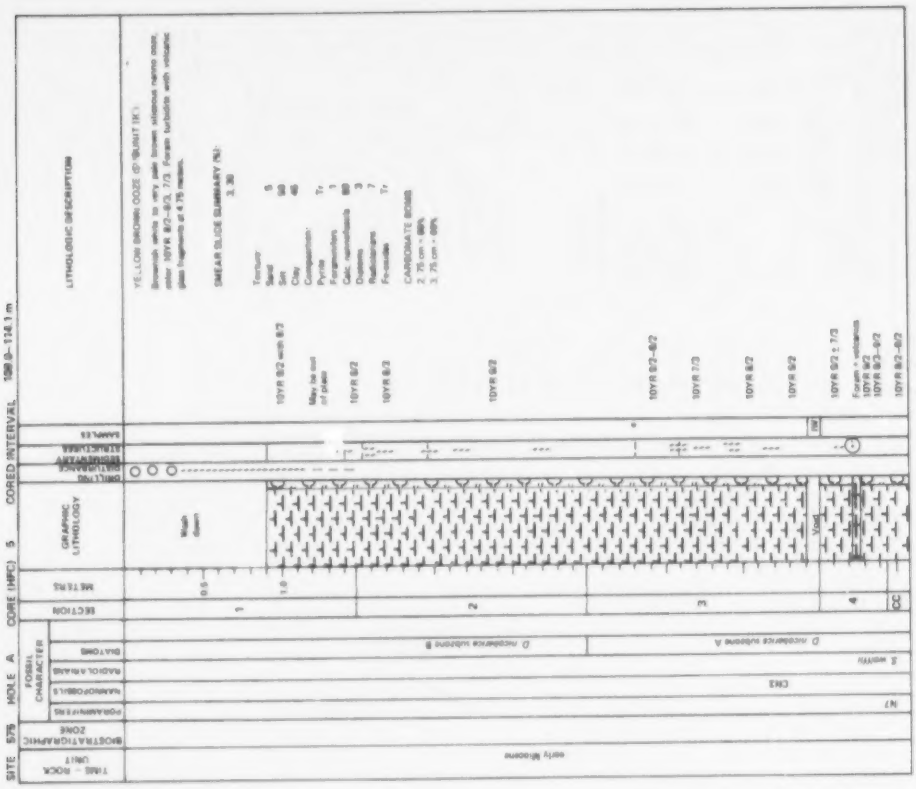

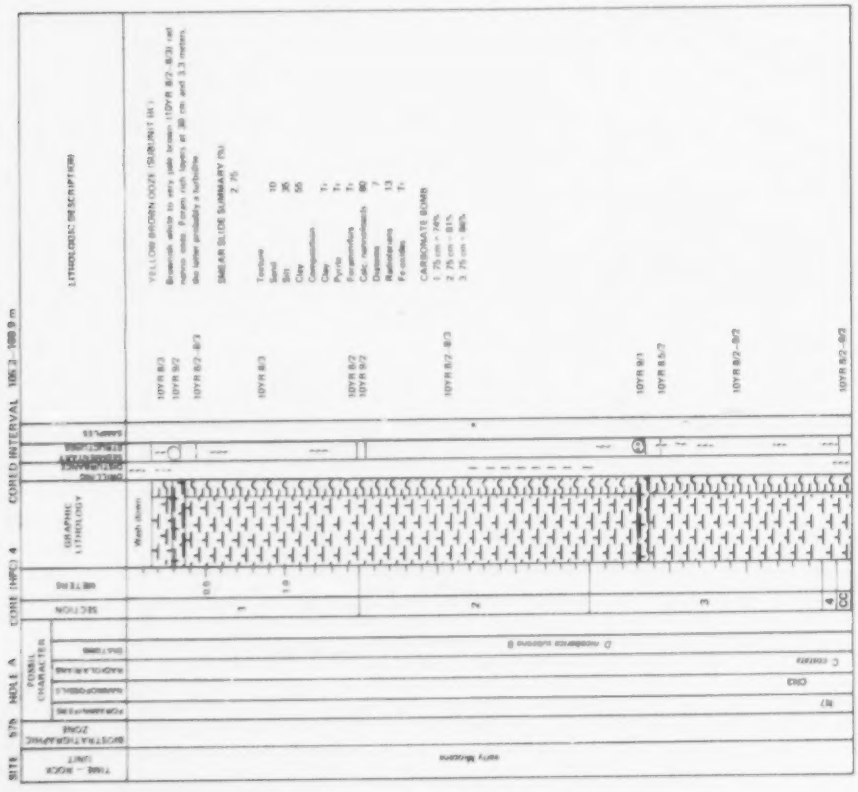

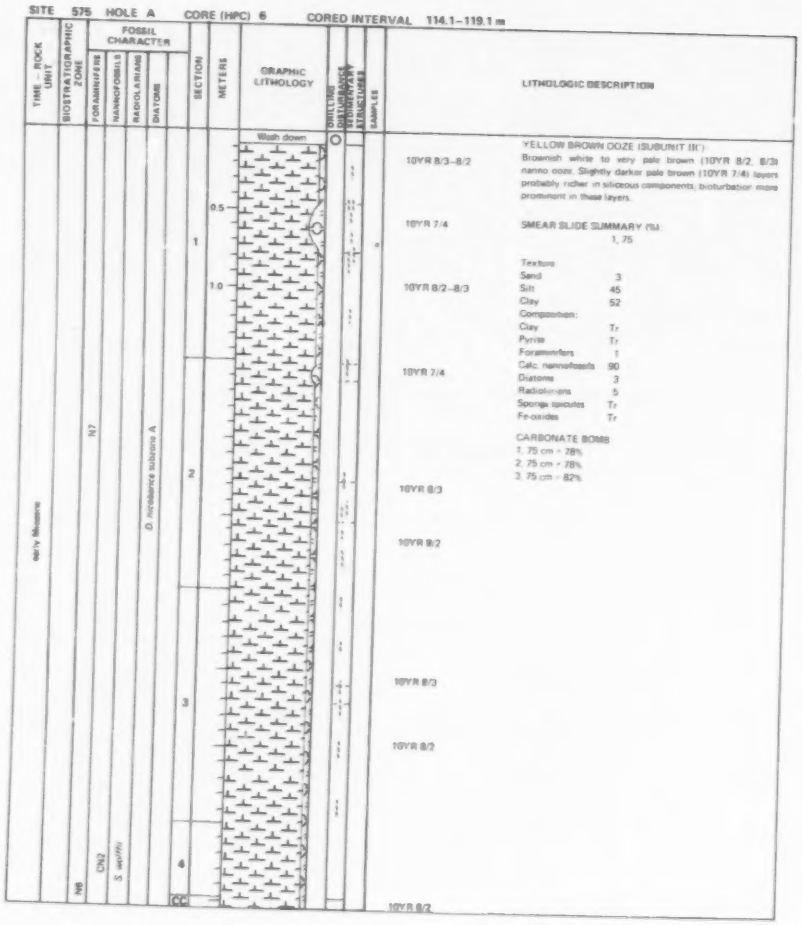
SITE 575 HOLE A CORE (HPC) 6 CORED INTERVAL 114.1–119.1 m
TIME – ROCK UNIT
BIOSTRATIGRAPHIC ZONE
FOSSIL CHARACTER
FORAMINIFERS
NANNOFOSSILS
RADIOLARIANS
DIATOMS
SECTION
METERS
GRAPHIC LITHOLOGY
DRILLING DISTURBANCE
SED. STRUCTURES
SAMPLES
LITHOLOGIC DESCRIPTION
early Miocene
N8
CN2
S. peplinii
D. nicobarica subzone A
Wash down
YELLOW BROWN OOZE (SUBUNIT IIC)
Brownish white to very pale brown (10YR 8/2, 8/3) nanno ooze. Slightly darker pale brown (10YR 7/4) layers probably richer in siliceous components, bioturbation more prominent in these layers.
SMEAR SLIDE SUMMARY (%)
1, 75
Texture
Sand 3
Silt 45
Clay 52
Composition:
Clay Tr
Pyrite Tr
Foraminifers 1
Calc. nannofossils 90
Diatoms 3
Radiolarians 5
Sponge spicules Tr
Fe-oxides Tr
CARBONATE BOMB
1, 75 cm = 78%
2, 75 cm = 78%
3, 75 cm = 82%
10YR 8/3–8/2
10YR 7/4
10YR 8/2–8/3
10YR 7/4
10YR 8/3
10YR 8/2
10YR 8/3
10YR 8/2
10YR 8/2

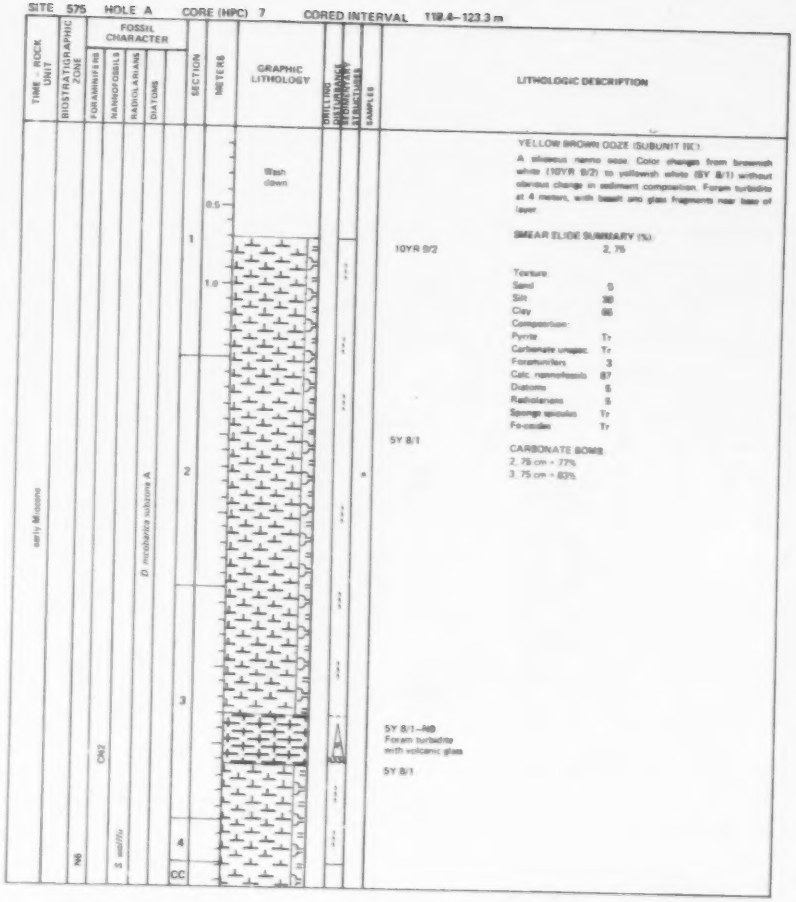
SITE 575 HOLE A CORE (HPC) 7 CORED INTERVAL 118.4–123.3 m
TIME – ROCK UNIT
BIOSTRATIGRAPHIC ZONE
FOSSIL CHARACTER
FORAMINIFERS
NANNOFOSSILS
RADIOLARIANS
DIATOMS
SECTION
METERS
GRAPHIC LITHOLOGY
DRILLING DISTURBANCE
SED. STRUCTURES
SAMPLES
LITHOLOGIC DESCRIPTION
early Miocene
N8
CN2
S. peplinii
D. nicobarica subzone A
Wash down
YELLOW BROWN OOZE (SUBUNIT IIC)
A siliceous nanno ooze. Color changes from brownish white (10YR 8/2) to yellowish white (5Y 8/1) without obvious change in sediment composition. Foram turbidite at 4 meters, with basalt and glass fragments near base of layer
SMEAR SLIDE SUMMARY (%)
2, 75
Texture
Sand 0
Silt 30
Clay 66
Composition:
Pyrite Tr
Carbonate unspec. Tr
Foraminifers 3
Calc. nannofossils 87
Diatoms 5
Radiolarians 5
Sponge spicules Tr
Fe-oxides Tr
CARBONATE BOMB
2, 75 cm = 77%
3, 75 cm = 83%
10YR 8/2
5Y 8/1
5Y 8/1–N8
Foram turbidite with volcanic glass
5Y 8/1

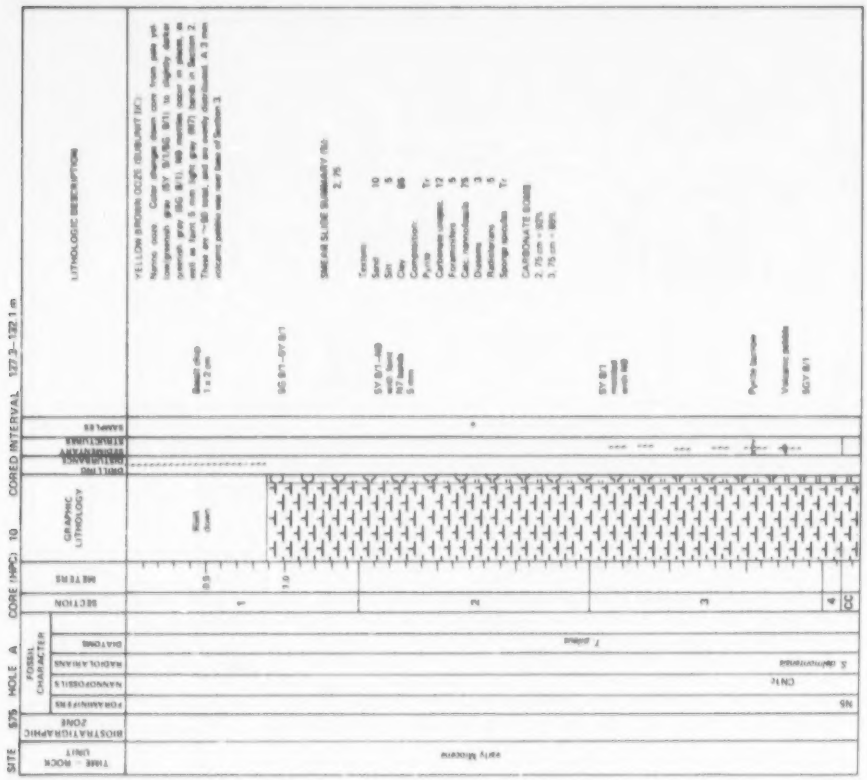

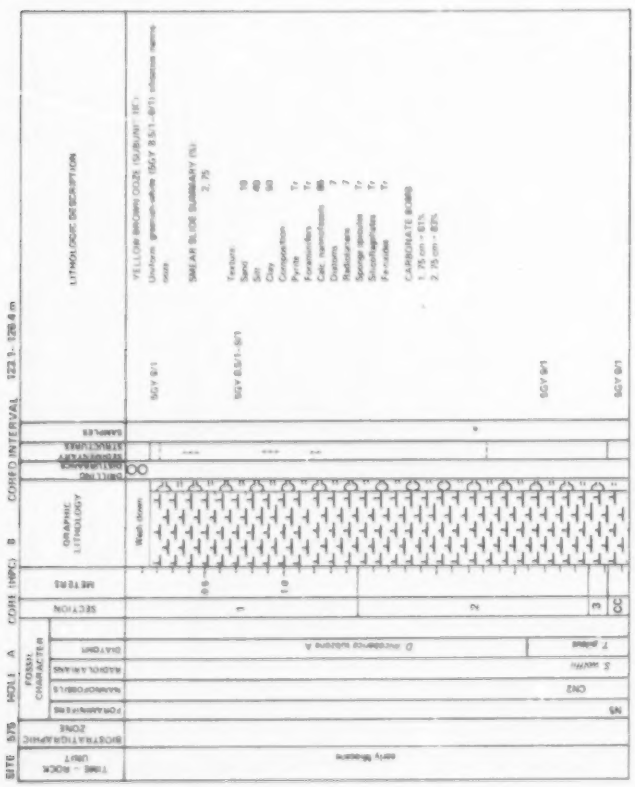

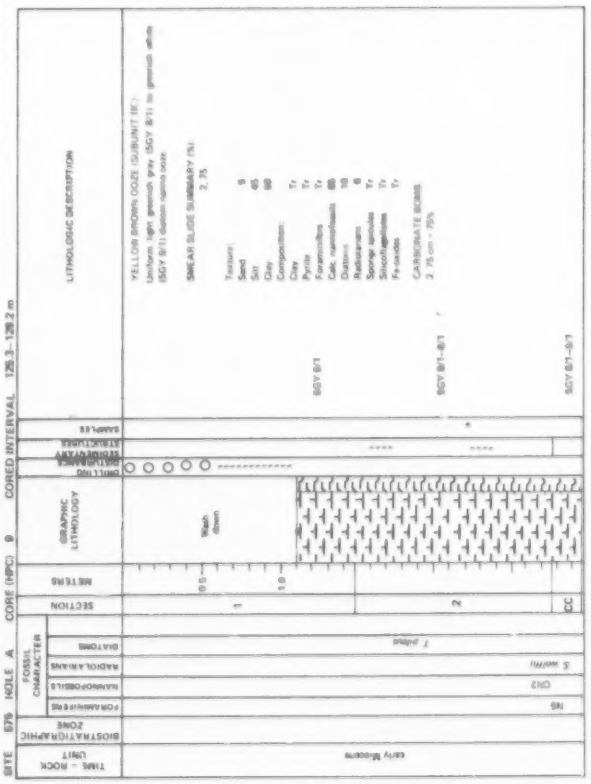

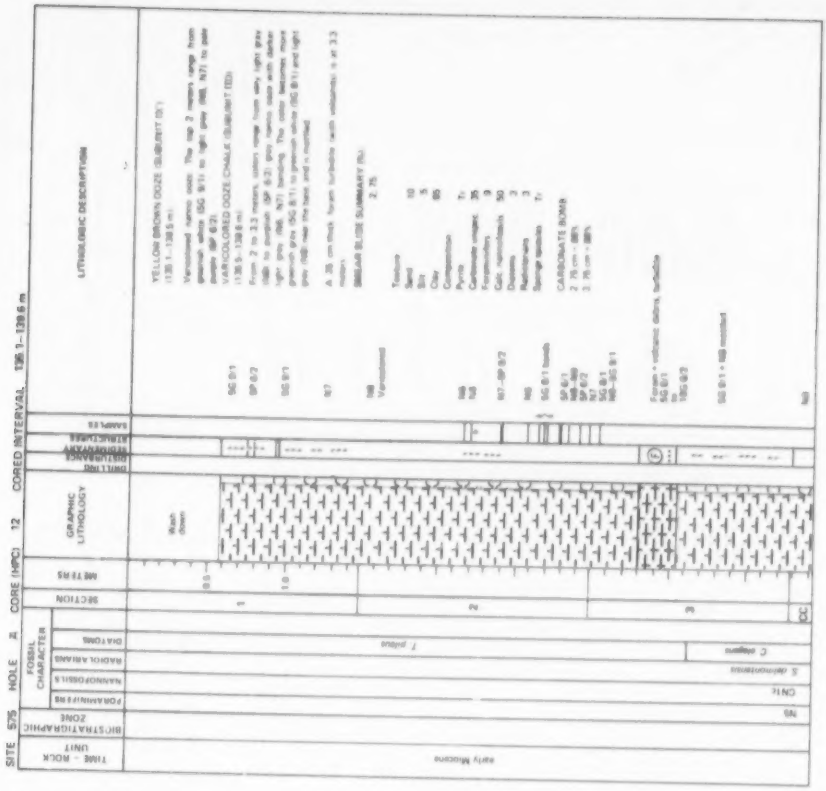

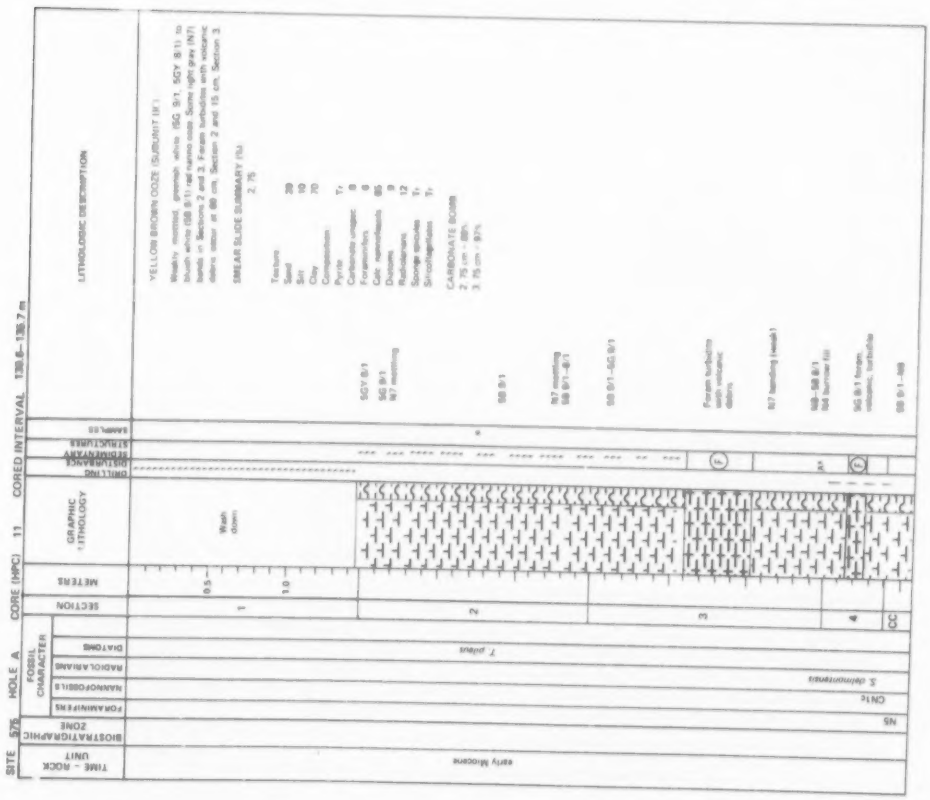

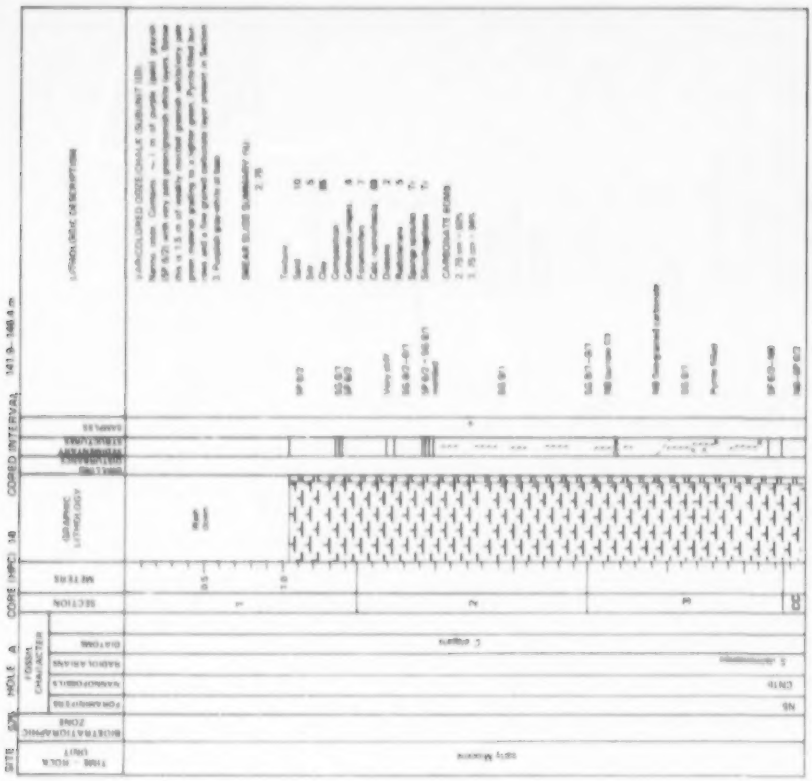

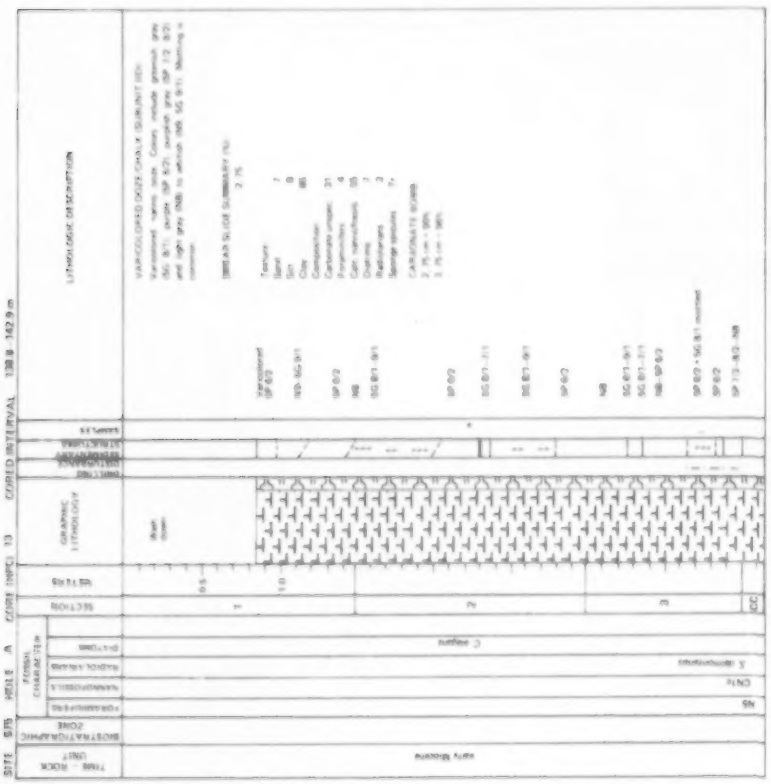

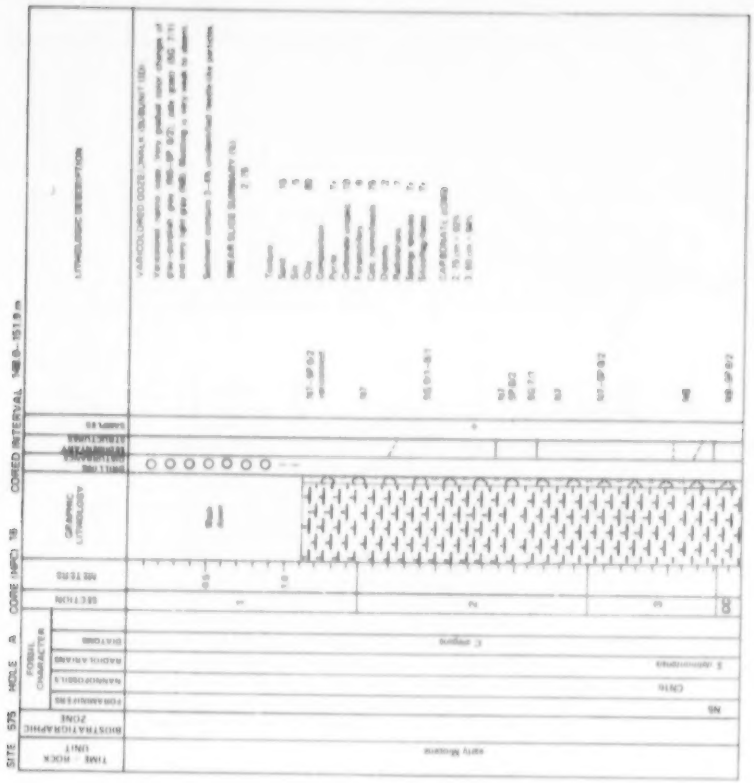

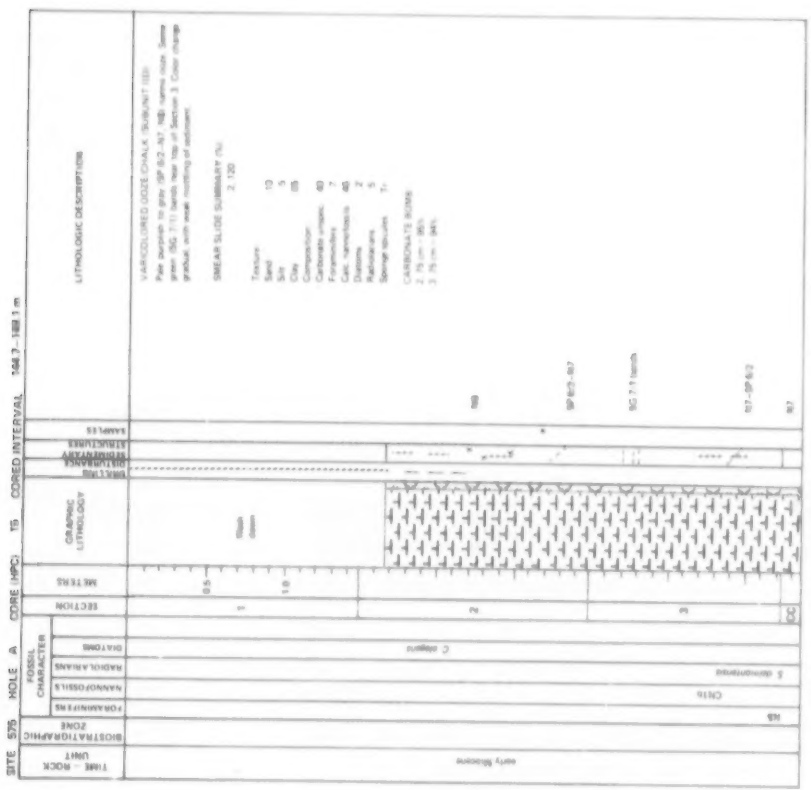

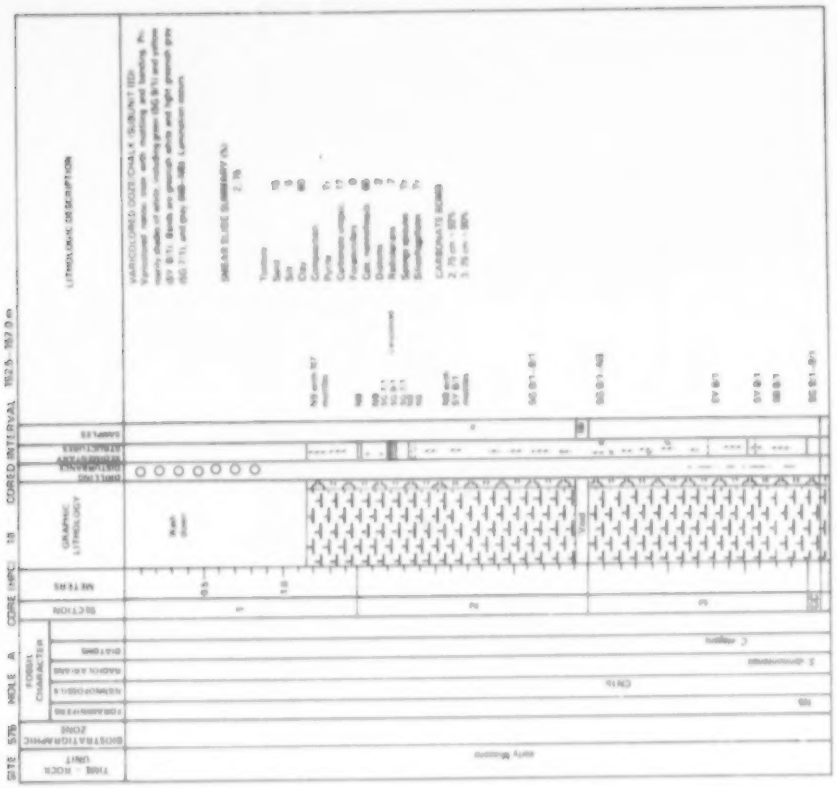

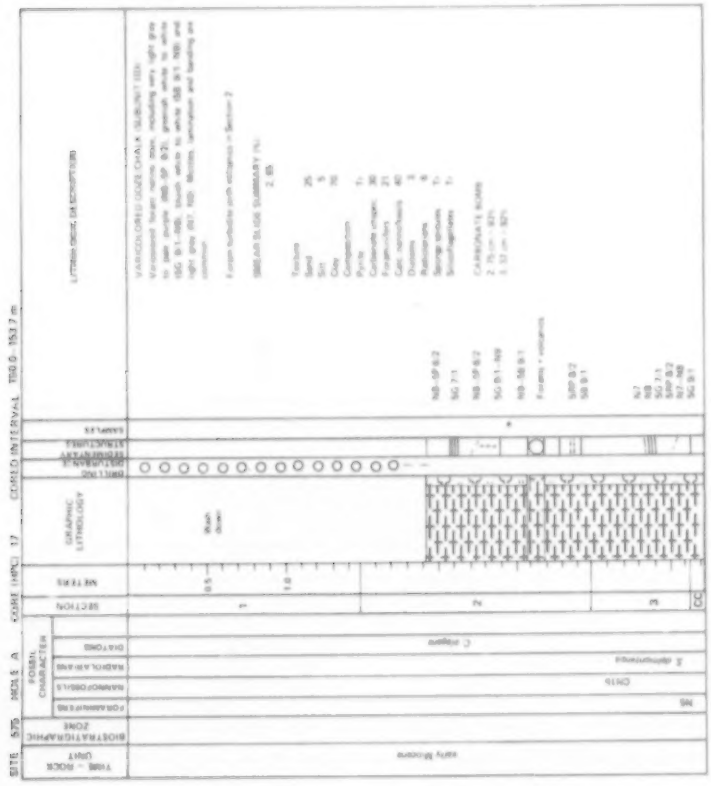

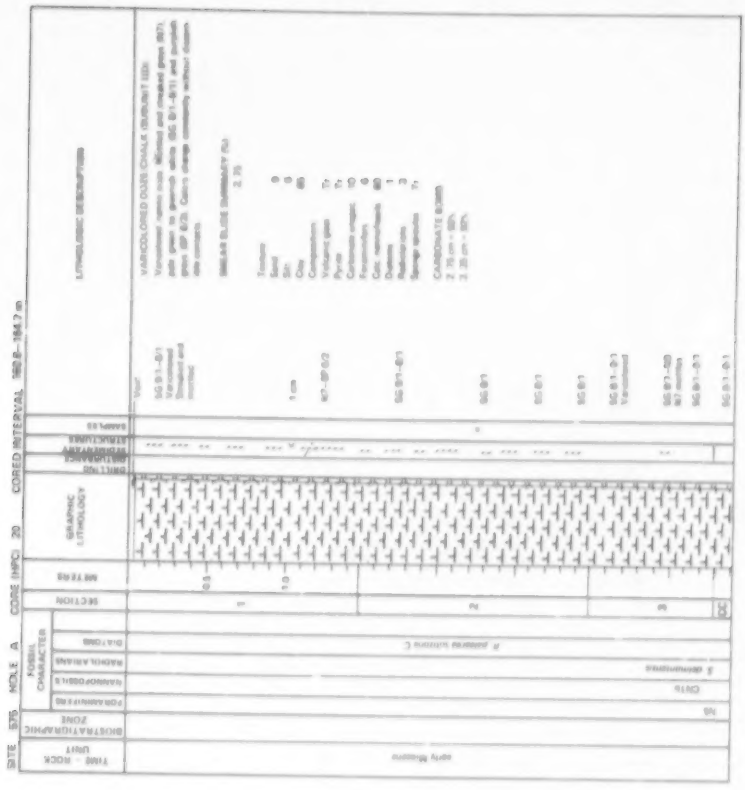

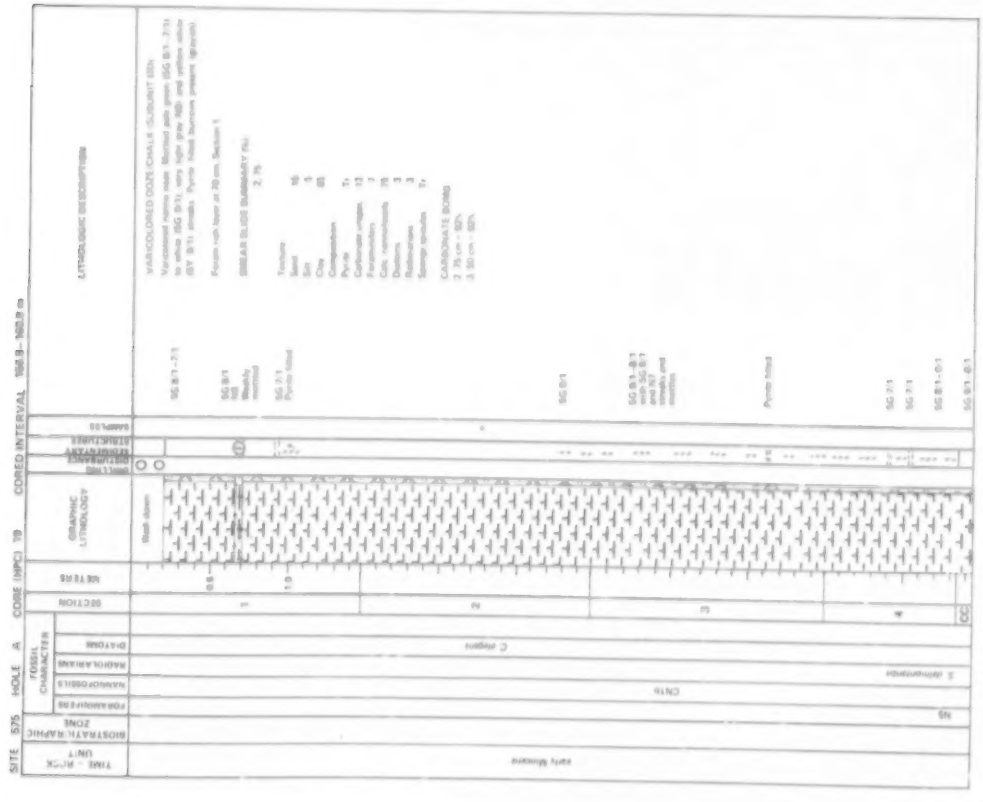

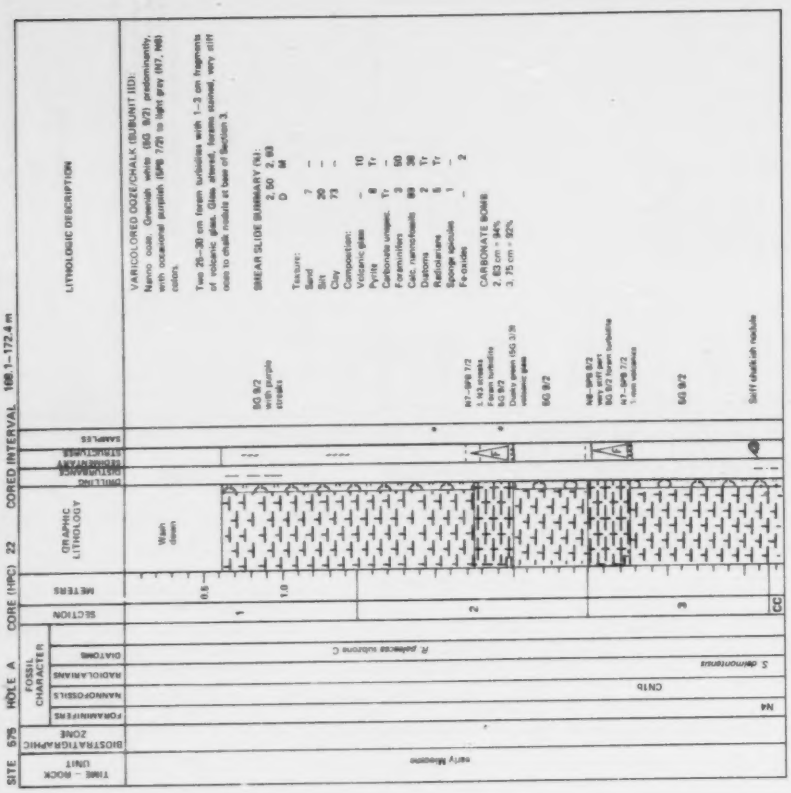

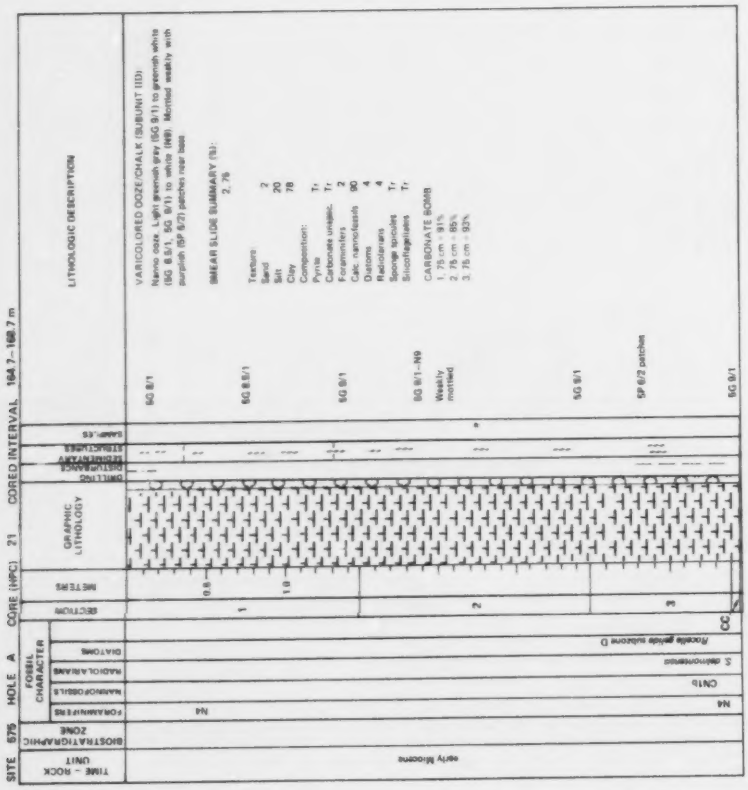

READEX FICHE best copy available

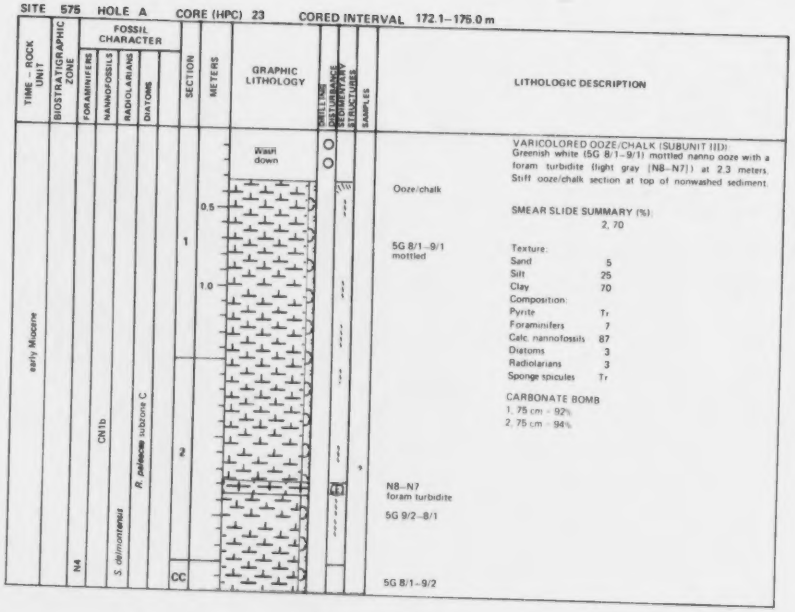
SITE 575 HOLE A CORE (HPC) 23 CORED INTERVAL 172.1–175.0 m
TIME – ROCK UNIT
BIOSTRATIGRAPHIC ZONE
FOSSIL CHARACTER
FORAMINIFERS
NANNOFOSSILS
RADIOLARIANS
DIATOMS
SECTION
METERS
GRAPHIC LITHOLOGY
DRILLING DISTURBANCE
SEDIMENTARY STRUCTURES
SAMPLES
LITHOLOGIC DESCRIPTION
early Miocene
N4
CN1b
S. delmontensis
R. pallacea subzone C
Wash down
Ooze/chalk
5G 8/1–9/1 mottled
N8–N7 foram turbidite
5G 9/2–8/1
5G 8/1–9/2
VARICOLORED OOZE/CHALK (SUBUNIT IIID):
Greenish white (5G 8/1–9/1) mottled nanno ooze with a foram turbidite (light gray (N8–N7)) at 2.3 meters. Stiff ooze/chalk section at top of nonwashed sediment.
SMEAR SLIDE SUMMARY (%):
2, 70
Texture:
Sand 5
Silt 25
Clay 70
Composition:
Pyrite Tr
Foraminifers 7
Calc. nannofossils 87
Diatoms 3
Radiolarians 3
Sponge spicules Tr
CARBONATE BOMB
1, 75 cm – 92%
2, 75 cm – 94%

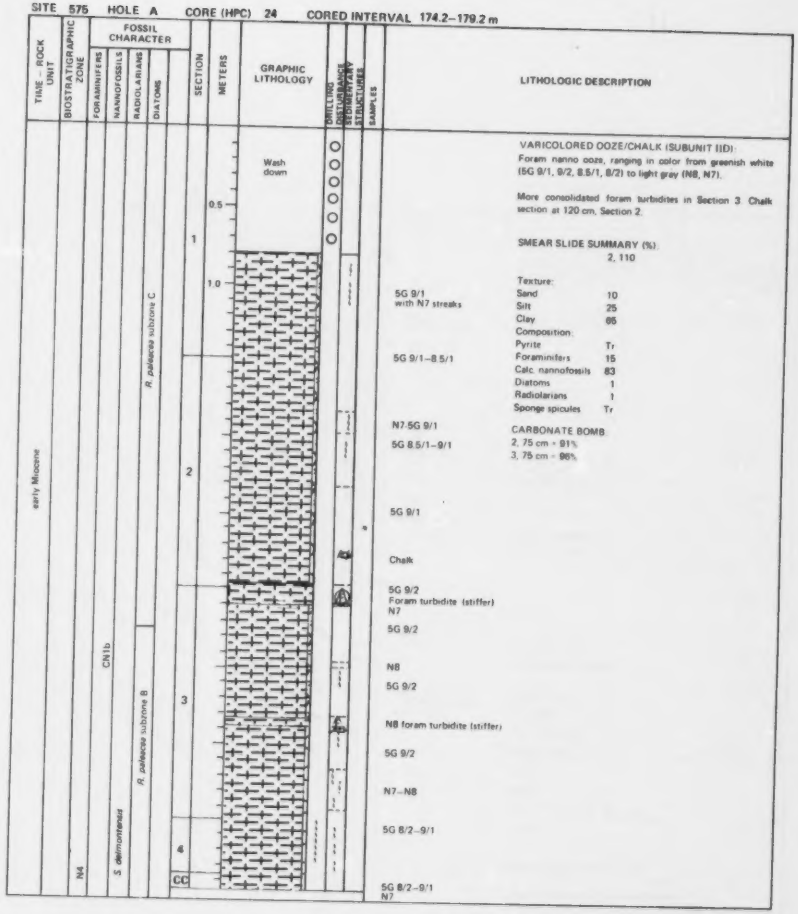
SITE 575 HOLE A CORE (HPC) 24 CORED INTERVAL 174.2–179.2 m
TIME – ROCK UNIT
BIOSTRATIGRAPHIC ZONE
FOSSIL CHARACTER
FORAMINIFERS
NANNOFOSSILS
RADIOLARIANS
DIATOMS
SECTION
METERS
GRAPHIC LITHOLOGY
DRILLING DISTURBANCE
SEDIMENTARY STRUCTURES
SAMPLES
LITHOLOGIC DESCRIPTION
early Miocene
N4
CN1b
S. delmontensis
R. pallacea subzone C
R. pallacea subzone B
Wash down
5G 9/1 with N7 streaks
5G 9/1–8.5/1
N7.5G 9/1
5G 8.5/1–9/1
5G 9/1
Chalk
5G 9/2 Foram turbidite (stiffer) N7
5G 9/2
N8
5G 9/2
N8 foram turbidite (stiffer)
5G 9/2
N7–N8
5G 8/2–9/1
5G 8/2–9/1 N7
VARICOLORED OOZE/CHALK (SUBUNIT IIID):
Foram nanno ooze, ranging in color from greenish white (5G 9/1, 9/2, 8.5/1, 8/2) to light gray (N8, N7).
More consolidated foram turbidites in Section 3. Chalk section at 120 cm, Section 2.
SMEAR SLIDE SUMMARY (%):
2, 110
Texture:
Sand 10
Silt 25
Clay 65
Composition:
Pyrite Tr
Foraminifers 15
Calc. nannofossils 83
Diatoms 1
Radiolarians 1
Sponge spicules Tr
CARBONATE BOMB
2, 75 cm – 91%
3, 75 cm – 98%

SITE 575 HOLE A CORE (HPC) 25 CORED INTERVAL 177.2–182.0 m

TIME – ROCK UNIT	BIOSTRATIGRAPHIC ZONE	FOSSIL CHARACTER: FORAMINIFERS	FOSSIL CHARACTER: NANNOFOSSILS	FOSSIL CHARACTER: RADIOLARIANS	FOSSIL CHARACTER: DIATOMS	SECTION	METERS	GRAPHIC LITHOLOGY	DRILLING DISTURBANCE	SEDIMENTARY STRUCTURES	SAMPLES	LITHOLOGIC DESCRIPTION
early Miocene	N4		CN1b	*S. delmontensis*	*R. palacea subzone B*	1	0.5	Wash down				VARICOLORED OOZE/CHALK (SUBUNIT IID): Greenish white (5G 9/1, 9/2) nanno ooze with some light grey (N7) streaks. Thin chalk sections at 3.75 and 4.75 meters. SMEAR SLIDE SUMMARY (%): 3, 75 — Texture: Sand 1; Silt 35; Clay 64. Composition: Volcanic glass Tr; Foraminifers 5; Calc. nannofossils 93; Diatoms 1; Radiolarians 1. CARBONATE BOMB: *3, 75 cm – 99%
							1.0					
						2						5G 8/2, N7 ± 5Y 8/1 Badly streaked
												Chalk, N8 5G 9/2
						3						5G 8/2–9/2 Very stiff
												5G 9/1 + N7 streaked
												Chalk 5G 9/1
						4						
						CC						5G 9/1

SITE 575 HOLE A CORE (HPC) 26 CORED INTERVAL 180.1–186.7 m

TIME – ROCK UNIT	BIOSTRATIGRAPHIC ZONE	FOSSIL CHARACTER: FORAMINIFERS	FOSSIL CHARACTER: NANNOFOSSILS	FOSSIL CHARACTER: RADIOLARIANS	FOSSIL CHARACTER: DIATOMS	SECTION	METERS	GRAPHIC LITHOLOGY	DRILLING DISTURBANCE	SEDIMENTARY STRUCTURES	SAMPLES	LITHOLOGIC DESCRIPTION
early Miocene	N4		CN1b	*S. delmontensis*	*R. palacea subzone B*	1	0.5	Wash down				VARICOLORED OOZE/CHALK (SUBUNIT IID): Greenish white (5G 9/1–9/2) to white (N9) nanno ooze. Foram turbidites at 1.56 and 4.0 meters. SMEAR SLIDE SUMMARY (%): 2, 75 — Texture: Sand 3; Silt 30; Clay 67. Composition: Pyrite Tr; Foraminifers 5; Calc. nannofossils 92; Diatoms 3; Radiolarians 2; Sponge spicules Tr; Fe-oxides Tr. CARBONATE BOMB: 2, 75 cm = 83%; 3, 75 cm = 94%
							1.0					5G 9/2
						2						N8 foram turbidite N8, 1 mm
												5G 9/1
												5G 8/2
												5G 9/2–9/1
						3						5G 9/1–N9
												Foram turbidite 5GY 8/1
												5G 9/2
								Void			IW	
						4						
						CC						5G 9/1–N7

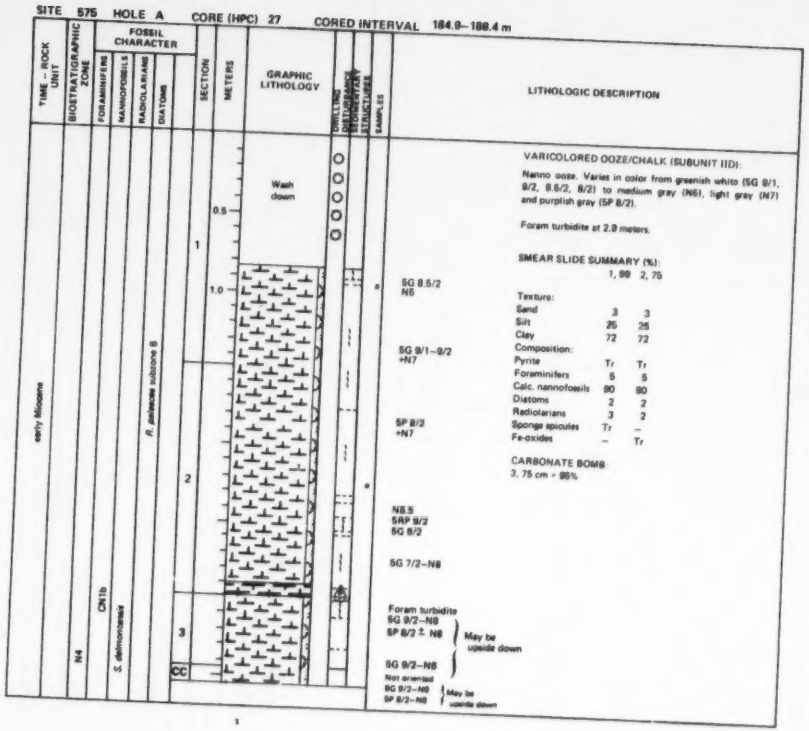
SITE 575 HOLE A CORE (HPC) 27 CORED INTERVAL 184.9–188.4 m
TIME – ROCK UNIT
BIOSTRATIGRAPHIC ZONE
FOSSIL CHARACTER
FORAMINIFERS
NANNOFOSSILS
RADIOLARIANS
DIATOMS
SECTION
METERS
GRAPHIC LITHOLOGY
DRILLING DISTURBANCE
SEDIMENTARY STRUCTURES
SAMPLES
LITHOLOGIC DESCRIPTION
early Miocene
N4
CN1b
S. delmontensis
R. pliskaiae subzone B
Wash down
VARICOLORED OOZE/CHALK (SUBUNIT IID):
Nanno ooze. Varies in color from greenish white (5G 9/1, 9/2, 8.5/2, 6/2) to medium gray (N6), light gray (N7) and purplish gray (5P 8/2).
Foram turbidite at 2.9 meters.
SMEAR SLIDE SUMMARY (%):
1, 99 2, 75
Texture:
Sand 3 3
Silt 25 25
Clay 72 72
Composition:
Pyrite Tr Tr
Foraminifers 5 5
Calc. nannofossils 90 90
Diatoms 2 2
Radiolarians 3 2
Sponge spicules Tr –
Fe-oxides – Tr
CARBONATE BOMB:
3, 75 cm = 96%
5G 8.5/2 N6
5G 9/1–9/2 +N7
5P 8/2 +N7
N8.5
5RP 8/2
5G 8/2
5G 7/2–N8
Foram turbidite
5G 9/2–N8
5P 8/2 ± N8
May be upside down
5G 9/2–N8
Not oriented
5G 9/2–N8
5P 8/2–N8
May be upside down

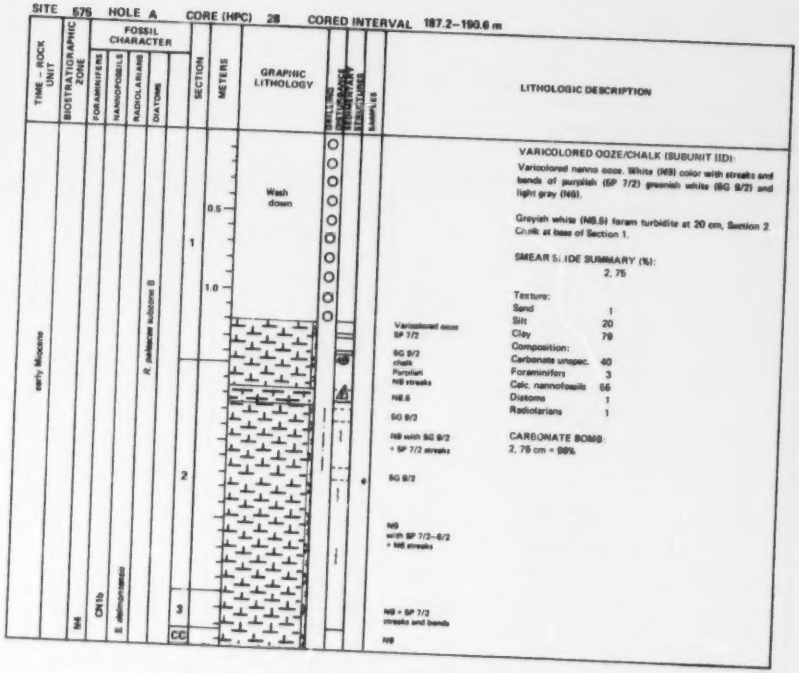
SITE 575 HOLE A CORE (HPC) 28 CORED INTERVAL 187.2–190.6 m
TIME – ROCK UNIT
BIOSTRATIGRAPHIC ZONE
FOSSIL CHARACTER
FORAMINIFERS
NANNOFOSSILS
RADIOLARIANS
DIATOMS
SECTION
METERS
GRAPHIC LITHOLOGY
DRILLING DISTURBANCE
SEDIMENTARY STRUCTURES
SAMPLES
LITHOLOGIC DESCRIPTION
early Miocene
N4
CN1b
S. delmontensis
R. pliskaiae subzone B
Wash down
VARICOLORED OOZE/CHALK (SUBUNIT IID):
Varicolored nanno ooze. White (N9) color with streaks and bands of purplish (5P 7/2) greenish white (5G 9/2) and light gray (N6).
Greyish white (N8.5) foram turbidite at 20 cm, Section 2.
Chalk at base of Section 1.
SMEAR SLIDE SUMMARY (%):
2, 75
Texture:
Sand 1
Silt 20
Clay 79
Composition:
Carbonate unspec. 40
Foraminifers 3
Calc. nannofossils 56
Diatoms 1
Radiolarians 1
CARBONATE BOMB:
2, 75 cm = 99%
Varicolored ooze 5P 7/2
5G 9/2 chalk
Pyrolusi
N9 streaks
N8.5
5G 9/2
N9 with 5G 9/2 + 5P 7/2 streaks
5G 9/2
N9 with 5P 7/2–8/2 + N8 streaks
N9 + 5P 7/2 streaks and bands
N9

SITE 575 HOLE A CORE (HPC) 29 CORED INTERVAL 189.7–193.7 m

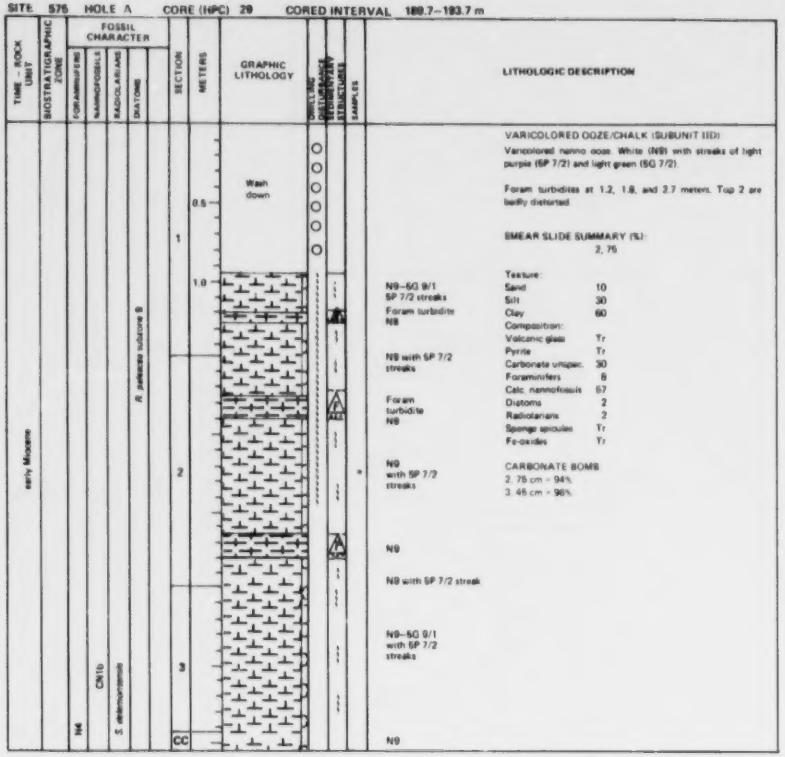

SITE 575 HOLE A CORE (HPC) 30 CORED INTERVAL 193.6–197.9 m

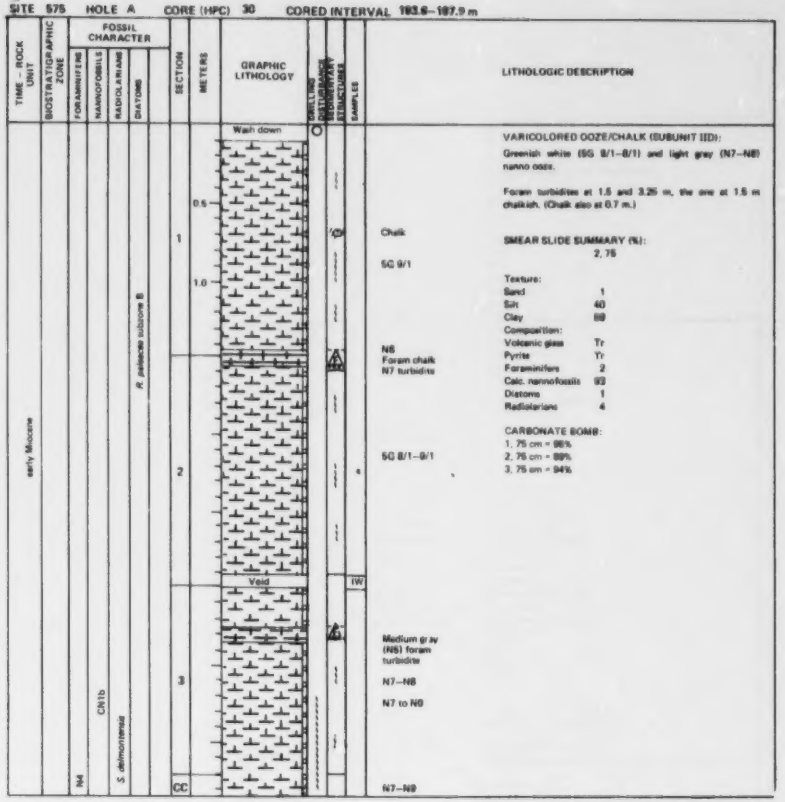

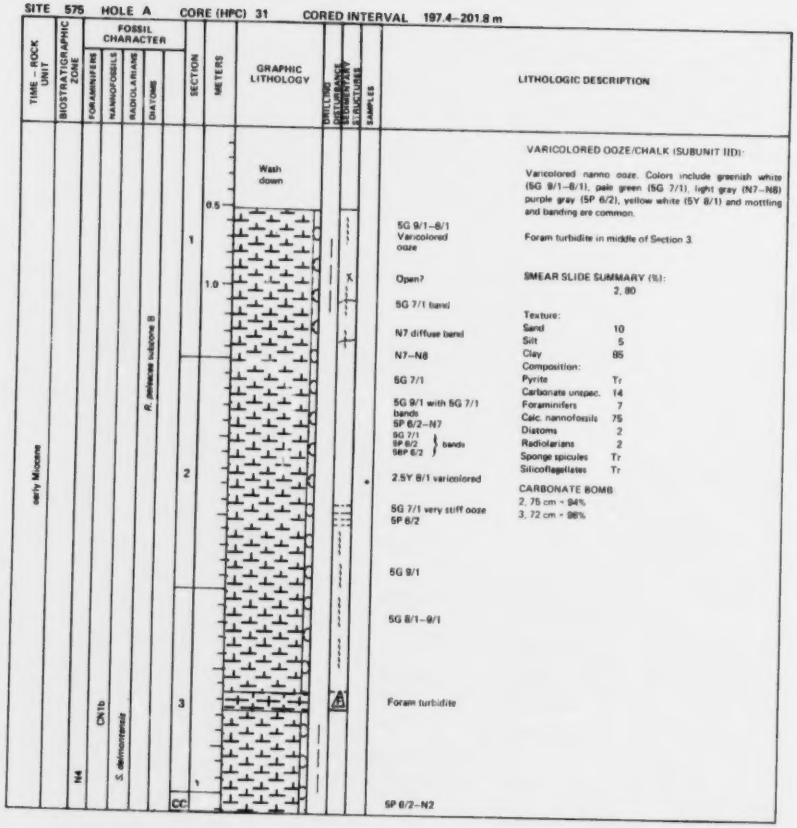
SITE 575 HOLE A CORE (HPC) 31 CORED INTERVAL 197.4–201.8 m
TIME – ROCK UNIT
BIOSTRATIGRAPHIC ZONE
FOSSIL CHARACTER
FORAMINIFERS
NANNOFOSSILS
RADIOLARIANS
DIATOMS
SECTION
METERS
GRAPHIC LITHOLOGY
DRILLING DISTURBANCE
SEDIMENTARY STRUCTURES
SAMPLES
LITHOLOGIC DESCRIPTION
early Miocene
N4
CN1b
S. delmontensis
R. petiacea subzone B
Wash down
5G 9/1–8/1 Varicolored ooze
Open?
5G 7/1 band
N7 diffuse band
N7–N8
5G 7/1
5G 9/1 with 5G 7/1 bands
5P 8/2–N7
5G 7/1
5P 8/2
5RP 8/2
bands
2.5Y 8/1 varicolored
5G 7/1 very stiff ooze
5P 8/2
5G 9/1
5G 8/1–9/1
Foram turbidite
5P 8/2–N2
VARICOLORED OOZE/CHALK (SUBUNIT IID):
Varicolored nanno ooze. Colors include greenish white (5G 9/1–8/1), pale green (5G 7/1), light gray (N7–N8) purple gray (5P 6/2), yellow white (5Y 8/1) and mottling and banding are common.
Foram turbidite in middle of Section 3.
SMEAR SLIDE SUMMARY (%):
2, 80
Texture:
Sand 10
Silt 5
Clay 85
Composition:
Pyrite Tr
Carbonate unspec. 14
Foraminifers 7
Calc. nannofossils 75
Diatoms 2
Radiolarians 2
Sponge spicules Tr
Silicoflagellates Tr
CARBONATE BOMB
2, 75 cm = 94%
3, 72 cm = 96%

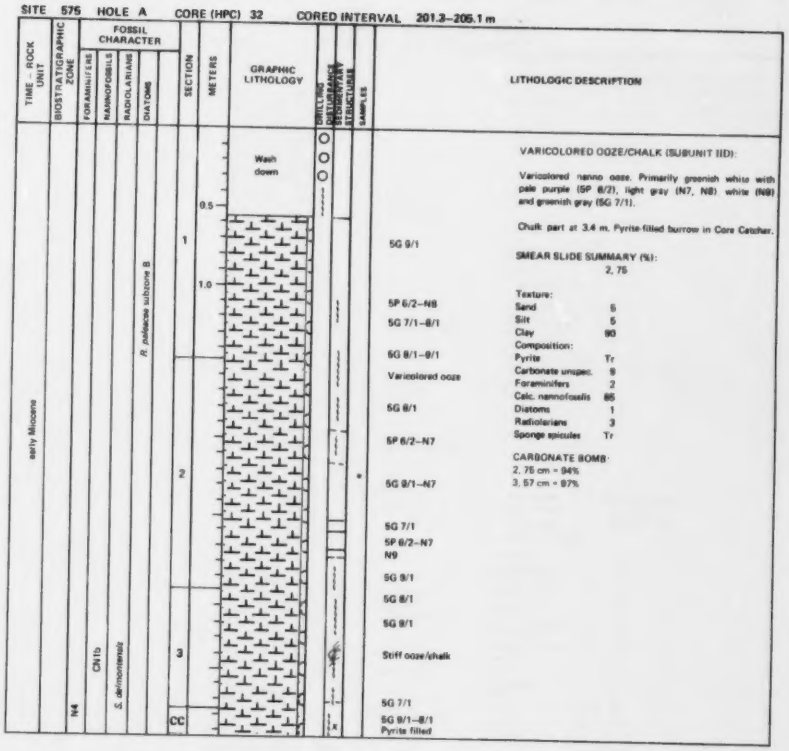
SITE 575 HOLE A CORE (HPC) 32 CORED INTERVAL 201.3–206.1 m
TIME – ROCK UNIT
BIOSTRATIGRAPHIC ZONE
FOSSIL CHARACTER
FORAMINIFERS
NANNOFOSSILS
RADIOLARIANS
DIATOMS
SECTION
METERS
GRAPHIC LITHOLOGY
DRILLING DISTURBANCE
SEDIMENTARY STRUCTURES
SAMPLES
LITHOLOGIC DESCRIPTION
early Miocene
N4
CN1b
S. delmontensis
R. petiacea subzone B
Wash down
5P 6/2–N8
5G 7/1–8/1
5G 8/1–9/1
Varicolored ooze
5G 8/1
5P 6/2–N7
5G 9/1–N7
5G 7/1
5P 8/2–N7
N9
5G 9/1
5G 8/1
5G 8/1
Stiff ooze/chalk
5G 7/1
5G 9/1–8/1
Pyrite filled
VARICOLORED OOZE/CHALK (SUBUNIT IID):
Varicolored nanno ooze. Primarily greenish white with pale purple (5P 8/2), light gray (N7, N8) white (N9) and greenish gray (5G 7/1).
Chalk part at 3.4 m. Pyrite-filled burrow in Core Catcher.
SMEAR SLIDE SUMMARY (%):
2, 75
Texture:
Sand 5
Silt 5
Clay 90
Composition:
Pyrite Tr
Carbonate unspec. 9
Foraminifers 2
Calc. nannofossils 86
Diatoms 1
Radiolarians 3
Sponge spicules Tr
CARBONATE BOMB:
2, 75 cm = 94%
3, 57 cm = 97%

SITE 575 HOLE A CORE (HPC) 33 CORED INTERVAL 204.3–208.4 m

TIME – ROCK UNIT	BIOSTRATIGRAPHIC ZONE	FOSSIL CHARACTER: FORAMINIFERS	NANNOFOSSILS	RADIOLARIANS	DIATOMS	SECTION	METERS	GRAPHIC LITHOLOGY	DRILLING DISTURBANCE	SEDIMENTARY STRUCTURES	SAMPLES	LITHOLOGIC DESCRIPTION
early Miocene	N4		Chiasmolithus oamaruensis		A. ingenua subsp. B	1	0.6	Wash down				
						2	1.0	Void			•	
						3						
						CC						

VARICOLORED OOZE/CHALK (SUBUNIT IID)

Varicolored nanno ooze. Greenish white (5G 8/1–8/1) with light greenish gray (5G 7/1) and blue gray (5B 8/1–N7) bands and pale purple (5P 8/2) streaks.

SMEAR SLIDE SUMMARY (%):

	2, 75
Texture:	
Sand	5
Silt	5
Clay	90
Composition:	
Pyrite	Tr
Carbonate unspec.	6
Foraminifers	3
Calc. nannofossils	85
Diatoms	1
Radiolarians	3
Sponge spicules	Tr

CARBONATE BOMB:
2, 75 cm = 91%
3, 75 cm = 91%

5G 8/1–8/1
5G 7/1
5B 8/1–8/1
5G 8/1–8/1
N7–5B 8/1
5G 8/1–8/1 with 5P 8/2 streaks and 10YR 8/2 mottling
5G 8/1

SITE 575 HOLE B CORE 1 CORED INTERVAL 3.3–12.8 m

TIME – ROCK UNIT	BIOSTRATIGRAPHIC ZONE	FOSSIL CHARACTER: FORAMINIFERS	NANNOFOSSILS	RADIOLARIANS	DIATOMS	SECTION	METERS	GRAPHIC LITHOLOGY	DRILLING DISTURBANCE	SEDIMENTARY STRUCTURES	SAMPLES	LITHOLOGIC DESCRIPTION
			R. p. (CN1?)	N. pseudo		1	0.5					
							1.0	Void				
						2						
						3						
						4						
						5						
						6						
						7						
						CC						

10YR 8/3
10YR 8/2
10YR 7/1
10YR 7/2
10YR 8/3 10YR 7/2
10YR 7/3 + 6/3 Foram sand + volcanics
10YR 8/4
10Y 5/4 + 10YR 7/3 mottled
10YR 3/2
10YR 7/3–4/4
10YR 3/3 + 8/2
Vertical color bands of 10YR 4/4 + 10YR 8/3–8/4
10YR 8/4 + 10YR 8/3
10YR 3/3 + 6/3 + 8/4
10YR 8/3, 6/3, 8/4
10YR 4/3 with 10YR 8/3 streaks
10YR 4/3

MOTTLED BROWN OOZE (SUBUNIT IA):

Highly deformed, mottled brownish siliceous nanno ooze. Colors range from very pale brown (10YR 8/3, 8/4, 7/3) to pale brown (10YR 6/3), yellowish brown (10YR 4/3; dark – 10YR 4/4), to very dark grayish brown (10YR 3/2). Rare clay was observed.

Also present near top of Section 2 is a foram turbidite with sharp base and volcanic debris.

SMEAR SLIDE SUMMARY (%):

	1, 75	2, 30
Texture:		
Sand	15	45
Silt	10	30
Clay	75	20
Composition:		
Clay	–	4
Pyrite	1	1
Carbonate unspec.	8	30
Foraminifers	8	20
Calc. nannofossils	70	15
Diatoms	4	9
Radiolarians	8	20
Sponge spicules	Tr	Tr
Silicoflagellates	–	Tr
Fe-oxides	1	1

CARBONATE BOMB:

1, 75 cm = 75%	4, 75 cm = 38%
2, 71 cm = 48%	5, 75 cm = 5%
3, 75 cm = 58%	6, 75 cm = 42%

NOTE: Graphic lithologies represent average compositions derived from smear slides and do not always reflect the detailed alternation of sediment types. Major lithologic boundaries are shown but gradational contacts, small-scale cyclicity and ooze-chalk alternations are represented schematically. Color changes approximate to lithologic changes.

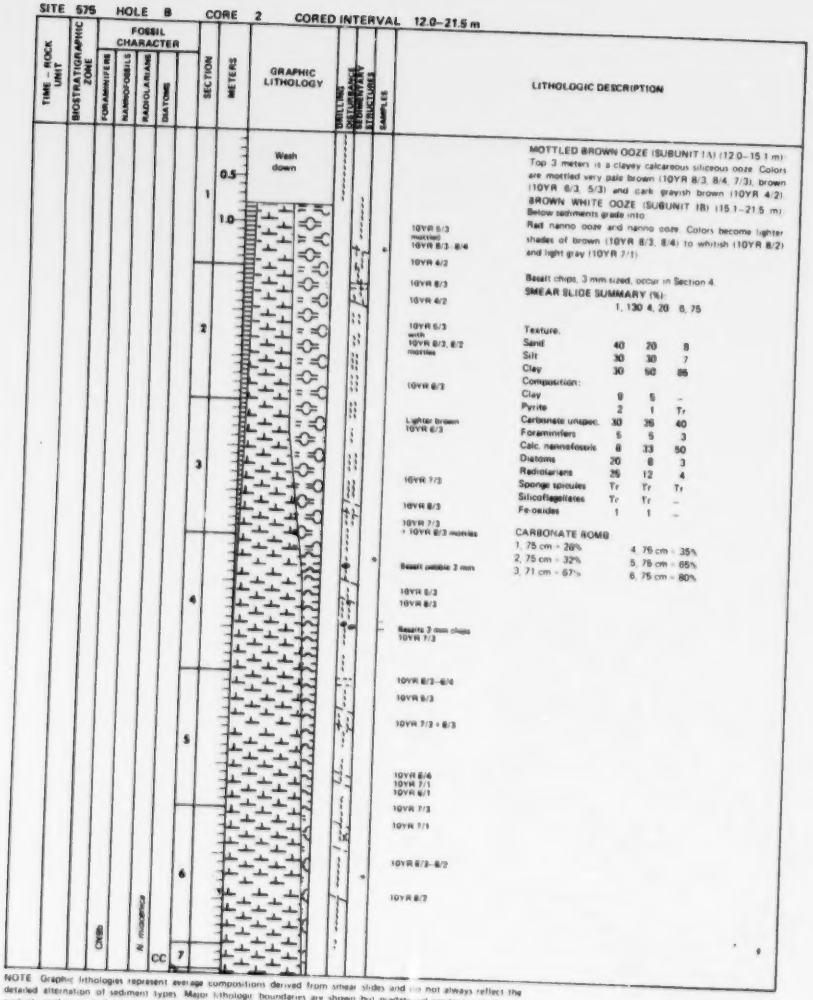
SITE 575 HOLE B CORE 2 CORED INTERVAL 12.0–21.5 m
TIME – ROCK UNIT
BIOSTRATIGRAPHIC ZONE
FOSSIL CHARACTER
FORAMINIFERS
NANNOFOSSILS
RADIOLARIANS
DIATOMS
SECTION
METERS
GRAPHIC LITHOLOGY
DRILLING DISTURBANCE
SED. STRUCTURES
SAMPLES
LITHOLOGIC DESCRIPTION
Wash down
CN8b
N. inflatina
CC
MOTTLED BROWN OOZE (SUBUNIT IA) (12.0–15.1 m):
Top 3 meters is a clayey calcareous siliceous ooze. Colors are mottled very pale brown (10YR 8/3, 8/4, 7/3), brown (10YR 6/3, 5/3) and dark grayish brown (10YR 4/2).
BROWN WHITE OOZE (SUBUNIT IB) (15.1–21.5 m):
Below sediments grade into
Rad nanno ooze and nanno ooze. Colors become lighter shades of brown (10YR 8/3, 8/4) to whitish (10YR 8/2) and light gray (10YR 7/1).
Basalt chips, 3 mm sized, occur in Section 4.
SMEAR SLIDE SUMMARY (%)
1, 130 4, 20 6, 75
Texture.
Sand 40 20 8
Silt 30 30 7
Clay 30 50 85
Composition:
Clay 9 5 –
Pyrite 2 1 Tr
Carbonate unspec. 30 25 40
Foraminifers 5 5 3
Calc. nannofossils 8 33 50
Diatoms 20 8 3
Radiolarians 25 12 4
Sponge spicules Tr Tr Tr
Silicoflagellates Tr Tr –
Fe-oxides 1 1 –
CARBONATE BOMB
1, 75 cm = 26%
2, 75 cm = 32%
3, 71 cm = 67%
4, 76 cm = 35%
5, 75 cm = 65%
6, 75 cm = 80%

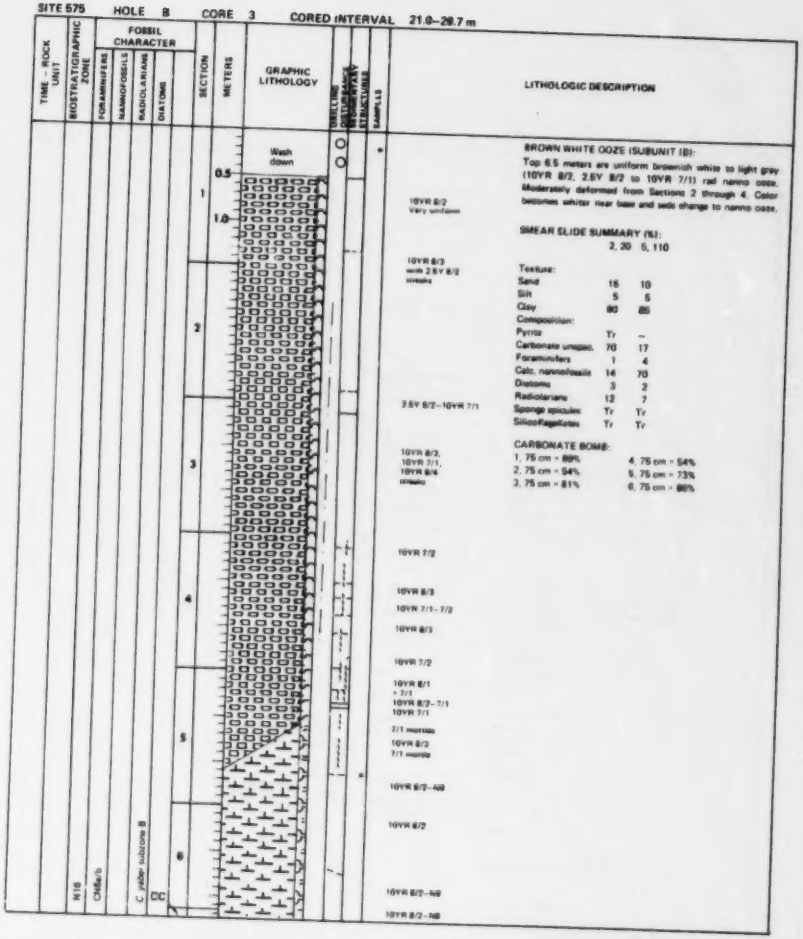

NOTE: Graphic lithologies represent average compositions derived from smear slides and do not always reflect the detailed alternation of sediment types. Major lithologic boundaries are shown but gradational contacts, small scale cyclicity and ooze-chalk alternations are represented schematically. Color changes approximate to lithologic changes.

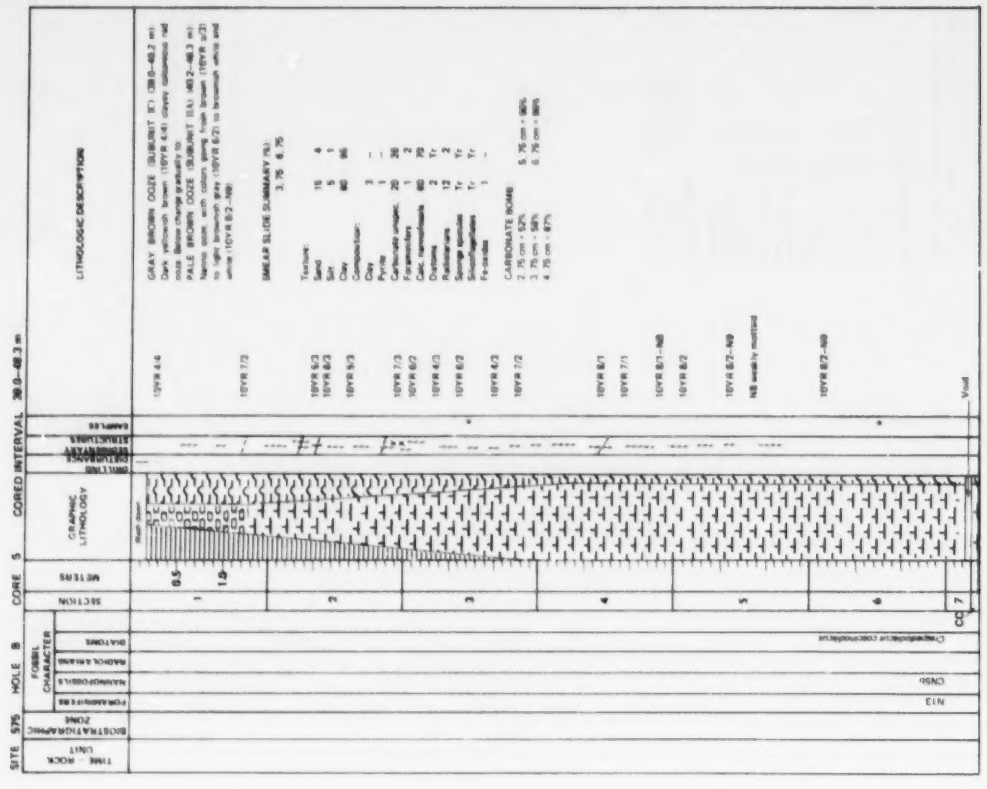

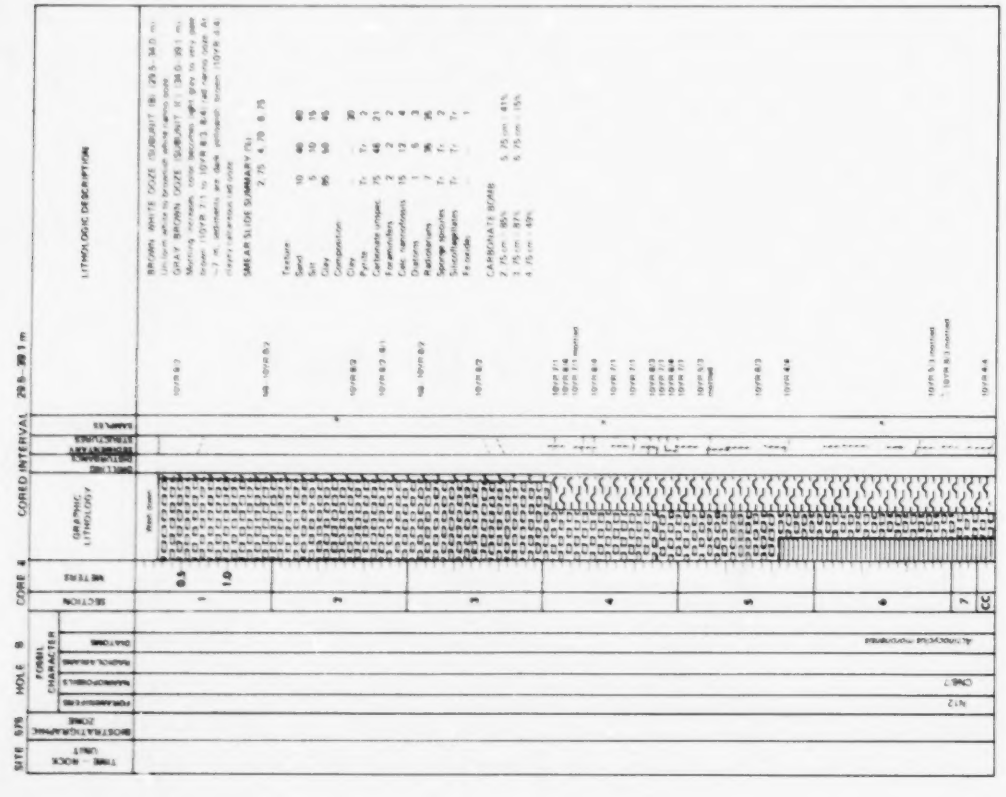

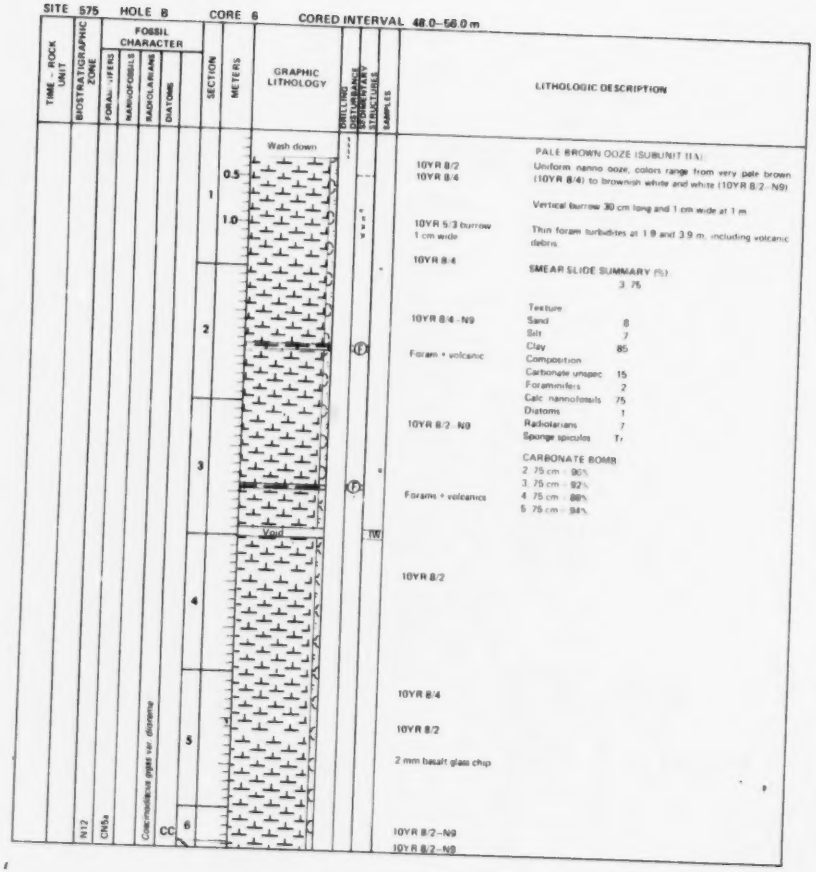
SITE 575 HOLE B CORE 6 CORED INTERVAL 48.0–56.0 m
TIME – ROCK UNIT
BIOSTRATIGRAPHIC ZONE
FOSSIL CHARACTER
FORAMINIFERS
NANNOFOSSILS
RADIOLARIANS
DIATOMS
SECTION
METERS
GRAPHIC LITHOLOGY
DRILLING DISTURBANCE
SEDIMENTARY STRUCTURES
SAMPLES
LITHOLOGIC DESCRIPTION
N12
CN5a
Coscinodiscus gigas var. diorama
Wash down
Void
CC
10YR 8/2
10YR 8/4
Vertical burrow 30 cm long and 1 cm wide at 1 m
10YR 5/3 burrow 1 cm wide
Thin foram turbidites at 1.9 and 3.9 m, including volcanic debris.
10YR 8/4
10YR 8/4 - N9
Foram + volcanic
10YR 8/2 - N9
Foram + volcanics
10YR 8/2
10YR 8/4
10YR 8/2
2 mm basalt glass chip
10YR 8/2 - N9
10YR 8/2 - N9
PALE BROWN OOZE (SUBUNIT IIA)
Uniform nanno ooze, colors range from very pale brown (10YR 8/4) to brownish white and white (10YR 8/2 - N9)
SMEAR SLIDE SUMMARY (%)
3, 75
Texture
Sand 8
Silt 7
Clay 85
Composition
Carbonate unspec 15
Foraminifers 2
Calc. nannofossils 75
Diatoms 1
Radiolarians 1
Sponge spicules Tr
CARBONATE BOMB
2, 75 cm - 96%
3, 75 cm - 92%
4, 75 cm - 88%
5, 75 cm - 94%

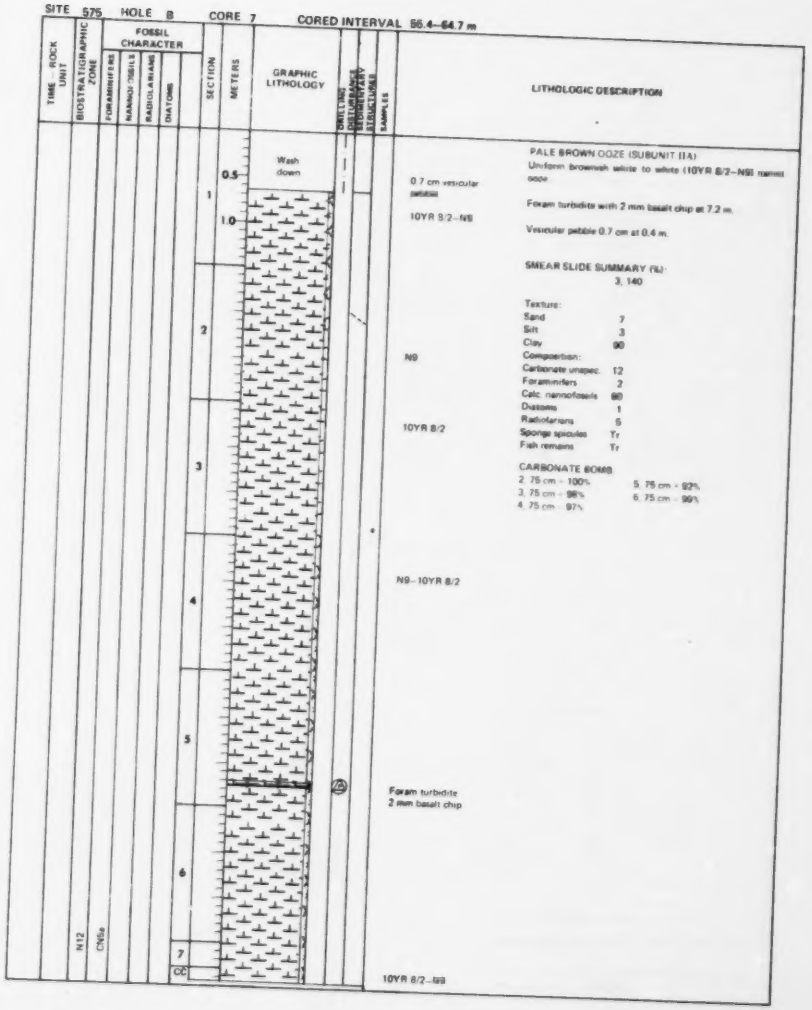
SITE 575 HOLE B CORE 7 CORED INTERVAL 56.4–64.7 m
TIME – ROCK UNIT
BIOSTRATIGRAPHIC ZONE
FOSSIL CHARACTER
FORAMINIFERS
NANNOFOSSILS
RADIOLARIANS
DIATOMS
SECTION
METERS
GRAPHIC LITHOLOGY
DRILLING DISTURBANCE
SEDIMENTARY STRUCTURES
SAMPLES
LITHOLOGIC DESCRIPTION
N12
CN5a
Wash down
CC
0.7 cm vesicular pebble
10YR 8/2 - N9
N9
10YR 8/2
N9 - 10YR 8/2
Foram turbidite
2 mm basalt chip
10YR 8/2 - N9
PALE BROWN OOZE (SUBUNIT IIA)
Uniform brownish white to white (10YR 8/2 - N9) nannof ooze
Foram turbidite with 2 mm basalt chip at 7.2 m.
Vesicular pebble 0.7 cm at 0.4 m.
SMEAR SLIDE SUMMARY (%)
3, 140
Texture:
Sand 7
Silt 3
Clay 90
Composition:
Carbonate unspec. 12
Foraminifers 2
Calc. nannofossils 80
Diatoms 1
Radiolarians 5
Sponge spicules Tr
Fish remains Tr
CARBONATE BOMB
2, 75 cm - 100%
3, 75 cm - 96%
4, 75 cm - 97%
5, 75 cm - 92%
6, 75 cm - 99%

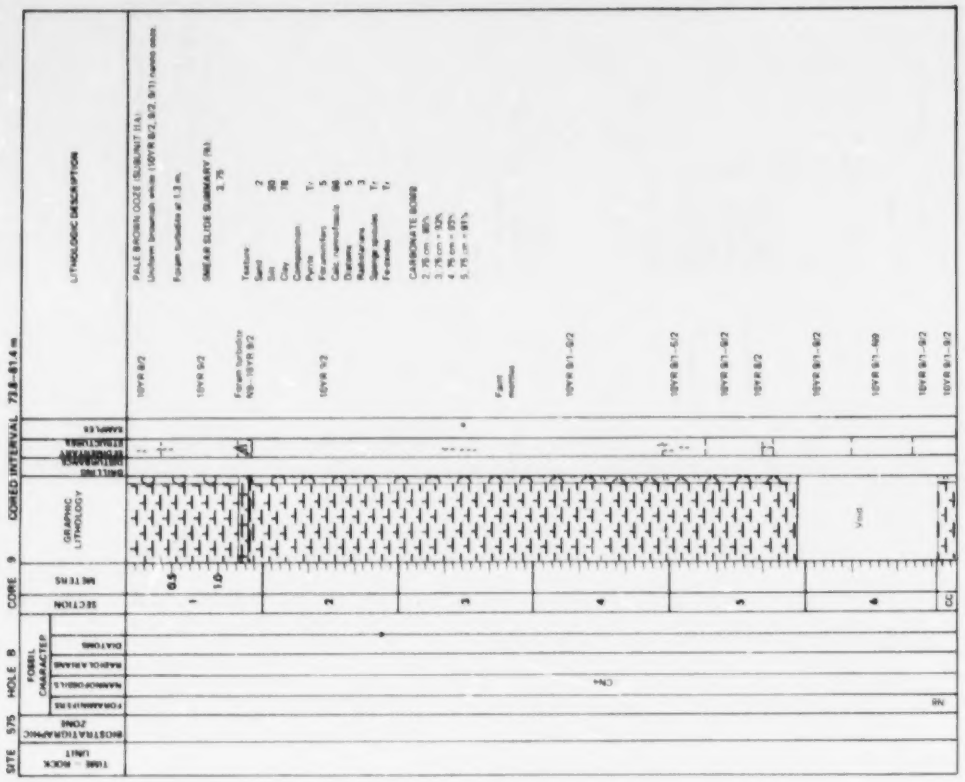

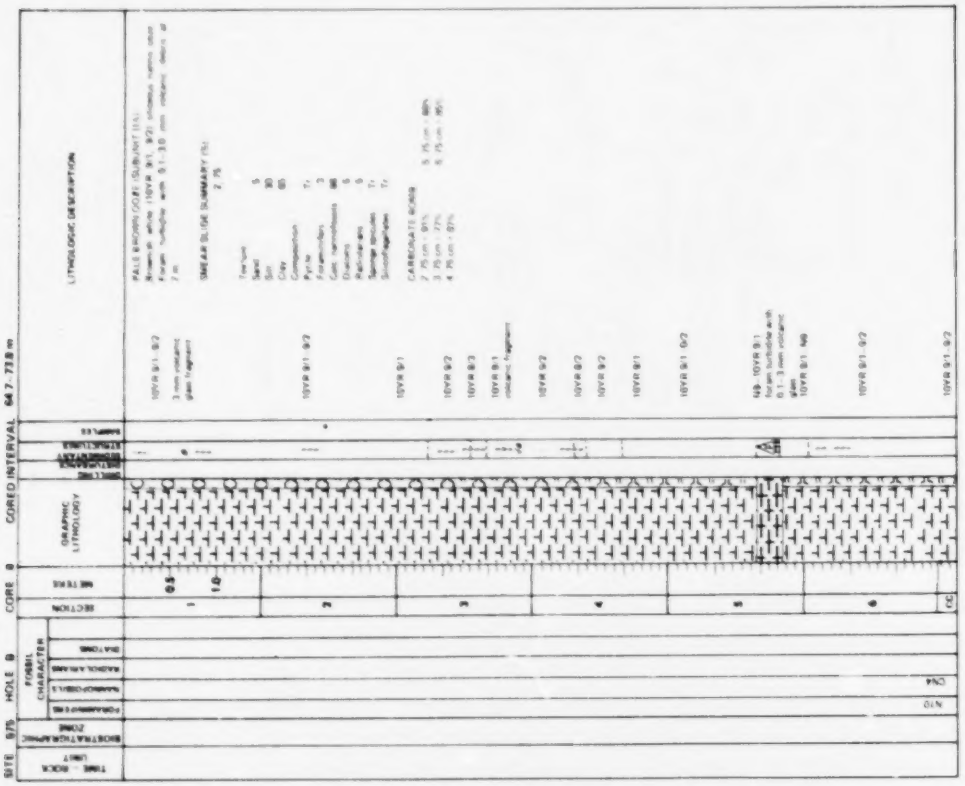

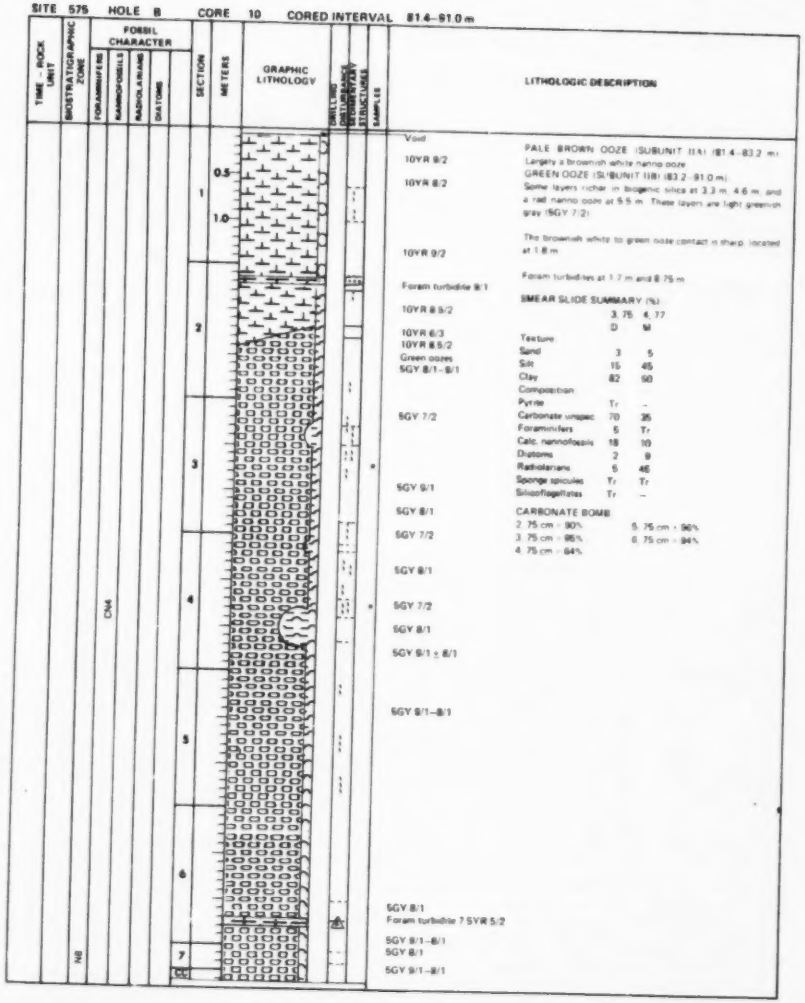
SITE 575 HOLE B CORE 10 CORED INTERVAL 81.4–91.0 m
TIME – ROCK UNIT
BIOSTRATIGRAPHIC ZONE
FOSSIL CHARACTER
FORAMINIFERS
NANNOFOSSILS
RADIOLARIANS
DIATOMS
SECTION
METERS
GRAPHIC LITHOLOGY
DRILLING DISTURBANCE
SEDIMENTARY STRUCTURES
SAMPLES
LITHOLOGIC DESCRIPTION
CN4
N8
Void
10YR 8/2
PALE BROWN OOZE (SUBUNIT IIA) (81.4–83.2 m):
Largely a brownish white nanno ooze
GREEN OOZE (SUBUNIT IIB) (83.2–91.0 m):
Some layers richer in biogenic silica at 3.3 m, 4.6 m, and a rad nanno ooze at 5.5 m. These layers are light greenish gray (5GY 7/2)
10YR 8/2
The brownish white to green ooze contact is sharp, located at 1.8 m
10YR 8/2
Foram turbidite 8/1
Foram turbidites at 1.7 m and 8.75 m
SMEAR SLIDE SUMMARY (%)
3, 75 D
4, 77 M
10YR 8.5/2
10YR 6/3
10YR 8.5/2
Green oozes
5GY 8/1–8/1
Texture
Sand 3 5
Silt 15 45
Clay 82 50
Composition
Pyrite Tr –
Carbonate unspec. 70 35
Foraminifers 5 Tr
Calc. nannofossils 18 10
Diatoms 2 9
Radiolarians 5 46
Sponge spicules Tr Tr
Silicoflagellates Tr –
5GY 7/2
5GY 8/1
CARBONATE BOMB
2, 75 cm – 90%
3, 75 cm – 86%
4, 75 cm – 84%
5, 75 cm – 96%
6, 75 cm – 94%
5GY 7/2
5GY 8/1
5GY 8/1 ± 8/1
5GY 8/1–8/1
5GY 8/1
Foram turbidite 7.5YR 5/2
5GY 8/1–8/1
5GY 8/1
5GY 8/1–8/1

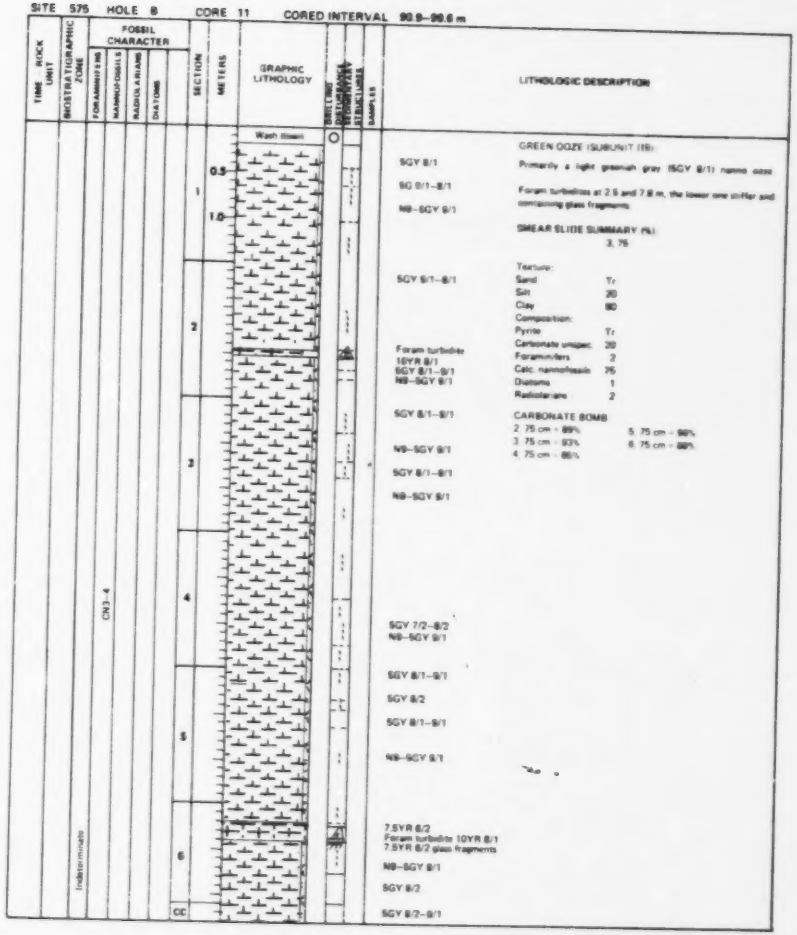
SITE 575 HOLE B CORE 11 CORED INTERVAL 90.9–99.6 m
TIME – ROCK UNIT
BIOSTRATIGRAPHIC ZONE
FOSSIL CHARACTER
FORAMINIFERS
NANNOFOSSILS
RADIOLARIANS
DIATOMS
SECTION
METERS
GRAPHIC LITHOLOGY
DRILLING DISTURBANCE
SEDIMENTARY STRUCTURES
SAMPLES
LITHOLOGIC DESCRIPTION
CN3–4
Indeterminate
Wash (foam)
GREEN OOZE (SUBUNIT IIB):
Primarily a light greenish gray (5GY 8/1) nanno ooze
Foram turbidites at 2.5 and 7.8 m, the lower one sitlier and containing glass fragments
SMEAR SLIDE SUMMARY (%)
3, 75
Texture:
Sand Tr
Silt 20
Clay 80
Composition:
Pyrite Tr
Carbonate unspec. 20
Foraminifers 2
Calc. nannofossils 75
Diatoms 1
Radiolarians 2
CARBONATE BOMB
2, 75 cm – 89%
3, 75 cm – 93%
4, 75 cm – 86%
5, 75 cm – 96%
6, 75 cm – 88%
5GY 8/1
5G 8/1–8/1
N8–5GY 8/1
5GY 8/1–8/1
Foram turbidite
10YR 8/1
5GY 8/1–8/1
N8–5GY 8/1
5GY 8/1–8/1
N8–5GY 8/1
5GY 7/2–8/2
N8–5GY 8/1
5GY 8/1–8/1
5GY 8/2
5GY 8/1–8/1
N8–5GY 8/1
7.5YR 8/2
Foram turbidite 10YR 8/1
7.5YR 8/2 glass fragments
N8–5GY 8/1
5GY 8/2
5GY 8/2–8/1

SITE 575 HOLE B CORE 12 CORED INTERVAL 99.6–109.2 m

TIME – ROCK UNIT	BIOSTRATIGRAPHIC ZONE	FOSSIL CHARACTER: FORAMINIFERS	FOSSIL CHARACTER: NANNOFOSSILS	FOSSIL CHARACTER: RADIOLARIANS	FOSSIL CHARACTER: DIATOMS	SECTION	METERS	GRAPHIC LITHOLOGY	DRILLING DISTURBANCE	SEDIMENTARY STRUCTURES	SAMPLES	LITHOLOGIC DESCRIPTION
			CN3–4			1	0.5					5GY 7/2
							1.0					5GY 8/1–G/1
						2						5GY 7/2 5GY 8/1–B/1 NB–5GY 8/1 5GY 8/1–B/1 NB–5GY 8/1
						3						Foram turbidite 7.5YR 8/2 5GY 7/2–8/2 NB–5GY 8/1 5GY 7/2–8/2 NB–5GY 8/1
						4						NB–5GY 8/1
						5						Foram turbidite + glass fragments NB–5GY 8/1 5Y 6/2–8/2 NB–5GY 8/1
			Inoperculata			6						5GY 8/1–B/1 5GY 7/2–8/2 5GY 8/1–B/1 NB–5GY 8/1
						7						5Y 6/2–8/2
						CC						NB–5GY 8/1

LITHOLOGIC DESCRIPTION

GREEN OOZE (SUBUNIT IIB)

Top 7 cm are light green gray to white (5GY 7/2–8/1, NB) nanno ooze. Below this are light olive gray to yellowish gray (5Y 6/2–8/1) clayey calcareous ooze layers at 7.5 and 9.1 m.

Foram turbidites at 4, 6.8, and 2.7 m

SMEAR SLIDE SUMMARY (%)

	3, 75 D	5, 130 M
Texture		
Sand	1	25
Silt	30	50
Clay	69	25
Composition		
Clay	–	15
Pyrite	Tr	Tr
Carbonate unspec.	30	15
Foraminifers	5	-
Calc. nannofossils	55	5
Diatoms	4	8
Radiolarians	4	50
Silicoflagellates	Tr	Tr
Fe-oxides	Tr	5

CARBONATE BOMB
2, 75 cm – 96%
3, 75 cm – 85%
4, 75 cm – 87%
5, 75 cm – 82%

SITE 575 HOLE B CORE (HPC) 13 CORED INTERVAL 109.2–114.1 m

TIME – ROCK UNIT	BIOSTRATIGRAPHIC ZONE	FOSSIL CHARACTER: FORAMINIFERS	FOSSIL CHARACTER: NANNOFOSSILS	FOSSIL CHARACTER: RADIOLARIANS	FOSSIL CHARACTER: DIATOMS	SECTION	METERS	GRAPHIC LITHOLOGY	DRILLING DISTURBANCE	SEDIMENTARY STRUCTURES	SAMPLES	LITHOLOGIC DESCRIPTION
						1	0.5					5GY–5Y 8/1–9/1
							1.0					
						2		Void			IW	5Y 8/1 5Y 8/2 5Y 8/1
		NB	CN3			3						5Y 8/1–8/1 5Y 7.5/2 5Y 7/2 5Y 7.5/2 5Y 8/1–8/1
						4						
						CC						

LITHOLOGIC DESCRIPTION

GREEN OOZE (SUBUNIT IIB)

Dominantly a greenish white to light greenish gray nanno ooze

Light olive gray (5Y 7/2) clayey calcareous ooze at 4 m.

SMEAR SLIDE SUMMARY (%)

	2, 60 D	3, 100 M
Texture		
Sand	2	25
Silt	30	50
Clay	78	25
Composition:		
Clay	–	5
Carbonate unspec.	35	35
Foraminifers	5	Tr
Calc. nannofossils	50	10
Diatoms	5	5
Radiolarians	5	55
Sponge spicules	Tr	Tr
Fe-oxides	Tr	Tr

CARBONATE BOMB
2, 75 cm – 73%
3, 75 cm – 83%

SITE 575 HOLE B CORE (HPC) 14 CORED INTERVAL 114.1–119.0 m
TIME – ROCK UNIT
BIOSTRATIGRAPHIC ZONE
FOSSIL CHARACTER
FORAMINIFERS
NANNOFOSSILS
RADIOLARIANS
DIATOMS
SECTION
METERS
GRAPHIC LITHOLOGY
DRILLING DISTURBANCE
SEDIMENTARY STRUCTURES
SAMPLES
LITHOLOGIC DESCRIPTION
Zone indeterminate
PM
CN3
Gretzbeus pliplum subzone A
5Y 8/1–8/1
GREEN OOZE (SUBUNIT IIB) (114.1–117.1 m)
Greenish white to yellowish white and yellow (5Y 8/1 to 2.5Y 7/2 to 2.5Y 7/4) siliceous nanno oozes
YELLOW BROWN OOZE (SUBUNIT IIA)
(117.1–119.0 m)
Layers of very pale brown (10YR 7/4) nanno rad ooze at 3.1 m and 4.2 m and 2.8 m. Ash turbidite at 2.9 m
N9–5Y 8/1
SMEAR SLIDE SUMMARY (%)
2.75 3.7
D M
2.5Y 7/2–8/2
Texture
Sand 3 25
Silt 25 50
Clay 72 25
2.5Y 8/2
Composition:
Clay – 5
Pyrite Tr Tr
Carbonate unspec. 10 20
Foraminifers 5 Tr
2.5Y 8/2–8/2
Calc. nannofossils 75 15
Diatoms 5 10
Radiolarians 5 50
Sponge spicules Tr Tr
Fe oxides Tr Tr
CARBONATE BOMB
2.75 cm = 91%
3.75 cm = 86%
3.5Y 7/2
2.5Y 7/4
2.5Y 7/2
2.5Y 9/2
10YR 7/4
10YR 8/2
10YR 8–8.5/2
10YR 8/4
10YR 8.5/2
10YR 8.5/2
CC

SITE 575 HOLE C CORE 1 CORED INTERVAL 0.0–8.5 m

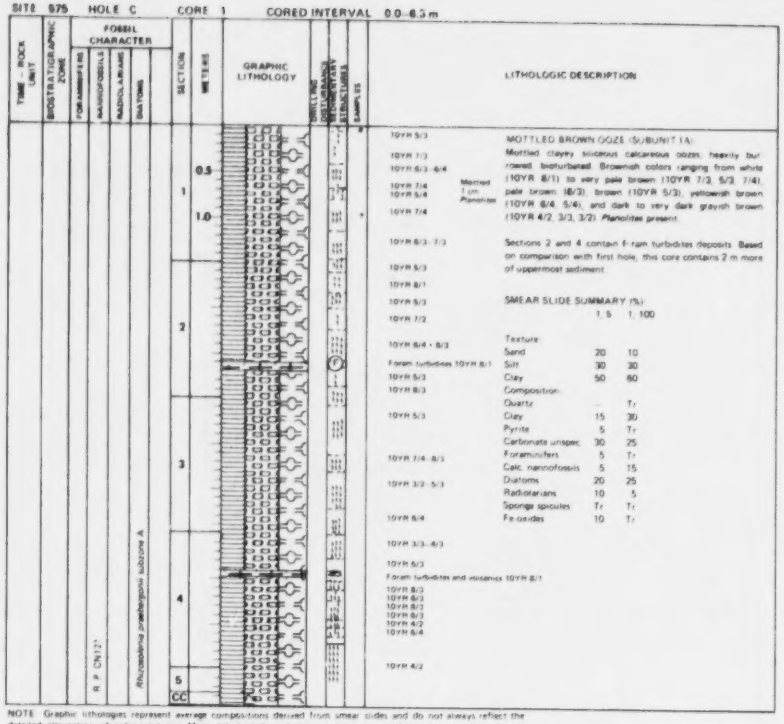

NOTE Graphic lithologies represent average compositions derived from smear slides and do not always reflect the detailed alternation of sediment types. Major lithologic boundaries are shown but gradational contacts, small-scale cyclicity and ooze/chalk alternations are represented schematically. Color changes approximate to lithologic changes.

SITE 575 HOLE C CORE 2 CORED INTERVAL 6.3–16.8 m

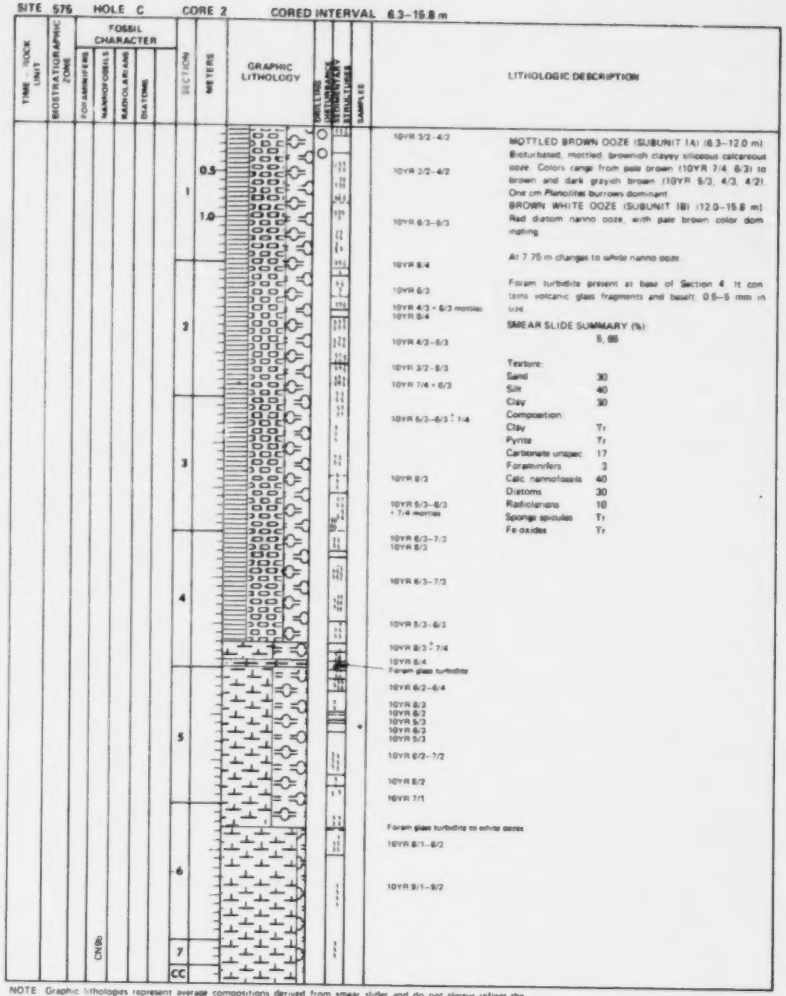

NOTE Graphic lithologies represent average compositions derived from smear slides and do not always reflect the detailed alternation of sediment types. Major lithologic boundaries are shown but gradational contacts, small-scale cyclicity and ooze/chalk alternations are represented schematically. Color changes approximate to lithologic changes.

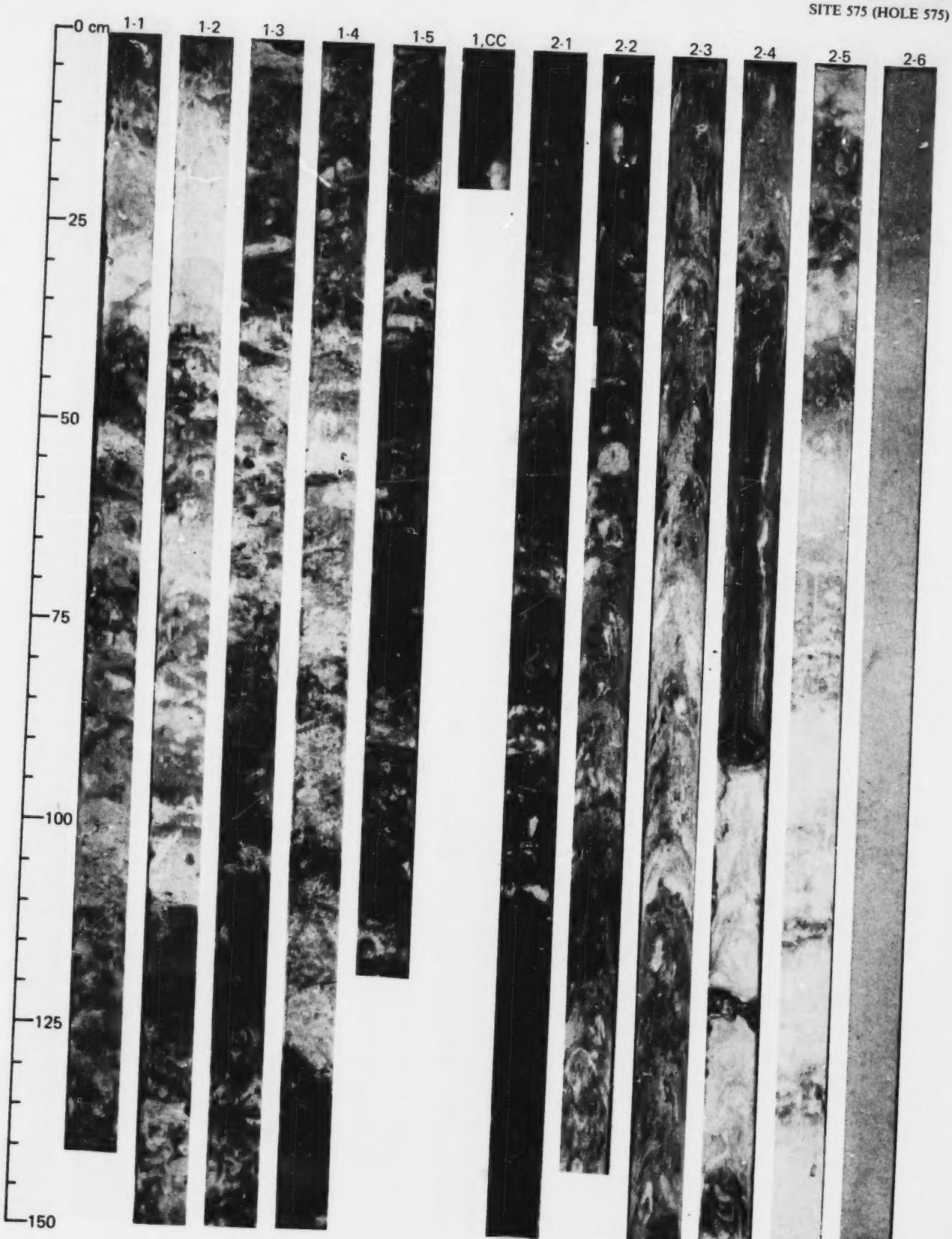
0 cm
1-1
1-2
1-3
1-4
1-5
1,CC
2-1
2-2
2-3
2-4
2-5
2-6
25
50
75
100
125
150

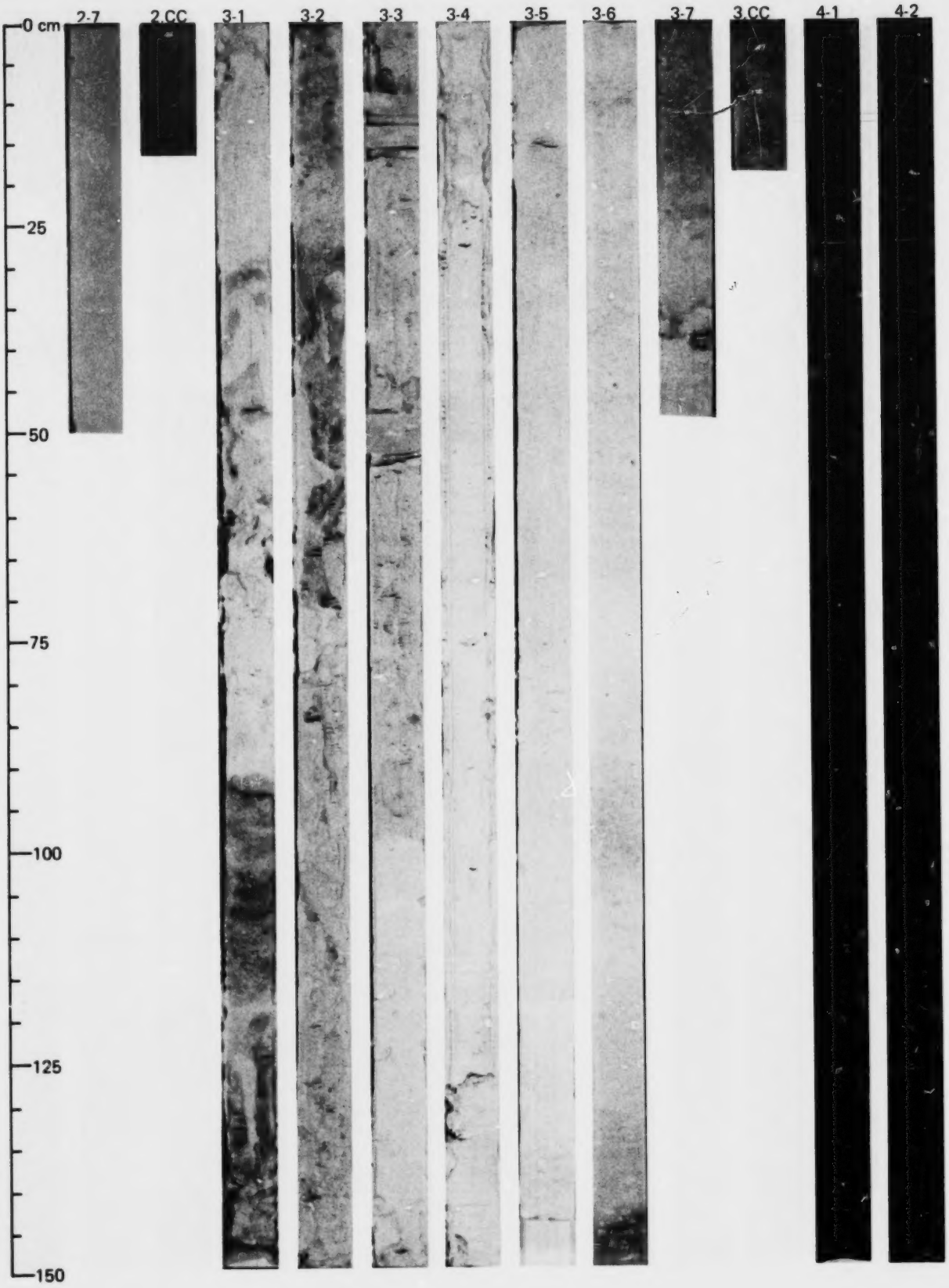
0 cm
25
50
75
100
125
150
2-7
2,CC
3-1
3-2
3-3
3-4
3-5
3-6
3-7
3,CC
4-1
4-2

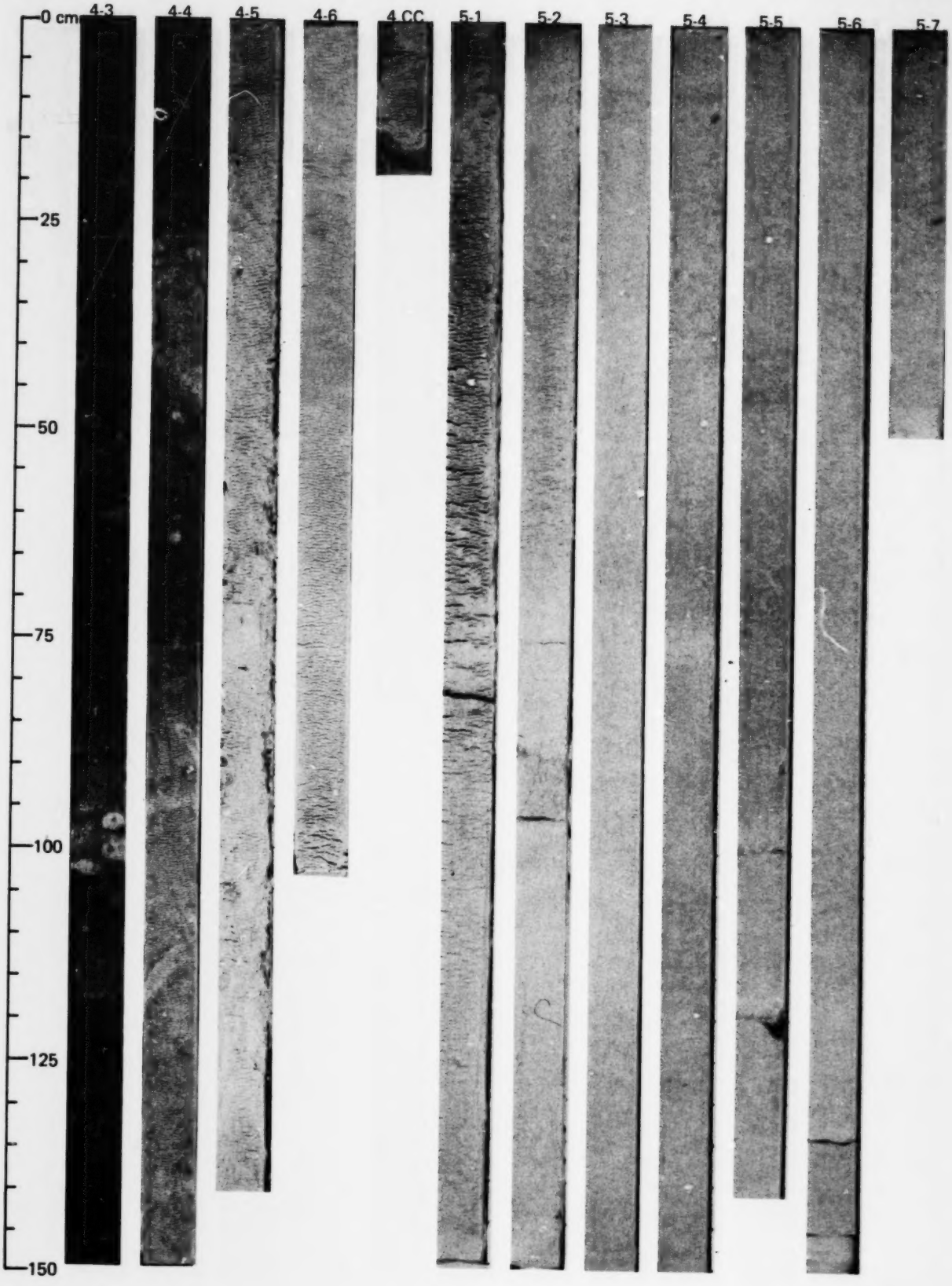
0 cm
4-3
4-4
4-5
4-6
4 CC
5-1
5-2
5-3
5-4
5-5
5-6
5-7
25
50
75
100
125
150

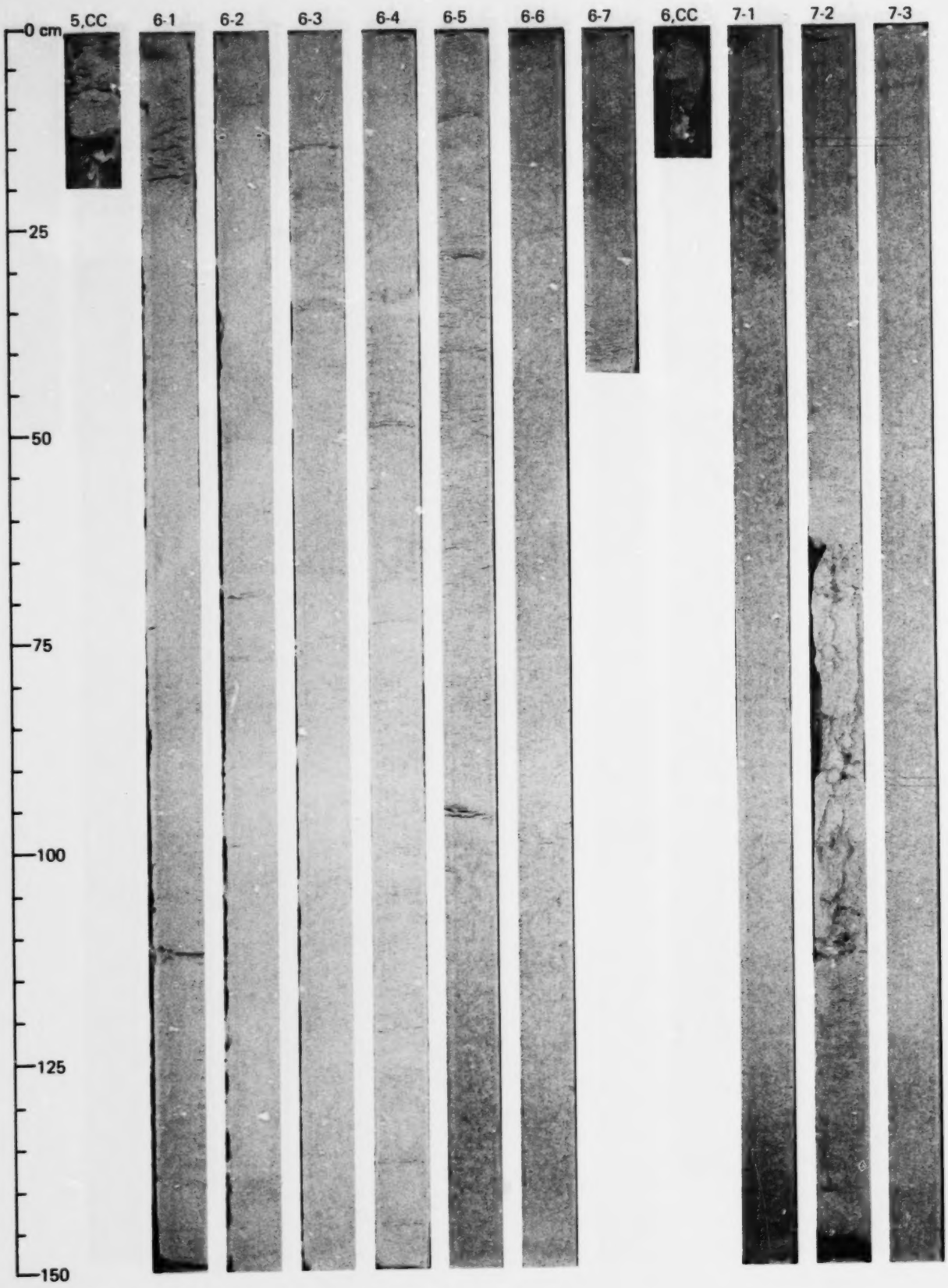
0 cm
5,CC
6-1
6-2
6-3
6-4
6-5
6-6
6-7
6,CC
7-1
7-2
7-3
25
50
75
100
125
150

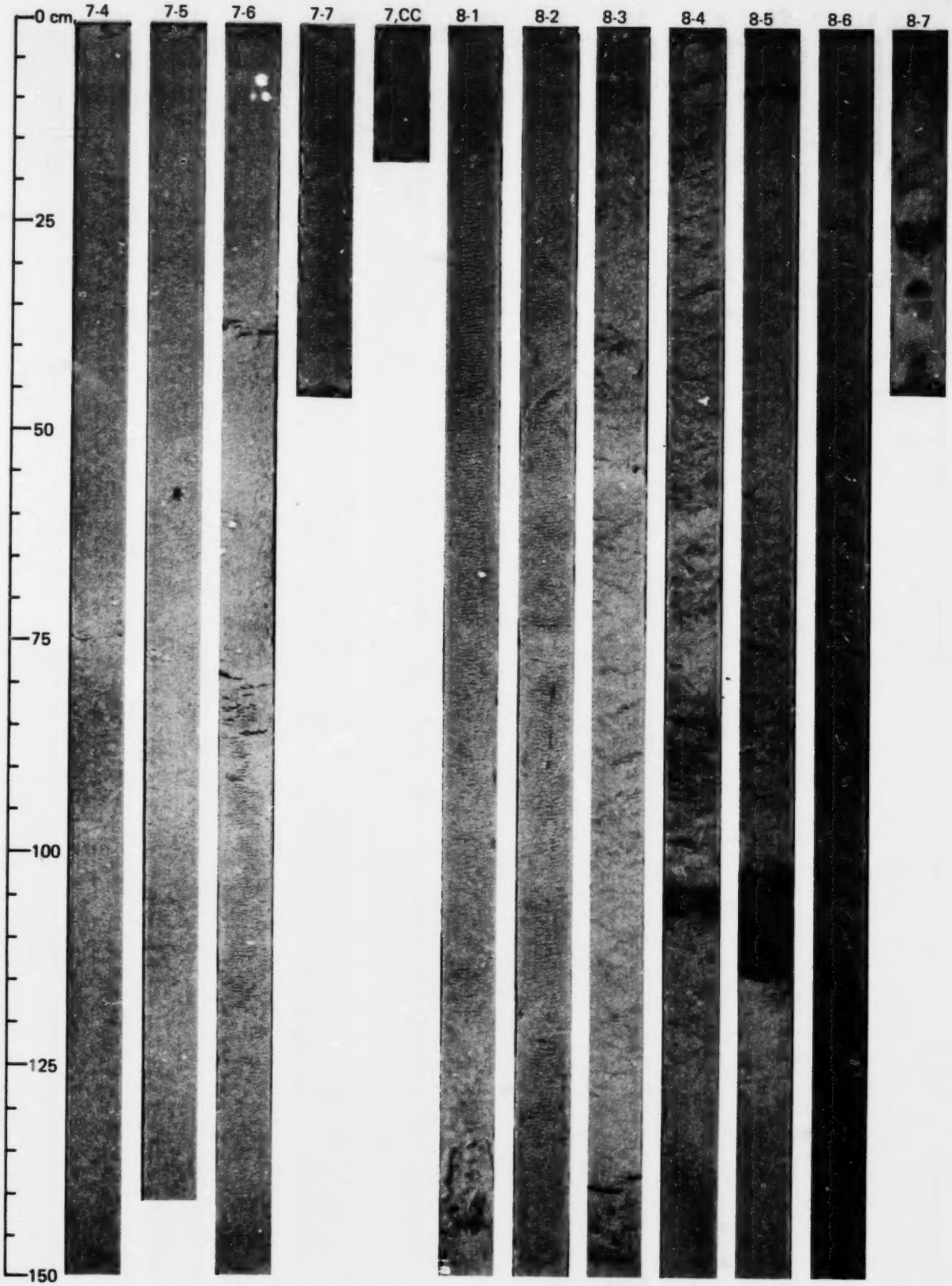
0 cm
25
50
75
100
125
150
7-4
7-5
7-6
7-7
7,CC
8-1
8-2
8-3
8-4
8-5
8-6
8-7

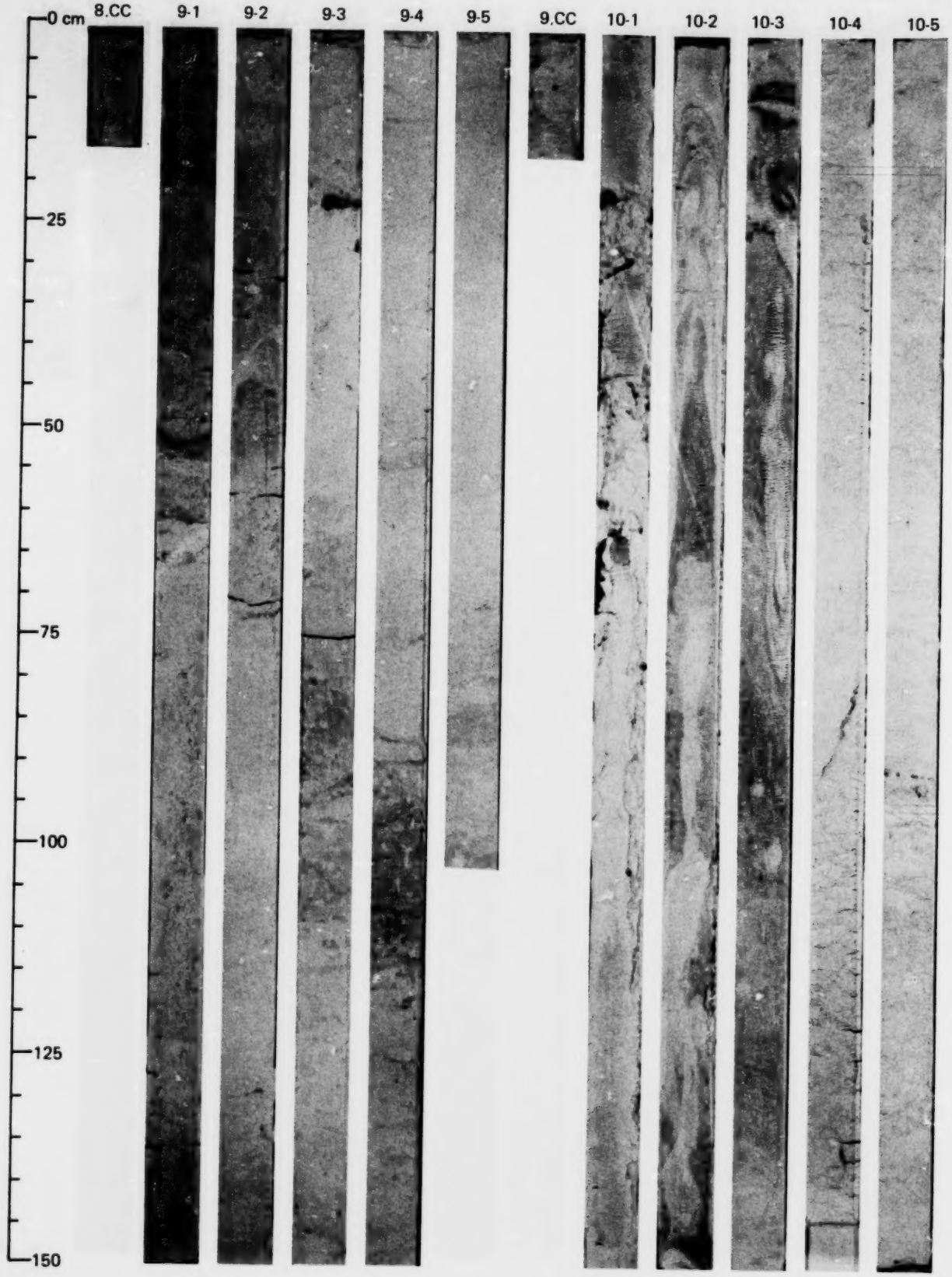
0 cm
8.CC
9-1
9-2
9-3
9-4
9-5
9.CC
10-1
10-2
10-3
10-4
10-5
25
50
75
100
125
150

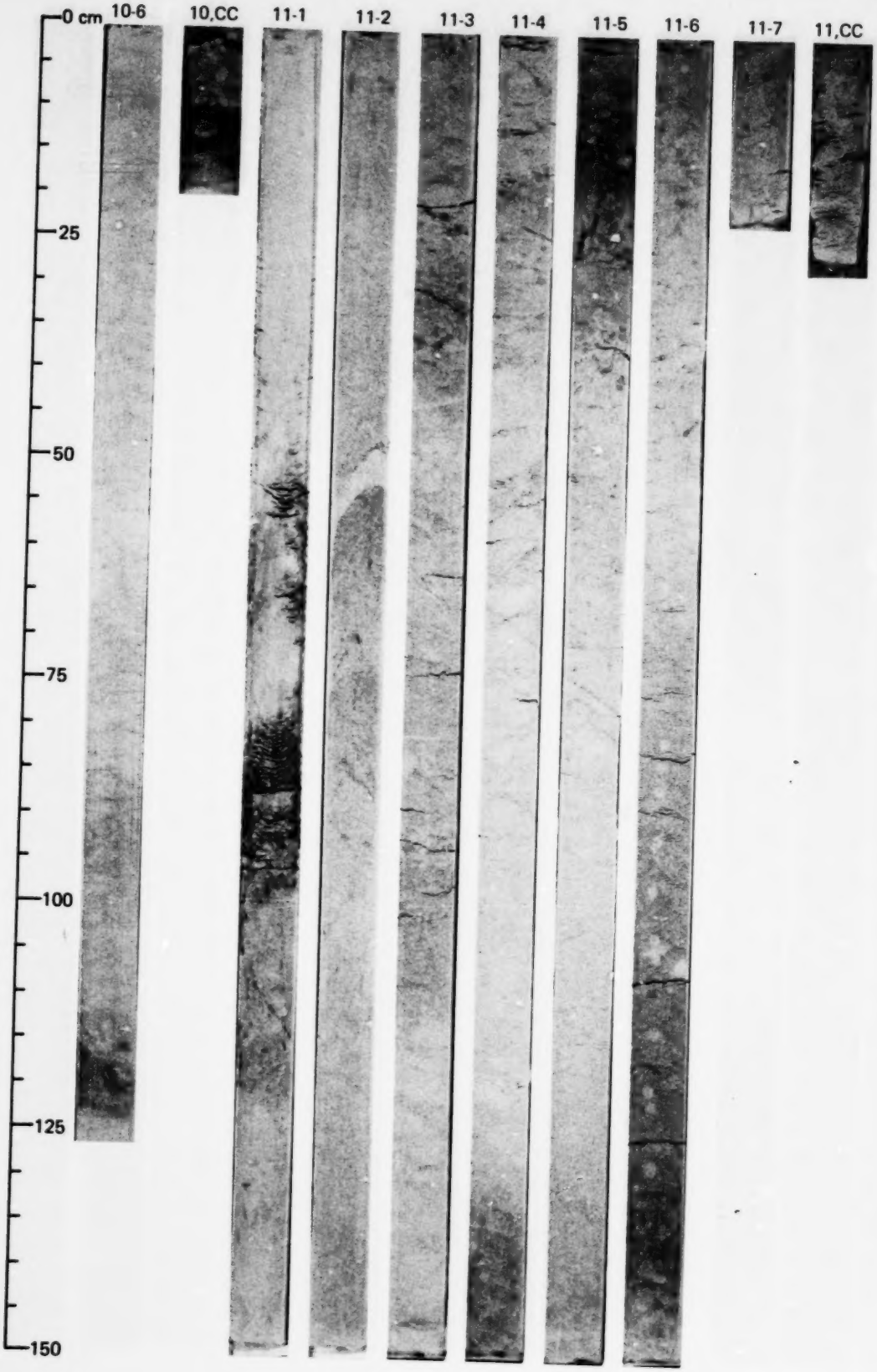
0 cm
10-6
10,CC
11-1
11-2
11-3
11-4
11-5
11-6
11-7
11,CC
25
50
75
100
125
150

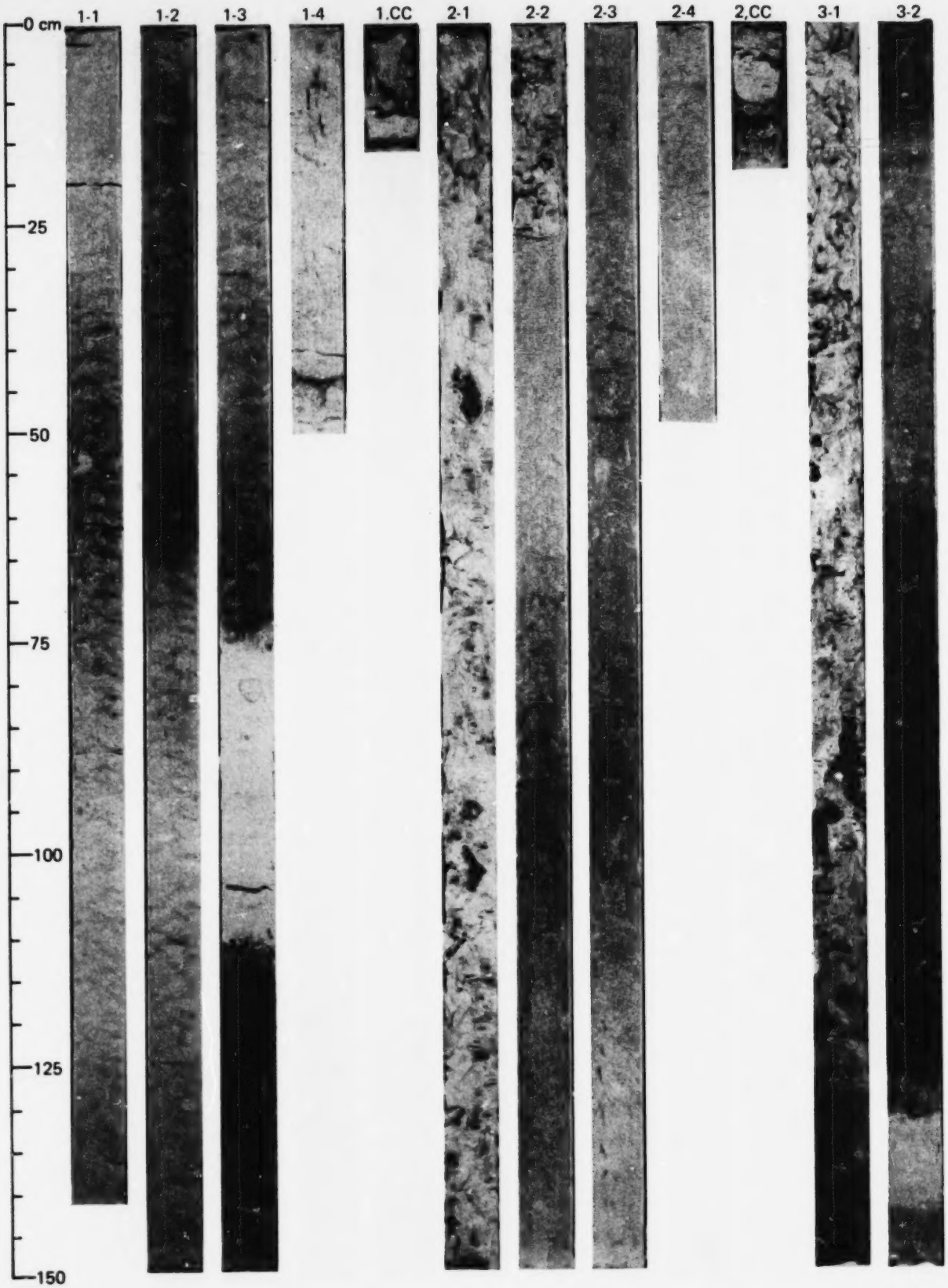
0 cm
25
50
75
100
125
150
1-1
1-2
1-3
1-4
1,CC
2-1
2-2
2-3
2-4
2,CC
3-1
3-2

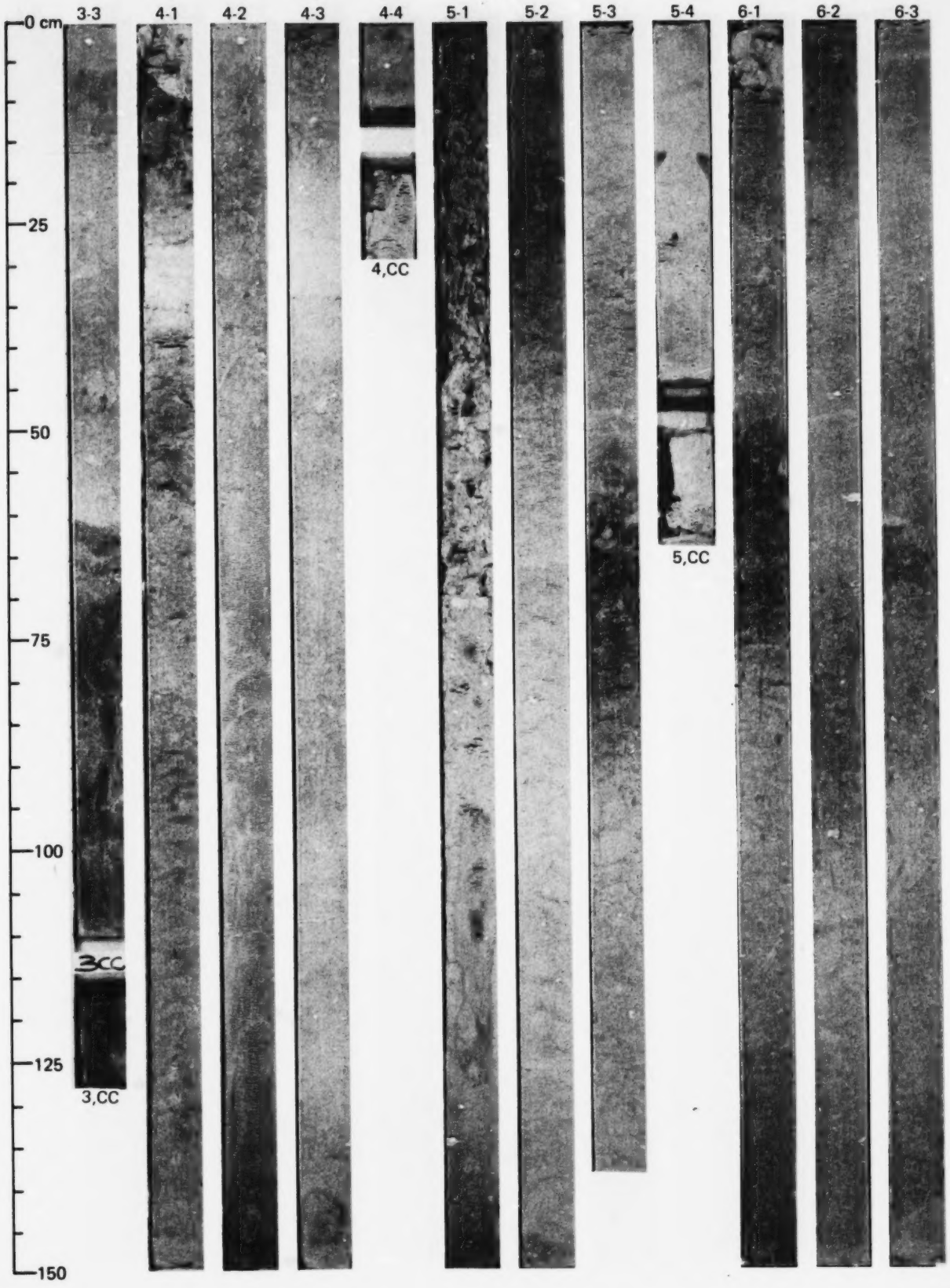
0 cm
25
50
75
100
125
150
3-3
4-1
4-2
4-3
4-4
5-1
5-2
5-3
5-4
6-1
6-2
6-3
4,CC
5,CC
3CC
3,CC

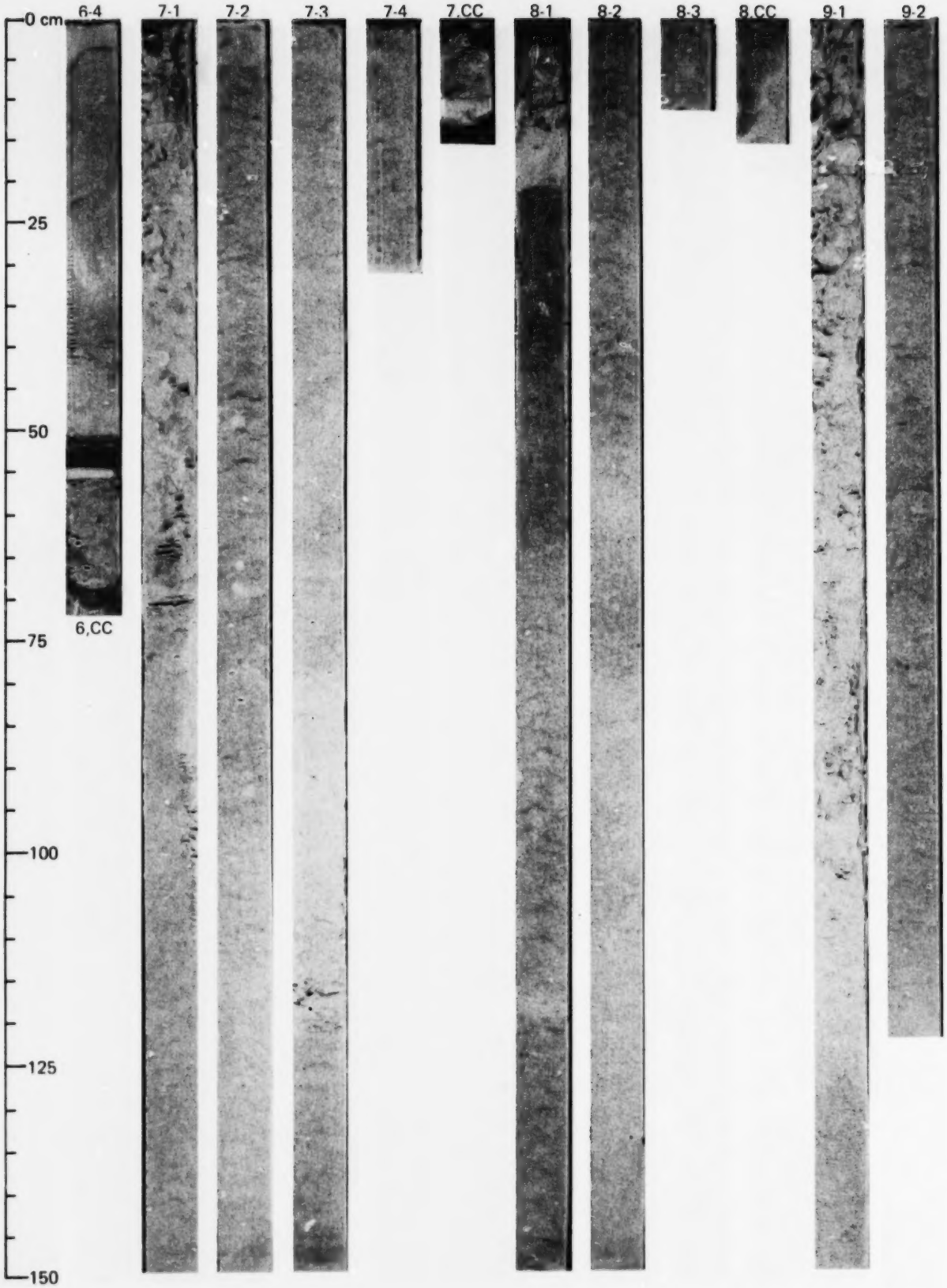
0 cm
25
50
75
100
125
150
6-4
6,CC
7-1
7-2
7-3
7-4
7,CC
8-1
8-2
8-3
8,CC
9-1
9-2

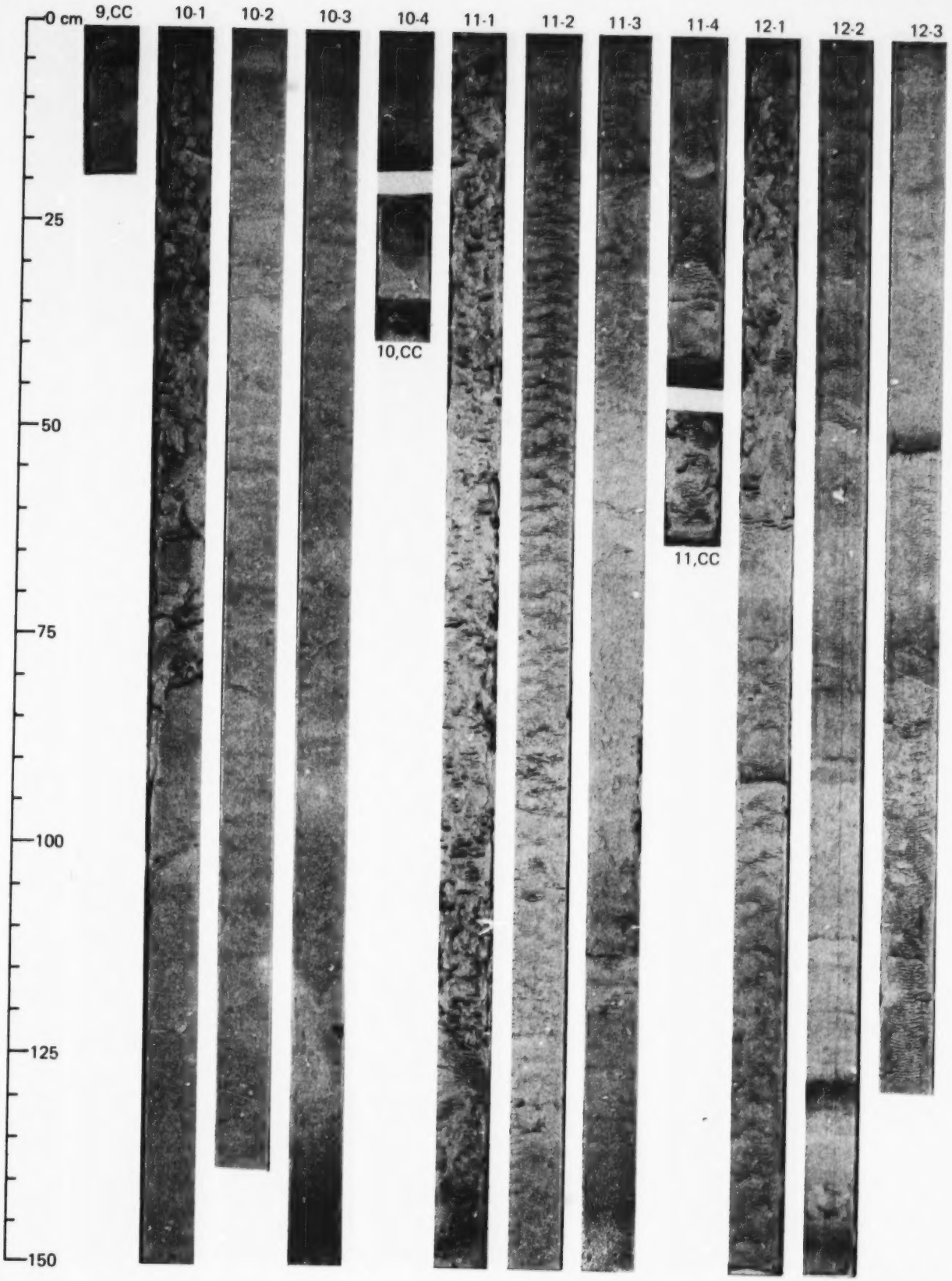
0 cm
25
50
75
100
125
150
9,CC
10-1
10-2
10-3
10-4
10,CC
11-1
11-2
11-3
11-4
11,CC
12-1
12-2
12-3

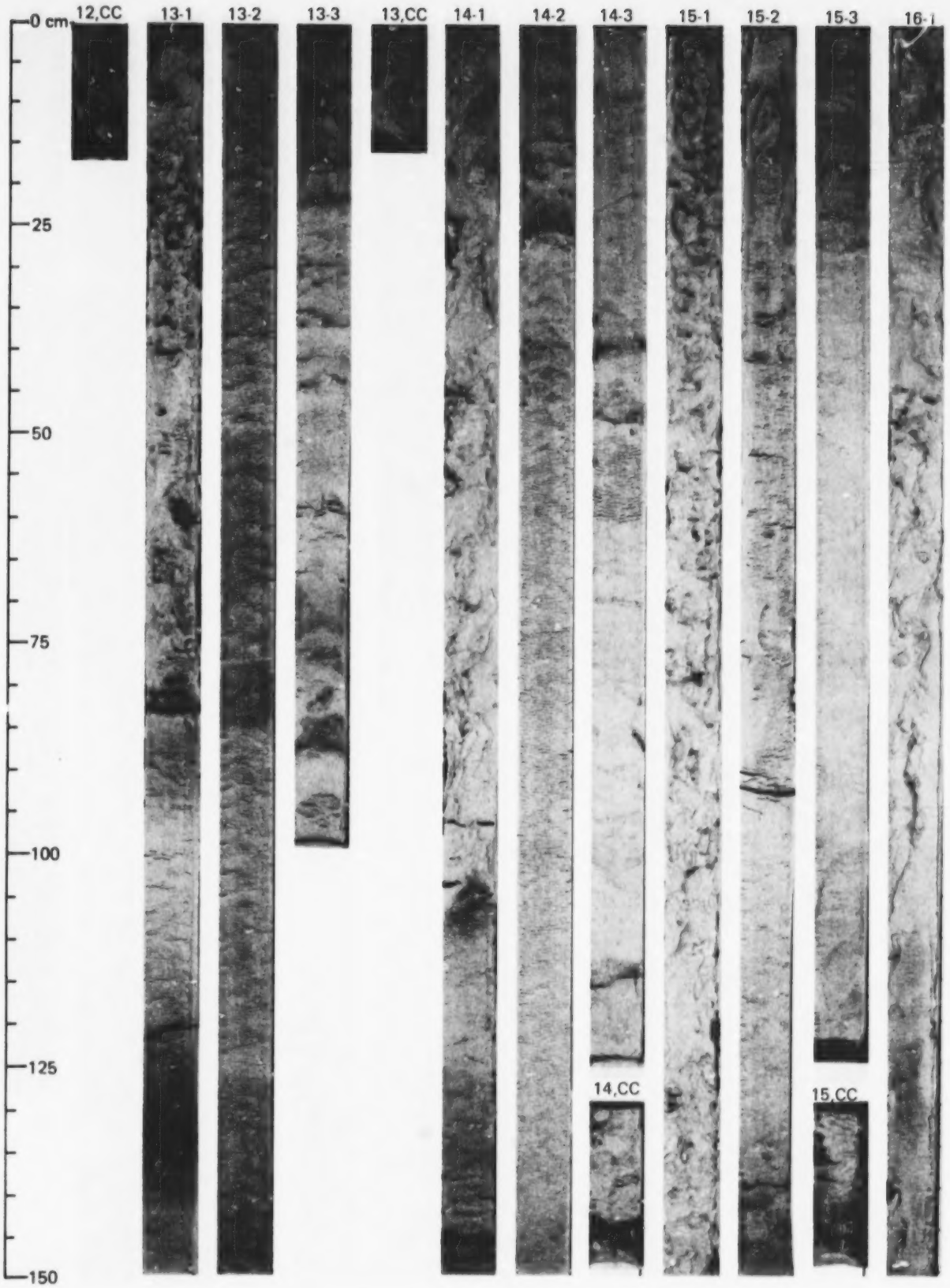
0 cm
25
50
75
100
125
150
12,CC
13-1
13-2
13-3
13,CC
14-1
14-2
14-3
14,CC
15-1
15-2
15-3
15,CC
16-1

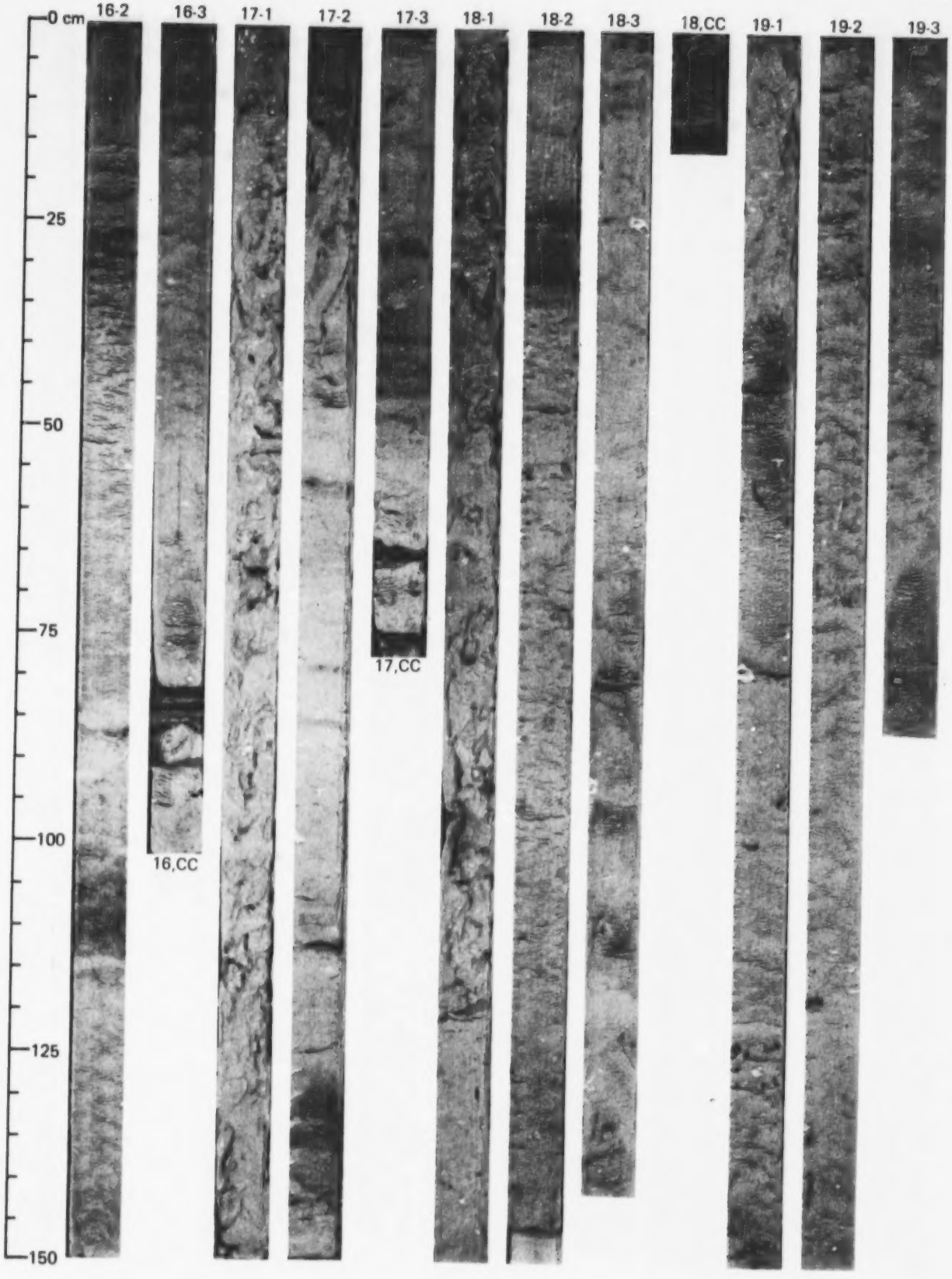
0 cm
25
50
75
100
125
150
16-2
16-3
16,CC
17-1
17-2
17-3
17,CC
18-1
18-2
18-3
18,CC
19-1
19-2
19-3

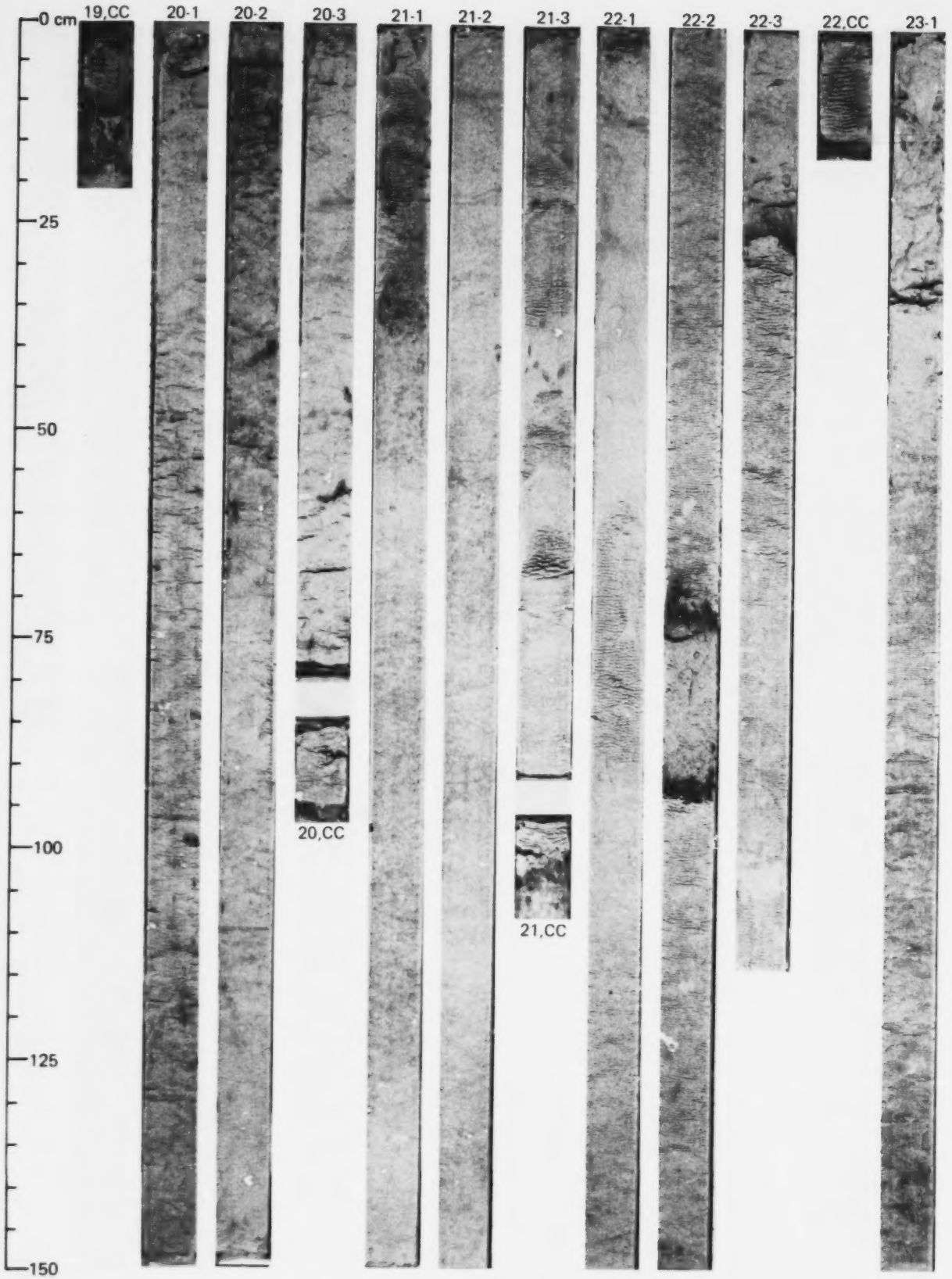
0 cm
25
50
75
100
125
150
19,CC
20-1
20-2
20-3
20,CC
21-1
21-2
21-3
21,CC
22-1
22-2
22-3
22,CC
23-1

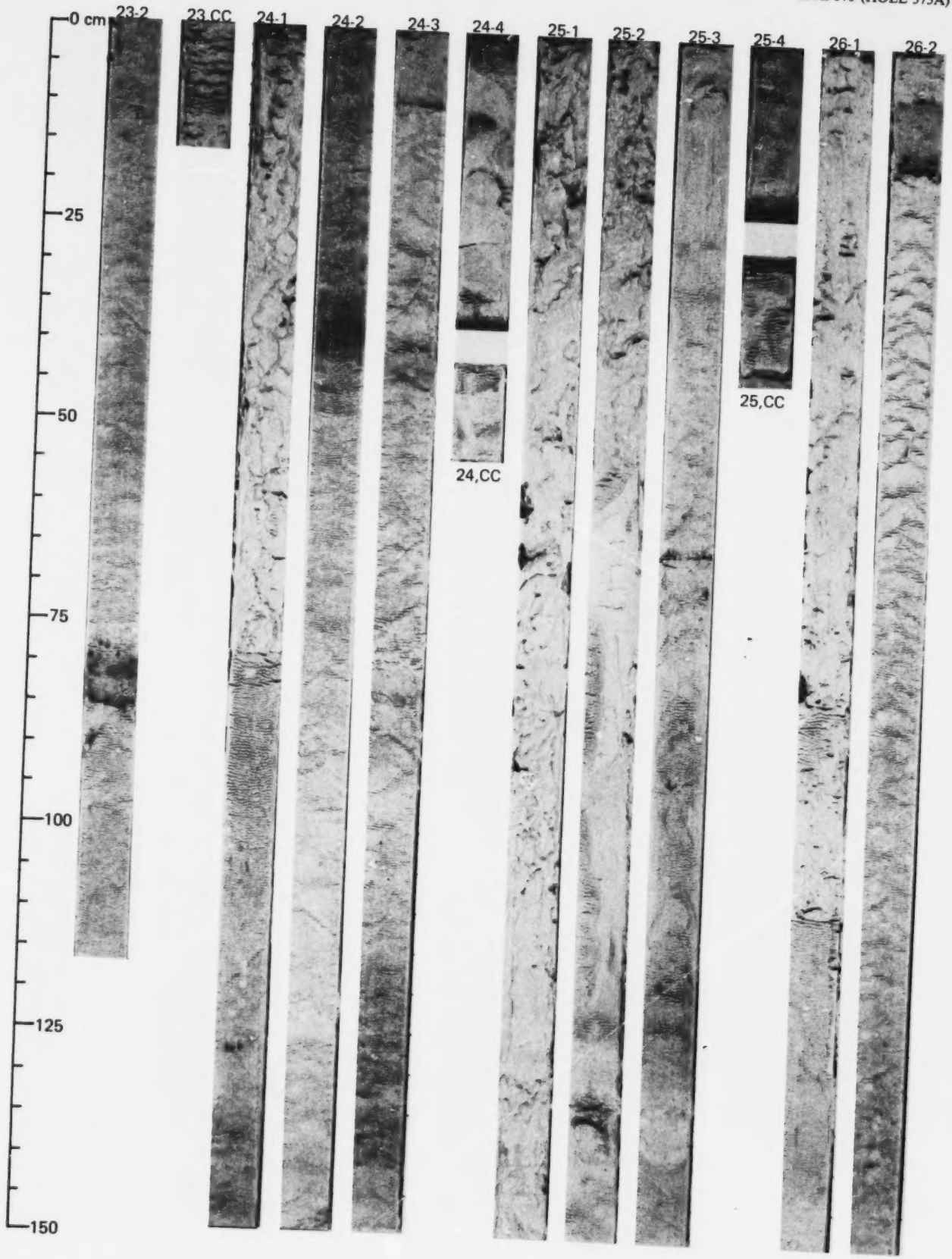
0 cm
25
50
75
100
125
150
23-2
23,CC
24-1
24-2
24-3
24-4
24,CC
25-1
25-2
25-3
25-4
25,CC
26-1
26-2

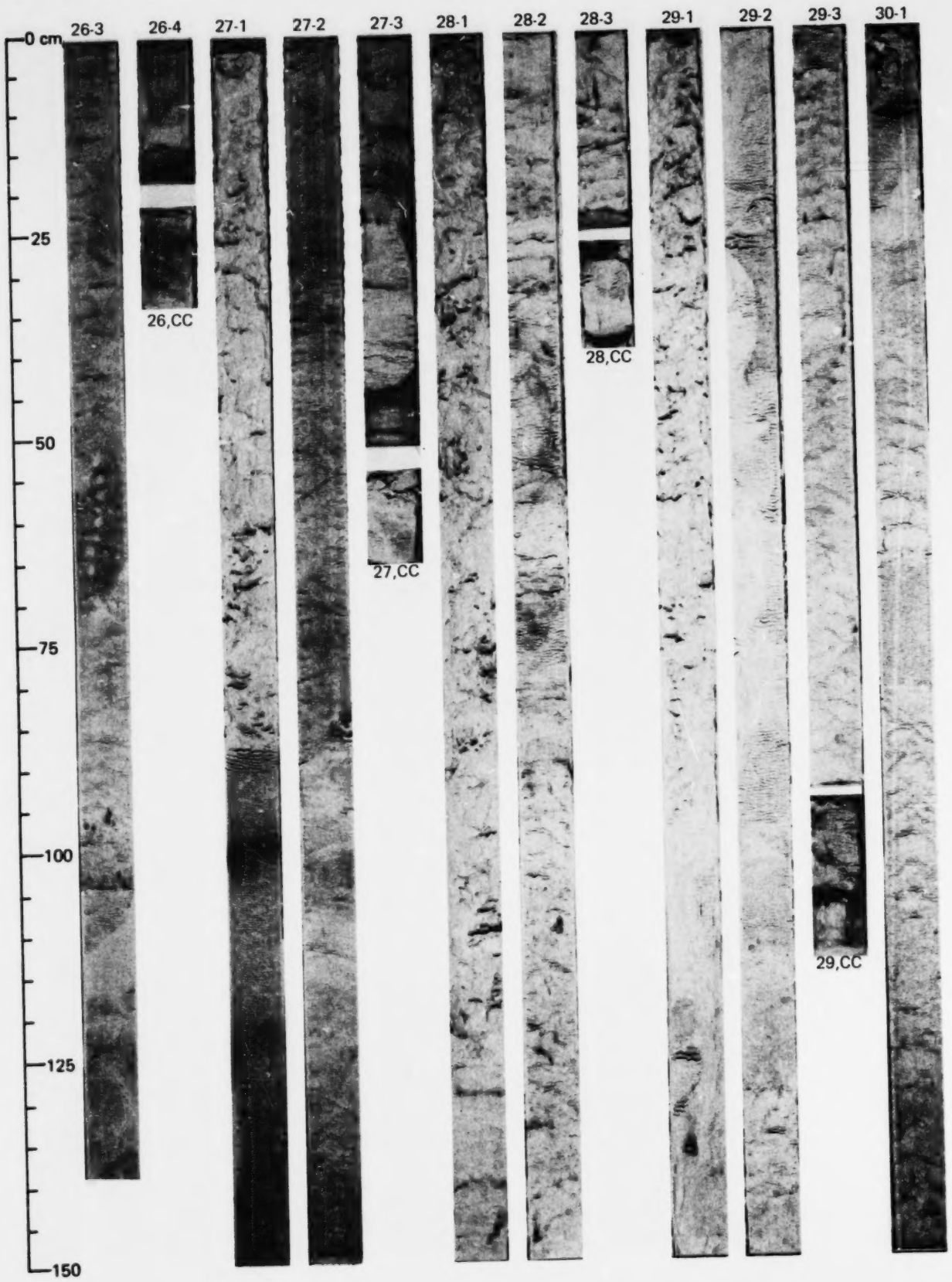
0 cm
25
50
75
100
125
150
26-3
26-4
26,CC
27-1
27-2
27-3
27,CC
28-1
28-2
28-3
28,CC
29-1
29-2
29-3
29,CC
30-1

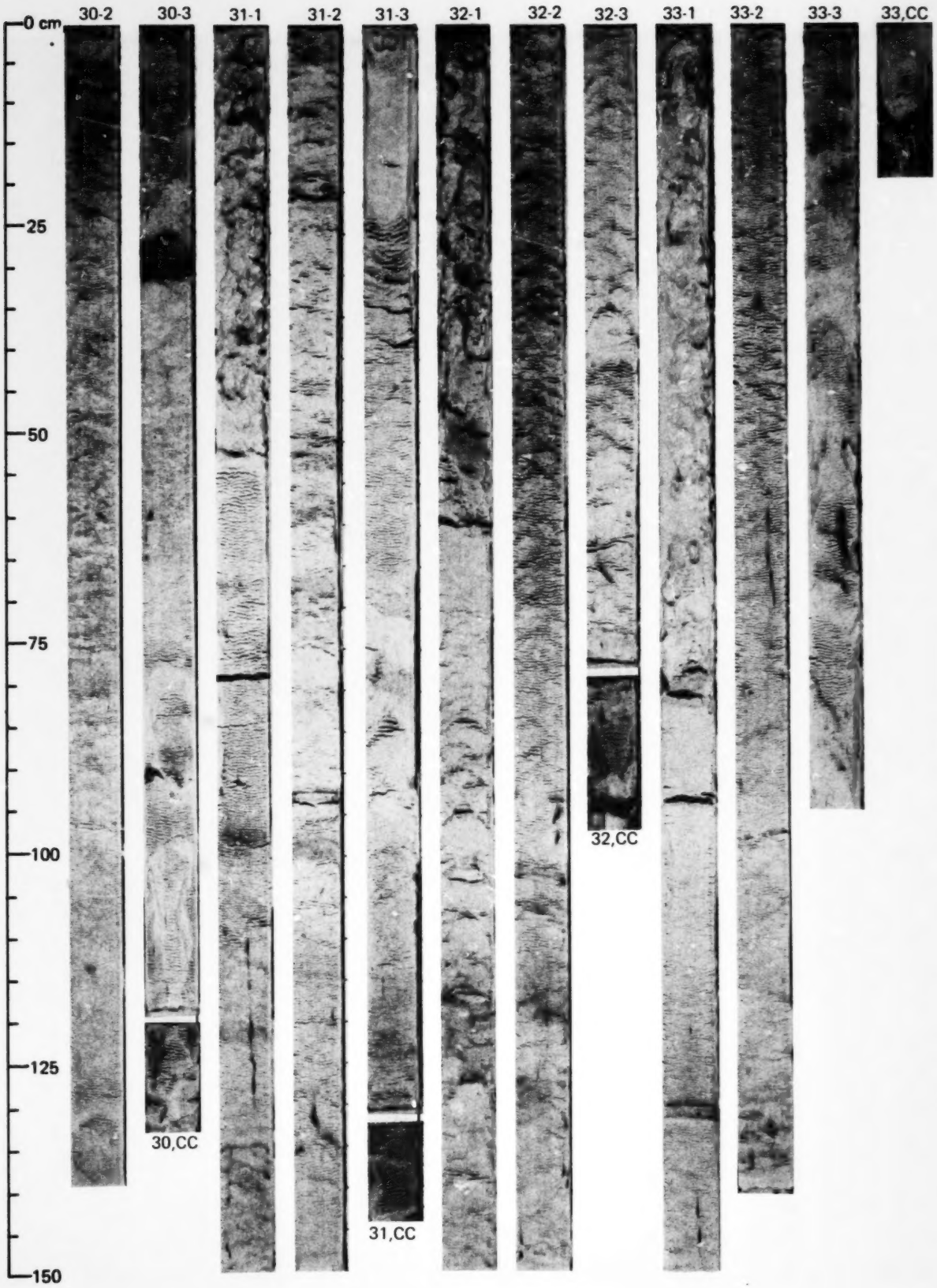
0 cm
25
50
75
100
125
150
30-2
30-3
30,CC
31-1
31-2
31-3
31,CC
32-1
32-2
32-3
32,CC
33-1
33-2
33-3
33,CC

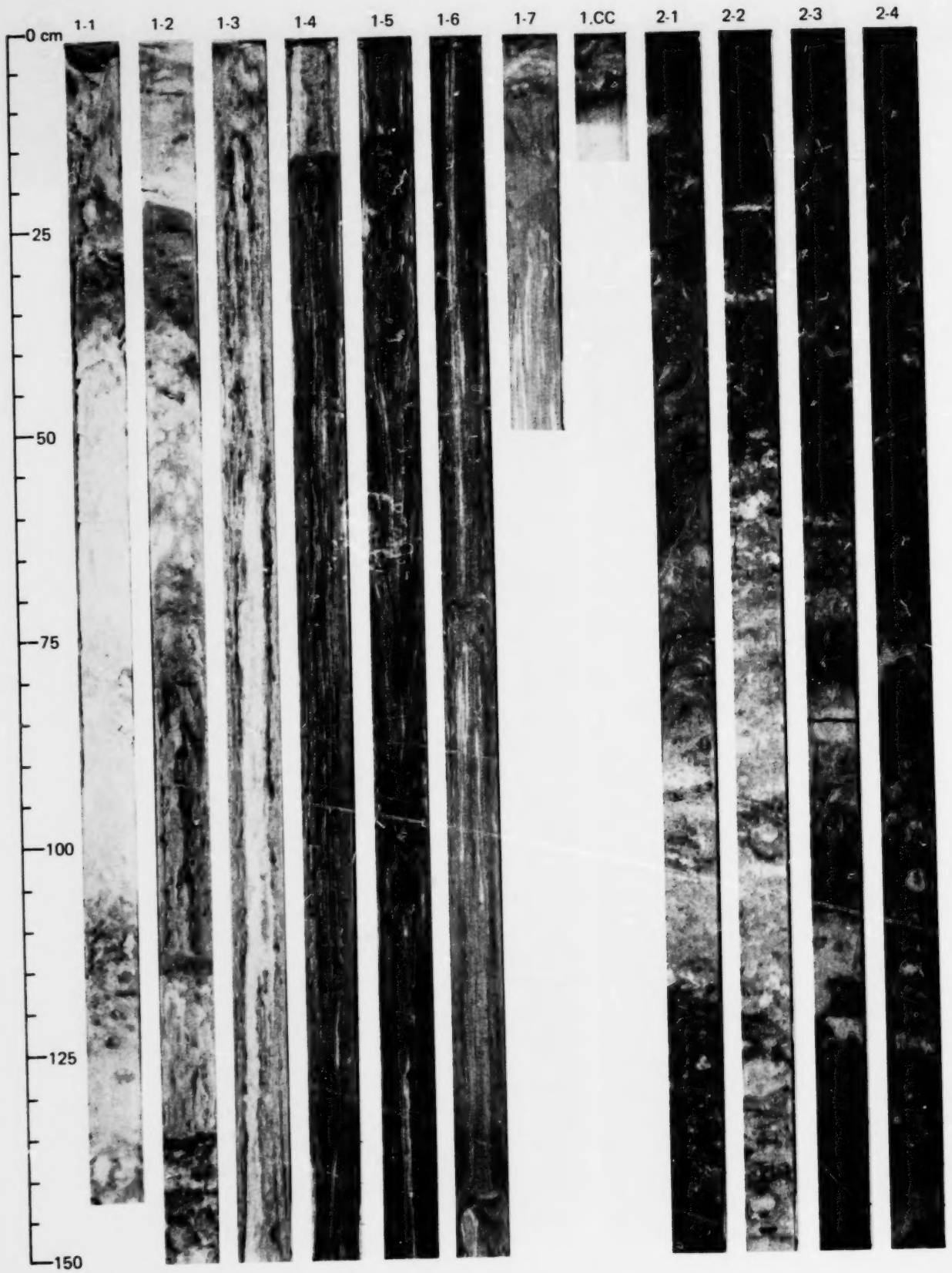
0 cm
25
50
75
100
125
150
1-1
1-2
1-3
1-4
1-5
1-6
1-7
1.CC
2-1
2-2
2-3
2-4

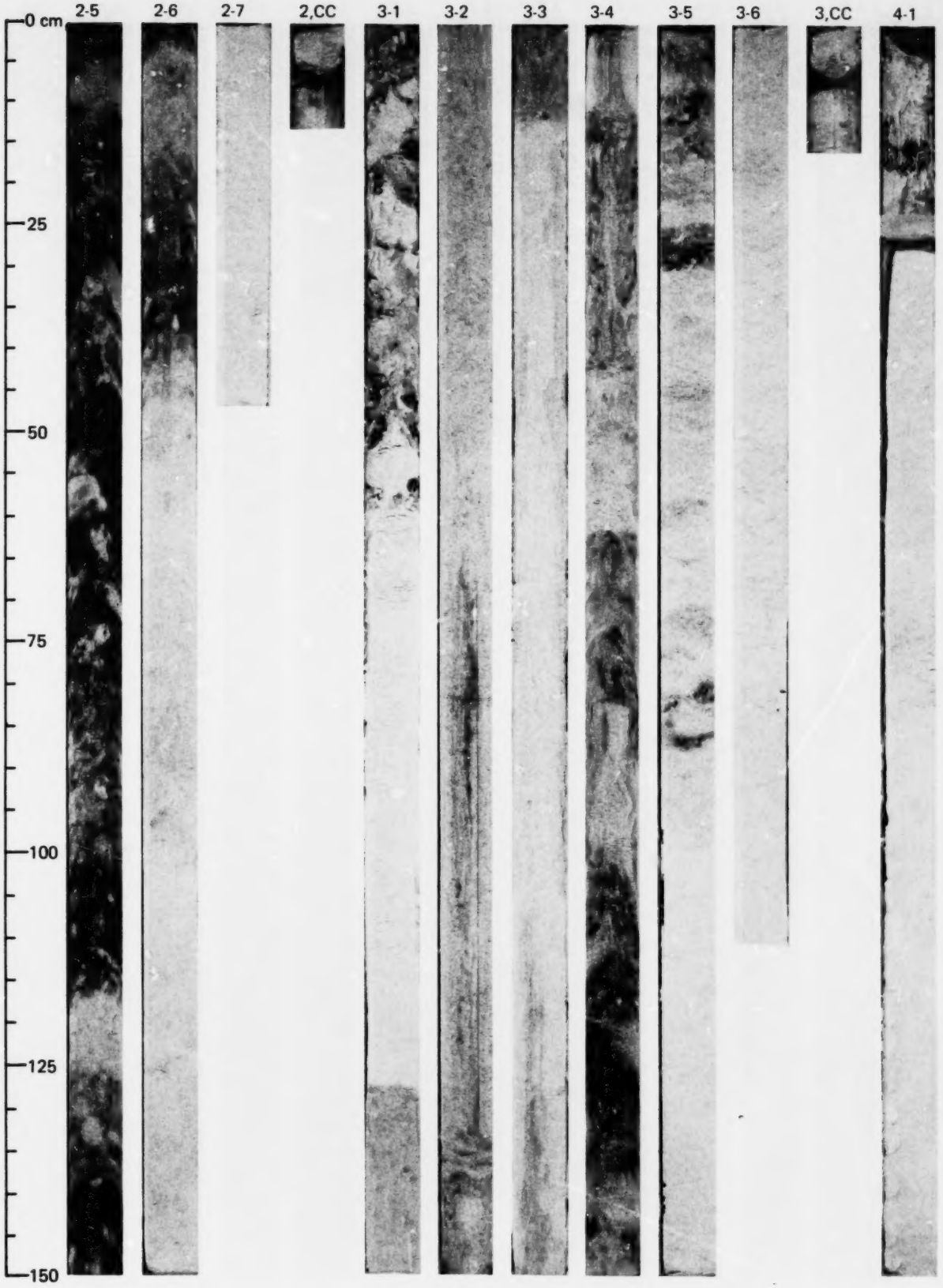
0 cm
25
50
75
100
125
150
2-5
2-6
2-7
2,CC
3-1
3-2
3-3
3-4
3-5
3-6
3,CC
4-1

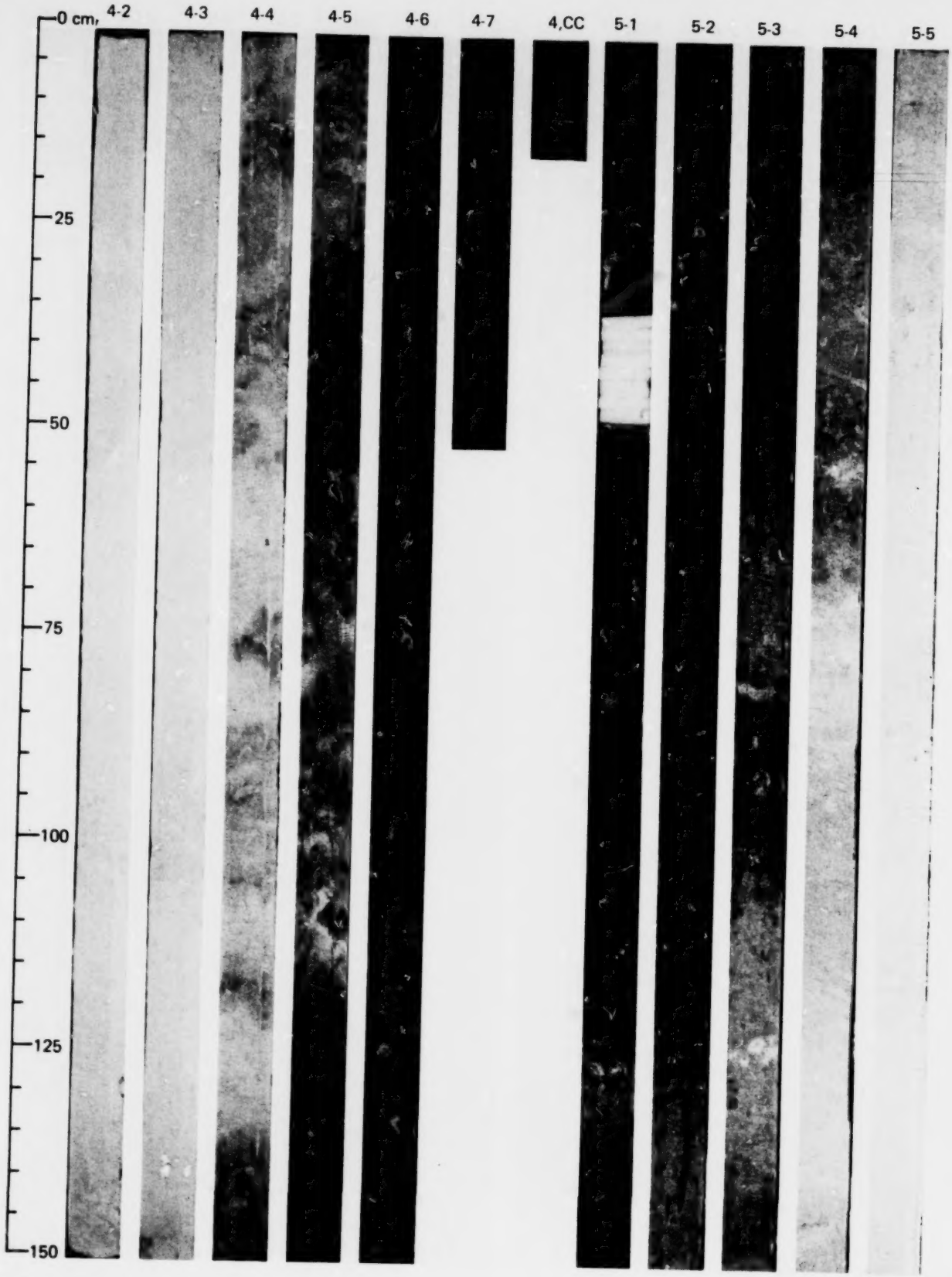
0 cm
25
50
75
100
125
150
4-2
4-3
4-4
4-5
4-6
4-7
4,CC
5-1
5-2
5-3
5-4
5-5

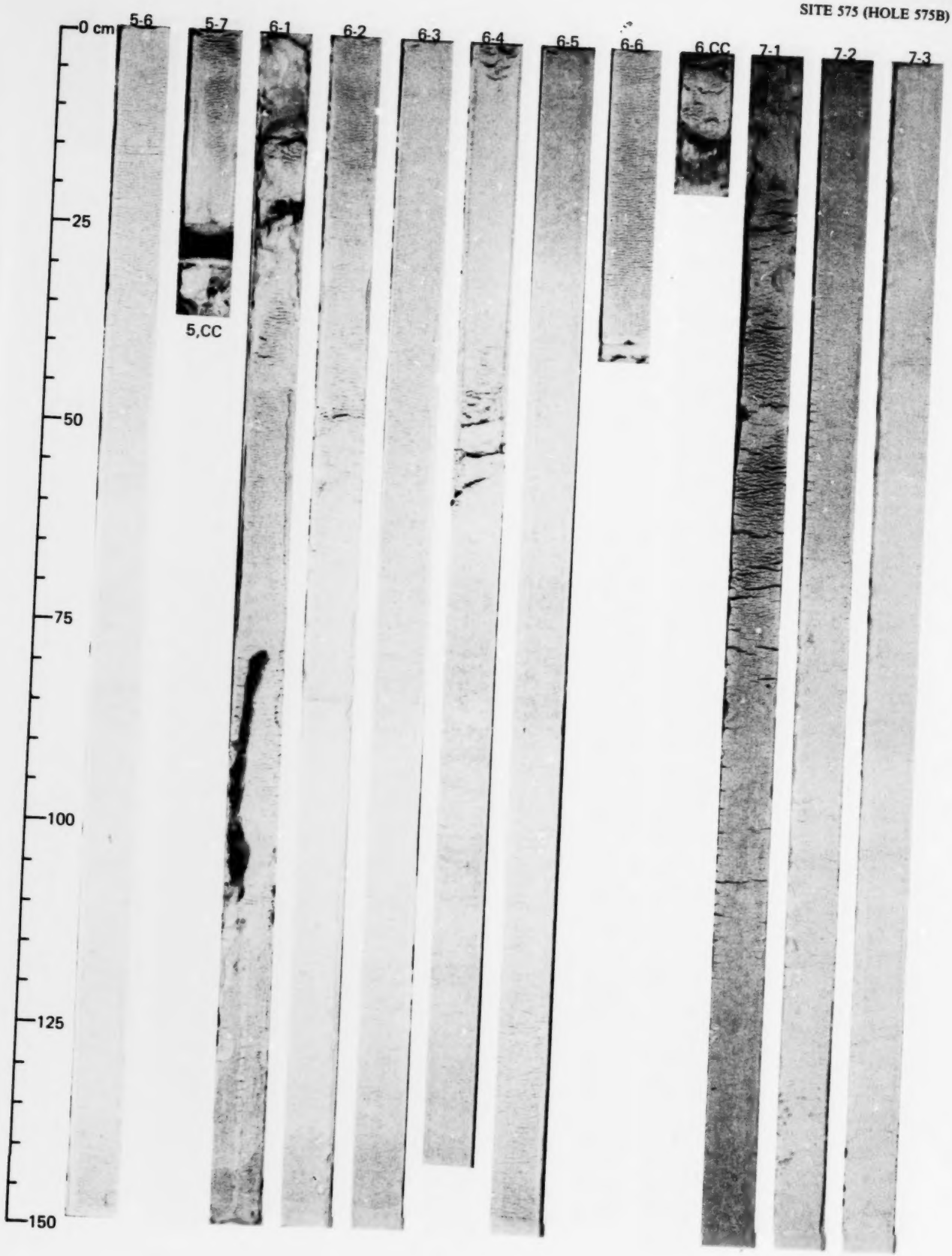
0 cm
25
50
75
100
125
150
5-6
5-7
5,CC
6-1
6-2
6-3
6-4
6-5
6-6
6,CC
7-1
7-2
7-3

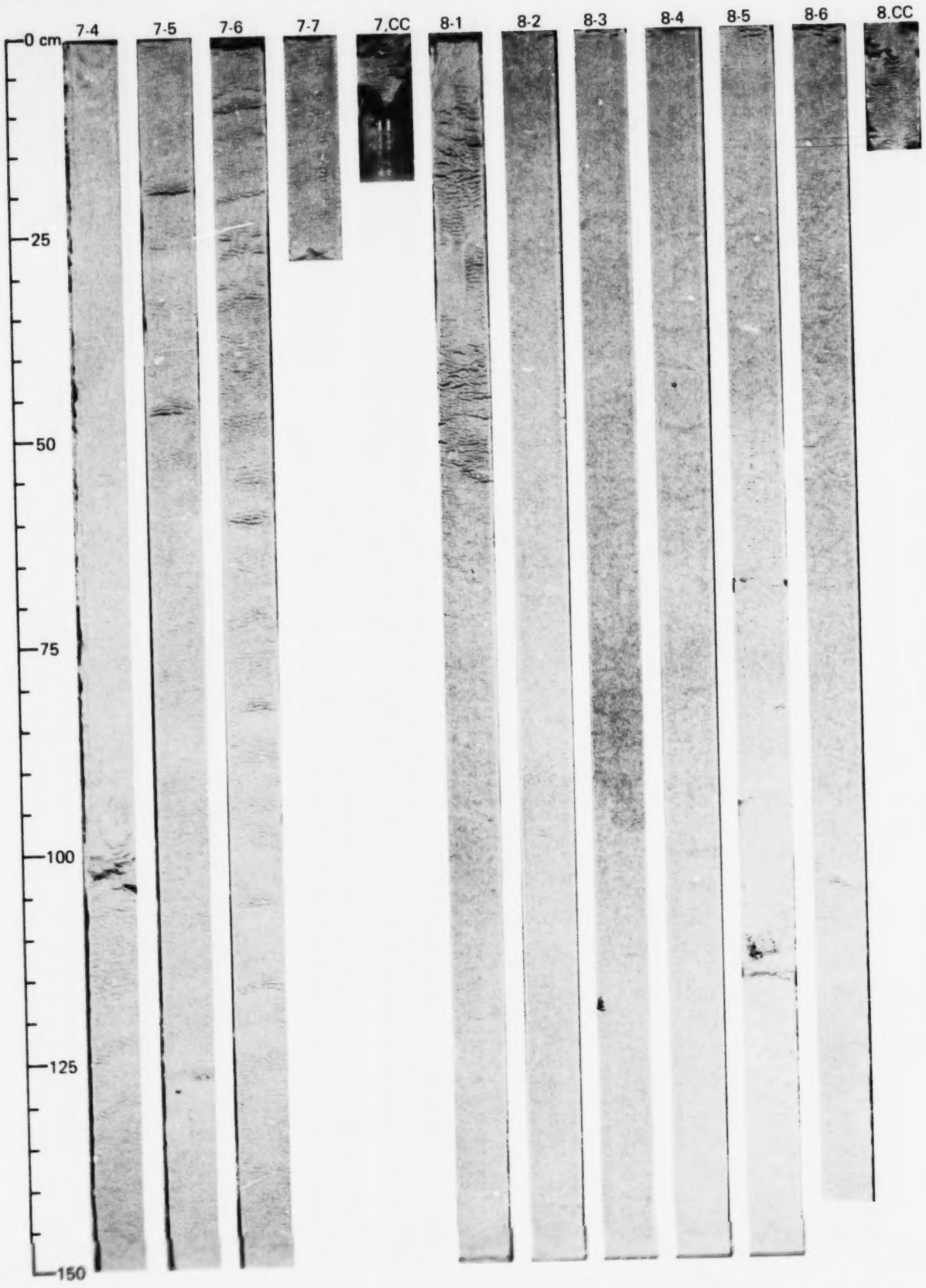
7-4
7-5
7-6
7-7
7,CC
8-1
8-2
8-3
8-4
8-5
8-6
8,CC
0 cm
25
50
75
100
125
150

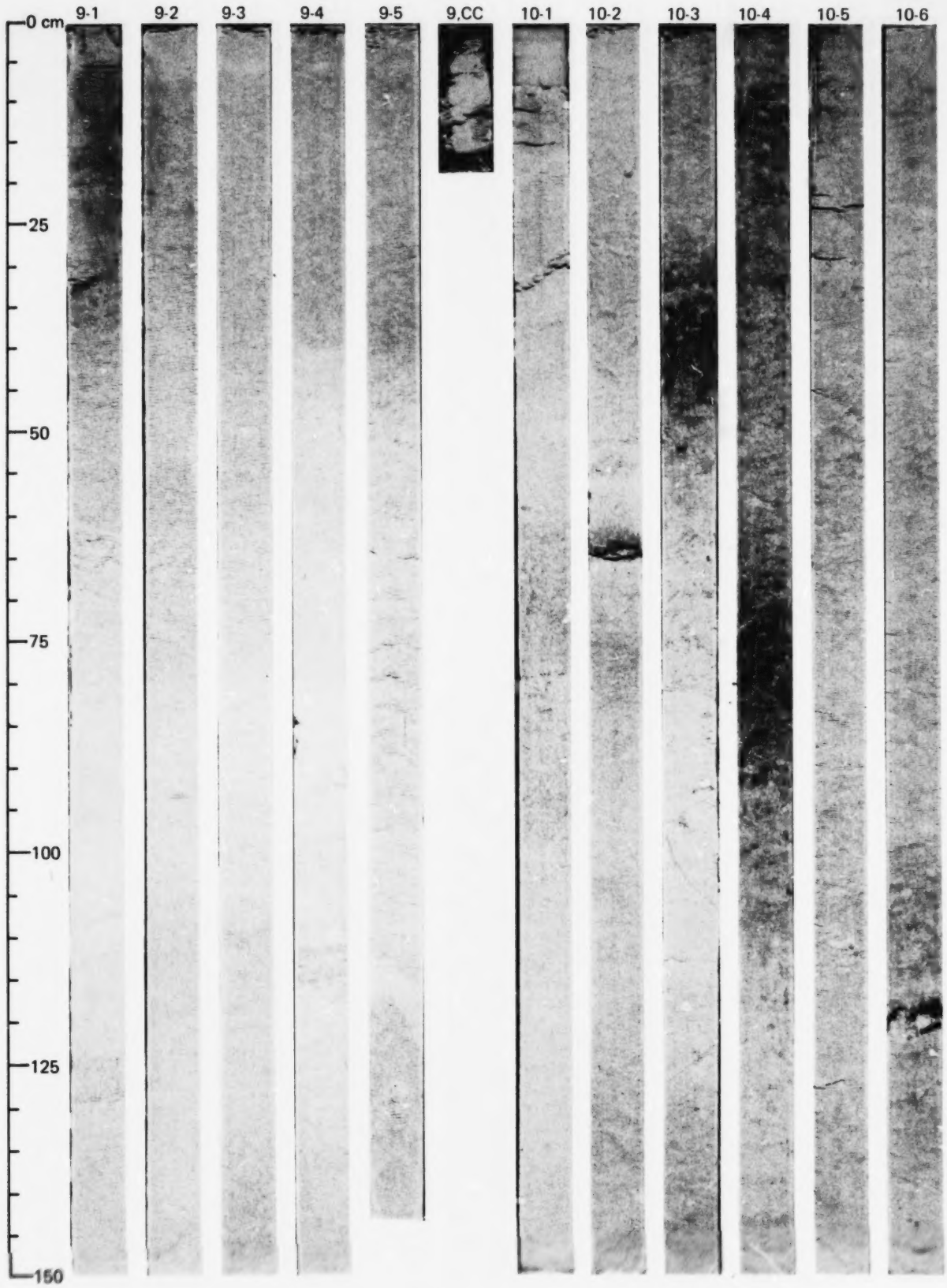
0 cm
25
50
75
100
125
150
9-1
9-2
9-3
9-4
9-5
9,CC
10-1
10-2
10-3
10-4
10-5
10-6

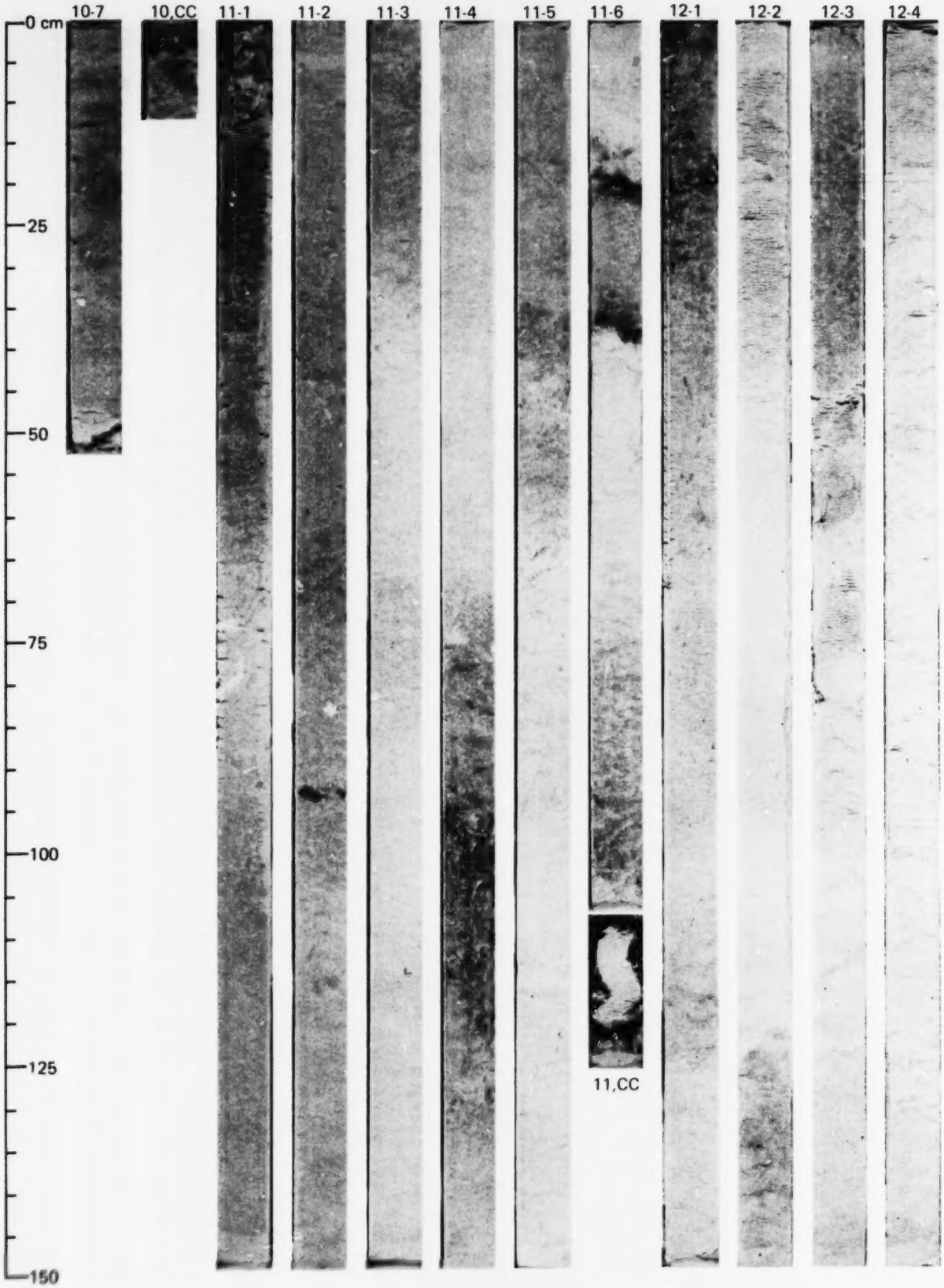
10-7
10,CC
11-1
11-2
11-3
11-4
11-5
11-6
12-1
12-2
12-3
12-4
0 cm
25
50
75
100
125
150
11,CC

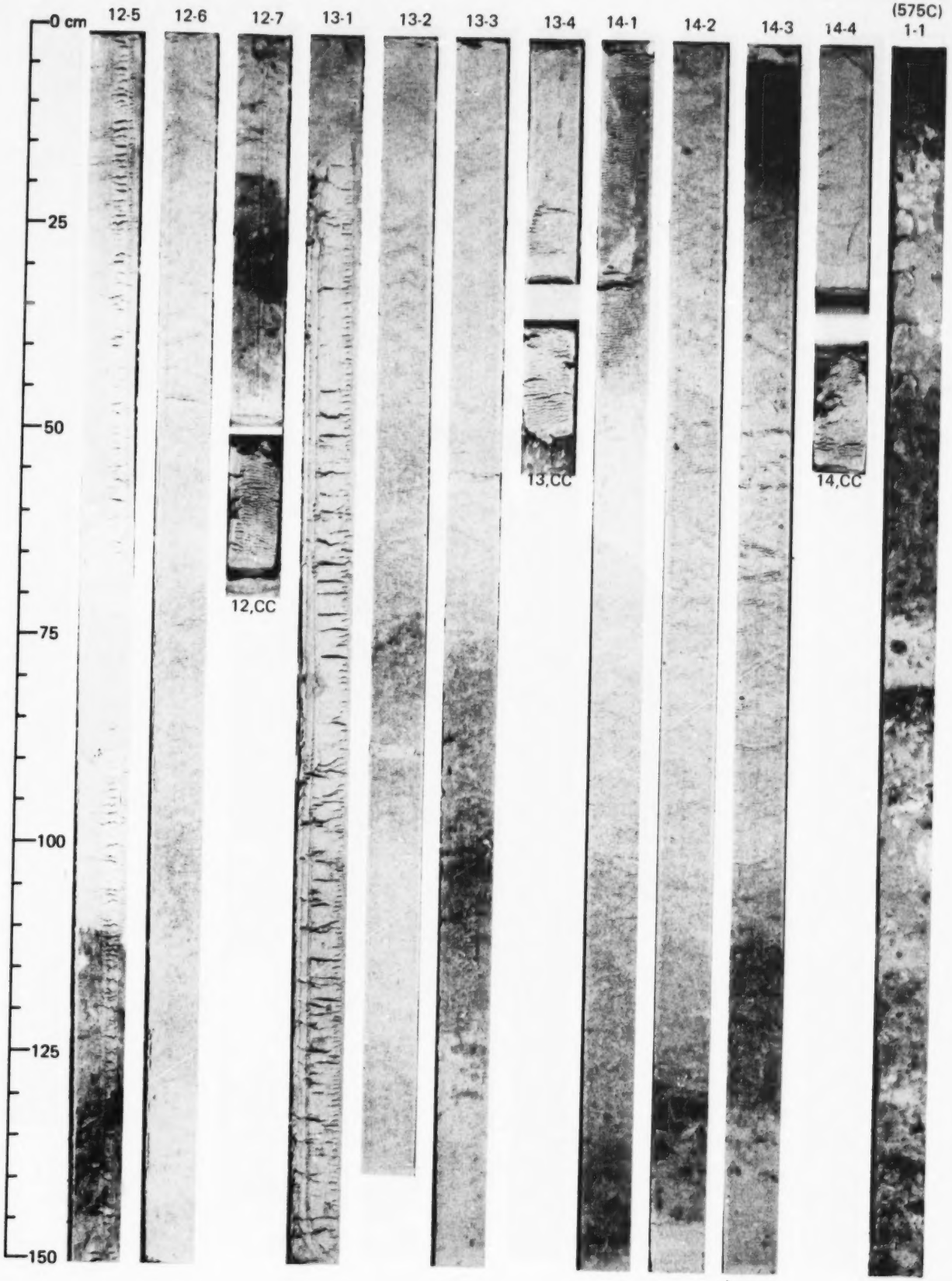
0 cm
25
50
75
100
125
150
12-5
12-6
12-7
13-1
13-2
13-3
13-4
14-1
14-2
14-3
14-4
(575C)
1-1
12,CC
13,CC
14,CC

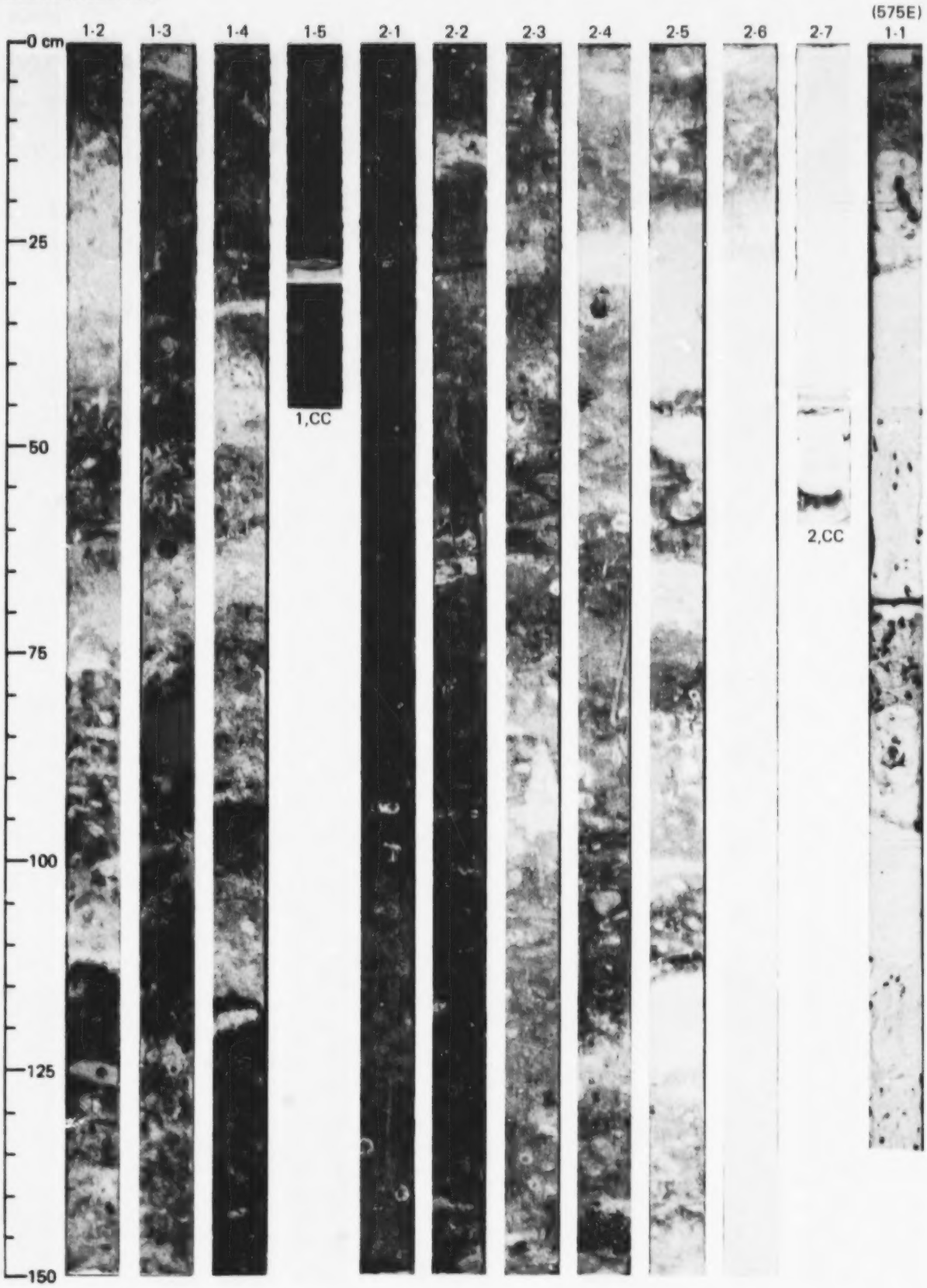
(575E)
1-1
1-2
1-3
1-4
1-5
2-1
2-2
2-3
2-4
2-5
2-6
2-7
0 cm
25
50
75
100
125
150
1,CC
2,CC

PART II: PALEONTOLOGY AND BIOSTRATIGRAPHY

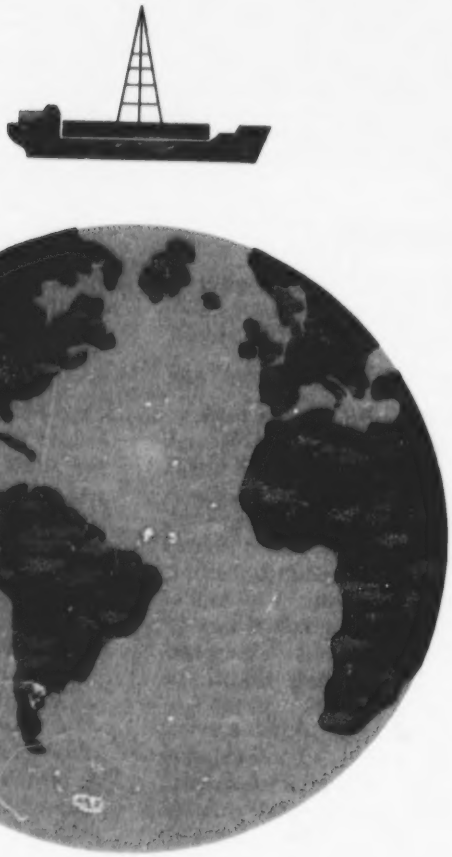

Reprinted from Mayer, L., Theyer, F., et al., 1985
Initial Reports of the Deep Sea Drilling Project, Volume LXXXV, Washington (U. S. Government Printing Office)

7. NEOGENE AND QUATERNARY DINOFLAGELLATE BIOSTRATIGRAPHY OF THE EASTERN EQUATORIAL PACIFIC: DEEP SEA DRILLING PROJECT LEG 85[1]

Ian Jarvis and Bruce A. Tocher, Department of Geology, City of London Polytechnic[2]

ABSTRACT

Samples from DSDP Leg 85 Sites 572–575 in the central equatorial Pacific were analyzed for palynomorph content; only those from Site 572 consistently yielded assemblages of Neogene–Quaternary dinoflagellate cysts. These assemblages are described and compared with coeval material from elsewhere in the world. Several of the 15 species identified are stratigraphically restricted, and comparison with published ranges suggests that they may provide worldwide stratigraphic indices. *Nematosphaeropsis labyrinthea* (Ostenfeld) Reid and identified species of the genus *Impagidinium* range from middle Miocene to Quaternary. *Palaeocystodinium golzowense* Alberti disappears in the middle Miocene and *Pyxidiella simplex* Harland is restricted to the basal upper Miocene. *Operculodinium* cf. *israelianum* Wall and *Spiniferites bentorii truncatus* (Rossignol) Lentin and Williams are Quaternary species. An increased abundance of dinoflagellate cysts in the uppermost Miocene at Site 572 is associated with the common occurrence of the diatom genera *Thalassionema* and *Thalassiothrix*, which are regarded as indicators of upwelling. The higher concentration of dinoflagellate cysts in this interval is related to the location of the site below the equatorial high productivity belt at a time of enhanced local upwelling in the eastern equatorial Pacific.

INTRODUCTION

One of the primary aims of DSDP Leg 85 was to recover undisturbed Neogene–Quaternary sediments in the central equatorial Pacific for detailed biostratigraphic analysis. This was accomplished using the newly developed hydraulic piston corer.

Previous attempts at recovering dinoflagellate cysts from equatorial Pacific sediments have proven unsuccessful (T. Saito, personal communication, 1982). We have processed 101 samples from Sites 572–575 of Leg 85 for biostratigraphic analysis using standard palynological techniques (Neves and Dale, 1963; Doher, 1980). The majority of samples (92%) from the central equatorial Pacific (Sites 573–575) were barren. However, all five holes drilled at Site 572, located at the eastern edge of the equatorial sediment bulge (Fig. 1), yielded assemblages of Neogene–Quaternary dinoflagellate cysts (only 7% barren). Spores and pollen were absent throughout. Biozonal correlations produced by shipboard paleontologists that were based on foraminifers, nannofossils, radiolarians and diatoms have been related (Barron et al., this volume) to the established magnetostratigraphy and chronostratigraphy of the central Pacific. This integrated stratigraphic framework was used to provide age assignments for the palynomorph assemblages recovered. Sample locations at Site 572 are plotted stratigraphically in Figure 2, and the positions of productive samples are listed in Tables 1 and 2.

BIOSTRATIGRAPHY

Fifteen species of dinoflagellate cysts have been identified in the present study (Fig. 2). The main species are figured in Plate 1.

Site 572

Most samples from Site 572 (Fig. 2; Table 1) contain *Impagidinium patulum* (Wall) Stover and Evitt, *I. sphaericum* (Wall) Lentin and Williams, and *Nematosphaeropsis labyrinthea* (Ostenfeld) Reid. Two further species of *Impagidinium* appear within the succession. *I. paradoxum* (Wall) Stover and Evitt occurs near the top of the middle Miocene (318 m sub-bottom depth) and ranges into the Pleistocene, whereas *I. aculeatum* (Wall) Lentin and Williams occurs only in the upper Pliocene and Pleistocene (above 50 m). Other genera have more restricted distributions.

Palaeocystodinium golzowense Alberti and *Spiniferites pseudofurcatus* (Klumpp) Sarjeant occur only in the middle Miocene (423 and 319 m, respectively). *Pyxidiella simplex* Harland is restricted to the base of the upper Miocene (262 m), and *Operculodinium centrocarpum* (Deflandre and Cookson) Wall and *Tectatodinium* occur in the Miocene and Pliocene. *Impagidinium* sp. A, *Operculodinium* cf. *israelianum* (Rossignol) Wall, *Spiniferites bentorii truncatus* (Rossignol) Lentin and Williams, and *S.* sp. A occur only in Pleistocene samples (above 5 m).

Other Sites

Impagidinium patulum, *I. paradoxum*, and *Nematosphaeropsis labyrinthea* occur rarely in the upper Miocene and lower Pliocene at Sites 573 and 574 (Table 2). A single specimen of *Spiniferites pseudofurcatus* was recorded from the lower Oligocene at Site 574.

[1] Mayer, L., Theyer, F., et al., *Init. Repts. DSDP*, 85: Washington (U.S. Govt. Printing Office).

[2] Addresses: Department of Geology, City of London Polytechnic, Walburgh House, Bigland Street, London E1 2NG, UK; (Jarvis, present address) Department of Geology, Kingston Polytechnic, Penrhyn Rd., Kingston-upon-Thames, Surrey KT1 2EE, United Kingdom; (Tocher, present address) Department of Environmental Sciences, Plymouth Polytechnic, Plymouth, Devon PL4 8AA, United Kingdom.

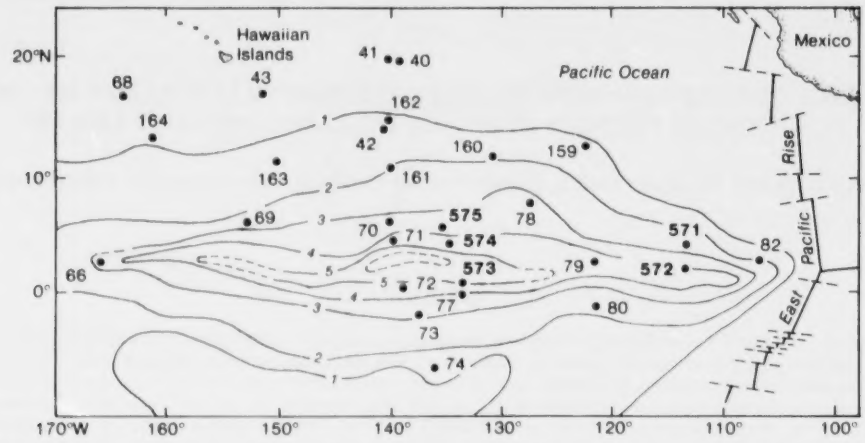

Figure 1. Location map of DSDP Site 572. Positions of other DSDP drill sites in the central Pacific are shown. Contours are in tenths of seconds of two-way traveltime.

DISCUSSION

The biostratigraphy and paleogeographical range of Neogene and Quaternary dinoflagellate cysts are still poorly known. Pioneering work on Quaternary species by Rossignol (1962, 1964, 1969) in the eastern Mediterranean, and by Wall (1967, 1970) in the Caribbean and western Europe, has been augmented by studies on the Neogene and Quaternary palynology of the Black Sea and the North Atlantic, particularly offshore eastern Canada (see Reid and Harland, 1977; Williams and Bujak, 1977; Harland, 1978, for reviews). We know of no comparable data from the equatorial Pacific, although Neogene and Quaternary dinoflagellates have been recorded in DSDP samples from off the coasts of southern California (Ballog and Malloy, 1981), Mexico (Fournier, 1982), and Peru (Wiseman, 1976).

Dinoflagellate Ranges and Zones

There is no formal dinoflagellate cyst zonation for the Neogene and Quaternary, although Williams (1975, 1979), Williams and Brideaux (1975), Gradstein and Williams (1976), and Williams and Bujak (1977) have developed an informal scheme based primarily on material from offshore eastern Canada. Other informal schemes have been proposed by Manum (1976) for the Tertiary of the Norwegian-Greenland Sea, by Harland (1978, 1979) for the Neogene and Quaternary of the Bay of Biscay, by Costa and Downie (1979) for the Cenozoic of the Rockall Plateau, and by Piasecki (1980) for the Miocene of Denmark. Our floras correspond most closely to those from the Bay of Biscay (Harland, 1979) but are less diverse.

Palaeocystodinium golzowense was recovered solely from the middle Miocene at Site 572, which supports records (Alberti, 1961; Williams and Bujak, 1977; Williams, 1979; Harland, 1979) suggesting that the species became extinct in the middle Miocene. *Pyxidiella simplex* occurs only in the basal upper Miocene, confirming data from the Bay of Biscay (Harland, 1979) that indicate that this species is restricted to that stratigraphic level. *Operculodinium centrocarpum* also only occurs in the Miocene at Site 572, but the species is a common constituent of Quaternary pelagic sediments in many areas (Wall, 1967; Wiseman, 1976; Reid and Harland, 1977) and certainly ranges back to the Eocene (Williams and Bujak, 1977; Williams, 1979). *Nematosphaeropsis labyrinthea* and three species of *Impagidinium (I. paradoxum, I. patulum,* and *I. sphaericum)* range from middle Miocene to Quaternary at Site 572, although *I. paradoxum* appears above the base of the succession. *I. aculeatum,* on the other hand, occurs only in the upper Pliocene and Quaternary. *N. labyrinthea* and *I. patulum* are known to range down into the upper Eocene in the eastern Atlantic (Williams, 1979; Costa and Downie, 1979), but *I. paradoxum* and *I. aculeatum* first appear in the middle Miocene (Stover and Evitt, 1978; Williams, 1979; Costa and Downie, 1979; Harland, 1978, 1979). We record *Spiniferites pseudofurcatus* from the middle Miocene at Site 572 and the lower Oligocene at Site 574 (Table 2), but the species is known to extend into the Eocene (Klumpp, 1953; Sarjeant, 1970; Williams and Bujak, 1977; Williams, 1979). *O.* cf. *israelianum* and *S. bentorii truncatus* occur only in the youngest sediment at Site 572, conforming with a Pleistocene age for these species (Rossignol, 1962, 1964; Wall, 1967; Wiseman, 1976), although a comparable form of *O. israelianum* is recorded as ranging down into the lower Eocene (Williams and Bujak, 1977; Williams, 1979).

Abundance and Diversity

The small number of species recorded here from the Neogene and Quaternary of the eastern equatorial Pacific is similar to the low diversity displayed by coeval pelagic assemblages from the Atlantic (Williams and Bujak, 1977; Williams, 1979; Harland, 1979) and off the Peruvian coast (Wiseman, 1976). The common occurrence of *Impagidinium aculeatum, I. paradoxum, I. patulum,* and *Nematosphaeropsis labyrinthea* supports the widely held view that these are tropical to temperate deep oceanic species (Reid and Harland, 1977; Wall et al., 1977; Harland, 1978, 1979).

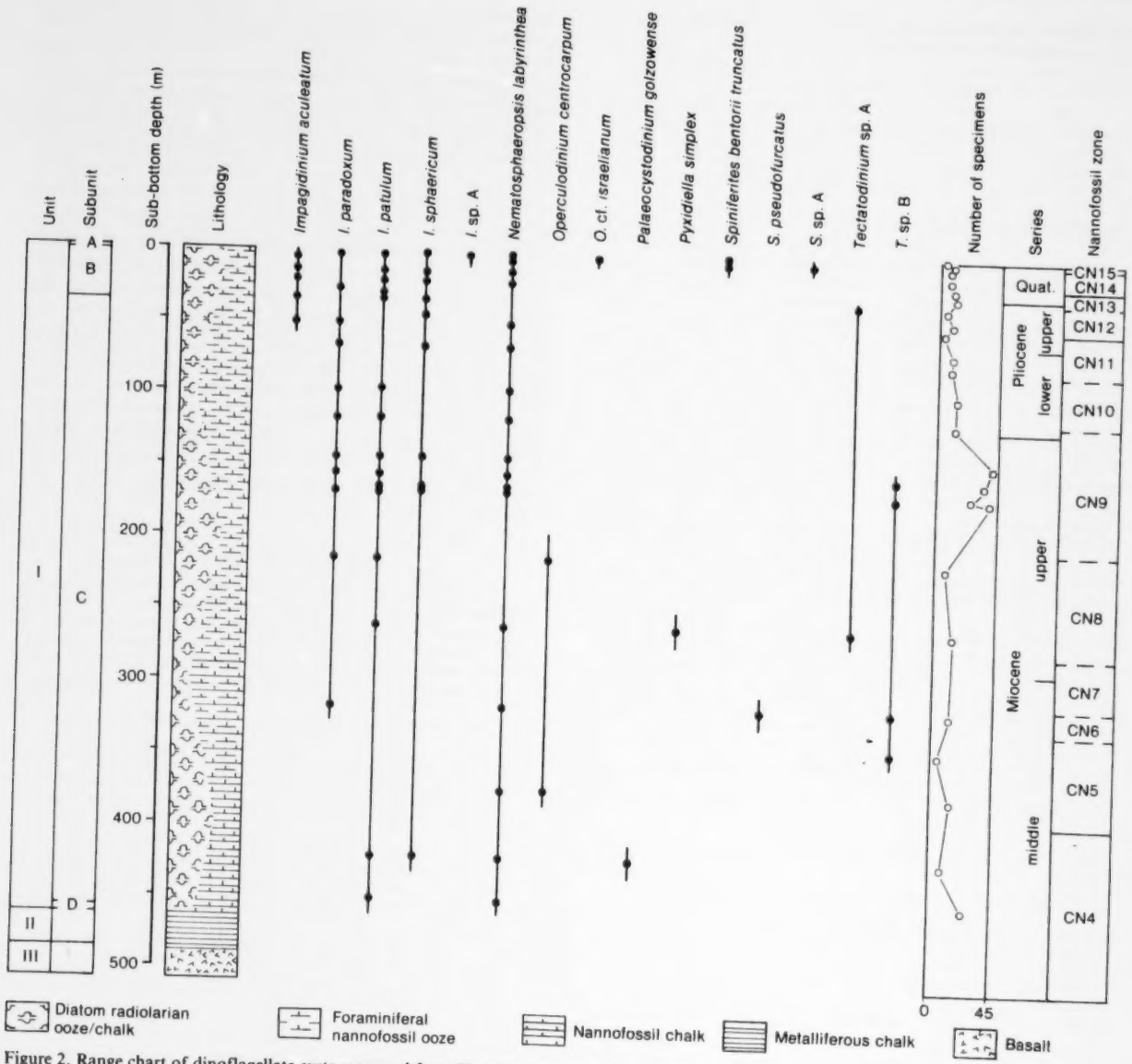

Figure 2. Range chart of dinoflagellate cysts recovered from Site 572. Lithostratigraphic units (left) are those distinguished by Leg 85 sedimentologists. Unit I (0–454.5 m): cyclic siliceous calcareous ooze/chalk; Subunit A, gray brown ooze; Subunit B, varicolored ooze; Subunit C, green varicolored ooze; Subunit D, yellow chalk. Unit II (464.5–?479.5 m): metalliferous chalk. Unit III (479.5–489.0 m): basalt. Chronostratigraphic subdivisions (right) are based on age assignments made by shipboard paleontologists using nannofossils, foraminifers, diatoms, and radiolarians. The nannofossil zonation is based on Pujos (this volume). Dinoflagellate cyst abundance can be gauged from the graph (○——○), which shows the number of specimens recovered from each 20 g sample of dry sediment.

Uppermost Miocene sediment (140–170 m sub-bottom depth) at Site 572 yielded larger numbers of dinoflagellate cysts than samples from other parts of the succession (Fig. 2), but there is no increase in diversity associated with this acme. The latest Miocene falls within a broader period (late Miocene to early Pliocene, 7.8–4.0 Ma) characterized at Site 572 by high sedimentation rates and the deposition of sediments with low carbonate contents (Pisias and Prell, this volume). These resulted primarily from high productivity as the site passed through the equator. The deposition of siliceous oozes resulted from the high proportion of siliceous microplankton and the apparently diagenetic dissolution of carbonate, which is indicated by the poor preservation of foraminifers and calcareous nannofossils. Dissolution was probably a consequence of the enhanced preservation of organic matter that resulted from the increased flux of biogenic debris to the seafloor. An increased input of organic matter is supported by the abundance of dinoflagellates. Subsequent oxidation of organic material during early diagenesis caused the dissolution of carbonate.

Table 1. Samples from Site 572 (27 samples, 2 barren) examined for dinoflagellate cysts.

Hole	Section (interval in cm)	Sub-bottom depth (m)	Age
Hole 572	1-1, 115-135	1.15-1.35	Quaternary
	1-2, 100-120	2.50-2.70	Quaternary
	1-3, 100-120	4.00-4.20	Quaternary
Hole 572A	1-1, 0-20	0.00-0.20	Quaternary
	1-4, 50-70	5.00-5.20	Quaternary
	2-1, 0-20[a]	9.50-9.70	Quaternary
	3-2, 115-135	21.65-21.85	Quaternary
	4-4, 95-115	34.05-34.25	up. Pliocene
	6-3, 85-105	49.75-49.95	up. Pliocene
	9-3, 85-105[a]	76.15-76.35	low. Pliocene
	13-5, 85-105	116.75-116.95	low. Pliocene
Hole 572B	2-3, 123-143	163.53-163.73	up. Miocene
Hole 572C	2-2, 144-150	13.04-13.10	Quaternary
	3-5, 144-150	27.14-27.20	Quaternary
	5-5, 144-150	46.34-46.40	up. Pliocene
	7-5, 144-150	65.54-65.60	low. Pliocene
	10-5, 144-150	97.34-97.40	low. Pliocene
	17-3, 144-150	144.74-144.80	up. Miocene
Hole 573D	1-3, 144-150	155.44-155.50	up. Miocene
	2-5, 144-150	167.94-168.00	up. Miocene
	7-5, 144-150	215.44-215.50	up. Miocene
	12-4, 144-150	261.44-261.50	up. Miocene
	18-4, 144-150	318.44-318.50	mid. Miocene
	21-4, 144-150	345.94-346.00	mid. Miocene
	24-5, 144-150	376.94-377.00	mid. Miocene
	29-4, 140-150	422.90-423.00	mid. Miocene
	32-4, 140-150	453.40-453.50	mid. Miocene

Note: Age assignments are based on nannofossil, foraminifer, radiolarian, and diatom determinations made by shipboard paleontologists. No *a priori* assumptions were made concerning the stratigraphic ranges of dinoflagellate cyst species. Species records are given in Figure 2.

[a] Barren sample.

Table 2. Samples from DSDP Sites 573-575 yielding dinoflagellate cysts.

Site/Hole	Section (interval in cm)	Sub-bottom depth (m)	Age	Species
Site 573 (28 samples processed, 24 barren)				
Hole 573	9-5, 140-150	74.10-74.20	low. Pliocene	*I. paradoxum* (1)
	12-5, 140-150	102.60-102.70	up. Miocene	*I. paradoxum* (1) *I. patulum* (2) *N. labyrinthea* (5)
	16-5, 140-150	137.70-137.80	up. Miocene	*I. paradoxum* (4) *N. labyrinthea* (1)
Hole 573A	6-4, 143-150	55.13-55.20	low. Pliocene	*I. paradoxum* (1) *I. patulum* (2)
Site 574 (29 samples processed, 27 barren)				
Hole 574A	7-4, 144-150	51.84-51.90	up. Miocene	*N. labyrinthea* (1)
Hole 574C	29-1, 135-150	461.85-462.00	low. Oligocene	*S. pseudofurcatus* (1)
Site 575 (17 samples processed, all barren)				

Note: Age assignments as in Table 1. Samples were identical to those used for pore-water analysis; see Stout (this volume) for further details of barren intervals. Number of specimens recovered are indicated in parentheses after each species.

The concentration of dinoflagellate cysts in Site 572 sediments cannot be related simply to the equatorial location of the site, since other Leg 85 sites yielded few dinoflagellates. Site 572 is unique among the sites examined, however, in having siliceous intervals characterized by sediments composed almost entirely of diatom species (particularly species of *Thalassionema* and *Thalassiothrix*), which are regarded as indicators of deep-water productivity and upwelling (Hasle, 1960; Hasle and de Mendiola, 1967; Bukry and Foster, 1973; Sancetta, 1982, 1983). Sediments of this type were deposited at Site 572 (Barron, this volume) during the late Miocene–early Pliocene (7.8–4.0 Ma) when the site crossed the equator and in the middle Miocene (13.0–11.8 Ma), which was an interval of high biogenic silica accumulation throughout the equatorial Pacific (Leinen, 1979). The occurrence of upwelling diatom assemblages has been related to periods of expanded Antarctic glaciation causing increased gyral circulation and increased upwelling throughout the eastern equatorial Pacific (Keller et al., 1982). We suggest, therefore, that Site 572 falls geographically in a broad area favorable to dinoflagellate productivity, but that during the latest Miocene (a period of enhanced upwelling) when the site was located immediately below the equatorial high productivity belt, there was a significant increase in the flux of dinoflagellate cysts to the seafloor.

ACKNOWLEDGMENTS

This work was completed under the tenure of an Inner London Education Authority postdoctoral research fellowship to I. J. and an ILEA research assistantship to B. A. T. Critical review by the referees greatly improved the original manuscript. Facilities and financial support provided by the ILEA, the Natural Environmental Research Council, and City of London Polytechnic are gratefully acknowledged.

REFERENCES

Alberti, G., 1961. Zur Kenntnis mesozoischer und alttertiärar Dinoflagellaten und Hystrichosphaerideen von Nord- und Mitteldeutschland sowie einigen anderen Europäischen Gebieten. *Palaeontographica*, 116A:1-58.

Ballog, R. A., and Malloy, R. E., 1981. Neogene palynology from the southern California continental borderland, Site 467, Deep Sea Drilling Project Leg 63. *In* Yeats, R. S., Haq, B. U., et al., *Init. Repts. DSDP*, 63: Washington (U.S. Govt. Printing Office), 565-576.

Bukry, D., and Foster, J. H., 1973. Silicoflagellate and diatom stratigraphy, Leg 16, Deep Sea Drilling Project. *In* van Andel, T. H., Heath, G. R., et al., *Init. Repts. DSDP*, 16: Washington (U.S. Govt. Printing Office), 815-872.

Costa, L. I., and Downie, C., 1979. Cenozoic dinocyst stratigraphy of Sites 403 to 406 (Rockall Plateau), IPOD, Leg 48. *In* Montadert, L., Roberts, D. G., et al., *Init. Repts. DSDP*, 48: Washington (U.S. Govt. Printing Office), 513-529.

Doher, L. I., 1980. Palynomorph preparation procedures currently used in the paleontology and stratigraphy laboratories, U.S. Geological Survey. *U.S. Geol. Surv. Circ. 830.*

Fournier, G. R., 1982. Palynostratigraphic analysis of cores from Site 493, Deep Sea Drilling Project Leg 66. *In* Watkins, J. S., Moore, J. C., et al., *Init. Repts. DSDP*, 66: Washington (U.S. Govt. Printing Office), 661-670.

Gradstein, F. M., and Williams, G. L., 1976. Biostratigraphy of the Labrador Shelf, part 1. *Geol. Surv. Canada Open File*, 349:1-39.

Harland, R., 1978. Quaternary and Neogene dinoflagellate cysts. *In* Thusu, B. (Ed.), *Distribution of Biostratigraphically Diagnostic Dinoflagellate Cysts and Miospores from the Northwest European Continental Shelf and Adjacent Area.* Continental Shelf Inst. Publ., 100:7-17.

———, 1979. Dinoflagellate biostratigraphy of Neogene and Quaternary sediments at Holes 400/400A in the Bay of Biscay (Deep Sea Drilling Project Leg 48). *In* Montadert, L., Roberts, D. G., et al., *Init. Repts. DSDP*, 48: Washington (U.S. Govt. Printing Office), 531-545.

Hasle, G. R., 1960. Phytoplankton and ciliate species from the tropical Pacific. *Skr. Nor. Vidensk. Akad. Math. Naturvis. Kl. (Oslo)*, 2:1–50.

Hasle, G. R., and de Mendiola, B. R. E., 1967. Fine structure of some *Thalassionema* and *Thalassiothrix* species. *Phycology*, 6:107–125.

Keller, G., Barron, J. A., and Burckle, L. H., 1982. North Pacific late Miocene correlations using microfossils, stable isotopes, percentage $CaCO_3$, and magnetostratigraphy. *Mar. Micropaleontol.*, 7: 327–357.

Klumpp, B., 1953. Beitrag zur Kenntnis der Mikrofossilien des mittleren und oberen Eozän. *Palaeontographica*, 103A:377–406.

Leinen, M., 1979. Biogenic silica accumulation in the central equatorial Pacific and its implication for Cenozoic paleoceanography. *Geol. Soc. Am. Bull.*, 90:1310–1376.

Manum, S. B., 1976. Dinocysts in Tertiary Norwegian–Greenland Sea sediments (Deep Sea Drilling Project Leg 38), with observations on palynomorphs and palynodebris in relation to environment. *In* Talwani, M., Udintsev, G., et al., *Init. Repts. DSDP*, 38: Washington (U.S. Govt. Printing Office), 897–919.

Neves, R., and Dale, B., 1963. A modified filtration system for palynological preparations. *Nature (London)*, 198:775–776.

Piasecki, S., 1980. Dinoflagellate cyst stratigraphy of the Miocene Hodde and Gram Formations, Denmark. *Geol. Surv. Denmark Bull.*, 29:53–76.

Reid, P. C., and Harland, R., 1977. Studies of Quaternary dinoflagellate cysts from the North Atlantic. *Am. Assoc. Strat. Palynol. Contrib.*, 5A:147–165.

Rossignol, M., 1962. Analyse pollinique de sédiments marins Quaternaires en Israël II: sédiments Pleistocènes. *Pollen Spores*, 4:121–148.

———, 1964. Hystrichosphères du Quaternaire en Méditerranée orientale, dans les sédiments Pleistocènes et les boues marines actuelles. *Revue Micropaléont.*, 7:83–99.

———, 1969. Sédimentation palynologique dans le domaine marin Quaternaire de Palestine: étude de paléoenvironnement: notes et mémoires sur le Moyen-Orient. *Mus. Nat. Hist. Natur. Paris*, 10: 1–272.

Sancetta, C. A., 1982. Diatom biostratigraphy and paleoceanography, Deep Sea Drilling Project Leg 68. *In* Press, W. L., Gardner, J. V., et al., *Init. Repts. DSDP*, 68: Washington (U.S. Govt. Printing Office), 301–309.

———, 1983. Biostratigraphic and paleoceanographic events in the eastern equatorial Pacific: results of Deep Sea Drilling Project Leg 69. *In* Cann, J. R., Langseth, M. G., Honnorez, J., Von Herzen, R. P., White, S. M., et al., *Init. Repts. DSDP*, 69: Washington (U.S. Govt. Printing Office), 311–319.

Sarjeant, W. A. S., 1970. The genus *Spiniferites* Mantell, 1850 (Dinophyceae). *Grana*, 10:74–78.

Stover, L. E., and Evitt, W. R., 1978. Analyses of pre-Pleistocene organic-walled dinoflagellates. *Stanford Univ. Publ. Geol. Sci.*, 15: 1–300.

Wall, D., 1967. Fossil microplankton in deep-sea cores from the Caribbean Sea. *Palaeontology*, 10:95–123.

———, 1970. Quaternary dinoflagellate micropaleontology: 1959–1969. *Proc. North Am. Paleont. Convention*, G:844–866.

Wall, D., Dale, B., Lohmann, G. P., and Smith, W. K., 1977. The environmental and climatic distribution of dinoflagellate cysts in modern marine sediments from regions in the North and South Atlantic Oceans and adjacent seas. *Mar. Micropalaeontol.*, 2:121–200.

Williams, G. L., 1975. Dinoflagellate and spore stratigraphy of the Mesozoic–Cenozoic, offshore eastern Canada. *Geol. Surv. Canada Paper*, 74-30, 2:107–161.

———, 1979. Palynological biostratigraphy, Deep Sea Drilling Project Sites 367 and 370. *In* Supko, P. R., Perch-Nielsen, K., et al., *Init. Repts. DSDP*, Suppl. to Vols. 38, 39, 40, and 41: Washington (U.S. Govt. Printing Office), 783–815.

Williams, G. L., and Brideaux, W. W., 1975. Palynological analysis of late Mesozoic–Cenozoic rocks of the Grand Banks off Newfoundland. *Geol. Surv. Canada Bull.*, 263:1–162.

Williams, G. L., and Bujak, J. P., 1977. Cenozoic palynostratigraphy of offshore eastern Canada. *Am. Assoc. Strat. Palynol. Contrib.*, 5A:14–47.

Wiseman, J. F., 1976. Palynological investigation of samples from Holes 319, 320, 320A and Site 321 of DSDP Leg 34. *In* Yeats, R. S., Hart, S. R., et al., *Init. Repts. DSDP*, 34: Washington (U.S. Govt. Printing Office), 741–742.

Date of Initial Receipt: 3 October 1983
Date of Acceptance: 26 April 1984

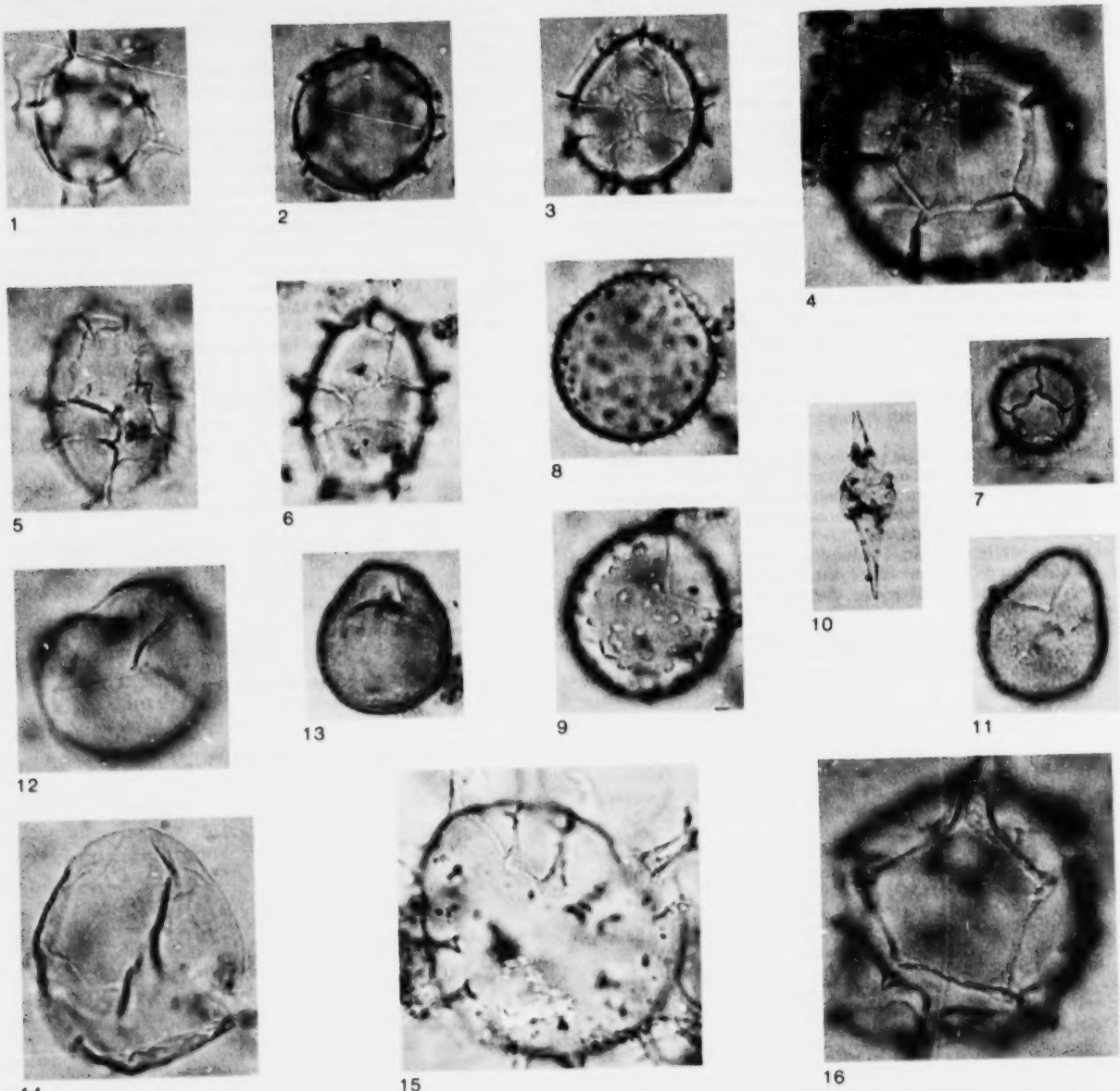

Plate 1. Dinoflagellate cysts from DSDP Site 572. (All figures magnified ×1000 unless otherwise indicated.) **1.** *Impagidinium aculeatum* (Wall) Lentin and Williams, Sample 572A-3-2, 115–135 cm, 21.65–21.85 m sub-bottom depth. **2–3.** *I. sphaericum* (Wall) Lentin and Williams, Sample 572C-2-2, 144–150 cm, 13.04–13.10 m. **4.** *I. patulum* (Wall) Stover and Evitt, Sample 572-1-3, 100–120 cm, 4.00–4.20 m. **5–6.** *I. paradoxum* (Wall) Stover and Evitt, Sample 572C-3-5, 144–150 cm, 27.14–27.10 m. **7.** *I.* sp. A, Sample 572-1-1, 115–135 cm, 1.15–1.35 m. **8–9.** *Operculodinium* cf. *israelianum* (Rossignol) Wall, Sample 572-1-1, 115–135 cm, 1.15–1.35 m. **10.** *Palaeocystodinium golzowense* Alberti, ×400, Sample 572D-29-4, 140–150 cm, 422.90–423,00 m. **11.** *Tectatodinium* sp. B, Sample 572D-12-4, 144–150 cm, 261.44–261.50 m. **12.** *T.* sp. A, Sample 572A-4-4, 95–115 cm, 34.05–34.25 m. **13.** *Pyxidiella simplex* Harland, Sample 572D-12-4, 144–150 cm, 261.44–261.50 m. **14.** Cyst (?*Protoperidinium*) sp. A, Sample 572C-5-5, 144–150 cm, 46.34–46.40 m. **15.** *Spiniferites* sp. A, Sample 572A-1-4, 50–70 cm, 5.00–5.20 m. **16.** *S. bentorii truncatus* (Rossignol) Wall and Dale, Sample 572A-1-4, 50–70 cm, 5.00–5.20 m.

Reprinted from Mayer, L., Theyer, F., et al., 1985
Initial Reports of the Deep Sea Drilling Project, Volume LXXXV, Washington (U.S. Government Printing Office)

8. LATE EOCENE TO HOLOCENE DIATOM BIOSTRATIGRAPHY OF THE EQUATORIAL PACIFIC OCEAN, DEEP SEA DRILLING PROJECT LEG 85[1]

John A. Barron, U.S. Geological Survey, Menlo Park[2]

ABSTRACT

Excellent reference sections for lower Oligocene through Holocene diatoms were recovered at DSDP Sites 572 to 575 in the central equatorial Pacific. Diatoms are generally common and well preserved at all sites, except in the upper Oligocene. These sections are zoned and correlated on the basis of diatoms, including the identification and correlation of 89 additional secondary datum levels in the Miocene and Pliocene. Paleomagnetic stratigraphy was obtained for the entire *Denticulopsis nicobarica* Zone (17.8 to 16.4 Ma) at Site 575, and upper lower Miocene diatom datum levels are correlated directly to paleomagnetic stratigraphy for the first time.

Quantitative diatom studies of upper lower Miocene to uppermost Miocene (18.0 to 6.2 Ma) of Sites 572, 574, and 575 are supplemented by quantitative diatom studies at Sites 77 and 158 to form transects across the central and eastern equatorial Pacific. Where the sampling interval is 100,000 yr. or less, quantitative trends in *Cestodiscus pulchellus, Coscinodiscus radiatus, Denticulopsis hustedtii, D. nicobarica*, and *Thalassiothrix longissima* are readily correlatable, thereby greatly enhancing biostratigraphic resolution. Comparison of species abundance reveals minor differences between the eastern and central equatorial Pacific. *Thalassionema nitzschioides, D. hustedtii*, and *D. nicobarica* show preferences for the eastern equatorial Pacific, whereas *C. pulchellus, Actinocyclus ellipticus, Coscinodiscus tuberculatus*, and *Nitzschia* spp. seem to prefer the central equatorial Pacific.

Five new diatom taxa are proposed: *Actinocyclus ellipticus* var. *spiralis* Barron, n. var., *Coscinodiscus lewisianus* var. *rhomboides* Barron, n. var., *C. koeblichii* Barron, n. sp., *C. yabei* var. *ellipticus* Barron, n. var., and *Thalassiosira tapponae* Barron, n. sp.

INTRODUCTION

The central equatorial Pacific has been a key area for biostratigraphic and paleoceanographic studies since the inception of the Deep Sea Drilling Project. Drilling has been carried out on four previous DSDP legs in the region (Legs 5, 8, 9, and 16), and nearly all major studies of Oligocene to Quaternary tropical microfossils and isotopes in the Pacific have utilized cores collected from the area. The section at DSDP Site 77 alone has figured in more such studies than any other Pacific DSDP section. The main purpose of Leg 85 was to revisit the central equatorial Pacific with the hydraulic piston corer (HPC) to recover a series of upper Eocene through Quaternary reference sections that are relatively free of the drilling disturbance associated with rotary coring. The HPC allows coring in the upper 100 to 300 m of sediment, making possible the collection of relatively undisturbed material having high sediment accumulation rates (15 m/m.y.), which is crucial to high-resolution stratigraphic and paleoceanographic studies. The five Leg 85 sites selected by the JOIDES Ocean Paleoenvironment Panel form transects from the eastern equatorial Pacific (Sites 571 and 572) to the central equatorial Pacific (Sites 573 to 575) and from south to north across equatorial high-productivity zones of the Oligocene to Holocene (Sites 573 to 575) (Fig. 1).

Diatoms are present throughout all five sections cored on Leg 85 (Sites 571 to 575). Only one core of the uppermost Quaternary *Pseudoeunotia doliolus* Zone was recovered at Site 571, but drilling at Sites 572 to 575 produced numerous cores with uppermost Eocene to Quaternary diatoms. Coring at Sites 572 and 575 terminated in the lower middle Miocene (about 15 Ma) and lower Miocene (about 22 Ma), respectively. Uppermost Eocene to Quaternary sections were cored at both Site 573 and Site 574. Diatom preservation was poor in the upper Oligocene, and most of the lower Miocene of Site 573 is barren of diatoms; otherwise, diatom preservation was typically good to excellent.

Previous studies of Oligocene to Quaternary diatom biostratigraphy in the area have been numerous. R. Kolbe (1954) pioneered diatom biostratigraphic work in the tropics with his study of piston cores collected by the Swedish Deep Sea Expedition. V. V. Mukhina and A. P. Jousé have led Russian diatomists in a major effort to document late Cenozoic equatorial diatom assemblages (Mukhina, 1963, 1965, 1966, 1969; Jousé, 1968, 1973, 1977). L. H. Burckle calibrated numerous late early Miocene to Quaternary diatom datum levels directly to paleomagnetic stratigraphy in piston cores collected from the area (Burckle, 1972, 1977, 1978; Burckle and Opdyke, 1977; Burckle and Trainer, 1979; Burckle et al., 1982; Opdyke et al., 1974). Deep Sea Drilling Project studies have included those of Milow (in Hays et al., 1972, Leg 9), Bukry (1973, Leg 17), Gombos (1975, DSDP Site 66), Barron (1981a, 1983), Barron and Burckle (in Keller et al., 1982, DSDP Site 77), and Harwood (1982, Oligocene to lower Miocene of DSDP Sites 65 and 77). Other studies within the easternmost equatorial Pacific have also been helpful in refining late Cenozoic diatom biostratigraphy in the area: Bukry and Foster (1973, Leg 16), Barron (1980a, Leg 54), Harper et al. (1982, Leg 67), and Sancetta (1982, 1983, Legs 68 and 69).

[1] Mayer, L., Theyer, F., et al., *Init. Repts. DSDP*, 85: Washington (U.S. Govt. Printing Office).
[2] Address: U.S. Geological Survey, 345 Middlefield Road, Menlo Park, CA 94025.

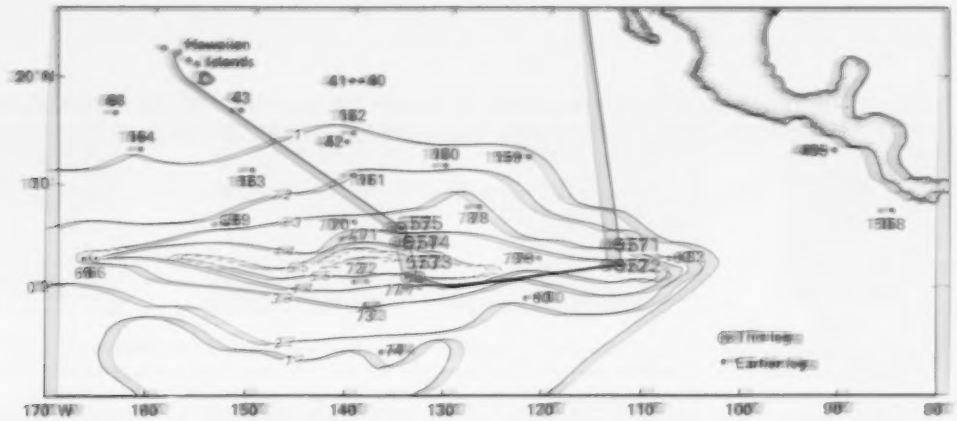

Figure 1. Locations of Leg 85 sites and other DSDP sites studied in the central and eastern equatorial Pacific. Contours represent two-way traveltime in tenths of seconds.

Leg 85 offers the opportunity to apply the knowledge gained from these and other studies of the low-latitude Atlantic Ocean (Fenner, in press) and Indian Ocean (Schrader, 1974) to develop an updated and refined late Cenozoic diatom biostratigraphy for the central equatorial Pacific. In addition, graphic correlation techniques and quantitative diatom biostratigraphy (Barron and Keller, 1983) might also be applied to refine late Cenozoic time to 100,000 yrs. or less, so that the gap between conventional biostratigraphy and high-resolution isotope and $CaCO_3$ stratigraphy could be bridged. Such high-resolution biostratigraphy is necessary for integrated paleoceanographic and paleoclimatic studies, and for understanding the nature and mechanisms of oceanic and climatic change.

METHODS

Typically, two to three samples per 9.5-m core were selected for study; in selected intervals, one sample per 1.5-m section was examined. Samples (3 to 5 cm^3) were treated with 10% hydrochloric acid to remove the calcium carbonate. Core-catcher samples, which were processed on ship, were then cleansed of acid by centrifuging at 2000 rpm for 2 min., decanting off the liquid, washing in distilled water, and repeating that cycle four or more times. Care was taken in selecting core-catcher samples from a single lithology in order to minimize possible contamination. Samples processed on shore were cleansed by washing in distilled water in a 250-ml beaker, settling for 2 hrs., and decanting the liquid away. Generally, four such cycles were necessary to remove the acid. Strewn slides were prepared by sampling the suspended sample with a pipette, spreading it on a 22 mm × 30 mm cover glass, drying on a hot plate, and mounting in Hyrax.

The entire microscope slide was scanned at 500× to check for the presence of biostratigraphic marker species. These marker species were selected from Burckle (1978), Fenner (in press), and the author's own studies (Barron, 1980a, b; 1981a, b; 1983; in press). Identifications of species were checked routinely at 1250×.

Quantitative studies were done at 1250×, using random traverses across the slide and counting the first 300 diatoms encountered. The counting techniques of Schrader and Gersonde (1978) were used, and resting spores were not counted.

The paleomagnetic time scale of Berggren et al. (in press) has been adopted for Leg 85 studies, and absolute ages obtained by first- and second-order calibrations to paleomagnetics reflect that time scale. The time scale adopted for Leg 85 utilizes Berggren et al.'s (in press) age estimates for the paleomagnetic anomalies, but it is based on the traditional Anomaly 5–Chron 9 correlation (Barron et al., this volume).

ZONATION

The diatom zonation used here (Table 1) is that proposed by Barron (in press) for the Miocene through Quaternary of the equatorial Pacific, and a modification of that of Fenner (in press) for the Oligocene. Barron's (in press) zonation consists of Burckle's (1972) upper Miocene through Quaternary zonation, Barron's (1983) lower

Table 1. Diatom zonation with defining marker taxa used for Leg 85 studies.

Zone	Subzone	Marker[a]
P. doliolus		T. *Nitzschia reinholdii*
Nitzschia reinholdii	B	T. *Rhizosolenia praebergonii* var. *robusta*
	A	B. *Pseudoeunotia doliolus*
Rhizosolenia praebergonii	C	T. *Thalassiosira convexa*
	B	T. *Nitzschia jouseae*
	A	B. *Rhizosolenia praebergonii*
Nitzschia jouseae		B. *Nitzschia jouseae*
Thalassiosira convexa	C	T. *Thalassiosira miocenica*
	B	T. *Thalassiosira praeconvexa*
	A	B. *Thalassiosira convexa*
Nitzschia miocenica	B	B. *Thalassiosira praeconvexa*
	A	B. *Nitzschia miocenica*
Nitzschia porteri	B	T. *Thalassiosira burckliana*
	A	T. *Coscinodiscus yabei (plicatus)*
Coscinodiscus yabei	B	B. *Thalassiosira burckliana*
	A	T. *Actinocyclus moronensis*
Actinocyclus moronensis		T. *Craspedodiscus coscinodiscus*
Craspedodiscus coscinodiscus		B. *Coscinodiscus temperei* var. *delicata*
Coscinodiscus gigas var. *diorama*		T. *Coscinodiscus lewisianus*
Coscinodiscus lewisianus		T. *Cestodiscus peplum*
Cestodiscus peplum	BB	T. *Actinocyclus oculatus*
	AA	B. *Cestodiscus peplum*
Denticulopsis maccollumii	BB	T. *Thalassiosira burckii*
	AA	B. *Denticulopsis maccollumii*
Triceratium pileus		T. *Craspedodiscus elegans*
Craspedodiscus elegans		T. *Bogorovia veniamini*
Rossiella paleacea	C	T. *Coscinodiscus oligocenicus*
	B	T. *Thalassiosira primulaboides*
	A	B. *Rossiella paleacea*
Rocella gelida		B. *Rocella gelida*
Bogorovia veniamini		B. *Bogorovia veniamini*
Rocella vigilans	B	T. *Cestodiscus mukhinae*
	A	T. *Coscinodiscus excavatus*
Coscinodiscus excavatus		B. *Coscinodiscus excavatus*

[a] B. = first occurrence (bottom); T. = last occurrence (top).

Miocene zonation, and new middle Miocene zones to bridge the gap between the two zonations.

Assignment of Leg 85 samples to this zonation is summarized on Table 2. All zonal and subzonal assignments were made using primary marker taxa. The zones themselves, their subzones and contained datum levels, and their correlation with other planktonic microfossil zones and with diatom zones are discussed thoroughly in the following section. Correlation of the various diatom zonations is shown on Figure 2 and 3. Table 3 shows the stratigraphic position of 8 secondary upper Cenozoic diatom datum levels that occur in two or more of the Leg 85 sections. Absolute ages have been obtained for these datum levels both by direct correlation with paleomagnetic stratigraphy and by extrapolation between the paleomagnetically calibrated datum levels in age-versus-depth plots for the four main Leg 85 sections. These methods will be discussed more thoroughly in a later section of this chapter.

Upper Eocene?

Sections 1 and 2 of Core 574C-34 contain *Cestodiscus robustus* Jousé, *C. mukhinae* Jousé, *C. pulchellus* sensu Jousé (1973), *Coscinodiscus decrescens* Grunow, *C. oligocenicus* Jousé, *Melosira architecturalis* Brun, and *Hemiaulus polycystinorum* Ehrenberg; but the sections lack *Coscinodiscus excavatus* Greville. According to the argument that follows, these sections are tentatively assigned to the upper Eocene, an assignment supported by data on calcareous nannofossils and benthic foraminifers. Study of planktonic foraminifers indicates assignment of these sections to the lower Oligocene (P18) (see site chapter).

***Coscinodiscus excavatus* Zone**

Category: Taxon-range zone

Author: Fenner (1984), modified here.

Definition: Interval of the total range of *Coscinodiscus excavatus*.

Age: Early Oligocene, about 36.5 to 33 Ma (extrapolated, Barron et al., this volume).

Remarks: Jousé (1973) and Fenner (1977) recognized the stratigraphic utility of *C. excavatus* in the tropical Pacific and subtropical South Atlantic respectively. This zonal definition is in contrast to that of Fenner (1984), who proposed the *C. excavatus* Zone as the interval between the first occurrence of *C. excavatus* and the first occurrence of *Cestodiscus reticulatus* Fenner, at DSDP Site 366 in the tropical Atlantic. She proposed the *Cestodiscus reticulatus* Zone for the overlying interval containing the total range of *C. reticulatus*, noting that the last occurrence of *Coscinodiscus excavatus* was near the top of that zone at DSDP Site 369. *C. excavatus* is a large, easily recognizable diatom, whereas *Cestodiscus reticulatus* can be easily confused with *Cestodiscus robustus* Jousé. For purposes of this preliminary report, these two *Cestodiscus* species were not separated, so the *Coscinodiscus excavatus* Range Zone has been utilized here without recognition of Fenner's (1984) *C. reticulatus* Zone.

Characteristic flora: *Cestodiscus robustus* (including *C. reticulatus*) is the most common constituent of the *C. excavatus* Zone floras; *Coscinodiscus excavatus*, *C. oligocenicus*, and *C.* sp. cf. *C. marginatus* Ehrenberg are the next most common species. Other characteristic species include *Cestodiscus mukhinae* and *C. pulchellus* sensu Jousé (1973). *Melosira architecturalis* Brun, *Coscinodiscus spiralis* Hajos, and *Hemiaulus polycystinorum* var. *mesolepta* Grunow are sporadic, being more characteristic of the lower part of the zone.

Correlation: Fenner (1984) places the first occurrence of *Coscinodiscus excavatus* within the upper part of the Eocene DSDP Core 366-10. This placement lies just above the CP16/CP15 calcareous nannofossil zonal boundary of Bukry (1978a) and just below the P17/P18 boundary of G. Keller (pers. comm., 1983) at Site 366. As such, this diatom datum very nearly coincides with the Eocene/Oligocene boundary of Berggren et al. (in press), which is the boundary used in the Leg 85 time scale. At Sites 573 and 574, the base of the *C. excavatus* Zone lies at or just above the CP16/CP15 zonal boundary, so it appears that the first occurrence of *C. excavatus* is isochronous between the tropical Atlantic and tropical Pacific.

At Site 369, Fenner (in press) places the last occurrence of *C. excavatus*, which defines the top of the *C. excavatus* Zone, near the base of CP17, within the *Globigerina ampliaperta* Zone (= P19-P20), and near the top of the *Thyrsocyrtis tuberosa* Zone of radiolarians. In Leg 85 material, the last *C. excavatus* in Samples 573B-34,CC and 574C-27,CC is correlative with the top of the *T. tuberosa* Zone but is slightly above the top of CP17. *C. excavatus* is sparse near its last occurrence, and its last occurrence in Leg 85 material was determined with sieved slides. Admittedly, such a procedure is not preferable for diatom biostratigraphy, and other biostratigraphic criteria, such as Fenner's (in press) last occurrence of *Cestodiscus reticulatus*, may, with further study, be a better zonal marker to use within this interval of the Oligocene.

Correlation with other diatom zones: As stated in the foregoing, the *C. excavatus* Zone is equivalent to the *C. excavatus* and the *Cestodiscus reticulatus* zones of Fenner (1984). It is also correlative with Jousé's (1973) *Cestodiscus pulchellus* Zone and at least part of her *C. mukhinae* Zone, and with the uppermost *Rylandsia inequiradiata* to lower *Rhizosolenia gravida* Zone of Gombos and Ciesielski (1983) (Fig. 2).

Rocella hannae Jousé is restricted to Subzone b of the *Cestodiscus reticulatus* Zone of Fenner (in press) and to the lower *R. gravida* Zone of Gombos and Ciesielski (1983). Although *R. hannae* was not observed in Leg 85 sediments, Fenner's (in press) correlation of its range with upper planktonic foraminiferal Zone P20 has been used to suggest correlation with the upper *C. excavatus* Zone of this chapter.

***Rocella vigilans* Zone**

Category: Interval zone.

Author: Fenner (1984), modified here.

Table 2. Assignment of Leg 85 samples to the diatom zonation.

Diatom zone and subzone	Age of boundary (Ma)[a]	Holes 573A, 573B	Holes 573C, 573D	Hole 573	Holes 573A, 573B
D. dichotoma			0/572A-2-3 (0/13.2)	0/573-2,CC (0/11.5)	
	0.85*		572A-2-4/572A-3-5 (14.7/25.7)	573-3-1/573-3,CC (12.8/20.8)	573A-1CC/573A-2,CC (14.0/22.0)
Nitzschia reinholdii	B		572C-2,CC (19.7)		
	1.95*				
	A/A		572A-3-6/572A-4-3 (27.2/32.3)	573-4-3 (25.3)	
	2.05*		572C-3,CC (29.3)		
	C/C		572A-4-4 (33.8)	573-4,CC/573-5-2 (30.5/33.1)	573A-3,CC (31.3)
	2.25*				
R. pseudokunyaensis	B/B		572A-4-6/572A-5-3 (36.5/39.6)	573-5-4 (36.1)	
	2.65*		572C-4,CC (38.8)		
	A/A		572A-5-6/572A-6-2 (41.5/44.1)	573-5-6/573-6-3 (38.9/43.4)	573A-4,CC (39.7)
	3.05*		572C-5,CC (40.4)		
N. jouseae			572A-6-5/572A-11-3 (49.6/95.1)	573-6-5/573-9-5 (46.4/73.4)	573A-5,CC/573A-6,CC (49.2/57.6)
	4.55*		572C-6,CC/572C-9,CC (58.1/86.6)		
	C/—		572A-11,CC/572A-14-5 (108.6/122.8)	573-9,CC (76.2)	
	5.15*		572C-10,CC/572C-13,CC (96.5/111.5)		
T. convexa	B/—		572A-14,CC/572A-16,CC (128.2/149.2)	573-10-1/573-12-1 (76.9/95.9)	
	5.85*		572C-14,CC/572C-16,CC (119.3/146.0)		
	A/—		572A-17,CC/572B-3,CC (154.1/168.7)	573-12-3/573-13-5 (98.9/110.7)	
	6.15*		572C-17,CC/572D-3-6 (148.0/175.2)		
	B/—		572B-4,CC (172.1)	573-13,CC (112.6)	
N. denticula	8.35*		572D-3,CC/572D-5-2 (179.7/191.2)		
	A/—		572D-5,CC/572D-6,CC (198.7/208.1)	573-14-2/573-15-5 (114.6/128.5)	
	7.35*		572D-7-1/572D-7,CC (208.5/217.6)	573-15,CC/573-16-2 (131.3/133.4)	
	B/—				
N. porteri	8.05*		572D-8-2/572D-8,CC (219.5/227.2)	573-16-5/573-16,CC (137.9/140.1)	
	A/—				
	8.65*		572D-9-1/572D-11,CC (227.5/255.7)	573-17-2/573-18,CC (142.2/152.9)	573B-1,CC/573B-3-1 (147.0/158.2)
	B/—				
C. vulnifer	10.5		572D-12-2/572D-14-2 (257.5/276.5)	573-19-1/573-19,CC (153.5/159.1)	573B-3-1/573B-3,CC (158.3/167.2)
	A/—				
	11.3*		572D-14-4/572D-18-3 (279.5/316.0)		573B-4-3/573B-5,CC (170.7/185.9)
A. moronensis	12.2*		572D-18,CC/572D-21,CCC (321.1/348.5)		573B-6-1/573B-6,CC (186.7/195.6)
C. coscinodiscus	12.8*		572D-22-1/572D-25-3 (350.5/382.5)		573B-7-3/573B-7,CC (199.2/203.4)
C. gigas var. *diorama*	13.5		572D-25,CC/572D-29-2,2 (388.7/419.0)		573B-8-4/573B-9-6 (210.2/222.7)
C. lewisianus	14.2*		572D-29,CC/572D-33,CCC (424.0/464.7)		573B-9,CC/573B-10,CC (224.1/232.8)
	B/—				573B-11,CC/573B-12,CC (242.9/250.2)
C. peplum	15.0*				
	A/—				573B-13-2/573B-14-3 (254.7/265.7)
	B/—				
D. mochtharia	17.0*				573B-14-4 (267.2)
	A/—				
	17.8*				573B-14-5 (268.7)
T. pileus	18.7*				
C. elegans	19.9*				
	C/—				
	20.6*				
R. praeporus	B/—				
	22.7*				
	A/—				
	22.7				573B-19,CC (312.7)
R. cedrus	24.5				573B-20,CC/573B-24,CC (328.2/362.2)
R. amicorum	26.5				573B-26,CC (383.7)
	B/—				
R. vigilans	28.5				573B-27,CC/573B-33,CC (392.5/450.7)
	A/—				
	34				573B-34,CC/573B-42-1 (454.4/520.5)
C. excavatus	36.5				

Note: Uppermost and lowermost section numbers assigned to each zone/subzone are separated by a slash. Numbers in parentheses are sub-bottom depths of these sections in meters. All zonal/subzonal assignments are based on primary markers.

[a] Asterisk indicates direct paleomagnetic calibration (see text).

Table 2. (Continued).

Hole 574	Holes 574A, 574B, 574C	Holes 575, 575A	Holes 575B, 575C
0/574-1,CC (0/4.5)		575-1-1 (0.5)	
574-2-2 (7.3)		575-1-3 (3.5)	
574-2-3/574-2-4 (8.3/9.4)			
		575-1-4 (5.0)	
574-2,CC (14.1)	574A-2,CC (15.4)	575-1-5 (6.5)	575C-1,CC (6.3)
574-3-2/574-4-4 (16.8/29.3)	574A-3,CC (23.9)	575-1,CC (7.3)	575B-1,CC (12.8)
574-4,CC (33.1)	574-4,CC (33.1)		
574-5-2/574-5,CC (34.9/42.5)	574A-5,CC (42.3)	575-2-1/575-2-3 (7.8/10.8)	
574-6-2 (44.4)		575-2-4 (12.3)	
574-6-4/574-6-6 (47.4/50.4)		575-2-5 (13.8)	
574-6,CC/574-7-2 (52.0/53.9)	574A-6,CC (51.9)	575-2-6/575-3-2 (15.3/18.8)	575B-2,CC (21.5)
574-7-4/574-7,CC (56.9/60.9)		575-3-3/575-3-5 (20.3/23.3)	575B-3-4/575B-3,CC (24.2/29.7)
574-8-1 (61.4)	574A-7,CC (61.3)		
574-8-3/574-8-7 (64.4/70.1)	574A-8,CC (70.4)	575-3-6/575-3,CC (24.8/26.3)	
574-8,CC/574-9-6 (70.5/76.4)		575-4-1 (26.8)	
574-9,CC/574-11-4 (80.0/94.4)	574A-9,CC/574A-10,CC (79.9/87.2)	575-4-2/575-4-5 (28.3/32.8)	575B-4,CC (39.1)
574-11,CC/574-13-2 (98.6/110.0)	574A-11,CC/574A-12,CC (98.8/108.2)	575-4-6/575-5-4 (34.3/39.9)	575B-5,CC (48.3)
574-13-4/574-16-2 (113.0/129.5)	574A-13,CC/574A-16,CC (113.1/127.1)	575-5,CC/575-6-4 (44.6/49.4)	575B-6,CC (55.9)
574-16,CC/574-20,CC (132.6/152.5)	574A-17,CC/574A-19,CC (132.7/150.9)	575-6,CC/575-8-2 (54.0/65.4)	
574-21-2/574-24,CC (154.4/172.5)	574A-20,CC/574A-21,CC (160.2/167.4)	575-8,CC/575-9-2 (73.0/74.9)	575B-11-1/575B-11-3 (79.4/82.4)
574-25-2/574-29-2 (174.4/194.2)	574A-22,CC/574B-1,CC (178.0/194.4)	575-9,CC/575A-1-1 (74.9/94.3)	575B-11-4/575B-13-1 (83.9/96.4)
574-29,CC/574-31,CC (197.2/206.5)	574C-1,CC/574C-2,CC (202.2/213.4)	575A-1-2/575A-4-1 (95.8/105.6)	575B-13-2/575B-14-3 (97.9/98.4)
	574C-3,CC/574C-4-2 (218.8/224.9)	575A-4-2/575A-7,CC (107.1/123.3)	
	574C-4,CC/574C-5-3 (226.7/235.9)	575A-8-1/575A-12-2 (123.5/137.0)	
	574C-5,CC/574C-8-1 (238.8/261.4)	575A-12,CC/575A-20-2 (139.6/162.7)	
	574C-8-3/574C-9,CC (264.4/275.3)	575A-20,CC/575A-24-2 (164.7/176.1)	
	574C-10-2/574C-12,CC (281.9/308.4)	575A-24,CC/575A-30-2 (179.2/196.0)	
	574C-13-2/574C-15,CC (310.4/336.8)	575A-30,CC/575A-33,CC (197.9/208.3)	
	574C-16-1/574C-17,CC (337.4/354.0)		
	574C-18-1/574C-19,CC (356.4/368.2)		
	574C-20,CC/574C-21,CC (384.2/390.6)		
	574C-22,CC/574C-26,CC (398.9/435.9)		
	574C-27,CC/574C-33,CC (446.9/506.0)		
	574C-34-1/574C-34-2		

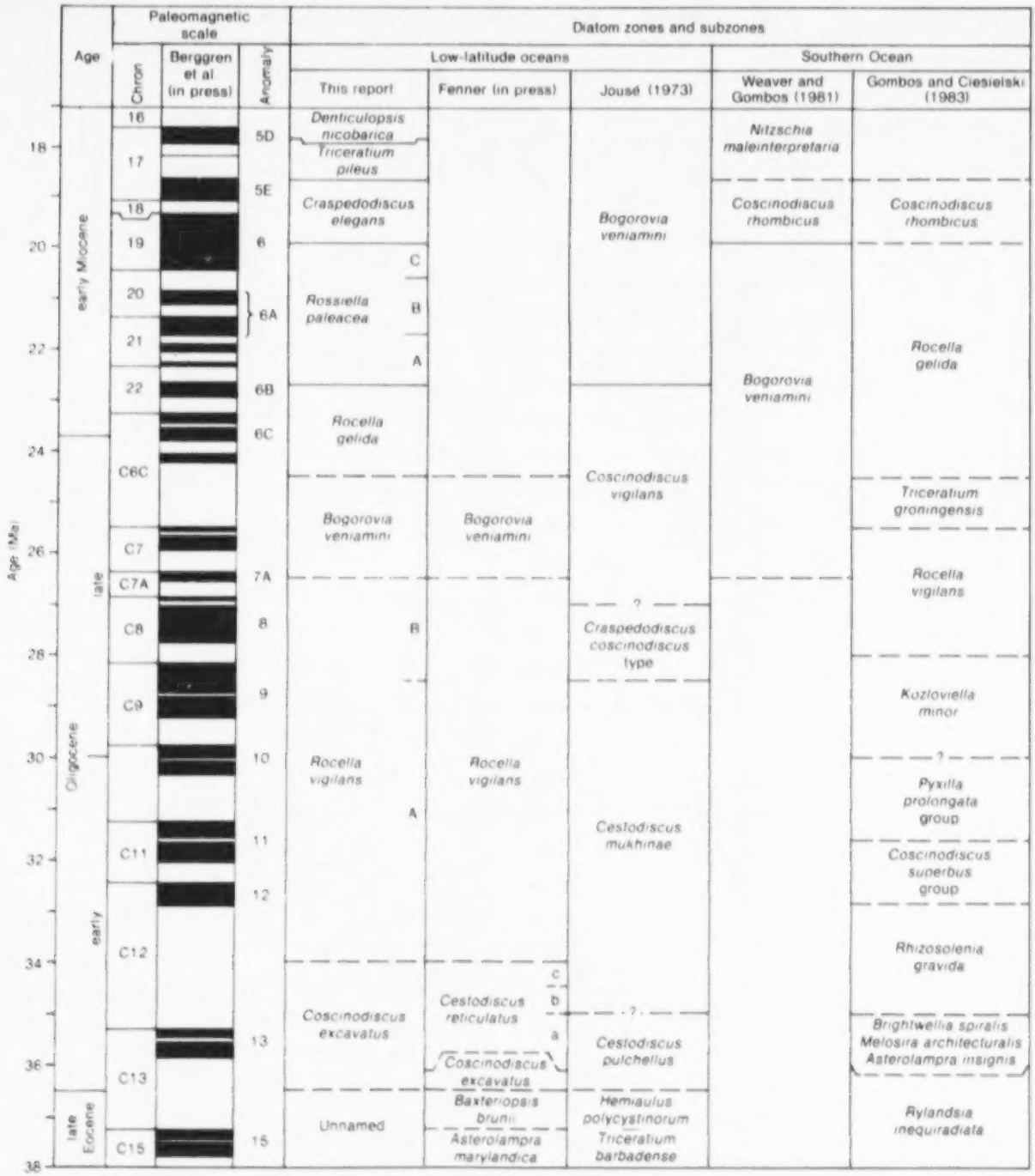

Figure 2. Correlation of the low-latitude diatom zonation of this report (Barron, 1983 and this report; Fenner, 1984) with the low-latitude diatom zonations of Fenner (in press) and Jousé (1973) and the Southern Ocean diatom zonations of Weaver and Gombos (1981) and Gombos and Ciesielski (1983) for the latest Eocene to middle early Miocene. Correlations are after Barron (1983) and this report.

Definition: Interval between the last occurrence of *Coscinodiscus excavatus* and the first occurrence of *Bogorovia veniamini*.

Subzones: Two subzones are proposed: Subzone A, from the base of the zone to the last occurrence of *Cestodiscus mukhinae*, and Subzone B, from the top of Subzone A to the top of the zone.

Age: Early to late Oligocene, about 33 to about 26.5 Ma. Subzone A/Subzone B boundary, about 28.5 Ma. (Ages extrapolated, Barron et al., this volume.)

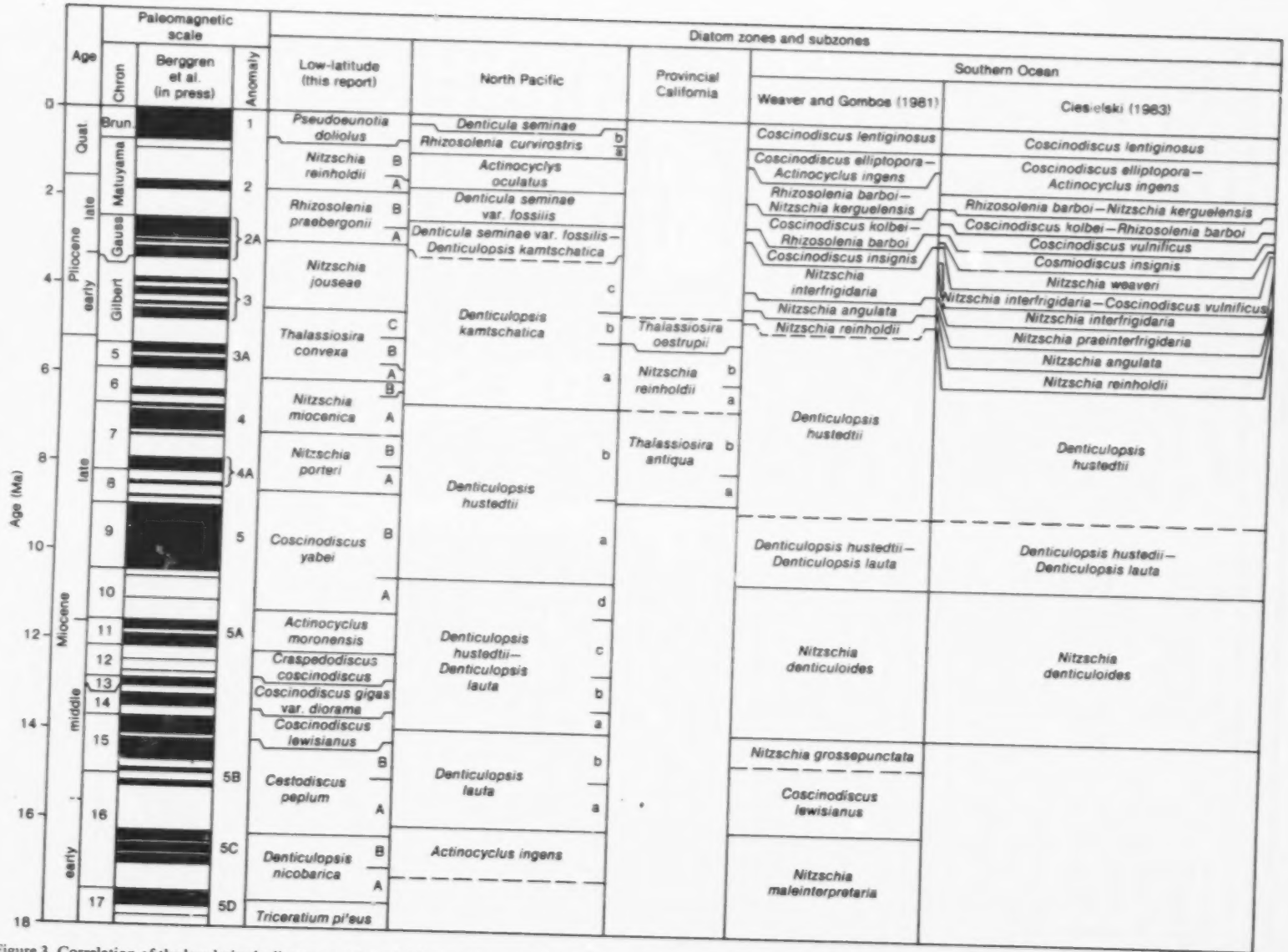

Figure 3. Correlation of the low-latitude diatom zonation of this report (Burckle, 1972; Barron, in press and 1983) with the North Pacific diatom zonation (Koizumi, 1973; Barron, 1980a; Barron and Keller, 1983), the provincial California diatom zonation for the latest Miocene to earliest Pliocene (Barron, 1981a), and the Southern Ocean diatom zonations of Weaver and Gombos (1981) and Ciesielski (1983) for the latest early Miocene through the Quaternary. Correlations are after Barron (in press), Ciesielski (1983), and this report.

Table 3. Correlation of secondary late Cenozoic diatom datum levels between Sites 572, 573, 574, and 575. Samples (Hole-Core-Section, level in cm) that constrain each datum level are separated by a slash.

Datum	Age (Ma)[a]	Site 572	Site 573	Site 574	Site 575
T. *Rhizosolenia matuyamai*	0.93 (1)	572A-2-5/572A-2-6			
B. *Rhizosolenia matuyamai*	1.0 (1)	572A-2-6/572A-2,CC			
T. *Rhizosolenia praebergonii*	1.82 (2)	572A-4-3/572A-4-4	573-4-3/573-4,CC	574-1,CC/574-2,CC	575-1-3/575-1-4
T. *Actinocyclus ellipticus* f. *lanceolata*	3.5–3.2	572A-7-1/572A-7-2	573-6-5/573-6,CC	574-3-2/574-3-4	575-1,CC/575-2-1
B. *Thalassiosira convexa* var. *convexa*	3.6 (2)	572A-7-2/572A-7-3	573-7-1/573-7-3	574-3-4/574-3,CC	575-1,CC/575-2-1
B. *Asteromphalus elegans*	3.9 (3)	572A-7-5/572A-7-6	573-8-1/573-8-5	574-3,CC/574-4-4	575-1,CC/575-2-1
T. *Nitzschia cylindrica*	4.3 (3)	572A-9,CC/572A-10-3	573-8-5/573-8,CC	574-4-4/574-4,CC	575-1,CC/575-2-1
B. *Thalassiosira oestrupii*	5.1 (3)	572A-13,CC/572A-14,CC	573-9,CC/573-10-1	574-4,CC/574-5-2	575-1,CC/575-2-1
T. *Asterolampra acutiloba*	5.35 (3)	572A-14,CC/572A-15-3	573-10-1/573-10,CC	574-5-5/574-5,CC	575-2-3/575-2-4
T. *Nitzschia miocenica*	5.55 (3)	572A-15,CC/572A-16-3	573-11-5/573-11,CC	574-5-5/574-5,CC	575-2-3/575-2-4
T. *Nitzschia miocenica* var. *elongata*	5.65 (4)	572A-16-3/572A-16,CC	573-11,CC/573-12-1	574-5,CC/574-6-2	575-2-3/575-2-4
T. *Rossiella praepaleacea*	6.0 (4)	572D-2,CC/572D-3,CC	573-12,CC/573-13-2	574-6-2/574-6-4	575-2-5/575-2-6
B. *Thalassiosira miocenica*	6.1 (3)	572D-3-4/572D-3,CC	573-13-5/573-13,CC	574-6-2/574-6-4	575-2-4/575-2-5
T. *Nitzschia porteri*	6.8	572D-5,CC/572D-6-1	573-14,CC/573-15-4	574-6,CC/574-7-2	575-3-2/575-3-3
T. *Rossiella paleacea*	7.4 (3)	572D-6,CC/572D-7-1	573-15-5/573-15,CC	574-7-2/574-7-4	575-3-2/575-3-3
T. *Coscinodiscus nodulifer* var. *cyclopus*	7.9	572D-7-5/572D-7,CC	573-16-2/573-16-5	574-7-2/574-7-4	575-3-3/575-3-4
B. *Nitzschia reinholdii* s. ampl.	8.0	572D-7,CC/572D-8-2	573-16-2/573-16-5	574-7-4/574-7-6	575-3-4/575-3-5
T. *Actinocyclus ellipticus* var. *javanicus*	8.0	572D-7,CC/572D-8-2	573-16-2/573-16-5	574-7-4/574-7-6	575-3-4/575-3-5
B. *Nitzschia marina*	8.2–8.1	572D-8-2/572D-8-4	573-16-5/573-16,CC	574-7,CC/574-8-1	575-3-5/575-3-6
B. *Nitzschia cylindrica* s. ampl.	8.7–8.6	572D-9-1/572D-9-3	573-17-2/573-17-5	574-7,CC/574-8-1	575-3,CC/575-4-1
B. *Coscinodiscus nodulifer* var. *cyclopus*	8.9–8.8	572D-9-3/572D-9,CC	573-17-2/573-17-5	574-8-3/574-8-5	575-3,CC/575-4-1
T. *Coscinodiscus yabei* var. *ellipticus*	9.5–9.4	572D-10-2/572D-10-4	573-17,CC/573-18-3	574-8-3/574-8-5	
T. *Coscinodiscus loeblichii*	9.5–9.4	572D-10-2/572D-10-4	573-17,CC/573-18-3	574-8-3/574-8-5	575-3,CC/575-4-1
T. *Coscinodiscus temperei* var. *delicata*	9.7	572D-10-6/572D-10,CC	573-18-3/573-18,CC	574-8-3/574-8-5	575-3-6/575-3,CC
B. *Nitzschia fossilis*	9.8	572D-10,CC/572D-11-1	573B-2,CC/573B-3-1, 81 and 573-18-3/573-18,CC	574-8-3/574-8-5	575-3,CC/575-4-1
B. *Coscinodiscus yabei* var. *ellipticus*	9.8	572D-10,CC/572D-11-1	573B-3-1, 71/573B-3-1, 81 and 573-18-3/573-18,CC	574-8-7/574-8,CC	
B. *Coscinodiscus loeblichii*	10.5–10.4	572D-11,CC/572D-12-2	573B-3-1, 71/573B-3-1, 81	574-8-7/574-8,CC	575-3,CC/575-4-1
T. *Denticulopsis hustedtii*	11.2–10.5	572D-11,CC/572D-12-2	573B-3,CC/573B-4-3	574-8-5/574-8-7	575-3,CC/575-4-1
T. *Coscinodiscus vetustissimus* v. *javanica*	10.7 (3)	572D-12-2/572D-12-4	573B-3-2/573B-3-4	574-8,CC/574-9-1	575-3,CC/575-4-1
B. *Coscinodiscus vetustissimus* v. *javanica*	11.2 (3)	572D-13-2/572D-13-4	573B-3,CC/573B-4-3	574-9-4/574-9,CC	575-4-1/575-4-2
B. *Actinocyclus ellipticus* f. *lanceolata*	11.4	572D-14-2/572D-14-4	573B-3,CC/573B-4-3	574-10-1/574-10-2	575-4-2/575-4-4
T. *Coscinodiscus tuberculatus*	12.0 (5)	572D-17,CC/572D-18-1	573B-4,CC/573B-5-1	574-10,CC/574-11-1	575-4-2/575-4-4
T. *Denticulopsis punctata* f. *hustedtii*	12.1 (5)	572D-17,CC/572D-18-1	573B-4,CC/573B-5-1	574-11-1/574-11-2	575-4-2/575-4-4
T. *Synedra jouseana*	12.3–12.1	572D-17,CC/572D-18-1	573B-5,CC/573B-6-1	574-11-1/574-11-2	575-4-6/575-4,CC
B. *Rossiella paleacea* var. *elongata*	12.3–12.2	572D-18-3/572D-18,CC	573B-5,CC/573B-6-1	574-11-2/574-11-4	575-4-4/575-4-5
B. *Thalassionema nitzschioides*	12.3–12.3	572D-18-3/572D-18,CC	573B-5,CC/573B-6-1	574-11-4/574-11,CC	575-4-4/575-4-5
T. *Coscinodiscus gigas* var. *diorama*	12.3	572D-19-1/572D-19-3	573B-5,CC/573B-6-1	574-11-4/574-11,CC	575-4-2/575-4-4
T. *Actinocyclus ellipticus* var. *spiralis*	12.4–12.3	572D-19,CC/572D-20-1	573B-5,CC/573B-6-1	574-11-4/574-11,CC	575-4,CC/575-5-2
B. *Hemidiscus cuneiformis*	12.5 (3)	572D-20-2/572D-20,CC	573B-5,CC/573B-6-1	574-12-2/574-12-4	575-5-2/575-5-4
B. *Rossiella praepaleacea*	12.7	572D-21-4/572D-21,CC	573B-6-5/573B-6,CC	574-12-4/574-12,CC	575-5-4/575-5,CC
T. *Actinocyclus ingens*	12.8–12.5	572D-21,CC/572D-22-1	573B-6-5/573B-6,CC	574-12-2/574-12-4	575-5-4/575-5,CC
B. *Nitzschia porteri*	13.1–12.9	572D-22-1/572D-22,CC	573B-6-5/573B-6,CC	574-14,CC/574-15-2	575-5,CC/575-6-2
T. *Denticulopsis nicobarica*	13.2	572D-23-3/572D-23,CC	573B-7,CC/573B-8-4	574-15-2/574-15,CC	575-6-2/575-6-4
T. *Annellus californicus*	13.5–13.4	572D-24-2/572D-24,CC	573B-8-4/573B-8,CC	574-15,CC/574-16-2	575-6-4/575-6,CC
T. *Coscinodiscus salisburyanus*	13.5–13.4	572D-24,CC/572D-25-3	573B-7,CC/573B-8-4	574-16-2/574-16,CC	575-6,CC/575-7-2
B. *Coscinodiscus gigas* var. *diorama*	13.6–13.5	572D-25-3/572D-25,CC	573B-7,CC/573B-8-4	574-17-2/574-17,CC	575-6,CC/575-7-2
T. *Cestodiscus pulchellus*	13.6–13.5	572D-25,CC/572D-26-3	573B-7,CC/573B-8-4	574-16-2/574-16,CC	575-6,CC/575-7-2
B. *Denticulopsis punctata* f. *hustedtii*	13.7	572D-25,CC/572D-26,CC	573B-8,CC/573B-9-4	574-16,CC/574-17-2	575-6,CC/575-7-2
B. *Coscinodiscus nodulifer*	13.8	572D-26,CC/572D-27-3	573B-8-4/573B-8,CC	574-17,CC/574-18-2	575-6,CC/575-7-2
T. *Thalassiosira lappanae*	13.8	572D-26,CC/572D-27-3	573B-8-4/573B-8,CC	574-17,CC/574-18-2	575-6,CC/575-7-2
B. *Coscinodiscus plicatus*	13.9–13.8	572D-26,CC/572D-27-3	573B-8-4/573B-8,CC	574-18,CC/574-19-2	575-7-2/575-7,CC
B. *Triceratium cinnamomeum*	13.9–13.8	572D-26,CC/572D-27-3	573B-8-4/573B-8,CC	574-19-2/574-19,CC	575-7-2/575-7,CC
T. *Cestodiscus pulchellus* var. *maculatus*	13.9	?	573B-8,CC/573B-9-4	574-19-3/574-19,CC	575-7-2/575-7,CC
B. *Denticulopsis hustedtii* (main)	13.9	572D-2?,CC/572D-28-2	573B-8,CC/573B-9-4	574-18,CC/574-19-2	575-7-2/575-7,CC
B. *Coscinodiscus tuberculatus*	14.0	572D-28-2/572D-28,CC	573B-8,CC/573B-9-4	574-19,CC/574-20-2	575-7-2/575-7,CC
B. *Actinocyclus ellipticus* var. *spiralis*	14.2–14.1	572D-29-2/572D-29,CC	573B-9-4/573B-9-6	574-20-2/574-20,CC	575-8-4/575-8,CC
B. *Denticulopsis hustedtii* (isolated)	14.2	572D-29,CC/572D-30-1	?	574-20,CC/574-21-2	?
B. *Actinocyclus ellipticus*	14.4–14.3	572D-30-1/572D-30,CC	573B-9,CC/573B-10-2	574-21,CC/574-22-2	575-8,CC/575-9-2
B. *Coscinodiscus blysmos*	14.4	572D-30,CC/572D-31-2	573B-9,CC/573B-10-2	574-21,CC/574-22-2	575-8,CC/575-9-2
B. *Thalassiosira lappanae*	14.4	572D-30,CC/572D-31-2	573B-9,CC/573B-10-2	574-22-2/574-22,CC	575-8,CC/575-9-2
T. *Coscinodiscus praenodulifer*	15.5–15.4		573B-11,CC/573B-12-2	574-26-2/574-26,CC	575-9,CC/575-10-2
B. *Actinocyclus ingens*	15.5		573B-10,CC/573B-11,CC	574-26,CC/574-27-2	575-10-2/575-10,CC
T. *Nitzschia maleinterpretaria*	15.6		573B-11,CC/573B-12-2	574-27,CC/574-28-1	575-10,CC/575-11-2
T. *Coscinodiscus lewisianus* var. *similis*	15.7		573B-12-2/573B-12-4	574-27,CC/574-28-1	575-10-2/575-10,CC and 575B-12-4/575B-12-5
Occurrence *Denticulopsis lauta*	15.9–15.8		573B-12-4	574-28,CC	575-10,CC
T. *Denticulopsis* cf. *kanayae*	16.0		573B-12-4/573B-12,CC	574-28,CC/574-29-2	575A-1-2/575A-1-3
T. *Thalassiosira fraga*	16.3–16.1		573B-13-2/573B-13-4	574-28,CC/574-29-2	575-11,CC/575A-1-1
T. *Synedra miocenica*	16.5 (6)		573B-13-2/573B-13-4	574-29-2/574-29,CC	575A-1-3/575A-1,CC
T. *Raphidodiscus marylandicus*	16.7 (6)		573B-13-4/573B-13,CC	574-30,CC/574-31-2	575A-2-3/575A-2-4
B. *Denticulopsis* cf. *kanayae*	16.9 (6)		583B-13-4/573B-13,CC	574C-2,CC/574C-3,CC	575A-2,CC/575A-3-2
Occurrence *Craspedodiscus rudei*	16.9 (6)		573B-14-1, ?	574C-2,CC	575A-3-2
B. *Coscinodiscus blysmos*	17.1 (6)		573B-14-1, ?/573B-14-1, 68	574C-2,CC/574C-3,CC	575A-4-2/575A-4-3
B. *Annellus californicus*	17.3 (6)		573B-14-1,?/573B-14-1, 68	574C-2,CC/574C-3,CC	575A-5-2/575A-5-3
B. *Craspedodiscus coscinodiscus* s.str.	17.3 (6)		?	?	575A-5-3/575A-5,CC
T. *Coscinodiscus lewisianus* var. *robustus*	17.4 (6)		573B-14-1, 68/573B-14-3	574C-2,CC/574C-3,CC	575A-5,CC/575A-6-1
B. *Coscinodiscus lewisianus* var. *similis*	17.4 (6)		573B-14-1, 68/573B-14-3	574C-2,CC/574C-3,CC	575A-5,CC/575A-6-1
B. *Cestodiscus pulchellus* var. *maculatus*	17.4 (6)		573B-14-1, 68/573B-14-3	574C-2,CC/574C-3,CC	575A-5,CC/575A-6-1
T. *Thalassiosira spumellaroides*	17.5 (6)			574C-2,CC/574C-3,CC	575A-6-2/575A-6-3
T. *Triceratium pileus*	17.6 (6)			574C-2,CC/574C-3,CC	575A-6-3/575A-6,CC
T. *Thalassiosira spinosa*	17.9 (6)			574C-4,CC/574C-5-1	575A-9-2/575A-9,CC
T. *Actinocyclus radionovae*	18.0 (6)			574C-5-1/574C-5-3	575A-9-2/575A-9,CC
B. *Nitzschia maleinterpretaria*	18.8			574C-5,CC/574C-6-2	575A-12,CC/575A-13-2
B. *Triceratium pileus*	18.8			574C-5,CC/574C-6-2	575A-12,CC/575A-13-2
T. *Actinocyclus hajosiae*	19.6			?	575A-18-2/575A-18,CC
B. *Thalassiosira fraga*	19.9			574C-8-1/574C-8-3	575A-20-2/575A-20,CC
B. *Coscinodiscus lewisianus* var. *robustus*	20.0			574C-8-3/574C-8,CC	575A-20-2/575A-20,CC
T. *Melosira architecturalis*	20.9–20.6			574C-10-4/574C-10,CC	575A-24-2/575A-24,CC
B. *Actinocyclus radionovae*	21.2			574C-10,CC/574C-11,CC	575A-26,CC/575A-27,CC
B. *Actinocyclus hajosiae*	22.0–21.6			574C-11,CC/574C-12,CC	575A-31,CC/575A-32,CC

[a] References indicate direct paleomagnetic calibration. (1) Burckle et al. (1978); (2) Burckle and Trainer (1979); (3) Burckle (1978); (4) Burckle (pers. comm., 1978); (5) Burckle et al. (1982); (6) Hole 575A—Barron interpretation. Ages of other datum levels from extrapolation. The paleomagnetic time scale of Berggren et al. (in press) is utilized.

Remarks: The interval of the *R. vigilans* Zone is generally poorly preserved in Leg 85 sediments. At Site 574, the first occurrence of *Rocella vigilans* Fenner coincides with the base of the zone, so the zone is exactly equivalent to the *R. vigilans* Zone of Fenner (1984). Poor preservation in the basal part of the zone at Site 573, however, obscures the first occurrence of *R. vigilans* there. At both Site 573 and Site 574, the first occurrence of *Synedra jouseana* Sheshukova-Poretzkaya corresponds to a restricted occurrence of *Kozloviella edita* Jousé and *K. minor* Jousé in Samples 573B-26,CC and 574C-21,CC at the base of Subzone B. The first occurrence of *Coscinodiscus rhombicus* Castracane, which marks the base of Fenner's (in press) Subzone C of her *R. vigilans* Zone, is in Sample 574C-20,CC, immediately below the first occurrence of *Bogorovia veniamini* in Sample 574C-19,CC, or top of the *R. vigilans* Zone. Preservation at Site 573 is too poor to allow recognition of the first-occurrence datum of *C. rhombicus*.

Characteristic flora: *Rocella vigilans* is the most consistently present species throughout the *R. vigilans* Zone, as it is robust and resistant to dissolution. *Cestodiscus mukhinae* is fairly consistent within Subzone A, and *Synedra jouseana* is fairly consistent within Subzone B. *Cestodiscus robustus* is present sporadically in the lower part of the zone at Site 573, as are *Coscinodiscus oligocenicus* and *Cestodiscus pulchellus* sensu Jousé (1973).

Correlation: As already stated, the *Coscinodiscus excavatus/Rocella vigilans* zonal boundary correlates with the lowermost part of calcareous nannofossil Zone CP18 and the base of the radiolarian *Dorcadospyris ateuchus* Zone. The Subzone A/Subzone B boundary falls within Zone P21 and the *D. ateuchus* Zone, and within either CP18 or CP19 (calcareous nannofossils) (Barron et al., this volume).

The *R. vigilans/Bogorovia veniamini* zonal boundary lies within Zone P22, Zone CP19, and in the upper part of the *D. ateuchus* Zone at Sites 573 and 574; this is slightly younger than Fenner's (in press) boundary at Site 369.

Correlation with other diatom zones: If the first occurrence of *Rocella vigilans* is truly coincident with the last occurrence of *Coscinodiscus excavatus*, the *R. vigilans* Zone is equivalent to Fenner's (1984) *R. vigilans* Zone. The *R. vigilans* Zone also correlates with the upper part of the *Cestodiscus mukhinae* Zone (= Subzone A), all of the *Craspedodiscus coscinodiscus* type Zone, and the lowermost part of the *Coscinodiscus vigilans* Zone of Jousé (1973) (Fig. 2). The ranges of *Kozloviella minor* and *Synedra jouseana* suggest that Subzone B of the *R. vigilans* Zone correlates with the *Kozloviella minor* and *Rocella vigilans* zones of Gombos and Ciesielski (1983). By superposition and the correlation suggested for the *C. excavatus* Zone, Subzone A of the *R. vigilans* Zone correlates with the upper *Rhizosolenia gravida* Zone to the middle *K. minor* Zone of Gombos and Ciesielski (1983) (Fig. 2).

Bogorovia veniamini Zone

Category: Partial-range zone

Author: Fenner (1984).

Definition: Interval from the first occurrence of *Bogorovia veniamini* to the first occurrence of *Rocella gelida* (Mann) Bukry.

Age: Late Oligocene, about 26.5 to 24.0 Ma. (Ages extrapolated, Barron et al., this volume.)

Remarks: Sediments assigned to the *Bogorovia veniamini* Zone at Sites 573 and 574 contain poorly preserved diatoms.

Characteristic flora: *Rocella vigilans* s. ampl. is the most common species in the *B. veniamini* Zone at Site 574, followed by *Synedra jouseana* and *S. jouseana* f. *linearis* Sheshukova-Poretzkaya. Other characteristic diatoms include *Coscinodiscus rhombicus, C. oligocenicus, C. lewisianus* var. *rhomboides* Barron, n. var., *Cestodiscus pulchellus*, and *Melosira architecturalis*.

Correlation: As stated, the *R. vigilans/B. veniamini* zonal boundary falls within planktonic foraminiferal Zone P22, calcareous nannofossil Zone CP19, and radiolarian *D. ateuchus* Zone. The *B. veniamini/Rocella gelida* zonal boundary is well represented at Site 574, where it is placed immediately below the first occurrence of *Rocella gelida* in Sample 574C-17,CC. As such, the upper boundary of the *B. veniamini* Zone occurs in the uppermost parts of Zones P22 and CP19 and within the lowermost part of the *Lychnocanoma elongata* Zone (radiolarians).

Correlation with other diatom zones: The *B. veniamini* Zone correlates with the middle part of the *Rocella vigilans* Zone of Jousé (1973), the lowermost part of the *Bogorovia veniamini* Zone of Weaver and Gombos (1981), and the upper *Rocella vigilans* Zone and the *Triceratium gronigensis* Zone of Gombos and Ciesielski (1983) (Fig. 2).

Rocella gelida Zone

Category: Partial-range zone.

Author: Barron (1983).

Definition: Interval from the first occurrence of *Rocella gelida* to the first occurrence of *Rossiella paleacea* (Grunow) Desikachary and Maheshwari.

Secondary markers: The last occurrence of *Rocella gelida* is a secondary marker for the top of the zone (Barron, 1983).

Age: Latest Oligocene to earliest Miocene, 24.0 to 22.7 Ma. (Ages extrapolated, Barron et al., in press and this volume.)

Remarks: Site 574 provides a seemingly complete section of the *R. gelida* Zone, in that it contains an interval below the first occurrence of *R. gelida* var. *schraderi* (Bukry) Barron (Sample 574-16,CC) and above the first occurrence of *R. gelida* s. ampl. (Sample 574C-17,CC). At Site 71, this interval is removed at a hiatus (hiatus PH of Keller and Barron, 1983) (Barron, 1983). *Rocella vigilans* last occurs within the upper part of the *R. gelida* Zone.

Characteristic flora: *Rocella gelida, Coscinodiscus oligocenicus*, and *Synedra jouseana* are the dominant diatoms of the *R. gelida* Zone. Other characteristic diatoms include *Coscinodiscus lewisianus* var. *rhomboides, C. rhombicus, Craspedodiscus coscinodiscus* sensu Jousé (1977) (coarse, indented form), *Bogorovia veniamini*, and *Actinodiscus barbadensis* sensu Jousé (1977).

Correlation: At Site 574, the base of the *R. gelida* Zone lies in the uppermost parts of planktonic foraminiferal Zone P22 and calcareous nannofossil Zone CP19, and within the lowermost part of the *L. elongata* Zone of radiolarians. The top of the *R. gelida* Zone falls within lower planktonic foraminiferal Zone N4 and the upper part of the *L. elongata* Zone, and it approximates the Subzone CN1a/Subzone CN1b boundary, a correlation consistent with the results of Barron (1983).

Correlation with other diatom zones: The *R. gelida* Zone correlates with the upper part of the *Coscinodiscus vigilans* Zone of Jousé (1973), the middle part of the *Bogorovia veniamini* Zone of Weaver and Gombos (1981), and the lower part of the *R. gelida* Zone of Gombos and Ciesielski (1983) (Fig. 2).

Rossiella paleacea Zone

Category: Concurrent-range zone.

Author: Barron (1983).

Definition: Interval from the first occurrence of *Rossiella paleacea* to the last occurrence of *Bogorovia veniamini*.

Subzones: The last occurrence of *Thalassiosira primalabiata* Gombos defines the Subzone A/Subzone B boundary. The last occurrence of *Coscinodiscus oligocenicus* marks the Subzone B/Subzone C boundary.

Secondary markers: At Site 574, the last occurrence of *Rocella gelida* coincides with the base of the *R. paleacea* Zone, a relationship observed by Barron (1983) at Site 71. As indicated by Barron (1983), the first occurrences of *Thalassiosira fraga* Schrader and *Coscinodiscus lewisianus* var. *robustus* Barron at Sites 574 and 575 closely approximate the top of the *R. paleacea* Zone (Tables 2 and 3); however, the last occurrence of *Actinocyclus hajosiae* Barron at Site 575 lies substantially above the top of the zone (Table 3).

Age: Early Miocene, 22.7 to 19.6 Ma. Subzone A/Subzone B boundary, 21.7 Ma; Subzone B/Subzone C boundary, 20.2 Ma. (Extrapolated ages, Barron et al., in press and this volume.)

Remarks: Sites 574 and 575 have good sequences of the *R. paleacea* Zone, although drilling at Site 575 was terminated in the upper part of Subzone A. Within Subzone A are the last occurrence of *Coscinodiscus lewisianus* var. *rhomboides* (Sample 574C-15,CC), near its base, and the first occurrences of *Coscinodiscus praenodulifer* Barron (Sample 574C-14,CC) and *Thalassiosira spumellaroides* Schrader (Sample 574C-13,CC). *Raphidodiscus marylandicus* and *Craspedodiscus elegans* Ehrenberg are too sparse and sporadic at Site 574 to determine whether their first occurrences fall within Subzone A, as is reported by Barron (1983).

The first occurrence of *Actinocyclus hajosiae* is within Subzone B at Site 574 (Sample 574C-11,CC) and within Subzone A at Site 575 (Sample 575A-31,CC) (Table 3). Either that datum or the last occurrence of *Thalassiosira primalabiata*, the top of Subzone A, is diachronous between Sites 574 and 575. Radiolarian biostratigraphy at Site 71 (Dunn, 1982, compared with Barron, 1983), Site 574, and Site 575 (Nigrini, this volume) suggests that the first occurrence of *A. hajosiae* is isochronous, occurring in the lowermost part of the *Stichocorys delmontensis* Zone at all three sites. Placement of the Subzone A/Subzone B boundary at Sites 71 and 575 is consistent with these results, but placement of the boundary at Site 574 may be as much as two cores too low. With further study, it may be found that the first occurrence of *Actinocyclus hajosiae* is a more consistent datum level to define the Subzone A/Subzone B boundary than the last occurrence of *Thalassiosira primalabiata*.

Subzone B contains the last occurrence of *Melosira architecturalis* (20.9 to 20.6 Ma) (Table 3), which varies somewhat between Sites 574 and 575, and the first occurrence of *Actinocyclus radionovae* Barron (21.2 Ma).

Characteristic flora: *Synedra jouseana* is the most consistently common diatom of the *R. paleacea* Zone. *Cestodiscus pulchellus* Greville, *Coscinodiscus marginatus, C. oligocenicus, C. rhombicus*, and *Bogorovia veniamini* also become important members of the assemblages in various parts of the zone.

Correlation: The correlations of Barron (1983) are supported in general by Leg 85 results at Sites 574 and 575. The base of the *R. paleacea* Zone falls in lower planktonic foraminiferal Zone N4 and the uppermost part of the *Lychnocanoma elongata* Zone of radiolarians, and approximates the CN1a/CN1b subzonal boundary of calcareous nannofossils. The top of the *R. paleacea* Zone correlates with Zone N5, upper Zone CN1, and middle *Stichocorys delmontensis* Zone at Site 574, but near the N4/N5 boundary at Site 575.

Correlation with other diatom zones: The *R. paleacea* Zone is equivalent to the lower part of the *Bogorovia veniamini* Zone of Jousé (1973), the upper part of the *B. veniamini* Zone of Weaver and Gombos (1981), and the upper part of the *Rocella gelida* Zone of Gombos and Ciesielski (1983) (Fig. 2).

Craspedodiscus elegans Zone

Category: Partial-range zone.

Author: Barron (1983).

Definition: Interval from the last occurrence of *Bogorovia veniamini* to the last occurrence of *Craspedodiscus elegans*.

Secondary markers: The first occurrences of *Thalassiosira fraga* (19.9 Ma) and *Coscinodiscus lewisianus* var. *robustus* (20.0 Ma) approximate the base of the *C. elegans* Zone. At Sites 574 and 575, the first occur-

rences of *Nitzschia maleinterpretaria* Schrader (18.8 Ma) and *Triceratum pileus* Ehrenberg (18.8 Ma) approximate the zone's top, ranges slightly younger than those reported by Barron (1983) at Sites 71 and 495.

Age: Early Miocene, 19.9 to 18.7 Ma (extrapolated ages, Barron et al., in press and this volume).

Remarks: Site 575 has an exceptionally thick (22 m), well preserved section of the *C. elegans* Zone.

Characteristic flora: *Thalassiosira fraga* is a common diatom within the *C. elegans* Zone, although *T. spinosa* Ehrenberg dominates over *T. fraga* in the lowermost part of the zone (Barron, 1983). *Synedra jouseana* and *Cestodiscus pulchellus* are secondarily common, and *Actinocyclus radionovae, Coscinodiscus rhombicus*, and *C. marginatus* are also characteristic.

Correlation: As reported by Barron (1983), the *C. elegans* Zone correlates with upper planktonic foraminiferal Zone N5, upper calcareous nanofossil Zone CN1, and the upper *Stichocorys delmontensis* Zone (radiolarians) at Site 575. Coincidence of the top of the *C. elegans* Zone with the tops of CN1 and the *S. delmontensis* Zone at Site 574 suggests a possible short hiatus there at about 237 m sub-bottom (Core 574C-5).

Correlation with other diatom zones: The *C. elegans* Zone is equivalent to the middle part of the *B. veniamini* Zone of Jousé (1973), and it closely approximates the limits of the *Coscinodiscus rhombicus* Zone of Weaver and Gombos (1981) and Gombos and Ciesielski (1983) (Barron, 1983) (Fig. 2).

Triceratium pileus Zone

Category: Interval zone.

Author: Barron (1983).

Definition: Interval containing *Triceratium pileus* between the last occurrence of *Craspedodiscus elegans* and the first occurrence of *Denticulopsis nicobarica* (Grunow) Simonsen.

Secondary markers: As stated, the first occurrences of *Nitzschia maleinterpretaria* and *Triceratium pileus* approximate the base of the *T. pileus* Zone in Leg 85 sediments. The last occurrence of *Triceratium pileus* (17.6 Ma) slightly postdates the zone's top.

Age: Early Miocene, 18.7 Ma (extrapolated age) to 17.8 Ma (paleomagnetic tie, Hole 575A).

Remarks: The *T. pileus* Zone is well represented at Sites 574 and 575, where it contains the last occurrences of *Thalassiosira spinosa* (17.9 Ma) and *Actinocyclus radionovae* (18.0 Ma).

Characteristic flora: *Cestodiscus pulchellus* and *Synedra jouseana* are common diatoms within the *T. pileus* Zone. Assemblages in the lower part of the zone at Site 575 are dominated by fragments of a diatom similar to *Ethmodiscus rex* (Wallich) Hendey (Samples 575A-9,CC through 575A-12,CC).

Correlation: At Site 575, the *T. pileus* Zone brackets the CN1c/CN2 (calcareous nannofossil) and *Stichocorys delmontensis/S. wolffii* (radiolarian) zonal boundaries, and is equivalent to the upper part of planktonic foraminiferal Zone N5; these correlations are consistent with the results of Barron (1983) and Barron et al. (in press).

Correlation with other diatom zones: The *T. pileus* Zone is equivalent to the upper middle part of the *Bogorovia veniamini* Zone of Jousé (1973) and the lower part of the *Nitzschia maleinterpretaria* Zone of Weaver and Gombos (1981) (Barron, 1983) (Fig. 2).

Denticulopsis nicobarica Zone

Category: Partial-range zone.

Author: Barron (1983).

Definition: Interval from the first occurrence of *Denticulopsis nicobarica* to the first occurrence of *Cestodiscus peplum*.

Subzones: The last occurrence of *Thalassiosira bukryi* Barron (17.0 Ma) marks the top of Subzone A and the base of Subzone B.

Secondary markers: The last occurrence of *Triceratium pileus* (17.6 Ma) approximates the base of the *D. nicobarica* Zone, and the last occurrences of *Synedra miocenica* Schrader (16.5 Ma) and *Thalassiosira fraga* (16.3 to 16.1 Ma) approximate the top of the zone.

Age: Early Miocene, 17.8 to 16.4 Ma (paleomagnetic calibration, Hole 575A).

Remarks: The *D. nicobarica* Zone also contains the last occurrences of *Thalassiosira spumellaroides* (17.5 Ma), *Coscinodiscus lewisianus* var. *robustus* (17.4 Ma), and *Raphidodiscus marylandicus* (16.7 Ma), and the first occurrences of *Cestodiscus pulchellus* var. *maculatus* (17.4 Ma), *Coscinodiscus lewisianus* var. *similis* Rattray (17.4 Ma), *Craspedodiscus coscinodiscus* Ehrenberg s. str. (17.3 Ma), *Annellus californicus* (17.3 Ma), and *Denticulopsis* sp. cf. *D. kanayae* Akiba (16.9 Ma) (Table 3; Barron, 1983).

Characteristic flora: See Table 4 (Hole 575A) and Table 5 (Hole 574) for quantitative diatom data on the *D. nicobarica* Zone.

Correlation: At Sites 573, 574, and 575, the *D. nicobarica* Zone correlates with upper Zone N6 to lower Zone N8 (planktonic foraminifers), upper Zone CN2 to upper Zone CN3 (calcareous nannofossils), and middle *Stichocorys wolffii* Zone to middle *Calocycletta costata* Zone (radiolarians), correlations supported by Barron (1983) and Barron et al. (in press).

Correlation with other diatom zones: The *D. nicobarica* Zone is correlative with the *Actinocyclus ingens* Zone of Barron (1980a) of the North Pacific and with the upper part of the *Nitzschia maleinterpretaria* Zone of Weaver and Gombos (1981) (Fig. 3).

Cestodiscus peplum Zone

Category: Taxon-range zone.

Author: Barron (1983).

Definition: Interval of the total range of *Cestodiscus peplum* Brun.

Subzones: The last occurrence of *Annellus californicus* Tempere within the *C. peplum* Zone (15.0 Ma) defines the top of Subzone A and the base of Subzone B.

Table 4. Percent planktonic diatoms through the *Denticulopsis nicobarica* Zone of Hole 575A.

Zone and subzone	Core-Section interval (cm)	Sub-bottom depth (m)	*Actinocyclus* aff. *ellipticus*	*Annellus californicus*	*Asteromphalus*/*Asteralampra*	*Cestodiscus peplum*	*C. pulchellus*	*C. pulchellus* var. *maculatus*	*Coscinodiscus blysmos*	*C. lewisianus*	*C. lewisianus* var. *similis*	*C. lewisianus* var. *robustus*	*C. praenodulifer*	*C. radiatus* s. ampl.	*C. rhombicus*	*C. salisburyanus*	*C. tabularis* s. ampl.	*C.* spp.	*Craspedodiscus coscinodiscus* s. str.	*C. ryderi*	*Denticulopsis nicobarica* s. ampl.	*Nitzschia maleinterpretaria*	*Raphidodiscus marylandicus*	*Rhizosolenia* spp.	*Rossiella paleacea*	*Synedra jouseana*/*S. miocenica*	*Thalassionema nitzschioides* s. ampl.	*Thalassiosira bukryi*	*T. fraga*	*T. lentiqua*	*T. spinosa*	*T. spumellaroides*	*Thalassiothrix longissima*	*Triceratium pileus*	Miscellaneous diatoms	Number counted	Estimated age (Ma) (from Fig. 5)
Cestodiscus peplum A	1-1, 50-51	94.3	—	+	1	1	40	—	—	5	—	—	—	1	—	4	8	+	—	—	2	—	—	+	4	15	11	—	+	—	—	—	5	—	—	150	16.3
	1-2, 50-51	95.8	—	—	3	—	47	+	—	2	+	—	3	6	—	5	+	+	—	—	1	—	—	—	2	20	4	—	+	—	—	—	4	—	—	300	16.5
	1-3, 50-51	97.3	—	1	+	—	40	—	—	4	+	—	—	4	—	2	4	+	+	—	2	1	—	—	3	17	10	—	1	—	—	—	10	—	—	200	16.6
B	2-2, 42-43	99.1	—	+	4	—	24	—	+	2	—	—	5	16	—	3	2	+	—	—	1	+	—	—	2	28	6	—	+	—	—	—	5	—	—	200	16.7
	2-3, 42-43	100.6	—	—	2	—	12	1	1	2	—	—	2	29	—	3	4	1	—	—	—	+	+	—	+	4	19	9	—	3	—	—	—	8	—	1	259	16.8
	2-4, 42-43	102.1	—	—	2	—	14	3	1	5	—	—	+	24	—	+	6	+	—	—	5	1	2	—	2	16	5	—	6	1	—	—	5	—	—	200	16.9
	3-2, 42-43	103.0	+	—	2	—	18	6	—	2	—	—	4	36	—	+	1	+	+	+	2	—	1	—	1	8	4	—	9	—	—	—	5	—	—	326	16.95
	3-3, 42-43	104.5	—	—	1	—	15	9	11	1	—	—	4	11	+	3	4	—	+	—	5	+	2	—	2	12	2	—	9	—	—	—	8	—	+	300	17.0
	4-1, 42-43	105.6	4	—	2	—	16	9	9	3	+	—	6	4	+	—	3	—	+	—	12	+	2	—	+	11	3	—	6	—	—	—	12	—	—	300	17.05
	4-2, 42-43	107.1	1	1	2	—	14	11	6	2	1	—	6	4	—	+	3	—	+	—	19	+	2	—	+	12	2	+	3	—	—	—	11	—	—	300	17.1
Denticulopsis nicobarica	4-3, 42-43	108.6	1	+	1	—	12	6	—	1	+	—	3	7	—	—	4	—	+	—	26	1	4	—	+	11	3	1	4	—	—	—	12	—	+	270	17.15
	4,CC	109.9	+	1	2	—	15	13	—	1	+	—	5	10	—	+	3	+	+	—	17	+	6	—	1	2	2	+	4	—	—	—	16	—	—	300	17.2
	5-2, 42-43	110.9	3	1	1	—	16	7	—	+	+	—	3	12	+	—	4	+	+	—	23	+	2	—	—	4	3	1	7	+	—	—	12	—	1	300	17.25
	5-3, 42-43	112.4	—	—	+	—	10	2	—	2	+	—	3	22	—	+	2	+	+	—	37	1	2	1	+	10	2	+	1	2	—	—	7	—	—	300	17.3
A	5,CC	114.1	+	—	1	—	24	+	—	—	+	—	2	14	—	+	1	—	—	—	35	+	3	—	—	7	1	+	+	1	—	—	8	—	+	300	17.35
	6-1, 42-43	114.5	—	—	2	—	25	—	—	+	—	+	6	+	+	—	3	+	—	—	33	9	2	—	+	6	+	+	+	2	—	—	9	—	1	300	17.4
	6-2, 42-43	116.0	—	—	+	—	47	—	—	1	—	15	2	+	—	1	3	1	—	—	7	—	+	—	+	5	10	1	1	—	—	—	5	—	—	200	17.45
	6-3, 42-43	117.5	—	—	1	—	34	—	—	—	—	9	5	+	—	+	4	1	—	—	6	—	3	—	1	6	16	2	2	—	—	+	6	—	2	300	17.5
	6,CC	119.1	—	—	1	—	30	—	—	—	—	8	+	7	—	—	2	—	—	—	31	2	2	—	+	4	5	+	1	+	—	+	3	+	—	300	17.6
	7-2, 43-44	120.3	—	—	2	—	42	—	—	1	—	6	3	4	—	+	1	+	—	—	3	7	1	—	—	11	7	2	+	+	+	—	11	+	+	300	17.7
	7-3, 43-44	121.8	—	—	2	—	30	—	—	2	—	7	2	10	+	—	+	—	—	—	+	4	2	—	—	6	5	2	+	+	—	—	16	+	3	200	17.75
Triceratium pileus	8-1, 42-43	123.5	—	—	2	—	39	—	—	3	—	7	4	8	+	—	2	—	—	—	—	6	+	—	+	1	3	1	—	2	—	—	15	+	+	200	17.85

Note: + means <1% or encountered after the count; — means not encountered.

Secondary markers: As stated, the last occurrences of *Synedra miocenica* (16.5 Ma) and *Thalassiosira fraga* (16.3 to 16.1 Ma) approximate the base of the *C. peplum* Zone. The first occurrence of *Actinocyclus ellipticus* var. *spiralis* Barron, n. var. (14.2 to 14.1 Ma) corresponds closely to the top of the zone.

Age: Latest early Miocene to early middle Miocene, 16.4 Ma (paleomagnetic calibration, Hole 575A) to 14.2 Ma (paleomagnetic calibration, Burckle, 1978).

Remarks: The following last occurrences are within the *C. peplum* Zone: *Denticulopsis* sp. cf. *D. kanayae* (16.0 Ma), *Coscinodiscus lewisianus* var. *similis* (15.7 Ma), *Nitzschia maleinterpretaria* (15.6 Ma), *Coscinodiscus praenodulifer* (15.5 to 15.4 Ma), and *C. blysmos* Barron (14.4 Ma). The first occurrences of *Actinocyclus ingens* Rattray in the tropics (15.5 Ma), *Thalassiosira tappanae* Barron, n. sp. (14.4 Ma), and *Actinocyclus ellipticus* (14.4 to 14.3 Ma) also fall within the *C. peplum* Zone. An isolated occurrence of the middle- to high-latitude species *Denticulopsis lauta* (15.9 to 15.9 Ma) in the lower part of the zone, reported by Barron (1983), has also been observed at Sites 573, 574, and 575 (Table 3). At Sites 572 and 574, isolated specimens of *Denticulopsis hustedtii* (Simonsen and Kanaya) Simonsen are observed as low as the 14.2-Ma level, the top of the *C. peplum* Zone. These occurrences more closely approximate the first occurrence of *D. hustedtii* in the middle- to high-latitude North Pacific (Barron, 1981a).

Characteristic flora: See Table 5 (Hole 574) and Table 6 (Hole 572D) for quantitative diatom data on the *C. peplum* Zone.

Correlation: In Leg 85 sediments, the *C. peplum* Zone correlates with lower Zone N8 to middle Zone N10 (planktonic foraminifers), middle Zone CN3 to upper Zone CN4 (calcareous nannofossils), and middle *Calocycletta costata* Zone to lower *Dorcadospyris alata* Zone (radiolarians). These results are generally consistent with those of Barron (1983) and Barron et al. (in press), although the top of CN4 appears relatively lower in Leg 85 sediments.

Correlation with other diatom zones: The *C. peplum* Zone correlates closely with the *Denticulopsis lauta* Zone (of Barron, 1980a, and Barron and Keller, 1983) of the North Pacific, and with the *Coscinodiscus lewisianus* and *Nitzschia grossepunctata* zones (Weaver and Gombos, 1981) of the Southern Ocean (Barron, in press) (Fig. 3).

Coscinodiscus lewisianus Zone

Category: Partial-range zone.

Author: Barron (in press).

Definition: Interval from the last occurrence of *Cestodiscus peplum* to the last occurrence of *Coscinodiscus lewisianus* Greville.

Secondary markers: The first occurrence of *Actinocyclus ellipticus* var. *spiralis* (14.2 to 14.1 Ma) approximates the base of the *C. lewisianus* Zone. The last occurrences of *Cestodiscus pulchellus* (13.6 to 13.5 Ma), *Coscinodiscus salisburyanus* Lohman (13.5 to 13.4 Ma), and *Annellus californicus* (13.5 to 13.4 Ma), and the first occurrence of *Coscinodiscus gigas* var. *diorama* (Schmidt) Grunow (13.6 to 13.5 Ma), all fall near the top of the zone.

Table 5. Percent planktonic diatoms in Cores 9 to 31 of Hole 574.

Zone and subzone	Core-Section, interval (cm)	Sub-bottom depth (m)	*Actinocyclus ehrenbergii*	*A. ellipticus* s. ampl.	*A. ingens*	*Asteromphalus/Asteralampra*	*Cestodiscus peplum*	*C. pulchellus*	*C. pulchellus* var. *maculatus*	*Coscinodiscus bysmos*	*C. lewisianus*	*C. marginatus*	*C. nodulifer*	*C. plicatus/C. yabei*	*C. praenodulifer*	*C. radiatus* s. ampl.	*C. salisburianus*	*C. tabularis* s. ampl.	*C. temperei* var. *delicata*	*C. tuberculatus*	*C.* spp.	*Craspedodiscus coscinodiscus*	*Annellus californicus*	*Denticulopsis hustedtii*	*D. nicobarica*	*D. praedimorpha*	*D. punctata* f. *hustedtii*	*Hemidiscus cuneiformis*	*Nitzschia maleinterpretaria*	*N.* spp.	*Raphidodiscus marylandicus*	*Rhizosolenia* spp.	*Roseisella pulnaeae*	*Roseisa* spp.	*Synedra jouseana*	*Thalassionema nitzschioides*	*T. nitzschioides* var. *parva*	*T. robusta*	*Thalassiosira fraga*	*T. lepidopus*	*T. tappanae*	*T.* spp.	*Thalassiothrix longissima*	*Actinopychus* spp.	*Melosira sulcata*	Miscellaneous diatoms	Estimated age (Ma) (from Fig. 4)
Coscinodiscus yabei, Subzone A	9-1, 9-10	70.6	—	2	—	5	—	—	—	—	—	3	7	4	—	1	—	5	4	+	+	—	—	—	—	—	—	1	—	7	—	+	—	+	—	14	23	—	—	3	—	+	17	—	—	2	10.8
	9-2, 43-45	72.4	+	6	—	1	—	—	—	—	—	—	9	2	—	+	—	+	3	—	2	—	—	1	—	—	—	4	—	10	—	+	—	—	—	16	36	5	—	+	—	+	6	—	—	—	10.95
	9-3, 43-45	73.9	+	3	—	+	—	—	—	—	—	—	9	+	—	+	—	+	+	+	+	—	—	2	—	—	—	5	—	14	—	+	—	—	—	9	46	+	—	+	—	2	7	—	—	—	11.05
	9-4, 43-45	75.4	—	2	—	+	—	—	—	—	—	1	12	1	—	1	—	1	2	+	2	—	—	+	—	—	—	1	—	48	—	+	—	—	—	5	12	—	—	+	—	+	6	—	—	3	11.15
	9-5, 43-44	76.9	—	1	—	+	—	—	—	—	—	—	8	2	—	—	—	+	1	—	—	—	—	15	—	—	—	4	—	15	—	+	—	—	—	20	22	—	—	+	—	+	8	—	—	+	11.2
	9-6, 43-45	78.4	—	3	+	+	—	—	—	—	—	—	8	1	—	+	—	—	3	—	1	—	—	17	—	—	—	4	—	6	—	+	+	—	—	11	26	+	—	1	—	1	13	—	—	1	11.3
	9,CC	80.0	+	4	—	+	—	—	—	—	—	—	10	2	—	1	—	—	3	+	+	+	—	10	—	—	—	1	—	6	—	+	—	—	—	9	39	+	—	+	—	1	8	—	—	1	11.4
	10-1, 43-45	80.4	—	7	—	+	—	—	—	—	—	—	7	2	—	—	—	—	6	—	—	—	—	24	—	—	—	2	—	1	—	+	1	—	—	10	18	1	—	3	—	+	16	—	—	—	11.45
	10-2, 43-45	81.9	—	9	—	1	—	—	—	—	—	—	6	1	—	—	—	—	2	+	1	1	—	33	—	+	1	—	—	2	—	+	1	+	—	7	16	—	—	2	—	—	14	—	—	—	11.5
	10-3, 43-45	83.4	+	4	—	—	—	—	—	—	—	—	10	2	—	—	—	—	2	2	+	+	—	52	—	—	—	1	—	3	—	+	3	—	—	4	7	+	—	—	—	—	7	—	—	+	11.6
	10-4, 43-45	84.9	—	5	—	1	—	—	—	—	—	—	6	1	—	—	—	—	6	1	—	—	—	39	—	—	—	2	—	5	—	+	2	+	—	5	14	+	—	3	—	+	3	—	—	+	11.7
	10-5, 43-45	86.4	+	4	—	+	—	—	—	—	—	—	6	2	—	+	—	—	5	2	1	1	—	7	—	+	+	—	21	—	—	—	—	—	1	—	6	26	6	—	—	—	—	9	—	—	—	11.8
	10-6, 43-45	87.9	2	4	—	1	—	—	—	—	—	—	9	5	—	+	—	—	5	2	+	+	—	5	—	—	+	2	—	6	—	+	3	+	—	4	25	11	—	2	—	—	10	—	—	—	11.9
	10,CC	89.3	—	9	—	1	—	—	—	—	—	—	+	2	—	—	—	—	1	+	—	—	—	64	—	—	—	+	—	5	—	+	1	—	—	3	9	5	—	—	—	—	4	—	—	2	11.95
	11-1, 43-45	89.9	3	2	—	+	—	—	—	—	—	—	10	2	—	1	—	—	2	2	1	1	—	27	—	1	—	1	—	7	—	—	1	2	—	4	17	10	—	1	—	—	3	—	—	1	12.0
	11-2, 43-45	91.4	10	1	—	1	—	—	—	—	—	+	1	2	—	—	—	—	7	2	4	+	—	3	—	—	+	1	—	4	—	—	2	—	2	7	25	10	—	2	—	—	9	+	—	4	12.1
	11-4, 43-45	94.4	2	5	—	1	—	—	—	—	—	2	4	4	—	—	—	—	3	1	36	+	—	2	—	—	—	+	—	8	—	—	1	—	1	2	17	2	+	—	—	—	5	—	3	12.2
	11,CC	98.6	+	1	—	1	—	—	—	—	—	—	8	2	—	—	—	—	2	1	21	+	—	3	—	—	—	+	—	6	—	+	1	—	1	5	41	—	—	—	—	—	3	—	1	12.35
	12-2, 43-45	100.5	+	4	—	2	—	—	—	—	—	1	2	1	—	—	—	—	1	3	—	+	—	10	+	3	—	—	—	7	—	+	1	—	+	3	29	—	—	—	—	—	6	1	—	2	12.45
	12-4, 43-45	103.5	+	4	+	2	—	—	—	—	—	—	5	+	27	1	2	—	9	—	—	—	—	5	—	23	2	—	—	2	—	—	1	—	3	1	17	—	—	2	—	—	6	—	—	4	12.5
	12,CC	108.1	3	6	2	+	—	—	—	—	—	1	10	+	3	—	—	—	5	—	1	2	—	5	—	7	—	+	—	+	—	+	1	—	1	10	23	—	—	+	—	—	6	—	—	3	12.7
	13-2, 43-45	110.0	3	13	2	1	—	—	—	—	—	2	10	1	6	+	2	—	5	—	1	2	—	—	—	2	—	+	—	4	—	9	16	—	—	+	—	+	11	1	—	+	12.75
	13-4, 43-45	113.0	7	10	+	—	—	—	—	—	—	2	9	3	9	+	3	—	+	—	—	2	—	—	—	—	—	—	+	—	2	4	24	—	—	1	—	—	6	+	—	3	12.85
	13-6, 43-45	116.0	+	12	—	3	—	—	—	—	—	—	15	—	2	1	+	—	4	—	3	7	—	—	—	—	—	—	—	+	—	2	4	24	—	—	1	—	—	14	—	—	1	13.0
	14-2, 42-43	119.5	5	6	5	1	—	1	—	—	+	1	3	8	—	+	—	—	4	—	2	+	3	—	—	5	—	+	—	1	—	5	—	4	10	21	—	—	2	—	—	4	—	—	1	13.1
	14,CC	122.5	6	6	1	1	—	—	—	—	—	2	2	2	—	+	—	—	7	—	3	+	3	—	5	24	—	1	—	—	—	—	+	3	—	+	6	13	—	—	2	2	—	4	—	1	13.2
	15-2, 42-43	124.5	8	13	+	1	—	—	—	—	—	1	2	5	—	+	—	—	12	—	6	1	+	—	5	—	—	+	—	—	1	—	1	—	2	4	35	—	—	+	—	—	4	1	—	2	13.2
	15,CC	128.7	10	21	1	4	—	—	—	—	—	1	17	—	11	+	+	—	1	—	—	+	—	—	—	—	—	—	—	—	—	—	1	—	+	5	26	—	—	1	—	—	4	—	—	1	13.25
	16-2, 42-43	129.5	+	6	11	2	—	—	—	—	—	1	3	2	—	—	—	—	7	—	8	+	—	—	7	1	+	—	—	—	—	—	3	—	2	5	13	—	—	4	—	—	6	1	—	1	13.4
	16,CC	132.6	+	4	16	2	—	3	—	+	3	3	8	—	—	1	+	+	15	3	—	1	—	—	—	—	—	—	—	1	—	—	2	+	2	6	19	—	—	6	—	+	7	+	—	1	13.45
	17-2, 42-43	134.5	+	7	3	1	—	+	—	—	1	1	2	1	—	2	+	6	—	+	2	3	+	2	22	—	+	—	—	+	+	+	—	—	3	3	9	—	—	3	1	+	5	—	2	13.55
	17,CC	137.6	+	7	4	1	—	—	—	—	3	8	3	2	—	+	+	10	—	+	2	+	—	46	—	—	—	—	—	—	—	—	2	+	+	2	10	—	—	5	—	+	3	—	—	1	13.6
	18-2, 42-43	139.5	—	4	9	+	—	2	—	—	3	—	4	—	+	+	+	4	—	1	+	4	—	8	31	—	—	—	—	—	—	—	+	—	+	3	8	—	—	2	—	+	5	—	—	1	13.65
	18,CC	142.2	—	2	13	2	—	9	—	—	4	2	10	—	+	+	1	+	6	32	—	—	—	—	—	+	—	+	4	—	+	2	6	—	—	3	4	—	—	6	—	—	13.75
	19-2, 43-44	144.5	—	2	2	2	—	5	—	—	3	6	2	—	—	—	+	+	24	—	—	—	—	—	—	—	—	+	2	—	+	3	5	—	—	2	1	—	7	+	—	1	13.85
	19,CC	148.2	+	7	+	+	—	3	+	—	1	6	8	—	—	—	+	+	19	—	—	—	—	—	—	—	—	—	1	+	3	1	10	—	—	3	15	—	10	1	—	+	13.9
	20-2, 43-44	149.5	—	5	—	+	—	3	—	—	4	1	2	—	—	—	+	—	28	—	—	—	—	—	—	—	—	—	—	+	+	5	12	—	—	5	6	+	6	—	—	8	14.0
	20,CC	152.5	—	2	2	+	—	3	+	—	3	2	1	—	—	—	1	+	15	—	—	—	—	—	—	—	—	—	—	—	+	—	1	+	5	31	—	—	1	12	+	9	+	—	1	14.1
	21-2, 43-44	154.4	—	2	—	+	+	2	1	—	3	1	9	—	—	1	+	—	+	52	—	—	—	—	—	—	—	—	—	2	+	+	9	3	—	—	—	—	—	10	—	+	14.15
	21,CC	157.5	—	+	15	+	2	4	—	—	2	3	16	—	—	1	+	—	42	—	—	—	—	—	—	—	—	—	—	—	+	—	3	11	—	—	—	3	+	9	—	2	14.2
	22-2, 43-44	159.4	—	—	22	2	+	2	+	1	2	1	16	—	—	1	+	—	25	—	—	—	—	—	—	—	—	—	—	+	—	—	2	2	—	—	+	5	—	9	—	2	14.3
B	22,CC	162.6	—	—	5	2	1	8	2	3	3	1	11	—	—	6	4	—	21	—	—	—	—	—	—	—	—	—	2	—	4	6	5	—	—	+	1	—	8	+	1	14.4
	23-2 43-44	164.4	—	—	31	—	4	3	3	1	1	+	12	—	—	6	+	—	24	—	—	2	—	2	—	—	—	—	+	—	11	5	7	—	2	+	—	—	7	—	+	14.5
	23,CC	167.5	—	—	6	2	2	5	2	+	2	1	12	—	—	11	6	—	13	—	—	—	—	—	—	—	—	—	+	—	3	1	+	—	—	—	—	—	8	—	1	14.6
	24-2, 43-44	169.4	—	—	55	1	1	1	2	+	—	—	4	—	—	17	7	—	27	—	—	—	—	—	—	—	—	—	+	+	3	2	1	—	—	+	—	—	17	—	+	14.7
Cestodiscus peplum	24,CC	172.5	—	—	11	1	+	2	—	+	+	+	2	—	—	6	6	—	10	—	—	—	—	—	—	—	—	—	+	—	6	2	2	—	—	—	—	—	5	—	—	14.8
	25-2, 43-44	174.4	—	—	1	+	+	3	1	1	—	3	—	—	—	3	7	—	35	—	—	—	—	—	—	—	—	—	2	—	1	6	5	—	—	—	—	+	15	+	1	14.95
	25,CC	177.8	—	—	3	+	—	4	+	—	—	3	—	—	—	22	4	—	33	—	—	—	—	—	—	—	—	—	1	—	+	6	+	—	—	—	—	—	14	—	+	15.05
	26-2, 42-43	179.4	—	—	4	1	+	18	+	—	1	+	—	—	—	15	3	9	—	1	+	+	—	18	—	—	—	—	—	—	—	—	—	—	2	3	5	—	—	—	—	—	26	+	—	5	15.2
A	26,CC	182.2	—	—	+	2	+	21	6	+	+	—	—	—	—	20	2	4	—	—	—	2	+	17	—	—	—	—	—	—	—	—	1	—	3	1	3	—	—	—	—	—	18	—	—	3	15.3
	27-2, 42-43	184.2	—	—	—	3	+	15	4	—	2	—	—	—	—	1	8	7	—	+	—	+	+	9	—	—	—	—	—	—	—	—	+	—	11	9	7	—	—	—	—	—	19	—	2	5	15.5
	27,CC	187.1	—	—	—	1	+	17	3	—	2	1	—	—	—	1	12	+	20	—	—	—	—	—	—	—	—	—	2	—	18	3	2	—	—	—	—	—	13	—	—	15.6
	28-1, 30-31	187.6	—	—	—	2	+	11	1	—	—	—	4	—	—	2	7	+	13	—	—	—	—	—	—	—	—	—	2	—	18	7	8	—	—	—	—	—	9	—	+	15.7
	28,CC	192.3	—	—	—	1	4	4	4	—	1	—	3	—	—	3	4	+	7	—	—	6	+	—	—	—	—	—	1	—	27	8	8	—	—	—	—	—	11	—	+	15.8
	29-2, 42-43	194.2	—	—	—	1	+	13	6	+	6	2	9	—	—	4	1	—	+	—	—	—	—	—	—	—	—	—	3	—	21	5	9	—	—	+	—	—	6	—	—	16.0
Denticulopsis nicobarica B	29,CC	197.2	—	—	2	—	—	7	3	—	7	—	6	—	—	3	+	+	2	—	—	—	—	—	—	—	—	—	3	—	19	6	6	—	+	—	—	—	10	—	+	16.1
	30-2, 42-43	199.2	—	—	3	—	—	16	3	—	3	—	13	—	—	4	7	+	2	—	—	—	—	—	—	—	—	—	2	—	2	—	+	6	—	18	4	8	—	1	—	—	—	8	—	1	1	16.3
	30,CC	202.2	—	—	2	—	—	12	9	2	3	+	2	—	—	3	4	+	2	—	—	—	—	—	—	—	—	—	2	—	2	—	1	2	—	20	5	8	—	—	—	—	9	—	16	1	16.4
	31-2, 42-43	204.2	—	—	3	—	—	8	3	—	3	+	1	—	—	1	10	—	1	—	—	+	—	—	—	—	—	—	+	—	38	2	5	—	—	—	—	—	11	—	+	16.6
	31,CC	206.5	—	—	3	—	—	8	9	2	3	1	—	—	2	17	—	3	23	1	—	+	—	—	—	—	—	—	1	—	23	3	6	—	3	1	—	—	11	—	+	16.7
													1	—	—	+	—	—	—	—	—	11	—	—	—	—	—	—	—	—	+	—	—	—	19	—	—	+	4	—	—	16.8

Note: + means < 1% or encountered after the count; — means not encountered. 300 specimens were counted.

Age: Middle Miocene, 14.2 Ma to 13.5 Ma (ages extrapolated, Barron et al., in press).

Remarks: Numerous datum levels are present within the relatively short (0.7 m.y. duration) *C. lewisianus* Zone, presumably reflecting response to global cooling and floral turnover in the early middle Miocene (Woodruff et al., 1981; Keller and Barron, 1983). First occurrences include *Coscinodiscus tuberculatus* Greville (14.0 Ma), *Triceratium cinnamomeum* Greville (13.9 to 13.8 Ma), *Coscinodiscus plicatus* Grunow (13.9 to 13.8 Ma), *Coscinodiscus nodulifer* Schmidt (13.7 Ma), and *Denticulopsis punctata* f. *hustedtii* (Schrader) Simonsen (13.7 Ma). *Cestodiscus pulchellus* var. *maculatus* (13.9 Ma) and *Thalassiosira tappanae* (13.8 Ma) have last occurrences within the *C. lewisianus* Zone. *Denticulopsis hustedtii* became established in the tropics about 13.9 Ma, after isolated incursions from middle latitudes around 14.2 Ma.

Characteristic flora: See Table 5 (Hole 574) and Table 6 (Hole 572D) for quantitative diatom data on the *C. lewisianus* Zone.

Correlation: In Leg 85 sediments, the *C. lewisianus* Zone is equivalent to upper Zone N10 and Zone N11 (planktonic foraminifers), upper Zone CN4 to lower Zone CN5 (calcareous nannofossils), and the middle part of the *Dorcadospyris alata* Zone (radiolarians). At Site 573, Nigrini (this volume) records the *Diartus petterssoni* Zone (radiolarians) relatively lower, with respect to the other microfossil zones, than in the other Leg 85 holes. These results are consistent with the cor-

Table 6. Percent planktonic diatoms in Cores 12 to 33 of Hole 572D.

Zone and subzone	Core-Section, interval (cm)	Sub-bottom depth (m)	*Actinocyclus ehrenbergii*	*A. ellipticus* s. ampl.	*A. ingens*	*Asteromphalus/Asteroliampra*	*Cestodiscus peplum*	*C. pulchellus* s. ampl.	*Coscinodiscus bysmas*	*C. lewisianus*	*C. marginatus*	*C. nodulifer*	*C. plicatus/C. yabei*	*C. radiatus* s. ampl.	*C. tabularis* s. ampl.	*C. temperei* var. *delicata*	*C. tuberculatus*	*C.* spp.	*Craspedodiscus coscinodiscus*	*Annellus californicus*	*Denticulopsis hustedtii*	*D. nicobarica*	*D. praedimorpha*	*D. punctata* f. *hustedtii*	*Hemidiscus cuneiformis*	*Nitzschia* spp.	*Rhizosolenia* spp.	*Rossiella paleacea*	*Rousia* spp.	*Synedra jouseana*	*Thalassionema nitzschioides*	*T. nitzschioides* var. *parva*	*T. robusta*	*Thalassiosira lepidopus*	*T. lappanae*	*T.* spp.	*Thalassiothrix longissima*	*Actinoptychus* spp.	Miscellaneous diatoms	Estimated age (Ma)
Coscinodiscus yabei, Subzone A	12-2, 50-52	257.5	+	+	—	+	—	—	—	—	—	5	1	1	2	2	—	1	—	—	3	—	—	8	7	—	+	+	—	24	31	—	—	—	1	5	—	3	10.7
	12,CC	261.8	—	1	—	+	—	—	—	—	+	4	+	—	1	1	—	+	—	—	+	—	—	3	20	3	—	—	+	23	44	—	+	—	—	4	—	2	10.85
	13-2, 50-52	267.0	—	+	—	—	—	—	—	—	—	1	—	—	—	—	—	—	—	—	—	—	—	+	7	—	+	—	—	52	33	—	—	—	—	4	—	1	11.15
	13-4, 50-52	270.0	—	+	—	—	—	—	—	—	+	3	2	+	2	—	—	—	—	—	9	—	—	2	15	+	—	—	—	20	37	—	+	—	—	7	—	1	11.2
	13,CC	272.4	—	1	—	+	—	—	—	—	—	1	+	—	—	1	—	1	—	—	39	—	—	3	7	+	—	—	—	17	21	—	—	—	1	6	—	1	11.25
	14-2, 50-52	276.5	—	2	—	—	—	—	—	—	+	4	3	—	4	—	—	1	—	—	6	—	—	1	1	+	—	—	—	13	42	6	+	—	—	15	—	+	11.35
	14-4, 50-52	279.5	+	2	—	+	—	—	—	—	—	10	1	—	4	1	—	+	—	—	18	—	—	2	1	+	3	—	—	11	38	—	—	—	+	6	—	1	11.4
	14,CC	281.9	1	3	—	+	—	—	—	—	—	7	1	—	4	—	—	1	—	—	26	—	—	1	4	+	1	+	+	11	22	—	1	—	2	8	—	3	11.45
	15-1, 50-52	284.5	+	6	—	1	—	—	—	—	+	4	4	—	2	1	—	3	—	—	22	—	—	+	3	+	1	+	+	4	42	—	1	—	1	16	—	2	11.5
	15,CC	287.8	—	2	—	+	—	—	—	—	—	1	1	—	1	—	—	+	—	—	68	—	—	—	3	—	1	—	—	3	12	—	—	—	1	5	—	+	11.55
Actinocyclus moronensis	16-2, 50-52	295.5	+	3	—	+	—	—	—	—	—	5	2	—	7	1	+	3	—	—	45	—	—	1	3	+	1	—	—	7	13	—	—	—	—	7	—	2	11.7
	16-4, 50-52	298.5	+	2	—	1	—	—	—	—	+	+	2	—	5	2	+	1	—	—	62	—	—	1	4	—	+	—	—	3	8	1	—	—	—	4	—	2	11.75
	16,CC	302.9	+	+	—	—	—	—	—	—	—	1	2	—	3	—	+	—	—	—	48	—	—	+	4	—	1	+	—	+	33	4	3	—	—	5	—	1	11.85
	17-1, 50-52	303.5	—	+	—	—	—	—	—	—	—	—	1	—	4	+	—	+	—	—	55	—	—	+	8	—	1	—	—	2	33	+	+	—	—	3	—	+	11.9
	17,CC	306.4	—	—	—	—	—	—	—	—	—	+	1	—	2	—	—	—	—	—	57	—	—	+	4	+	1	—	—	1	20	2	—	—	—	8	—	2	11.95
	18-1, 50-52	313.0	10	2	—	1	—	—	—	—	2	2	3	+	8	1	2	+	—	—	5	—	—	+	2	3	—	—	+	4	37	7	—	—	—	5	+	4	12.05
	18-3, 50-52	316.0	+	+	—	+	—	—	—	—	—	10	3	+	5	+	5	+	—	—	12	—	—	+	4	—	+	+	+	12	34	+	+	—	+	9	+	2	12.15
	18,CC	321.1	+	1	—	1	—	—	—	—	1	3	2	2	6	2	34	+	+	—	5	—	—	+	+	10	—	1	+	1	20	—	+	—	—	5	+	4	12.2
	19-1, 50-52	322.5	+	2	—	+	—	+	—	—	—	4	1	—	3	—	12	+	—	—	3	—	6	—	9	—	+	—	—	1	51	—	—	—	+	2	—	2	12.25
	19-3, 50-52	325.5	+	3	+	—	—	—	—	—	—	2	2	—	5	+	9	+	—	—	17	—	—	+	1	4	+	—	—	1	48	—	—	—	—	4	—	1	12.3
Craspedodiscus coscinodiscus	19,CC	325.7	—	2	—	+	—	—	—	—	—	2	1	—	7	3	24	—	1	—	13	—	—	+	—	5	+	2	—	1	2	27	—	—	—	—	3	+	+	12.35
	20-2, 50-52	333.5	—	1	—	+	—	—	—	—	—	+	2	—	3	+	4	+	+	—	13	—	—	1	4	—	+	—	1	3	57	—	—	—	—	5	—	1	12.5
	20,CC	335.0	2	12	—	2	—	—	—	—	3	3	1	—	9	+	5	+	+	—	16	—	—	3	—	5	—	+	+	5	2	14	—	1	—	8	1	1	12.55
	21-3, 50-52	344.5	3	1	—	+	—	—	—	—	2	4	2	—	7	1	6	+	1	—	6	—	—	+	—	3	+	2	—	3	5	39	—	+	—	+	12	+	+	12.7
	21-4, 50-52	346.0	4	1	—	+	—	—	—	—	1	3	3	+	10	+	5	—	—	—	10	—	—	2	—	4	+	—	2	3	31	—	—	—	1	13	+	2	12.75
	21,CC	348.5	1	5	—	3	—	—	—	—	2	3	3	—	12	1	5	+	2	—	18	—	1	3	—	3	+	+	—	2	3	25	—	—	—	+	6	—	1	12.8
	22-1, 50-52	351.0	—	1	2	+	—	—	—	—	+	—	3	—	5	—	—	+	1	—	18	—	6	6	—	2	—	+	+	3	11	40	—	—	—	+	3	—	+	12.85
Coscinodiscus gigas var. *diorama*	22,CC	354.7	2	3	—	1	—	—	—	—	1	—	7	+	12	—	1	+	1	—	10	—	—	3	—	3	+	2	2	5	3	22	—	+	—	—	7	—	+	12.9
	23-3, 50-52	363.5	+	11	7	+	—	—	—	—	5	1	4	1	9	—	—	1	+	—	7	—	—	1	—	+	1	2	—	1	11	11	—	2	—	—	20	2	+	13.1
	23,CC	369.4	10	8	1	2	—	—	—	—	—	—	7	—	13	—	6	+	2	—	2	+	—	+	—	1	—	3	—	4	8	20	—	4	—	—	4	2	1	13.2
	24-2, 50-52	371.5	6	9	+	2	—	—	—	—	2	+	6	+	12	—	1	+	+	—	12	1	—	—	—	—	—	1	—	1	7	25	—	3	—	—	5	2	2	13.25
	24,CC	378.6	+	4	36	1	—	—	—	—	+	+	2	+	4	—	1	+	1	+	16	1	—	+	—	—	—	—	—	3	4	14	—	2	—	—	8	+	+	13.4
	25-3, 50-52	382.5	—	6	9	+	—	—	—	—	+	4	4	+	5	—	—	+	1	—	6	4	—	—	—	+	—	1	—	+	20	21	—	3	—	+	6	—	3	13.5
	25,CC	388.7	—	2	8	1	—	—	5	2	—	—	—	+	4	—	4	+	1	+	26	31	—	+	—	—	—	2	—	1	1	3	—	+	—	—	7	—	+	13.6
	26-3, 50-52	392.0	—	3	2	2	—	3	—	1	+	+	+	+	4	—	1	1	4	1	6	51	—	—	—	+	+	—	—	—	6	6	—	2	—	—	4	—	1	13.65
	26,CC	397.0	—	—	4	2	—	1	—	2	—	+	+	+	6	—	1	—	5	+	9	49	—	—	—	—	+	+	—	1	3	4	—	1	—	+	7	—	4	13.75
Coscinodiscus lewisianus	27-3, 50-52	401.5	—	+	1	1	—	2	—	1	+	—	—	—	2	—	+	+	2	—	+	56	—	—	—	2	—	3	—	+	2	14	—	1	+	—	6	2	1	13.8
	27,CC	407.6	—	4	2	+	—	2	—	1	2	—	—	—	5	6	—	3	2	10	1	+	21	—	—	—	—	—	+	—	—	3	13	—	+	6	+	13	2	2	13.9
	28-2, 50-52	409.5	—	6	+	1	—	2	—	+	—	—	—	—	1	+	—	+	2	—	—	44	—	—	—	+	—	1	—	—	5	19	—	+	6	—	8	—	+	13.95
	28,CC	414.7	—	+	11	1	—	—	—	—	1	—	—	—	4	+	—	—	—	+	—	61	—	—	—	—	—	—	—	—	3	+	—	—	—	—	16	—	2	14.05
	29-2, 50-52	419.0	—	+	+	—	—	—	5	—	—	—	—	—	2	3	—	+	1	—	1	56	—	—	—	—	—	—	—	1	7	14	—	+	—	—	6	—	1	14.1
Cestodiscus peplum	29,CC	424.0	—	—	2	+	+	1	—	—	2	—	—	1	+	—	—	—	—	—	1	62	—	—	—	—	—	—	—	—	10	2	—	—	—	—	15	—	2	14.2
	30-1	427.0	—	+	—	—	—	—	—	—	+	—	—	—	1	—	—	—	—	—	—	77	—	—	—	—	—	+	—	—	2	12	—	—	—	—	7	—	+	14.25
	30,CC	433.8	—	—	13	+	—	1	—	+	+	—	—	3	7	—	—	+	—	—	—	50	—	—	—	—	—	—	—	+	10	+	—	—	2	+	11	—	+	14.4
	31-2, 65-66	438.2	—	—	26	1	+	12	1	+	—	—	—	23	15	—	—	—	+	—	—	8	—	—	—	—	—	—	—	1	3	+	—	—	—	—	6	—	1	14.5
	31,CC	444.4	—	—	7	+	—	12	3	+	—	—	—	7	4	—	—	+	+	+	—	6	—	—	—	—	—	1	—	19	15	2	—	—	—	—	20	—	+	14.55
	32-1, 65-66	446.2	—	—	+	2	1	27	—	1	2	—	—	14	4	—	—	—	+	+	—	2	—	—	—	—	—	+	—	15	3	4	—	—	—	—	20	—	2	14.6
	32-2, 65-66	447.7	—	—	5	+	—	+	+	+	—	—	—	4	2	—	—	—	—	—	—	73	—	—	—	—	—	—	—	2	6	+	—	—	—	—	4	—	1	14.65
	32,CC	454.0	—	—	53	—	+	3	—	2	+	—	—	15	3	—	—	—	+	—	—	6	—	—	—	—	—	+	—	1	7	+	—	—	—	—	7	—	+	14.75
	33,CC	464.7	—	—	6	+	+	5	+	—	6	—	—	34	5	—	—	—	1	—	—	3	—	—	—	—	—	—	—	+	8	1	—	—	—	—	27	1	+	14.95

Note: + means < 1% or encountered after the count; — means not encountered. 300 specimens were counted.

relations of Barron et al. (in press), although the CN4/CN5 boundary appears slightly higher in Leg 85 sediments.

Correlation with other diatom zones: The *C. lewisianus* Zone correlates with the uppermost part of the *Denticulopsis lauta* Zone and Subzone a of the *D. hustedtii–D. lauta* Zone (of Barron, 1980a, and Barron and Keller, 1983) of the North Pacific, and with the uppermost *Nitzschia grossepunctata* to lowermost *N. denticuloides* zones (Weaver and Gombos, 1981) of the Southern Ocean (Barron, in press) (Fig. 3).

Coscinodiscus gigas var. *diorama* Zone

Category: Interval zone.

Author: Barron (in press).

Definition: Interval containing *Coscinodiscus gigas* var. *diorama* between the last occurrence of *Coscinodiscus lewisianus* and the first occurrence of *C. temperei* var. *delicata* Barron.

Secondary markers: The last occurrences of *Cestodiscus pulchellus, Coscinodiscus salisburyanus*, and *Annellus californicus* and the first occurrence of *C. gigas* var. *diorama* approximate the base of the *C. gigas* var. *diorama* Zone, and the last occurrence of *Actinocyclus ingens* (12.8 to 12.5 Ma) in the tropics is near the top of the zone.

Age: Middle Miocene, 13.5 Ma (extrapolated, Barron et al., in press) to 12.8 Ma (paleomagnetic calibration, Burckle et al., 1982).

Remarks: The *C. gigas* var. *diorama* Zone contains the first occurrence of *Nitzschia porteri* sensu Burckle (1972) (13.1 to 12.9 Ma) and the last occurrence of *Denticulopsis nicobarica* (13.2 Ma).

Characteristic flora: See Table 5 (Hole 574) and Table 6 (Hole 572D) for quantitative diatom data on the *C. gigas* var. *diorama* Zone.

Correlation: In Leg 85 sediments, the *C. gigas* var. *diorama* Zone is equivalent to Zone N12 (planktonic for-

aminifers), and it brackets the CN5a/CN5b subzonal boundary of calcareous nannofossils. At Sites 574 and 575, the *C. gigas* var. *diorama* Zone correlates with the upper *Dorcadospyris alata* Zone of radiolarians, whereas at Sites 572 and 573 a correlation with the lower *Diartus petterssoni* Zone is suggested. Correlation with the upper *D. alata* Zone is favored by Barron et al. (in press); comparison of the various microfossil biostratigraphies (Barron et al., this volume) suggests that the *D. alata/D. petterssoni* zonal boundary is diachronous between Sites 572–573 and Sites 574–575.

Correlation with other diatom zones: The *C. gigas* var. *diorama* Zone correlates with Subzone b of the *Denticulopsis hustedtii–D. lauta* Zone of the North Pacific, and with a lower part of the *Nitzschia denticuloides* Zone of the Southern Ocean (Barron, in press) (Fig. 3).

Craspedodiscus coscinodiscus Zone

Category: Concurrent-range zone.
Author: Barron (in press).
Definition: Interval from the first occurrence of *Coscinodiscus temperei* var. *delicata* to the last occurrence of *Craspedodiscus coscinodiscus*.
Secondary markers: The last occurrence of *Actinocyclus ingens* in the tropics approximates the base of the *C. coscinodiscus* Zone. The last occurrences of *Coscinodiscus gigas* var. *diorama* (12.3 Ma) and *Synedra jouseana* (12.3 to 12.1 Ma) and the first occurrences of *Thalassionema robusta* Schrader (12.3 to 12.2 Ma) and *Rossiella paleacea* var. *elongata* Barron (12.3 to 12.2 Ma) all nearly coincide with the zone's top.
Age: Middle Miocene, 12.8 Ma (paleomagnetic calibration, Burckle et al., 1982) to 12.2 Ma (extrapolated age, Barron et al., in press).
Remarks: The first occurrences of *Rossiella praepaleacea* (Schrader) Gersonde (12.7 Ma) and *Hemidiscus cuneiformis* Wallich (12.5 Ma) and the last occurrence of *Actinocyclus ellipticus* var. *spinulis* (12.4 to 12.3 Ma) are within the *C. coscinodiscus* Zone.
Characteristic flora: See Table 5 (Hole 574) and Table 6 (Hole 572D) for quantitative diatom data on the *C. coscinodiscus* Zone.
Correlation: The *C. coscinodiscus* Zone is equivalent to planktonic foraminiferal Zone N13, calcareous nannofossil Subzone CN5b to lower Zone CN6, and the lower *Diartus petterssoni* Zone of radiolarians in Leg 85 sediments. These correlations are supported by Barron et al. (in press).
Correlation with other diatom zones: The lower part of Subzone c of the *Denticulopsis hustedtii–D. lauta* Zone of the North Pacific, and a middle part of the *Nitzschia denticuloides* Zone of the Southern Ocean, are correlative with the *C. coscinodiscus* Zone (Barron, in press) (Fig. 3).

Actinocyclus moronensis Zone

Category: Partial-range zone.
Author: Barron (in press).
Definition: Interval from the last occurrence of *Craspedodiscus coscinodiscus* to the last occurrence of *Actinocyclus moronensis* Deby.
Secondary markers: The last occurrences of *Coscinodiscus gigas* var. *diorama* and *Synedra jouseana* and the first occurrences of *Thalassionema robusta* and *Rossiella paleacea* var. *elongata* correspond closely to the base of the *A. moronensis* Zone. The first occurrence of *Actinocyclus ellipticus* f. *lanceolata* Kolbe (11.4 Ma) slightly predates the top of the zone.
Age: Latest middle Miocene to earliest late Miocene, 12.2 Ma (extrapolated age, Barron et al., in press) to 11.3 Ma (paleomagnetic calibration, Burckle, 1978).
Remarks: The last occurrence of *Denticulopsis punctata* f. *hustedtii* (12.1 Ma) and the last consistent occurrence of *Coscinodiscus tuberculatus* (12.0 Ma) fall within the *A. moronensis* Zone.
Characteristic flora: See Table 5 (Hole 574) and Table 6 (Hole 572D) for quantitative diatom data on the *A. moronensis* Zone.
Correlation: The *A. moronensis* Zone is equivalent to planktonic foraminiferal Zones N14 and N15, calcareous nannofossil Zone CN7, and the middle part of the *Diartus petterssoni* Zone of radiolarians in Leg 85 sediments. These correlations are supported by Barron et al. (in press).
Correlation with other diatom zones: The *A. moronensis* Zone correlates with the upper part of Subzone C of the *Denticulopsis hustedtii–D. lauta* Zone of the North Pacific and with the upper part of the *Nitzschia denticuloides* Zone of the Southern Ocean (Barron, in press) (Fig. 3).

Coscinodiscus yabei Zone

Category: Partial-range zone.
Author: Burckle, 1972 (top); Barron, in press (base).
Definition: Interval from the last occurrence of *Actinocyclus moronensis* to the last occurrence of *Coscinodiscus yabei* Kanaya.
Subzones: Barron (in press) proposed the first occurrence of *Thalassiosira burckliana* to define the Subzone A/Subzone B boundary.
Secondary markers: The first occurrence of *Actinocyclus ellipticus* f. *lanceolata* slightly predates the base of the zone, and the first occurrence of *Nitzschia cylindrica* Burckle s. ampl. (8.7 to 8.6 Ma) coincides with the top of the zone.
Age: Late Miocene, 11.3 to 8.6 Ma (paleomagnetic calibrations, Burckle, 1978).
Remarks: Restricted ranges of *Coscinodiscus vetustissimus* var. *javanica* Reinhold (11.2 to 10.7 Ma, Burckle, 1978), *C. loeblichii* Barron, n. sp. (about 10.5 to 9.4 Ma), and *C. yabei* var. *ellipticus* Barron, n. var. (about 9.8 to 9.4 Ma) all fall within the *C. yabei* Zone. *Nitzschia fossilis* (Frenguelli) Kanaya (9.8 Ma) and *Coscinodiscus nodulifer* var. *cyclopus* Jousé (8.9 to 8.8 Ma) have first occurrences within the *C. yabei* Zone, and *Denticulopsis hustedtii* last occurs (11.2 to 10.5 Ma) within the tropics within the zone.
Burckle (1978) correlated the first occurrence of *Thalassiosira burckliana* with the uppermost part of

paleomagnetic Chron 9 in the equatorial Pacific, but admitted that Chron 9 appears greatly abbreviated in many of his piston cores (L. H. Burckle, pers. comm., 1981). Hiatus NH5 of Keller and Barron (1983) removes sediments equivalent to Chron 9 throughout the equatorial Pacific, so it is possible that Burckle's calibration of the first occurrence of *T. burckliana* to paleomagnetics was affected by a hiatus in his piston cores. On Figure 2, the sediment accumulation rate curve for Site 572, the middle late Miocene trend established by paleomagnetically calibrated diatom datums has been continued to intersect the late middle Miocene trend established by diatom datums, and the extrapolated age of 10.5 Ma (Table 3) has been obtained for the first occurrence of *T. burckliana*. Site 572 was within the high-productivity zone along the equator in the eastern Pacific during the early late Miocene, and it is the most likely of the Leg 85 sites to have a complete section representing that interval. Indeed, compression of datum levels within the 10.5 to 9.8 Ma interval at Sites 573, 574, and 575 (Table 3) indicates the likelihood of hiatuses there. However, see also Barron et al. (this volume).

Characteristic flora: See Tables 5 and 7 (Hole 574) and Tables 6 and 7 (Hole 572D) for quantitative diatom data through the *C. yabei* Zone.

Correlation: The *C. yabei* Zone is equivalent to planktonic foraminiferal Zone N16 to lowermost Zone N17, calcareous nannofossil Subzone CN8, and upper *Diartus petterssoni* Zone to lower *Didymocyrtis antepenultima* Zone (radiolarians) in Leg 85 sediments.

Correlation with other diatom zones: The *C. yabei* Zone correlates with Subzone d of the *Denticulopsis hustedtii–D. lauta* Zone through Subzone a of the *D. hustedtii* Zone of the North Pacific, and with the uppermost *Nitzschia denticuloides* Zone through the *D. hustedtii–D. lauta* Zone of the Southern Ocean (Barron, in press; Ciesielski, 1983) (Fig. 3).

Nitzschia porteri Zone

Category: Interval zone.

Author: Burckle (1972).

Definition: Interval containing *Nitzschia porteri* between the last occurrence of *Coscinodiscus yabei* and the first occurrence of *Nitzschia miocenica*.

Subzones: Barron (in press) proposed the last occurrence of *Thalassiosira burckliana* (8.0 Ma) to define the Subzone A/Subzone B boundary.

Secondary markers: The first occurrence of *Nitzschia cylindrica* s. ampl. approximates the base of the *N. porteri* Zone, and the last occurrence of *Rossiella paleacea* (7.4 Ma) slightly predates the top of the zone.

Age: Late Miocene, 8.6 to 7.3 Ma (paleomagnetic calibrations, Burckle, 1978).

Remarks: The *N. porteri* Zone contains the first occurrences of *Nitzschia reinholdii* Kanaya and Koizumi s. ampl. (8.0 Ma) and *N. miocenica* Grunow (8.2 to 8.1 Ma) and the last occurrences of *Actinocyclus ellipticus* var. *javanica* Reinhold (8.0 Ma) and *Coscinodiscus vetulifer* var. *cyclopus* (7.9 Ma—within the Miocene). The first occurrence of *N. reinholdii* predates by more than 1 m.y. Burckle's (1978) calibration of that datum with lower paleomagnetic Chron 6, but it is consistent with the results of Sancetta (1982), who found *N. reinholdii* to range to the equivalent of the middle of Chron 7 at DSDP Site 503 in the eastern equatorial Pacific.

Characteristic flora: See Table 7 (Holes 574 and 572D) for quantitative diatom data on the *N. porteri* Zone.

Correlation: In Leg 85 sediments, the *N. porteri* Zone is equivalent to lower planktonic foraminiferal Zone N17 and to part of calcareous nannofossil Zone CN8, and it brackets the *Didymocyrtis antepenultima/D. penultima* zonal boundary of radiolarians. The calcareous nannofossil correlation appears somewhat old, because elsewhere in the Pacific, the *N. porteri* Zone contains the CN8/CN9 boundary within Subzone A (Barron et al., in press; Keller et al., 1982) (Fig. 3).

Correlation with other diatom zones: The *N. porteri* Zone correlates with the lower part of Subzone B of the *Denticulopsis hustedtii* Zone of the North Pacific, the lower part of Barron's (1981b) *Thalassiosira antiqua* Zone of the California area, and the lower part of the *D. hustedtii* Zone of the Southern Ocean (Barron, in press).

Nitzschia miocenica Zone

Category: Partial-range zone.

Author: Burckle (1972).

Definition: Interval between the first occurrence of *Nitzschia miocenica* Burckle and the first occurrence of *Thalassiosira convexa* Mukhina.

Subzones: The first occurrence of *Thalassiosira praeconvexa* Burckle (6.3 Ma) defines the Subzone A/Subzone B boundary (Burckle, 1972).

Secondary markers: The last occurrence of *Rossiella paleacea* slightly predates the base of the *N. miocenica* Zone, and the first occurrence of *Thalassiosira miocenica* (6.1 Ma) closely approximates the zone's top.

Age: Late Miocene, 7.3 to 6.1 Ma (paleomagnetic calibration, Burckle, 1978).

Remarks: *Nitzschia porteri* sensu Burckle (1972) has its last occurrence within the *N. miocenica* Zone (at about 6.8 Ma). Burckle (1978) noted only a slight overlap between the first occurrence of *N. miocenica* (7.3 Ma) and the last occurrence of *N. porteri*. At DSDP Site 503 in the eastern equatorial Pacific, Sancetta (1982) records an overlap of more than three cores between the two species, but Sancetta's (1982) extinction level for *N. porteri* coincides with the first occurrence of *Thalassiosira praeconvexa* (6.3 Ma). Thus, the Leg 85 result for the extinction level of *N. porteri* lies approximately halfway between the results of Burckle (1978) and Sancetta (1982).

Characteristic flora: See Table 7 (Holes 574 and 572D) for quantitative diatom data on Subzone A and Baldauf (this volume; Holes 573, 572A, and 572D) for quantitative diatom data on Subzone B of the *N. miocenica* Zone.

Correlation: The *N. miocenica* Zone is equivalent to middle planktonic foraminiferal Zone N17, upper calcareous nannofossil Zone CN8, and the upper *Didymocyrtis penultima* Zone (radiolarians) in Leg 85 sediments. Elsewhere in the Pacific, the zone is restricted

Table 7. Percent planktonic diatoms in Cores 5 to 11 of Hole 572D and Sample 574-6-6, 43–44 cm and Cores 7 and 8 of Hole 574.

Zone and subzone		Core-Section, interval (cm)	Sub-bottom depth (m)	*Actinocyclus ehrenbergii*	*A. ellipticus* s. ampl.	*Asteromphalus/Asteralampra*	*Coscinodiscus marginatus*	*C. nodulifer*	*C. plicatus/C. yabei*	*C. radiatus* s. ampl.	*C. tabularis* s. ampl.	*C. temperei* var. *deticata*	*C.* spp.	*Hemidiscus cuneiformis*	*Nitzschia cylindrica* s. ampl.	*N. fossilis*	*N. marina*	*N. miocenica* s. ampl.	*N. porteri*	*N. praereinholdii*	*N. reinholdii* s. ampl.	*N.* spp.	*Rhizosolenia* spp.	*Rossiella paleacea* s. ampl.	*R. praepaleacea*	*Rousia* spp.	*Thalassionema nitzschioides*	*T. nitzschioides* var. *parva*	*T. robusta*	*Thalassiosira kuerkiana*	*T. eccentrica*	*T. lentiginosa*	*T. praeconvexa*	*T.* spp.	*Thalassiothrix longissima*	*Thrinattium obtusatum*	Miscellaneous diatoms	Est. mated age (Ma)
		Hole 572D																																				
	B	5-2, 70-72	39.2	—	—	—	—	—	—	—	—	—	—	—	—	—	—	—	—	—	—	—	—	—	—	—	—	—	—	—	—	—	—	—	—	—	—	—
		5-4, 70-72	39.2	+	+	+	—	+	—	—	—	—	+	+	+	+	+	+	—	—	—	+	+	—	—	—	—	—	—	—	—	—	—	—	—	—	—	—
Nitzschia reinholdii		5-CC	39.7	+	+	+	—	+	—	—	—	—	+	+	+	+	+	+	—	—	—	+	+	—	—	—	—	—	—	—	—	—	—	—	—	—	—	—
	A	6-2, 70-72	39.5	+	+	+	—	+	—	—	—	—	+	+	+	+	+	+	—	—	—	+	+	—	—	—	—	—	—	—	—	—	—	—	—	—	—	—
		6-3, 70-72	39.9	+	+	+	—	+	—	—	—	—	+	+	+	+	+	+	—	—	—	+	+	—	—	—	—	—	—	—	—	—	—	—	—	—	—	—
		6-CC	40.1	+	+	+	—	+	—	—	—	—	+	+	+	+	+	+	—	—	—	+	+	—	—	—	—	—	—	—	—	—	—	—	—	—	—	—
	B	7-1, 70-72	39.5	+	+	+	—	+	—	—	—	—	+	+	+	+	+	+	—	—	—	+	+	—	—	—	—	—	—	—	—	—	—	—	—	—	—	—
		7-3, 70-72	41.5	+	+	+	—	+	—	—	—	—	+	+	+	+	+	+	—	—	—	+	+	—	—	—	—	—	—	—	—	—	—	—	—	—	—	—
Nitzschia porteri		7-CC	41.7	+	+	+	—	+	—	—	—	—	+	+	+	+	+	+	—	—	—	+	+	—	—	—	—	—	—	—	—	—	—	—	—	—	—	—
	A	8-2, 70-72	43.5	+	+	+	—	+	—	—	—	—	+	+	+	+	+	+	—	—	—	+	+	—	—	—	—	—	—	—	—	—	—	—	—	—	—	—
		8-4, 70-72	46.5	+	+	+	—	+	—	—	—	—	+	+	+	+	+	+	—	—	—	+	+	—	—	—	—	—	—	—	—	—	—	—	—	—	—	—
		8-6, 70-72	49.5	+	+	+	—	+	—	—	—	—	+	+	+	+	+	+	—	—	—	+	+	—	—	—	—	—	—	—	—	—	—	—	—	—	—	—
		8-CC	49.7	+	+	+	—	+	—	—	—	—	+	+	+	+	+	+	—	—	—	+	+	—	—	—	—	—	—	—	—	—	—	—	—	—	—	—
		9-1, 70-72	49.1	+	+	+	—	+	—	—	—	—	+	+	+	+	+	+	—	—	—	+	+	—	—	—	—	—	—	—	—	—	—	—	—	—	—	—
		9-3, 70-72	52.1	+	+	+	—	+	—	—	—	—	+	+	+	+	+	+	—	—	—	+	+	—	—	—	—	—	—	—	—	—	—	—	—	—	—	—
		9-CC	52.3	+	+	+	—	+	—	—	—	—	+	+	+	+	+	+	—	—	—	+	+	—	—	—	—	—	—	—	—	—	—	—	—	—	—	—
Coscinodiscus yabei	B	10-2, 70-72	52.5	+	+	+	—	+	—	—	—	—	+	+	+	+	+	+	—	—	—	+	+	—	—	—	—	—	—	—	—	—	—	—	—	—	—	—
		10-4, 70-72	55.5	+	+	+	—	+	—	—	—	—	+	+	+	+	+	+	—	—	—	+	+	—	—	—	—	—	—	—	—	—	—	—	—	—	—	—
		10-6, 70-72	58.5	+	+	+	—	+	—	—	—	—	+	+	+	+	+	+	—	—	—	+	+	—	—	—	—	—	—	—	—	—	—	—	—	—	—	—
		10-CC	58.7	+	+	+	—	+	—	—	—	—	+	+	+	+	+	+	—	—	—	+	+	—	—	—	—	—	—	—	—	—	—	—	—	—	—	—
		11-1, 70-72	58.1	+	+	+	—	+	—	—	—	—	+	+	+	+	+	+	—	—	—	+	+	—	—	—	—	—	—	—	—	—	—	—	—	—	—	—
		11-2, 77-78	59.8	+	+	+	—	+	—	—	—	—	+	+	+	+	+	+	—	—	—	+	+	—	—	—	—	—	—	—	—	—	—	—	—	—	—	—
		11-4, 70-71	61.5	+	+	+	—	+	—	—	—	—	+	+	+	+	+	+	—	—	—	+	+	—	—	—	—	—	—	—	—	—	—	—	—	—	—	—
		11-CC	63.7	+	+	+	—	+	—	—	—	—	+	+	+	+	+	+	—	—	—	+	+	—	—	—	—	—	—	—	—	—	—	—	—	—	—	—
		Hole 574																																				
	B	6-6, 43-44	50.4	—	6	3	—	13	—	—	1	—	—	2	—	—	1	19	—	—	1	5	—	—	2	—	19	6	—	—	2	4	+	—	12	2	—	6.3
Nitzschia miocenica		7-2, 43-45	53.9	—	3	3	—	20	—	+	+	—	—	2	+	+	+	8	+	—	+	2	—	+	+	—	24	6	—	—	1	+	—	+	30	1	—	6.8
	A	7-4, 43-45	56.9	+	3	3	—	5	—	—	—	—	—	3	2	1	2	—	+	—	+	3	1	2	+	+	28	11	—	—	1	+	—	+	6	+	+	7.4
		7-6, 43-45	59.9	—	6	2	—	3	—	—	—	—	—	3	2	1	2	—	3	1	—	3	1	+	—	+	28	11	—	—	3	+	—	+	7	2	+	7.9
Nitzschia porteri	B	7-CC	60.9	—	2	2	—	15	—	—	+	—	+	2	2	1	—	—	5	—	—	5	+	+	—	+	42	10	1	—	+	1	—	+	2	4	3	+	8.1
	A	8-1, 43-45	61.4	+	+	1	—	12	—	+	1	—	+	2	2	—	—	23	—	—	4	+	—	—	—	—	27	30	+	1	+	1	—	—	7	3	+	8.2
		8-3, 42-43	64.4	—	2	1	—	6	—	+	1	+	+	+	+	—	—	33	—	—	2	+	—	—	—	—	33	2	—	1	+	1	—	—	9	2	—	8.7
Coscinodiscus yabei	B	8-5, 110-111	67.4	2	3	3	—	11	—	+	4	+	2	3	—	—	—	13	—	—	2	—	3	1	+	31	+	—	1	+	1	—	—	3	13	1	1	9.3
		8-7, 20-21	70.2	+	1	+	+	4	2	+	1	+	+	+	—	—	—	32	2	—	1	+	1	2	+	25	15	—	—	—	—	—	—	1	9	+	—	9.8

Note: + means <1% or encountered after the count; — means not encountered. 300 specimens were counted.

to Zone CN9 and brackets the CN9a/CN9b boundary (Keller et al., 1982; Barron, in press; Haq et al., 1980). It therefore appears that the CN8/CN9 boundary is placed substantially above its generally accepted position in Leg 85 sediments.

Correlation with other diatom zones: The *Nitzschia miocenica* Zone correlates with the upper part of Subzone b of the *D. hustedtii* Zone to lowermost *D. kamtschatica* Zone of the North Pacific, the upper part of the *Thalassiosira antiqua* Zone to lowermost *Nitzschia reinholdii* Zone (Barron, 1981b) of the California area, and the middle part of the *D. hustedtii* Zone of the Southern Ocean (Barron, in press; Ciesielski, 1983) (Fig. 3).

Thalassiosira convexa Zone

Category: Partial-range zone.

Author: Burckle (1972).

Definition: Interval from the first occurrence of *Thalassiosira convexa* to the first occurrence of *Nitzschia miocenica* Burckle.

Subzones: Burckle (1972) defined three subzones: Subzone A, from the base of the zone to the last occurrence of *Thalassiosira praeconvexa* (5.8 Ma); Subzone B, from the top of Subzone A to the last occurrence of *Thalassiosira miocenica* Schrader (5.1 Ma); and Subzone C, from the top of Subzone B to the top of the zone.

Secondary markers: The first occurrence of *Thalassiosira miocenica* closely approximates the base of the *T. convexa* Zone.

Age: Latest Miocene to earliest Pliocene, 6.1 to 4.6 Ma (paleomagnetic calibrations, Burckle, 1978). The Subzone B/Subzone C boundary coincides with the Miocene/Pliocene boundary (Burckle, 1978).

Remarks: The *Thalassiosira convexa* Zone contains the last occurrences of *Rossiella praepaleacea* (6.0 Ma), *Nitzschia miocenica* Burckle (5.6 Ma), *Nitzschia miocenica* var. *elongata* Burckle (5.65 Ma), and *Asteralampra acutiloba* Forti (5.35 Ma). *Thalassiosira oestrupii* (Ostenfeld) Proshkina-Lavrenko ss. str. first occurs at the Subzone B/Subzone C boundary or Miocene/Pliocene boundary (5.1 Ma).

Correlation: The *Thalassiosira convexa* Zone is equivalent to upper planktonic foraminiferal Zone N17 to lower N19 and to calcareous nannofossil Zone CN9

through Subzone CN10b, and it closely approximates the *Stichocorys peregrina* Zone of radiolarians in Leg 85 sediments.

Correlation with other diatom zones: The *T. convexa* Zone correlates with most of Subzones a and b of the *Denticulopsis kamtschatica* Zone of the North Pacific, with the upper *Nitzschia reinholdii* Zone to lower *Thalassiosira oestrupii* Zone (Barron, 1981b) of the California area, and the upper *D. hustedtii* Zone of the Southern Ocean (Barron, in press; Ciesielski, 1983) (Fig. 3).

Nitzschia jouseae Zone

Category: Partial-range zone.

Author: Burckle (1972).

Definition: Interval from the first occurrence of *Nitzschia jouseae* to the first occurrence of *Rhizosolenia praebergonii* Mukhina.

Age: Early Pliocene to early late Pliocene, 4.5 to 3.0 Ma (paleomagnetic calibration, Burckle, 1978).

Remarks: Within the *N. jouseae* Zone are the last occurrences of *Nitzschia cylindrica* (4.4 Ma) and *Actinocyclus ellipticus* f. *lanceolata* (3.5 to 3.2 Ma; oldest at Site 572—Table 3) and the first occurrences of *Asterolampra elegans* Greville (3.9 Ma) and *Thalassiosira convexa* var. *convexa* Schrader (3.6 Ma). Burckle (1978) also records the first occurrence of *Coscinodiscus africanus* Janisch at about 3.7 Ma, but this datum was not searched for in Leg 85 sediments.

Characteristic flora: See Baldauf (this volume) for quantitative diatom data from the *N. jouseae* Zone of Sites 572 and 573.

Correlation: In Leg 85 sediments, the *Nitzschia jouseae* Zone is equivalent to upper planktonic foraminiferal Zone N19, Subzone CN10c and Zone CN11 of calcareous nannofossils, and the *Spongaster pentas* Zone of radiolarians.

Correlation with other diatom zones: The *N. jouseae* Zone correlates with Subzone c of the *Denticulopsis kamtschatica* Zone of the North Pacific. For the Southern Ocean, the *N. jouseae* Zone is equivalent to the *Nitzschia reinholdii* to upper *N. interfrigidaria* zones of Weaver and Gombos (1981) and the *Nitzschia reinholdii* to middle *N. interfrigidaria–Coscinodiscus vulnificus* zones of Ciesielski (1983) (Barron, in press; Ciesielski, 1983) (Fig. 3).

Rhizosolenia praebergonii Zone

Category: Partial-range zone.

Author: Burckle (1972).

Definition: Interval from the first occurrence of *Rhizosolenia praebergonii* to the first occurrence of *Pseudoeunotia doliolus* Wallich.

Subzones: Burckle (1972) defined three subzones: Subzone A, from the base of the zone to the last occurrence of *Nitzschia jouseae* (2.6 Ma); Subzone B, from the top of Subzone A to the last occurrence of *Thalassiosira convexa* (2.1 Ma); and Subzone C, from the top of Subzone B to the top of the zone.

Secondary markers: The last occurrence of *Rhizosolenia praebergonii* (1.8 Ma) slightly predates the top of the zone (Burckle and Trainer, 1979).

Age: Late Pliocene, 3.0 to 1.8 Ma (paleomagnetic calibrations, Burckle, 1978).

Characteristic flora: Quantitative diatom data for the *R. praebergonii* Zone of Sites 572 and 573 are given in Baldauf (this volume).

Correlation: The *R. praebergonii* Zone is equivalent to planktonic foraminiferal Zone N21 and to calcareous nannofossil Zone CN12, and it brackets the *Spongaster pentas/Pterocanium prismaticum* zonal boundary of radiolarians in Leg 85 sediments.

Correlation with other diatom zones: The *R. praebergonii* Zone correlates with the *Denticulopsis seminae* var. *fossilis–D. kamtschatica* and *D. seminae* var. *fossilis* zones of the North Pacific. For the Southern Ocean, the *R. praebergonii* Zone correlates with the upper part of the *Nitzschia interfrigidaria* through *Coscinodiscus kolbei–Rhizosolenia barboi* zones of Weaver and Gombos (1981), and with the upper *N. interfrigidaria–C. vulnificus* through *Coscinodiscus kolbei–Rhizosolenia barboi* zones of Ciesielski (1983) (Barron, in press; Ciesielski, 1983) (Fig. 3).

Nitzschia reinholdii Zone

Category: Concurrent-range zone.

Author: Burckle (1977).

Definition: Interval from the first occurrence of *Pseudoeunotia doliolus* to the last occurrence of *Nitzschia reinholdii*.

Subzones: Burckle (1977) proposed two subzones, A and B, with the last occurrence of *Rhizosolenia praebergonii* var. *robusta* Burckle and Trainer (1.55 Ma) defining the subzonal boundary.

Secondary markers: The last occurrence of *Rhizosolenia praebergonii* var. *praebergonii* slightly predates the base of the *P. doliolus* Zone (Burckle and Trainer, 1979).

Age: Latest Pliocene to Quaternary, 1.8 to 0.65 Ma (paleomagnetic calibration, Burckle, 1978). The Subzone A/Subzone B boundary closely approximates the Pliocene/Quaternary boundary.

Remarks: Although Sancetta (1982) reported that *Nitzschia reinholdii* disappeared just below the Jaramillo Event of the Matuyama paleomagnetic Chron at DSDP 503 in the eastern equatorial Pacific, its extinction in Leg 85 sediments is within the lower part of the Brunhes Chron (Table 3 and Weinreich and Theyer, this volume), consistent with the results of Burckle (1977) and Burckle and Opdyke (1977).

Characteristic flora: *Thalassionema nitzschioides* Grunow and *Coscinodiscus nodulifer* are common diatoms within the *N. reinholdii* Zone; *Pseudoeunotia doliolus, Nitzschia marina*, and *N. reinholdii* are frequent species. *Rhizosolenia praebergonii* var. *robusta* is fairly common within Subzone A.

Correlation: The *N. reinholdii* Zone is equivalent to planktonic foraminiferal Zone N22, lower calcareous nannofossil Zone CN13 to middle Zone CN14, and the upper part of the *Pterocanium prismaticum* Zone to uppermost *Amphirhopalum ypsilon* Zone of radiolarians in Leg 85 sediments.

Correlation with other diatom zones: The *N. reinholdii* Zone correlates with the *Actinocyclus oculatus* Zone through Subzone a of the *Rhizosolenia curvirostris*

Zone of the North Pacific, and with the *Rhizosolenia barboi–Nitzschia kerguelensis* and *Coscinodiscus elliptopora–Actinocyclus ingens* zones of the Southern Ocean (Barron, in press; Ciesielski, 1983) (Fig. 3).

***Pseudoeunotia doliolus* Zone**

Category: Partial-range zone.
Author: Burckle (1972, 1977).
Definition: Interval above the last occurrence of *Nitzschia reinholdii* containing *Pseudoeunotia doliolus*.
Age: Late Quaternary, 0.65 to 0 Ma (paleomagnetic calibration, Burcke, 1977).
Remarks: See comments under *N. reinholdii* Zone.
Characteristic flora: Assemblages are dominated by *Coscinodiscus nodulifer* and *Thalassiosira oestrupii*. *Nitzschia marina, Pseudoeunotia doliolus, Thalassiosira nitzschioides*, and *Asteromphalus* spp. are secondarily common.
Correlation: The *P. doliolus* Zone is equivalent to upper planktonic foraminiferal Zone N22 and Zone N23, upper calcareous nannofossil Zone CN14 and Zone CN15, and the *Collosphaera tuberosa* and *Buccinosphaera invaginata* zones of radiolarians in Leg 85 sediments.
Correlation with other diatom zones: The *P. doliolus* Zone correlates with Subzone b of the *Rhizosolenia curvirostris* Zone and the *Denticulopsis seminae* Zone of the North Pacific, and with the *Coscinodiscus lentigenosus* Zone of the Southern Ocean (Barron, in press; Ciesielski, 1983) (Fig. 3).

AGE-VERSUS-DEPTH PLOTS

Estimated ages of diatom datum levels that have been calibrated directly and indirectly with paleomagnetic stratigraphy (Tables 1 to 3) and direct Leg 85 paleomagnetic stratigraphy (Weinreich and Theyer, this volume) have been used on Figure 4 to construct age-versus-depth plots for the upper Cenozoic of Sites 572 to 575. The datums used include those of Burckle (1978), along with additions and modifications suggested by Barron et al. (in press). As stated in the preceding section, these plots allow the ages of secondary datum levels to be extrapolated and compared within the Leg 85 sections. In addition, rates of sediment accumulation can be compared between the sites, and hiatuses and greatly compressed intervals can be detected.

Sediment Accumulation Rates

Figure 4 shows that rates of sediment accumulation at eastern equatorial Site 572 were at least 1.7 times greater than those at central equatorial Sites 573 to 575 throughout the middle Miocene, late Miocene, and earliest Pliocene. Of the three central equatorial sites, Site 573 shows the highest rates of sediment accumulation between 0 and 11 Ma, reflecting its present position with the equatorial region of high productivity. Sediment accumulation rates between 1 and 4 Ma are roughly comparable (15 m/m.y.) between eastern Site 572 and central Site 573. For the middle Miocene (15.5 to 11 Ma), the central equatorial Pacific rates are higher (20 to 30 m/m.y.) at Site 574 than at Sites 573 and 575, corresponding to a time when Site 574 was within the high-productivity zone and Sites 573 and 575 were not. Early Miocene sediment accumulation rates were relatively high (18 to 20 m/m.y.) at Sites 574 and 575, indicating that both those sites were then within the region of high productivity.

Hiatuses

The near coincidence of the last occurrences of *Craspedodiscus elegans* (18.7 Ma; Sample 574C-5,CC) and *Actinocyclus radionovae* (18.0 Ma; Sample 574C-5-3, 43–45 cm) indicates the possibility of a hiatus at about 235 m sub-bottom at Site 574. This hiatus would correspond in part to hiatus NH1 of Keller and Barron (1983), which is present throughout much of the central equatorial Pacific.

Compression of diatom datum levels in the upper part of Core 573B-14 (Table 3) suggests a hiatus from about 17.6 to 17.0 Ma at Site 573 (Fig. 4). This hiatus (NH1b) has also been recognized at nearby Site 77 by Keller and Barron (1983). A sharp lithologic contact at 262.1 m sub-bottom in upper Core 573B-14, where white radiolarian–nannofossil oozes rest on white to very light brown radiolarian–nannofossil oozes and chalks and siliceous nannofossil oozes and chalks (see site chapter), is consistent with this hiatus.

Keller and Barron (1983) also proposed a second hiatus (NH1a) at Site 77, approximately 20 m below NH1b, at the base of Core 77B-30. Poor preservation of diatoms below 270 m at Site 573 hinders recognition of this second hiatus, which spans the interval of Subzone A of the *Rossiella paleacea* Zone (20.6 to 19.9 Ma), according to Barron et al. (in press); but a sharp lithologic contact in uppermost Core 573B-17 (290.6 m), between light brown nannofossil oozes above and white nannofossil oozes below, may correspond to this hiatus.

At Site 575 sediment accumulation rates decreased dramatically between 15.5 and 14.4 Ma (82 to 74 m sub-bottom depth). This is also indicated by a relatively compressed planktonic foraminiferal Zone N9 at Site 575 (Saito, this volume). Although no hiatus is apparent, this interval does correspond in part with widespread hiatus NH2 (16.0 to 15.0 Ma) of Keller and Barron (1983).

Figure 4 also shows decreased sediment accumulation rates for Site 573 between 12.0 and 11.4 Ma, corresponding to the compression of the last-occurrence datum level of *Coscinodiscus tuberculatus* (12.0 Ma) (Sample 573B-5-1, 68–70 cm) and the last common occurrence of *Denticulopsis hustedtii* (11.5 Ma; see section on quantitative stratigraphy) (Sample 573B-4-5, 68–70 cm). This compressed interval corresponds in part to hiatus NH4 of Keller and Barron (1983) (12.0 to 11.0 Ma), which is widespread in the northeast Pacific, and also coincides with severe calcium carbonate dissolution at all the Leg 85 sites.

Hiatuses between 10.5 and 9.8 Ma (hiatus NH4 of Keller and Barron, 1983) are present at Sites 573, 574, and 575 (Fig. 4), although Core 572D-11 (255.5 to 246 m sub-bottom) apparently is complete across that interval (Fig. 2). Compression of diatom datum levels in Section 1 of Core 573B-3, in lowermost Core 574-8, and in low-

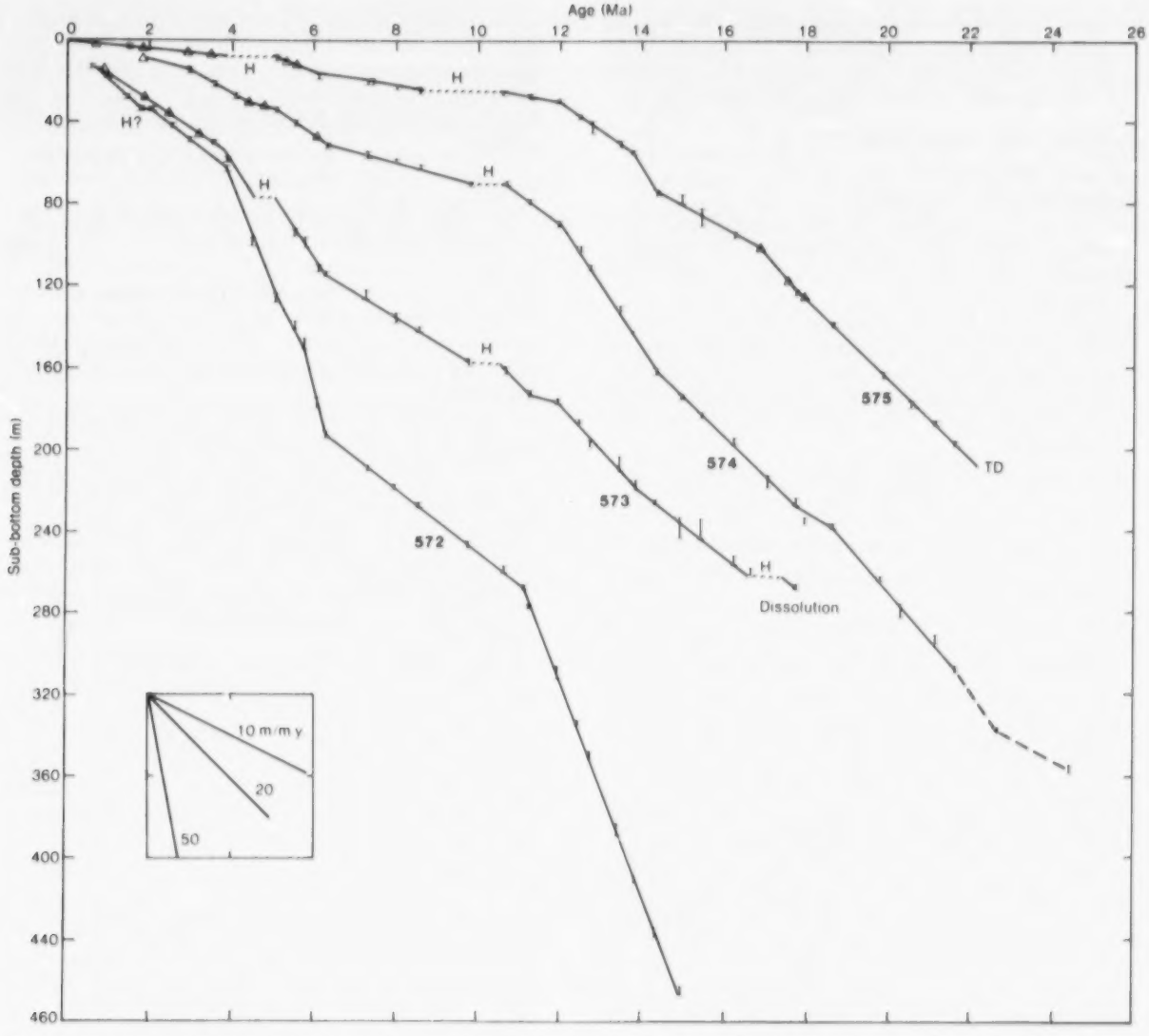

Figure 4. Age-versus-depth curves for the upper Cenozoic of DSDP Sites 572 to 575. △ = paleomagnetic calibrations after Weinreich and Theyer (this volume); H = hiatus; TD = total depth. Vertical bars represent depth intervals in which diatom datums occur (see Tables 2 and 3). See also Barron et al. (this volume).

ermost Core 575-3 (Table 3) indicates hiatuses. At Sites 573 and 574, the hiatuses coincide with distinctive purple-banded sediment units (see site chapters), but such a unit was not observed at Site 575, where the hiatus is more extensive (10.5 to 8.6 Ma).

Near coincidence of the last occurrence of *Thalassiosira miocenica* (5.1 Ma; Sample 573-10-1, 65–66 cm) with the first occurrence of *Nitzschia jouseae* (4.5 Ma; Sample 573-9-5, 67–68 cm) indicates the probability of a hiatus (NH7 of Keller and Barron, 1983) at 76 m subbottom at Site 573. At Site 574, paleomagnetic stratigraphy suggests that this interval is present (Weinreich and Theyer, this volume; Fig. 4), but it is much compressed. At Site 575 a more extensive hiatus (5.1 to 3.6 Ma) removes sediments at the interval between Samples 575-2-1, 52–53 cm and 575-1,CC.

Finally, a possible hiatus or greatly compressed interval is present in Section 4 of Core 572A-4, as indicated by the near coincidence of the last occurrence of *Thalassiosira convexa* (2.1 Ma; Sample 572A-4-5, 66–67 cm) and the first occurrence of *Pseudoeunotia doliolus* (1.8 Ma; Sample 572A-4-3, 66–67 cm).

PALEOMAGNETIC CORRELATION, HOLE 575A

On Figure 5 the paleomagnetic data of Weinreich and Theyer (this volume) for Cores 1 to 10 of Hole 575A are correlated with the polarity sequence from the middle of paleomagnetic Chron 16 (Anomaly 5C) to middle Chron 17 (Anomaly 5D). This interpretation supports paleomagnetic calibrations for the N6/N7 planktonic foraminiferal zonal boundary and the CN2/CN3 calcareous nannofossil zonal boundary proposed by Ryan et al.

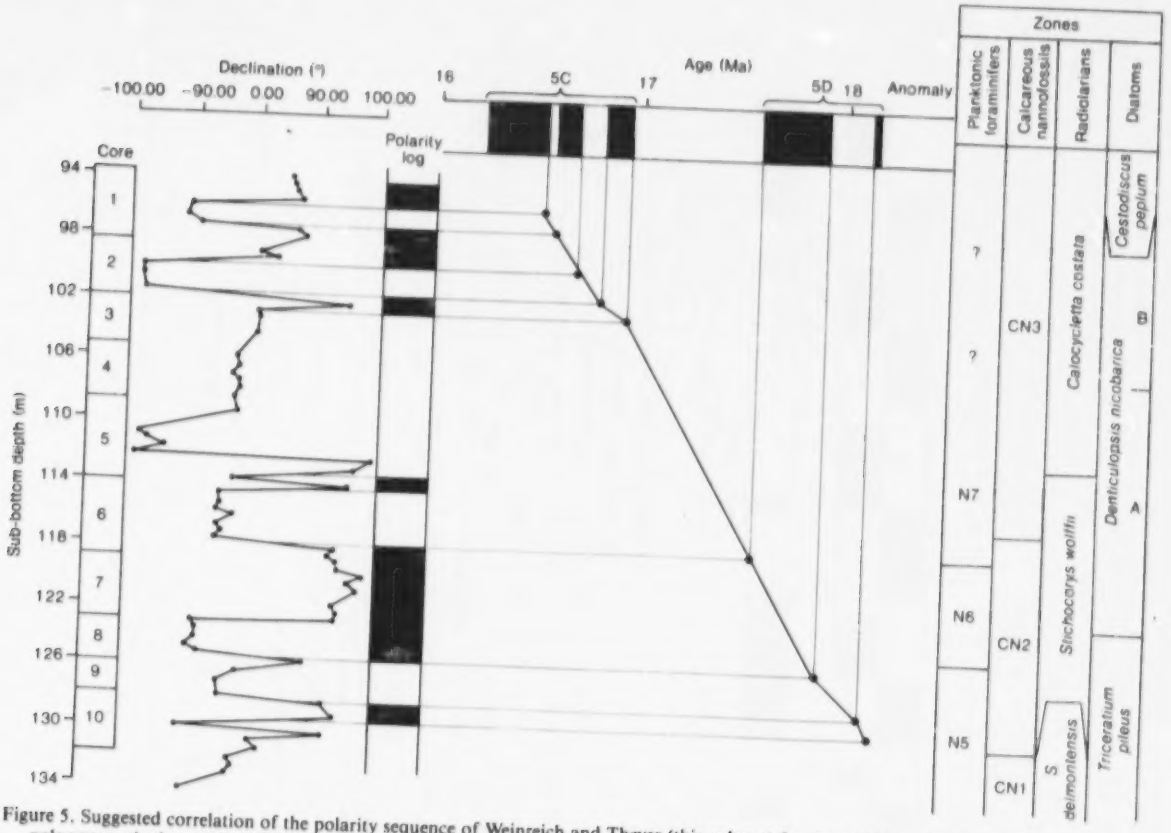

Figure 5. Suggested correlation of the polarity sequence of Weinreich and Theyer (this volume) for Cores 575A-1 through 575A-10 with the paleomagnetic time scale of Berggren et al. (in press). Planktonic foraminifer, calcareous nannofossil, and radiolarian zones are after the site chapter.

(1974) and Berggren (1981). It also is compatible with the paleomagnetic correlations (Poore et al., 1983) of planktonic foraminiferal Zone N8 and calcareous nannofossil Zones CN3 and CN4 with the upper reversed event of paleomagnetic Chron 16. In addition, the correlation of Figure 5 produces a relatively straight age-versus-depth curve for the lower Miocene of Sites 574 and 575 when coupled with younger diatom datum levels tied directly to paleomagnetics (by Burckle, 1978) and older diatom datum levels calibrated indirectly with paleomagnetics (by Barron et al., in press).

The ranges of key diatoms in Cores 1 to 10 of Hole 575A are presented on Figure 6. The sequence of datums in the interval from the middle part of the *Triceratium pileus* Zone to the lowermost *Cestodiscus peplum* Zone agrees well with the sequence at Sites 574 and 575 (Table 3), and with the sequences at Sites 71, 77, and 495 (Barron, 1983). As discussed by Barron (1983), Burckle's (1978) correlations of the first occurrence of *Annellus californicus* with upper Chron 16 and of the first occurrence of *Cestodiscus peplum* with uppermost Chron 17 are discounted, because these datums consistently occur in the reverse order. The *Annellus californicus* first-occurrence datum of Burkle (1978), however, may represent a recurrence, because the species becomes sparse to absent above its initial occurrences (Barron, 1983). The remaining diatom datum levels on Figure 6 are correlated directly with paleomagnetic stratigraphy for the first time. Occurrence data are presented, in part, on Table 4. The *Thalassiosira spinosa* and *T. spumellaroides* last-occurrence datums are regarded with some doubt, because they represent isolated sparse occurrences. The other datum levels are placed above or below continuous occurrences, although *Annellus californicus, Craspedodiscus coscinodiscus* s. str., and *Triceratium pileus* are generally sparse.

QUANTITATIVE DIATOM BIOSTRATIGRAPHY

Quantitative diatom data for the late early Miocene to latest Miocene (17.8 to 6.3 Ma) of Sites 572, 574, and 575 are presented on Tables 4 to 7. These data are supplemented by data from DSDP Sites 77 (within 10 km of Site 573) and 158 (Tables 8 to 10) to complete a transect from the easternmost equatorial Pacific to the central Pacific (Fig. 1). For the late early and middle Miocene, one to two samples per 100,000-yr. span in the section were counted from Sites 158, 572, 574, and 575. For the late Miocene and for Site 77, sampling intervals average one per 200,000 to 300,000 yrs. The age-versus-depth curves (Figs. 4 and 5) were used to assign absolute ages

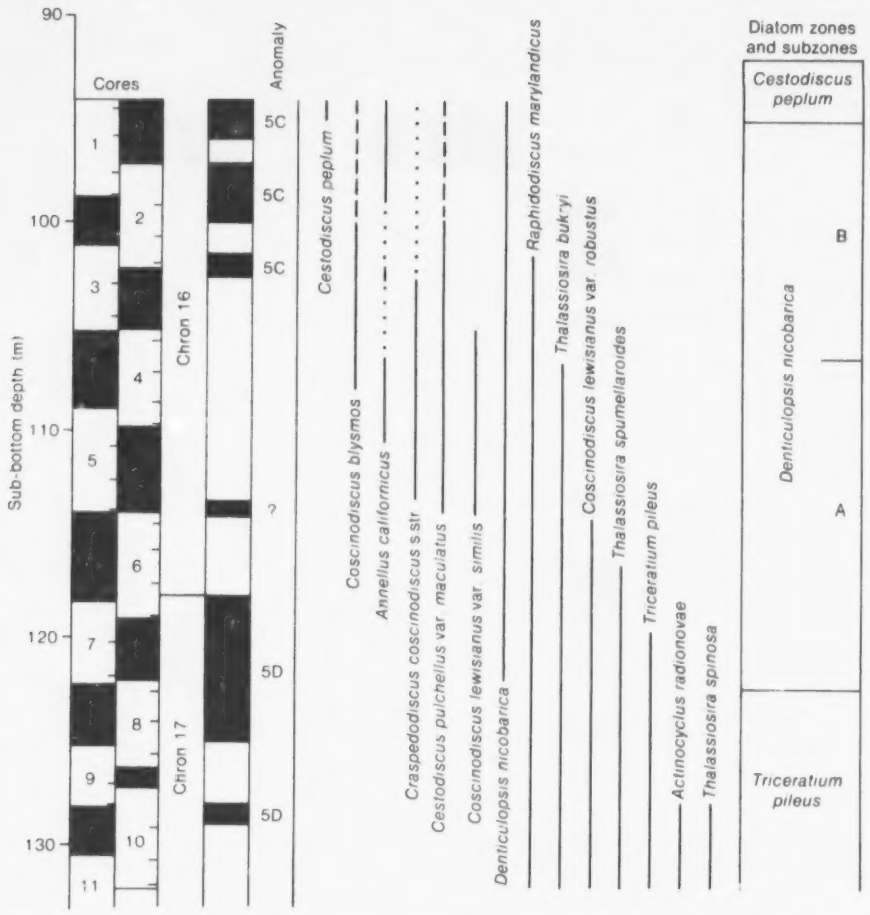

Figure 6. Correlation of diatom ranges in Cores 575A-1 through 575A-10 with paleomagnetic stratigraphy. Refer to Figure 5 and Table 3.

to the Leg 85 samples, whereas curves constructed with the same datums and time scale (Barron et al., in press) were used to assign ages to the Site 77 and Site 158 samples. These ages, therefore, are assigned solely by diatom datum level and paleomagnetic control, and they provide a framework for evaluating the abundance trends of individual diatom species and assessing their use for biostratigraphy. Where quantitative changes have been induced by abrupt region-wide changes in paleoceanography, these changes should approach isochroneity in the equatorial Pacific sections (Burckle and Trainer, 1979; Barron and Keller, 1983). In addition, quantitative data obtained from the sections can be useful in directly establishing the paleogeography of individual species during the late early Miocene to latest Miocene in the equatorial Pacific, and in determining paleoceanographic and paleoclimatic changes.

In the following section, quantitative trends of individual species will be discussed in the light of their stratigraphic value, and differences in the abundance of these species across the equatorial Pacific will be noted. Paleoceanographic and paleoclimatic interpretations are treated in Barron (this volume). The error in assigning absolute ages to the samples from the age-versus-depth curves is believed to be as much as 100,000 yrs., so that distinctive quantitative changes occurring at two or more sites within 100,000 yrs. of each other will be treated as isochronous. It is hoped that $CaCO_3$ and isotope stratigraphy will provide the stratigraphic resolution necessary to test the isochroneity of these changes.

Actinocyclus ehrenbergii has two brief abundance spikes in the middle Miocene, where abundance values double to triple. One event at about 13.2 Ma is apparent at Site 574 (Table 5) and Site 572 (Table 6), where *A. ehrenbergii* increases to 10% of the assemblage. This event seems more abrupt at Site 572, so it may be more distinctive in the eastern equatorial Pacific. The event was apparently missed by the broader sampling interval at Site 77, and it predates the Site 158 sedimentary record. The second *A. ehrenbergii* abundance spike at about 12.1 Ma is recognizable at Sites 547, 77, 572, and 158 (Tables 5, 6, 8, and 9). Again, abundance values reach 8

Table 8. Percent planktonic diatoms in Cores 17 to 28 of Hole 77B.

Zone and subzone	Core-Section, interval (cm)	Sub-bottom depth (m)	*Actinocyclus ehrenbergii*	*A. ellipticus* s. ampl.	*A. ingens*	*Asteromphalus/Asteromphalus*	*Cestodiscus peplum*	*C. pulchellus*	*C. pulchellus* var. *maculatus*	*Coscinodiscus blysmos*	*C. lewisianus*	*C. marginatus*	*C. nodulifer*	*C. plicatus/C. yabei*	*C. radiatus*	*C. salisburyanus*	*C. tabularis* s. ampl.	*C. temperei* var. *delicata*	*C. tuberculatus*	*C.* spp.	*Craspedodiscus coscinodiscus*	*Annellus californicus*	*Denticulopsis hustedtii*	*D. nicobarica*	*D. praedimorpha*	*D. punctata* f. *hustedtii*	*Hemidiscus cuneiformis*	*Nitzschia maleinterpretans*	*N.* spp.	*Raphidodiscus marylandicus*	*Rhizosolenia* spp.	*Rossiella paleacea* s. ampl.	*Rouxia* spp.	*Synedra jouseana/S. miocenica*	*Thalassionema nitzschioides* s. ampl.	*T. robusta*	*Thalassiosira fraga*	*T. lepidopus*	*T. lappanae*	*Thalassiothrix longissima*	Miscellaneous diatoms	Estimated age (Ma) (after Barron et al., in press)
Coscinodiscus yabei A	17-1, 18-20	155.6	+	1	—	+	—	—	—	—	—	+	7	—	—	—	—	1	—	1	—	—	+	—	—	1	—	14	—	+	+	—	—	57	12	—	+	—	2	2	10.8
	17-4, 100–104	158.8	+	1	—	+	—	—	—	—	—	+	7	+	—	—	1	+	—	2	—	—	+	—	—	6	—	13	—	2	—	—	—	53	2	—	+	—	6	2	11.0
	17-6, 23–25	160.9	—	1	—	+	—	—	—	—	—	+	7	2	+	—	+	+	—	—	—	—	—	—	—	—	—	18	—	—	—	—	—	59	—	—	1	—	2	+	11.2
	18-2, 23–25	163.3	—	2	—	+	—	—	—	—	—	5	7	2	+	—	+	1	—	2	—	—	—	9	—	—	—	10	—	+	+	—	—	50	3	—	+	—	6	2	11.3
Actinocyclus moronensis	18-4, 100–104	167.1	+	1	+	—	—	—	—	—	—	1	7	2	—	—	3	1	—	—	—	—	—	10	—	—	1	15	—	2	+	—	—	52	+	—	—	—	3	2	11.5
	18-6, 38–40	169.5	—	3	—	+	—	—	—	—	—	+	3	2	—	—	2	1	—	—	—	—	—	24	—	—	1	6	—	—	2	—	—	40	—	—	+	—	2	3	11.65
	19-2, 38–40	172.5	1	1	—	1	—	—	—	—	—	+	5	4	—	—	5	—	—	2	—	—	—	13	—	—	2	—	—	+	4	1	—	43	7	—	—	—	6	2	11.8
	19-4, 100–104	176.1	8	1	—	3	—	—	—	—	—	2	5	2	+	—	6	1	2	—	—	—	—	3	—	—	1	4	—	+	2	—	—	35	14	—	1	—	8	2	12.0
	19-6, 38–40	178.5	2	4	—	+	—	—	—	—	—	+	2	3	—	—	8	1	2	—	—	—	—	13	—	—	2	—	—	+	—	—	—	44	11	—	1	—	3	1	12.15
Craspedodiscus coscinodiscus	20-2, 38–40	181.6	+	1	—	+	—	—	—	—	—	+	4	1	+	—	15	1	3	2	—	—	—	1	—	—	+	—	—	—	—	—	—	27	—	—	—	—	4	2	12.3
	20-4, 30–31	184.5	—	7	+	+	—	—	—	—	—	—	7	4	+	—	16	+	29	—	+	—	—	4	—	—	+	—	—	—	—	—	—	23	—	—	+	—	6	2	12.45
	20-6, 38–40	187.6	2	6	—	—	—	—	—	—	—	—	2	2	2	—	29	+	11	—	2	—	—	6	—	—	+	+	—	—	—	—	—	28	—	—	1	—	5	3	12.6
Coscinodiscus gigas var. *diorama*	21-2, 38–40	190.9	—	6	43	+	—	—	—	—	—	—	1	2	1	—	10	+	+	+	—	—	—	14	—	24	—	—	—	—	2	—	—	20	—	—	—	—	3	1	12.6
	21-5, 90–94	195.9	7	4	27	1	—	—	—	—	—	8	—	1	1	—	6	—	9	—	—	—	—	1	—	—	—	—	—	—	—	—	—	20	—	—	—	—	3	—	12.9
	21-6, 35–37	196.9	+	4	11	—	—	—	—	—	—	7	+	2	—	—	13	—	9	—	1	—	—	1	—	—	+	—	—	—	—	—	—	28	—	—	+	—	5	+	13.05
	22-2, 35–37	200.0	—	7	14	+	—	—	—	—	—	3	1	4	3	—	11	—	6	—	—	—	—	2	—	—	+	—	—	—	1	—	—	44	—	—	+	—	5	—	13.1
Coscinodiscus lewisianus	22-5, 102–106	205.1	—	4	26	2	—	—	—	—	—	+	1	2	+	—	11	—	—	1	3	+	—	17	7	—	+	—	—	—	1	—	—	26	—	—	3	—	3	—	13.3
	22-6, 35–37	206.0	+	5	7	—	—	—	—	—	1	+	+	1	+	—	14	—	+	+	+	+	—	2	29	—	+	—	—	—	1	—	—	12	—	—	+	—	6	1	13.5
	23-2, 35–37	209.1	+	2	41	1	—	—	—	—	+	2	—	1	+	—	15	—	—	+	+	+	—	3	48	—	+	—	—	—	+	2	+	1	7	—	—	+	—	2	+	13.6
	23-4, 23–24	211.9	—	4	6	+	—	—	—	—	+	1	—	—	2	—	7	—	+	8	—	—	—	—	—	—	—	—	—	—	+	—	—	12	—	—	+	—	11	+	13.75
	23-6, 35–37	215.1	—	6	4	—	—	—	—	—	3	+	—	—	+	+	2	—	—	3	—	+	—	25	—	—	—	—	—	—	+	—	—	40	—	—	—	5	6	+	13.9
	24-2, 35–37	218.2	—	—	38	+	3	12	—	—	—	2	—	—	51	—	4	—	—	2	—	—	—	—	2	—	—	—	—	—	+	—	—	15	—	—	1	7	6	—	14.05
B	24-4, 100–104	221.8	—	—	8	1	2	4	—	+	1	2	—	—	3	+	7	—	—	+	+	—	—	—	26	—	—	—	—	—	+	—	1	—	—	—	3	2	—	14.25
Cestodiscus peplum	24-6, 20–22	224.0	—	—	6	—	+	3	—	—	2	2	—	—	3	+	18	—	—	—	—	—	—	—	51	—	—	—	—	—	+	—	—	20	—	—	—	1	4	—	14.55
	25-2, 20–22	227.3	—	—	—	+	1	7	—	—	3	+	—	—	20	—	4	—	—	—	2	+	—	—	40	—	—	—	—	—	+	—	—	42	—	—	—	—	7	—	14.75
A	25-4, 94–98	231.1	—	—	2	+	—	4	—	+	+	2	—	—	42	—	7	—	—	—	—	—	—	—	21	—	—	—	—	—	+	—	—	22	—	—	—	—	2	—	15.0
	25-6, 20–22	233.3	—	—	—	+	+	24	4	+	1	1	—	—	22	—	2	—	—	—	—	+	—	—	8	—	—	—	—	—	+	—	—	5	—	—	—	—	29	—	15.3
	26-2, 20–22	236.3	—	—	—	+	+	40	12	7	+	2	—	—	4	—	1	—	—	—	+	+	—	—	2	—	—	—	—	—	—	—	—	5	2	—	—	—	24	—	15.5
B	26-4, 92–96	240.0	—	—	—	+	+	22	2	—	2	5	—	—	5	1	2	—	—	—	—	—	—	—	1	—	—	6	—	—	—	2	—	33	10	—	—	—	6	+	15.8
	26-6, 42–44	242.5	—	—	—	2	—	41	+	—	5	—	—	—	2	1	1	—	—	—	—	—	—	—	1	—	—	1	+	—	—	2	—	23	15	—	—	—	6	—	16.2
	27-2, 92–96	246.2	—	—	—	2	—	43	—	—	3	+	—	—	2	3	+	—	—	—	—	—	—	—	—	—	—	+	—	—	+	1	—	28	6	—	—	—	7	—	16.3
Denticulopsis nicobarica A	27-4, 92–94	249.2	—	—	—	5	—	3	+	—	4	—	—	—	11	2	1	—	—	+	—	+	—	—	+	—	—	+	—	—	—	—	—	50	16	—	+	—	14	+	16.6
	27-6, 30–31	251.6	—	—	—	+	—	15	1	+	2	—	—	—	5	+	1	—	—	—	1	1	—	—	2	—	—	—	—	—	—	+	2	31	16	—	+	—	19	—	16.8
	28-2, 28–30	254.8	—	—	—	2	—	2	2	—	1	+	—	—	—	5	+	—	—	—	—	—	—	—	22	—	—	+	—	4	—	2	—	8	10	—	14	—	12	—	17.1
	28-4, 92–96	258.4	—	—	—	+	—	31	—	—	1	2	—	—	—	+	+	—	—	—	—	—	—	—	62	—	—	3	—	2	—	—	—	2	2	—	3	—	11	1	17.3
	28-6, 28–30	260.8	—	—	—	+	—	63	—	—	1	+	—	—	2	+	+	—	—	—	—	—	—	—	22	—	—	2	—	2	—	—	—	2	12	—	+	—	22	—	17.5
																								3	—	—	+	—	+	—	—	—	11	—	1	—	—	6	—	17.7

Note: + means < 1% or encountered after the count; — means not encountered. 300 specimens were counted.

to 10%, with the exception of Site 158, where values reach 6%. Overall, *A. ehrenbergii* seems slightly more abundant in the west than in the east.

Actinocyclus ellipticus s. ampl. shows no distinctive trends for biostratigraphy, although it is generally most common in the *Coscinodiscus gigas* var. *diorama* Zone (13.5 to 12.8 Ma) at all sites, and exhibits a slight preference for the western sites.

Actinocyclus ingens was introduced to the tropics from middle latitudes (Barron, 1983), and it was excluded from the tropics before its extinction at higher latitudes (Burckle, 1978). It is generally present in low numbers (< 10%) in middle Miocene sediment, but it reaches values of 20 to 50% in isolated samples from the middle Miocene of Sites 574, 77, 572, and 158 (Tables 5, 6, 8, and 9). Some of these events appear to be roughly isochronous (about 50% at 14.8 Ma, Sites 574 and 572; about 25 to 30% at 14.5 Ma, Sites 574 and 572; and about 30% at 13.5 Ma, Sites 77 and 574). Other isolated abundance spikes, especially those at Site 77, show little comparison in site-to-site correlations. *Actinocyclus ingens* is a robust diatom that would be concentrated by dissolution of other less resistant diatoms. Dissolution, however, is not solely responsible for the abundance spikes of *A. ingens*, because other resistant diatoms such as *Cestodiscus pulchellus* and *Coscinodiscus radiatus* are not concentrated in the same samples and less resistant species (*Denticulopsis* spp.) are not selectively removed from the same samples. Core 77B-21 (13.1 to 12.9 Ma) and Sample 158-34-1, 50–51 cm (12.65 Ma) do, however, appear to have dissolved assemblages along with increased numbers of *A. ingens*.

Quantitative trends for *Cestodiscus pulchellus* and *C. pulchellus* var. *maculatus* are shown on Figure 7. Sites 575 and 77 show good comparison in abundance trends of *C. pulchellus* s. ampl. between 18 and 16 Ma, with abundant *C. pulchellus* s. ampl. at 17.5 Ma declining sharply by one half or more (to 10 to 20%) by 17.3 Ma. *Cestodiscus pulchellus* s. ampl. increases again at about 16.6 Ma to values around 40% of the assemblage at Sites 575 and 77, but it declines abruptly at 15.4 to 15.2 Ma to values that remain low (< 10%) for the remainder of its range. Where they can be compared, Sites 575 and 77 have similar abundances of *C. pulchellus* s. ampl., but Site 574 has abundances roughly half of those sites between 16.6 and 15.3 Ma. These lower values at Site 574 possibly reflect the site's position at 16.6 to 15.3 Ma: just south of the equator, within the area corre-

Table 9. Percent planktonic diatoms in Cores 22 to 34 of Hole 158.

Zone and subzone	Core-Section, interval (cm)	Sub-bottom depth (m)	*Actinocyclus ehrenbergii*	*A. ellipticus* s. ampl.	*A. ingens*	*Asteromphalus/Asterolampra*	*Coscinodiscus marginatus*	*C. nodulifer*	*C. plicatus/C. yabei*	*C. radiatus* s. ampl.	*C. tabularis* s. ampl.	*C. temperei* var. *delicata*	*C. tuberculatus*	*C.* spp.	*Craspedodiscus coscinodiscus* s. str.	*Denticulopsis hustedtii*	*D. punctata* f. *hustedtii*	*Hemidiscus cuneiformis*	*Nitzschia* spp.	*Rhizosolenia* spp.	*Rossiella paleacea* s. ampl.	*Rouxia* spp.	*Synedra jouseana*	*Thalassionema nitzschioides*	*T. nitzschioides* var. *parva*	*T. robusta*	*Thalassiosira leptopus*	*T.* spp.	*Thalassiothrix longissima*	*Actinoptychus* spp.	Miscellaneous diatoms	Estimated age (Ma)
Coscinodiscus yabei, Subzone A	22-2, 30–32	190.8	—	6	—	1	1	2	4	6	4	1	—	—	—	2	—	+	7	+	—	—	—	38	6	—	—	—	18	—	3	10.8
	22-6, 30–32	196.8	—	4	—	1	+	4	8	4	9	1	—	+	—	1	—	3	5	—	+	—	—	18	6	—	4	1	26	—	4	10.9
	23-2, 30–32	199.8	—	2	—	+	+	7	+	3	3	—	—	1	—	+	—	13	3	1	—	—	—	28	19	—	2	+	15	—	2	10.95
	23-5, 30–32	204.3	—	+	—	—	7	9	2	1	1	+	—	1	—	3	—	1	15	2	—	—	—	21	17	—	1	+	19	—	+	11.05
	24-1, 108–110	208.1	—	+	—	+	—	2	—	+	1	+	—	—	—	17	—	2	2	—	—	—	—	44	18	—	—	+	9	—	1	11.1
	24-3, 30–32	210.3	—	+	+	—	—	1	2	+	+	+	—	+	—	8	—	2	1	1	—	—	—	39	27	—	+	—	15	—	+	11.15
	25-2, 30–32	217.8	—	+	—	—	—	3	+	+	2	—	—	—	—	9	—	+	+	+	+	—	—	26	28	7	+	3	16	+	+	11.25
	25-6, 30–32	223.8	—	2	—	—	—	3	7	+	6	—	—	1	—	10	—	2	—	—	+	—	—	24	13	5	+	—	22	+	2	11.35
	26-2, 30–32	226.8	—	3	—	+	—	3	+	—	+	—	—	+	—	50	—	+	+	+	1	—	—	9	11	—	+	+	14	—	3	11.4
	26-6, 30–32	232.8	+	3	—	—	—	4	1	—	1	—	—	—	—	35	—	+	1	—	+	—	—	9	10	—	1	—	24	—	1	11.5
	27-2, 30–32	235.8	—	1	—	+	—	3	+	+	+	+	—	+	—	22	—	+	—	—	+	—	—	42	20	—	—	—	9	—	—	11.55
Actinocyclus moronensis	27-6, 30–32	241.8	—	—	—	—	—	2	1	—	1	+	—	—	—	70	—	+	+	—	—	—	+	7	7	—	—	—	11	—	1	11.65
	28-1, 30–32	243.3	—	3	—	+	—	1	3	1	3	+	1	+	—	61	—	—	+	+	—	—	—	8	9	—	1	—	10	—	—	11.7
	28-3, 30–32	246.3	—	1	—	—	+	2	2	—	2	1	+	+	—	68	—	+	1	+	+	—	—	5	9	+	—	—	6	—	+	11.75
	29-3, 30–32	255.3	—	2	—	+	—	+	3	—	3	+	—	+	—	61	—	+	1	+	+	—	—	1	9	2	+	+	11	—	2	11.95
	30-1, 30–32	261.3	+	1	—	—	4	2	5	13	5	1	1	1	—	1	—	1	2	—	—	—	—	34	11	1	1	—	15	—	1	12.05
	30-5, 30–32	267.3	2	3	—	+	3	8	2	+	2	+	18	1	—	2	+	1	+	—	+	—	1	12	25	7	+	—	3	—	2	12.15
	31-1, 30–32	270.3	6	2	—	1	3	3	3	2	3	2	4	2	—	4	2	+	2	+	1	+	+	22	15	3	—	+	11	—	7	12.2
	32-2, 30–32	280.8	+	3	+	—	+	5	3	—	3	—	17	+	+	5	+	—	2	—	2	—	+	9	42	—	+	—	7	—	+	12.35
Craspedodiscus coscinodiscus	32-4, 30–32	283.8	+	1	+	+	—	4	4	+	7	+	13	1	1	7	+	+	+	—	+	+	—	11	29	+	—	—	13	—	5	12.4
	33-2, 30–32	288.3	4	+	—	+	+	1	3	1	7	2	9	1	+	2	+	—	+	+	—	—	+	17	23	—	—	—	18	+	2	12.5
	34-1, 50–51[a]	296.5	2	15	23	1	7	—	4	1	1	1	10	1	—	1	1	—	1	—	—	—	1	17	5	—	—	—	11	—	1	12.65

Note: + means <1% or encountered after the count; — means not encountered. 300 specimens were counted.
[a] 200 specimens were counted.

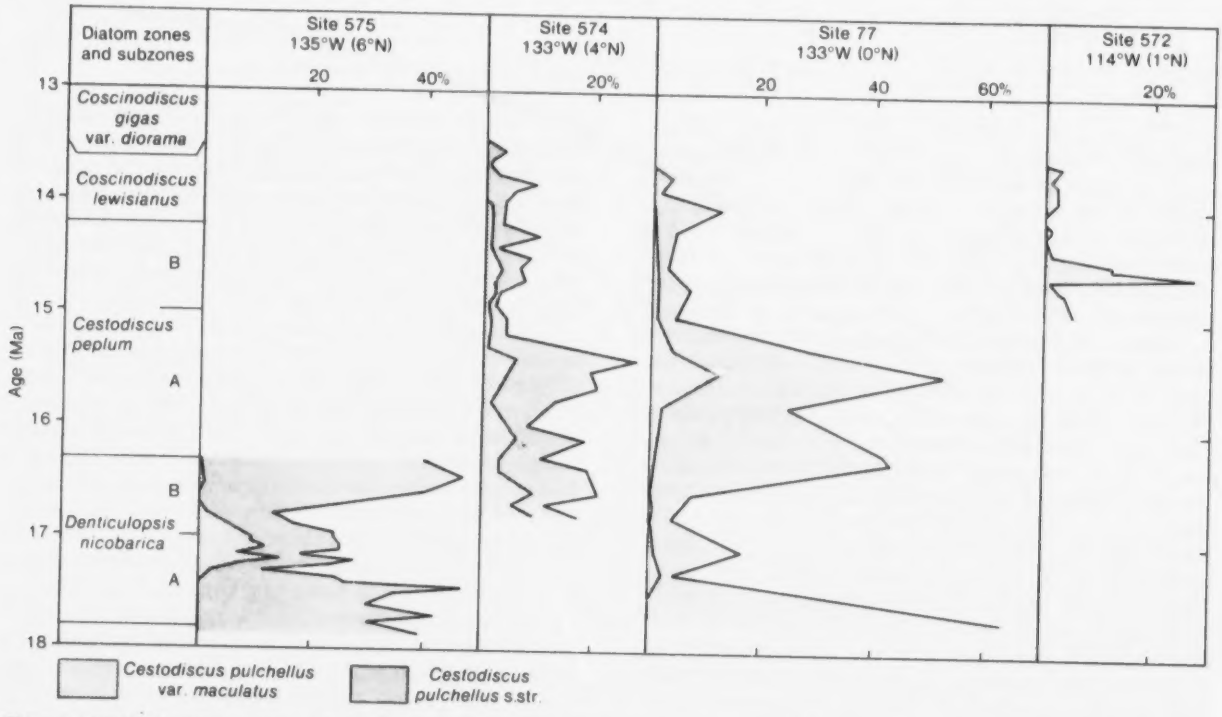

Figure 7. Relative abundance of *Cestodiscus pulchellus* and *C. pulchellus* var. *maculatus* at DSDP Sites 575, 574, 77, and 572 (after 17.8 Ma), plotted against age. Refer to Tables 4, 5, 6, and 8.

sponding to maximum primary productivity and opal accumulation in the Holocene ocean (van Andel et al., 1975). *Cestodiscus pulchellus* var. *maculatus* typically makes up less than half of the *C. pulchellus* s. ampl. populations, except between 17.2 and 17.0 Ma at Site 575, where it is roughly equivalent in numbers with the type form.

Quantitative trends of *Coscinodiscus nodulifer* s. ampl. across the equatorial Pacific are shown on Figure 8. *C. nodulifer* is typically less than 10% of the assemblage for the middle Miocene and most of the late Miocene, and it shows no definitive abundance peaks that can be correlated between the four sites. At about 8 Ma, however, *C. nodulifer* approaches values of 20% at easternmost Site 158, and it remains at comparable values through 6.2 Ma. During this same interval (8.0 to 6.2 Ma), values of *C. nodulifer* at the other sites are generally half of those at Site 158. L. H. Burckle (pers. comm., 1983) relates *C. nodulifer* to equatorial upwelling in the modern Pacific Ocean, so it is possible that the greater values of *C. nodulifer* after 8 Ma at easternmost Site 158 reflect enhanced upwelling there with respect to the more western sites.

The quantitative trends of *Coscinodiscus radiatus* s. ampl. before 14.2 Ma are shown on Figure 9. Late early Miocene and early middle Miocene forms tabulated as *C. radiatus* s. ampl. may include some forms allied with *C. blysmos*, which differs from *C. radiatus* only by the presence of a central indentation. The *C. radiatus* morphology is relatively simple, and it is entirely possible that different species can achieve it independently. The biostratigraphically most definitive trends in *C. radiatus* abundance include abundance spikes (20% or more) at 17.0 to 16.7 Ma at Sites 575 and 574 (not as pronounced

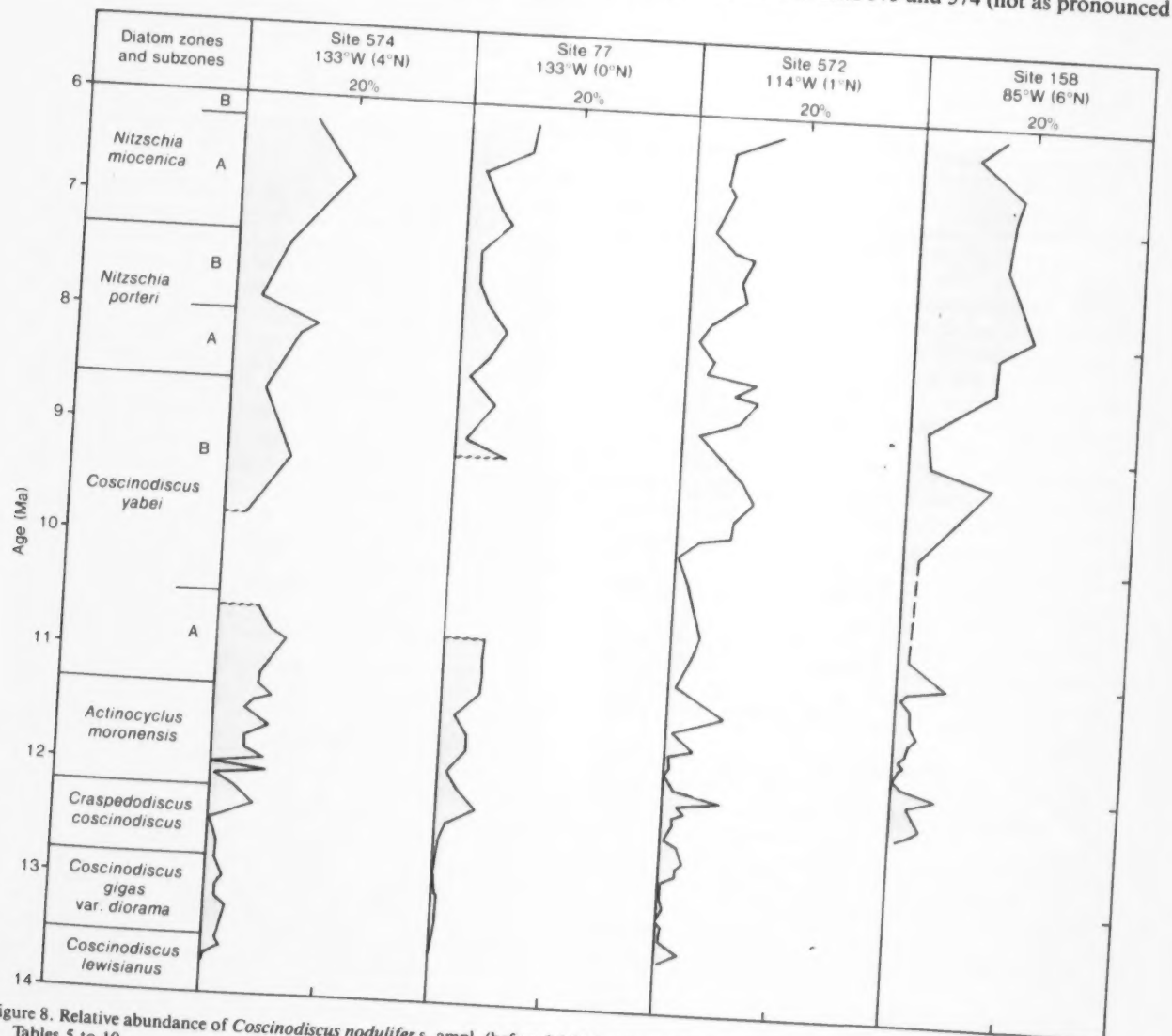

Figure 8. Relative abundance of *Coscinodiscus nodulifer* s. ampl. (before 6.1 Ma) at DSDP Sites 574, 77, 572, and 158, plotted against age. Refer to Tables 5 to 10.

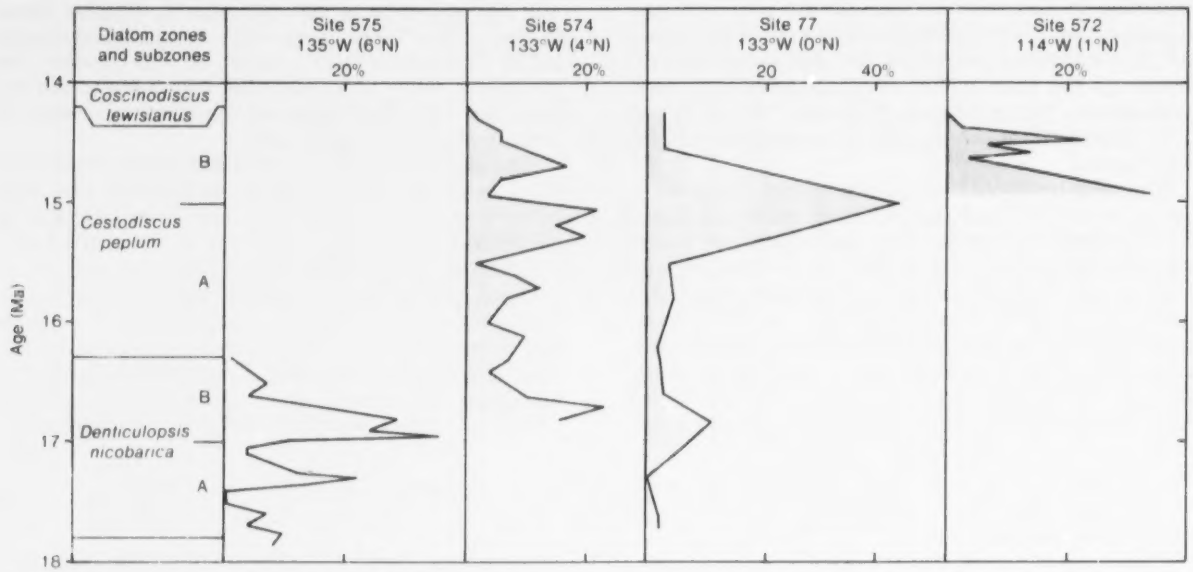

Figure 9. Relative abundance of *Coscinodiscus radiatus* s. ampl. (between 17.8 and 14.2 Ma) at DSDP Sites 575, 574, 77, and 572, plotted against age. Refer to Tables 4, 5, 6, and 8.

at Site 77) and at about 15.3 to 14.7 Ma at Sites 574, 77, and 572. *Coscinodiscus radiatus* is robust and relatively resistant to dissolution, but other less resistant diatoms (including *Denticulopsis* spp.) do not appear to have been selectively removed in samples containing common *C. radiatus*, and dissolution alone cannot explain the abundance spikes. *Coscinodiscus radiatus* s. ampl. shows no noticeable differences in its abundance at the various sites, although the abundance spikes (e.g., 16.8 and 15.0 Ma) at Site 574 are typically one half the size of the corresponding spikes at Sites 575 and 77. It should also be pointed out that between 18 and 14.5 Ma there appears to be an antithetical relationship between the abundance peaks for *Coscinodiscus radiatus* and *Cestodiscus pulchellus* (compare Figs. 7 and 9).

Coscinodiscus tabularis s. ampl. generally is most common (10% or more) between 13.5 and 12.5 Ma at Sites 574, 77, and 572, although it is also typically common between 14.6 and 13.7 Ma at Site 574. The species appears to show a slight preference for the central Pacific after 12.5 Ma, as compared with easternmost Pacific Site 158.

Coscinodiscus tuberculatus remains generally sparse to few (10% or less) throughout much of its range (14.0 to 12.0 Ma), but it abruptly increases in abundance to 20 to 36% at 12.4 to 12.2 Ma, immediately before its last consistent occurrence (12.0 Ma). Abundance values are somewhat greater at the western sites (574 and 77) and least of all at easternmost Site 158. At all four sites (574, 77, 572, and 158), *C. tuberculatus* declines sharply in abundance to values of 1 to 2% between 12.2 and 12.1 Ma.

Figure 10 gives the quantitative trends of *Denticulopsis hustedtii* across the equatorial Pacific. As discussed by Burckle (1978) and Barron (in press), this high- to middle-latitude species was introduced into the tropics in the middle middle Miocene and was excluded from the tropics by the early late Miocene, well before its extinction at higher latitudes in the early Pliocene. After a brief incursion into low latitudes at about 14.2 Ma (Sites 572 and 574), *D. hustedtii* became established in the region by about 13.9 Ma. Thereafter, *D. hustedtii* persisted at relatively low abundances (5 to 10% at Sites 574 and 77; 10 to 15% at Site 572) until about 12.0 Ma, when the abundance increased dramatically to 50 to 60% at all sites except Site 77. The lack of such a dramatic increase at Site 77 either reflects the greater sample spacing there or may indicate a hiatus (see greatly reduced sediment accumulation rate between 12.0 and 11.5 Ma at nearby Site 573, Fig. 2). At about 11.5 Ma, *D. hustedtii* declines just as abruptly to values of 10%. By 11.1 Ma it has dropped to 2% or less, and by 10.5 Ma it has disappeared from the tropical Pacific. *Denticulopsis hustedtii* is more abundant at the eastern sites (Sites 572 and 159) even during its abundance spike (12.0 to 11.5 Ma), where only two single points at Site 574 exceed 50% abundance and values at 11.9 to 11.8 Ma drop abruptly but briefly to below 10%.

Denticulopsis nicobarica exhibits a curiously bimodal distribution in its range (17.8 to 13.2 Ma) in the equatorial Pacific (Fig. 11). It is generally common to abundant (>20%) between 17.5 and 17.1 Ma, but drops off sharply in abundance to values of 5% or less for the interval from 16.9 to 15.7 Ma. Between 15.5 and 15.0 Ma, *D. nicobarica* increases gradually in abundance to 30 to 50%, and it remains abundant through 13.6 Ma. Thereafter, *D. nicobarica* decreases abruptly to values of 5% or less by 13.4 Ma. Undoubtedly, dissolution and/or winnowing of the small, relatively fragile *D. nicobarica* tests are responsible for much of the decline of *D. nicobarica* between 16.9 and 15.7 Ma, because other small delicate species (*Nitzschia* spp., *Thalassionema* spp.,

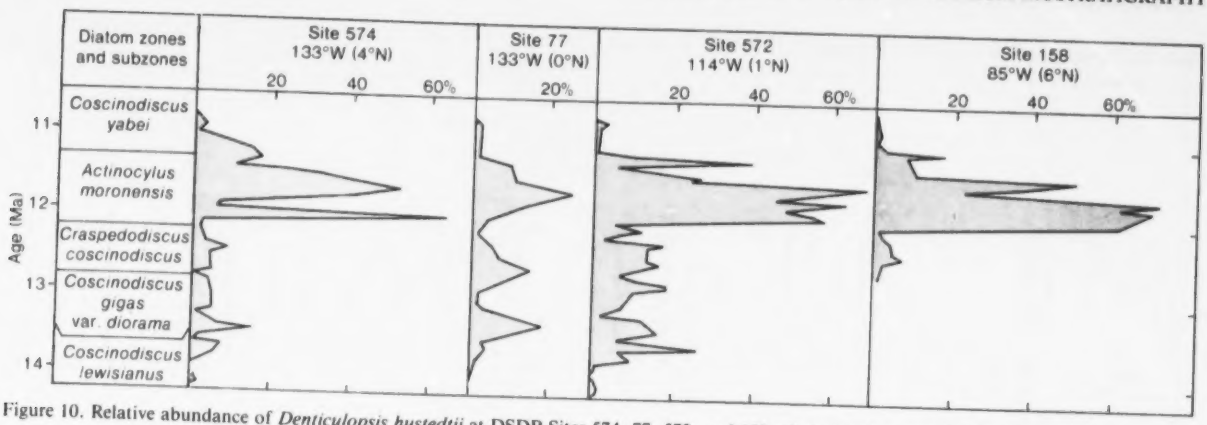

Figure 10. Relative abundance of *Denticulopsis hustedtii* at DSDP Sites 574, 77, 572, and 158, plotted against age. Refer to Tables 5, 6, 8, and 9.

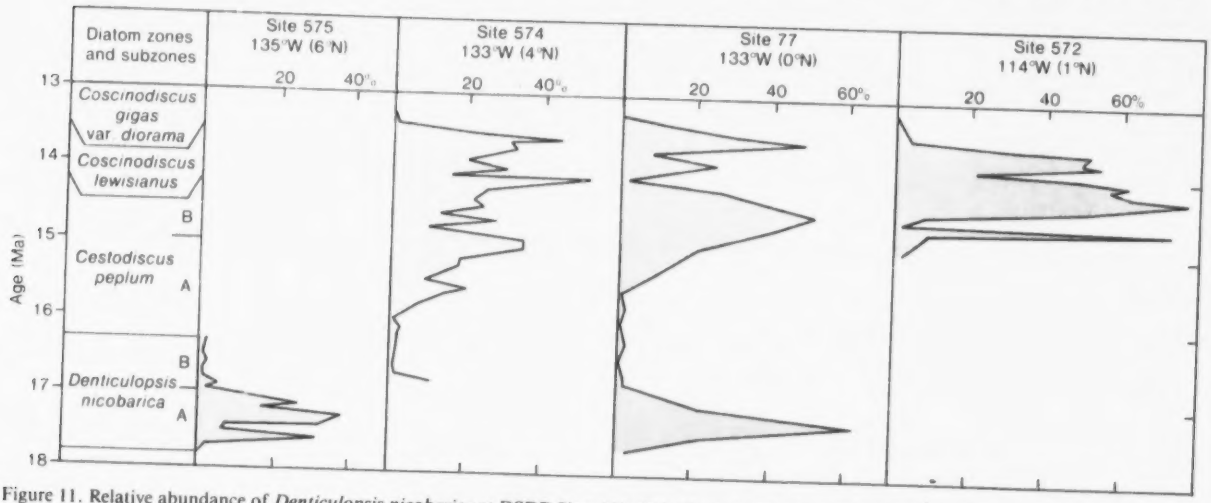

Figure 11. Relative abundance of *Denticulopsis nicobarica* at DSDP Sites 575, 574, 77, and 572, plotted against age. Refer to Tables 4, 5, 6, and 8.

and *Thalassiothrix* spp.) are also sparse in that interval. This decline in *D. nicobarica* abundance corresponds to the interval of warmest isotopic temperatures of the Miocene (Savin et al., 1981) and may reflect decreased opal productivity caused by decreased equatorial upwelling (Barron, this volume).

Denticulopsis praedimorpha is a high- to middle-latitude diatom which had a brief incursion into the tropics between 12.9 and 12.6 Ma (Tables 5, 6, and 8). The most pronounced incursion is at about 12.6 Ma; values of 20% or more are encountered at the corresponding level at Sites 574 and 77. This horizon was not observed at eastern Sites 572 and 158, possibly because of its brevity and the sampling interval. Alternatively, concentration of *D. nicobarica* at this horizon at the western sites may reflect transportation of the species from higher southern latitudes by bottom waters, because hiatus NH3 of Keller and Barron (1983) was more dominant in the western Pacific than in the eastern Pacific at that time.

Hemidiscus cuneiformis is generally rare throughout its early range, but it triples in abundance (to about 10%) at about 11.0 Ma at Sites 574, 77, and 158. Abundance values are typically greatest at easternmost Site 158, especially in the late Miocene (Tables 7 and 10).

Figure 12 shows the abundance trends for *Nitzschia porteri* sensu Burckle (1972) and *N. miocenica* between 10 and 6.2 Ma. (*N. porteri* was not separated from other *Nitzschia* species below the 10-Ma level.) The record at Site 572 indicates an abundance spike (40% or more) for *N. porteri* between 10.3 and 9.8 Ma. This interval is removed by hiatuses at Sites 574 and 77 (Fig. 4 and Barron et al., in press) and is greatly compressed at Site 158 (Keller et al., 1982); but the Site 574 and Site 158 curves both show a decline in abundance of *N. porteri* from 9.8 Ma (20 to 30%) to 9.3 Ma (4 to 12%). The *N. porteri* curves between 9 and 7 Ma show little correlation between the sites, possibly reflecting the relatively broad (200,000 to 300,000 yrs.) sampling interval; *N. porteri* appears to be slightly more common at the western sites in this interval. From 7.4 to 6.8 Ma, *N. porteri* declines in abundance as *N. miocenica* develops and expands, reflecting the evolutionary transition between the two species proposed by Burckle (1972). *N. miocenica* also seems

Table 10. Percent planktonic diatoms in Sample 158-15-6, 30–32 cm and Cores 16 to 21 of Hole 158 and in Cores 12 to 16 of Hole 77B.

Zone and subzone		Core-Section, interval (cm)	Sub-bottom depth (m)	*Actinocyclus ehrenbergii*	*A. ellipticus* s. ampl.	*Asteromphalus/Asteralampra*	*Coscinodiscus marginatus*	*C. nodulifer*	*C. plicatus/C. yabei*	*C. radiatus* s. ampl.	*C. tabularis* s. ampl.	*C. temperei* var. *deticata*	*C.* spp.	*Hemidiscus cuneiformis*	*Nitzschia cylindrica* s. ampl.	*N. fossilis*	*N. marina*	*N. miocenica* s. ampl.	*N. porteri*	*N. praereinholdii*	*N. reinholdii* s. ampl.	*N.* spp.	*Rhizosolenia* spp.	*Rossiella paleacea* s. ampl.	*R. praepaleacea*	*Roussa* spp.	*Thalassionema nitzschioides*	*T. nitzschioides* var. *parva*	*T. robusta*	*Thalassiosira burckliana*	*T. eccentrica*	*T. lentopus*	*T. praeconvexa*	*T.* spp.	*Thalassiothrix longissima*	*Triceratium cinnamomeum*	Miscellaneous diatoms	Estimated age (Ma) (after Barron et al., in press)
		Hole 158																																				
Nitzschia miocenica	B	15-6, 30-32	133.8	—	2	2	—	15	—	+	+	—	—	2	—	1	2	1	—	—	1	2	5	—	+	—	36	6	—	—	3	+	1	1	15	1	1	6.2
		16-2, 30-32	136.8	—	3	1	—	10	—	—	+	—	2	3	—	—	+	4	—	—	1	1	1	—	6	—	36	3	—	—	1	+	—	+	21	1	3	6.35
	A	16-6, 30-32	142.8	—	2	2	—	18	—	—	1	—	+	4	—	1	+	8	—	—	—	2	4	—	2	—	31	2	—	—	4	+	—	—	14	2	+	6.7
		17-2, 30-32	145.8	—	4	1	+	17	—	—	1	—	—	4	—	1	+	2	+	—	+	+	2	—	3	—	27	5	—	—	—	7	—	+	27	+	+	6.9
		17-6, 30-32	151.8	—	+	1	—	16	—	—	+	—	1	1	+	1	1	3	3	—	1	3	5	—	4	+	39	1	—	—	—	+	—	—	17	+	+	7.3
Nitzschia porteri	B	18-2, 30-32	154.8	+	2	2	—	18	—	+	+	—	+	8	1	2	+	—	1	—	1	5	1	2	1	—	27	6	—	—	—	2	—	—	18	—	+	7.55
		18-6, 30-32	160.8	1	4	+	—	21	—	+	1	—	+	6	3	+	1	—	3	—	+	4	1	+	+	+	19	4	—	—	+	2	—	+	22	—	3	7.9
	A	19-2, 30-32	163.8	—	4	3	—	15	—	1	4	—	2	2	1	1	+	—	1	—	—	4	5	2	—	—	29	2	—	+	—	2	—	2	27	1	1	8.05
		19-6, 30-32	169.8	—	3	+	—	14	—	2	4	—	+	5	+	+	—	—	1	—	—	1	2	—	—	—	35	13	1	—	—	2	—	+	14	1	1	8.45
Coscinodiscus yabei	B	20-3, 30-32	174.3	—	2	3	—	3	+	+	2	—	+	2	1	1	—	—	5	—	—	2	10	—	+	—	24	14	1	1	—	1	—	+	23	+	1	8.8
		20-6, 30-32	178.8	—	3	+	—	4	+	1	2	—	+	+	—	1	—	—	6	+	—	5	5	—	—	—	53	3	—	+	+	+	—	2	10	—	2	9.1
		21-2, 30-32	181.8	—	7	1	1	15	3	2	16	—	1	5	—	—	—	—	3	+	—	2	1	+	+	—	15	1	—	1	—	1	—	+	15	4	1	9.25
		21-5, 30-32	186.3	—	2	+	—	3	5	1	7	+	1	+	—	—	—	—	17	+	—	2	+	3	1	—	27	3	—	+	—	+	—	+	20	1	3	9.9
		Hole 77B																																			
Nitzschia miocenica	B	12-3, 94-98	113.6	+	1	1	—	12	—	+	+	—	+	+	+	+	+	19	—	—	—	3	1	—	1	—	34	7	—	—	1	+	+	1	12	1	2	6.25
		12-6, 30-32	117.4	—	2	+	—	11	—	—	+	—	—	1	+	+	1	23	—	—	+	4	+	—	1	—	29	8	—	—	1	1	—	2	11	1	3	6.5
	A	13-2, 30-32	120.6	+	3	+	—	3	—	—	1	—	—	+	+	4	1	5	—	—	2	5	1	—	3	—	54	7	—	—	1	+	—	2	5	+	2	6.7
		13-4, 102-106	124.3	+	2	3	—	6	—	—	1	—	—	2	+	+	+	6	3	—	1	4	1	—	3	—	49	4	—	—	2	1	—	+	8	2	1	7.0
		13-6, 30-32	126.6	+	3	3	—	8	—	—	+	—	1	+	+	+	+	6	5	—	4	7	1	—	2	1	38	2	—	—	1	1	—	+	14	1	—	7.15
Nitzschia porteri	B	14-2, 30-32	129.8	+	+	+	—	4	—	+	2	—	—	+	3	3	2	—	14	+	+	10	2	+	—	—	30	23	—	—	+	1	—	+	4	2	—	7.4
		14-4, 90-94	133.4	+	1	+	—	3	—	—	1	—	+	3	3	+	1	—	22	—	+	6	1	1	+	—	18	25	—	—	+	1	—	1	7	1	4	7.7
		14-6, 30-32	135.8	+	3	+	—	4	-	—	2	—	+	+	+	2	+	—	13	+	—	6	1	1	—	+	30	29	—	—	+	2	—	+	5	+	+	7.85
	A	15-2, 30-32	138.9	+	+	+	—	8	—	—	1	—	+	+	+	+	—	—	13	+	—	6	+	+	—	1	36	21	2	+	+	5	—	1	2	3	—	8.1
		15-4, 100-104	142.6	+	+	+	—	5	—	—	4	—	+	+	+	+	—	—	31	+	—	6	—	—	+	+	31	10	2	1	+	3	—	—	3	3	+	8.35
		15-6, 23-25	144.8	+	+	1	—	2	—	—	+	—	+	+	—	2	—	—	31	+	—	9	—	3	2	5	25	10	+	2	+	2	—	2	2	1	2	8.5
Coscinodiscus yabei	B	16-2, 23-25	147.9	—	+	+	—	7	+	+	+	—	1	+	+	2	—	—	23	+	—	2	+	+	1	+	37	10	—	1	+	3	—	—	6	+	3	8.75
		16-4, 100-104	151.7	—	+	+	—	2	+	—	7	—	—	+	—	+	—	—	12	2	—	1	1	—	—	1	28	26	—	3	+	2	—	1	3	1	1	9.05
		16-6, 23-25	153.9	—	1	1	—	9	2	—	3	—	2	+	+	+	—	—	18	2	—	4	+	—	+	+	45	6	—	1	+	3	—	—	6	+	—	9.2

Note: + means < 1% or encountered after the count; — means not encountered. 300 specimens were counted.

to prefer the western sites (574 and 77) and central site (572) over the easternmost site (158).

Quantitative trends for *Synedra jouseana* are shown on Figure 13. The prominent abundance spikes at 16.6 and 15.8 Ma, where *S. jouseana* increases to 30% or more of the assemblage, are the most noticeable features of the *S. jouseana* curves. The interval of common (≥ 20%) *Synedra jouseana* (16.8 to 15.7 Ma) coincides precisely with the interval of sparse *Denticulopsis nicobarica* (Fig. 11) in the latest early Miocene. After about 15.3 Ma, *S. jouseana* is typically sparse (5% or less) at all sites. Early middle Miocene abundance values are greatest at Site 77, the site farthest from the equator (about 5°S) at that time.

Thalassionema nitzschioides becomes a dominant equatorial Pacific diatom in the late middle Miocene between 14.2 and 12.2 Ma, where abundance values increase from about 10% to 40–50% (Fig. 14). Close sampling intervals (100,000 yrs. or less) at Sites 572 and 574 reveal considerable variability in *T. nitzschioides* abundance during the late middle Miocene, so that individual abundance spikes are difficult to correlate. There is some suggestion, however, that abundance peaks at about 14.0 Ma and 13.2 Ma, and a generalized abundant interval between 12.4 and 11.9 Ma, are correlative. Between about 11.2 and 11.0 Ma, *T. nitzschioides* reaches its greatest numbers (60 to 70%) for the Miocene interval investigated (18.2 to 6.2 Ma) at all sites (possibly earlier at Site 77). Middle Miocene assemblages are dominated by shorter forms of *T. nitzschioides* (length-to-width ratios < 3) (= *T. nitzschioides* var. *parva* s. ampl.). Longer forms (length-to-width ratios ≥ 3) (= *T. nitzschioides* s. str.) are more important in the late Miocene. Sites 574, 77, and 572 all show a generalized abundance peak for *T. nitzschioides* var. *parva* s. ampl. between 8.2 and 7.3 Ma, but Site 158 shows no such peak. Other late Miocene trends in *T. nitzschioides* are difficult to correlate, which may again reflect high variability and relatively broad sampling intervals.

Thalassionema robusta shows a minor abundance peak between 12.15 and 12.0 Ma at all sites (Tables 5, 6, 8, and 9), with values at the western sites (574 and 77) slightly higher than those at the eastern sites (572 and 158).

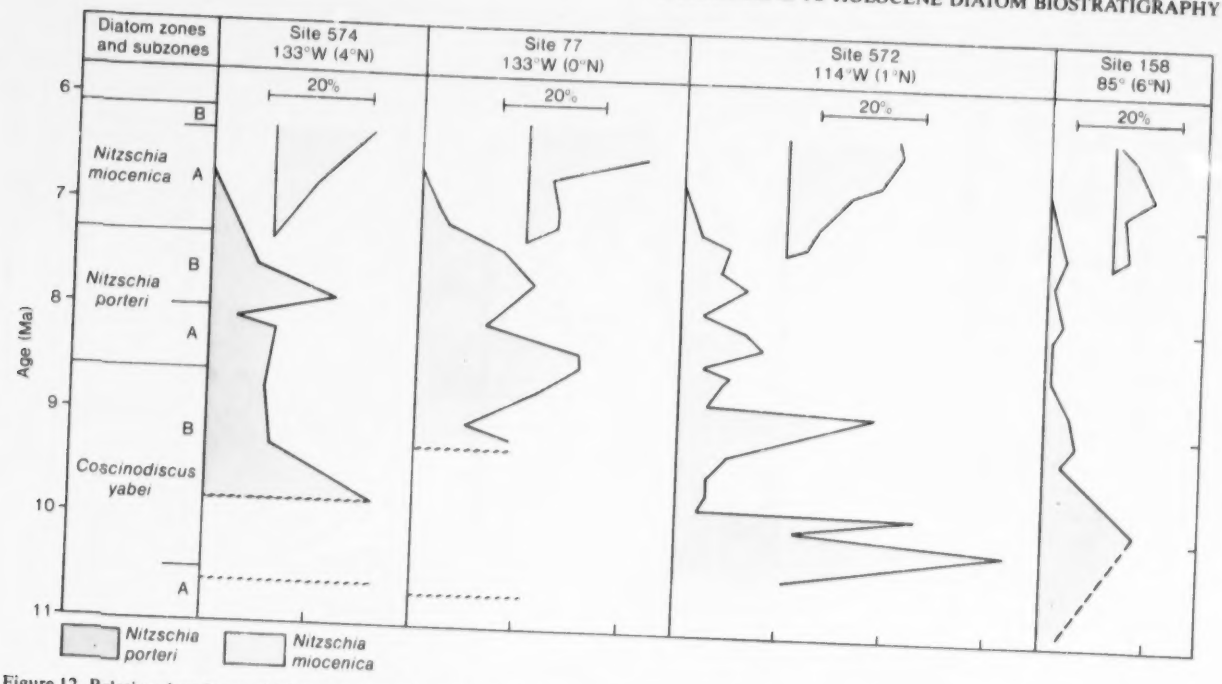

Figure 12. Relative abundance of *Nitzschia porteri* and *N. miocenica* s. ampl. (between 10.8 and 6.2 Ma) at DSDP Sites 574, 77, 572, and 158, plotted against age. Refer to Tables 7 and 10.

Quantitative trends for *Thalassiothrix longissima* (Fig. 15) reveal numerous correlative abundance spikes (labeled A to F) between the early middle Miocene and the earliest late Miocene (15.3 to 10.9 Ma). These peaks are most recognizable in the curves with the closest sampling intervals (Sites 574, 572, and 158), and they are strongly supportive of the diatom datum-level correlations between the sites (Tables 1 and 2). Estimated ages for these spikes are as follows: A, 15.2 Ma; B, 14.7 Ma; C, 13.0 Ma; C′, 12.7 Ma; D, 12.1 Ma; D′, 11.9 Ma; E, 11.5 Ma; E′, 11.3 Ma; and F, 10.9 Ma. Absolute abundance values are comparable (5 to 20%) at Sites 574, 77, and 572, but slightly greater (10 to 25%) at easternmost Site 158.

REWORKING

Horizons of reworked diatoms are rare at Sites 572 and 573 and more common at Sites 574 and 575. The Quaternary through upper Miocene section (0 to 26 m) of Site 575 accumulated at a very slow rate (Fig. 4), and reworked middle Miocene to Oligocene diatoms are typically present in low numbers. Core 575B-3 (about 7.5 Ma) contains an anomalously thick sequence, and it is dominated by reworked diatoms from the upper middle Miocene, including *Coscinodiscus tuberculatus* and *Denticulopsis punctata* f. *hustedtii*.

At Site 574, upper lower Miocene diatoms are reworked into the lower middle Miocene (Samples 574-25,CC and 574-22,CC), and lower middle Miocene diatoms are reworked into the upper middle Miocene (Samples 574-16,CC and 574-14-2, 42–43 cm) (Table 5). Lower and middle Miocene diatoms are also present in upper Miocene (Samples 574A-7,CC and 574A-8,CC) and Pliocene (Samples 574-2,CC; 574A-3,CC; and 574-4,CC) horizons.

SUMMARY

Excellent upper Eocene to Holocene reference sections were recovered on Leg 85 at four sites (572 to 575) in the central equatorial Pacific. Diatoms are generally common and well preserved at all sites, except in the upper Eocene and upper Oligocene. The upper Cenozoic diatom zonation of Barron (in press), which consists of the upper Miocene to Holocene zonation of Burckle (1972, 1977) and the lower Miocene zonation of Barron (1983), is readily applicable. In addition, 89 secondary datum levels have been identified in the Miocene and Pliocene and correlated between the sites. The Oligocene zonation used is a modification of Fenner's (in press), wherein the upper Oligocene zones are simplified to allow for the relatively poor diatom preservation in that interval. Paleomagnetic stratigraphy was obtained for the entire *Denticulopsis nicobarica* Zone at Site 575, from the middle of paleomagnetic Chron 17 to the middle of Chron 16, and 13 upper lower Miocene diatom datum levels are calibrated directly with paleomagnetic stratigraphy for the first time.

Site 572 in the east (114°W) contains a thick sequence of lower middle Miocene to Quaternary diatom-rich sediment. Sites 573 to 575 (133° to 135°W) have more carbonate-rich sediments accumulated at rates that were, at most, 60% those of Site 572. Hiatuses are more com-

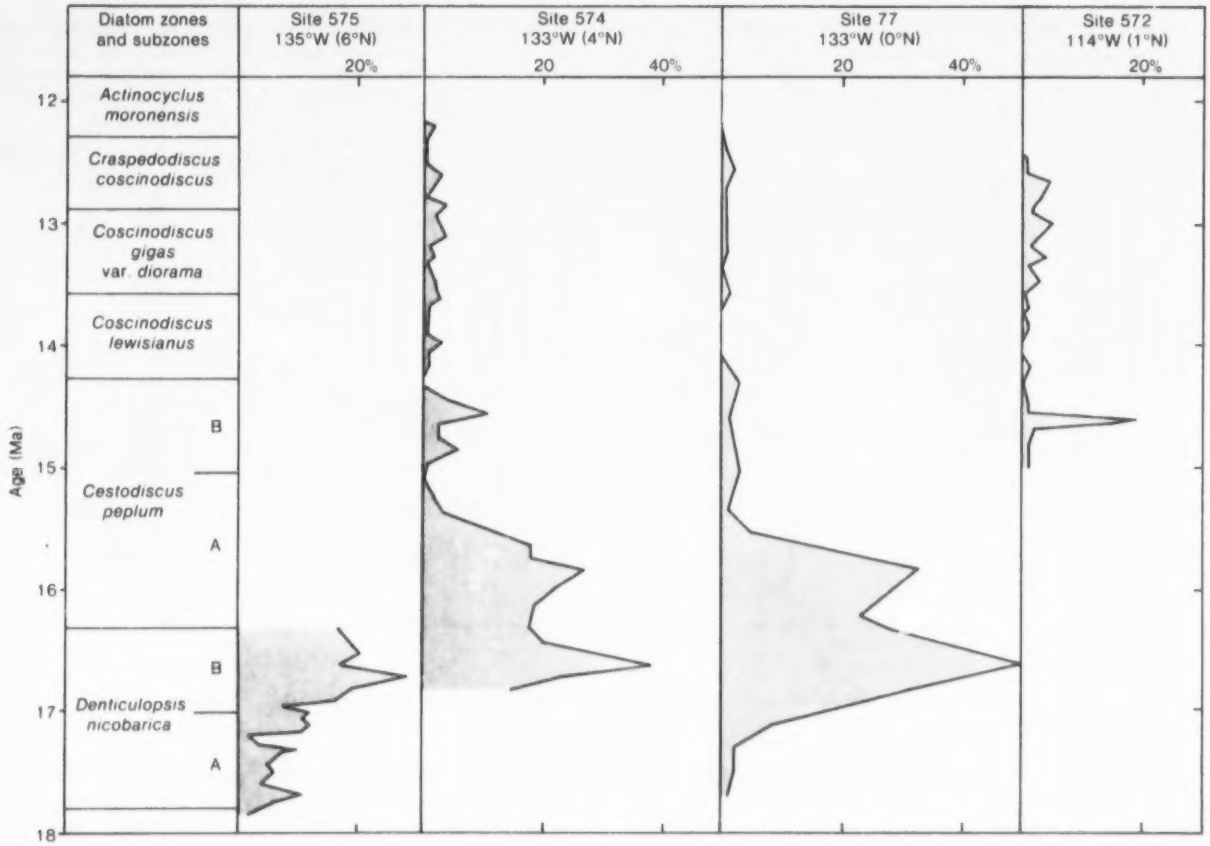

Figure 13. Relative abundance of *Synedra jouseana* s. ampl. (after 17.8 Ma) at DSDP Sites 575, 574, 77, and 572, plotted against age. Refer to Tables 4, 5, 6, and 8.

mon at the western sites, specifically in the intervals between about 18 and 17 Ma (NH1), 10.5 and 9.8 Ma (NH5), and 5.1 and 4.5 Ma (NH7).

Quantitative diatom studies of the upper lower Miocene to uppermost Miocene (18.0 to 6.2 Ma) of Sites 572, 574, and 575 are supplemented by quantitative diatom studies at Site 77 (about 10 km from Site 573) and Site 158 (85°W) to form transects across the eastern and central equatorial Pacific. Where the sampling interval represents 100,000 yrs. or less (lower Miocene of Sites 574 and 575 and middle Miocene of Sites 158, 572, and 574), quantitative trends in species such as *Cestodiscus pulchellus, Coscinodiscus radiatus, Denticulopsis hustedtii, D. nicobarica*, and *Thalassiothrix longissima* are readily correlatable, and greatly enhance the biostratigraphic resolution. Sampling intervals for the late Miocene represent an average of 200,000 to 300,000 yrs., and correlation of the individual peaks and troughs of the species abundance curves is more difficult. Comparison of species abundance reveals relatively minor differences between the eastern and western sites, especially in the lower and middle Miocene. *Thalassionema nitzschioides, Denticulopsis hustedtii*, and *D. nicobarica* show general eastern preferences, whereas *Cestodiscus pulchellus, Actinocyclus ellipticus, Coscinodiscus tuberculatus*, and *Nitzschia* spp. seem to prefer the western area.

DESCRIPTION OF NEW DIATOM TAXA

The taxonomy below follows that of Barron (1980a, b; 1981a, b; 1983; in press) for the uppermost Oligocene through Holocene, and that of Jousé (1977) and Fenner (in press) for the Oligocene.

Genus *ACTINOCYCLUS* Ehrenberg

***Actinocyclus ellipticus* Grunow *in* Van Heurck, 1883**
***Actinocyclus ellipticus* var. *spiralis* n. var.**
(Plate 7, Figs. 9–10; Plate 9, Fig. 5)

Description. This variety is distinguished from other forms of *A. ellipticus* Grunow by its areolation pattern, which closely resembles that of *Coscinodiscus lewisianus* Greville. Kolbe (1954) characterizes this *C. lewisianus*-type areolation as "apical straight or slightly rounded rows parallel to the apical axis; transapical rows curved and diverging from the transapical axis; central space forming irregular circular figures." Well-developed hyaline fields are present in the valve's center. At low power this taxon closely resembles *C. lewisianus*, but it is easily distinguished by the presence of a marginal pseudonodule. The valves of this variety are not as robust as those of *C. lewisianus*; and smaller specimens, comparable in size to *C. lewisianus*, have apices more tapered than those of *C. lewisianus*. Observed valve sizes range from 40 × 11 μm (length × width) to 70 × 55 μm.

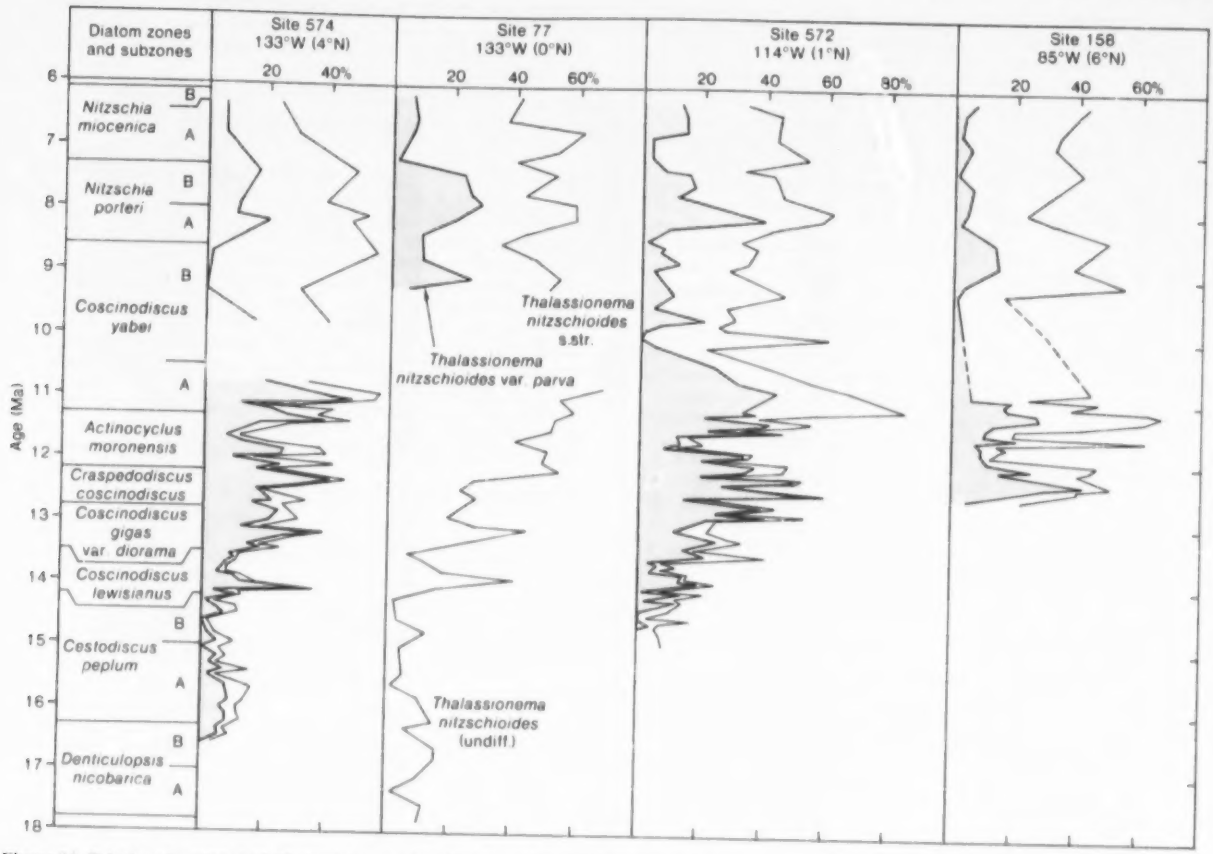

Figure 14. Relative abundance of *Thalassionema nitzschioides* and *T. nitzschiodes* var. *parva* (between 17.8 and 6.2 Ma) at DSDP Sites 574, 77, 572, and 158, plotted against age. Refer to Tables 5 to 10.

Remarks. This variety is separated because it is restricted to the middle Miocene (about 14.2 to 12.3 Ma) (Table 3). Burckle (1978) reported *C. lewisianus* to range above *Denticulopsis nicobarica* (Grunow) Simonsen in the equatorial Pacific, which conflicts with the results of Barron (1981a, b) and this report. It is possible that Burckle (1978) included *A. ellipticus* var. *spiralis* in this concept of *C. lewisianus*.

Holotype. USNM 370301. Plate 9, Figure 5. DSDP Sample 575-5-5, 43–44 cm. Length 57 μm.

Genus *COSCINODISCUS* Ehrenberg

Coscinodiscus lewisianus Greville 1866 *Coscinodiscus lewisianus* var. *rhomboides*, n. var.

(Plate 7, Figs. 2, 3)

Coscinodiscus lewisianus var. *similis* Rattray, Kolbe, 1954, pl. 2, fig. 22.
C. lewisianus var. *similis* Rattray, Kanaya, 1971, pl. 40.5, figs. 7, 8.
C. lewisianus var. *similis* Rattray, Jousé, 1977, pl. 57, figs. 8, 20–23.
C. lewisianus var. *similis* Rattray, Barron, 1983, p. 512, pl. 1, fig. 8.

Description. This variety has distinctly rhombic valves ranging in size from 60 × 30 μm to 120 × 50 μm (length × width). It has been confused in the literature with *C. lewisianus* var. *similis* Rattray, which is also rhombic in shape, although much less so (compare Plate 7, Figs. 2, 3, 6). In addition to being more elliptical in outline, *C. lewisianus* var. *similis* possesses a distinct, finely areolated margin, which is much broader than the finely areolated margin of *C. lewisianus* var. *rhomboides*. *C. lewisianus* var. *rhomboides* is mainly an upper Oligocene diatom which ranges into the lowermost Miocene, whereas *C. lewisianus* var. *similis* is restricted to the upper lower Miocene (about 17.4 to 15.7 Ma).

Remarks. Barron (1983) recognized the two rhombic forms of *C. lewisianus*, but mistakenly called the older form *C. lewisianus* var. *similis* Rattray and the younger form *C. lewisianus* ("late early Miocene form resembling *C. lewisianus* var. *similis*").

Holotype. USNM 370299. DSDP Sample 71-39-2, 87–89 cm. Length 114 μm.

Coscinodiscus loeblichii, n. sp.

(Plate 4, Figs. 1–3)

Stictodiscus truanii Witt, Jousé, 1977, pl. 48, fig. 13.

Description. Circular valve 14 to 40 μm in diameter with a large, asymmetric indentation at its center. The indentation is not as abrupt as that which is typical of *Craspedodiscus*, and typically makes up about 4/5 of the valve's face. On opposing sides of the valve, the raised marginal rim varies in thickness by a factor of 2. The areolar pattern is sublinear, and the polygonal areolae range from 9 per 10 μm on the valve's margin to 13 in 10 μm near the valve's center. Within the indentation itself, a small area near the valve's center is raised slightly above the surrounding area of the indentation. The valve's margin is simple and without spines.

Remarks. *Coscinodiscus loeblichii* has a brief range (representing about 10.5 to 9.4 Ma) in the lower upper Miocene of the equatorial Pacific.

Holotype: USNM 370304. Plate 4, Figure 1. DSDP Sample 572D-10,CC. Diameter 28 μm.

Isotypes. USNM 370305 and 370306. Plate 4, Figures 2, 3. Diameter 23 μm and 30 μm.

Derivation of name. Named in honor of Dr. Alfred R. Loeblich of the University of California at Los Angeles.

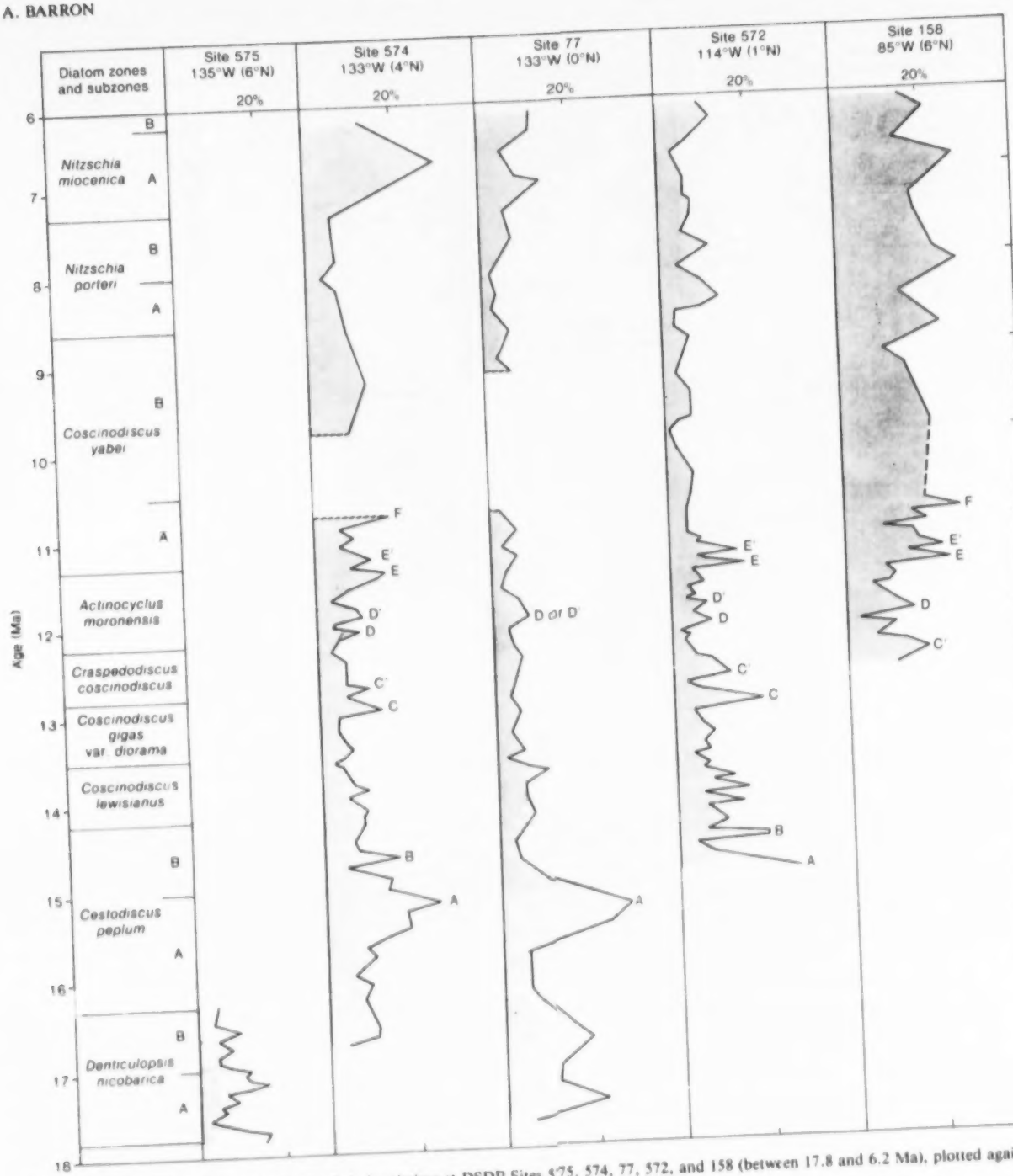

Figure 15. Relative abundance of *Thalassiothrix longissima* at DSDP Sites 575, 574, 77, 572, and 158 (between 17.8 and 6.2 Ma), plotted against age. Refer to Tables 4 to 10. Correlative abundance peaks are labeled A to F (see text).

Coscinodiscus yabei Kanaya, 1957
***Coscinodiscus yabei* var. *ellipticus*, n. var.**
(Plate 4, Fig. 9; Plate 9, Fig. 1)

Cymatotheca temperei (Brun) Hendey, Jousé, 1977, pl. 50, fig. 5.

Description. This variety is distinguished by its distinctive elliptical shape. Observed valves range in size from 42 × 23 μm to 96 × 57 μm (length × width). The plication is always along the transapical (shorter) axis of the valve, in contrast to *C. temperei* Brun, which is always plicated along the apical (longer) axis. Smaller specimens of *C. yabei* var. *ellipticus* have their axis of plication at a slight angle to the transapical axis, producing an asymmetrical appearance of the plications. Larger specimens have flattened margins covering 1/5 of the transapical axis, with the plication restricted to the center of the valve.

Remarks. *C. yabei* var. *ellipticus* has a short range (representing 9.8 to 9.4 Ma) in the lower upper Miocene (Table 3).

Holotype. USNM 370307. Plate 4, Figure 9. DSDP Sample 572D-10-4, 50–52 cm. Length 63 μm.
Isotype. USNM 370308. Plate 9, Figure 1. Length 46 μm.

Genus *THALASSIOSIRA* Cleve

***Thalassiosira tappanae*, n. sp.**
(Plate 6, Figs. 1–5, 7)

?Stephanopyxis sp., Bukry, 1978b, pl. 19, fig. 10.
Coscinodiscus sp. of Burckle (1978), Barron, 1981a, p. 139.
Description. Small (10 to 14 μm diameter), circular valves which are robust and slightly convex. Subpolygonal areolae are arranged in a linear to slightly eccentric pattern, and range in size from 9 per 20 μm near the valve center to 11 per 10 μm near the valve margin. Characteristic "gear-like" margin contains robust double spines (1 μm long) dispersed every 1.5 to 2 μm along a hyaline 1-μm-wide margin. There are typically 15 to 18 such spines per valve. Seven marginal strutted processes and one possible labiate process were observed on the interior face of the valve (Plate 6, Fig. 3).
Remarks. *T. tappanae* has a short range (representing 14.4 to 13.8 Ma) in the middle middle Miocene of the tropical Pacific. It was referred to as *Coscinodiscus* sp. by Burckle (1978) but was not described or figured.
Holotype. USNM 370309. Plate 6, Figure 7. DSDP Sample 572D-28-2, 50–52 cm. Diameter 12.5 μm.
Isotype. USNM 370310. Plate 6, Figure 5. Diameter 13 μm.
Derivation of name. Named in honor of Dr. Helen Tappan of the University of California at Los Angeles.

OTHER DIATOM TAXA OBSERVED

Actinocyclus ehrenbergii Ralfs
A. ellipticus Grunow
A. ellipticus f. *lanceolata* Kolbe
A. ellipticus var. *javanica* Reinhold
A. hajosiae Barron
A. ingens Rattray
A. moronensis Deby
A. radionovae Barron
Actinoptychus undulatus (Bailey) Ralfs
Annellus californicus Tempére
Asterolampra acutiloba Frenguelli
Asteromphalus elegans Greville
Bogorovia veniamini Jousé
Cestodiscus peplum Brun
C. pulchellus Greville
C. pulchellus Greville sensu Jousé, 1973
C. mukhinae Jousé
C. robustus Jousé
Coscinodiscus africanus Janisch
C. blysmos Barron
C. excavatus Ralfs
C. gigas var. *diorma* (Schmidt) Grunow
C. lewisianus Greville
C. lewisianus var. *robustus* Barron
C. lewisianus var. *similis* Rattray
C. marginatus Ehrenberg
C. nodulifer A. Schmidt
C. nodulifer var. *cyclopus* Jousé
C. oligocenicus Jousé
C. plicatus Grunow
C. praenodulifer Barron
C. radiatus Ehrenberg
C. rhombicus Castracane
C. salisburyanus Lohman
C. tabularis Grunow
C. temperei var. *delicata* Barron
C. tuberculatus Greville
C. vetustissimus var. *javanica* Reinhold
C. yabei Kanaya
Craspedodiscus coscinodiscus Ehrenberg
C. elegans Ehrenberg
C. rydei Barron
Denticulopsis hustedtii (Simonsen and Kanaya) Simonsen
K. kanayae (Aliba) Barron
D. lauta (Bailey) Simonsen
D. nicobarica (Grunow) Simonsen
D. praedimorpha (Akiba) Akiba
D. punctata f. *hustedtii* (Schrader) Simonsen
Hemidiscus cuneiformis Wallich
Lisitzinia ornata Jousé
Melosira architecturalis Brun
M. sulcata (Ehrenberg) Kutzing
Nitzschia cyclindrica Burckle
N. fossilis (Frenguelli) Kanaya and Koizumi
N. jouseae Burckle
N. maleinterpretaria Schrader
N. marina Grunow
N. miocenica Burckle
N. miocenica var. *elongata* Burckle
N. porteri Frenguelli sensu Burckle (1972)
N. praereinholdii Schrader
N. reinholdii Kanaya and Koizumi
Pseudoeunotia doliolus (Wallich) Grunow
Raphidodiscus marylandicus Christian
Rhizosolenia matuyamai Burckle
R. praebergonii Mukhina
R. praebergonii var. *robusta* Burckle and Trainer
Rocella gelida (Mann) Bukry
R. gelida var. *schraderi* (Bukry) Barron
R. vigilans Fenner
Rossiella paleacea (Grunow) Desikachary and Maheshwari
R. paleacea var. *elongata* (Barron)
R. praepaleacea (Schrader) Gersonde
Rouxia spp.
Synedra miocenica Schrader
S. jouseana Sheshukova-Poretzkaya
S. jouseana f. *linearis* Sheshukova-Poretzkaya
Thalassionema nitzschioides Grunow
T. nitzschioides var. *parva* Heiden and Kolbe
T. robusta Schrader
Thalassiosira bukryi Barron
T. burckliana Schrader
T. convexa Mukhina
T. convexa var. *aspinosa* Schrader
T. eccentrica (Ehrenberg) Cleve
T. fraga Schrader
T. leptopus (Grunow) Hasle and Fryxell
T. miocenica Schrader
T. oestrupii (Ostenfeld) Proshkina-Lavrenko
T. praeconvexa Burckle
T. primalabiata Gombos
T. spinosa Schrader
T. spumellaroides Schrader
Thalassiothrix longissima Cleve and Grunow
Triceratium cinnamomeum Greville
T. pileus Ehrenberg

ACKNOWLEDGMENTS

I thank the Leg 85 Co-Chiefs, Larry Mayer and Fritz Theyer, and the entire staff for making Leg 85 rewarding and successful. This manuscript benefited from the reviews of William H. Abbott and Lloyd H. Burckle. Jack G. Baldauf and David Bukry provided helpful comments. Robert Oscarson of the U. S. Geological Survey assisted with scanning electron microscope studies. Samples were made available for study by the NSF through the Deep Sea Drilling Project.

REFERENCES

Barron, J. A., 1980a. Miocene to Quaternary diatom biostratigraphy of DSDP Leg 57, off northeast Japan. *In* Scientific Party, *Init. Repts. DSDP*, 56, 57, Pt. 2: Washington (U.S. Govt. Printing Office), 641–685.

_____, 1980b. Upper Pliocene and Quaternary diatom biostratigraphy of Deep Sea Drilling Project Leg 54, tropical eastern Pacific. *In* Rosendahl, B. R., Hekinian, R., et al., *Init. Repts. DSDP*, 54: Washington (U.S. Govt. Printing Office), 455–485.

_____, 1981a. Late Cenozoic diatom biostratigraphy and paleoceanography of the middle-latitude eastern North Pacific. *In* Yeats, R.

S., Haq, B. U., et al., *Init. Repts. DSDP*, 63: Washington (U.S. Govt. Printing Office), 507–538.

_____, 1981b. Middle Miocene diatom biostratigraphy of DSDP Site 77B in the eastern equatorial Pacific. *Geosci. J.*, 2(2):137–144.

_____, 1983. Latest Oligocene through early middle Miocene diatom biostratigraphy of the eastern tropical Pacific. *Mar. Micropaleontol.*, 7:487–515.

_____, in press. Miocene to Quaternary planktic diatom biostratigraphy. *In* Bolli, H. M., and Saunders, J. B. (Eds.), *Biostratigraphy by Marine Plankton*: Cambridge (Cambridge Univ. Press).

Barron, J. A., and Keller, G., 1983. Paleotemperature oscillations in the middle and late Miocene of the northeastern Pacific. *Micropaleontology*, 29(2):150–181.

Barron, J. A., Keller, G., and Dunn, D. A., in press. A multiple microfossil biochronology for the Miocene. *In* Kennett, J. P. (Ed.), *The Miocene Ocean: Paleoceanography and Biogeography*. Mem. Geol. Soc. Am. 163.

Berggren, W. A., 1981. Correlation of Atlantic, Mediterranean, and Indo-Pacific Neogen stratigraphies: geochronology and chronostratigraphy. *Proc. IGCP Project 114: Internat. Workshop Pacific Neogene Biostratig.* (Nov. 25–29, 1981, Osaka and Kobe, Japan), pp. 29–60.

Berggren, W. A., Kent, D. V., and Flynn, J. J., in press. Paleogene geochronology and chronostratigraphy. *In* Snelling, N. J. (Ed.), *Geochronology and the Geologic Time Scale*.

Bukry, D., 1973. Phytoplankton stratigraphy, central Pacific Ocean, Deep Sea Drilling Project Leg 17. *In* Winterer, E. L., Ewing, J. I., et al., *Init. Repts. DSDP*, 17: Washington (U.S. Govt. Printing Office), 871–887.

_____, 1978a. Cenozoic coccolith and silicoflagellate stratigraphy, offshore northwest Africa, Deep Sea Drilling Project Leg 41. *In* Lancelot, Y., Seibold, E., et al., *Init. Repts. DSDP*, 41: Washington (U.S. Govt. Printing Office), 689–707.

_____, 1978b. Cenozoic coccolith, silicoflagellate, and diatom stratigraphy, Deep Sea Drilling Project Leg 44. *In* Benson, W. E., Sheridan, R. E., et al., *Init. Repts. DSDP*, 44: Washington (U.S. Govt. Printing Office), 807–863.

Bukry, D., and Foster, J. H., 1973. Silicoflagellate and diatom stratigraphy, Leg 16, Deep Sea Drilling Project. *In* van Andel, T. H., Heath, G. R., et al., *Init. Repts. DSDP*, 16: Washington (U.S. Govt. Printing Office), 815–871.

Burckle, L. H., 1972. Late Cenozoic planktonic diatom zones from the eastern equatorial Pacific. *Nova Hedwigia*, 39:217–246.

_____, 1977. Pliocene and Pleistocene diatom datum levels from the equatorial Pacific. *Quat. Res.*, 7:330–340.

_____, 1978. Early Miocene to Pliocene diatom datum levels for the equatorial Pacific. *Proc. Second Working Group Mtg., Biostratig. Datum-Planes Pacific Neogene, IGCP Project 114* (Bandung, Indonesia, May 30–June 1, 1977). Spec. Publ. Geol. Res. Dev. Ctr., 1:25–44.

Burckle, L. H., Hammond, S. R., and Seyb, S. M., 1978. A stratigraphically important new diatom from the Pleistocene of the North Pacific. *Pacific Sci.*, 32(2):209–214.

Burckle, L. H., Keigwin, L. D., and Opdyke, N. D., 1982. Middle and late Miocene stable isotope stratigraphy: correlation to the paleomagnetic reversal record. *Micropaleontology*, 28(4):329–334.

Burckle, L. H., and Opdyke, N. D., 1977. Late Neogene diatom correlations in the circum-Pacific. *Proc. First Internat. Congr. Pacific Neogene Stratig.* (Tokyo, 1976): Tokyo (Kaiyo Shuppan Co. Ltd.), pp. 255–284.

Burckle, L. H., and Trainer, J., 1979. Middle and late Pliocene diatom datum levels from the central Pacific. *Micropaleontology*, 25(3): 281–293.

Ciesielski, P. F., 1983. The Neogene and Quaternary diatom biostratigraphy of subantarctic sediments, Deep Sea Drilling Project Leg 71. *In* Ludwig, W. J., and Krasheninnikov, V. A., et al., *Init. Repts. DSDP*, 71: Washington (U.S. Govt. Printing Office), 635–665.

Dunn, D. A., 1982. Miocene sediments of the Pacific Ocean: carbonate stratigraphy and dissolution history [Ph.D. dissert.]. Univ. Rhode Island, Narragansett.

Fenner, J., 1977. Cenozoic diatom biostratigraphy of the equatorial and Southern Atlantic Ocean. *In* Supko, P. R., Perch-Nielsen, K., et al., *Init. Repts. DSDP*, Suppl. to Vols. 38, 39, 40, and 41: Washington (U.S. Govt. Printing Office), 491–624.

_____, 1984. Eocene–Oligocene planktic diatom stratigraphy in the low latitudes and high southern latitudes. *Micropaleontology*, 30(4):319–342.

_____, in press. Paleogene and Late Cretaceous planktic diatom stratigraphy. *In* Bolli, H. M., and Saunders, J. B. (Eds.), *Biostratigraphy by Marine Plankton*: Cambridge (Cambridge Univ. Press).

Gombos, A. M., Jr., 1975. Fossil diatoms from Leg 7, Deep Sea Drilling Project. *Micropaleontology*, 21(3):306–333.

_____, 1976. Paleogene and Neogene diatoms from the Falkland Plateau and Malvinas Outer Basin: Leg 36, Deep Sea Drilling Project. *In* Barker, P., Dalziel, I. W. D., et al., *Init. Repts. DSDP*, 36: Washington (U.S. Govt. Printing Office), 575–687.

Gombos, A. M., Jr., and Ciesielski, P. F., 1983. Late Eocene to early Miocene diatoms from the southwest Atlantic. *In* Ludwig, W. J., Krasheninnikov, V. A., et al., *Init. Repts. DSDP*, 71: Washington (U.S. Govt. Printing Office), 583–634.

Haq, B. U., Worsley, J. R., Burckle, L. H., Douglas, R. G., Keigwin, L. D., et al., 1980. Late Miocene marine carbon-isotope shift and synchroneity of some phytoplanktic biostratigraphic events. *Geology*, 8:427–431.

Harper, H. E., Jr., Rider, J., and Abbott, W. H., 1982. Diatom biostratigraphy of Sites 495, 496, and 497, Deep Sea Drilling Project Leg 67. *In* Aubouin, J., von Huene, R., et al., *Init. Repts. DSDP*, 67: Washington (U.S. Govt. Printing Office), 447–454.

Harwood, D. M., 1982. Oligocene–Miocene diatom biostratigraphy from the equatorial to the Antarctic Pacific [Master's thesis]. Florida State University, Tallahassee.

Hays, J. D., et al., 1972. *Init. Repts. DSDP*, 9: Washington (U.S. Govt. Printing Office).

Jousé, A. P., 1968. New species of diatoms in bottom sediments of the Pacific and the Sea of Okhotsk. *Nov. System. Plant. non Vascular 1968*, Akad. Nauk. SSSR, 3:12–21. (In Russian.)

_____, 1973. Diatoms in the Oligocene–Miocene biostratigraphic zones of the tropical areas of the Pacific Ocean. *Nova Hedwigia*, 45:333–364.

_____, 1977. *Atlas of Microorganisms in Bottom Sediments of the Oceans: Diatoms, Radiolaria, Silicoflagellates, and Coccoliths:* Moscow (Nauka).

Kanaya, T., 1971. Some aspects of pre-Quaternary diatoms in the oceans. *In* Riedel, W. R., and Funnell, W. M. (Eds.), *Micropaleontology of the Oceans*: Cambridge (Cambridge Univ. Press), pp. 545–565.

Keller, G., and Barron, J. A., 1983. Paleoceanographic implications of Miocene deep sea hiatuses. *Geol. Soc. Am. Bull.*, 94:590–613.

Keller, G., Barron, J. A., and Burckle, L. H., 1982. Paleomagnetic, stable isotope, carbonate, and microfossil stratigraphies in upper Miocene sediments in the North Pacific Ocean. *Mar. Micropaleontol.*, 7:327–357.

Koizumi, I., 1973. The late Cenozoic diatoms of Sites 183–193, Leg 19. *In* Creager, J. S., Scholl, D. W., et al., *Init. Repts. DSDP*, 19: Washington (U.S. Govt. Printing Office), 805–855.

Kolbe, R., 1954. Diatoms from the equatorial Pacific cores. *Rep. Swed. Deep Sea Exped., 1947–1948*, 6:1–49.

Mukhina, V. V., 1963. Biostratigraphic analysis of bottom sediments from Station 3802 in the equatorial zone of the Pacific Ocean. *Okeanologiya*, 3:861–869. (In Russian.)

_____, 1965. New species of diatoms from bottom sediments of the equatorial region of the Pacific. *Nov. System. Plant. non Vascularium*, Bot. Inst. Akad. Nauk. SSSR, pp. 22–25. (In Russian with systematic description of species in Latin.)

_____, 1966. The boundary between sediments of Quaternary and Tertiary age in the Pacific (on the basis of diatom analysis). *Oceanology*, 6:99–110.

_____, 1969. Biostratigraphy of sediments and some questions of paleogeography of the tropical region of Pacific and Indian oceans *In* Jousé, A. P. (Ed.), *Micropaleontology and Organogenous Sedimentation in the Oceans*: Moscow (Izd. Nauka), 52–84.

Opdyke, N. D., Burckle, L. H., and Todd, A., 1974. The extension of the magnetic time scale in sediments of the central Pacific Ocean. *Earth Planet. Sci. Lett.*, 22:300–306.

Poore, R. Z., Tauxe, L., Percival, S. F., Jr., LaBrecque, J. L., Wright, R., et al., 1983. Late Cretaceous—Cenozoic magnetostratigraphic and biostratigraphic correlations of the South Atlantic Ocean: DSDP Leg 73. *Palaeogeogr. Palaeoclim. Palaeoecol.*, 42:127–149.

Ryan, W. B. F., Cita, M. B., Rawson, M. D., Burckle, L. H., and Saito, T., 1974. A paleomagnetic assignment of Neogene stage boundaries and the development of isochronous datum planes between the Mediterranean, the Pacific and Indian oceans in order to investigate the response of the world ocean to the Mediterranean "salinity crisis." *Riv. Ital. Paleontol.*, 80:631–688.

Sancetta, C. A., 1982. Diatom biostratigraphy and paleoceanography, Deep Sea Drilling Project Leg 68. *In* Prell, W. L., Gardner, J. V., et al., *Init. Repts. DSDP*, 68: Washington (U.S. Govt. Printing Office), 301–310.

———, 1983. Biostratigraphic and paleoceanographic events in the eastern equatorial Pacific: results of Deep Sea Drilling Project Leg 69. *In* Cann, J. R., Langseth, M. G., Honnorez, J., Von Herzen, R. P., White, S. M., et al., *Init. Repts. DSDP*, 69: Washington (U.S. Govt. Printing Office), 311–342.

Savin, S. M., Douglas, R. G., Keller, G., Killingley, J. S., Shaughnessy, L., et al., 1981. Miocene benthic foraminiferal isotope records: a synthesis. *Mar. Micropaleontol.*, 6:423–450.

Schrader, H. J., 1974. Cenozoic marine planktonic diatom stratigraphy of the tropical Indian Ocean. *In* Fisher, R. L., Bunce, E. T., et al., *Init. Repts. DSDP*, 24: Washington (U.S. Govt. Printing Office), 887–967.

Schrader, H. J., and Gersonde, R., 1978. Diatoms and silicoflagellates. *Utrecht Micropal. Bull.*, 17:1129–1176.

van Andel, T. H., Heath, G. R., and Moore, T. C., Jr., 1975. Cenozoic history and paleoceanography of the central equatorial Pacific Ocean. *Mem. Geol. Soc. Am. 143.*

Weaver, F. M., and Gombos, A. M., Jr., 1981. Southern high-latitude diatom biostratigraphy. *Spec. Publ. Soc. Econ. Paleontol. Mineral.*, 32:445–470.

Woodruff, F., Savin, S. M., and Douglas, R. G., 1981. Miocene stable isotope record: a detailed deep Pacific Ocean study and its paleoclimatic implications. *Science*, 212:665–668.

Date of Initial Receipt: 10 October 1983
Date of Acceptance: 6 March 1984

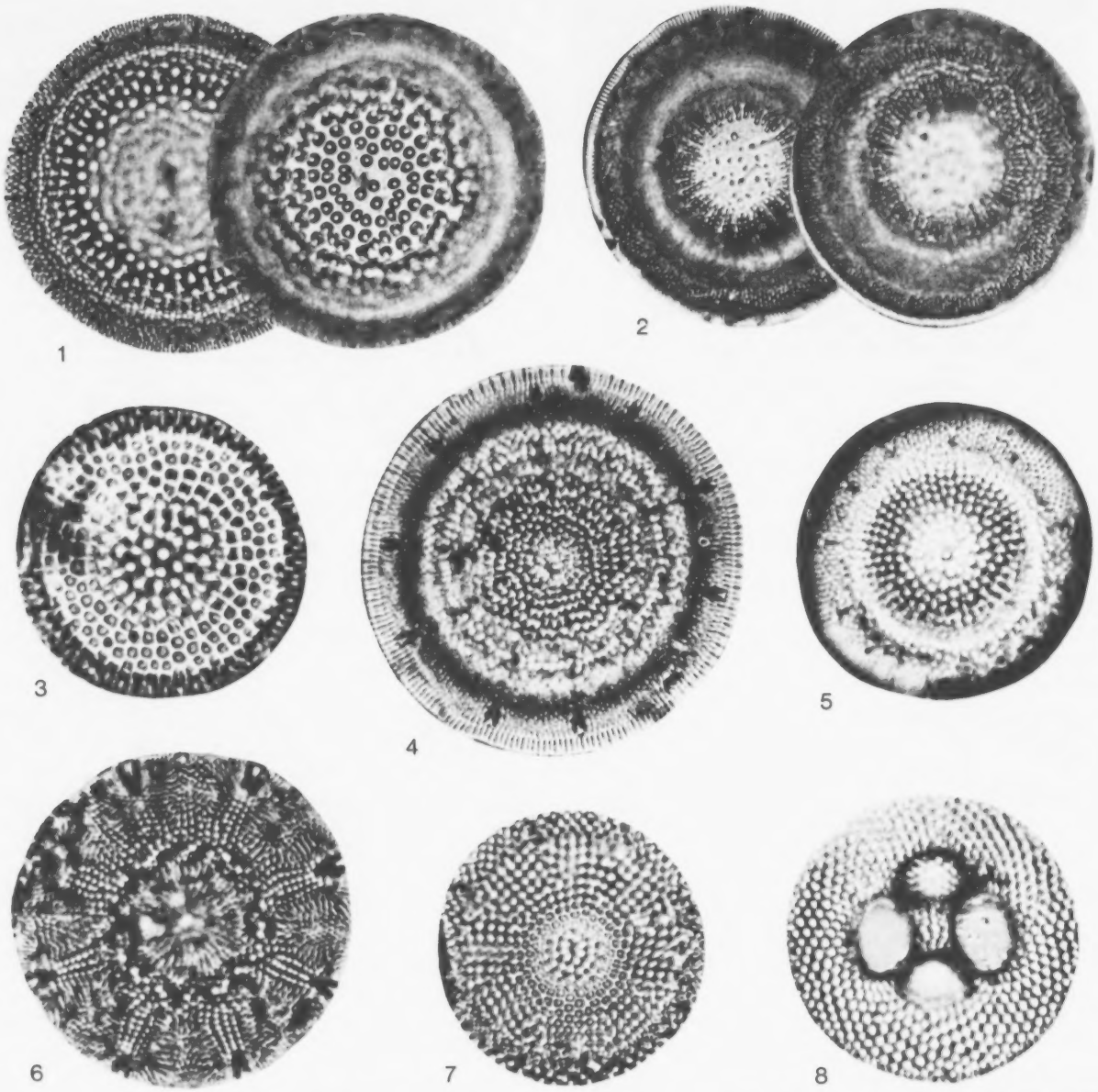

Plate 1. **1.** *Cestodiscus robustus* Jousé, low and high focus, diameter 92 μm, Sample 574C-28,CC. **2.** *Actinocyclus radionovae* Barron, low and high focus, diameter 75 μm, Sample 574C-6-2, 43–45 cm. **3.** *Cestodiscus mukhinae* Jousé, diameter 33 μm, Sample 574C-22,CC. **4.** *Cestodiscus pulchellus* var. *maculatus* Kolbe, diameter 40 μm, Sample 77B-28-2, 28–30 cm. **5.** *Cestodiscus pulchellus* Greville sensu Jousé (1977), diameter 52 μm, Sample 574C-31,CC. **6.** *Aulacodiscus* sp. (figured by Jousé [1977] as *Actinodiscus barbadensis* Greville), diameter 54 μm, Sample 574C-17,CC. **7.** *Cestodiscus pulchellus* Greville, diameter 41 μm, Sample 77B-25-6, 20–22 cm. **8.** *Coscinodiscus excavatus* Ralfs, diameter 130 μm, Sample 573B-37,CC.

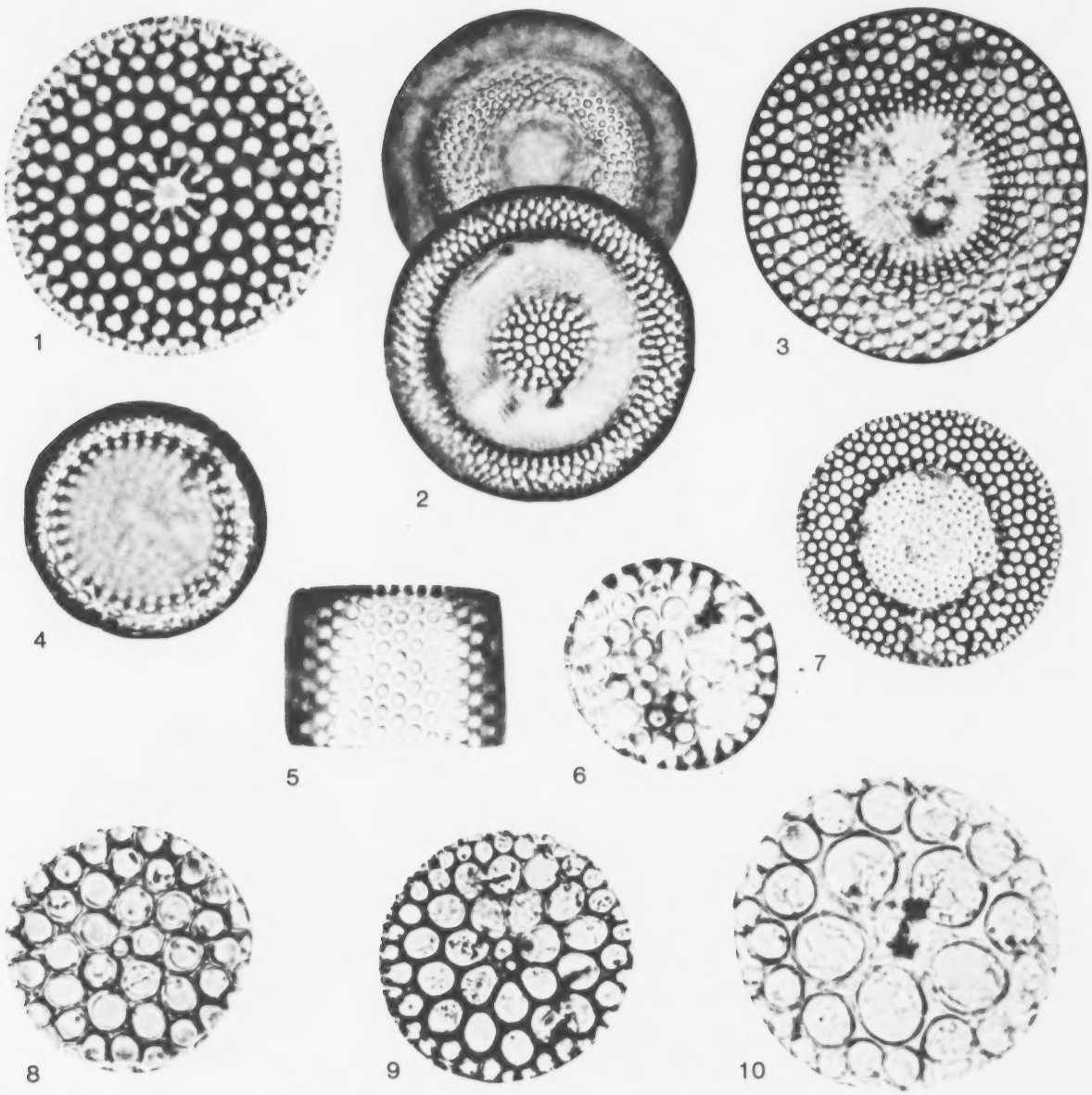

Plate 2. **1.** *Coscinodiscus blysmos* Barron, diameter 40 μm, Sample 575A-2-3, 42–43 cm. **2.** *Craspedodiscus elegans* Ehrenberg, low and high focus, diameter 107 μm, Sample 575A-17,CC. **3.** *Craspedodiscus coscinodiscus* Ehrenberg s. ampl., coarse indented form of the late Oligocene, diameter 148 μm, Sample 574C-17-2, 43–45 cm. **4.** *Craspedodiscus rydei* Barron, diameter 34 μm, Sample 575A-3-2, 42–43 cm. **5.** *Annellus californicus* Tempère, width 39 μm, Sample 575B-12-6, 105–106 cm. **6.** *Rocella vigilans* (Schmidt) Fenner, plicate form, diameter 30 μm, Sample 574C-17,CC. **7.** *Craspedodiscus coscinodiscus* Ehrenberg s. str., diameter 72 μm, Sample 574-16-2, 42–43 cm. **8–9.** *Rocella gelida* (Mann) Bukry, (8) diameter 34 μm, Sample 574C-17,CC, (9) diameter 66 μm, Sample 574C-17-2, 43–45 cm. **10.** *Rocella gelida* var. *schraderi* (Bukry) Barron, diameter 47 μm, Sample 574C-16,CC.

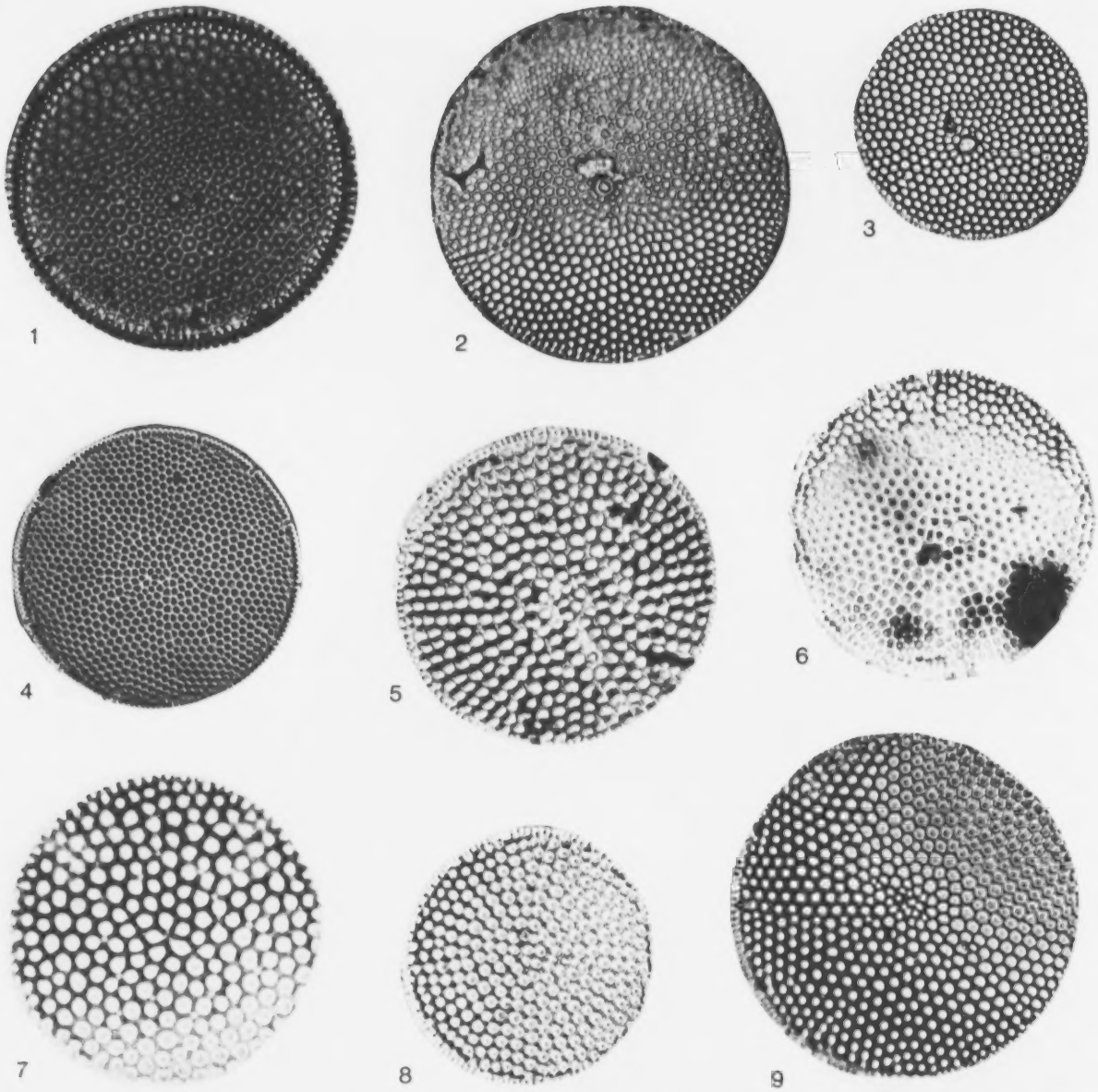

Plate 3. **1.** *Coscinodiscus nodulifer* A. Schmidt, diameter 54 μm, Sample 572A-6-3, 42–43 cm. **2.** *Coscinodiscus nodulifer* var. *cyclopus* Jousé, Miocene form, clear area above center is bubble in mounting medium; diameter 91 μm, Sample 574-8-1, 43–45 cm. **3.** *Coscinodiscus nodulifer* var. *cyclopus* Jousé s. str., diameter 60 μm, Sample 573-8,CC. **4.** *Coscinodiscus tabularis* Grunow, diameter 46 μm, Sample 574-10-6, 43–45 cm. **5.** *Coscinodiscus oligocenicus* Jousé, diameter 39 μm, Sample 574C-31,CC. **6.** *Coscinodiscus vetustissimus* var. *javanica* Reinhold, diameter 29 μm, Sample 77B-17-1, 18–20 cm. **7.** *Coscinodiscus radiatus* Ehrenberg, diameter 59 μm, Sample 574-20,CC. **8.** *Coscinodiscus tuberculatus* Greville, diameter 36 μm, Sample 574-11-4, 43–45 cm. **9.** *Coscinodiscus salisburyanus* Lohman, diameter 47 μm, Sample 574-20-2, 43–44 cm.

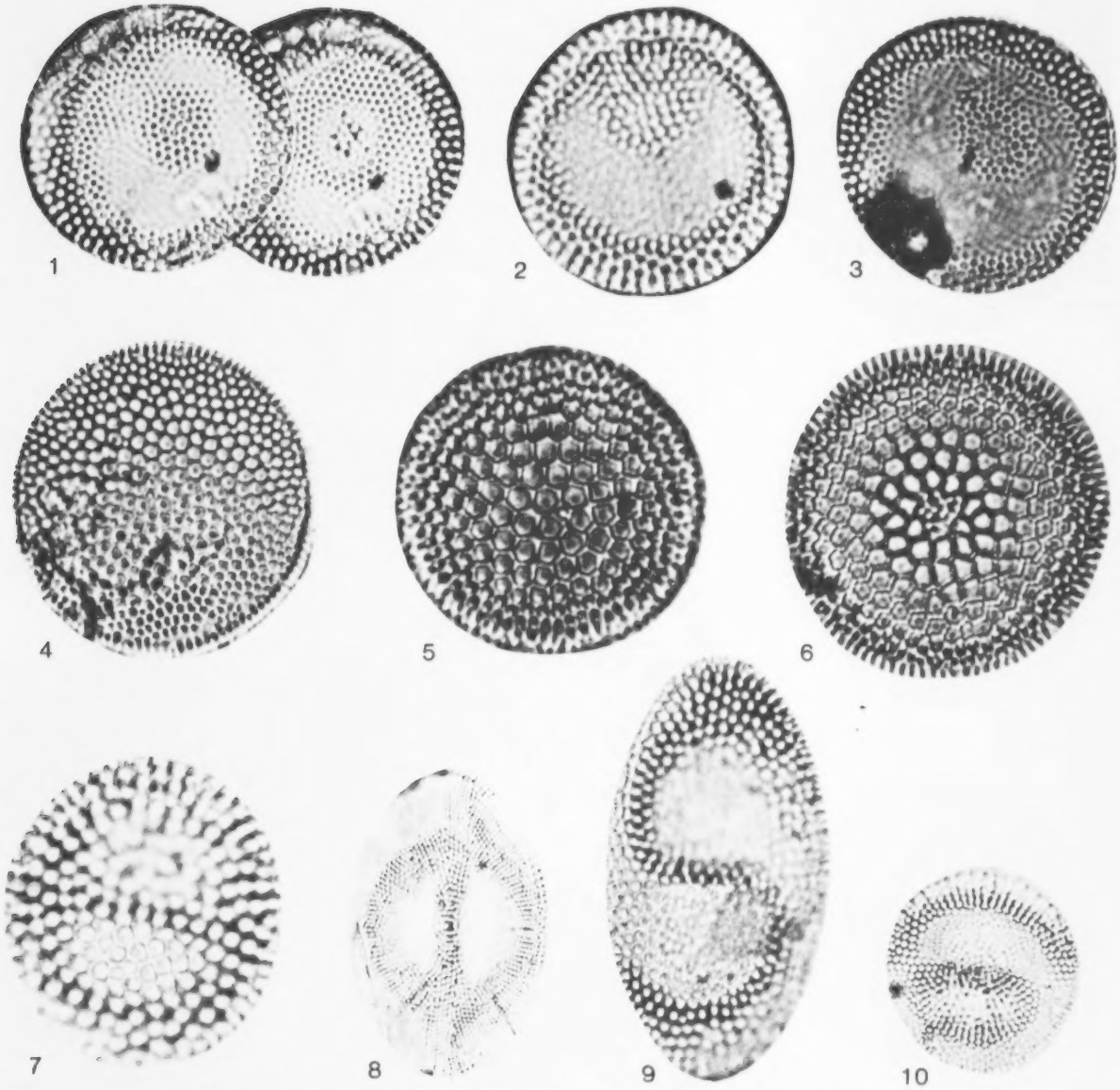

Plate 4. **1-3.** *Coscinodiscus loeblichii* Barron, n. sp., Sample 572D-10,CC, (1) Holotype USNM 370304, high and low focus, diameter 28 μm, (2) Isotype USNM 370305, diameter 23 μm, (3) Isotype USNM 370306, diameter 30 μm. **4.** *Thalassiosira bukryi* Barron, diameter 33 μm, Sample 575A-6-3, 42-43 cm. **5.** *Thalassiosira oestrupii* (Ostenfeld) Proshkina-Lavrenko, diameter 24 μm, Sample 572A-1-3, 67-68 cm. **6.** *Thalassiosira burckliana* Schrader, diameter 15 μm, Sample 77B-15-6, 23-25 cm. **7.** *Coscinodiscus yabei* Kanaya, diameter 24 μm, Sample 574-8,CC. **8.** *Coscinodiscus temperi* var. *delicata* Barron, length 57 μm, Sample 574-10-5, 43-45 cm. **9.** *Coscinodiscus yabei* var. *ellipticus* Barron, n. var., Holotype USNM 370307, length 63 μm, Sample 572D-10-4, 50-52 cm. **10.** *Coscinodiseus plicatus* Grunow, diameter 46 μm, Sample 574-10-5, 43-45 cm.

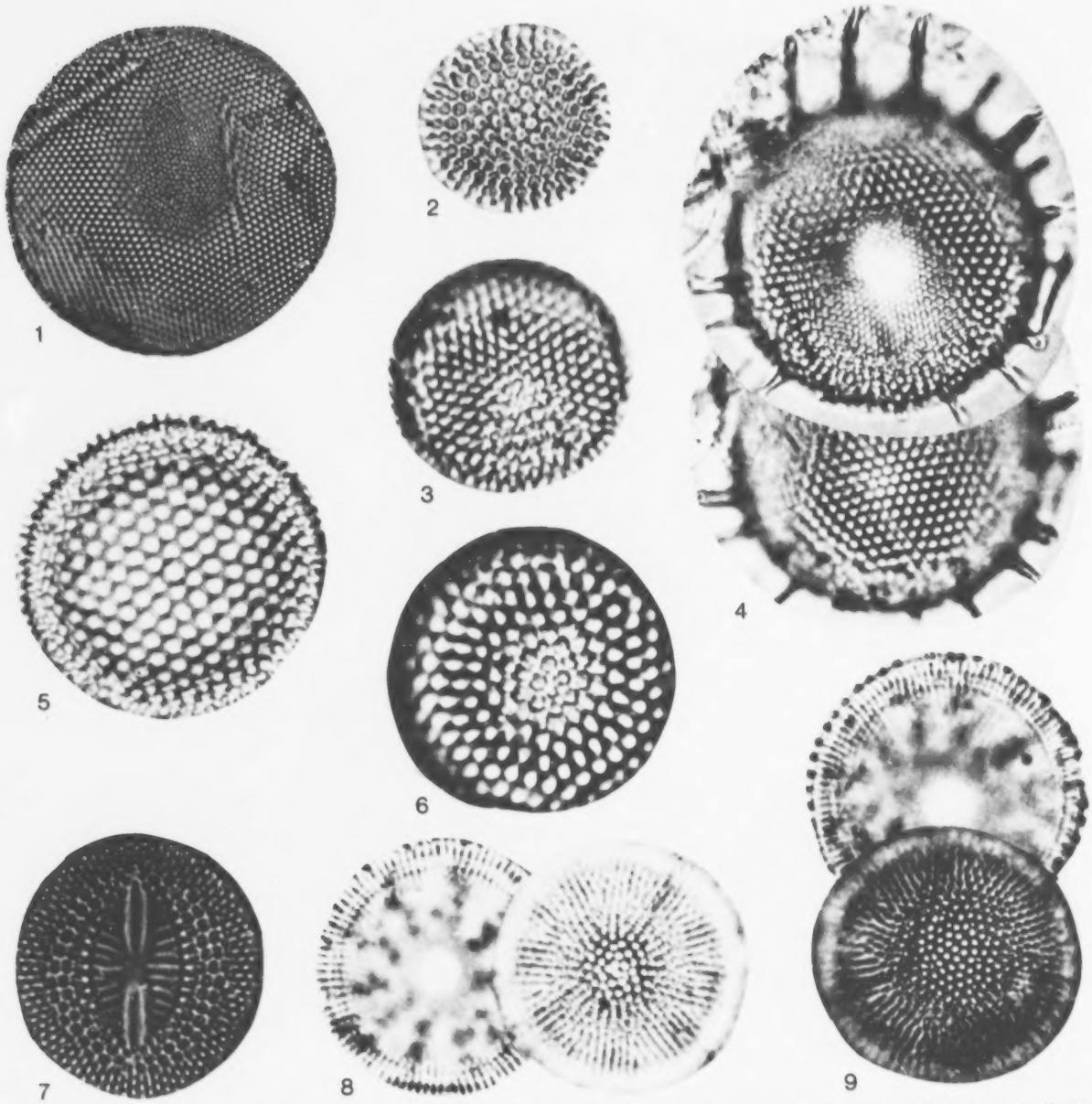

Plate 5. **1.** *Thalassiosira eccentrica* (Ehrenberg) Cleve, diameter 78 μm, Sample 572A-4-3, 66–67 cm. **2.** *Thalassiosira fraga* Schrader, diameter 18 μm, Sample 575A-1-1, 50–51 cm. **3.** *Thalassiosira praeconvexa* Burckle, diameter 15 μm, Sample 573-12,CC. **4.** *Thalassiosira spumellaroides* Schrader, low and high focus, diameter 34 μm, Sample 574C-7-2, 43–45. **5.** *Thalassiosira leptopus* (Grunow) Hasle and Fryxell, diameter 35 μm, Sample 574-18-2, 42–43 cm. **6.** *Thalassiosira miocenica* Schrader, diameter 16 μm, Sample 77B-10-6, 30–32 cm. **7.** *Raphidodiscus marylandicus* Christian, length 24 μm, Sample 575A-7-3, 43–44 cm. **8.** *Thalassiosira convexa* var. *aspinosa* Schrader, low and high focus, diameter 34 μm, Sample 574-3-4, 129–130 cm. **9.** *Thalassiosira convexa* var. *convexa* Mukhina, low and high focus, diameter 38 μm, Sample 574-3-4, 129–130 cm.

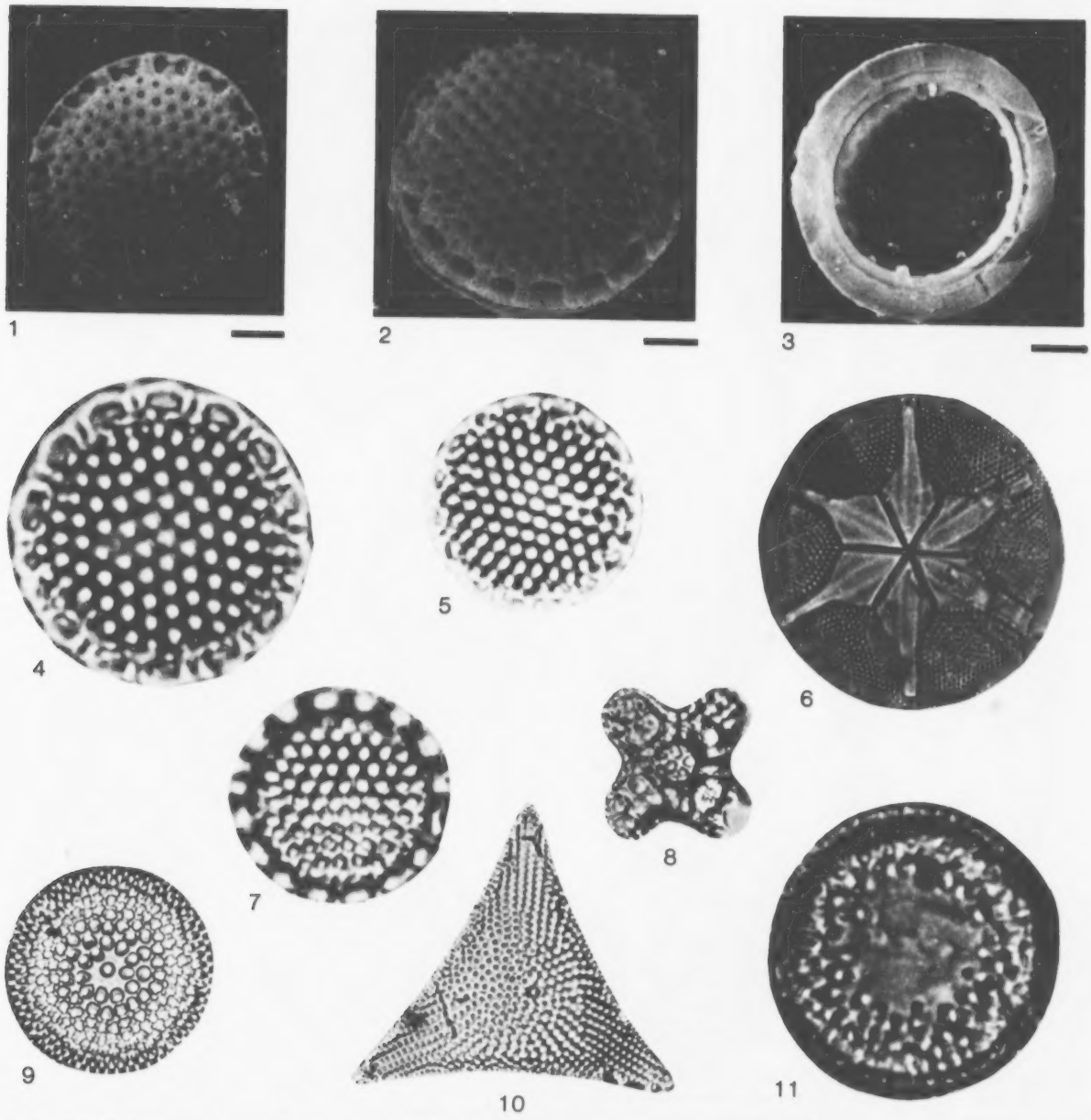

Plate 6. **1–3.** *Thalassiosira tappanae* Barron, n. sp., scanning electron microscope pictures, Sample 574-19-2, 43–44 cm (scale bar = 3 μm), (1) USNM 370311, showing small accessory pore midway along radius at 3 o'clock position, (2) USNM 370312, (3) USNM 370313, internal view of valve showing marginal strutted processes and single labiate process at 7 o'clock position. **4, 5, 7.** *Thalassiosira tappanae* Barron, n. sp., (4) diameter 14 μm, Sample 572-20-2, 43–44 cm, (5) Isotype USNM 370310, diameter 13 μm, Sample 572D-28-2, 50–52 cm, (7) Holotype USNM 370309, diameter 12.5 μm, Sample 572D-28-2, 50–52 cm. **6.** *Asterolampra acutiloba* Frenguelli, diameter 48 μm, Sample 573-12,CC. **8.** *Lisitzinia ornata* Jousé, side 27 μm, Sample 574C-17-2, 43–45 cm. **9.** *Actinocyclus ingens* Rattray, diameter 35 μm, Sample 574-16-2, 42–43 cm. **10.** *Triceratium pileus* Ehrenberg, side 71 μm, Sample 575A-7-2, 43–44 cm. **11.** *Melosira architecturalis* Brun, diameter 18 μm, Sample 574C-22,CC.

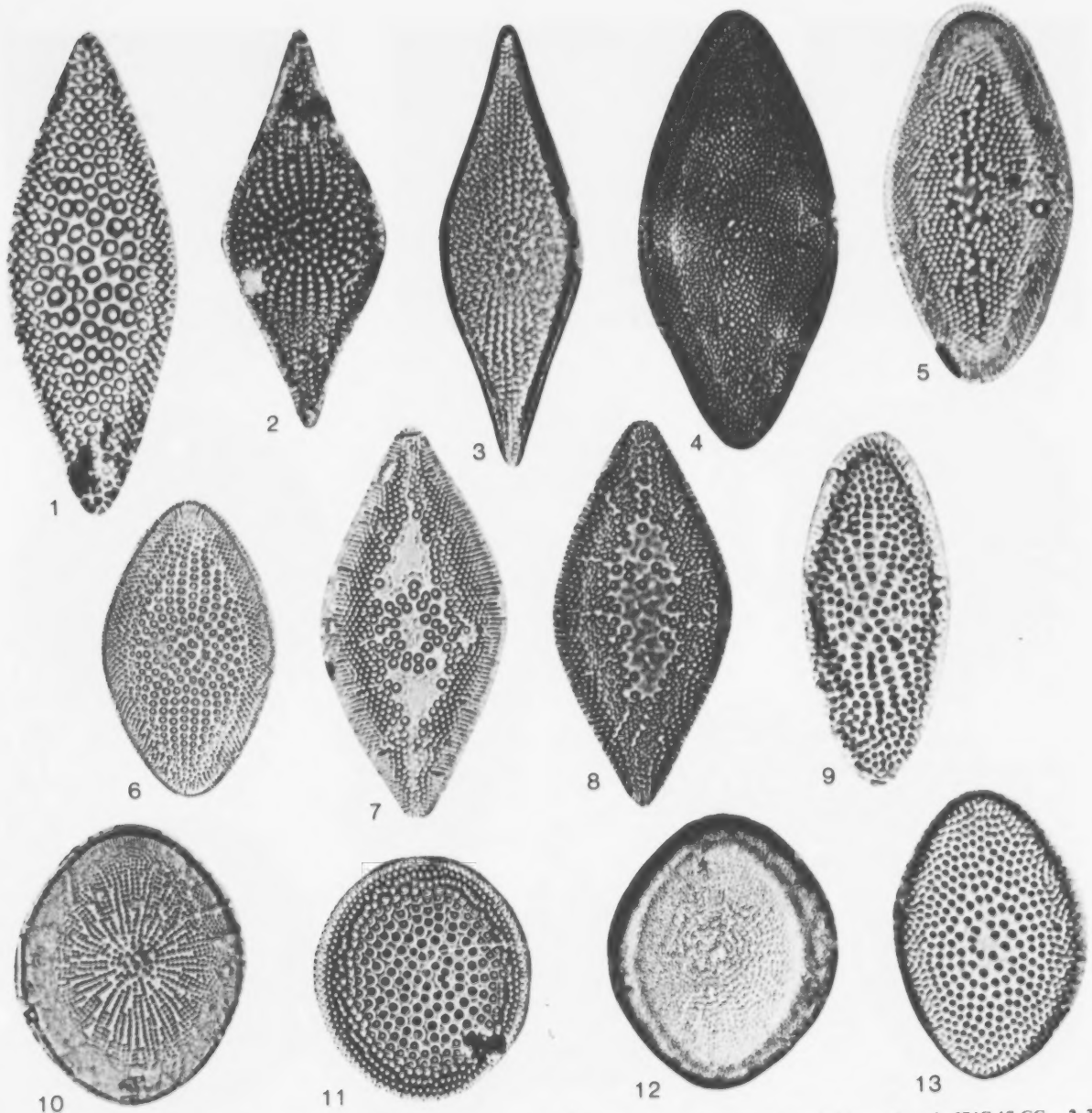

Plate 7. (All pseudonodules are at the 3 o'clock position.) **1.** *Coscinodiscus rhombicus* Castracane, length 54 μm, Sample 574C-17,CC. **2–3.** *Coscinodiscus lewisianus* var. *rhomboides* Barron, n. var., (2) Holotype USNM 370299, length 114 μm, Sample 71-39-2, 87–89 cm, (3) USNM 370300, length 116 μm, Sample 574C-20,CC. **4.** *Actinocyclus ellipticus* f. *lanceolata* Kolbe, length 63 μm, Sample 77B-12-1, 62–66 cm. **5.** *Actinocyclus moronensis* Deby, length 44 μm, Sample 574-11-4, 43–44 cm. **6.** *Coscinodiscus lewisianus* var. *similis* Rattray, length 65 μm, Sample 575A-4-3, 42–43 cm. **7–8.** *Cestodiscus peplum* Brun, (7) length 75 μm, Sample 575B-11-1, 106–107 cm, (8) length 59 μm, Sample 574-22-2, 43–44 cm. **9–10.** *Coscinodiscus lewisianus* var. *spiralis* Barron, n. var., Sample 575-5-2, 43–44 cm, (9) USNM 370302, length 38 μm, (10) USNM 370303, length 70 μm. **11.** *Coscinodiscus lewisianus* var. *robustus* Barron, length 56 μm, Sample 575A-6-3, 42–43 cm. **12.** *Actinocyclus ellipticus* var. *javanica* Reinhold, length 79 μm, Sample 572D-11-1, 50–52 cm. **13.** *Actinocyclus* sp. cf. *A. ellipticus* Grunow, early Miocene form, length 25 μm, Sample 575A-5-2, 42–43 cm.

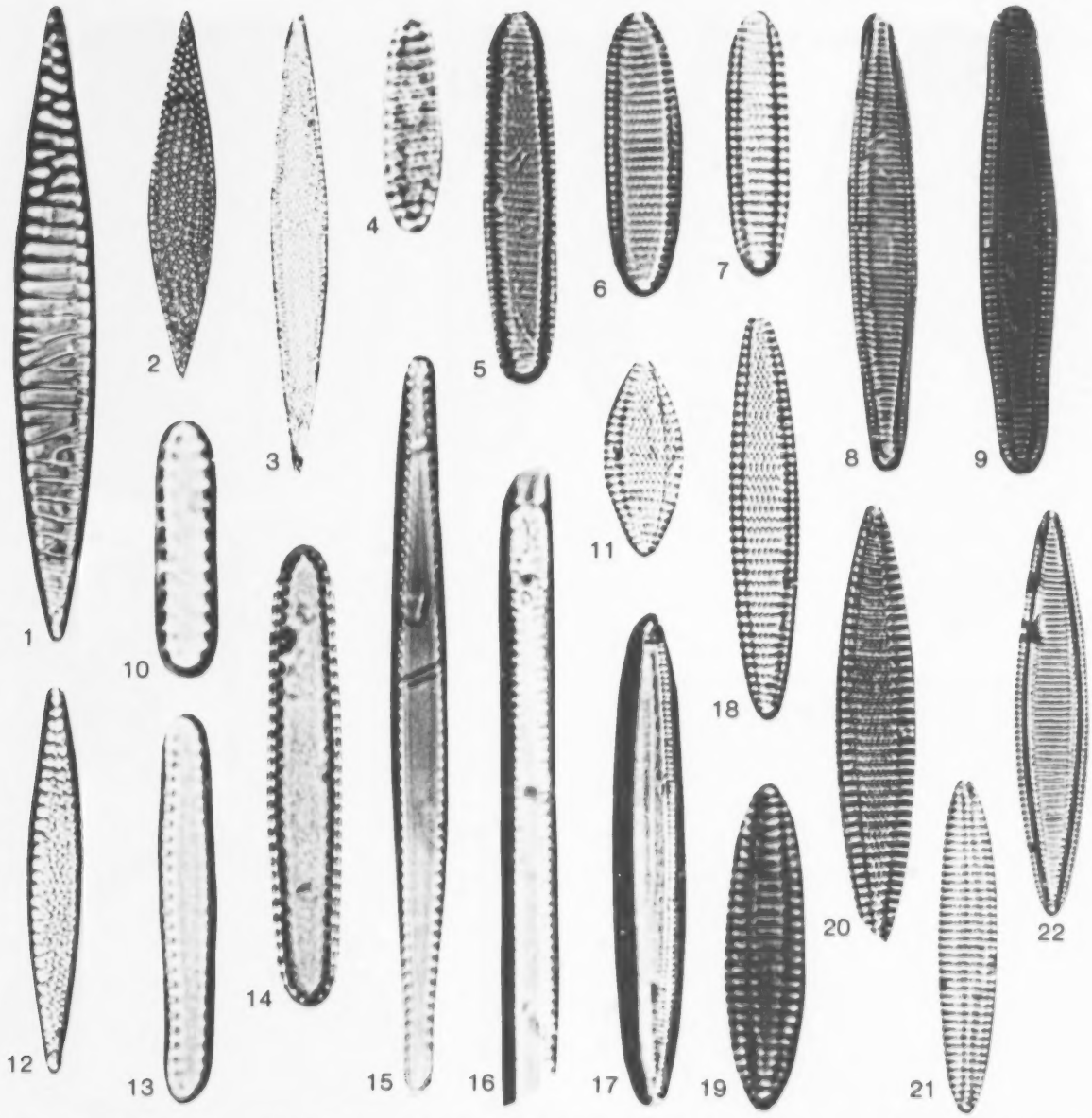

Plate 8. **1.** *Rossiella praepaleacea* (Schrader) Gersonde, length 49 μm, Sample 572D-6,CC. **2.** *Rossiella paleacea* (Grunow) Desikachary and Maheshwari, length 69 μm, Sample 77B-28-2, 28–30 cm. **3.** *Rossiella paleacea* var. *elongata* (Barron) Barron, n. comb., length 92 μm, Sample 574-10-6, 43–45 cm. **4.** *Nitzschia porteri* Frenguelli sensu Burckle (1972), length 14 μm, Sample 573D-11-1, 50–52 cm. **5–6.** *Nitzschia cyclindrica* Burckle s. ampl., Sample 573-17-2, 62–63 cm, (5) length 34 μm, (6) length 28 μm. **7.** *Nitzschia cyclindrica* Burckle s. str., length 28 μm, Sample 573-12,CC. **8–9.** *Nitzschia fossilis* (Frenguelli) Kanaya and Koizumi, (8) length 48 μm, Sample 572D-10,CC, (9) length 42 μm, Sample 573-13,CC. **10.** *Thalassionema nitzschioides* var. *parva* Heiden and Kolbe, length 12 μm, Sample 574-12-4, 43–45 cm. **11, 18.** *Nitzschia jouseae* Burckle, (11) length 27 μm, Sample 574-3-4, 129–130 cm, (18) elongated form, length 50 μm, Sample 572A-6-3, 66–67. **12.** *Bogorovia veniamini* Jousé, length 57 μm, Sample 575A-22,CC. **13, 15.** *Thalassionema nitzschioides* Grunow, (13) length 27 μm, Sample 574-20-2, 43–44 cm, (15) length 65 μm, Sample 572D-6-2, 50–52 cm. **14.** *Thalassionema robusta* Schrader, length 41 μm, Sample 574-11-2, 43–45 cm. **16.** *Thalassiothrix longissima* Cleve and Grunow, width 5 μm, Sample 574-20-2, 43–44 cm. **17.** *Synedra jouseana* Sheshukova-Poretzkaya, length 51 μm, Sample 574C-17,CC. **19.** *Nitzschia miocenica* Burckle, length 22 μm, Sample 77B-12-6, 30–32 cm. **20.** *Nitzschia praereinholdii* Schrader, length 57 μm, Sample 572D-10,CC. **21.** *Nitzschia miocenica* var. *elongata* Burckle, length 42 μm, Sample 573-12,CC. **22.** *Nitzschia reinholdii* Kanaya and Koizumi, length 56 μm, Sample 572A-6-3, 66–67 cm.

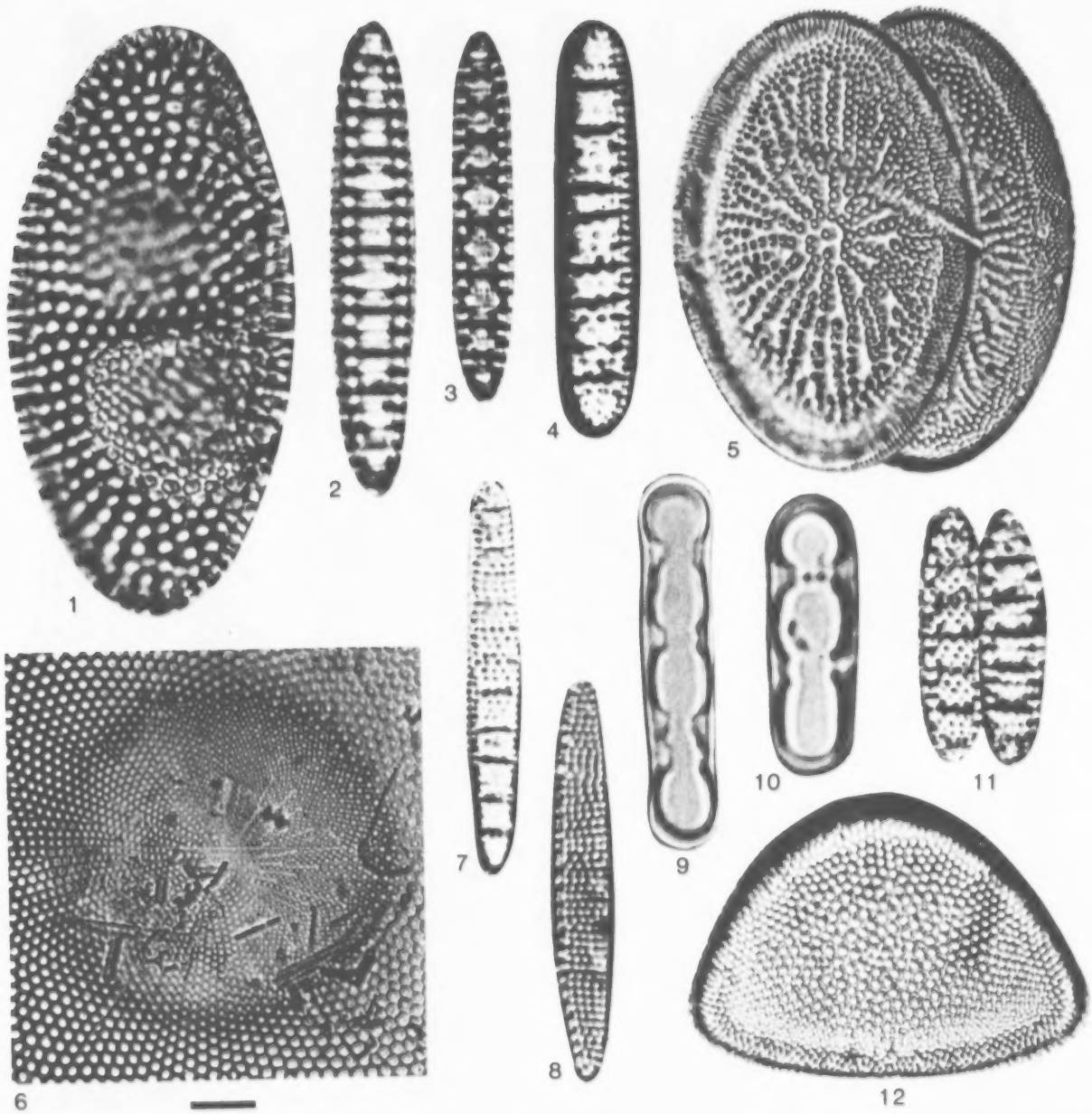

Plate 9. **1.** *Coscinodiscus yabei* var. *ellipticus* Barron, n. sp., Isotype USNM 370308, length 46 μm, Sample 572D-10-4, 50–52 cm. **2–3.** *Denticulopsis hustedtii* (Simonsen and Kanaya) Simonsen, (2) length 44 μm, Sample 572D-19-3, 50–52 cm, (3) length 35 μm, Sample 574-10-6, 43–45 cm. **4.** *Denticulopsis* sp. cf. *D. kanayae* (Akiba) Barron, length 36 μm, Sample 575A-1-1, 50–51 cm. **5.** *Coscinodiscus lewisianus* var. *spiralis* Barron, n. var., Holotype USNM 370301, high and low focus (note pseudonodule at 3 o'clock position), length 57 μm, Sample 575-5-4, 43–44 cm. **6.** *Coscinodiscus gigas* var. *diorama* (Schmidt) Grunow, central area (scale bar = 20 μm), Sample 574-14,CC. **7.** *Denticulopsis nicobarica* (Grunow) Simonsen, length 33 μm, Sample 575A-1,CC. **8.** *Nitzschia maleinterpretaria* Schrader, length 35 μm, Sample 575A-6-1, 42–43 cm. **9–10.** *Denticulopsis praedimorpha* (Akiba) Akiba, Sample 574-12-4, 43–45 cm, (9) length 21 μm, (10) length 16 μm. **11.** *Denticulopsis punctata* f. *hustedtii* (Schrader) Simonsen, low and high focus, length 25 μm. **12.** *Hemidiscus cuneiformis* Wallich, length 46 μm, Sample 572D-10,CC.

Reprinted from Mayer, L., Theyer, F., et al., 1985
Initial Reports of the Deep Sea Drilling Project, Volume LXXXV, Washington (U. S. Government Printing Office)

9. A HIGH RESOLUTION LATE MIOCENE–PLIOCENE DIATOM BIOSTRATIGRAPHY FOR THE EASTERN EQUATORIAL PACIFIC[1]

Jack G. Baldauf, U.S. Geological Survey, Menlo Park, and Department of Paleontology, University of California at Berkeley[2]

ABSTRACT

Quantitative procedures are used here for DSDP Sites 572, 573, and 503 to refine the stratigraphic resolution for upper Neogene sediments of the eastern equatorial Pacific Ocean. As a result, six new diatom events are defined for the stratigraphic interval 6.2 to 1.5 Ma. The carbonate minimums 5e, Gu3, and M21, as well as the carbonate maximums 5f and 5d, are correlated to diatom datums and are useful in refining the stratigraphic resolution of the upper Neogene.

In addition to allowing stratigraphic refinement, quantitative procedures aid in determining paleoceanographic conditions. The greater abundance of *Coscinodiscus nodulifer* at Site 503 as compared with Sites 572 and 573 suggests that this species is associated with equatorial upwelling. The greater abundance of *Thalassionema nitzschioides* at Site 572 suggests that this species is associated with the Equatorial Undercurrent. Furthermore, the gradual decline in the abundance of *T. nitzschioides* between 4.2 and 3.7 Ma at Sites 572 and 503 may have resulted from restriction in surface-water communication between the Atlantic and Pacific Oceans as a result of the emergence of the Isthmus of Panama.

INTRODUCTION

Numerous biostratigraphic studies of the equatorial Pacific (in particular, Burckle, 1969, 1972, 1977, 1978; Barron, in press) have resulted in the development and adoption of a middle Miocene–Holocene low-latitude diatom zonation. This zonal scheme, defined principally by Burckle (1972, 1977), is based on biostratigraphic events. With the exception of one event, these events are based on the first or last occurrences of selected, easily recognizable species that have a consistent stratigraphic range and a wide geographic distribution. The single exception is the evolutionary transition of *Rhizosolenia praebergonii* to *R. praebergonii* var. *robusta*, which is a stratigraphically useful event. These events have been correlated with magnetostratigraphy by Burckle (1972, 1977, 1978), Burckle and Trainer (1979), and Barron et al. (in press).

Figure 1 presents the diatom datums defined (previously and in this paper) for the interval 6.5 to 1.5 Ma and their correlation to the paleomagnetic scale of Berggren et al. (in press). The occurrence of 25 datums within this 5-m.y. interval (Column 1, Fig. 1) indicates that the average temporal resolution is 1 datum per 0.2 m.y. However, this resolution is not uniform because the datums are generally concentrated within specific time intervals. For example, only two datums occur within the Gauss paleomagnetic chron, whereas six datums are defined for an equivalent duration of time within the older part of the Matuyama paleomagnetic chron.

The use of changes in relative abundances in addition to first and last occurrences results in an increase in the number of definable datums, thereby increasing the available temporal resolution (Column 2, Fig. 1). Quantitative procedures using diatoms were first made popular by Burckle (1977), who defined two diatom events for the Quaternary. These Quaternary datums are based on the progressive upward increase in abundance of *Thalassiosira oestrupii* from 5 to 20% of the overall diatom assemblage and by a distinct acme in *Roperia tesselata* var. *ovata*.

Burckle and Trainer (1979) subsequently defined six additional datums for the interval including the upper Gilbert Chron to slightly above the Olduvai Subchron within the Matuyama Chron. These datums defined by Burckle and Trainer are based on the disappearance and reappearance of *T. convexa* and *Coscinodiscus nodulifer* var. *cyclopus* in Core V28-179 from the equatorial Pacific.

To further refine the stratigraphic resolution of the middle and upper Neogene, the quantitative biostratigraphic approach used by Burckle and Trainer (1979) is here extended to older floras through the lower Pliocene and uppermost Miocene sequences on the basis of samples recovered from three sites located within the eastern equatorial Pacific (Fig. 2).

At least three factors should be taken into consideration if stratigraphic correlations based on fluctuations in fossil abundance are to be valid. First, species abundance is influenced by environment and will vary with fluctuations in climate, the migration of water masses, nutrient limitations, and biological factors (i.e., predation and competition). For a correlation between abundance peaks to be valid, the main environmental conditions that affect diatom abundance must be similar in the regions of interest. Second, abundance fluctuations may be cyclical, and the frequency of the fluctuations may be unknown, so a sampling program may be insufficient to document all the fluctuations in the abundance of a given species. To be valid, correlated abundance peaks must be coeval, and to ensure that they are re-

[1] Mayer, L., Theyer, F., et al., *Init. Repts. DSDP*, 85: Washington (U.S. Govt. Printing Office).

[2] Present address: Ocean Drilling Program, Texas A&M University, College Station, TX 77843.

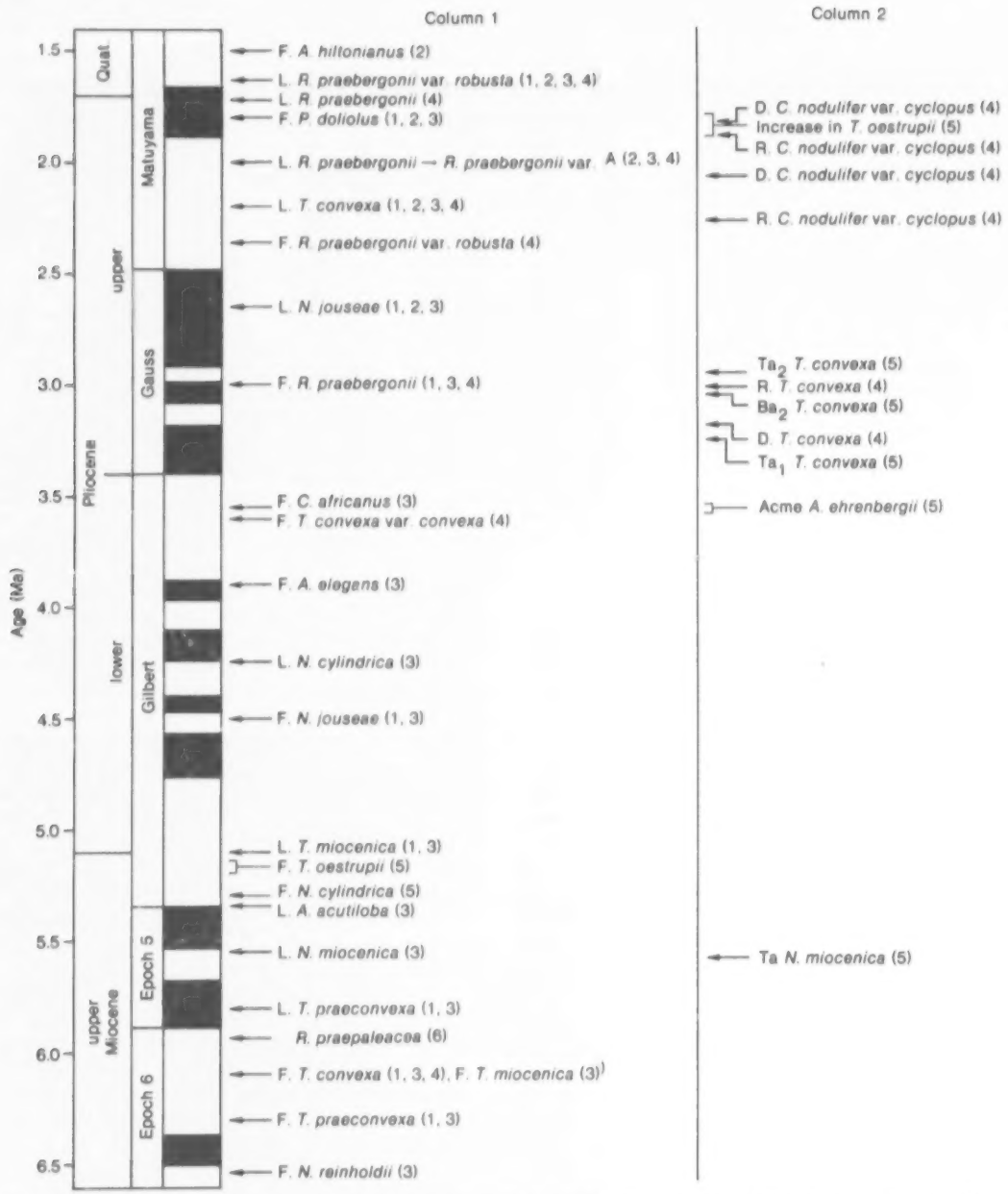

Figure 1. Correlation of useful diatom datums to the paleomagnetic scale of Berggren et al. (in press). Column 1 consists of datums defined on the first or last occurrence of specific species (with the exception of the evolutionary transition of *R. praebergonii*). Column 2 consists of diatom datums resulting from quantitative analysis. Ta = top of abundance interval; D = disappearance; Ba = bottom of abundance interval; R = recurrence. References: (1) Burckle, 1972; (2) Burckle, 1977; (3) Burckle, 1978; (4) Burckle and Trainer, 1979; (5) this paper; (6) Barron et al., in press.

quires a large number of stratigraphically closely spaced samples and an independent stratigraphic control (isotopes, paleomagnetism, or other fossil groups). Third, it is necessary to know the stratigraphic and counting precision to ensure that correlated peaks in abundance are coeval.

These constraints limit the usefulness of fluctuations in abundance for purposes of stratigraphic correlation; the results of this study are preliminary. The author intends to use these results to determine major fluctuations of a species within specific stratigraphic intervals and to study these intervals further with more closely spaced samples from the same geographic region.

Sites 573, 572, and 503 form a west–east transect from the central Pacific (Site 573), characterized by low surface-water productivity, to the Guatemala basin region (Site 503), characterized by high surface-water productivity (Fig. 2). The intermediate site (572) is located at

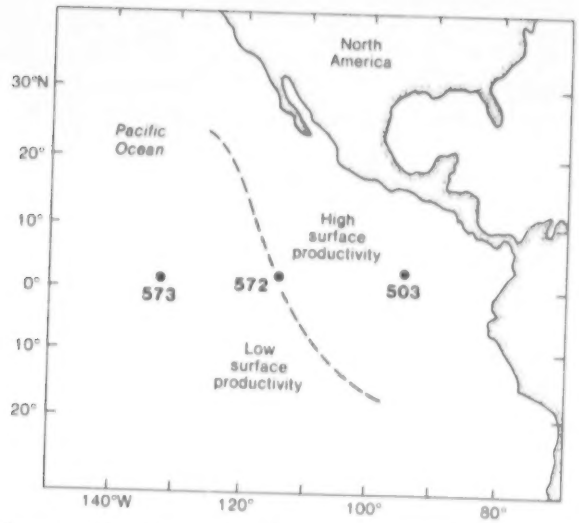

Figure 2. Geographic locations of Sites 573, 572 (Leg 85), and 503 (Leg 68). Dashed line represents inferred boundary between areas of high and low productivity.

the westernmost fringe of the high productivity region. Because of the geographic position of these sites, this study provides information on the paleoceanography of the region in addition to a refinement of the stratigraphy.

METHODOLOGY

At least one sample was examined for each 0.1-m.y. period within the time interval 6.2 to 1.5 Ma, except when recovery was poor or when hiatuses were present. The length of each 0.1-m.y. period was extrapolated from sediment accumulation rate curves derived from paleomagnetic and paleontologic data. When available, more than one sample was examined for each 0.1-m.y. period. For the interval younger than 3.5 Ma, the sediment accumulation curve is based on both paleomagnetic and biostratigraphic data; age estimates are carried to two digits after the decimal. For the interval older than 3.5 Ma, the sediment accumulation curve is based solely on biostratigraphic data. Age estimates are, therefore, carried to one digit after the decimal. The precision is greatest when the stratigraphy is based on biostratigraphic, paleomagnetic, and isotopic data. Use of biostratigraphic data alone for the interval older than 3.5 Ma assumes isochroneity of biostratigraphic datums, an assumption that cannot be tested without independent (e.g., paleomagnetic or isotopic) stratigraphies. Further studies are required to determine if a 0.1-m.y. age difference between two abundance peaks in different cores is significant for this time interval.

Samples were processed and strewn slides were prepared following the procedures outlined in Baldauf (1985). Strewn slides were examined in their entirety. The first 300 diatoms observed at ×1250 were tabulated. The remaining portion of the slide was examined at ×500 for additional stratigraphically useful species. The counting procedures of Schrader and Gersonde (1978) were used. The age assigned to each sample (see Tables 1 to 3) is extrapolated from the sedimentation accumulation curves shown in Figure 3. For taxonomic descriptions and figures of species discussed in this report, the reader is referred to Barron (this volume) and Baldauf (1985).

RESULTS

Tables 1 through 3 show the relative frequency of species recorded at each site. The first or last occurrences of stratigraphically useful species are used in determining the sediment accumulation rate curves (Fig. 3). In addition, the paleomagnetic results of Hailwood and Rees (1982, Site 503) and Weinreich and Theyer (this volume, Site 573) are used where applicable.

With the exception of two hiatuses having durations of about 0.5 m.y., a continuous sedimentary sequence is present at all sites. However, no sediment was recovered from Cores 503A-25, -26, and -28; thus, with the exception of Sample 503A-27,CC, no samples in the stratigraphic interval representing 4.8 to 4.4 Ma were examined at Site 503. The oldest hiatus occurs within the lower Pliocene at Site 573, approximately between the last occurrence of *Thalassiosira miocenica* and the first occurrence of *Nitzschia jouseae*. This hiatus occurs from approximately 5.1 to 4.5 Ma, which suggests that it corresponds to the NH7 hiatus of Barron and Keller (1982) and Keller and Barron (1983). The NH7 hiatus extends from 5.2 to 4.7 Ma, an interval noted by Barron and Keller (1982) as corresponding to a period of diatom dissolution in the eastern equatorial Pacific. The early Pliocene hiatus observed at Site 573 is also recognized by Barron (this volume) at Site 575. A stratigraphic compression of this same interval occurs at Site 574 and could have resulted from a reduced sedimentation rate rather than from erosion or dissolution. At Site 575 the early Pliocene hiatus is expanded and extends upward to the first occurrence of *Rhizosolenia praebergonii* (3.0 Ma). The second hiatus is late Pliocene in age and is observed at Site 572. This hiatus occurs within the interval between the last occurrence of *T. convexa* Group at 2.2 Ma and the first occurrence of *Pseudoeunotia doliolus* at 1.8 Ma.

Although sedimentation rates are slightly different at each site (see Fig. 3), similarities are observed between sites. First, an abrupt change in the sedimentation rate from 73.0 m/m.y. to 39.5 m/m.y. occurs at Site 572 (~5.6 Ma) and at Site 503 (~5.8 Ma). Second, a change in the sedimentation rate from 39.5 m/m.y. to 15.0 m/m.y. also occurs at Site 572 (~3.6 Ma) and at Site 573 (~3.9 Ma).

Figures 4 through 12 present the fluctuation in the relative frequency of selected species. As a result of this quantitative analysis, six datums are defined for the interval 6.2 to 1.5 Ma on the basis of acmes of individual species.

Peak in the Abundance of *Nitzschia miocenica*

Figures 4 to 6 show the relative frequency of *Nitzschia miocenica* from the samples examined. At both Sites 572 and 503 (Figs. 4 and 5), *N. miocenica* ordinarily composes 10 to 15% of the overall diatom assemblage throughout its stratigraphic range. However, a decline in abundance from approximately 15% to less than 5% is observed near the top of the stratigraphic range of *N. miocenica*. Approximately 0.2 m.y. above the start of this decline *N. miocenica* becomes extinct. This peak in abundance has an extrapolated age of 5.6 Ma at both Sites 572 and 503.

At Site 573 (Fig. 6) a similar decline in abundance from approximately 20% to less than 5% is observed. The peak in abundance, however, occurs at approximately 5.8 Ma, which differs from the extrapolated age. This

Table 1. Relative frequency of species encountered during examination of samples from Site 572.

Diatom zonation		Sample interval (cm)	Depth (m)	*Actinocyclus curvatulus*	*A. divisus*	*A. ehrenbergii*	*A. ellipticus*	*Actinocyclus* "Group"	*Actinoptychus undulatus*	*Asterolampra* "Group"	*Asteromphalus* "Group"	*Coscinodiscus marginatus*	*C. nodulifer*	*C. nodulifer* var. *cyclopus*	*C. tabularis*	*Coscinodiscus* "Group"	*Hemidiscus cuneiformis*	*Nitzschia cylindrica*	*N. fossilis*	*N. jouseae*	*N. marina*	*N. miocenica*
		Hole 572A																				
Pseudoeunotia doliolus		3-6, 68-69	27.2	–	+	+	–	–	–	–	2	1	5	+	4	1	4	–	9	–	–	–
		3,CC	28.6	1	–	–	–	1	–	1	4	1	5	1	1	–	3	–	5	–	3	–
		4-1, 68-69	29.3	–	+	–	–	–	–	+	2	–	2	–	3	–	3	–	11	–	1	–
		4-2, 66-67	30.8	–	+	1	1	–	–	–	4	–	8	–	4	1	3	–	14	–	2	–
		4-3, 66-67	32.3	–	1	2	2	–	–	–	5	1	6	2	4	1	2	–	7	–	1	–
Rhizosolenia praebergonii	c	4-4, 66-67	33.8	–	1	–	–	+	–	–	e	+	5	1	2	1	3	–	18	–	1	–
		4-5, 66-67	35.3	1	+	1	1	+	–	1	5	–	12	3	2	1	6	–	8	–	+	–
	b	4,CC	36.2	1	–	1	1	+	–	–	2	1	3	–	2	1	3	–	7	–	4	–
		5-1, 66-67	37.0	+	1	1	1	–	–	–	4	+	6	–	6	+	2	–	12	–	1	–
		5-2, 66-67	38.5	–	+	+	1	–	–	+	3	1	12	2	3	+	4	–	9	–	1	–
		5-3, 66-67	40.0	1	+	1	1	+	–	–	2	+	5	–	3	–	4	–	10	–	2	–
		5-4, 66-67	41.5	+	1	1	1	–	–	–	3	–	5	–	3	–	1	–	7	2	1	–
		5-5, 66-67	43.0	–	–	1	1	–	–	+	5	+	7	–	5	1	4	–	8	3	1	–
	a	5-6, 66-67	44.5	–	+	1	5	–	–	–	1	+	11	+	3	1	7	–	10	9	2	–
		5,CC	45.8	+	–	+	1	1	–	–	2	1	4	–	1	+	4	–	4	6	3	–
		6-1, 66-67	46.6	–	1	–	+	–	–	–	3	–	8	1	3	1	3	–	6	5	+	–
		6-2, 66-67	48.1	–	–	–	3	–	–	–	1	–	8	–	2	–	1	–	3	7	–	–
Nitzschia jouseae		6-3, 66-67	49.6	1	–	+	5	–	–	–	4	1	12	1	5	1	9	–	7	4	2	–
		6-4, 66-67	51.1	1	1	–	2	–	–	–	1	–	2	1	1	+	2	–	4	10	–	–
		6-5, 66-67	52.6	–	+	+	1	+	–	–	1	+	5	–	6	–	3	–	2	6	–	–
		6-6, 66-67	54.1	–	–	1	1	–	–	–	1	–	5	+	6	1	–	–	4	11	–	–
		6,CC	55.1	–	–	+	1	+	–	–	1	1	6	–	1	+	3	–	3	8	1	–
		7-1, 66-67	55.9	–	–	3	1	–	+	–	1	–	10	+	2	–	2	–	2	5	+	–
		7-2, 66-67	57.4	+	+	14	2	+	–	–	1	–	11	1	2	1	4	–	3	13	1	–
		7-3, 66-67	58.9	–	–	+	3	–	–	–	2	+	11	1	1	1	1	–	2	10	+	–
		7-4, 66-67	60.4	–	–	3	4	–	–	–	6	+	10	+	1	+	3	–	4	10	+	–
		7-5, 66-67	61.9	1	1	–	3	–	1	1	5	–	9	2	3	1	2	–	2	13	1	–
		7-6, 66-67	63.4	+	–	+	7	+	4	1	3	–	7	1	2	+	2	–	8	14	3	–
		7,CC	64.0	1	–	1	3	–	4	–	1	1	4	–	2	+	+	–	5	8	1	–
		8-3, 66-67	67.8	–	–	1	3	–	–	–	1	+	2	1	1	+	–	–	13	10	1	–
		8,CC	72.3	1	–	–	2	+	1	–	1	–	1	–	–	–	2	–	9	6	1	–
		9-3, 66-67	76.0	1	1	–	–	–	–	–	–	1	–	–	–	+	–	–	7	5	1	–
		9,CC	81.7	1	–	–	3	–	+	–	1	1	5	2	+	–	1	–	4	4	+	–
		10-3, 66-67	85.5	–	–	+	1	–	–	+	+	+	6	–	1	+	2	3	1	8	–	–
		10,CC	91.4	+	–	–	–	–	–	+	+	–	1	–	–	–	–	1	4	3	–	–
Thalassiosira convexa	c	11-3, 67-68	95.1	–	+	+	2	–	–	1	1	–	3	–	–	–	1	4	6	–	–	–
		11,CC	100.6	–	1	+	2	–	–	+	1	+	3	–	+	+	1	12	6	–	1	–
		12,CC	109.6	–	+	+	+	–	–	–	+	–	1	–	–	–	+	5	2	–	1	–
		13-3, 66-67	113.6	1	–	+	+	–	–	–	+	–	1	–	–	–	1	7	3	–	–	–
		13,CC	119.1	+	+	+	+	2	–	+	2	+	2	–	1	–	1	11	7	–	2	–
	b	14,CC	128.2	+	1	1	1	+	–	1	1	+	12	3	1	–	3	–	5	–	2	–
		15-3, 68-69	132.0	–	–	–	3	+	–	+	–	+	4	–	+	–	+	–	2	–	+	–
		15,CC	136.7	–	1	1	1	–	+	1	1	–	4	–	+	+	5	–	3	–	1	+
		16-3, 66-67	140.8	–	–	+	1	1	–	–	–	2	4	–	–	+	3	–	1	–	1	4
		16,CC	145.2	–	1	1	+	–	–	–	1	+	5	1	+	1	+	–	1	–	1	18
		17,CC	154.1	–	1	–	2	–	–	1	1	–	2	–	–	–	–	–	3	–	1	16
		Hole 572D																				
	a	1,CC	156.3	–	–	1	1	–	–	1	+	1	3	–	1	–	+	–	1	–	1	15
		2-2, 70-72	162.7	–	1	–	1	–	1	1	1	1	1	–	+	–	1	–	2	–	1	12
		2,CC	170.3	–	+	–	+	–	1	–	+	+	1	–	–	–	1	–	+	–	+	11
		3,CC	179.7	–	1	–	1	–	–	1	1	+	4	–	–	–	2	–	1	–	1	7
Nitzschia miocenica	b	4,CC	189.0	+	–	–	2	–	–	2	1	–	1	–	–	–	+	–	2	–	2	9

Notes: The abundance of each species is rounded to the nearest percentage. Samples are correlated to the diatom zonation of Burckle (1972, 1977). The age of each sample is extrapolated from the sediment accumulation curve. + = <1% of the assemblage; ± = reworked specimens composing <1% of the assemblage.

Table 1. (Continued).

N. reinholdii	*Nitzschia* sp. 1	*Nitzschia* "Group"	*Pseudoeunotia doliolus*	*Rhizosolenia bergonii*	*R. praebergonii*	*R. styliformis*	*Rossiella praepaleacea*	*T. nitzschioides* var. *parva*	*T. nitzschioides* s. ampl.	*Thalassiosira convexa* s. str.	*T. convexa* var. *aspinosa*	*T. eccentrica*	*T. lentiginosa*	*T. miocenica*	*T. nativa*	*T. oestrupii*	*T. praeconvexa*	*Thalassiosira* "Group"	*Thalassiothrix longissima*	*Triceratium cinnamomeum*	Other	Total number counted	Extrapolated age (Ma)
3	–	3	8	3	4	3	–	2	15	–	–	3	2	–	–	19	–	1	7	4	–	309	1.50
1	–	2	2	3	4	2	–	9	5	–	–	5	3	–	–	16	–	2	12	1	2	293	1.62
1	–	2	6	2	4	3	–	5	15	–	–	7	2	–	–	16	–	2	10	2	1	296	1.66
3	–	4	7	1	2	1	–	2	12	–	–	4	5	–	–	13	–	1	4	4	1	299	1.70
3	–	3	3	+	1	1	–	13	13	–	–	4	2	–	–	13	–	1	6	2	1	301	1.78
+	1	3	–	2	4	–	–	7	21	–	–	6	4	–	–	4	–	2	8	1	1	304	1.90
+	1	2	–	2	2	3	–	5	20	–	+	3	2	–	–	3	–	1	11	2	1	302	2.23
1	–	3	–	+	4	+	–	11	17	4	3	4	1	–	–	5	–	3	16	–	2	303	2.26
3	–	12	–	1	4	+	–	5	18	–	+	2	3	–	–	5	–	2	5	2	1	294	2.33
1	–	6	–	2	7	1	–	5	15	2	6	3	3	–	–	3	–	1	6	4	1	311	2.43
2	–	5	–	+	3	–	–	14	26	1	4	4	2	–	–	4	–	2	2	1	1	299	2.50
2	–	8	–	+	2	–	–	17	22	1	7	6	3	–	–	+	–	1	3	2	+	306	2.60
3	–	4	–	+	3	–	–	9	21	1	2	6	2	–	–	5	–	+	5	1	–	298	2.70
4	–	2	–	1	4	–	–	2	15	+	1	4	2	–	–	3	–	1	9	–	1	309	2.80
+	–	3	–	+	3	–	–	23	17	3	3	2	1	–	–	1	–	1	12	–	1	294	2.87
2	–	1	–	1	4	+	–	20	15	4	8	2	1	–	–	2	–	+	8	+	1	304	2.92
+	–	3	–	1	5	1	–	12	23	4	6	3	1	–	–	3	–	–	12	–	+	284	3.00
8	–	1	–	6	–	1	–	6	7	–	1	3	2	–	–	4	–	1	6	1	2	301	3.10
1	3	2	–	1	–	1	–	11	34	1	+	5	3	–	–	4	–	1	6	1	1	298	3.20
3	+	3	–	1	–	–	–	8	9	9	20	3	1	–	–	–	–	2	12	2	+	303	3.27
1	3	1	–	+	–	–	–	7	25	8	11	3	2	–	–	3	–	1	2	2	1	294	3.37
–	–	1	–	–	–	–	–	16	31	1	6	1	+	–	–	5	–	–	10	–	1	253	3.43
+	2	–	–	1	–	–	–	6	39	3	8	1	1	–	–	2	–	+	9	+	–	275	3.47
2	1	1	–	1	–	–	–	5	22	+	1	4	1	–	–	2	–	3	1	1	1	294	3.56
2	2	+	–	1	–	–	–	8	36	–	3	4	2	–	–	3	–	1	4	–	1	305	3.61
3	4	1	–	1	–	+	–	14	16	–	1	5	3	–	–	2	–	4	4	+	+	311	3.63
2	3	1	–	+	–	+	–	9	18	–	1	8	1	–	+	4	–	3	2	2	1	306	3.70
1	4	1	–	+	–	+	–	13	14	–	–	4	1	–	–	1	–	3	4	1	1	298	3.73
–	–	4	–	2	–	1	–	29	15	–	1	4	1	–	–	2	–	2	7	+	2	301	3.74
1	–	1	–	1	–	–	–	12	35	–	–	1	+	–	–	1	–	+	13	1	+	296	3.83
1	–	3	–	–	–	–	–	24	16	–	+	4	–	–	–	3	–	1	20	1	2	293	3.94
–	+	–	–	–	–	+	–	20	37	–	–	5	1	–	–	1	–	2	14	2	1	300	4.04
+	–	1	–	+	–	–	–	37	15	–	1	3	+	–	–	3	–	1	13	1	1	306	4.18
1	–	1	–	–	–	1	–	26	33	–	+	4	1	–	–	2	–	1	6	+	1	304	4.27
+	–	2	–	–	–	–	–	70	6	–	+	1	–	–	–	2	–	–	6	–	+	271	4.41
1	–	1	–	–	–	+	–	20	38	–	+	4	1	–	+	3	–	–	11	–	1	295	4.50
1	–	2	–	–	–	–	–	27	26	–	–	2	1	–	–	5	–	1	4	1	3	298	4.64
–	–	+	–	–	–	1	–	50	27	–	+	2	+	–	–	4	–	–	3	+	2	297	4.87
1	–	2	–	–	–	–	–	8	49	–	1	2	+	–	1	5	–	1	16	1	1	296	4.95
1	–	2	–	–	–	–	–	11	38	–	–	3	3	–	–	5	–	1	5	1	1	295	5.08
1	–	1	–	+	–	2	–	18	32	–	+	6	1	+	–	–	–	+	4	3	1	303	5.30
1	–	1	–	1	–	–	–	14	53	–	1	3	–	3	2	–	–	1	7	1	2	303	5.40
2	–	1	–	–	–	–	–	31	24	–	3	5	+	2	–	–	–	1	6	1	–	299	5.53
1	–	2	–	1	–	–	–	8	41	–	3	5	+	7	2	–	–	1	9	–	2	306	5.58
2	–	5	–	+	–	–	–	30	14	–	3	3	1	1	+	–	–	1	4	–	2	306	5.64
1	–	1	–	–	–	–	–	31	22	–	3	2	1	2	+	–	–	1	7	1	2	293	5.76
+	–	1	–	–	–	–	–	41	9	–	3	2	–	2	+	–	1	1	12	+	1	274	5.79
1	–	–	–	–	–	2	+	31	22	–	4	2	1	1	–	–	2	1	9	+	2	300	5.88
+	–	2	–	–	–	–	–	37	24	–	1	2	1	1	–	–	–	–	13	+	1	292	5.98
1	–	+	–	+	–	–	1	21	22	–	1	1	1	–	–	–	1	1	27	–	3	292	6.09
+	–	–	–	–	–	+	2	16	17	–	–	4	+	–	+	–	2	2	25	–	2	286	6.20

Table 2. Relative frequency of species encountered during examination of samples from Hole 503A.

Diatom zonation		Sample interval (cm)	Depth (m)	*Actinocyclus curvatulus*	*A. divisus*	*A. ehrenbergii*	*A. ellipticus*	*Actinocyclus* "Group"	*Actinoptychus undulatus*	*Asterolampra* "Group"	*Asteromphalus* "Group"	*Coscinodiscus marginatus*	*C. nodulifer*	*C. nodulifer* var. *cyclopus*	*C. tabularis*	*Coscinodiscus* "Group"	*Hemidiscus cuneiformis*	*Nitzschia cylindrica*	*N. fossilis*	*N. jouseae*	*N. marina*	*N. miocenica*
		Hole 503A																				
Rhizosolenia praebergonii	b	12-2, 101–102	48.2	1	+	–	5	–	–	1	2	+	26	3	2	1	4	–	8	–	3	–
		12,CC	49.7	1	2	2	3	·	1	+	3	1	20	+	2	1	13	–	6	–	2	–
	a	13-3, 90–92	54.0	–	+	1	3	+	1	1	3	–	18	1	3	–	11	–	7	+	1	–
		13,CC	54.4	–	2	+	+	–	–	–	5	–	11	–	4	1	7	–	4	4	1	–
		14-2, 60–62	55.9	1	2	+	2	–	–	–	4	–	8	–	4	1	5	–	10	3	2	–
		14-3, 58–60	57.3	1	2	2	2	–	–	+	2	7	8	–	2	1	15	–	9	9	2	–
		15-1, 90–92	59.9	1	3	1	2	–	–	–	3	–	11	1	3	1	10	–	8	7	1	–
		15-2, 88–90	61.4	1	2	+	1	–	–	–	2	–	10	–	1	3	7	–	3	10	2	–
Nitzschia jouseae		15,CC	63.0	1	1	+	3	–	–	1	4	–	14	–	1	1	1	–	6	4	1	⊕
		16-2, 66–68	65.6	–	2	2	2	–	–	–	3	–	18	–	3	2	5	–	3	7	1	–
		16,CC	66.5	+	2	–	3	+	–	–	1	–	8	–	4	+	12	–	+	10	1	–
		17-2, 10–12	69.1	1	1	+	2	–	–	–	1	+	11	1	1	1	10	–	5	11	2	–
		17,CC	69.3	1	1	–	2	+	–	1	2	–	7	1	3	–	11	–	4	11	1	–
		18,CC	72.3	+	+	1	2	+	–	+	3	+	5	3	4	1	6	–	4	5	1	–
		19-2, 111–113	79.0	–	1	13	1	–	–	2	3	–	22	2	2	1	11	–	1	5	3	–
		19,CC	79.8	1	–	10	2	–	–	1	2	+	19	1	+	1	5	–	5	7	1	–
		20-2, 100–102	83.3	1	2	–	2	–	–	+	1	1	25	3	2	1	5	–	1	7	2	–
		20,CC	85.4	+	1	1	1	–	–	–	2	1	35	3	3	1	8	–	3	4	2	–
		21-2, 112–114	88.0	4	2	1	3	–	2	1	3	–	14	6	4	+	7	–	3	7	2	–
		21,CC	89.6	+	+	+	4	–	1	+	1	+	13	2	3	1	3	–	4	5	3	⊕
		23-2, 100–112	98.7	+	+	4	2	–	1	+	2	+	20	+	2	+	2	–	4	8	1	–
		24-1, 60–62	99.2	+	+	1	1	–	–	–	–	1	12	2	2	1	4	–	3	4	–	①
		24-1, 100–102	99.6	1	1	1	2	–	5	1	4	–	6	3	2	1	2	–	5	6	1	–
		24-2, 101–103	101.2	1	1	1	3	+	–	1	1	+	10	1	1	1	4	–	3	3	1	⊕
		24,CC	102.7	1	1	2	5	+	–	–	3	+	9	4	1	1	5	–	4	5	1	–
		27,CC	112.7	–	+	+	1	–	+	1	2	–	4	–	+	1	2	4	3	2	1	⊕
Thalassiosira convexa	c	29-2, 101–103	123.1	1	1	2	2	1	–	2	1	–	11	3	+	–	1	8	4	–	+	–
		29,CC	124.8	+	1	1	2	–	–	–	1	1	36	6	1	–	2	3	2	–	1	–
		30-1, 94–95	125.9	1	1	1	2	1	–	1	+	1	13	1	+	2	2	8	5	–	+	–
		30-2, 86–88	127.1	–	+	1	1	–	–	1	+	–	9	1	+	+	3	4	3	–	–	①
		30,CC	127.9	1	–	3	2	–	+	1	2	–	16	2	+	1	2	8	4	–	1	①
		31-2, 111–113	132.0	1	1	1	3	+	–	+	+	+	19	1	1	+	2	5	3	–	1	–
		31-3, 100–103	133.4	–	–	2	3	–	–	+	1	–	6	+	2	1	2	10	3	–	1	–
		32-1, 61–66	134.4	1	1	2	2	–	–	+	1	–	16	1	1	2	3	8	4	–	1	–
	b	33-1, 100–102	139.2	–	1	2	3	–	–	+	1	–	14	–	3	1	1	7	6	–	1	–
		33,CC	139.4	–	1	3	1	–	–	+	1	–	9	+	1	1	2	2	1	–	+	⊕
		34-2, 58–60	144.4	1	1	1	1	+	–	–	1	–	5	–	1	2	1	1	1	–	+	⊕
		34,CC	146.2	–	+	1	1	+	–	1	1	+	9	–	2	1	2	–	4	–	–	–
		35-1, 24–26	147.2	–	1	+	2	–	–	1	+	+	21	1	–	2	4	–	2	–	2	⊕
		35,CC	147.8	+	–	+	2	–	–	–	1	–	23	4	1	+	3	–	2	–	+	–
		36-2, 81–83	153.6	–	1	+	2	–	–	1	–	–	13	2	+	+	1	–	1	–	+	–
		36,CC	154.8	–	1	–	1	–	–	+	1	–	11	1	1	1	3	–	2	–	1	–
		37-1, 124–125	157.0	1	+	+	3	3	–	3	1	–	11	+	+	2	4	–	–	–	–	+
		37-2, 90–92	158.1	1	+	1	+	+	–	–	1	+	12	+	1	+	2	–	1	–	1	5
		37,CC	158.5	1	1	1	2	–	–	1	1	1	13	–	–	1	1	–	1	–	1	3
		38,CC	160.7	+	1	+	2	–	+	–	–	–	9	–	1	–	5	–	1	–	–	15
	a	39-2, 91–92	166.8	+	+	–	–	–	–	1	+	–	3	–	1	–	1	–	1	–	–	17
		39,CC	167.5	–	2	2	1	–	–	1	1	–	5	–	1	+	+	–	+	–	1	13
		40-1, 100–102	170.0	1	–	–	1	–	1	1	1	+	17	+	1	+	2	–	1	–	+	14
		40,CC	170.5	+	–	1	1	+	–	1	1	–	9	–	1	–	1	–	1	–	–	20
		41-2, 120–122	176.2	–	1	–	2	–	1	3	1	–	7	–	1	–	1	–	1	–	+	11
		41,CC	177.6	+	1	–	1	–	1	–	+	–	5	–	1	+	1	–	+	–	–	15
		42-3, 38–40	180.4	1	–	–	1	–	–	1	+	–	3	+	1	–	1	–	1	–	–	8
		42,CC	181.8	–	–	+	2	–	+	1	1	–	6	–	1	+	2	–	2	–	1	10
		43-1, 94–95	183.1	+	+	–	2	–	+	1	+	–	10	–	–	1	1	–	1	–	+	12
		43-2, 101–103	184.0	–	–	–	2	–	+	+	1	+	6	–	1	+	2	–	+	–	1	10
		43,CC	185.7	+	+	1	2	–	+	+	1	–	8	+	+	1	1	–	–	–	1	15
		44-1, 64–65	187.2	1	–	+	1	–	–	1	1	+	6	–	+	1	3	–	1	–	+	10
		44-2, 124–125	189.6	–	1	–	3	–	+	1	1	–	5	–	+	1	1	–	1	–	–	13

Notes: The depth of each sample is recorded in meters. The abundance of each species is rounded to the nearest percentage. Samples are correlated to the diatom zonation of Burckle (1972, 1977). The age of each sample is extrapolated from the sediment accumulation curve. + = <1% of the assemblage. ⊕ = reworked specimens composing <1% of the assemblage; ① = reworked specimens composing 1% of the assemblage; ② = reworked specimens composing 2% of the assemblage.

READEX FICHE best copy available

Table 2. (Continued).

N. reinholdii	*Nitzschia* sp. 1	*Nitzschia* "Group"	*Pseudoeunotia doliolus*	*Rhizosolenia barbai*	*Rhizosolenia bergonii*	*R. praebergonii*	*R. styliformis*	*Rossiella praepaleacea*	*T. nitzschioides* var. *parva*	*T. nitzschioides* s. ampl.	*Thalassiosira convexa* s. str.	*T. convexa* var. *aspinosa*	*T. eccentrica*	*T. leptopus*	*T. miocenica*	*T. nativa*	*T. oestrupii*	*T. praeconvexa*	*Thalassiosira* "Group"	*Thalassiothrix longissima*	*Triceratium cinnamomeum*	Other	Total number counted	Extrapolated age (Ma)
3	–	1	–	–	1	1	1	–	2	9	1	2	4	7	–	–	2	–	1	8	1	+	299	2.52
1	–	1	–	–	2	4	1	–	2	11	–	1	4	4	–	–	2	–	+	8	1	–	298	2.56
3	–	2	–	–	+	4	1	–	3	14	1	4	4	2	–	–	1	–	+	7	+	1	296	2.75
5	1	3	–	–	1	5	1	–	3	12	1	9	8	2	–	–	1	–	–	5	4	–	301	2.78
3	–	2	–	–	–	2	–	–	2	20	1	6	6	4	–	–	2	–	1	8	1	1	300	2.85
3	–	1	–	–	1	1	1	–	1	15	3	6	7	+	–	–	+	–	1	5	+	2	300	2.91
2	–	1	–	–	1	3	+	–	3	13	1	4	8	4	–	–	1	–	1	5	1	1	299	2.95
1	1	3	–	–	1	2	–	–	3	14	7	7	4	2	–	–	–	–	+	12	1	1	290	2.98
3	–	1	–	–	1	–	–	–	2	17	5	9	6	3	–	–	1	–	+	6	1	1	305	3.00
3	1	1	–	–	2	–	+	–	3	11	5	12	3	2	–	–	2	–	2	5	–	1	301	3.10
2	–	2	–	1	1	+	1	–	5	17	1	5	6	2	–	–	3	–	2	10	–	1	298	3.14
2	–	4	–	–	1	–	–	–	4	8	5	15	3	2	–	–	1	–	1	7	+	1	302	3.25
2	–	2	–	–	2	–	–	–	2	9	5	16	4	3	–	–	2	–	2	6	1	1	300	3.28
2	–	1	–	–	1	–	1	–	2	19	5	11	7	2	–	–	1	–	2	8	1	2	300	3.36
6	–	1	–	–	2	–	+	–	+	8	+	2	2	2	–	–	–	–	+	9	–	2	305	3.58
3	+	2	–	–	3	–	1	–	2	13	–	1	8	1	–	–	1	–	1	4	–	1	302	3.60
2	–	1	–	–	1	–	–	–	3	13	–	5	10	2	–	–	1	–	1	8	+	1	300	3.68
2	–	1	–	–	1	–	–	–	3	10	–	3	5	2	–	–	1	–	+	5	+	1	300	3.72
3	–	+	–	–	1	–	–	–	3	13	–	+	8	1	①	–	1	–	1	3	1	2	299	3.84
2	–	1	–	–	1	–	1	–	7	15	–	2	7	3	–	+	1	–	1	15	1	2	299	3.89
2	+	1	–	–	+	–	1	–	3	23	–	+	5	1	–	–	+	–	1	9	3	+	291	3.99
1	–	2	–	–	+	–	–	–	19	24	–	2	7	2	–	+	1	–	1	6	+	1	300	4.13
+	–	3	–	–	–	–	–	–	7	24	–	+	7	1	–	–	1	–	1	14	2	1	301	4.14
2	–	2	–	–	1	–	1	–	12	30	–	2	8	1	–	+	2	–	–	9	1	+	311	4.15
2	+	3	–	–	–	–	+	–	1	11	–	3	8	1	–	+	3	–	1	14	5	1	300	4.21
1	–	2	–	–	–	–	1	–	26	32	–	1	3	1	–	1	1	–	1	8	1	1	302	4.46
1	–	3	–	–	1	–	–	–	9	28	–	+	4	1	⊕	1	–	–	1	11	2	+	301	4.69
1	–	1	–	–	–	–	–	–	4	19	–	+	3	1	–	+	+	–	+	12	2	–	300	4.78
1	–	4	–	–	+	–	1	–	9	29	–	+	2	+	–	–	+	–	2	12	1	1	298	4.81
1	–	2	–	–	1	–	–	–	10	41	–	1	2	–	②	1	+	–	1	9	1	1	300	4.83
2	–	1	–	–	–	–	–	–	10	23	–	+	6	1	⊕	–	1	–	–	12	–	+	302	4.86
2	–	2	–	–	–	–	1	–	7	30	–	+	2	1	–	1	2	–	1	10	2	1	303	4.95
1	–	7	–	–	+	–	+	–	5	28	–	1	6	1	–	–	3	–	1	8	2	2	294	4.97
1	–	2	–	–	–	–	1	–	7	27	–	1	4	4	–	–	1	–	1	6	4	1	310	5.02
2	–	3	–	–	1	–	+	–	8	22	–	+	7	2	+	+	2	–	+	11	3	+	301	5.13
–	–	1	–	–	–	–	–	–	12	50	–	1	5	+	–	–	1	–	1	6	2	+	305	5.14
2	1	2	–	–	+	–	+	–	11	46	–	+	6	2	–	+	–	–	+	11	3	+	304	5.26
1	+	2	–	–	–	–	+	–	10	41	–	1	3	1	+	+	–	–	+	14	2	1	302	5.32
1	1	2	–	–	–	–	+	–	4	33	–	3	4	1	3	1	–	–	+	8	3	1	301	5.34
1	2	2	–	–	–	–	1	–	5	32	–	2	4	1	1	+	–	–	1	9	1	1	298	5.37
1	2	1	–	–	–	–	+	–	8	47	–	1	6	2	+	+	–	–	–	7	+	1	303	5.51
1	2	1	–	–	+	–	+	–	10	39	–	3	4	1	3	2	–	–	–	12	1	1	304	5.53
1	–	+	–	–	1	–	1	–	3	38	–	2	3	1	3	–	–	–	2	13	1	1	299	5.60
2	–	4	–	–	+	–	–	–	3	28	–	5	2	2	7	–	–	–	1	16	1	1	309	5.62
1	–	3	–	–	1	–	–	–	3	25	–	5	7	2	8	1	–	–	–	13	2	2	297	3.64
2	–	1	–	–	+	–	–	–	19	24	–	3	2	1	3	–	–	–	–	9	–	1	298	5.69
2	–	2	–	–	–	–	–	–	20	21	–	6	2	2	7	–	–	3	–	3	–	1	328	5.82
1	–	2	–	–	+	–	–	–	17	25	–	5	4	2	4	–	–	1	–	10	1	3	302	5.83
2	–	1	–	–	1	–	–	–	16	14	–	6	3	2	3	+	–	1	–	10	1	1	306	5.85
1	–	1	–	–	1	–	+	–	11	26	–	1	4	+	3	–	–	1	–	11	1	2	290	5.86
1	–	3	–	–	1	–	–	1	10	33	–	4	3	1	2	–	–	1	–	9	–	3	301	5.92
1	–	1	–	–	1	–	+	+	16	34	–	1	3	1	1	–	–	1	1	10	1	2	299	5.94
1	–	3	–	–	2	–	1	–	16	34	–	2	4	1	2	–	–	3	+	9	1	1	301	5.98
1	–	1	–	–	1	–	+	–	25	18	–	1	2	–	2	–	–	3	1	16	1	1	292	5.99
1	–	–	–	–	–	–	1	1	8	29	–	2	2	1	2	–	–	3	1	20	1	1	296	6.00
2	–	2	–	–	–	–	+	+	11	38	–	3	3	+	1	–	–	2	–	11	–	1	294	6.02
2	–	–	–	–	–	–	–	–	11	35	–	1	2	1	–	–	–	2	–	12	1	1	301	6.03
1	–	1	–	–	–	–	–	1	9	39	–	+	3	–	2	–	–	+	1	15	–	1	300	6.06
2	–	2	–	–	+	–	+	–	5	33	–	2	2	1	2	–	–	4	1	18	+	1	302	6.00

Table 3. Relative frequency of species encountered during examination of samples from Hole 573.

Diatom zonation		Sample interval (cm)	Depth (m)	*Actinocyclus curvatulus*	*A. divisus*	*A. ehrenbergii*	*A. ellipticus*	*Actinocyclus* "Group"	*Actinoptychus undulatus*	*Asterolampra* "Group"	*Asteromphalus* "Group"	*Coscinodiscus marginatus*	*C. nodulifer*	*C. nodulifer* var. *cyclopus*	*C. tabularis*	*Coscinodiscus* "Group"	*Hemidiscus cuneiformis*	*Nitzschia cylindrica*	*N. fossilis*	*N. jouseae*	*N. marina*
		Hole 573																			
Pseudoeunotia doliolus	a	4-1, 131-132	22.3	1	1	⊕	1	–	–	1	2	1	6	2	3	3	1	–	3	–	1
		4-3, 131-132	25.3	–	1	–	+	–	+	–	2	–	5	–	3	+	6	–	5	–	1
Rhizosolenia praebergonii	c	4,CC	30.5	–	+	–	–	–	+	–	3	–	11	+	4	3	1	–	10	–	2
	b	5-2, 131-132	33.1	+	+	+	–	–	–	+	5	+	12	1	5	2	5	–	10	–	2
		5-4, 131-132	36.1	+	+	1	1	+	–	–	2	–	5	–	3	1	+	–	9	–	1
	a	5-6, 109-110	38.9	–	1	1	1	–	–	–	1	–	5	–	3	1	2	–	5	1	1
		5,CC	39.3	1	+	1	1	–	–	–	2	–	6	+	4	1	4	–	5	6	1
		6-1, 132-133	40.4	1	2	+	3	–	–	+	2	+	3	+	4	2	2	–	6	8	1
		6-3, 131-132	43.4	+	–	1	+	1	–	–	2	–	10	+	1	1	3	–	4	6	1
Nitzschia jouseae		6-5, 131-132	46.4	–	1	1	1	–	–	1	3	–	8	1	6	+	6	–	6	16	1
		6,CC	48.0	–	–	–	1	–	1	–	2	–	5	–	2	+	2	–	3	6	1
		7-1, 130-131	49.1	–	+	–	1	–	+	–	–	1	4	+	2	2	1	–	1	9	+
		7-3, 131-132	52.1	–	+	5	4	+	–	+	1	–	12	–	3	–	4	–	3	11	+
		7-5, 130-131	55.11	+	–	–	2	–	3	1	3	–	11	3	4	–	3	–	3	8	2
		7,CC	57.1	1	1	+	3	–	1	1	1	+	6	1	2	–	2	–	1	12	1
		8-1, 70-71	57.7	–	+	–	8	–	–	–	1	–	3	1	1	+	1	–	5	8	2
		8-3, 70-71	60.7	+	–	1	3	–	10	+	+	1	8	+	2	1	1	–	3	14	1
		8-5, 70-71	63.7	+	+	3	1	+	1	–	1	+	3	1	–	1	1	–	2	7	1
		8,CC	66.6	+	1	–	4	–	1	–	1	–	5	+	5	1	5	1	4	10	+
		9-1, 67-68	67.4	+	1	+	5	–	–	1	2	1	13	5	2	1	5	2	2	5	+
		9-3, 67-68	70.4	+	1	1	4	–	+	1	1	–	11	1	1	1	1	1	3	10	–
		9-5, 67-68	73.4	1	1	+	+	–	–	1	2	–	4	–	–	+	2	6	4	1	1
Thalassiosira convexa	c	9,CC	76.2	–	1	–	4	+	–	–	2	–	4	–	+	–	1	6	2	–	2
	b	10-3, 65-66	79.9	+	1	1	5	–	–	1	1	+	15	2	–	1	1	8	3	–	+
		10-5, 65-66	82.9	1	1	4	1	1	–	2	1	+	5	–	1	+	+	6	2	–	–
		10,CC	85.8	–	–	+	2	–	–	1	1	–	5	–	1	+	1	–	3	–	–
		11-1, 65-66	86.4	–	+	2	3	–	–	1	–	–	4	–	+	1	1	2	2	–	+
		11-3, 65-66	89.4	–	+	–	1	+	–	1	+	–	10	1	–	1	1	–	3	–	–
		11-5, 66-67	92.4	+	–	2	2	+	–	⊕	+	–	7	–	1	1	1	–	1	–	+
		11,CC	95.0	1	1	–	3	2	–	2	2	–	21	1	+	+	2	–	1	–	+
		12-1, 65-66	95.9	1	+	–	3	–	–	1	2	–	10	–	+	1	1	–	+	–	1
		12-3, 65-66	98.9	–	+	1	2	–	–	2	–	–	5	–	–	+	2	–	2	–	+
	a	12-5, 65-66	101.9	+	–	–	2	–	–	3	+	1	7	+	1	–	1	–	1	–	–
		12,CC	104.2	+	–	–	2	1	–	1	1	–	6	+	1	1	+	–	2	–	+
		13-2, 68-69	106.2	–	–	–	2	+	1	2	1	+	3	–	+	–	1	–	1	–	+
		13-3, 68-69	107.7	–	–	–	+	–	–	2	–	–	10	1	+	1	2	–	1	–	2
		13-5, 68-69	110.7	+	+	–	2	–	–	3	–	1	11	1	+	+	1	–	1	–	–
Nitzschia miocenica	b	13,CC	112.6	+	1	–	–	–	4	3	–	–	6	–	1	–	1	–	1	–	+
		14-2, 68-69	114.6	+	+	1	6	–	+	2	1	–	13	–	–	+	2	–	3	–	1

Notes: The abundance of each species is rounded to the nearest percentage. Samples are correlated to the diatom zonation of Burckle (1972, 1977). The depth of each sample is recorded in meters. The age of each sample is extrapolated from the sediment accumulation curve. + = <1% of the assemblage. ⊕ = reworked specimens composing <1% of the assemblage.

age difference may result from paleoceanographic provincialism, which may be supported by examination of the abundance of *Thalassiosira miocenica* over the same time interval. At both Sites 572 and 503, *T. miocenica* increases approximately 5% between the peak in abundance and the last occurrence of *N. miocenica*. This slight increase in *T. miocenica* is also observed at Site 573, but when compared to the range of *N. miocenica* at Sites 503 and 572, the increase occurs over a longer period of time and approximately 0.15 m.y. prior to its occurrence at the other sites (Figs. 4 to 6). The peak in abundance of *N. miocenica* is therefore useful in the high productivity region of the equatorial Pacific and is assigned a tentative age of 5.6 Ma. The greater age (5.8 Ma) extrapolated for this event at Site 573 may be useful in the low productivity zone of the eastern equatorial Pacific. However, further documentation of this event is required before it can be considered stratigraphically useful in this region.

Acme of *Actinocyclus ehrenbergii*

Actinocyclus ehrenbergii typically composes 1% of the overall diatom assemblage (see Tables 1 to 3). However, in Sample 572A-7-2, 66–67 cm, 503A-19-2, 111–113 cm, and 503A-19,CC, *A. ehrenbergii* attains 14, 13, and 10% of the overall assemblage, respectively. This acme of *A. ehrenbergii* approximates the first occurrence of *Thalassiosira convexa* var. *convexa* (Figs. 7 and 8). The extrapolated ages for these samples are 3.6 Ma (572A-7-2), 3.6 Ma (503A-19-2), and 3.60 Ma (503A-19,CC).

Table 3. (Continued).

N. miocenica	*N. reinholdii*	*Nitzschia* sp. 1	*Nitzschia* "Group"	*Pseudoeunotia doliolus*	*Rhizosolenia bergonii*	*R. praebergonii*	*R. styliformis*	*Rossiella praepaleacea*	*T. nitzschioides* var. *parva*	*T. nitzschioides* s. ampl.	*Thalassiosira convexa* s. str.	*T. convexa* var. *aspinosa*	*T. eccentrica*	*T. leptopus*	*T. miocenica*	*T. nativa*	*T. oestrupii*	*T. praeconvexa*	*Thalassiosira* "Group"	*Thalassiothrix longissima*	*Triceratium cinnamomeum*	Other	Total number counted	Extrapolated age (Ma)
–	3	4	3	1	3	1	1	–	8	11	–	–	8	1	–	–	13	–	1	6	3	+	300	1.50
–	1	2	2	3	1	2	2	–	9	16	–	–	8	2	–	–	12	–	3	4	5	2	302	1.63
–	3	+	–	–	2	14	+	–	3	15	–	–	12	2	–	–	1	–	1	10	3	1	302	2.10
–	3	2	3	–	3	4	–	–	1	20	–	+	11	2	–	–	2	–	2	1	4	1	281	2.30
–	1	13	1	–	1	3	–	–	7	28	1	2	5	3	–	–	3	–	3	3	2	1	303	2.50
–	2	7	1	–	2	4	+	–	–	34	1	3	4	2	–	–	2	–	6	5	2	1	295	2.60
–	3	3	1	–	2	5	+	–	11	19	1	4	7	2	–	–	+	–	2	6	2	1	297	2.73
–	3	5	3	–	1	4	–	–	8	20	1	4	8	2	–	–	1	–	2	3	3	+	302	2.80
–	2	2	1	–	3	1	–	–	7	13	8	10	5	2	–	–	2	–	1	7	1	1	292	2.97
–	1	1	1	–	2	–	–	–	–	13	2	17	3	3	–	–	1	–	+	3	2	+	294	3.25
–	1	3	–	–	1	–	–	–	10	41	3	7	3	1	–	–	+	–	1	5	2	+	296	3.38
–	+	1	2	–	3	–	+	–	12	37	5	8	2	1	–	–	1	–	+	5	1	1	302	3.43
–	1	1	1	–	2	–	–	–	8	24	–	–	3	1	–	–	1	–	2	5	4	1	299	3.67
–	+	–	3	–	2	–	7	–	–	25	–	3	4	3	–	–	1	–	2	5	+	+	300	3.90
–	1	5	1	–	1	–	+	–	22	22	–	1	3	2	–	–	1	–	2	5	1	+	296	3.96
–	+	7	3	–	–	–	–	–	–	35	–	1	5	1	–	–	2	–	2	6	2	3	295	4.00
–	+	–	1	–	+	–	1	–	8	22	–	3	7	1	–	–	1	–	+	5	3	1	303	4.06
–	1	–	1	–	+	–	–	–	19	38	–	+	2	1	–	–	2	–	–	10	4	1	302	4.15
–	–	1	+	–	–	–	1	–	7	13	–	1	17	3	–	–	2	–	1	12	4	1	301	4.25
–	+	–	1	–	–	–	–	–	2	16	–	6	7	2	–	–	3	–	3	8	5	2	300	4.28
–	–	1	1	–	–	–	–	–	8	26	–	2	9	1	–	–	3	–	2	6	3	+	301	4.38
–	2	+	1	–	–	–	–	–	11	26	–	1	7	1	–	–	2	–	3	9	1	1	303	4.47
–	2	–	–	–	–	–	–	–	14	44	–	2	3	+	–	–	+	–	1	10	1	–	301	5.10
–	1	2	1	–	–	–	+	–	2	36	–	1	5	2	1	1	–	–	1	5	1	1	299	5.20
⊕	2	2	1	–	–	–	1	–	4	45	–	1	4	1	1	2	–	–	4	7	5	1	302	5.27
–	1	–	6	–	–	–	–	–	4	65	–	–	2	1	+	–	–	–	–	6	1	1	301	5.35
⊕	1	–	1	–	–	–	–	–	–	71	–	–	2	1	–	1	–	–	1	5	2	–	300	5.38
–	2	–	2	–	–	–	+	–	12	47	–	1	6	3	2	1	–	–	1	5	1	1	300	5.44
–	1	3	2	–	–	–	–	–	9	57	–	2	5	–	1	–	–	–	1	4	1	+	301	5.51
2	1	–	1	–	–	–	–	–	4	22	–	1	7	3	3	1	–	–	2	13	2	1	302	5.60
14	1	–	1	–	–	–	1	–	11	23	–	1	11	2	3	–	–	–	1	12	1	–	303	5.65
16	+	–	2	–	+	–	–	–	–	36	–	4	3	+	8	–	–	–	3	7	3	1	287	5.75
23	1	1	–	–	–	–	–	–	8	22	–	4	1	+	7	+	–	1	1	12	–	1	301	5.83
16	+	–	1	–	–	–	1	–	17	20	–	2	5	1	5	–	–	4	1	8	+	2	302	5.88
16	1	–	1	–	+	–	–	+	15	32	–	2	3	+	3	–	–	3	+	10	1	2	293	5.95
12	1	2	–	–	–	–	1	+	–	32	–	2	3	2	3	–	–	3	1	19	1	1	302	5.98
10	1	–	1	–	1	–	1	+	1	36	–	2	5	1	–	+	–	4	1	15	2	1	300	6.06
15	1	–	1	–	–	–	+	–	5	36	–	–	5	1	–	–	–	3	1	11	2	1	299	6.12
22	1	–	8	–	–	–	+	+	2	14	–	–	7	3	–	–	–	–	2	9	2	1	298	6.18

Unfortunately, the geographic extent of this datum is presently unknown. This datum was not observed at Site 573 because no samples were examined from this time interval.

First Peak in Abundance of *Thalassiosira convexa* Group

Stratigraphically below the first occurrence of *Thalassiosira convexa* var. *convexa* at 3.6 Ma, *T. convexa* var. *aspinosa* commonly makes up less than 3% of the diatom assemblage. Directly above the first occurrence of *T. convexa* var. *convexa*, the abundance of *T. convexa* Group (*T. convexa* var. *aspinosa* and *T. convexa* var. *convexa*) increases gradually from less than 3% at 3.6 Ma to between 20 and 30% at 3.27 Ma. A sharp decline in abundance of *T. convexa* Group occurs in younger material. This peak in abundance is observed at all sites (Figs. 7 to 9) and has an extrapolated age of 3.25 Ma at Site 573 and of 3.27 Ma at Sites 572 and 503.

Base of the Second Abundance Interval of *Thalassiosira convexa* Group

This datum was originally defined by Burckle and Trainer (1979) as the "reoccurrent appearance" of *Thalassiosira convexa*. They placed this event directly below the first occurrence of *Rhizosolenia praebergonii* (3.0 Ma) and within the Mammoth Subchron. An age of approximately 3.03 Ma was assigned by Burckle and Trainer (1979) to this event. Adjustment of this date to more current ages given for the Mammoth Subchron (bottom at 3.17 Ma, top at 3.07 Ma; Berggren et al., in press) indicates that the age of this datum is most likely slightly older than originally estimated.

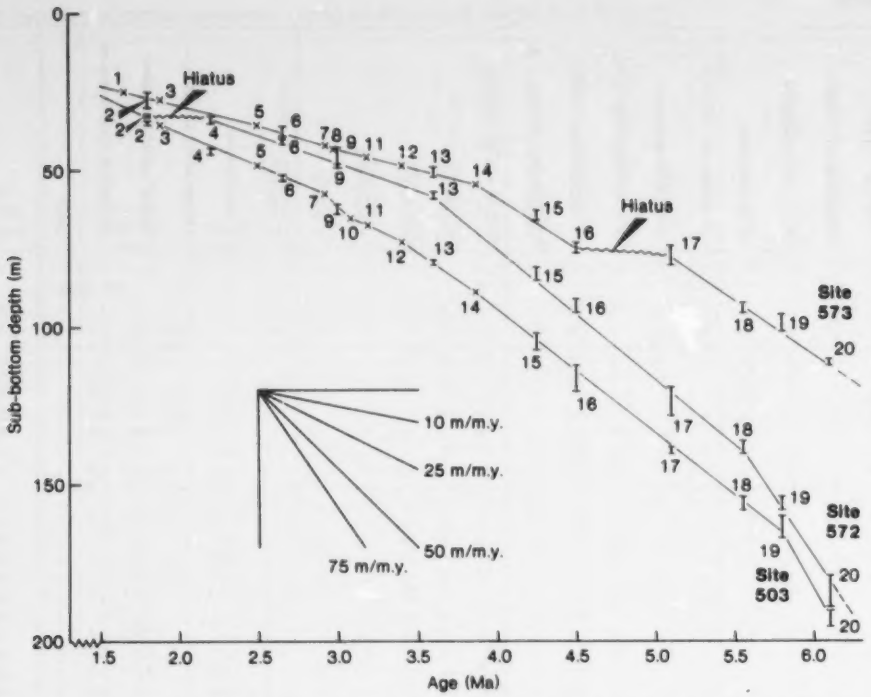

Figure 3. Sediment accumulation curves for Sites 572, 573, and 503. 1. top of Olduvai; 2. first *P. doliolus*; 3. base of Olduvai; 4. last *T. convexa*; 5. top of Gauss; 6. last *N. jouseae*; 7. top of Kaena; 8. base of Kaena; 9. first *R. praebergonii*; 10. top of Mammoth: 11. base of Mammoth; 12. Gilbert/Gauss boundary; 13. first *T. convexa* var. *convexa*; 14. top of Cochiti; 15. last *N. cyclindrica*; 16. first *N. jouseae*; 17. last *T. miocenica*; 18. last *N. miocenica*; 19. last *T. praeconvexa*; 20. first *T. convexa* and *T. miocenica*. × = magnetostratigraphic boundaries. Vertical bars indicate range of uncertainty in sample depth.

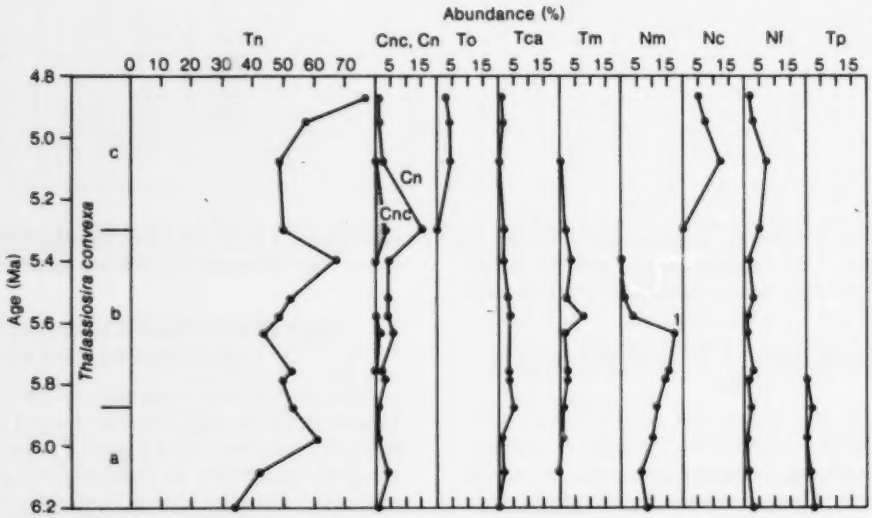

Figure 4. Fluctuations in abundance (percentage) of selected species from Site 572 for the interval 6.2 to 4.8 Ma. Tn = *T. nitzschioides*; Cnc = *C. nodulifer* var. *cyclopus*; Cn = *C. nodulifer*; To = *T. oestrupii*; Tca = *T. convexa* var. *aspinosa*; Tm = *T. miocenica*; Nm = *N. miocenica* (1, peak in abundance of *N. miocenica*); Nc = *N. cylindrica* s. str.; Nf = *N. fossilis*; Tp = *T. praeconvexa*. The diatom zones figured are from Burckle (1972, 1977). Ages of samples are extrapolated from the sediment accumulation curves (Fig. 3).

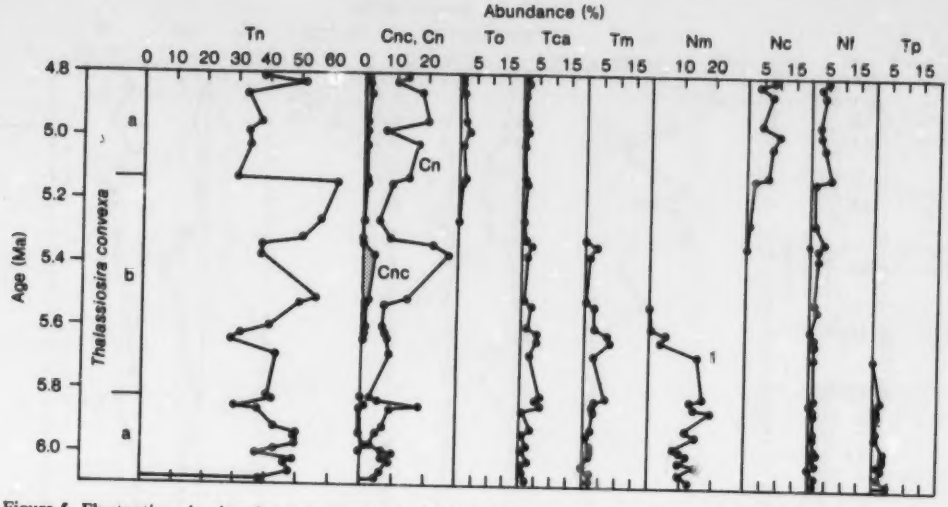

Figure 5. Fluctuations in abundance (percentage) of selected species from Site 503 for the interval 6.2 to 4.8 Ma. Abbreviations and notes same as for Figure 4.

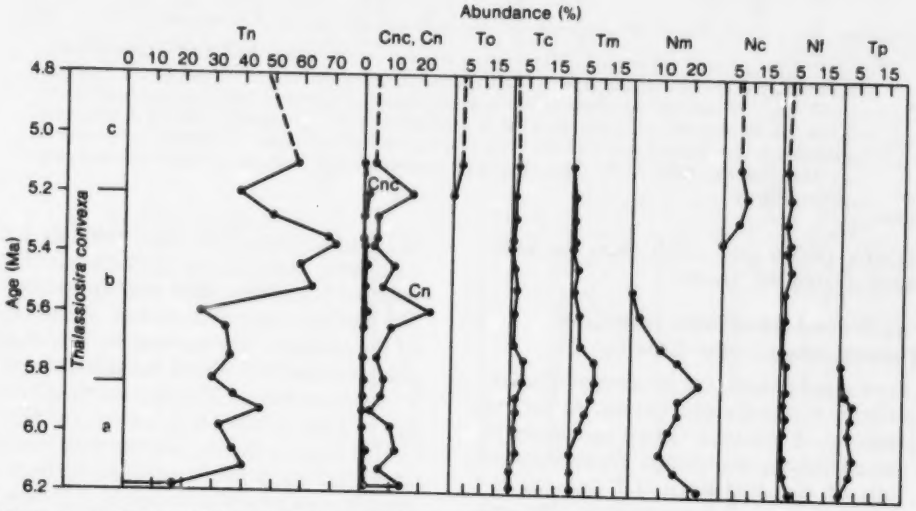

Figure 6. Fluctuations in abundance (percentage) of selected species from Site 573 for the interval 6.2 to 4.8 Ma. Dashed line represents duration of observed hiatus. Abbreviations and notes same as for Figure 4.

At Sites 572 (Fig. 10) and 503 (Fig. 11), a second abundance interval of *T. convexa* Group is observed between 2.9 and 3.1 Ma. The recurrence of *T. convexa*, as described by Burckle and Trainer (1979), corresponds to the base of this second abundance interval. At Site 572 the base of this second interval occurs between 3.0 and 3.1 Ma. At Site 503 this event occurs between 3.1 and 3.15 Ma. Therefore, a tentative age of 3.10 Ma is assigned to this datum. As a result of the sampling interval used in this study, this event can not be recognized at Site 573.

Burckle and Trainer (1979, p. 255) noted that *T. convexa* disappears slightly above the Gilbert/Gauss boundary in Core V28-179 from the equatorial Pacific and suggested that this disappearance may be a useful secondary datum. They assigned an approximate age of 3.2 Ma to this event, indicating that it should occur between the first peak in abundance of *T. convexa* Group (3.27 Ma) and the base of the second abundance interval of *T. convexa* Group (3.1 Ma). The disappearance of the *T. convexa* Group described by Burckle and Trainer (1979) is not observed in this study. The *T. convexa* Group composes less than 1 to 5% of the diatom assemblage in samples from this interval examined at Sites 503 and 572. Samples from this interval were not examined at Site 573. The nonrecognition of the event observed by

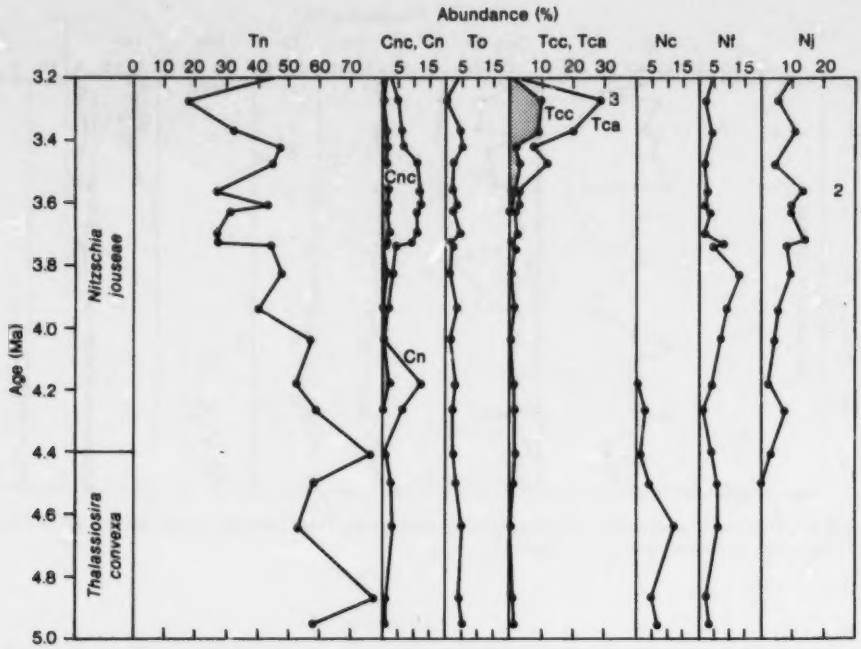

Figure 7. Fluctuations in abundance (percentage) of selected species from Site 572 for the interval 5.0 to 3.2 Ma. Tn = *T. nitzschioides*; Cnc = *C. nodulifer* var. *cyclopus*; Cn = *C. nodulifer*; To = *T. oestrupii*; Tcc = *T. convexa* var. *convexa*; Tca = *T. convexa* var. *aspinosa* (3, first peak in abundance of *T. convexa* Group); Nc = *N. cylindrica*; Nf = *N. fossilis*; Nj = *N. jouseae* (2, acme of *Actinocyclus ehrenbergii*). See Tables 1 and 2 for the acme of *Actinocyclus ehrenbergii*. The diatom zones figured are from Burckle (1972, 1977). Ages of samples are extrapolated from the sediment accumulation curves (Fig. 3).

Burckle and Trainer (1979) may result from the sampling interval used during this study.

Top of the Second Abundance Interval of *Thalassiosira convexa* Group

The top of the second abundance interval of *Thalassiosira convexa* Group is also a useful datum. At the top of this second interval, *T. convexa* Group composes 10 to 20% of the overall diatom assemblage. Directly above the top of this interval, the abundance of *T. convexa* declines to 5% or less of the overall assemblage. The age of this datum is 2.97 Ma at Site 503 and between 2.93 and 3.0 Ma at Site 572. Due to the sampling interval, this datum is not recognized at Site 573. An age of 2.97 Ma seems most reliable for this datum since Site 503 has four data points between 2.9 and 3.0 Ma. Although Burckle and Trainer (1979) did not recognize this datum as being useful, it does appear in their figure 1 and has an age similar to that observed in this study.

Increase in the Abundance of *Thalassiosira oestrupii*

At Site 573 an increase in abundance of *Thalassiosira oestrupii* occurs between 1.9 and 1.8 Ma (Figs. 10 and 12). Below this interval *T. oestrupii* consistently composes less than 5% of the diatom assemblage. Above this interval *T. oestrupii* composes 10 to 20% of the diatom assemblage. An increase is also observed at Site 572, but a hiatus from approximately 2.2 to 1.8 Ma occurs there, and thus the exact placement of this increase remains a problem. The corresponding interval at Site 503 was not examined because of the poor preservation of the samples. The increase in *T. oestrupii* can only be placed tentatively within the interval approximating the first occurrence of *Pseudoeunotia doliolus*. A tentative age of 1.90 to 1.80 Ma is assigned to this event. Burckle (1977) noted a second increase in abundance of *T. oestrupii* just below the Matuyama/Bruhnes boundary. This event has an approximate age of 0.75 Ma (Burckle, 1977) and is therefore different from the event defined in this study.

Table 4 presents the datums that are considered to be stratigraphically useful and their extrapolated ages. The first occurrence of *Coscinodiscus africanus*, placed by Burckle (1978) within the upper part of the Gilbert Chron (Fig. 1), is not included because *C. africanus* is too sporadic after its first occurrence to be useful for stratigraphic correlation. The first occurrence of *C. africanus* may be applicable within a specific geographic province, but further studies are required.

The first occurrence of *T. miocenica* is defined by Burckle (1972, 1978) to occur stratigraphically below the first appearance of *T. convexa* within the upper part of paleomagnetic chron 6. The order of appearance of these two species is reversed according to Sancetta (1982); while

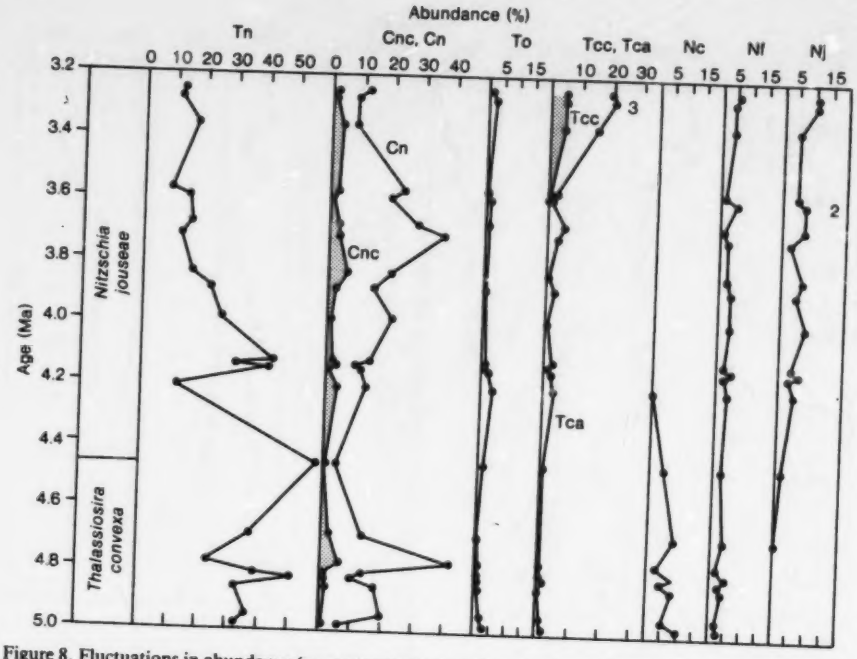

Figure 8. Fluctuations in abundance (percentage) of selected species from Site 503 for the interval 5.0 to 3.2 Ma. Abbreviations and notes same as for Figure 7.

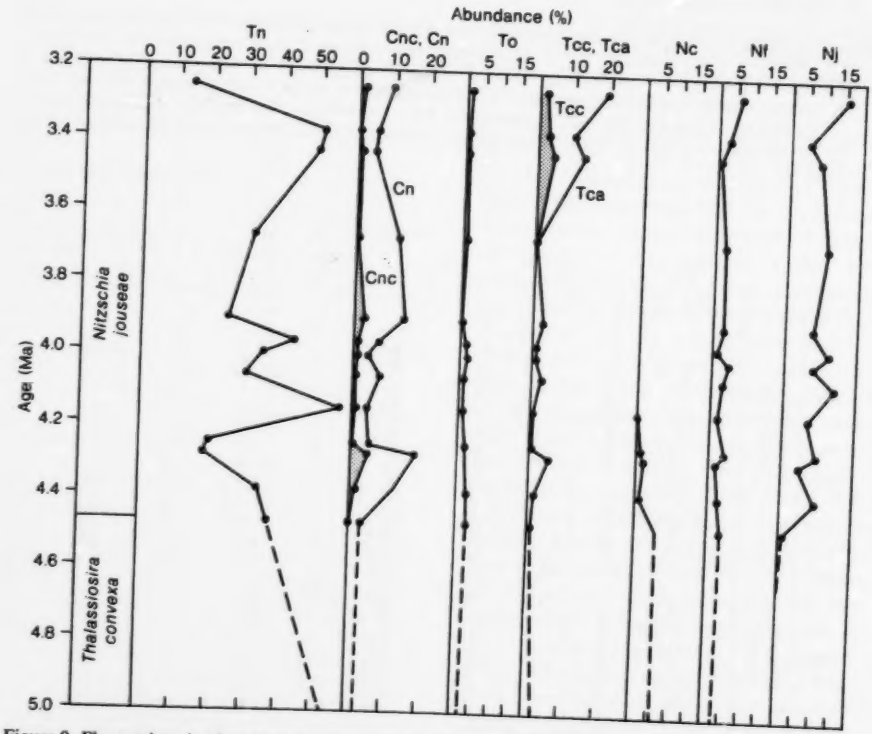

Figure 9. Fluctuations in abundance (percentage) of selected species from Site 573 for the interval 5.0 to 3.2 Ma. Dashed line represents the duration of the observed hiatus. Abbreviations and notes same as for Figure 7.

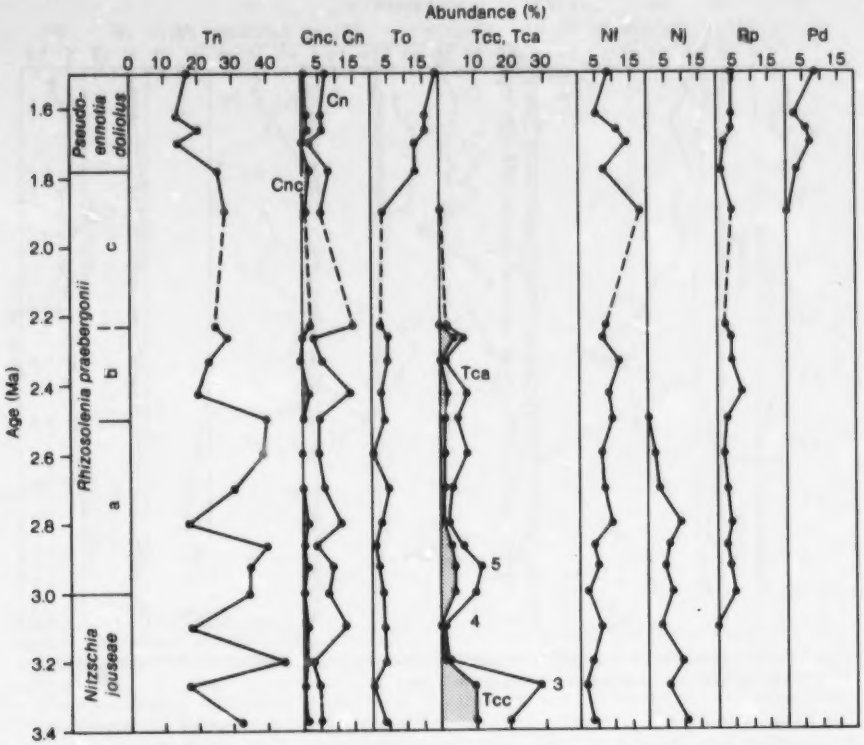

Figure 10. Fluctuations in abundance (percentage) of selected species from Site 572 for the interval 3.4 to 1.5 Ma. Tn = *T. nitzschioides*; Cnc = *C. nodulifer* var. *cyclopus*; Cn = *C. nodulifer*; To = *T. oestrupii*; Tcc = *T. convexa* var. *convexa*; Tca = *T. convexa* var. *aspinosa* (3, first peak in abundance of *T. convexa* Group; 4, base of second interval of abundance; 5, second peak in abundance); Nf = *N. fossilis*; Nj = *N. jouseae*; Rp = *R. praebergonii*; Pd = *P. doliolus*. Dashed line represents the duration of the observed hiatus. Ages of samples are extrapolated from the sediment accumulation curves (Fig. 3).

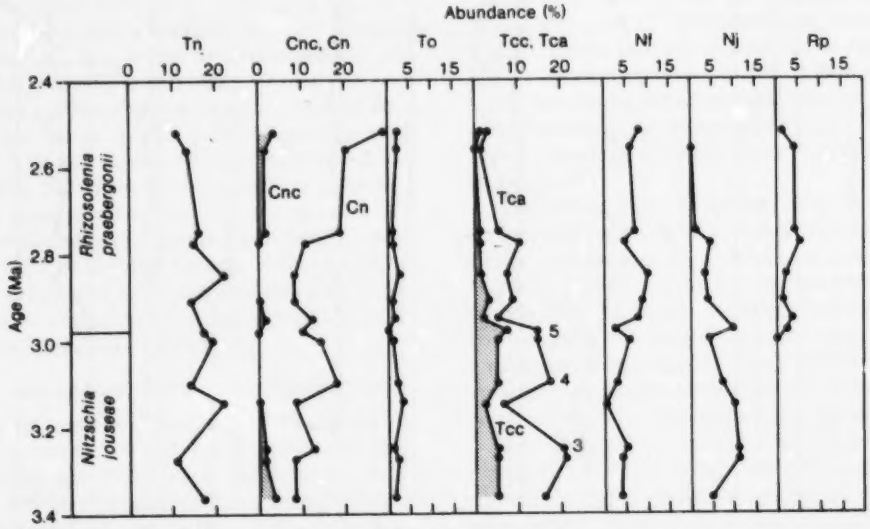

Figure 11. Fluctuations in abundance (percentage) of selected species from Site 503 for the interval 3.4 to 1.5 Ma. Abbreviations and notes same as for Figure 10.

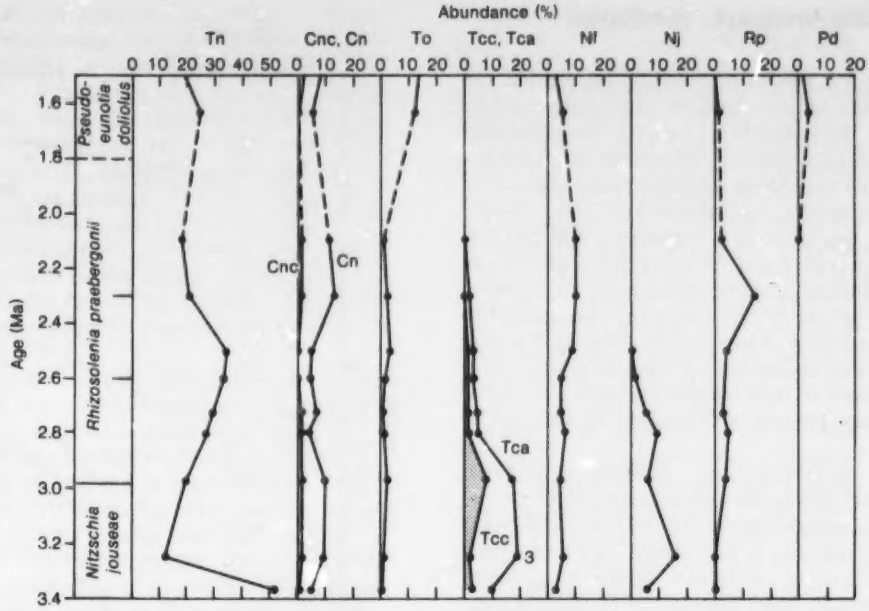

Figure 12. Fluctuations in abundance (percentage) of selected species from Site 573 for the interval 3.4 to 1.5 Ma. Dashed line represents an interval of uncertainty resulting from the sampling interval. Abbreviations and notes same as for Figure 10.

Table 4. Useful diatom datums recognized within the upper Neogene of the eastern equatorial Pacific and their extrapolated ages.

Datum	Diatoms	Age (Ma)	References
L.	*R. praebergonii* var. *robusta*	1.55	3, 4, 5
F.	*P. doliolus*	1.80	1, 3, 4, 5
L.	*R. praebergonii*	1.85	2, 3
In.	*T. oestrupii*	1.8–1.9	6
Tr.	*R. praebergonii* → *R. praebergonii* var. *robusta*	2.00	1
L.	*T. convexa*	2.20	3
F.	*R. praebergonii* var. *robusta*	2.36	3
L.	*N. jouseae*	2.60	3, 5
Ta_2	*T. convexa*	2.97	6
F.	*R. praebergonii*	3.00	3, 5
Ba_2	*T. convexa*	3.10	6
Ta_1	*T. convexa*	3.27	6
F.	*T. convexa* var. *aspinosa*	3.60	3, 5
Ac.	*A. ehrenbergii*	3.5–3.6	6
F.	*A. elegans*	3.9	2, 5
L.	*N. cylindrica*	4.2	2
F.	*N. jouseae*	4.5	2, 5
L.	*T. miocenica*	5.1	2
F.	*T. oestrupii*	5.1–5.2	6
F.	*N. cylindrica*	5.3	6
L.	*A. acutiloba*	5.3	2
L.	*N. miocenica*	5.5	2, 6
Ta	*N. miocenica*	5.6	6
L.	*R. praepaleacea*	5.7	7
L.	*T. praeconvexa*	5.8	5
F.	*T. convexa*	6.1	2, 5
F.	*T. miocenica*	6.1	2, 4, 5
F.	*T. praeconvexa*	6.3	2

Notes: 1. Burckle, 1977; 2. Burckle, 1978; 3. Burckle and Trainer, 1979; 4. Barron, 1980; 5. Barron, this volume; 6. Baldauf, this paper; 7. Burckle, in Vincent, 1981. L = last occurrence; F = first occurrence; In = increase in abundance; Tr = evolutionary transition; Ta = top of abundance interval; Ba = bottom of abundance interval; Ac = acme.

both Baldauf (1985) and Barron (in press) recognize the first occurrences of *T. miocenica* and *T. convexa* var. *aspinosa* as being synchronous. The difference in the stratigraphic relationship and placement of these datums probably represents differences in taxonomic concepts.

Although the last occurrence of *Nitzschia cylindrica* is described by Burckle (1978) as a useful secondary datum for low latitudes, no mention is made of the stratigraphic potential of this species' first occurrence. Sancetta (1982) suggests that the total stratigraphic range of *N. cylindrica* is useful, thereby suggesting that the first occurrence of this species is also useful. The present study indicates that the first occurrence of *N. cylindrica* s.s. is useful within the equatorial Pacific (Fig. 7 to 9). An age of 5.3 Ma is extrapolated for this event.

The first occurrence of *T. oestrupii* is a useful stratigraphic marker, as indicated by previous work. Burckle (1978) places the first occurrence in the equatorial Pacific slightly above the top of paleomagnetic chron 5. Barron (1981) defined the base of his *T. oestrupii* Zone as the first occurrence of this taxon. Barron (1981) placed this datum within the lowermost reversed interval of the Gilbert Chron and suggested that it occurred approximately at the Miocene/Pliocene boundary. The results of the present study also indicate that the first occurrence of *T. oestrupii* approximates the Miocene/Pliocene boundary as dated by Berggren et al. (in press) (Figs. 4 to 6). An age of 5.1 to 5.2 Ma is assigned to this first occurrence. A slight stratigraphic overlap exists between the range of *T. oestrupii* and *T. miocenica* (Figs. 4 to 6). The last occurrence of *T. miocenica* is placed at 5.1 Ma.

Calcium Carbonate Stratigraphy and Diatom Correlation

Three factors are generally cited as responsible for fluctuations in the relative calcium carbonate content preserved within the sedimentary record. These include variation in the productivity of calcareous microplankton, dissolution of calcareous materials, and dilution by noncarbonate sediments. Unfortunately, little is understood about the mechanisms controlling these factors, although Vincent (1981) and Dunn (1982) suggest that carbonate fluctuations tend to correspond to climatic oscillations. Arrhenius (1952) originally discussed the correlation of carbonate content and climatic fluctuations. He associated sediments having a high carbonate content with periods of cold climate and sediments having a low carbonate content with periods of warmer climate.

Although understanding the relationship between fluctuations in the carbonate content and climate oscillation is difficult, recognition of synchronous carbonate minima and maxima over a geographic region is useful in refining stratigraphic resolution. Figure 13 presents the upper Miocene to lower Pleistocene carbonate stratigraphy for Sites 572 and 573 (site chapters, this volume). The correlation of carbonate maxima and minima between sites is based on diatom datums observed at both sites.

Vincent (1981) used datums of diatom taxa in addition to those of other microfossils to correlate the Neogene carbonate stratigraphy of the Hess Rise region of the central North Pacific to the equatorial Pacific region. Comparison of the results of the present study to those of Vincent (1981) allows correlation of the carbonate stratigraphy to the diatom datums. Two distinct intervals of carbonate fluctuations can be readily correlated between Sites 572 and 573 and can be dated using diatom datums. The first interval occurs in the upper Miocene and approximates the last occurrence of *Nitzschia miocenica*. The second interval occurs in the upper Pliocene and corresponds to the interval between the last occurrences of *Rhizosolenia praebergonii* and *Thalassiosira convexa*.

The last occurrence of *N. miocenica* is at a depth of 140.8 m at Site 572 and 95.0 m at Site 573. This datum correlates at both sites to the transition between the carbonate maximum 5d and the carbonate minimum 5e (Fig. 13). Directly below the last occurrence of *N. miocenica* is the peak in abundance of *N. miocenica* that correlates to the transition between the carbonate minimum 5e and carbonate maximum 5f. Vincent (1981) correlates the carbonate event 5d with the last occurrence of *N. miocenica* in Core RC12-66 in the central North Pacific Ocean. The slight difference between the correlation by Vincent (1981) and this study (approximately 50,000 yr.) is the probable result of sampling differences and biostratigraphic resolution.

The upper Pliocene sequence, within which 3 diatom datums occur (first *R. praebergonii*; last *N. jouseae*; and last *T. convexa*), is easily correlated between Sites 572 and 573 and occurs from 47 to 35 m at Site 572 and from 43 to 33 m at Site 573. These datums allow the correlation of the carbonate minima Gu3 and M21 between these sites (Fig. 13).

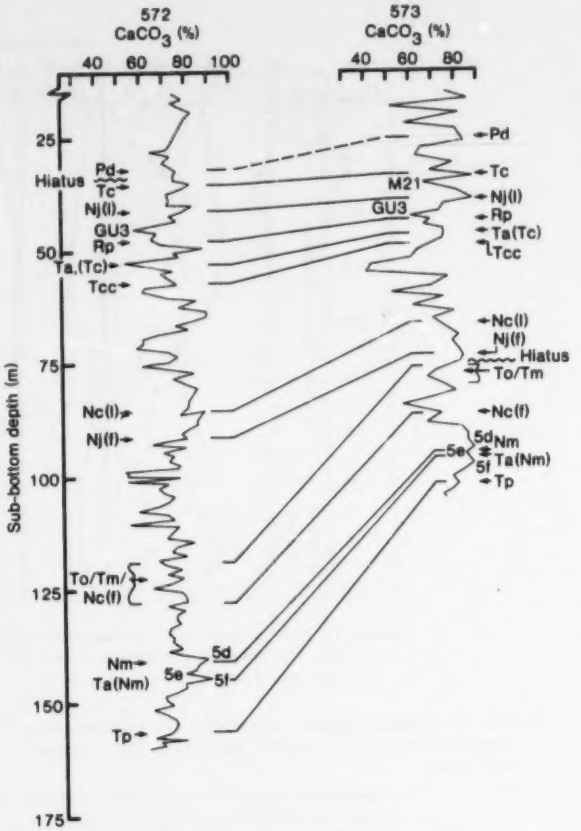

Figure 13. Correlation of the carbonate stratigraphy from Sites 572 and 573 (site chapters, this volume) to the late Neogene diatom datums observed at both sites. The carbonate peaks are labeled following Vincent (1981). Tp = last *T. praeconvexa*; Ta(Nm) peak of abundance of *N. miocenica*; Ta(Tc) peak of abundance of *T. miocenica*; Nm = last *N. miocenica*; To = first *T. oestrupii*; Tm = last *T. miocenica*; Nc(f) = first *N. cylindrica*; Nj(f) = first *N. jouseae*; Nc(l) = last *N. cylindrica*; Tcc = first *T. convexa* var. *convexa*; Rp = first *R. praebergonii*; Nj(l) = last *N. jouseae*; Tc = last *T. convexa*; Pd = first *P. doliolus*.

Carbonate minimum Gu3 occurs at 45 m depth at Site 572 and at 42 m at Site 573, directly above the first occurrence of *R. praebergonii* at 47.5 m at Site 572 and 43 m at Site 573. Vincent (1981) correlates the Gu3 carbonate minimum at Site RC12-66 and DSDP Site 157 in the central North Pacific with the first occurrence of *R. praebergonii* var. *A*. However, it is clear from the rest of her data that Gu3 coincides with the first occurrence of *R. praebergonii*, which is in agreement with observations at Sites 572 and 573.

Other carbonate peaks shown in Figure 13 are not discussed here because of the uncertainty of their correlation. The use of only diatom datums for correlation of these carbonate peaks results in this uncertainty.

Diatom Abundance Stratigraphy

Coscinodiscus nodulifer has a greater average abundance at Site 503 than at Sites 573 and 572 (Figs. 4–12).

At Site 503 *C. nodulifer* composes an average of 15% of the total diatom assemblage. Occasional peaks of 30 to 40% are also observed. At Site 573 the average abundance of *C. nodulifer* is slightly less, having an average of 10%. The occasional peaks observed for this site are also less and have a maximum value of 20%. The lowest average abundance of *C. nodulifer* occurs at Site 572, where values of 5% are common. The abundance peaks at this site are further reduced, with a maximum value of 15%. The abundance of *C. nodulifer* at Site 572 may be influenced not only by the effects of equatorial upwelling but also by the Peru–Chile Current. This is suggested by the abundance of *Thalassionema nitzschioides* at Site 572.

Site 503 is geographically situated within the Guatemala Basin, which is a region characterized by equatorial upwelling. The greater abundance of *C. nodulifer* at Site 503 suggests that *C. nodulifer* favors equatorial upwelling conditions. A similar conclusion was reached by Cooke-Poferl et al. (1975) on the basis of three diatom assemblages that were recognized from 180 core tops in the eastern equatorial Pacific region. They recognized an assemblage dominated by *C. nodulifer* that was associated with equatorial upwelling. The additional assemblages recognized by Cooke-Poferl et al. (1975) include an assemblage dominated by *T. nitzschioides* (associated with the Peru–Chile Current) and an assemblage dominated by *Pseudoeunotia doliolus* and *T. oestrupii* (associated with the North Equatorial Counter Current).

The fluctuations in the relative frequency of *T. nitzschioides* also merit discussion. *T. nitzschioides* has the greatest average abundance at Site 572, where it averages 40% of the total diatom assemblage (see Fig. 14). At Sites 573 and 503 the abundance of *T. nitzschioides* is slightly less, averaging 36 and 32%, respectively. Previous studies have associated *T. nitzschioides* with coastal upwelling (Schuette and Schrader, 1979). In addition, Cooke-Poferl et al. (1975) associate the dominance of *T. nitzschioides* in the eastern equatorial Pacific with the northward-flowing Peru–Chile Current. This study suggests that *T. nitzschioides* is also associated with the upwelling of the Equatorial Undercurrent.

Site 572, at the western edge of the productivity region, has the greatest abundance of *T. nitzschioides*, which can be divided into three intervals (Fig. 14). The first interval extends from 6.1 to ~4.2 Ma. Within this interval, *T. nitzschioides* composes 50 to 65% of the total diatom assemblage. Between 4.2 and 3.8 Ma the abundance of *T. nitzschioides* declines from 65 to 40%. Above this interval *T. nitzschioides* composes between 15 and 40% of the assemblage.

Although the average abundance of *T. nitzschioides* is less at Site 503, a trend in abundance similar to that at Site 572 is observed within the high productivity region (Fig. 14). Between 6.1 and ~4.1 Ma, *T. nitzschioides* composes from 30 to 55% of the assemblage. A gradual decline in abundance from 30 to 15% is observed between 4.1 and 3.9 Ma. Stratigraphically above this decline, *T. nitzschioides* composes from 10 to 20% of the diatom assemblage (Fig. 14).

The trend in abundance is not as pronounced at Site 573 in the low productivity region (Fig. 14). The abundance of *T. nitzschioides* at Site 573 ranges from 20 to 65%. A distinct pulse of *T. nitzschioides* (from 40 to 65%) is observed at 5.4 Ma. Although at Site 573 *T. nitzschioides* shows a slight decline near the top of the examined interval, a decline in abundance similar to that at Sites 503 and 572 between 4.2 and 3.7 Ma is not observed. The gradual decline in abundance of *T. nitzschioides* at both Sites 572 and 503 in the easternmost Pacific may represent a change in oceanographic circulation between 4.2 and 3.7 Ma. The absence of a similar decline at Site 573 suggests that the effects of this oceanographic change (if responsible) would have been restricted, or at least most extreme, within the easternmost equatorial Pacific.

Prior to the closing of the Isthmus of Panama, *T. nitzschioides* may have been associated with not only the Peru–Chile Current but also with the zone of mixing that may have resulted from the influx and interaction of warm, high-salinity Atlantic surface water with cooler, lower salinity Equatorial Undercurrent water. If this hypothesis is correct, *T. nitzschioides* would have had a greater abundance in the region of Sites 572 and 503 while communication between the two oceans remained open. Once this communication was severed (as a result of the emergence of the Isthmus of Panama), water masses within the easternmost equatorial Pacific would have had to reorganize. In particular, the geographic location of the upwelling of the eastern Equatorial Undercurrent would have been affected. This would presumably have resulted in conditions less favorable to *T. nitzschioides* and thus in a decline in its abundance. Although the above model presents a reasonable explanation for the fluctuation in the abundance of *T. nitzschioides*, further evidence should be evaluated.

CONCLUSION

The stratigraphic resolution for the upper Neogene of the eastern equatorial Pacific is refined by the recognition of six new diatom events. Recognition of these datums is the result of quantitative methods. In addition, stratigraphic resolution is improved in the equatorial Pacific by the correlation of diatom events to the carbonate events 5f, 5e, 5d, Gu3, and M21.

The fluctuations in abundance revealed by quantitative methods suggest changes in paleoceanographic circulation. The decline in abundance of *T. nitzschioides* between 4.2 and 3.7 Ma in the easternmost sites may be related to the restriction in communication between the Atlantic and Pacific resulting from emergence of the Isthmus of Panama. The absence of a decline in *T. nitzschioides* at the more westerly Site 573 during the same time interval suggests that the easternmost Pacific was most affected by this closure. Fluctuations in abundances of species also allow inferences to be made about the association of species to ecological conditions. The association of *C. nodulifer* with equatorial upwelling and *T. nitzschioides* with the Peru–Chile Current and

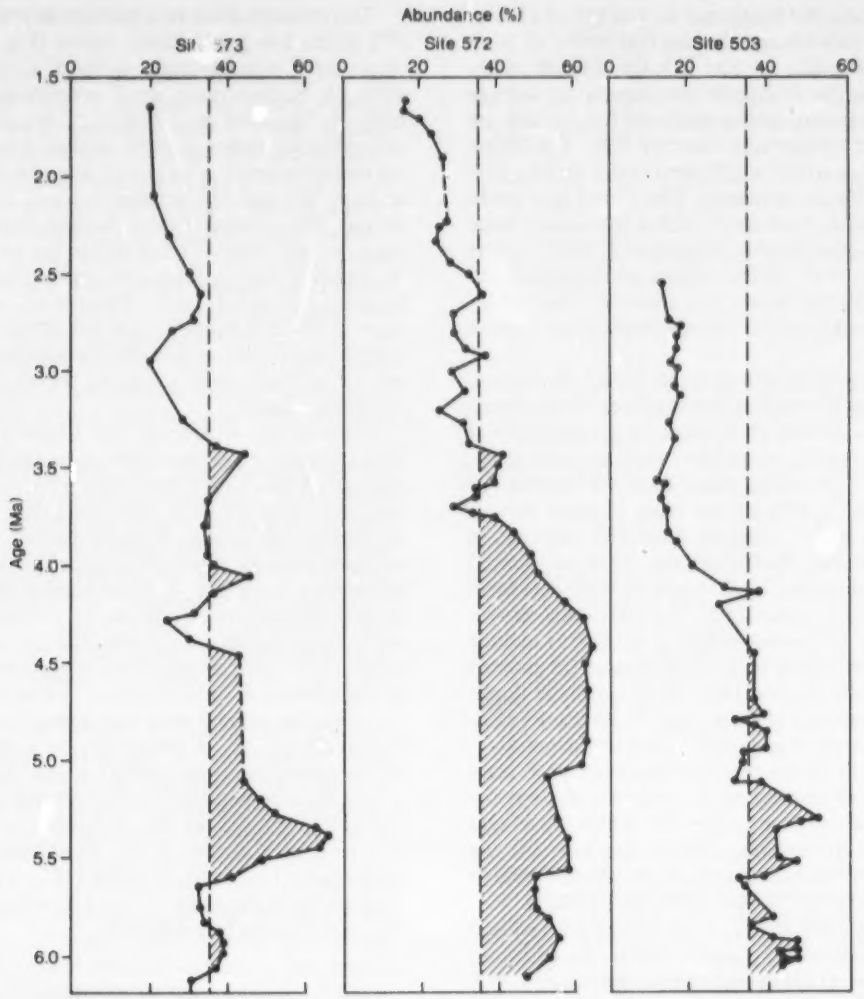

Figure 14. Correlation of the fluctuations in abundance (percentage) of *T. nitzschioides* for Sites 573, 572, and 503. The ages of the samples are extrapolated from the sediment accumulation curves (Fig. 3). Vertical dashed lines are a frame of reference to show the decline in abundance at Sites 572 and 503 between 4.2 and 3.7 Ma.

the Equatorial Undercurrent suggest changes in circulation related to the uplift of the Isthmus of Panama.

ACKNOWLEDGMENTS

I wish to thank John Barron, Charles Blome, Charlotte Brunner, Dave Bukry, and Charles Repenning for reviewing this manuscript. In addition, I would like to express my thanks to John Barron for his helpful discussion during this study. Appreciation is further due to John Barron, James Gardner, and the National Science Foundation for providing the samples examined.

REFERENCES

Arrhenius, G., 1952. Sediment cores from the east Pacific. *Rep. Swed. Deep Sea Exped., 1947–1948*, 5:1–202.

Baldauf, J. G., 1985. Cenozoic diatom biostratigraphy and paleoceanography of the Rockall Plateau Region, North Atlantic, Deep Sea Drilling Project Leg 81. *In* Roberts, D., Schnitker, D., et al., *Init. Repts. DSDP*, 81: Washington (U.S. Govt. Printing Office), 439–478.

Barron, J. A., 1980. Upper Pliocene and Quaternary diatom biostratigraphy of the Deep Sea Drilling Project Leg 54. *In* Rosendahl, B. R., Hekinian, R., et al., *Init. Repts. DSDP*, 54: Washington (U.S. Govt. Printing Office), 455–485.

_____, 1981. Late Cenozoic diatom biostratigraphy and paleoceanography of the middle latitude eastern North Pacific, Deep Sea Drilling Project Leg 63. *In* Yeats, R. S., Haq, B. U., et al., *Init. Repts. DSDP*, 63: Washington (U.S. Govt. Printing Office), 507–538.

_____, in press. Neogene planktic diatom biostratigraphy. *In* Saunders, J. B., and Bolli, H. M., (Eds.), *Biostratigraphy by Marine Plankton:* Cambridge (Cambridge Univ. Press).

Barron, J. A., and Keller, G., 1982. Widespread Miocene deep-sea hiatuses: Coincidence with periods of global cooling. *Geology*, 10: 577–581.

Barron, J. A., Keller, G., Dunn, D. A., Kennett, J. P., Lombari, G., Burckle, L. H., and Vinvent, E., in press. A multiple microfossil

biochronology for the Miocene. *In* Savin, S. M. (Ed.), *Cenozoic Paleoceanographic Synthesis (CENOP)*, Geol. Soc. Am. Mem.

Berggren, W. A., Kent, D. V., and Flynn, J. J., in press. Neogene geochronology and chronostratigraphy. *Geochronology and the Geological Record*, Geol. Soc. London Spec. Pap.

Burckle, L. H., 1969. Late Cenozoic planktonic diatom zones in equatorial Pacific sediments. *Geol. Soc. Am. Abstr. Progr.*, 7:24. (Abstract)

———, 1972. Late Cenozoic planktic diatom zones from the eastern equatorial Pacific. *Nova Hedwigia*, 39:150–217.

———, 1977. Pliocene and Pleistocene diatom datum levels from the equatorial Pacific. *Quat. Res. (NY)*, 7:330–340.

———, 1978. Early Miocene to Pliocene diatom datum levels for the equatorial Pacific. *Proc. Second Working Group Mtg., Biostratigraphic Datum Planes of the Pacific Neogene, IGCP Project 114*: Bandung, Indonesia (Geol. Res. Dev. Ctr.), 1:25–44.

Burckle, L. H., and Trainer, J., 1979. Middle Miocene and late Pliocene diatom datum levels from the Central Pacific. *Micropaleontology*, 25(3):281–293.

Cooke-Poferl, K., Burckle, L. H., and Riley, S., 1975. Diatom evidence bearing on late Pleistocene climatic changes in the equatorial Pacific. *Geol. Soc. Am. Ann. Meet.*, 1038–1039.

Dunn, D. A., 1982. Changes from "Atlantic-type" to "Pacific-type" carbonate stratigraphy in middle Pliocene equatorial Pacific ocean. *Mar. Geol.*, 50:41–60.

Hailwood, E. A., and Rees, A. I., 1982. Magnetic properties of sediments from Hole 503A. *In* Prell, W. L., Gardner, J. V., et al., *Init. Repts. DSDP*, 68: Washington (U.S. Govt. Printing Office), 441–444.

Keller, G., and Barron, J. A., 1983. Paleoceanographic implications of Miocene deep-sea hiatuses. *Geol. Soc. Am. Bull.*, 94:590–613.

Sancetta, C., 1982. Diatom biostratigraphy and paleoceanography, Deep Sea Drilling Project Leg 68. *In* Prell, W. L., Gardner, J. V., et al., *Init. Repts. DSDP*, 68: Washington (U.S. Govt. Printing Office), 301–310.

Schrader, H. J., and Gersonde, R., 1978. Diatoms and silicoflagellates. *Utrect Micropaleonotol. Bull.*, 17:129–176.

Schuette, G., and Schrader, H. J., 1979. Diatom taphocenoses in the coastal upwelling area off western South America. *Nova Hedwigia*, 64:359–378.

Vincent, E., 1981. Neogene carbonate stratigraphy of the Hess Rise (central north Pacific) and paleoceanographic implications. *In* Thiede, J., Vallier, T. L., et al., *Init. Repts. DSDP*, 62: Washington (U.S. Govt. Printing Office), 571–606.

Date of Initial Receipt: 10 October 1983
Date of Acceptance: 28 February 1984

Reprinted from Mayer, L., Theyer, F., et al., 1985
Initial Reports of the Deep Sea Drilling Project, Volume LXXXV, Washington (U. S. Government Printing Office)

10. TROPICAL PACIFIC SILICOFLAGELLATE ZONATION AND PALEOTEMPERATURE TRENDS OF THE LATE CENOZOIC[1]

David Bukry, United States Geological Survey, Scripps Institution of Oceanography[2]

ABSTRACT

Quantitative study of late Cenozoic silicoflagellates at tropical Pacific DSDP Sites 572 and 575 shows that the greatest amplitude of fluctuation in relative paleotemperature values occurred in the late Miocene. The coolest minimum paleotemperature values (near *Ts* = 30) also occurred in the late Miocene. The warmest intervals (*Ts* = 80 to 100) occurred in the middle Miocene and late Pliocene to Quaternary. In detail, the silicoflagellate relative paleotemperature curve correlates fairly well with the eustatic sea-level curve and deep-sea hiatus sequence.

The only upper Cenozoic low-latitude biostratigraphic units not identified are the *Distephanus speculum haliomma* Subzone and *Naviculopsis quadrata* Zone, owing to the absence of the nominative species, which probably had nontropical ecologic preference. Several *Naviculopsis* occurrence events within the *Naviculopsis ponticula* Zone correlate between DSDP Hole 575A and DSDP Hole 495 off Guatemala. Many local and regional biostratigraphic events are recognized.

New taxa identified from DSDP Leg 85 include *Dictyocha nola* Bukry, n. sp., *Distephanus stradneri* var. *grandis* Bukry, n. var., *Mesocena elliptica* var. *rhomboidea* Bukry, n. var., and *Naviculopsis obtusarca* var. *acicula* Bukry, n. var.

INTRODUCTION

A composite section of upper Cenozoic sediment, rich in siliceous skeletons, from the equatorial Pacific at DSDP Sites 572 and 575 was studied quantitatively for silicoflagellate relative-paleotemperature trends and biostratigraphic zonation. This composite section (Hole 572A, Cores 1 to 17; Hole 572D, Cores 1 to 33; and Hole 575A, Cores 1 to 33) provides a tropical and open-ocean comparison with the previous quantitative studies of silicoflagellates recovered nearer the Pacific coast, from California to Ecuador (DSDP Legs 63 to 69). Relations examined in this study include the correlation of early Miocene *Naviculopsis* between DSDP Site 495, off Guatemala, and DSDP Site 575; the paleotemperature significance of *Naviculopsis;* and the distribution of silicoflagellates through the lower Miocene, which has been poorly known in the Pacific area. Also examined are the pattern of the *Ts* paleotemperature curve relative to Pacific currents and eustatic sea-level changes. The possible changing significance of certain silicoflagellate morphologies, such as quadrate and hexagonal *Distephanus*, for paleotemperature is discussed with reference to previous DSDP investigations for higher latitudes.

Early occurrence data on tropical eastern Pacific silicoflagellates for DSDP Leg 9 sites were provided by D. Milow and published in Volume 9 of the *Initial Reports*[3]; those data, however, were nonquantitative. Similarly, a subsequent study of DSDP eastern Pacific silicoflagellates by Ling (1977) examined some tropical sites to provide a biostratigraphic framework, but yielded no quantitative data needed for paleoecological comparison or correlation. Quantitative data for upper Cenozoic silicoflagellate assemblages are available in Volumes 16, 54, and 67 to 69 of the *Initial Reports*.

METHODS AND MATERIALS

Acid-residue strewn slides were prepared for 136 samples from DSDP Holes 572A, 572D, and 575A. Light-microscope counts of silicoflagellates were made at the generic level for Holes 572A and 572D; some stratigraphic and ecologic key species also were counted. The light-microscope counts of silicoflagellates were made at more detailed subgeneric levels for Hole 575A, but diversity was low in these less abundant assemblages.

Identifications were made at magnifications of 250× to 500×. Broken specimens possessing the apical structure were counted as whole specimens, but other broken segments were not counted; breakage was minor, though (typically less than 5%). Counts of 300 specimens or one complete slide area (22 × 40 mm) were made to compute percentages. For the sparse assemblages of Hole 575A, counts were terminated at the round figures of 50 or 100 if only a little slide area remained uncounted. Percentages were not calculated for populations of less than 50 specimens because of the unlikelihood of consistent rankings.

Many of the Leg 85 samples examined are the same sample preparations used, aboard ship and ashore, for diatom studies (Barron, this volume). These samples, kindly made available by John A. Barron, permit better age control and correlation of the silicoflagellates with diatoms for Leg 85 and other eastern Pacific cruises, such as Legs 54 and 67 to 69. Diatom ages for Leg 85 were provided by John A. Barron (personal communication, 1983).

The basis for relative paleotemperature values (*Ts*) and biostratigraphic zonation for silicoflagellates has been given by Bukry (1981a, 1981b, and 1983). Species distributions are compared against those at other DSDP sites in the eastern Pacific region (Fig. 1) and more distant Pacific and Atlantic sites.

COMMENTS ON SILICOFLAGELLATE ZONES

Low-latitude zones (Table 1) can be applied through the lower Miocene to the Quaternary composite section formed by DSDP Holes 572A, 572D, and 575A (Tables 2 to 5). The only missing biostratigraphic units, defined

[1] Mayer, L., Theyer, F., et al., *Init. Repts. DSDP*, 85: Washington (U.S. Govt. Printing Office).

[2] Address: United States Geological Survey, Scripps Institution of Oceanography, La Jolla, CA 92093.

[3] Hays et al. (1972), pp. 79–82, 237, 240, 346–348, 420, 421, 468, 469, 507–510, 558–561, and 636–640.

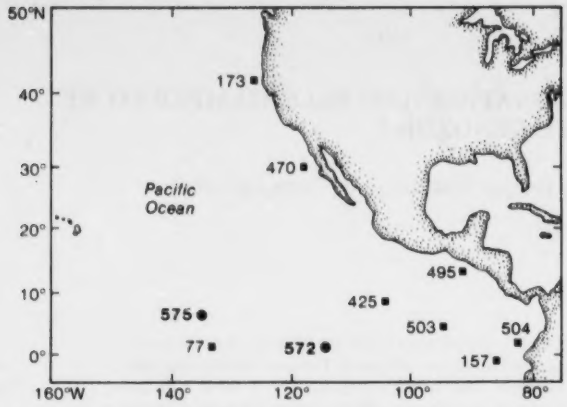

Figure 1. Locations of silicoflagellate-rich DSDP sites in the eastern Pacific, referred to in text. DSDP Leg 85 sites are shown by circles.

Table 1. Late Cenozoic low-latitude silicoflagellate zonation (Bukry, 1981b and 1983).

Age	Zone	Subzone
Quaternary	*Dictyocha aculeata*	
	Mesocena quadrangula	
late Pliocene	*Dictyocha stapedia*	*Dictyocha delicata*
		Dictyocha ornata ornata
early Pliocene	*Dictyocha fibula*	*Dictyocha angulata*
		Dictyocha pulchella
late Miocene		*Dictyocha neonautica*
	Dictyocha brevispina	
middle Miocene	*Corbisema triacantha*	*Distephanus stauracanthus*
		—
early Miocene	*Naviculopsis ponticula*	
	Naviculopsis quadrata[a]	
	Naviculopsis lata	
Oligocene	*Naviculopsis biapiculata*	*Distephanus speculum haliomma*[a]
		—

[a] Not identified at DSDP Leg 85 sites.

for low to middle latitudes (Bukry, 1981b), are the *Naviculopsis quadrata* Zone and the *Distephanus speculum haliomma* Subzone. The guide species for these zones are missing from the tropical assemblages of Leg 85, but are present at middle and high latitudes (e.g., DSDP Legs 38, 41, and 49). Comments on the Leg 85 zonal assemblages follow.

Naviculopsis biapiculata Zone

The zonal assemblages of the *Naviculopsis biapiculata* Zone are sparse, with no *Corbisema* or *Mesocena* (Table 2). *Distephanus speculum patulus, Naviculopsis biapiculata* s. ampl., and *N. constricta* are the most distinctive taxa present at Hole 575A. No specimens of subzonal guide taxa *Distephanus speculum haliomma* or *D. speculum hemisphaericus* are present at Hole 575A, suggesting that they are more useful for biostratigraphy at middle or high latitudes, where their occurrence is more consistent. One new variety, *Distephanus stradneri* var. *grandis*, n. var., is limited here to the *N. biapiculata* Zone.

Naviculopsis lata Zone

A transition from *Distephanus schauinslandii* to *D. crux scutulatus* appears to occur in the *N. lata* Zone of Hole 575A (Plate 3, Figs. 2–5, 7, 8). *D. speculum patulus* is prominent, along with *N. biapiculata* s. ampl. and *N. lata* (Table 3). The absences of *Corbisema triacantha* and the *Mesocena apiculata* group contrast with high-latitude assemblages preserved at DSDP Site 407 west of Iceland. *N. lata* is more abundant at tropical DSDP Site 575 (Hole 575A) than at higher-latitude sites, suggesting that *N. lata* had a warm-water preference, which makes it a good biostratigraphic guide for low latitudes.

Naviculopsis quadrata Zone

The interval between the first *Naviculopsis quadrata* and the first *N. ponticula* or the last *N. quadrata* defines the *Naviculopsis quadrata* Zone (Bukry and Foster, 1974; Bukry, 1981a). Owing to the very poor silicoflagellate assemblage in Core 13 of Hole 575A and the absence of *N. quadrata*, no *N. quadrata* Zone can be identified at Hole 575A (Table 3). The tropical location of Leg 85 sites probably precludes good representation of the *N. quadrata* Zone, because *N. quadrata* favors cooler regions. For example, high-latitude DSDP Site 338, off Norway, has up to 16% *N. quadrata*, whereas coeval assemblages at mid-latitude DSDP Site 369, off northwest Africa, contain a maximum of only 1% *N. quadrata*.

The higher abundance of *N. quadrata* and the lower abundance of *N. lata* (1 or 2%) at high latitude, seen for DSDP Sites 338 and 369, show a trend that is supported by the high (48%) abundance of *N. lata* and by the absence of *N. quadrata* at tropical Hole 575A. If this indicated difference in paleogeographic preference is confirmed at other lower Miocene localities, then the biostratigraphic application of *Naviculopsis* would be linked closely with paleoceanographic interpretations of the assemblages. Whole-assemblage taxonomy and *Ts* calculation may be needed to help define the lower Miocene *Naviculopsis* stratigraphy (see the section on Silicoflagellate *Ts* Comparison).

Naviculopsis ponticula Zone

At Hole 575A, the *Naviculopsis ponticula* Zone is identified by the range of *N. ponticula*. *N. ponticula spinosa* is the dominant *Naviculopsis* at the top of the zone, but maximum numbers of *N. ponticula* occur in the lower part of the zone. *N. ponticula* is missing in the middle part of the zone, where the *Naviculopsis* population is dominated sequentially by *N. obtusarca* and *N. contraria* (Table 3). A similar distribution was recorded off Guatemala in the *N. ponticula* Zone of DSDP Site

Table 2. Early Miocene silicoflagellate biostratigraphy, relative paleotemperature values (*Ts*), and percent distribution of various genera and morphologic subgroups, with remarks on significant occurrences for Hole 575A.

Zone	Core-Section, interval (cm)	Sub-bottom depth (m)	Total specimens	*Ts* value	Generic percents								Noteworthy occurrences
					Corbisema	*Dictyocha*	*Distephanus* (quadrate)	*Distephanus* (nonquadrate)	*Mesocena* (quadrate)	*Mesocena* (nonquadrate)	*Naviculopsis*	*Octactis*	
C. triacantha	1,CC	99	50	98		96	4						Only asperoid *Dictyocha*
	2,CC	102	18	—									
	3,CC	105	7	—									
	4,CC	110	100	51		1	99						
	5,CC	114	50	46	2	2	84	8					
N. ponticula	6,CC	119	100	61	8		38	20			34		*Naviculopsis ponticula spinosa* (30%) acme
	7-2, 42–43	121	50	44			74	16	6		4		
	7-3, 24–25	122	100	53	3		57	17	4		19		
	7,CC	123	50	50			48	16	20		16		
	8-1, 42–43	124	24	—									
	8-2, 42–43	125	50	51			4	28	38		30		Solution-thinned specimens
	8,CC	126	200	90		1	4	9			87		
	9-2, 42–43	127	100	72			6	25			69		*Naviculopsis contraria* (87%) acme
	9,CC	128	300	81			10	2	22		65		
	10-2, 42–43	129	100	96			7	1			92		
	10-3, 42–43	130	50	96			4	2			94		
	10,CC	132	30	—									*Naviculopsis obtusarca* (66%) acme
	11-3, 24–25	134	100	82		2	32	2			64		
	11,CC	136	100	86			25				73		
	12,CC	139	100	49			94	4			2		
—	13,CC	143	10	—									
N. lata	14,CC	146	100	73			1	27			72		
	15,CC	149	50	72		20	10	22			47		
	16,CC	152	50	91		16	10	4			70		Second acme of *Naviculopsis lata*
	17,CC	154	300	74		6	38	8			49		*Distephanus crux scutulatus* evolved from *D. schauinslandii*
	18,CC	157	100	65			44	12			43		
	19,CC	161	100	72			1	28			71		First acme of *Naviculopsis lata*
	20,CC	165	12	—									
N. biapiculata	21,CC	169	80	91			1	9			90		
	23,CC	175	100	93		2	1	7			90		
	27,CC	188	9	—									
	29,CC	194	17	—									
	33,CC	208	27	—									Only *Distephanus* occurs

Note: Species distribution for Hole 575A is shown in Table 3. The top of Hole 575A in Core 1 is older by about 1 m.y. than the base of Hole 572D, according to diatom and paleomagnetic correlation (John Barron, personal communication, 22 Aug. 1983).

495 (Bukry, 1982a). The two stratigraphic sequences differ in the presence of an *N. lacrima* acme horizon at Site 495 and the greater abundance of *N. ponticula* near the top of the zone at Hole 575A. There is an unusual positive correlation between the two sites in the exceptionally high abundance of cruxoid *Distephanus* just above the lower zone boundary (85% at Site 495 and 94% at Hole 575A) and just above the upper zone boundary (83% at Site 495 and 84% at Hole 575A). *Mesocena elliptica* var. *rhomboidea*, n. var. is also essentially limited to the zone at both sites. These distinctive silicoflagellate stratigraphic similarities and the fast plate-tectonic spreading in the region of Site 495 and Hole 575A (van Andel and Bukry, 1973) suggest that Sites 495 and 575 were in much closer proximity during the early Miocene.

Corbisema triacantha Zone

Corbisema triacantha is sparse and sporadic at Hole 575A, but the extinction of *Naviculopsis*, defining the base of the *Corbisema triacantha* Zone, is distinct. Preservation and diversity deteriorate upward through the zone. Sample 575A-1,CC (Table 3), the highest sample studied from Hole 575A, is dominated by *Dictyocha brevispina ausonia*, and contains sparse specimens of *Dictyocha pons*, which marks a short interval just above the *Naviculopsis ponticula* Zone at DSDP Hole 416A off northwest Africa (Bukry, 1980a). No deflandroid *Dictyocha pulchella* were recorded at Hole 575A, so the strata assigned to the *C. triacantha* Zone must represent a short interval at the base of the zone. The absence of any *Distephanus stauracanthus* or well-developed *Dictyocha pulchella*, which characterize the upper *C. triacantha* Zone at the base of Hole 572D, also support an assignment of the Hole 575A assemblages to the lower part of the zone.

A somewhat higher stratigraphic level within the zone, with more diversity, is preserved in a thick (116 m) section at Hole 572D. A distinctive acme of short-ranging,

Table 3. Occurrences (%) of early Miocene silicoflagellates in samples from Hole 575A.

Zone	Core-Section, interval (cm)	Sub-bottom depth (m)	Total specimens	*Corbisema triacantha*	*Dictyocha brevispina ausonia*	*D. brevispina brevispina*	*D. fibula*	*D. pons*	*D.* sp. cf. *D. pulchella*	*Distephanus crux crux* s. ampl.	*D. crux parvus*	*D. crux scutulatus*	*D. hannai*	*D. schauinslandii*	*D. speculum paradus*	*D.* sp. cf. *D. speculum patulus*	*D. stradneri*	*D. stradneri* var. *grandis*	*Mesocena elliptica*	*M. elliptica* var. *rhomboidea*	*Naviculopsis biapiculata* s. ampl.	*N. constricta*	*N. constricta* (semibarred)	*N. contraria*	*N.* sp. aff. *N. contraria*	*N.* sp. aff. *N. lacrima*	*N. lata*	*N. lata* (narrow)	*N. navicula*	*N. obtusarca*	*N. obtusarca* var. *acicula*	*N. ponticula*	*N. ponticula spinosa*	*N.* spp.
Corbisema triacantha	1,CC	99	50		54	20		4	18	4																							
	2,CC	102	18	X	⊗					X		X	X																				
	3,CC	105	7				X				X	⊗			X																		
	4,CC	110	100			1				43		56																					
	5,CC	114	50	2		2				70		14			8																		
Naviculopsis ponticula	6,CC	119	100	8						8		30			20							1									3	30	
	7-2, 42–43	121	50							4		70			16				6												4		
	7-3, 24–25	122	100	3							1	56			17					4											19		
	7,CC	123	50							6		42			16					20											8	8	
	8-1, 42–43	124	24									X			X				X	X											⊗		
	8-2, 42–43	125	50							4					28				2	36				24							6		
	8,CC	126	200			1				3	1				9									87									
	9-2, 42–43	127	100							2	2	1			25		1							68					1				
	9,CC	128	300								1	9			2					22				65		<1							
	10-2, 42–43	129	100							3		4			1									75		8				8			1
	10-3, 42–43	130	50							4					2																		
	10,CC	132	30								X	X			X														70	24			
	11-3, 24–25	134	100			2					1	28		2	2		1			X				X			X			⊗	X	X	
	11,CC	136	100							1	1	23										1					9			7	3	36	8
	12,CC	139	100							1		83		10	4													1	1			72	
—	13,CC	143	10						X			⊗																				1	
Naviculopsis lata	14,CC	146	100									1			27						33	1					7	23					
	15,CC	149	50		2	18						10			22						30					1		8					8
	16,CC	152	50			16						10			4						4				14		48						8
	17,CC	154	300			6						36		2	8						34			1			11	3		2			2
	18,CC	157	100									4		40	12						4						33	6					
	19,CC	161	100							1					25	3					17						40	14					
	20,CC	165	12			X									X	X											⊗						
Naviculopsis biapiculata	21,CC	169	80							1					9						65	20	3										2
	23,CC	175	100			2				1					7						6	53	20										11
	27,CC	188	9			⊗										X																	
	29,CC	194	17		X	X										⊗																	
	33,CC	208	27												X	X		⊗															

Note: For samples where silicoflagellates are too sparse for meaningful percents, presence (X) and predominance (⊗) are shown by symbols. See Table 2 for comparisons of relative paleotemperature values (*Ts*).

Table 4. Late and middle Miocene silicoflagellate biostratigraphy, relative paleotemperature values (*Ts*), and percent distribution of various genera and morphologic subgroups, with remarks on significant occurrences for Hole 572D.

Age	Zone or Subzone		Core-Section, interval (cm)	Sub-bottom depth (m)	Total specimens	*Ts* value	Generic percents								Noteworthy occurrences
							Corbisema	*Dictyocha*	*Distephanus* (quadrate)	*Distephanus* (nonquadrate)	*Mesocena* (quadrate)	*Mesocena* (nonquadrate)	*Naviculopsis*	*Octactis*	
late Miocene	*D. fibula*		1,CC	156	300	86		85	1	15					
			2,CC	170	300	93		93		7					No *Dictyocha pulchella*
			3,CC	180	300	91		91		9					
			4,CC	189	300	84		84		16					
			5-3, 70-72	193	300	53		52	2	46					*Distephanus speculum tenuis* 38% acme
			5-4, 70-72	194	300	32		32		67					
			5,CC	199	300	56		56		45					Fibuloid ≫ asperoid *Dictyocha*
			6-5, 50-52	202	300	37		37		63					
			6,CC	205	300	30		30		70					First *Dictyocha longa*
	D. brevispina		7-1, 50-52	209	300	61		61		39					
			7,CC	218	300	82		82		18					Asperoid *Dictyocha* predominant
			8,CC	227	300	65		65		34					First *Distephanus speculum tenuis*
			9-3, 50-52	231	300	74		74		26					Fibuloid ≫ asperoid *Dictyocha*
			9,CC	232	300	74		74		26		<1			Asperoid *Dictyocha* predominant
			10-2, 50-51	239	300	60		60		40					
			10-4, 50-52	242	300	32		32		68					
			10-6, 50-52	245	300	43		42	1	57					
			10,CC	246	300	64		64	<1	35		<1			
			11-1, 50-51	247	300	52		52		48		<1			
			11-4, 50-52	250	300	42		40	3	56		1			*Mesocena circulus* 1%
			11,CC	256	300	44		44	<1	54		1			
			12-2, 50-52	258	300	36		36		63		1			
			12,CC	262	300	51		51		48		<1			<1% pentagonal *Distephanus*
			13-4, 50-52	270	300	88		86	3	11		<1			5% pentagonal *Distephanus*
			13,CC	272	300	78		78		22		1			7% pentagonal *Distephanus*
			14-2, 50-52	277	50	96		96		4					Dilution by diatom *Thalassiothrix*
			14,CC	282	300	68		68		32					*Dictyocha pulchella* predominant
			15-1, 50-52	285	300	58		18	80	1					Low diversity
			15,CC	288	300	85		81	7	12					*Dictyocha pulchella* predominant
			16,CC	303	300	79		79	<1	21					
			17-1, 50-52	304	300	72		71	1	28					
			17,CC	306	300	89		89		11					Consistently shaped *Dictyocha pulchella* predominant
			18-1, 50-52	313	300	81		81		19					No fibuloid *Dictyocha*
			18,CC	321	300	63		62	2	36					
			19,CC	326	300	83		74	17	8	<1	<1			
			20,CC	335	300	92		91	2	7					
middle Miocene		*D. stauracanthus*	21,CC	349	300	88	4	76	15	5	1				
			22,CC	355	300	80	14	54	23	9		1			*Dictyocha pulchella* predominant
			23,CC	369	200	75	12	41	44	3		1			*Distephanus stauracanthus* 5%, top. Two *D. polyactis*.
			24,CC	379	300	77	3	52	38	1	5	2			
			25,CC	389	300	95	8	82	9	1					
			26,CC	397	300	71	18	28	49	5					*Dictyocha pulchella* predominant
	C. triacantha	—	27,CC	408	300	94	18	69	12	1	1				First *Distephanus stauracanthus* 14%
			28,CC	415	300	82	38	34	19	6					
			29,CC	424	100	98	5	92	1	2					No fibuloid *Dictyocha*
			30,CC	434	200	99	22	75	4	1					Deflandroid *Dictyocha pulchella* 38%
			31,CC	444	100	87	39	44	7	10					Deflandroid *Dictyocha pulchella* 1%
			32,CC	454	200	98	2	96		3					
			33,CC	465	100	100	3	97							Equal numbers of asperoid and fibuloid *Dictyocha*

Note: Silicoflagellate data support the correlation between the top of Hole 572D (Core 1) and the base of Hole 572A (Core 17); see Table 5.

deflandroid *Dictyocha pulchella* in Sample 572D-29,CC accounts for 38% of the assemblage (Table 4). This value approaches 41%, the maximum recorded, in the *Corbisema triacantha* Zone of DSDP Site 543 northeast of Barbados in the tropical North Atlantic (Bukry, in press b).

The section at Hole 572D is distinguished by a thick *Distephanus stauracanthus* Subzone occupying the top 48 m of the zone. *Distephanus stauracanthus* is a persistent meager (5%) to common (14%) member of the assemblages in Cores 572D-22 to 572D-26. An indication that the phenotypic shift from apical ring dominance in early populations of *D. stauracanthus* to apical bar dominance in later populations could be of stratigraphic use for eastern Pacific Site 470 (Bukry, 1981a) is only partly evident at Hole 572D. Ring specimens predominate in Cores 572D-22 and 572D-26 (Plate 3, Fig. 6), whereas bar specimens predominate in the intervening Cores 572D-23 to 572D-25, gainsaying a consistent, one-way shift at this oceanic site.

Dictyocha brevispina Zone

The assemblages between the extinction of *Corbisema* and the appearance of *Dictyocha longa* are characterized at Hole 572D by low diversity, asperoid-bar dominance within *Dictyocha*, and the predominance of *Dictyocha pulchella* among asperoid *Dictyocha* (often exceeding 90%) (Table 4). Aside from a mid-zone cool-

ing marked by the entry of sparse *Mesocena circulus* into the assemblages, there are few stratigraphically significant changes.

Dictyocha fibula Zone

The first *Dictyocha longa* of Hole 572D defines the base of the *Dictyocha fibula* Zone and coincides with a locally permanent change from asperoid- to fibuloid-bar dominance in *Dictyocha* (compare Martini, 1971). The lower zonal assemblages of Hole 572D are characterized by low diversity, persistent *Distephanus speculum tenuis*, the appearance of *Dictyocha longa* var. *paxilla* in Sample 572D-2,CC, and the scarcity or absence of *D. pulchella* in Cores 572D-1 to 572D-3 (Tables 4 and 5). Similar basal assemblages from Cores 16 and 17 of Hole 572A suggest correlation between the two holes at this interval. The best evidence of correlation is the predominance of *D. longa*, presence of *D. speculum tenuis*, and decline of *D. pulchella*. The paleotemperature correlation is also supportive of stratigraphic occurrences.

The lower interval of the zone in Cores 15 to 17 of Hole 572A, below the *Dictyocha neonautica* Subzone, contains persistent *D. longa*, *D. longa* var. *paxilla*, and *Distephanus speculum tenuis* (Table 5). A distinct increase in *Distephanus* in Core 572A-15 suggests that the stratigraphic appearance of *Dictyocha neonautica* at the top of the core is related to a cool-water event.

Only two closely spaced samples contain *Dictyocha neonautica* Subzone assemblages. A possibly compressed section is indicated by the dominance of *D. neonautica*, which characterizes the lower part of the subzone, in Sample 572A-15-1, 68–69 cm, and by the contrasting dominance of younger *D. neonautica* var. *cocosensis*, just above in Sample 572A-14,CC. Both samples contain fibuloid *Dictyocha*, but the asperoid *D. brevispina*/*D. pulchella* group is very sparse (< 1 to 3%). This relationship suggests that *D. neonautica* filled the asperoid niche at Hole 572A.

The *Dictyocha pulchella* Subzone is not well defined at Hole 572A, because of the sporadic and sparse occurrence of *Dictyocha pulchella*. *D. brevispina* predominates among asperoid *Dictyocha*.

Dictyocha angulata, a guide fossil for the *Dictyocha angulata* Subzone, occurs in Cores 7, 9, and 10 of Hole 572A, but is most abundant at the top of the subzone in Core 7. A minor, rarely encountered species, *Dictyocha orbiculata*, occurs only in Sample 572A-7,CC (Table 5). This provides a local horizon correlation with Sample 77B-6-5, 100–101 cm, where *D. orbiculata* was first described (Ling, 1977).

Fibuloid *Dictyocha* species, including *D. longa* var. *paxilla*, *D. perfecta*, and *D. perlaevis*, dominate the assemblages at the top of the *D. fibula* Zone in Cores 572A-6 and 572A-7. No particular morphologic type is diagnostic for this interval between the last *D. angulata* and the first *D. flexatella* and *D. ornata africana* or *D. ornata ornata*.

Dictyocha stapedia stapedia Zone

The late Pliocene silicoflagellate guide species *Dictyocha flexatella* and the *D. ornata* group (Bukry, 1982a) occur in close order in Samples 572A-6-1, 66–67 cm and 572A-5,CC, and indicate the base of the *Dictyocha ornata ornata* Subzone. Early *Dictyocha stapedia stapedia*, which first occurs in Sample 572A-6-3, 66–67 cm, is a consistent member of assemblages in Sample 572A-6-1, 66–67 cm and above. The *D. ornata* group is sparse and sporadic, but the companion species *D. flexatella* is more ubiquitous, although it is abundant (37%) only in Core 572A-5 (Table 5). *Dictyocha calida calida* and *Distephanus mesophthalmus* occur in the top sample of the *D. ornata ornata* Subzone. A similar occurrence in Sample 157-11,CC, recovered to the east, has the conjunction of these two species plus *D. ornata africana*, signifying the stratigraphic potential of short-term conjunctions for correlation in the eastern equatorial Pacific. Both samples are assigned to the highest coccolith subzone of the upper Pliocene (CN12d).

The *Dictyocha delicata* Subzone of the *D. stapedia stapedia* Zone is identified in the lower part of Core 572A-3. Because *Octactis pulchra* is present in this interval with *Dictyocha delicata*, a Quaternary assignment is made. Minor occurrences of *Mesocena quadrangula* in the subzone presage the consistent presence of this species above, in the *Mesocena quadrangula* Zone.

Mesocena quadrangula Zone

The common occurrence of *Mesocena quadrangula* above the range of *Dictyocha delicata* defines the *M. quadrangula* Zone in Cores 2 and 3 of Hole 572A. *Dictyocha stapedia stapedia* is abundant, but *D. aculeata* is absent or sparse up to Sample 572A-2-3, 68–69 cm, where *D. aculeata* constitutes a third of the assemblage though *D. stapedia stapedia* (47%) still predominates.

Dictyocha aculeata Zone

At Hole 572A, *Dictyocha aculeata* is present throughout the *Dictyocha aculeata* Zone, but diversity is very low, and, aside from Sample 572A-1-5, 68–69 cm, *D. stapedia stapedia* predominates. Solution-thinning and small-sized specimens are most prominent in this zone, suggesting reduced silica and increased solution relative to DSDP Site 425, which is farther to the east (Bukry, 1980b), where higher sedimentation rates and fossil diversity are indicated in this zonal interval.

SILICOFLAGELLATE *Ts* COMPARISON

The lower Miocene silicoflagellate assemblages of DSDP Hole 575A are significant in relative-paleotemperature (*Ts*) studies, especially because of the near absence of *Corbisema*, the scarcity of *Dictyocha*, and the high abundance of *Naviculopsis*. Previous work on Pacific lower Miocene silicoflagellates at DSDP Site 495 had questioned the paleotemperature significance of *Naviculopsis* (Bukry, 1982a), because no living relatives or similarly formed taxa survived into the Quaternary and the known fossil record suggested a cosmopolitan range with greater productivity in cool regions. But the generally high abundances of *Naviculopsis* through the lower Miocene and the displacement of regular *Dictyocha* species by naviculopsoid *D. neonautica* in the upper Miocene (Hole 572A) show that *Naviculopsis* and *Navicu-*

Table 5. Late Miocene to Quaternary silicoflagellate biostratigraphy, relative paleotemperature values (*Ts*), and percent distribution of various genera and morphologic subgroups, with remarks on significant occurrences for Hole 572A.

Age	Zone or Subzone		Core-Section, interval (cm)	Sub-bottom depth (m)	Total specimens	*Ts* value	Generic percents							Noteworthy occurrences
							Corbisema	*Dictyocha*	*Distephanus* (quadrate)	*Distephanus* (nonquadrate)	*Mesocena* (quadrate)	*Mesocena* (nonquadrate)	*Naviculopsis*	*Octactis*	
Quaternary	*D. aculeata*		1-1, 105-106	1	300	100		100							*D. stapedia stapedia* 98%
			1-3, 67-68	4	300	99		99						1	
			1-5, 68-69	7	300	99		99						1	*D. aculeata* > *D. stapedia stapedia*
			1,CC	9	200	96		96						4	*D. stapedia stapedia*
			2-1, 68-69	10	300	99		99						1	*D. stapedia stapedia* 84%
	M. quadrangula		2-2, 68-69	12	300	96		94			4			2	*D. stapedia stapedia* and last *M. quadrangula*
			2-3, 68-69	13	300	95		90			10			<1	*D. stapedia stapedia* > *D. aculeata*
			2-4, 68-69	15	300	87		74			26			<1	
			2-5, 68-69	16	300	75		54	<1	2	42			2	
			2-6, 68-69	18	300	73		46		<1	53			<1	*D. stapedia stapedia*
			2,CC	19	300	71		44		2	53			1	
			3-1, 68-69	20	300	66		35		3	61			<1	*D. stapedia stapedia* 98% of *Dictyocha*
			3-2, 68-69	21	300	89		83		2	12			4	
	D. stapedia	*D. delicata*	3-3, 16-17	22	300	93		88		1	9			3	*Dictyocha delicata* 9%
			3-4, 68-69	24	300	98		97	<1	2				<1	*D. delicata* 23%
			3-5, 68-69	26	300	92		92		8				1	*D. delicata* 8%
			3-6, 68-69	27	300	93		93	<1	7					*D. delicata* 39%
			3,CC	28	300	94		93		6	1			<1	
late Pliocene		*D. ornata ornata*	4-3, 23-24	32	300	93		88	10	2					*Dictyocha calida calida* and *Distephanus mesophthalmus*
			4,CC	36	300	97		97		3		<1			*Dictyocha flexatella* 4%, top
			5-3, 16-17	39	300	91		91		9					*D. flexatella* 37%; no *D. ornata* group.
			5,CC	45	300	92		92		8		<1			*D. brevispina* 1%, top. Two *D. ornata africana*.
			6-1, 66-67	46	300	88		88		12					*D. flexatella* 1%
early Pliocene	*D. fibula*	—	6-3, 17-18	49	300	76		76		24					*Dictyocha* more equant than elongate, solution thinning.
			6-3, 66-67	50	300	93		93		7		<1			Solution thinning
			6-5, 66-67	53	300	79		79		21					*Dictyocha longa* var. *paxilla* predominant
			6,CC	55	300	80		80		20					Low diversity (4 species), no asperoid *Dictyocha*
			7-2, 66-67	57	100	89		89	1	10					
			7-3, 19-20	58	300	93		92	2	17					No asperoid *Dictyocha*
		D. angulata	7-4, 66-67	60	300	90		90		10					*Dictyocha angulata* ~ 50%, no *D. pulchella*
			7,CC	64	300	81		80	1	19		<1			*Dictyocha orbiculata* 1%
			8-3, 16-17	67	300	58		57	1	41		1			Small *Distephanus speculum speculum*
			8-3, 66-67	68	300	60		59	1	39		1			
			8,CC	72	300	45		45		43		12			No *Dictyocha pulchella*, only two asperoid specimens
			9-3, 66-67	76	300	61		61	<1	39		<1			
			9,CC	82	300	90		87	6	6		<1			*D.* sp. cf. *D. angulata*
			10-3, 66-67	85	300	72		72	<1	18		10			*D.* sp. cf. *D. angulata*; small *Mesocena circulus*.
		—	10,CC	91	300	56		51	6	40	3				Only one asperoid *Dictyocha*
			11-3, 67-68	95	300	44		40	5	53	3				Low diversity
			11-5, 67-68	98	300	83		82	<1	18	<1				
		D. pulchella	11,CC	101	300	82		82	<1	17					
			12-2, 68-69	103	300	67		66	2	32					
			12,CC	110	300	52		51	2	46					
			13-3, 66-67	114	300	49		45	1	47	6				
			13,CC	119	300	52		48	2	43	7				One *Distephanus polyactis*
			14-3, 18-19	122	300	60		59	1	39	1				
		D. neonautica	14,CC	128	300	74		73	1	26					*Distephanus xenus* 6%
			15-1, 68-69	129	300	66		66		33					*Dictyocha neonautica* var. *cocosensis* 63%
late Miocene		—	15-3, 19-20	132	300	44		43	1	56					*D. neonautica* 38%
			15,CC	137	300	29		28	2	69	<1				*Distephanus speculum tenuis* 3%, top
			16-2, 66-67	139	300	71		71	<1	29					*D. speculum tenuis* 17%
			16-3, 19-20	140	300	81		80	2	18					*D. speculum tenuis* 7%
			16,CC	145	300	88		83	9	8					*D. speculum tenuis* 5%
			17,CC	154	300	84		83	2	15					*D. speculum tenuis* 1%
															D. speculum tenuis 3%

Note: Silicoflagellate data support the correlation between the base of Hole 572A (Core 17) and the top of Hole 572D (Core 1); see Table 4.

lopsis-like forms occupied a paleotemperature niche similar to that of *Dictyocha* at tropical Sites 572 and 575.

New *Naviculopsis* paleotemperature information is indicated by the absence of the stratigraphic guide species *Naviculopsis quadrata* at Hole 575A. The first *N. quadrata* can be used to distinguish a zonal interval above the *N. lata* Zone (Bukry, 1981b). To account for its absence, sites at high latitude (Site 338) and low latitude (Site 369) in the Atlantic were compared. *Naviculopsis quadrata* was quantitatively more abundant than *N. lata* at high latitude, whereas at low latitude *N. lata* far outnumbered *N. quadrata*. Therefore, the very high abundances of *N. lata* (up to 48%) at Hole 575A, and the complete absence of *N. quadrata*, show that the distribution of certain species within *Naviculopsis* can probably be used effectively for relative-paleotemperature comparisons.

Calculation of *Ts* values for Hole 575A yields fluctuations of considerable amplitude in the lower Miocene, with values from *Ts* 44 to *Ts* 96 (Fig. 2). *Naviculopsis*

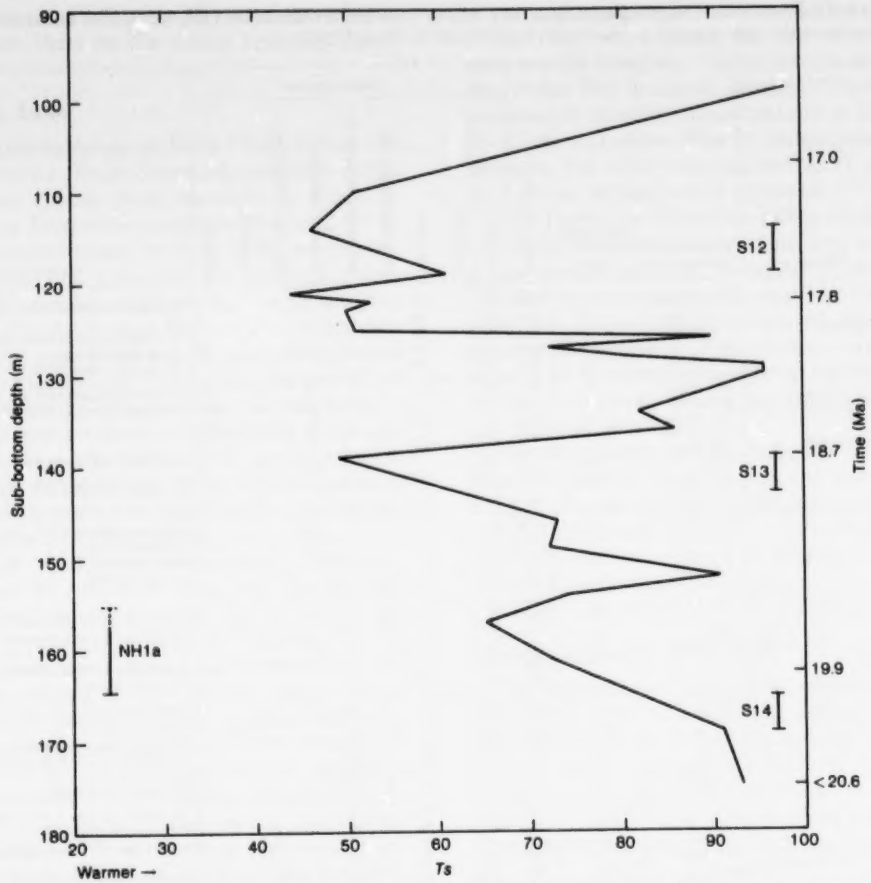

Figure 2. Silicoflagellate relative paleotemperature curve for Hole 575A samples. The chronology shown is based on diatom ages (Ma); see Barron (this volume). Silicoflagellate data for the curve are available in Table 3. Useful silicoflagellate events: S12 = last *Naviculopsis ponticula ponticula;* S13 = first *Naviculopsis ponticula ponticula;* S14 = first *Naviculopsis lata.* A deep-sea hiatus (NH1a) interval, representing a cool-water event beginning at 20.0 Ma (Keller and Barron, 1983), is shown.

was counted as warm, filling the niche occupied by *Dictyocha* in younger Neogene strata. Surprisingly, the cool troughs within Cores 7, 12, and 18 of Hole 575A are not the levels of maximum abundance for cool-water indicator *Distephanus* (hexagonal). Instead, these *Ts* minima are dominated by the temperate-water indicator *Distephanus* (quadrate). Because the *Ts* paleotemperature model was designed for middle Miocene and younger assemblages (Bukry, 1981a), it is possible that the paleotemperature significance of older species in the genera cited was not the same. In other words, Oligocene and early Miocene *Distephanus* (quadrate) could have been an indicator of cool water, instead of temperate, whereas *Distephanus* (hexagonal) could have been a temperate- and not a strictly cool-water indicator. There is some evidence supporting such a paleotemperature transition, beyond the record at Hole 575A, in the abundances of *Distephanus* (quadrate versus hexagonal) at different latitudes during the Oligocene and early Miocene. Quadrate specimens equal or outnumber the hexagonal at high-latitude DSDP Holes 173, 267, 274, 278, 280A, 328B, 338, and 407. Hexagonal specimens of *Distephanus* achieved continuing dominance over quadrate first at higher-latitude sites, such as Site 278 (Bukry, 1975) in the early Miocene, and somewhat later at lower-latitude sites, such as nearshore Site 470 in the late Miocene and offshore Hole 572D in the late middle Miocene (see Table 4). Therefore, hexagonal *Distephanus* can be the cool-water indicator for the late Miocene to Holocene, but for the Oligocene and part of the early Miocene, quadrate *Distephanus* and probably *Mesocena* may be the better cool-water indicators.

Corbisema has been used as a warm-water indicator because of its great abundance during the Paleocene and Eocene thermal highs and subsequent extinction at the beginning of a sharp thermal drop in the middle Miocene (see Shackleton, 1982). However, the last few species of the genus in the Miocene are nearly absent at tropical Hole 575A. The record and abundance at Hole 572D are better, with some values almost as high as the 58% recorded at Site 407 between Iceland and Greenland. Other high abundances of *C. triacantha* appear to

occur at temperate coastal sites, such as DSDP Sites 415 and 470 (Bukry, in press b), where the maximum values are 48 and 23%, respectively. By contrast, the values for *Corbisema* at cool-water sites such as DSDP Sites 173 and 278 are very low, from 0 to 12% and from 0 to 3%, respectively. Also, at DSDP Site 407, up to 17% of the *Corbisema* specimens belong to *C. flexuosa*, which is also present at high-latitude Site 278 but missing at most low- or mid-latitude sites.

Although temperature seems to affect the abundance of *Corbisema*, other fertility-enhancing conditions, such as nitrogen or phosphorus enrichment, must have contributed to the high abundances at Sites 407 and 415 in the Atlantic.

A major cooling of *Ts* relative-paleotemperature values in the lower Miocene of Hole 575A occurs from the middle of the *Naviculopsis ponticula* Zone up into the lower *Corbisema triacantha* Zone in Cores 4 to 9. This cool portion of the *Ts* curve corresponds to an interval of increased foraminifer dissolution (see Fig. 2 and site chapter for Site 575) and deep-sea hiatus NH1b (Barron and Keller, 1982; Keller and Barron, 1983). The association of effects suggests a global cooling event corresponding to a level near the extinction of *Naviculopsis* at the base of the *Corbisema triacantha* Zone.

Quadrate *Distephanus* have two levels of maximum abundance in the lower Miocene at Holes 575A and 495. The samples just above the base of the *Naviculopsis ponticula* Zone and just above the top have the highest percentages (84 to 99%) recorded for quadrate *Distephanus* at Hole 575A. At Site 495, the sampling interval was less detailed, but a similar occurrence pattern for quadrate *Distephanus* is recorded, showing the highest percentages (81 and 82%) at the boundaries of the *N. ponticula* Zone.

The *Ts* relative-paleotemperature curves for the *Naviculopsis ponticula* Zone at Holes 575A and 495 show the same major trends (Figs. 2 and 3). There are cool values of *Ts* = 49 to 53 for the upper and lower parts of the zone, bracketing a pronounced warm peak (*Ts* = 88 to 96) in the middle. This close correspondence between biostratigraphic and paleotemperature records at Holes 575A and 495 indicates a much closer proximity of these sites or much more uniform conditions in the eastern Pacific during the early Miocene.

Oxygen-isotope thermometry from benthic foraminifers shows a steep decline in paleotemperatures of world oceans from about 15 Ma to 8 Ma (Shackleton, 1982). The long-term record of silicoflagellate relative-paleotemperature values, *Ts*, for Holes 572A and 572D encompasses the last 15 m.y. of the Cenozoic and shows a fluctuating decline (major cool events progressively cooler) from about 15 Ma to 7 Ma, followed by a fluctuating increase (major cool events progressively warmer) after 7 Ma (Figs. 4 and 5). Within the interval of declining paleotemperature, from the *Corbisema triacantha* Zone to the lower *Dictyocha fibula* Zone, there was a lower part below 321 m sub-bottom where lower-amplitude fluctuations prevailed, principally in the *C. triacantha* Zone. The upper part of the decline, mainly within the *D. brevispina* Zone, has higher-amplitude fluctuations, as the coolest points diverge further from the intervening warm points.

Comparison of the upper part of the *Ts* curve for Hole 572D to that for Hole 503A (farther east) shows corresponding cool points at about 7.3 Ma and warm points at 6.0 to 6.1 Ma. The *Ts* values of these warm points are in close agreement at *Ts* = 93 and *Ts* = 97, respectively. But the cool point at Hole 572D (*Ts* = 30) is considerably cooler than the coeval point at Hole 503A (*Ts* = 67), suggesting a greater westward—versus northward—vector of Peru Current waters or related systems. The paleotemperature contrast is evidenced by the 70% abundance of hexagonal *Distephanus* for Hole 572D, versus only 29% for Hole 503A. This paleotemperature contrast between the oceanographic regimes at the two

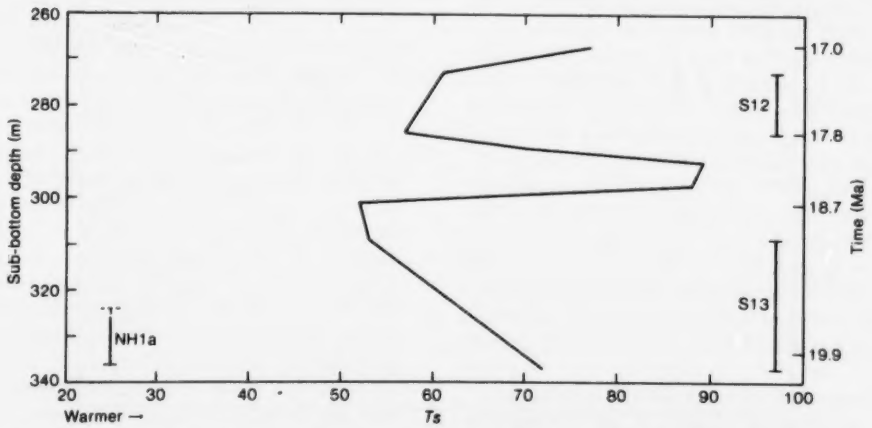

Figure 3. Silicoflagellate relative paleotemperature curve for Hole 495 samples. The chronology shown is based on diatom ages (Ma); see Barron (1983 and this volume). Silicoflagellate data for the curve are available in Bukry (1982a). Useful silicoflagellate events: S12 = last *Naviculopsis ponticula ponticula;* S13 = first *Naviculopsis ponticula ponticula.* A deep-sea hiatus (NH1a) interval, representing a cool-water event beginning at 20.0 Ma (Keller and Barron, 1983), is shown.

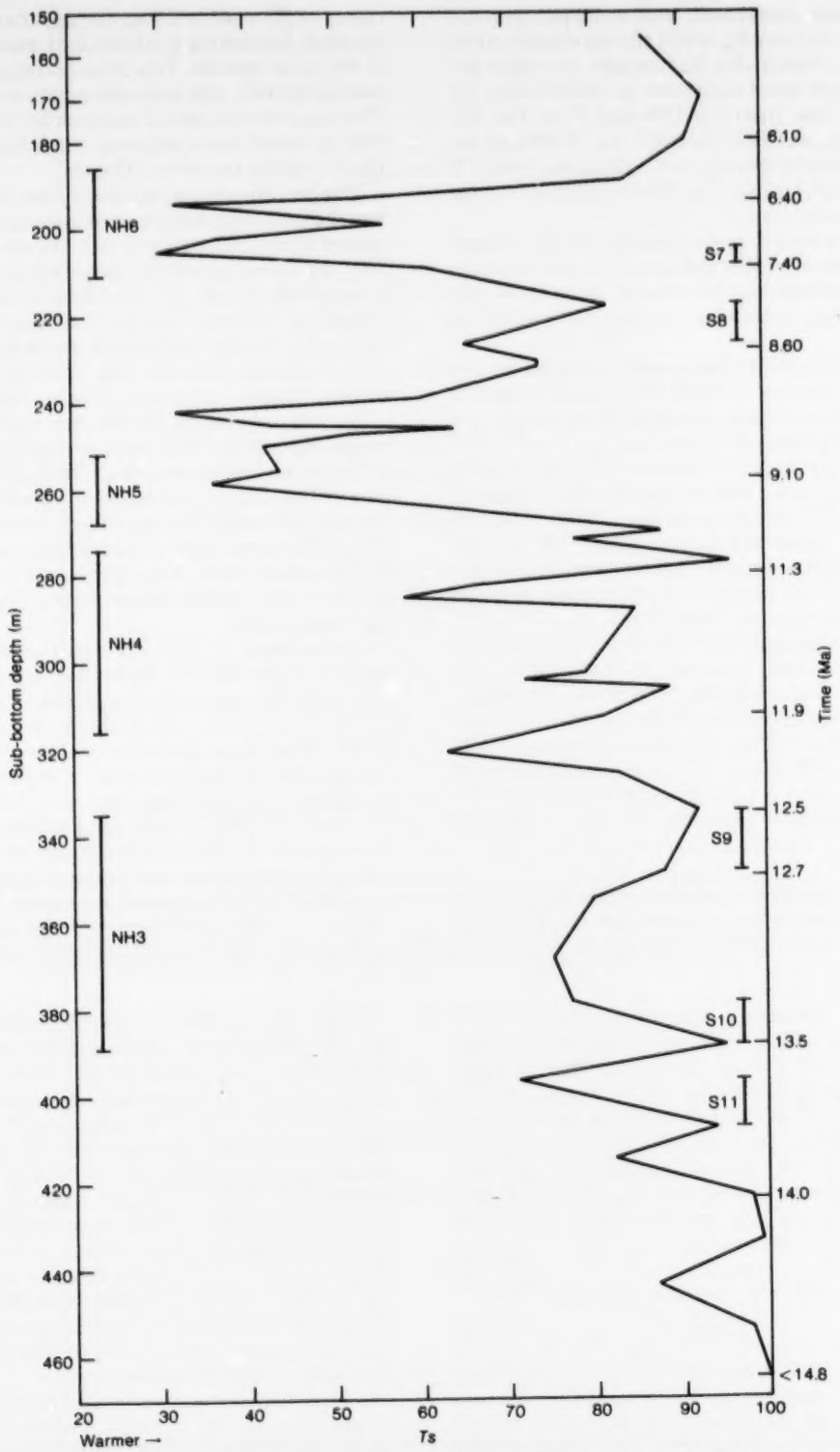

Figure 4. Silicoflagellate relative paleotemperature curve for Hole 572D samples. The chronology shown is based on diatom ages (Ma); see Barron (this volume). Silicoflagellate data for the curve are available in Table 4. Useful silicoflagellate events: S7 = first *Dictyocha longa;* S8 = first *Distephanus speculum tenuis;* S9 = last *Corbisema triacantha;* S10 = first *Mesocena circulus;* S11 = first *Distephanus stauracanthus*. Deep-sea hiatus (NH3 to NH6) intervals, representing cool-water events (Keller and Barron, 1983), are shown.

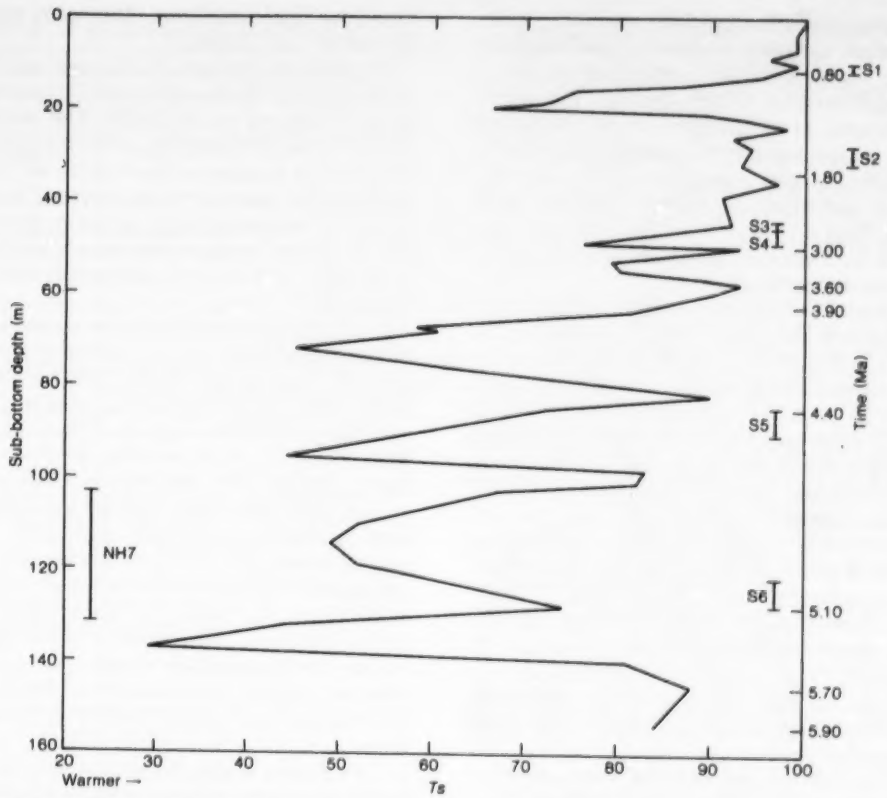

Figure 5. Silicoflagellate relative paleotemperature curve for Hole 572A samples. The chronology shown is based on diatom ages (Ma); see Baldauf (this volume) and Barron (this volume). Silicoflagellate data for the curve are available in Table 5. Useful silicoflagellate biostratigraphic events: S1 = last *Mesocena quadrangula;* S2 = first *Octactis pulchra;* S3 = first *Dictyocha ornata africana;* S4 = first *Dictyocha stapedia stapedia;* S5 = first *Dictyocha angulata;* S6 = last *Dictyocha neonautica* var. *cocosensis.* A deep-sea hiatus (NH7) interval, representing a cool-water event or events between 4.7 and 5.2 Ma (Keller and Barron, 1983), is shown.

locations persisted for a considerable period because cool-water indicator *Mesocena circulus* is recorded at Hole 572D but missing from Hole 503A.

The Miocene/Pliocene boundary warm peak (about 5.0 Ma) is present at Holes 572A and 503A, but like the 6.0-Ma warm peak the Hole 572A assemblage yields a cooler (*Ts* = 74) value than that of Hole 503A (*Ts* = 92). A nearly 20-point difference is also seen for the *Dictyocha pulchella/Dictyocha angulata* cool peak at about 4.5 Ma in Core 11 of Hole 572A (*Ts* = 44) and Cores 24 to 27 of Hole 503A (*Ts* = 68). The following *Dictyocha angulata* warm peak (3.4 to 3.8 Ma) occurs in the middle of Core 7 of Hole 572A, and the *Ts* value of 93 is nearly identical to the correlative *Ts* value of 97 for Hole 503A. Above this level the values are very similar. Therefore, between 7.3 and 3.8 Ma the *Ts* values at Hole 572A gradually changed from much cooler (Δ37) to cooler (Δ24) to nearly identical (Δ4), at fairly high values in the 80s and 90s. A weakening of the westward component of the Peru Current, combined with the oceanic effects resulting from the closing of the Panamanian Land Bridge, could have contributed to this convergence of relative-paleotemperature records.

A possibly analogous modern feature is the eastern equatorial tongue of cool surface waters, below 21°C, that in July and August extends as far west as Site 572 (Bernstein and Morris, 1983). The tongue is maintained by westward advection of cool water from coastal South America and by locally wind-driven equatorial upwelling (Bernstein and Morris, 1983). Site 503 lies slightly north of this cool tongue, in the latitudinal band of warmest temperatures, where isotherms are compressed and rise as high as 27°C. Shifting of these temperature zones in response to oceanographic changes could be responsible for the exceptional contrast in cool and warm values portrayed by the *Ts* relative-paleotemperature curve.

Above the *Dictyocha angulata* warm peak, the high amplitudes (*Ts* = Δ30 to Δ50) of the upper Miocene and lower Pliocene relative-paleotemperature fluctuations at Hole 572A are remarkably diminished to amplitudes of less than *Ts* = Δ24, typically less than *Ts* = Δ5. The

major event in the upper Pliocene and Quaternary is the acme and extinction of *Mesocena quadrangula* at about 1 Ma. Although the acme of *M. quadrangula* occurs at low latitude and is missing at high latitude, the paleotemperature character of *M. quadrangula* is considered to be temperate at low latitude because an upper Miocene bloom of this species coincides with locally elevated numbers of cool-water *Distephanus speculum speculum* at DSDP Sites 157 and 504. This supports the presumption that later occurrences of the same morphology reflect similar temperature trends.

Owing to a general decline of cool-water indicator *D. speculum speculum* in the Quaternary of tropical areas, *M. quadrangula* is thought to indicate relatively cool or temperate paleotemperatures. The few *D. speculum speculum* at Hole 572A in the *M. quadrangula* acme have a distribution of 2 specimens and 5 specimens just below the acme, 9 specimens at the acme, and 5 specimens, followed by 0 specimens, above, in the interval of the decline of *M. quadrangula* to extinction.

The coolest value (*Ts* = 66) for the Quaternary is assigned to the *Mesocena quadrangula* acme at Hole 572A. Correlative *M. quadrangula* acme *Ts* values are *Ts* = 65 at Site 157 and *Ts* = 63 at Site 504. Silicoflagellates indicate close similarity in paleotemperature response for the eastern tropical Pacific region at that time.

In the Atlantic, an especially cool event, producing 63% *D. speculum speculum*, coincides with a reduced acme of *M. quadrangula* at Site 397 (*Ts* = 28). Just above the acme at Site 397, the value is more similar to that for the Pacific, at *Ts* = 69 (Bukry, 1979b).

The general trend of the upper Cenozoic eustatic sea-level curve, constrained by Midway Island stratigraphy (Major and Matthews, 1983), shows a long-term decline for the Pacific between 13 and 6.7 Ma. Although the Midway evidence reduces the amplitudes of eustatic sea-level fluctuation (Major and Matthews, 1983), the principal times of rapid change of sea level (Vail et al., 1977) are corroborated. The end of a highstand of sea level at about 13 Ma corresponds to a warming trend (*Ts* = 76 to 92) on the silicoflagellate relative-paleotemperature curve for Cores 572D-23 to 572D-20, at the base of the *Dictyocha brevispina* Zone. A sharp decline in *Ts* values from *Ts* = 96 to *Ts* = 36 occurs between about 11.3 and 10.7 Ma, and is the first major cooling event within the late Miocene. This was also the time of one of the maximum declines of eustatic sea level at about 11 Ma, and indicates that marine temperature response (measured by silicoflagellate *Ts*) to rapid sea-level changes is similarly rapid.

After the maximum lowering at about 6.7 Ma, the eustatic sea level has an average upward trend that is overlain by higher-frequency oscillations. The general average trend for *Ts* values is also inflected upward between 6 and 7 Ma toward warmer *Ts* values at Site 572. A broad warming across the Miocene/Pliocene boundary has been shown by *Ts* values for Holes 503A and 504 in the eastern Pacific and for Hole 552A in the North Atlantic. At Hole 572A this warming is abbreviated near a stratigraphically compressed section that reduced the upper and lower *Dictyocha neonautica* Zone to a short 1-m section.

Correlations between the Pliocene and Pleistocene eustatic sea-level fluctuations and *Ts* fluctuations are less positive than for the Miocene. The sea-level decline at about 3.0 Ma is distinguished as a major event comparable to the maximum lowering at 6.7 Ma. Many biostratigraphic events, such as the first *Dictyocha flexatella* and *D. ornata africana*, occur at about 3.0 Ma. It is one of the last times of depressed *Ts* values (*Ts* = 76) at Hole 572A, following the *Dictyocha angulata* warm peak (*Ts* = 93).

Comparison of the *Ts* relative-paleotemperature curve of silicoflagellates to the sequence of Neogene deep-sea hiatuses (Barron and Keller, 1982; Keller and Barron, 1983) shows good correlation between cool *Ts* minima and hiatus intervals such as NH1a, NH3, NH6, and NH7 (Figs. 2 to 5). Also, some of the major declines in Pacific eustatic level (Major and Matthews, 1983) occur at the same times as *Ts* minima and deep-sea hiatuses, such as NH3 and Eustatic Event (EE) 1 after 13 Ma, and NH6 and EE3 at about 6.7 Ma (Fig. 4). The rising sea level at EE5 correlates with the warming *Ts* values from about 5.2 Ma to 5.1 Ma at Hole 572A (Fig. 5). Such correlations suggest that paleoceanographic changes linking cool paleotemperatures, lowered sea levels, and deep-sea hiatuses may be detected in the *Ts* relative-paleotemperature record of shallow-dwelling siliceous phytoplankton such as silicoflagellates.

The paleoecologic signal to be derived from absolute and relative comparisons of silicoflagellate *Ts* values is significant enough to consider such information a useful addition to other chemical and physical measures for paleoceanography. The silicoflagellate photosynthetic habitat in surface waters and the temperature-sensitive variation in generic proportions make silicoflagellates valuable indicators for changes in marine paleotemperature in areas where their productivity has been sufficient.

SYSTEMATIC PALEONTOLOGY OF NEW TAXA

Genus *DICTYOCHA* Ehrenberg, 1837

***Dictyocha nola* Bukry, n. sp.**
(Plate 2, Figs. 1–5)

Description. *Dictyocha nola* has a moderate-sized, generally wide, oblong basal ring with slightly protruding minor-axis portals and short spines. The outer margins of portals are squared off, and the basal pikes are close to the strut junctions. The short to moderate apical bar is oriented along the minor axis of the basal ring. A few specimens have apiculate basal rings or lack minor-axis spines.

Remarks. *Dictyocha nola* is distinguished from other taxa with the same structural elements, such as *Dictyocha brevispina ausonia*, *D. brevispina brevispina*, and *D. pulchella*, by a combination of different proportions. The flattened ends of the major-axis portals (resembling the top of a large bell) and the subparallel sides of the portal yield an oblong outline missing in the other taxa. The larger, protruding, minor-axis portals and basal pike location distinguish *D. nola* from *D. brevispina ausonia*. The other asperoid taxa have a more rhomboid than oblong outline. The squared-off portals of *D. nola* are an effect similar to that seen in the smaller, fibuloid species *D. angulata*, which occurs just above *D. nola* in Cores 7 to 10 of Hole 572A.

Occurrence. *Dictyocha nola* accounts for 20% of the *Dictyocha* specimens in Sample 572A-11-3, 67–68 cm (95 m), which is assigned to the lower Pliocene *Dictyocha fibula* Zone, between 4.40 and 5.10 Ma,

according to diatom ages. It was not identified in other samples, and may represent a useful, short-lived, horizon species.

Size. Maximum inner diameter 25 to 33 μm (holotype 31 μm).

Holotype. USNM 371373 (Plate 2, Fig. 3).

Isotypes. USNM 371374 to 371377.

Type locality. Eastern equatorial Pacific, Sample 572A-11-3, 67–68 cm (95 m sub-bottom).

Genus *DISTEPHANUS* Stöhr, 1880

Distephanus stradneri (Jerkovic) Bukry var. *grandis* Bukry, n. var.

(Plate 4, Figs. 1–7)

Description. *Distephanus stradneri* var. *grandis* has a large, elongate-rhomboid basal ring and a small, slightly oblong apical ring, connected together by symmetric struts. The major-axis spines are two to four times the length of the minor-axis spines, but all spines are short. Minor-axis portals are less angular than major-axis portals because of rhomboid elongation. Elongation, measured by the ratio of major- and minor-axis inner diameters, ranges from 1.13 to 1.29, and the outer-diameter ratio (including spines) ranges from 1.30 to 1.44. Some specimens show small basal pikes next to the strut junctions.

Remarks. *Distephanus stradneri* var. *grandis* is distinguished from *D. stradneri*, including *D. pusillus* (see Bukry, 1982a), by the rhomboid elongation of the basal ring, shown by the inner-diameter ratio, which is higher (1.13 to 1.29, average 1.16) for *D. stradneri* var. *grandis* and lower (1.00, 1.04, and 1.08) for *D. stradneri* (including *D. pusillus*). The small pikes present on some *D. stradneri* var. *grandis* are absent on *D. stradneri*. The short spines may also help to distinguish *D. stradneri* var. *grandis*.

Occurrence. *Distephanus stradneri* var. *grandis* occurs in the lower Miocene *Naviculopsis biapiculata* Zone, Core 33 of Hole 575A. Ling (1977) illustrated a square-ringed *D. stradneri* from the lower Miocene of the eastern Pacific, which also has short spines but is slightly older than *D. stradneri* var. *grandis*, according to diatom correlations (Barron, 1983 and this volume), and which is probably a lineal source of the elongate evolution evidenced by *D. stradneri* var. *grandis*.

Size. Maximum inner diameter 35 to 45 μm (holotype 41 μm).

Holotype. USNM 371378 (Plate 4, Fig. 2).

Isotypes. USNM 371379 to 371384.

Type locality. Eastern equatorial Pacific, DSDP Sample 575A-33,CC (208 m sub-bottom).

Genus *MESOCENA* Ehrenberg, 1843

Mesocena elliptica (Ehrenberg) Ehrenberg var. *rhomboidea* Bukry, n. var.

(Plate 5, Figs. 1–6)

Mesocena elliptica (Ehrenberg), Bukry, 1978a, p. 698, pl. 2, fig. 16.

Description. *Mesocena elliptica* var. *rhomboidea* has a straight-sided, elongate, rhomboid-shaped basal ring with angular corners and four short, nearly equal spines at the corners. The elongation of the basal ring, measured by the ratio of major and minor axes, ranges from 1.2 to 1.5, with an average of 1.4.

Remarks. *Mesocena elliptica* var. *rhomboidea* is distinguished from *Mesocena elliptica* (see Ehrenberg, 1840, 1854) by its rhomboid basal ring with straight sides, instead of curved, elliptic, or oval basal ring. It is distinguished from *Mesocena quadrangula* by having an elongate rhomboid ring, instead of a square ring. *M. elliptica* var. *rhomboidea* is classified with *M. elliptica* because of short, nearly equant spines and stratigraphic similarities.

Locker's (1974) designation of a rhomboidal lectotype for *M. elliptica* is considered superfluous because Ehrenberg described *M. elliptica* as an elliptic form from Zante, Greece (Ehrenberg, 1840) and illustrated a group of elliptic specimens from Zante, Greece (Ehrenberg, 1854). Therefore, Ehrenberg's species concept was adequately fixed in the last century. Designation of Ehrenberg's (1854) pl. 20, fig. 44b as the lectotype for *M. elliptica* is preferred to the subsequent rhomboid specimen illustrated in 1974 by Locker.

Occurrence. *Mesocena elliptica* var. *rhomboidea* occurs in the lower Miocene *Naviculopsis ponticula* Zone in Cores 7 to 10 of DSDP Hole 575A in the Pacific and in Core 3 of DSDP Hole 370 in the Atlantic. It occurs below and with *M. elliptica* sensu Ehrenberg at DSDP Hole 575A. Therefore, the presently known range is upper lower Miocene.

Size. Maximum inner diameter 40 to 50 μm (holotype 49 μm).

Holotype. USNM 371385 (Plate 4, Fig. 1).

Isotypes. USNM 371386 to 371390.

Type locality. Equatorial Pacific Ocean, DSDP Sample 575A-8-2, 42–43 cm (125 m sub-bottom).

Genus *NAVICULOPSIS* Frenguelli, 1940

Naviculopsis obtusarca Bukry var. *acicula* Bukry, n. var.

(Plate 6, Figs. 5–9)

Naviculopsis sp. cf. *N. obtusarca* Bukry, Bukry, 1982a, p. 444, pl. 8, figs. 6, 8–10.

Description. *Naviculopsis obtusarca* var. *acicula* has a boat-shaped basal ring with narrow, protruding ends that are rounded. The apical bar is aligned with the minor axis of the ring. The lengths of the solid end-points of the ring are about equal to the maximum width of the ring opening along the minor axis. There are no spines developed, and the end points may have an oblong hyaline area oriented along the major axis.

Remarks. *Naviculopsis obtusarca* var. *acicula* is distinguished from *N. obtusarca* by the single, narrow ends of the ring, instead of the blunt or doubly pointed concave ends for *N. obtusarca*. Also, the hyaline area at the end of *N. obtusarca* var. *acicula* shows elongation along the major axis, not across it. *N. obtuscarca* var. *acicula* is distinguished from *N. ponticula* by the bowed sides of the basal ring and the protruding, long, narrow ends, and from *N. navicula* by the protruding ends with hyaline areas.

Occurrence. *Naviculopsis obtusarca* var. *acicula* occurs in lower Miocene *Naviculopsis ponticula* Zone Cores 10 and 11 of DSDP Hole 575A and in Core 32 of DSDP Hole 495. Both sources are in the eastern Pacific, on opposite sides of the East Pacific Rise, and probably represent the same or contiguous populations. Populations of *N. obtusarca* from Austria, illustrated by Stradner (1961) and Bachmann (1970), did not reveal specimens of this new variety.

Size. Maximum inner diameter 50 to 60 μm (holotype 51 μm).

Holotype. USNM 371391 (Plate 6, Fig. 5).

Isotypes. USNM 371392 to 371395.

Type locality. Eastern equatorial Pacific, DSDP Sample 575A-10-2, 42–43 cm (129 m sub-bottom).

SYSTEMATIC PALEONTOLOGY OF NEW COMBINATIONS

Genus *DICTYOCHA* Ehrenberg, 1837

Dictyocha flexatella (Bukry) Bukry, n. comb.

Dictyocha perlaevis flexatella Bukry, 1979b, p. 984, pl. 3, figs. 1–3.

AUTHORSHIP AND ILLUSTRATION REFERENCES TO PUBLISHED LITERATURE FOR CITED TAXA

Corbisema triacantha (Ehrenberg) Hanna—Bukry, 1979a
Dictyocha aculeata (Lemmermann) Dumitrică—Bukry, 1980b
D. angulata Bukry—Bukry, 1982a
D. brevispina ausonia (Deflandre) Bukry—Bukry, 1978a
D. brevispina brevispina (Lemmermann) Bukry—Bukry, 1981a
D. calida calida Poelchau—Poelchau, 1976
D. delicata (Bukry) Bukry—Bukry, 1980b
D. fibula Ehrenberg—Bukry, 1980a
D. longa Bukry—Bukry, 1982a
D. longa var. *paxilla* Bukry—Bukry, 1982a
D. neonautica Bukry—Bukry, 1981a
D. neonautica var. *cocosensis* Bukry—Bukry, 1981a
D. orbiculata Ling—Ling, 1977
D. ornata africana Bukry—Bukry, 1982a
D. ornata ornata (Bukry) Bukry—Bukry, 1982a
D. pons Ehrenberg—Bukry, 1980a
D. pulchella Bukry—Bukry, 1980a
D. stapedia stapedia Haeckel—Bukry, 1980b
Distephanus crux crux (Ehrenberg) Haeckel—Ehrenberg, 1854
D. crux parvus (Bachmann) Bukry emend.—Bukry, 1982a
D. crux scutulatus Bukry—Bukry, 1982a
D. hannai (Bukry) Bukry—Bukry, 1975
D. mesophthalmus (Ehrenberg) Haeckel—Bukry, 1982a
D. polyactis (Ehrenberg) Deflandre—Bukry, 1981a

D. schauinslandii Lemmermann—Lemmermann, 1901
D. speculum haliomma (Ehrenberg) Bukry—Bukry, 1978a
D. speculum hemisphaericus (Ehrenberg) Bukry—Bukry, 1978a
D. speculum patulus Bukry—Bukry, 1982a
D. speculum speculum (Ehrenberg) Haeckel—Bukry, 1980b
D. speculum tenuis Bukry—Bukry, 1982b
D. stauracanthus (Ehrenberg) Haeckel—Dumitrică, 1973
D. stradneri (Jerkovíc) Bukry—Stradner, 1961
D. xenus Bukry—Bukry, in press a
Mesocena apiculata apiculata (Schulz) Hanna—Schulz, 1928
M. circulus (Ehrenberg) Ehrenberg—Bukry, 1979b
M. elliptica (Ehrenberg) Ehrenberg—Bukry, 1978b
M. quadrangula Ehrenberg ex Haeckel—Bukry, 1978b
Naviculopsis biapiculata (Lemmermann) Frenguelli—Bukry, 1975
N. constricta (Schulz) Bukry emend.—Barron et al., in press
N. contraria Bukry—Bukry, 1982a
N. lacrima Bukry—Bukry, 1982a
N. lata (Deflandre) Frenguelli—Bukry, 1978b
N. navicula (Ehrenberg) Deflandre—Bukry, 1982a
N. obtusarca Bukry—Bukry, 1982a
N. ponticula ponticula (Ehrenberg) Bukry—Bukry, 1982a
N. ponticula spinosa Bukry—Bukry, 1982a
N. quadrata (Ehrenberg) Ling—Bukry, 1979a
Octactis pulchra Schiller—Bukry, 1980b

CONCLUSIONS

Silicoflagellates provide a useful relative paleotemperature record that reflects major paleoceanographic events for the lower Miocene to Holocene of Leg 85 sites. For purposes of comparison, the tropical, oceanic setting for the lower Miocene of Hole 575A provides corroboration of major latitudinal trends in silicoflagellate morphology. For example, the virtual absence of fibuloid *Dictyocha* at high- and middle-latitude Holes 407, 391A, 370, 369A, and 278 is a cosmopolitan relation because they are, likewise, absent at tropical Hole 575A. Thus, Neogene populations of fibuloid *Dictyocha* did not become established anywhere until the middle Miocene *Corbisema triacantha* Zone. This happens to coincide with the time of major transition in silicoflagellate morphologies, which was much more extreme than at the earlier worldwide boundary between Neogene and Paleogene.

The lack of fibuloid *Dictyocha* in the lower Miocene suggests, further, that no direct lineages exist between the small populations of fibuloid *Dictyocha* in the Paleogene and those extensive populations of the Neogene, above the lower Miocene.

The early Miocene record of Holes 575A and 495 is distinguished by the absence of the *Mesocena apiculata* group, which is present at nontropical sites and is most abundant at the coldest site, 278 (Bukry, 1975), south of New Zealand. Because of the absence of *Corbisema triacantha* in the lower Miocene of Holes 575A and 495, its presence in the lower middle Miocene of Hole 572D, and its lower Miocene occurrences at middle and high latitudes, *C. triacantha* shows a mixed pattern that is less clear than that of *Mesocena apiculata*.

A pattern of changing paleotemperature values (*Ts*) and species arrays in the *Naviculopsis ponticula* Zone of Hole 575A is practically the same as at Site 495 off Guatemala. Quantitative silicoflagellate data show that tectonic backtracking across the East Pacific Rise should place these two sites in the same vicinity during the period 17 to 19 Ma.

High-amplitude fluctuation in silicoflagellate relative-paleotemperature values characterizes the upper Miocene of Hole 572D, which is situated to the east of Hole 575A and at the westernmost position of a modern tongue of cool equatorial waters advected from coastal South America. The substantial populations of cool-water indicator taxon *Distephanus speculum speculum* suggest the presence of an analogous cool-water tongue as long ago as the late middle Miocene. Following the maximum coolings in the late late Miocene, a general warming trend and reduction in the amplitude of *Ts* fluctuation occurred. The latest major cooling (below *Ts* = 50) occurred in the early Pliocene. Aside from the mid-Quaternary cooling (*Ts* = 71) associated with the acme of *Mesocena quadrangula*, warm *Ts* values of 80 to 100 are typical for the late Pliocene and Quaternary of Hole 572A.

The low-latitude, open-ocean application of the *Ts* relative-paleotemperature technique appears to be successful for Leg 85, as shown by cool peaks matching deep-sea hiatuses in conjunction with fluctuations of cool and warm currents in the area during the late Cenozoic. Both absolute and relative comparisons of *Ts* values for Leg 85 correlate well within the eastern equatorial Pacific and also reflect global paleoceanographic changes.

ACKNOWLEDGMENTS

I thank Gerta Keller and Jack G. Baldauf, U.S. Geological Survey, for their helpful reviews of this paper. John A. Barron, U.S. Geological Survey, provided additional samples and excellent background information on diatom correlations for Leg 85, which helped to make a detailed silicoflagellate analysis feasible. I thank Dorothy L. Blackstock, U.S. Geological Survey, for excellent manuscript and figure typing and for proofing the paper.

REFERENCES

Bachmann, A., 1970. Silicoflagellaten aus dem oberösterreichischen Egerien (Oberoligozän). *Österreichische Geol. Bundesanst. Verh.*, 2:275–305.

Barron, J. A., 1983. Latest Oligocene through early middle Miocene diatom biostratigraphy of the eastern tropical Pacific. *Mar. Micropaleontol.*, 7:487–515.

Barron, J. A., Bukry, D., and Poore, R. Z., in press. Correlation of the middle Eocene Kellog Shale of northern California. *Micropaleontology.*

Barron, J. A., and Keller, G., 1982. Widespread Miocene deep-sea hiatuses: Coincidence with periods of global cooling. *Geology*, 10: 577–581.

Bernstein, R. L., and Morris, J. H., 1983. Tropical and mid-latitude North Pacific sea surface temperature variability from the SEASAT SMMR. *J. Geophys. Res.*, 88:1877–1891.

Bukry, D., 1975. Silicoflagellate and coccolith stratigraphy, Deep Sea Drilling Project Leg 29. *In* Kennett, J. P., Houtz, R. E., et al., *Init. Repts. DSDP*, 29: Washington (U.S. Govt. Printing Office), 845–872.

_____, 1978a. Cenozoic coccolith and silicoflagellate stratigraphy, offshore northwest Africa, Deep Sea Drilling Project Leg 41. *In* Lancelot, Y., Seibold, E., et al., *Init. Repts. DSDP*, 41: Washington (U.S. Govt. Printing Office), 689–707.

_____, 1978b. Cenozoic coccolith, silicoflagellate, and diatom stratigraphy, Deep Sea Drilling Project Leg 44. *In* Benson, W. E., Sheridan, R. E., et al., *Init. Repts. DSDP*, 44: Washington (U.S. Govt. Printing Office), 807–863.

_____, 1979a. Coccolith and silicoflagellate stratigraphy, northern Mid-Atlantic Ridge and Reykjanes Ridge, Deep Sea Drilling Project Leg 49. *In* Luyendyk, B. P., Cann, J. P., et al., *Init. Repts. DSDP*, 49: Washington (U.S. Govt. Printing Office), 551–581.

———, 1979b. Comments on opal phytoliths and stratigraphy of Neogene silicoflagellates and coccoliths at Deep Sea Drilling Project Site 397 off northwest Africa. *In* Luyendyk, B. P., Cann, J. R., et al., *Init. Repts. DSDP*, 49: Washington (U.S. Govt. Printing Office), 977–1009.

———, 1980a. Miocene *Corbisema triacantha* Zone phytoplankton from Deep Sea Drilling Project Sites 415 and 416, off northwest Africa. *In* Lancelot, Y., Winterer, E. L., et al., *Init. Repts. DSDP*, 50: Washington (U.S. Govt. Printing Office), 507–523.

———, 1980b. Silicoflagellate biostratigraphy and paleoecology in the eastern equatorial Pacific, Deep Sea Drilling Project Leg 54. *In* Rosendahl, B. R., Hekinian, R., et al., *Init. Repts. DSDP*, 54: Washington (U.S. Govt. Printing Office), 545–573.

———, 1981a. Silicoflagellate stratigraphy of offshore California and Baja California, Deep Sea Drilling Project Leg 63. *In* Yeats, R. S., Haq, B. U., et al., *Init. Repts. DSDP*, 63: Washington (U.S. Govt. Printing Office), 539–557.

———, 1981b. Synthesis of silicoflagellate stratigraphy for Maestrichtian to Quaternary marine sediment. *Soc. Econ. Paleontol. Mineral. Spec. Publ.*, 32:433–444.

———, 1982a. Cenozoic silicoflagellates from offshore Guatemala, Deep Sea Drilling Project Site 495. *In* Aubouin, J., von Huene, R., et al., *Init. Repts. DSDP*, 67: Washington (U.S. Govt. Printing Office), 425–445.

———, 1982b. Neogene silicoflagellates of the eastern equatorial Pacific, Deep Sea Drilling Project Hole 503A. *In* Prell, W. L., Gardner, J. V., et al., *Init. Repts. DSDP*, 68: Washington (U.S. Govt. Printing Office), 311–323.

———, 1983. Upper Cenozoic silicoflagellates from offshore Ecuador, Deep Sea Drilling Project Site 504. *In* Cann, J. R., Langseth, M. G., Honnorez, J., Von Herzen, R. P., White, S. M., et al., *Init. Repts. DSDP*, 69: Washington (U.S. Govt. Printing Office), 321–342.

———, in press a. Cenozoic silicoflagellates from Rockall Plateau, Deep Sea Drilling Project Leg 81. *In* Roberts, D. G., Schnitker, D., et al., *Init. Repts. DSDP*, 81: Washington (U.S. Govt. Printing Office).

———, in press b. Neogene silicoflagellates from DSDP Site 543, western tropical Atlantic Ocean. *In* Hyndman, R. D., Salisbury, M. H., et al., *Init. Repts. DSDP*, 78B: Washington (U.S. Govt. Printing Office).

Bukry, D., and Foster, J. H., 1974. Silicoflagellate zonation of Upper Cretaceous to lower Miocene deep-sea sediment. *U.S. Geol. Surv. J. Res.*, 2:303–310.

Dumitrică, P., 1973. Paleocene, late Oligocene and post-Oligocene silicoflagellates in southwestern Pacific sediments cored on DSDP Leg 21. *In* Burns, R. E., Andrews, J. E., et al., *Init. Repts. DSDP*, 21: Washington (U.S. Govt. Printing Office), 837–883.

Ehrenberg, C. G., 1840. 274 Blätter von ihm selbst ausgeführter Zeichnungen von ebenso vielen Arten. *K. Preuss. Akad. Wiss. Berlin Ber. Jahrg.*, 1840(Nov.):197–219.

———, 1854. *Mikrogeologie:* Leipzig (Leopold Voss), pp. 1–374.

Hays, J. D., et al., 1972. *Init. Repts. DSDP*, 9: Washington (U.S. Govt. Printing Office).

Keller, G., and Barron, J. A., 1983. Paleoceanographic implications of Miocene deep-sea hiatuses. *Geol. Soc. Am. Bull.*, 94:590–613.

Lemmermann, E., 1901. Silicoflagellatae. *Deutsche. Bot. Gesell. Ber.*, 19:247–271.

Ling, H. Y., 1977. Late Cenozoic silicoflagellates and ebridians from the eastern North Pacific region. *First Internat. Congr. Pacific Neogene Stratigraphy Proc.* (Tokyo), pp. 205–233.

Locker, S., 1974. Revision der Silicoflagellaten aus der Mikrogeologischen Sammlung von C. G. Ehrenberg. *Eclogae Geol. Helvetiae*, 67:631–646.

Major, R. P., and Matthews, R. K., 1983. Isotopic composition of bank margin carbonates on Midway Atoll: Amplitude constraint on post-early Miocene eustasy. *Geology*, 11:335–338.

Martini, E., 1971. Neogene silicoflagellates from the equatorial Pacific. *In* Winterer, E. L., Riedel, W. R., et al., *Init. Repts. DSDP*, 7, Pt. 2: Washington (U.S. Govt. Printing Office), 1695–1708.

Poelchau, H. S., 1976. Distribution of Holocene silicoflagellates in North Pacific sediments. *Micropaleontology*, 22:164–193.

Schulz, P., 1928. Beiträge zur Kenntnis fossiler und rezenter Silicoflagellaten. *Bot. Archiv*, 21:225–292.

Shackleton, N. J., 1982. The deep-sea sediment record of climate variability. *Prog. Oceanogr.*, 11:199–218.

Stradner, H., 1961. Über fossile Silicoflagelliden und die Möglichkeit ihrer Verwendung in der Erdölstratigraphie. *Erdol Kohle*, 14:87–92.

Vail, P. R., Mitchum, R. M., Jr., and Thompson, S., 1977. Global cycles of relative changes of sea level. *In* Payton, C. E. (Ed.), *Seismic stratigraphy—applications to hydrocarbon exploration:* Tulsa (Am. Assoc. Pet. Geol.), pp. 83–98.

van Andel, T. H., and Bukry, D., 1973. Basement ages and basement depths in the eastern equatorial Pacific from Deep Sea Drilling Project Legs 5, 8, 9, and 16. *Geol. Soc. Am. Bull.*, 84:2361–2370.

Date of Initial Receipt: 28 October 1983
Date of Acceptance: 6 March 1984

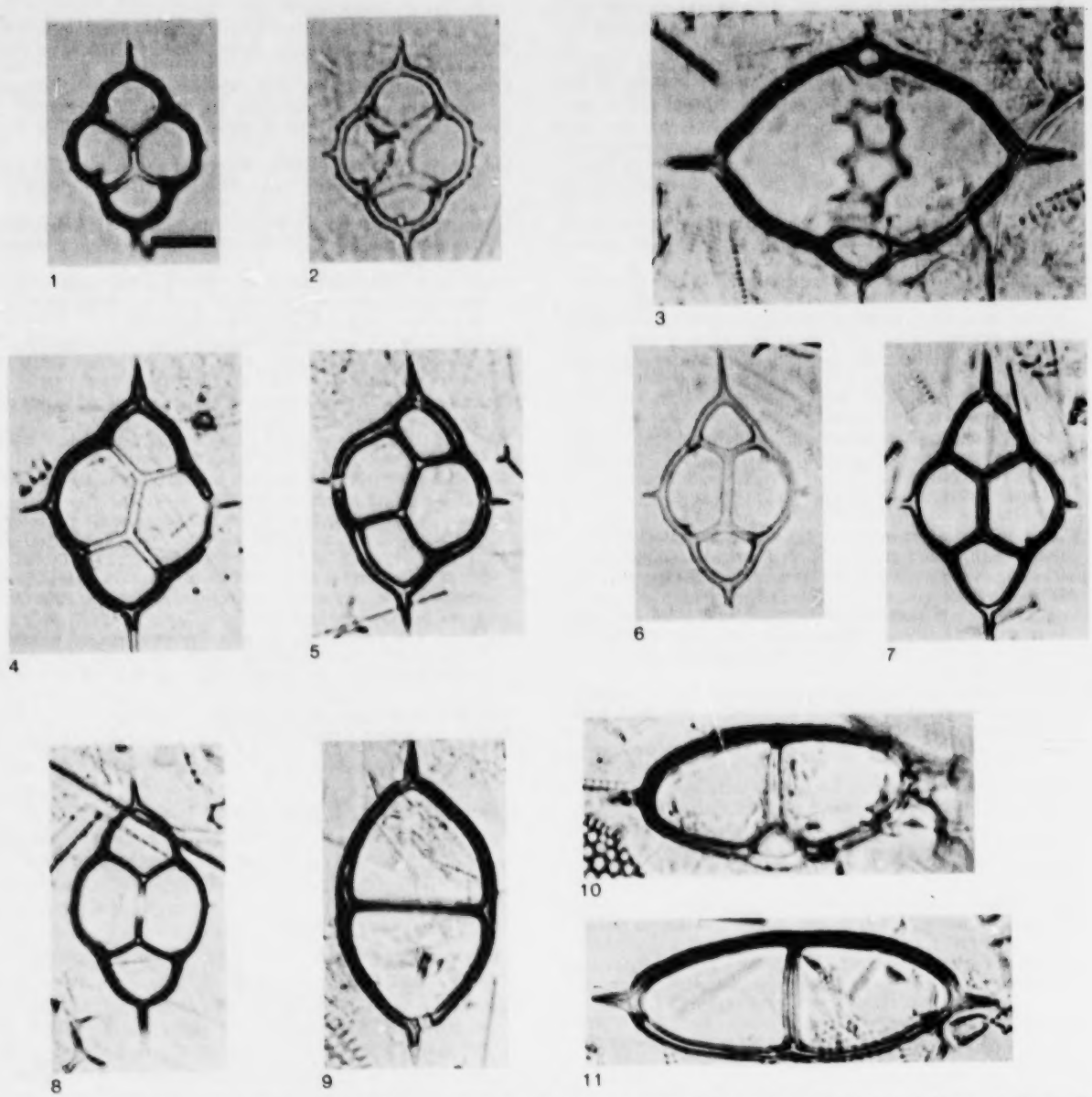

Plate 1. Silicoflagellates from DSDP Leg 85. (Scale bar = 10 μm.) **1–2.** *Dictyocha angulata* Bukry, Sample 572A-7-4, 66–67 cm. **3.** *Dictyocha brevispina* (Lemmermann) (no bar), Sample 572A-10,CC. A form identical to the coeval (approx. 4.5 Ma) population in Section 504-45-1 (Bukry, 1983), which also lacks barred asperoid specimens. **4–5.** *Dictyocha flexatella* (Bukry), Sample 572A-5-3, 16–17 cm. **6–8.** *Dictyocha longa* Bukry, (6) Sample 572A-8-3, 66–67 cm, (7) Sample 572A-8-3, 16–17 cm, (8) rounded ends, Sample 572A-8-3, 16–17 cm. **9.** *Dictyocha neonautica* var. *cocosensis* Bukry, Sample 572A-14,CC. **10–11.** *Dictyocha neonautica* Bukry, Sample 572A-15-1, 68–69 cm, (10) transitional specimen, (11) normal specimen.

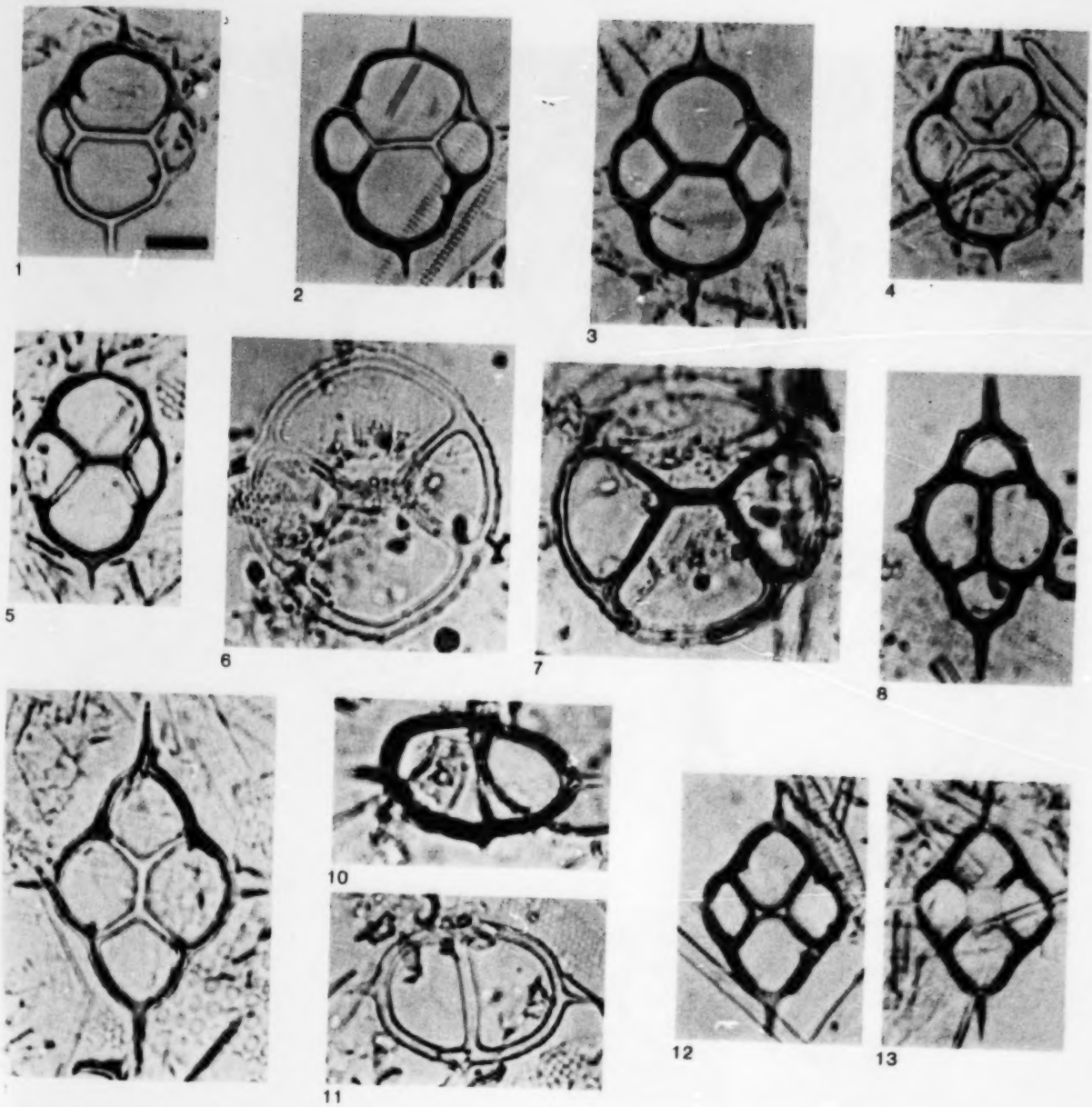

e 2. Silicoflagellates from DSDP Leg 85. (Scale bar = 10 μm.) **1–5.** *Dictyocha nola* Bukry, n. sp., Sample 572A-11-3, 67–68 cm, (1) USNM 371374, (2) USNM 371375, (3) holotype, USNM 371373, (4) USNM 371376, (5) USNM 371377. **6–7.** *Dictyocha orbiculata* Ling, Sample 572A-7,CC. **8.** *Dictyocha ornata africana* (Bukry), Sample 572A-5,CC. **9.** *Dictyocha perfecta* Bukry, Sample 572A-8-3, 66–67 cm. **10–11.** *Dictyocha pons* Ehrenberg, Sample 575A-1,CC. **12–13.** *Dictyocha pulchella* Bukry, Sample 572D-18,CC, (12) normal specimen, (13) deflanroid specimen.

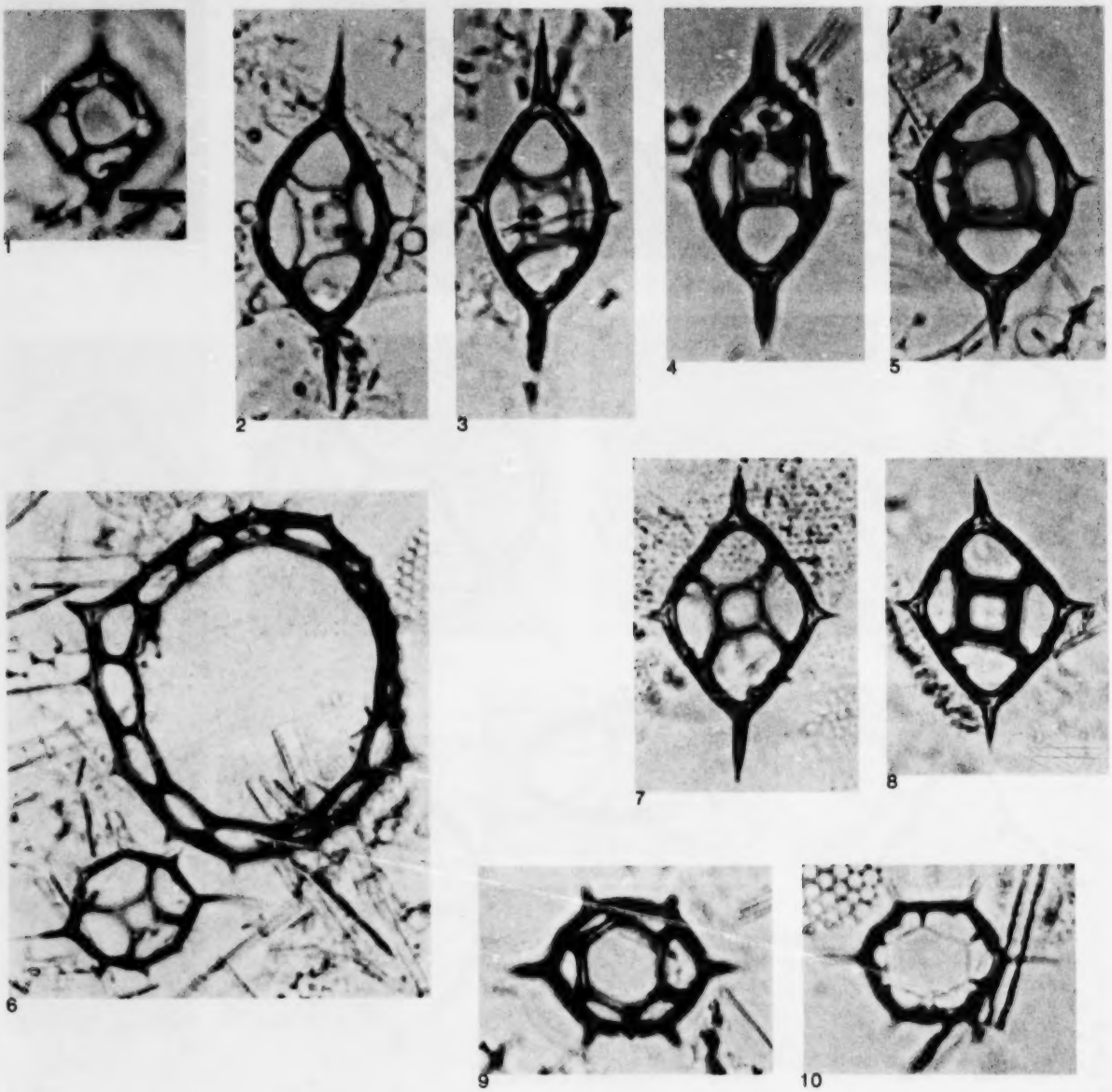

Plate 3. Silicoflagellates from DSDP Leg 85. (Scale bar = 10 μm.) **1.** *Distephanus mesophthalmus* (Ehrenberg), Sample 572A-15-3, 19–20 cm. **2–5.** *Distephanus schauinslandii* Lemmermann, (2) Sample 575A-18,CC, (3) Sample 575A-11-3, 24–25 cm, (4) Sample 575A-18,CC, (5) Sample 575A-17,CC. **6.** *Distephanus polyactis* (Ehrenberg) above *Distephanus stauracanthus* (Ehrenberg), Sample 572D-22,CC. **7–8.** *Distephanus crux scutulatus* Bukry, (7) Sample 575A-12,CC, (8) Sample 575A-7-2, 42–43 cm. **9.** *Distephanus speculum patulus* Bukry, Sample 575A-19,CC. **10.** *Distephanus speculum tenuis* Bukry, Sample 572A-16-3, 19–20 cm.

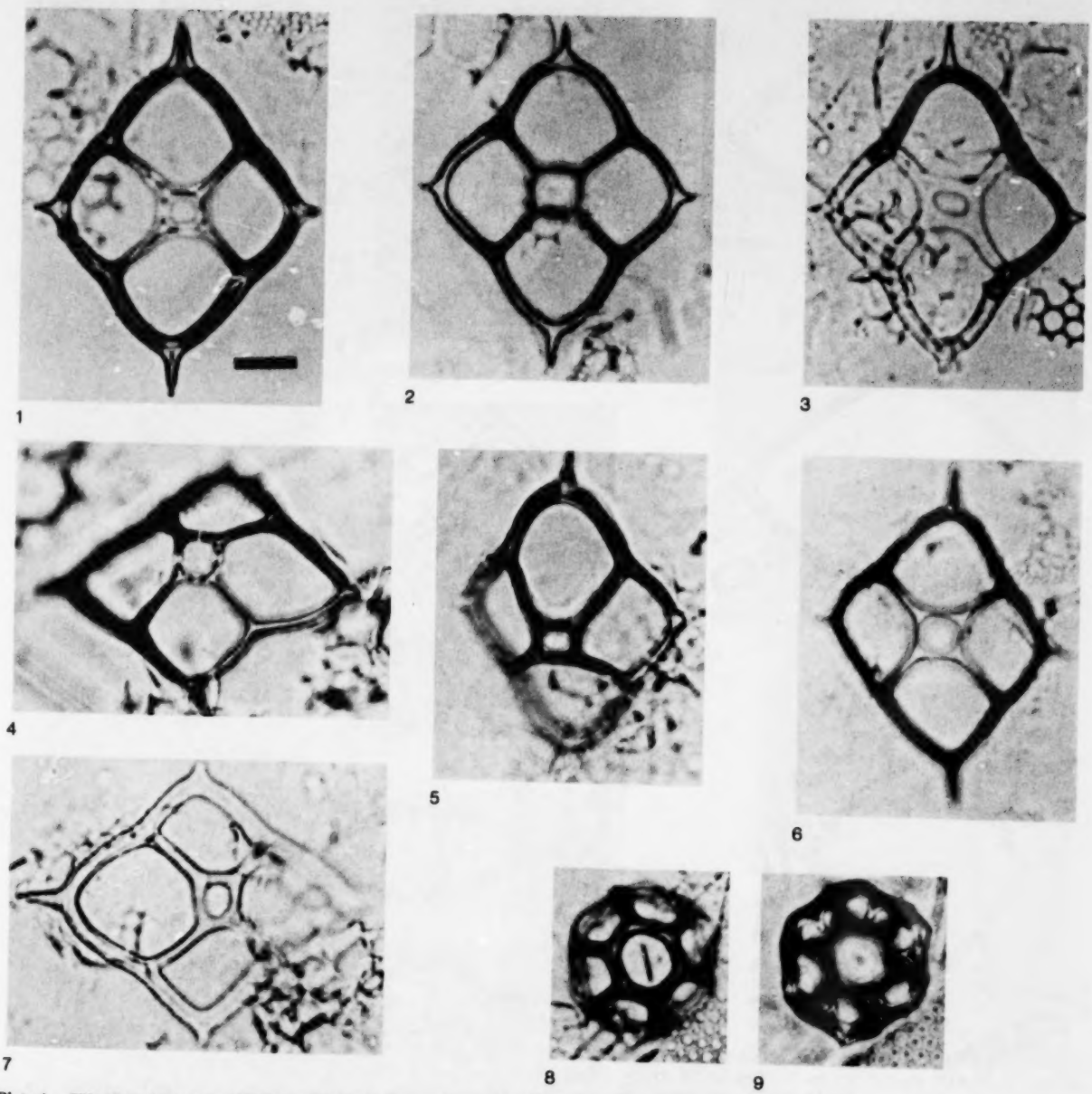

Plate 4. Silicoflagellates from DSDP Leg 85. (Scale bar = 10 μm.) 1–7. *Distephanus stradneri* var. *grandis* Bukry, n. var., Sample 575A-33,CC, (1) USNM 371379, (2) holotype, USNM 371378, (3) USNM 371380, (4) USNM 371381, (5) USNM 371382, (6) USNM 371383, (7) USNM 371384. 8–9. *Distephanus xenus* Bukry, Sample 572A-14-3, 18–19 cm, (8) apical focus, (9) basal focus.

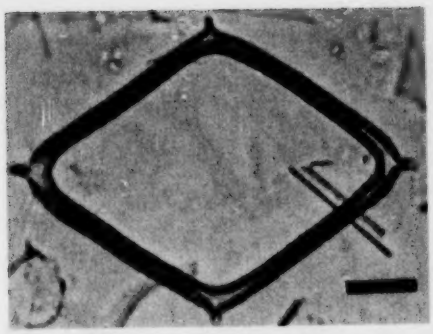
1

2

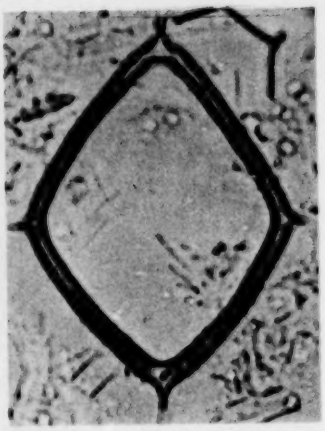
3

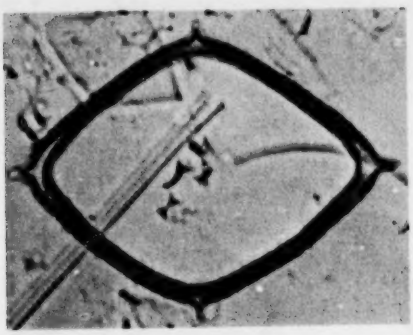
4

5

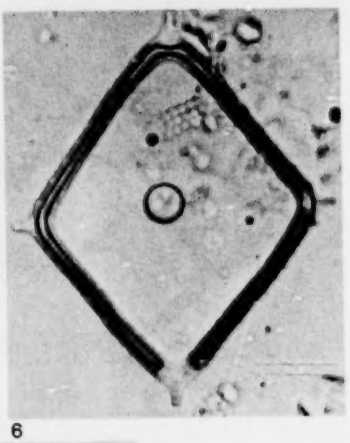
6

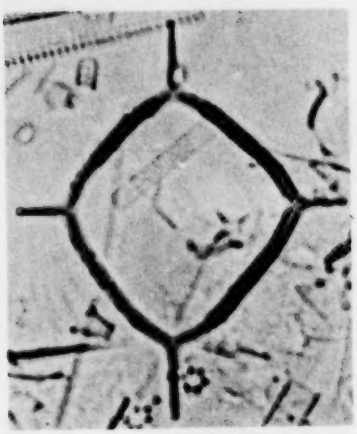
7

8

9

Plate 5. Silicoflagellates from DSDP Leg 85. (Scale bar = 10 μm.) **1–6.** *Mesocena elliptica* var. *rhomboidea* Bukry, n. var., (1) holotype, USNM 371385, Sample 575A-8-2, 42–43 cm, (2) USNM 371386, Sample 575A-9,CC, (3) USNM 371387, Sample 575A-7-3, 24–25 cm, (4) USNM 371388, Sample 575A-8-2, 42–43 cm, (5) USNM 371389, Sample 575A-7,CC, (6) USNM 371390, Sample 575A-10,CC. **7.** *Mesocena quadrangula* Ehrenberg ex Haeckel, Sample 572A-3-1, 68–69 cm. **8–9.** *Naviculopsis biapiculata* (Lemmermann) s. ampl., (8) Sample 575A-19,CC, (9) Sample 575A-17,CC.

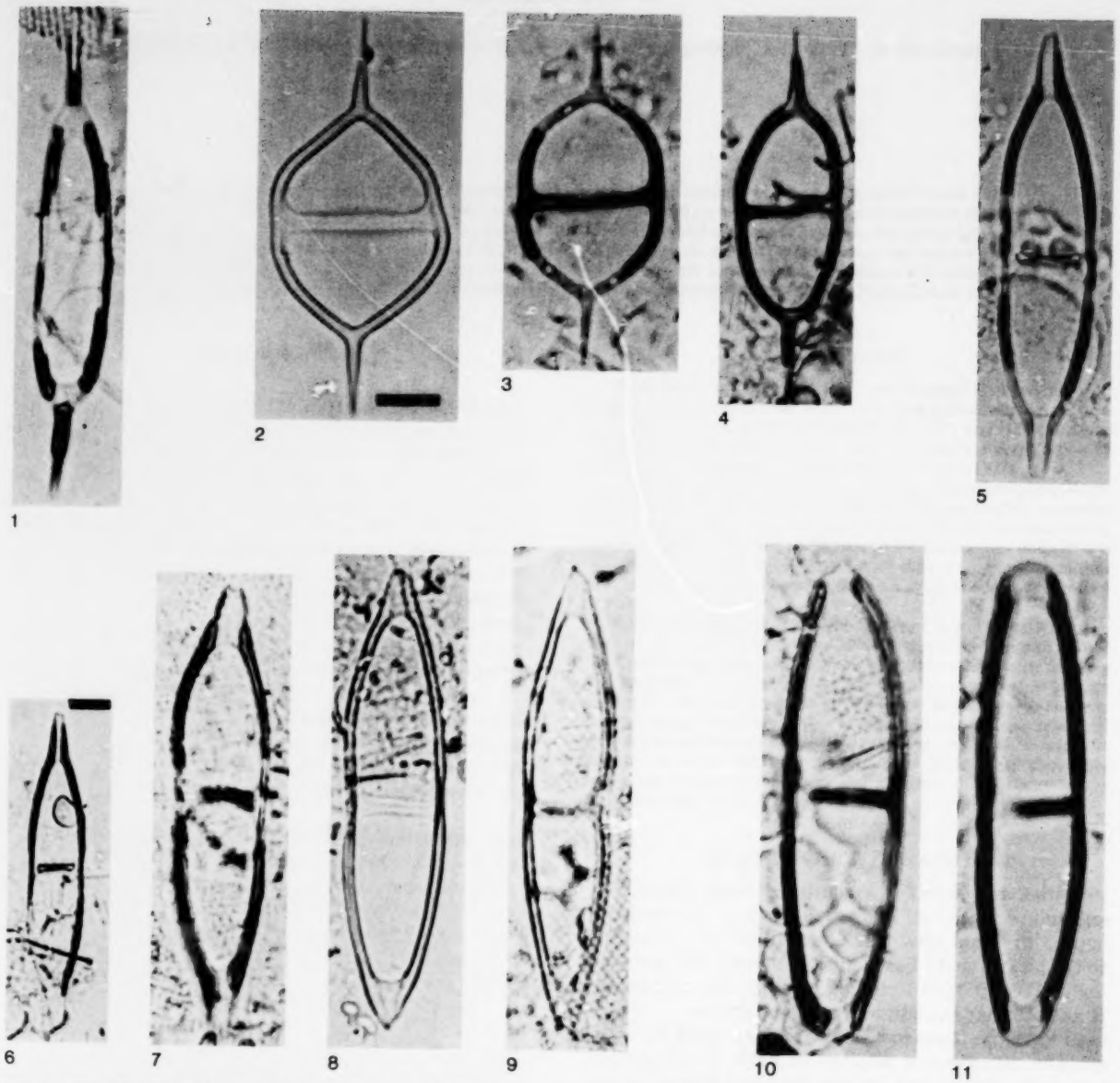

Plate 6. Silicoflagellates from DSDP Leg 85. (Scale bar for Figs. 1–5 and 7–11 = 10 μm. Scale bar for Fig. 6 = 20 μm.) **1.** *Naviculopsis contraria* Bukry, Sample 575A-9,CC. **2–4.** *Naviculopsis lata* (Deflandre), (2) hexagonal, Sample 575A-20,CC, (3) normal, Sample 575A-19,CC, (4) narrow, Sample 575A-19,CC. **5–9.** *Naviculopsis obtusarca* var. *acicula* Bukry, n. var., (5) holotype, USNM 371391, Sample 575A-10-2, 42–43 cm, (6) USNM 371392, Sample 575A-10-2, 42–43 cm, (7) USNM 371393, Sample 575A-10-2, 42–43 cm, (8) USNM 371394, Sample 575A-10-3, 42–43 cm, (9) USNM 371395, Sample 575A-10-3, 42–43 cm. **10–11.** *Naviculopsis ponticula* (Ehrenberg), (10) vestigial spine, Sample 575A-7-2, 42–43 cm, (11) smooth end, Sample 575A-7-3, 24–25 cm.

Reprinted from Mayer, L., Theyer, F., et al., 1985
Initial Reports of the Deep Sea Drilling Project, Volume LXXXV, Washington (U. S. Government Printing Office)

11. QUATERNARY RADIOLARIANS FROM THE EQUATORIAL PACIFIC, DEEP SEA DRILLING PROJECT LEG 85[1]

Monique Labracherie, Département de Géologie et Océanographie, Université de Bordeaux I[2]

ABSTRACT

Quaternary radiolarians are common and rather well preserved in the sections recovered from DSDP Holes 571, 572A, and 573. The assemblages from Hole 575C are less abundant and contain high concentrations of reworked specimens. Twelve first occurrences, extinction levels, and transitions, some of which are already known in the equatorial Pacific area, are recognized in the interval between the top of the Olduvai and the present (approximately between the Pliocene/Pleistocene boundary and the Holocene). These radiolarian events are compared and correlated with both the paleomagnetic time scale and the carbonate content determined from an undisturbed section with a high sediment accumulation rate.

INTRODUCTION

Numerous biostratigraphic studies have shown the usefulness of radiolarian species for interpretation of the Quaternary. Nigrini's (1971) Quaternary radiolarian zonation of the tropical Pacific presented the main stratigraphic markers. Later, Johnson and Knoll (1975) proposed age estimates for zonal boundaries of this zonation by correlation with paleomagnetic stratigraphy. Recently, Goll (1980) did not apply Nigrini's zonation to the eastern province of the equatorial Pacific, because of the absence of some biostratigraphic indicator taxa. The presence of radiolarians more typical of eastern equatorial assemblages gave him the opportunity to establish a new biozonation with a high resolution. One of the disadvantages of the fourfold Quaternary zonation proposed by Nigrini (1971) is indeed the relatively long time-range of biozones 3 and 4 (the *Amphirhopalum ypsilon* Interval-Zone and the *Anthocyrtidium angulare* Range-Zone).

Leg 85 coring recovered sediments containing especially diverse and abundant Quaternary radiolarians. Radiolarian assemblages were examined in 4 of 17 holes on Leg 85. These four holes (571, 572A, 573, and 575C) are situated in two regions of the equatorial Pacific: Holes 573 and 575C at approximatively 0°N, 134°W and 5°N, 134°W, respectively, and Holes 572A and 571 at about 1°N, 114°W and 4°N, 114°W, respectively toward the East Pacific Rise (Fig. 1).

All radiolarian datum levels of Johnson and Knoll (1975) and some biohorizons or evolutionary lineages of Goll (1980) are easily recognizable in Leg 85 sediments. They correlate directly with stratigraphies based upon paleomagetism (Weinreich and Theyer, this volume) and/or carbonate content (Pujos, this volume).

PROCEDURES

Cores from Holes 571 and 575C were sampled at 20-cm intervals. In cores from Holes 573 and 572A, only three or four samples per core were analyzed. Sediments were treated with H_2O_2 and HCl and sieved through a 45-μm screen. Strewn slides were also prepared, following the procedures outlined by Riedel and Sanfilippo (1977).

In the Quaternary stratigraphic zonation schemes based on the radiolarian fauna, the definition of limits of species range is somewhat ambiguous because of (1) low abundances of the marker taxa, resulting from their usually strong dilution in the biosiliceous (radiolarian) assemblages, (2) fragility of skeletons of some stratigraphic indicator radiolarians, causing poor preservation and (3) the possibility of reworking.

In this investigation of radiolarians from Leg 85 Quaternary sequences, for each sample, about 500 specimens were counted on one slide, along several horizontal traverses, and the main species found in this geographic area were noted. Six categories were used to indicate the relative abundances of selected taxa (see Tables 1 to 4). The level for each species event was chosen as the lowermost or uppermost sample—bounding an interval of regular presence—in which the taxon occurs; in the ideal cases, these samples show an increased abundance (above the first-occurrence level) and a decreased abundance (below extinction level) of the taxon, respectively.

QUATERNARY ZONATION

The main faunal constituents of Leg 85 radiolarian assemblages are typically equatorial and tropical; but species more specifically associated with the Peru coastal upwelling are present (Romine and Moore, 1981). The low-latitude radiolarian zonation of Nigrini (1971) is applied as a starting point to describe the radiolarians at each site (Table 5). The radiolarian zonal sequence used to characterize these Pleistocene assemblages includes events identified in both central and eastern equatorial provinces of the Pacific Ocean. The paleomagnetism record is used as the basis for the chronostratigraphy, and fluctuations in carbonate content are used for the local correlations.

Site 571

Core 571-1 contains Quaternary assemblages of good to moderate preservation (Table 1). Changes in the preservation of biogenic silica can be correlated with impor-

[1] Mayer, L., Theyer, F., Thomas, E., et al., *Init. Repts. DSDP*, 85: Washington (U.S. Govt. Printing Office).

[2] Address: Département de Géologie et Océanographie, Laboratoire associé au C.N.R.S. no. 197, Université de Bordeaux I, Avenue des Facultés, 33405 Talence Cedex, France.

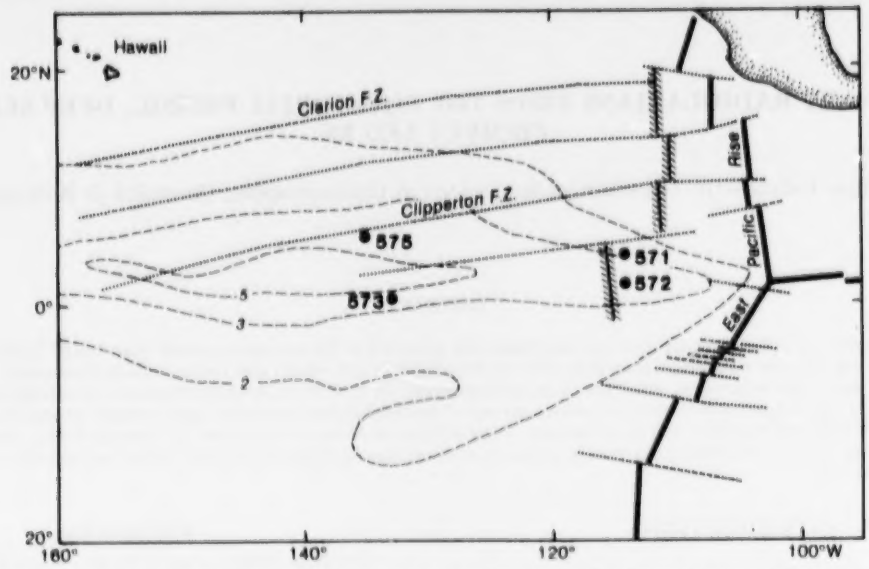

Figure 1. Locations of Sites 571, 572, 573, and 575 (Leg 85) in relation to sediment thickness (broken contours) and fracture zones. Contour intervals are in tenths of seconds of two-way traveltime.

tant fluctuations in the carbonate content. Minima and maxima in the carbonate content at Site 571 are given by Pujos (this volume). Radiolarians from carbonate-rich sediments are abundant, well preserved, and diluted by centric diatoms. Assemblages are generally more poorly preserved within intervals where the carbonate content is minimal. Samples 571-1-2, 41–43 cm, 571-1-3, 18–20 cm, and 571-1-4, 118–120 cm yielded many broken forms, associated sometimes with numerous *Ethmodiscus* fragments, whereas centric diatoms become rare or absent in the fraction greater than 45 μm. Radiolarians are diluted by clay aggregates, which may be trapped inside skeletons.

Hole 571 reached only the uppermost levels of the Quaternary. Abundances of some radiolarians are shown in Table 1. Specimens indicative of the uppermost two Quaternary zones of Nigrini's (1971) zonation are common throughout the top meter. These species decrease or disappear below the minima in the carbonate content. The uppermost samples (571-1-5, 21–23 cm through 571-1,CC, 20 cm) containing *Axoprunum angelinum* (= *Stylatractus universus*) can be considered older than 410,000 yrs. (age estimated by Hays and Shackleton [1976] for the extinction level of this species over the whole of its geographic distribution). The date of its last appearance has been differently estimated at 320,000 yrs. ago in the equatorial Pacific (Johnson and Knoll, 1975).

Site 572

Sediments from the upper 26 m of Hole 572A (Cores 572A-1 through 572A-3) represent a continuous record throughout the Quaternary of the eastern equatorial Pacific. Sediments contain well-preserved to moderately well preserved radiolarian assemblages diluted with diatoms. Reworking is minor and occasional (Table 2). The high diversity of assemblages reveals biogeographic correlations with the radiolarian fauna from DSDP sites of the East Pacific Rise and the Galapagos Spreading Center (Goll, 1980); species belonging to the genus *Acrosphaera* are always more scarce, however.

The four Quaternary zones of Nigrini's (1971) tropical zonation can be recognized, but some events described by Goll (1980), using data from Leg 54 sites, are also represented in the assemblages from Hole 572A. Approximately the uppermost 43 cm are from the *Buccinosphaera invaginata* Zone, and the underlying 5 m are from the *Collosphaera tuberosa* Zone. Samples 572A-1-5, 117–119 cm (7.17 m sub-bottom) and 572A-2-3, 118–120 cm (13.70 m) contained the uppermost occurrences of *Axoprunum angelinum* and *Amphispyris roggentheni*, respectively. This latter species, described by Goll (1980), was originally reported in the eastern Pacific, where it became extinct about 650,000 yrs. ago. The transition from *Androspyris anthropiscus* to *A. huxleyi* can be placed between Samples 572A-2-2, 37–39 cm (last occurrence of *A. anthropiscus*) and 572A-1-6, 76–78 cm (first occurrence of *A. huxleyi*). There is a gap between the two events, which occurs between the uppermost occurrences of *A. angelinum* and *A. roggentheni*. Sporadic occurrences of *Androspyris* specimens have been mentioned by Goll (1980), and can explain why it is difficult to place exactly the limit of the *A. anthropiscus–A. huxleyi* transition in Hole 572A. Goll (1980) gave it a date of about 500,000 yrs. ago. Samples 572A-2-6, 117–119 cm through 572A-3-2, 142–144 cm have been assigned to the *Anthocyrtidium angulare* Zone. The uppermost occurrence of *Pterocanium prismatium*, between Samples 572A-3-5, 118–120 cm and 572A-3-5, 141–143 cm, places the Pliocene/Pleistocene boundary near 26 m sub-bottom.

Table 1. Ranges and frequency of selected radiolarian species, DSDP Hole 571.

Core-Section (interval in cm)	Preservation	Reworking	Zone	*Buccinosphaera invaginata*	*Collosphaera tuberosa*	*Collosphaera orthoconna*	*Androspyris haxtoni*	*Diolenia* spp.	*Lamprocyrtis nigriniae*	*Pterocorys hertwigii*	*Axoprunum angelinium* (*S. universus*)	*Lithopera bacca*	*Androspyris anthropiscus*	*Amphispyris roggentheni*	*Anthocyrtidium angulare*	*Lamprocyrtis neoheteroporos*	*Lamprocyrtis heteroporos*	*Theocorythium trachelium* gr.	*Theocorythium vetulum*	*Pterocanium prismatium*	*Amphirhopalum ypsilon*
1-1, 0-2	MG	•		r	R	—	—	F	—	R								F			R
1-1, 20-22	M			—	F	—	—	C	—	r								r			R
1-1, 40-42	MG			r	C	r	—	C	—	r								r			r
1-1, 60-62	G	•		r	F	r	—	C	—	r								—			r
1-1, 81-83	GM		*B. invaginata*	r	R	r	—	F	—	r								—			r
1-1, 101-103	M	•		—	F	r	—	F	—	R								—			R
1-1, 121-123	MG	•		+	R	r	—	F	—	r								—			r
1-2, 1-3	M	•		—	R	—	—	R	—	r								r			r
1-2, 21-23	MG	•		—	—	r	—	R	—	r								r			R
1-2, 41-43	P	•		—	—	—	—	—	—	r								r			—
1-2, 81-83	G			+	—	r	r	F	—	r								—			r
1-2, 102-104	MG	•		!	—	F	r	F	—	r								—			r
1-2, 120-122	MG			—	r	—	—	F	R	r								—			R
1-2, 137-139	P	•	*C. tuberosa*	r!	R	—	—	C	R	—								r			R
1-3, 18-20	P			—	R	—	—	R	—	r								r			r
1-3, 56-58	M			—	+	—	—	F	—	—								R			r
1-3, 98-100	M	•		—	r	r	+	F	—	R								r			r
1-3, 118-120	P	•			R	R	—	C	—	r								—			R
1-4, 3-5	G				—	r	—	F	—	—								r			R
1-4, 36-38	MP				—	—	—	F	—	r	—							—			R
1-4, 98-100	MP	•			—	—	—	F	—	—	—							r			F
1-4, 137-139	P	•			—	—	—	r	+	—	—							r			R
1-5, 4-6	G				—	—	—	r	—	r	—	—	—					F			F
1-5, 21-23	M	•	*A. ypsilon*		—	—	—	r	—	r	r	—	—	—				r			R
1-5, 40-42	M					—	r	R	r	r	r	—	—	—				r			R
1-5, 61-63	M	•				+	—	r	—	r	R	—	—	—				—			R
1-5, 81-83	P					—	—	R	—	—	R	—	—	—				—			R
1,CC (1-3)	MG					—	—	—	—	r	R	r	—	—				r			F
1,CC (17-19)	MG					—	—	—	—	—	R	—	—	—				—			F

Note: Species abundances: — = species sought but not found; + = present (<0.15% of the encountered radiolarians with a constant species numeration, generally about 1 specimen per slide); r = very rare specimens (0.15–0.99%); R = rare specimens (1–2.99%); F = few specimens (3–9.99%); C = common (>10% or more than about 60 specimens per slide); ! = reworking. Preservation of the assemblage: P = poor; M = moderate; G = good. Reworking: • = low.

Site 573

Hole 573 was drilled farther west in the equatorial Pacific, and is the southernmost hole of Leg 85. The magnetostratigraphy provided by the major polarity-reversal events in this hole (Weinreich and Theyer, this volume) places the base of the Quaternary between Samples 573-4-3, 88 cm and 573-4-3, 136 cm, at the top of the Olduvai event (Berggren et al., 1980). A record of fluctuations in calcium carbonate content is also available from this same hole (Pujos, this volume).

On average, radiolarians are moderately well preserved, abundant to common, and somewhat diluted by diatoms, with a very small number of reworked Pliocene and Miocene species. Pliocene radiolarians (especially *Spongaster pentas*) occur in well-preserved Pleistocene assemblages. Older forms are mixed into more poorly preserved assemblages. Relative abundances of radiolarians, and the zonation, are shown in Table 3. Preservation is very good at the top (Cores 573-1 and 573-2). The *Buccinosphaera invaginata* and *Collosphaera tuberosa* zones occupy about the upper 0.70 and 4.5 m, respectively. The first-occurrence level of *C. tuberosa* lies above poorly preserved samples. The *Amphirhopalum ypsilon* Zone is quite thick (about 14 m). Within this broad interval, the last occurrence of *Axoprunum angelinum* (= *Stylatractus universus*) is between Samples 573-2-3, 145–147 cm and 573-2-4, 36–40 cm. The average relative-abundance curve of this taxon seems to indicate that its upper limit could have been truncated, because the progressive final decline (Hays and Shackleton, 1976) was not observed. Only two samples contain *Androspyris anthropiscus*, and the last occurrence of *Amphispyris roggentheni* is between Sample 573-3-2, 35–37 cm and 573-3-2, 85–87 cm. The *Anthocyrtidium angulare* Range Zone is bounded by both the extinction levels of *A. angulare* and *Lamprocyrtis neoheteroporos*, at the top, and the first occurrence of *A. angulare*, just above the uppermost occurrence of *Pterocanium prismatium* at the base. In Hole 573, this last species is very abundant in its uppermost occurrence, which coincides exactly with the top of the Olduvai.

Table 2. Ranges and frequency of selected radiolarian species, DSDP Hole 572A.

Core-Section (interval in cm)	Preservation	Reworking	Zone	*Buccinosphaera invaginata*	*Collosphaera tuberosa*	*Collosphaera orthoconus*	*Andropyris huxleyi*	*Dictyomitra* spp.	*Lamprocyrtis nigriniae*	*Pterocorys hertwigii*	*Axoprunum angelinum (S. universa)*	*Lithopera bacca*	*Andropyris anthropiscus*	*Amphipyris roggenthini*	*Acrhocyrtidium angulare*	*Lamprocyrtis neoheteroporos*	*Lamprocyrtis heteroporos*	*Theocorythium trachelium* gr.	*Theocorythium vetulum*	*Pterocanium prismatium*	*Amphirhopalum ypsilon*
1-1, 2-4	G			r	R	—	—	R	r	R								R			R
1-1, 21-23	M		*B. invaginata*	r	R	r	—	F	r	R								—			R
1-1, 41-43	GM			r	R	—	—	F	r	+								—			r
1-1, 61-63	GM			—	R	—	—	R	r	R								r			r
1-1, 90-101	G			—	R	r	—	R	—	R								r			r
1-1, 141-143	M			—	F	r	—	r	r	r								R			R
1-2, 37-39	G			—	r	—	—	+	r	r								R			r
1-2, 77-79	G			—	—	—	r	r	—	r								r			r
1-2, 117-119	GM		*C. tuberosa*	—	r	—	—	R	r	r								—			R
1-3, 37-38	MG			—	r	—	—	R	r	r								—			r
1-3, 77-79	G			—	+	—	+	R	r	+								R			r
1-3, 118-119	GM			+!	—	—	—	R	—	R								r			R
1-3, 137-139	G			—	R	r	—	R	—	R								r			+
1-4, 36-38	M			—	r	—	—	R	—	r	—							—			R
1-4, 117-119	P	•		—	—	—	—	R	—	r	—							—			R
1-4, 137-139	MP	•		—	—	—	—	R	r	r	—							r			R
1-5, 36-38	G			—	—	—	—	R	—	r	—	—						—			R
1-5, 76-78	G				—	—	—	r	r	r	—	—						r			R
1-5, 117-119	G	•			—	—	—	R	—	R	+	—						R			R
1-5, 137-139	G				—	—	—	r	r	r	r	—	—					—			r
1-6, 36-38	P				—	—	—	r	—	R	R	—	—					—			R
1-6, 76-78	M				—	—	r	R	R	—	r	—	—	—				—			R
1-6, 137-139	G					+!	—	R	—	R	r	r	—	—				+			R
2-1, 37-39	G					—	—	R	—	r	r	r	—	—				r			R
2-1, 117-119	G	•				r	—	r	—	+	r	r	—	—				r			F
2-2, 37-39	M	•	*A. ypsilon*			—	—	+	—	—	R	—	—	—				R			R
2-2, 117-119	MG	•				—	—	—	—	—	r	—	—	—				r			R
2-3, 38-40	MG					—	—	—	—	—	r	—	+	—				R			R
2-3, 118-120	M					—	—	—	—	—	r	r	—	+				R			R
2-3, 141-143	G					—	—	+	—	—	r	—	r	r				R			R
2-4, 77-79	G					—	—	+	—	+	R	r	—	—	—	—		R			r
2-4, 142-144	GM							r	—	r	—	—	—	r	—	—		R			R
2-5, 37-39	G							r	—	r	r	+	—	+	—	—	—	R			R
2-5, 77-79	G							—	—	—	R	R	r	—	—	—	—	R			R
2-5, 142-144	G							r	—	+	r	r	—	+	—	—	—	R			r
2-6, 82-84	GM							—	—	—	R	—	r	+	—	—	—	r			+
2-6, 117-119	GM							—	—	+	r	+	+	—	+	r	—	r	—		R
2-6, 142-144	G							—	—	+	r	r	+	—	R	+	—	—	—	—	—
3-1, 37-39	G							r	—	—	r	—	+	—	R	r	—	F	—		R
3-1, 82-84	G							r	—	—	r	+	—	r	R	r	—	R	—		R
3-1, 117-119	M							—	—	—	R	r	—	—	r	r	r	r	r		—
3-1, 142-144	G							R	—	—	R	r	—	+	r	+	—	R	R		R
3-2, 37-39	G							+	—	—	r	r	+	—	F	r	—	R	r		R
3-2, 81-83	G							r		—	R	—	—	r	F	—	—	R	+		R
3-2, 142-144	G							r		—	r	r	r	r	R	r	r	R	R		R
3-3, 81-83	G		*A. angulare*					—			F	—	—	—	r	R	—	r	F		F
3-3, 141-143	G							—			F	—	—	—	r	—	r	r	R		R
3-4, 37-39	G							—			F	r	—	—	R	—	r	r	F		R
3-4, 81-83	G							—			F	R	—	—	r	—	r	+	R		r
3-4, 118-120	M							—			F	—	—	—	r	—	F	—	F		r
3-4, 141-143	M							—			R	r	—	r	—	r	R	—	F	—	r
3-5, 37-39	G							r			r	—	r	—	—	—	r	+	F	—	r
3-5, 81-83	G							+			R	r	—	r	—	—	R	—	R	—	R
3-5, 118-120	M							r			R	r	—	—	—	—	R	+	F	—	R
3-5, 141-143	M							R			R	—	+	—	—	?	r	—	F	r	R
3-6, 82-84	M		*P. prismatium*					R			R	—	—	—	—	—	r	—	F	R	r
3-6, 118-120	GM							R			R	—	—	—	—	r!	r	—	F	R	r

Note: Symbols for species abundances, preservation, and reworking as in Table 1; ? = doubtful.

Table 3. Ranges and frequency of selected radiolarian species, DSDP Hole 573.

Core-Section (interval in cm)	Preservation	Reworking	Zone	*Buccinosphaera invaginata*	*Collosphaera tuberosa*	*Collosphaera orthoconus*	*Androspyris huxleyi*	*Disolenia* spp.	*Lamprocyrtis nigriniae*	*Pterocorys hertwigii*	*Axoprunum angelinum (S. universa)*	*Lithopera bacca*	*Androspyris anthropiscus*	*Amphispyris roggenthieni*	*Anthocyrtidium angulare*	*Lamprocyrtis neoheteroporos*	*Lamprocyrtis heteroporos*	*Theocorythium trachelium* gr.	*Theocorythium vetulum*	*Pterocanium prismatium*	*Amphirhopalum ypsilon*
1-1, 30-33	G		*B. invaginata*	r	R	—	—	C	r	F								r			r
1-1, 70-72	G	•		r	R	r	—	F	r	F								—			r
1-1, 110-113	GM			—	r	r	—	F	r	F								r			r
1-2, 20-22	G			—	r	—	—	r	—	R								R			R
2-1, 145-147	G		*C. tuberosa*	—	r	r	—	F	r	R								R			r
2-2, 38-40	M				R	R	—	r	r	F	—								r			R
2-2, 95-97	M				+	+	—	R	r	R	—								—			R
2-2, 145-137	P	•			—	—	—	r	r	R	—	—							—			F
2-3, 38-40	P				—	—	—	F	r	R	—	—	—						—			R
2-3, 95-97	M				—	—	—	R	R	R	—	—	—						—			R
2-3, 145-147	PM				—	—	—	R	—	r	R	—	—						—			R
2-4, 36-40	M						—	—	r	R	R	r	—						r			R
2-4, 95-97	G	•					?	R	R	F	r	—	—						—			r
2-4, 145-147	M						—	R	r	F	r	r	—						—			F
2-5, 36-40	M						—	r	r	R	R	—	—						r			F
2-5, 95-97	MG							r	—	r	R	r	—						—			F
2-5, 143-145	M							r	r	R	r	—	—	—					—			F
2-6, 36-38	P	•						R	r	R	R	—	—	—					—			F
2-6, 95-97	M							r	+	R	r	—	+	—					—			F
2-6, 138-140	G							r	r	R	r	—	+	—					—			F
2-7, 36-38	P	•						r	+	R	r	—	+	—					—			F
3-1, 8-10	MP	•	*A. ypsilon*					r	r	F	r	—	—	—					r			F
3-1, 68-70	M							r	r	R	r	—	—	—	—	—		R	R			F
3-1, 125-127	P							—	r	R	r	—	—	—	—	—		R	R			F
3-1, 146-147	M	•						—	+	r	R	—	+	—	—	—		R	R			F
3-2, 35-37	GM							r	r	—	R	—	—	—	—	—		R	F			F
3-2, 85-87	GM							r	—	—	R	—	—	r	—	—	—	F	F			F
3-2, 135-137	M	•						r	r	—	R	—	—	—	—	—		F	F			F
3-3, 35-37	MG							R	+	—	r	—	—	—	—	—		F	F			F
3-3, 85-87	MG							r	r	—	R	r	—	r	—	—	—	F	F			F
3-3, 135-137	MG							r	r	—	R	R	—	r	—	—	—	F	F			F
3-4, 35-37	P							R	—	—	r	—	—	—	—	—	—	R	F			F
3-4, 85-87	M							—	r	—	r	R	—	r	—	—	—	F	F			F
3-4, 135-137	GM	•						—	r	—	r	—	—	r	r	—	—	F	F	—		F
3-5, 6-8	GM							r	—	—	r	r	—	—	—	r	—	F	F	—		F
3-5, 35-37	G							—	—	—	r	—	—	—	—	r	—	F	F	—		F
3-5, 85-87	G							R	+	—	R	r	—	r	F	—	r	F	F	—		R
3-5, 135-137	MG							R	—	—	R	R	—	r	F	R	—	F	F	—		F
3-6, 36-37	G							r	—	—	R	R	—	r	F	r	R	F	F	—		r
3-6, 85-87	G							—	—	—	r	r	—	—	F	r	—	R	R	r		F
3-6, 135-137	MG							—	—	—	R	r	—	—	C	r	—	R	r	—	r	F
4-1, 103-105	M	•						r	—	—	R	r	—	—	F	F	+	+	r	—	r	R
4-1, 144-146	M	•	*A. angulare*					+	—	—	R	r	—	—	F	R	—	r	R	—	r	R
4-2, 36-37	G							r	—	—	R	r	—	—	F	R	—	r	r	—	r	R
4-2, 135-137	G							—	—	—	R	r	—	+	F	R	r	r	r	—	r	R
4-3, 3-10	G	•						—	—	—	r	r	—	r	R	R	r	—	r	—	r	R
4-3, 35-37	G							r	—	—	R	—	—	+	R	—	r	—	r	—	r	R
4-3, 87-89	G		*P. prismatium*					R	—	—	r	—	—	—	r	—	r	R	r	—	r	R

Note: Symbols for species abundances, preservation, and reworking as in Table 2.

Site 575

Hole 575C, at 6°N near the Clipperton Fracture Zone, is the northernmost site of Leg 85. Magnetic stratigraphy was established (Weinreich and Theyer, this volume) and the Pliocene/Pleistocene boundary placed between Samples 575C-1-3, 106 cm and 575C-1-3, 116 cm. Hole 575C reached the uppermost level of the Pliocene at 4.11 m sub-bottom. Percentages of calcium carbonate were not determined. Pleistocene sedimentation appears to have been strongly influenced by bottom currents. The rate of sediment accumulation was lower in this hole, even though it was drilled in the high-productivity area, and the sediments contain very high proportions of reworked Tertiary radiolarians throughout the entire section. Reworking is especially important near the Pliocene/Pleistocene and Brunhes/Matuyama boundaries; it dominates the younger assemblages in the upper part of the Brunhes, except those of some uppermost levels. Preservation of Pleistocene radiolarians is regularly poor

Table 4. Ranges and frequency of selected radiolarian species, DSDP Hole 575C.

Core-Section (interval in cm)	Preservation	Reworking	Zone	*Buccinosphaera invaginata*	*Collosphaera tuberosa*	*Collosphaera orthoconus*	*Androspyris haxleyi*	*Disolenia* spp.	*Lamprocyrtis nigriniae*	*Pterocorys hertwigii*	*Axoprunum angelinum (S. universus)*	*Lithopera bacca*	*Androspyris anthropiscus*	*Amphispyris roggenthieni*	*Anthocyrtidium angulare*	*Lamprocyrtis neoheteroporos*	*Lamprocyrtis heteroporos*	*Theocorythium trachelium* gr.	*Theocorythium vetulum*	*Pterocanium prismatium*	*Amphirhopalum ypsilon*
1-1, 5–7	M	*	*B. invaginata*	+	r	—	—	F	—	—								—			+
1-1, 25–27	M	*		+	R	—	—	r	—	—								—			—
1-1, 45–47	M	**	*C. tuberosa*	—	r	r	—	r	—	—	—	—						—			r
1-1, 65–67	P	***		—	+	—	—	r	r	—	—	—						—			r
1-1, 85–87	P	***			?	—	?	r	—	—	—	—						r			—
1-1, 105–107	P	***			?	R	—	—	+	—	—	—						r			r
1-1, 125–127	M	***			—	r	—	—	+	—	r	r						R			R
1-1, 145–147	P	***			—	—	—	—	—	—	r	r						r			F
1-2, 15–17	MP	**				r	—	—	—	—	r	—						r			F
1-2, 35–37	MP	*				r	—	—	—	—	r	—						—			F
1-2, 55–57	M	*	*A. ypsilon*			—	—	—	—	—	r	—	—	—				—			R
1-2, 85–87	M	*									r	—	—	—				r			F
1-2, 95–97	M	***									r	—	—	—				F			F
1-2, 115–117	MG	**									r	r	—	+	—			F			r
1-2, 135–137	M	*									r	—	—	+	—	—		r			r
1-2, 145–147	MG	**									—	r	—	r	—	r		R			r
1-3, 5–7	P	**									r	r	—	r	—	r	—	r			r
1-3, 25–27	P	**									—	—	—	r	r	r	—	—	—		+
1-3, 45–47	MG	***	*A. angulare*								r	r	—	r	R	R	—	r	—		F
1-3, 65–67	MG	***									r	r	—	—	R	r	r	r	—	—	r
1-3, 85–87	P	***									r	—	—	r	r	—	r	r	r	—	+
1-3, 105–107	P	***									r	—	—	—	—	+	r	—	r	—	—
1-3, 115–117	P	***	*P. prismatium*								r	r	—	—	r	—	r	r	—	r	—

Note: Species abundances are estimated. Symbols for abundance, preservation, and reworking as in Table 2. (Additional symbols for reworking: ** = moderate; *** = high.)

to moderate, and may explain the discontinuous occurrences. All stratigraphic indicator species are scarce, but the different radiolarian zones or events could be observed (Table 4). *Buccinosphaera invaginata* is confined to a thin surface layer about 25 cm thick, and *Collosphaera tuberosa* occurs within the topmost meter. The genus *Acrosphaera* is exceptionally abundant at the top of the Quaternary sequence. The *Anthocyrtidium angulare* Zone occupies a short interval, and the first and the last occurrences of *A. angulare* are recorded in poorly preserved samples. The extinction level of *Pterocanium prismatium* coincides with the upper boundary of the Olduvai event.

CORRELATIONS AND DISCUSSION

Discussion of the correlations of sequences here proceeds from the base (Pliocene/Pleistocene boundary) to the top (the present). Hole 573 was chosen as the reference Quaternary section for Leg 85 because levels of lowermost and uppermost occurrence can be compared with both the paleomagnetism record (Weinreich and Theyer, this volume) and the calcium carbonate curve (Pujos, this volume). Moreover, Hole 573 yielded an almost undisturbed succession having a high sediment accumulation rate (Figs. 2 and 3).

The Pliocene/Pleistocene boundary is placed near the top of the Olduvai polarity event according to Berggren et al. (1980); it is very close to the extinction level of *Pterocanium prismatium* (about 1.65 Ma). It seems necessary, however, to discuss the exact characteristics of the upper limit of the *Pterocanium prismatium* Zone emended by Riedel and Sanfilippo (1977). Goll (1980) mentioned that the last appearance of *P. prismatium* was diachronous in the equatorial Pacific; that is, there was a gap between this event and the first appearance of *Lamprocyrtis nigriniae*, and consequently there is no radiolarian biohorizon for the Pliocene/Pleistocene boundary.

In Holes 573 and 575C the upper limit of *Pterocanium prismatium* coincides with the Pliocene/Pleistocene boundary and the first occurrence of *Anthocyrtidium angulare*. These events mark also the top of carbonate-dissolution cycle M17, which has been correlated with the top of the Olduvai (Hays et al., 1969 and Gardner, 1982). The last occurrence of *Theocorythium vetulum* is higher in the section. In Hole 572A *P. prismatium* becomes extinct at the top of carbonate stage M17, but there is a gap between this extinction level and the first occurrence of *A. angulare*, which lies higher in the sequence.

Farther east (Goll, 1980), *A. angulare* is even scarcer, and its lower limit is higher in the Pleistocene sequence. This may reflect a true diachronism in the appearance of this species. Interpretation of its morphologic limits becomes more difficult toward the eastern regions of the

Table 5. Radiolarian zones and events, Holes 571, 572A, 573, and 575C.

Age	Radiolarian zone (Nigrini, 1971)	Radiolarian "event"	Hole 571	Hole 572A	Hole 573	Hole 575C
			Core-Section (interval in cm)			
Quaternary	*B. invaginata*	FO *B. invaginata*	1-1, 121-123 1-2, 1-3	1-1, 41-43 1-1, 61-63	1-1, 70-73 1-1, 110-113	1-1, 25-27 1-1, 35-37
	C. tuberosa	FO *C. tuberosa*	1-3, 118-120 1-4, 3-5	1-4, 36-38 1-4, 117-119	2-2, 95-97 2-2, 145-147	1-1, 65-67 1-1, 85-87
	A. ypsilon	LO *A. angelinum* (= *S. universus*)	1-5, 21-23 1-5, 40-42	1-5, 76-78 1-5, 117-119	2-3, 145-147 2-4, 36-40	1-1, 105-107 1-1, 125-127
		LO *L. bacca*	1-5, 81-83 1,CC (1-3)	1-6, 76-78 1-6, 137-139	2-4, 36-40 2-4, 95-97	1-1, 105-107 1-1, 125-127
		A. anthropiscus → *A. huxleyi*	Not reached	1-6, 137-139 2-2, 117-119	Upper to 2-6, 138-140	Species sought but not found
		LO *A. roggentheni*		2-3, 118-120 2-3, 141-143	3-2, 35-37 3-2, 85-87	1-2, 95-97 1-2, 115-117
	A. angulare	LO *A. angulare*		2-6, 82-84 2-6, 117-119	3-5, 35-37 3-5, 85-87	1-3, 5-7 1-3, 25-27
		LO *L. neoheteroporos*		2-6, 82-84 2-6, 117-119	3-5, 85-87 3-5, 135-137	1-2, 135-137 1-2, 145-147
		FO acme *T. trachelium* LO *T. vetulum*		3-1, 82-84 3-1, 117-119	3-6, 35-37 3-6, 85-87	1-3, 5-7 1-3, 85-87
		L. heteroporos → *L. neoheteroporos*		3-3, 81-83 3-3, 141-143	3-6, 135-137 4-1, 103-105	1-3, 65-67 1-3, 85-87
		FO *A. angulare*		3-4, 118-120 3-4, 141-143	4-3, 35-37 4-3, 87-89	1-3, 85-87 1-3, 105-107
Pliocene	*P. prismatium*	LO *P. prismatium*		3-5, 118-120 3-5, 141-143	4-3, 35-37 4-3, 87-89	1-3, 105-107 1-3, 115-117

Note: FO = first occurrence; LO = last occurrence.

Pacific; this explains why Goll has not used the range of *A. angulare* in his stratigraphy of the easternmost Pacific. Unfortunately, the first occurrence of *Collosphaera huxleyi*, reported by Goll (1980) as marker for the base of the Pleistocene, cannot be useful in this part of the equatorial Pacific, because its occurrences are too sporadic.

Johnson and Knoll (1975) dated the last appearance of *A. angulare* at about 940,000 yrs. ago, whereas Goll (1980) has estimated that this species became extinct about 900,000 yrs. ago. The last occurrence in Hole 573 occurs just below the Jaramillo polarity event and marks carbonate-dissolution cycle M5. The extinction occurs at a level similar to that in the other holes, in higher latitudes (Hole 575C) as well as toward the eastern region (Hole 572A); it indicates a date somewhat earlier than the first estimates (approximately 1.05 Ma, calculated on the basis of magnetic reversals). This extinction event may be a reliable boundary marker in the equatorial Pacific.

Significant changes occur among the radiolarian assemblages within the *A. angulare* Zone of Nigrini (1971), and they could be useful to informally divide it into upper and lower parts. The first occurrence of *Theocorythium trachelium* could be an eventual marker for the Pliocene/Pleistocene boundary in the equatorial Pacific, but this species occurs in very low numbers in the lowermost Pleistocene. Other workers have reported its extension below the Pliocene/Pleistocene boundary (Johnson, 1974). On the other hand, Nigrini (1971) and Riedel and Westberg (1982) did not find any specimens of *T. trachelium* in the *P. prismatium* Zone. At Leg 85 sites, *T. trachelium* does show an increased abundance (acme), coincident with the extinction level of *Theocorythium vetulum*. This occurs within carbonate-dissolution cycle M7 in both Hole 573 and Hole 572A, and may be used to divide the *Anthocyrdium angulare* Zone into separate parts. The lower part is distinguished by the presence of *T. vetulum*, associated with infrequent *T. trachelium* and *A. angulare*. The evolution from *Lamprocyrtis heteroporos* to *L. neoheteroporos* occurs in this subdivision. The upper part is bounded at the bottom by the lowest occurrence of abundant *T. trachelium*, and is identified by the presence of *L. neoheteroporos* and very common *A. angulare* and *T. trachelium* specimens. The highest occurrence of *L. neoheteroporos* falls very close to the extinction level of *A. angulare*. In Hole 575C the expression of these events is probably masked by the much lower sedimentation rate and the reworking.

Goll has used the extinction level of *Amphispyris roggentheni* in his zonation of the easternmost equatorial Pacific. The occurrence in Holes 572A, 573, and 575C are the first reported for the central Pacific. In both the east and the central region, this species is always scarce and sporadic; to be certain of its presence, one must study several slides. I consider that in both Hole 573 and Hole 575C the extinction level of *A. roggentheni* occurs just below the Brunhes/Matuyama boundary, and that in Holes 573 and 572A it marks the transition between carbonate-dissolution cycles M1 and B17. This extinction may be a reliable marker in the equatorial Pa-

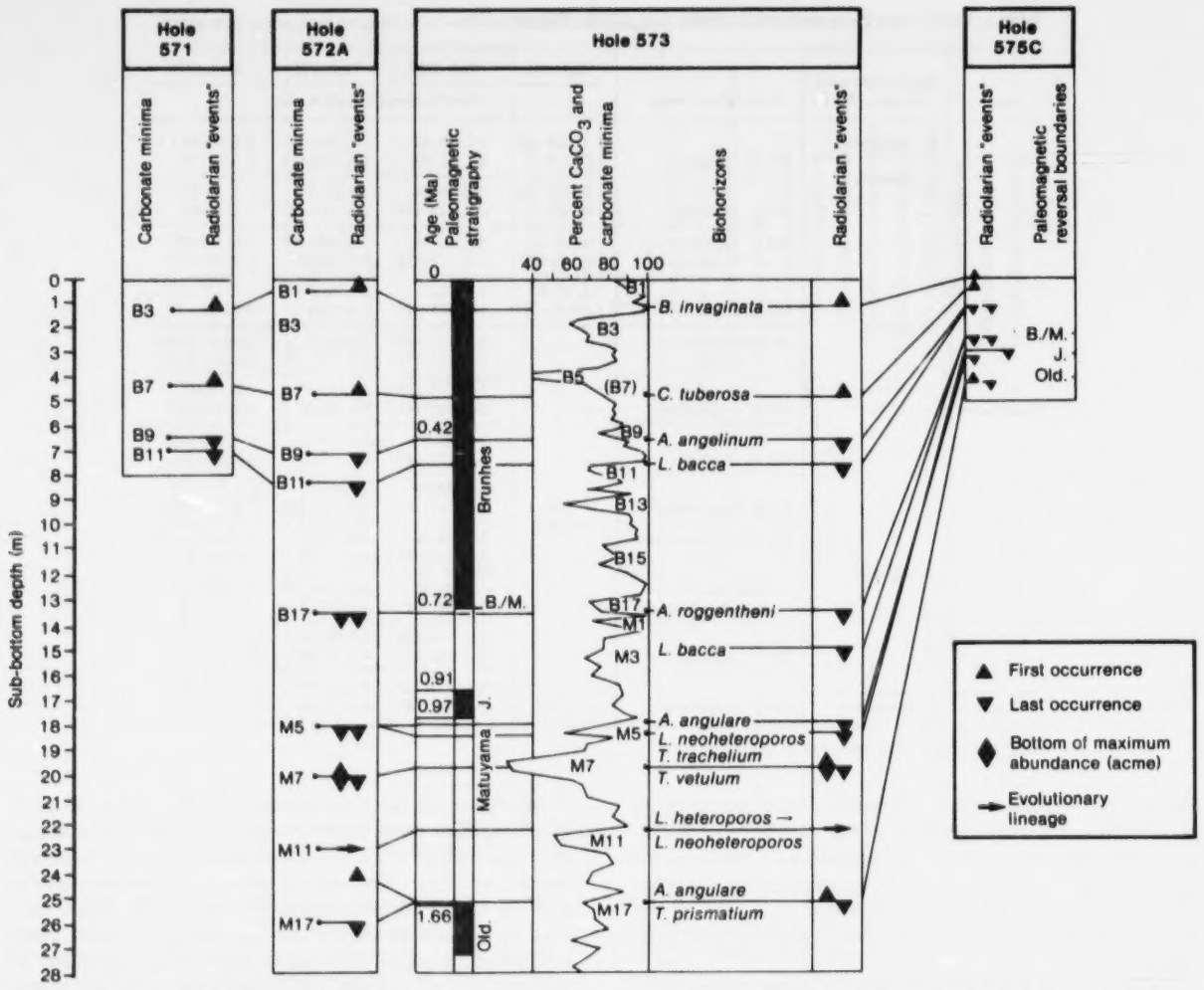

Figure 2. Pleistocene radiolarian biohorizons (events), calcium carbonate fluctuations, and paleomagnetics, Hole 573. Carbonate-minima data from Pujos (this volume). Paleomagnetic stratigraphy from Weinreich and Theyer (this volume). Correlations between four holes of Leg 85.

cific near the Brunhes/Matuyama boundary, although the scarcity of the species will have to be taken into account when attempting correlations. The timing of this extinction and the possibility of a west–east diachronism will also have to be addressed by further work, because Goll (1980) has estimated this event to be about 650,000 yrs. old in the eastern Pacific. In that region Goll (1980) has reported the highest (last) occurrence of *Lithopera bacca* just below the highest (last) occurrence of *A. roggentheni*. *L. bacca* always occurred rather infrequently. A first (i.e., older) highest occurrence level lies at or very close to the extinction level of *A. roggentheni*. However, *L. bacca* recurs in a short interval in the Brunhes. The second (younger) highest occurrence lies just below the highest occurrence of *Axoprunum angelinum*.

The date of the extinction level of *Axoprunum angelinum* (= *Stylatractus universus* Hays) has been estimated in two ways, using (1) a constant accumulation rate between the Brunhes/Matuyama boundary and the present and (2) an astronomical base for the time control. In accord with Hays et al. (1969), the upper limit is synchronous with the top of carbonate maximum peak B10 in the three holes where the carbonate content has been recorded (Pujos, this volume).

This limit occurs in an interval where the radiolarian assemblages are always well preserved. In correlations between carbonate and oxygen-isotope stratigraphies (Berggren et al., 1980; Gardner, 1982), the transition between carbonate stages B9 and B10 has been correlated with the boundary of isotopic stages 11 to 12. The age of 421,000 yrs. can be considered as the definitive estimate of the age of this isotopic stage boundary (Morley and Hays, 1981). If one uses this age for the upper limit of *Axoprunum angelinum*, and if one considers the surface level as representing the Recent sedimentation, it becomes evident that an assumption of a constant accumulation rate between 720,000 yrs. ago and the present is untenable.

The first appearance of *Collosphaera tuberosa* and *Buccinosphaera invaginata* correspond to dates presum-

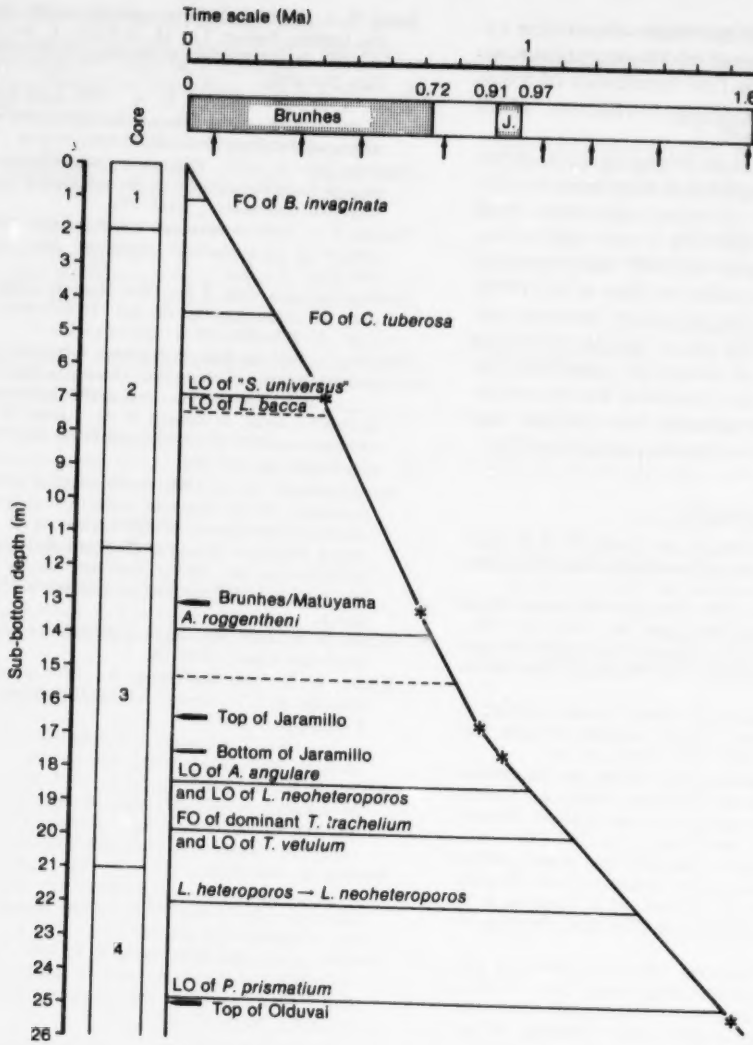

Figure 3. Calibration of Pleistocene radiolarian events, Hole 573. Ages are obtained by extrapolating the sediment accumulation rates between the paleomagnetic boundaries determined by Weinreich and Theyer (this volume) and the estimated date of last occurrence of "*S. universus*," based on time scale of Morley and Hays (1981). FO = first occurrence; LO = last occurrence; asterisks = data points used to construct sedimentation rate curve.

ably later than those reported by Johnson and Knoll (1975). The first occurrence of *C. tuberosa* often falls above rather poorly preserved samples, and coincides in all cases with the top of carbonate stage B7, which has been correlated (Berggren et al., 1980) with the base of ^{18}O Stage 8 and dated at about 279,000 yrs. (Morley and Hays, 1981). The distribution of *Buccinosphaera invaginata* coincides with the two upper carbonate stages in Holes 571 and 573. In Hole 572A, calcium carbonate fluctuations seem more complicated.

The first appearance of *B. invaginata* is estimated here at about 65,000 to 72,000 yrs. ago—that is, later than the date determined by Goll (1980). We might have to reconsider the use of these two species for datum levels, because their preservation threshold is very low.

SUMMARY

Quaternary radiolarians from 4 of the 17 Leg 85 holes were studied intensively. Twelve datum levels, biohorizons, or evolutionary lineages were compared and calibrated using the magnetostratigraphy and carbonate-dissolution cycles of the last 1.7 m.y.

Radiolarians that become extinct in the section representing this interval are *Pterocanium prismatium* (just above the Olduvai event), *Anthocyrtidium angulare* and *Lamprocyrtis neoheteroporos* (just below the Jaramillo event), and *Amphispyris roggentheni* (just below the Brunhes/Matuyama boundary).

Throughout the Matuyama, the evolutionary lineage from *Lamprocyrtis heteroporos* to *Lamprocyrtis neohet-*

eroporos occurs at the top of carbonate-dissolution cycle M11, and the last occurrence of *Theocorythium vetulum* is synchronous with the first occurrence of maximum abundance of *Theocorythium trachelium*, which marks carbonate minimum M7.

Within sediments interpreted as belonging to the Brunhes, *Lithopera bacca* and *Axoprunum angelinum* (= *Stylatractus universus*) bracket carbonate-maximum peak B10. The upper limit of *A. angelinum* is now well known, although it had previously been variously dated between 320,000 and 440,000 yrs.; according to Hays et al. (1969), this extinction occurs near the boundary between carbonate cycles B9 and B10. The use of species belonging to the genus *Collosphaera* is somewhat unreliable because of their low preservation threshold. But the occurrence of *Buccinosphaera invaginata* demonstrates that sediments are younger than carbonate minimum B3.

REFERENCES

Berggren, W. A., Burckle, L. H., Cita, M. B., Cooke, H. B. S., Funnel, B. M., et al., 1980. Towards a Quaternary time scale. *Quat. Res.*, 13:277–302.

Campbell, A. S., and Clark, B. L., 1944. Miocene radiolarian faunas from southern California. *Spec. Pap. Geol. Soc. Am.*, 51:1–76.

Caulet, J. P., 1971. Contribution à l'étude de quelques radiolaires nasselaires des boues de la Méditerranée et du Pacifique. *Cah. Micropaleontol.*, ser. 2, 10:1–10.

_____, 1979. Les dépots à Radiolaires d'âge Pliocène supérieur à Pléistocène dans l'océan Indien central: nouvelle zonation biostratigraphique. *Mem. Mus. Hist. Nat.*, 43(C):119–141.

Ehrenberg, C. G., 1872. Mikrogeologischen Studien als Zusammenfassung seiner Beobachtungen des Kleinsten Lebens der Meeres-Tiefgründe aller Zonen und dessen geologischen Einfluss. *Monatsber. Kgl. Preuss. Akad. Wiss. Berlin Jahrg.*, pp. 265–322.

Gardner, J. V., 1982. High-resolution carbonate and organic-carbon stratigraphies for the late Neogene and Quaternary from the western Caribbean and eastern Pacific. *In* Prell, W. L., Gardner, J. V., et al., *Init. Repts. DSDP*, 68: Washington (U.S. Govt. Printing Office), 347–364.

Goll, R. M., 1980. Pliocene–Pleistocene radiolarians from the East Pacific Rise and the Galapagos Spreading Center, Deep Sea Drilling Project Leg 54. *In* Rosendahl, B. R., Hekinian, R. et al., *Init. Repts. DSDP*, 54: Washington (U.S. Govt. Printing Office), 425–453.

Haeckel, E., 1887. Report on the Radiolaria collected by H.M.S. *Challenger* during the years 1873–76. *Rep. Sci. Results Voyage H.M.S.* Challenger, *Zoology*, 18:1–1303.

Hays, J. D., 1965. Radiolaria and late Tertiary and Quaternary history of Antarctic seas: biology of the Antarctic Seas. II. *Antarct. Res. Ser.*, 5:125–184.

_____, 1970. Stratigraphy and evolutionary trends of radiolaria in North Pacific deep sea sediments. *In* Hays J. D. (Ed.), *Geological Investigations of the North Pacific. Mem. Geol. Soc. Am.*, 126: 185–218.

Hays, J. D., Saito, T., Opdyke, N. D., and Burckle, L. H., 1969. Pliocene–Pleistocene sediments of the equatorial Pacific: their paleomagnetic, biostratigraphic, and climatic record. *Geol. Soc. Am. Bull.*, 80:1481–1514.

Hays, J. D., and Shackleton, N. J., 1976. Globally synchronous extinction of the radiolarian *Stylatractus universus*. *Geology*, 4: 649–652.

Hedberg, H. D., 1976. *International Stratigraphic Guide: A Guide to Stratigraphic Classification, Terminology and Procedure*: New York (Wiley-Interscience).

Johnson, D. A., 1974. Radiolaria from the eastern Indian Ocean, DSDP Leg 22. *In* von der Borch, C. C., Sclater, J. G., et al., *Init. Repts. DSDP*, 22: Washington (U.S. Govt. Printing Office), 521–575.

Johnson, D. A., and Knoll, A. H., 1975. Absolute ages of Quaternary radiolarian datum levels in the equatorial Pacific. *Quat. Res.*, 5: 99–110.

Kling, S. A., 1973. Radiolaria from the eastern North Pacific, Deep Sea Drilling Project, Leg 18. *In* Kulm, L. D., von Huene, R., et al., *Init. Repts. DSDP*, 18: Washington (U.S. Govt. Printing Office), 617–672.

Knoll, A. H., and Johnson, D. A., 1975. Late Pleistocene evolution of the collosphaerid radiolarian *Buccinosphaera invaginata* Haeckel. *Micropaleontology*, 21(1):60–68.

Molina-Cruz, A., 1977. Radiolarian assemblages and their relationship to the oceanography of the subtropical southeastern Pacific. *Mar. Micropaleontol.*, 2:315–352.

Morley, J. J., 1980. Analysis of the abundance variations of the subspecies of *Cycladophora davisiana*. *Mar. Micropaleontol.*, 5: 205–214.

Morley, J. J., and Hays, J. D., 1981. Towards a high resolution, global, deep sea chronology for the last 750,000 years. *Earth Planet Sci. Lett.*, 53:279–295.

Nigrini, C., 1967. Radiolaria in pelagic sediments from the Indian and Atlantic oceans. *Scripps Inst. Oceanogr. Bull. 11.*

_____, 1971. Radiolarian zones in the Quaternary of the equatorial Pacific Ocean. *In* Funnell, B. M., Riedel, W. R. (Eds.), *The Micropalaeontology of the Oceans*: Cambridge (Cambridge University Press), pp. 443–461.

Petrushevskaya, M. G., 1968. Radiolarians of orders Spumellaria and Nasselaria of the Antarctic region (from material of the Soviet Antarctic expedition). *In* Andriyashev, A. P., and Ushakov, P. V. (Eds.), *Biological Report of the Soviet Antarctic Expedition (1955–1958)* (Leningrad, 1967 [Isdatel'stp "Nanka"]): Jerusalem (Israel Program for Scientific Translations), pp. 9–156. (Transl. from Russian.)

Riedel, W. R., 1957. Radiolaria: a preliminary stratigraphy. *Rep. Swed. Deep-Sea Exped.*, 6:59–96.

Riedel, W. R., and Sanfilippo, A., 1977. Cenozoic Radiolaria. *In* Ramsay, A. T. S., *Oceanic Micropaleontology*: London (Academic Press), pp. 847–912.

_____, 1978. Stratigraphy and evolution of tropical Cenozoic radiolarians. *Micropaleontology*, 24(1):61–96.

Riedel, W. R., and Westberg, M. J., 1982. Neogene radiolarians from the eastern tropical Pacific and Caribbean, Deep Sea Drilling Project, Leg 68. *In* Prell, W. L., Gardner, J. V., et al., *Init. Repts. DSDP*, 68: Washington (U.S. Govt. Printing Office), 289–300.

Romine, K., and Moore, T. C., Jr., 1981. Radiolarian assemblage distribution and paleoceanography of the eastern equatorial Pacific Ocean during the last 127,000 years. *Palaeogeogr., Palaeoclimatol., Paleoecol.*, 35:281–314.

Strelkov, A. A., and Reshetnyak, V. V., 1971. Colonial Spumellarian radiolarians of the world ocean. *In* Strelkov, A. A. (Ed.), *Exploration of the Fauna of the Seas*: Moscow (Zool. Inst., Acad. of Sci., U.S.S.R.), 9(17):295–373.

Date of Initial Receipt: 7 November 1983
Date of Acceptance: 22 April 1984

APPENDIX
Species List with Bibliography for Taxa Cited[3]

***Androspyris anthropiscus* Haeckel**

Androspyris anthropiscus Haeckel, 1887, p. 1093, pl. 83, fig. 8; Goll, 1980, p. 436, pl. 4, figs. 2–3.

***Androspyris huxleyi* (Haeckel)**

Lamprospyris huxleyi Haeckel, 1887, p. 1094, pl. 89, fig. 14.
Androspyris huxleyi (Haeckel) Goll, 1980, p. 436. pl. 4, figs. 4–5.

***Amphirhopalum ypsilon* Haeckel**

Amphirhopalum ypsilon Haeckel, 1887, p. 522; Nigrini, 1971, p. 447, pl. 34.1, figs. 7a–c.

***Amphispyris roggentheni* Goll**

Amphispyris roggentheni Goll, 1980, p. 437, pl. 6, figs. 1, 3, 4, pl. 7, figs. 4–6.

***Anthocyrtidium angulare* Nigrini**

Anthocyrtidium angulare Nigrini, 1971, p. 445, pl. 34.1, figs. 3a–b.

[3] See References for full bibliographic data on sources given here.

***Axoprunum angelinum* (Campbell and Clark)**

Stylosphaera angelina Campbell and Clark, 1944, p. 12, pl. 1, figs. 14–20.
Stylatractus universus Hays, 1970, p. 215, pl. 1, figs. 1–2.
Axoprunum angelinum (Campbell and Clark) Kling, 1973, p. 634, pl. 1, figs. 13–16, pl. 6, figs. 14–18.

***Buccinosphaera invaginata* Haeckel**

Buccinosphaera invaginata Haeckel, 1887, p. 99, pl. 5, fig. 11; Nigrini, 1971, p. 445, pl. 34.1, fig. 2; Knoll and Johnson, 1975, p. 63, pl. 1, figs. 3–6.

***Collosphaera orthoconus* (Haeckel)**

Conosphaera orthoconus Haeckel, 1887, p. 221, pl. 12, fig. 2.
Collosphaera sp. A, Knoll and Johnson, 1975, p. 103, pl. 1, fig. 1.
Collosphaera orthoconus (Haeckel) Goll, 1980, p. 436, pl. 1, figs. 10–11.

***Collosphaera tuberosa* Haeckel**

Collosphaera tuberosa Haeckel, 1887, p. 97; Nigrini, 1971, p. 445, pl. 34.1, fig. 1; Strelkov and Reshetnyak, 1971, pp. 336–337, pl. 4, figs. 24–25; Knoll and Johnson, 1975, p. 63, pl. 2, figs. 1–3.

***Cycladophora* (?) *davisiana* Ehrenberg**

Cycladophora davisiana Ehrenberg, 1872, p. 297; Petrushevskaya, 1968, p. 120, figs. 69–70; Morley, 1980, pl. 1.

***Disolenia* spp.**

Different species belonging to the genus *Disolenia*.

***Lamprocyrtis heteroporos* (Hays)**

Lamprocyclas heteroporos Hays, 1965, p. 179, pl. 3, fig. 1.
Lamprocyrtis heteroporos (Hays) Kling, 1973, p. 639, pl. 5, figs. 19–21, pl. 15, fig. 6.

***Lamprocyrtis neoheteroporos* Kling**

Lamprocyrtis neoheteroporos Kling, 1973, p. 639, pl. 5, figs. 17–18, pl. 15, figs. 4–5.

***Lamprocyrtis nigriniae* (Caulet)**

Conarachnium nigriniae Caulet, 1971, p. 3, pl. 3, figs. 1–4, pl. 4, figs. 1–4.
Lamprocyrtis haysi Kling, 1973, p. 639, pl. 5, figs. 15–16, pl. 15, figs. 1–3.
Lamprocyrtis nigriniae (Caulet) Kling, 1973, p. 217, pl. 1, fig. 17.

***Lithopera bacca* Ehrenberg**

Lithopera bacca Ehrenberg, 1872, p. 314; Riedel and Sanfilippo, 1978, p. 70, pl. 6, fig. 9.

***Pterocanium prismatium* Riedel**

Pterocanium prismatium Riedel, 1957, p. 87, pl. 3, figs. 4–5; Riedel and Sanfilippo, 1978, p. 72, pl. 9, fig. 1.

***Pterocorys hertwigii* (Haeckel)**

Eucyrtidium hertwigii (Haeckel), 1887, p. 1491, pl. 80, fig. 12.
Pterocorys hertwigii (Haeckel) Caulet, 1979, pl. 3, fig. 4.

***Theocorythium trachelium* (Ehrenberg)**

Eucyrtidium trachelius Ehrenberg, 1872, p. 312.
Theocorythium trachelium (Ehrenberg) Nigrini, 1967, p. 77, pl. 8, figs. 1–2, pl. 9, figs. 1–2, Riedel and Sanfilippo, 1978, p. 76, pl. 9, fig. 17.

***Theocorythium vetulum* Nigrini**

Theocorythium vetulum Nigrini, 1971, p. 447, pl. 34.1, figs. 6a–b.

Reprinted from Mayer, L., Theyer, F., et al., 1985
Initial Reports of the Deep Sea Drilling Project, Volume LXXXV, Washington (U. S. Government Printing Office)

12. RADIOLARIAN BIOSTRATIGRAPHY IN THE CENTRAL EQUATORIAL PACIFIC, DEEP SEA DRILLING PROJECT LEG 85[1]

Catherine A. Nigrini[2]

ABSTRACT

The radiolarian fauna found at the five sites drilled on Leg 85 ranges from Recent to uppermost Eocene and is both abundant and well preserved in almost all the recovered sediments. Detailed lists of 133 radiolarian events and range charts, comprising the upper and lower morphotypic limits of 73 species of Radiolaria, are presented for Sites 572, 573, 574, and 575.

Of the 133 events, 96 are consistently in order in the 12 Leg 85 holes. Twenty-five additional events are out of sequence in $<30\%$ of the holes, but are still considered to be reliable and reproducible in the central equatorial Pacific. The remaining 12 events are out of sequence in $\geq 30\%$ of the holes in which they occur. Of these, 3 are artifacts of insufficient data or coring disturbance. The remaining 9 events (T *Spirocyrtis subtilis*, B *Cyrtocapsella japonica*, T *Lychnodictyum audax*, T *Botryostrobus bramlettei*, T *Didymocyrtis laticonus*, B *Lithopera neotera*, B *Phormostichoartus corbula*, B *Dictyocoryne ontongensis*, and B *Carpocanopsis cristata* s.s.) are more or less suspect for a variety of reasons.

Contrary to expectations, the percentage of out-of-sequence events, relative to the number of events tracked in various holes, is not noticeably lower in the hydraulic-piston-cored holes.

INTRODUCTION

Radiolarians were recovered from virtually all levels of the five DSDP sites drilled in the central equatorial Pacific on Leg 85 (Fig. 1). The upper portion of each site (down to maximum depth of 206.5 m in Hole 574) was double cored by using the hydraulic piston corer (HPC). Sites 572, 573, and 574 were then rotary drilled, with continuous coring, from a depth approximately equal to the maximum penetration of the HPC on down to basement. Site 575 was drilled with the HPC only, and basement was not reached. A single mudline core was recovered at Site 571. The locations and water depths of the sites are as follows:

Site	Location	Water depth (m)
571	3°59.84′N, 114°08.53′W	3962
572	1°26.09′N, 113°50.52′W	3893
573	0°29.91′N, 113°18.57′W	4301
574	4°12.52′N, 133°19.81′W	4561
575	5°51.00′N, 135°02.16′W	4536

Radiolarian assemblages range from uppermost Eocene to Recent (Fig. 2), and the fauna is both well preserved and prolific in almost all the recovered sediments.

PROCEDURES

One sample was taken from each section of core recovered during the first penetration of the HPC and the rotary drilling phase of the operation. Only core-catcher samples were taken from the second HPC penetration. Sediments were prepared in the usual manner, sieved at 63 μm, and mounted on strewn slides. For this report every core-catcher sample, and usually one intermediate sample from each core, was examined.

RADIOLARIANS AT EACH SITE

In this section, the radiolarian findings for each site are summarized. Detailed lists of events for Sites 572, 573, 574, and 575 are presented in Appendix A; range charts, plotted against depth of penetration, are presented in Figures 3 to 10. Raw data are presented in Appendix B. Unlike other DSDP reports (e.g., Westberg and Riedel, 1982), this chapter does not report abundances, but rather evaluates species on their presence or absence only. Some evolutionary transitions have been noted, but the bulk of the data presented are based on morphotypic first- and last-occurrence datum levels. In the events list, samples are designated by core and section number, and the sample depths below the seafloor are given in meters. Events and absolute ages that are inconsistent with the majority of the data collected are bracketed in the tables of events. Absolute ages are those used by the shipboard party to calculate sediment accumulation rates (see Table 1, Introduction, this volume). In the range charts, a heavy line indicates maximum confirmed range of species, and the dashed line indicates the interval between the first or last sample examined in which the species is present and the nearest sample examined in which the species is not present. An asterisk indicates a first or last occurrence that is inconsistent with the majority of the data collected. The epoch boundaries conform to those of Barron et al. (this volume). Abundances and conditions of preservation are almost always "common" and "good," so only exceptions to this general condition are noted in the text for each site.

The radiolarian zones used in this chapter for the Tertiary are those of Riedel and Sanfilippo (1978). The Quaternary zones used are those defined by Nigrini (1971).

[1] Mayer, L., Theyer, F., et al., *Init. Repts. DSDP*, 85: Washington (U.S. Govt. Printing Office).

[2] Address: 510 Papyrus Drive, La Habra Heights, CA 90631.

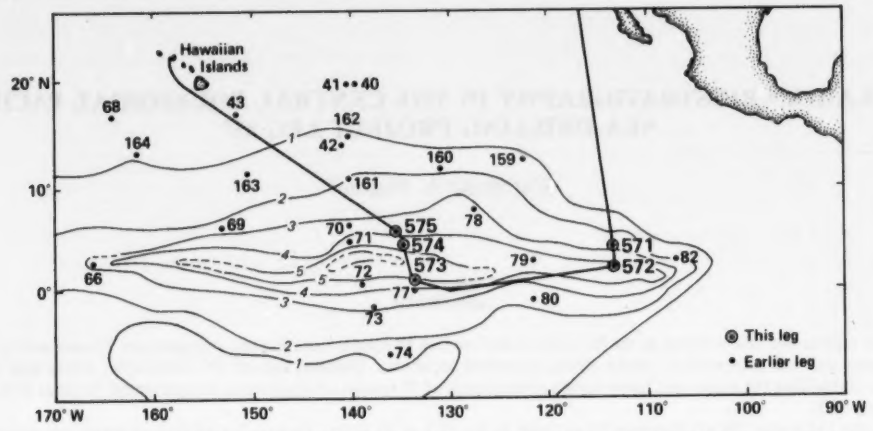

Figure 1. Location of Leg 85 and earlier drill sites. Sediment thickness is in tenths of two-way traveltime.

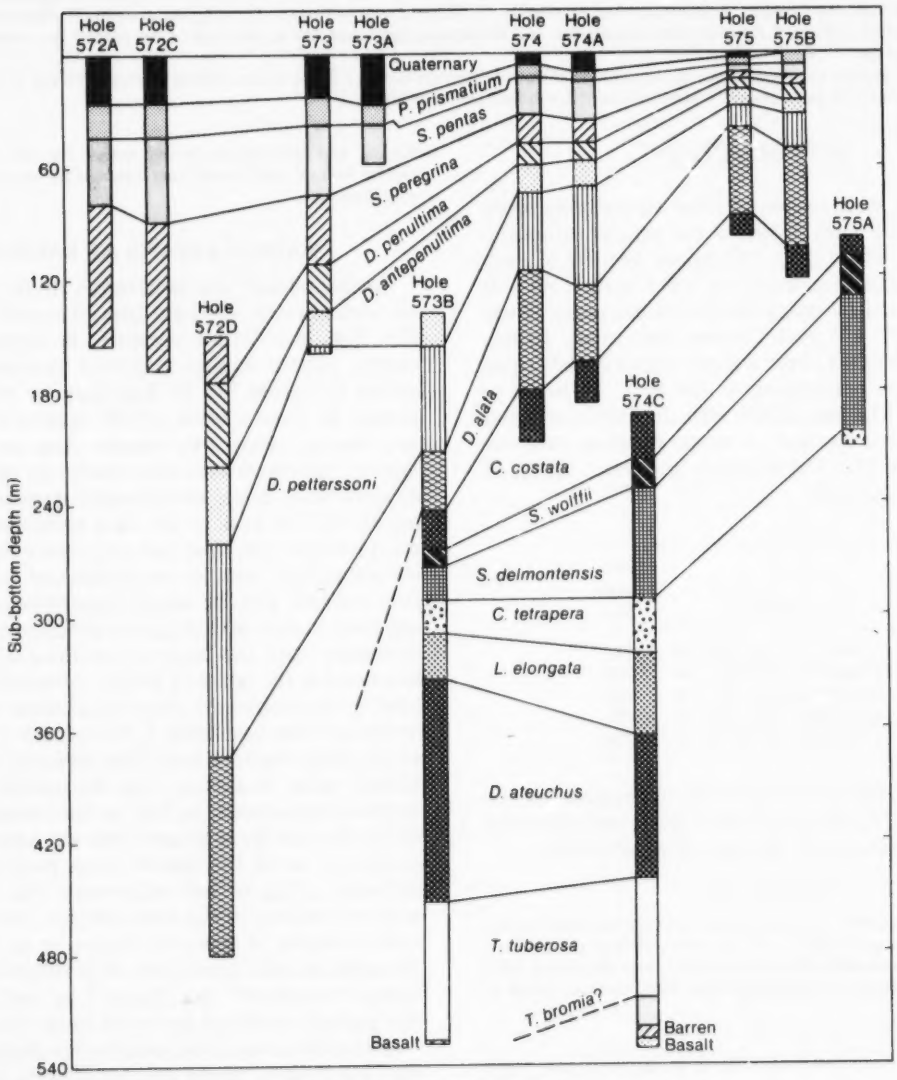

Figure 2. Summary chart of radiolarian zonation for DSDP Leg 85, Sites 572 to 575.

Site 571

Site 571 was occupied primarily for the collection of heat-flow data. In the process, a single 7.11-m mudline core was recovered. It contains common, well-preserved, and diverse Quaternary radiolarians; the oldest sediment belongs to the *Amphirhopalum ypsilon* Zone (Quaternary).

Site 572

Site 572 is on the eastern edge of the equatorial high-productivity zone, slightly south and west of DSDP Site 81. Three of the five holes drilled at this site (572A, 572C, and 572D) are sufficiently long to contain useful stratigraphic information. Holes 572A and 572C are parallel HPC sequences, both of which end in the *Stichocorys peregrina* Zone (upper Miocene). Hole 572D was rotary drilled and continuously cored to basement (479.5 m sub-bottom) and was still within the *Dorcadospyris alata* Zone (middle Miocene) just above the basalt. The *Stichocorys peregrina* Zone is unusually thick at this site, owing to a very high rate of sediment accumulation caused by an abundant upwelling diatom flora. As a result, there is some dilution of the radiolarian fauna between 572A-8,CC and 572D-7,CC (72 to 218 m sub-bottom). A list of radiolarian events for Site 572 is presented in Appendix A, Table 1. Figures 3 and 4 are range charts for Holes 572A and 572D.

Site 573

Site 573 is near DSDP Site 77 in the eastern equatorial Pacific. Holes 573 and 573A are parallel HPC holes, but Hole 573A was abandoned prematurely. Hole 573B was rotary drilled and continuously cored to basement

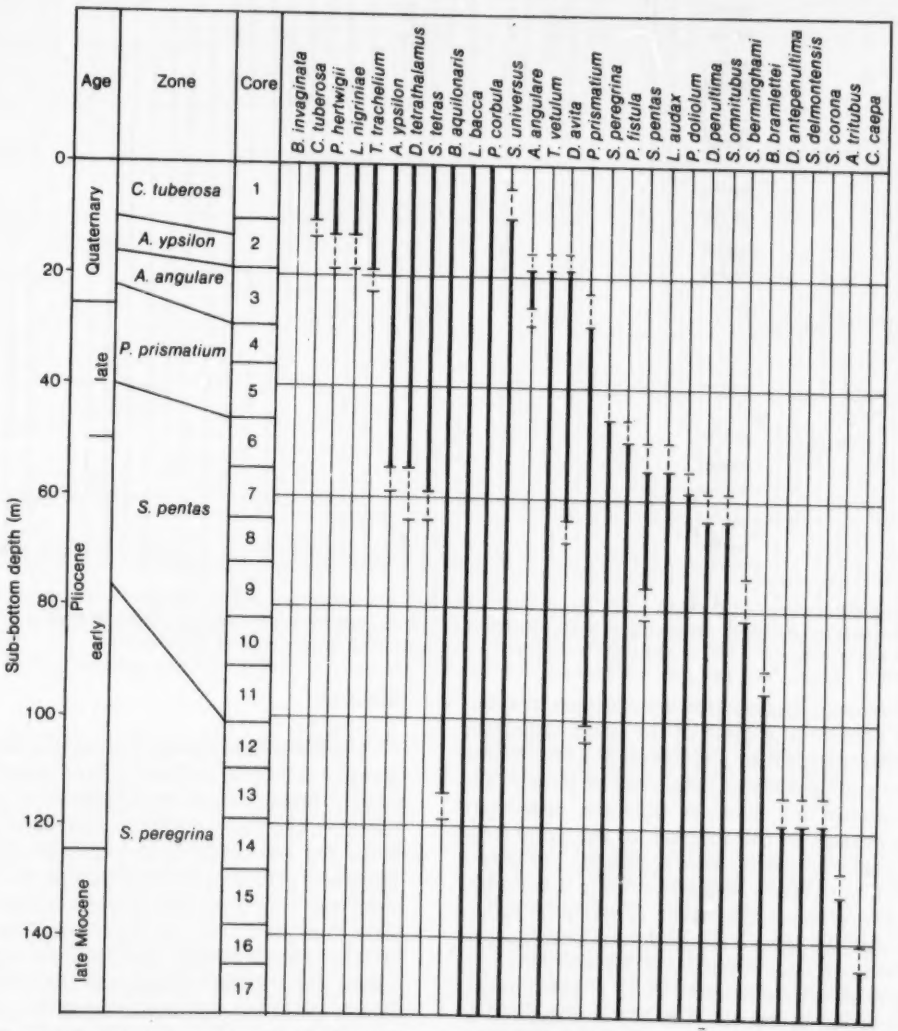

Figure 3. Radiolarian range chart for Hole 572A. Heavy vertical line indicates maximum confirmed range of a species. Dashed line interval between the first or last sample examined in which the species is present and the nearest sample examined in which the species is not present.

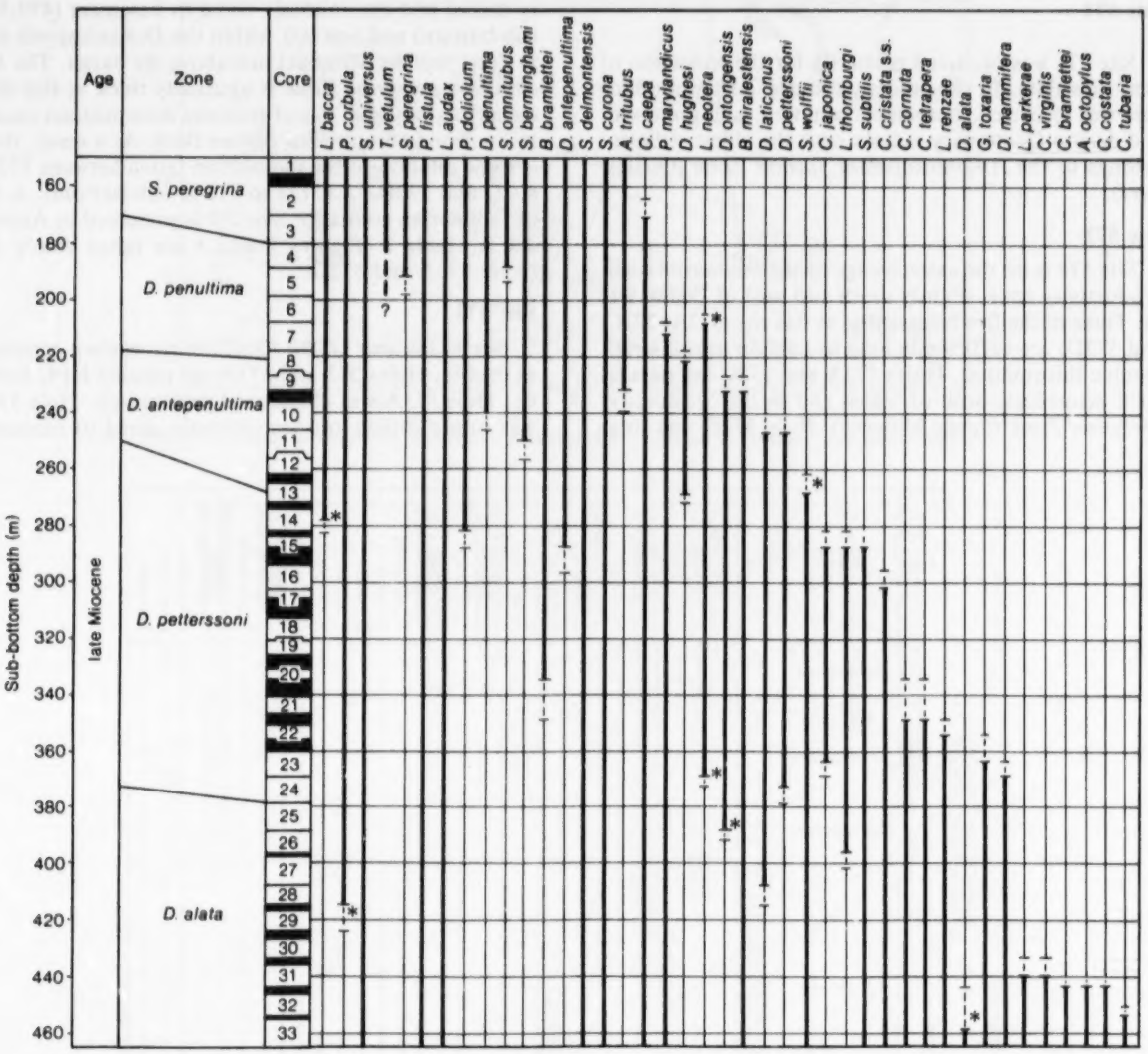

Figure 4. Radiolarian range chart for Hole 572D. Heavy vertical line indicates maximum confirmed range of a species. Dashed line interval between the first or last sample examined in which the species is present and the nearest sample examined in which the species is not present. Asterisk indicates a first or last occurrence that is inconsistent with the majority of data obtained.

(528.0 m sub-bottom). Radiolarians are common to abundant and well preserved in most of the cored sequence, which ranges from Recent to uppermost Eocene. In the lower Miocene and uppermost Oligocene of Hole 573B, however, abundance and diversity decrease, and many specimens are broken. In this interval, orosphaerid fragments and spyroid radiolarians are common. The oldest moderately well preserved radiolarian fauna is found in 573B-40,CC and is lower Oligocene (*Theocyrtis tuberosa* Zone) in age; an impoverished fauna belonging to the same radiolarian zone occurs in 573B-42-1, 0–1 cm, but radiolarians are absent from 573B-42-1, 149–150 cm. A list of radiolarian events for Site 573 is presented in Appendix A, Table 2. Figures 5 and 6 are range charts for Holes 573 and 573B.

Site 574

Site 574 is the second of three sites along a latitudinal transect at 133°W across the equatorial high-productivity belt. Hole 574 and its parallel HPC hole, 574A, bottomed in the *Calocycletta costata* Zone (lower Miocene). Hole 574 was rotary drilled and continuously cored to basement (532.5 m sub-bottom). Radiolarians are common and well preserved in most of the material recovered, but Core 574C-35 is barren of radiolarians.

The oldest sediments recovered are uppermost Eocene, and a good Eocene/Oligocene boundary sequence was cored. Although Hardenbol and Berggren (1978) show the *Theocyrtis tuberosa/Thyrsocyrtis bromia* zonal boundary to lie within P19 (lower Oligocene), most ra-

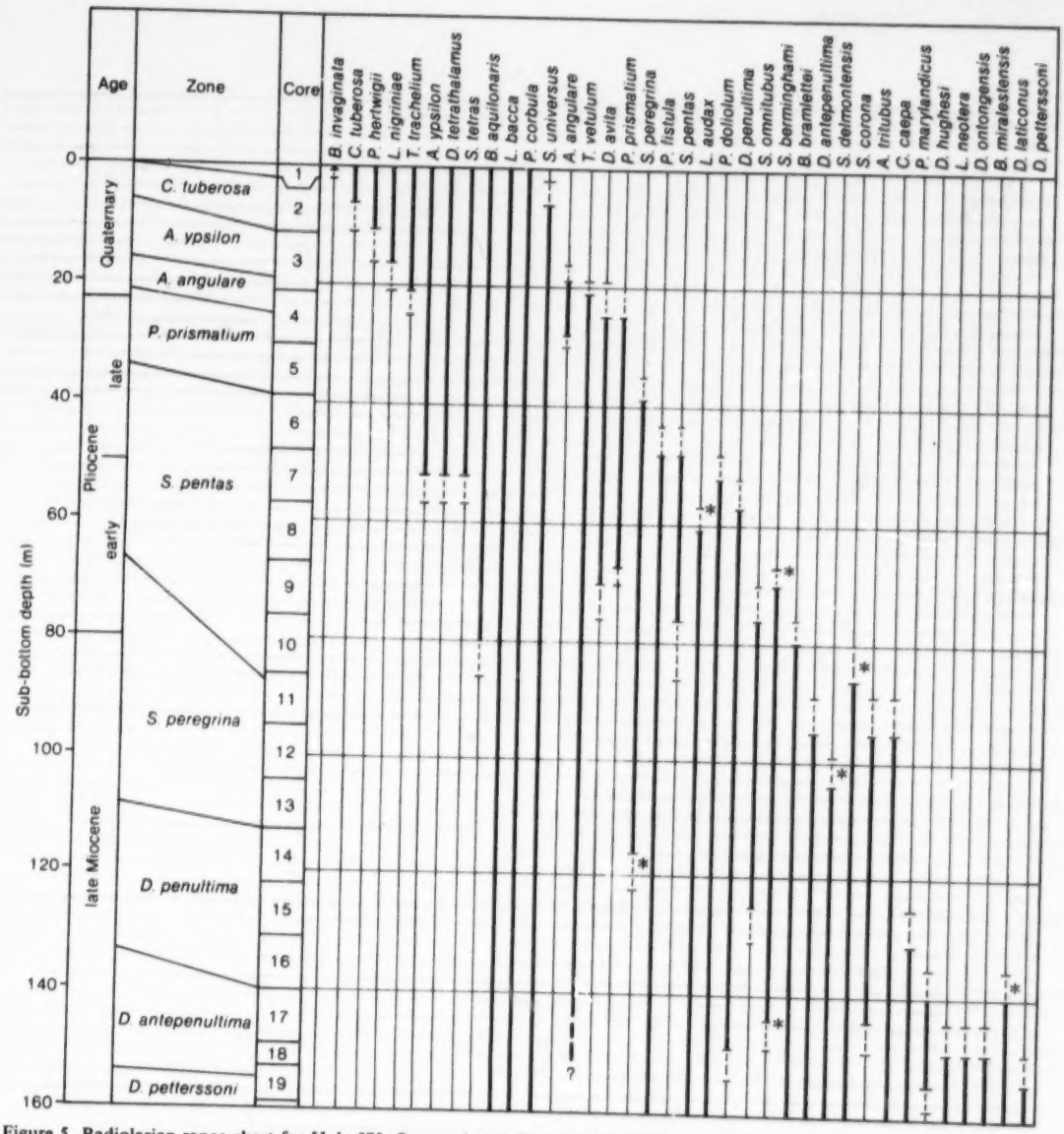

Figure 5. Radiolarian range chart for Hole 573. See caption to Figure 4 for explanation. Top, unlabeled, zone is *B. invaginata* Zone.

diolarian workers have, until recently, accepted Riedel and Sanfilippo's (1978) placement of that boundary as coincident with the Eocene/Oligocene boundary. Unpublished work by Riedel and Sanfilippo (personal communication, 1982) on the Bath Cliff section (Barbados) suggests, however, that a revision of the uppermost Eocene radiolarian zones is in order. Once this zonation can be tied to the foraminiferal sequence in the Bath Cliff section, and hence to the European stratotype, the Eocene/Oligocene boundary can be precisely located with respect to the radiolarian fauna. In the present work, the boundary is tentatively placed between 574C-33-4, 49–51 cm (503.5 m sub-bottom) and 574C-33-5, 57–59 cm (505.08 m sub-bottom). A list of radiolarian events for Site 574 is presented in Appendix A, Table 3. Figures 7 and 8 are range charts for Holes 574 and 574C.

Site 575

Site 575 is the northernmost site of a three-site transect at 133°W. Radiolarians ranging from Recent to lower Miocene (*Calocycletta costata* Zone) are common and well preserved. At the top of the cored sequences (Hole 575 and its parallel HPC hole, 575B), there is considerable reworking of Miocene and Oligocene species. Quaternary and Pliocene zones are either missing or greatly compressed in the upper two cores of both holes. In addition, some drilling disturbance is indicated, making the sequence of events in these sections questionable.

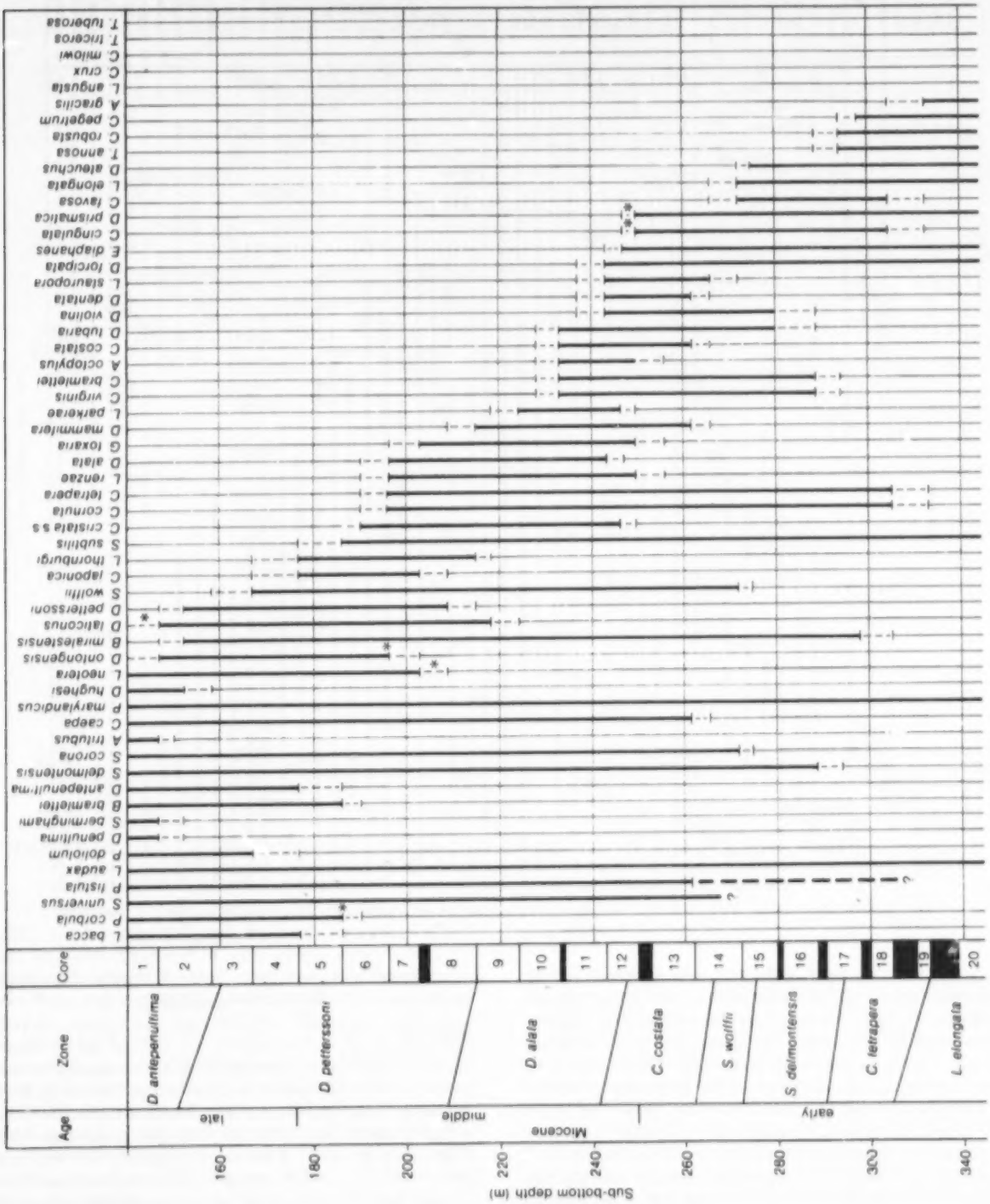
T. tuberosa
T. inceros
C. miowi
C. crux
L. angusta
A. gracilis
C. pegetum
C. robusta
T. annosa
D. atlouchus
L. elongata
C. tavosa
D. prismatica
C. cingulata
E. diaphanes
D. torcipata
L. staurogora
D. dentata
D. violina
D. tubaria
C. costata
A. octopylus
C. bramlettei
C. virginis
L. parkerae
D. mammifera
G. foxaria
D. alata
L. renzae
C. tetrapera
C. cornuta
C. cristata s.s.
S. subtilis
L. thornburgi
C. japonica
S. wolffii
D. petterssoni
D. laticonus
B. mirabestensis
D. ontongensis
L. neotera
D. hughesi
P. maryblandicus
C. carpa
A. tritubus
S. corona
S. delmontensis
D. antepenultima
B. bramlettei
S. berminghami
D. penultima
P. doliolum
L. audax
P. fistula
S. universus
P. corbula
L. bacca
Core
Zone
D. antepenultima
D. petterssoni
D. alata
C. costata
S. wolffii
S. delmontensis
C. tetrapera
L. elongata
Age
late
middle
early
Miocene
Sub-bottom depth (m)

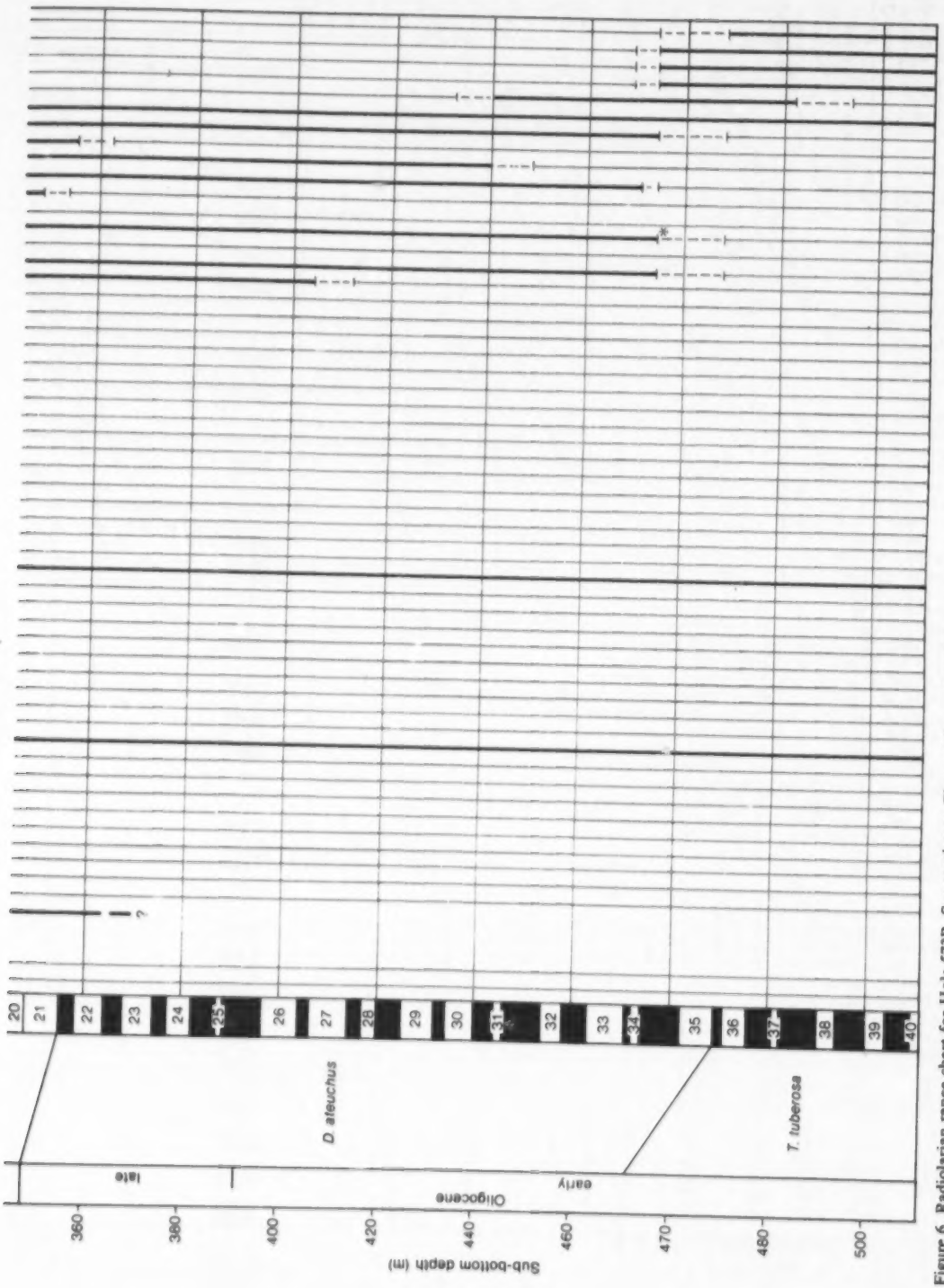

Figure 6. Radiolarian range chart for Hole 573B. See caption to Figure 4 for explanation.

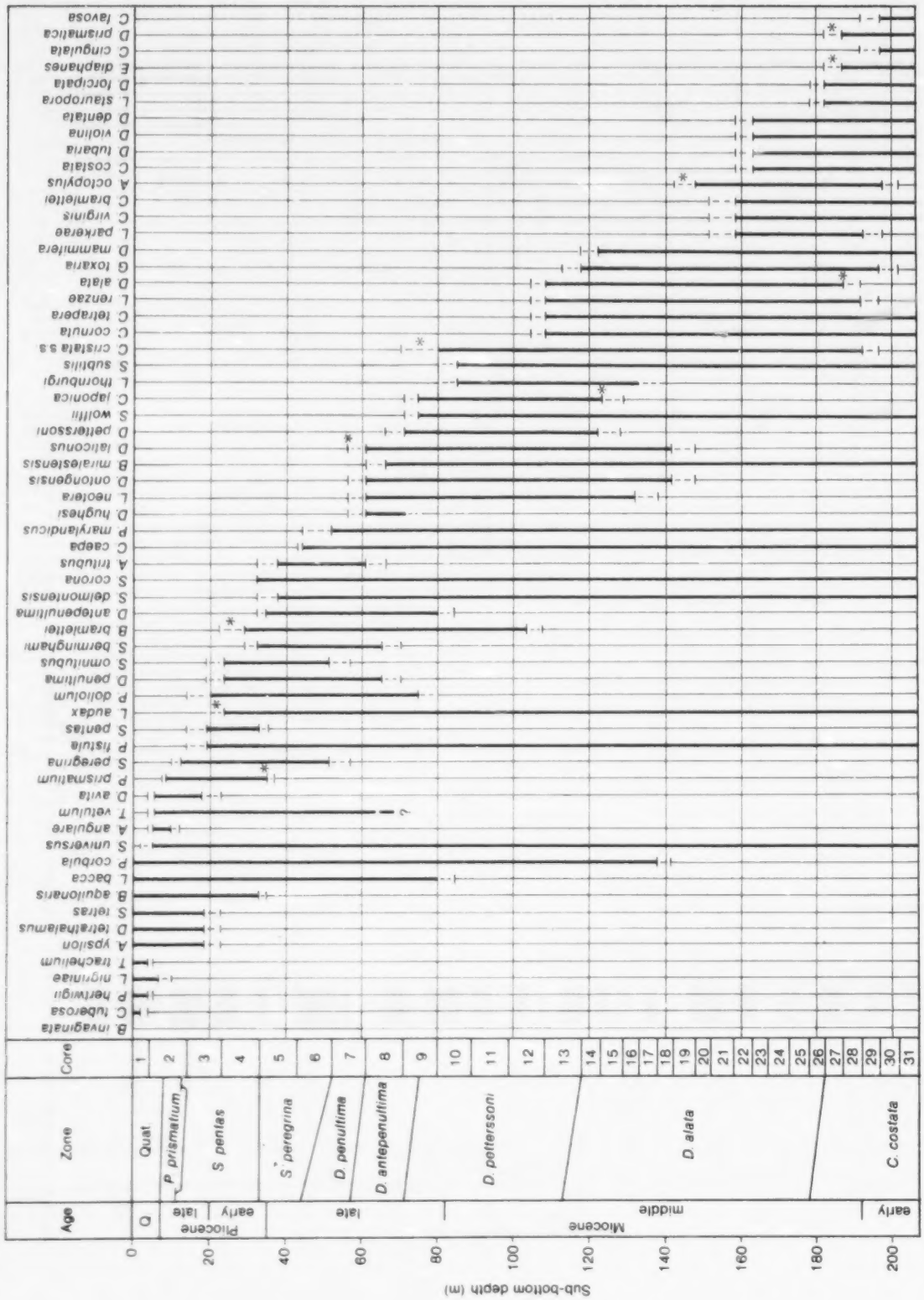

Figure 7. Radiolarian range chart for Hole 574. See caption to Figure 4 for explanation.

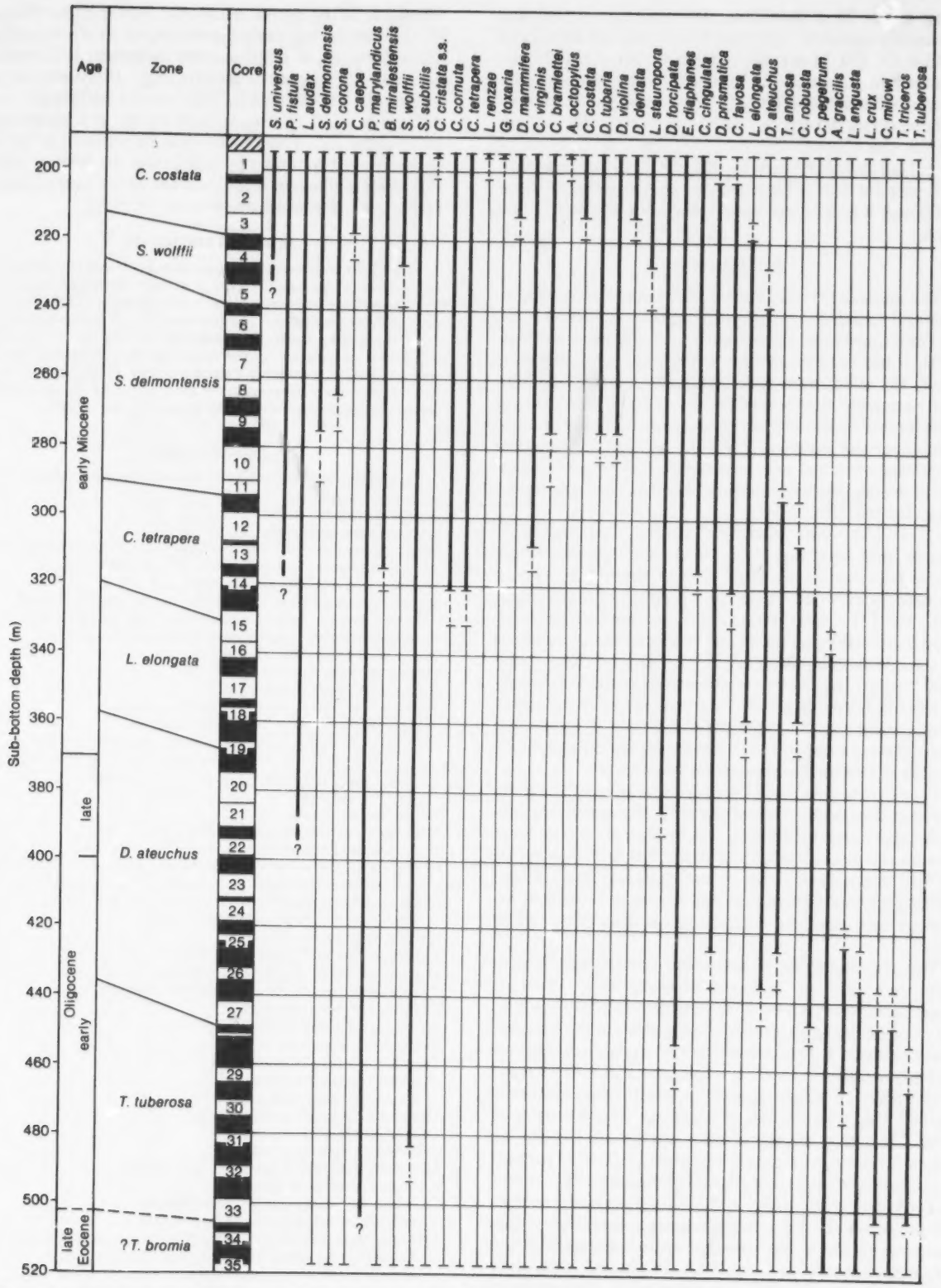

Figure 8. Radiolarian range chart for Hole 574C. See caption to Figure 3 for explanation.

From about 20 m downhole, all zones are present and apparently complete. Between 575B-5,CC (48.28 m) and 575B-8,CC (73.74 m), radiolarian events are highly irregular (see Appendix A, Table 4). Hole 575A was continuously cored using HPC to the *Cyrtocapsella tetrapera* Zone (lower Miocene), but basement was not reached. See the site chapter (this volume) for a description of the coring technique used at this site. A list of radiolarian events for Site 575 is presented in Appendix A, Table 4. Figures 9 and 10 are range charts for Holes 575 and 575A.

SUMMARY

The material from DSDP Leg 85 has provided an abundant and well-preserved tropical radiolarian fauna ranging from uppermost Eocene to Recent. By using this material, it has been possible to catalogue, in considerable detail, 133 radiolarian events (primarily morphotypic tops and bottoms). The reproducibility of the sequence of these events is remarkably good, considering the close spacing of the samples. Contrary to expectations, the percentage of out-of-sequence events, relative to the number of events tracked in various holes, is not noticeably lower for the HPC holes.

Of the 133 events charted in 12 holes 37 are out of sequence in at least one hole. Of these 37 events, 25 are out of sequence in less than 30% of the holes in which the event occurs (see Table 1). A number of these events (e.g., top [T] *Stichocorys wolffii*, T *Calocycletta virginis*, T *Carpocanopsis bramlettei*) are only out of sequence by a single sample. Others (e.g., T *Theocorythium vetulum*, bottom [B] *Dictyocoryne ontongensis*, T *Lithopera renzae*) occur in a core that was found to be either greatly compressed or disturbed. Overall, it is felt that these 25 events can still be considered reliable and reproducible in the central equatorial Pacific.

Four events were out of sequence in 30% of the holes in which they occur. One of these (T *Dorcadospyris alata*) involves a disturbed core, but in Hole 572D the event is seriously out of order (by about 100 m). Another of the four events (T *Lychnocanoma elongata*) shows a high out-of-sequence percentage, but this may be an artifact of poor data, since the event occurs in only three Leg 85 holes.

The remaining eight events are out of sequence in more than 30% of the holes in which they occur. Of these eight, one (B *Didymocyrtis prismatica*) occurs in only two of the holes studied. Three other events (B *Lithopera neotera*, B *Phormostichoartus corbula*, B *Dictyocoryne ontongensis*) are out of sequence in 30% or more of the holes in which they occur, even if one discounts the fact that they are out of sequence in the section of Hole 575B that shows serious mixing of radiolarian events. These events cluster around the *Diartus petterssoni/Dorcadospyris alata* zonal boundary. Two events (T *Lychnodictyum audax* and T *Botryostrobus bramlettei*) fall below the 30% out-of-sequence boundary if one discounts the fact that they are out of sequence in the compressed section of Hole 574A. In general, these eight events, with the possible exception of B *Didymocyrtis prismatica*, cannot be considered reproducible, and are unreliable in the central equatorial Pacific either because (1) they are evolutionary events subject to errors in identification (e.g., T *Didymocyrtis laticonus*, B *Lithopera neotera*); (2) the species are rare (e.g., *Dictyocoryne ontongensis*); (3) the species may not be sufficiently well defined (e.g., T *Lychnodictyum audax*, B *Carpocanopsis cristata*, s.s., T *Botryostrobus bramlettei*); or (4) the species occur sporadically well below the level at which they are a well-established member of the faunal assemblage (e.g., B *Phormostichoartus corbula*).

ACKNOWLEDGMENTS

I should like to express my sincere appreciation to the Chevron Oil Field Research Company for the use of their laboratory facilities for processing all my radiolarian samples. In particular, Carlton Ford and Kevin Kirwan were helpful and pleasant laboratory companions. As usual, the drilling, marine, and technical crews of the *Glomar Challenger* were consistently helpful and supportive during the recovery and processing of a remarkable amount of core. Finally, my thanks also go to my family for making my participation in Leg 85 possible, and to my children for learning to make their own lunches.

SPECIES LIST

Descriptions and illustrations of the following species can be found in Nigrini and Lombari (1984).

Acrobotrys tritubus Riedel
Botryostrobus aquilonaris (Bailey)
Botryostrobus bramlettei (Campbell and Clark). Note: The upper limit of this species does not appear to be a reliable datum.
Botryostrobus miralestensis (Campbell and Clark)
Calocycletta caepa Moore. Note: The lower limit of this species is not clearly defined, because of the difficulty in distinguishing it from *C. virginis* when the abdominal segment is incomplete.
Calocycletta costata Riedel
Calocycletta robusta Moore
Calocycletta virginis (Haeckel)
Carpocanopsis bramlettei Riedel and Sanfilippo
Carpocanopsis cingulata Riedel and Sanfilippo
Carpocanopsis cristata (Carnevale). Note: This species is used in a restricted sense herein. Only specimens resembling those figured by Riedel and Sanfilippo, 1971, plate 1G, figure 16 and plate 2G, figure 1, are included.
Carpocanopsis favosa (Haeckel)
Cyclampterium(?) pegetrum Sanfilippo and Riedel
Cyrtocapsella cornuta (Haeckel). Note: The upper limit of this species was found to be coincident (within the range of the sample interval) with the upper limit of *C. tetrapera* at all Leg 85 sites.
Cyrtocapsella japonica (Nakaseko). Note: The lower limit of this species appears to be an unreliable datum.
Cyrtocapsella tetrapera (Haeckel)
Diartus hughesi (Campbell and Clark)
Diartus petterssoni (Riedel and Sanfilippo)
Didymocyrtis antepenultima (Riedel and Sanfilippo)
Didymocyrtis laticonus (Riedel)
Didymocyrtis mammifera (Haeckel)
Didymocyrtis penultima (Riedel)
Didymocyrtis prismatica (Haeckel)
Didymocyrtis tubaria (Haeckel)
Didymocyrtis violina (Haeckel)
Dorcadospyris ateuchus (Ehrenberg)
Dorcadospyris dentata Haeckel
Dorcadospyris forcipata (Haeckel)
Eucyrtidium diaphanes Sanfilippo and Riedel
Liriospyris stauropora (Haeckel)
Lithopera thornburgi Sanfilippo and Riedel
Lychnocanoma elongata (Vinassa de Regny)
Lychnodictyum audax Riedel. Note: This species was not observed below the *D. ateuchus* Zone. However, Sanfilippo et al. (in press) show its lower morphotypic limit to be within the *T. tuberosa* Zone.
Phormostichoartus corbula (Harting). Note: The lower limit of this species was found to be an unreliable datum because of sporadic

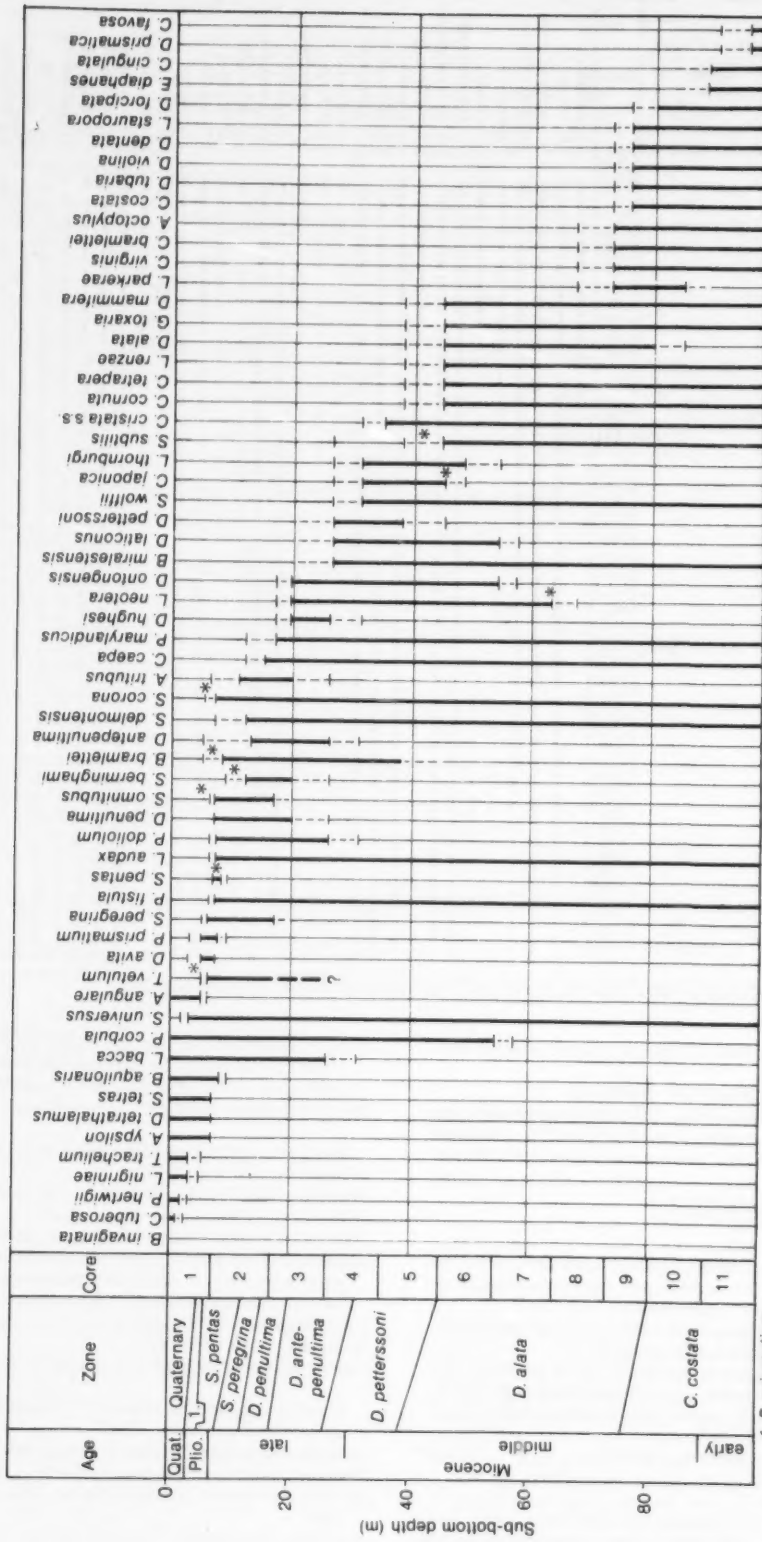

Figure 9. Radiolarian range chart for Hole 575. See caption to Figure 4 for explanation.

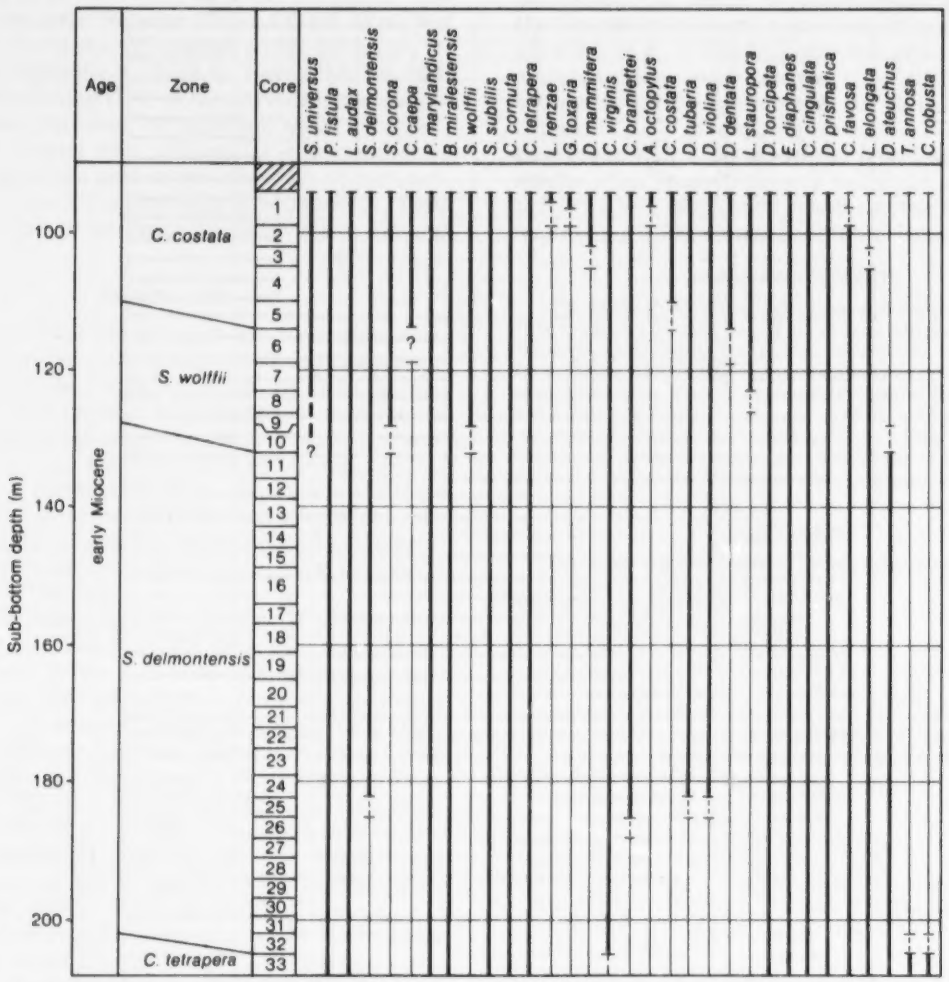

Figure 10. Radiolarian range chart for Hole 575A. See caption to Figure 3 for explanation.

occurrences well below the level at which it is found to occur with some consistency.

Phormostichoartus doliolum (Riedel and Sanfilippo)

Phormostichoartus fistula Nigrini. Note: This species was found only sporadically below the *C. costata* Zone in Hole 573B and below the *C. tetrapera* Zone in 574C. The lower limit could not be well defined.

Phormostichoartus marylandicus (Martin)

Pterocanium prismatium (Riedel)

Siphostichartus corona (Haeckel)

Solenosphaera omnitubus omnitubus Riedel and Sanfilippo. Note: The range of *S. omnitubus procera* is similar to, but somewhat narrower than, that of the nominate subspecies.

Spirocyrtis subtilis Petrushevskaya. Note: This species ranges considerably lower than was reported by Nigrini (1977).

Spongaster berminghami (Campbell and Clark). Note: Both this species and *S. pentas* are rather rare in Leg 85 sediments, making definition of the *S. peregrina/S. pentas* zonal boundary difficult.

Spongaster pentas (Riedel and Sanfilippo)

Stichocorys delmontensis (Campbell and Clark)

Stichocorys peregrina (Riedel)

Stichocorys wolffii (Haeckel)

Stylatractus universus Hays (= *Axoprunum angelinum*). Note: The lower limit of this species is not defined herein. Specimens are found in sediments at least as old as the *S. wolffii* Zone.

Theocorythium vetulum Nigrini. Note: The lower limit of this species is not defined herein, because the relationship between it and various species of *Lamprocyclas* is not presently understood.

Theocyrtis annosa (Riedel)

Descriptions and illustrations of the following species can be found in Nigrini and Moore (1979).

Amphirhopalum ypsilon Haeckel

Collosphaera tuberosa Haeckel

Didymocyrtis tetrathalamus (Haeckel) (= *Ommatartus tetrathalamus*)

Lamprocyrtis nigriniae (Caulet). Note: The closely related species *L. heteroporus* and *L. neoheteroporus* were found to be unreliable stratigraphic markers in the latitudes covered by Leg 85.

Peterocorys hertwigii (Haeckel)

Spongaster tetras Ehrenberg

Theocorythium trachelium (Ehrenberg)

Descriptions and illustrations of the following species may be found in the publications cited.

Acrocubus octopylus Haeckel; Haeckel, 1887; Goll, 1972

Anthocyrtidium angulare Nigrini; Nigrini, 1971

Artophormis gracilis (Riedel), Riedel, 1959; Riedel and Sanfilippo, 1970

Buccinosphaera invaginata Haeckel; Nigrini, 1971, and Knoll and Johnson, 1975

Table 1. Summary of out-of-sequence radiolarian events.

	Radiolarian event[a]	Out of sequence				Possible explanation		
		Frequency	Percentage	By 1 sample	By >1 sample	Rare species	Member of evolutionary sequence	Disturbed or compressed core
T	*Theocorythium vetulum*	1 in 7	14	✓				
T	*Phormostichoartus fistula*	1 in 8	12	✓			✓	✓ (575)
T	*Spongaster pentas*	2 in 8	25	✓				✓ (574A)
T	*Solenosphaera omnitubus*	2 in 7	28	✓	✓	✓	✓	✓ (575)
B	*Didymocyrtis avita*	1 in 7	14	✓				✓ (575)
T	*Spongaster berminghami*	2 in 7	28				✓	✓ (574A)
B	*Pterocanium prismatium*	1 in 7	14	✓	✓	✓	✓	
T	*Didymocyrtis antepenultima*	1 in 7	14			✓[b]		
T	*Stichocorys delmontensis*	1 in 7	14					
T	*Siphostichartus corona*	1 in 7	14		✓		✓	
B	*Solenosphaera omnitubus*	1 in 6	17	✓				✓ (575)
T	*Lithopera neotera*	1 in 6	17		✓			
B	*Spongaster berminghami*	1 in 7	14		✓		✓	
T	*Stichocorys wolffii*	1 in 6	17	✓		✓		
B	*Lithopera bacca*	1 in 6	17	✓			✓	
T	*Lithopera renzae*	1 in 6	17		✓		✓	
T	*Didymocyrtis mammifera*	1 in 6	17		?		✓	✓ (575B)[c]
B	*Lithopera thornburgi*	1 in 6	17		?			✓ (575B)[c]
T	*Calocycletta virginis*	1 in 6	17		?	✓		✓ (575B)[c]
T	*Carpocanopsis bramlettei*	1 in 6	17	✓			✓[d]	
T	*Dorcadospyris dentata*	1 in 5	20	✓				
T	*Eucyrtidium diaphanes*	1 in 5	20	✓				
T	*Didymocyrtis prismatica*	1 in 5	20	✓				
T	*Carpocanopsis favosa*	1 in 6	17		✓			
B	*Lithopera renzae*	1 in 5	20	✓	✓			
T	*Spirocyrtis subtilis*	2 in 6	30	✓	✓			
T	*Dorcadospyris alata*	2 in 6	30		✓[e]			✓ (575B)[c]
B	*Cyrtocapsella japonica*	2 in 6	30	✓				
T	*Lychnocanoma elongata*	1 in 3	30[f]	✓				
T	*Lychnodictyum audax*	3 in 8	37	✓	✓			✓ (574A)
T	*Botryostrobus bramlettei*	3 in 7	43	✓	✓		?	✓ (574A, 575)
T	*Didymocyrtis laticonus*	3 in 7	43	✓	✓		✓	
B	*Lithopera neotera*	4 in 6	67	✓	✓			✓ (575B)[c]
B	*Phormostichoartus corbula*	4 in 6	67	✓	✓			✓ (575B)[c]
B	*Dictyocoryne ontongensis*	3 in 6	50		✓	✓		✓ (575B)[c]
B	*Carpocanopsis cristata* s.s.	2 in 5	40	✓				
B	*Didymocyrtis prismatica*	1 in 2	50[f]	✓				

Note: Rules are used to separate events that are out sequence in <30%, 30%, and >30% of the holes in which the event occurs (see text).

[a] T = top; B = bottom.
[b] At lower end of range.
[c] A large section of Hole 575B shows serious mixing of radiolarian events, although no disturbance is indicated on the barrel sheets.
[d] Requires complete specimen for identification.
[e] Out of sequence by about 100 m in Hole 572D.
[f] Event occurs in 3 or fewer holes.

Cyclampterium(?) milowi Sanfilippo and Riedel; Sanfilippo and Riedel, 1970

Dictyocoryne ontongensis Riedel and Sanfilippo; Riedel and Sanfilippo, 1971. Note: The lower limit of this species is difficult to place because specimens are so rare.

Didymocyrtis avita (Riedel); Riedel, 1953

Dorcadospyris alata (Riedel); *Brachiospyris alata* in Riedel, 1959; Riedel and Sanfilippo, 1970. Note: The upper limit of this species is seriously misplaced in Hole 572D.

Giraffospyris toxaria (Haeckel); Goll, 1969

Giriospyris parkerae Riedel and Sanfilippo; Riedel and Sanfilippo, 1971

Lithocyclia angusta (Riedel); *Trigonactura angusta* in Riedel, 1959; Riedel and Sanfilippo, 1970

Lithocyclia crux Moore; Moore, 1971

Lithopera bacca Ehrenberg; Nigrini, 1967

Lithopera neotera Sanfilippo and Riedel; Sanfilippo and Riedel, 1970. Note: The lower limit of this species appears to be an unreliable datum.

Lithopera renzae Sanfilippo and Riedel; Sanfilippo and Riedel, 1970

Theocyrtis tuberosa Riedel; Riedel 1959, and Riedel and Sanfilippo, 1971

Tristylospyris triceros (Ehrenberg); Haeckel, 1887

REFERENCES

Goll, R. M., 1969. Classification and phylogeny of Cenozoic Trissocyclidae (Radiolaria) in Pacific and Caribbean basins. Part II. *J. Paleontol.*, 43(2):322–339.

———, 1972. Radiolaria. *In* Hayes, J. D., et al., *Init. Repts. DSDP*, 9: Washington (U.S. Govt. Printing Office), 947–1058.

Haeckel, E., 1887. Report on the Radiolaria collected by H.M.S. *Challenger* during the years 1873–1876. *Report Scientific Results, Voyage H.M.S. Challenger, Zoology* (Vol. 18, 2 pts.).

Hardenbol, J., and Berggren, W. A., 1978. A new Paleogene numerical time scale. *Stud. Geol.*, 6:213–214.

Knoll, A., and Johnson, D., 1975. Late Pleistocene evolution of the collosphaerid radiolarian *Buccinosphaera invaginata* Haeckel. *Micropaleontology*, 21:60–68.

Moore, T. C., 1971. Radiolaria. *In* Tracey, J. I., Jr., Sutton, G. H., et al., *Init. Repts. DSDP*, 8: Washington (U.S. Govt. Printing Office), 727–775.

Nigrini, C., 1967. Radiolaria in pelagic sediments from the Indian and Atlantic oceans. *Bull. Scripps Inst. Oceanogr.*, 11:1–125.

_____, 1971. Radiolarian zones in the Quaternary of the equatorial Pacific Ocean. *In* Funnell, B. M., and Riedel, W. R. (Eds.), *Micropaleontology of Oceans:* Cambridge (Cambridge Univ. Press), pp. 443–461.

_____, 1977. Tropical Cenozoic Artostrobiidae (Radiolaria). *Micropaleontology*, 23(3):241–269.

Nigrini, C., and Lombari, G., 1984. A guide to Miocene Radiolaria. *Cushman Found. Spec. Publ.*, 22:1–308.

Nigrini, C., and Moore, T. C., 1979. A guide to modern Radiolaria. *Cushman Found. Spec. Publ.*, 16:1–260.

Riedel, W. R., 1953. Mesozoic and late Tertiary Radiolaria of Rotti. *J. Paleontol.*, 27(6):805–813.

_____, 1959. Oligocene and lower Miocene Radiolaria in tropical Pacific sediments. *Micropaleontology*, 5(3):285–302.

Riedel, W. R., and Sanfilippo, A., 1970. Radiolaria, Leg 4, Deep Sea Drilling Project. *In* Bader, R. G., Gerard, R. D., et al., *Init. Repts. DSDP*, 4: Washington (U.S. Govt. Printing Office), 503–575.

_____, 1971. Cenozoic Radiolaria from the western tropical Pacific, Leg 7. *In* Winterer, E. L., Riedel, W. R., et al., *Init. Repts. DSDP*, 7, Pt. 2: Washington (U.S. Govt. Printing Office), 1529–1672.

_____, 1978. Stratigraphy and evolution of tropical Cenozoic radiolarians. *Micropaleontology*, 24(1):61–96.

Sanfilippo, A., and Riedel, W. R., 1970. Post-Eocene "closed" theoperid radiolarians. *Micropaleontology*, 16(4):446–462.

Sanfilippo, A., Westberg-Smith, M. J., and Riedel, W. R., in press. Cenozoic Radiolaria. *In* Bolli, H. M., Saunders, J. B., and Perch-Nielsen, K. (Eds.), *Biostratigraphy by Marine Plankton* (provisional title): Cambridge (Cambridge Univ. Press).

Westberg, M. J., and Riedel, W. R., 1982. Radiolaria from the Middle America Trench off Guatemala, Deep Sea Drilling Project Leg 67. *In* Aubouin, J., von Huene, R., et al., *Init. Repts. DSDP*, 67: Washington (U.S. Govt. Printing Office), 401–424.

Date of Initial Receipt: 3 November 1983
Date of Acceptance: 8 March 1984

APPENDIX A
Radiolarian Events, Sites 572 to 575

Table 1. List of radiolarian events for Site 572.[a]

Zone	Age (Ma)	Top or bottom	Species	Hole 572A Core-Section	Hole 572A Sub-bottom depth (m)	Hole 572C Core-Section	Hole 572C Sub-bottom depth (m)	Hole 572D Core-Section	Hole 572D Sub-bottom depth (m)
B. invaginata	0.3	B	*Buccinosphaera invaginata*						
C. tuberosa	0.44	T	*Stylatractus universus*	1-3	3.70				
				1,CC	9.57	1,CC	9.50		
		B	*Collosphaera tuberosa*	1,CC	9.57	1,CC	9.50		
				2-3	13.20	2,CC	19.67		
		B	*Pterocorys hertwigii*	2-3	13.20	1,CC	9.50		
				2,CC	18.59	2,CC	19.67		
A. ypsilon	1.1	T	*Anthocyrtidium angulare*	2-5	16.20	1,CC	9.50		
				2,CC	18.59	2,CC	19.67		
A. angulare		T	*Theocorythium vetulum*	2-5	16.20	2,CC	19.67		
				2,CC	18.59	3,CC	29.33		
		T	*Didymocyrtis avita*	2-5	16.20	2,CC	19.67		
				2,CC	18.59	3,CC	29.33		
		B	*Lamprocyrtis nigriniae*	2,CC	18.59	2,CC	19.67		
				3-3	22.91	3,CC	29.33		
	1.35	B	*Theocorythium trachelium*	2,CC	18.59	2,CC	19.67		
				3-3	22.91	3,CC	29.33		
P. prismatium	1.5	T	*Pterocanium prismatium*	3-3	22.91	2,CC	19.67		
				3,CC	28.56	3,CC	29.33		
		B	*Anthocyrtidium angulare*	3-5	25.91	2,CC	19.67		
				3,CC	28.56	3,CC	29.33		
S. pentas	2.4	T	*Stichocorys peregrina*	5-3	40.01	4,CC	38.77		
				5,CC	45.84	5,CC	48.44		
		T	*Phormostichoartus fistula*	5,CC	45.84	4,CC	38.77		
				6-3	49.61	5,CC	48.44		
	3.4	T	*Spongaster pentas*	6-3	49.61	5,CC	48.44		
				6,CC	55.13	6,CC	58.07		
		T	*Lychnodictyum audax*	6-3	49.61	5,CC	48.44		
				6,CC	55.13	6,CC	58.07		
		T	*Phormostichoartus doliolum*	6,CC	55.13	5,CC	48.44		
				7-3	58.91	6,CC	58.07		
		B	*Amphirhopalum ypsilon*	6,CC	55.13	6,CC	58.07		
				7-3	58.91	7,CC	67.75		

[a]Pairs of levels (sections and the corresponding depths in meters below the sediment surface) bracket the level at which an event occurs. Events and absolute ages in brackets are inconsistent with the majority of data collected.

Table 1. (Continued).

Zone	Age (Ma)	Top or bottom	Species	Hole 572A Core-Section	Hole 572A Sub-bottom depth (m)	Hole 572C Core-Section	Hole 572C Sub-bottom depth (m)	Hole 572D Core-Section	Hole 572D Sub-bottom depth (m)
S. pentas		B	*Didymocyrtis tetrathalamus*	6,CC 7,CC	55.13 63.99	6,CC 7,CC	58.07 63.99		
	3.6	B	*Spongaster tetras*	7-3 7,CC	58.91 63.99	6,CC 7,CC	58.07 67.75		
	3.69	T	*Didymocyrtis penultima*	7-3 7,CC	58.91 63.99	6,CC 7,CC	58.07 67.75		
		T	*Solenosphaera omnitubus*	7-3 7,CC	58.91 63.99	[5,CC 6,CC	48.44] 58.07		
		B	*Didymocyrtis avita*	7,CC 8-3	63.99 67.81	8,CC 9,CC	77.24 86.62		
		T	*Spongaster berminghami*	9-3 9,CC	76.01 81.71	[10,CC 11,CC	94.46] 101.01		
			S. berminghami → *S. pentas*	9-3 9,CC	76.01 81.71	8,CC 11,CC	77.24 101.01		
S. peregrina	4.3	B	*Spongaster pentas*	9-3 9,CC	76.01 81.71	8,CC 9,CC	77.24 86.62		
		T	*Botryostrobus bramlettei*	10,CC 11-3	91.38 95.19	8,CC 9,CC	77.24 86.62		
	4.8	B	*Pterocanium prismatium*	11,CC 12-3	100.63 104.39	10,CC 11,CC	96.46 101.01		
		B	*Botryostrobus aquilonaris*	13-3 13,CC	113.61 119.08	12,CC 13,CC	106.39 111.46		
		T	*Didymocyrtis antepenultima*	13-3 13,CC	113.61 119.08	12,CC 13,CC	106.39 111.46		
		T	*Stichocorys delmontensis*	13-3 13,CC	113.61 119.08	12,CC 13,CC	106.39 111.46		
		T	*Siphostichartus corona*	13-3 13,CC	113.61 119.08	13,CC 14,CC	111.46 119.34		
	5.0	T	*Acrobotrys tritubus*	14,CC 15-3	128.23 132.01	15,CC 16,CC	130.23 139.99		
		T	*Calocycletta caepa*	16-3 16,CC	140.82 145.20	15,CC 16,CC	130.23 139.99	2-3 2,CC	164.15 170.24
			S. delmontensis → *S. peregrina*					2,CC 3,CC	170.24 179.71
D. penultima		T	*Phormostichoartus marylandicus*					6,CC 7-3	208.07 211.61
	6.55	B	*Solenosphaera omnitubus*					[4,CC 5-4	189.02] 194.15
	[6.4]	B	*Stichocorys peregrina*					7-3 7,CC	211.61 217.62
D. antepenultima	8.2	T	*Diartus hughesi*					7,CC 8-3	217.62 221.11
		T	*Lithopera neotera*					[6-5 6,CC	205.11] 208.07
		T	*Dictyocoryne ontongensis*					8,CC 9,CC	227.23 231.97
		T	*Botryostrobus miralestensis*					8,CC 9,CC	227.23 231.97
	[11.2]	B	*Acrobotrys tritubus*					9,CC 10-3	231.97 240.11
		T	*Didymocyrtis laticonus*					10-3 10,CC	240.11 246.10
	8.2	B	*Didymocyrtis penultima*					10-3 10,CC	240.11 246.10
	9.7	T	*Diartus petterssoni*					10,CC 11-3	246.10 249.61

Table 1. (Continued).

Zone	Age (Ma)	Top or bottom	Species	Hole 572A Core-Section	Hole 572A Sub-bottom depth (m)	Hole 572C Core-Section	Hole 572C Sub-bottom depth (m)	Hole 572D Core-Section	Hole 572D Sub-bottom depth (m)
D. antepenultima		B	*Spongaster berminghami*					11-3 11,CC	249.61 255.68
			D. petterssoni → *D. hughesi*					11-3 13-3	249.61 268.61
D. petterssoni	11.5	B	*Diartus hughesi*					13-3 13,CC	268.61 272.45
	11.6	T	*Stichocorys wolffii*					[12,CC 13-3	261.79] 268.61
		T	*Cyrtocapsella japonica*					14,CC 15,CC	281.87 287.83
		B	*Phormostichoartus doliolum*					14,CC 15,CC	281.87 287.83
		T	*Lithopera thornburgi*					14,CC 15,CC	281.83 287.83
		T	*Spirocyrtis subtilis*					14,CC 15,CC	281.83 287.83
		B	*Didymocyrtis antepenultima*					15,CC 16-3	287.83 297.11
		B	*Lithopera bacca*					[14-3 14,CC	278.11] 281.83
		T	*Carpocanopsis cristata* s.s.					16-3 16,CC	297.11 302.93
		B	*Botryostrobus bramlettei*					20,CC 21,CC	334.96 348.54
	11.8	T	*Cyrtocapsella cornuta*					20,CC 21,CC	334.96 348.54
	[12.5]	T	*Cyrtocapsella tetrapera*					20,CC 21,CC	334.96 348.54
		T	*Lithopera renzae*					21,CC 22,CC	348.54 354.70
	11.8	T	*Dorcadospyris alata*					[31,CC 32-3	444.45] 458.61
		T	*Giraffospyris toxaria*					22,CC 23-3	354.70 363.61
		B	*Cyrtocapsella japonica*					23-3 23,CC	363.61 369.40
		T	*Didymocyrtis mammifera*					23-3 23,CC	363.61 369.40
	12.3	B	*Diartus petterssoni*					24-3 24,CC	373.11 378.58
D. alata	14.2	B	*Lithopera neotera*					[23,C 24-3	369.40] 373.11
		B	*Lithopera thornburgi*					26,CC 27-3	397.03 401.61
		B	*Phormostichoartus corbula*					[28,CC 29,CC	414.68] 423.99
		B	*Dictyocoryne ontongensis*					[25,CC 26-3	388.69] 392.11
	[13.8]	B	*Didymocyrtis laticonus*					27,CC 28,CC	407.61 414.68
		T	*Liriospyris parkerae*					30,CC 31-3	433.83 439.61
	14.75	T	*Calocycletta virginis*					30,CC 31-3	433.83 439.61
		T	*Carpocanopsis bramlettei*					31-3 31,CC	439.61 444.45

Table 1. (Continued).

Zone	Age (Ma)	Top or bottom	Species	Hole 572A Core-Section	Hole 572A Sub-bottom depth (m)	Hole 572C Core-Section	Hole 572C Sub-bottom depth (m)	Hole 572D Core-Section	Hole 572D Sub-bottom depth (m)
D. alata		T	*Acrocubus octopylus*					31-3 31,CC	439.61 444.45
	15.35	T	*Calocycletta costata*					31-3 31,CC	439.61 444.45
		T	*Didymocyrtis tubaria*					32-4 32,CC	450.61 454.03

Table 2. List of radiolarian events for Site 573.

Zone	Age (Ma)	Top or bottom	Species	Hole 573 Core-Section	Hole 573 Sub-bottom depth (m)	Hole 573A Core-Section	Hole 573A Sub-bottom depth (m)	Hole 573B Core-Section	Hole 573B Sub-bottom depth (m)
B. invaginata	0.3	B	*Buccinosphaera invaginata*	1-1 1,CC	0.09 1.97				
C. tuberosa	0.44	T	*Stylatractus universus*	1,CC 2-3	1.97 6.31	1,CC	0.00 14.09		
		B	*Collosphaera tuberosa*	2-3 2,CC	6.31 11.46				
		B	*Pterocorys hertwigii*	2,CC 3-3	11.46 15.81	1,CC 2,CC	14.09 22.00		
A. ypsilon	1.1	T	*Anthocyrtidium angulare*	3-3 3-5	15.81 18.81	1,CC 2,CC	14.09 22.00		
A. angulare		T	*Theocorythium vetulum*	3-5 3,CC	18.81 20.76	1,CC 2,CC	14.09 22.00		
		T	*Didymocyrtis avita*	3-5 4-3	18.81 25.31	1,CC 2,CC	14.09 22.00		
		B	*Lamprocyrtis nigriniae*	3-3 3,CC	15.81 20.76	1,CC 2,CC	14.09 22.00		
	1.35	B	*Theocorythium trachelium*	3,CC 4-3	20.76 25.31	1,CC 2,CC	14.09 22.00		
P. prismatium	1.5	T	*Pterocanium prismatium*	3,CC 4-3	20.76 25.31	2,CC 3,CC	22.00 31.32		
		B	*Anthocyrtidium angulare*	4-3 4-5	25.31 28.31	2,CC 3,CC	22.00 31.32		
S. pentas	2.4	T	*Stichocorys peregrina*	5-3 5,CC	34.61 39.25	3,CC 4,CC	31.32 39.73		
		T	*Phormostichoartus fistula*	6-3 6,CC	43.41 48.01	4,CC 5,CC	39.73 49.16		
	3.4	T	*Spongaster pentas*	6-3 6,CC	43.41 48.01				
		T	*Lychnodictyum audax*	[7,CC 8-3	57.09] 60.70]	4,CC 5,CC	39.73 49.16		
		T	*Phormostichoartus doliolum*	6,CC 7-3	48.01 52.10	5,CC 6,CC	39.73 49.16		
		B	*Amphirhopalum ypsilon*	7-3 7,CC	52.10 57.09				
		B	*Didymocyrtis tetrathalamus*	7-3 7,CC	52.10 57.09				
	3.6	B	*Spongaster tetras*	7-3 7,CC	52.10 57.09				
	3.69	T	*Didymocyrtis penultima*	7-3 7,CC	52.10 57.09				

Table 2. (Continued).

Zone	Age (Ma)	Top or bottom	Species	Hole 573 Core-Section	Hole 573 Sub-bottom depth (m)	Hole 573A Core-Section	Hole 573A Sub-bottom depth (m)	Hole 573B Core-Section	Hole 573B Sub-bottom depth (m)
S. penias		T	*Solenosphaera omnitubus*	9-3 9,CC	70.39 76.18				
		B	*Didymocyrtis avita*	9-3 9,CC	70.39 76.18				
		T	*Spongaster berminghami*	[8,CC 9-3	66.60] 70.39				
			S. berminghami → *S. penias*	8,CC 10,CC	66.60 85.76				
S. peregrina	4.3	B	*Spongaster penias*	9,CC 10,CC	76.18 85.76				
		T	*Botryostrobus bramlettei*	9,CC 10-3	76.18 79.99				
	4.8	B	*Pterocanium prismatium*	8,CC 9-3	66.60 70.39				
		B	*Botryostrobus aquilonaris*	10-3 10,CC	79.88 85.76				
		T	*Didymocyrtis antepenultima*	[11-3 11,CC	89.34] 94.98				
		T	*Stichocorys delmontensis*	[12-3 12,CC	98.89] 104.15				
		T	*Siphostichartus corona*	10-3 10,CC	79.88 85.76				
	5.0	T	*Acrobotrys tritubus*	11-3 11,CC	89.34 94.98				
		T	*Calocycletta caepa*	11-3 11,CC	89.34 94.98				
			S. delmontensis → *S. peregrina*	13-4 13,CC	109.16 112.57				
D. penultima		T	*Phormostichoartus marylandicus*	15-3 15,CC	125.45 131.29				
	6.55	B	*Solenosphaera omnitubus*	15-3 15,CC	125.45 131.29				
	[6.4]	B	*Stichocorys peregrina*	14-3 14,CC	116.06 122.00				
D. antepenultima	8.2	T	*Diartus hughesi*	16-3 16,CC	134.91 140.07				
		T	*Lithopera neotera*	17-3 17,CC	143.72 148.99				
		T	*Dictyocoryne ontongensis*	17-3 17,CC	143.72 148.99			1-1 1,CC	139.12 147.01
		T	*Botryocyrtis miralestensis*	17-3 17,CC	143.72 148.99			1,CC 2-3	147.01 151.62
	[11.2]	B	*Acrobotrys tritubus*	17-3 17,CC	143.72 148.99			1,CC 2-3	147.01 151.62
		T	*Didymocyrtis laticonus*	[16-3 16,CC	134.91] 140.07			[1-1 1,CC	139.12] 147.01
	8.2	B	*Didymocyrtis penultima*	17,CC 18,CC	148.99 153.54			1,CC 2-3	147.01 151.62
	9.7	T	*Diartus petterssoni*	17,CC 18,CC	148.99 153.54			1,CC 2-3	147.01 151.62
		B	*Spongaster berminghami*	[17-3 17,CC	143.72] 148.99			1,CC 2-3	147.01 151.62
			D. petterssoni → *D. hughesi*	18,CC 19-2	153.54 155.02			2-3 2,CC	151.62 157.61
D. petterssoni	11.5	B	*Diartus hughesi*	19-2 19,CC	155.02 159.07			2-3 2,CC	151.62 157.61

Table 2. (Continued).

Zone	Age (Ma)	Top or bottom	Species	Hole 573 Core-Section	Hole 573 Sub-bottom depth (m)	Hole 573A Core-Section	Hole 573A Sub-bottom depth (m)	Hole 573B Core-Section	Hole 573B Sub-bottom depth (m)
D. pettersoni	11.6	T	*Stichocorys wolffii*					2,CC 3,CC	157.61 167.20
		T	*Cyrtocapsella japonica*					3,CC 4,CC	167.20 176.58
		B	*Phormostichoartus doliolum*					3,CC 4,CC	167.20 176.58
		T	*Lithopera thornburgi*					3,CC 4,CC	167.20 176.58
		T	*Spirocyrtis subtilis*					4,CC 5,CC	176.58 185.86
		B	*Didymocyrtis antepenultima*					4,CC 5,CC	176.58 185.86
		B	*Lithopera bacca*					4,CC 5,CC	176.58 185.86
		T	*Carpocanopsis cristata* s.s.					5,CC 6-3	185.86 189.62
		B	*Botryostrobus bramlettei*					5,CC 6-3	185.86 189.62
	11.8	T	*Cyrtocapsella cornuta*					6-3 6,CC	189.62 195.65
	[12.5]	T	*Cyrtocapsella tetrapera*					6-3 6,CC	189.62 195.65
		T	*Lithopera renzae*					6-3 6,CC	189.62 195.65
	11.8	T	*Dorcadospyris alata*					6-3 6,CC	189.62 195.65
		T	*Giraffospyris toxaria*					6,CC 7,CC	195.65 203.43
		B	*Cyrtocapsella japonica*					7,CC 8-3	203.43 208.62
		T	*Didymocyrtis mammifera*					8-3 8,CC	208.62 214.72
		B	*Diartus petterssoni*					8-3 8,CC	208.62 214.72
D. alata	14.2	B	*Lithopera neotera*					[7,CC 8-3]	[203.43 208.62]
		B	*Lithopera thornburgi*					8,CC 9-3	214.72 218.12
		B	*Phormostichoartus corbula*					[5,CC 6-3]	[185.86 189.62]
		B	*Dictyocoryne ontongensis*					[6,CC 7,CC]	[195.65 203.43]
	[13.8]	B	*Didymocyrtis laticonus*					9-3 9,CC	218.12 224.08
		T	*Liriospyris parkerae*					9-3 9,CC	218.12 224.08
	14.75	T	*Calocycletta virginis*					10-3 10,CC	227.62 232.76
		T	*Carpocanopsis bramlettei*					10-3 10,CC	227.62 232.76
		T	*Acrocubus octopylus*					10-3 10,CC	227.62 232.76
	15.35	T	*Calocycletta costata*					10-3 10,CC	227.62 232.76
		T	*Didymocyrtis tubaria*					10-3 10,CC	227.62 232.76

Table 2. (Continued).

Zone	Age (Ma)	Top or bottom	Species	Hole 573 Core-Section	Hole 573 Sub-bottom depth (m)	Hole 573A Core-Section	Hole 573A Sub-bottom depth (m)	Hole 573B Core-Section	Hole 573B Sub-bottom depth (m)
D. alata		T	*Didymocyrtis violina*					11-3 11,CC	237.12 242.88
	15.8	T	*Dorcadospyris dentata*					11-3 11,CC	237.12 242.88
		T	*Liriospyris stauropora*					11-3 11,CC	237.12 242.88
			L. stauropora → *L. parkeri*					11-3 12,CC	237.12 250.25
		T	*Dorcadospyris forcipata*					11-3 11,CC	237.12 242.88
			D. dentata → *D. alata*					11,CC 12-3	242.88 246.62
C. costata	15.7	B	*Dorcadospyris alata*					11,CC 12-3	242.88 246.62
		T	*Eucyrtidium diaphanes*					11,CC 12-3	242.88 246.62
		B	*Liriospyris parkerae*					12-3 12,CC	246.62 250.25
		T	*Carpocanopsis cingulata*					12-3 12,CC	246.62 250.25
	16.2	T	*Didymocyrtis prismatica*					12-3 12,CC	246.62 250.25
		B	*Carpocanopsis cristata* s.s.					12-3 12,CC	246.62 250.25
		T	*Carpocanopsis favosa*					[14-3 14,CC	265.62] 271.59
		B	*Lithopera renzae*					12,CC 13-3	250.25 256.12
		B	*Acrocubus octopylus*					12,CC 13-3	250.25 256.12
		B	*Giraffospyris toxaria*					12,CC 13-3	250.25 256.12
	16.5	T	*Lychnocanoma elongata*					[14-3 14,CC	265.62] 271.59
		B	*Didymocyrtis mammifera*					13,CC 14-3	262.11 265.62
	17.3	B	*Calocycletta costata*					13,CC 14-3	262.11 265.62
S. wolffii	17.1	B	*Dorcadospyris dentata*					13,CC 14-3	262.11 265.62
		B	*Calocycletta caepa*					13,CC 14-3	262.11 265.62
		B	*Liriospyris stauropora*					14-3 14,CC	265.62 271.59
	[20.4]	T	*Dorcadospyris alauchus*					14,CC 15-3	271.59 275.12
	17.6	B	*Stichocorys wolffii*					14,CC 15-3	271.59 275.12
S. delmontensis		B	*Siphostichartus corona*					14,CC 15-3	271.59 275.12
	19.25	N	*Didymocyrtis violina*					15,CC 16,CC	279.93 288.73
		B	*Didymocyrtis tubaria*					15,CC 16,CC	279.93 288.73
	20.3		*Stichocorys delmontensis*					16,CC 17-3	288.73 294.11

Table 2. (Continued).

Zone	Age (Ma)	Top or bottom	Species	Hole 573 Core-Section	Hole 573 Sub-bottom depth (m)	Hole 573A Core-Section	Hole 573A Sub-bottom depth (m)	Hole 573B Core-Section	Hole 573B Sub-bottom depth (m)
S. delmontensis		B	*Carpocanopsis bramlettei*					16,CC 17-3	288.73 294.11
C. tetrapera	21.3	T	*Theocyrtis annosa*					16,CC 17-3	288.73 294.11
		T	*Calocycletta robusta*					16,CC 17-3	288.73 294.11
	21.35	B	*Calocycletta virginis*					16,CC 17-3	288.73 294.11
		T	*Cyclampterium pegetrum*					17-3 17,CC	294.11 298.24
		B	*Botryostrobus miralestensis*					17,CC 18,CC	298.24 304.62
		B	*Carpocanopsis cingulata*					18,CC 19,CC	304.62 312.74
	22.2	B	*Cyrtocapsella cornuta*					18,CC 19,CC	304.62 312.74
	22.2	B	*Cyrtocapsella tetrapera*					18,CC 19,CC	304.62 312.74
L. elongata		B	*Carpocanopsis favosa*					18,CC 19,CC	304.62 312.74
	22.5	T	*Artophormis gracilis*					18,CC 19,CC	304.62 312.74
	25.9	B	*Lychnocanoma elongata*					20,CC 21,CC	328.25 334.99
D. ateuchus		B	*Calocycletta robusta*					21,CC 22,CC	334.99 343.99
		B	*Dorcadospyris forcipata*					26,CC 27,CC	383.71 392.46
		T	*Lithocyclis angusta*					29,CC 30,CC	411.87 420.38
		B	*Theocyrtis annosa*					30,CC 31,CC	420.38 437.50
		T	*Lithocyclis crux*					33,CC 34,CC	450.68 454.43
		B	*Didymocyrtis prismatica*					[34,CC 35,CC]	454.43 468.95
		T	*Cyclampterium milowi*					33,CC 34,CC	450.68 454.43
		T	*Tristylospyris triceros*					33,CC 34,CC	450.68 454.43
			T. triceros → *D. ateuchus*					33,CC 35,CC	450.68 468.95
T. tuberosa	33.0	B	*Dorcadospyris ateuchus*					33,CC 34,CC	450.68 454.43
		B	*Cyclampterium pegetrum*					34,CC 35,CC	454.43 468.95
		T	*Theocyrtis tuberosa*					34,CC 35,CC	454.43 468.95
		B	*Eucyrtidium diaphanes*					34,CC 35,CC	454.43 468.95
		B	*Lithocyclia angusta*					37,CC 38,CC	482.28 494.41

Note: Pairs of levels and brackets as defined in Table 1 of this appendix.

Table 3. List of radiolarian events for Site 574.

Zone	Age (Ma)	Top or bottom	Species	Hole 574 Core-Section	Hole 574 Sub-bottom depth (m)	Hole 574A Core-Section	Hole 574A Sub-bottom depth (m)	Hole 574C Core-Section	Hole 574C Sub-bottom depth (m)
B. invaginata	0.3	B	*Buccinosphaera invaginata*						
C. tuberosa	0.44	T	*Stylatractus universus*	1-2 1,CC	2.41 4.48	 1,CC	0.00 6.30		
		B	*Collosphaera tuberosa*	1-2 1,CC	2.41 4.48				
		B	*Pterocorys hertwigii*	1,CC 2-1	4.48 5.25	1,CC 2,CC	6.30 15.45		
A. ypsilon	1.1	T	*Anthocyrtidium angulare*	1,CC 2-1	4.48 5.25				
A. angulare		T	*Theocorythium vetulum*	1,CC 2-1	4.48 5.25	1,CC 2,CC	6.30 15.45		
		T	*Didymocyrtis avita*	1,CC 2-1	4.48 5.25				
		B	*Lamprocyrtis nigriniae*	1,CC 2-1	4.48 5.25	1,CC 2,CC	6.30 15.45		
	1.35	B	*Theocorythium trachelium*	2-2 2-4	6.75 9.75	1,CC 2,CC	6.30 15.45		
P. prismatium	1.5	T	*Pterocanium prismatium*	2-2 2-3	6.75 8.25	1,CC 2,CC	6.30 15.45		
		B	*Anthocyrtidium angulare*	2-5 2-6	11.25 12.75				
S. pentas	2.4	T	*Stichocorys peregrina*	2-5 2-6	11.25 12.75	1,CC 2,CC	6.30 15.45		
		T	*Phormostichoartus fistula*	2,CC 3-4	14.07 19.20	[3,CC 4.CC	23.92] 33.13		
	3.4	T	*Spongaster pentas*	2,CC 3-4	14.07 19.20	2,CC 3,CC	15.45 23.92		
		T	*Lychnodictyum audax*	[3-4 3,CC	19.20] 23.48	[4,CC 5,CC	33.13] 42.34		
		T	*Phormostichoartus doliolum*	2,CC 3-4	14.07 19.20	2,CC 3,CC	15.45 23.92		
		B	*Amphirhopalum ypsilon*	3-4 3,CC	19.20 23.48	2,CC 3,CC	15.45 23.92		
		B	*Didymocyrtis tetrathalamus*	3-4 3,CC	19.20 23.48	2,CC 3,CC	15.45 23.92		
	3.6	B	*Spongaster tetras*	3-4 3,CC	19.20 23.48	2,CC 3,CC	15.45 23.92		
	3.69	T	*Didymocyrtis penultima*	3-4 3,CC	19.20 23.48	2,CC 3,CC	15.45 23.92		
		T	*Solenosphaera omnitubus*	3-4 3,CC	19.20 23.48	3,CC 4,CC	23.92 33.13		
		B	*Didymocyrtis avita*	3-4 3,CC	19.20 23.48	[—			
		T	*Spongaster berminghami*	4-4 4,CC	28.73 33.10	3,CC 4,CC	23.92 33.13		
			S. berminghami → *S. pentas*	4,CC 5-1	33.10 33.44	4,CC 5,CC	33.13 42.34		
S. peregrina	4.3	B	*Spongaster pentas*	5-1 5-2	33.44 34.94	4,CC 5,CC	33.13 42.34		
		T	*Botryostrobus bramlettei*	[3,CC 4-4	23.48] 28.73	[3,CC 4,CC	23.92] 33.13		
	4.8	B	*Pterocanium prismatium*	[5-2 5-4	34.94] 37.94	4,CC 5,CC	33.13 42.34		
		B	*Botryostrobus aquilonaris*	5-1 5-2	33.44 34.94	4,CC 5,CC	33.13 42.34		
		T	*Didymocyrtis antepenultima*	4,CC 5-2	33.10 34.94	4,CC 5,CC	33.13 42.34		

Table 3. (Continued).

Zone	Age (Ma)	Top or bottom	Species	Hole 574 Core-Section	Hole 574 Sub-bottom depth (m)	Hole 574A Core-Section	Hole 574A Sub-bottom depth (m)	Hole 574B Core-Section	Hole 574B Sub-bottom depth (m)
S. peregrina		T	*Stichocorys delmontensis*	4,CC 5-4	33.10 37.94	4,CC 5,CC	33.13 42.34		
		T	*Siphostichartus corona*	4,CC 5-1	33.10 33.44	4,CC 5,CC	33.13 42.34		
	5.0	T	*Acrobotrys tritubus*	4,CC 5-4	33.10 37.94	4,CC 5,CC	33.13 42.34		
		T	*Calocycletta caepa*	5,CC 6-2	42.54 44.42	5,CC 6,CC	42.34 51.92		
			S. delmontensis → *S. peregrina*	6-2 6,CC	44.42 52.00	5,CC 6,CC	42.34 51.92		
D. penultima		T	*Phormostichoartus marylandicus*	6-2 6,CC	44.42 52.00	6,CC 7,CC	51.92 61.26		
	6.55	B	*Solenosphaera omnitubus*	6,CC 7-4	52.00 56.92	6,CC 7,CC	51.92 61.26		
	[6.4]	B	*Stichocorys peregrina*	6,CC 7-4	52.00 56.92	6,CC 7,CC	51.92 61.26		
D. antepenultima	8.2	T	*Diartus hughesi*	7-4 7,CC	56.92 60.93	6,CC 7,CC	51.92 61.26		
		T	*Lithopera neotera*	7-4 7,CC	56.92 60.93	6,CC 7,CC	51.92 61.26		
		T	*Dictyocoryne ontongensis*	7-4 7,CC	56.92 60.93	6,CC 7,CC	51.92 61.26		
		T	*Botryostrobus miralestensis*	7,CC 8-4	60.93 65.92	7,CC 8,CC	61.26 70.42		
	[11.2]	B	*Acrobotrys tritubus*	7,CC 8-4	60.93 65.92	7,CC 8,CC	61.26 70.42		
		T	*Didymocyrtis laticonus*	[7-4 7,CC	56.92] 60.93]	7,CC 8,CC	61.26 70.42		
	8.2	B	*Didymocyrtis penultima*	8-4 8,CC	65.92 70.52	7,CC 8,CC	61.26 70.42		
	9.7	T	*Diartus petterssoni*	8-4 8,CC	65.92 70.52	7,CC 8,CC	61.26 70.42		
		B	*Spongaster berminghami*	8-4 8,CC	65.92 70.52	7,CC 8,CC	61.26 70.42		
			D. petterssoni → *D. hughesi*	8,CC 9-4	70.52 75.42	7,CC 9,CC	61.26 79.87		
D. petterssoni	11.5	B	*Diartus hughesi*	8,CC 9-4	70.52 75.42	8,CC 9,CC	70.42 79.87		
	11.6	T	*Stichocorys wolffii*	8,CC 9-4	70.52 75.42	8,CC 9,CC	70.42 79.87		
		T	*Cyrtocapsella japonica*	8,CC 9-4	70.52 75.42	8,CC 9,CC	70.42 79.87		
		B	*Phormostichoartus doliolum*	9-4 9,CC	75.42 79.96	8,CC 9,CC	70.42 79.87		
		T	*Lithopera thornburgi*	9,CC 10-4	79.96 84.92	8,CC 9,CC	70.42 79.87		
		T	*Spirocyrtis subtilis*	9,CC 10-4	79.96 84.92	8,CC 9,CC	70.42 79.87		
		B	*Didymocyrtis antepenultima*	9,CC 10-4	79.96 84.92	8,CC 9,CC	70.42 79.87		
		B	*Lithopera bacca*	9,CC 10-4	79.96 84.92	9,CC 10,C	79.87 87.19		
		T	*Carpocanopsis cristata* s.s.	[9-4 9,CC	70.50] 79.96]	9,CC 10,CC	79.87 87.19		
		B	*Botryostrobus hramlettei*	12-4 12,CC	103.52 108.14	11,CC 12,CC	98.91 108.17		

Table 3. (Continued).

Zone	Age (Ma)	Top or bottom	Species	Hole 574 Core-Section	Hole 574 Sub-bottom depth (m)	Hole 574A Core-Section	Hole 574A Sub-bottom depth (m)	Hole 574B Core-Section	Hole 574B Sub-bottom depth (m)
D. petterssoni	11.8	T	*Cyrtocapsella cornuta*	12-4 12,CC	103.52 108.14	12,CC 13,CC	108.17 113.08		
	[12.5]	T	*Cyrtocapsella tetrapera*	12-4 12,CC	103.52 108.14	12,CC 13,CC	108.17 113.08		
		T	*Lithopera renzae*	12-4 12,CC	103.02 108.14	12,CC 13,CC	108.17 113.08		
	11.8	T	*Dorcadospyris alata*	12-4 12,CC	103.52 108.14	12,CC 13,CC	108.17 113.08		
		T	*Giraffospyris toxaria*	13-4 13,CC	113.02 117.65	13,CC 14,CC	113.08 118.03		
		B	*Cyrtocapsella japonica*	14,CC 15,CC	122.53 128.73	[12,CC 13,CC	108.17] 113.08		
		T	*Didymocyrtis mammifera*	14,CC 15,CC	122.53 128.73	15,CC 16,CC	122.68 127.08		
	12.3	B	*Diartus petterssoni*	14,CC 15,CC	122.53 128.73	15,CC 16,CC	122.68 127.08		
D. alata	14.2	B	*Lithopera neotera*	16,CC 17,CC	132.56 137.57	16,CC 17,CC	127.08 132.66		
		B	*Lithopera thornburgi*	16,CC 17,CC	132.56 137.57	16,CC 17,CC	127.08 132.66		
		B	*Phormostichoartus corbula*	17,CC 18,CC	137.57 142.18	[15,CC 16,CC	122.68] 127.08		
		B	*Dictyocoryne ontongensis*	18,CC 19,CC	142.18 148.24	17,CC 18,CC	132.66 141.43		
	[13.8]	B	*Didymocyrtis laticonus*	18,CC 19,CC	142.18 148.24	18,CC 19,CC	141.43 150.90		
		T	*Liriospyris parkerae*	20,CC 21,CC	152.48 157.52	19,CC 20,CC	150.90 160.17		
	14.75	T	*Calocycletta virginis*	20,CC 21,CC	152.48 157.52	[20,CC 21,CC	160.17] 167.38		
		T	*Carpocanopsis bramlettei*	20,CC 21,CC	152.48 157.52	19,CC 20,CC	150.90 160.17		
		T	*Acrocubus octopylus*	[18,CC 19,CC	142.18] 148.24	19,CC 20,CC	150.90 160.17		
	15.35	T	*Calocycletta costata*	21,CC 22,CC	157.52 162.55	20,CC 21,CC	160.17 167.17		
		T	*Didymocyrtis tubaria*	21,CC 22,CC	157.52 162.55	20,CC 21,CC	160.17 167.17		
		T	*Didymocyrtis violina*	21,CC 22,CC	157.52 162.55	20,CC 21,CC	160.17 167.17		
	15.8	T	*Dorcadospyris dentata*	21,CC 22,CC	157.52 162.55	20,CC 21,CC	160.17 167.17		
		T	*Liriospyris stauropora*	25,CC 26,CC	177.79 182.19	20,CC 21,CC	160.17 167.17		
			L. stauropora → *L. parkeri*	25,CC 29,CC	177.79 197.18	20,CC 23,CC	160.17 186.23		
		T	*Dorcadospyris forcipata*	25,CC 26,CC	177.79 182.19	20,CC 21,CC	160.17 167.17		
			D. dentata → *D. alata*	25,CC 26,CC	177.79 182.19	20,CC 21,CC	160.17 167.17		
C. costata	15.7	B	*Dorcadospyris alata*	27,CC 28,CC	187.14 192.27	21,CC 22,CC	167.17 178.00		
		T	*Eucyrtidium diaphanes*	[26,CC 27,CC	182.19] 187.14	22,CC 23,CC	178.00 186.23		
		B	*Liriospyris parkerae*	28,CC 29,CC	192.27 197.18	22,CC 23,CC	178.00 186.23		

Table 3. (Continued).

Zone	Age (Ma)	Top or bottom	Species	Hole 574 Core-Section	Hole 574 Sub-bottom depth (m)	Hole 574A Core-Section	Hole 574A Sub-bottom depth (m)	Hole 574B Core-Section	Hole 574B Sub-bottom depth (m)
C. costata		T	*Carpocanopsis cingulata*	28,CC 29,CC	192.27 197.18				
	16.2	T	*Didymocyrtis prismatica*	[26,CC 27,CC	182.19] 187.14			1-2 1,CC	196.42 202.21
		B	*Carpocanopsis cristata* s.s.	28,CC 29,CC	192.27 197.18			1-2 1,CC	196.42 202.21
		T	*Carpocanopsis favosa*	28,CC 29,CC	192.27 197.18			1-2 1,CC	196.42 202.21
		B	*Lithopera renzae*	28,CC 29,CC	192.27 197.18			1-2 1,CC	196.42 202.21
		B	*Acrocubus octopylus*	29,CC 30,CC	197.18 202.16			1-2 1,CC	196.42 202.21
		B	*Giraffospyris toxaria*	29,CC 30,CC	197.18 202.16			1-2 1,CC	196.42 202.21
	16.5	T	*Lychnocanoma elongata*					2,CC 3,CC	213.38 218.78
		B	*Didymocyrtis mammifera*					2,CC 3,CC	213.38 218.78
	17.3	B	*Calocycletta costata*					2,CC 3,CC	213.38 218.78
S. wolffii	17.1	B	*Dorcadospyris dentata*					2,CC 3,CC	213.38 218.78
		B	*Calocycletta caepa*					3,CC 4,CC	218.78 226.67
		B	*Liriospyris stauropora*					4,CC 5,CC	226.67 238.79
	[20.4]	T	*Dorcadospyris ateuchus*					4,CC 5,CC	226.67 238.79
	17.6	B	*Stichocorys wolffii*					4,CC 5,CC	226.67 238.79
S. delmontensis		B	*Siphostichartus corona*					8,CC 9,CC	265.85 275.28
	19.25	B	*Didymocyrtis violina*					9,CC 10-3	275.28 283.42
		B	*Didymocyrtis tubaria*					9,CC 10-3	275.28 283.42
	20.3	B	*Stichocorys delmontensis*					9,CC 10,CC	275.28 289.54
		B	*Carpocanopsis bramlettei*					9,CC 10,CC	275.28 289.54
C. tetrapera	21.3	T	*Theocyrtis annosa*					10,CC 11,CC	289.54 294.00
		T	*Calocycletta robusta*					11,CC 12,CC	294.00 308.39
	21.35	B	*Calocycletta virginis*					12,CC 13,CC	308.39 314.94
		T	*Cyclampterium pegetrum*					13,CC 14,CC	314.94 321.38
		B	*Botryostrobus miralestensis*					13,CC 14,CC	314.94 321.38
		B	*Carpocanopsis cingulata*					13,CC 14,CC	314.94 321.38
	22.2	B	*Cyrtocapsella cornuta*					14,CC 15-3	321.38 330.92
	22.2	B	*Cyrtocapsella tetrapera*					14,CC 15-3	321.38 330.92

Table 3. (Continued).

Zone	Age (Ma)	Top or bottom	Species	Hole 574 Core-Section	Hole 574 Sub-bottom depth (m)	Hole 574A Core-Section	Hole 574A Sub-bottom depth (m)	Hole 574B Core-Section	Hole 574B Sub-bottom depth (m)
L. elongata		B	*Carpocanopsis favosa*					14,CC 15-3	321.38 330.92
	22.5	T	*Artophormis gracilis*					15-3 15,CC	330.92 336.85
	25.9	B	*Lychnocanoma elongata*					18,CC 19,CC	358.48 368.17
D. ateuchus		B	*Calocycletta robusta*					18,CC 19,CC	358.48 368.17
		B	*Dorcadospyris forcipata*					20,CC 21,CC	384.25 390.65
		T	*Lithocyclia angusta*					24,CC 25,CC	419.47 424.51
		B	*Theocyrtis annosa*					25,CC 26,CC	424.51 435.90
		T	*Lithocyclia crux*					25,CC 26,CC	424.51 435.90
		B	*Didymocyrtis prismatica*					25,CC 26,CC	424.51 435.90
		T	*Cyclampterium milowi*					26,CC 27,CC	435.90 446.86
		T	*Tristylospyris triceros*					26,CC 27,CC	435.90 446.86
			T. triceros → *D. ateuchus*					26,CC 27,CC	435.90 446.86
T. tuberosa	*33.0*	*B*	*Dorcadospyris ateuchus*					26,CC 27,CC	435.90 446.86
		B	*Cyclampterium pegetrum*					27,CC 28,CC	446.86 451.57
		T	*Theocyrtis tuberosa*					28,CC 29,CC	451.57 465.27
		B	*Eucyrtidium diaphanes*					28,CC 29,CC	451.57 465.27
		B	*Lithocyclia angusta*					29,CC 30,CC	465.27 474.85
		B	*Spirocyrtis subtilis*					31,CC 32,CC	483.15 493.19
		B	*Cyclampterium milowi*					33-4 33-5	503.50 505.08
		B	*Theocyrtis tuberosa*					33-4 33-5	503.50 505.08

Note: Pairs of levels and brackets as defined in Table 1 of this appendix.

Table 4. List of radiolarian events for Site 575.

Zone	Age (Ma)	Top or bottom	Species	Hole 575 Core-Section	Hole 575 Sub-bottom depth (m)	Hole 575A Core-Section	Hole 575A Sub-bottom depth (m)	Hole 575B Core-Section	Hole 575B Sub-bottom depth (m)
B. invaginata	0.3	B	*Buccinosphaera invaginata*						
C. tuberosa	0.44	T	*Stylatractus universus*	1-2 1-3	1.92 3.42				
		B	*Collosphaera tuberosa*	1-1 1-2	0.42 1.92				
		B	*Pterocorys hertwigii*	1-2 1-3	1.92 3.42				

Table 4. (Continued).

Zone	Age (Ma)	Top or bottom	Species	Hole 575 Core-Section	Hole 575 Sub-bottom depth (m)	Hole 575A Core-Section	Hole 575A Sub-bottom depth (m)	Hole 575B Core-Section	Hole 575B Sub-bottom depth (m)
A. ypsilon	1.1	T	*Anthocyrtidium angulare*						
A. angulare		T	*Theocorythium vetulum*	[1-4 1-5	4.92] 6.42				
		T	*Didymocyrtis avita*	1-3 1-4	3.42 4.92			1,CC	0.00 12.85
		B	*Lamprocyrtis nigriniae*	1-3 1-4	3.42 4.92				
	1.35	B	*Theocorythium trachelium*	1-3 1-4	3.42 4.92				
P. prismatium	1.5	T	*Pterocanium prismatium*	1-3 1-4	3.42 4.92				
		B	*Anthocyrtidium angulare*	1-4 1-5	4.92 6.42				
S. pentas	2.4	T	*Stichocorys peregrina*	1-4 1-5	4.92 6.42			1,CC	0.00 12.85
		T	*Phormostichoartus fistula*	1-5 1,CC	6.42 7.27			1,CC 2,CC	12.85 21.50
	3.4	T	*Spongaster pentas*	[1,CC 2-1	7.27] 7.30			1,CC	0.00 12.85
		T	*Lychnodictyum audax*	1-5 1,CC	6.42 7.27			1,CC 2,CC	12.85 21.50
		T	*Phormostichoartus doliolum*	1-5 1,CC	6.42 7.27			1,CC	0.00 12.85
		B	*Amphirhopalum ypsilon*	1,CC 2-1	7.27 7.30			1,CC 2,CC	12.85 21.50
		B	*Didymocyrtis tetrathalamus*	1,CC 2-1	7.27 7.30				
	3.6	B	*Spongaster tetras*	1,CC 2-1	7.27 7.30			1,CC	0.00 12.85
	3.69	T	*Didymocyrtis penultima*	1,CC 2-1	7.27 7.30			1,CC	0.00 12.85
		T	*Solenosphaera omnitubus*	[1-5 1,CC	6.42] 7.27			1,CC	0.00 12.85
		B	*Didymocyrtis avita*	1,CC 2-1	7.27 7.30			1,CC 2,CC	12.85 21.50
		T	*Spongaster berminghami*	2-2 2-4	9.23 12.23			1,CC 2,CC	12.85 21.50
			S. berminghami → *S. pentas*	2-1 2-4	7.73 12.23				
S. peregrina	4.3	B	*Spongaster pentas*	2-1 2-2	7.73 9.23			1,CC 2,CC	12.85 21.50
		T	*Botryostrobus bramlettei*	[1-4 2-1	4.92] 7.73			1,CC 2,CC	12.85 21.50
	4.8	B	*Pterocanium prismatium*	2-1 2-2	7.73 9.23			1,CC 2,CC	12.85 21.50
		B	*Botryostrobus aquilonaris*	2-1 2-2	7.73 9.23			1,CC 2,CC	12.85 21.50
		T	*Didymocyrtis antepenultima*	1,CC 2-5	7.27 13.73			1,CC 2,CC	12.85 21.50
		T	*Stichocorys delmontensis*	1,CC 2-4	7.27 12.23			1,CC 2,CC	12.85 21.50
		T	*Siphostichartus corona*	[1-4 1,CC	4.92] 7.27			1,CC 2,CC	12.85 21.50
	5.0	T	*Acrobotrys tritubus*	1-5 2-3	6.42 10.73			1,CC	0.00 12.85

Table 4. (Continued).

Zone	Age (Ma)	Top or bottom	Species	Hole 575 Core-Section	Hole 575 Sub-bottom depth (m)	Hole 575A Core-Section	Hole 575A Sub-bottom depth (m)	Hole 575B Core-Section	Hole 575B Sub-bottom depth (m)
S. peregrina		T	*Calocycletta caepa*	2-4 2-6	12.23 15.23			 1,CC	0.00 12.85
			S. delmontensis → S. peregrina	2-4 2-6	12.23 15.23			1,CC 2,CC	12.85 21.50
D. penultima		T	*Phormostichoartus marylandicus*	2-4 2,CC	12.23 16.89			1,CC 2,CC	12.85 21.50
	6.55	B	*Solenosphaera omnitubus*	2,CC 3-3	16.89 20.23			2,CC 3,CC	21.50 29.66
	[6.4]	B	*Stichocorys peregrina*	2,CC 3-3	16.89 20.23			2,CC 3,CC	21.50 29.66
D. antepenultima	8.2	T	*Diartus hughesi*	2,CC 3-3	16.89 20.23			2,CC 3,CC	21.50 29.66
		T	*Lithopera neotera*	2,CC 3-3	16.89 20.23			2,CC 3,CC	21.50 29.66
		T	*Dictyocoryne ontongensis*	2,CC 3-3	16.89 20.23			2,CC 3,CC	21.50 29.66
		T	*Botryocyrtis miralestensis*	3-3 3,CC	20.23 26.40			2,CC 3,CC	21.50 29.66
	[11.2]	B	*Acrobotrys tritubus*	3-3 3,CC	20.23 26.40			2,CC 3,CC	21.50 29.66
		T	*Didymocyrtis laticonus*	3-3 3,CC	20.23 26.40			2,CC 3,CC	21.50 29.66
	8.2	B	*Didymocyrtis penultima*	3-3 3,CC	20.23 26.40			3,CC 4,CC	29.66 39.08
	9.7	T	*Diartus petterssoni*	3-3 3,CC	20.23 26.40			3,CC 4,CC	29.66 39.08
		B	*Spongaster berminghami*	3-3 3,CC	20.23 26.40			3,CC 4,CC	29.66 39.08
			D. petterssoni → D. hughesi	3,CC 4-4	26.40 31.23			3,CC 4,CC	29.66 39.08
D. petterssoni	11.5	B	*Diartus hughesi*	3,CC 4-4	26.40 31.23			3,CC 4,CC	29.66 39.08
	11.6	T	*Stichocorys wolffii*	3,CC 4-4	26.40 31.23			3,CC 4,CC	29.66 39.08
		T	*Cyrtocapsella japonica*	3,CC 4-4	26.40 31.23			3,CC 4,CC	29.66 39.08
		B	*Phormostichoartus doliolum*	3,CC 4-4	26.40 31.23			3,CC 4,CC	29.66 39.08
		T	*Lithopera thornburgi*	3,CC 4-4	26.40 31.23			3,CC 4,CC	29.66 39.08
		T	*Spirocyrtis subtilis*	[5-3 5,CC]	[38.43 44.55]			[4,CC 5,CC	[39.08 48.28]
		B	*Didymocyrtis antepenultima*	3,CC 4-4	26.40 31.23			3,CC 4,CC	29.66 39.08
		B	*Lithopera bacca*	3,CC 4-4	26.40 31.23			3,CC 4,CC	29.66 39.08
		T	*Carpocanopsis cristata* s.s.	4-4 4,CC	31.23 34.93			3,CC 4,CC	29.66 39.08
		B	*Botryostrobus bramlettei*	5-3 5,CC	38.43 44.55			3,CC 4,CC	29.66 39.08
	11.8	T	*Cyrtocapsella cornuta*	5-3 5,CC	38.43 44.55			3,CC 4,CC	29.66 39.08
	[12.5]	T	*Cyrtocapsella tetrapera*	5-3 5,CC	38.43 44.55			3,CC 4,CC	29.66 39.08
		T	*Lithopera renzae*	5-3 5,CC	38.43 44.55			[6,CC 7,CC	[55.95 64.74]

Table 4. (Continued).

Zone	Age (Ma)	Top or bottom	Species	Hole 575 Core-Section	Hole 575 Sub-bottom depth (m)	Hole 575A Core-Section	Hole 575A Sub-bottom depth (m)	Hole 575B Core-Section	Hole 575B Sub-bottom depth (m)
D. petterssoni	11.8	T	*Dorcadospyris alata*	5-3 5,CC	38.43 44.55			[8,CC 9,CC]	73.74 81.33
		T	*Giraffospyris toxaria*	5-3 5,CC	38.43 44.55			5,CC 6,CC	48.28 55.95
		B	*Cyrtocapsella japonica*	[5,CC 6-3]	44.55 47.92]			5,CC 6,CC	48.28 55.95
		T	*Didymocyrtis mammifera*	5-3 5,CC	38.43 44.55			[7,CC 8,CC]	64.73 73.74]
	12.3	B	*Diartus petterssoni*	5-3 5,CC	38.43 44.55			5,CC 6,CC	48.28 55.95
D. alata	14.2	B	*Lithopera neotera*	[7,CC 8-3]	63.54 66.92]			[7,CC 8,CC]	64.73 73.74]
		B	*Lithopera thornburgi*	6-3 6,CC	47.92 53.98			[7,CC 8,CC]	64.73 73.74]
		B	*Phormostichoartus corbula*	6,CC 7-3	53.98 57.42			[6,CC 7,CC]	55.95] 64.73]
		B	*Dictyocoryne ontongensis*	6,CC 7-3	53.98 57.42			[6,CC 7,CC]	55.95] 64.73]
	[13.8]	B	*Didymocyrtis laticonus*	6,CC 7-3	53.98 57.42			8,CC 9,CC	73.74 81.33
		T	*Liriospyris parkerae*	8-3 8,CC	66.92 72.99			8,CC 9,CC	73.74 81.33
	14.75	T	*Calocycletta virginis*	8-3 8,CC	66.92 72.99			8,CC 9,CC	73.74 81.33
		T	*Carpocanopsis bramlettei*	8-3 8,CC	66.92 72.99			[10,CC 11,CC]	90.98] 99.53]
		T	*Acrocubus octopylus*	8-3 8,CC	66.92 72.99			9,CC 10,CC	81.33 90.98
	15.35	T	*Calocycletta costata*	8,CC 9-3	72.99 76.42			9,CC 10,CC	81.33 90.98
		T	*Didymocyrtis tubaria*	8,CC 9-3	72.99 76.42			10,CC 11,CC	90.98 99.53
		T	*Didymocyrtis violina*	8,CC 9-3	72.99 76.42			10,CC 11,CC	90.98 99.53
	15.8	T	*Dorcadospyris dentata*	8,CC 9-3	72.99 76.42			[11,CC 12,CC]	99.53] 90.98]
		T	*Liriospyris stauropora*	8,CC 9-3	72.99 76.42			10,CC 11,CC	90.98 99.53
			L. stauropora → *L. parkeri*	8,CC 10,CC	72.99 89.01			10,CC 13,CC	90.98 114.04
		T	*Dorcadospyris forcipata*	9-3 9,CC	76.42 80.14			11,CC 12,CC	99.53 109.15
			D. dentata → *D. alata*	9-3 9,CC	76.42 80.14			11,CC 12,CC	99.53 109.15
C. costata	15.7	B	*Dorcadospyris alata*	9,CC 10-4	80.14 85.12			11,CC 12,CC	99.53 109.15
		T	*Eucyrtidium diaphanes*	10-4 10,CC	85.12 89.01			11,CC 12,CC	99.53 109.15
		B	*Liriospyris parkerae*	10-4 10,CC	85.12 89.01			12,CC 13,CC	109.15 114.04
		T	*Carpocanopsis cingulata*	10-4 10,CC	85.12 89.01			12,CC 13,CC	109.15 114.04
	16.2	T	*Didymocyrtis prismatica*	11-3 11,CC	92.51 98.45			12,CC 13,CC	109.15 114.04
		B	*Carpocanopsis cristata* s.s.	[—]				[—]	

Table 4. (Continued).

Zone	Age (Ma)	Top or bottom	Species	Hole 575 Core-Section	Hole 575 Sub-bottom depth (m)	Hole 575A Core-Section	Hole 575A Sub-bottom depth (m)	Hole 575B Core-Section	Hole 575B Sub-bottom depth (m)
C. costata		T	*Carpocanopsis favosa*	11-3 11,CC	92.51 98.45	1-2 1,CC	95.72 98.86	12,CC 13,CC	114.04 114.04
		B	*Lithopera renzae*			1-1 1-2	94.22 95.72	[—]	
		B	*Acrocubus octopylus*			1-2 1,CC	95.72 98.86	13,CC 14,CC	114.04 118.97
		B	*Giraffospyris toxaria*			1-2 1,CC	95.72 98.86	13,CC 14,CC	114.04 114.04
	16.5	T	*Lychnocanoma elongata*			2,CC 3,CC	102.26 105.28		
		B	*Didymocyrtis mammifera*			2,CC 3,CC	102.26 105.28		
	17.3	B	*Calocycletta costata*			4,CC 5,CC	109.87 114 00		
S. wolffii	17.1	B	*Dorcadospyris dentata*			5,CC 6,CC	114.00 119 17		
		B	*Calocycletta caepa*			5,CC 6,CC	114.00 119.17		
		B	*Liriospyris stauropora*			7,CC 8,CC	123.25 126.29		
	[20.4]	T	*Dorcadospyris ateuchus*			9,CC 10,CC	128.14 132.01		
	17.6	B	*Stichocorys wolffii*			9,CC 10,CC	128.14 132.01		
S. delmontensis		B	*Siphostichartus corona*			9,CC 10,CC	128.14 132.01		
	19.25	B	*Didymocyrtis violina*			25,CC 26,CC	181.96 184.80		
		B	*Didymocyrtis tubaria*			25,CC 26,CC	181.96 184.88		
	20.3	B	*Stichocorys delmontensis*			25,CC 26,CC	181.96 184.80		
		B	*Carpocanopsis bramlettei*			26,CC 27,CC	184.80 188.41		
C. tetrapera	21.3	T	*Theocyrtis annosa*			31,CC 32,CC	201.75 205.13		
		T	*Calocycletta robusta*			31,CC 32,CC	201.75 205.13		
	21.35	B	*Calocycletta virginis*			32,CC 33,CC	205.13 208.30		

Note: Pairs of levels and brackets as defined in Table 1 of this appendix.

APPENDIX B
Raw Data for the Leg 85 Holes

The following appendix comprises tables of raw data for each of the Leg 85 holes. Unlike other DSDP reports (e.g., Westberg and Riedel, 1982) this study does not record species abundances, but rather notes only presence or absence. Radiolarian abundances and conditions of preservation are almost always "common" and "good." Exceptions to this general rule are noted in the text for each site.

Table 1. Raw data for Hole 572A.

Core-Section (interval in cm)	*B. invaginata*	*C. tuberosa*	*P. hertwigii*	*L. nigriniae*	*T. trachelium*	*A. ypsilon*	*D. tetrathelamus*	*S. tetras*	*B. equilonaris*	*L. bacca*	*P. corbula*	*S. universus*	*A. angulare*	*T. vetulum*	*D. avita*	*P. prismatium*	*S. peregrina*	*P. fistula*	*S. pentas*	*L. audax*	*P. doliolum*	*D. penultima*	*S. omnitubus*	*S. berminghami*	*B. bramlettei*	*D. antepenultima*	*S. delmontensis*	*S. corona*	*A. tribulus*	*C. caepa*
1-1, 108–109	—	P	P	P		P	P	P	P		P																			
1-3, 69–70		P	P	P	P	P	P	P	P		P	—																		
1,CC		+	P	P	P	P	P	P	P	P	P	P																		
2-3, 70–71		—	P	P	P	P	P	P	P		P	P	—	—	—															
2-5, 70–71							P						—	—	—															
2,CC			—	+	P	P	P	P	P	P	P	P	P	P	+				—											
3-3, 90–92			—	—	—	P	P		P	P	P	P	P	P	+	—														
3-5, 90–92													P	P																
3,CC				—	+	P	P	P	P	—	P	P	—	P	+	P			+											
4-3, 70–71					—		P	P		P	P			P		P														
4,CC				+	—	P	P	P	P	P	P	P		P	+	P														
5-3, 70–71			—			P	P	P	P		P	P		P	+	P	—		+						—					
5,CC			—			P	P	P	P	P	P	P		P		P	P		—											
6-3, 70–71						P			P		P	P		P		P	P	P	—	+					—					
6,CC						P	+	P	P	P	P	P		P	P	P	P	P	+	P	—		—		+					
7-3, 70–71						—		P				P		P	P	P	P	P	+	P		—								
7,CC							—	+	—	P	P	P		P	P	P	P	P	+	P	P		—							
8-3, 70–71								—		P				P	—	P	P	P	—		P	P	+		—					
8,CC										P				P		P	P	P			P			—						
9-3, 70–71									—	P	P	P		P		P	P	—		P	P		P	—	—					
9,CC																P	P	P	+	+	P			—						
10,CC								P	P		P	P		P	+	P	P	—		P	P	P	—	P						
11-3, 78–79								P			P				+	P	P	+		P	P	P	—	P	—					
11,CC								P	P		P	P		P		P	P			P	P	P	—	P	+					
12-3, 68–69								+							+	P	P			P	P	P	P	P	+					
12,CC								P	P		P	P		P	—									P	+					
13-3, 70–71								P			P	P			—	P	P	P	+	P	P	P	—	+	+	—	—			
13,CC								—	P		P	P		P	—	P				P	P			P	—	—	—			
14-3, 70–71								—	P			P		P	—	P	P	P	+	P	P	P	P	+	P	P	P	—		
14,CC									P		P	P		P	—	P				P	P	P	P	P			P	—		
15-3, 70–71									P		P				—	P	P	P		P	P	P	P	—	P	P	P	—		
15,CC									P		P	P		P		P	P		P	P	P	P	P	P	P		P		
16-3, 72–73									P		P	P		P		P	P		P	P	P	P	P	P	P	P	P	P	—
16,CC											P	P		P		P	P		P	P	P	P	P	P	P		P	—	—
17,CC									P		P	P		P		P	P		P	P	P	P	P	P	P	P	P	P	P

Note: P = present; + = rare (one or two specimens); — = searched for and found to be absent.

Table 2. Raw data for Hole 572C (for explanation of symbols see note to this appendix, Table 1).

Section	*B. invaginata*	*C. tuberosa*	*P. kerrwigii*	*L. nigriniae*	*T. trochelium*	*A. ypsilon*	*D. tetrathalamus*	*S. tetras*	*B. aquilonaris*	*L. bacca*	*P. corbula*	*S. universus*	*A. angulare*	*T. vetulum*	*D. avita*	*P. prismatium*	*S. peregrina*	*P. fistula*	*S. penlas*	*L. audax*	*P. doliolum*	*D. penultima*	*S. omnitubus*	*S. berminghami*	*B. bramlietei*	*D. antepenultima*	*S. delmontensis*	*S. corona*	*A. tribulus*	*C. caepa*
1,CC	—	+	P	P	+	P	P	P		—	P	P				—							+							
2,CC		—	—	P	P	P	P	P	P	P	P	P	P																	
3,CC			—	—	—	P	P	P	P	—	P	P	—	P	+	P														
4,CC			—			P	P	P	P	P	P	P	+	P	P	P	—	—					+							
5,CC						P	P	P	P	P	P	P	+	P	P	P	P	P	—	—	—		—							
6,CC						P	P	P	—	P	P	P		P	P	P	P	P	+	P	P	—	P							
7,CC						—	—	—	P	P	P	P		P	P	P	P	P	+	P	P	P	P							
8,CC									P	P	P	P		P	P	P	P	P	+	P	P	P	P	—	—					
9,CC									+	P	P	P		P	+		P	P	—	P	P	P		—	+					
10,CC									P	P	P	P		P	—	+	P	P	—	P	P	P	P	—	P	+	+			
11,CC									P	P	P	P		P		—	P		—	P	P	P	—	P	P	+		—		
12,CC									+		P	P					P	P		P	P	P	P	—	P	—	—	—		
13,CC									—	P	P	P					P	P		P	P	P	P	P	P	P	P	—		
14,CC										P	P	P					P	P		P	P	P	P	P						
15,CC											P	P					P	P		P	P	+	P		P	P	P	—	—	
16,CC										P	P						P	P		P	P		P	P	P	P	P	P	P	P
17,CC										P	P						P			P	P	P	P	P	P	P	P	P	P	P
18,CC										P	P						P			P	P	P	P	P	P	P	P	P	P	P
19,CC										P	P						P	P		P	P	P	P	P	P	P	P	P	—	
20,CC											P						P	P		P	P	P	P	P	P	P	P		—	

Table 3. Raw data for Hole 572D (for explanation of symbols see note to this appendix, Table 1).

Core-Section (interval in cm)	*L. barra*	*P. corbula*	*S. universa*	*T. venulum*	*S. peregrina*	*P. fistula*	*L. mitra*	*P. dolodum*	*D. penultima*	*S. omnitubus*	*S. hermughusi*	*B. bramlettei*	*D. antepenultima*	*S. delmontensis*	*S. cornuta*	*A. irwini*	*C. carpa*	*P. marylandica*	*D. hughesi*	*L. inversa*	*D. ontongensis*	*B. nuttalli*	*D. laticonus*	*D. petterssoni*	*S. wolffii*	*C. japonica*	*L. thornburgi*	*S. subtilis*	*C. cristata* s.l.	*C. cornuta*	*C. irregularis*	*L. recta*	*D. alata*	*G. tosana*	*D. mammifera*	*L. parkerae*	*C. virgulta*	*C. humilicrus*	*A. octopylus*	*C. costata*	*D. tuberosa*	*D. violina*	*D. devisa*	*L. staurogonia*	*D. forcipata*	*E. diaphanes*	*C. cingulata*	*D. prismatica*	*C. fossa*
1,CC	P	P			P	P	P	P	P	P	P	P	P	P	P	P	—																														
2-3, 64-66		P			P				P			P	P	P																																
2,CC		P			P				P			P	P	P			—																														
3,CC	P	P		P	P	P	P	P	P	P		P	P	P			P																														
4,CC	P	P			P	P	P	P	P	—	P	P	P	P	P	P	P																																
5-4, 64-66		P			P	P	P	P	P	—	P	P	P	P	P	P	P																																
5,CC	P	P				P	P	P	P	—		P		P	P		P																																
6-5, 60-62	P	P			•	P	P	P	P	—	P	P	P	P	P	P	P	—	—																												
6,CC	P	P			•	P	P	P	P	—	•	P		P	P	P	P	—	—																														
7-3, 60-62	P	P			•	P		P	P	•	P	P	P	P	P	P	P	P		•																												
7,CC	—	P									P									•																												
8-3, 60-62	P	P				P	P	P	P		P	P	P	P	P	P	P	P	—																														
8,CC	P					P	P	P	P		P	P	P	P	P	P	P	—	P																														
9,CC	P	P			•	P		P	P		P	P	P	P	P		P	P	P	P																												
10-3, 60-62	P	P			•			—	P		P	P	P	P	P	P	P	P	P	P	P	—	—	—																						
10,CC	P	P				P	P																																									
11-3, 60-62	P	P			•	P	P	P	P		P	•	P	P	P	—	P	•	P	P	P	•	—																								
11,CC	P	P				P	P	P	P		P	P	P	P	P		P	P	P	P	P	•	P																								
12,CC	P	P						P	P		—	•	P	P	P		P	P	P	•	P	P	P																								
13-3, 60-62	—										—	•	P	P	P		P	P	F		P	P	P	—																								
13,CC	P																																														
14-3, 60-62	•							P					P	P	P				—		P	P	P	P																								
14,CC	—	P																		P	P																										
15,CC		P			P		—	•			—	P	P	P	P	P	P			P	P	P	P	—																								
16-3, 60-62					P		P					P	P	P	P	P	P			P	P	P	P	—	P	P	—																		
16,CC		P			P																P																										
17,CC		P					P						P	P		P	P			P	P				P																					
18,CC		P			P		P				P		P	P		P				P	P																									
19,CC		P					P				P		P	P		P				P	P																									
20,CC		P			P		P				•		P	P		P	P			P	P																									
21,CC		P																																												
22,CC					P		P				—		P	P		P	P			P	P																									
23-3, 60-62							P						P	P		P	P			P	P																									
23,CC		P			P		P																																						
24-3, 60-62													P	P		P	P			P	P																									
24,CC		P																																											
25,CC		P			P		P						P	P		P	P			P	P																									
26,CC					P		P						P	P		P	P			P	P																									
27-3, 60-62		P											P	P		P	P																													
27,CC					P		P						P	P		P	P																													
28,CC		P																																											
29,CC		—											P	P		P				P	P																									
30,CC		—					P						P	P		P	P			P	P																									
31-3, 60-62					P								P	P		P	P						P																						
31,CC		—			P		P						P	P		P	P						P																						
32-3, 60-62					P		P							P		P							P																						
32,CC					P		P						P	P		P							P																						
33,CC					P		P							P		P				P			P																						

Table 4. Raw data for Hole 573 (for explanation of symbols see note to this appendix, Table 1).

Core-Section (interval in cm)	*B. inaequalis*	*C. tuberosa*	*P. hertwigii*	*L. nigriniae*	*T. trochelium*	*A. spinifer*	*D. tetrathalamus*	*S. ianus*	*B. aequilonaris*	*L. bacca*	*P. corbula*	*S. universa*	*A. angulare*	*T. vetulum*	*D. avita*	*P. praematurum*	*S. peregrina*	*P. fistula*	*S. persiana*	*L. sadai*	*P. dolioliformis*	*D. penultima*	*S. omnivallata*	*S. hermighami*	*B. bramlettei*	*D. asymmetrica*	*S. delmontensis*	*S. corona*	*A. tricuspis*	*C. carpa*	*P. marylandica*	*D. hughesi*	*L. necrona*	*D. ontongensis*	*D. miradentensis*	*D. laticonus*	*D. petterssoni*
1-1, 8-10	P	P	P	P	P	P	P	P	P	—	P	—																									
1,CC	—	P	P	P	P	P	P	P	P	P	P	+																									
2-3, 130-131	—	P	P	P		P	P	P	P	P	P	P			+																						
2,CC		—	P	+	P	P	P	P	P	P	P	P			+				—																		
3-3, 130-131			—	P	P	P	P	P	P	P	P	P	—	—	+																						
3-5, 130-131					P								P	—	—																						
3,CC				—	P	P	P	P	P	P	P	P	P	P	—	—			+																		
4-3, 130-131					—	P	P	P	P		P	P	P	P	+	P																					
4,CC					—	P	P	P	P	P	P	P	—	P	P	P																					
5-3, 130-131			—			P		P	P	P	P	P		P		P	—																				
5,CC						P	P	P	P	P	P	P		P	P	P	P																				
6-3, 130-131			—			P	P	P	P	P	P				P	P	P	—	—																		
6,CC						P	P	P	P	P	P	P		P	P	P	P	P	P				+														
7-3, 129-130						P	P	P			P	P		P	P	P	P	P	—				—														
7,CC						—	—	—	P	P	P	P			P	P	P	P	—		P	P															
8-3, 69-70									P	P	P	P			P	P	P	P	+		P				+												
8,CC							—		P		P	P		P	P	P	P	P	+		P	P	—	—	P												
9-3, 68-69									P			P			P	+	—	P	+		+	P	P	P	P	—												
9,CC									P	P	P	P			—	—	P		P		P	P	P	—	P												
10-3, 67-68									+	P	P	P		P		—	P	P			P	P	P	P	P												
10,CC									—		P	P			—		P	P	—	P	P	P	P	P	P			P	—								
11-3, 63-64										P	P	P					P			P	P	P	P	P		—	—	P	—	—							
11,CC										P		P					P	P			P	P	P	P		+		P	—	P							
12-3, 68-69											P	P					P	P		P	P	P	P	P	P	P	+	P	—	P							
12,CC											P	P					P	P	+	P	P	P	P	P		P	+	P	P	P							
13-4, 65-66													P				P	P		P	P	P	P	P	P	P	P	P	P	P							
13,CC										P	P	P	P	P			P	P	◇	P	P	P	P	P		P	P	P	P	P							
14-3, 65-66											P	P		P			P			P	P	P	P	P		P	P	P	P	P							
14,CC										P	P	P		P			—			P	P	P	P	P		P	P	P	P	P							
15-3, 54-55											P						+				P		+	P		P	P	P	P	P	—						
15,CC										P	P						+			P	P	P	P			P	P	P	P	P							
16-3, 60-61										P			P					P		P	P	P	—	P	P	P	P	P	P	P		—			+	—
16,CC										P	P							P		P	P	P	P	P	P	P	P	—	P	P	—	P	—		P	—
17-3, 61-62										P	P			P				P		P	P	P	P	—	P	P	P	+	P	P	P	P	P			—
17,CC										P	P						+	P		P	P	P	—		—	P	P	—	P	P			P		P	P
18,CC										P	P							P		P	P	P				P	P	P	P	P	P				P	P
19-2, 61-62										P	P									P	P	P				P	P	P	P	P	P	P	P	P	P	P
19,CC										P	P						+	P		P	P			—	P	P	P	P	P	P	—	P	P	P	P	P

Table 5. Raw data for Hole 572A (for explanation of symbols see note to this appendix, Table 1).

Section	*B. inaequalis*	*C. tuberosa*	*P. hertwigii*	*L. nigriniae*	*T. trochelium*	*A. spinifer*	*D. tetrathalamus*	*S. ianus*	*B. aequilonaris*	*L. bacca*	*P. corbula*	*S. universa*	*A. angulare*	*T. vetulum*	*D. avita*	*P. praematurum*	*S. peregrina*	*P. fistula*	*S. persiana*	*L. sadai*	*P. dolioliformis*	*D. penultima*
1,CC	—	—	P	P	P	P	P	P			P	P	—	—	—							
2,CC			—	—	—	P	P	P		P	P	P	P	P	+	—						
3,CC			—			P	P	P	P	P	P	P	—		+	P	P	—				
4,CC						P	P	P	P		P	P		P	+	P	P	P	—	+	—	+
5,CC						P		P		P	P			P	P	P	P	P	—	P	P	
6,CC						P		P		P	P			P	P	P	P	P	—	P	P	

Table 6. Raw data for Hole 576B (for explanation of symbols see note to this appendix, Table 1).

| Core-Section (interval in cm) | L. barbui | P. carpbula | S. universus | P. flustula | L. awdax | P. dolioloides | D. penultima | S. berminghami | B. tumidistri | D. antepenultima | S. delmontensis | S. crassa | A. tribulus | C. carpa | P. moyamadarus | D. hughesi | L. neotera | D. onondagensis | B. mylnefarmeri | D. laticonus | D. petterssoni | S. woodi | C. japonica | L. thornburgi | S. subtilis | C. crassata s.l. | C. cornuta | H. tetrapera | L. mitra | D. alata | G. toxaria | D. mammifera | L. penultima | C. virgula | C. bumsteini | A. octopylus | C. costata | D. tubaria | D. wolfini | D. dentata | L. staurospora | D. furcipata | E. diaphanes | C. cinguiata | D. pyramidina | C. fyrosa | L. elongata | D. asterias | T. annosa | C. robusta | C. petrinum | A. brevilis | L. angusta | L. crux | C. milowi | T. inserta | T. tuberosa |
|---|---|---

Table 7. Raw data for Hole 574 (for explanation of symbols see note to this appendix, Table 1).

| Core-Section (interval in cm) | *B. invaginata* | *C. tuberosa* | *P. hertwigii* | *L. nigriniae* | *T. trochelium* | *A. ypsilon* | *D. tetrathalamus* | *S. istrus* | *B. aquilonaris* | *L. bacca* | *P. corbula* | *S. universus* | *A. angulare* | *T. vetulum* | *D. avita* | *P. prismatium* | *S. peregrina* | *P. fistula* | *S. penias* | *L. audax* | *R. dolioloides* | *D. penultima* | *S. omnitubus* | *S. bermudezi* | *B. bramletti* | *D. antepenultima* | *S. delmontensis* | *S. corona* | *A. tribulus* | *C. carpe* | *R. macfadyeni* | *D. hughesi* | *L. neoiana* | *D. ontongensis* | *B. miralestensis* | *D. falconus* | *D. petterssoni* | *S. wolffii* | *C. japonica* | *L. thornburgi* | *S. subtilis* | *C. cristata s.s.* | *C. cornuta* | *C. tetrapera* | *L. renzae* | *D. alata* | *G. ixoxera* | *D. mammifera* | *L. carinata* | *C. vitrea* | *C. braarudi* | *A. octopylus* | *C. costata* | *D. tubaria* | *D. violina* | *D. dentata* | *L. staurogona* | *D. forcipata* | *E. diaphanes* | *C. cingulata* | *D. prismatica* | *C. javana* |
|---|---|---

Table 8. Raw data for Hole 574A (for explanation of symbols see note to this appendix, Table 1).

| Core-Section (interval in cm) | B. invaginata | C. tuberosa | P. hertwigii | L. nigriniae | T. trachelium | A. ypsilon | D. tetrathalamus | S. tetras | B. aquilonaris | L. baccia | P. corbula | S. universus | A. angulare | T. vetulum | D. avita | P. prismatium | S. peregrina | P. fistula | S. petasus | L. audax | P. dolioluum | D. penultima | S. omnitubus | S. berminghami | B. bermudezi | D. antepenultima | S. delmontensis | S. corona | A. tritubus | C. ceepa | P. marylandicus | D. hughesi | L. neotera | D. ontongensis | B. mutationensis | D. laticornus | D. petterssoni | S. woodi | C. japonica | L. thornburgi | S. subtilis | C. crassata s.s. | C. cornuta | C. tetraspera | L. renzae | D. elata | G. tosaria | D. mammiferus | L. parkerae | C. virginis | C. bramlettei | A. octopylus | C. costata | D. tubaria | D. violina | D. denticulata | L. staurospora | D. forcipata | E. diaphanes | C. clavigulata | D. prismatica | C. javorsae |
|---|---|---

Table 9. Raw data for Hole 574C (for explanation of symbols see note to this appendix, Table 1).

Core-Section (interval in cm)	*S. universus*	*P. fistula*	*L. sadax*	*S. delmontensis*	*S. corona*	*C. caepa*	*P. marylandicus*	*B. miralestensis*	*S. wolffii*	*S. subtilis*	*C. cristata* s.s.	*C. cornuta*	*C. tetrapera*	*L. rezae*	*G. tauria*	*D. mammifera*	*C. virginis*	*C. bramlettei*	*A. octopylus*	*C. castata*	*D. ruberia*	*D. violina*	*D. denisia*	*L. staurospora*	*D. forcipata*	*E. diaphanes*	*C. cingulata*	*D. prismatica*	*C. fossa*	*L. elongata*	*D. strelchus*	*T. annosa*	*C. robusta*	*C. pegetrum*	*A. gracilis*	*L. arcuata*	*L. crux*	*C. milowi*	*T. tricerus*	*T. tuberosa*
1-1, 41–43					P	P		P	P	P			P			P					P				P	P													
1-2, 41–43		P	P	P		P	P	P	P	P	P	P	P	P	P	P	P	P	P	P	P	P	P	P	P	P	P	P	P	P	P								
1,CC				P		P	P	P			—	P	P	—		P	P	P	—	P	P	P	P	P	P		P	—	P	P										
2,CC				P	—	P	P		P	P		P	P			P	P	P		P	P	P	P	—	P		P	—	P	P										
3,CC		P		P		P			P	P		P	P			—	P	P		—	P			P	P				P	—										
4,CC		P	P		P	+		P	P	P		P	P			—	P	P		P	P			P	P		P		P	+	P									
5,CC		P	P	P		—			—	P		P	—				P			—	P	P		—	P		P	—	P	P										
6,CC				P	P			P	—	P		P	P				P			+	P	P			P		P		P	P										
7,CC		P		P	P	+	P			P		P	P								P	P			P		P		P	P		—								
8,CC				P	P	+				P		P	P								P	P			P		P		P	P										
9,CC				P	—		P			P		P	P					P			P	P			P		P		P	P										
10-3, 41–43										P		P	P								—	—			P		P		P	P	—	P								
10,CC		P	P	—		+				P		P	P								—	—			P			P	P	P		P								
11,CC			P	—				P		P		P	P				P				+				P			P	P	P		P								
12,CC		P	P					P		P		P	P				+							P	P			P	P	P		P								
13,CC		P	P					P		P		P	P				—								P			P	P	P		P								
14,CC			P					—		P		P	P				—								P				P	P		P								
15-3, 41–43												—	—												P				P	P		P								
15,CC												—	—												P				+	P		P								
16,CC																														P	P		P							
17,CC							P			P														P	P		P		P	P		P								
18,CC			P							P														P	P		P		P	P		P								
19,CC			P							P														P	P		P		P	P		P								
20,CC										P														P	+		P		P	P		P								
21,CC			P							P															—		P		P	P		P								
22,CC																									—	P				P		P								
23,CC										P																	P		P	P		P								
24,CC																														P		P								
25,CC																												P							P				
26,CC		—	—							—																P		—		P					—	+				
27,CC			—				—			P																P				—	+					P	P			
28,CC		—	—							—																P				P						P	P			
29,CC		—	—				—			—																—										P	P			
30,CC										P																										P	P			
31,CC										P																														
32-1, 41–43																																								
32-2, 39–41																																								
32,CC										—																														
33-1, 42–44																																								
33-2, 42–44																																								
33-4, 49–51																																								
33-5, 57–59																																								
33,CC																																								
34-1, 59–61																																								
34-1																																								
34-2, 59–61																																								
34,CC	—									—																														

Table 10. Raw data for Hole 575 (for explanation of symbols see note to this appendix, Table 1).

| Core-Section (interval in cm) | B. invaginata | C. tuberosa | P. hertwigii | L. nigriniae | T. trachelium | A. ypsilon | D. tetrathalamus | S. ireta | B. aquilonaris | L. bacca | P. corbula | S. universus | A. angulare | T. vetulum | D. avita | P. prismatium | S. peregrina | P. fistula | S. penta | L. awdax | P. dolioluni | D. penultima | S. omnituhus | S. bermudaensis | B. bramlette | D. antepenultima | S. delmontensis | S. corona | A. trilobus | C. carpe | P. marylandicus | D. hughesi | L. neotera | O. ontongensis | B. mutatesiensis | D. laticonus | D. petterssoni | S. wolffii | C. japonica | L. thornburgi | S. subtilis | C. cristata s.s. | C. cornuta | C. tetrapera | L. inretae | D. alata | G. ioxaria | D. mammulfera | L. parkerae | C. virginis | C. hamiltoni | A. octopylus | C. costata | D. lusaria | D. violina | D. dentata | L. staurospor. | D. forcipata | E. diaphanes | C. cingulata | D. prismatica | C. javosa |
|---|---|---

Table 11. Raw data for Hole 572A (for explanation of symbols see note to this appendix, Table 1).

Core-Section (interval in cm)	*S. universus*	*P. fistula*	*L. audax*	*S. delmontensis*	*S. corona*	*C. caepa*	*P. marylandicus*	*B. mirulestensis*	*S. wolffii*	*S. subtilis*	*C. cornuta*	*C. tetrapera*	*L. renzae*	*G. toxaria*	*D. mammifera*	*C. virginis*	*C. bramlettei*	*A. octopylus*	*C. costata*	*D. tuberia*	*D. violina*	*D. denisia*	*L. stauropora*	*D. forcipata*	*E. diaphanes*	*C. cingulata*	*D. prismatica*	*C. favosa*	*L. elongata*	*D. ateuchus*	*T. annosa*	*C. robusta*
1-1, 41–42				P	P	P	P		P		P	P	+	—		P	P	P	P		P	P	P		P	P	P	—				
1-2, 41–42		P		P	P	P	P	P	P		P	P	—	P		P	—	P	P		P	P	P		P	—	P	—				
1,CC		P	P	P	P	P			P		P	P		—	P	P	P	—	P	P	P	P	P	P	P	P		+	—			
2,CC				P		P	P	P	P	P	P	P	—	—	P	P		—	P	P	P	P	P	P	P	P		P	—			
3,CC		P	P		P	P	P		P		P	P			—	P	P		P	P	P	P	P	P	P	P	P		P			
4,CC				P	+	+			P	P	P	P				P	P		+	P	P	P	P	P	P	P	P	P	P			
5-2, 41–42		P			+		P		P	P						P			—	P			P		P			—				
5-3, 41–42	P	P		P			P		P							P	P		—	P		P	P		P		P					
5,CC					—	+			P	P	P	P				P	P		—	P	P	P	P	P	P	P		—				
6-1, 41–42						—			P		P	P				P			—	P			P									
6-2, 41–42						—	P	+	P		P	P				P			—	P	P	—		P	P			—				
6-3, 41–42	P	P			—				P		P	P				P	P		—	P		—	P	P	P			—				
6,CC						—	P				P	P				P	P			P	P	—	P	P	P		P	P	P				
7-2, 41–42									P											P	P		P	P			P		—			
7-3, 41–41									P											P				P			P		—			
7,CC			P	P					P	P	P					P							P	P	P	P	P		—			
8-1, 41–42									P											P			—	P			P		—			
8-2, 41–42									P											P			—	P			P		+			
8,CC			P	P					P	P	P	P				P	P			P				P	P	P	P					
9,CC			P	P	P				P	P	P					P	P		—	P				P	P	P	P	P	—			
10-2, 41–42					—				—														—	—				—	—			
10,CC		P	P	P	—		P	P	—		P	P				P					P			P		P		P	P			
11-3, 41–42																				P				P				P				
11,CC		P		P						P	P					P	P			P	P			P	P			P	P			
12,CC											P	P																				
13,CC				P			P	P		P	P	P				P	P				P			P	P	P		P	P			
14,CC																																
15,CC			P	P				P		P	P	P				P					P		P	P		P			P			
16,CC																																
17,CC				P				P		P		P				P	P			P	P					P	P	P	P			
18,CC																																
19,CC		P		P				P			P	P				P				P	P			P	P	P	P	P				
20,CC																																
21,CC		P	P	P			P			P	P	P				P	P			P			P		P	P	P					
22,CC																																
23,CC		P		P				P			P	P				P				P	P		P	P	P	P	P	P	P			
24,CC											P	P																				
25,CC			P	P			P	P								P	P			P	P		P	P	P	P	P	P	P			
26,CC				—						P							P		—	—			P	P		P						
27,CC			P	—				P		P	P	P				P	—		—	—			P	P		P		P	P			
28,CC																																
29,CC			P	—						P	P	P				P							P	P	P	P		P		—		
30,CC																																—
31,CC		P	P				P			P	P	P				P							P		P	P	P	P	—	P	
32,CC			—							P	P					+							P		P	P		P	P	P	
33,CC		P	—				P	P		P	P	P				—							P	P		P	P	P		P		

Table 12. Raw data for Hole 575B (for explanation of symbols see note to this appendix, Table 1).

| Section | B. invaginata | C. tuberosa | P. hermesi | L. nigriniae | T. tracheliu | A. ypsilon | D. tetrathalamus | S. tetras | B. aquilonaris | L. baccu | P. corbula | S. universus | A. angulare | T. wetzlim | D. avita | P. prismatium | S. pererina | P. fistula | S. penias | L. audax | P. dolioli | D. penultima | S. omnitubus | S. berminghami | B. bramletti | D. antepenultima | S. delmontensis | S. corona | A. trifidus | C. ceepa | P. marylandicus | D. hueberi | L. neoter | D. ontongensis | B. miralestrensis | D. laticonus | D. petterssoni | S. wolffii | C. japonica | L. thornburgi | S. subtilis | C. cristata s.s. | C. cornuta | C. tetrapera | L. renzae | D. alata | G. toxaria | D. mammifera | L. parkerae | C. virginis | C. bramlettei | A. octopylus | C. costata | D. tuberia | D. violina | D. dentata | L. staurospora | D. forcipata | E. diaphanes | C. cingulata | D. prismatica | C. javosa |
|---|---|---

13. NANNOFOSSILS FROM QUATERNARY DEPOSITS IN THE HIGH-PRODUCTIVITY AREA OF THE CENTRAL EQUATORIAL PACIFIC, DEEP SEA DRILLING PROJECT LEG 85[1]

Annick Pujos, Département de Géologie et Océanographie, Institut de Géologie du Bassin d'Aquitaine[2]

ABSTRACT

During Leg 85, drilling was undertaken at DSDP Sites 571 to 575 in the high-productivity area of the central equatorial Pacific. Nannofossil-rich Quaternary sediment was recovered at the five sites, and provided adequate material for a detailed study of coccoliths. Various species and variants were found; the most important of them are briefly described and are used for a precise determination of stratigraphy. Besides conventional datums, some additional markers (*Gephyrocapsa ericsonii, Gephyrocapsa oceanica* s. s., *Gephyrocapsa doronicoides* s. ampl., *Crenalithus productus, Cyclococcolithina* sp. cf. *C. macintyrei, Coccolithus pelagicus*) proved useful for correlating sites and for correlating Leg 85 sites with other Quaternary sections. In addition, nannofossil total abundance is often close to $CaCO_3$ content, and so can be used for locating carbonate cycles; carbonate cycles represent a standard stratigraphic tool in the equatorial Pacific. Finally, carbonate dissolution is commonly strong in this area. In the most dissolved samples, the almost exclusive presence of reworked coccoliths might be explained by the episodic influence of a corrosive water mass (possibly a deep current from Antarctica).

INTRODUCTION

The central equatorial Pacific is well known as an area of high biologic productivity. Siliceous (diatoms, radiolarians, silicoflagellates) and calcareous (foraminifers and nannofossils) organisms are very abundant, generally in the same samples, and they commonly show good preservation. In spite of the great importance of this productive area, very few Quaternary high-resolution studies have been published. Hays et al. (1969) studied planktonic foraminifers and radiolarians in various short cores with a low rate of sedimentation, from the equatorial Pacific; the carbonate curve of Core RC 11-209 (with cycles named after Arrhenius's results [1952]) is considered now to be a standard record of the Pacific. Shackleton and Opdyke (1973, 1976) gave oxygen-isotope measurements from two cores of the western tropical Pacific, which are standard records for isotopes. DSDP Site 77 of Leg 9 (Bukry, 1972; Hays et al., 1972) is considered a reference for the equatorial Pacific, but Quaternary sediments at this site were disturbed by rotary drilling.

Quaternary nannofossils were even less studied. Okada and Honjo (1973) and Geitzenauer et al. (1977) described Recent nannoplankton of most of the Pacific, with ecologic and nomenclatural objectives. On Leg 68, Rio (1982) made a detailed study of Quaternary nannofossils of DSDP Site 503, in the Panama Basin. In this study, Rio did not use some important taxa (especially the group of *Gephyrocapsa caribbeanica, Gephyrocapsa doronicoides,* some small *Gephyrocapsa*, etc.), so that comparison with Italian sections has to be confirmed. Finally, radiolarians and nannofossils permit dating of an upper Quaternary section cored close to DSDP Site 77 (Labracherie et al., 1981).

On Leg 85, coring was conducted at five sites along two transects (east–west and south–north) across the northern part of the equatorial high-productivity area (Fig. 1). All sites proved to have reasonably abundant Quaternary nannofossils (site chapters, this volume). These sections are of interest because of their medium to high carbonate contents, their high rates of sediment accumulation, without big gaps, and their apparently undisturbed character. Such material is appropriate for a study of Quaternary nannofossils that tries to establish a high-resolution stratigraphy for this area.

METHODS

All the Quaternary sections were sampled in detail, usually each 20 or 40 cm; at DSDP Site 575, the study on board showed that the sediment accumulation rate was very low, and cores from this site were sampled each 10 cm.

For most of the work, I used smear slides, studied with a light microscope at a magnification of 1200×. Some samples were studied with a scanning electron microscope (SEM) to identify and study details of morphology of the smallest coccoliths; but generally the use of the light microscope was sufficient.

To evaluate the nannofossil total and specific abundances on smear slides, a semiquantitive method, fairly close to that described by Backman and Shackleton (1983, p. 146: first mean), was used. In the present work I used equal quantities of sediments for the smear slides, so that nannofossil abundances are comparable for all the samples. Total abundances were estimated on one field of view, using the same magnification (1200×). Fairly abundant or very abundant species were roughly counted or estimated in a semiquantitative way, on ten fields of view, using the count scale drawn on Figures 2 to 9. For rare species, specimens were counted exactly, always on ten fields of view. In using this method (equivalent-sized sediments; equal number of fields of view at the same magnification), I obtained absolute data which proved to be "surprisingly accurate...from slides made by a single experienced worker. [The method]...represents a fast and highly accurate way to gather biostratigraphic information" (Backman and Shackleton, 1983).

In addition, for two holes (572A and 573), the $CaCO_3$ content of the bulk sediment was measured in the same samples that were used in the study of nannofossils. Percent $CaCO_3$ was determined with a Bernard calcimeter (method described in Vatan, 1967). The carbonate content at Site 571 was measured on board (see site chapter).

[1] Mayer, L., Theyer, F., et al., *Init. Repts. DSDP,* 85: Washington (U.S. Govt. Printing Office).

[2] Address: Institut de Géologie du Bassin d'Aquitaine, Université de Bordeaux I, Avenue des Facultés, 33405 Talence Cedex, France.

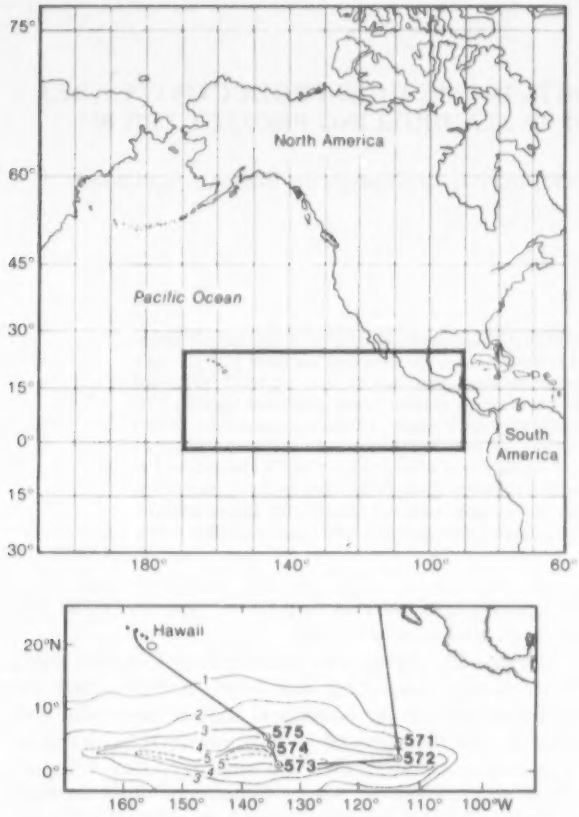

Figure 1. Locations of Leg 85 sites in relation to sediment thickness (contours in tenths of seconds of two-way traveltime). *Glomar Challenger* course to Hawaii is shown in inset, indicated on main figure by bold outline.

PRESERVATION

The preservation of nannofossils varies strongly in the Quaternary material. In many samples, the composition of nannofossil associations seems not to be disturbed by dissolution, and coccoliths are abundant. But even in these associations, dissolution is obvious. In a few samples, the $CaCO_3$ content is low, and some species are lacking, especially those which are not solution-resistant (Berger, 1973a, b, c). In samples with a minimum of $CaCO_3$, almost all the coccoliths are dissolved, and only some "ghosts" can be seen. This gradient of dissolution is given with more accuracy by a "solution index" (Bukry, 1973a). Six steps of increasing dissolution of coccoliths are defined and summarized in Table 1.

The five sites can be separated into two groups according to dissolution. Sites 571, 572, and 573 show an alternation of nondissolved and dissolved sections, with the nondissolved greatly predominant. At Sites 574 and 575, dissolution is stronger, and the dissolved sections are predominant. In some cases, dissolution obscures stratigraphy (lower Pleistocene at Site 575); dissolution is always much more severe in the Matuyama than in the Brunhes.

REWORKING

There is some reworking at all the sites, but it is always more pronounced in the Matuyama than in the Brunhes. From east to west and from south to north, there is a gradation in reworking. It increases from Site 571 to Site 575:

Hole 571: Scarce specimens of the Miocene *Discoaster* spp. in the middle of Core 571-1 (in $CaCO_3$ cycles B7 and B6).

Hole 572C: Few *Reticulofenestra* spp. throughout the Brunhes; common specimens of only one species of *Reticulofenestra* in one sample of the Matuyama (572C-3-1, 120 cm).

Hole 573: No reworking in the Brunhes; various *Reticulofenestra* in the Matuyama.

Hole 574: Some *Reticulofenestra* in the Brunhes, which become common in the Matuyama.

Hole 575C: Reworking is especially pronounced in this hole, as indicated by various species from various periods. Medium-sized coccoliths from the Oligocene–Miocene (*Cyclicargolithus abisectus, Cyclicargolithus floridanus, Coccolithus miopelagicus*) are common in the Brunhes. In the upper part of the Brunhes and mostly in the Matuyama there are some *Reticulofenestra. Discoasters* (especially *D. deflandrei*) are present throughout the Quaternary, and they are common in the Matuyama.

STRATIGRAPHIC METHODS, QUATERNARY OF THE PACIFIC OCEAN

Various stratigraphic methods are used to study the Quaternary in the Pacific Ocean. Paleomagnetic stratigraphy is important in stratigraphic studies; for Leg 85, it is crucial (Weinreich and Theyer, this volume). The isotopic record would also be useful, but for the Quaternary of Leg 85, no oxygen isotope measurements were made.

In the equatorial Pacific, and especially in the high-productivity zone, carbonate stratigraphy is often used. The carbonate content of sediments shows global variations attributed to climate. The interpretation of these fluctuations in the Pacific Ocean was first made by Arrhenius (1952), who correlated $CaCO_3$ minima with interglacial periods and maxima with glacial periods. This pioneer was followed by Olausson (1961) and many other researchers; one of the most important papers is by Hays et al. (1969), who studied several Pliocene–Pleistocene cores and gave "names" to some characteristic $CaCO_3$ minima related to the magnetostratigraphy: B1 to B17 are the minima in the Brunhes, and M1, M3, M5, M7, M11, and M17 are those in the Matuyama. One of the cores (RC 11-209) studied by Hays et al. (1969) is usually considered a standard Pacific carbonate record. Using this core and Site 503, Gardner (1982) correlated carbonate minima with isotopic stages, although "the carbonate response always lags behind the oxygen isotope response by about 1 to 5 ky." Thus, carbonate cycles can be used for dating.

Short-term variations in carbonate content are "cyclic fluctuations" (Gardner, 1982), with a period of about

Table 1. Nannofossil solution index.

	Dissolution	Abundance of intact coccoliths	Taxonomic diversity	State of solution-resistant structures	State of non-solution-resistant structures
−1	Few coccoliths slightly dissolved	Almost 100%	Normal	Good	Good
−2	Most coccoliths slightly dissolved	About 70%	Normal	Good	Beginning of solution
−3	Most coccoliths moderately dissolved	More than 40%	Few genera and/or species absent	Some central structures missing	Strongly dissolved or missing
−4	Most coccoliths strongly dissolved	About 20%	Weak	Many central structures missing	
−5	Very strong; almost noncalcareous sediment	No intact coccolith	Mono- or bi-specific		
−6	Total dissolution; no calcareous sediment	Barren sediment			

Note: Adapted from Bukry (1973a).

0.5 m.y. They were delineated mostly from late Miocene through early Pliocene. In the Pleistocene, Gardner found shorter periodicities, about 0.095 m.y. for "S-cycles" and 0.041 m.y. for "C-cycles."

The carbonate content was measured in material from three holes (571, 572A, and 573). In the same samples, the nannofossil total abundance was estimated with accuracy. A curve of nannofossil total abundance is a useful stratigraphic tool that reflects climatic changes (in the Atlantic, DSDP Leg 80: Pujos, in press) or varies with bulk $CaCO_3$ content (in the equatorial Pacific: Labracherie et al., 1981).

Although carbonate dissolution is connected with the $CaCO_3$ content, in the complex Pacific environment (and especially in this high-productivity area), interpretation of dissolution has to be partly separated from interpretation of carbonate content. Dissolution has its "solution index" (see the previous section on preservation and Table 1), and shows important fluctuations. Fluctuations in dissolution of planktonic foraminifers were interpreted as "Pacific terminations" (Thompson and Saito, 1974). The term "Pacific terminations" is now considered to be isotopic terminology. But (1) no Quaternary isotopic stratigraphy was established on Leg 85, and (2) "terminations" can be used to date and correlate Pleistocene sections in a well-defined area. So I use the term "Pacific terminations" in this study.

In the Quaternary of the Pacific Ocean, siliceous organisms (diatoms and radiolarians) give more detailed stratigraphic data than do carbonate organisms. For nannofossils, very useful zonations were established, subdividing the Quaternary into three or five zones/subzones (Bukry, 1973b; Okada and Bukry, 1980), but nannofossil Quaternary markers are rare: the first appearance of *Emiliania huxleyi* is not easy to use in a light-microscope study; the *Pseudoemiliania lacunosa* last appearance is at 0.475 Ma (Berggren et al., 1980). Leg 85 Quaternary sections are often rich in nannofossils, which show strong variations in quantity and quality. One purpose of this study is to try to find nannofossil species and associations which could be used as stratigraphic markers of the Quaternary, at least in this part of this ocean.

The appendix provides a complete list of the nannofossil species found in the Leg 85 Quaternary sediments.

SITE SUMMARIES

At Sites 571 to 575, the uppermost sediments contain abundant Quaternary coccoliths. Their abundances were estimated with accuracy, and specimens were named, especially various species and variants belonging to the genus *Gephyrocapsa*. Details of the distribution are shown in Figures 2, 3, 5, 6, and 8, and do not require much explanation. The following descriptions of the five sites are restricted to characteristics of the area and a few significant details.

Site 571 (03°59.84′N, 114°08.53′W; water depth 3969.5 m)

This very short section (Fig. 2) is restricted to one 7.11-m core representing the uppermost Quaternary. Nannofossils are alternately very abundant and rather scarce, giving a good curve of total abundance. Carbonate minima are evident, from B1 to B11. Dissolution is never important, and "terminations" are not very obvious.

Most of the Quaternary nannofossil species are abundant, chiefly *Emiliania huxleyi* and various *Gephyrocapsa*. *Pseudoemiliania lacunosa* is present in the lowermost part of the section. Some common Quaternary species were not found (*Umbellosphaera irregularis, Gephyrocapsa ericsonii, Helicopontosphaera neogranulata*). These absences do not seem to be due to dissolution in this section, but perhaps to environmental factors: Site 571 is situated near the northeastern edge of the high-productivity area, in a zone where some upwelling phenomena occur, leading to special environmental features. The presence at the top of the section, of very rare *Coccolithus pelagicus*, unusual in equatorial waters, corroborates this hypothesis.

Sedimentation at Site 571 is continuous between the top (Holocene) and the bottom (which can be dated at about 0.5 Ma). Reworking is very rare and restricted to

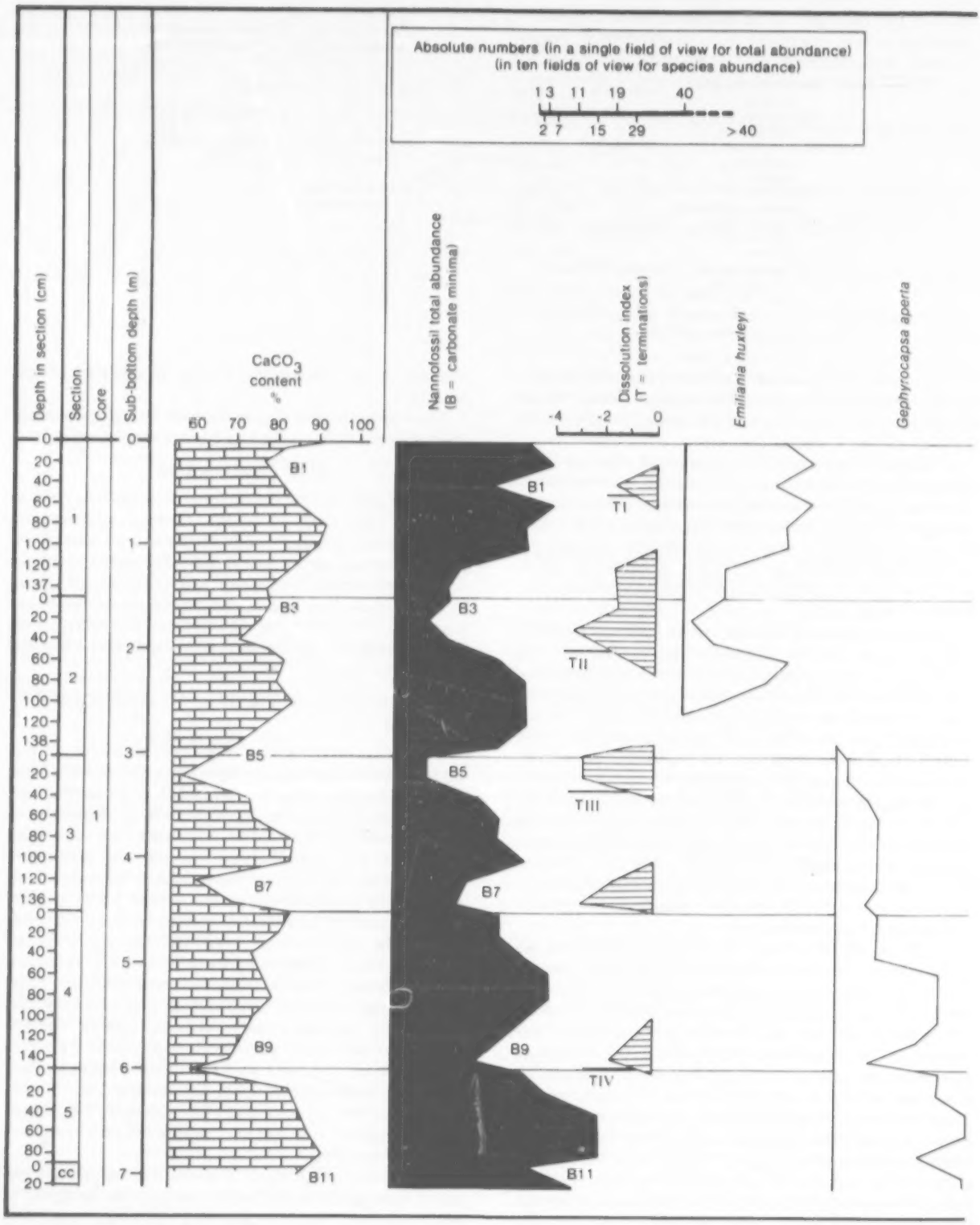

Figure 2. Nannofossils, Hole 571.

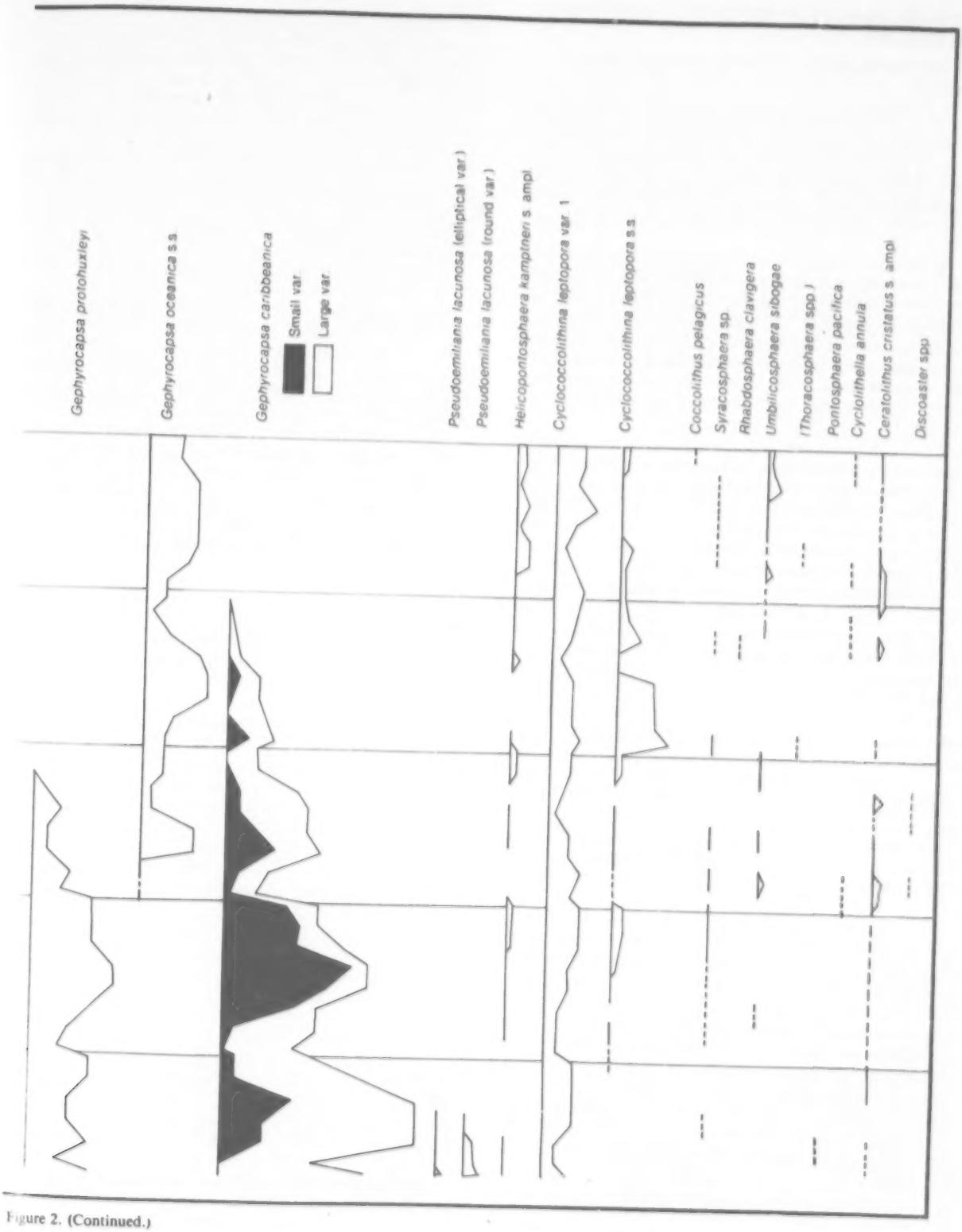

Figure 2. (Continued.)

scarce *Discoaster* spp. in Section 571-1-3 (carbonate cycles B6 to B7).

Site 572 (01°26.09′N, 113°50.52′W; water depth 3903 m)

Site 572 (Fig. 3) was cored in the vicinity of Site 81, in the eastern part of the high-productivity area. Five holes were drilled and cored, but only Holes 572, 572A, and 572C yielded Quaternary sediments. Hole 572A was selected for a detailed nannofossil study of the Quaternary, which corresponds to the upper 26 m of the section.

At this site, magnetic intensity is too weak to establish a magnetic stratigraphy; variations of $CaCO_3$ content give a tentative stratigraphy. The main cycles are easily recognizable on the $CaCO_3$ curve (Fig. 3) and on the nannofossil total abundance curve. Major cyclic variations (Gardner, 1982) are evident, mostly in the upper part of the section, with a periodicity of about 0.5 m.y. (which would agree with Gardner's long cycles in the Tertiary, but not in the Quaternary).

The results from the two uppermost sections of Core 572A-1 are not very clear, perhaps as a result of slight coring disturbance. The carbonate curve shows strong variations, unlike the comparatively constant nannofossil total abundance. Nevertheless, the nannofossil associations with *Emiliania huxleyi* suggest that the top of Hole 572A is Holocene ($CaCO_3$ cycle B1).

Nannofossils are almost always abundant, especially between 572A-1-3, 100 cm and 572A-2-4, 80 cm; below, dissolution of coccoliths has much more influence, and the total abundance decreases strongly. This change in the abundance and dissolution occurs between $CaCO_3$ cycles M2 and M3.

Various species of *Gephyrocapsa* appear and disappear throughout the section, and can be used as stratigraphic markers. *G. doronicoides* and its five variants are very useful (see discussion in subsequent section). "Small *Gephyrocapsa*" (Gartner, 1977) are almost always abundant from 572A-1-2, 60 cm to the Pliocene/Pleistocene boundary; they consist of the species *G. aperta*. I recognized no special "small *Gephyrocapsa*" Zone, which does not seem to be useful in this part of the Pacific.

The Quaternary of Hole 572 can be correlated with that of Hole 572A by means of the nannofossil total abundance, solution index, and some nannofossil markers (Fig. 4). The very top of the section is lacking in Hole 572, where the youngest sediments belong to $CaCO_3$ cycle B2; the oldest sediments (Section 572-1,CC) are older than cycle M1. The difference in the rate of sediment accumulation is obvious if we compare the two holes: between cycles B2 and M2, there is 12.70 m in Hole 572A and 9.5 m in Hole 572. This difference in thickness is not due to a hiatus in Hole 572, where all the $CaCO_3$ cycles and the main nannofossil events can be recognized.

Site 573 (00°29.91′N, 133°18.57′W; water depth 4311.5 m)

Site 573 (Fig. 5) is the southernmost Leg 85 site, and lies south of the crest of maximum sediment accumulation. It is very close to DSDP Site 77 (Leg 9), which was considered a reference section for the Pacific Neogene (Hays et al., 1972). But at Site 77, Quaternary sediments were not studied in detail. Therefore, special attention was paid to Site 573, which was chosen as the reference section of this study. Three holes were drilled at this site; only Holes 573 and 573B cored Quaternary sediments. Nannofossils of Hole 573 were studied in detail.

A good magnetic stratigraphy (Weinreich and Theyer, this volume) gives the main stratigraphic framework of the Quaternary, and situates the Pliocene/Pleistocene boundary at 573-4-3, 112 cm, at the top of the Olduvai (Berggren et al., 1980).

All $CaCO_3$ cycles are very clear, but the major cycles (of 0.5 m.y.) are less evident than at Site 572.

The nannofossil total abundance curve shows well-defined maxima compared with the $CaCO_3$ curve. Nannofossils are almost always abundant, especially between 573-2-1, 120 cm and 573-3-5, 40 cm. Below (between $CaCO_3$ cycles M4 and M5), dissolution of coccoliths is severe, and strongly reduces the total abundance.

Various species of nannofossils may be used as stratigraphic markers; the succession of species and variants of *Gephyrocapsa* is shown in Fig. 5. Reworking is almost absent, so that Hole 573 provides a good reference section for Quaternary stratigraphy of nannofossils.

Site 574 (04°12.52′N, 133°19.81′W; water depth 4571 m)

Site 574 (Fig. 6) is situated north of Site 573 and to the north of the axis of the high-productivity zone. It was cored in the vicinity of DSDP Site 71 (Leg 8). Four holes were drilled at this site, two with Quaternary sediments. Hole 574 was chosen for detailed study of nannofossils.

Quaternary magnetostratigraphy (Weinreich and Theyer, this volume) of Hole 574 shows the Olduvai event clearly, but the Jaramillo is not clearly delimited: there is a normal event between the top of the hole and 574-2-1, 15 cm, above a reversed event which extends down to 574-2-3, 30–55 cm (Weinreich, personal communication, 1983). It is not possible to name the inversion at 574-2-1, 15 cm. The study of nannofossils allows assignment of all of Core 574-1 to the Brunhes. The top of Core 574-2 (between 574-2-1, 0 cm and 574-2-1, 60 cm) seems to be mixed by drilling disturbance, and this agrees with the description of sediments (see site chapter); below 574-2-1, 60 cm, the nannofossil associations indicate an age older than the Jaramillo (mostly because of the first occurrences of *Gephyrocapsa doronicoides* var. 4 and *Gephyrocapsa caribbeanica*).

The $CaCO_3$ content was not measured at this site. The nannofossil total abundance curve shows strong variations corresponding to $CaCO_3$ cycles. Thus, it is possible to situate B1 through B14 (B14 seems not to be complete—its lowest part is lacking); below the mixed sediments, M4 to M17 can be located.

These strong fluctuations in nannofossil abundance are the result of dissolution stronger than at Sites 571, 572, and 573, as shown by the solution index curve. Solution is especially strong below the Brunhes: in the mixed part (574-2-1, 0 cm to 574-2-1, 60 cm) and lower, cocco-

liths are reduced in quantity and quality, and difficult to use for precise stratigraphy. In this part of the hole, the smallest species of *Gephyrocapsa* are almost absent, and some *Crenalithus productus* and *G. doronicoides* are present at some levels; solution-resistant *Cyclococcolithina* spp. (Berger, 1973c) are rather abundant.

In general, reworking is unimportant in this hole, but slightly more important in Core 574-2, which contains some small and some big *Reticulofenestra*.

I have tried to correlate the Quaternary of Holes 574 and 574A. Core 1 of Hole 574A has 25 cm of (mixed?) sediment; the upper part of Core 574A-2 is easily correlated with the upper part of Core 2 from Hole 574, using the nannofossil total abundance curve and some nannofossil markers (Fig. 7).

Site 575 (05°51.00′N, 135°02.16′W, water depth 4550 m)

Site 575 (Fig. 8) is the northernmost site of Leg 85. It is situated on the northern edge of the high-productivity area, south of the Clipperton Fracture Zone. Three holes were drilled at Site 575. Hole 575C was chosen for the nannofossil study because its two cores seem not to be disturbed.

Magnetic polarity (Weinreich and Theyer, this volume) gives a good stratigraphy of Hole 575C, with the Pliocene/Pleistocene boundary at Sample 575C-1-3, 106–116 cm, the Jaramillo between 575C-1-3, 16-26 cm and 575C-1-3, 6–16 cm, and the Brunhes/Matuyama boundary at 575C-1-2, 106–116 cm.

The $CaCO_3$ content was not measured in material from Hole 575C. The nannofossil total abundance curve shows clear fluctuations, which can be interpreted as $CaCO_3$ cycles. The top of the hole is situated in B3; all the Brunhes cycles can be recognized. In the Matuyama, carbonate dissolution is always very strong, so we cannot recognize the M-cycles. Gardner's (1982) major cycles are evident in the upper part of this curve, with a cyclicity of about 0.5 m.y.

At Site 575, nannofossil associations can be used in the Brunhes only, and mostly above B14. Below, and throughout the Matuyama, most of the coccoliths are dissolved, leaving only some solution-resistant species (*Cyclococcolithina* spp. and *Coccolithus pelagicus*).

Reworking is very important at Site 575, with some Oligocene–Miocene species in the Brunhes, several discoasters (mostly *D. deflandrei*) throughout the Quaternary (common in the Matuyama), and various *Reticulofenestra* in the Matuyama.

The Quaternary sections of Holes 575 and 575C can be correlated (Fig. 9). Nannofossil total abundances are very similar; strong dissolution occurs in the lower Brunhes and in the Matuyama in both holes. Nannofossil markers can be used in the Brunhes; in the Matuyama only the solution-resistant species *Cyclococcolithina macintyrei* is usable.

MORPHOLOGICAL AND STRATIGRAPHIC CHARACTERISTICS OF SOME SELECTED NANNOFOSSILS

The same taxa are present at almost all the sites. Some of them have already proved useful as stratigraphic markers, and were correlated with chronostratigraphic scales (Bukry, 1971, 1973a, b; Gartner, 1977; Thierstein et al., 1977; Pujos-Lamy, 1976, 1977; Pujos, in press; Okada and Bukry, 1980; Backman and Shackleton, 1983/1984). Therefore, only certain taxa will be discussed in detail, chosen because they are generally not described precisely, or because new variants must be distinguished to allow a more precise nannofossil stratigraphy, or because they can be regarded as typical of this high productivity zone. Their distribution will be related to the magnetostratigraphy and/or the carbonate stratigraphy.

The *Gephyrocapsa* Complex

This group can be subdivided into three major groups (Gartner, 1977), previously described in detail for DSDP Leg 80 (Pujos, in press); only the most important morphological features are mentioned here. The distinction between groups and species is established mostly according to the size of the central area (after Gartner, 1977 and Bukry, 1973a), the dimensions of the outer shield, and/or the aspect of elements. The crossbar is also taken into account (see the variants of *Gephyrocapsa doronicoides*), but not the angle of the bar, because (1) this angle can be measured only when the coccolith lies strictly flat on the slide, which happens very rarely, and (2) it seems to fluctuate greatly within a group or a species. I conclude that the use of bar angles to distinguish species complicates the study of *Gephyrocapsa* and is not really useful in stratigraphy (Pujos, in press).

The Small *Gephyrocapsa*

Gartner (1977) used this name for a group of very small *Gephyrocapsa* (coccolith length < 2 μm) delimiting a stratigraphic zone between 0.92 and 1.22 Ma (below Jaramillo). A similar acme was not found at the sites of Leg 85.

***Gephyrocapsa aperta* Kamptner.** Two variants were previously described (Pujos-Lamy, 1976), but could not be distinguished at Leg 85 sites, perhaps because of dissolution. This group of *G. aperta* makes up most of the small *Gephyrocapsa* at Leg 85 sites, and is always abundant throughout the Pleistocene, below B3 (Plate 1, Figs. 10–11).

***Gephyrocapsa ericsonii* McIntyre and Bé.** This is a small species with an elevated bar. It is very rare, but has a very short range (limited to cycle B4), which makes it useful in stratigraphy.

***Gephyrocapsa protohuxleyi* McIntyre.** This species is characteristized by the indentations of the outer shield. It was not possible to find—with the SEM—a perfectly characteristic coccolith of the species. Perhaps this aspect of the shield under a light microscope is due to moderate dissolution of another species (possibly *G. caribbeanica*, which has almost the same distribution). Therefore, "*G. protohuxleyi*" is not taken into account in the stratigraphy.

The Open *Gephyrocapsa*

***Gephyrocapsa oceanica* Kamptner s. s.** (Plate 1, Figs. 1b, 2a, 4a). This medium-sized species (the most important open *Gephyrocapsa*) is moderately abundant in the upper Quaternary; it appears in cycle B10 and is present in sediments up to Recent.

I have described this open *Gephyrocapsa* elsewhere (Pujos, in press).

***Gephyrocapsa oceanica* Kamptner W** (warm) (Plate 1, Figs. 2b, 3). This variant is larger than the species s. s. (greatest length = 2.4 to 3.2 μm for *G. oceanica* s. s. and 4 μm for the warm variant), and it has a larger central opening (opening diameter = 1.2 to 1.8 μm for *G. oceanica* s. s. and about 2.5 μm for the variant). The bar orientation is not taken into account, although it seems to be ecologically significant within this group of open *Gephyrocapsa*. But stratigraphy is the objective of the present paper, and different angles of the crossbar in this species do not seem to be stratigraphically significant (thus *G. omega* Bukry and *G. oceanica* Kamptner var. *californiensis* Kamptner can be considered as ecophenotypic variants of *G. oceanica*).

At Leg 85 sites this large type has a distribution very close to that of *G. oceanica* s. s., but it appears earlier, at about the Brunhes/Matuyama boundary.

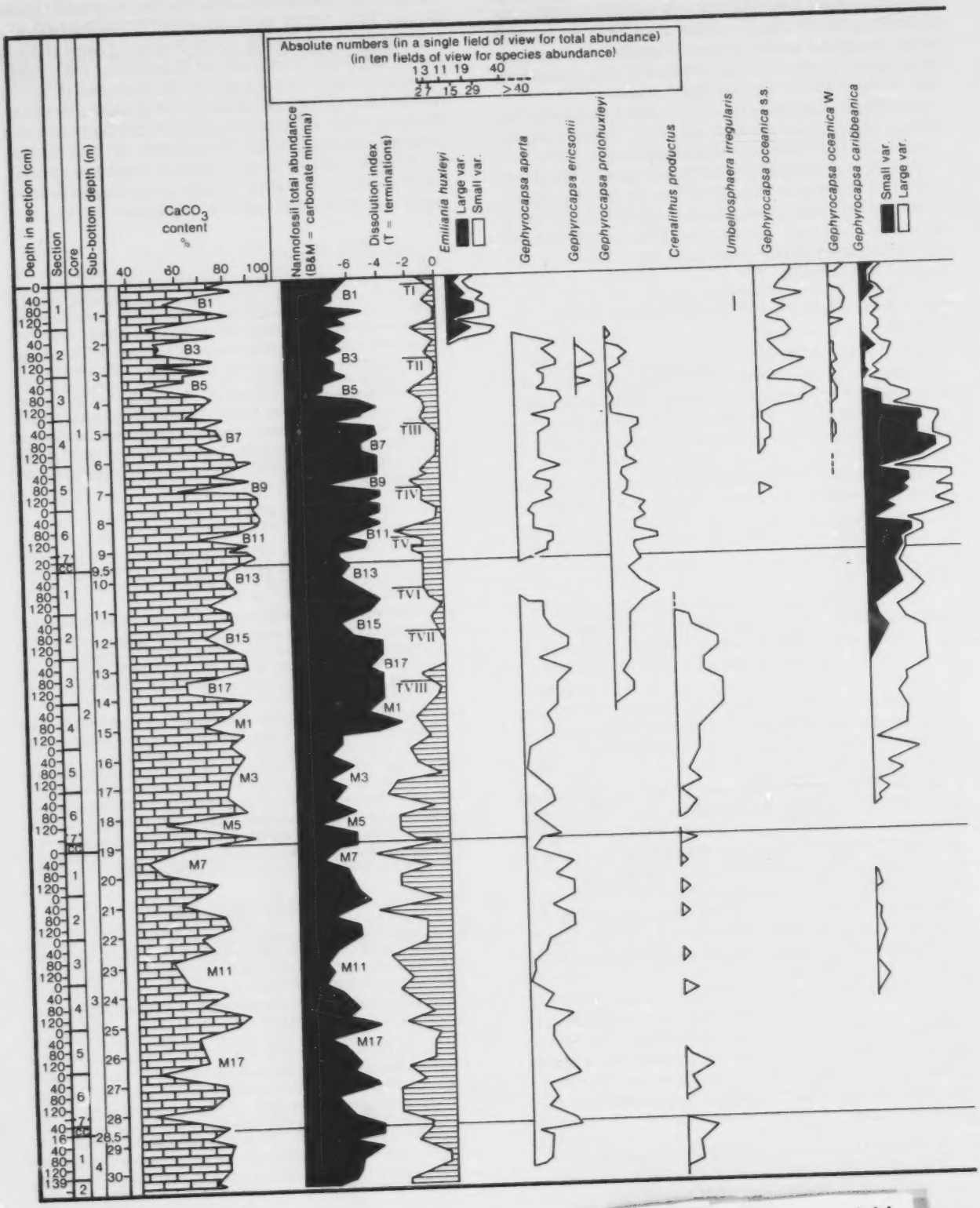

Figure 3. Nannofossils, Hole 572A.

READEX FICHE best copy available

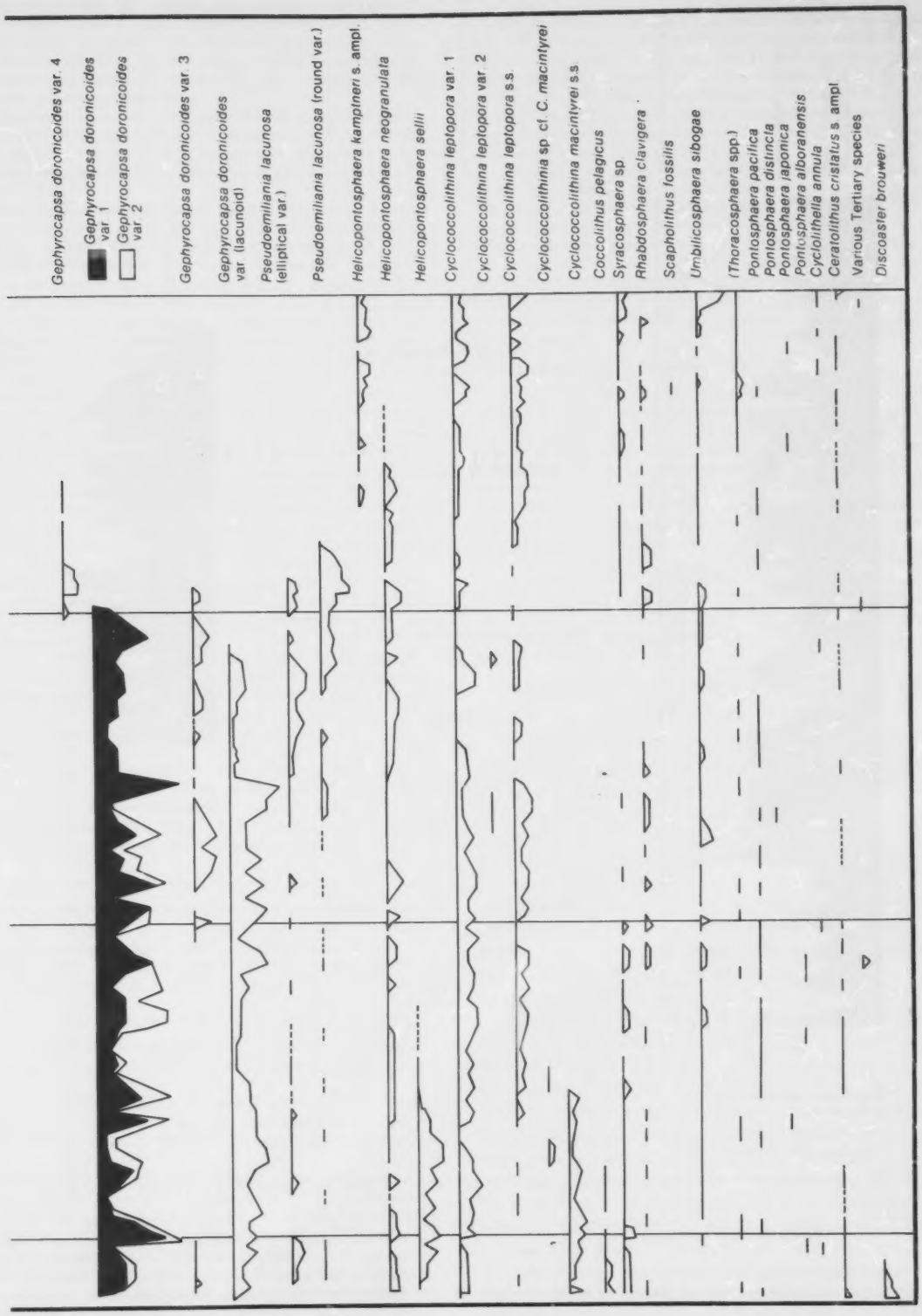

Figure 3. (Continued.)

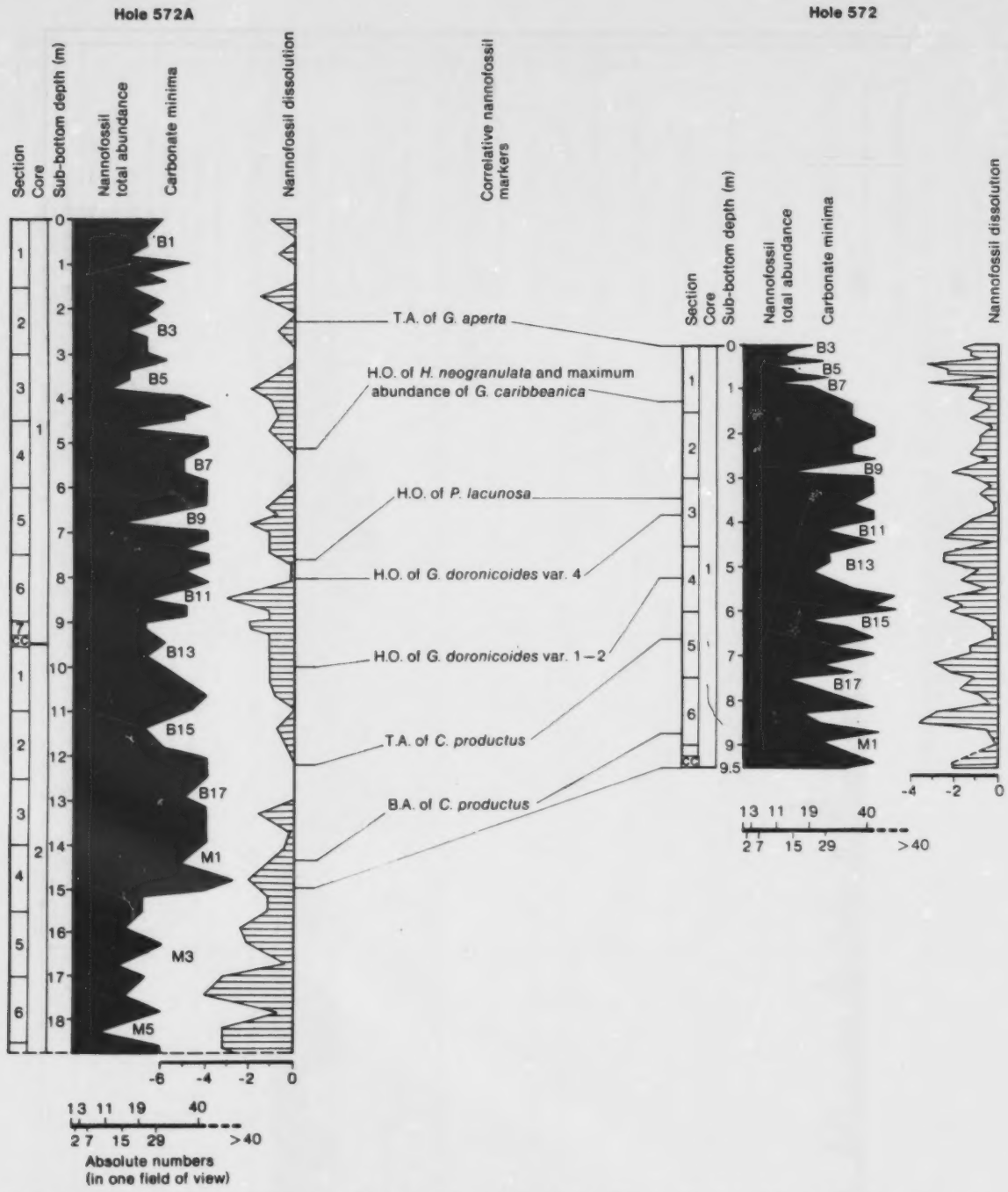

Figure 4. Correlation of Holes 572 and 572A. T.A. = top of acme; H.O. = highest occurrence; B.A. = bottom of acme.

The Closed *Gephyrocapsa*

This is the most abundant group of Quaternary nannofossils.

***Gephyrocapsa caribbeanica* Boudreaux and Hay** (Plate 1, Fig. 7). This is a medium-size *Gephyrocapsa* with a crossbar more or less well developed and a slightly open central area. It appears near the boundary between cycles M4 and M5, and it is present till the Holocene. Its acme characterizes the middle part of the Brunhes; the bottom of the acme is in B15 and its top is in B7 (which agrees with the age of 0.268 Ma given for this event by Thierstein et al., 1977).

***Crenalithus productus* (Kamptner) n. comb.** (Plate 1, Figs. 4b, 5, 6): ***Ellipsoplacolithus productus* Kamptner, 1963**, p. 172, pl. 8, figs. 42–44. This *Crenalithus* is placed within the "*Gephyrocapsa* complex" because it resembles *G. caribbeanica*, of which it is probably the ancestor, despite the complete absence of the crossbar. In a previous paper, I therefore named it *Gephyrocapsa producta* (Pujos,

in press), as Bukry did (1973a). It is completely closed, with a slit along the major axis of the coccolith, and is small to medium-sized (greatest length = 3 to 4.5 μm). Because of this appearance, these specimens might be placed in the species *C. productellus* Bukry (1975). Backman (1980, p. 49) wrote that "the specific epithet *productellus* is a junior synonym of *productus*." So I name this taxon *Crenalithus productus* (Kamptner).

C. productus is rare in the Pleistocene; its maximum abundance is between M4 and B15. It disappears in B15. Bukry (1980) situates common specimens of "*Crenalithus productellus*" in his *Crenalithus doronicoides* Zone, which may be equivalent to the period M4 to B15.

***Gephyrocapsa doronicoides* (Black and Barnes).** This is a complex taxon. Its generic attribution is not easy. It was first described as a *Coccolithus*, and this name was used by various authors till 1973, when Roth described a new combination: *Crenalithus doronicoides*. This new name could be all right for various specimens of the species. But as I described in detail (Pujos, in press), some variants have a beginning of a true crossbar (a characteristic of the genus *Gephyrocapsa*); the variants cannot be dissociated from each other but must be placed in the same taxon. The variants have stratigraphic significance.

G. doronicoides var. 1 and 2 (Plate 2, Figs. 2–3) are medium-size coccoliths (greatest length = 5 to 6 μm) with a large (diameter = 2.5 μm, var. 1) or a small (diameter = 1 to 1.5 μm, var. 2) central opening. They usually have a crossbar. They are present in the lowermost Pleistocene and are rather abundant until B12/B13, where they disappear. At Leg 85 sites, it seems that dissolution may have destroyed some parts of the central opening, so that the difference in size of the central opening (which is the distinguishing characteristic) is destroyed. Variants 1 and 2 are therefore not always distinguished from each other in the present study.

G. doronicoides var. 3 (Plate 2, Fig. 4) is the giant of the species (greatest length = 8 to 9 μm), and its size is its characteristic distinction. It is never abundant, but has a useful short range, between M2 and M5.

G. doronicoides var. 4 (Plate 2, Fig. 1) is a small coccolith (greatest length = 2.8 μm) with a small central opening; a crossbar is not always present. The variant may be considered as the end of the lineage. It was found between B8 and B13 (at Sites 571, 572, and 573) and between B9 and B11 (at Sites 574 and 575).

G. doronicoides var. (lacunoid) (Plate 2, Figs. 5–6) has a morphology and a size close to that of variant 1 (greatest length = 3.6 to 4 μm). It can be distinguished by the presence of several slits, giving it the aspect of *Pseudoemiliania lacunosa* when observed with a light microscope; it is present at the bottom of the Pleistocene, and is rare to common till its disappearance at B14/15.

Pseudoemiliania lacunosa (Kamptner) (Plate 2, Fig. 7)

Two types (round and elliptical) are present, and commonly alternate. This species disappears in B10, as was already observed by Hays et al. (1969). The disappearance is dated at 0.474 Ma, worldwide, by Berggren et al. (1980), and can be used for establishing rates of sediment accumulation (discussed in a later section).

The *Helicopontosphaera* Complex (Plate 2, Figs. 8–9)

I chose this name of *Helicopontosphaera*, following the arguments of Hay (Hay, 1977; Pujos, in press). Three species are present in Leg 85 material:

***Helicopontosphaera neogranulata* Gartner.** This species was tentatively taken as an additional marker at Leg 80 sites (where it disappears at 0.42 Ma); its last appearance occurs at various ages at Leg 85 sites.

***Helicopontosphaera sellii* Bukry and Bramlette.** Considered as an additional marker by Gartner (1977), it disappears in M7, which agrees with the date this author gives for the event (1.22 Ma), but which is later than the date given by Backman and Shackleton (1983/1984) for this event in the equatorial zone (1.37 Ma).

***Helicopontosphaera kamptneri* Hay and Mohler.** The species is taken in its s. ampl., as in Leg 80 material (Pujos, in press). I include in this name some rare specimens of *H. wallichi* (Lohmann), which, according to Haq (1973), is similar in morphology to *H. kamptneri*. *H. kamptneri* s. ampl. occurs sporadically throughout the Quaternary of Leg 85 sites.

***Cyclococcolithina macintyrei* (Bukry and Bramlette)** (Plate 3, Fig. 4)

The two species *leptopora* and *macintyrei* belong to the same genus. This genus cannot be *Calcidiscus* (*Cyclococcolithina* is a "subjective senior synonym because the type species *Calcidiscus quadriforatus* Kamptner is a fragment of *Cyclococcolithina*" [Hay, 1977]) or *Cyclococcolithus* (considered as illegitimate by Loeblich and Tappan, 1970). So the two species (and their variants) are attributed to the genus *Cyclococcolithina*, as established by Wilcoxon (1970), Hay (1977), and Loeblich and Tappan (1971).

Berggren et al. (1980) situate the last appearance of *C. macintyrei* within the Olduvai, Gartner (1977) puts it at 1.51 Ma in the early Pleistocene, and Backman and Shackleton (1983/1984) place it at 1.45 Ma, well after the Olduvai. At Leg 85 sites, this event occurred always after the Olduvai, between M11 and M12, at about 1.50 Ma.

A type of *Cyclococcolithina* is slightly different from the species *macintyrei* s. s.: it is somewhat smaller, with numerous elements and a smaller central opening. I named it *C.* sp. cf. *C. macintyrei*. It disappeared later than the species s. s., and may be the end of the lineage (Plate 3, Fig. 3).

***Coccolithus pelagicus* (Wallich)** (Plate 3, Fig. 5)

Except for DSDP Site 571, where it is present at the top of the recovered interval, *C. pelagicus* occurs in the Olduvai only, at all sites of Leg 85. It has its last appearance in M17, and does occur in the Pliocene. The distribution of this species was studied in detail by Bukry (1980), who followed its disappearance along a longitudinal transect, in a tropical area situated to the east of the high-productivity zone. The extinction of *C. pelagicus* occurs in the *Emiliania ovata* Subzone (about 0.8 Ma) in the Galapagos area (longitude 86°W); this event has an earlier date to the west, and is situated between the *C. macintyrei* and *Discoaster pentaradiatus* subzones (about 2 Ma) in the Siqueiros area (longitude 106°W). Thus, the last appearance of *C. pelagicus* took place either in the earliest Pleistocene or in the latest Pliocene (see discussion following). At Leg 85 sites, it occurs in the upper part of the Olduvai, which is close to the Pliocene/Pleistocene boundary (about 1.65 Ma).

SEDIMENT ACCUMULATION RATES AND NANNOFOSSIL MARKERS

Sediment accumulation rate curves (Fig. 10) can be drawn using dates of (1) Quaternary magnetic polarity events (Weinreich and Theyer, this volume) for Holes 573, 574, and 575C, (2) extinction of *Pseudoemiliania lacunosa* at 0.474 Ma (Berggren et al., 1980) at the five sites, and (3) some $CaCO_3$ minima: carbonate minima are used for Hole 572A, where magnetostratigraphy could not be established. Precise dates are not given for carbonate events, but only their positions close to some polarity event: cycle B17 occurs just above the Brunhes/Matuyama boundary, M3 above the top of Jaramillo, and M17 in the upper Olduvai.

Holes 571, 572A, and 573 have very similar curves, with rates of sediment accumulation between 10 and 25 m/m.y. Hole 574 has a rate between about 4.5 and 16 m/m.y. and the rate for Hole 575C is between 1 and 4 m/m.y. In each case the lowest rate is in the Matuyama and the highest one is between the extinction of *P. lacunosa* and the Brunhes/Matuyama boundary.

By using sediment accumulation rate curves, it is possible to plot a chronological scale for each Quaternary site (Fig. 11 and Table 2) and to date nannofossil markers.

The succession of nannofossil events is shown in Figure 11. The events consist of highest and lowest occurrences, of tops and bottoms of acmes, and a change in dominance of two species. Some of these markers are usually taken as datums in the literature: highest occurrences of *Pseudoemiliania lacunosa*, *Cyclococcolithina*

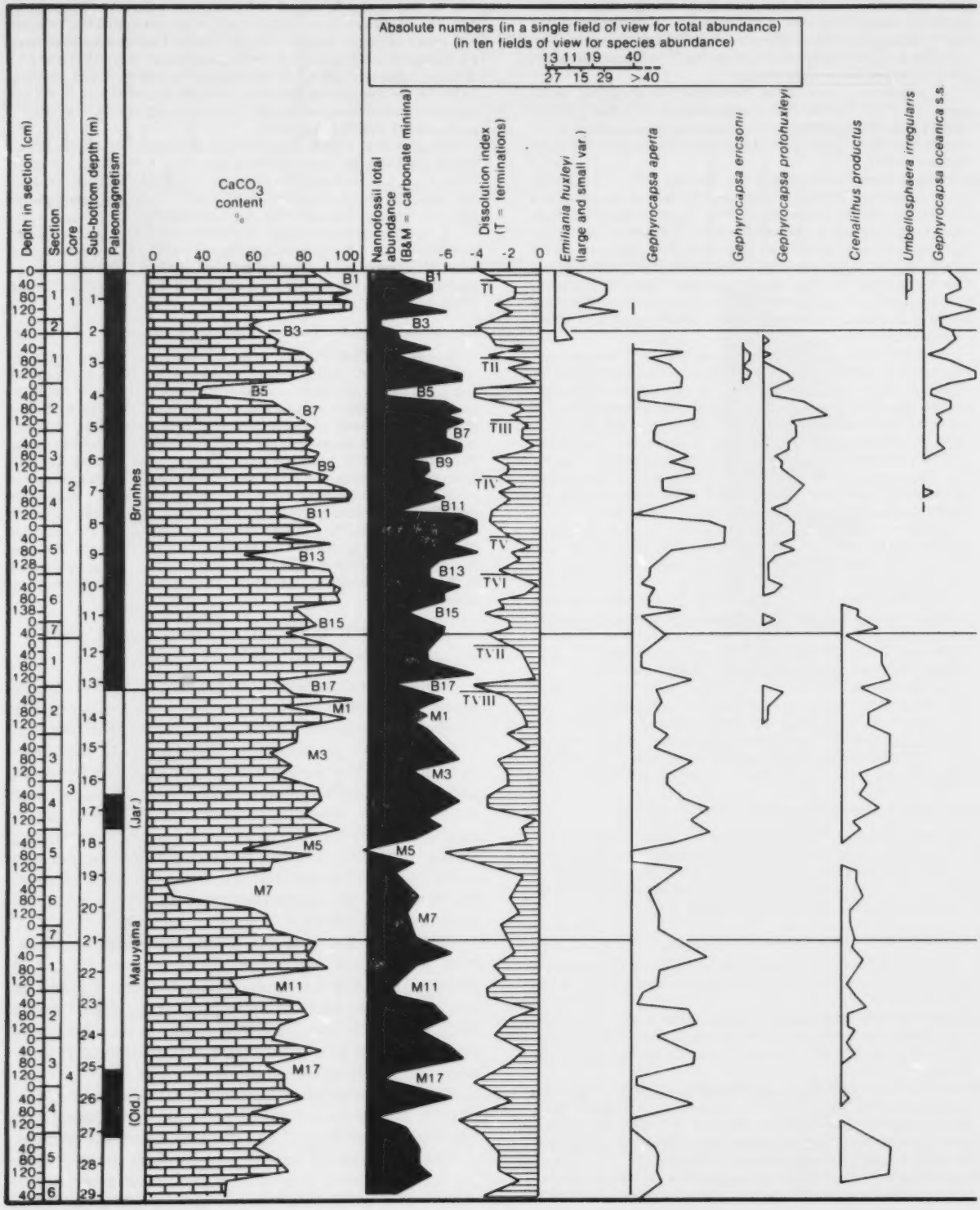

Figure 5. Nannofossils, Hole 573.

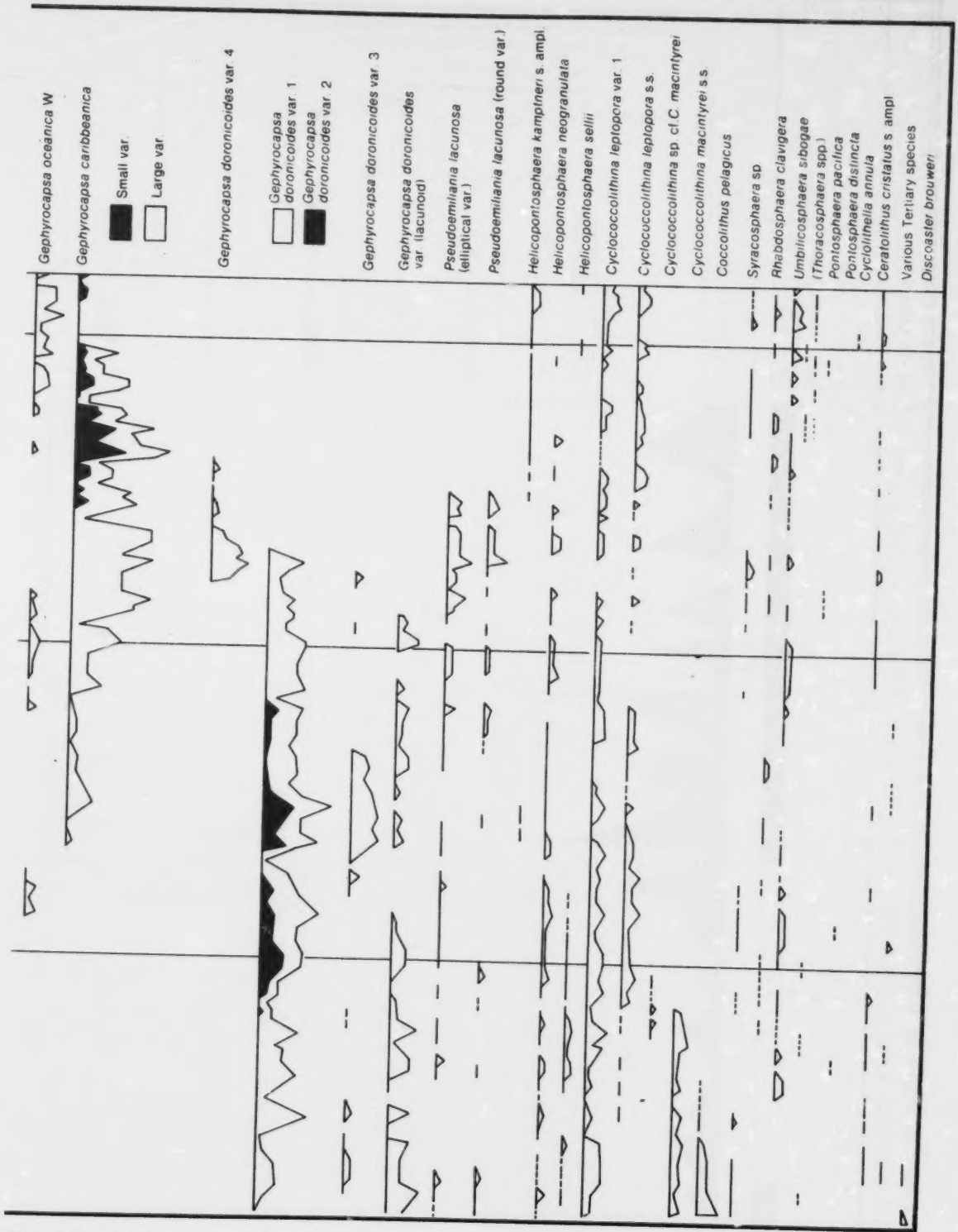

Figure 5. (Continued.)

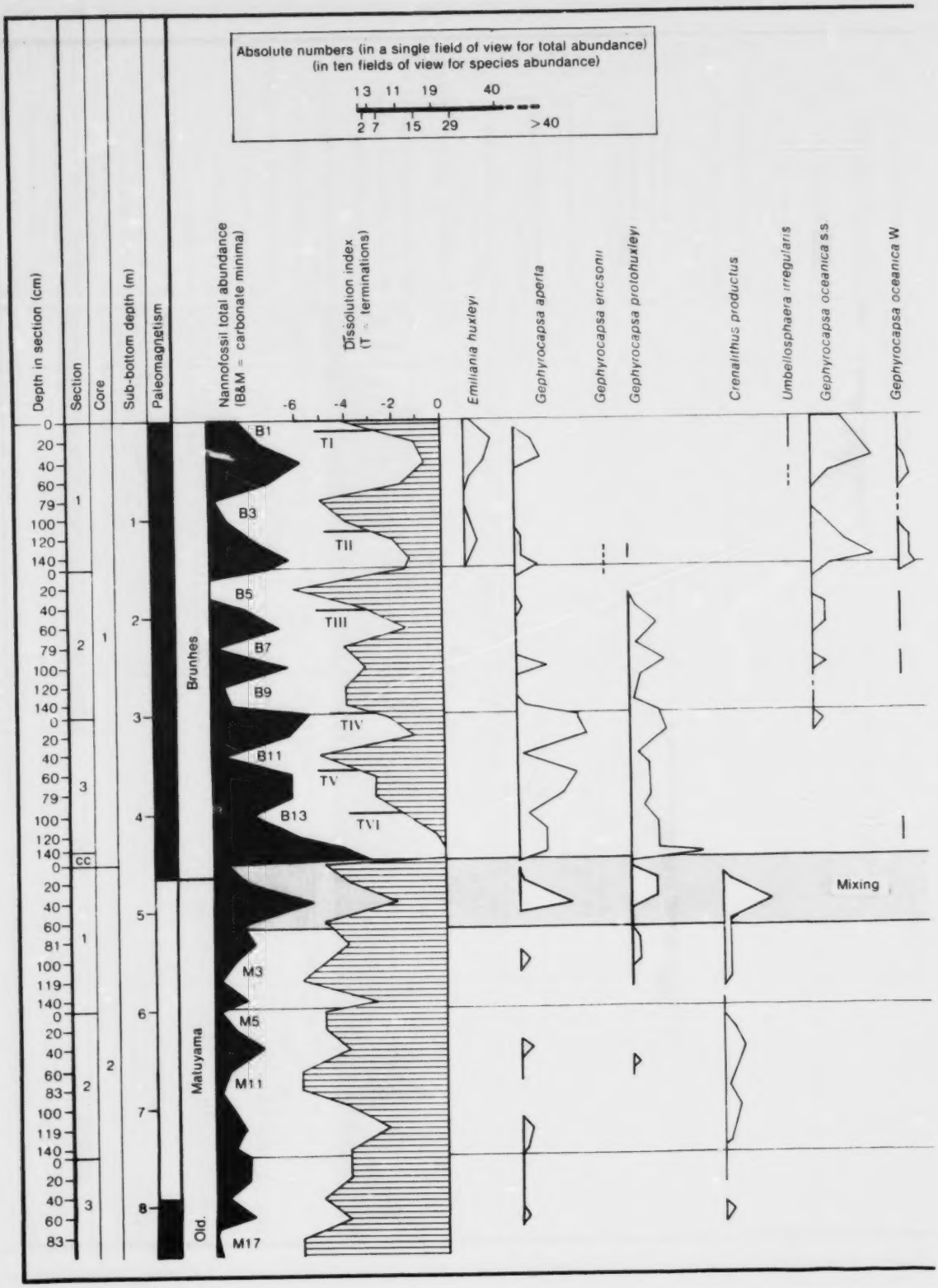

Figure 6. Nannofossils, Hole 574.

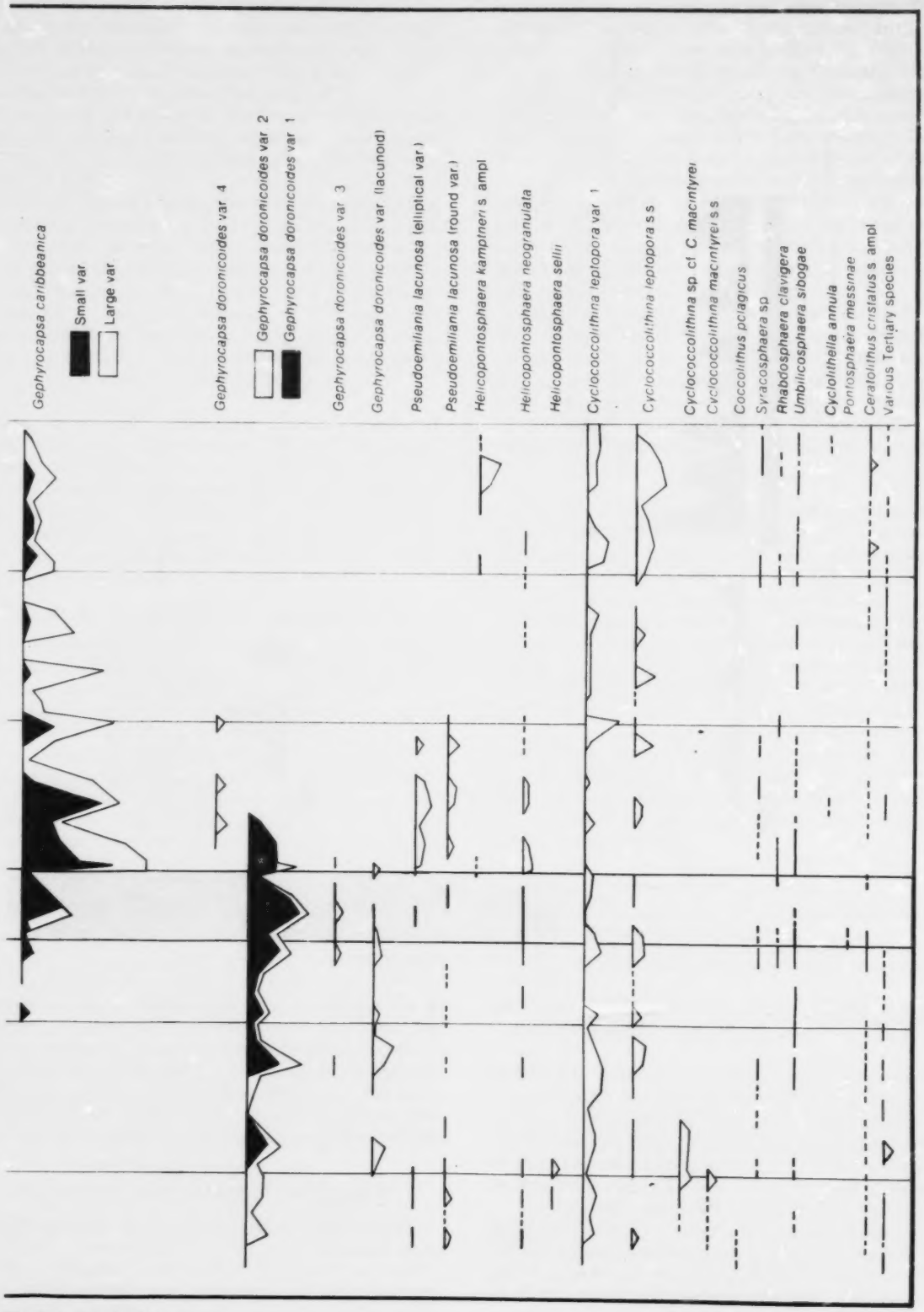

Figure 6. (Continued.)

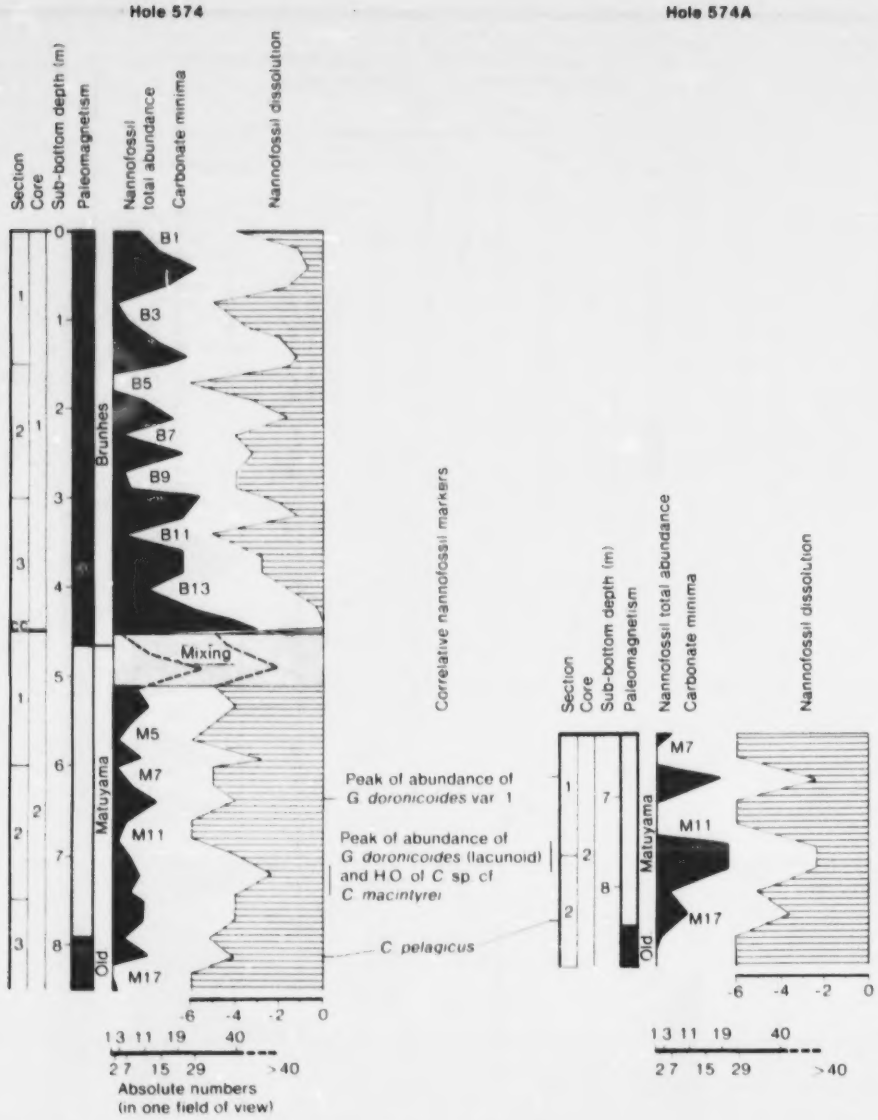

Figure 7. Correlation of Holes 574 and 574A. H.O. = highest occurrence.

macintyrei, and *Discoaster brouweri*. For the two latter taxa, see the section on the Pliocene/Pleistocene boundary.

Some conventional markers were found: the change in dominance of *Emiliania huxleyi* and *Gephyrocapsa caribbeanica* (about 0.11 Ma, Thierstein et al., 1977), and the extinction of *Helicopontosphaera sellii* (about 1.22 Ma, Gartner, 1977). Some of these markers can be used only at Sites 571, 572, and 573; they are absent at Sites 574 and 575, because of stronger dissolution.

Some additional markers, previously described using material recovered in the northeastern Atlantic Ocean (Pujos, in press: DSDP Leg 80), are found also at Leg 85 sites, at about the same chronostratigraphic levels as at Leg 80 sites (Table 2). These are *Gephyrocapsa oceanica* s. s., *Gephyrocapsa doronicoides* s. ampl., *Crenalithus productus, Cyclococcolithina* sp. cf. *C. macintyrei,* and *Coccolithus pelagicus*. They may be considered as cosmopolitan markers. Some other markers—mostly the "small *Gephyrocapsa*" of Gartner's zonation (1977)—were not recognized in the present study; this may be due to the environmental conditions in the equatorial Pacific, which may make these markers less reliable.

THE PROBLEM OF THE PLIOCENE/PLEISTOCENE BOUNDARY

Nannofossil characteristics of the Pliocene/Pleistocene boundary have been often discussed. Usually the extinction of *Discoaster brouweri* is assumed to be synchronous with this boundary; this disappearance occurs often at the top of the Olduvai or within it (Berggren et al., 1980). In the equatorial Pacific, Hays et al. (1969)

observed "a sharp reduction in number [of *D. brouweri*] just above the base of the Olduvai event, or [it] disappears well below the Olduvai, probably because of solution." At Leg 85 sites, *D. brouweri* disappears distinctly below the Olduvai, even when dissolution is weak (Holes 572A and 573). According to Backman and Shackleton (1983), "*D. brouweri* shows a consistent extinction datum immediately below the base of the Olduvai subchron," at 1.88 Ma.

Bizon and Müller (1978) proposed *Cyclococcolithina macintyrei* as the marker species for the boundary in the Mediterranean, the extinction of this taxon being dated at 1.51 Ma by Gartner (1977) and at 1.45 Ma by Backman and Shackleton (1983). Bukry (1980) reviewed various papers on this disappearance, which may occur from the middle of the Olduvai to far above this event. At the Leg 85 sites, *C. macintyrei* disappears well above the Olduvai, at about the extinction date given by Gartner.

Thus, the Pliocene/Pleistocene boundary at the Leg 85 sites must be situated between these two nannofossil markers: the disappearance of *D. brouweri* well below the Olduvai and the disappearance of *C. macintyrei* well above the Olduvai. There is about 0.5 m.y. between them. So the position of Berggren et al. (1980) seems to be the wiser one; they place the Pliocene/Pleistocene boundary at the extreme top of the Olduvai.

CORRELATION OF THE FIVE LEG 85 SITES

The detailed study of nannofossils provides various stratigraphic criteria. Site 571 is different from the four others because only the uppermost Quaternary was cored, and also because its location, on the edge of the high-productivity area, induces different environmental conditions. Therefore, some nannofossil events were not observed at this site. At the four other sites, correlation is easy, using nannofossil markers and nannofossil total abundance only. The discussion below starts with Site 573, which has the most complete succession of events. It is possible to distinguish two groups of sites.

Sites 573 and 572 (and 571)

In the section on rates of sediment accumulation, these three sites were grouped together. Holes 572A and 573 have almost the same thickness of Quaternary sediments, but some differences are evident, mostly in the Matuyama. Some events are distinct at Hole 573, and were not found at separate levels in Hole 572A: bottom of the acme of *Crenalithus productus*, lowest occurrence of *Gephyrocapsa caribbeanica*, and bottom of the acme of *Gephyrocapsa doronicoides*. This may be attributable to a hiatus of about 0.12 m.y. in Hole 572A, or to special environmental conditions.

Sites 572 and 573 are similar in nannofossil total abundance. They show a high-frequency alternation of minima and maxima, with a relatively low amplitude.

Sites 574 and 575

Quaternary sediments are reduced in thickness at Sites 574 and 575. This leads to the apparent superposition of some nannofossil events in the same sample. But the general succession of events is the same as at the other Leg 85 sites, and can be used in the same way.

The nannofossil total abundance fluctuates strongly; especially at the $CaCO_3$ minima, the abundance is very low, and sometimes completely nil. In such samples the only nannofossils present are usually reworked Tertiary. These two coincident features (near absence of Quaternary plankton and presence of reworked specimens) are probably caused by the same phenomenon. Only a deep current (AABW) could explain the nannofossil composition in the $CaCO_3$ minima of the cycles; it has dissolved the *in situ* flora and brought in Tertiary coccoliths and discoasters.

Major carbonate cycles can be observed easily in the sections from Holes 574 and 575C, with the most important maximum in cycle B14 and the less important maximum in B5. In these two holes, dissolution is dominant below B14, even in maxima cycles; this interval corresponds to a thin section of sediments in the Matuyama, and carbonate cycles are very difficult to determine.

CONCLUSION

The use of nannofossils in correlating Quaternary sections gives detailed and precise results. Besides conventional datums, various additional markers proved useful for regional stratigraphy. A synthesis of the most important stratigraphic results is given in Table 2, where these results are also related to Okada and Bukry's (1980) nannofossil zonation. Supplementary markers were previously used in the northeastern Atlantic Ocean (DSDP Leg 80: Pujos, in press), where they were found in the same succession but sometimes at different age levels. This problem of correlating events of different ages according to location is inherent in Quaternary nannofossils. The solution of this problem will necessitate the study of many Quaternary sections at various latitudes; we can test whether the supplementary nannofossil events can be used worldwide.

REFERENCES

Arrhenius G., 1952. Sediment cores from the east Pacific. *Rep. Swed. Deep-Sea Exped. 1947–1948*, 5:1–227.

Backman, J., 1980. Miocene–Pliocene nannofossils and sedimentation rates in the Hatton–Rockall Basin, NE Atlantic Ocean. *Stockholm Contrib. Geol. 36.*

Backman, J., and Shackleton, N. J., 1983. Quantitative biochronology of Pliocene and early Pleistocene calcareous nannofossils from the Atlantic, Indian, and Pacific oceans. *Mar. Micropaleontol.*, 8(2): 141–170.

Berger, W. H., 1973a. Cenozoic sedimentation in the eastern tropical Pacific. *Geol. Soc. Bull.*, 84:1941–1954.

_____, 1973b. Deep-sea carbonates: Pleistocene dissolution cycles. *J. Foraminiferal Res.*, 3:187–195.

_____, 1973c. Deep-sea carbonates: evidence for a coccolith lysocline. *Deep-Sea Res.*, 20:917–921.

Berggren, W. A., Burckle, L. H., Cita, M. B., Cooke, H. B. S., Funnel, B. M., et al., 1980. Towards a Quaternary time scale. *Quat. Res.*, 13:277–302.

Bizon, G., and Müller, C., 1978. Remarks on the determination of the Pliocene–Pleistocene boundary in the Mediterranean. *In* Hsü, K. J., Montadert, L., et al., *Init. Repts. DSDP*, 42, Pt. 1: Washington (U.S. Govt. Printing Office), 847–853.

Bukry, D., 1971. Cenozoic calcareous nannofossils from the Pacific Ocean. *Trans. San Diego Soc. Nat. Hist.*, 16:303–328.

_____, 1972. Coccolith stratigraphy, Leg 9, Deep Sea Drilling Project. *In* Hays, J. D., et al., *Init. Repts. DSDP*, 9: Washington (U.S. Govt. Printing Office), 817–832.

_____, 1973a. Coccolith stratigraphy, eastern equatorial Pacific, Leg 16, Deep Sea Drilling Project. *In* van Andel, T. M., Heath, G. R., et al., *Init. Repts. DSDP*, 16: Washington (U.S. Govt. Printing Office), 653–711.

_____, 1973b. Low-latitude coccolith biostratigraphic zonation. *In* Edgar, N. T., Saunders, J. B., et al., *Init. Repts. DSDP*, 15: Washington (U.S. Govt. Printing Office), 685–703.

_____, 1975. Coccolith and silicoflagellate stratigraphy, northwest Pacific Ocean, Deep Sea Drilling Project Leg 32. *In* Larson, R. L., Moberly, R., et al., *Init. Repts. DSDP*, 32: Washington (U.S. Govt. Printing Office), 677–701.

_____, 1976. Coccolith stratigraphy of Manihiki Plateau, central Pacific, Deep Sea Drilling Project Site 317. *In* Schlanger, S. O., Jackson, E. D., et al., *Init. Repts. DSDP*, 33: Washington (U.S. Govt. Printing Office), 493–501.

_____, 1980. Coccolith stratigraphy, tropical eastern Pacific Ocean, Deep Sea Drilling Project Leg 54. *In* Rosendahl, B. R., Hekinian, R., et al., *Init. Repts. DSDP*, 54: Washington (U.S. Govt. Printing Office), 535–543.

Gardner, J. V., 1982. High-resolution carbonate and Quaternary organic-carbon stratigraphies for the late Neogene and Quaternary from the western Caribbean and eastern equatorial Pacific. *In* Prell, W. L., Gardner, J. V., et al., *Init. Repts. DSDP*, 68: Washington (U.S. Govt. Printing Office), 347–364.

Gartner, S., 1977. Calcareous nannofossils biostratigraphy and revised zonation of the Pleistocene. *Mar. Micropaleontol.*, 2:1–25.

Geitzenauer, K. R., Roche, M. B., and McIntyre, A., 1977. Coccolith biogeography from North Atlantic and Pacific surface sediments. A comparison of species distribution and abundances. *In* Ramsay, A. T. S. (Ed.), *Oceanic Micropaleontology* (2): London (Academic Press), 973–1008.

Haq, B. U., 1973. Evolutionary trends in the Cenozoic coccolithophore genus *Helicopontosphaera*. *Micropaleontology*, 19:32–52.

Hay, W. W., 1977. Calcareous nannofossils. *In* Ramsey, A. T. S. (Ed.), *Oceanic Micropaleontology* (2): London (Academic Press), 1055–1200.

Hays, J. D., et al., 1972. Site 77. *In* Hays, J. D., et al., *Init. Repts. DSDP*, 9: Washington (U.S. Govt. Printing Office), 43–208.

Hays, J. D., Saito, T., Opdyke, N. D., and Burkle, L. H., 1969. Pliocene-Pleistocene sediments of the eastern equatorial Pacific, their paleomagnetic, biostratigraphic and climatic record. *Geol. Soc. Am. Bull.*, 80:1481–1514.

Labracherie, M., Moyes, J., and Pujos-Lamy, A., 1981. Mission COPANO: Etude stratigraphique et apport des organismes à la connaissance de l'environnement sédimentaire. *Rapport Deleg. Générale Rech. Scientifique Technique*, 78.7.0014.

Loeblich, A. R., Jr., and Tappan, H., 1970. Annotated index and bibliography of the calcareous nannoplankton IV. *J. Paleontol.*, 44: 558–574.

_____, 1971. Annotated index and bibliography of the calcareous nannoplankton VI. *Phycologia*, 10:309–339.

Ness, G., Levi, S., and Couch, R., 1980. Marine magnetic anomaly timescales for the Cenozoic and Late Cretaceous: a précis, critique, and synthesis. *Rev. Geophys. Space Phys.*, 18(4):753–770.

Okada, H., and Bukry, D., 1980. Supplementary modification and introduction of code numbers to the low-latitude coccolith biostratigraphic zonation (Bukry, 1973–1975). *Mar. Micropaleontol.*, 5: 321–325.

Okada, H., and Honjo, S., 1973. The distribution of oceanic coccolithophorids in the Pacific. *Deep-Sea Res.*, 20:355–374.

Olausson, E., 1961. Remarks on some Cenozoic core sequences from the central Pacific, with a discussion of the role of coccolithophorids and foraminifera in carbonate deposition. *Göteborgs Kungl. Vet. Vitt. Sam. Handl.*, B, 8:1–35.

Pujos, A., in press. Quaternary nannofossils from Goban Spur, eastern North Atlantic Ocean, Deep Sea Drilling Project Holes 548 and 549A. *In* Graciansky, P. C. de, Poag, C. W., et al., *Init. Repts. DSDP*, 80, Pt. 2: Washington (U.S. Govt. Printing Office), 767–792.

Pujos-Lamy, A., 1976. *Emiliania* et *Gephyrocapsa* (nannoplancton calcaire): biométrie et intérêt biostratigraphique dans le Pleistocène supérieur marin des Açores. *Rev. Espan. Micropaleontol.*, 9:69–84.

_____, 1977. Essai d'établissement d'une biostratigraphie du nannoplancton calcaire dans le Pleistocène de l'Atlantique nord-oriental. *Boreas*, 6:323–331.

Rio, D., 1982. The fossil distribution of Coccolithophore genus *Gephyrocapsa* Kamptner and related Plio-Pleistocene chronostratigraphic problems. *In* Prell, W. L., Gardner, J. V., et al., *Init. Repts. DSDP*, 68: Washington (U.S. Govt. Printing Office), 325–343.

Roth, P. H., 1973. Calcareous nannofossils—Leg 17, Deep Sea Drilling Project. *In* Winterer, E. L., Ewing, J. I., et al., *Init., Repts. DSDP*, 17: Washington (U.S. Govt. Printing Office), 695–795.

Shackleton, N. J., and Opdyke, N. D., 1973. Oxygen isotope and paleomagnetic stratigraphy of equatorial Pacific core V28-238: Oxygen isotope temperatures and ice volumes on a 10^3 year and 10^6 year scale. *Quat. Res.*, 3:39–55.

_____, 1976. Oxygen isotope and paleomagnetic stratigraphy of Pacific core V28-239, late Pliocene to latest Pleistocene. *Mem. Geol. Soc. Am.*, 145:449–465.

Thierstein, H. R., Geitzenauer, K. R., Molfino, B., and Shackleton, N. J., 1977. Global synchronicity of late Quaternary coccolith datum levels: validation by oxygen isotopes. *Geology*, 5:400–404.

Thompson, P. R., and Saito, T., 1974. Pacific Pleistocene sediments: planktonic foraminifera dissolution cycles and geochronology. *Geology*, 2:333–335.

Vatan, A., 1967. *Manuel de Sédimentologie*: Paris (Ed. Technip).

Wilcoxon, J. A., 1970. *Cyclococcolithina* Wilcoxon nom. nov. (nom. subst. pro *Cyclococcolithus* Kamptner, 1954). *Tulane Stud. Geol. Paleontol.*, 8:82–83.

Date of Initial Receipt: 29 August 1983
Date of Acceptance: 22 April 1984

APPENDIX

List of Quaternary and Tertiary Nannofossils Found in Quaternary Sediments of DSDP Leg 85 (in alphabetic order of species names)

Quaternary Species

Pontosphaera alboranensis Bartolini, 1970
Cyclolithella annula (Cohen) Cohen and Reinhardt, 1968
Gephyrocapsa aperta Kamptner, 1963
Gephyrocapsa caribbeanica Boudreaux and Hay, 1967
Rhabdosphaera clavigera Murray and Blackman, 1898
Ceratolithus cristatus Kamptner, 1950
Gephyrocapsa doronicoides (Black and Barnes) Pujos, in press
Gephyrocapsa ericsonii McIntyre and Bé, 1967
Scapholithus fossilis Deflandre, 1954
Emiliania huxleyi (Lohmann) Hay and Mohler, 1967
Umbellosphaera irregularis Paasche, 1955
Pontosphaera japonica (Takayama) Burns, 1973
Helicopontosphaera kamptneri Hay and Mohler, 1867
Pseudoemiliania lacunosa (Kamptner) Gartner, 1969
Cyclococcolithina leptopora (Murray and Blackman) Wilcoxon, 1970
Pontosphaera messinae Bartolini, 1970
Cyclococcolithina macintyrei (Bukry and Bramlette) Hay, 1977
Helicopontosphaera neogranulata Gartner, 1977
Gephyrocapsa oceanica Kamptner, 1943
Pontosphaera pacifica Burns, 1973
Coccolithus pelagicus (Wallich) Schiller, 1930
Crenalithus productus (Kamptner) n. comb.
Gephyrocapsa protohuxleyi McIntyre, 1970
Helicopontosphaera sellii Bukry and Bramlette, 1969
Umbilicosphaera sibogae (Weber and van Bosse) Gaarder, 1970
Helicopontosphaera wallichi (Lohmann) Boudreaux and Hay, 1969

Tertiary Species

Cyclicargolithus abisectus (Müller) Wise, 1973
Discoaster brouweri Tan Sin Hok, 1927
Discoaster deflandrei Bramlette and Riedel, 1954
Amaurolithus delicatus Gartner and Bukry, 1975
Cyclicargolithus floridanus (Roth and Hay) Bukry, 1971
Coccolithus miopelagicus Bukry, 1971
Reticulofenestra pseudoumbilica (Gartner) Gartner, 1969

Table 2. Correlation between nannofossil zonation of Okada and Bukry (1980), nannofossil events, chronologic scale, carbonate cycles, and some isotopic stages in the Pacific (Leg 85) and in the Atlantic (Leg 80).

Okada and Bukry (1980) low-latitude zonation		Nannofossil conventional (marked [conv.]) and additional markers				
		Leg 85			Leg 80	
Zones	Subzones	Estimated ages (Ma)	Carbonate cycles	Nannofossil events	Climatic (= isotopic) cycles	Estimated ages (Ma)
CN15 *E. huxleyi*		0.13–0.17	B3/B4	Change of dominance between *E. huxleyi* and *G. caribbeanica* [conv.]	5	0.11
0.2 Ma		0.15	Top B4	HO of *G. ericsonii*		
	CN14b *Ceratolithus cristatus*	0.23	Bottom B4	LO of *G. ericsonii*		
	0.3 Ma	0.3–0.4	B7/B8	Acme top of *G. caribbeanica*	7/8	0.25
		0.32	Top B7	HO of *H. neogranulata*	12	0.42
		0.38–0.45	B8 to B10	HO of *G. doronicoides* var. 4		0.32
		0.475	B10	HO of *P. lacunosa* [conv.]	12/13	0.475
CN14 *G. oceanica*		0.4–0.5	B10/B11	LO of *G. oceanica* [conv.]		0.63
	CN14a *Emiliania ovata*	0.55	B12	HO of *G. doronicoides* var. 1–2	12	0.45
		0.58	B12/B13	LO of *G. doronicoides* var. 4	12	0.45
		0.62	B14/B15	HO of *G. doronicoides* (lacunoid)		0.55
		0.63	B14/B15	HO of *C. productus*		0.58[a]
		0.65	B15	Acme bottom of *G. caribbeanica*		0.63
0.9 Ma		0.8	M2/M3	Acme top of *G. doronicoides* var. 3		
		0.96	M4/M5	Acme bottom of *C. productus*		1.22[a]
		0.98	M4/M5	LO of *G. caribbeanica*		1.22
	CN13b *G. caribbeanica*	1.050	M5	Acme bottom of *G. doronicoides* var. 3		
CN13 *G. doronicoides*		1.230	M7	HO of *H. sellii* [conv.]		1.22
		1.350–1.450	M10/M11	HO of *C.* sp. cf. *C. macintyrei* [conv.]		1.51
	1.6 Ma	1.500	M11/M12	HO of *C. macintyrei*		1.65
	CN13a *Emiliania annula*	1.650	M16/M17	HO of *C. pelagicus*		1.63
1.8 Ma		1.750	M17/M18	Acme bottom of *G. doronicoides* var. 1–2		
CN12 *D. brouweri*	CN12d *C. macintyrei*	>2.0		HO of *D. brouweri*		

Note: HO = highest occurrence; LO = lowest occurrence.
[a] On Leg 80, a distinction was established between *C. productus* s. s. and *G. sinuosa* (which may be a variant of *C. productus*).

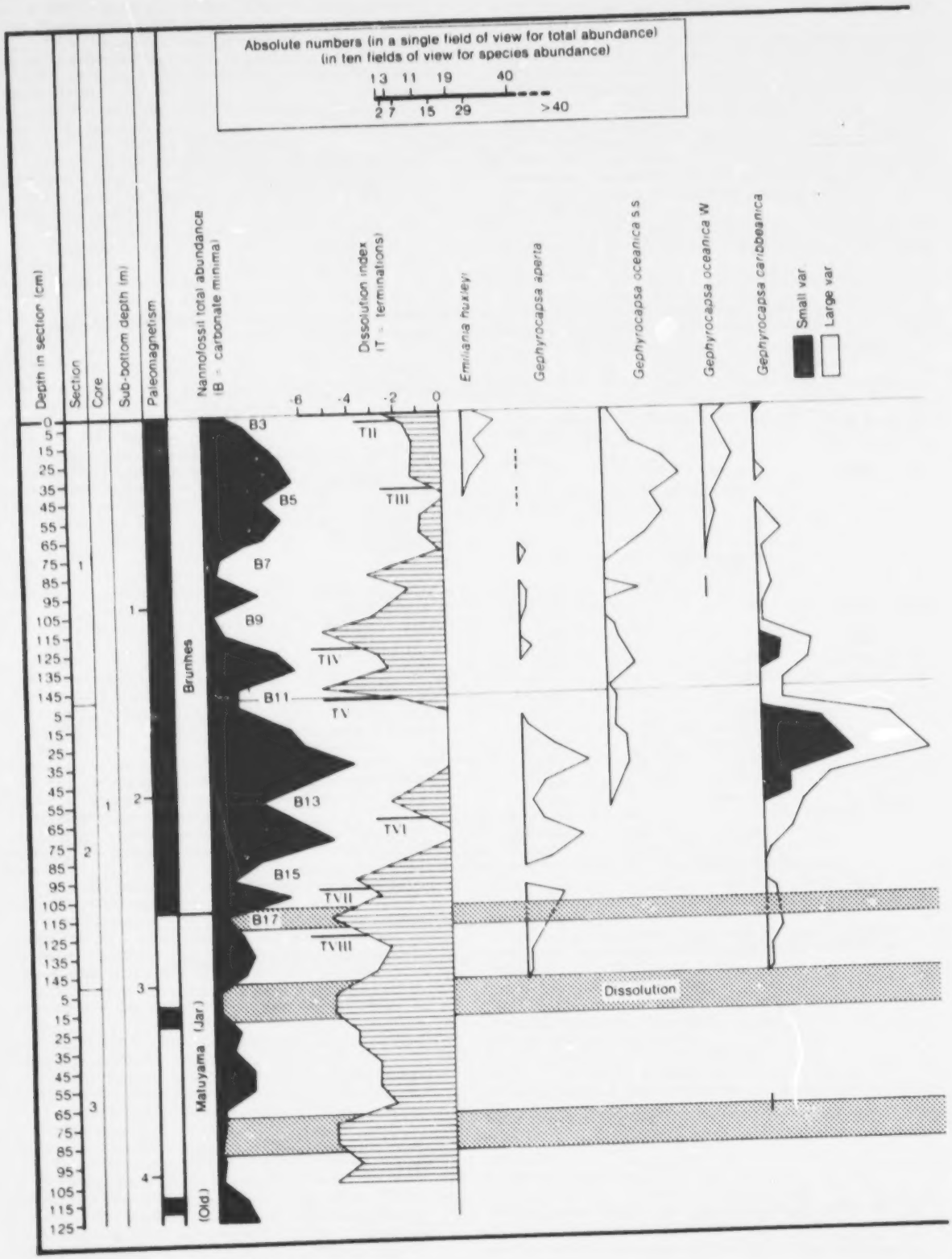

Figure 8. Nannofossils, Hole 575C.

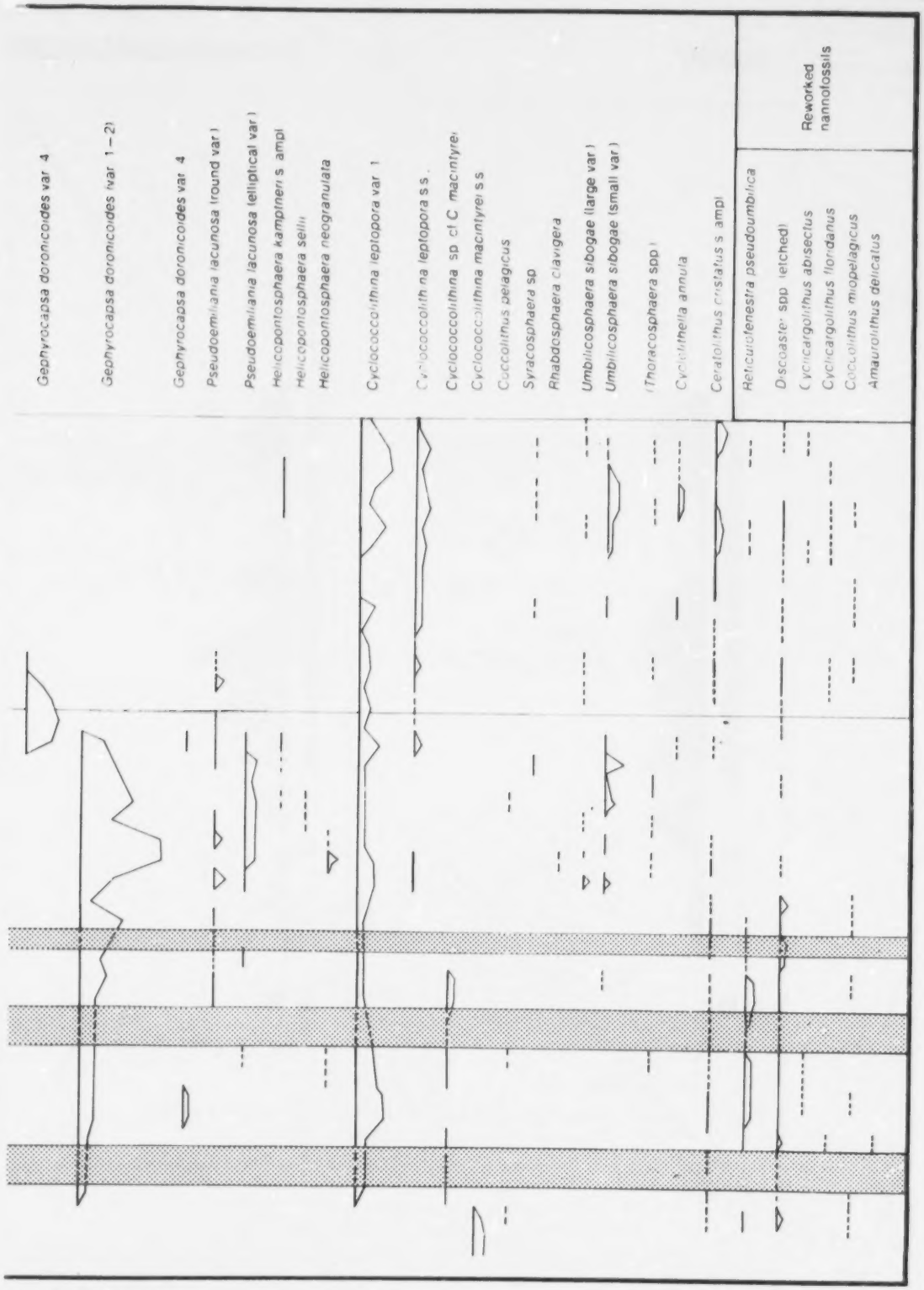

Figure 8. (Continued.)

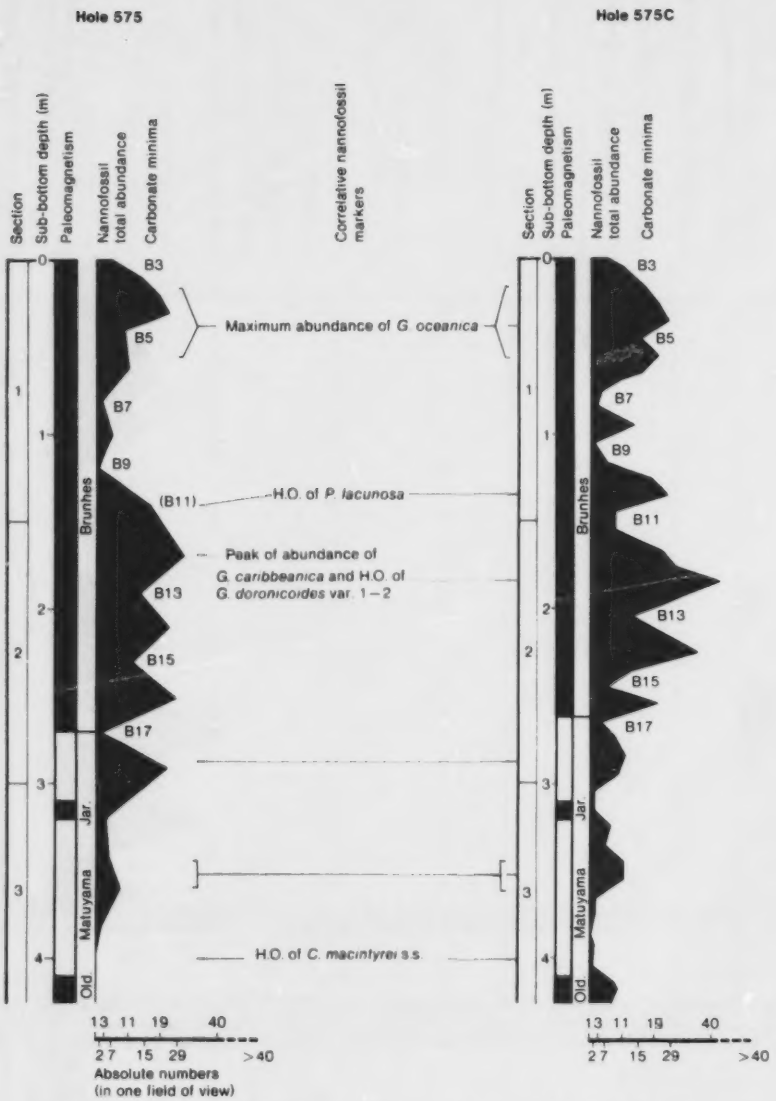

Figure 9. Correlation of Holes 575 (Core 1) and 575C (Core 1). H.O. = highest occurrence.

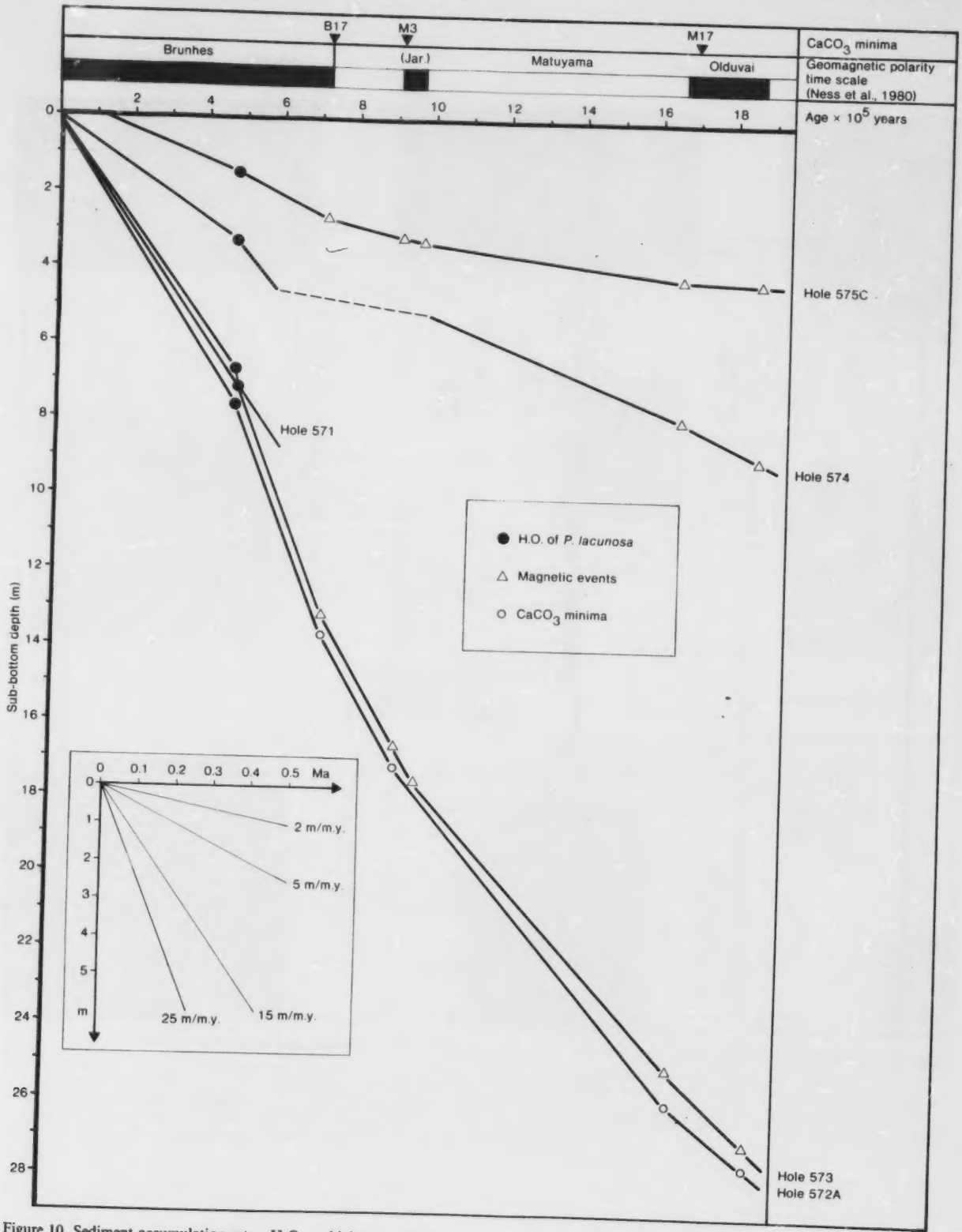

Figure 10. Sediment accumulation rates. H.O. = highest occurrence.

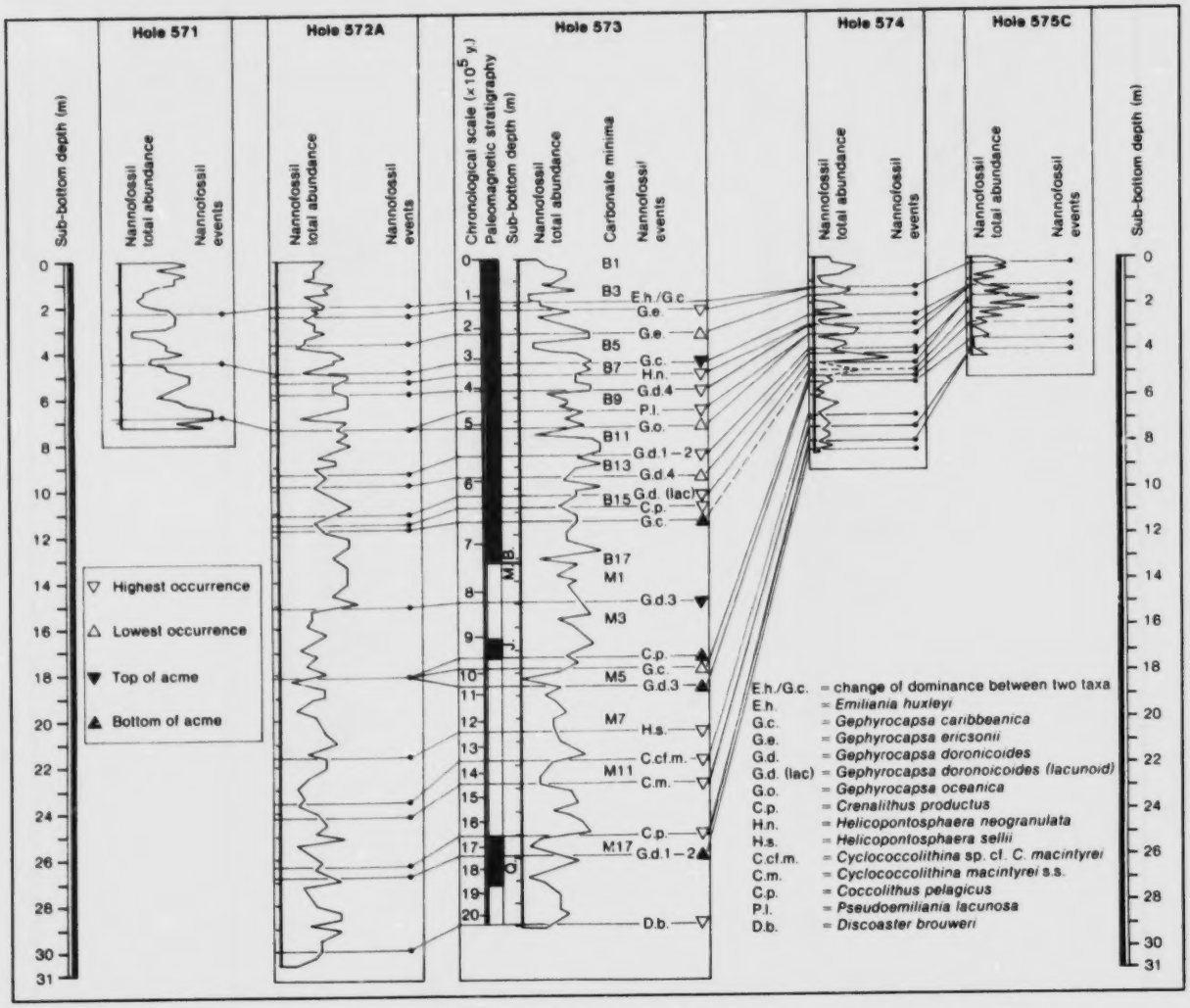

Figure 11. Correlation of Holes 571, 572A, 573, 574, and 575C, using nannofossil total abundance and nannofossil markers.

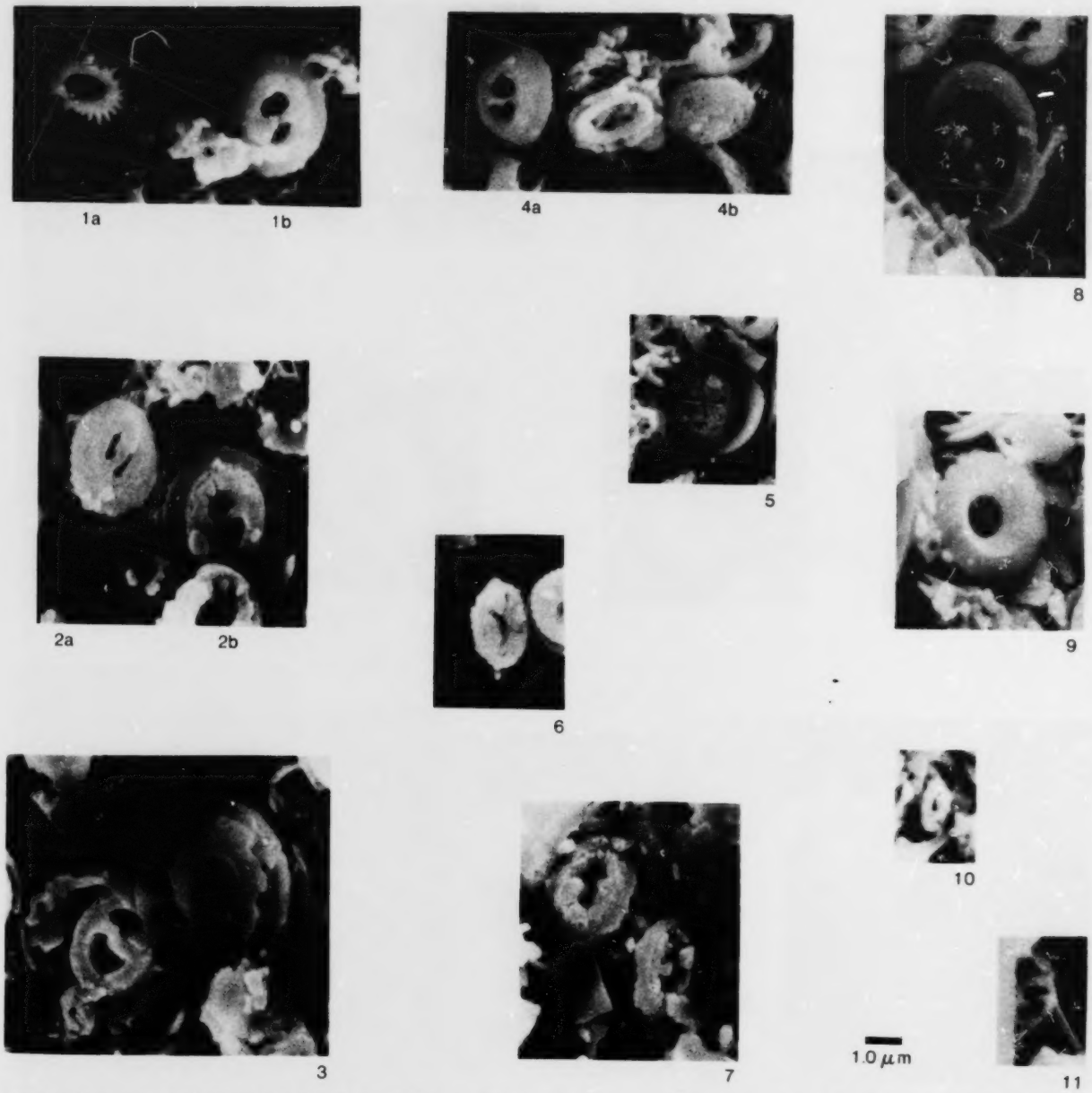

Plate 1. Quaternary nannofossils from Leg 85 sites. (SEM; magnification ×6000.) **1a.** *Emiliania huxleyi*, 573-1-1, 40 cm. **1b, 2a, 4a.** *Gephyrocapsa oceanica* s. s., (1b) 573-1-1, 40 cm, (2a) 573-2-6, 40 cm, (4a) 573-2-6, 138 cm. **2b, 3.** *Gephyrocapsa oceanica* W, 573-2-6, 40 cm, (3) includes a *Cyclococcolithina leptopora* var. 1. **4b, 5–6.** *Crenalithus productus*, (4b) 573-2-6, 138 cm, (5) 573-3-1, 120 cm, (6) 573-3-3, 40 cm. **7.** *Gephyrocapsa caribbeanica*, slightly dissolved specimens, 573-2-5, 40 cm. **8.** *Syracosphaera* sp., 573-2-5, 40 cm. **9.** *Umbilicosphaera sibogae*, 573-3-3, 40 cm. **10–11.** *Gephyrocapsa aperta*, (10) 573-3-3, 40 cm, (11) 573-2-2, 100 cm.

1.0 μm

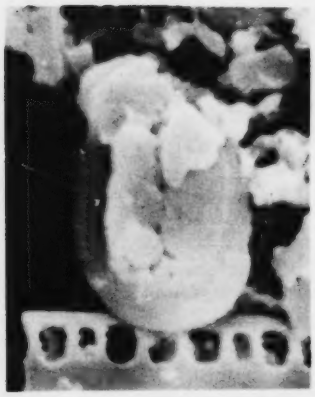

Plate 2. Quaternary nannofossils from Leg 85 sites. (SEM; magnification ×6000.) **1–6.** *Gephyrocapsa doronicoides* (1) var. 4, 573-2-5, 40 cm, (2) var. 1, distal side, 573-2-6, 40 cm, (3) var. 2, proximal side, 573-3-2, 40 cm, (4) var. 3, 573-3-3, 40 cm, (5–6) (lacunoid, 5, sample 573-2-7, 40 cm; 6, sample 573-4-5, 60 cm). **7.** *Pseudoemiliania lacunosa*, elliptical type, 573-3-3, 40 cm. **8.** *Helicopontosphaera kamptneri* s. ampl., 573-1-1, 40 cm. **9.** *Helicopontosphaera sellii*, 573-4-5, 60 cm.

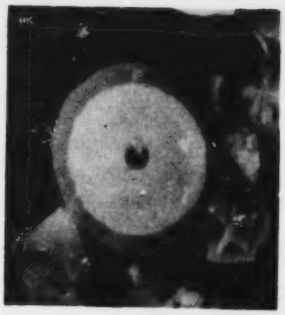

1

1.0 μm

5

2

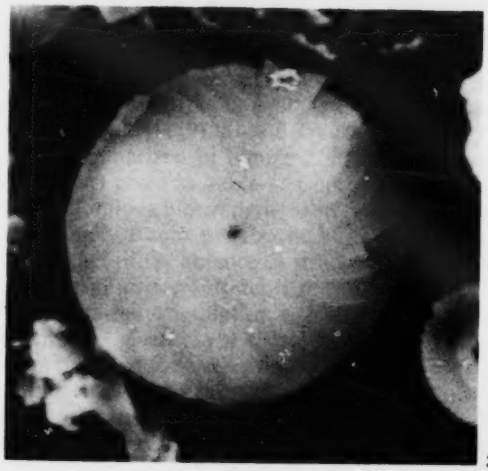

3

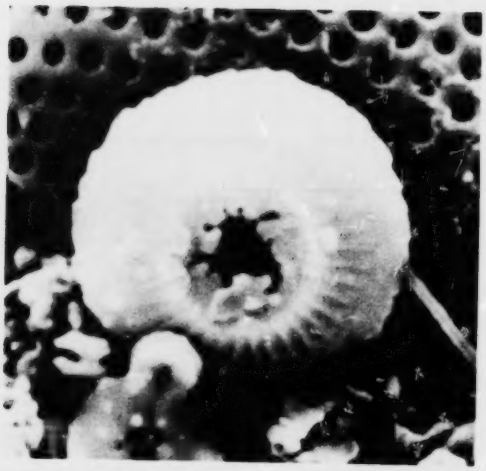

4

Plate 3. Quaternary nannofossils from Leg 85 sites (SEM; magnification ×6000.) **1.** *Cyclococcolithina leptopora* var. 1, distal side, 573-3-3, 40 cm. **2.** *Cyclococcolithina leptopora* s. s., 573-3-3, 40 cm. **3.** *Cyclococcolithina* sp. cf. *C. macintyrei*, 573-4-1, 120 cm. **4.** *Cyclococcolithina macintyrei*, 573-4-5, 60 cm. **5.** *Coccolithus pelagicus*, 573-4-5, 60 cm.

14. CENOZOIC NANNOFOSSILS, CENTRAL EQUATORIAL PACIFIC, DEEP SEA DRILLING PROJECT LEG 85[1]

Annick Pujos, Département de Géologie et Océanographie, Institut de Géologie du Bassin d'Aquitaine[2]

ABSTRACT

Leg 85 of the Deep Sea Drilling Project recovered Cenozoic nannofossils from the central and eastern parts of the Pacific equatorial high-productivity area. The low-latitude zonation of Bukry (1973a) was used for dating uppermost Eocene to uppermost Pliocene samples. At two sites (573 and 574) the Eocene/Oligocene boundary was reached, enabling accurate study in spite of an unconformity and strong calcite dissolution. Some unconformities and/or intervals of very low rates of sedimentation are described in detail and correlated from one site to another. The high abundance of species belonging to *Reticulofenestra* and *Dictyococcites* permitted the accurate study of these taxa; their morphologic differences and their stratigraphic occurrences are described in detail. A short, tentative, ecological study was made by using the nannofossil dissolution index, the total nannofossil abundance, and the abundance of some taxa. The easternmost site (Site 572) contains some species that are restricted to this site and are characteristic of upwelling areas. Discoasters are totally absent in a sediment interval apparently deposited during a period of unstable climate when glacial to interglacial oscillations were occurring in Antarctica.

INTRODUCTION

Leg 85 of the Deep Sea Drilling Project began at San Pedro, California, and ended at Honolulu, Hawaii (Fig. 1). Five sites were drilled, but only four of them provided Cenozoic material (Sites 572 to 575). A light microscope (with a phase contrast and a Nomarski interferential system) was used for studying about 1000 nannofossil samples with the smear-slide technique. All the slides were quickly reviewed for determining zonal boundaries; abundances of nannofossils were estimated on most of them, and the abundance of a few taxa was estimated with more precision for ecological studies (see range charts for count scales). The species (and a few genera for which the species were indeterminate) are listed in alphabetic order in the Appendix. Coccolith zonation is based on Bukry (1973a) and Okada and Bukry (1980) and is summarized in Figure 2. Nannofossil zonal assignment is given in Table 1. Coccoliths provide an almost continuous biostratigraphic record at the four sites. Occasionally, a zone or subzone is not well defined, usually because of the absence of stratigraphic markers. Few unconformities were evident; they are indicated in the site summaries. Dissolution was also estimated; the solution index given in the Quaternary study (Pujos, this volume) is used for the placoliths only. The usual scarcity of discoasters does not allow the precise study of dissolution and/or etching on these *incertae sedis*. Nannofossil total abundance was evaluated by observing two fields (×100). Variations in abundance are not directly related to nannofossil dissolution and therefore may provide information on productivity and ecology.

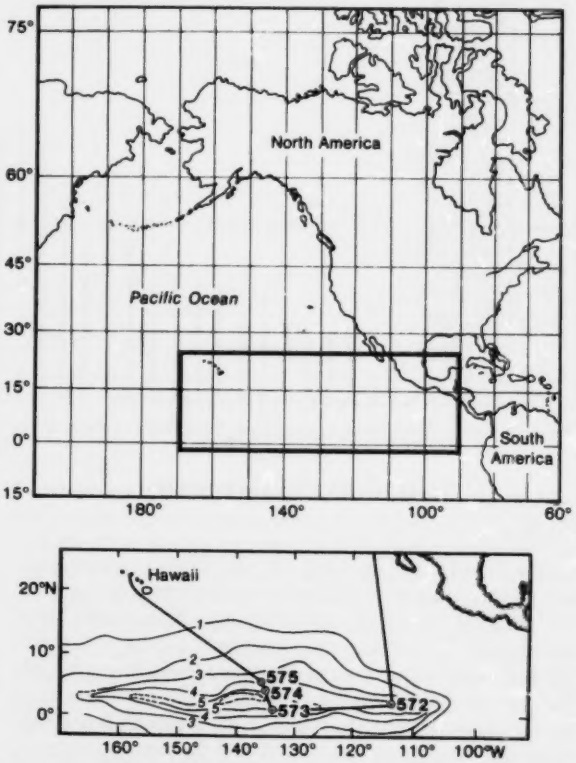

Figure 1. Location of DSDP Leg 85 in the equatorial high-productivity area, with blow-up at bottom showing detailed location of sites.

Species identification and abundance estimates were made in approximately 1000 samples; the results for selected samples, which were chosen as being typical of the various assemblages, are reported in Tables 2 to 5.

[1] Mayer, L., Theyer, F., et al., *Init. Repts. DSDP*, 85: Washington (U.S. Govt. Printing Office).

[2] Address: Institut de Géologie du Bassin d'Aquitaine, Université de Bordeaux I, Avenue des Facultés, 33405 Talence Cedex, France.

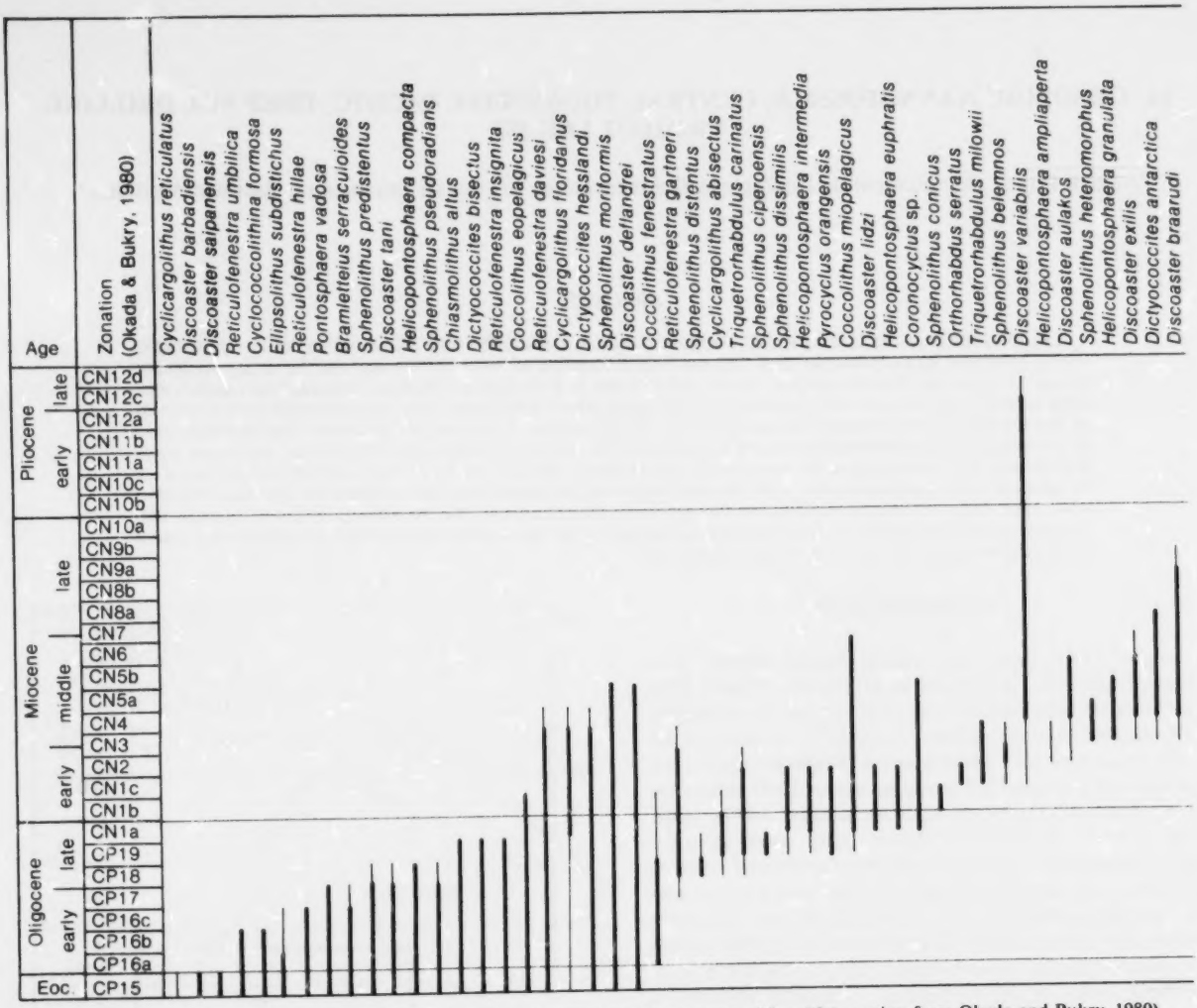

Figure 2. Stratigraphic ranges of selected nannofossils present in the Cenozoic sequence of Leg 85 (zonation from Okada and Bukry, 1980).

SUMMARY OF THE SITES

Site 572

Site 572 (Table 2 and Fig. 3) was cored in the eastern part of the equatorial high-productivity area (1°26.1′N, 113°50.5′W; 3903 m sub-bottom). Five holes were drilled and 76 cores were recovered. Holes 572A and 572D provide a continuous sequence from lower middle Miocene to the top of the Pliocene. Coccoliths are usually common to very abundant in all samples, but dissolution has resulted in significant and frequent variations. Placoliths are occasionally very poorly preserved (e.g., Cores 572A-7, 572D-14, and 572D-17), and sometimes they do not show any sign of dissolution (Cores 572A-10, 572A-15, 572A-16, 572D-5, and 572D-16). This complete absence of dissolution at some levels is exceptional in the high-productivity area, where calcite is usually not well preserved. The excellent state of preservation at Site 572 may be due to its location at the periphery of the productive area, where the ecological factors causing calcite dissolution are not effective continuously. Discoasters are especially scarce at this site; they are usually completely absent or represented by less than 0.5% of the whole population. Thus, they cannot be used for zonation except in the *Sphenolithus neoabies* and *Discoaster asymmetricus* subzones (including *D. brouweri, D. surculus*, and *D. decorus*), in the *D. berggrenii* Subzone (having a small bloom of the zonal species), and in the *D. bellus* Subzone (containing frequent *D. bollii*). Reworked coccoliths from the Eocene/Oligocene boundary are common in the middle Miocene (from the bottom of Hole 572D up to Core 572D-24). Above the *Coccolithus miopelagicus* Subzone, reworking is sporadic.

Most of the zones from the middle Miocene to the top of the Pliocene were identified biostratigraphically. This identification was not always easy because of the dominance of various members of the Gephyrocapsaceae family in all samples. Besides common species such as *Reticulofenestra pseudoumbilica, R. doronicoides, R. haquii*, and *R. minutula*, there is a huge abundance of

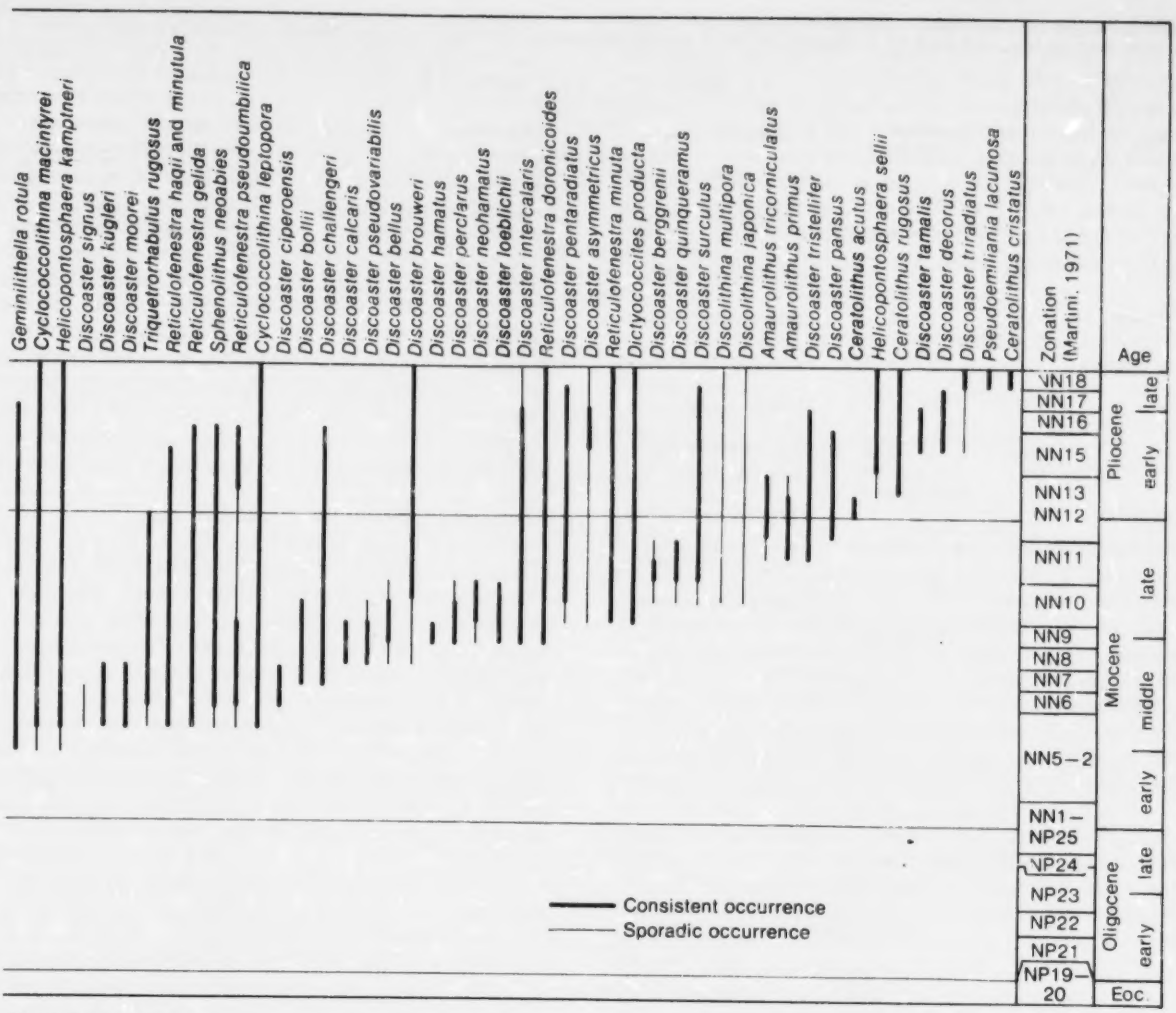

Figure 2. (Continued).

small elliptical coccoliths belonging to *R. minuta* and *"R." tagana*, which tend to hide the other taxa throughout the stratigraphic column. This abundance of small *Reticulofenestra* and the reduced number of discoasters are considered by Lohmann and Carlson (1981) to be characteristic of cooler waters. Moreover, *"R." tagana* has been noted only in upwelling areas (Fonseca, 1976, in Portugal; Bukry, 1981, in sediments off the coast of California and Mexico). Therefore, nannofossil assemblages at Site 572 are apparently strongly influenced by special ecological factors such as upwelling (Barron, this volume). This may explain the presence of some taxa that are completely absent from the other sites of Leg 85: some *Pontosphaera* spp. (e.g., *P. multipora* and *P. japonica*), *Scyphosphaera* spp., and *Syracosphaera* spp. have a sporadic distribution, whereas *Geminithella rotula* is almost continuously present in all cores.

The *Catinaster calyculus* and *Discoaster bellus* subzones are condensed to a thin interval of sediment, probably resulting from a very low rate of sedimentation. Furthermore, there is evidence that a low rate of sedimentation occurred throughout the Pliocene and the late Miocene. A strong change in this rate apparently occurred between middle and late Miocene: for the interval from Core 572D-16 to the bottom of the hole, the rate of sedimentation was apparently very high.

The oldest zone identified at Site 572 is the *Sphenolithus heteromorphus* Zone (14 to 15 Ma). The same age was attributed to the bottom sediment recovered at most of the sites of Leg 63, which were drilled at about the same longitude (but at much higher latitudes). This result is in accordance with the tectonic setting of the area.

Site 573

Site 573 (Table 3 and Fig. 3) is located in the eastern part of the equatorial high-productivity area (00°29.9′N, 133°18.57′W; 4317 m sub-bottom), in the vicinity of Site 77 of Leg 9. Three holes were drilled, providing 68 cores dated from latest Eocene to Pleistocene. Nannofossils were studied in Holes 573 and 573B.

Table 1. Summary of nannofossil zonal assignments for Leg 85. In the last four columns, the two numbers given for each zonal interval represent the hole, core, section, and depth of the highest and lowest samples delineating that zone or subzone (zonation of Okada and Bukry, 1980).

Age		Zones	Subzones	Site 572	Site 573	Site 574	Site 575
Pleistocene		CN13 *Crenalithus doronicoides*	CN13a *Emiliania annula*	572A-4-1, 139 cm	573-4-6, 40 cm	574-2-3, 100 cm	575-1-3, 120 cm
Pliocene	late	CN12 *Discoaster brouweri*	CN12d *Cyclococcolithus macintyrei*	572A-4-2, 20 cm 572A-4-3, 20 cm	573-4-6, 60 cm 573-5,CC	574-2-3, 120 cm 574-2-4, 60 cm	575-1-3, 140 cm 575-1-4, 60 cm
			CN12c *Discoaster pentaradiatus*	572A-4-4, 20 cm 572A-5-3, 0 cm	573-6-2, 0 cm 573-6-5, 0 cm	574-2-4, 80 cm 574-2-6, 60 cm	575-1-4, 140 cm 575-1-5, 60 cm
			CN12a *Discoaster tamalis*	572A-5-4, 0 cm 572A-6-6, 0 cm	573-7-2, 0 cm 573-7-3, 0 cm	574-2-6, 83 cm 574-3-5, 27 cm	575-1,CC 575-2-1, 35 cm
	early	CN11 *Reticulofenestra pseudoumbilica*	CN11b *Discoaster asymmetricus*	572A-6-7, 0 cm 572A-7-3, 0 cm	573-7-4, 0 cm	574-3-6, 27 cm	575-2-1, 115 cm
			CN11a *Sphenolithus neoabies*	572A-8-3, 0 cm ?Dissolution	573-8-6, 0 cm	574-4-3, 27 cm	575-2-3, 115 cm
		CN10 *Amaurolithus tricorniculatus*	CN10c *Ceratolithus rugosus*	572A-10-3, 0 cm	573-8-7, 0 cm	574-4-4, 27 cm	575-2-4, 35 cm 575-2-4, 35 cm
			CN10b *Ceratolithus acutus*	572A-10,CC			575-2-4, 115 cm
Miocene	late		CN10a *Triquetrorhabdulus rugosus*	572A-13,CC	573-10-5, 0 cm	574-5-2, 29 cm	575-3-1, 35 cm
		CN9 *Discoaster quinqueramus*	CN9b *Amaurolithus primus*	572A-14-3, 0 cm 572A-17-3, 0 cm	573-10,CC 573-12-2, 0 cm	574-5-3, 29 cm Dissolution	575-3-2, 35 cm
			CN9a *Discoaster berggrenii*	572A-17,CC 572D-2,CC	573-12-3, 0 cm 573-13-1, 0 cm	574-6-1, 29 cm	575-3-4, 35 cm
		CN8 *Discoaster neohamatus*	CN8b *Discoaster neorectus*	572D-3-1, 50 cm	573-13-2, 0 cm 573-15-3, 0 cm	574-6-2, 28 cm	575-3-5, 35 cm 575-3-6, 35 cm
			CN8a *Discoaster hellus*	572D-14-3, 55 cm	573-15-4, 0 cm 573B-4-2, 15 cm	574-8,CC	575-3,CC 575-4-1, 28 cm
		CN7 *Discoaster hamatus*		572D-14-4, 55 cm 572D-16-3, 55 cm	573B-4-3, 15 cm 573B-4,CC	574-9-1, 49 cm 574-10-3, 49 cm	575-4-2, 35 cm
	middle	CN6 *Catinaster coalitus*		572D-16-4, 55 cm 572D-19-2, 47 cm	573B-5-1, 15 cm 573B-6-2, 15 cm	574-10-4, 49 cm 574-12-1, 49 cm	575-4-3, 35 cm 575-4-6, 35 cm
		CN5 *Discoaster exilis*	CN5b *Discoaster kugleri*	572D-19-3, 47 cm 572D-24-2, 55 cm	573B-6-3, 15 cm 573B-7-1, 15 cm	574-12-2, 49 cm 574-13-2, 49 cm	575-5-1, 35 cm 575-5-4, 35 cm
			CN5a *Coccolithus miopelagicus*	572D-24-3, 55 cm 572D-27,CC	573B-7-2, 15 cm 573B-9-3, 15 cm	574-14-3, 49 cm 573-16-2, 34 cm	575-5-5, 35 cm 575-8-3, 35 cm
		CN4 *Sphenolithus heteromorphus*		572D-28,CC	573B-9-4, 15 cm 573B-12-4, 15 cm	574-16-3, 34 cm 574-28-3, 49 cm	575-8-4, 35 cm 575-9-4, 35 cm
	early	CN3 *Helicopontosphaera ampliaperta*		Not reached	573B-12-5, 15 cm 573B-14-2, 15 cm	574-28,CC 574C-3-2, 49 cm	575-9,CC 575A-6-1, 51 cm
		CN2 *Sphenolithus belemnos*			573B-14-3, 15 cm 573B-17-2, 15 cm	574C-3-3, 49 cm 574C-5-3, 49 cm	575A-6-2, 51 cm 575A-7-3, 51 cm
		CN1 *Triquetrorhabdulus carinatus*	CN1c *Discoaster druggii*		573B-17-3, 15 cm 573B-20-6, 25 cm	574C-5-4, 49 cm 574C-10-1, 49 cm	575A-8-2, 51 cm 575A-13,CC
			CN1b *Discoaster deflandrei*		573B-20,CC	574C-10-2, 49 cm 574C-16-3, 49 cm	575A-14-2, 5 cm
			CN1a *Cyclicargolithus abisectus*		573B-20,CC	574C-16,CC 574C-17-2, 49 cm	Not reached
Oligocene	late	CP19 *Sphenolithus ciperoensis*			573B-21-1, 30 cm 573B-26-1, 15 cm	574C-17-3, 49 cm 574C-23-1, 39 cm	
		CP18 *Sphenolithus distentus*			573B-26-2, 17 cm 573B-34-2, 19 cm	574C-23-2, 39 cm 574C-27-2, 27 cm	
	early	CP17 *Sphenolithus predistentus*			573B-35,CC 573B-38-2, 27 cm	574C-27-3, 25 cm 574C-29-1, 35 cm	
		CP16 *Helicopontosphaera reticulata*	CP16c *Reticulofenestra hillae*		573B-38-3, 27 cm 573B-41,CC	574C-29-2, 34 cm 574C-32-2, 49 cm	
			CP16b *Coccolithus formosus*		573B-42-1, 20 cm 573B-42-2, 50 cm	574C-32-3, 49 cm	
			CP16a *Coccolithus subdistichus*		573B-42-4, 71 cm	574C-33-4, 114 cm	
Eocene		CP15 *Discoaster barbadiensis*			573B-42-4, 58 cm 573B-42-4, 135 cm	574C-33-5, 5 cm	

Note: No nannofossils were found at 573B-42-4, 10 cm (dashed boundary).

Coccolith assemblages are usually abundant and diverse but often dissolved. Nannofossils in the Eocene sediments of this site are rare and usually show much dissolution and/or etching. Oligocene and early middle Miocene coccoliths are common to very abundant and are moderately dissolved. Coccoliths are less abundant and more dissolved in the upper Miocene. There is a thin section containing abundant and well-preserved coccoliths in the lowermost Pliocene. Rapid and continuous evolution can be recognized up to the upper middle

Pliocene, where dissolution has destroyed almost all coccoliths. The uppermost Pliocene shows the opposite situation; the top of the Cenozoic section is rich in well preserved nannofossils.

Discoasters are not abundant at this site. When present, they are often dissolved and/or etched, and most of them cannot be identified to the species level, nor are they useful for zonation. In only one case was the general morphologic outline useful: from the top of the Cenozoic to the *Sphenolithus heteromorphus* Zone (early middle Miocene), the discoaster assemblages are dominated by long-rayed specimens. Below this level (from the *Helicopontosphaera ampliaperta* Zone), short-rayed discoasters are much more abundant, and they are often the only discoasters present. This differentiation is also useful for the other sites. Reworking is not common at this site, although some Eocene coccoliths or discoasters are found sporadically below the middle upper Miocene.

Almost all zones of Bukry's zonation were found between Zone CP15b (latest Eocene) and CN12d (latest Pliocene). Some subzones could not be identified clearly in the lower Pliocene (within the *Reticulofenestra pseudoumbilica* Zone and the *Amaurolithus tricorniculatus* Zone) because of the absence or scarcity of the subzonal markers (e.g., *Triquetrorhabdulus rugosus, Ceratolithus acutus, C. primus, Discoaster asymmetricus, D. tamalis*, and *D. decorus*). At the same levels, some species indicative of cooler water, such as *D. variabilis*, are frequent. The apparent arrival of cool water may explain the absence of cosmopolitan and warm water taxa. The rate of sedimentation appears to have been constant throughout this interval.

By using the nannofossil occurrences and the rates of sedimentation, it is possible to identify three periods of hiatus, or at least very low rates of sedimentation. (1) The rate of sedimentation was apparently low in the early late Miocene, from 9 to 13 Ma, but the corresponding nannofossil zones do exist for this interval. If there actually is a hiatus here, it may occur within a single zone, more specifically in the earliest part of the *D. bellus* Subzone. This phenomenon is noted not only at Sites 574 and 575, but also in wide areas of the Pacific (Keller, 1981). (2) The *Cyclicargolithus abisectus* Subzone is missing and the *D. deflandrei* Subzone is present in the uppermost Oligocene only between Sample 573D-20,CC and 573D-21-1, 30–31 cm. The underlying zone (*Sphenolithus ciperoensis* Zone) is apparently almost complete. The hiatus occurs approximately between 21 and 24 Ma, as was already noted by Hays et al. (1972) at Site 77. (3) The lowermost hiatus corresponds to a barren, metalliferous claystone unit. There are no coccoliths or discoasters between 573D-42-4, 10 cm and 573D-42-2, 71 cm. Above this barren unit, at the interval between 573D-42-2, 71 cm and 573D-42-1, 20–21 cm, abundant nannofossils characterize the lower Oligocene (*Coccolithus formosus* Subzone), but the lowermost Oligocene subzone (*C. subdistichus* Subzone) is absent. Below the barren sediment, a thin layer of sediment (573D-42-4, 58–135 cm) is attributed to the Eocene; nannofossils are scarce and poorly preserved in this interval, and discoasters are strongly etched. *Isthmolithus recurvus* was not found. Bukry (1975) noted that this species "can be considered a consistent marker fossil only at latitudes higher than 30° north or south. It is typically absent at tropical sites and is best considered a restricted subzonal marker." The attribution of these samples to *D. barbadiensis* Zone is based on the presence of a few *D. saipanensis* in the interval 573D-42-4, 58–105 cm and *D. saipanensis* and *D. barbadiensis* in the interval 573D-42-4, 110–135 cm. In summary, the oldest sediments of Hole 573D present this succession:

573D-42-2, 50 cm	Subzone CP16b		Oligocene
573D-42-2, 71 cm to 573D-42-4, 10 cm	Barren sediment		
573D-42-4, 58-105 cm	*D. saipanensis*	Zone CP15	Eocene
573D-42-4, 110–135 cm	*D. saipanensis* and *D. barbadiensis*		

It is not possible to date the barren sediment precisely in this succession. In addition to Subzone CP16a (which is not represented in the nannofossil associations), most of Subzone CP16b and the uppermost part of Zone CP15 may be also missing. In observing the marked change in the sedimentation rate corresponding to this period (Fig. 3), it becomes obvious that it is much more than simply a hiatus in the biozonation, but a real unconformity in sedimentation that can be more precisely defined as occurring between 573D-42-2, 50 cm and 573D-42-4, 58 cm.

Such a succession is typical in the equatorial eastern Pacific (Bukry, pers. comm., 1983), where the Eocene/Oligocene boundary commonly occurs within barren sediment. This hiatus is known to be extensive in the Pacific (Kennett et al., 1975). For Bukry (1973a), Subzone CP16a "may be missing as a result of ecological factors." Kennett et al. (1975) link it with the beginning of Antarctic glaciation, which caused increased circulation of Antarctic Bottom Water.

Site 574

Site 574 (Table 4 and Fig. 3) was drilled within the central Pacific high-productivity area, just north of the crest of the sediment bulge (4°12.52′N, 139°19.81′W; 4548 m sub-bottom). The four holes of the site provided 92 cores. Holes 574 and 574C were chosen for the study of Cenozoic nannofossils ranging from the uppermost Eocene to the uppermost Pliocene. From the lowest Oligocene to the upper middle Miocene, coccoliths are often abundant and moderately etched; above this section, nannofossils are extensively etched and are common to rare. This advanced dissolution that appears at the top of the middle Miocene (~13 Ma) most likely is related to the end of the time of equatorial crossing (van Andel et al., 1975). From the end of the middle Miocene, Site 574 was located north of the equator under the influence of corrosive waters. Only the most resistant of the solution-resistant species can be found in the section representing this time. For example, *Coccolithus pelagicus* is usually absent in the upper Miocene and the Plio-

Table 2. Occurrence and estimated abundance of nannofossils in selected samples from Site 572.

Hole-Core-Section	Upper depth of sample (cm)	Sub-bottom depth (m)	Coccolith total abundance	Coccolith dissolution	Discoaster abundance	Zonation (Okada and Bukry, 1980)	Age		*Reticulofenestra minuta*	*"Reticulofenestra" lagana*	*Coccolithus radiatus*	*Coccolithus pelagicus*	*Cyclococcolithina macintyrei*	*Cyclococcolithina leptopora*	*Discoaster brouweri*
572A-4-2	20	30.30	C	−5	R	12d			R	●	●	●	R	F	R
4-3	20	31.80	A	−4	●	12d			A	●		F	R	F	●
4-4	20	33.30	A	−4	R	12c			C	●	●	F	R	R	●
5-3	0	39.30	A	−2	●	12c		late	C	●	●	F	●	R	●
5-4	0	40.80	C	−3	R	12a			F	●	●	R	F	R	●
6-6	0	53.40	C	−5	R	12a			C	●	●		R	F	R
6-7	0	54.90	C	−4	R	11b	Pliocene		C	●	●		R	F	R
7-3	0	58.20	F	−5	R	11b			F	F			●	●	●
8-3	0	67.10	C	−3	F	11a			C	C	●	●	●	●	R
9-3	0	75.30	C	−1	●	11a		early	C	R	●	●	●	●	●
10-3	0	84.80	A	/	●	11a			A	C		●	●	R	
11-3	0	94.40	F	−5	●	10b			F	R		●	●		●
12-3	0	103.70	C	−3	●	10			F	●		R	R	F	
13-3	0	112.90	A	−2	●	10			C	R		●	F	F	
14-3	0	122.10	A	−2	/	9b			C	F		●	F	F	
15-3	0	131.30	C	/	●	9b			C	C			●	R	
16-3	0	140.10	A	/	●	9b			C	F		R		R	●
17-3	0	148.30	C	−1	R	9b			F	R		●	●	●	R
572D-1-3	20	154.20	A	−2	F	9a			A	C		R	R	R	R
2-3	50	163.50	F	−4	R	8a			F	●		R	●	R	R
3-3	50	173.50	C	−2	R	8a		late	F	R		●	●		
4-3	50	183.00	C	−1	R	8a			F	R		R	●		●
5-3	60	192.60	A	/	/	8a			C	R		R	●	R	
6-2	55	200.55	A	−3	R	8a			C	R		R	●	F	●
7-3	55	211.55	A	−2	●	8a			C	F		F	●	R	
10-3	55	240.05	A	−3	F	8a			C	R		F	R	●	
14-3	55	278.05	F	−5	R	8a				C			●		
15-3	55	287.55	F	−4	●	7	Miocene			R		●			
16-3	55	297.05	A	/	R	7				R		●			
17-2	55	305.05	F	−6	R	6				R				●	
18-3	55	316.05	C	−3	●	6				R		R	●	●	
19-3	47	325.47	A	/	●	5b				R		●		●	
21-3	47	344.47	C	−4	●	5b				R		R	●		
23-3	55	363.55	C	−1	●	5b				●		R	●		
24-3	55	373.05	C	−1	/	5a		middle		●		R			
26-3	55	392.05	C	−3	●	5a				●		R	●		
27-3	55	401.55	A	−3	●	5a				●		F			
29-3	55	420.55	F	−1	●	4				●		R			
30,CC		433.83	F	−3	R	4				R		R			
31-1	49	439.49	A	−2	●	4				F		F	●		
572D-33,CC		464.66	C	−4	/	4				R		F			

Notes: Abundance of species is indicated as follows: ● = very rare, R = rare = one specimen in >10 fields of view; F = few = at least one specimen in 5 to 10 fields of view; C = common = at least one specimen in 1 field of view; A = abundant = numerous specimens in 1 field of view; ( ) = reworked specimens; * = cf. Index of solution is as follows (see discussion of Quaternary, Pujos, this volume): / = no dissolution, −1 = few coccoliths slightly dissolved, −2 = most coccoliths are slightly dissolved, −3 = most coccoliths are moderately dissolved, −4 coccoliths are strongly dissolved, −5 = no intact coccoliths, and −6 only ghosts of coccoliths.

cene, while *Cyclococcolithina leptopora* and *C. macintyrei* still persist.

Discoasters are not abundant at this site. They are very scarce in the *Sphenolithus heteromorphus* Zone, although *Coccolithus pelagicus* is common. This assemblage is attributable to the influence of cool waters. In the *Amaurolithus tricorniculatus* Zone and the *Reticulofenestra pseudoumbilica* Zone, discoasters are more abundant. This is most likely due to the acme of certain species, such as *Discoaster tristellifer* and *D. pentaradiatus*, which are warmer water species, and *D. variabilis* and *D. intercalaris*, which are cooler water species. This specific duality may reflect a climatic duality controlled by the ecological complexity of the area.

Reworking occurs throughout the section at Site 574 but is never significant. It is, however, noteworthy in three intervals: (1) in the middle Miocene, the *Coccolithus miopelagicus* Subzone contains abundant *Reticulofenestra hillae* reworked from the Eocene/Oligocene boundary; (2) in the lower middle Miocene, there is a notable number of coccoliths reworked from the Oligocene/Miocene boundary; and (3) there is a constant reworking of Eocene nannofossils in all the Oligocene assemblages.

Table 2. (Continued).

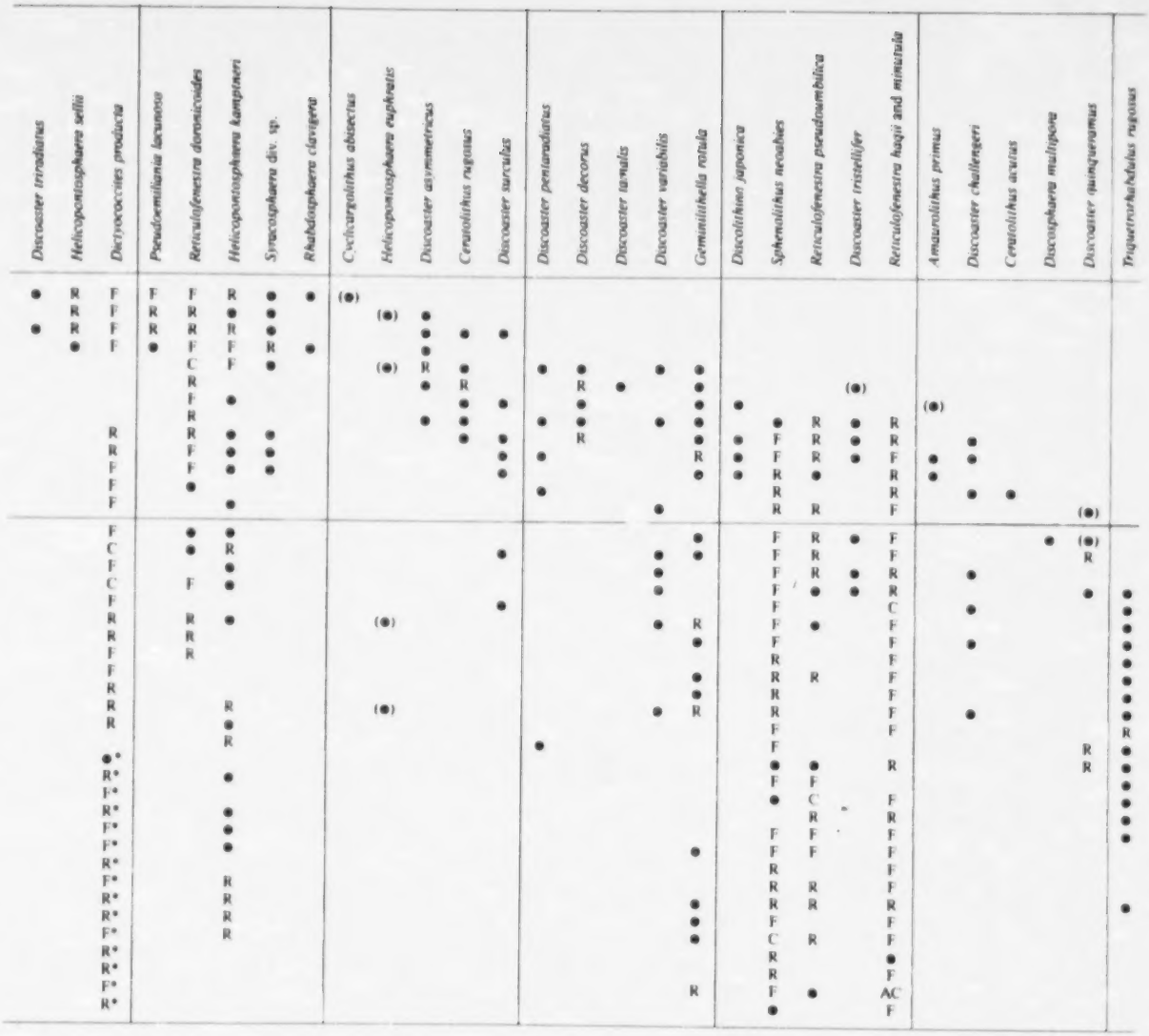

Almost all the zones from the zonation of Bukry (1973a) can be found at Site 574. On the basis of the sedimentation rates, the stratigraphic column can be divided into four parts:

1. From the top of the Pliocene to the section at about 10.6 Ma, the rate is low. Most of the zones are represented by very few samples, and the scarcity of nannofossils and the low specific diversity do not facilitate the biostratigraphy. It is interesting to note the presence of *D. tristellifer*, which Bukry (1981) considers to be a warm water species of the lower Pliocene. At Site 572, it is present in the *Ceratolithus acutus* Subzone and in the *C. rugosus* Subzone, which agrees with Bukry's assignment. But in the *Reticulofenestra pseudoumbilica* zone and in the *D. tamalis* Subzone, some specimens are attributable to *"Catinaster mexicanus"* Bukry. This *"Catinaster"* has a morphology similar to that of the knobbed center of *D. tristellifer*. There could also be some reworked and dissolved specimens of *D. tristellifer* present, so in the present study the two "taxa" are given under the same name.

2. Between about 10.6 and 13 Ma, there is an unconformity corresponding to the lower part of the *D. bellus* Subzone and to the *D. hamatus* Zone. An unconformity corresponding to this interval may also be present at Site 573.

3. Below this unconformity and down to the middle lower Oligocene, the rate of sedimentation appears to have been high, as it was at Site 573 for the same period. In the lower to middle Miocene section, *Sphenolithus moriformis* specimens are usually abundant and are commonly in the form of large sphenoliths, whereas at Site 574 they are rare and most of them are small. *S. heteromorphus* is also very rare in its nominate Zone CN4,

Table 2. (Continued).

Hole-Core-Section	*Discoaster berggrenii*	*Discoaster bollii*	*Amaurolithus delicatus*	*Discoaster intercalaris*	*Cyclococcolithina formosa*	*Discoaster bellus*	*Cyclicargolithus reticulatus*	*Pyrocyclus orangensis*	*Dictyococcites antarctica*	*Discoaster perclarus*	*Discoaster pseudovariabilis*	*Coccolithus miopelagicus*	*Discosphaera* sp.	*Discoaster kugleri*	*Discoaster braarudi*	*Discoaster aulakos*	*Coronocyclus* sp.	*Reticulofenestra hillae*	*Sphenolithus moriformis*	*Helicopontosphaera granulata*	*Discoaster exilis*	*Scyphosphaera* sp.	*Discoaster subsurculus*	*Cyclicargolithus floridanus*	*Sphenolithus heteromorphus*	*Reticulofenestra daviesi*
572A-4-2																										
4-3																										
4-4																										
5-3																										
5-4																										
6-6																										
6-7																										
7-3																										
8-3																										
9-3																										
10-3																										
11-3																										
12-3																										
13-3																										
14-3																										
15-3		(●)																								
16-3																										
17-3																										
572D-1-3	R																									
2-3	●	R																								
3-3		R																								
4-3		R	●																							
5-3																				(●)						
6-2																										
7-3		●		●	(●)																					
10-3				●		F					●															
14-3		●				●	(●)	(●)	R	●	R	(●)														
15-3		●					(R)		R		●	(●)														
16-3		●					(●)	(●)																		
17-2		●											●													
18-3							(●)		F			R														
19-3							(●)		F			R		●												
21-3									F			F		●	●											
23-3									R			R	●	●		●										
24-3									R			R	●				●	(●)	●	●		●		(●)		
26-3								(●)	R			R		●			●			●	●					
27-3									F			R	R						●				●			
29-3							(●)		F			●					●				●			●	F	●
30,CC									R			R				●				R	■			R	F	R
31-3								(●)	R			●				●				R				F	F	F
572D-33,CC									F			F							●	F		●			F	F

while *S. conicus* (which is almost absent at the other sites) is common. In the same interval *Coccolithus pelagicus* is abundant; the presence of this cool water species may explain the absence of warm water sphenoliths.

4. The lowermost Oligocene section below 34 Ma is very thick; it begins with a thin *Coccolithus formosus* Subzone. The deepest sediments at Hole 574C are attributable to the Eocene *Discoaster barbadiensis* Zone according to the presence of poorly preserved *D. saipanensis*, alone or with *D. barbadiensis*. Between the Oligocene and the Eocene sections there are metalliferous sediments. At Site 573, the metalliferous sediments are completely barren of nannofossils. At Site 574, some very rare and poorly preserved specimens of *D. saipanensis* were found at just below the Oligocene boundary (574C-35-5, 5 cm). This observation allowed me to place the Eocene/Oligocene boundary between 504.14 and 504.55 m, in the upper part of the metalliferous sediments. This succession can be schematized as follows:

574C-33-4, 114 cm	No *D. saipanensis*		Subzone CP16b Oligocene
574C-33-5, 5 cm 574C-33-5, 47 cm	Scarce *D. saipanensis*	Metalliferous sediment	Zone CP15? Eocene?
574C-33-5, 65 cm 574C-34-1, 120 cm	No *D. saipanensis*		
574C-34-2, 6 cm 547C-34-2, 60 cm	*D. saipanensis*		Zone CP15 Eocene
574C-34-2, 93 cm 574C-35,CC	*D. saipanensis* and *D. barbadiensis*		

As at Site 573, the Eocene/Oligocene boundary occurs in the barren metalliferous sediment. The succes-

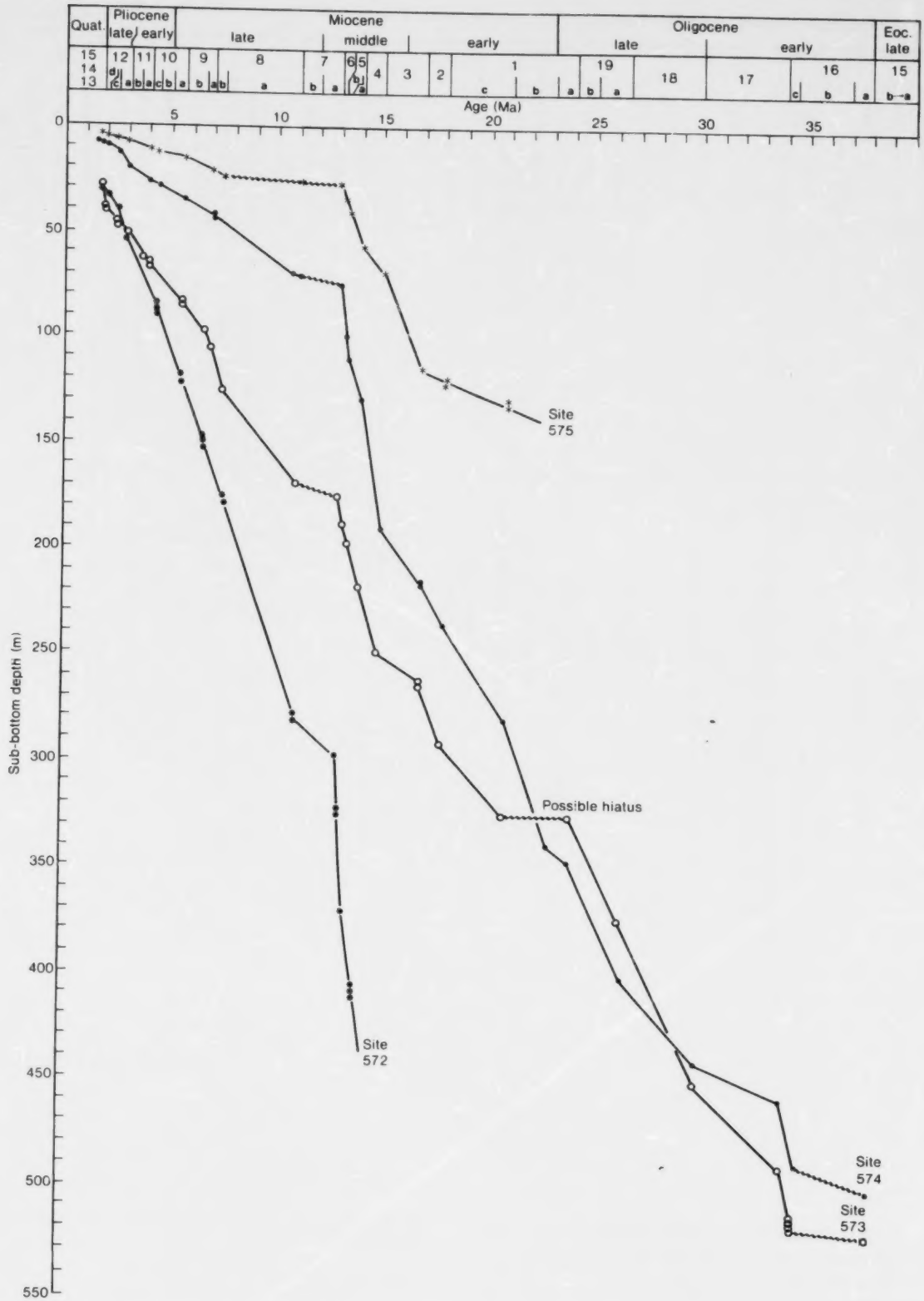

Figure 3. Rate of sedimentation at the four sites using ages estimated from Bukry's zonation (Okada and Bukry, 1980).

Table 3. Occurrence and estimated abundance of nannofossils in selected samples from Site 573. Symbols same as for Table 2.

| Hole-Core-Section | Upper depth of sample (cm) | Sub-bottom depth (m) | Coccolith total abundance | Coccolith dissolution | Discoaster abundance | Zonation (Okada and Bukry, 1980) | Age | *Helicopontosphaera ampliaperta* | *Cruciplacolithus tenuis* | *Sphenolithus heteromorphus* | *Helicopontosphaera ampliaperta* | *Helicopontosphaera kamptneri* | *Helicopontosphaera kamptneri* | *Helicopontosphaera kamptneri

Table 3. (Continued).

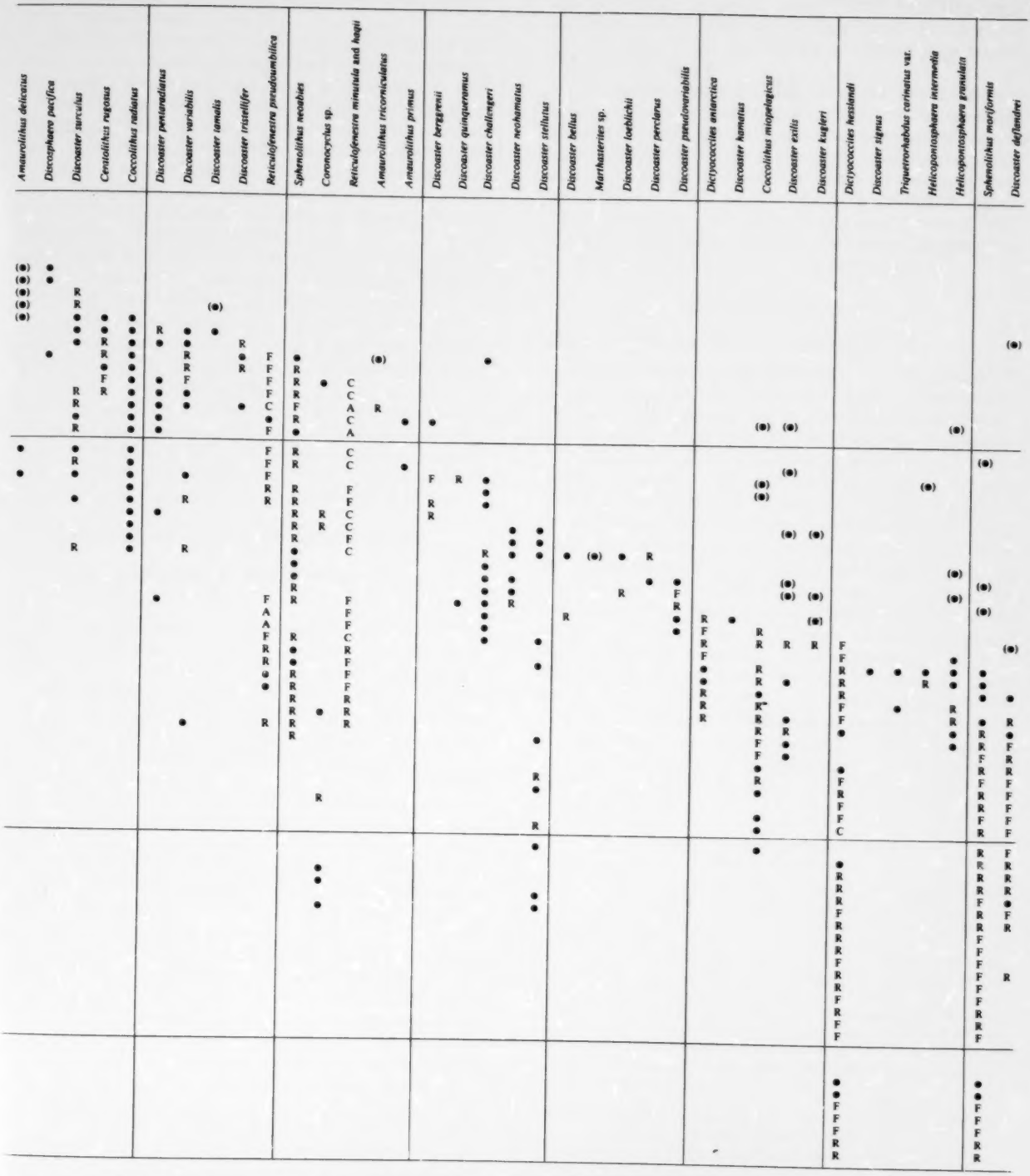

51.00′N, 135°02.16′W; 4536 m sub-bottom) in the vicinity of the Clipperton Fracture Zone. Four holes were drilled; 60 cores were recovered. The basement was not reached. Site 575 presents an almost continuous succession from the lowermost Miocene to the upper Pliocene.

Nannofossils were studied in Holes 575 and 575A. Coccoliths fluctuate in abundance between abundant and rare in the Miocene; they are usually scarce in the Pliocene. The degree of dissolution also fluctuates (from strong to weak) up through lower middle Miocene. In

Table 3. (Continued).

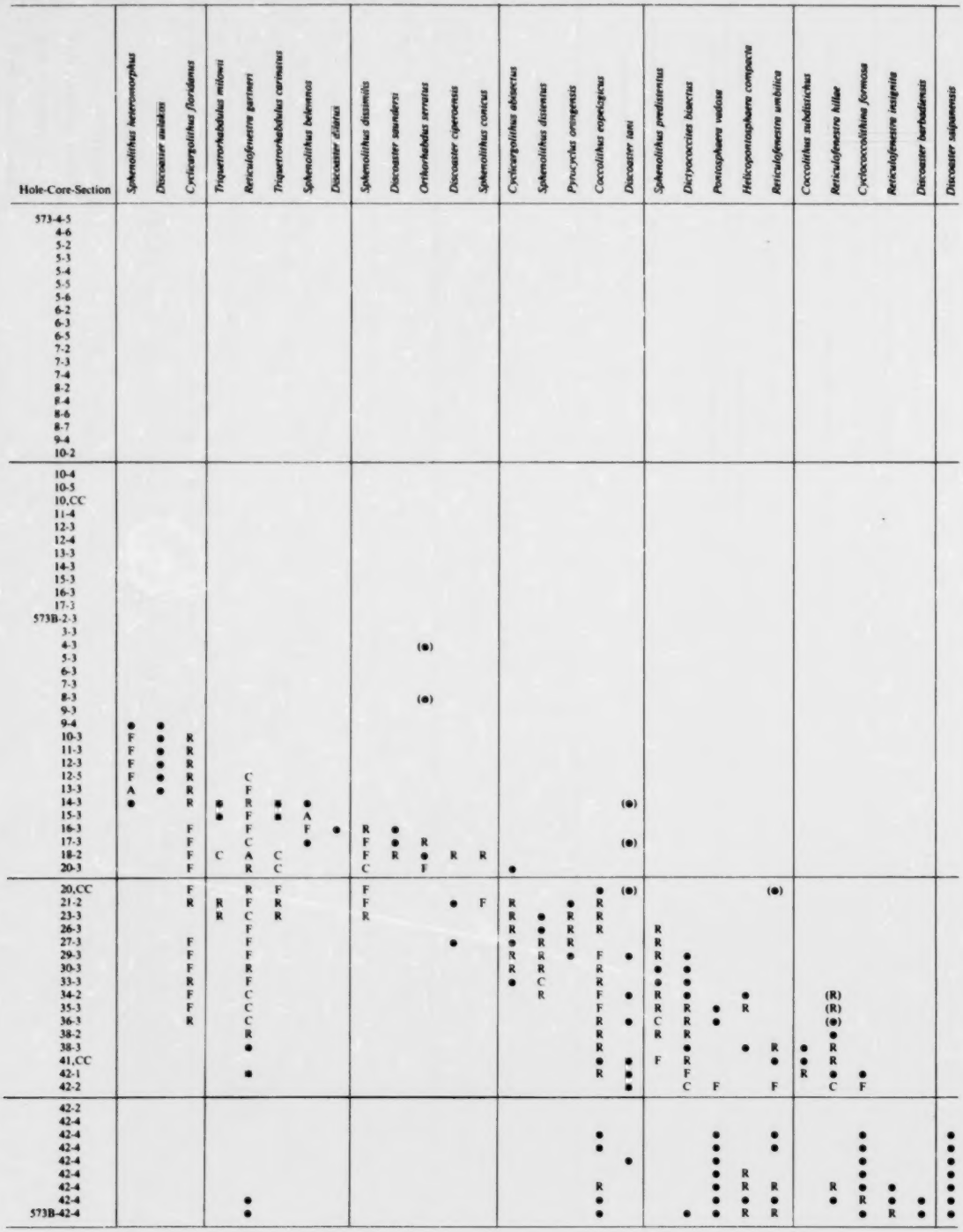

the section representing the past 13 Ma, cycles of dissolution correspond to various environmental changes. Discoasters are usually rare except for some short acme periods: *Discoaster variabilis* at the top of the *Helicopontosphaera ampliaperta* Zone, *D. surculus* in the *Amaurolithus tricorniculatus* Zone, *D. berggrenii* in the *Reticulofenestra pseudoumbilica* Zone, and *D. loeblichii* in the *D. quinqueranus* Zone.

Reworking is significant throughout Site 575; reworked Eocene–Pliocene specimens are mixed with *in situ* as-

semblages at almost all levels. This continuous reworking and the thick sections showing dissolution characterize the sediments at Site 575.

The Plio-Pleistocene boundary occurs within a section in which nannofossils are strongly dissolved (see the Quaternary study by Pujos, this volume), but at 575-1-3, 140–141 cm, the assemblage is characteristic of the *Cyclococcolithus macintyrei* Subzone, which corresponds to the uppermost Pliocene. (1) From the latest Pliocene to middle late Miocene (*D. neohamatus* Zone), the sedimentation rate appears to have been low. From about 7.5 to 13 Ma, there was apparently almost no sedimentation. This interval may correspond to the hiatus found at Sites 573 and 574, but it is even longer here at Site 575 than at the previous two sites. The low sedimentation rate may have resulted from an intensification of the currents in this area, which is evidenced by the extent of reworking at this site. (2) In middle and late early Miocene, the rate of sedimentation apparently increased considerably and was about the same as at the other sites. All the corresponding zones are well represented. (3) In the early Miocene, the rate of sedimentation appears to have dropped to as low as it was in the upper part of the section at this site. The oldest nannofossils recovered here belong to the *D. deflandrei* Subzone.

TAXONOMIC NOTES ON SOME SPECIES

Small- and Medium-Sized *Reticulofenestra* and *Dictyococcites*

Reticulofenestra and *Dictyococcites* are two genera that, according to Hay (1977), belong to the family of Gephyrocapsaceae, along with the genera *Gephyrocapsa, Pseudoemiliania, Emiliania*, and others. *Reticulofenestra* and *Dictyococcites* resemble one another closely. The main difference in the construction of their coccoliths is that *Dictyococcites* has its center spanned by a grid. Its form is that of a completely closed or slitted central area when observed under crossed nicols. In contrast, coccoliths of *Reticulofenestra* have an open central area, which may be spanned by a reticulated grid. Elements of the grid are independent of those of the shields, and between crossed nicols there is usually a dark empty space in the center of the coccolith or a thin structure that is not easy to distinguish.

Thus, the difference between these two genera can be described as being between a "closed" (*Dictyococcites*) and an "open" variety (*Reticulofenestra*). It is the same kind of characteristic that is used to distinguish the closed and open forms of *Gephyrocapsa* from the Quaternary (Pujos, this volume). In fact, it can be considered the same problem: the late Pliocene *Dictyococcites* or *Reticulofenestra* may be the ancestor of *Gephyrocapsa*. For example, it is not easy to separate *R. minuta* from *G. aperta*, especially when the cross-bar of *G. aperta* is dissolved. The problem of *"R." tagana* will be discussed below; its small coccoliths have a cross-bar, usually a characteristic element of the genus *Gephyrocapsa*. *D. producta* is also of the same lineage as *G. producta*. Some closed and very small placoliths were also found at Site 572. Under a light microscope, what looks like a cross-bar appears. These forms look like small specimens of *G. sinuosa*, although their taxonomy is not yet clear; SEM observation is necessary to further clarify the problem.

The largest species of *Dictyococcites* and *Reticulofenestra*, namely *D. bisectus, R. hillae*, and *R. umbilica*, are well documented and are used as stratigraphic markers for the Cenozoic. It is therefore unnecessary to discuss them here. Thus, only the small- and medium-sized specimens of these genera will be described in detail. These species are not well known; Haq (1968 and 1971) and Backman (1980) established distinctions between these small specimens (< 11 to 12 μm in length).

Reticulofenestra Species

Miocene–Pliocene Reticulofenestrids

Miocene–Pliocene reticulofenestrids were studied in detail by Backman (1980); he accurately measured many specimens belonging to five species (*Reticulofenestra gelida, R. haqii, R. minuta, R. minutula*, and *R. pseudoumbilica*), and he used these measurements in various statistical methods. His purpose was to define the relationships and differences between these species more clearly. Backman concluded that it was possible to distinguish the various species by using some simple criteria: the length of the placolith along the long axis, and the relative size of the central opening to the overall size. Other more sophisticated criteria are less useful; for example, he found that the number of elements of the shields varies as a function of the increasing length of the coccoliths, and thus it was not necessary to count these elements. The study of this group is therefore possible only with light microscope observations. Most of the discriminating criteria are drawn in a simplified manner on Plate 1. The appearance of the coccoliths under crossed nicols is shown along with the silhouette (drawn to scale).

Reticulofenestra minuta Roth, 1970
(Plate 1, figs. 1a, b)

This is the smallest species of the group. Its minute size and distribution make it difficult to separate this species from the smallest *Gephyrocapsa* (especially *G. aperta*) of the lower Pleistocene. It appears at Leg 85 sites in the lower upper Miocene in the lower part of Zone CN8a, and it is common up to the very top of the Neogene. Nevertheless, it disappears in Subzone CN10c at Site 574 and is completely absent from Site 575 because of dissolution.

According to Haq (1976) this species is biogeographically important: it dominates nannofossil assemblages in the middle and high latitudes. However, *R. minuta* is often common in the equatorial area. Cita et al. (1978) found it as a dominant taxon in Miocene sediments of the western Mediterranean Sea.

Reticulofenestra minutula (Gartner) Haq and Berggren, 1978, and *R. haqii* Backman, 1978
(Plate 1, figs. 2a, b and 3a, b)

Usually in the literature, these two species are grouped and named together as small *Reticulofenestra pseudoumbilica*. It is true that the two species are very difficult to distinguish from one other. In his biometrical study, Backman (1980) grouped them and concluded that the only difference was the slightly larger central opening of *R. minutula*, which could be an environmental (latitudinal) effect. *R. minutula* and

Table 4. Occurrence and estimated abundance of nannofossils in selected samples from Site 574. Symbols same as for Table 2.

Hole-Core-Section	Upper depth of sample (cm)	Sub-bottom depth (m)	Coccolith total abundance	Coccolith dissolution	Discoaster abundance	Zonation (Okada and Bukry, 1980)	Age	*Dictyococcites productus*	*Cyclococcolithus leptoporus*	*Discoaster brouweri*	*Ceratolithus cristatus*	*Cyclococcolithus macintyrei*	*Coccolithus radiatus*	*Reticulofenestra doronicoides*	*Coccolithus pelagicus*	*Ceratolithus rugosus*	*Discoaster pentaradiatus*	*Discoaster triradiatus*	*Discoaster tamalis*	*Discoaster asymmetricus*	*Reticulofenestra minuta*	*Discoaster surculus*
574-2-3	100	8.50	R	−6	●	12d		●	●	●	●	●	●									
2-4	100	10.00	F	−6	●	12c		●	●	R		R	●	F	R	●	●					
2-5	100	11.50	●	−6	●	12c				●		●		●		●		●				
2-6	100	13.00	F	−6	F	12a	late	●	R	F		R	●	F		R	●					
3-3	27	17.27	F	−6	F	12a				F		R		R		●	●	●	●	R	R	R
3-4	27	18.77	●	−6	●	12a	Pliocene			●		●					●					
3-5	27	20.27	/	−6	●	12a				●												
3-6	27	21.77	●	−6	●	11				●												
4-3	27	26.77	F	−6	F	11			R	F		R					R	●			F	●
4-4	27	28.27	R	−6	F	10c	early	●	●			●						●				
4-5	27	29.77	F	−4	F	10b		R	F			●						R				
5-3	29	36.29	F	−6	R	9b		●	R			●										
6-2	28	44.28	F	−5	F	8		●	●													
7-3	49	55.49	F	−5	F	8	late			●					R			●				
8-3	49	64.49	C	−4	R	8			R	●		●	●		R							
9-1	49	70.99	F	−6	●	7			●	●		●	●									
9-4	49	75.49	F	−6	●	7			●			●	●									
10-4	49	84.49	C	−4	F	6																
11-3	49	92.99	A	−2	R	6																
12-3	49	102.09	C	−3	R	5b						●			R							
12-6	49	106.59	F	−2	●	5b						R			R							
13-4	49	111.99	A	−3	R	5a									F							
14-3	49	121.09	A	−4	●	5a						●			F							
15-3	34	125.94	C	−4	R	5a						●			R							
16-3	34	130.94	C	−1	/	4	middle								F							
17-2	34	134.44	C	−2	●	4																
19-2	34	144.44	C	−1	●	4						●			F							
21-2	34	154.34	A	−3	●	4																
23-2	34	164.34	C	−3	●	4									R							
25-2	34	174.34	C	−4	●	4	Miocene					●			R							
27-2	49	184.19	C	−5	R	4									R							
28,CC		192.27	F	−4	F	4/3																
29-1	49	192.69	C	−2	F	3									F							
31-2	49	204.19	A	−4	F	3																
574C-2-3	49	207.49	F	−3	F	3									F							
3-3	49	216.99	C	−2	F	2									F							
4-3	49	226.49	A	−1	F	2									F							
5-4	49	237.49	F	−3	●	1c									F							
6-2	49	243.99	C	−4	F	1c	early								F							
7-3	49	254.99	A	−1	R	1c									F							
10-2	49	281.99	F	−4	R	1b									F							
12-3	49	302.49	A	−3	R	1b									●							
15-3	49	330.99	F	−3	●	1b									●							
16,CC		341.88	A	−1	F	1a									●							
17-3	49	349.99	C	−1	F	19									F							
18-2	49	357.99	A	−3	F	19	late								●							
19-2	49	367.49	C	−4	R	19									R							
23-2	39	405.39	C	−4	R	18	Oligocene								R							
24-3	41	416.41	A	−4	F	18									F							
27-3	25	444.75	A	−3	R	17									●							
29-2	34	462.34	A	−2	R	16c	early								R							
32-3	49	492.49	C	−4	/	16b									R							
33-4	111	504.11	C	−4	/	16b									R							
33-5	5	504.55	C	−5	●	15?									R							
34-1	60	508.60	F	−4		15?	Eocene								F							
34-2	60	510.10	C	−4	●	15									F							
35-1	13	517.63	F	−5	R	15									R							

R. haqii are grouped together in the present study. They occur at all sites in the interval between lower middle Miocene (lower part of Zone CN4) and lower Pliocene (Zones CN10c or CN11).

Some authors (Roth, 1973; Backman, 1980) place *R. doronicoides* in the synonymy of *R. minutula*, but the two species can be easily distinguished even with a light microscope. *R. doronicoides* is clearly larger and has a less open central area than *R. minutula* and *R. haqii*.

Reticulofenestra doronicoides (Black and Barnes) n. comb. (Plate 1, figs. 7a, b)

Backman (1980) placed the species *doronicoides* in the genus *Dictyococcites*; I do not agree with this assignment because of the open central area of the coccoliths. Roth (1973) combined this species into *Crenalithus*, but as does Backman (1980), I consider *Crenalithus* to be a junior synonym of *Reticulofenestra*.

R. doronicoides is often confused with *R. minutula* (see above), but they can easily be distinguished by comparing their dimensions. *R. doronicoides* is present at all sites of Leg 85 except Site 575. Its absence at the latter site is probably due to strong dissolution. At Site 574 it first appears in Subzone CN12a (middle Pliocene), and at Sites 572 and 573 it starts appearing in Zone CN8 (upper Miocene). When present, this species ranges up into the uppermost Pliocene.

"Reticulofenestra" tagana (Fonseca) n. comb. (Plate 1, figs. 4a, b)

Assigned as a species of *Coccolithus* by Fonseca (1976) in the Atlantic Ocean, this species was renamed as a species of *Crenalithus* by Bukry (1981) in his study of the Pacific coast of Mexico and California. Backman (1980) considers *Crenalithus* to be a junior synonym of *Reticulofenestra*. It is problematic to place this species within the genus *Reticulofenestra*, because *"R." tagana* has a notable cross-bar that is a characteristic feature of the genus *Gephyrocapsa*. This problem is the same as for some other *"Reticulofenestra"* (*R. doronicoides*) and for some *"Dictyococcites"* (*D. producta*).

"R." tagana was found at Site 572 only from the lowest part of the section (Zone CN4) up to the upper Pliocene (Zone CN12); in this in-

Table 4. (Continued).

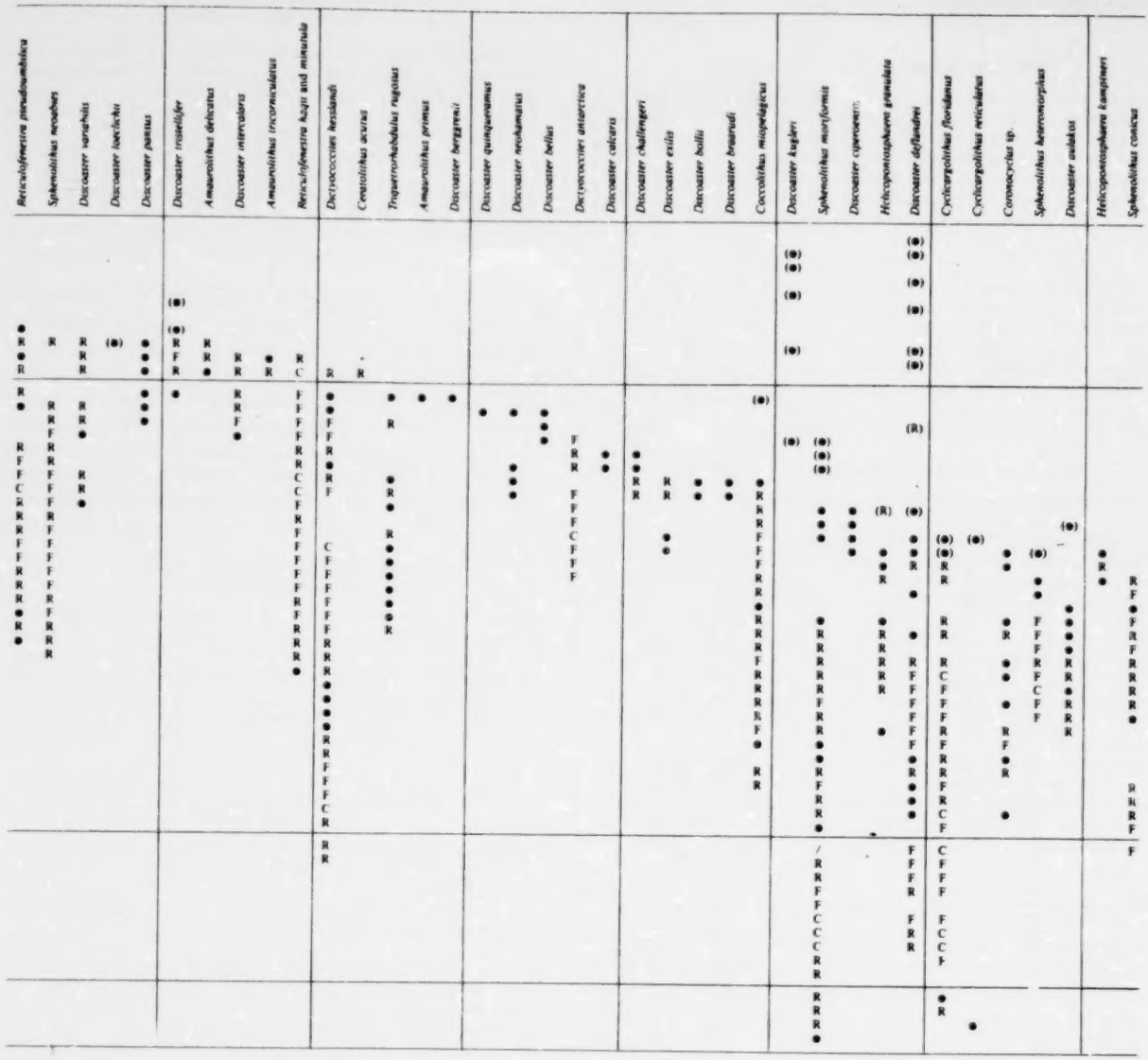

terval it is often abundant. *"R." tagana* has been reported mainly from Portugal and from sediments recovered during Leg 63; in these two areas upwelling is common.

"R. tagana" coexists with abundant small coccoliths having closed central areas and cross-bars. This species can be placed between typical small *Reticulofenestra* and *"R. tagana;"* it is very similar to the small type of the Quaternary *Gephyrocapsa sinuosa*. For Leg 85, the two taxa are put under the same name of *"R." tagana*. A further detailed study might resolve the ambiguity.

Reticulofenestra gelida (Geitzenauer) Backman, 1978, and *Reticulofenestra pseudoumbilica* (Gartner) Gartner, 1969 (Plate 1, figs. 5a, b and 6a, b)

According to Backman, it is not possible to separate these two species by biometry: *Reticulofenestra gelida* could be the winter ecotype of *R. pseudoumbilica*. Lohmann and Carlson (1981) also group these two taxa "to minimize taxonomic problems," and they conclude that together the two taxa could be indicative of cooler waters, especially when they are associated with *Coccolithus pelagicus* (which is usually the case). In the present study, the two species are not distinguished from one other, and the group is named *R. pseudoumbilica*. Abundant at all the sites, they appear in the lower middle Miocene (Zone CN4) and become extinct in the upper lower Pliocene (Zone CN11). This taxon is usually absent between Zones CN8 and CN10b, which is consistent with its usual appearance in tropical and equatorial areas (Bukry, 1972; 1973a,b).

Eocene–Oligocene Reticulofenestrids

Eocene–Oligocene reticulofenestrids were not studied by Backman (1980). In his detailed low-latitude zonation, Bukry (1973a) used *R. gartneri* for a common medium-sized placolith. A larger and a smaller form are

Table 4. (Continued).

Hole-Core-Section	*Triquetrorhabdulus milowii*	*Reticulofenestra gartneri*	*Sphenolithus belemnos*	*Orthorhabdus serratus*	*Sphenolithus dissimilis*	*Triquetrorhabdulus carinatus*	*Cyclicargolithus ?abisectus*	*Helicopontosphaera euphratis*	*Reticulofenestra daviesi*	*Discoaster lodoensis*	*Coccolithus eopelagicus*	*Pyrocyclus orangensis*	*Reticulofenestra insignita*	*Sphenolithus distentus*	*Sphenolithus cyperoensis*	*Dictyococcites bisectus*	*Helicopontosphaera intermedia*	*Chiasmolithus altus*	*Sphenolithus predistentus*	*Helicopontosphaera compacta*	*Reticulofenestra hillae*	*Reticulofenestra umbilica*	*Ponsaltzara vaticus*	*Cyclococcolithina formosa*	*Braarudosphaera serraculoides*	*Discoaster gemmifer*	*Ellipsolithus subdisticha*	*Discoaster saipanensis*	*Discoaster barbadiensis*	*Discoaster tani*
574-2-3																														
2-4																														
2-5																														
2-6																														
3-3																														
3-4																														
3-5																														
3-6																														
4-3																														
4-4																														
4-5																														
5-3																														
6-2																														
7-3																														
8-3																														
9-1																														
9-4																														
10-4																					(●)									
11-3																														
12-3																														
12-6																														
13-4																														
14-3	(●)																				(R)									
15-3	(R)																				(R)									
16-3	(R)																													
17-2	(●)								R																					
19-2									R																					
21-2				(●)					F																					
23-2	(●)							(●)	R																					
25-2									F																					
27-2									●																					
28,CC									●																					
29-1	●	F							●																					
31-2	●	F																												
574C-2-3	●	F																												
3-3	R	F	R																											
4-3	R	C	F					(●)																						
5-4	●	F		●	●	●	●		●	●																				
6-2	R	F		R	F	●	R	●	F	F																				
7-3	R	C		R	F	F	R		●	R																				
10-2		F			F	R	R	●		R																				
12-3	R	R			F	R			F	R	●																			
15-3		R		●	●	R			F	●	●																			(●)
16,CC		C			F	C	R			●	●					(●)														
17-3		C			R	F	●		R		R		R																	
18-2		A				R	R		F		●		F	R	R	R	R													
19-2		F				R	R		R		R	●	R	●	R	R		●												
23-2		R					R		R		●	●	R	●		R			R											(●)
24-3		F					R		R		R	●	R	●		R			F											
27-3		F							R		R	●	R			●			R											
29-2									C		●	●	R			●			R			●	●	(●)						
32-3									F		R	R	●			R			R		R	●	R	R	R	(●)	●			
33-4									F		●	R	●			F			R		R	R	R	R			R			
33-5									●		●	●	●			R			●		●	●		●	●		●	●		
34-1									●		R	R	●			F			R		R	●		R	R		●	R		
34-2									F		●	R	R			R		●			R	●		R			R	●		
35-1											R	R	F			R		●			R	R		R	●		●	R	●	R

observed in the Paleogene sediments at Leg 85 and are identified as *R. daviesi* and *R. insignita*, respectively.

Reticulofenestra insignita Roth and Hay, 1967 (Plate 1, figs. 8a, b)

This small species was found for the first time in the *Reticulofenestra laevis* Zone of the Blake Plateau. Some dissolved specimens are present between Zones CP15 and CP19 at Site 574 and only in the uppermost Eocene sediments (Zone CP15b) at Site 573.

Reticulofenestra gartneri Roth and Hay, 1967 (Plate 1, figs. 9a, b)

This marker species has been found at low latitudes by Bukry (1973a) and on Leg 85 between the middle Oligocene (Zones CP17 or CP18) and the upper lower Miocene (Zones CN2 or CN3). It is present only in Subzone CN1c at Site 575, which may be due to some special environment. Because of its morphology and distribution, *R. gartneri* may be considered a possible ancestor of *R. pseudoumbilica*.

Reticulofenestra daviesi (Haq) Haq, 1971 (Plate 1, figs. 10a, b)

This species was combined into *Dictyococcites* by Perch-Nielsen (1971); Haq (1971) transferred it to *Reticulofenestra*. But it is obvious that there is an ambiguity in its generic attribution, which may be why I confused it with *D. hesslandi* (see below). *R. daviesi* is present at the Eocene/Oligocene boundary (Zones CP15/CP16), and it persists perhaps up into the lower Miocene.

Dictyococcites Species

Miocene–Pliocene Dictyococcites *Species*

The only *Dictyococcites* found in the upper Miocene to Pliocene is *D. producta*.

Dictyococcites producta (Kamptner) Backman, 1980 (Plate 1, figs. 13a, b)

The problem of the generic attribution of the species *producta* was explained above. It is obvious that the same species is present in the Cenozoic and Quaternary. But in the Neogene specimens, the crossbar (which is common in the Pleistocene forms) seems to be absent. Therefore, it is necessary to use the generic name *Dictyococcites*. This taxonomic problem will be described in detail in a future study of the Neogene and lower Pleistocene assemblages.

D. producta is the smallest *Dictyococcites* described for Leg 85. Its placoliths are always smaller than 4.5 μm in length. As is true for *R. doronicoides*, *D. producta* is absent from Site 575. It appears in Zone CN8 and persists up to the Quaternary at other sites.

Oligocene–Miocene Dictyococcites *Species*

The Oligocene–Miocene *Dictyococcites* are represented by the *D. antarctica–hesslandi* complex. Backman (1980) notes that there is a gradation in the measured parameters of the placoliths of these two species from Miocene to Pliocene; thus, it could be difficult to separate them. Nevertheless, a characteristic extinction figure, a notable difference in size, and a different distribution usually make their distinction easy (see Plate 1 and discussion below).

Dictyococcites antarctica Haq, 1976 (Plate 1, figs. 12a, b)

D. antarctica may be the ancestor of *D. producta*. Backman (1980) showed the continuous evolution from *D. antarctica* (medium-sized placoliths of the middle lower Miocene) to *D. producta* (small-sized placoliths of the Pliocene). As for *R. minutula–haqii*, the distinction from *D. hesslandi* is easy (see Plate 1): placoliths of *D. antarctica* are longer than 4 μm. It is present between Zones CN3/4 and CN8 (middle Miocene) at all Leg 85 sites except Site 575, where it was not found.

Dictyococcites hesslandi (Haq) Haq and Lohmann, 1976 (Plate 1, figs. 11a, b)

Dictyococcites hesslandi is the senior synonym of *D. scrippsae* Bukry, which is a marker species at low latitudes (Bukry, 1973a). According to Backman (1980), it is possible to follow the evolution of this taxon through the Miocene using the length of its placoliths: 3 to 5 μm long in lower Miocene sections and 3 to 8 μm long in upper lower Miocene.

This morphologic instability and severe dissolution at some sites may explain why it was not possible to separate *D. hesslandi* from *R. daviesi*. It seems wiser to group these two taxa together to avoid stratigraphic problems. *D. hesslandi* and *R. daviesi* are already present at the Eocene/Oligocene boundary (Zones CP15 or CP16) and persist up through lower middle Miocene (Zones CN4/5). At Site 574, there are some morphologic variations within the *D. hesslandi–daviesi* group: open coccoliths (*R. daviesi* ?) are predominant from Zone CP15 to CN1c, and closed coccoliths (*D. hesslandi* ?) are found from the upper part of Zone CP19 to Subzone CN10b. This observation, however, is tentative because of the influence of dissolution, which can remove the central area of the placoliths and transform a closed *Dictyococcites* into a form that resembles an open *Reticulofenestra*.

Medium-Sized Five-Rayed Discoasters

The group of five-rayed discoasters discussed here is restricted to a period younger than middle Miocene. Of course, prior to that time some five-rayed discoasters occurred, and some of them are marker species, such as *D. hamatus*, a large umbrella-like discoaster restricted to Zone CN7. Five species of *Discoaster* found in lower upper Miocene sediment are exclusively five-rayed. They succeed one another, and their distinction is not always easy. It is therefore necessary to document their morphologic differences and their stratigraphic ranges (Bukry, 1973a).

Discoaster pentaradiatus Tan Sin Hok, 1927

This is the largest species of the group (usually about 15 to 20 μm long). It is characterized by a sharp bifurcation at the end of each ray and by each ray being a crystal of calcite. The discoaster is composed of five distinct crystals that do not become extinguished at the same time under crossed nichols, whereas most of the other discoasters are made of a single crystal. *D. pentaradiatus* is rare in Zone CN8a, and it is present between Subzones CN8b and CN12c.

Discoaster asymmetricus Gartner, 1969

This slender discoaster is characterized by unequal angles between some of its rays. In spite of this distinctive character, it can be confused with *D. bellus*. Bukry (1973a) reports that in his Zone CN8a, the first rare specimens of *D. asymmetricus* are perhaps variants of *D. bellus*, which then disappear in the next Zone (CN8b). Thus Bukry thinks that *D. bellus* could perhaps be the ancestor of *D. asymmetricus*. *D. asymmetricus* is 12 to 15 μm in length, and it occurs from Zone CN8a to CN12d, being abundant in Zones CN11b and CN12a.

Discoaster bellus–quinqueramus–berggrenii Group

These species are very similar, and they can occur in the same samples.

D. bellus Bukry and Percival, 1971, occurs from Zone CN6 to CN8b. It is small to medium in size (6 to 11 μm long). Rays are almost blunt and they are strong and slightly bulging. The central area has no distinctive structure. The species may be the ancestor of *D. asymmetricus* and *D. quinqueramus*.

D. quinqueramus Gartner, 1969, has a restricted occurrence, from Zone CN8b to CN9b. *D. quintanus* is a junior synonym. Its length is about 10 μm. It is close to *D. bellus*, but it has a small, rough knob in the central area. Its rays are strong at their base and sharp at their ends, with straight edges, and inter-rays are usually angular.

D. berggrenii Bukry, 1971, has the same occurrence as *D. quinqueramus* and becomes very abundant in some samples of Zone CN9a. Such erratic occurrence may reflect some special localized environment. It is a small species (no more than 10 μm long) with short, blunt rays. The center is often large, sometimes appearing as a rough pentagonal plate with a big knob, and the inter-rays are so large that they seem to be bi-angular.

TENTATIVE ECOLOGICAL INTERPRETATION

Nannofossils are planktonic organisms and should be considered good indicators of climatic and hydrologic changes. Some authors have tried to understand fluctuations in recent and living nannoplankton ecologically (Geitzenauer et al., 1977; Okada et al., 1977; Lohmann et al., 1981; Roth et al., 1982). The results are often disappointing, because quantitative relations could not be observed between species abundance and common parameters, such as surface temperature and salinity, in the same way as they can be for planktonic foraminifers. As a consequence, their usefulness for precise Cenozoic ecological interpretation is *a priori* questionable.

Nevertheless, nannofossil assemblages in Pacific oceanic sediments can be used for global estimates of environment. Dissolution and total abundance of coccoliths can reflect hydrology and climate, especially in the high-productivity areas. Bukry (in his various DSDP papers, particularly those for Leg 63, 1981) used the following nannofossil criteria for ecological interpretation: *Discoaster/Coccolithus* ratio (which cannot be used for Leg 85 because of the scarcity of discoasters); the presence of some warm water or cool water discoasters; and the abundance of *Coccolithus pelagicus* and *Cyclococco-*

Table 5. Occurrence and estimated abundance of nannofossils in selected samples from Site 575. Symbols same as for Table 2.

Hole-Core-Section	Upper depth of sample (cm)	Sub-bottom depth (m)	Coccolith total abundance	Coccolith dissolution	Discoaster abundance	Zonation (Okada and Bukry, 1980)	Age	*Discoaster berggrenii*	*Cyclococcolithina macintyrei*	*Cyclococcolithina leptopora*	*Discoaster intercalaris*	*Ceratolithus cristatus*	*Coccolithus pelagicus*	*Discoaster tani*	*Ceratolithus rugosus*	*Discoaster pentaradiatus*	*Discoaster crassus*	*Cyclococcolithus formosus*	*Cyclicargolithus floridanus*	*Discoaster tuculus*	*Discoaster asymmetricus*	*Discoaster variabilis*
575-1-3	140	4.50	F	−4	R	12d		R	R	R	•	R	•	(•)	•	•	•	(•)				
1-4	60	5.10	C	−3	F	12d		F	F	F		•	R		•		•		(•)	(•)		
1-4	140	5.90	F	−3	F	12c		F	F	F		•	R		•		•					
1-5	60	6.60	•	−5	F	12c	late	F	•			•					•					
1,CC		7.27	•	−6	R	12a		F	•		•						•			•	•	•
2-1	35	7.65	F	−1	C	12a		•	•	•	•									•		
2-1	115	8.45	F	−3	R	11		•		F	•		•		•		•		(•)	F	•	R
2-2	35	9.15	R	−5	F	11			•	•			•			•	•			R		R
2-2	115	9.95	F	−3	F	11			•				•	(•)		•	•					R
2-3	35	10.65	C	−4	F	11	Pliocene	•	•		R		R							•	•	
2-3	115	11.45	F	−3	F	11		•	R				•			•				R		
2-4	35	12.15	F	−2	C	10c		•	R		•										•	
2-4	115	12.95	F	−2	C	10b	early	F	•				•	(•)		•	•			F		
2-5	35	13.65	F	−4	C	10b		F	R				R			•	•			R		R
2-5	115	14.45	F	−4	F	10b		R	•				•			•				R		
2-6	35	15.15	A	−5	F	10b		F	F				F							R		•
2-6	115	15.95	A	−5	F	10b		R	F				F				•			R		•
3-1	35	17.15	A	−5	F	10b		R	F				F				•					
3-2	35	18.65	F	−5	C	9		•	R				R							•		•
3-3	35	20.15	C	−4	R	9		R	R				R							•		
3-4	35	21.65	C	−3	F	9		F	R				R							•		R
3-5	35	23.15	F	−2	C	8b	late	R	R				F	(•)						•		R
3-6	35	24.65	F	−3	C	8b		R	F				F	(•)						•		F
4-1	28	26.58	A	−5	F	8a		R	R				R			R		(•)		•		R
4-2	35	28.15	F	−6	F	7			•				•									R
4-3	35	29.65	F	−5	R	6			•				•									
4-4	35	31.15	C	−4	/	6			•				•									
4-5	35	32.65	A	−1	/	6			•				•									
4-6	35	34.15	F	−4	•	6			•				•									
5-1	35	35.35	A	−2	R	5b			•				•									
5-2	35	36.85	F	−3	•	5b			•				•									•
5-3	35	38.35	F	−4	•	5b			•				R									
5-4	35	39.85	C	/	•	5b			•				R	(•)								
5-5	35	41.35	C	−4	•	5b			R				R									
5-6	35	42.85	F	−2	R	5a			•				R									
5-7	35	44.35	C	−1	•	5a			R				R									
6-1	35	44.85	C	−1	•	5a			•				R									
6-2	35	46.35	F	−2	•	5a			•				R									
6-3	35	47.85	C	−1	/	5a			R				R									
6-4	35	49.85	A	/	•	5a							R									
6-5	35	50.85	C	/	/	5a							R									
6-6	35	52.35	C	−1	•	5a							•									
7-1	35	54.35	A	−3	•	5a							•									
7-2	35	55.85	A	−3	•	5a			•				R	(•)					(•)			
7-3	35	57.35	C	−4	•	5a							R									
7-4	35	58.85	C	−3	R	5a							•									
7-5	35	60.35	A	−4	•	5a							•									
7-6	35	61.85	A	−4	•	5a							•									
8-1	35	63.85	C	−2	•	5a							F									•
8-2	35	65.35	C	−2	•	5a							F						R			•
8-3	35	66.85	C	−2	•	5a	middle						F						•			
8-4	35	68.35	F	−2	•	4							F						R			
8-5	35	69.85	C	−3	•	4			•				R						•			
8-6	35	71.35	C	−1	R	4							R	(•)					R			
9-2	35	74.85	F	−4	R	4							R						R			
9-4	35	77.85	A	−3	F	4							R						R			
10-2	35	82.05	C	/	F	3							R						R			•
10-4	35	85.05	A	−2	C	3			•				R						F			R
10-6	35	88.05	F	−3	•	3							F						C			F
11-2	35	90.95	A	−1	R	3							•						R			•
11-4	35	93.95	F	/	•	3							F						F			R
11-6	35	96.95	C	/	•	3	Miocene						R						R			•
575A-1-1	51	94.31	F	−4	R	3							•						R			•
1-3	51	97.31	F	−4	R	3							•						R			•
2-2	51	99.21	A	−3	•	3							•						R			•
3-2	51	103.11	C	−3	R	3							•						R			•
4-2	51	107.21	F	−4	R	3							•	(•)					R			•
5-2	51	111.01	F	−2	R	3							•						R			•
6-2	51	116.11	C	/	F	2							•						R			•
7-2	51	120.41	C	−4	F	2							F						R			R
8-2	51	125.11	C	−1	•	1c							F						R			R
9-2	51	127.31	A	−4	•	1c							F						F			•
10-2	51	129.31	A	−5	F	1c							F						F			•
11-2	5	132.15	F	−3	R	1c							F									•
12-2	5	136.65	C	−4	R	1c							R									
13-2	5	140.35	C	−4	R	1c							•									
14-2	5	143.45	F	−5	•	1b	early												•			
16,CC		151.88	C	−3	F	1b							R						•			
18,CC		156.93	F	−2	R	1b							•						F			
20,CC		164.65	C	−1	F	1b													F			
22,CC		172.34	A	−3	R	1b													R			
23,CC		174.91	C	−2	F	1b							R						F			
25,CC		181.96	F	−3	•	1b							•						F			
26,CC		184.80	A	−4	R	1b							•						F			
28,CC		190.50	C	−5	R	1b							R						F			
29,CC		193.69	F	−4	•	1b							•						F			
575A-32,CC		205.13	F	−4	•	1b							•						R			

Table 5. (Continued).

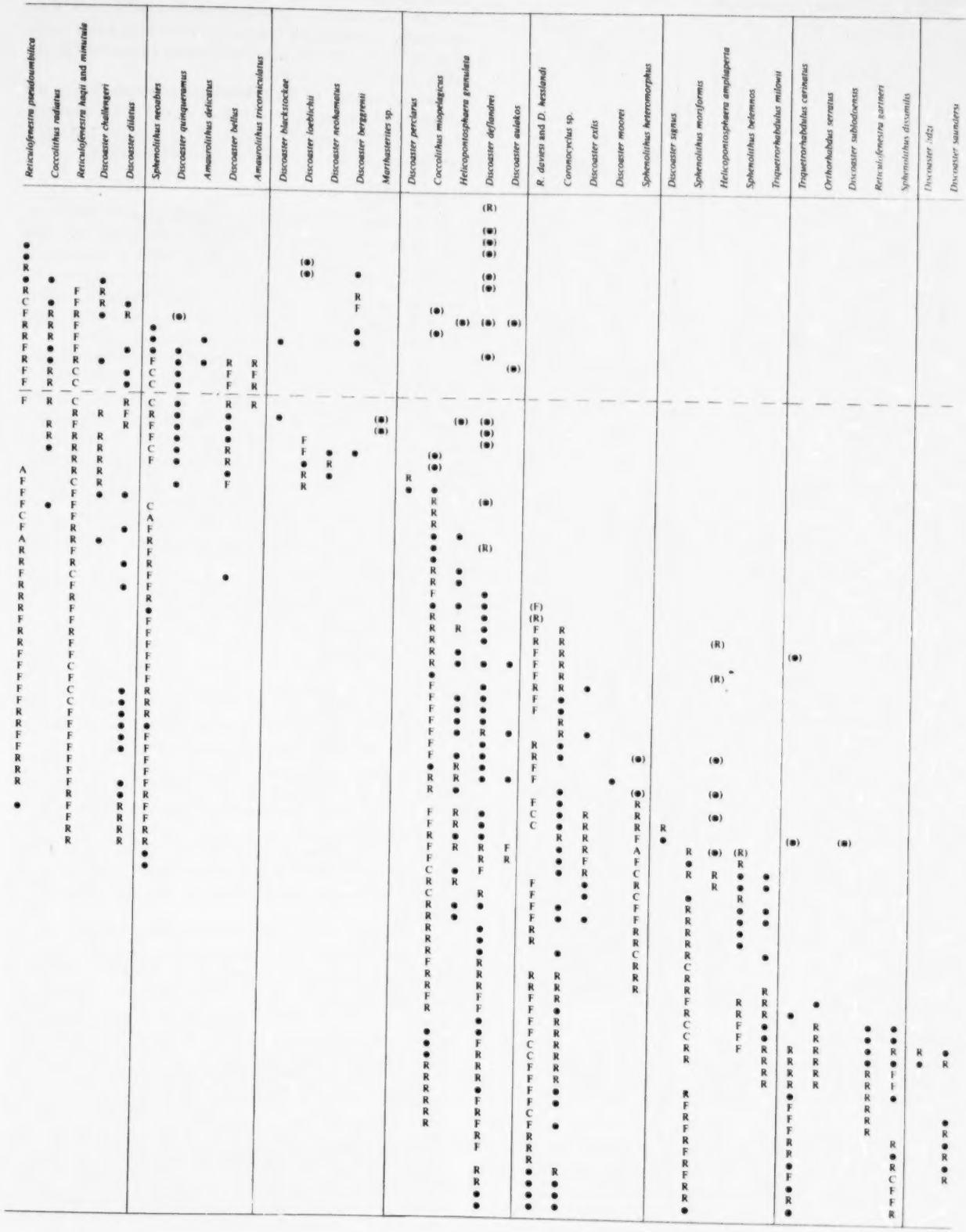

Table 5. (Continued).

Hole-Core-Section	*Cyclicargolithus abiscatus*	*Helicopontosphaera intermedia*	*Pyrocyclus orangensis*	*Coccolithus* aff. *fenestratus*
575-1-3				
1-4				
1-4				
1-5				
1,CC				
2-1				
2-1				
2-2				
2-2				
2-3				
2-3				
2-4				
2-4				
2-5				
2-5				
2-6				
2-6				
3-1				
3-2				
3-3				
3-4				
3-5				
3-6				
4-1				
4-2				
4-3				
4-4				
4-5				
4-6				
5-1				
5-2				
5-3				
5-4				
5-5				
5-6				
5-7				
6-1				
6-2				
6-3				
6-4				
6-5				
6-6				
7-1				
7-2				
7-3				
7-4	(●)			
7-5				
7-6				
8-1				
8-2	(●)			
8-3	(●)			
8-4				
8-5	(●)			
8-6	(●)			
9-2				
9-4				
10-2	(R)			
10-4				
10-6				
11-2	(●)			
11-4				
11-6				
575A-1-1	(●)			
1-3	(●)			
2-2	(R)			
3-2				
4-2	(●)			
5-2	(●)			
6-2				
7-2				
8-2	(R)			
9-2	(R)			
10-2	(R)			
11-2				
12-2	(R)			
13-2	(R)			
14-2	R	●		
16,CC	R			
18,CC	R	●		
20,CC	R			
22,CC	●		●	
23,CC	R		●	
25,CC	●			
26,CC	R			
28,CC	R	R		●
29,CC	●	●		R
575A-32,CC	●	●		●

iithina div. sp. (which are both solution resistant, *Cyclococcolithina* more so than *Coccolithus pelagicus*). Furthermore, *C. pelagicus* is usually taken as a good index of cool water, even in pre-Quaternary sediments (Lohmann and Carlson, 1981).

Various aspects of the occurrence of nannofossils are presented in Figure 4, which also shows some geologic features such as unconformities or periods of low sedimentation rate and periods of equator crossing.

Stratigraphic Unconformities

Detailed descriptions of hiatuses or periods of reduced sedimentation are presented in Barron et al. (this volume). These intervals were recognized as changes in sedimentation rate (Fig. 2). Two of these changes were observed at Sites 573 and 574 (Eocene/Oligocene boundary and Oligocene/Miocene boundary), and another (middle upper Miocene) was recognized at four sites.

1. The Eocene/Oligocene boundary represents a time of global climatic cooling (Kennett et al., 1975) and is the beginning of modern climate. A world-wide Oligocene unconformity at the Eocene/Oligocene boundary was apparently caused by the increase in bottom water circulation at the onset of Antarctic glaciation. This bottom water was formed by the sinking of cold, dense surface water in Antarctic coastal regions; its temperature is estimated to have been 0 to 3°C (Woodruff et al., 1981; Keigwin and Keller, in press; Miller and Thomas, this volume).

A hiatus corresponding to a few meters of barren metalliferous sediment occurs at Sites 573 and 574 at the Eocene/Oligocene boundary. Most of the upper Eocene is present, and the hiatus seems to have begun in the latest Eocene at about 38–38.5 Ma. The oldest Oligocene nannofossil assemblages correspond to the upper part of Subzone CP16b at about 34.5 Ma. This hiatus is thus attributed to the beginning of the Antarctic glaciation.

2. At the Oligocene/Miocene boundary at Site 573 there is a hiatus representing a time period from 24 to 21 Ma. The phenomenon is less significant at Site 574 where there is only a decrease in the sedimentation rate (and not a true hiatus) of much shorter duration (between 24 and 23 Ma). Thus, the beginning of the period of slow sedimentation is synchronous at both sites, but the phenomenon lasted longer at Site 573 than at Site 574.

This hiatus is a widespread phenomenon in the Pacific (Keller and Barron, 1982) and also at many places in the Southern Ocean. Kennett et al. (1975) assume that the opening of the deep Drake Passage occurred between 25 and 22 Ma. This event may have resulted in major climatic changes, which, in turn, may have caused the Oligocene/Miocene hiatus.

3. The third hiatus occurred in the middle–early late Miocene. According to Kennett et al. (1975), a major ice sheet developed on East Antarctica during this period (10 to 13 Ma). Woodruff et al. (1981) analyzed isotopic fluctuations of benthic foraminifers of the Miocene of the Ontong Java Plateau area. They concluded that during the early Miocene, polar glaciation was limited and deep water was warmer than it is today. Keller and Bar-

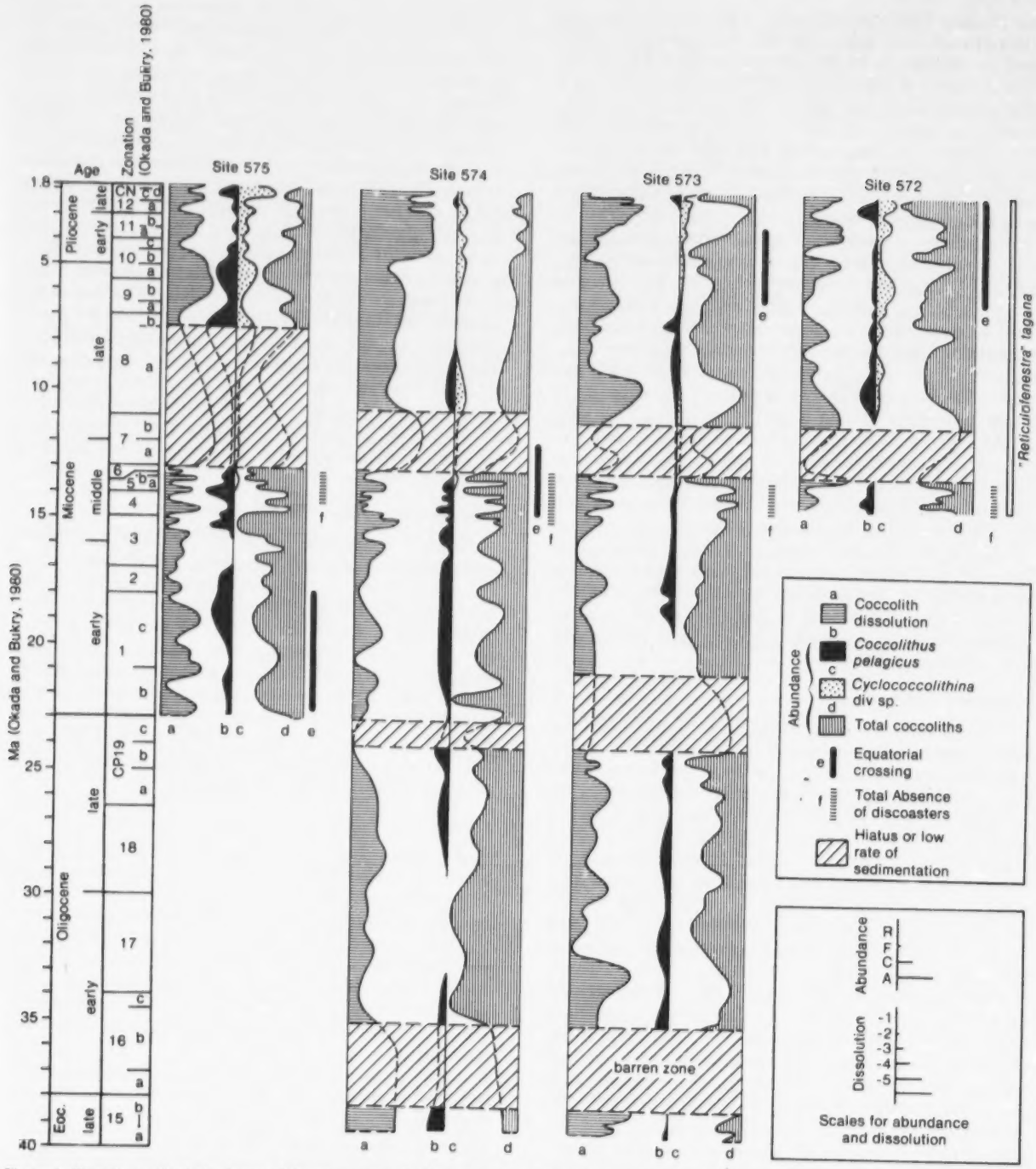

Figure 4. Tentative ecological scheme of the sequence at the four sites. The ecology is based on the following criteria: (a) the amount of coccolith dissolution, which is based on the nannofossil index of solution (see footnote to Table 2); (b) abundance of *Coccolithus pelagicus*; (c) abundance of *Cyclococcolithina* div. sp.; (d) total abundance of nannofossils (see footnote to Table 2); (e) times of equatorial crossings; and (f) total absence of discoasters.

ron (1982) argue that at the same time, there was an increase in the water mass stratification, which could strongly influence nannofossil distributions. In most of the lower Miocene cores of Leg 85, nannofossils are abundant and are not affected much by dissolution. This observation seems to suggest a strong productivity without the existence of corrosive deep water.

The most important climatic change occurred in the middle Miocene between 16.5 and 13 Ma, which was "a transition from a relatively unglaciated world to one sim-

ilar to today" (Woodruff et al., 1981). At this time, the Antarctic ice sheet was expanding and caused changes in oceanic circulation (Woodruff et al., 1981). This evolution occurred in three steps. (1) Between 16.5 and 14.8 Ma, equatorial surface waters were warmer; nannofossils were abundant and dissolution was restricted at Sites 573 and 575. (2) Woodruff et al. (1981) think that between 14.8 and 14.0 Ma, the Earth's climatic system became extremely unstable, oscillating between glacial and interglacial periods. Nannofossils recorded these climatic fluctuations at each site of Leg 85, especially discoasters, which disappeared almost completely during this period. Discoasters seem not to be able to withstand strong and rapid climatic variation caused by advances of glaciation. The same environmental change may have caused the definitive disappearance of this group in the early Pliocene. (3) After 14 Ma, the trend of glaciation was definitively established; this period corresponds to an unconformity and/or a period of a very low sedimentation rate at the Leg 85 sites. At Sites 572 and 573, the hiatus occurred between 13 and 11 Ma, whereas at Sites 574 and 575 it took place at 10.5 Ma and 13 to 7.5 Ma, respectively. Like the Oligocene/Miocene hiatus, the arrival of Antarctic deep water was synchronous (13 Ma) at all the sites, although it ended later toward the western direction. This can be interpreted either as an influence of the Antarctic Bottom Water (AABW) lasting longer in the area of Site 575, or as a consequence of another phenomenon, such as an erosive current, at about 7.5 Ma.

Equator Crossing

It has been well documented that new crust generated at the East Pacific Rise moved from southeast to northwest (van Andel et al., 1975). All the Leg 85 sites crossed the equator during the Cenozoic at various times depending on their location (see site chapters, this volume): Site 572 from ~6 to 2 Ma; Site 573 from ~6 to 3.2 Ma; Site 574 from ~14.6 to 13 Ma; and Site 575 from ~22.8 to 18 Ma. The equatorial area of the middle and eastern Pacific Ocean is one of the most productive regions in the world because of the presence of warm water masses at the surface and diverging and converging subsurface currents.

Nannofossils observed in the Leg 85 cores seem to have been affected by this crossing of the equator. At each site, this event is marked by very high total abundance and fluctuating dissolution that indicates very high productivity. In this area of the Pacific, that very high productivity causes strong calcite dissolution due to the sinking of too much organic matter, which in turn creates corrosive bottom water due to oxidation of organic matter to CO_2. Calcite skeletons tend to be dissolved. At these sites, nannofossil productivity is so high that, even with strong dissolution, many coccoliths remain in the sediment, although they become barely recognizable. This solution affects all nannofossils, even the most resistant ones such as *Coccolithus pelagicus*.

Upwelling at Site 572

Upwelling occurs often in high-productivity areas and is caused by the complex current system at the surface of the ocean. It is especially dominant in the eastern part of the area, where presently the Peru Current (in the southern part) and the California Current (in the northern part) are known to cause upwelling. Site 572 is located near the northeastern edge of the area in the vicinity of the Peru Current. Nannofossils are abundant during many time intervals at this site. Assemblages are strongly dominated by very small ellipsoidal placoliths that can be interpreted as being (1) indicative of cooler waters that are brought to the surface as upwelling waters and (2) characteristic of very strong upwelling, because most of these coccoliths are *"Reticulofenestra" tagana* and related forms. The species *tagana* was found in the Miocene of Portugal by Fonseca (1976) and in the Cenozoic off California by Bukry (1981). These two places are characterized by an almost permanent upwelling. Hence, the continuous presence of *"R." tagana* at Site 572 has been interpreted as the result of a permanent presence of upwelling waters in this area, at least since 14.5 Ma. *"R." tagana* was not found at the other sites of Leg 85, where upwelling was probably less frequent or nonexistent.

Bottom Currents at Site 575

Site 575 is characterized by several dissolution cycles and evidence of constant reworking. Furthermore, some marker reticulofenestrids are completely absent at this site; this absence is attributed to strong dissolution, rather than to ecological factors. These three phenomena (dissolution, reworking, and scarcity of reticulofenestrids) could be due to strong bottom currents of corrosive water that can rework nannofossils. It is well known that the Antarctic Bottom Water today flows over the area of present-day Site 575 (Wirrmann, 1980); it is likely that it has influenced the distribution of nannofossils at this site since early Miocene.

Conclusions

As explained at the beginning of this section, attempting to use nannofossils as ecological indicators can be disappointing. It was not possible to use them for temperature interpretation because (1) most of the cool water or warm water taxa used for such a purpose are solution prone, or else they are species of *Discoaster*, a group that is often scarce at Leg 85 sites; and (2) most of the published ecological studies deal only with the Neogene, which makes the interpretation of older assemblages difficult.

Nevertheless, nannofossils give us interesting information on the progression of Antarctic Deep Water in the central equatorial Pacific and hence on the development of Antarctic glaciation at three time periods during the Cenozoic. In addition, it is evident that the presence or absence of discoasters can be interpreted as the stability or unstability of global climate factors. *"Reticulofenestra" tagana* and related forms must be taken as indicators of prolonged upwelling; Site 572 is very likely located in an area of almost permanent upwelling. Site 575 is situated in an area where Antarctic Bottom Water persisted for a longer period during Antarctic glaciations. It is also apparent that the presence of a permanent Antarctic Bottom Water caused strong solution cy-

cles and a constant and significant reworking at Site 575 since 22.5 Ma.

REFERENCES

Backman, J., 1980. Miocene–Pliocene nannofossils and sedimentation rates in the Hatton–Rockall Basin, NE Atlantic Ocean. *Stockholm Contrib. Geol. 36.*

Bukry, D., 1972. Coccolith stratigraphy, Leg 9, Deep Sea Drilling Project. *In* Hays, J. D., et al., *Init. Repts. DSDP*, 9: Washington (U.S. Govt. Printing Office), 817–832.

———, 1973a. Low-latitude coccolith biostratigraphic zonation. *In* Edgar, N. T., Saunders, J. B., et al., *Init. Repts. DSDP*, 15: Washington (U.S. Govt. Printing Office), 685–703.

———, 1973b. Coccolith stratigraphy, eastern equatorial Pacific, Leg 16, Deep Sea Drilling Project. *In* van Andel, T. H., Heath, G. R., et al., *Init. Repts. DSDP*, 16: Washington (U.S. Govt. Printing Office), 653–711.

———, 1975. Coccolith and silicoflagellate stratigraphy, northwestern Pacific Ocean, Deep Sea Drilling Project, Leg 32. *In* Larson, R. L., Moberly, R., et al., *Init. Repts. DSDP*, 32: Washington (U.S. Govt. Printing Office), 677–701.

———, 1981. Pacific coast coccolith stratigraphy between Point Conception and Cabo Corrientes, Deep Sea Drilling Project, Leg 63. *In* Yeats, R. S., Haq, B. U., et al., *Init. Repts. DSDP*, 63: Washington (U.S. Govt. Printing Office), 445–471.

Cita, M. B., Colalongo, M. L., d'Onofrio, S., Iaccarino, S., and Salvatorini, G., 1978. Biostratigraphy of Miocene deep sea sediments (Sites 372 and 375), with special reference to the Messinian/pre-Messinian interval. *In* Hsü, K. J., Montadert, L., et al., *Init. Repts. DSDP*, 42, Pt. 1: Washington (U.S. Govt. Printing Office), 671–708.

Fonseca, B., 1976. *Coccolithus taganus*, nouvelle espèce de coccolithophoridé du Miocène de Lisbonne. *Bol. Soc. Geol. Portugal*, 20:29–32.

Geitzenauer, K. R., Roche, M. B., and McIntyre, A., 1977. Coccolith biogeography from North Atlantic and Pacific surface sediments. A comparison of species distribution and abundances. *In* Ramsay, A. T. S. (Ed.), *Oceanic Micropaleontology* (Vol. 2): New York (Academic Press), pp. 973–1008.

Haq, B. U., 1968. Studies on upper Eocene calcareous nannoplankton from N.W. Germany. *Stockholm Contrib. Geol.*, 18:13–74.

———, 1971. Paleogene calcareous nannoflora. Parts I–IV. *Stockholm Contrib. Geol.*, 25:1–158.

———, 1976. Early Cenozoic nannoplankton biogeography of the Atlantic Ocean. *Mar. Micropal.*, 1:119–194.

Hay, W. W., 1977. Calcareous nannofossils. *In* Ramsay, A. T. S. (Ed.), *Oceanic Micropaleontology*, (Vol. 2): New York (Academic Press), pp. 1055–1200.

Hays, J. D., Cook, H. E., III, Jenkins, D. G., Cook, F. M., Fuller, J. T., Goll, R. M., Milow, E. D., and Orr, W. N., 1972. Site 77. *In* Hays, J. D., et al., *Init. Repts. DSDP*, 9: Washington (U.S. Govt. Printing Office), 43–208.

Keigwin, L. D., and Keller, G., in press. Middle Oligocene climatic range from equatorial Pacific DSDP Site 77B. *Geology*.

Keller, G., 1981. Miocene biochronology and paleoceanography of the North Pacific. *Mar. Micropal.*, 6:535–551.

Keller, G., and Barron, J., 1982. Paleoceanographic implications of Miocene deep sea hiatuses. *Geol. Soc. Am. Bull.*, 94:590–613.

Kennett, J. P., Houtz, R. E., Andrews, P. B., Edwards, A. R., Gostin, V. A., Hajos, M., Hampton, M., Jenkins, D. G., Margolis, S. V., Ovenshine, A. T., and Perch-Nielsen, K., 1975. Cenozoic paleoceanography in the southwest Pacific Ocean, Antarctic glaciation, and the development of the circum-Antarctic current. *In* Kennett, J. P., Houtz, R. E., et al., *Init. Repts. DSDP*, 29: Washington (U.S. Govt. Printing Office), 1155–1169.

Lohmann, G. P., and Carlson, J. J., 1981. Oceanographic significance of Pacific late Miocene calcareous nannoplankton. *Mar. Micropal.*, 6:553–579.

Martini, E., 1971. Standard Tertiary and Quaternary calcareous nannoplankton zonation. *Proc. Second Planktonic Conf.*, pp. 739–785.

Okada, H., and Bukry, D., 1980. Supplementary modification and introduction of code numbers to the low-latitude coccolith biostratigraphic zonation (Bukry, 1973–1975). *Mar. Micropal.*, 5:321–325.

Okada, H., and McIntyre, A., 1977. Modern coccolithophores of the Pacific and North Atlantic Oceans. *Micropaleontology*, 23:1–55.

Perch-Nielsen, K., 1971. Elektronen mikroskopische Untersuchungen an Coccolithen und verwandten Formen aus dem Eozän von Dänemark. *Biol. Skr. K. Dan. Vidensk. Selsk.*, 18:1–76.

Roth, P. H., 1973. Calcareous nannofossils. Leg 17, Deep Sea Drilling Project. *In* Winterer, E. L., Ewing, J. I., et al., *Init. Repts. DSDP*, 17: Washington (U.S. Govt. Printing Office), 695–795.

Roth, P. H., and Coulbourn, W. T., 1982. Floral and solution patterns of coccoliths in surface sediments of the North Pacific. *Mar. Micropal.*, 7:1–52.

van Andel, T. H., Heath, G. R., and Moore, Jr., T. C., 1975. Cenozoic history and paleoceanography of the central equatorial Pacific ocean. *Mem. Geol. Soc. Am.*, 143:1–134.

Wirrmann, D., 1980. Les sédiments superficiels de la zone "Clarion–Clipperton" (Pacifique tropical nord): sédimentologie–minéralogie [Thèse 3° cycle]. Université Louis Pasteur, Strasbourg.

Woodruff, F., Savin, S. M., and Douglas, R. G., 1981. Miocene stable isotope record: a detailed Pacific ocean study and its paleoclimatic implications. *Science*, 212:665–668.

Date of Initial Receipt: 25 October 1983
Date of Acceptance: 22 April 1984

APPENDIX
Nannofossil Taxa Found at Leg 85 Sites

Cyclicargolithus abisectus (Müller, 1970) Bukry, 1973
Ceratolithus acutus Gartner and Bukry, 1974
Chiasmolithus altus Bukry and Percival, 1971
Helicopontosphaera ampliaperta (Bramlette and Wilcoxon, 1967) Bukry, 1970
Dictyococcites antarctica Haq, 1976
Discoaster asymmetricus Gartner, 1969
Discoaster aulakos Gartner, 1967
Discoaster barbadiensis Tan, 1927
Sphenolithus belemnos Bramlette and Wilcoxon, 1967
Discoaster bellus Bukry and Percival, 1971
Discoaster berggrenii Bukry, 1971
Dictyococcites bisectus (Hay, Mohler, and Wade, 1966) Bukry and Percival, 1971
Discoaster blackstockae Bukry, 1973
Discoaster bollii Martini and Bramlette, 1963
Discoaster braarudi Bukry, 1971
Discoaster brouweri Tan, 1927
Discoaster calcaris Gartner, 1967
Triquetrorhabdulus carinatus Martini, 1965
Discoaster challengeri Bramlette and Riedel, 1954
Discoaster ciperoensis = *Discoaster* sp. (*ciperoensis* group) Martini, 1965
Sphenolithus ciperoensis Bramlette and Wilcoxon, 1967
Rhabdosphaera clavigera Murray and Blackman, 1898
Helicopontosphaera compacta (Bramlette and Wilcoxon, 1967) Hay, 1970
Sphenolithus conicus Bukry, 1971
Ceratolithus cristatus Kamptner, 1954
Reticulofenestra daviesi (Haq, 1968) Haq, 1971
Discoaster decorus (Bukry, 1971) Bukry, 1973
Discoaster deflandrei Bramlette and Riedel, 1954
Amaurolithus delicatus Gartner and Bukry, 1975
Discoaster dilatus Hay, 1967
Sphenolithus dissimilis Bukry and Percival, 1971
Sphenolithus distentus (Martini, 1965) Bramlette and Wilcoxon, 1967
Pontosphaera distincta (Bramlette and Sullivan, 1961) Burns, 1973
Reticulofenestra doronicoides (Black and Barnes, 1961) n. comb.
Coccolithus eopelagicus (Bramlette and Riedel, 1954) Bramlette and Sullivan, 1961
Helicopontosphaera euphratis (Haq, 1966) Martini, 1969
Discoaster exilis Martini and Bramlette, 1963
Coccolithus fenestratus (Deflandre and Fert, 1968) Bukry, 1971
Cyclicargolithus floridanus (Roth and Hay, 1967) Bukry, 1971
Cyclococcolithina formosa (Kamptner, 1963) Wilcoxon, 1970
Reticulofenestra gartneri Roth and Hay, 1967

Reticulofenestra gelida (Geitzenauer, 1972) Backman, 1978
Discoaster gemmifer Stradner, 1961
Helicopontosphaera granulata Bukry and Percival, 1971
Discoaster hamatus Martini and Bramlette, 1963
Reticulofenestra haqii Backman, 1978
Dictyococcites hesslandi (Haq, 1966) Haq and Lohmann, 1976
Sphenolithus heteromorphus Deflandre, 1953
Reticulofenestra hillae Bukry and Percival, 1971
Reticulofenestra insignita Roth and Hay, 1967
Discoaster intercalaris Bukry, 1971
Helicopontosphaera intermedia (Martini, 1965) Hay and Mohler, 1967
Discolithina japonica Takayama, 1967
Helicopontosphaera kamptneri Hay and Mohler, 1967
Discoaster kugleri Martini and Bramlette, 1963
Pseudoemiliania lacunosa (Kamptner, 1963) Gartner, 1969
Cyclococcolithina leptopora (Murray and Blackman, 1898) Wilcoxon, 1970
Discoaster lidzi Hay, 1967
Discoaster loeblichii Bukry, 1971
Cyclococcolithina macintyrei (Bukry and Bramlette, 1969) Bukry, 1973
Triquetrorhabdulus milowii Bukry, 1971
Reticulofenestra minuta Roth, 1970
Reticulofenestra minutula (Gartner, 1967) Haq and Berggren, 1978
Coccolithus miopelagicus Bukry, 1971
Discoaster moorei Bukry, 1971
Sphenolithus moriformis (Brönnimann and Stradner, 1960) Bramlette and Wilcoxon, 1967
Discolithina multipora (Kamptner, 1948) Martini, 1965
Sphenolithus neoabies Bukry and Bramlette, 1969
Discoaster neohamatus Bukry and Bramlette, 1969
Pyrocyclus orangensis (Bukry, 1971) Backman, 1980
Pontosphaera pacifica Burns, 1973
Discoaster pansus (Bukry and Percival, 1971) Bukry, 1973
Coccolithus pelagicus (Wallich, 1877) Schiller, 1930
Discoaster pentaradiatus Tan, 1927
Discoaster perclarus Hay, 1967
Sphenolithus predistentus Bramlette and Wilcoxon, 1967
Amaurolithus primus (Bukry and Percival, 1971) Gartner and Bukry, 1975
Dictyococcites producta (Kamptner, 1963) Backman, 1980
Sphenolithus pseudoradians Bramlette and Wilcoxon, 1967
Reticulofenestra pseudoumbilica (Gartner, 1967) Gartner, 1969
Discoaster pseudovariabilis Martini and Worsley, 1971
Discoaster quinqueramus Gartner, 1969
Coccolithus radiatus Kamptner, 1955
Cyclicargolithus reticulatus (Gartner and Smith, 1967) Bukry, 1971
Geminilithella rotula (Kamptner, 1956) Backman, 1980
Ceratolithus rugosus Bukry and Bramlette, 1968
Triquetrorhabdulus rugosus Bramlette and Wilcoxon, 1967
Discoaster saipanensis Bramlette and Riedel, 1954
Discoaster saundersi Hay, 1967
Helicopontosphaera sellii Bukry and Bramlette, 1969
Orthorhabdus serratus Bramlette and Wilcoxon, 1967
Bramletteius serraculoides Gartner, 1969
Discoaster signus Bukry, 1971
Discoaster stellutus Gartner, 1967
Ellipsolithus subdistichus Roth and Hay, 1967
Discoaster sublodoensis Bramlette and Sullivan, 1961
Discoaster subsurculus Gartner, 1967
Discoaster surculus Martini and Bramlette, 1963
"Reticulofenestra" tagana (Fonseca, 1976) n. comb.
Discoaster tamalis Kamptner, 1967
Discoaster tani Bramlette and Riedel, 1954
Amaurolithus tricorniculatus (Gartner, 1967) Gartner and Bukry, 1975
Discoaster triradiatus Tan, 1927
Discoaster tristellifer Bukry, 1976
Reticulofenestra umbilica (Levin, 1965) Martini and Ritzkowski, 1968
Pontosphaera vadosa Hay, Mohler, and Wade, 1966
Discoaster variabilis Martini and Bramlette, 1963
Coronocyclus sp.
Scyphosphaera sp.
Syracosphaera sp.

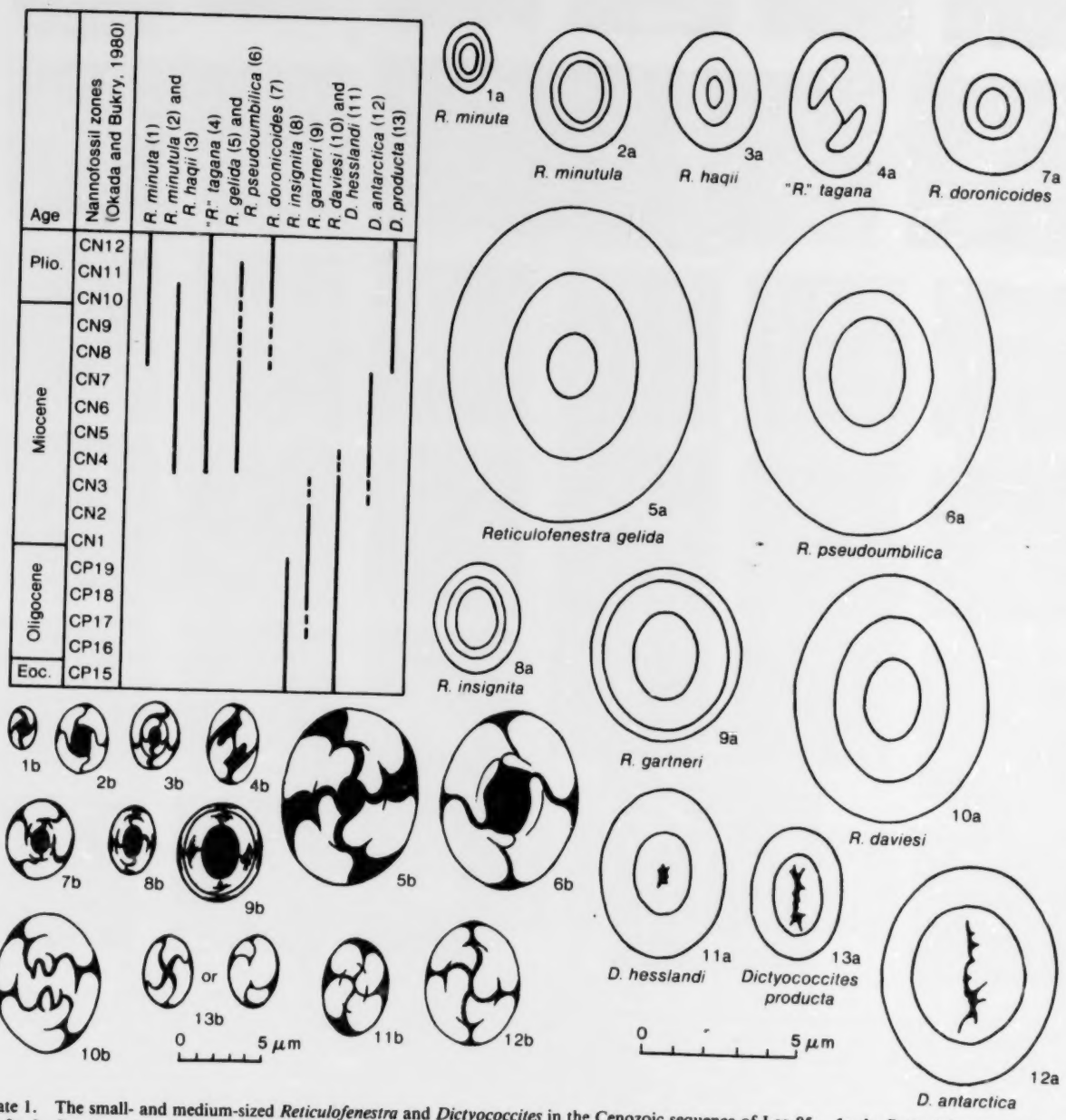

Plate 1. The small- and medium-sized *Reticulofenestra* and *Dictyococcites* in the Cenozoic sequence of Leg 85. **1a, b.** *Reticulofenestra minuta*. **2a, b.** *R. minutula*. **3a, b.** *R. haqii*. **4a, b.** *"R." tagana*. **5a, b.** *R. gelida*. **6a, b.** *R. pseudoumbilica*. **7a, b.** *R. doronicoides*. **8a, b.** *R. insignita*. **9a, b.** *R. gartneri*. **10a, b.** *R. daviesi*. **11a, b.** *Dictyococcites hesslandi*. **12a, b.** *D. antarctica*. **13a, b.** *D. producta*. (a = archetype-scheme of the coccolith; b = figure in polarized light.)

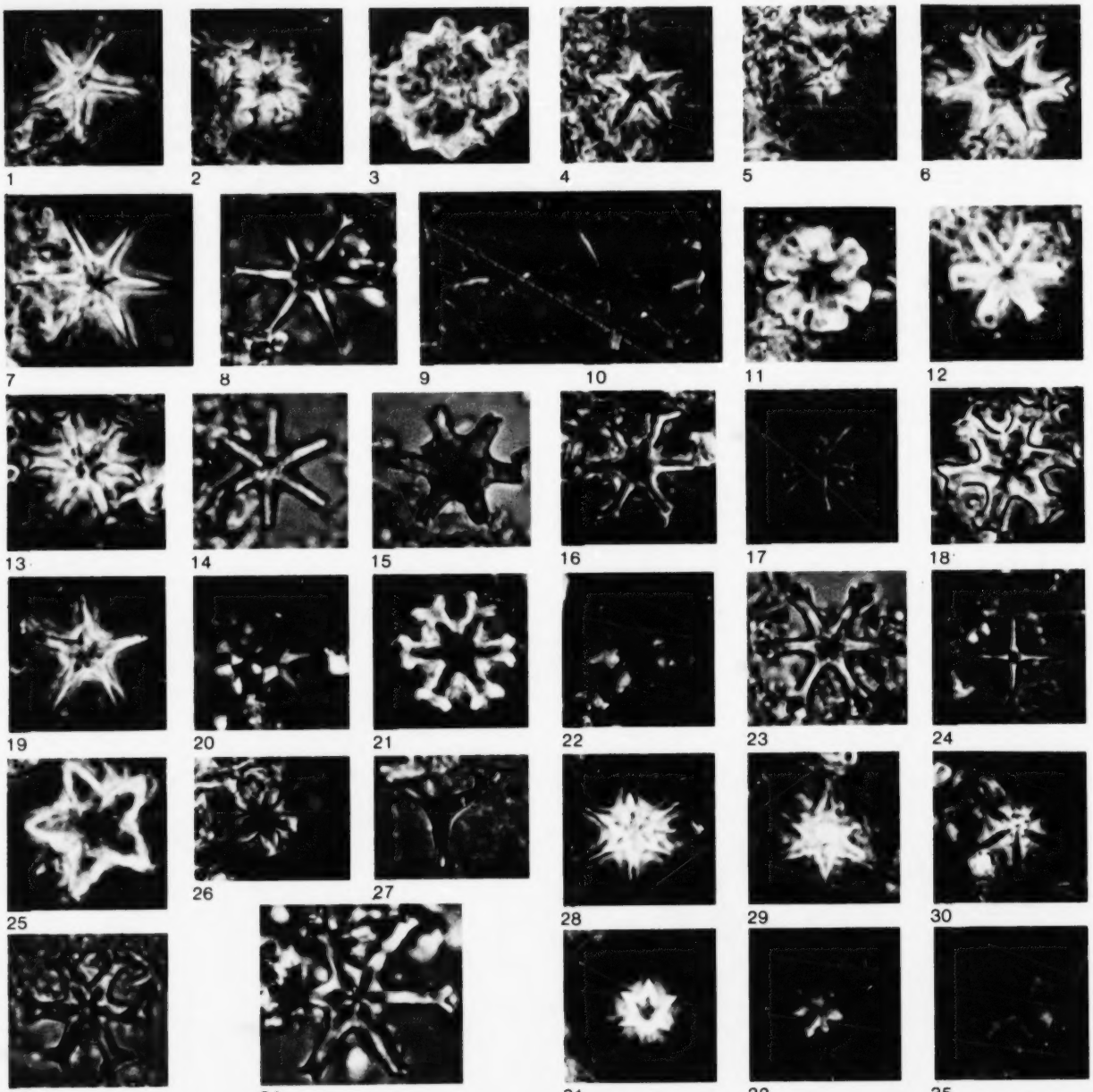

Plate 2. (About × 1300; unless stated otherwise, the photographs were taken with a Nomarski interferential system.) **1.** *Discoaster asymmetricus*, 572A-6-6, 0–1 cm (CN12a). **2.** *D. aulakos*, 572A-14-3, 0–1 cm (CN9a). **3.** *D. barbadiensis*, 573B-42-4, 135 cm (CP15). **4.** *D. bellus*, 573B-4-3, 15–16 cm (CN7). **5.** *D. berggrenii*, 573-12-4, 0–1 cm (CN9a). **6.** *D. bollii*, 572A-14-3, 0–1 cm (CN9b). **7.** *D. brouweri*, 573-7-2, 0–1 cm (CN12a). **8.** *D. calcaris*, 573-7-2, 0–1 cm (CN12a). **9.** *D. ciperoensis*, bright field, 574-2-6, 100–101 cm (CN12a). **10.** *D. druggi*, bright field, 574-2-6, 100–101 cm (CN12a). **11.** *D. deflandrei*, 573B-12-5, 15–16 cm (CN3). **12.** *D. dilatus*, 573B-4-3, 15–16 cm (CN7). **13.** *D. exilis*, 574-4-4, 27–28 cm (CN10c). **14.** *D. intercalaris*, bright field, 572D-7-3, 55–56 cm (CN8a). **15.** *D. kugleri*, bright field, 572D-21-3, 47–48 cm (CN5b). **16.** *D. loeblichii*, 573B-2-3, 15–16 cm (CN8a). **17.** *D. moorei*, bright field, 574-13-4, 49–50 cm (CN5a). **18.** *D. pansus*, 574-4-3, 27–28 cm (CN11). **19.** *D. pentaradiatus*, 574-4-5, 27–28 cm (CN10b). **20.** *D. pentaradiatus*, polarized light, 573-7-3, 0–1 cm (CN12a). **21.** *D. pseudovariabilis*, 573B-2-3, 15–16 cm (CN8a). **22.** *D. saipanensis*, bright field, 573B-42-4, 116 cm (CP15). **23.** *D. surculus*, bright field, 572D-10-3, 55–56 cm (CN8a). **24.** *D. tamalis*, bright field, 574-2-6, 100–101 cm (CN12a). **25.** *D. tani*, 573B-18-2, 15–16 cm (CN1c). **26.** *D. tani*, 574C-35-1, 13–14 cm (CP15). **27.** *D. triradiatus*, 574-2-5, 100–101 cm (CN12c). **28.** *D. tristellifer*, 574-4-4, 27–28 cm, low focus (CN10c). **29.** *D. tristellifer*, 574-4-5, 27–28 cm, middle focus (CN10b). **30.** *D. tristellifer*, 574-4-4, 27–28 cm, high focus (CN10c). **31.** *D. tristellifer*, 573-8-7, 0–1 cm, slightly dissolved specimen (CN10). **32.** *D. tristellifer*, polarized light, 573-7-3, 0–1 cm, very dissolved specimen (CN12a). **33.** *D. variabilis*, bright field, 574-4-3, 27–28 cm (CN11). **34.** *D. decorus*, bright field, 573-7-4, 0–1 cm (CN11). **35.** Undetermined etched discoaster.

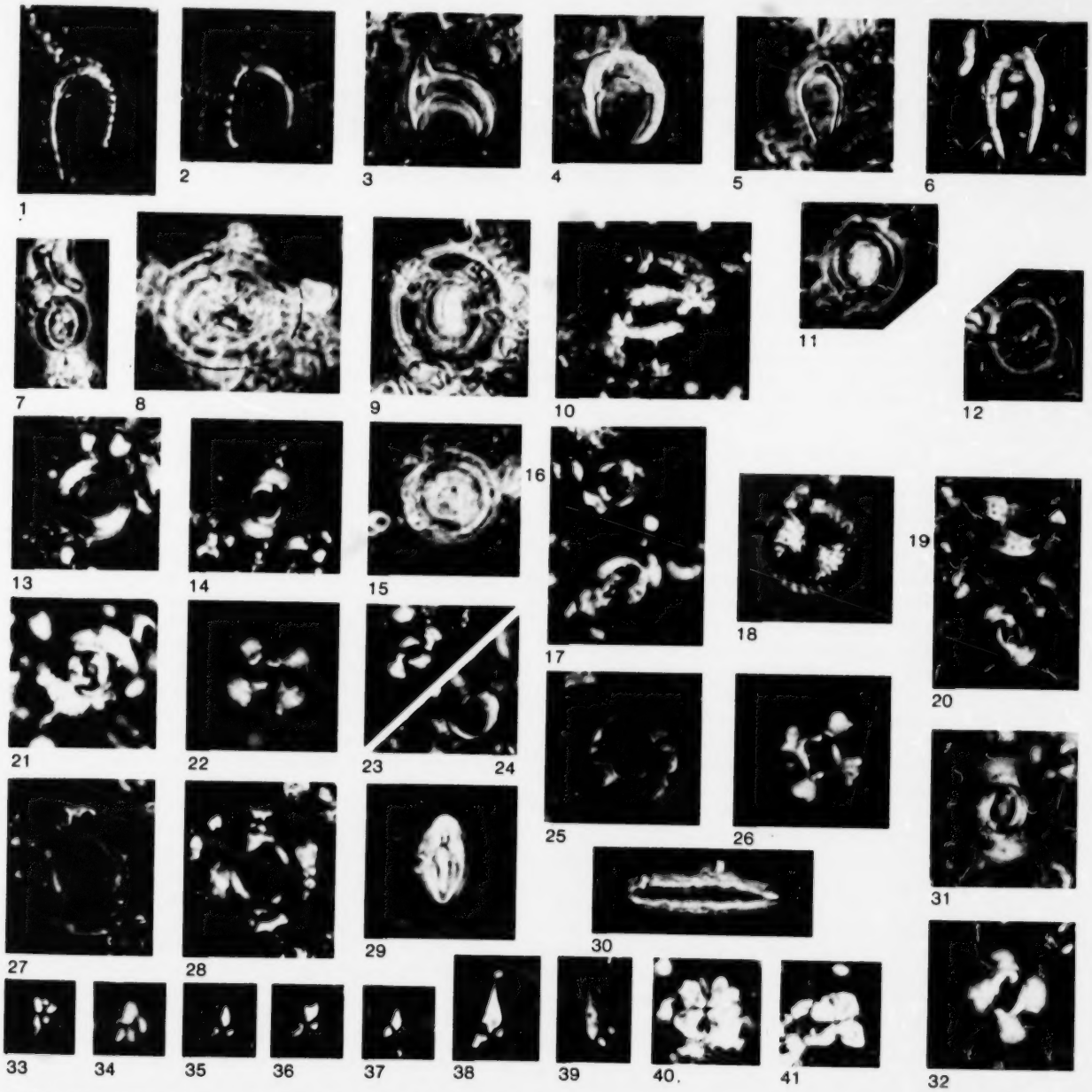

Plate 3. (About ×1300; unless stated otherwise, the photographs were taken with a Nomarski inferential system.) **1.** *Ceratolithus cristatus*, bright field, 575-1-3, 140–141 cm (CN12d). **2.** *Amaurolithus amplificus*, bright field, 575-1-3, 140–141 cm (CN12d). **3.** *Amaurolithus tricorniculatus*, 574-4-5, 27–28 cm (CN10b). **4.** *Amaurolithus primus*, 573-10-5, 0–1 cm (CN10). **5.** *Amaurolithus delicatus*, 574-4-4, 27–28 cm (CN10c). **6.** *Ceratolithus rugosus*, bright field, 574-2-4, 100–101 cm (CN12c). **7.** *Ellipsolithus subdistichus*, 573B-38-3, 27–28 cm (CP16). **8.** *Chiasmolithus altus*, 573B-38-3, 27–28 cm (CP16c). **9.** *Coccolithus eopelagicus*, 573B-30-3, 15–16 cm (CP18). **10.** *Coccolithus miopelagicus*, polarized light, 573B-5-3, 15–16 cm (CN6). **11.** *Coccolithus pelagicus*, 572A-14-3, 0–1 cm (CN9b). **12.** *Coccolithus radiatus*, 573B-18-2, 15–16 cm (CN1c). **13.** *Coronocyclus* sp., bright field, 575A-6-2, 51–52 cm (CN2). **14.** *Cyclicargolithus floridanus*, polarized light, 573B-13-3, 15–16 cm (CN3). **15.** *Cyclococcolithina formosa*, 573B-42-4, 135–136 cm (CP15). **16.** *Cyclococcolithina formosa*, polarized light, 573B-42-2, 50–51 cm (CP15). **17.** *Dictyococcites bisectus*, polarized light, 573B-42-2, 50–51 cm (CP15). **18.** *Cyclococcolithina macintyrei*, bright field, 573-10-3, 0–1 cm (CN10). **19.** *Discolithina multipora*, 572D-27-3, 55–56 cm (CN5a). **20.** *Reticulofenestra daviesi*, 572D-27-3, 55–56 cm (CN5a). **21.** *Cyclicargolithus abisectus*, bright field, 575A-23,CC (CN1b). **22.** *Cyclicargolithus abisectus*, polarized light, 575A-23,CC (CN1b). **23.** *Pyrocyclus orangensis*, polarized light, 573B-27-3, 15–16 cm (CP18). **24.** *Pyrocyclus orangensis*, bright field, 573B-27-3, 15–16 cm (CP18). **25.** *Reticulofenestra hillae*, bright field, 574C-34-2, 93–94 cm (CP15). **26.** *Reticulofenestra hillae*, polarized light, 574C-34-2, 93–94 cm (CP15). **27.** *Reticulofenestra umbilica*, bright field, 573B-42-2, 50–51 cm (CP16b). **28.** *Reticulofenestra umbilica*, polarized light, 573B-42-2, 50–51 cm (CP16b). **29.** *Triquetrorhabdulus milowii*, 573B-17-3, 15–16 cm (CN1c). **30.** *Triquetrorhabdulus carinatus*, 573B-18-2, 15–16 cm (CN1c). **31.** *Reticulofenestra pseudoumbilica*, 572D-19-3, 47–48 cm (CN5b). **32.** *Reticulofenestra pseudoumbilica*, polarized light, 572D-19-3, 47–48 cm (CN5b). **33.** *Sphenolithus belemnos*, polarized light, 575A-8-2, 51–52 cm (CN2). **34.** *Sphenolithus belemnos*, bright field, 575A-6-2, 51–52 cm (CN2). **35.** *Sphenolithus conicus*, polarized light, 573B-21-2, 30–31 cm (CP19). **36.** *Sphenolithus dissimilis*, polarized light, 574C-5-4, 49–50 cm (CN1c). **37.** *Sphenolithus distentus*, polarized light, 573B-23-3, 35–36 cm (CP19). **38.** *Sphenolithus heteromorphus*, polarized light, 574-28-2, 49–50 cm (CN4). **39.** *Sphenolithus predistentus*, polarized light, 573B-38-3, 27–28 cm (CP16c). **40.** *Sphenolithus moriformis*, polarized light, 575A-6-2, 51–52 cm (apical view) (CN2). **41.** *Sphenolithus moriformis*, polarized light, 575A-6-2, 51–52 cm (lateral view) (CN2).

Reprinted from Mayer, L., Theyer, F., et al., 1985
Initial Reports of the Deep Sea Drilling Project, Volume LXXXV, Washington (U. S. Government Printing Office)

15. CALCAREOUS NANNOFOSSIL BIOSTRATIGRAPHY, DEEP SEA DRILLING PROJECT LEG 85, EASTERN EQUATORIAL PACIFIC[1]

Stefan Gartner and Jinder Chow, Texas A&M University[2]

ABSTRACT

Pelagic sediments recovered during Leg 85 span the uppermost Eocene to Pleistocene interval in a series of fairly continuous sections. The calcareous nannofossils are normally not very well preserved in the cores from this leg; coccoliths, discoasters, and other morphologic types have been corroded and overgrown by secondary calcite. Poor preservation in some cases precludes a sharp and precise biostratigraphy at the subzonal level, although remarkably, most zones can be clearly identified. Middle Miocene markers are the most consistently troublesome, and it is suggested that *Coronocyclus nitescens* be introduced as an additional useful marker in this interval.

INTRODUCTION

During Leg 85, tropical deep-water pelagic sediments were cored in the equatorial Pacific. Four sites (572 to 575) in particular were cored extensively, and multiple holes were drilled at each site (Fig. 1). The sediment at each of these sites consists principally of pelagic, biogenic constituents, both calcareous and siliceous. In total, 217 samples from the four sites (two holes from each site) were used in biostratigraphic analysis. This chapter presents the results of these analyses. The scope of this study is to provide a concise biostratigraphic framework that is developed from the calcareous nannofossils and based on a limited number of samples. It is not intended to be a comprehensive regional study.

Age assignments are mostly made according to the zonation scheme of Bukry (Bukry, 1975; Okada and Bukry, 1980), with minor modifications where a given zonation proved inadequate or unsuitable. One such case is Pleistocene, but it was not sampled in sufficient detail to present serious problems. A second instance is the Miocene/Pliocene boundary, which, according to the best data available, should probably be placed at the extinction of *Discoaster quinqueramus* (Gartner et al., 1983). A third area of difficulty introduced by Bukry's zonation is his use of the beginning or end of an acme to delimit zones. The beginning or end of an acme can be rendered meaningless by differential dissolution because the abundance of a species can be decreased or enhanced greatly depending on its susceptibility to dissolution. Finally, the first appearance of *Sphenolithus distentus* cannot be used as a marker where indicated by Bukry because the species occurs consistently at a much lower level.

One recommendation for improving existing zonations of the middle Miocene where several of the designated markers are notably sporadic and unreliable is to use the highest occurrence of *Coronocyclus nitescens* as a marker. This species is distinctive and hence easy to recognize and identify. It is consistent in its occurrence in pelagic and hemipelagic sediments and relatively resistant to dissolution. Although the species is rarely a major constituent of the assemblage, it is in all other respects a nearly ideal marker species. The bio-horizon marked by the last or highest occurrence of this species is above the highest occurrence of *Sphenolithus heteromorphus* and below the first appearance of *Catinaster coalitus*. It probably occurs within the lower part of magnetic polarity epoch 13 and has an age of about 13 Ma. In Hole 572D *C. nitescens* last occurs somewhat below the CN5a/CN5b zonal boundary; in Holes 573B and 574 its last occurrence is imprecisely known because the accepted marker species are not present. In Hole 574C the highest occurrence of the species may not have been recovered, and in Hole 575 *C. nitescens* disappears just below the CN5a/CN5b zonal boundary. It should be noted that the apparent inconsistencies in the highest occurrence of *C. nitescens* can partly be explained by inconsistent occurrences of designated markers but could also reflect the relatively wide sample spacing of this study.

A summary overview of the zonal and age assignments of the cores from Leg 85 is given on Table 1.

METHODS

Smear slides were prepared for each sample from unprocessed material. The slides were examined with a light microscope at approximately ×1600 magnification using cross-polarized light, differential interference constrast, and phase contrast optics. Abundance estimates were made on optimum density areas of the slides, that is, areas where most of the field was covered with sample material without appreciable piling of specimens or sample material. The abundance code translates as follows: A (abundant), usually more than 10 specimens occurring per field; C (common), 1 to 10 specimens per field; F (few), 1 specimen per 1 to 10 fields; R (rare), 1 specimen per more than 10 fields.

SITE 572

Holes 572A and 572C

Forty-nine samples were examined from Site 572. Seventeen samples are from Holes 572A and 572C; four of

[1] Mayer, L., Theyer, F., et al., *Init. Repts. DSDP*, 85: Washington (U.S. Govt. Printing Office).

[2] Address: Department of Oceanography, Texas A&M University, College Station, TX 77843.

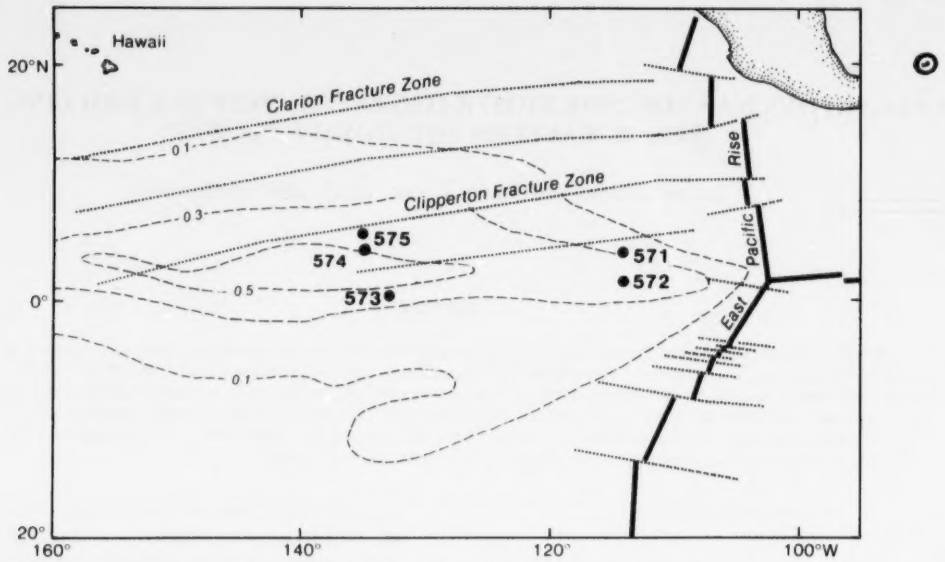

Figure 1. Location of DSDP Leg 85 sites in the eastern equatorial Pacific. Contours show sediment thickness in seconds (two-way traveltime).

these are core-catcher samples. The two samples from Hole 572C (Cores 1 and 2) are combined on one chart with fifteen samples from Hole 572A (Cores 3 through 17). The calcareous nannofossil checklist for these samples is given in Table 2. Preservation of nannofossils is fair to poor throughout the interval, and the biostratigraphy lacks sharp definition because marker species are usually present only sporadically. Nevertheless, the age determinations given are considered accurate and reliable.

Samples 572C-1,CC through 572A-3,CC are of Pleistocene age (Zones CN14 and CN13) and extend from the middle to the upper Pleistocene in the topmost sample and down to the lower Pleistocene in the lowermost sample. Conspicuous markers include *Pseudoemiliania lacunosa* and *Calcidiscus tropicus* (= *C. macintyrei*).[3]

Sample 572A-4-5, 139–140 cm is uppermost Pliocene; it contains the lone asterolith species *Discoaster brouweri* characteristic of this level (Zone CN12d). The Pliocene extends through Core 10 (Sample 572A-10-7, 40–41 cm), the Miocene/Pliocene boundary being in the next lower core. The Pliocene succession is complete, although poor preservation prevents recognition of all subzones. Zones 12, 11, and 10 are, however, recognizable as distinct units.

Sample 572A-11-6, 140–141 cm contains *D. quinqueramus* and thus is assigned to the uppermost Miocene *D. quinqueramus* Zone (Zone CN9). This zone continues to the bottom of the section (Sample 572A-17-6, 8–9 cm) where the presence of *Amaurolithus amplificus* indicates an age probably not older than Zone CN9b, which corresponds to the upper part of the *D. quinqueramus* Zone.

[3] The name *Calcidiscus tropicus* (Kamptner) is used in preference to *C. macintyrei* (Bramlette and Bukry). The latter is considered a junior synonym (Gartner et al., 1983).

Hole 572D

The 32 samples from Hole 572D extended from the lower Pliocene (Zone CN10) to the lower middle Miocene (Zone CN4) (Table 3). Poor preservation makes accurate biostratigraphic subdivision of this hole difficult, although most of the zones and several subzones can be recognized. The Pliocene/Miocene boundary is tentatively placed within Core 5 because the sample immediately above it (Sample 4,CC) contains the birefringent *Ceratolithus armatus*, whereas the base of the next lower core (Sample 5,CC) lacks birefringent ceratoliths. *Discoaster quinqueramus*, the extinction of which marks the top of the Miocene, was encountered only lower (Sample 8, CC) where it co-occurs with *D. loeblichii*, a species that does not occur above the middle part of the upper Miocene.

Within the upper Miocene Subzones 9b, 9a, and 8b are recognizable, but below that zones and subzones are less clearly distinguishable. The marker species *D. hamatus* and *Catinaster coalitus* (for Zones CN7 and CN6, respectively) are very rare and both occur in only one (and the same) sample (15,CC). Immediately below Zone CN6, markers are lacking until *D. kugleri* is encountered in Samples 19,CC and 21,CC. This marks Zone CN5b, the *D. kugleri* Subzone. The next lower zone (CN5a) has no distinctive marker of its own, but its lower limit is recognizable by the last occurrence of *Sphenolithus heteromorphus* (Sample 28,CC), which continues to the bottom of the section (Sample 32,CC).

SITE 573

Hole 573

Nineteen core-catcher samples were examined from Hole 573 (Table 4). Calcareous nannofossils are common to abundant in all samples, but preservation is most-

Table 1. Summary of zonal and age assignments of Leg 85 cores based on calcareous nannofossils from Holes 572 through 575. Nannofossil zonal numbers are those of Okada and Bukry (1980). For more detailed age assignments see Tables 2 through 9.

Age		Nannofossil zones	572A	572C	572D	573	573B	574C	575	575A
Pleistocene		CN15 to CN13	3,CC	1,CC 2,CC		1,CC/ 3,CC				
Pliocene		CN12	4,CC 5,CC			4,CC 6,CC			1,CC	
		CN11 to CN10	6,CC 10-7		1,CC/4,CC	7,CC 9,CC			2,CC	
Miocene	late	CN9	11-6 17-6		5,CC 7,CC	10,CC 18,CC			3,CC	
		CN8			8,CC	19,CC	1,CC/4,CC			
	middle	CN7					5,CC			
		CN6								
		CN5			27,CC		8,CC	1,CC	7,CC	
		CN4			28,CC 32,CC		9,CC	2,CC	8,CC 11,CC	1,CC
		CN3					13,CC	3,CC		5,CC
	early	CN2					14,CC	4,CC		6,CC 9,CC
		CN1					15,CC	5,CC		10,CC
							20,CC	17,CC		33,CC
Oligocene	late	CP19					21,CC 30,CC	18,CC 20,CC		
	early	CP18					31,CC	21,CC		
		CP17					37,CC	28,CC		
		CP16					38,CC 40,CC	29,CC 34,CC		
Eocene	late	CP15						35,CC		

ly fair to poor. Only in the uppermost three core-catcher samples is nannofossil preservation fair to good. Both dissolution and overgrowth are noticeable, and the low species diversity of some samples suggests that some species have probably been removed by corrosion.

The 19 samples extend from the upper Pleistocene at the top (Zone CN14b) to the upper Miocene *Discoaster neohamatus* Zone (Zone CN8) at the bottom. All of the intervening zones can be recognized, and in several cases subzones can be distinguished as well. The Pliocene/Pleistocene boundary is placed within Core 4; the base of that core contains the upper Pliocene marker *D. brouweri*. The next higher sample (3,CC) lacks discoasters. The Pliocene zones appear to be of uneven spans (e.g., CN11 and CN12), which could be the result of poor preservation of some marker species or notably different sediment accumulation rates, possibly stemming from differential dissolution of biogenic carbonate. However, it may be entirely an artifact introduced by the wide spacing between adjacent samples.

The Miocene/Pliocene boundary is placed at the highest occurrence of *D. quinqueramus*, which is within Core 10. The upper Miocene *D. quinqueramus* Zone (Zone CN9) is more expanded than the Pliocene zones, although nannofossil preservation is not notably better.

Hole 573B

Forty samples, all but one of them core-catcher samples, were examined from Hole 573B (Table 5), and these extend from the upper Miocene at the top to upper Oli-

Table 2. Occurrence of calcareous nannofossils in core-catcher samples, DSDP Holes 572A and 572C, Leg 85.

Age	Sample (interval in cm)	Preservation	Nannofossil zones	*Gephyrocapsa oceanica*	*Pseudoemiliania lacunosa*	*Crenalithus productellus*	*Gephyrocapsa caribbeanica*	*Calcidiscus leptoporus*	*Ceratolithus cristatus*	*Helicosphaera carteri*	*Umbilicosphaera sibogae*	*Reticulofenestra minutulus*	*Ceratolithus rugosus*	*Ceratolithus telesmus*	*Calcidiscus tropicus*	*Helicosphaera sellii*	*Coccolithus pelagicus*
Pleist.	572C-1,CC	F	CN14	C	C	A	C	C		C	F						
	2,CC	F-P	to	F	A	C	C	C	F	F	C	C	F	F	C	C	
	572A-3,CC	F-P	CN13		A		F	C	R	C	C	A	F		C		F
Pliocene	4-5, 139-140	F-P	CN12 d/a		C			F		F		A	R		A	A	
	5,CC, 14-15	F-P							F	F		F	F		A	F	A
	6-6, 140-141	F-P			F				F			A			A		
	7-6, 100-101	P	CN11									C	F		C		C
	8-6, 59-60	P							R			A	R		C		F
	9-6, 140-144	P-F	CN10			C				C		A			C		
	10-7, 40-41	F-P				F		F		C		A			C		R
Miocene	11-6, 140-141	P-F						F		R		A			R		
	12-6, 140-141	P-F						F		C		A			C		
	13-6, 140-141	P-F						C		F		A			C		C
	14-6, 140-141	P-F	CN9					F		C		A					F
	15-6, 100-101	P-F						C		R		A			C		
	16-6, 40-41	P-F								R		C				R	F
	17-6, 8-9	F-P						R		F		C					A

Note: A = abundant; C = common; F = few; R = rare. See text for further explanation. Preservation: F = fair; P = poor.

gocene at the bottom of this hole. Not all intervening zones are identifiable, again resulting from poor preservation and the absence of certain key marker species. The youngest zone represented is the upper Miocene *Discoaster neohamatus* Zone (Zone CN8). The middle Miocene Zones CN7, CN6, and CN5 cannot be differentiated, although all three may be represented in the interval of Cores 5 through 8. The two critical markers for this interval, *Catinaster coalitus* and *D. hamatus*, were not found in the samples. Zones CN4 and CN3, which are the *Sphenolithus heteromorphus* and *Helicosphaera ampliaperta* Zones, together cover the interval of Cores 9 through 13. The marker species for differentiating these two zones, however, were not considered reliable over this interval.

The Oligocene/Miocene boundary cannot be placed precisely (it does not correspond to a nannofossil biohorizon used in Bukry's zonation), although the interval in which it is contained, the *Triquetrorhabdulus carinatus* Zone (Zone CN1), is well developed from Cores 15 through 20. The Oligocene Zones CP19 through CP16, which are the *Sphenolithus ciperoensis* through *Helicosphaera reticulata* Zones, are represented from Cores 21 through 40. Zones CP18 and CP17 cannot be separated because the marker species *Sphenolithus distentus* extends well below the next lower marker, an apparent internal inconsistency in Bukry's zonation. There is a break in the range of *S. distentus* (Cores 33 and 34), and it is tempting to place the zonal boundary at this level; however, that interpretation of the data would be incorrect.

SITE 574

Two suites of samples were examined from Site 574: one from Hole 574 consists of 30 core-catcher samples, and the second from Hole 574C consists of 35 core-catcher samples. The two sections combined extend from the Pleistocene at the top of Hole 574 to the uppermost Eocene at the bottom (Core 35) of Hole 574C. The section appears to be continuous over the entire interval to the extent that it can be resolved given the sample spacing and the poor preservation of much of the section.

Hole 574

The 30 samples from Hole 574 are from the core catchers of each of the 31 successive cores, except for Core 23 from which no sample was available (Table 6). The upper Neogene (upper Miocene, Pliocene, and Pleistocene) is represented in only the uppermost 7 cores (Zones CN8 through CN14), whereas the middle Miocene is represented in Cores 8 through 31 (Zones CN4 through CN7). This great difference in thickness probably indicates a pronounced change in sedimentation rates; however, the preservation of the nannofossils is poor throughout and thus does not reflect the different sedimentation rates perfectly. Preservation is rendered poor by both dissolution of some species and overgrowth of others, often within the same sample.

The Pleistocene is represented in Core 1 and possibly the upper part of Core 2, although the base of Core 2 is Pliocene as are Cores 3 through 5. The three zones of

	Discoaster brouweri	*Discoaster pentaradiatus*	*Discoaster tamalis*	*Discoaster surculus*	*Discoaster asymmetricus*	*Discoaster variabilis*	*Ceratolithus armatus*	*Reticulofenestra pseudoumbilica*	*Sphenolithus abies*	*Ceratolithus acutus*	cf. *Catinaster* sp.	*Discoaster intercalaris*	*Amaurolithus primus*	*Amaurolithus delicatus*	*Amaurolithus tricorniculatus*	*Discoaster quinqueramus*	*Discoaster berggrenii*	*Discoaster sanmiguelensis*	*Triquetrorhabdulus rugosus*	*Discoaster neohamatus*	*Amaurolithus amplificus*	*Helicosphaera parallela*
F A		A	R	F	R	F																
F C C		F		F		F C C	R	R C C	F C	cf.	F											
C F		C F	R	F F		F F	R	A C	C C	R R		F R	R	R	R							
C R F C C F		R F R		C R F R C R		F R C R		C C C A C C A	C C A A C C			R cf.	R R F R	 R 	 	R R R C F R	F R R F R	C	R	 R 	 R R	 R

the Pliocene (CN12 through CN10b) are represented but subzones cannot be identified consistently. The upper Miocene zones can only be identified imperfectly. Subzone CN10a was not identified, although it may be present within an unsampled interval of Core 6. The bottom of Core 6 (Sample 6,CC) belongs to Zone CN9. The interval from the *Discoaster neohamatus* Zone through the *D. exilis* Zone (Zones CN8, CN7, CN6, and CN5) is reasonably complete, but the boundary between the lower two zones is unclear because of the absence in the samples of the marker species *Catinaster coalitus*.

The boundary between Zone CN5 and CN4 is also unclear because of the rare but unambiguous occurrence of *Sphenolithus heteromorphus* in Core 16. This species is not found in the three immediately subjacent cores but does occur in much greater abundance from Cores 20 through 31. Thus the occurrence of the species in Core 16 is suspect. If the occurrence of *Sphenolithus heteromorphus* in Core 16 is spurious, as assumed here, then the sedimentation rate change in the section implied by the spacing of nannofossil bio-horizons occurred somewhat later and was less intense than indicated by the actually documented last occurrence of *Sphenolithus heteromorphus*.

Hole 574C

The 35 core-catcher samples from Hole 574C (Table 7) extend from the middle Miocene *Sphenolithus heteromorphus* Zone (CN5) to the upper Eocene *Discoaster barbadiensis* Zone (CP15). Although not all zones and subzones can be clearly identified, primarily resulting from poor preservation of marker species, the section appears to be continuous. The lower to middle Miocene *Helicosphaera ampliaperta* Zone (CN3) cannot be clearly identified. Similarly the Miocene/Oligocene boundary remains somewhat ambiguous because it is not possible to clearly identify the marker horizon, the acme of *Cyclicargolithus abisectus*. The boundary is placed within Core 17; however, it could be somewhat higher because specimens intermediate between *C. abisectus* and the smaller *C. floridanus* are common.

The Paleogene interval from *Sphenolithus ciperoensis* Zone through the *D. barbadiensis* Zone (Zones CP19 through CP15) are well represented. The boundary between the *S. distentus* Zone (CP18) and the *S. predistentus* Zone (CP17), however, cannot be determined because the marker species *S. distentus* ranges well below the level implied by the zonation scheme. Clearly the Oligocene zonal succession merits further study, including identification of some additional nannofossil marker species.

The Eocene/Oligocene boundary is within Core 35 because the base of that core contains the distinctive *D. barbadiensis* and *D. saipanensis*, both characteristic of the upper Eocene, along with several other upper Eocene species.

SITE 575

Two suites of sample were examined from Site 575: one from Hole 575 consists of 11 samples, and the second from Hole 575A consists of 33 samples. All of the samples are from core-catcher material. The total interval represented by the two sections includes part of the Pliocene and nearly all of the Miocene. Pleistocene nannofossil assemblages were not identified; the youngest sample, although nearly barren, appears to be Pliocene

Table 3. Occurrence of calcareous nannofossils in core-catcher samples, DSDP Hole 572D, Leg 85.

Age	Sample	Preservation	Nannofossil zones	*Sphenolithus abies*	*Reticulofenestra pseudoumbilica*	*Coccolithus pelagicus*	*Calcidiscus leptoporus*	*Discoaster variabilis*	*Discoaster brouweri*	*Discoaster pentaradiatus*	*Helicosphaera carteri*	*Discoaster surculus*	*Amaurolithus primus*	*Calcidiscus tropicus*	*Ceratolithus armatus*	*Amaurolithus tricorniculatus*	*Helicosphaera sellii*	*Discoaster challengeri*	*Discoaster loeblichii*	*Discoaster quinqueramus*	*Helicosphaera granulata*	*Discoaster bellus*	*Discoaster neohamatus*	*Helicosphaera parallela*	*Catinaster coalitus*	*Discoaster hamatus*	*Discoaster bollii*	*Discoaster kugleri*	*Discoaster deflandrei*	*Discoaster exilis*	*Triquetrorhabdulus rugosus*	*Coronocyclus nitescens*	*Cyclicargolithus floridanus*	*Sphenolithus heteromorphus*
Pliocene	572D-1,CC	F-P	CN10	C	A	C	C	C	F		R	R	R	R																				
	2,CC	F-P		A	A	C	C	C	F		R	R	R	R																				
	3,CC	P		C	A	A	C	C			F																							
	4,CC	F-P		A	A	A	C	C			F		R	R																				
	5,CC	P	CN9b	A	A	C	A	C	F		C	C		C																				
	6,CC	F-P	CN9a	A	A	C	C	C	C		C	F	F	F																				
	7,CC	P		C	A	C	C	R	R	R	R	R	R	R																				
Miocene	8,CC	P	CN8b	A	C	C	C	C	C		C	C		C																				
	9,CC	P-F		C	C	F	C	C	F		C	F		F																				
	10,CC	F	CN8a	A	A	C	C	C	C		C	F		F																				
	11,CC	F		A	C	C	R	F	C		R	F		F																				
	12,CC	F	?	A	VA	F	R	R	C		R	F		F																				
	13,CC	P		C	C	R	R	R	F		R	F		F																				
	14,CC	F	CN7	C	A	C	C	R	R		R	F		F	cf.																			
	15,CC	F		C	A	C	C	R	F		R	F		F	cf.																			
	16,CC	F-P		C	A	C	C	F	F		F	F		F																				
	17,CC	F-P		C	A	C	C	F	F		F	F		F																				
	18,CC	F-P		A	A	C	F	C	F		F	F		F																				
	19,CC	F-P	?	F	A	A	C	C	F		F	F		F																				
	20,CC	F-P		C	A	A	C	C	R		R	F		F																				
	21,CC	F-P		C	A	C	C	C	F		F	F		F																				
	22,CC	F-P	CN5b	C	C	C	C	C	F		C	F		F																				
	23,CC	F-P		C	A	C	C	R	F		R	F		F																				
	24,CC	F-P		C	A	C	C	F	F		R	F		F																				
	25,CC	F-P	CN5a	A	A	C	C	R	F		R	F		F																				
	26,CC	F-P		A	A	C	C	R	F		R	F		F																				
	27,CC	F-P		C	C	C	R	R	F		F	F		F																				
	28,CC	F	CN4	C	C	F	R				R																							C
	29,CC	F-P		F	C	C					R																							C
	30,CC	P-F		R	A	C					R																							A
	31,CC	F-P		C	C	C					F																							C
	32,CC	F-P		F	F	C	R				F																							F

Note: Symbols as in Table 2.

Table 4. Occurrence of calcareous nannofossils in core-catcher samples, DSDP Hole 573, Leg 85.

Age	Sample	Preservation	Nannofossil zones	*Gephyrocapsa oceanica*	*Gephyrocapsa caribbeanica*	*Calcidiscus leptoporus*	*Helicosphaera carteri*	*Umbilicosphaera sibogae*	*Cenatolithus crassus*	*Thoracosphaera* sp.	*Pseudoemiliania lacunosa*	*Helicosphaera sellii*	*Discoaster brouweri*	*Discoaster brouweri* (3 rays)	*Coccolithus pelagicus*	*Calcidiscus tropicus*	*Discoaster pentaradiatus*	*Discoaster tamalis*	*Discoaster asymmetricus*	*Cenatolithus rugosus*	*Reticulofenestra minutulus*	*Discoaster variabilis*	*Sphenolithus abies*	*Reticulofenestra pseudoumbilica*	*Discoaster surculus*	cf. *Discoaster sanmiguelensis*	*Amaurolithus primus*	*Amaurolithus tricorniculatus*	*Cenatolithus acutus*	*Amaurolithus delicatus*	*Discoaster quinqueramus*	*Amaurolithus amplificus*	*Discoaster berggrenii*	*Discoaster loeblichii*	*Discoaster bellus*	*Discoaster challengeri*
Pleist.	573-1,CC	F-G	CN14 b	A	A	C	F	R	R																										
	2,CC	F-G	a	A	A	C	F		R		C	A																							
	3,CC	F-G	CN13	C	A	C	F	R	R			A	F																						
Pliocene	4,CC	F	CN12			F	R		R			A	C	R	C	C																			
	5,CC	F				F	C			F			F		C	C	F	F	R															
	6,CC	P				A	F		R			C	F	R			R		R	R	A	F													
	7,CC	F	CN11			C	R		F				A		C	F			R	R	A	R	A	A	R	R									
	8,CC	F	CN10						F				C		C	C	F		R	F	A	R	A	A	F	R	R								
	9,CC	P				C									A	C	R					R	C	A	C		R	R							
Miocene	10,CC	P-F					R						F		C	C	C					C	A	A	C	R			R	C					
	11,CC	F											C		C		R					R	C	C	C	R			R	R	R				
	12,CC	F-P	b										F		A		R					C	A	C					R	R	R				
	13,CC	F-P				F	R						F	R	C	C					C	F			F					R	R		F			
	14,CC	F-P	CN9 —				R						F		C	C					C	F			F					R	R	R				
	15,CC	F-P				F	R						F		C	C					C	F	C							R	R				
	16,CC	F-P				C							C		C	C					C	F	C												
	17,CC	F-P	a			C	R						C	R	C	C					A	C	C	R	F										
	18,CC	F-P				C							A	R	C	C					F	A	A	R	F						R				
															F	R	F					A	C	A						R					
	19,CC	F-P	CN8			C							F		C	C						F	A	C											

Note: Symbols as in Table 2.

in age (see below). Preservation of nannofossils is rather poor throughout both sections, with notable evidence for corrosion and overgrowth.

Hole 575

Hole 575 (Table 8) extends possibly from Pliocene (the core-catcher sample of Core 1 yielded only very rare *Discoaster brouweri*) to the middle Miocene *Sphenolithus heteromorphus* Zone (CN4). From Cores 2 through 7 the *D. quinqueramus* through *D. exilis* Zones (Zones CN10c through CN5) are represented, but the assemblages are too poorly preserved to allow more refined zonal assignments. Marker species are not present, and even some of the most resistant species are notably sporadic in their occurrence. Samples from Cores 8 through 11 yielded abundant *Sphenolithus heteromorphus*, and these cores are thus assigned to the *S. heteromorphus* Zone (CN4).

Hole 575A

The samples from Hole 575A (Table 9) extend from the *Sphenolithus heteromorphus* Zone (CN4) through the *Triquetrorhabdulus carinatus* Zone (CN1). The *S. heteromorphus* Zone grades into the subjacent *Helicosphaera ampliaperta* Zone (CN3) from which, however, it cannot be separated because of inadequate preservation of marker species. The next lower zone, the *S. belemnos* Zone (CN2), extends from Cores 6 through 9. The remaining interval, Cores 10 through 33, is assigned to the *Triquetrorhabdulus carinatus* Zone (CN1). Further subdivision of the relatively long Zone CN1 is not practical in this section because the two critical marker species *Discoaster druggii* and *Cyclicargolithus abisectus* are unreliable. The first is a generalized asterolith species that is particularly susceptible to overgrowth and alteration; the second is a solution-resistant form whose abundance is enhanced in a residual assemblage, and hence, a true acme is not necessarily recognizable.

One line of evidence that may indicate that Hole 575A penetrated into the uppermost Oligocene is the presence of *Helicosphaera recta* in Core 31; however, that is an isolated occurrence and may be spurious.

REFERENCES

Bukry, D., 1975. Coccolith and silicoflagellate stratigraphy, northwestern Pacific Ocean, Deep Sea Drilling Project Leg 32. *In* Larson, R. L., Moberly, R., et al., *Init. Repts. DSDP*, 32: Washington (U.S. Govt. Printing Office), 677–701.

Gartner, S., Chen, M. P., and Stanton, R. J., 1983. Late Neogene nannofossil biostratigraphy and paleoceanography of the northeastern Gulf of Mexico and adjacent areas. *Mar. Micropaleontol.*, 8:17–50.

Okada, H., and Bukry, D., 1980. Supplementary modification and introduction of code numbers to the low latitude coccolith biostratigraphic zonation (Bukry, 1973; 1975). *Mar. Micropalentol.*, 5: 321–325.

Date of Initial Receipt: 28 October 1983
Date of Acceptance: 6 April 1984

Table 5. Occurrence of calcareous nannofossils in core-catcher samples, DSDP Hole 573B, Leg 85.

Age	Sample (interval in cm)	Preservation	Nannofossil zones	*Calcidiscus leptoporus*	*Sphenolithus abies*	*Coccolithus pelagicus*	*Discoaster variabilis*	*Reticulofenestra pseudoumbilica*	*Discoaster brouweri*	*Discoaster loeblichii*	*Discoaster bellus*	*Helicosphaera granulata*	*Discoaster neohamatus*	*Discoaster bollii*	*Cronomyckus nitescens*	*Helicosphaera parallela*	*Sphenolithus heteromorphus*	*Cyclicargolithus floridanus*	*Discoaster exilis*	*Discoaster deflandrei*	*Coccolithus miopelagicus*	*Discoaster calculosus*	*Sphenolithus belemnos*	*Triquetrorhabdulus carinatus*	*Sphenolithus conicus*	*Sphenolithus morjformis*	*Sphenolithus dissimilis*	*Cyclicargolithus abisectus*	*Sphenolithus ciperoensis*	*Helicosphaera intermedia*	*Sphenolithus distentus*	*Discoaster tani*	*Reticulofenestra bisecta*	*Sphenolithus pseudoradians*	*Helicosphaera compacta*	*Sphenolithus predistentus*	*Helicosphaera reticulata*	*Helicosphaera euphratis*	*Reticulofenestra umbilica*	*Lepidolithus larvalis*
Miocene	573B-1,CC	F-P	CN8	C	A	C	C	F	F	F	R			R																										
	2,CC	P		C	C	F	F	F	F	R	C		R																											
	3,CC	P		F	C	E	F	R	R																															
	4,CC	P	— —	C	C	F	F	A																															
	5,CC	P	CN7 to CN5	C	F	F	A	A	F			R	R	F	R	R																								
	6,CC	P		R	C	F	F	A																																
	7,CC	P		C	A	C		A																																
	8,CC	P		C		C		A				R																												
	9,CC	P	CN4 to CN3	R	A	C		A			C	C		C			C	F	F																					
	10,CC	P		R	F	C	C	C			F	R		R			A	C	C	F	R																			
	11,CC	P		R	C	C	C	C						R			C	C	cf.	cf.	F																			
	12,CC	P		cf.	C	C	C	F						C			C	C	cf.	C																				
	13,CC	P		cf.	C	C	C	F						C			C	C	cf.	C																				
	14,CC	P	CN2		C	C		F						C	F				F		F	R	F																
Oligocene	15,CC	P	CN1	C	C	C		F	F					F	F			C	F	R	F			C	C														
	16,CC	P-F		C	C	C		F						F	F			C	F	C				C	C														
	17,CC	P-F		C	C	C								F				A	F	A				C	C														
	18,CC	P-F		C	C	C												C	F	A				C	C														
	19,CC	P-F		C	C	C								F				C	F	C		F		C	C														
	20,CC	P-F		C	C	C		F						C				A	C	A				C	A														
	21,CC	P-F	b	C		R		R						A				A	F	A				C	F				R										
	22,CC	P-F				R		R						A				A	F	A				C	F				R										
	23,CC	P-F				R								C				C	F	C				C	F				R										
	24,CC	P				C								C				C	F	C				C	F				R										
	25,CC	P	CP19 —			C								C				C	F	C				C	F				R										
	26,CC	P				C		F						C				C	F	C				C	F				R										
	27,CC	P	a			C								C				C	F	C				C	F				R										
	28,CC	P				C		F						A		R		A	F	A				C	F				R										
	29,CC	P				C								C		C		C	F	C				C	F				R										
	30,CC	P				C								C				C	F	C				C	F				R										
	31,CC	P	CP18 to CP17	C		C		C						A				A	F	A				C	F				R										
	32,CC	P		C		C		F						C				C	F	C				C	F				R										
	33,CC	P		C		C		C						C				C	F	C				C	F				R										
	34,CC	P		C		C		C						C				C	F	C				C	F				R										
	35,CC	P		C		C		C						C				C	F	C				C	F				R										
	36,CC	P		C		C		C						C				C	F	C				C	F				R										
	37-2, 23–24	P	— —	C		C		C						C				C	F	C				C	F				R										
	38,CC	P	CP16	C		C		C																					R										
	39,CC	P		C		C		C						C				C											C										
	40,CC	P		C		C		C																					C										

Note: Symbols as in Table 2.

Table 6. Occurrence of calcareous nannofossils in core-catcher samples, DSDP Hole 574, Leg 85.

Age	Sample	Preservation	Nannofossil zones	*Gephyrocapsa oceanica*	*Pseudoemiliania lacunosa*	*Calcidiscus leptoporus*	*Calcidiscus tropicus*	*Discoaster brouweri*	*Discoaster iamalis*	*Cenatolithus crisatus*	*Discoaster pentaradiatus*	*Coccolithus pelagicus*	*Discoaster surculus*	*Discoaster variabilis*	*Sphenolithus abies*	*Reticulofenestra pseudoumbilica*	*Helicosphaera carteri*	*Discoaster asymmetricus*	*Discoaster brouweri* (5 rays)	*Cenatolithus acutus*	*Amaurolithus primus*	*Discoaster quinqueramus*	*Discoaster berggrenii*	*Triquetrorhabdulus rugosus*	*Amaurolithus delicatus*	*Discoaster bellus*	*Discoaster loeblichii*	*Helicosphaera granulata*	*Discoaster challengeri*	*Discoaster hamatus*	*Discoaster prepentaradiatus*	*Discoaster kugleri*	*Discoaster bollii*	*Discoaster exilis*	*Cornococtus nitescens*	*Discoaster deflandrei*	*Sphenolithus heteromorphus*	*Coccolithus miopelagicus*	*Discoaster druggii*	*Cyclicargolithus floridanus*
Pleist.	574-1,CC	P	CN14a	R	C	F	C																																	
Plio.	2,CC	P	CN12		C		F	C	R	R	R	R	R	R																										
	3,CC	P	CN11				C	C		R		C	F		R	C	C	R		R	R																		
	4,CC	P					C	C							C	C	C																						
	5,CC	P	CN10 c/b				F	C				F	F		R	A	C	R			F																		
	6,CC	P	CN9				C	C				C			A							R	F	R	R														
	7,CC	P	CN8b				C	C				C			F	A	C	R				A		R		F	F	F										
	8,CC	P	CN7				C	C							C	R	C		R			A		F														
	9,CC	P					F	C				C			C	A	C					A																	
Miocene	10,CC	P	CN6 to CN5b			F						C			C	F	C							cf.	R								F						
	11,CC	P				C						C			F	A	C	R															R						
	12,CC	P					R					C			R	A	C	F						R									R						
	13,CC	P			F	F	R					C			R	A	A	A						R									R						
	14,CC	P			F	aff.						C			C	A	A	R															R						
	15,CC	P			F		cf.					C			A	A	C	R															R						
	16,CC	P			F	aff.						C			R	A	C	R															R						
	17,CC	P	CN5a		F					C		C			C	A																	F	F					
	18,CC	P			F	R				C		C			C	A																	F	F					
	19,CC	P			C	F				A		A			R	A								R									R	R					
	20,CC	P	CN4							A		A			A	A																	R	R					
	21,CC	P								C		C			A	C		F						R									R						
	22,CC	P				F				C		C			C	C																	R	C	A	F			
	24,CC	P					aff.			C		C			C	C		F															R	C	C	F			
	25,CC	P								C		C			C	C		F															R						
	26,CC	P								C		C			F	C	F							R									R	A	R				
	27,CC	P								A		C			F	C	F							R									R	F	A	R			
	28,CC	P								C		A			cf.	C	R																F	C	F				
	29,CC	P								A		C			cf.	A								F									R	C	A	R			
	30,CC	P								C		A			C	C								cf.									R	C	A	R			
	31,CC	P				F						C																											

Note: Symbols as in Table 2.

Table 7. Occurrence of calcareous nannofossils in core-catcher samples, DSDP Hole 574C, Leg 85.

Age	Sample	Preservation	Nannofossil zones	*Discoaster exilis*	*Coccolithus miopelagicus*	*Coccolithus pelagicus*	*Discoaster deflandrei*	*Sphenolithus morjformis*	*Cribrocrvcus Jordanus*	*Cyrtocrvcus nitescens*	*Discoaster calcitrosus*	*Sphenolithus heteromorphus*	*Discoaster variabilis*	*Calcidiscus leptoporus*	*Sphenolithus belemnos*	*Sphenolithus abies*	*Reticulofenestra pseudoumbilica*	*Helicosphaera granulata*	*Triquetrorhabdulus carinatus*	*Sphenolithus conicus*	*Helicosphaera intermedia*	*Triquetrorhabdulus milowii*	*Cribrocrvcus absecrtus*	*Sphenolithus cyperensis*	*Helicosphaera wilcoxoni*	*Dictyococcites bisectus*	*Sphenolithus dissimilis*	*Lepidocyclus larvalis*	*Chiasmolithus altus*	*Helicosphaera truncata*	*Helicosphaera parallela*	*Discoaster tani*	*Helicosphaera compacta*	*Sphenolithus predistentus*	*Sphenolithus pseudoradians*	*Reticulofenestra umbilica*	*Braarudosphaera serraculoides*	*Cricocoscolithus formosus*	*Isthmolithus recurvus*	*Helicosphaera euphratis*	*Discoaster barbadiensis*	*Cribrocentrum reticulatum*	*Discoaster saipanensis*	*Helicosphaera reticulata*
Miocene	574C-1,CC	P	CN5	F	R	C	C	C	C	R	F			C																														
	2,CC	P	CN4	R		C	C	C	C	R	F	C	C	R		C	F	R	C																									
	3,CC	P	CN3			C	C	C	C	C	F	R	C																															
	4,CC	P	CN2		R	A	C	C	C	F	F			C			F		C																									
	5,CC	P	c/b		C	F	C	C	F	R	F	F	F	C		C	C		R	F																								
	6,CC	P				C	C	C	C	C	R	F	F	C		C	C		R	F																								
	7,CC	P				C	C	C	C	C	R	R	F	C		C	C		R	R																								
	8,CC	P					C	F	C	C	R	R	F	C		C	C		R	R																								
	9,CC	P				R	C	C	C	C	R	R	F	C		C	C		R	R																								
	10,CC	P	CN11				F	C	C	C	VA	R	R	C		C	C		R	R	F																							
	11,CC	P					C	C	C	C	VA	R	R	C		F	F		R	F	F																							
	12,CC	P						F	F	C	C	A	R	C		F	F		R	F	F																							
	13,CC	P						C	F	F	C	C	A	F		F	F		R	F	F		cf.																					
	14,CC	P	a?						C	F	C	C	A	F	R		F		R	C	F		cf.																					
	15,CC	P							C	C	C	C	A	F	R		cf.		R	C	F	R	cf.																					
	16,CC	P								C	C	C	A	C	C		cf.		R	C	C		cf.																					
	17,CC	P									C	C	A	C	A		cf.		R	C	C		C																					
	18,CC	F	CP19				C	C	A	A							cf.		R					C	R																			
	19,CC	P					A	R	C	C	R						cf.							F	R																			
	20,CC	P					C	R	C	C	F						cf.							F	R																			
Oligocene	21,CC	P	CP18 to CP17				C	C	A	F																																		
	22,CC	P					C	F	C	C	A	R	R																															
	23,CC	P					C	C	C	A	A	R	R																															
	24,CC	F					C	C	C	A	A	R	R								R																						
	25,CC	F					C	F	C	A	A	F	C	A																														
	26,CC	P					C	F	A	C	A																																	
	27,CC	P					F	A	C	A																																		
	28,CC	F					C	A	C	A																																		
	29,CC	P	c				C	R	C	C																																		
	30,CC	P					C	C	C	F																																		
	31,CC	P	CP16				C	C	C																																			
	32,CC	P	b/a				C	C	F	F																																		
	33,CC	P					C	F	A	C																																		
	34,CC	P					C	F	A	C																																		
Eoc	35,CC	P	CP15			A		F																		F						R			C	R	C					

Note: Symbols as in Table 2.

Table 8. Occurrence of calcareous nannofossils in core-catcher samples, DSDP Hole 575, Leg 85.

Age	Sample	Preservation	Nannofossil zones	*Discoaster brouweri*	*Coccolithus pelagicus*	*Reticulofenestra minutulus*	*Calcidiscus tropicus*	*Discoaster surculus*	*Calcidiscus leptoporus*	*Sphenolithus abies*	*Discoaster pentaradiatus*	*Ceratolithus rugosus*	*Discoaster variabilis*	*Reticulofenestra pseudoumbilica*	*Discoaster asymmetricus*	*Discoaster quinqueramus*	*Discoaster deflandrei*	*Helicosphaera granulata*	*Coccolithus miopelagicus*	*Helicosphaera carteri*	*Cyclicargolithus floridanus*	*Coronocyclus nitescens*	*Sphenolithus heteromorphus*	*Discoaster exilis*
Plio.	575-1,CC	VP	CN12-	VR																				
	2,CC	P	CN10c	P	C	A	C	F	R	F	R	R	R	C	R									
Miocene	3,CC	P		P	C				C	F	F		F	C		A								
	4,CC	P	CN9b	P	C		F		C	C			R	C										
	5,CC	P	to	P	C				C	C			cf	A			F	R	R					
	6,CC	P	CN5 b/a	P	C				C	A			cf	A			F	F						
	7,CC	P		P	A				R	A			cf	A			R			F	C	R		
	8,CC	P		P	A				R					A			R	F			C	R	A	R
	9,CC	P	CN4	P	A				R	A				C			R	F			C		A	R
	10,CC	P		P	C				R	C				C			R	C			C		A	R
	11,CC	P		P	C				F	C				C			F	F		R	C	F	A	

Note: Symbols as in Table 2; V = very.

Table 9. Occurrence of calcareous nannofossils in core-catcher samples, DSDP Hole 575A, Leg 85.

Age	Sample	Preservation	Nannofossil zones	*Discoaster exilis*	*Coccolithus pelagicus*	*Sphenolithus morjformis*	*Cyclicargolithus floridanus*	*Coronocyclus nitescens*	*Reticulofenestra pseudoumbilica*	*Sphenolithus heteromorphus*	*Discoaster deflandrei*	*Coccolithus miopelagicus*	*Helicosphaera intermedia*	*Sphenolithus belemnos*	*Triquetrorhabdulus carinatus*	*Sphenolithus abies*	*Cyclicargolithus abisectus*	*Orthorhabdus serratus*	*Sphenolithus dissimilis*	*Helicosphaera granulata*	*Helicosphaera parallela*	*Helicosphaera obliqua*	*Sphenolithus capricornutus*	*Sphenolithus conicus*	*Helicosphaera recta*
	575A-1,CC	P		R	C	C	A	R	C	A															
	2,CC	P	CN4	R	C	C	A	F	C	A	F														
	3,CC	P	to	R	C	C	A	F	C	C	C														
	4,CC	P	CN3	R	C	C	C	F	C	C		R													
	5,CC	P			C	C	C	F	C	C		R	R												
	6,CC	P			C	C	C	F	C		C			F											
	7,CC	P	CN2		C		F	F	C					A	F	C									
	8,CC	P			C	C	C	F	C		F	R		C											
	9,CC	P			C	F	C	F	C		R			F		C	R								
	10,CC	P			C	C	C	F	C		R				R	R	F	C	F						
	11,CC	P			C	C	R	F	A						R	R	F	F	F						
	12,CC	P			A	C	C	F	C		C	F				F	F	cf.	F						
	13,CC	P			C	C		F	A		F				F	A	F			F					
	14,CC	P			A	C	C	F	C		C					A	F								
Miocene	15,CC	P			C	C	C		A						C	A	F			R					
	16,CC	P			C	F	C		A		F				F	C	F								
	17,CC	P			C	C	C		A		C				C	C	C								
	18,CC	P			C	C	C		cf.								F								
	19,CC	P			C	C	C				C				F	F	C								
	20,CC	P			C	C	A	R	cf.		C	cf.					C								
	21,CC	P	CN1		C	C	A	R	F		F	C			R	R	C								
	22,CC	P			A	C	A	R	C		F	C			R	C	F								
	23,CC	P			F	C	A	F	C		F	C			F		F								
	24,CC	P			C	C	A	R	R		A	C			R	A	C								
	25,CC	P			F	C	A	R	F		C	C			F	A	C			R	R				
	26,CC	P			C	C	A	R	F		C	F			F	A	C			R					
	27,CC	P			F	R	A	R	R		C	C			F	A	C				R				
	28,CC	P			F	C	A	R	R						R	A	C			R					
	29,CC	P			F	C	A	R	R						R	F	C			R		R	R		
	30,CC	P			F	F	A	R			F				R	A	C			R					
	31,CC	P			C	C	A	R	F		C		R		R	C	C			R				R	R
	32,CC	P			C	F	A	R	F		F		R		F	C	C			R		R		R	
Oligo.?	33,CC	P			C	C	A	R	F				R		F		C		F	R				R	

Note: Symbols as in Table 2.

16. PLANKTONIC FORAMINIFERAL BIOSTRATIGRAPHY OF EASTERN EQUATORIAL PACIFIC SEDIMENTS, DEEP SEA DRILLING PROJECT LEG 85[1]

Tsunemasa Saito, Department of Earth Sciences, Yamagata University[2]

ABSTRACT

Tropical planktonic foraminifers occur throughout the sequences at all sites of Leg 85, and the standard planktonic foraminiferal zonation of Blow (1969) is applicable to most of the recovered sequences. However, the abundance and state of preservation of foraminifers decline markedly in certain intervals because of the effects of dissolution. Although siliceous microfossils studied on this leg indicate recovery of nearly complete records for the Pleistocene to Oligocene interval, the planktonic foraminiferal biostratigraphy is interrupted by strongly dissolved sections at all sites. Particularly, faunas assignable to Zone N7 (early Miocene) and Zone N15–16 (early late Miocene) are almost totally unrecognizable throughout the eastern equatorial Pacific. Well-preserved and diverse planktonic foraminifers occur in the lower middle Miocene, where the evolutionary developments of *Orbulina universa* d'Orbigny and *Globorotalia fohsi* Cushman and Ellisor are well represented. The *Orbulina* first appearance datum is observed to be nearly coincident with the last occurrence level of the diatom *Annellus californicus* Tempère, thus establishing an age of 15 Ma for this datum by using the paleomagnetic calibration of the diatom datum. Moderately well-preserved late Eocene planktonic foraminifers occur in the carbonate sediments immediately overlying the basalt basement at Sites 573 and 574. The Eocene–Oligocene faunal transition, however, is masked at both sites by an intercalation of metalliferous layers containing no planktonic foraminifers.

INTRODUCTION

With the use of a newly developed hydraulic piston corer (HPC), Leg 85 attempted to recover from the eastern equatorial Pacific undisturbed Cenozoic sequences suitable for high-resolution biostratigraphy. The region covered by Leg 85 is in the equatorial high-productivity zone, where steady accumulation of siliceous and carbonate shells of planktonic microorganisms has created a belt of thick sediment piles on the seafloor. The crest of this belt lies slightly north of the equator (4°N at 180°W) and trends toward the equator to the east. Four earlier DSDP cruises (Legs 5, 8, 9, and 16) drilled into this belt of sediment piles, and Leg 85 established five additional drill sites (Fig. 1 and Table 1).

A large body of knowledge now exists on the planktonic foraminiferal biostratigraphy of this region. Although the pioneering work of the Swedish Deep Sea Expedition was the first to thoroughly describe the sediment types of this region, it was Parker (1967) who first established a planktonic foraminiferal zonation for the upper Miocene to Pleistocene sediments of the tropical Pacific region. Subsequent studies by Hays et al. (1969) and Saito et al. (1975) integrated microfaunal successions with geomagnetic reversal sequences down to upper Miocene and were able to paleomagnetically calibrate microfossil first and last appearances within a time resolution of several hundred thousand years. These earlier studies are all based on piston cores, and hence research was limited to upper Neogene sections.

The first successful attempt to study older Cenozoic sediments in this belt of thick sediment piles was made during Leg 8. Sediments as old as middle Eocene were recovered on this cruise by intermittent coring. Beckman (1971) described and illustrated most of the zonal marker species of planktonic foraminifers used for age determination. One nearly continuous calcareous record was obtained during Leg 9 from Hole 77B. The foraminiferal biostratigraphy of Hole 77B was initially described by Jenkins and Orr, who also illustrated many species (Jenkins and Orr, 1972, pls. 1 to 41). The sedimentary record at Hole 77B has since become a focus of intensive study by many micropaleontologists; six papers on planktonic foraminifers alone have been written, mostly by Keller and co-authors (cited in Keller and Barron, 1983).

Although the foraminiferal sequence at Hole 77B provides one of the few nearly complete Neogene faunal records, its foraminiferal assemblages are severely affected by dissolution. The effects of dissolution were such that Jenkins and Orr (1972) developed a new zonation (distinct from the one defined by Blow [1969]), which was largely based on solution-resistant species. Keller (1980, 1981), however, was able to apply Blow's zones to at least the Miocene sequence.

Dissolution of planktonic foraminifers is also a factor in most of the sequences cored during Leg 85. One exception is the lower middle Miocene interval covering the evolutionary development of *Globorotalia fohsi* and its subspecies from their ancestor *G. peripheroronda*. To aid age assignments and comparisons of the results of Leg 85 with studies of other areas, I have applied, as well as possible, the standard zonation of Blow (1969) to the planktonic foraminiferal assemblages in Leg 85 samples. There are a few instances, however, where I have used a second-order correlation to approximate the

[1] Mayer, L., Theyer, F., et al., *Init. Repts. DSDP*, 85: Washington (U.S. Govt. Printing Office).

[2] Address: Department of Earth Sciences, Faculty of Science, Yamagata University, Yamagata, 990 Japan.

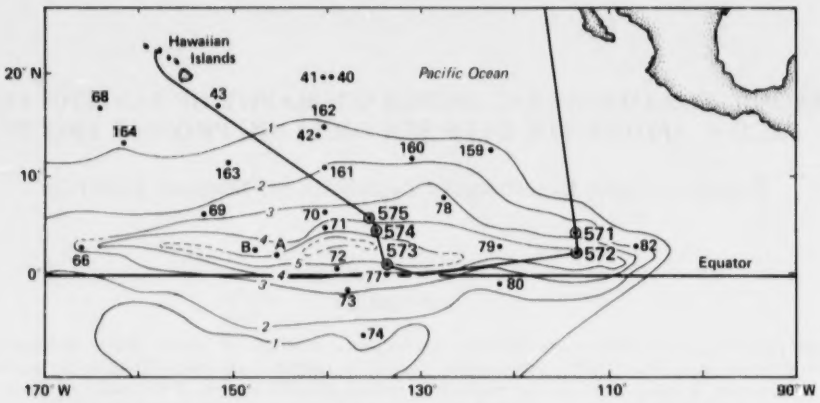

Figure 1. Cruise track and locations of Leg 85 drill sites in the eastern equatorial Pacific. Contours in tenths of seconds of two-way traveltime. Previous holes drilled on Legs 5 (Sites 40–43), 8 (Sites 66–74), 9 (Sites 77–82), and 16 (Sites 159–164) are also shown, in addition to the locations of two piston cores, V24-59 (A) and RC12-66 (B), for which Hays et al. (1969) and Saito et al. (1975), respectively, established a combined microfossil and paleomagnetic stratigraphy.

Table 1. Leg 85 site data.

Hole	Latitude	Longitude	Water depth (m)	Sub-bottom depth (m)	Number of cores	Total sediment recovered (m)	Oldest sediment cored
571	03°59.84′N	114°08.53′W	3962	0–7.11	1	7.11	Pleistocene
572	01°26.09′N	113°50.52′W	3893	0–18.7	2	9.25	Pleistocene
572A	01°26.09′N	113°50.52′W	3893	0–154	17	154.35	up. Miocene
572B	01°26.09′N	113°50.52′W	3893	154–169.4	4	19.95	up. Miocene
572C	01°26.09′N	113°50.52′W	3893	0–169.5	20	161.56	up. Miocene
572D	01°26.09′N	113°50.52′W	3893	151–489.0	34	258.87	mid. Miocene
573	00°29.91′N	133°18.57′W	4301	0–158.6	19	159.4	up. Miocene
573A	00°29.91′N	133°18.57′W	4301	14.0–57.7	6	53.5	low. Pliocene
573B	00°29.91′N	133°18.57′W	4301	138.5–529.0	43	279.7	up. Eocene
574	04°12.52′N	133°19.81′W	4561	0–206.5	31	208.93	low. Miocene
574A	04°12.52′N	133°19.81′W	4561	6.0–186.2	23	180.74	low. Miocene
574B	04°12.52′N	133°19.81′W	4561	185.0–194.0	1	9.45	low. Miocene
574C	04°12.53′N	133°19.81′W	4561	194.5–532.5	37	197.35	low. Eocene
575	05°51.00′N	135°02.16′W	4536	0–98.6	11	99.35	low. Miocene
575A	05°51.00′N	135°02.16′W	4536	93.8–208.4	33	140.53	low. Miocene
575B	05°51.00′N	135°02.16′W	4536	3.3–119.0	14	118.68	low. Miocene
575C	05°51.00′N	135°02.16′W	4536	0–15.8	2	15.91	up. Miocene

standard zonal boundary. Tables 2 through 6 present the stratigraphic distribution of planktonic foraminifers, their state of preservation, and abundances. Since so much is already known about the planktonic foraminifers of this region, only a few taxonomic comments are added to those taxa pertinent to discussion (see Appendix), and the plate illustrations cover only selected species.

METHODS

The planktonic foraminiferal biostratigraphy presented in this paper is based primarily on the onboard examination of core-catcher samples. When a foraminiferal zone boundary occurred between two core-catcher samples, additional samples from each core section were examined on shore to narrow the boundary. Samples of approximately 10 cm^3 were washed through a 250-mesh screen (0.62-μm opening) and dried. Unconsolidated sediments were soaked in water, and when necessary, disaggregation was facilitated by the addition of small amounts of hydrogen peroxide. Hydrogen peroxide was also routinely added to more consolidated sediments. Much more consolidated or semi-indurated sediments encountered in the lower parts of the sedimentary columns were disaggregated by using a petroleum solvent, Varsol or Naphtha. In this technique, samples are thoroughly oven dried at about 130°C and are soaked with the solvent while they are still hot. After the excess fluid is drained, the solvent-soaked sediments are boiled in water containing a small quantity of sodium metaphosphate until complete disaggregation occurs. In the final washing process, the solvent can be easily driven off from both the sample and the washing screen by applying a jet of multisurface spray cleaner, such as Fantastik®

Quantitative analyses of species abundance shown in Tables 2 through 6 were made with the aid of the visual percentage estimation chart of Terry and Chilingar (1955; reproduced in Scholle, 1979, p. vii). (See the footnotes to Tables 2 and 3 for explanations of the abbreviations.)

I have attempted to graphically illustrate the varying degrees of foraminiferal dissolution by calculating for each assemblage the 10-point foraminifer solution code of Berger and von Rad (1972), in which a high solution-code number indicates stronger dissolution. These plots can be found in the site chapters and are not reproduced here.

Saito (1976) showed that systematic changes with time in the coiling direction of the planktonic foraminiferal genus *Pulleniatina* provide useful datum levels for interregional correlation of Pliocene–Pleistocene sediments. To establish additional criteria for the biostratigraphy, counts of *Pulleniatina* coiling direction were made for Holes 572C and 573 (Fig. 2). More than 100 specimens were randomly picked whenever possible from each assemblage, and the percentages of right-coiling and left-coiling individuals were determined.

Table 2. Occurrence and estimated abundance of planktonic foraminifers at Site 571.

Age	Zone	Sample (interval in cm)	Abundance	*Globigerinella aequilateralis*	*Globigerinella calida*	*Beella digitata*	*Globigerina falconensis*	*Globigerina rubescens*	*Globigerinoides conglobatus*	*Globigerinoides ruber elongatus*	*Globigerinoides ruber ruber (pink)*	*Globigerinoides ruber ruber (white)*	*Globigerinoides sacculifer*	*Orbulina universa*	*Sphaeroidinella dehiscens*	*Globigerinita glutinata*	*Globigerinita iota*	*Globorotaloides hexagona*	*Globoquadrina conglomerata*	*Globoquadrina pseudofoliata*	*Pulleniatina finalis*	*Pulleniatina obliquiloculata*	*Neogloboquadrina eggeri*	*Globorotalia crassula*	*Globorotalia eastropacia*	*Globorotalia inflata*	*Globorotalia menardii*	*Globorotalia scitula*	*Globorotalia tumida tumida*	*Globorotalia truncatulinoides*	*Globorotalia ungulata*
Pleistocene	N23	571-1-1, 140–144	A	F	T	T		T	T			F	R	F		R	T		R		R	F	C			R	F		C		C
		1-2, 119–120	A	R	T			R	R	R		F	F	T	R	R	T	T	F		R	F	F	T		C	T		R		R
		1-2, 131–132	A	R	R			R	R	R	T	R	F	R	T	R	R	T	R	R	R	F	F	T		C	T		F		
		1-3, 14–15	F	T	T					T			R	T						R		R	T			F			R		
		1-3, 42–43	F	T					T			T	F	T	T				F	T	R	R	R			C			R		
		1-3, 101–102	A	F				R	R	T	R	R	F	R		R	R	T	F	T	R	F	F	T			C			F		T
		1-3, 143–145	A	F	T						R		F	R		T		T	R	F	F	F	F				F			C		F
		1-4, 65–66	A	R	T	T		T	T	F		F	F	R		F		T	R	R	F	C	C				F			F		R
		1,CC, 11–12	A	R	T		T		R			F	F	F	T	T			F	F	C	C	F				C	T	C	T	T

Note: A = abundant (>10% of assemblage); C = common (3–10%); F = few (0.5–3%); R = rare (<0.5%); T = trace (only one or two specimens in entire assemblage).

MODIFICATION TO THE STANDARD ZONATION

The dissolution of planktonic foraminifers observed in certain intervals of the sequences recovered on Leg 85 necessitates a second-order correlation to approximate the standard zonal boundary proposed by Blow (1969).

I have placed the top boundary of Zone N19 at the extinction level of *Sphaeroidinellopsis seminulina* (Schwager). This cortex-covered species is fairly resistant to solution and provides a reliable correlation datum. The top of Zone N19 was initially defined by Banner and Blow (1965) as the last occurrence level of *Globoquadrina altispira* (Cushman and Jarvis). According to the paleomagnetic stratigraphy of Saito et al. (1975), the extinction level of *S. seminulina* occurs at the top of the Mammoth Subchron (3.08 Ma) and that of *G. altispira* at the top of the Kaena Subchron (2.92 Ma), both in the Gauss Chron. They are indeed very close. Furthermore, I have excluded Zone N20 from the Leg 85 sequences for several reasons. In their initial proposal of the Neogene numerical zonation, Banner and Blow (1965) defined Zone N20 to be the interval following the extinction of *G. altispira* and before the first appearance of *G. tosaensis*. Both Parker (1967) and Hays et al. (1969), however, showed that the ranges of these two species actually overlap in the tropical Indo-Pacific, which precludes the establishment of a zone based on the absence of these two species. Blow (1969) subsequently redefined Zone N20 by introducing two new subspecies, *Globorotalia acostaensis pseudopima* and *G. tosaensis tenuitheca*. The first occurrence of the former defines the lower limit of the zone, and the first occurrence of the latter marks the upper limit. Blow (1970) further justified his 1969 redefinition in yet another discussion on the standard zonation. This definition of Zone N20, however, poses two correlation problems. One is the uncertainty of taxonomically recognizing these two zonal index taxa, both of which were erected at a subspecific level. The second is the stratigraphic position of the zonal reference section chosen for Zone N20. Blow (1969) designated the locality and level of Sample ER.156, within the Bowden Formation of Jamaica, West Indies, as the primary reference section. The prefix "ER." stands for E. Robinson of the University of the West Indies, who collected samples for Blow and who described the Neogene section of Jamaica (Robinson, 1969). I have examined planktonic foraminifers of this sample, which was kindly supplied by Dr. Robinson, and found among others *Globorotalia crassaformis* (Galloway and Wissler), *G. exilis* Blow, *G. miocenica* Palmer, *G. truncatulinoides* (d'Orbigny), *Neogloboquadrina dutertrei* (d'Orbigny), and *Globigerinoides fistulosus* (Schubert). The joint occurrence of *Globorotalia exilis, G. miocenica*, and *G. truncatulinoides* enables a correlation of Sample ER.156 with the uppermost Matuyama Chron of the paleomagnetic stratigraphy at about the Olduvai Subchron. Zone N21 is, however, defined as the interval prior to the first appearance of *G. truncatulinoides*, an event that occurred shortly before Olduvai Subchron time. Thus, the Zone N20 reference section is in reality younger than Zone N21. To circumvent this stratigraphic dilemma, I excluded Zone N20 from the zonal scheme and placed Zone N21 to directly overlie Zone N19 at the extinction level of *S. seminulina*.

The first appearance level of *Globigerinatella insueta* Cushman and Stainforth occurs in a solution-affected interval at both Sites 574 and 575. This level defines the N5/N6 zonal boundary. The last appearance level of *Globigerina binaiensis* Koch is instead used to approximate this boundary. In carbonate-rich sequences, these two paleontologic events are shown to occur within a close stratigraphic interval (Srinivasan and Kennett, 1981).

Zone N4 as defined by Blow (1969) is the second example where his original definition came to be nonwork-

Table 3A. Occurrence and estimated abundance of planktonic foraminifers, Holes 572 and 572A.

Age	Zone	Sample (interval in cm)	Abundance	Preservation	*Globigerinella aequilateralis*	*Globigerinella calida*	*Globigerinella praecalida*	*Beella digitata*	*Beella praedigitata*	*Globigerina bulloides*	*Globigerina decoraperta*	*Globigerina druryi*	*Globigerina falconensis*	*Globigerina nepenthes*	*Globigerina pachyderma*	*Globigerina rubescens*	*Globigerinoides conglobatus*	*Globigerinoides fistulosus*	*Globigerinoides obliquus*	*Globigerinoides obliquus extremus*	*Globigerinoides ruber elongatus*	*Globigerinoides ruber pyramidalis*
Quaternary	N23	**Hole 571**																				
		1-1, 2-5	A	G	F	T									T	T	R					R
		1-1, 147-149	C	G		R		T					R				R					
		1-2, 147-149	C	M	R	T											R					
	N22	1,CC	C	G	F	R									R		R				R	
		2,CC	C	G	R		T	T									T				T	
	N23	**Hole 572A**																				
		1,CC	A	G	F		T								R		R				R	
	N22	2,CC	A	G	F		R				R						R					
		3,CC	A	M	R		R		T								T	R			T	
Pliocene	N21	4,CC	A	G						T									R			
		5,CC	C	M	R		R										T	T	R			
	N19	6,CC	C				T				R						R		R	R		
		7,CC	C	M	R		T										T		R			
		8,CC	C	M	R		R							R			R		F			
		9,CC	C	M	R		R							R					R			
		10,CC	C	M	T		R							T			T		F	R		
late Miocene	N18	11,CC	F	M										R					R			
	N17	12,CC	F	M										T					T			
		13,CC	F	M	R		T					T		T								
		14,CC	C	M													R		T			
		15,CC	C	M	P									R			T		R			
		16,CC	C				R							T					R			
		17,CC	F	M	T																	

Note: G = good; M = moderate; P = poor. Other symbols as in Table 2. (L) = left coiling; (R) = right coiling.

able. Blow (1969) defined Zone N4 as based on concurrent ranges of *Globigerinoides quadrilobatus primordius* and *Globorotalia kugleri*. He believed that the first appearance of the former postdates the first appearance of the latter, thereby enabling two divisions of the range of *G. kugleri*. Zone N4 of Blow represents the younger part of the range of *G. kugleri* subsequent to the first appearance of *Globigerinoides*. Since then, many authors (e.g., Stainforth and Lamb, 1981; Srinivasan and Kennett, 1983; Berggren, 1984) have convincingly demonstrated that *G. quadrilobatus primordius* actually evolved earlier than *G. kugleri*. The usage of Zone N4 in this report is a modified one, defined as the total range zone of *G. kugleri*. Species of the genus *Globigerinoides* are susceptible to solution, and little contribution can be made by the Leg 85 sequences regarding the evolutionary development of *Globigerinoides* in the Oligocene–Miocene interval.

SITE SUMMARIES

Site 571

Site 571 is located near the eastern terminus of the equatorial Pacific high-sedimentation belt (Fig. 1). The only core (7.11 m) taken at this site consists of light, yellow brown, foraminifer–nannofossil ooze. Planktonic foraminifers are generally abundant and well preserved throughout the cored sequence, although we noted faunas affected by marked dissolution at intervals 571-1-1, 140–144 cm and 1-3, 41–43 cm. *Globorotalia menardii* is the most dominant element of the planktonic foraminiferal assemblages. *Pulleniatina obliquiloculata* also commonly occurs in most of the horizons.

In Core 571-1-2, between 119–120 and 131–132 cm, *Globoquadrina pseudofoliata* becomes extinct. The extinction datum of *Globorotalia tosaensis* was apparently not reached at this site because assemblages containing this species were not recognized. The paleomagnetically dated deep-sea sequence from the same eastern equatorial Pacific region (Saito et al., 1975; Thompson and Saito, 1977) places the extinction datum levels of *Globoquadrina pseudofoliata* and *Globorotalia tosaensis* at 0.22 and 0.60 Ma, respectively. Thus, the entire core is assignable to the Brunhes Chron of the paleomagnetic stratigraphy, and the base of the core is no older than 0.6 Ma.

Site 572

This site is nearly due south of Site 571 and is also situated near the eastern edge of the equatorial high-productivity zone. Site 81 of Leg 9 is approximately due east of this site.

Five holes were drilled at Site 572, yielding 170 m of a continuously double-piston-cored sequence, and below that, 300 m of an almost continuously rotary-drilled se-

Table 3A. (Continued).

Globigerinoides ruber ruber (pink)	*Globigerinoides ruber ruber (white)*	*Globigerinoides sacculifer*	*Orbulina bilobata*	*Orbulina universa*	*Sphaeroidinella dehiscens*	*Sphaeroidinellopsis seminulina*	*Globigerinita glutinata*	*Globigerinita iota*	*Globorotaloides hexagona*	*Globoquadrina altispira altispira*	*Globoquadrina conglomerata*	*Globoquadrina pseudofoliata*	*Globoquadrina venezuelana*	*Pulleniatina finalis*	*Pulleniatina obliquiloculata*	*Pulleniatina praecursor*	*Pulleniatina primalis*	*Pulleniatina spectabilis*	*Neogloboquadrina eggeri*	*Neogloboquadrina humerosa*	*Globorotalia acostaensis*	*Globorotalia cibaoensis*	*Globorotalia continuosa = opima*	*Globorotalia crassaformis*	*Globorotalia crassula*
F	F	F		F	T		T				F	R		R	F				C						T
R	R			R			R				R	R		T	C				C						
					R							F		R	F				C						
	F	F		R	F			T			R	F		R	F	T									T
		F					T					R		R	F	T			C						
	F	F		R	R						R	C		F	C				C						
R	C	C		R	R							F		R	F	R			C						
		R		R	F		R					R			F	F									
	F	F		R	R							R			F	R				C					T
		F		F	F		R		T	R		R			F	R				C				R	T
	R					R										(L+R)	R							R	T
		R		R		F	R		F	T	R	R				R				F				R	
	F	F			T	F	R		T	R	T	T			F(L)		F	T			T		T		
	R	R		F		F			R	R	T						R(L)								
	F	T		T		F			F	R	F						R								
	R			R		F											R(L)			R					
	F			R		F			R	T	T		R				T(L)					T			
	R	T		T	F	F			T				F				T(L)					T			
	F			R	R	C					T		R							T					
	R			T	F				R	R			C				T								
	F	R		R	F	F			T	T			F												
	R	R		F	F				R				R												

quence. A sediment/basalt basement contact was reached at 479.5 m in Hole 572D.

Hole 572A was continuously piston cored to a sub-bottom depth of 154 m. Hole 572B was washed down to 154 m, and coring began from that level to 172.1 m sub-bottom. Hole 572C duplicated 572A, yielding a continuously piston-cored sequence from the mudline to 168.5 m sub-bottom. Hole 572D was rotary drilled to the basalt basement after washing down to 151 m sub-bottom.

The state of preservation of planktonic foraminifers makes it possible to divide the 170-m-thick piston-cored sequence into two units. The upper unit, from Cores 1 through 17 in both Holes 572A and 572C, contains abundant and well-preserved assemblages, whereas the lower unit yields moderately well-preserved, but rather monotonous, assemblages. These monotonous assemblages consist largely of such solution-resistant forms as robust *Globoquadrina*, keeled *Globorotalia*, and cortex-covered sphaeroidinellids. The downhole change from the upper, rich assemblages to the lower solution-affected assemblages is sharp and occurs between Cores 572C-17 and -18. Planktonic species are practically absent in Sample 572-19,CC. The upper foraminifer-rich sequence can be correlated precisely with the paleomagnetically dated deep-sea sequence to the west of this site in the equatorial Pacific (Hays et al., 1969; Saito et al., 1975). Such a correlation places the base of the Quaternary, as marked by the extinction of *Globigerinoides obliquus*, between Samples 2,CC and 3,CC in both Holes 572A and C. The disappearance of *Sphaeroidinellopsis seminulina* in Hole 572C between Samples 6-4, 50–52 cm and 6-5, 100–102 cm is used to draw the upper limit of Zone N19.

Since systematic changes with time in the coiling direction of *Pulleniatina* have been shown to provide useful datum levels for inter-regional correlation, we plotted coiling direction patterns in assemblages from Holes 572C and 573. The sharp left-to-right coiling direction change, termed L9 by Saito (1976) and known to occur shortly after the Cochiti Subchron of the Gilbert Reversed Chron (~3.6 Ma), occurs in the upper part of Core 572C-7 (Fig. 2).

Although dissolution of foraminifers becomes increasingly evident downsection starting from Core 10 of both Holes 572A and 572C, the first appearance of *Globorotalia tumida* accompanied by the extinction of *Globoquadrina dehiscens* between Samples 13,CC and 14,CC enables the placement of the Pliocene/Miocene boundary at this level.

The rotary-cored sequence of Hole 572D yields moderately well-preserved but impoverished middle and upper Miocene foraminiferal assemblages. The effect of dissolution makes it difficult to establish time–rock divisions for this hole based solely on planktonic foraminifers. Two intervals of marked dissolution characterize the middle of the cored sequence (Cores 572D-2 to -8 and -11 to -18), whereas a well-preserved and diverse assemblage is present toward the basement in Cores 572D-30 through -33. The basal sediment of this hole, Sample

Table 3A. (Continued).

Age	Zone	Sample (interval in cm)	Abundance	Preservation	*Globorotalia esnrogacia*	*Globorotalia kessi*	*Globorotalia margaritae*	*Globorotalia margaritae primitiva*	*Globorotalia menardii*	*Globorotalia merotumida*	*Globorotalia multicamerata*	*Globorotalia plesiotumida*	*Globorotalia "praescitropiana"*	*Globorotalia scitula*	*Globorotalia tosaensis*	*Globorotalia truncatulinoides*	*Globorotalia tumida flexuosa*	*Globorotalia tumida tumida*	*Globorotalia ungulata*	*Streptochilus tokelauae*
		Hole 572																		
	N23	1-1, 2-5	A	G	T				C								T	R	R	
		1-1, 147-149	C	G															R	
		1-2, 147-149	C	M														C		
Quaternary	N22	1,CC	C	G		F			F						R			F		
		2,CC	C	G		R			R						R	T		C	T	
	N23	**Hole 572A**																		
		1,CC	A	G					R						R	F		F	RT	
	N22	2,CC	A	G					F					C	R	R	T	R		
		3,CC	A	M													T	C		
	N21	4,CC	A	G							C				R		R	C		
		5,CC	C	M													R	C	R	
Pliocene	N19	6,CC	C						F		R			T			R	C		
		7,CC	C	M			T							T			R	C		
		8,CC	C	M													C	C		T
		9,CC	C	M													$F_{(L)}$			
		10,CC	C	M				T	$R_{(L)}$		R			T			R	C		
	N18	11,CC	F	M							$R_{(L)}$	R	T					$F_{(L)}$		
		12,CC	F	M					$R_{(L)}$			$T_{(L)}$								
late Miocene	N17	13,CC	F	M					F			R		T						
		14,CC	C	M					R			F		R						
		15,CC	C	M						R		T								
		16,CC	C							R		R		T						
		17,CC	F	M						T										

33,CC, contains rare specimens of *Orbulina universa* in association with *Globorotalia peripheroronda* and *G. praemenardii* and is assigned to Zone N9, the lowest middle Miocene zone. Paleontologists on Leg 9 assigned the basal sediment of Hole 81 to the uppermost lower Miocene Zone N8 (Hays et al., 1972). Their zonal assignment was not based on the occurrence of the zonal marker species *Globigerinoides bisphericus*, but rather on the presence of *Hastigerinella bermudezi* (referred to as *Clavatorella bermudezi* in the present report). Since Blow (1969) reported that *H. bermudezi* ranges from the uppermost part of Zone N8 through the lower part of Zone N10, the basal sediment in Hole 81 could well be of Zone N8 age. However, the same Leg 9 report shows the range of *H. bermudezi* in a more continuously cored sequence at Site 77 (about 960 km due west of Site 572 in the eastern equatorial Pacific) to be restricted to the middle Miocene in zones equivalent to N9 and N10. At Site 572, *H. bermudezi* occurs in association with the Zone N9 assemblage. Therefore, the basal sediment at Site 81 is here reinterpreted to be of Zone N9 age, in agreement with our findings.

Site 573

This site represents the southernmost of a three-site latitudinal transect along 133°W across the equatorial high-productivity belt and was chosen to sample the maximum sediment accumulation along the equator. Coring was also intended to duplicate the well-studied section recovered at Site 77 of Leg 9 (Fig. 1).

The upper 160 m of the sedimentary column at this site were piston cored in Holes 573 and 573A, and the remaining 370 m were rotary cored in Hole 573B. Hole 573A duplicates the upper 60-m section of Hole 573. Hole 573B penetrated a baked sediment/basalt contact at 528.0 m sub-bottom. An approximate 1.6-m-thick Eocene biogenic limestone layer and 3.5-m-thick metalliferous claystone layer overlie the basalt.

The site yielded upper Eocene through Pleistocene planktonic foraminifers in varying abundances. Most of the fossil assemblages exhibit some alteration by dissolution, which caused such solution-resistant forms as keeled *Globorotalia*, robust *Globoquadrina*, sphaeroidinellids, and *Catapsydrax* to be dominant in the faunas. However, all the species present show a good state of preservation throughout the entire sequence. Two intervals, 112 to 186 and 252.5 to 366.5 m sub-bottom, show a marked decrease in foraminiferal abundance and correspond to those intervals in which diatom and nannofossil data indicate the presence of stratigraphic hiatuses.

Because of the effect of dissolution, many interesting evolutionary lineages of planktonic foraminifers known from the tropical latitudes are not recorded at this site. One exception is the *Globorotalia fohsi* evolutionary lineage, which occurs in consecutive order from Core 573B-11 to -6. Since the *Orbulina* datum is not recorded, the

Table 3B. Occurrence and estimated abundance of planktonic foraminifers, Holes 572C and 572D.

Age	Zone	Sample (interval in cm)	Abundance	Preservation	*Globigerinella aequilateralis*	*Globigerinella calida*	*Globigerinella praecalida*	*Beella digitata*	*Beella praedigitata*	*Globigerina bulloides*	*Globigerina decoraperta*	*Globigerina falconensis*	*Globigerina nepenthes*	*Globigerinoides bellii*	*Globigerinoides conglobatus*	*Globigerinoides conglobatus*	*Globigerinoides fistulosus*	*Globigerinoides obliquus extremus*	*Globigerinoides obliquus obliquus*	*Globigerinoides quadrilobatus*	*Globigerinoides ruber (pink)*	*Globigerinoides ruber ruber (white)*	*Globigerinoides sacculifer*	*Globigerinoides subquadratus*	*Globigerinoides trilobus*	*Orbulina bilobata*
Quat	N22	**Hole 572C**																								
		1,CC	A	G	R	F		R								R					T	F	C			
		2,CC	A	G	F		T		T	T						F							F			
		3,CC	A	G	F		R		T	T						R	C		R			F	F			
		4(5), 100–102	A	G	T	T						T				R						F	R			
	late	4,CC	C	M	R	R					R					R	F					F	F			
		5(4), 49–51	C	M																			R			
		5(5), 140–142	A	G																			T			
		5,CC	A	G	R		R				R					R			R			F	F			
		6(4), 50–52	C	M												T						T	R			
		6(5), 100–102	C	M																			R			
Pliocene		6,CC	C	M	R		R												R				T			
		7(4), 100–102	C	M	T		T									R										
	N19	7-5, 100–102	C	M	T	T					T		T				T						R			
		7,CC	F	M			T						R			T			R				R			
		8,CC	C	M	R		R						T			R			R				F			
	early	9,CC	C	M	R		T					R	T						R				F			
		10(5), 50–52	C	M					T				T										F			
		10,CC	C	M	R		T						T			R			R	R			R			
	N18	11-2, 50–52	R	M															R				F			
		11,CC	R	M									T													
		12,CC	F	M	R																					
		13,CC	F	M			R				R				T				R				R			
		14,CC	F	M																						
		15,CC	F	M	R		T												RF				F			R
		16,CC	C	M			R												R				F			
		17,CC	C	M			T						R						R				F			
		18,CC	F	M												R			F				F			
		19,CC	R	M										T					R							T
		20,CC	F	M							T	R	T			T			R				R			
	N17	**Hole 572D**																								
		1,CC	R	P									T										T			
		2,CC	R	M																						
late		3,CC	R	M									R						T				T			
Miocene		4,CC	F	M							T		T													
		5,CC	R	P									T						R							
		6,CC	R	M									T													
		7,CC	R	M									T						R				T			
		8,CC	F	M	T																		F			
		9,CC	R	M							R		R				T		R				F			
		10,CC	F	M	R									R	R								F			
	N16	11,CC	R	M			T						T						T				R			
		12,CC	R	M															T				R			
	?	13,CC	F	M																						
		14,CC	R	M																						
	N15	15,CC	R	P									T						T							
	N14	16,CC	R	M									T	T					T							
		17,CC	C	M																						
		18,CC	C	M															R				R	T		
		19,CC	F	M																			R			
		20,CC	C	M																			F			
	N13	21,CC	R	M																						
		22,CC	F	M																						
	N12	23,CC	C	M								F										F			T	
middle	N11?	24,CC	R	M																						
Miocene		25,CC	R	M																						
		26,CC	F	M																						
	N10	27,CC	F	M																		R				
		28,CC	F	M										T								R	T			
		29,CC	R	M																						
		30,CC	C	M																		T				
	N9	31,CC	C	M																					F	
		32,CC	C	M																		R	F		R	
		33,CC	C	M																		R	R		R	

Note: G = good; M = moderate; P = poor. Other symbols as in Table 2. Precise location of diagonal boundary could not be determined.

Table 3B. (Continued).

Age	Zone	Sample (interval in cm)	Abundance	Preservation	*Orbulina suturalis*	*Orbulina universa*	*Spheroidinella dehiscens*	*Spheroidinellopsis seminulina*	*Spheroidinellopsis subdehiscens*	*Globigerinita glutinata*	*Globoconella kugleri*	*Globoquadrina dehiscens altispira*	*Globoquadrina conglomerata*	*Globoquadrina dehiscens advena*	*Globoquadrina dehiscens dehiscens*	*Globoquadrina larmeni*	*Globoquadrina pseudofoliata*	*Globoquadrina venezuelana*	*Clavatorella bermudezi*	*Pulleniatina finalis*	*Pulleniatina obliquiloculata*	*Pulleniatina praecursor*	*Pulleniatina primalis*	*Pulleniatina spectabilis*	*Neogloboquadrina eggeri*	*Neogloboquadrina humerosa*
		Hole 572C																								
Quat	N22	1,CC	A	G		R	R				R	R					C			F	C				F	
		2,CC	A	G		C	R				R	R					R			R	F	R			C	
		3,CC	A	G		F	R				F	R					R					F	F			C
		4(5), 100–102	A	G		T	F				T										R	R	R			R
		4,CC	C	M		F	R					R		R			R					R	R			
	late	5(4), 49–51	C	M			T																			
	N21	5(5), 140–142	A	G		R	F						T				T									
		5,CC	A	G		R						R	R				R				F		F			F
		6(4), 50–52	C	M		F	F							R									T			T
		6(5), 50–52	C	M		T	F				T	T	T				T									T
		6(5), 100–102	C	M		T	T	T			T		T				T									T
		6,CC	C	M			R	F					R	R			R						F			R
Pliocene		7(4), 100–102	C	M		R		R			T	T	R										T			
	N19	7-5, 100–102	C	M		R		R	T	T	T		R					T				T	R			T
		7,CC	F	M				R				R	R	F				R					R			
		8,CC	C	M		R	R	F				R	R				R	R					R			
	early	9,CC	C	M			R	F				R	R	F				C					R	R			
		10(5), 50–52	C	M		R		F	R								T	R								
		10,CC	C	M		R		F			T	R	R					F					R			
	N18	11-2, 50–52	R	M		T				T								T								
		11,CC	R	M																						
		12,CC	F	M				R							T			F					R	T		
		13,CC	F	M		R		F				R	R					F					R			
		14,CC	F	M		R		F					R					F					R			
		15,CC	F	M		R		R					R					F					T			
		16,CC	C	M		F		R				R	R					C					T			
		17,CC	C	M		F		R				R	F					C					T			
		18,CC	F	M				C					T		T			R								
		19,CC	R	M				T									T									
		20,CC	F	M				R					R				T									
		Hole 572D																								
	N17	1,CC	R	P				R					T				R									
late		2,CC	R	M									T				T									
Miocene		3,CC	R	M		T					T		T				T	T								
		4,CC	F	M		R		R									R									
		5,CC	R	P			R						T					T								
		6,CC	R	M		T		R					R				T	T								
		7,CC	R	M									T				T	R								
		8,CC	F	M				R						F			R									
		9,CC	R	M		R		R										F								
		10,CC	F	M		R		F		R			R					F								
	N16	11,CC	R	M		T		F					T					R								
		12,CC	R	M				R			T							R								
	?	13,CC	F	M																						
		14,CC	R	M														T								
	N15	15,CC	R	F									T				T									
	N14	16,CC	R	M		T												R								
		17,CC	C	M																						
		18,CC	C	M				F										C								
		19,CC	F	M				R										F								
		20,CC	C	M		R		R					F		F			C								
	N13	21,CC	R	M		R							R					R								
		22,CC	F	M		R							R		R			F								
	N12	23,CC	C	M		R												C								
		24,CC	R	M																						
middle	N11?	25,CC	R	M		R		F										F								
Miocene		26,CC	F	M								R	F					F								
		27,CC	F	M		R		F										C								
	N10	28,CC	F	M				R					R					F								
		29,CC	R	M									T					R								
		30,CC	C	M											F			C								
	N9	31,CC	C	M												F		C								
		32,CC	C	M	R			F					R		R			C	F							
		33,CC	C	M		R												F								

Table 3B. (Continued).

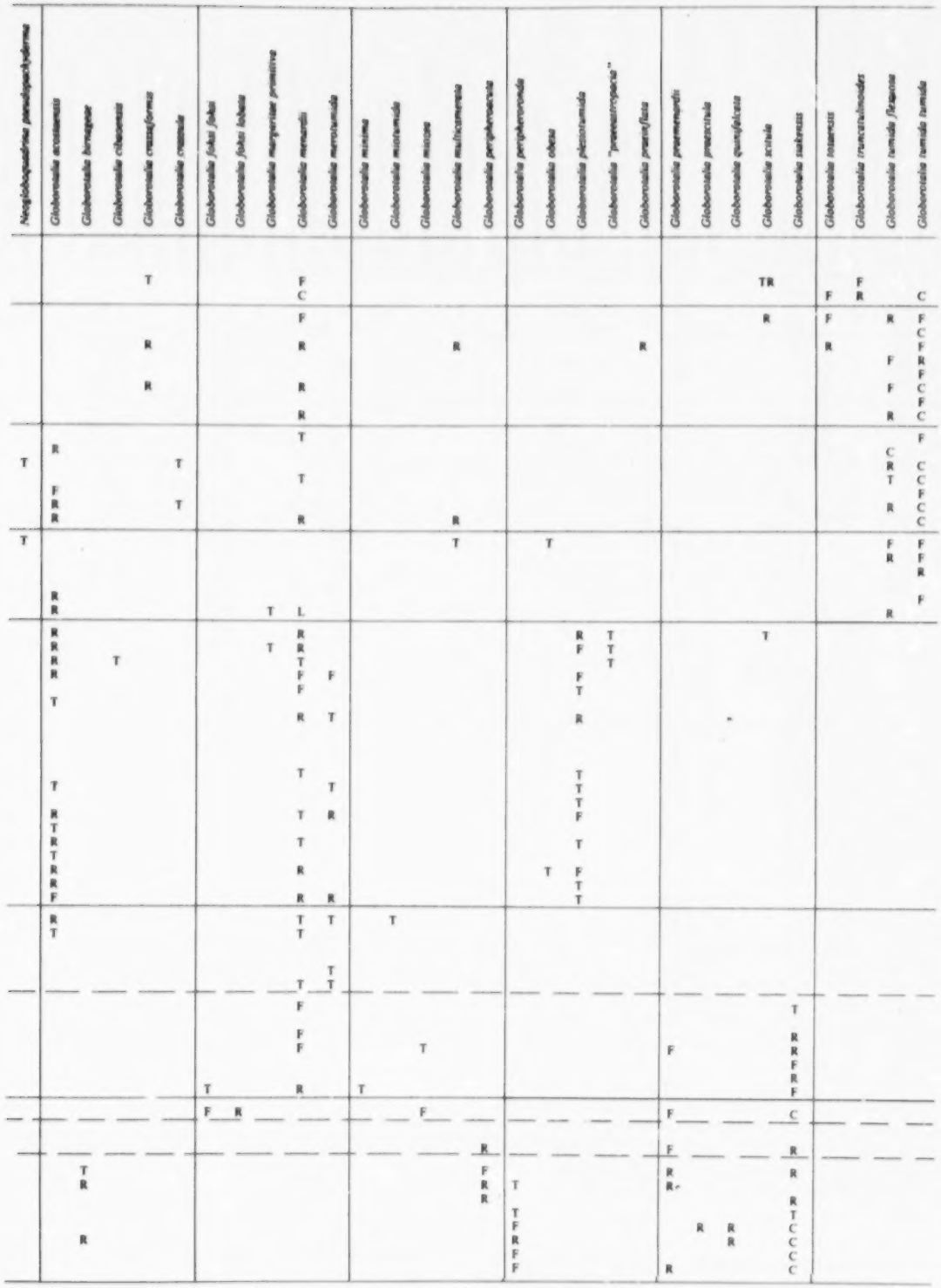

Table 4. Occurrence and estimated abundance of planktonic foraminifers at Site 573.

Age	Zone	Sample (interval in cm)	Abundance	Preservation	*Globigerinella aequilateralis*	*Globigerinella calida*	*Globigerinella praecalida*	*Beella digitata*	*Beella praedigitata*	*Globigerina angulisuturalis*	*Globigerina angustiumbilicata*	*Globigerina decoraperta*	*Globigerina nepenthes*	*Globigerina praebulloides*	*Globigerina rubescens*	*Globigerinoides bollii*	*Globigerinoides conglobatus*	*Globigerinoides fistulosus*	*Globigerinoides obliquus obliquus*	*Globigerinoides quadrilobatus*	*Globigerinoides ruber ruber* (white)	*Globigerinoides ruber cyclostomus*	*Globigerinoides ruber elongatus*	*Globigerinoides sacculifer*	*Globigerinoides sicanus*	*Globigerinoides subquadratus*	*Globigerinoides trilobus*	*Orbulina suturalis*	*Orbulina universa*	*Sphaeroidinella dehiscens*	*Sphaeroidinella dehiscens immatura*	*Sphaeroidinellopsis seminulina*	*Sphaeroidinellopsis subdehiscens*	*Candeina nitida*	*Globigerinita bradyi-uvula*	*Globigerinita glutinata*
	N23	**Hole 573**																																	
		1-1, 50–52	A	G	R	T		T							R		T				R			R					R						R
		1,CC	C	M																				T					T						
		2,CC	A	G	R		R														R			R				T	F						R
Quaternary	N22	3,CC	A	G													T				R			R				R	F						
		4-4, 10–12	A	G														T											F						T
		4-6, 10–12	A	G											T	R	T	T	T	R		T					T		F						T
		4,CC	FC	M					T							T	T						R	R				R	R						R
		5,CC	C	M	R											T	R	T			T			T				R	F						
	N21	6(2), 90–93	C	M																				T					F						
		6-2, 110–112	C	M																				T					F						
		6-3, 62–63	A	M	R														T									R	C						
		6-4, 10–11	F	M	T																			T				T	F						
		6-4, 29–30	C	M	R		T																	R					T		F				
		6-4, 110–111	C	M	T		T											R	T		T			F				T	F		T				T
		6-5, 10–11	F	M																									F						
		6-5, 110–112	C	M			T												R		T			R					F		T				T
Pliocene	N19	6,CC	C	G	T		T												R		T			F					F		T				
		7-1, 22–23	C	M			T												R		T			R					R		T		T		
		7,CC	C	M	T		T		T				T						T					R							R				T
		8,CC	A	G	F								R				R		R					R						T	F				
		9,CC	C	M	R																			R				R			R				
		10-4, 106–107	C	M																R											R	T			
	N18	10-5, 106–107	C	M							R	T				R								T							R				T
		10,CC	FC	M	T														R					R				R			F				
		11,CC	C	M			R						R			R			R					R				R			F				
	b	12,CC	C	M	T		T				T								R					R							F				T
		13,CC	F	M									F						R					R				T			T				
		14,CC	R	M															T					T				T			T				
		15,CC	F	M															T					T							R				
		16,CC	F	M									T											R							T				T
	N17	17,CC	R	M	T														R					F							T				T
	a	18,CC	R	M															T					R											
late Miocene		19,CC	F	M																											T				
		Hole 573B																																	
		1,CC	R	PM	T														T					F							F				
		2,CC	R	M	T																			R				R			R				
		3,CC	R	M																											T				
	N16	4,CC	R	P																															
	?	5,CC	F	M									T							R											R				
	N13	6,CC	F	M																T					T						T				
		7,CC	A	G										R										F	R			T			F				R
middle Miocene	N12	8(2), 112–114	A	G																															
	N11	8(3), 112–114	A	G																															
		8(4), 112–114	A	G																															
		8,CC	F	M																															
		9(2), 112–114	M	G																															

Note: Symbols as in Tables 2 and 3. Species looked for and not found: *Globigerina binaiensis, G. bulloides, G. druryi, G. falconensis, G. pachyderma, G. woodi, Globigerinoides canimarensis, G. japonicus, G. obliquus extremus, G. primordius, Praeorbulina glomerosa curva, P. glomerosa glomerosa, Orbulina bilobata, Globigerinita iota, Globoegerinatella insueta, Globorotaloides* aff. *suteri, Globorotalia conomiozea, G. fohsi robusta, G. margaritae primitiva, G. minima, G. miotumida, G. obesa, G. opima continuosa, G. quinifalcata, G. ungulata, Globigerina ciperoensis, G. gortanii, G. tripartita, G. winkleri, Globigerinita africana, Globoquadrina sellii Globigerinatheka barri, Globigerapsis mexicana, Pseudohastigerina micra, Cribrohantkenina inflata* subsp. *bermudezi*, and *Hantkenina primitiva*.

[a] AT.
[b] F–C.
[c] FR.

middle/lower Miocene boundary is approximated at the last appearance level of *Globigerinoides sicanus* between Samples 573B-12-5, 112–114 cm and -12,CC. The first appearance datum of *Globorotalia kugleri* is between Samples 573B-20-4, 110–112 cm and -20-6, 110–112 cm. Since the Oligocene/Miocene boundary is slightly younger than the *G. kugleri* datum, a possible unconformity, recognized in Core 573B-22 or -21 on the basis of nan-

Table 4. (Continued).

Globigerinita incrusta	*Globigerinita uvula*	*Globorotaloides hexagona*	*Globorotaloides suteri*	*Globorotaloides variabilis*	*Globoquadrina altispira altispira*	*Globoquadrina conglomerata*	*Globoquadrina dehiscens advena*	*Globoquadrina dehiscens dehiscens*	*Globoquadrina eximia*	*Globoquadrina larmeui*	*Globoquadrina praedehiscens*	*Globoquadrina pseudofoliata*	*Globoquadrina venezuelana*	*Pulleniatina finalis*	*Pulleniatina obliquiloculata*	*Pulleniatina praecursor*	*Pulleniatina primalis*	*Pulleniatina spectabilis*	*Neogloboquadrina eggeri*	*Neogloboquadrina humerosa*	*Neogloboquadrina pseudopachyderma*	*Catapsydrax dissimilis*	*Catapsydrax stainforthi*	*Catapsydrax unicavus*	*Clavatorella bermudezi*	*Globorotalia acostaensis*	*Globorotalia aemiliana*	*Globorotalia birnageae*	*Globorotalia cibaoensis*	*Globorotalia continuosa = opima continuosa*	*Globorotalia crassaformis*	*Globorotalia crassula*	*Globorotalia eastropacia*	*Globorotalia foksi foksi*	*Globorotalia foksi lobata*	*Globorotalia incisa*	*Globorotalia kugleri*	*Globorotalia margaritae*	*Globorotalia menardii*	*Globorotalia merotumida*	*Globorotalia minuta*	*Globorotalia minutissima*	*Globorotalia miozea*	*Globorotalia multicamerata*	*Globorotalia opima nana*	*Globorotalia peripheroacuta*
					F								C	C				F												F								F							
	R				R							F	F	F				F	C																		F							
												R	F	C				C	F																		R							
												T	F	C	R			R	R																		T							
	R				T							R	R		R	T	R	F	F												R						T				R			
												R			R																R													
	T					F												T			T										T													
	T					R						F			R		R																				T	T						
						R	T					R				R	R				R																								
	T					R	R					R				T	T				R																								
						F	R					F									R																								
	F					F	F					R						R	R		R																								
	T					R							F					R									F																		
																											T																		
	T					R		R					R					T			T																								
	T					R		R					R					T			T																								
	T					R		F					F					T																											
								R																																				
								F																																				
								R																																				
								F																																				
								R

Table 4. (Continued).

Age	Zone	Sample (interval in cm)	Abundance	Preservation	*Globigerinella aequilateralis*	*Globigerinella calida*	*Globigerinella praecalida*	*Beella digitata*	*Beella praedigitata*	*Globigerina anguisuturalis*	*Globigerina angustiumbilicata*	*Globigerina decoraperta*	*Globigerina nepenthes*	*Globigerina praebulloides*	*Globigerina rubescens*	*Globigerinoides bollii*	*Globigerinoides conglobatus*	*Globigerinoides fistulosus*	*Globigerinoides obliquus obliquus*	*Globigerinoides quadrilobatus*	*Globigerinoides ruber ruber (white)*	*Globigerinoides ruber cyclostomus*	*Globigerinoides ruber elongatus*	*Globigerinoides sacculifer*	*Globigerinoides scanus*	*Globigerinoides subquadratus*	*Globigerinoides trilobus*	*Orbulina suturalis*	*Orbulina universa*	*Sphaeroidinella dehiscens*	*Sphaeroidinella dehiscens immatura*	*Sphaeroidinellopsis seminulina*	*Sphaeroidinellopsis subdehiscens*	*Candeina nitida*	*Globigerinita bradyi-wyvilli*	*Globigerinita glutinata*
		Hole 573B (Cont.)																																		
	N10	9(3), 112–114	M	G																			R			F				R					R
		9,CC	C	M																			R												
middle Miocene	N9	10(1), 113–114	C	M																															
		10(2), 113–114	C	M																															
		10(3), 112–114	C	M																															
		10,CC	C	M																															
		11(4), 112–114	C	M																															
		11,CC	A	M																	R														
		12(3), 112–114	C	M																						R	R								R
	N8	12(5), 112–114	C	M																					T										
		12,CC	C	M																															
	?	13,CC	F	M																															
	?	14,CC	F	M																															
		15,CC	F	M																															
		16(1), 108–110	F	M																															
		16(1), 108–110	F	M																														F	R
	N6	16(2), 108–110	F	M																															
		16(3), 108–110	F	M																															
early Miocene	N5	16(5), 108–110	F	M																															
		16,CC	R	M																															R
	N4	17-1, 37–39	F	M						T	T																								
		17(1), 110–112	F	M																															
		17(3), 110–112	F	M																															
		17(3), 110–112	F	M																															
		17(5), 110–112	F	M																															
		17,CC	F	M																															
		18,CC	F																																
		19,CC	F	M							R																								
		20(4), 110–112	F	M																															
		20-5, 13–15	F	M																															
		20(6), 110–112	F	M							F																								
		20,CC	F	M							F																								
	P22	21,CC	F	M							C			R																					
		22,CC	F																																
		23,CC	R	M																															
		24,CC	F	M							R																								
		25,CC	C	M							C																								
		26,CC	A	G																															
	P21	27,CC	A	M						(c)																									
		28,CC	C	M																															
Oligocene		29,CC	C	P																															
		30,CC	C	M																															
		31,CC	F	M																															
	P20	32,CC	F	M																															
		33,CC	F	M																															
		34,CC	R	M																															
		35,CC	F	P																															
	P19	36,CC	C	P																															
		37,CC	C	PM																															
		38,CC	C	P																															
	P18	39,CC	C	M																															
		40,CC	C	M																															
		42-1, 135–137	C	M																															
	?	42-2, 5–8	A	P																															
late Eocene		42-4, 116–119	F																																
		42-4, 123–124	A	M																															
	P16	42-4, 140–144	C	M													F																		

Table 4. (Continued).

Globigerinita incrusta	*Globigerinita uvula*	*Globoturborotalita hexagona*	*Globoturborotaloides suteri*	*Globoturborotaloides variabilis*	*Globoquadrina altispira altispira*	*Globoquadrina conglomerata*	*Globoquadrina dehiscens advena*	*Globoquadrina dehiscens dehiscens*	*Globoquadrina eximia*	*Globoquadrina larmeui*	*Globoquadrina praedehiscens*	*Globoquadrina pseudofoliata*	*Globoquadrina venezuelana*	*Pulleniatina finalis*	*Pulleniatina obliquiloculata*	*Pulleniatina praecursor*	*Pulleniatina primalis*	*Pulleniatina spectabilis*	*Neogloboquadrina eggeri*	*Neogloboquadrina humerosa*	*Neogloboquadrina pseudopachyderma*	*Catapsydrax dissimilis*	*Catapsydrax stainforthi*	*Catapsydrax unicavus*	*Clavatorella bermudezi*	*Globorotalia acostaensis*	*Globorotalia acrostoma*	*Globorotalia birnagea*	*Globorotalia ciperoensis*	*Globorotalia continuosa = opima continuosa*	*Globorotalia crassaformis*	*Globorotalia crassula*	*Globorotalia extropaea*	*Globorotalia foksi foksi*	*Globorotalia foksi lobata*	*Globorotalia incisa*	*Globorotalia kugleri*	*Globorotalia margaritae*	*Globorotalia menardii*	*Globorotalia merotumida*	*Globorotalia minuta*	*Globorotalia mutartissima*	*Globorotalia miocea*	*Globorotalia multicamerata*	*Globorotalia opima nana*	*Globorotalia peripheroacuta*
					F			F					R													F		R																F C
	R				C			F F					F C																R														F
F			R		F			C	R F T	R R			F C T C									F	R																					
			R		R					R			F									R		T																		T	
R			R R R					R T	R	R			R R T T									R R T R T	T	R												F (b) C F F C F T T			T			R T	
			C R								R		R									F F R C	R	F																			R	
			F F																			F F		F R																			F F	
			R F R																			R F R F		R F R F																				
																						F		F																				

Table 4. (Continued).

Age	Zone	Sample (interval in cm)	Abundance	Preservation	*Globorotalia perpheroronda*	*Globorotalia plesiotumida*	*Globorotalia praefohsi*	*Grobrotalia praemenardii*	*Globorotalia praescitula*	*Globorotalia pseudokugleri*	*Globorotalia ronda = crassaformis ronda*	*Globorotalia scitula*	*Globorotalia siakensis*	*Globorotalia tosaensis*	*Globorotalia truncatulinoides*	*Globorotalia tumida flexuosa*	*Globorotalia tumida tumida*	*Globigerina ampliapertura*	*Globigerina angiporoides*	*Globigerina limaperta*	*Globigerina ouachitaensis*	*Globigerina pera*	*Globigerina praesepis*	*Globigerina pseudovenezuelana*	*Globigerina tapuriensis*	*Globigerina yeguaensis*	*Globigerapsis index*	*Globorotalia centralis*	*Globorotalia opima opima*	*Globorotalia postcretacea*	*Pseudohastigerina barbadoensis*	*Cassigerinella chipolensis forma gigantea*	*Cassigerinella chipolensis*	*Chiloguembelina cubensis*	*Chiloguembelina martini*
		Hole 573																																	
	N23	1-1, 50–52	A	G													C																		
		1,CC	C	M													C																		
Quaternary	N22	2,CC	A	G										R	F		C																		
		3,CC	A	G													C																		
		4-4, 10–12	A	G												T	A																		
		4-6, 10–12	A	G							T						A																		
		4,CC	FC	M										T			C																		
		5,CC	C	M													C																		
	N21	6(2), 90–93	C	M												R	C																		
		6-2, 110–112	C	M												T	C																		
		6-3, 62–63	A	M										T		F	A																		
		6-4, 10–11	F	M													C																		
		6-4, 29–30	C	M												R	C																		
		6-4, 110–111	C	M								T				F	C																		
		6-5, 10–11	F	M													C																		
		6-5, 110–112	C	M												F	C																		
Pliocene	N19	6,CC	C	G												T	C																		
		7-1, 22–23	C	M												R	C																		
		7,CC	C	M												R	C																		
		8,CC	A	G												R	C																		
		9,CC	C	M												R	C																		
		10-4, 106–107	C	M		R											R																		
	N18	10-5, 106–107	C	M													R																		
		10,CC	FC	M		C											R																		
		11,CC	C	M		R						R					R																		
	b	12,CC	C	M																															
		13,CC	F	M		F																													
		14,CC	R	M		T																													
		15,CC	F	M		R																													
		16,CC	F	M		F																													
	N17	17,CC	R	M		T																													
	a	18,CC	R	M		R																													
late Miocene		19,CC	F	M																															
		Hole 573B																																	
		1,CC	R	PM		T																													
		2,CC	R	M																															
		3,CC	R	M		T																													
	N16	4,CC	R	P									R																						
	?	5,CC	F	M																															
	N13	6,CC	F	M									F																						
		7,CC	A	G				F	T				A																						
middle Miocene	N12	8(2), 112–114	A	G																															
		8(3), 112–114	A	G			F	F					C																						
	N11	8(4), 112–114	A	G																															
		8,CC	F	M		R							C																						
		9(2), 112–114	M	G		R	R																												

77, where only one species, *G. insolita*, was found to be diagnostic of a late Eocene age (Jenkins and Orr, 1972). The abundance of Eocene foraminifers diminishes upward as the metalliferous layer is approached, and no foraminifers occur in that layer. Sample 573B-42-2, 48–50 cm, which was taken immediately above the metalliferous layer, contains a rich benthic foraminiferal fauna dominated by calcareous forms, a fauna that suggests severe dissolution of planktonic species at this level. At 40 cm above this sample, an Oligocene planktonic assemblage assignable to the upper P18 Zone is present. These observations suggest that the Eocene/Oligocene boundary at Site 573 is marked by a break in the foraminiferal sequence, in which at least the P17 and lower P18 assemblages are not present. Also, just prior to and immediately subsequent to the deposition of the metalliferous layer, some mechanism appears to have dissolved planktonic foraminifers, calcareous nannoplankton, and

Table 4. (Continued).

Age	Zone	Sample (interval in cm)	Abundance	Preservation	*Globoturalia perpheroronda*	*Globoturalia plesiotumida*	*Globoturalia praefoksi*	*Globoturalia praemenardii*	*Globoturalia praescitula*	*Globoturalia pseudokugleri*	*Globoturalia ronda = crassaformis ronda*	*Globoturalia scitula*	*Globoturalia siakensis*	*Globoturalia tosaensis*	*Globoturalia truncatulinoides*	*Globoturalia tumida flexuosa*	*Globoturalia tumida tumida*	*Globigerina ampliapertura*	*Globigerina angulporoides*	*Globigerina limaperta*	*Globigerina ouachitaensis*	*Globigerina pera*	*Globigerina pressaepis*	*Globigerina pseudovenezuelana*	*Globigerina tapuriensis*	*Globigerina yeguaensis*	*Globigerinopsis index*	*Globorotalia cerroazulensis*	*Globorotalia opima opima*	*Globorotalia postcretacea*	*Pseudohastigerina barbadoensis*	*Cassigerinella chipolensis forma gigantea*	*Cassigerinella chipolensis*	*Chiloguembelina cubensis*	*Chiloguembelina martini*
		Hole 573B (Cont.)																																	
	N10	9(3), 112–114	M	G								C																							
		9,CC	C	M				R				C																							
middle Miocene	N9	10(1), 113–114	C	M																															
		10(2), 113–114	C	M																															
		10(3), 112–114	C	M				R				C																							
		10,CC	C	M	C							C																							
		11(4), 112–114	C	M																															
		11,CC	A	M	C							(a)																							
		12(3), 112–114	C	M																															
early Miocene	N8	12(5), 112–114	C	M																															
		12,CC	C	M	F							?																							
	?	13,CC	F	M																															
	?	14,CC	F	M																															
		15,CC	F	M								R																							
		16(1), 108–110	F	M																															
	N6	16(1), 108–110	F	M																															
		16(2), 108–110	F	M																															
		16(3), 108–110	F	M																															
	N5	16(5), 108–110	F	M																															
		16,CC	R	M								F																							
	N4	17-1, 37–39	F	M								F																							
		17(1), 110–112	F	M								C																							
		17(3), 110–112	F	M																															
		17(3), 110–112	F	M																															
		17(5), 110–112	F	M								C																							
		17,CC	F	M						R																									
		18,CC	F									R																							
		19,CC	F	M																															
		20(4), 110–112	F	M																															
		20-5, 13–15	F	M								R																							
Oligocene	P22	20(6), 110–112	F	M								C																							
		20,CC	F	M								C																						T	
		21,CC	F	M	R							F									R														
		22,CC	F																																
		23,CC	R	M																															
		24,CC	F	M																			R						R	F					
	P21	25,CC	C	M								R									R		R					C	C			R			
		26,CC	A	G								F																	C		F		A	C	
		27,CC	A	M																									C						
		28,CC	C	M																			F						F	C					
	P20	29,CC	C	P																															
		30,CC	C	M																															
		31,CC	F	M																									C	R					
		32,CC	F	M																		R													
		33,CC	F	M																									C	C					
	P19	34,CC	R	M																															
		35,CC	F	P													R					R									F				
		36,CC	C	P																	R	F	F										T		
		37,CC	C	PM																					R				C	C			C		
	P18	38,CC	C	P													R						C							T	C		C		
		39,CC	C	M													F	R				R									C		R	F	
		40,CC	C	M													F	R						R							F				
		42-1, 135–137	C	M														F													C				
late Eocene	?	42-2, 5–8	A	P													F						R		R				C		C				
		42-4, 116–119	F																												C		F	C	
	P16	42-4, 123–124	A	M																															
		42-4, 140–144	C	M															F							R	F							C	

Table 5. Occurrence and estimated abundance of planktonic foraminifers at Site 574.

Age	Zone	Sample (interval in cm)	Abundance	Preservation	Globigerinella aequilateralis	Globigerinella calida	Globigerinella praecalida	Globigerina angustiumbilicata	Globigerina angulisuturalis	Globigerina bulloides	Globigerina falconensis	Globigerina rubescens	Globigerina praebulloides	Globigerinoides altiaperturus	Globigerinoides bollii	Globigerinoides conglobatus	Globigerinoides immaturus	Globigerinoides obliquus obliquus	Globigerinoides primordius	Globigerinoides quadrilobatus	Globigerinoides ruber cyclostomus	Globigerinoides ruber ruber	Globigerinoides sacculifer	Globigerinoides trilobus	Globigerinoides subquadratus	Globoquadrina dehiscens	Praeorbulina glomerosa circularis	Praeorbulina glomerosa curva	Praeorbulina glomerosa glomerosa	Praeorbulina glomerosa praeglomerosa	Orbulina bilobata	Orbulina suturalis	Orbulina universa	Sphaeroidinella dehiscens dehiscens	Sphaeroidinellopsis seminulina	Sphaeroidinellopsis subdehiscens	Globigerinita bradyi-wvula
Quat		**Hole 574**																																			
	N22	1,CC	A	G	F	T										R					R	R											R				
Plio.	?	2,CC	F	M																													R				
	N19	3,CC	F	M																																	
		4,CC	F	M																													T		C	C	
late Miocene	N17	5,CC	F	M	T													R													T		T		F	F	
		6,CC	F	M																															F	R	
		7,CC	F	G								R				R							F										R		F		
		8-4, 107–110	F	G	T													R					R												R	R	
		8(5), 107–110	F	G								R						R					R										T		R	T	
		8(6), 107–110	F	G	T							T						T					R										R		R	R	
	N16	8,CC	R	M								T						R		T													R		R	R	
	?	9,CC	R	M																																	
		10,CC	R	M																																	
	N14	11,CC	R	M																															T	T	
	N13	12,CC	F	G																																	
	N12	13,CC	C	G																C				F	F								F				
		14,CC	A	G											F					F				F	R												
		15,CC	A	G																F				F	F								R		F		
		16,CC	R	G																				R											R		
		17(2), 108–110	F	F																																	
middle Miocene	N11	17(3), 108–110	M	M																													T		R		
		17,CC	F	M																R															R		
		18,CC	F	M																R															R		
		19(2), 50–53	F	M																															R		
		19(3), 50–53	F	M																																	
	N10	19,CC	F	G										T						F											T				R		
		20,CC	F	G																															R		
		21(2), 107–110	C	G																																	
	N9	21(3), 107–110	C	G																																	
		21,CC	C	M																															T		
		22-3, 140–141	C	G																																	
		22,CC	F	M																																	
		23,CC	C	M																R													T		F		
		24,CC	R	M																T			R	R									T				
early Miocene	N8	25(1), 107–110	C	M																				R	R	R	R										
		25-3, 107–110	C	M																T			T	R	T												
		25,CC	C	M																				F	R												
		26,CC	F	M																																	
		27(1), 61–64	C	M																			R	F													
		27(2), 61–64	C	M																																	
		27-3, 61–66	C	M			R																F	F		R			T							
		27,CC	C	G																			F	F				R								
		28,CC	A	G																R			F	F	R											
		29,CC	A	G																				T											R		
	?	30,CC	A	G																			T														
	?	31,CC	R	M																																	

Note: Symbols as in Tables 2 and 3.

some or most of the benthic foraminifers. The metalliferous layer was thus most likely deposited during a time when dissolution was prevalent in the area. Recent studies indicate that ocean ridge-crest hydrothermal activity is responsible for the generation of metalliferous layers (e.g., Edmond et al., 1982). The absence of foraminifers and other microfossils in and around the metalliferous layer could argue for corrosion of biogenic material by a hydrothermal solution.

Site 574

Site 574, about 350 km north of Site 573, is the second site of the three-site latitudinal transect and is situated just north of the crest of the equatorial sediment belt. Four holes were drilled at this site. The upper 206 m of sediments were piston cored in a duplicate set in Holes 574 and 574A, and the remaining 224 m were rotary cored in Hole 574D. Only one rotary-cored se-

Table 5. (Continued).

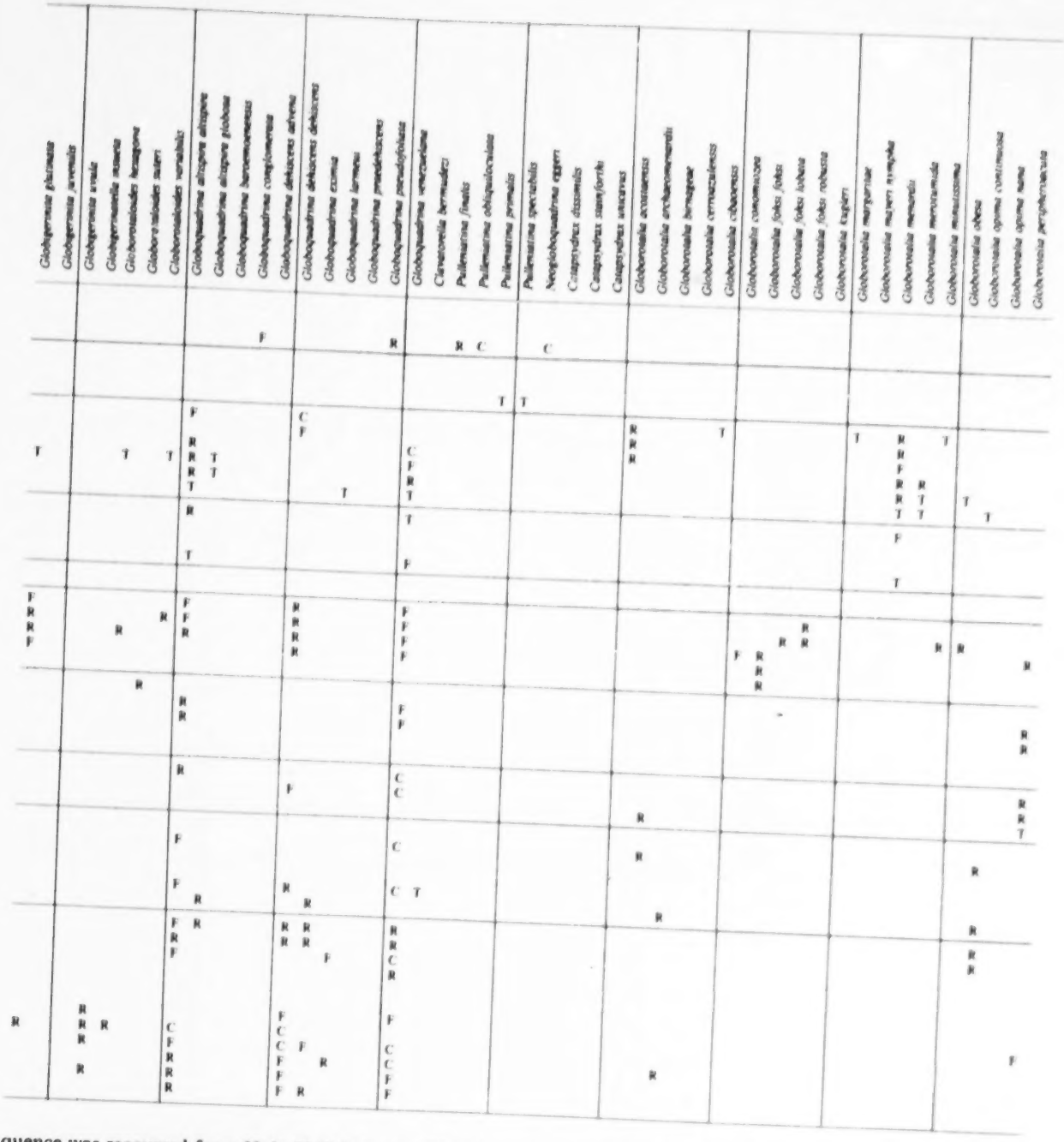

quence was recovered from Hole 574B between 185 and 194.5 m sub-bottom. Hole 574D ended in basalt at 520 m sub-bottom.

The recovered sequence yields planktonic foraminiferal faunas from upper Eocene through Pleistocene. Owing to severe dissolution of planktonic foraminifers, however, this fossil group provides good stratigraphic control for only three sections of the sequence, from 110 to 190 m (Zones N8 through N12), from 230 to 440 m (Zones N4 through N6), and from 517.5 m to the base at 520 m (Zone P17). Other intervals contain rare assemblages; their zonal assignments were established only after consultation with paleontologists studying other microfossil groups.

The sedimentary sequence recovered from the two parallel HPC holes yielded rich and well-preserved assemblages recording two important events in planktonic foraminiferal evolution. One is the well-known "*Globoro-*

Table 5. (Continued).

Age	Zone	Sample (interval in cm)	Abundance	Preservation	*Globigerinella aequilateralis*	*Globigerinella calida*	*Globigerinella praecalida*	*Globigerina angulisuturalis*	*Globigerina angustiumbilicata*	*Globigerina bimaensis*	*Globigerina falconensis*	*Globigerina nepenthes*	*Globigerina praebulloides*	*Globigerinoides altiaperturus*	*Globigerinoides bollii*	*Globigerinoides conglobatus*	*Globigerinoides immaturus*	*Globigerinoides obliquus obliquus*	*Globigerinoides primordius*	*Globigerinoides quadrilobatus*	*Globigerinoides ruber cyclostomus*	*Globigerinoides sacculifer*	*Globigerinoides sicanus*	*Globigerinoides subquadratus*	*Globigerinoides trilobus*	*Praeorbulina glomerosa circularis*	*Praeorbulina glomerosa curva*	*Praeorbulina glomerosa glomerosa*	*Praeorbulina transitoria*	*Orbulina bilobata*	*Orbulina suturalis*	*Orbulina universa*	*Sphaeroidinella dehiscens*	*Sphaeroidinella dehiscens immaturus*	*Sphaeroidinellopsis seminulina*	*Sphaeroidinellopsis subdehiscens*	*Globigerinita bradyi-uvula*
		Hole 574C																																		
	N8	1,CC	R	M																																
	?	2,CC	R	M																																
	?	3,CC	F	M																																
		4,CC	C	M																																
	N6	5,CC	C	M									F	T				T																T		
		6,CC	C	M													R						R												T	
	N5	7-1, 110–112	C	M						T	T		T	T						T					F											
		7,CC	A	G						T							R																			C
		8,CC	A	M										R																						
		9,CC	C	P					T									T																		
early Miocene		10-5, 110–112	C	M						R																										
		10-6, 110–112	C	M						R									T																	
		10,CC	C	M					R																											
		11,CC	A	M				F		R			R						R																	
		12,CC	C	M				R		R							R																			
		13,CC	F	M																																
	N4	14,CC	C	M																																R
		15,CC	C	M					R																											
		16(1), 110–112	C	M																																
		16,CC	R	M																																
		17(2), 110–112	F	M																																
		17(4), 110–112	F	M																																
		17,CC	F	M				R	C																											
	P22	18,CC	C	M				R	C																											
		19,CC	F	M																																
		20,CC	C	M				R																												
		21,CC	A	G																																
	P21	22,CC	C	M																																
		23,CC	A	M				F																												
		24,CC	A	M																																
	P20	25,CC	A	G																																
		26,CC	F	P																																
	P19	27,CC	C	M																																
		28,CC	F	M																																
Oligocene	?	29,CC	A	M																																
		30,CC	F	M																																
		31,CC	F	P																																
	P19	32,CC	A	M																																
		33-4, 80–82	R	M																																
		33-5, 58–59	R	M																																
	?	33,CC	R	M																																
		34-2, 29–30	R	M																																
		34-2, 75–76	R	M																																
		34,CC	R	P																																
Eocene	P17	35-1, 126–128	F	M																																
		35-2, 54–55	F	M																																
		35,CC	C	M																																

talia fohsi lineage" which underwent rapid development in the tropical region during the early middle Miocene from the small, nonkeeled ancestor *G. peripheroronda* via the medium-sized and weakly keeled *G. praefohsi* to the robust, well-keeled *G. fohsi robusta* (Bolli, 1950; Blow and Banner, 1966). These species are zonal markers for Zones N9 through N12 and provide an excellent means of establishing a precise global correlation. Another event of significant stratigraphic importance is the evolutionary lineage of the genus *Orbulina*. The first appearance of *Orbulina suturalis* from its immediate ancestor *Praeorbulina* occurs at the lower/middle Miocene boundary in the European type section and coincides with the foraminiferal zonal boundary between Zones N8 and N9 (Berggren and Van Couvering, 1974).

The *G. fohsi* evolutionary lineage is traceable in Cores 574-12 through -21. The Zone N11/N12 boundary is recognized between Samples 17-3, 108–110 cm and 17-2, 108–110 cm; the Zone N10/N11 boundary between 19,CC and 19-3, 50–53 cm; and the Zone N9/N10 boundary

Table 5. (Continued).

Globigerinita glutinata	*Globigerinita juvenilis*	*Globigerinita uvula*	*Globigerinatella insueta*	*Globoturborotalita hexagona*	*Globoturborotalita tuerri*	*Globoturborotalita venabilis*	*Globoquadrina altispira altispira*	*Globoquadrina altispira globosa*	*Globoquadrina baroemoenensis*	*Globoquadrina conglomerata*	*Globoquadrina dehiscens advena*	*Globoquadrina dehiscens dehiscens*	*Globoquadrina exima*	*Globoquadrina larmeui*	*Globoquadrina praedehiscens*	*Globoquadrina pseudofoliata*	*Globoquadrina venezuelana*	*Clavatorella bermudezi*	*Pulleniatina finalis*	*Pulleniatina obliquiloculata*	*Pulleniatina primalis*	*Pulleniatina spectabilis*	*Neogloboquadrina eggeri*	*Catapsydrax dissimilis*	*Catapsydrax stainforthi*	*Catapsydrax unicavus*	*Globorotalia acostaensis*	*Globorotalia archaeomenardii*	*Globorotalia birnageae*	*Globorotalia cerroazulensis*	*Globorotalia cibaoensis*	*Globorotalia conomiozea*	*Globorotalia foshi foshi*	*Globorotalia foshi lobata*	*Globorotalia foshi robusta*	*Globorotalia kugleri*	*Globorotalia margaritae*	*Globorotalia mayeri nympha*	*Globorotalia menardii*	*Globorotalia merotumida*	*Globorotalia miozea miozea*	*Globorotalia obesa*	*Globorotalia opima continuosa*	*Globorotalia opima nana*	*Globorotalia peripheroacuta*
T	F				F		T					R		R			F						T																			
F					T		R					F		T			F							R											R							
T							F				F						C							T																			
							F				R						F																										
R							F	R	T		R	R	R				R							R	T	F														T			
R							F				F						F							F	R	R																
F		T			R						F	R		T			F							R	T	R										T						
											R						F							R	R	R																
											F																															
F		F			R			R				R	R		R		R							F	T	R																
F												R			R		F							F	R	R																
R					F																			F	R	R																
R																	F							F	R	R																
F																								F	R	R																
F																								F	R	R																
C												R					F							F	R	R																
					F												F							F		R																
					R		R																		R	R																
																	F							F		F																
					R																			C	R	F																
					F																			F	C	F																
					F																			F	F	F																
					F																			F	F	F																
					F																			F	R	F																
					R																			F	R	F																
																								R	R	R																
																								F																		
					F																			C		F																
																								C		R			T													

between 21-3, 107–110 and 21-2, 107–110 cm. The evolutionary development of the genus *Orbulina* is recorded in Cores 574-26 and -22. The first appearance datum of *Orbulina* lies between Samples 574-24,CC and -25-1, 107–110 cm and Samples 574A-22-6, 144–147 cm and 77–79 cm. At least three sections consisting almost exclusively of reworked Oligocene planktonic foraminiferal faunas occur in the middle Miocene interval: an approximately 9-m-thick section from 574A-17-3, 105–108 cm to -18-7, 27–29 cm; a 6-m-thick section from 574-21-2, 138–140 cm to -21,CC; and a 4-m-thick section from 574A-22-2, 19–20 cm to -22-4, 141–144 cm. A similar section also occurs in the basal part of Core 574-22. Characteristic features common to all of these sections are that (1) the sediment consists predominantly of grains smaller than 150 μm, and (2) the three species of Oligocene planktonic foraminifers, *Chiloguembelina cubensis*, *Cassigerinella chipolensis*, and *Globorotalia postcretacea*, almost exclusively make up the sediment fraction greater than 63 μm. *Chiloguembelina cubensis* somewhat

Table 5. (Continued).

Age	Zone	Sample (interval in cm)	Abundance	Preservation	*Globorotalia periphroronda*	*Globorotalia plesiotumida*	*Globorotalia praefohsi*	*Globorotalia praemenardii*	*Globorotalia praescitula*	*Globorotalia pseudokugleri*	*Globorotalia quinifalcata*	*Globorotalia siakensis*	*Globorotalia truncatulinoides*	*Globorotalia tumida flexuosa*	*Globorotalia tumida tumida*	*Globigerina ampliapertura*	*Globigerina angiporoides*	*Globigerina aff. corpulenta*	*Globigerina galavisi*	*Globigerina gortanii*	*Globigerina nepenthes*	*Globigerina pera*	*Globigerina praebulloides*	*Globigerina pseudovenezuelana*	*Globigerina sipuriensis*	*Globigerina tripartita*	*Globigerina winkleri*	*Globigerina yeguaensis*	*Globoquadrina altispira*	*Globoquadrina spinea spinea*	*Globorotalia postcretacea*	*Pseudohastigerina micra*	*Pseudohastigerina barbadoensis*	*Pseudohastigerina naperimcheusis*	*Cribrohantkenina inflata subsp. bermudezi*	*Hantkenina primitiva*	*Cassigerinella chipolensis*	*Chiloguembelina cubensis*
		Hole 574																																			
Quat	N22	1,CC	A	G									R		A																						
Plio.	?	2,CC	F	M											F																						
	N19	3,CC	F	M																																	
		4,CC	F	M										R	F																						
late Miocene	N17	5,CC	F	M		F																															
		6,CC	F	M		C																															
		7,CC	F	G		R																															
		8-4, 107-110	F	G		R																															
		8(5), 107-110	F	G		F																															
		8(6), 107-110	F	G		T																															
	N16	8,CC	R	M																																	
	?	9,CC	R	M																																	
		10,CC	R	M																																	
	N14	11,CC	R	M								R																									
	N13	12,CC	F	G																																F	
middle Miocene	N12	13,CC	C	G				R				C																									
		14,CC	A	G				F	R			A																									
		15,CC	A	G				R				C																									
		16,CC	R	G			R					F																									
		17(2), 108-110	F	F				R																													
	N11	17(3), 108-110	M	M			F	R				C																									
		17,CC	F	M			R	R				C																									
		18,CC	F	M				T				C																									
		19(2), 50-53	F	M																																	
		19(3), 50-53	F	M	R		T																														
	N10	19,CC	F	G				R	R			C																									
		20,CC	F	G								F																									
		21(2), 107-110	C	G																																	
	N9	21(3), 107-110	C	G																																	
		21,CC	C	M	R			T				C																									
		22-3, 140-141	C	G																																	
		22,CC	F	M																																	
		23,CC	C	M	R							A																									
		24,CC	R	M	T				T																												
early Miocene	N8	25(1), 107-110	C	M	R						T	F																									
		25-3, 107-110	C	M	R							F																									
		25,CC	C	M	F			R				C																									
		26,CC	F	M	F							C																									
		27(1), 61-64	C	M																																	
		27(2), 61-64	C	M																																	
		27-3, 61-66	C	M	R			T				C																									
		27,CC	C	G								C																									
		28,CC	A	G	F							A																									
		29,CC	A	G	R							C																									
	?	30,CC	A	G	F							A																									
	?	31,CC	R	M	R							C																									

resembles *Streptochilus globigera* (Schwager), which ranges from middle Miocene to Pliocene. *Cassigerinella chipolensis* also ranges up to middle Miocene. Thus, an argument could be made that these layers are simply anomalously fine-grained middle Miocene sediments. However, *C. chipolensis*, one of the most easily recognizable species, appears to have become extinct earlier in this part of the Pacific, in early Miocene. Jenkins and Orr (1972, p. 1084), in their study of nearby Site 77 of Leg 9, also described a shortened stratigraphic range of *C. chipolensis*. One plausible explanation for the origin of such homogeneous reworked layers is that an active bottom current winnowed fine carbonate fractions out of some seafloor Oligocene exposures and transported these fine-grained carbonates to the present site as a flocculation load.

The *Globorotalia kugleri* total range zone, here defined as Zone N4, is unusually thick at this site, span-

Table 5. (Continued).

Age	Zone	Sample (interval in cm)	Abundance	Preservation	*Globorotalia perspheronda*	*Globorotalia plesiotumida*	*Globorotalia praefohsi*	*Globorotalia praemenardii*	*Globorotalia praescitula*	*Globorotalia pseudokugleri*	*Globorotalia quinifalcata*	*Globorotalia siakensis*	*Globorotalia truncatulinoides*	*Globorotalia tumida flexuosa*	*Globorotalia tumida tumida*	*Globigerina angiporoides*	*Globigerina aff. corpulenta*	*Globigerina galavisi*	*Globigerina gortanii*	*Globigerina ouachitaensis*	*Globigerina pera*	*Globigerina praesiakensis*	*Globigerina pseudovenezuelana*	*Globigerina tapuriensis*	*Globigerina triparnita*	*Globigerina woodi jenkinsi*	*Globigerina yeguaensis*	*Globoquadrina selli*	*Globorotalia opima opima*	*Globorotalia postcretacea*	*Pseudohastigerina micra*	*Pseudohastigerina barbadoensis*	*Pseudohastigerina naguewichiensis*	*Cribrohantkenina inflata subsp. bermudezi*	*Hantkenina primitiva*	*Cassigerinella chipolensis*	*Chiloguembelina cubensis*
		Hole 574C																																	
early Miocene	N8	1,CC	R	M																															
	?	2,CC	R	M																															
	?	3,CC	F	M								F																							
		4,CC	C	M							T	F																							
	N6	5,CC	C	M								C																							
		6,CC	C	M								C																							
	N5	7-1, 110-112	C	M								C													T										
		7,CC	A	G								A																							
		8,CC	A	M								A													F										
		9,CC	C	P								C																							
		10-5, 110-112	C	M								C																							
	N4	10-6, 110-112	C	M								A						T																R	
		10,CC	C	M								C					R																		
		11,CC	A	M						F		C													F										
		12,CC	C	M								C																							
		13,CC	F	M								F													F	R									
		14,CC	C	M								F									T														
		15,CC	C	M								F													R										
		16(1), 110-112	C	M																															
		16,CC	R	M																															
		17(2), 110-112	F	M																															
		17(4), 110-112	F	M																															
	P22	17,CC	F	M						R		C													R										
		18,CC	C	M								F													F										
		19,CC	F	M																					R		R								
		20,CC	C	M								R													R			R							
	P21	21,CC	A	G								R						R			R				F			A						F	R
		22,CC	C	M								F																C	R					F	C
		23,CC	A	M																					F			C							
	P20	24,CC	A	M																		F			R			C	C						C
		25,CC	A	G												T			R	R		F			R			R	C					C	A
		26,CC	P	P													R																			R
Oligocene	P19	27,CC	C	M																			R				R	C	F		F				
		28,CC	F	M																		R			R			F							F
	?	29,CC	A	M												R	C					F		T											
		30,CC	F	M												C	R					R									F				C
		31,CC	F	P																															
	P19	32,CC	A	M												F	F		F			F					R		F	C		C			C
		33-4, 80-82	R	M																												R			
		33-5, 58-59	R	M																															F
	?	33,CC	R	M																			R			F					T				
		34-2, 29-30	R	M													T				T				F				R						
		34-2, 75-76	R	M																															
		34,CC	R	P															R																
Eocene	P17	35-1, 126-128	F	M												R														F			T		
		35-2, 54-55	F	M																									F	T		F	T		
		35,CC	C	M															F														R		T

ning eight cores from 574C-17 through -10. Keller (1981a, b) documented similarly expanded sections all over the equatorial Pacific based on her study of Sites 55, 71, 77, and 292. Despite this expanded section of Zone N4, the evolutionary radiation of the genus *Globigerinoides* cannot be analyzed in detail, because specimens of this genus are almost absent at this site, possibly as the result of dissolution. The first appearance of the genus *Globigerinoides* had long been thought to mark the Oligocene/Miocene boundary (Berggren, 1972), but it is now considered to have evolved during the late Oligocene. This genus underwent rapid radiation during the early Miocene (Lamb and Stainforth, 1976; Keller, 1980; Srinivasan and Kennett, 1983).

The position of the Oligocene/Miocene boundary in planktonic microfossil sequences has long been debated (see Stainforth and Lamb, 1981; Keller, 1980; Steininger, 1981; Srinivasan and Kennett, 1983). If we accept the Oligocene/Miocene boundary as marked by the initial appearance of *Globorotalia kugleri*, it would occur be-

Table 6. Occurrence and estimated abundance of planktonic foraminifers at Site 575.

Age		Zone	Sample (interval in cm)	Abundance	Preservation	*Globigerinella aequilateralis*	*Globigerinella calida*	*Globigerinella praecalida*	*Beella digitata*	*Globigerina angustiumbilicata*	*Globigerina bulloides*	*Globigerina decoraperta*	*Globigerina falconensis*	*Globigerina nepenthes*	*Globigerina praebulloides*	*Globigerina rubescens*	*Globigerinoides altiaperturus*	*Globigerinoides conglobatus*	*Globigerinoides diminutus*	*Globigerinoides immaturus*	*Globigerinoides obliquus*	*Globigerinoides primordius*
			Hole 575																			
Plio-Pleist.			1-4, 51-52	A	G													R				
			1,CC	R	M																	
	late	N17	2,CC	F	M																	
		N15	3,CC	R	M																	
		N13	4,CC	C	G																	
		N12	5(2), 92-95	C	G																	
			5,CC	C	G																T	
			6,CC	A	G																	
	middle	N11	7-1, 128-129	A	G																	
			7(2), 104-105	A	G																	
			7(3), 121-124	A	G																	
			7,CC	C	M																	
		N10	8(1), 121-124	C	M																	
			8,CC	A	G							T									T	
			9(1), 121-124	A	G																	
		N9	9(2), 21-23	A	G																	
			9(2), 121-124	A	G																	
			9-4, 121-124	A	G																	
		N8	9(5), 21-23	A	G																	
			9(5), 121-124	A	G																	
			9(3), 21-23	A	G																	
			9(4), 70-72	A	G																	
			9(5), 70-72	A	G																	
			9,CC	A	G																	
			10,CC	A	G														T			
			11,CC	C	G																	
			Hole 575A																			
			1,CC	A	G																	
		?	2,CC	A	G																	
			3,CC	R	M																	
			4,CC	F	M																	
Miocene			5,CC	F	M																	
		N7	6(2), 110-113	R	M																	
		N6	6(3), 110-112	R	M																	
			6,CC	R	M																	
			7,CC	C	G						T											
			8,CC	F	M						R											
	early	N5	9,CC	F	M										T							
			10,CC	F	M						T				T							
			11,CC	C	M						R				T					T		
			12,CC	A	G						F						R					
			13,CC	A	G						R				R		R				T	R
			14,CC	A	M						R				R							
			15,CC	A	M						R						R					
			16,CC	A	G						R				R		R					
			17,CC	A	G						R						F					
			18,CC	A	G						R						T					
			19,CC	A	G						R				R		R					
			20,CC	C	M						R				T							T
		N4	21(1), 110-113	C	M																	
			21,CC	C	M					R	T											
			22,CC	C	M												T					
			23,CC	C	M						R											
			24,CC	A	G										T		R					R
			25,CC	C	M										R		R					
			26,CC	A	G												R					
			27,CC	A	G				T						T							R
			28,CC	A	G						T		R				?					
			29,CC	A	G										R		T					
			30,CC	A	G				R						R		R					
			31,CC	C	M				R	R												
			32,CC	A	G					R					T							R
			33,CC	A	G						T											R

Note: Symbols as in Tables 2 and 3.

Table 6. (Continued).

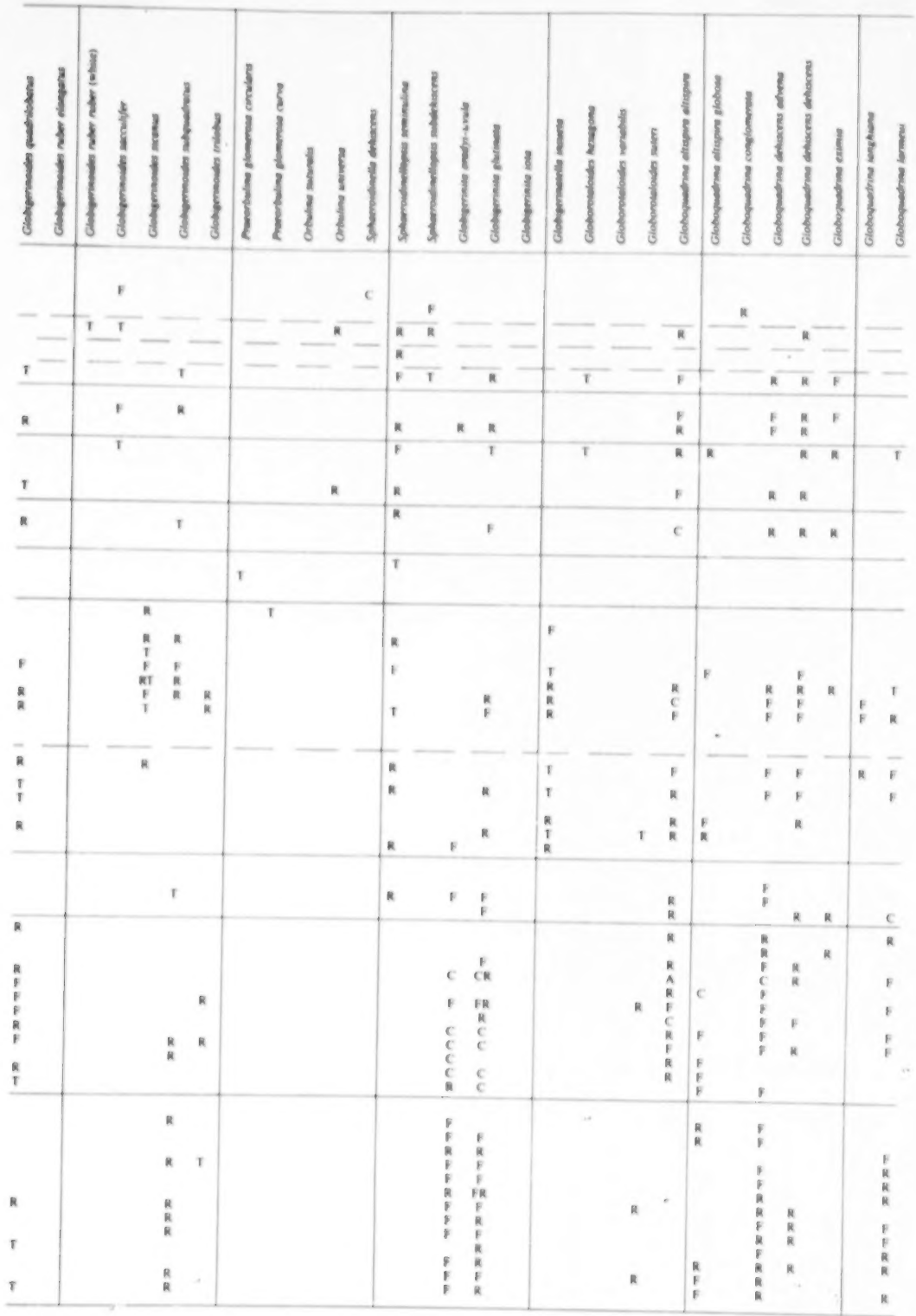
Globigerinoides quadrilobatus
Globigerinoides ruber elongatus
Globigerinoides ruber ruber (white)
Globigerinoides sacculifer
Globigerinoides trilobus
Globigerinoides obliquus extremus
Globigerinoides ruber (pink)
Orbulina universa
Orbulina suturalis
Praeorbulina glomerosa curva
Praeorbulina glomerosa circularis
Sphaeroidinella dehiscens
Sphaeroidinellopsis seminulina
Sphaeroidinellopsis subdehiscens
Globigerina bulloides
Globigerina falconensis
Globigerina praebulloides
Globigerina nepenthes
Globigerina angustiumbilicata
Globigerina venezuelana
Globigerina druryi
Globigerina ciperoensis ciperoensis
Globigerina ciperoensis angustiumbilicata
Globigerina ampliapertura
Globigerina sellii
Globigerina labiacrassata
Globigerina eocaena
Globigerina eocaena gortanii
Globigerina eocaena eocaena
Globigerina eocaena inflata
Globigerina eocaena index
Globigerina eocaena labiacrassata
Globigerina eocaena leroyi
Globigerina eocaena micra
Globigerina eocaena praecursoria
Globigerina eocaena reticulata
Globigerina eocaena turgida
Globigerina eocaena ciperoensis
Globigerina eocaena gnaucki
Globigerina eocaena sellii
Globigerina eocaena venezuelana
Globigerina eocaena ampliapertura
Globigerina eocaena nepenthes
Globigerina eocaena praebulloides
Globigerina eocaena bulloides
Globigerina eocaena falconensis
Globigerina eocaena druryi
Globigerina eocaena angustiumbilicata
Globigerina eocaena labiacrassata
Globigerina eocaena eocaena
Globigerina eocaena inflata
Globigerina eocaena index

Table 6. (Continued).

Age		Zone	Sample (interval in cm)	Abundance	Preservation	*Globoquadrina praedehiscens*	*Globoquadrina pseudofoliata*	*Globoquadrina venezuelana*	*Clavatorella bermudezi*	*Pullenatina finalis*	*Pullenatina obliquiloculata*	*Neogloboquadrina eggeri*	*Catapsydrax dissimilis*	*Catapsydrax stainforthi*	*Catapsydrax unicavus*	*Globorotalia acostaensis*	*Globorotalia archaeomenardii*	*Globorotalia birnageae*	*Globorotalia conomiozea*	*Globorotalia crassula*	*Globorotalia eastropacia*	*Globorotalia flexuosa = tumida flexuosa*	*Globorotalia fohsi fohsi*
Plio-Pleist.			**Hole 575**																				
			1-4, 51-52	A	G					T													
			1,CC	R	M																		
	late	N17	2,CC	F	M			F								T							
		N15	3,CC	R	M																		
		N13	4,CC	C	G			C											R				
		N12	5(2), 92-95	C	G																		R
			5,CC	C	G			C															F
			6,CC	A	G			C	T														
	middle	N11	7-1, 128-129	A	G			F															
			7(2), 104-105	A	G																		
			7(3), 121-124	A	G																		
			7,CC	C	M			C															
		N10	8(1), 121-124	C	M																		
			8,CC	A	G			F									R						
			9(1), 121-124	A	G																		
		N9	9(2), 21-23	A	G												R						
			9(2), 121-124	A	G												R						
			9-4, 121-124	A	G																		
		N8	9(5), 21-23	A	G																		
			9(3), 121-124	A	G																		
			9(3), 21-23	A	G													R					
			9(4), 70-72	A	G												T						
			9(5), 70-72	A	G																		
			9,CC	A	G			C															
			10,CC	A	G			F															
			11,CC	C	G			C										R					
			Hole 575A																				
			1,CC	A	G			R															
		?	2,CC	A	G			C															
			3,CC	R	M			F															
			4,CC	F	M			F															
Miocene			5,CC	F	M			T						T									
		N7	6(2), 110-113	R	M									R									
			6(3), 110-112	R	M																		
		N6	6,CC	R	M			F					R										
			7,CC	C	G			C					F										
			8,CC	F	M			F					T										
			9,CC	F	M			F						T									
			10,CC	F	M			F															
			11,CC	C	M			F					F	R									
			12,CC	A	G								F										
	early		13,CC	A	G			C					T										
		N5	14,CC	A	M									R									
			15,CC	A	M																		
			16,CC	A	G	F		F															
			17,CC	A	G			F					R	R									
			18,CC	A	G	C		F					R		T								
			19,CC	A	G	F		F					F										
			20,CC	C	M	F		F					R	T									
			21(1), 110-113	C	M																		
			21,CC	C	M	F							R	T									
			22,CC	C	M	F		R					R	R									
			23,CC	C	M	F		F					R										
			24,CC	A	G	F		F					R										
			25,CC	C	M	F							F										
			26,CC	A	G	F		F					F			R							
		N4	27,CC	A	G	F		R					R										
			28,CC	A	G	F		F					R										
			29,CC	A	G	F		F															
			30,CC	A	G	F		F					F	T	R								
			31,CC	C	M	F							R		R								
			32,CC	A	G	F		F					F										
			33,CC	A	G	F		F															

Table 6. (Continued).

Globorotalia foksi lobata	*Globorotalia foksi robusta*	*Globorotalia gigantea = scitula gigantea*	*Globorotalia kugleri*	*Globorotalia mayeri nympha*	*Globorotalia menardii*	*Globorotalia menardii limbata*	*Globorotalia merotumida*	*Globorotalia minutissima*	*Globorotalia multicamerata*	*Globorotalia opima continuosa*	*Globorotalia opima nana*	*Globorotalia peripheroacuta*	*Globorotalia peripheroronda*	*Globorotalia plesiotumida*	*Globorotalia praefoksi*	*Globorotalia praemenardii*	*Globorotalia praescitula*	*Globorotalia siakensis*	*Globorotalia tumida flexuosa*	*Globorotalia tumida tumida*	*Globorotalia truncatulinoides*	*Globorotalia ungulata*	*Globigerina* aff. *corpulenta*	*Globigerina gortanii*	*Globigerina praesepis*	*Globigerina winkleri*	*Orbulinatikenina inflata* subsp. *bermudez*	*Cassigerinella chipolensis*	*Cassigerinella martinezpicoi*
																			F	A F									
					T				T					F															
					T		T																						
																		R											
R R	R														R			A											
								T				R			R T	R		C											
		R										R			F	R	R	C											
		F										R	F		T			C											T
																		C											
													R R F F			R T		F F C C C C											
													F					C											
													F					C C R C C C											
				F							R							C F											
											F R F F			T				R F C C A-C C C C A					F R R					F F F	
			F R R R R F R C F C								R R F R							C F C C A C A A C C C C					R			R T T R R R	R	R R	

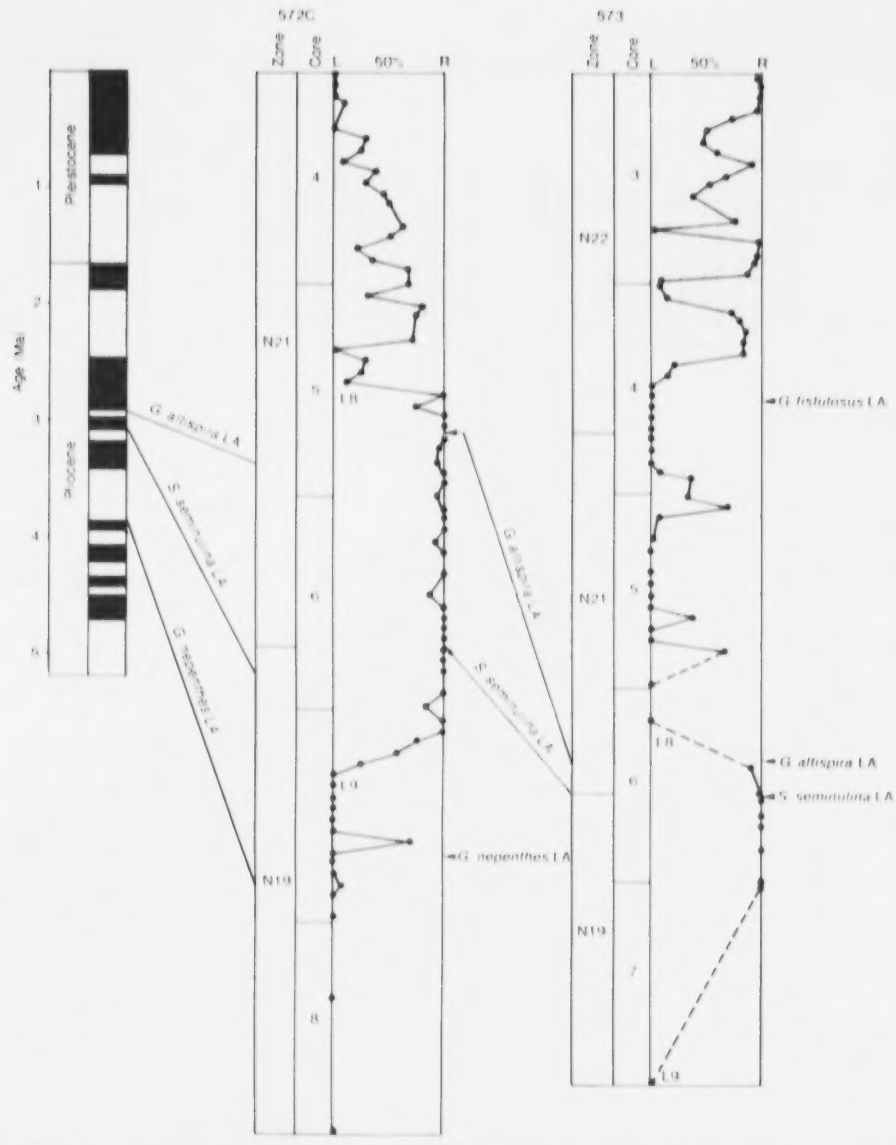

Figure 2. Biostratigraphic correlation of Holes 572C and 573 based on planktonic foraminiferal datum levels and the preferred direction of coiling in *Pulleniatina* populations. Correlation of these foraminiferal events with the paleomagnetic stratigraphy is based on Hays et al. (1969) and Saito et al. (1975). L8 and L9 mark the prominent horizons dominated by the left-coiling population of *Pulleniatina* as established by Saito (1976) in the Gilbert–Gauss (3–5 Ma) interval. Paleomagnetic stratigraphy after LaBrecque et al. (1977). LA = last appearance.

tween Samples 574-17-4, 110–112 cm and -17,CC. However, if we accept Srinivasan and Kennett's (1983) suggestion to draw the boundary below the first appearance level of *G. dehiscens*, it would lie between Samples 574C-14,CC and 574-15,CC.

Downhole encrustation of foraminifers by sediment particles progressively increases in the Oligocene sequence; this state of preservation makes it difficult to establish precise zonal assignments for the Oligocene assemblages. Cores 574-31 through -34 yield sparse assemblages. Moderately well-preserved upper Eocene planktonic foraminifers occur both in Cores 35-1 and -2. These assemblages include rare specimens of *Hantkenina primitiva* and *Globorotalia cerroazulensis* and are assigned to Zone P17 in the uppermost Eocene. The species belonging to the genera *Globigerinatheka* and *Globigerapsis*, which characterize the Eocene fauna at Site 573, are not observed at Site 574. Because sediments yielding the Zone P17 fauna underlie a sparsely foraminiferous, metalliferous chalk, the Eocene/Oligocene boundary was not identified on the basis of foraminiferal evidence. Hardenbol and Berggren (1978) regard the extinction level

of both *H. primitiva* and *G. cerroazulensis* to be one of the criteria that marks the Eocene/Oligocene boundary, and this extinction level occurs between Core 34,CC and -35-1, 126–128 cm. However, dissolution of foraminifers in the metalliferous layer also could have produced the disappearance of these two species.

Site 575

This northernmost site of the three-site transect is located just south of the Clipperton Fracture Zone. Four HPC holes were drilled at this site. Holes 575 (11 cores, 0 to 98.6 m sub-bottom), 575B (14 cores, 3.3 to 119.0 m), and 575C (2 cores, 0 to 15.8 m) make up a triplicate set representing the upper sedimentary column at this site. Hole 575A, drilled with a short 3-m core barrel, recovered the lower sedimentary column from 93.8 to 208.4 m sub-bottom and produced 33 cores. Basement was not reached at this site.

Planktonic foraminifers are abundant to common with good to moderate preservation throughout the cored sequence except for the uppermost 25 m (Cores 575-1 through -3) and a short section from 102 to 108 m sub-bottom (Cores 575A-3 and -4 and 575B-14). The foraminiferal succession is readily zonable from middle Miocene Zone N13 to early Miocene Zone N4, with the exception of the Zone N7/N8 boundary, which falls within an interval affected by intense dissolution.

The two important foraminiferal evolutionary events useful for global stratigraphic correlation, which were recognized at Site 574, were also found at this site. These are the evolutionary lineage of *Globorotalia fohsi* recorded in Cores 575-4 through -9 and that of the genus *Orbulina* in Core 575-9. The Zone N12/N13 boundary, which is nearly coincident with the extinction level of the *G. fohsi* lineage, is recognizable between Samples 575-4,CC and -5-2, 94–95 cm. The Zone N11/N12 boundary, as defined by the first appearance of *G. fohsi* sensu lato, occurs between Samples 575-6,CC and -7-1, 128–129 cm. The Zone N10/N11 boundary marked by the evolutionary development of *G. praefohsi* lies between Samples 575-7,CC and -8-1, 121–124 cm and the N9/N10 boundary as defined by the first appearance of *G. peripheroacuta* between Samples 575-9-1, 121–124 cm and -9-2, 21–23 cm.

The evolutionary appearance datum of the genus *Orbulina* is placed between Samples 575-9-4, 70–72 cm and -9-5, 21–23 cm. The interval from Zones N6 through N8 appears to be greatly condensed, whereas both the overlying Zones N9 through N12 and the underlying Zones N4 and N5 are much expanded. The deepest sedimentary layer cored at this site is from Zone N4, which is characterized by the common occurrence of *G. kugleri*.

One of the interesting aspects of the Zone N4 fauna at Sites 574 and 575 is the frequent occurrence of *Globigerinita uvula* (Ehrenberg) and *G. glutinata* (Egger). Akers and Dorman (1964) included *G. naparimaensis* Brönnimann, *G. incrusta* Akers and *Tinophodella ambitacrena* Loeblich and Tappan in the synonymy of *G. glutinata*. I consider *Globigerina juvenilis* Bolli also to be a junior synonym of *Globigerinita glutinata*, making this species one of the long-ranging planktonic foraminifers in the Neogene. In the distribution chart of Tables 4 to 7, however, the occurrences of *G. glutinata* are listed under these separate species names to show the various developmental stages of umbilical bulla and infralaminal openings. Stainforth and Lamb (1981) noted the common occurrence of *Globigerinita incrusta* (= *G. glutinata* of this chapter) in the *G. ciperoensis* Zone (= Zone P22) and in the lower half of the *Globorotalia kugleri* Zone (= Zone N4 of the present paper). Apparently, little attention has so far been given to the lower stratigraphic range of *Globigerinita uvula*. In modern oceans, this species is common in temperate and subpolar assemblages. Its small, smooth, high trochospiral test is common to both the modern and early Miocene forms.

Numerous discrete layers of foraminiferal sand, exhibiting a distinct downward increase in grain size, occur throughout the recovered sequence. The turbidite layers present in the uppermost part of the sequence (e.g., Sample 575-1-4, 51–52 cm) contain a mixed assemblage including taxa indicative of Zones N12 through N17. On the other hand, turbidites in the lower part of the sequence (e.g., Sample 575A-31-3, 70–71 cm) contain a Zone P21 assemblage. In general, reworked assemblages in a given turbidite layer are a few to several zones older than the respective *in situ* sediments. These turbidites were probably derived from an approximately 1000-m-high seamount located 10 km north of the present site (see Fig. 1 in Site 575 chapter, this volume).

THE *ORBULINA* DATUM

The first appearance of *Orbulina suturalis* Brönnimann has long been recognized as providing a datum level for globally correlating the early/middle Miocene boundary (Van Couvering and Berggren, 1977; Ryan et al., 1974). In the planktonic foraminiferal zonation, this event marks the base of Zone N9 (Blow, 1969; Jenkins et al., 1981). Studies of the European stratotype fauna by Cita and Blow (1969) place this event in the middle part of the Langhian.

However, arguments still continue regarding the calibration of the *Orbulina* datum with the radiometric time scale and the geomagnetic reversal sequences. This may be partly because only preliminary results of the studies of geomagnetic reversal sequences of the European Neogene stratotype sections have been published (Nakagawa et al., 1974). For instance, age estimates by Berggren and Van Couvering have varied from 18 Ma (Berggren, 1969) to 16 Ma (Van Couvering, 1972; Berggren, 1972) and 14 Ma (Van Couvering and Berggren, 1974). A later paper (Van Couvering and Berggren, 1977), however, advocates the date of 15 Ma based on several lines of evidence, the most important of which are the following: (1) radiometric dating by Page and McDougall (1970) using K/Ar on a volcanic sequence in New Guinea above the *Orbulina* datum gives a 13- to 15-Ma range; (2) similar dating of Japanese volcanic rocks bracketing the *Orbulina* datum gives a number of consistent ages of 14 to 16 Ma; and (3) Opdyke et al. (1974) and Theyer and Hammond (1974) come to a close agreement with an age of 15 Ma for levels very close to the *Orbulina* datum in deep-sea cores.

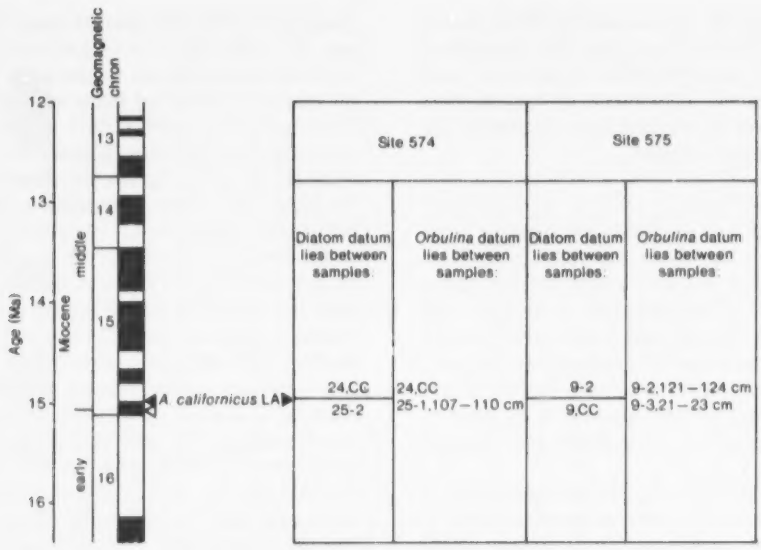

Figure 3. Comparison of stratigraphic levels of the *Orbulina* first appearance datum with the last appearance datum of *Annellus californicus* (solid triangle) at Sites 574 and 575. Paleomagnetic scales after LaBrecque et al. (1977) with radiometric dates revised by Mankinen and Dalrymple (1979). The open triangle denotes the stratigraphic position of the first appearance level of *Orbulina* spp. as indicated by Poore et al. (1983).

Our examination of planktonic foraminifers and diatoms (Barron, this volume) in the continuously HPC-cored sequences of Leg 85 sheds additional light on the age and geomagnetic calibration of the *Orbulina* datum. We examined the evolutionary development of the genus *Orbulina* from its ancestor *Globigerinoides sicanus* (de Stefani) through the few species belonging to the genus *Praeorbulina* in Holes 574, 574A, and 575. The first appearance datum of *O. suturalis* is identified precisely in these holes and occurs at the following levels: between 574-24,CC and -25-1, 107–110 cm; between 574-22-6, 77–79 cm and -22-6, 141–144 cm; and between 575-9-4, 70–72 cm and -9-5, 21–23 cm.

Barron (this volume) used a secondary correlation and tied some diatom datum levels recognized in the Leg 85 cores to the geomagnetic reversal record. In recent years, several authors (e.g., Opdyke et al., 1974; Burckle, 1978) have succeeded in directly integrating sequences of diatom datum levels with the geomagnetic reversal records, mainly by using piston cores. Fortunately for diatomists, many cores that are suitable for paleomagnetic study also yield good diatom assemblages.

Figure 3 compares the *Orbulina* datum level recognized at Sites 574 and 575 with diatom datum levels of Barron (this volume). At both sites, the *Orbulina* datum falls within an interval where Barron draws the last occurrence horizon of *Annellus californicus* Tempère. In terms of geomagnetic reversal sequences, as discussed by Ness et al. (1980), the *A. californicus* extinction datum lies in the middle of Anomaly 5B in the lower part of geomagnetic Chron 15. This correlation would give an age of 14.8 Ma for the *Orbulina* datum.

Burckle (1978) also discussed the position of the *Orbulina* datum relative to geomagnetic reversal records by using the range of *A. californicus* in two paleomagnetically dated cores, RC13-22 and RC13-24 from the equatorial Pacific. In Core RC13-24, *A. californicus* first appears in geomagnetic Chron 16 and disappears in the lower part of Chron 15 (Burckle cited in Opdyke et al., 1974). Burckle in the same paper also examined the range of this species in Leg 9 cores (Site 77) and established its last appearance level in Section 77B-24-2. The foraminiferal study by Jenkins and Orr (1972) had shown that the first appearance level of *O. universa* d'Orbigny is in the core-catcher sample of Core 23, immediately above the core section that was shown by Burckle to record the top of the range of *A. californicus*.

Thus, all the evidence available from Sites 77, 574, and 575 points to a remarkable coincidence between the extinction level of *A. californicus* and the first appearance of *O. suturalis* and *O. universa*. This line of evidence further indicates that the *Orbulina* datum must lie within the lower part of geomagnetic Chron 15 with an approximate age of 15 Ma.

Poore et al. (1983) recently made direct calibrations of magnetostratigraphy and biostratigraphy for much of the latest Cretaceous to Cenozoic sequence based on HPC cores recovered during Leg 73. Their text-figure 4 indicates that the first appearance level of *Orbulina* spp. does indeed occur in Chron 15 within the normal polarity interval of Anomaly 5B.

REFERENCES

Akers, W. H., 1955. Some planktonic foraminifera of the American Gulf Coast and suggested correlations with the Caribbean Tertiary. *J. Paleontol.*, 29:647–664.

Akers, W. H., and Dorman, J. H., 1964. Pleistocene foraminifera of the Gulf Coast. *Tulane Stud. Geol. and Paleontol.*, 3:1–93.

Banner, F. T., and Blow, W. H., 1965. Progress in the planktonic foraminiferal biostratigraphy of the Neogene. *Nature (London)*, 208: 1164–1169.

Beckman, J. P., 1971. The foraminifera of Sites 68 to 75. *In* Tracey, J. I., Jr., Sutton, G. H., et al., *Init. Repts. DSDP*, 8: Washington (U.S. Govt. Printing Office), 713–726.

Berger, W. H., and von Rad, U., 1972. Cretaceous and Cenozoic sediments from the Atlantic Ocean. *In* Hayes, D. E., Pimm, A. C., et al., *Init. Repts. DSDP*, 14: Washington (U.S. Govt. Printing Office), 787–954.

Berggren, W. A., 1969. Paleogene biostratigraphy and planktonic foraminifera of northern Europe. *In* Brönnimann, P., and Renz, H. H. (Eds.), *Proc. First Internat. Conf. Planktonic Microfossils:* Leiden (Brill), pp. 121–160.

_____, 1972. A Cenozoic time-scale—some implications for regional geology and palaeobiogeography. *Lethaia*, 5:195–215.

_____, 1984. Correlation of Atlantic, Mediterranean, Indo-Pacific Neogene stratigraphics: geochronology and chronostratigraphy. *In* Ikebe, N., and Tsuchi, R. (Eds.), *Pacific Neogene Datum Planes*: Tokyo (Univ. Tokyo Press), pp. 93–110.

Berggren, W. A., and Van Couvering, J. A., 1974. The late Neogene: biostratigraphy, geochronology and paleoclimatology of the last 15 million years in marine and continental sequences. *Palaeogeogr. Palaeoclimatol. Palaeoecol.*, 16:1–216.

Bermudez, P. J., and Seiglie, G. A., 1967. A new genus and species of foraminifer from the early Miocene of Puerto Rico. *Tulane Stud. Geol. and Paleontol.*, 5:177–179.

Blow, W. H., 1956. Origin and evolution of the foraminiferal genus *Orbulina* d'Orbigny. *Micropaleontology*, 2:57–70.

_____, 1965. *Clavatorella*, a new genus of the Globorotaliidae. *Micropaleontology*, 11:365–368.

_____, 1969. Late middle Eocene to Recent planktonic foraminiferal biostratigraphy. *In* Brönnimann, P., and Renz, H. H. (Eds.), *Proc. First Internat. Conf. Planktonic Microfossils:* Leiden, (Brill), pp. 199–422.

_____, 1970. Validity of biostratigraphic correlations based on the Globigerinacea. *Micropaleontology*, 16:257–268.

Blow, W. H., and Banner, F. T., 1962. Part 2: The mid-Tertiary (upper Eocene to Aquitanian) Globigerinaceae. *In* Eames, F. E., Banner, F. T., Blow, W. H., and Clarke, W. J., (Eds.), *Fundamentals of Mid-Tertiary Stratigraphical Correlation:* Cambridge (Cambridge Univ. Press), pp. 61–151.

_____, 1966. The morphology, taxonomy and biostratigraphy of *Globorotalia barisanensis* LeRoy, *Globorotalia fohsi* Cushman and Ellisor, and related taxa. *Micropaleontology*, 12:286–302.

Bolli, H. M., 1950. The direction of coiling in the evolution of some Globorotaliidae. *Cushman Found. Foram. Res. Contrib.*, 1:82–89.

_____, 1957. Planktonic foraminifera from the Oligocene–Miocene Cipero and Lengua Formations of Trinidad, B. W. I. *U.S. Nat. Mus. Bull.*, 215:97–124.

Brönnimann, P., 1951. *Globigerinita naparimaensis* n. gen., n. sp. from the Miocene of Trinidad, B. W. I. *Cushman Found. Foram. Res. Contrib.*, 2:16–18.

Burckle, L. H., 1978. Early Miocene to Pliocene diatom datum levels for the equatorial Pacific. *In* Wiryosujono, S., and Marks, E. (Eds.), *Proc. Second Working Group Mtg., IGCP Project 114 (Bandung, Indonesia)*, pp. 25–44.

Cita, M. B., and Blow, W. H., 1969. The biostratigraphy of the Langhian, Serravallian and Tortonian stages in the type-sections in Italy. *Riv. Ital. Paleont. Strat.*, 75:549–603.

Cushman, J. A., and Jarvis, P. W., 1929. New foraminifera from Trinidad. *Cushman Lab. Foram. Res. Contrib.*, 5:6–17.

Cushman, J. A., and Stainforth, R. M., 1945. The foraminifera of the Cipero Marl Formation of Trinidad, British West Indies. *Spec. Publ. Cushman Lab. Foram. Res.*, 14:1–75.

de Stefani, T., 1952. Su alcune manifestizioni di idrocarburi in provincia di Palermo e descrizione di foraminiferi nuovi. *Plinia, Palermo, Italy*, 3(1950–1951):1–12.

Edmond, J. M., von Damm, K. L., McDuff, R. E., and Measures, C. I., 1982. Chemistry of hot springs on the East Pacific Rise and their effluent dispersal. *Nature (London)*, 297:187–191.

Egger, J. G., 1893. Foraminiferen aus Meeresgrundproben, gelothet von 1874 bis 1876 von S. M. Sch. Gazelle. *Abh. K. Bayer. Akad. Wiss. München, Math. Physik. Kl.*, 18:193–458.

Ehrenberg, C. G. 1861. Elemente des tiefen Meeresgrundes in Mexikanischen Golfströme bei Florida; über die Tiefgrund-Verhältnisse des Ozeans am Eingänge der Davisstrasse und bei Island. *Monatsber. K. Preuss. Akad. Wiss. Berlin*, pp. 222–240, 275–315.

Hardenbol, J., and Berggren, W. A., 1978. A new Paleogene numerical time scale. *Am. Assoc. Pet. Geol. Stud. Geol.*, 6:213–214.

Hays, J. D., Saito T., Opdyke, N. D., and Burckle, L. H., 1969. Pliocene–Pleistocene sediments of the equatorial Pacific: their paleomagnetic, biostratigraphic and climatic record. *Geol. Soc. Am. Bull.*, 80:1481–1514.

Hays, J. D., and Shipboard Scientific Party, 1972. An interpretation of the geologic history of the eastern equatorial Pacific from the drilling results of the *Glomar Challenger*, Leg 9. *In* Hays, J. D., et al., *Init. Repts. DSDP*, 9: Washington (U.S. Govt. Printing Office), 909–931.

Jenkins, D. G., and Orr, W. N., 1972. Planktonic foraminiferal biostratigraphy of the eastern equatorial Pacific—DSDP Leg 9. *In* Hays, J. D., et al., *Init. Repts. DSDP*, 9: Washington (U.S. Govt. Printing Office), 1059–1193.

Jenkins, D. G., Saunders, J. B., and Cifelli, R., 1981. The relationship of *Globigerinoides bisphericus* Todd 1954 to *Praeorbulina sicana* (de Stefani) 1952. *J. Foraminiferal Res.*, 11:262–267.

Keller, G., 1980. Early to middle Miocene planktonic foraminifera datum levels of the equatorial and subtropical Pacific. *Micropaleontology*, 26:372–391.

_____, 1981a. Miocene biochronology and paleoceanography of the North Pacific. *Mar. Micropaleontol.*, 6:535–551.

_____, 1981b. The genus *Globorotalia* in the early Miocene of the equatorial and northwestern Pacific. *J. Foraminiferal Res.*, 11: 118–132.

Keller, G., and Barron, J. A., 1983. Paleoceanographic implications of Miocene deep-sea hiatuses. *Geol. Soc. Am. Bull.*, 94:590–613.

Koch, R. E., 1926. Mitteltertiäre Foraminiferen aus Bulongan, Ost-Borneo. *Eclogae Geol. Helvetiae*, 19:722–751.

_____, 1935. Namensänderung einiger Tertiär–Foraminiferen aus Niederländisch Ost-Indien. *Eclogae Geol. Helvetiae*, 28:557–558.

LaBrecque, J. L., Kent, D. V., and Cande, S. C., 1977. Revised magnetic polarity time scale for Late Cretaceous and Cenozoic time. *Geology*, 5:330–335.

Lamb, J. L., and Stainforth, R. M., 1976. Unreliability of the *Globigerinoides* datum. *Am. Assoc. Pet. Geol. Bull.*, 60:1564–1569.

Loeblich, A. R., Jr., and Tappan, H., 1957. The new planktonic foraminiferal genus *Tinophodella*, and an emendation of *Globigerinita* Brönnimann. *J. Washington Acad. Sci.*, 47:112–116.

Mankinen, E. A., and Dalrymple, G. B. 1979. Revised geomagnetic polarity time scale for the interval 0–5 m.y.B.P. *J. Geophys. Res.*, 84:615–626.

Nakagawa, H., Niitsuma, N., Kitamura, N., Matoba, Y., Takayama, T., and Asano, K., 1974. Preliminary results on magnetostratigraphy of Neogene stage stratotype sections in Italy. *Riv. Ital. Paleontol. Strat.*, 80:615–630.

Ness, G., Levi, S., and Couch, R., 1980. Marine magnetic anomaly timescales for the Cenozoic and Late Cretaceous: prècis, critique, and synthesis. *Rev. Geophys. Space Phys.*, 18:753–770.

Opdyke, N. D., Burckle, L. H., and Todd, A., 1974. The extension of the magnetic time scale in sediments of the central Pacific Ocean. *Earth Planet. Sci. Lett.*, 22:300–306.

Page, R. W., and McDougall, I., 1970. Potassium–argon dating of the Tertiary F1-2 stage in New Guinea and its bearing on the geological time-scale. *Am. J. Sci.*, 269:321–342.

Parker, F. L., 1967. Late Tertiary biostratigraphy (planktonic foraminifera) of tropical Indo-Pacific deep-sea cores. *Bull. Am. Paleont.*, 52:115–208.

Poore, R. Z., Tauxe, L., Percival Jr., S. F., LaBrecque, J. L., Wright, R., Petersen, N. P., Smith, C. C., Tucker, P. and Hsü, K. J., 1983. Late Cretaceous–Cenozoic magnetostratigraphic and biostratigraphic correlations of the South Atlantic Ocean: DSDP Leg 73. *Palaeogeogr. Palaeoclimat. Palaeoecol.*, 42:127–149.

Quilty, P. G., 1976. Planktonic foraminifera DSDP Leg 34—Nazca Plate. *In* Yeats, R. S., Hart, S. R., et al., *Init. Repts. DSDP*, 34: Washington (U.S. Govt. Printing Office), 629–703.

Robinson, E., 1969. Geological field guide to Neogene sections in Jamaica West Indies. *J. Geol. Soc. Jamaica*, 10:1–24.

Ryan, W. B. F., Cita, M. B., Dreyfus-Rauson, M., Burckle, L. H., and Saito, T., 1974. A paleomagnetic assignment of Neogene stage boundaries and the development of isochronous datum planes between the Mediterranean, the Pacific and Indian oceans in order to investigate the response of the world ocean to the Mediterranean "salinity crisis." *Riv. Ital. Paleontol. Strat.*, 80:631–688.

Saito, T., 1976. Geologic significance of coiling direction in the planktonic foraminifera *Pulleniatina*. *Geology*, 4:305–309.
Saito, T., and Biscaye, P. E., 1977. Emendation of *Riveroinella martinezpicoi* Bermudez and Seiglie, 1967, and synonymy of *Riveroinella* with *Cassigerinella* Pokorny, 1955. *Micropaleontology*, 23: 319–329.
Saito, T., Burckle, L. H., and Hays, J. D., 1975. Late Miocene to Pleistocene biostratigraphy of equatorial Pacific sediments. *In* Saito, T., and Burckle, L. H. (Eds.), *Late Neogene Epoch Boundaries:* New York (Am. Mus. Nat. Hist.), pp. 226–244.
Saito, T., Thompson, P. R., and Breger, D., 1976. Skeletal ultra-microstructure of some elongate-chambered planktonic foraminifera and related species. *In* Takayanagi, Y., and Saito, T. (Eds.), *Progress in Micropaleontology:* New York (Micropaleontology Press, Am. Mus. Nat. Hist.), pp. 278–304.
_____, 1981. *Systematic Index of Recent and Pleistocene Planktonic Foraminifera:* Tokyo (Univ. Tokyo Press).
Scholle, P. A., 1979. A color guide to sandstones: a color illustrated guide to constituents, textures, cements, and porosities of sandstone and associated rocks. *Mem. Am. Assoc. Pet. Geol.*, 28:1–201.
Spraul, G., 1963. Current status of the upper Eocene foraminiferal guide fossil, *Cribrohantkenina*. *J. Paleontol.*, 37:366–370.
Srinivasan, M. S., and Kennett, J. P., 1981. A review of Neogene planktonic foraminiferal biostratigraphy: applications in the equatorial and South Pacific. *In* Warme, T. E., Douglas, R. C., and Winterer, E. L. (Eds.), *The Deep Sea Drilling Project: A Decade of Progress*. Spec. Publ. Soc. Econ. Paleontol. Mineral., 32:395–431.
_____, 1983. The Oligocene–Miocene boundary in the South Pacific. *Geol. Soc. Am. Bull.*, 94:798–812.
Stainforth, R. M., and Lamb, J. L., 1981. An evaluation of planktonic foraminiferal zonation of the Oligocene. *Univ. Kans. Paleontol. Contrib.*, 104:1–42.
Stainforth, R. M., Luterbacher, H., Beard, J. H., and Jeffords, R. M., 1975. Cenozoic planktonic foraminiferal zonations and characteristics of index forms. *Univ. Kans. Paleontol. Contrib.*, 62: 1–425.
Steininger, F. F., 1981. The working group of the Palaeogene/Neogene boundary. *G. Geol.*, 64:15–24.
Thalmann, H. E., 1942. Foraminiferal genus *Hantkenina* and its subgenera. *Am. J. Sci.*, 240:809–820.
Theyer, F., and Hammond, S. R., 1974. The Cenozoic magnetic time scale in deep-sea cores: completion of the Neogene. *Geology*, 2: 487–492.
Thompson, R. R., and Saito, T., 1977. Pacific Pleistocene sediments: planktonic foraminifera dissolution cycles and geochronology. *Geology*, 2:333–335.
Todd, R., 1957. Smaller foraminifera. *Geology of Saipan, Mariana Islands: Pt. 3, Paleontology.* U.S. Geol. Surv., Prof. Paper, 280-H: 265–320.
Van Couvering, J. A., 1972. Radiometric calibration of the European Neogene. *In* Bishop, W. W., and Miller, J. A. (Eds.), *Calibration of Hominoid Evolution:* Edinburgh (Scottish Acad. Press), pp. 247–271.
Van Couvering, J. A., and Berggren, W. A., 1977. Biostratigraphical basis of the Neogene time scale. *In* Kauffman, E. G., and Hazel, J. E. (Eds.), *Concepts and Methods of Biostratigraphy:* Stroudsburg, PA (Dowden, Hutchinson & Ross), pp. 283–306.
Wiesner, H., 1931. Die Foraminiferen der deutschen Südpolar—Expedition 1901–1903. *In* von Drygalski, E. (Ed.), *Deutsche Südpolar Expedition 1901–1903:* Berlin (de Gruyter), 10:53–165.

Date of Initial Receipt: 15 September 1983
Date of Acceptance: 23 August 1984

APPENDIX
Taxonomic Notes

Because most of the species identified in Tables 2 through 6 are commonly recognized and have been treated fully elsewhere, only those taxa pertinent to discussion are selected for discussion and to provide a reference for the original description. For the Recent and Pleistocene planktonic foraminifers, a complete taxonomic treatment can be found in Saito et al. (1981).

Cribrohantkenina inflata (Howe) subsp. *bermudezi* (Thalmann)
(Plate 1, Fig. 2)

Hantkenina (Cribrohantkenina) bermudezi Thalmann, 1942, pp. 812, 815, 819.

Remarks. Spraul (1963) reillustrated and reviewed all the known species of the genus *Cribrohantkenina*. This species is distinct in that each of its succeeding chambers is progressively inflated, with the final chamber becoming greatly inflated and bulbose in shape. It possesses an equatorially located primary aperture with supplementary areal apertures above.

Hantkenina primitiva Cushman and Jarvis
(Plate 1, Fig. 1)

Hantkenina alabamensis Cushman var. *primitiva* Cushman and Jarvis, 1929, p. 16, pl. 3, figs. 2, 3.

Remarks. This is an interesting species of *Hantkenina* whose earlier one or few chambers in the last whorl lack the characteristic spines of *Hantkenina*. Previous records of this species are from Virginia and Alabama of the United States, Trinidad, Morocco, Italy, Ecuador, and Tanzania.

Cassigerinella martinezpicoi Bermudez and Seiglie

Riveroinella martinezpicoi Bermudez and Seiglie, 1967, pp. 177–178, pl. 1, figs. 1–6.
Cassigerinella martinezpicoi (Bermudez and Seiglie) Saito and Biscay, 1977, pp. 322–324, pl. 1, figs. 1–8; pl. 2, figs. 1, 2, 4.

Remarks. This species, originally defined as a benthic foraminifer under the genus *Riveroinella*, has since been reassigned to the planktonic foraminiferal genus *Cassigerinella*. Quilty (1976) reported this species from Hole 319 (middle Miocene, Zone N9) and Hole 321 (late Oligocene, Zone P19) of Leg 34 under the names of *Globorotalia (Turborotalia) scitula* (Brady), n. subsp. and *Cassigerinella* sp., respectively. Hole 319 and 321 are also located in the eastern equatorial Pacific but at a latitude of about 10°S.

Globigerinita glutinata (Egger)
(Plate 2, Figs. 5, 6)

Globigerina glutinata Egger, 1893, p. 371, pl. 13, figs. 19–21.
Globigerinita naparimaensis Brönnimann, 1951, p. 18, figs. 1–14.
Tinophodella ambitacrena Loeblich and Tappan, 1957, p. 114, figs. 2–3.
Globigerinita incrusta Akers, 1955, p. 655, pl. 65, figs. 2A–D.
Globigerina juvenilis Bolli, 1957, p. 110, pl. 24, figs. 5a–6.

Remarks. One of the unexpected findings in the planktonic foraminiferal biostratigraphy of Leg 85 sequences is the frequent occurrence of *G. glutinata* and *G. uvula* in the lower Miocene (Zone N4) sections at Sites 574 and 575. These small species, with their smooth, glassy tests develop an umbilical cover plate called bulla or, in many instances, a full-grown supplementary chamber. The great variability of bulla gives *G. glutinata* many morphologic variations even within a single sample, ranging from *G. juvenilis*, which lacks a bulla, to *T. ambitacrena* and *G. naparimaensis*, both of which possess a fully inflated bulla with multiple infralaminal openings. *G. incrusta* has a medium-built, rectangular bulla with only four openings. *G. juvenilis*, as described from Miocene sediments containing *G. fohsi robusta*, is a well-lobulated form and shows a thin-lipped primary aperture. Forms representing these various morphologies are tabulated in Tables 2 through 6 under their respective species names to show the extent of morphologic variations.

Globigerinita uvula (Ehrenberg)
(Plate 2, Figs. 1–4)

Pylodexia uvula Ehrenberg, 1861, pp. 276–277, 308.
Globigerina bradyi Wiesner, 1931, pp. 133–134.
Globigerinita uvula (Ehrenberg) Saito, Thompson, and Breger, 1981, pp. 81–82, pl. 24, figs. 3a–d.

Remarks. This species is common in temperate and subpolar assemblages of Recent seas. The frequent occurrence of this species in the equatorial assemblages of Leg 85 cores was quite unexpected. The species is most numerous in the Zone N4 assemblages and rapidly diminishes in other intervals.

Clavatorella bermudezi (Bolli)
(Plate 1, Figs. 3, 4)

Hastigerinella bermudezi Bolli, 1957, p. 112, pl. 25, figs. 1a–c.
Clavatorella bermudezi (Bolli) Blow, 1965, pp. 367–368, figs. 1–5.

Remarks. Blow (1965) thought that *Clavatorella* evolved from a globorotaliid ancestor and thus erected a new genus with *H. bermudezi* Bolli as its type species. Saito et al. (1976) showed that the genus *Clavatorella* developed from *Globorotaloides hexagona* (Natland) in the early Miocene by developing clavate chambers that extend in a radial direction. This species is also distinct in having coalesced umbilical flaps resembling a webbed foot. This species has been reported from equatorial DSDP sites from the Atlantic, Indian, and Pacific oceans.

Globorotalia kugleri Bolli
(Plate 1, Figs. 5, 6)

Globorotalia kugleri Bolli, 1957, p. 118, pl. 28, figs. 5, 6.

Remarks. This biochronologically important species has received much attention and has been widely recorded from the tropics to temperate areas. Keller (1981) analyzed in detail morphologic variations and abundances of this species in the equatorial and northwestern Pacific regions.

Globoquadrina eximia (Todd)
(Plate 1, Figs. 8–10)

Globigerina eximia Todd, 1957, p. 300, pl. 78, figs. 8a–c.

Remarks. Three inflated globular chambers make up the last whorl of this species, giving rise to its rounded, triangular equatorial profile. These three chambers in the last whorl increase very rapidly in size, and they constitute a large portion of the test. This species has an umbilical tooth and is herein reassigned to the genus *Globoquadrina*. Another three-chambered form is *Globigerina tripartita* Koch, which ranges from the upper Eocene to possibly lower Miocene. However, *G. tripartita* differs from *G. eximia* in having a subquadrate equatorial profile and a narrower, semi-closed umbilicus. Also, *G. eximia* has a much younger stratigraphic range, occurring in sediments as young as the middle Miocene Zone N13. Since it was first described from the island of Saipan, this species has received only limited acceptance.

Globigerina binaiensis Koch

Globigerina? aspera Koch, 1926, p. 746, figs. 22a–c.
Globigerina binaiensis Koch, 1935, p. 558.

Remarks. This species is a unique and very distinct planktonic foraminifer characterized by its remarkably flattened apertural face. Its last chamber is extraordinarily large compared with all the earlier chambers combined. The presence of a weak but distinct umbilical tooth suggests its taxonomic affinity with the genus *Globoquadrina*.

Globigerina pseudovenezuelana Blow and Banner
(Plate 2, Figs. 7–9)

Globigerina yeguaensis Weinzierl and Applin subsp. *pseudovenezuelana* Blow and Banner, 1962, pp. 100–101, pl. 11, figs. J–L, N, O.

Stainforth et al. (1975) considered *G. pseudovenezuelana* to be one of the species representing a closely knit plexus of integrating species from the form known as *G. eocaena* Guembel (= *G. yeguaensis* Weinzierl and Applin) to the three-chambered *G. tripartita* Koch. They placed *G. pseudovenezuelana* in synonymy with *G. venezuelana* Hedberg. *G. pseudovenezuelana* is here distinguished in having more rounded chambers and more deeply depressed sutures than those of *G. venezuelana*. This species characterizes upper Eocene and Oligocene sequences of Leg 85.

Globigerinoides sicanus (de Stefani)

Globigerinoides conglobatus (Brady), Cushman and Stainforth, 1945, p. 68, pl. 13, fig. 6.
Globigerinoides sicana de Stefani, 1952, p. 9.

De Stefani (1952) erected *G. sicanus* with the designation as its type species of the specimen identified and figured by Cushman and Stainforth (1945) as *G. conglobatus* (Brady). The name *G. sicanus* remained in relative obscurity until Blow (1969) described it as having a taxonomic priority over the then widely used species *G. bisphericus* Todd. Since then, there has been a mixture of usage, some preferring *G. sicanus* and some favoring the old name *G. bisphericus*. Jenkins et al. (1981) examined the holotype specimens of these two species and concluded that *G. sicanus* should be classified under the genus *Praeorbulina* because of its possession of four slitlike apertures at the base of the final chamber. There is a possibility that *G. sicanus* is a senior synonym of *P. glomerosa* (Blow), because Blow (1956) included in the morphologic variation of his new species those forms having four slitlike apertures. Therefore, *G. sicanus* as used in this report follows the definition given by Stainforth et al. (1975) and includes those forms previously classified as *G. bisphericus* Todd.

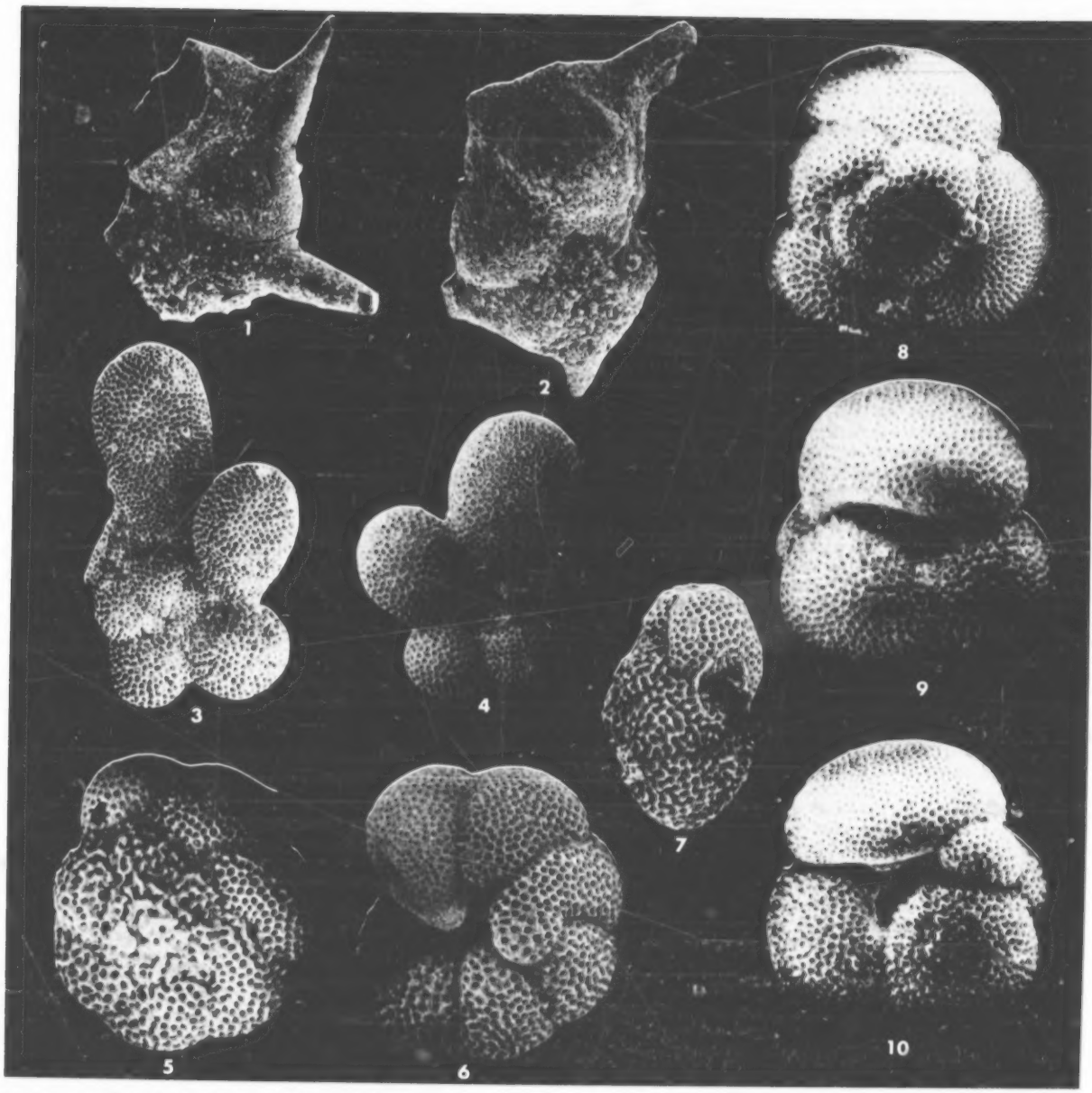

Plate 1. Cenozoic planktonic foraminifera. **1.** *Hantkenina primitiva* Cushman and Jarvis, side view, ×146, Sample 573B-42-4, 140–144 cm, upper Eocene. **2.** *Cribrohantkenina inflata bermudezi* (Thalmann), side view, ×146, Sample 573B-42-4, 123–124 cm, upper Eocene. **3–4.** *Clavatorella bermudezi* (Bolli), spiral and umbilical side views, ×107, Sample 574A-20,CC, middle Miocene. **5–7.** *Globorotalia kugleri* Bolli, spiral side, umbilical side, and side views ×230, Sample 575A-33,CC, lower Miocene. **8–10.** *Globoquadrina eximia* (Todd), spiral side, umbilical side, and umbilical side views, ×107, Sample 574-28,CC, lower Miocene.

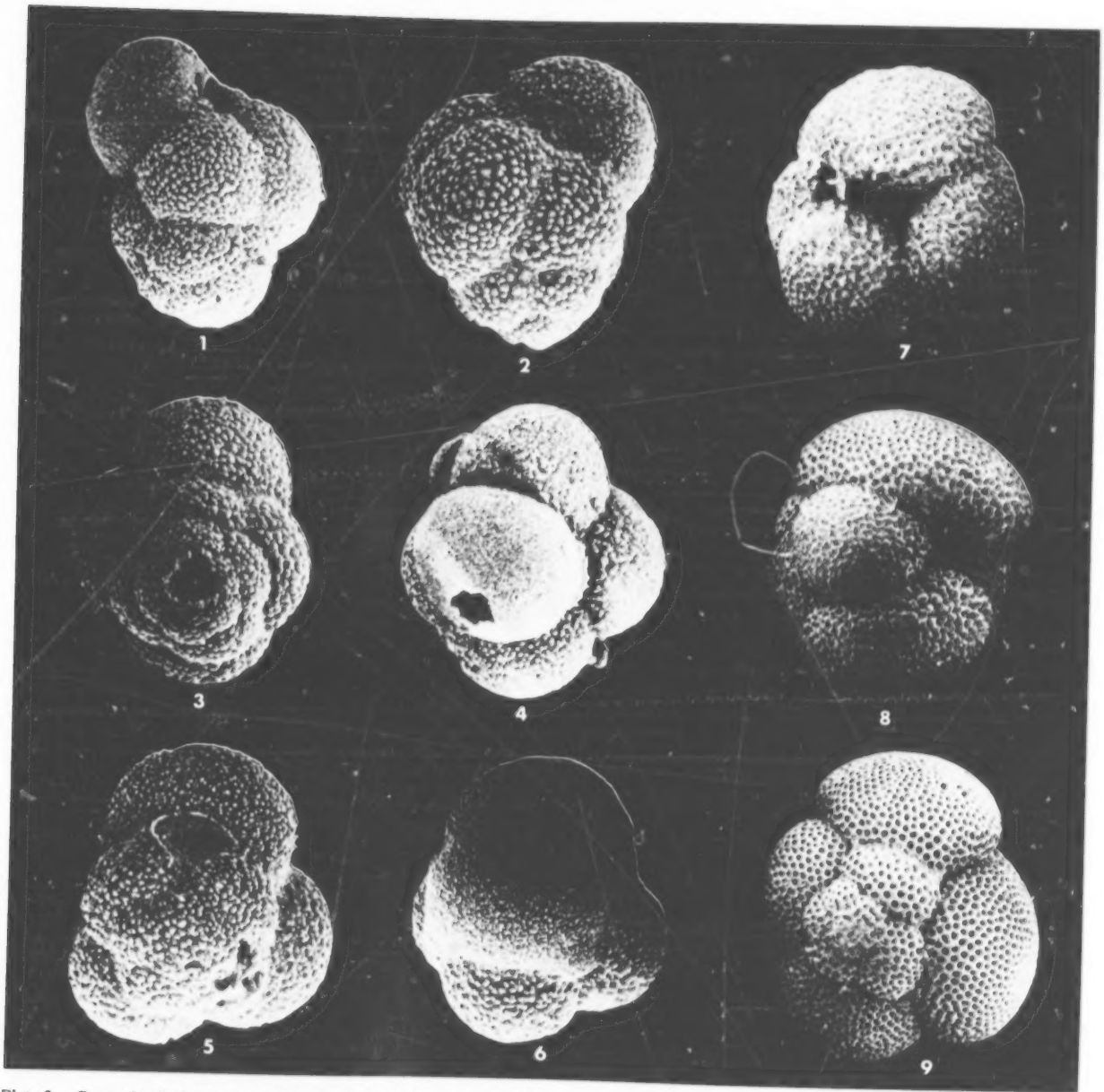

Plate 2. Cenozoic planktonic foraminifera. **1-4.** *Globigerinita uvula* (Ehrenberg), two side, spiral side, and umbilical (covered by a bulla) side views, ×338, Sample 575A-33,CC, lower Miocene. **5-6.** *Globigerinita glutinata* (Egger), ×338, Sample 575A-33,CC, lower Miocene (5, specimen resembling *Globigerinita parkerae* (Bermudez) in having a bulla-covered supplementary aperture on spiral side; 6, umbilical side view of specimen having a bulla with four infralaminal apertures). **7-9.** *Globigerina pseudovenezuelana* Blow and Banner, umbilical side, side, and spiral side views, ×107, Sample 574C-29,CC, lower Oligocene.

Reprinted from Mayer, L., Theyer, F., et al., 1985
Initial Reports of the Deep Sea Drilling Project, Volume LXXXV, Washington (U. S. Government Printing Office)

17. LATE EOCENE TO RECENT DEEP-SEA BENTHIC FORAMINIFERS FROM THE CENTRAL EQUATORIAL PACIFIC OCEAN[1]

Ellen Thomas, Scripps Institution of Oceanography[2]

ABSTRACT

Benthic foraminifers were studied in upper Eocene to Recent core-catcher samples from DSDP Sites 573, 574, and 575. The sites are on a north-south transect from the equator to about 05°N at about 133°W, water depth 4300 to 4600 m. At Site 574 additional samples were used to study the Eocene/Oligocene boundary in detail. About 200 specimens were counted per sample.

The fauna is highly diverse (about 50 to 70 species per sample) and is of low dominance. The diversity is not related to age or sub-bottom depth. Many species are cosmopolitan and probably have wide environmental tolerances. Fluctuations in frequency of some taxa (e.g., *Nuttallides umbonifera*, *Epistominella exigua*, and *Uvigerina* spp.) cannot be correlated from one site to another.

Several common species (e.g., *Oridorsalis umbonatus* and *Globocassidulina subglobosa)* range from late Eocene to Recent. First and last appearances are generally difficult to define precisely because many species are rare. For some species these datums differ from one site to another, but several datum levels are within 1 m.y. at all sites. First and last appearances are most numerous in two intervals, the late Eocene to early Oligocene (about 32 to 37 Ma) and the early to middle Miocene (about 13 to 18.5 Ma).

Isotopic events occur within each of these periods of benthic faunal change, but the isotopic events have a shorter duration and start after the initiation of the changes in the fauna. Changes in deep-sea benthic faunal composition are not directly related to short-term oceanographic changes as expressed in isotopic records.

INTRODUCTION

The knowledge of deep-sea benthic foraminifers has increased rapidly since 1968, when the Deep Sea Drilling Project began to recover Cenozoic abyssal sediments. Several review papers have been published recently on deep-sea benthic foraminifers, such as those by Douglas and Woodruff (1981), who include many previously unpublished data on Pacific faunas; Schnitker (1980), who covers Quaternary faunas; and Miller (1982). Only a few papers, notably those by Woodruff and Douglas (1981) and Tjalsma and Lohmann (1983), have quantitatively described the benthic foraminiferal fauna in long sections (spanning more than a few millions of years).

Benthic faunas from the eastern Pacific (Nazca Plate) have been described by Ingle (1973), Resig (1976, 1981), Coulbourn (1980), and Boltovskoy (1981b); from the western Pacific by Boltovskoy (1980a,b, 1981b), Woodruff and Douglas (1981), and Culp-Burke (1981); and from the central Pacific by Douglas (1973). An important discussion of Miocene benthic faunas from 25 sites distributed over the entire Pacific Ocean is presented by Woodruff (in press). The comparison of results of different authors is generally complicated by varying taxonomic concepts. Deep-sea benthic foraminiferal faunas are extremely diverse and contain many rare species, and taxonomic confusion is rampant.

The use of deep-sea benthic foraminifers in biostratigraphy is under current investigation. Detailed zonations comparable to those of planktonic microorganisms are not possible using benthic foraminifers. Boltovskoy (1976, 1978, 1980a,b, 1981a,b) found that abyssal benthic foraminifers are of limited value in biostratigraphy; his arguments were based on his work on hundreds of samples (late Eocene to Recent) from the Pacific, Indian, and south Atlantic oceans. Miller (1982) stressed that biozones based on benthic foraminifers tend to be diachronous because of the relationship between benthic faunas and the local environment. Several authors (e.g., Douglas and Woodruff, 1981; Tjalsma and Lohmann, 1983), however, agree that during times of relatively rapid change in benthic faunas, these faunas can be used for biostratigraphy, although their use is limited by geographic and depth migration of species and by taxonomic problems.

Studies of benthic foraminifers have contributed significantly to paleoclimatic and paleoceanographic reconstructions. Benthic foraminifers are rare in most samples from the deep ocean (mainly because of dilution with the skeletons of more numerous planktonic organisms), but they are generally the only bottom dwellers found in significant numbers in deep-sea cores. Therefore, they are the most important fossil group used in the reconstruction of bottom-water movements and changes in deep-water circulation (e.g., Boltovskoy et al., 1980).

Assemblages of benthic foraminifers were found to be correlated with specific water masses in the present oceans (see Boltovskoy, 1959; Streeter, 1973; Schnitker, 1974; Boltovskoy, 1976; Lohmann, 1978, for the Atlantic Ocean; Belanger and Streeter, 1980, for the Norwegian–Greenland Sea; Corliss, 1979a, for the Indian Ocean; Boltovskoy, 1976; Ingle et al., 1980, for the southeast Pacific Ocean). Unfortunately, exact relationships between

[1] Mayer, L., Theyer, F., et al., *Init. Repts. DSDP*, 85: Washington (U.S. Govt. Printing Office).

[2] Present address: Lamont-Doherty Geological Observatory, Columbia University, Palisades, N.Y. 10964.

benthic species and properties of the water masses are not yet clear. For instance, Miller (1983) and Tjalsma and Lohmann (1983) describe that *Nuttallides umbonifera* is abundant in old, sluggish, oxygen-poor bottom waters, whereas Woodruff and Douglas (1981) conclude that this species (*Epistominella umbonifera* in their nomenclature) is indicative of young, oxygenated bottom waters in the western Pacific.

The records of carbon and oxygen isotopic ratios, which are based on analyses of tests of benthic foraminifers, also document changes in bottom-water conditions. The relationships, however, between the carbon and oxygen isotopic records and the record of changes in the composition of benthic faunas are not straightforward.

A major shift in oxygen and carbon isotopic ratios in planktonic and benthic foraminifers occurred worldwide in the earliest Oligocene, just above the Eocene/Oligocene boundary (e.g., see Kennett and Shackleton, 1976; Keigwin, 1980; Keller, 1983; Keigwin and Keller, 1984; Miller and Thomas, this volume). Corliss (1981) documents that changes in the benthic faunas at that time were minor. Schnitker (1979) used DSDP material from the Bay of Biscay and concluded that a faunal turnover in the benthic foraminifers did occur at the Eocene/Oligocene boundary, but Miller (1983) studied material from the same sites and found that major changes took place between the middle Eocene and the Oligocene. These changes, however, cannot be dated unequivocally in the Bay of Biscay because of hiatuses in the upper Eocene. Tjalsma and Lohmann (1983), Tjalsma (1983), and Clark and Wright (1984) studied material from the Atlantic Ocean. They concluded that there was no major crisis in abyssal benthic faunas close to the Eocene/Oliogocene boundary, but that there were gradual changes from the middle Eocene through the early Oligocene (i.e., mainly before the major shift in isotopic ratios). In agreement with the conclusions of the papers cited above are reports by Miller (1983), Miller et al. (in press), and Snyder et al. (1984) who describe deep-sea benthic faunas from the southwest Atlantic Ocean and the Bay of Biscay. Wood et al. (in press) come to similar conclusions in their paper on the benthic faunas from the Oceanic Formation on Barbados.

A major increase in oxygen isotopic ratios of benthic and planktonic foraminifers at high latitudes occurred in the middle Miocene. The increase in benthic foraminiferal oxygen isotopic ratios is recognized worldwide (Savin et al., 1981) and is well documented in the Pacific Ocean (Shackleton and Kennett, 1975; Woodruff and Douglas, 1981). The latter authors report that a major change in benthic faunal composition occurred at the same time as the isotopic shift. Woodruff (in press) describes that migratory and evolutionary changes in benthic faunas from 25 sites all over the Pacific Ocean occurred at the same time as the shift in oxygen isotopic ratios. However, the "main phase of benthic evolution" occurred between 16.5 and 13.2 Ma (Woodruff, in press), whereas the main shift in oxygen isotopes started later and had a much shorter duration (14.0 to 14.8 Ma, Woodruff et al., 1981; see also Pisias and Shackleton, this volume; Vincent and Killingley, this volume). Berggren (1972) noted a change in the benthic faunal composition in the middle Miocene in the Atlantic Ocean, but he does not present isotopic data, nor does he give a more precise age for the event than "middle Miocene."

A worldwide increase in carbon isotopic ratios in benthic and planktonic foraminifers predates the shift in oxygen isotopic ratios (Savin et al., 1981; Vincent and Berger, 1984; Vincent et al. 1983; Vincent and Killingley, this volume). No comparison between the time of this shift and the composition of benthic faunas has been made as yet.

The late Miocene shift in carbon isotopic ratios has likewise been recognized worldwide (Savin et al., 1981; Haq et al., 1980; Keigwin, 1979; Bender and Keigwin, 1979; Vincent et al., 1980). None of the authors describing the shift gives details concerning the composition of the benthic faunas before and after the event, although Vincent et al. (1980) report a sharp peak in abundance of *Uvigerina* spp. just below the shift.

In summary, there appears to be a general relationship between changes in the composition of benthic faunas and changes in carbon and oxygen isotopic ratios, but the relationship is not straightforward: faunal changes have a longer duration and start earlier. Several authors describe the isotopic events at the Leg 85 sites (Miller and Thomas, this volume, late Eocene and Oligocene; Vincent and Killingley, this volume, early Miocene; Pisias and Shackleton, this volume, middle Miocene; Prell, this volume, Pliocene). This makes it possible to compare the isotopic records at Sites 573, 574, and 575 with the composition of the benthic fauna.

MATERIAL AND METHODS

I used material from DSDP Sites 573 (00°29.91′N, 133°18.57′W, 4301 m water depth), 574 (04°12.52′N, 133°19.81′W, 4561 m depth), and 575 (05°51.00′N, 135°02.16′W, 4536 m depth) (Fig. 1). The basement age at all sites is late Eocene. At Sites 573 and 574 basement was recovered, but at Site 575 the oldest sediment recovered was lower Miocene. Assuming that the initial depth of deposition at the ridge crest was approximately 2700 m (Berger, 1973), Sites 573, 574, and 575 backtrack (see Berger and Winterer, 1974, for methodology) from their present positions to about 3900 m depth in the early Miocene.

The sediments at all sites are siliceous nannofossil oozes and chalks. The preservation of benthic foraminifers varies from good to poor. Calcite overgrowth is rare or absent, but some dissolution does commonly occur. In many samples, especially in the older sediments, specimens show etching of the walls and detached last chambers (see Plates 1 to 15). Some samples (upper part of Holes 574 and 575) do not contain sufficient calcareous microfossils for study because of strong dissolution.

At Sites 573 and 574 core-catcher samples (about 20 cm^3) were used from one HPC hole and from the deeper rotary-drilled hole (573B and 574C, respectively). At Site 575 core-catcher samples were used from two HPC holes (575 and 575A). All core-catcher samples from these holes were studied, except those from the lower part of Hole 575A in which cores are shorter than 4 m. In this interval every second core-catcher sample was used. The sampling interval is about 0.5 m.y. averaged over the complete section, but the use of equally spaced samples does not mean that the samples are equally spaced in time. At Site 574 (Hole 574C), the lower part of the section, which spans the Eocene/Oligocene boundary, was studied in detail. From Core 574C-29 down to 547C-32 one sample per section was used, and from Core 574C-33 downward as many as five samples per section were used. The volume of these additional samples was 10 cm^3.

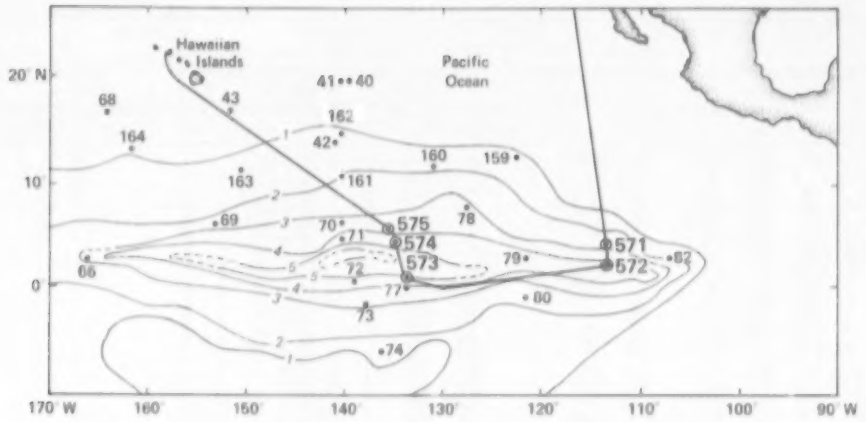

Figure 1. Track and locations of sites drilled on DSDP Leg 85 (●) in relationship to sediment thickness (contours in tenths of seconds of two-way traveltime) and to DSDP holes drilled previously (Legs 5, 8, 9, and 16).

All samples were dried and washed through a 63-μm sieve. Samples from the indurated chalks in the lower part of the section were dried and then soaked in kerosene. The kerosene was poured off and the sample heated in water.

Species-specimen plots were constructed for several samples by plotting the number of species versus the number of specimens while counting the specimens (Fig. 2). The species-specimen curves start to become parallel to the species axis at about 180 specimens; in other words, many extra specimens have to be counted to find a few extra species. Therefore, I decided to obtain about 200 specimens per sample and not use samples in which considerably fewer specimens were present. I made a strewing on a 5 × 9 cm picking tray to determine how abundant benthic foraminifers were in each sample. If fewer than five specimens were present in the strewing, the sample was not used. If more than five specimens were found, the amount of sample needed to obtain 200 specimens was estimated and a split of that size was made. If not enough specimens were found in the split, extra splits were made as needed. In the additional samples from Hole 574C, I counted all benthic foraminifers present, and samples with fewer than 180 specimens (total) were excluded from the analysis. All specimens counted were picked and mounted on Cushman slides.

Most core-catcher samples contained sufficient specimens for study (200), with the exception of samples from the upper 95 m at Site 574 and the upper 30 m at Site 575, which represent the latest 10.9 and 12.4 m.y., respectively. These sediments show strong dissolution.

The entire size fraction larger than 63 μm was used, mainly because inconsistent results were obtained when the fraction larger than 125 μm was separated. Some samples have numerous specimens of *Pleurostomella* spp. and *Stilostomella* spp., and these linear specimens can pass through the 125-μm sieve. The number of specimens that actually pass, however, turned out to depend on the way in which the sieve is shaken (how vigorously and for how long). Since the majority of the benthic foraminifers are larger than about 120 μm, the results of this study can be compared with studies in which the larger than 125-μm fraction was used, but not with studies in which the larger than 250-μm fraction was studied.

RESULTS AND DISCUSSION

The counts of benthic foraminifers for all sites are presented in Appendix A, and the taxonomy is discussed in Appendix B. The relative abundances (percent frequencies) of the most common species and species groups are shown plotted versus sub-bottom depth in Figures 3 (Site 573), 4 (Site 574), and 5 (Site 575). Figure 6 shows some of the data on Figures 3, 4, and 5 plotted versus time for the three sites combined. The time scale used to construct this figure was taken from the sedimentation rate curves in Barron et al. (this volume), and is based on the time scale by Berggren et al. (in press). (Note that a correlation of Anomaly 5 with Chron 11 has been assumed.)

Figure 7 shows stratigraphic ranges for selected species at all three sites plotted versus time. Figures 8 and 9 show relative abundances and stratigraphic ranges for selected species for the interval in Hole 574C that was studied in more detail.

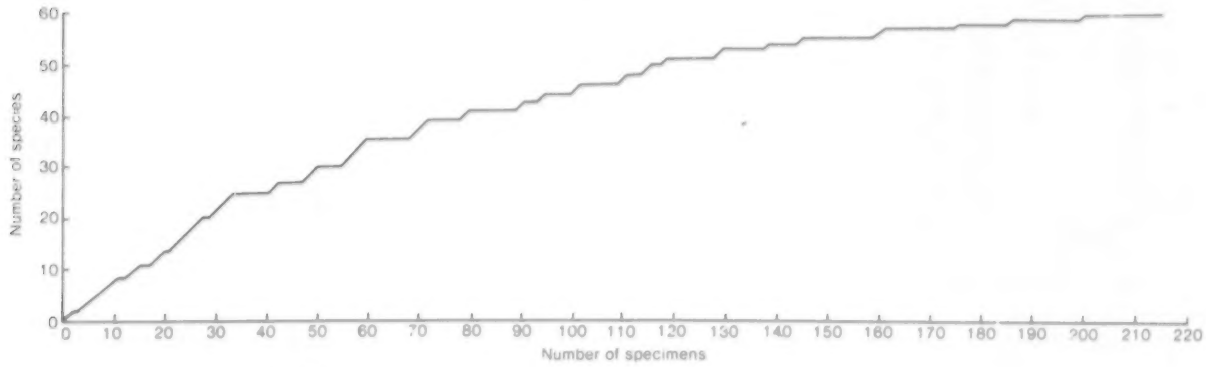

Figure 2. Species-specimen plot for Sample 573-4,CC.

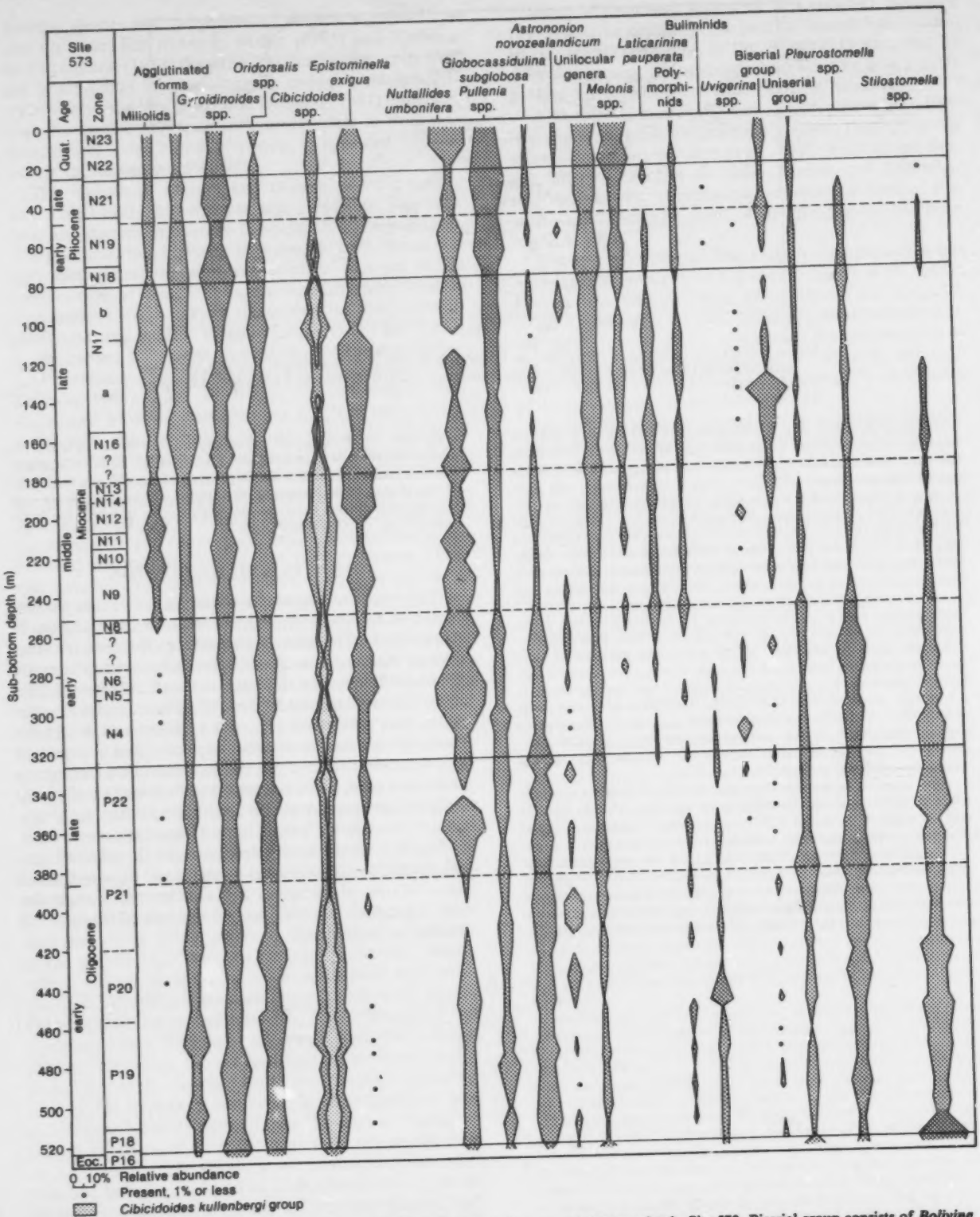

Figure 3. Relative abundances of selected species and species groups plotted versus sub-bottom depth, Site 573. Biserial group consists of *Bolivina* spp., *Fursenkoina* spp., *Stainforthia complanata*, and *Francesita advena*. Buliminids consist of *Bulimina* spp. and *Buliminella* spp. Uniserial group consists of uniserial lagenids.

READEX FICHE best copy available

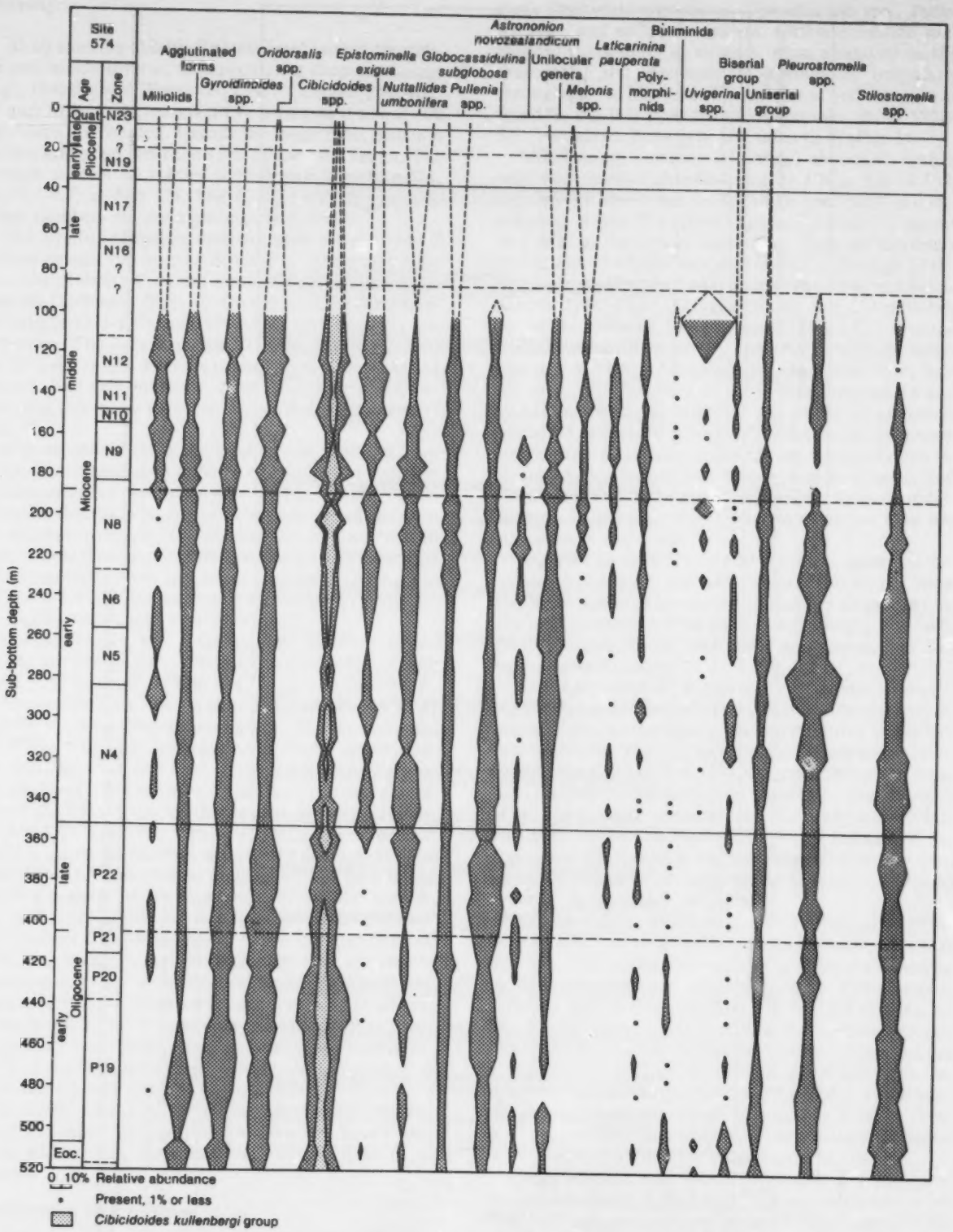

Figure 4. Relative abundances of selected species and species groups plotted versus sub-bottom depth, Site 574. Biserial group consists of *Bolivina* spp., *Fursenkoina* spp., *Stainforthia complanata*, and *Francesita advena*. Buliminids consist of *Bulimina* spp. and *Buliminella* spp. Uniserial group consists of uniserial lagenids.

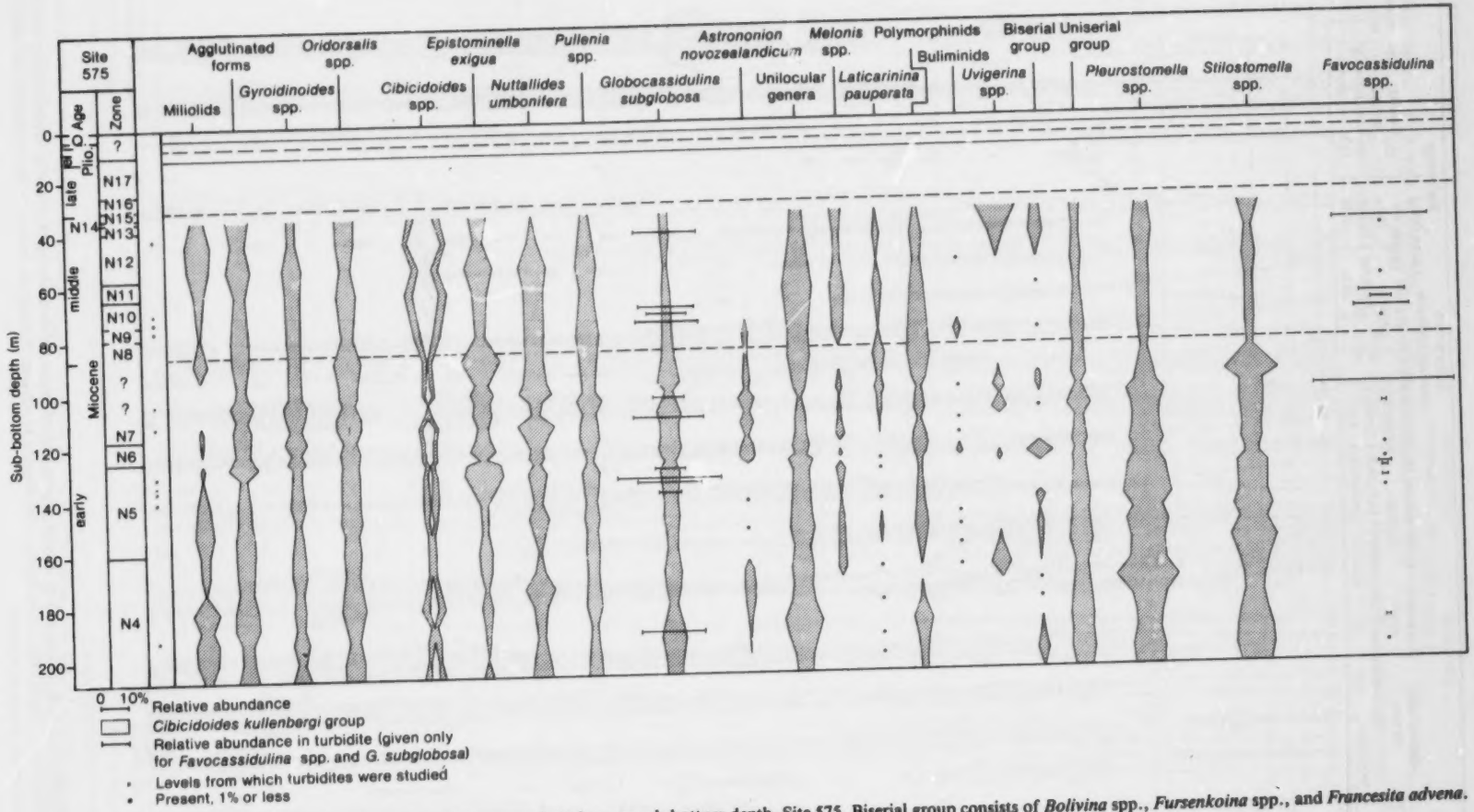

Figure 5. Relative abundances of selected species and species groups plotted versus sub-bottom depth, Site 575. Biserial group consists of *Bolivina* spp., *Fursenkoina* spp., and *Francesita advena*. Buliminids consist of *Bulimina* spp. and *Buliminella* spp. Uniserial group consists of uniserial lagenids.

Diversity

At all sites the benthic foraminiferal faunas are similar and highly diverse, as expected for deep-sea faunas (e.g., Douglas and Woodruff, 1981). Generally, between 50 and 70 taxa are recognized in a sample if about 200 specimens are counted. Usually the single most common species makes up less than 15% of the total fauna. The average number of species is 58.0 (±6.1) at Site 573, 58.8 (±6.7) at Site 574, and 63.4 (±5.5) at Site 575. These numbers are not significantly different.

The number of species does not show a clear trend if plotted against sub-bottom depth (Fig. 10) or time (Fig. 11). The diversity does not markedly decrease in more indurated sediments (Fig. 10). On the contrary, the youngest samples (573-1,CC and 574-1,CC) have relatively low diversities. The data from Site 573 (Fig. 11) suggest that the diversity might decrease overall from about 6 Ma to present. The data, however, show considerable fluctuation, and this recent decrease in diversity is not unequivocal.

It is improbable that the fluctuations in the number of species are caused completely by the slight differences in the number of specimens counted per sample. Figure 12 shows that there is no significant correlation between the number of species and the number of specimens in each sample if more than 200 specimens are counted. Of course, counting more specimens gives more species, but only very few additional species are found for many extra specimens counted over 200 (Fig. 2).

Samples with a low diversity (less than 50 species found) are 574-11,CC, 574-18,CC, 574C-9,CC, 574C-28,CC, 573B-3,CC, 573B-16,CC, and 573B-29,CC. These samples have little in common. Sample 574-9,CC contains abundant *Pleurostomella* spp. (27.1%), and Sample 573B-16,CC has abundant *Nuttallides umbonifera* (24.5%). Both samples have similar ages (19 to 20 Ma). Sample 574-11,CC contains abundant *Uvigerina graciliformis* (28.6%), a species that is also common in Sample 575-4,CC (14.6%). These two samples are the first samples below the interval with severe dissolution. The other relatively less diverse samples do not have a low diversity because of the dominance of a single species, but many species that are rare in other samples are absent. Sample 573B-9,CC is just below a hiatus (Barron et al., this volume), and the sediments were apparently deposited at a slow sedimentation rate. This sample and Sample 574-28,CC show severe dissolution in planktonic foraminifers (see site chapters, this volume); in those samples the low diversity may be caused by dissolution. None of the samples with a relatively low diversity has an extraordinarily low $CaCO_3$ content.

Generally speaking, there does not seem to be any one single cause for relatively low diversity. Both dissolution and primary environmental effects appear to be causes.

Composition of the Fauna

Abundant Taxa

Several species and species groups are common throughout the interval studied at all sites. These include *Oridorsalis umbonatus, Gyroidinoides* spp., *Pullenia* spp., and unilocular genera. *Globocassidulina subglobosa* is common at all sites, most abundant in the Oligocene, and decreases in abundance irregularly throughout the Miocene. The species is not common at Site 573, but it is present in most samples above 573B-5,CC (at about Zone N16 and upsection) (Fig. 3).

Miliolids are common to (rarely) abundant, with a maximum relative abundance of 16.1% in 573-14,CC, but they are absent (except for single specimens in a few samples) at Site 573 below Sample 573B-12,CC (about 16.5 Ma, at the top of Zone N8). They are extremely rare at Site 574 from Sample 574-29,CC through 574C-4,CC (about 18 to 16.5 Ma, Zones N6 to N8) and below Sample 574C-25,CC (Zone P20). At Site 575 miliolids are all but absent from Sample 575A-1,CC through -10,CC (about 18 to 16 Ma, Zone N6 through the lower part of Zone N8). (All zonal assignments are from Barron et al., this volume.) In the interval between 16 and 18 Ma in which the miliolids are absent or extremely rare at all sites there is strong dissolution of planktonic foraminifers at all sites. Miliolids are reportedly less resistant to dissolution than hyaline species (Corliss and Honjo, 1981), and thus the first appearances of miliolids may be dependent on preservation rather than immigration or evolution.

Agglutinant taxa are rare to common, generally between 5 and 15% of the total fauna. They do not show major fluctuations in relative abundance (Figs. 3 to 5). The most common species are *Eggerella bradyi, Trochammina globigeriniformis, Textularia agglutinans*, and *Siphotextularia catenata*.

Both *Epistominella exigua* and *Nuttallides umbonifera* show strong fluctuations in relative abundances. *E. exigua* is present throughout the section, from upper Eocene to Recent. The species is extremely rare below Sample 573B-22,CC and 574C-19,CC (upper Oligocene, Zone P22). Higher in the section its maximum abundance is 16%. The increase in abundance of *E. exigua* in the late Oligocene may be related to the depth increase at the sites, since this species is mainly described from the deep ocean (although it has been found in shallow, brackish water by Boltovskoy et al., 1980).

N. umbonifera, with a maximum abundance of 25%, is fairly common to abundant throughout the section at Site 573, with strong fluctuations in relative abundance in the upper lower and upper Oligocene. The species is generally less abundant at Sites 574 and 575 (Fig. 6). At Site 574 *N. umbonifera* is rare in the lower Oligocene and upper Eocene. A modest peak in abundance occurs in Samples 573B-33,CC and -34,CC (10.6 and 9.4%, respectively) and in Sample 574C-27,CC (9.6%). These samples are approximately coeval (about 32 to 33 Ma). There is no evident correlation between the relative abundance of *N. umbonifera* and the paleodepths of the sites.

Pleurostomella spp. and *Stilostomella* spp. are common to abundant in the lower part of the section at all sites. Both taxa decrease in abundance from Sample 573B-10,CC upward, from 574-25,CC upward, and from 575-10,CC upward (14.8 to 15.8 Ma). *Pleurostomella* spp. is most abundant at Site 574 in the lower Miocene (Zone N5).

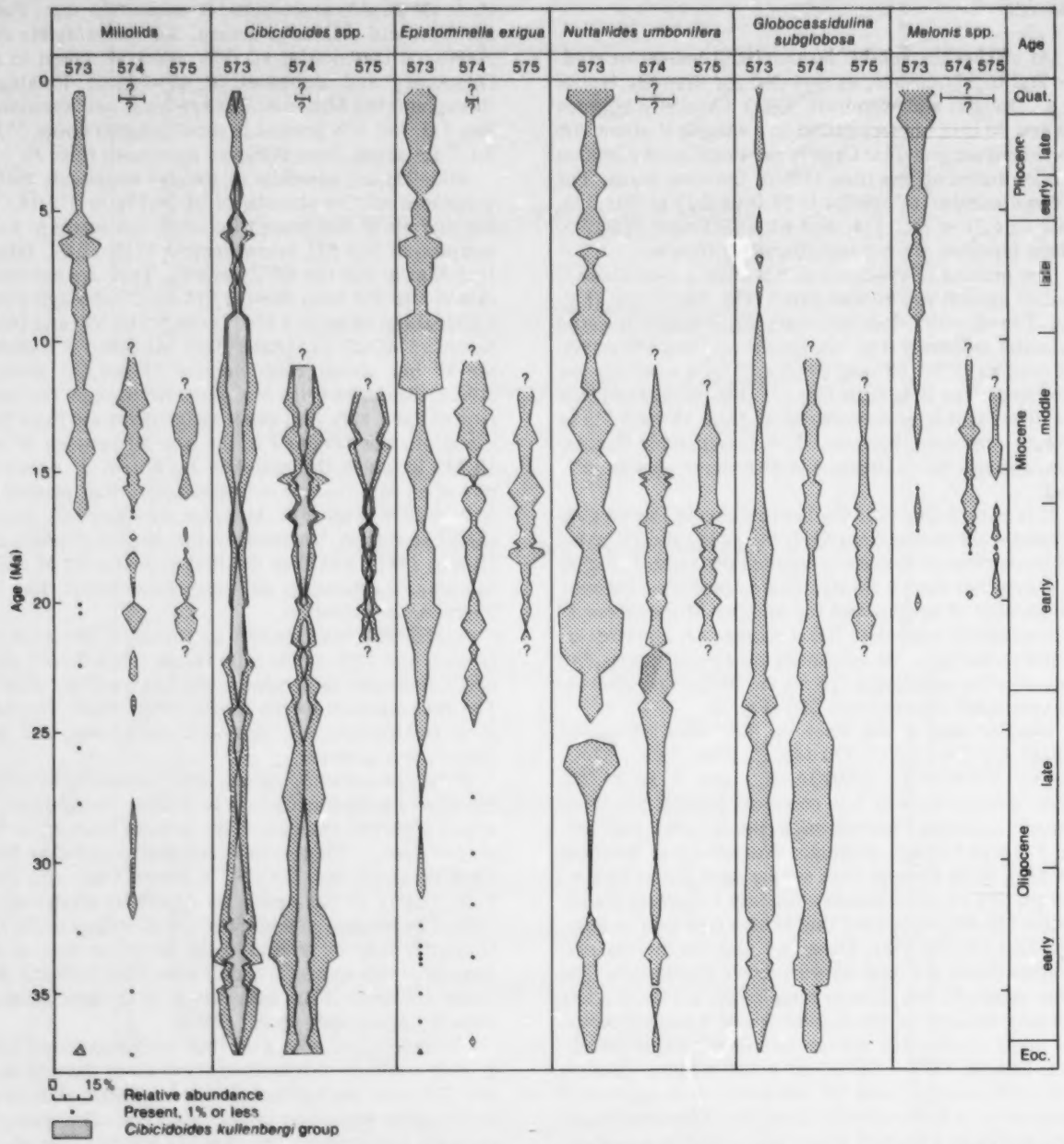

Figure 6. Relative abundances of selected species and species groups plotted versus time, Sites 573, 574, and 575. Data from Barron et al. (this volume) were used to construct the age model. Biserial group consists of *Bolivina* spp., *Fursenkoina* spp., *Stainforthia complanata*, and *Francesita advena*. Buliminids consist of *Bulimina* spp. and *Buliminella* spp.

The *Cibicidoides kullenbergi* group is present throughout the section at all sites. It decreases in abundance at Sites 573 and 574 in the upper Oligocene and increases again in the Miocene (Fig. 6). Other fluctuations in abundance of the *Cibicidoides* group cannot be correlated between the sites. The taxon is common to abundant at all sites, but it is the most abundant at Site 574 in the upper Oligocene (upper Zones P19 to P20).

Uvigerina spp., *Bolivina* spp., and *Bulimina* spp. are generally rare but common to abundant in a few samples. Abundant *Uvigerina graciliformis* occurs just below the level of strong dissolution at Sites 574 and 575; no other fluctuations in abundance of these taxa can be correlated between the sites.

Stratigraphic Ranges

The first appearances (FAs) and last appearances (LAs) of selected species at all sites are plotted versus time in Figure 7, and the timing of these events is given in Table 1. Data are given for all species with fairly continuous

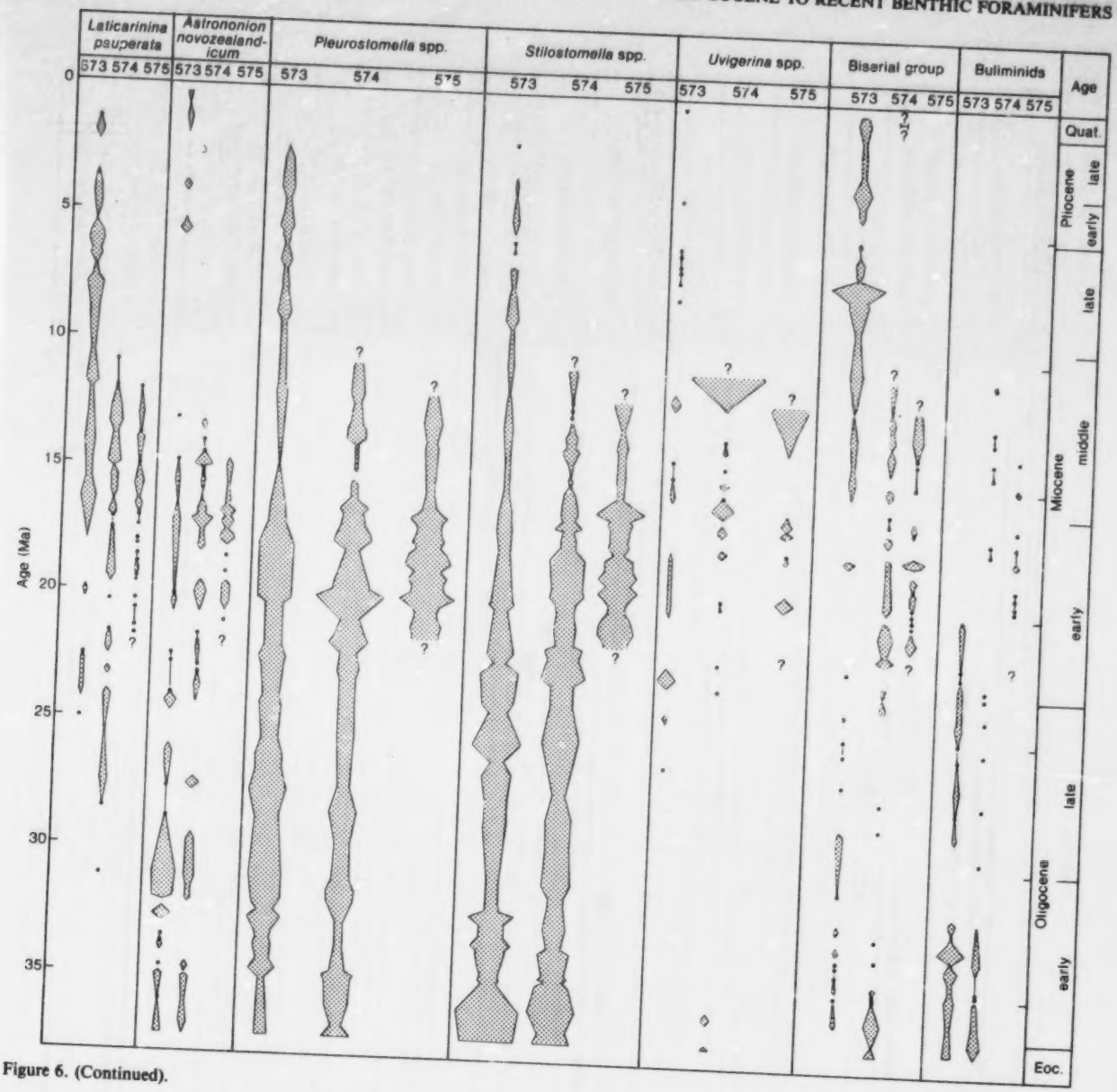

Figure 6. (Continued).

ranges of occurrence. Determining the FAs and LAs is problematic in deep-sea benthic foraminiferal faunas because many species that have FAs or LAs are rare and thus have discontinuous occurrences (Fig. 7, Appendix A). Chance may be the main determinant for the exact range of rare species.

FAs and LAs can be either evolutionary (evolution–extinction) or migratory (immigration–emigration). Migration can be either geographic migration or depth migration (or both). Evolution, extinction, and depth migration may be worldwide (although not necessarily synchronous), but study of sites in a small area cannot give information on geographic consistency of datum levels. It is not clear which of the observed FAs and LAs are local and which ones (if any) are useful for correlation over a larger area. Clustering of events (FAs and LAs) at specific levels, however, suggests that major changes in the environment of the deep sea occurred at those times, either on a local or more widespread scale.

Many species do not have similar occurrences at the three sites, and thus their FAs or LAs are not consistent even within a relatively small area in the equatorial Pacific. Some species have a continuous occurrence at one of the sites and are rare or absent at the other sites (e.g., *Bulimina microcostata* occurs at Site 573 only, and *Cibicidoides* aff. *mundulus* is common at Site 574 but extremely rare at Site 573). Probably some differences in LAs and FAs from one site to another are caused by uncertainties in biostratigraphic correlation, but there is no consistent offset in ages between the sites. Some of the

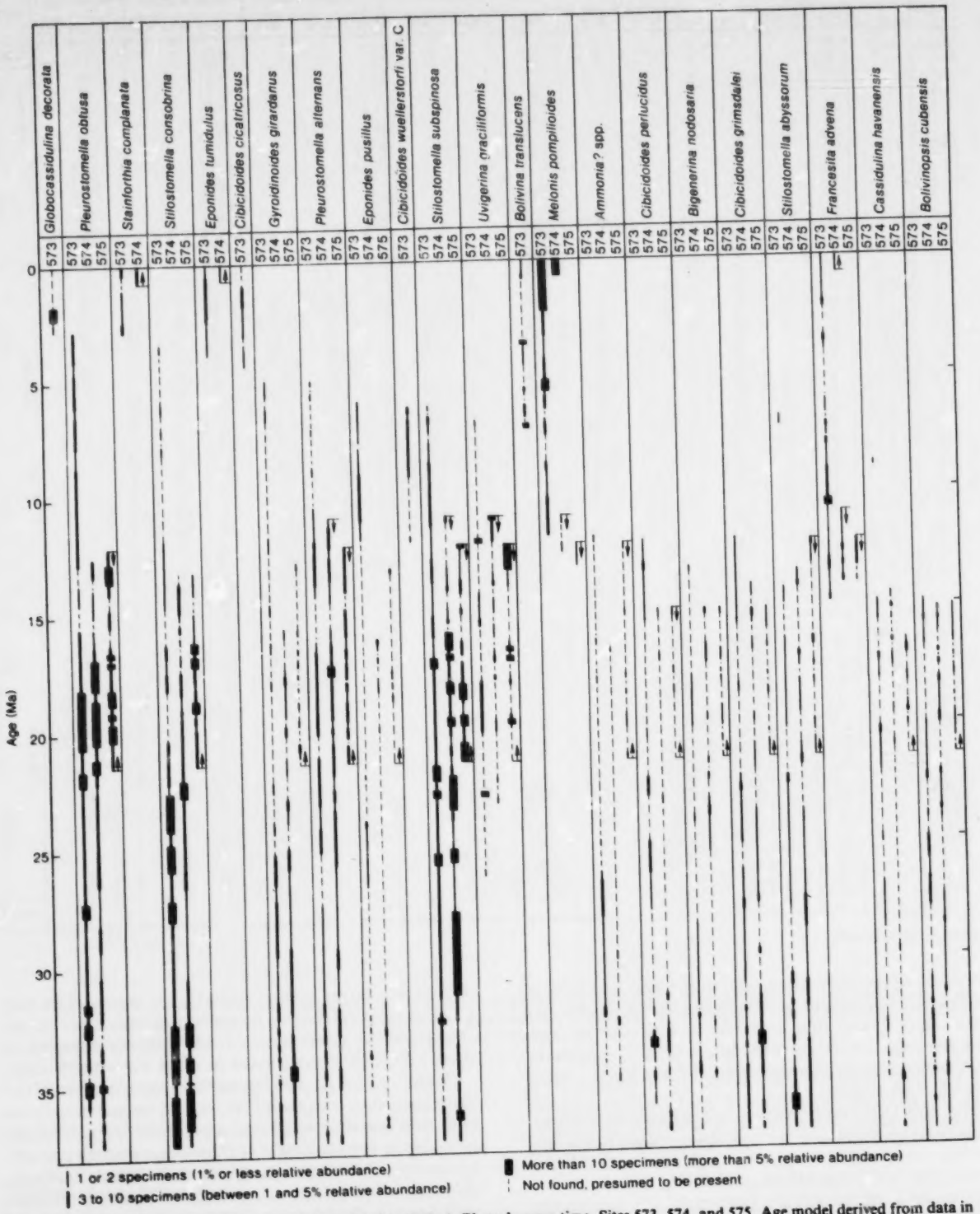

Figure 7. Stratigraphic ranges of some species tabulated in Table 1. Plotted versus time, Sites 573, 574, and 575. Age model derived from data in Barron et al. (this volume).

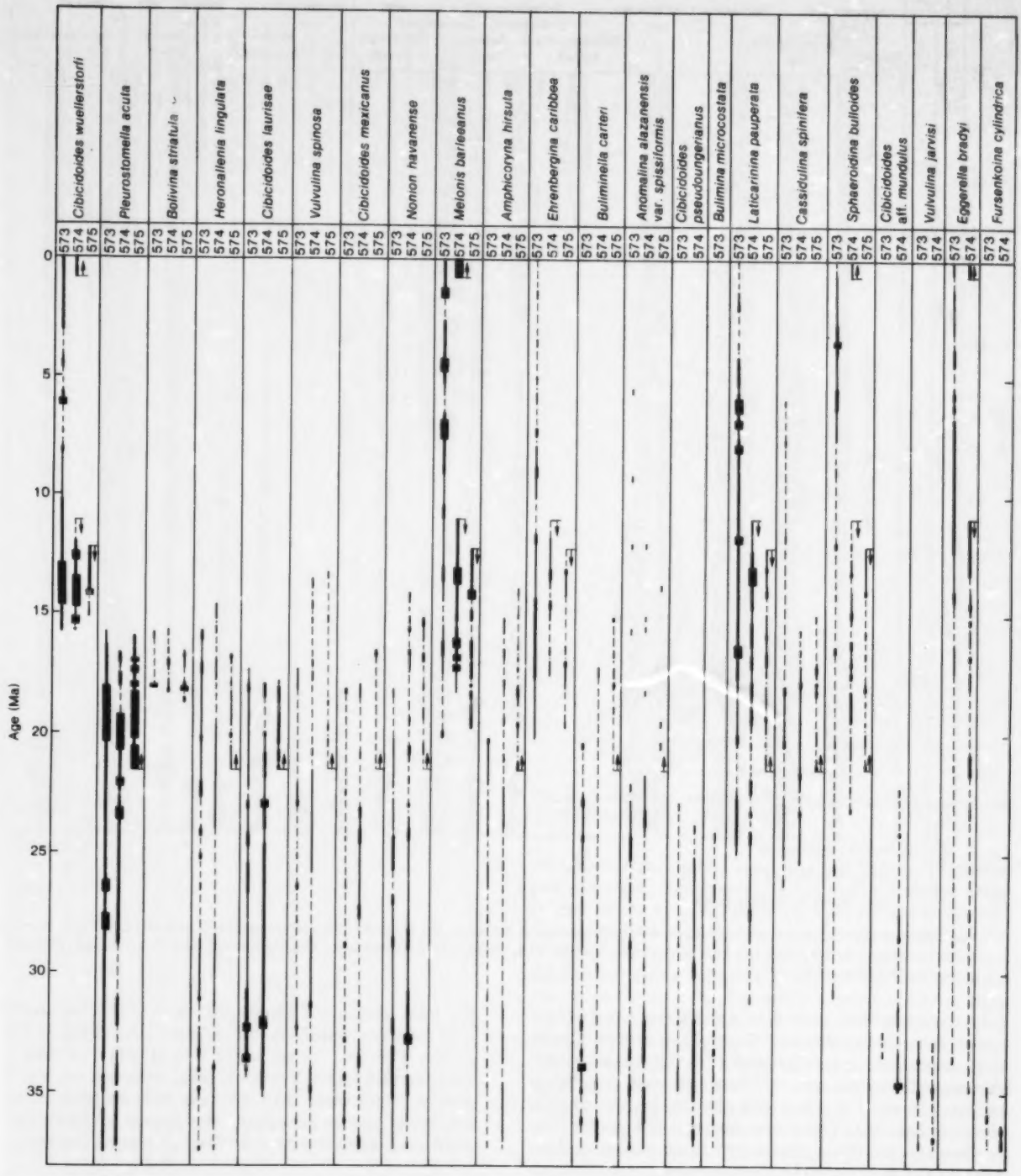

Figure 7. (Continued).

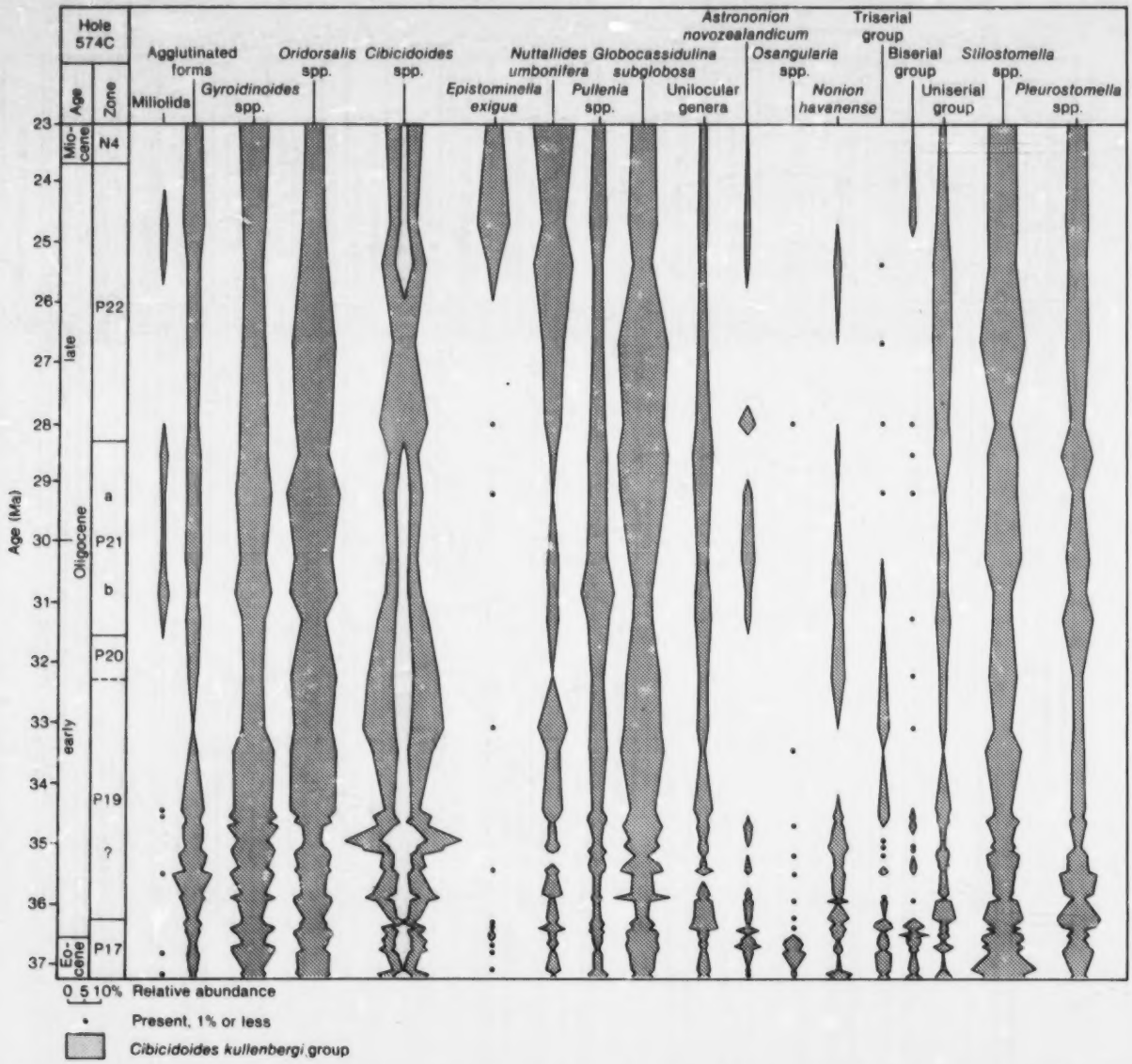

Figure 8. Relative abundances of selected species and species groups in the upper Eocene and Oligocene (Hole 574C), plotted versus time. Biserial group consists of *Bolivina* spp. and *Fursenkoina* spp. Triserial group consists of *Bulimina* spp., *Buliminella* spp., and *Uvigerina* spp. Uniserial group consists of uniserial lagenids.

LAs are apparently caused by local processes, because they appear to be related to dissolution. Several species (e.g., *Stilostomella lepidula* and *Pleurostomella obtusa*) disappear below the interval showing strong dissolution at Sites 574 and 575 but extend into much younger sediments at Site 573, where dissolution is less severe (Fig. 7). Possibly the disappearance of these species at Sites 574 and 575 was caused by the same changes in the environment that later caused strong dissolution and not by differential dissolution, as is shown by the species not appearing to be solution-prone in samples lower in the section.

Although there is no evident correlation between diversity and time or sub-bottom depth (as described above), the total number of species decreases with time. At all sites there are more LAs than FAs (32 LAs versus 19 FAs at Site 573, 29 LAs versus 15 FAs at Site 574, and 16 LAs versus 6 FAs at Site 575); thus, there is a net loss of species. Since more than 200 taxa were recognized, the number of species per sample may appear to remain constant even when the total number of species declines.

Stratigraphic Events

Late Eocene to Oligocene

At Site 574 datum levels (FAs and LAs) cluster between 32 and 37 Ma (Figs. 8 and 13). At Site 573 few data are available for this period, because there is a fora-

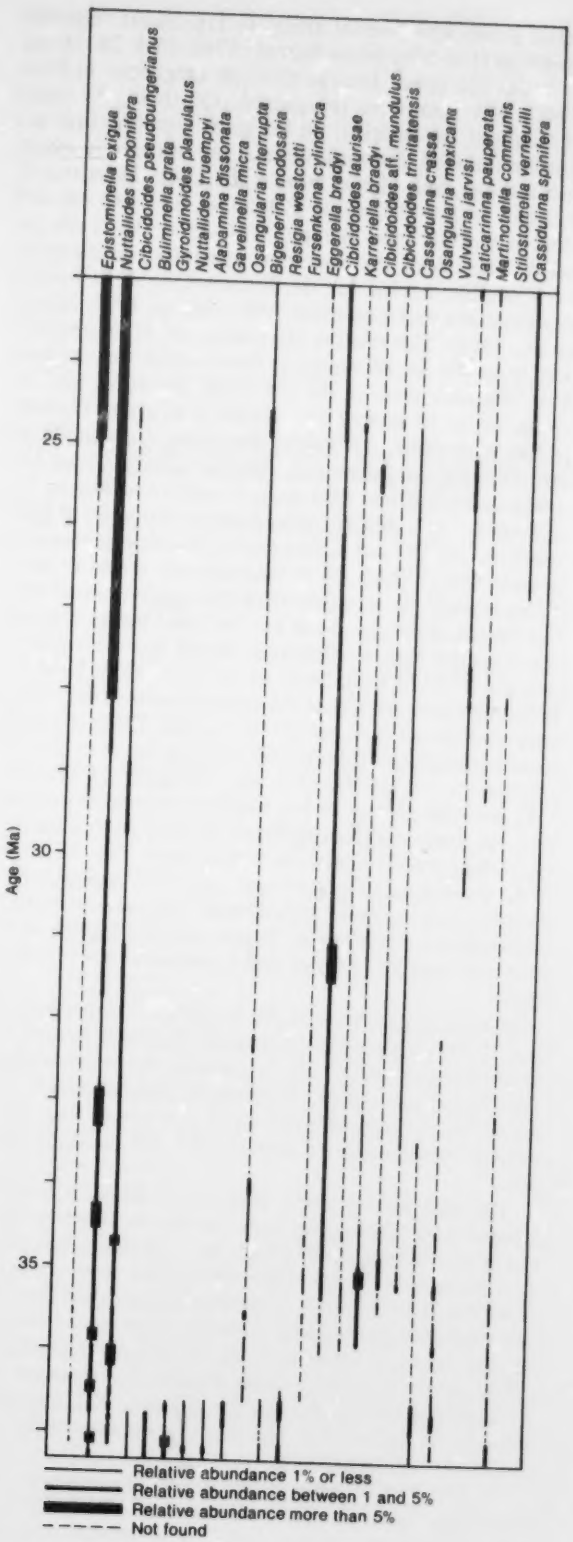

Figure 9. Stratigraphic ranges of selected species in the upper Eocene–Oligocene (Hole 574C). See also Table 1.

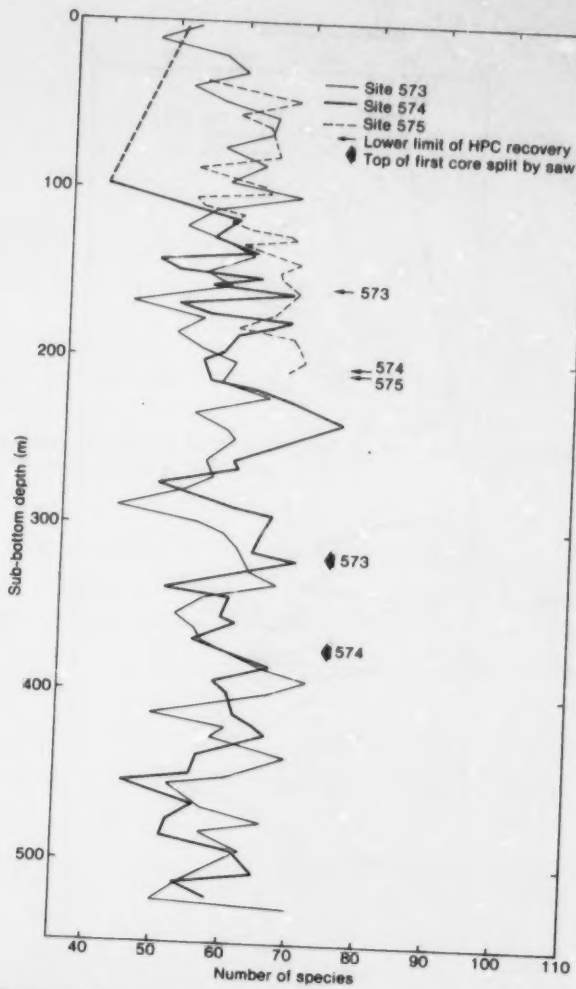

Figure 10. Diversity (number of species) plotted versus sub-bottom depth for Sites 573, 574, and 575.

minifer-barren interval spanning the Eocene/Oligocene boundary (see site chapter, this volume). Relative abundances of the most common taxa are shown in Figure 8 and stratigraphic ranges of selected species in Figure 9.

The most common taxa in Eocene and Oligocene are *Globocassidulina subglobosa* and *Oridorsalis umbonatus*, both present throughout this period. Other common taxa are the *Cibicidoides kullenbergi* group (see Appendix B for taxonomy), *C. pseudoungerianus, C. grimsdalei, Anomalina spissiformis, Nonion havanense, Pullenia* spp., *Gyroidinoides* spp., *Pleurostomella* spp., and *Stilostomella* sp. *Epistominella exigua* is rare below Sample 574C-18,CC but present throughout the interval. *Nuttallides umbonifera* is likewise found throughout the interval but is most common (relative abundance 6 to 14%) above Sample 574C-19,CC. Below this level its relative abundance is generally less than 6%, except in Samples 574C-27,CC (9.6%), 574C-32-1, 102–104 cm (6.6%), and 574C-33-4, 39–41 cm (9.5%). *Uvigerina senticosa, Bulimina alazanensis*, and *Fursenkoina cylindrica* (tri-

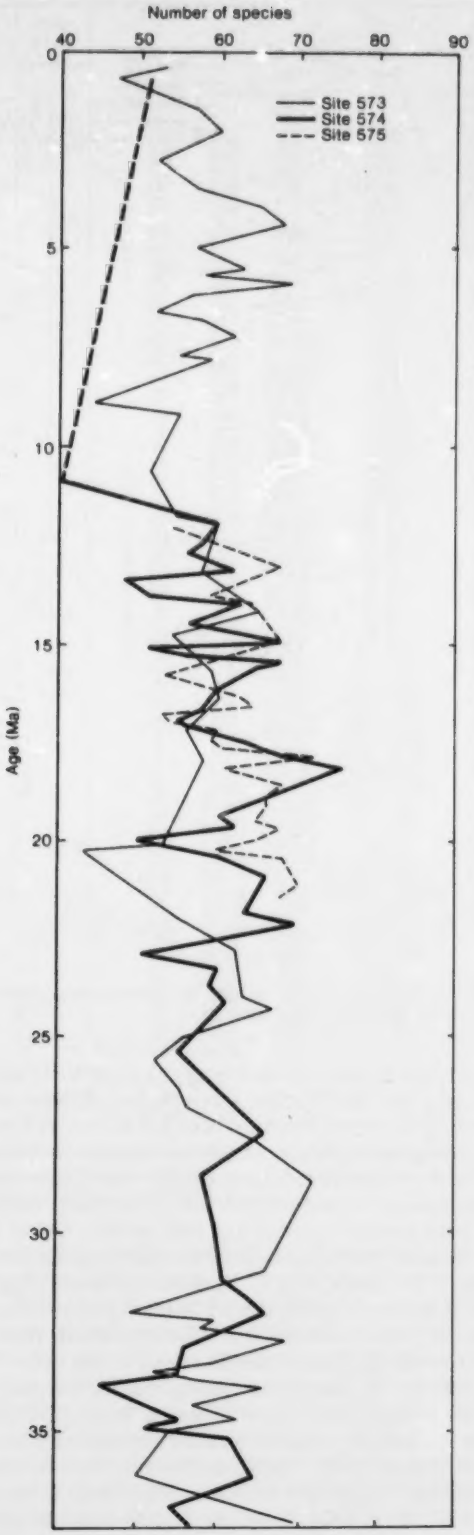

Figure 11. Diversity (number of species) plotted versus time for Sites 573, 574, and 575.

serial group and biserial group in Fig. 8) are relatively common (1 to 5%) below Sample 574C-33-5, 26–28 cm.

From the upper Eocene through Oligocene in Hole 574C, 168 taxa were recognized. Of these, 85 range throughout the interval; all the most common taxa are among these 85. In total, 60 taxa are too rare to establish a range, and 11 taxa have a LA. *Nuttallides truempyi* has its LA in Sample 574C-33-4, 141–143 cm and does not occur from Sample 574C-33-4, 90–92 cm upward. The LA of this species is generally considered to be a reliable marker for the Eocene/Oligocene boundary (Tjalsma and Lohmann, 1983; Miller, 1983; Snyder et al., 1984). The relative abundance of *N. truempyi* is less than 8% in all samples. Seven other species have LAs relatively close to the LA of *N. truempyi*, i.e., between about 35 and 37 Ma: *Buliminella grata, Gyroidinoides planulatus, Alabamina dissonata, Gavelinella micra, Osangularia interrupta, Resigia westcotti*, and *Fursenkoina cylindrica. Osangularia mexicana* has its LA in Sample 574C-20,CC, *Stilostomella verneuilli* in Sample 574C-20,CC and *Cibicidoides pseudoungerianus* in Sample 574C-17,CC. All of these species, except *C. pseudoungerianus*, are rare (less than 6% relative abundance, but usually less than 1 to 3%). The two *Osangularia* species together have a maximum abundance of 9.5% (in Sample 574C-34,CC). Most of the LAs are of local significance only, given that the species occur in the Oligocene elsewhere (Douglas, 1973; Corliss, 1981). *Gyroidinoides planulatus* extends into the Oligocene at Site 573 (Appendix A). At Site 574 the clustering of FAs and LAs between 32 and 37 Ma might have been influenced by a relatively rapid water-depth increase during this period when the site was close to the ridge. The extinction of *N. truempyi* and *Resigia* spp., however, represents the extinction of endemic abyssal taxa that were important constituents of the earlier Eocene abyssal faunas in the Atlantic Ocean (Tjalsma and Lohmann, 1983; Miller, 1983).

Several species have a FA in the period between 35 and 37 Ma: *Bigenerina nodosaria, Eggerella bradyi, Cibicidoides laurisae, C.* aff. *mundulus, Karreriella bradyi,* and *Cassidulina crassa. Cibicidoides laurisae* and *C.* aff. *mundulus* are the only species in this group that attain relative abundances of greater than 5% in some samples.

The high-diversity, low-dominance fauna at Site 574 resembles the coeval deep-water faunas described by Tjalsma and Lohmann (1983) from the Caribbean and south Atlantic and by Miller (1983) and Miller et al. (in press) from the Bay of Biscay. This fauna was called the *Globocassidulina subglobosa–Gyroidinoides* spp.*–Oridorsalis* spp. fauna by these authors. In the Atlantic this assemblage replaced the middle Eocene *N. truempyi* fauna near the end of the middle Eocene. The transition was not found at Site 574 because no middle Eocene sediments were recovered.

At Site 574 *N. umbonifera* is not as abundant as in the Oligocene in the Bay of Biscay (as much as 25% relative abundance; Miller, 1983). The species is present throughout the section, but it has only modest peaks in abundance (9.5%) in Sample 574C-27,CC (Zone P19)

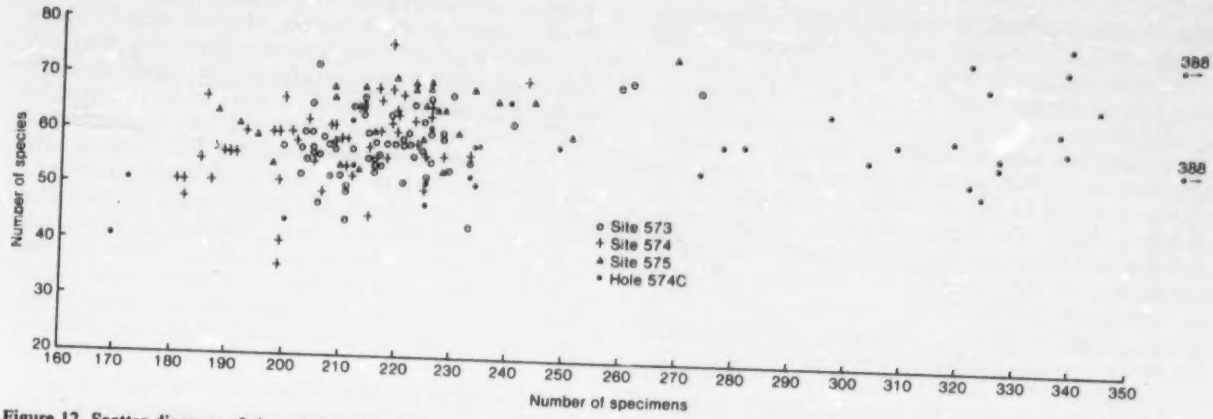

Figure 12. Scatter diagram of the number of species versus the number of specimens for all samples (Sites 573, 574, and 575). Data are included from the additional samples used in the detailed study of the Eocene/Oligocene boundary in Hole 574C.

Table 1. Timing of first and last appearance datums.

Event		Sample, Site 573	Approximate age (Ma)	Sample, Site 574	Approximate age (Ma)	Sample, Site 575	Approximate age (Ma)	Age range (Ma)
FAD	*Globocassidulina decorata*	573-5,CC	2.8					
LAD	*Pleurostomella obtusa*	573-5,CC	2.8	574-14,CC	12.5			2.8–12.5
FAD	*Stainforthia complanata*	573-5,CC	2.8					
LAD	*Stilostomella consobrina*	573-6,CC	3.5	574-17,CC	13.2	575-5,CC	13.1	3.5–13.2
FAD	*Eponides tumidulus*	573-7,CC	3.9					
FAD	*Cibicidoides cicatricosus*	573-8,CC	4.4					
LAD	*Gyroidinoides girardanus*	573-9,CC	5.0	574-27,CC	15.6	575-6,CC	13.8	5.0–13.7
LAD	*Pleurostomella alternans*	573-9,CC	5.0					
LAD	*Eponides pusillus*	573-12,CC	5.9	574-28,CC	16.1	575-5,CC	13.1	5.9–16.1
LAD	*Cibicidoides wuellerstorfi*, var. *C*	573-13,CC	6.2					
LAD	*Stilostomella subspinosa*	573-13,CC	6.2					
LAD	*Uvigerina graciliformis*	573-15,CC	6.8					
FAD	*Bolivina translucens*	573-16,CC	7.2					
FAD	*Melonis barleeanus*	573B-6,CC	11.8	574-14,CC	12.5	575-5,CC	13.1	11.8–13.1
LAD	*Cibicidoides perlucidus*	573B-7,CC	12.0	574-23,CC	15.0	575-9,CC	15.0	12.0–15.0
FAD	*Cibicidoides wuellerstorfi*, var. *C*	573B-7,CC	12.0					
LAD	*Bigenerina nodosaria*	573B-8,CC	13.2	574-23,CC	15.0	575-9,CC	15.0	13.2–15.0
LAD	*Cibicidoides grimsdalei*	573B-9,CC	14.2	574-20,CC	14.0	575-9,CC	15.0	14.0–15.0
LAD	*Stilostomella abyssorum*	573B-9,CC	14.2	574-18,CC	13.4			12.1–14.2
FAD	*Francesita advena*	573B-10,CC	14.8	574-20,CC	14.0	575-7,CC	14.0	14.0–14.8
LAD	*Cassidulina havanensis*	573B-10,CC	14.8	574-21,CC	14.5	575A-1,CC	16.4	14.5–16.4
LAD	*Bolivinopsis cubensis*	573B-10,CC	14.8	574-24,CC	15.1	575-9,CC	15.0	14.8–15.1
FAD	*Cibicidoides wuellerstorfi*	573B-11,CC	15.6	574-18,CC	15.6	575-9,CC	15.0	15.0–15.6
LAD	*Pleurostomella acuta*	573B-11,CC	15.6	574-29,CC	16.5	575-10,CC	15.8	15.6–16.5
LAD	*Bolivina striatula*	573B-11,CC	15.6	574-26,CC	15.5	575A-1,CC	16.4	15.5–16.4
LAD	*Heronallenia lingulata*	573B-11,CC	15.6	574-21,CC	14.5	575A-2,CC	16.6	14.5–16.6
LAD	*Cibicidoides laurisae*	573B-13,CC	17.2	574C-4,CC	17.8	575A-7,CC	17.7	17.2–17.8
LAD	*Vulvulina spinosa*	573B-13,CC	17.2	574-18,CC	13.4	575-5,CC	13.1	13.1–17.2
LAD	*Cibicidoides mexicanus*	573B-14,CC	18.0	574C-4,CC	17.8			16.4–18.0
LAD	*Nonion havanense*	573B-14,CC	18.0	574-20,CC	14.0	575-9,CC	15.0	14.0–18.0
FAD	*Bolivina striatula*	573B-14,CC	18.0	574C-5,CC	18.2	575A-13,CC	18.6	18.0–18.6
FAD	*Melonis barleeanus*	573B-15,CC	20.1	574C-5,CC	18.2	575A-21,CC	19.7	18.2–20.1
LAD	*Amphicoryna hirsuta*	573B-15,CC	20.1	574-26,CC	15.5	575-6,CC	13.8	13.8–20.1
FAD	*Ehrenbergina caribbea*	573B-15,CC	20.1	574C-3,CC	17.5	575A-21,CC	19.7	17.5–20.1
LAD	*Buliminella carteri*	573B-16,CC	20.3					
LAD	*Anomalina alazanensis*, var. *spissiformis*	573B-17,CC	22.0	574C-12,CC	21.6			21.6–22.0
LAD	*Cibicidoides pseudoungerianus*			574C-17,CC	23.7			
LAD	*Bulimina microcostata*	573B-20,CC	24.0					
FAD	*Laticarinina pauperata*	573B-22,CC	25.0	574C-23,CC	31.2			
FAD	*Cassidulina spinifera*	573B-24,CC	26.3	574C-19,CC	25.4			25.0–31.2
FAD	*Uvigerina graciliformis*	573B-24,CC	26.3	574C-16,CC	23.2			25.4–26.3
FAD	*Sphaeroidina bulloides*			574C-16,CC	23.2			23.2–26.3
LAD	*Cibicidoides* aff. *mundulus*			574C-14,CC	22.2			
LAD	*Vulvulina jarvisi*	573B-34,CC	32.7	574C-26,CC	32.8			
FAD	*Cibicidoides* aff. *mundulus*			574C-32-1, 102–104 cm	34.9			32.7–32.8
FAD	*Cibicidoides laurisae*	573B-37,CC	34.3	574C-32,CC	35.1			
LAD	*Fursenkoina cylindrica*			574C-33-3, 113–115 cm	36.3			34.3–35.1
FAD	*Cibicidoides pseudoungerianus*	573B-39,CC	34.9	574C-35-1, 126–128 cm	37.2			
FAD	*Ammonia*? sp.	573B-39,CC	34.9	574C-35-2, 99–100 cm	37.3			
FAD	*Eponides pusillus*	573B-40,CC	35.0	574C-35-1, 97–98 cm	37.2			34.9–37.3
LAD	*Buliminella grata*	573B-42-4, 140–144 cm	36.6	574C-34-1, 138–140 cm	36.8			35.0–37.2
LAD	*Nuttallides truempyi*	573B-42-4, 140–144 cm	36.6	574C-33-5, 141–143 cm	36.6			
LAD	*Resigia westcotti*			574C-33-4, 139–140 cm	36.5			
LAD	*Gavelinella micra*			574C-33-4, 139–140 cm	36.5			
LAD	*Alabamina dissonata*	573B-42-4, 140–144 cm	36.6	574C-33-5, 90–92 cm	36.6			
LAD	*Osangularia mexicana*	573B-42-4, 140–144 cm	36.6	574C-28,CC	33.8			

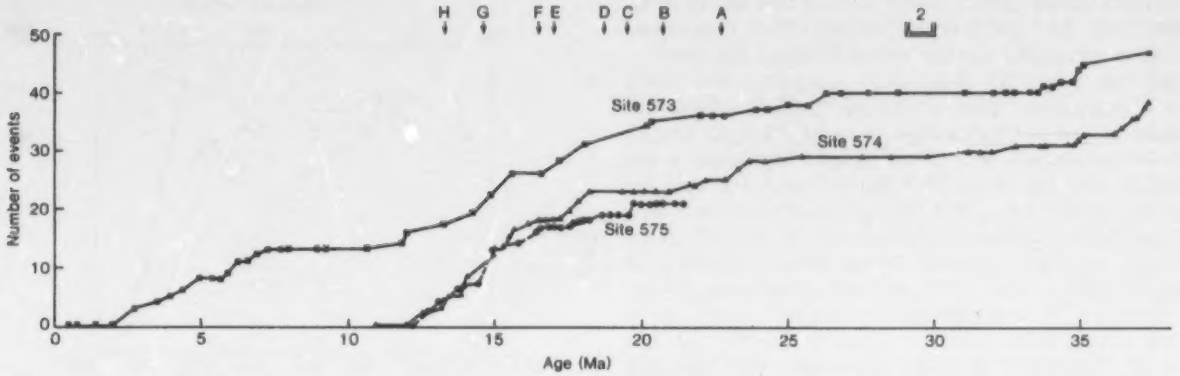

Figure 13. Cumulative plot of first and last appearances at Sites 573, 574, and 575. The letters A through H indicate events in the isotopic and $CaCO_3$ records of Sites 573 to 575 described by Vincent and Killingley (this volume). An interval of relatively heavy $\delta^{13}C$ occurs between 22.7 and 20.7 Ma (events A and B); a warming trend begins at 19.5 Ma (event C); more severe dissolution and a lower $CaCO_3$ content begin at 18.7 Ma (event D); a shift to heavier $\delta^{13}C$ values is centered at 17 Ma (event E); the peak of a warming trend (i.e., the lightest $\delta^{18}O$ value) is at 16.5 Ma (event F); a shift toward heavier $\delta^{18}O$ values is centered at 14.6 Ma (event G); strong dissolution begins at 13.3 Ma (event H). Events 1 and 2 are shifts in oxygen isotopic values described by Miller and Thomas (this volume); 1 is shift to heavy values of $\delta^{18}O$, and 2 indicates period of enrichment in $\delta^{18}O$.

and just above the LA of *N. truempyi* (Zone P17). *Stilostomella* spp. and *Pleurostomella* spp. are more abundant at Site 574 than in the Bay of Biscay.

The fauna at Site 574 also resemble the fauna described by Corliss (1981) from DSDP Site 277 (southwest Pacific). A notable difference is the abundance of *N. umbonifera*, which at Site 277 has a peak in abundance (25 to 30%) at about the same level as a shift in oxygen isotopic ratios. The modest peak in abundance of this species at Site 574 is just below the shift in oxygen isotopic ratios (Miller and Thomas, this volume).

Coeval faunas described by Tjalsma (1983) from DSDP Site 516 in the south Atlantic (paleodepth less than 1700 m) resemble the Site 574 faunas in that they contain abundant *Cibicidoides* spp. and *Oridorsalis umbonatus* and common *Pullenia* spp. and *Gyroidinoides* spp. *Bulimina* spp. and *Uvigerina* spp., however, are much more common at Site 516, whereas *Pleurostomella* spp. and *Stilostomella* spp. are more abundant at Site 574.

Generally, the observations at Site 574 agree well with Corliss (1981), Miller (1983), Clark and Wright (1984), Snyder et al. (1984), Miller et al. (in press), and Wood et al. (in press) in that no major changes occurred at the Eocene/Oligocene boundary in the dominant species of benthic foraminifers, although some relatively rare species have FAs or LAs close to the boundary.

The dominant species do not show large variations in relative abundance between 32 and 37 Ma. There were, however, considerable shifts in oxygen and carbon isotopic ratios (Miller and Thomas, this volume): 0.9 and 0.6‰, respectively, between Samples 574C-33-1, 113–115 cm and 574C-33-3, 113–115 cm, which corresponds to a period of about 0.4 m.y. (Fig. 13, event 1). There was no change in composition of the benthic fauna in the late Oligocene (29 to 30 Ma), which is the time of another shift toward heavier oxygen isotopic ratios (Keigwin and Keller, 1984; Miller and Thomas, this volume). This suggests that the fauna had wide environmental tolerances, which is also indicated by the dominant species being long ranging and cosmopolitan and occurring over a large depth range in the present-day oceans. The tolerant character of the fauna is also shown by the lack of change in the dominant species while the water depth increased by more than 1000 m.

Some of the fluctuations in relative abundance may be the effect of differential dissolution. According to Corliss and Honjo (1981), *Gyroidinoides* spp. is more solution resistant than *C. kullenbergi, O. umbonatus*, and *N. umbonifera*, which are about equally resistant. *Globocassidulina subglobosa* is also resistant (Woodruff and Douglas, 1981). However, dissolution effects probably do not completely obscure the faunal compositional fluctuations. The abundance of *Gyroidinoides* spp., a resistant group, is similar to the abundance of this taxon in the Bay of Biscay (Miller, 1983). Furthermore, the less resistant *Cibicidoides* spp. are abundant throughout the lower Oligocene, where dissolution of planktonic foraminifers is usually severe (Saito, this volume). *Stilostomella* spp., described as "least preservable" by Woodruff and Douglas (1981), is common in all samples.

Early to Middle Miocene

Many FAs and LAs cluster in the upper lower to middle Miocene. The exact limits of this period of change in the benthic faunal composition are not easy to locate. At Site 573 the upper limit is at about 13 Ma, the lower limit between 18.0 and 20.1 Ma (no data are available between these data points). The lower limit is at about 18.2 Ma at Site 574, where the precise position of the upper limit cannot be determined because of strong dissolution in the upper part of the section. At Site 575 the upper limit cannot be determined because of strong dissolution, and the position of the lower limit is not clear. The changes appear to start more gradually here than at Site 574, between 20.5 and 18.5 Ma (Fig. 13). When the data for the three sites are combined, it appears that the majority of the FAs and LAs occur between 13 and 18.5 Ma. The event rates, that is, the number of FAs and LAs per time unit, are comparable at the three sites at about 4 events/m.y.

Since many FAs and LAs occur in the period between about 13 and 18.5 Ma, faunas from before and after that period are easily distinguished (Fig.6 and Table 1), although many abundant and common species have ranges extending from Eocene to Recent. "Modern" species, that is, species that have FAs between about 13 and 18.5 Ma, include *Cibicidoides wuellerstorfi* (FA at 15.0 to 15.6 Ma), *Francesita advena* (FA at 14.0 to 14.8 Ma), and *Melonis pompilioides* (FA at 11.8 to 13.1 Ma). A less common "modern" species is *Ehrenbergina caribbea* (FA at 17.5 to 20.1 Ma). *M. barleeanus* (FA at 18.2 to 20.1 Ma), *Sphaeroidina bulloides* (FA at about 23 Ma), and *Laticarinina pauperata* (FA at 25.0 to 31.2 Ma) might be included in the "modern" group, but have earlier FAs.

"Old" species that have their LAs in the early to middle Miocene include *Cibicidoides grimsdalei* (LA at 14.0 to 15.0 Ma), *C. mexicanus* (LA at 16.4 to 18.0 Ma), *C. perlucidus* (LA at 12.0 to 15.0 Ma), *Vulvulina spinosa* (LA at 13.1 to 17.2 Ma), *Nonion havanense* (LA at 14.0 to 18.0 Ma), *Bolivinopsis cubensis* (LA at 14.8 to 15.1 Ma), and *Pleurostomella acuta* (LA at 15.6 to 16.5 Ma). The LAs are not all precise, since the "old" species decline in abundance and become very rare before they finally disappear. *Anomalina spissiformis* is extremely rare in the interval younger than 21.6 to 22.0 Ma; the rare occurrences higher in the section might be due to reworking. Typically, *Pleurostomella* spp. and *Stilostomella* spp. are much more common in the "old" than in the "modern" fauna at these Pacific sites (Fig. 6, decrease in abundance at about 16.5 Ma). *Bolivina striatula* is found only in the interval of maximum change in benthic faunal composition (FA at 18.0 to 18.6 Ma; LA at 15.5 to 16.4 Ma).

From the range of ages found for the first and last appearances, it is evident that detailed benthic foraminiferal biostratigraphy using the present data set is not possible within the interval between 13 and 18.5 Ma. The detailed sequence of FAs and LAs is somewhat different at all sites (Table 1 and Fig. 7) (see also Barron et al., this volume). Detailed patterns in the relative abundances can generally not be correlated between the sites because the time resolution as given by the sampling interval is not precise enough. The fauna at the three sites is similar, but many details are different, such as the fluctuations in the abundance of *Epistominella exigua* and *Nuttallides umbonifera* and some fluctuations in the abundance of *Pleurostomella* spp. (Fig. 6). Therefore, fluctuations in abundance observed at one site must be interpreted with care and cannot be seen as results of general changes in bottom-water circulation.

It must also be emphasized that the total relative abundance of specimens belonging to species that have FAs and LAs is generally between 20 and 40% of the total fauna and that between 60 and 80% of all specimens in the fauna belong to long-ranging species. Thus, Boltovskoy (e.g., 1980a,b) was able to conclude that the benthic deep-sea fauna has a stable character and shows hardly any changes since the late Eocene. Woodruff and Douglas (1981) and Woodruff (in press), on the other hand, emphasize the less abundant taxa and conclude that a major faunal turnover in benthic faunas occurred in the middle Miocene. The "turnover" is definitely observed at Sites 573 to 575, but it affects less than half of the fauna. In addition, the "old" species are not completely replaced by "modern" species, as is seen from an increase in the relative abundance of the long-ranging species from an average of about 62% to an average of about 75% between about 18 and 17 Ma. A maximum of 80% of the specimens in present-day faunas and about 50% of the species in the deep equatorial Pacific belong to species that have been around since the late Eocene.

During the interval from 13 to 18.5 Ma, several isotopic events were recognized. A shift in oxygen isotopic composition of benthic foraminifers occurs at 155 m subbottom depth at Site 574 (Pisias and Shackleton, this volume). The duration of the event is about 30,000 yr., and the age is estimated as 14.6 Ma, using data from Barron et al. (this volume). This agrees well with the estimate of Woodruff et al. (1981) for the age of the largest shift in oxygen isotopic ratios at 14.0 to 14.8 Ma.

Vincent and Killingley (this volume) recognize several events in the isotopic and calcium carbonate records from Sites 573 to 575. They describe a period of $\delta^{13}C$ enrichment in planktonic foraminifers between 22.7 and 20.7 Ma (see events A and B on Fig. 13); the beginning of a warming trend. i.e., lighter values of $\delta^{18}O$ at 19.5 Ma (event C, Fig. 13); the beginning of increasing dissolution and lower $CaCO_3$ content at 18.7 Ma (event D); a major shift toward heavier $\delta^{13}C$ values centered at 17 Ma (event E); the peak in the warming trend (i.e., the lowest values of $\delta^{18}O$ at 16.5 Ma; event F); a shift toward heavier $\delta^{18}O$ values at 14.6 Ma, which is the shift also recognized by Pisias and Shackleton (this volume) (event G); and stronger dissolution at 13.3 Ma (event H).

The isotopic events (a carbon shift at 17 Ma and an oxygen shift at 14.6 Ma) postdate the beginning of the changes in the benthic faunas and are within the period of change in the faunas. The beginning of the faunal changes seems to be best correlated with (i.e., slightly later than) the increase in dissolution (event D, Fig. 13) at 18.7 Ma, which reflects a change in bottom-water properties.

Woodruff and Douglas (1981) describe a major change in benthic faunas in the western Pacific (Site 289) that is coeval with the shift in oxygen isotopes at 14.0 to 14.8 Ma. The benthic fauna at Sites 573 to 575 resembles the fauna at Site 289 in overall characteristics, although Site 289 was considerably shallower (paleodepth 2300 to 2400 m, Woodruff [in press], versus 3900 to 4100 m at Sites 573 to 575). *Epistominella exigua* is much more common in the lower Miocene section at Sites 573 to 575 than at Site 289, as are *Pleurostomella* spp. and *Stilostomella* spp. The events in most species of the *Cibicidoides* group are difficult to compare because of the complicated taxonomy, but *C. wuellerstorfi* has a FA at 16 Ma at Site 289, which agrees well with a FA at 15.0 to 15.6 Ma at Sites 573 to 575. *Melonis barleeanus* has a FA at about 14.3 Ma at Site 289, much later than at Sites 573 to 575, where it has a FA at 18.4 to 21.1 Ma.

In general, the faunal events described for Site 289 by Woodruff and Douglas (1981) and for the deep Pacific

in general by Woodruff (in press) are similar to the events as described in this paper. Woodruff and Douglas, however, conclude that the timing of the faunal changes correlates well with the timing of the shift in oxygen isotopic ratios, although the greatest isotopic change (14.0 to 14.8 Ma, Woodruff et al., 1981) predates and is of shorter duration than the main faunal change (13.2 to 16.5 Ma, Woodruff, in press). The difference in opinion as to the beginning of the main faunal change (at about 18.5 Ma in this paper) may be caused by several factors, including the difficulty in determining the precise level of FAs and LAs of rare species. Furthermore, not all age models for the sites described by Woodruff (in press) are well restrained. In addition, the part of the section deposited at Site 289 between 16.9 and 18.5 Ma was apparently deposited at very low sedimentation rates (about 6.3 m/m.y.) (data from Savin et al., 1981, p. 445), and Woodruff and Douglas do not present data from this time interval. Similarly, Woodruff (in press) presents relatively few data from the interval between 16 and 19 Ma: for paleodepths of more than 3 km, she gives data on 40 samples between 13 and 16 Ma and on 11 samples between 16 and 19 Ma.

In conclusion, data from Sites 573 to 575 suggest that changes in the benthic fauna occur roughly in the same time interval as changes in isotopic ratios, but the faunal changes start earlier and have a longer duration. The beginning of the faunal changes may be related to the beginning of increased dissolution at about 18.7 Ma. Keller (1981) suggests that a major change in bottom-water circulation occurred at about 20 Ma: after the opening of the Drake Passage, Antarctic Bottom Water reached the equatorial Pacific. Either this event occurred later than suggested by Keller (1981), or the benthic foraminifers took about 1.5 m.y. to react to the changes in the bottom-water masses, which seems unlikely when contrasted with the fast reactions of benthic faunas to glacial–interglacial events (Schnitker, 1980). It is also possible that another event caused the faunal changes and increased dissolution. The short-term changes in isotopic ratios may represent a sudden adjustment to changes in ocean circulation resulting from positive feedback processes (Berger et al., 1981). However, these sudden adjustments do not seem to occur at the same time as major changes in bottom water as perceived by deep-water benthic foraminifers.

Post–Middle Miocene

Data on the last 12 Ma are available from Site 573 only because of strong dissolution at the other two sites. The data from Site 573 cannot be compared with the data from Site 289 (Woodruff and Douglas, 1981), where an important change in the benthic fauna occurred around 9 to 10 Ma. At this time *Uvigerina* spp. increased sharply in abundance, probably because the site fell under the influence of the deep oxygen-minimum zone.

At Site 573 the number of FAs and LAs per time unit is relatively low between 12 and 7 Ma (Fig. 13), is higher between 7 and 5.5 Ma, and remains relatively high until the Recent. These data suggest that further research on benthic foraminifers from this period could prove interesting, because the increase in the event rate of the benthic fauna at 7 Ma occurs close to the time of an important shift in carbon isotopic ratios (e.g., Savin et al., 1981) at 6.2 Ma.

Foraminiferal Turbidites

At Site 575 a number of distinctive, coarse-grained, fining-upward foraminiferal turbidites were recognized (see Site 575 chapter, this volume) which were probably derived from a nearby seamount with a present-day elevation of about 1000 m above the seafloor (water depth at the top of the seamount about 3500 m). Benthic faunas in samples from the turbidites are distinct from the *in situ* faunas (Fig. 5 and Appendix A).

Most of the turbidites contain abundant large, thick-walled specimens. The abundance of these large specimens is apparently the result of size sorting in the turbidites, but the specimens of some species in the turbidites are much larger than any specimen found in the pelagic samples (e.g., *Globocassidulina subglobosa, Favocassidulina favus*, and *Eggerella bradyi*). These observations suggest that these species attained larger sizes at shallower depths on the seamount. A similar depth-size correlation in *G. subglobosa* has been observed by Corliss (1979b,c) in the Indian Ocean. The hypothesis that some species of benthic foraminifers are smaller at greater depths (more than 4000 m) is supported by the observation that the specimens at Sites 573 to 575 are overall smaller than specimens of the same species from shallower depths (e.g., Douglas, 1973).

In most turbidites *G. subglobosa* is more abundant (relative abundance up to 38.6%) than in pelagic samples (Fig. 5), and *F. favus* and *F. subfavus* are abundant (relative abundance up to 53.4%) in turbidites from Sample 575A-3-2, 142–144 cm upward (above 110 m sub-bottom depth). *E. caribbea* is common (11.8%) in a turbidite sampled at 575A-8-5, 110–112 cm. Several species are absent or extremely rare in the pelagic samples but are frequent in the turbidites, including species that have been described from stratigraphic intervals lower than the ones in which they are found. These include *Bulimina jarvisi* (Oligocene), *Hanzawaia cushmani* (Eocene), *Planulina renzi* (Eocene–Oligocene), and *Buliminella* sp. (Oligocene) (all from Douglas, 1973). All these species were found in lower to middle Miocene turbidites at Site 575. *Eggerella propinqua* and *Uvigerina spinulosa* were found only in the turbidites.

CONCLUSIONS

1. Many common to abundant species in deep-sea benthic foraminiferal faunas in the equatorial Pacific have long ranges and probably wide environmental tolerances. Taxa with limited stratigraphic ranges generally make up between 20 and 40% of the total fauna.

2. Diversity is high (50 to 70 species per 200 specimens) and not correlatable with time or sub-bottom depth, although the total number of species decreases with time; in other words, there are more last appearances than first appearances.

3. First and last appearances of taxa (whether they are evolutionary or migratory) are concentrated in two

periods: in the late Eocene to early Oligocene (32 to 37 Ma) and in the early to middle Miocene (13 to 18.5 Ma).

4. "Old" species are partly replaced by "modern" species and partly by long-ranging species. The latter increase in abundance from about 62 to 75% between 17 and 18 Ma.

5. Post–middle Miocene faunas are readily distinguished from early Miocene and older faunas, but the transition is slow (about 6 m.y.). Characteristic "modern" species are *Melonis barleeanus, Francesita advena, M. pompilioides*, and *Cibicicodes wuellerstorfi*. "Old" species include *C. grimsdalei, C. mexicanus, C. laurisae, Bolivinopsis cubensis*, and *Pleurostomella acuta. Stilostomella* spp. and *Pleurostomella* spp. are more abundant in the "old" fauna.

6. First and last appearances of the above taxa are within 1 to 2 m.y. at the three sites, but the first and last appearances of many other species differ widely in age at the different sites. No data are available to assess whether some of the events are correlatable on a larger scale. Some events (FA of *C. wuellerstorfi*) correlate well with the western Pacific, while others do not (FA of *M. barleeanus*).

7. Carbon and oxygen isotopic events occur within the periods of relatively high rates of change in the benthic faunal composition, but the isotopic events start after the initiation of the faunal changes and have a shorter duration. The beginning of the faunal change can possibly be correlated with a period of increased dissolution of $CaCO_3$.

8. Data from foraminiferal turbidites (Site 575) suggest that several species (e.g., *Globocassidulina subglobosa*) attain a larger size at shallower depths (about 3,500 km versus 4,500 km).

ACKNOWLEDGMENTS

I thank J. Resig and E. Boltovskoy for reviewing the manuscript, F. Woodruff for stimulating discussion, and all scientists from the shipboard party of Leg 85 for their contribution to this successful cruise. Financial support from the Scripps Industrial Associates and from NSF (Grant OCE-8310518) made this study possible. I also thank J. C. Varekamp and the Department of Earth and Environmental Sciences at Wesleyan University (Middletown, Conn.) for their support.

REFERENCES

Barker, R. W., 1960. *Taxonomic Notes, etc.* Spec. Publ. Soc. Econ. Paleontol. Mineral. 9.

Beckmann, J. P., 1953. Die Foraminiferen der Oceanic Formation (Eocaen–Oligocaen) von Barbados, Kl. Antillen. *Eclogae Geol. Helv.*, 46:301–412.

Belanger, P. E., and Streeter, S. S., 1980. Distribution and ecology of benthic foraminifera in the Norwegian–Greenland Sea. *Mar. Micropaleontol.*, 5:401–428.

Bender, M. L., and Keigwin, L. D., Jr., 1979. Speculations about the upper Miocene change in abyssal Pacific dissolved bicarbonate ^{13}C. *Earth Planet. Sci. Lett.*, 45:383–393.

Berger, W. H., 1973. Cenozoic sedimentation in the eastern tropical Pacific. *Geol. Soc. Am. Bull.*, 84:1941–1951.

Berger, W. H., Vincent, E., and Thierstein, H. R., 1981. The deep-sea record: major steps in Cenozoic ocean evolution. *Spec. Publ. Soc. Econ. Paleontol. Mineral.*, 32:489–504.

Berger, W. H., and Winterer, E. L., 1974. Plate stratigraphy and the fluctuating carbonate line. *In* Hsü, K. J., and Jenkyns, H. C. (Eds.), *Pelagic Sediments on Land and Under the Oceans*: Cambridge (Cambridge Univ. Press), pp. 693–809.

Berggren, W. A., 1972. Cenozoic biostratigraphy and paleobiogeography of the North Atlantic. *In* Laughton, A. S., Berggren, W. A., et al., *Init. Repts. DSDP*, 72: Washington (U.S. Govt. Printing Office), 965–1002.

Berggren, W. A., Kent, D. V., and Flynn, J. J., in press. Paleogene geochronology and chronostratigraphy. *In* Snelling, N. J. (Ed.), *Geochronology and the Geological Record*: London (Geol. Soc. London).

Boltovskoy, E., 1959. La corriente de Malvinas (un estudio en base a la investigación de foraminíferos). *Argent. Serv. Hidr. Nav.*, H1005: 1–120.

———, 1976. Distribution of Recent foraminifera of the South American region. *In* Hedley, R. H., and Adams, C. G. (Eds.), *Foraminifera* (Vol. 2): New York (Academic Press), pp. 717–736.

———, 1978. Late Cenozoic foraminifera of the Ninety-east Ridge, Indian Ocean. *Mar. Geol.*, 26:139–175.

———, 1980a. On the benthonic bathyal zone foraminifera as stratigraphic guide fossils. *J. Foraminiferal Res.*, 10:163–172.

———, 1980b. Benthonic foraminifera of the bathyal zone from Oligocene through Quaternary. *Rev. Esp. Micropaleontol.*, 12: 283–304.

———, 1981a. Foraminíferos bentonicos del Sitio 360 del "Deep Sea Drilling Project" (Eoceno medio–Plioceno inferior). *Assoc. Geol. Argent. Rev.*, 36:389–423.

———, 1981b. Benthic late Cenozoic foraminifera of DSDP Site 173 and comparison with the same faunas of other sites. *Rev. Micropaleontol.*, 23:212–217.

Boltovskoy, E., Giussani, G., Watanabe, S., and Wright, R., 1980. *Atlas of Benthic Shelf Foraminifera of the Southwest Atlantic*: The Hague (Junk).

Clark, M. W., and Wright, R. C., 1984. Paleogene abyssal foraminifers from the Cape and Angola Basin. *In* Hsü, K. J., LaBrecque, J. L., et al., *Init. Repts. DSDP*, 73: Washington (U.S. Govt. Printing Office), 459–480.

Corliss, B. H., 1979a. Recent deep-sea benthonic foraminiferal distributions in the southeast Indian Ocean: inferred bottom-water routes and ecological implications. *Mar. Geol.*, 31:115–138.

———, 1979b. Size variation in the deep-sea benthonic foraminifer *Globocassidulina subglobosa* (Brady) in the southeast Indian Ocean. *J. Foraminiferal Res.*, 9:50–60.

———, 1979c. Taxonomy of Recent deep-sea benthonic foraminifera from the southeast Indian Ocean. *Micropaleontology*, 25: 1–19.

———, 1981. Deep-sea benthonic foraminiferal faunal turnover near the Eocene/Oligocene boundary. *Mar. Micropaleontol.*, 6: 367–384.

Corliss, B. H., and Honjo, S., 1981. Dissolution of deep-sea benthonic foraminifera. *Micropaleontology*. 27:356–378.

Coulbourn, W. T., 1980. Relationship between the distribution of foraminifera and geologic structures of the Arica Bight, South America. *J. Paleontol.*, 54:696–718.

Culp-Burke, S., 1981. Recent benthic foraminifera of the Ontong–Java Plateau. *J. Foraminiferal Res.*, 11:1–19.

Cushman, J. A., 1918–1931. *Foraminifera of the North Atlantic Ocean.* U.S. Nat. Mus. Bull. 104, Pts. 1–8.

Cushman, J. A., and Stainforth, R. M., 1945. The foraminifera of the Cipero Marl Formation of Trinidad, B. W. I. *Spec. Publ. Cushman Foraminiferal Res.*, 14:1–74.

Cushman, J. A., and Todd, R., 1945. Miocene foraminifera from Buff Bay, Jamaica. *Spec. Publ. Foraminiferal Res.*, 15:1–73.

Douglas, R. G., 1973. Benthonic foraminiferal biostratigraphy in the central north Pacific. *In* Winterer, E. L., Ewing, J. L., et al., *Init. Repts. DSDP*, 17: Washington (U.S. Govt. Printing Office), 607–671.

Douglas, R. G., and Woodruff, F., 1981. Deep-sea benthic foraminifera. *In* Emiliani, C. (Ed.), *The Sea* (Vol. 7): New York (Wiley–Interscience), pp. 1233–1327.

Haq, B. U., Worsley, T. R., Burckle, L. M., Douglas, R. G., Keigwin, L. D., Jr., Opdyke, N. D., Savin, S. M., Sommer, M. A., Vincent, E., and Woodruff, F., 1980. Late Miocene marine carbon isotopic shift and synchroneity of some phytoplanktonic biostratigraphic events. *Geology*, 8:427–431.

Ingle, J. C., Jr., 1973. Neogene foraminifera from the northeastern Pacific Ocean, Leg 18, Deep Sea Drilling Project. *In* Kulm, L. D.,

von Huene, R., et al., *Init. Repts. DSDP*, 18: Washington (U.S. Govt. Printing Office), 517–567.

Ingle, J. C., Keller, G., and Kolpack, R. L., 1980. Benthic foraminiferal biofacies, sediments, and water masses of the southern Peru-Chile Trench area, southeastern Pacific Ocean. *Micropaleontology*, 26:113–150.

Keigwin, L. D., Jr., 1979. Late Cenozoic stable isotope stratigraphy and paleoceanography of DSDP sites from the east equatorial and central Pacific Ocean. *Earth Planet. Sci. Lett.*, 45:361–382.

_____, 1980. Paleoceanographic change at the Eocene/Oligocene boundary. *Nature (London)*, 287:722–725.

Keigwin, L. D., Jr., and Keller, G., 1984. Middle Oligocene cooling from equatorial Pacific DSDP Site 77. *Geology*, 12:16–19.

Keller, G., 1981. Planktonic foraminiferal faunas of the equatorial Pacific suggest early Miocene origin of present oceanic circulation. *Mar. Micropaleontol.*, 6:269–295.

_____, 1983. Paleoclimatic analysis of middle Eocene through Oligocene planktic foraminiferal faunas. *Palaeogeogr. Palaeoclimatol. Palaeoecol.*, 43:73–94.

Kennett, J. P., and Shackleton, N. J., 1976. Oxygen isotopic evidence for the development of the psychrosphere 38 m.y. ago. *Nature (London)*, 260:513–515.

Lipps, J. H., 1965. Revision of the foraminiferal family Pseudoparrellidae voloshinova. *Tulane Stud. Geol.*, 3(2):117–147.

Lohmann, G. P., 1978. Abyssal benthic foraminifera as hydrographic indicators in the western South Atlantic Ocean. *J. Foraminiferal Res.*, 8:6–34.

Miller, K. G., 1982. Cenozoic benthic foraminifera, case histories of paleoceanographic and sea-level changes. *In* Gupta, B. S., and Buzas, M. (Eds.), *Short Course on Foraminifera, Geol. Soc. Am. Ann. Mtg.*, pp. 107–126.

_____, 1983. Eocene–Oligocene paleoceanography of the deep Bay of Biscay: benthic foraminiferal evidence. *Mar. Micropaleontol.*, 7:403–440.

Miller, K. G., Curry, W. B., and Ostermann, D. R., in press. Late Paleogene (Eocene to Oligocene) benthic foraminiferal oceanography of the Goban Spur Region, Deep Sea Drilling Project Leg 80. *In* Graciansky, P. C. de, Poag, C. W., et al., *Init. Repts. DSDP*, 80, Pt. 1: Washington (U.S. Govt. Printing Office), 505–538.

Nuttall, W. L. F., 1930. Eocene foraminifera from Mexico. *J. Paleontol.*, 4:271–293.

_____, 1932. Lower Oligocene foraminifera from Mexico. *J. Paleontol.*, 6:3–35.

Phleger, F. B., and Parker, F. L., 1951. Ecology of foraminifera, northwest Gulf of Mexico. *Mem. Geol. Soc. Am.*, 46(2):1–64.

Phleger, F. B., Parker, F. L., and Peirson, J. F., 1953. North Atlantic foraminifera. *Rept. Swed. Deep Sea Exped. 1947–1948*, 7:1–121.

Resig, J. M., 1976. Benthic foraminiferal stratigraphy, eastern margin, Nazca Plate. *In* Yeats, R. S., Hart, S. R., et al., *Init. Repts. DSDP*, 34: Washington (U.S. Govt. Printing Office), 743–759.

_____, 1981. Biogeography of benthic foraminifera of the northern Nazca Plate. *Mem. Geol. Soc. Am.*, 154:629–666.

Savin, S. M., Douglas, R. G., Keller, G., Killingley, J. S., Shaughnessy, L., Sommer, M. A., Vincent, E., and Woodruff, F., 1981. Miocene benthic foraminiferal isotopic records: a synthesis. *Mar. Micropaleontol.*, 6:423–450.

Schnitker, D., 1974. West Atlantic abyssal circulation during the past 120,000 years. *Nature (London)*, 248:385–387.

_____, 1979. Cenozoic deep-water benthic foraminifera. *In* Montadert, L., Roberts, D. G., et al., *Init. Repts. DSDP*, 48: Washington (U.S. Govt. Printing Office), 377–413.

_____, 1980. Quaternary deep-sea benthic foraminifers and bottom-water masses. *Annu. Rev. Earth Planet. Sci.*, 8:343–370.

Shackleton, N. S., and Kennett, J. P., 1975. Paleotemperature history of the Cenozoic and the initiation of Antarctic glaciation: oxygen and carbon isotope analyses in DSDP Sites 277, 279, and 281. *In* Kennett, J. P., Houtz, R. E., et al., *Init. Repts. DSDP*, 29: Washington (U.S. Govt. Printing Office), 743–756.

Snyder, S. W., Müller, C., and Miller, K. G., 1984. Eocene–Oligocene boundary: biostratigraphic recognition and gradual paleoceanographic change at DSDP Site 549. *Geology*, 12:112–115.

Streeter, S. S., 1973. Bottom water and benthonic foraminifera in the North Atlantic—glacial-interglacial contrasts. *Quat. Res. (N.Y.)*, 3:131–141.

Thomas, E., 1980. *Details of Uvigerina Development in the Cretan Mio-Pliocene*. Utrecht Micropaleontol. Bull. 23.

Tjalsma, R. C., 1983. Eocene to Miocene benthic foraminifers from Deep Sea Drilling Project Site 516, Rio Grande Rise, South Atlantic. *In* Barker, P. F., Carlson, R. L., Johnson, D. A., et al., *Init. Repts. DSDP*, 72: Washington (U.S. Govt. Printing Office), 731–755.

Tjalsma, R. C., and Lohmann, G. P., 1983. *Paleocene–Eocene Bathyal and Abyssal Benthic Foraminifera from the Atlantic Ocean*. Micropaleontology Spec. Pub. 4.

Vincent, E., and Berger, W. H., in press. Carbon dioxide and Antarctic ice build-up in the Miocene: the Monterey hypothesis. *In* Sundquist, E. T., and Broecher, W. (Eds.), *Chapman Conf. Natural Variations in Carbon Dioxide and the Carbon Cycle*. Am. Geophys. Union Monogr. Ser.

Vincent, E., Killingley, J. S., and Berger, W. H., 1980. The magnetic Epoch-6 carbon shift: a change in the ocean's $^{13}C/^{12}C$ ratio 6.2 m.y. ago. *Mar. Micropaleontol.*, 5:185–203.

_____, 1983. The Chron-16 carbon event in the Miocene Indian Ocean. *Geol. Soc. Am. Abstr. Progr.*, 15(6):712. (Abstract)

Wood, K. C., Miller, K. G., and Lohmann, G. P., in press. Middle Eocene to Oligocene benthic foraminifera from the Oceanic Formation, Barbados. *Micropaleontology*.

Woodruff, F., in press. Changes in deep-sea benthic foraminiferal distribution in the Pacific Ocean: relationship to paleoceanography. *In* Kennett, J. P. (Ed.), *Cenozoic Paleoceanography (CENOP)*, Mem. Geol. Soc. Am.

Woodruff, F., and Douglas, R. G., 1981. Response of deep-sea foraminifera to Miocene paleoclimatic events, DSDP Site 289. *Mar. Micropaleontol.*, 6:617–632.

Woodruff, F., Savin, S. M., and Douglas, R. G., 1981. Miocene stable isotope record: a detailed deep Pacific Ocean study and its paleoclimatic implications. *Science (Washington, D.C.)*, 212:665–668.

Date of Initial Receipt: 27 October 1983
Date of Acceptance: 25 April 1984

APPENDIX A
Counts of Benthic Foraminifer Specimens for All Samples Studied, Sites 573, 574, and 575[3]

APPENDIX B
Taxonomy

***Alabamina dissonata* (Cushman and Renz).** *Pulvinulinella atlantisae* Cushman, var. *dissonata* Cushman and Renz, 1948, *Spec. Publ. Cushman Lab. Foraminiferal Res.*, v. 24, p. 35, pl. 7, figs. 11, 12.

***Allomorphina trigona* Reuss, 1850,** *Denkschr. K. Akad. Wiss. Wien, Math. Naturwiss. Kl.*, v. 1, p. 380.

***Allomorphinella contraria* Reuss, 1841,** *Haidinger's Naturwiss. Abh.*, v. 4, p. 43.

***Alveolophragmium subglobosum* (Cushman).** *Haplophragmoides subglobosum* Cushman, 1910, *Bull. U.S. Nat. Mus.*, v. 71, p. 105, figs. 162–164.

***Ammonia*? sp.** Plate 15, Figs. 1, 2. Test free, calcareous, perforate, generally between 300 and 500 μm, trochospiral with slightly evolute ventral side, 5–7 chambers in last whorl. Flattened with almost parallel sides, slightly depressed umbo, and broadly rounded, somewhat lobulate to smooth periphery. Sutures flush to slightly depressed, generally indistinct. Chambers increase in size gradually. Wall thick, hyaline, extremely smooth. Primary aperture is an elongate, low slit bordered by a narrow lip, extending from just outside the umbo to the periphery. Secondary apertures (rounded or L-shaped) along the spiral suture on the dorsal side and on the junctions of spiral and cameral sutures. On slightly evolute ventral side secondary apertures are on cameral sutures close to umbo or on spiral suture. The species superficially resembles an indistinct species of *Eponides* and has a close resemblance to *Gyroidinoides lamarckianus* in its flattened shape. Its actual affinity is unknown

[3] This appendix is in the back pocket.

until a more detailed study of the internal structure is completed. For the time being it is tentatively assigned to the genus *Ammonia* because of its similarity to juvenile *A. tepida* or *A. beccarii*, in which the spiral fissure system is not yet fully developed. If the species belongs in the genus *Ammonia*, its abyssal habitat is remarkable, since *Ammonia* species are generally shallow-water dwellers.

Stratigraphic Range. Late Eocene–early middle Miocene.

***Amphicoryna hirsuta* (d'Orbigny).** Plate 1, Fig. 12. *Nodosaria hirsuta* d'Orbigny, 1826, *Ann. Sci. Nat., Ser. 1*, v. 7, p. 87, no. 7.

***Anomalina alazanensis*, var. *spissiformis* Cushman and Stainforth, 1945.** Plate 12, Figs. 4, 5. *Spec. Publ. Cushman Lab. Foraminiferal Res.*, v. 14, p. 77, pl. 14, fig. 5.

***Anomalinoides acutus* (Plummer).** Plate 12, Figs. 10, 11. *Anomalina anomalinoides* (Reuss), var. *acuta* Plummer, 1947, *Univ. Texas Bull.*, no. 2644, p. 149, pl. 10, fig. 2.

***Anomalinoides dorri*, var. *aragonensis* (Nuttall).** *Anomalina dorri* Cole var. *aragonensis* Nuttall, 1930, *J. Paleontol.*, v. 4, p. 291, pl. 24, fig. 18.

***Anomalinoides globulosus* (Chapman and Parr).** Plate 12, Figs. 6, 7. *Anomalina globulosa* Chapman and Parr, 1937, *Rep. Australasian Antarctic Exped.*, C, v. 1, p. 119, pl. 9, fig. 27.

***Anomalinoides semicribratus* (Beckmann).** Plate 12, Figs. 8, 9. *Anomalina pompilioides* Galloway and Heminway var. *semicribrata* Beckmann, 1953, *Eclogae Geol. Helv.*, v. 10, pp. 400–401, pl. 27, fig. 3, text figs. 24, 25.

***Astacolus crepidulus* (Fichtel and Moll).** *Nautilus crepidulus* Fichtel and Moll, 1798, *Test. Microsc.*, p. 107, pl. 19, figs. g–i.

***Astacolus reniformis* (d'Orbigny).** *Cristellaria reniformis* d'Orbigny, 1846, *Foraminifères fossiles du Bassin Tertiaire de Vienne*, pp. 88–89, pl. 3, figs. 39, 40.

***Astrononion novozealandicum* Cushman and Edwards, 1937,** Plate 4, Fig. 9. *Contrib. Cushman Lab Foraminiferal Res.*, v. 13, pt. 1, p. 35, pl. 3, fig. 18.

***Bigenerina nodosaria* d'Orbigny, 1826,** Plate 1, Fig. 6. *Ann. Sci. Nat., Ser. 1*, v. 7, p. 261, pl. 11, figs. 9–12.

***Bolivina capitata* Cushman, 1933,** Plate 3, Fig. 2. *Contrib. Cushman Lab. Foraminiferal Res.*, v. 9, pt. 4, p. 80, pl. 8, figs. 12a,b.

***Bolivina huneri* Howe, 1939,** Plate 3, Fig. 1. *Geol. Bull. Louisiana Geol. Surv.*, v. 14, p. 66, pl. 9, figs. 3, 4.

***Bolivina silvestrina* Cushman, 1936,** *Spec. Publ. Cushman Lab Foraminiferal Res.*, v. 6, p. 56, pl. 8, fig. 5.

***Bolivina spathulata* (Williamson).** *Textularia variabilis*, var. *spathulata* Williamson, 1858, *Recent Foraminifera of Great Britain*, p. 76, pl. 6, figs. 164, 165.

***Bolivina striatula* Cushman, 1922,** Plate 3, Fig. 3. *Carnegie Inst. Washington Publ. 311*, p. 27, pl. 3, fig. 10. Resembles *B. subaenariensis* Cushman, but the latter species has parallel sides and an angular periphery, whereas *B. striatula* is a flattened oval in cross section.

***Bolivina tectiformis* Cushman, 1926,** *Contrib. Cushman Lab. Foraminiferal Res.* v. 1, p. 83, pl. 12, fig. 6.

***Bolivina translucens* Phleger and Parker, 1951,** Plate 3, Fig. 4. *Mem. Geol. Soc. Am.*, v. 46, pt. 2, p. 15, pl. 7, figs. 13, 14. *B. translucens* is flat in cross section and has a narrow aperture. *B. seminuda* Cushman is round in cross section. *B. pseudopunctata* Hoeglund has a wide aperture.

***Bolivinopsis cubensis* (Cushman and Bermudez).** Plate 1, Fig. 1. *Spiroplectoides cubensis* Cushman and Bermudez, 1937, *Contrib. Cushman Lab. Foraminiferal Res.*, v. 13, pt. 1, pl. 1, figs. 44, 45.

***Bolivinopsis trinitatensis* (Cushman and Renz).** *Spiroplectammina trinitatensis* Cushman and Renz, 1948, *Spec. Publ. Cushman Lab. Foraminiferal Res.*, v. 24, p. 11, pl. 2, figs. 13, 14.

***Bulimina alazanensis* Cushman, 1927,** Plate 2, Fig. 6. *J. Paleontol.*, v. 1, p. 161, pl. 25, fig. 4. There is considerable confusion between *B. alazanensis* and *B. rostrata* Brady. *B. alazanensis* has a reticulate pattern of costae, whereas in *B. rostrata* the costae do not touch. *B. semicostata* resembles *B. alazanensis* closely, but the costae do not cover the last chamber.

***Bulimina fijensis* Cushman, 1933,** *Contrib. Cushman Lab. Foraminiferal Res.*, v. 9, p. 79, pl. 8, figs. 7a–c.

***Bulimina jarvisi* Cushman and Parker, 1936,** *Contrib. Cushman Lab. Foraminiferal Res.*, v. 12, p. 39, pl. 7, fig. 1. Found mainly in turbidites, Site 575.

***Bulimina macilenta* Cushman and Parker, 1939,** *Contrib. Cushman Lab. Foraminiferal Res.*, v. 15, p. 93.

***Bulimina microcostata* Cushman and Parker, 1936,** Plate 2, Fig. 5. *Contrib. Cushman Lab. Foraminiferal Res.*, v. 12, p. 39, pl. 7, figs. 2a–c. Resembles *B. alazanensis*, but has less well-developed costae.

***Bulimina simplex* Terquem, 1882,** *Mem. Soc. Geol. Fr.*, ser. 3, v. 2, p. 109, pl. 11, figs. 23, 24.

***Bulimina tarda* Parker and Bermudez, 1937,** *J. Paleontol.*, v. 11, p. 514, pl. 58, figs. 6a–c.

***Bulimina translucens* Phleger, Parker and Peirson, 1953,** *Rep. Swed. Deep Sea Exped. 1947–1948*, v. 7, p. 33, pl. 6, figs. 30, 31.

***Bulimina trihedra* Cushman, 1926,** *Am. Assoc. Pet. Geol. Bull.*, v. 10, p. 591, pl. 17, figs. 6a,b.

***Buliminella carteri* Bhatia, 1955,** Plate 2, Fig. 7. *J. Paleontol.*, v. 29, p. 678, pl. 66, fig. 10. Resembles *B. grata* Parker and Bermudez, but the sutures are not scalloped.

***Buliminella grata* Parker and Bermudez, 1937,** *J. Paleontol.*, v. 11, p. 515, pl. 59, figs. 6a–c.

***Buliminella* sp. Douglas, 1973,** *Init. Repts. DSDP*, v. 17, p. 634, pl. 7, fig. 5. Found only in turbidites, Site 575.

***Cassidulina crassa* d'Orbigny, 1846,** *Foraminifères fossiles du Bassin Tertiaire de Vienne*, pp. 212–213, pl. 21, figs. 42, 43.

***Cassidulina havanensis* Cushman and Bermudez, 1936,** Plate 7, Figs. 1, 2. *Contrib. Cushman Lab. Foraminiferal Res.*, v. 12, p. 36, pl. 6, fig. 11.

***Cassidulina laevigata* d'Orbigny, 1826,** *Ann. Sci. Nat., Ser. 1*, v. 7, p. 282, pl. 15, figs. 4, 5, 5b.

***Cassidulina spinifera* Cushman and Jarvis, 1929,** Plate 7, Fig. 3. *Contrib. Cushman Lab. Foraminiferal Res.*, v. 5, pt. 1, p. 17, pl. 3, figs. 1a,b.

***Cassidulina translucens* Cushman and Hughes, 1925,** *Contrib. Cushman Lab. Foraminiferal Res.*, v. 1, pt. 1, p. 15, pl. 2, figs. 5a–c.

***Cassidulinoides bradyi* (Norman).** *Cassidulina bradyi* Norman, 1881, *Q. J. Microsc. Sci.*, new ser., v. 21, p. 59.

***Chilostomella ovoidea* Reuss, 1850,** *Denkschr. K. Akad. Wiss. Wien, Math. Naturwiss. Kl.*, v. 1, p. 380, pl. 48, fig. 12.

***Chrysalogonium tenuicostatum* Cushman and Bermudez, 1936,** *Contrib. Cushman Lab. Foraminiferal Res.*, v. 12, pt. 2, p. 27, 28, pl. 5, figs. 3–5.

***Cibicidoides alleni* (Plummer).** *Cibicides alleni* Plummer, 1927, *Univ. Texas Bull.*, no. 2644, p. 144, pl. 10, fig. 4.

***Cibicidoides bradyi* (Trauth).** Plate 10, Figs. 7, 8. *Truncatulina bradyi* Trauth, 1884, *Denkschr. K. Akad. Wiss. Wien, Math. Naturwiss. Kl.*, v. 95, p. 235, pl. 4, figs. 7–9.

***Cibicidoides cicatricosus* (Schwager).** *Anomalina cicatricosa* Schwager, 1866, *Novara Exp. Geol. Theil.*, v. 2, p. 260, pl. 7, fig. 108. Not the same as *C. cicatricosus* in Resig, 1981, *Mem. Geol. Soc. Am.*, v. 154, pl. 8, figs. 13, 14. These figures show a more acute periphery.

***Cibicidoides dickersoni* (Bermudez).** *Cibicides dickersoni* Bermudez, 1937, *Mem. Soc. Cubana Hist. Nat.*, v. 11, p. 244, pl. 21, figs. 8, 9.

***Cibicidoides grimsdalei* (Nuttall).** Plate 9, Figs. 1, 2. *Cibicides grimsdalei* Nuttall, 1930, *J. Paleontol.*, v. 4, p. 291, pl. 25, figs. 7, 8, 11.

***Cibicidoides havanensis* (Cushman and Bermudez).** *Cibicides havanensis* Cushman and Bermudez, 1937, *Contrib. Cushman Lab. Foraminiferal Res.*, v. 13, pt. 1, p. 28, pl. 3, figs. 1–3.

***Cibicidoides kullenbergi* (Phleger, Parker and Peirson).** Plate 8, Figs. 1, 2. *Cibicides kullenbergi* Phleger, Parker and Peirson, 1953, *Rep. Swed. Deep Sea Exped., 1947–1948*, v. 7, p. 49, pl. 11, figs. 7, 8. This species shows considerable variability. In my opinion, it is closely related to *C. mundulus* (Brady, Parker, and Jones), *C. mollis* (Phleger and Parker), *C. kullenbergi*, var. *S.* (this study), *C.* aff. *mundulus* (this study), and *C. pseudoungerianus* (Cushman). This classification does not take into account bi- or planconvexity of the test, since this varies considerably in type material of *C. kullenbergi*. I call specimens *C. kullenbergi* if they have a keel and if the sutures on the involute side are curved strongly and thus join the keel tangentially. *C. kullenbergi*, var. *S.* also has strongly curved sutures on the involute side, but there is a kink in each suture close to the umbo, and the sutures do not join the keel tangentially. The species is keeled. *C. mundulus* also has a keel, but the sutures on the involute side are not or hardly curved. In *C. mollis* the later chambers of the last whorl are not keeled, but inflated; the sutures on the involute side in these inflated chambers are not curved. *C. pseudoungerianus* does not have a keel. *C.* aff. *mundulus* resembles *C. mundulus*, but the keel tends to be lobate and very thick; the specimens are larger. Generally, *C. kullenbergi* has more cham-

bers per whorl (about 13) than the other species (9 to 11). *C. wuellerstorfi* juveniles strongly resemble *C. kullenbergi*. I include in *C. wuellerstorfi* all forms that have strongly curved sutures on the evolute side. Although problematic individuals certainly occur, this taxonomic scheme proved to be useful.

Cibicidoides kullenbergi*, var. *S. Plate 8, Figs. 3, 4. See *C. kullenbergi*.

***Cibicidoides laurisae* (Mallory).** Plate 10, Figs. 3, 4. *Cibicides laurisae* Mallory, 1959, *Lower Tertiary Biostratigraphy of the California Coast Ranges: Am. Assoc. Pet. Geol., Tulsa, Okla.*, p. 267, pl. 24, figs. 8a–c. This is probably the same species as *Anomalinoides* sp. 1, Douglas, 1973, *Init. Repts. DSDP*, v. 17, pl. 19, figs. 4, 5.

***Cibicidoides mexicanus* (Nuttall).** Plate 9, Figs. 3, 4. *Cibicides mexicanus* Nuttall, 1932, *J. Paleontol.*, v. 6, p. 33, pl. 9, figs. 7–9. *C. mexicanus* resembles *C. perlucidus* in its thickened, glassy wall on the evolute side, but has a much more highly convex involute side.

***Cibicidoides mollis* (Phleger and Parker).** Plate 8, Figs. 7, 8. *Cibicides mollis* Phleger and Parker, 1951, *Mem. Geol. Soc. Am.*, v. 46, pt. 2, p. 30. See *C. kullenbergi*.

***Cibicidoides mundulus* (Brady, Parker and Jones).** Plate 8, Figs. 5, 6. *Truncatulina mundula* Brady, Parker and Jones, 1888, *Trans. Zool. Soc. London*, v. 12, p. 228, pl. 45, fig. 25. See *C. kullenbergi*.

***Cibicidoides* aff. *mundulus*.** Plate 8, Figs. 9, 10. See *C. kullenbergi*.

***Cibicidoides perlucidus* (Nuttall).** Plate 9, Figs. 5, 6. *Cibicides perlucida* Nuttall, 1932, *J. Paleontol.*, v. 6, p. 33, pl. 8, figs. 10–12. See *C. mexicanus*.

***Cibicidoides pseudoungerianus* (Cushman).** Plate 11, Figs. 5, 6. *Truncatulina pseudoungeriana* Cushman, 1922, *U.S. Geol. Surv. Prof. Pap.*, v. 129E, p. 97, pl. 20, fig. 9.

***Cibicidoides robertsonianus* (Brady).** Plate 10, Figs. 5, 6. *Truncatulina robertsoniana* Brady, 1881, *Q. J. Microsc. Sci.*, new ser., v. 21, p. 65.

***Cibicidoides trinitatensis* (Nuttall).** Plate 10, Figs. 1, 2. *Truncatulina trinitatensis* Nuttall, 1928, *Q. J. Geol. Soc. London*, v. 84, p. 97, pl. 7, figs. 3, 5–6. This species is the same as *C. trincherasensis* Beckmann, not Bermudez, *Eclogae Geol. Helv.*, 1953, v. 46, p. 656, pl. 18, figs. 4–6; the species that Beckmann names *C. trinitatensis* is completely different.

***Cibicidoides wuellerstorfi* (Schwager).** Plate 11, Figs. 1, 2, 3, 4. *Anomalina wuellerstorfi* Schwager, 1866, *Novara Exp. Geol. Theil.*, v. 2, p. 258, pl. 7, figs. 105–107. See *C. kullenbergi*.

Cibicidoides wuellerstorfi*, var. *C. Plate 11, Figs. 7, 8. This form resembles the nominate species in overall shape and chamber arrangement, but the evolute side does not show the thick ridges. On the involute side the sutures are less thickened and glassy.

***Cyclammina cancellata* Brady, 1876,** *in* Norman, *Proc. Roy. Soc. London*, v. 25, p. 214.

***Dentalina communis* d'Orbigny.** *Nodosaria* (*Dentalina*) *communis* d'Orbigny, 1826, *Ann. Sci. Nat., Ser. 1*, v. 7, p. 254.

***Dentalina intorta* (Dervieux).** *Nodosaria intorta* Dervieux, 1893–94, *Boll. Soc. Geol. Ital.*, v. 12, p. 610.

***Dentalina reussi* Neugeboren, 1856,** *Denkschr. K. Akad. Wiss. Wien, Math. Naturwiss. Kl.*, v. 12 (Abt. 2), p. 85, pl. 3, figs. 6–7.

***Dentalina subsoluta* (Cushman).** *Nodosaria subsoluta* Cushman, 1923, *Bull. U.S. Nat. Mus.*, v. 104, pt. 4, p. 74, pl. 13, fig. 1.

***Dorothia brevis* Cushman and Stainforth, 1945,** *Spec. Publ. Cushman Lab. Foraminiferal Res.*, v. 14, p. 18, pl. 2, fig. 5.

***Dorothia scabra* (Brady).** *Gaudryina scabra* Brady, 1884, *Rep. Voy. Challenger, Zool.*, v. 9, pl. 46, figs. 7a,b.

***Eggerella bradyi* (Cushman).** Plate 1, Fig. 4. *Verneullina bradyi* Cushman, 1911, *Bull. U.S. Nat. Mus.*, v. 71, pt. 2, p. 54, text figs. 87a,b.

Eggerella propinqua (Brady). *Verneuillina propinqua* Brady, 1884, *Rep. Voy. Challenger, Zool.*, v. 9, p. 383, pl. 47, figs. 8–12. Only in turbidites, Site 575.

***Ehrenbergina caribbea* Galloway and Heminway, 1941,** Plate 7, figs. 7, 8. *N.Y. Acad. Sci., Scientific Surv. Porto Rico and Virgin Islands*, v. 3, pt. 4, p. 426, pl. 32, figs. 4a–d.

***Eilohedra weddellensis* (Earland).** Plate 13, Figs. 5, 6. *Eponides weddellensis* Earland, 1936, *Discovery Repts.*, v. 13, p. 57, pl. 1, figs. 65–67. This species closely resembles *Eponides pusillus* Parr in chamber arrangement and small size. However, the aperture in *E. pusillus* is at the base of the last chamber. In *E. weddellensis* it extends into the apertural face parallel to the periphery. *Epistominella levicula* Resig was designated as the type species of the genus *Eilohedra* by Lipps (1965). However, I consider *E. levicula* to be a junior synonym of *E. weddellensis*, which makes *E. weddellensis* the type species of *Eilohedra*.

***Ellipsobulimina* sp.** Resembles *E. seguenzai* Silvestri, but is much more slender.

***Ellipsodimorphina subcompacta* Liebus, 1922,** *Lotos (Praga)*, v. 70, p. 57, pl. 2, fig. 13.

***Ellipsoglandulina exponens* (Brady).** *Ellipsoidina exponens* Brady, 1892, *Q. J. Geol. Soc. London*, v. 48, p. 198.

***Ellipsoglandulina laevigata* Silvestri, 1900,** *Mem. R. Accad. Sci., Lett. Arti degli Zelanti, Cl. Sci.*, Nuova Ser., v. 10, p. 12.

***Ellipsoglandulina multicostata* Galloway and Morrey, 1929,** *Bull. Am. Geol.*, v. 15, no. 55, p. 42, pl. 6, fig. 13.

***Ellipsoglandulina* aff. *fragilis* Bramlette.** *Ellipsoglandulina* sp., aff. *fragilis* Bramlette, Beckmann, 1953, *Eclogae Geol. Helv.*, v. 46, p. 379, pl. 28, fig. 7.

***Ellipsoglandulina* sp.** Very strongly depressed sutures, inflated chambers.

***Ellipsopolymorphina* sp.** Last chamber more enveloping than in *E. fornasinii*, first chambers more elongate than in *E. schlichtii*.

***Epistominella exigua* (Brady).** Plate 13, figs. 3, 4. *Pulvinulina exigua* Brady, 1884, *Rep. Voy. Challenger, Zool.*, v. 9, p. 696, pl. 103, figs. 13a–c, 14a–c.

***Eponides pusillus* Parr, 1950,** *BANZ Antarctic Res. Exp.*, v. 5, pt. 6, p. 360, pl. 14, figs. 16a–c. See *Eilohedra weddellensis*.

***Eponides regularis* Phleger and Parker, 1951,** *Mem. Geol. Soc. Am.*, v. 46, pt. 2, p. 21, pl. 11, figs. 3a,b, 4a–c.

***Eponides tumidulus* (Brady).** *Truncatulina tumidula* Brady, 1884, *Rep. Voy. Challenger, Zool.*, v. 9, p. 666, pl. 95, figs. 8a–d.

***Favocassidulina favus* (Brady).** *Pulvinulina favus* Brady, 1877, *Suppl. Notes Foram. Chalk, New Britain Group, Geol. Mag. London*, new ser., v. 4, no. 12, p. 535.

***Favocassidulina subfavus* Resig, 1982,** Plate 7, Figs. 6. *J. Paleontol.*, v. 56, pp. 979–980, pl. 7, figs. 6–8.

***Francesita advena* (Cushman).** Plate 2, Fig. 8. *Virgulina*(?) *advena* Cushman, 1922, *Bull. U.S. Nat. Mus.*, v. 104, pt. 3, p. 120, pl. 25, figs. 1–3.

***Fursenkoina bradyi* (Cushman).** Plate 3, Fig. 7. *Virgulina bradyi* Cushman, 1922, *Bull. U.S. Nat. Mus.*, v. 104, pt. 3, p. 115, pl. 24, fig. 1.

***Fursenkoina ciperana* (Cushman and Stainforth).** Plate 3, Fig. 6. *Virgulina ciperana* Cushman and Stainforth, 1945, *Contrib. Cushman Lab. Foraminiferal Res.*, v. 14, p. 46, 47, pl. 7, fig. 10.

***Fursenkoina compressa* (Bailey).** *Bulimina compressa* Bailey, 1851, *Smithsonian Contrib.*, v. 2, art. 3, p. 12, pl. 12, figs. 35–37.

***Fursenkoina cylindrica* (Cushman and Bermudez).** Plate 3, Fig. 8. *Virgulina cylindrica* Cushman and Bermudez, 1936, *Contrib. Cushman Lab. Foraminiferal Res.*, v. 12, pt. 2, p. 30, 31, pl. 5, figs. 15a–c.

***Fursenkoina pauciloculata* (Brady).** Plate 3, Fig. 5. *Virgulina pauciloculata* Brady, 1884, *Rep. Voy. Challenger, Zool.*, v. 9, p. 414, pl. 52, figs. 4, 5.

***Gavelinella micra* (Bermudez).** Plate 11, Figs. 11, 12. *Cibicides micrus* Bermudez, 1949, *Spec. Publ. Cushman Lab. Foraminiferal Res.*, v. 25, p. 302, pl. 24, figs. 34–36.

***Globobulimina ovata* (d'Orbigny).** *Bulimina ovata* d'Orbigny, 1846, *Foraminifères fossiles du Bassin Tertiaire de Vienne*, p. 185, pl. 11, figs. 13, 14.

***Globocassidulina decorata* (Sidebottom).** Plate 7, Fig. 5. *Cassidulina decorata* Sidebottom, 1910, *J. Quekett Microsc. Club*, ser. 2, v. 11, no. 67, p. 107, pl. 4, figs. 2a–c.

***Globocassidulina subglobosa* (Brady).** Plate 7, Fig. 4. *Cassidulina subglobosa* Brady, 1884, *Rep. Voy. Challenger, Zool.*, v. 9, p. 430, pl. 54, figs. 17a–c.

***Globulina minuta* (Roemer).** *Polymorphina minuta* Roemer, 1838, *Neues Jahrb. Mineral.*, v. 20, p. 386, pl. 3, fig. 35.

***Gravellina narivaensis* Brönnimann, 1953,** Plate 1, Fig. 7. *Contrib. Cushman Found. Foraminiferal Res.*, v. 4, pt. 1, p. 88, text fig. 1, pl. 15, fig. 8.

***Gyroidinoides acutus* (Boomgaart).** Plate 6, Figs. 4, 5, 6. *Gyroidina neosoldanii* Brotzen var. *acuta* Boomgaart, 1949, Univ. Utrecht doctoral dissert., p. 124, pl. 9, figs. 1a–c. I think that this species is closely related to *G. soldanii* (d'Orbigny). Probably this species is the same as *G. zealandica* (Finlay) *in* Resig, 1981, *Mem. Geol. Soc. Am.*, v. 154, pl. 8, figs. 3–4, and as *G. zealandica* in Douglas, 1973, *Init. Repts. DSDP*, v. 17, p. 644, pl. 12, partim, figs. 7–9,

not figs. 4–6. The type figure of *G. zealandica* Finlay, 1939, *Trans. R. Soc. N.Z.*, v. 67, p. 323, pl. 28, figs. 138–140, shows much more convex sides and the periphery is less acute. I use the name *G. acutus* for forms with somewhat concave evolute side, acute periphery, and about triangular on cross section.

***Gyroidinoides girardanus* (Reuss).** Plate 6, Figs. 1, 2, 3. *Rotalina girardana* Reuss, 1851, *Dtsch. Geol. Ges.*, v. 3, p. 73, pl. 5, fig. 34.

***Gyroidinoides globosus* (Hagenow).** Plate 5, Figs. 7, 8. *Nonionina globosa* Hagenow, 1842, *Neues Jahrb. Mineral.*, p. 574.

***Gyroidinoides lamarckianus* (d'Orbigny).** Plate 5, Figs. 1, 2. *Rotalina lamarckiana* d'Orbigny, 1839, *Hist. Nat. Iles Canaries*, v. 2, pt. 2, p. 131, pl. 2, figs. 13–15. *G. lamarckianus* is a flat form, in which the involute side is not strongly convex and the periphery is broadly rounded. The species is probably the same as that named *G. orbicularis* by Corliss, 1979, *Micropaleontology*, v. 25, p. 9, pl. 5, figs. 1–3 and by Pflum and Frerichs, 1976, *Spec. Publ. Cushman Found. Foraminiferal Res.*, v. 14, pl. 5, figs. 5–7. *G. orbicularis* d'Orbigny, 1826, *Ann. Sci. Nat.*, v. 7, p. 278, no. 1, modelès no. 13 has a much more acute periphery and a more convex involute side.

***Gyroidinoides mediceus* (Emiliani).** Plate 5, Figs. 5, 6. *Gyroidina medicea* Emiliani, 1954, *Paleontographica Italiana*, v. 48, p. 136, pl. 24, fig. 6.

***Gyroidinoides planulatus* (Cushman and Renz).** Plate 5, Figs. 3, 4. *Gyroidina planulata* Cushman and Renz, 1941, *Contrib. Cushman Lab. Foraminiferal Res.*, v. 17, p. 23, pl. 4, fig. 1.

***Gyroidinoides soldanii* (d'Orbigny).** Plate 6, Figs. 7, 8. *Gyroidina soldanii* d'Orbigny, 1826, *Ann. Sci. Nat.*, v. 7, p. 298, no. 5, modèles no. 36. This is probably the same species as *G. zealandica* (Finlay), Douglas, 1973, *Init. Repts. DSDP*, v. 17, p. 644, pl. 12, partim, figs. 4–6, not figs. 7–9 (see *G. acutus*).

***Guttulina problema* d'Orbigny, 1826,** *Ann. Sci. Nat.*, v. 6, p. 266, no. 14.

***Guttulina seguenziana* (Brady).** *Polymorphina seguenziana* Brady, 1884, *Rep. Voy. Challenger, Zool.*, v. 9, p. 567, pl. 72, figs. 16, 17.

***Hanzawaia cushmani* (Nuttall).** *Cibicides cushmani* Nuttall, 1930, *J. Paleontol.*, v. 4, p. 291, pl. 25, figs. 3, 5, 6.

***Heronallenia lingulata* (Burrows and Holland).** Plate 13, Fig. 7. *Discorbina lingulata* Burrows and Holland, 1896, *in* Jones, *Foram. Crag*, pt. 3, p. 297, pl. 7, fig. 33.

***Involutina tenuis* Brady, 1884,** *Rep. Voy. Challenger, Zool.*, v. 9, pl. 38, figs. 5, 6.

***Karreriella bradyi* (Cushman).** *Gaudryina bradyi* Cushman, 1911, *Bull. U.S. Nat. Mus.*, v. 71, pt. 2, p. 67, fig. 107.

***Laticarinina pauperata* (Parker and Jones).** Plate 11, Fig. 10. *Pulvinellina repanda* var. *menardii* subvar. *pauperata* Parker and Jones, 1865, *Philos. Trans. R. Soc. London*, v. 155, p. 395, pl. 16, figs. 50–51.

***Lenticulina gibba* (d'Orbigny).** *Cristellaria gibba* d'Orbigny, 1826, *Ann. Sci. Nat.*, v. 7, p. 292, no. 7.

***Lenticulina mexicana* (Cushman).** *Cristellaria mexicana* Cushman, 1925, *Am. Assoc. Pet. Geol. Bull.* v. 9, p. 299, pl. 7, figs. 1, 2.

***Lenticulina* sp. juv.** This includes all juvenile specimens having only 2–3 chambers present that cannot be assigned to a species.

***Marginulina costata* (Montagu).** *Nautilus costatus* Montagu, 1803, *Test. Britt.*, p. 199, pl. 14, fig. 5.

***Marginulina glabra* var. *obesa* Cushman.** *Marginulina glabra* d'Orbigny var. *obesa* Cushman, 1923, *Bull. U.S. Nat. Mus.*, v. 104, pt. 4, p. 128, pl. 37, fig. 1.

***Marginulina suberecta* Franke, 1927,** *Dan. Geol. Unders.*, v. 2, Raekke nr. 46, p. 19, pl. 1, fig. 28.

Martinotiella communis (d'Orbigny). *Clavulina communis* d'Orbigny, 1826, *Ann. Sci. Nat.*, v. 7, p. 268, no. 4.

***Martinotiella petrosa* (Cushman and Bermudez).** *Listerella petrosa* Cushman and Bermudez, 1937, *Contrib. Cushman Lab. Foraminiferal Res.*, v. 13, p. 5, pl. 1, figs. 24–26.

***Melonis barleeanus* (Williamson).** Plate 12, Fig. 3. *Nonionina barleeana* Williamson, 1858, *Recent Foraminifera of Great Britain*, p. 32, pl. 3, figs. 68–69.

***Melonis pompilioides* (Fichtel and Moll).** Plate 12, Figs. 1, 2. *Nautilus pompilioides* Fichtel and Moll, 1798, *Test. Microsc.*, p. 31, pl. 2, figs. a–c.

***Nodosaria albatrossi* Cushman.** *Nodosaria vertebralis* Batsch var. *albatrossi* Cushman, 1924, *Bull. U.S. Nat. Mus.*, v. 104, pt. 4, p. 87, pl. 15, fig. 1.

***Nodosaria filiformis* d'Orbigny, 1826,** *Ann. Sci. Nat.*, v. 7, p. 2543, no. 14.

***Nodosaria fusiformis* Silvestri, 1872,** *Accad. Gioenia Sci. Nat. Catania, Atti*, ser. 3, v. 7, p. 99, fig. 34.

***Nodosaria lamnulifera* Boomgaart, 1950,** *Contrib. Cushman Found. Foraminiferal Res.*, v. 1, p. 42.

***Nodosaria longiscata* d'Orbigny, 1846,** *Foraminifères fossiles du Bassin Tertiaire de Vienne*, p. 32, pl. 1, figs. 10–12.

***Nodosaria pyrula* d'Orbigny, 1826,** *Ann. Sci. Nat.*, v. 7, p. 253, no. 13.

***Nodosaria vertebralis* (Batsch).** *Nautilus* (*Orthoceras*) *vertebralis* Batsch, 1791, *Conchyl. Seesandes*, p. 3, no. 6, pl. 2, fig. 6.

***Nodosarella subnodosa* (Guppy).** *Ellipsoidina subnodosa* Guppy, 1894, *Proc. Zool. Soc. London*, p. 650, pl. 61, fig. 12.

***Nonion havanense* Cushman and Bermudez, 1937,** Plate 4, Figs. 10, 11. *Contrib. Cushman Lab. Foraminiferal Res.*, v. 13, p. 19, pl. 2, figs. 13, 14.

***Nonionellina labradorica* (Dawson).** *Nonionina labradorica* Dawson, 1860, *Can. Naturalist*, v. 5, p. 191, fig. 4.

***Nuttallides truempyi* (Nuttall).** *Eponides truempyi* Nuttall, 1930, *J. Paleontol.*, v. 4, p. 271, pl. 24, figs. 9, 13, 14.

***Nuttallides umbonifera* (Cushman).** Plate 13, Figs. 1, 2. *Pulvinulinella umbonifera* Cushman, 1933, *Contrib. Cushman Lab. Foraminiferal Res.*, v. 9, pt. 4, pl. 9, figs. 9a–c.

***Ophthalmidium pusillum* (Earland).** *Spiroloculina pusilla* Earland, 1934, *Discovery Repts.*, v. 10, p. 47, pl. 1, figs. 3, 4.

***Oridorsalis tener* (Brady).** Plate 4, Figs. 5, 6. *Truncatulina tenera* Brady, 1884, *Rep. Voy. Challenger, Zool.*, v. 9, p. 665, pl. 95, figs. 11a–c.

***Oridorsalis umbonatus* (Reuss).** Plate 4, Figs. 7, 8. *Rotalina umbonata* Reuss, 1851, *Z. Dtsch. Geol. Ges.*, v. 3, p. 75, pl. 5, figs. 35a–c.

***Orthomorphina calomorpha* (Reuss).** *Nodosaria* (*Nodosaria*) *calomorpha* Reuss, 1886, *Denkschr. K. Akad. Wiss. Wien, Math. Naturwiss. Kl.*, v. 25, p. 129, pl. 1, figs. 15–19.

***Orthomorphina doliolaris* (Parr).** *Nodosaria doliolaris* Parr, 1950, *BANZ Antarctic Res. Exp.*, ser. B, v. 5, p. 290, pl. 12, fig. 2.

***Orthomorphina glandigena* (Schwager).** *Nodosaria glandigena* Schwager, 1866, *Novara Exp. Geol. Theil.*, v. 2, p. 219, pl. 5, fig. 46.

***Osangularia culter* (Parker and Jones).** *Planorbulina culter* Parker and Jones, 1865, *Philos. Trans. R. Soc. London*, v. 155, p. 421, pl. 19, fig. 1.

***Osangularia interrupta* (Cushman).** *Pulvinulinella interrupta* Cushman, 1927, *Contrib. Cushman Lab. Foram. Res.*, v. 3, p. 115, figs. 10a–c.

***Osangularia mexicana* (Cole).** *Pulvinulinella culter* Parker and Jones var. *mexicana* Cole, 1927, *Bull. Am. Paleontol.*, v. 14, no. 51, p. 31, pl. 1, figs. 15, 16.

***Planulina marialana* Hadley, 1934,** *Bull. Am. Paleontol.*, v. 20, no. 70A, p. 27, pl. 4, figs. 4–6.

***Planulina renzi* Cushman and Stainforth, 1945,** Plate 11, Fig. 9. *Spec. Publ. Cushman Lab. Foraminiferal Res.*, v. 14, p. 72, pl. 15, fig. 1.

***Planulinoides biconcavus* (Jones and Parker).** *Discorbina biconcava* Jones and Parker, 1861, *in* Carpenter, Parker, and Jones, *Intro. Study Foram.*, p. 201, fig. 32g.

***Plectofrondicularia alazanensis* Cushman, 1927,** *Contrib. Cushman Lab. Foraminiferal Res.*, v. 3, p. 113, pl. 22, fig. 12.

***Pleurostomella acuminata* Cushman, 1922,** *Bull. U.S. Nat. Mus.*, v. 104, pt. 3, p. 50, pl. 19, fig. 6.

***Pleurostomella acuta* Hantken, 1875,** Plate 14, Figs. 1, 2. *K. Ungar. Geol. Anst. Mitt.*, v. 4, pt. 1, p. 44, pl. 13, fig. 18.

***Pleurostomella alternans* Schwager, 1866,** Plate 14, Fig. 5. *Novara Exp. Geol. Theil.*, v. 2, p. 238, pl. 6, fig. 79.

***Pleurostomella bierigi* Palmer and Bermudez, 1936,** *Mem. Soc. Cubana Hist. Nat.*, v. 10, p. 294, pl. 17, figs. 7, 8.

***Pleurostomella bolivinoides* Schubert, 1911,** *Geol. Reichsanst. Wien Abh.*, v. 20, pt. 4, p. 57, pl. 4.

***Pleurostomella fusiformis* Reuss, 1860,** *Sitzungsber. Kais. Akad. Wiss. Wien, Math. Naturwiss. Kl.*, v. 40, p. 205, pl. 8, fig. 1.

***Pleurostomella obtusa* Berthelin, 1880,** Plate 14, Figs. 3, 4. *Mem. Soc. Geol. Fr.*, ser. 3, v. 1, pt. 5, p. 29, pl. 1, fig. 9.

***Pleurostomella rimosa* Cushman and Bermudez, 1937,** *Contrib. Cushman Lab. Foraminiferal Res.*, v. 13, pt. 1, p. 17, pl. 1, figs. 62–63.

***Polymorphina lactea* (Walker and Jacob).** *Serpula lactea* Walker and Jacob, 1798, *Adam's Essays*, ed. 2, p. 634, pl. 24, fig. 4.

***Pseudoparrella* sp.** This species resembles *P. subperuviana* (Cushman) closely in shape of the chambers on the evolute side, but it is more flattened and has a broadly rounded periphery. *P. garrisoni* Lipps has wider chambers and less curved sutures on the evolute side. See Lipps (1965).

***Pullenia bulloides* (d'Orbigny).** *Noniona bulloides* d'Orbigny, 1846, *Foraminifères fossiles du Bassin Tertiaire de Vienne*, p. 107, pl. 5, figs. 9, 10. 4–4½ chambers, spheroid, smooth outline.

***Pullenia quadriloba* Reuss.** Plate 4, Fig. 1. *Pullenia compressiuscula* Reuss var. *quadriloba* Reuss, 1867, *Denkschr. K. Akad. Wiss. Wien, Math. Naturwiss. Kl.*, ser. B, v. 55, p. 87, pl. 3, fig. 8. 4–4½ chambers, flattened, lobate periphery.

***Pullenia quinqueloba* (Reuss).** Plate 4, Fig. 2. *Nonionina quinqueloba* Reuss, 1857, *Z. Disch. Geol. Ges.*, v. 3, p. 47, pl. 5, fig. 31. 5–5½ chambers, flattened, lobate periphery.

***Pullenia salisburyi* Stewart and Stewart, 1930,** Plate 4, Fig. 4. *J. Paleontol.*, v. 4, p. 72, pl. 8, figs. 2a–b. 6–8 chambers, more flattened than *P. quinqueloba*, lobate periphery.

***Pullenia subcarinata* (d'Orbigny).** Plate 4, Fig. 3. *Nonionina subcarinata* d'Orbigny, 1839, *Voy. Amer. Merid.*, v. 5, p. 28, pl. 5, figs. 23, 24. 5–5½ chambers, lenticular, smooth outline.

***Pullenia trinitatensis* Cushman and Stainforth, 1945,** *Spec. Publ. Cushman Lab. Foraminiferal Res.*, v. 14, p. 66, pl. 12, fig. 11. 6–7 chambers, outline pronounced lobate, chambers inflated, umbo depressed.

***Pyrgo elongata* (d'Orbigny).** *Biloculina elongata* d'Orbigny, 1826, *Ann. Sci. Nat.*, v. 7, p. 298, no. 4.

***Pyrgo murrhina* (Schwager).** Plate 1, Fig. 10. *Biloculina murrhina* Schwager, 1866, *Novara Exp. Geol. Theil.*, v. 2, p. 203, pl. 4, figs. 15a–c.

***Pyrulina angusta* (Egger).** *Polymorphina* (*Globulina*) *angusta* Egger, 1857, *Neues Jahrb. Min. Geogn. Geol. Petrof.-kunde*, p. 290, pl. 13, figs. 13–15.

***Pyrulina cylindroides* (Roemer).** *Polymorphina cylindroides* Roemer, 1838, *Neues Jahrb. Min. Geogn. Geol. Petrof.-kunde*, p. 385, pl. 3, figs. 26a–b.

***Pyrulina extensa* (Cushman).** *Polymorphina extensa* Cushman, 1923, *Bull. U.S. Nat. Mus.*, v. 104, pt. 4, p. 156, pl. 41, figs. 7–8.

***Pyrulina fusiformis* (Roemer).** *Polymorphina fusiformis* Roemer, 1838, *Neues Jahrb. Min. Geogn. Geol. Petrof.-kunde*, p. 386, pl. 3, figs. 37a–b.

***Quadrimorphina allomorphinoides* (Reuss).** *Valvulina allomorphinoides* Reuss, 1860, *Sitzungsber. Kais. Akad. Wiss. Wien, Math. Naturwiss. Kl.*, v. 40, p. 223.

***Quinqueloculina lamarckiana* d'Orbigny, 1839,** *in* de la Sagra, *Hist. Phys. Pol. Nat. Cuba*, p. 189, pl. 11, figs. 14, 15.

***Quinqueloculina pygmaea* Reuss, 1850,** *Denkschr. K. Akad. Wiss. Wien, Math. Naturwiss. Kl.*, v. 1, p. 384, pl. 50, fig. 3.

***Quinqueloculina venusta* Karrer, 1868,** *Sitzungsber. Kais. Akad. Wiss. Wien, Math. Naturwiss. Kl.*, v. 58, Abt. 1, p. 147, pl. 2, fig. 6.

***Quinqueloculina* cf. *weaveri* Rau.** Plate 1, Fig. 11. *Quinqueloculina* cf. *weaveri* Phleger, Parker and Peirson, 1953, *Rep. Swed. Deep Sea Exped. 1947–1948*, v. 7, p. 28, pl. 5, figs. 13, 14.

***Reophax dentaliniformis* Brady, 1884,** *Rep. Voy. Challenger, Zool.*, v. 9, p. 299, pl. 30, figs. 21, 22.

***Reophax nodulosus* Brady, 1879,** *Q. J. Microsc. Sci.*, v. 19, p. 52, pl. 4, figs. 7, 8.

***Resigia westcotti* Schnitker and Tjalsma, 1980,** *J. Foraminiferal Res.*, v. 10, p. 240, pl. 1, figs. 22–27.

***Rhabdammina* sp.** Only found as fragments; I did not try to assign a species.

***Robertina subcylindrica* (Brady).** *Bulimina subcylindrica* Brady, 1879, *Q. J. Microsc. Sci.*, v. 19, p. 56.

***Saracenaria arcuata* var. *ampla* Cushman and Todd.** *Saracenaria arcuata* d'Orbigny var. *ampla* Cushman and Todd, 1945, *Spec. Publ. Cushman Lab. Foraminiferal Res.*, v. 15, p. 31, pl. 5, figs. 5, 6.

***Saracenaria italica* de France, 1824,** *Dict. Sci. Nat.*, v. 32, p. 177.

***Sigmoilina tenuis* (Czjzek).** *Quinqueloculina tenuis* Czjzek, 1848, *Haidinger's Naturw. Abh.*, v. 2, pt. 1, p. 149, pl. 13, figs. 31–34.

***Siphotextularia catenata* (Cushman).** *Textularia catenata* Cushman, 1911, *Bull. U.S. Nat. Mus.*, v. 71, pt. 2, p. 23, figs. 39–40. I agree with Corliss, 1979, *Micropaleontology*, v. 25, p. 5, pl. 1, figs. 1, 2, that *S. rolshauseni* (Phleger and Parker) is a junior synonym of *S. catenata*.

***Sphaeroidina bulloides* d'Orbigny, 1826,** *Ann. Sci. Nat.*, v. 7, p. 267, modèles no. 65.

***Spiroloculina canaliculata* d'Orbigny, 1846,** *Foraminifères fossiles du Bassin Tertiaire de Vienne*, pp. 269–270, pl. 16, figs. 10–12.

***Spiroplectammina biformis* (Parker and Jones).** *Textularia agglutinans* d'Orbigny var. *biformis* Parker and Jones, 1865, *Philos. Trans. R. Soc. London*, v. 155, p. 370.

***Stainforthia complanata* (Egger).** Plate 2, Fig. 9. *Virgulina schreibersiana* Czjzek var. *complanata* Egger, 1893, *Abh. Bayer. Akad. Wiss., Math-Phys. Naturwiss. Kl.*, p. 292, pl. 8, figs. 91, 92.

***Stilostomella abyssorum* (Brady).** Plate 14, Fig. 9. *Nodosaria abyssorum* Brady, 1881, *Q. J. Microsc. Sci.*, new ser., v. 21, p. 63.

***Stilostomella consobrina* (d'Orbigny).** Plate 14, Figs. 6, 7. *Dentalina consobrina* d'Orbigny, 1846, *Foraminifères fossiles du Bassin Tertiaire de Vienne*, p. 46, pl. 2, figs. 1–3. There consists considerable confusion in the nomenclature within *Stilostomella*. I use *S. consobrina* for forms in which the last chambers are elongated, *S. lepidula* for forms with rounded chambers, with a ridge or ring of spines along the lower edge of each chamber, and *S. subspinosa* for forms with rounded chambers, covered with spines. *S. consobrina* may have delicate spines randomly distributed over its chambers.

***Stilostomella lepidula* (Schwager).** Plate 14. Fig. 8. *Nodosaria lepidula* Schwager, 1866, *Novara Exp. Geol. Theil.*, v. 2, pp. 210–211, pl. 5, figs. 27, 28. See *S. consobrina*. I think that *S. antillea* (Cushman), 1923, *Bull. U.S. Nat. Mus.*, v. 104, pt. 4, p. 91, pl. 14, fig. 9 is a junior synonym.

***Stilostomella subspinosa* (Cushman).** Plate 14, Fig. 10. *Ellipsonodosaria subspinosa* Cushman, 1943, *Contrib. Cushman Lab. Foraminiferal Res.*, v. 19, p. 92, pl. 16, figs. 16, 17. See *S. consobrina*.

***Stilostomella verneuilli* (d'Orbigny).** *Dentalina verneuilli* d'Orbigny, 1846, *Foraminifères fossiles du Bassin Tertiaire de Vienne*, p. 48, pl. 2, figs. 7, 8.

***Textularia agglutinans* d'Orbigny, 1839,** Plate 1, Fig. 5. *In* de la Sagra, *Hist. Phys. Pol. Nat. Cuba*, p. 136, pl. 1, figs. 17, 18, 32, 34.

***Textularia leuzengeri* Cushman and Renz,** 1941, *Contrib. Cushman Lab. Foraminiferal Res.*, v. 17, p. 3, pl. 1, fig. 2.

***Textularia porrecta* Brady.** *Textularia agglutinans* d'Orbigny var. *porrecta* Brady, 1884, *Rep. Voy. Challenger, Zool.*, v. 9, p. 364, pl. 43, fig. 4.

***Textularia pseudogramen* Chapman and Parr, 1937,** *Sci. Rep. Australian Antarctic Exp.*, v. 1, p. 153.

***Triloculina trigonula* (Lamarck).** *Miliolites trigonula* Lamarck, 1804, *Ann. Mus. Nat. Hist. Nat. Paris*, pt. 5, p. 351, pl. 17, fig. 4.

***Trochammina globigeriniformis* (Parker and Jones).** Plate 1, Figs. 2, 3. *Lituola nautiloidea* Lamarck, var. *globigeriniformis* Parker and Jones, 1865, *Philos. Trans. R. Soc. London*, v. 155, pl. 17, fig. 96.

***Trochammina squamata* Jones and Parker, 1860,** *Q. J. Geol. Soc. London*, v. 16, p. 304.

***Trochamminoides proteus* (Karrer).** *Trochammina proteus* Karrer, 1865, *Sitzungsber. Kais. Akad. Wiss. Wien*, v. 52, Abt. 1, p. 494, fig. 8 (not figs. 1–7).

Unilocular genera. I did not try to assign specific names to any of the occasionally common unilocular specimens. However, I grouped them and counted the number of species to which they belonged. This number was used in counting the total number of species.

***Uvigerina cylindrica* (d'Orbigny).** Plate 2, Fig. 4. *Clavulina cylindrica* d'Orbigny, 1852, *Prodr. Pal. Strat.*, v. 3, p. 94. For discussion of taxonomy, see Thomas (1980).

***Uvigerina graciliformis* Papp, 1953,** Plate 2, Fig. 3. *Jahrb. Geol. Bundesanst.*, v. 16, p. 122, pl. 5A, figs. 5–7.

***Uvigerina peregrina* Cushman, 1923,** *Bull. U.S. Nat. Mus.*, v. 104, pt. 4, p. 166, pl. 42, figs. 7–10.

***Uvigerina senticosa* Cushman, 1927,** Plate 2, Fig. 1. *Scripps Inst. Techn. Ser. Bull.*, v. 1, p. 159, pl. 3, fig. 14.

***Uvigerina spinulosa* Hadley.** Plate 2, Fig. 2. *Uvigerina canariensis* d'Orbigny var. *spinulosa* Hadley, 1934, *Am. Paleontol. Bull.*, v. 20, p. 18, pl. 2, fig. 17. Occurs only in turbidites, Site 575.

Vaginulina advena **Cushman, 1923,** *Bull. U.S. Nat. Mus.*, v. 104, pt. 4, p. 134–135, pl. 39, figs. 1–4.

Vaginulina elegans **d'Orbigny, 1826,** *Ann. Sci. Nat.*, v. 7, p. 257, no. 1, modèles no. 54.

Vaginulina insolita **(Schwager).** *Cristellaria insolita* Schwager, 1866, *Novara Exp. Geol. Theil.*, v. 2, p. 242, pl. 6, fig. 85.

Vaginulina pacifica **Cushman and Hanzawa.** *Polymorphinella pacifica* Cushman and Hanzawa, 1936, *Contrib. Cushman Lab. Foraminiferal Res.*, v. 12, pt. 2, p. 47.

Vaginulina subelegans **Parr, 1950,** *BANZ Antarctic Res. Exp.*, ser. B, v. 5, pt. 6, p. 326, pl. 11, figs. 20a–b.

Vaginulina sublegumen **(Parr).** *Vaginulinopsis sublegumen* Parr, 1950, *BANZ Antarctic Res. Exp.*, ser. B, v. 5, pt. 6, p. 325, pl. 11, figs. 18a–b.

Vulvulina jarvisi **Cushman, 1932,** Plate 1, Fig. 8. *Contrib. Cushman Lab. Foraminiferal Res.*, v. 8, p. 84, pl. 10, fig. 10. In *V. jarvisi* the biserial portion is flat-sided, whereas *V. spinosa* is biconvex (see Douglas, 1973).

Vulvulina spinosa **Cushman, 1927,** Plate 1, Fig. 9. *Contrib. Cushman Lab. Foraminiferal Res.*, v. 3, pt. 2, p. 111, pl. 23, fig. 1. See *V. jarvisi*.

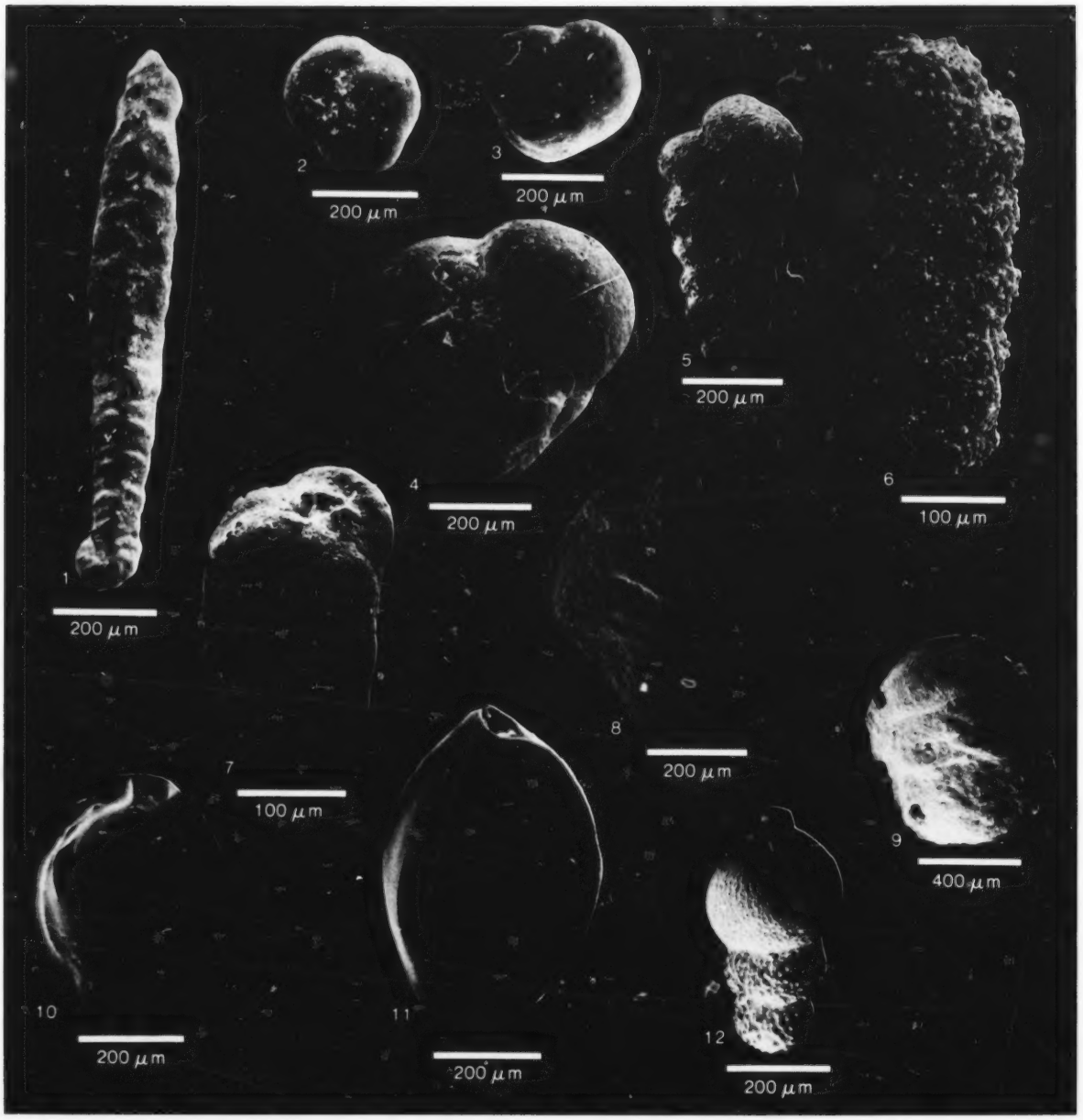

Plate 1. **1.** *Bolivinopsis cubensis*, Sample 573B-15,CC. **2–3.** *Trochammina globigeriniformis*, Sample 573-15,CC. **4.** *Eggerella bradyi*, Sample 574-25,CC. **5.** *Textularia agglutinans*, Sample 573-13,CC. **6.** *Bigenerina nodosaria* (juv.), Sample 574C-17,CC. **7.** *Gravellina narivaensis*, Sample 574C-30-1, 110–112 cm. **8.** *Vulvulina jarvisi*, Sample 574C-30,CC. **9.** *V. spinosa*, Sample 573B-30,CC. **10.** *Pyrgo murrhina*, Sample 573-16,CC. **11.** *Quinqueloculina* cf. *weaveri*, Sample 572A-14,CC. **12.** *Amphicoryna hirsuta*, Sample 573B-15,CC.

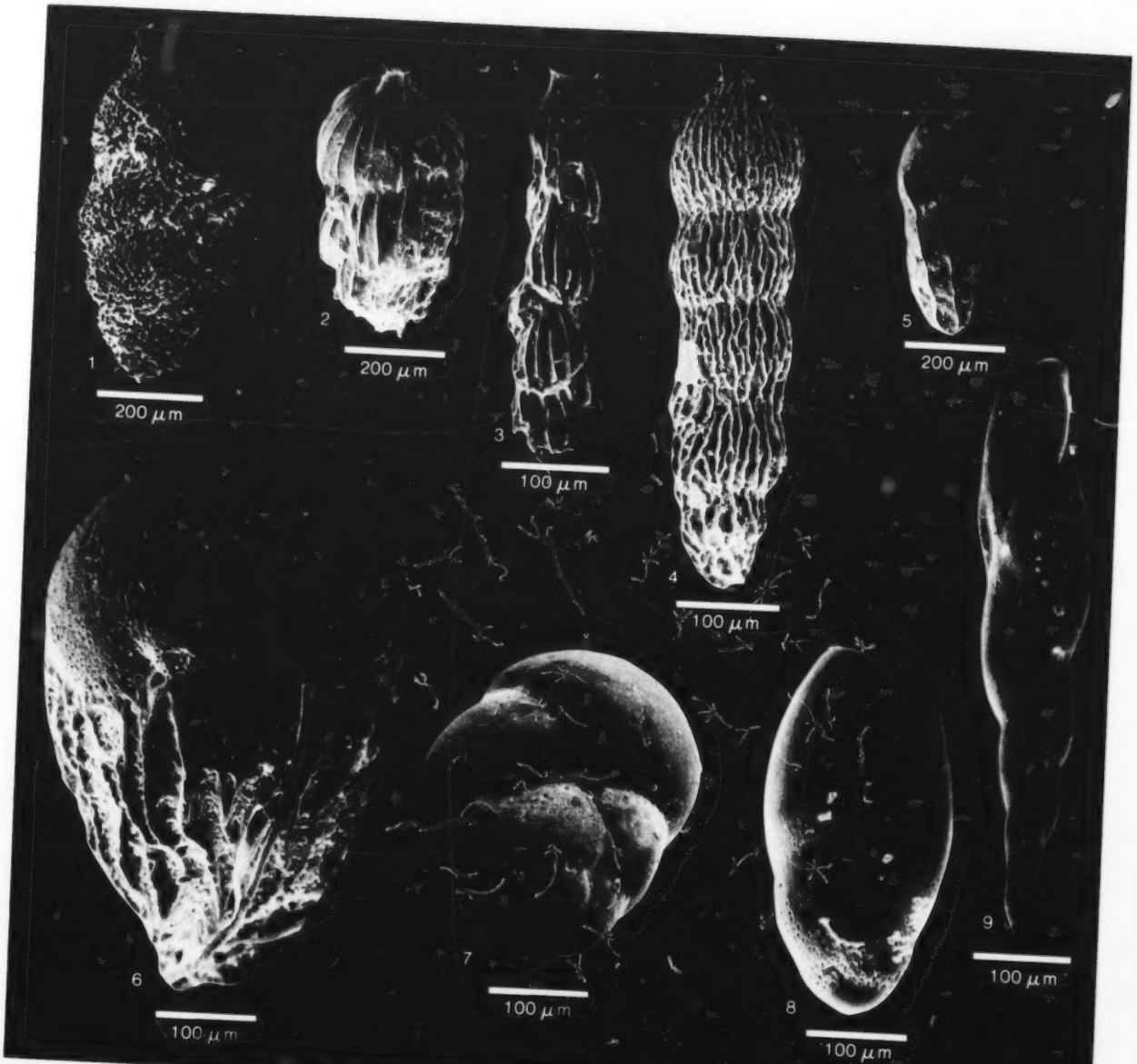

Plate 2. **1.** *Uvigerina senticosa*, Sample 572A-14,CC. **2.** *U. spinulosa*, Sample 575A-11-3, 109–111 cm. **3.** *U. graciliformis*, Sample 574-11,CC. **4.** *U. cylindrica*, Sample 573B-2,CC. **5.** *Bulimina microcostata*, Sample 573B-33,CC. **6.** *B. alazanensis*, Sample 574C-34-1, 138-140 cm. **7.** *Buliminella carteri*, Sample 575A-8,CC. **8.** *Francesita advena*, Sample 573-1,CC. **9.** *Stainforthia complanata*, Sample 573-1,CC.

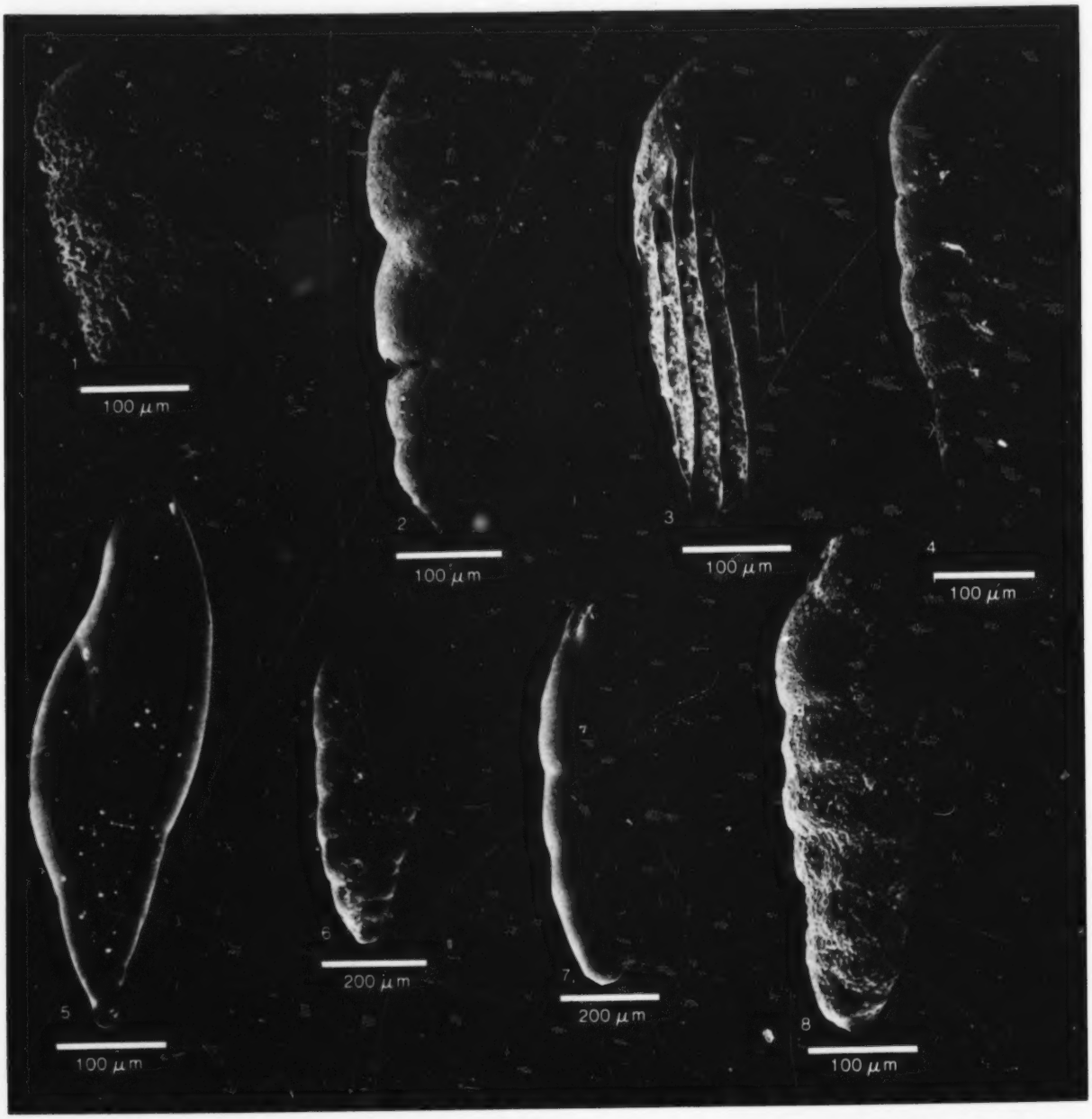

Plate 3. **1.** *Bolivina huneri*, Sample 573B-31,CC. **2.** *B. capitata*, Sample 575A-8,CC. **3.** *B. striatula*, Sample 573B-14,CC. **4.** *B. translucens*, Sample 573-16,CC. **5.** *Fursenkoina pauciloculata*, Sample 573-1,CC. **6.** *F. ciperana*, Sample 574C-30-2, 110–112 cm. **7.** *F. bradyi*, Sample 573-17,CC. **8.** *F. cylindrica*, Sample 574C-35-1, 6–8 cm.

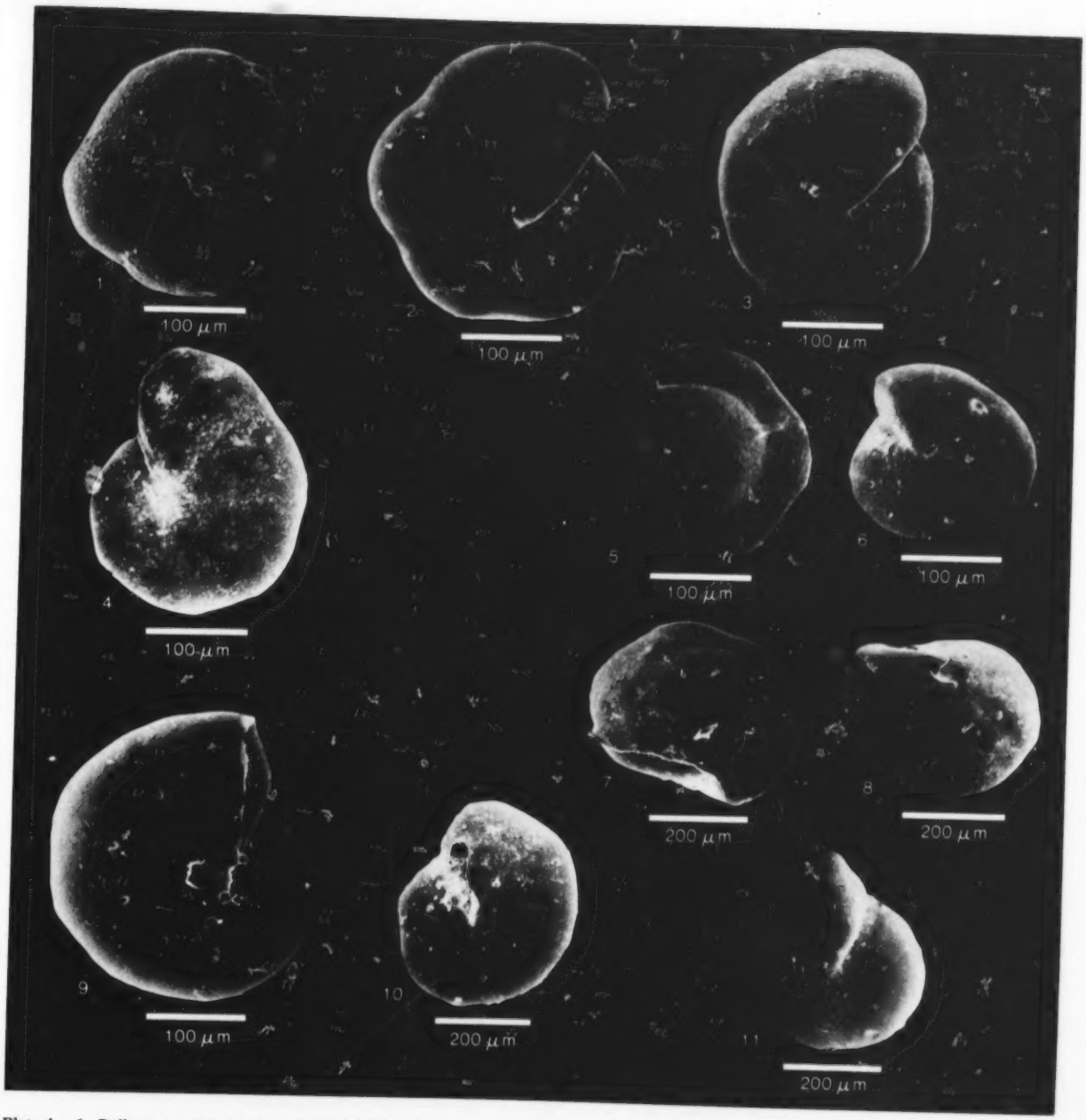

Plate 4. **1.** *Pullenia quadriloba*, Sample 574C-30-2, 110–112 cm. **2.** *P. quinqueloba*, Sample 574C-29-3, 96–98 cm. **3.** *P. subcarinata*, Sample 574C-29-3, 96–98 cm. **4.** *P. salisburyi*, Sample 573B-13,CC. **5–6.** *Oridorsalis tener*, Sample 573-17,CC. **7–8.** *O. umbonatus*, Sample 572A-14,CC. **9.** *Astrononion novozealandicum*, Sample 573-2,CC. **10–11.** *Nonion havanense*, (10) Sample 573B-37,CC, (11) Sample 573B-38,CC.

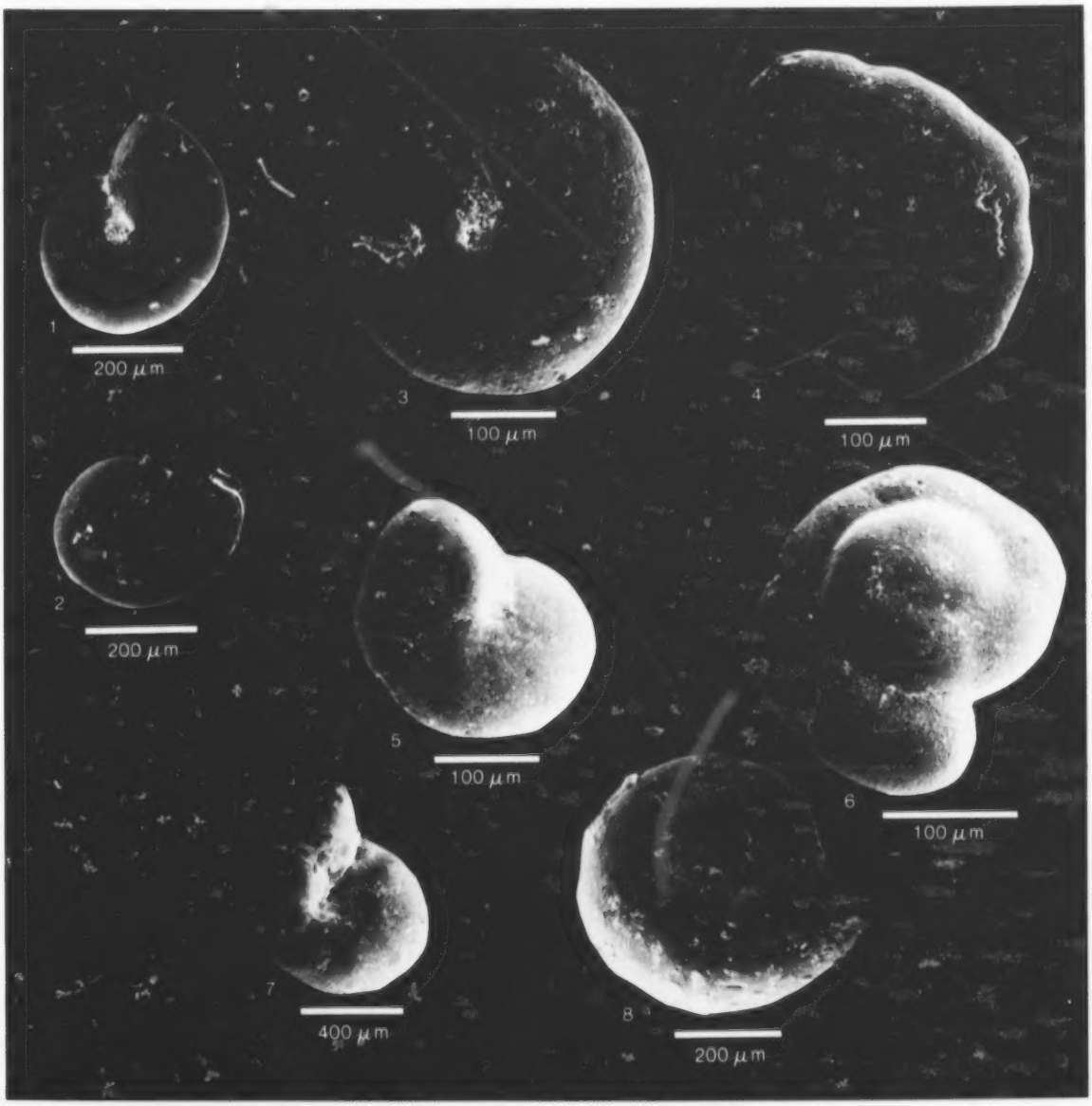

Plate 5. **1–2.** *Gyroidinoides lamarckianus*, Sample 573B-37,CC. **3–4.** *G. planulatus*, Sample 574C-34-1, 138–140 cm. **5–6.** *G. mediceus*, Sample 573B-9,CC. **7–8.** *G. globosus*, Sample 573B-40,CC.

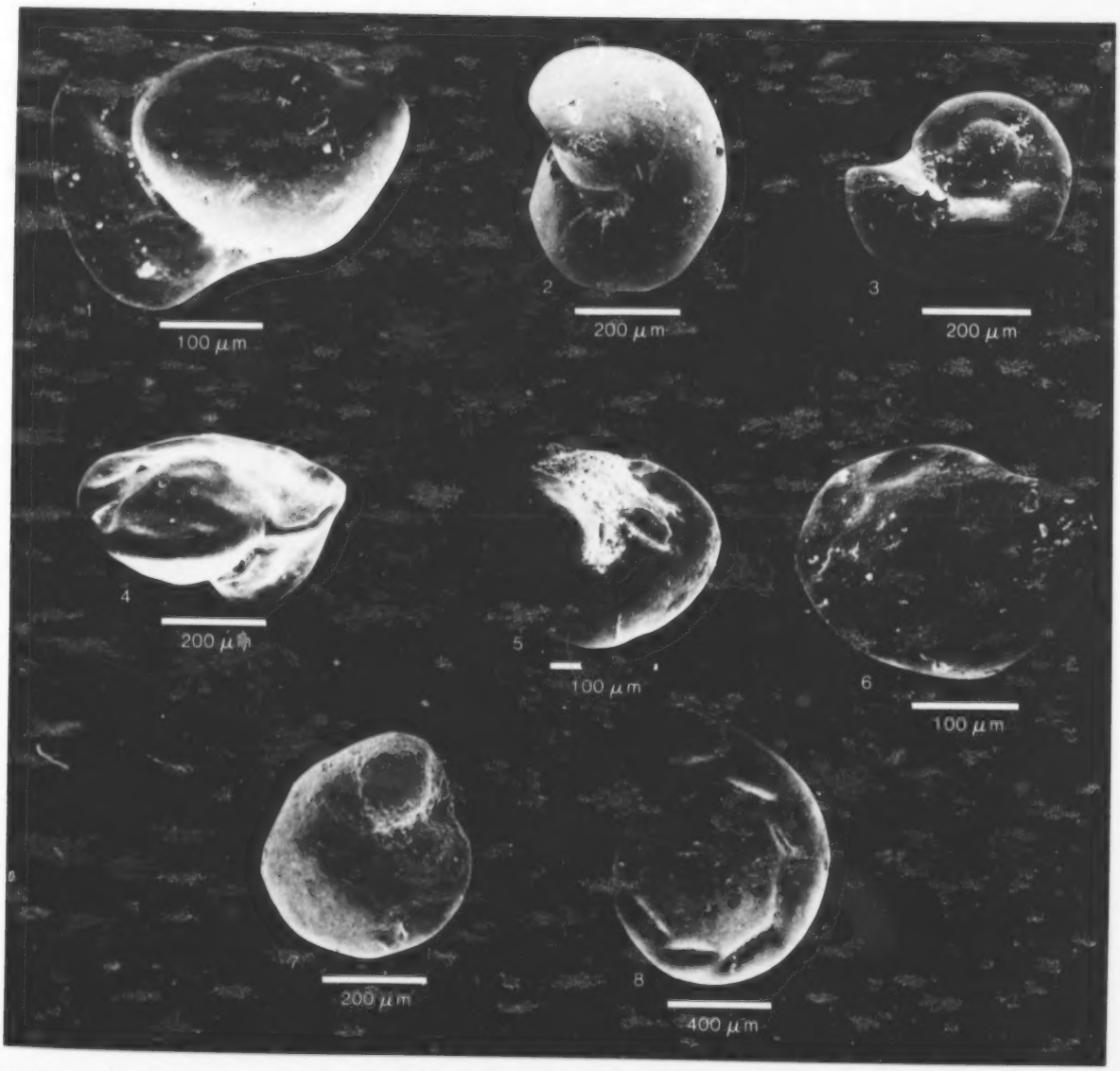

Plate 6. **1–3.** *Gyroidinoides girardanus*, Sample 574C-30-2, 110–112 cm. **4–6.** *G. acutus*, (4) Sample 573-2,CC, (5) Sample 573B-37,CC, (6) Sample 573B-37,CC. **7–8.** *G. soldanii*, Sample 573B-9,CC.

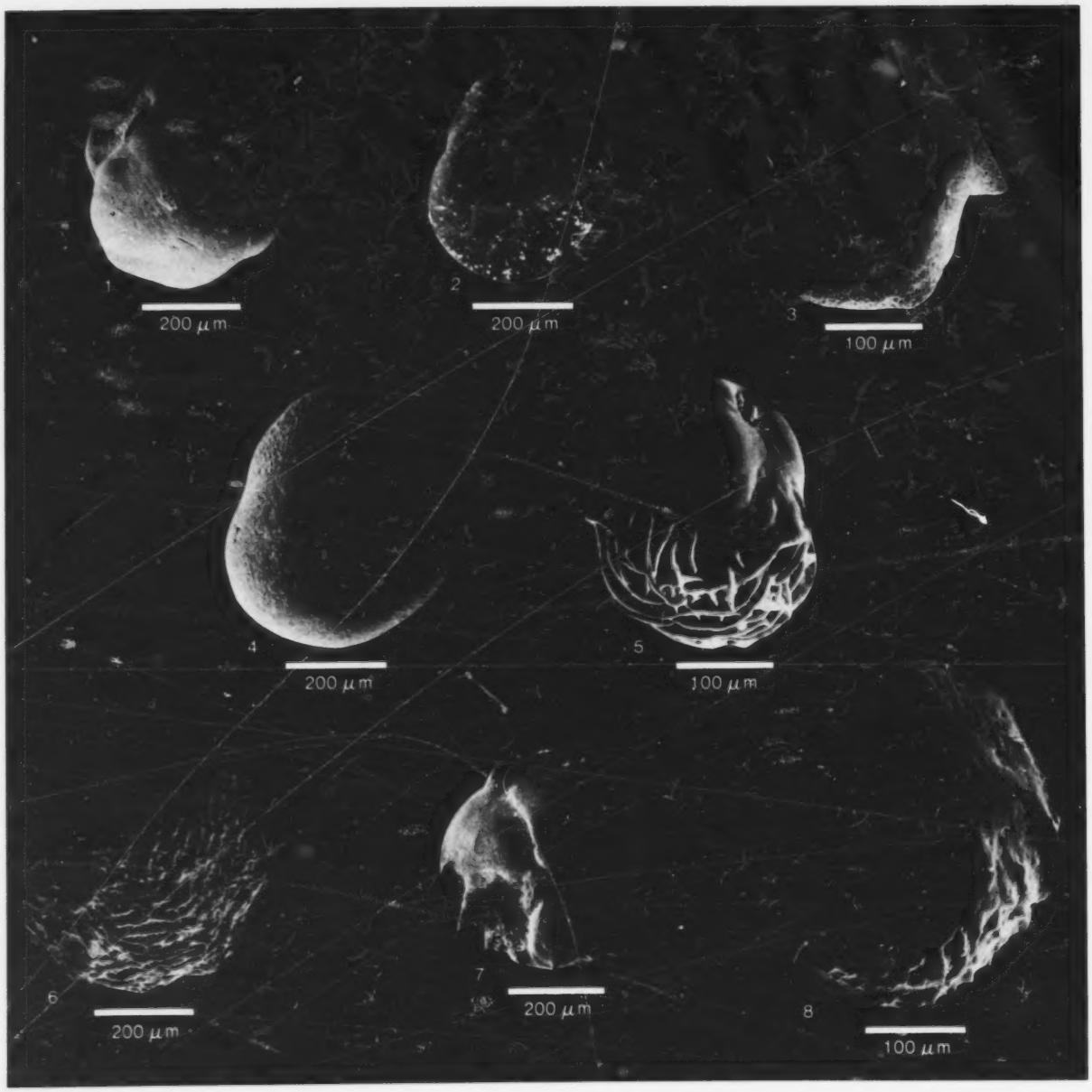

Plate 7. **1-2.** *Cassidulina havanensis*, Sample 573B-37,CC. **3.** *C. spinifera*, Sample 573B-16,CC. **4.** *Globocassidulina subglobosa*, Sample 573B-13,CC. **5.** *G. decorata*, Sample 573-4,CC. **6.** *Favocassidulina subfavus*, Sample 574-25,CC. **7.** *Ehrenbergina caribbea*, Sample 573-16,CC. **8.** *E. caribbea*, Sample 573B-13,CC.

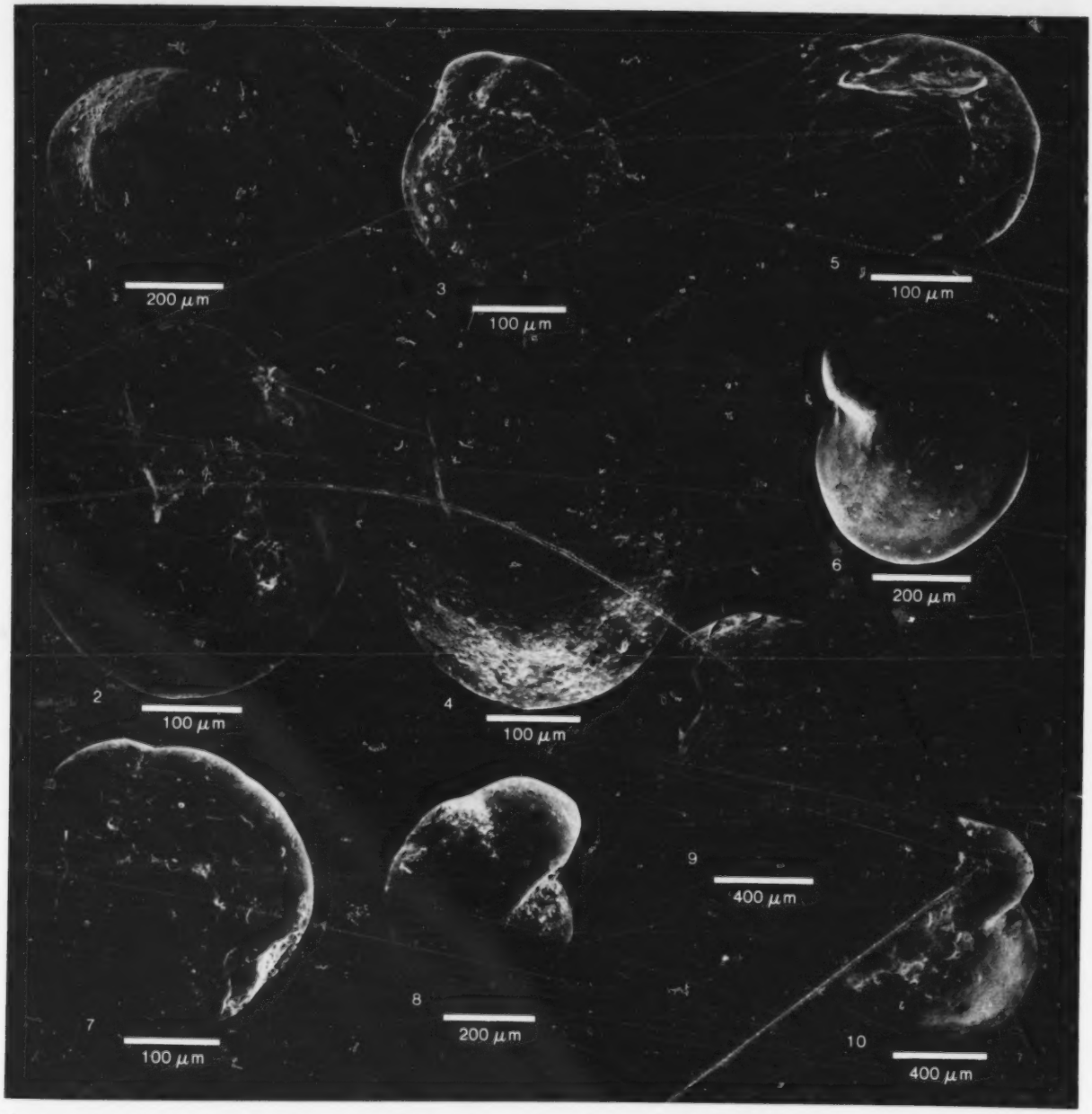

Plate 8. **1–2.** *Cibicidoides kullenbergi*, Sample 574C-30-1, 110–112 cm. **3–4.** *C. kullenbergi* var. *S.*, Sample 574-25,CC. **5–6.** *C. mundulus*, Sample 573-13,CC. **7–8.** *C. mollis*, Sample 574-23,CC. **9–10.** *Cibicidoides* aff. *mundulus*, Sample 574C-30-1, 110–112 cm.

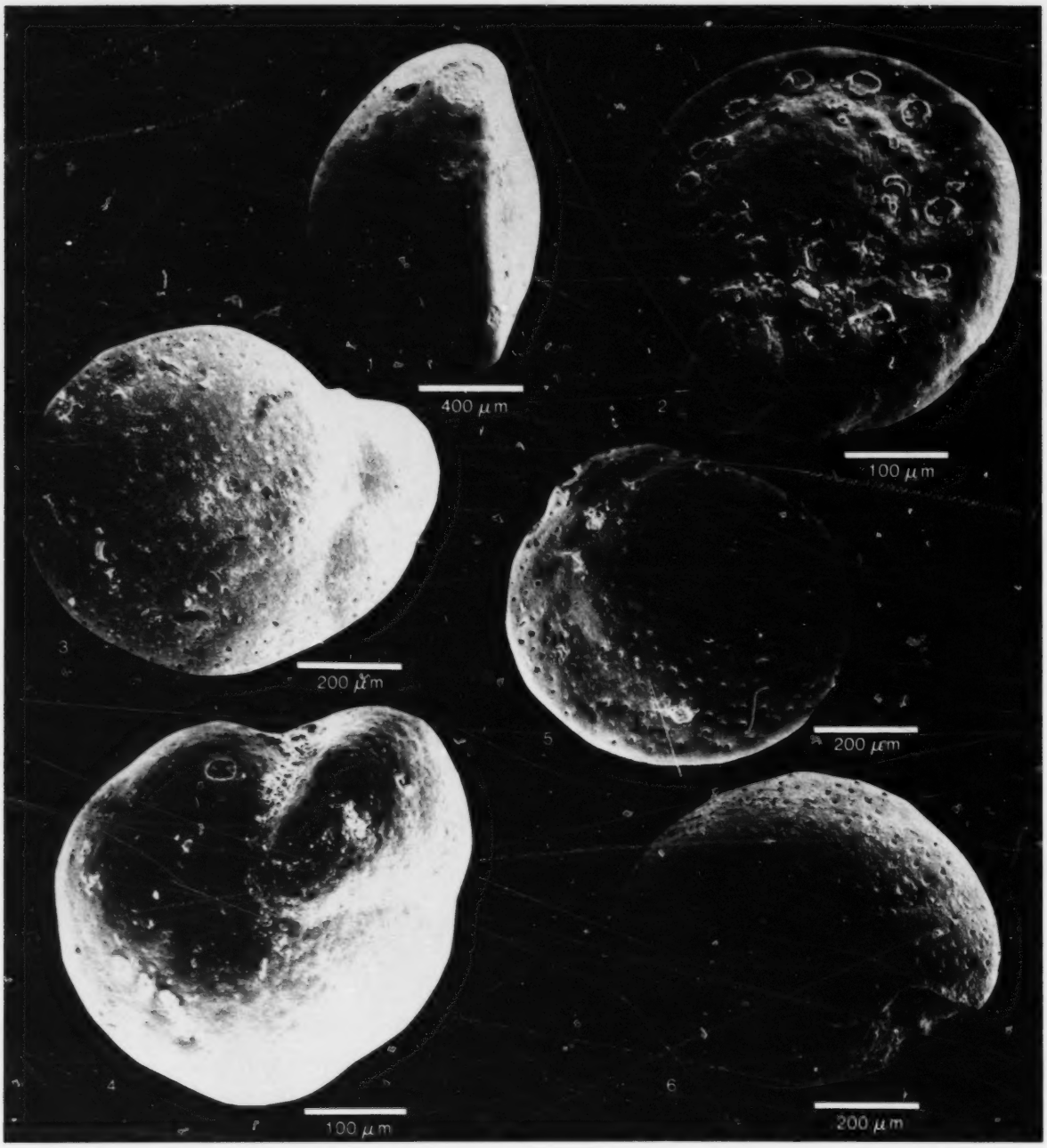

Plate 9. **1–2.** *Cibicidoides grimsdalei*, (1) side view, Sample 573-9,CC, (2) juvenile, Sample 574C-30-3, 110–112 cm. **3–4.** *C. mexicanus*, Sample 573B-37,CC. **5–6.** *C. perlucidus*, (5) Sample 574C-30-1, 110–112 cm, (6) Sample 574C-35-1, 109–111 cm.

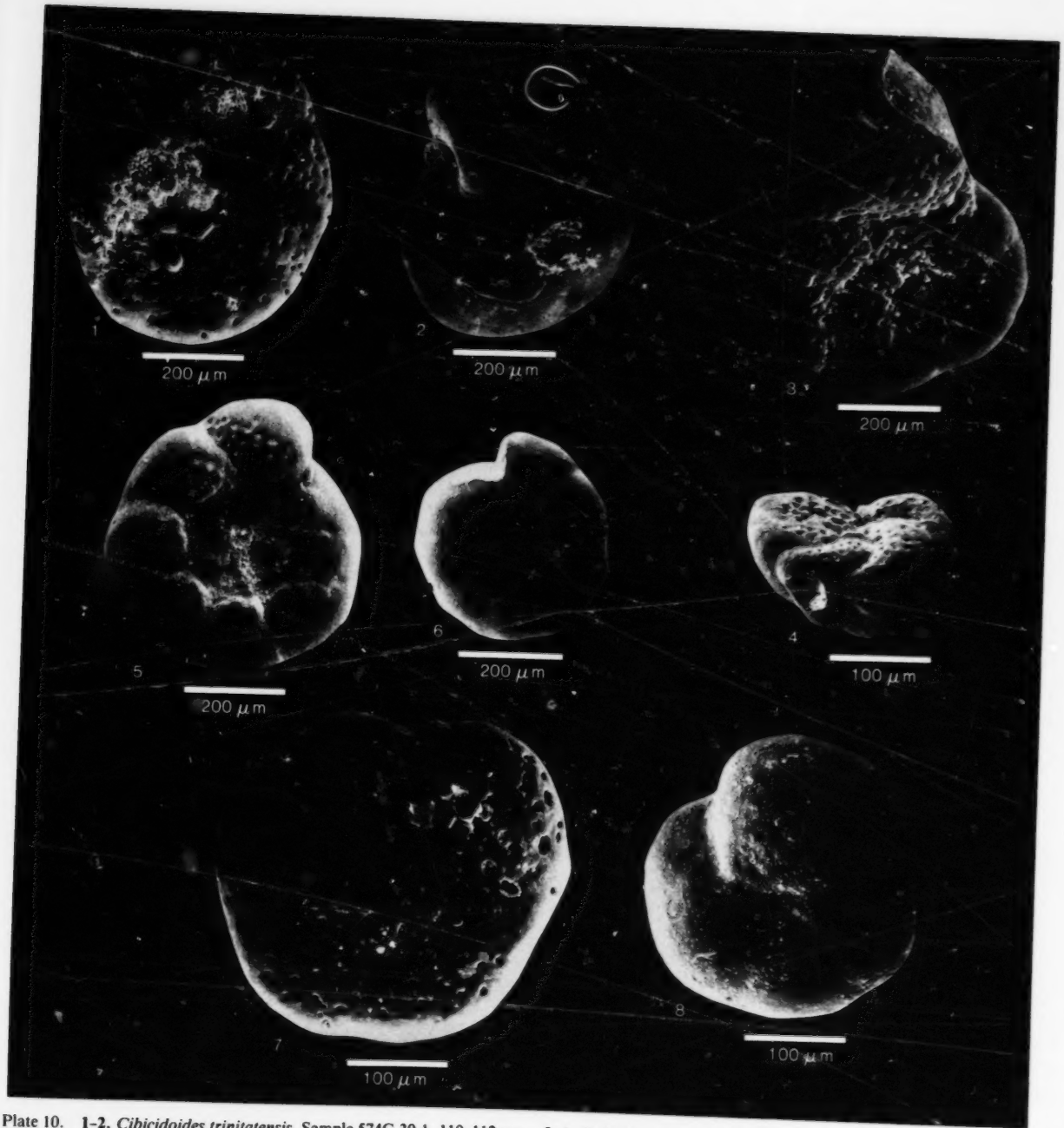

Plate 10. **1–2.** *Cibicidoides trinitatensis*, Sample 574C-30-1, 110–112 cm. **3–4.** *C. laurisae*, Sample 574C-30-2, 110–112 cm. **5–6.** *C. robertsonianus*, Sample 574C-30-2, 110–112 cm. **7–8.** *C. bradyi*, Sample 572-14,CC.

Plate 11. **1–2.** *Cibicidoides wuellerstorfi* (specimens from indurated sediments), Sample 574-25,CC. **3–4.** *C. wuellerstorfi* ("clean" specimen), Sample 573-3,CC. **5–6.** *C. pseudoungerianus*, Sample 573B-37,CC. **7–8.** *C. wuellerstorfi* var. *C.*, Sample 573-14,CC. **9.** *Planulina renzi*, Sample 575A-29-2, 128–130 cm (turbidite). **10.** *Laticarinina pauperata*, Sample 574-17,CC. **11–12.** *Gavelinella micra*, Sample 574C-35-1, 109–111 cm.

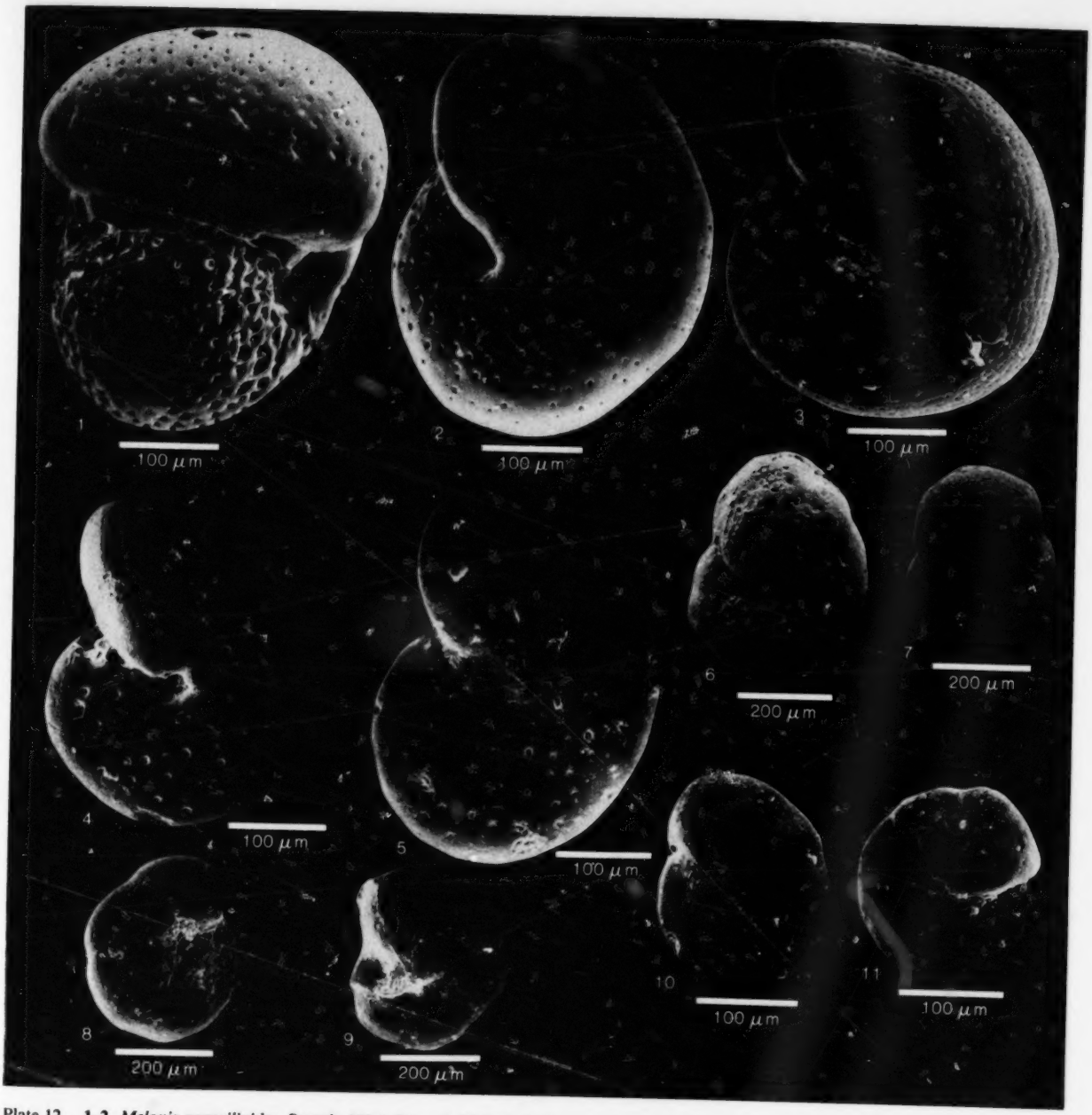

Plate 12. **1–2.** *Melonis pompilioides*, Sample 573-1,CC. **3.** *Melonis barleeanus*, Sample 572A-14,CC. **4–5.** *Anomalina alazanensis* var. *spissiformis*, Sample 574C-30-2, 110–112 cm. **6–7.** *Anomalinoides globulosus*, Sample 574C-34-1, 138–140 cm. **8–9.** *A. semicribratus*, Sample 573-9,CC. **10–11.** *A. acutus*, Sample 573B-28,CC.

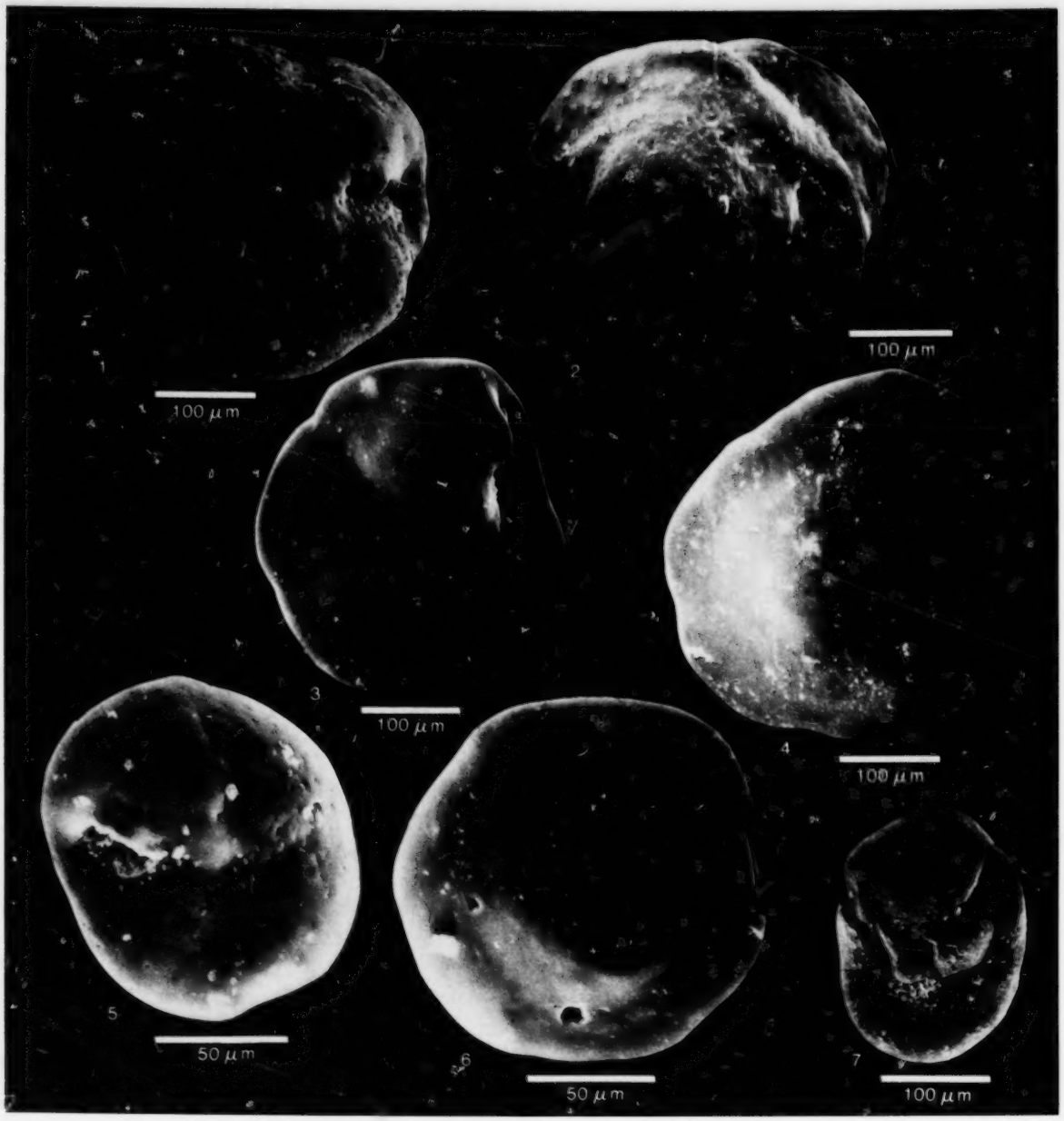

Plate 13. **1–2.** *Nuttallides umbonifera*, Sample 573-3,CC. **3–4.** *Epistominella exigua*, Sample 573-3,CC. **5–6.** *Eilohedra weddellensis*, Sample 573-3,CC. **7.** *Heronallenia lingulata*, Sample 573B-13,CC.

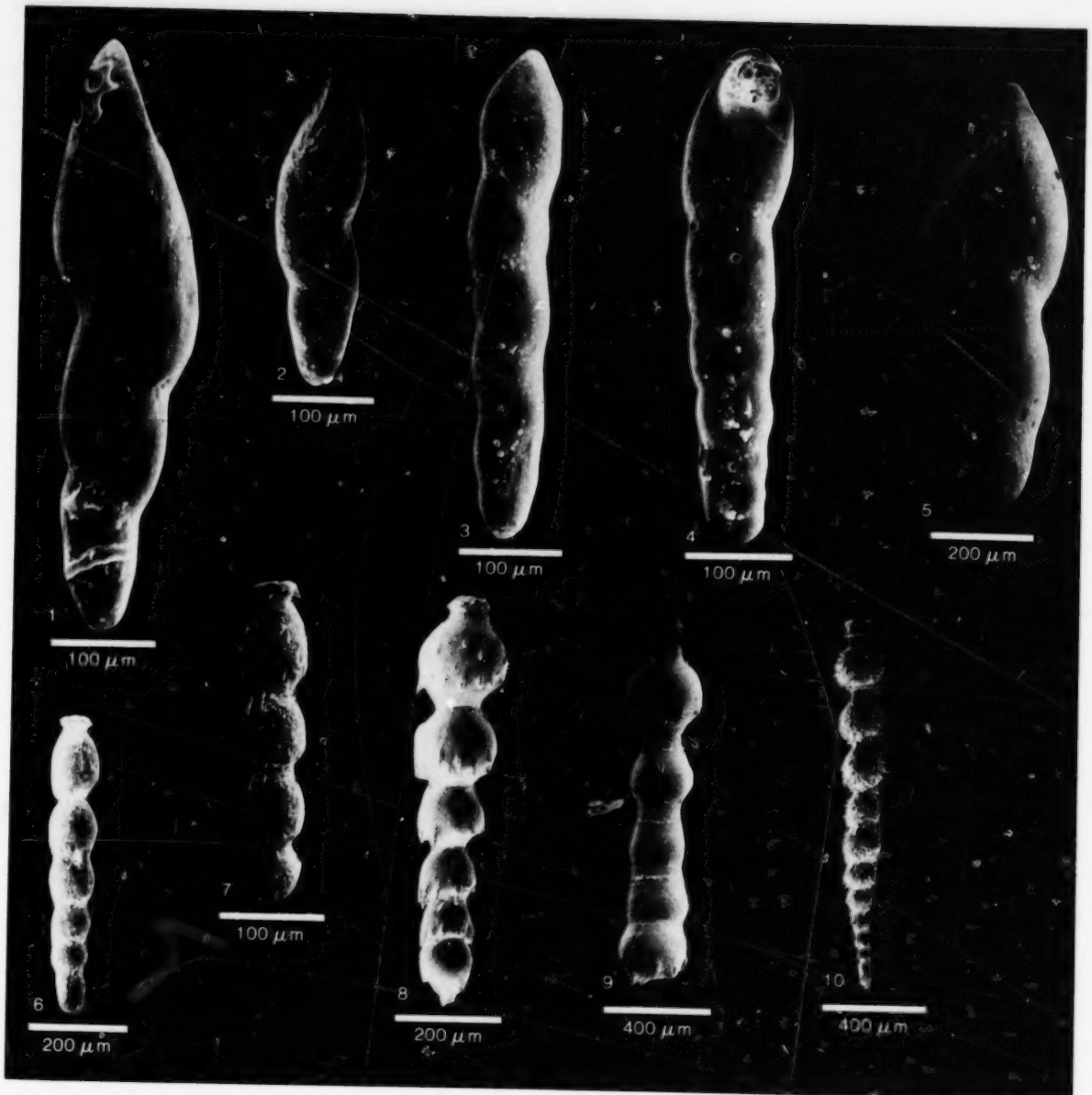

Plate 14. **1–2.** *Pleurostomella acuta*, Sample 573B-14,CC. **3–4.** *P. obtusa*, Sample 573B-37,CC. **5.** *P. alternans*, Sample 574-17,CC. **6–7.** *Stilostomella consobrina*, Sample 573-15,CC. **8.** *S. lepidula*, Sample 575A-19,CC. **9.** *S. abyssorum*, Sample 574C-35-1, 6–8 cm. **10.** *S. subspinosa*, Sample 574-11,CC.

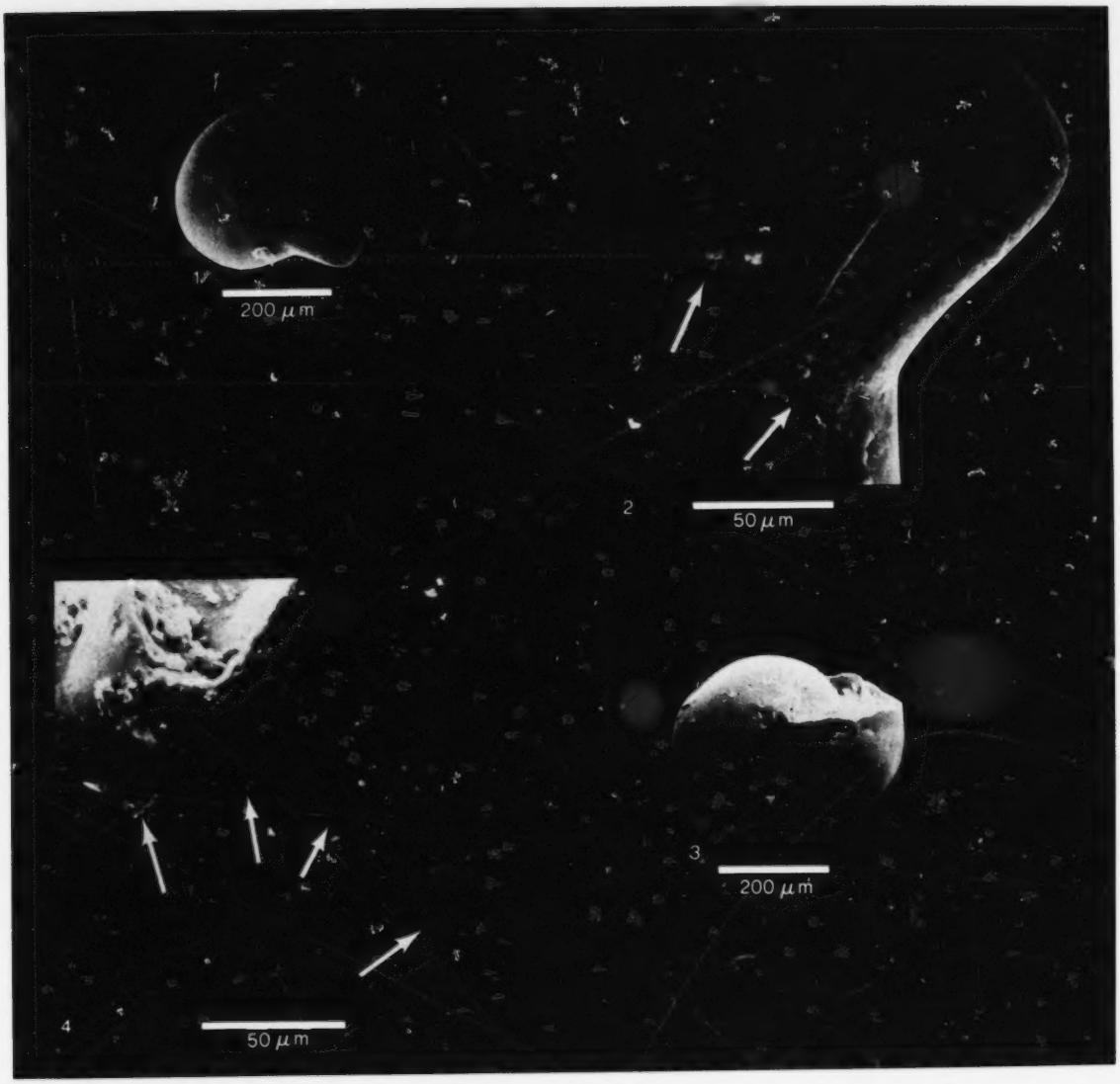

Plate 15. **1–2.** *Ammonia*(?) sp., Sample 574C-35-2, 51–53 cm, (1) dorsal side, (2) detail from (1). Arrows indicate secondary apertures. **3–4.** *Ammonia*(?) sp., Sample 574C-22,CC, (3) ventral side, (4) detail from (3). Arrows indicate secondary apertures.

Reprinted from Mayer, L., Theyer, F., et al., 1985
Initial Reports of the Deep Sea Drilling Project, Volume LXXXV, Washington (U. S. Government Printing Office)

18. STRATIGRAPHIC RESOLUTION OF LEG 85 DRILL SITES: AN INITIAL ANALYSIS[1]

Nicklas G. Pisias, Oregon State University
John A. Barron, U.S. Geological Survey, Menlo Park
Catherine A. Nigrini
and
Dean A. Dunn, University of Southern Mississippi[2]

ABSTRACT

Biostratigraphic datums determined from the study of radiolarian and diatom microfossils are combined with variations in calcium carbonate content to provide an estimate of stratigraphic resolution for the Leg 85 drill sites. These data sets are used to correlate sites, utilizing techniques which consider the sampling resolution of the primary data. The graphic correlation procedure of Shaw (1964) provides an objective means for estimating the line of correlation between sites. The two microfossil groups are used independently to define two lines of correlation. The inverse mapping technique of Martinson et al. (1982) is used to correlate sites from calcium carbonate data. Comparison of the lines of correlation determined from these three data sets suggests that stratigraphic resolution is on the order of 125,000 to 380,000 yrs. However, these limits of resolution are of the same order as the sampling density for the biostratigraphic and carbonate analyses. This suggests that a higher degree of stratigraphic resolution is possible at these important hydraulically piston-cored sites.

INTRODUCTION

One of the primary objectives of Leg 85 and other hydraulic-piston-coring (HPC) cruises aboard *Glomar Challenger* was to provide high-quality, continuous sediment sections for "high-resolution" stratigraphic and paleoceanographic studies. The ability to carry out such detailed studies depends in part on the quality of the stratigraphic framework into which sediment sections can be placed.

On Leg 85, five sites were drilled in the eastern and central equatorial Pacific. Coring at four sites, 572, 573, 574, and 575, recovered at least 150 m of sediment using the hydraulic piston corer. By double piston coring most of the upper portion of the sediment column, continuous high-quality sediment sections were recovered. Stratigraphic correlation of these sites is based primarily on biostratigraphic datums. Magnetic stratigraphy is available only in the intervals at Sites 573, 574, and 575 where sediment accumulation rate was lower; thus, it provides only limited stratigraphic resolution (Weinreich and Theyer, this volume). Barron et al. (this volume) have summarized the paleontological and magnetic stratigraphy available for sites drilled during Leg 85. In this chapter we use a different approach to address the question of stratigraphic resolution. We try to define the precision of correlation attainable for Leg 85 sites and present a strategy for defining high-resolution stratigraphies for marine sediment sections using biostratigraphic and carbonate stratigraphies.

METHODS

Our strategy is to correlate all sites in detail, using diatoms and radiolarians, and to correlate using the characteristics of the calcium carbonate records of these pelagic sediment sections. The radiolarian and diatom data are used independently to provide two estimates of the correlation between sites. Correlations based on variations in calcium carbonate content provide a third estimate of stratigraphic correlation between sites. These three stratigraphies enable us to estimate the precision with which sites can be correlated. In all cases, we try to account for the sampling resolution of the biostratigraphic and carbonate data.

BIOSTRATIGRAPHIC CORRELATIONS

The biostratigraphic data used for correlating sites are the first and last occurrences of numerous radiolarian and diatom species. In general, we have not used datums based on evolutionary transitions or changes in relative-abundance estimates. Such datums are more likely to be related to changes in local oceanographic conditions and may not represent synchronous events. Evolutionary transitions may also reflect differing taxonomic concepts of different investigators. The datums used in this summary, and the depth ranges in which they occur at each site, are listed in Tables 1 and 2. Each of the 91 datums was assigned a number, with the convention that a number with a zero to the right of the decimal place represents a last occurrence and a number with a 1 to the right of the decimal place represents a first occurrence. The depth ranges listed in Tables 1 and 2 were determined from the two samples used to define the event. For a last occurrence, the topmost sample in which the species was found defines the base of the depth range, and the next (overlying) sample (in which the species is absent) defines the top of the depth range.

Detailed stratigraphic correlations based on the biostratigraphic data were made by using the graphic correlation technique developed by Shaw (1964) and recently

[1] Mayer, L., Theyer, F., et al., *Init. Repts. DSDP*, 85: Washington (U.S. Govt. Printing Office).

[2] Addresses: (Pisias) College of Oceanography, Oregon State Univ., Corvallis, OR 97331; (Barron) U.S. Geological Survey, Menlo Park, CA 94205; (Nigrini) 510 Papyrus Drive, La Habra Heights, CA; (Dunn) Department of Geological Science, Univ. So. Miss., Hattiesburg, MS 39406.

Table 1. Radiolarian datums used in graphic-correlation analysis of Leg 85 sites.

Event code[a]	Species	Lower-limit depth (m)[b]	Upper-limit depth (m)[c]
	Site 572		
41.1	*Buccinosphaera invaginata*	9.5	0.0
42.0	*Stylatractus universus*	9.59	3.70
43.1	*Collosphaera tuberosa*	13.20	9.57
44.0	*Anthocyrtidium angulare*	18.59	13.20
45.0	*Lamprocyrtis neoheteroporus*	18.59	13.20
46.0	*Theocorythium vetulum*	18.59	13.20
47.0	*Didymocyrtis avita*	18.59	13.20
48.1[d]	*Lamprocyrtis nigriniae*	22.91	18.59
49.1	*Theocorythium trachelium*	22.91	18.59
50.0	*Pterocanium prismatium*	28.56	22.91
51.1	*Anthocyrtidium angulare*	28.56	19.70
52.1	*Pterocorys hertwigii*	40.01	36.20
53.1	*Pterocanium praetextum*	48.40	32.30
54.1	*Lamprocyrtis neoheteroporus*	40.01	36.20
55.0[d]	*Lamprocyrtis heteroporus*	45.84	40.01
56.0[e]	*Stichocorys peregrina*	45.84	40.01
57.0	*Phormostichoartus fistula*	49.61	45.84
58.0	*Spongaster pentas*	55.13	49.61
59.0	*Lychnodictyum audax*	55.13	49.61
60.0	*Phormostichoartus doliolum*	58.91	55.13
61.1	*Amphirhopalum ypsilon*	58.91	55.13
62.1	*Didymocyrtis tetrathalamus*	63.99	55.13
63.1	*Spongaster tetras*	63.99	58.91
64.0	*Didymocyrtis penultima*	63.99	58.91
65.1	*Lamprocyrtis heteroporus*	63.99	58.91
66.0	*Solenosphaera omnitubus*	63.99	58.91
67.1[d]	*Didymocyrtis avita*	67.81	63.99
69.0	*Spongaster berminghami*	81.71	76.01
70.1[d]	*Spongaster pentas*	81.71	76.01
71.0[d]	*Botryostrobus bramlettei*	95.19	91.38
72.1[d]	*Pterocanium prismatium*	104.39	100.63
73.1[d]	*Botryostrobus aquilonaris*	119.08	113.61
74.0	*Stichocorys delmontensis*	119.08	113.61
75.0[d]	*Didymocyrtis antepenultima*	119.08	113.61
76.0	*Siphostichartus corona*	119.08	113.61
77.0	*Acrobotrys tritubus*	132.01	128.23
78.0	*Calocycletta caepa*	145.20	140.82
80.1	*Stichocorys peregrina*	179.1	170.2
81.1	*Solenosphaera omnitubus*	194.2	189.0
82.1	*Didymocyrtis penultima*	246.1	240.1
83.0	*Diartus hughesi*	221.1	217.6
84.0	*Diartus petterssoni*	249.6	246.1
85.1	*Acrobotrys tritubus*	240.1	232.0
87.1	*Diartus hughesi*	272.5	268.6
88.0	*Stichocorys wolffii*	268.6	261.8
88.3	*Didymocyrtis antepenultima*	297.1	287.8
89.0	*Cyrtocapsella cornuta*	348.54	334.96
90.0	*Dorcadospyris alata*	458.6	444.68
91.1[d]	*Diartus petterssoni*	378.6	373.1
92.0[d]	*Cyrtocapsella tetrapera*	348.5	335.0
93.1[d]	*Didymocyrtis laticonus*	414.7	407.6
94.1[d]	*Lithopera neotera*	373.1	369.4
95.0	*Calocycletta virginis*	439.6	433.8
	Site 573		
41.1	*Buccinosphaera invaginata*	1.97	0.09
42.0	*Stylatractus universus*	6.31	1.97
43.1	*Collosphaera tuberosa*	11.46	6.31
44.0	*Anthocyrtidium angulare*	20.76	15.81
45.0	*Lamprocyrtis neoheteroporus*	20.76	15.81
46.0	*Theocorythium vetulum*	20.76	15.81
48.1	*Lamprocyrtis nigriniae*	20.76	15.81
49.1	*Theocorythium trachelium*	25.31	20.76
50.0	*Pterocanium prismatium*	25.31	20.76
51.1	*Anthocyrtidium angulare*	31.32	22.0
52.1	*Pterocorys hertwigii*	34.61	30.48
53.1	*Pterocanium praetextum*	43.41	39.25
54.1[e]	*Lamprocyrtis neoheteroporus*	48.01	43.41
55.0[d]	*Lamprocyrtis heteroporus*	57.09	52.10
56.0	*Stichocorys peregrina*	39.25	34.61
57.0	*Phormostichoartus fistula*	48.01	43.41

Table 1. (Continued).

Event code[a]	Species	Lower-limit depth (m)[b]	Upper-limit depth (m)[c]
	Site 573 (Cont.)		
58.0	*Spongaster pentas*	48.01	43.41
60.0	*Phormostichoartus doliolum*	52.10	48.01
61.1	*Amphirhopalum ypsilon*	57.09	52.10
62.1	*Didymocyrtis tetrathalamus*	57.09	52.10
63.1	*Spongaster tetras*	57.09	52.10
64.0	*Didymocyrtis penultima*	57.09	52.10
65.1	*Lamprocyrtis heteroporus*	60.70	57.09
66.0	*Solenosphaera omnitubus*	76.18	70.39
67.1[d]	*Didymocyrtis avita*	76.18	70.39
69.0	*Spongaster berminghami*	70.39	66.60
70.1[d]	*Spongaster pentas*	85.76	76.18
71.0[d]	*Botryostrobus bramlettei*	79.99	76.18
72.1[d]	*Pterocanium prismatium*	70.39	66.60
73.1[d]	*Botryostrobus aquilonaris*	85.76	79.88
74.0[e]	*Stichocorys delmontensis*	104.15	98.89
75.0[d]	*Didymocyrtis antepenultima*	94.98	89.34
76.0	*Siphostichartus corona*	85.76	79.88
77.0	*Acrobotrys tritubus*	94.98	89.34
78.0[e]	*Calocycletta caepa*	94.98	89.34
80.1	*Stichocorys peregrina*	122.1	122.6
81.1	*Solenosphaera omnitubus*	131.29	125.45
82.1	*Didymocyrtis penultima*	151.62	147.01
83.0	*Diartus hughesi*	140.07	134.91
84.0	*Diartus petterssoni*	151.62	147.01
85.1	*Acrobotrys tritubus*	151.62	147.01
87.1	*Diartus hughesi*	157.6	151.62
88.0	*Stichocorys wolffii*	167.2	157.6
88.3	*Didymocyrtis antepenultima*	185.9	176.6
89.0	*Cyrtocapsella cornuta*	195.7	189.6
90.0	*Dorcadospyris alata*	195.7	189.6
91.1[d]	*Diartus petterssoni*	214.7	208.6
92.0[d]	*Cyrtocapsella tetrapera*	195.6	189.6
93.1[d]	*Didymocyrtis laticonus*	224.1	218.1
94.1[d]	*Lithopera neotera*	208.6	204.3
95.0	*Calocycletta virginis*	232.8	227.6
96.0	*Calocycletta costata*	232.8	227.6
97.1	*Dorcadospyris alata*	246.6	242.8
	Site 574		
42.0	*Stylatractus universus*	4.48	2.41
43.1	*Collosphaera tuberosa*	4.48	2.41
44.0	*Anthocyrtidium angulare*	5.25	4.48
45.0	*Lamprocyrtis neoheteroporus*	5.25	4.48
46.0	*Theocorythium vetulum*	5.25	4.48
48.1[d]	*Lamprocyrtis nigriniae*	5.25	4.48
49.1	*Theocorythium trachelium*	9.75	6.75
50.0	*Pterocanium prismatium*	8.25	6.75
51.1	*Anthocyrtidium angulare*	12.75	11.25
52.1	*Pterocorys hertwigii*	12.75	11.25
53.1	*Pterocanium praetextum*	12.75	11.25
54.1	*Lamprocyrtis neoheteroporus*	14.07	12.75
55.0	*Lamprocyrtis heteroporus*	12.75	8.25
56.0	*Stichocorys peregrina*	12.75	11.25
57.0	*Phormostichoartus fistula*	19.20	14.07
58.0	*Spongaster pentas*	19.20	14.07
60.0	*Phormostichoartus doliolum*	19.20	14.07
61.1[e]	*Amphirhopalum ypsilon*	23.48	19.20
63.1	*Spongaster tetras*	23.48	19.20
64.0	*Didymocyrtis penultima*	23.48	19.20
65.1	*Lamprocyrtis heteroporus*	19.20	14.07
66.0[e]	*Solenosphaera omnitubus*	23.48	19.20
67.1[d]	*Didymocyrtis avita*	23.48	19.20
69.0	*Spongaster berminghami*	33.10	28.73
70.1[d]	*Spongaster pentas*	34.94	33.44
71.0[d]	*Botroystrobus bramlettei*	28.73	23.48
72.1[d]	*Pterocanium prismatium*	37.94	34.94
73.1[d]	*Botryostrobus aquilonaris*	34.94	33.44
74.0	*Stichocorys delmontensis*	37.94	33.10
75.0[d]	*Didymocyrtis antepenultima*	34.94	33.10
76.0	*Siphostichartus corona*	33.44	33.10
77.0	*Acrobotrys tritubus*	42.34	33.13

Table 1. (Continued).

Event code[a]	Species	Lower-limit depth (m)[b]	Upper-limit depth (m)[c]
	Site 574 (Cont.)		
78.0	*Calocycletta caepa*	51.92	42.34
79.1	*Spongodiscus ambus*	42.54	34.94
80.1	*Stichocorys peregrina*	52.0	42.5
81.1	*Solenosphaera omnitubus*	56.92	52.00
82.1	*Didymocyrtis penultima*	70.52	65.9
83.0	*Diartus hughesi*	60.93	56.92
84.0	*Diartus petterssoni*	70.52	65.92
85.1	*Acrobotrys tritubus*	65.92	60.93
87.1	*Diartus hughesi*	75.42	70.52
88.0	*Stichocorys wolffii*	75.42	70.52
88.3	*Didymocyrtis antepenultima*	84.92	79.87
89.0	*Cyrtocapsella cornuta*	108.14	103.52
90.0	*Dorcadospyris alata*	108.1	103.5
91.1[d]	*Diartus petterssoni*	127.1	122.7
92.0[d]	*Cyrtocapsella tetrapera*	108.14	103.52
93.1[d]	*Didymocyrtis laticonus*	150.9	142.2
94.1[d]	*Lithopera neotera*	137.6	132.6
95.0	*Calocycletta virginis*	157.5	152.5
96.0	*Calocycletta costata*	162.6	157.5
97.1	*Dorcadospyris alata*	192.3	187.1
	Site 575		
42.0	*Stylatractus universus*	3.42	1.92
43.1	*Collosphaera tuberosa*	1.92	0.42
46.0	*Theocorythium vetulum*	6.42	4.92
48.1[d]	*Lamprocyrtis nigriniae*	4.92	3.42
49.1	*Theocorythium trachelium*	4.92	3.42
50.0	*Pterocanium prismatium*	4.92	3.42
51.1	*Anthocyrtidium angulare*	6.42	4.92
52.1	*Pterocorys hertwigii*	6.42	4.92
53.1	*Pterocanium praetextum*	6.42	4.92
55.0[d]	*Lamprocyrtis heteroporus*	4.92	3.42
56.0	*Stichocorys peregrina*	6.42	4.92
57.0	*Phormostichoartus fistula*	7.27	6.42
58.0	*Spongaster pentas*	7.30	7.27
59.0	*Lychnodictyum audax*	7.27	6.42
60.0	*Phormostichoartus doliolum*	7.27	6.42
61.1	*Amphirhopalum ypsilon*	7.30	7.27
63.1	*Spongaster tetras*	7.30	7.27
64.0	*Didymocyrtis penultima*	12.9	7.3
66.0[e]	*Solenosphaera omnitubus*	7.27	6.42
69.0	*Spongaster berminghami*	12.23	9.23
70.1[d]	*Spongaster pentas*	9.23	7.73
71.0[d]	*Botryostrobus bramlettei*	7.73	4.92
72.1[d]	*Pterocanium prismatium*	9.23	7.73
73.1[d]	*Botryostrobus aquilonaris*	9.23	7.73
74.0	*Stichocorys delmontensis*	12.23	7.27
76.0	*Siphostichartus corona*	7.27	4.92
77.0	*Acrobotrys tritubus*	10.73	6.42
78.0	*Calocycletta caepa*	15.23	12.23
80.1	*Stichocorys peregrina*	26.3	16.8
81.1	*Solenosphaera omnitubus*	20.23	16.89
82.1	*Didymocyrtis penultima*	26.40	20.23
83.0	*Diartus hughesi*	20.23	16.89
84.0	*Diartus petterssoni*	26.40	20.23
85.1	*Acrobotrys tritubus*	26.40	20.23
87.1	*Diartus hughesi*	31.23	26.40
88.0	*Stichocorys wolffii*	31.23	26.40
88.3	*Didymocyrtis antepenultima*	31.23	26.40
89.0	*Cyrtocapsella cornuta*	44.55	38.43
90.0	*Dorcadospyris alata*	44.5	38.4
91.1[d]	*Diartus petterssoni*	44 55	38.43
92.0[d]	*Cyrtocapsella tetrapera*	44.55	38.43
93.1[d]	*Didymocyrtis laticonus*	57.4	54.0
94.1[d]	*Lithopera neotera*	66.9	63.5
95.0	*Calocycletta virginis*	73.0	66.9
96.0	*Calocycletta costata*	76.4	73.0
97.1	*Dorcadospyris alata*	85.1	80.2

[a] Event code: x.1 = FAD; x.0 = LAD.
[b] Depth of sample used to determine lowest limit of datum.
[c] Depth of sample used to determine highest limit of datum.
[d] Datums excluded from graphic correlation of all sites.
[e] Datums excluded only for individual sites.

Table 2. Diatom datums used in graphic-correlation analysis of Leg 85 sites.

Event code[a]	Species	Lower-limit depth (m)[b]	Upper-limit depth (m)[c]
	Site 572		
1.0	*Nitzschia reinholdii*	14.7	13.2
2.0	*Rhizosolenia matuyamaii*	17.7	16.2
3.1	*Rhizosolenia matuyamaii*	19.0	17.7
4.0	*Rhizosolenia praebergonii* v. *robusta*	27.2	25.7
5.1	*Pseudoeunotia doliolus*	33.8	32.3
6.0	*Thalassiosira convexa*	35.3	33.8
7.0	*Nitzschia jouseae*	41.5	40.0
8.1	*Rhizosolenia praebergonii*	49.6	48.1
9.1	*Thalassiosira convexa* v. *convexa*	58.9	57.4
10.1	*Asteromphalus elegans*	63.4	61.9
11.0	*Nitzschia cylindrica*	85.5	81.8
12.1	*Nitzschia jouseae*	100.7	95.1
13.0	*Thalassiothrix miocenica*	128.3	125.7
14.0	*Asterolampra acutiloba*	132.0	128.3
15.0	*Nitzschia miocenica*	140.8	136.7
16.0	*Thalassiosira praeconvexa*	154.1	145.3
17.1	*Thalassiosira convexa*	179.5	176.7
18.1	*Thalassiosira praeconvexa*	198.5	192.7
19.1	*Nitzschia miocenica*	208.7	208.0
20.0	*Rossiella paleacea*	208.7	208.0
21.0	*Thalassiosira burckliana*	219.7	217.5
22.0	*Coscinodiscus yabei*	227.7	227.0
23.1[d]	*Thalassiosira burckliana*	257.7	255.5
24.0	*Coscinodiscus vetustissimus* v. *javanica*	260.7	257.7
25.1	*Coscinodiscus vetustissimus* v. *javanica*	270.2	267.2
26.0	*Asteromphalus moronensis*	279.7	276.7
27.0	*Coscinodiscus tuberculatus*	313.2	312.5
28.0	*Denticula punctata* v. *hustedtii*	313.2	312.5
29.0	*Craspedodiscus coscinodiscus*	322.0	316.2
30.1	*Hemidiscus cuneiformis*	341.0	333.7
31.1	*Coscinodiscus temperei* v. *delicata*	351.2	350.5
32.0[d]	*Denticula nicobarica*	369.4	363.5
33.0	*Coscinodiscus lewisianus*	388.5	382.7
34.1	*Denticula hustedtii*	408.7	407.5
35.0	*Cestodiscus peplum*	426.5	419.2
	Site 573		
1.0	*Nitzschia reinholdii*	12.2	11.5
4.0	*Rhizosolenia praebergonii* v. *robusta*	24.7	21.0
5.1	*Pseudoeunotia doliolus*	30.5	24.7
6.0	*Thalassiosira convexa*	35.7	32.7
7.0	*Nitzschia jouseae*	39.3	35.7
8.1	*Rhizosolenia praebergonii*	46.0	43.0
9.1	*Thalassiosira convexa* v. *convexa*	51.7	48.7
10.1	*Asteromphalus elegans*	63.7	57.7
11.0	*Nitzschia cylindrica*	66.7	63.2
12.1	*Nitzschia jouseae*	76.2	73.4
13.0	*Thalassiothrix miocenica*	76.9	76.2
14.0	*Asterolampra acutiloba*	85.7	76.2
15.0	*Nitzschia miocenica*	95.2	92.4
16.0	*Thalassiosira praeconvexa*	98.9	95.9
17.1	*Thalassiosira convexa*	112.6	110.7
18.1	*Thalassiosira praeconvexa*	114.6	112.6
19.1	*Nitzschia miocenica*	131.3	128.8
20.0	*Rossiella paleacea*	131.3	128.8
21.0	*Thalassiosira burckliana*	138.0	133.5
22.0	*Coscinodiscus yabei*	140.1	142.2
23.1[d]	*Thalassiosira burckliana*	156.2	154.0
24.0	*Coscinodiscus vetustissimus* v. *javanica*	167.0	158.2
25.1	*Coscinodiscus vetustissimus* v. *javanica*	170.7	167.0
26.0	*Asteromphalus moronensis*	170.7	167.2
27.0	*Coscinodiscus tuberculatus*	177.2	176.5
28.0	*Denticula punctata* v. *hustedtii*	177.2	176.5
29.0	*Craspedodiscus coscinodiscus*	186.7	186.0
30.1	*Hemidiscus cuneiformis*	186.7	185.9
31.1	*Coscinodiscus temperei* v. *delicata*	199.2	195.5
32.0[d]	*Denticula nicobarica*	210.2	205.0
33.0	*Coscinodiscus lewisianus*	210.2	205.0
34.1	*Denticula hustedtii*	219.7	214.5
35.0	*Cestodisdcus peplum*	224.0	222.7
36.0	*Anaulus californicus*	243.0	233.5
37.1	*Cestodiscus peplum*	254.7	252.5

Table 2. (Continued).

Event code[a]	Species	Lower-limit depth (m)[b]	Upper-limit depth (m)[c]
	Site 573 (Cont.)		
38.0	*Thalassiosira fraga*	256.2	254.7
39.0	*Thalassiosira bukryi*	267.2	265.7
40.1	*Denticula nicobarica*	268.7	267.2
	Site 574		
1.0	*Nitzschia reinholdii*	6.7	4.5
4.0	*Rhizosolenia praebergonii* v. *robusta*	8.2	6.7
5.1	*Pseudoeunotia doliolus*	14.0	9.7
6.0	*Thalassiosira convexa*	14.0	9.7
7.0	*Nitzschia jouseae*	14.0	9.7
8.1	*Rhizosolenia praebergonii*	16.2	14.0
9.1	*Thalassiosira convexa* v. *convexa*	23.5	19.2
10.1[e]	*Asteromphalus elegans*	29.7	23.5
11.0	*Nitzschia cylindrica*	33.0	29.7
12.1	*Nitzschia jouseae*	33.0	29.7
13.0	*Thalassiothrix miocenica*	35.2	33.0
15.0	*Nitzschia miocenica*	42.5	39.7
16.0	*Thalassiosira praeconvexa*	44.7	42.5
17.1	*Thalassiosira convexa*	52.0	44.7
18.1	*Thalassiosira praeconvexa*	52.0	44.7
19.1	*Nitzschia miocenica*	57.2	54.2
20.0	*Rossiella paleacea*	57.2	54.2
21.0	*Thalassiosira burckliana*	61.4	60.9
22.0	*Coscinodiscus yabei*	64.7	61.7
23.1[d]	*Thalassiosira burckliana*	70.5	70.1
24.0	*Coscinodiscus vetustissimus* v. *javanica*	72.2	70.5
25.1	*Coscinodiscus vetustissimus* v. *javanica*	80.0	75.7
26.0	*Asteromphalus moronensis*	80.0	78.7
27.0	*Coscinodiscus tuberculatus*	90.2	89.0
28.0	*Denticula punctata* v. *hustedtii*	91.7	90.2
29.0	*Craspedodiscus coscinodiscus*	98.6	93.2
30.1	*Hemidiscus cuneiformis*	103.5	100.5
31.1	*Coscinodiscus temperei* v. *delicata*	113.0	110.3
32.0[d]	*Denticula nicobarica*	128.7	124.5
33.0	*Coscinodiscus lewisianus*	132.6	129.8
34.1	*Denticula hustedtii*	144.8	142.6
35.0	*Cestodiscus peplum*	154.7	152.5
36.0	*Anaulus californicus*	177.5	172.5
37.1	*Cestodiscus peplum*	197.2	194.4
38.0	*Thalassiosira fraga*	194.2	192.3
39.0	*Thalassiosira bukryi*	223.0	213.5
40.1	*Denticula nicobarica*	226.7	224.9
	Site 575		
1.0	*Nitzschia reinholdii*	3.7	0.7
4.0	*Rhizosolenia praebergonii* v. *robusta*	5.2	3.7
5.1	*Pseudoeunotia doliolus*	5.2	3.7
6.0	*Thalassiosira convexa*	5.2	3.7
7.0	*Nitzschia jouseae*	6.5	5.0
8.1	*Rhizosolenia praebergonii*	7.3	6.7
12.1	*Nitzschia jouseae*	7.8	7.3
13.0	*Thalassiothrix miocenica*	7.8	7.3
15.0	*Nitzschia miocenica*	12.5	11.0
16.0	*Thalassiosira praeconvexa*	12.5	11.0
17.1	*Thalassiosira convexa*	15.3	13.8
19.1	*Nitzschia miocenica*	20.5	19.0
20.0	*Rossiella paleacea*	20.5	19.0
21.0	*Thalassiosira burckliana*	25.0	23.5
22.0	*Coscinodiscus yabei*	25.0	23.5
23.1[d]	*Thalassiosira burckliana*	27.0	26.3
26.0	*Asteromphalus moronensis*	28.5	27.0
27.0	*Coscinodiscus tuberculatus*	31.5	28.5
28.0	*Denticula punctata*	35.0	34.5
29.0	*Craspedodiscus coscinodiscus*	34.3	32.8
30.1	*Hemidiscus cuneiformis*	39.9	36.9
31.1	*Coscinodiscus temperei* v. *delicata*	44.5	40.2
32.0[d]	*Denticula nicobarica*	49.7	46.7
33.0	*Coscinodiscus lewisianus*	54.0	49.7
34.1	*Denticula hustedtii*	63.5	56.2
35.0	*Cestodiscus peplum*	73.0	65.7
36.0	*Anaulus californicus*	80.2	75.2

Table 2. (Continued).

Event code[a]	Species	Lower-limit depth (m)[b]	Upper-limit depth (m)[c]
	Site 575 (Cont.)		
37.1	*Cestodiscus peplum*	98.6	91.3
38.0	*Thalassiosira fraga*	98.6	91.3
39.0[d]	*Thalassiosira bukryi*	107.4	105.9
40.1	*Denticula nicobarica*	123.8	123.3
44.0	*Coscinodiscus oligocenicus*	179.2	177.9
45.0	*Thalassiosira primalabiata*	197.9	197.3

[a] Event code: x.1 = FAD; x.0 = LAD.
[b] Depth of sample used to determine lowest limit of datum.
[c] Depth of sample used to determine highest limit of datum.
[d] Datums excluded from graphic correlation of all sites.
[e] Datums excluded for individual sites.

modified and applied to deep-sea sediments (Pisias et al., 1984). In this technique, all cores are compared to a "standard" section. We have used the section at Site 573 as the standard because of its length and relatively high sediment accumulation rates. A Miocene/Pliocene hiatus or interval of low accumulation rate at about 80 m sub-bottom, and the possible short hiatuses in the upper and middle Miocene (Barron et al., this volume) at this site, do, however, limit the usefulness of this site in parts of the Miocene.

We have assumed that the biostratigraphic events listed in Tables 1 and 2 represent synchronous events, so that the graphic correlation plots can be used to determine relative changes in sedimentation and the presence of sedimentation anomalies. In Figures 1 and 2, the depth ranges of the diatom and radiolarian datums are plotted for Sites 572, 574, and 575 versus the depth ranges at Site 573. Ideally, if all datums are synchronous and the first or last occurrence of a species in a sediment section represents its true evolutionary appearance or extinction, then the "line" of correlation between any site and the standard site would pass through all correlation boxes. As seen in Figures 1 and 2, the correlation "line" between any one site and Site 573 can be described by a few line segments. Line segments were drawn by hand so that as few segments as possible were used to connect the largest number of correlation boxes.

Several explanations are possible for an event that does not fall on a correlation "line." A last appearance of a species may occur too soon or a first appearance may be delayed because of local environmental conditions. The original graphic correlation method developed by Shaw (1964) assumes that any one site does not necessarily contain the true first or last occurrence, and that by correlating many sites into the standard section the "true" relative position of an event will be defined. In this analysis we deviate from Shaw's (1964) original approach by assuming that, for the most part, the biostratigraphic events represented in each core are the true first or last appearances of a given species. There are several events for which this cannot be so, and these are eliminated from the detailed correlation analysis.

As described by Shaw (1964), changes in the slopes of these line segments represent changes in relative sedi-

ment accumulation rates between sites, and any offsets in the lines reflect a hiatus in one section and/or expanded accumulation rates in the other. By comparing many sections to the standard, it is possible to determine which is the likely cause of any one observed offset.

In Figures 1 and 2, a number of offsets, some common to both microfossil groups, can be seen. The diatom graphic correlation plot for Site 572 (Fig. 2A) shows a marked offset at about 80 m sub-bottom at Site 573, suggesting a hiatus at Site 573, which is represented by at least 30 m of section at Site 572. The radiolarian datums do not clearly show this hiatus, although several datums in this depth interval apparently represent nonsynchronous behavior in the datums. An offset at about 60 m sub-bottom at Site 572 is seen in both the radiolarian and diatom plots (Figs. 1A and 2A). This offset suggests a short hiatus at Site 572, or a slightly expanded section at Site 573 at about 70 m sub-bottom. An expanded section at Site 573 is not inconsistent with the Site 574 correlation plots (Figs. 1B and 2B). Thus, it is possible that a hiatus is present at both Site 574 and Site 572 in this interval or that Site 573 has a slightly expanded section at about 70 m sub-bottom. Unfortunately, the very low sediment accumulation rates or hiatuses at Site 575 in this interval do not allow the use of this site to clarify the cause of the offset in Figures 1A and 2A.

A similar situation is observed for the offset in the graphic correlation plot for Site 572 at about 35 m sub-bottom at that site. The diatom correlation shows a possible hiatus at Site 572 or an expanded section at Site 573 (Fig. 2A). Inspection of the Site 574 plot (Fig. 2B) shows a similar compression at Site 574 as compared with Site 573. The radiolarian data do not indicate an offset at 35 m sub-bottom at Site 572 (Fig. 1A), but do show either a compressed section at Site 574 or an expansion at Site 573 in this same interval (Figs. 1B and 2B; 35 to 40 m sub-bottom at Site 573). Without other sites for comparison, the simplest assumption is that Site 573 has a slightly higher sediment accumulation rate and expanded section in this interval, and that Sites 572 and 574 have complete sections. It is possible that the diatom datum, the first appearance of *Pseudoeunotia doliolus* at Site 572, is diachronous (Barron et al., this volume).

The correlation plots for Site 575 suggest that the interval of low accumulation rate noted in the upper section at this site (site chapter, this volume), is made up of several short hiatuses separated by intervals of low sediment accumulation rates.

Finally, it is important to note that the major offset and apparent hiatus at Site 573 at 80 m sub-bottom is not evident in the Site 574 plots (Figs. 1B and 2B). Thus, if this is a hiatus at Site 573, then it must be present at Site 574 as either a hiatus or a period of greatly reduced accumulation rate. For further discussion of possible hiatuses at Leg 85 sites, see Barron et al. (this volume).

To refine the correlation between all sites and the standard section (Site 573), we utilized Prell's (pers. comm.) modification of the graphic correlation technique, as applied to late Pleistocene isotopic records by Pisias et al. (1984). From each correlation plot and set of correlation lines, the depth ranges of all datum levels defined at Sites 572, 574, and 575 can be expressed in terms of depth at Site 573. These depth ranges were determined from least-squares regression lines calculated from the event "boxes" contained within the interval spanned by the line segments drawn in the graphic correlation plots (Figs. 1 and 2).

The depth intervals calculated for the biostratigraphic events were then plotted as in Figure 3 to determine the interval common to all the sites. The common depth interval is considered to be the "best" estimate of where the biodatum should occur within the standard section. Not all events have overlapping depth intervals when projected onto the standard section. This may reflect nonsynchronous behavior of a stratigraphic datum, or the inadequacy of the correlation "line" for an individual site. Datums that clearly cannot represent synchronous events at any one site (datums that predict unrealistic relative accumulation-rate patterns, such as negative slopes in the line of correlation) were removed from further calculations. In some cases, new line segments were drawn and the projected depth intervals of all events were recalculated. The events that had overlapping intervals are indicated in Tables 1 and 2.

Given the depth interval common to all sites, the midpoint is used as the estimate of the true position of the biostratigraphic event in the standard section. The least-squares regression lines used to define each line of correlation between Site 573 and all other sites allow this depth estimate to be expressed in terms of the sub-bottom depth at Sites 572, 573, and 575. Thus, the diatom and radiolarian datums produce independent correlation lines for all sites with Site 573 (Fig. 4). Note that by using graphic correlation, we have incorporated the resolution with which datums were determined in the correlation estimates.

CARBONATE CORRELATIONS

The carbonate data used in this summary are from the carbonate-bomb analyses done on board ship for percent $CaCO_3$. The results of the high-resolution studies of Sites 572 and 574 (Pisias and Shackleton, this volume; Pisias and Prell, this volume) suggest that the shipboard data have some limitations in resolving part of the true variability in calcium carbonate deposition at the equatorial Pacific sites, but many similar features in the carbonate signatures of these sites can be resolved by the low-resolution shipboard data and used for stratigraphic purposes.

To provide an objective means of correlation, the inverse mapping technique described by Martinson et al. (1982) was used to correlate Sites 572, 574, and 575 with the standard section at Site 573. This technique utilizes an inverse procedure to find a line of correlation (referred to as a mapping function) which maximizes the correlation coefficient between the two records being correlated. The mapping function is parameterized by a series of weighted sine functions, and the weights are calculated to maximize the linear correlation coefficient between the carbonate records being compared. Thus, the

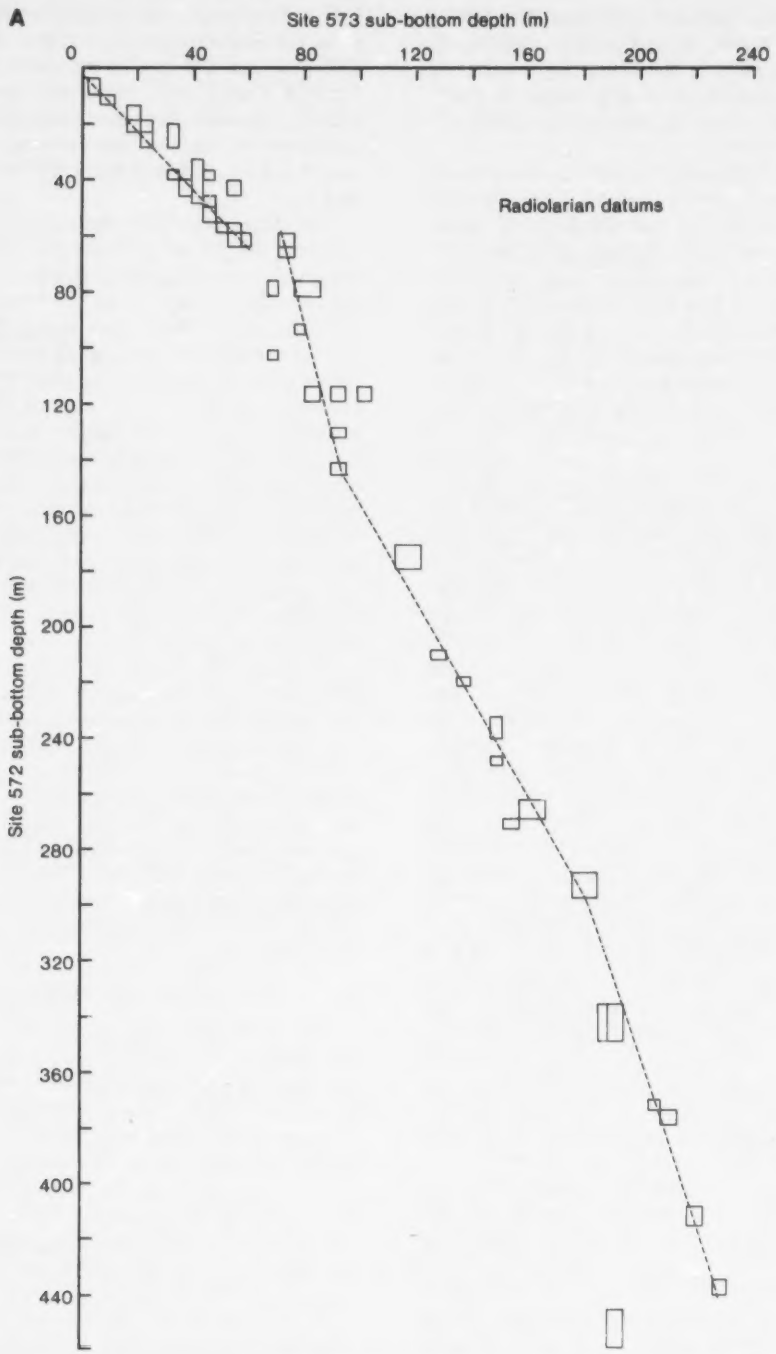

Figure 1. Shaw plots showing correlation of Leg 85 sites based on radiolarian datums given in Table 1. A. Site 572 versus Site 573. B. Site 574 versus Site 573. C. Site 575 versus Site 573.

carbonate records are aligned on the basis of their common characteristics, with regard to both the number of events in an interval and the relative amplitudes of these events. Because the technique has the potential of converging to "local" maxima in the correlation coefficient (Martinson et al., 1982), and because of the large differences in sediment accumulation rates observed for the Leg 85 sites, the inverse-mapping calculations were made using the biostratigraphic data as initial guesses for the true mapping function. Thus, the estimated line of cor-

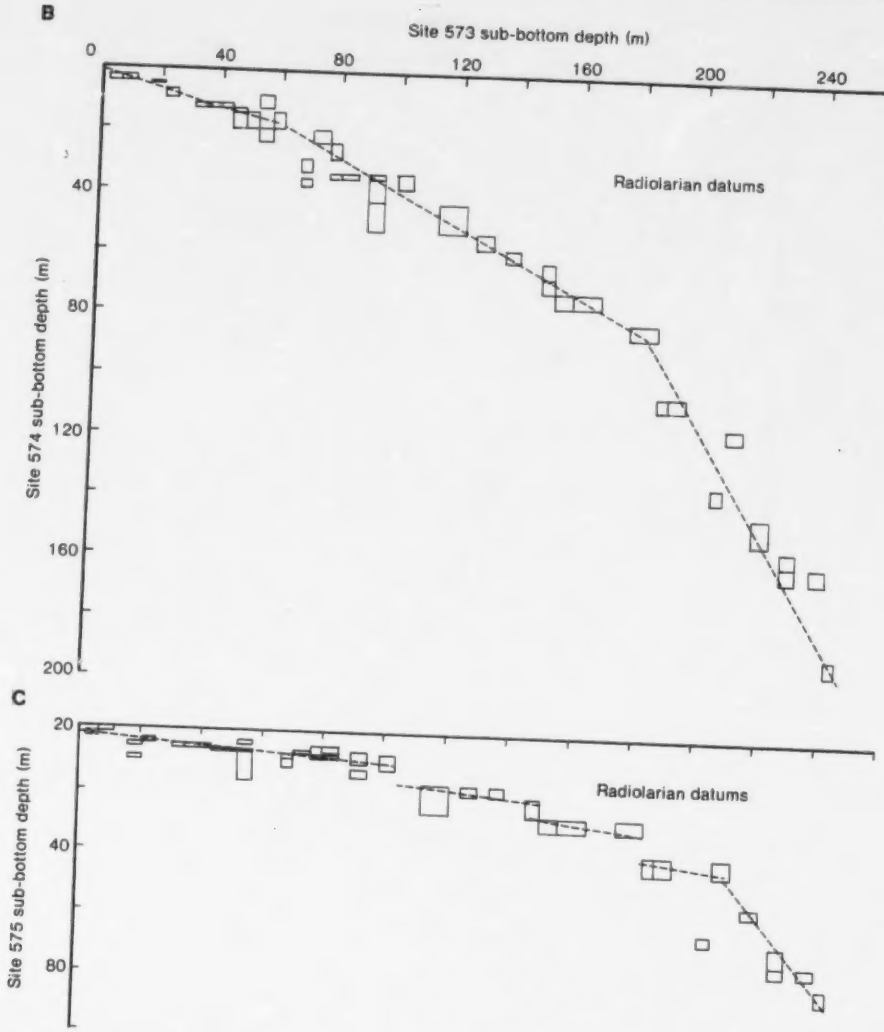

Figure 1. (Continued).

relation from the carbonate data is not independent of the biostratigraphic data.

The inverse-mapping calculations were made twice, each time a different fossil group provided the initial correlation. The results of correlating Sites 574 and 573, using the radiolarian data as an initial guess, are shown in Figure 5. The final correlation coefficients obtained between the Site 573 carbonate record and Sites 572, 574, and 575 were 0.21, 0.75, and 0.65, respectively. Except for Site 572, the correlation maps calculated from the two different starting guesses were essentially identical. Because of this convergence in the inverse calculations, we assume that the carbonate correlation provides a third estimate for the true lines of correlation between Sites 573, 574, and 575. Because of the low total correlation and the lack of convergence for the Site 572 data, we do not use the carbonate correlation for this site to estimate the precision of correlation for Site 572.

RESULTS AND DISCUSSION

The results of both the biostratigraphic and carbonate correlations for Sites 572, 574, and 575 are shown in Figure 4. We have used these plots to estimate the precision of correlation at each site. These estimates were made by tabulating the ranges (in meters at Site 573) defined by the diatom, radiolarian, and carbonate lines of correlation. Estimates were made at each level where a diatom or radiolarian event occurred at both sites. For Site 572 these ranges are defined from the biostratigraphic data only. These intervals are represented as horizontal lines in Figure 3. The general statistics of these intervals of resolution are given in Table 3. The data presented in Table 3 suggest that the resolution of correlation for these sites is on the order of 4 m depth at Site 573. For example, a given depth at Site 574 can be correlated with a depth interval at Site 573 within a mean error of

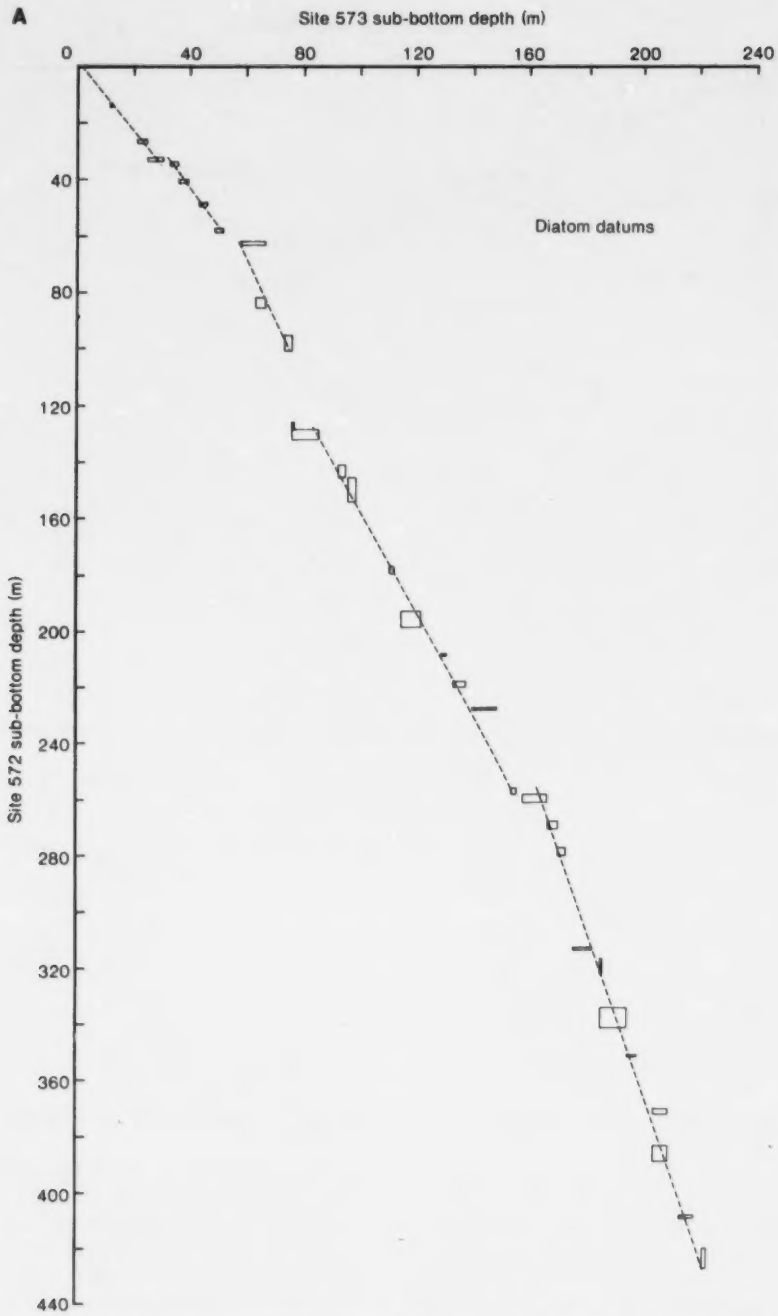

Figure 2. Shaw plots showing correlation of Leg 85 sites based on diatom datums given in Table 2. A. Site 572 versus Site 573. B. Site 574 versus Site 573. C. Site 575 versus Site 573.

±3.8 m (Table 3). Given the mean sediment accumulation rates at these sites, this indicates that a stratigraphic resolution on the order of 125,000 to 380,000 yrs. is possible. The error of correlation for Site 575 is larger than for the other sites. If, however, we exclude the interval of lowered accumulation rates or possible hiatuses, the mean stratigraphic error is also close to 4 m.

There are two primary limiting factors to the stratigraphic resolution based on biostratigraphic datums: (1) the number of datums within the interval being correlated and (2) the precision with which the stratigraphic datums are defined.

The estimated resolution of 125,000 to 380,000 yrs. (based on the datums considered in this study and the

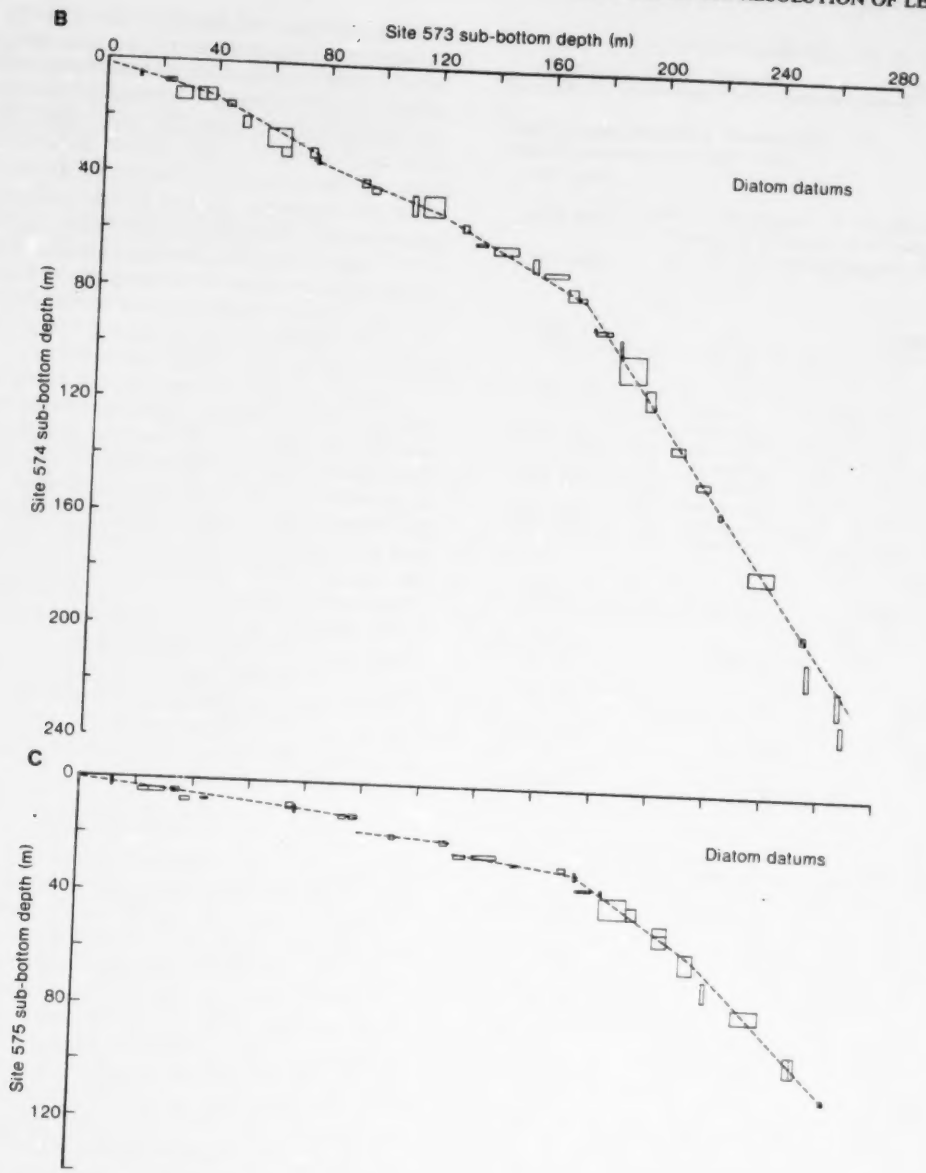

Figure 2. (Continued).

sampling intervals) is not unlike estimated stratigraphic resolution based on studies of isotopic records (Loutit et al., 1983) and that based on analysis of the distribution and number of biodatums in the Neogene (Moore and Romine, 1981). This range of correlation is not satisfactory, however, for the type of high-resolution studies that can be completed on HPC material. It is important, though, to consider the resolution of the data used for stratigraphy. Table 4 summarizes the resolution of the biodatums for each site. Note that the range to which datums are determined is very similar to the estimated stratigraphic resolution. Also, the mean sample interval of the carbonate data from Site 573 limits the resolution of correlation based on carbonate records to about 3.8 m (twice the mean sampling interval).

Thus, the precision to which the biodatums are determined appears to be an important factor limiting the precision of correlation, as might be expected. This is encouraging, given the lack of detailed magnetic stratigraphy for the Leg 85 drill sites. The results suggest that problems associated with biostratigraphic markers may not severely limit our ability to correlate these equatorial Pacific sites in detail and that it may be possible, with more precise biostratigraphic studies, to determine a high-resolution stratigraphic framework for Leg 85 sites.

To provide an estimate of stratigraphic resolution, we have used the biostratigraphic and carbonate data independently. Theoretically, combining the data should increase the possible stratigraphic resolution (assuming that all datums are reliable and that unique features of the

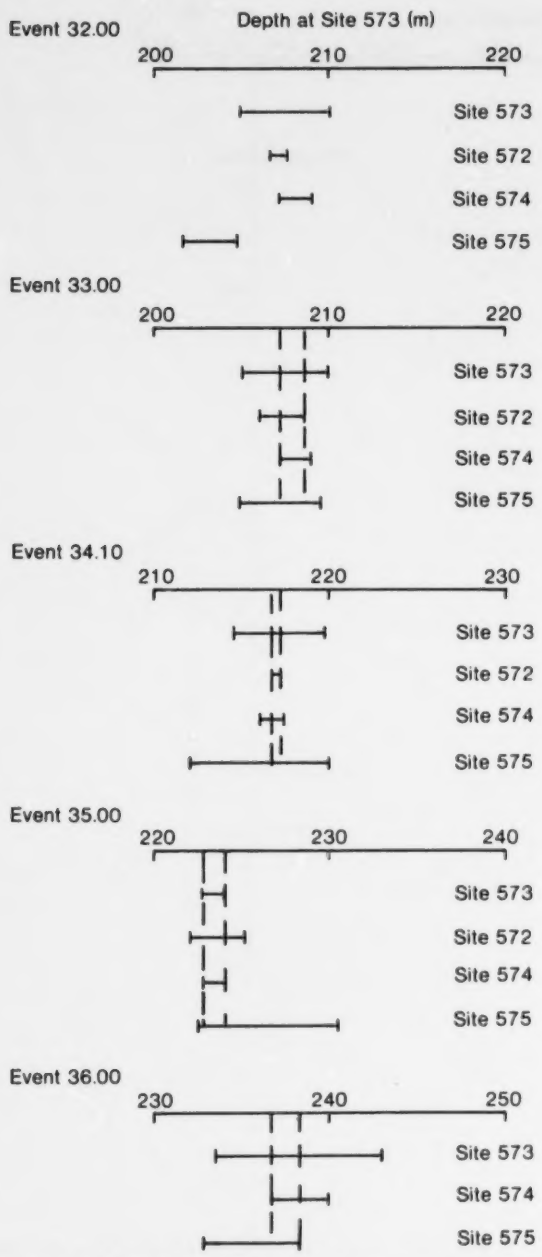

Figure 3. Example of overlapping ranges of datums projected into Site 573.

carbonate variations can be identified). For example, radiolarian and diatom biostratigraphies provide over 91 datums in the 250 m from Site 573 examined in this analysis. If these datums were uniformly distributed, then correlation to within 2.5 m depth at Site 573 should be possible. As already noted above, however, this is a finer scale than the sampling resolution for this site.

One of the initial assumptions of the study was that the biostratigraphic datums determined for the Leg 85 sites represented time-correlative events. The graphic correlation analysis used here provides a means to evaluate datums that may not satisfy this assumption. Tables 1 and 2 indicate species that did not form overlapping intervals within the graphic correlation analysis. Inconsistent stratigraphic occurrences were noted for several of these species (Nigrini, this volume; Barron, this volume). Some of these datums are based on species that proved to be rare at some of the Leg 85 sites (radiolarians: *Spongaster pentas*, *Pterocanium prismatium* [at the lower end of its range]; diatoms: *Thalassiosira burckliana*), which makes determination of their first or last occurrences difficult. Diatom species *Asteromphalus elegans* and *Denticulopsis nicobarica* are relatively fragile, so the dissolution of silica may affect their datums.

Though we have not used datums based on evolutionary transitions, several radiolarian events are based on species that make up well-known lineages. A number of these datum levels proved to be inconsistent. *Didymocyrtis penultima*, *D. avita*, and the lineage *Lamprocyrtis heteroporus* and *L. neoheteroporus* all showed inconsistent behavior (note that Nigrini, this volume, excluded the ancestors of *L. nigriniae* from her analysis because these species were very rare in tropical sediments). Detailed analysis of the *Lamprocyrtis* group at Site 573 shows that the occurrence of some of these species is sporadic, and there seem to be some inconsistencies in defining the distinguishing characteristics of *L. heteroporus* and *L. neoheteroporus*. It is possible that some of the inconsistencies in datums result from hiatuses at some of the Leg 85 sites.

CONCLUSION

Because of time limitations and the amount of new biostratigraphic data being generated from material collected during Leg 85, this summary does not contain all datums determined from the study of radiolarians (Nigrini, this volume) and diatoms (Barron, this volume) or all datums based on calcareous microfossils. Also, we have not fully used the graphic stratigraphy of Shaw (1964) to develop a standard section for the equatorial Pacific. To develop an estimate of stratigraphic resolution, this step was not necessary. Before developing a standard, it would be important to include data from the many other equatorial sites. Finally, it it likely that Site 573 is not the "best" site to use as a standard for Leg 85; but to make as objective an estimate of resolution as possible, we chose to use a single site rather than a composite section from a number of sites. This initial analysis of stratigraphic resolution does strongly suggest, however, that sampling resolution is the primary limiting factor in controlling the degree to which the HPC sites in the equatorial Pacific can be correlated.

ACKNOWLEDGMENTS

This research was supported in part by National Science Foundation Grant OCE83-15471, through the Submarine Geology and Geophysics Section of Ocean Sciences.

REFERENCES

Loutit, T. S., Pisias, N. G., and Kennett, J. P., 1983. Pacific Miocene carbon isotope stratigraphy using benthic foraminifera. *Earth Planet. Sci. Lett.*, 66:48–62.

Martinson, D. G., Menke, W., and Stoffa, P., 1982. An inverse approach to signal correlation. *J. Geophys. Res.*, 87:4807–4818.
Moore, T. C., Jr., and Romine, K., 1981. In search of biostratigraphic resolution. *Soc. Econ. Paleontol. Mineral. Spec. Publ.*, 32:317–334.
Pisias, N. G., Martinson, D. G., Moore, T. C., Jr., Shackleton, N. J., Prell, W., et al., 1984. High resolution stratigraphic correlation of benthic oxygen isotope records spanning the last 300,000 years. *Mar. Geol.*, 56:119–136.
Shaw, A. B., 1964. *Time in Stratigraphy:* New York (McGraw-Hill).

Date of Initial Receipt: 6 March 1984
Date of Acceptance: 19 June 1984

Table 3. Stratigraphic resolution for Leg 85 drill sites (ranges of correlation based on radiolarian, diatom, and carbonate stratigraphies).

Site		Mean (m at Site 573)	Standard deviation (m at Site 573)
572	(all)	3.4	2.9
572	(Pliocene only)	3.3	1.0
574	(all)	3.8	2.5
575	(all)	9.8	7.1
575	(below 160 m)	3.6	1.2

Table 4. Resolution of biodatums (general statistics for depth ranges over which biodatums were determined).

Site	Fossil group	Mean (m)	Standard deviation (m)
572	Diatoms	2.8	0.7
572	Radiolarians	6.0	2.9
573	Diatoms	4.0	2.7
573	Radiolarians	6.2	2.2
574	Diatoms	4.0	2.5
574	Radiolarians	5.3	3.0
575	Diatoms	2.7	2.2
575	Radiolarians	3.6	2.4

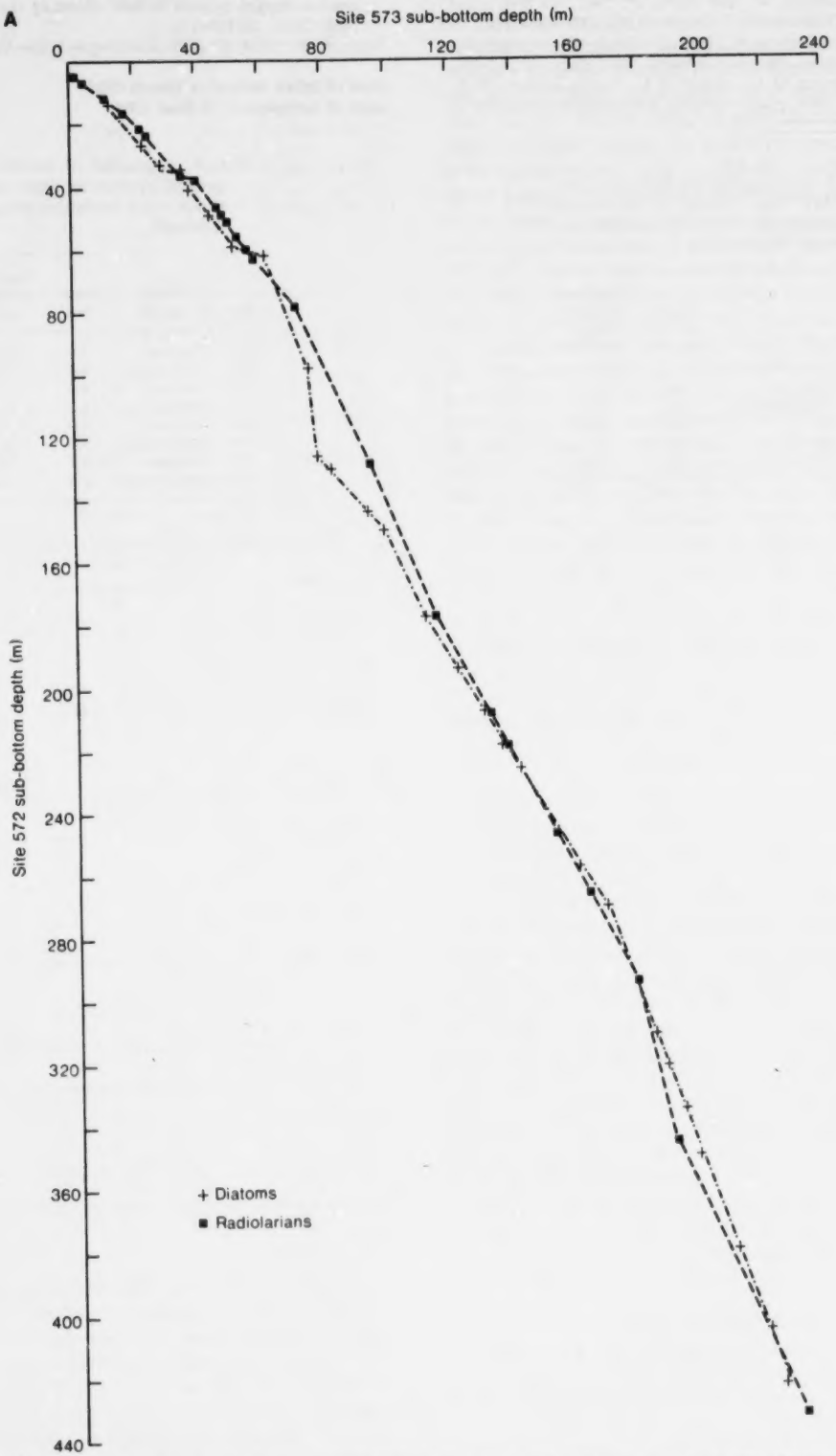

Figure 4. Lines of correlation determined from both biodatums and carbonate records. A. Site 572 versus Site 573. B. Site 574 versus Site 573. C. Site 575 versus Site 573.

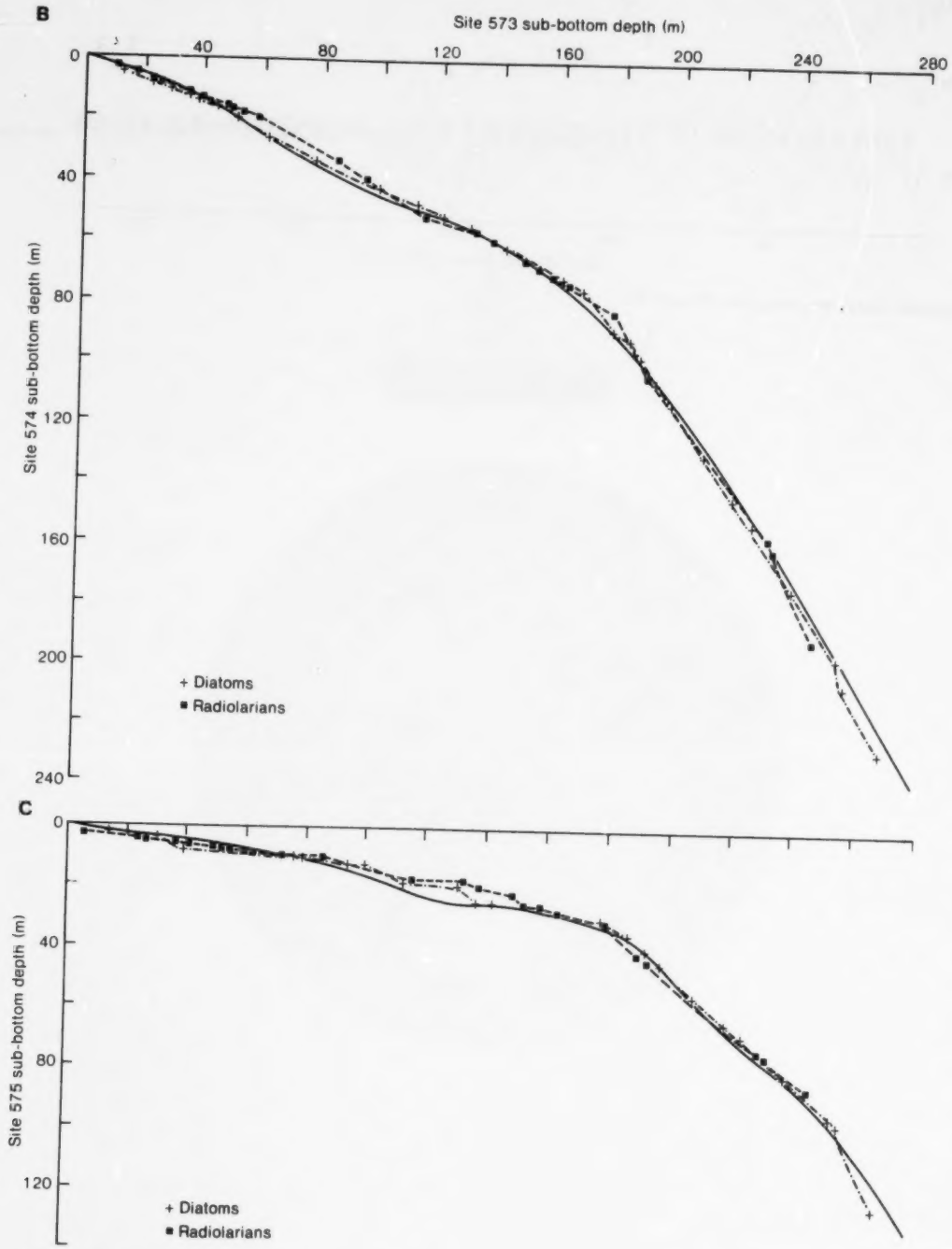

Figure 4. (Continued).

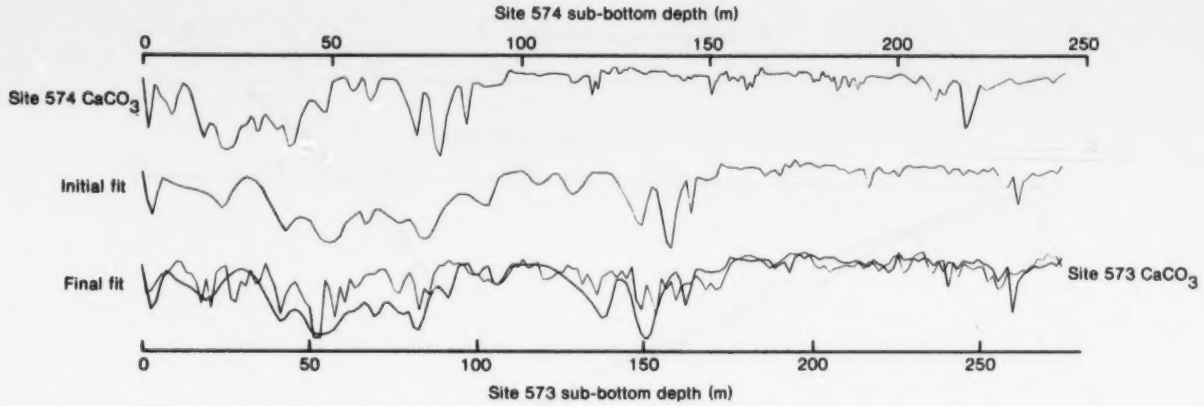

Figure 5. Carbonate plots comparing Sites 574 and 573.

PART III: ISOTOPIC AND CARBONATE STRATIGRAPHY

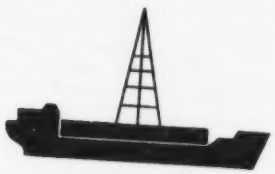

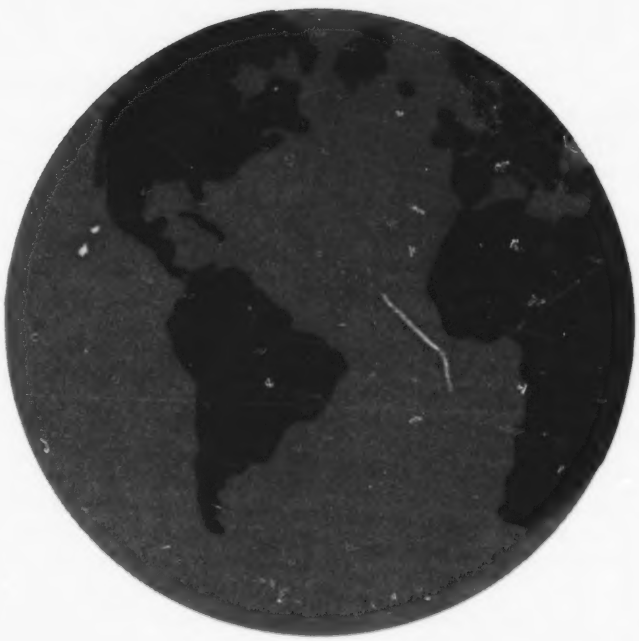

Reprinted from Mayer, L., Theyer, F., et al., 1985
Initial Reports of the Deep Sea Drilling Project, Volume LXXXV, Washington (U. S. Government Printing Office)

19. HIGH RESOLUTION CARBONATE RECORDS FROM THE HYDRAULIC PISTON CORED SECTION OF SITE 572[1]

Nicklas G. Pisias, College of Oceanography, Oregon State University
and
Warren L. Prell, Department of Geological Sciences, Brown University[2]

ABSTRACT

At Site 572, located at 1°N, 114°W (3903 m water depth), we recovered a continuous hydraulic piston cored section of upper Miocene to upper Pleistocene pelagic sediments. The sediment is composed of biogenic carbonate and silica with nonbiogenic material as a minor component. Detailed analysis of the calcium carbonate content shows that the degree of variability in carbonate deposition apparently changed markedly between the late Miocene and Pliocene at this equatorial Pacific site. During this interval carbonate mass accumulation rates decreased from 2.6 to 0.8 g/cm^2 per 10^3 yr. If we assume that variations in $CaCO_3$ content reflect changes in the degree of dissolution, then the detailed carbonate analysis would suggest that the degree of variability in carbonate deposition decreases by a factor of 5 as the dominant wavelength of variations increases significantly. However, if the variability in carbonate concentration is described in terms of changes in mean mass accumulation, calculations then suggest that relatively small changes in noncarbonate rates may be important in controlling the observed carbonate records. In addition, the analysis suggests that the degree of variability observed in pelagic carbonate data may in part reflect total accumulation rates. Intervals with high sedimentation rates show lower amplitude variations in concentration than intervals with lower sedimentation rates for the same degree of change in the carbonate accumulation rate.

INTRODUCTION

Variations in calcium carbonate content have been used by marine geologists and paleoceanographers as a tool for stratigraphic correlation (Prell, 1978; Dunn and Moore, 1981; Hays et al., 1969) and as an indicator of oceanic response to global climate change. In general, the resolution attained in studies of calcium carbonate deposition reflects the quality and sedimentation rate of the sediment sections available.

Studies of Pleistocene sediments typically attain sampling resolution on the order of a few thousand years, and stratigraphic resolution on the order of 50,000 yr. is possible, as shown by Hays et al. (1969). These studies used samples of undisturbed sediment collected by standard piston coring techniques. The availability of undisturbed sections of pre-Pleistocene sediments was severely limited until the development of the hydraulic piston coring capability on the *Glomar Challenger*. Thus, most studies of carbonate variation in pre-Pleistocene sediments have used samples from either rotary drilled sections or the few piston cores that sampled areas where much of the Pleistocene section had been removed by erosion. Studies of carbonate variations in pre-Pleistocene sections (e.g., Dunn and Moore, 1981; Vincent, 1981) typically have sample spacing of several tens of thousands of years and demonstrate stratigraphic resolution on the order of 100,000 to 500,000 yr. A few studies have examined carbonate variations in pre-Pleistocene sediments at a time resolution comparable to that in Pleistocene studies (Dean et al., 1981; Gardner, 1982; Moore et al., 1982), but the coverage in time and space is still extremely limited.

Because of the limited resolution of available Cenozoic carbonate records, it has been difficult to evaluate whether the ocean's carbonate system has displayed the same high degree of variability in the more remote geologic past as that observed in the last 1 m.y. Detailed stable isotope records from the Miocene and Pliocene (Woodruff et al., 1981; Pisias and Shackleton, this volume; Prell, 1982 and this volume) suggest a high degree of climatic variability and lead us to expect variations in carbonate sedimentation as well. Detailed sampling was completed in a number of cores from Site 572 to examine the variability of carbonate deposition in the equatorial Pacific. In this report we present high resolution carbonate analyses from the hydraulic piston cored section of Site 572.

SAMPLING STRATEGY AND METHODS

At Site 572 (01°26.09′N, 113°50.52′W, water depth, 3903 m), the hydraulic piston corer (HPC) recovered sediments to 154 m sub-bottom and provided a high quality, undisturbed, sediment section spanning the last 6 m.y. During this period Site 572 has always been within the equatorial divergence zone. Hence, sedimentation rates have been high throughout much of its history, with sedimentation rates of 13 to 21 m/m.y. in the upper 68 m increasing to 50 m/m.y. between 68 and 208 m sub-bottom (Table 1).

Selected intervals were sampled at 10-cm spacing to examine the sedimentary response to oceanographic and climatic variability in the latest Miocene and Pliocene in

[1] Mayer, L., Theyer, F., et al., *Init. Repts. DSDP*, 85: Washington (U.S. Govt. Printing Office).

[2] Addresses: (Pisias) College of Oceanography, Oregon State University, Corvallis, OR 97331; (Prell) Department of Geological Sciences, Brown University, Providence, RI 02901.

Table 1. Sedimentation and mass accumulation rate estimates for the HPC section of Site 572.

Sub-bottom depth (m)	Age (Ma)	Rate (m/m.y.)	Mean density (g/cm^3)	Mean $CaCO_3$ (%)	Mass accumulation rate (g/cm^2 per 10^3 yr.)	
					$CaCO_3$	Non-$CaCO_3$
9.5	0.55					
		13	0.57	79	0.58	0.16
29.0	2.0					
		21	0.61	73	0.93	0.35
49.0	2.95					
		15.2	0.70	75	0.80	0.20
68.0	4.2					
		50.0	0.72	73	2.60	1.00
208.0	6.95					

detail. The intervals were selected on the basis of four criteria: (1) high sedimentation rates (so that high resolution records could be obtained); (2) shipboard evaluation of carbonate fossil preservation (to ensure adequate numbers of foraminiferal tests for later stable isotopic analyses); (3) intervals that spanned major paleoclimatic or paleoceanographic events; and (4) at least 15 m of continuous good recovery so that a long enough sequence could be sampled for detailed time and frequency domain statistical analysis.

Three intervals from Site 572 were sampled in detail: Cores 572C-4 to 572C-7, 29 to 68 m sub-bottom; Cores 572A-11 and 12, 92 to 110 m sub-bottom; and Cores 572C-15 and 16, 121 to 134 m sub-bottom. The first sample interval represents the time interval from 2 to 4.6 Ma and spans the time when major glaciation supposedly began in the Northern Hemisphere (Shackleton et al., 1984). A detailed stable isotopic analysis of this section is presented by Prell (this volume). The sedimentation rate in this interval is about 15 m/m.y. so that the sampling resolution is on the order of 6000 yr.

The sedimentation rate below 68 m sub-bottom is estimated to be ~50 m/m.y. Thus, the intervals from 92 to 110 m and 121 to 134 m sub-bottom provided very high resolution records of carbonate variations in the latest Miocene. These intervals sample the time periods of about 4.6 to 5 Ma and 5.2 to 5.3 Ma with a sample resolution of 2000 yr. Stable isotopic analyses for these intervals are in progress.

Analyses of calcium carbonate in samples from 29 to 68 m sub-bottom were completed on paired samples for isotopic analysis by using a modified version of the Jones and Kaiteris (1983) vacuum–gasometric technique. In the system used for this study, reactions are measured at atmospheric pressure and measurements are made with a differential pressure gauge. Analytic precision is estimated to be ~0.5% from replicate analyses. Calcium carbonate was determined in the interval from 92 to 134 m sub-bottom using the carbonate bomb technique as modified by Dunn (1980). Analytic precision based on homogenized sample splits is 1% $CaCO_3$, and on samples split without homogenization it is 2% $CaCO_3$. All carbonate analyses are listed in Table 2 and plotted as a function of sub-bottom depth in Figures 1 and 2.

RESULTS AND DISCUSSION

Sample Aliasing

Included in Figures 1 and 2 are the carbonate data obtained on board the *Glomar Challenger*. Shipboard analyses were made using the carbonate bomb technique. In general, two samples per core section (at about 75 cm sample spacing) were analyzed on board ship. All shipboard analyses shown are from Hole 572A. Therefore, only in the interval from 92 to 110 m sub-bottom are the high resolution samples from the same cores as the shipboard data. Where data from the high resolution studies come from the same hole (572A) as the shipboard data, agreement is very good (see Fig. 3B). If we assume that sub-bottom depths are calculated correctly, then differences between the data sets from two different holes, as over the interval from 29 to 68 m, reflect inhomogeneity in the horizontal distribution of calcium carbonate within the distance between the different holes at Site 572. More important, this can also reflect the effect of sample aliasing that results from the marked difference in resolution of the two data sets.

Aliasing, as applied to sampling in the time domain, (or in the depth domain, as with deep-sea sediments), results from sampling at a resolution too low for the wavelength of variation. In effect, short-wavelength components that are sampled at long sampling intervals appear as long-wavelength variations. For example, in Figure 3A a hypothetical carbonate record with a wavelength of 1.25 m is shown. If the core is sampled at 145-cm intervals, the resulting data look like a long-period component of 11 m. Thus, the true information in the data set is "aliased" as a signal of much lower frequency. Note that in this example the true amplitude of variations can be determined from the aliased data.

An example of aliasing from the Site 572 data is shown in Figure 3B. The shipboard data at 75-cm intervals would suggest an interval of relatively constant (±5%) $CaCO_3$ content between 100 and 110 m sub-bottom. The detailed sampling, however, shows variations on the order of ±10% $CaCO_3$. The low-resolution sampling aliased variability of 15% $CaCO_3$ with a wavelength of 1 cycle/m to a constant signal of very low frequency. In this case, the 15,000-yr. sampling represented by the shipboard analyses lost essentially all the information about the $CaCO_3$ variations, not even recovering the amplitude of variation.

The effect of aliasing on a data set cannot be determined from that data set. Information not contained in the data set is needed to evaluate aliasing, and only high-resolution sampling can reveal the effects of short-wavelength components on the aliased "low frequencies."

Depth Versus Time Domain

The data from Site 572 span almost 4 m.y., from the latest Miocene through most of the Pliocene. In general, the depth series are very similar in their general appearance and statistical properties (Table 3; Figs. 1 and 2). The mean values for four intervals range from 69 to

Table 2. $CaCO_3$ percentages in all samples analyzed at Site 572.

Sub-bottom depth (m)	Sample (level in cm)	$CaCO_3$ (%)	Sub-bottom depth (m)	Sample (level in cm)	$CaCO_3$ (%)	Sub-bottom depth (m)	Sample (level in cm)	$CaCO_3$ (%)
29.74	572C-4-1, 44	73.15	37.34	572C-4-6, 54	85.43	45.94	572C-5-5, 104	78.55
29.84	572C-4-1, 54	80.23	37.44	572C-4-6, 64	80.32	46.04	572C-5-5, 114	77.46
29.94	572C-4-1, 64	78.86	37.54	572C-4-6, 74	72.65	46.14	572C-5-5, 124	85.23
30.04	572C-4-1, 74	80.37	37.64	572C-4-6, 84	69.63	46.24	572C-5-5, 134	86.27
30.14	572C-4-1, 84	77.34	37.74	572C-4-6, 94	80.17	46.44	572C-5-6, 4	83.66
30.24	572C-4-1, 94	78.00	37.84	572C-4-6, 104	76.44	46.54	572C-5-6, 14	79.42
30.34	572C-4-1, 104	77.47	38.14	572C-4-6, 134	76.28	46.64	572C-5-6, 24	79.19
30.44	572C-4-1, 114	67.75	38.24	572C-4-6, 144	75.31	46.74	572C-5-6, 34	76.74
30.54	572C-4-1, 124	72.61	38.34	572C-4-7, 4	72.61	46.84	572C-5-6, 44	61.55
30.64	572C-4-1, 134	73.36	38.44	572C-4-7, 14	72.96	46.94	572C-5-6, 54	58.01
30.74	572C-4-1, 144	73.82	38.54	572C-4-7, 24	80.26	47.04	572C-4-5, 64	65.47
30.84	572C-4-2, 4	73.57	38.64	572C-4-7, 34	83.48	47.11	572C-5-6, 71	62.27
30.94	572C-4-2, 14	70.64	38.94	572C-5-1, 4	76.81	47.24	572C-5-6, 84	58.82
31.04	572C-4-2, 24	73.74	39.04	572C-5-1, 14	78.58	47.34	572C-5-6, 94	57.45
31.14	572C-4-2, 34	71.40	39.24	572C-5-1, 34	65.40	47.44	572C-5-6, 104	80.05
31.24	572C-4-2, 44	75.24	39.34	572C-5-1, 44	81.09	47.54	572C-5-6, 114	77.80
31.34	572C-4-2, 54	75.87	39.44	572C-5-1, 54	84.36	47.64	572C-5-6, 124	79.57
31.44	572C-4-2, 64	78.65	39.54	572C-5-1, 64	84.49	47.74	572C-5-6, 134	81.61
31.54	572C-4-2, 74	76.30	39.61	572C-5-1, 71	81.90	47.84	572C-5-6, 144	76.70
31.64	572C-4-2, 84	76.02	39.74	572C-5-1, 84	81.14	47.94	572C-5-7, 4	73.27
31.74	572C-4-2, 94	79.80	39.84	572C-5-1, 94	80.60	48.04	572C-5-7, 14	72.47
31.84	572C-4-2, 104	77.87	39.94	572C-5-1, 104	79.51	48.14	572C-5-7, 24	82.30
31.94	572C-4-2, 114	80.61	40.04	572C-5-1, 114	73.49	48.24	572C-5-7, 34	81.20
32.04	572C-4-2, 124	82.55	40.14	572C-5-1, 124	76.06	48.54	572C-6-1, 4	78.56
32.14	572C-4-2, 134	84.72	40.24	572C-5-1, 134	78.20	48.64	572C-6-1, 14	76.44
32.24	572C-4-2, 144	86.33	40.34	572C-5-1, 144	75.92	48.74	572C-6-1, 24	71.72
32.34	572C-4-3, 4	85.84	40.44	572C-5-2, 4	74.91	48.84	572C-6-1, 34	81.60
32.44	572C-4-3, 14	82.62	40.54	572C-5-2, 14	72.12	48.98	572C-6-1, 48	81.18
32.54	572C-4-3, 24	85.74	40.64	572C-5-2, 24	73.04	49.04	572C-6-1, 54	84.46
32.64	572C-4-3, 34	83.48	40.74	572C-5-2, 34	75.86	49.14	572C-6-1, 64	86.48
32.74	572C-4-3, 44	81.78	41.11	572C-5-2, 71	84.18	49.23	572C-6-1, 73	87.64
32.84	572C-4-3, 54	83.73	41.24	572C-5-2, 84	86.59	49.34	572C-6-1, 84	84.32
32.94	572C-4-3, 64	79.33	41.34	572C-5-2, 94	86.68	49.44	572C-6-1, 94	84.36
33.04	572C-4-3, 74	79.99	41.44	572C-5-2, 104	75.93	49.54	572C-6-1, 104	85.63
33.14	572C-4-3, 84	82.82	41.54	572C-5-2, 114	80.62	49.64	572C-6-1, 114	84.98
33.24	572C-4-3, 94	83.08	41.64	572C-5-2, 124	85.67	49.74	572C-6-1, 124	73.97
33.34	572C-4-3, 104	82.14	41.74	572C-5-2, 134	85.09	49.84	572C-6-1, 134	86.30
33.44	572C-4-3, 114	79.24	41.84	572C-5-2, 144	86.04	49.94	572C-6-1, 144	84.73
33.54	572C-4-3, 124	78.21	41.94	572C-5-3, 4	87.81	50.04	572C-6-2, 4	81.85
33.64	572C-4-3, 134	81.36	42.04	572C-5-3, 14	85.26	50.14	572C-6-2, 14	86.16
33.74	572C-4-3, 144	82.07	42.14	572C-5-3, 24	88.03	50.24	572C-6-2, 24	83.60
33.84	572C-4-4, 4	81.36	42.24	572C-5-3, 34	83.67	50.34	572C-6-2, 34	75.72
33.94	572C-4-4, 14	80.89	42.34	572C-5-3, 44	86.94	50.44	572C-5-2, 44	75.51
34.04	572C-4-4, 24	73.76	42.44	572C-5-3, 54	86.61	50.54	572C-6-2, 54	78.59
34.14	572C-4-4, 34	73.65	42.54	572C-5-3, 64	84.33	50.64	572C-6-2, 64	79.10
34.24	572C-4-4, 44	84.74	42.61	572C-5-3, 71	81.23	50.73	572C-6-2, 73	80.73
34.34	572C-4-4, 54	78.19	42.84	572C-5-3, 94	81.32	50.84	572C-6-2, 84	77.56
34.44	572C-4-4, 64	75.02	42.94	572C-5-3, 104	82.75	50.94	572C-6-2, 94	85.01
34.57	572C-4-4, 77	79.73	43.04	572C-5-3, 114	79.98	51.04	572C-6-2, 104	84.12
34.64	572C-4-4, 84	77.93	43.24	572C-5-3, 134	78.02	51.14	572C-6-2, 114	85.76
34.74	572C-4-4, 94	79.59	43.34	572C-5-3, 114	78.89	51.24	572C-6-2, 124	82.71
34.84	572C-4-4, 104	81.28	43.44	572C-5-4, 4	83.64	51.34	572C-6-2, 134	83.23
34.94	572C-4-4, 114	82.74	43.55	572C-5-4, 15	80.25	51.44	572C-6-2, 144	80.65
35.04	572C-4-4, 124	84.33	43.64	572C-5-4, 24	73.25	51.54	572C-6-3, 4	81.04
35.14	572C-4-4, 134	83.69	43.74	572C-5-4, 34	75.25	51.64	572C-6-3, 14	75.62
35.24	572C-4-4, 144	83.28	43.84	572C-5-4, 44	78.91	51.74	572C-6-3, 24	67.46
35.34	572C-4-5, 4	86.35	43.94	572C-5-4, 54	76.00	51.84	572C-6-3, 34	62.70
35.44	572C-4-5, 14	82.40	44.04	572C-5-4, 64	80.68	51.94	572C-6-3, 44	64.75
35.54	572C-4-5, 24	86.66	44.11	572C-5-4, 71	75.08	52.04	572C-6-3, 54	69.74
35.64	572C-4-5, 34	88.68	44.24	572C-5-4, 84	75.37	52.14	572C-6-3, 64	69.97
35.74	572C-4-5, 44	92.48	44.34	572C-5-4, 94	79.65	52.23	572C-6-3, 73	70.31
35.84	572C-4-5, 54	90.42	44.44	572C-5-4, 104	84.89	52.34	572C-6-3, 84	69.79
35.94	572C-4-5, 64	87.93	44.54	572C-5-4, 114	80.88	52.44	572C-6-3, 94	71.02
36.04	572C-4-5, 74	85.79	44.64	572C-5-4, 124	83.87	52.54	572C-6-3, 104	72.90
36.14	572C-4-5, 84	79.72	44.74	572C-5-4, 134	81.97	52.64	572C-6-3, 114	78.62
36.24	572C-4-5, 94	79.94	44.84	572C-5-4, 144	83.23	52.74	572C-6-3, 124	80.02
36.34	572C-4-5, 104	79.44	44.94	572C-5-5, 4	85.54	52.84	572C-6-3, 134	81.62
36.44	572C-4-5, 114	84.32	45.04	572C-5-5, 14	83.20	52.94	572C-6-3, 144	83.20
36.54	572C-4-5, 124	88.10	45.14	572C-5-5, 24	86.67	53.04	572C-6-4, 4	71.10
36.64	572C-4-5, 134	85.71	45.24	572C-5-5, 34	86.57	53.14	572C-6-4, 14	73.15
36.74	572C-4-5, 144	81.29	45.34	572C-5-5, 44	74.12	53.24	572C-6-4, 24	75.86
36.84	572C-4-6, 4	79.92	45.44	572C-5-5, 54	56.76	53.34	572C-6-4, 34	56.32
36.94	572C-4-6, 14	76.58	45.54	572C-5-5, 64	59.32	53.44	572C-6-4, 44	48.61
37.04	572C-4-6, 24	81.63	45.61	572C-5-5, 71	56.58	53.54	572C-6-4, 54	68.67
37.14	572C-4-6, 34	77.36	45.74	572C-5-5, 84	60.24	53.64	572C-6-4, 64	83.12
37.24	572C-4-6, 44	85.97	45.84	572C-5-5, 94	66.45	53.73	572C-6-4, 73	81.63

Table 2. (Continued).

Sub-bottom depth (m)	Sample (level in cm)	$CaCO_3$ (%)
53.84	572C-6-4, 84	76.66
53.94	572C-6-4, 94	74.44
54.04	572C-6-4, 104	64.87
54.14	572C-6-4, 114	60.10
54.34	572C-6-4, 134	83.70
54.44	572C-6-4, 144	88.52
54.54	572C-6-5, 4	88.58
54.64	572C-6-5, 14	90.37
54.74	572C-6-5, 24	86.54
54.84	572C-6-5, 34	78.96
54.94	572C-6-5, 44	76.83
55.04	572C-6-5, 54	84.19
55.14	572C-6-5, 64	83.70
55.23	572C-6-5, 73	86.88
55.34	572C-6-5, 84	86.41
55.44	572C-6-5, 94	79.89
55.54	572C-6-5, 104	70.20
55.64	572C-6-5, 114	76.02
55.74	572C-6-5, 124	75.41
55.84	572C-6-5, 134	75.98
55.94	572C-6-5, 144	75.25
56.04	572C-6-6, 4	72.89
56.14	572C-6-6, 14	75.76
56.24	572C-6-6, 24	73.00
56.34	572C-6-6, 34	74.20
56.44	572C-6-6, 44	83.82
56.54	572C-6-6, 54	83.27
56.64	572C-6-6, 64	76.97
56.73	572C-6-6, 73	61.27
56.84	572C-6-6, 84	59.84
56.94	572C-6-6, 94	59.60
57.04	572C-6-6, 104	68.19
57.14	572C-6-6, 114	71.46
57.24	572C-6-6, 124	67.22
57.34	572C-6-6, 134	32.20
57.44	572C-6-6, 144	66.97
57.54	572C-6-7, 4	80.19
57.64	572C-6-7, 14	75.83
57.74	572C-6-7, 24	79.79
57.84	572C-6-7, 34	79.47
58.14	572C-7-1, 4	65.13
58.24	572C-7-1, 14	58.22
58.34	572C-7-1, 24	54.18
58.44	572C-7-1, 34	63.96
58.54	572C-7-1, 44	68.06
58.64	572C-7-1, 54	66.64
58.74	572C-7-1, 64	68.82
58.83	572C-7-1, 73	74.74
58.94	572C-7-1, 84	78.41
59.04	572C-7-1, 94	77.53
59.14	572C-7-1, 104	75.39
59.24	572C-7-1, 114	76.17
59.34	572C-7-1, 124	71.62
59.44	572C-7-1, 134	74.31
59.54	572C-7-1, 144	71.94
59.64	572C-7-2, 4	68.83
59.74	572C-7-2, 14	66.92
59.84	572C-7-2, 24	65.52
59.94	572C-7-2, 34	64.07
60.04	572C-7-2, 44	76.75
60.14	572C-7-2, 54	77.43
60.24	572C-7-2, 64	76.35
60.33	572C-7-2, 73	77.97
60.44	572C-7-2, 84	78.42
60.54	572C-7-2, 94	88.16
60.64	572C-7-2, 104	86.16
60.74	572C-7-2, 114	85.80
60.84	572C-7-2, 124	84.69
60.94	572C-7-2, 134	85.00
61.04	572C-7-2, 144	88.71
61.14	572C-7-3, 4	84.13
61.24	572C-7-3, 14	85.07
61.34	572C-7-3, 24	86.44
61.44	572C-7-3, 34	83.81
61.54	572C-7-3, 44	84.60
61.64	572C-7-3, 54	86.24
61.74	572C-7-3, 64	86.54
61.84	572C-7-3, 74	87.74
61.94	572C-7-3, 84	87.32
62.04	572C-7-3, 94	87.59
62.14	572C-7-3, 104	90.36
62.24	572C-7-3, 114	89.72
62.34	572C-7-3, 124	86.40
62.44	572C-7-3, 134	84.43
62.54	572C-7-3, 144	89.43
62.64	572C-7-4, 4	87.35
62.74	572C-7-4, 14	83.00
62.84	572C-7-4, 24	84.66
62.94	572C-7-4, 34	85.85
63.04	572C-7-4, 44	75.57
63.14	572C-7-4, 54	72.67
63.24	572C-7-4, 64	85.92
63.33	572C-7-4, 73	85.99
63.44	572C-7-4, 84	86.90
63.54	572C-7-4, 94	88.01
63.64	572C-7-4, 104	88.34
63.74	572C-7-4, 114	88.89
63.84	572C-7-4, 124	86.28
63.94	572C-7-4, 134	90.39
64.14	572C-7-5, 4	86.16
64.24	572C-7-5, 14	73.01
64.34	572C-7-5, 24	73.35
64.44	572C-7-5, 34	70.95
64.54	572C-7-5, 44	80.02
64.64	572C-7-5, 54	85.36
64.74	572C-7-5, 64	85.90
64.83	572C-7-5, 73	80.14
64.94	572C-7-5, 84	71.53
65.04	572C-7-5, 94	85.74
65.14	572C-7-5, 104	84.73
65.24	572C-7-5, 114	84.52
65.34	572C-7-5, 124	90.72
65.44	572C-7-5, 134	89.09
65.54	572C-7-5, 144	89.66
65.64	572C-7-6, 4	89.15
65.74	572C-7-6, 14	83.93
65.84	572C-7-6, 24	89.56
65.94	572C-7-6, 34	88.67
66.04	572C-7-6, 44	89.80
66.14	572C-7-6, 54	89.68
66.24	572C-7-6, 64	91.28
66.35	572C-7-6, 75	88.34
66.44	572C-7-6, 84	86.74
66.54	572C-7-6, 94	83.11
66.64	572C-7-6, 104	79.28
66.74	572C-7-6, 114	74.16
66.84	572C-7-6, 124	73.93
66.94	572C-7-6, 134	70.40
67.04	572C-7-6, 144	69.74
67.14	572C-7-7, 4	68.68
67.24	572C-7-7, 14	76.01
67.34	572C-7-7, 24	80.79
67.44	572C-7-7, 34	81.67
91.53	572A-11-1, 13	73.73
91.73	572A-11-1, 33	70.52
91.83	572A-11-1, 43	74.81
91.93	572A-11-1, 53	68.37
92.03	572A-11-1, 63	69.44
92.11	572A-11-1, 71	69.23
92.23	572A-11-1, 83	67.83
92.33	572A-11-1, 93	66.55
92.43	572A-11-1, 103	67.30
92.53	572A-11-1, 113	61.18
92.63	572A-11-1, 123	57.64
92.73	572A-11-1, 133	52.82
92.83	572A-11-1, 143	65.15
92.93	572A-11-2, 3	75.27
93.03	572A-11-2, 13	68.76
93.13	572A-11-2, 23	75.81
93.23	572A-11-2, 33	77.33
93.33	572A-11-2, 43	82.32
93.43	572A-11-2, 53	80.04
93.53	572A-11-2, 63	83.73
93.59	572A-11-2, 69	82.97
93.73	572A-11-2, 83	78.30
93.83	572A-11-2, 93	76.24
93.93	572A-11-2, 103	75.59
94.03	572A-11-2, 113	72.88
94.13	572A-11-2, 123	72.88
94.23	572A-11-2, 133	71.47
94.33	572A-11-2, 143	68.22
94.43	572A-11-3, 3	65.93
94.53	572A-11-3, 13	64.31
94.63	572A-11-3, 23	70.23
94.73	572A-11-3, 33	67.54
94.83	572A-11-3, 43	67.00
94.93	572A-11-3, 53	76.15
95.03	572A-11-3, 63	70.23
95.10	572A-11-3, 70	71.63
95.23	572A-11-3, 83	72.93
95.33	572A-11-3, 93	75.07
95.43	572A-11-3, 103	76.15
95.53	572A-11-3, 113	74.32
95.63	572A-11-3, 123	73.46
95.73	572A-11-3, 133	72.92
95.83	572A-11-3, 143	68.08
96.03	572A-11-4, 13	70.77
96.13	572A-11-4, 23	71.63
96.23	572A-11-4, 33	71.63
96.33	572A-11-4, 43	64.31
96.43	572A-11-4, 53	68.08
96.53	572A-11-4, 63	68.94
96.61	572A-11-4, 71	72.38
96.73	572A-11-4, 83	75.07
96.83	572A-11-4, 93	75.61
96.93	572A-11-4, 103	72.38
97.03	572A-11-4, 113	68.94
97.13	572A-11-4, 123	70.77
97.23	572A-11-4, 133	66.25
97.33	572A-11-4, 143	65.93
97.53	572A-11-5, 13	87.43
97.63	572A-11-5, 23	67.54
97.73	572A-11-5, 33	99.99
97.83	572A-11-5, 43	94.06
97.93	572A-11-5, 53	75.05
98.03	572A-11-5, 63	71.41
98.11	572A-11-5, 71	68.64
98.23	572A-11-5, 83	78.04
98.33	572A-11-5, 93	85.22
98.43	572A-11-5, 103	83.01
98.53	572A-11-5, 113	62.02
98.63	572A-11-5, 123	68.09
98.73	572A-11-5, 133	68.09
98.83	572A-11-5, 143	64.10
98.93	572A-11-6, 3	40.87
99.03	572A-11-6, 13	38.11
99.13	572A-11-6, 23	51.94
99.33	572A-11-6, 43	44.75
99.53	572A-11-6, 63	67.42
99.59	572A-11-6, 69	66.32
99.73	572A-11-6, 83	47.51
100.03	572A-11-6, 113	76.83
100.13	572A-11-6, 123	74.06
100.23	572A-11-6, 133	74.95
100.33	572A-11-6, 143	77.38
100.43	572A-11-7, 3	75.72
100.73	572A-12-1, 3	55.13
100.73	572A-12-1, 3	45.85
100.83	572A-12-1, 13	52.91
100.93	572A-12-1, 23	57.34
101.03	572A-12-1, 33	66.21
101.03	572A-12-1, 33	41.43
101.13	572A-12-1, 43	72.86
101.23	572A-12-1, 53	75.08
101.33	572A-12-1, 63	69.53
101.33	572A-12-1, 63	75.72
101.40	572A-12-1, 70	70.64

Table 2. (Continued).

Sub-bottom depth (m)	Sample (level in cm)	$CaCO_3$ (%)	Sub-bottom depth (m)	Sample (level in cm)	$CaCO_3$ (%)	Sub-bottom depth (m)	Sample (level in cm)	$CaCO_3$ (%)
101.43	572A-12-1, 73	74.95	108.83	572A-12-6, 63	77.38	127.21	572C-15-5, 11	79.39
101.53	572A-12-1, 83	73.19	108.90	572A-12-6, 70	74.35	127.30	572C-15-5, 20	80.55
101.63	572A-12-1, 93	72.86	109.03	572A-12-6, 83	72.45	127.41	572C-15-5, 31	82.11
101.73	572A-12-1, 103	65.66	109.13	572A-12-6, 93	68.50	127.50	572C-15-5, 40	81.79
101.83	572A-12-1, 113	65.10	109.23	572A-12-6, 103	76.95	127.62	572C-15-5, 52	83.54
101.93	572A-12-1, 123	71.75	109.33	572A-12-6, 113	76.38	127.70	572C-15-5, 60	82.20
102.03	572A-12-1, 133	70.42	109.43	572A-12-6, 123	73.80	127.81	572C-15-5, 71	78.02
102.13	572A-12-1, 143	69.53	109.43	572A-12-6, 123	73.80	127.90	572C-15-5, 80	81.19
102.33	572A-12-2, 13	63.99	109.53	572A-12-6, 133	79.23	128.01	572C-15-5, 91	74.63
102.43	572A-12-2, 23	67.65	109.63	572A-12-6, 143	79.64	128.10	572C-15-5, 100	80.24
102.53	572A-12-2, 33	66.21	109.73	572A-12-7, 3	62.56	128.21	572C-15-5, 111	80.99
102.63	572A-12-2, 43	68.43				128.30	572C-15-5, 120	77.52
102.73	572A-12-2, 53	68.43	121.10	572C-15-1, 0	75.03	128.42	572C-15-5, 132	79.14
102.83	572A-12-2, 63	67.32	121.21	572C-15-1, 11	83.10	128.50	572C-15-5, 140	71.94
103.23	572A-12-2, 103	68.98	121.30	572C-15-1, 20	76.73	128.60	572C-15-5, 150	71.75
103.43	572A-12-2, 123	62.88	121.41	572C-15-1, 31	65.17	128.71	572C-15-6, 11	79.81
103.53	572A-12-2, 133	64.88	121.50	572C-15-1, 40	50.88	128.80	572C-15-6, 20	78.17
103.63	572A-12-2, 143	71.20	121.70	572C-15-1, 60	64.23	128.91	572C-15-6, 31	80.93
103.83	572A-12-3, 13	78.40	121.81	572C-15-1, 71	75.64	128.91	572C-15-6, 31	80.93
103.93	572A-12-3, 23	76.74	121.90	572C-15-1, 80	72.70	129.00	572C-15-6, 40	82.34
104.03	572A-12-3, 33	78.40	122.01	572C-15-1, 91	73.07	129.12	572C-15-6, 52	84.81
104.03	572A-12-3, 33	77.29	122.10	572C-15-1, 100	72.32	129.20	572C-15-6, 60	81.57
104.13	572A-12-3, 43	79.51	122.21	572C-15-1, 111	71.39	129.24	572C-15-6, 64	75.98
104.33	572A-12-3, 63	71.20	122.30	572C-15-1, 120	72.18	129.31	572C-15-6, 71	78.33
104.40	572A-12-3, 70	70.64	122.42	572C-15-1, 132	77.47	129.35	572C-15-6, 75	74.28
104.53	572A-12-3, 83	68.98	122.50	572C-15-1, 140	81.95	129.40	572C-15-6, 80	81.46
104.63	572A-12-3, 93	65.66	122.60	572C-15-2, 0	82.25	129.44	572C-15-6, 84	71.81
104.73	572A-12-3, 103	75.08	122.71	572C-15-2, 11	81.07	129.51	572C-15-6, 91	77.05
104.83	572A-12-3, 113	80.06	122.80	572C-15-2, 20	86.03	129.55	572C-15-6, 95	74.32
104.93	572A-12-3, 123	77.29	122.91	572C-15-2, 31	79.65	129.60	572C-15-6, 100	74.76
105.03	572A-12-3, 133	77.29	123.00	572C-15-2, 40	81.53	129.65	572C-15-6, 105	71.61
105.13	572A-12-3, 143	75.08	123.12	572C-15-2, 52	75.37	129.71	572C-15-6, 111	76.45
105.23	572A-12-4, 3	66.21	123.20	572C-15-2, 60	73.19	129.74	572C-15-6, 114	80.73
105.33	572A-12-4, 13	60.67	123.31	572C-15-2, 71	75.03	129.80	572C-15-6, 120	74.41
105.43	572A-12-4, 23	68.98	123.40	572C-15-2, 80	77.66	129.85	572C-15-6, 125	81.68
105.53	572A-12-4, 33	72.86	123.51	572C-15-2, 91	73.77	129.92	572C-15-6, 132	77.54
105.63	572A-12-4, 43	80.62	123.60	572C-15-2, 100	66.40	129.94	572C-15-6, 134	74.54
105.73	572A-12-4, 53	73.97	123.71	572C-15-2, 111	66.24	130.00	572C-15-6, 140	77.02
105.83	572A-12-4, 63	76.19	123.80	572C-15-2, 120	64.96	130.04	572C-15-6, 144	72.88
105.90	572A-12-4, 70	76.19	123.92	572C-15-2, 132	67.47	130.15	572C-15-7, 5	64.81
106.03	572A-12-4, 83	66.21	124.00	572C-15-2, 140	66.04	130.24	572C-15-7, 14	74.76
106.13	572A-12-4, 93	67.65	124.10	572C-15-3, 0	62.18	130.36	572C-15-7, 26	74.32
106.23	572A-12-4, 103	62.33	124.21	572C-15-3, 11	59.80	130.44	572C-15-7, 34	72.69
106.33	572A-12-4, 113	63.99	124.30	572C-15-3, 20	58.34	130.55	572C-15-7, 45	76.58
106.43	572A-12-4, 123	63.44	124.41	572C-15-3, 31	59.07	130.65	572C-15-7, 55	76.68
106.53	572A-12-4, 133	71.75	124.50	572C-15-3, 40	64.37	131.00	572C-16-1, 30	73.92
106.63	572A-12-4, 143	74.52	124.70	572C-15-3, 60	72.00	131.10	572C-16-1, 40	72.82
106.73	572A-12-5, 3	72.18	124.81	572C-15-3, 71	74.56	131.20	572C-16-1, 50	71.18
106.83	572A-12-5, 13	67.33	124.90	572C-15-3, 80	75.66	131.40	572C-16-1, 70	72.33
106.93	572A-12-5, 23	56.89	125.01	572C-15-3, 91	70.53	131.60	572C-16-1, 90	73.32
107.03	572A-12-5, 33	58.32	125.10	572C-15-3, 100	78.54	131.70	572C-16-1, 100	75.16
107.13	572A-12-5, 43	63.98	125.21	572C-15-3, 111	78.04	131.82	572C-16-1, 112	74.29
107.23	572A-12-5, 53	78.94	125.30	572C-15-3, 120	74.63	131.90	572C-16-1, 120	73.01
107.33	572A-12-5, 63	70.45	125.42	572C-15-3, 132	68.03	132.01	572C-16-1, 131	69.70
107.40	572A-12-5, 70	64.72	125.50	572C-15-3, 140	79.01	132.10	572C-16-1, 140	69.74
107.53	572A-12-5, 83	67.66	125.60	572C-15-4, 0	80.54	132.20	572C-16-2, 0	66.77
107.63	572A-12-5, 93	64.39	125.71	572C-15-4, 11	81.96	132.40	572C-16-2, 20	68.40
107.73	572A-12-5, 103	65.79	125.80	572C-15-4, 20	82.92	132.51	572C-16-2, 31	70.64
107.83	572A-12-5, 113	47.64	126.00	572C-15-4, 40	82.92	132.60	572C-16-2, 40	71.85
107.93	572A-12-5, 123	69.05	126.12	572C-15-4, 52	80.15	132.70	572C-16-2, 50	69.38
108.03	572A-12-5, 133	70.52	126.20	572C-15-4, 60	75.11	132.80	572C-16-2, 60	69.55
108.13	572A-12-5, 143	66.51	126.31	572C-15-4, 71	85.12	132.80	572C-16-2, 60	73.27
108.23	572A-12-6, 3	63.07	126.40	572C-15-4, 80	78.04	132.90	572C-16-2, 70	64.58
108.33	572A-12-6, 13	67.01	126.51	572C-15-4, 91	88.18	133.00	572C-16-2, 80	64.45
108.43	572A-12-6, 23	67.19	126.60	572C-15-4, 100	80.15	133.10	572C-16-2, 90	63.02
108.53	572A-12-6, 33	79.84	126.71	572C-15-4, 111	78.70	133.20	572C-16-2, 100	73.93
108.63	572A-12-6, 43	80.92	126.92	572C-15-4, 132	71.58	133.20	572C-16-2, 100	81.77
108.73	572A-12-6, 53	79.16	127.00	572C-15-4, 140	78.30	133.40	572C-16-2, 120	53.89
108.73	572A-12-6, 53	72.41	127.10	572C-15-5, 0	78.21	133.51	572C-16-2, 131	87.24

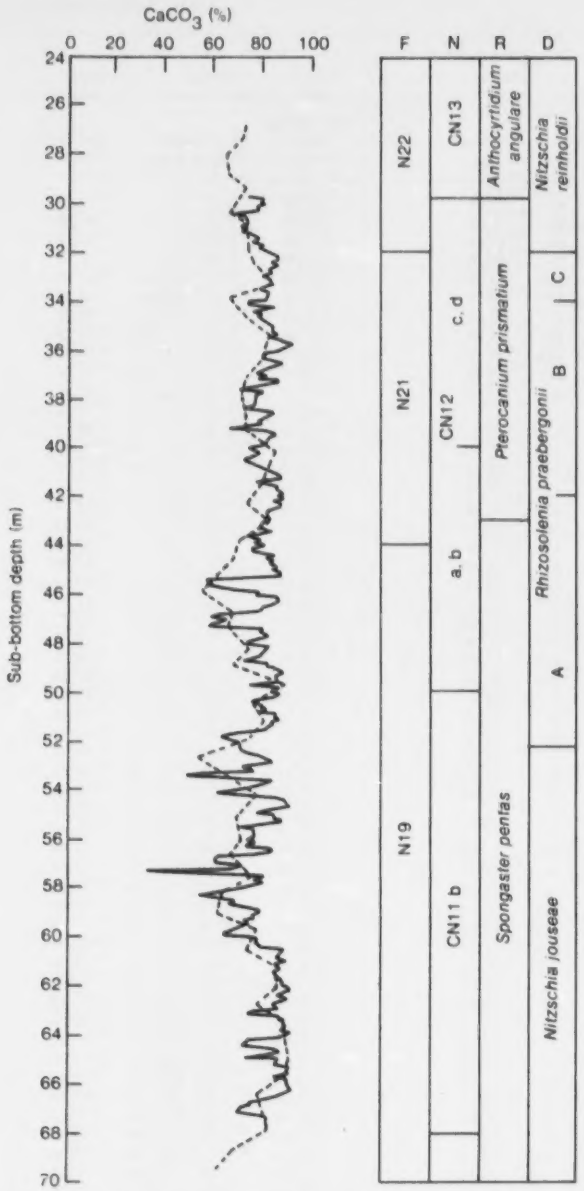

Figure 1. Calcium carbonate versus sub-bottom depth (27 to 70 m) in HPC Site 572. Detailed, high resolution carbonate data from Hole 572C are shown as solid line. Dashed line shows shipboard analyses from Hole 572A. Biostratigraphy is from Site 572 chapter (this volume). F = planktonic foraminiferal zonation; N = calcareous nannofossil zonation; R = radiolarian zonation; D = diatom zonation.

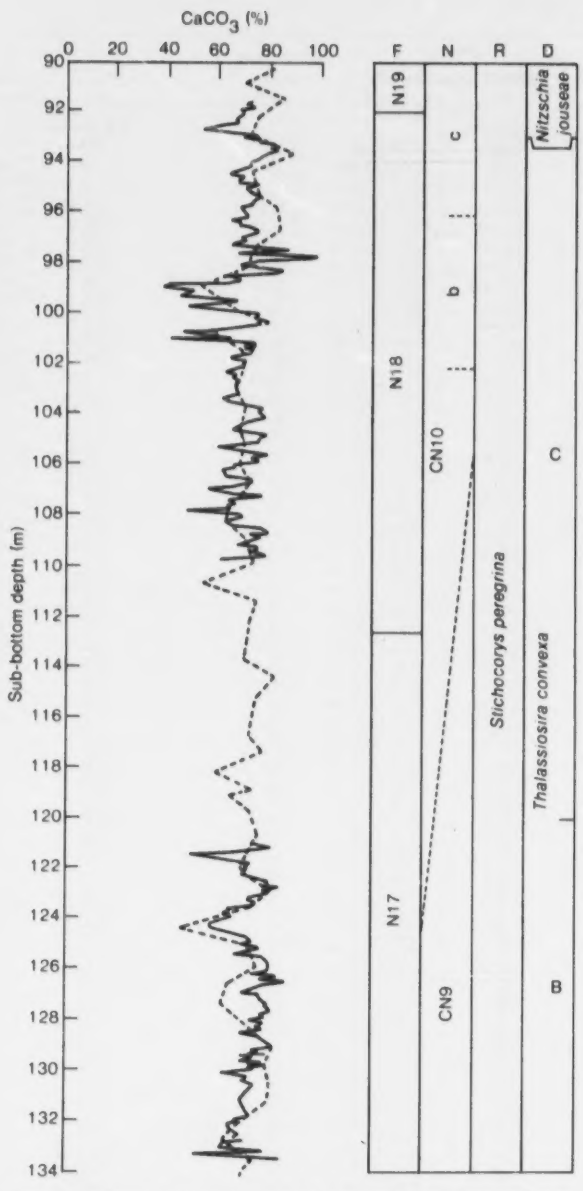

Figure 2. Calcium carbonate versus sub-bottom depth (90 to 134 m) in HPC Site 572. Detailed high resolution carbonate data from Hole 572A (92 to 110 m) and Hole 572C (121 to 134 m) are shown as solid line. Dashed line shows shipboard analyses from Hole 572A. Biostratigraphy plotted from Site 572 chapter (this volume). F, N, R, D as defined in Fig. 1.

79% $CaCO_3$, with the standard deviations of the intervals ranging from 6.6 to 9.2% carbonate. (The interval from 30 to 68 m was divided into two parts, with the number of data points in each approximately equal to the other depth intervals sampled.) Differences between the extreme values of the mean and variance are significant only at the 10% level (Table 3). The average wavelength of variations in all sections is on the order of 20 to 50 samples per cycle, with secondary fluctuations on the order of 10 samples per cycle (e.g., Fig. 3B).

Although the depth series are remarkably similar, there are significant differences when the data are plotted against age. In Figure 4 the carbonate data are plotted versus ages determined from the sedimentation rates for Site 572 (Table 1). The differences in the frequency of

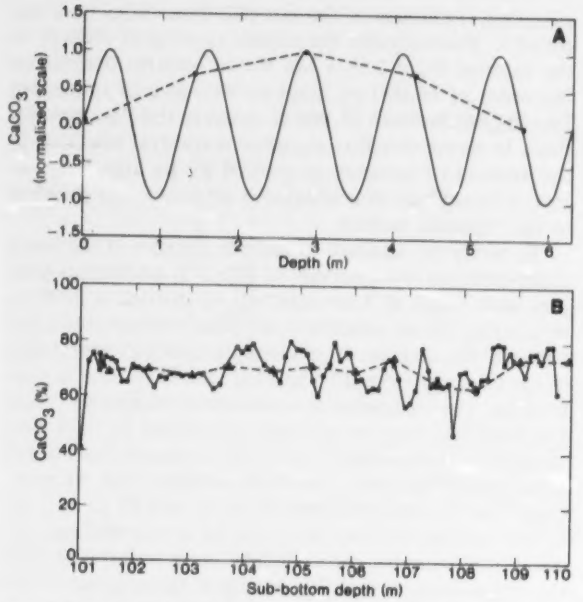

Figure 3. Effects of sample aliasing. A. The effect of sampling a pure sine function with a wavelength of 6 units at a sampling interval of 7 units (1.166 wavelengths). The observed signal is a sine function of 36 units. B. Aliasing of the variations in carbonate as measured by shipboard sampling at 75-cm intervals (dashed line) versus detailed 10-cm interval sampling (solid line). Data points are indicated by squares (detailed data) and triangles (shipboard data).

Table 3. General statistics for high resolution calcium carbonate records from Site 572.

Hole	Depth interval (m)	Time interval (Ma)	Number of samples	Mean value (% $CaCO_3$)	Variance (%^{2})	Range (% $CaCO_3$)
572C	30–50	2–3	178	75	44	35
572C	50–90	3–4	180	79	85	59
572A	92–110	4.7–5	178	69	75	61
572C	121–134	5.2–5.6	141	75	45	37

carbonate variations are striking when the intervals from 4.7 to 5.0 Ma and from 2 to 4 Ma are compared (Fig. 4). (The potential of aliasing of the 2-to-4-Ma record will be discussed later.) These differences are best quantified by considering the frequency domain characteristics. In Figure 5 the variance spectra for the intervals 2 to 3 Ma and 4.7 to 5 Ma are shown. The results of analyses of all four intervals represented in Table 3 are summarized in Table 4. The sample resolution in the 2-to-3-Ma interval is on the order of 6000 to 7000 yr., so the highest frequency resolved is equivalent to a 12,000-to-14,000-yr. period. In this interval (2 to 3 Ma), the spectrum is dominated by three spectral components centered at periods of about 300,000, 67,000, and 35,000 yr. (Fig. 5A). Analysis of both the 2-to-3- and 3-to-4-Ma intervals shows that the amplitudes of the carbonate variation associated with these components (where amplitude is defined as 2 × variance$^{1/2}$ associated with the spectral

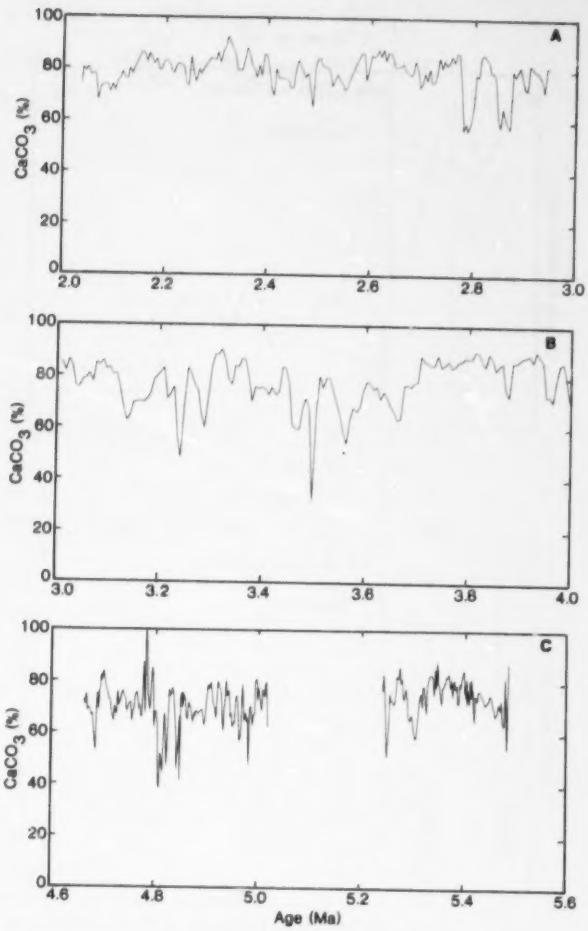

Figure 4. Detailed carbonate data from Site 572 plotted versus age. Age estimates from Site 572 chapter (this volume).

component) are 8 to 12%, 7.5 to 9%, and 2 to 5%, respectively.

In the interval from 4.7 to 5.6 Ma the spectrum shows a significant amount of variance associated with very high frequencies (Fig. 5B). From 12 to 20% of the total variance in the intervals 4.7 to 5 and 5.2 to 5.6 Ma is found at frequencies equivalent to 16,000-yr. periods. The dominant spectral component, containing 50 to 60% of the variance, centers at periods of about 40,000 to 50,000 yr. In these late Miocene records, the resolution of long periods is hindered by the limited length of record (about 400,000 yr.). However, the fact that the spectra do not show a continual increase in variance with decreasing frequency of periods over 40,000 yr. suggests that long periods are not major contributors to the variance of the intervals analyzed.

To determine whether the differences between these intervals represent real changes in the variability of the carbonate system of the latest Miocene and Pliocene, we must consider a number of problems. As mentioned above, sample aliasing may be important, because the

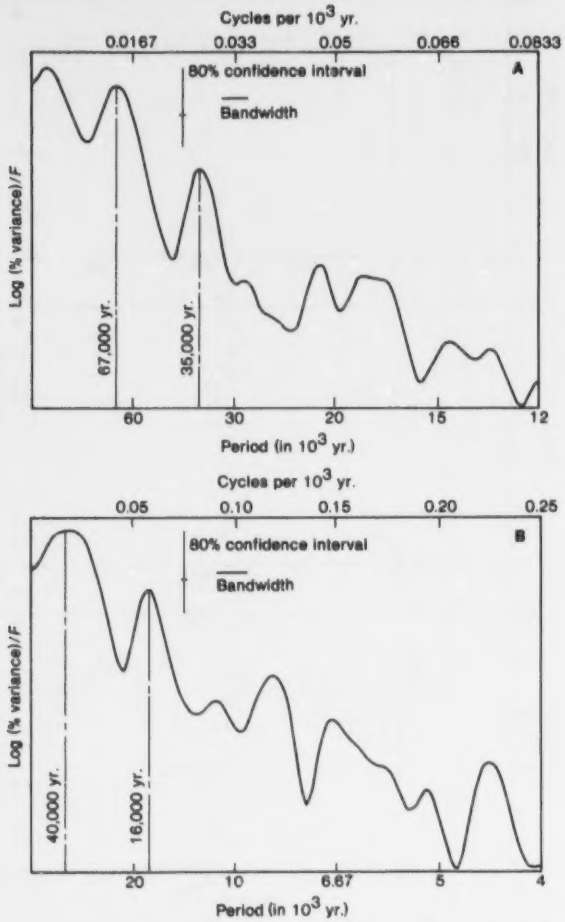

Figure 5. Variance spectra from Site 572 carbonate data. Spectra are plotted on a linear frequency scale and a log variance scale. Confidence interval is for the 80% level; horizontal bar gives the bandwidth of spectral calculations. Frequencies are in cycles per 10^3 yr. and periods in 10^3 yr. A. Spectra for 2-to-3-Ma interval, Hole 572C (data shown in Fig. 4A). B. Spectra for 4.7-to-5-Ma interval, Hole 572A (data shown in Fig. 4C).

Table 4. Summary of spectral results for detailed calcium carbonate time series from Site 572.

Interval (Ma) [m]	Variance with frequency bands (10^3-yr. periods) ∞–142	142–42	42–30	Total	Sample interval (yr.)
2–3 [30–50]	15	14	2	35	6000
3–4 [50–90]	37	21	6	71	6000
	142–23	23–12.5	12.5–7	Total	Sample interval (yr.)
4.7–5 [92–110]	34	10	6	62	2000
5.2–5.6 [121–134]	20	8	3	41	2000

sampling resolution of the Site 572 data varies by a factor of 3. Theoretically, the sample spacing of 6000 yr. in the interval from 2 to 4 Ma should resolve periods on the order of 16,000 yr. Since no evidence of important periods shorter than 35,000 yr. exists in the Pliocene records, in terms of either significant spectral peaks or in the amount of variance accounted for by high frequencies, it is unlikely that aliasing is an important problem in the Pliocene section.

To verify the absence of sample aliasing in the lower sedimentation rate intervals of Site 572, additional samples were taken at 3-cm intervals to provide a 2000-yr. resolution. These additional samples (two samples taken between the original 10-cm sample spacing) were taken in the intervals from 30.5 to 33.0 and 35 to 36.5 m sub-bottom. The carbonate concentrations measured (using the modified vacuum–gasometric system) in these new samples are very close to the values expected from linear interpolation between the 10-cm samples (Fig. 6), especially for the intervals from 32 to 33 and 35 to 36.5 m. In the interval between 30.5 and 32 m sub-bottom, the additional samples show slightly more variability than the original 10-cm samples. However, comparison of the means and variance of these intervals estimated from the 10-cm and 3-cm sample sets shows no significant differences. It should be noted that the similarity between the samples at 10-cm intervals and the data set sampled at 3-cm intervals, reflects, in part, the mixing of pelagic sediments by benthic organisms.

In addition to sample aliasing as a possible cause for an apparent difference between the Miocene and Pliocene records, there may be significant error in the mean sedimentation rates used to determine the time scales for these records. Magnetic stratigraphy is not available for Site 572, and sedimentation rate estimates were made by using radiolarian and diatom datums that have been correlated to the geomagnetic time scale by a number of investigators (see Barron et al., this volume). Stratigraphic analysis of all sites drilled on Leg 85 suggests that correlations to within a few meters are possible throughout the Pliocene and Miocene sections of Sites 573 and 572. Thus, it is possible to correlate accurately the magnetic stratigraphy of Site 573 with the Site 572 data (Pisias et al., this volume; Prell, this volume). Such correlations also support the estimated sedimentation rate estimates used in this study.

If the change in sedimentation rates estimated between the intervals from 68 to 208 m and 29 to 68 m sub-bottom is correct, the mass accumulation rate of calcium carbonate changes from 3.5 to 1 g/cm^2 per 10^3 yr., respectively. Associated with this threefold decrease in mass accumulation rate (Table 1) is a marked decrease in high-frequency variations in carbonate content. Thus, if the carbonate variations are converted to mass accumulation rates, the latest Miocene carbonate record at Site 572 requires not only high-frequency variations of carbonate content but also very high amplitude variations in the total mass of carbonate dissolved or preserved as compared to the Pliocene interval. However, these mass accumulation rate differences may have an effect on the nature of the variability of the carbonate content in a sediment column.

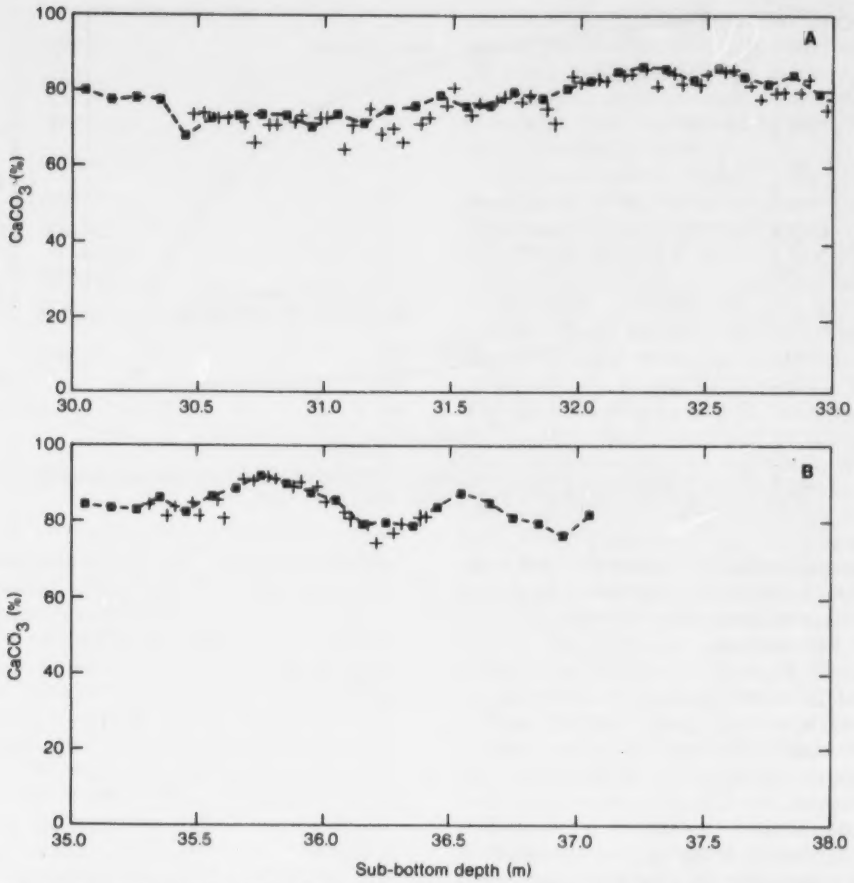

Figure 6. Detailed sampling of Hole 572C done to determine whether sample aliasing was present. Solid squares represent samples at 10-cm sample spacing, and crosses represent additional samples taken at about 3-cm intervals. Note the close agreement of 3-cm samples and values expected from linear interpolation (dashed line) between the 10-cm samples in the intervals 32 to 33 and 35 to 36.5 m sub-bottom. All samples analyzed with high precision carbonate analysis technique described in text. A. Sub-bottom depths 30 to 33 m. B. Sub-bottom depths 35 to 37 m.

Causes of Carbonate Fluctuations—A Mass Accumulation Rate Approach

A useful review of the hypotheses for variation in calcium carbonate concentrations is given by Volat et al. (1980). The weight percentage of calcium carbonate in pelagic sediments reflects the balance between the rate of input of calcium carbonate to the sediment surface, the rate of carbonate dissolution, and rate of accumulation of non-carbonate diluents. The major noncarbonate sediment at Site 572 is biogenic silica (opal), so the rate of noncarbonate deposition reflects the rate of input versus the rate of dissolution of opal.

The effects of the factors controlling carbonate deposition can be modeled as in Figure 7 (Heath and Culberson, 1970; Dean et al., 1981; Gardner, 1982). In Figure 7 it is assumed that the initial pelagic rain is 85% carbonate and 15% noncarbonate. (Note that the assumption of an initial pelagic rain of 85% would require some dissolution of noncarbonate material at the sediment surface to account for higher $CaCO_3$ contents in some of the Site 572 samples.) Variations in the concentration of calcium carbonate can result from changes in dilution by non-$CaCO_3$ or from changes in the percentage of calcium carbonate dissolved. The percentage of dilution D needed to produce the observed calcium carbonate C_f from the initial carbonate content C_i (Gardner, 1975) is

$$D = 100([C_i/C_f] - 1)/(1 - C_i)$$

The percentage carbonate lost (L) to dissolution needed to produce the observed noncarbonate fraction N_f from the initial fraction N_i is

$$L = 100(1 - [N_i/N_f])/(1 - N_i)$$

Analyses of late Pleistocene sediments (Volat et al., 1980) and Cenozoic sections (Dean et al., 1981; Dunn and Moore, 1981) suggest that dissolution rather than dilution plays the dominant role in controlling carbonate variations. In the following discussion we infer that dissolution plays an important role in controlling pre-

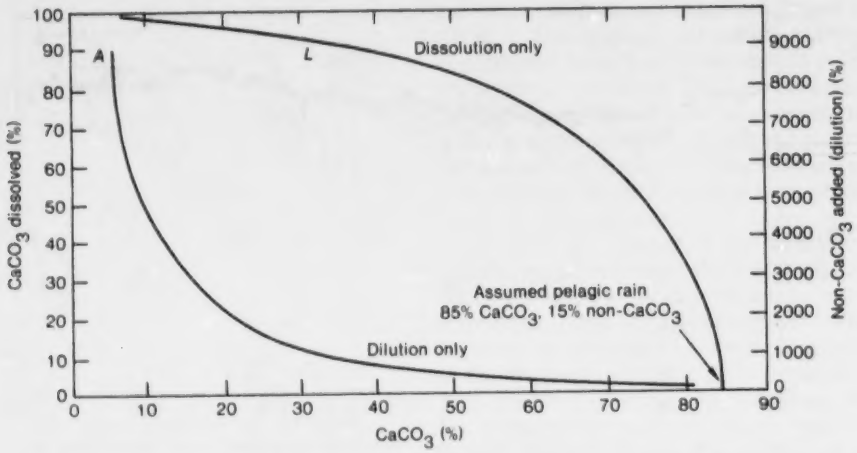

Figure 7. Curves for the loss of carbonate by dissolution (*L*) and addition of noncarbonate dilutents (*A*) to an initial carbonate rain of 85% $CaCO_3$ (after Dean et al., 1981).

Pleistocene carbonate variations in Site 572, but without detailed studies of carbonate preservation we cannot eliminate variations in biogenic silica deposition or preservation as important controls.

As is apparent in Figure 7, changing the observed carbonate content from an initial 85% to a value of 80% by dissolution alone requires a minimum of 30% of the initial carbonate to be dissolved. If we compare two different sediment records, as in the case of the Pliocene and Miocene at Site 572, and calculate the percentage dissolution required to describe the individual records, we have inherently assumed that dissolution is the only process responsible for changes in carbonate content (i.e., there are no changes in supply or dilution by other sediment fractions) and that the system is steady-state over each interval. This implies that for a given change in $CaCO_3$ content, the proportion of $CaCO_3$ that has been dissolved is constant and is independent of the absolute rate of dissolution. For example, the change from 85 to 80% $CaCO_3$ would require three times the rate of dissolution for a sediment column with a carbonate deposition rate of 3 g/cm^2 per 10^3 yr. as it would for one with a rate of 1 g/cm^2 per 10^3 yr. For the Site 572 data, this assumption of dissolution-controlled variation would suggest that the amplitude of variation in $CaCO_3$ percentages in the uppermost Miocene sediment (which is similar to the Pliocene data) would represent a calcium carbonate dissolution rate of three times that needed to produce the observed carbonate percentage variations in the Pliocene sediment. Thus, not only was the wavelength of carbonate variations much shorter during the Miocene, but the variations in the total mass of carbonate dissolved were significantly higher.

Since the mass of carbonate preserved, or the rate of dissolution, provides more information than $CaCO_3$ percentages, we suggest a different approach to describing changes in carbonate content. It is our belief that changes from the mean concentration of calcium carbonate caused by specific changes in oceanographic processes are best described in terms of changing rates of dissolution rather than simply changing proportions of carbonate preserved at any one location.

An example of an important consequence of this approach is to consider the amplitude of carbonate variations associated with the 67,000-yr. spectral component of the 2-to-3-Ma carbonate record of Site 572 (Fig. 5A). The amplitude of this frequency component is about 10% $CaCO_3$ in the intervals with mean sediment accumulation rates of 1.00 g/cm^2 per 10^3 yr. and a mean carbonate content of 75% (Table 1). If we assume that the supply of non-$CaCO_3$ sediment has remained constant, a change in the mass accumulation of $CaCO_3$ of 0.2 g/cm^2 per 10^3 yr. is required to produce the observed 10% carbonate content signal. The value of 0.2 g/cm^2 per 10^3 yr. is the amplitude of the change in accumulation rate associated with the 67,000-yr. frequency component and may reflect changes in dissolution as well as production. If the total mass accumulation rate was 3.5 g/cm^2 per 10^3 yr. as in the 5.2-to-5.6-Ma interval, the 0.2 g/cm^2 per 10^3 yr. change in carbonate deposition would produce a carbonate content change of only 4%.

The relationship between the amplitude of the change in the carbonate concentration and the mean mass accumulation rate can be calculated for a given mean carbonate percentage (75% is used in Fig. 8A). Two values for the net change in carbonate mass accumulation rates (0.2 and 0.35 g/cm^2 per 10^3 yr.) are shown in Figure 8A. A mean of 75% was chosen, because this is a typical value for the mean carbonate value of all sites drilled on Leg 85 in the equatorial Pacific. As shown in Figure 8A, for mass accumulation rates of 0.5 to 2.0 g/cm^2 per 10^3 yr. (sedimentation rates on the order of 1 to 3 cm/10^3 yr.), a 0.2 g/cm^2 per 10^3 yr. rate change in carbonate deposition is reflected in carbonate concentration as a variation by a factor of 5 (from 40 to 8% $CaCO_3$).

Thus far we have assumed that changes in carbonate concentrations reflect changes in net carbonate mass accumulation rates (i.e., our supply–dissolution model). If we consider that changes in calcium carbonate content at Site 572 reflect changes in noncarbonate (dilu-

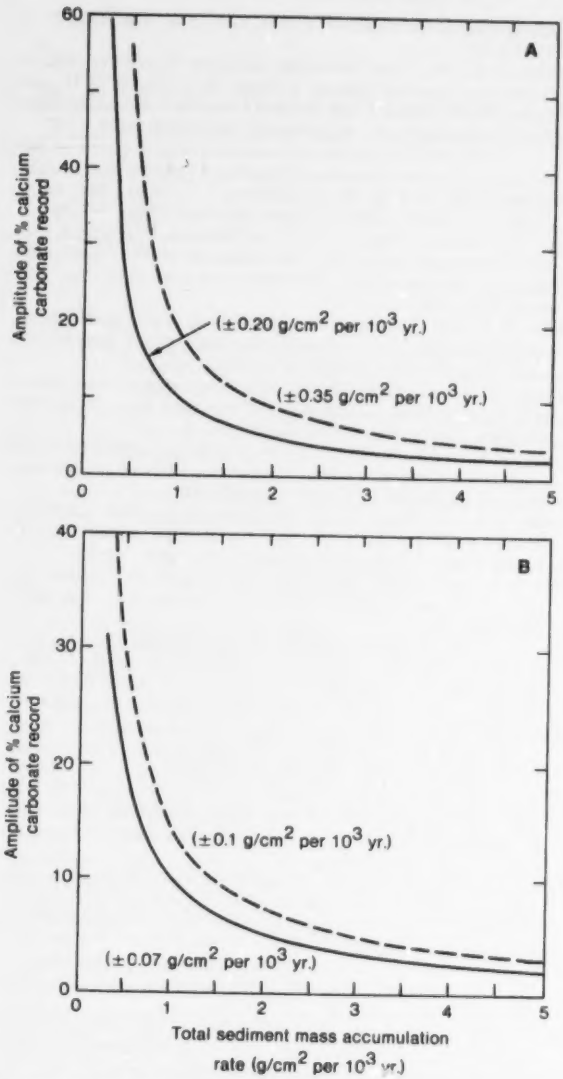
A
Amplitude of % calcium carbonate record
(±0.20 g/cm² per 10³ yr.)
(±0.35 g/cm² per 10³ yr.)
B
(±0.1 g/cm² per 10³ yr.)
(±0.07 g/cm² per 10³ yr.)
Total sediment mass accumulation rate (g/cm² per 10³ yr.)

Figure 8. Amplitude of the carbonate concentration record versus total mean accumulation rates for a given response in the net accumulation rate of carbonate or noncarbonate. A. Calculations made assuming a mean carbonate concentration of 75%, a constant noncarbonate flux, and a change in net carbonate deposition of 0.20 and 0.35 g/cm² per 10^3. B. Calculations assume a mean carbonate concentration of 75%, a constant carbonate flux, and a change in net noncarbonate accumulation of 0.07 and 0.10 g/cm² per 10^3 yr.

tion), we can calculate the change in the mass accumulation necessary to produce carbonate fluctuations. If we use the same starting values (a mean mass accumulation rate of 1 g/cm² per 10^3 yr. and a mean carbonate content of 75%), a change in net noncarbonate accumulation of 0.07 g/cm² per 10^3 yr. is required to produce a 10% $CaCO_3$ amplitude in the carbonate record. Although this value is less than half of the change needed if only variations in carbonate supply and dissolution are considered, it represents 30% of the mean noncarbonate accumulation. As shown in Figure 8B, the amplitude of carbonate variations caused by changes in noncarbonate deposition also varies as a function of total mean accumulation. An increase in the amplitude of variations in carbonate content with decreasing sedimentation rates is produced by variation in noncarbonate accumulation rates.

Without detailed studies of the degree of carbonate dissolution in the sediments from Site 572 or detailed time control to constrain very short-term changes in sedimentation rates, it is difficult to evaluate the ultimate cause of the carbonate content fluctuations in this equatorial Pacific site. However, one possible constraint is supplied by the variance spectrum calculated from these data. If changes in the $CaCO_3$ records reflect changes in carbonate supply and/or dissolution, then we would expect significant changes in the short-term mass accumulation rates. In Figure 9 the percentage change in the total accumulation rate associated with the estimated 0.2 and 0.07 g/cm² per 10^3 yr. rate changes in carbonate and noncarbonate accumulation is plotted as a function of mean sedimentation rates. For a mean rate of 1 g/cm² per 10^3 yr., changes in noncarbonate deposition would produce a 15% change in the total accumulation, as opposed to a 40% change if carbonate deposition is controlling the carbonate concentrations. In Figure 4 the carbonate minima tend to occur over shorter depth intervals relative to maxima. This could reflect reduced sedimentation rates during intervals of decreased carbonate concentration. This type of sedimentation rate distortion would produce harmonics in the variance spectra associated with important periodic components (Holman and Pisias, 1983). In the 2-to-3-Ma interval of the Site 572 data, the secondary spectral peak (35,000 yr.) is very close to the predicted harmonic of the 67,000-yr. com-

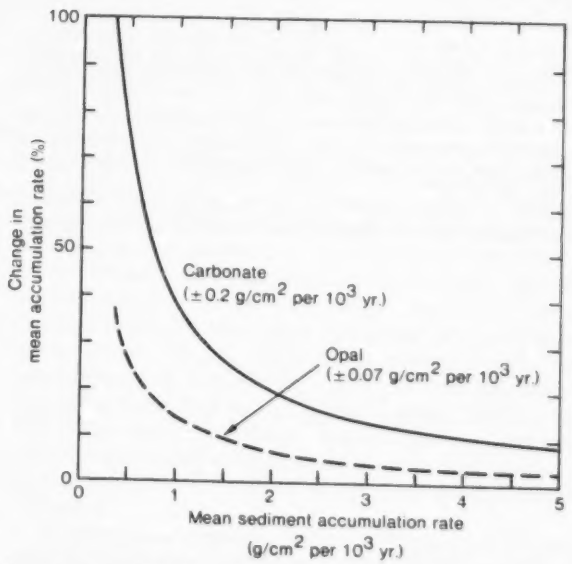

Figure 9. Percentage change in mean accumulation rate versus mean accumulation rate for a 0.07 g/cm² per 10^3 yr. change in the noncarbonate accumulation rate (dashed line) and a 0.2 g/cm² per 10^3 yr. change in the carbonate accumulation rate (solid line).

ponent. Further study is necessary to evaluate whether the variance and phase of the 35,000-yr. component is consistent with sedimentation rate changes on the order of 67,000 yr.

These calculations of carbonate content changes relative to mass accumulation rates have important implications for the resolution of carbonate records from lower sedimentation rate intervals. As sedimentation rates decrease and/or sampling intervals increase, then aliasing becomes an important problem. If the amplitude of the carbonate variation also tends to increase with decreasing sedimentation rates, the effect of aliasing becomes even more exaggerated.

CONCLUSIONS

Detailed analysis of calcium carbonate concentrations in the HPC sections of Site 572 shows a significant difference between the nature of carbonate deposition at this equatorial site during the late Miocene and during the Pliocene. Both the degree of variability of carbonate deposition and the total sediment and carbonate accumulation rates were markedly higher in the late Miocene than in the Pliocene intervals. The present data set, however, does not allow us to determine the nature of the transition between these two regimes of carbonate deposition.

Calculations of changes in mass accumulation rates suggest that the nature of a carbonate concentration record is controlled in part by total mass accumulation rates and that small changes in the mass accumulation of noncarbonate material have a significant effect on the carbonate concentration data. Thus, without detailed analysis of the changes in mass accumulation rates or the influence of dissolution, it is difficult to determine the true causes of the carbonate variations observed.

REFERENCES

Dean, W. E., Gardner, J. V., and Čepek, P., 1981. Tertiary carbonate-dissolution cycles on the Sierra Leone Rise, eastern equatorial Atlantic Ocean. *Mar. Geol.*, 39:81–101.

Dunn, D. A., 1980. Revised technique for quantitative calcium carbonate analysis using the "Karbonat-Bombe" and correlations to other quantitative carbonate analysis methods. *J. Sediment. Petrol.*, 50:631–637.

Dunn, D. A., and Moore, T. C., Jr., 1981. Late Miocene–Pliocene (Magnetic Epoch 9–Gilbert Magnetic Epoch) calcium carbonate stratigraphy of the equatorial Pacific. *Geol. Soc. Am. Bull.*, Pt. I, 92:104–107.

Gardner, J. V., 1975. Late Pleistocene carbonate dissolution cycles in the eastern equatorial Atlantic. *In* Sliter, W. V., Bé, A. W. H., and Berger, W. H. (Eds.), *Dissolution of Deep-Sea Carbonates*. Spec. Publ. Cushman Found. Foraminiferal Res., 13:129–141.

_____, 1982. High-resolution carbonate and organic-carbon stratigraphies for the late Neogene and Quaternary from the eastern equatorial Pacific. *In* Prell, W. L., Gardner, J. V., et al., *Init. Repts. DSDP*, 68: Washington (U.S. Govt. Printing Office), 347–364.

Hays, J. D., Saito, T., Opdyke, N. D., and Burckle, L. H., 1969. Pliocene–Pleistocene sediments of the equatorial Pacific: their paleomagnetic, biostratigraphic, and climatic record. *Geol. Soc. Am. Bull.*, 80(8):1481–1514.

Heath, G. R., and Culberson, C., 1970. Calcite: degree of saturation, rate of dissolution and compensation depth in the deep oceans. *Geol. Soc. Am. Bull.*, 81(10):3157–3160.

Holman, R. A., and Pisias, N. G., 1983. Geologic time series: distortion due to periodic variations in sedimentation rates. *Trans. Am. Geophys. Union*, 64(45):738. (Abstract)

Jones, G. A., and Kaiteris, P., 1983. A vacuum-gasometric technique for rapid and precise analysis of calcium carbonate in sediments and soils. *J. Sediment. Petrol.*, 53(2):655–659.

Moore, T. C., Jr., Pisias, N. G., and Dunn, D. A., 1982. Carbonate time series of the Quaternary and late Miocene sediments in the Pacific Ocean: a spectral comparison. *Mar. Geol.*, 46:217.

Prell, W. L., 1978. Upper Quaternary sediments of the Colombia Basin: spatial and stratigraphic variations. *Geol. Soc. Am. Bull.*, 89(8):1241–1255.

_____, 1982. Oxygen and carbon isotope stratigraphy for the Quaternary of Hole 502B: evidence for two modes in isotopic variability. *In* Prell, W. L., Gardner, J. V., et al., *Init. Repts. DSDP*, 68: Washington (U.S. Govt. Printing Office), 455–464.

Shackleton, N. J., Backman, J., Zimmerman, H., Kent, D. V., Hall, M. A., Roberts, D. G., Schnitker, D., Baldauf, J. G., Desprairies, A., Homrighausen, R., Huddlestun, P., Keene, J. B., Kaltenback, A. J., Krumsiek, K. A. O., Morton, A. C., Murray, J. W., and Westberg-Smith, J., 1984. Oxygen isotope calibration of the onset of ice-rafting and history of glaciation in the North Atlantic region. *Nature*, 307:620–623.

Vincent, E., 1981. Neogene carbonate stratigraphy of Hess Rise (central North Pacific) and paleoceanographic implications. *In* Thiede, J., Vallier, T. L., et al., *Init. Repts. DSDP*, 62: Washington (U.S. Govt. Printing Office), 571–606.

Volat, J. L., Pastouret, L., and Vergnaud Grazzini, C., 1980. Dissolution and carbonate fluctuations in Pleistocene deep-sea cores: a review. *Mar. Geol.*, 34:1–28.

Woodruff, F., Savin, S. M., and Douglas, R. G., 1981. Miocene stable isotope record: a detailed deep Pacific Ocean study and its paleoclimatic implications. *Science*, 212:665–668.

Date of Initial Receipt: 28 October 1983
Date of Acceptance: 18 April 1984

Reprinted from Mayer, L., Theyer, F., et al., 1985
Initial Reports of the Deep Sea Drilling Project, Volume LXXXV, Washington (U. S. Government Printing Office)

20. PLIOCENE STABLE ISOTOPE AND CARBONATE STRATIGRAPHY (HOLES 572C AND 573A): PALEOCEANOGRAPHIC DATA BEARING ON THE QUESTION OF PLIOCENE GLACIATION[1]

Warren L. Prell, Department of Geological Sciences, Brown University[2]

ABSTRACT

Holes 572C and 573A provide high resolution (~5000-yr. sampling interval) records of oxygen and carbon isotope stratigraphy (*Globigerinoides sacculifera*) and carbonate stratigraphy for the Pliocene of the equatorial Pacific. These data enable detailed correlation of carbonate events between sites and provide additional resolution to the previous carbonate stratigraphy. Comparison of calcium carbonate and $\delta^{18}O$ data reveal a "Pacific-type" carbonate stratigraphy throughout the Pliocene. The $\delta^{18}O$ data have two modes of variability with a boundary at 2.9 Ma. The planktonic $\delta^{18}O$ record does not have a steplike enrichment at 3.2 Ma, which is observed in benthic records elsewhere, suggesting that this event does *not* represent the proposed initiation of northern hemispheric glaciation. Hole 572C does record a distinct $\delta^{18}O$ enrichment event at about 2.4 Ma, which has been previously associated with the onset of major ice rafting in the North Atlantic.

INTRODUCTION

Leg 85 provides an opportunity to study high resolution records of carbonate-rich sediments from the equatorial Pacific. Although this area has been extensively sampled in the past, previous cores were not suitable for high resolution work. Soft sediments in cores from earlier DSDP sites in this area (summarized in van Andel et al., 1975; Vincent, 1981) are disturbed by drilling, which rendered detailed work nearly impossible. The piston cores from this area (Hays et al., 1969; Saito et al., 1975) have relatively continuous records but very low accumulation rates (<5 m/m.y.). Hence, many details of the carbonate and isotopic records from the equatorial Pacific are obscured by low sample density, drilling disturbances and bioturbation. The multiple hydraulic piston cores of Leg 85 provide records of continuous, undisturbed Neogene sediments having moderate to high rates of accumulation.

The sediments of the equatorial Pacific have been important in deciphering the paleoceanography of the Neogene. Specifically, they have been used to establish temporal variations of calcium carbonate content and the relationship of carbonate stratigraphy to climatic changes. They have also been used to develop the oxygen and carbon isotopic record of Neogene foraminifers, which has been used to establish the temporal sequence of glaciation in the Northern Hemisphere.

This study uses Pliocene sediments at Sites 572 and 573 to provide a detailed record of isotopic and carbonate variations during the Pliocene from about 4.0 to 2.0 Ma. The specific objective is to construct a high resolution (~5000-yr. sample interval) time series of planktonic $\delta^{18}O$ and total carbonate and to compare that record to the benthic isotopic and carbonate record of equatorial Pacific piston Core V28-179 (Shackleton and Opdyke, 1977). Specifically, I seek to establish the pattern of planktonic $\delta^{18}O$ variability prior to, during, and after the proposed initiation of Northern Hemisphere glaciation at about 3.2 Ma (Shackleton and Opdyke, 1977). I also wish to compare the record of calcium carbonate dissolution events (for summary, see Vincent, 1981) to the planktonic and benthic isotopic records to determine the correlation in the timing of glacial–sea level events and the carbonate preservation in the equatorial Pacific.

DATA AND METHODS

Samples were selected from Hole 572C (3893 m water depth) and Hole 573A (4301 m water depth) because these holes were at the shallowest sites and offered the best possibility for good carbonate preservation. Specifically, samples were analyzed at 10-cm intervals in Cores 4, 5, 6, and 7 (29.3 to 67.7 m) in Hole 572C and at 15- to 20-cm intervals in Cores 5 and 6 (39.8 to 57.7 m) in Hole 573A. All samples were analyzed for coarse fraction content and calcium carbonate content, and the isotopic composition of *Globigerinoides sacculifera* (300 to 355 μm) was analyzed in samples from Hole 572C.

All samples were disaggregated in tap water and wet sieved through a 150 μm sieve and dried at 50°C. Coarse fraction values are the weight percentage of the fraction greater than 150 μm. Calcium carbonate content was measured using a modified version of the gasometric apparatus described by Jones and Kaiteris (1983). The Brown University carbonate system uses a differential pressure gauge rather than vacuum gauge and routinely attains a precision of about 0.5% (based on duplicate analyses).

The oxygen and carbon isotopic composition of foraminifers were measured on approximately 10 to 20 individuals of *G. sacculifera* that were cleaned in an ultrasonic bath to remove fine fraction contamination. All samples were roasted under a vacuum at 370°C for 1 hr. H_2O and CO_2 were extracted from the carbonate reac-

[1] Mayer, L., Theyer, F., et al., *Init. Repts. DSDP*, 85: Washington (U.S. Govt. Printing Office).
[2] Address: Department of Geological Sciences, Brown University, Providence, RI 02912.

tion with orthophosphoric acid at 50°C and separated by a series of three transfer steps; the CO_2 was analyzed in an online VG Micromass 602D Mass Spectrometer. All data are referred to PDB by the standard δ notation (Craig, 1957). Calibration to PDB is through three intermediate laboratory standards. Agreement among all calibration standards is ±0.2 ‰. Analytic precision indicated by the first acceptable analysis of the working carbonate standard before each analytical session (31 days) is ±0.09 ‰ (1 σ) for oxygen and ±0.06 ‰ for carbon. Analytic precision based on 41 blind duplicate analyses run on separate days is ±0.09 ‰ (average $\frac{1}{2}\Delta\delta^{18}O$) and ±0.14 ‰ (average $\frac{1}{2}\Delta\delta^{13}C$). The coarse fraction, carbonate, $\delta^{18}O$, and $\delta^{13}C$ data for Hole 572C are plotted versus core depth in Figure 1 and are summarized in Table 1. The carbonate data for Hole 573A are shown in Figure 2 and are given in Table 2. Carbonate data for Core V28-179 (Fig. 2) are from Dunn (1982).

RESULTS

Carbonate and Magnetostratigraphy

One objective of this study is to compare the carbonate and isotopic records of Site 572 to the magnetostratigraphy of other equatorial Pacific cores, such as V24-59 (Hays et al., 1969), RC12-66 (Saito et al., 1975), and V28-179 (Shackleton and Opdyke, 1977). Unfortunately, a reliable magnetostratigraphy could not be established for Site 572 (Weinreich and Theyer, this volume). Therefore, carbonate and isotopic records of Site 572 have been correlated to the magnetostratigraphy of Site 573 and Core V28-179. Initially, Site 572 was correlated to

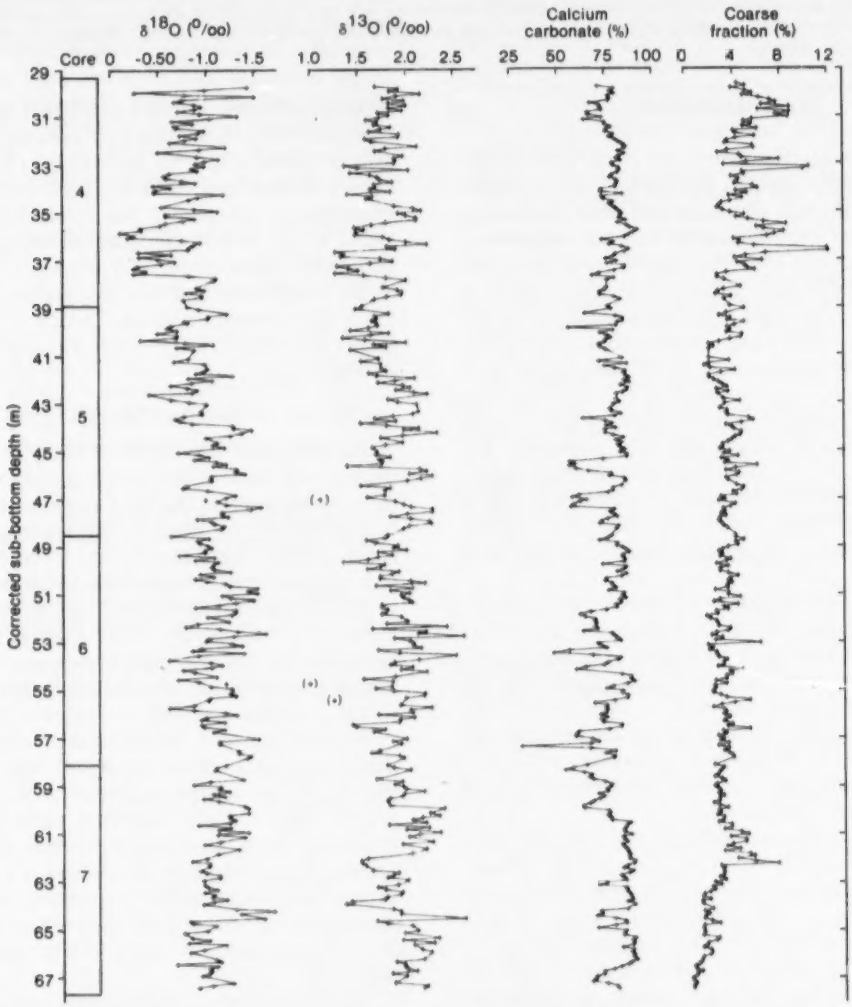

Figure 1. Oxygen and carbon isotope stratigraphy (PDB, *G. sacculifera*) and calcium carbonate and coarse fraction stratigraphy for Hole 572C (Cores 4, 5, 6, and 7). Averages of duplicates are plotted and values in parentheses are suspect but are not eliminated because they have not been duplicated more than once. All data are given in Table 1.

Table 1. Coarse fraction (>150 μm), calcium carbonate and oxygen and carbon isotopic data (PDB) for Hole 572C (Cores 4, 5, 6, and 7).

Sample (level in cm)	Sub-bottom depth (m)	Coarse fraction (%)	Calcium carbonate (%)	*G. sacculifera* $\delta^{18}O$ (‰)	*G. sacculifera* $\delta^{13}C$ (‰)
4-1, 36	29.64	4.5	—	—	—
4-1, 45	29.74	5.2	71.86*	−1.44	1.69
4-1, 55	29.84	4.0	80.23	−0.99	1.93
4-1, 65	29.94	5.2	78.33*	−0.26	1.84
4-1, 75	30.04	5.8	80.37	−0.78	2.16
4-1, 85	30.14	5.0	77.34	−1.51	1.91
4-1, 95	30.24	6.4	78.00	−0.75	1.77
4-1, 105	30.34	7.3	77.47	−0.79	2.10
4-1, 105				−0.54	1.88
4-1, 115	30.44	7.8	67.75	−0.88	1.83
4-1, 125	30.54	6.6	72.61	−0.95	2.01
4-1, 135	30.64	8.9	73.36	−0.88	1.83
4-1, 145	30.74	6.3	73.82	−0.87	2.08
4-1, 145				−0.56	1.86
4-2, 5	30.84	8.9	66.54*	−0.94	1.72
4-2, 15	30.94	7.8	66.90*	−1.33	1.83
4-2, 25	31.04	8.8	73.74	−1.04	1.73
4-2, 35	31.14	5.8	64.47*	−0.70	1.61
4-2, 35				−0.61	1.58
4-2, 45	31.24	5.1	75.24	−0.86	1.71
4-2, 55	31.34	5.7	75.87	−0.67	1.68
4-2, 65	31.44	5.0	78.65	−0.63	1.78
4-2, 65				−0.76	1.92
4-2, 75	31.54	6.2	76.30	−0.98	1.74
4-2, 85	31.64	4.2	76.02	−0.92	1.63
4-2, 95	31.74	4.4	79.80	−0.73	1.94
4-2, 105	31.84	6.0	77.87	−1.03	1.73
4-2, 105				−0.77	2.12
4-2, 115	31.94	4.4	80.61	−0.78	1.59
4-2, 125	32.04	3.7	82.55	−0.63	1.65
4-2, 135	32.14	3.5	84.72	—	—
4-2, 145	32.24	5.8	86.33	−1.24	2.15
4-2, 145				−1.16	2.11
4-3, 5	32.34	5.9	85.84	−0.93	1.80
4-3, 15	32.44	3.7	82.62	−0.50	1.69
4-3, 25	32.54	2.9	85.76	—	—
4-3, 35	32.64	4.7	83.48	−0.91	1.98
4-3, 45	32.74	4.9	81.78	−1.13	1.89
4-3, 55	32.84	8.0	83.73	−0.99	1.90
4-3, 65	32.94	5.3	79.33	−0.81	1.83
4-3, 65				−0.97	1.95
4-3, 75	33.04	3.4	79.99	−0.98	1.37
4-3, 85	33.14	10.5	82.82	−0.85	1.50
4-3, 95	33.24	10.0	83.08	−0.91	2.04
4-3, 105	33.34	4.9	82.14	−0.62	1.43
4-3, 115	33.44	5.1	79.24	−0.59	1.54
4-3, 115				−0.53	1.74
4-3, 125	33.54	4.0	78.21	−0.59	1.71
4-3, 135	33.64	4.6	81.36	−0.75	1.74
4-3, 145	33.74	4.5	82.07	−0.89	1.87
4-4, 5	33.84	4.3	81.36	−0.45	1.68
4-4, 15	33.94	5.8	80.89	−0.63	1.69
4-4, 25	34.04	6.2	73.69*	−0.47	1.64
4-4, 35	34.14	4.4	73.47*	−0.46	1.85
4-4, 45	34.24	5.3	84.74	−1.18	1.40
4-4, 55	34.34	3.8	73.93*	−0.91	1.66
4-4, 65	34.44	4.9	75.02	−0.82	1.60
4-4, 79	34.57	3.9	79.73	—	—
4-4, 85	34.64	3.2	77.93	—	—
4-4, 95	34.74	3.0	79.59	−0.54	1.89
4-4, 105	34.84	2.8	81.28	−0.88	2.09
4-4, 115	34.94	3.3	82.74	−1.12	2.17
4-4, 125	35.04	3.9	84.33	−0.58	1.93
4-4, 135	35.14	5.1	83.69	−0.58	2.01
4-4, 145	35.24	4.4	83.28	−0.83	2.02
4-4, 145				−0.94	2.22
4-5, 5	35.34	5.4	86.35	−0.66	1.94
4-5, 5				−0.87	2.30
4-5, 15	35.44	6.7	82.40	−0.81	1.73
4-5, 15		6.7	82.40	−0.35	1.86
4-5, 25	35.54	8.6	86.66	−0.65	1.45
4-5, 25				−0.40	1.85
4-5, 35	35.64	6.1	88.68	−0.11	1.48
4-5, 35		6.1	88.68	−0.52	1.45

Table 1. (Continued).

Sample (level in cm)	Sub-bottom depth (m)	Coarse fraction (%)	Calcium carbonate (%)	*G. sacculifera* $\delta^{18}O$ (‰)	*G. sacculifera* $\delta^{13}C$ (‰)
4-5, 45	35.74	6.7	92.48	−0.11	1.48
4-5, 45				−0.54	1.66
4-5, 55	35.84	8.4	90.42	0.02	1.47
4-5, 55				−0.21	1.51
4-5, 65	35.94	7.6	87.93	0.06	1.42
4-5, 65				−0.53	1.55
4-5, 75	36.04	7.0	85.79	−0.19	1.78
4-5, 75				−0.16	1.75
4-5, 85	36.14	4.2	74.04*	−0.69	1.63
4-5, 85				−0.80	2.04
4-5, 95	36.24	4.7	79.94	−0.71	2.01
4-5, 95				−1.16	2.01
4-5, 105	36.34	4.6	77.95*	−0.73	2.13
4-5, 105				−1.01	2.33
4-5, 115	36.44	5.9	84.32	−0.83	1.81
4-5, 125	36.54	12.0	88.10	−0.81	1.90
4-5, 135	36.64	12.1	85.71	−0.29	1.27
4-5, 145	36.74	6.9	81.29	−0.64	1.36
4-6, 5	36.84	5.2	79.92	−0.30	1.33
4-6, 15	36.94	4.3	76.01*	−0.50	1.74
4-6, 25	37.04	6.6	81.63	−0.67	1.87
4-6, 35	37.14	4.5	76.58*	−0.53	1.64
4-6, 45	37.24	5.1	85.97	−0.28	1.29
4-6, 55	37.34	5.3	85.43	−0.24	1.41
4-6, 65	37.44	6.0	80.32	−0.37	1.51
4-6, 75	37.54	3.6	72.34*	−0.24	1.27
4-6, 85	37.64	2.8	68.87*	−0.82	1.57
4-6, 95	37.74	2.8	80.17	−1.10	1.80
4-6, 105	37.84	3.4	76.44	−1.08	2.01
4-6, 135	38.14	4.8	76.28	−0.65	1.87
4-6, 135				−1.15	1.68
4-6, 145	38.24	3.4	75.31	−0.98	1.92
4-7, 5	38.34	2.9	72.61	−0.79	1.97
4-7, 15	38.44	2.7	72.96	−0.93	1.96
4-7, 25	38.54	4.0	80.26	−0.95	1.81
4-7, 35	38.64	3.4	83.48	−0.76	1.68
5-1, 6	38.94	3.9	76.81	−0.80	1.55
5-1, 16	39.04	5.1	78.58	−0.92	1.48
5-1, 36	39.24	3.6	65.07*	−1.21	1.83
5-1, 46	39.34	3.0	81.09	−1.02	1.68
5-1, 56	39.44	3.9	84.36	−0.98	1.63
5-1, 56				−1.03	1.78
5-1, 66	39.54	3.7	84.49	−0.77	1.65
5-1, 73	39.61	5.1	81.90	−0.80	1.69
5-1, 86	39.74	4.3	81.14	−0.63	1.71
5-1, 96	39.84	3.7	56.19*	−0.59	1.62
5-1, 106	39.94	3.9	79.51	−0.67	1.64
5-1, 106				−0.70	1.22
5-1, 116	40.04	3.6	72.88*	−0.49	1.83
5-1, 126	40.14	4.9	76.06	−0.69	1.64
5-1, 136	40.24	4.8	78.20	−0.43	1.61
5-1, 136				−0.92	1.10
5-1, 146	40.34	3.9	75.92	−0.31	1.58
5-2, 6	40.44	3.0	74.91	−0.78	2.01
5-2, 16	40.54	2.1	72.12	−1.07	1.67
5-2, 26	40.64	2.5	73.04	−0.69	1.80
5-2, 36	40.74	2.1	75.86	−0.87	1.43
5-2, 73	41.11	2.1	84.18	−0.81	1.72
5-2, 86	41.24	3.8	72.38*	−0.66	1.54
5-2, 96	41.34	2.1	86.68	−0.98	1.74
5-2, 106	41.44	1.7	75.28*	—	—
5-2, 116	41.54	2.2	80.62	−1.01	1.75
5-2, 126	41.64	4.3	85.67	−0.97	1.80
5-2, 136	41.74	3.1	85.09	−0.89	1.62
5-2, 146	41.84	2.1	86.04	−1.27	1.70
5-3, 6	41.94	2.1	87.81	−0.81	2.10
5-3, 16	42.04	2.5	85.26	−0.80	1.91
5-3, 16				−1.31	1.87
5-3, 26	42.14	2.9	88.03	−0.84	1.71
5-3, 36	42.24	3.2	83.45*	−0.63	1.97
5-3, 46	42.34	3.6	86.94	−0.80	2.05
5-3, 56	42.44	2.7	86.61	−0.90	1.90

Table 1. (Continued).

Sample (level in cm)	Sub-bottom depth (m)	Coarse fraction (%)	Calcium carbonate (%)	*G. sacculifera* $\delta^{18}O$ (‰)	*G. sacculifera* $\delta^{13}C$ (‰)
5-3, 66	42.54	3.7	84.33	−0.85	2.09
5-3, 73	42.61	2.8	81.23	−0.40	2.23
5-3, 96	42.84	3.3	81.32	−0.63	1.82
5-3, 106	42.94	4.7	82.75	−0.82	1.92
5-3, 116	43.04	3.4	79.98	−1.00	2.12
5-3, 136	43.24	3.0	78.02	—	—
5-3, 146	43.34	3.6	78.89	−0.94	2.14
5-4, 6	43.44	3.5	83.64	−0.95	2.08
5-4, 16	43.54	3.7	80.25	−0.76	1.87
5-4, 26	43.64	5.4	63.87*	−0.41	1.81
5-4, 26				−0.92	1.54
5-4, 36	43.74	5.8	75.25	−0.72	1.90
5-4, 46	43.84	4.8	78.91	−0.85	1.53
5-4, 56	43.94	3.5	76.00	−1.27	1.80
5-4, 66	44.04	4.0	80.68	−1.28	2.14
5-4, 73	44.11	4.2	75.08	−1.47	1.98
5-4, 86	44.24	4.8	75.37	−1.36	2.33
5-4, 96	44.34	4.7	79.65	−1.24	2.09
5-4, 96				−1.25	1.85
5-4, 106	44.44	4.3	84.89	−0.99	1.74
5-4, 116	44.54	4.0	80.88	—	—
5-4, 126	44.64	3.7	83.87	−1.11	1.97
5-4, 136	44.74	3.2	81.97	−0.97	1.93
5-4, 136				−1.15	1.65
5-4, 146	44.84	3.2	83.23	−1.18	1.65
5-5, 6	44.94	3.0	85.54	—	—
5-5, 16	45.04	3.8	83.20	−0.70	1.70
5-5, 26	45.14	3.3	86.67	−0.92	1.69
5-5, 36	45.24	4.5	86.57	−1.02	1.84
5-5, 46	45.34	3.1	74.12	−0.87	1.72
5-5, 56	45.44	3.7	56.76	−1.10	1.76
5-5, 66	45.54	3.4	59.32	−1.22	2.00
5-5, 66				−1.18	1.48
5-5, 73	45.61	6.1	56.58	−1.07	1.39
5-5, 86	45.74	4.3	60.24	−1.31	2.15
5-5, 96	45.84	3.5	66.45	−1.30	2.22
5-5, 106	45.94	4.6	78.55	−1.40	2.04
5-5, 116	46.04	4.4	77.46	−1.05	2.28
5-5, 126	46.14	3.5	85.23	−1.04	2.16
5-5, 136	46.24	3.7	86.27	−0.95	2.45
5-5, 136				−1.14	1.60
5-6, 6	46.44	4.4	83.66	−0.78	1.53
5-6, 16	46.54	5.0	79.42	−0.75	1.84
5-6, 26	46.64	4.8	79.19	−1.01	1.78
5-6, 36	46.74	4.1	76.74	—	—
5-6, 46	46.84	4.4	61.55	−1.30	1.78
5-6, 56	46.94	3.1	58.01	−1.20	1.60
5-6, 66	47.04	3.4	65.47	−1.29	1.06
5-6, 66				−0.68	1.16
5-6, 73	47.11	2.9	62.27	−1.11	1.89
5-6, 86	47.24	4.3	58.82	−1.20	1.98
5-6, 96	47.34	3.9	57.45	−1.57	2.06
5-6, 106	47.44	3.3	80.05	−1.46	2.28
5-6, 116	47.54	3.4	77.80	−1.16	2.28
5-6, 126	47.64	3.1	79.57	−1.16	2.02
5-6, 136	47.74	3.5	81.61	−1.22	1.84
5-6, 146	47.84	3.0	76.70	−0.90	2.05
5-7, 6	47.94	2.9	73.27	−1.05	2.25
5-7, 16	48.04	3.1	72.47	−1.08	2.27
5-7, 26	48.14	3.3	82.30	−1.18	2.04
5-7, 36	48.24	3.6	81.20	−1.15	1.98
6-1, 6	48.54	4.3	78.56	−0.63	1.81
6-1, 16	48.64	4.3	78.44	−1.02	1.78
6-1, 26	48.74	5.0	72.23*	−0.90	1.59
6-1, 36	48.84	4.3	81.60	−0.93	1.68
6-1, 46	48.94	4.5	81.18	−1.01	1.92
6-1, 56	49.04	3.7	84.48	−1.05	1.87
6-1, 66	49.14	3.2	86.48	−0.98	2.01
6-1, 75	49.23	2.9	87.64	−0.98	1.71
6-1, 86	49.34	3.2	84.32	−0.71	1.86
6-1, 96	49.44	3.0	84.36	−1.08	1.71
6-1, 106	49.54	3.9	85.63	−0.88	1.61
6-1, 116	49.64	3.5	84.98	−1.12	1.35
6-1, 126	49.74	2.7	73.90*	−1.07	1.78
6-1, 136	49.84	3.7	86.30	−1.05	1.73

Table 1. (Continued).

Sample (level in cm)	Sub-bottom depth (m)	Coarse fraction (%)	Calcium carbonate (%)	*G. sacculifera* $\delta^{18}O$ (‰)	*G. sacculifera* $\delta^{13}C$ (‰)
6-1, 146	49.94	3.0	84.73	−1.17	1.80
6-1, 146				−0.99	1.40
6-2, 6	50.04	3.0	81.34*	−1.25	1.93
6-2, 16	50.14	3.7	86.16	−0.93	1.86
6-2, 26	50.24	4.5	83.60	−1.02	1.73
6-2, 26				−1.12	1.73
6-2, 36	50.34	3.9	75.72	−0.88	1.73
6-2, 46	50.44	3.7	75.09*	−1.00	2.05
6-2, 56	50.54	4.0	78.59	−1.19	2.20
6-2, 66	50.64	3.6	79.10	−1.24	1.69
6-2, 73	50.73	3.6	80.73	−1.53	2.07
6-2, 86	50.84	2.6	77.03*	−1.43	1.84
6-2, 96	50.94	3.7	85.01	−1.53	2.04
6-2, 106	51.04	3.7	84.12	−1.08	1.92
6-2, 106				−1.24	1.99
6-2, 116	51.14	4.7	85.76	−1.25	1.98
6-2, 126	51.24	3.0	82.71	−1.49	2.03
6-2, 136	51.34	2.5	83.23	−1.30	2.07
6-2, 146	51.44	4.5	80.65	−1.13	1.75
6-3, 6	51.54	3.3	81.04	−0.88	1.75
6-3, 16	51.64	3.7	75.62	−1.30	1.81
6-3, 26	51.74	2.7	67.46	−1.30	1.79
6-3, 36	51.84	2.8	62.12*	−1.26	1.75
6-3, 46	51.94	1.9	64.75	−1.01	1.95
6-3, 56	52.04	2.2	69.74	—	—
6-3, 66	52.14	2.7	69.97	−1.23	2.02
6-3, 75	52.23	2.8	70.31	−0.90	1.80
6-3, 86	52.34	2.9	69.79	−0.78	2.43
6-3, 96	52.44	3.9	71.02	−1.40	1.93
6-3, 96				−0.87	1.37
6-3, 106	52.54	3.7	63.89*	−1.32	2.21
6-3, 116	52.64	2.7	78.62	−1.62	2.13
6-3, 126	52.74	2.3	80.02	−1.28	2.61
6-3, 136	52.84	3.2	81.62	−1.11	2.04
6-3, 136				−0.94	1.72
6-3, 146	52.94	2.6	83.20	−0.99	2.04
6-4, 6	53.04	6.4	71.10	−1.26	2.08
6-4, 16	53.14	2.0	73.05	−1.37	2.08
6-4, 26	53.24	2.4	75.86	−0.95	2.16
6-4, 36	53.34	2.1	56.32	−0.85	1.71
6-4, 46	53.44	2.7	48.32*	−1.39	1.93
6-4, 56	53.54	2.7	68.67	−0.91	2.53
6-4, 66	53.64	2.9	83.12	—	—
6-4, 75	53.73	3.6	81.63	−0.61	2.14
6-4, 86	53.84	3.3	76.66	−1.04	1.88
6-4, 96	53.94	3.3	74.44	−1.16	1.84
6-4, 106	54.04	2.8	64.87	−1.05	2.07
6-4, 116	54.14	4.9	59.96*	−0.48	2.14
6-4, 116				−1.03	1.77
6-4, 126	54.24	3.8	—	−0.87	2.22
6-4, 136	54.34	4.0	83.70	—	—
6-4, 146	54.44	3.5	88.52	—	—
6-4, 146				−1.10	1.89
6-5, 6	54.54	3.5	88.58	−0.70	1.56
6-5, 16	54.64	2.6	90.37	−0.91	1.86
6-5, 26	54.74	3.5	86.54	−1.16	1.38
6-5, 26				−1.25	0.62
6-5, 36	54.84	2.5	78.96	−1.04	1.85
6-5, 46	54.94	2.6	75.83*	−1.26	1.68
6-5, 56	55.04	2.4	84.19	−1.26	1.87
6-5, 66	55.14	2.4	83.70	−1.24	2.20
6-5, 70	55.23	3.0	86.88	−1.30	2.19
6-5, 86	55.34	3.5	86.41	−1.03	2.00
6-5, 96	55.44	5.5	79.89	−0.90	2.02
6-5, 96				−1.13	0.48
6-5, 106	55.54	4.2	69.65*	—	—
6-5, 116	55.64	3.1	76.02	−0.86	1.94
6-5, 126	55.74	2.4	75.41	−0.61	2.27
6-5, 136	55.84	3.3	75.98	−0.86	2.05
6-5, 146	55.94	3.5	75.25	−1.19	2.07
6-6, 6	56.04	3.3	72.89	−1.31	1.71
6-6, 16	56.14	3.8	75.76	−0.99	2.09
6-6, 26	56.24	3.5	73.00	−0.94	1.94
6-6, 36	56.34	3.3	74.20	—	—
6-6, 36				−1.18	1.93

Table 1. (Continued).

Sample (level in cm)	Sub-bottom depth (m)	Coarse fraction (%)	Calcium carbonate (%)	*G. sacculifera* $\delta^{18}O$ (‰)	*G. sacculifera* $\delta^{13}C$ (‰)
6-6, 46	56.44	4.0	83.82	−0.94	1.44
6-6, 56		3.6	83.27	−1.01	1.64
6-6, 56	56.54	3.6	83.27	−0.93	1.33
6-6, 66	56.64	5.5	76.97	−1.18	1.78
6-6, 75	56.73	3.2	61.27	−1.07	1.66
6-6, 86	56.84	3.5	59.90	—	—
6-6, 96	56.94	2.8	59.60	—	—
6-6, 106	57.04	3.3	68.19	−1.54	2.01
6-6, 116	57.14	3.0	71.46	−1.00	2.06
6-6, 116				−1.25	1.66
6-6, 126	57.24	3.7	67.22	−1.13	1.95
6-6, 136	57.34	2.8	31.47*	—	—
6-6, 146	57.44	3.7	66.97	—	—
6-7, 6	57.54	3.3	80.19	−1.33	1.72
6-7 16	57.64	3.7	75.17*	−1.33	1.64
6-7, 26	57.74	4.0	79.79	−1.46	1.93
6-7, 36	57.84	4.1	79.47	−1.42	1.98
7-1, 6	58.14	2.5	65.13	−1.19	1.80
7-1, 16	58.24	3.3	58.22	−1.09	1.92
7-1, 16				−1.10	1.82
7-1, 26	58.34	3.1	54.18	−1.08	2.05
7-1, 36	58.44	2.9	63.96	—	—
7-1, 46	58.54	2.8	67.96*	—	—
7-1, 56	58.64	2.5	66.64	—	—
7-1, 66	58.74	3.1	68.82	−1.38	1.69
7-1, 75	58.83	3.4	74.74	−1.03	1.96
7-1, 86	58.94	2.7	78.41	−0.86	1.88
7-1, 96	59.04	2.5	77.53	−1.14	1.97
7-1, 106	59.14	2.8	75.78*	−1.12	2.00
7-1, 116	59.24	3.0	76.17	−1.23	2.19
7-1, 126	59.34	2.8	71.62	−1.06	1.98
7-1, 136	59.44	3.3	74.31	−1.18	1.96
7-1, 146	59.54	2.9	71.94	−0.96	1.83
7-2, 6	59.64	2.9	68.83	−1.12	1.80
7-2, 16	59.74	2.4	66.92	—	—
7-2, 26	59.84	2.9	63.52	−1.39	1.83
7-2, 36	59.94	3.6	64.07	−1.43	2.40
7-2, 46	60.04	2.8	76.75	—	—
7-2, 56	60.14	3.0	77.43	−1.43	2.25
7-2, 66	60.24	2.7	76.35	−1.23	2.35
7-2, 75	60.33	3.3	77.97	−1.24	2.17
7-2, 86	60.44	3.2	78.42	−1.29	2.07
7-2, 96	60.54	2.8	88.16	−1.23	2.21
7-2, 106	60.64	3.9	86.16	−0.91	1.82
7-2, 116	60.74	3.9	85.80	−1.24	2.24
7-2, 126	60.84	3.3	84.69	−1.12	2.00
7-2, 136	60.94	4.7	85.00	−1.43	2.36
7-2, 146	61.04	5.3	88.71	−1.11	2.14
7-3, 6	61.14	3.8	84.13	−1.39	2.03
7-3, 16	61.24	5.1	85.07	—	—
7-3, 26	61.34	5.1	86.44	−1.13	2.28
7-3, 36	61.44	4.0	83.81	−0.97	1.96
7-3, 46	61.54	3.5	84.60	—	—
7-3, 56	61.64	4.6	86.24	−1.33	2.21
7-3, 66	61.74	3.3	86.53	—	—
7-3, 75	61.84	5.4	87.74	−1.11	2.06
7-3, 86	61.94	5.8	87.32	—	—

Site 573 on the basis of shipboard biostratigraphy. Magnetostratigraphy is available for Site 573 from the Brunhes Chron to the Cochiti Subchron of the Gilbert Chron (Weinreich and Theyer, this volume). Fine-scale correlation of the interval from about 42 to 62 m in Hole 572C was accomplished by aligning the carbonate maxima and minima with comparable events in the interval from 39 to 57 m in Hole 573C (Fig. 2). The same carbonate events were also correlated to piston Core V28-179 (Fig. 2), which has both isotopic stratigraphy and magnetostratigraphy (Shackleton and Opdyke, 1977).

Table 1. (Continued).

Sample (level in cm)	Sub-bottom depth (m)	Coarse fraction (%)	Calcium carbonate (%)	*G. sacculifera* $\delta^{18}O$ (‰)	*G. sacculifera* $\delta^{13}C$ (‰)
7-3, 96	62.04	4.4	87.59	−0.99	1.60
7-3, 106	62.14	5.8	90.36	−0.84	1.53
7-3, 116	62.24	7.8	89.72	−1.02	1.54
7-3, 126	62.34	3.0	86.40	−1.02	1.58
7-3, 136	62.44	3.3	84.43	—	—
7-3, 146	62.54	3.2	89.43	−0.93	1.65
7-4, 6	62.64	3.3	87.35	−0.99	1.92
7-4, 16	62.74	3.2	83.00	−1.13	1.86
7-4, 26	62.84	2.9	84.66	−1.13	1.80
7-4, 36	62.94	3.4	85.85	−0.96	2.02
7-4, 46	63.04	2.5	75.29	—	—
7-4, 56	63.14	3.0	71.59*	−0.97	1.91
7-4, 66	63.24	2.3	85.92	−1.01	1.70
7-4, 75	63.33	2.5	85.99	−1.10	1.78
7-4, 86	63.44	2.1	86.90	−0.97	1.96
7-4, 96	63.54	1.6	88.01	−1.07	1.94
7-4, 106	63.64	1.5	88.34	−1.05	1.80
7-4, 116	63.74	2.1	88.89	−1.20	1.77
7-4, 126	63.84	1.4	86.28	−1.06	1.43
7-4, 136	63.94	1.5	90.39	−0.96	1.38
7-5, 6	64.14	2.3	86.16	−1.30	1.86
7-5, 16	64.24	1.6	72.67*	−1.70	1.94
7-5, 26	64.34	2.0	73.10*	−1.35	1.94
7-5, 36	64.44	1.7	70.43*	—	—
7-5, 46	64.54	1.6	80.02	−1.60	2.62
7-5, 56	64.64	2.2	85.36	−0.82	1.69
7-5, 66	64.74	2.9	85.90	−0.85	1.80
7-5, 75	64.83	1.6	80.14	−1.09	2.06
7-5, 86	64.94	1.5	71.14*	—	—
7-5, 96	65.04	1.6	85.74	−1.00	2.12
7-5, 106	65.14	1.6	84.73	−0.76	1.98
7-5, 116	65.24	1.5	84.52	—	—
7-5, 126	65.34	2.8	90.72	−0.84	2.34
7-5, 136	65.44	2.6	89.09	−1.02	1.96
7-5, 146	65.54	1.9	89.66	−0.80	2.29
7-6, 6	65.64	1.8	89.15	−1.19	2.08
7-6, 16	65.74	1.5	83.86*	—	—
7-6, 26	65.84	2.1	89.56	−0.96	2.16
7-6, 36	65.94	2.2	88.67	−0.82	2.26
7-6, 46	66.04	2.1	89.80	—	—
7-6, 56	66.14	1.5	89.68	—	—
7-6, 66	66.24	1.4	91.28	−1.09	2.18
7-6, 76	66.35	1.3	88.34	−1.14	1.89
7-6, 86	66.44	1.1	86.74	−0.68	1.98
7-6, 96	66.54	0.8	83.11	−1.10	1.98
7-6, 106	66.64	0.9	79.28	−1.02	2.01
7-6, 116	66.74	1.4	74.16	−1.04	2.11
7-6, 126	66.84	1.0	73.93	−1.01	1.85
7-6, 136	66.94	0.9	70.40	−0.94	2.00
7-6, 146	67.04	0.6	69.74	—	—
7-7, 6	67.14	0.7	68.11*	—	—
7-7, 16	67.24	0.9	76.01	−1.27	1.88
7-7, 26	67.34	0.7	80.79	−1.05	2.22
7-7, 36	67.44	0.7	81.67	−0.91	2.18

Notes: Replicate sample numbers indicate replicate $\delta^{18}O$ and $\delta^{13}C$ analyses. Dashes indicate that isotopic analyses could not be made. Asterisks indicate the average of several carbonate measurements.

The mean carbonate content of these three equatorial cores is related to water depth. Site 572 is the shallowest (3893 m) and has a mean carbonate content of 78.4%. Site 573 is 4301 m deep and has a mean carbonate content of 66.2%. Core V28-179 is the deepest core (4509 m) and has a mean carbonate content of 48.4%. Although the mean carbonate content is different for the various sites, several intervals of high and low carbonate form distinctive events that can be correlated between these and other equatorial Pacific cores (Hays et al., 1969; Kaneps, 1973; Vincent, 1981).

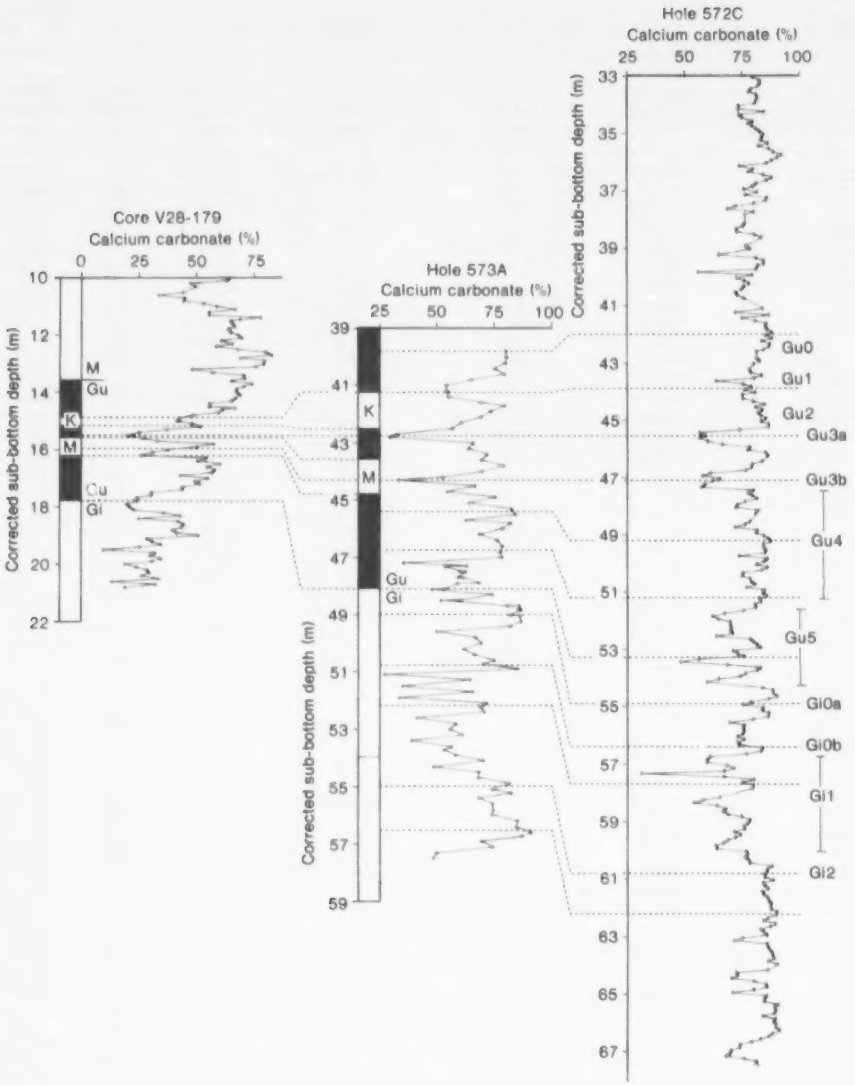

Figure 2. Calcium carbonate content and magnetostratigraphy for Core V28-179 and Hole 573A and carbonate stratigraphy for Hole 572C. All records are aligned on carbonate event Gu3a. Correlations between Hole 573A and Hole 572C are the basis for assigning ages to Hole 572C (see Table 3). Nomenclature of carbonate events follows that of Hays et al. (1969) with modifications for higher resolution events (see text for discussion). K = Kaena Subchron; M = Mammoth Subchron.

The most prominent event in the mid-Pliocene is the Gu3 event of Hays et al. (1969). This low carbonate "dissolution" event occurs near the Mammoth Subchron (Hays et al., 1969; Kaneps, 1973; Vincent, 1981). In the higher resolution records of this study, event Gu3 is observed to be a twin dissolution event, with the younger event (Gu3a) located just below the Kaena Subchron and the older event (Gu3b) occurring within the Mammoth Subchron (Fig. 2). This distinctive twin event is a key datum level for the correlation of Hole 572C to other cores. In Figure 2, the cores are aligned on event Gu3a. Above Gu3 there is an intermediate carbonate low centered at 43.9 m (Gu1 in Fig. 2) and an interval having consistently high values centered at 42.2 m (Gu0 in Fig. 2) that can be correlated between cores (Fig. 2). These upper Gauss designations are preliminary because the data do not cover the complete interval that is equivalent to the Gauss, and the available data indicate that previous records may have missed important details.

Below event Gu3, the Gauss contains an interval of high carbonate with small-scale variability (Gu4) and a complex low carbonate interval with several subevents (here grouped as Gu5) (Fig. 2). The Gauss/Gilbert boundary falls within event Gu5 at Site 573 and in Core V28-179, and its equivalent depth in Hole 572C is 53.3 m (Fig. 2). This placement of the Gauss/Gilbert boundary

Table 2. Calcium carbonate content for Hole 573A (Cores 5 and 6).

Sample (level in cm)	Sub-bottom depth (m)	Carbonate (%)	Sample (level in cm)	Sub-bottom depth	Carbonate (%)
5-1, 0	39.80	79.82	5-6, 120	48.50	51.77*
5-1, 20	40.00	80.37*	5-6, 139	48.69	80.65
5-1, 40	40.20	79.72	5-6, 140	48.70	85.66
5-1, 60	40.40	75.01*	5-7, 0	48.80	85.34
5-1, 80	40.60	79.27*	5-7, 2	48.82	86.31
5-1, 100	40.80	64.91	5-7, 20	49.00	81.73*
5-1, 120	41.00	54.07	6-1, 3	49.23	86.40
5-1, 140	41.20	54.22	6-1, 19	49.39	81.75
5-2, 0	41.40	55.09	6-1, 39	49.59	49.84*
5-2, 20	41.60	69.21	6-1, 59	49.79	66.67
5-2, 40	41.70	79.25*	6-1, 79	49.99	69.06
5-2, 60	41.90	73.42	6-1, 99	50.19	61.49
5-2, 80	42.10	69.10*	6-1, 119	50.39	66.08
5-2, 100	42.30	60.62	6-1, 139	50.59	74.65
5-2, 120	42.50	56.69	6-2, 2	50.72	69.99
5-2, 140	42.70	32.06	6-2, 19	50.89	84.93*
5-3, 0	42.80	29.43	6-2, 39	51.09	27.30*
5-3, 20	43.00	65.79*	6-2, 57	51.27	64.26*
5-3, 40	43.20	63.60	6-2, 79	51.49	34.94*
5-3, 60	43.40	71.70	6-2, 99	51.69	65.44*
5-3, 80	43.60	69.39	6-2, 119	51.89	33.60*
5-3, 100	43.80	78.96*	6-2, 138	52.08	71.38
5-3, 120	44.00	69.43*	6-3, 2	52.22	69.03
5-3, 140	44.20	52.52	6-3, 19	52.39	70.45
5-4, 0	44.30	33.33*	6-3, 59	52.59	41.23*
5-4, 20	44.50	66.44*	6-3, 60	52.80	58.16
5-4, 70	44.70	54.55*	6-3, 79	52.99	55.65
5-4, 60	44.90	75.30*	6-3, 99	53.19	61.04
5-4, 80	45.10	63.80*	6-3, 119	53.39	39.04*
5-4, 100	45.30	82.23	6-3, 141	53.61	56.13*
5-4, 120	45.50	84.19	6-4, 2	53.72	53.37
5-4, 140	45.70	62.56*	6-4, 19	53.89	58.02
5-5, 0	45.80	81.98	6-4, 39	54.09	70.05
5-5, 20	46.00	78.37*	6-4, 61	54.31	48.58*
5-5, 40	46.20	68.54*	6-4, 80	54.50	68.23
5-5, 60	46.40	76.07	6-4, 99	54.69	67.99
5-5, 80	46.60	78.32*	6-4, 119	54.89	81.39
5-5, 100	46.80	77.28	6-4, 139	55.09	74.10*
5-5, 120	47.00	77.99	6-5, 2	55.22	82.25
5-5, 140	47.20	35.44*	6-5, 19	55.39	68.24*
5-6, 0	47.30	62.88	6-5, 39	55.59	74.22
5-6, 2	47.32	53.63*	6-5, 61	55.81	74.46*
5-6, 19	47.49	60.06	6-5, 78	55.98	73.96
5-6, 20	47.50	62.35	6-5, 99	56.19	85.15
5-6, 39	47.69	59.19	6-5, 119	56.39	84.55
5-6, 40	47.70	61.20	6-5, 138	56.58	90.98
5-6, 59	47.89	68.07*	6-6, 2	56.72	86.78
5-6, 60	47.90	58.95*	6-6, 19	56.89	69.34*
5-6, 80	48.10	53.10*	6-6, 39	57.09	74.35*
5-6, 82	48.12	47.86	6-6, 60	57.30	49.94
5-6, 100	48.30	74.07*	6-6, 78	57.48	48.53
5-6, 119	48.49	60.21*			

Note: Asterisk indicates average of several carbonate analyses.

within the carbonate stratigraphy is consistent with its location in Cores V24-59 and RC12-66, which have much less detail.

Below the Gauss/Gilbert boundary, at about 54.9 m, Site 572 contains a short, unrecognized, high-carbonate-content event with a twin peak (Gi0a). This event is clear at about 48.99 m at Site 573, but the split peak is less obvious (Fig. 2). A second carbonate maximum (Gi0b) occurs at about 56.4 m in Hole 572C and 50.78 m in Hole 573A. This nomenclature is used to preserve the previously numbered events within the Gilbert. Below the proposed Gi0 subevents there is an interval of low carbonate (57 to 60 m) that has several discrete subevents. This entire interval is probably equivalent to Gi1, because it is observed in Cores V24-59 and RC11-62 and at DSDP Sites 310 and 157 (Vincent, 1981). Below Gi1 there is an interval of high carbonate content at about 61 to 63 m at Site 572 and 55 to 57 m at Site 573 that is equivalent to Gi2 (Fig. 2).

The above correlations between Sites 572 and 573 have been used along with two shipboard biostratigraphic age datum levels to construct an age model for the Hole 572C record (Table 3). The age models for Site 573 and Core V28-179 are based directly on their magnetostratigraphy.

Coarse Fraction Stratigraphy

The coarse fraction record of Site 572 is characterized by two distinct regimes of variability (Fig. 1 and Table 1). The upper section (29.5 to 37.5 m in Hole 572C) is highly variable (6% standard deviation) and has several distinct cycles about 2 m in length. The lower section (37.5

Table 3. Age models for Pliocene sections of Holes 572C and 573A.

Hole	Level	Depth in hole (m)	Age (m.y.)	Magnetostratigraphy
572C	1	29.5	2.00	
	2	37.5	2.40	
	3	42.0	2.84	
	4	43.9	2.92	
	5	45.5	3.01	
	6	47.1	3.14	
	7	49.2	3.22	
	8	51.2	3.31	
	9	54.9	3.47	
	10	56.4	3.61	
	11	57.7	3.72	
	12	60.8	3.94	
	13	62.2	4.06	
573A		41.25	2.92	upper Kaena
		42.52	2.99	lower Kaena
		43.58	3.08	upper Mammoth
		44.80	3.18	lower Mammoth
		48.10	3.40	Gauss/Gilbert
		53.96	3.86	upper Cochiti

Notes: Hole 572C: Levels 1 and 2 are from the shipboard biostratigraphy used to calculate accumulation rates. Levels 3 to 13 are carbonate stratigraphy correlations to Hole 573A (see Fig. 2). Ages for these levels are derived from the magnetostratigraphy of Hole 573A. Hole 573A: Ages of chron and subchron boundaries are from LaBrecque et al. (1977) and are updated by Mankinen and Dalrymple (1979) and summarized for Leg 68 by Keigwin (1982a).

to 63.0 m in Hole 572C) is characterized by low amplitude (1 to 2‰), high-frequency variations superimposed on a longer periodicity. The boundary between these two regimes is recognized as the color and lithofacies boundary between cyclic siliceous and calcareous, varicolored ooze in the upper section and green varicolored ooze in the lower section. The boundary between the lithofacies and coarse fraction regimes is estimated to be at about 2.4 Ma on the basis of shipboard biostratigraphy and at about 2.5 Ma on the basis of extrapolation from the nearest paleomagnetic–carbonate correlation datum.

Oxygen and Carbon Isotope Stratigraphy

The planktonic $\delta^{18}O$ record of the Pliocene of Site 572 is characterized by two intervals with different patterns of isotopic variability, which are separated by a sharp increase upward at about 44 m sub-bottom depth (Fig. 1). The lower interval (67 to 44 m) is characterized by lower $\delta^{18}O$ values ($\bar{x} = -1.10$ ‰) and low variability ($\sigma = 0.21$ ‰). Within this interval, events with low values reach about -1.5 ‰ and events with high values reach about -0.75 ‰ (Fig. 1). The maxima and minima in the lower section are lower than comparable events in the upper section. Cyclic variability on the scale of 1 and 2 m is observed within this lower section. Preliminary spectral analysis of this interval reveals concentrations of variance near 250,000, 100,000, 26,000, and 19,000 yr. The transition to the upper section occurs at 44 m and is observed as a rapid increase in $\delta^{18}O$. The age of this transition is about 2.9 Ma. A similar transition is observed in the benthic record from North Atlantic Hole 552A (Shackleton et al., 1984).

The upper section (44 to 29 m) displays higher $\delta^{18}O$ values ($\bar{x} = -0.77$ ‰) and higher variability ($\sigma = 0.27$ ‰) than the lower section. Within this interval the minimum events are about -1.2 ‰, whereas the maximum events reach about -0.40 ‰ (Fig. 1). The largest and most distinctive event in this interval occurs from about 37.5 to 35.5 m, which is equivalent to about 2.4 to 2.3 Ma. This event has a characteristic two-peak structure that is similar to but lower in amplitude than the benthic isotopic event associated with the onset of major ice rafting found in North Atlantic Hole 552A (Shackleton et al., 1984). Preliminary analysis of the $\delta^{18}O$ data of the upper section indicates that it contains a long-period component between 300,000 and 500,000 yr. and weaker components near 100,000 and 47,000 yr.

The carbon isotope stratigraphy also displays long-term variability but does not naturally fall into two intervals as do the $\delta^{18}O$ data. However, if the divisions defined by the $\delta^{18}O$ data are used, the $\delta^{13}C$ of the lower section (67 to 44 m) is somewhat higher ($\bar{x} = 1.92$ ‰) and more variable ($\sigma = 0.25$) than the $\delta^{13}C$ of the upper section ($\bar{x} = 1.77$ ‰, $\sigma = 0.22$ ‰). The $\delta^{13}C$ record also displays a definite long-period variability of about 215,000 yr. in the upper section and both 500,000 and 120,000 yr. in the lower section. This strong low-frequency variability is more evident in the $\delta^{13}C$ record than in the $\delta^{18}O$ record.

Comparison of the $\delta^{18}O$ and $\delta^{13}C$ records reveals numerous intervals or events that have strong negative co-variation. Specific examples of this co-variation are the intervals from 35 to 38 m, 44 to 48 m, 48 to 52 m (a lower amplitude variation), and 60 to 65 m. Some of these intervals also correlate to events in the carbonate or coarse fraction records, especially the interval from 44 to 48 m, which coincides with the twin dissolution event Gu3.

DISCUSSION

Pliocene Glaciation

The Pliocene is often thought to contain the first major Cenozoic glaciation of the Northern Hemisphere. Much of the evidence supporting the timing of this proposed glaciation has come from deep-sea sediments and includes ice-rafted sediments (Berggren, 1972; Poore, 1981; Blanc et al., 1983; Shackleton et al., 1984), faunal indices (Thunell and Belyea, 1982; Kennett, 1978), and enrichment trends in the isotope composition of benthic foraminifers (Shackleton and Kennett, 1975; Shackleton and Opdyke, 1977; Keigwin, 1979; Blanc et al., 1983; Shackleton et al., 1984). Prior to the use of hydraulic piston cores, the highest quality isotopic record relevant to this question was that of Core V28-179 from the equatorial Pacific (Shackleton and Opdyke, 1977). This record contains a 0.4 ‰ increase in the average benthic $\delta^{18}O$ at approximately 3.2 Ma. This baseline shift separates an interval of low variability and relatively low isotopic values, called the preglacial Pliocene, from an interval of greater and more variable isotopic values (Shackleton and Opdyke, 1977). The more variable and enriched values are interpreted to indicate a changing isotopic com-

position of the ocean related to increased terrestrial ice volume from the presumed Northern Hemisphere continental glaciation. A second increase in the mean isotopic composition occurs at about 2.4 Ma (Shackleton and Opdyke, 1977). This latter event is also observed in the planktonic record of Site 572 and in the benthic record of Shackleton et al. (1984).

If these mean isotopic increases (especially the one previously proposed for 3.2 Ma) do represent permanent additions to the mean volume of continental glaciers, the isotopic composition of the entire ocean should have been increased. Therefore, the $\delta^{18}O$ observed in benthic records should also be observed in the isotopic composition of surface-dwelling planktonic foraminifers. Although surface $\delta^{18}O$ values may be modified by local temperature and salinity, the planktonic isotopic records should still contain the ubiquitous ice volume $\delta^{18}O$ signature.

Comparison of the time series of benthic $\delta^{18}O$ in Core V28-179 with the planktonic record from Site 572 (Fig. 3) reveals that the planktonic record does not have a step-like enrichment of the mean values at 3.2 Ma as does the benthic record. The planktonic record does show a broad interval of enriched $\delta^{18}O$ of about 0.4 ‰ between about 3.3 and 3.15 Ma, but the values do not remain enriched as they do for the benthic data (Fig. 3). The mean $\delta^{18}O$ from 2.9 to 3.3 Ma is -1.08 ‰, which is close to the mean of -1.11 ‰ from 3.3 to 4.5 Ma. Hence, the planktonic record does not contain the enriched mean values that are required by the glacial initiation hypothesis.

Shackleton et al. (1984) have recently interpreted a high resolution benthic isotopic record from Hole 552A to indicate that no significant Northern Hemisphere glaciation is required between 3.2 and 2.4 Ma. Although their record does not show a distinct event at 3.2 Ma, the age model for Core 552A-11 is equivocal. In this core, the documentation of the Mammoth Subchron is questionable, and large sedimentation rate changes are required within this section. Hence, the magnetic data are apparently disturbed and the isotopic record may also be affected. In this connection, a large number of benthic records do show an enrichment at about 3.2 Ma (e.g., Keigwin, 1982b; Hodell et al., 1983; Leonard et al., 1983; Weissert et al., 1984; Shackleton and Cita, 1979). Hence, the Hole 552A record may be not definitive for this interval.

Two explanations of these data are possible. If the benthic isotopic composition does indicate a permanent, but variable, increase in ice volume, the surface waters must have either warmed or become less saline in order to compensate for the increased $\delta^{18}O$ composition of the ocean. An alternate explanation is that no permanent addition of ice volume was initiated at about 3.2 Ma, although the co-variation of the planktonic and benthic records suggests that a short ice growth event may have occurred. This explanation requires that the benthic record reflect colder bottom waters to account for the $\delta^{18}O$ enrichment observed at 3.2 Ma and that this colder bottom water be a permanent feature of the bottom circulation.

These data cannot resolve this apparent paradox, but other low-latitude planktonic data (see Prell, 1984) have patterns similar to data from Hole 572C and thus suggest that a global warming is required to explain the planktonic patterns. Since this mechanism seems unlikely, cooler bottom waters are a more plausible alternative. In any case, the data indicate that the initiation of Northern Hemisphere glaciation is not a simple event. Further, the 3.2 Ma event may be more related to bottom water production near Antarctica, as suggested by Backman (1979), than to glaciation in the Northern Hemisphere. We are presently analyzing the benthic isotopic composition in Site 572 to establish both records in the same core.

However, comparison of the planktonic record from equatorial Pacific Hole 572C with the benthic record from North Atlantic Hole 552A suggests the possibility of some ice volume variation. Both records are distinctly lower in $\delta^{18}O$ prior to 2.9 Ma and show similar patterns of variability (although strict co-variation cannot be evaluated at this time). In general, the co-variation of benthic and planktonic records is the best evidence for ice volume changes in the isotopic composition of the ocean. Hence, glacial variability may be indicated over the length of these records from 2.9 to 3.5 Ma. Note that Hole 572C exhibits a fairly uniform pattern of $\delta^{18}O$ variability back to about 4.5 Ma.

The Coincidence of Carbonate and Isotopic Events

Pleistocene sediments of the equatorial Pacific show a strong co-variance of carbonate and oxygen isotopic variations, with high carbonate values occurring during glacial (increased $\delta^{18}O$) intervals. The lower carbonate contents of interglacial intervals are widely interpreted to indicate increased carbonate dissolution. This general Pacific-type pattern of carbonate and isotopic records is thought to apply to the entire Pleistocene of the equatorial Pacific. However, several low carbonate (dissolution) events in the Pliocene have been correlated with increased $\delta^{18}O$ and climatic cooling or "deterioration" at approximately 2.4 and 3.1 Ma (Vincent, 1981). A decrease in benthic $\delta^{13}C$ values is also associated with some carbonate events. Hence, in the equatorial Pacific, the climatic associations of Pliocene dissolution events appear to be opposite to those of the Pleistocene.

The detailed record from Site 572, along with the less detailed records from Site 573 and Core V28-179, indicate that the timing and character of the Gu3 dissolution event do not coincide with increased $\delta^{18}O$ events in the isotopic record (Figs. 2 and 3). The carbonate dissolution event Gu3 is observed in all three carbonate records as a complex two-peak event, with each dissolution event (Gu3a and Gu3b) lasting about 30,000 yr. The age of the midpoint of each event is about 3.02 Ma for Gu3a and 3.13 Ma for Gu3b. Hence, the detailed carbonate and isotopic records of these cores show that the dissolution events are not coincident with the isotopic enrichments and that the patterns of isotopic enrichment are not consistent between benthic and planktonic records. Detailed examination of the carbonate and oxy-

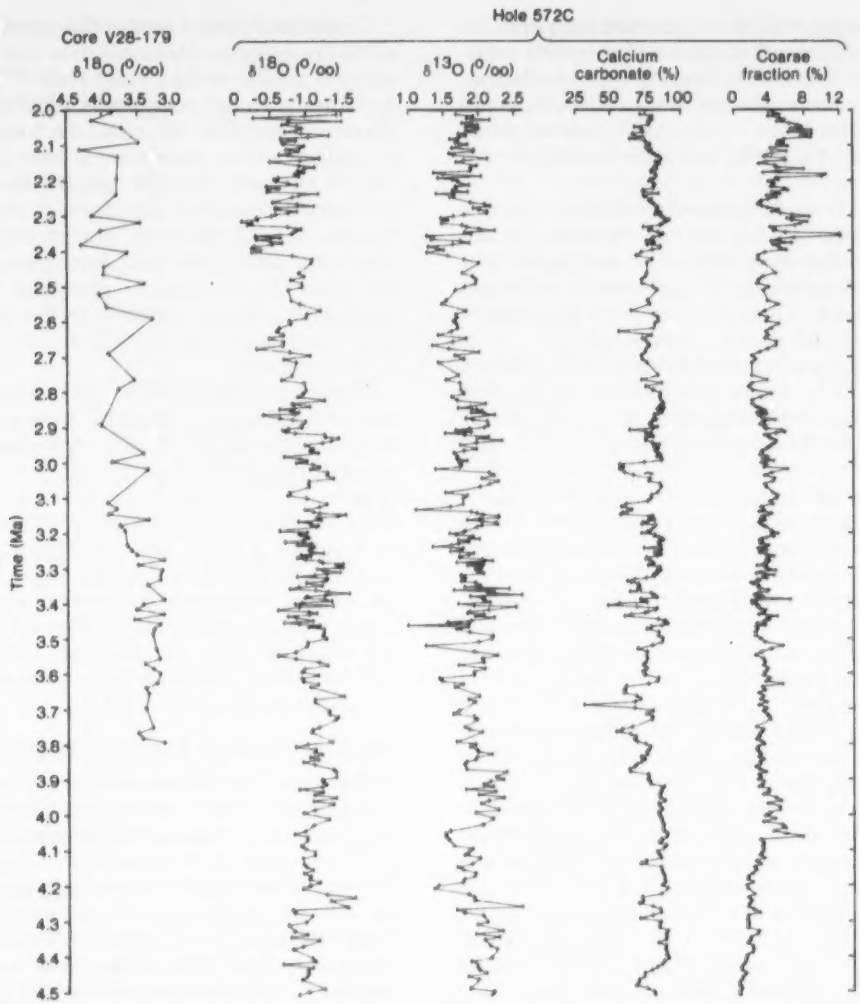

Figure 3. Time series of benthic $\delta^{18}O$ in Core V28-179 and planktonic $\delta^{18}O$ and $\delta^{13}C$, calcium carbonate, and coarse fraction data for Hole 572C. The age model for Hole 572C is given in Table 3 and discussed in the text.

gen isotopic data of Hole 572C reveals that the co-variation is positive, with low carbonate values being coincident with depleted isotopic values (i.e., interglacial intervals). Thus, the detailed record shows that event Gu3 is consistent with the Pacific-type pattern of carbonate variability. Although this striking event is probably associated with the climatic deterioration within the middle Gauss, it is not coincident with the initial isotopic enrichments observed in both the planktonic and benthic records. Thus, any mechanism proposed to link the dissolution and isotope events must take into account a lag of more than 100,000 yr. between them.

Dunn (1982) has proposed that the carbonate record (Core V28-179) of the equatorial Pacific changes from an "Atlantic-type" (high carbonate values associated with low $\delta^{18}O$ during interglacial intervals) to a Pacific-type (high carbonate values associated with increased $\delta^{18}O$ during glacial intervals) during the early Gauss Chron. He suggests that this change may be related to changes in orbital parameters or to intensification of Antarctic bottom water. The paired carbonate and $\delta^{18}O$ samples of Site 572 provide a high resolution record to test this hypothesis. The Site 572 time series has a 5000-yr. sample interval, whereas the Core V28-179 time series has a 15,000 to 30,000 yr. sample interval. I used spectral analysis techniques identical to those of Dunn (1982) to examine the correlation of carbonate and $\delta^{18}O$ over the interval from 3.0 to 4.5 Ma, a time when the Atlantic-type pattern should be evident.

The results of this preliminary cross-correlation analysis indicates that the lower Pliocene carbonate stratigraphy is characterized by a clear but weak association of low carbonate and low $\delta^{18}O$ (interglacial) events (Fig. 4). Hence, Site 572 exhibits Pacific-type variation (compare fig. 4 and fig. 3 of Dunn, 1982) rather than Atlantic-type variation as proposed by Dunn (1982). This type of analysis calculates the correlation between carbonate and $\delta^{18}O$ values at all frequency bands, i.e., the total record.

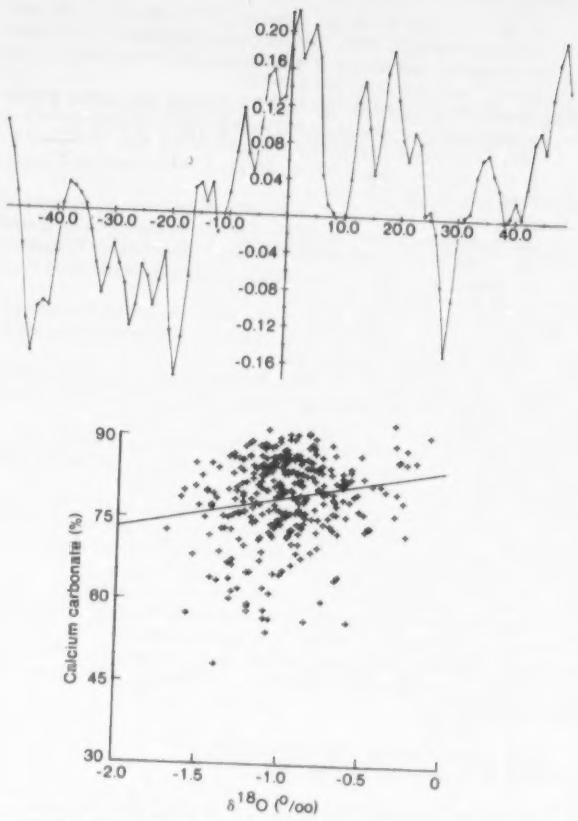

Figure 4. Cross-correlation and scatter plot of calcium carbonate (%) and $\delta^{18}O$ values in Hole 572C for the interval from 3.0 to 4.5 Ma. The vertical axis in the upper plot is the correlation coefficient. Positive values indicate correlation of higher carbonate values with increased (glacial) $\delta^{18}O$ values, i.e., the "Pacific-type" pattern. Horizontal axis indicates that $\delta^{18}O$ variations lead or lag the carbonate variations. A small lag (about 5,000 yr.) is indicated. The scatter plot reveals the weak correlation but also shows the Pacific-type pattern.

The coherence (correlation over a specific frequency band at 0 phase) and phase spectra for these data reveal that no frequency band with significant coherence has a phase of 180° (i.e., the Atlantic-type pattern). This preliminary analysis also reveals no significant coherence between carbonate and $\delta^{18}O$ at or near the frequency band equivalent to 100,000 yr. These comparisons and preliminary analyses indicate that the equatorial Pacific did not have an Atlantic-type carbonate stratigraphy during the early Pliocene. Further, these findings suggest that the concept of Atlantic-type and Pacific-type carbonate variations is too simplistic, especially in the absence of a dominant frequency band such as the 100,000-yr. cycle in the late Pleistocene. Because this concept relies on the total records, it combines information from all frequency bands that may have vastly different coherence and phase. In retrospect, Dunn's (1982) results may reflect aliasing and the absence of higher frequency components.

CONCLUSIONS

1. Hole 572C provides a detailed (5000-yr. sample interval) of planktonic $\delta^{18}O$ and $\delta^{13}C$ values and total calcium carbonate content for much of the Pliocene (4.5 to 2.0 Ma) of the equatorial Pacific.

2. The equatorial Pacific carbonate events of Hays et al. (1969) can be correlated with Sites 572 and 573. The detailed record of Hole 572C provides greater resolution and shows that the Gu3 event is a two-peak event.

3. The planktonic $\delta^{18}O$ of Hole 572C reveals that, first, the Pliocene has two $\delta^{18}O$ modes with different mean values and variability. At about 2.9 Ma, $\delta^{18}O$ values increase and become more variable. This division is also apparent in the benthic $\delta^{18}O$ record of North Atlantic Hole 552A (Shackleton et al., 1984). Hence, similar patterns of planktonic and benthic variability indicate some ice volume changes prior to 2.9 Ma. This idea must be tested with data from the same core or better age models. Second, a distinct two-peak enrichment is observed at 2.4 to 2.3 Ma and is coincident with a similar event in the North Atlantic, which is associated with the onset of major ice rafting. The strong co-variation of planktonic and benthic records clearly identifies this glacial event. Third, the planktonic $\delta^{18}O$ record of Hole 572C does not show a steplike enrichment of mean values at 3.2 Ma. This lack of co-variation with benthic records suggests that increased glaciation is not the cause of the benthic isotopic change at 3.2 Ma. An alternative suggestion is that bottom waters cooled at this time (probably from a southern source).

4. Comparison of high resolution $\delta^{18}O$ records and carbonate records from Hole 572C reveals that the lower Pliocene of the equatorial Pacific is characterized by a Pacific-type carbonate stratigraphy.

REFERENCES

Backman, J., 1979. Pliocene biostratigraphy of DSDP Sites 111 and 116 from the North Atlantic Ocean and the age of Northern Hemisphere glaciation. *Stockholm Contrib. Geol.*, 32:115–137.

Berggren, W. A., 1972. Late Pliocene–Pleistocene glaciation. *In* Laughton, A. S., Berggren, W. A., et al., *Init. Repts. DSDP*, 12: Washington (U.S. Govt. Printing Office), 953–963.

Blanc, P. L., Fontugne, M. R., and Duplessy, J. C., 1983. The time-transgressive initiation of boreal ice-caps: continental and ocean evidence reconciled. *Palaeogeogr. Palaeoclimatol. Palaeocol.*, 42: 211–224.

Craig, H., 1957. Isotopic standards for carbon and oxygen and correction factors for mass-spectrometric analysis of carbon dioxide. *Geochim. Cosmochim. Acta*, 12:133–140.

Dunn, D. A., 1982. Change from "Atlantic-type" to "Pacific-type" carbonate stratigraphy in the middle Pliocene equatorial Pacific Ocean. *Mar. Geol.*, 80:41–60.

Hays, J. D., Saito, T., Opdyke, N. D., et al., 1969. Pliocene–Pleistocene sediments of the equatorial Pacific: their paleomagnetic, biostratigraphic, and climatic record. *Geol. Soc. Am. Bull.*, 80: 1481–1514.

Hodell, D. A., Kennett, J. P., and Leonard, K. A., 1983. Climatically induced changes in vertical water mass structure of the Vema Channel during the Pliocene: evidence from Deep Sea Drilling Project Holes 516A, 517, and 518. *In* Barker, P. F., Carlson, R. L., Johnson, D. A., et al., *Init. Repts. DSDP*, 72: Washington (U.S. Govt. Printing Office), 907–919.

Jones, A., and Kaiteris, P., 1983. A vacuum-gasometric technique for rapid and precise analysis of calcium carbonate in sediments and soils. *J. Sediment. Petrol.*, 53(2):655–660.

Kaneps, A. G., 1973. Carbonate chronology for Pliocene deep-sea sediments. *In* van Andel, T. H., Heath, G. R., et al., *Init. Repts. DSDP*, 16: Washington (U.S. Govt. Printing Office), 873–881.

Keigwin, L. D., Jr., 1979. Late Cenozoic stable isotope stratigraphy and paleoceanography of DSDP sites from the east equatorial and central North Pacific Ocean. *Earth Planet. Sci. Lett.*, 45:361–382.

_____, 1982a. Appendix: basis for age assignments at Deep Sea Drilling Project Sites 502 and 503. *In* Prell, W. L., Gardner, J. V., et al., *Init. Repts. DSDP*, 68: Washington (U.S. Govt. Printing Office), 493–495.

_____, 1982b. Stable isotope stratigraphy and paleoceanography of Sites 502 and 503. *In* Prell, W. L., Gardner, J. V., et al., *Init. Repts. DSDP*, 68: Washington (U.S. Govt. Printing Office), 445–453.

Kennett, J. P., 1978. The development of planktonic biogeography in the Southern Ocean during the Cenozoic. *Mar. Micropaleontol.*, 3:301–345.

LaBrecque, J. L., Kent, D. V., and Cande, S. C., 1977. Revised magnetic polarity time scale for Late Cretaceous and Cenozoic time. *Geology*, 5:330–335.

Leonard, K. A., Williams, D. F., and Thunell, Robert C., 1983. Pliocene paleoclimatic and paleoceanographic history of the South Atlantic Ocean: stable isotopic records from Leg 72 Deep Sea Drilling Project Holes 516A and 517. *In* Barker, P. F., Carlson, R. L., Johnson, D. A., et al., *Init. Repts. DSDP*, 72: Washington (U.S. Govt. Printing Office), 895–906.

Mankinen, E. A., and Dalrymple, G. B., 1979. Revised geomagnetic time scale for interval 0–5 m.y. B.P. *J. Geophys. Res.*, 84:615–626.

Poore, R. Z., 1981. Temporal and spatial distribution of ice-rafted mineral grains in Pliocene sediments of the North Atlantic: implications for late Cenozoic climatic history. *Spec. Publ. Soc. Econ. Paleontol. Mineral.*, 32:505–515.

Prell, W. L., 1984. Covariance patterns of foraminiferal $\delta^{18}O$: an evaluation of Pliocene ice volume changes near 3.2 million years ago. *Science*, 226:692–693.

Saito, T., Burckle, L. H., and Hays, J. D., 1975. Late Miocene to Pleistocene biostratigraphy of equatorial Pacific sediments.*In* Saito, T., and Burckle, L. H. (Eds.), *Late Neogene Epoch Boundaries*: New York (Micropaleontology Press), pp. 226–244.

Shackleton, N. J., Backman, J., Zimmerman, H., Kent, D. V., Hall, M. A., Roberts, D. G., Schnitker, D., Baldauf, J. G., Desprairies, A., Homrighausen, R., Huddlestun, P., Keene, J. B., Kaltenback, A. J., Krumsiek, K. A. O., Morton, A. C., Murray, J. W., and Westberg-Smith, J., 1984. Oxygen isotope calibration of the onset of ice-rafting and history of glaciation in the North Atlantic Region. *Nature (London)*, 307:620–623.

Shackleton, N. J., and Cita, M. B., 1979. Oxygen and carbon isotope stratigraphy of benthic foraminifers at Site 397: detailed history of climatic change during the late Neogene. *In* von Rad, U., Ryan, W. B. F., et al., *Init. Repts. DSDP*, 47, Pt. 1: Washington (U.S. Govt. Printing Office), 433–445.

Shackleton, N. J., and Kennett, J. P., 1975. Late Cenozoic oxygen and carbon isotopic changes at DSDP Site 284: implications for glacial history of the Northern Hemisphere and Antarctica. *In* Kennett, J. P., Houtz, R. E., et al., *Init. Repts. DSDP*, 29: Washington (U.S. Govt. Printing Office), 801–807.

Shackleton, N. J., and Opdyke, N. D., 1977. Oxygen isotope and paleomagnetic evidence for early Northern Hemisphere glaciation. *Nature (London)*, 270:216–219.

Thunell, R., and Belyea, P., 1982. Neogene planktonic foraminiferal biogeography of the Atlantic Ocean. *Micropaleontology*, 28(4): 381–398.

van Andel, T. H., Heath, G. R., and Moore, T. C., 1975. Cenozoic tectonics, sedimentation and paleoceanography of the central equatorial Pacific. *Mem. Geol. Soc. Am.*, 143:1–134.

Vincent, E. 1981. Neogene carbonate stratigraphy of Hess Rise (central north Pacific) and paleoceanographic implications. *In* Thiede, J., Vallier, T. L., et al., *Init. Repts. DSDP*, 62: Washington (U.S. Govt. Printing Office), 571–606.

Weissert, H. J., McKenzie, J. A., Wright, R. C., Clark, M., Oberhänsli, H., and Casey, M., 1984. Paleoclimatic record of the Pliocene at Deep Sea Drilling Project Sites 519, 521, 522, and 523 (Central South Atlantic). *In* Hsü, K. J., LaBrecque, J. L., et al., *Init. Repts. DSDP*, 73: Washington (U.S. Govt. Printing Office), 701–715.

Date of Initial Receipt: 28 October 1983
Date of Acceptance: 31 May 1984

Reprinted from Mayer, L., Theyer, F., et al., 1985
Initial Reports of the Deep Sea Drilling Project, Volume LXXXV, Washington (U. S. Government Printing Office)

21. STABLE ISOTOPE AND CALCIUM CARBONATE RECORDS FROM HYDRAULIC PISTON CORED HOLE 574A: HIGH-RESOLUTION RECORDS FROM THE MIDDLE MIOCENE[1]

Nicklas G. Pisias, College of Oceanography, Oregon State University
and
Nicholas J. Shackleton and Michael A. Hall, The Godwin Laboratory, University of Cambridge[2]

ABSTRACT

Detailed stable isotopic and calcium carbonate records (with a sampling resolution of 3000 yr.) from the middle Miocene section of hydraulic piston corer (HPC) Hole 574A provide a sequence that records the major shift in the oxygen isotopic composition of the world's oceans that occurred at about 14 Ma. The data suggest that this transition was rapid and spans about 30,000 yr. of sediment deposition. In intervals before and after the shift, the mean $\delta^{18}O$ values are characterized by a constant mean with a high degree of variability. The degree of variability in both the $\delta^{18}O$ and $\delta^{13}C$ records is comparable to that observed for the Pliocene and earliest Pleistocene and does not show a significant change before or after the major shift in the $\delta^{18}O$ record. Whereas the oxygen isotopic record is characterized by relatively stable mean values before and after the middle Miocene event, the $\delta^{13}C$ record shows a number of significant offsets in the mean value separated by intervals of high-frequency variations.

Time and frequency domain analysis of all records from Hole 574A indicate that the frequency components shown to be related to orbital changes in the Pleistocene record are also present in the middle Miocene. The high variability observed in the Site 574 isotopic records places important constraints on models describing the role of formation of the Antarctic ice sheet during the middle Miocene climatic transitions. Thus, HPC Hole 574A provides a valuable sequence for detailed study of climatic variability during an important time in the Earth's history, although we cannot provide a definitive explanation of the major oxygen isotopic event of the middle Miocene.

INTRODUCTION

Site 574 was drilled at a location that was within the equatorial divergence zone in the early and middle Miocene. As would be expected in this oceanographic setting, sedimentation rates during the middle Miocene at Site 574 were relatively high (30 to 35 m/m.y.). In Hole 574A the hydraulic piston corer (HPC) was used to recover sediments to 186 m sub-bottom depth to provide a high-quality sediment section spanning the last 16.5 m.y. To make a detailed examination of the oceanographic and climatic variability during the Miocene, selected intervals were sampled at 10-cm spacing. In selecting the intervals for detailed analysis, the following criteria were considered: (1) high sedimentation rates so that records with resolution better than 5000 yr. could be obtained; (2) shipboard evaluation of carbonate fossil preservation indicating that adequate numbers of foraminiferal tests would be available for stable isotopic analyses; (3) intervals that spanned major paleoclimatic or paleoceanographic events of particular importance; and (4) at least 15 m of good continuous recovery to provide a sequence long enough for statistical analysis.

In Hole 574A three intervals in the middle Miocene section were sampled at 10-cm intervals providing a resolution of 3000 to 5000 yr.: 100–115 m, 140–160 m, and 168–186 m sub-bottom. The latter two intervals span the foraminiferal biostratigraphic Zones N9 and N10. A major shift in the mean oxygen isotopic composition of the ocean, which has been associated with the onset of major glaciation in Antarctica, occurred during this interval (Woodruff et al., 1981; Shackleton and Kennett, 1975). Detailed analysis of the sections from Hole 574A provides high-resolution records of the variability in the stable isotopic composition and deposition of calcium carbonate in the deep central equatorial Pacific.

METHODS

The analytical methods used in stable isotope studies of foraminifers from deep-sea sediments are essentially standardized. Samples were disaggregated by shaking them on a commercial orbital shaker in distilled water and were then washed through a 150-μm sieve. Although both the coarse fraction and the dried fine residue were weighed, we do not present the data here because the coarse fraction in these sediments is not invariably dominated by foraminifers. Thus, the percentage of coarse material may not be a useful indication of the extent of dissolution. Benthic foraminifers for isotopic analysis were picked from the coarse fraction. In order to minimize the effect of sample selection on the variance of the isotope record, we aimed to pick similar species of similar size over long intervals of the core. The majority of the analyses are of *Planulina (= Cibicidoides) wuellerstorfi*, and many of the remainder are *Cibicidoides kullenbergi* and similar forms. The number of individuals analyzed was controlled almost entirely by the number present in the samples available; the average number is about six. Occasionally other species were analyzed, chiefly to increase the number of comparisons available. In particular *Oridorsalis* sp. was picked in a long run of samples, and *Globocassidulina subglobosa, Gyroidina* sp., and *Cibicidoides havanensis* were also picked occasionally.

The picked specimens were crushed and cleaned ultrasonically to remove adhering fine-grained material before being roasted *in vacuo* at about 410°C for 30 min. to remove possible organic contaminants. Carbon dioxide was released by the action of 100% orthophosphoric acid in the extraction line shown by Shackleton et al. (1984) and analyzed in a VG Micromass 903 mass spectrometer. Analytical precision is about ±0.07‰. The analyses shown in Table 1 have been normalized for genetically controlled departure from isotopic equilibrium using the adjustment factors given in the footnote to Table 1.

[1] Mayer, L., Theyer, F., et al., *Init. Repts. DSDP*, 85: Washington (U.S. Govt. Printing Office).

[2] Addresses: (Pisias) College of Oceanography, Oregon State University, Corvallis, OR 97331; (Shackleton and Hall) The Godwin Laboratory, University of Cambridge, Free School Lane, Cambridge CB2 3RS, United Kingdom.

Table 1. Stable isotopic data from HPC Hole 574A.

Sample (level in cm)	Sub-bottom depth (m)	Species	$\delta^{18}O$ (‰)	$\delta^{13}C$ (‰)
574-A-12-3, 80	102.50	*Oridorsalis* sp.	2.88	0.91
574A-12-3, 100	102.70	*Oridorsalis* sp.	2.66	1.28
574A-12-3, 100	102.70	*C. kullenbergi*	2.96	1.02
574A-12-3, 120	102.90	*G. subglobosa*	2.82	0.97
574A-12-3, 140	103.10	*G. subglobosa*	2.70	0.66
574A-12-3, 140	103.10	*C. kullenbergi*	2.87	0.81
574A-12-4, 0	103.20	*Oridorsalis* sp.	2.92	0.67
574A-12-4, 0	103.20	*C. kullenbergi*	3.00	1.14
574A-12-4, 20	103.40	*Oridorsalis* sp.	2.91	0.68
574A-12-4, 20	103.40	*C. kullenbergi*	2.91	1.03
574A-12-4, 40	103.60	*C. kullenbergi*	2.67	1.02
574A-12-4, 60	103.80	*Oridorsalis* sp.	2.70	1.03
574A-12-4, 60	103.80	*C. kullenbergi*	2.75	1.05
574A-12-4, 80	104.00	*Oridorsalis* sp.	2.93	0.95
574A-12-4, 80	104.00	*C. kullenbergi*	3.02	0.94
574A-12-4, 100	104.20	*Oridorsalis* sp.	3.21	0.74
574A-12-4, 100	104.20	*C. kullenbergi*	3.06	0.86
574A-12-4, 120	104.40	*Oridorsalis* sp.	3.05	0.70
574A-12-4, 120	104.40	*C. kullenbergi*	3.20	0.65
574A-12-4, 140	104.60	*Oridorsalis* sp.	2.96	0.75
574A-12-4, 140	104.60	*C. kullenbergi*	2.73	0.97
574A-12-5, 0	104.70	*C. kullenbergi*	3.02	0.67
574A-12-5, 0	104.70	*Oridorsalis* sp.	2.91	0.65
574A-12-5, 20	104.90	*C. kullenbergi*	2.73	1.06
574A-12-5, 40	105.10	*C. kullenbergi*	2.86	0.98
574A-12-5, 60	105.30	*C. kullenbergi*	2.70	0.78
574A-12-5, 80	105.50	*C. kullenbergi*	2.97	0.70
574A-12-5, 100	105.70	*Oridorsalis* sp.	3.03	0.74
574A-12-5, 120	105.90	*C. kullenbergi*	2.97	0.75
574A-12-5, 120	105.90	*Oridorsalis* sp.	2.85	0.85
574A-12-5, 140	106.10	*Oridorsalis* sp.	2.79	0.69
574A-12-6, 0	106.20	*Oridorsalis* sp.	2.69	0.84
574A-12-6, 0	106.20	*C. kullenbergi*	2.73	0.99
574A-12-6, 20	106.40	*Oridorsalis* sp.	2.89	0.58
574A-12-6, 20	106.40	*C. kullenbergi*	2.84	1.07
574A-12-6, 40	106.60	*Oridorsalis* sp.	2.69	0.64
574A-12-6, 40	106.60	*Oridorsalis* sp.	2.94	0.67
574A-12-6, 40	106.60	*Oridorsalis* sp.	2.47	0.72
574A-12-6, 60	106.80	*Oridorsalis* sp.	2.81	0.89
574A-12-6, 60	106.80	*Gyroidina* sp.	2.71	0.04
574A-12-6, 60	106.80	*C. kullenbergi*	2.80	0.97
574A-12-6, 80	107.00	*P. wuellerstorfi**	2.91	0.79
574A-12-6, 80	107.00	*Oridorsalis* sp.	2.83	0.51
574A-12-6, 100	107.20	*P. wuellerstorfi*	3.13	0.88
574A-12-6, 100	107.20	*C. kullenbergi*	2.84	0.87
574A-12-6, 120	107.40	*Oridorsalis* sp.	2.90	1.31
574A-12-6, 120	107.40	*P. wuellerstorfi**	2.54	0.87
574A-12-6, 140	107.60	*Oridorsalis* sp.	2.82	0.54
574A-12-6, 140	107.60	*P. wuellerstorfi**	3.12	0.81
574A-12-7, 0	107.70	*C. kullenbergi*	2.70	0.65
574A-12-7, 0	107.70	*P. wuellerstorfi**	2.75	0.80
574A-12-7, 20	107.90	*C. kullenbergi*	2.86	0.80
574A-12-7, 20	107.90	*P. wuellerstorfi*	2.77	0.93
574A-13-1, 100	109.20	*C. kullenbergi*	2.66	0.79
574A-13-1, 120	109.40	*C. kullenbergi*	2.50	0.48
574A-13-1, 140	109.60	*C. kullenbergi*	2.38	0.34
574A-13-2, 0	109.70	*P. wuellerstorfi*	2.93	0.64
574A-13-2, 20	109.90	*C. kullenbergi*	2.74	0.41
574A-13-2, 20	109.90	*P. wuellerstorfi*	2.94	0.73
574A-13-2, 40	110.10	*C. kullenbergi*	2.08	0.51
574A-13-2, 60	110.30	*Oridorsalis* sp.	2.36	0.74
574A-13-2, 60	110.30	*P. wuellerstorfi*	2.62	0.57
574A-13-2, 80	110.50	*C. kullenbergi*	2.85	0.50
574A-13-2, 100	110.70	*G. subglobosa*	2.90	0.48
574A-13-2, 100	110.70	*C. kullenbergi*	2.79	0.67
574A-13-2, 120	110.90	*C. kullenbergi*	2.78	0.75
574A-13-2, 140	111.10	*C. kullenbergi*	2.66	0.56
574A-13-2, 140	111.10	*Oridorsalis* sp.	2.71	0.53
574A-13-3, 0	111.20	*Oridorsalis* sp.	2.96	0.63
574A-13-3, 0	111.20	*C. kullenbergi*	2.97	0.61
574A-13-3, 20	111.40	*Oridorsalis* sp.	2.77	1.20
574A-13-3, 40	111.60	*Oridorsalis* sp.	2.79	0.64
574A-13-3, 40	111.60	*C. kullenbergi*	2.62	0.67
574A-13-3, 60	111.80	*C. kullenbergi*	2.57	0.61
574A-13-3, 80	112.00	*C. kullenbergi*	2.98	0.78
574A-13-3, 80	112.00	*Oridorsalis* sp.	2.81	0.72

Table 1. (Continued).

Sample (level in cm)	Sub-bottom depth (m)	Species	$\delta^{18}O$ (‰)	$\delta^{13}C$ (‰)
574A-13-3, 100	112.20	*C. kullenbergi*	2.83	0.89
574A-13-3, 100	112.20	*C. kullenbergi*	2.75	0.80
574A-13-3, 120	112.40	*C. kullenbergi*	2.38	0.69
574A-13-3, 140	112.60	*C. kullenbergi*	2.70	0.49
574A-13-3, 140	112.60	*C. kullenbergi*	2.70	0.72
574A-13-4, 0	112.70	*Oridorsalis* sp.	2.93	0.36
574A-13-4, 0	112.70	*C. kullenbergi*	3.00	0.80
574A-13-4, 20	112.90	*C. kullenbergi*	2.53	0.80
574A-14-1, 0	113.10	*Oridorsalis* sp.	2.78	0.57
574A-14-1, 0	113.10	*C. kullenbergi*	2.88	0.90
574A-14-1, 20	113.30	*C. kullenbergi*	2.81	0.87
574A-14-1, 40	113.50	*C. kullenbergi*	2.78	0.78
574A-14-1, 60	113.70	*C. kullenbergi*	2.75	0.92
574A-14-1, 80	113.90	*C. kullenbergi*	2.66	0.84
574A-14-1, 100	114.10	*C. kullenbergi*	2.72	0.82
574A-14-1, 120	114.30	*C. kullenbergi*	2.70	0.87
574A-14-1, 140	114.50	*C. kullenbergi*	2.80	0.80
574A-14-2, 0	114.60	*C. kullenbergi*	2.69	0.87
574A-14-2, 17	114.77	*C. kullenbergi*	2.73	0.89
574A-14-2, 40	115.00	*C. kullenbergi*	2.72	0.93
574A-14-2, 60	115.20	*C. havanensis*	2.83	0.56
574A-14-2, 60	115.20	*C. kullenbergi*	2.87	0.95
574A-14-2, 80	115.40	*C. kullenbergi*	2.73	0.88
574A-19-1, 1	141.41	*C. kullenbergi*	2.60	1.27
574A-19-1, 11	141.51	*C. kullenbergi*	2.52	1.15
574A-19-1, 21	141.61	*C. kullenbergi*	2.36	1.04
574A-19-1, 31	141.71	*C. kullenbergi*	2.37	0.84
574A-19-1, 41	141.81	*C. kullenbergi*	2.64	0.82
574A-19-1, 51	141.91	*C. kullenbergi*	2.83	1.04
574A-19-4, 11	146.01	*C. kullenbergi*	2.54	1.13
574A-19-1, 61	142.01	*C. kullenbergi*	2.63	1.17
574A-19-4, 21	146.11	*C. kullenbergi*	2.21	1.26
574A-19-1, 71	142.11	*C. kullenbergi*	2.79	1.20
574A-19-1, 81	142.21	*C. kullenbergi*	2.85	1.36
574A-19-1, 91	142.31	*C. kullenbergi*	2.79	1.23
574A-19-1, 101	142.41	*C. kullenbergi*	2.75	1.23
574A-19-1, 108	142.48	*C. kullenbergi*	2.75	1.28
574A-19-1, 112	142.52	*Oridorsalis* sp.	2.51	1.37
574A-19-1, 121	142.61	*C. kullenbergi*	2.45	1.04
574A-19-1, 131	142.71	*C. kullenbergi*	2.50	1.18
574A-19-1, 141	142.81	*C. kullenbergi*	2.59	1.06
574A-19-2, 1	142.91	*C. kullenbergi*	2.38	0.98
574A-19-2, 11	143.01	*C. kullenbergi*	2.41	1.05
574A-19-2, 21	143.11	*C. kullenbergi*	2.39	0.84
574A-19-2, 31	143.21	*C. kullenbergi*	2.63	1.20
574A-19-2, 41	143.31	*C. kullenbergi*	2.61	1.12
574A-19-2, 51	143.41	*C. kullenbergi*	2.68	1.20
574A-19-2, 61	143.51	*C. kullenbergi*	2.65	1.17
574A-19-2, 71	143.61	*C. kullenbergi*	2.64	1.14
574A-19-2, 81	143.71	*C. kullenbergi*	2.65	1.14
574A-19-2, 91	143.81	*C. kullenbergi*	2.67	0.81
574A-19-2, 101	143.91	*C. kullenbergi*	2.54	1.08
574A-19-2, 111	144.01	*C. kullenbergi*	2.63	0.89
574A-19-2, 121	144.11	*C. kullenbergi*	2.62	1.15
574A-19-2, 131	144.21	*C. kullenbergi*	2.41	1.12
574A-19-2, 141	144.31	*C. kullenbergi*	2.44	1.24
574A-19-3, 1	144.41	*C. havanensis*	2.37	1.21
574A-19-3, 1	144.41	*P. wuellerstorfi*	2.42	1.27
574A-19-3, 11	144.51	*C. kullenbergi*	2.32	1.16
574A-19-3, 31	144.71	*C. kullenbergi*	2.58	1.27
574A-19-3, 41	144.81	*C. kullenbergi*	2.37	1.17
574A-19-3, 61	145.01	*C. kullenbergi*	2.41	1.22
574A-19-3, 61	145.01	*P. wuellerstorfi*	2.46	1.33
574A-19-3, 71	145.11	*C. kullenbergi*	2.25	1.08
574A-19-3, 81	145.21	*C. kullenbergi*	2.47	1.17
574A-19-3, 91	145.31	*C. kullenbergi*	2.47	1.24
574A-19-3, 101	145.41	*C. kullenbergi*	2.60	1.29
574A-19-3, 111	145.51	*C. kullenbergi*	2.56	0.97
574A-19-3, 111	145.51	*C. kullenbergi*	2.50	1.26
574A-19-3, 121	145.61	*C. kullenbergi*	2.60	1.18
574A-19-3, 131	145.71	*C. kullenbergi*	2.58	1.15
574A-19-3, 141	145.81	*P. wuellerstorfi*	2.63	1.11
574A-19-4, 1	145.91	*C. kullenbergi*	2.62	1.14
574A-19-4, 31	146.21	*P. wuellerstorfi*	2.41	1.13
574A-19-4, 41	146.31	*P. wuellerstorfi*	2.20	0.93
574A-19-4, 51	146.41	*C. kullenbergi*	2.25	0.77

Table 1. (Continued).

Sample (level in cm)	Sub-bottom depth (m)	Species	$\delta^{18}O$ (‰)	$\delta^{13}C$ (‰)
574A-19-4, 61	146.51	*P. wuellerstorfi*	2.40	1.09
574A-19-4, 61	146.51	*C. kullenbergi*	2.12	0.60
574A-19-4, 71	146.61	*P. wuellerstorfi*	2.54	1.18
574A-19-4, 71	146.61	*C. kullenbergi*	1.97	0.84
574A-19-4, 81	146.71	*P. wuellerstorfi*	2.66	1.31
574A-19-4, 91	146.81	*P. wuellerstorfi*	2.48	1.27
574A-19-4, 101	146.91	*P. wuellerstorfi*	2.43	1.13
574A-19-4, 111	147.01	*P. wuellerstorfi*	2.96	1.38
574A-19-4, 121	147.11	*C. kullenbergi*	2.55	1.35
574A-19-4, 131	147.21	*C. kullenbergi*	2.59	1.28
574A-19-4, 141	147.31	*P. wuellerstorfi*	2.52	1.16
574A-19-5, 1	147.41	*P. wuellerstorfi*	2.77	1.29
574A-19-5, 11	147.51	*P. wuellerstorfi*	2.84	1.32
574A-19-5, 21	147.61	*P. wuellerstorfi*	2.70	1.18
574A-19-5, 31	147.71	*P. wuellerstorfi*	2.56	1.31
574A-19-5, 41	147.81	*P. wuellerstorfi*	2.54	1.32
574A-19-5, 51	147.91	*P. wuellerstorfi*	2.64	1.38
574A-19-5, 61	148.01	*P. wuellerstorfi*	2.46	1.14
574A-19-5, 71	148.11	*P. wuellerstorfi*	2.39	1.18
574A-19-5, 81	148.21	*P. wuellerstorfi*	2.40	1.10
574A-19-5, 91	148.31	*P. wuellerstorfi*	2.24	1.02
574A-19-5, 101	148.41	*P. wuellerstorfi*	2.23	0.95
574A-19-5, 111	148.51	*C. kullenbergi*	2.29	0.89
574A-19-5, 121	148.61	*C. kullenbergi*	2.42	0.96
574A-19-5, 131	148.71	*C. kullenbergi*	2.09	1.19
574A-19-5, 141	148.81	*C. kullenbergi*	2.12	0.98
574A-19-6, 1	148.91	*C. kullenbergi*	2.54	1.11
574A-19-6, 1	148.91	*C. havanensis*	2.43	0.64
574A-19-6, 11	149.01	*C. kullenbergi*	2.55	1.32
574A-19-6, 21	149.11	*C. kullenbergi*	2.44	1.47
574A-19-6, 31	149.21	*C. kullenbergi*	2.49	1.43
574A-19-6, 41	149.31	*C. kullenbergi*	2.54	1.34
574A-19-6, 51	149.41	*C. kullenbergi*	2.48	1.30
574A-19-6, 61	149.51	*C. kullenbergi*	2.40	1.29
574A-19-6, 71	149.61	*C. kullenbergi*	2.23	1.36
574A-19-6, 81	149.71	*C. kullenbergi*	2.54	1.31
574A-19-6, 91	149.81	*C. kullenbergi*	2.32	1.17
574A-19-6, 101	149.91	*C. kullenbergi*	2.40	1.46
574A-19-6, 111	150.01	*C. kullenbergi*	2.11	1.34
574A-19-6, 121	150.11	*C. kullenbergi*	2.31	1.38
574A-19-6, 131	150.21	*C. kullenbergi*	2.55	1.58
574A-19-6, 141	150.31	*C. kullenbergi*	2.67	1.68
574A-19-7, 1	150.41	*C. kullenbergi*	2.45	1.70
574A-19-7, 11	150.51	*C. kullenbergi*	2.72	1.74
574A-19-7, 21	150.61	*C. kullenbergi*	2.72	1.81
574A-19-7, 21	150.61	*Oridorsalis* sp.	2.35	1.73
574A-19-7, 31	150.71	*C. kullenbergi*	2.46	1.59
574A-19-7, 41	150.81	*C. kullenbergi*	2.64	1.81
574A-20-1, 61	151.51	*C. kullenbergi*	2.46	1.75
574A-20-1, 71	151.61	*C. kullenbergi*	2.75	1.96
574A-20-1, 71	151.61	*Oridorsalis* sp.	2.46	1.95
574A-20-1, 81	151.71	*C. kullenbergi*	2.59	1.95
574A-20-1, 81	151.71	*Oridorsalis* sp.	2.59	2.04
574A-20-1, 91	151.81	*C. kullenbergi*	2.55	1.84
574A-20-1, 91	151.81	*Oridorsalis* sp.	2.74	1.88
574A-20-1, 101	151.91	*C. kullenbergi*	2.73	2.01
574A-20-1, 101	151.91	*Oridorsalis* sp.	2.66	1.78
574A-20-1, 111	152.01	*Oridorsalis* sp.	2.74	1.71
574A-20-1, 111	152.01	*C. kullenbergi*	2.77	2.03
574A-20-1, 121	152.11	*C. kullenbergi*	2.61	1.83
574A-20-1, 121	152.11	*Oridorsalis* sp.	2.61	1.67
574A-20-1, 131	152.21	*C. kullenbergi*	2.80	2.01
574A-20-1, 131	152.21	*Oridorsalis* sp.	2.31	1.48
574A-20-1, 141	152.31	*C. kullenbergi*	2.72	1.69
574A-20-1, 141	152.31	*Oridorsalis* sp.	2.53	1.64
574A-20-2, 1	152.41	*C. kullenbergi*	2.80	1.93
574A-20-2, 1	152.41	*Oridorsalis* sp.	2.66	2.06
574A-20-2, 11	152.51	*C. kullenbergi*	2.74	1.85
574A-20-2, 21	152.61	*C. kullenbergi*	2.75	1.98
574A-20-2, 21	152.61	*Oridorsalis* sp.	2.67	1.93
574A-20-2, 31	152.71	*C. kullenbergi*	2.63	1.79
574A-20-2, 41	152.81	*C. kullenbergi*	2.64	1.74
574A-20-2, 41	152.81	*Oridorsalis* sp.	2.53	1.56
574A-20-2, 51	152.91	*C. kullenbergi*	2.53	1.64
574A-20-2, 51	152.91	*Oridorsalis* sp.	2.59	1.56
574A-20-2, 61	153.01	*C. kullenbergi*	2.58	1.70

Table 1. (Continued).

Sample (level in cm)	Sub-bottom depth (m)	Species	$\delta^{18}O$ (‰)	$\delta^{13}C$ (‰)
574A-20-2, 61	153.01	*Oridorsalis* sp.	2.60	1.75
574A-20-2, 71	153.11	*C. kullenbergi*	2.76	1.82
574A-20-2, 81	153.21	*C. kullenbergi*	2.64	1.74
574A-20-2, 81	153.21	*Oridorsalis* sp.	2.65	1.73
574A-20-2, 91	153.31	*C. kullenbergi*	2.52	1.72
574A-20-2, 101	153.41	*C. kullenbergi*	2.59	1.79
574A-20-2, 101	153.41	*Oridorsalis* sp.	2.74	1.88
574A-20-2, 111	153.51	*C. kullenbergi*	2.57	1.80
574A-20-2, 111	153.51	*Oridorsalis* sp.	2.57	1.80
574A-20-2, 121	153.61	*P. wuellerstorfi*	2.60	1.21
574A-20-2, 121	153.61	*C. kullenbergi*	2.72	1.17
574A-20-2, 131	153.71	*C. kullenbergi*	2.69	1.04
574A-20-2, 141	153.81	*C. kullenbergi*	2.56	1.76
574A-20-2, 141	153.81	*Oridorsalis* sp.	2.56	1.68
574A-20-3, 1	153.91	*C. kullenbergi*	2.81	1.83
574A-20-3, 11	154.01	*Oridorsalis* sp.	2.80	1.73
574A-20-3, 11	154.01	*C. kullenbergi*	2.68	1.70
574A-20-3, 21	154.11	*Oridorsalis* sp.	2.62	1.99
574A-20-3, 31	154.21	*C. kullenbergi*	2.82	1.77
574A-20-3, 31	154.21	*Oridorsalis* sp.	2.69	1.75
574A-20-3, 41	154.31	*C. kullenbergi*	2.64	1.88
574A-20-3, 41	154.31	*Oridorsalis* sp.	2.64	1.75
574A-20-3, 61	154.51	*C. kullenbergi*	2.61	1.80
574A-20-3, 71	154.61	*Oridorsalis* sp.	2.63	1.62
574A-20-3, 81	154.71	*C. kullenbergi*	2.45	1.56
574A-20-3, 91	154.81	*Oridorsalis* sp.	2.37	1.98
574A-20-3, 91	154.81	*C. kullenbergi*	2.64	1.87
574A-20-3, 101	154.91	*Oridorsalis* sp.	2.57	1.61
574A-20-3, 101	154.91	*C. kullenbergi*	2.78	1.72
574A-20-3, 111	155.01	*C. kullenbergi*	2.69	1.65
574A-20-3, 121	155.11	*C. kullenbergi*	2.55	1.62
574A-20-3, 131	155.21	*C. kullenbergi*	2.63	1.70
574A-20-3, 141	155.31	*C. kullenbergi*	2.72	1.70
574A-20-3, 141	155.31	*Oridorsalis* sp.	2.45	1.75
574A-20-4, 1	155.41	*C. kullenbergi*	2.57	1.64
574A-20-4, 11	155.51	*C. kullenbergi*	2.53	1.54
574A-20-4, 21	155.61	*C. kullenbergi*	2.41	1.64
574A-20-4, 31	155.71	*C. kullenbergi*	2.06	1.40
574A-20-4, 41	155.81	*C. kullenbergi*	2.21	1.22
574A-20-4, 41	155.81	*Oridorsalis* sp.	2.14	1.11
574A-20-4, 51	155.91	*C. havanensis*	2.34	1.04
574A-20-4, 61	156.01	*C. kullenbergi*	2.06	1.56
574A-20-4, 71	156.11	*C. havanensis*	1.95	0.92
574A-20-4, 71	156.11	*Oridorsalis* sp.	2.02	1.20
574A-20-4, 81	156.21	*C. havanensis*	1.85	1.39
574A-20-4, 91	156.31	*P. wuellerstorfi*	1.88	1.30
574A-20-4, 91	156.31	*Oridorsalis* sp.	1.50	1.26
574A-20-4, 101	156.41	*P. wuellerstorfi*	2.39	1.41
574A-20-4, 101	156.41	*C. kullenbergi*	2.22	0.89
574A-20-4, 111	156.51	*C. kullenbergi*	2.02	1.35
574A-20-4, 121	156.61	*C. kullenbergi*	1.93	1.43
574A-20-4, 121	156.61	*Oridorsalis* sp.	1.65	1.19
574A-20-4, 141	156.81	*P. wuellerstorfi*	2.19	1.16
574A-20-5, 1	156.91	*P. wuellerstorfi*	2.28	1.17
574A-20-5, 11	157.01	*C. kullenbergi*	2.26	1.17
574A-20-5, 21	157.11	*C. kullenbergi*	2.10	1.56
574A-20-5, 31	157.21	*Oridorsalis* sp.	2.13	1.08
574A-20-5, 41	157.31	*C. havanensis*	2.06	1.31
574A-20-5, 51	157.41	*P. wuellerstorfi*	2.08	1.33
574A-20-5, 61	157.51	*C. kullenbergi*	2.20	1.10
574A-20-5, 71	157.61	*C. kullenbergi*	1.99	1.33
574A-20-5, 71	157.61	*Oridorsalis* sp.	2.07	1.25
574A-20-5, 81	157.71	*C. havanensis*	2.04	1.24
574A-20-5, 91	157.81	*P. wuellerstorfi*	2.03	1.38
574A-20-5, 41	157.31	*C. kullenbergi*	1.87	1.45
574A-20-5, 91	157.81	*P. wuellerstorfi*	2.03	1.38
574A-20-5, 101	157.91	*P. wuellerstorfi*	1.90	1.28
574A-20-5, 101	157.91	*Oridorsalis* sp.	1.69	1.41
574A-20-5, 111	158.01	*P. wuellerstorfi*	2.24	1.29
574A-20-5, 111	158.01	*Oridorsalis* sp.	1.93	1.34
574A-20-5, 121	158.11	*P. wuellerstorfi*	2.43	1.33
574A-20-5, 131	158.21	*P. wuellerstorfi*	2.53	1.41
574A-20-5, 141	158.31	*Oridorsalis* sp.	2.26	1.26
574A-20-5, 141	158.31	*P. wuellerstorfi*	2.52	1.44
574A-20-6, 1	158.41	*P. wuellerstorfi*	2.65	1.51
574A-20-6, 11	158.51	*C. kullenbergi*	2.38	1.25

Table 1. (Continued).

Sample (level in cm)	Sub-bottom depth (m)	Species	$\delta^{18}O$ (‰)	$\delta^{13}C$ (‰)
574A-20-6, 11	158.51	*Oridorsalis* sp.	2.41	1.41
574A-20-6, 21	158.61	*Oridorsalis* sp.	2.13	1.67
574A-20-6, 21	158.61	*C. kullenbergi*	2.18	1.60
574A-20-6, 31	158.71	*C. kullenbergi*	2.13	1.59
574A-20-6, 41	158.81	*C. kullenbergi*	1.82	1.29
574A-20-6, 51	158.91	*Oridorsalis* sp.	2.00	1.37
574A-20-6, 61	159.01	*Oridorsalis* sp.	2.07	1.32
574A-20-6, 61	159.01	*C. kullenbergi*	2.05	1.30
574A-20-6, 71	159.11	*C. kullenbergi*	2.33	1.39
574A-20-6, 81	159.21	*C. kullenbergi*	2.11	1.22
574A-20-6, 91	159.31	*C. kullenbergi*	2.28	1.47
574A-20-6, 101	159.41	*C. kullenbergi*	2.10	1.51
574A-20-6, 111	159.51	*C. kullenbergi*	2.10	1.58
574A-20-6, 121	159.61	*C. kullenbergi*	2.10	1.62
574A-20-6, 131	159.71	*Oridorsalis* sp.	1.92	1.56
574A-20-6, 141	159.81	*C. kullenbergi*	1.85	1.41
574A-22-1, 1	168.41	*C. kullenbergi*	1.79	1.30
574A-22-1, 1	168.41	*P. wuellerstorfi*	2.13	1.63
574A-22-1, 11	168.51	*P. wuellerstorfi*	2.21	1.66
574A-22-1, 21	168.61	*C. kullenbergi*	1.85	1.58
574A-22-1, 31	168.71	*P. wuellerstorfi*	2.07	1.83
574A-22-1, 41	168.81	*P. wuellerstorfi*	1.72	1.74
574A-22-1, 61	169.01	*P. wuellerstorfi*	1.65	1.78
574A-22-1, 71	169.11	*P. wuellerstorfi*	1.88	1.80
574A-22-1, 81	169.21	*P. wuellerstorfi*	1.85	1.73
574A-22-1, 91	169.31	*P. wuellerstorfi*	1.94	1.70
574A-22-1, 101	169.41	*P. wuellerstorfi*	1.95	1.57
574A-22-1, 111	169.51	*P. wuellerstorfi*	2.08	1.56
574A-22-1, 21	168.61	*P. wuellerstorfi*	2.14	1.80
574A-22-1, 121	169.61	*P. wuellerstorfi*	1.88	1.50
574A-22-1, 131	169.71	*P. wuellerstorfi*	2.14	1.64
574A-22-1, 141	169.81	*P. wuellerstorfi*	2.16	1.71
574A-22-2, 1	169.91	*P. wuellerstorfi*	2.16	1.62
574A-22-2, 11	170.01	*P. wuellerstorfi*	2.04	1.96
574A-22-2, 21	170.11	*P. wuellerstorfi*	1.91	1.88
574A-22-2, 31	170.21	*P. wuellerstorfi*	1.84	1.93
574A-22-2, 41	170.31	*C. kullenbergi*	1.55	1.76
574A-22-2, 41	170.31	*P. wuellerstorfi*	1.76	1.75
574A-22-2, 51	170.41	*C. kullenbergi*	1.65	1.65
574A-22-2, 61	170.51	*P. wuellerstorfi*	1.67	1.66
574A-22-2, 71	170.61	*C. kullenbergi*	2.20	1.56
574A-22-2, 71	170.61	*P. wuellerstorfi*	1.82	1.73
574A-22-2, 81	170.71	*P. wuellerstorfi*	1.89	1.61
574A-22-2, 91	170.81	*P. wuellerstorfi*	2.30	1.69
574A-22-2, 101	170.91	*P. wuellerstorfi*	2.10	1.71
574A-22-2, 111	171.01	*P. wuellerstorfi*	2.12	1.63
574A-22-2, 121	171.11	*P. wuellerstorfi*	2.38	1.68
574A-22-2, 131	171.21	*P. wuellerstorfi*	2.16	1.67
574A-22-2, 146	171.36	*P. wuellerstorfi*	2.14	1.73
574A-22-3, 1	171.41	*P. wuellerstorfi*	2.14	1.90
574A-22-3, 11	171.51	*P. wuellerstorfi*	1.99	1.71
574A-22-3, 21	171.61	*Gyroidina* sp.	1.78	0.73
574A-22-3, 21	171.61	*C. kullenbergi*	2.07	1.80
574A-22-3, 21	171.61	*P. wuellerstorfi*	1.97	1.88
574A-22-3, 31	171.71	*C. kullenbergi*	2.13	1.62
574A-22-3, 31	171.71	*P. wuellerstorfi*	2.17	1.84
574A-22-3, 41	171.81	*C. kullenbergi*	2.03	1.89
574A-22-3, 51	171.91	*P. wuellerstorfi*	2.15	1.74
574A-22-3, 61	172.01	*P. wuellerstorfi*	1.99	1.74
574A-22-3, 71	172.11	*P. wuellerstorfi*	2.10	1.92
574A-22-3, 81	172.21	*P. wuellerstorfi*	1.94	1.53
574A-22-3, 91	172.31	*P. wuellerstorfi*	1.94	1.51
574A-22-3, 101	172.41	*P. wuellerstorfi*	1.88	1.49
574A-22-3, 111	172.51	*C. kullenbergi*	1.96	0.99
574A-22-3, 121	172.61	*P. wuellerstorfi*	2.17	1.47
574A-22-3, 131	172.71	*C. kullenbergi*	1.94	1.48
574A-22-3, 141	172.81	*P. wuellerstorfi*	1.75	1.40
574A-22-4, 1	172.91	*P. wuellerstorfi*	1.84	1.16
574A-22-4, 11	173.01	*P. wuellerstorfi*	1.76	1.65
574A-22-4, 21	173.11	*P. wuellerstorfi*	1.57	1.36
574A-22-4, 31	173.21	*P. wuellerstorfi*	1.82	1.60
574A-22-4, 41	173.31	*P. wuellerstorfi*	1.77	1.33
574A-22-4, 51	173.41	*P. wuellerstorfi*	1.94	1.62
574A-22-4, 61	173.51	*P. wuellerstorfi*	1.85	1.59
574A-22-4, 71	173.61	*P. wuellerstorfi*	1.78	1.27
574A-22-4, 81	173.71	*P. wuellerstorfi*	2.17	1.56

Table 1. (Continued).

Sample (level in cm)	Sub-bottom depth (m)	Species	$\delta^{18}O$ (‰)	$\delta^{13}C$ (‰)
574A-22-4, 91	173.81	*P. wuellerstorfi*	2.43	1.49
574A-22-4, 101	173.91	*P. wuellerstorfi*	2.42	1.54
574A-22-4, 111	174.01	*P. wuellerstorfi*	2.31	1.52
574A-22-4, 121	174.11	*P. wuellerstorfi*	2.08	1.36
574A-22-4, 131	174.21	*P. wuellerstorfi*	1.85	1.23
574A-22-4, 146	174.36	*C. kullenbergi*	1.83	1.18
574A-22-5, 61	175.01	*P. wuellerstorfi*	2.16	1.53
574A-22-5, 71	175.11	*P. wuellerstorfi*	1.79	1.35
574A-22-5, 81	175.21	*P. wuellerstorfi*	1.88	1.40
574A-22-5, 91	175.31	*P. wuellerstorfi*	1.81	1.55
574A-22-5, 101	175.41	*C. kullenbergi*	1.76	1.34
574A-22-5, 111	175.51	*P. wuellerstorfi**	1.53	1.19
574A-22-5, 121	175.61	*P. wuellerstorfi*	1.92	1.47
574A-22-5, 131	175.71	*P. wuellerstorfi**	1.78	1.41
574A-22-5, 141	175.81	*P. wuellerstorfi**	1.80	1.17
574A-22-6, 1	175.91	*P. wuellerstorfi**	1.70	1.28
574A-22-6, 11	176.01	*P. wuellerstorfi*	1.97	1.40
574A-22-6, 21	176.11	*P. wuellerstorfi*	1.85	1.37
574A-22-6, 21	176.11	*C. kullenbergi*	1.65	1.07
574A-22-6, 31	176.21	*P. wuellerstorfi*	2.16	1.45
574A-22-6, 41	175.31	*P. wuellerstorfi*	2.15	1.54
574A-22-6, 61	176.51	*P. wuellerstorfi*	2.10	1.63
574A-72-6, 71	176.61	*P. wuellerstorfi*	1.90	1.50
574A-22-6, 81	176.71	*P. wuellerstorfi**	1.74	1.27
574A-22-6, 91	176.81	*P. wuellerstorfi**	1.70	1.36
574A-22-6, 101	176.91	*P. wuellerstorfi**	1.82	1.31
574A-22-6, 111	177.01	*P. wuellerstorfi*	1.92	1.47
574A-22-6, 111	177.01	*C. kullenbergi*	1.55	1.13
574A-22-6, 121	177.11	*P. wuellerstorfi*	1.93	1.36
574A-22-6, 131	177.21	*P. wuellerstorfi*	1.70	1.26
574A-22-6, 141	177.31	*P. wuellerstorfi*	1.83	1.33
574A-22-7, 1	177.41	*C. kullenbergi*	1.86	1.21
574A-22-7, 11	177.51	*P. wuellerstorfi*	2.10	1.44
574A-22-7, 21	177.61	*P. wuellerstorfi*	2.00	1.40
574A-22-7, 31	177.71	*P. wuellerstorfi*	2.06	1.38
574A-22-7, 41	177.81	*P. wuellerstorfi*	2.02	1.32
574A-23-1, 6	177.96	*C. kullenbergi*	1.94	1.31
574A-23-1, 6	177.96	*P. wuellerstorfi*	1.84	1.28
574A-23-1, 21	178.11	*P. wuellerstorfi*	1.76	1.54
574A-23-1, 31	178.21	*P. wuellerstorfi*	1.62	1.50
574A-23-1, 41	178.31	*P. wuellerstorfi**	1.63	1.42
574A-23-1, 41	178.31	*C. kullenbergi*	1.62	0.94
574A-23-1, 51	178.41	*P. wuellerstorfi*	1.70	1.52
574A-23-1, 71	178.61	*P. wuellerstorfi*	1.59	1.32
574A-23-1, 1	177.91	*P. wuellerstorfi*	2.11	1.49
574A-23-1, 11	178.01	*P. wuellerstorfi*	1.97	1.29
574A-23-1, 21	178.11	*P. wuellerstorfi*	1.91	1.24
574A-23-1, 31	178.21	*P. wuellerstorfi*	1.73	1.24
574A-23-1, 41	178.31	*P. wuellerstorfi*	2.05	1.44
574A-23-1, 51	178.41	*P. wuellerstorfi*	1.89	1.43
574A-23-1, 61	178.51	*P. wuellerstorfi*	1.77	1.41
574A-23-1, 81	178.71	*P. wuellerstorfi*	1.80	1.29
574A-23-1, 91	178.81	*P. wuellerstorfi*	1.68	1.29
574A-23-1, 101	178.91	*P. wuellerstorfi*	1.92	1.30
574A-23-1, 111	179.01	*P. wuellerstorfi*	1.85	1.30
574A-23-1, 121	179.11	*P. wuellerstorfi*	1.89	1.40
574A-23-1, 132	179.22	*P. wuellerstorfi*	1.76	1.35
574A-23-1, 147	179.37	*P. wuellerstorfi*	1.55	1.32
574A-23-2, 21	179.61	*P. wuellerstorfi*	1.39	1.24
574A-23-2, 11	179.51	*C. kullenbergi*	1.59	1.25
574A-23-2, 21	179.61	*C. kullenbergi*	1.59	1.34
574A-23-2, 31	179.71	*C. kullenbergi*	1.36	1.04
574A-23-2, 41	179.81	*C. kullenbergi*	1.84	1.12
574A-23-2, 51	179.91	*C. kullenbergi*	1.45	1.12
574A-23-2, 51	179.91	*P. wuellerstorfi*	1.72	1.31
574A-23-2, 61	180.01	*C. kullenbergi*	1.73	1.37
574A-23-2, 61	180.01	*P. wuellerstorfi*	1.70	1.00
574A-23-2, 71	180.11	*P. wuellerstorfi*	2.08	1.37
574A-23-2, 81	180.21	*P. wuellerstorfi*	1.99	1.39
574A-23-2, 91	180.31	*P. wuellerstorfi*	1.99	1.42
574A-23-2, 101	180.41	*C. kullenbergi*	1.84	1.19
574A-23-2, 111	180.51	*C. kullenbergi*	1.69	1.32
574A-23-2, 111	180.51	*C. kullenbergi*	1.89	1.37
574A-23-2, 121	180.61	*P. wuellerstorfi*	1.69	1.31
574A-23-2, 132	180.72	*C. kullenbergi*	1.58	1.42
574A-23-2, 147	180.87	*P. wuellerstorfi*	2.15	1.38

Table 1. (Continued).

Sample (level in cm)	Sub-bottom depth (m)	Species	$\delta^{18}O$ (‰)	$\delta^{13}C$ (‰)
574A-23-3, 1	180.91	*P. wuellerstorfi*	1.85	1.46
574A-23-3, 11	181.01	*P. wuellerstorfi*	2.02	1.55
574A-23-3, 21	181.11	*P. wuellerstorfi*	2.11	1.63
574A-23-3, 31	181.21	*P. wuellerstorfi*	1.89	1.35
574A-23-3, 41	181.31	*P. wuellerstorfi*	2.14	1.66
574A-23-3, 51	181.41	*P. wuellerstorfi*	2.02	1.19
574A-23-3, 61	181.51	*P. wuellerstorfi*	2.10	1.53
574A-23-3, 71	181.61	*P. wuellerstorfi*	2.22	1.50
574A-23-3, 81	181.71	*P. wuellerstorfi*	2.01	1.52
574A-23-3, 91	181.81	*P. wuellerstorfi*	1.66	1.37
574A-23-3, 101	181.91	*P. wuellerstorfi*	1.69	1.46
574A-23-3, 112	182.02	*P. wuellerstorfi*	1.90	1.61
574A-23-3, 132	182.22	*P. wuellerstorfi*	1.55	1.31
574A-23-3, 147	182.37	*P. wuellerstorfi*	1.65	1.20
574A-23-4, 1	182.41	*P. wuellerstorfi*	2.24	1.34
574A-23-4, 11	182.51	*P. wuellerstorfi*	2.23	1.47
574A-23-4, 21	182.61	*P. wuellerstorfi*	2.17	1.60
574A-23-4, 31	182.71	*P. wuellerstorfi*	2.18	1.55
574A-23-4, 41	182.81	*P. wuellerstorfi*	2.11	1.57
574A-23-4, 51	182.91	*P. wuellerstorfi*	2.10	1.76
574A-23-4, 61	183.01	*P. wuellerstorfi*	2.13	1.78
574A-23-4, 71	183.11	*P. wuellerstorfi*	2.04	1.75
574A-23-4, 81	183.21	*P. wuellerstorfi*	1.98	1.63
574A-23-4, 91	183.31	*P. wuellerstorfi*	2.01	1.59
574A-23-4, 101	183.41	*P. wuellerstorfi*	2.32	1.66
574A-23-4, 111	183.51	*P. wuellerstorfi*	2.24	1.57
574A-23-4, 121	183.61	*P. wuellerstorfi*	2.31	1.70
574A-23-4, 132	183.72	*P. wuellerstorfi*	2.31	1.75
574A-23-4, 147	183.87	*C. kullenbergi*	1.76	1.70
574A-23-5, 1	183.91	*P. wuellerstorfi*	1.86	1.79
574A-23-5, 11	184.01	*C. kullenbergi*	1.53	1.47
574A-23-5, 21	184.11	*P. wuellerstorfi*	1.70	1.73
574A-23-5, 31	184.21	*P. wuellerstorfi*	1.63	1.50
574A-23-5, 41	184.31	*P. wuellerstorfi*	2.04	1.76
574A-23-5, 51	184.41	*P. wuellerstorfi*	2.05	1.85
574A-23-5, 61	184.51	*P. wuellerstorfi*	1.68	1.61
574A-23-5, 71	184.61	*P. wuellerstorfi*	1.91	1.36
574A-23-5, 81	184.71	*P. wuellerstorfi*	2.31	1.88
574A-23-5, 91	184.81	*P. wuellerstorfi*	2.44	1.79
574A-23-5, 101	184.91	*P. wuellerstorfi*	2.41	1.54
574A-23-5, 111	185.01	*P. wuellerstorfi*	2.07	1.48
574A-23-5, 121	185.11	*P. wuellerstorfi*	2.27	1.69
574A-23-5, 132	185.22	*C. kullenbergi*	2.11	1.63
574A-23-5, 132	185.22	*Oridorsalis* sp.	2.06	1.79
574A-23-5, 147	185.37	*C. kullenbergi*	1.95	1.72
574A-23-5, 147	185.37	*P. wuellerstorfi*	2.22	1.85
574A-23-5, 147	185.37	*Oridorsalis* sp.	2.02	1.95
574A-23-6, 1	185.41	*P. wuellerstorfi*	2.01	1.72
574A-23-6, 11	185.51	*C. kullenbergi*	1.89	1.62
574A-23-6, 11	185.51	*Oridorsalis* sp.	1.73	1.53
574A-23-6, 21	185.61	*P. wuellerstorfi*	2.19	1.81
574A-23-6, 31	185.71	*P. wuellerstorfi*	2.18	1.81
574A-23-6, 41	185.81	*P. wuellerstorfi*	2.14	1.62
574A-23-6, 51	185.91	*P. wuellerstorfi*	2.15	1.72
574A-23-6, 61	186.01	*P. wuellerstorfi*	2.23	1.69

Note: Asterisks identify samples run with some specimens of *Cibicidoides* spp. All $\delta^{18}O$ analyses have been normalized to values of *Uvigerina* sp., and $\delta^{13}C$ analyses have been normalized to values of *Cibicidoides* spp., by the corrections given below:

$\delta^{18}O$ (‰)	$\delta^{13}C$ (‰)	Species
0.64	0.00	*P. wuellerstorfi*
0.00	1.00	*Oridorsalis* sp.
−0.10	0.50	*G. subglobosa*
0.50	0.00	*C. kullenbergi*
0.50	0.00	*C. havanensis*
0.50	0.00	*P. wuellerstorfi* with *Cibicidoides* spp.
0.00	0.00	*Gyroidina* sp.

RESULTS

All isotopic analyses are given in Table 1 and the calcium carbonate data in Table 2. The data are plotted versus sub-bottom depth in Figure 1. The general statistics for the sampled intervals of Hole 574A are listed in Tables 3 and 4. Data from other isotopic sequences are shown in Table 3 for comparison.

Oxygen Isotopes

The oxygen isotopic record (Fig. 1) appears to be characterized by two intervals of relatively constant means separated by a rapid transition at 155 m sub-bottom. The shift in the mean oxygen isotopic ratio in Hole 574A at 155 m occurs within 11 samples and spans a 1.1-m interval. Within each of these intervals of constant means, the high-frequency variability is quite similar and is well above the analytical noise level. In the intervals above 155 m and below 155 m the variation around the means is similar, but the difference between the means is about 0.6‰. As shown in Table 3 the variance of these records is comparable to Pliocene benthic isotopic records from the North Atlantic (Site 552), and the range of the Hole 574A data is more than half that observed for the upper Pleistocene.

Carbon Isotopes

The carbon isotopic record shows a degree of variability similar to that observed for the oxygen data, but it displays considerable low-frequency variations rather than a steplike change in the time-averaged mean value (Fig. 1). In the interval between 168 and 186 m sub-bottom there appears to be a long-term trend with values of about 1.7‰ at 186 m decreasing to values of about 1.4‰ at 172 m. At about 172 m sub-bottom $\delta^{13}C$ values increase sharply (within 50 cm of section) to values near 1.9‰. The oxygen isotopic values do not show a similar shift in this interval, although the high-frequency correlation between $\delta^{13}C$ and $\delta^{18}O$ is greater in this interval than in the other intervals examined (Table 3).

At 155 m sub-bottom the carbon isotopic values show a further increase of about 0.4‰, which is coincident with the shift in the time-averaged $\delta^{18}O$ values. This interval of maximal $\delta^{13}C$ values spans about 6 m of section, and at about 151 m sub-bottom $\delta^{13}C$ values become lower, decreasing to a mean of about 1.1‰. This transition in $\delta^{13}C$ values (about 0.6‰) spans an interval of about 2 m.

Above the transition in the $\delta^{13}C$ values at 148 m sub-bottom, the carbon isotopic values show variations on the order 0.20 to 0.80‰, which are comparable to variations observed in the deeper part of the section. The variability in the interval between 100 and 115 m is significantly less than in the deeper intervals, having a mean value of about 0.8‰.

Calcium Carbonate

Whereas the isotopic data from Hole 574A show significant shifts in the mean value over the interval examined, the calcium carbonate records show an essentially constant mean of about 85% (Fig. 1), and no interval

Table 2. Detailed calcium carbonate analyses for Holes 574 and 574A.

Sub-bottom depth (m)	Sample (level in cm)	$CaCO_3$ (%)
61.00	574-8-1, 0	72.82
61.20	574-8-1, 20	76.83
61.40	574-8-1, 40	85.56
61.60	574-8-1, 60	85.95
62.00	574-8-1, 100	84.17
62.40	574-8-1, 140	79.35
62.50	574-8-2, 0	73.90
62.70	574-8-2, 20	83.47
62.90	574-8-2, 40	83.19
63.10	574-8-2, 60	80.18
63.30	574-8-2, 80	84.68
63.50	574-8-2, 100	84.24
63.70	574-8-2, 120	86.41
63.90	574-8-2, 140	88.53
64.00	574-8-3, 0	86.58
64.20	574-8-3, 20	84.63
64.40	574-8-3, 40	85.01
64.60	574-8-3, 60	80.03
64.80	574-8-3, 80	80.42
65.00	574-8-3, 100	80.29
65.20	574-8-3, 120	78.07
65.40	574-8-3, 140	73.78
65.50	574-8-4, 0	68.36
65.70	574-8-4, 20	77.88
65.90	574-8-4, 40	82.90
66.10	574-8-4, 60	82.31
66.30	574-8-4, 80	86.99
66.50	574-8-4, 100	88.58
66.70	574-8-4, 120	85.33
66.90	574-8-4, 140	84.43
67.00	574-8-5, 0	80.87
67.20	574-8-5, 20	73.18
67.40	574-8-5, 40	85.13
67.60	574-8-5, 60	76.37
67.80	574-8-5, 80	66.05
68.00	574-8-5, 100	62.82
68.20	574-8-5, 120	44.95
68.40	574-8-5, 140	34.74
68.50	574-8-6, 0	25.43
68.70	574-8-6, 20	51.24
68.90	574-8-6, 40	56.19
69.10	574-8-6, 60	49.33
69.30	574-8-6, 80	56.24
69.50	574-8-6, 100	57.31
69.70	574-8-6, 120	61.91
69.90	574-8-6, 140	45.45
70.00	574-8-7, 0	51.58
70.20	574-8-7, 20	64.58
70.40	574-8-7, 40	68.85
70.50	574-9-1, 0	64.91
70.70	574-9-1, 20	56.85
70.90	574-9-1, 40	56.21
71.10	574-9-1, 60	21.55
71.30	574-9-1, 80	12.43
71.50	574-9-1, 100	40.12
71.70	574-9-1, 120	46.83
71.90	574-9-1, 140	43.73
72.00	574-9-2, 0	42.81
72.20	574-9-2, 20	34.46
72.40	574-9-2, 40	38.95
72.60	574-9-2, 60	53.67
72.80	574-9-2, 80	60.13
73.00	574-9-2, 100	51.61
73.20	574-9-2, 120	53.86
73.40	574-9-2, 140	54.79
73.50	574-9-3, 0	48.14
73.70	574-9-3, 20	58.82
73.90	574-9-3, 40	74.69
74.10	574-9-3, 60	76.87
74.30	574-9-3, 80	74.17
74.70	574-9-3, 120	65.61
74.90	574-9-3, 140	55.70
75.00	574-9-4, 0	49.03
75.20	574-9-4, 20	15.07
75.40	574-9-4, 40	25.34
75.60	574-9-4, 60	27.65
75.80	574-9-4, 80	15.30
76.00	574-9-4, 100	34.80
76.20	574-9-4, 120	35.78
76.40	574-9-4, 140	27.34
76.50	574-9-5, 0	41.32
76.70	574-9-5, 20	12.44
76.90	574-9-5, 40	16.37
77.30	574-9-5, 80	1.69
77.50	574-9-5, 100	6.24
77.70	574-9-5, 120	53.35
77.90	574-9-5, 140	46.34
78.00	574-9-6, 0	15.59
78.20	574-9-6, 20	38.66
78.40	574-9-6, 40	73.76
78.60	574-9-6, 60	43.91
78.80	574-9-6, 80	44.42
79.00	574-9-6, 100	35.87
79.20	574-9-6, 120	33.71
79.40	574-9-6, 140	67.53
79.50	574-9-7, 0	62.14
79.70	574-9-7, 20	26.99
79.90	574-9-7, 40	41.49
80.00	574-10-1, 0	71.11
80.20	574-10-1, 20	73.37
80.40	574-10-1, 40	83.41
80.60	574-10-1, 60	73.48
80.80	574-10-1, 80	73.28
81.00	574-10-1, 100	71.02
81.20	574-10-1, 120	78.39
81.40	574-10-2, 140	68.77
81.50	574-10-2, 0	59.18
81.70	574-10-2, 20	66.19
81.90	574-10-2, 40	72.07
82.10	574-10-2, 60	72.83
82.30	574-10-2, 80	74.14
82.50	574-10-2, 100	73.77
82.70	574-10-2, 120	30.76
82.90	574-10-2, 140	45.91
83.00	574-10-3, 0	45.53
83.20	574-10-3, 20	63.75
83.40	574-10-3, 40	59.55
83.60	574-10-3, 60	64.63
83.80	574-10-3, 80	25.88
84.00	574-10-3, 100	27.97
84.20	574-10-3, 120	40.69
84.40	574-10-3, 140	43.59
84.50	574-10-4, 0	26.15
84.70	574-10-4, 20	39.28
84.90	574-10-4, 40	65.97
85.10	574-10-4, 60	75.87
85.30	574-10-4, 80	79.15
85.50	574-10-4, 100	75.12
85.70	574-10-4, 120	60.22
85.90	574-10-4, 140	83.99
86.00	574-10-5, 0	81.44
86.20	574-10-5, 20	86.87
86.40	574-10-5, 40	76.43
86.60	574-10-5, 60	71.07
86.80	574-10-5, 80	73.30
87.00	574-10-5, 100	67.07
87.20	574-10-5, 120	64.68
87.40	574-10-5, 140	61.08
87.50	574-10-6, 0	59.28
87.70	574-10-6, 20	76.47
87.90	574-10-6, 40	82.47
88.10	574-10-6, 60	78.17
88.30	574-10-6, 80	71.58
88.50	574-10-6, 100	69.74
88.70	574-10-6, 120	66.59
88.90	574-10-6, 140	58.62
89.00	574-10-7, 0	53.61
89.19	574-10-7, 19	25.34
89.90	574-11-1, 40	39.62
90.10	574-11-1, 60	81.08
90.30	574-11-1, 80	76.85
90.50	574-11-1, 100	81.56
90.70	574-11-1, 120	80.43
90.90	574-11-1, 140	79.51
91.00	574-11-2, 0	82.73
91.20	574-11-2, 20	82.52
91.40	574-11-2, 40	73.98
91.60	574-11-2, 60	81.79
91.80	574-11-2, 80	79.72
92.00	574-11-2, 100	78.49
92.20	574-11-2, 120	67.96
92.40	574-11-2, 140	75.13
92.50	574-11-3, 0	70.72
92.70	574-11-3, 20	76.10
92.90	574-11-3, 40	69.94
93.10	574-11-3, 60	69.54
93.30	574-11-3, 80	81.81
93.50	574-11-3, 100	82.92
93.70	574-11-3, 120	88.00
93.90	574-11-3, 140	88.25
94.00	574-11-4, 0	89.41
94.20	574-11-4, 20	84.10
94.40	574-11-4, 40	89.34
94.60	574-11-4, 60	91.42
94.80	574-11-4, 80	93.35
95.00	574-11-4, 100	92.07
95.20	574-11-4, 120	92.39
95.40	574-11-4, 140	93.03
95.50	574-11-5, 0	93.74
95.70	574-11-5, 20	89.85
95.90	574-11-5, 40	89.21
96.10	574-11-5, 60	93.12
96.30	574-11-5, 80	89.77
96.50	574-11-5, 100	84.57
96.70	574-11-5, 120	85.51
96.90	574-11-5, 140	84.79
97.00	574-11-6, 0	93.36
97.20	574-11-6, 20	93.17
97.40	574-11-6, 40	90.08
97.60	574-11-6, 60	90.64
97.80	574-11-6, 80	90.98
98.00	574-11-6, 100	87.09
98.20	574-11-6, 120	86.24
98.40	574-11-6, 140	84.79
98.60	574-12-1, 0	83.84
98.80	574-12-1, 20	86.80
99.00	574-12-1, 40	88.31
99.20	574-12-1, 60	87.10
99.40	574-12-1, 80	84.63
99.60	574-12-1, 100	82.55
99.80	574-12-1, 120	90.07
100.00	574-12-1, 140	88.11
100.10	574-12-2, 0	91.28
100.30	574-12-2, 20	88.08
100.50	574-12-2, 40	90.84
100.70	574-12-2, 60	95.11
100.90	574-12-2, 80	91.14
101.10	574-12-2, 100	87.91
101.30	574-12-2, 120	86.26
101.50	574-12-2, 140	82.42
101.60	574-12-3, 0	88.52
101.80	574-12-3, 20	86.82
102.00	574-12-3, 40	85.61
102.20	574-12-3, 60	87.05
102.40	574-12-3, 80	85.31
102.60	574-12-3, 100	84.02
102.80	574-12-3, 120	84.02
103.00	574-12-3, 140	84.84
103.10	574-12-4, 0	86.89
103.30	574-12-4, 20	77.28
103.50	574-12-4, 40	87.28
103.70	574-12-4, 60	87.62
103.90	574-12-4, 80	89.92
104.10	574-12-4, 100	89.42
104.30	574-12-4, 120	88.96
104.50	574-12-4, 140	83.81
104.60	574-12-5, 0	82.88
104.80	574-12-5, 20	88.82
105.00	574-12-5, 40	92.03
105.20	574-12-5, 60	90.54
105.40	574-12-5, 80	86.91
105.60	574-12-5, 100	85.43
105.80	574-12-5, 120	84.56
106.00	574-12-5, 140	88.71
106.10	574-12-6, 0	85.99
106.30	574-12-6, 20	88.78
106.50	574-12-6, 40	87.31
106.70	574-12-6, 60	89.06
106.90	574-12-6, 80	90.23
107.10	574-12-6, 100	89.46
107.30	574-12-6, 120	89.14
107.50	574-12-6, 140	90.94
107.60	574-12-7, 0	88.08
107.80	574-12-7, 20	91.37
108.00	574-12-7, 40	99.99
108.70	574A-13-1, 50	89.25
108.90	574A-13-1, 70	87.27
109.30	574A-13-1, 110	89.21
109.50	574A-13-1, 130	88.55
109.70	574A-13-2, 0	87.43
109.90	574A-13-2, 20	85.03
110.00	574A-13-2, 30	84.98
110.20	574A-13-2, 50	88.50
110.40	574A-13-2, 70	86.99
110.60	574A-13-2, 90	80.34
110.80	574A-13-2, 110	82.68
111.00	574A-13-2, 130	78.92
111.20	574A-13-3, 0	82.41
111.40	574A-13-3, 20	87.66
111.50	574A-13-3, 30	83.03
111.70	574A-13-3, 50	79.50
111.90	574A-13-3, 70	85.96
112.10	574A-13-3, 90	84.30
112.30	574A-13-3, 110	82.11
112.50	574A-13-3, 130	82.07
112.70	574A-13-4, 0	82.60
112.90	574A-13-4, 20	77.80
113.00	574A-13-4, 30	81.30
113.20	574A-14-1, 10	86.09
113.46	574A-14-1, 30	87.35
113.60	574A-14-1, 50	88.96
113.80	574A-14-1, 70	89.00
114.00	574A-14-1, 90	89.79
114.20	574A-14-1, 110	58.59
114.40	574A-14-1, 130	87.68
114.60	574A-14-2, 0	87.84
114.80	574A-14-2, 20	88.02
114.90	574A-14-2, 30	86.55
115.10	574A-14-2, 50	89.95
115.30	574A-14-2, 70	88.61
115.50	574A-14-2, 90	85.04
115.70	574A-14-2, 110	80.42
115.90	574A-14-2, 130	78.20
116.10	574A-14-3, 0	66.11
116.30	574A-14-3, 20	75.28
116.40	574A-14-3, 30	78.16
116.80	574A-14-3, 70	82.67
117.00	574A-14-3, 90	82.40
117.20	574A-14-3, 110	80.74
117.60	574A-14-4, 0	71.19
117.80	574A-14-4, 20	85.68
117.90	574A-14-4, 30	89.52
118.10	574A-15-1, 0	89.43
118.10	574A-15-1, 0	91.73
118.30	574A-15-1, 20	94.20
118.50	574A-15-1, 40	93.06
118.50	574A-15-1, 40	92.99
118.70	574A-15-1, 60	93.40
118.90	574A-15-1, 80	92.67
119.10	574A-15-1, 100	92.69
119.30	574A-15-1, 120	89.82
119.60	574A-15-2, 0	92.89
119.80	574A-15-2, 20	91.74
120.00	574A-15-2, 40	88.90

Table 2. (Continued).

Sub-bottom depth (m)	Sample (level in cm)	$CaCO_3$ (%)
120.20	574A-15-2, 60	94.82
120.40	574A-15-2, 80	91.19
120.60	574A-15-2, 100	90.23
120.80	574A-15-2, 120	88.61
121.00	574A-15-2, 140	93.02
121.10	574A-15-3, 0	93.13
121.30	574A-15-3, 20	98.42
121.50	574A-15-3, 40	91.76
121.70	574A-15-3, 60	93.16
121.90	574A-15-3, 80	93.66
122.10	574A-15-3, 100	99.51
122.30	574A-15-3, 120	95.64
122.50	574A-15-3, 140	96.98
122.60	574A-15-4, 0	88.14
123.40	574A-16-1, 60	94.21
123.60	574A-16-1, 80	90.53
123.80	574A-16-1, 100	92.37
124.00	574A-16-1, 120	92.11
124.20	574A-16-1, 140	87.80
124.30	574A-16-2, 0	93.58
124.50	574A-16-2, 20	93.97
124.70	574A-16-2, 40	93.17
124.90	574A-16-2, 60	95.27
125.10	574A-16-2, 80	93.19
125.30	574A-16-2, 100	96.46
125.50	574A-16-2, 120	92.99
125.70	574A-16-2, 140	96.29
125.80	574A-16-3, 0	97.95
126.00	574A-16-3, 20	95.52
126.20	574A-16-3, 40	90.89
126.40	574A-16-3, 60	95.39
126.60	574A-16-3, 80	95.61
126.80	574A-16-3, 100	91.76
127.00	574A-16-3, 120	94.48
127.80	574A-17-1, 0	78.18
128.00	574A-17-1, 20	85.67
128.20	574A-17-1, 40	87.03
128.40	574A-17-1, 60	86.30
128.60	574A-17-1, 80	79.77
128.80	574A-17-1, 100	81.60
129.00	574A-17-1, 120	79.72
129.20	574A-17-1, 140	83.86
129.30	574A-17-2, 0	82.98
129.50	574A-17-2, 20	84.99
129.70	574A-17-2, 40	86.71
129.90	574A-17-2, 60	84.96
130.10	574A-17-2, 80	83.67
130.30	574A-17-2, 100	85.22
130.50	574A-17-2, 120	86.79
130.70	574A-17-2, 140	87.37
130.80	574A-17-3, 0	88.66
131.00	574A-17-3, 20	87.78
131.20	574A-17-3, 40	85.94
131.40	574A-17-3, 60	88.71
131.60	574A-17-3, 80	89.08
131.80	574A-17-3, 100	86.66
131.90	574A-18-1, 0	79.68
132.10	574A-18-1, 20	81.26
132.30	574A-18-1, 40	80.91
132.50	574A-18-1, 60	78.80
132.70	574A-18-1, 80	78.66
133.10	574A-18-1, 120	74.99
133.30	574A-18-1, 140	72.27
133.40	574A-18-2, 0	71.91
133.60	574A-18-2, 20	75.86
133.80	574A-18-2, 40	72.03
134.00	574A-18-2, 60	65.42
134.20	574A-18-2, 80	74.92
134.40	574A-18-2, 100	75.94
134.60	574A-18-2, 120	81.96
134.80	574A-18-2, 140	83.31
134.90	574A-18-3, 0	81.21
135.30	574A-18-3, 40	77.19
135.50	574A-18-3, 60	82.96
135.70	574A-18-3, 80	78.88
135.90	574A-18-3, 100	77.01
136.10	574A-18-3, 120	79.63
136.30	574A-18-3, 140	78.01
136.40	574A-18-4, 0	98.63
136.60	574A-18-4, 20	88.76
136.80	574A-18-4, 40	84.99
137.00	574A-18-4, 60	97.89
137.20	574A-18-4, 80	89.61
137.40	574A-18-4, 100	88.93
137.60	574A-18-4, 120	85.87
137.80	574A-18-4, 140	80.98
137.90	574A-18-5, 0	84.14
138.10	574A-18-5, 20	81.90
138.30	574A-18-5, 40	85.49
138.50	574A-18-5, 60	82.58
138.70	574A-18-5, 80	81.78
138.90	574A-18-5, 100	97.65
139.10	574A-18-5, 120	84.25
139.30	574A-18-5, 140	85.20
139.40	574A-18-6, 0	86.16
139.60	574A-18-6, 20	87.52
139.80	574A-18-6, 40	88.62
140.00	574A-18-6, 60	89.38
140.20	574A-18-6, 80	88.20
140.40	574A-18-6, 100	83.98
140.60	574A-18-6, 120	81.63
140.90	574A-18-7, 0	77.72
141.10	574A-18-7, 20	81.34
141.30	574A-18-7, 40	83.57
141.40	574A-19-1, 0	85.75
141.50	574A-19-1, 10	85.39
141.60	574A-19-1, 20	86.84
141.70	574A-19-1, 30	81.74
141.80	574A-19-1, 40	85.59
141.90	574A-19-1, 50	85.91
142.00	574A-19-1, 60	88.11
142.10	574A-19-1, 70	85.39
142.20	574A-19-1, 80	87.34
142.30	574A-19-1, 90	94.64
142.40	574A-19-1, 100	87.99
142.50	574A-19-1, 110	86.25
142.60	574A-19-1, 120	85.53
142.70	574A-19-1, 130	85.44
142.80	574A-19-1, 140	85.25
142.90	574A-19-2, 0	82.75
143.00	574A-19-2, 10	87.40
143.10	574A-19-2, 20	86.26
143.10	574A-19-2, 20	88.09
143.20	574A-19-2, 30	87.99
143.30	574A-19-2, 40	88.31
143.40	574A-19-2, 50	90.31
143.50	574A-19-2, 60	86.57
143.60	574A-19-2, 70	91.95
143.70	574A-19-2, 80	89.91
143.80	574A-19-2, 90	85.85
143.90	574A-19-2, 100	89.11
144.00	574A-19-2, 110	93.71
144.10	574A-19-2, 120	86.89
144.20	574A-19-2, 130	83.96
144.30	574A-19-2, 140	88.35
144.40	574A-19-3, 0	91.78
144.50	574A-19-3, 10	88.61
144.70	574A-19-3, 30	88.37
144.80	574A-19-3, 40	87.85
144.90	574A-19-3, 50	89.47
145.00	574A-19-3, 60	86.80
145.10	574A-19-3, 70	85.11
145.20	574A-19-3, 80	88.26
145.30	574A-19-3, 90	86.54
145.40	574A-19-3, 100	88.26
145.50	574A-19-3, 110	89.83
145.60	574A-19-3, 120	89.53
145.70	574A-19-3, 130	86.12
145.80	574A-19-3, 140	87.13
145.90	574A-19-4, 0	85.48
146.00	574A-19-4, 10	80.53
146.10	574A-19-4, 20	85.19

Table 2. (Continued).

Sub-bottom depth (m)	Sample (level in cm)	$CaCO_3$ (%)
146.20	574A-19-4 30	90.90
146.30	574A-19-4, 40	85.02
146.40	574A-19-4, 50	86.27
146.50	574A-19-4, 60	78.61
146.60	574A-19-4, 70	79.75
146.70	574A-19-4, 80	76.21
146.80	574A-19-4, 90	74.91
146.90	574A-19-4, 100	67.53
147.00	574A-19-4, 110	74.44
147.10	574A-19-4, 120	77.07
147.20	574A-19-4, 130	84.05
147.30	574A-19-4, 140	83.62
147.40	574A-19-5, 0	84.85
147.50	574A-19-5, 10	80.95
147.60	574A-19-5, 20	80.66
147.70	574A-19-5, 30	80.95
147.80	574A-19-5, 40	78.17
147.90	574A-19-5, 50	68.07
148.00	574A-19-5, 60	84.07
148.10	574A-19-5, 70	76.50
148.20	574A-19-5, 80	79.89
148.30	574A-19-5, 90	79.91
148.40	574A-19-5, 100	84.79
148.50	574A-19-5, 110	75.48
148.60	574A-19-5, 120	74.71
148.70	574A-19-5, 130	67.62
148.80	574A-19-5, 140	78.34
148.90	574A-19-6, 0	80.70
149.00	574A-19-6, 10	87.24
149.10	574A-19-6, 20	90.33
149.20	574A-19-6, 30	89.81
149.30	574A-19-6, 40	88.26
149.40	574A-19-6, 50	88.28
149.50	574A-19-6, 60	88.15
149.60	574A-19-6, 70	87.13
149.70	574A-19-6, 80	93.55
149.80	574A-19-6, 90	88.62
149.90	574A-19-6, 100	89.14
150.00	574A-19-6, 110	93.23
150.10	574A-19-6, 120	88.24
150.20	574A-19-6, 130	92.01
150.30	574A-19-6, 140	89.06
150.40	574A-19-7, 0	90.74
150.50	574A-19-7, 10	91.13
150.60	574A-19-7, 20	91.84
150.70	574A-19-7, 30	93.51
150.80	574A-19-7, 40	90.42
151.50	574A-20-1, 60	82.34
151.70	574A-20-1, 80	80.86
151.90	574A-20-1, 100	86.18
152.10	574A-20-1, 120	86.29
152.30	574A-20-1, 140	90.17
152.40	574A-20-2, 0	90.08
152.60	574A-20-2, 20	87.91
152.80	574A-20-2, 40	87.97
153.00	574A-20-2, 60	83.91
153.20	574A-20-2, 80	87.67
153.40	574A-20-2, 100	85.82
153.60	574A-20-2, 120	82.15
153.80	574A-20-2, 140	84.57
153.90	574A-20-3, 0	87.72
154.10	574A-20-3, 20	86.53
154.30	574A-20-3, 40	86.92
154.50	574A-20-3, 60	88.11
154.70	574A-20-3, 80	88.87
154.90	574A-20-3, 100	87.66
155.10	574A-20-3, 120	86.66
155.30	574A-20-3, 140	88.22
155.40	574A-20-4, 0	87.65
155.60	574A-20-4, 20	82.72
155.80	574A-20-4, 40	82.20
156.00	574A-20-4, 60	63.10
156.20	574A-20-4, 80	73.98
156.40	574A-20-4, 100	76.33
156.60	574A-20-4, 120	81.01
156.80	574A-20-4, 140	86.32
156.90	574A-20-5, 0	79.23
157.10	574A-20-5, 20	82.93
157.30	574A-20-5, 40	77.46
157.70	574A-20-5, 80	76.74
157.90	574A-20-5, 100	87.16
158.10	574A-20-5, 120	90.13
158.30	574A-20-5, 140	89.99
158.40	574A-20-6, 0	90.73
158.60	574A-20-6, 20	89.85
158.80	574A-20-6, 40	87.38
159.00	574A-20-6, 60	91.54
159.20	574A-20-6, 80	95.93
159.40	574A-20-6, 100	93.49
159.60	574A-20-6, 120	99.99
159.80	574A-20-6, 140	93.51
159.90	574A-21-1, 0	93.22
160.10	574A-21-1, 20	92.58
160.30	574A-21-1, 40	91.66
168.40	574A-22-1, 0	85.99
168.60	574A-22-1, 20	88.44
168.80	574A-22-1, 40	89.81
169.00	574A-22-1, 60	88.25
169.20	574A-22-1, 80	92.67
169.40	574A-22-1, 100	93.30
169.60	574A-22-1, 120	89.72
169.80	574A-22-1, 140	90.05
169.90	574A-22-2, 0	88.79
170.10	574A-22-2, 20	93.34
170.30	574A-22-2, 40	86.95
170.50	574A-22-2, 60	89.77
170.70	574A-22-2, 80	68.87
170.90	574A-22-2, 100	93.97
171.10	574A-22-2, 120	99.99
171.30	574A-22-2, 140	94.43
171.40	574A-22-3, 0	99.99
171.60	574A-22-3, 20	91.65
171.80	574A-22-3, 40	91.47
172.00	574A-22-3, 60	91.69
172.20	574A-22-3, 80	91.87
172.40	574A-22-3, 100	90.21
172.60	574A-22-3, 120	95.44
172.80	574A-22-3, 140	92.43
172.90	574A-22-4, 0	86.92
173.10	574A-22-4, 20	82.78
173.30	574A-22-4, 40	79.18
173.50	574A-22-4, 60	86.36
173.70	574A-22-4, 80	85.48
173.90	574A-22-4, 100	85.22
174.10	574A-22-4, 120	86.55
174.30	574A-22-4, 140	84.54
174.40	574A-22-5, 0	85.03
174.60	574A-22-5, 20	79.62
174.80	574A-22-5, 40	84.70
175.00	574A-22-5, 60	94.41
175.20	574A-22-5, 80	98.03
175.40	574A-22-5, 100	93.14
175.60	574A-22-5, 120	87.09
175.80	574A-22-5, 140	88.30
175.90	574A-22-6, 0	91.72
176.10	574A-22-6, 20	89.94
176.30	574A-22-6, 40	90.24
176.50	574A-22-6, 60	91.66
176.70	574A-22-6, 80	91.77
176.90	574A-22-6, 100	89.31
177.10	574A-22-6, 120	86.18
177.30	574A-22-6, 140	83.68
177.40	574A-22-7, 0	83.85
177.60	574A-22-7, 20	81.80
177.80	574A-22-7, 40	87.46
177.90	574A-23-1, 0	87.42
178.00	574A-23-1, 10	90.45
178.10	574A-23-1, 20	92.89
178.20	574A-23-1, 30	92.22
178.30	574A-23-1, 40	88.23
178.40	574A-23-1, 50	87.79
178.50	574A-23-1, 60	87.69

Table 2. (Continued).

Sub-bottom depth (m)	Sample (level in cm)	$CaCO_3$ (%)
178.60	574A-23-1, 70	87.75
178.70	574A-23-1, 80	83.32
178.80	574A-23-1, 90	75.64
178.90	574A-23-1, 100	79.94
179.00	574A-23-1, 110	81.88
179.10	574A-23-1, 120	73.10
179.19	574A-23-1, 129	73.60
179.30	574A-23-1, 140	59.95
179.30	574A-23-1, 140	59.95
179.40	574A-23-2, 0	57.71
179.50	574A-23-2, 10	60.84
179.60	574A-23-2, 20	87.96
179.70	574A-23-2, 30	82.11
179.80	574A-23-2, 40	84.76
179.90	574A-23-2, 50	77.28
180.00	574A-23-2, 60	82.29
180.10	574A-23-2, 70	88.53
180.20	574A-23-2, 80	88.43
180.30	574A-23-2, 90	88.23
180.40	574A-23-2, 100	86.49
180.50	574A-23-2, 110	85.18
180.60	574A-23-2, 120	90.01
180.69	574A-23-2, 129	84.91
180.80	574A-23-2, 140	90.27
180.90	574A-23-3, 0	80.41
181.00	574A-23-3, 10	84.71
181.10	574A-23-3, 20	86.46
181.20	574A-23-3, 30	85.04
181.30	574A-23-3, 40	86.37
181.40	574A-23-3, 50	87.69
181.50	574A-23-3, 60	85.31
181.60	574A-23-3, 70	87.86
181.70	574A-23-3, 80	88.16
181.80	574A-23-3, 90	68.48
181.90	574A-23-3, 100	70.49
182.00	574A-23-3, 110	63.55
182.10	574A-23-3, 120	68.27
182.19	574A-23-3, 129	87.59
182.30	574A-23-3, 140	78.27
182.40	574A-23-4, 0	84.84
182.50	574A-23-4, 10	87.04
182.60	574A-23-4, 20	82.91
182.70	574A-23-4, 30	87.09
182.80	574A-23-4, 40	84.46
182.90	574A-23-4, 50	85.18
183.00	574A-23-4, 60	87.89
183.10	574A-23-4, 70	85.91
183.20	574A-23-4, 80	86.20
183.30	574A-23-4, 90	90.75
183.40	574A-23-4, 100	89.02
183.50	574A-23-4, 110	89.00
183.60	574A-23-4, 120	87.16
183.69	574A-23-4, 129	85.93
183.80	574A-23-4, 140	83.43
183.90	574A-23-5, 0	81.77
184.00	574A-23-5, 10	74.99
184.10	574A-23-5, 20	77.69
184.20	574A-23-5, 30	83.91
184.30	574A-23-5, 40	68.19
184.40	574A-23-5, 50	75.12
184.50	574A-23-5, 60	78.64
184.60	574A-23-5, 70	77.63
184.70	574A-23-5, 80	84.49
184.80	574A-23-5, 90	84.93
184.90	574A-23-5, 100	84.52
185.00	574A-23-5, 110	84.23
185.10	574A-23-5, 120	83.99
185.19	574A-23-5, 129	79.76
185.30	574A-23-5, 140	76.19
185.40	574A-23-6, 0	81.68
185.50	574A-23-6, 10	82.21
185.60	574A-23-6, 20	82.61
185.70	574A-23-6, 30	77.14
185.80	574A-23-6, 40	74.40
185.90	574A-23-6, 50	82.22

Table 3. General statistics for Hole 574A isotopic data.

Hole or Core	Interval	Mean	Variance	Standard deviation	Range	Correlation $\delta^{18}O$ vs. $\delta^{13}C$
574A	100–115 m	2.78 (0.78)	0.031 (0.03)	0.18 (0.17)	1.1 (0.86)	0.1
574A	140–160 m	2.44 (1.36)	0.064 (0.08)[a]	0.25 (0.28)	1.3 (1.22)	0.2
574A	168–188 m	1.94 (1.51)	0.049 (0.04)[a]	0.22 (0.20)	1.1 (0.97)	0.4
552[b]	1–2 Ma	— —	0.148 (0.12)	0.38 (0.35)	1.7 (1.60)	0.6
552[b]	2.5–3.5 Ma	— —	0.063 (0.07)[a]	0.25 (0.25)	1.5 (2.0)	−0.0
289[c]	Core 55	— —	0.062[a]	0.24	0.9	
V22-174[d]	0–1 Ma	— —	0.150	0.40	1.8	

Note: Values given are for $\delta^{18}O$ and, in parentheses, for $\delta^{13}C$.
[a] Pair-wise F-test shows that these values are not significantly different.
[b] Data from Shackleton et al. (1982).
[c] Data from Shackleton (1980).
[d] Data from Imbrie et al. (1984).

Table 4. General statistics for high-resolution calcium carbonate data from Hole 574A.

Interval (m)	Number of samples	Mean	Variance	Standard deviation	Range	Correlation $CaCO_3$ vs. $\delta^{18}O$	Correlation $CaCO_3$ vs. $\delta^{13}C$
126–137	54	83.0	49.0	6.5	33	a	a
140–160	142	85.7	34.0	5.8	37	0.32	0.26
168–186	133	84.6	60.0	7.7	42	0.27	0.15

[a] Overlap with isotope record insufficient for meaningful calculations.

shows a significant change in the mean (Table 4). Between 128 and 137 m there is an interval of reduced calcium carbonate, with values being particularly low (below 80%) between 132 and 134 m. Isotopic data have not yet been obtained for this interval.

The calcium carbonate records also display little high-frequency variability and can be described as having relatively small-amplitude fluctuations with a number of short "events" of reduced $CaCO_3$. This is especially evident below 135 m sub-bottom.

The relationship between the isotopic records and the calcium carbonate data is weak. The correlation coefficients between these data sets are relatively low (Table 4), with a positive correlation between $\delta^{18}O$ and calcium carbonate. In general, carbonate events (times of reduced carbonate) tend to occur during intervals of increased $\delta^{18}O$ values; however, not all $\delta^{18}O$ maxima correspond to marked carbonate minima. Offsets in the isotopic records do tend to coincide with "events" in the calcium carbonate data; the offset in $\delta^{18}O$ values at 155 m is accompanied by a marked decrease in $CaCO_3$. The change in $\delta^{13}C$ at 150 m is marked by a series of carbonate events (Fig. 1), although the offset in $\delta^{13}C$ at 172 m is not clearly reflected in the $CaCO_3$ data.

DISCUSSION OF RESULTS

Correlation with Middle Miocene Data from Site 289

The isotopic records from benthic foraminifers from DSDP Site 289 (Woodruff et al., 1981; Shackleton, 1982) are the most detailed data available for comparison with the Hole 574A data. Although the sedimentation rate at Site 289 is one to two times that in Hole 574A, the sampling interval used in our study is closer than that in the best studied cores from Site 289. Thus, in general, our resolution is better than that available for Site 289. In making a comparison of the Site 289 data (Fig. 2) (Wood-

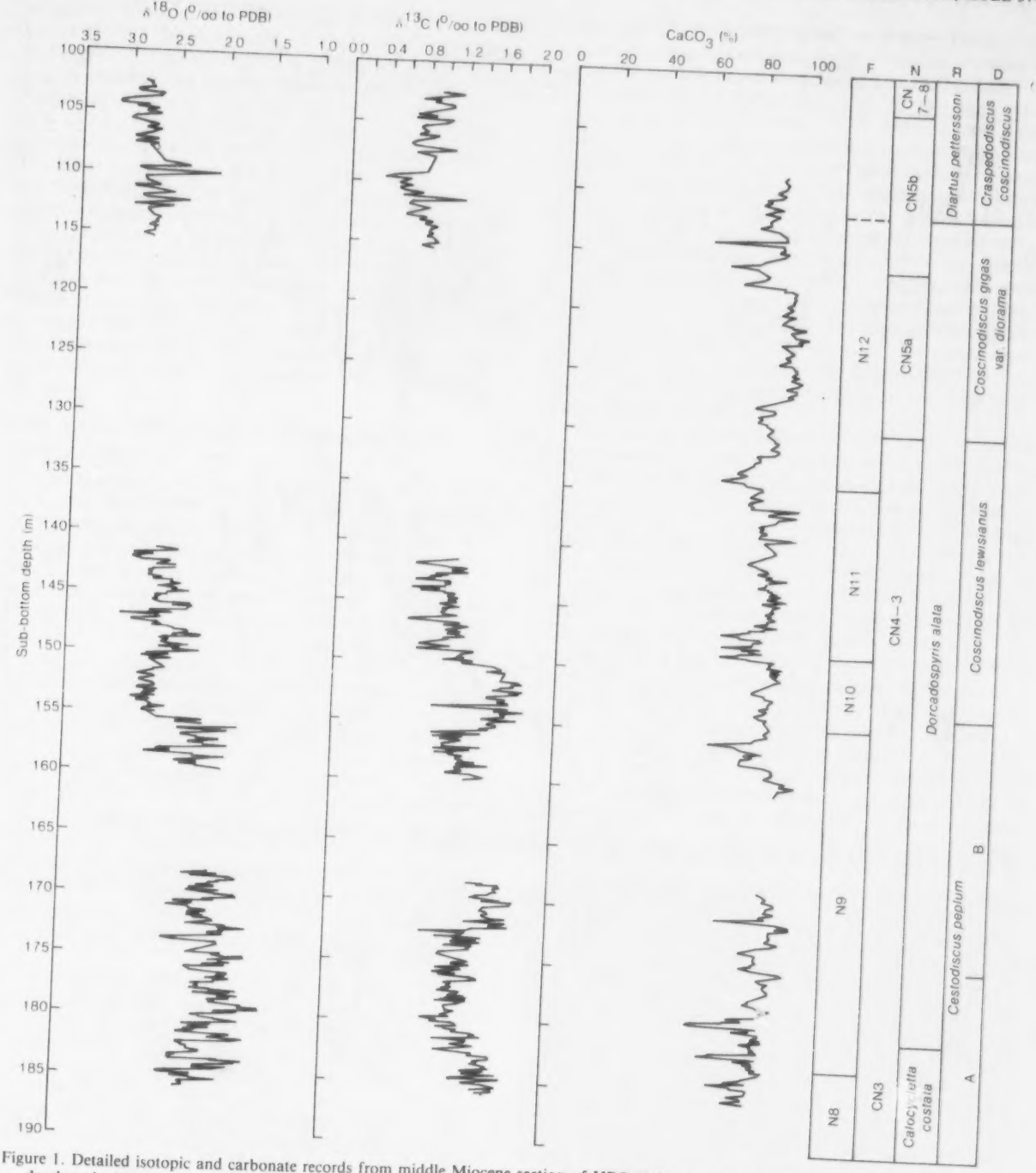

Figure 1. Detailed isotopic and carbonate records from middle Miocene section of HPC Hole 574A. Data are plotted versus sub-bottom depth and with microfossil stratigraphic zones as defined in the site chapter (this volume).

ruff et al., 1981) and the Hole 574A data, one must be aware that the apparent differences may reflect errors in biostratigraphic uncertainties, different water depths, different sampling resolutions, and possible drilling disturbance at Site 289.

The Site 289 data suggest that the transition in isotopic composition is associated with increased variability (an observation that may, however, result from a strong sampling bias). Close examination of the Site 289 data shows an interval of variable isotopic values within foraminiferal Zones N8 through N10 preceding a sharp break at the N10/N11 zonal boundary, which is followed by another interval of variable $\delta^{18}O$ and $\delta^{13}C$ values. In Hole 574A the transitions in $\delta^{18}O$ and $\delta^{13}C$ values ap-

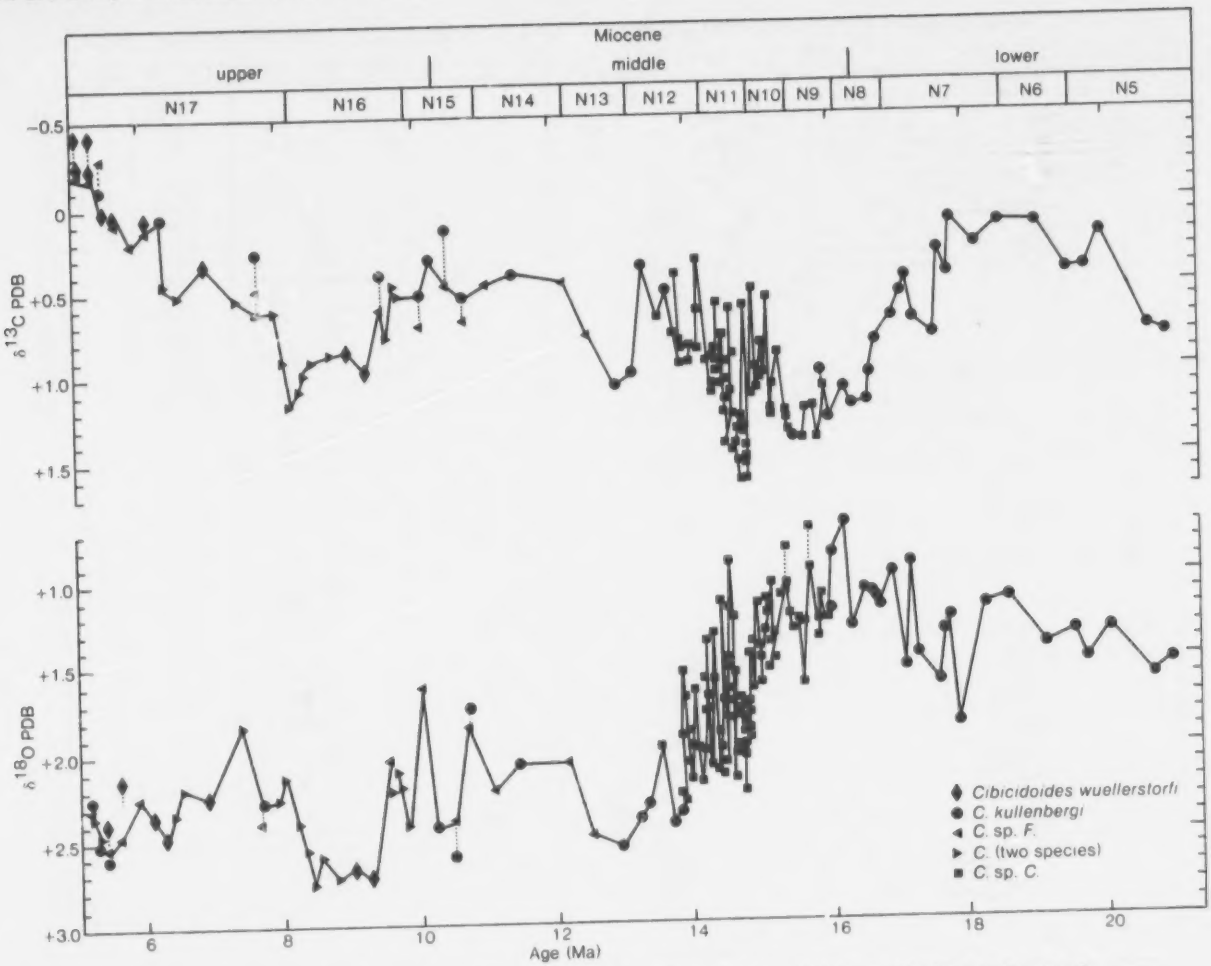

Figure 2. Detailed stable isotopic analysis from DSDP Site 289. Figure from Woodruff et al. (1981); copyright 1981 by the AAAS.

pear to occur at the N9/N10 zonal boundary with no significant offset at the N10/N11 boundary. The offset in the $\delta^{18}O$ values in Hole 574A is about 0.7 to 0.8‰, a value consistent with the Site 289 data at the N10/N11 zonal boundary. In the Site 289 data there appears to be an increase in the $\delta^{18}O$ values during the interval following Zone N11. Much of this interval has not been analyzed in Hole 574A, but the interval at 100 m sub-bottom, which spans the later part of Zone N12 and the beginning of N13, does not show a marked decrease in the mean $\delta^{18}O$ value (Table 3). Thus, from the Site 289 data, Woodruff et al. (1981) suggest that the transition in benthic isotopes spanned an interval of between 16.5 and 13 Ma, with the greatest change between approximately 14.8 and 14.0 Ma. The transition in Hole 574A seems to occur more rapidly, over 1.1 m of section, and from the long-term sedimentation rate estimates for Site 574, this represents about 30,000 to 100,000 yr.

At the transition in the $\delta^{18}O$ record of Hole 574A, the carbon isotopic values show an increase of 0.4‰, which in general is opposite to the carbon isotopic trend defined for the Site 289 data. However, in the Site 289 data, there is a similar increase in $\delta^{13}C$ at the N10/N11 zonal boundary, which is then followed by a decrease in carbon isotopic values. The carbon and oxygen isotopic data from Zone N11 at Site 289 are similar in both direction and magnitude to the Hole 574A data from foraminiferal Zone N10.

We suggest that the lack of correlation implied by the foraminiferal zonation is not real. The diatom stratigraphy from both sites shows that this transition occurs near the same diatom zonal boundary (Barron et al., this volume). A lag of approximately several hundred thousand years between the response of the deep Pacific (Site 574) and the intermediate waters (Site 289) is oceanographically unreasonable given the mixing times of the ocean. Thus, it seems possible that the disagreement in the foraminiferal stratigraphies reflects the increased dissolution of calcareous fossils at Site 574. In many intervals, dissolution prevents the precise location of both foraminifers and calcareous nannofossil zonal boundaries (Barron et al., this volume).

A possible explanation for the differences in the rapidity of the middle Miocene oxygen isotopic event recorded at Sites 289 and 574 is that the section in Hole 574A is not complete. Comparison of the length of fo-

raminiferal zones in Hole 574A and at Site 289 shows that at Hole 574A the length of Zone N10 is smaller than expected as compared to N11. Zone N9 is relatively long in Hole 574A, supporting the suggested drop in sedimentation rate in Zone N10 (above 155 m sub-bottom) at Site 574. However, in view of the reservations expressed above on the problems in foraminiferal zonation, such comparisons may not be meaningful.

Comparison of Sites 574 and 289 carbonate records (Site 574 chapter, this volume) suggests that the carbonate record at Site 574 is as complete as at Site 289. Given the continuity suggested by the carbonate records from Sites 574 and 289 and the similarity in the isotopic response of both the $\delta^{18}O$ and $\delta^{13}C$ records at both sites, we suggest that the Hole 574A data may give a reasonable representation of the important transition in the oceanic oxygen isotopic composition during the middle Miocene.

Stable Isotope Records and Implication for Middle Miocene Paleoceanography

The high-resolution oxygen isotopic data from Hole 574A span the interval of the middle Miocene during which a major paleoceanographic and climatic event apparently occurred. The shift in the benthic and planktonic isotopic records from high-latitude sites during the middle Miocene has been inferred to represent the onset of major glaciation in Antarctica (Shackleton and Kennett, 1975). It has been assumed that before this event little ice was present and that changes in $\delta^{18}O$ values of foraminifers reflected changes in oceanic temperatures. This assumption has recently been questioned by Matthews and Poore (1980; see Miller and Thomas, this volume), who suggest that the isotopic shift represents a major cooling of oceanic deep-water masses.

The data from Hole 574A provide some limitations on both of these models. There are a number of mechanisms that can change the benthic isotopic composition in the ocean as measured at any one location. The most important are (1) changes in the volume of water stored as ice sheets; (2) changes in the temperature of the waters overlying the seafloor at the site[3]; and (3) changes in the origin of the overlying waters that may affect the isotopic composition of the water without affecting temperature. Mechanisms (2) and (3) are related but the processes required to change the average temperature of the Pacific Basin as a whole and those required to change the site of deep- and bottom-water mass formation are not necessarily the same.

If we assume that there was no major ice before the middle Miocene event, then the high degree of variability measured in the interval from 168 to 186 m of Hole 574A represents changes either in the benthic temperatures or the benthic water mass at Site 574, or both. The range in $\delta^{18}O$ of 1.1‰ at this time would represent changes in temperatures of over 4°C. Using the estimated sedimentation rates for this site, the dominant frequency of variation is on the order of 40,000 yr. (see below). Because Site 574 is at 4400 m in the central Pacific, we would conclude that on time scales of tens of thousands of years the bottom-water temperatures in the deep Pacific have changed about 2 to 4°C. If the deep-water structure of the Pacific were similar today, a very large volume of water would be responding to changing oceanographic conditions over relatively short periods of time. Thus, if there were no major fluctuations in ice volume during the earliest middle Miocene, the benthic isotopic data from Hole 574A would require considerable variability in the deep-water structure of the Pacific Ocean. Multiple sources of deep water, with contributions varying on time scales similar to the variations seen in Pleistocene records, are suggested. The high correlation between the $\delta^{18}O$ and $\delta^{13}C$ records within the oldest interval studied (Table 3) supports the hypothesis that these records reflect the changing character of the deep-water masses of the Pacific.

A second alternative, however, is that a significant and varying amount of ice was present prior to the middle Miocene isotopic shift. If so, then a major change in the deep-water structure of the Pacific during the middle Miocene is not a necessary requirement, and the high degree of variability observed in the benthic isotopic values of both Sites 289 (Shackleton, 1982) and 574 can be explained by changes in ice volume. The Hole 574A data would then suggest that the volume of ice varied on time scales of a few tens of thousands of years.

The rapidity of the transition is not inconsistent with the hypothesis of significant ice growth. Pleistocene records show that ice sheets, equivalent to a 1.8‰ isotopic shift, waxed and waned on a time scale of 100,000 yr., not unlike the rate estimated from Hole 574A. As pointed out by Matthews and Poore (1980), however, the middle Miocene isotopic enrichment is not seen in tropical planktonic records. By assuming that tropical temperatures have remained constant with time, they conclude that the middle Miocene isotopic shift is a change in deep-ocean temperatures and not an ice-volume signal. However, if it is assumed that the $\delta^{18}O$ values for *Globoquadrina altispira* analyzed in Core 55 of Site 289 correspond to a surface-water temperature of 28°C as implied by the Matthews and Poore (1980) model, this would require ice volumes during the early Miocene greater than that observed during the Pleistocene (Shackleton, 1982).

The uniform magnitude in the isotopic shift observed at Sites 289 and 574 would require a similar temperature change throughout much of the water column of the Pacific. But if the assumption of Matthews and Poore is correct, this temperature change would not be reflected at low latitudes.

The high-resolution data from Site 574 do not allow us to conclusively state which hypothesis concerning the cause of the middle Miocene isotopic shift is correct, but the degree and nature of the variability of the data do place constraints on the oceanographic conditions in the Pacific during the middle Miocene.

Statistical Analysis of Middle Miocene Time Series

One of the original objectives of sampling the HPC section of Site 574 was to obtain long, continuous, paleoceanographic records of high time resolution for de-

[3] Note that we do not use the term *bottom water* to avoid confusion with oceanic bottom-water masses, such as the present-day Antarctic Bottom Water. Sites such as 289 at 2200 m have never experienced true bottom water.

tailed time series work. Time series analysis of high-resolution records available from Pleistocene sediments have been instrumental in developing models describing the causes of climatic change during the past 1 m.y. (Imbrie et al., 1984). These studies have shown that a significant fraction of the variability in the climate and oceans of the Pleistocene reflects a response to the changing configuration of the Earth's orbit (Hays et al., 1976; Kominz et al., 1979; Imbrie et al., 1984). During the late Pleistocene, the nature of the response of the climatic system to orbital forcing was partially related to the response of large Northern Hemisphere ice sheets. During this interval, the long-period component of the Earth's orbit, which is the eccentricity having a dominant 100,000-yr. period of variation, is most strongly reflected in the climate records. During the early Pleistocene when the Northern Hemisphere ice sheets were smaller, the tilt component (a period of 41,000 yr.) of the Earth's orbit geometry dominated the variance spectra of the isotopic records (Pisias and Moore, 1981; Shackleton et al., 1982). Thus, changes in variance spectra of paleoceanographic records have proved useful in developing an understanding of the causes of climate change.

Since variations in the Earth's orbit are not unique to the Pleistocene, we can use HPC material from pre-Pleistocene sections to determine whether variations in oceanographic parameters occur at frequencies similar to those in the Pleistocene, and if time-scale resolution improves, whether such variations are related to responses of the Earth's climate system to orbital changes.

Of the data presently available from Site 574, the interval from 168 to 186 m provides an interval suitable for an initial analysis. In this interval there are no major changes in the means of the oxygen isotopic and carbonate values, and the $\delta^{13}C$ data below the offset at 172 m are a long enough series to provide statistically useful results. The data were converted from a depth sequence to a time series using the sedimentation rate of 32 m/m.y. (site chapter, this volume). This is consistent with additional detailed diatom stratigraphic data from this site (Barron, this volume). The data are plotted versus absolute age in Figure 3. The variance spectra for these data are shown in Figure 4. The method used for calculating the spectra is given in Pisias et al. (1973).

The most striking feature of these spectra is the dominance of a frequency component corresponding to a period of 40,000 yr. in the $\delta^{18}O$ record (Fig. 4A). The similarity of this frequency to that of the orbital tilt component is suggestive of a significant response to orbitally induced changes in solar insolation in the middle Miocene. The presence of this spectral peak, however, is not conclusive proof that orbital variations did cause climate change in this time interval.

The $\delta^{13}C$ spectrum shows a dominance of very long period components in the data. This component is also observed in Plio-Pleistocene $\delta^{13}C$ records and probably relates to the long residence time of carbon in the ocean (100,000 yr.; Broecker, 1974). In addition to the very low frequency component, the carbon isotope spectrum contains spectral components at 46,000 and 26,000 yr. and a high frequency component at 14,000 yr. The latter is also present in the oxygen isotopic data, and cross spectra calculations show that they are related with a coherence of ove- 0.95. This suggests that during the interval represented by these data, very high frequency variations affecting both the carbon and oxygen isotopic composition of the deep Pacific were present in the middle Miocene. The 26,000-yr. component is near the frequency of variation in orbital precession (23,000 yr. at present-day) and is suggestive of a possible cause. More importantly, the data suggest a response in the carbon isotopic system that is independent of the oxygen isotopes, which do not display this frequency component (Figs. 2 and 3).

The spectrum of the calcium carbonate data displays a pattern very similar to that of Pleistocene records, with a dominant 100,000-yr. component and indications of frequency components at 40,000 and 25,000 yr. The general form of this spectrum is similar to that of upper Pleistocene oxygen isotope records. Again, these results strongly suggest significant variability in the middle Miocene oceans and the possibility that orbitally induced variations in solar insolation (the Milankovitch hypothesis of climate change) was operating at times remote from the late Pleistocene.

CONCLUSIONS

The detailed isotopic and carbonate data from Site 574 clearly show that a high degree of oceanic variability occurred in the early part of the middle Miocene. Initial time series analysis shows that the amplitude and frequency characteristics of the paleoclimate records from Site 574 are comparable to records from the Pliocene and lower Pleistocene. This suggests that the processes controlling climate change during late Cenozoic are likely to have been important prior to 16 Ma.

The detailed analysis of the major shift in the oxygen isotopic composition of the ocean during the middle Miocene shows that this oceanic "event" occurred over a time interval of approximately 30,000 yr. The degree of oceanic variability implied by these data is the same before and after the event. The high degree of variability prior to the middle Miocene must be accounted for in models describing the presence or absence of major continental ice sheets during this interval. Significant variations in ice volume prior to 16 Ma could explain the high degree of variability observed. If ice sheets were not of importance prior to 16 Ma, then the data would suggest a significantly different deep-water structure in the Pacific during the early Miocene.

Finally, the high degree of variability observed in these high-resolution records show the importance of detailed sampling of high-quality sediment sections to aid in defining the true nature of oceanic and climatic variability.

REFERENCES

Hays, J. D., Imbrie, J., and Shackleton, N. J., 1976. Variations in the earth's orbit: pacemaker of the ice ages. *Science*, 194:1121–1132.

Imbrie, J., Shackleton, N. J., Pisias, N. G., Morley, J. J., Prell, W. L., Martinson, D. G., Hays, J. D., McIntyre, A., and Mix, A. C., 1984. The orbital theory of Pleistocene climate: support from a revised chronology of the marine $\delta^{18}O$ record. *In* Imbrie, J., and Berger, A. (Eds.), *Milankovitch and Climate Change*: Amsterdam, (Elsevier Sci. Publ. Co.), pp. 269–305.

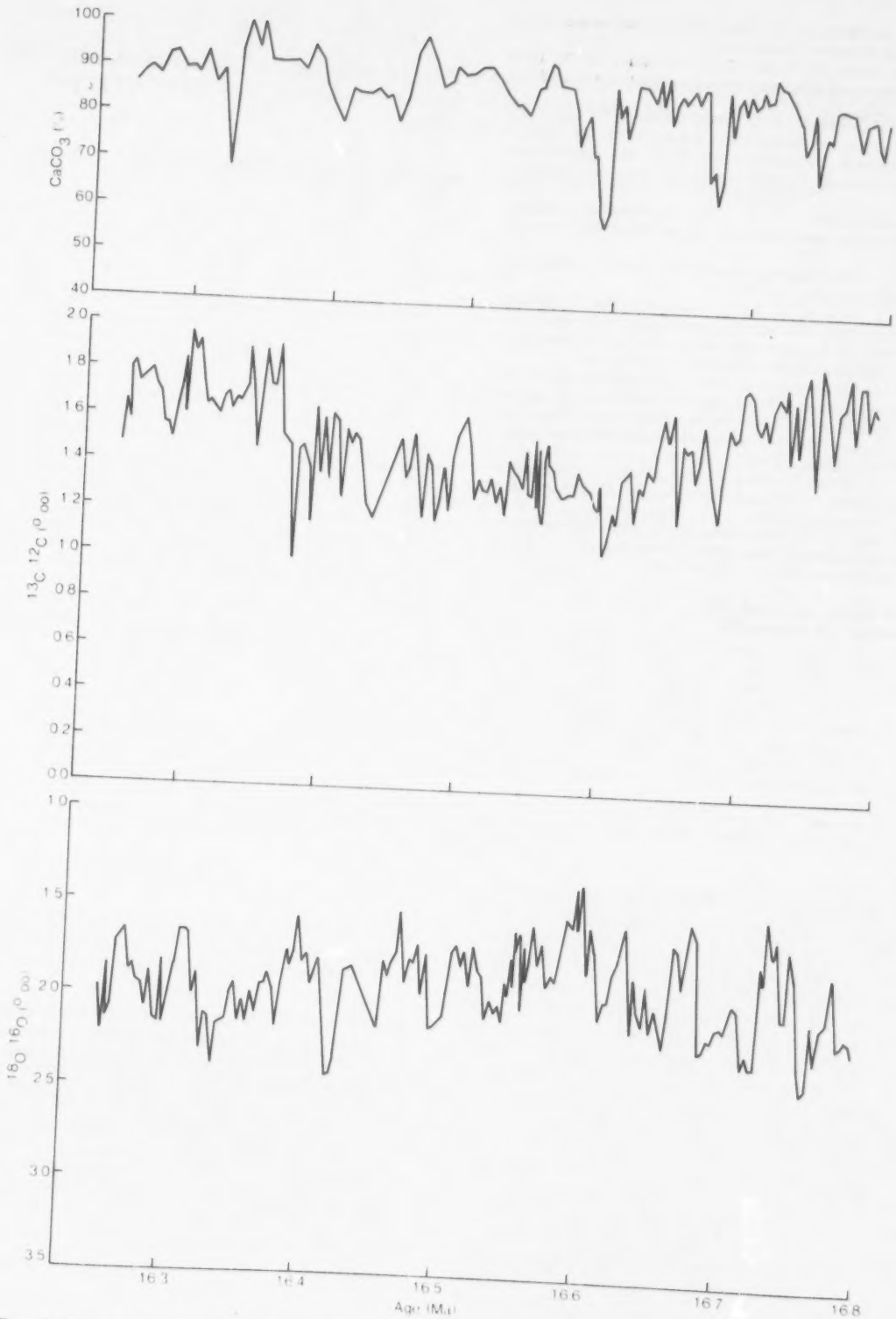

Figure 3. Detailed isotopic and carbonate data for sub-bottom depths from 168 to 188 m (16.2 to 16.8 Ma) in Hole 574A. Ages were derived from sedimentation rate estimates made in the site chapter (this volume).

Jenkins, G. M., and Watts, D. G., 1968. *Spectral Analysis and its Application*: San Francisco (Holden-Day).

Kominz, M. A., Heath, G. R., Ku, T.-L., and Pisias, N. G., 1979. Brunhes time scales an the interpretation of climatic change. *Earth Planet. Sci. Lett.*, 45:394–410.

Matthews, R. K., and Poore, R. Z., 1980. Tertiary $\delta^{18}O$ record and glacio-eustatic sea-level fluctuation. *Geology*, 8:501–504.

Pisias, N. G., Dauphin, J. P., and Sancetta, C. S., 1973. Spectral analysis of late Pleistocene–Holocene sediments. *Quat. Res. (N.Y.)*, 3: 3–9.

Pisias, N. G., and Moore, T. C., Jr., 1981. The evolution of Pleistocene climate: a time series approach. *Earth Planet. Sci. Lett.*, 52: 450–458.

Shackleton, N. J., 1982. The deep-sea sediment record of climate variability. *Prog. Oceanogr.*, 11:199–218.

Shackleton, N. J., Hall, M. A., and Boersma, A., 1984. Oxygen and carbon isotope data from Leg 74 Foraminifera. *In* Moore, T. C., Jr., Rabinowitz, P. D., et al., *Init. Repts. DSDP*, 74: Washington (U.S. Govt. Printing Office), 599–612.

Shackleton, N. J., and Kennett, J. P., 1975. Late Cenozoic oxygen and carbon isotopic changes at DSDP Site 284: implications for glacial history of the Northern Hemisphere and Antarctica. *In* Kennett, J. P., Houtz, R. E., et al., *Init. Repts. DSDP*, 29: Washington (U.S. Govt. Printing Office), 801–807.

Shackleton, N. J., Pisias, N., Prell, W., and Imbrie, J., 1982. Evolution of the climate response to orbital forcing. *EOS Trans. Am. Geophys. Union*, 63(45):996.

Woodruff, F., Savin, S. M., and Douglas, R. G., 1981. Miocene stable isotope record: a detailed deep Pacific Ocean study and its paleoclimatic implications. *Science*, 212:665–668.

Date of Initial Receipt: 14 August 1983
Date of Acceptance: 22 August 1984

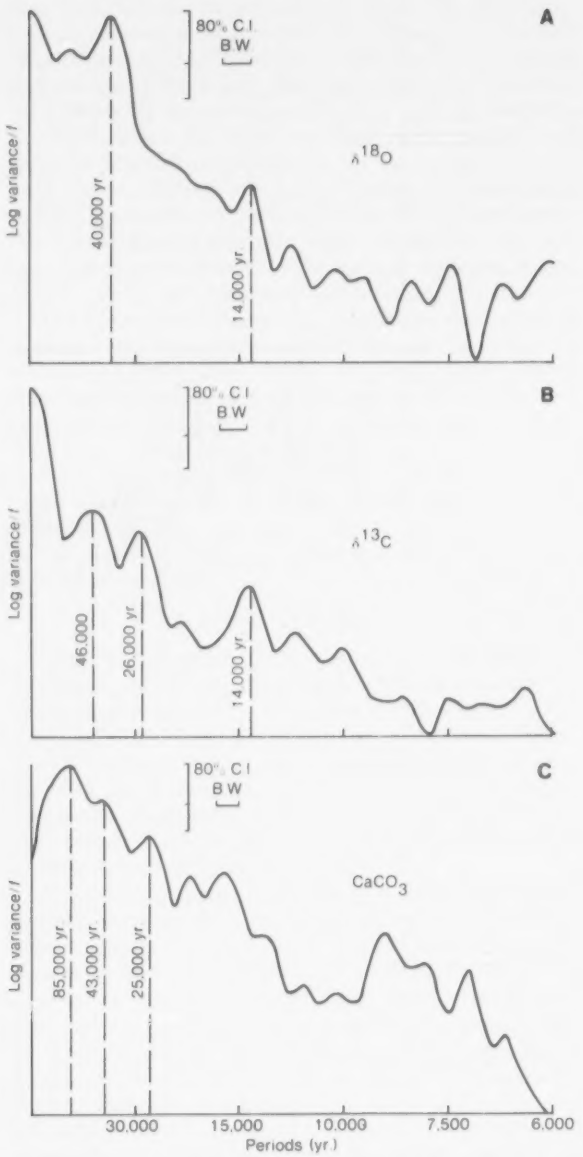

Figure 4. Variance spectra for $\delta^{18}O$, $\delta^{13}C$, and $CaCO_3$ data for 16.2 to 16.8 Ma plotted in Figure 3. Spectra were calculated from 41 lags of the auto-covariance function (Jenkins and Watts, 1968). Time series contained 145 data points sampled at 3,000-yr. intervals. All spectra are plotted on a linear frequency scale versus log variance. Shown are the 80% confidence interval (C.I.) of spectral estimates and the bandwidth (B.W.) used to calculate smoothed spectra. A. Variance spectra for $\delta^{18}O$ record showing the 40,000-yr. spectral peak. B. Variance spectra for $\delta^{13}C$ showing important 46,000, 26,000, and 14,000-yr. peaks and long period components. C. Variance spectra for $CaCO_3$.

22. OXYGEN AND CARBON ISOTOPE RECORD FOR THE EARLY AND MIDDLE MIOCENE IN THE CENTRAL EQUATORIAL PACIFIC (LEG 85) AND PALEOCEANOGRAPHIC IMPLICATIONS[1]

Edith Vincent and John S. Killingley, Scripps Institution of Oceanography[2]

ABSTRACT

Oxygen and carbon isotope stratigraphies are given for the planktonic foraminifer *Globoquadrina venezuelana* (a deep-dwelling species) at three DSDP sites located along a north–south transect at approximately 133°W across the Pacific equatorial high-productivity zone. The records obtained at Sites 573 and 574 encompass the lower Miocene. At Site 575 the record includes the middle Miocene and extends into the lowermost lower Miocene. The time resolution of the planktonic foraminifer isotope record varies from 50,000 to 500,000 yr. The benthic foraminifer *Oridorsalis umbonatus* was analyzed for isotope composition at a few levels of Site 575. Isotope stratigraphies for all three sites are compared with carbonate, foraminifer preservation, and grain size records. We identified a number of chemostratigraphic signals that appear to be synchronous with previously recognized signals in the western equatorial Pacific and the tropical Indian Ocean, and thus provide useful tools for chronostratigraphic correlations. The sedimentary sequence at Site 573 is incomplete and condensed, whereas the sequences from Sites 574 and 575 together provide a complete lower Miocene record. The expanded nature of this record, which was recovered with minimum disturbance and provides excellent calcareous and siliceous biostratigraphic control, offers a unique opportunity to determine the precise timing of early Miocene events. Paleomagnetic data from the hydraulic piston cores at Site 575 for the first time allow late early Miocene paleoceanographic events to be tied directly to the paleomagnetic time scale.

The multiple-signal stratigraphies provide clues for paleoceanographic reconstruction during the period of preconditioning before the major middle Miocene cooling. In the lowermost lower Miocene there is a pronounced shift toward greater $\delta^{13}C$ values (by ~1‰) within magnetic Chron 16 (between approximately 17.5 and 16.5 Ma). The "Chron 16 Carbon Shift" coincides with the cessation of an early Miocene warming trend visible in the $\delta^{18}O$ signals. Values of $\delta^{13}C$ remain high until approximately 15 Ma, then decrease toward initial (early Miocene) values near 13.5 Ma. The broad lower to middle Miocene $\delta^{13}C$ maximum appears to correlate with the deposition of organic-carbon-rich sediments around the margin of the northern Pacific in the Monterey Formation of California and its lateral equivalents. The sediments rimming the Pacific were probably deposited under coastal upwelling conditions that may have resulted from the development of a strong permanent thermocline. Deposition in the upwelling areas occurred partly under anaerobic conditions, which led to the excess extraction of organic carbon from the ocean. The timing of the middle Miocene cooling, which began after the Chron 16 Carbon Shift, suggests that the extraction of organic carbon preconditioned the ocean–atmosphere system for subsequent cooling.

A major carbonate dissolution event in the late early Miocene, starting at approximately 18.7 Ma, is associated with the enrichment in ^{13}C. The maximum dissolution is coeval with the Chron 16 Carbon Shift. It corresponds to a prominent acoustic horizon that can be traced throughout the equatorial Pacific.

INTRODUCTION

Among Cenozoic paleoceanographic events, the middle Miocene oxygen isotope step is of prime importance, because it probably marks the onset of modern ocean conditions, that is, ocean basins filled with water masses generated at high latitudes. The step consists of a sharp ^{18}O enrichment in benthic foraminifers representing a shift of about +1‰. This shift has been interpreted as reflecting a major buildup of Antarctic ice and a drop in surface-water temperatures on the Antarctic coast (Savin et al., 1975; Shackleton and Kennett, 1975; Woodruff et al., 1981). The concept of ice buildup at this time has been widely accepted, although there is disagreement about the amount of ice that was present before the middle Miocene (Matthews and Poore, 1980; Keigwin and Keller, 1984; Miller and Thomas, this volume). The cause of the proposed rapid increase in volume of the Antarctic ice sheet remains unknown; its explanation is a prime challenge of Cenozoic paleoceanography. Berger et al. (1981) pointed out that the rapidity of the glaciation suggests positive feedback within the system, presumably tied to albedo effects or to the CO_2 budget (Berger, 1982). Blanc et al. (1980), Schnitker (1980a, b), and Berggren and Schnitker (1983) have suggested that the Antarctic glaciation was triggered by a fundamental rearrangement of the North Atlantic circulation system that occurred when the Iceland Ridge subsided below a critical depth, an event that linked the entire north polar sea as a heat sink to the world ocean. More recently, Vincent et al. (1983) and Vincent and Berger (1984) have suggested that the extraction of organic carbon at the ocean margins in the latest early Miocene preconditioned the ocean–atmosphere for subsequent middle Miocene cooling. These authors suggest that the buildup of organic-carbon-rich sediments around the edge of the northern Pacific reduced the CO_2 concentration in the atmosphere and thus fostered the subsequent growth of ice in Antarctica.

The reconstruction of environmental conditions during the period before the middle Miocene cooling is crucial to an understanding of this event. To date, however,

[1] Mayer, L., Theyer, F., et al., *Init. Repts. DSDP*, 85: Washington (U.S. Govt. Printing Office).

[2] Addresses: (Vincent, present address) Département de Géologie Dynamique, Université Pierre et Marie Curie, 4 Place Jussieu, 75230 Paris Cedex 05, France; (Killingley) Scripps Institution of Oceanography, University of California at San Diego, La Jolla, CA 92093.

paleoceanographic studies of the early Miocene have been hampered by the paucity of complete and undisturbed sedimentary sequences. The recovery of expanded lower Miocene sections, with minimum disturbance and excellent calcareous and siliceous biostratigraphic control, during DSDP Leg 85 in the central equatorial Pacific offers a unique opportunity to investigate the environmental conditions prevailing during the early Miocene. The sequence at Site 575, which was recovered by hydraulic piston coring, is of special interest. Paleomagnetic data for the uppermost lower Miocene at this site permit for the first time biostratigraphic and paleoceanographic events to be tied directly to the paleomagnetic time scale.

MATERIAL OF STUDY

The sediments analyzed in this study were recovered at Sites 573, 574, and 575 in the central equatorial Pacific during DSDP Leg 85. These three sites are located along a north–south transect across the equatorial high-productivity zone along approximately 133°W. They lie at water depths ranging from 4300 to 4555 m near the crest of the equatorial sediment bulge (Table 1; Fig. 1). The three sites have migrated from south of the equator to deeper, more western locations at or north of the equator. The changes in productivity that accompanied the equatorial crossings (which occurred for the different sites at different times during the Miocene) are reflected in the sediments in changes in accumulation rates, siliceous microfossil abundance, and foraminiferal preservation. The basic patterns of Pacific equatorial sedimentation have been outlined by Berger and Winterer (1974), and models relating sedimentation and equatorial crossing have been elaborated by various authors (Winterer, 1973; van Andel et al., 1975; Lancelot, 1978). Sites 574 and 575 crossed the equator during the early Miocene, Site 573 during the late Miocene (Weinreich and Theyer, this volume). Previous DSDP holes drilled in this area include Sites 71 and 77, which provided valuable sections for Miocene paleoceanographic studies.

Lower Miocene sequences were recovered at Sites 573 and 574 by rotary coring. Disturbance was minor because of the induration of the sediments. The sequences are ~75 and 160 m thick, respectively, and they overlie Oligocene sediments. At Site 575, a 120-m-thick lower Miocene sequence was recovered by hydraulic piston corer (HPC); the section ended in lowermost lower Miocene sediments assigned an age of approximately 22 Ma. We recovered the stable isotope stratigraphies for the lower Miocene at these three sites. Other studies in this volume provide stable isotope stratigraphies for Site 574 for Oligocene (Miller and Thomas, this volume) and middle Miocene (Pisias et al., this volume) sediments. Our sampling ranges from the uppermost Oligocene to the lowermost middle Miocene at Sites 573 and 574. At Site 575 it encompasses the middle Miocene and was extended into the upper Miocene to obtain a continuous isotope record for the early to middle Miocene time interval.

The sediments consist of calcareous ooze and chalk with a high calcium carbonate content of 80 to 96% throughout most of the lower and middle Miocene. An interval with decreased calcium carbonate content occurs at all three sites in the uppermost lower Miocene with pronounced minima as low as 40 to 60% (Figs. 2 to 4). This interval of decreased $CaCO_3$ content (in the middle of the *Denticulopsis nicobarica* Zone, near 17 Ma) appears to correspond to a prominent and laterally traceable acoustic horizon (Mayer et al., this volume). At Site 575, centimeter-thick sandy turbidite layers containing mostly sand-sized foraminifers and volcanic debris are intercalated throughout the section. These layers were carefully skipped during sampling.

The abundance of both calcareous and siliceous microfossils throughout the sequences permits a multiple biostratigraphic zonation (Figs. 2 to 4). The ages indicated in Figures 2 to 4 are derived from diatom zonal boundaries and the time scale given by Barron et al. (this volume) and Barron et al. (in press), which is based on the paleomagnetic time scale of Berggren et al. (in press). Paleomagnetic data obtained from the upper lower Miocene in Hole 575A (Weinreich and Theyer, this volume) allow the identification of magnetic Anomalies 5C and 5D (Fig. 4). Biostratigraphic datums and paleoceanographic events of the late early Miocene can thus be directly tied for the first time to the magnetostratigraphy encompassing the middle of Chron 17 to the middle of Chron 16.

The average accumulation rate for the entire lower Miocene is approximately 9.7 m/m.y. at Site 573, 20.8 m/m.y. at Site 574, and 20 m/m.y. at Site 575. Middle Miocene sediments accumulated at Site 575 at an average rate of about 9 m/m.y., upper Miocene sediments at an average reduced rate of about 4.7 m/m.y. Our sampling interval, which is 1 m, thus corresponds to a time interval of roughly 103,000, 48,000, and 50,000 yr. for the lower Miocene at Sites 573, 574, and 575, respectively. For the middle Miocene at Site 575 it corresponds to 110,000 yr. and for the upper Miocene, to 212,000 yr. (Barron et al., this volume).

All samples (20 cm^3) were dried, weighed, soaked in buffered Calgon solution, washed on a 63-μm sieve, and cleaned ultrasonically to remove fine particles from inside the foraminifer test. Residues were then dried and weighed. Results of grain size analyses are listed in Table 2 and plotted in Figures 2 to 4. Calcium carbonate con-

Table 1A. Site locations.

Site	Location	Longitude	Water depth (m)
573	00°29.91'N	133°18.57'W	4.301
574	04°12.52'N	133°19.81'W	4.561
575	05°51.00'N	135°02.16'W	4.536

Table 1B. Material studied.

Hole	Cores	Coring method
573B	11 to 23	Rotary
574	25 to 31	HPC
574C	1 to 21	Rotary
575A	1 to 33	HPC
575B	2 to 14	HPC

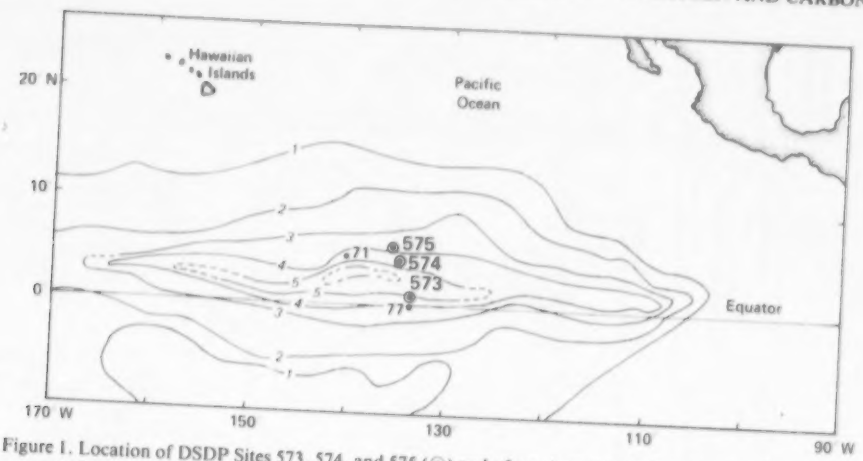

Figure 1. Location of DSDP Sites 573, 574, and 575 (⊙) and of previous DSDP Sites 71 and 77 (●) in the central equatorial Pacific in relationship to sediment thickness (contours in tenths of seconds of two-way traveltime).

tents obtained from shipboard carbonate bomb analyses at 1.5-m intervals (see site chapters, this volume) are plotted in Figures 2 to 4. Because of time constraints, not all samples were analyzed for isotope composition. Approximately 200 samples were analyzed for both oxygen and carbon isotopes by following our standard procedure (Berger and Killingley, 1977). The time resolution of our isotope stratigraphies is roughly 500,000, 170,000, and 50,000 yr. for the early Miocene at Sites 573, 574, and 575, respectively. For the middle Miocene at Site 575 it is roughly 280,000 yr., and for the late Miocene it is 700,000 yr.

Foraminifers are abundant throughout the sequences; preservation is good to moderate. Fluctuations in the preservation of planktonic foraminifers are indicated by the foraminifer preservation curves constructed by Saito (this volume) from core-catcher samples using the codes of Berger and von Rad (1972) (Figs. 2 to 4). Throughout the lower Miocene, preservation is better at Site 575 than at Sites 573 and 574, probably because of the earlier equatorial crossing of Site 575 during the early Miocene. At all three sites there is an interval with poorer foraminifer preservation in the uppermost lower Miocene in the N6–N8 zonal interval, which corresponds to the interval of decreased $CaCO_3$ content. The elimination of solution-susceptible species in this interval precludes the identification of Zone N7.

We established continuous isotope stratigraphies for the deep-dwelling planktonic foraminifer *Globoquadrina venezuelana*. To minimize the effect of ontogenetic development on the isotope composition of the test (Berger et al., 1978), specimens were selected from a restricted size range (350 to 420 μm). We chose *G. venezuelana* because this species is common throughout the sequences. Furthermore, our various studies have shown this species to be the most reliable deep-dwelling planktonic foraminifer for Neogene reconstruction (Vincent et al., 1980; in press). We can thus compare our results with isotope stratigraphies obtained from the same species in the Miocene of the tropical Indian Ocean (Vincent et al., in press), where we also obtained an isotope record from shallow-dwelling planktonic and benthic foraminifers. Because of the time constraints of this study, benthic foraminifers (*Oridorsalis umbonatus*) were analyzed at only a few levels of Site 575.

RESULTS

Isotope Stratigraphy

Isotope values of *Globoquadrina venezuelana* are given in Table 3 and are plotted versus depth and biostratigraphic zonation in Figures 2 to 4. Despite the problems that occurred as the result of varying sampling density, general trends could be identified and isotope events could be correlated between sites. The isotope curves reveal a succession of stratigraphic intervals with distinct isotopic signatures. The levels marking the boundaries between these intervals have been labeled in a stratigraphic order from bottom to top with capital letters (A to H). Their biostratigraphic position is given in Figure 5.

Oxygen Isotope Stratigraphy

Throughout the uppermost Oligocene and the lower half of the lower Miocene, up to level C, there is no definite trend in the oxygen isotope record of *Globoquadrina venezuelana*. The $\delta^{18}O$ values range between 0.5 and 1.5‰, with rather large fluctuations (up to 0.8‰). From level C to level F, throughout the upper half of the lower Miocene, there is a regular and steady decrease in the $\delta^{18}O$ values from approximately 1‰ to 0‰. Variations in this interval are of low amplitude. At level F, in the uppermost lower Miocene, the $\delta^{18}O$ values are the lowest of the entire record (−0.2‰). Immediately above this level, there is an abrupt enrichment in ^{18}O of over 1‰ within 2 m.

Above this offset, the isotope stratigraphy can be followed at Site 575 only. In the interval between levels F and G, which spans the lower/middle Miocene boundary, $\delta^{18}O$ values decrease slightly, with a mean of about 0.8‰. In the lower half of this interval, there is little variability at Site 575, in contrast to results from Site 574, where large-amplitude fluctuations occur. In the next

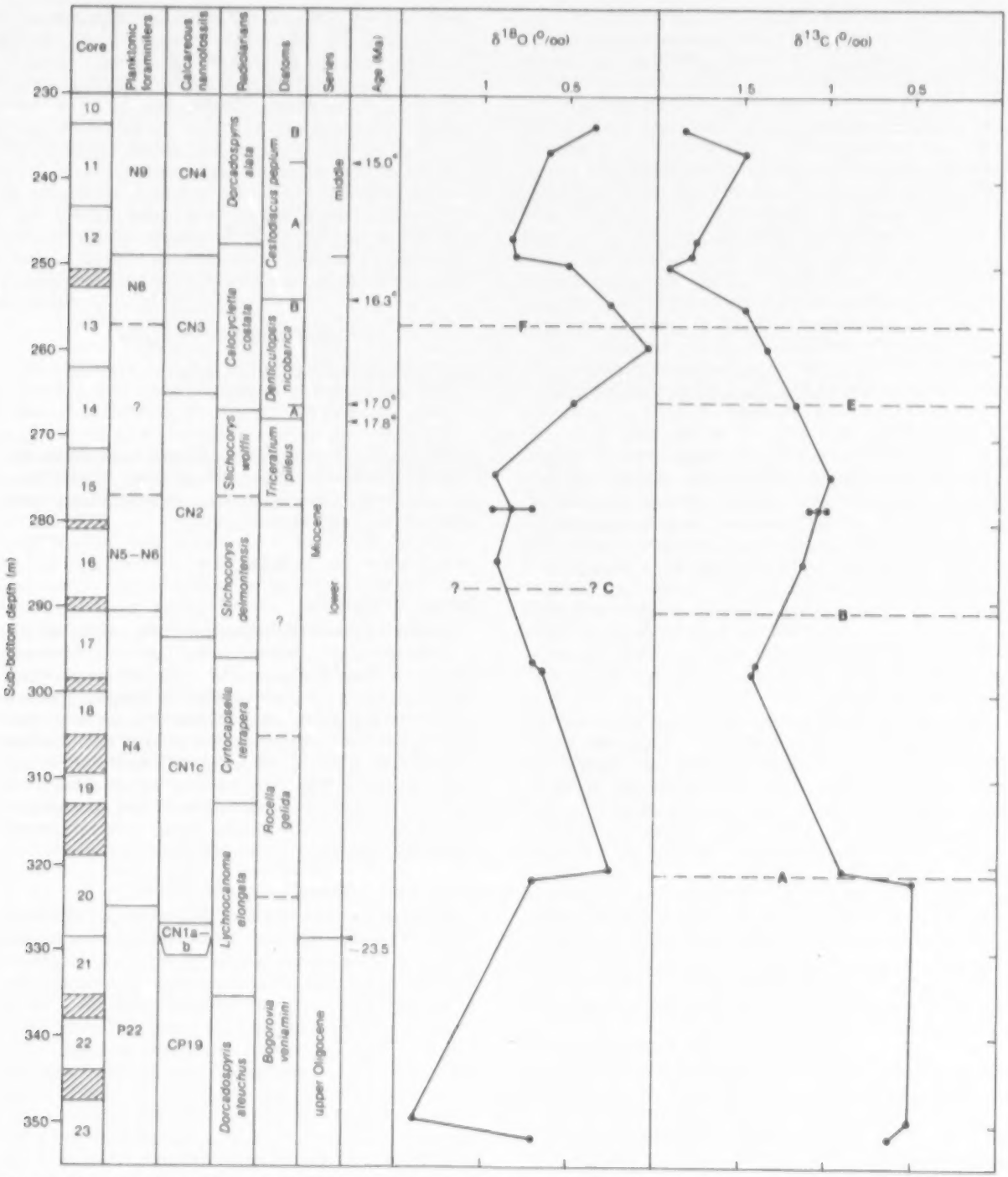

Figure 2. Biostratigraphy and changes at Site 573 in stable isotope composition of the deep-dwelling planktonic foraminifer *Globoquadrina venezuelana*, in sand fraction (>63 μm) content, in $CaCO_3$ content, and in foraminiferal solution (FS). Biostratigraphy at left is a composition column established from the various holes at this site by Saito (this volume) for foraminifers, Pujos (this volume) for calcareous nannofossils, Nigrini (this volume) for radiolarians, and Barron (this volume) for diatoms. Except for the earliest age at the Oligocene/Miocene boundary, ages are from diatom zonal boundaries according to Barron (this volume) and Barron et al. (in press). Asterisks indicate those derived from direct paleomagnetic calibration. Oxygen and carbon isotope data are from Table 3 and those for sand fraction content from Table 2. Calcium carbonate data are from shipboard analyses (site chapters, this volume). Foraminiferal solution data are from Saito (site chapters, this volume) following the codes of Berger and von Rad (1972). Increasing values indicate more pronounced dissolution. Stratigraphic levels A to G are defined in Figure 5.

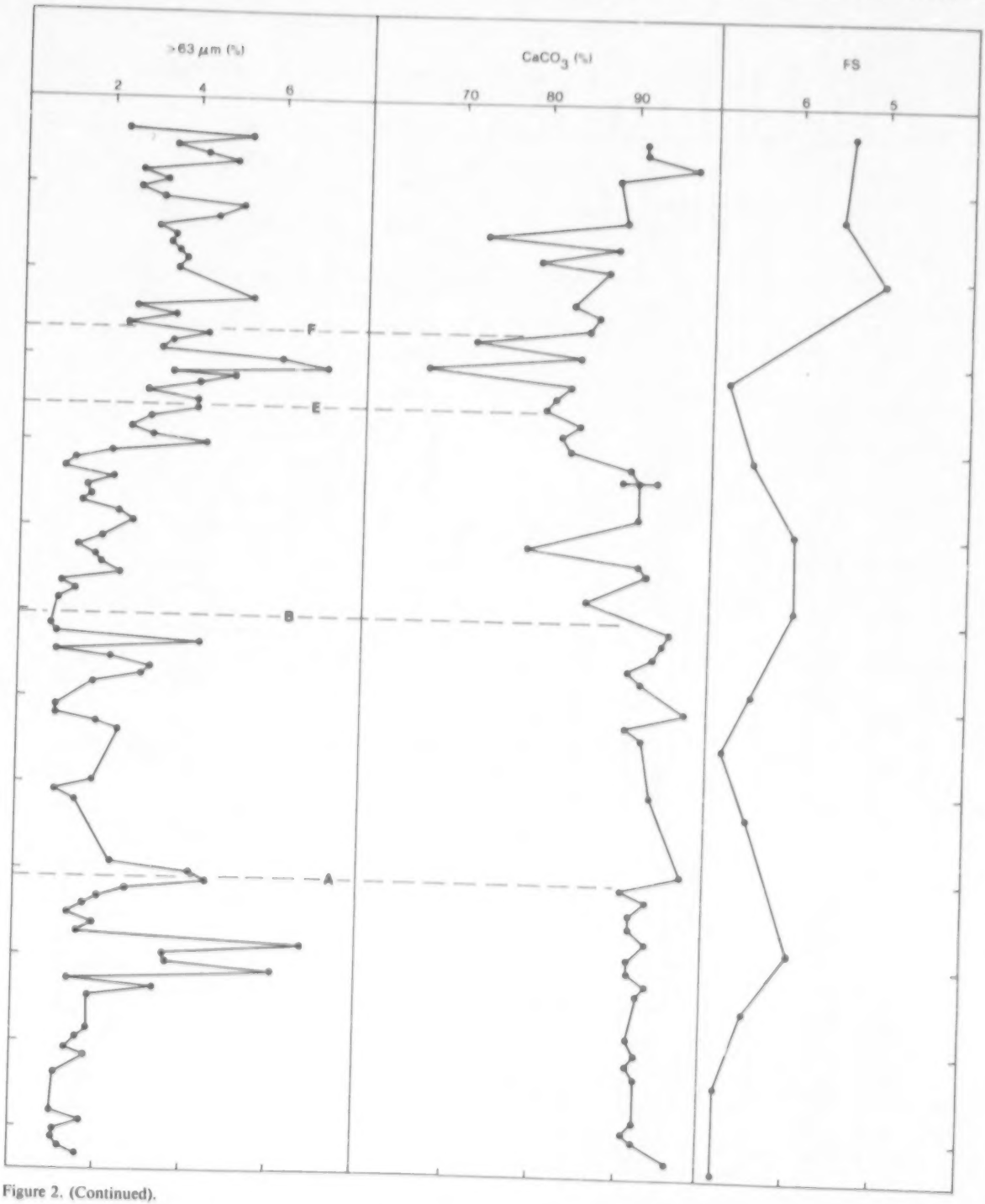

Figure 2. (Continued).

interval, from levels G to H in the middle Miocene, $\delta^{18}O$ values show high-amplitude, high-frequency fluctuations, with an overall increase in $\delta^{18}O$ of approximately 0.7‰. Above level H, $\delta^{18}O$ values show a significant decrease of about 1‰ throughout the remainder of the middle Miocene to values near 0.7‰. In the upper Miocene $\delta^{18}O$ remains close to this value. The upper Miocene sequence at Site 575 is condensed and incomplete and is not well suited to detailed stratigraphy (note the low carbonate values).

A detailed comparison between the planktonic and benthic foraminifer isotope records at Site 575 cannot

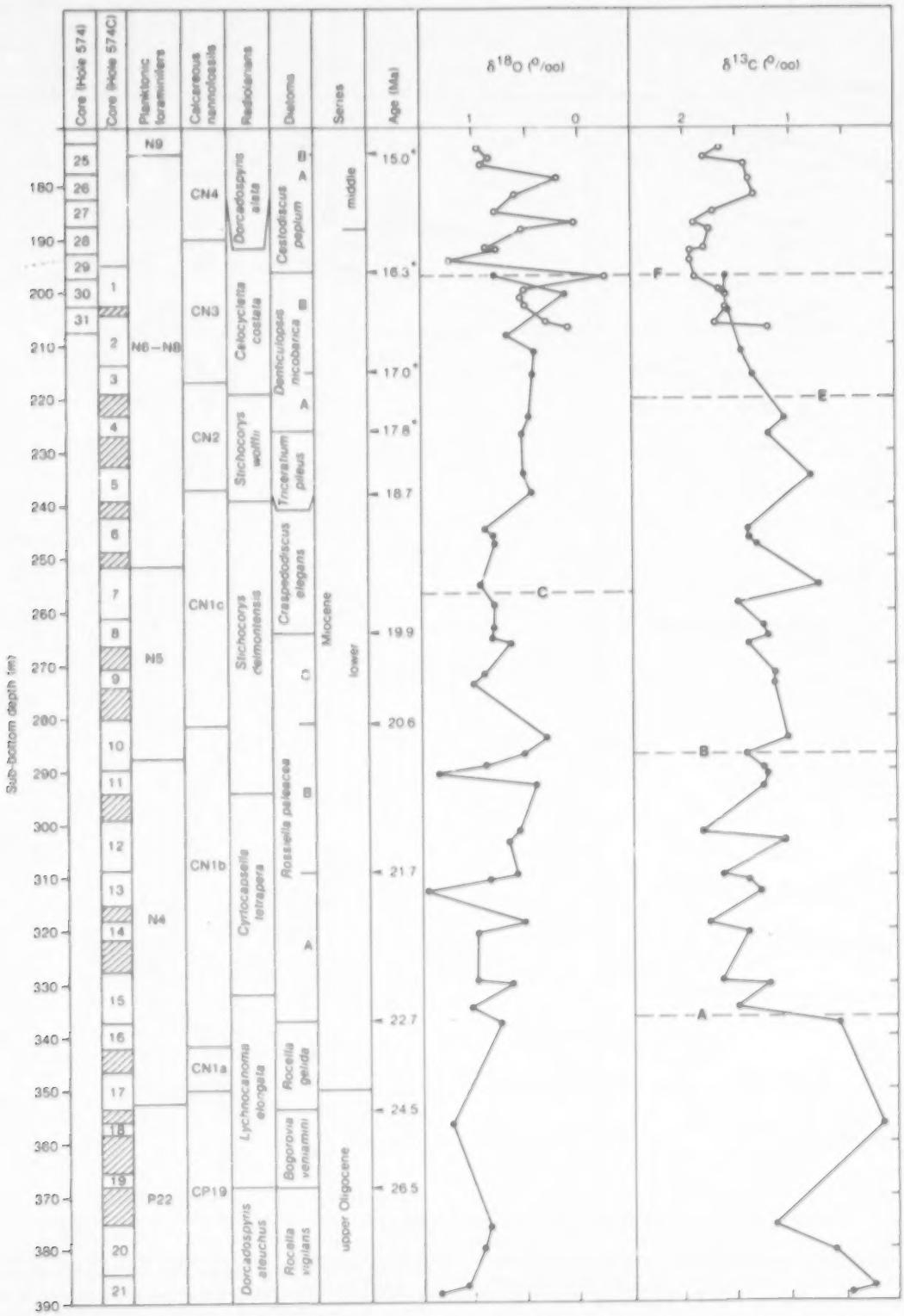

Figure 3. Biostratigraphy and changes at Site 574 in stable isotope composition of *Globoquadrina venezuelana*, in sand fraction content, in $CaCO_3$ content, and in foraminiferal solution (FS). See Figure 2 legend for data origin and other details. Solid black dots indicate data from Hole 574C, open dots data from Hole 574.

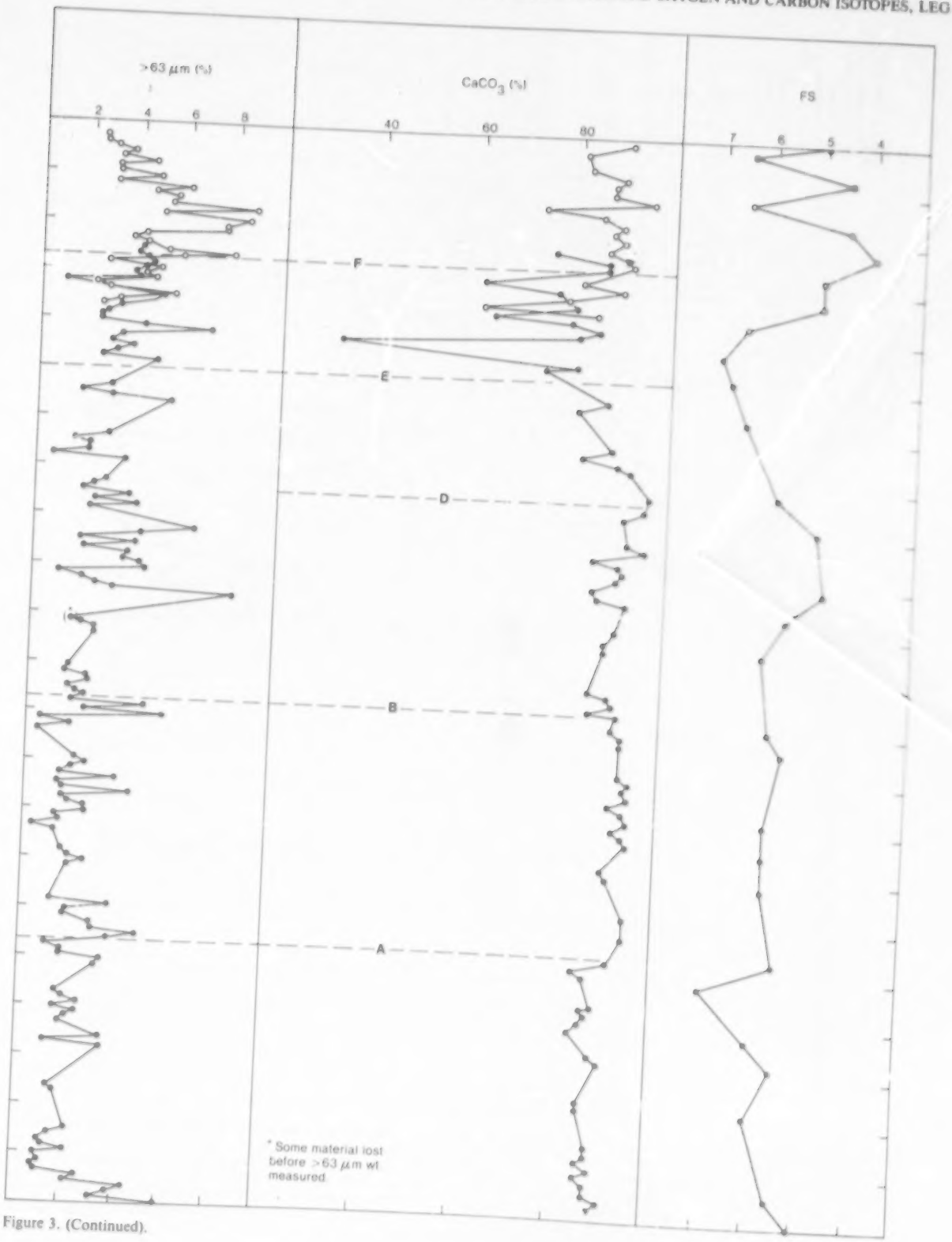

Figure 3. (Continued).

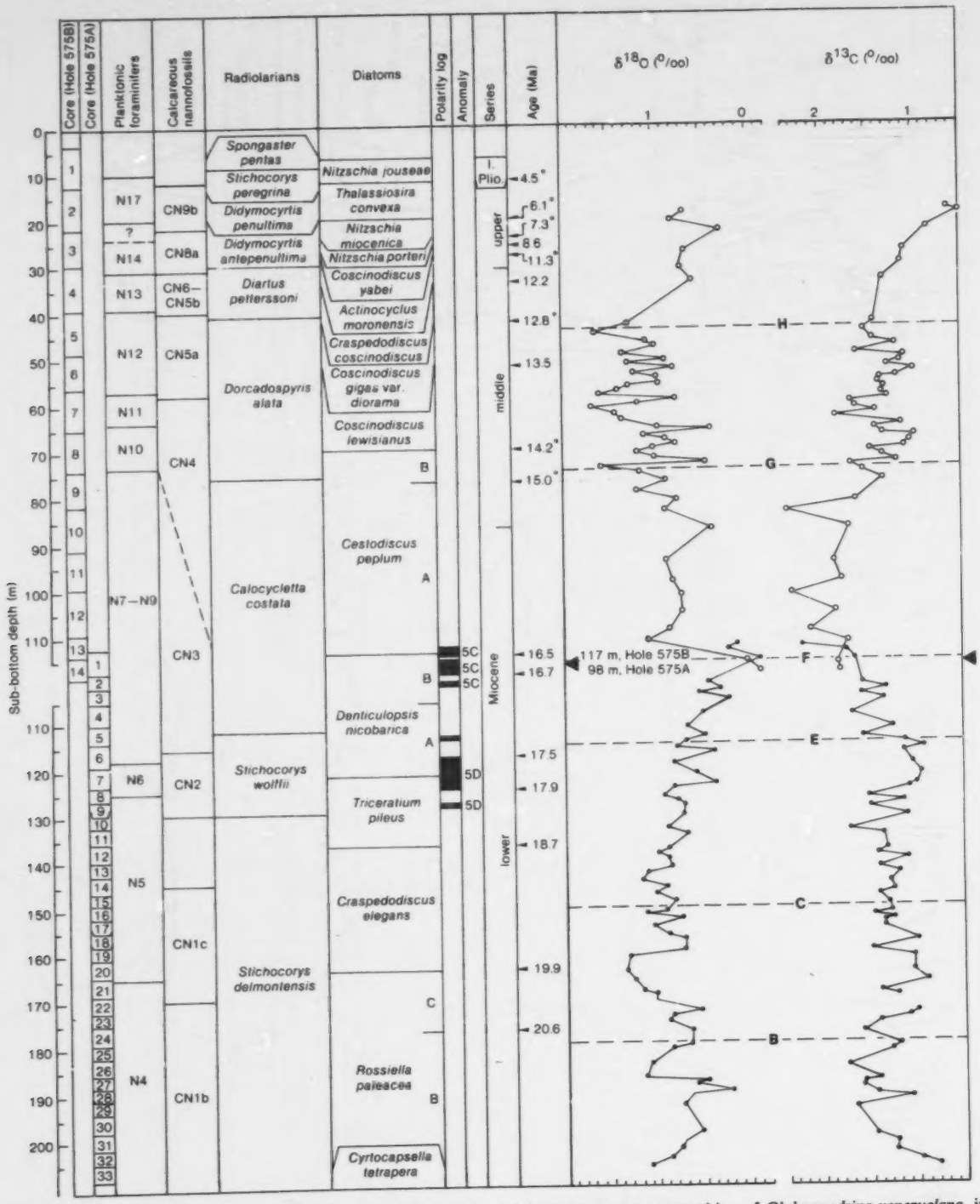

Figure 4. Biostratigraphy, magnetostratigraphy, and changes at Site 575 in stable isotope composition of *Globoquadrina venezuelana*, in sand fraction content, in $CaCO_3$ content, and in foraminiferal solution (FS). See Figure 2 legend for data origin and other details. The magnetic polarity log in the interval between Cores 575A-1 and 575A-10 is from Weinreich and Theyer (this volume). Ages given in this interval are derived from the boundaries between revised and normal intervals. Solid black dots indicate data from Hole 575A, open dots data from Hole 575B. There is a 19-m offset in the sub-bottom depths given for the cores of Hole 575A as compared with Hole 575B. To obtain the real sub-bottom depths of these cores, a value of 19 m should be added to the nominal depths indicated at the left of Hole 575A. A correlation point between Holes 575A and 575B is obtained by a turbidite horizon in Core 575B-14 (117 m sub-bottom) and Core 575A-1 (98 m nominal sub-bottom). This horizon is indicated with a solid triangle. This correlation between the two holes is in good agreement with the isotope, sand content, and carbonate data within the interval of overlap and with biostratigraphic data given in the site chapters (this volume).

READEX FICHE best copy available

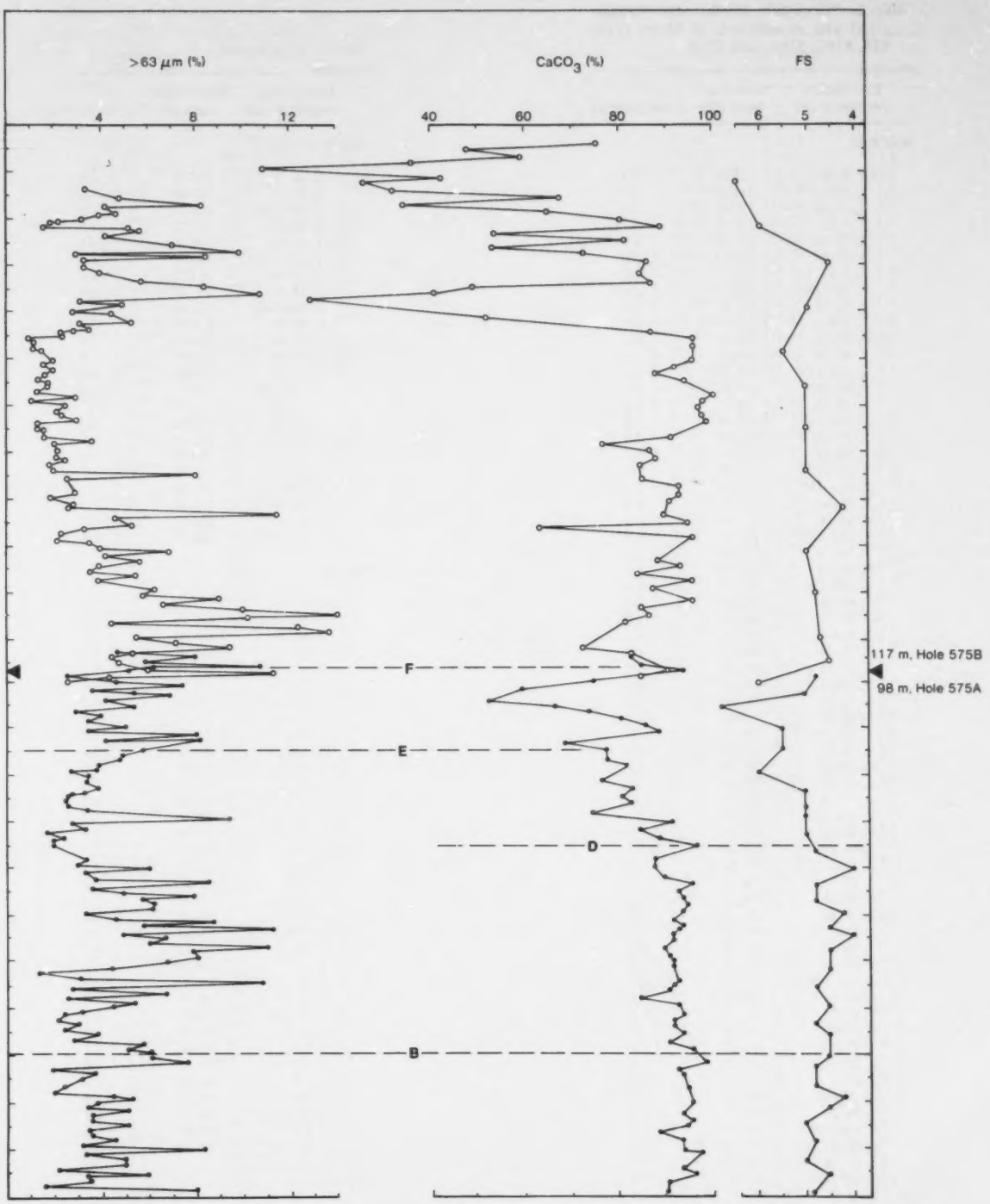

Figure 4. (Continued).

be made because of the wide spacing between the benthic data (Table 4; Fig. 6). However, a few features are apparent. The $\delta^{18}O$ values of *Oridorsalis umbonatus* show a slight upwardly decreasing trend in the lower Miocene interval between levels C and E. The trend parallels the decreasing trend of *G. venezuelana*. In the interval between levels F and G, which spans the lower/middle Miocene boundary, the benthic foraminifers have a constant $\delta^{18}O$ value of 2‰. At level G in the middle Miocene the signature of the *G. venezuelana* record changes

Table 2. Percentages of the sand fraction (>63 μm) in sediments of Holes 573B, 574, 574C, 575A, and 575B.

Core-Section (interval in cm)	Sub-bottom depth (m)	>63 μm (%)
Hole 573B		
11-1, 6-10	233.58	2.4
1, 103-107	234.55	5.1
2, 50-54	235.52	3.5
3, 7-11	236.59	4.2
3, 98-102	237.50	4.9
4, 50-54	238.52	2.6
5, 5-9	239.57	3.3
5, 101-105	240.53	2.6
6, 49-53	241.51	3.2
7, 5-9	242.57	5.1
12-1, 92-96	243.94	4.4
2, 46-50	244.98	3.0
2, 146-150	245.98	3.5
3, 98-102	247.00	3.4
4, 50-54	248.02	3.6
4, 146-150	248.98	3.7
5, 98-102	250.00	3.5
13-1, 80-84	253.32	5.3
2, 28-32	254.30	2.6
2, 130-134	255.32	3.6
3, 80-84	256.32	2.4
4, 32-36	257.34	4.3
4, 133-137	258.35	3.4
5, 78-80	259.29	3.1
6, 30-34	260.32	6.0
6, 130-134	261.32	7.1
7, 46-50	261.98	3.5
14-1, 28-30	262.29	5.0
1, 129-133	263.31	4.1
2, 75-79	264.27	2.9
3, 21-25	265.23	4.1
3, 120-124	266.22	4.1
4, 78-82	267.30	2.9
5, 28-32	268.30	2.5
5, 127-131	269.29	3.1
6, 73-77	270.25	4.3
7, 26-30	271.28	2.1
15-1, 64-68	272.16	1.3
2, 17-21	273.19	1.0
2, 118-122	274.20	2.2
3, 65-69	275.17	1.5
4, 18-22	276.20	1.7
4, 119-123	277.21	1.5
5, 71-75	278.23	2.3
6, 25-29	279.27	2.6
16-1, 38-42	281.40	1.9
1, 138-140	282.39	1.3
2, 86-90	283.38	1.7
3, 36-40	284.38	1.9
3, 145-149	285.47	2.4
4, 95-99	286.47	1.0
5, 49-53	287.51	1.4
6, 6-10	288.58	0.9
17-1, 95-99	291.47	0.8
2, 50-54	292.52	0.9
3, 3-7	293.55	4.1
3, 101-105	294.53	0.9
4, 50-54	295.52	2.2
4, 146-150	296.48	3.1
5, 82-86	297.34	2.9
6, 15-19	298.17	1.8
18-1, 100-104	301.02	0.9
2, 45-49	301.97	0.9
2, 146-150	302.98	1.9
3, 98-102	304.00	2.4
19-1, 48-52	310.00	1.8
1, 144-148	310.96	0.9
2, 100-104	312.02	1.4
20-1, 16-20	319.18	2.3
1, 119-123	320.21	4.1
2, 74-78	321.26	4.5
3, 20-24	322.22	2.5
3, 121-125	323.23	1.9

Table 2. (Continued).

Core-Section (interval in cm)	Sub-bottom depth (m)	>63 μm (%)
Hole 573B (Cont.)		
4, 68-72	324.20	1.7
5, 27-31	325.29	1.3
5, 130-134	326.32	1.9
6, 80-84	327.32	1.5
21-1, 18-22	328.70	6.8
1, 120-124	329.72	3.5
2, 75-79	330.77	3.6
3, 28-32	331.80	6.0
3, 136-140	332.88	1.3
4, 88-92	333.90	3.3
5, 30-34	334.82	1.8
22-1, 80-84	338.82	1.8
2, 31-35	339.83	1.5
2, 130-134	340.82	1.3
3, 76-80	341.78	1.7
4, 30-34	342.82	2.8
4, 129-133	343.81	1.0
23-1, 80-84	347.50	0.9
2, 36-40	349.38	1.7
2, 134-138	350.36	1.1
3, 90-94	351.42	1.0
4, 30-34	352.32	1.2
4, 130-134	353.32	1.6
Hole 574		
25-1, 11-14	172.63	2.5
1, 114-117	173.66	2.5
2, 64-69	174.67	2.9
3, 14-19	175.67	3.6
3, 124-128	176.76	3.2
26-1, 31-40	177.86	4.6
1, 130-137	178.84	3.0
2, 73-80	179.76	4.7
3, 32-39	180.86	3.1
3, 130-138	181.84	3.0
27-1, 65-72	182.89	6.1
2, 21-28	183.95	4.5
2, 123-129	184.96	5.5
3, 82-89	186.06	5.2
4, 22-29	186.96	8.8
28-1, 89-97	188.13	5.0
2, 41-47	189.14	8.5
3, 3-9	190.26	7.6
3, 92-99	191.16	7.6
4, 42-50	192.16	4.2
29-1, 100-107	193.24	3.6
2, 50-57	194.24	4.3
3, 2-9	195.26	5.2
3, 93-100	196.17	7.9
4, 33-40	197.07	5.8
30-1, 94-100	198.17	2.7
2, 51-58	199.25	4.8
3, 2-9	200.26	4.2
3, 102-107	201.25	4.6
31-1, 2-9	202.26	2.2
1, 101-109	203.25	2.8
2, 48-56	204.22	5.5
3, 2-8	205.25	3.2
3, 101-109	206.25	2.5
Hole 574C		
1-1, 75-79	195.27	4.1
2, 25-29	196.27	4.0
2, 125-129	197.27	4.2
3, 80-84	198.32	4.5
4, 30-34	199.32	4.2
4, 131-135	200.33	3.8
5, 80-84	201.32	4.0
6, 7-11	202.09	1.0
2-1, 100-104	205.02	5.0
2, 52-56	206.04	4.6

Table 2. (Continued).

Core-Section (interval in cm)	Sub-bottom depth (m)	>63 μm (%)
Hole 574C (Cont.)		
3, 2–6	207.04	3.2
3, 101–105	208.03	2.9
4, 53–57	209.05	2.5
5, 3–7	210.05	2.4
5, 101–105	211.03	4.2
6, 46–50	211.98	7.0
7, 2–6	213.04	3.3
3-1, 67–71	214.19	2.9
2, 15–19	215.17	3.8
2, 116–120	216.18	3.1
3, 68–72	217.20	2.6
4, 16–20	218.18	4.8
4-1, 34–38	223.36	2.9
1, 135–139	224.37	1.8
2, 83–87	225.35	3.0
3, 49–53	226.51	5.4
5-1, 100–104	233.52	2.9
2, 50–54	234.52	1.5
3, 2–6	235.54	2.2
3, 96–100	236.48	2.1
4, 52–56	237.54	0.6
5, 2–6	238.54	3.6
6-1, 80–84	242.82	2.9
2, 30–34	243.82	2.4
2, 131–135	244.83	1.9
3, 82–135	245.84	3.8
4, 30–34	246.82	2.4
4, 129–133	247.81	4.2
5, 30–34	248.32	2.2
7-1, 100–104	252.52	6.6
2, 52–56	253.54	4.4
3, 3–7	254.55	1.9
3, 102–106	255.54	4.2
4, 51–55	256.53	2.0
5, 2–6	257.54	3.9
5, 100–104	258.52	3.7
6, 51–55	259.53	4.3
7, 8–12	260.60	4.6
8-1, 53–57	261.55	1.1
2, 2–6	262.54	2.1
2, 100–104	263.52	2.5
3, 51–55	264.53	3.3
4, 3–7	265.55	7.3
9-1, 68–72	271.20	1.6
2, 26–30	272.28	2.0
2, 125–129	273.27	2.6
3, 72–76	274.24	2.6
10-1, 80–84	280.82	1.6
2, 28–32	281.80	1.4
2, 130–134	282.82	2.3
3, 80–84	283.82	2.4
4, 30–34	284.82	1.6
4, 131–135	285.83	1.9
5, 74–79	286.76	2.2
6, 26–30	287.78	1.7
6, 125–129	288.77	4.7
7, 43–47	289.45	2.3
11-1, 96–100	290.48	5.6
2, 51–55	291.53	0.5
3, 3–7	292.55	1.7
3, 101–105	293.53	0.5
12-1, 52–56	299.54	2.0
2, 2–6	300.54	2.4
2, 105–109	301.57	1.8
3, 55–59	302.57	1.4
3, 146–150	303.48	3.7
4, 94–98	304.46	1.2
5, 50–54	305.52	1.5
6, 3–7	306.55	4.3
6, 101–105	307.53	1.5
7, 30–34	308.32	1.7
13-1, 94–98	309.46	2.4
2, 31–35	310.33	2.5
2, 135–139	311.37	1.2
3, 90–94	312.42	1.4

Table 2. (Continued).

Core-Section (interval in cm)	Sub-bottom depth (m)	>63 μm (%)
Hole 574C (Cont.)		
4, 36–40	313.38	0.3
4, 131–135	314.33	1.2
14-1, 35–39	318.37	1.6
1, 136–140	319.38	1.8
2, 78–82	320.30	2.4
3, 30–34	321.32	1.8
15-1, 100–104	328.52	1.2
2, 37–41	329.39	3.5
2, 138–142	330.40	1.8
3, 80–84	331.32	1.8
4, 26–30	332.28	2.4
4, 129–133	333.31	2.8
5, 81–85	334.33	2.9
6, 29–33	335.31	4.8
6, 136–140	336.38	3.7
16-1, 55–59	337.57	1.1
2, 4–8	338.56	1.7
2, 103–107	339.55	1.6
3, 54–58	340.56	3.3
4, 32–36	341.84	3.1
17-1, 81–85	347.33	1.5
2, 32–36	348.34	1.8
2, 133–137	349.35	2.4
3, 76–80	350.28	1.5
4, 26–30	351.28	2.3
4, 131–135	352.33	2.0
5, 70–74	353.22	1.7
18-1, 25–74	356.27	3.4
1, 120–124	357.22	1.1
2, 74–78	358.26	3.5
19-1, 86–90	366.38	1.4
2, 33–37	367.35	1.5
20-1, 30–34	375.32	2.1
1, 125–129	376.27	1.4
2, 87–91	377.39	1.0
3, 44–48	378.46	1.1
4, 2–6	379.54	2.2
4, 100–104	380.52	1.0
5, 51–55	381.53	1.1
5, 146–150	382.48	0.8
6, 93–97	383.45	0.9
21-1, 30–34	384.82	2.6
1, 134–138	385.86	2.1
2, 80–84	386.82	4.6
3, 30–34	387.82	2.9
3, 131–135	388.83	3.3
4, 79–83	389.81	6.0
Hole 575A		
1-1, 2–9	93.85	4.7
1, 102–109	94.85	8.0
2, 61–68	95.94	5.9
3, 10–17	96.93	10.8
3, 134–141	98.18	6.2
4, 43–50	98.76	5.2
2-2, 31–38	99.05	2.6
2, 130–137	100.04	4.6
3, 81–88	101.05	7.5
4, 32–36	102.04	3.7
3-1, 130–137	102.43	5.4
2, 53–60	103.17	6.9
3, 10–19	104.24	4.2
4-1, 21–29	105.45	5.4
1, 122–128	106.45	3.0
2, 81–88	107.55	4.0
3, 45–52	108.69	3.5
4, 2–9	109.76	4.5
5-1, 142–149	110.46	3.5
2, 94–100	111.47	8.0
3, 52–59	112.56	4.3
4, 2–9	113.56	8.2
6-1, 61–68	114.74	5.8
2, 21–28	115.85	4.9
2, 121–128	116.85	4.4

Table 2. (Continued).

Core-Section (interval in cm)	Sub-bottom depth (m)	>63 μm (%)
Hole 575A (Cont.)		
3, 81–88	117.94	3.9
4, 41–48	119.05	3.8
7-1, 101–108	119.45	2.8
2, 52–59	120.46	3.5
2, 142–149	121.36	3.4
3, 130–138	122.74	3.9
8-1, 53–60	123.67	3.3
1, 102–109	124.15	2.9
8-2, 2–9	124.65	2.6
2, 102–109	125.65	2.5
9-1, 122–129	126.56	2.6
2, 81–88	127.64	3.4
10-1, 93–100	128.26	3.4
2, 49–56	129.33	9.5
3, 2–9	130.35	2.8
3, 104–111	131.38	3.3
11-2, 7–14	132.21	1.8
2, 102–109	133.15	2.4
3, 35–41	133.98	2.0
3, 131–138	134.94	2.0
12-1, 72–80	135.86	
2, 27–35	136.91	
2, 134–141	137.97	3.3
3, 94–101	139.07	3.0
13-1, 101–108	139.85	6.0
2, 50–57	140.84	2.7
3, 6–13	141.89	3.8
14-1, 111–118	143.05	8.6
2, 64–71	144.08	3.6
3, 13–20	145.07	5.0
3, 104–111	145.98	7.9
15-2, 25–31	146.48	5.8
2, 125–131	147.48	6.3
3, 89–97	148.63	6.2
16-2, 8–15	149.62	3.4
2, 104–111	150.58	4.6
3, 54–61	151.58	8.8
17-2, 53–60	152.07	5.9
3, 8–15	153.12	11.3
18-1, 128–135	153.82	5.0
2, 68–75	154.72	6.7
3, 28–35	155.82	6.0
3, 129–136	156.83	11.1
19-1, 89–86	157.72	8.0
2, 49–56	158.83	8.1
3, 2–9	159.85	6.8
20-1, 22–29	161.06	4.5
1, 128–135	162.12	1.4
2, 88–95	163.22	3.1
3, 49–56	164.33	10.9
21-1, 82–89	165.56	2.8
2, 30–37	166.54	6.8
2, 131–138	167.55	2.6
3, 81–88	168.55	5.4
22-1, 102–109	169.15	4.5
2, 44–52	170.08	3.2
2, 133–140	170.97	2.4
3, 92–99	172.06	2.2
23-1, 92–99	173.06	3.1
2, 51–58	174.14	2.5
24-1, 101–109	175.25	3.9
2, 52–59	176.26	2.8
3, 12–19	177.36	5.8
3, 102–109	178.26	5.1
4, 22–29	178.96	6.1
25-2, 143–150	180.17	6.1
3, 103–110	181.27	7.7
26-1, 132–139	181.46	2.7
2, 90–97	182.53	1.9
3, 31–38	183.44	2.7
3, 130–137	184.43	3.2
27-1, 130–137	186.24	2.4
2, 88–97	187.33	2.0
3, 30–37	188.24	4.5
28-1, 143–150	188.67	5.3

Table 2. (Continued).

Core-Section (interval in cm)	Sub-bottom depth (m)	>63 μm (%)
Hole 575A (Cont.)		
2, 100–107	189.74	3.8
3, 14–21	190.38	3.4
29-1, 141–148	191.15	5.1
2, 101–109	192.25	3.6
3, 52–59	193.26	3.6
30-1, 63–70	194.26	5.1
2, 23–30	195.36	3.5
2, 130–137	196.43	3.6
3, 90–97	197.53	4.7
31-1, 128–135	198.72	3.2
2, 65–72	199.59	8.3
3, 13–20	200.57	3.3
3, 101–108	201.45	5.0
32-1, 143–150	202.76	5.0
2, 92–100	203.76	2.2
3, 48–55	204.81	5.9
33-1, 92–99	205.26	3.4
2, 50–57	206.34	3.5
3, 2–9	207.35	1.6
3, 85–92	208.18	8.8
Hole 575B		
2-2, 67–71	14.19	5.4
3, 116–120	16.18	4.8
4, 86–90	17.38	8.2
5, 6–10	18.08	4.2
5, 117–121	19.19	4.6
6, 8–12	19.60	3.9
6, 107–111	20.59	3.2
7, 36–40	21.38	1.8
3-1, 123–127	22.25	1.6
1, 143–147	22.45	5.2
2, 45–49	22.97	5.4
3, 18–22	24.20	4.2
4, 54–58	26.06	7.0
5, 63–67	27.65	9.8
5, 103–107	28.05	3.0
5, 3–7	28.55	8.4
6, 101–105	29.53	3.3
4-1, 123–127	30.75	3.3
2, 76–80	31.78	2.9
3, 24–28	32.76	
3, 128–132	33.80	5.7
4, 80–84	34.82	8.4
5, 90–94	36.42	10.7
6, 120–124	38.22	3.1
7, 20–24	38.72	4.8
5-1, 128–132	40.30	2.8
2, 26–30	40.78	4.4
3, 13–17	42.15	5.2
3, 113–117	43.15	3.1
4, 3–7	43.55	3.2
4, 69–73	44.21	2.8
4, 144–148	44.96	2.3
5-5, 3–7	45.05	2.3
5, 103–107	46.05	1.0
6, 50–54	47.02	1.1
7, 3–7	48.05	1.1
6-1, [illegible]–69	48.67	1.5
2, 24–28	49.76	1.6
2, 123–127	50.75	1.9
3, 69–73	51.71	1.6
4, 25–29	52.77	1.9
4, 124–128	53.76	1.6
5, 85–89	54.87	1.4
6, 32–36	55.84	1.7
-1, 93–97	56.35	1.6
2, 47–51	57–39	1.3
3, 3–7	58.45	2.8
3, 95–99	59.37	1.1
4, 50–54	60.42	2.4
5, 3–7	61.45	2.1
5, 105–109	62.47	2.3
6, 50–54	63.42	2.9

Table 2. (Continued).

Core-Section (interval in cm)	Sub-bottom depth (m)	>63 μm (%)
Hole 575B (Cont.)		
7, 7–11	64.49	1.3
8-1, 62–66	65.34	1.3
1, 130–134	66.02	1.5
2, 88–92	67.10	1.6
3, 29–33	68.01	3.5
3, 126–130	68.98	2.0
4, 80–84	70.02	2.1
5, 30–34	71.02	2.1
5, 130–134	72.02	2.4
6, 90–94	73.12	1.8
9-1, 30–34	74.12	1.9
1, 135–139	75.17	7.9
2, 91–95	76.23	2.5
3, 33–37	77.15	
9-3, 134–138	78.16	
4, 90–94	79.22	2.9
5, 35–38	80.17	1.8
5, 135–139	81.17	2.8
10-1, 10–17	81.54	2.6
1, 107–114	82.51	5.0
2, 44–51	83.38	11.4
3, 2–9	84.46	4.7
3, 105–112	85.49	5.3
4, 47–54	86.41	3.2
5, 2–9	87.46	2.3
5, 104–111	88.48	2.2
6, 44–51	89.38	3.6
7, 4–11	90.48	4.0
11-1, 46–52	91.39	6.9
2, 3–10	92.47	4.2
2, 106–113	93.50	3.6
3, 43–50	94.37	3.9
4, 3–10	95.47	3.6
4, 104–111	96.48	5.4
5, 47–54	97.41	4.0
6, 2–9	98.46	5.4
6, 92–99	99.36	6.2
12-1, 93–100	100.56	5.8
2, 47–54	101.60	8.9
3, 3–10	102.67	6.7
3, 126–133	103.87	10.0
4, 65–72	104.78	14.0
5, 13–20	105.76	10.2
5, 107–114	106.71	4.4
6, 46–53	107.60	12.4
6, 132–139	108.46	13.7
13-1, 43–50	109.67	5.4
2, 3–10	110.77	7.1
2, 106–113	111.80	9.5
3, 62–69	112.86	5.2
4, 10–17	113.84	4.4
14-1, 92–99	115.06	4.7
2, 45–52	116.09	6.0
3, 5–12	117.18	11.3
3, 91–98	118.05	4.3
4, 12–19	118.76	2.6

Table 3. Oxygen and carbon isotope composition (‰, PDB) of *Globoquadrina venezuelana* (350 to 420 μm) in cores of Holes 573B, 574, 574C, 575A, and 575B.

Core-Section (interval in cm)	Sub-bottom depth (m)	$\delta^{18}O$ (‰)	$\delta^{13}C$ (‰)
Hole 573B			
11-1, 6–10	233.58	0.36	1.85
3, 7–11	236.59	0.62	1.49
12-3, 98–102	247.00	0.83	1.78
4, 146–150	248.98	0.81	1.81
5, 98–102	250.00	0.51	1.94

Table 3. (Continued).

Core-Section (interval in cm)	Sub-bottom depth (m)	$\delta^{18}O$ (‰)	$\delta^{13}C$ (‰)
Hole 573B (Cont.)			
13-2, 28–32	254.30	0.26	1.48
5, 78–80	259.29	0.05	1.36
14-3, 120–124	266.22	0.47	1.19
15-2, 118–122	274.20	0.93	0.98
5, 71–75	278.23	0.95	1.10
16-3, 36–40	284.38	0.92	1.14
17-4, 146–150	296.48	0.71	1.42
5, 82–86	297.34	0.65	1.44
20-1, 119–123	320.21	0.26	0.80
2, 74–78	321.26	0.71	0.50
23-2, 36–40	349.38	1.40	0.52
3, 90–94	351.42	0.70	0.63
Hole 574			
25-1, 11–14	172.63	0.96	1.63
64–69	174.67	0.85	1.80
3, 14–19	175.67	0.92	1.41
26-1, 130–137	178.84	0.20	1.37
3, 130–138	181.84	0.59	1.32
27-2, 123–129	184.96	0.78	1.71
4, 22–29	186.96	0.04	1.89
28-1, 89–97	188.13	0.54	1.75
3, 92–99	191.16	0.87	1.79
4, 42–50	192.16	0.79	1.93
29-2, 50–57	194.24	1.22	1.93
4, 33–40	197.07	−0.26	1.87
30-2, 51–58	199.25	0.52	1.64
3, 2–9	200.26	0.53	1.60
31-1, 2–9	202.26	0.51	1.57
3, 2–8	205.25	0.31	1.69
3, 101–109	206.25	0.11	1.19
Hole 574C			
1-2, 125–129	195.27	0.80	1.59
4, 131–135	200.33	0.12	1.61
2-3, 101–105	208.03	0.67	1.56
5, 101–105	211.03	0.42	1.45
3-2, 15–19	215.17	0.43	1.34
4-1, 34–38	223.36	0.47	1.04
3, 49–53	226.51	0.53	1.21
5-2, 50–54	234.52	0.52	0.77
4, 52–56	237.54	0.45	0.99
6-2, 131–135	244.83	0.89	1.48
3, 82–86	245.84	0.81	1.48
4, 129–133	247.81	0.80	1.28
7-3, 3–7	254.55	0.93	0.72
5, 100–104	258.52	0.81	1.49
8-2, 2–6	262.54	0.80	1.24
3, 51–55	264.53	0.82	1.20
4, 3–7	265.55	0.70	1.38
9-2, 26–30	272.28	0.88	1.13
3, 72–76	274.24	0.98	1.13
10-3, 80–84	283.82	0.27	1.01
5, 74–79	286.76	0.51	1.40
7, 43–47	289.45	0.88	1.25
11-1, 96–100	290.48	1.34	1.19
3, 3–7	292.55	0.39	1.23
12-2, 105–109	301.57	0.56	0.82
3, 146–150	303.48	0.65	1.04
13-1, 94–98	309.46	0.57	1.62
2, 31–35	310.33	0.82	1.37
3, 90–94	312.42	1.43	1.26
14-1, 35–39	318.37	0.50	1.76
2, 78–82	320.30	0.95	1.38
15-2, 37–41	329.39	0.96	1.63
2, 138–142	330.40	0.61	1.20
5, 81–85	334.33	1.01	1.50
16-1, 55–59	337.57	0.73	0.54
18-1, 25–29	356.27	1.19	0.12
20-1, 30–34	375.32	0.84	0.15
4, 2–6	379.54	0.89	0.61
21-2, 80–84	386.82	1.04	0.19
3, 30–34	387.82	1.30	0.44

Table 3. (Continued).

Core-Section (interval in cm)	Sub-bottom depth (m)	$\delta^{18}O$ (‰)	$\delta^{13}C$ (‰)
Hole 575A			
1-1, 2-9	93.85	0.15	2.24
1, 102-109	94.85	0.25	1.75
3, 10-17	96.93	−0.09	1.64
2-4, 32-36	102.04	0.46	1.57
3-2, 53-60	103.17	0.32	1.33
3, 10-19	104.24	0.56	1.59
4-1, 21-29	105.45	0.24	1.35
3, 45-52	108.69	0.52	1.68
5-2, 94-100	111.47	0.69	1.25
4, 2-9	113.56	0.50	1.56
6-1, 61-68	114.74	0.72	1.13
2, 21-28	115.85	0.81	0.93
2, 121-128	116.85	0.40	1.14
7-1, 101-108	119.45	0.84	1.03
2, 142-149	121.36	0.57	0.95
8-1, 53-60	123.67	0.38	1.00
2, 2-9	124.65	0.83	1.08
9-1, 122-129	126.56	0.94	1.31
2, 81-88	127.64	0.78	1.15
10-1, 93-100	128.26	0.72	1.48
3, 2-9	130.35	0.73	1.10
11-2, 102-109	133.15	0.91	1.71
3, 131-138	134.94	0.69	1.35
12-2, 134-141	137.97	0.89	1.32
3, 94-101	139.07	1.01	1.40
13-1, 101-108	139.85	0.88	1.10
3, 6-13	141.89	0.86	1.38
14-1, 111-118	143.05	1.22	1.19
3, 13-20	145.07	1.18	1.28
15-2, 25-31	146.58	0.95	1.24
2, 125-131	147.48	1.06	1.40
16-2, 8-15	149.62	0.85	1.28
3, 54-61	151.58	0.96	1.27
17-2, 53-60	152.07	1.16	1.47
3, 8-15	153.12	0.78	1.24
18-2, 68-75	154.72	1.09	1.36
3, 129-136	156.83	0.93	1.26
19-1, 89-96	157.72	0.74	1.01
3, 2-9	159.85	0.75	1.47
20-1, 22-29	161.06	1.35	1.05
3, 49-56	164.33	1.38	1.05
21-2, 30-37	166.54	1.30	0.90
3, 81-88	168.55	1.21	1.38
22-1, 102-109	169.15	1.08	1.23
2, 133-140	170.97	1.08	1.06
23-1, 92-99	173.06	0.59	1.01
2, 51-58	174.14	0.92	1.10
24-1, 101-109	175.25	0.94	1.42
3, 12-19	177.36	0.70	1.59
25-2, 143-150	180.17	0.71	1.20
3, 103-110	181.27	0.90	1.30
26-1, 132-139	181.46	0.63	1.49
3, 130-137	184.43	1.14	1.74
27-2, 88-97	187.33	1.19	1.43
3, 30-37	188.24	0.52	1.59
28-1, 143-150	188.67	0.64	1.61
3, 14-21	190.38	0.22	1.49
29-1, 141-148	191.15	0.69	1.09
3, 52-59	193.26	0.80	1.67
31-2, 65-72	199.59	0.56	1.48
3, 101-108	201.45	0.78	1.24
32-1, 143-150	202.76	0.83	1.26
3, 48-55	204.81	0.91	0.99
33-2, 50-57	206.34	1.10	0.81
Hole 575B			
2-5, 117-121	19.19	0.69	0.58
6, 107-111	20.59	0.80	0.50
3-2, 45-49	22.97	0.31	0.83
5, 63-67	27.65	0.67	1.07
4-1, 123-127	30.75	0.72	1.13
3, 128-132	33.80	0.58	1.32
5-3, 113-117	43.15	1.30	1.42
4, 144-148	44.96	1.64	1.52
6, 50-54	47.02	1.08	1.44

Table 3. (Continued).

Core-Section (interval in cm)	Sub-bottom depth (m)	$\delta^{18}O$ (‰)	$\delta^{13}C$ (‰)
Hole 575B (Cont.)			
7, 3-7	48.05	1.01	1.18
6-2, 24-28	49.76	1.35	1.60
2, 123-127	50.75	0.87	1.10
3, 69-73	51.71	1.31	1.13
4, 25-29	52.77	0.81	1.27
4, 124-128	53.76	1.25	1.01
5, 85-89	54.87	0.99	1.15
6, 32-36	55.84	0.97	1.37
7-1, 93-97	56.35	1.29	1.37
2, 47-51	57.39	1.42	1.32
3, 3-7	58.45	1.61	1.33
3, 95-99	59.37	0.79	1.28
4, 50-54	60.42	1.20	1.67
5, 3-7	61.45	1.70	1.63
5, 105-109	62.47	1.44	1.42
6, 50-54	63.42	1.37	1.83
8-1, 62-66	65.34	0.98	1.16
1, 130-134	66.02	0.43	1.41
2, 88-92	67.10	1.15	1.34
3, 29-33	68.01	0.91	1.00
3, 126-130	68.98	0.81	1.05
4, 80-84	70.02	1.03	1.10
5, 30-34	71.02	1.22	1.46
5, 130-134	72.02	1.01	1.32
6, 90-94	73.12	0.49	1.17
9-1, 30-34	74.12	1.60	1.67
1, 135-139	75.17	1.20	1.56
3, 33-37	77.15	0.92	1.34
4, 90-94	79.22	1.21	1.48
5, 135-139	81.17	0.80	1.62
10-2, 44-51	83.38	0.90	2.38
5, 2-9	87.46	0.41	1.70
11-3, 43-50	94.37	0.90	1.87
6, 2-9	98.46	0.83	1.81
12-2, 47-54	101.60	0.73	2.32
5, 13-20	105.76	0.73	1.86
13-1, 43-50	109.67	0.86	2.13
2, 106-113	111.80	1.11	1.73
14-2, 45-52	116.09	0.05	1.82
3, 91-98	118.05	−0.09	1.82

from less variable below to high-frequency, high-amplitude variability above, and the benthic foraminifers show a marked increase in $\delta^{18}O$ of about 0.7‰. This increase can be correlated with an abrupt increase in the benthic foraminifer oxygen isotope record of the same amplitude at 155 m at Site 574 (Pisias et al., this volume, and Fig. 5).

Above this sharp ^{18}O enrichment the $\delta^{18}O$ values of *O. umbonatus* continue to increase to values close to 3‰ at a level slightly above level H in the middle Miocene. They retain this high value through the remainder of the section, whereas the ^{18}O values of *G. venezuelana* decrease sharply. The oxygen isotope gradient between *O. umbonatus* and *G. venezuelana* ($\Delta\delta^{18}O_{B-P}$; Table 4) increases progressively from about 1‰ in the F–G interval to about 2‰ in the G–H interval and 2.5‰ at the top of the middle Miocene.

Carbon Isotope Stratigraphy

In the uppermost Oligocene and lowermost Miocene (below level A), the carbon isotope record of *Globoquadrina venezuelana* at Site 574 shows depleted $\delta^{13}C$ values (values less than 1‰). At level A, there is a sharp increase of about 1‰. An interval of enrichment, with mean $\delta^{13}C$ values near 1.5‰, occurs between levels A

Levels	Biostratigraphic and magnetostratigraphic position	Approximate age (Ma)	Chemical signals (decrease ↔ increase)			Position in cores					
						Site 573		Site 574		Site 575	
			$\delta^{18}O$	$\delta^{13}C$	$CaCO_3$	Hole-Core	Depth (m)	Hole-Core	Depth (m)	Hole-Core	Depth (m)
H	Within *Coscinodiscus gigas* var. *diorama* Zone Within upper *Dorcadospyris alata* Zone Within Zone CN5a Within Zone N12	12.5	PF						~112 m (Pisias and Shackleton, this volume)	575B-5	43
G	Within Subzone B of *Cestodiscus peplum* Zone Within lower *Dorcadospyris alata* Zone Within Zone CN4 Approximates the N9/N10 boundary	14.6	BF						155 (Pisias and Shackleton, this volume)	upper 575B-9	75
F	Approximates the *Denticulopsis nicobarica/Cestodiscus peplum* boundary Within the middle of the *Calocycletta costata* Zone Within Zone CN3 Within undifferentiated N6—N8 interval Within magnetic Anomaly 5C	16.5	PF minimum			573B-13	257	574-29/30	197	575A-1 and 575B-14	115
E	Within Subzone A of *Denticulopsis nicobarica* Zone Approximates the *Stichocorys wolffii/Calocycletta costata* boundary Approximates the CN2/CN3 zonal boundary Within undifferentiated N6—N8 interval Within lower reversed interval of magnetic Anomaly 5C	17.5		BF + PF		573B-14	267	574C-3/4	220	575A-6	134 (115 + 19)
D	Approximates the *Craspedodiscus elegans/Triceratium pileus* boundary Within uppermost *Stichocorys delmontensis* Zone Within uppermost Zone CN1c Within Zone N5	18.7						574C-6	244	lower 575A-11	154 (135 + 19)
C	Within lowermost *Craspedodiscus elegans* Zone Within *Stichocorys delmontensis* Zone Within Zone CN1c Within Zone N5	19.5	PF			573B-16 (?)	288	574C-7	257	lower 575A-16	170 (151 + 19)
B	Slightly below the B/C boundary in *Rossiella paleacea* Zone Within lower *Stichocorys delmontensis* Zone Within CN1b Within upper Zone N4	20.7		PF		573B	291	lower 574C-10	287	575-25	199 (180 + 19)
A	Approximates the *Rocella gelida/Rossiella paleacea* boundary Within *Lychnocanoma elongata* Zone Within lower Zone CN1b Within Zone N4	22.7		PF		upper 573B-20	320	574-15/16	335		

Figure 5. Biostratigraphic and magnetostratigraphic position of levels marking changes in the signature of the isotope and carbonate records at DSDP Sites 573, 574, and 575. Ages are derived from the Barron et al. (in press) time scale based on the paleomagnetic time scale of Berggren et al. (in press). BF = benthic foraminifers; PF = planktonic foraminifers.

Table 4. Oxygen and carbon isotope composition (‰, PDB) of the benthic species *Oridorsalis umbonatus* (>250 μm) in cores of Holes 575A and 575B and the difference between $\delta^{18}O$ values of *O. umbonatus* and *G. venezuelana* ($\Delta\delta^{18}O_{B-P}$).

Core-Section (interval in cm)	Sub-bottom depth (m)	$\delta^{18}O$	$\delta^{13}C$	$\Delta\delta^{18}O_{B-P}$
Hole 575B				
2-5, 6-10	18.08	3.13	−2.43	
3-6, 101-105	29.53	2.84	−2.34	
4-3, 128-132	33.80	3.22	−1.35	2.64
6-6, 32-36	55.84	2.98	−0.83	2.01
9-1, 135-139	75.17	2.64	0.05	1.44
10-3, 105-112	85.49	2.10	1.03	
11-3, 43-50	94.37	2.04	0.28	1.14
12-3, 126-133	103.89	2.03	0.31	
Hole 575A				
4-3, 45-52	108.69	2.10	−0.12	1.58
5-[illegible] 2-9	113.56	2.24	−0.61	1.74
6-[illegible], 81-88	117.94	1.68	−0.42	
8-1, 53-60	123.67	2.26	−0.76	1.88
8-1, 102-109	124.15	2.17	−0.12	
12-1, 72-80	135.86	2.13	−0.18	
18-3, 129-136	156.83	2.50	−0.38	1.57
25-3, 103-110	181.27	2.25	−1.13	1.35
31-2, 65-72	199.59	2.56	−0.24	2.00

and B in the lower lower Miocene. These two levels are tentatively identified at Site 573, and level B is placed at Site 575 in the lower part of the sequence. In the next interval, between levels B and E, $\delta^{13}C$ values have slightly decreased averages of about 1.2 to 1.3‰.

Above level E in the upper lower Miocene, there is a marked enrichment in ^{13}C of approximately 1‰ which takes place progressively between levels E and F. This enrichment is directly tied to the reversed interval in lower magnetic Anomaly 5C (lower magnetic Chron 16), which is apparent in cores from Hole 575A and which we have referred to as the Chron 16 Carbon Shift (Vincent et al., 1983). Values of $\delta^{13}C$ remain high (from 1.7‰ to 2.4‰) throughout a large part of the interval between levels F and G, which spans the lower/middle Miocene boundary, then decrease just below level G toward values similar to the preceding lower Miocene values, that is, values averaging 1.2 to 1.3‰. This average characterizes the remainder of the middle Miocene; the values then show a pronounced decrease in the upper Miocene.

Carbonate Stratigraphy

Throughout the uppermost Oligocene and most of the lower Miocene, up to level D, the calcium carbonate records at all three sites display a relatively constant $CaCO_3$ content, with a mean of about 90% and small-amplitude fluctuations. There are no pronounced changes in this interval. However, in the expanded record of Site 574 a slight variation is apparent. The interval of enriched ^{13}C between levels A and B corresponds to an interval of slightly increased carbonate content (Figs. 3 and 5). In this interval the mean $CaCO_3$ content is about 92%, whereas below level A it is about 88%, and above level B up to level D, it is about 90%. The A–B interval of slightly increased $CaCO_3$ percentages is tentatively identified in the condensed record of Site 573 and its upper part at Site 575 (Figs. 2 and 4).

Above level D in the upper lower Miocene, the $CaCO_3$ content decreases markedly, reaching a pronounced minimum of 32 to 65 percent at 114 m, 212 m, and 261 m at Sites 575, 574, and 573, respectively. This pronounced minimum, which occurs between levels E and F in the uppermost lower Miocene, correlates with the Chron 16 Carbon Shift. Above the Chron 16 carbonate minimum, the calcium carbonate content increases again to values of about 90% throughout the remainder of the middle Miocene. However, the fluctuations in this interval are of higher amplitude than in the Oligocene to lower Miocene interval (see site chapters, this volume, for middle Miocene $CaCO_3$ records at Sites 573 and 574).

The uppermost lower Miocene interval of decreased carbonate content is correlated with an interval of reduced preservation of foraminifers (see Figs. 2 to 4). However, the wide sampling interval used for the foraminiferal preservation stratigraphy does not allow a detailed correlation with carbonate stratigraphy.

Near the middle/upper Miocene boundary the carbonate curves at all three sites show a marked change (Fig. 4 and site chapters, this volume). Above this level (throughout the upper Miocene to the Quaternary), there are high-amplitude cyclic fluctuations between high-carbonate and low-carbonate sediments that are paralleled by fluctuations in the abundance of siliceous sediments. This pronounced change in sedimentary regime is widespread in the central equatorial Pacific, where it is seismically traceable (Mayer et al., this volume).

Grain Size Stratigraphy

A detailed analysis of our grain size data is beyond the scope of this chapter. Further, data obtained from paired samples, which are preferable for a statistical analysis of the relationship between sand-sized content and calcium-carbonate content, are unavailable for this study. However, long-term cycles are apparent from a visual examination of the sand-sized content curves in Figures 2 to 4. The cycles are defined by the alternation of (1) intervals of high-amplitude fluctuations with pronounced maxima and higher average values and (2) intervals of low-amplitude fluctuations with smaller average values. An interval of type 1, present at all three sites, occurs just below the boundary between lower Miocene and middle Miocene, immediately above the Chron 16 Carbon Shift and the pronounced decrease in $CaCO_3$ content. Another interval of type 1 at the top of the Site 575 sequence is clearly associated with the high-amplitude carbonate fluctuations.

DISCUSSION

Reading the Record

The stratigraphic signals available refer to the physical state of the ocean and the hydrologic cycle in general, and to the ocean's carbon chemistry, which is affected by life processes and geochemical cycles. Physical conditions are reflected mainly in the $\delta^{18}O$ record, and chemical conditions predominantly in $\delta^{13}C$, carbonate

content, and foraminiferal preservation. Of the various signals, the reasons for the fluctuations in $CaCO_3$ preservation are the simplest to interpret (they are due mainly to saturation of the bottom water), and the reasons for the fluctuations in $\delta^{13}C$ are the most complex. The reasons for grain size fluctuations are also complex. All signals are strongly interdependent, because there is an intimate connection between the physical, chemical, and biological aspects of the system. These matters have been discussed elsewhere (e.g., van Andel et al., 1975; Bender and Keigwin, 1979; Vincent et al., 1980; Berger, 1981; Berger and Vincent, 1981; Vincent and Berger, 1981, in press).

We used the following guidelines in reading the record, which are gleaned, in the main, from the references cited (we do not suggest that our methods are preferable to more detailed analysis):

1. *$\delta^{18}O$* reflects changes in water temperature at the time of growth of the shells, as well as changes in the $^{18}O/^{16}O$ ratio of the surrounding water (which is affected by regional and/or global salinity and the presence or absence of ice caps). The formula of Epstein et al. (1953) applies. The temperature effect is roughly 0.2‰ change in $\delta^{18}O$ per 1°C change in water temperature. To change $\delta^{18}O$ through ice buildup, a change in sea level of between 10 and 20 m (depending on the composition of the ice; see Emiliani, 1955) is necessary to cause a change in $\delta^{18}O$ of about 0.1‰.

2. *$\delta^{13}C$* is regionally influenced by carbon fixation (which increases $\delta^{13}C$) and respiration (which decreases it). The $\delta^{13}C$ value reflects net productivity at the surface and oxygen utilization at depth. Regional patterns are governed by mixing processes in the ocean as well as by chemical processes. Global changes are effected by changes in the overall carbon cycle, notably changes in the ratio of inorganic to organic carbon in source- and sink-terms.

3. *Sand content* is a function of (a) productivity and the relative proportion of large, robust deep-dwelling microfossils, (b) winnowing (which increases sand content) and dilution by fines (which decreases it), and (c) carbonate dissolution (decreases sand content).

4. *Carbonate content* is affected by the rates of supply, dilution, and dissolution of $CaCO_3$. Of these, dissolution is probably the most important in any given interval.

5. *Foraminiferal preservation* is affected by the saturation of bottom waters in carbonate and the supply of organic matter to the seafloor.

The interdependence of these signals is obvious. Hence, we shall adopt the hypothesis that events (peaks or shifts) in different signals that are closely associated in time have a common cause or are part of a causal chain. Because a change in each individual signal can be produced by a number of factors, we need a number of signals to be able to narrow the choices down to the most likely cause. Clearly, the considerable effort that is necessary to establish such multiple-signal stratigraphies can best be justified for continuous records of high resolution, in regions that record events of global significance.

In this respect we are satisfied that the expanded record at Sites 573 to 575 has excellent potential for the paleoceanographic reconstruction of the early to middle Miocene.

A more detailed "multichannel" isotope stratigraphy than could be prepared for this study will be necessary to resolve many paleoceanographic questions. We especially need to complement the isotope record obtained in this study, which was from a deep-living planktonic foraminifer (subsurface water), with a record for the ocean properties at the surface (shallow-dwelling planktonic foraminifers) and at the seafloor (benthic foraminifers).

Correlation between Biostratigraphy and Chemostratigraphy

The levels of change in the isotope and carbonate records summarized in Figure 5 correlate well from site to site through biostratigraphy (Figs. 2 to 4). The age of these levels can thus be estimated with reasonable confidence despite minor discrepancies between the various microfossil zonations at the three sites (Barron et al., this volume).

The sedimentary sequences from Sites 574 and 575 together provide a complete lower Miocene record. The record at Site 573 is incomplete and condensed, and several hiatuses were recognized (see Barron et al. and Theyer et al., both this volume). Because of sediment condensation and the wide sampling interval, the exact position of levels A to H could not be determined at the latter site. Several of these levels are identifiable, however, with even a low-resolution chemostratigraphy when placed in a biostratigraphic framework (Fig. 2).

Other isotope records that are available for comparison with this study are shown in Figure 6 (in back pocket).

Miocene benthic foraminifer isotope records from the equatorial Pacific have been published by Savin et al. (1981) and Woodruff et al. (1981) for DSDP Sites 71, 77, and 289. The first two of these sites are in the same area as the Leg 85 sites (see Fig. 1). The lower and middle Miocene sedimentary sequence at Site 71, to the west of Sites 574 and 575, accumulated at an average rate of approximately 32 m/m.y., which is similar to accumulation rates at the latter two sites (Barron et al., in press). The benthic foraminifer isotope record from Site 71, however, was not obtained from monospecific samples, and it does not encompass more than the lowermost middle Miocene. The section from Site 77, like that from nearby Site 573, is condensed and contains several hiatuses. Site 289, which is on the Ontong Java Plateau in the western equatorial Pacific (latitude: 0°29′S; longitude: 158°30′E; water depth: 2224 m), provides an expanded continuous record of the upper lower Miocene and the entire middle Miocene; the section accumulated at an average rate of approximately 33 m/m.y., varying from 20 m/m.y. to 50 m/m.y. (Andrews et al., 1975; Barron et al., in press). The detailed benthic foraminifer isotope stratigraphy obtained at this site by Savin et al. (1981) and Woodruff et al. (1981) is reproduced in Figure 6.

Vincent et al. (in press) used benthic foraminifers as well as shallow-dwelling and deep-living planktonic foraminifers to establish multiple isotope stratigraphies throughout the Miocene for four DSDP sites in the tropical Indian Ocean. The trends in the isotope stratigraphies for the four sites are similar. Of these four sites we selected Site 216 (on the Ninetyeast Ridge, latitude: 1°27′N; longitude: 90°12′E; water depth: 2247 m) for comparison with the Pacific records (Fig. 6), because the sedimentary sequence at this site, despite its condensation (an average accumulation rate of 5 m/m.y.), provides the most complete and undisturbed record for the early and middle Miocene (Vincent et al., in press). It is also the only site that yielded siliceous biostratigraphic control throughout the interval.

We have made no attempt here to present data plotted against time, because as of this writing discrepancies between the time scales used by various authors have not been resolved. The middle Miocene time scale has been revised since the start of this study (see the differences between the time scales used in the site chapters and in Barron et al., this volume), and we felt it inappropriate to attempt to work out detailed correlations between various records at this time.

Berggren et al. (in press) have recently proposed the correlation of Anomaly 5 with Chron 11 (as originally proposed by Foster and Opdyke, 1970), instead of correlating Anomaly 5 with Chron 9, the correlation many authors have utilized in constructing time scales during the last 10 yr. Berggren's proposed revision results in age estimates approximately 1.5 to 2 m.y. younger for biostratigraphic datum levels in the interval between approximately 6.5 and 13.8 Ma. It also implies considerable changes in previously published sedimentation rate profiles.

Despite the varying sampling density and varying biostratigraphic resolution of the various records shown in Figures 2 to 4 and Figure 6, a number of the chemostratigraphic markers A to H can be identified in all records. These thus provide signals of the utmost importance for chronostratigraphic correlation. Careful stacking of chemostratigraphic signals from different records will greatly enhance the precision of correlation between different ocean basins and will provide a precious tool for global paleoceanographic reconstruction. Once a chemostratigraphic signal is shown to be global, it becomes a superior time marker, and one to which biostratigraphy must defer. An example of discrepancies in the biostratigraphic position of a global chemostratigraphic marker, seen in Figure 6, is discussed below.

Level G marks an abrupt step in the benthic foraminifer $\delta^{18}O$ record toward higher values. The step occurs within the mid-Miocene oxygen enrichment. This level corresponds to the N9/N10 foraminiferal zonal boundary identified by Saito (this volume) at both Sites 575 and 574 (see Figs. 5 and 6). From an examination of Figure 6, however, it appears that level G has a higher stratigraphic position with respect to the foraminiferal zonation at Site 289 and a lower one at Site 216. At Site 289 level G, at approximately 450 m, falls in Core 48, in the upper part of Zone N10 identified by Srinivasan and Kennett (1981a, b), whereas at Site 216 it lies in the uppermost part of an undifferentiated N8–N9 interval as given by Berggren et al. (1974) (Fig. 6).

The precise placement of foraminiferal zonal boundaries is often made difficult by taxonomic ambiguities and/or the rarity of zonal nominate taxa. Zonal boundaries defined by the FAD (first appearance datum) of a species are placed by many biostratigraphers at the level of first appearance of a morphotype of this species, which is older than the level of "evolutionary appearance" of that species. The latter has been defined as "the level at which more than half of the individuals in the population have the character(s) that distinguishes the species from its ancestor or descendant" (Riedel and Sanfilippo, 1971, p. 1530). Different interpretations of foraminiferal data by various workers in identifying levels of first appearance may be responsible for discrepancies in zonal assignments.

The N9/N10 boundary is defined by the FAD of *Globorotalia peripheroacuta* (Blow, 1969; Srinivasan and Kennett, 1981a, b). Saito (this volume) places the N9/N10 boundary at the first morphotypic appearance of *G. peripheroacuta* at approximately 155 m at Site 574 (between Sections 2 and 3 of Core 574-21) and approximately 74 m at Site 575 (between Sections 1 and 2 of Core 575-9), that is, at a level that nearly coincides with the depth of level G at both sites. Srinivasan and Kennett (1981a, b) may have given the N9/N10 boundary at Site 289 a lower stratigraphic position with respect to level G because their interpretation of the FAD of *G. peripheroacuta* was different from Saito's. Srinivasan and Kennett report "the first evolutionary appearance" of this species at Site 289 in Core 49 (Srinivasan and Kennett, 1981a, p. 425), and their generalized range chart (Srinivasan and Kennett, 1981b, p. 502) shows the bottom of continuous occurrence of *G. peripheroacuta* in Core 49. However, no detailed chart of species occurrences has been published by these authors.

Although the N9/N10 boundary at Site 216, as drawn on Figure 6, has a stratigraphic position relative to level G higher than at Sites 574 and 575, foraminiferal data from this site support the correlation of level G with the N9/N10 boundary. This boundary is placed on Figure 6 in the middle of Core 216A-5, as originally drawn by Berggren et al. (1974) and followed by Vincent (1977), at the base of the common occurrence of *G. peripheroacuta*. Rare specimens referable to this species, however, are reported on Berggren et al.'s (1974) range charts below that stratigraphic horizon, ranging down to lower Core 5A near level G.

At all sites examined here, level G falls within the calcareous nannofossil Zone CN4 and the *Dorcadospyris alata* radiolarian Zone. At both Sites 574 and 575, level G is slightly below the *Cestodiscus peplum/C. lewisianus* diatom zonal boundary (Barron, this volume). This boundary is marked by the LAD of *C. peplum*, which has been paleomagnetically dated within magnetic Chron 15 (Burckle, 1978) and occurs at approximately 14.1 Ma according to the Barron et al. (in press) time scale used in this study. There is no biostratigraphic control from diatom data at either Site 289 or 216. The siliceous rec-

ord at Site 289 is very poor and barren of diagnostic diatoms (Barron, pers. comm., 1983), and diatom data from Site 216 are not yet available.

The importance of obtaining biostratigraphic and chemostratigraphic data from paired samples for the precise timing of chemostratigraphic signals should be emphasized. Hole-to-hole correlations at a single site that are based solely on sub-bottom depth often require offsets because of the uncertainty of the mudline position. Such offsets had to be made between several Leg 85 holes (see, for example, the 19-m offset between Holes 575A and 575B, as explained in the Fig. 4 caption). The isotope stratigraphies presented in this study (Figs. 2 to 4) are plotted against a composite biostratigraphic column (one established from the various holes at each site; Barron et al., this volume); the holes used in establishing the composite are not always the same as those used in our own analyses. Discrepancies in the correlation of the stratigraphies at the various sites should be resolved when higher resolution biostratigraphic and chemostratigraphic studies can be conducted from paired samples.

PALEOCEANOGRAPHIC IMPLICATIONS OF EARLY MIOCENE EVENTS

The data presented in Figures 2 to 4 and 6 clearly show the succession of events preceding the middle Miocene ^{18}O enrichment and allow the timing of these events to be established.

During the warming trend that characterized the second half of the early Miocene (between approximately 19.5 and 16.5 Ma, or between levels C and F), the following succession of events took place. Fluctuations in $\delta^{18}O$ values are subdued, and the $\delta^{13}C$ record is uneventful. At the same time, sand content decreases (C to D); then $CaCO_3$ preservation and carbonate content decrease (D to E). We suggest that warming (as revealed by the $\delta^{18}O$ signal) is associated with declining bottom current activity (as evidenced by winnowing, which is reflected in the sand content), and that a sea level rise associated with warming (D to E) tends to remove carbonate to the shelves, increasing dissolution on the deep-sea floor (shelf–basin fractionation, which is indicated by $CaCO_3$ content and foraminiferal preservation).

After these events, there is a sharp increase in carbonate dissolution near level E that coincides with the onset of the Chron 16 Carbon Shift, where $\delta^{13}C$ values become higher. The presence of a shift in both the planktonic and benthic foraminifer records suggests that a change in the composition of the ocean is involved, that is, a change in the entire geochemical cycle. We propose that the production of organic carbon increases at this point, at the expense of carbonate. The underlying mechanism might be increased upwelling due to thermocline development (which is evidenced by the first appearance of *Sphaeroidinellopsis* and other planktonic forms with heavy cortices in the tropics at this time). The increased deposition of organic carbon on widely flooded shelves with the shelf edge intersecting the oxygen minimum might also be appealed to. Both thermocline development and equatorial upwelling may be reflected in the increasing sand content, which may result from an increase in heavy, deep-dwelling species. Increased bottom current activity also may contribute to this trend.

The Chron 16 Carbon Shift marks the levels E and F. It lasts about 1 m.y., beginning approximately at 17.5 Ma. After the carbon shift ends, the middle Miocene cooling begins, a sequence that suggests the above-mentioned geochemical preconditioning of the ocean–atmosphere system for entry into a modern, glacier-dominated world.

The pattern of cooling is not easily decipherable from the $\delta^{18}O$ records. A cooling step is clearly indicated immediately after the 16.5 Ma level (just above level F) in both the benthic foraminifer records (see Sites 216 and 289 in Fig. 6) and the planktonic foraminifer records (see Sites 216 and 575 in Fig. 6), but it is short, and warming recurs between 16.5 and 14.6 Ma (between levels F and G). Within the F–G interval, there is a pronounced excursion toward lower $\delta^{18}O$ values in the *Globoquadrina venezuelana* isotope record from the tropical Indian Ocean (DSDP Sites 216 and 238; Fig. 6). During the period immediately following F (end of carbon shift, first cooling pulse), the system seems to have been unstable, as recorded in large fluctuations in sand content and carbonate content. A relaxation toward pre-E conditions is then indicated in all signals except $\delta^{13}C$, which remains unusually positive.

At 14.6 Ma (level G), a sharp step in ^{18}O enrichment in benthic foraminifers coincides with the change in regime in the *G. venezuelana* $\delta^{18}O$ record at Site 575. The increase in instability shown by the planktonic foraminifer record (high-amplitude, high-frequency fluctuations) above this level may be an effect of ice buildup at this time. However, this change in regime is not apparent in the *G. venezuelana* record from the Indian Ocean.

An increase in $\delta^{18}O$ of 1‰ or more is clear in all benthic foraminifer records between 14.6 and 12.5 Ma (from levels G to H). There is also an overall increase in $\delta^{18}O$ values in the planktonic foraminifer isotope records in this interval, but it is of much smaller amplitude. Whereas above level H the $\delta^{18}O$ benthic foraminifer values remain high, the $\delta^{18}O$ planktonic foraminifer values decrease. Thus, if ice buildup caused the ^{18}O enrichment it must have been counteracted by the warming of tropical surface waters. In the absence of such counteraction no more than about one-third of the 1‰ $\delta^{18}O$ increase can be attributed to an ice buildup. Therefore, the evidence for a large ice buildup (one causing more than 20 m of sea level change) is not convincing at this time.

The $\delta^{18}O$ records through the middle and late Miocene are characterized by the increasing separation of benthic and planktonic foraminifer $\delta^{18}O$ values. The separation reflects an increase in the planetary temperature gradient during that time interval, and the increased temperature gradient resulted in a more stably stratified ocean, presumably one with a stronger thermocline and hence increased equatorial and coastal upwelling. We have discussed these trends before (Berger et al., 1981; Vincent and Berger, 1981; Vincent et al., in press).

After the Chron 16 Carbon Shift the $\delta^{13}C$ values of both the benthic and planktonic foraminifers remain high during most of the interval between levels F and G and

then relax progressively to early Miocene values. This broad lower to middle Miocene carbon maximum, which we call the "Monterey Carbon Excursion" (Vincent and Berger, in press), appears to be correlated with the deposition of organic-carbon-rich sediments around the margin of the North Pacific in the Monterey Formation of California and its equivalents. We have elaborated elsewhere on the significance of this correlation (Vincent and Berger, in press). The organic-carbon-rich Monterey rocks and equivalents are the result of coastal upwelling, which arose because of the development of a permanent strong thermocline. The sediments in the upwelling areas were deposited, in part, under anaerobic conditions, which led to the excess extraction of organic carbon from the ocean. A decrease in the rate of carbon extraction (due to the exhaustion of nutrient phosphorus) would have allowed relaxation toward initial values. Alternatively, or concurrently, a drop in sea level due to ice buildup would have led to the increased erosion of shallow areas, with the preferential erosion of organic matter. This process could have helped shift the $\delta^{13}C$ signal back toward negative values. From a simple geochemical balance model, Vincent and Berger (in press) estimated the amount of excess organic carbon extracted during the course of the Monterey event to be between 40 and 80 atmospheric carbon masses. This amount corresponds to that present in the ocean, that is, one ocean carbon mass.

It is remarkable that a major carbonate dissolution event is associated with the heavy carbon excursion. The same situation occurs at two other equatorial Pacific DSDP sites (71 and 289), where a pronounced carbonate minimum ("16 g" of Dunn, 1982) occurs in the same relative position with respect to the carbon shift shown by Savin et al. (1981) and Woodruff et al. (1981). It corresponds to a prominent traceable acoustic horizon throughout the equatorial Pacific, the "Lavender" reflector of Mayer et al. (this volume). The maximum dissolution is coeval with the Chron 16 Carbon Shift (see the pronounced carbonate minima between levels E and F in Figs. 2 to 4; at Site 289 the pronounced carbonate minimum identified by Dunn, pers. comm., 1983, occurs between levels E and F, as marked in Fig. 6). The dissolution increase, however, appears to precede the ^{13}C enrichment, as evidenced by the inflection point on the carbon curves at level D. The diatom biostratigraphy for Site 573 suggests that there is a hiatus at this time (Barron, this volume). This short hiatus, which corresponds to NH1b of Barron and Keller (1982), has been observed in a number of deep-sea sequences in other parts of the Pacific.

A decrease in carbonate deposition tied to an increase in ^{13}C is opposite to what one would expect from Broecker's (1982) model, in which increased $\delta^{13}C$ is tied with increased $CaCO_3$ deposition. We used an argument similar to Broecker's when we discussed the association of the late Miocene Chron 6 Carbon Shift toward light $\delta^{13}C$ values with a carbonate dissolution event (Vincent et al., 1980).

The relationship between $CaCO_3$ content and ^{13}C signals is obviously far from simple. The complexity of the interactions is illustrated in this study by the occurrence of high ^{13}C with either dissolution (as in the Chron 16 Carbon Shift interval E–F) or increased $CaCO_3$ (as in the earlier A–B interval) (Figs. 3 and 5). Different mechanisms must be involved. In principle, it seems safe to say that a change in the state of the system, in whatever direction, should lead to the redistribution of carbonate and other chemically active sediments. Thus, hiatus formation must occur in some places whenever there is change, as long as the change is large enough and the sediment is mostly carbonate. If this is correct, any strong global shift of $\delta^{18}O$ and/or $\delta^{13}C$, in either direction, becomes a candidate for hiatus formation.

CONCLUSIONS

Because causes precede effects, it is important for an understanding of the mechanisms involved in the evolution of ocean conditions to identify with precise timing the sequential order of events. In this respect, the sedimentary sequences studied here are the best acquired to date for high-resolution paleoceanographic reconstruction during the period of preconditioning before the major middle Miocene cooling.

It is premature to attempt to identify causes for all paleoceanographic changes. Our explanations should be considered hypotheses only. The development of additional detailed multichannel stratigraphies (chemostratigraphies combined with biostratigraphy and changes in faunal and floral composition), which permit the separation of the numerous variables involved in changes in environmental conditions, will allow a better understanding of the mechanisms involved in changes in the ocean–atmosphere system.

ACKNOWLEDGMENTS

We are very grateful to Wolf Berger for many stimulating discussions and for reviewing our manuscript. Our work is supported by NSF Grants OCE83-10518 and OCE83-14984.

REFERENCES

Andrews, J. E., Packham, G., et al., 1975. *Init. Repts. DSDP*, 30: Washington (U.S. Govt. Printing Office).

Barron, J. A., and Keller, G., 1982. Widespread Miocene deep-sea hiatuses: coincidence with periods of global cooling. *Geology*, 10: 577–581.

Barron, J. A., Keller, G., and Dunn, D. A., in press. A multiple microfossil biochronology for the Miocene. *In* Kennett, J. P. (Ed.), *The Miocene Ocean: Paleoceanography and Biogeography*. Mem. Geol. Soc. Am. 163.

Bender, M. L., and Keigwin, L. D., Jr., 1979. Speculations about the upper Miocene change in abyssal Pacific dissolved bicarbonate $\delta^{13}C$. *Earth Planet. Sci. Lett.*, 45:383–393.

Berger, W. H., 1981. Paleoceanography: the deep-sea record. *In* Emiliani, C. (Ed.), *The Oceanic Lithosphere: The Sea* (Vol. 7): New York (Wiley-Interscience), 1437–1519.

_____, 1982. Deep-sea stratigraphy: Cenozoic climate steps and the search for chemo-climatic feedback. *In* Einsele, G., and Seilacher, A. (Eds.), *Cyclic and Event Stratification:* Berlin (Springer Verlag), 121–157.

Berger, W. H., and Killingley, J. S., 1977. Glacial Holocene transition in deep-sea carbonates: selective dissolution and the stable isotope signal. *Science*, 197:563–566.

Berger, W. H., Killingley, J. S., and Vincent, E., 1978. Stable isotopes in deep-sea carbonates: Box Core ERDC-92, west equatorial Pacific. *Oceanologica Acta*, 1:203–216.

Berger, W. H., and Vincent, E., 1981. Chemostratigraphy and biostratigraphic correlation: exercises in systematic stratigraphy. *Proc.*

26th Internat. Geol. Congress, Geology of Oceans Symposium (Paris, 1980). Spec. Publ. Oceanologica Acta, 115–127.

Berger, W. H., Vincent, E., and Thierstein, H. R., 1981. The deep-sea record: major steps in Cenozoic ocean evolution. *Spec. Publ. Soc. Econ. Paleontol. Mineral.*, 32:489–504.

Berger, W. H., and von Rad, U., 1972. Cretaceous and Cenozoic sediments from the Atlantic Ocean. *In* Hayes, D. E., Pimm, A. C., et al., *Init. Repts. DSDP*, 14: Washington (U.S. Govt. Printing Office), 787–954.

Berger, W. H., and Winterer, E. L., 1974. Plate stratigraphy and the fluctuating carbonate line. *In* Hsü, K. J., and Jenkyns, H. (Eds.), *Pelagic Sediments on Land and Under the Sea*. Spec. Publ. Internat. Assoc. Sedimentol., 11–48.

Berggren, W. A., Kent, D. V., and Van Couvering, J. A., in press. Neogene geochronology and chronostratigraphy. *In* Snelling, N. J. (Ed.), *Geochronology and the Geological Records*. Spec. Pap. Geol. Soc. London.

Berggren, W. A., Lohmann, G. P., and Poore, R. Z., 1974. Shore laboratory report on Cenozoic planktonic foraminifera: Leg 22. *In* von der Borch, C. C., Sclater, J. G., et al., *Init. Repts. DSDP*, 22: Washington (U.S. Govt. Printing Office), 635–655.

Berggren, W. A., and Schnitker, D., 1983. Cenozoic marine environments in the North Atlantic and Norwegian–Greenland Sea. *In* Bott, M. H. P., Saxon, S., Talwani, M., and Thiede, J. (Eds.), *Structure and Development of the Greenland–Scotland Ridge:* Plenum, 495–548.

Blanc, P. L., Rabussier, D., Vergnaud Grazzini, C., and Duplessy, J. C., 1980. North Atlantic deep water formed by the later middle Miocene. *Nature*, 289:553–555.

Blow, W. H., 1969. Late middle Eocene to Recent planktonic foraminiferal biostratigraphy. *In* Brönniman, P., and Renz, H. H. (Eds.), *Proc. First Internat. Conf. Planktonic Microfossils* (Geneva, 1967): Leiden (Brill), 199–421.

Broecker, W. S., 1982. Glacial to interglacial changes in ocean chemistry. *Prog. Oceanogr.*, 11:151–197.

Bukry, D., 1975. Phytoplankton stratigraphy, southwest Pacific, Deep Sea Drilling Project, Leg 30. *In* Andrews, J. E., Packham, G., et al., *Init. Repts. DSDP*, 30: Washington (U.S. Govt. Printing Office), 539–547.

Burckle, L. H., 1978. Early Miocene to Pliocene diatom datum levels for the equatorial Pacific. *Proc. Second Working Group Mtg., Biostratigr. Datum-Planes Pacific Neogene, IGCP Project 114* (Bandung, Indonesia, May 30–June 1, 1977). Spec. Publ. Geol. Res. Dev. Ctr., 1:25–44.

Dunn, D. A., 1982. Miocene sediments of the equatorial Pacific Ocean: carbonate stratigraphy and dissolution history [Ph.D. dissert.]. Univ. Rhode Island, Narragansett.

Emiliani, C., 1955. Pleistocene temperatures. *J. Geol.*, 63:538–578.

Epstein, S., Buchsbaum, R., Lowenstam, H. A., and Urey, H. C., 1953. Revised carbonate-water isotopic temperature scale. *Geol. Soc. Am. Bull.*, 64:1315–1326.

Foster, J. H., and Opdyke, N. D., 1970. Upper Miocene to Recent magnetic stratigraphy in deep-sea sediments. *J. Geophys. Res.*, 75: 4465–4473.

Holdsworth, B. K., 1975. Cenozoic Radiolaria biostratigraphy: Leg 30: tropical and equatorial Pacific. *In* Andrews, J. E., Packham, G., et al., *Init. Repts. DSDP*, 30: Washington (U.S. Govt. Printing Office), 499–537.

Johnson, D. A., 1974. Radiolaria from the eastern Indian Ocean, DSDP Leg 22. *In* von der Borch, C. C., Sclater, J. G., et al., *Init. Repts. DSDP*, 22: Washington (U.S. Govt. Printing Office), 521–575.

Keigwin, L. D., and Keller, G., 1984. Middle Oligocene climatic change from equatorial Pacific DSDP Site 77. *Geology*, 12:16–19.

Lancelot, Y., 1978. Relations entre évolution sédimentaire et tectonique de la Plaque Pacifique depuis le Crétacé Inférieur. *Mem. Soc. Geol. Fr. 134.*

Matthews, R. K., and Poore, R. Z., 1980. Tertiary $\delta^{18}O$ record and glacio-eustatic sea-level fluctuations. *Geology*, 8:501–504.

Riedel, W. R., and Sanfilippo, A., 1971. Cenozoic Radiolaria from the western tropical Pacific, Leg 7. *In* Winterer, E. L., et al., *Init. Repts. DSDP*, 7: Washington (U.S. Govt. Printing Office), 1529–1672.

Savin, S. M., Douglas, R. G., Keller, G., Killingley, J. S., Shaughnessy, L., Sommer, M. A., Vincent, E., and Woodruff, F., 1981. Miocene benthic foraminiferal isotope records: a synthesis. *Mar. Micropaleontol.*, 6:423–450.

Savin, S. M., Douglas, R. G., and Stehli, F. G., 1975. Tertiary marine paleotemperatures. *Geol. Soc. Am. Bull.*, 86:1499–1510.

Schnitker, D., 1980a. North Atlantic oceanography as possible cause of Antarctic glaciation and eutrophication. *Nature*, 284:615–616.

_____, 1980b. Global paleoceanography and its deep water linkage to the Antarctic glaciation. *Earth Sci. Rev.*, 16:1–20.

Shackleton, N. J., and Kennett, J. P., 1975. Paleotemperature history of the Cenozoic and the initiation of Antarctic glaciation: oxygen and carbon isotope analyses in DSDP Sites 277, 279 and 281. *In* Kennett, J. P., Houtz, R. E., et al., *Init. Repts. DSDP*, 29: Washington (U.S. Govt. Printing Office), 743–756.

Srinivasan, M. S., and Kennett, J. P., 1981a. A review of Neogene planktonic foraminiferal biostratigraphy: applications in the equatorial and South Pacific. *In* Warme, J. E., Douglas, R. G., and Winterer, E. L. (Eds.), *The Deep Sea Drilling Project: A Decade of Progress*. Spec. Publ. Soc. Econ. Paleontol. Mineral., 32:395–432.

_____, 1981b. Neogene planktonic foraminiferal biostratigraphy and evolution: equatorial to subantarctic South Pacific. *Mar. Micropaleontol.*, 6:499–533.

van Andel, T. H., Heath, G. R., and Moore, T. C., Jr., 1975. Cenozoic history and paleoceanography of the central equatorial Pacific. *Mem. Geol. Soc. Am. 143.*

Vincent, E., 1977. Indian Ocean Neogene planktonic foraminiferal biostratigraphy and its paleoceanographic implications. *In* Heirtzler, J. R., Bolli, H. M., Davies, T. A., Saunders, J. B., et al. (Eds.), *Indian Ocean Geology and Biostratigraphy:* Washington, D.C. (Am. Geophys. Un.), 469–584.

Vincent, E., and Berger, W. H., 1981. Planktonic foraminifera and their use in paleoceanography. *In* Emiliani, C. (Ed.), *The Oceanic Lithosphere: The Sea* (Vol. 7): New York (Wiley Interscience), 1025–1119.

_____, 1984. Carbon dioxide and Antarctic ice-buildup in the Miocene: the Monterey hypothesis. *Chapman Conf. on Natural Variations in Carbon Dioxide and the Carbon Cycle* (Tarpon Springs, Florida, Jan. 9–13, 1984). (Abstract)

_____, in press. Carbon dioxide and polar cooling in the Miocene: the Monterey hypothesis. *In* Sundquist, E. T., and Broecker, W. S. (Eds.), *The Carbon Cycle and Atmospheric CO_2: Natural Variations Archaean to Present*. Monogr. Ser. Am. Geophys. Union 32.

Vincent, E., Killingley, J. S., and Berger, W. H., 1980. The magnetic epoch-6 carbon shift: a change in the ocean's $^{13}C/^{12}C$ ratio 6.2 million years ago. *Mar. Micropaleontol.*, 5:185–203.

_____, 1983. The Chron-16 Carbon Event in the Miocene Indian Ocean. *Geol. Soc. Am. Abstr. Progr.*, 15:712. (Abstract)

_____, in press. Miocene oxygen and carbon isotope stratigraphy of the tropical Indian Ocean. *In* Kennett, J. (Ed.), *The Miocene Ocean: Paleoceanography and Biogeography*. Mem. Geol. Soc. Am. 163.

Winterer, E. L., 1973. Sedimentary facies and plate tectonics of equatorial Pacific. *Am. Assoc. Pet. Geol. Bull.*, 57:265–282.

Woodruff, F., Savin, S. M., and Douglas, R. G., 1981. Miocene stable isotope record: a detailed deep Pacific Ocean study and its paleoclimatic implications. *Science*, 212:665–668.

Date of Initial Receipt: 30 January 1984
Date of Acceptance: 6 March 1985

23. LATE EOCENE TO OLIGOCENE BENTHIC FORAMINIFERAL ISOTOPIC RECORD, SITE 574, EQUATORIAL PACIFIC[1]

Kenneth G. Miller, Lamont-Doherty Geological Observatory, Columbia University
and
Ellen Thomas, Scripps Institution of Oceanography, University of California, San Diego[2]

ABSTRACT

Oxygen and carbon isotopic data from mixed species of the benthic foraminifer *Cibicidoides* at Site 574 in the equatorial Pacific are compared with benthic foraminiferal isotopic data from equatorial Pacific Site 77 (Keigwin and Keller, 1984) and western North Atlantic Site 563 (Miller and Fairbanks, 1983, in press). *Cibicidoides* within the age range of ~33 to 35 Ma (within the early Oligocene) at the Pacific sites were lower in $\delta^{13}C$ than those of the same age from the North Atlantic site. For those from ~26 to 33 Ma (late early to late Oligocene), the equatorial Pacific and western North Atlantic $\delta^{13}C$ values were similar, whereas for those from ~26 to 12 Ma (latest Oligocene to Miocene) (see Miller and Fairbanks, 1983), Pacific values were lower. We suggest that this reflects bottom-water production analogous to modern North Atlantic Deep Water (NADW) in the early Oligocene and latest Oligocene to Miocene and reduced production of "NADW" in the late early to late Oligocene. High $\delta^{18}O$ values (approximately 2.0‰) were recorded at Site 574 for *Cibicidoides* at 36 Ma (earliest Oligocene); high, oscillating $\delta^{18}O$ values occurred from 30 to 29 Ma (near the early/late Oligocene boundary). These intervals of high $\delta^{18}O$ values apparently represent either bottom waters colder than at present or the presence of significant continental ice sheets. We suggest that major periods of continental glaciation occurred at approximately 36 and from 29 to 30 Ma.

INTRODUCTION

Isotopic studies of Tertiary benthic foraminifers have emphasized $\delta^{18}O$ history and have used these records as indicators of past ice volume (hence sea level) and bottom-water temperatures (Shackleton and Kennett, 1975; Savin et al., 1975, 1981; Savin, 1977; Woodruff et al., 1981). Although carbon isotopic records have been used successfully in stratigraphy (e.g., Keigwin, 1979; Vincent et al., 1980; Haq et al., 1980; Savin et al., 1981), their utility as paleoenvironmental indicators has been hindered by the numerous possible interpretations of the relatively small variations in the $\delta^{13}C$ records of deep and bottom waters (Berger et al., 1981). Deep-water benthic foraminiferal $\delta^{13}C$ variations may be due to either global changes in the ^{13}C budget (Shackleton, 1977; Broecker, 1982) or changes in abyssal circulation. (Kroopnick et al., 1972; Kroopnick, 1974, 1980; Bender and Keigwin, 1979; Belanger et al., 1981; Curry and Lohmann, 1982, 1983). Most studies of North Atlantic Tertiary $\delta^{13}C$ records have been restricted to bathyal locations, and therefore may only represent changes in intermediate water (Blanc et al., 1980; Blanc and Duplessy, 1982). Tertiary carbon isotopic comparisons also have been hampered by most data being based on analyses of benthic assemblages or taxa (such as *Oridorsalis* spp.) that do not accurately record modern deep-sea $\delta^{13}C$ distributions (Belanger et al., 1981).

Curry and Lohmann (1982, 1983) isolated abyssal circulation changes from global $\delta^{13}C$ changes for the late Quaternary by examining synoptic benthic foraminiferal $\delta^{13}C$ records over a wide bathymetric range from a small geographic region. Such core coverage is lacking in the Tertiary, but it is possible to make comparisons of $\delta^{13}C$ from different ocean basins to isolate global changes from abyssal circulation changes. This method assumes that the records compared are representative of bottom-water $\delta^{13}C$ conditions for the basins examined.

Miller and Fairbanks (1983) noted three cycles in the Oligocene to middle Miocene benthic foraminiferal $\delta^{13}C$ record. These cycles were observed in benthic foraminifers from the North Atlantic (Miller and Curry, 1982; Miller and Fairbanks, 1983, in press), the South Atlantic (Poore and Matthews, 1984; Shackleton et al., 1984), and the Pacific (Savin et al., 1981; Keigwin and Keller, 1984). They were also observed in planktonic foraminifers (Shackleton et al., in press; Miller and Fairbanks, in press), suggesting that these $\delta^{13}C$ cycles resulted from global changes in the ^{13}C budget (Miller and Fairbanks, 1983, in press).

Synoptic offsets in $\delta^{13}C$ between basins can be used to infer abyssal circulation. The interpretations of such interbasinal comparisons are based on analogy with the modern ocean. Today, basin-basin fractionation (Berger, 1970) results in Pacific bottom water having $\delta^{13}C$ values lower by approximately 1.0‰ than Atlantic bottom water, which is influenced by production of young, ^{13}C-enriched North Atlantic Deep Water (NADW) (Kroopnick et al., 1972; Kroopnick, 1974, 1980). Miller and Fairbanks (1983) measured an offset between Atlantic and Pacific benthic foraminiferal $\delta^{13}C$ records from the latest Oligocene (~26 Ma) to middle Miocene (~12 Ma) that was similar to the modern offset. They concluded that the production of bottom water analogous to modern NADW began prior to the latest Oligocene.

[1] Mayer, L., Theyer, F., et al., *Init. Repts. DSDP*, 85: Washington (U.S. Govt. Printing Office).

[2] Addresses: (Miller; and Thomas, present address) Lamont-Doherty Geological Observatory, Columbia University, Palisades, NY 10964.

They could not extend their comparison further back in time because of a lack of suitable data from the Oligocene of the Pacific.

We attempt to isolate the Oligocene global $\delta^{13}C$ signal from abyssal circulation $\delta^{13}C$ changes by making interbasinal (North Atlantic versus Pacific) comparisons of $\delta^{13}C$ records. Oligocene oxygen and carbon isotopic data from Site 574 in the equatorial Pacific (03°59.24′N, 114°8.53′W; 4561 m present water depth; this study) are compared with records from Site 77 in the equatorial Pacific (00°28.90′N, 133°13.70′W; 4291 m present water depth; Keigwin and Keller, 1984) and Site 563 in the western North Atlantic (33°38.53′N, 43°46.04′W; 3496 m present water depth; Miller and Fairbanks, 1983). These comparisons demonstrate that higher $\delta^{13}C$ values occurred at the Atlantic site from 33 to 35 Ma (within the early Oligocene) and from 26 to 12 Ma (latest Oligocene to Miocene) (Miller and Fairbanks, 1983). However, $\delta^{13}C$ values were similar (with variations being $< 0.3‰$) at all three locations between about 26 and 33 Ma (late early to late Oligocene).

METHODS

Isotopic analyses were performed on mixed species of the benthic foraminiferal taxon *Cibicidoides*. This taxon secretes calcite tests that have a constant offset from $\delta^{18}O$ equilibrium equal to 0.65‰ (Shackleton and Opdyke, 1973; Duplessy et al., 1980; Woodruff et al., 1980; Belanger et al., 1981; Graham et al., 1981). Studies of Holocene core tops demonstrated that *Cibicidoides* accurately reflects the distribution of $\delta^{13}C$ of ΣCO_2 in the modern ocean (Belanger et al., 1981; Graham et al., 1981).

Samples were washed with sodium hexametaphosphate and/or hydrogen peroxide in tap water through a 63 μm sieve and air dried. Specimens for isotopic analyses were ultrasonically cleaned in distilled water for 10 to 20 s, crushed, and roasted at 370°C in a vacuum to remove organic matter. The $CaCO_3$ was reacted with H_3PO_4 at 50°C, and the gas was analyzed on a VG Micromass 903E mass spectrometer at Lamont-Doherty Geological Observatory (see Table 1; Fig. 1). Ages are reported using the Berggren et al. (in press) time scale by interpolation between datum levels (see Figs. 2 and 3).

Sites 574, 77, and 563 were located at abyssal depths (greater than 2000 m) during the Oligocene. Site 563 can be "backtracked" (Sclater et al., 1971; Berger and Winterer, 1974; Sclater et al., 1977; Parsons and Sclater, 1977) using the empirical western North Atlantic age versus subsidence curve (Tucholke and Vogt, 1979) to about 2200 m during the earliest Oligocene (36 Ma) and 3100 m during the latest Oligocene (24 Ma). Backtrack estimates are 3200 and 2700 m during the earliest Oligocene (36 Ma) and 3900 and 3600 m during the latest Oligocene (24 Ma) for Sites 574 and 77, respectively (using the empirical Pacific age–subsidence curve of Sclater et al., 1977).

RESULTS AND DISCUSSION

We sampled approximately one sample per core (29 samples); thus, for the 14 m.y. interval studied, our average sampling interval is approximately 0.5 m.y. If high-frequency changes similar to those of the Quaternary are present (on the order of 10^4 to 10^5 yr.), our sampling would introduce aliasing. However, the oxygen and carbon isotopic records from Site 574 (Fig. 1) show patterns and magnitudes that are remarkably similar to records from Site 77 (Fig. 2) (Keigwin and Keller, 1984). This consistency exists between sites with different sampling intervals (Fig. 2). Thus, we believe that our sampling interval is sufficient to resolve isotopic changes on the order of 10^6 to 10^7 yr.

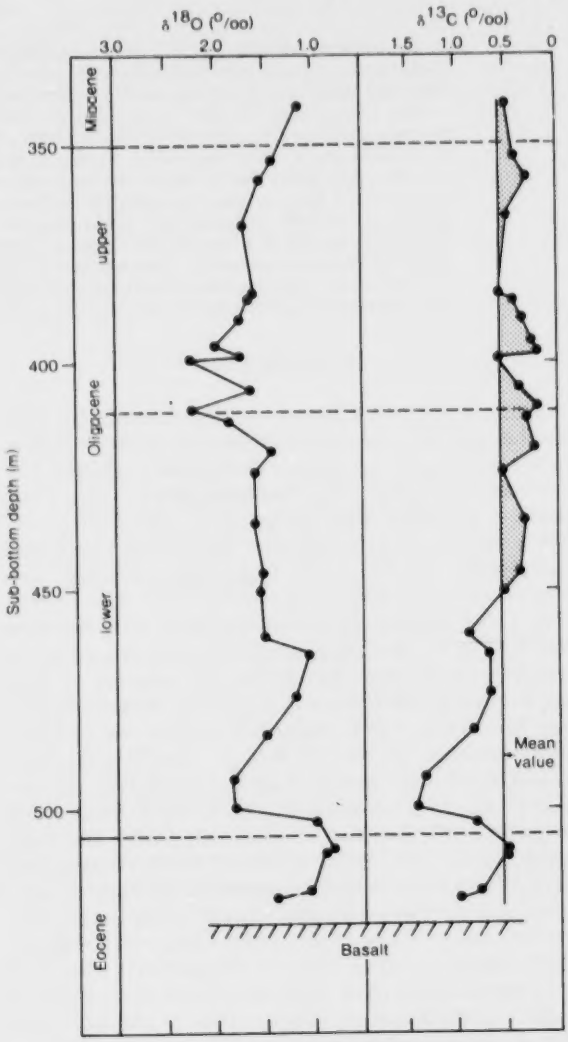

Figure 1. Oxygen and carbon isotopic values for the benthic foraminiferal taxon *Cibicidoides* at Site 574. Vertical line on left indicates the mean of ^{13}C values at 0.6‰ (see Table 1); depleted intervals are indicated with stipples. The Eocene/Oligocene boundary is drawn at the last occurrence of *Nuttallides truempyi*, although nannofossils suggest that it may be above this by ~2 m; the lower/middle Oligocene boundary is drawn on the basis of estimates from interpolation of sedimentation rates.

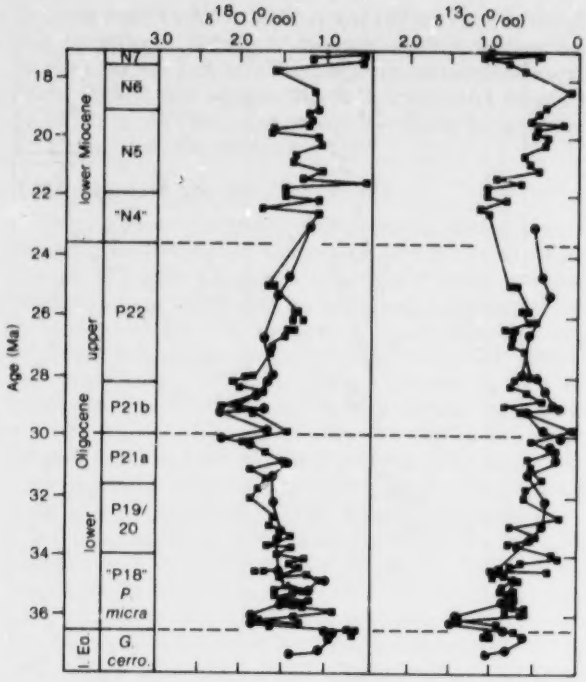

Figure 2. Age comparison of the records of Site 574 (dots) and Site 77 (squares). Site 77 data: Oligocene, after Keigwin and Keller (1984); Miocene, after Savin et al. (1981). Age assignments for Site 77 obtained by interpolating between the following datum levels: first occurrence (FO), *Praeorbulina*, 241 m sub-bottom, 16.6 Ma; FO, *G. kugleri*, 317 m, 23.6 Ma; last occurrence (LO), *Chiloguembelina*, 375 m, 30.0 Ma; LO, *Pseudohastigerina*, 413.5 m, 34.0 Ma; oxygen isotopic enrichment, 470 m, 36.4 Ma. Biostratigraphic datum levels after Keller (1981) and Hays et al. (1972). Age assignments for Site 574 after Site 574 chapter, this volume.

It is possible for diagenesis to alter the original isotopic record in such cases as this (e.g., Arthur et al., 1979; Miller and Curry, 1982; Killingley, 1983). However, this appears not to have occurred here. The close agreement between the $\delta^{18}O$ records at Site 574 and 77 (Fig. 2) occurs at sites with different burial depths (corresponding sections at Site 574 are approximately 50 m deeper). In addition, the oxygen values noted at these sites are similar to Oligocene values reported elsewhere (Keigwin, 1980; Miller and Curry, 1982; Poore and Matthews, 1984; Belanger and Matthews, in press; Shackleton et al., 1984). The correspondence of $\delta^{18}O$ values among sites with a wide range of burial depths and preservational states suggests that the records have not been altered significantly by diagenesis.

Oxygen Isotopes

The $\delta^{18}O$ record at Site 574 shows a major increase (~0.9‰ between 503 and 500 m sub-bottom depth) just above the Eocene/Oligocene boundary (~504–506 m) (Fig. 1). Keigwin (1980), Snyder et al. (1984), and Miller, Curry, et al. (in press) demonstrated that a similar increase at Sites 277 (Southern Ocean), 289 (Pacific), and 549 (northeastern North Atlantic) occurred immediately following the extinction of planktonic foraminifers used to recognize the Eocene/Oligocene boundary (i.e., *Hantkenina* spp. and *Globorotalia cerroazulensis cerroazulensis*) and also occurred within Zone NP21. Thus, if the extinctions were synchronous, then the previously reported enrichments should correlate in time (Miller, Curry, et al., in press). The best estimate for the timing of this enrichment is in the middle of Zone NP21 at approximately 36 ± 0.5 Ma (time scale of Berggren et al., in press); this is in good agreement with the estimate obtained at Site 574 (36.4 Ma) by interpolation of sedimentation rates. Such interpolations suggest that the oxygen isotopic enrichment between 500 and 503 m sub-bottom at Site 574 occurred in less than a 0.2-m.y interval.

At Site 574, the $\delta^{18}O$ increase occurred immediately after the last occurrence (LO) of *Nuttallides truempyi* (LO, Sample 33-5, 141–143 cm; 506 m sub-bottom (Thomas, this volume). The $\delta^{18}O$ increase also postdated the LO of *Discoaster saipanensis* (namely, within Zone NP21; LO, between Sample 33-5, 5–7 cm, 504.14 m sub-bottom and Sample 33-4, 114–116 cm, 504.55 m sub-bottom). *D. barbadiensis* has its LO between 574C-34-2, 93 cm and 574C-34-2, 60 cm (Barron et al., this volume). *N. truempyi* apparently became extinct at the end of the Eocene (Tjalsma and Lohmann, 1983; Wood et al., in press), suggesting that the increase occurred in the earliest Oligocene. This is consistent with the assignment of the increase to Zone NP21 because this zone straddles the Eocene/Oligocene boundary (Snyder et al., 1984; Miller, Curry, et al., in press).

At Site 77, a similar $\delta^{18}O$ increase was noted (Keigwin and Keller, 1984); this enrichment also occurred just following the extinction of *D. saipanensis* and *D. barbadiensis*, namely, within Zone NP21 (Hays et al., 1972). Unfortunately, diagnostic planktonic foraminifers are missing from the uppermost Eocene to lowermost Oligocene sections at Site 77 due to dissolution, and precise biostratigraphic correlation (with resolution better than 1 m.y.) is therefore lacking. Because of this, we constrained our age model for Site 77 to the interval from 34 to 36 Ma (Fig. 2) using the earliest Oligocene oxygen isotopic enrichment as an interpolation point.

Magnetostratigraphic data are needed to establish first-order magnetostratigraphic, biostratigraphic, and isotopic correlations and the isochrony of the earliest Oligocene $\delta^{18}O$ increase. Our biostratigraphic and isotopic correlations suggest that the increase should correlate with the reversed interval of Chron C13 (i.e., between Anomalies 13 and 15) (chron terminology of LaBrecque et al., 1983; see also Barron et al., this volume). The only primary correlation has been made at Site 522 (Poore and Matthews, 1984; Oberhänsli et al., 1984), and is limited by sample resolution. At Site 522, the enrichment could have occurred either in the normal interval of Chron C13 (i.e., 35.3 to 35.9 Ma) or immediately before it.

Oxygen isotopic values at Site 574 are relatively constant between 424 and 465 m sub-bottom (lower Oligocene) (Fig. 1; Table 1). A $\delta^{18}O$ increase and associated series of oscillations occurs between 419 and 389 m near the lower/middle Oligocene boundary in the upper part of Zone NP23 to Zone NP24 and in Zone P21 to lower Zone P22 (Site 574 chapter, this volume). This increase

biostratigraphically correlates with a similar $\delta^{18}O$ change noted at Site 77 in Zone P21 (Fig. 2) (Keigwin and Keller, 1984). Values in the interval from ~30 to 29 Ma ("middle" Oligocene) at Sites 574 and 77 are higher than those noted in the lower Oligocene section; some values exceed 2.0‰ (Table 1). Oxygen isotopic values subsequently decrease in the uppermost Oligocene section. Resolution in the uppermost Oligocene at both sites is limited at present.

A comparison (Fig. 3) of the isotopic records at western North Atlantic Site 563 (Miller and Fairbanks, 1983) with Sites 574 and 77 shows that the "middle" Oligocene $\delta^{18}O$ increase is absent at Site 563. However, magnetobiostratigraphic comparisons (Miller, Aubry, et al., in press) show that the "middle" Oligocene at Site 563 is condensed or missing, specifically Chron C8R and perhaps portions of Chrons C10 and C11 are missing (chron terms of Berggren et al., in press).

Carbon Isotopes

The carbon isotopic record at Site 574 shows an enrichment in the lowermost Oligocene at the same level as the ^{18}O enrichment; a similar enrichment was noted at Site 77 (Fig. 2) (Keller and Keigwin, 1984). Between 461 and 499 m sub-bottom (lower lower Oligocene), $\delta^{13}C$ values are high (>0.6‰) compared with values between 451 and 341 m sub-bottom (upper lower and upper Oligocene), which are less than 0.7‰ (Fig. 1). This pattern of decreasing $\delta^{13}C$ in benthic foraminifers from early to late Oligocene was noted at Site 77 (Keigwin and Keller, 1984), Site 563 (Miller and Fairbanks, 1983), South Atlantic Site 522 (Poore and Matthews, 1984), Leg 74 (South Atlantic) sites (Shackleton et al., 1984), Gulf of Mexico Site 540 (Belanger and Matthews, in press), and Sites 119 and 400 in the Bay of Biscay (Miller and Curry, 1982). In addition, this $\delta^{13}C$ change has been noted in planktonic foraminifers (Shackleton et al., 1984; Miller and Fairbanks, in press), implying that the decrease resulted from a change in the global ^{13}C budget.

Comparison of western North Atlantic (Site 563) and Pacific (Sites 574 and 77) $\delta^{13}C$ records shows that the Pacific sites were depleted in ^{13}C from about 33 to 35 Ma (early Oligocene) and from 18 to 26 Ma (latest Oligocene to Miocene). However, there appears to have been little difference between the Atlantic and the Pacific sites from about 26 to 33 Ma (late early to late Oligocene). Our interpretation of the carbon isotopic record is that in the early Oligocene and latest Oligocene to Miocene, nutrient-depleted, ^{13}C-enriched bottom waters formed in the North Atlantic and/or its marginal seas. This circulation pattern resulted in ^{13}C-enriched bottom waters

Table 1. Oxygen and carbon isotopic values for mixed species of *Cibicidoides*, Site 574 (reported to PDB standard).

Sample (interval in cm)	Sub-bottom depth (m)	Age (Ma)	$\delta^{18}O$ (‰)	$\delta^{13}C$ (‰)
16,CC	341.88m	23.0	1.15	0.49
17,CC	353.97	24.7	1.46	0.40
18,CC	358.48	25.3	1.54	0.28
19,CC	368.17	26.7	1.71	0.55
20,CC	384.25	28.0	1.61	0.62
21-1, 79-81	385.29	28.1	1.67	0.43
21-4, 88-93	389.88	28.5	1.75	0.35
22-2, 47-53	395.97	29.0	2.01	0.24
22-3, 125-130	398.20	29.1	1.73	0.17
22,CC	398.87	29.2	2.27	0.60
23-2, 96-101	405.96	29.8	1.65	0.38
23-5, 87-92	410.37	30.1	2.23	0.18
23,CC	412.47	30.3	1.87	0.31
24,CC	419.47	30.9	1.43	0.21
25,CC	424.51	31.3	1.61	0.56
26,CC	435.90	32.2	1.61	0.34
27,CC	446.86	33.1	1.51	0.40
28,CC	451.57	33.5	1.55	0.56
29-1, 80-83	461.32	34.5	1.53	0.94
29,CC	465.27	34.8	1.05	0.71
30,CC	474.85	35.2	1.19	0.72
31,CC	483.15	35.6	1.51	0.90
32,CC	493.19	36.0	1.86	1.40
33-1, 113-115	499.64	36.3	1.84	1.48
33-3, 113-115	502.64	36.5	0.99	0.89
34-1, 71-73	508.72	36.7	0.83	0.57
34-2, 25-27	509.76	36.8	0.96	0.58
35-1, 97-98	518.48	37.2	1.05	0.83
35-2, 99-100	520.00	37.3	1.41	1.06

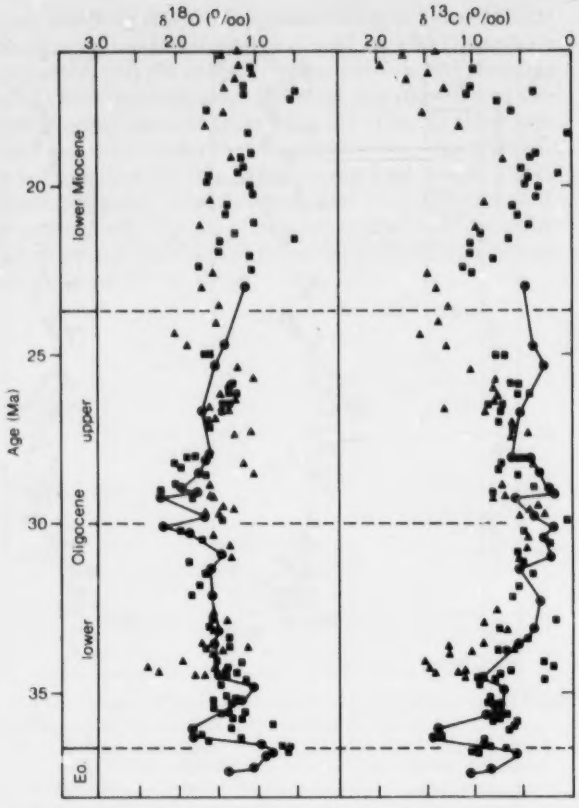

Figure 3. Comparison of $\delta^{18}O$ and $\delta^{13}C$ values for *Cibicidoides* at western North Atlantic Site 563 (triangles), Pacific Site 574 (dots), and Pacific Site 77 (squares). Age assignments for Site 563 based on interpolation and extrapolation of sedimentation rates between the following datum levels: top of Chron C5DN, 260.0 m sub-bottom, 17.57 Ma; base of Chron C5DN, 267.0 m, 18.14 Ma; unconformity 270.5 m at 18.42–19.41 Ma; base of Chron C6N, 277.5 m, 20.45 Ma; top of Chron C6CN, 296.5 m, 23.27 Ma; LO, *Chiloguembelina*, 326.0 m, 30.0 Ma; base of Chron C12N, 339.0 m, 32.9 Ma; LO, *Pseudohastigerina*, 353.5 m, 34.0 Ma.

in the western North Atlantic relative to the Pacific, which is a situation analogous to modern conditions. Similarly, the apparent lack of $\delta^{13}C$ difference between the equatorial Pacific and western North Atlantic sites from 26 to 33 Ma in the Oligocene indicates reduced bottom-water formation analogous to NADW.

Glacio-Eustacy and the $\delta^{18}O$ Record

What caused the major $\delta^{18}O$ increases that occurred at about 36 Ma (earliest Oligocene) and 29–30 Ma (near the early/middle Oligocene boundary)? Most isotopic studies have assumed that no significant continental ice existed prior to a $\delta^{18}O$ increase of the middle Miocene (Shackleton and Kennett, 1975; Savin et al., 1975, 1981; Woodruff et al., 1981). However, Matthews and Poore (1980) suggested that significant ice volume may have existed prior to the middle Miocene. Miller and Fairbanks (1983) and Keigwin and Keller (1984) supported this by noting that bottom waters must have been as cold or colder than today if little or no ice was present in the Oligocene. High $\delta^{18}O$ values (>1.9‰) at about 36 and from 29 to 30 Ma at Site 574 supply further evidence for ice volume at these times. Modern values for *Cibicidoides* at Site 574 would be 1.6‰, assuming an ice-free world (Graham et al., 1981; Shackleton and Kennett, 1975). Therefore, if the Oligocene were ice free, then bottom waters at Site 574 would have been 1–2°C colder than today during the earliest Oligocene and near the early/late Oligocene boundary. We believe that such cold bottom-water temperatures (and the inferred cold source region) are incompatible with an ice-free world and suggest that the $\delta^{18}O$ increases resulted from a combination of ice-volume increases and bottom-water temperature drops.

Significant ice-volume increases would have resulted in a glacio-eustatic lowering of sea level. The covariance of planktonic and benthic foraminiferal $\delta^{18}O$ is used in the Quaternary as an indicator of ice-volume changes (e.g., Shackleton and Opdyke, 1973). Keigwin (1980) and Keigwin and Keller (1984) noted approximately 0.3 and 0.4‰ covariance in planktonic and benthic foraminiferal $\delta^{18}O$ increases for the earliest Oligocene and "middle" Oligocene, respectively. If it is assumed that 0.3 to 0.4‰ of the increases are attributable to ice-volume changes, sea level would have changed by 30 to 40 m (according to the Quaternary ice volume–$\delta^{18}O$ calibration of Fairbanks and Matthews, 1978) in both the earliest and "middle" Oligocene.

Vail et al. (1977) and Vail and Mitchum (1980) noted that a major coastal offlap occurred in the "middle" Oligocene; they suggested that this was related to a major low stand of eustatic sea level. We estimate that the $\delta^{18}O$ increase that occurred near the early/late Oligocene boundary at Sites 574 and 77 represents approximately 30 to 40 m of glacio-eustatic sea-level lowering. The maximum $\delta^{18}O$ values at these sites (inferred minimum glacio-eustatic sea level) occurred in the upper part of undifferentiated Zone P21. The offlap event of Vail et al. (1977) and Vail and Mitchum (1980) occurred in Zone P21a at approximately 31 Ma (time scale of Berggren et al., in press). Therefore, it apparently pre-dated the inferred age of the minimum glacio-eustatic sea level (= maximum $\delta^{18}O$ values) which is estimated as 29 to 30 Ma. This offset of 1 to 2 m.y. is difficult to evaluate at present due to uncertainties in Oligocene biostratigraphy. If this difference is real, however, it may be resolved by noting that the inferred glacio-eustatic lowering may have begun prior to 30 Ma (Fig. 2). Thus, the continental margin may not be responding directly to eustatic sea level, but rather to the rate of change of eustatic sea level (Pitman, 1978; Pitman and Golovchenko, 1983; Thorne and Watts, in press; Miller et al., 1985).

CONCLUSIONS

Two increases in benthic foraminiferal $\delta^{18}O$ occurred in the Oligocene at Pacific Site 574: one at about 36 Ma (earliest Oligocene) and the other at 29 to 30 Ma (near the early/late Oligocene boundary). These increases are interpreted as having resulted from a combination of ice-volume increases and bottom-water temperature drops.

The $\delta^{13}C$ record at Site 574 provides evidence for two important conclusions. First, high $\delta^{13}C$ values occurred in the early Oligocene, then decreased later in the Oligocene (after about 33 Ma). This pattern in benthic foraminifers has been noted in other Pacific, North Atlantic, and South Atlantic locations. The presence of a similar pattern in planktonic foraminifers (Shackleton et al., 1984; Miller and Fairbanks, in press) suggest that it resulted from global changes in the ^{13}C budget. Second, the Pacific was depleted in ^{13}C relative to the western North Atlantic from about 33 to 35 Ma (within the early Oligocene) and from 26 to 18 Ma (latest Oligocene to Miocene). Miller and Fairbanks (1983) noted a similar offset between 26 Ma and 12 Ma (latest Oligocene to Miocene). There was little $\delta^{13}C$ difference between the Atlantic and Pacific from about 26 to 32 Ma (late early to late Oligocene). This pattern suggests production of bottom water in the North Atlantic and/or its marginal seas (analogous to present-day NADW) during part of the early Oligocene (33 to 35 Ma) and latest Oligocene to Miocene (26 to 12 Ma) and reduction of production from 32 to 26 Ma.

Our $\delta^{13}C$ comparisons involve only one Atlantic record and therefore must be considered tentative. In addition, coverage of the latest Oligocene at Sites 574 and 77 is limited at present. Further comparisons of Atlantic and Pacific abyssal benthic foraminiferal $\delta^{13}C$ records are needed to demonstrate that the $\delta^{13}C$ differences observed here reflect abyssal circulation changes.

ACKNOWLEDGMENTS

We thank W. B. Curry, R. G. Fairbanks, T. R. Janecek, L. D. Keigwin, W. F. Ruddiman, and N. J. Shackleton for reviewing the manuscript; R. G. Fairbanks for numerous discussions and use of the L-DGO mass spectrometer; W. B. Curry and L. D. Keigwin for discussions of $\delta^{13}C$–abyssal circulation and $\delta^{18}O$–ice volume relationships; and G. Kolibas for performing all isotopic analyses. L. D. Keigwin supplied data from Site 77. Samples were provided by DSDP. This research was supported by a postdoctoral fellowship from L-DGO, NSF Grant OCE 83-10086, and a grant from the ARCO Foundation (KGM).

This is Lamont-Doherty Geological Observatory Contribution number 3783. E.T.'s research was partially funded by NSF grant OCE 83-10518.

REFERENCES

Arthur, M. A., Scholle, P. A., and Hasson, P., 1979. Stable isotopes of oxygen and carbon in carbonates from Sites 398 and 116 of the

Deep Sea Drilling Project. *In* Sibuet, J.-C., Ryan, W. B. F., et al., *Init. Repts. DSDP*, 47, Pt. 2: Washington (U.S. Govt. Printing Office), 477–491.

Belanger, P. E., Curry, W. B., and Matthews, R. K., 1981. Core-top evaluation of benthic foraminiferal isotopic ratios for paleo-oceanographic interpretations. *Palaeogeogr., Palaeoclimatol., Palaeoecol.*, 33:205–220.

Belanger, P. E., and Matthews, R. K., in press. The foraminiferal isotopic record across the Eocene/Oligocene boundary at Deep Sea Drilling Project Site 540. *In* Buffler, R. T., Schlager, W., et al., *Init. Repts. DSDP*, 77: Washington (U.S. Govt. Printing Office), 589–592.

Bender, M. L., and Keigwin, L. D., 1979. Speculations about the upper Miocene change in abyssal Pacific dissolved bicarbonate $\delta^{13}C$. *Earth Planet. Sci. Lett.*, 45:383–393.

Berger, W. H., 1970. Biogenous deep-sea sediments: fractionation by deep-sea circulation. *Geol. Soc. Am. Bull.*, 81:1385–1402.

Berger, W. H., Vincent, E., and Thierstein, H. R., 1981. The deep-sea record: major steps in Cenozoic ocean evolution. *In* Warme, T. E., Douglas, R. C., and Winterer, E. L. (Eds.), *The Deep-Sea Drilling Project: A Decade of Progress*. Soc. Econ. Paleontol. Mineral. Spec. Publ., 32:489–504.

Berger, W. H., and Winterer, E. L., 1974. Plate stratigraphy and the fluctuating carbonate line. *In* Hsü, K. J., and Jenkyns, H. C. (Eds.), *Pelagic Sediments on Land and Under the Sea*. Int. Assoc. Sediment. Spec. Pub., 1:11–48.

Berggren, W. A., Kent, D. V., and Flynn, J., in press. Paleogene geochronology and chronostratigraphy. *Geol. Soc. London Spec. Pub.*

Blanc, P.-L., and Duplessy, J. C., 1982. The deep-water circulation during the Neogene and the impact of the Messinian salinity crisis. *Deep Sea Res.*, 29A:1391–1414.

Blanc, P.-L., Rabussier, D., Vergnaud Grazzini, C., and Duplessy, J. C., 1980. North Atlantic deep water formed by the later middle Miocene. *Nature (London)*, 283:553–555.

Broecker, W. S., 1982. Ocean chemistry during glacial time. *Geochim. Cosmochim. Acta*, 46:1689–1705.

Curry, W. B., and Lohmann, G. P., 1982. Carbon isotopic changes in benthic foraminifera from the western South Atlantic: reconstruction of glacial abyssal circulation patterns. *Quat. Res. (NY)*, 18: 218–235.

_____, 1983. Reduced advection into Atlantic Ocean deep eastern basins during last glacial maximum. *Nature (London)*, 306:577–580.

Duplessy, J.-C., Moyes, J., and Pujol, C., 1980. Deep water formation in the North Atlantic during the last ice age. *Nature (London)*, 286:479–482.

Fairbanks, R. G., and Matthews, R. K., 1978. The marine oxygen isotopic record in Pleistocene coral, Barbados, West Indies. *Quat. Res. (NY)*, 10:181–196.

Graham, D. W., Corliss, B. H., Bender, M. L., and Keigwin, L. D., 1981. Carbon and oxygen isotopic disequilibria of Recent benthic foraminifera. *Mar. Micropaleontol.*, 6:483–497.

Haq, B. U., Worsley, T. R., Burkle, L. H., Douglas, R. G., Keigwin, L. D., Opdyke, N. D., Savin, S. M., Sommer, M. A., Vincent, E., and Woodruff, F., 1980. Late Miocene marine carbon isotopic shift and synchroneity of some phytoplanktonic biostratigraphic events. *Geology*, 8:437–431.

Hays, J. D., et al., 1972. *Init. Repts. DSDP*, 9: Washington (U.S. Govt. Printing Office).

Keigwin, L. D., 1979. Late Cenozoic stable isotopic stratigraphy and paleoceanography of DSDP sites from the east equatorial and central Pacific Ocean. *Earth Planet. Sci. Lett.*, 45:361–382.

_____, 1980. Palaeoceanographic change in the Pacific at the Eocene–Oligocene boundary. *Nature (London)*, 287:722–725.

Keigwin, L. D., and Keller, G., 1984. Middle Oligocene climatic change from equatorial Pacific DSDP Site 77. *Geology*, 12:16–19.

Keller, G., 1981. Miocene biochronology and paleoceanography of the North Pacific. *Mar. Micropaleontol.*, 6:535–552.

Killingley, J. S., 1983. Effects of diagenetic recrystallization of $^{18}O/^{16}O$ values of deep-sea sediments. *Nature (London)*, 301:594–597.

Kroopnick, P., 1974. Correlation between ^{13}C and CO_2 in surface waters and atmospheric CO_2. *Earth Planet. Sci. Lett.*, 22:397–403.

_____, 1980. The distribution of ^{13}C in the Atlantic Ocean. *Earth Planet. Sci. Lett.*, 49:469–484.

Kroopnick, P., Weiss, R. F., and Craig, H., 1972. Total CO_2, ^{13}C, and dissolved oxygen-^{18}O at Geosecs II in the North Atlantic. *Earth Planet. Sci. Lett.*, 16:103–110.

LaBrecque, J. L., Hsü, K. J., Carman, M. F., Jr., Karpoff, A. M., McKenzie, J. A., et al., 1983. Contributions to Paleogene stratigraphy in nomenclature, chronology, and sedimentation rates. *Palaeogeogr., Palaeoclimatol., Palaeoecol.*, 42:92–125.

Matthews, R. K., and Poore, R. Z., 1980. Tertiary $\delta^{18}O$ record and glacio-eustatic sea-level fluctuations. *Geology*, 8:501–504.

Miller, K. G., Aubrey, M. P., Khan, M. J., Melillo, A. J., Kent, D. V., and Berggren, W. A., in press. Oligocene–Miocene biostratigraphy, magnetostratigraphy, and isotopic stratigraphy of the western North Atlantic. *Geology*.

Miller, K. G., and Curry, W. B., 1982. Eocene to Oligocene benthic foraminiferal isotopic record in the Bay of Biscay. *Nature (London)*, 296:347–350.

Miller, K. G., Curry, W. B., and Ostermann, D. R., in press. Late Paleogene (Eocene to Oligocene) benthic foraminiferal oceanography of the Goban Spur Region, Deep Sea Drilling Project Leg 80. *In* Graciansky, P. C. de, Poag, C. W., et al., *Init. Repts. DSDP*, 80, Pt. 1: Washington (U.S. Govt. Printing Office), 505–538.

Miller, K. G., and Fairbanks, R. G., 1983. Evidence for Oligocene–Middle Miocene abyssal circulation changes in the western North Atlantic. *Nature (London)*, 306:250–253.

_____, in press. Oligocene–Miocene global carbon and abyssal circulation changes. *In* Sunquist, E., and Broecker, W. (Eds.), *Chapman Conference on Natural Variations in Carbon Dioxide and the Carbon Cycle*. Am. Geophys. Union Monograph Series.

Miller, K. G., Mountain, G. S., and Tucholke, B. E., 1985. Oligocene glacioeustasy and erosion on the margins of the North Atlantic. *Geology*, 13:10–13.

Oberhänsli, H., McKenzie, J., Toumarkine, M., and Weissert, H., 1984. A paleoclimatic and paleoceanographic record of the Paleogene in the central South Atlantic (Leg 73, Sites 522, 523, and 524). *In* Hsü, K. J., LaBrecque, J., et al., *Init. Repts. DSDP*, 73: Washington (U.S. Govt. Printing Office), 737–747.

Parsons, B., and Sclater, J. G., 1977. An analysis of the variation of ocean floor bathymetry and heat flow with age. *J. Geophys. Res.*, 82:803–827.

Pitman, W. C., 1978. Relationship between eustacy and stratigraphic sequences of passive margins. *Geol. Soc. Am. Bull.*, 89:1389–1403.

Pitman, W. C., and Golovchenko, X., 1983. The effect of sea-level change on the shelf edge and slope of passive margins. *Soc. Econ. Paleontol. Min. Spec. Pub.*, 33:41–58.

Poore, R. Z., and Matthews, R. K., 1984. Late Eocene–Oligocene oxygen- and carbon-isotope record from South Atlantic Ocean, Deep Sea Drilling Project Site 522. *In* Hsü, K. J., LaBrecque, J. L., et al., *Init. Rept. DSDP*, 73: Washington (U.S. Govt. Printing Office), 725–735.

Savin, S. M., 1977. The history of the earth's surface temperature during the last 100 million years. *Annu. Rev. Earth Planet. Sci.*, 5: 319–355.

Savin, S. M., Douglas, R. G., Keller, G., Killingley, J. S., Shaughnessy, L., Sommer, M. A., Vincent, E., and Woodruff, F., 1891. Miocene benthic foraminiferal isotope records: a synthesis. *Mar. Micropaleontol.*, 6:423–450.

Savin, S. M., Douglas, R. G., and Stehli, F. G., 1975. Tertiary marine paleotemperatures. *Geol. Soc. Am. Bull.*, 86:1499–1510.

Sclater, J. G., Abbott, D., and Thiede, J., 1977. Paleobathymetry of sediments of the Indian Ocean. *In* Heirtzler, J. R., Bolli, H. M., and Davies, T. A. (Eds.), *Indian Ocean Geology and Biostratigraphy:* Washington (Am. Geophys. Union), 25–59.

Sclater, J. G., Anderson, R. N., and Bell, N. L., 1971. Elevation of ridges and the evolution of the central eastern Pacific. *J. Geophys. Res.*, 76:7888–7915.

Shackleton, N. J., 1977. Carbon-13 in *Uvigerina:* tropical rain forest history and the equatorial Pacific carbonate dissolution cycles. *In* Anderson, N. R., and Malahoff, A. (Eds.), *The Fate of Fossil Fuel CO_2 in the Oceans*. New York (Plenum Press), 401–427.

Shackleton, N. J., Hall, M. A., and Boersma, A., 1984. Oxygen and carbon isotope data from Leg 74 foraminifers. *In* Moore, T. C., Jr., Rabinowitz, P. D., et al., *Init. Repts. DSDP*, 74: Washington (U.S. Govt. Printing Office), 599–612.

Shackleton, N. J., and Kennett, J. P., 1975. Paleotemperature history of the Cenozoic and the initiation of Antarctic glaciation: oxygen and carbon isotopic analyses in DSDP Sites 277, 279, and 281. *In* Kennett, J. P., Houtz, R. E., et al., *Init. Repts. DSDP*, 29: Washington (U.S. Govt. Printing Office), 743–755.

Shackleton, N. J., and Opdyke, N. D., 1973. Oxygen isotopic and palaeomagnetic stratigraphy of equatorial Pacific Core V28-238: oxygen isotope temperatures and ice volume on a 10^5 and 10^6 year scale. *Quat. Res. (NY)*, 3:39–55.

Snyder, S. W., Müller, C., and Miller, K. G., 1984. Biostratigraphy and paleoceanography across the Eocene/Oligocene boundary at Deep Sea Drilling Project Site 549. *Geology*, 12:112–115.

Thorne, J., and Watts, A. B., in press. Seismic reflectors and unconformities at passive continental margins. *Nature (London)*.

Tjalsma, R. C., and Lohmann, G. P., 1983. Paleocene–Eocene bathyal and abyssal benthic foraminifera from the Atlantic Ocean. *Micropaleontology Press Spec. Pub. 4*.

Tucholke, B. E., and Vogt, P. R., 1979. Western North Atlantic: sedimentary evolution and aspects of tectonic history. *In* Tucholke, B. E., Vogt, P. R., et al., *Init. Rept. DSDP*, 43: Washington (U.S. Govt. Printing Office), 791–825.

Vail, P. R., and Mitchum, R. M., 1980. Global cycles of sea-level change and their role in exploration. *Proc. Tenth World Petrol. Congress, 2, Expl. Supply and Demand*, pp. 95–104.

Vail, P. R., Mitchum, R. M., Jr., Todd, R. G., Widmier, J. M., Thompson, S. III, Sangree, J. B., Bubb, J. N., and Hatelid, W. G., 1977. Seismic stratigraphy and global changes of sea level. *In* Payton, C. E. (Ed.), *Seismic Stratigraphy—Applications to Hydrocarbon Exploration*. Am. Assoc. Petrol. Geol. Mem., 26:49–205.

Vincent, E., Killingley, J., and Berger, W. H., 1980. The magnetic epoch 6 carbon shift: a change in the ocean's $^{13}C/^{12}C$ ratio 6.2 million years ago. *Mar. Micropaleontol.*, 5:185–203.

Wood, K. C., Miller, K. G., and Lohmann, G. P., in press. Middle Eocene to Oligocene benthic foraminifera from the Oceanic Formation, Barbados. *Micropaleontology*.

Woodruff, F., Savin, S. M., and Douglas, R. G., 1980. Biological fractionation of oxygen and carbon isotopes by Recent benthic foraminifera. *Mar. Micropaleontol.*, 5:3–13.

_____, 1981. Miocene stable isotopic record: a detailed deep Pacific ocean study and its paleoclimatic implications. *Science (Washington, D. C.)*, 212:665–668.

Date of Initial Receipt: 14 November 1983
Date of Acceptance: 12 March 1984

PART IV: GEOCHEMISTRY

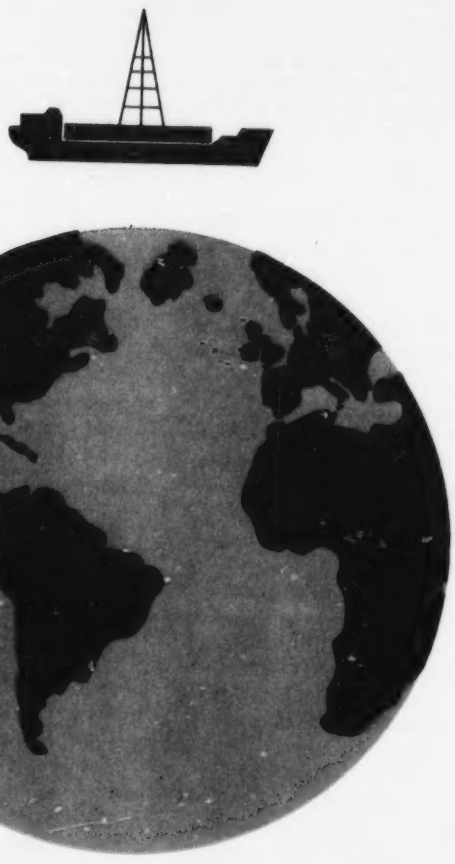

24. GEOCHEMISTRY AND ORIGIN OF EOCENE-OLIGOCENE METALLIFEROUS SEDIMENTS FROM THE CENTRAL EQUATORIAL PACIFIC: DEEP SEA DRILLING PROJECT SITES 573 AND 574[1]

Ian Jarvis, Department of Geology, City of London Polytechnic[2]

ABSTRACT

Eocene-Oligocene metalliferous sediments and associated lithologies from the central equatorial Pacific are described in detail. Geochemical analyses of 54 sediment and 2 basalt samples are presented for 34 elements. Detailed stratigraphic and statistical analyses of these data, combined with mineralogic studies, indicate the presence of volcanic glass and seven main mineral phases: biogenic calcite and opal, Fe smectite, goethite, δMnO_2, carbonate fluorapatite, and barite. Fe smectite formed by reactions between Fe oxyhydroxides and biogenic opal, causing the dissolution of calcite and the precipitation of barite. Diagenesis was oxic. Sediments have rare earth element distributions similar to those in seawater. The metal content of the sediments is related to competition between the supply rates of hydrothermal and biogenic particles, but has been enhanced by early diagenetic processes. Eocene-Oligocene metalliferous sediments compare closely to those currently being deposited in the Bauer Basin and on the flanks of the East Pacific Rise. There is, however, no evidence that they were deposited in close proximity to an active hydrothermal system.

INTRODUCTION

It has been known for some time that sediments near the East Pacific Rise are strongly enriched in Fe, Mn, and other transition metals relative to normal pelagic sediments (Murray and Renard, 1891; Revelle, 1944; Boström and Peterson, 1966; Boström et al., 1969; Bender et al., 1971). It is generally accepted that the metals were leached from the basaltic crust by seawater hydrothermal systems (Corliss, 1971; Bonatti et al., 1972; Dymond et al., 1973; Piper, 1973; Bonnatti, 1975; Dymond and Veeh, 1975; Cronan, 1980; Dymond, 1981; Thompson, 1983), which subsequently deposited them as authigenic precipitates on the seafloor. Studies of the mineralogy, geochemistry, and origin of metalliferous sediments in the central Pacific (Fig. 1) have concentrated on the recent sediments of the East Pacific Rise (Sayles and Bischoff, 1973; Heath and Dymond, 1977, 1981; Lyle, 1981; Marchig and Gundlach, 1982; Marchig et al., 1982), the Bauer Deep (Sayles et al., 1975; Dymond and Veeh, 1975; Heath and Dymond, 1977; Dymond, 1981; McMurtry et al., 1981; Lyle, 1981; Field et al., 1981), and the Galapagos Hydrothermal Mounds Field (Corliss et al., 1978; Hekinian et al., 1978; Edmond, Measures, McDuff, et al., 1979; Edmond, Measures, Mangum, et al., 1979; Williams et al., 1979; Varnavas and Cronan, 1981; Honnorez et al., 1981; Honnorez, Von Herzen, et al., 1983; Barrett and Friedrichsen, 1982; Moorby, 1983). Relatively few data are available on the ancient analogs of these deposits that have been cored by DSDP to the west of the East Pacific Rise.

Eocene-Oligocene metalliferous sediments occur in the central Pacific (Fig. 1) in the base of the sediment column at DSDP Sites 74 and 75 (Tracey et al., 1971; von der Borch et al., 1971), Sites 77 and 78 (Hays et al., 1972), and Sites 159, 160, and 162 (van Andel, Heath, et al., 1973; Cronan, 1973). Miocene metalliferous sediments occur in the base of the sediment column at Site 81 (Hays et al., 1972) and in the upper part of the sediment column at Sites 74 (von der Borch et al., 1971) and 159 (Cronan, 1973). No study of these deposits has been published since the work of Cronan (1973, 1976; Cronan and Garrett, 1973), although Leinen (1981) described similar material from the northeast Pacific. Comparable Eocene-Oligocene sediments were collected on DSDP Leg 85 at Sites 573 and 574, and a stratigraphic succession including 54 sediment and 2 basalt samples was collected from these two localities for geochemical analysis. In this chapter, I describe the geochemistry of these samples, discuss the partitioning of elements between different mineral phases in the sediment, and examine the constraints these data place on the origin of the ferromanganese component.

MINERALOGY

Pelagic sediments in the eastern equatorial Pacific are composed dominantly of calcium carbonate (low-Mg calcite), biogenic opal, and clay minerals. Common accessory phases include quartz, feldspar, barite, apatite (fish debris), zeolites (phillipsite and clinoptilolite), and volcanic glass. Metalliferous sediments contain these components admixed with varying proportions of ferromanganese minerals. The ferromanganese phase was initially regarded as being X-ray amorphous (Boström and Peterson, 1966, 1970; von der Borch and Rex, 1970; von der Borch et al., 1971; Bender et al., 1971), but the application of ultraslow scan X-ray diffraction (XRD) and other techniques has shown that a number of discrete mineral phases can be recognized (Dasch et al., 1971; Dymond et al., 1973; Sayles and Bischoff, 1973; Sayles et al., 1975; Heath and Dymond, 1977; Dymond and Ek-

[1] Mayer, L., Theyer, F., et al., *Init. Repts. DSDP*, 85: Washington (U.S. Govt. Printing Office).

[2] Present address: Department of Geology, Kingston Polytechnic, Penrhyn Road, Kingston-upon-Thames, Surrey KT1 2EE, United Kingdom.

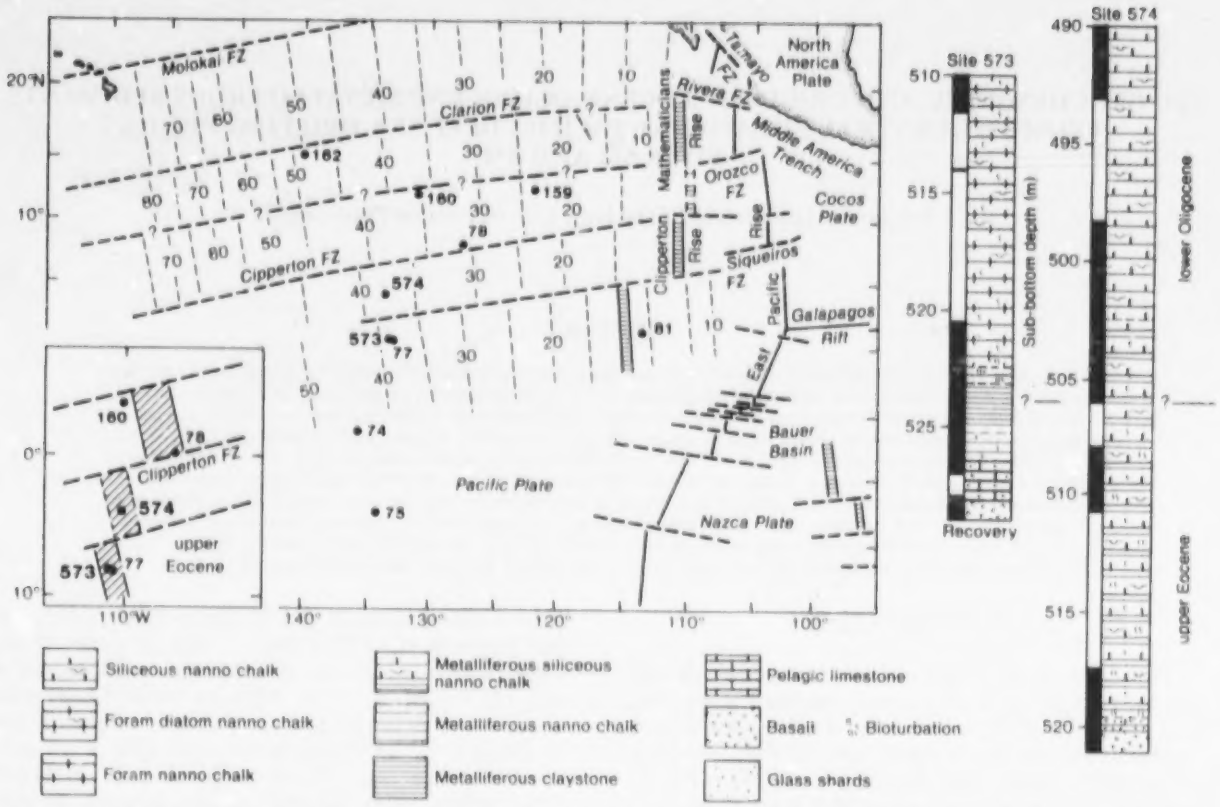

Figure 1. Location and stratigraphy of metalliferous sediments from DSDP Sites 573 and 574. The base map is a tectonic and basement isochron chart of the central equatorial Pacific (after van Andel et al., 1975). Bold numbers and dots indicate DSDP drilling sites where metalliferous sediments have been recovered. Solid line represents the ridge crest; broad striped zone is extinct ridge crest; heavy dashed lines are fracture zones (FZ). Light dashed lines with numbers 10 to 80 are basement isochrons, expressed in millions of years. Inset shows a reconstruction of the late Eocene ridge crest and the location of drilling sites based on the back-track model of van Andel et al. (1975). Stratigraphic columns are shown to the right; dark stripes indicate recovered intervals; light stripes indicate no recovery.

lund, 1978). A brown Fe smectite (generally identified as Fe montmorillonite) is an important, and commonly dominant, component in many deposits. Nontronite (a yellow-green, aluminum-poor Fe smectite) is the major iron-bearing phase in the Galapagos Hydrothermal Mounds Field (Honnorez et al., 1981; Honnorez, Von Herzen et al., 1983), and authigenic Fe montmorillonite is an important constituent in recent pelagic clays throughout the eastern and central Pacific (Aoki et al., 1974; Hein et al., 1979). Other minerals identified in metalliferous sediments include goethite (the dominant phase in some basal deposits), psilomelane, δMnO_2, birnessite, and todorokite. The wide range of manganese mineralogy reflects the inclusion of manganese micronodules and crusts in many deposits.

Preliminary mineralogic analysis of Leg 85 samples indicates the occurrence of varying proportions of calcite, poorly crystallized Fe smectite and goethite, δMnO_2, carbonate-fluorapatite, barite, quartz, and plagioclase feldspar.

MATERIAL

Eocene–Oligocene metalliferous sediments vary from pale-brown, metalliferous nannofossil chalks (composed of variable amounts of radiolarians, diatoms, and foraminifers) that are tens of meters thick and contain only a small percentage of Fe_2O_3, to dark-brown, metalliferous claystones only a few meters thick with greater than 30 wt.% Fe_2O_3. These metalliferous sediments either immediately overlie basalt or are separated from igneous rocks by a decimeter-thick bed of strongly indurated pelagic limestone containing abundant volcanic debris. The deposits have either sharp or transitional bottoms and tops and are commonly bioturbated. At Sites 74 and 75 decimeter thick metalliferous units are interbedded with pelagic oozes and have sharp but burrowed contacts; elsewhere (e.g., Sites 573 and 574) only a single metalliferous unit is present.

The holes cored continuously to basement on Leg 85 (at Sites 573 and 574) contained metalliferous sediments at the base of the sediment column. In both cases the deposits span the Eocene/Oligocene boundary (Barron et al., this volume), although the exact position of the boundary (Fig. 1) is difficult to determine because of the absence of microfossils (Site 573) or because of disparity in its position when defined using different fossil groups (Site 574). Hole 573B contains 4 m of metalliferous claystone and chalk overlying 1.4 m of strongly in-

durated, upper Eocene pelagic limestone and basalt (Fig. 1). Hole 574C contains 7.5 m of metalliferous chalks resting on basalt (Fig. 1). The top of the metalliferous unit at Site 573 displays numerous burrows (Planolites, Chondrites, and Zoophycos) filled with lighter colored sediment. The metalliferous chalks at Site 574 are burrow mottled throughout. The metalliferous component consists predominantly of dark brown, clay-sized grains and silt-sized aggregates mixed in varying proportions with biogenic debris. Scattered 0.5 to 3 mm glass shards and small 0.5 mm ferromanganese micronodules occur at both sites and are most abundant toward the base of the sections.

METHODS

Samples were taken on board the *Glomar Challenger* at approximately 20 cm intervals through the recovered interval of metalliferous sediment. In addition, representative material was selected from the pelagic sediments above and below the metalliferous units and from the underlying basalt. Disturbed sections and sediment near the core liners were avoided to minimize possible contamination.

Samples were dried at 60°C for 24 hr., and crushed in an agate mortar and pestle. Powders were desalinated by stirring in 500 ml of warm deionized water for 2 hr. followed by filtration and rinsing with fresh deionized water. Samples were redried and crushed prior to storage in glass vials.

The mineralogy of selected samples was determined by X-ray diffraction (XRD) at the Institute of Oceanographic Sciences (Wormley, Surrey, U.K.). Powders were reground in a tungsten–carbide tema to minimize grain-size variations between samples and then mounted in random-aggregate cavity mounts. Analyses were performed using Cu-Kα radiation at 40 kV/20 mA and a Philips PW1050 goniometer with AMR monochromator. Scan speeds of 0.25° 2θ/min were used throughout.

Geochemical analyses were performed on 54 sediment and 2 basalt samples. Three separate solution methods were applied to 0.5 g subsamples of the processed powders: (1) Fusion with lithium–metaborate in carbon crucibles and digestion of the hot fusion beads in 0.5 *N* HNO_3; (2) Open digestion in PTFE beakers using $HClO_4$ and HF followed by $HClO_4$ and H_3BO_3 acids; final solutions were made up in 1 *N* HCl; and (3) Partial digestion for 30 min. in warm 1 *N* HCl; solutions were filtered immediately and made up to volume with additional 1 *N* HCl.

Fusion solutions were analyzed simultaneously for Si, Fe, Mn, and Ca using a Philips PV8210 Inductively Coupled Plasma (ICP) Spectrometer at the Department of Geology, King's College, London. The open and partial digestions were analyzed simultaneously by ICP for Al, Fe, Mg, Mn, Ca, Na, K, P, Ba, Cr, Co, Cu, Li, Ni, Sc, Ti, V, and Zn. The HCl-soluble solutions were additionally analyzed for B. Values of K were checked by atomic absorption (AA) spectrometry. The rare earth elements (REE) and Y were extracted from solutions prepared by a separate HF–$HClO_4$ open digestion and using a cation separation procedure modified from Walsh et al. (1981). La, Ce, Pr, Nd, Sm, Eu, Gd, Dy, Ho, Er, Yb, Lu, and Y were determined simultaneously by ICP. Calibration curves were constructed using artificial composite standards (made from BDH and Eldrich standard solutions for atomic absorption and from Specpure chemicals) and were calculated to match closely the range of values expected for each element in the unknowns. Careful matching of matrices was essential to minimize interference effects. Raw intensity data were processed on a Digital PDP 11-34 computer, utilizing a program developed by the author, which incorporates drift and blank corrections. The REE data were additionally corrected for interelement interferences by Ba, Ca, Sr, Ti, and Zr to compensate for the small proportion of these elements that remained after the cation exchange procedure was completed.

Analytical precision as determined by replicate analyses is better than ± 5% for most elements and better than ± 3% for all of the REE present in amounts >0.2 ppm. Elements with poorer precisions are B, Ba, Ni (± 10%), and Cr (± 20%). Detection limits are below 5 ppm for all trace elements. Detection limits for the REE are below chondritic levels. By reference to international standards, absolute accuracy is judged to be within the limits indicated by the precision.

Fe, Mn, and Ca values obtained from the fusion and open-digestion solutions were averaged prior to further data reduction. The REE and Y were not determined on the HCl-soluble portions, and levels of Cr were generally below detection limits in these solutions. Finally, HCl-soluble values were compared with their corresponding whole-sediment values to determine whether any elements had been extracted completely by the differential leaching. It was concluded that Ca, P, and Sr (plus Ba at Site 574) values were indistinguishable (within the limits of the precision) between the two data sets, and values were averaged for each sample. Analytical results are presented in Appendixes A to D.

The metalliferous sediments generally contain little Ca, but the transitional sediments above and below them are characterized by highly variable Ca contents (e.g., Site 573, 3.04–54.70% CaO; Appendix A). Comparisons between the carbonate content and the percentage Ca in pelagic sediments from the eastern Pacific (Sayles et al., 1975; Dymond et al., 1976) have shown that <2% CaO occurs in the noncarbonate fraction. Pelagic clays generally contain <1% CaO (Turekian and Wedepohl, 1961; Chester, 1965; Dymond and Eklund, 1978; Barrett et al., 1983). Other elements (with the notable exception of Sr) vary inversely with the amount of Ca, indicating that although calcium carbonate has a major effect on the bulk composition of the sediments, it does not control the distribution of minor and trace elements. Compositional variations in the noncarbonate fraction are best assessed, therefore, if the data are recalculated on a carbonate-free basis (CFB). It is simplest to assume that all Ca occurs as $CaCO_3$ since the small percentage of Ca that does occur in other minerals (zeolites, feldspar, apatite, and clay minerals) should have no significant effect on the recalculated data. Where the carbonate content is high, however, small errors in Ca determinations produce large variations in the CFB values of other elements (Boström et al., 1976; Dymond et al., 1976). Calcium values reported here (Appendix A) were determined from three separate dissolutions of each sample; nevertheless, possible inaccuracies must be considered when interpreting CFB data.

RESULTS

The sampling scheme was devised to allow a stratigraphic assessment of interelement variation and was used in conjunction with the application of statistical techniques. Statistical techniques have proven to be a valuable tool in assessing interelement correlations and in determining the partitioning of elements between different mineral phases (Cronan, 1969b, 1972, 1976; Sayles et al., 1975; Marchig and Gundlach, 1982), but both methods are necessary to delimit possible postdepositional mobilization of elements in the sediment (e.g., Heath and Dymond, 1981). Consequently, stratigraphic analysis of geochemical data at Sites 573 and 574 has been combined in this study with an assessment of interelement variations.

Site 573

Sediments analyzed at Site 573 vary from white foraminifer diatom nannofossil chalk and pelagic limestone to dark brown metalliferous claystone (Figs. 1 and 2). The geochemical variation reflects this wide range in lithology.

Major Elements

Major element data (Fig. 2 and Appendix A) indicate a number of independent trends. Fe, Mn, and P have similar distributions, forming broad symmetric peaks that reach maxima in the middle of the metalliferous claystone (~524 m sub-bottom depth) and gradually drop

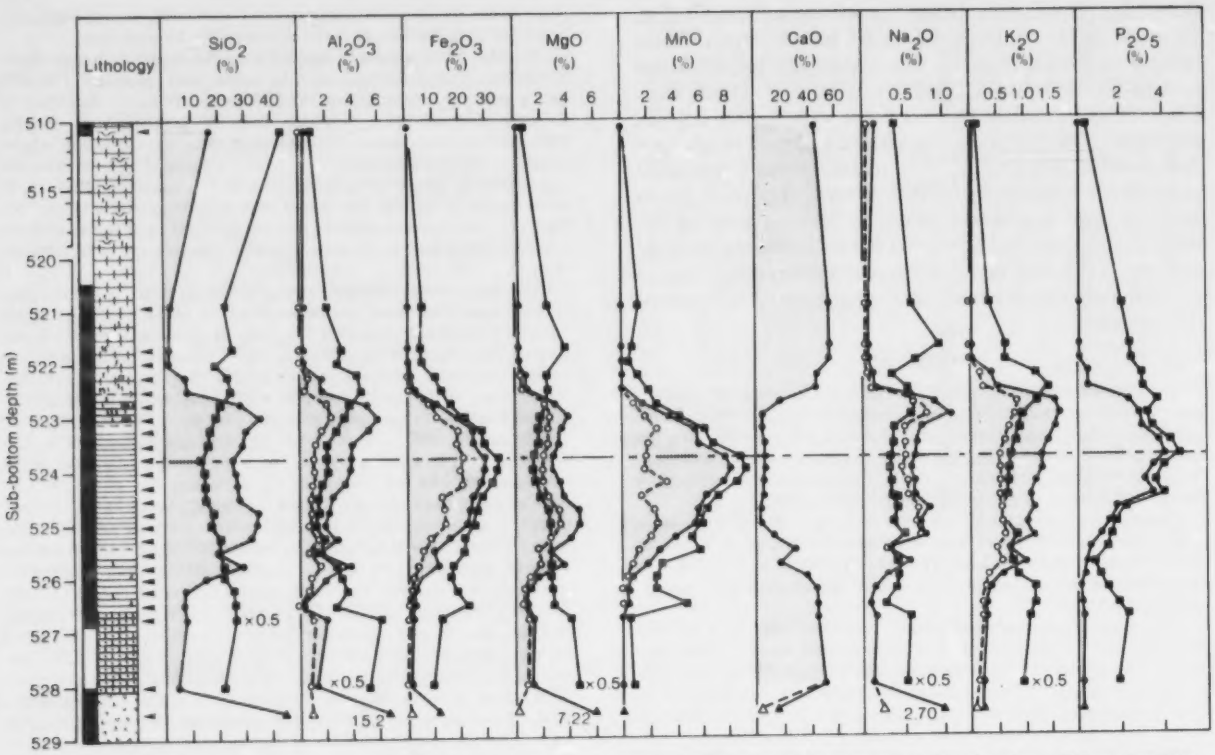

Figure 2. Stratigraphic variation of major elements in metalliferous sediments and associated lithologies at Site 573. For key to lithostratigraphic symbols see Figure 1. Stippled areas and black dots indicate bulk compositions; circles are HCl-soluble values. Squares are bulk compositions recalculated on a CFB; they represent the composition of the noncarbonate fraction. Scale factors (e.g., ×0.5) relate to CFB data; filled triangles indicate the bulk composition of the tholeiitic basalt and open triangles the HCl-soluble values for the basalts.

off to low concentrations at the base and top of the unit. Their distribution is reflected in the darker color of the sediment. Si, Al, Mg, Na, and K also show large increases within the metalliferous unit but display approximately bimodal distributions that peak at the top and toward the base of the unit. Ca has a distribution that is the inverse of the Si group of elements. These major groupings may be loosely ascribed to ferromanganese, aluminosilicate, and carbonate phases in the sediment. The relative amplitude of the two peaks displayed by the aluminosilicate group varies between different elements in the group. Al, Na, and K all display maxima at the top of the metalliferous unit, Mg reaches a maximum at the base of the unit, and the two Si peaks have approximately the same amplitude. This indicates that there are at least two separate mineral phases controlling the interelement variation within the aluminosilicate group. Concentrations of Al, Fe, Mg, Na, and K are higher in the Eocene limestone beneath the metalliferous unit than in the Oligocene chalk above. The underlying basalt (Fig. 2 and Appendix D) is strongly enriched in Al, Mg, and Na relative to the sediments.

The HCl-soluble values (Fig. 2 and Appendix A) do not simply follow the whole-sediment data. Fe and Mn have very different distributions (see below) indicating the presence of separate Fe- and Mn-bearing minerals. Smaller proportions of the total Al, Na, and K are HCl soluble in the upper part of the metalliferous unit, confirming the presence of two distinct aluminosilicate phases.

When expressed on a carbonate-free basis (Fig. 2), the whole-sediment data display essentially the same relationships within the metalliferous unit but the aluminosilicate group peaks are shifted even closer toward the top and bottom of the unit. The CFB data confirm that the noncarbonate component of the Eocene limestone is enriched in Al, Fe, Mg, and K relative to the Oligocene chalks.

Bivariate statistical analysis of the primary whole-sediment data (Table 1) demonstrates a strong negative correlation of all elements with Ca that overshadows the interrelationships between other elements. (Only samples of metalliferous sediment [522.25–526.45 m sub-bottom

Table 1. Correlation coefficients for major elements in metalliferous sediments at Site 573.

	SiO_2	Al_2O_3	Fe_2O_3	MnO	MgO	CaO	Na_2O	K_2O	P_2O_5
SiO_2									
Al_2O_3	0.67								
Fe_2O_3	0.77	0.54							
MnO	0.68	—	0.98						
MgO	0.97	—	0.74	0.66					
CaO	−0.95	−0.67	−0.93	−0.87	−0.91				
Na_2O	0.95	0.81	0.69	0.58	0.86	−0.88			
K_2O	0.87	0.91	0.77	0.67	0.73	−0.88	0.93		
P_2O_5	0.61	0.68	0.88	0.85	—	−0.80	0.65	0.81	

Note: Sample population = 18. Minimum significant correlation at 99% confidence level = 0.50; — indicates correlation coefficient is <0.50.

depth; Appendix A, Samples 573B-42-2, 25–26 cm to 42-4, 125–126 cm] were used in the bivariate analysis because the inclusion of other sediment types causes the correlation coefficients to be biased toward samples with large CFB recalculation factors or to be masked by a negative correlation with biogenic silica.) When recalculated on a CFB (Table 2), it can be demonstrated that Fe is strongly positively correlated with Mn and weakly positively associated with P and that this group is negatively correlated with the other major elements. Si is positively correlated with Al, Mg, and K, but Al variation does not correlate significantly with Mg; Na does not correlate significantly with any other element.

Table 2. Correlation coefficients for major elements in Site 573 metalliferous sediments recalculated on a carbonate-free basis.

	SiO_2	Al_2O_3	Fe_2O_3	MnO	MgO	Na_2O	K_2O	P_2O_5
SiO_2								
Al_2O_3	0.63							
Fe_2O_3	−0.83	−0.70						
MnO	−0.85	−0.75	0.97					
MgO	0.83	—	−0.59	−0.59				
Na_2O	—	—	−0.51	−0.55	—			
K_2O	0.73	0.93	−0.66	−0.71	—	—		
P_2O_5	−0.66	—	0.52	—	−0.91	—	—	

Note: Sample population = 18. Minimum significant correlation at 99% confidence level = 0.50; — indicates correlation coefficient is <0.50.

Trace Elements

The stratigraphic distribution of trace element data (Figs. 3 and 4 and Appendixes A and C) corresponds closely with the major element groups. B, Co, Cr, Cu, Ni, V, and Zn have similar distributions to the ferromanganese group. Li and Ti have strongly bimodal distributions with peaks of approximately equal amplitude; Sc has a bimodal distribution that reaches a maximum at the top of the metalliferous unit. The peaks of the bimodally distributed elements correspond in position with those of the aluminosilicate group (~523 and 526 m sub-bottom depth) defined by the major element data. Ce, La, and Y have distributions that correspond most closely to the ferromanganese group but have secondary peaks that match the upper peak of the aluminosilicate group. Sr has a distribution that is similar to Ca, but it is strongly depleted in the Eocene limestone and enriched in the upper part of metalliferous unit, Ba has an irregular distribution that does not relate closely to any other element; it reaches its highest concentration toward the base of the metalliferous sediments. The basalt is strongly enriched in Cr, Sc, and Ti relative to the overlying sediments.

The HCl-soluble distributions (Figs. 3 and 4 and Appendix A) broadly follow the whole-sediment values. Ti is relatively insoluble but Cu, Ni, and Zn are highly soluble in HCl. Other elements show intermediate solubilities.

The CFB recalculated data (Figs. 3 and 4) display significantly different distributions. B, Cu, Ni, V, Zn, and, to a lesser extent, Co and Cr all have high values in the

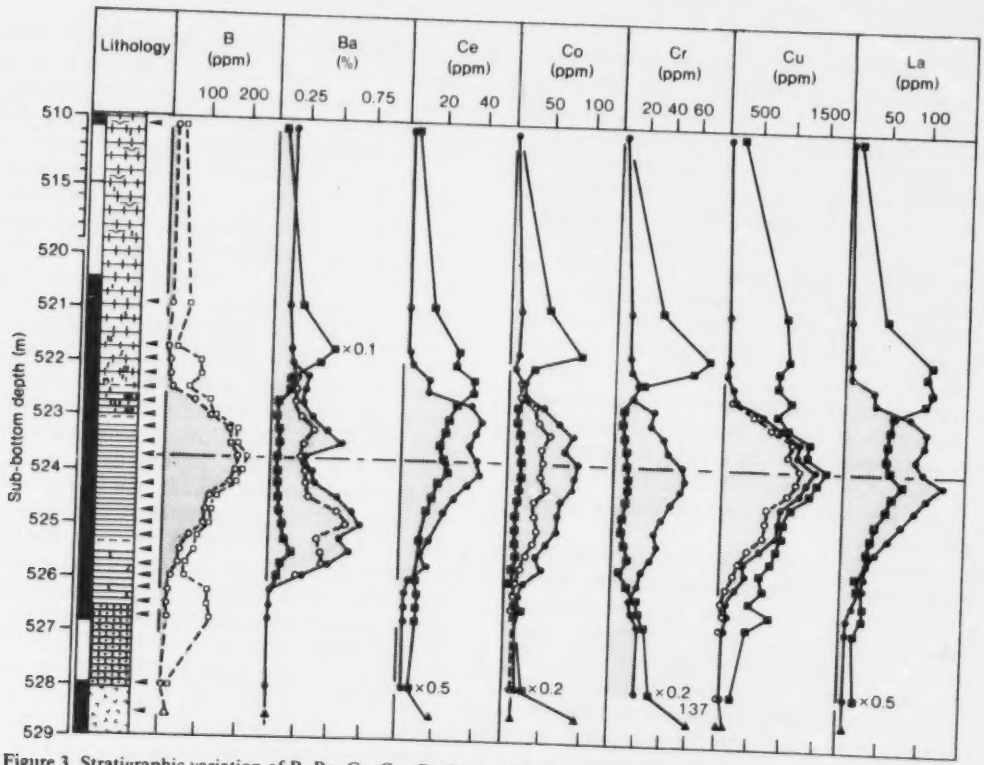

Figure 3. Stratigraphic variation of B, Ba, Ce, Co, Cr, Cu, and La in metalliferous sediments and associated lithologies, Site 573. Open squares are HCl-soluble values recalculated on a CFB; vertical scale and other symbols as in Figure 2.

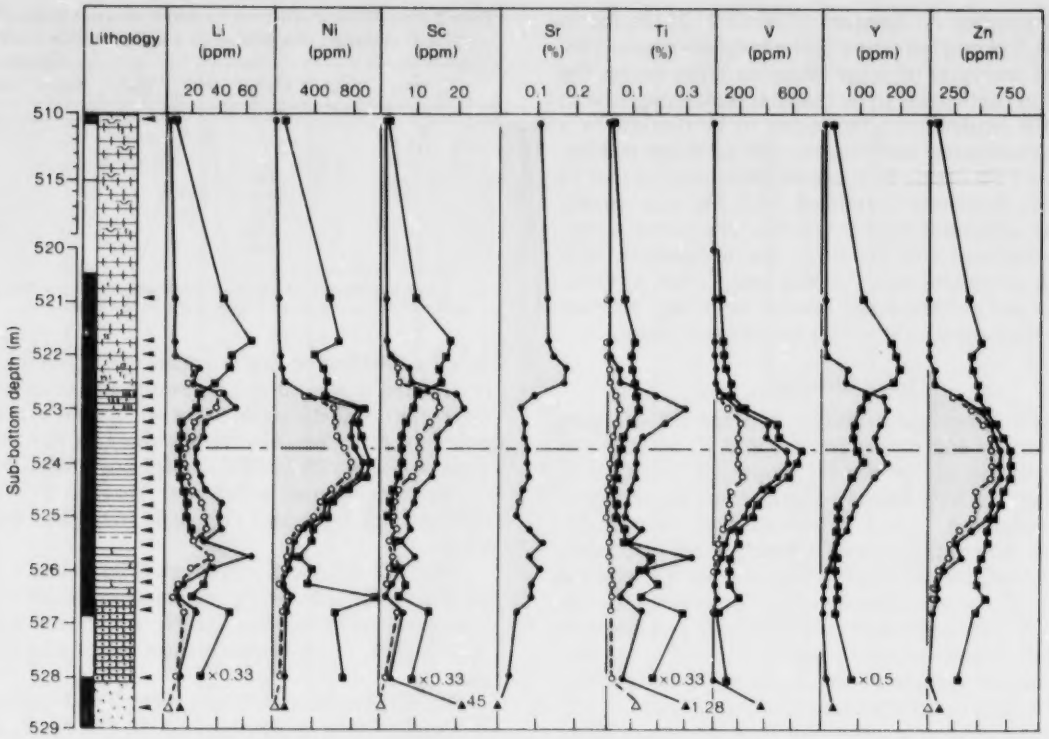

Figure 4. Stratigraphic variation of Li, Ni, Sc, Ti, V, Y, and Zn in metalliferous sediments and associated lithologies at Site 573. Vertical scale and symbols as in Figure 2.

middle of the metalliferous sediment unit relative to its top and base, confirming a correlation with the ferromanganese component. Ce, La, Sc, and Y are strongly enriched in the noncarbonate fraction at the top of the metalliferous unit relative to its middle and base. Cr and Li values expressed on a CFB are higher at the base and top of the metalliferous sediments than in the middle, which indicates a correlation with the aluminosilicate group of the major element data. Ti values increase markedly toward the base of the succession. The noncarbonate fraction in the Eocene limestone is enriched in Cr, Li, Sc, and Ti relative to that in the metalliferous sediments. Ba, Co, Cr, La, Li, Sc, and Y are all strongly enriched in the noncarbonate fraction of the three samples from immediately above the metalliferous unit. This trend must be interpreted with caution, however, because these samples have very high Ca values (>94% $CaCO_3$), which may have resulted in an overestimation of the CFB values at this level.

Bivariate analysis of the trace element data (Table 3) from the metalliferous sediments demonstrates strong negative correlations between Ca and all trace elements except Sr (which co-varies), Li, and Ti (both of which show no significant correlation). Fe and Mn have very strong positive correlations (coefficients of >0.90) with Co, Cr, Cu, Ni, V, and Zn (Fig. 5) and are also both significantly positively correlated with Ce, La, and Y. Correlation of the HCl-soluble data displays essentially the same trends (Fig. 5), but the correlation between Mn and Fe is much poorer, suggesting that the elements occur in different mineral phases. P correlates best with Ce, Co, Cu, La, Ni, V, and Y. Al and K co-vary with Sc (Fig. 6). The elements Ba, Li, and Ti correlate only weakly with each other and other elements, but most trace elements exhibit strong positive interelement correlations.

When trace element data are recalculated on a CFB (Table 4), the number of significant correlations is greatly reduced and many elements display negative rather than positive coefficients. Fe and Mn retain significant positive correlations with only B, Cu, Ni, V, and Zn and show significant negative correlations with Li, Sc, and Ti. Either Al or K (and sometimes both) are positively correlated with Ce, Co, Cr, Li, Sc, Ti, and Y and have negative coefficients with V and Zn. Both Si and Mg positively correlate with Li and Ti and negatively correlate with B, Cu, V, and Zn. P correlates with B, Ce, Cu, La, Ni, V, Y, and Zn; Na exhibits no positive trends.

The trace element data can be interpreted within the framework of the groups defined by the major elements. The ferromanganese phases (Fe and Mn) control the distribution of B, Cu, Ni, V, and Zn and affect the Co and Cr content of the sediment. The minerals represented by the aluminosilicate group (Si, Mg, Al, Na, and K) control the distribution of Co and Cr. Close examination of the data indicates, however, that the group contains two distinct phases. The first, indicated by the distribution of Si and Mg, also controls Li and Ti; the second is defined by Al and K, which co-vary with Sc. The carbonate phase (Ca) controls only Sr. P is strongly related to the ferromanganese group of elements but also affects

Table 3. Correlation coefficients for trace elements in Site 573 metalliferous sediments.

	Ba	Ce	Co	Cr	Cu	La	Li	Ni	Sc	Sr	Ti	V	Y	Zn
SiO_2	0.69	0.70	0.78	0.63	0.72	0.67	0.70	0.67	0.60	−0.70	0.52	0.55	0.65	0.82
Al_2O_3	—	0.87	0.66	—	0.64	0.74	0.55	0.68	0.96	—	0.80	—	0.81	0.56
Fe_2O_3	0.51	0.81	0.99	0.94	0.98	0.87	—	0.92	0.54	−0.64	—	0.95	0.77	0.99
MnO	—	0.74	0.96	0.96	0.96	0.84	—	0.89	—	−0.59	—	0.96	0.72	0.97
MgO	0.77	0.56	0.71	0.57	0.64	0.56	0.68	0.57	—	−0.73	—	—	0.50	0.79
CaO	−0.64	−0.82	−0.93	−0.82	−0.90	−0.83	—	−0.84	−0.63	0.70	—	−0.78	−0.78	−0.96
Na_2O	—	0.77	0.73	0.57	0.70	0.71	0.70	0.68	0.76	−0.61	0.60	0.50	0.73	0.74
K_2O	—	0.73	0.84	0.70	0.82	0.83	0.52	0.80	0.89	−0.54	0.60	0.66	0.86	0.79
P_2O_5	—	0.92	0.91	0.88	0.93	0.94	—	0.94	0.74	—	—	0.90	0.92	0.86
Ba														
Ce	—													
Co	—	0.88												
Cr	—	0.76	0.93											
Cu	—	0.89	0.99	0.94										
La	—	0.97	0.91	0.85	0.92									
Li	—	—	—	—	—	—								
Ni	—	0.90	0.94	0.86	0.96	0.94	—							
Sc	—	0.93	0.66	0.52	0.69	0.83	—	0.71						
Sr	—	—	−0.58	—	−0.55	—	—	−0.56	—					
Ti	—	—		—	—	—	0.77	—	0.64	—				
V	—	0.79	0.94	0.95	0.97	0.87	—	0.93	0.53	—	—			
Y	—	0.99	0.84	0.76	0.86	0.98	—	0.88	0.91	—	—	0.78		
Zn	0.56	0.80	0.98	0.92	0.96	0.87	—	0.91	0.55	−0.66	—	0.91	0.77	

Note: Sample population = 18. Minimum significant correlation at 99% confidence level = 0.50; — indicates correlation coefficient is <0.50.

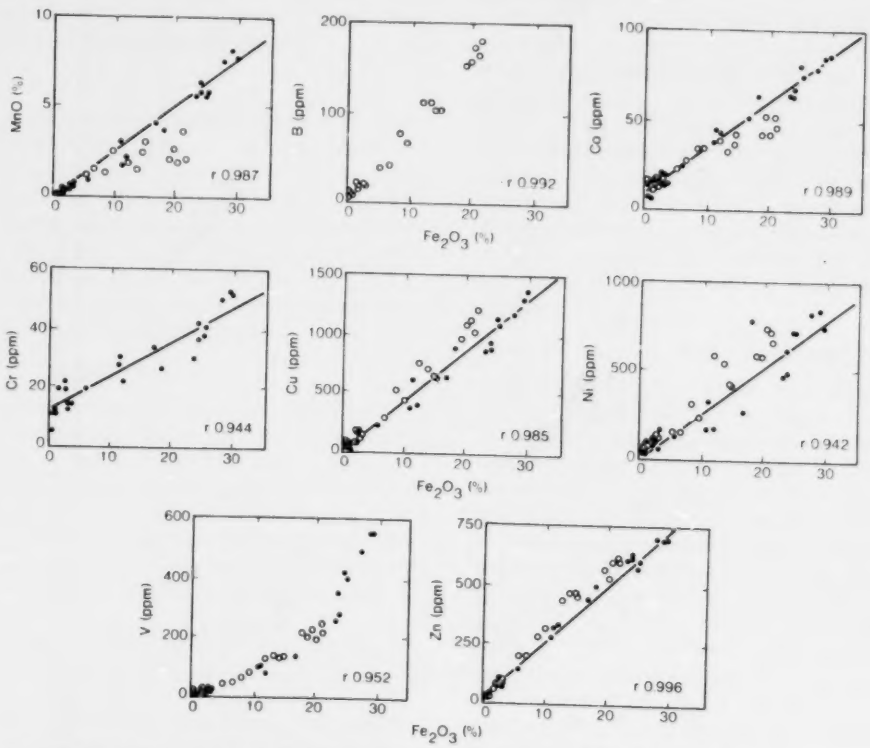

Figure 5. Variation diagrams of MnO and trace elements B, Co, Cr, Cu, Ni, V, and Zn with Fe_2O_3 in basal sediments at Site 573. Dots represent bulk compositions; circles represent HCl-soluble data. Only elements having highly significant correlations with Fe_2O_3 (>0.90) are shown. Regression lines and correlation coefficients relate only to bulk compositions; they incorporate all analyses of sediments at Site 573 and consequently differ slightly from those in Tables 1 and 3.

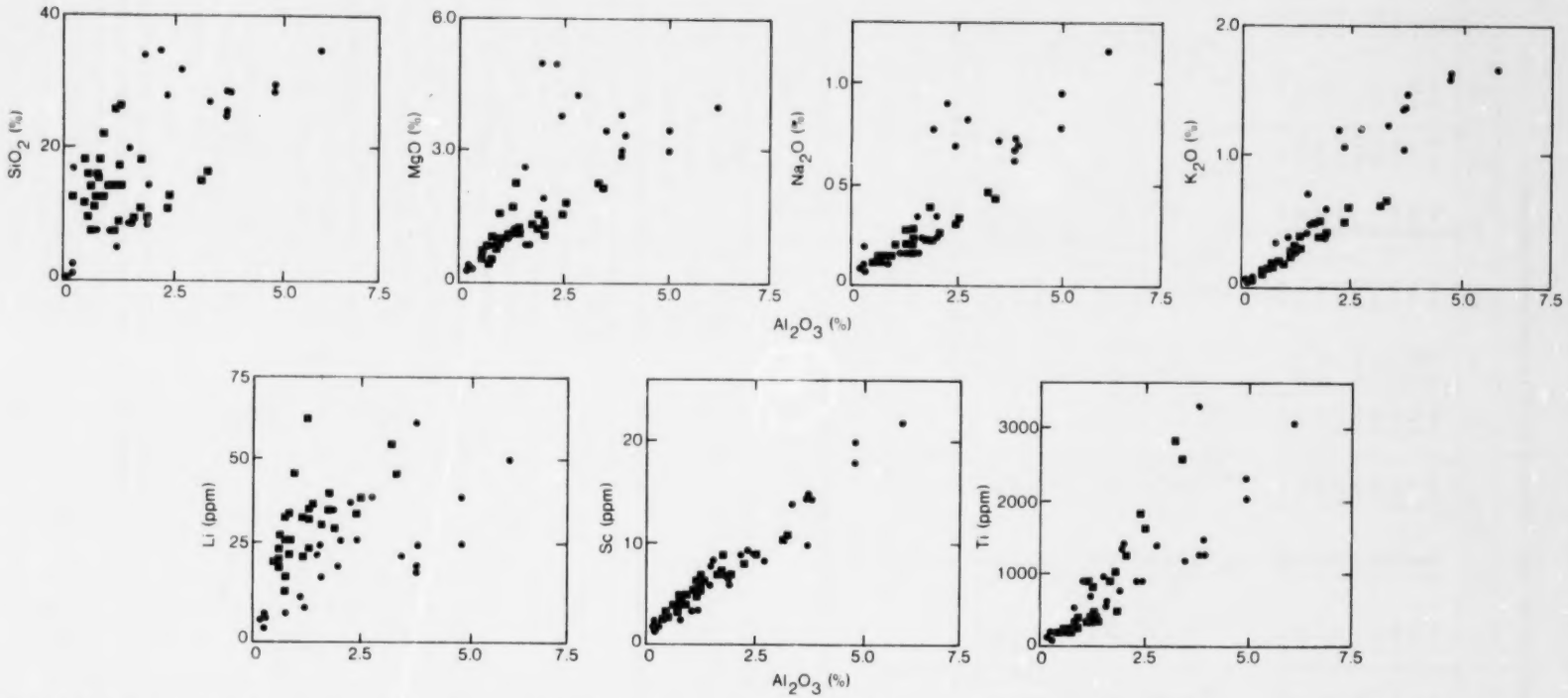

Figure 6. Variation diagrams of some major and trace elements with Al_2O_3 in basal sediments from Sites 573 and 574. Only elements that are strongly associated with Al are shown. Dots represent bulk compositions from Site 573; filled squares are bulk compositions from Site 574.

Table 4. Correlation coefficients for trace elements in Site 573 metalliferous sediments recalculated on a carbonate-free basis.

	B	Ba	Ce	Co	Cr	Cu	La	Li	Ni	Sc	Ti	V	Y	Zn
SiO_2	−0.77	—	—	—	0.55	−0.81	—	0.78	—	—	0.75	−0.89	—	−0.88
Al_2O_3	—	—	0.59	0.51	0.50	—	—	0.75	—	0.90	0.71	−0.50	0.62	−0.70
Fe_2O_3	0.86	−0.50	—	—	—	0.74	—	−0.92	0.66	−0.63	−0.63	0.94	—	0.96
MnO	0.79	—	—	—	—	0.74	—	−0.90	0.62	−0.63	−0.73	0.92	—	0.97
MgO	−0.79	—	−0.57	—	—	−0.92	−0.58	0.51	−0.52	—	0.56	−0.81	—	0.66
Na_2O	—	—	—	—	—	—	—	—	—	—	—	—	—	—
K_2O	—	—	—	0.54	0.62	—	—	0.64	—	0.82	0.65	−0.53	0.53	−0.69
P_2O_5	0.77	—	0.59	—	—	0.86	0.60	—	0.64	—	—	0.72	0.50	0.57
B														
Ba	−0.51													
Ce	—	—												
Co	—	—	0.55											
Cr	—	—	—	0.73										
Cu	0.84	—	—	—	—									
La	—	0.50	0.97	0.63	—	—								
Li	−0.77	0.56	—	—	—	−0.63	—							
Ni	0.74	−0.53	—	—	—	0.67	—	−0.65						
Sc	—	—	0.85	0.59	—	—	0.80	0.69	—					
Ti	—	—	—	—	—	—	—	−0.65	—	0.66				
V	0.93	—	—	—	—	0.90	—	−0.83	0.70	—	−0.64			
Y	—	0.54	0.98	0.60	—	—	0.98	—	—	0.89	—	—		
Zn	0.81	—	—	—	—	0.81	—	−0.88	0.64	−0.54	−0.74	0.95	—	

Note: Sample population = 18. Minimum significant correlation at 99% confidence level = 0.50; — indicates correlation coefficient is <0.50. B is determined from HCl-soluble portion only.

the distribution of Ce, La, and Y. This suggests the occurrence of a separate P-bearing phase in the sediment. Ba does not relate to any major or trace element and must also reside in a discrete mineral phase.

Site 574

Metalliferous sediments recovered from Site 574 do not show the extremes of lithologic variation observed at Site 573. The succession consists of white, siliceous nannofossil chalks underlain by a thick sequence of pale-brown, metalliferous, siliceous nannofossil chalks resting on basalt (Figs. 1 and 7). The basal 50 cm of sediment contains numerous shards of volcanic glass. The metalliferous sediments display relatively little geochemical variation (see Figs. 7–9; Appendix B).

Major Elements

With the exception of Si and Ca, most elements display progressive enrichment toward the base of the sediment column (Fig. 7; Appendix B). Differences between the distribution of different elements are less distinct than at Site 573. Ca and Sr values show small variations that are the inverse of those displayed by other elements. Recalculation of the data on a CFB smooths out minor fluctuations but does not markedly affect the overall trends.

Most elements are enriched below 510 m sub-bottom depth. Al, Na, and K (and to a lesser extent Fe and Mg) all peak at ~505 m but are highest in the basal 2 m of sediment. Mn and P also peak at ~505 m but exhibit their highest concentrations of ~518 m, tailing-off below that. Si decreases progressively toward the base of the section. Fe, Mg, Mn, and K are less HCl soluble and Na is more HCl soluble in the sediment below 510 m than above it. This indicates different mineralogic controls on these elements in the upper and lower parts of the section. The basalt (Fig. 7; Appendix D) is strongly enriched in Si, Al, Fe, Mg, and Na compared with the overlying sediments.

Bivariate analysis of the CFB major element data (Table 5) demonstrates strong negative correlations between Si and all other elements, which are themselves significantly positively correlated. (Only CFB matrices will be discussed since they differ little from those derived from the primary data, and they were found to be better indicators of mineralogic control at Site 573. Ca has a strong negative correlation with all elements except Sr.) There is evidence, therefore, for discrete carbonate, silica, and "metalliferous" phases, but subdivision of this last category is not possible using the major element analyses.

Trace Elements

Stratigraphic plots of the trace element data (Figs. 8 and 9; Appendixes B to D) display (with the exception of Ba and Sr) marked enrichments below ~510 m sub-bottom depth. This enrichment is greatest for B, Co, Cu, Sc, Ti, V, and Zn. Li, Sc, and Ti all peak at ~505 m and increase markedly toward the base in the lowest 2 m of sediment (518 to 520 m). Ti is enriched in the basal sediment by an order of magnitude. These trends correspond to the distribution of Al, Na, and K in the sediment. B, Ce, Cr, Cu, La, Ni, V, Y, and Zn also display peaks at ~505 m but reach their highest concentrations at ~518 m before tailing-off. This corresponds to the distribution of Mn and P. Ba does not display any significant trend. Irregularities in the distributions of Cr are partly related to the low levels of this element in the sediment. Recalculation on a CFB (Figs. 8 and 9) does not significantly alter these trends. The underlying basalt is strongly enriched in B, Co, Cr, Sc, Ti, V, and Zn relative to the sediments.

Cu, Ni, Sc, and Zn are less HCl soluble in the basal part of the section than in the sediment above. Most of

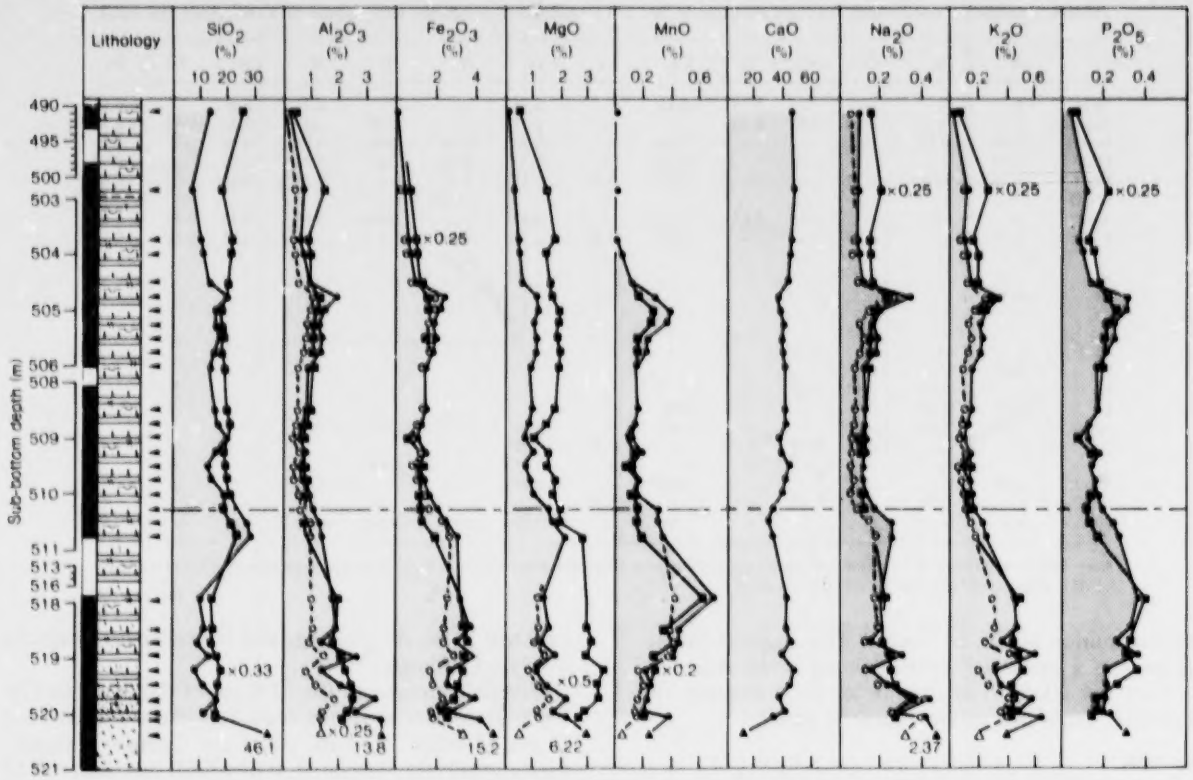

Figure 7. Stratigraphic variations of major elements in metalliferous sediments and associated lithologies at Site 574. Symbols as in Figure 2. The vertical scale is contracted for intervals where no sediment was recovered, allowing easier evaluation of interelement trends.

Table 5. Correlation coefficients for major elements in Site 574 metalliferous sediments recalculated on a carbonate-free basis.

	SiO_2	Al_2O_3	Fe_2O_3	MnO	MgO	Na_2O	K_2O	P_2O_5
SiO_2								
Al_2O_3	−0.73							
Fe_2O_3	−0.80	0.85						
MnO	−0.68	0.51	0.80					
MgO	−0.70	0.88	0.94	0.64				
Na_2O	−0.56	0.92	0.69	—	0.74			
K_2O	−0.75	0.95	0.93	0.68	0.89	0.85		
P_2O_5	−0.59	0.62	0.79	0.84	0.66	0.47	0.77	

Note: Sample population = 30. Minimum significant correlation at 99% confidence level = 0.40; -- indicates correlation coefficient is <0.40.

the Co, Cu, Li, and Ni is soluble in HCl throughout the succession, while Ti is relatively insoluble.

Bivariate analysis of the CFB data (Table 6) indicates that Si is either uncorrelated or negatively correlated with all trace elements. Most elements are positively correlated, and it is difficult to differentiate distinct interelement associations. Correlations of Fe and Mn with trace elements at Site 574 do not correspond as closely as at Site 573 (Fig. 10). Fe correlates best with B, Co, V, and Zn, and Mn appears to control Cu and Ni. Comparison of the interelement correlations of Fe at Site 573 with those at Site 574 (Fig. 10) indicates very similar linear trends for most elements suggesting that the ferromanganese phases at two sites have comparable mineralogies and diagenetic histories. Al and K have strong positive correlations with Co, Sc, Ti, V, and Zn, which also correspond closely to the trends displayed by the aluminosilicate group at Site 573 (Fig. 6). P correlates strongly with B, Ce, Cu, La, Ni, V, Y, and Zn. The absence of clear groups of elements may be attributed to the lack of lithologic end-members in the succession. Further interpretation of the data requires consideration of the mineralogic constraints and comparison with other deposits.

DISCUSSION

The East Pacific Rise is a relatively young feature (Sclater et al., 1971; Herron, 1972; van Andel et al., 1975). Previously the eastern boundary of the Pacific Plate was located along a series of fossil ridge crests referred to as the Galapagos, Clipperton, and Mathematicians' rises (Fig. 1). Seafloor spreading patterns and other geologic data indicate that these ridges became extinct at 5–12 Ma (van Andel et al., 1975). Basement ages and paleomagnetic data demonstrate that Sites 573 and 574 were located at the ridge crests during the late Eocene (Fig. 1). This is consistent with the hypothesis that the formation of the basal metalliferous sediments at the two sites is related to ridge crest hydrothermal activity (e.g., see Cronan, 1976), but it does not necessarily prove that the sediments were deposited in the immediate vicinity of an active hydrothermal vent system. Metalliferous sediments at Site 573 contain the highest concentra-

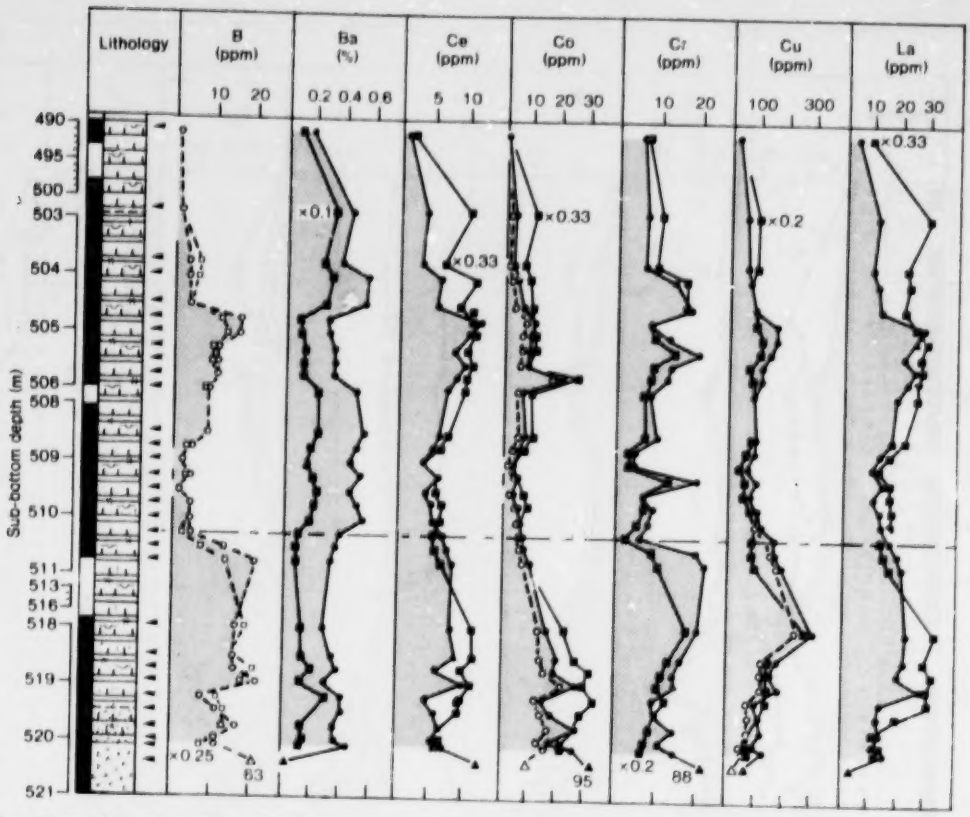

Figure 8. Stratigraphic variation of B, Ba, Ce, Co, Cr, Cu, and La in metalliferous sediments and associated lithologies at Site 574. Open squares are HCl-soluble values recalculated on a CFB; vertical scale and other symbols as in Figure 7.

tion of ferromanganese material but rest on Eocene limestone containing little noncarbonate sediment. Sediments at Site 574 are dominantly pelagic oozes and contain only an accessory ferromanganese component. Comparison with recent metalliferous sediments is necessary to provide a framework to interpret the origin of the Eocene–Oligocene deposits.

Modern Analogs

Recent metalliferous sediments in the eastern Pacific can be subdivided into three main sediment types based on deposits exemplified by three classic areas: (1) the Galapagos Mounds, (2) the East Pacific Rise, and (3) the Bauer Basin.

Galapagos Mounds Sediments

The sediments of the Galapagos Mounds (Corliss et al., 1978; Hekinian et al., 1978; Edmond et al., 1979a,b; Williams et al., 1979) are composed dominantly of nontronite-rich, aluminum-poor, Fe smectite sediment in lenticular masses up to a few meters thick and tens of meters across (Honnorez, Von Herzen et al., 1981, 1983). Lenses of nontronite are interbedded with pelagic sediments beneath hydrothermal mounds and ridges 25 to 50 m across, which form positive topographic features on the seafloor (Klitgord and Mudie, 1974; Lonsdale, 1977). It has been suggested (Corliss et al., 1978; Hekinian et al., 1978) that nontronite forms from reducing, metal-rich hydrothermal fluids leached from basalt, which replace pelagic sediments during early diagenesis (Honnorez, Von Herzen et al., 1981, 1983; Moorby, 1983). Suboxic conditions below the seafloor (Bender, 1983) result in the mobilization of Mn that has reprecipitated as Mn-oxide crusts near the sediment/water interface. The resulting metalliferous sediments therefore display strong fractionation between the Fe and Mn phases. Nontronite-rich layers are strongly enriched in Si and Fe but have very low Al, Mn, Ca, and trace element contents (Tables 7 and 8). Mn crusts are relatively depleted in Si and Fe but enriched in Mn and trace elements (Moorby and Cronan, 1983). Basal sediments are less pure, having substantial Al contents due to admixture of detrital phases (Varnavas and Cronan, 1981; Moorby and Cronan 1983; Varnavas et al., 1983).

East Pacific Rise Sediments

The metalliferous sediments of the East Pacific Rise are composed primarily of amorphous ferromanganese oxyhydroxides (Boström and Peterson, 1966; Boström, Peterson, et al., 1969; Boström, Joensuu, et al., 1976; Horowitz, 1970; Bender et al., 1972; Piper, 1973; Dymond and Veeh, 1975; Heath and Dymond, 1977, 1981) that recrystallize to goethite (Marchig and Gundlach, 1982) during early diagenesis. They form extensive de-

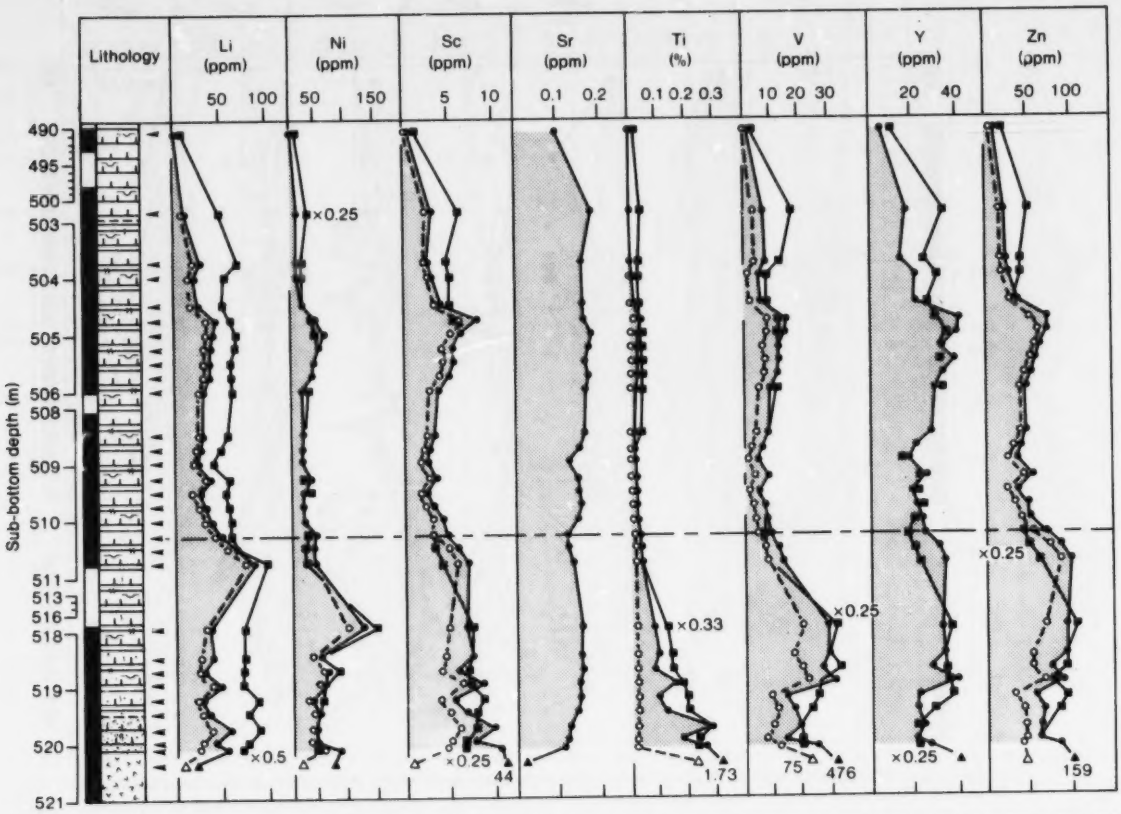

Figure 9. Stratigraphic variation of Li, Ni, Sc, Sr, Ti, V, Y, and Zn in metalliferous sediments and associated lithologies from Site 574. Vertical scale and symbols as in Figure 7.

Table 6. Correlation coefficients for trace elements in Site 574 metalliferous sediments recalculated on a carbonate-free basis.

	B	Ba	Ce	Co	Cr	Cu	La	Li	Ni	Sc	Ti	V	Y	Zn
SiO_2	−0.62		−0.41	−0.72	—	−0.52	—	—	−0.62	−0.67	−0.68	−0.68	—	−0.70
Al_2O_3	0.68		0.44	0.88	—	0.47	—	0.56	0.54	0.95	0.93	0.75	0.43	0.77
Fe_2O_3	0.86		0.49	0.92	0.40	0.69	0.51	0.65	0.70	0.85	0.80	0.90	0.53	0.95
MnO	0.80		0.51	0.64	0.48	0.90	0.60	0.41	0.92	0.56	0.41	0.81	0.56	0.88
MgO	0.78		—	0.88	—	0.57	—	0.80	0.57	0.86	0.86	0.78	0.41	0.90
Na_2O	0.60		—	0.74	—	—	—	0.44	0.41	0.86	0.88	0.61	—	0.62
K_2O	0.75		0.50	0.92	0.43	0.65	0.50	0.52	0.69	0.95	0.88	0.89	0.53	0.88
P_2O_5	0.78		0.77	0.72	0.58	0.90	0.88	0.46	0.82	0.75	0.41	0.89	0.86	0.92
B														
Ba	—													
Ce	0.62	—												
Co	0.75	—	0.46											
Cr	0.43	—	0.53	—										
Cu	0.71	—	0.63	0.56	0.62									
La	0.62	—	0.91	0.49	0.54	0.74								
Li	0.63	—	—	0.53	—	0.45	—							
Ni	0.68	—	0.51	0.59	0.55	0.94	0.61	—						
Sc	0.72	—	0.61	0.86	0.47	0.60	0.56	0.62	0.60					
Ti	0.55	—	—	0.83	—	—	—	0.49	0.41	0.82				
V	0.80	—	0.58	0.84	0.51	0.81	0.70	0.44	0.79	0.82	0.63			
Y	0.63	—	0.94	0.51	0.55	0.70	0.98	—	0.57	0.61	—	0.67		
Zn	0.85	—	0.60	0.85	0.53	0.86	0.69	0.67	0.81	0.83	0.69	0.92	0.69	

Note: Sample population = 30. Minimum significant correlation at 99% confidence level = 0.40; — indicates correlation coefficient is <0.40. B is determined from HCl-soluble portion only.

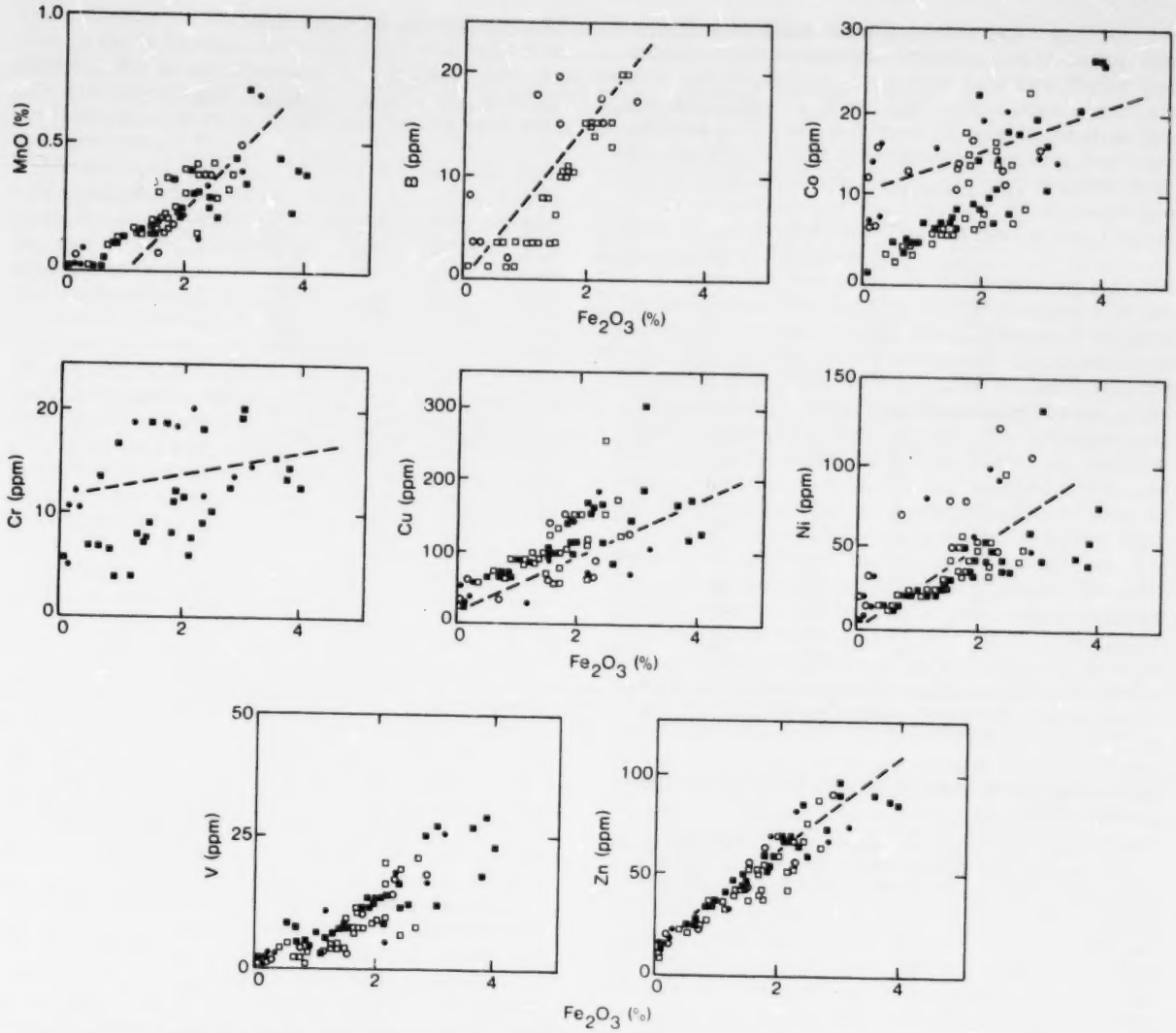

Figure 10. Variation diagrams of MnO and trace elements B, Co, Cr, Cu, Ni, V, and Zn with Fe_2O_3 in basal sediments at Site 574. Filled squares indicate bulk compositions; open squares represent HCl-soluble data. Dots and open circles are corresponding values from sediments at Site 573. Regression lines are based on bulk compositions at Site 573 (Figure 5). There is a strong similarity in the interelement trends between the two sites.

posits on the ridge crest and generally overlie basalt; on the flanks of the ridge they are mixed with increasing amounts of biogenic material and smectite. It is believed (Zelenov, 1964) that the oxyhydroxides form where reducing, metal-rich hydrothermal solutions mix with seawater, producing a precipitate that settles out of suspension. Suboxic diagenesis has resulted in mobilization of some Mn which is depleted in the lower part of the sediment column (Heath and Dymond, 1981). The predominance of oxyhydroxides is partly related to the high rate of deposition of the metalliferous component (Dymond and Veeh, 1975; McMurtry et al., 1981) on the ridge crest, which swamps biogenic and other particulate phases. The resulting metalliferous sediments are strongly enriched in both Fe and Mn but depleted in Si and Al relative to other types (Table 7). The sediments of the East Pacific Rise are enriched in trace elements relative to the Galapagos Mounds nontronites.

Bauer Basin Sediments

The metalliferous sediments of the Bauer Basin contain up to 90% Fe smectite (Sayles et al., 1975; Dymond et al., 1976; Dymond and Eklund, 1978; Heath and Dymond, 1977, 1981) mixed with varying proportions of ferromanganese oxyhydroxides and mixed-layer clay minerals (Sayles and Bischoff, 1973; Cronan, 1980; Dymond, 1981; Marchig et al., 1982). They form laterally extensive deposits that accumulate slowly in deep basins immediately below the calcite compensation depth (CCD). The Fe smectite (commonly identified as Fe montmorillonite) is probably authigenic (hydrogenous), formed by a reaction between Fe oxyhydroxides (brought into the

Table 7. Major and trace element composition of metalliferous sediments from the eastern Pacific.

	Site 573 basal n = 18 (1)	Site 574 basal n = 28 (2)	East Pacific Rise surface n = 20 (3)	DSDP Pacific Basal n = 25 (4)	DSDP Pacific Basal n = 12 (5)	Bauer Deep Surface n = 59 (6)	Bauer Deep Basal n = 11 (7)	Galapagos Mounds Nontronite n = 13 (8)	Galapagos Mounds Basal n = 9 (9)
Major elements (%)									
SiO_2	40.30	54.80	7.49	23.10	45.60	37.40	15.00	52.60	41.30
Al_2O_3	5.32	5.09	0.68	5.16	9.85	5.06	2.23	0.38	9.07
Fe_2O_3	23.20	7.58	40.20	28.70	16.30	23.00	34.10	29.90	8.86
MnO	5.21	0.91	11.90	7.83	2.08	6.73	8.37	0.04	1.03
MgO	4.87	4.37	2.23	3.45	6.05	4.24	—	4.30	5.31
CaO	CFB	CFB	CFB	2.06	CFB	CFB	CFB	0.37	CFB
Na_2O	0.86	0.69	0.67	3.45	—	1.01	—	2.51	—
K_2O	1.79	1.01	0.25	1.39	—	1.06	—	3.22	1.10
P_2O_5	2.68	0.79	2.62	—	—	—	—	—	0.41
Trace elements (ppm)									
Ba	6150	16000	2100	6230	3850	19000	9250	350	—
Ce	35	24	13	—	—	51	44	—	—
Co	85	45	111	82	59	176	134	—	50
Cr	57	45	30	—	—	32	26	14	110
Cu	979	461	1300	790	293	1160	1440	20	240
La	100	65	107	—	—	216	144	—	—
Ni	608	147	600	460	232	1010	565	13	260
Sc	19	20	—	—	—	19	11	—	—
Ti	2460	2340	300	—	—	—	—	120	2950
V	289	52	1920	—	—	—	—	12	240
Y	156	99	110	—	—	—	—	—	—
Zn	590	220	394	470	231	450	555	35	310

Note: Sources for (1) and (2) this work; (3) Marchig and Gundlach, 1982; (4) Cronan, 1976; (5) Leinen, 1981; (6) Sayles et al., 1975; Dymond et al., 1976; Heath and Dymond, 1981; (7) Dymond et al., 1976; (8) Honnorez et al., 1983; (9) Moorby and Cronan, 1983. n = number of analyses; CFB = carbonate-free basis; — = not reported.

Table 8. Major element composition of Fe-rich clay minerals from the eastern Pacific.

Major elements (%)	Average Pacific clay (bulk sediment) n = 26 (1)	Northeastern Pacific Fe montmorillonite (bulk sediment) n = 5 (2)	Bauer Deep Fe smectite (microprobe) n = 10 (3)	Galapagos Mounds nontronite (microprobe) n = 11 (4)
SiO_2	53.50	51.70	52.30	52.20
Al_2O_3	17.70	8.13	2.44	0.19
Fe_2O_3	7.23	14.70	29.70	30.30
MnO	0.62	0.29	0.64	0.06
MgO	2.92	4.21	6.10	3.90
CaO	0.92	0.15	0.47	0.38
Na_2O	1.59	1.21	0.60	0.94
K_2O	3.23	0.71	2.04	3.74
P_2O_5	0.24	nd	nd	nd
Total	87.95	81.10	94.29	91.71

Note: Sources of data are (1) Turekian and Wedepohl, 1961; Chester, 1965; Cronan, 1969; (2) Aoki et al., 1974; (3) Dymond and Eklund, 1978; (4) Barrett et al., 1983. n = number of analyses; nd = not determined.

basin by currents from the East Pacific Rise) and biogenic silica (Lyle et al., 1977; Heath and Dymond, 1977; Dymond and Eklund 1978; Bischoff, Heath, et al., 1979; Bischoff, Piper, et al., 1979; Hein et al., 1979; Lyle, 1981). Early diagenesis is oxic, and there is no evidence of Mn migration (Lyle, 1981; Heath and Dymond, 1981). The resulting metalliferous sediments are characterized by Al contents that are higher than in either nontronites or East Pacific Rise deposits and by intermediate Si contents (Tables 7 and 8). They display the greatest degree of trace element enrichment (Table 7) of the three types, probably because they accumulated more slowly (Dymond and Veeh, 1975; McMurtry et al., 1981) near the sediment/water interface where oxyhydroxides and/or smectite could absorb transition metals from seawater (Toth, 1980). Basal sediments in Bauer Basin directly overlie basalt (Dymond et al., 1976) and have lower A' and Si contents (Table 7), suggesting that they are more akin to the East Pacific Rise deposits.

In addition to the three main categories, local seafloor deposits of metal sulfides occur at 21°N on the East Pacific Rise (Edmond, Measures, McDuff, et al., 1979; Edmund, Measures, Mangum, et al., 1979; Francheteau et al., 1979; Hekinian et al., 1980), and hydrothermal vents also precipitate sulfides in the Galapagos Mounds Hydrothermal Field (Corliss et al., 1979; Edmond, Measures, Mangum, et al., 1979). These are, however, very localized deposits that are mineralogically distinct from the others considered here. There is no evidence of sulfides in the Leg 85 material. It has been speculated, however, that oxidation of sulfides suspended in the water column provides an alternative mechanism for the formation of dispersed oxyhydroxides (Dymond, 1981; Michard et al., 1983; Shearme et al., 1983).

Mineralogy and Composition

Comparison between the mineralogy and average CFB bulk chemistry of Leg 85 metalliferous sediments and their modern analogs (Table 7) indicates that the sediments at Site 573 closely resemble those from the Bauer Basin and that they are not dissimilar to basal sediments recovered at other DSDP sites in the eastern Pacific. Metalliferous sediments at Site 574 contain substantially more Si and are depleted in Fe and Mn relative to other sites, reflecting a greater abundance of biogenic silica here.

The sediments at Sites 573 and 574 contain more Al than do the Galapagos Mounds or the East Pacific Rise deposits; they are enriched in Si relative to the East Pacific Rise deposits and to most basal sediments, and they are strongly enriched in trace elements compared with the nontronites.

Metalliferous sediments of the Bauer Basin are composed predominantly of Fe smectite, yet at Site 573 Fe displays a strong negative correlation with Si, Al, Mg, Na, and K in the noncarbonate fraction (Table 2). This apparent anomaly can be explained if the major element data are examined in more detail. Lithostratigraphic analysis has demonstrated that the composition of the noncarbonate fraction varies considerably between the middle and the margins of the metalliferous unit. If representative sample analyses from these three portions (Table 9) are compared with analyses of Fe-rich clay minerals from the eastern Pacific (Table 8), it becomes apparent that the noncarbonate fraction from the base and top of the metalliferous unit has a comparison similar to Fe montmorillonite from the northeast Pacific (Aoki et al., 1974) but that it contains excess Mn and P. This composition is intermediate between Fe smectite from the Bauer Basin (Dymond and Eklund, 1978) and average Pacific clay (Turekian and Wedepohl, 1961; Chester 1965; Cronan, 1969).

Sediment from the middle of the metalliferous unit at Site 573 contains a far higher percentage of Fe, Mn, and P but less of the other major elements than do the top and base of the unit. This difference in composition is explained by XRD data that indicate an increased admixture of ferromanganese oxyhydroxides (including goethite and δMnO_2), similar to that in the East Pacific Rise deposits (Table 7). Thus, the oxyhydroxide phases are enriched in Fe, Mn, and P but depleted in the other major elements relative to Fe smectite, resulting in a negative correlation between the two groups of elements. Metalliferous sediments at Site 574 show less variation and have compositions (Tables 7 and 9) that indicate the predominance of Fe smectite.

Table 9. Compositional variation in the noncarbonate fraction of metalliferous sediments at Sites 573 and 574.

	573B-42-2, 50–51 cm	573B-42-3, 25–26 cm	573B-42-2, 125–126 cm	574C-35-2, 26–27 cm
Major elements (%)				
SiO_2	51.10	29.20	53.00	54.50
Al_2O_3	9.68	4.56	7.58	9.05
Fe_2O_3	13.70	34.90	19.20	13.40
MnO	1.96	9.00	2.69	1.42
MgO	5.05	3.34	6.34	7.42
Na_2O	1.12	0.77	0.90	0.97
K_2O	2.79	1.57	2.44	2.09
P_2O_5	2.88	4.72	1.40	1.41
Total	88.20	88.06	93.55	90.26
Trace elements (ppm)				
B	61.7	212.0	118.0	43.8
Ba	14300.0	2780.0	366.0	28300.0
Ce	70.9	42.8	19.9	28.0
Co	118.0	103.0	95.8	103.0
Cr	69.7	59.6	93.0	61.5
Cu	1080.0	1610.0	488.0	706.0
La	204.0	114.0	50.6	96.9
Li	105.0	23.3	79.2	165.0
Ni	512.0	867.0	326.0	228.0
Sc	46.0	16.4	21.4	34.6
Ti	3050.0	1360.0	5810.0	5860.0
V	112.0	649.0	111.0	101.0
Y	348.0	173.0	85.8	146.0
Zn	479.0	794.0	442.0	372.0

Note: Total Fe expressed as Fe_2O_3; B determined from HCl-soluble portion only.

It is possible, therefore, to assign most of the Si in the metalliferous sediments at Site 573 to smectite, which would appear to indicate the virtual absence of biogenic opal. In addition, the Ca content of the metalliferous claystone is very low (Fig. 2), which indicates that the sediment contains little or no biogenic carbonate, a conclusion confirmed by XRD analysis. This is in sharp contrast to other sediments at the site, which are predominantly biogenic. A decline in the biogenic component could be explained by: (1) a reduced influx of biogenic detritus, (2) increased input of the metalliferous component, (3) dissolution of biogenic silica and carbonate, or (4) a combination of these three processes. Biostratigraphic evidence (Barron et al., this volume) indicates that the metalliferous claystone at Site 573 was deposited at a greatly reduced rate of deposition and probably contains a depositional hiatus corresponding to the Eocene/Oligocene boundary. A comparable hiatus is widespread throughout the Pacific (Kennett et al., 1975), although it apparently does not occur at Site 574. Clearly, a massive influx of ferromanganese oxyhydroxides and Fe smectite did not swamp normal biogenic sedimentation, although fluctuation in the supply of ferromanganese minerals may have been a contributory factor.

The state of preservation of microfossils within the metalliferous sediments at Site 573 indicates that both calcareous (planktonic foraminifers and nannofossils) and siliceous (diatoms and radiolarians) forms have undergone severe dissolution in the transitional sediments and that they are entirely absent in the metalliferous claystone. The claystone contains only an impoverished fauna of benthic foraminifers. A positive correlation between dissolution of microfossils and Fe content is also apparent at Site 574. It may be concluded that dissolution, probably combined with reduced biogenic sedimentation, was a major process in the formation of these metalliferous sediments.

There is no evidence for a detrital source for Fe smectite (Griffin et al., 1968), and it has been suggested (Lyle et al., 1977; Heath and Dymond, 1977; Dymond and Eklund, 1978; Bischoff et al., 1979; Hein et al., 1979; Lyle, 1981) that the mineral is authigenic, formed by the low-temperature interaction of Fe oxyhydroxides and biogenic silica. This reaction is favored thermodynamically by the high surface energies of oxyhydroxides (Bischoff, Piper, et al., 1979) and has been demonstrated experimentally by Harder (1976). Silica and probably Al are provided by the dissolution of biogenic opal, with other major cations being sequestered from seawater, so that the reaction is limited by the availability of either Fe

oxyhydroxide and/or opal. Self-regulation of the reaction may partly explain the gross compositional variation seen at Site 573. It is envisaged that:

1. A gradual reduction in biogenic sedimentation during the latest Eocene, combined with an increased influx of ferromanganese oxyhydroxides, led to the formation of increasing amounts of authigenic Fe smectite in the sediment. Protons formed as a byproduct of the reaction (cf. Honnorez et al., 1981; Honnorez, Von Herzen, et al., 1983; Moorby, 1983) and caused the dissolution of biogenic carbonate.

2. The proportion of oxyhydroxides continued to increase until all biogenic opal was consumed and an excess of ferromanganese oxyhydroxides (goethite and δMnO_2) remained in the sediment. Biogenic carbonate was removed almost completely as a consequence of smectite formation.

3. Biogenic sedimentation increased during the early Oligocene. This was probably coincident with a waning in the supply of oxyhydroxides and led to the return of transitional sediments containing mainly Fe smectite as the noncarbonate phase.

Excess oxyhydroxide deposition never occurred at Site 574, which records a simple history of a steadily declining supply of ferromanganese oxyhydroxides.

The presence of two Fe minerals does not explain the strong correlation between Fe and Mn in Leg 85 metalliferous sediments, which occurs despite the ease of separation of the two elements by sedimentary processes (Krauskopf, 1957; Bonatti et al., 1972; Elderfield, 1977). Furthermore, partition analysis and mineralogic data indicate that Fe occurs principally in Fe smectite and goethite, while Mn occurs in δMnO_2. The association of Fe and Mn in the primary oxyhydroxide phase indicates that either they have a common source or, possibly, precipitation of one element catalyzes the precipitation of the other (Cronan, 1980). The smectite structure does not accommodate Mn^{4+} ions (Weaver and Pollard, 1973); thus Mn must recrystallize into secondary oxide phases on the sediment, either as micronodules or as interlaminations within recrystallized Fe oxyhydroxides. The former process is indicated by the occurrence of micronodules in Leg 85 metalliferous sediments. A strong association of δMnO_2 with goethite is confirmed by the lower Fe:Mn ratios in the middle of the metalliferous unit at Site 573, but a small amount of δMnO_2 also co-exists with Fe smectite and explains the high Mn content of the transitional sediments. The lack of evidence of Mn migration during early diagenesis (cf. Bauer Basin) indicates that the sediment remained oxic (Berner, 1981) throughout the history of the two sites.

Biogenic apatite (fish debris) is the main site of P in pelagic sediments (Arrhenius, 1963), but P can also be absorbed or co-precipitated on Fe oxyhydroxides (Berner, 1973; Froelich et al., 1977). The positive correlations between Fe, Mn, and P at Site 573 (Tables 1 and 2) suggest that the latter may be a significant process. Concentrations of biogenic apatite, however, are common in attenuated successions because of the higher density and lower solubility of apatite compared with calcite. There is a broad correlation between phosphorus content and the proportion of carbonate fluorapatite in Leg 85 sediments, thus it must be concluded that biogenic apatite is the primary site of P.

In addition to Fe smectite, partition analysis and statistical data indicate the occurrence of a second aluminosilicate phase distinguished by its effect on Si, Mg, Li, and Ti. These elements are most enriched in the noncarbonate fraction of the Eocene limestone and basal metalliferous sediment. Comparison with the composition of the underlying basalt and, in particular, the high Ti values suggest that this phase is volcanic glass, which is known to be abundant at the bases of both sections.

A final mineral phase indicated by the geochemical data solely affects the distribution of Ba. This has been identified as barite, a common constituent of metalliferous sediments from the eastern Pacific (Heath and Dymond, 1977; Toth, 1980; Dymond, 1981).

Trace Element Partitioning

Geochemical variation in Leg 85 basalt sediments can be explained in terms of eight main mineral and lithic phases: biogenic calcite and opal, Fe smectite, goethite, δMnO_2, volcanic glass, barite, and carbonate fluorapatite. The relationship, however, between mineralogy and trace element composition is not always clear.

Fe smectite and ferromanganese oxyhydroxides are both known to strongly partition trace elements (James and MacNaughton, 1977; Hein et al., 1979). My data indicate that the formation of authigenic Fe smectite has relatively little effect on the bulk trace element composition of the sediment. Many elements (B, Co, Cr, Cu, Ni, and Zn) show consistent linear trends (Fig. 5) between sediments in which the noncarbonate fraction is mainly Fe smectite (transition sediments) and those containing appreciable goethite (metalliferous claystone). An exception to this is displayed by V, which although correlating strongly with Fe, shows a very sharp upward deflection of the trend line at $\sim 20\%$ Fe_2O_3 (Fig. 5). This suggests that V is strongly partitioned by goethite.

Statistical and stratigraphic data indicate, however, that Fe smectite is the main control on the distribution of Co and Cr, while ferromanganese oxyhydroxides control the distribution of B, Cu, Ni, V, and Zn. The relative effect of goethite and δMnO_2 on individual trace elements is impossible to gauge from the Leg 85 data because Fe and Mn are themselves so strongly correlated. The association between Sc and Al indicates that the former element is concentrated during the formation of smectite, although a proportion of both probably resides in volcanic glass. Ti is strongly enriched in the volcaniclastic fraction, but it also occurs, along with Li, in smectite.

Ca correlates well with Sr, which indicates the presence of Sr in calcite. There are, however, significant differences between the distributions of Ca and Sr at Site 573; Sr is markedly depleted in the Eocene limestone compared with the Oligocene chalks. Large-scale Sr depletion such as this has been observed as the normal process that accompanies the dissolution and reprecipitation of pelagic carbonates during burial diagenesis (Matter et al., 1975; Sayles and Manheim, 1975). Thus, the

low Sr content of the Eocene limestone reflects its more extensive recrystallization and cementation, probably a consequence of the high heat flow that most likely occurred during the intrusion of the basalt (cf. Scholle, 1974). Late diagenetic depletion of Sr in pelagic carbonates is accompanied by Mg enrichment, and this may partly account for the high Mg content of the Eocene limestone, although volcanic glass and smectite probably provide more significant contributions.

Ba is believed to occur predominantly in barite. Ba has strong biogenic associations (Goldberg and Arrhenius, 1958; Church and Wolgemuth, 1972; Boström, 1976; Boström et al., 1978; Gurvich et al., 1978) and is relatively refractory; consequently, it has been suggested (by Heath and Dymond, 1977; Toth, 1980; Dymond, 1981) that Ba could be utilized as an index of dissolution. Ba is strongly enriched in metalliferous sediments at Site 573, but its distribution does not correlate well with the amount of dissolution observed from biogenic particles. This suggests that diagenetic processes have redistributed Ba prior to the precipitation of barite. Alternatively, its distribution may have been affected by an additional hydrothermal source of Ba (Arrhenius and Bonatti, 1965; Bonatti et al., 1972; Boström et al., 1973; Bonatti, 1975).

The distributions of the REE (represented by La and Ce), Sc, and Y do not compare closely with any single mineral phase. The REE and Y correlate best with P and are known to be partitioned by biogenic apatite during diagenesis (Dymond and Eklund, 1978), but significant positive correlations with elements controlled by Fe smectite suggest that REE and Y are also associated with the metalliferous component of the sediment. Co-precipitation of REE with Fe oxyhydroxides is a standard procedure for removing these elements from solution without fractionation (e.g., Elderfield and Greaves, 1982) so their enrichment in metalliferous sediments is not unexpected. The large ionic radii of the REE, Sc, and Y, however, preclude their substitution in either the tetrahedral or octahedral lattice sites of the smectite structure; therefore, they must be released into solution during the formation of Fe smectite.

The strong enrichment of the REE, Sc, and Y in the noncarbonate fraction at the top of the metalliferous unit at Site 573 can thus be explained by diagenetic processes that accompany the formation of Fe smectite. REE, Sc, and Y were mobilized during the mineralogic transformation of the ferromanganese component and by the dissolution of biogenic calcite and opal, and they were subsequently assimilated by biogenic apatite (cf. Elderfield et al., 1981). The effectiveness of the absorption process depends on the pH. A low pH within the metalliferous claystone during early diagenesis is indicated by dissolution of carbonate; this would have inhibited the removal of the REE, Sc, and Y from solution. Buffering associated with the increased carbonate content at the top of the metalliferous sediment would have raised the pH of the pore water sufficiently to allow more effective removal of the REE, Sc, and Y by biogenic apatite and other phases. Enrichment of the noncarbonate fraction at this level in Ba, B, Co, Cr, and Li may also be related to the readsorption or co-precipitation of trace elements mobilized during early diagenesis.

Marchig et al. (1982) suggested that hydrothermally dominated metalliferous sediments of the East Pacific Rise can be distinguished from authigenic deposits of the Bauer Basin on the basis of the relationship between the REE, Sc, Y, and P. East Pacific Rise deposits have low REE, Sc, and Y values that do not correlate with P. Bauer Basin deposits have higher REE, Sc, and Y values that correlate with P. This is because in rapidly deposited hydrothermal sediments P is co-precipitated with Fe oxyhydroxide (Berner, 1973; Froelich et al., 1977), while in authigenic deposits P is associated with biogenic apatite that has been enriched in REE by diagenetic processes. Leg 85 metalliferous sediments correspond with the characteristics of the authigenic group, which is consistent with the conclusions derived from the major element data.

Rare Earth Element Patterns

The REE distributions of recent metalliferous sediments are broadly similar to deep ocean seawater (Bender et al., 1971; Dymond et al., 1973; Piper and Graef, 1974; Toth, 1980; Marchig et al., 1982). They show comparatively little variation despite strong fractionation of the REE (particularly Ce and Eu) at different depths in the water column (Elderfield and Greaves, 1982; De Baar et al., 1983). Shale-normalized patterns are characterized by enrichment in the heavy (HREE) relative to the light (LREE) rare earth elements, and they display a marked depletion in Ce relative to its neighbors La and Pr. This Ce anomaly (Ce^*) can be quantified as:

$$Ce^* = \log [Ce_{sh}/\tfrac{1}{2}(La_{sh} + Pr_{sh})]$$

where Ce_{sh}, La_{sh}, and Pr_{sh} are the shale normalized values of each element.

Eocene limestone from the base of Site 573 has a low REE content and a pattern ($Ce^* = -0.70$) that is very similar to foraminiferal calcite (Elderfield et al., 1981) and oceanic seawater at ~3000 m depth (Goldberg et al., 1963; Høgdahl et al., 1968; Elderfield and Greaves, 1981, 1982; De Baar et al., 1983). Associated tholeiitic basalts (Appendix D) have higher REE abundances, exhibit no Ce anomaly, and display less HREE enrichment (Fig. 11). A sample from the top of the Eocene limestone (Sample 573B-42-5, 26–27 cm) also has a smaller Ce anomaly ($Ce^* = -0.44$) and is less enriched in the HREE. The high Ti content of this sample (Fig. 4; Appendix A) indicates the inclusion of a significant quantity of volcanic glass. The REE distribution is the result, therefore, of the primary seawater-like pattern being overprinted by an igneous REE distribution.

The REE patterns of Eocene–Oligocene metalliferous sediments (Appendix C) compare closely to their recent analogs. They are remarkably uniform considering that the absolute concentration of the REE varies by an order of magnitude (0.5 to 5 times that of shale) between the margins and center of the metalliferous unit at Site 573 (Figs. 3, 4, and 11). The patterns have strong negative Ce anomalies ($Ce^* = -0.72$) and are slightly en-

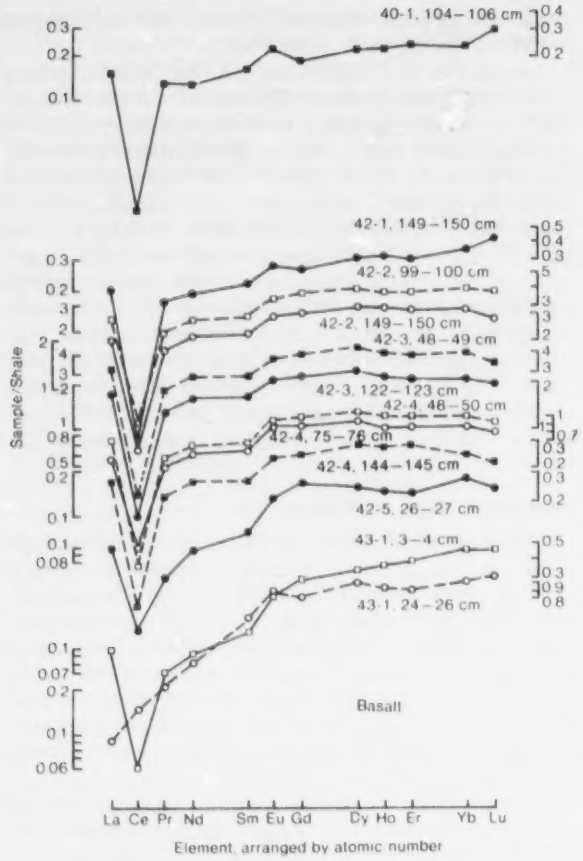

Figure 11. Rare earth element distributions of metalliferous sediments and associated lithologies at Site 573. Values are normalized to average shale (Haskin and Haskin, 1966; Piper 1974b). Samples are plotted stratigraphically to aid the visual separation of patterns; consequently, vertical scales vary. Absolute concentrations are given in Appendix C. Metalliferous sediments from Site 574 display essentially the same trends.

riched in the HREE relative to the LREE. The pattern is similar to sediments of the Bauer Basin type from the flanks of the East Pacific Rise (Piper and Graef, 1974), to authigenic montmorillonite from the southern Pacific (Piper, 1974b), and to ferromanganese nodules and crusts from the Bauer Basin (Elderfield and Greaves, 1981). Metalliferous sediments from the crest of the East Pacific Rise have lower REE contents and show stronger HREE enrichment over the LREE (Piper and Graef, 1974; Marchig et al., 1982). The pattern contrasts markedly with that of pelagic clays (montmorillonite) from the northern Pacific, which have flat patterns with no Ce anomalies (Piper, 1974a,b; Elderfield et al., 1981).

Oligocene chalks have lower REE contents and stronger Ce anomalies ($Ce^* = -0.88$) and are relatively enriched in the HREE compared with metalliferous sediments, although the HREE patterns are flatter than those of the Eocene limestone at Site 573.

Geochemical and mineralogic considerations suggest that the REE were originally sequestered from seawater. A hydrothermal source is rejected because REE distributions in hydrothermal solutions from the East Pacific Rise are characterized by large positive Eu anomalies (Michard et al., 1983) and are strongly depleted in the HREE relative to the LREE. Metalliferous sediments with patterns of this type are known from the Red Sea (Courtois and Treuil, 1977). A primary seawater source is also indicated by the $^{143}Nd/^{144}Nd$ ratios of metalliferous sediments from the eastern Pacific (O'Nions et al., 1978; Piepgras et al., 1979; Elderfield et al., 1981; Goldstein and O'Nions, 1981), which have seawater values.

The REE, however, are mobilized during early diagenesis (see above) and probably now reside in biogenic apatite. Mobilization of REE also occurs during the formation of ferromanganese nodules (Elderfield and Greaves, 1981, 1982; Elderfield et al., 1981; Murphy and Dymond, 1984) in the northern Pacific. Partition analysis of these nodules (Elderfield et al., 1981) indicates that the REE occur in separate Fe- and P-rich carrier phases. The P-rich phase (in the nodules) is enriched in the HREE relative to the Fe-rich component, which is HREE depleted. By contrast, the flatter pattern of Leg 85 metalliferous sediments compared with other lithologies probably reflects REE fractionation during their incorporation by apatite. Fractionation must be the result of diagenesis because deposits of the East Pacific Rise type, which are composed dominantly of ferromanganese oxyhydroxides, have seawater-like HREE-enriched patterns (Piper and Graef, 1974).

CONCLUSIONS

Upper Eocene–lower Oligocene metalliferous sediments occur at the base of the sediment columns at Sites 573 and 574 in the central equatorial Pacific. These sediments are strongly enriched in Fe, Mn, and other transition metals. The deposition of metalliferous sediments is related to the proximity to a source of ferromanganese oxyhydroxides (an active, mid-ocean ridge hydrothermal system) and low biogenic sedimentation rates across the Eocene/Oligocene boundary. Initially high metal contents were enhanced substantially by authigenic and diagenetic processes.

Geochemical and mineralogic data indicate that Fe smectite is the main Fe-bearing phase in these sediments but that it co-exists with goethite and δMnO_2. Fe smectite apparently formed by the reaction between hydrothermal ferromanganese oxyhydroxides and biogenic opal but was limited by the availability of opal in the most metalliferous sediments at Site 573. Diagenesis remained oxic. Mn liberated from mixed ferromanganese phases during the formation of smectite was reprecipitated to form Mn oxyhydroxide micronodules dispersed throughout the sediment. Carbonate was dissolved as a byproduct of smectite formation, producing sediments severely depleted in biogenic material. Most biogenic carbonate and silica was removed in solution from the metalliferous claystone at Site 573. Barite probably formed following the liberation of Ba absorbed onto biogenic opal.

Metalliferous sediments at Site 574 and transition sediments at Site 573 contain substantially less Fe and Mn. Here the metalliferous components are diluted by biogenic material (calcite, opal, and apatite) reflecting

higher rates of biogenic sedimentation. The noncarbonate component, however, is essentially similar to that in more metalliferous sediments. Volcanic glass is an important accessory at the base of both metalliferous successions.

Variations in trace element composition may be explained by a combination of mineralogic controls and diagenetic reactions. Fe smectite exerts a major control on the distribution of Co, Cr, and Sc, while ferromanganese oxyhydroxides control B, Cu, Ni, V, and Zn. The relative effects of goethite and δMnO_2 are impossible to gauge because Fe and Mn are themselves strongly correlated. Barite controls Ba, calcite controls Sr, and volcanic glass controls Ti and possibly Li. Strontium depletion in the Eocene limestone at Site 573 is apparently related to recrystallization of carbonate that accompanied the intrusion of basalt.

The REE are strongly enriched in metalliferous sediments. The REE had a seawater source suggesting that they were sequestered by Fe oxyhydroxides as they precipitated in the water column. The REE were mobilized during early diagenesis and now reside predominantly in a P-rich phase, probably biogenic apatite. The seawater-like distribution of REE in the primary ferromanganese oxyhydroxides was modified during the formation of smectite resulting in slight depletion in the heavy REE, which remained in solution because of the greater stability of their soluble compounds.

Comparison with recent analogs demonstrates that the Eocene–Oligocene deposits most closely resemble deposits in the Bauer Basin and on the flanks of the East Pacific Rise. This indicates that Sites 573 and 574 were never in close proximity to an active hydrothermal system. Even during the late Eocene, when the sites were located at the ridge crest, they received hydrothermal sediments from another part of the ridge system, possibly several hundred kilometers away. The difference in metal contents between the two sites is related predominantly to differences in local rates of biogenic sedimentation and does not indicate distance from hydrothermal source.

ACKNOWLEDGMENTS

Dr. Nick Walsh kindly provided the use of the Inductively Coupled Plasma (ICP) Spectrometer at King's College, London, and gave invaluable advice concerning analytical techniques. Laboratory assistance was given by Ms. Siobhan McKeown, Ms. Kym Hockings, and Dr. Alistair Baxter. The work was carried out under the tenure of an ILEA postdoctoral research fellowship at City of London Polytechnic.

REFERENCES

Aoki, S., Kohyama, N., and Sudo, T., 1974. An iron-rich montmorillonite in a sediment core from the northeastern Pacific. *Deep Sea Res.*, 21:865–875.

Arrhenius, G., 1963. Pelagic sediments. *In* Hill, M. N. (Ed.), *The Sea* (Vol. 3): New York (Wiley-Interscience), pp. 655–727.

Arrhenius, G., and Bonatti, E., 1965. Neptunism and volcanoes in the ocean. *In* Sears, M. (Ed.), *Progress in Oceanography:* Oxford (Pergamon Press), pp. 7–22.

Barrett, T. J., and Friedrichsen, H., 1982. Element and isotopic compositions of some metalliferous and pelagic sediments from the Galapagos Mounds area, DSDP Leg 70. *Chem. Geol.*, 36:275–298.

Barrett, T. J., Friedrichsen, H., and Fleet, A. J., 1983. Elemental and stable isotopic compositions of some metalliferous and pelagic sediments from the Galapagos Mounds area, Deep Sea Drilling Project Leg 70. *In* Honnorez, J., Von Herzen, R. P., et al., *Init. Repts. DSDP*, 70: Washington (U.S. Govt. Printing Office), 315–323.

Bender, M. L., 1983. Pore-water chemistry, Sites 506-509, Deep Sea Drilling Project. *In* Honnorez, J., Von Herzen, R. P., et al., *Init. Repts. DSDP*, 70: Washington (U.S. Govt. Printing Office), 343–353.

Bender, M. L., Brocker, W., Gornitz, V., Middel, U., Kay, R., Sun, S. S., and Biscay, P., 1971. Geochemistry of three cores from the East Pacific Rise. *Earth Planet. Sci. Lett.*, 12:425–433.

Berner, R. A., 1973. Phosphate removal from seawater by adsorption on volcanogenic ferric oxides. *Earth Planet. Sci. Lett.*, 18:77–86.

———, 1981. A new geochemical classification of sedimentary environments. *J. Sed. Petrol.*, 51:359–365.

Bischoff, J. L., Heath, G. R., and Leinen, J., 1979. Geochemistry of deep-sea sediments from the Pacific manganese nodule province: DOMES sites A, B and C. *In* Bischoff, J. L., and Piper, D. Z. (Eds.), *Marine Geology and Oceanography of the Pacific Manganese Nodule Province:* New York (Plenum), pp. 397–436.

Bischoff, J. L., Piper, D. Z., and Quinterno, P., 1979. Nature and origin of metalliferous sediment in DOMES site C, Pacific manganese nodule province. *In* Lalou, C. (Ed.), *International Colloquium on the Genesis of Manganese Nodules:* Paris (Coll. Int. CNRS), pp. 119–137.

Bonatti, E., 1975. Metallogenesis at oceanic spreading centers. *Annu. Rev. Earth Planet. Sci.*, 3:401–431.

Bonatti, E., Kraemer, T., and Rydell, H., 1972. Classification and genesis of submarine iron-manganese deposits. *In* Horn, D. R. (Ed.), *Ferromanganese Deposits on the Ocean Floor:* Washington (NSF), pp. 149–166.

Boström, K., 1976. Particulate and dissolved matter as sources for pelagic sediments. *Stockholm Contrib. Geol.*, 30:15–79.

Boström, K., Joensuu, O., Moore, C., Bostrom, B., Dalziel, K., and Horowitz, A., 1973. Geochemistry of barium in pelagic sediments. *Lithos*, 6:159–174.

Boström, K., Joensuu, O., Valdes, S., Charm, W., and Glaccum, R., 1976. Geochemistry and origin of east Pacific sediments sampled during DSDP Leg 34. *In* Yeats, R. S., Hart, S. R., et al., *Init. Repts. DSDP*, 34: Washington (U.S. Govt. Printing Office), 559–574.

Boström, K., Lysen, L., and Moore, C., 1978. Biological matter as a source of authigenic matter in pelagic sediments. *Chem. Geol.*, 23: 11–20.

Boström, K., and Peterson, M. N. A., 1966. Precipitates from hydrothermal exhalations of the East Pacific Rise. *Econ. Geol.*, 61: 1258–1265.

Boström, K., Peterson, M. N. A., Joensuu, O., and Fisher, D. E., 1969. Aluminium-poor ferromanganese sediments on active ocean ridges. *J. Geophys. Res.*, 74:3261–3270.

Chester, R., 1965. Elemental geochemistry of marine sediments. *In* Riley, J. P., and Skirrow, G. (Eds.), *Treatise on Chemical Oceanography* (Vol. 2): New York (Academic Press), pp. 23–80.

Church, T. M., and Wolgemuth, K., 1972. Marine barite saturation. *Earth Planet. Sci. Lett.*, 15:35–44.

Courtois, C., and Treuil, M., 1977. Distribution des terres rares et de quelques éléments en trace dans les sédiments récents des fosses de la Mer Rouge. *Chem. Geol.*, 20:57–72.

Corliss, J. B., 1971. The origin of metal-bearing hydrothermal solutions. *J. Geophys. Res.*, 76:8128–8138.

Corliss, J. B., Dymond, J., Gordon, L. E., Edmond, J. M., Von Herzen, R. P., Ballard, R. D., Green, K., Williams, D., Bainbridge, A. E., Crane, K., and van Andel, T. H., 1979. Submarine thermal springs in the Galapagos Rift. *Science*, 203:1073–1083.

Corliss, J. B., Lyle, M., Dymond, J., and Crane, K., 1978. The chemistry of hydrothermal mounds near the Galapagos Rift. *Earth Planet. Sci. Lett.*, 40:12–24.

Cronan, D. S., 1969a. Average abundances of Mn, Fe, Ni, Co, Cu, Pb, Mo, V, Cr, Ti, and P in Pacific pelagic clays. *Geochim. Cosmochim. Acta*, 33:1562–1565.

———, 1969b. Interelement associations in some pelagic deposits. *Chem. Geol.*, 5:99–106.

———, 1972. The Mid-Atlantic Ridge near 45°N, XVII: Al, As, Hg, and Mn in ferruginous sediments from the median valley. *Can. J. Earth Sci.*, 9:319–323.

_____, 1973. Basal ferruginous sediments cored during Leg 16, Deep Sea Drilling Project. *In* van Andel, T. H., Heath, G. R., et al., *Init. Repts. DSDP*, 16: Washington (U.S. Govt. Printing Office), 601–604.

_____, 1976. Basal metalliferous sediments from the eastern Pacific. *Geol. Soc. Am. Bull.*, 87:928–934.

_____, 1980. *Underwater Minerals:* London (Academic Press).

Cronan, D. S., and Garrett, D. A., 1973. Distribution of elements in metalliferous Pacific sediments collected during the Deep Sea Drilling Project. *Nature Phys. Sci.*, 242:88–89.

Dasch, E. J., Dymond, J. R., and Heath, G. R., 1971. Isotopic analysis of metalliferous sediments from the East Pacific Rise. *Earth Planet. Sci. Lett.*, 13:175–180.

De Baar, H. J. W., Bacon, M. P., and Brewer, P. G., 1983. Rare-earth distributions with a positive Ce anomaly in the western North Atlantic Ocean. *Nature*, 301:324–327.

Dymond, J., 1981. Geochemistry of Nazca Plate surface sediments: an evaluation of hydrothermal, biogenic, detrital, and hydrogenous sources. *Mem. Geol. Soc. Am.*, 154:133–173.

Dymond, J., Corliss, J. B., Heath, G. R., Field, C. W., Dasch, E. J., and Veeh, H. H., 1973. Origin of metalliferous sediments from the Pacific Ocean. *Geol. Soc. Am. Bull.*, 84:3355–3372.

Dymond, J., Corliss, J. B., and Stillinger, R., 1976. Chemical composition and metal accumulation rates of metalliferous sediments from Sites 319, 320, and 321. *In* Yeats, R. S., Hart, S. R., et al., *Init. Repts. DSDP*, 34: Washington (U.S. Govt. Printing Office), 575–588.

Dymond, J., and Eklund, W., 1978. A microprobe study of metalliferous sediment components. *Earth Planet. Sci. Lett.*, 40:243–251.

Dymond, J., and Veeh, H. H., 1975. Metal accumulation rates in the southeast Pacific and the origin of metalliferous sediments. *Earth Planet. Sci. Lett.*, 28:13–22.

Edmond, J. M., Measures, C., McDuff, R. E., Chan, L. H., Collier, R., Grant, B., Gordon, L. I., and Corliss, J. B., 1979. Ridge crest hydrothermal activity and the balances of the major and minor elements in the Ocean: the Galapagos data. *Earth Planet. Sci. Lett.*, 46:1–18.

Edmond, J. M., Measures, C., Mangum, B., Grant, B., Sclater, F. R., Collier, R., Hudson, A., Gordon, L. I., and Corliss, J. B., 1979. On the formation of metal-rich deposits at ridge crests. *Earth Planet. Sci. Lett.*, 46:19–30.

Elderfield, H., 1977. The form of manganese and iron in marine sediments. *In* Glasby, G. P. (Ed.), *Marine Manganese Deposits:* Amsterdam (Elsevier), pp. 269–289.

Elderfield, H., and Greaves, M. J., 1981. Negative cerium anomalies in the rare-earth element patterns of oceanic ferromanganese nodules. *Earth Planet. Sci. Lett.*, 55:163–170.

_____, 1982. The rare-earth elements in seawater. *Nature*, 296: 214–219.

Elderfield, H., Hawkesworth, C. J., Greaves, M. J., and Calvert, S. E., 1981. Rare-earth element geochemistry of oceanic ferromanganese nodules and associated sediments. *Geochim. Cosmochim. Acta*, 45:513–528.

Field, C. W., Wetherell, D. G., and Dasch, E. J., 1981. Economic appraisal of Nazca Plate metalliferous sediments. *Mem. Geol. Soc. Am.*, 154:315–320.

Francheteau, J., Needham, H. D., Choukroune, P., Juteau, P., Seguret, M., Ballard, R. D., Fox, P. J., Normark, W., Carranza, A., Cordoba, D., Guerrero, J., Rangin, C., Bougault, H., Cambon, O., and Hekinian, R., 1979. Massive deep-sea sulphide ore deposits discovered on the East Pacific Rise. *Nature*, 227:523–528.

Froelich, P. N., Bender, M. L., and Heath, G. R., 1977. Phosphate accumulation rates in metalliferous sediments on the East Pacific Rise. *Earth Planet. Sci. Lett.*, 34:351–359.

Goldberg, E. D., and Arrhenius, G. O. S., 1958. Chemistry of Pacific pelagic sediments. *Geochim. Cosmochim. Acta*, 13:153–212.

Goldberg, E. D., Koide, M., Schmitt, R. A., and Smith, R. H., 1963. Rare-earth distributions in the marine environment. *J. Geophys. Res.*, 68:4209–4217.

Goldstein, S. L., and O'Nions, R. K., 1981. Nd and Sr isotopic relationships in pelagic clays and ferromanganese deposits. *Nature*, 292:324–327.

Griffin, J. J., Windom, H., and Goldberg, E. D., 1968. The distribution of clay minerals in the World Ocean. *Deep Sea Res.*, 15: 433–459.

Gurvich, Y. G., Boganov, Y. A., and Lisitsin, A. P., 1978. Behaviour of barium in recent sedimentation in the Pacific. *Geokhimiya*, 3: 359–374.

Harder, H., 1976. Nontronite synthesis at low temperatures. *Chem. Geol.*, 18:169–180.

Haskin, M. A., and Haskin, L. A., 1966. Rare earths in European shales: a redetermination. *Sciences*, 154:507–509.

Hays, J. D., Cook, H. E., Jenkins, G., Cook, F. M., Fuller, J. T., Goll, R. M., Milow, D., and Orr, W. N., 1972. *Init. Repts. DSDP*, 9: Washington (U.S. Govt. Printing Office).

Heath, G. R., and Dymond, J., 1977. Genesis and transformation of metalliferous sediments from the East Pacific Rise, Bauer Deep, and Central Basin, northwest Nazca Plate. *Geol. Soc. Am. Bull.*, 88:723–733.

_____, 1981. Metalliferous sediment deposition in time and space: East Pacific Rise and Bauer Basin, northern Nazca Plate. *Mem. Geol. Soc. Am.*, 154:175–197.

Hein, J. R., Veh, H. W., and Alexander, E., 1979. Origin of iron-rich montmorillonite from the manganese nodule belt of the north equatorial Pacific. *Clays Clay Min.*, 27:185–194.

Hekinian, R., Rosendahl, B. R., Cronan, D. S., Dmitriev, Y., Fodor, R. V., Goll, R. M., Hoffert, M., Humphris, S. E., Mattey, D. P., Natland, J., Peterson, W., Roggenthen, W., Schrader, E., Scrivastava, R. K., and Warren, N., 1978. Hydrothermal deposits and associated basement rocks from the Galapagos Spreading Center. *Oceanol. Acta*, 1:473–482.

Herron, E. M., 1972. Seafloor spreading and the Cenozoic history of the east-central Pacific. *Geol. Soc. Am. Bull.*, 83:1671–1692.

Høgdahl, Ø., Melson, S., and Bowen, V., 1968. Neutron activation analysis of lenthanide elements in sea water. *Adv. Chem.*, 73: 308–325.

Honnorez, J., Von Herzen, R. P., Barrett, T., Becker, K., Borella, P., Hubberten, H. W., Jones, S., Karato, S., Laverne, C., Levi, S., Migdisov, A. A., Moorby, S. A., and Schrader, E., 1981. Hydrothermal mounds and young oceanic crust of the Galapagos: preliminary Deep Sea Drilling results, Leg 70. *Geol. Soc. Am. Bull.*, 92:457–472.

Honnorez, J., Von Herzen, R. P., et al., 1983. *Init. Repts. DSDP*, 70: Washington (U.S. Govt. Printing Office).

Horowitz, A., 1970. The distribution of Pb, Ag, Sn, Ti, and Zn in sediments on active ocean ridges. *Mar. Geol.*, 9:241–259.

James, P. O., and MacNaughton, M. G., 1977. The adsorption of aqueous heavy metals on inorganic compounds. *Geochim. Cosmochim. Acta*, 41:1549–1555.

Kennett, J. P., Houtz, R. E., Andrews, P. B., Edwards, A. R., Gostin, V. A., Hajos, M., Hampton, M., Jenkins, D. G., Margolis, S. V., Ovenshine, A. T., and Perch-Nielsen, K., 1975. Cenozoic paleoceanography in the southwest Pacific Ocean, Antarctic glaciation, and the development of the Circum-Antartic current. *In* Kennett, J. P., Houtz, R. E., et al., *Init. Repts. DSDP*, 29: Washington (U.S. Govt. Printing Office), 1155–1169.

Klitgord, K. D., and Mudie, J. D., 1974. The Galapagos Spreading Center: a near-bottom geophysical survey. *Geophys. J. R. Astron. Soc.*, 38:563–586.

Krauskopf, K. B., 1957. Separation of manganese and iron in sedimentary processes. *Geochim. Cosmochim. Acta*, 12:61–84.

Leinen, M., 1981. Metal-rich basal sediments from northeastern Pacific Deep Sea Drilling Project sites. *In* Yeats, R. S., Haq, B. U., et al., *Init. Repts. DSDP*, 63: Washington (U.S. Govt. Printing Office), 667–676.

Lonsdale, P., 1977. Deep-tow observations at the mounds abyssal hydrothermal field, Galapagos Rift. *Earth Planet. Sci. Lett.*, 36: 92–110.

Lyle, M., 1981. Formation and growth of ferromanganese oxides on the Nazca Plate. *Mem. Soc. Am.*, 154:269–293.

Lyle, M., Dymond, J., and Heath, G. R., 1977. Copper-nickel-enriched ferromanganese nodules and associated crust from the Bauer Basin, northwest Nazca Plate. *Earth Planet. Sci. Lett.*, 35:55–64.

McMurtry, G. M., Veeh, H. H., and Moser, C., 1981. Sediment accumulation rate patterns on the northwest Nazca Plate. *Mem. Geol. Soc. Am.*, 154:211–249.

Marchig, V., and Gundlach, H., 1982. Iron-rich metalliferous sediments on the East Pacific Rise—prototype of undifferentiated metalliferous sediments in divergent plate boundaries. *Earth Planet. Sci. Lett.*, 58:361–382.

Marchig, V., Gundlach, H., Moller, P., and Schley, F., 1982. Some geochemical indicators for discriminating between diagenetic and hydrothermal metalliferous sediments. *Mar. Geol.*, 50:241–256.

Matter, A., Douglas, R. G., and Perch-Nielsen, K., 1975. Fossil preservation, geochemistry, and diagenesis of pelagic carbonates from Shatsky Rise, northwest Pacific. *In* Larsen, R. L., Moberly, R., et al., *Init. Repts. DSDP*, 32: Washington (U.S. Govt. Printing Office), 891–921.

Michard, A., Albarede, F., Michard, G., Minster, J. F., and Charlou, J. L., 1983. Rare-earth elements and uranium in high-temperature solutions from East Pacific Rise hydrothermal vent field (13°N). *Nature*, 303:795–797.

Moorby, S. A., 1983. The geochemistry of transitional sediments recovered from the Galapagos Hydrothermal Mounds Field during DSDP Leg 70—implications for mounds formation. *Earth Planet. Sci. Lett.*, 62:367–376.

Moorby, S. A., and Cronan, D. S., 1983. Chemical composition of sediments from Sites 506, 507, 508, and 509, Leg 70, DSDP. *In* Honnorez, J., Von Herzen, R. P., et al., *Init. Repts. DSDP*, 70: Washington (U.S. Govt. Printing Office), 269–275.

Murphy, K., and Dymond, J., 1984. Rare earth element fluxes and geochemical budget in the eastern equatorial Pacific. *Nature*, 307: 444–447.

Murray, J., and Renard, A. F., 1891. *Deep Sea Deposits: Report of the Scientific Results of the HMS Challenger, 1873–1876:* London (HMSO).

O'Nions, R. K., Carter, S. R., Cohen, R. S., Evensen, N. M., and Hamilton, P. J., 1978. Pb, Nd, and Sr isotopes in oceanic ferromanganese deposits and ocean floor basalt. *Nature*, 273:435–438.

Piepgras, D. J., Wasserberg, G. J., and Dasch, E. J., 1979. The isotopic composition of Nd in different ocean masses. *Earth Planet. Sci. Lett.*, 45:223–236.

Piper, D. Z., 1973. Origin of metalliferous sediments from the East Pacific Rise. *Earth Planet. Sci. Lett.*, 19:75–82.

———, 1974a. Rare-earth elements in ferromanganese nodules and other marine phases. *Geochim. Cosmochim. Acta*, 38:1007–1022.

———, 1974b. Rare-earth elements in sedimentary cycle: a summary. *Chem. Geol.*, 14:285–304.

Piper, D. Z., and Graef, P. A., 1974. Gold and rare-earth elements in sediments from the East Pacific Rise. *Mar. Geol.*, 17:287–297.

Revelle, R., 1944. Marine bottom samples collected in the Pacific Ocean by the *Carnegie* on its seventh cruise. *Carnegie Inst. Washington Publ.*, 556:1–180.

Sayles, F. L., and Bischoff, J. L., 1973. Ferromanganese sediments in the equatorial east Pacific. *Earth Planet. Sci. Lett.*, 19:330–336.

Sayles, F. L., Ku, T. L., and Bowker, P. C., 1975. Chemistry of ferromanganese sediment of the Bauer Deep. *Geol. Soc. Am. Bull.*, 86: 1423–1431.

Sayles, F. L., and Manheim, F. T., 1975. Interstitial solutions and diagenesis in buried marine sediments: results from the Deep Sea Drilling Project. *Geochim. Cosmochim. Acta*, 39:103–127.

Scholle, P. A., 1974. Diagenesis of Upper Cretaceous chalks from England, Northern Ireland, and the North Sea. *In* Hsü, K. J., and Jenkyns, H. C. (Eds.), *Pelagic Sediments: On Land and under the Sea*, Spec. Publ. Int. Assoc. Sedimentol., 1:177–210.

Sclater, J. G., Andersen, R. N., and Bell, M. L., 1971. Elevation of ridges and evolution of the central eastern Pacific. *J. Geophys. Res.*, 76:7888–7915.

Shearme, S., Cronan, D. S., and Rona, P. A., 1983. Geochemistry of sediments from the TAG hydrothermal field, MAR at latitude 26°N. *Mar. Geol.*, 51:269–291.

Thompson, G., 1983. Hydrothermal fluxes in the Ocean. *In* Riley, J. P., and Chester, R. (Eds.), *Chemical Oceanography* (Vol. 8): London (Academic Press), pp. 271–337.

Toth, J. R., 1980. Deposition of submarine hydrothermal iron and evidence for hydrothermal input of volatile elements to the oceans. *Geol. Soc. Am. Bull.*, 91:44–54.

Tracey, J. I., Jr., Sutton, G. H., et al., 1971. *Init. Repts. DSDP*, 8: Washington (U.S. Govt. Printing Office).

Turekian, K. K., and Wedepohl, K. H., 1961. Distribution of elements in some major units of the Earth's crust. *Bull. Geol. Soc. Am.*, 72: 175–192.

van Andel, T. H., Heath, G. R., et al., 1973. *Init. Repts. DSDP*, 16: Washington (U.S. Govt. Printing Office).

van Andel, T. H., Heath, G. R., and Moore, T. C., 1975. Cenozoic history and paleoceanography of the central equatorial Pacific. *Mem. Geol. Soc. Am.*, 143.

Varnavas, S. P., and Cronan, D. S., 1981. Partition geochemistry of sediments from DSDP Site 424 in the Galapagos Hydrothermal Mounds Field. *Min. Mag.*, 44:325–331.

Varnavas, S. P., Moorby, S A., and Cronan, D. S., 1983. Partition geochemistry of sediments from Holes 506 and 509B, DSDP Leg 70. *In* Honnorez, J., Von Herzen, R. P., et al., *Init. Repts. DSDP*, 70: Washington (U.S. Govt. Printing Office), 297–302.

von der Borch, C. C., Nesteroff, W. D., and Galehouse, J., 1971. Iron-rich sediments cored during Leg 8 of the Deep Sea Drilling Project. *In* Tracey, J. I., Jr., Sutton, G. H., et al., *Init. Repts. DSDP*, 8: Washington (U.S. Govt. Printing Office), 829–835.

von der Borch, C. C., and Rex, R. W., 1970. Amorphous iron oxide precipitates in sediments cored during Leg 5, Deep Sea Drilling Project. *In* McManus, D. A., Burns, R. E., et al., *Init. Repts. DSDP*, 5: Washington (U.S. Govt. Printing Office), 541–544.

Walsh, J. N., Buckley, F., Barker, J., 1981. The simultaneous determination of the rare-earth elements in rocks using inductively coupled plasma source spectrometry. *Chem. Geol.*, 33:141–153.

Weaver, C. E., and Pollard, L. D., 1973. *The Chemistry of Clay Minerals.* New York (Elsevier).

Williams, D. L., Green, K., van Andel, T. H., Von Herzen, R. P., Dymond, J. R., and Crane, K., 1979. The hydrothermal mounds of the Galapagos Rift: observations with DSRV *Alvin* and detailed heat flow studies. *J. Geophys. Res.*, 84:7467–7484.

Zelenov, K. K., 1964. Iron and manganese in exhalations of the submarine Banu Wuhu Volcano, Indonesia. *Akad. Nauk. SSSR Doklady*, 155:94–96.

Date of Initial Receipt: 27 September 1983
Date of Acceptance: 3 May 1984

APPENDIX A
Major and Trace Element Composition of Basal Sediments from Hole 573B

	40-1 104–106 cm	42-1 45–46 cm	42-1 125–126 cm	42-1 149–150 cm	42-2 25–26 cm	42-2 50–51 cm	42-2 76–77 cm	42-2 99–100 cm	42-2, 125–126 cm	42-2, 149–150 cm	42-3, 25–26 cm	42-3, 48–49 cm
Major elements (%)												
SiO_2	17.00	2.64	1.59	1.57	8.23	8.86	29.00	35.00	30.30	29.50	25.20	26.50
Al_2O_3	0.26 (0.15)	0.24 (0.15)	0.19 (0.08)	0.24 (0.13)	1.57 (0.68)	1.68 (0.57)	5.05 (2.13)	6.13 (2.42)	5.01 (1.88)	3.97 (1.42)	3.93 (1.21)	3.93 (1.30)
Fe_2O_3	0.10 (0.09)	0.30 (0.21)	0.16 (0.06)	0.25 (0.19)	1.97 (1.60)	2.37 (1.78)	11.20 (8.30)	18.20 (12.42)	25.20 (19.90)	25.40 (19.40)	30.10 (21.70)	29.50 (20.60)
MnO	0.02 (0.02)	0.09 (0.04)	0.03 (0.02)	0.02 (0.01)	0.23 (0.20)	0.34 (0.19)	1.65 (1.13)	3.59 (1.88)	5.62 (2.67)	5.88 (2.10)	7.76 (1.99)	8.30 (1.90)
MgO	0.20 (0.20)	0.31 (0.29)	0.24 (0.20)	0.25 (0.23)	0.82 (0.75)	0.88 (0.71)	3.05 (2.33)	4.05 (2.75)	3.43 (2.58)	3.42 (2.65)	2.88 (2.15)	3.00 (2.21)
CaO	45.20	52.70	54.30	53.50	46.10	46.30	18.20	5.26	5.44	6.93	7.70	6.78
Na_2O	0.15 (0.07)	0.07 (0.07)	0.06 (0.06)	0.06 (0.06)	0.14 (0.09)	0.20 (0.14)	0.90 (0.70)	1.11 (0.83)	0.72 (0.51)	0.66 (0.53)	0.67 (0.54)	0.58 (0.50)
K_2O	0.07 (0.03)	0.04 (0.03)	0.04 (0.02)	0.05 (0.03)	0.42 (0.21)	0.49 (0.26)	1.64 (0.89)	1.68 (0.84)	1.61 (0.73)	1.49 (0.70)	1.35 (0.58)	1.35 (0.59)
P_2O_5	0.10	0.13	0.07	0.10	0.52	0.50	2.49	2.88	3.02	3.81	4.07	3.51
Trace elements (ppm)												
B	(8.0)	(3.5)	(0.8)	(3.5)	(15.6)	(10.7)	(74.3)	(110)	(158)	(154)	(183)	(176)
Ba	1560 (1430)	1220 (1050)	1420 (1130)	1410 (1390)	2760 (1830)	2490 (2490)	2230 (1590)	2490 (2250)	4060 (3430)	5390 (2560)	2400 (2180)	3120 (2750)
Ce	1.5	1.7	1.7	2.2	12.8	12.3	35.4	39.9	38.5	33.0	36.9	38.9
Co	6.5 (6.0)	16.1 (15.8)	13.7 (12.2)	7.0 (6.0)	19.0 (14.0)	20.4 (16.7)	45.2 (33.5)	64.9 (38.8)	81.1 (52.1)	75.4 (42.3)	88.8 (45.0)	85.5 (41.4)
Cr	4.8	11.1	11.0	12.4	19.0	12.1	30.3	26.4	36.9	40.9	51.4	53.0
Cu	49.5 (49.5)	55.6 (53.5)	31.1 (25.6)	35.6 (33.6)	149 (141)	187 (153)	588 (518)	882 (739)	1150 (1070)	1090 (963)	1390 (1190)	1290 (1120)
La	5.1	5.9	6.4	8.2	37.5	35.4	81.9	101	98.0	86.9	98.3	128
Li	3.6 (3.6)	7.3 (6.6)	5.6 (4.2)	5.6 (5.5)	23.4 (19.9)	18.2 (14.7)	42.3 (39.5)	52.3 (36.2)	27.7 (20.2)	27.2 (19.1)	20.1 (12.0)	21.5 (12.5)
Ni	10.3 (9.3)	32.7 (32.7)	19.8 (19.8)	16.4 (16.3)	57.1 (52.0)	88.9 (78.5)	316 (290)	784 (570)	713 (573)	718 (575)	748 (656)	835 (735)
Sc	1.1 (1.0)	1.6 (1.4)	1.7 (1.3)	2.1 (1.9)	7.6 (6.2)	8.0 (5.8)	19.5 (14.9)	21.6 (15.6)	17.5 (13.7)	14.2 (10.5)	14.1 (10.0)	14.5 (9.9)
Sr	1010	1170	1240	1330	1740	1690	999	632	715	745	796	754
Ti	81.9 (66.4)	127 (84.4)	104 (66.4)	112 (74.4)	510 (152)	529 (142)	1960 (369)	3040 (526)	2210 (429)	1400 (242)	1170 (123)	1180 (98.4)
V	0.9 (0.1)	3.5 (1.1)	2.3 (0.5)	2.9 (0.7)	13.6 (7.8)	19.4 (11.2)	93.0 (55.7)	203 (125)	427 (221)	413 (188)	560 (202)	566 (184)
Y	10.4	12.4	11.1	15.6	69.1	60.3	154	164	151	133	149	171
Zn	14.1 (7.7)	22.8 (20.0)	15.4 (10.2)	17.9 (13.9)	70.1 (58.7)	83.1 (64.9)	309 (268)	490 (431)	574 (531)	606 (575)	685 (603)	685 (607)

	42-3, 75–76 cm	42-3, 100–101 cm	42-3, 122–123 cm	42-3, 145–146 cm	42-4, 25–26 cm	42-4, 48–50 cm	42-4, 75–76 cm	42-4, 100–101 cm	42-4, 125–126 cm	42-4, 144–145 cm	42-5, 26–27 cm	43-1, (Piece 1, 3–4 cm)
Major elements (%)												
SiO_2	27.50	28.20	35.60	34.70	32.60	20.20	29.20	14.90	7.96	7.32	8.80	5.17
Al_2O_3	3.52 (1.21)	2.45 (0.94)	2.29 (1.03)	1.93 (0.90)	2.82 (1.62)	1.61 (0.91)	3.89 (1.67)	2.00 (1.06)	1.14 (0.85)	0.82 (0.55)	2.06 (1.29)	1.29 (0.81)
Fe_2O_3	28.10 (21.50)	24.30 (13.50)	24.00 (14.80)	23.60 (15.10)	16.70 (9.83)	10.70 (6.48)	12.00 (5.09)	5.56 (2.91)	2.89 (2.28)	3.21 (2.36)	2.19 (1.56)	1.19 (0.74)
MnO	7.65 (3.52)	6.41 (1.44)	5.78 (2.50)	5.66 (2.91)	3.95 (2.42)	2.96 (1.42)	2.01 (1.04)	0.86 (0.51)	0.40 (0.39)	0.69 (0.38)	0.12 (0.05)	0.13 (0.08)
MgO	3.53 (2.56)	3.82 (2.60)	5.01 (3.37)	5.02 (3.51)	4.27 (2.90)	2.67 (1.87)	3.89 (2.11)	1.87 (1.18)	0.95 (0.86)	0.89 (0.78)	1.44 (1.19)	1.22 (1.03)
CaO	5.90	6.71	3.62	3.04	13.40	29.00	18.90	38.20	47.60	48.20	47.00	52.40
Na_2O	0.67 (0.54)	0.64 (0.61)	0.85 (0.75)	0.71 (0.68)	0.78 (0.78)	0.30 (0.29)	0.62 (0.62)	0.29 (0.28)	0.14 (0.13)	0.08 (0.08)	0.20 (0.20)	0.13 (0.12)
K_2O	1.25 (0.58)	1.10 (0.54)	1.20 (0.65)	1.04 (0.63)	1.21 (0.72)	0.73 (0.47)	1.04 (0.62)	0.58 (0.36)	0.37 (0.30)	0.32 (0.23)	0.34 (0.27)	0.23 (0.19)
P_2O_5	3.13	3.55	1.92	1.55	1.11	0.66	0.48	0.35	0.21	0.27	0.36	0.21
Trace elements (ppm)												
B	(167)	(110)	(105)	(105)	(65.4)	(38.9)	(37.4)	(17.8)	(17.8)	(15.6)	(20.5)	(2.1)
Ba	3320 (2650)	5150 (2790)	6210 (5080)	6920 (6140)	5220 (3600)	6180 (4780)	4370 (4240)	2080 (1760)	55.0 (55.0)	64.0 (52.0)	9.2 (< 5.0)	20.0 (< 5.0)
Ce	31.8	24.9	21.6	nd	14.0	9.3	12.9	4.8	3.0	2.0	2.3	1.4
Co	80.9 (52.1)	68.7 (31.7)	63.9 (36.1)	63.9 (41.4)	51.9 (34.4)	38.1 (25.5)	43.4 (22.8)	23.0 (15.8)	14.4 (13.1)	14.0 (11.3)	14.1 (10.5)	15.6 (13.1)
Cr	50.6	41.7	36.3	30.6	33.8	27.9	21.4	18.8	14.0	14.8	21.2	19.5
Cu	1180 (1020)	925 (678)	860 (642)	851 (638)	615 (427)	368 (272)	394 (215)	212 (126)	73.4 (61.8)	104 (85.2)	71.3 (53.2)	31.3 (25.7)
La	101	87.3	70.3	nd	40.0	30.0	22.7	13.8	7.6	6.9	3.7	4.1
Li	24.3 (15.5)	27.8 (17.9)	19.9 (15.4)	16.8 (26.0)	41.3 (30.5)	26.3 (18.2)	63.2 (33.5)	29.2 (17.5)	11.9 (9.7)	7.4 (5.3)	21.2 (13.7)	8.8 (6.8)
Ni	812 (714)	614 (537)	478 (427)	459 (398)	261 (218)	162 (131)	154 (134)	119 (105)	49.0 (47.9)	158 (124)	98.8 (79.3)	80.7 (69.2)
Sc	13.4 (8.8)	8.9 (5.0)	8.6 (4.0)	6.6 (3.5)	7.9 (4.7)	5.4 (3.2)	9.4 (4.0)	5.6 (3.4)	3.2 (2.9)	1.9 (1.6)	5.8 (4.7)	2.9 (1.9)
Sr	770	690	583	477	767	1120	702	1020	796	807	436	222
Ti	1100 (146)	824 (54.4)	825 (55.4)	670 (48.4)	1350 (192)	890 (169)	3240 (129)	1240 (128)	874 (282)	465 (210)	1360 (171)	611 (195)
V	502 (239)	364 (132)	278 (125)	256 (124)	129 68.3)	92.1 (41.9)	70.5 (35.0)	33.1 (18.5)	16.7 (15.0)	26.5 (17.8)	5.4 (3.4)	11.2 (4.1)
Y	133	116	90.2	nd	57.0	42.9	33.0	21.4	12.9	9.9	10.8	20.1
Zn	702 (616)	612 (461)	633 (468)	593 (451)	431 (309)	270 (190)	336 (195)	142 (93.5)	66.4 (66.4)	76.0 (58.7)	67.0 (45.7)	33.4 (21.4)

Note: Total Fe is expressed as Fe_2O_3. Values in parentheses are the HCl-soluble portion of the sample. nd = not determined.

APPENDIX B
Major and Trace Element Composition of Basal Sediments from Hole 574C

	32-2, 54–55 cm	33-1, 56–57 cm	33-4, 73–74 cm	33-4, 102–103 cm	33-5, 2–3 cm	33-5, 34–35 cm	33-5, 61–62 cm	33-5, 74–75 cm	33-5, 100–102 cm	33-5, 120–122 cm	33-5, 148–149 cm	34-1, 47–48 cm	34-1, 75–76 cm	34-1, 97–98 cm	34-1, 121–122 cm
Major elements (%)															
SiO_2	13.10	7.69	10.20	12.00	13.00	19.10	15.30	15.10	17.80	15.20	13.20	15.50	16.50	19.10	16.30
Al_2O_3	0.21 (0.13)	0.77 (0.47)	0.57 (0.38)	0.75 (0.49)	0.89 (0.56)	1.89 (1.18)	1.41 (0.91)	1.20 (0.77)	1.38 (0.87)	1.25 (0.74)	0.93 (0.57)	0.81 (0.55)	0.63 (0.45)	0.54 (0.37)	0.78 (0.55)
Fe_2O_3	0.07 (0.04)	0.51 (0.40)	0.63 (0.56)	0.72 (0.64)	1.02 (0.90)	2.20 (1.99)	2.12 (1.99)	1.80 (1.72)	1.95 (1.83)	1.88 (1.71)	1.46 (1.29)	1.52 (1.41)	1.18 (1.14)	0.91 (0.83)	1.53 (1.44)
MnO	0.01 (0.01)	0.01 (0.01)	0.01 (0.01)	0.04 (0.04)	0.12 (0.12)	0.30 (0.30)	0.40 (0.40)	0.37 (0.36)	0.23 (0.23)	0.22 (0.22)	0.16 (0.16)	0.15 (0.15)	0.14 (0.14)	0.11 (0.10)	0.18 (0.18)
MgO	0.19 (0.19)	0.41 (0.41)	0.54 (0.54)	0.52 (0.52)	0.67 (0.67)	1.20 (1.20)	1.17 (1.17)	1.04 (1.04)	1.12 (1.12)	1.08 (1.08)	0.88 (0.88)	0.91 (0.91)	0.77 (0.77)	0.65 (0.65)	0.98 (0.98)
CaO	46.70	48.70	47.50	45.90	44.00	36.10	39.50	40.60	38.80	40.60	42.90	41.40	41.20	37.00	39.00
Na_2O	0.11 (0.06)	0.11 (0.09)	0.09 (0.06)	0.11 (0.07)	0.12 (0.10)	0.35 (0.26)	0.20 (0.14)	0.16 (0.10)	0.18 (0.12)	0.17 (0.10)	0.13 (0.08)	0.13 (0.08)	0.13 (0.07)	0.13 (0.05)	0.12 (0.07)
K_2O	0.4 (0.04)	0.15 (0.11)	0.10 (0.08)	0.14 (0.10)	0.16 (0.12)	0.36 (0.26)	0.26 (0.18)	0.21 (0.14)	0.24 (0.16)	0.22 (0.13)	0.16 (0.10)	0.15 (0.10)	0.12 (0.09)	0.11 (0.07)	0.15 (0.10)
P_2O_5	0.05	0.13	0.08	0.11	0.15	0.31	0.31	0.24	0.25	0.22	0.18	0.18	0.14	0.12	0.18
Trace elements (ppm)															
B	(0.8)	(0.08)	(3.5)	(3.5)	(3.5)	(15.6)	(15.6)	(10.6)	(10.7)	(10.7)	(8.0)	(8.0)	(3.5)	(0.8)	(3.5)
Ba	1810 (1810)	4650 (4650)	3980 (3980)	5720 (5720)	5510 (5510)	2880 (2880)	3010 (3010)	3410 (3410)	3430 (3430)	3250 (3250)	5120 (5120)	5510 (5510)	5050 (5050)	4540 (4540)	5230 (5230)
Ce	0.9	4.0	3.0	6.1	5.3	11.7	9.8	8.1	9.5	8.0	6.7	5.8	4.4	3.5	5.4
Co	0.5 (0.5)	4.3 (2.9)	3.1 (1.9)	4.9 (3.7)	6.7 (4.5)	10.7 (8.0)	9.7 (6.4)	8.9 (7.3)	8.1 (5.9)	22.0 (18.2)	7.3 (5.7)	8.3 (5.4)	6.1 (4.4)	4.1 (2.3)	6.3 (5.3)
Cr	5.9	6.9	6.6	14.2	17.6	7.9	12.1	19.6	12.4	11.3	7.8	9.5	3.9	3.9	19.5
Cu	21.8 (21.4)	60.5 (59.0)	61.3 (61.3)	73.3 (71.9)	91.0 (86.6)	164 (153)	166 (157)	142 (136)	114 (108)	110 (99.0)	90.8 (84.3)	100 (92.4)	84.5 (80.6)	84.9 (63.4)	98.4 (98.4)
La	4.1	11.8	9.7	12.3	13.7	27.8	25.2	21.5	25.0	21.7	19.0	17.3	13.6	10.7	14.9
Li	3.4 (2.9)	13.9 (13.9)	20.9 (20.9)	18.4 (16.2)	23.4 (20.7)	42.5 (36.8)	38.5 (35.1)	34.0 (32.1)	37.0 (35.7)	34.7 (32.6)	28.5 (26.8)	29.1 (27.9)	26.1 (24.4)	22.7 (20.8)	34.9 (31.7)
Ni	5.8 (5.8)	15.2 (15.2)	12.3 (12.3)	15.4 (15.4)	25.1 (25.1)	46.8 (46.8)	55.1 (55.1)	50.7 (50.7)	42.2 (42.2)	37.3 (37.3)	24.6 (24.6)	23.3 (23.3)	20.4 (20.4)	19.8 (19.8)	28.7 (28.7)
Sc	0.8 (0.7)	3.2 (2.6)	2.9 (2.7)	3.6 (3.1)	4.3 (3.7)	8.4 (7.1)	5.9 (5.2)	5.0 (4.5)	5.3 (4.7)	4.7 (4.0)	3.7 (3.2)	3.4 (2.9)	2.9 (2.5)	2.4 (2.0)	3.5 (2.9)
Sr	1060	1850	1600	1600	1670	1680	1790	1710	1660	1750	1700	1630	1550	1260	1490
Ti	68.7 (46.6)	167 (87.4)	131 (85.4)	157 (92.6)	189 (98.9)	392 (180)	302 (155)	278 (145)	328 (166)	314 (153)	241 (130)	239 (138)	173 (118)	149 (85.8)	206 (129)
V	1.8 (0.5)	8.6 (3.8)	8.0 (4.6)	5.1 (2.0)	6.6 (2.8)	15.0 (8.8)	14.3 (9.2)	11.8 (7.5)	12.9 (8.0)	12.4 (7.7)	9.4 (5.4)	8.3 (4.6)	6.2 (3.1)	4.2 (1.3)	8.0 (3.8)
Y	6.0	17.5	14.1	21.2	20.2	41.4	40.1	31.7	37.7	32.3	29.3	27.4	19.0	15.9	24.3
Zn	12.3 (6.5)	24.7 (22.5)	(24.7 (20.0)	26.6 (23.9)	37.7 (36.3)	70.1 (61.2)	70.1 (69.8)	60.7 (53.6)	58.9 (55.0)	54.5 (50.0)	44.0 (38.8)	47.7 (42.5)	42.8 (36.3)	34.7 (26.3)	53.9 (41.3)

	34-2, 3–4 cm	34-2, 24–25 cm	34-2, 50–51 cm	34-2, 74–75 cm	34-2, 100–101 cm	34-2, 121–122 cm	35-1, 9–10 cm	35-1, 100–101 cm	35-1, 124–125 cm	35-2, 2–3 cm	35-2, 28–27 cm	35-2, 49–50 cm	35-2, 75–76 cm	35-2, 97–98 cm	35,CC 0–2 cm
Major elements (%)															
SiO_2	12.80	14.60	19.10	23.20	26.70	27.80	9.91	12.00	8.98	13.50	7.70	10.10	15.90	12.00	17.00
Al_2O_3	0.52 (0.34)	0.69 (0.46)	0.88 (0.59)	0.99 (0.59)	1.30 (0.91)	1.38 (0.986)	1.75 (1.11)	1.87 (1.01)	1.34 (0.90)	2.56 (1.42)	1.28 (0.81)	2.01 (1.10)	3.33 (1.73)	2.48 (1.40)	3.44 (1.29)
Fe_2O_3	0.87 (0.76)	1.29 (1.13)	1.43 (1.28)	2.16 (1.53)	2.45 (2.45)	3.03 (2.72)	3.05 (2.46)	3.61 (2.21)	2.87 (2.18)	3.85 (2.76)	1.90 (1.54)	2.40 (1.76)	3.80 (2.21)	2.54 (1.74)	4.02 (1.73)
MnO	0.11 (0.11)	0.16 (0.16)	0.15 (0.15)	0.30 (0.30)	0.29 (0.29)	0.33 (0.32)	0.73 (0.41)	0.45 (0.39)	0.44 (0.42)	0.40 (0.38)	0.20 (0.16)	0.24 (0.20)	0.22 (0.14)	0.19 (0.14)	0.38 (0.14)
MgO	0.67 (0.67)	0.88 (0.88)	1.01 (1.01)	1.57 (1.57)	1.71 (1.71)	2.26 (2.15)	1.34 (1.17)	1.52 (1.16)	1.25 (1.05)	1.78 (1.37)	1.05 (0.84)	1.36 (1.10)	2.23 (1.52)	1.57 (1.15)	2.17 (1.12)
CaO	43.80	41.80	38.90	31.90	30.50	33.00	43.10	41.50	44.90	38.90	48.10	44.40	37.40	41.20	34.40
Na_2O	0.10 (0.05)	0.11 (0.07)	0.13 (0.06)	0.18 (0.08)	0.25 (0.15)	0.26 (0.17)	0.19 (0.19)	0.20 (0.19)	0.15 (0.15)	0.31 (0.29)	0.14 (0.13)	0.22 (0.18)	0.44 (0.42)	0.27 (0.27)	0.42 (0.42)
K_2O	0.10 (0.06)	0.13 (0.08)	0.14 (0.10)	0.16 (0.10)	0.23 (0.16)	0.25 (0.18)	0.46 (0.30)	0.48 (0.31)	0.36 (0.26)	0.58 (0.41)	0.30 (0.20)	0.36 (0.27)	0.58 (0.43)	0.46 (0.35)	0.64 (0.460)
P_2O_5	0.14	0.16	0.17	0.18	0.25	0.28	0.37	0.33	0.25	0.36	0.20	0.29	0.21	0.19	0.23
Trace elements (ppm)															
B	(0.8)	(3.5)	(3.5)	(3.5)	(12.9)	(20.5)	(15.6)	(14.2)	(15.6)	(20.5)	(6.2)	(10.6)	(15.6)	(10.7)	(10.7)
Ba	4480 (4480)	5110 (5110)	5420 (5420)	3900 (3900)	3460 (3460)	3260 (3260)	2710 (2710)	3230 (3230)	3740 (3740)	2750 (2750)	4150 (4150)	4070 (4070)	3610 (3610)	3360 (3360)	4210 (4210)
Ce	3.5	4.8	5.2	6.6	7.0	8.0	7.5	8.6	5.6	9.7	4.0	5.5	6.2	4.8	6.7
Co	4.5 (3.4)	6.5 (5.2)	6.7 (5.4)	6.7 (5.7)	7.7 (6.5)	10.7 (8.2)	16.2 (14.0)	20.4 (14.0)	19.0 (15.8)	26.0 (22.8)	14.0 (13.1)	18.0 (14.9)	26.5 (16.7)	17.5 (14.0)	26.0 (11.3)
Cr	6.5	8.7	7.9	5.9	19.0	21.2	30.0	16.0	13.2	15.1	8.7	9.5	14.0	10.5	13.0
Cu	69.7 (62.7)	97.0 (87.8)	104 (96.4)	154 (125)	166 (157)	189 (175)	306 (256)	168 (113)	148 (122)	178 (127)	99.8 (73.4)	110 (76.7)	119 (65.7)	87.2 (55.6)	126 (55.8)
La	10.9	13.4	14.2	16.6	19.5	20.8	23.3	22.3	18.8	27.0	13.7	12.3	13.1	11.2	14.9
Li	22.6 (19.5)	30.1 (25.8)	36.0 (31.3)	48.6 (45.5)	64.5 (59.6)	82.7 (75.8)	32.6 (30.0)	36.8 (26.8)	25.4 (21.6)	40.6 (32.9)	23.4 (18.1)	31.0 (23.1)	56.4 (33.6)	36.6 (25.1)	48.1 (21.5)
Ni	19.5 (19.5)	19.9 (19.9)	22.5 (22.5)	40.7 (40.7)	35.4 (35.4)	41.3 (41.3)	135 (97.4)	45.3 (39.2)	59.7 (55.3)	54.1 (49.2)	32.3 (30.1)	41.4 (36.4)	38.9 (32.6)	35.5 (31.5)	74.5 (57.5)
Sc	2.4 (2.0)	3.3 (2.6)	4.2 (3.4)	4.6 (3.3)	6.0 (5.1)	6.7 (5.8)	6.4 (4.8)	7.2 (4.2)	5.4 (4.0)	8.6 (6.0)	4.9 (3.8)	6.5 (4.7)	9.8 (5.9)	7.3 (4.9)	10.4 (4.7)
Sr	1510	1540	1430	1260	1260	1360	1560	1510	1530	1440	1470	1370	1210	1260	1110
Ti	161 (100)	216 (135)	270 (167)	361 (129)	315 (214)	433 (265)	820 (195)	975 (150)	745 (227)	1570 (253)	928 (191)	1170 (231)	2710 (104)	1720 (174)	2520 (90.4)
V	4.7 (2.0)	7.0 (3.4)	8.4 (4.3)	9.2 (4.4)	12.2 (7.2)	13.2 (8.3)	29.1 (20.4)	29.3 (17.1)	26.9 (20.5)	31.2 (21.7)	14.3 (9.8)	17.2 (11.0)	18.6 (9.9)	13.4 (7.6)	25.2 (12.0)
Y	17.5	21.7	23.0	25.0	30.4	33.6	32.3	33.4	26.4	40.7	20.7	20.5	22.5	20.3	26.8
Zn	34.0 (23.9)	48.3 (32.6)	50.8 (41.3)	68.2 (53.7)	86.8 (74.9)	98.0 (87.3)	91.0 (67.4)	90.5 (52.5)	71.9 (52.5)	88.1 (66.2)	52.6 (36.3)	64.5 (41.3)	nd (42.5)	58.9 (41.0)	84.4 (37.6)

Note: Total Fe is expressed as Fe_2O_3. Values in parentheses are the HCl-soluble portion of the sample. nd = not determined.

APPENDIX C
Rare Earth Element Composition (ppm) of Basal Sediments from Holes 573B and 574C

	La	Ce	Pr	Nd	Sm	Eu	Gd	Dy	Ho	Er	Yb	Lu
Hole 573B												
40-1, 104–106 cm	5.33	1.50	1.38	4.98	1.25	0.37	1.23	1.27	0.31	0.91	0.82	0.19
42-1, 45–46 cm	5.92	1.67	1.65	5.88	1.41	0.41	1.56	1.51	0.37	0.95	0.97	0.20
42-1, 125–126 cm	6.41	1.74	1.21	5.22	1.16	0.31	1.35	1.33	0.31	0.90	0.92	0.18
42-1, 149–150 cm	8.19	2.16	1.75	7.08	1.65	0.47	1.67	1.79	0.44	1.18	1.28	0.26
42-2, 25–26 cm	37.50	12.80	7.87	34.30	7.26	2.04	8.64	8.35	1.92	5.34	5.44	0.88
42-2, 50–51 cm	35.40	12.30	7.30	33.60	6.83	1.90	8.15	7.91	1.79	5.03	4.78	0.77
42-2, 76–77 cm	81.90	35.40	18.20	83.20	17.00	4.93	20.60	19.30	4.37	12.10	12.50	2.00
42-2, 99–100 cm	101.00	39.90	19.80	89.80	18.40	5.30	22.40	21.80	4.97	13.60	13.80	2.24
42-2, 125–126 cm	98.00	38.50	21.00	92.60	18.70	5.56	21.80	20.60	4.59	12.50	12.90	2.00
42-2, 149–150 cm	86.90	33.00	19.30	84.50	16.80	5.01	19.60	18.70	4.15	11.40	11.60	1.77
42-3, 25–26 cm	98.30	36.90	22.30	98.50	19.40	5.80	22.50	21.30	4.69	12.70	12.70	1.91
42-3, 48–49 cm	128.00	38.90	24.00	110.00	21.40	6.09	25.20	24.70	5.51	14.90	14.40	2.21
42-3, 75–76 cm	101.00	31.80	19.40	87.30	16.70	4.94	19.60	19.20	4.28	11.70	11.50	1.74
42-3, 100–101 cm	87.30	24.90	15.70	71.90	13.80	3.99	16.70	16.60	3.73	10.10	9.79	1.54
42-3, 122–123 cm	70.30	21.60	12.90	58.30	11.50	3.36	13.90	13.30	2.96	7.84	7.62	1.20
42-4, 25–26 cm	40.00	14.00	7.94	34.70	6.94	2.15	8.19	8.04	1.82	4.93	5.07	0.80
42-4, 48–50 cm	30.00	9.28	5.66	25.80	5.12	1.54	6.98	6.14	1.37	3.82	3.76	0.56
42-4, 75–76 cm	22.70	12.90	4.98	22.40	4.58	1.46	5.64	5.29	1.16	3.18	3.07	0.47
42-4, 100–101 cm	13.80	4.81	2.60	12.50	2.48	0.78	3.35	3.32	0.75	2.27	2.09	0.31
42-4, 125–126 cm	7.60	2.99	1.56	7.30	1.50	0.47	2.93	2.07	0.45	1.42	1.26	0.18
42-4, 144–145 cm	6.93	2.00	1.30	6.44	1.23	0.36	1.55	1.59	0.35	1.10	0.94	0.13
42-5, 26–27 cm	3.71	2.33	0.64	3.62	0.89	0.34	1.65	1.35	0.31	0.80	0.99	0.15
42-5, (Piece 1, 3–4 cm)	4.08	1.38	0.66	3.43	0.95	0.36	1.80	1.83	0.47	1.41	1.68	0.28
Hole 574C												
32-2, 54–55 cm	4.06	0.93	0.69	3.20	0.68	0.19	0.86	0.78	0.17	0.49	0.54	0.09
33-3, 56–57 cm	11.80	3.97	2.24	10.50	2.25	0.63	2.66	2.36	0.52	1.44	1.44	0.25
33-4, 73–74 cm	9.71	3.01	1.64	7.93	1.74	0.49	2.04	1.80	0.39	1.10	1.18	0.21
33-4, 102–103 cm	12.30	6.05	2.15	9.93	2.18	0.61	2.57	2.29	0.51	1.38	1.46	0.27
33-5, 2–3 cm	13.70	5.26	2.49	11.70	2.52	0.71	2.96	2.62	0.56	1.55	1.66	0.28
33-5, 34–35 cm	27.80	11.70	5.52	25.00	5.34	1.49	6.24	5.42	1.17	3.15	3.18	0.53
33-5, 61–62 cm	25.20	9.82	4.34	20.20	4.43	1.28	5.35	4.57	1.00	2.78	2.98	0.51
33-5, 74–75 cm	21.50	8.11	4.01	18.50	4.02	1.14	4.76	4.05	0.87	2.37	2.40	0.42
33-5, 100–102 cm	25.00	9.53	4.84	22.00	4.71	1.35	5.64	4.84	1.04	2.82	2.82	0.48
3-5, 120–122 cm	21.70	8.00	4.14	19.00	4.02	1.15	4.80	4.10	0.89	2.38	2.36	0.40
33-5, 148–149 cm	19.00	6.73	3.38	15.50	3.32	0.95	3.93	3.43	0.74	2.05	2.05	0.35
34-1, 47–48 cm	17.30	5.75	3.08	14.30	3.04	0.88	3.69	3.12	0.68	1.84	1.86	0.32
34-1, 75–76 cm	13.60	4.38	2.48	11.60	2.44	0.71	2.92	2.50	0.55	1.52	1.52	0.27
34-1, 97–98 cm	10.70	3.50	1.88	8.77	1.87	0.53	2.24	2.01	0.44	1.24	1.32	0.23
34-1, 121–122 cm	14.90	5.40	2.67	12.70	2.74	0.79	3.21	2.93	0.65	1.74	1.83	0.31
34-2, 3–4 cm	10.90	3.52	1.84	9.13	1.96	0.56	2.35	2.11	0.48	1.31	1.37	0.23
34-2, 24–25 cm	13.40	4.78	2.35	11.40	2.51	0.73	3.01	2.65	0.58	1.73	1.59	0.27
34-2, 50–51 cm	14.20	5.20	2.73	12.80	2.78	0.80	3.12	2.91	0.65	1.87	1.79	0.29
34-2, 74–75 cm	16.60	6.63	3.06	14.70	3.20	0.93	3.61	3.24	0.70	2.05	1.91	0.32
34-2, 100–101 cm	19.50	6.95	3.74	17.40	3.75	1.06	4.26	3.97	0.86	2.50	2.43	0.40
34-2, 121–122 cm	20.80	8.04	3.97	18.50	4.01	1.17	4.63	4.26	0.94	2.68	2.65	0.45
35-1, 9–10 cm	23.30	7.52	4.64	21.60	4.53	1.32	5.63	4.71	1.02	2.90	2.78	0.42
35-1, 100–101 cm	22.30	8.58	4.96	21.00	4.43	1.36	5.80	4.66	1.01	2.71	2.79	0.41
35-1, 124–125 cm	18.80	5.60	3.53	16.90	3.54	1.02	4.54	3.82	0.83	2.37	2.22	0.35
35-2, 2–3 cm	27.00	9.70	4.99	23.70	5.15	1.56	7.44	5.41	1.18	3.08	3.30	0.51
35-2, 26–27 cm	13.70	3.96	2.50	12.50	2.63	0.77	3.28	2.94	0.64	1.86	1.77	0.28
35-2, 49–50 cm	12.30	5.45	1.79	11.20	2.45	0.74	3.30	2.93	0.68	1.93	1.77	0.29
35-2, 75–76 cm	13.10	6.16	2.50	12.60	2.88	0.91	3.80	3.31	0.72	2.07	1.96	0.30
35-2, 97–98 cm	11.20	4.82	2.24	10.80	2.41	0.79	4.05	2.87	0.64	1.72	1.82	0.27
35,CC (0–2 cm)	14.90	6.66	3.05	15.10	3.37	1.05	4.69	4.14	0.90	2.57	2.41	0.37

APPENDIX D
Major and Trace Element Composition of Tholeiitic Basalts

	573B-43-1 (Piece 2, 24–26 cm)	574C-36-1 (Piece 5, 34–39 cm)
Major elements (%)		
SiO_2	41.20	46.10
TiO_2	2.14	2.88
Al_2O_3	15.20 (1.09)	13.80 (1.27)
Fe_2O_3	12.40 (1.68)	15.20 (3.22)
MnO	0.21 (0.01)	0.22 (0.01)
MgO	7.22 (0.26)	6.22 (0.17)
CaO	12.00 (0.87)	10.50 (0.85)
Na_2O	2.70 (0.27)	2.37 (0.23)
K_2O	0.22 (0.11)	0.36 (0.13)
P_2O_5	0.16 (0.07)	0.18 (0.10)
H_2O	0.83	1.53
CO_2	0.00	0.04
Total	100.28	99.40
Trace elements (ppm)		
B	(12.4)	(63.4)
Ba	30.0 (15.0)	22.0 (< 10)
Co	98.2 (13.0)	94.5 (9.6)
Cr	137.0 (< 10)	88.0 (< 10)
Cu	75.4 (26.8)	63.4 (24.3)
Li	9.6 (0.3)	10.1 (1.2)
Ni	76.7 (< 5)	69.2 (< 5)
Sc	45.0 (0.7)	44.4 (0.2)
Sr	85.0 (< 10)	65.0 (< 10)
Ti	12800.0 (1340)	17300.0 (2530)
V	368.0 (29.1)	476.0 (75.2)
Y	35.7	40.0
Zn	124.0 (27.6)	159.0 (44.0)
Rare earth elements (ppm)		
La	3.80	2.89
Ce	12.10	12.10
Pr	2.16	2.00
Nd	11.10	11.40
Sm	4.31	4.18
Eu	1.44	1.55
Gd	5.23	5.72
Dy	5.91	6.68
Ho	1.29	1.45
Er	3.47	3.82
Yb	3.71	4.26
Lu	0.70	0.73

Note: Total Fe expressed as Fe_2O_3. Values in parentheses are the HCl-soluble portion of the sample.

Reprinted from Mayer, L., Theyer, F., et al., 1985
Initial Reports of the Deep Sea Drilling Project, Volume LXXXV, Washington (U. S. Government Printing Office)

25. INTERSTITIAL WATER CHEMISTRY AND DIAGENESIS OF BIOGENIC SEDIMENTS FROM THE EASTERN EQUATORIAL PACIFIC, DEEP SEA DRILLING PROJECT LEG 85[1]

Paul M. Stout, Scripps Institution of Oceanography

ABSTRACT

The concentration changes in pore waters of dissolved calcium, magnesium, sulfate, strontium, and silica and of alkalinity are controlled by diagenetic reactions occurring within the biogenic sediments of DSDP Sites 572, 573, and 574. Downcore increases in dissolved Sr^{2+} indicate recrystallization of calcite, and increases in dissolved SiO_2 reflect dissolution of amorphous silica. Minor gradients in dissolved Ca^{2+} and Mg^{2+} suggest little if any influence from reactions involving volcanic sediments or basalt. Differences in interstitial water profiles showing the downhole trends of these chemical species mark variations in carbonate and silica diagenesis, sediment compositions, and sedimentation rate histories among the sites.

The location and extent of carbonate diagenesis in these sediments are determined from Sr/Ca distributions between the interstitial waters and the bulk carbonate samples. Pore water strontium increases in the upper 100 to 250 m of sediment are assumed to reflect diffusion from underlying zones where calcite recrystallization has occurred. On the basis of calculations of dissolved strontium production and comparisons between observed and calculated "equilibrium" Sr/Ca ratios of the solids, approximately 30 to 50% of the carbonate has recrystallized in these deeper intervals. These estimates agree with the observed amounts of chalk at these sites. Variations in Sr/Ca ratios of these carbonates reflect differences in calcareous microfossil content, in diagenetic history, and, possibly, in changes in seawater Sr/Ca with time.

Samples of porcelanite recovered below 300 m at Site 572 suggest formation at temperatures 20 to 30°C greater than ones estimated assuming oceanic geothermal gradients from sedimentary sections similar to those recovered on Leg 85. The higher temperatures may partially account for higher Sr/Ca ratios determined for recrystallized carbonates from this site.

INTRODUCTION

Recovery of complete and undisturbed sedimentary sections by the *Glomar Challenger* has enabled detailed investigations of the physical and chemical changes that transform unconsolidated marine sediments into lithified rocks. These transformations include the progression from calcareous ooze to chalk and limestone, and from siliceous ooze to porcelanite and chert.

Several previous studies on diagenesis of calcareous deposits from DSDP sites in the Pacific Ocean concentrated on textural evidence to examine downhole recrystallization of carbonates (e.g., Schlanger and Douglas, 1974; Matter et al., 1975; van der Lingen and Packham, 1975). Recently, Baker et al. (1982) and Elderfield et al. (1982) used a geochemical approach to examine carbonate diagenesis from the same regions. Concentration distributions of calcium, magnesium, strontium, and variations in $^{87}Sr/^{86}Sr$ and $\delta^{18}O$ between the solid phases and interstitial waters were compared to assess the amount of diagenetic alteration. Baker et al. (1982) demonstrated that significant calcite recrystallization occurs at subbottom depths less than 200 m. They showed how Sr/Ca ratios in sediments progressively change downhole, in accordance with predicted equilibrium distributions, in response to calcite recrystallization. Elderfield et al. (1982) further substantiated these conclusions with strontium isotope data. Identical values of $^{87}Sr/^{86}Sr$ ratios were determined for the carbonates and interstitial waters at the same depths where Sr/Ca ratios agreed with predicted equilibrium distributions.

Leg 85 afforded an opportunity to expand our understanding of diagenetic changes within calcareous deposits (Fig. 1). Use of the variable length hydraulic piston corer, combined with complete coring of sections drilled to basement and closely spaced interstitial water sampling, enabled more detailed examination of earlier stages of diagenesis than was possible with rotary drilling methods. The overall objective of the leg, which was to conduct a detailed investigation of the paleoceanographic and paleoclimatic history of the region, allowed us to consider the influences that varying oceanographic and tectonic conditions have on diagenetic processes (and have had in the past). The effects of diagenetic processes on paleoceanographic reconstructions could also be examined.

The sedimentary successions cored during this leg are almost exclusively biogenic, composed predominantly of calcareous nannofossils and varying mixtures of foraminifers, radiolarians, and diatoms (Fig. 2). The sediments accumulated nearly continuously, with only short intervals of nonaccumulation or erosion (Fig. 3). This chapter presents data on the chemistry of interstitial waters and the Sr/Ca distributions between the carbonate sediments and interstitial waters. These data are used to interpret and identify the extent of diagenetic alteration within the sediments and to determine the important factors that control the observed distributions and trends. Results and discussions are for Sites 572, 573, and 574, the three sites drilled to basement (Figs. 2 and 3).

[1] Mayer, L., Theyer, F., et al., *Init. Repts. DSDP*, 85: Washington (U.S. Govt. Printing Office).

[2] Address: Scripps Institution of Oceanography, University of California, San Diego, La Jolla, CA 92093.

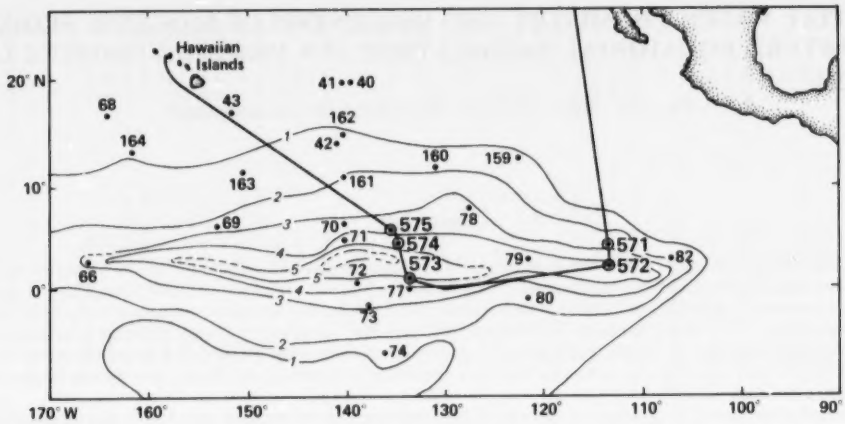

Figure 1. Cruise track and site locations of Leg 85 in relationship to acoustic sediment thicknesses (contours in tenths of seconds of two-way travel-time) and previous DSDP operations (Legs 5, 8, 9, and 16). ● = Leg 85; ◉ = other DSDP legs.

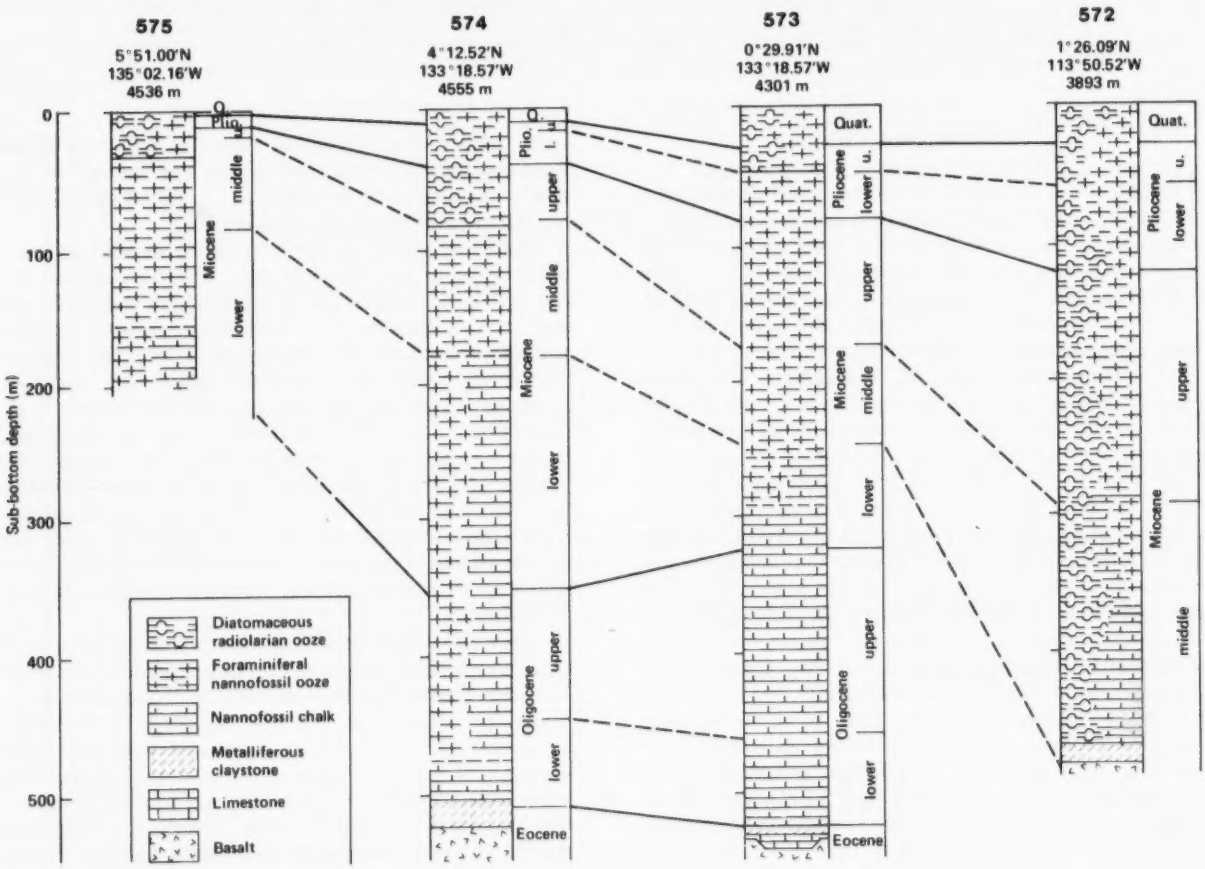

Figure 2. Lithologic columns and stratigraphy of Sites 572, 573, 574, and 575.

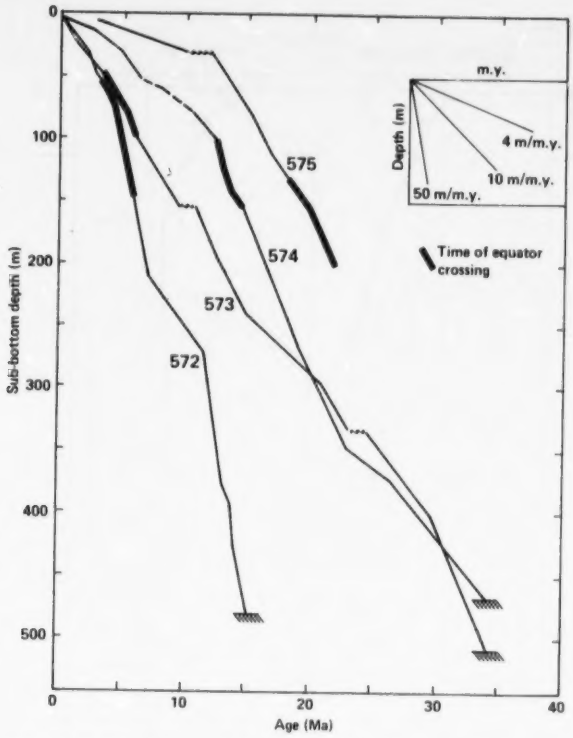

Figure 3. Sediment accumulation rates at Sites 572, 573, 574, and 575, as determined on board ship.

The time scale used is as discussed in the Introduction (this volume); sedimentation rate curves are as determined on board ship.

METHODS

Interstitial water samples were obtained at intervals between 1 and 30 m for all sites. Slightly larger intervals (50 m) were required in a few places because of concern about sampling major stratigraphic boundaries. Shipboard processing of samples and analytical techniques for the various ions are reported elsewhere (Gieskes, 1973, 1974; Gieskes et al., 1982). All squeezing of samples on board was performed at room temperature. We usually recovered about 50 ml of fluid, except in a few cases where induration was extreme and/or drilling disturbance was severe, but at least 15 ml were always recovered.

Concentrations of calcium and strontium in carbonate samples were determined following leaching of powdered samples by an acetic acid–sodium acetate solution (pH 5). Calcium was determined by EGTA titration and strontium by flame atomic absorption. No corrections were made for salt content resulting from drying (60°C). Experience has shown that for squeezed samples, corrections for strontium and calcium are insignificant (J. Gieskes, pers. comm., 1983) The influence of ion exchange reactions for strontium concentrations, which has not been adequately studied (Gieskes, 1978), is assumed to be small due to negligible amounts of clay minerals.

Insoluble residues of the carbonates were quantitatively determined, and the samples were analyzed by X-ray diffraction (XRD). Selected samples of the acid-leached sediment and original sediments and rocks were examined by petrographic and scanning electron microscopy (SEM) having an attached X-ray energy dispersive unit. A thorough examination of sediment texture and composition has not been completed. Data on porosities, weight percentage calcium carbonate, electrical conductivity (used to determined sediment diffusion coefficients), and microfossil abundances are from shipboard results reported elsewhere in this volume.

INTERSTITIAL WATER CHEMISTRY

Concentration versus depth profiles for Sites 572, 573, and 574 are plotted in Figures 4, 5, and 6. Table 1 contains sample location data and the concentrations determined for all species analyzed. Profiles for dissolved calcium, strontium, magnesium, silica, and sulfate and for alkalinity are presented. In general, the profiles from all sites show similar trends and similar changes in magnitude going downhole from overlying seawater. Maximum and minimum values, however, do not occur at the same depths. The slight contrasts in concentration changes and the different locations of maxima and minima reflect differences in sediment composition and in the loci of intervals undergoing enhanced diagenetic alterations.

The strontium profiles reveal steady concentration increases until near the maximum value, where an interval of roughly constant concentration occurs. Below these intervals, the values steadily decrease as basement is approached. I use these similar trends in dissolved strontium to divide each sedimentary section into three zones. Zone I corresponds to the interval where the concentrations steadily increase, Zone II to the intervals where the concentrations are approximately constant at maxima, and Zone III to the lowest sections, where concen rations steadily decrease. The depth relationships for each zone are summarized in Table 2. The sediment sections are divided in this manner for purposes of interpreting the carbonate recrystallization histories of these sites (discussed in detail below).

The observed increases in dissolved strontium are attributed to diagenetic recrystallization of calcite. Calcareous microfossils incorporate more strontium into their skeletons than predicted from equilibrium distribution coefficients for inorganic calcite (Katz et al., 1972; Baker et al., 1982). During recrystallization of calcite, the calcite dissolved and reprecipitated with lesser amounts of strontium, generating the observed strontium increase in pore waters (e.g., Sayles and Manheim, 1975; Gieskes, 1981). Other possible sources for strontium increases in solution include alteration of volcanic matter in the sediments or alteration of the underlying basaltic layer (Elderfield et al., 1982; Elderfield and Gieskes, 1982). However, such sources are not present here; the amount of volcanic sediment is negligible, and the gradients in dissolved calcium and magnesium are very slight. In deep-sea sections where extensive alteration of oceanic layer II is important, fivefold or greater increases in calcium and decreases in magnesium are observed (Lawrence et al., 1975; Gieskes, 1981; Gieskes and Lawrence, 1981).

The trends in alkalinity resemble those for strontium at each site. Sulfate profiles, in contrast, display opposite trends. Increases in alkalinity probably represent production from bacterial sulfate reduction. Sulfate decreases and alkalinity increases are largest at Site 572, for which sediment accumulation rates are highest (Figs. 3 to 4). The possible relationships between sulfate, alkalinity, and strontium profiles and sedimentation rate histories cannot be explained definitively at present. However, Sayles and Manheim (1975) and Gieskes and Johnson (1985) suggested that higher sedimentation rates cause

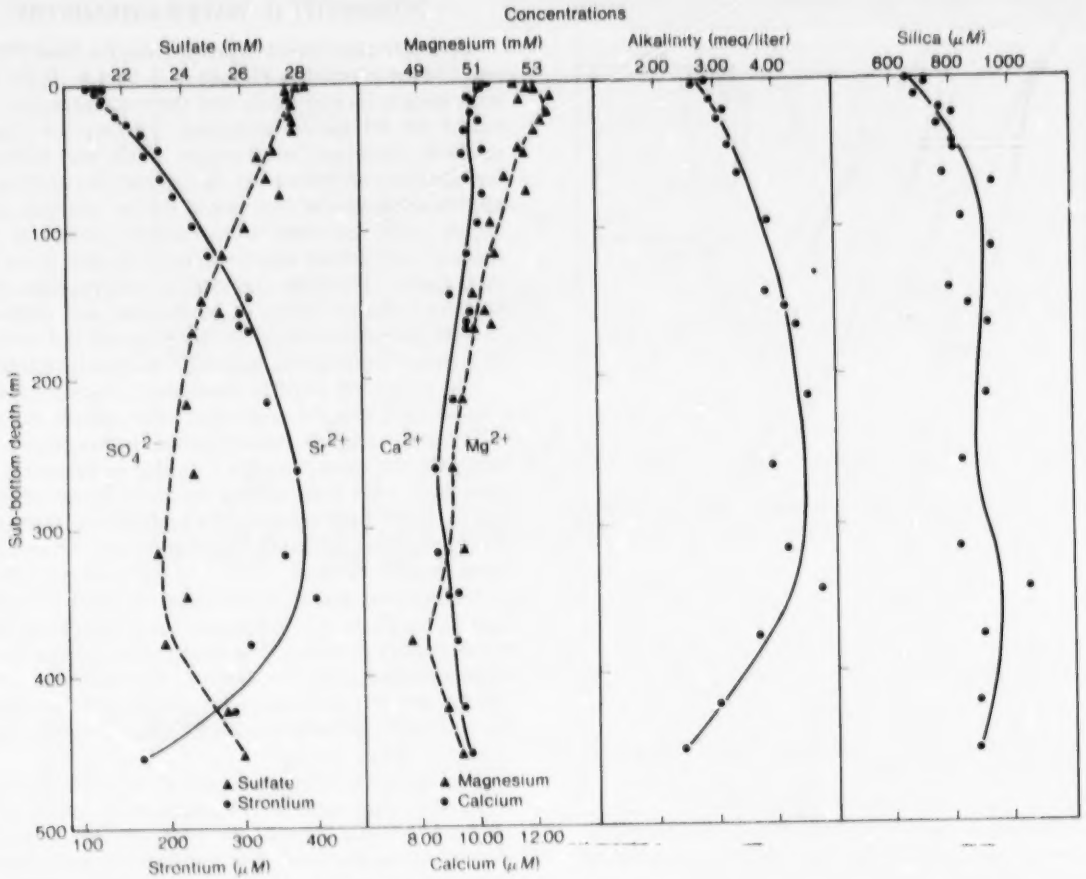

Figure 4. Interstitial water chemistry for Site 572.

burial of more organic matter, which in turn leads to more sulfate reduction and possibly higher rates of carbonate recrystallization. The increase in carbonate recrystallization is manifest by increases in dissolved strontium. The connection between sedimentation rate and carbonate diagenesis is discussed more fully in following sections of this chapter.

The dissolved silica profiles for the three sites are similar. The values increase from near-surface lows of about 600 μM to concentrations between 800 and 1000 μM. Some of the scatter in silica concentrations over short depth ranges is caused by differences in squeezing temperatures and by the amount of siliceous components in the sediments. In some samples taken at identical depths, and which contain similar percentages of noncarbonate components, the dissolved silica concentrations were 15 to 25% higher for sediments having higher temperatures (10 to 15°C) at time of squeezing. There is agreement between the average dissolved silica concentrations and the average percentages of noncarbonate in the sediments from which the pore waters were recovered. I assume that most noncarbonate material is biogenic silica; this is supported by petrographic observations and XRD results that indicate only trace amounts of nonbiogenic components. Site 572 had the highest values: 836 μM dissolved silica and 27% noncarbonate. Site 572 was intermediate with 776 μM silica and 20% noncarbonate; Site 573 had the lowest with 723 μM silica and 16% noncarbonate. Site 572, the easternmost site, also had the highest individual dissolved silica concentration of all samples: a value of 1055 μM SiO_2 was found for a sample from 345 m sub-bottom. Small pieces (several centimeters in diameter) of laminated porcelanite were recovered below 300 m at irregular intervals at this site. At Site 574, silica concentrations between 380 and 480 m are close to the maximum values of Site 572, yet no porcelanite was recovered. This may reflect nonrecovery of samples that may have been present at Site 574. Alternatively, the absence of porcelanite may result from a higher geothermal gradient at Site 572.

Sr/Ca DISTRIBUTIONS OF CARBONATES AND INTERSTITIAL WATERS

The strontium and calcium distributions between the pore fluids and sediments are compared to determine the extent of carbonate diagenesis in these sediments. Following the approach of Baker et al. (1982), "equilibrium" values for the Sr/Ca ratios are calculated and

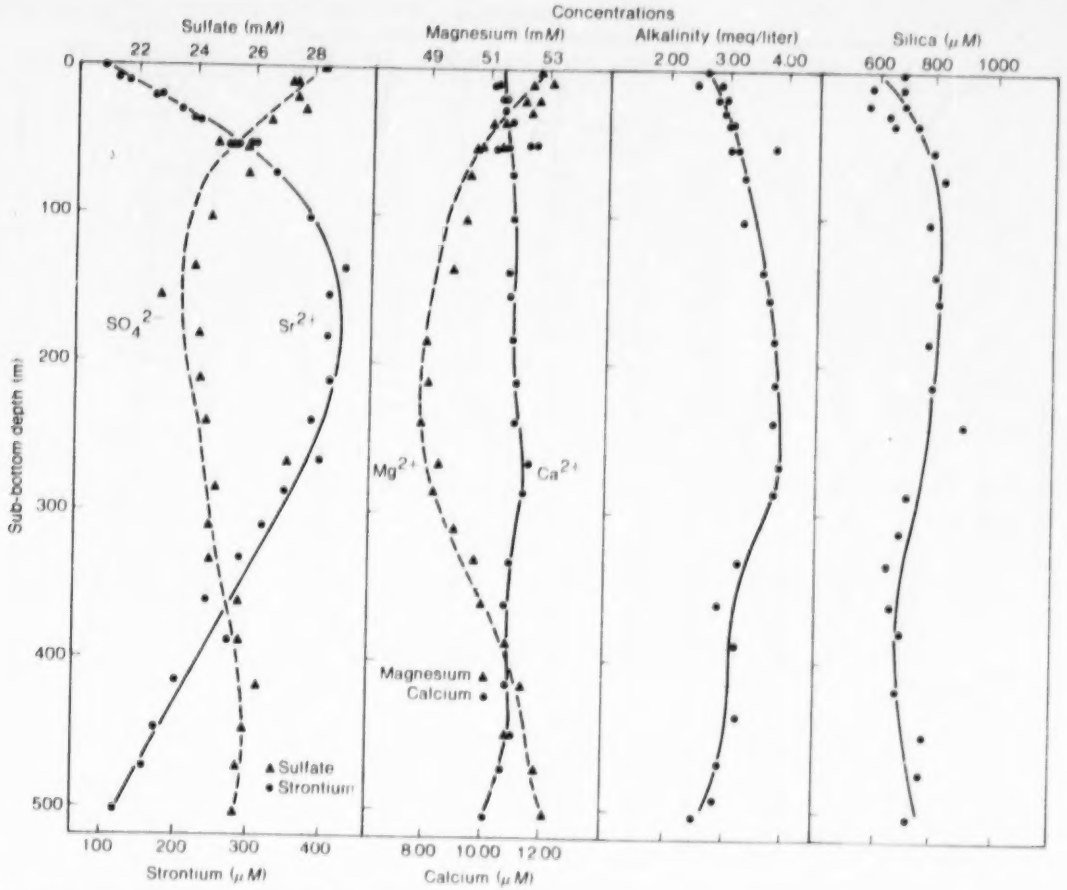

Figure 5. Interstitial water chemistry for Site 573.

plotted with the ratios determined for the leached bulk samples. The "equilibrium" values are calculated from the equation

$$Sr/Ca = k_{Sr}(Sr^{2+}/Ca^{2+})$$

where

Sr/Ca	=	molar ratio in carbonates
k_{Sr}	=	experimentally determined distribution coefficient for strontium in low-Mg calcite
Sr^{2+}/Ca^{2+}	=	molar ratio in interstitial waters

The distribution coefficient k_{Sr} was corrected for temperature and solution composition after Baker et al. (1982) assuming a 40°C/km geothermal gradient (Sites 71 and 72, Von Herzen et al., 1971).

There is continued disagreement on the appropriate value of k_{Sr} for inorganic calcite. Recent results by Mucci and Morse (1983), extrapolated to low-Mg calcite, support early values reported by Kinsman (1969) and Holland et al. (1964), which are an order of magnitude higher than those determined by Katz et al. (1972) and Baker et al. (1982). The experiments conducted by the latter groups were performed at very slight calcite supersaturation values, a situation that more closely resembles diagenetic conditions occurring in deep-sea carbonate sediments. Furthermore, if the larger distribution coefficient were appropriate in these sediments, one would not expect to see strontium increases in pore waters, nor would one observe the decreases in the Sr/Ca ratios in the solids, which has been clearly documented (Baker et al., 1982; Elderfield et al., 1982).

The calculated Sr/Ca equilibrium ratios and the observed ratios in bulk carbonate values are plotted in Figures 7, 8, and 9 and included in Table 3. The curves for the Sr/Ca equilibrium values closely resemble the dissolved strontium profiles (Figs. 4, 5, 6), reflecting the minor changes with depth in interstitial calcium concentrations. Overall, the dissolved calcium decreases slightly with depth at Site 572 but increases with depth at the other two sites. The slight changes in dissolved calcium affect the maximum Sr/Ca equilibrium values estimated for each site. For example, the maximum equilibrium value is 2.02×10^{-3} at Site 572, compared to 1.48×10^{-3} for Site 574. In contrast, the maximum observed dissolved strontium concentrations at these two sites are

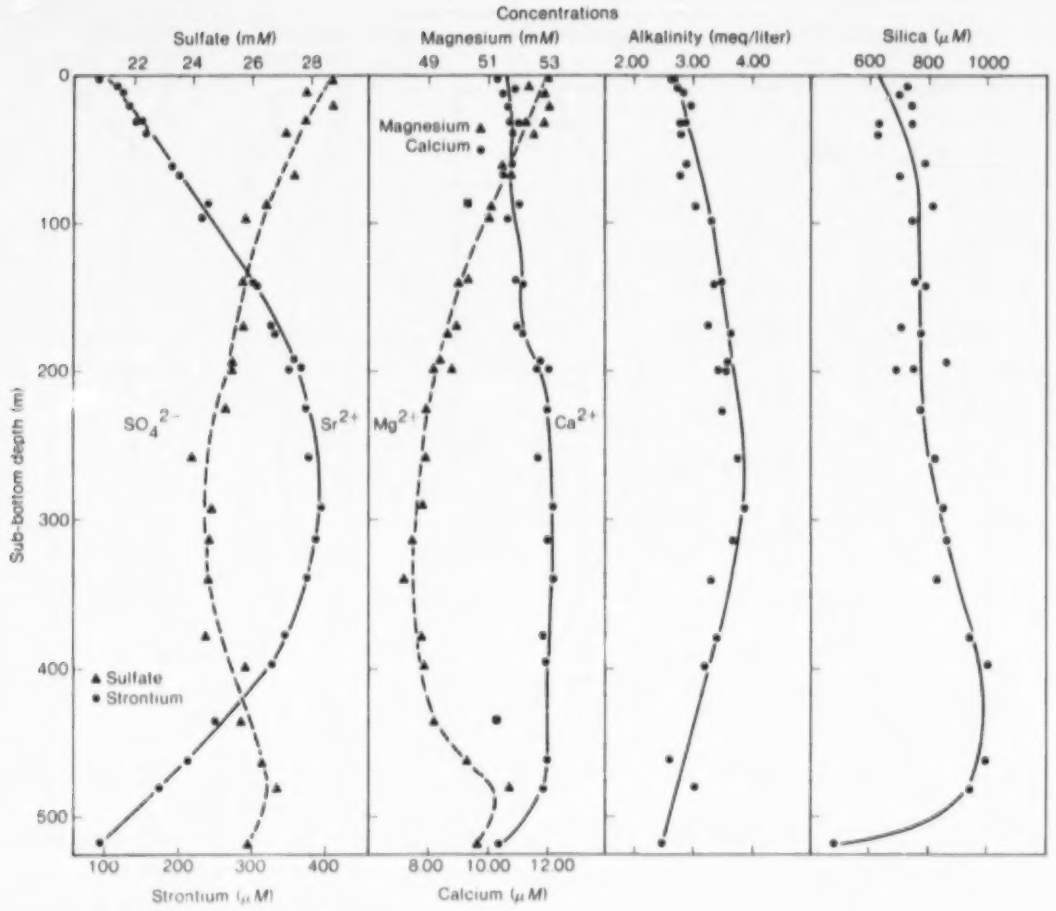

Figure 6. Interstitial water chemistry for Site 574.

virtually identical: 397 μM Sr^{2+} for Site 572 and 391 μM Sr^{2+} for Site 574. The reasons for the slight variations in calcium are unknown. Whatever the reasons, the interstitial calcium variations strongly influence the predicted Sr/Ca ratios and thus the interpretation of calcite recrystallization at each site.

There is little agreement between the observed Sr/Ca ratios and the calculated equilibrium values for the three sites (Figs. 7 to 9). Except for a few isolated points, the measured values are significantly higher than the predicted values. The observed values more closely approach the equilibrium ratios in the 100 to 150-m-thick zones near the predicted Sr/Ca maxima where the dissolved Sr^{2+} concentrations reach approximately constant values (compare Figs. 4 to 6 with 7 to 9). These zones correspond to Zone II of Table 2. The closest agreement between the observed and predicted equilibrium values in this zone implies that carbonate recrystallization is occurring most actively over these depth intervals. In Zone III, the larger disparity between predicted and observed ratios suggests that carbonate recrystallization is presently less active and that the Sr/Ca values in the carbonates reflect older diagenetic conditions. In sediments within the uppermost zone, the differences between predicted and observed ratios suggest that carbonate recrystallization has not been significant.

The Sr/Ca ratios measured from the bulk carbonate leaches vary over a wide range throughout the three sites. The variations may be attributed to numerous factors, the more important ones including (1) differences in calcareous microfossil compositions of the sediments (variations in the nannofossil/foraminifer ratio); (2) chemical paleoceanographic effects, such as variations in the Sr/Ca ratio or in the temperature of seawater with age, and consequently the Sr/Ca ratios incorporated during growth of skeletal calcite; and (3) the amount of recrystallized calcite and the specific physicochemical conditions under which recrystallization occurred.

Concerning the first factor, chemical analyses of individual species of foraminifers reveal Sr/Ca ratios in calcite ranging from 1.2×10^{-3} to 1.7×10^{-3} (Bender et al., 1975; Lorens et al., 1977; Elderfield et al., 1982). The bulk carbonate sediment samples are consistently higher in measured Sr/Ca ratios than individual species of foraminifers of the same age. The bulk samples invariably contain nannofossils, implying that nannofos-

Table 1. Interstitial water data, Leg 85.

Sample (interval in cm)	Sub-bottom depth (m)	pH	Alkalinity (meq/liter)	SO_4^{2-} (m*M*)	SiO_2 (μM)	Ca^{2+} (m*M*)	Mg^{2+} (m*M*)	Sr^{2+} (μM)	Cl (‰)	S (‰)
Hole 572										
1-1, 115-135	1	7.49	2.87	28.2	—	10.49	52.25	96	19.14	35.2
1-2, 100-120	2.5	7.58	2.64	27.7	—	10.19	52.67	101	19.34	35.2
1-3, 100-120	4	7.48	2.65	27.7	—	10.18	52.76	116	19.34	35.2
Hole 572A										
1-1, 0-20	0.5	7.58	2.63	27.9	653	10.39	52.81	96	19.14	35.2
1-4, 50-70	5	7.60	2.38	27.5	716	10.08	53.03	101	19.12	35.2
2-1, 0-20	9.5	7.56	2.25	27.5	—	9.70	53.48	116	19.24	35.4
3-2, 115-135	22	7.51	3.16	27.6	765	9.84	53.46	131	19.36	35.5
4-4, 95-115	34	7.57	2.49	27.7	757	9.63	53.02	161	19.60	35.4
6-3, 85-105	50	7.46	2.60	26.5	816	9.47	52.64	167	19.51	35.2
9-3, 85-105	76	7.46	3.25	27.3	941	10.12	52.71	208	19.51	35.5
13-5, 85-105	117	7.40	3.47	25.4	939	9.64	51.61	255	19.31	35.2
Hole 572B										
2-3, 123-143	164	7.50	3.99	—	—	9.66	51.50	296	19.27	35.2
Hole 572C										
2-2, 144-150	13	7.38	2.93	27.6	685	9.89	52.44	113	19.10	—
3-5, 144-150	27	7.39	3.09	27.7	810	10.08	53.26	142	19.31	35.5
5-5, 144-150	46	7.39	3.23	27.0	816	9.47	52.64	185	19.39	35.5
7-5, 144-150	66	7.41	3.39	26.8	778	9.65	52.04	190	19.49	35.5
10-5, 144-150	97	7.43	3.92	26.1	833	10.03	51.46	231	19.19	—
17-3, 144-150	145	7.40	3.87	24.6	795	9.04	50.93	309	18.92	—
Hole 572D										
1-3, 144-150	155	7.39	4.20	25.2	856	9.74	51.31	296	19.24	35.2
2-5, 144-150	168	7.34	4.37	24.2	922	9.61	50.96	308	19.25	35.2
7-5, 144-150	215	7.35	4.58	24.0	916	9.16	50.51	331	19.26	35.1
12-4, 144-150	261	7.43	3.93	24.2	835	8.53	50.09	372	19.26	34.9
18-4, 144-150	318	7.43	4.22	23.1	822	8.64	50.48	356	19.17	34.9
21-4, 144-150	346	7.43	4.76	24.0	1055	9.14	49.89	397	19.32	34.9
24-5, 144-150	377	7.38	3.70	23.3	906	9.20	48.67	308	19.14	34.6
29-4, 140-150	423	7.53	3.02	25.4	887	9.43	49.94	285	19.29	35.1
32-4, 140-150	454	7.54	2.43	26.0	887	9.69	50.32	161	19.34	35.2
Hole 573										
1-1, 144-150	1.5	7.39	2.61	28.4	679	10.42	52.68	93	19.18	35.2
2-6, 144-150	11	7.29	2.84	27.3	678	10.22	53.37	128	19.20	35.2
3-6, 144-150	20.5	7.33	2.97	—	691	10.60	52.15	173	19.43	35.2
5-5, 144-150	38	7.31	3.05	—	732	10.59	52.68	222	19.42	35.2
In situ I	53	7.66	3.76	—	819	11.40	51.52	295	19.39	35.2
In situ II	53	—	—	24.8	675	11.51	50.77	301	—	—
7-5, 140-150	55	7.30	3.18	25.8	781	10.70	50.77	276	19.35	35.2
9-5, 140-150	74	7.24	3.29	25.8	821	10.81	50.38	331	19.27	35.2
12-5, 140-150	103	7.35	3.24	24.5	778	10.83	50.25	378	19.23	35.2
16-5, 140-150	138	7.25	3.60	24.0	797	10.79	49.82	424	19.18	34.9
Hole 573A										
1-4, 144-150	10.5	7.38	2.48	27.2	580	10.34	53.04	113	19.32	35.2
2-4, 144-150	21	7.33	2.83	27.5	568	10.43	52.58	164	19.36	35.2
3-5, 143-150	30	7.28	2.93	27.7	633	10.51	52.35	203	19.36	35.2
4-4, 143-150	37	7.30	3.00	26.6	650	10.64	51.08	219	19.46	35.2
6-4, 143-150	55	7.33	3.01	25.3	779	10.21	50.54	266	19.19	35.2
Hole 573B										
2-5, 143-150	156	7.31	3.70	22.9	802	10.83	—	407	19.26	34.9
5-5, 144-150	184	7.30	3.78	24.1	779	10.83	48.93	404	19.14	34.6
8-5, 140-150	212	7.22	3.85	24.3	790	10.99	49.00	407	19.09	34.8
11-4, 140-150	239	7.24	3.80	24.4	895	10.96	48.78	381	19.15	34.9
14-4, 140-150	268	7.31	3.90	27.2	—	11.42	49.41	390	19.12	35.1
16-4, 140-150	287	7.31	3.78	24.8	707	11.26	49.24	345	19.19	35.1
19-2, 65-95	312	—	—	24.5	687	—	49.83	315	—	35.1
21-3, 140-150	333	7.37	3.22	24.5	647	10.82	50.62	286	19.32	35.2
24-3, 140-150	361	7.41	2.89	25.6	658	10.64	50.90	243	19.41	35.2
27-2, 140-150	388	7.34	3.17	25.6	690	10.67	51.69	268	19.41	35.2
30-2, 140-150	417	7.31	3.21	26.2	678	10.74	52.25	209	19.32	35.2
33-5, 140-150	450	7.32	2.95	25.8	778	10.95	51.78	169	19.42	35.2

Table 1. (Continued).

Sample (interval in cm)	Sub-bottom depth (m)	pH	Alkalinity (meq/liter)	SO_4^{2-} (mM)	SiO_2 (μM)	Ca^{2+} (mM)	Mg^{2+} (mM)	Sr^{2+} (μM)	Cl (‰)	S (‰)
Hole 573B (Cont.)										
36-1, 135-150	472	7.47	2.85	25.6	762	10.59	52.74	156	19.40	35.4
39-2, 135-150	502	7.45	2.50	25.5	724	10.04	53.02	117	19.49	35.1
Hole 574										
1-1, 144-150	1.5	7.45	2.61	28.7	599	10.33	53.03	93	19.24	35.2
2-5, 144-150	12	7.44	2.78	27.8	692	10.59	52.94	123	19.31	35.2
3-4, 144-150	20	7.44	2.91	28.8	732	10.70	53.10	131	19.34	35.4
4-5, 144-150	31	7.44	2.77	—	620	10.76	52.93	147	19.49	35.5
5-4, 144-150	39	7.40	2.78	27.1	620	10.81	52.60	154	19.49	35.4
8-4, 144-150	67	7.42	2.76	27.4	692	10.50	51.80	199	19.38	35.2
11-5, 140-150	97	7.33	3.27	25.7	732	10.70	51.04	230	19.43	35.2
18-2, 140-150	141	7.30	3.46	25.7	742	11.01	50.32	301	19.30	35.2
24-2, 140-150	171	7.27	3.23	—	770	11.17	49.66	327	19.20	35.2
28-2, 140-150	199	7.27	3.54	25.2	686	12.04	49.81	365	19.25	35.2
Hole 574A										
2-5, 144-150	8	7.39	2.74	—	714	10.92	52.41	115	19.25	35.5
4-5, 144-150	32	7.38	2.81	27.8	735	11.01	52.27	144	19.48	35.4
7-4, 144-150	60	7.44	2.84	—	780	10.80	51.55	189	19.38	35.4
10-5, 144-150	87	7.37	3.03	26.5	809	11.04	51.16	237	19.32	35.2
18-6, 140-150	141	7.29	3.37	—	771	11.19	49.99	305	19.22	35.2
22-5, 144-150	175	7.33	3.61	—	770	11.17	49.66	365	19.17	35.1
Hole 574B										
1-5, 144-150	193	7.30	3.57	25.3	859	11.80	49.36	359	19.24	35.2
Hole 574C										
1-3, 144-150	199	7.29	3.38	—	738	11.65	49.20	346	19.21	35.2
4-2, 144-150	226	7.28	3.48	25.1	765	12.01	48.89	375	19.21	35.3
7-5, 144-150	259	7.26	3.73	24.0	811	11.68	48.89	378	19.19	35.2
11-1, 140-150	291	7.21	3.83	24.6	836	12.19	48.82	391	19.19	35.2
13-4, 140-150	314	7.31	3.69	24.5	857	12.06	48.47	384	19.19	35.2
16-2, 140-150	340	7.28	3.43	24.5	827	12.22	48.12	378	19.17	35.2
20-3, 140-150	379	7.32	3.44	24.3	938	11.90	48.73	344	19.26	35.2
22-2, 140-150	397	7.36	3.17	25.7	994	11.97	48.76	324	19.32	35.2
26-2, 140-150	435	7.46	1.58	25.5	—	10.32	49.04	249	19.41	35.2
29-1, 135-150	462	7.44	2.56	26.2	989	11.01	50.26	211	19.46	35.2
31-1, 135-150	481	7.37	2.98	26.8	933	10.90	51.70	173	19.46	35.8
35-1, 135-150	519	7.46	2.45	25.7	470	10.43	50.58	93	19.04	34.9
Hole 575										
1-1, 144-150	1.5	7.44	2.61	27.9	—	10.78	52.35	110	19.16	35.2
2-2, 144-150	10	7.41	2.62	28.2	—	10.64	52.85	117	19.29	35.2
3-5, 144-150	24	7.34	2.81	29.0	—	10.62	52.75	157	19.53	35.5
4-5, 144-150	34	7.25	2.96	26.7	—	10.60	51.94	167	19.41	35.4
5-5, 144-150	43	7.34	2.96	26.4	—	10.84	51.37	187	19.36	35.2
7-5, 144-150	61	7.30	3.14	25.1	—	11.14	50.47	222	19.29	35.2
10-4, 144-150	86	7.26	3.21	25.9	—	11.55	50.05	268	19.31	35.2
Hole 575A										
1-1, 144-150	95	7.35	3.11	25.6	—	11.77	49.74	259	19.24	35.2
5-3, 140-150	114	7.28	3.27	25.5	—	11.94	49.26	285	19.16	35.2
10-2, 140-150	130	7.34	3.18	25.2	—	11.84	49.16	294	19.17	35.2
18-2, 140-150	155	7.33	3.25	26.0	—	12.28	48.74	311	19.21	35.2
26-3, 140-150	185	7.25	3.17	24.9	—	11.93	48.40	347	19.20	34.9
30-2, 140-150	197	7.29	3.52	25.0	—	12.64	48.14	357	19.14	34.9
33-2, 140-150	207	7.20	3.58	24.5	—	12.20	48.10	374	19.18	35.1
Hole 575B										
1-1, 144-150	5	7.39	2.64	28.3	—	10.41	52.26	101	19.10	35.2
6-4, 144-150	54	7.39	2.91	26.4	—	10.87	51.75	181	19.43	35.2
13-2, 140-150	112	7.34	3.25	26.3	—	11.76	49.77	273	19.17	35.2

Note: — indicates that sample was not analyzed.

Table 2. Thicknesses of sedimentary zones divided on the basis of dissolved-Sr^{2+} profiles.

Site	Zone I (m)	Zone II (m)	Zone III (m)
572	0–260	260–360	360–480
573	0–110	110–270	270–520
574	0–200	200–340	340–510

Note: Zone I = depth interval of increasing dissolved Sr^{2+} concentrations. Zone II = depth interval of approximately constant maximum dissolved Sr^{2+} concentrations. Zone III = Depth interval of decreasing dissolved Sr^{2+} concentrations.

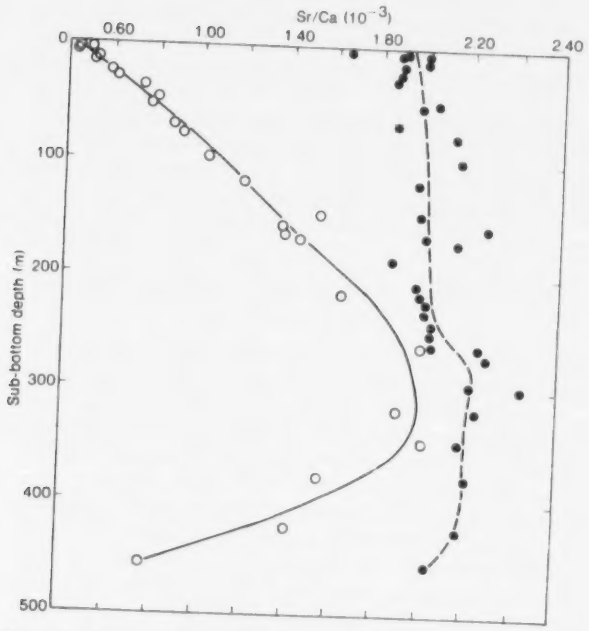

Figure 7. Calculated equilibrium Sr/Ca ratios (○) and observed ratios (●) for bulk carbonates for Site 572.

sils have higher strontium concentrations in their skeletal calcite than foraminifers.

Regarding the second factor, studies have suggested that the Sr/Ca ratio of seawater varies with age (Graham et al., 1982). Such chemical changes could influence the strontium distribution in biogenic calcite. Graham et al. (1982) presented data on variations in Sr/Ca ratios in planktonic foraminifers extending back to the Mesozoic. They suggested that the observed changes in Sr/Ca ratios with respect to geologic age resulted from basin-to-shelf fractionation between Sr-rich aragonite and less Sr-rich calcite. They suggested that the age differences may also reflect changing calcium fluxes varying in response to different rates of seafloor spreading. Cronblad and Malmgren (1981) showed that in Quaternary sediments, the strontium concentrations of two forami-

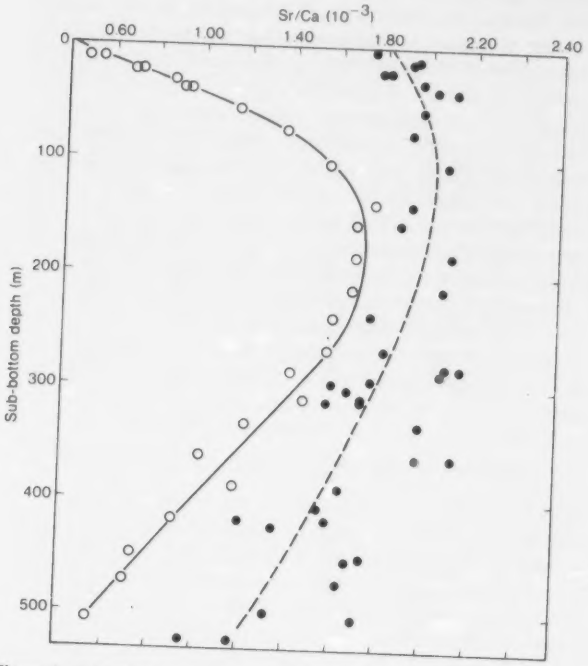

Figure 8. Calculated equilibrium Sr/Ca ratios (○) and observed ratios (●) for bulk carbonates for Site 573.

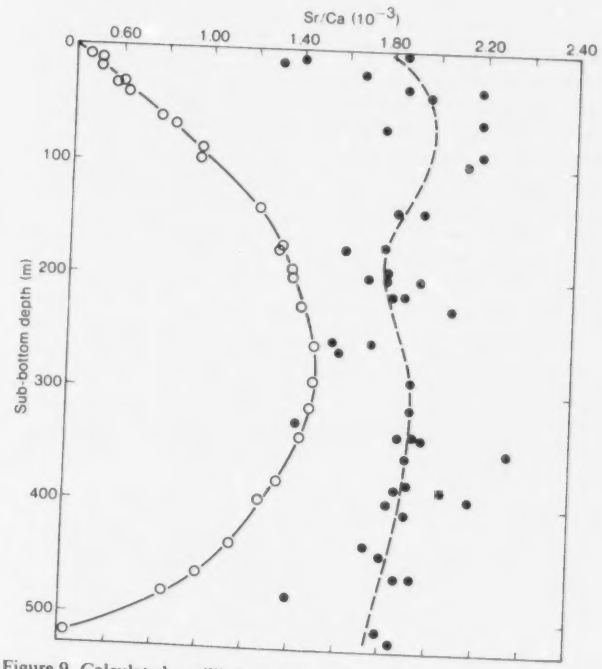

Figure 9. Calculated equilibrium Sr/Ca ratios (○) and observed ratios (●) for bulk carbonates for Site 574.

Table 3. Sr/Ca ratios of carbonate samples and calculated equilibrium Sr/Ca ratios derived from interstitial water profiles.

Sample (interval in cm)	Sub-bottom depth (m)	Age (Ma)	Sr/Ca (10^3)	Sr/Ca_{equil} (10^3)
Hole 572				
1-1, 115–135	1	0.1	1.90	0.40
1-2, 100–120	2.5	0.2	1.99	0.44
1-3, 100–120	4	0.2	1.88	0.50
Hole 572A				
1-1, 0–20	0.5	0.1	1.65	0.41
1-4, 50–70	5	0.3	1.88	0.44
2-1, 0–20	9.5	0.6	1.99	0.53
3-2, 115–135	22	1.5	1.87	0.59
4-4, 95–115	34	2.2		0.74
6-3, 85–105	50	3.0	1.97	0.78
9-3, 85–105	76	4.4	2.12	0.92
13-5, 85–105	117	5.2	1.97	1.19
Hole 572B				
2-3, 123–143	164	6.1	2.01	1.38
Hole 572C				
2-2, 144–150	13	0.8	1.89	0.51
3-5, 144–150	27	1.9	1.86	0.62
5-5, 144–150	46	2.8	2.04	0.80
7-5, 144–150	66	4.1	1.87	0.88
10-5, 144–150	97	4.8	2.15	1.03
17-3, 144–150	145	5.7	1.98	1.54
Hole 572D				
1-3, 144–150	155	5.9	2.27	1.37
2-5, 144–150	168	6.2	2.14	1.45
4-4, 78–80	185	6.5	1.86	—
6-6, 80–82	207	6.9	1.97	—
7-5, 144–150	215	7.5	1.99	1.64
8-3, 100–102	222	8.0	2.01	—
9-3, 100–102	231	8.7	2.00	—
10-3, 100–102	241	9.4	2.04	—
11-3, 100–102	250	10.1	2.03	—
12-3, 100–102	260	10.8	2.04	—
12-4, 144–150	261	10.8	2.24	2.00
13-3, 100–102	269	11.5	2.28	—
16-1, 58–60	294	12.0	2.22	—
16-3, 100–102	298	12.1	2.44	—
18-4, 144–150	318	12.3	2.24	1.90
21-4, 144–150	346	12.7	2.18	2.02
24-5, 144–150	377	13.3	2.21	1.56
29-4, 140–150	423	14.1	2.18	1.42
32-4, 140–150	454	14.6	2.05	0.78
Hole 573				
1-4, 144–150	1.5	0.2	1.74	0.39
2-6, 144–150	11	0.7	1.91	0.55
3-6, 144–150	20.5	1.3	1.78	0.72
5-5, 144–150	38	2.6	2.11	0.94
7-5, 140–150	55	3.9	1.97	1.15
9-5, 140–150	74	4.9	1.92	1.37
12-5, 140–150	103	6.1	2.08	1.56
16-5, 140–150	138	8.5	1.93	1.77
Hole 573A				
1-4, 144–150	10.5	0.7	1.94	0.48
2-4, 143–150	21	1.3	1.82	0.69
3-5, 143–150	30	2.0	1.96	0.86
4-4, 143–150	37	2.6	2.03	0.91
6-4, 143–150	55	3.9		1.16
Hole 573B				
2-5, 143–150	156	9.7	1.88	1.69
5-5, 144–150	184	12.4	2.11	1.69
8-5, 140–150	212	13.7	2.08	1.68
11-4, 140–150	239	15.0	1.75	1.59

Table 3. (Continued).

Sample (interval in cm)	Sub-bottom depth (m)	Age (Ma)	Sr/Ca (10^3)	Sr/Ca_{equil} (10^3)
Hole 573B (Cont.)				
14-4, 140–150	268	17.7	1.82	1.57
16-2, 10–12	283	19.2	2.09	—
16-2, 49–51	283	19.2	2.15	—
16-4, 140–150	287	19.7	2.07	1.41
17-3, 51–53	294	20.4	1.76	—
17-5, 68–70	297	20.7	1.59	—
19-2, 65–95	312	21.8	1.72	1.47
21-3, 140–150	333	23.3	1.98	1.22
24-3, 140–150	361	26.7	1.99	1.06
27-2, 140–150	388	28.8	1.63	1.17
30-2, 140–150	417	30.8	1.20	0.91
33-5, 140–150	450	32.2	1.73	0.73
36-1, 140–150	472	33.2	1.64	0.70
39-2, 135–150	502	34.5	1.71	0.55
42-2, 30–32	522	37.0	2.19	—
42-3, 74–76	525	37.3	7.98	—
43-3, 128–130	526	37.8	1.16	—
Hole 574				
1-1, 144–150	1.5	0.2	1.85	0.40
2-5, 144–150	12	2.2	1.31	0.51
3-4, 144–150	20	3.5	1.67	0.51
4-5, 144–150	31	4.8	2.18	0.61
5-4, 144–150	39	5.4	1.96	0.63
8-4, 144–150	67	9.0	1.76	0.84
11-5, 140–150	97	12.1	2.13	0.96
18-2, 140–150	141	13.4	1.84	1.23
24-2, 144–150	171	16.0	1.78	1.33
28-2, 140–150	199	17.0	1.71	1.38
Hole 574A				
2-5, 144–150	8	1.4	1.40	0.46
4-5, 144–150	32	4.9	1.86	0.58
7-4, 144–150	60	6.7	2.18	0.78
10-5, 144–150	87	11.3	2.19	0.96
18-6, 144–150	141	13.4	1.84	1.23
22-5, 144–150	175	16.2	1.60	1.32
Hole 574B				
1-5, 144–150	193	16.8	1.79	1.38
Hole 574C				
1-3, 144–155	199	17.0	1.79	1.38
1-5, 37–39	201	17.0	1.94	—
3-1, 126–128	215	17.5	1.87	—
3-2, 6–8	215	17.5	1.81	—
4-2, 140–150	226	17.8	2.08	1.42
7-5, 144–150	259	18.9	1.73	1.48
11-1, 140–150	291	20.1	1.92	1.48
13-4, 140–150	314	21.2	1.91	1.47
16-1, 71–73	338	22.3	1.86	—
16-1, 95–97	338	22.3	1.92	—
16-2, 140–150	340	22.5	1.96	1.43
17-4, 120–122	352	24.0	2.33	—
17-4, 124–126	352	24.0	2.33	—
18-2, 54–56	358	24.8	1.89	—
20-3, 140–150	379	27.1	1.91	1.34
21 1, 60–62	385	27.6	2.05	—
21-1, 50–52	385	27.6	1.85	—
22-1, 19–21	394	28.3	2.18	—
22-2, 140–150	397	28.7	1.81	1.26
23-3, 82–84	407	29.4	1.89	—
26-2, 140–150	435	31.6	1.72	1.14
27-2, 75–77	444	32.4	1.80	
29-1, 135–150	462	33.9	1.93	0.90
29-2, 56–58	462	33.9	1.86	
31-1, 135–150	481	35.1	1.40	0.75
34-1, 120–122	509	—	1.99	
35-1, 135–140	519	37.5	2.03	0.42

Note: — indicates that no interstitial water sample was taken at this depth.

niferal species co-varied with paleoclimatic indices. They claimed that changes in the temperature of seawater accounted for the strontium variations.

The third important factor, the extent and the physicochemical conditions of recrystallization during diagenesis, also contributes to variations in Sr/Ca ratios in the carbonates. Large intervals of closely spaced, interlayered chalks and oozes were observed throughout Leg 85 cores and have been reported in many deep-sea carbonate studies (e.g., Schlanger and Douglas, 1974; Garrison, 1981). These differences imply that calcite recrystallization occurs more rapidly in some layers than in others. Suggested explanations include preburial halmyrolitic and early diagenetic influences, such as variations in sedimentation rates and the amount of dissolution of labile species at the benthic boundary layer. Postburial diagenetic processes can also vary. For example, experimental evidence (deep-sea sediments reacting at elevated temperatures) indicate that the amount of clay minerals and biogenic silica may affect the rate of calcite recrystallization (Baker et al., 1980).

I now discuss how these different factors may account for the observed trends from Leg 85 sites and compare these with results from other DSDP sites drilled in the equatorial Pacific. I also present an estimate of the amount of calcite recrystallization that has occurred at Sites 572, 573, and 574.

VARIATIONS IN CALCAREOUS MICROFOSSIL COMPOSITION

I examined the relationship between the Sr/Ca ratios measured for the bulk carbonates and the calcareous microfossil percentages of adjacent sediments, which are taken from shipboard smear-slide results. The Sr/Ca ratios are compared with the nannofossil/foraminifer ratios. With the exception of three samples from Site 574, all samples contained more nannofossils than foraminifers. The results are summarized in Table 4. The average Sr/Ca ratios, the mean nannofossil/foraminifer ratios, and a correlation coefficient (r) for a linear regression analysis of the data are presented. Values of these parameters are given for each of the three zones (as defined above and described in Table 2), which divide the sediment section according to trends in the dissolved strontium profiles. The best positive correlation coefficient for each site occurs in Zone I, which is the depth interval for which the Sr/Ca distributions between observed and predicted values suggest that calcite recrystallization has been minor. An extrapolated value for the Sr/Ca ratios, corresponding to a sample composed exclusively of nannofossils, is presented for this upper zone (Table 4). All three regression analyses extrapolate to a similar value, and this Sr/Ca ratio is slightly higher than any observed ratio, except for two samples. These results suggest that much of the Sr/Ca variations in carbonates from Zone I can be attributed to different proportions of calcareous microfossils, and they support the implication that nannofossils incorporate more strontium in their skeletal structures than foraminifers. The lower values for the correlation coefficients for Zones II and III suggest that the Sr/Ca variations are controlled largely by calcite recrystallization and, to a much lesser extent, by microfossil content.

Table 4. Sr/Ca ratios in bulk carbonates versus calcareous microfossil contents.

Site	Zone	Mean Sr/Ca (10^3)	Mean log N/F[a]		Sr/Ca nanno[b] (10^3)
572	I	1.96 ± 0.13	1.01 ± 0.5	0.765	2.35
	II	2.01 ± 0.03	1.77 ± 0.1	0.525	
	III	2.01 ± 0.10	1.22 ± 0.6	0.489	
573	I	1.93 ± 0.12	0.81 ± 0.5	0.613	2.43
	II	1.93 ± 0.14	1.74 ± 0.3	0.189	
	III	1.77 ± 0.31	1.26 ± 0.6	0.153	
574	I	1.82 ± 0.3	0.74 ± 0.7	0.823	2.34
	II	1.84 ± 0.12	1.71 ± 0.7	0.579	
	III	1.92 ± 0.19	1.44 ± 0.3	−0.052	

[a] Log N/F = $\log \frac{\%\ \text{Nannofossils}}{\%\ \text{Foraminifers}}$

[b] Sr/Ca nanno = extrapolated value, assuming sediments composed of 100% nannofossils.

CHEMICAL OCEANOGRAPHIC FACTORS

The Sr/Ca ratios for all sediment samples from Leg 85 are plotted versus age in Figure 10. Also plotted are data from Site 289, drilled on the Ontong–Java Plateau, reported by Elderfield et al. (1982). Some of the large differences observed in Sr/Ca values from samples of similar ages result from variations in calcareous microfossil content. The low values at 1.4, 2.7, and 3.5 Ma for Site 574 and the overall lower ratios for Sites 575 and 289 are attributable to higher foraminifer contents. Despite these differences, there appears to be an age control on the Sr/Ca ratios, at least from early Miocene to the Recent. Older sediments are more extensively recrystallized. The most important fact to note in Figure 10 is that all curves have relatively low Sr/Ca ratios for sediments deposited during the late Miocene and near the boundary of early/middle Miocene and relatively higher Sr/Ca ratios for middle Miocene sediments. These results resemble those of Graham et al. (1982) for planktonic foraminifers. These data also help explain at least some of the variations in Sr/Ca ratios in Zone I of the three sites studied (Figs. 7 to 9; Tables 3 and 4). In addition, some of the observed variations in the older, more extensively recrystallized sediments in Zones II and III may reflect primary differences in the calcareous deposits—differences that were controlled by paleochemical fluctuations in seawater Sr/Ca ratios. In principle, diagenetic reactions do not necessarily obliterate paleoceanographic signals, although they undoubtedly modify them.

VARIATIONS IN CARBONATE DIAGENESIS

The Sr/Ca ratios in the carbonates from Sites 572, 573, and 574 differ in overall trend and in the extent of divergence from equilibrium ratios within the depth interval where calcite recrystallization is apparent (Zones II and III) (Figs. 7 to 9; Tables 3 and 4). These data indicate differences in diagenetic histories among the three sites. The average Sr/Ca ratios in carbonates from Sites 572 and 574 increase slightly with depth, whereas the ratios decrease with depth at Site 573. There is also less

scatter in observed Sr/Ca values from Sites 572 and 574 as compared with Site 573, especially in Zone III. Site 573 is also unique in that a general trend of observed Sr/Ca ratios approaching equilibrium values with depth is apparent (Fig. 8).

At Site 572, there seems to be a correlation between the carbonate Sr/Ca ratios and the carbonate accumulation rates. The high Sr/Ca ratios, which approach a constant value of 2.2×10^{-3} in the depth interval below 260 m (Fig. 7), coincide with large carbonate mass accumulation rates, ranging from 2.4 to 5.0 g/cm^2 per thousand years as determined on board ship. More solution-susceptible species of calcareous microfossils and more organic material are buried at times of high accumulation rates. This might enhance diagenetic reactions because the biogenic calcite might dissolve at faster rates. The higher Sr/Ca ratios in the solids at this site may thus reflect greater rates of strontium production, which in turn generates more dissolved Sr^{2+} in interstitial waters. Consequently, more strontium is incorporated into the inorganically produced calcite. Carbonate accumulation rates were lower at Sites 573 and 574, and the overall Sr/Ca ratios are not as high as those at Site 572 (Figs. 7 to 9; Tables 3 and 4). Also, a higher temperature gradient at Site 572 may have contributed to the higher Sr/Ca values in these sediments.

The Sr/Ca ratios from intervals containing closely spaced ooze and chalk layers from Sites 573 and 574 were determined. Care was taken when sampling to ensure that the induration variations were not artifacts of drilling. The data are summarized in Table 5. The chalks were significantly lower than the oozes in Sr/Ca concentrations in only two of the intervals studied.

The disagreement between the predicted and observed Sr/Ca distributions in Zone III at each site illustrates a problem inherent in comparing present interstitial water data with measurements from adjacent solids. The Sr/Ca values in solids from these deeper intervals most probably reflect recrystallization at times when pore water concentrations were significantly different from those at present. The higher Sr/Ca ratios of the carbonates versus the equilibrium values in Zone III may represent recrystallization that occurred in the past when dissolved Sr^{2+} concentrations were higher. The predominance of chalk in sediments from this zone indicates that carbonate diagenesis has already been significant (Fig. 2). The decreasing, roughly linear, dissolved strontium gradient in Zone III suggests that the pore water profile repre-

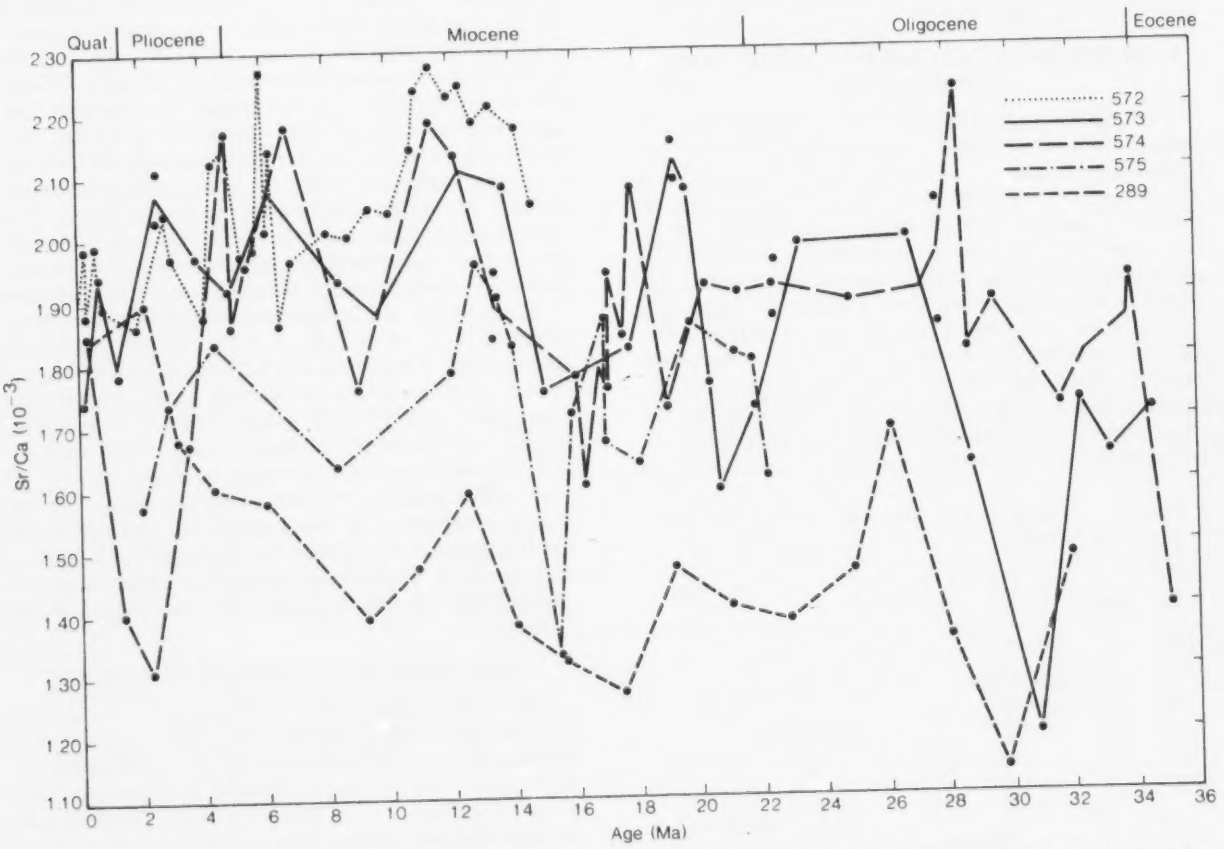

Figure 10. Sr/Ca ratios of bulk carbonates versus age for DSDP sites from the equatorial Pacific. Site 289 data are from Elderfield et al. (1982) for sediments from the Ontong–Java plateau, Leg 30.

Table 5. Sr/Ca ratios in pairs of adjacent chalk and ooze layers.

Sample (interval in cm)	Sr/Ca (10^3)	Sediment type
Hole 573B		
16-2, 10–12	2.09	Ooze
16-2, 49–51	2.15	Chalk
17-3, 51–53	1.76	Ooze
17-5, 6–8	1.59	Chalk
Hole 574C		
3-1, 136–137	1.87	Ooze
3-2, 6–7	1.81	Chalk
16-1, 95–97	1.92	Ooze
16-1, 71–72	1.86	Chalk
17-4, 120–121	2.33	Ooze
17-4, 124–125	2.33	Chalk
21-1, 60–61	2.05	Ooze
21-1, 50–51	1.85	Chalk

sents diffusion downward toward the basement from overlying sediments in which recrystallization is occurring most actively at present and also suggests some strontium sink. Consequently, using the pore water Sr/Ca values to predict "equilibrium" values for these deeper sediments may be inappropriate because processes controlling the Sr^{2+}/Ca^{2+} distributions may be unrelated to previously recrystallized carbonates. It follows that the driving forces for continuous recrystallization and re-equilibration with interstitial fluids in this zone are inadequate under existing diagenetic conditions. There is evidence, however, for some deeper diagenesis, particularly at Site 573, where there is an overall Sr/Ca decrease in the solids and where there is a very low value in the limestone interval (Sr/Ca = 0.95×10^{-3}) at 525 m sub-bottom depth.

EXTENT OF CALCITE RECRYSTALLIZATION

To quantify the extent of recrystallization in the calcareous sediments from Leg 85, a model based largely on observed strontium pore water profiles is presented. It assumes that (1) production of strontium resulting from biogenic calcite recrystallization occurs exclusively in the depth interval of maximum Sr^{2+} concentration (Zone II, Table 2); (2) only diffusive processes operate in Zones I and III; (3) calculated diffusive fluxes for the present have been the same in the past, since the time recrystallization initiated at each site; and (4) recrystallization did not start until a sufficiently large amount of carbonate had accumulated at each site.

Diffusive fluxes are calculated by determining diffusion coefficients and gradients from observed profiles using shipboard electrical resistivity and porosity data and appropriate temperature corrections assuming a 40°C/km geothermal gradient (Manheim, and Waterman, 1974; McDuff and Gieskes, 1976; Berner, 1980; Baker et al., 1982). Pertinent data used for calculations, the present diffusive fluxes, the Sr^{2+} production rates, and the carbonate mass accumulation rates for sediments from Zones II and III are presented in Tables 6 and 7.

Table 6. Diffusion coefficients and porosities used to calculate dissolved strontium fluxes from Zone II.

Site	Zone	D_b avg[a]	ϕ avg[b]
572	I	3.4	0.70
	III	3.5	0.63
573	I	2.6	0.71
	III	3.2	0.52
574	I	2.7	0.70
	III	2.9	0.53

[a] D_b avg = average bulk diffusion coefficient (10^6/cm^2/sec).
[b] ϕ avg = average porosity.

Table 7. Production of dissolved Sr^{2+} from carbonate recrystallization.

Site	Time recryst.[a] (Ma)	J Sr^{2+} [b] (mol/cm^2/sec)	Σ Sr^{2+} [c] (mol/cm^2)	Rate Sr^{2+} [d] (mol/cm^3/sec)	Carb. accum. rate[e] (g/cm^2/1000 yr.)
572	10	6.38×10^{-17}	2.56×10^{-2}	3.70×10^{-21}	2.82
573	33.4	7.65×10^{-17}	8.58×10^{-2}	1.98×10^{-21}	1.35
574	29.4	5.27×10^{-17}	5.45×10^{-2}	1.84×10^{-21}	1.63

[a] Time recryst. = time since onset of recrystallization.
[b] J Sr^{2+} = present strontium diffusive flux.
[c] Σ Sr^{2+} = total dissolved strontium produced since onset of recrystallization.
[d] Rate Sr^{2+} = production rate of dissolved strontium from carbonates, Zones II and III.
[e] Carb. accum. rate = average carbonate mass accumulation rates for sediments from Zones II and III.

The onset of recrystallization at each site is assumed to have occurred at the following times: Site 572—10 Ma; Site 573—33.4 Ma; and Site 574—29.4 Ma. These ages represent the time period during which the same amount of carbonate as that found in Zone I had accumulated at each site, according to past accumulation rates. These ages also represent the number of years over which the present diffusive flux is assumed to have operated, which is used to estimate the total dissolved strontium production. This reasoning follows from my assumption that calcite recrystallization is not occurring in Zone I. Approximately 130 m of sediment would have accumulated at Site 573 before recrystallization originated. This approximation is consistent with the present dissolved Sr^{2+} profile in that the strontium maximum there (i.e., the depth below which recrystallization occurs) is located at 110 m sub-bottom. Similar comparisons hold for the other sites.

Recrystallization estimates based on Sr/Ca distributions are given in Table 8, along with estimates of the amount of chalk present in Zones II and III for each site. The percent recrystallization is a comparison between the amount of Sr^{2+} produced from Zones II and III since recrystallization initiated and the amount of Sr^{2+} available in the carbonates from these same zones. The amount of strontium available represents the total dissolved strontium produced in the interstitial waters by carbonate recrystallization plus the amount of strontium greater than the calculated equilibrium value. This is derived from the calculated equilibrium profiles, which compare the average equilibrium and the average ob-

Table 8. Estimates of calcite recrystallization from Sr/Ca distributions.

Site	$\Sigma CaCO_3$[a] (mol)	ΔSr[b] (mol)	$\Sigma Sr^{2+}_{avail.}$[c] (mol)	Recryst.[d] (%)	Chalk[e] (%)
572	1.48×10^2	0.2×10^{-3}	5.5×10^{-2}	46	50
573	3.87×10^2	0.2×10^{-3}	1.63×10^{-1}	53	60
574	3.25×10^2	0.4×10^{-3}	1.84×10^{-1}	30	40

[a] $\Sigma CaCO_3$ = moles of calcite in Zones II and III.
[b] ΔSr = difference between Sr/Ca ratios, mean of observed values and mean of calculated equilibrium in Zone II.
[c] $\Sigma Sr^{2+}_{avail.}$ = amount of Sr^{2+} produced from calcite recrystallization (ΣSr^{2+}, Table 6) plus amount Sr^{2+} in solids above calculated equilibrium value: $\Sigma Sr^{2+}_{avail.} = (\Sigma CaCO_3 \times \Delta Sr) + \Sigma Sr^{2+}$.
[d] Recryst. = amount of calcite recrystallization: Recryst. (%) = $\frac{\Sigma Sr^{2+}}{\Sigma Sr_{avail.}} \times 100$.
[e] Chalk = observed percentages of chalk in sediments from Zones II and III.

served value within Zone II of each site. The chalk estimates represent the thicknesses of all-chalk sections plus one-third of the thicknesses of the intervals of chalk and ooze interlayering, which is an approximation determined from the visual core descriptions.

The highest strontium production rate occurs at Site 572 (Table 7). The carbonate accumulation rate is the highest at this site as well, which supports the contention that high accumulation rates can enhance diagenesis. Overall, the Sr^{2+} production rates are similar to those reported by Baker et al. (1982) for carbonate-rich DSDP sites drilled in plateau regions in the western Pacific and southern Atlantic. Production rates from 1.8 to 7.6 $\times$ 10^{-21} mol $Sr^{2+}/cm^3/sec$ were calculated from downhole changes in Sr/Ca ratios of bulk carbonate samples according to their model. These values were recalculated to be expressed in units of moles per cubic centimeter of bulk sediment, as shown in Table 7. These slightly higher production rates may reflect differences in solution susceptibility of calcareous microfossil assemblages. The plateau areas, which lie higher above the lysocline than the sites drilled on Leg 85, should contain a higher proportion of delicate calcareous microfossils. Consequently, higher reaction rates and greater strontium production may be expected there.

The percentage of recrystallization calculated from the Sr/Ca distributions shows very good agreement with the estimated percentage of chalk (Table 8). Detailed petrographic study of the sediments from these sites, coupled with more rigorous and constrained modeling of the Sr/Ca distributions, should allow for improved estimates of calcite recrystallization. It is especially important to determine if significant recrystallization occurs at shallower burial depths than is assumed in the model proposed here. Modeling the dissolved Sr^{2+} profiles will determine if the increases in Zone I are due solely to diffusion from deeper zones.

BIOGENIC SILICA DIAGENESIS

Centimeter-thick pieces of finely laminated porcelanite were recovered at Site 572. X-ray diffraction analyses indicate that the main silica phase present in these indurated sediments is opal-CT (Jones and Segnit, 1971). Scanning electron microscopic examination of these samples revealed that the opal-CT occurs predominantly as the massive type (Keene, 1976).

The first sample of porcelanite was found in a core taken at 315 m corresponding to an age of 12 Ma (see Site 572 chapter). Assuming a 40°C/km geothermal gradient and a 1°C bottom-water temperature, the projected temperature at this depth is about 14°C. The low temperature and young age are at odds with most observed occurrences of opal-CT from other DSDP sites. Kastner (1981) derived two equations relating time and temperature to the opal-A to opal-CT transition by using data from 37 DSDP legs. Applying a temperature of 14°C, the corresponding age estimates are 50 and 46 Ma (± 5 to ± 10), respectively, for the two equations. The oldest sediment recovered at this site (which was drilled to basement) was less than 16 Ma in age. The carbonate content and sedimentation rates at this site are such that transformation of opal-A to opal-CT should be fostered. However, higher temperatures than those assumed from typical oceanic geothermal gradients would be required to occur or to have occurred in the past. Using the ages of the sediments in the interval where the porcelanites are found (12 to 15 Ma), temperature estimates of about 35 and 45°C would be needed according to the two equations. Similar temperature estimates are indicated by data compiled from deep-sea siliceous deposits throughout the circum-Pacific area (Hein et al., 1978).

If the higher temperatures implied from the age-temperature relationships of the opal-A to opal-CT transformation actually occurred, they would have greatly enhanced any other diagenetic reactions occurring in these sediments. This is especially important in carbonate recrystallization. The higher temperatures would help explain the high Sr/Ca ratios observed in the deeper zones of this site. For example, if a temperature of 40°C were applicable to the observed Sr/Ca distributions in pore waters, using the temperature-corrected distribution coefficients, the calculated equilibrium values would equal the observed near-constant Sr/Ca ratios of $\sim 2.2 \times 10^{-3}$ in the carbonates at Site 572 (Figure 7, Table 3). Whether or not similarly higher temperatures help explain the Sr/Ca distributions at the other sites is uncertain. However, it is clear that the possible causes of the high temperatures, and the temporal and spatial significance of the mechanisms and processes causing the higher thermal gradients, deserve further attention and investigation.

SUMMARY AND CONCLUSIONS

The interstitial water chemistry from sediments recovered during Leg 85 reflects influences from diagenetic reactions common in deep-sea biogenic deposits. Increases in dissolved strontium and silica result from calcite recrystallization and dissolution of amorphous silica, respectively. Minor decreases in sulfate concentrations and increases in alkalinity most likely indicate degradation of buried organic material. Small gradients in calcium and magnesium imply minor or no influence from alteration of volcanic matter or oceanic layer II. The chemical gradients of all species determined are of similar steepness and magnitude; the maxima and min-

ima, however, occur at different depths. The differences are attributable to variations in diagenetic alterations, sediment composition, and sedimentation rate histories among the sites.

Comparisons between Sr/Ca distribution profiles of interstitial waters and bulk carbonate sediments are used to infer locations of calcite recrystallization and allow for calculations of the extent of recrystallization at each site. In the uppermost, nonrecrystallized sediments, variations in dissolved Sr^{2+} in pore waters are assumed to result from diffusive processes from the underlying zones of active recrystallization. The varying Sr/Ca ratios in solids reflect differences in calcareous microfossil content, in diagenetic histories, and possibly in changes in seawater Sr/Ca with time. A model estimating the amount of carbonate recrystallization at each site is based on interpretations of dissolved strontium profiles and comparisons between predicted equilibrium and observed Sr/Ca ratios in the solids. Accordingly, in zones having experienced recrystallization, between 30 and 53% of the carbonates have been altered diagenetically. These estimates agree with observed amounts of chalk in the same sediments. At Site 573, more recrystallization is apparent, and it has occurred at shallower depths than at other sites.

Small pieces of laminated porcelanite occur below 300 m sub-bottom at Site 572. The depth-age relationships of these samples imply significantly higher temperatures than ones inferred from typical oceanic geothermal gradients, possibly by as much as 20 to 30°C. These higher temperatures may help explain the relatively high Sr/Ca in the altered carbonates observed at this site.

ACKNOWLEDGMENTS

I thank all those responsible for the success of DSDP Leg 85. Special thanks are extended to Mr. Ken Thomson, shipboard chemist, for his excellent work, despite having a tremendous work load during the cruise. Drs. Miriam Kastner and Joris Gieskes, SIO, Paul A. Baker, Duke University, and Ken Johnson, University of California, Santa Barbara, provided stimulating discussions and helpful comments on the topics covered in this report. Financial support for this research came from ONR Contract No. USN N00014-80-C-0440 to M. Kastner.

REFERENCES

Baker, P. A., Gieskes, J. M., and Elderfield, H., 1982. Diagenesis of carbonates in deep-sea sediments—evidence from Sr/Ca ratios and interstitial dissolved Sr^{2+} data. *J. Sediment. Petrol.*, 52:71–82.

Baker, P. A., Kastner, M., Byerlee, J. D., and Lockner, D. A., 1980. Pressure solution and hydrothermal recrystallization of carbonate sediments—an experimental study. *Mar. Geol.*, 38:185–203.

Bender, M. L., Lorens, R. E., and Williams, D. F., 1975. Sodium, magnesium and strontium in the tests of planktonic foraminifera. *Micropaleontology*, 21:448–459.

Berner, R. A., 1978. Rate control of mineral dissolution under earth surface conditions. *Am. J. Sci.*, 278:1235–1252.

———, 1980. *Early Diagenesis: A Theoretical Approach:* Princeton (Princeton Univ. Press).

Cronblad, H. G., and Malmgren, B. A., 1981. Climatically controlled variation of Sr and Mg in Quaternary planktonic foraminifera. *Nature (London)*, 291:61–64.

Elderfield, H., and Gieskes, J. M., 1982. Sr isotopes in interstitial waters of marine sediments from Deep Sea Drilling Project cores. *Nature (London)*, 300:493–497.

Elderfield, H., Gieskes, J. M., Baker, P. A., Oldfield, R. K., Hawkesworth, C. J., and Miller, R., 1982. $^{87}Sr/^{86}Sr$ and $^{18}O/^{16}O$ ratios, interstitial water chemistry and diagenesis in deep-sea carbonate sediments of the Ontong Java Plateau. *Geochim. Cosmochim. Acta*, 46:2259–2268.

Garrison, R. E., 1981. Diagenesis of oceanic carbonate sediments: A review of the DSDP perspective. *In* Warme, T. E., Douglas, R. C., and Winterer, E. L. (Eds.), *The Deep Sea Drilling Project: A Decade of Progress*. Soc. Econ. Paleontol. Mineral. Spec. Publ., 32: 181–207.

Gieskes, J. M., 1973. Interstitial water studies, Leg 15—alkalinity, pH, Mg, Ca, Si, PO_4. *In* Heezen, B. C., MacGregor, I. D., et al., *Init. Repts. DSDP*, 20: Washington (U.S. Govt. Printing Office), 813–829.

———, 1974. Interstitial water studies, Leg 25. *In* Simpson, E. S. W., Schlich, R., et al., *Init. Repts. DSDP*, 25: Washington (U.S. Govt. Printing Office), 361–394.

———, 1975. Chemistry of interstitial waters of marine sediments. *Annu. Rev. Earth Planet. Sci. Lett.*, 3:433–453.

———, 1978. Reactions controlling strontium abundances in natural waters. *In* Wedepohl, K. H. (Ed.), *Handbook of Geochemistry*, II/4, 38-H:1–5.

———, 1981. Deep Sea Drilling interstitial water studies: Implications for chemical alteration of the oceanic crust, layers I and II. *In* Warme, J. E., Douglas, R. G., and Winterer, E. L. (Eds.), *The Deep Sea Drilling Project: A Decade of Progress*, Soc. Econ. Paleontol. Mineral. Spec. Publ., 32:149–167.

Gieskes, J. M., Elderfield, H., Lawrence, J. R., Johnson, J., Meyers, B., and Campbell, A., 1982. Geochemistry of interstitial waters and sediments, Leg 64, Gulf of California. *In* Curray, J. R., Moore, D. G., et al., *Init. Repts. DSDP*, 64: Washington (U.S. Govt. Printing Office), 675–694.

Gieskes, J. M., and Johnston, K., 1985. Interstitial water studies, Leg 81. *In* Roberts, D. G., Schnitker, D., et al., *Init. Repts. DSDP*, 81: Washington (U.S. Govt. Printing Office), 829–836.

Gieskes, J. M., and Lawrence, J. R., 1981. Alteration of volcanic matter in deep-sea sediments: Evidence from the chemical composition of interstitial waters from deep sea drilling cores. *Geochim. Cosmochim. Acta*, 45:1687–1703.

Graham, D. W., Bender, M. L., Williams, D. F., and Keigwin, Jr., L. D., 1982. Strontium–calcium ratios in Cenozoic planktonic foraminifera. *Geochim. Cosmochim. Acta*, 46:1281–1292.

Hein, J. R., Scholl, D. W., Barron, J. A., Jones, M. G., and Miller, J., 1978. Diagenesis of late Cenozoic diatomaceous deposits and formation of the bottom simulating reflector in the southern Bering Sea. *Sedimentology*, 25:155–182.

Holland, H. D., Holland, H. J., and Munoz, J. L., 1964. The coprecipitation of cations with $CaCO_3$-II. The coprecipitation of Sr^{2+} with calcite between 90 and 100°C. *Geochim. Cosmochim. Acta*, 28:1287–1302.

Jones, J. B., and Segnit, E. R., 1971. The nature of opal. I. Nomenclature and constituent phases. *J. Geol. Soc. Austr.*, 18:56–68.

Kastner, M., 1981. Authigenic silicates in deep-sea sediments: Formation and diagenesis. *In* Emiliani, C. (Ed.), *The Sea (Vol. 7), The Oceanic Lithosphere:* New York (Wiley).

Katz, A., Sass, E., Starinsky, A., and Holland, H. D., 1972. Strontium behavior in the aragonite–calcite transformation: An experimental study at 40–98°C. *Geochim. Cosmochim. Acta*, 36:481–496.

Keene, J. B., 1976. The Distribution, Mineralogy, and Petrography of Biogenic and Authigenic Silica from the Pacific Basin [Ph.D. dissert.]. Scripps Institution of Oceanography, La Jolla.

Kinsman, D. J., 1969. Interpretation of Sr^{2+} concentration in carbonate minerals and rocks. *J. Sediment. Petrol.*, 39:486–508.

Lawrence, J. R., Gieskes, J. M., and Broecker, W. S., 1975. Oxygen isotope and cation composition of DSDP pore water and the alteration of layer II basalts. *Earth Planet. Sci. Lett.*, 27:1–10.

Lorens, R. B., Bender, M. L., and Williams, D. F., 1977. The early nonstructural chemical diagenesis of foraminiferal calcite. *J. Sediment. Petrol.*, 47:1602–1609.

McDuff, R. E., and Gieskes, J. M., 1976. Calcium and magnesium profiles in DSDP interstitial waters: Diffusion or reaction? *Earth Planet. Sci. Lett.*, 33:1–10.

Manheim, F. T., and Waterman, L. S., 1974. Diffusimetry (diffusion constant estimation) on sediment cores by resistivity probe. *In* von der Borch, C. C., Sclater, J. G., et al., *Init. Repts. DSDP*, 22: Washington (U.S. Govt. Printing Office), 663–670.

Matter, A., Douglas, R. G., and Perch-Nielsen, K., 1978. Fossil preservation, geochemistry and diagenesis of carbonates from the Shatsky Rise, N.W. Pacific. *In* Larson, R. L., Moberly, R., et al., *Init. Repts. DSDP*, 32: Washington (U.S. Govt. Printing Office), 891–921.

Mucci, A., and Morse, J. W., 1983. The incorporation of Mg^{2+} and Sr^{2+} into calcite overgrowths: Influences of growth rate and solution composition. *Geochim. Cosmochim. Acta*, 47:217–233.

Sayles, F. L., and Manheim, F. T., 1975. Interstitial solutions and diagenesis in deeply buried marine sediments: Results from the Deep Sea Drilling Project. *Geochim. Cosmochim. Acta*, 39:103–127.

Schlanger, S. O., and Douglas, R. G., 1974. The pelagic ooze-chalk-limestone transition and its implications for marine stratigraphy. *In* Hsü, K. J., and Jenkyns, H. C. (Eds.), *Pelagic Sediments: On Land and Under the Sea*. Internat. Assoc. Sedimentologists Spec. Publ., 1:117–148.

van der Lingen, G. J., and Packham, G. H., 1975. Relationships between diagenesis and physical properties of biogenic sediments of the Ontong–Java Plateau (Sites 288 and 289, Deep Sea Drilling Project). *In* Andrews, J. E., Packham, G., et al., *Init. Repts. DSDP*, 30: Washington (U.S. Govt. Printing Office), 443–481.

Von Herzen, R. P., Fiske, R. J., and Sutton, G. H., 1971. Geothermal gradients on Leg 8. *In* Tracey, J. I., Jr., Sutton, G. H., et al., *Init. Repts. DSDP*, 8: Washington (U.S. Govt. Printing Office), 837–849.

Date of Initial Receipt: 14 September 1983
Date of Acceptance: 29 March 1984

Reprinted from Mayer, L., Theyer, F., et al., 1985
Initial Reports of the Deep Sea Drilling Project, Volume LXXXV, Washington (U. S. Government Printing Office)

26. COMPOSITION AND SOURCES OF PUMICES IN LEG 85 CORES[1]

Haraldur Sigurdsson and A. N. Davis, Graduate School of Oceanography, University of Rhode Island[2]

Pumice and volcanic ash in oceanic sediments can provide indications of wind and ocean current directions in the geologic past. In favorable cases the good stratigraphic control in deep-sea cores can also provide dating of volcanic events in the subaerial volcanic source region if the drilled volcanic deposits can be correlated to the source region. Such correlations can be made on the basis of chemical composition and should ideally involve a large number of elements.

The occurrence of pumice, dispersed volcanic ash, and a few volcanic ash layers in Leg 85 cores indicates that one or more volcanic source regions contributed to this depositional regime. We have studied the composition of pumices from Hole 573B to evaluate their possible source regions. A 10-mm pumice fragment from Section 573B-29-5 (90–92 cm) occurs in lower Oligocene white chalk. The highly vesicular pumice contains rare microlites of plagioclase. The other pumice fragment studied is 23 mm in diameter and occurs in lower Miocene brown ooze from Section 573B-15-3 (56–57 cm). It is a gray, pipe-vesicular pumice that contains rare microphenocrysts of plagioclase.

The composition of the pumice glass was determined by microprobe analysis. The glasses suffered severe sodium loss under the electron beam, and consequently, Na was determined by the method of Nielsen and Sigurdsson (1981). The average compositions of the two pumices are shown in Table 1, along with standard deviations. The standard deviations are within analytical error, indicating that the pumices are homogeneous. The oxide totals in the microprobe analyses are low for both pumices. We assume that this is an indication of 3–4% water dissolved in the silicic glass, probably resulting from posteruption hydration.

The glass composition of the two pumices from Hole 573B is markedly different and indicates two contrasting petrographic provinces or source regions. The lower Miocene pumice (Section 573B-15-3) is a quartz trachyte of the type associated with tholeiite-icelandite-quartz trachyte-rhyolite provinces. In the Pacific Ocean such markedly siliceous differentiates are confined to ridge-centered hotspots, such as Easter Island and the Galapagos Islands, lying along the crest of the East Pacific Rise. The lower Miocene pumice (Table 1, column 3) compares rather closely with a siliceous trachyte pumice from the Alcedo Volcano in the Galapagos Islands (Table 1, column 4). The Galapagos Islands may be the source region for the lower Miocene pumice, which is consistent with the Miocene age found for some of the islands themselves (Durham, 1965). An Easter Island source cannot be ruled out on basis of the composition, but the Miocene age is not consistent with the younger age of Easter Island.

Table 1. Microprobe analyses of glass in pumices from Site 573, with comparisons.

	1	2	3	4
SiO_2	66.76 (0.43)	66.81	69.07 (0.43)	66.87
TiO_2	0.43 (0.05)	0.26	0.30 (0.03)	0.66
Al_2O_3	22.34 (0.20)	22.08	12.68 (0.22)	12.55
FeO[a]	2.46 (0.06)	2.41	4.67 (0.26)	4.20
MgO	0.22 (0.03)	0.21	0.14 (0.02)	0.60
MnO	0.21 (0.03)	0.06	0.22 (0.04)	0.09
CaO	2.06 (0.10)	0.93	1.30 (0.04)	1.10
Na_2O	8.44 (0.25)	9.26	5.25 (0.14)	5.32
K_2O	5.06 (0.26)	5.46	2.47 (0.10)	3.08
	96.98		96.10	
Norms				
Q	—	—	23.73	19.79
Or	30.83	33.41	15.19	19.27
Ab	33.13	32.05	66.23	47.65
An	8.38	2.46	3.89	1.38
Ne	21.95	26.68	—	—
Wo	0.99	0.97	1.18	1.85
En	0.11	0.12	0.36	1.58
Fs	0.87	0.95	8.83	7.19
Fo	0.32	0.30	—	—
Fa	2.67	2.56	—	—
Il	0.84	0.51	0.59	1.33

Notes: 1. White pumice from Section 573B-29-5, 90–92 cm. Microprobe analysis of glass, average of 10 analyses. Standard deviation in parentheses. 2. Phonolite lava from Tahiti (McBirney and Aoki, 1968). 3. Gray pumice from Section 573B-15-3, 56–57 cm. Microprobe analysis of glass, average of 13 analyses. Standard deviation in parentheses. 4. Siliceous trachyte pumice, Alcedo Volcano, Albemarle Island, Galapagos (McBirney and Williams, 1969).

[a] Total Fe measured as FeO.

The lower Oligocene pumice from Section 573B-29-5 is of phonolitic composition (Table 1, column 1). This phonolite is of the type found in the strongly undersaturated basanite-alkali basalt-phonolite provinces, typical of many offaxis or intraplate oceanic islands. The composition of a phonolite lava from Tahiti is shown for comparison (Table 1, column 2); the two phonolites are virtually identical, except for calcium content. Although Tahiti seems a likely source region for the lower Oligocene phonolite pumice, we cannot rule out other undersaturated volcanic provinces in the region, such as the Marquesas Islands (see Bishop and Woolley, 1983).

The pumice fragments in Leg 85 cores are much too large to have been transported to the site by winds. Thus, no past wind directions can be derived from the presented data. It is more likely that the pumices were transported by surface ocean currents. The petrologic evi-

[1] Mayer, L., Theyer, F., et al., *Init. Repts. DSDP*, 85: Washington (U.S. Govt. Printing Office).

[2] Address: Graduate School of Oceanography, University of Rhode Island, Kingston, RI 02881.

dence is consistent with derivation of the lower Miocene pumice from the Galapagos Islands. This is also in agreement with present-day prevailing surface current directions, that is, with the Pacific South Equatorial Current flowing to the west of the Galapagos Islands at a velocity of about 1 knot (Fig. 1). The lower Miocene pumice would have taken about 100 days to reach Site 573 at this drift rate. Derivation of the lower Oligocene pumice by drift in prevailing surface currents from the strongly undersaturated phonolite-producing volcanic islands in the Southern Pacific is highly problematic (Fig. 1). The possible source regions of Marquesas Islands, Tahiti, and Christmas Island all lie upstream of the site within the prevailing summer and winter flow of the Pacific South Equatorial Current. A southerly shift of 5° latitude of the east-flowing Pacific Equatorial Countercurrent in Oligocene time, however, could account for drift of this pumice from Christmas Island to Site 573. The Equatorial Countercurrent, however, is believed to have developed in early–middle Miocene (15–23 Ma) (Haq, 1981; van Andel et al., 1976) during closing of the Central American Seaway in late Cenozoic time. In light of the postulated absence of the Equatorial Countercurrent in late Oligocene time, transport of the phonolite pumice cannot be attributed to any known Oligocene surface currents from likely sources, and therefore the source of this pumice remains unknown at this time.

REFERENCES

Bishop, A. C., and Wooley, A. R., 1973. A basalt–trachyte–phonolite series from Ua Pua, Marquesas Islands, Pacific Ocean. *Contrib. Miner. Petrol.*, 39:309–326.

Durham, J. W., 1965. Geology of the Galapagos. *Pacific Discovery*, 18:3–6.

Haq, B. U., 1981. Paleogene paleoceanography—early Cenozoic oceans revisited. *Oceanol. Acta. 4.*

McBirney, A. R., and Williams, H., 1969. Geology and petrology of the Galapagos Islands. *Mem. Geol. Soc. Am. 118.*

Nielsen, C. H., and Sigurdsson, H., 1981. Quantitative methods for electron microprobe analysis of sodium in natural and synthetic glasses. *Am. Mineral.*, 66:547–552.

van Andel, T. H., Heath, G. R., and Moore, T. C., Jr., 1976. Cenozoic history of the central equatorial Pacific: a synthesis based on Deep Sea Drilling Project data. *The Geophysics of the Pacific Ocean Basin and its Margins, Geophysical Monogr.* Am. Geophys. Union, 19:281–296.

U.S. Navy Marine Climatic Atlas of the World (Vol. V), South Pacific Ocean, 1979. Washington (U.S. Govt. Printing Office).

Date of Initial Receipt: 18 January 1984
Date of Acceptance: 20 January 1984

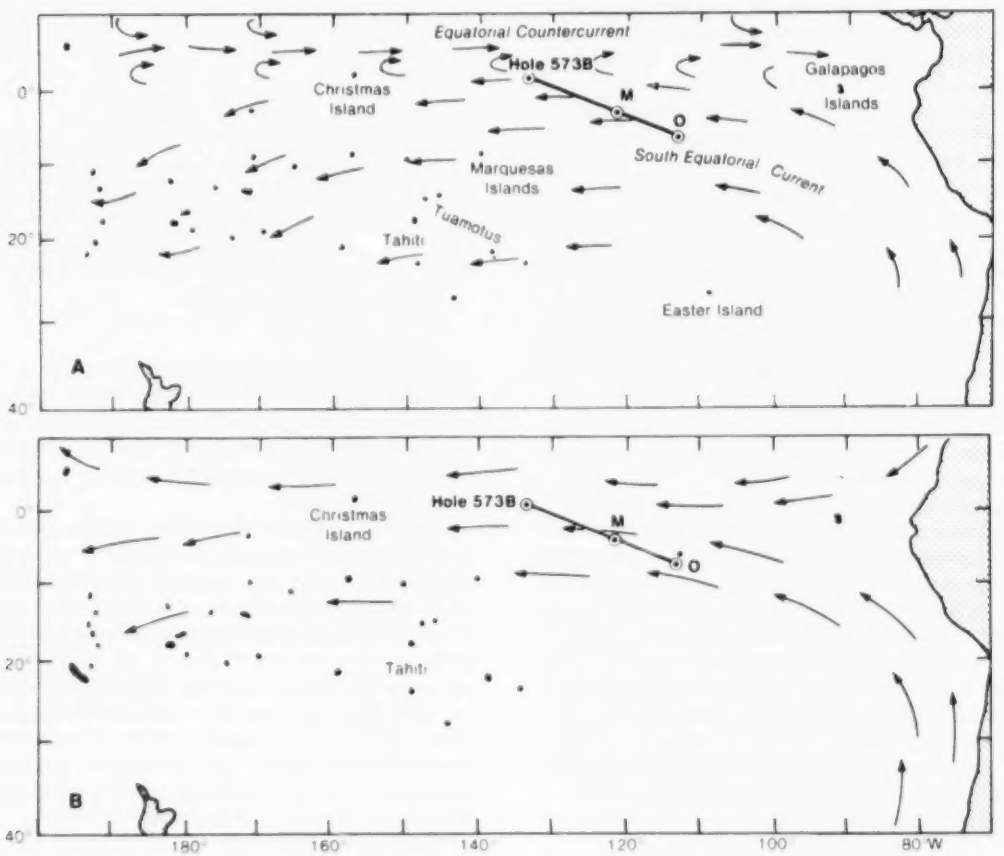

Figure 1. Circulation patterns of surface waters in the equatorial and southern Pacific. A. Present-day winter (June–August) surface currents (*U.S. Navy Marine Climatic Atlas of the World*, 1979). B. Postulated Oligocene surface currents (35 Ma). Note the open Central American Seaway and the absence of the Equatorial Countercurrent (after Haq, 1981; van Andel et al., 1976). M and O show the back-tracked position of Site 573 in Miocene and Oligocene times, respectively.

PART V: GEOPHYSICS

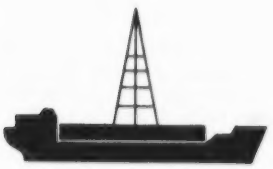

Reprinted from Mayer, L., Theyer, F., et al., 1985
Initial Reports of the Deep Sea Drilling Project, Volume LXXXV, Washington (U. S. Government Printing Office)

27. SEABEAM BATHYMETRIC AND WATER-GUN SEISMIC REFLECTION SURVEYS IN THE EQUATORIAL PACIFIC[1]

T. H. Shipley, Institute for Geophysics, The University of Texas at Austin
E. L. Winterer, Scripps Institution of Oceanography
M. Goud, Woods Hole Oceanographic Institution
and
S. J. Hills, C. V. Metzler, C. K. Paull, and J. T. Shay, Scripps Institution of Oceanography[2]

ABSTRACT

Five potential drilling sites in the equatorial Pacific were surveyed on the *Thomas Washington* in January and February, 1982, and three of them, Sites 573, 574, and 575, were then drilled on Leg 85 of the Deep Sea Drilling Project. At each of the survey sites we collected Seabeam bathymetry and high-resolution seismic reflection data, which were used to construct charts of bathymetry, navigation adjusted by best fit of the bathymetry, sediment thickness, and basement depth. For completeness, we also constructed similar charts for Site 572 from a 1970 survey. These surveys illustrate the bathymetry, sediment thickness, and basement structure and their interrelationship. They also reveal significant areas of erosion and redeposition (departures from the simple pelagic sequences) to be avoided in detailed siting of the drill holes. These data were used to locate the optimum pelagic sections for the paleoceanographic sampling objectives of Leg 85.

INTRODUCTION

This chapter summarizes the data collected at five equatorial Pacific (EQ) survey sites on the ARIADNE Expedition of the *Thomas Washington* in January and early February of 1982. For each site, four charts have been constructed: Seabeam bathymetry, sediment thickness, basement depth, and navigation. Data from a 1970 SCAN Expedition of the *Thomas Washington* were used to construct charts in the vicinity of Site 572. The purpose of these surveys was to investigate the local history around each proposed site and locate areas with maximum normal section and minimal erosional or depositional unconformities. Besides the maximum-section criterion, the paleoceanographic results would be enhanced if the drill sites were located as far as possible from areas of redeposition, such as those associated with infilling of local bathymetric lows. We designed a survey program to achieve these objectives using Seabeam swath-mapping and high-resolution seismic profiling (Fig. 1). Together, these tools provide a powerful three-dimensional image of the seafloor and subsurface.

The regional objectives included two N–S transects of the equatorial high-productivity zone between the Clipperton and Galapagos fracture zones. One track was between existing DSDP Sites 71, 72, and 73, the other between the EQ sites proposed for Leg 85. We will not report on the results of these more regional surveys. The purpose of the drilling program was to investigate the cyclicity of biogenic sedimentation, the low-latitude signals of climatic variations, and general high-resolution Cenozoic biostratigraphy.

METHODS

Seabeam is a 16-narrow-beam echo sounder that provides bathymetric information for a swath parallel to the ship track, with a width equal to about 80% of the water depth and relief resolution of better than 20 m. Using this system we were able to obtain nearly complete bathymetric coverage within the areas surveyed. Our most significant problem constructing internally consistent bathymetric charts involved the navigational inaccuracies resulting largely from dead-reckoning uncertainties between satellite fixes. We found that better navigation was produced by shifting tracks slightly—but within the error ellipses of the satellite fixes—until unique bathymetric features from overlapping swaths matched. This corrected navigation was used in subsequent analyses. See Renard and Allenou (1979) and references therein for a complete description of the Seabeam system.

The subsurface was explored with a single-channel seismic reflection system using an 80-in.^{3}, 2000-psi water-gun as the sound source (French and Henson, 1978). This source has a much broader bandwidth (Fig. 2A) than conventional air-guns, and does not produce bubble reverberations, since it is an implosive source (Fig. 2B). This source is still not ideal, because it is band-limited, though less so than the air-gun, and it generates a low-amplitude precursor about 20 ms in front of the main pulse. The data were digitally recorded with amplitude preservation for later processing and display. All seismic sections displayed in this chapter were bandpass-filtered 30 to 250 Hz and displayed at the same constant plotting gain. Time-varying and trace-varying amplitude adjustments were not applied to these data, so that amplitudes could be used in the interpretations. Subsurface data were digitized at 5-min. intervals (nominally 500 to 700 m along track) for presentation as charts shown elsewhere in this chapter.

SITE 573 (EQ-3)

This is the southernmost site along the N–S transect across the Pacific equatorial high-productivity zone. The survey comprised several E–W tracks of about 30 km each and two roughly N–S tracks of about 15 km each (Fig. 3). Adjacent track lines were separated by 1 to 3 km. Navigation during the survey was based on seven satellite fixes and dead reckoning. Owing to the strong drift

[1] Mayer, L., Theyer, F., et al., *Init. Repts. DSDP*, 85: Washington (U.S. Govt. Printing Office).

[2] Addresses: (Shipley) Institute for Geophysics, The University of Texas at Austin, Austin, TX 78712; (Winterer, Hills, Metzler, Paull, and Shay) Scripps Institution of Oceanography, University of California, San Diego, La Jolla, CA 92093; (Goud) Woods Hole Oceanographic Institution, Woods Hole, MA 02543.

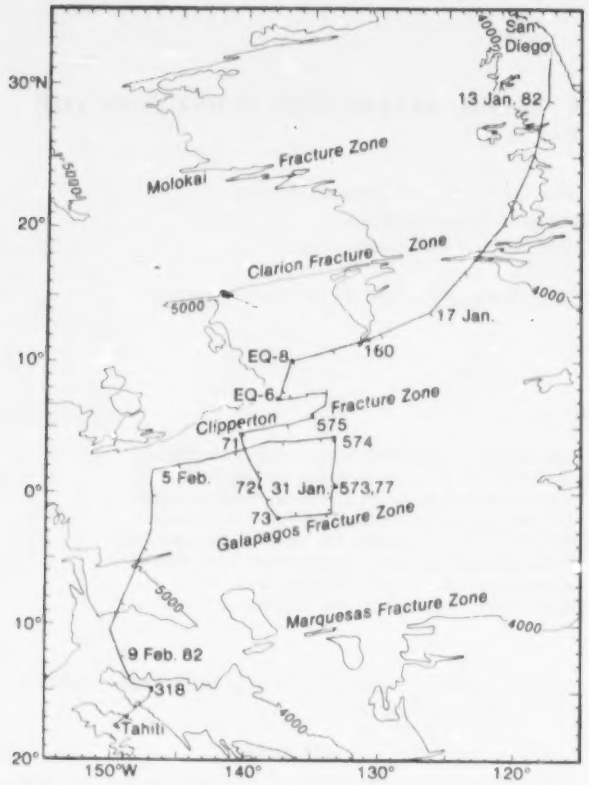

Figure 1. Cruise track of the *Thomas Washington* ARIADNE Expedition Leg 1.

in the survey area and to relatively few satellite fixes, compounded by the temporary failure of the ship's gyro system, the navigation is considered only fair.

The survey area is one of generally low relief, between 4200 and 4330 m, with a single major hill rising to 4020 m. The overall structural trend in the area is northwesterly. The sediment thickness ranges up to 0.55 s; depth to basement ranges from 5.5 to 6.35 s. The survey area can be divided into three regions: a western region, which is a thickly sedimented basin; a broad central, gently sloping region with thick sediments; and an eastern, hilly region with thinner sediments. Each of these regions is discussed here in terms of structure, sediment thickness, and bathymetry.

The western region is a broad basin, trending NW–SE, which deepens to the northwest, where it extends out of the survey area. Depths range between 4200 and 4330 m and generally mimic the basement relief; basement depths range from 6.20 to 6.35 s. Sediment thickness ranges from 0.40 to 0.55 s. The seismic reflection profiles show a section of basin-filling sediment, just above acoustic basement, which is not present elsewhere in the EQ-3 survey area (Figs. 4 to 6). Overlying the basin-filling deposits are thick sheet-drape deposits, which contain more highly reflective layers toward the top of the section. Site 573 was located in this western area to provide the maximum sediment thickness, and was the only location where the oldest sedimentary unit is present.

The central region is broad and slopes gently to the west, with depths of 4200 to 4300 m. Basement has subdued relief and ranges from 6.10 to 6.30 s. The sedimentary section in this region probably consists primarily of sheet-drape deposits. Although not possessing the lowest unit of the western region, the sediments are nonetheless quite th[ick] (0.35 to 0.5 s) and apparently undisturbed. DSDP Sit[e], drilled in this region, is easily correlated with Site 573.

The eastern region contains bathymetric and basement highs. Depths generally range from 4200 to 4230 m; there is a single prominent hill 300 m high. Basement depths range from 6.15 to about 5.5 s. The sedimentary section ranges in thickness from nil to 0.5 s, thinning over the highs and apparently absent from the prominent hill. The sediment distribution pattern shows substantial redeposition associated with the hill; a minor erosional moat is present at the base of the west-southwest side.

SITE 574 (EQ-4)

At this site a total of 260 km of tracklines was run, consisting of nine E–W lines, each separated by 2 to 3 km, and two N–S tie lines (Fig. 7). Eleven satellite fixes were obtained during the survey, with the resulting absolute (external) navigational uncertainties probably less than 2 to 3 km. One wide-angle reflection seismic profile was collected from a sonobuoy dropped overboard at the southern end of a N–S line along 133°19′W (Fig. 7D).

The area has low relief; the bathymetry consists of three broad ridges trending N–S and separated by troughs of similar size. The total relief in the area is about 160 m. The acoustic basement is rough (Figs. 8, 9); the sampling and contour intervals of the charts (Figs. 7B, 7C) are too coarse to resolve the local features accurately (Figs. 8, 9). Despite this lack of resolution, gross trends in the basement of the area follow the seafloor bathymetry; elongate lows underlie the seafloor lows and elongate basement highs underlie the broad ridges. Aside from a circular basement low, which extends below 6.7 s, in the NW part of the area, the deepest part of the survey is the trough in the center.

In general, sediment is thickest over basement lows. Notably less sediment is present under the seafloor channel in the western portion of the area, where the youngest part of the section is missing. The most complete section appears to be under the central valley, where the section thickness is about 0.55 s and there is somewhat less high-frequency basement topography. This was the position ultimately chosen for Site 574 (Fig. 10).

SITE 575 (EQ-5)

The northernmost survey area may be divided, for descriptive purposes, into a northern half and a southern half. The northern half was traversed by four E–W tracklines totaling about 130 km. The southern half was traversed by an equal number of E–W tracklines totaling about 110 km. Adjacent E–W lines were separated by 2 to 3 km, and the whole area was tied by two N–S ties (Fig. 11). One wide-angle reflection seismic profile was recorded from a sonobuoy dropped overboard at the southern end of a N–S line along 135°01′W. Fifteen sat-

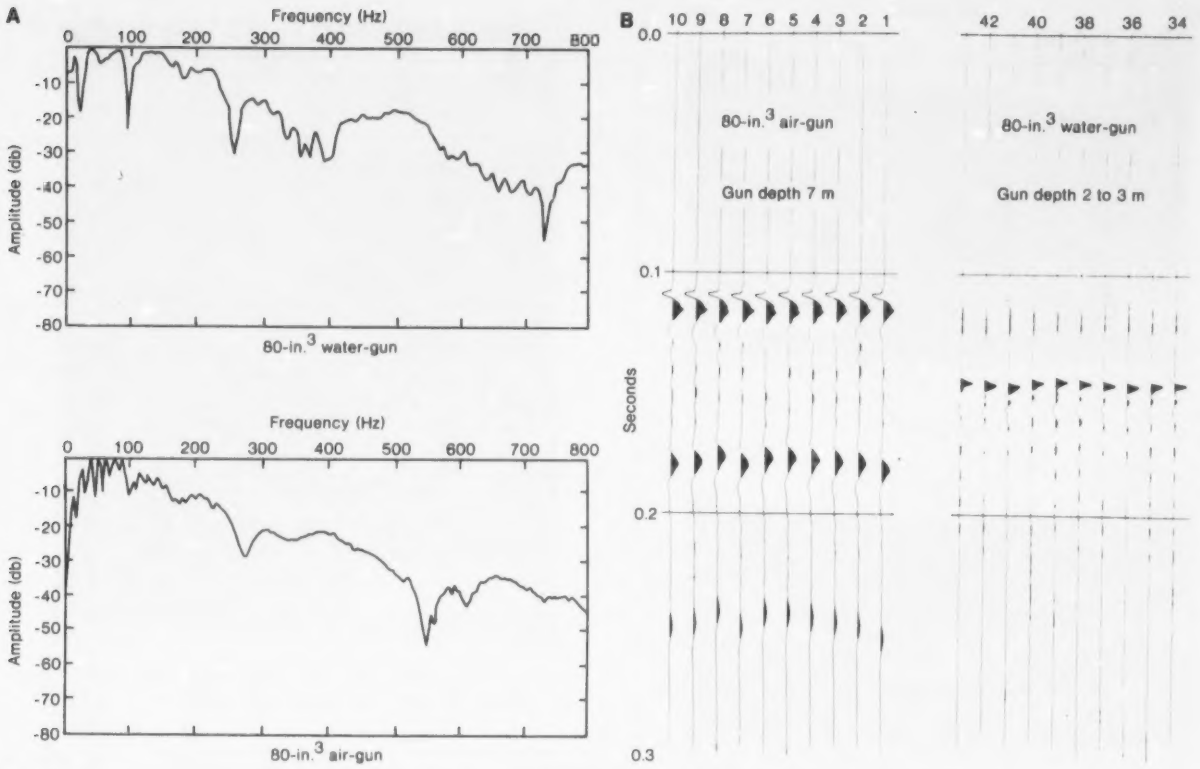

Figure 2. A. Frequency spectra of source-phone data for air-gun and water-gun at a depth of 10 ft. (3 m). The 6-db point is at 90 Hz for the air-gun and 220 Hz for the water-gun. B. Source signatures recorded at 1/4-ms sample period, source phone at 1000 ft. (300 m). Relative amplitudes between air-gun and water-gun have been adjusted for the display.

ellite fixes were recorded, and absolute navigational uncertainties are not more than 1 to 2 km.

The bathymetry of the northern half of the survey area shows low relief in the west, but is dominated in the east by an elongate seamount with relief of over 1000 m. The seamount trends NW–SE and rises from about 4500 m water depth to two separate peaks. The summit of the peak to the northwest reaches less than 3700 m depth; the summit of the southeast peak rises to about 3500 m depth. The detailed morphology of the seamount is unknown, owing to poor Seabeam performance over terrain where the slope parallel to the ship's track is steep. The seafloor to the west of the seamount ranges from 4500 to 4790 m depth. Seismic profiles show truncation of reflectors at the seafloor in this area as the bathymetry deepens toward a centrally located low trending N–S (Fig. 12). This appears to be a channel where more than 0.1 s of sediment has been eroded. The seafloor rises to the western edge of the survey area.

The survey was expanded farther south in an attempt to find an area with a more complete section. Both the bathymetry and basement show much less relief in the southern half of the survey area than in the northern half. The center of the area is an elongated shelf about 8 km wide, extending roughly 12 km southwest of the seamount and ranging in depth from 4540 to 4560 m. Along the western edge of this southern half of the area, the gradient steepens as the seafloor drops into the southerly extension of the channel observed in the northern half. Basement deepens under the channel to the southwest, and seismic reflectors are truncated along its eastern margin (Figs. 13, 14).

The basement below the elongate shelf is similarly low in relief, with only broad, undulatory topography. The sediments are generally about 0.5 s thick, but one notable exception occurs over a basement low along the north central edge of the shelf. Here the sediments are over 0.55 s thick, and the upper units observed in the seismic records are thicker than elsewhere in the survey area. Site 575 was eventually located about 10 km from the base of the seamount.

EQ-6 SITE

Site EQ-6, the next northerly site along the transect, was not drilled. Here the survey consisted of six E–W lines spaced about 2 km apart and two tie-lines oriented NNE and NNW (Fig. 15). Sea conditions were moderate for the duration of the survey, making the 3.5-kHz records unusably noisy. Ten satellite fixes during the survey provided good navigational control.

The EQ-6 bathymetry shows a series of three NNW- to northerly-trending ridges and valleys with a 10-km wavelength. Total depth varies from 4660 to 4850 m. The crests of ridges and floors of valleys tend to be wide and gently sloping, but are separated by more steeply dipping ridge flanks. A subtle ENE trend is superimposed

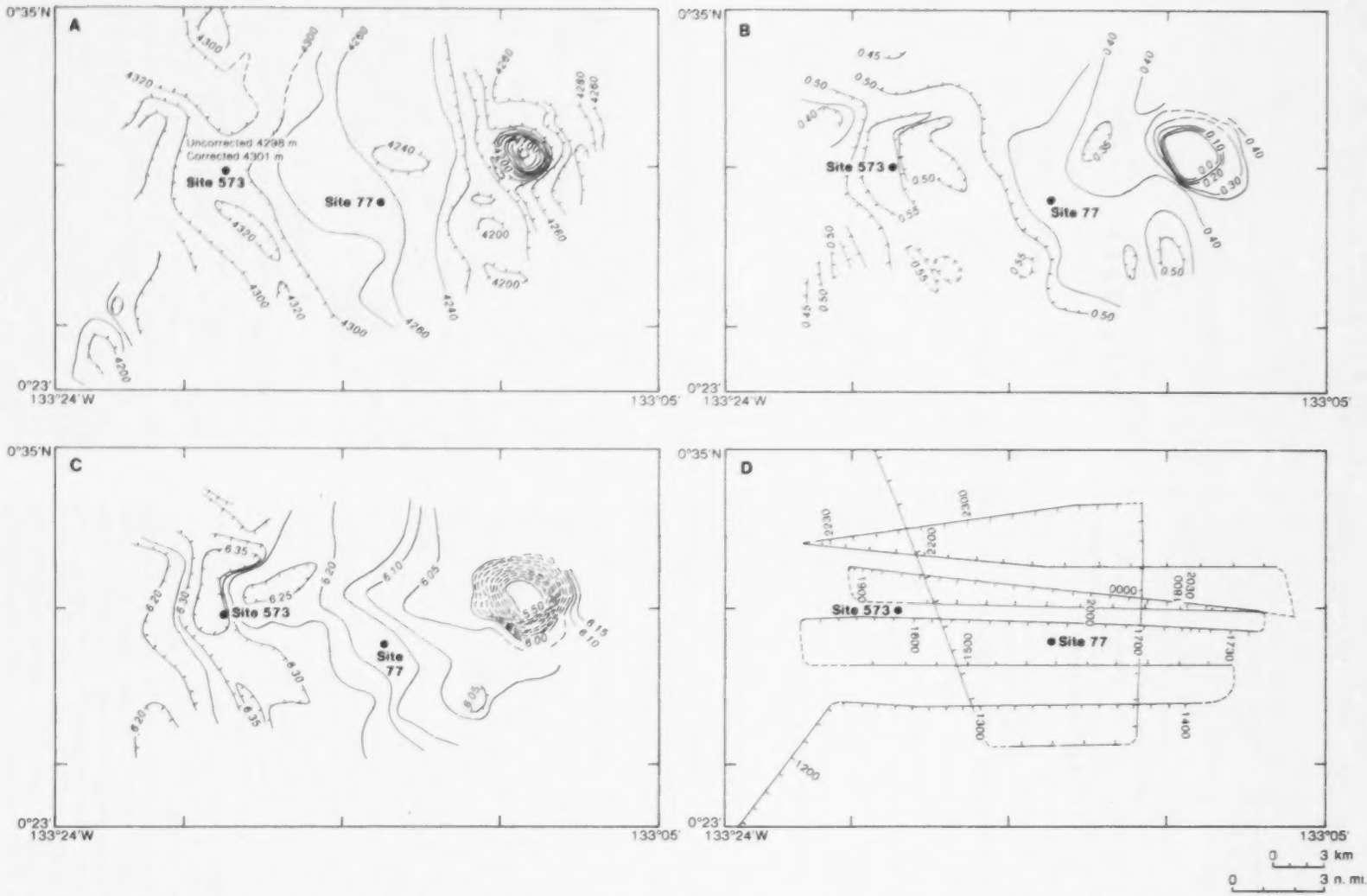

Figure 3. A. Site 573 Seabeam bathymetry. A moat exists on the southwest side of the hill. Contour interval = 20 m. Uncorrected depth: velocity = 1.5 km/s. B. Sediment thickness in seconds of two-way traveltime. Drilling at Site 573 sampled thicker section than at Site 77. Contour interval = 0.05 s. C. Total depth to basement in seconds of two-way traveltime. Contour interval = 0.05 s. D. Track chart after adjustment to make Seabeam data internally consistent. Tick marks at 5-min. intervals.

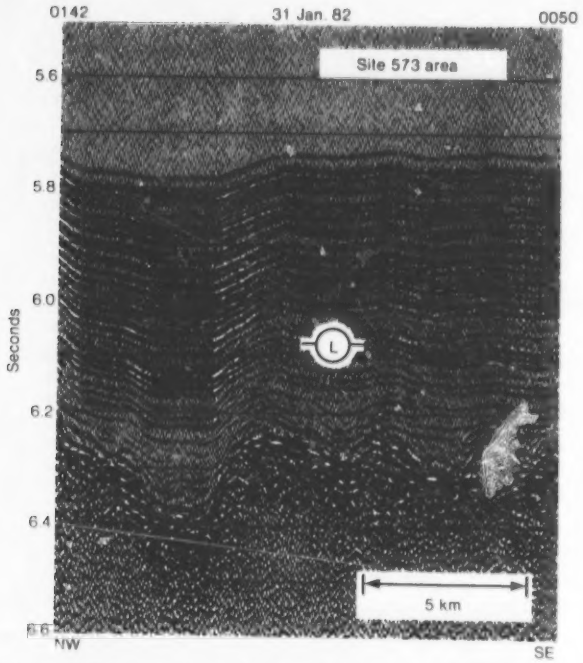

Figure 4. Water-gun seismic data in the vicinity of Site 573. "L" is a reference reflection traced throughout the equatorial Pacific.

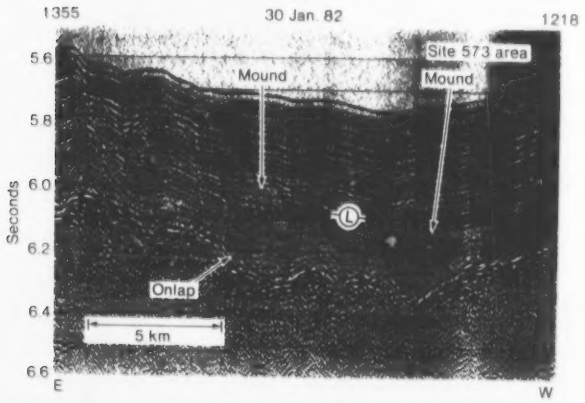

Figure 5. Another seismic profile in the Site 573 area showing the characteristic mounds and basement onlap of the earliest sedimentary deposits.

on the dominant NNW trend. Basement shows a series of NNW-trending ridges, with intervening valleys, and a subtler ENE trend, both similar to the bathymetric trends. The isopach map shows that the total sediment thickness varies between 0.25 and 0.40 s, with most areas having slightly more than 0.3 s of sediment which uniformly drapes the basement. Much of the variation in sediment thickness occurs on the flanks of the ridges.

The acoustic stratigraphy of the EQ-6 site is characterized by a fairly uniform section, which drapes over basement and lacks significant unconformities. It may be divided into four subunits: (1) an upper transparent layer, up to 0.03 s thick, present on the gentler flanks of ridges

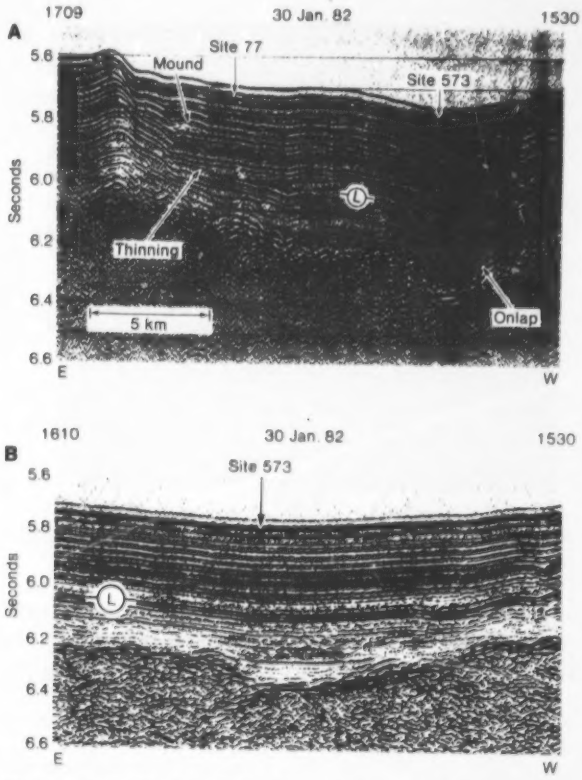

Figure 6. A. Profile through Site 77 and Site 573, showing that coring at Site 77 did not sample the earliest sediments deposited in this area. Note thinning onto the high. B. Migrated portion of Figure 6A, illustrating that even with removal of most hyperbolae associated with the acoustic basement there is still no evidence for a deeper basement at Site 573.

and in valleys but not identified on ridge crests; (2) an upper strong reflective unit, 0.05 to 0.12 s thick, consisting of 3 to 6 wavelets; (3) a transparent unit, 0.10 to 0.25 s thick, without significant reflectors; and (4) an interval with two or three moderately strong reflectors, spaced about 0.05 s apart, which overlie basement. The boundaries between the lower three units are poorly defined.

EQ-8 SITE

EQ-8 is the northernmost of the survey sites. Our survey consisted of seven E–W lines spaced about 2 km apart and two tielines oriented NNW (Fig. 16). Sea conditions caused the 3.5-kHz records to be noisy and effectively useless. Ten satellite fixes during the survey provided good control on absolute position.

The bathymetric trend is NNW and total relief is only 160 m. The eastern section of the survey area is dominated by a broad high, which reaches 4690 m in the southeast corner, the shallowest portion of the area. The seafloor descends to the west to about 4830 m; in the central region the seafloor varies from about 4800 to about 4580 m, in an irregular pattern. The western edge of this central low is marked by a NNW-trending low at least 4840 m deep. The low rises toward the west to a NNW-trending high, which reaches 4710 m.

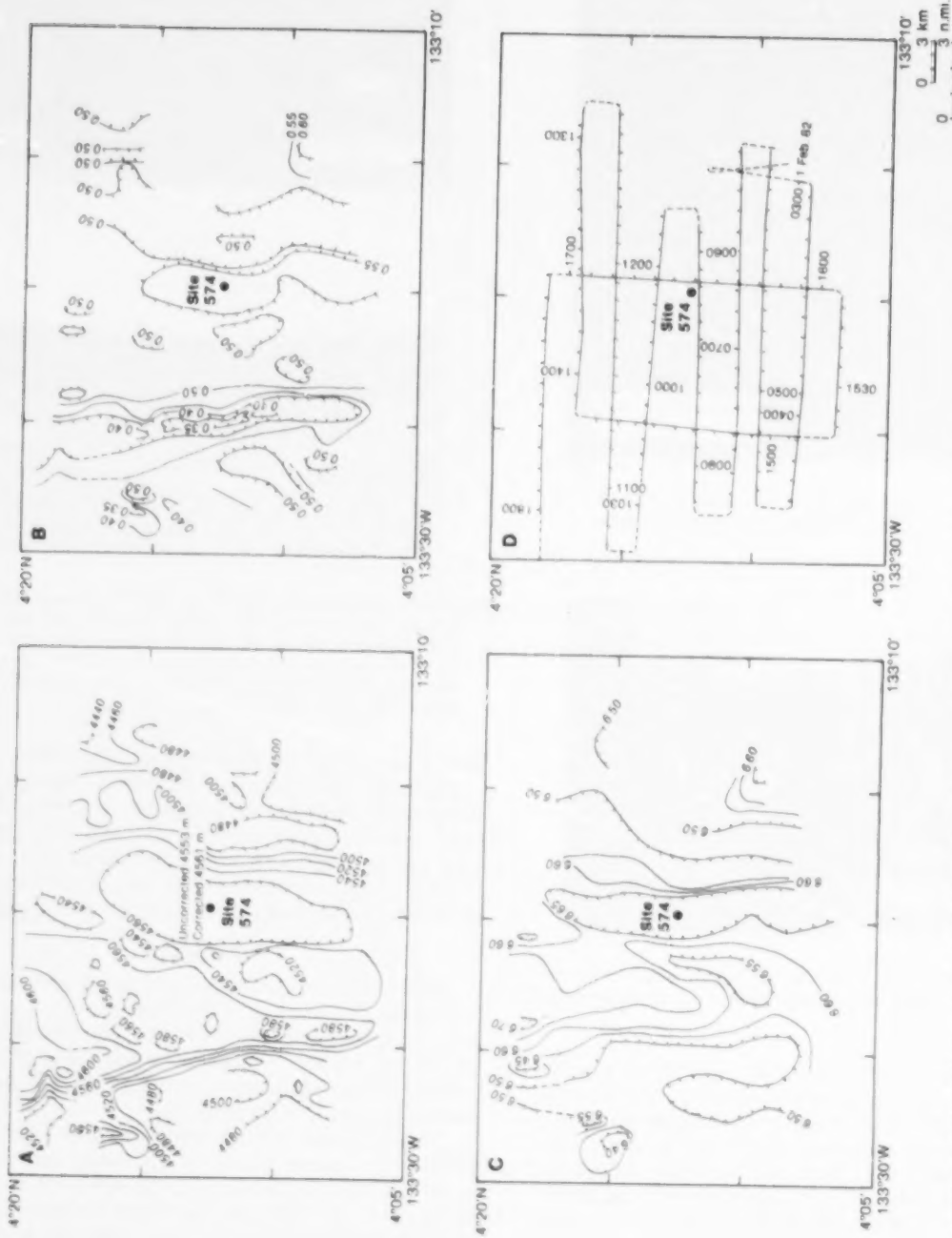

Figure 7. A. Seabeam bathymetry in the vicinity of Site 574. Contour interval = 20 m. Uncorrected depth; velocity = 1.5 km/s. B. Sediment thickness in two-way traveltime based on the seismic data collected along tracks shown in Figure 7D. Contour interval = 0.05 s. C. Total depth to basement in seconds of two-way traveltime. Contour interval = 0.05 s. D. Track chart after the corrections to make the Seabeam bathymetry internally consistent. Tick marks at 5-min. intervals.

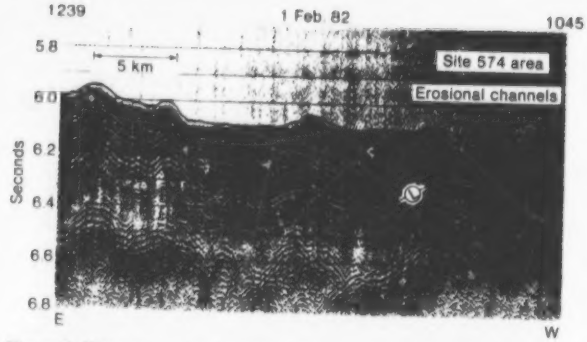

Figure 8. Water-gun seismic section in the vicinity of Site 574. "L" is a reference reflection annotated on most seismic sections from this region.

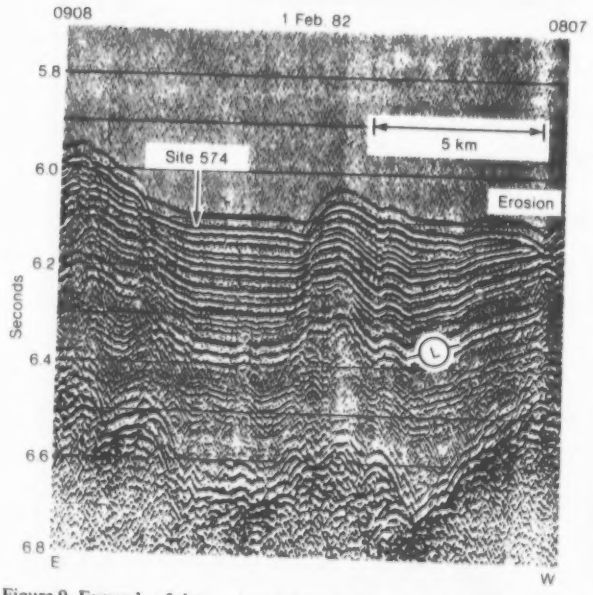

Figure 9. Example of the erosional channels that have removed significant portions of the younger sediments in the vicinity of Site 574.

The broad, NNW-trending pattern of bathymetric highs and lows generally mimics the basement relief, but with some preferential infilling of lows. The most prominent basement feature is a NNW-trending scarp, which truncates the eastern high, dropping into a narrow trough containing the thickest sediments in the area. The seismic facies is generally sheet-drape with no prominent reflectors. The thickness of the section varies from about 0.10 to 0.30; the lower values occur over the basement highs and the higher values occur in some of the low areas. Basement relief in the area is 0.3 s (about 250 m); the seafloor relief is only 160 m. The sediment distribution effectively attenuates the basement relief.

SITE 572 (EQ-1A)

EQ-1A was surveyed of the *Thomas Washington* SCAN Expedition by H. Craig in early 1970. This survey was a post-drilling investigation of Site 81. Standard navigation, magnetics, 12-kHz echo-sounding, and analog seismic profiles were obtained. These data were used to prepare charts of the bathymetry, sediment thickness, and basement relief (Fig. 17).

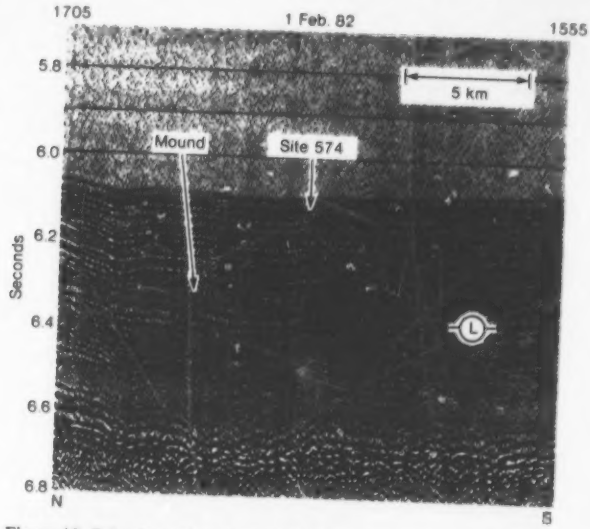

Figure 10. Seismic section at Site 574. Note the appearance of smooth basement in the N–S profile.

The bathymetric relief is about 80 m, and has a NNW trend. Sediment thickness averages about 0.45 s, and is 50 m thicker in basement lows. The preferential infilling of the basement lows has attenuated the effects of basement relief on the seafloor bathymetry.

Site 572 was located in one of the basement lows where the sediment cover is thickest. Site 81 was located just to the northeast, where the sediment thickness was about 50 to 75 m thinner.

DISCUSSION

The mean plate-fabric orientation varies by as much as 25° between the different survey areas, which is more than had been expected. Between the Clipperton and Galapagos fracture zones, the mean trends are N20°W at Site 573, N5°E at Site 574, and N10°W(?) at Site 575, and between the Clipperton and Clarion fracture zones they are N10°W at EQ-6 and N15°W at EQ-8. These trends, the fabric imparted to the crust at or soon after its formation, vary more than the N10°W predicted from the geometry of the major transforms. Similar 20 to 30° swings in trend are also evident in the Seabeam data along the track from San Diego to EQ-8 (Fig. 1). The amplitude and wavelength of the fabric also vary from site to site; amplitude ranges from about 130 to 315 m, and the wavelength varies from 4 to 8 km. Apparently the ridge-crest segments are much smaller than the gross geometry defined by the major fracture zones, and impart a variant to the fabric orientation. These variations are of the same magnitude as those observed by Lonsdale (1983) along the active East Pacific Rise crest, where individual rise crest segments do not always trend normal to the major fracture zones. Although the fabric observed here is probably of similar origin, propagating

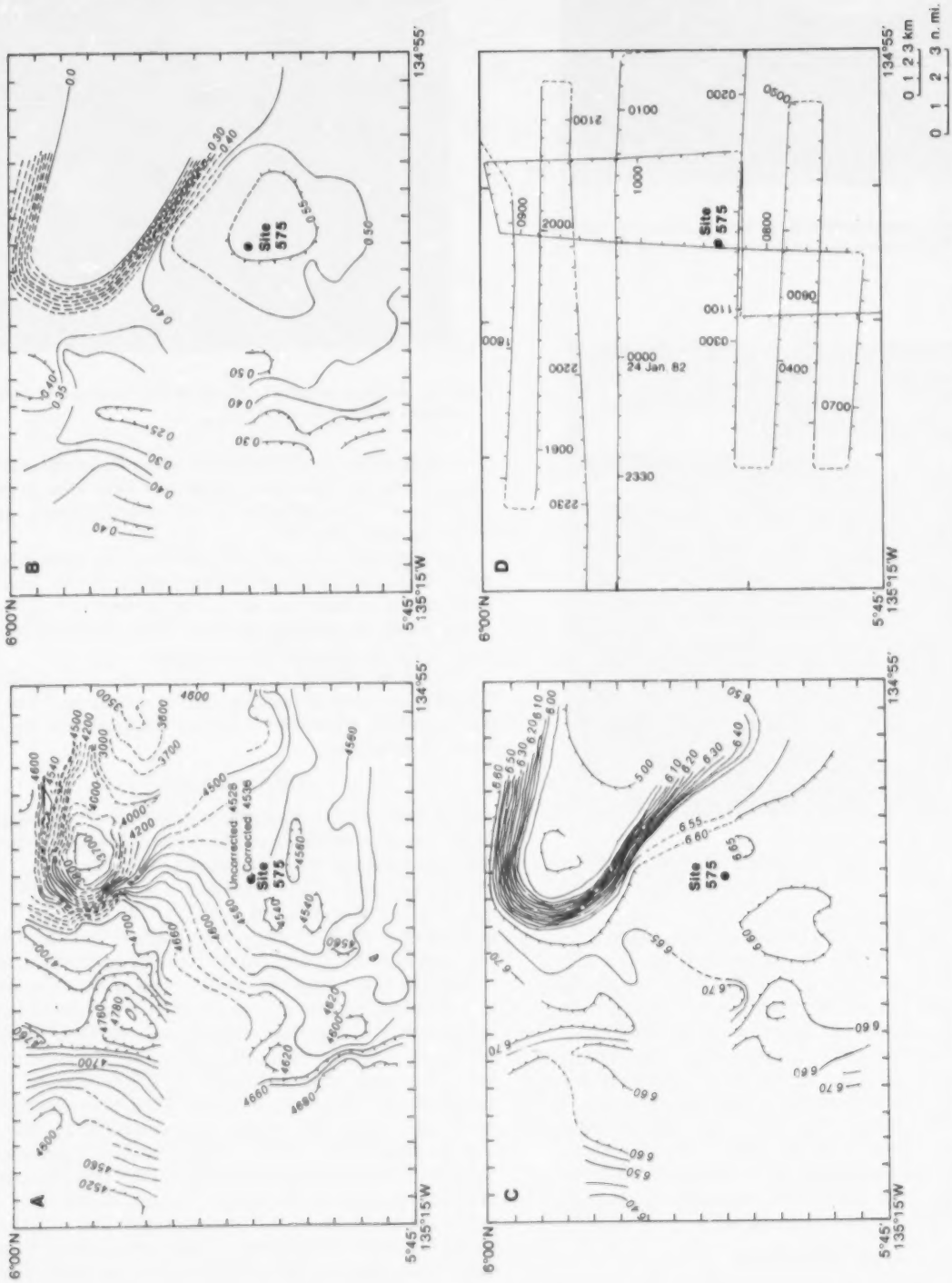

Figure 11. A. Seabeam bathymetry near Site 575. Significant erosion of the seafloor is occurring to the west of the high, and a moat has formed along the northern side of the high. Contours at intervals of 20 m; 100 m when depth < 4500 m. Uncorrected depth: velocity = 1.5 km/s. B. Site 575 was situated where the sediment section was thickest. Sediment thickness in seconds of two-way traveltime. Contours at 0.05-s intervals. C. Depth to basement in seconds of two-way traveltime. Contours at intervals of 0.05 s; 0.50 s when <6.00. D. Adjusted navigation resulting from matching overlapping Seabeam bathymetric swaths. Tick marks at 5-min. intervals.

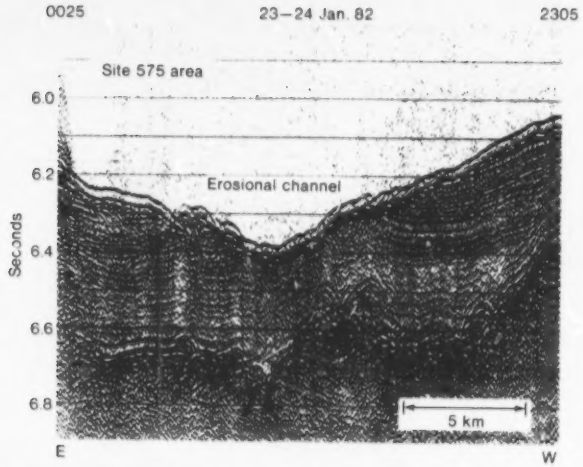

Figure 12. Seismic section to the west of the high, illustrating the seafloor erosion associated with the channel in the Site 575 area.

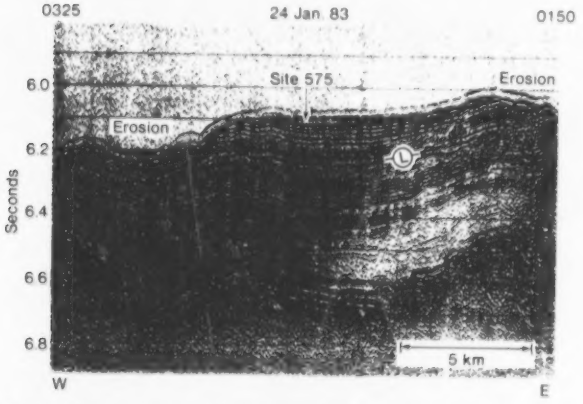

Figure 13. Seismic section illustrating the relationship between the erosional areas and the drill site location.

rifts (Hey et al., 1980) could also be expected to produce similar anomalies in the fabric.

The site surveys provide abundant evidence of recent seafloor erosion. Some, such as erosional moats that have formed at the base of isolated highs (Figs. 3, 11, 12), result from current intensification caused by bottom-water flow around bathymetric obstructions. Others are well-defined channels, located either on basement highs or within lows (Figs. 7 to 9, 11, 13, 14). In a Deep-Tow survey of one of these erosional channels, Mayer (1981) showed that the channels are of very limited extent, unlike some mid-ocean channels; curiously, the one studied by Mayer actually follows the crest of a basement structural high. These erosional features emphasize that there is much redeposition of the sediments within the equatorial Pacific, even if the transport occurs only over a short distance.

The sediment isopach charts show that the sediment thickness varies within a single survey area by 20 to 30%, a significant departure from simple pelagic drape. Most of the variation in sediment thickness results from recent seafloor erosion as well as basin-filling within the low-

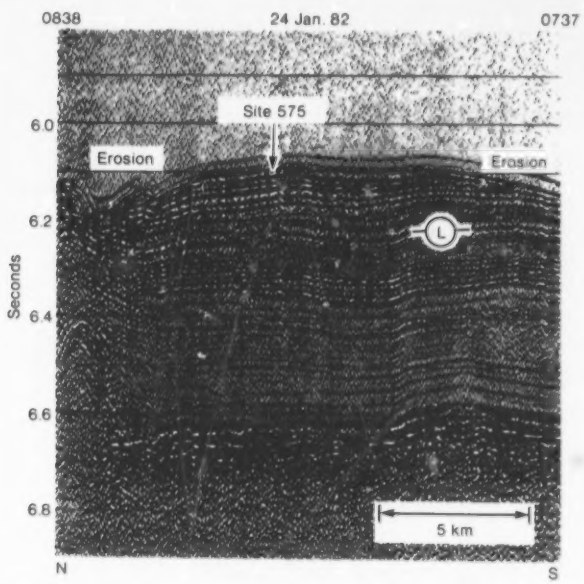

Figure 14. Water-gun seismic section at Site 575. Note that volcanic basement, probably at about 6.67 s, is nearly masked by a shallower reflection at 6.64 s.

ermost (Eocene/Oligocene) sediment intervals. The onlapping character of the basin-filling is illustrated in Figures 5 and 6. Early in their history, depressions act as sediment traps, and only after partial filling and reduction of the seafloor gradients does sediment draping become established.

If erosional episodes and early preferential redeposition in basement depressions are factored out, remaining sediment-thickness anomalies are less than 0.05 s (less than 50 m). Within the sediment section, the seismic reflection data reveal episodes of onlapping and other erosion and mound development. Some episodes appear to be regional in timing and extent, whereas others are apparently localized departures from the pelagic depositional pattern. An example of the thinning by onlap is shown in Figure 6A. This is not an uncommon event, but appears to occur mainly at one stratigraphic level. The simplest explanation for this geometry is an episode of redeposition of sediment from surrounding highs that occurred in association with bottom-current intensification, though other episodes of erosional truncation are found throughout the regional survey data. They are often related to seafloor relief, and few seem to be regionally continuous or synchronous. We are still investigating the possible significance of several regional reflections which at some localities appear as unconformities.

Another depositional feature that accounts for local anomalies in sediment thickness is a mound, lobate in cross section, and usually with no detectable internal structure. Mounds of this type have well-defined tops, often with high-amplitude diffractions. They are fairly common; examples are shown in Figures 5, 6A, and 10. Seldom are such mounds more than 4 km wide in apparent profile; nor are they often more than 20 to 30 m thick. In contrast with the onlapping fill, the relationship between

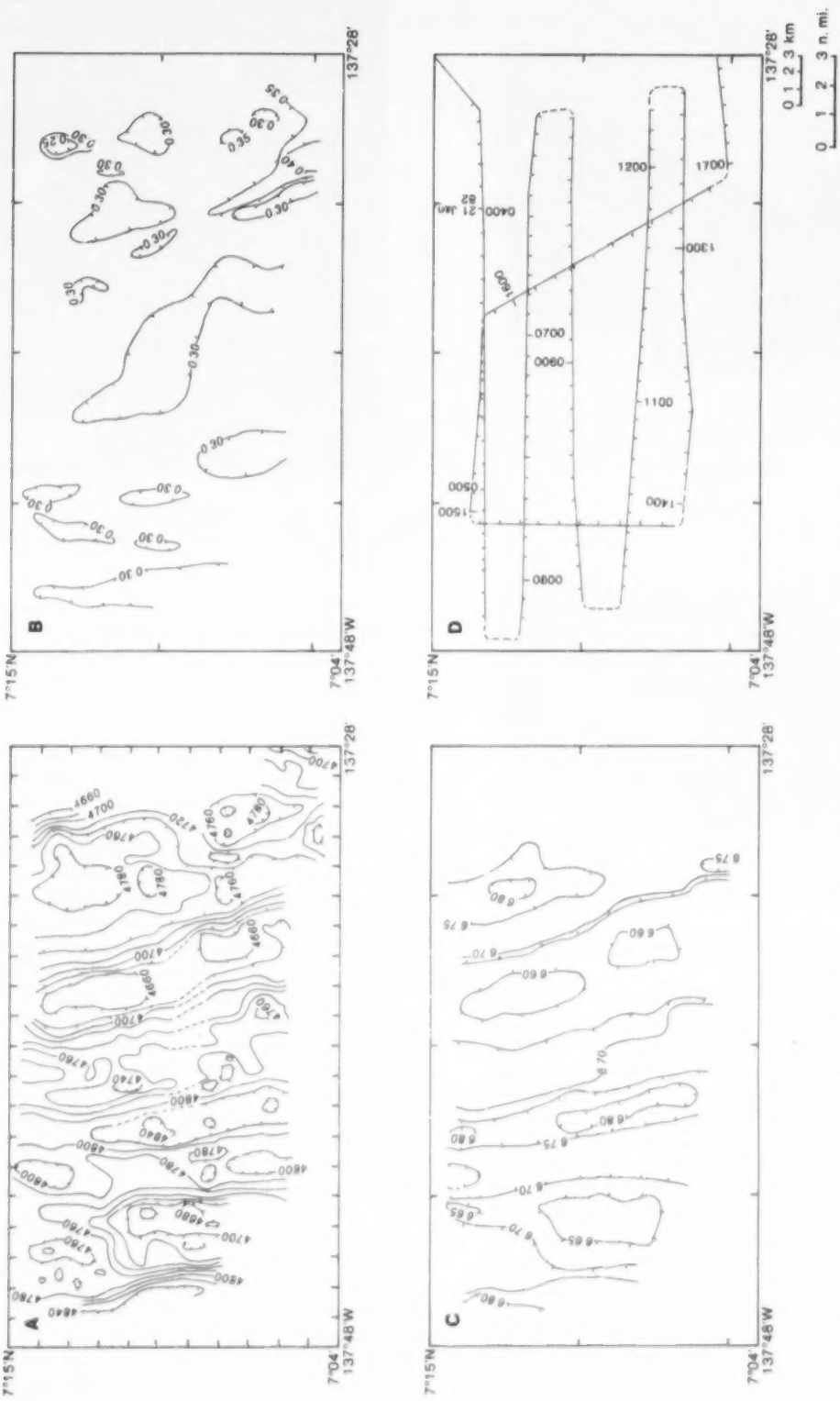

Figure 15. A. Seabeam bathymetry at EQ-6 survey area. Contours at intervals of 20 m. Uncorrected depth: velocity = 1.5 km/s. This site was not drilled on Leg 85. B. Sediment thickness in seconds of two-way traveltime. Contours at 0.05-s intervals. C. Depth to basement in seconds of two-way traveltime. The sediment thickness mimics the basement relief. Contours at 0.05-s intervals. D. Navigation adjusted for best fit of the Seabeam swaths. Tick marks at 5-min. intervals.

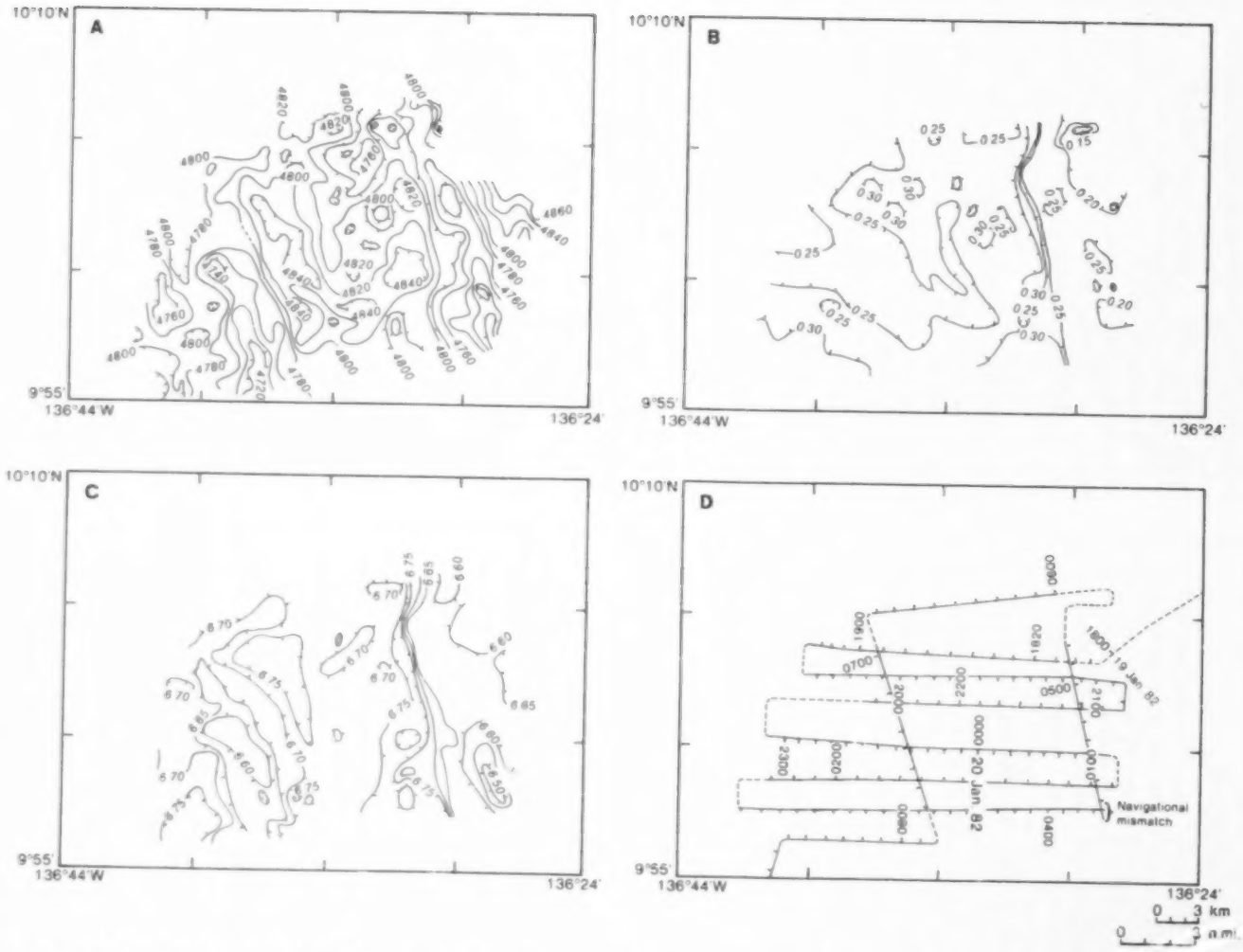

Figure 16. A. Seabeam bathymetry in the EQ-8 survey area. Contours at intervals of 20 m. Uncorrected depth: velocity = 1.5 km/s. This site was not drilled on Leg 85. B. Total sediment thickness in seconds of two-way traveltime. Contours at 0.05-s intervals. C. Total depth in seconds of two-way traveltime. Contours at 0.05-s intervals. D. Navigation adjusted for best fit of Seabeam swaths. Tick marks at 5-min. intervals.

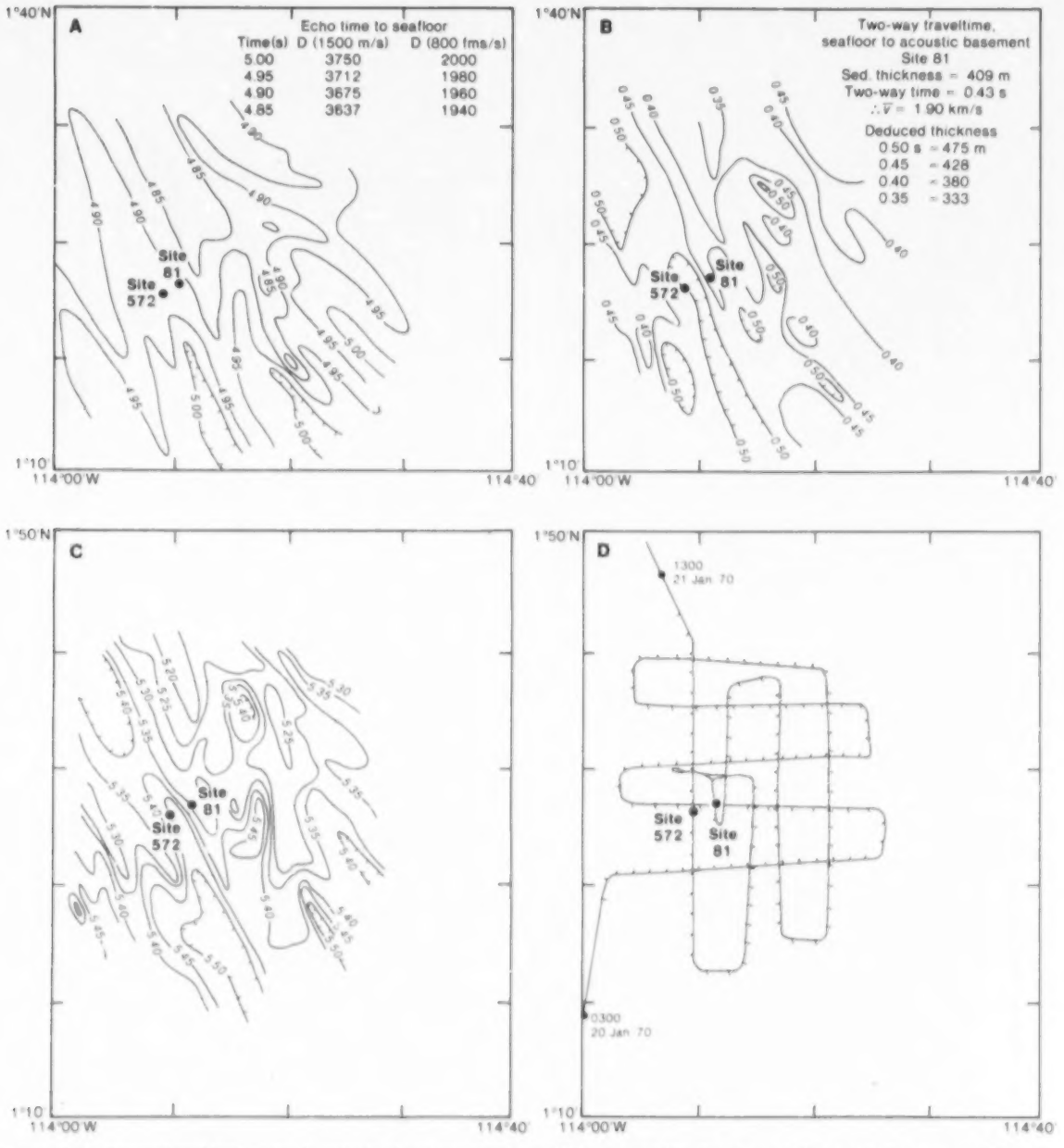

Figure 17. A. Conventional bathymetry in seconds of two-way traveltime at Sites 81 and 572. Based on a 1970 post-drilling survey of Site 81. B. Sediment thickness in seconds of two-way traveltime. C. Basement relief in seconds of two-way traveltime. D. SCAN 10 track chart in vicinity of Site 572 and Site 81, showing data points (ticks) used in preparing bathymetric and isopach maps.

these mounds and thinning within the same stratigraphic interval nearby is imperfect.

Since these depositional and erosional features are so common, the concept of a simple pelagic sediment blanket does not seem appropriate for much of the sedimentary history of this region. Earlier investigations have shown that the sediments on the slopes are thinner than in the lows and on the highs in abyssal hill terrain (e.g., Luyendyk, 1970; Mudie et al., 1972). We find that over a much longer time interval these simple slope-related processes are insignificant compared with other sedimentological processes that are redistributing much of the pelagic sediments.

Isolated volcanic highs were encountered at Sites 573 and 575. The one in the Site 573 area is typical of a class of volcanoes observed in the transits between sites. This particular hill rises 160 m above the seafloor and over 500 m above the surrounding basement, and is nearly conical, 6 km wide at its base with a nearly flat top 1 to 2 km wide (Fig. 3). It is probably a volcano generated

near a ridge crest, dormant since the early spreading phase. A second, larger volcano in the Site 575 area caused us to relocate our survey area to the south, away from the sediment-redeposition influence of the high. This hill extends about 1000 m above the seafloor, 1300 m above general basement depth, and at its base is at least 8 km wide and may be elongated toward the southeast (Fig. 11). It represents a class of larger, distinctly more complex, composite volcanic cones. They may be slightly larger than the smaller conical hills because of slightly prolonged volcanism, but still near the ridge crest, or they could result from a more recent off-axis volcanic event. The drilling at Site 575 indicated that the volcano has been influencing sedimentation since at least the early Miocene, represented at the bottom of the drill hole (see Site 575 chapter).

Possibly related to these volcanic episodes are very high-amplitude reflection anomalies encountered in a number of different areas within the regional surveys. Figure 18 shows one example of such an anomaly. The section is true amplitude—all recording gains have been removed—and was bandpass-filtered 30 to 250 Hz and displayed at a constant gain. The anomaly is in fact two wavelets wide, and partially masks reflections from beneath it. They appear to be limited to particular stratigraphic intervals, usually beneath "L" level (Fig. 18). The sharp edges of the features produce strong diffraction hyperbolae, and seismic windows into the deeper section are common (Fig. 18). Because of the very restricted nature of these events, their abrupt terminations, and their ability to mask deeper events, we believe that they may be volcanic sills or flows. (Davis [1982] has reported similar features in the northeastern Pacific.) They could also be diagenetic horizons, perhaps related to turbidites originating from nearby highs, judging from the abrupt termination of the horizons. Our surveying time was insufficient to allow investigation of the spatial form of any of these occurrences and their relationship to adjacent volcanic highs.

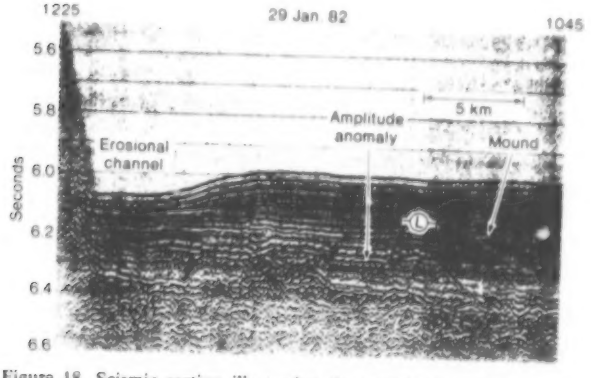

Figure 18. Seismic section illustrating the amplitude anomalies encountered at several locations in transits between the survey sites. Refer to Figure 1 for approximate location.

CONCLUSIONS

The preliminary results of our surveys indicate that the geology, on a scale of a few kilometers, is more complex than the simple model for the pelagic environment would predict. Seafloor erosion, recent and ancient, has sculptured the sedimentary deposits, mostly on a very local scale related to basement highs and channels, but also more regionally in specific stratigraphic intervals. Onlapping fill, general thinning and thickening of sedimentary intervals, and mound development have been widespread in time and space. All of these effects are encountered in the sedimentary section, so they must be recognized and taken into account in reconstructing the paleoceanography of each drill site.

ACKNOWLEDGMENTS

Time for this project was severely limited because drilling was scheduled within weeks after the site survey cruise. It was successful only because of the help of numerous students and staff. The water-gun program succeeded largely because of the efforts of P. Crampton. Shore-based seismic data processing was guided by P. Henkart. Seabeam data processing, much of it accomplished on board ship, was the work of J. Charters and L. Abbott. The work was supported by JOI, Inc. contract no. 42-81. This chapter represents The University of Texas Institute for Geophysics Contribution No. 617.

REFERENCES

Davis, E. E., 1982. Evidence for extensive basalt flows on the seafloor. *Geol. Soc. Am. Bull.*, 93:1023–1029.

French, W. S., and Henson, C. G., 1978. Signature measurements on the water-gun marine seismic source. *Proc. Ann. Offshore Technol. Conf.*, 1:631–638.

Hey, R. N., Duennebier, F. K., and Morgan, W. J., 1980. Propagating rifts on mid-ocean ridges. *J. Geophys. Res.*, 85:3649–3558.

Lonsdale, P., 1983. Overlapping rift zones at the 5.5°S offset of the East Pacific Rise. *J. Geophys. Res.*, 88:9393–9406.

Luyendyk, B. P., 1970. Origin and history of abyssal hills in the northeast Pacific Ocean. *Geol. Soc. Am. Bull.*, 81:2237–2260.

Mayer, L., 1981. Erosional troughs in deep-sea carbonates and their relationship to basement structure. *Mar. Geol.*, 39:59–80.

Mudie, J. D., Grow, J. A., and Bessey, J. S., 1972. A near-bottom survey of lineated abyssal hills in the equatorial Pacific. *Mar. Geophys. Res.*, 1:397–411.

Renard, V., and Allenou, J.-P., 1979. Sea Beam multi-beam echosounding in "Jean Charcot" description, evaluation and first results. *Int. Hydrogr. Rev. Monaco*, 56:35–67.

Date of Initial Receipt: 3 November 1983
Date of Acceptance: 2 June 1984

Reprinted from Mayer, L., Theyer, F., et al., 1985
Initial Reports of the Deep Sea Drilling Project, Volume LXXXV, Washington (U. S. Government Printing Office)

28. PHYSICAL PROPERTIES OF EQUATORIAL PACIFIC SEDIMENTS[1]

R. H. Wilkens, Earth Resources Laboratory, Department of Earth, Atmospheric, and Planetary Sciences, Massachusetts Institute of Technology
and
T. Handyside, Department of Geology, University of Newcastle-upon-Tyne[2]

ABSTRACT

The relationships between acoustic velocity, bulk density, grain density, porosity, carbonate content, thermal conductivity, and electrical conductivity (formation factor) in sediments from a single equatorial Pacific site from DSDP Leg 85 are examined. Bulk density and porosity are controlled by both compaction and composition. Silica-rich sediments are less dense because of lower grain density values and the grain shapes, which tend to hold the sediment framework open. Velocity increases slowly and uniformly with depth in the unconsolidated sediments and then increases in both magnitude and variability as lithification increases in the lower levels of the section. Density (and thus composition) controls acoustic impedance in the unconsolidated sediments, and the degree of lithification controls acoustic impedance lower in the section. Thermal conductivity values are in general agreement with theoretical values when composition is taken into account. Thermal conductivity and formation factor show a high degree of correlation. A comparison of vertical and horizontal values of formation factor indicates that horizontal electrical paths in the sediment are systematically more conductive than vertical paths. Both depth-dependent and time-dependent (synchronous) changes can be seen in all sites when downhole data are plotted versus first depth and then age.

INTRODUCTION

Measurements of the physical properties of marine sediments in combination with other observations from DSDP boreholes reveal information that can lead to a better understanding of the processes of sedimentation and lithification in the deep ocean. The primary goal of Leg 85 of the Deep Sea Drilling Project was to recover undisturbed sections of equatorial Pacific sediments by using the hydraulic piston corer (HPC) in soft sediments and by rotary coring in the deeper, partially lithified sections. The drilling presented an opportunity to investigate various physical properties of these sediments in great detail and to combine these data with the results of other investigations, such as the reflection seismic data from the site surveys, the lithostratigraphic descriptions of the recovered core, and the general paleoceanographic history of the individual sites as revealed in studies of carbonate content and microfossil assemblages.

In the course of the cruise, several thousand measurements were made on recovered core. The techniques and measurements included the gamma ray attenuation porosity evaluator (GRAPE) determination of fine-scale variations in porosity (Boyce, 1976); the gravimetric determination of wet-bulk density, water content, and porosity (Boyce, 1976); the measurement of compressional wave acoustic velocity (Boyce, 1977); the needle probe measurement of thermal conductivity (Von Herzen and Maxwell, 1959); the four-probe measurement of electrical conductivity, which was used to yield the ratio of seawater to sediment electrical conductivity (formation factor; Manheim and Waterman, 1974); and the determination of sediment shear strength by using the Wykeham-Farrance vane shear apparatus (Boyce, 1977). A complete tabulation of the resulting measurements is presented in the appendix to this volume.

These properties are plotted versus depth in the site chapters. This chapter does not repeat the results but rather examines the relationships among the properties at a single location, Site 574. We chose the Site 574 data for two reasons: (1) the sediments from Site 574 covered wide ranges of depth (0 to 520 m), age (0 to 39 Ma), and carbonate content (5 to 95%), and (2) the data for all of the properties measured are highly reliable, unlike the data for the other sites, into which one or another of the measurement procedures may have introduced some error. The trends apparent at Site 574 are much the same as at the other sites. We have chosen not to consider either the GRAPE or the shear strength data in this chapter. The GRAPE results are in good agreement with the gravimetric determinations of porosity for the HPC cores, but they do not add significant information to a study in which measurements at given levels (instead of downhole trends) are compared. Furthermore, the GRAPE results from the deeper, rotary cored sections of the sites are not generally reliable because the measurements involve passing a gamma ray beam through the cores, and many of the core liners for the deeper cores are partially empty. It should be noted, however, that the GRAPE results from the hydraulic-piston-cored section may be extremely useful in future studies of the details of the variations of porosity and density in the softer sediments. Vane shear measurements were not made with the frequency of the other measurements, and we believe that the shear strength of the sediments should be studied in more detail before the existing data are presented.

[1] Mayer, L., Theyer, F., et al., *Init. Repts. DSDP*, 85: Washington (U.S. Govt. Printing Office).

[2] Addresses: (Wilkens) Massachusetts Institute of Technology, Cambridge, MA 02139; (Handyside) University of Newcastle-upon-Tyne, United Kingdom.

We did not make any corrections to the laboratory data to attempt to restore *in situ* conditions, although we realize that relationships for this purpose exist. We did not want to bias any of the measurements by correction factors that would not apply to every property. Thus, the data presented here were acquired at standard room temperature and pressure conditions.

SITE 574

We have discussed the downhole changes in physical properties in the Site 574 chapter (this volume) in some detail, but it is useful to review the data here before we look at the relationships among the various parameters. Figure 1 shows a plot of porosity, wet-bulk density, carbonate content, vertical formation factor, thermal conductivity, and compressional wave velocity versus depth for Site 574; the data for the upper 200 m are derived from HPC cores, and the data from 200 m to basement at approximately 520 m are derived from rotary cores. The measurements of formation factor and thermal conductivity were terminated at levels somewhat above basement because the probes used in making the measurements became unable to penetrate the sediments, which grew increasingly more competent as a result of lithification as depth increased.

The porosity and density plots, which essentially result from the same measurement, are mirror images of one another. Both properties are variable in the upper 100 m

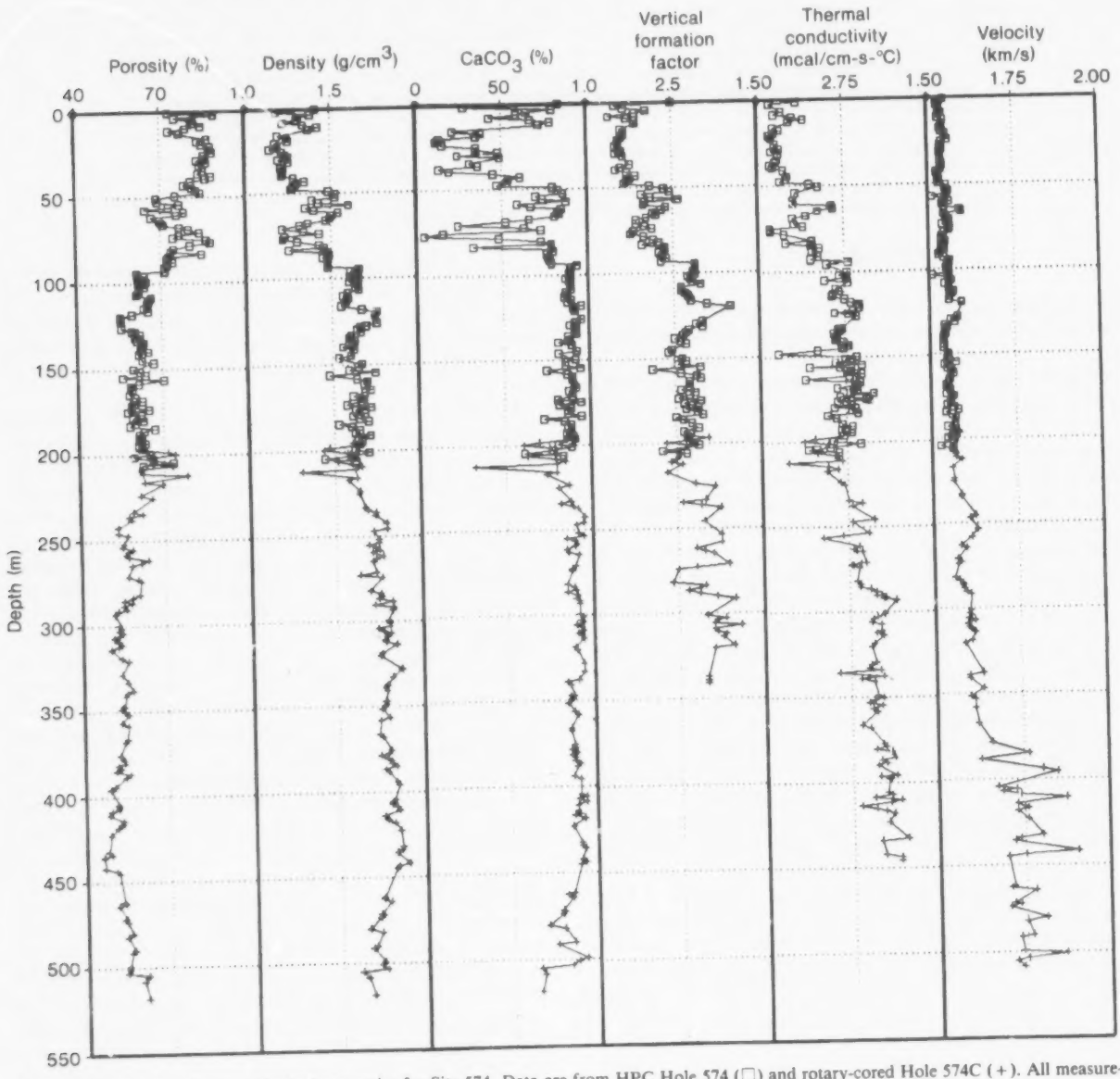

Figure 1. Depth plotted versus physical properties for Site 574. Data are from HPC Hole 574 (□) and rotary-cored Hole 574C (+). All measurements were made at room temperature and pressure.

of the sediment column and generally become more uniform with increasing depth. In some cases single points or groups of points show local maxima or minima within relatively constant sections. Especially in the case of the single points it is tempting to doubt the accuracy of the values and to attribute them to analytical error; however, these data are supported by independent measurements at the same level, such as carbonate content or thermal conductivity, and they represent true excursions in the profile.

Carbonate content is also extremely variable in the upper 100 m of sediment. It is included here with the physical properties because of the control of carbonate content on the porosity and density values, which are discussed in detail below. Most samples below a depth of 100 m had carbonate contents in excess of 80%, and almost all of the low-carbonate samples are from the unconsolidated ooze near the top of the section.

Both formation factor and thermal conductivity generally increase with increasing depth. They show the same general trends, and the changes correspond somewhat to the changes in wet-bulk density and porosity. Compressional wave velocity is the only property measured that does not appear to be variable over the shallow depth range. Velocities slowly increase with depth to about 380 m, where they exhibit a general increase and variability, in marked contrast to the smoothly varying values above 350 m.

Site 574 was piston cored twice to depths near 200 m to ensure the recovery of important biostratigraphic datums. To provide a check on the data, duplicate measurements were made on the second HPC core, although generally only two measurements were made per core rather than one per section (about one-third the number of measurements). Data from the two deep HPC holes at Site 574 are displayed in Figure 2, with an offset of the porosity values of Hole 574A by 25% to facilitate comparison. The values are in excellent agreement and could easily be taken for duplicate measurements on the same core instead of measurements on different cores from the same site. Another point of interest is the amount of detail that is lost by enlarging the sampling interval by a factor of 3. It is clear that data taken only once or twice per core can indicate only general trends in the data and that the sediment cannot be assumed to be uniform between data points.

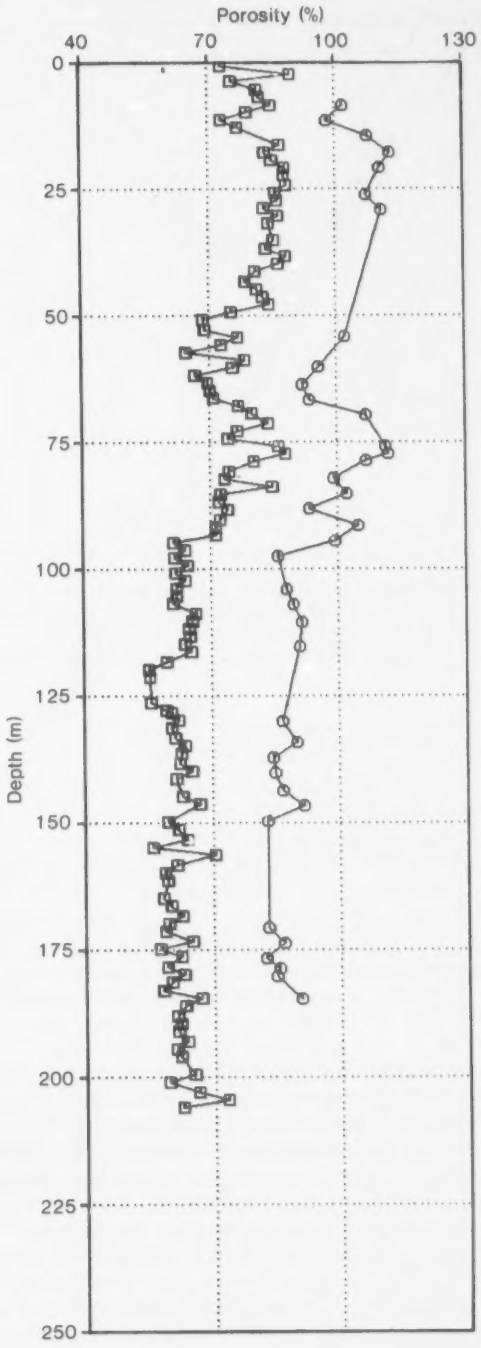

Figure 2. Depth plotted versus porosity for HPC Hole 574 (□) and Hole 574A (○). Values for Hole 574A are offset by +25% to facilitate comparison. All measurements were made at room temperature and pressure.

Density and Porosity

The basic controls on wet-bulk density in marine sediments are porosity and grain density. In the central equatorial Pacific Ocean, almost all of the sediment grains are biogenic, and the average grain densities reflect a mixture of biogenic silica (ρ_g = 2.1 to 2.3 g/cm^3; Baas Becking and Moore, 1959) and biogenic calcite (ρ_g = 2.72 g/cm^3). A plot of wet-bulk density versus porosity for Site 574 is shown in Figure 3. Superimposed on the plot are calculated lines of constant grain density for ρ_g = 2.4, 2.6, and 2.8 g/cm^3. In general, wet-bulk density appears to decrease smoothly with increasing porosity.

Figure 3 also shows a more subtle trend: grain density tends to decrease as porosity increases. The grain densities of samples with porosity less than 75% are generally between 2.6 and 2.7 g/cm^3, whereas samples with porosity greater than 75% tend to have grain densities less than 2.6 g/cm^3. Mayer (1979, 1982) observed the same

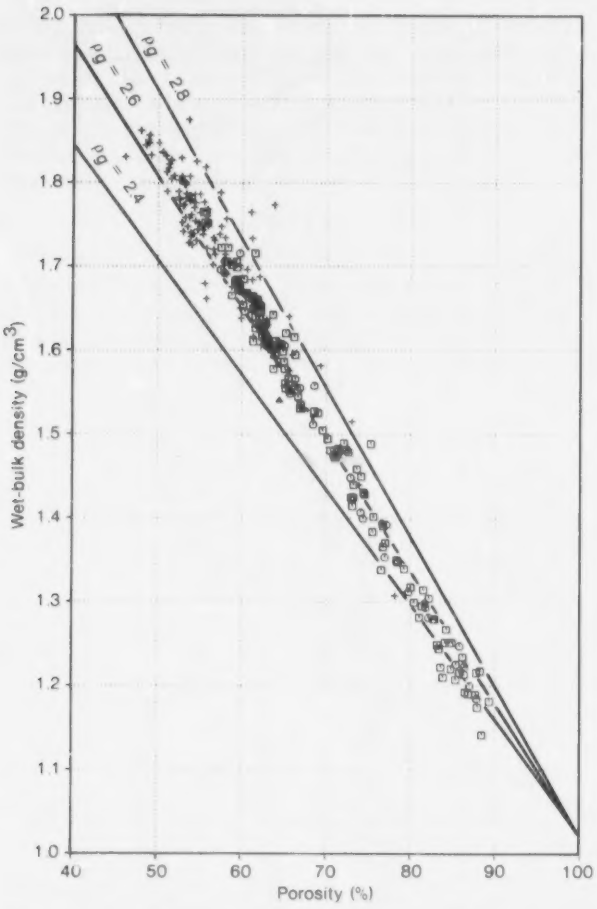

Figure 3. Wet-bulk density plotted versus porosity for Site 574. Data are from Holes 574 (□), 574A (○), 574B (△), and 574C (+). Lines are calculated relationships for constant grain density (ρ_g) of 2.4, 2.6, and 2.8 g/cm^3. All measurements were made at room temperature and pressure.

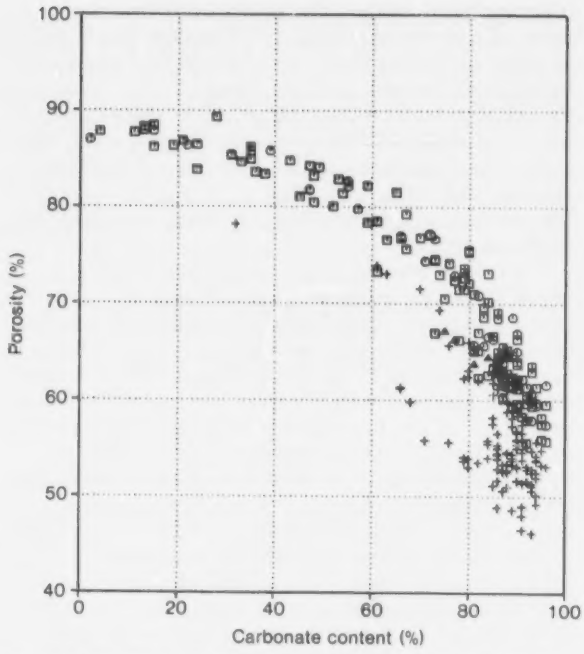

Figure 4. Porosity plotted versus carbonate content for Site 574. Symbols as in Figure 3. All measurements were made at room temperature and pressure.

trends in eastern equatorial Pacific sediments. Higher density sediments are composed predominantly of platy calcareous nannofossil tests, whereas lower density (higher porosity) samples contain a relatively greater amount of siliceous open-work radiolarian tests. These radiolarian tests lower the sediment density by both lowering the average grain density and keeping the framework of the sediment open as the result of the voids inside the grains.

The effect of carbonate content on porosity is illustrated in Figure 4, a plot of percent porosity versus percent carbonate. Sediments low in carbonate have the highest porosities, suggesting that the siliceous components of the sediments tend to hold the framework open. The effects of compaction are also apparent in the distribution of the data. For a given compositional range the samples from deeper in the sediment column have lower porosities (Hole 574C).

Velocity

The relationship between compressional wave velocity and porosity is shown in Figure 5. For values of porosity greater than approximately 60%, velocities remain fairly close to 1.55 km/s. These values reflect a fluid-dominated system of relatively unconsolidated sediment particles. Velocities increase dramatically as porosity decreases below about 55%, an effect of the onset of the lithification of the sediments. Gradually, as the sediment is buried, connective links form between sediment grains. The links substantially increase both the bulk modulus and the ridigity of the material, changes that in turn increase velocity. It is interesting that in sedimentary rocks on land, porosity is an important controlling factor in the value of compressional velocity (Wyllie et al., 1958), whereas in marine sediments velocity may remain relatively constant over a range of porosities or vary greatly within a limited porosity range.

The velocity–porosity relationship influences seismic stratigraphy, because the acoustic impedance of a sediment is the product of velocity and density, and in this case density and porosity are linearly related. Mayer (1979) showed that in soft sediments with relatively constant velocity it is density that controls acoustic impedance. Thus, the density contrasts in the upper sections of Site 574 (Fig. 1) will produce seismic reflections. In the lower part of the hole, however, the situation is reversed. Density and porosity remain relatively constant in comparison with velocity, which varies. The velocity variation is probably a response to the degree of lithification of any particular layer of sediment. Thus, at Site 574 the seismic reflectors near the surface (where increased carbonate deposition is correlated with increased density) may be the result of depositional environment, and the seismic reflectors near the basement (where increased lithi-

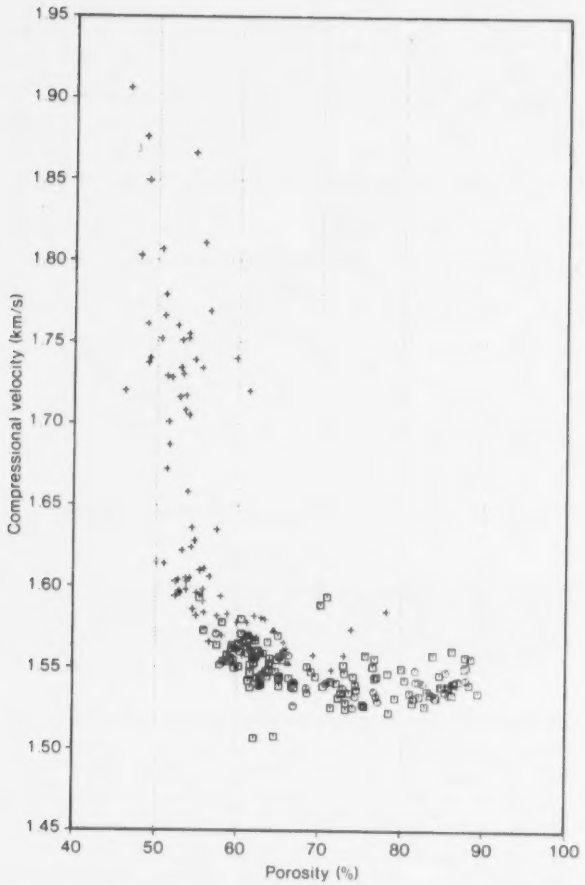

Figure 5. Compressional velocity plotted versus porosity for Site 574. Symbols as in Figure 3. All measurements were made at room temperature and pressure.

fication is correlated with increased velocity) may be the result of diagenetic state.

Thermal Conductivity and Formation Factor

Thermal conductivity and formation factor are measurements of the ability of the sediments to conduct heat and electricity, respectively. Because they are both conductive properties, it is not surprising that they have similar relationships to bulk sediment properties. A plot of thermal conductivity versus porosity is shown in Figure 6. The lines in the plot represent theoretical values of thermal conductivity that were calculated by using the weighted geometric mean equation of Woodside and Messmer (1961). This equation describes the conductivity of unconsolidated two-phase media with random distributions of the phases and has the form

$$K = K_f^{\varphi} K_s^{(1-\varphi)},$$

where K is the thermal conductivity, K_f is the fluid conductivity, K_s is the solid conductivity, and φ is the porosity, expressed as a fraction. The upper line in Figure 6

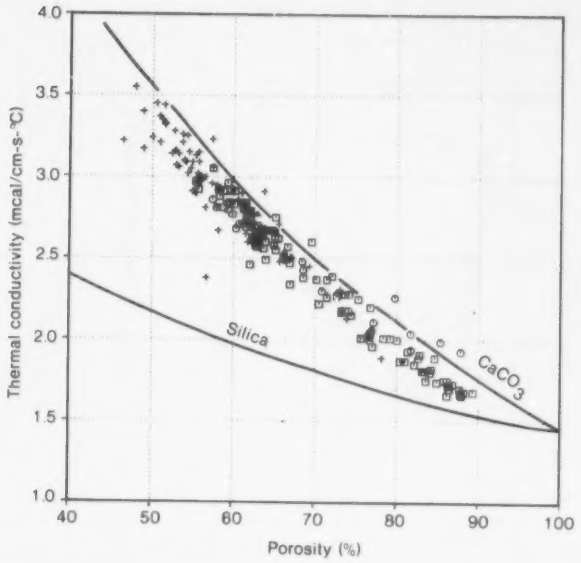

Figure 6. Thermal conductivity plotted versus porosity for Site 574. Symbols as in Figure 3. Lines are theoretical relationships of Woodside and Messmer (1961) for calcite and fused quartz. All measurements were made at room temperature and pressure.

represents a mixture of calcite and seawater (K_f = 1.46, K_s = 8.58 mcal/cm-s-C°; Horai and Simmons, 1969), and the lower line represents fused silica and seawater (K_s = 3.25 mcal/cm-s-°C). The measured values of thermal conductivity generally fall close to the curve calculated for a calcite–seawater mixture. As porosity increases, however, silica content increases, and as a result the data fall off the calcite line and approach the silica line.

Formation factor was measured both horizontally (with probes normal to the core axis) and vertically (with probes parallel to the core axis). The values of the vertical and horizontal measurements are plotted against one another in Figure 7, along with the line $x = y$. Two observations may be made about the distribution of the data: (1) formation factor measured vertically is uniformly greater than formation factor measured horizontally, and (2) the difference between the two measurements is larger in the deeper samples (those from Hole 574C). Both of these observations can be related to the pore geometry of the sediments. The platy calcareous nannofossils are aligned horizontally when they are deposited on the seafloor and produce an overlapping structure much like brickwork. Horizontal formation factor is measured in the plane of these layers, whereas vertical formation factor is measured normal to them. An overlapping structure of platy grains would tend to keep conductive seawater paths open within the plane of the layering but to close those paths normal to the layering. The contrast between the two directions becomes more pronounced as the lithification of the deeper samples proceeds; the overlapping grains bond at the grain-to-grain contacts and the overall porosity of the sediment decreases through compaction. The data suggest that

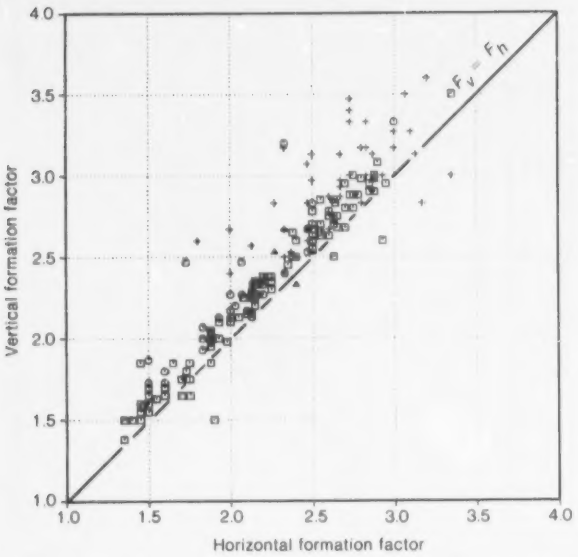

Figure 7. Vertical formation factor (F_v) plotted versus horizontal formation factor (F_h) for Site 574. Symbols as in Figure 3. Line is the relationship $F_v = F_h$. All measurements were made at room temperature and pressure.

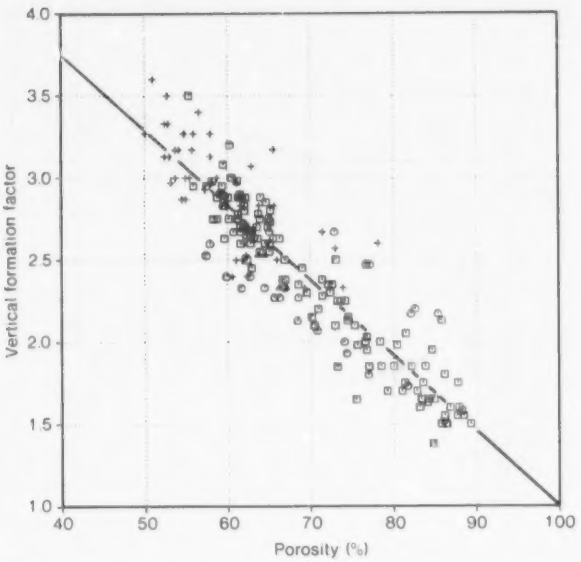

Figure 8. Vertical formation factor plotted versus porosity for Site 574. Symbols as in Figure 3. Line is linear least-squares fit to data; equation is given in text. All measurements were made at room temperature and pressure.

the conductive paths in the plane of layering are kept open longer than those perpendicular to the plane of layering.

We display the relationship between the vertical and horizontal formation factor and porosity in Figures 8 and 9. Least-square regressions of the data have the form:

$$F_v = -0.0456\varphi + 5.5680,\ r^2 = 0.84,\ N = 195$$

$$F_h = -0.0421\varphi + 5.1679,\ r^2 = 0.84,\ N = 195$$

where F is formation factor, φ is porosity (%), r^2 is the coefficient of determination, and N is the number of measurements. Both data fields have similar distributions about their respective regression values. There is some indication that measurements of deep samples in the vertical sense depart slightly more than the horizontal values from their respective regression lines.

Because formation factor can be measured continuously *in situ* in a borehole by using electric logging techniques and thermal conductivity cannot, it is interesting to crosscorrelate the two properties to develop the empirical relationship between them. The relationship at Site 574 (Fig. 10) is as follows:

$$F_v = 0.772K + 0.577,\ r^2 = 0.82,\ N = 175.$$

While the scatter is not negligible, for most points the relationship holds to ±10%, which is within the realm of combined error in the measurements themselves. Moreover, an examination of the pore structure and mineralogy of the sediments at different levels might explain why some data deviate from the regression equation values.

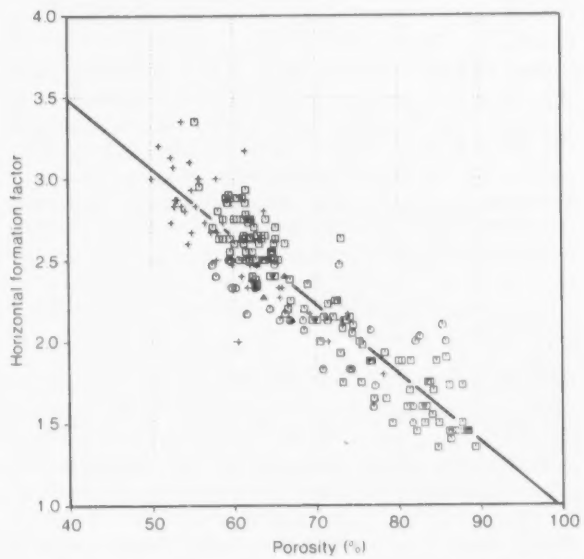

Figure 9. Horizontal formation factor plotted versus porosity for Site 574. Symbols as in Figure 3. Line is linear least-squares fit to data; equation is given in text. All measurements were made at room temperature and pressure.

INTERSITE COMPARISONS

Of the data available, we elected to compare the porosity and compressional velocity data for Sites 572 to 575. The relationships between porosity and density, formation factor, and thermal conductivity are generally lin-

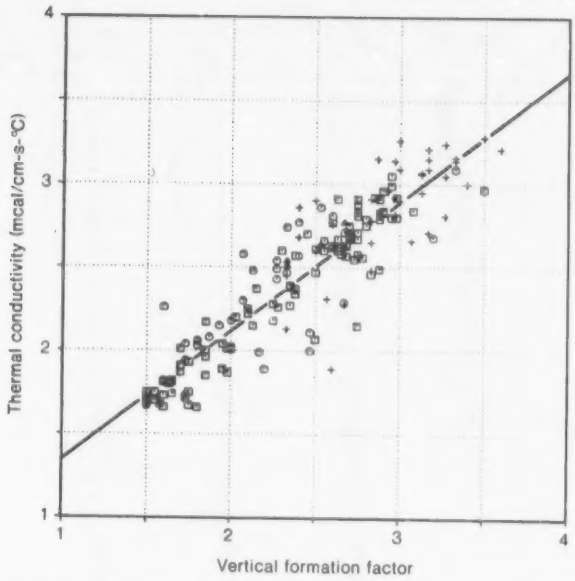

Figure 10. Thermal conductivity plotted versus vertical formation factor for Site 574. Symbols as in Figure 3. Line is linear least-squares fit to data; equation is given in text. All measurements were made at room temperature and pressure.

ear, so intersite comparisons of all these properties would tend to mimic one another. As demonstrated above, velocity is not simply related to porosity and therefore deserves separate analysis. As discussed above, these two factors also affect the acoustic impedance and therefore the acoustic stratigraphy of the sediments. We first examine the changes in each of these properties with increasing depth at each site and then, by using the sedimentation rates from the site chapters to convert the depth data to age data, examine how these properties changed at each site over time.

Depth

Porosity and velocity data for Sites 572 to 575 are plotted versus depth in Figures 11 and 12, respectively. The drilling at Site 575 did not reach basement (which was estimated from seismic survey data to be at a depth of approximately 500 m), so the data for that site do not reflect the entire sedimentary column. The sites do appear to have some characteristics in common.

There is a general variability of porosity in the uppermost 100 m or so of sediment. The values tend to decrease with depth, although the rate of decrease varies from site to site. The porosities of the near-surface sediments are around 80% at all of the sites, and the Site 572 values remain near 70% to depths in excess of 400 m. At the other sites the porosity values are less than 70% at depths greater than 175 m. Thus, mechanical loading operates differently on the porosity of the sediment column at Site 572 than at the other sites. Sites 573 and 574 are predominantly calcareous at greater depths, but the silica content remains between 30 and 40% for much of the Site 572 sediment column, so the radiolarian tests may increase porosity by holding the sediment framework open.

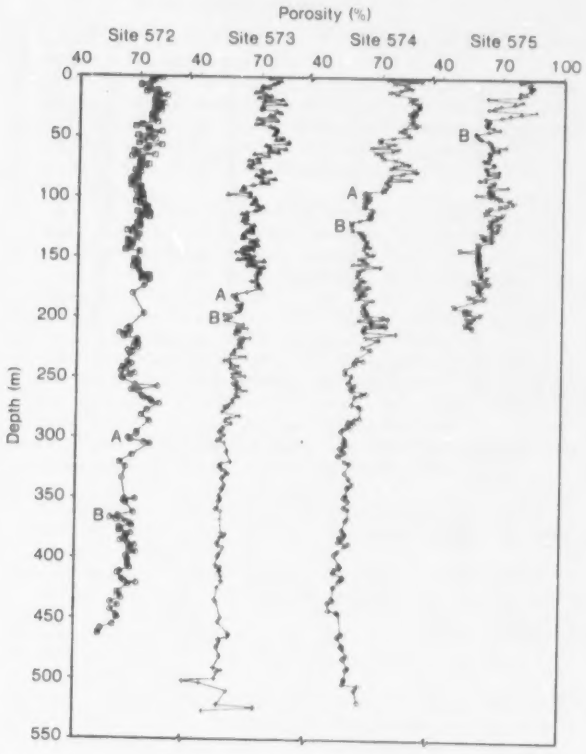

Figure 11. Depth plotted versus porosity for Sites 572, 573, 574, and 575. Data are from Holes 572C (□), 572D (○), 573 (△), 573B (+), 574 (×), 574C (◇), 575 (†), 575A (x). Letters A and B represent events of similar age discussed in text. All measurements were made at room temperature and pressure.

The change in velocity with increasing depth (Fig. 12) is very similar at all four sites: velocity increases very gradually for most of the sections. Abrupt changes in velocity take place that are attributed to increasing lithification, but they do not occur at the same level at each site. At Sites 572 and 573 the change takes place somewhere within 50 m of basement, whereas at Site 574 the change takes place well over 100 m above basement.

Age

We used the sedimentation rates derived from the biostratigraphy at each site to convert the depth of each measurement into an age. Age data are as given in the site chapters and the introduction to the volume and are not adjusted to later data as given in Barron et al. (this volume). Porosity values versus age for the four sites are plotted in Figure 13. We have only displayed the data for the past 25 m.y. because only two of the four sites reached sediment older than that age. Because our sampling was carried out at regular depth intervals, the spacing of the data with respect to time is controlled by sedimentation rate. Thus, in the upper sections of Sites 572 and 573 the data are closely spaced, reflecting the present position of the sites in the equatorial high-productivity zone. Sites 574 and 575 have moved north out of the axis of high productivity. Their uppermost sections show longer time intervals between samples as the result of

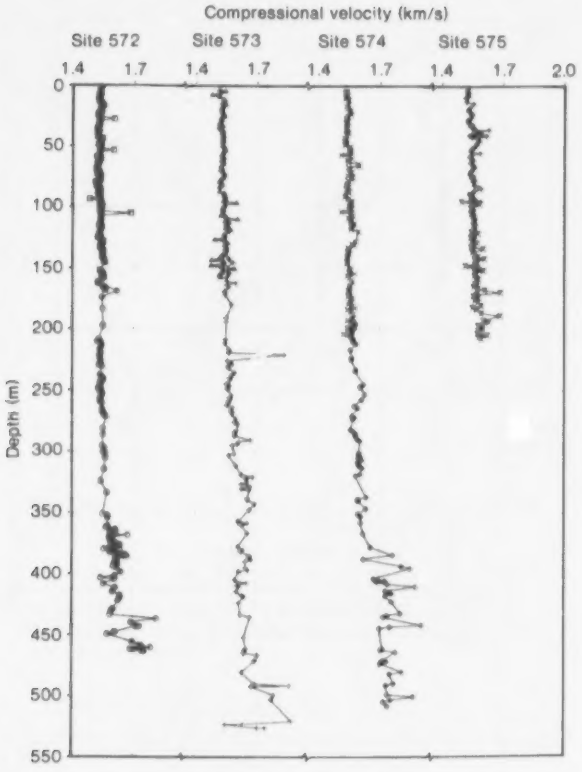

Figure 12. Depth plotted versus velocity for Sites 572, 573, 574, and 575. Symbols as in Figure 11. All measurements were made at room temperature and pressure.

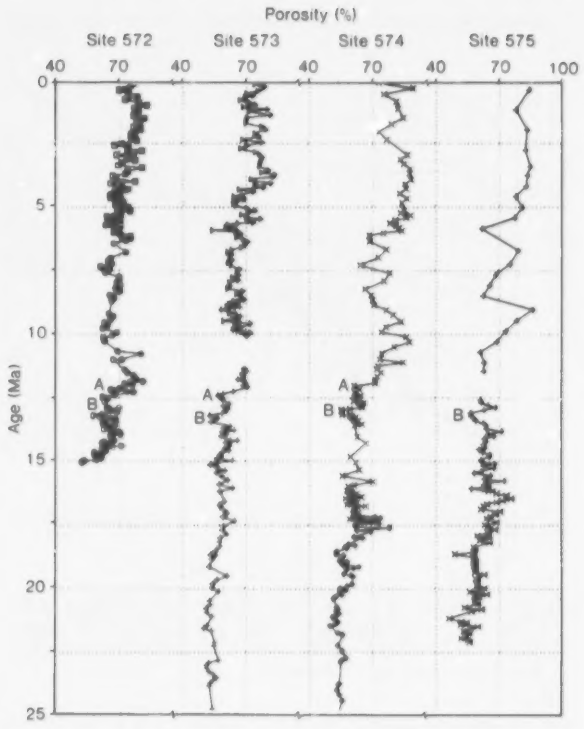

Figure 13. Age plotted versus porosity for Sites 572, 573, 574, and 575. Symbols as in Figure 11. Letters A and B represent events of similar age discussed in text. All measurements were made at room temperature and pressure.

the lower sedimentation rate, although deeper in the sections the data density increases, indicating the time in the past when these sites were within the high-productivity zone. Gaps between 10 and 12.5 Ma Sites 573 and 575 are hiatuses or perhaps erosional events not seen at the other sites.

An examination of velocity versus age (Fig. 14) shows that sediments younger than 25 Ma that have undergone sufficient lithification to enhance compressional velocity occur only at Site 572. The change in lithification occurs at Site 573 at about 490 m depth, which is equivalent to about 38 Ma, while that at Site 574 occurs at 380 m, which is equivalent to about 28 Ma. The age of lithification is different at each site, and, more important, except at the very bottom of Site 572 the sediments younger than 25 Ma show only the generally uniform, gradual rise in velocity with age reflected in the velocity–depth relationships.

In the time frame considered, porosity (density) controls the seismic reflection profile. Thus, at the levels at which abrupt changes in porosity occur that can be correlated between sites we would expect to find time-equivalent reflectors. An example of such a change occurs at around 12 to 13 Ma (Fig. 13). Sites 572, 573, and 574 all show decreases in porosity at around 12 Ma; then all four sites have another decrease near 13 Ma. We call the 12-Ma event A and the 13-Ma event B and have indicated their position in the actual sediment column in Figure 11. Event A occurs at depths of a little over 300 m at Site 572, at 175 m at 573, at 90 m at 574, and is not present as the result of a hiatus or erosional episode at Site 575. Event B is at a depth of 365 m at Site 572, 190 m at 573, 120 m at 574, and 40 m at Site 575.

It is beyond the scope of this study to explain these sets of correlatable changes in sediment properties. Rather, we point out that these two events, and several others, are probably responsible for continuous or nearly continuous reflectors that reach from site to site in the seismic survey data (see also Mayer et al., this volume). In view of the nature of the interval, they appear to define some environmental event that affected carbonate production and through it the eventual degree of sediment porosity. We also see events that may be more local in nature; that is, they affect Sites 573 to 575 but are absent 1000 km to the east at Site 572. An examination of the sediments deposited during these events, in combination with an indication of their extent from seismic reflections, should provide new information about paleoceanographic change in equatorial Pacific sedimentation.

ACKNOWLEDGMENTS

The authors would like to thank B. Charlotte Schreiber, Marcus Langseth, and N. Christensen for their reviews of this paper. It has benefited greatly from their comments.

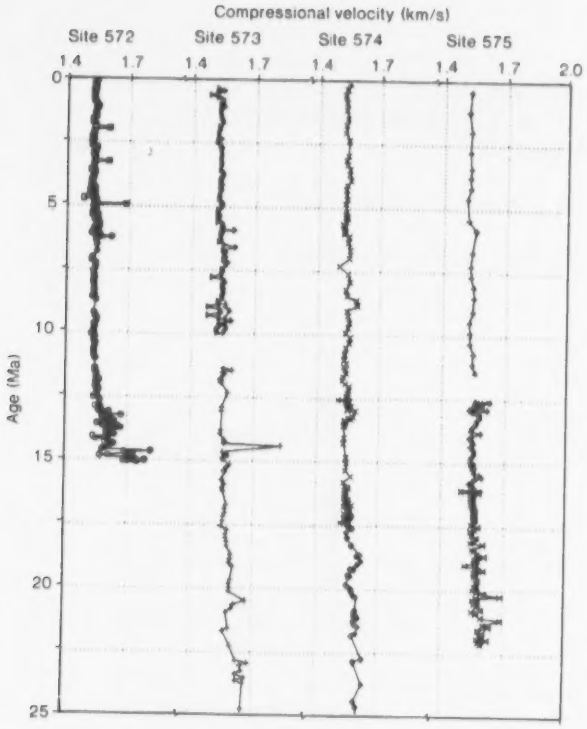

Figure 14. Age plotted versus compressional wave velocity for Sites 572, 573, 574, and 575. Symbols as in Figure 11. All measurements were made at room temperature and pressure.

REFERENCES

Baas Becking, L. G. M., and Moore, D., 1959. Density distribution in sediments. *J. Sediment. Petrol.*, 29:45–55.

Boyce, R. E., 1976. Definitions and laboratory techniques of compressional sound velocity parameters and wet-water content, wet-bulk density, and porosity parameters by gravimetric and gamma ray attenuation techniques. *In* Schlanger, S. O., Jackson, E. D., et al., *Init. Repts. DSDP*, 33: Washington (U.S. Govt. Printing Office), 931–958.

_____, 1977. Deep Sea Drilling Project procedures for shear strength measurement of clayey sediment using modified Wykeham Farrance Laboratory vane apparatus. *In* Barker, P. F., Dalziel, I. W. D., et al., *Init. Repts. DSDP*, 36: Washington (U.S. Govt. Printing Office), 1059–1068.

Horai, K., and Simmons, G., 1969. Thermal conductivity of rock forming minerals. *Earth Planet. Sci. Lett.*, 6:359–368.

Manheim, F. T., and Waterman, L. S., 1974. Diffusimetry (diffusion constant estimation) on sediment cores by resistivity probe. *In* von der Borch, C. C., Sclater, J. G., et al., *Init. Repts. DSDP*, 22: Washington (U.S. Govt. Printing Office), 663–670.

Mayer, L. A., 1979. Deep sea carbonates: acoustical, physical, and stratigraphic properties. *J. Sediment. Petrol.*, 49:819–836.

_____, 1982. Physical properties of sediment recovered on Deep Sea Drilling Project Leg 68 with the hydraulic piston corer. *In* Prell, W. L., Gardner, J. V., et al., *Init. Repts. DSDP*, 68: Washington (U.S. Govt. Printing Office), 365–382.

Von Herzen, R. P., and Maxwell, A. E., 1959. The measurement of thermal conductivity of deep-sea sediments by a needle probe method. *J. Geophys. Res.*, 64:1557–1563.

Woodside, W., and Messmer, J. H., 1961. Thermal conductivity of porous media. I. Unconsolidated sediments. *J. Appl. Phys.*, 32: 1688–1699.

Wyllie, M. R. J., Gregory, A. R., and Gardner, G. H. F., 1958. An experimental investigation of factors affecting elastic wave velocities in porous media. *Geophysics*, 23:459–493.

Date of Initial Receipt: 3 November 1984
Date of Acceptance: 22 April 1984

Reprinted from Mayer, L., Theyer, F., et al., 1985
Initial Reports of the Deep Sea Drilling Project, Volume LXXXV, Washington (U. S. Government Printing Office)

29. PALEOMAGNETISM OF DEEP SEA DRILLING PROJECT LEG 85 SEDIMENTS: NEOGENE MAGNETOSTRATIGRAPHY AND TECTONIC HISTORY OF THE CENTRAL EQUATORIAL PACIFIC[1]

Norbert Weinreich, Institut für Geophysik, Ruhr-Universität Bochum
and
Fritz Theyer, Hawaii Institute of Geophysics, University of Hawaii[2]

ABSTRACT

On Leg 85, 16 holes were cored at five sites. Thirteen of the holes were cored with the hydraulic piston corer (HPC) or the variable-length hydraulic piston corer (VLHPC) or both; the remainder were rotary drilled. Partially duplicating stratigraphic sections were successfully recovered by hydraulic piston coring at Sites 572 to 575. Sub-bottom penetration was deepest (about 210 m) at HPC Hole 575A, which bottomed in lower Miocene sediments. Penetration by hydraulic piston coring was limited at all sites not by the failure of the corer to stroke out but by the excessive force (overpull) necessary to retrieve the core barrel from the hole. The sediments recovered are relatively uniform siliceous-calcareous oozes to calcareous ooze-chalks. Paleomagnetic measurements were made at all stratigraphic levels, but magnetostratigraphic sequences could be resolved only for the Pleistocene-Pliocene and for brief upper, middle, and lower Miocene sections.

In the younger and less consolidated sediments, the declination often shows large-scale azimuthal rotations downcore. These smooth trends vary from core to core, indicating either rotation between the sediment and the core liner or the rotation of the core barrel during the coring or retrieval process. Thus, azimuthal orientation of the samples was impossible even though a Kuster azimuthal orientation tool was used during the hydraulic piston coring.

At all sites, the downhole shift from mainly siliceous to mainly calcareous ooze-chalk coincided with a decrease in NRM intensity of at least one order of magnitude, to 1.0×10^{-8} G. Diagenesis is the probable reason for this behavior, although the dilution of magnetic carriers as the result of higher accumulation rates may also be a factor. A tectonic analysis using data from samples with stable remanence indicates a northward plate motion of about 0.3°/m.y. during the last 18 m.y., a rate that agrees with most previous reconstructions of Pacific Plate motion.

INTRODUCTION

The primary objective of Leg 85 of the Deep Sea Drilling Project was to analyze sediments from holes that formed a transect of the central equatorial Pacific high-productivity belt. The study was undertaken because it was hoped that the use of a tool then relatively new, the variable-length hydraulic piston corer (VLHPC), would permit the recovery of largely undisturbed sediment from as deep as 300 m sub-bottom; undisturbed sediment was desired because it would permit the highest possible stratigraphic resolution of the cored material. The study of paleomagnetism was considered central to the studies to be undertaken, especially those using the pre-Pliocene sequences, for which correlation between calcareous nannofossil datums and magnetic reversals is incomplete.

The VLHPC had been used for paleomagnetic research in the Atlantic (Kent and Spariosu, 1982a, b; Tauxe et al., 1983), but it had never been used before in this part of the Pacific, although successful paleomagnetic work has been done in the central equatorial Pacific with conventional piston cores (Hays et al., 1969; Opdyke, 1972; Hammond et al., 1974; Opdyke et al., 1974; Theyer and Hammond, 1974; Theyer et al., 1978). The rotary-drilled cores acquired during four previous DSDP cruises to the central Pacific have yielded meager paleomagnetic results. It has generally been thought that drilling disturbance has been responsible for the poor results, although workers also observed that the older, highly calcareous oozes yielded very weak intensities. By using the VLHPC we hoped to establish magnetostratigraphic reference profiles for the entire section, including the Neogene, for this region. Unfortunately, our aims were thwarted, not by drilling disturbance or operational difficulties but by the nature of the magnetic remanence of the older sediments.

MATERIALS AND METHODS

Square, plastic boxes with a capacity of approximately 7 cm^3 were used to sample the working half of each core. We wanted to achieve a stratigraphic resolution of about 0.05 to 0.1 m.y. at all levels. Therefore, except where the sediment was disturbed, we acquired samples at roughly equal time intervals, using shipboard-derived rates of sedimentation to adjust the sampling intervals. Where possible we also preferentially sampled horizons that showed horizontal bedding in order to avoid parts of the section that might be affected by subtle coring-induced disturbance. The directions and intensities of NRM_0 (untreated natural remanent magnetization) were measured on board on selected samples by using a Digico spinner magnetometer; the results of this preliminary work are reported in the site chapters (this volume). For the present study, samples from about upper Miocene to Recent were analyzed at the Ruhr-Universität Bochum

[1] Mayer, L., Theyer, F., et al., *Init. Repts. DSDP*, 85: Washington (U.S. Govt. Printing Office). Contribution No. 1463 of the Hawaii Institute of Geophysics.

[2] Addresses: (Weinreich) Institut für Geophysik, Ruhr-Universität Bochum, 4630 Bochum, Federal Republic of Germany; (Theyer, present address) Department of Geological Sciences, University of Southern California, Los Angeles, CA 90089.

(RUB), and samples older than about upper Miocene were analyzed at the Hawaii Institute of Geophysics (HIG). All except a few measurements were made by using cryogenic magnetometers (Goree and Fuller, 1976). Alternating-field (AF) demagnetization studies were performed at RUB by using a Schonstedt GSD-1 single-axis demagnetizer and at HIG by using a three-axis sample tumbler, which was also driven by a GSD-1. For the sediments measured at RUB (upper Miocene and younger), systematic stepwise AF demagnetization series were carried out on each sample in addition to the NRM_0 measurement. All these series were taken to the median destructive field (MDF), and most were taken to the 500-Oe level. The direction of the stable remanent magnetization (RM) was then determined for each sample by analyzing its demagnetization behavior. For this purpose plots of the normalized intensity of magnetization (J/J_{NRM}) versus the applied demagnetization field, vector diagrams (Zijderveld, 1967), and stereographic projections of total vector and of difference vectors of magnetization (Hoffman and Day, 1978) were studied. The stable RM direction for each sample was then determined by finding the mean of at least three consecutive demagnetization steps which showed the least directional dispersion during Fisherian (Fisher, 1953) analysis (Appendix A). We interpret this stable RM direction as the magnetic component that carries the Earth's paleofield information.

Because the samples from the older sediments (those studied at HIG) were generally characterized by uniformity and extremely low intensities, they were treated in a different way. NRM_0 was measured for only some of the holes and for only some depth intervals, and progressive AF demagnetization was performed solely on selected samples. After we reviewed the demagnetization series, we demagnetized all the HIG samples by applying an alternating field of 50 Oe, a level we hoped would leave measurable magnetization yet remove some viscous components. The resulting data are listed in Appendix B.

All the Leg 85 sites lie near the equator. Therefore, most of the inclination data scattered within a few degrees of zero, and 180° variations in the declination data were used to define polarity changes. This made the determination of the true polarity of the samples difficult, especially since the azimuthal orientation was unknown. At first we hoped that the Kuster single-shot orientation device, which we used during VLHPC operation, would provide azimuthal orientation. This device takes a photograph, just before the VLHPC barrel strokes out, of the position with respect to a compass needle of a double line marked on the core liner. The camera is triggered as the corer falls through a nonmagnetic collar in the drill string, an arrangement that makes the exact chronological relationship between the coring and the orientation photograph uncertain. Many mechanical, photographic, and handling difficulties were encountered with the Kuster tool, but about 57% of the slides recorded data. Unfortunately, onshore paleomagnetic analysis made it obvious that there are systematic rotations in the declination data that wholly negate the device's usefulness for azimuthal orientation purposes. For example, the downhole declination data for Cores 4 and 5 of Hole 573 show continuous clockwise and anticlockwise rotations of different magnitudes in addition to the 180° polarity offsets (Fig. 1). In Core 4 there is an anticlockwise rotation of approximately 120°; in Core 5 there is a clockwise rotation of about 200°; and neither rotation is constant. These variations are due to relative motion between the sediment, core liner, and possibly even the VLHPC barrel itself. Therefore, only the uppermost part of a VLHPC core may be oriented as shown by the Kuster photo, and even that is open to question, because neither the vertical position of the camera nor the exact time at which the camera takes the photo is known (motion between sediment, core liner,

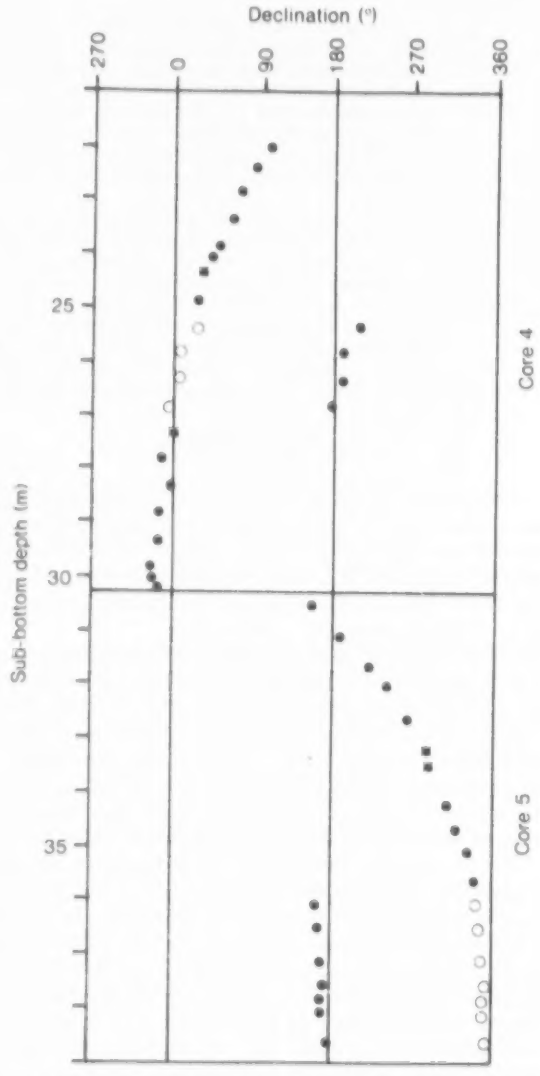

Figure 1. Downcore variation of the uncorrected declination data for Cores 4 and 5 of Hole 573, showing rotation produced during VLHPC coring. See text for details. Solid circles indicate actual data; open circles are 180° projections made to provide visual continuity in the trends.

and barrel, may occur between the time when the photograph is exposed and the actual coring process). In other words, the photo shows the azimuthal orientation of the core liner at a certain instant, but the azimuthal orientation may change before or as the coring actually takes place. In this report, therefore, only relative declination directions are used (those found by referring to the position of the line marked on the core liner).

The younger cores (those measured at RUB) yielded acceptable magnetic data, and the declination data are mostly well grouped azimuthally (180° shifts indicate polarity changes). Thus, average declinations were calculated for these cores as described by Kent and Spariosu (1982a). We did not do this for the sediments analyzed at HIG, because these older sediments displayed weak NRM intensities and were consequently nearly useless for magnetostratigraphy. Arbitrary declinations are shown from core to core for these sediments. All data, corrected and uncorrected, are listed in Appendixes A and B.

The data in Appendixes A and B provide the basis for our magnetostratigraphic and tectonic interpretations. The polarity sequences were constructed by assuming that the topmost interval of continuous polarity is the Brunhes Normal Chron and that the first 180° shift of declination is the Brunhes/Matuyama boundary at 0.72 Ma (Ness et al., 1980). The underlying cores were interpreted by assuming that 180° changes between two cores resulted not from changes in polarity but rather from the rotation of the cores themselves. The azimuthal average of the uppermost (Brunhes) declination sequence was then arbitrarily set at 0°, which resulted in an azimuthal average of 180° for the reversed Matuyama sequence that followed below. Subsequent downcore 180° swings of declination were then used to define the magnetostratigraphy. In some intervals this method failed, and the interpretation of polarity was guided by inclination behavior and biostratigraphy. Finally, a few intervals were so difficult to interpret that the sequence of polarities can only be considered an estimate.

RESULTS AND DISCUSSION

Magnetic Behavior of Sediments

The direction of the stable RM may be overprinted by weaker magnetic components of low coercivity (Kent and Lowrie, 1974). Figure 2 illustrates a sample from a cyclic siliceous–calcareous lithologic unit in Hole 573A (Core 2) that carries multiple components of magnetization with almost antiparallel directions. The components are revealed by the increase in the normalized magnetization from an NRM_0 level of 5.8×10^{-6} G (Fig. 2A) and by the wide scatter in the total vector of magnetization in the stereographic projection (Fig. 2C). After about 200 Oe these weaker components are removed, and the very high MDF of 652 Oe indicates the high stability of the stable RM (Fig. 2A). The vector diagram (Fig. 2B) and the difference-vector projection (Fig. 2D) show the multiple components of the system in more detail. One weaker component is removed at about 50 Oe and another at 200 Oe. This behavior is reflected in both the xy- and the yz-planes (Fig. 2B). The ensuing monotonous decrease of the orthogonal components toward zero suggests that there are no other components. The weak component of the sample of Figure 2 can be identified as a viscous magnetization acquired during the Brunhes Chron, whereas the stable component reflects the reversed direction of the Matuyama Chron.

Figure 3 shows the response of Sample 574C-34-2, 109–111 cm, which is from a metalliferous sediment layer overlying basalt. The sample is characterized by a relatively high NRM_0 intensity (7.4×10^{-6} G). The increase in the normalized intensity curve (Fig. 3A) and the vector diagram (Fig. 3B) suggest that it too may contain separate components of magnetization. The weaker component persists to about 100 Oe, and the MDF of the components with higher stability lies at 310 Oe. Even though the stereographic projection of the total vector of magnetization shows only one direction (Fig. 3C), the difference-vector diagram (Fig. 3D) allows a qualitative and quantitative definition of the two antiparallel directions of the sample. The inclination data define the polarity of the low-coercivity component (0 to 100 Oe) as reversed and that of the stable component as normal (Fig. 3D).

Sample 573A-1-3, 90–92 cm, which is from a siliceous–calcareous lithologic unit of Brunhes age, carries an NRM_0 intensity of 2.5×10^{-6} G. Its behavior (Fig. 4) suggests a single component. The normalized intensity shows a continuous decrease during stepwise AF cleaning (Fig. 4A). The vector diagram (Fig. 4B) and the stereographic projections (Figs. 4C, D) show a single pattern, and the MDF of 270 Oe reflects the inherent stability of the component.

Finally, Figure 5 gives an example of useless data obtained on a weakly magnetized sample. This material (Sample 575A-18-1, 144–146 cm) is from highly calcareous ooze and had an NRM_0 intensity of 6.7×10^{-7} G. Although the stereographic projection in Figure 5C suggests stability, the other diagrams (Figs. 5A, B, D) reveal its erratic behavior upon AF treatment. This sample was typical of the highly calcareous (older than uppermost Miocene) sediments recovered during Leg 85.

Leg 85 Magnetostratigraphy

A satisfactory magnetostratigraphy was derived for the Pliocene and Pleistocene sediments, which had intensities that were in a reasonable range ($> 10^{-8}$ G) for measurement on the cryogenic magnetometer, even after AF demagnetization. In contrast, the calcareous oozes from the Miocene and below allowed the determination of magnetostratigraphic sequences at only a few intervals. The boundary between usable and unusable data coincided with the boundary between cyclic siliceous–calcareous ooze and calcareous ooze. Within the lower, highly calcareous sediments, the weakness of the NRM_0 intensities made AF demagnetization impossible, and the NRM_0 data alone did not contain coherent stratigraphies.

Polarity boundaries had to be inferred from 180° shifts of declination because of the shallowness of the inclinations. However, some of the sites crossed the equator, and in the absence of azimuthal orientation neither declination nor inclination was an unequivocal guide to po-

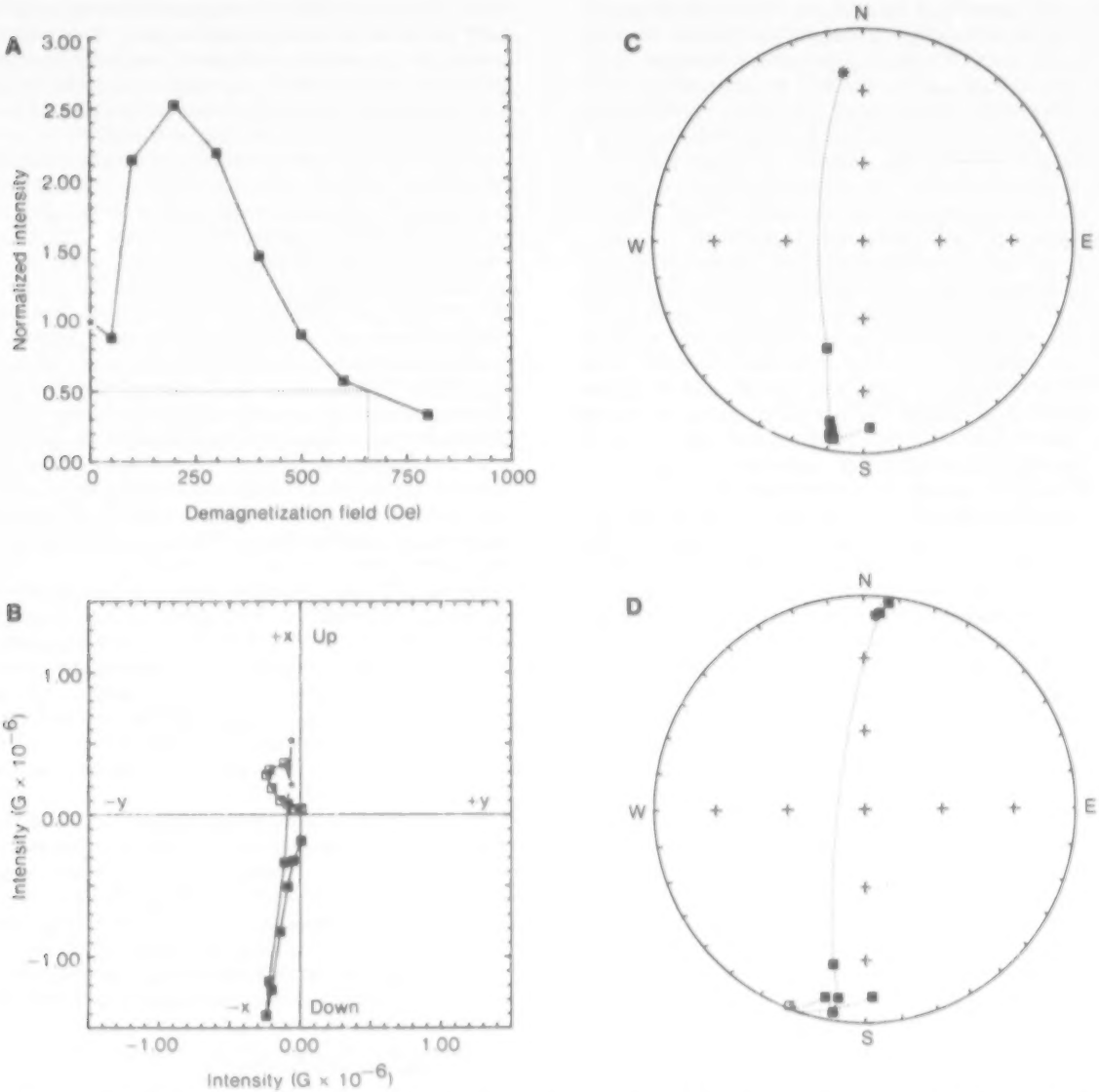

Figure 2. Behavior of the magnetization of Sample 573A-2-3, 67-69 cm, taken from a cyclic siliceous-calcareous lithologic unit, during successive AF demagnetization. A. Normalized intensity of magnetization plotted against the applied demagnetization field. Dotted line indicates the MDF. Asterisk indicates NRM_0. B. Vector diagram of the orthogonal components (x, y, z) of magnetization. Closed symbols represent the horizontal (x, y) plane, open symbols the vertical (z, y) plane. Asterisk indicates NRM_0 components. C. Stereographic projection of the total vector of magnetization. Closed symbols indicate normal, open reversed polarity. Asterisk indicates NRM_0 direction. All directions are connected by great-circles. D. Stereographic projection of the difference vectors. Closed symbols indicate normal, open symbols reversed polarity. The starting point is marked by an asterisk.

larity. We developed our magnetostratigraphy for these sites by (1) comparing the relative lengths of the polarity intervals with the known polarity sequence and (2) referring to biostratigraphy. In the metalliferous sediment layer at Site 574 (which contains the Eocene/Oligocene boundary), intensities increased to about 10^{-5} G, but despite the apparent stability of most of the samples from this layer (see the AF demagnetization series in Fig. 3), the directions (especially the inclinations) fail to indicate a coherent stratigraphic pattern.

Site 571

Only one core (7.10 m) was recovered at Site 571. Shipboard paleomagnetic analysis of NRM_0 indicates that the polarity pattern is coherent throughout this core. Biostratigraphic dating defined the core as Quaternary, from Recent to about 0.46 Ma. Thus, it correlates with the Brunhes Chron. NRM_0 intensities vary from 2.4×10^{-6} G to 7.4×10^{-6} G, with a geometric mean of 4.7×10^{-6} G. The AF-cleaned data, especially the inclina-

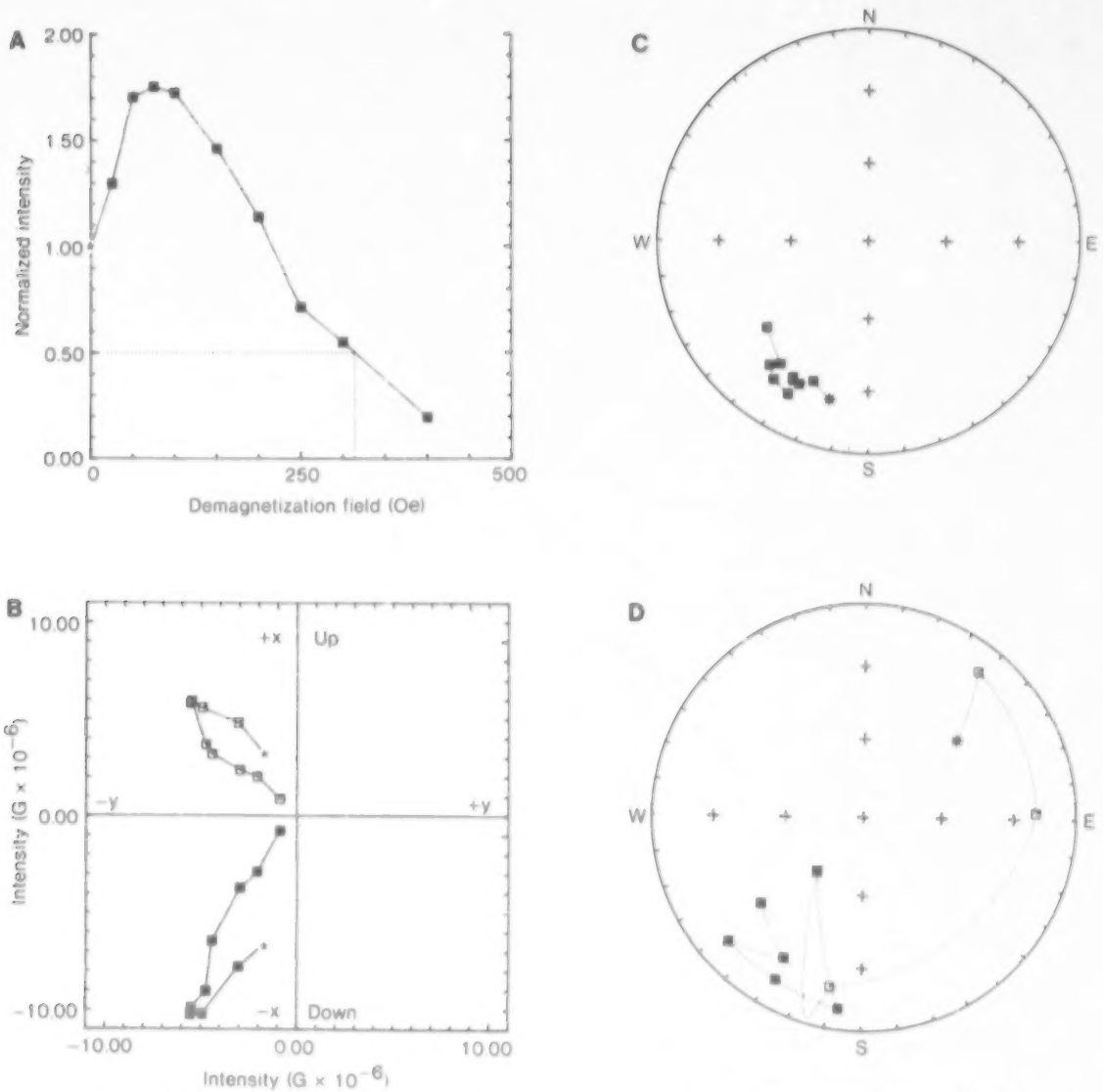

Figure 3. Behavior of Sample 574C-34-2, 109–111 cm. This sample was rotary drilled from the metalliferous sediments overlying basement at Site 574. See Figure 2 caption for details.

tions, show very stable behavior; we were able to derive a mean stable inclination of 7.6°, which gives a dipole paleolatitude of 3.8°N. This is in good agreement with the present site latitude of 4.0°N.

Site 572

No magnetostratigraphy could be established for Site 572. Most of the NRM_0 intensities of the sediments recovered with the HPC were at the noise level of the cryogenic magnetometer, so that demagnetization studies were pointless. In addition, the NRM_0 directional data show almost random scatter. Although some intervals in the older, rotary-drilled sediments show high intensities, their inclinations are scattered about zero, and AF cleaning did not improve the results. The data are therefore presented in tabular form only (Appendix B).

Site 573

Site 573 is the southernmost site in a three-site north-south transect along about 133°W. The transect cuts across the north-central region of the equatorial high-productivity zone. Two holes were cored with the VLHPC at Site 573, and one was rotary drilled to basement (which was at a sub-bottom depth of 529 m; Table 1). Both the sediment (which ranged in age from Quaternary to upper Eocene) and the basalt were sampled for paleomagnetic analysis. A drastic decrease in intensity occurs at about 45 m sub-bottom in both Holes 573 and 573A

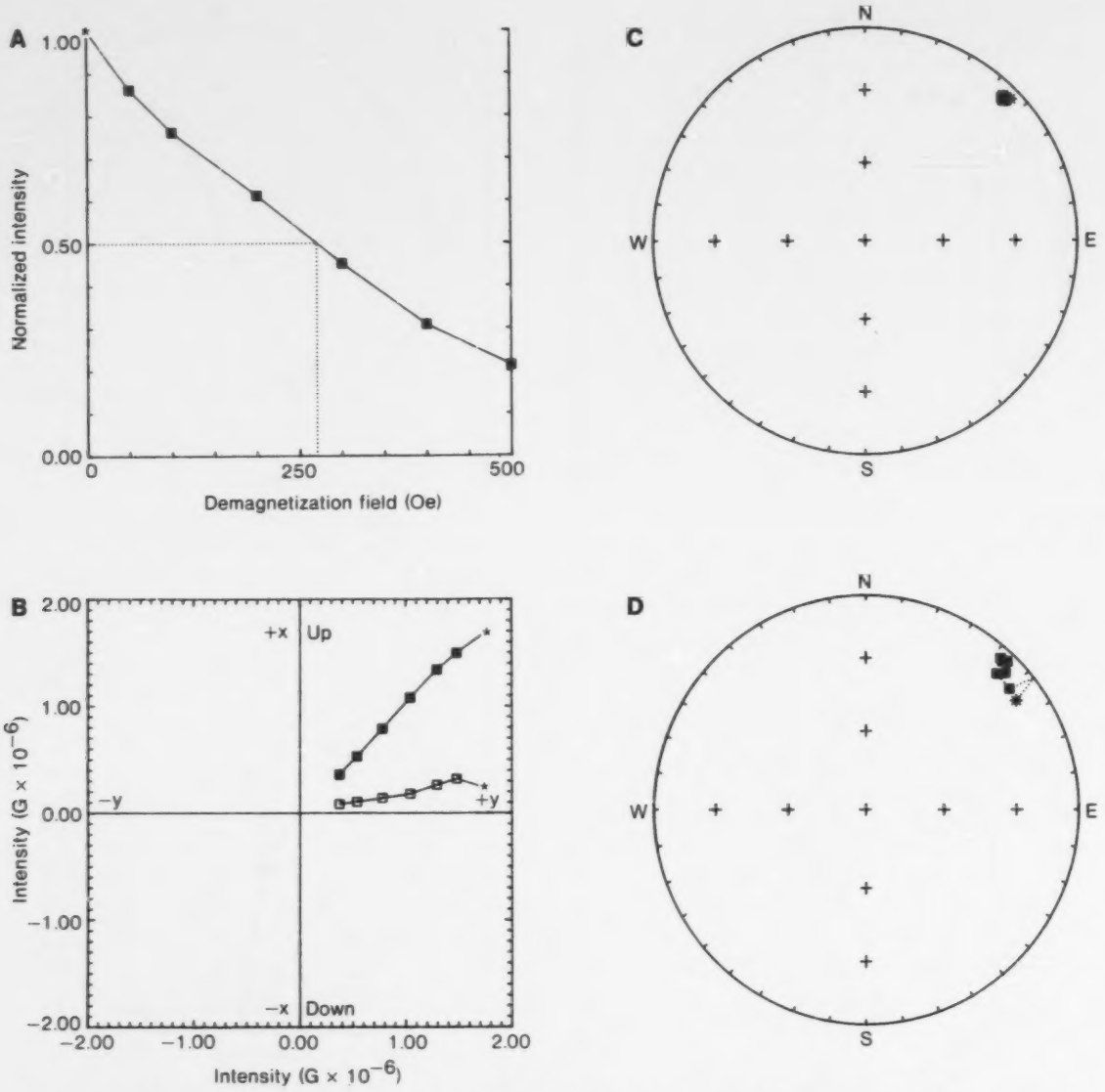

Figure 4. Behavior of Sample 573A-1-3, 90–92 cm. This sample was taken from Brunhes-age siliceous–calcareous sediments. See Figure 2 caption for details.

(Fig. 6); it defines the lower limit of the interpretable data and coincides with a change in lithology from cyclic siliceous–calcareous ooze (Unit I) to calcareous ooze (Unit II). The decrease in intensity exceeds one order of magnitude. The intensities throughout lithologic Unit I show a variation about a mean of $2.31 \pm 1.74 \times 10^{-6}$ G, a mean similar to that at Site 571. The intensities exhibited by other Neogene siliceous–calcareous pelagic sediments are comparable (Kent and Spariosu, 1982a, b; Tauxe et al., 1983). Throughout the underlying lithostratigraphic Unit II (from 45.1 m to 520.0 m sub-bottom), there are intervals of remarkably constant intensities that average about 10^{-7} G, but these intervals do not provide interpretable data. Within the metalliferous chalk to claystone unit (lithologic Unit III, from 520.0 m to 526.6 m sub-bottom) and the short upper Eocene sequence of pelagic limestone (lithologic Unit IV, 526.6 m to 529.0 m sub-bottom), the intensities increase to a maximum of about 10^{-3} G, but the data are useless for magnetostratigraphic work because of their almost random scatter. The inclinations, which during the latest Eocene and early Oligocene are expected to reflect a southerly latitude of some 7 to 10°, do not allow the identification of polarity sequences. The NRM_0 intensities of the six basalt samples measured have a mean of $3.7 \pm 2.7 \times 10^{-4}$ G, which is typical of such material (Petersen and Roggenthen, 1980).

The magnetostratigraphies developed for the uppermost parts of Holes 573 and 573A are shown in Figure 6. Core-to-core interpretation was straightforward because

READEX FICHE best copy available

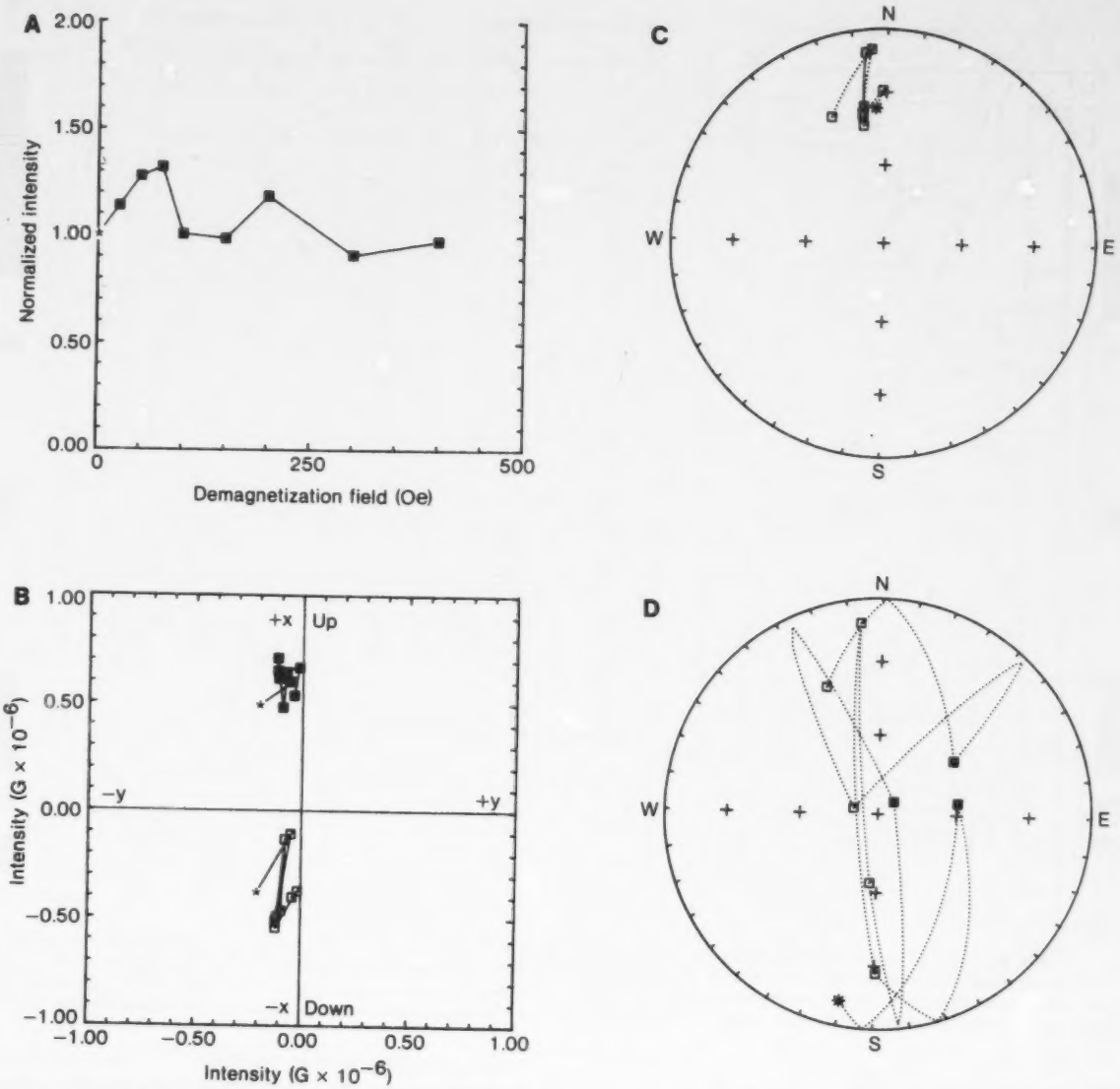

Figure 5. Behavior of Sample 575A-18-1, 144–146 cm. This sample represents the majority of sediments encountered on Leg 85. It comes from a highly calcareous unit and is very weakly magnetized, its NRM intensity being 6.7×10^{-7} G. See Figure 2 caption for details.

of the 180° declination shifts in Hole 573. In both holes the record spans from the lower Mammoth transition at 3.19 Ma (Ness et al., 1980) to the Brunhes/Matuyama boundary. Table 2 lists the depths of polarity changes found in both holes; it also gives the position of the last sample of the upper polarity sequence and the first sample of the lower sequence, thus defining the depth-uncertainty range for each polarity change (Fig. 7, dotted intervals). As shown in Table 2 and Figure 7, the stratigraphically equivalent 180° shifts in declination occur at different depths in the holes. In Figure 7, the points that define the same polarity transition in the holes plot along three 45° line segments, and the top segment is offset from zero. Within the depth intervals indicated by each 45° line segment, the drilling-related displacement of material is absent and the net sedimentation rate is constant. The breaks between the line segments may be explained in three ways: (1) net sedimentation rates may have changed from hole to hole, although such variation is unlikely, given the general uniformity of the region's seismic properties and sedimentation rates; (2) coring procedures may have introduced disturbances in the form of missing material and partial core recovery; and (3) shifts in the magnetic boundaries may have been introduced by reworking, direct disturbance, or postdepositional effects (Løvlie, 1976).

The top line segment may be offset from zero because the top of the section in Hole 573A is missing. However, we believe that solution or erosion caused the sediment sequence from the Brunhes Chron in Hole 573A to be

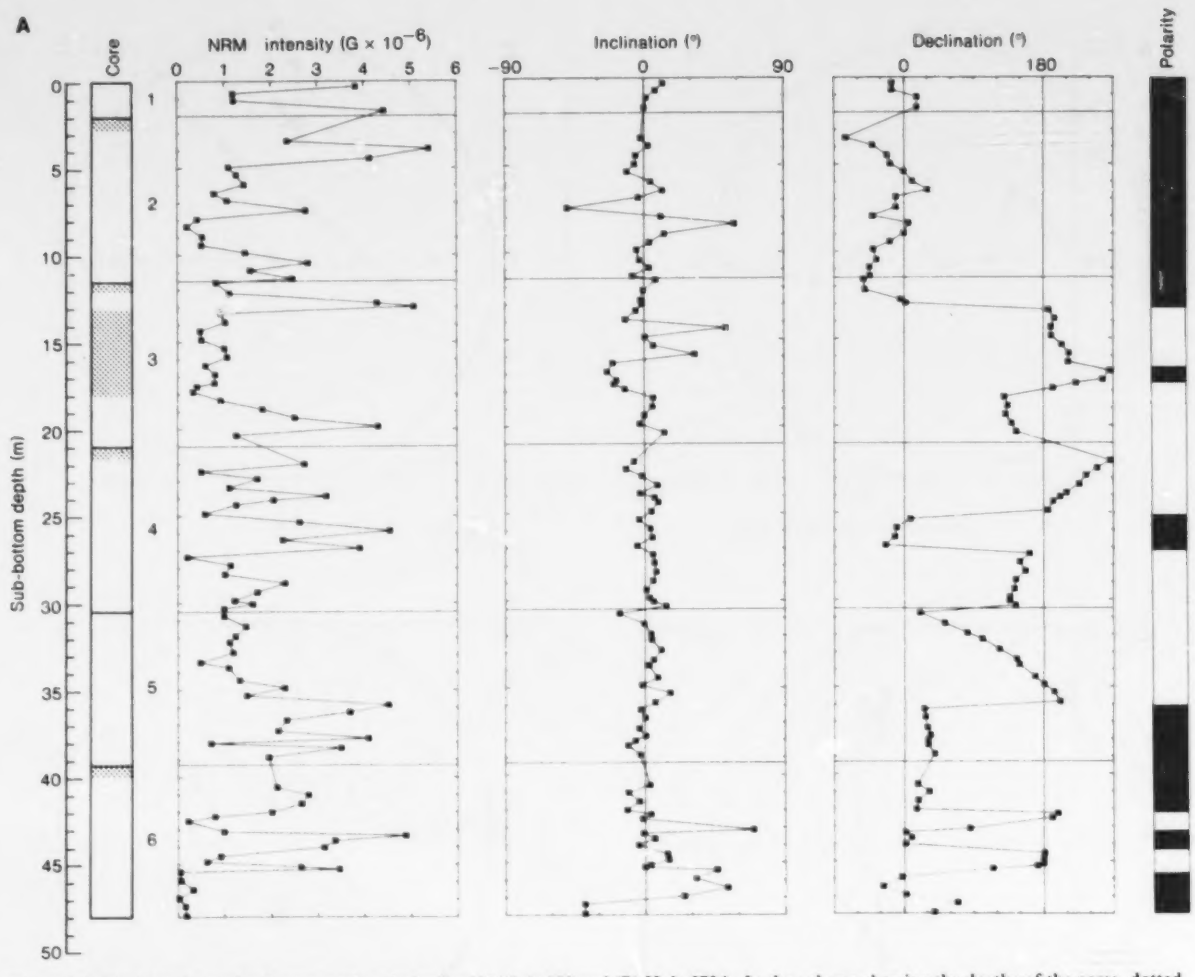

Figure 6. NRM intensity and paleomagnetic polarity for (A) Hole 573 and (B) Hole 573A. In the column showing the depths of the cores, dotted intervals are those identified on the barrel sheets as disturbed by drilling. The remaining columns show the downhole variation of NRM intensity; stable inclination and corrected declination (see text for details); and paleomagnetic polarity (derived from 180° shifts in the declination data). Black indicates intervals of normal polarity, white intervals of reversed polarity, and striping intervals that could not be interpreted.

Table 1. Summary of Leg 85 coring.

Site	Location	Maximum depth of penetration (m)	Hole	Interval cored (m sub-bottom)	Estimated age of oldest sediment (Ma)	Nature of basement
571	114°08.53′W, 3°59.84′N	7.1	571	0-7.1	0.46	Not reached
572	113°50.52′W, 1°26.09′N	486.0	572	0-19.0	14-15	Basalt
			572A	0-154.0		
			572B	154.0-172.1		
			572C	0-169.5		
			572D[a]	151.0-486.0		
573	133°18.57′W, 0°29.91′N	529.0	573	0-158.6	38-39	Basalt
			573A	0-53.2		
			573B[a]	138.5-529.0		
574	133°19.81′W, 4°12.52′N	532.5	574	0-206.5	38-39	Basalt
			574A	0-180.2		
			574B[a]	185.0-204.0		
			574C[a]	194.5-532.5		
575	135°02.16′W, 5°51.00′N	208.3	575	0-98.6	22	Not reached
			575A	0-208.3		
			575B	3.3-119.0		
			575C	0-15.8		

[a] Rotary drilled.

more compressed than in Hole 573, an interpretation consistent with the shortness of both the first reversed interval of the Matuyama Chron and the Jaramillo subchron in Hole 573A. On the other hand, both the Jaramillo subchron and the Brunhes/Matuyama boundary in Hole 573 fall within an interval disturbed by coring (Fig. 6A).

The first break in the 45° line (Fig. 7) occurs in the early part of the Matuyama Chron. It too can be interpreted as a compaction effect, because again there is some shortening in Hole 573A, but in this case it is more likely to be due to the coring process. The Jaramillo, Olduvai, and all the polarity changes in the Gauss Chron follow the predicted sequence. Between the Matuyama/Gauss boundary and the beginning of the Olduvai subchron, there is a second break in the 45° line (Fig. 7); it occurs at the boundary between Cores 4 and 5 in Hole 573 and between Cores 3 and 4 in Hole 573A. It is likely that sediments were lost between those cores:

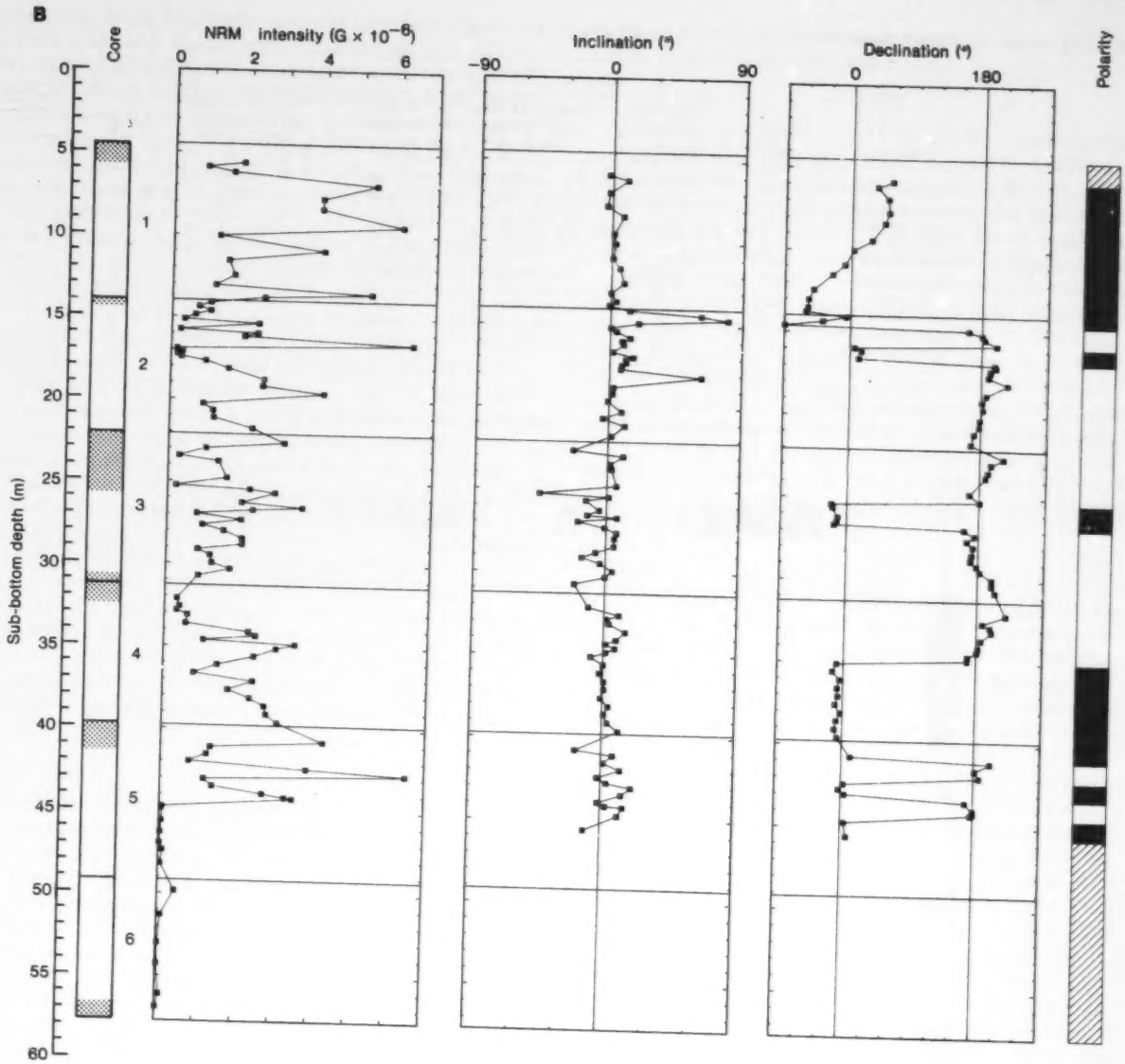

Figure 6. (Continued).

adding about 1 m of sediment between Cores 4 and 5 in Hole 573 and between Cores 3 and 4 in Hole 573A would produce a straight line from the Gauss/Gilbert boundary to the Jaramillo subchron.

Site 574

Site 574, at 4°12.52′N and 133°19.81′W, was near the northern edge of the high-productivity belt. A sediment sequence from upper Eocene to Quaternary was recovered, as well as a few pieces of basalt drilled from basement. All cores were sampled (Appendixes A and B), although only the samples from the uppermost 10 cores of Holes 574 and 574A are discussed here because of the low intensities lower in the section. The intensities are characteristic of lithologic Unit I (cyclic siliceous–calcareous ooze) down to about 84 m sub-bottom; they show significant variations that are in accord with the lithostratigraphic subunits (site chapters, this volume). For Subunit IA (Hole 574), a mean intensity of $3.93 \pm 2.94 \times 10^{-6}$ G was obtained. In both holes there is a very sharp decrease in intensity of more than one order of magnitude at the transition from Subunit IA to Subunit IB. The intensities of the sediments in Subunit IC are slightly lower than in Subunit IA ($2.12 \pm 1.14 \times 10^{-6}$ G in Hole 574 and $1.56 \pm 1.16 \times 10^{-6}$ G in Hole 574A). Throughout lithologic Unit II (calcareous ooze-chalk), the intensities are in the range of 10^{-7} G (Fig. 8), and the resulting data are not usable for magnetostratigraphy. With few exceptions, the magnetic directions and the intensities to 520 m sub-bottom are either randomly

Table 2. Magnetostratigraphy for Holes 573 and 573A.

Boundary	Age (Ma)[a]	Hole 573		Hole 573A	
		Depth of boundary (m sub-bottom)[b]	Uncertainty range (Core-Section, level in cm)[c]	Depth of boundary (m sub-bottom)[b]	Uncertainty range (Core-Section, level in cm)[c]
Brunhes/Matuyama	0.72	13.17	3-1, 147/3-2, 36	14.63	2-1, 38/2-1, 88
upper Jaramillo	0.91	16.61	3-4, 36/3-4, 86	15.98	2-2, 28/2-2, 68
lower Jaramillo	0.97	17.47	3-4, 136/3-5, 7	16.96	2-2, 113/2-3, 28
upper Olduvai	1.66	25.12	4-3, 88/4-3, 136	25.48	3-3, 173/3-3, 58
lower Olduvai	1.87	27.11	4-4, 136/4-5, 36	26.77	3-3, 147/3-4, 36
Matuyama/Gauss	2.47	35.97	5-4, 86/5-4, 128	35.19	4-3, 33/4-3, 84
upper Kaena	2.91	42.05	6-2, 123/6-2, 147	41.25	5-1, 99/5-1, 131
lower Kaena	2.98	43.15	6-3, 84/6-3, 106	42.52	5-2, 69/5-2, 114
upper Mammoth	3.07	44.19	6-24, 23/6-4, 74	43.58	5-3, 26/5-3, 69
lower Mammoth	3.17	45.58	6-5, 13/6-5, 62	44.80	5-3, 144/5-4, 46

[a] Ness et al. (1980).
[b] Interpolated from coring summary (site chapter).
[c] Last sample of upper polarity sequence/first sample of lower polarity sequence.

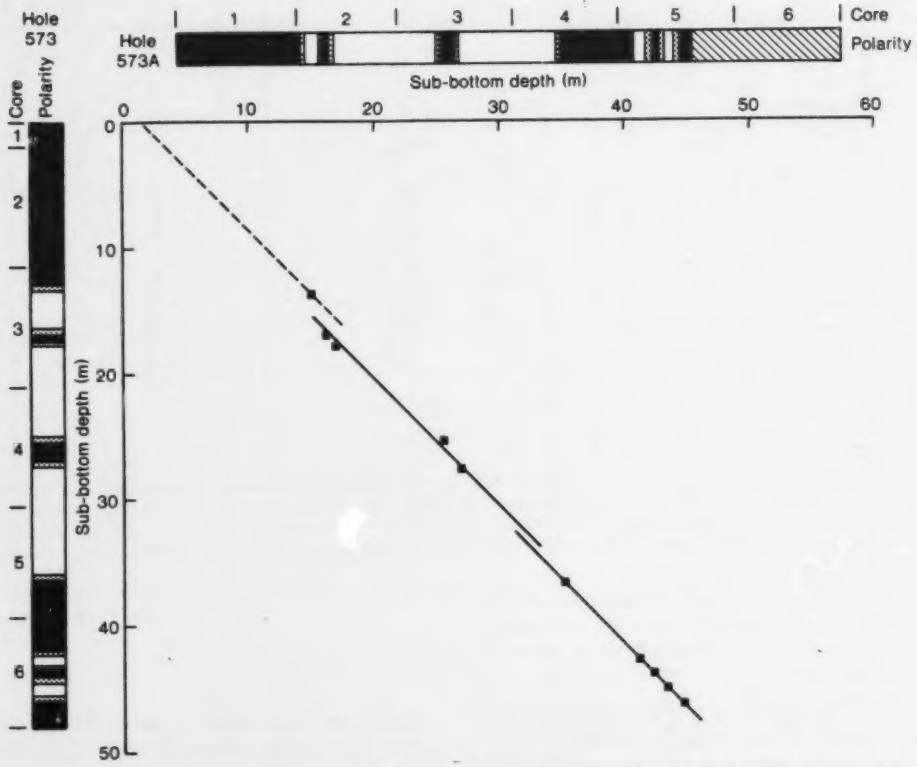

Figure 7. Comparison of paleomagnetic polarity logs for Holes 573 and 573A. Correlative polarity transitions are plotted. The dotted intervals above and below the transitions indicate lack of samples and thus the uncertainty in the depth of a boundary. Black indicates intervals of normal polarity, white intervals of reversed polarity, and striping intervals that were not interpreted.

scattered or remain virtually constant for considerable depth intervals, and both of these patterns preclude coherent interpretation. Typically, both the declinations and the intensities follow this pattern, possibly indicating remagnetization or chemical alteration of the magnetic carriers (Henshaw and Merrill, 1980). In the upper Eocene metalliferous chalk unit (Unit III), we measured stronger intensities (in the range of some 10^{-5} G), but the inclination data did not allow the establishment of a meaningful stratigraphic pattern.

Hole 574

The magnetostratigraphy for the upper 10 cores of Site 574 (Figs. 8A and B) is coherent, although it contains a gap as the result of the very low intensities of Cores 6 to 8 in lithologic Subunit IB. The polarity se-

quence in Hole 574 starts with the Brunhes Chron in Core 1 (Fig. 8A). Core 2 contains Matuyama sediments (as defined by inclination data), and the next interval of normal polarity indicates the Olduvai subchron; the Brunhes/Matuyama boundary and the Jaramillo subchron are missing in this hole. The normal section at the bottom of Core 2 marks the top of the Gauss Chron. Throughout the upper part of Core 3, coring disturbance prohibits interpretation; the Gauss/Gilbert boundary alone is well defined. The first normal subchron within the Gilbert Chron, the Cochiti subchron, is poorly expressed in Core 4, but the lower three Gilbert subchrons can easily be identified (Fig. 8A). The transition (reversed to normal) in Core 5 defines the Gilbert/Chron 5 boundary, and the Chron 5/Chron 6 boundary can be distinguished in Core 6. Farther below, a brief normal subchron may occur, but it is not clearly indicated because of the low intensity and the noise in the inclination data. From Section 574-6-4 to Section 574-9-4 no stratigraphy is discernible. The polarity sequence in Cores 9 and 10 indicates the presence of the youngest normal subchron in Chron 8 and the transition from Chron 8 to Chron 9. This interpretation disagrees, however, with the biostratigraphic dating of this depth interval and may well be erroneous: the polarity sequence is discontinuous with that above Core 9, and the inclination data give no indication of polarity. Our interpretation is based on a linear extrapolation and on a comparison to the length of the polarity intervals of the actual time scale (Ness et al., 1980).

Hole 574A

Hole 574A (Fig. 8B) is similar to Hole 574 (Fig. 8A). No paleomagnetic data are available from Core 1 because of poor recovery, but Core 2 correlates with the Matuyama Chron, and the first interval of normal polarity is interpreted as the Olduvai subchron. The next, poorly defined transition from reversed to normal may be the Matuyama/Gauss boundary at 2.47 Ma (Ness et al., 1980). The initial polarity of Core 3 is interpreted as reversed only because of its length. If this interpretation is accurate, Core 3 is of Gilbert age and the older part of the Gauss Chron (between Cores 2 and 3) is missing. Consequently, the transition at the lower part of Core 3 may be the younger boundary of the Cochiti subchron at 3.86 Ma, and Core 4 may contain the four normal subchrons of the Gilbert Chron. The Gilbert/Chron 5 boundary can be identified in Core 5, and the Chron 5/Chron 6 boundary can be identified in Core 6. Because the older normal polarity interval of Chron 5 is very short, however, material might have been lost between Cores 5 and 6. From the lower part of Core 6 down to Core 9 (lithologic Subunit IB), the low intensity precludes the determination of any polarity change from either the inclination or declination data, as in Hole 574 (Fig. 8B). Cores 9 and 10 are interpreted as containing the Chron 8/Chron 9 transition and parts of Chron 9. The data from the lower part of Core 10 are poor and must be interpreted by extrapolation, as for Hole 574. Table 3 shows the polarity changes in Holes 574 and 574A by depth and age (Ness et al., 1980). The possible reasons for the differences in depth of some polarity transitions are discussed above.

Site 575

Site 575, at 5°51.00′N, 135°02.16′W, constitutes the northernmost of three sites drilled in a north–south transect across the equatorial high-productivity belt. Miocene to Quaternary sediments were recovered at this site; basement was not reached. The entire set of cores was sampled for paleomagnetic analysis, and a magnetostratigraphy into the lower Miocene was established, although unfortunately it has some gaps due to weak magnetization in the lower to middle Miocene (Fig. 9). The intensities throughout lithologic Unit I at Holes 575, 575B, and 575C show large-scale variations ranging from 10^{-7} G to about 10^{-6} G, with constant averages. The magnetization properties of the Site 575 sediments are similar to those at the other sites. The lower Miocene sequence, which is characterized by a pale brown ooze (lithologic Subunit IIA), provided intensities with a mean of $8.97 \pm 7.81 \times 10^{-6}$ G.

Hole 575

If we assume that no polarity boundaries occur between cores, the magnetostratigraphic interpretation of the data for Hole 575 is straightforward. We correlate the uppermost polarity sequence with the Brunhes Normal Chron (Table 4A; Fig. 9A), a correlation supported by the inclination data. Lower we distinguish the Matuyama and Gauss Chrons, as documented by the declination data and, at 10.27 m sub-bottom, the Gilbert/Chron 5 transition (5.41 Ma; Ness et al., 1980), in agreement with the biostratigraphic results (Barron et al., this volume). Thus, the entire sequence of the Gilbert normal subchrons appears to be missing as the result of a hiatus. The normal polarity interval ranging from 10.27 to 13.17 m sub-bottom is interpreted as Chron 5. The magnetic record of the underlying normal polarity sequence (that from 16.15 to 22.77 m sub-bottom) is poor because of the disturbance of the sediments. The transition at 22.77 m appears to be the Chron 7/Chron 8 boundary (at 8.18 Ma; Ness et al., 1980). We assume that most of Chron 9 is missing as the result of a prominent hiatus (see Barron et al., this volume), but otherwise the polarity record down to the upper part of Chron 12 (Core 4) is reasonably well developed (Fig. 9A, Table 4A).

Hole 575C

The two cores that constitute Hole 575C provide an excellent record of the upper Miocene to Quaternary polarity sequence (Fig. 9C, Table 4C). As clearly indicated by the inclination data, the uppermost sequence of uniform declination can be interpreted as the Brunhes Chron. The Brunhes/Matuyama boundary occurs at 2.61 m sub-bottom in Core 1 and is followed by the Jaramillo and Olduvai subchrons (Table 4C). Between the termination and the onset of the Gauss Chron, both the Kaena and Mammoth subchrons are present (Fig. 9C; Table 4C). As in Hole 575 (see above), the polarity transition following the Gauss/Gilbert boundary (Core 575C-2; 9.91 m)

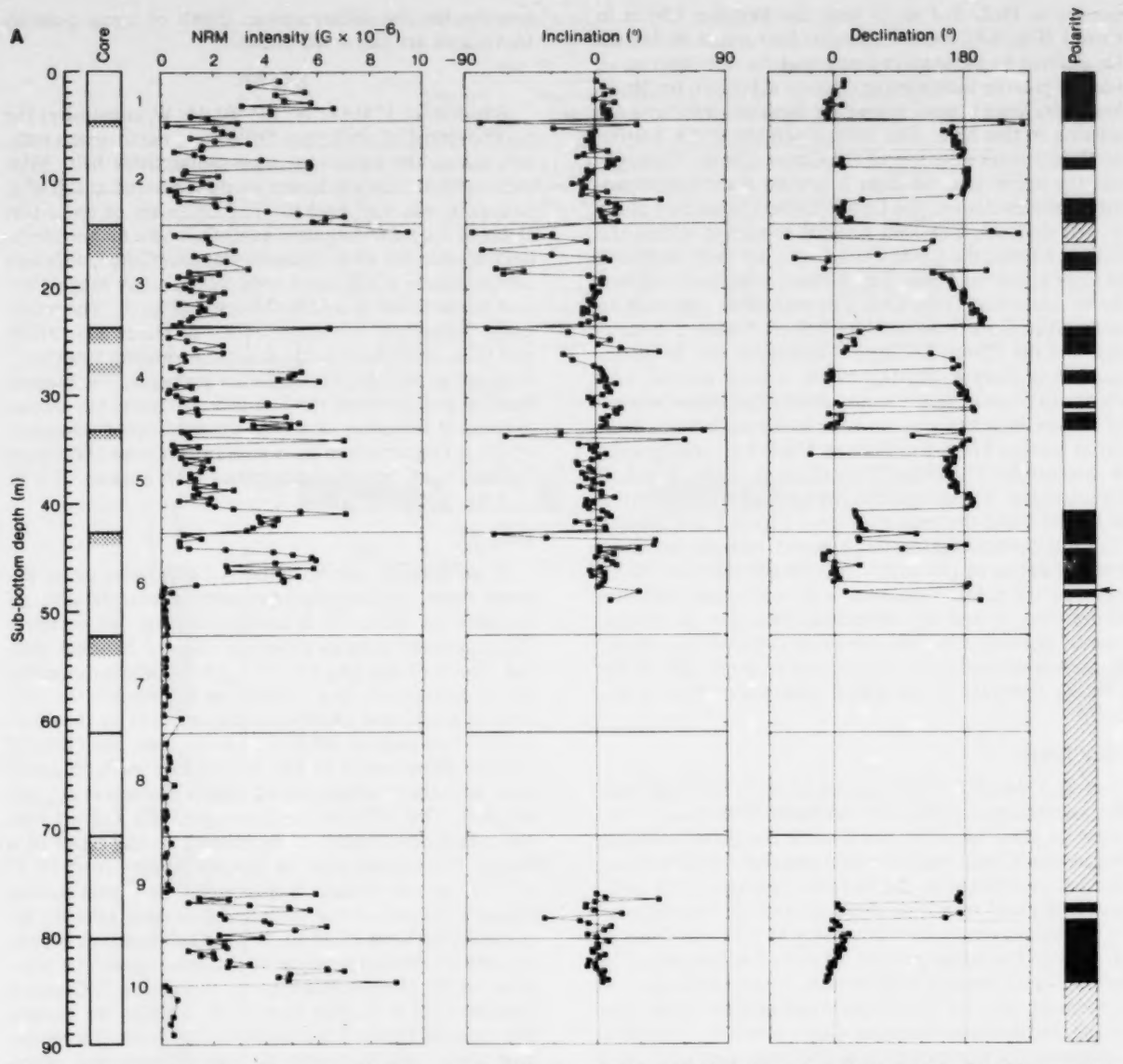

Figure 8. NRM intensity and paleomagnetic polarity logs for (A) Hole 574 and (B) Hole 574A. In the column showing the depths of the cores, dotted intervals are those identified on the barrel sheets as disturbed by drilling. The remaining columns show the downhole variation of NRM intensity; stable inclination and corrected declination (see text for details); and paleomagnetic polarity (derived from 180° shifts in the declination data). Black indicates intervals of normal polarity and white intervals of reversed polarity. Striping shows intervals where only erratic and NRM_0 data were available; these intervals were not interpreted. Arrows indicate polarity changes documented by one data point only.

is correlative to the Gilbert/Chron 5 boundary, a correlation that requires there to be a hiatus during the Gilbert Chron. All the polarity transitions in Chron 5 can be identified (Fig. 9C). The erratic 180° shifts in the declination data that occur in the lower normal interval of Chron 5 are caused by volcanic detritus (see site chapters, this volume). The polarity change at 15.57 m sub-bottom (Core 575C-2) agrees well with the N-R transition dated at 6.42 Ma (Ness et al., 1980).

Hole 575B

In contrast, the record of late Miocene to Quaternary magnetostratigraphy in Hole 575B is poor (Fig. 9B). Core 575B-1 begins in the Brunhes Chron. The Brunhes/Matuyama boundary at 4.96 m sub-bottom is followed by the Jaramillo subchron (Fig. 9B). At 6.41 m the sampling of the first core was discontinued because of the severe disturbance of the sediments. Sampling was resumed at 12.81 m, at the top of Core 2, within an interval of normal polarity as indicated by the inclination data. The uppermost polarity change in Core 2, at 13.06 m, is correlated to the Gauss/Gilbert boundary (3.40 Ma). Since we assumed that there is a hiatus centered on the Gilbert Chron (see discussion above), the two intervals of normal polarity that follow are interpreted as Chron 5. Its upper boundary (5.41 Ma) occurs

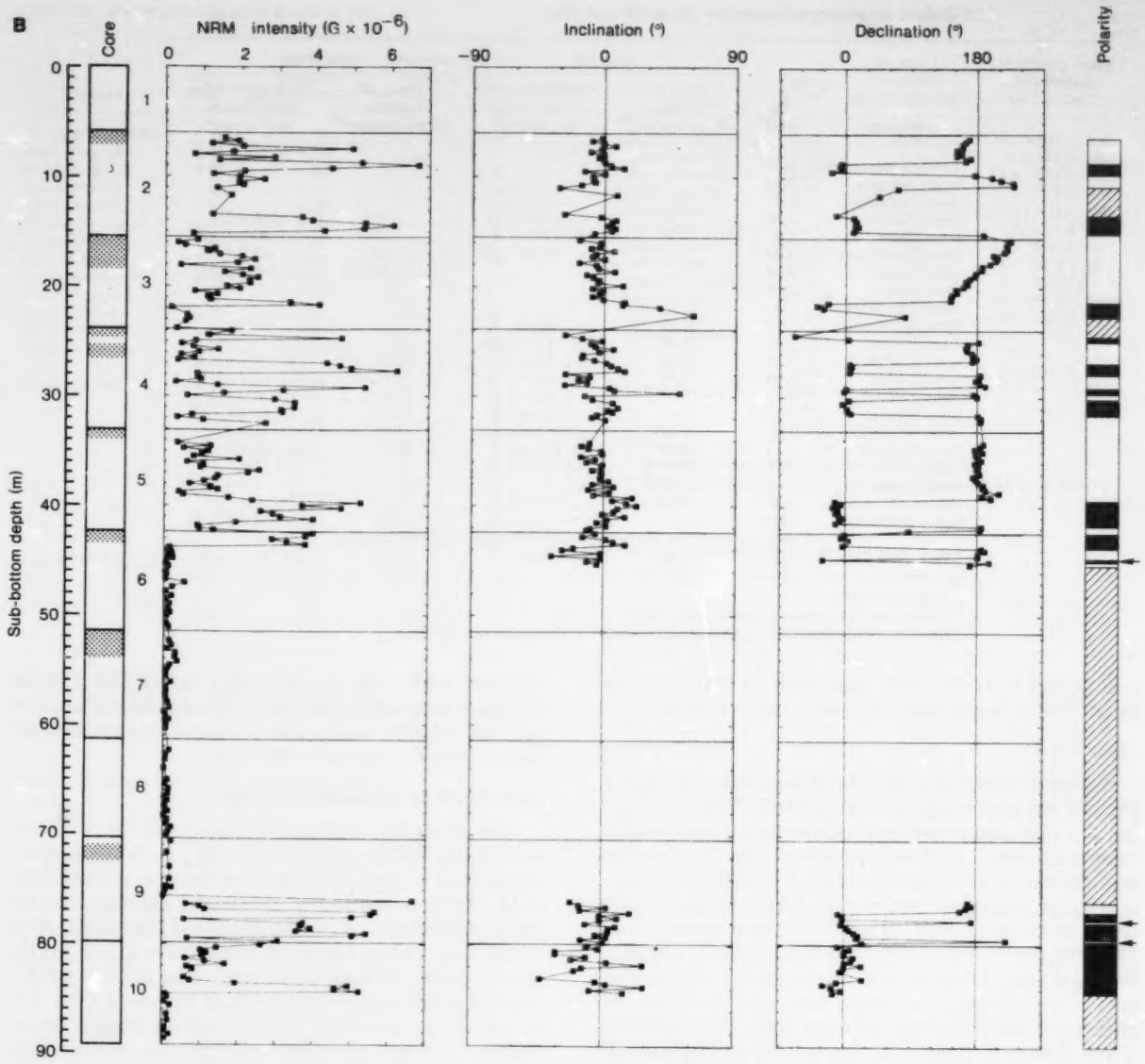

Figure 8. (Continued).

at 14.68 m, and its lower boundary occurs at 18.18 m sub-bottom. Erratic declinations occur in the lower interval of normal polarity of Chron 5, in a position stratigraphically correlative with those that occur in Core 575C-2 and for the same reason (volcanic detritus). The polarity change at 21.03 m sub-bottom in Core 575B-2 correlates with the N–R transition in Hole 575C that is dated at 6.42 Ma (Ness et al., 1980). The first 180° shift of declination identified in Core 575B-3 at 22.70 m, therefore, appears to be the transition at 6.55 Ma. Unfortunately, further magnetostratigraphic interpretation is impossible because of the weak intensities and erratic inclination and declination data that characterize the underlying sediments.

A comparison of the depths of polarity transitions in Holes 575C and 575B indicates a depth displacement. Stratigraphically correlative intervals bounded by 180° shifts in declination (those from the Brunhes/Matuyama boundary down to the Chron 5/Chron 6 boundary and those in the intervals of volcanic detritus) were used to calculate a regression with a correlation coefficient, r^2, of 0.997. This displacement between the holes amounts to 1.63 m, instead of the 3.30 m suggested by the coring logs (which show an offset of that amount between the mudline and the top of Core 575B-1). The determination of the depth of the top of each core was made difficult by the presence of both this within-hole displacement and the overcoring technique used in Holes 575B and 575A (see Site 575 chapter). For this study the length of the interval that was overcored (which is called washdown in the barrel sheets) was subtracted from the length of each core. The good correlation between the polarity

Table 3. Magnetostratigraphy for Holes 574 and 574A.

Boundary	Age (Ma)[a]	Hole 574		Hole 574A	
		Depth of boundary (m sub-bottom)[b]	Uncertainty range (Core-Section, level in cm)[c]	Depth of boundary (m sub-bottom)[b]	Uncertainty range (Core-Section, level in cm)[c]
Brunhes/Matuyama	0.72				
upper Jaramillo	0.91				
lower Jaramillo	0.97				
upper Olduvai	1.66	7.92	2-3, 30/2-3, 55	8.58	2-2, 66/2-2, 9
lower Olduvai	1.87	8.92	2-3, 130/2-4, 5	9.59	2-3, 16/2-3, 42
Matuyama/Gauss	2.47	11.67	2-5, 105/2-5, 130	12.10	2-3, 142/2-5, 110
upper Kaena	2.91			15.02	2-6, 110/2-6, 135
lower Kaena	2.98				
upper Mammoth	3.07				
lower Mammoth	3.17	16.89	3-2, 88/3-3, 40		
Gauss/Gilbert	3.40	18.46	3-3, 113/3-4, 30		
upper Cochiti	3.86	23.86	3-7, 30/4-1, 92	21.28	3-4, 115/3-4, 141
lower Cochiti	3.98	26.32	4-2, 49/4-3, 65	24.83	4-1, 81/4-1, 104
upper Nunivak	4.12	27.52	4-3, 90/4-3, 115	26.82	4-2, 130/4-3, 5
lower Nunivak	4.26	28.67	4-4, 55/4-4, 80	27.83	4-3, 81/4-3, 105
upper Sidufjall	4.41	30.42	4-5, 80/4-5, 105	29.08	4-4, 55/4-4, 81
lower Sidufjall	4.49	30.92	4-5, 130/4-6, 5	29.57	4-4, 105/4-4, 130
upper Thvera	4.59	31.47	4-6, 30/4-6, 55	30.12	4-5, 5/4-5, 38
lower Thvera	4.79	33.57	4-7, 28/5-1, 135	31.57	4-6, 6/4-6, 28
Gilbert/Chron 5	5.41	40.42	5-5, 130/5-6, 5	39.38	5-5, 15/5-5, 41
Chron 5/Chron 6	6.07	47.17	6-4, 5/6-4, 30	43.69	6-1, 116/6-1, 142
	Core 6 to Core 9 data did not allow identification of specific reversals				
Chron 8/Chron 9	8.98	78.22	9-6, 10/9-6, 35	76.94	9-5, 42/9-5, 67

[a] Ness et al. (1980).
[b] Interpolated from coring summary (site chapter).
[c] Last sample of upper polarity sequence/first sample of lower polarity sequence.

boundaries in Holes 575C and 575B (if the offset of Hole 575B is disregarded) supports this procedure.

Hole 575A

We could develop a reasonable magnetostratigraphy for only the uppermost 10 cores of Hole 575A. Overcoring was also used in this hole, so the actual core lengths were recalculated as described above. The stratigraphy was derived by defining the mean declination for each core. This mean was then used to arbitrarily align each core's declination with either 0° (normal polarity) or 180°. Figure 9D shows the resulting polarity pattern. We emphasize, however, that without usable inclination data it is impossible to define the polarity of the sequence on paleomagnetic grounds alone. The interpretation shown in Figure 9D was guided by the general biostratigraphic age of the sediments. Because of the age range of the interval (about 16 to 18 Ma), this interpretation of polarity also fits the anomaly pattern much better than would the opposite polarity solution. The uppermost sequence with uniform declination data, which starts at 93.80 m sub-bottom (the top of Core 1) was arbitrarily set at 0° or normal polarity. The three intervals of normal polarity that can be identified in Cores 1 to 3 are interpreted as Anomaly 5C (Mankinen and Dalrymple, 1979; Ness et al., 1980), which begins at 102.64 m sub-bottom (16.71 Ma). At the bottom of Core 5 (113.54 m) there is a 180° shift to 0°, and at the top of Core 6 (114.59 m) the declination shifts back to 180°. This normal polarity interval cannot be correlated to the geomagnetic time scale (Ness et al., 1980). The transition at 118.09 m sub-bottom is interpreted as the younger limit of Anomaly 5D (17.28 Ma), and the polarity change at 125.59 m (17.60 Ma; Ness et al., 1980) is interpreted as its older limit. This interpretation agrees well with the accepted time scales and the biostratigraphy (Barron et al., this volume); and it also yields reasonable sedimentation rates for the lower Miocene.

Discussion of Magnetostratigraphy

The magnetostratigraphy of the Leg 85 sites is summarized in Figure 10. It was derived from the polarity boundaries of each hole by using the time scale of Ness et al. (1980) as a reference. Alternative geomagnetic time scales (McDougall, 1977; Mankinen and Dalrymple, 1979) would produce no significant differences in age for the late Neogene. The sedimentation rates defined by this magnetostratigraphy decrease from the south (Site 573) to the north (Site 575). The northward motion of the Pacific Plate and the migration of the sites into the high-productivity belt of the equatorial region (Winterer, 1973; van Andel et al., 1975) is generally confirmed by the increase in sedimentation rate that occurs as depth in Sites 574 and 575 increases.

The sedimentation rates at Site 573 are surprisingly constant at about 18.2 m/m.y. At Site 574, the rates change significantly at approximately 3 Ma (during the Gauss Chron), from about 5.5 m/m.y. above to about 12.2 m/m.y. below. Below the Chron 5/Chron 6 boundary, the sedimentation rates are poorly documented, however, because we lack reliable data. There should be a significant hiatus at about 9 to 10 Ma (Moore et al., 1978; Barron and Keller, 1972). The oldest polarity change determined at this site (at about 80 m sub-bottom) is interpreted here as the Chron 8/Chron 9 boundary. This interpretation disagrees with the biostratigraphic dating, which places the Chron 10/Chron 11 boundary at this level (Barron et al., this volume). Site 575 shows a more

Table 4A. Magnetostratigraphy for Hole 575.

Boundary	Age (Ma)[a]	Depth of boundary (m sub-bottom)[b]	Uncertainty range (Core-Section, level in cm)[c]
Brunhes/Matuyama	0.72	2.70	1-2, 115/1-2, 125
upper Jaramillo	0.91	3.10	1-3, 5/1-3, 15
lower Jaramillo	0.97	3.20	1-3, 15/1-3, 25
upper Olduvai	1.66	4.10	1-3, 105/1-3, 115
lower Olduvai	1.87	4.30	1-3, 125/1-3, 135
Matuyama/Gauss	2.47	5.40	1-4, 85/1-4, 95
upper Kaena	2.91	6.60	1-5, 55/1-5, 65
lower Kaena	2.98	6.90	1-5, 85/1-5, 95
upper Mammoth	3.07	7.19	1-5, 115/1-5, 123
lower Mammoth	3.17	7.31	1-5, 128/2-1, 4
Gauss/Gilbert	3.40	7.65	2-1, 30/2-1, 40
Gilbert/Chron 5	5.41	10.27	2-2, 140/2-3, 4
Chron 5/Chron 6	6.07	13.17	2-4, 128/2-4, 145
	6.42	16.15	2-6, 130/2-6, 140
Chron 7/Chron 8	8.18	22.77	3-4, 139/3-5, 5
	8.40	25.80	3-6, 140/3-7, 10
	8.49	26.05	3-7, 10/3-7, 20
	10.42	26.85	4-1, 50/4-1, 60
	10.47	27.11	4-1, 70/4-1, 91
	10.89	28.00	4-2, 7/4-2, 3
	10.96	28.42	4-2, 33/4-2, 90
Chron 10/Chron 11	11.42	29.32	4-2, 134/4-3, 20
	11.58	29.75	4-3, 40/4-3, 50
	11.71	30.65	4-3, 130/4-3, 140
Chron 11/Chron 12	11.98	31.50	4-4, 65/4-4, 75
	12.28	32.10	4-4, 125/4-4, 135
	12.32	32.67	4-5, 9/4-5, 65
	12.40	33.43	4-5, 91/4-5, 134
	12.45	34.24	4-6, 39/4-6, 48

[a] Ness et al. (1980).
[b] Interpolated from coring summary (site chapter).
[c] Last sample of upper polarity sequence/first sample of lower polarity sequence.

Table 4B. Magnetostratigraphy for Hole 575B.

Boundary	Age (Ma)[a]	Depth of boundary (m sub-bottom)[b]	Uncertainty range (Core-Section, level in cm)[c]
Brunhes/Matuyama	0.72	4.96	1-2, 11/1-2, 21
upper Jaramillo	0.91	5.46	1-2, 61/1-2, 71
lower Jaramillo	0.97	5.72	1-2, 71/1-2, 113
Gauss/Gilbert	3.40	13.06	2-1, 101/1-1, 111
Gilbert/Chron 5	5.41	14.68	2-2, 113/2-2, 123
	5.70	15.75	2-3, 73/2-3, 83
	5.78	16.58	2-4, 3/2-4, 13
Chron 5/Chron 6	6.07	18.18	2-5, 13/2-5, 23
	6.42	21.03	2-6, 143/2-7, 13
	6.55	22.70	3-2, 9/3-2, 31[d]

[a] Ness et al. (1980).
[b] Interpolated from coring summary (site chapter) and corrected with regard to each core's washdown.
[c] Last sample of upper polarity sequence/first sample of lower polarity sequence.
[d] Correlation with the known polarity sequence was not possible in the rest of Core 3 or in Core 4.

Table 4C. Magnetostratigraphy for Hole 575C.

Boundary	Age (Ma)[a]	Depth of boundary (m sub-bottom)[b]	Uncertainty range (Core-Section, level in cm)[c]
Brunhes/Matuyama	0.72	2.61	1-2, 106/1-2, 116
upper Jaramillo	0.91	3.11	1-3, 6/1-3, 16
lower Jaramillo	0.97	3.21	1-3, 16/1-3, 26
upper Olduvai	1.66	4.11	1-3, 106/1-3, 116
lower Olduvai	1.87	4.21	1-3, 116/1-3, 126
Matuyama/Gauss	2.47	5.31	1-4, 76/1-4, 86
upper Kaena	2.91	6.66	2-1, 26/2-1, 46
lower Kaena	2.98	6.91	2-1, 56/2-1, 66
upper Mammoth	3.07	7.11	2-1, 76/2-1, 86
lower Mammoth	3.17	7.41	2-1, 106/2-1, 116
Gauss/Gilbert	3.40	8.01	2-2, 16/2-2, 26
Gilbert/Chron 5	5.41	9.91	2-3, 56/2-3, 66
	5.70	10.91	2-4, 6/2-4, 16
	5.78	11.51	2-4, 66/2-4, 76
Chron 5/Chron 6	6.07	12.71	2-5, 36/2-5, 46
	6.42	15.51	2-7, 16/2-7, 26

[a] Ness et al. (1980).
[b] Interpolated from coring summary (site chapter).
[c] Last sample of upper polarity sequence/first sample of lower polarity sequence.

Table 4D. Magnetostratigraphy for Hole 575A.

Boundary	Age (Ma)[a]	Depth of boundary (m sub-bottom)[b]	Uncertainty range (Core-Section, level in cm)[c]
	16.25	95.79	1-1, 29/1-1, 69
	16.29	97.29	1-3, 29/1-3, 69
	16.46	99.69	2-1, 49/2-1, 109
	16.53	101.74	2-2, 109/2-3, 9
Anomaly 5C onset	16.71	102.64	3-1, 9/3-1, 59
	?	113.59	5-3, 39/5-3, 97
	?	114.59	6-1, 29/6-1, 69
Anomaly 5D termination	17.28	118.09	6-3, 69/6-3, 129
Anomaly 5D onset	17.60	125.59	8-2, 49/8-2, 109
	17.81	128.44	10-1, 1/10-1, 46
	17.83	129.83	10-1, 134/10-2, 41

[a] Ness et al. (1980).
[b] Interpolated from coring summary (site chapter) and corrected with regard to each core's washdown.
[c] Last sample of upper polarity sequence/first sample of lower polarity sequence.

complex pattern of accumulation rates. The rates are very low at the top (less than 3 m/m.y.), and there are two possible hiatuses. The youngest prominent hiatus seems to occur between about 3.6 and 5.3 Ma (Barron et al., this volume), so almost the entire Gilbert Chron may be missing at this site. The magnetic data from about 16 to 23 m sub-bottom (≈6.4 Ma) are uncertain because of coring disturbance. Shipboard biostratigraphy suggests that a second hiatus affects the record of Chron 9. If so, the polarity pattern of Chrons 10 to 12 correlates with the measured magnetostratigraphy. From about 34.5 m to 93.8 m sub-bottom, very weak intensities again precluded the development of a coherent magnetostratigraphy. The polarity pattern established throughout the upper 10 cores of Hole 575A (Fig. 9D) is interpreted here as being correlated with Anomalies 5C and 5D (about 16 to 18 Ma; Ness et al., 1980), an interpretation that is generally compatible with biostratigraphic results (Barron et al., this volume). Despite the poor control, an increase in sedimentation rates up to 21.5 m/m.y. can be detected in the older sediments.

The transition at all Leg 85 sites from cyclic siliceous-calcareous oozes to highly calcareous oozes is accompanied by a remarkable decrease in NRM intensities that may be caused by a significant reduction in the proportion of magnetic grains in the Miocene and older sediments. It is more likely, however, that the magnetic carriers have been altered (Kent and Lowrie, 1974; Henshaw and Merrill, 1980). The alteration may be related to the change from mainly calcareous (foram-nanno)

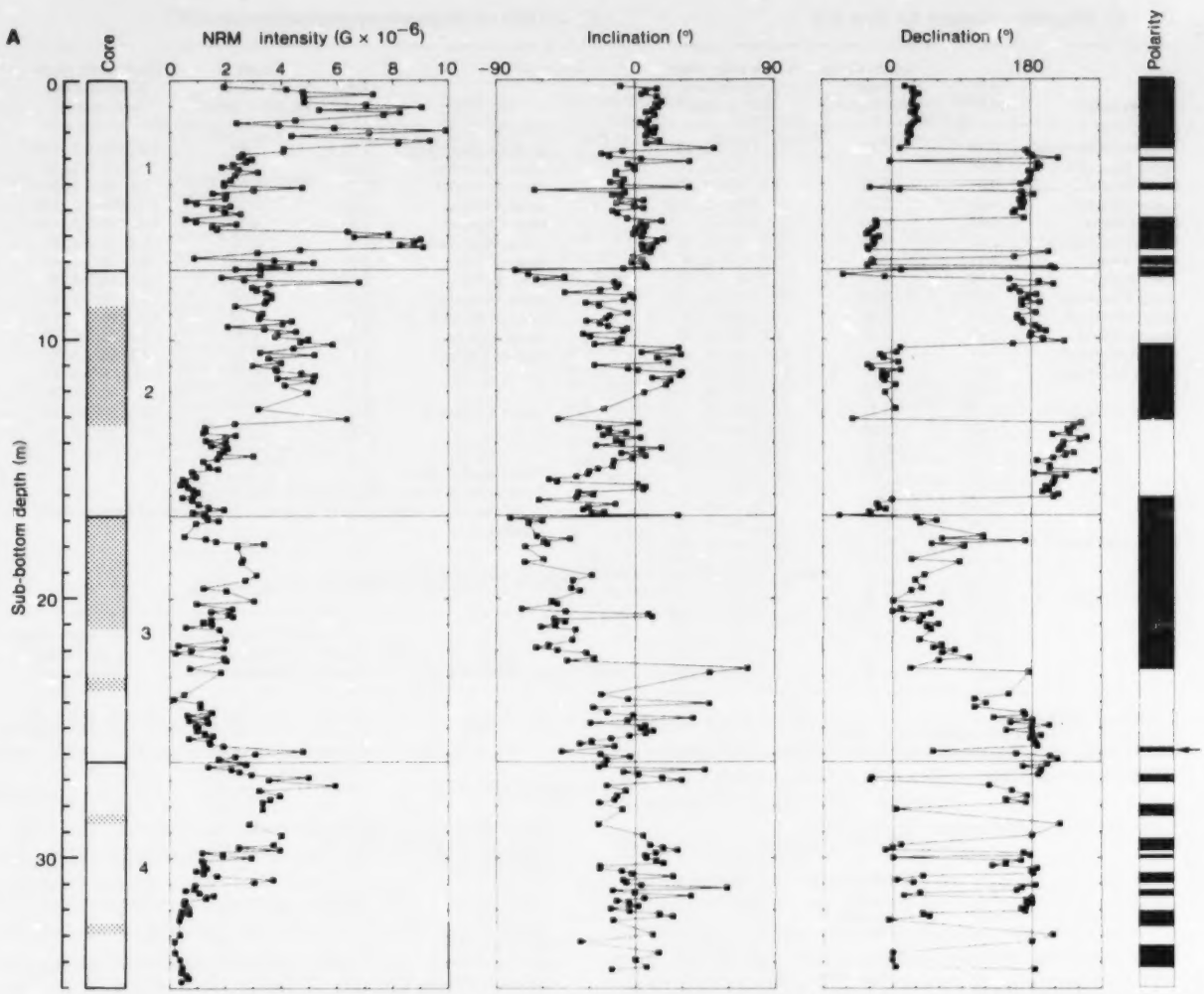

Figure 9. Polarity and NRM intensity logs for (A) Hole 575, (B) 575B, (C) Hole 575C, and (D) Hole 575A. See Figure 8 caption for further explanation.

oozes below to more siliceous sediments above or to diagenetic changes that begin at some 40 to 80 m sub-bottom at these sites. It is possible, of course, that all three of the conditions mentioned above are at work simultaneously. We performed no rock-magnetic analyses, so none of these ideas is supported by experimental evidence. However, Kent (1982) has shown that there is a correlation between low biogenic carbonate and high silica content and high NRM intensity. We noted an empirical relation between large-scale carbonate content variations and NRM intensity changes in the cyclic units of the Leg 85 sites, although no direct correlation was attempted. This relation may reflect a climatically driven, complex interaction between these parameters (Kent, 1982). No prominent changes in sedimentation rate or porosity were noted in these cyclic intervals (site chapters), so the amounts or properties of the magnetic materials (Hamano, 1980) are unlikely to be strongly affected by these factors. In contrast, the poor quality of the data in the metalliferous sediment layers overlying basement at Sites 573 and 574 is in all probability caused by erratic chemical and thermal magnetic overprints due to hydrothermal alteration.

Tectonic Analysis

The Pacific Plate has moved northwest at the rate of a little less than 1°/m.y. during the Mesozoic and Cenozoic. Different authors have used various methods to infer this motion. The methods include the study of the thickness of equatorial pelagic facies (Hays et al., 1969; Winterer, 1973; van Andel et al., 1975), basement age comparisons (Hays et al., 1972), hotspot traces (Minster et al., 1974; Epp, 1978; Gordon and Cape, 1981), the study of seamount magnetization (Sager, 1983), the study of magnetic anomaly patterns (Atwater and Menard, 1970; Herron, 1972), and the analysis of the paleomagnetism of central Pacific sedimentary cores (Hammond et al., 1974, 1975, 1979). Although our data are limited, we have attempted to study the northward component of plate motion by using Leg 85 paleomagnetic results. We divided the usable data from Sites 573, 574, and 575 into the time intervals or ranges listed in Table 5. These

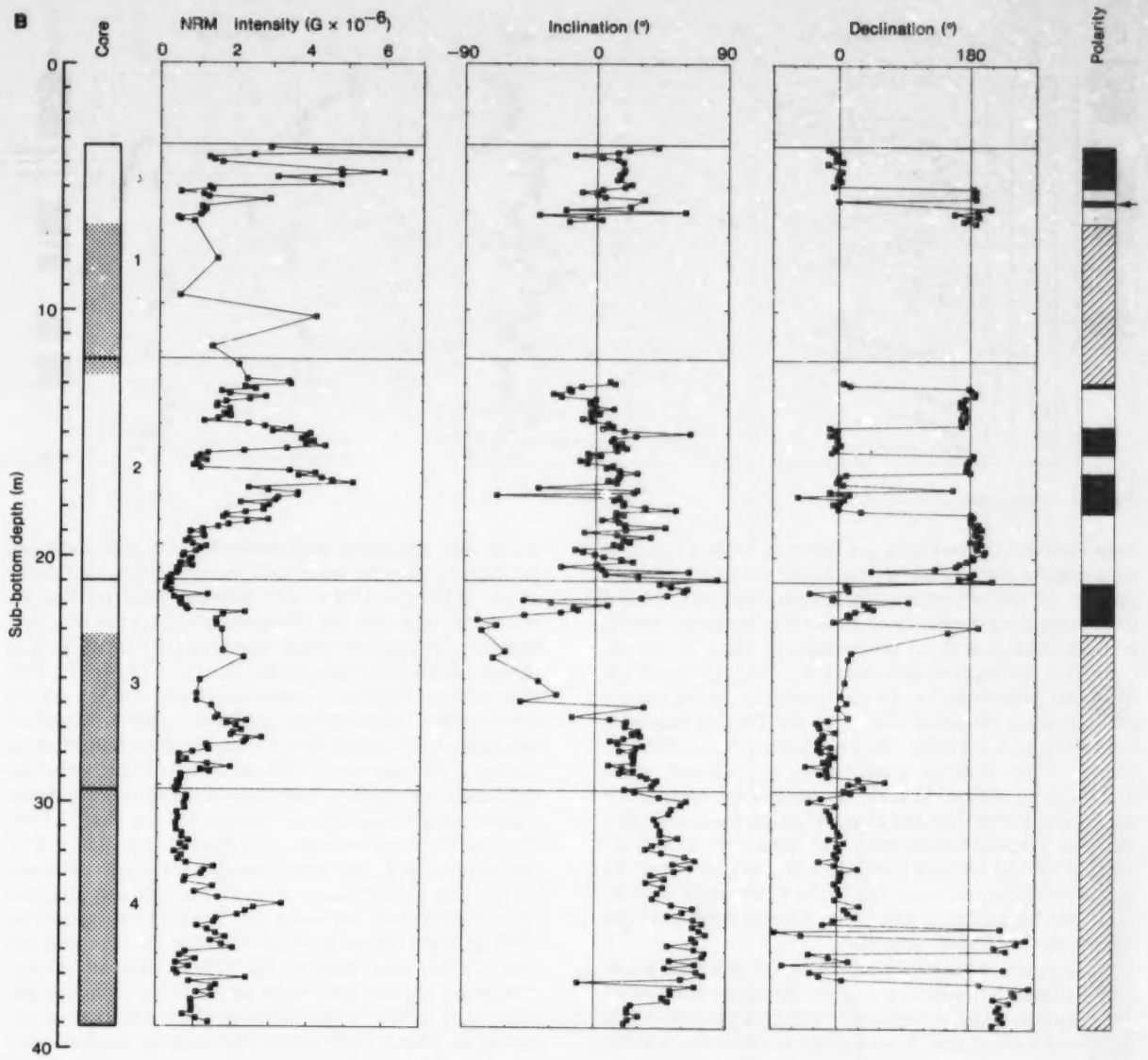

Figure 9. (Continued).

particular intervals were chosen because the resolution of our data varies (resolution is highest in the youngest intervals and lowest in the oldest sediments). Hiatuses, or inferred gaps, also influenced the choices. Thus, the Plio–Pleistocene data for Site 574, for example, were divided at the Gauss/Gilbert boundary into two intervals; an upper Miocene interval was also used. In the data for Site 575 a Pliocene hiatus was used as a boundary between two data sets; and a third interval between about 16 and 18 Ma was also analyzed (see previous discussion of Hole 575A). Using inclination data only, we averaged data from correlative intervals of parallel holes at each site (Fig. 10). We then calculated mean dipole paleolatitudes for each time interval by using statistics developed by Kono (1980), which provide 95% confidence limits. The mean paleolatitude for each time interval was then normalized for present site latitudes, and a latitude differential, or δ latitude, was derived. The latter was plotted (Table 5, Fig. 11) against the mean age of the interval as shown in Bleil (1981). The regression coefficient of 0.99 indicates a good linear fit (Fig. 11), and the slope of the curve expresses a northward motion of 0.29°/m.y., which agrees in general with previous approaches. (Figure 11 also supports our interpretation of the upper Miocene polarity sequence at Site 574. If that interval were as old as suggested by the biostratigraphy [Chron 8], the curve's fit would deteriorate.)

Paleolatitudes for Leg 85 sites were also calculated by using the rotation poles derived from a hotspot analysis (Epp, 1978). The backtracked positions of Sites 573 to 575 are shown in 1-m.y. steps in Figure 12. The hotspot paleolatitudes corresponding to the mean ages of the

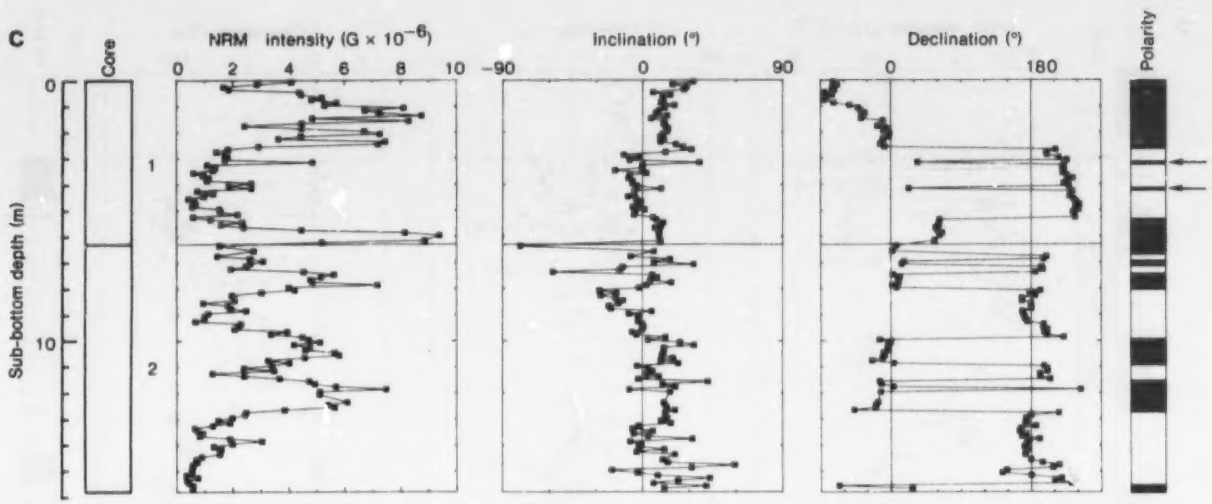

Figure 9. (Continued).

time intervals chosen here are listed in Table 5 together with present site latitude minus dipole paleolatitude and present site latitude minus hotspot paleolatitude. Table 5 shows that the hotspot-based differences are always smaller than those based on paleomagnetic data. If we assume that the hotspot data carry only tectonic information, this difference can be interpreted as an expression of oscillatory far-sided effects of the Earth's magnetic field (Epp et al., 1983). The regression (r^2 = 0.99) calculated from hotspot data shows a shallower slope (0.23°/m.y., indicating a slower northward motion for the Pacific Plate) than the slope resulting from a hotspot reference system, a conclusion that Epp et al. (1983) arrived at on the basis of central Pacific piston cores. As the authors pointed out, the differences could also be explained by assuming that the hotspot is not fixed with respect to the Earth's spin axis.

In addition to the above paleolatitude analysis, we also calculated paleo-pole positions for some time intervals. Gordon and Cox developed a technique (1980) that calculates a mean pole from a given model pole by using an iterative least-squares method. With this procedure it is possible to use heterogeneous (unoriented as well as azimuthally oriented) magnetic and paleomagnetic data to define paleo-pole positions. Because the Leg 85 data are confined to virtually one point on the Pacific and thus result in large uncertainties, paleomagnetic data from several HIG conventional piston cores (CPCs) were added. The CPCs, which were acquired 30 to 40° west of Leg 85's sites (at similar latitudes), span the same time interval as the Leg 85 data. Most of the CPC data have the advantage of being azimuthally oriented (Seyb et al., 1977), which improves the resolution of the Gordon and Cox (1980) method. We arbitrarily divided the entire data set into three age groups: Recent to about 6 Ma, 8 to approximately 11 Ma, and 15 to about 18 Ma (Table 6). Paleo-pole positions were then calculated (with Gordon and Cox's procedure) together with their semi-axes of the 95% oval of confidence (Table 6). These geographically well separated and internally coherent data sets produced relatively small and discrete 95% confidence ovals, although for the early Miocene pole the data are less numerous and the constraints are correspondingly broader. An apparent polar wander path (APWP) could thus be derived for the interval from 0 to 18 Ma (Fig. 13) that substantiates the overall northwest motion of the Pacific Plate. Our APWP shows a larger longitudinal and latitudinal displacement than the data published by Gordon and Cape (1981) for the Pacific Plate, although the trends are similar. Our paleo-pole latitudes indicate a northward component of motion for the Pacific Plate of about 0.59 ± 0.08°/m.y. during the last 18 m.y. This migration exceeds our earlier calculations, which are based on the Leg 85 inclination data alone. One can interpret this difference as reflecting the longitudinal separation (on the same plate) between the Leg 85 sites and the HIG CPCs. Hammond et al. (1979) gave an average northward motion calculated on the basis of inclination data from CPCs (which included the cores used in this paper) of about 0.59°/m.y. Our tectonic analysis also shows that low-latitude inclination data, previously often considered to be useless, can be employed with significant success for tectonic work. Finally, the study confirms the results of previous work that had pointed out that Tertiary paleomagnetic data may contain appreciable components of long- and short-term paleofield variations in addition to tectonic information (Epp et al., 1983; Theyer et al., 1983).

ACKNOWLEDGMENTS

We thank all persons responsible for the success of DSDP Leg 85, especially the JOIDES Ocean Paleoenvironmental Panel, who were the original "movers" behind it all. Special appreciation is given to U. Bleil and V. Spiess for discussions and valuable comments. D. Wilson, S. Hammond, D. Epp, and W. Sager, all formerly at HIG, stimulated and helped with the paleomagnetic-tectonic phase. J. Barron and C. Nigrini assisted with stratigraphic data and discussions. N. Shackleton suggested changes in an early version of the manuscript, and two anonymous reviewers offered many suggestions for improvements. R.

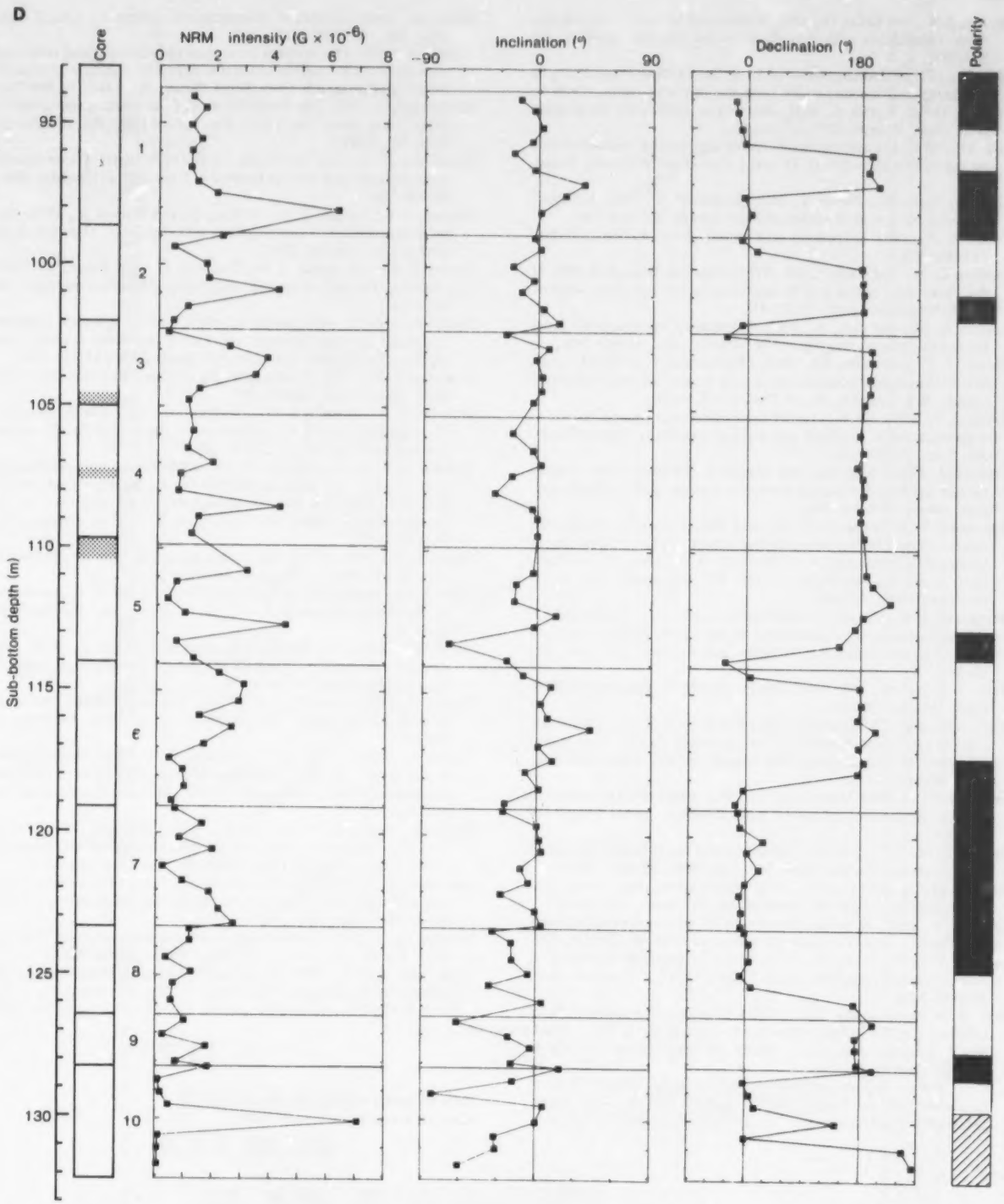

Figure 9. (Continued).

Pujalet also assisted with editorial advice. J. Tuthill helped develop tectonic software. We are also grateful to the members of the HIG Core Analysis Laboratory for their support.

N.W. thanks the Deutsche Forschungsgemeinschaft for support. F.T.'s research was in part supported under National Science Foundation Grant OCE81-17997. The HIG Core Analysis Laboratory is supported under NSF Grant OCE82-0196. This paper is HIG Contribution No. 1463.

REFERENCES

Atwater, T., and Menard, H. W., 1970. Magnetic lineations in the northwest Pacific. *Earth Planet. Sci. Lett.*, 7:445–450.

Barron, J. A., and Keller, G., 1982. Widespread Miocene deep-sea hiatuses: coincidence with periods of global cooling. *Geology*, 10: 577–581.

Bleil, U., 1981. Paleomagnetism of Deep Sea Drilling Project Leg 60 sediments and igneous rocks from the Mariana region. *In* Hussong, D. M., Uyeda, S., et al., *Init. Repts. DSDP*, 60: Washington (U.S. Govt. Printing Office), 855–873.

Epp, D., 1978. Age and tectonic relationships among volcanic chains on the Pacific plate [Ph.D. Dissert.]. University of Hawaii, Honolulu.

Epp, D., Sager, W., Theyer, F., and Hammond, S., 1983. Hotspot/spin axis motion or far-sided effects? *Nature*, 303:318–320.

Fisher, R. A., 1953. Dispersion on a sphere. *Proc. R. Soc. London*, 217:295–305.

Gordon, G. G., and Cape, C. D., 1981. Cenozoic latitudinal shift of the Hawaiian hotspot and its implications for true polar wander. *Earth Planet. Sci. Lett.*, 55:37–47.

Gordon, G. G., and Cox, A., 1980. Calculating paleomagnetic poles for oceanic plates. *Geophys. J. R. Astron. Soc.*, 63:619–640.

Goree, W. S., and Fuller, M., 1976. Magnetometers using RF-driven SQUIDS and their applications in rock magnetism and paleomagnetism. *Rev. Geophys. Space Phys.*, 14:591–608.

Hamano, Y., 1980. An experiment on the post-depositional remanent magnetization in artificial and natural sediments. *Earth Planet. Sci. Lett.*, 51:221–232.

Hammond, S. R., Epp, D., and Theyer, F., 1979. Neogene relative motion between the Pacific plate, the mantle, and the Earth spin axis. *Nature*, 278:309–312.

Hammond, S. R., Kroenke, L. W., and Theyer, F., 1975. Northward motion of the Ontong-Java plateau between -110 and -30 my: a paleomagnetic investigation of Site 289. *In* Andrews, J. E., Packham, G., et al., *Init. Repts. DSDP*, 30: Washington (U.S. Govt. Printing Office), 415–418.

Hammond, S. R., Theyer, F., and Sutton, G. H., 1974. Paleomagnetic evidence of northward movement of the Pacific Plate in deep-sea cores from the central Pacific basin. *Earth Planet. Sci. Lett.*, 22: 22–28.

Hays, J. D., et al., 1972. *Init. Repts. DSDP*, 9: Washington (U.S. Govt. Printing Office).

Hays, J. D., Saito, T., Opdyke, N. D., and Burckle, L. H., 1969. Pliocene–Pleistocene sediments of the equatorial Pacific: their paleomagnetic, biostratigraphic, and climatic record. *Geol. Soc. Am. Bull.*, 80:1481–1514.

Henshaw, P. C., and Merrill, R. T., 1980. Magnetic and chemical changes in marine sediments. *Rev. Geophys. Space Phys.*, 18: 483–504.

Herron, E. M., 1972. Sea-floor spreading and the Cenozoic history of the east central Pacific. *Geol. Soc. Am. Bull.*, 83:1671–1692.

Hoffman, K. A., and Day, R., 1978. Separation of multi-component NRM, a general method. *Earth Planet. Sci. Lett.*, 40:433–438.

Kent, D. V., 1982. Apparent correlation of paleomagnetic intensity and climatic records in deep-sea sediments. *Nature*, 299:538–539.

Kent, D. V., and Lowrie, W., 1974. Origin of magnetic instability in sediment cores from the central North Pacific. *J. Geophys. Res.*, 79:2987–3000.

Kent, D. V., and Spariosu, D. J., 1982a. Magnetostratigraphy of equatorial Pacific Site 503 hydraulic piston cores. *In* Prell, W. L., Gardner, J. V., et al., *Init. Repts. DSDP*, 68: Washington (U.S. Govt. Printing Office), 435–440.

_____, 1982b. Magnetostratigraphy of Caribbean Site 502 hydraulic piston cores. *In* Prell, W. L., Gardner, J. V., et al., *Init. Repts. DSDP*, 68: Washington (U.S. Govt. Printing Office), 419–433.

Kono, M., 1980. Statistics of paleomagnetic inclination data. *J. Geophys. Res.*, 85:3878–3882.

Løvlie, R., 1976. The intensity pattern of post-depositional remnance acquired in some marine sediments deposited during a reversal of the external magnetic field. *Earth Planet. Sci. Lett.*, 30:209–214.

McDougall, I., 1977. *The Present Status of the Geomagnetic Polarity Time Scale:* Austr. Nat. Univ., Res. School Earth Sci. (Canberra), Publ. No. 1288.

Mankinen, E. A., and Dalrymple, G. B., 1979. Revised geomagnetic polarity time scale for the interval 0–5 my B.P. *J. Geophys. Res.*, 84:615–626.

Minster, J. B., Jordan, T. H., Molnar, P., and Haines, E., 1974. Numerical modeling of instantaneous plate tectonics. *Geophys. J. R. Astron. Soc.*, 36:541–576.

Moore, T. C., van Andel, T. H., Sancetta, C., and Pisias, N., 1978. Cenozoic hiatuses in pelagic sediments. *Micropaleontology*, 24: 113–138.

Ness, G., Levi, S., and Couch, R., 1980. Marine magnetic anomaly timescales for the Cenozoic and Late Cretaceous: a precis, critique, and synthesis. *Rev. Geophys. Space Phys.*, 18:753–770.

Opdyke, N. D., 1972. Paleomagnetism of deep-sea cores. *Rev. Geophys. Space Phys.*, 10:213–249.

Opdyke, N. D., Burckle, L. H., and Todd, A., 1974. The extension of the magnetic time scale in sediments of the central Pacific ocean. *Earth Planet. Sci. Lett.*, 22:300–306.

Petersen, N., and Roggenthen, W. M., 1980. Rock- and paleomagnetism of Deep Sea Drilling Project Leg 54 basalts—East Pacific Rise and Galapagos Rift. *In* Rosendahl, B. R., Hekinian, R., et al., *Init. Repts. DSDP*, 54: Washington (U.S. Govt. Printing Office), 865–877.

Sager, W. W., 1983. A late Eocene paleomagnetic pole for the Pacific plate. *Earth Planet. Sci. Lett.*, 63:408–422.

Seyb, S. M., Hammond, S. R., and Gilliard, T., 1977. A new device for recording the behavior of a piston corer. *Deep Sea Res.*, 24: 943–950.

Tauxe, L., Tucker, P., Petersen, N., and LaBrecque, J., 1983. The magnetostratigraphy of Leg 73 sediments. *Palaeogeogr. Palaeclimatol., Palaeoecol.*, 42:65–90.

Theyer, F., and Hammond, S. R., 1974. Cenozoic magnetic time scale in deep-sea sediments: completion of the Neogene. *Geology*, 2: 487–492.

Theyer, F., Mato, C. Y., and Hammond, S. R., 1978. Paleomagnetic and geochronologic calibration of latest Oligocene to Pliocene radiolarian events, equatorial Pacific. *Mar. Micropaleontol.*, 3: 377–395.

Theyer, F., Weinreich, N., and Bleil, U., 1983. Neogene polar wander path for the Pacific: plate motion and field behavior. Internat. Union Geol. Geophys. Gral. Assembly, Hamburg. (Abstract)

van Andel, T. H., Heath, G. R., and Moore, T. C., 1975. Cenozoic history and paleoceanography of the central equatorial Pacific Ocean. *Mem. Geol. Soc. Am.*, 143:1–134.

Winterer, E. L., 1973. Sedimentary facies and plate tectonics of equatorial Pacific. *Am. Assoc. Pet. Geol. Bull.*, 57:265–282.

Zijderveld, J. D. A., 1967. AC demagnetization of rocks: analysis of results. *In* Collison, D. W., Creer, K. M., and Runcorn, S. K. (Eds.), *Methods in Paleomagnetism:* Elsevier (N.Y.), pp. 254–286.

Date of Initial Receipt: 18 August 1983
Date of Acceptance: 4 April 1984

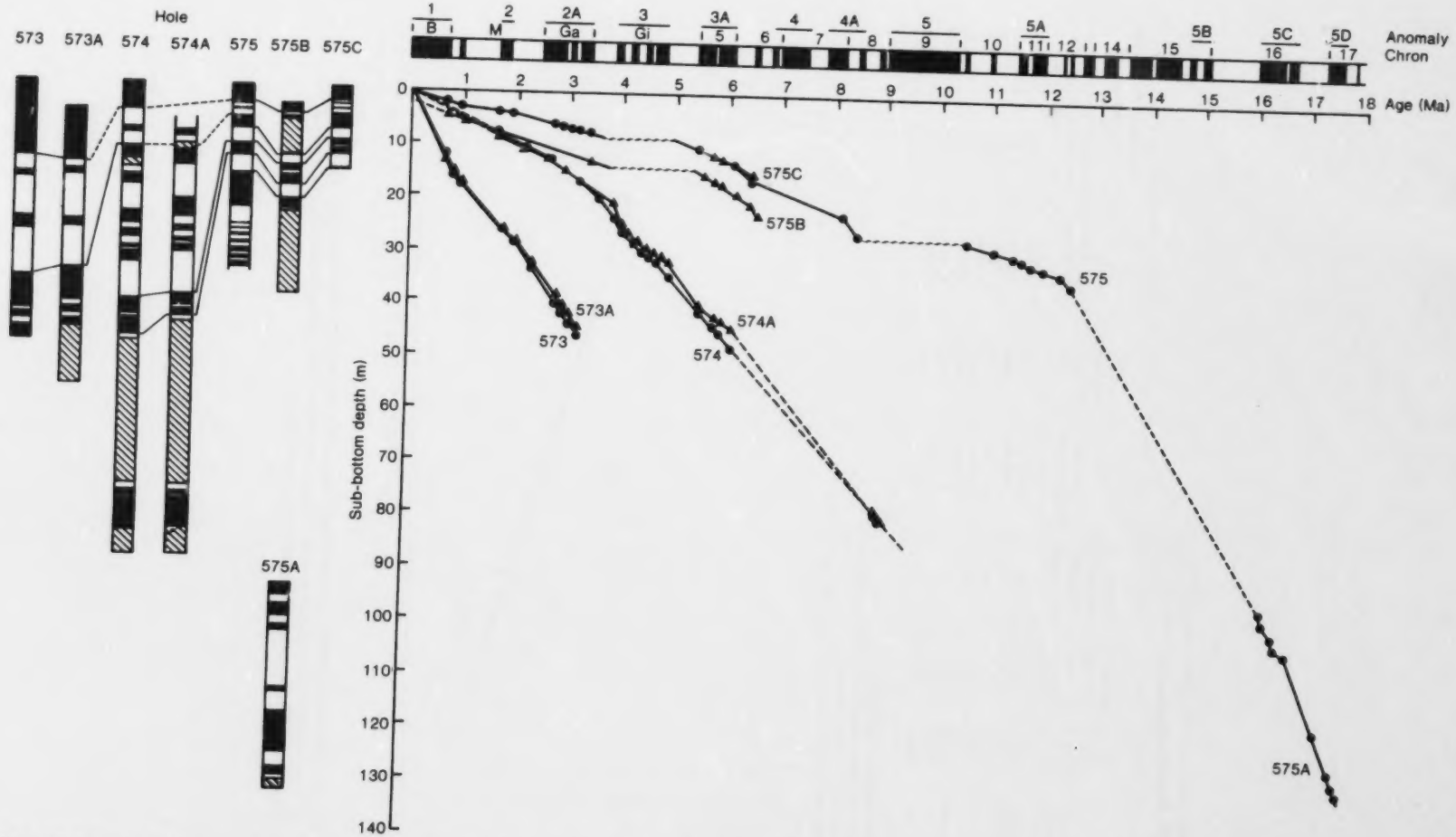

Figure 10. Summary of magnetostratigraphy and sedimentation rates for the sections at Sites 573, 574, and 575. Sediment depth and polarity are plotted against the geomagnetic time scale of Ness et al. (1980). The major marine magnetic anomalies are also shown (Mankinen and Dalrymple, 1979). The circles and triangles in the sedimentation curves distinguish data from different holes. Wavy lines indicate hiatuses. The dashed lines (Sites 574 ar 575) indicate lack of data. Black indicates intervals of normal polarity, white intervals of reversed polarity, and striping intervals that could not be interpreted. B = Brunhes, M = Matuyama, Ga = Gauss, Gi = Gilbert Chron.

Table 5. Summary of tectonic parameters.

Site	Location	Age range (Ma)[a]	Arithmetic mean of age range (Ma)	Number of data used to calculate paleolatitude	Dipole paleolatitude[b]	95% confidence limit (°)[c]	Hotspot paleolatitude[d]	Difference (°) between present site and	
								Dipole paleolatitude	Hotspot paleolatitude
573	0.5°N, 133.3°W	0–3.3	1.7	162	0.81°S	±0.78	0.36°S	1.31	0.86
574	4.2°N, 133.3°W	0–3.4	1.7	74	2.95°N	±0.86	3.43°N	1.25	0.77
		3.4–6.2	4.8	182	1.91°N	±0.66	2.63°N	2.29	1.57
		8.7–10	9.4	58	0.30°N	±1.39	1.15°N	3.90	3.03
575	5.9°N, 135.0°W	0–3.4	1.7	125	4.13°N	±0 58	5.05°N	1.72	0.80
		5–6.4	5.7	102	3.21°N	±1.25	4.04°N	2.64	1.81
		16–18	17.0	50	0.06°N	±1.67	1.70°N	5.79	4.15

[a] Age range used for tectonic calculations.
[b] Calculated by using the dipole formula and Kono's (1980) statistics.
[c] Calculated by using Kono's (1980) method.
[d] Calculated by using Epp's (1978) rotation poles for the Pacific Plate.

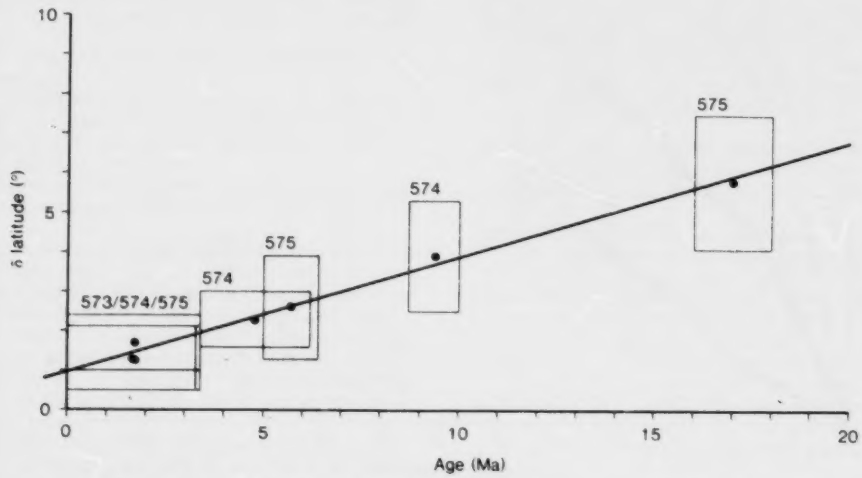

Figure 11. Delta latitude (site's present latitude minus its paleolatitude) versus age (Ma). Boxes represent the size of the error in latitude (which is based on Kono's [1980] statistics [Table 5]) and range of the error in age. The solid line is the regression curve (Table 5).

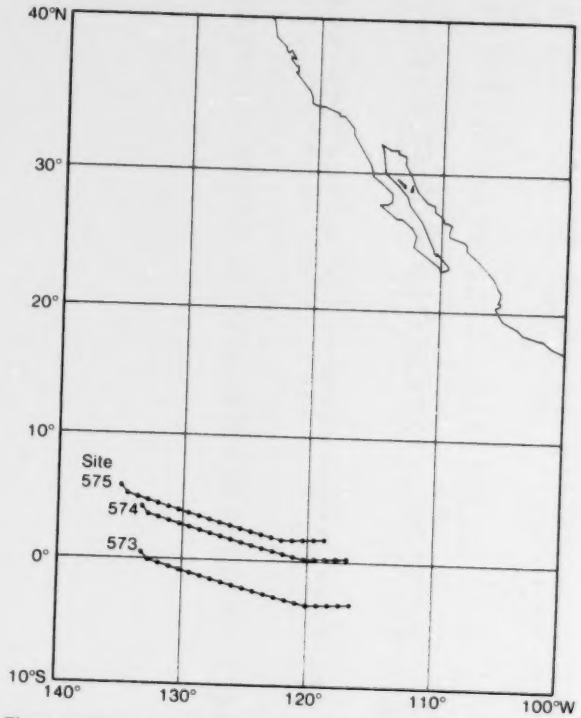

Figure 12. Stereographic projection of the migration of Sites 573, 574 and 575. Site positions (in 1-m.y. steps) were calculated by using the rotation poles for the Pacific Plate that Epp (1978) derived from the movement of Pacific island chains.

Table 6. Pliocene to early Miocene paleo-pole positions for the Pacific Plate derived from Leg 85 sites and HIG piston cores, using the method of Gordon and Cox (1980).

Number of DSDP site or HIG piston core	Present longitude, latitude	Age range used to calculate pole position (Ma)	Paleo-pole position	dp[a]	dm[a]	Number of samples
573	0.5°N, 133.3°W	0–3.3				
574	4.2°N, 133.3°W	0–6.2				
575	5.9°N, 135.0°W	0–6.4	87.9°N, 59.6°E	0.9°	3.3°	106
K78-5-11	7.5°N, 169.7°W	1.7–5.3				
K76-1-07	2.8°S, 177.9°E	3–4.8				
574	4.2°N, 133.3°W	8.7–10				
K76-1-11	0.9°N, 178.6°W	8–11	85.1°N, 4.7°E	2.3°	4.2°	71
K76-1-17	4.6°N, 176.6°W	8–11.5				
575	5.9°N, 135.0°W	16–18				
K78-5-18	8.7°N, 166.9°W	15–18	79.5°N, 31.7°W	2.9°	7.0°	35
K72-36	2.4°S, 177.8°W	16–19				

[a] Semi-axes of the 95% oval for the calculated pole position.

Figure 13. Apparent polar wander path determined on the basis of Leg 85 and HIG piston core paleomagnetic data. Poles and their 95% ovals are calculated for three time intervals (0 to 6 Ma, 8 to 11 Ma, 16 to 18 Ma) using the method of Gordon and Cox (1980). Crosses show HIG locations (Table 6), and triangles indicate Sites 573 to 575.

APPENDIX A
Paleomagnetic Data Derived from Late Miocene to Recent Leg 85 Samples (samples were measured at RUB)

Core-Section (interval in cm)	Sub-bottom depth (m)	J_{NRM} (G)	I_{NRM}	D_{NRM}	I_{stable}	D_{stable}	Polarity	MDF (Oe)
Hole 573								
1-1, 30–32	0.31	3.83 E-6	+12.0	343.1	+12.1	343.7	N	498
1-1, 70–72	0.71	1.19 E-6	+8.8	343.2	+7.2	343.4	N	388
1-1, 111–113	1.12	1.20 E-6	+0.0	17.3	+1.5	16.2	N	350
1-2, 20–22	1.71	4.43 E-6	+0.7	15.8	+0.1	16.0	N	281
2-1, 145–147	3.46	2.35 E-6	+0.3	282.2	−2.3	283.8	N	382
2-2, 38–40	3.89	5.40 E-6	+0.3	319.0	+2.6	318.8	N	347
2-2, 95–97	4.46	4.12 E-6	−7.3	338.7	−5.6	337.7	N	275
2-2, 145–147	4.96	1.09 E-6	−4.5	343.3	−6.4	341.7	N	411
2-3, 38–40	5.39	1.26 E-6	−9.4	357.3	−11.4	359.0	N	374
2-3, 95–97	5.96	1.43 E-6	+0.9	14.2	+4.0	10.2	N	308
2-3, 145–147	6.46	7.78 E-7	+0.8	12.5	+11.6	29.7	N	300
2-4, 36–38	6.87	1.06 E-6	−11.7	352.2	−3.9	349.0	N	325
2-4, 95–97	7.46	2.75 E-6	−48.4	356.8	−49.9	349.2	N	265
2-4, 145–147	7.96	4.14 E-7	+7.7	322.7	+10.6	318.7	N	389
2-5, 36–38	8.37	2.00 E-7	+59.0	13.5	+58.0	5.4	N	>400
2-5, 95–97	8.96	5.32 E-7	−3.3	351.7	+12.7	359.2	N	233
2-5, 143–145	9.44	5.11 E-7	−9.7	343.3	+3.3	341.3	N	399
2-6, 36–38	7.87	1.45 E-6	−5.8	319.8	−5.1	319.6	N	330
2-6, 95–97	10.46	2.80 E-6	−4.1	324.6	−3.4	324.1	N	310
2-6, 138–140	10.89	1.56 E-6	+0.9	314.7	+3.1	314.8	N	309
2-7, 36–38	11.37	2.47 E-6	−9.9	314.0	−7.9	315.2	N	345
3-1, 8–10	11.59	8.23 E-7	+3.6	308.0	+7.4	307.2	N	378
3-1, 68–70	12.19	1.11 E-6	−0.0	308.7	−0.8	308.9	N	371
3-1, 125–127	12.76	4.28 E-6	−2.1	355.3	−2.5	354.6	N	297
3-1, 146–148	12.97	5.07 E-6	+0.6	323.3	−1.9	1.8	N	176
3-2, 35–37	13.36	9.23 E-7	−20.6	189.8	−5.7	185.9	R	559
3-2, 85–87	13.86	1.02 E-6	−13.6	193.6	−12.5	193.4	R	499
3-2, 135–137	14.36	4.77 E-7	+3.6	129.3	+52.3	189.0	R	466
3-3, 35–37	14.86	5.04 E-7	−7.3	196.8	+0.2	189.4	R	390
3-3, 85–87	15.36	9.97 E-7	−4.6	213.1	+5.6	202.7	R	463
3-3, 135–137	15.86	1.06 E-6	+13.7	212.1	+32.4	212.1	R	472
3-4, 35–37	16.36	5.89 E-7	−30.5	265.4	−20.6	211.0	R	368
3-4, 85–87	16.86	8.03 E-7	−29.3	271.8	−24.2	264.4	N	338
3-4, 135–137	17.36	7.90 E-7	−22.5	261.4	−18.1	255.6	N	365
3-5, 6–8	17.57	4.06 E-7	−14.4	303.5	−19.9	221.0	R	198
3-5, 35–37	17.86	3.20 E-7	−20.6	209.1	−12.8	191.2	R	397
3-5, 85–87	18.36	9.21 E-7	+22.1	154.7	+5.5	128.6	R	478
3-5, 135–137	18.86	1.82 E-6	+2.5	131.9	+5.0	133.0	R	399
3-6, 35–37	19.36	2.51 E-6	−0.4	128.9	−0.2	130.5	R	347
3-6, 85–87	19.86	4.30 E-6	−9.2	138.2	−3.1	138.0	R	361
3-6, 135–137	20.36	1.25 E-6	+6.4	148.0	+12.6	144.1	R	433
4-1, 101–103	22.02	2.72 E-6	−7.4	265.9	−7.1	265.2	R	420
4-1, 144–146	22.45	5.00 E-7	−32.9	242.2	−12.4	248.4	R	572
4-2, 35–37	22.86	1.71 E-6	−2.0	234.8	−1.9	234.0	R	386
4-2, 87–89	23.38	1.11 E-6	+6.1	225.9	+8.1	225.2	R	408
4-2, 135–137	23.86	3.19 E-6	−2.1	213.5	−3.4	208.7	R	388
4-3, 8–10	24.09	2.05 E-6	+6.8	204.4	+6.0	200.5	R	364
4-3, 35–37	24.36	1.25 E-6	+13.3	194.0	+8.4	191.6	R	398
4-3, 87–89	24.88	5.77 E-7	+1.2	179.3	+4.0	184.7	R	454
4-3, 135–137	25.36	2.61 E-6	+0.5	359.5	−4.1	7.5	N	154
4-4, 35–37	25.86	4.55 E-6	+4.0	349.0	+3.3	349.8	N	260
4-4, 87–89	26.38	2.25 E-6	+6.2	349.6	+4.6	347.5	N	256
4-4, 135–137	26.86	3.90 E-6	−7.0	333.7	−5.3	335.4	N	248
4-5, 35–37	27.36	1.98 E-7	+20.3	184.4	+5.0	161.2	R	>700
4-5, 82–84	27.83	1.13 E-6	+13.4	176.7	+5.8	148.6	R	456
4-5, 135–137	28.36	1.01 E-6	+1.2	153.3	+7.2	155.9	R	384
4-6, 35–37	28.86	2.30 E-6	+1.6	144.4	+5.2	143.4	R	441
4-6, 87–89	29.38	1.70 E-6	+11.7	142.8	+0.8	141.9	R	432
4-6, 135–137	29.86	1.21 E-6	−6.8	134.3	+2.9	135.8	R	473
4-7, 5–7	30.06	1.61 E-6	+2.3	132.3	+5.5	135.4	R	369
4-7, 32–34	30.33	9.87 E-7	+17.4	141.9	+13.6	143.3	R	426
5-1, 25–27	30.76	9.86 E-7	−17.9	18.5	−16.7	19.6	R	449
5-1, 84–86	31.35	1.46 E-6	−1.3	49.3	−0.7	51.5	R	393
5-1, 141–143	31.92	1.23 E-6	+1.9	81.5	+3.9	80.8	R	403
5-2, 25–27	32.26	1.11 E-6	+15.2	94.3	+4.2	100.3	R	487
5-2, 84–86	32.85	1.18 E-6	+23.8	116.0	+10.4	122.2	R	537
5-2, 141–143	33.42	4.73 E-7	+7.0	144.6	+5.4	144.8	R	422
5-3, 22–24	33.73	1.09 E-6	+4.7	148.3	+2.4	148.0	R	415

Appendix A. (Continued).

Core-Section (interval in cm)	Sub-bottom depth (m)	J_{NRM} (G)	I_{NRM}	D_{NRM}	I_{stable}	D_{stable}	Polarity	MDF (Oe)
Hole 573 (Cont.)								
5-3, 93–95	34.44	1.32 E-6	+15.3	165.4	+8.1	168.4	R	388
5-3, 137–139	34.88	2.29 E-6	−0.7	178.1	−1.9	180.1	R	440
5-4, 31–33	35.32	1.47 E-6	+42.8	199.3	+16.2	193.1	R	583
5-4, 85–87	35.86	4.52 E-6	+7.9	200.7	+6.5	200.9	R	485
5-4, 127–129	36.28	3.69 E-6	−1.0	24.9	−2.9	25.1	N	471
5-5, 23–25	36.74	2.33 E-6	+4.5	23.8	+0.2	26.8	N	263
5-5, 85–87	37.36	2.15 E-6	−7.7	27.9	−3.7	29.6	N	218
5-5, 127–129	37.78	4.09 E-6	−2.6	30.9	+0.4	33.1	N	260
5-6, 6–8	38.07	7.06 E-7	+9.2	19.3	−6.3	30.3	N	142
5-6, 32–34	38.33	3.51 E-6	−6.3	32.3	−11.0	30.5	N	164
5-6, 85–87	38.86	1.95 E-6	−1.3	38.7	−3.1	38.5	N	191
6-1, 128–130	40.59	2.12 E-6	−0.7	14.7	+3.0	16.6	N	235
6-2, 22–24	41.03	2.80 E-6	−11.6	32.7	−10.9	31.8	N	226
6-2, 72–74	41.53	2.65 E-6	−2.7	19.4	−3.7	17.2	N	232
6-2, 122–124	42.03	2.01 E-6	−6.4	16.4	−11.8	14.9	N	201
6-2, 146–148	42.27	7.91 E-7	−1.2	203.6	+3.7	197.8	R	>500
6-3, 22–24	42.53	2.12 E-7	−46.6	63.6	−1.6	190.4	R	>1000
6-3, 83–85	43.14	9.83 E-7	+10.7	8.8	+69.5	84.3	R	63
6-3, 105–107	43.36	4.89 E-6	−3.3	2.8	−1.1	1.4	N	268
6-3, 135–137	43.66	3.36 E-6	−0.3	7.1	+6.2	9.0	N	177
6-4, 22–24	44.03	3.13 E-6	−2.0	2.5	−4.3	1.0	N	208
6-4, 73–75	44.54	9.15 E-7	+31.3	174.1	+14.3	180.5	R	391
6-4, 105–107	44.86	6.15 E-7	+32.1	175.5	+15.0	179.1	R	494
6-4, 135–137	45.16	2.63 E-6	+6.7	177.7	+3.3	178.8	R	384
6-4, 147–149	45.28	3.46 E-6	+0.9	173.7	−0.3	171.2	R	352
6-5, 12–14	45.43	4.32 E-8	+46.0	134.4	+46.2	113.9	R	>200
6-5, 61–63	45.92	6.56 E-8	+7.5	350.7	+32.4	356.9	N	>200
6-5, 114–116	46.45	3.27 E-7	+55.3	331.4	+53.0	332.4	N	223
6-6, 12–14	46.93	2.18 E-8	+18.8	12.4	+24.9	2.1	N	98
6-6, 57–59	47.38	1.59 E-7	−47.6	65.7	−38.9	68.7	N	>300
6-6, 112–114	47.93	1.77 E-7	−41.5	40.8	−38.8	38.2	N	189
Hole 573A								
1-1, 113–115	5.64	1.82 E-6	−6.2	203.5	−5.8	8.3	N	169
1-1, 138–140	5.89	8.74 E-7	+0.9	58.0	−2.6	54.4	N	408
1-2, 20–22	6.21	1.56 E-6	+9.1	36.7	+10.2	33.9	N	385
1-2, 94–96	6.95	5.37 E-6	−4.4	49.9	−2.1	48.6	N	332
1-3, 27–29	7.78	3.95 E-6	−3.3	50.3	−3.7	49.9	N	455
1-3, 90–92	8.41	3.94 E-6	+5.4	46.1	+7.6	44.4	N	270
1-4, 45–47	9.46	6.09 E-6	+2.3	28.8	+1.2	27.1	N	257
1-4, 105–107	10.06	1.22 E-6	+2.8	3.3	+2.6	2.6	N	302
1-5, 45–47	10.96	4.02 E-6	−1.1	350.4	+0.9	350.8	N	303
1-5, 105–107	11.56	1.48 E-6	+5.7	334.6	+5.6	334.4	N	373
1-6, 45–47	12.46	1.64 E-6	+8.2	309.1	+8.7	309.1	N	337
1-6, 105–107	13.06	1.14 E-6	+6.2	302.9	−0.1	302.4	N	358
1-7, 5–7	13.56	5.30 E-6	+2.9	300.6	+3.5	301.2	N	292
1-7, 29–31	13.80	2.46 E-6	+1.4	298.1	−1.0	298.6	N	241
2-1, 11–13	14.12	1.03 E-6	+4.1	354.7	+12.9	353.9	N	326
2-1, 37–39	14.38	7.13 E-7	+59.3	315.4	+61.8	322.0	N	396
2-1, 63–65	14.64	1.03 E-6	+81.8	245.3	+80.2	270.1	R	371
2-1, 87–89	14.88	6.17 E-7	+32.3	158.4	+19.2	161.8	R	567
2-1, 115–117	15.16	3.28 E-7	+23.2	152.6	+0.3	180.3	R	747
2-1, 138–140	15.39	2.32 E-6	+4.1	182.9	+4.1	183.7	R	654
2-2, 27–29	15.78	2.30 E-7	+76.9	318.5	+13.7	200.4	R	>1000
2-2, 47–49	15.98	2.30 E-6	+7.1	7.8	+8.0	6.0	N	169
2-2, 67–69	16.18	1.95 E-6	+6.5	14.6	+9.3	15.2	N	219
2-2, 112–114	16.63	6.43 E-6	+0.5	11.6	+1.9	11.9	N	276
2-2, 144–146	16.95	1.50 E-7	+45.6	192.5	+16.0	197.7	R	>500
2-3, 9–11	17.10	2.99 E-7	+29.9	230.3	+10.9	199.5	R	>500
2-3, 27–29	17.28	1.62 E-7	+35.8	33.2	+11.2	192.6	R	>600
2-3, 43–45	17.44	2.74 E-7	+46.9	34.6	+8.3	191.2	R	>500
2-3, 67–69	17.68	9.23 E-7	+21.3	353.3	+7.6	189.5	R	658
2-3, 112–114	18.13	1.54 E-6	+3.2	4.9	+62.9	215.8	R	86
2-4, 27–29	18.78	2.49 E-6	+2.7	186.0	+2.9	186.7	R	384
2-4, 67–69	19.18	2.46 E-6	+1.4	178.3	+2.4	181.2	R	360
2-4, 112–114	19.63	4.09 E-6	−4.2	183.5	−0.7	182.6	R	398
2-5, 27–29	20.28	8.83 E-7	+9.9	176.3	+8.8	178.8	R	365
2-5, 67–69	20.68	1.15 E-6	−8.4	178.8	−4.0	177.7	R	389

Appendix A. (Continued).

Core-Section (interval in cm)	Sub-bottom depth (m)	J_{NRM} (G)	I_{NRM}	D_{NRM}	I_{stable}	D_{stable}	Polarity	MDF (Oe)
Hole 573A (Cont.)								
2-5, 112–114	21.13	1.18 E-6	+17.4	159.6	+11.3	170.8	R	542
2-6, 25–27	21.76	2.21 E-6	+1.3	163.2	+2.0	167.1	R	478
3-1, 53–55	22.64	3.07 E-6	−19.4	212.0	−23.5	212.2	R	407
3-1, 88–90	22.99	9.93 E-7	+10.0	194.6	+10.6	195.1	R	412
3-1, 135–137	23.46	2.85 E-7	−17.0	203.2	+1.8	191.0	R	534
3-2, 17–19	23.78	1.34 E-6	−2.4	188.3	+2.9	187.6	R	426
3-2, 117–119	24.78	1.57 E-6	+11.1	159.7	+6.3	166.4	R	414
3-3, 16–18	25.27	2.24 E-7	−62.9	114.4	−45.6	180.6	R	584
3-3, 36–38	25.47	2.19 E-6	+7.8	339.0	+1.3	338.7	N	79
3-3, 57–59	25.68	2.87 E-6	−15.5	338.3	−14.1	340.8	N	197
3-3, 116–118	26.27	1.98 E-6	−5.0	343.9	−5.0	347.5	N	187
3-3, 146–148	26.57	3.59 E-6	-12.1	347.3	−13.0	346.1	N	217
3-4, 11–13	26.72	2.28 E-6	+6.5	346.1	+7.2	342.9	N	64
3-4, 35–37	26.96	7.99 E-7	−55.0	71.6	−19.4	160.3	R	452
3-4, 71–73	27.32	1.98 E-6	+3.5	182.7	−1.0	174.2	R	383
3-4, 103–105	27.64	9.47 E-7	+19.3	156.9	+7.2	164.1	R	365
3-4, 138–140	27.99	1.51 E-6	+10.6	180.1	+5.7	172.9	R	352
3-5, 35–37	28.46	2.01 E-6	+12.2	176.6	+5.5	171.0	R	438
3-5, 71–73	28.82	2.01 E-6	−8.3	161.6	−6.9	169.5	R	416
3-5, 103–105	29.14	8.40 E-7	−60.5	102.8	−16.1	177.8	R	494
3-5, 137–139	29.48	1.17 E-6	−16.8	185.5	−3.8	182.2	R	444
3-6, 35–37	29.96	1.22 E-6	−8.5	206.8	+4.8	199.0	R	366
3-6, 71–73	30.32	1.71 E-6	+4.1	191.7	−0.2	199.1	R	478
3-6, 113–115	30.74	8.73 E-7	−11.3	217.4	−20.9	203.8	R	399
4-1, 83–85	32.14	3.23 E-7	−20.7	217.7	−10.9	219.3	R	451
4-1, 131–133	32.62	3.96 E-7	−3.7	15.8	+10.1	187.4	R	71
4-2, 5–7	32.86	3.20 E-7	+0.9	207.8	+1.7	197.9	R	536
4-2, 32–34	33.13	6.14 E-7	+7.6	198.3	+3.2	200.1	R	440
4-2, 83–85	33.64	5.71 E-7	+14.6	183.4	+14.5	185.9	R	387
4-2, 131–133	34.12	2.24 E-6	+11.6	180.6	+8.4	182.2	R	473
4-3, 5–7	34.36	2.43 E-6	+6.0	177.7	+1.2	180.6	R	490
4-3, 32–34	34.63	1.05 E-6	+6.3	166.3	+7.8	168.1	R	554
4-3, 57–59	34.88	3.49 E-6	+2.3	168.5	+1.6	167.7	R	471
4-3, 83–85	35.14	2.99 E-6	−4.5	348.6	−8.4	350.8	N	275
4-3, 131–133	35.62	2.40 E-6	+1.2	339.3	+0.1	345.3	N	238
4-4, 32–34	36.13	1.43 E-6	−3.7	0.8	−2.5	355.4	N	188
4-4, 83–85	36.64	8.16 E-7	+7.8	341.0	+0.8	352.2	N	93
4-4, 131–133	37.12	2.39 E-6	−0.5	354.2	+0.9	353.2	N	308
4-5, 32–34	37.63	1.73 E-6	+4.3	348.8	−1.2	349.7	N	175
4-5, 83–85	38.14	2.32 E-6	+10.2	350.4	+4.0	357.0	N	185
4-5, 131–133	38.62	2.71 E-6	−9.1	355.0	+1.2	351.4	N	232
4-6, 32–34	39.13	2.76 E-6	−3.1	354.2	+3.5	349.1	N	250
4-6, 83–85	39.64	3.07 E-6	+6.1	349.2	+11.1	353.2	N	242
5-1, 98–100	40.79	4.30 E-6	−17.1	14.4	−18.1	11.6	N	232
5-1, 130–132	41.11	1.31 E-6	+20.5	211.1	+7.9	201.9	R	551
5-2, 25–27	41.56	1.21 E-6	+5.4	174.0	+1.4	181.3	R	421
5-2, 68–70	41.99	7.47 E-7	−3.5	8.0	+12.9	187.2	R	32
5-2, 113–115	42.44	3.87 E-6	−1.7	6.0	−2.6	3.0	N	200
5-2, 146–148	42.77	6.50 E-6	+2.8	354.8	+3.8	356.8	N	267
5-3, 25–27	43.06	1.15 E-6	−1.3	9.2	+20.5	4.7	N	40
5-3, 68–70	43.49	1.38 E-6	+13.4	160.1	+14.1	168.8	R	363
5-3, 113–115	43.94	2.71 E-6	−6.0	181.3	−1.9	179.5	R	447
5-3, 136–138	44.17	3.31 E-6	+6.0	181.3	+3.3	179.9	R	383
5-3, 143–145	44.24	3.51 E-6	+17.0	171.6	+15.2	176.8	R	439
5-4, 45–47	44.76	7.14 E-8	+14.8	2.4	no stable			399
5-4, 131–133	45.62	6.23 E-8	−15.1	6.5	no stable			277
5-5, 51–53	46.32	3.96 E-8	+58.7	283.8	no stable			
5-5, 115–117	46.96	2.60 E-8	+74.3	345.5	no stable			
5-6, 8–10	47.39	1.04 E-7	+35.3	1.4	no stable			
5-6, 90–92	48.21	6.26 E-8	+8.9	118.5	no stable			
6-1, 65–67	49.86	4.45 E-7	−8.8	177.2	no stable			105
6-2, 61–63	51.32	9.76 E-8	+71.4	254.1	no stable			31
6-3, 81–83	53.02	3.52 E-8	+57.0	289.6	no stable			
6-4, 58–60	54.29	2.96 E-8	−42.6	294.0	no stable			
6-5, 90–92	56.11	1.05 E-7	+82.6	336.5	no stable			
6-6, 18–20	56.89	2.15 E-8	+15.8	323.0	no stable			
Hole 574								
1-1, 79–81	0.80	4.54 E-6	−1.5	16.2	+0.9	14.0	N	250
1-1, 129–131	1.30	3.37 E-6	+6.2	16.0	+5.5	13.9	N	201

Appendix A. (Continued).

Core-Section (interval in cm)	Sub-bottom depth (m)	J_{NRM} (G)	I_{NRM}	D_{NRM}	I_{stable}	D_{stable}	Polarity	MDF (Oe)
Hole 574 (Cont.)								
1-2, 29-31	1.80	5.51 E-6	+12.0	5.5	+12.4	1.6	N	156
1-2, 54-56	2.05	4.39 E-6	+11.1	4.2	+6.8	1.0	N	147
1-2, 104-106	2.55	4.72 E-6	+2.8	0.7	−0.6	356.7	N	196
1-2, 129-131	2.80	5.75 E-6	+15.0	336.5	+13.6	348.9	N	225
1-3, 4-6	3.05	3.10 E-6	+4.9	12.1	+5.6	11.3	N	198
1-3, 29-31	3.30	6.61 E-6	+0.1	355.5	+5.5	353.8	N	216
1-3, 54-56	3.55	4.20 E-6	+24.4	351.5	+9.5	352.9	N	95
1-3, 79-81	3.80	4.21 E-6	+7.1	355.3	+6.0	347.2	N	131
1-3, 104-106	4.05	1.14 E-6	−7.2	38.5	+10.6	351.5	N	464
1-3, 129-131	4.30	1.78 E-6	+7.2	345.9	+8.9	350.8	N	280
2-1, 14-16	4.65	2.93 E-6	−68.5	242.7	−79.5	231.4	R	290
2-1, 37-39	4.88	2.27 E-7	−63.2	277.8	+28.9	261.0	R	19
2-1, 67-69	5.18	2.05 E-6	+18.9	202.1	−28.9	164.1	R	285
2-1, 94-96	5.45	2.34 E-6	+2.9	149.0	−0.1	151.3	R	418
2-1, 119-121	5.70	2.73 E-6	−3.8	157.4	−3.3	161.0	R	508
2-2, 4-6	6.05	1.13 E-6	−8.4	328.9	−2.2	167.5	R	510
2-2, 29-31	6.30	2.06 E-6	−5.6	165.5	−6.1	165.9	R	388
2-2, 54-56	6.55	3.37 E-6	+3.4	176.5	−2.4	172.3	R	434
2-2, 79-81	6.80	1.58 E-6	+4.0	152.5	−1.3	166.0	R	468
2-2, 104-106	7.05	1.53 E-6	−1.0	172.0	−2.5	171.9	R	429
2-2, 129-131	7.30	5.01 E-7	+2.8	163.3	+8.7	179.7	R	521
2-3, 4-6	7.55	1.28 E-6	−0.2	178.1	−7.9	179.0	R	442
2-3, 29-31	7.80	1.60 E-6	−14.3	164.7	−12.4	174.2	R	421
2-3, 54-56	8.05	3.84 E-6	19.7	9.6	+5.8	10.7	N	121
2-3, 79-81	8.30	5.66 E-6	+9.7	10.3	+9.1	11.1	N	161
2-3, 104-106	8.55	5.73 E-6	+10.4	3.9	+12.6	4.9	N	173
2-3, 129-131	8.80	5.68 E-6	+5.4	8.0	+8.4	12.3	N	171
2-4, 4-6	9.05	9.31 E-7	−12.4	184.2	−5.7	185.6	R	467
2-4, 29-31	9.30	8.64 E-7	+0.3	193.7	−1.6	181.3	R	456
2-4, 54-56	9.55	2.19 E-6	+3.2	195.1	−4.9	185.2	R	398
2-4, 79-81	9.80	4.39 E-7	−29.7	354.7	−6.6	183.5	R	552
2-4, 104-106	10.05	1.57 E-6	−10.7	185.5	−9.8	185.2	R	416
2-4, 129-131	10.30	1.91 E-6	−31.5	186.4	−15.8	184.3	R	392
2-5, 4-6	10.55	1.16 E-6	+5.8	182.0	−6.8	184.1	R	440
2-5, 29-31	10.80	3.12 E-7	+9.3	168.8	−8.6	180.1	R	560
2-5, 54-56	11.05	5.70 E-7	+20.6	214.9	+8.3	179.0	R	599
2-5, 79-81	11.30	5.49 E-7	−4.5	177.8	−9.6	178.0	R	493
2-5, 104-106	11.55	2.64 E-6	+0.8	152.6	+1.5	161.1	R	431
2-5, 129-131	11.80	6.73 E-7	+14.5	5.8	+45.5	38.7	N	49
2-6, 4-6	12.05	2.05 E-6	+11.3	1.2	+8.8	14.0	N	144
2-6, 29-31	12.30	2.09 E-6	+14.0	10.9	+14.3	13.0	N	186
2-6, 54-56	12.55	2.61 E-6	+3.6	357.9	+16.7	3.6	N	74
2-6, 79-81	12.80	4.06 E-6	+8.1	9.2	+3.1	13.2	N	75
2-6, 104-106	13.05	5.25 E-6	+10.8	359.2	+13.8	8.1	N	135
2-6, 129-131	13.30	7.02 E-6	+5.2	8.7	+4.6	11.0	N	159
2-7, 4 6	13.55	6.30 E-6	+5.4	18.1	+6.4	23.1	N	103
2-7, 29-31	13.80	5.80 E-6	+11.1	15.9	+15.7	17.4	N	95
3-1, 75-77	14.76	9.45 E-6	−86.2	249.2	−85.0	217.7	R	274
3-1, 97-99	14.98	5.15 E-7	+11.2	321.5	-29.5	254.8	R	348
3-1, 118-120	15.19	1.74 E-6	−39.0	330.4	−41.8	295.1	R	217
3-2, 16-18	15.67	1.83 E-6	−17.8	126.3	−6.1	137.2	R	388
3-2, 87-89	16.38	2.81 E-6	−80.5	130.1	−78.2	125.5	R	321
3-2, 136-138	16.87	1.25 E-6	−61.8	65.3	−30.0	60.4	N	315
3-3, 15-17	17.16	1.67 E-6	+14.6	332.3	+6.2	305.9	N	88
3-3, 39-41	17.40	2.49 E-6	+11.6	352.8	+9.8	351.8	N	208
3-3, 112-114	18.13	3.34 E-6	−66.3	335.4	−68.8	346.5	N	300
3-3, 136-138	18.37	1.06 E-6	−46.2	231.8	−49.5	210.9	R	299
3-4, 8-10	18.59	2.20 E-6	−67.4	115.9	−63.7	136.2	R	284
3-4, 29-31	18.80	6.45 E-7	−18.0	147.6	−4.6	148.5	R	449
3-4, 54-56	19.05	1.52 E-6	+2.5	146.0	+5.3	152.3	R	462
3-4, 79-81	19.30	1.16 E-6	+0.7	153.9	+3.7	160.4	R	418
3-4, 104-106	19.55	2.62 E-7	+79.6	239.4	+4.6	162.6	R	>1000
3-4, 129-131	19.80	9.06 E-7	−5.5	159.9	−2.2	164.0	R	498
3-5, 4-6	20.05	1.13 E-6	−3.0	144.1	−1.5	165.3	R	443
3-5, 29-31	20.30	2.41 E-6	+8.2	179.6	+2.7	180.4	R	424
3-5, 54-56	20.55	1.54 E-6	1.3	171.5	+0.1	177.6	R	384
3-5, 75-77	20.76	1.99 E-6	+2.9	181.4	−0.9	181.0	R	390
3-5, 104-106	21.05	1.87 E-6	+0.7	179.2	−4.9	178.0	R	396
3-5, 129-131	21.30	6.86 E-7	+8.4	133.4	−3.1	179.0	R	495
3-6, 4-6	21.55	1.51 E-6	+5.3	174.6	−0.6	189.5	R	437
3-6, 29-31	21.80	1.67 E-6	−12.3	186.2	−8.7	191.0	R	449
3-6, 54-56	22.05	1.42 E-6	−4.5	193.1	−5.3	197.4	R	401
3-6, 79-81	22.30	2.39 E-6	−13.6	180.0	−8.9	190.3	R	424

Appendix A. (Continued).

Core-Section (interval in cm)	Sub-bottom depth (m)	J_{NRM} (G)	I_{NRM}	D_{NRM}	I_{stable}	D_{stable}	Polarity	MDF (Oe)
Hole 574 (Cont.)								
3-6, 104–106	22.55	1.17 E-6	−5.7	193.5	+0.8	202.2	R	500
3-6, 129–131	22.80	1.06 E-6	+57.8	86.5	+6.3	207.7	R	487
3-7, 4–6	23.05	7.27 E-7	−44.5	193.2	−4.8	202.9	R	532
3-7, 29–31	23.30	4.60 E-7	+4.3	105.3	−10.0	204.2	R	694
4-1, 12–14	23.63	6.45 E-6	−80.7	40.9	−75.0	62.9	N	307
4-1, 50–52	24.01	7.09 E-7	−1.3	50.2	−18.8	35.3	N	267
4-1, 91–93	24.42	2.76 E-7	−2.4	13.5	−3.0	7.8	N	287
4-1, 123–125	24.74	9.82 E-7	+18.5	18.9	+10.1	27.2	N	273
4-2, 15–17	25.16	2.36 E-6	+13.5	17.1	+1.8	28.5	N	142
4-2, 48–50	25.49	1.29 E-6	+21.0	15.2	+17.5	17.2	N	176
4-2, 85–87	25.86	2.37 E-6	+64.3	345.8	+44.0	13.0	N	304
4-2, 102–104	26.03	8.50 E-7	−31.9	320.1	−22.3	133.9	R	341
4-3, 6–8	26.57	9.37 E-7	+35.5	332.7	−15.8	164.0	R	23
4-3, 64–66	27.15	3.66 E-7	+39.2	226.8	−1.0	172.3	R	676
4-3, 89–91	27.40	7.21 E-7	+49.7	15.9	+3.2	164.5	R	378
4-3, 114–116	27.65	5.37 E-6	+6.1	350.0	+4.8	355.6	N	130
4-3, 139–141	27.90	5.10 E-6	+8.8	350.2	+4.9	351.2	N	189
4-4, 4–6	28.05	4.91 E-6	+4.5	354.3	+5.9	358.1	N	235
4-4, 29–31	28.30	4.47 E-6	+5.3	348.6	+7.2	354.9	N	159
4-4, 54–56	28.55	6.05 E-6	+4.7	346.3	+2.9	350.2	N	188
4-4, 79–81	28.80	5.49 E-7	+42.6	2.8	+14.2	169.4	R	48
4-4, 104–106	29.05	1.16 E-6	+51.5	178.3	+7.1	173.1	R	393
4-4, 129–131	29.30	3.06 E-7	+32.6	231.9	+8.8	176.5	R	699
4-5, 4–6	29.55	2.54 E-7	+70.0	201.3	+10.4	182.8	R	699
4-5, 29–31	29.80	5.82 E-7	+62.0	125.9	+4.8	173.5	R	499
4-5, 54–56	30.05	1.33 E-6	+22.1	186.4	−4.9	183.0	R	403
4-5, 79–81	30.30	7.84 E-7	+11.7	167.6	−2.4	185.9	R	476
4-5, 104–106	30.55	4.08 E-6	+4.5	357.4	−2.2	3.5	N	86
4-5, 129–131	30.80	5.74 E-6	+7.8	0.6	+7.0	8.1	N	160
4-6, 4–6	31.05	1.34 E-6	+25.6	332.0	+17.4	191.9	R	47
4-6, 29–31	31.30	7.32 E-7	+25.0	308.0	+13.5	193.9	R	>500
4-6, 54–56	31.55	1.40 E-6	+6.7	359.4	+14.8	352.4	N	56
4-6, 79–81	31.80	4.78 E-6	+5.1	6.3	+8.5	9.8	N	205
44-6, 104–106	32.05	3.09 E-6	+1.6	0.8	+4.2	9.1	N	121
4-6, 139–141	32.40	5.28 E-6	+9.4	5.5	+7.1	4.7	N	234
4-7, 4–6	32.55	3.51 E-6	−19.3	354.1	+7.3	355.4	N	199
4-7, 27–29	32.78	4.94 E-6	−0.7	337.1	+3.7	350.1	N	123
5-1, 14–16	33.15	7.77 E-7	+69.5	260.0	+74.5	177.6	R	314
5-1, 36–38	33.37	9.93 E-7	−26.5	200.3	−24.4	176.4	R	431
5-1, 60–62	33.61	1.07 E-6	−35.7	74.5	−62.5	108.7	R	72
5-1, 100–102	34.01	7.00 E-6	+60.3	186.4	+61.2	186.7	R	47
5-1, 134–136	34.35	4.17 E-7	+25.0	311.1	−11.9	178.4	R	635
5-2, 4–6	34.55	1.43 E-6	+20.1	221.8	+0.4	176.6	R	464
5-2, 29–31	34.80	5.26 E-7	−4.9	332.9	−3.7	167.7	R	706
5-2, 54–56	35.05	4.56 E-7	+20.4	229.1	−1.1	161.9	R	680
5-2, 79–81	35.30	7.00 E-6	−42.6	298.5	+7.1	326.9	R	214
5-2, 104–106	35.55	7.35 E-7	+14.1	199.3	+2.0	166.8	R	772
5-2, 129–131	35.80	1.79 E-6	+21.7	342.7	−2.8	154.7	R	49
5-3, 4–6	36.05	9.19 E-7	−25.7	299.9	−13.3	165.7	R	496
5-3, 29–31	36.30	1.57 E-6	−36.3	209.9	−12.3	159.9	R	526
5-3, 54–56	36.55	1.96 E-6	−2.0	187.3	−4.5	156.7	R	433
5-3, 79–81	36.80	1.51 E-6	+43.4	2.0	−1.6	153.6	R	418
5-3, 104–106	37.05	1.09 E-6	−36.8	171.9	−9.7	162.4	R	677
5-3, 129–131	37.30	1.11 E-6	+24.0	171.8	+9.2	157.0	R	604
5-4, 4–6	37.55	1.30 E-6	−35.2	63.9	−6.9	161.7	R	462
5-4, 29–31	37.80	6.97 E-7	−20.6	329.6	−1.8	165.4	R	762
5-4, 54–56	38.05	2.04 E-6	+52.8	316.9	+4.4	169.8	R	485
5-4, 79–81	38.30	1.27 E-6	−63.2	315.2	−11.4	160.9	R	597
5-4, 104–106	38.55	2.77 E-6	+11.4	188.0	−2.9	169.5	R	446
5-4, 129–131	38.80	1.41 E-6	+66.1	310.6	+4.0	170.1	R	506
5-5, 4–6	39.05	1.22 E-6	+44.4	298.8	+3.6	187.2	R	572
5-5, 29–31	39.30	1.90 E-6	+16.8	43.3	+13.0	183.9	R	347
5-5, 54–56	39.55	6.69 E-7	−38.3	241.0	−6.7	191.5	R	575
5-5, 79–81	39.80	1.81 E-6	+27.1	340.4	−1.3	192.0	R	347
5-5, 104–106	40.05	2.05 E-6	+26.0	358.0	−7.5	190.0	R	27
5-5, 129–131	40.30	2.76 E-6	+13.3	3.0	−4.9	182.7	R	31
5-6, 4–6	40.55	5.32 E-6	−1.7	19.2	+4.6	28.1	N	81
5-6, 29–31	40.80	7.06 E-6	+11.8	20.2	+7.9	28.8	N	175
5-6, 54–56	41.05	3.71 E-6	−1.1	19.0	+10.4	30.4	N	71
5-6, 79–81	41.30	4.45 E-6	−0.2	23.4	+2.8	34.2	N	90
5-6, 104–106	41.55	3.80 E-6	+6.8	21.4	−14.1	35.0	N	66
5-6, 129–131	41.80	4.31 E-6	+5.0	23.9	−5.1	36.6	N	87

Appendix A. (Continued).

Core-Section (interval in cm)	Sub-bottom depth (m)	J_{NRM} (G)	I_{NRM}	D_{NRM}	I_{stable}	D_{stable}	Polarity	MDF (Oe)
Hole 574 (Cont.)								
5-7, 4–6	42.05	3.51 E-6	+2.2	23.1	+6.3	35.2	N	81
5-7, 29–31	42.30	3.27 E-6	−1.4	35.7	+6.8	43.2	N	153
6-1, 15–17	42.66	8.54 E-7	−32.2	316.4	−70.6	113.7	N	484
6-1, 52–54	43.03	1.53 E-6	+3.5	19.7	−34.2	32.8	N	179
6-1, 77–79	43.28	6.82 E-7	+29.8	0.7	+40.8	34.3	N	124
6-1, 119–121	43.70	7.06 E-7	−30.6	332.9	+39.8	182.3	R	28
6-1, 142–144	43.93	1.05 E-6	+2.2	173.9	+2.2	160.8	R	703
6-2, 4–6	44.05	2.45 E-6	+24.0	2.5	+29.4	94.0	N	40
6-2, 29–31	44.30	4.28 E-6	+5.5	351.7	+1.8	352.7	N	227
6-2, 54–56	44.55	5.03 E-6	+11.8	337.1	+12.4	344.4	N	181
6-2, 79–81	44.80	5.75 E-6	+4.5	348.1	−0.5	346.9	N	92
6-2, 104–106	45.05	5.92 E-6	+7.6	340.3	+7.4	344.7	N	208
6-2, 129–131	45.30	4.35 E-6	+10.0	347.3	+11.4	0.7	N	86
6-3, 4–6	45.55	2.47 E-6	−5.8	349.2	+14.2	35.4	N	47
6-3, 29–31	45.80	5.83 E-6	+0.6	353.4	+2.9	359.5	N	285
6-3, 54–56	46.05	2.54 E-6	−1.8	345.6	−4.6	2.3	N	50
6-3, 79–81	46.30	4.48 E-6	+3.6	350.5	+5.9	356.1	N	158
6-3, 104–106	46.55	5.24 E-6	−6.4	358.3	−3.3	4.1	N	139
6-3, 129–131	46.80	4.65 E-6	+6.2	0.9	+6.0	7.3		138
6-4, 4–6	47.05	4.68 E-6	+5.4	359.1	+5.3	358.8	N	150
6-4, 29–31	47.30	1.33 E-6	+10.8	187.1	+3.4	186.1	R	473
6-4, 54–56	47.55	8.94 E-8	−36.0	174.1	+0.8	182.3	R	>300
6-4, 79–81	47.80	4.05 E-8	+27.1	348.4	no stable			
6-4, 99–101	48.00	4.08 E-7	+17.1	16.6	+29.5	15.8	N	387
6-4, 129–131	48.30	1.11 E-8	−17.7	236.7	no stable			
6-5, 30–32	48.81	1.93 E-7	+19.7	132.7	+9.6	202.0	R	23
6-5, 70–72	49.21	8.84 E-8	+44.7	202.5	no stable			
6-5, 116–118	49.67	1.46 E-7	−41.4	254.9	no stable			
6-6, 30–32	50.31	1.45 E-7	−27.8	261.9	no stable			
6-6, 70–72	50.71	1.57 E-7	−31.0	241.9	no stable			
6-6, 116–118	51.17	2.34 E-7	−59.2	258.7	no stable			
6-7, 30–32	51.81	1.84 E-7	−55.8	258.3	no stable			44
7-1, 85–87	52.86	2.60 E-7	+0.7	2.0	no stable			
7-2, 56–58	54.07	1.46 E-7	−5.2	36.5	no stable			
7-2, 65–67	54.16	1.75 E-7	−52.4	194.7	no stable			
7-2, 130–132	54.81	1.59 E-7	+2.0	61.0	no stable			
7-3, 55–57	55.56	1.73 E-7	+2.3	38.8	no stable			19
7-4, 15–17	56.66	1.59 E-7	+12.9	37.5	no stable			73
7-4, 65–67	57.16	1.38 E-7	−37.1	174.2	no stable			
7-4, 97–99	57.48	2.68 E-7	+14.6	24.1	no stable			18
7-5, 34–36	58.35	1.30 E-7	+75.7	57.5	no stable			
7-5, 133–135	59.34	7.38 E-8	+1.1	36.2	no stable			
7-6, 13–15	59.64	7.62 E-7	+2.1	53.7	no stable			14
8-1, 92–94	61.93	1.59 E-7	+15.6	45.9	no stable			
8-2, 69–71	63.20	2.73 E-7	+2.0	48.5	no stable			17
8-2, 115–117	63.66	3.05 E-7	+3.4	32.9	no stable			126
8-3, 33–35	64.34	2.44 E-7	−7.8	40.7	no stable			
8-3, 113–115	65.14	1.33 E-7	−37.1	168.3	no stable			
8-4, 29–31	65.80	4.81 E-7	+29.2	202.2	no stable			205
8-4, 130–132	66.81	1.46 E-7	−7.3	28.2	no stable			
8-5, 117–119	68.18	1.58 E-7	+19.6	46.5	no stable			
8-6, 9–11	68.60	1.95 E-7	+11.6	34.5	no stable			
8-6, 38–40	68.89	1.08 E-7	−32.7	172.2	no stable			
8-6, 125–127	69.76	1.65 E-7	+12.0	41.0	no stable			
9-1, 65–67	71.16	3.64 E-7	−0.3	44.8	no stable			
9-2, 5–7	72.06	1.90 E-7	+12.8	26.8	no stable			
9-2, 34–36	72.35	1.40 E-7	−43.9	72.1	no stable			43
9-2, 30–32	73.81	2.58 E-7	+14.8	35.8	no stable			
9-3, 144–146	74.95	2.20 E-7	+7.1	32.4	no stable			38
9-4, 35–37	75.36	3.65 E-7	+0.2	76.6	no stable			
9-4, 58–60	75.59	1.61 E-7	−44.5	100.8	no stable			85
9-4, 85–87	75.86	5.88 E-6	−0.3	172.8	−0.6	173.0	R	288
9-4, 118–120	76.19	1.41 E-6	+29.2	152.9	+5.6	169.8	R	>1000
9-4, 135–137	76.36	2.55 E-6	+18.9	351.6	+42.4	169.2	R	69
9-5, 9–11	76.60	1.00 E-6	−8.8	52.0	−1.6	172.8	R	361
9-5, 34–36	76.85	3.34 E-6	−3.5	16.2	−7.9	3.7	N	52
9-5, 58–60	77.09	4.86 E-6	−4.4	10.2	−8.1	3.8	N	69
9-5, 85–87	77.36	5.66 E-6	−4.1	18.0	−2.3	9.8	N	97
9-5, 118–120	77.69	2.22 E-6	+0.9	31.0	+17.0	173.0	R	31
9-6, 9–11	78.10	2.40 E-6	−12.4	24.0	−36.3	152.7	R	27

Appendix A. (Continued).

Core-Section (interval in cm)	Sub-bottom depth (m)	J_{NRM} (G)	I_{NRM}	D_{NRM}	I_{stable}	D_{stable}	Polarity	MDF (Oe)
Hole 574 (Cont.)								
9-6, 34-36	78.35	3.91 E-6	−10.0	6.9	−11.9	357.0	N	99
9-6, 58-60	78.59	4.13 E-6	−7.8	9.7	−6.0	1.7	N	97
9-6, 85-87	78.86	6.29 E-6	+4.4	16.7	+9.6	6.8	N	128
9-6, 118-120	79.19	5.09 E-6	+4.5	4.0	+4.8	354.9	N	105
9-7, 9-11	79.60	2.20 E-6	−9.8	33.7	−6.8	19.8	N	46
9-7, 34-36	79.85	3.82 E-6	−3.9	24.2	−0.3	10.1	N	89
10-1, 23-25	80.24	1.81 E-6	+8.1	9.6	+7.7	13.2	N	151
10-1, 50-52	80.51	2.38 E-6	+0.8	10.1	−0.1	10.4	N	204
10-1, 77-79	80.78	2.50 E-6	+2.7	4.6	+0.5	4.8	N	163
10-1, 102-104	81.03	1.01 E-6	−4.1	10.0	−3.6	13.2	N	57
10-1, 125-127	81.26	1.97 E-6	+0.4	2.0	−3.2	2.2	N	150
10-1, 147-149	81.48	1.47 E-6	+5.3	357.2	+5.4	6.0	N	180
10-2, 23-25	81.74	2.01 E-6	−0.1	2.0	+1.2	5.6	N	182
10-2, 50-52	82.01	2.58 E-6	−9.6	0.0	−6.0	0.3	N	245
10-2, 77-79	82.28	3.36 E-6	−2.6	352.1	−1.4	353.9	N	238
10-2, 102-104	82.53	2.51 E-6	−5.7	354.0	−7.1	359.9	N	76
10-2, 125-127	82.76	6.32 E-6	−2.2	346.4	−0.8	351.2	N	93
10-2, 147-149	82.98	6.98 E-6	+0.3	345.9	+4.9	353.2	N	157
10-3, 23-25	83.24	4.90 E-6	+0.8	351.5	+2.6	353.6	N	188
10-3, 50-52	83.51	4.45 E-6	−2.0	344.4	+3.6	349.2	N	122
10-23, 77-79	83.78	4.84 E-6	+1.0	340.2	+7.6	350.7	N	73
10-3, 102-104	84.03	8.96 E-6	+4.0	343.1	+3.5	347.6	N	131
10-3, 125-127	84.26	1.32 E-7	+43.1	308.2	no stable			
10-4, 13-15	84.64	2.91 E-7	+7.8	292.8	no stable			
10-4, 103-105	85.54	6.03 E-7	−7.2	305.0	no stable			
10-5, 115-117	87.16	4.49 E-7	−3.0	285.7	no stable			
10-6, 30-32	87.81	3.45 E-7	+14.2	262.8	no stable			
10-6, 129-131	88.80	4.62 E-7	+2.6	283.5	no stable			
Hole 574A								
2-1, 14-16	6.45	1.53 E-6	+0.7	172.2	−1.7	168.4	R	536
2-1, 40-42	6.71	1.90 E-6	−7.2	166.9	−8.6	163.4	R	478
2-1, 64-66	6.95	1.20 E-6	+6.5	160.8	−0.5	159.6	R	410
2-1, 89-91	7.20	2.02 E-6	+6.2	161.7	+7.5	159.0	R	440
2-1, 114-116	7.45	4.95 E-6	−2.1	152.0	−2.3	151.4	R	361
2-1, 140-142	7.71	1.76 E-6	−17.6	166.5	−9.6	157.7	R	406
2-2, 15-17	7.96	7.68 E-7	−6.8	158.9	−0.6	151.1	R	444
2-2, 41-43	8.22	2.86 E-6	+1.7	173.9	−4.2	170.1	R	380
2-2, 65-67	8.46	1.39 E-6	+2.2	166.7	−0.6	163.4	R	398
2-2, 90-92	8.71	5.20 E-6	+0.7	345.1	+0.1	353.4	N	111
2-2, 115-117	8.96	6.70 E-6	+7.7	347.6	+4.2	351.4	N	191
2-2, 141-143	9.22	4.39 E-6	+13.2	351.6	+13.1	354.8	N	231
2-3, 15-17	9.46	2.05 E-6	−0.4	335.0	−13.8	340.4	N	38
2-3, 41-43	9.72	1.23 E-6	+7.7	197.9	+0.1	175.8	R	426
2-3, 65-67	9.96	1.93 E-6	−7.6	220.7	−8.2	199.4	R	401
2-3, 90-92	10.21	2.59 E-6	−8.3	201.9	−7.9	211.6	R	365
2-3, 115-117	10.46	1.90 E-6	−16.7	213.9	−6.4	228.2	R	370
2-3, 141-143	10.72	2.03 E-6	−24.1	217.7	−15.9	229.4	R	358
2-4, 18-20	10.99	1.33 E-6	−24.7	64.1	−30.9	71.2	N	294
2-4, 85-87	11.66	1.70 E-6	+13.7	44.1	+8.5	45.5	N	224
2-5, 109-111	13.40	1.22 E-6	−25.3	351.3	−27.6	346.7	N	214
2-5, 134-136	13.65	3.61 E-6	−4.1	2.8	−2.6	10.8	N	164
2-6, 14-16	13.95	3.88 E-6	+8.0	14.0	+7.9	14.5	N	202
2-6, 40-42	14.21	5.30 E-6	+0.2	7.2	+4.9	13.0	N	178
2-6, 64-66	14.45	6.05 E-6	+6.9	16.2	+2.5	17.6	N	238
2-6, 89-91	14.70	5.26 E-6	+12.6	13.4	+7.5	12.1	N	225
2-6, 109-111	14.90	4.20 E-6	+2.5	10.5	+4.9	10.2	N	226
2-6, 134-136	15.15	7.31 E-7	+13.7	190.4	+6.8	188.3	R	488
3-1, 24-26	15.75	8.50 E-7	−31.2	223.0	−16.9	225.6	R	430
3-1, 49-51	16.00	3.32 E-7	+38.8	246.0	−2.4	221.0	R	638
3-1, 74-76	16.25	5.26 E-7	+14.3	223.4	−2.9	219.9	R	523
3-1, 100-102	16.51	1.28 E-6	−6.4	227.6	−9.1	220.9	R	388
3-1, 124-126	16.75	1.10 E-6	+17.7	222.8	+6.8	217.1	R	397
3-2, 2-4	17.03	1.41 E-6	−1.6	204.1	−5.8	201.8	R	437
3-2, 24-26	17.25	2.01 E-6	−2.8	211.0	−8.3	207.6	R	373
3-2, 49-51	17.50	2.35 E-6	+0.7	207.4	+0.3	205.1	R	423
3-2, 80-82	17.81	1.88 E-6	−20.0	200.4	−17.3	197.5	R	419
3-2, 104-106	18.05	4.04 E-7	+6.5	225.5	−5.5	186.7	R	496
3-2, 134-136	18.35	2.24 E-6	−0.6	194.4	−3.9	186.0	R	375
3-3, 14-16	18.65	1.53 E-6	+17.4	185.2	+7.1	177.9	R	408
3-3, 40-42	18.91	2.02 E-6	−12.2	182.6	−12.3	175.9	R	395

Appendix A. (Continued).

Core-Section (interval in cm)	Sub-bottom depth (m)	J_{NRM} (G)	I_{NRM}	D_{NRM}	I_{stable}	D_{stable}	Polarity	MDF (Oe)
Hole 574A (Cont.)								
3-3, 64–66	19.15	2.43 E-6	−1.1	177.0	−7.7	169.7	R	403
3-3, 89–91	19.40	2.20 E-6	−0.2	175.6	−3.6	164.0	R	420
3-3, 114–116	19.65	2.22 E-6	+12.8	184.6	−4.4	166.6	R	440
3-3, 139–141	19.90	1.59 E-6	+41.0	151.2	+12.8	160.6	R	476
3-4, 14–16	20.15	1.95 E-6	−11.9	156.3	−8.2	150.4	R	439
3-4, 40–42	20.41	7.77 E-7	+15.0	235.6	−0.9	152.3	R	459
3-4, 64–66	20.65	1.35 E-6	−2.9	141.5	−3.6	145.2	R	441
3-4, 89–91	20.90	1.11 E-6	−14.1	298.6	−8.3	143.2	R	338
3-4, 114–116	21.15	1.18 E-6	+0.0	162.2	−0.8	143.5	R	476
3-4, 140–142	21.41	3.31 E-6	+16.7	334.2	+13.9	336.2	N	82
3-5, 14–16	21.65	4.08 E-6	+14.1	325.3	+12.5	321.0	N	117
3-5, 40–42	21.91	1.57 E-7	+30.7	332.8	+38.0	329.6	N	514
3-5, 108–110	22.59	5.75 E-7	+74.0	84.1	+61.0	81.1	N	377
3-5, 136–138	22.87	6.40 E-7	+38.4	113.0	no stable			311
3-6, 14–16	23.15	5.36 E-7	−53.0	249.7	no stable			
3-6, 80–82	23.81	3.00 E-7	−11.1	226.8	no stable			
4-1, 10–12	24.01	1.74 E-6	−63.2	154.7	no stable			334
4-1, 49–51	24.40	1.14 E-6	−56.8	167.8	−26.5	290.9	N	46
4-1, 80–82	24.71	4.68 E-6	−8.0	359.4	−14.8	4.1	N	144
4-1, 103–105	24.94	8.13 E-7	+46.5	220.9	−1.2	182.1	R	463
4-1, 129–131	25.20	4.33 E-7	+23.1	238.7	−8.7	166.4	R	>500
4-2, 4–6	25.45	7.53 E-7	+41.3	216.6	−6.0	164.3	R	529
4-2, 29–31	25.70	1.39 E-6	+44.9	197.1	+6.6	166.0	R	496
4-2, 54–56	25.95	8.99 E-7	+47.1	335.7	−3.2	172.6	R	451
4-2, 80–82	26.21	4.22 E-7	−11.3	303.8	−14.4	174.0	R	539
4-2, 104–106	26.45	7.76 E-7	−6.4	162.0	−15.2	179.0	R	532
4-2, 129–131	26.70	3.40 E-7	−23.1	236.2	−6.5	173.3	R	584
4-3, 4–6	26.95	4.29 E-6	+10.8	5.5	+1.7	5.8	N	108
4-3, 29–31	27.20	4.63 E-6	+12.1	7.3	+5.0	8.5	N	142
4-3, 54–56	27.45	4.94 E-6	+10.5	8.2	+9.7	6.1	N	211
4-3, 80–82	27.71	6.16 E-6	+15.5	5.0	+14.3	5.6	N	208
4-3, 104–106	27.95	8.60 E-7	−18.2	194.3	−26.3	184.4	R	486
4-3, 129–131	28.20	8.74 E-7	+5.1	187.2	−9.5	182.2	R	439
4-4, 4–6	28.45	9.54 E-7	+10.2	2.2	−17.4	177.6	R	42
4-4, 29–31	28.70	2.85 E-7	+33.7	197.8	−11.3	182.7	R	600
4-4, 54–56	28.95	1.38 E-6	−10.1	3.9	−26.7	190.8	R	30
4-4, 80–82	29.21	5.31 E-6	+10.5	356.1	+3.8	0.9	N	117
4-4, 104–106	29.45	3.13 E-6	+13.3	357.6	+7.2	357.9	N	68
4-4, 129–131	29.70	1.55 E-6	+22.5	350.4	+52.1	175.3	R	48
4-5, 4–6	29.95	5.96 E-7	+26.6	11.1	−13.0	179.9	R	461
4-5, 37–39	30.28	2.90 E-6	+6.4	0.4	−7.7	4.8	N	73
4-5, 68–70	30.59	3.44 E-6	+4.1	356.8	+6.2	355.4	N	120
4-5, 113–115	31.04	3.43 E-6	+12.6	2.4	+9.8	1.8	N	189
4-5, 135–137	31.26	3.07 E-6	+6.6	3.7	+2.7	2.3	N	90
4-6, 5–7	31.46	3.10 E-6	+4.0	4.3	+6.1	6.8	N	139
4-6, 27–29	31.68	7.23 E-7	+17.4	162.6	−4.6	180.9	R	417
4-6, 51–53	31.92	3.25 E-7	+10.6	181.8	−8.2	185.2	R	472
4-6, 75–77	32.16	1.02 E-6	+26.3	128.7	+1.1	184.9	R	312
4-6, 104–106	32.45	2.67 E-6	+48.4	111.9	no stable			266
5-1, 115–117	34.26	3.34 E-7	+42.4	290.6	−9.5	188.3	R	>600
5-1, 142–144	34.53	1.20 E-6	−32.7	176.3	−15.3	183.9	R	513
5-2, 14–16	34.75	5.04 E-7	+55.2	356.0	−10.4	176.5	R	550
5-2, 40–42	35.01	1.14 E-6	+33.4	172.2	−1.5	187.7	R	480
5-2, 64–66	35.25	9.91 E-7	+19.4	281.4	−0.6	178.0	R	522
5-2, 89–91	35.50	7.74 E-7	−9.0	127.9	−15.5	180.7	R	553
5-2, 114–116	35.75	1.96 E-6	+14.5	197.2	−5.6	185.7	R	488
5-2, 140–142	36.01	5.97 E-7	+20.2	194.3	−11.7	176.7	R	496
5-3, 14–16	36.25	1.03 E-6	+21.4	143.6	−0.6	181.6	R	577
5-3, 40–42	36.51	9.56 E-7	−4.6	178.2	−1.6	178.8	R	625
5-3, 64–66	36.75	2.50 E-6	−10.2	176.4	−7.8	180.8	R	517
5-3, 89–91	37.00	2.20 E-6	+4.6	173.6	−1.3	183.4	R	488
5-3, 114–116	37.25	1.40 E-6	−15.7	179.1	−1.8	174.2	R	497
5-3, 140–142	37.51	1.33 E-6	−3.9	170.0	−2.4	178.1	R	571
5-4, 14–16	37.75	1.06 E-6	+21.3	177.7	+3.5	181.4	R	615
5-4, 40–42	38.01	6.63 E-7	+41.6	217.7	−7.5	188.5	R	630
5-4, 64–66	38.25	1.21 E-6	+70.5	49.6	+7.1	186.9	R	471
5-4, 89–91	38.50	1.40 E-6	−28.0	174.3	−10.6	191.5	R	522
5-4, 114–116	38.75	3.84 E-7	+29.6	297.8	+3.9	210.1	R	>800
5-4, 140–142	39.01	4.96 E-7	+6.8	189.0	−6.7	185.7	R	>800
5-5, 14–16	39.25	1.68 E-6	+31.1	345.1	+19.7	199.0	R	33
5-5, 40–42	39.51	2.31 E-6	+2.5	347.8	+6.0	345.7	N	85
5-5, 64–66	39.75	5.20 E-6	+10.3	1.0	+15.6	353.7	N	180

Appendix A. (Continued).

Core-Section (interval in cm)	Sub-bottom depth (m)	J_{NRM} (G)	I_{NRM}	D_{NRM}	I_{stable}	D_{stable}	Polarity	MDF (Oe)
Hole 574A (Cont.)								
5-5, 89-91	40.00	3.65 E-6	+24.0	357.9	+22.8	342.6	N	73
5-5, 114-116	40.25	4.69 E-6	+15.4	347.3	+9.7	349.8	N	165
5-5, 140-142	40.51	2.54 E-6	+3.0	354.8	+7.1	346.1	N	82
5-6, 14-16	40.75	2.87 E-6	+1.3	5.5	−0.8	350.6	N	89
5-6, 40-42	41.01	3.07 E-6	+13.0	3.1	+14.8	355.6	N	97
5-6, 64-66	41.25	3.95 E-6	+9.9	349.4	+2.5	352.2	N	181
5-6, 89-91	41.50	1.88 E-6	+8.7	6.1	−4.6	346.5	N	70
5-6, 122-124	41.83	8.82 E-7	+33.5	32.6	+1.9	185.9	R	42
5-6, 144-146	42.05	9.30 E-7	+16.6	148.2	−9.0	184.0	R	635
5-7, 9-11	42.20	1.29 E-6	−63.3	333.0	−11.5	86.2	R	328
6-1, 13-15	42.54	3.94 E-6	−0.4	358.2	−5.3	358.5	N	133
6-1, 41-43	42.82	3.75 E-6	−0.3	354.0	−14.2	353.9	N	129
6-1, 65-67	43.06	2.84 E-6	+3.3	319.8	+1.9	4.3	N	85
6-1, 90-92	43.31	3.25 E-6	+6.9	1.3	+6.7	1.4	N	197
6-1, 115-117	43.56	3.74 E-6	+16.1	355.7	+15.1	356.3	N	150
6-1, 141-143	43.82	1.48 E-7	−17.1	181.9	−20.5	185.8	R	362
6-2, 11-13	44.02	1.14 E-7	−27.7	189.2	−28.0	190.6	R	>400
6-2, 41-43	44.32	2.07 E-7	−38.9	181.8	−1.9	180.9	R	353
6-2, 65-67	44.56	1.11 E-7	−11.0	177.4	−35.4	180.7	R	463
6-2, 90-92	44.81	2.41 E-7	+6.6	334.8	−1.8	329.0	N	381
6-2, 115-117	45.06	6.41 E-8	−24.7	195.9	−11.3	196.7	R	87
6-2, 140-142	45.31	4.40 E-8	−52.8	138.5	−4.2	170.0	R	20
6-3, 13-15	45.54	1.20 E-7	+51.0	248.4	no stable			68
6-3, 41-43	45.82	6.06 E-8	−4.1	165.2	no stable			
6-3, 68-70	46.09	3.54 E-8	−66.5	8.0	no stable			
6-3, 85-87	46.26	6.98 E-8	+80.6	194.9	no stable			39
6-3, 130-132	46.71	4.46 E-8	−65.6	39.9	no stable			
6-4, 13-15	47.04	5.50 E-7	+13.4	80.3	no stable			
6-4, 55-57	47.46	2.20 E-7	+13.1	95.6	no stable			
6-4, 95-97	47.86	4.63 E-8	+36.2	216.3	no stable			
6-4, 137-139	48.28	2.07 E-7	+31.6	106.3	no stable			
6-5, 13-15	48.54	5.70 E-8	+18.6	88.9	no stable			
6-5, 57-59	48.98	1.49 E-7	−68.7	56.4	no stable			
6-5, 105-107	49.46	1.06 E-7	−53.2	121.7	no stable			
6-5, 137-139	49.78	1.63 E-7	−80.5	143.3	no stable			
6-6, 13-15	50.04	8.01 E-8	−10.0	156.7	no stable			
6-6, 84-86	50.75	6.56 E-8	+35.1	88.8	no stable			
6-6, 118-120	51.09	1.28 E-7	−62.0	125.2	no stable			
7-1, 85-87	52.76	1.44 E-7	−48.3	149.9	no stable			
7-1, 126-128	53.17	2.06 E-7	+51.1	187.4	no stable			
7-2, 8-10	53.49	9.96 E-8	−46.1	23.6	no stable			
7-2, 45-47	53.86	3.14 E-7	−63.0	45.6	no stable			
7-2, 85-87	54.26	2.95 E-7	−83.4	354.9	no stable			
7-2, 125-127	54.66	3.64 E-7	−52.9	42.4	no stable			
7-3, 8-10	54.99	1.61 E-7	−59.9	302.7	no stable			
7-3, 35-37	55.26	1.03 E-7	+63.4	259.8	no stable			
7-3, 69-71	55.60	6.60 E-8	+39.5	348.7	no stable			
7-3, 108-110	55.99	5.80 E-8	−31.0	111.3	no stable			
7-4, 15-17	56.56	1.87 E-7	−35.9	253.0	no stable			
7-4, 51-53	56.92	5.78 E-8	−46.4	38.4	no stable			
7-4, 86-88	57.27	6.61 E-8	+41.0	83.5	no stable			
7-4, 121-123	57.62	4.95 E-8	−63.7	142.7	no stable			
7-5, 15-17	58.06	6.47 E-8	+26.5	173.4	no stable			
7-5, 51-53	58.42	1.19 E-7	+51.7	153.3	no stable			
7-5, 96-98	58.87	1.50 E-7	−55.9	180.1	no stable			
7-5, 134-136	59.25	2.05 E-8	+31.3	234.5	no stable			
7-6, 17-19	59.58	5.44 E-8	+46.7	185.5	no stable			
7-6, 53-55	59.94	1.45 E-7	+80.6	234.9	no stable			
7-6, 65-67	60.06	4.36 E-8	−19.5	99.6	no stable			
7-6, 97-99	60.38	7.05 E-8	−78.1	105.5	no stable			
7-6, 134-136	60.75	5.98 E-8	−69.9	15.0	no stable			
8-1, 95-97	62.36	1.50 E-7	−80.6	263.0	no stable			
8-1, 134-136	62.75	5.86 E-8	+27.5	90.4	no stable			
8-2, 32-34	63.23	4.74 E-8	−20.2	324.9	no stable			
8-2, 108-110	63.99	1.96 E-8	−15.5	22.7	no stable			
8-3, 64-66	65.05	1.10 E-7	−16.2	264.6	no stable			
8-3, 103-105	65.44	4.54 E-8	−30.7	55.0	no stable			
8-3, 144-146	65.85	1.40 E-7	+52.7	81.3	no stable			
8-4, 44-46	66.35	1.29 E-7	−51.2	239.5	no stable			
8-4, 68-70	66.59	2.99 E-8	−1.0	43.9	no stable			
8-4, 103-105	66.94	1.21 E-7	−38.3	165.7	no stable			

Appendix A. (Continued).

Core-Section (interval in cm)	Sub-bottom depth (m)	J_{NRM} (G)	I_{NRM}	D_{NRM}	I_{stable}	D_{stable}	Polarity	MDF (Oe)
Hole 574A (Cont.)								
8-4, 145-147	67.36	3.71 E-8	+54.5	356.3	no stable			
8-5, 23-25	67.64	6.01 E-8	-24.1	336.6	no stable			
8-5, 32-54	67.93	1.35 E-7	-70.1	94.3	no stable			
8-5, 91-93	68.32	1.77 E-8	-53.5	28.3	no stable			
8-5, 123-125	68.64	1.12 E-7	-75.9	98.0	no stable			
8-6, 15-17	69.06	9.21 E-8	-35.5	260.9	no stable			
8-6, 46-48	69.37	2.18 E-7	+23.0	180.1	no stable			
8-6, 78-80	69.69	1.46 E-7	+77.8	174.5	no stable			
8-6, 112-114	70.03	1.04 E-7	+37.3	356.4	no stable			
9-1, 25-27	70.66	2.27 E-7	+19.6	204.9	no stable			
9-1, 128-130	71.69	1.21 E-7	-50.6	174.7	no stable			
9-2, 105-107	72.96	1.93 E-7	+14.4	227.0	no stable			
9-3, 67-69	74.08	1.87 E-7	+3.4	222.9	no stable			
9-3, 135-137	74.76	9.09 E-8	+32.1	266.1	no stable			
9-3, 143-145	74.84	2.43 E-7	-9.4	211.0	no stable			
9-4, 26-28	75.17	6.87 E-8	-16.2	72.8	no stable			
9-4, 70-72	75.61	2.38 E-8	-56.3	38.8	no stable			
9-4, 115-117	76.06	6.65 E-6	-21.6	168.0	-21.0	169.0	R	287
9-4, 144-146	76.35	6.34 E-7	+48.0	355.3	-15.1	173.7	R	>600
9-5, 15-17	76.56	9.82 E-7	+23.4	316.7	+3.5	166.5	R	366
9-5, 41-43	76.82	1.13 E-6	+4.4	334.1	-14.2	158.7	R	28
9-5, 66-68	77.07	5.66 E-6	+15.7	345.8	+19.5	352.1	N	127
9-5, 90-92	77.31	5.56 E-6	-1.0	350.1	-1.0	358.3	N	124
9-5, 114-116	77.55	5.05 E-6	+4.6	356.2	+11.1	358.1	N	89
9-5, 135-137	77.76	5.85 E-7	-3.2	211.6	-0.8	174.0	R	462
9-6, 15-17	78.06	3.74 E-6	-3.9	351.4	-10.7	355.8	N	84
9-6, 41-43	78.32	3.67 E-6	+7.4	357.6	+9.9	3.3	N	184
9-6, 66-68	78.57	3.94 E-6	+1.6	1.7	+5.1	7.2	N	153
9-6, 90-92	8.81	3.56 E-6	-0.7	6.9	+4.7	13.9	N	90
9-6, 114-116	79.05	5.43 E-6	-2.8	16.4	-3.8	19.6	N	177
9-6, 135-137	79.26	5.06 E-6	+0.6	15.5	+3.7	17.1	N	203
9-7, 8-10	79.49	6.69 E-7	+4.2	351.7	-13.8	220.9	R	35
9-7, 32-34	79.73	3.07 E-6	-4.4	23.0	+1.5	24.8	N	219
10-1, 15-17	80.06	2.61 E-6	-2.3	352.1	-9.9	351.7	N	177
10-1, 41-43	80.32	1.44 E-6	+0.9	8.7	-1.7	8.3	N	198
10-1, 65-67	80.56	1.03 E-6	-27.6	355.5	-30.9	0.6	N	228
10-1, 90-92	80.81	1.17 E-6	-29.3	353.2	-31.0	0.5	N	214
10-1, 115-117	81.06	1.07 E-6	-6.2	2.3	-10.1	13.4	N	250
10-1, 141-143	81.32	6.12 E-7	-1.4	352.6	-20.2	10.5	N	198
10-2, 15-17	81.56	1.13 E-6	+8.9	357.8	+4.1	1.2	N	224
10-2, 41-43	81.82	1.66 E-6	+17.6	60.9	+28.5	24.2	N	115
10-2, 65-67	82.06	6.62 E-7	-21.7	354.5	-12.8	360.0	N	281
10-2, 90-92	82.31	8.09 E-7	-20.0	348.8	-17.9	355.3	N	282
10-3, 15-17	83.06	5.81 E-7	-49.6	82.5	-41.4	25.1	N	195
10-3, 41-43	83.32	7.34 E-7	-0.2	343.3	-3.5	350.5	N	230
10-3, 65-67	83.56	1.94 E-6	+1.2	329.0	+3.5	331.3	N	255
10-3, 90-92	83.81	4.95 E-6	+31.4	339.0	+28.9	343.3	N	203
10-3, 119-121	84.10	4.59 E-6	-11.8	349.9	-7.7	356.0	N	199
10-3, 143-145	84.34	5.24 E-6	+15.1	342.7	+15.3	345.3	N	96
10-4, 15-17	84.56	9.25 E-8	+14.1	336.4	no stable			
10-4, 45-47	84.86	1.34 E-7	+8.7	352.9	no stable			
10-4, 87-89	85.28	5.72 E-8	+52.5	4.4	no stable			
10-4, 117-119	85.58	2.18 E-7	+33.5	354.3	no stable			
10-5, 50-52	86.41	1.26 E-7	+81.9	321.3	no stable			
10-5, 107-109	86.98	1.52 E-7	+51.6	343.0	no stable			
10-6, 18-20	87.59	7.61 E-8	-85.1	337.4	no stable			
10-6, 51-53	87.92	5.89 E-8	-52.3	311.7	no stable			
10-6, 83-85	88.24	1.85 E-7	+70.5	2.3	no stable			
10-6, 118-120	88.59	6.76 E-8	+53.2	339.6	no stable			
11-1, 45-47	89.66	1.80 E-7	+25.9	14.5	no stable			
11-1, 95-97	90.16	1.38 E-7	+84.4	319.9	no stable			
11-1, 115-117	90.36	2.83 E-7	-5.6	42.0	no stable			
11-2, 64-66	91.35	1.76 E-7	-15.0	64.9	no stable			
11-2, 95-97	91.66	1.05 E-7	+62.4	5.9	no stable			
11-3, 95-97	93.16	3.46 E-7	+51.7	5.8	no stable			
11-3, 144-146	93.65	1.74 E-7	-1.4	42.8	no stable			
11-4, 10-12	93.81	1.95 E-7	+13.1	10.8	no stable			
11-4, 95-97	94.66	1.35 E-7	+77.5	349.5	no stable			
11-5, 30-32	95.51	1.64 E-7	-14.3	42.1	no stable			
11-5, 95-97	96.16	1.66 E-7	+68.1	20.4	no stable			
11-6, 95-97	97.66	6.17 E-8	-29.5	196.9	no stable			
11-6, 131-133	98.02	9.20 E-8	+64.1	80.5	no stable			

Appendix A. (Continued).

Core-Section (interval in cm)	Sub-bottom depth (m)	J_{NRM} (G)	I_{NRM}	D_{NRM}	I_{stable}	D_{stable}	Polarity	MDF (Oe)
Hole 575								
1-1, 24–26	0.25	1.94 E-6	−25.5	48.0	−9.4	17.3	N	187
1-1, 34–36	0.35	4.17 E-6	+26.1	21.0	+14.4	28.1	N	287
1-1, 44–46	0.45	4.76 E-6	−5.3	15.3	+7.0	27.1	N	276
1-1, 54–56	0.55	7.30 E-6	−5.3	39.0	+4.4	35.4	N	259
1-1, 64–66	0.65	4.80 E-6	+22.4	21.0	+14.3	28.7	N	289
1-1, 84–86	0.85	4.81 E-6	+29.1	29.3	+17.5	27.1	N	225
1-1, 94–96	0.95	7.04 E-6	+29.0	22.6	+13.5	26.3	N	238
1-1, 104–106	1.05	9.05 E-6	+24.9	36.0	+15.2	33.0	N	231
1-1, 114–116	1.15	5.35 E-6	+14.7	26.4	+11.6	30.4	N	254
1-1, 124–126	1.25	8.26 E-6	+0.9	37.0	+7.2	25.1	N	156
1-1, 134–136	1.35	7.67 E-6	+8.7	42.4	+13.0	30.2	N	185
1-2, 4–6	1.55	4.50 E-6	+4.5	28.6	+8.9	34.6	N	254
1-2, 14–16	1.65	2.39 E-6	−0.4	23.6	+3.4	29.4	N	260
1-2, 24–26	1.75	3.90 E-6	−2.8	31.9	+7.1	26.0	N	227
1-2, 34–36	1.85	5.91 E-6	+17.7	13.1	+13.4	22.1	N	254
1-2, 44–46	1.95	9.89 E-6	+20.0	20.5	+8.4	24.0	N	225
1-2, 54–56	2.05	7.15 E-6	+3.1	13.9	+12.5	20.7	N	238
1-2, 64–66	2.15	4.36 E-6	−1.8	30.8	+6.9	24.9	N	194
1-2, 84–86	2.35	9.35 E-6	+14.9	11.4	+16.0	20.8	N	253
1-2, 94–96	2.45	8.20 E-6	−6.1	20.8	+7.4	20.9	N	174
1-2, 114–116	2.65	4.08 E-6	+21.2	23.7	+51.4	10.7	N	45
1-2, 124–126	2.75	4.06 E-6	+13.6	150.6	−7.9	173.5	R	353
1-2, 134–136	2.85	2.61 E-6	−43.5	140.8	−21.8	177.1	R	322
1-2, 144–146	2.95	2.49 E-6	−32.2	243.4	−16.6	182.1	R	315
1-3, 4–6	3.05	2.95 E-6	+43.5	299.1	+4.0	215.8	R	33
1-3, 14–16	3.15	2.74 E-6	−13.7	3.1	+35.4	357.8	N	57
1-3, 24–26	3.25	2.26 E-6	+34.2	228.7	−4.6	188.8	R	323
1-3, 34–36	3.35	1.85 E-6	+26.6	263.4	−0.4	192.5	R	256
1-3, 44–46	3.45	2.46 E-6	+40.3	267.8	+0.1	188.4	R	267
1-3, 54–56	3.55	3.16 E-6	−41.0	137.5	−12.2	177.2	R	305
1-3, 64–66	3.65	2.34 E-6	−11.0	218.6	−12.3	180.4	R	373
1-3, 84–86	3.85	2.18 E-6	−8.8	201.2	−7.0	178.9	R	407
1-3, 94–96	3.95	1.93 E-6	−20.4	209.7	−15.9	176.1	R	380
1-3, 104–106	4.05	1.93 E-6	−23.1	140.1	−8.9	167.0	R	350
1-3, 114–116	4.15	4.75 E-6	+15.9	312.5	+35.1	331.8	N	43
1-3, 124–126	4.25	3.01 E-6	+33.9	33.9	−65.0	10.2	N	36
1-3, 134–136	4.35	1.52 E-6	−59.8	220.0	−6.4	168.2	R	435
1-3, 144–146	4.45	2.01 E-6	−48.5	250.9	−14.7	184.0	R	301
1-4, 4–6	4.55	1.98 E-6	−30.1	173.5	−9.1	169.4	R	345
1-4, 14–16	4.65	5.91 E-7	+19.7	181.2	+5.8	165.5	R	401
1-4, 24–26	4.75	9.48 E-7	−51.5	235.4	−12.0	171.4	R	371
1-4, 34–36	4.85	2.16 E-6	+8.8	191.9	−0.3	167.6	R	405
1-4, 44–46	4.95	1.52 E-6	+32.0	249.5	+5.8	169.3	R	360
1-4, 55–57	5.06	1.95 E-6	−1.6	198.3	−14.6	159.7	R	406
1-4, 64–66	5.15	2.54 E-6	−29.7	148.3	−11.4	156.9	R	344
1-4, 84–86	5.35	5.58 E-7	+18.5	207.5	−4.9	171.4	R	357
1-4, 94–96	5.45	9.33 E-7	+4.5	4.2	+17.5	339.1	N	142
1-4, 104–106	5.55	2.39 E-6	−7.3	344.6	+3.9	340.8	N	161
1-4, 114–116	5.65	1.51 E-6	−11.2	351.1	+7.4	340.0	N	155
1-4, 124–126	5.75	1.69 E-6	−9.8	328.2	+0.4	335.2	N	87
1-4, 134–136	5.85	6.39 E-6	+14.4	320.5	+5.8	330.1	N	93
1-4, 144–146	5.95	7.86 E-6	−5.7	315.7	−1.1	327.1	N	76
1-5, 4–6	6.05	6.62 E-6	−6.8	352.2	+4.5	343.9	N	197
1-5, 14–16	6.15	9.01 E-6	+28.0	319.9	+18.6	336.1	N	79
1-5, 24–26	6.25	8.78 E-6	+26.5	329.9	+14.2	338.0	N	125
1-5, 34–36	6.35	8.26 E-6	−3.9	327.3	+4.5	336.3	N	164
1-5, 44–46	6.45	9.10 E-6	+17.2	319.8	+11.6	328.4	N	130
1-5, 54–56	6.55	4.68 E-6	−18.3	336.3	+5.1	329.6	N	86
1-5, 64–66	6.65	3.14 E-6	+29.0	304.1	+10.3	203.3	R	30
1-5, 84–86	6.85	8.66 E-7	+46.4	284.7	−1.6	158.9	R	33
1-5, 94–96	6.95	3.75 E-6	−12.8	343.0	+4.9	333.9	N	155
1-5, 104–106	7.05	5.17 E-6	−11.4	340.2	−1.9	336.3	N	153
1-5, 114–116	7.15	3.23 E-6	−2.4	328.2	+6.4	328.5	N	137
1-5, 122–124	7.23	4.32 E-6	+15.0	220.0	+7.7	206.3	R	107
1-5, 127–129	7.28	2.35 E-6	−4.9	209.0	−7.4	211.4	R	46
2-1, 3–5	7.34	3.25 E-6	−84.3	39.1	−77.3	12.4	N	267
2-1, 19–21	7.50	3.25 E-6	−44.8	282.4	−68.9	296.8	N	44
2-1, 29–31	7.60	1.85 E-6	−37.4	54.8	−45.5	350.9	N	37
2-1, 39–41	7.70	2.67 E-6	+51.4	21.3	−63.8	152.5	R	30
2-1, 49–51	7.80	6.81 E-6	−21.6	276.3	−13.2	190.4	R	39
2-1, 59–61	7.90	3.56 E-6	+20.7	288.8	−10.3	209.7	R	24
2-1, 69–71	8.00	2.95 E-6	+40.5	73.4	−11.8	158.9	R	45
2-1, 79–81	8.10	3.11 E-6	−5.3	64.7	−22.4	153.2	R	39

Appendix A. (Continued).

Core-Section (interval in cm)	Sub-bottom depth (m)	J_{NRM} (G)	I_{NRM}	D_{NRM}	I_{stable}	D_{stable}	Polarity	MDF (Oe)
Hole 575 (Cont.)								
2-1, 89–91	8.20	3.45 E-6	−66.6	1.4	−45.3	166.2	R	23
2-1, 99–101	8.30	3.65 E-6	+33.8	286.3	−3.0	187.7	R	45
2-1, 109–111	8.40	3.65 E-6	+66.6	307.5	−0.8	176.4	R	39
2-1, 119–121	8.50	3.47 E-6	+6.3	95.3	−7.2	168.1	R	250
2-1, 129–131	8.60	3.41 E-6	−56.7	291.7	−31.9	192.0	R	44
2-1, 140–142	8.71	2.34 E-6	+29.4	62.7	−23.2	168.1	R	41
2-2, 19–21	9.00	3.33 E-6	−21.3	260.8	−4.4	186.8	R	246
2-2, 29–31	9.10	3.23 E-6	−13.0	69.1	−16.3	162.3	R	274
2-2, 39–41	9.20	3.20 E-6	−18.2	66.4	−18.6	162.3	R	43
2-2, 49–51	9.30	4.38 E-6	−75.4	0.9	−31.5	167.7	R	45
2-2, 59–61	9.40	4.03 E-6	−58.3	80.1	−22.7	169.6	R	228
2-2, 69–71	9.50	2.07 E-6	−48.3	334.6	−17.4	185.5	R	286
2-2, 79–81	9.60	3.39 E-6	+36.8	291.2	−4.9	190.6	R	243
2-2, 89–91	9.70	4.34 E-6	+24.0	297.2	−7.5	199.8	R	35
2-2, 99–101	9.80	3.86 E-6	−53.8	41.5	−33.5	180.2	R	33
2-2, 109–111	9.90	3.78 E-6	−63.9	43.6	−28.9	178.5	R	39
2-2, 119–121	10.00	4.97 E-6	+56.3	315.5	−8.3	195.8	R	29
2-2, 129–131	10.10	4.68 E-6	+37.3	304.0	−10.9	223.6	R	30
2-2, 139–141	10.20	5.85 E-6	+11.9	81.0	−26.2	156.8	R	32
2-3, 3–5	10.34	4.44 E-6	+29.6	11.9	+28.4	10.7	N	38
2-3, 20–22	10.51	3.25 E-6	+0.7	2.2	+4.4	6.3	N	83
2-3, 29–31	10.60	5.20 E-6	+52.6	315.1	+29.8	344.6	N	44
2-3, 41–43	10.72	3.53 E-6	+60.3	3.5	+14.4	349.3	N	38
2-3, 59–61	10.90	4.00 E-6	+38.2	31.8	+21.7	8.6	N	50
2-3, 69–71	11.00	2.96 E-6	+11.1	305.8	−26.2	328.3	N	36
2-3, 82–84	11.13	3.79 E-6	+16.5	304.5	−4.5	333.3	N	36
2-3, 89–91	11.20	3.84 E-6	−2.7	60.6	+2.0	11.4	N	42
2-3, 99–101	11.30	4.72 E-6	+42.2	317.4	+30.5	347.1	N	46
2-3, 109–111	11.40	5.21 E-6	+66.6	10.2	+29.0	353.0	N	38
2-3, 119–121	11.50	3.87 E-6	+21.9	315.1	+11.3	347.2	N	42
2-3, 129–131	11.60	5.15 E-6	+51.8	319.4	+23.1	350.3	N	37
2-3, 146–148	11.77	4.12 E-6	+14.4	350.2	+20.3	5.0	N	69
2-4, 25–27	12.06	4.95 E-6	+18.8	329.9	+6.1	350.9	N	52
2-4, 87–89	12.68	3.17 E-6	+13.4	0.4	−20.1	4.7	N	73
2-4, 127–129	13.08	6.37 E-6	−62.1	305.4	−49.7	308.5	N	402
2-4, 144–146	13.25	2.34 E-6	+22.7	321.2	+2.7	245.2	R	32
2-5, 9–11	13.40	1.26 E-6	+7.4	325.4	−23.3	235.0	R	45
2-5, 19–21	13.50	1.28 E-6	−13.3	310.8	−16.7	227.6	R	47
2-5, 29–31	13.60	1.19 E-6	−1.9	316.0	−5.4	230.4	R	322
2-5, 39–41	13.70	2.38 E-6	−58.7	77.5	−20.7	207.8	R	252
2-5, 49–51	13.80	2.00 E-6	+52.8	353.3	+3.7	252.0	R	29
2-5, 59–61	13.90	1.28 E-6	+8.1	335.8	−12.2	242.8	R	36
2-5, 69–71	14.00	2.01 E-6	+12.8	276.8	−8.3	221.8	R	303
2-5, 79–81	14.10	1.48 E-6	−38.7	307.9	−25.2	221.7	R	331
2-5, 89–91	14.20	2.09 E-6	+55.8	344.2	+17.1	218.2	R	31
2-5, 99–101	14.30	1.94 E-6	+61.6	284.3	+4.3	215.6	R	46
2-5, 109–111	14.40	1.79 E-6	−23.6	330.9	−8.8	235.4	R	29
2-5, 119–121	14.50	3.01 E-6	+53.2	302.3	+7.0	224.3	R	34
2-5, 129–131	14.60	1.70 E-6	+63.1	11.8	−1.8	208.5	R	42
2-5, 139–141	14.70	1.19 E-6	−40.7	97.7	−13.7	187.1	R	343
2-6, 9–11	14.90	1.39 E-6	+9.4	264.5	−14.3	204.1	R	49
2-6, 19–21	15.00	1.74 E-6	−38.9	257.3	−24.0	203.9	R	282
2-6, 29–31	15.10	7.88 E-7	+25.2	318.8	−29.7	262.1	R	38
2-6, 39–41	15.20	8.46 E-7	−32.8	99.0	−30.6	183.5	R	269
2-6, 49–51	15.30	9.38 E-7	−19.5	318.5	−38.0	224.8	N	49
2-6, 59–61	15.40	4.57 E-7	−40.4	51.2	−55.6	210.3	N	39
2-6, 69–71	15.50	5.63 E-7	−73.5	30.7	−50.5	209.5	N	40
2-6, 79–81	15.60	3.73 E-7	+33.1	279.9	+1.7	207.4	R	306
2-6, 89–91	15.70	6.53 E-7	+66.7	265.8	+6.8	198.3	R	258
2-6, 99–101	15.80	8.37 E-7	+88.5	58.1	+5.4	202.8	R	317
2-6, 109–111	15.90	1.00 E-6	−69.2	338.8	−36.7	194.2	R	35
2-6, 119–121	16.00	8.54 E-7	+0.4	292.0	−27.0	215.3	R	38
2-6, 129–131	16.10	4.44 E-7	−19.3	12.6	−37.9	208.8	R	42
2-6, 139–141	16.20	8.01 E-7	−42.8	41.9	−62.3	359.6	N	40
2-7, 5–7	16.36	1.04 E-6	+23.8	347.0	−12.7	339.7	N	50
2-7, 16–18	16.47	1.39 E-6	−41.9	336.9	−30.2	342.0	N	50
2-7, 25–27	16.56	1.95 E-6	−42.5	353.4	−33.7	351.7	N	66
2-7, 36–38	16.67	8.27 E-7	−33.7	349.2	−20.0	329.7	N	43
2-7, 45–47	16.76	1.24 E-6	−12.3	322.7	−28.2	332.0	N	41
2-7, 49–51	16.80	1.27 E-6	+57.9	0.7	+27.7	291.5	N	142
3-1, 9–11	16.90	1.35 E-6	−78.6	82.8	−80.8	31.2	N	49
3-1, 19–21	17.00	1.76 E-6	−58.0	55.2	−59.9	57.4	N	62
3-1, 29–31	17.10	9.40 E-7	−70.3	36.1	−69.0	35.9	N	74

Appendix A. (Continued).

Core-Section (interval in cm)	Sub-bottom depth (m)	J_{NRM} (G)	I_{NRM}	D_{NRM}	I_{stable}	D_{stable}	Polarity	MDF (Oe)
Hole 575 (Cont.)								
3-1, 79–81	17.60	5.24 E-7	−11.4	54.3	−63.6	117.9	N	203
3-1, 89–91	17.70	1.30 E-6	−30.3	61.3	−42.1	64.1	N	146
3-1, 99–101	17.80	1.66 E-6	−23.5	279.7	−59.1	172.2	N	208
3-1, 109–111	17.90	3.39 E-6	−54.2	350.6	−56.7	50.6	N	46
3-1, 119–121	18.00	2.43 E-6	−70.5	47.1	−71.3	93.1	N	117
3-2, 19–21	18.50	2.63 E-6	−50.4	25.0	−59.1	24.7	N	45
3-2, 29–31	18.60	2.57 E-6	−19.0	43.8	−71.5	87.0	N	44
3-2, 79–81	19.10	3.12 E-6	−42.0	41.0	−27.9	41.4	N	45
3-2, 99–101	19.30	2.71 E-6	−31.4	46.0	−40.4	29.4	N	73
3-2, 129–131	19.60	1.21 E-6	+32.0	344.2	−41.5	38.3	N	299
3-2, 139–141	19.70	2.03 E-6	+52.2	336.3	−35.7	24.3	N	42
3-3, 29–31	20.10	3.03 E-6	−26.1	21.8	−54.1	0.9	N	83
3-3, 39–41	20.20	9.58 E-7	−19.3	20.2	−50.3	61.9	N	292
3-3, 59–61	20.40	2.25 E-6	−31.0	298.9	−73.5	10.6	N	94
3-3, 69–71	20.50	1.48 E-6	−3.4	289.0	−45.0	360.0	N	190
3-3, 79–81	20.60	2.12 E-6	+34.3	8.6	+8.5	49.4	N	41
3-3, 89–91	20.70	2.27 E-6	+47.5	41.6	+10.9	38.8	N	45
3-3, 99–101	20.80	1.48 E-6	−50.6	319.1	−52.4	13.9	N	61
3-3, 109–111	20.90	1.19 E-6	−42.5	54.4	−45.3	34.4	N	85
3-3, 119–121	21.00	1.52 E-6	−45.3	43.4	−51.9	59.5	N	72
3-3, 129–131	21.10	5.68 E-7	+24.7	26.8	−61.1	44.1	N	268
3-3, 139–141	21.20	1.79 E-6	−59.5	37.2	−38.6	49.7	N	50
3-4, 29–31	21.60	2.00 E-6	−69.4	39.1	−40.8	34.7	N	95
3-4, 49–51	21.80	3.01 E-7	−11.4	99.1	−56.2	63.3	N	546
3-4, 59–61	21.90	1.93 E-6	−46.9	42.8	−64.2	52.2	N	90
3-4, 69–71	22.00	7.68 E-7	−71.8	211.9	−50.4	80.5	N	286
3-4, 79–81	22.10	2.01 E-7	−75.5	87.4	−31.8	63.4	N	549
3-4, 99–101	22.30	1.95 E-6	−26.7	86.8	−26.8	98.8	N	58
3-4, 109–111	22.40	2.04 E-6	−50.9	59.1	−44.2	59.2	N	48
3-4, 138–140	22.69	7.13 E-7	+45.3	70.2	+72.5	22.7	N	187
3-5, 4–6	22.85	1.84 E-6	+47.8	176.0	+47.8	176.0	R	42
3-5, 89–91	23.70	5.16 E-7	+83.7	179.0	−22.5	150.0	R	41
3-5, 107–109	23.88	1.42 E-7	+30.1	317.7	−4.9	105.3	R	376
3-5, 123–125	24.04	1.10 E-6	+82.0	83.2	+47.7	120.7	R	41
3-5, 139–141	24.20	1.10 E-6	−51.4	45.9	−27.5	105.5	R	38
3-6, 9–11	24.40	1.52 E-6	−14.7	62.1	−18.3	169.2	R	35
3-6, 19–21	24.50	6.28 E-7	−19.4	53.0	−1.6	171.6	R	36
3-6, 29–31	24.60	1.33 E-6	+49.4	43.5	+37.1	130.4	R	43
3-6, 39–41	24.70	6.92 E-7	+64.9	289.2	−5.2	181.0	R	40
3-6, 49–51	24.80	1.39 E-6	−30.0	48.8	−29.2	152.1	R	33
3-6, 59–61	24.90	9.39 E-7	+89.3	28.2	+6.3	202.6	R	143
3-6, 69–71	25.00	1.02 E-6	+42.2	78.3	+3.2	179.3	R	39
3-6, 79–81	25.10	9.72 E-7	+26.6	65.9	+11.6	146.8	R	35
3-6, 89–91	25.20	1.26 E-6	+58.3	235.5	+6.6	180.3	R	41
3-6, 99–101	25.30	1.56 E-6	−55.8	73.2	−3.9	192.0	R	258
3-6, 109–111	25.40	6.86 E-7	+44.3	240.5	−15.7	177.8	R	46
3-6, 119–121	25.50	1.43 E-6	−28.5	64.8	−28.4	182.9	R	42
3-6, 129–131	25.60	1.45 E-6	−25.0	70.5	−36.1	185.3	R	259
3-6, 139–141	25.70	1.93 E-6	−4.3	71.5	−13.4	187.5	R	278
3-7, 9–11	25.90	4.79 E-6	−5.0	50.3	−47.8	51.7	N	37
3-7, 19–21	26.00	3.07 E-6	+27.7	57.1	−22.7	159.8	R	32
3-7, 29–31	26.10	2.36 E-6	−16.4	73.1	−3.4	203.7	R	40
3-7, 39–41	26.20	1.76 E-6	−71.8	101.8	−18.8	213.0	R	310
4-1, 9–11	26.40	2.75 E-6	−37.7	345.0	−19.8	199.8	R	93
4-1, 18–20	26.49	1.38 E-6	−25.7	221.8	−23.8	168.0	R	428
4-1, 29–31	26.60	2.22 E-6	+38.9	355.7	+44.9	192.1	R	832
4-1, 38–40	26.69	2.50 E-6	−70.7	44.2	−7.8	190.9	R	41
4-1, 49–51	26.80	2.94 E-6	+49.9	19.0	+1.8	188.2	R	36
4-1, 59–61	26.90	4.99 E-6	+24.4	322.1	+17.2	322.4	N	40
4-1, 69–71	27.00	3.56 E-6	−14.2	318.6	+30.0	330.1	N	47
4-1, 90–92	27.21	5.94 E-6	−13.9	142.3	−18.8	124.6	R	47
4-1, 110–112	27.41	3.21 E-6	−5.5	158.9	−6.2	153.8	R	67
4-1, 130–132	27.61	3.96 E-6	+8.5	159.4	−11.9	173.4	R	91
4-1, 145–147	27.76	3.61 E-6	−7.1	150.1	−13.6	145.9	R	78
4-2, 6–8	27.87	3.34 E-6	−2.9	182.0	−23.7	172.1	R	67
4-2, 32–34	28.13	3.34 E-6	+14.8	16.5	−8.3	4.0	N	56
4-2, 89–91	28.70	2.84 E-6	−26.2	209.9	−24.1	216.5	R	429
4-2, 133–135	29.14	4.02 E-6	+5.2	176.6	+5.0	180.0	R	104
4-3, 19–21	29.50	3.73 E-6	+9.3	357.2	+9.4	10.7	N	150
4-3, 29–31	29.60	2.48 E-6	+10.9	347.3	+17.7	359.4	N	70
4-3, 39–41	29.70	3.96 E-6	+42.1	340.2	+27.2	350.3	N	48
4-3, 49–51	29.80	1.17 E-6	−14.6	28.4	+13.1	169.2	R	37
4-3, 59–61	29.90	1.91 E-6	+46.6	345.8	+6.0	177.7	R	32
4-3, 69–71	30.00	2.93 E-6	−4.9	355.0	+7.0	0.7	N	57

Appendix A. (Continued).

Core-Section (interval in cm)	Sub-bottom depth (m)	J_{NRM} (G)	I_{NRM}	D_{NRM}	I_{stable}	D_{stable}	Polarity	MDF (Oe)
Hole 575 (Cont.)								
4-3, 79–81	30.10	1.15 E-6	+39.6	41.7	+13.5	166.1	R	30
4-3, 89–91	30.20	1.22 E-6	+37.4	343.7	+18.3	145.9	R	33
4-3, 99–101	30.30	1.22 E-6	−6.5	342.9	−23.2	128.4	R	36
4-3, 109–111	30.40	1.34 E-6	+42.3	317.5	−23.2	186.8	R	30
4-3, 119–121	30.50	9.44 E-7	−23.0	282.6	−8.9	179.2	R	317
4-3, 129–131	30.60	1.21 E-6	+39.0	83.3	−2.4	181.7	R	34
4-3, 139–141	30.70	1.70 E-6	+29.1	57.3	+24.3	39.1	N	34
4-4, 4–6	30.85	3.72 E-6	−4.4	353.4	−8.1	5.3	N	48
4-4, 14–16	30.95	3.04 E-6	+8.7	31.9	−6.0	26.6	N	46
4-4, 24–26	31.05	9.17 E-7	+21.3	67.0	+3.8	184.7	R	40
4-4, 34–36	31.15	8.89 E-7	+42.8	191.0	+59.1	167.1	R	35
4-4, 44–46	31.25	5.61 E-7	−15.7	1.0	−14.8	160.3	R	35
4-4, 54–56	31.35	1.07 E-6	−5.3	40.2	−0.5	35.5	N	37
4-4, 64–66	31.45	1.59 E-6	+34.8	20.3	+35.9	14.4	N	35
4-4, 74–76	31.55	1.31 E-6	+29.7	346.9	+4.8	179.9	R	30
4-4, 84–86	31.65	5.42 E-7	−16.5	55.7	−12.2	173.0	R	36
4-4, 94–96	31.75	5.07 E-7	+19.8	332.9	−4.1	180.4	R	28
4-4, 104–106	31.85	6.04 E-7	−5.8	56.6	+1.8	172.2	R	39
4-4, 114–116	31.95	6.91 E-7	+40.3	340.9	−16.0	166.0	R	29
4-4, 124–126	32.05	4.28 E-7	−42.2	342.5	−3.8	171.6	R	22
4-4, 134–136	32.15	7.12 E-7	+26.7	40.1	+15.4	38.8	N	36
4-4, 144–146	32.25	3.85 E-7	+22.2	41.7	+24.3	47.5	N	41
4-5, 8–10	32.39	3.48 E-7	−57.8	211.6	−14.6	354.6	N	>250
4-5, 64–66	32.95	3.70 E-7	+11.2	207.4	+11.2	207.4	R	46
4-5, 90–92	33.21	1.76 E-7	−39.4	177.0	−35.8	180.0	N	26
4-5, 133–135	33.64	1.98 E-7	+32.2	2.2	+15.0	0.1	N	>300
4-6, 10–12	33.91	3.75 E-7	−1.6	342.8	−0.2	359.3	N	>300
4-6, 38–40	34.19	4.46 E-7	+20.9	188.9	+7.0	3.6	N	37
4-6, 47–49	34.28	4.55 E-7	+61.2	27.8	−15.6	183.9	R	30
4-6, 59–61	34.40	4.07 E-7	+25.7	77.2	−33.0	158.3	R	42
4-6, 70–72	34.51	6.09 E-7	−10.2	78.0	+31.1	143.7	R	45
4-6, 82–84	34.63	6.95 E-7	−64.0	347.4	−5.9	167.0	R	45
4-6, 94–96	34.75	4.24 E-7	+56.0	325.9	−14.1	181.7	R	389
4-6, 94–96	34.75	4.24 E-7	+56.0	325.9	−14.1	181.7	R	389
Hole 575B								
1-1, 10–12	3.41	3.76 E-6	+30.7	346.0	+41.9	345.0	N	159
1-1, 20–22	3.51	5.23 E-6	+17.2	350.2	+22.0	351.5	N	97
1-1, 30–32	3.61	8.52 E-6	+13.7	358.4	+14.2	357.9	N	135
1-1, 40–42	3.71	3.19 E-6	−10.2	354.4	−15.1	357.6	N	128
1-1, 50–52	3.81	1.66 E-6	+6.7	3.9	+3.6	355.4	N	249
1-1, 60–62	3.91	1.83 E-6	+14.0	358.4	+14.3	4.9	N	188
1-1, 70–72	4.01	2.11 E-6	+24.6	337.7	+17.9	344.2	N	284
1-1, 100–102	4.31	6.17 E-6	+15.3	1.9	+18.7	4.1	N	206
1-1, 110–112	4.41	7.63 E-6	+11.0	3.5	+18.1	359.9	N	279
1-1, 120–122	4.51	6.19 E-6	+10.4	359.7	+15.5	358.8	N	126
1-1, 130–132	4.61	4.00 E-6	+11.8	357.0	+16.0	357.4	N	172
1-1, 140–142	4.71	5.20 E-6	+8.4	2.8	+13.6	3.1	N	163
1-2, 10–12	4.91	6.17 E-6	+15.3	343.0	+23.8	352.0	N	50
1-2, 20–22	5.01	1.67 E-6	+39.4	351.3	+19.1	184.1	R	339
1-2, 30–32	5.11	1.77 E-6	+28.8	2.0	+3.7	187.9	R	344
1-2, 40–42	5.21	6.93 E-7	−16.2	200.0	−10.3	186.2	R	645
1-2, 50–52	5.31	1.47 E-6	+29.4	183.6	+0.4	185.4	R	525
1-2, 60–62	5.41	1.64 E-6	+9.7	6.6	+5.4	187.7	R	349
1-2, 70–72	5.51	3.74 E-6	+5.6	13.7	+32.4	359.5	N	43
1-2, 100–102	5.81	1.42 E-6	−47.5	46.9	+22.6	207.7	R	31
1-2, 112–114	5.93	1.55 E-6	−69.3	20.6	−21.3	188.7	R	379
1-2, 122–124	6.03	1.45 E-6	+55.7	317.0	+60.6	157.7	R	187
1-2, 133–135	6.14	1.38 E-6	−67.6	277.0	−39.4	191.5	R	349
1-2, 144–146	6.25	6.05 E-7	−29.7	183.0	−4.7	176.8	R	497
1-3, 2–4	6.33	6.91 E-7	+15.8	231.5	+3.4	170.5	R	317
1-3, 10–12	6.41	1.16 E-6	−44.0	259.2	−19.0	187.0	R	266
1-4, 13–15	7.94	1.96 E-6	−49.9	287.9	−55.3	340.3	N	83
1-5, 12–14	9.43	6.84 E-7	−26.0	252.3	no stable			>500
1-5, 97–99	10.28	5.35 E-6	−7.0	2.5	no stable			40
1-6, 69–71	11.50	1.79 E-6	−38.7	276.7	no stable			254
1-6, 141–143	12.22	2.71 E-6	−10.1	306.5	no stable			75
2-1, 80–82	12.81	3.01 E-6	+8.1	43.6	+40.5	32.4	N	38
2-1, 90–92	12.91	4.43 E-6	+6.3	30.6	+9.6	6.3	N	50
2-1, 100–102	13.01	4.50 E-6	+12.3	32.3	+13.0	15.4	N	43
2-1, 110–112	13.11	2.93 E-6	+7.4	39.1	−9.9	178.1	R	29
2-1, 120–122	13.21	3.29 E-6	+12.4	35.9	−18.6	181.8	R	28
2-1, 130–132	13.31	2.12 E-6	+4.4	54.8	−17.0	186.9	R	48

Appendix A. (Continued).

Core-Section (interval in cm)	Sub-bottom depth (m)	J_{NRM} (G)	I_{NRM}	D_{NRM}	I_{stable}	D_{stable}	Polarity	MDF (Oe)
Hole 575B (Cont.)								
2-1, 140–142	13.41	2.40 E-6	−9.7	47.3	−29.2	186.1	R	43
2-2, 2–4	13.53	3.65 E-6	+20.5	71.0	−23.8	173.0	R	43
2-2, 12–14	13.63	3.09 E-6	+28.8	55.4	−0.2	166.6	R	46
2-2, 22–24	13.73	2.28 E-6	+27.5	71.5	−4.3	170.1	R	325
2-2, 32–34	13.83	1.98 E-6	+23.0	84.2	−3.9	166.1	R	355
2-2, 42–44	13.93	1.95 E-6	+24.4	77.5	−0.4	173.5	R	339
2-2, 52–54	14.03	2.41 E-6	+41.0	86.5	+12.2	172.7	R	341
2-2, 62–64	14.13	2.41 E-6	+17.3	113.8	−3.7	170.1	R	365
2-2, 72–74	14.23	2.21 E-6	+27.5	98.8	+2.4	174.0	R	352
2-2, 82–84	14.33	2.44 E-6	+8.2	111.7	−3.5	167.3	R	342
2-2, 92–94	14.43	2.01 E-6	+2.1	110.4	−9.5	173.2	R	345
2-2, 102–104	14.53	1.54 E-6	−1.0	65.7	−3.0	168.1	R	381
2-2, 112–114	14.63	3.05 E-6	+7.8	23.6	+8.3	168.2	R	33
2-2, 122–124	14.73	3.61 E-6	−2.5	15.9	+11.5	347.4	N	43
2-2, 132–134	14.83	4.49 E-6	−1.8	20.8	+4.4	358.3	N	64
2-2, 142–144	14.93	3.88 E-6	+4.6	15.2	+19.3	355.6	N	56
2-3, 2–4	15.03	5.17 E-6	+30.4	23.7	+64.3	347.8	N	36
2-3, 12–14	15.13	5.03 E-6	+22.9	21.5	+27.2	358.7	N	44
2-3, 22–24	15.23	4.87 E-6	+17.6	18.1	+12.0	357.6	N	48
2-3, 32–34	15.33	5.29 E-6	+15.6	15.3	+10.5	358.9	N	53
2-3, 42–44	15.43	5.02 E-6	+15.4	22.3	+17.5	2.7	N	63
2-3, 52–54	15.53	5.68 E-6	+17.3	13.1	+13.3	355.0	N	79
2-3, 62–64	15.63	4.37 E-6	+13.4	18.6	+21.1	356.2	N	67
2-3, 72–74	15.73	2.90 E-6	+10.8	19.0	+14.4	350.2	N	55
2-3, 82–84	15.83	1.67 E-6	+6.3	35.4	−5.6	184.8	R	41
2-3, 92–94	15.93	1.42 E-6	+13.3	47.0	+3.2	183.6	R	41
2-3, 102–104	16.03	1.29 E-6	−0.9	81.8	−5.0	178.6	R	337
2-3, 112–114	16.13	1.63 E-6	−7.4	118.4	−10.8	176.4	R	329
2-3, 122–124	16.23	1.29 E-6	−14.4	97.4	−5.9	174.9	R	314
2-3, 132–134	16.33	1.18 E-6	+5.1	65.7	+11.7	176.6	R	40
2-3, 142–144	16.43	1.42 E-6	−3.3	46.5	+7.1	174.0	R	41
2-4, 2–4	16.53	4.47 E-6	+26.7	35.6	+16.1	180.3	R	32
2-4, 12–14	16.63	5.35 E-6	+16.5	24.5	+28.2	10.1	N	43
2-4, 22–24	16.73	4.77 E-6	+12.5	24.2	+16.4	1.1	N	50
2-4, 32–34	16.83	5.57 E-6	16.6	21.4	+15.2	359.4	N	58
2-4, 42–44	16.93	5.93 E-6	+12.9	18.7	+8.2	357.4	N	74
2-4, 52–54	17.03	6.63 E-6	+13.3	19.7	+14.2	6.0	N	84
2-4, 72–74	17.23	3.07 E-6	+0.5	47.8	−39.3	156.4	N	37
2-4, 82–84	17.33	3.74 E-6	+18.3	20.2	+28.2	348.1	N	54
2-4, 92–94	17.43	4.77 E-6	+20.7	31.9	+26.1	15.0	N	81
2-4, 102–104	17.53	4.75 E-6	−45.5	11.4	−67.6	304.4	N	374
2-4, 122–114	17.63	4.08 E-6	+11.7	19.8	+16.1	7.5	N	93
2-4, 122–124	17.73	3.99 E-6	+10.7	25.9	+12.5	2.2	N	97
2-4, 132–134	17.83	2.81 E-6	+11.6	20.3	+19.1	352.7	N	99
2-4, 142–144	17.93	3.77 E-6	+11.3	25.9	+18.6	359.7	N	127
2-5, 2–4	18.03	3.59 E-6	+33.9	41.6	+33.5	359.7	N	45
2-5, 12–14	18.13	3.59 E-6	+32.8	54.9	+54.5	30.7	N	40
2-5, 22–24	18.23	2.97 E-6	+36.7	74.0	+13.8	181.3	R	34
2-5, 32–34	18.33	2.32 E-6	+22.7	47.1	+19.0	184.8	R	34
2-5, 42–44	18.43	2.20 E-6	+18.6	41.9	+13.7	180.7	R	31
2-5, 52–54	18.53	3.75 E-6	+24.8	51.6	+4.2	180.6	R	31
2-5, 62–64	18.63	3.02 E-6	+28.1	52.2	+15.8	191.7	R	34
2-5, 72–74	18.73	2.39 E-6	+34.0	62.5	+19.9	186.5	R	38
2-5, 82–84	18.83	2.03 E-6	+27.5	42.0	+47.5	196.3	R	43
2-5, 92–94	18.93	1.52 E-6	+25.3	51.7	+20.4	188.4	R	39
2-5, 102–104	19.03	1.09 E-6	+20.9	94.0	−7.8	186.6	R	364
2-5, 112–114	19.13	1.54 E-6	+31.9	76.4	+14.6	194.5	R	270
2-5, 122–124	19.23	1.58 E-6	+38.2	64.0	+37.5	192.0	R	88
2-5, 132–134	19.33	1.06 E-6	+16.2	69.5	+18.9	180.1	R	49
2-5, 142–144	19.43	9.28 E-7	+29.1	87.0	+23.3	195.4	R	316
2-6, 2–4	19.53	1.17 E-6	+38.9	79.8	+12.2	188.5	R	46
2-6, 12–14	19.63	1.64 E-6	+26.8	60.6	+17.3	189.6	R	40
2-6, 22–24	19.73	1.43 E-6	+22.8	73.6	−14.0	200.9	R	31
2-6, 32–34	19.83	1.28 E-6	+24.4	75.2	−8.7	199.2	R	36
2-6, 42–44	19.93	8.76 E-7	+30.4	98.0	−0.5	182.7	R	300
2-6, 52–54	20.03	8.29 E-7	+19.4	112.6	+5.5	185.0	R	44
2-5, 62–64	20.13	1.15 E-6	+24.6	120.1	+17.6	175.3	R	74
2-6, 72–74	20.23	1.07 E-6	+11.5	59.0	+25.5	165.7	R	44
2-6, 82–84	20.33	7.47 E-7	+16.6	68.4	+0.5	161.0	R	349
2-6, 92–94	20.43	1.17 E-6	−3.1	70.7	−23.5	132.6	R	38
2-6, 102–104	20.53	6.39 E-7	+4.2	45.0	+4.2	45.0	R	333
2-6, 112–114	20.63	7.04 E-7	+15.3	56.7	+63.7	185.4	R	48
2-6, 122–124	20.73	6.29 E-7	+16.1	78.3	+6.8	180.4	R	37
2-6, 132–134	20.83	4.46 E-7	+11.9	89.4	+29.0	164.8	R	118
2-6, 142–144	20.93	3.29 E-7	+14.4	65.0	+83.0	210.6	R	90

Appendix A. (Continued).

Core-Section (interval in cm)	Sub-bottom depth (m)	J_{NRM} (G)	I_{NRM}	D_{NRM}	I_{stable}	D_{stable}	Polarity	MDF (Oe)
Hole 575B (Cont.)								
2-7, 2–4	21.03	3.48 E-7	+29.0	67.8	no stable			
2-7, 12–14	21.13	4.43 E-7	+45.3	9.5	+43.6	10.0	N	63
2-7, 22–24	21.23	2.95 E-7	+45.5	9.4	+51.3	12.9	N	99
2-7, 32–34	21.33	2.57 E-7	+64.3	15.4	+62.7	14.2	N	134
2-7, 42–44	21.43	4.44 E-7	+56.2	327.3	+60.3	320.8	N	213
3-1, 58–60	21.59	1.70 E-6	+47.1	43.4	+48.9	353.2		37
3-1, 68–70	21.69	5.34 E-7	+38.7	356.9	+31.2	352.4		220
3-1, 78–80	21.79	7.86 E-6	+12.3	46.4	−49.1	96.4		41
3-1, 88–90	21.89	7.37 E-7	+1.4	39.1	−30.4	35.3		65
3-1, 98–100	21.99	7.82 E-7	+7.2	45.8	+8.3	40.4		97
3-1, 108–110	22.09	9.46 E-7	+12.2	51.8	−15.0	48.2		75
3-1, 118–120	22.19	9.97 E-7	−6.2	25.7	−11.9	23.2		109
3-1, 128–130	22.29	2.97 E-6	−3.0	14.5	−23.6	12.6		61
3-1, 138–140	22.39	2.21 E-6	−14.7	23.0	−48.6	15.5		97
3-2, 8–10	22.59	1.98 E-6	−3.2	23.3	−80.6	353.6		37
3-2, 30–32	22.81	2.00 E-6	+4.4	29.7	−67.4	192.0		34
3-2, 50–52	23.01	2.19 E-6	+7.5	30.3	−77.9	150.1		33
3-2, 136–138	23.87	2.22 E-6	−29.0	23.4	−61.6	18.0		98
3-3, 12–14	24.13	2.94 E-6	−23.7	15.7	−70.0	13.7		74
3-3, 106–108	25.07	1.44 E-6	−8.5	4.2	−38.8	9.3		220
3-4, 11–13	25.62	1.33 E-6	−12.1	11.9	−26.4	3.8		52
3-4, 39–41	25.90	1.32 E-6	−18.2	15.3	−51.0	12.4		47
3-4, 59–61	26.10	1.84 E-6	+16.5	18.0	+33.5	359.7		139
3-4, 100–102	26.51	2.06 E-6	−3.6	1.8	−15.6	14.5		96
3-4, 110–112	26.61	1.96 E-6	−0.5	1.6	+10.3	346.2		93
3-4, 120–122	26.71	3.04 E-6	+17.4	352.9	+21.6	330.9		99
3-4, 130–132	26.81	2.36 E-6	+18.2	346.2	+20.6	334.3		89
3-4, 140–142	26.91	2.68 E-6	+17.1	347.3	+20.7	335.0		91
3-5, 8–10	27.09	2.86 E-6	+41.7	16.3	+29.7	356.2		42
3-5, 18–20	27.19	2.58 E-6	+41.7	5.8	+25.5	339.3		51
3-5, 28–30	27.29	2.51 E-6	+45.0	25.6	+31.2	340.4		48
3-5, 38–40	27.39	3.56 E-6	+16.9	352.9	+19.5	335.7		64
3-5, 48–50	27.49	3.02 E-6	+11.2	349.6	+10.3	332.7		98
3-5, 58–60	27.59	2.94 E-6	+13.5	346.5	+15.7	334.2		107
3-5, 68–70	27.69	1.66 E-6	+21.2	359.1	+32.7	351.0		71
3-5, 78–80	27.79	1.72 E-6	+19.5	349.7	+27.9	332.2		96
3-5, 88–90	27.89	1.76 E-6	+12.3	349.5	+16.7	337.1		205
3-5, 98–100	27.99	1.20 E-6	+23.9	353.5	+26.9	350.3		177
3-5, 108–110	28.09	7.34 E-7	+16.4	7.1	+25.4	356.5		228
3-5, 118–120	28.19	7.57 E-7	+8.8	356.8	+26.7	348.3		208
3-5, 128–130	28.29	9.83 E-7	+12.5	355.0	+26.6	340.4		246
3-5, 138–140	28.39	7.31 E-7	+22.1	359.4	+26.3	348.3		235
3-5, 146–148	28.47	1.71 E-6	+12.4	292.8	+9.3	316.0		87
3-6, 8–10	28.59	2.50 E-6	+25.4	6.2	+18.6	344.2		75
3-6, 18–20	28.69	1.47 E-6	+17.7	6.4	+26.5	345.4		98
3-6, 28–30	28.79	1.79 E-6	+14.1	353.8	+16.7	335.1		178
3-6, 38–40	28.89	7.94 E-7	+24.7	7.6	+31.8	346.4		163
3-6, 48–50	28.99	8.12 E-7	+30.0	34.6	+35.8	28.5		99
3-6, 58–60	29.09	7.92 E-7	+27.6	53.7	+42.7	64.9		137
3-6, 68–70	29.19	6.77 E-7	+30.2	42.7	+40.7	15.1		188
3-6, 82–84	29.33	7.48 E-7	+48.5	51.5	+39.0	35.5		213
3-6, 95–97	29.46	6.08 E-7	+7.1	7.7	+20.4	8.5		145
3-6, 105–107	29.56	6.55 E-7	+2.3	18.1	+27.4	18.2		173
4-1, 26–28	29.77	10.0 E-7	+22.8	21.4	+44.2	337.7		149
4-1, 41–43	29.92	9.75 E-7	+22.0	13.8	+62.8	320.6		120
4-1, 56–58	30.07	9.25 E-7	+27.2	5.8	+59.0	357.9		173
4-1, 74–76	30.25	9.52 E-7	+25.3	352.1	+52.5	345.3		223
4-1, 92–94	30.43	6.79 E-7	+32.4	0.2	+50.8	349.4		255
4-1, 114–116	30.65	7.22 E-7	+24.1	5.2	+40.7	351.3		309
4-1, 136–138	30.87	6.48 E-7	+33.7	359.3	+42.8	355.6		313
4-2, 11–13	31.12	6.62 E-7	+31.6	2.7	+45.0	0.7		207
4-2, 26–28	31.27	8.57 E-7	+31.7	10.1	+44.9	3.9		286
4-2, 41–43	31.42	8.55 E-7	+35.2	3.5	+57.2	348.2		291
4-2, 56–58	31.57	1.10 E-6	+46.7	5.4	+46.0	9.1		266
4-2, 71–73	31.72	7.94 E-7	+36.3	1.1	+39.7	359.3		298
4-2, 86–88	31.87	1.00 E-6	+41.0	11.5	+34.9	2.9		316
4-2, 101–103	32.02	5.92 E-7	+46.6	358.3	+45.9	355.9		355
4-2, 116–118	32.17	8.46 E-7	+69.3	37.0	+61.8	359.7		305
4-2, 131–133	32.32	7.28 E-7	+83.7	81.7	+69.0	334.7		328
4-2, 146–148	32.47	1.01 E-6	+57.3	46.0	+53.7	355.9		306
4-3, 11–13	32.62	1.96 E-6	+52.2	24.3	+65.0	28.5		50
4-3, 26–28	32.77	1.61 E-6	+46.7	10.3	+54.7	5.1		97
4-3, 41–43	32.92	1.52 E-6	+35.1	11.7	+38.7	4.8		163

Appendix A. (Continued).

Core-Section (interval in cm)	Sub-bottom depth (m)	J_{NRM} (G)	I_{NRM}	D_{NRM}	I_{stable}	D_{stable}	Polarity	MDF (Oe)
Hole 575B (Cont.)								
4-3, 56–58	33.07	9.81 E-7	+37.9	16.2	+48.1	2.9		236
4-3, 71–73	33.22	9.30 E-7	+25.4	5.8	+35.3	356.1		195
4-3, 91–93	33.42	1.93 E-6	+44.2	13.7	+46.9	1.0		239
4-3, 114–116	33.65	1.29 E-6	+34.1	12.2	+43.0	4.0		208
4-3, 136–138	33.87	2.10 E-6	+37.1	16.5	+39.8	356.8		235
4-4, 11–13	34.12	4.29 E-6	+42.9	12.1	+52.8	30.6		45
4-4, 26–28	34.27	3.32 E-6	+55.9	3.5	+67.4	9.8		100
4-4, 41–43	34.42	3.05 E-6	+52.2	10.8	+60.1	15.2		171
4-4, 56–58	34.57	2.77 E-6	+49.9	19.9	+50.3	24.8		203
4-4, 71–73	34.72	2.04 E-6	+54.7	331.5	+67.8	354.9		215
4-4, 86–88	34.87	1.97 E-6	+68.1	8.6	+73.5	340.7		198
4-4, 101–103	35.02	1.39 E-6	+81.3	242.3	+67.2	223.0		260
4-4, 116–118	35.17	1.75 E-6	+82.8	279.1	+71.7	274.9		276
4-4, 131–133	35.32	2.04 E-6	+82.0	32.9	+76.2	311.4		265
4-4, 146–148	35.47	2.37 E-6	+81.2	242.3	+66.5	257.9		261
4-5, 11–13	35.62	1.84 E-6	+81.2	225.0	+69.4	244.5		222
4-5, 26–28	35.77	2.24 E-6	+53.0	175.7	+50.3	214.8		210
4-5, 41–43	35.92	2.62 E-6	+62.9	163.4	+68.4	230.4		180
4-5, 56–58	36.07	9.97 E-7	+84.0	66.1	+75.3	321.4		277
4-5, 71–73	36.22	8.08 E-7	+68.2	45.8	+74.0	348.9		306
4-5, 86–88	36.37	1.35 E-6	+50.8	32.6	+51.7	16.1		269
4-5, 101–103	36.52	6.71 E-7	+83.3	35.0	+69.0	285.5		264
4-5, 116–118	36.67	1.13 E-6	+40.3	195.0	+48.4	228.0		292
4-5, 131–133	36.82	6.27 E-7	+49.8	130.2	+69.9	323.5		358
4-5, 146–148	36.97	7.31 E-7	+43.3	107.5	+74.4	335.6		280
4-6, 11–13	37.12	3.07 E-6	+52.4	8.9	+59.4	7.3		40
4-6, 26–28	37.27	1.13 E-6	+84.2	231.2	−11.2	194.3		388
4-6, 41–43	37.42	2.05 E-6	+64.6	359.9	+68.7	262.6		56
4-6, 56–58	37.57	1.88 E-6	+76.0	336.7	+52.0	239.4		85
4-6, 71–73	37.72	1.38 E-6	+79.6	327.4	+52.3	243.0		121
4-6, 86–88	37.87	1.92 E-6	+76.9	173.9	+46.6	213.6		130
4-6, 101–103	38.02	1.20 E-6	+72.2	186.2	+50.5	235.3		142
4-6, 116–118	38.17	1.21 E-6	+57.2	202.1	+25.2	221.9		235
4-6, 131–133	38.32	1.22 E-6	+54.5	190.8	+22.8	217.8		219
4-6, 146–148	38.47	1.22 E-6	+51.1	179.8	+22.6	225.1		191
4-7, 11–13	38.62	9.08 E-7	+51.2	200.5	+30.4	221.7		241
4-7, 26–28	38.77	1.36 E-6	+40.0	202.9	+23.1	227.2		191
4-7, 41–43	38.92	1.79 E-6	+37.2	176.6	+20.6	212.4		88
Hole 575C								
1-1, 5–7	0.06	4.10 E-6	+34.2	307.1	+32.5	286.0	N	310
1-1, 15–17	0.16	2.86 E-6	+24.1	314.6	+19.1	291.1	N	287
1-1, 25–27	0.26	1.66 E-6	+32.2	305.1	+28.2	284.9	N	289
1-1, 35–37	0.36	1.85 e-6	+19.5	304.7	+26.5	287.4	N	281
1-1, 45–47	0.46	4.37 E-6	+16.6	294.3	+6.6	274.7	N	242
1-1, 55–57	0.56	4.44 E-6	+18.5	300.0	+17.8	284.5	N	175
1-1, 65–67	0.66	5.18 E-6	+19.6	300.4	+12.7	276.3	N	197
1-1, 75–77	0.76	4.81 E-6	+21.6	291.9	+13.3	274.4	N	268
1-1, 85–87	0.86	5.71 E-6	+19.7	307.8	+11.7	286.5	N	210
1-1, 95–97	0.96	5.27 E-6	+20.2	338.1	+20.5	307.1	N	209
1-1, 105–107	1.06	8.11 E-6	+15.1	330.6	+14.1	318.0	N	203
1-1, 115–117	1.16	6.72 E-6	+8.2	339.4	+10.5	321.2	N	194
1-1, 125–127	1.26	7.24 E-6	+6.6	337.2	+8.5	326.6	N	221
1-1, 135–137	1.36	8.75 E-6	+16.3	335.2	+15.7	324.5	N	227
1-1, 145–147	1.46	4.84 E-6	+4.5	335.2	+5.3	321.8	N	183
1-2, 5–7	1.56	8.28 E-6	+14.6	358.1	+13.9	349.6	N	132
1-2, 15–17	1.66	4.46 E-6	+12.1	5.8	+13.3	349.5	N	154
1-2, 25–27	1.76	2.42 E-6	+11.3	352.9	+14.6	342.8	N	224
1-2, 35–37	1.86	4.46 E-6	+10.1	4.7	+16.4	354.1	N	221
1-2, 45–47	1.96	6.70 E-6	+15.8	359.7	+15.7	350.7	N	214
1-2, 55–57	2.06	7.26 E-6	+9.4	5.4	+13.1	358.1	N	179
1-2, 65–67	2.16	4.43 E-6	+6.4	12.3	+11.3	357.3	N	157
1-2, 75–77	2.26	3.62 E-6	+3.6	9.6	+13.6	350.3	N	194
1-2, 85–87	2.36	7.45 E-6	+5.4	356.3	+11.4	349.6	N	226
1-2, 95–97	2.46	7.19 E-6	+9.7	358.4	+21.5	346.5	N	242
1-2, 105–107	2.56	2.92 E-6	−9.1	17.8	+26.1	351.8	N	103
1-2, 115–117	2.66	1.83 E-6	−13.8	61.4	+31.5	211.5	R	50
1-2, 125–127	2.76	1.41 E-6	−15.7	96.5	+14.6	199.5	R	394
1-2, 135–137	2.86	1.73 E-6	−64.4	142.4	−12.3	200.4	R	394
1-2, 145–147	2.96	1.81 E-6	−33.3	192.0	−2.7	215.2	R	418
1-3, 5–7	3.06	1.71 E-6	+13.2	40.4	−8.4	226.0	R	330
1-3, 15–17	3.16	4.84 E-6	+11.6	36.0	+36.5	34.1	N	58
1-3, 25–27	3.26	1.08 E-6	−9.2	54.1	−0.1	222.1	R	413
1-3, 35–37	3.36	1.37 E-6	−9.1	51.8	−0.3	220.3	R	381

Appendix A. (Continued).

Core-Section (interval in cm)	Sub-bottom depth (m)	J_{NRM} (G)	I_{NRM}	D_{NRM}	I_{stable}	D_{stable}	Polarity	MDF (Oe)
Hole 575C (Cont.)								
1-3, 45-47	3.46	1.29 E-6	−57.6	71.4	−17.8	222.1	R	450
1-3, 55-57	3.56	5.91 E-7	+2.7	64.0	+2.4	220.4	R	629
1-3, 65-67	3.66	9.33 E-7	−47.1	202.8	−8.3	226.2	R	561
1-3, 75-77	3.76	1.13 E-6	−56.6	215.5	−9.1	233.4	R	491
1-3, 85-87	3.86	1.08 E-6	−26.4	209.2	−6.5	226.2	R	466
1-3, 95-97	3.96	2.66 E-6	−13.6	215.6	−6.6	221.9	R	374
1-3, 105-107	4.06	1.86 E-6	−13.1	217.4	−3.6	228.3	R	432
1-3, 115-117	4.16	2.66 E-6	−8.7	51.5	+12.0	22.6	N	33
1-3, 125-127	4.26	7.32 E-7	−48.7	132.3	−5.5	232.8	R	478
1-3, 135-137	4.36	1.31 E-6	−28.9	70.0	−5.2	230.4	R	339
1-3, 145-147	4.46	9.68 E-7	−45.8	211.9	−9.4	229.7	R	417
1-4, 5-7	4.56	4.20 E-7	−47.0	155.0	−4.1	234.7	R	498
1-4, 15-17	4.66	6.27 E-7	−16.7	88.8	−0.9	237.8	R	449
1-4, 25-27	4.76	6.67 E-7	+27.4	265.4	−2.8	241.7	R	555
1-4, 35-37	4.86	5.49 E-7	−21.0	126.9	−6.4	237.0	R	452
1-4, 45-47	4.96	1.52 E-6	−19.1	222.9	+1.3	241.1	R	424
1-4, 55-57	5.06	1.56 E-6	−25.6	227.6	−4.9	233.7	R	411
1-4, 65-67	5.16	2.17 E-6	−22.9	226.4	−5.5	235.4	R	413
1-4, 75-77	5.26	5.38 E-7	−21.2	224.5	+6.8	236.4	R	428
1-4, 85-87	5.36	1.21 E-6	−9.2	71.6	+8.9	62.2	N	109
1-4, 95-97	5.46	2.34 E-6	−2.5	72.7	+13.3	61.7	N	107
1-4, 105-107	5.56	1.58 E-6	−5.1	71.8	+11.9	61.2	N	95
1-4, 115-117	5.66	2.39 E-6	−12.5	71.7	+7.9	57.2	N	79
1-4, 125-127	5.76	4.45 E-6	−6.7	70.0	+10.9	59.7	N	84
1-4, 135-137	5.86	8.15 E-6	−4.8	76.9	+10.8	65.4	N	113
1-4, 145-147	5.96	9.39 E-6	−7.5	69.6	+10.6	62.4	N	95
1-5, 15-17	6.16	8.85 E-6	−6.0	66.8	+11.4	55.8	N	86
1-5, 22-24	6.23	5.18 E-6	−18.5	341.1	no stable			174
2-1, 5-7	6.36	1.51 E-6	−35.9	41.5	−78.7	6.5	N	56
2-1, 25-27	6.56	2.74 E-6	+3.1	6.9	+7.2	1.7	N	96
2-1, 45-47	6.76	1.45 E-6	+51.9	345.7	−7.6	199.6	R	47
2-1, 55-57	6.86	2.61 E-6	+40.5	6.8	+17.7	195.5	R	30
2-1, 65-67	6.96	3.08 E-6	+16.8	19.9	+7.3	16.4	N	37
2-1, 75-77	7.06	2.62 E-6	+40.2	14.9	+32.9	13.6	N	48
2-1, 85-87	7.16	2.47 E-6	+36.1	40.6	−12.7	193.4	R	22
2-1, 95-97	7.26	1.92 E-6	+54.9	9.2	−14.5	194.8	R	356
2-1, 105-107	7.36	4.53 E-6	−20.3	28.2	−57.7	185.5	R	36
2-1, 115-117	7.46	5.61 E-6	−13.0	21.6	+6.3	2.4	N	48
2-1, 125-127	7.56	5.15 E-6	−10.7	25.8	+9.4	11.1	N	51
2-1, 135-137	7.66	4.76 E-6	−17.7	21.8	+5.0	9.4	N	43
2-1, 145-147	7.76	4.84 E-6	−15.2	27.0	+18.6	9.5	N	42
2-2, 5-7	7.86	7.17 E-6	+13.5	356.2	+2.6	1.8	N	41
2-2, 15-17	7.96	3.98 E-6	+4.3	329.3	−2.4	7.2	N	48
2-2, 25-27	8.06	4.20 E-6	+3.8	354.8	−27.8	191.9	R	32
2-2, 35-37	8.16	3.01 E-6	−11.8	10.8	−16.7	177.9	R	29
2-2, 45-47	8.26	1.96 E-6	+33.5	6.4	−27.0	185.1	R	47
2-2, 55-57	8.36	2.04 E-6	+20.4	23.4	−17.2	167.7	R	433
2-2, 65-67	8.46	2.06 E-6	+37.1	50.3	−12.4	167.8	R	469
2-2, 75-77	8.56	9.32 E-7	+7.0	131.1	−15.6	179.7	R	375
2-2, 85-87	8.66	1.83 E-6	+21.2	0.6	−21.8	180.2	R	42
2-2, 95-97	8.76	1.92 E-6	+19.4	13.5	−20.3	179.7	R	324
2-2, 105-107	8.86	2.48 E-6	−2.9	18.3	+5.9	168.1	R	34
2-2, 115-117	8.96	1.11 E-6	−24.8	22.2	−8.9	169.4	R	386
2-2, 125-127	9.06	9.84 E-7	−22.3	35.9	−2.8	171.2	R	446
2-2, 135-137	9.16	9.72 E-7	−35.4	72.1	−2.9	172.4	R	472
2-2, 145-147	9.26	6.54 E-7	−35.3	85.1	−2.8	174.8	R	541
2-3, 5-7	9.36	2.29 E-6	+13.6	12.2	−0.2	196.1	R	363
2-3, 15-17	9.46	2.19 E-6	+8.8	22.2	+0.7	195.1	R	363
2-3, 25-27	9.56	2.06 E-6	+2.8	10.0	−0.3	200.7	R	382
2-3, 35-37	9.66	3.94 E-6	−5.4	21.5	−6.8	196.7	R	29
2-3, 45-47	9.76	3.35 E-6	+39.2	355.0	−4.0	200.2	R	29
2-3, 55-57	9.86	4.48 E-6	+27.9	357.8	+14.7	221.8	R	34
2-3, 65-67	9.96	4.71 E-6	+19.7	351.7	+3.5	345.4	N	43
2-3, 75-77	10.06	5.12 E-6	+26.7	6.7	+24.0	359.4	N	48
2-3, 85-87	10.16	4.18 E-6	+33.1	0.4	+33.0	356.1	N	37
2-3, 95-97	10.26	4.74 E-6	+22.7	1.5	+13.7	355.7	N	48
2-3, 105-107	10.36	4.58 E-6	+1.6	12.5	+13.8	356.5	N	44
2-3, 115-117	10.46	5.63 E-6	+0.1	4.1	+13.3	350.3	N	49
2-3, 125-127	10.56	5.80 E-6	+2.4	357.9	+12.5	351.9	N	51
2-3, 135-137	10.66	4.56 E-6	+6.3	359.0	+19.7	349.3	N	47
2-3, 145-147	10.76	3.25 E-6	+1.2	345.1	+11.7	335.2	N	41
2-4, 5-7	10.86	4.01 E-6	+16.0	10.2	+23.0	3.3	N	35
2-4, 15-17	10.96	3.38 E-6	+10.9	5.3	−3.5	196.4	R	28
2-4, 25-27	11.06	2.39 E-6	+19.6	359.7	+3.5	200.8	R	293

Appendix A. (Continued).

Core-Section (interval in cm)	Sub-bottom depth (m)	J_{NRM} (G)	I_{NRM}	D_{NRM}	I_{stable}	D_{stable}	Polarity	MDF (Oe)
Hole 575C (Cont.)								
2-4, 35–37	11.16	3.47 E-6	+21.9	358.4	+6.4	201.2	R	30
2-4, 45–47	11.26	1.27 E-6	+22.9	286.0	+2.9	191.0	R	293
2-4, 55–57	11.36	2.41 E-6	+62.7	320.4	+10.6	191.3	R	258
2-4, 65–67	11.46	3.66 E-6	+42.5	348.6	−2.8	204.3	R	32
2-4, 75–77	11.56	4.72 E-6	+35.5	356.6	+42.0	345.4	N	41
2-4, 85–87	11.66	4.93 E-6	+20.7	342.5	+13.0	347.6	N	49
2-4, 95–97	11.76	5.69 E-6	+23.2	354.0	+21.2	2.8	N	61
2-4, 105–107	11.86	7.48 E-6	−6.9	281.3	−8.5	243.6	N	897
2-4, 115–117	11.96	5.11 E-6	+5.8	1.6	+17.9	346.6	N	44
2-4, 125–127	12.06	5.09 E-6	−24.1	338.4	no stable			91
2-5, 5–7	12.36	6.09 E-6	−9.8	359.2	+13.6	343.4	N	49
2-5, 15–17	12.46	5.41 e-6	+9.4	350.3	+14.6	340.8	N	54
2-5, 25–27	12.56	5.64 E-6	+9.2	350.1	+15.7	340.4	N	61
2-5, 35–37	12.66	3.85 E-6	+7.2	353.9	+21.0	312.6	N	41
2-5, 45–47	12.76	2.47 E-6	+13.6	313.4	+14.7	215.6	R	40
2-5, 55–57	12.86	2.42 E-6	+44.0	337.2	+14.5	180.1	R	34
2-5, 65–67	12.96	1.98 E-6	+43.6	330.9	+16.2	173.0	R	42
2-5, 75–77	13.06	1.48 E-6	+43.7	332.2	+11.8	173.8	R	46
2-5, 85–87	13.16	1.90 E-6	+42.6	335.9	+18.3	172.0	R	36
2-5, 95–97	13.26	1.29 E-6	+27.0	333.1	−2.7	186.2	R	34
2-5, 105–107	13.36	6.36 E-7	−16.8	33.9	−6.5	166.5	R	455
2-5, 115–117	13.46	7.46 E-7	+3.8	66.4	+6.7	164.8	R	494
2-5, 125–127	13.56	9.29 E-7	−7.2	12.6	−5.7	173.6	R	34
2-5, 135–137	13.66	8.16 E-7	+2.6	31.2	+3.6	168.1	R	378
2-5, 145–147	13.76	1.90 E-6	+0.3	357.2	+32.1	190.8	R	42
2-6, 5–7	13.86	3.04 E-6	+21.2	345.4	−7.9	175.5	R	30
2-6, 15–17	13.96	1.99 E-6	+12.4	345.1	−0.8	173.8	R	29
2-6, 25–27	14.06	1.32 E-6	+7.9	349.2	−2.4	171.0	R	28
2-6, 35–37	14.16	1.58 E-6	+17.5	344.2	+14.1	176.8	R	30
2-6, 45–47	14.26	1.54 E-6	+0.4	357.7	−3.8	173.2	R	34
2-6, 55–57	14.36	1.53 E-6	+12.8	0.8	+20.9	171.9	R	35
2-6, 65–67	14.46	8.90 E-7	+1.0	346.4	no stable			42
2-6, 75–77	14.56	6.84 E-7	+9.1	347.7	+12.8	179.5	R	34
2-6, 85–87	14.66	7.30 E-7	+8.9	345.1	+16.2	194.3	R	39
2-6, 95–97	14.76	5.82 E-7	+12.1	353.5	+59.2	215.9	R	40
2-6, 105–107	14.86	5.51 E-7	+6.1	351.1	+31.6	208.0	R	43
2-6, 115–117	14.96	5.46 E-7	−8.0	350.4	−19.7	148.5	R	30
2-6, 125–127	15.06	5.33 E-7	−1.8	19.2	−3.1	142.7	R	38
2-5, 135–137	15.16	3.40 E-7	+32.0	5.5	+9.7	179.9	R	369
2-6, 145–147	15.26	7.58 E-7	+9.6	3.8	+43.2	218.8	R	43
2-7, 5–7	15.36	3.70 E-7	+38.1	30.9	+22.8	210.1	R	298
2-7, 15–17	15.46	4.36 E-7	+12.7	34.1	+6.9	231.6	R	39
2-7, 25–27	15.56	5.84 E-7	+13.9	37.2	+40.9	293.2	N	49
2-7, 35–37	15.66	5.59 E-7	−4.3	73.1	+13.8	27.3	N	61

Notes: J = intensity; I = inclination, D = declination (+ = downward, − = upward); polarity is as derived from stable inclinations and declinations (N = normal, R = reversed).

APPENDIX B
Paleomagnetic Data Derived from Oligocene to Late Miocene Leg 85 Samples (samples were measured at HIG, after demagnetization at 50 Oe)

Sub-bottom depth (m)	Declination (°)	Inclination (°)	Intensity (G)
Hole 572A			
120.00	−30.75	−33.14	0.4140 E-6
121.11	−9.93	7.01	0.1202 E-5
122.61	−8.75	27.17	0.7416 E-6
124.11	−32.03	−13.53	0.6314 E-6
125.61	−11.06	−0.03	0.7462 E-6
127.11	−84.24	−13.65	0.9357 E-6
129.17	−24.49	−16.97	0.6278 E-6
130.33	−16.79	−17.00	0.6634 E-6
131.81	−176.09	−26.31	0.3915 E-5
133.31	2.04	−3.32	0.9725 E-6
134.81	−6.53	6.61	0.9195 E-6
136.31	−15.47	3.35	0.6878 E-6
139.09	−14.29	19.42	0.1012 E-5
140.59	−2.18	12.06	0.5413 E-6
142.09	48.59	−6.87	0.2807 E-5
143.59	−9.26	9.35	0.6088 E-6
145.09	−25.83	6.86	0.7711 E-6
145.80	−79.61	21.75	0.8132 E-5
147.30	−20.03	−27.25	0.9364 E-6
148.80	−1.25	8.03	0.9587 E-6
150.30	−20.42	−12.81	0.7407 E-6
151.80	−133.48	−17.92	0.6038 E-6
153.30	−16.85	17.63	0.9806 E-6
Hole 572B			
154.11	−31.58	−3.65	0.8671 E-6
154.51	−55.50	81.87	0.2193 E-4
155.31	−2.58	−13.63	0.7255 E-6
155.41	−79.98	1.14	0.2373 E-5
155.61	−17.23	−21.52	0.1098 E-5
156.01	−4.34	−5.84	0.1374 E-5
156.41	−13.61	−19.50	0.1121 E-5
156.81	−37.85	−0.95	0.7004 E-6
157.11	12.39	−35.88	0.7492 E-6
157.51	−14.07	20.42	0.1170 E-5
157.91	−13.78	−9.99	0.1745 E-5
158.31	−36.01	42.77	0.2268 E-5
158.61	46.52	−24.13	0.5915 E-5
159.78	−9.95	8.73	0.9883 E-6
161.28	−0.51	3.84	0.8560 E-6
163.32	−120.34	58.39	0.6165 E-5
164.70	−68.68	8.22	0.1372 E-5
166.20	−4.29	−0.79	0.1081 E-5
167.70	−63.76	−12.48	0.2251 E-5
169.29	0.88	15.08	0.7037 E-6
170.79	10.01	−14.63	0.6568 E-6
Hole 572C			
121.40	−8.39	3.66	0.6006 E-6
121.80	−178.13	−50.26	0.1208 E-5
122.40	−19.47	−6.02	0.9384 E-6
122.90	−13.51	−2.08	0.1071 E-5
123.30	48.00	−56.07	0.8916 E-6
123.90	−14.94	−19.92	0.9925 E-6
124.40	−24.54	−17.11	0.4741 E-6
124.80	−21.71	−16.45	0.5465 E-6
125.40	−17.22	−12.78	0.1005 E-5
125.90	−6.50	−0.03	0.9885 E-6
126.30	−15.13	5.02	0.9938 E-6
126.90	−1.16	0.02	0.1164 E-5
127.40	−8.24	−1.76	0.8270 E-6
127.80	−2.11	−19.44	0.1110 E-5
128.40	−10.85	0.93	0.1046 E-5
128.90	−15.52	2.04	0.7333 E-6
129.30	−15.32	−12.64	0.9309 E-6
129.90	−17.16	−12.20	0.7775 E-6
131.19	−30.40	−14.41	0.6704 E-6
131.69	−21.07	−18.65	0.9621 E-6

Appendix B. (Continued).

Sub-bottom depth (m)	Declination (°)	Inclination (°)	Intensity (G)
Hole 572C (Cont.)			
132.19	−32.58	−35.89	0.4285 E-6
132.69	−22.28	−17.31	0.6186 E-6
133.19	−11.94	−28.12	0.8788 E-6
133.69	−20.07	2.97	0.8102 E-6
134.19	−16.21	3.71	0.7840 E-6
134.69	−18.81	−18.69	0.8381 E-6
135.19	−25.23	0.56	0.1240 E-5
135.69	−32.16	−19.57	0.6772 E-6
136.19	−11.76	−19.97	0.1198 E-5
136.69	−5.75	−30.89	0.7144 E-6
137.19	−52.12	62.14	0.1279 E-5
137.69	−11.48	−2.73	0.7534 E-6
138.19	−11.70	−4.61	0.1042 E-5
138.69	−33.83	25.88	0.5139 E-6
139.19	−11.53	7.91	0.9498 E-6
139.69	−11.38	−4.01	0.9837 E-6
140.77	−4.19	−8.91	0.9177 E-6
140.80	−12.22	1.04	0.8669 E-6
141.29	−7.29	20.13	0.8724 E-6
142.30	−13.14	3.52	0.7377 E-6
142.79	−2.13	−10.84	0.8356 E-6
143.28	−13.44	4.43	0.7186 E-6
144.00	−10.69	−6.76	0.9705 E-6
144.70	−28.97	−2.50	0.5550 E-6
145.10	−12.16	3.56	0.8993 E-6
145.62	−6.63	−4.89	0.9526 E-6
150.73	−8.89	−0.78	0.1100 E-5
151.35	−10.10	2.13	0.8162 E-6
151.89	−38.46	63.84	0.8778 E-6
152.39	−12.47	15.45	0.6561 E-6
152.85	36.43	−51.98	0.5028 E-6
153.39	−12.34	−9.72	0.7096 E-6
153.89	−10.87	7.47	0.9266 E-6
154.35	−2.11	5.25	0.1255 E-5
154.89	−12.30	−23.57	0.1481 E-5
155.39	−7.84	12.71	0.7945 E-6
155.85	−19.01	−28.72	0.4982 E-6
156.39	−24.48	−28.81	0.8046 E-6
156.89	−16.39	−37.02	0.5728 E-6
157.35	−8.40	2.59	0.1009 E-5
157.70	−45.08	−26.67	0.2735 E-6
158.25	−4.34	−14.06	0.8719 E-6
158.61	−167.35	−39.02	0.7069 E-6
163.89	−14.38	−3.12	0.1297 E-5
164.24	−17.10	−16.14	0.1020 E-5
164.65	−39.85	−13.52	0.5896 E-6
165.01	−18.33	−17.82	0.9418 E-6
165.48	−13.68	−16.83	0.8960 E-6
165.92	−12.09	−32.99	0.9920 E-6
166.33	−10.31	14.86	0.7394 E-6
166.85	−49.97	1.01	0.1625 E-5
167.35	−41.09	−1.07	0.1269 E-5
167.83	−11.07	−6.81	0.8448 E-6
168.24	−33.38	−1.47	0.6688 E-6
Hole 572D			
155.21	−3.82	53.57	0.3624 E-5
155.71	−38.52	−37.92	0.4579 E-6
160.70	−15.98	−31.89	0.1086 E-5
161.41	−11.58	−8.63	0.5493 E-6
166.46	−8.68	−14.22	0.7600 E-6
167.33	−18.01	−23.65	0.7482 E-6
170.15	5.01	−14.65	0.2276 E-5
174.88	−17.08	−14.75	0.7485 E-6
179.61	−14.80	−13.99	0.3772 E-6
195.17	−15.52	−27.21	0.8771 E-6
196.56	−31.45	26.45	0.4452 E-6
206.71	−18.77	−30.71	0.5987 E-6
207.29	−16.08	−13.08	0.5534 E-6

Appendix B. (Continued).

Sub-bottom depth (m)	Declination (°)	Inclination (°)	Intensity (G)
Hole 572D (Cont.)			
207.81	−16.52	−20.30	0.6360 E-6
209.85	−9.52	−24.14	0.7813 E-6
210.81	−7.75	−1.15	0.5789 E-6
211.85	−2.28	−21.83	0.7976 E-6
212.43	−12.73	−5.40	0.6967 E-6
213.17	−17.53	−18.95	0.8165 E-6
215.20	−22.97	18.59	0.4700 E-6
215.91	−14.07	−7.39	0.6630 E-6
216.59	−13.90	−36.75	0.8534 E-6
217.70	−67.48	−15.51	0.1477 E-5
218.90	−20.94	−8.88	0.5221 E-6
219.58	−14.39	−21.04	0.8489 E-6
221.33	−1.23	−42.77	0.3744 E-6
221.75	−13.96	−29.20	0.5950 E-6
222.96	−33.83	−27.70	0.3443 E-6
224.27	−20.36	−34.81	0.6797 E-6
224.78	−16.39	−7.72	0.7839 E-6
225.57	−9.91	−35.13	0.5328 E-6
226.00	−68.72	9.64	0.1311 E-5
226.42	−9.87	−14.00	0.5632 E-6
227.26	8.46	−19.50	0.7741 E-6
227.71	−22.81	−22.63	0.7773 E-6
228.82	12.18	−29.71	0.6925 E-6
229.67	−20.08	−23.08	0.9788 E-6
230.61	−18.42	−18.40	0.7743 E-6
231.25	−8.98	−21.49	0.6186 E-6
231.75	−19.82	0.46	0.4861 E-6
236.61	−20.27	−4.66	0.6795 E-6
237.34	0.12	−15.09	0.6262 E-6
238.84	−14.81	−16.79	0.6937 E-6
240.73	−11.52	−13.60	0.4501 E-6
241.30	−25.25	−22.29	0.7709 E-6
241.84	−16.91	−15.83	0.5727 E-6
242.78	0.39	21.02	0.7595 E-6
243.58	−11.07	16.97	0.6840 E-6
244.41	34.50	−18.63	0.3768 E-6
245.35	−22.48	−19.93	0.5722 E-6
245.78	−19.38	−25.11	0.5653 E-6
246.05	−42.82	−7.09	0.6969 E-6
247.03	−26.75	−18.28	0.4328 E-6
248.38	−90.44	1.06	0.8393 E-4
249.69	1.80	−2.46	0.8809 E-6
250.87	−7.92	25.23	0.8604 E-6
251.66	−10.69	24.56	0.5116 E-6
252.68	−159.02	39.25	0.2302 E-6
253.45	−26.03	−14.16	0.7069 E-6
254.18	10.47	−19.19	0.1020 E-5
254.90	−3.75	−2.36	0.4406 E-6
255.47	−22.86	−15.24	0.7378 E-6
255.67	−6.19	−26.16	0.9569 E-6
256.75	−0.07	−5.65	0.1362 E-4
257.21	−60.13	−28.01	0.9167 E-5
257.82	157.88	−17.59	0.1356 E-4
258.25	−1.74	−25.32	0.8024 E-6
259.29	−16.69	−11.11	0.6727 E-6
260.21	33.21	4.53	0.2305 E-5
261.12	7.33	−4.43	0.7210 E-5
265.63	37.35	−7.17	0.1404 E-5
267.51	−0.35	−21.99	0.4359 E-6
267.61	14.02	5.31	0.1126 E-5
268.40	−7.66	−15.32	0.9872 E-6
270.72	17.49	−51.30	0.6518 E-5
272.32	−3.35	0.12	0.1596 E-5
277.35	83.04	10.26	0.3377 E-4
279.31	−24.17	2.89	0.1902 E-4
281.15	−140.64	−1.92	0.1147 E-4
281.74	9.48	−7.15	0.2453 E-4
284.14	4.36	−5.18	0.1032 E-5
287.41	−0.23	−29.87	0.9808 E-6
294.08	−152.02	4.50	0.6370 E-5
295.23	79.83	−1.39	0.2974 E-4
296.20	−47.31	−8.45	0.2746 E-4
296.71	59.33	6.36	0.2152 E-4
297.24	179.33	−33.50	0.3539 E-5

Appendix B. (Continued).

Sub-bottom depth (m)	Declination (°)	Inclination (°)	Intensity (G)
Hole 572D (Cont.)			
297.76	88.49	−0.95	0.2232 E-4
298.21	37.56	−8.58	0.1265 E-4
299.17	−10.25	−13.36	0.7184 E-6
299.75	−0.23	−7.25	0.6949 E-6
300.56	14.08	−37.07	0.8316 E-6
301.25	42.67	−2.65	0.2334 E-5
302.73	−6.59	−24.36	0.7178 E-6
303.27	−2.32	4.13	0.1181 E-5
304.16	−1.69	−42.06	0.7279 E-6
304.77	−20.14	−49.43	0.6524 E-6
306.20	71.75	−33.87	0.9729 E-6
312.82	−11.89	12.27	0.5565 E-6
313.82	−2.27	−17.47	0.6279 E-6
314.45	−6.03	−13.49	0.6298 E-6
314.93	−14.27	−24.38	0.5363 E-6
315.94	−10.78	−12.21	0.5764 E-6
316.54	−12.43	−12.81	0.5911 E-6
317.44	−16.07	−23.90	0.5329 E-6
318.94	−17.59	−26.50	0.5720 E-6
319.59	−2.07	3.86	0.4699 E-6
320.44	−9.79	−6.63	0.6976 E-6
322.40	−19.62	−16.64	0.6988 E-6
324.25	0.18	−39.53	0.6960 E-6
332.60	149.09	−35.53	0.2580 E-5
333.68	6.39	−19.14	0.6672 E-5
334.66	14.93	−58.26	0.5477 E-5
350.76	4.80	−67.87	0.8096 E-6
351.90	−2.52	−48.04	0.9978 E-6
353.40	−16.92	−42.49	0.1132 E-5
353.77	−5.51	−48.53	0.1057 E-5
354.51	1.20	−42.32	0.9772 E-6
360.77	−31.21	−46.29	0.8072 E-6
360.78	−37.95	−41.04	0.5761 E-6
361.42	−30.14	−31.41	0.4309 E-6
361.76	−11.99	−21.42	0.6691 E-6
362.85	−94.32	−25.47	0.2501 E-5
363.30	−149.29	−22.49	0.6058 E-5
363.73	−50.64	5.85	0.5503 E-5
364.38	−113.67	2.46	0.1272 E-4
364.63	37.70	−11.31	0.1325 E-4
365.27	41.58	−13.36	0.6311 E-5
365.74	−4.31	−31.31	0.6006 E-5
366.21	−17.64	−25.08	0.3020 E-5
367.39	−101.55	−16.96	0.1570 E-5
369.85	101.21	−17.11	0.6478 E-5
370.36	85.91	19.77	0.1123 E-4
370.81	176.37	12.82	0.1045 E-4
371.15	−45.87	−2.95	0.2160 E-4
372.46	58.66	3.92	0.7981 E-5
372.52	105.06	−2.49	0.1124 E-4
373.47	−154.67	−3.41	0.1896 E-4
375.37	−129.14	−8.00	0.1711 E-4
376.23	125.76	5.12	0.2589 E-4
376.37	−156.34	2.18	0.3179 E-4
377.33	61.67	5.57	0.7119 E-5
377.98	54.95	−5.27	0.4237 E-4
379.46	−18.95	4.64	0.1736 E-4
380.06	19.66	5.84	0.2397 E-4
381.36	71.52	−12.66	0.1707 E-4
381.89	125.02	−6.01	0.4127 E-5
382.99	−82.29	−11.77	0.1304 E-4
383.39	116.50	0.92	0.7968 E-5
383.83	73.63	−15.91	0.3317 E-4
384.96	22.98	7.39	0.3002 E-4
385.39	135.63	−72.27	0.3861 E-5
386.21	130.77	−9.36	0.1759 E-4
386.59	162.53	8.45	0.2731 E-4
387.85	−150.65	−4.91	0.2652 E-4
388.27	89.50	−17.95	0.2685 E-4
388.93	−144.08	0.62	0.2755 E-4
389.45	−24.05	−22.78	0.6259 E-5
389.96	−156.88	−20.57	0.2103 E-4
390.26	177.93	−6.46	0.1528 E-4
390.82	−170.43	−2.12	0.1305 E-4

Appendix B. (Continued).

Sub-bottom depth (m)	Declination (°)	Inclination (°)	Intensity (G)
Hole 572D (Cont.)			
391.46	−89.16	−12.73	0.2910 E-4
391.60	−11.69	−11.06	0.2916 E-4
392.47	−5.17	−16.95	0.5982 E-5
392.81	−42.85	−20.42	0.1181 E-4
393.41	168.78	−72.74	0.5074 E-5
393.98	74.84	−9.07	0.1589 E-4
394.44	57.33	−0.95	0.2508 E-4
396.03	−50.87	−7.89	0.2516 E-4
396.31	−62.94	−26.79	0.4312 E-5
396.55	−39.29	−49.79	0.3632 E-5
397.45	−40.25	−60.94	0.1318 E-5
398.24	−140.23	3.26	0.1535 E-4
398.69	−62.93	11.04	0.1686 E-4
399.14	150.05	17.28	0.1288 E-4
399.76	−130.77	11.69	0.1786 E-4
400.31	98.51	−6.22	0.1764 E-4
400.73	23.20	−10.12	0.2191 E-4
401.22	−6.49	−2.11	0.2828 E-4
401.81	3.82	−6.78	0.3381 E-4
402.22	137.23	−18.17	0.2363 E-4
402.73	−178.00	1.76	0.1924 E-4
403.21	103.32	−43.26	0.4757 E-5
403.72	75.32	−4.21	0.1925 E-4
404.24	−78.95	−13.28	0.2303 E-4
404.76	46.58	−4.72	0.2728 E-4
405.24	−127.99	−11.63	0.1532 E-4
405.74	134.91	22.31	0.1872 E-4
406.26	−173.93	11.89	0.1482 E-4
406.74	−54.19	13.15	0.2112 E-4
407.24	−78.33	−1.88	0.2048 E-4
407.59	97.09	−0.89	0.2335 E-4
407.93	−23.41	−0.92	0.4579 E-5
408.51	−158.76	34.16	0.3397 E-5
409.22	−81.47	5.65	0.2485 E-5
409.63	66.65	0.82	0.3848 E-4
410.07	56.95	−1.68	0.7768 E-5
410.59	133.86	−6.82	0.2093 E-4
411.16	70.15	−2.24	0.2894 E-4
411.57	−109.14	−12.89	0.7080 E-5
412.09	15.58	24.43	0.2724 E-5
412.87	54.80	−8.48	0.6336 E-5
413.38	148.94	−12.43	0.8179 E-5
413.86	−124.15	−17.40	0.3058 E-4
414.36	99.58	2.04	0.8275 E-5
417.32	98.54	−23.62	0.6353 E-5
417.85	178.02	−12.27	0.3399 E-5
418.35	−38.30	4.25	0.2667 E-4
418.83	−162.49	−31.43	0.2654 E-4
419.34	175.35	4.65	0.2616 E-4
419.85	−125.56	−4.44	0.1622 E-4
420.35	73.75	−9.61	0.2971 E-4
420.84	−40.35	3.36	0.2615 E-4
421.27	86.85	−14.11	0.2953 E-4
421.85	20.22	−9.65	0.6591 E-5
422.34	80.44	−7.40	0.2809 E-4
422.83	−12.24	−2.45	0.1523 E-4
423.38	−72.92	8.32	0.2177 E-4
427.76	−45.64	1.60	0.1204 E-4
429.08	−10.27	−33.85	0.1698 E-4
429.55	50.94	−40.31	0.2571 E-5
430.13	176.79	−26.51	0.8744 E-5
430.58	137.05	−7.67	0.9320 E-5
431.05	45.85	−17.25	0.1393 E-4
431.63	92.42	−12.47	0.2017 E-4
432.08	14.73	−25.41	0.1083 E-4
432.55	61.16	−3.76	0.1575 E-4
433.13	−60.18	−13.79	0.1636 E-4
433.58	115.41	−27.16	0.1550 E-4
434.05	76.03	−11.87	0.2365 E-4
434.63	71.58	−27.52	0.1131 E-4
436.13	−6.23	−6.49	0.5424 E-5
436.71	107.11	0.81	0.3451 E-4
437.22	96.46	−10.45	0.1157 E-4
437.62	128.74	−4.40	0.4012 E-4

Appendix B. (Continued).

Sub-bottom depth (m)	Declination (°)	Inclination (°)	Intensity (G)
Hole 572D (Cont.)			
438.51	46.73	0.51	0.5201 E-4
438.78	−78.05	2.87	0.3231 E-4
439.27	83.08	−6.39	0.6410 E-4
439.83	−141.86	5.24	0.3502 E-4
441.02	45.37	13.30	0.4477 E-4
441.61	53.81	−1.41	0.1811 E-4
442.20	61.70	0.51	0.3093 E-4
443.18	−171.07	17.29	0.2928 E-4
443.81	−126.31	12.38	0.4142 E-4
445.63	30.23	13.44	0.4874 E-4
446.32	−71.31	−36.34	0.7333 E-5
446.69	−11.51	−23.65	0.7505 E-6
447.31	23.53	−35.48	0.9180 E-6
448.49	−118.56	−2.09	0.4200 E-5
450.41	14.08	0.98	0.3600 E-4
451.02	76.11	−5.69	0.3831 E-4
451.38	−14.94	2.83	0.5979 E-4
451.61	136.38	−18.41	0.4659 E-4
452.01	163.55	−2.47	0.4647 E-4
452.55	−60.05	5.24	0.4595 E-4
452.94	48.25	−6.44	0.7193 E-4
453.15	−85.56	1.03	0.4306 E-4
453.64	−130.66	3.68	0.3380 E-4
455.31	−63.25	−0.78	0.5773 E-4
455.71	−50.25	−0.61	0.5391 E-4
456.18	166.31	1.99	0.3136 E-4
456.61	−50.23	−11.23	0.2431 E-4
457.31	6.88	−17.91	0.2098 E-4
457.56	66.30	0.24	0.3146 E-4
458.73	17.09	−18.95	0.2549 E-4
459.38	−69.94	12.30	0.5609 E-5
459.91	−106.51	21.59	0.2369 E-5
461.00	−21.26	21.40	0.1292 E-5
461.91	95.69	−3.38	0.1422 E-4
462.33	−162.62	0.72	0.1164 E-4
463.36	−63.33	1.89	0.3102 E-4
463.96	−71.69	−1.50	0.4524 E-4
464.16	−95.37	3.56	0.3286 E-4
464.41	−80.51	3.40	0.8191 E-5
Hole 573			
86.21	23.72	−19.22	0.9955 E-6
87.81	27.88	−19.91	0.1026 E-5
88.54	24.77	−16.80	0.1072 E-5
89.15	28.41	−5.22	0.8568 E-6
89.43	24.21	−8.47	0.9709 E-6
89.85	23.55	−14.10	0.1104 E-5
90.51	22.69	−7.38	0.1111 E-5
90.92	30.24	−22.56	0.1188 E-5
91.32	33.94	−6.29	0.8573 E-6
92.01	25.22	−11.98	0.1053 E-5
92.43	27.47	−3.91	0.9334 E-6
92.82	21.10	−14.77	0.8963 E-6
93.01	26.90	−22.95	0.9816 E-6
93.93	25.43	−14.17	0.9546 E-6
94.32	23.73	−19.88	0.9472 E-6
95.64	24.91	−10.49	0.9491 E-6
96.03	16.62	−14.74	0.9864 E-6
96.44	25.62	−11.32	0.1093 E-5
97.01	32.12	−9.29	0.8938 E-6
97.43	41.21	−0.47	0.9953 E-6
97.94	21.35	−13.89	0.1012 E-5
98.51	31.04	−7.38	0.8489 E-6
98.93	23.04	−3.07	0.9959 E-6
99.44	59.54	−18.85	0.7823 E-6
100.01	42.33	8.23	0.7683 E-6
100.43	30.72	−2.32	0.8443 E-6
100.94	34.81	−9.78	0.8179 E-6
101.51	23.96	−21.32	0.1053 E-5
101.93	44.61	−5.53	0.1017 E-5
102.44	43.06	−41.63	0.8287 E-6
103.01	25.43	−13.11	0.9394 E-6
103.43	35.21	−23.91	0.8869 E-6

Appendix B. (Continued).

Sub-bottom depth (m)	Declination (°)	Inclination (°)	Intensity (G)
Hole 573 (Cont.)			
103.94	35.85	9.47	0.9653 E-6
105.40	25.45	0.96	0.9804 E-6
105.82	31.99	6.00	0.8664 E-6
106.22	27.52	−17.34	0.9700 E-6
106.63	31.45	12.87	0.9875 E-6
107.32	31.51	−0.87	0.9585 E-6
107.72	13.01	−4.14	0.8362 E-6
108.13	26.22	3.83	0.9893 E-6
108.82	76.76	−9.58	0.1185 E-5
109.22	39.59	13.03	0.7803 E-6
109.63	19.69	2.05	0.1078 E-5
110.31	26.58	2.99	0.9746 E-6
110.72	22.80	2.98	0.9987 E-6
111.82	20.95	−11.44	0.8673 E-6
112.22	24.11	2.60	0.9206 E-6
112.63	30.47	−3.26	0.8608 E-6
113.04	49.52	10.16	0.1032 E-5
113.45	27.40	3.48	0.7606 E-6
113.87	38.93	34.22	0.9630 E-6
114.54	21.83	9.72	0.9329 E-6
114.95	24.04	−6.69	0.9261 E-6
115.37	27.16	30.72	0.1442 E-5
116.04	2.25	−18.19	0.4428 E-6
116.45	31.44	12.46	0.9073 E-6
116.87	37.53	−14.76	0.7448 E-6
117.54	32.80	20.03	0.8411 E-6
117.95	29.00	5.21	0.1104 E-5
118.37	32.30	6.29	0.9178 E-6
119.04	45.01	1.69	0.2398 E-5
119.45	24.29	7.48	0.9006 E-6
119.87	28.06	1.50	0.9696 E-6
120.54	21.75	5.83	0.1006 E-5
120.95	51.48	−2.96	0.1089 E-5
121.37	33.07	0.96	0.8907 E-6
121.72	34.28	2.15	0.9283 E-6
122.41	22.64	5.30	0.9404 E-6
122.82	61.89	37.45	0.7244 E-6
123.22	44.85	33.44	0.6481 E-6
123.91	−46.36	−33.53	0.1648 E-5
124.32	40.05	−6.55	0.8978 E-6
124.72	69.17	1.57	0.3192 E-5
125.41	20.61	−26.06	0.8318 E-6
125.82	26.05	8.35	0.1318 E-5
126.22	31.07	26.91	0.1052 E-5
126.91	42.66	27.79	0.1101 E-5
127.32	29.47	7.04	0.1297 E-5
127.72	18.92	−20.03	0.1878 E-5
128.41	33.21	3.78	0.1601 E-5
128.82	26.15	13.52	0.1567 E-5
129.22	10.43	14.17	0.1365 E-5
129.91	9.68	−7.14	0.1353 E-5
130.32	19.98	14.18	0.1084 E-5
130.72	16.39	11.46	0.1040 E-5
431.61	39.01	24.43	0.1875 E-5
132.01	17.06	−11.45	0.3362 E-5
132.53	7.31	5.15	0.1368 E-5
133.52	15.21	8.16	0.1292 E-5
135.02	6.37	4.74	0.1430 E-5
136.52	14.48	14.71	0.1188 E-5
138.02	5.75	−2.56	0.1616 E-5
139.52	11.62	−7.76	0.1586 E-5
140.81	19.50	4.25	0.7739 E-6
142.38	7.54	1.80	0.1501 E-5
143.87	9.36	1.80	0.1467 E-5
145.37	3.58	7.59	0.1055 E-5
146.81	8.17	8.97	0.1459 E-5
148.37	12.30	14.41	0.1075 E-5
150.69	5.30	8.20	0.1670 E-5
152.11	10.16	3.56	0.1565 E-5
153.61	12.11	5.64	0.1432 E-5
154.36	5.80	−18.86	0.1494 E-5
155.86	7.10	−6.06	0.1502 E-5
157.77	20.82	−12.47	0.1587 E-5
158.84	14.42	−13.32	0.1059 E-5

Appendix B. (Continued).

Sub-bottom depth (m)	Declination (°)	Inclination (°)	Intensity (G)
Hole 573B			
142.36	−3.48	16.36	0.7763 E-6
143.97	−27.05	33.28	0.6505 E-6
144.97	−2.55	19.79	0.5568 E-6
152.29	−13.15	−14.26	0.7916 E-6
155.27	12.83	−23.12	0.5982 E-6
158.74	−9.33	−13.35	0.1085 E-5
164.77	−7.16	−5.92	0.8191 E-6
176.03	−16.11	−7.67	0.9562 E-6
194.51	6.41	5.01	0.2402 E-5
195.49	−13.09	1.49	0.1063 E-5
195.83	−10.46	−16.54	0.9053 E-6
208.21	−5.61	−10.90	0.8185 E-6
211.58	−15.07	−13.18	0.1155 E-5
218.47	−9.28	−14.07	0.9271 E-6
222.52	−5.57	−12.21	0.8315 E-6
226.47	−9.48	2.97	0.8793 E-6
229.48	17.52	−15.09	0.1660 E-5
232.34	−7.49	−9.08	0.1147 E-5
235.39	−9.14	−4.67	0.1034 E-5
238.39	75.72	−41.19	0.6343 E-6
245.23	−0.67	5.27	0.9579 E-6
247.91	−13.44	−6.62	0.9069 E-6
254.47	−2.46	−8.96	0.8465 E-6
257.27	−43.96	−3.59	0.3488 E-6
262.71	126.90	−67.92	0.3921 E-5
263.18	152.60	1.97	0.8968 E-5
263.85	158.01	12.83	0.1067 E-4
264.34	10.55	10.97	0.3819 E-5
264.84	−92.07	−9.79	0.3357 E-5
265.83	12.11	4.09	0.1434 E-4
265.85	−113.28	−1.23	0.8724 E-5
266.34	−81.93	2.62	0.7963 E-6
266.79	−66.41	20.68	0.1091 E-4
267.39	22.03	−19.93	0.2294 E-5
267.92	−133.81	12.03	0.6803 E-5
268.19	−24.30	3.25	0.3354 E-5
268.86	31.36	−2.32	0.1702 E-5
269.33	−91.14	−35.33	0.1746 E-5
269.79	44.14	18.83	0.2735 E-5
270.30	38.93	5.04	0.8556 E-5
270.88	−93.38	−9.58	0.8369 E-5
271.31	−51.93	4.44	0.2675 E-5
271.75	−68.92	2.29	0.6279 E-5
272.47	73.34	−0.71	0.3252 E-5
272.65	29.95	54.79	0.1649 E-3
273.30	1.27	−14.26	0.2003 E-5
273.85	61.17	−21.78	0.1701 E-5
274.43	14.31	21.77	0.1156 E-5
274.84	109.63	1.37	0.2742 E-5
275.49	−158.77	17.87	0.9944 E-6
276.70	24.78	−0.03	0.2334 E-5
277.03	−134.29	−15.78	0.3077 E-5
277.77	169.35	−17.68	0.6023 E-5
278.65	36.79	−9.31	0.1965 E-5
279.69	−75.92	0.74	0.3634 E-5
281.06	−71.61	11.08	0.2286 E-5
281.73	103.88	−4.28	0.5347 E-5
282.21	35.24	−2.86	0.7671 E-5
282.82	−87.06	−5.26	0.5426 E-5
283.32	−40.73	−8.96	0.3548 E-5
283.92	36.47	−5.45	0.2603 E-5
284.54	−27.46	−5.29	0.1903 E-5
285.27	37.00	−27.47	0.9356 E-6
286.17	−54.40	34.91	0.1466 E-5
286.62	−114.84	−2.39	0.5767 E-5
287.13	175.08	−1.11	0.4377 E-5
287.57	172.02	4.80	0.9397 E-5
288.40	23.10	10.87	0.4489 E-5
290.63	−125.40	−36.20	0.1221 E-5
291.10	−34.57	−12.26	0.2990 E-5
291.67	37.29	−7.48	0.1681 E-5
292.09	−90.20	37.44	0.1097 E-5
292.89	159.39	16.11	0.2984 E-5
293.12	−9.91	1.68	0.4774 E-5

Appendix B. (Continued).

Sub-bottom depth (m)	Declination (°)	Inclination (°)	Intensity (G)
Hole 573B (Cont.)			
293.69	162.76	15.20	0.3546 E-5
296.11	−131.53	2.90	0.1730 E-5
300.35	−73.17	26.28	0.7788 E-6
301.70	169.34	1.56	0.2245 E-5
302.44	−110.61	−6.75	0.3257 E-5
303.05	1.45	−13.76	0.1619 E-5
303.62	−54.66	3.74	0.2483 E-5
304.06	−81.02	−4.04	0.2845 E-5
309.66	91.88	24.74	0.1601 E-5
310.13	85.09	41.56	0.2700 E-5
312.34	−25.76	−20.87	0.1287 E-5
312.65	−26.14	6.13	0.3160 E-5
319.31	72.29	−5.06	0.3639 E-5
319.75	−15.43	11.99	0.1200 E-4
320.21	−107.50	−20.09	0.3259 E-5
320.73	−154.99	14.37	0.1337 E-4
321.18	178.93	7.22	0.9509 E-5
321.67	−40.87	6.66	0.1291 E-5
322.28	−149.77	−4.70	0.1373 E-4
322.61	88.39	−10.42	0.6825 E-5
324.73	−110.58	−7.28	0.1464 E-4
325.19	147.45	−10.71	0.9675 E-5
325.93	−121.45	18.05	0.2280 E-5
326.76	159.89	24.15	0.1566 E-4
327.83	26.56	12.56	0.8943 E-4
328.10	−147.20	6.68	0.9576 E-5
328.62	14.25	4.48	0.1614 E-4
329.52	50.84	−3.84	0.2894 E-4
329.95	−61.68	2.59	0.2324 E-4
330.05	128.47	−3.28	0.5178 E-5
331.74	40.22	2.22	0.5733 E-5
332.64	−125.41	−29.77	0.1772 E-5
338.06	−70.58	−10.66	0.4178 E-5
338.58	−51.32	−11.75	0.8574 E-5
339.56	−134.77	−10.71	0.1148 E-4
340.58	−160.80	−9.96	0.6950 E-5
342.61	−101.35	3.46	0.1970 E-4
343.11	−98.33	−5.13	0.9847 E-5
348.75	104.53	1.69	0.6326 E-5
350.81	−146.67	−23.11	0.6124 E-5
352.54	−171.57	−38.14	0.2393 E-5
357.23	35.25	−55.40	0.3830 E-6
357.81	−133.69	−15.61	0.1155 E-4
358.86	−116.82	−29.49	0.5531 E-5
359.87	8.59	−68.75	0.1017 E-5
360.29	−145.86	−28.99	0.2135 E-5
360.64	−46.90	−1.57	0.7405 E-5
361.36	−53.66	−12.91	0.2598 E-5
361.54	74.01	−28.51	0.1542 E-5
366.69	−94.48	−17.81	0.2459 E-5
367.29	104.72	2.06	0.3896 E-5
367.65	6.12	−45.35	0.7391 E-6
377.66	−127.01	23.13	0.8867 E-6
378.06	−122.70	1.47	0.3539 E-5
378.55	−36.81	9.35	0.8119 E-5
379.12	2.85	−1.35	0.1317 E-5
379.88	−15.36	−14.50	0.9022 E-6
380.21	−171.80	19.88	0.7166 E-6
380.64	56.45	−17.48	0.5820 E-5
381.50	12.81	−43.76	0.2222 E-6
382.23	135.31	−15.02	0.4045 E-5
383.05	5.73	−23.06	0.8870 E-6
385.66	−98.72	−17.65	0.5337 E-6
386.25	−127.45	−20.58	0.6318 E-5
386.88	−7.57	−18.02	0.1104 E-5
387.53	129.43	9.31	0.4779 E-6
388.03	−6.74	−12.52	0.1541 E-5
388.57	−82.63	−24.86	0.9358 E-6
389.07	−20.34	−16.57	0.4100 E-6
389.77	22.88	−23.60	0.1440 E-5
390.47	−153.11	−15.11	0.5431 E-6
390.98	14.63	−2.53	0.1817 E-5

Appendix B. (Continued).

Sub-bottom depth (m)	Declination (°)	Inclination (°)	Intensity (G)
Hole 573B (Cont.)			
391.46	71.43	14.77	0.1064 E-5
391.92	−35.39	−3.71	0.7785 E-6
396.34	−26.35	−17.69	0.3195 E-5
396.99	0.36	−12.71	0.1076 E-5
398.75	−19.46	3.32	0.5444 E-6
399.24	12.90	18.20	0.2169 E-5
404.57	102.67	10.02	0.3522 E-5
404.98	−121.21	30.19	0.6779 E-6
405.73	105.01	−59.02	0.6213 E-6
406.29	8.36	−13.91	0.2309 E-5
406.86	13.34	2.93	0.1580 E-5
407.43	−108.95	13.77	0.6658 E-6
408.36	12.57	−10.04	0.6624 E-6
408.61	2.04	−6.00	0.3624 E-6
409.19	−20.50	−34.89	0.5770 E-6
410.01	−11.80	−5.94	0.5892 E-6
410.91	16.57	−21.89	0.6050 E-6
411.23	17.62	−14.97	0.7586 E-6
414.33	−14.49	−31.00	0.6793 E-6
415.25	4.45	−33.34	0.4999 E-6
418.28	−32.64	1.81	0.4464 E-6
418.79	11.05	−35.19	0.5381 E-6
424.07	175.16	23.15	0.1697 E-5
424.64	71.38	−37.83	0.3329 E-6
425.45	−146.19	−20.66	0.5830 E-6
433.25	−29.70	−32.21	0.5071 E-6
434.30	2.04	−49.06	0.4829 E-6
435.07	−21.80	−15.24	0.1427 E-5
435.48	−2.84	−13.51	0.9517 E-6
435.80	−23.32	−21.05	0.4468 E-6
436.06	5.14	−37.47	0.6220 E-6
436.57	13.63	−23.41	0.3267 E-6
442.74	52.58	−10.44	0.7661 E-6
447.69	−65.33	8.87	0.6548 E-6
452.15	24.65	−21.61	0.6318 E-6
452.55	66.18	−12.20	0.8267 E-6
453.36	39.78	13.17	0.2101 E-5
453.63	−29.45	12.52	0.1961 E-5
453.97	22.36	−12.31	0.2094 E-5
461.69	−32.23	−27.03	0.8095 E-6
462.51	−4.80	−2.12	0.4820 E-6
463.53	−29.01	−1.70	0.6072 E-6
464.96	−27.17	−61.94	0.8356 E-6
465.59	−3.83	−47.50	0.1450 E-5
466.12	−14.14	−48.15	0.9443 E-6
466.51	5.19	−39.94	0.1039 E-5
467.01	1.05	−36.00	0.6648 E-6
467.61	−18.21	−31.69	0.9446 E-6
468.43	−31.19	34.48	0.8813 E-6
471.27	−34.38	19.41	0.9195 E-6
471.70	−5.71	28.11	0.9408 E-6
472.30	−11.41	−36.00	0.1291 E-5
473.96	−19.03	−37.41	0.1375 E-5
474.03	−35.68	−39.57	0.1206 E-5
480.62	−23.28	1.75	0.4327 E-6
490.14	−161.24	7.57	0.1907 E-5
492.43	−28.98	4.98	0.7220 E-6
494.02	−21.97	−8.18	0.7251 E-6
499.77	−152.15	−15.96	0.5986 E-5
501.14	−108.37	−3.21	0.1513 E-5
502.02	−32.39	8.87	0.9539 E-5
502.85	−39.21	15.21	0.2282 E-5
503.37	−79.10	11.46	0.1810 E-4
503.58	−102.37	14.02	0.1488 E-4
510.24	61.41	14.09	0.2007 E-4
520.63	−110.70	1.02	0.1584 E-4
521.07	−112.64	2.11	0.1954 E-4
521.47	−112.67	−1.46	0.1341 E-4
521.91	−111.50	4.88	0.1761 E-4
522.37	−40.59	6.42	0.2150 E-4
523.65	−89.88	−0.25	0.8600 E-4
526.06	−114.01	−13.11	0.3485 E-3

Appendix B. (Continued).

Sub-bottom depth (m)	Declination (°)	Inclination (°)	Intensity (G)
Hole 573B (Cont.)			
526.35	−139.06	−47.52	0.6530 E-4
526.55	179.56	10.27	0.2383 E-4
527.00	−128.69	−1.69	0.1553 E-4
Hole 574			
93.34	15.74	5.72	0.1262 E-5
96.39	16.33	10.50	0.1451 E-5
100.22	8.63	3.83	0.1533 E-5
101.74	6.54	−1.58	0.1547 E-5
103.79	10.15	−7.07	0.1410 E-5
110.69	11.50	4.71	0.1534 E-5
113.86	8.98	−13.74	0.8777 E-6
115.96	10.66	2.42	0.1459 E-5
117.16	11.24	1.57	0.1482 E-5
121.02	7.91	4.56	0.1419 E-5
127.71	12.05	11.96	0.1402 E-5
127.96	9.52	11.38	0.1352 E-5
128.26	−5.33	8.55	0.1327 E-5
128.48	9.91	−2.16	0.1145 E-5
128.91	11.32	0.52	0.1216 E-5
129.40	−12.44	6.81	0.1391 E-5
129.98	75.68	0.99	0.5927 E-6
130.40	51.12	−13.05	0.4902 E-6
130.90	10.50	1.62	0.1269 E-5
131.48	10.91	13.06	0.1313 E-5
131.90	43.68	−7.80	0.3600 E-6
133.54	52.54	−41.28	0.8282 E-6
135.04	20.80	6.69	0.1650 E-5
136.54	18.67	−16.38	0.1537 E-5
138.54	20.72	2.04	0.1580 E-5
140.04	28.60	−1.38	0.1246 E-5
141.54	21.22	−1.05	0.1569 E-5
145.01	26.74	−8.48	0.1283 E-6
146.34	30.94	−2.09	0.1590 E-5
148.91	21.38	−5.81	0.1716 E-5
150.41	21.95	−3.68	0.1374 E-5
151.91	33.03	7.32	0.1461 E-5
153.81	52.13	−6.86	0.1003 E-5
155.31	26.84	−8.26	0.1368 E-5
156.81	30.68	8.71	0.1570 E-5
158.81	54.74	−37.27	0.1014 E-5
160.31	55.51	−35.46	0.9009 E-6
161.81	61.59	−42.07	0.7480 E-6
163.81	50.98	−27.94	0.8071 E-6
165.31	78.09	−27.78	0.6284 E-6
166.66	60.62	−38.43	0.8329 E-6
166.81	69.09	−39.44	0.8563 E-6
168.81	59.61	−28.17	0.7275 E-6
170.31	66.36	−40.39	0.8703 E-6
171.81	79.49	−35.24	0.7439 E-6
173.35	47.42	−28.84	0.1023 E-5
175.16	65.70	−35.96	0.8586 E-6
179.88	44.65	−41.10	0.8922 E-6
183.24	48.12	−41.15	0.8318 E-6
183.77	49.38	−36.07	0.9404 E-6
184.63	−116.99	17.83	0.2612 E-5
185.66	−16.54	−2.83	0.9616 E-6
187.35	−43.85	−28.84	0.1156 E-5
188.85	−34.53	−23.40	0.8712 E-6
193.74	7.48	7.14	0.1429 E-5
196.83	15.04	−10.59	0.8767 E-6
197.02	119.67	−41.13	0.4188 E-6
199.64	−37.39	−13.28	0.2298 E-5
199.85	51.17	−8.44	0.2696 E-5
200.05	49.67	−8.47	0.2832 E-5
200.32	46.45	9.63	0.1254 E-5
200.50	87.35	−0.38	0.4257 E-4
200.86	38.04	7.48	0.1288 E-5
201.16	52.76	17.87	0.1883 E-5
201.36	−58.98	−13.46	0.3352 E-5
201.56	−97.02	−0.05	0.1598 E-4
201.77	−110.41	−3.22	0.2250 E-4
201.98	−71.31	19.98	0.1186 E-4

Appendix B. (Continued).

Sub-bottom depth (m)	Declination (°)	Inclination (°)	Intensity (G)
Hole 574 (Cont.)			
202.53	128.58	−24.90	0.6949 E-5
202.76	137.30	9.33	0.1053 E-4
203.06	122.50	−11.86	0.6840 E-5
203.36	117.13	10.45	0.5108 E-5
203.66	79.40	−11.10	0.3030 E-5
204.03	97.01	−15.92	0.1374 E-4
204.26	87.75	−7.32	0.9311 E-5
204.56	78.33	15.84	0.1846 E-4
205.16	41.16	9.38	0.2323 E-5
205.53	4.90	−14.65	0.1995 E-5
205.76	10.50	−41.27	0.2302 E-5
206.06	15.46	−53.03	0.2849 E-5
206.36	31.17	−55.06	0.6456 E-5
206.48	32.42	−53.28	0.4737 E-5
Hole 574A			
96.26	57.22	19.11	0.1344 E-5
99.26	2.57	25.44	0.3752 E-6
102.96	11.36	15.44	0.2959 E-6
104.65	3.37	−13.70	0.3964 E-6
106.15	0.10	−14.01	0.1102 E-5
112.25	−27.76	16.08	0.8613 E-6
116.04	−13.75	18.23	0.1077 E-5
122.71	66.28	67.55	0.8800 E-6
125.44	5.50	16.16	0.8511 E-6
128.34	21.48	8.02	0.8496 E-6
132.03	34.39	9.02	0.1317 E-5
135.69	37.87	23.39	0.1267 E-5
140.15	31.75	21.00	0.1223 E-5
141.89	16.96	26.89	0.1232 E-5
144.02	64.65	0.00	0.1219 E-5
149.87	3.28	24.47	0.1346 E-5
150.27	16.27	8.68	0.1146 E-5
150.71	15.70	6.90	0.1248 E-5
150.98	21.93	17.60	0.1424 E-5
151.37	24.16	14.25	0.1682 E-5
151.77	45.03	−34.33	0.1335 E-5
163.27	59.35	−28.65	0.1173 E-5
164.77	−5.12	−19.41	0.8764 E-6
166.29	60.75	−30.69	0.1191 E-5
167.80	48.41	−28.92	0.1368 E-5
169.30	51.77	−25.34	0.1315 E-5
170.80	64.21	−33.14	0.1182 E-5
173.21	53.88	−18.97	0.8601 E-6
174.71	50.05	−34.16	0.1202 E-5
176.21	−89.00	−0.61	0.2962 E-4
177.71	45.59	1.14	0.1392 E-5
179.21	39.35	−15.31	0.1620 E-5
180.05	41.46	−4.99	0.1458 E-5
Hole 574B			
186.21	43.34	−5.10	0.1609 E-5
187.76	41.93	13.73	0.1428 E-5
189.11	24.59	0.60	0.2102 E-5
190.59	40.12	3.67	0.1511 E-5
192.22	51.53	1.62	0.1694 E-5
193.71	41.94	10.06	0.1368 E-5
Hole 574C			
195.18	60.55	−47.36	0.8097 E-6
196.48	60.42	−43.81	0.8281 E-6
197.06	59.90	−51.40	0.1160 E-5
197.84	55.94	−37.40	0.1028 E-5
198.12	49.85	−45.53	0.9664 E-6
198.43	53.28	−65.64	0.9683 E-6
198.83	113.16	−53.32	0.7672 E-6
199.21	117.42	−35.87	0.1927 E-5
199.61	−129.81	−46.78	0.1616 E-5
199.93	143.11	−60.74	0.5775 E-6
201.61	−100.36	−7.76	0.1163 E-4
201.91	−87.73	−19.54	0.1750 E-4

Appendix B. (Continued).

Sub-bottom depth (m)	Declination (°)	Inclination (°)	Intensity (G)
Hole 574C (Cont.)			
202.05	52.20	−11.79	0.1599 E-4
204.07	−66.66	−16.84	0.1311 E-4
204.80	127.55	−14.10	0.1285 E-4
205.89	66.55	19.15	0.1796 E-4
206.80	37.74	−8.74	0.2284 E-4
208.28	55.26	−47.60	0.9504 E-6
210.39	30.91	−85.21	0.1353 E-5
210.78	101.92	13.53	0.4225 E-5
210.98	97.06	6.03	0.1121 E-4
211.28	124.61	−8.36	0.1525 E-4
211.74	42.01	−7.62	0.1055 E-4
212.05	83.59	1.37	0.2425 E-4
212.40	79.06	10.21	0.3348 E-4
213.16	−137.98	−0.20	0.1528 E-4
216.70	−0.01	−52.32	0.1026 E-5
217.14	28.65	−37.64	0.1986 E-5
217.56	−0.72	−7.82	0.1356 E-4
217.76	−5.81	11.17	0.5048 E-6
218.31	13.34	−70.21	0.1746 E-5
218.61	−154.22	−19.59	0.3892 E-5
223.14	24.59	−0.34	0.1511 E-5
223.93	173.44	5.07	0.2008 E-5
224.31	−0.45	−1.56	0.2345 E-5
224.58	−77.21	−1.41	0.1626 E-5
224.91	114.23	−26.87	0.1224 E-5
225.14	155.20	−20.41	0.3134 E-5
225.43	−65.60	−30.80	0.2426 E-5
225.81	126.05	3.60	0.7823 E-5
226.14	−73.97	−31.49	0.2212 E-5
226.55	119.82	−3.79	0.2855 E-6
232.64	61.59	−23.97	0.3427 E-6
233.11	106.10	−26.34	0.8366 E-6
233.84	45.86	37.80	0.2831 E-6
234.31	−24.30	27.01	0.4259 E-6
234.61	100.40	−9.90	0.8560 E-6
234.90	29.76	39.02	0.5207 E-6
236.86	−93.76	−6.29	0.7998 E-6
237.11	−90.95	0.55	0.4208 E-4
252.29	53.06	−9.47	0.2306 E-6
258.23	70.21	−12.73	0.8032 E-6
261.29	48.24	−46.37	0.1080 E-5
263.12	59.15	−57.03	0.1080 E-5
264.04	48.41	−49.88	0.7906 E-6
271.74	171.81	−10.20	0.1638 E-6
273.35	26.71	−55.26	0.1007 E-5
274.37	51.37	−45.97	0.1076 E-5
280.21	−10.02	−43.03	0.9234 E-6
282.90	25.60	8.09	0.1345 E-5
282.93	3.35	−15.88	0.9385 E-6
284.02	41.75	−1.98	0.1350 E-5
285.67	43.39	7.14	0.1399 E-5
286.31	33.27	4.77	0.1507 E-5
287.29	32.28	−11.16	0.1435 E-5
287.68	29.46	11.76	0.1506 E-5
288.62	33.36	0.42	0.1413 E-5
290.71	18.58	25.87	0.5799 E-6
291.59	40.41	7.46	0.1562 E-5
292.80	42.25	1.37	0.1388 E-5
293.71	27.54	−15.39	0.1552 E-5
299.17	38.47	12.85	0.2522 E-5
300.26	29.53	−8.61	0.1313 E-5
301.62	23.97	−18.47	0.1662 E-5
302.52	30.20	−18.77	0.1320 E-5
303.41	27.77	−8.25	0.1290 E-5
303.83	23.93	−21.54	0.1417 E-5
304.63	20.74	−29.43	0.1502 E-5
305.12	35.76	1.54	0.1327 E-5
306.02	29.45	−25.87	0.1597 E-5
307.05	47.30	−14.14	0.1213 E-5
307.75	32.59	8.63	0.1254 E-5
309.06	47.90	14.66	0.1298 E-5
310.41	−5.62	−55.95	0.6842 E-6
311.09	26.45	−34.24	0.9832 E-6
312.04	−5.61	−23.51	0.6033 E-5

Appendix B. (Continued).

Sub-bottom depth (m)	Declination (°)	Inclination (°)	Intensity (G)
Hole 574C (Cont.)			
312.75	2.84	−41.94	0.8577 E-6
313.94	−2.14	−42.67	0.7843 E-6
318.11	−11.98	−45.66	0.8622 E-6
320.17	−19.52	−43.65	0.7608 E-6
320.90	−1.29	−32.89	0.9536 E-6
327.72	5.57	−54.42	0.6613 E-6
333.94	−9.42	−53.42	0.1048 E-5
336.78	−5.70	−34.58	0.7271 E-6
338.25	−164.93	−74.77	0.1213 E-5
339.39	−65.57	−21.21	0.3826 E-5
340.85	14.24	−9.68	0.1965 E-5
346.68	−33.25	−52.19	0.1028 E-5
350.52	46.30	−26.72	0.1337 E-5
351.65	−122.44	−24.31	0.2946 E-5
358.33	0.31	−7.65	0.4370 E-5
366.76	−64.51	−13.82	0.1579 E-5
375.17	153.65	−20.03	0.1403 E-4
375.63	52.62	3.28	0.1632 E-4
376.39	−22.44	24.18	0.4732 E-5
384.57	−1.62	11.65	0.1188 E-5
348.79	−43.67	−5.75	0.1897 E-6
385.01	−15.51	−1.26	0.5421 E-6
385.78	−63.01	−7.23	0.9591 E-6
394.15	−24.26	25.83	0.2262 E-5
395.68	103.04	−48.27	0.5252 E-6
396.23	87.75	−6.61	0.5772 E-5
396.68	−155.64	−22.51	0.2848 E-5
403.64	−38.37	22.28	0.7695 E-5
404.97	3.51	44.37	0.1415 E-5
406.34	−136.99	62.10	0.6916 E-6
408.46	−55.06	43.24	0.1312 E-5
409.92	1.83	13.98	0.1447 E-5
414.95	12.27	12.00	0.1541 E-5
416.52	−22.45	13.95	0.1383 E-5
418.36	−99.63	20.55	0.1317 E-5
422.76	18.26	17.62	0.1684 E-5
423.73	−147.43	−14.83	0.1827 E-5
432.24	−63.79	17.12	0.1981 E-5
432.90	−17.03	9.66	0.4725 E-5
433.27	−10.67	6.39	0.7738 E-5
434.41	−48.50	−3.76	0.2565 E-5
434.86	−62.87	4.55	0.3776 E-5
435.07	−91.93	−27.16	0.8642 E-6
435.78	−167.00	−16.53	0.3390 E-5
441.65	−86.57	3.77	0.1183 E-5
442.40	−61.07	30.56	0.5119 E-5
442.76	109.96	9.53	0.8783 E-5
443.14	7.92	58.99	0.3506 E-6
443.81	85.22	13.28	0.5486 E-5
444.46	71.22	22.28	0.1142 E-4
444.63	−140.18	26.24	0.3159 E-5
445.19	127.89	34.43	0.4085 E-5
445.84	30.72	16.50	0.3527 E-5
446.30	−2.81	−3.84	0.1814 E-5
451.29	−139.49	−16.81	0.3040 E-4
460.57	49.47	27.35	0.2052 E-4
461.24	−169.78	−2.94	0.1708 E-4
461.73	80.28	6.84	0.1323 E-4
462.11	127.51	13.31	0.8898 E-5
462.71	21.12	10.28	0.6760 E-5
463.29	−64.44	23.81	0.1332 E-4
463.68	178.52	22.96	0.2193 E-5
464.28	−24.65	31.18	0.1195 E-5
464.92	−20.61	16.86	0.1578 E-5
470.06	−52.13	7.79	0.8996 E-6
470.40	22.56	8.73	0.2109 E-5
470.77	−85.33	−10.21	0.1322 E-5
479.63	−75.18	−29.90	0.4698 E-6
480.03	98.18	−5.03	0.1753 E-5
480.28	−7.03	−14.33	0.5751 E-6
480.61	−10.33	15.17	0.1388 E-5
481.13	−6.61	10.35	0.1724 E-5
481.53	−13.12	−6.16	0.1059 E-5
481.86	−37.98	−21.11	0.6720 E-6

Appendix B. (Continued).

Sub-bottom depth (m)	Declination (°)	Inclination (°)	Intensity (G)
Hole 574C (Cont.)			
482.13	−18.59	8.83	0.8269 E-6
482.86	−22.85	3.41	0.2190 E-5
489.07	−5.24	−14.83	0.5807 E-6
490.17	−9.85	−10.53	0.1276 E-5
490.84	−5.15	16.89	0.1506 E-5
491.20	−6.34	−3.81	0.8450 E-6
491.41	−16.22	−7.91	0.1172 E-5
491.86	−51.99	−4.37	0.4625 E-6
492.64	−6.45	−0.41	0.2556 E-5
498.57	−32.06	22.74	0.8648 E-6
498.77	−2.99	−1.98	0.1185 E-5
499.05	−1.33	23.09	0.9921 E-6
499.54	−38.40	15.09	0.8277 E-6
499.97	−8.78	25.79	0.1269 E-5
500.23	−11.81	24.94	0.6042 E-6
500.60	−30.62	27.16	0.7612 E-6
500.99	−51.21	38.99	0.6702 E-6
501.37	13.20	−30.67	0.8634 E-6
501.70	−17.76	−0.08	0.1623 E-5
502.19	−28.28	1.53	0.5164 E-6
502.72	−90.72	6.35	0.1302 E-5
503.16	−76.54	19.96	0.1533 E-5
503.40	−0.47	10.48	0.2513 E-5
503.93	−14.59	15.38	0.4226 E-5
504.40	121.50	66.10	0.4311 E-4
504.77	−108.40	−13.90	0.7935 E-4
505.05	101.60	−65.70	0.4581 E-4
505.23	−133.10	−63.80	0.7238 E-4
505.92	−103.20	−22.40	0.5667 E-4
508.40	96.80	−07.00	0.7053 E-4
508.72	101.70	37.30	0.3732 E-4
509.05	−104.90	−04.60	0.1367 E-4
509.39	−92.80	−48.70	0.5195 E-4
509.76	98.00	24.30	0.1961 E-4
510.30	0.98	8.18	0.2011 E-4
510.61	−154.19	26.19	0.1264 E-4
517.57	78.00	63.20	0.8394 E-4
518.48	69.10	53.60	0.8369 E-4
518.77	93.50	55.70	0.7338 E-4
519.52	−077.20	−37.40	0.2965 E-5
520.00	−085.40	−21.60	0.4318 E-4
Hole 575			
35.31	−132.23	−40.33	0.3275 E-5
35.91	30.01	1.64	0.7878 E-6
36.38	30.57	−33.43	0.2323 E-5
36.81	6.00	−13.37	0.4402 E-5
37.39	44.58	−72.20	0.5699 E-6
37.88	16.75	−18.17	0.2509 E-5
38.31	123.23	−75.13	0.7707 E-6
38.81	35.06	−16.40	0.4074 E-5
39.38	15.85	−17.24	0.5058 E-5
39.81	29.11	−4.70	0.5978 E-5
40.31	15.28	6.54	0.1040 E-4
41.31	−165.24	4.31	0.8456 E-5
41.81	−171.23	−1.21	0.6947 E-5
42.38	0.68	−5.84	0.5870 E-5
42.81	0.45	0.60	0.4508 E-5
43.31	5.14	−14.79	0.2149 E-5
43.88	168.28	−2.33	0.4982 E-5
44.31	−174.24	1.96	0.3889 E-5
44.81	65.25	−38.57	0.1766 E-5
45.31	68.29	−1.37	0.1177 E-5
45.88	145.21	−8.08	0.2724 E-5
46.31	90.55	−7.71	0.2369 E-5
46.81	82.22	−13.13	0.1981 E-5
47.38	68.71	−19.75	0.1242 E-5
47.81	−13.25	−28.74	0.8124 E-6
48.31	−1.18	−20.98	0.6653 E-6
48.88	−9.99	−33.96	0.7818 E-6
49.25	1.15	−32.17	0.8997 E-6
49.74	23.17	−39.85	0.4713 E-6
50.38	27.19	−59.34	0.1331 E-5

Appendix B. (Continued).

Sub-bottom depth (m)	Declination (°)	Inclination (°)	Intensity (G)
Hole 575 (Cont.)			
50.81	1.89	−23.08	0.4949 E-6
51.31	19.28	−45.25	0.6055 E-6
51.88	−14.80	−21.33	0.8629 E-6
52.31	−8.19	−15.71	0.6173 E-6
52.81	2.93	−52.25	0.4420 E-6
53.38	21.92	−12.56	0.5383 E-6
53.81	27.90	−31.70	0.5439 E-6
54.31	23.53	−10.51	0.5020 E-6
54.81	−12.35	−23.90	0.9652 E-6
55.31	0.29	−39.52	0.9079 E-6
55.81	−9.21	−36.53	0.9259 E-6
56.81	−23.30	−22.30	0.1030 E-5
57.31	−8.86	−20.84	0.7780 E-6
57.81	−6.62	−12.77	0.8860 E-6
58.31	−12.70	−31.21	0.6390 E-6
58.81	−25.28	−8.84	0.5837 E-6
59.31	−147.25	−68.27	0.3380 E-6
59.81	−14.78	−25.54	0.5255 E-6
60.31	15.64	10.33	0.6936 E-6
60.81	−12.53	−16.07	0.6049 E-6
61.31	−27.53	−35.50	0.4338 E-6
61.81	−52.16	−40.55	0.3788 E-6
62.81	−15.23	−2.99	0.6925 E-6
63.81	−25.07	−18.11	0.9862 E-6
64.61	−20.47	−25.52	0.8706 E-6
65.31	−13.54	−14.16	0.8028 E-6
66.11	−17.86	−28.15	0.5747 E-6
66.81	30.21	−15.42	0.4612 E-6
67.61	−13.40	−33.70	0.7146 E-6
68.31	−47.45	−11.13	0.1023 E-5
69.11	−61.65	−6.77	0.5349 E-6
69.81	−50.61	−17.31	0.8744 E-6
70.81	−146.23	−8.01	0.3055 E-5
71.31	−50.51	−20.75	0.9244 E-6
72.31	−167.56	12.88	0.1068 E-4
73.11	112.81	15.29	0.3307 E-4
73.46	114.11	7.62	0.2180 E-4
73.86	109.84	−20.94	0.2048 E-5
74.06	80.60	1.14	0.2191 E-5
74.61	87.13	−37.73	0.2834 E-5
75.01	88.99	4.44	0.5569 E-5
75.56	49.13	−44.97	0.4593 E-5
75.96	83.77	−22.12	0.4000 E-5
76.11	73.25	−2.26	0.3183 E-5
76.71	−93.09	−12.89	07775 E-5
77.06	−103.64	−5.71	0.6628 E-5
77.46	−75.88	−37.91	0.1364 E-5
78.01	55.09	7.18	0.3255 E-5
78.56	58.85	1.60	0.2543 E-4
78.96	52.10	−5.54	0.3630 E-5
79.30	68.71	−0.51	0.4731 E-5
79.93	−117.90	−35.53	0.7902 E-5
84.51	171.22	−25.81	0.4558 E-5
85.01	4.01	−11.51	0.9678 E-6
85.62	−30.33	−41.84	0.3782 E-6
85.99	−26.42	−34.29	0.5776 E-6
86.51	−26.55	−2.19	0.3996 E-6
87.06	−19.90	−26.83	0.5451 E-6
87.49	−12.94	−18.76	0.5183 E-6
Hole 575A			
94.09	46.91	−14.27	0.4029 E-5
94.49	50.13	−3.48	0.9490 E-5
95.09	56.08	2.89	0.6587 E-5
95.59	62.36	−5.36	0.8648 E-5
95.99	−97.36	−19.58	0.6722 E-5
96.59	−102.62	−3.36	0.6496 E-5
97.09	−86.56	35.92	0.7884 E-5
97.49	60.58	21.11	0.1183 E-4
98.09	71.76	1.55	0.3652 E-4
98.99	4.54	−3.42	0.1298 E-4
99.39	28.45	1.57	0.3044 E-5
99.99	−166.22	−20.38	0.9745 E-5

Appendix B. (Continued).

Sub-bottom depth (m)	Declination (°)	Inclination (°)	Intensity (G)
Hole 575A (Cont.)			
100.49	−164.99	−3.88	0.1021 E-4
100.89	−163.03	−13.43	0.2448 E-4
101.49	−163.62	3.98	0.5921 E-5
101.99	5.40	16.31	0.2991 E-5
102.39	137.23	−25.54	0.2033 E-5
102.89	6.25	8.22	0.1458 E-4
103.29	7.11	−1.49	0.2232 E-4
103.89	3.44	3.39	0.1986 E-4
104.39	3.63	2.60	0.8409 E-5
104.79	−5.49	−3.87	0.6198 E-5
105.87	−25.75	−19.98	0.7246 E-5
106.49	−20.50	−3.84	0.6080 E-5
106.99	−30.44	2.43	0.1126 E-4
107.39	−21.15	−20.45	0.4619 E-5
107.99	−19.55	−33.84	0.4231 E-5
108.54	−24.50	−4.23	0.2497 E-4
108.89	−24.33	−0.43	0.8369 E-5
109.49	−18.87	−0.17	0.6972 E-5
110.79	−164.29	−3.49	0.1832 E-4
111.19	−154.46	−16.78	0.3999 E-5
111.79	−126.48	−18.25	0.2192 E-5
112.29	−169.33	14.68	0.5741 E-5
112.69	177.97	−2.64	0.2623 E-4
113.29	153.35	−69.57	0.4002 E-5
113.87	−26.07	−23.92	0.7485 E-5
114.39	142.97	−10.88	0.1279 E-4
114.79	−44.85	11.02	0.1783 E-4
115.39	−42.33	2.94	0.1678 E-4
115.89	−48.54	8.38	0.8713 E-5
116.29	−20.22	42.01	0.1532 E-4
116.89	−47.25	0.97	0.9641 E-5
117.39	−39.11	12.09	0.2598 E-5
117.79	−48.58	−9.06	0.5359 E-5
118.39	131.96	1.61	0.5687 E-5
118.89	119.40	−25.28	0.3092 E-5
119.17	133.43	−26.52	0.3820 E-5
119.69	136.97	0.21	0.9366 E-5
120.19	173.42	2.25	0.4720 E-5
120.59	147.86	3.93	0.1153 E-4
121.19	166.54	−12.30	0.1347 E-5
121.69	144.69	−6.23	0.5368 E-5
122.09	135.63	−28.00	0.1082 E-4
122.69	138.85	−0.81	0.1277 E-4
123.19	138.02	4.02	0.1580 E-4
123.39	−77.57	−34.25	0.6874 E-5
123.79	−70.72	−19.20	0.6944 E-5
124.39	−70.40	−18.80	0.2046 E-5
124.89	−84.47	−6.00	0.7238 E-5
125.29	−66.81	−36.58	0.3555 E-5
125.89	94.03	4.88	0.3131 E-5
126.59	−7.00	−62.15	0.5840 E-5
127.09	−34.14	−21.30	0.1440 E-5
127.49	−33.97	−3.81	0.1026 E-4
128.03	−31.33	−18.84	0.4055 E-5
128.21	−35.19	19.16	0.1060 E-4
128.66	122.84	−17.65	0.4536 E-6
129.11	132.28	−81.47	0.1043 E-5
129.54	140.63	6.25	0.2655 E-5
130.11	−92.24	0.52	0.4117 E-4
130.61	125.30	−32.15	0.5678 E-6
131.04	12.80	−31.12	0.4453 E-6
131.61	28.53	−60.73	0.4245 E-6
132.26	−14.25	−15.57	0.3794 E-6
132.76	−9.03	−29.52	0.9063 E-6
133.26	−17.55	−20.18	0.6959 E-6
133.76	−89.93	1.77	0.4232 E-4
134.76	−17.57	−28.50	0.6724 E-6
135.42	−22.97	−67.61	0.9312 E-6
135.80	8.91	−8.42	0.1559 E-5
136.41	87.80	−1.30	0.4177 E-4
136.73	−16.90	−31.54	0.6977 E-6
137.31	64.47	−54.39	0.1251 E-5
137.91	−90.20	0.37	0.4224 E-4
138.26	−18.09	−23.70	0.6456 E-6

Appendix B. (Continued).

Sub-bottom depth (m)	Declination (°)	Inclination (°)	Intensity (G)
Hole 575A (Cont.)			
139.01	6.11	−45.89	0.6391 E-6
139.95	−46.26	−6.20	0.2427 E-5
140.46	−25.90	−28.55	0.8430 E-6
141.04	−30.42	−40.59	0.9949 E-6
141.44	−24.37	−33.18	0.6581 E-6
141.96	−14.63	−38.48	0.7713 E-6
142.71	−131.56	−5.92	0.5062 E-5
143.20	−15.68	−31.65	0.8875 E-6
143.71	−17.00	−13.29	0.8446 E-6
144.26	−30.83	−69.62	0.1275 E-5
144.86	−8.15	−18.29	0.6746 E-6
145.16	−16.56	−9.83	0.5855 E-6
145.61	−12.11	−16.73	0.6973 E-6
145.76	126.20	−31.37	0.2952 E-7
146.06	35.00	−5.66	0.1235 E-5
147.11	−7.89	−21.31	0.1222 E-5
147.66	−13.20	−17.08	0.6800 E-6
148.01	−10.93	−37.50	0.1335 E-5
149.81	−5.64	−37.66	0.4633 E-6
150.35	−25.56	−37.34	0.6518 E-6
150.96	0.99	15.91	0.9398 E-6
151.31	−19.04	−20.17	0.7237 E-6
151.71	−16.26	−22.43	0.8365 E-6
152.06	−15.51	−31.34	0.6051 E-6
152.46	−9.02	−33.64	0.6866 E-6
152.96	−11.91	−29.47	0.7326 E-6
153.16	−5.81	−25.20	0.7660 E-6
153.51	−12.97	−26.34	0.7771 E-6
153.96	−10.34	−39.50	0.8570 E-6
154.31	−30.10	−40.18	0.8498 E-6
154.86	−14.95	−18.39	0.9572 E-6
155.31	−4.72	−36.31	0.6784 E-6
155.66	−22.36	−34.28	0.5156 E-6
156.06	−22.98	−23.17	0.9095 E-6
156.46	−10.22	−42.70	0.7463 E-6
157.31	−21.97	−40.22	0.5130 E-6
157.71	−10.03	−4.24	0.3095 E-6
158.11	54.24	−35.22	0.1181 E-5
158.61	66.83	−48.62	0.1454 E-5
159.16	89.50	−64.41	0.1348 E-5
159.76	17.70	−74.18	0.1455 E-5
160.11	19.43	2.61	0.9537 E-6
160.51	−34.77	−72.29	0.1509 E-5
161.11	42.96	−16.53	0.1177 E-5
161.66	60.39	−70.93	0.1698 E-5
162.26	36.37	−11.38	0.1378 E-5
162.61	27.53	−14.02	0.1531 E-5
163.16	−31.42	−1.02	0.1044 E-5
163.76	−38.36	−12.32	0.4906 E-6
163.96	−9.71	−50.92	0.6072 E-6
164.51	−28.62	−62.75	0.7096 E-6
164.99	11.40	−27.43	0.8673 E-6
165.39	17.43	−34.06	0.6178 E-6
165.99	2.22	−21.21	0.7960 E-6
166.49	12.86	−21.48	0.1490 E-5
166.89	3.33	−30.88	0.1469 E-5
167.49	6.52	−27.04	0.1054 E-5
167.99	−6.19	−55.41	0.1181 E-5
168.39	14.47	−50.37	0.6947 E-6
168.79	−4.35	−44.73	0.5452 E-6
169.39	−8.16	−34.11	0.7868 E-6
169.89	−9.31	−29.47	0.4717 E-6
170.29	−12.21	−36.50	0.8016 E-6
170.89	81.88	−4.26	0.6930 E-5
171.39	−13.43	−41.40	0.6439 E-6
171.79	−12.51	−37.82	0.9849 E-6
172.39	−3.64	−52.40	0.7415 E-6
172.79	−5.10	−41.37	0.9638 E-6
173.39	−7.78	−45.22	0.6168 E-6
174.29	−19.21	−41.25	0.8716 E-6
175.49	−13.88	−70.59	0.5769 E-6
175.99	−39.15	−64.36	0.1071 E-5
176.39	−15.47	−39.26	0.9960 E-6
176.89	−2.89	−38.15	0.7263 E-6

Appendix B. (Continued).

Sub-bottom depth (m)	Declination (°)	Inclination (°)	Intensity (G)
Hole 575A (Cont.)			
177.49	28.18	−44.11	0.7518 E-6
177.89	−18.89	−38.70	0.6630 E-6
178.49	3.44	−49.64	0.6612 E-6
178.99	−1.42	−42.86	0.8350 E-6
179.99	−10.18	−42.37	0.8043 E-6
180.89	−5.95	−69.22	0.8150 E-6
181.49	16.59	−64.68	0.6790 E-6
182.19	−4.05	−59.13	0.8538 E-6
183.69	0.49	−14.23	0.4606 E-6
184.59	−2.61	−19.76	0.4839 E-6
186.19	10.47	−26.50	0.4911 E-6
187.69	6.90	−30.06	0.5668 E-6
188.99	11.86	−45.23	0.8030 E-6
189.99	−3.08	−41.56	0.1133 E-5
193.39	2.70	−41.90	0.7166 E-6
195.79	−9.15	−43.40	0.8092 E-6
198.31	−2.23	−42.84	0.8488 E-6
199.76	−2.90	−40.86	0.7369 E-6
201.52	11.96	−46.23	0.8036 E-6
202.41	−14.28	−49.89	0.8254 E-6
205.01	−3.00	−39.99	0.1015 E-5
205.41	−9.15	−49.72	0.9256 E-6
206.91	9.10	−40.05	0.5588 E-6
Hole 575B			
39.51	−79.29	−21.35	0.2461 E-4
39.76	−68.60	−10.73	0.2979 E-4
40.01	−56.86	10.94	0.2714 E-4
40.24	−57.44	−5.41	0.2191 E-4
40.47	−57.02	1.06	0.2174 E-4
40.60	−60.05	−0.64	0.2301 E-4
40.86	−60.88	3.86	0.2307 E-4
41.09	−55.41	3.40	0.2023 E-4
41.36	−55.00	2.12	0.1724 E-4
41.61	−52.92	−5.51	0.1235 E-4
41.86	−75.09	−5.88	0.2153 E-4
42.10	−67.92	−7.98	0.2929 E-4
42.36	−65.75	1.24	0.3816 E-4
42.59	−43.03	−5.58	0.6883 E-5
42.86	−4.82	38.21	0.2249 E-5
43.11	−13.51	40.94	0.2964 E-5
43.36	−14.59	7.86	0.2973 E-5
43.60	112.07	−3.31	0.5084 E-5
43.86	−38.65	4.78	0.1060 E-4
44.09	−23.02	7.86	0.6013 E-5
44.36	−96.49	0.72	0.6921 E-5
44.61	−76.42	−8.74	0.1251 E-4
44.86	−74.93	−5.38	0.3289 E-5
45.10	−46.73	7.09	0.3172 E-5
45.36	−21.72	5.83	0.1885 E-5
45.59	−26.12	9.05	0.2234 E-5
45.86	−3.28	33.20	0.2271 E-5
46.11	106.79	1.05	0.1273 E-5
46.36	100.76	29.05	0.1186 E-5
46.60	69.03	6.34	0.5959 E-6
46.86	−121.47	22.26	0.2994 E-5
47.09	−94.56	18.45	0.3989 E-5
47.36	−73.05	17.69	0.2109 E-5
47.61	−49.99	47.70	0.3226 E-5
47.86	−26.67	23.84	0.1326 E-5
48.46	−24.59	−28.28	0.4139 E-5
48.75	−11.40	−4.03	0.2573 E-5
49.16	−23.53	−6.11	0.4615 E-5
49.46	−9.45	−44.96	0.4950 E-5
49.66	−41.85	−1.12	0.4654 E-5
49.96	−70.19	26.48	0.4693 E-5
50.28	−66.58	21.64	0.3239 E-5
50.56	−56.51	26.60	0.2572 E-5
50.86	53.54	29.52	0.2446 E-5
51.16	−39.21	17.79	0.2284 E-5
51.46	76.65	−17.21	0.1847 E-5
51.78	50.38	−32.39	0.1072 E-5
52.06	70.34	19.41	0.1518 E-5

Appendix B. (Continued).

Sub-bottom depth (m)	Declination (°)	Inclination (°)	Intensity (G)
Hole 575B (Cont.)			
52.36	54.27	37.69	0.2865 E-5
52.66	24.37	29.18	0.1860 E-5
52.96	138.50	36.09	0.3997 E-5
53.28	114.24	73.40	0.6093 E-5
53.56	81.35	20.54	0.4892 E-5
53.86	−52.34	6.56	0.9651 E-5
54.16	−54.80	4.65	0.1058 E-4
54.46	−46.47	28.63	0.1040 E-4
54.78	−4.19	10.10	0.1339 E-5
55.06	74.24	5.10	0.2921 E-5
55.66	4.06	13.41	0.2414 E-5
56.16	107.71	7.33	0.2675 E-5
56.46	−43.31	21.95	0.4141 E-5
56.76	−42.15	9.45	0.1069 E-4
57.16	−30.07	11.20	0.5584 E-5
57.46	−22.08	1.84	0.7635 E-5
57.76	−10.18	2.09	0.2852 E-5
58.06	−6.04	4.77	0.2567 E-5
58.36	2.29	19.29	0.1752 E-5
58.66	−7.70	38.37	0.1918 E-5
58.96	−19.97	5.44	0.2862 E-5
59.26	−0.11	−2.10	0.3586 E-5
59.56	9.13	16.12	0.3122 E-5
59.86	3.15	17.58	0.2341 E-5
60.16	−6.18	31.90	0.2400 E-5
60.46	9.23	20.67	0.2117 E-5
60.76	7.63	31.78	0.2346 E-5
61.06	1.84	−5.88	0.6080 E-6
61.36	−18.70	−2.21	0.6506 E-6
61.66	−1.68	11.85	0.1143 E-5
61.96	−16.55	6.49	0.9023 E-6
62.26	2.11	10.18	0.6143 E-6
62.56	−7.08	6.71	0.7528 E-6
62.86	−10.29	13.27	0.7168 E-6
63.16	−13.77	15.64	0.7226 E-6
63.46	−4.30	8.95	0.7998 E-6
63.76	−4.82	−12.58	0.1221 E-5
64.06	−31.03	−21.57	0.8960 E-6
64.36	0.99	26.70	0.1221 E-5
65.26	−19.54	−14.57	0.7907 E-6
65.56	−37.93	−28.08	0.1174 E-5
65.86	−0.68	−14.25	0.5836 E-6
66.16	−8.36	−12.74	0.1132 E-5
66.46	−2.24	−7.59	0.1100 E-5
66.76	−40.40	−16.08	0.5730 E-6
67.06	−46.99	−22.00	0.9893 E-6
67.36	−28.90	−22.63	0.6940 E-6
67.66	−40.34	−24.20	0.9952 E-6
67.96	−13.94	12.94	0.2398 E-5
68.26	4.68	−7.39	0.5811 E-5
68.56	12.81	−8.67	0.1207 E-4
68.86	−15.38	−31.82	0.5909 E-6
69.16	−36.63	−13.25	0.1825 E-5
69.46	−22.47	1.48	0.9839 E-6
69.76	10.50	−4.56	0.2184 E-5
70.06	7.62	−16.42	0.1160 E-5
70.36	−7.99	−21.01	0.8531 E-6
70.66	−7.14	−17.05	0.1001 E-5
70.96	−6.28	−15.04	0.1307 E-5
71.26	−38.94	−15.48	0.6867 E-6
71.56	−0.90	−0.11	0.7850 E-6
71.96	−9.45	−35.85	0.9126 E-6
72.16	−23.92	4.48	0.5764 E-6
72.46	24.06	12.24	0.4894 E-6
72.76	4.95	28.30	0.4658 E-6
73.06	−20.15	19.87	0.4327 E-6
73.36	−28.56	−30.04	0.8948 E-6
74.06	−90.43	0.17	0.4064 E-4
74.36	−13.37	−15.10	0.7696 E-6
74.66	−29.44	−12.55	0.1080 E-5
74.96	−0.76	0.85	0.1254 E-5
75.26	−13.18	−12.39	0.9283 E-6
75.86	−26.76	−14.11	0.1404 E-5
76.16	−16.21	−18.59	0.1106 E-5

Appendix B. (Continued).

Sub-bottom depth (m)	Declination (°)	Inclination (°)	Intensity (G)
Hole 575B (Cont.)			
76.46	−10.90	−22.29	0.1367 E-5
76.76	−8.00	−12.59	0.1769 E-5
77.06	−6.46	−21.96	0.1377 E-5
77.36	−13.31	−9.59	0.6332 E-6
77.66	−25.10	−12.18	0.9532 E-6
77.96	−82.82	2.57	0.1424 E-5
78.26	−17.19	−14.61	0.1169 E-5
78.56	1.01	−3.93	0.1600 E-5
78.86	−59.17	−20.35	0.1300 E-5
79.16	−0.80	−7.88	0.1201 E-5
79.46	−21.53	−14.54	0.7287 E-6
79.76	−30.55	−10.79	0.7325 E-6
80.06	−66.67	6.52	0.1545 E-5
80.36	−34.79	−14.49	0.1739 E-5
80.66	−29.33	−0.65	0.1132 E-5
80.96	−10.81	11.35	0.1788 E-5
81.26	−11.71	−13.77	0.9595 E-6
81.56	−14.35	−14.06	0.8809 E-6
81.66	−18.93	−10.93	0.1317 E-5
81.96	−34.99	0.68	0.1219 E-5
82.86	−23.84	13.90	0.1250 E-5
83.16	19.77	−6.70	0.1522 E-5
83.42	−7.59	−10.74	0.8915 E-6
83.76	1.75	−5.61	0.1242 E-5
84.06	3.32	−9.99	0.1252 E-5
84.36	35.49	−0.32	0.1812 E-5
84.66	70.37	3.80	0.7487 E-5
84.96	57.09	4.27	0.2568 E-5
85.26	33.18	15.33	0.1448 E-5
85.56	58.77	2.78	0.2919 E-5
85.86	84.94	6.36	0.2389 E-4
86.16	89.82	1.76	0.3007 E-4
86.46	91.93	−7.88	0.1799 E-4
86.76	84.18	2.16	0.2245 E-4
87.06	−24.97	16.88	0.2725 E-5
87.36	−71.72	9.86	0.9756 E-5
87.66	−40.84	7.16	0.4260 E-5
87.96	83.85	−11.33	0.4756 E-5
88.26	−22.24	25.09	0.5686 E-5
88.56	102.97	57.54	0.3542 E-5
88.86	66.35	−11.05	0.3495 E-5
89.16	32.50	8.77	0.2541 E-5
89.46	−46.89	24.29	0.7547 E-5
89.76	−71.71	45.53	0.6058 E-5
90.06	18.51	19.75	0.1815 E-5
90.36	55.82	5.41	0.6397 E-5
90.66	29.97	2.82	0.5057 E-5
91.16	146.45	−7.14	0.8780 E-5
91.46	145.40	8.99	0.7528 E-5
91.76	76.89	−60.75	0.1491 E-5
92.06	127.81	−17.86	0.5163 E-5
92.36	133.17	−20.26	0.6041 E-5
92.66	157.33	−10.46	0.1373 E-4
92.96	157.63	−4.13	0.9955 E-5
93.26	157.81	−12.11	0.2681 E-5
93.56	155.85	−13.21	0.1977 E-5
93.86	−117.09	−45.19	0.4498 E-5
94.16	−19.78	7.09	0.7326 E-5
94.46	132.45	−6.88	0.5738 E-6
94.76	−9.05	22.01	0.2779 E-5
95.06	−6.60	−64.02	0.1746 E-5
95.36	144.25	19.96	0.2065 E-5
95.66	−0.46	5.15	0.2929 E-5
95.96	−0.74	13.59	0.3015 E-5
96.26	−10.14	11.93	0.1482 E-4
96.56	−6.51	3.07	0.2065 E-4
96.86	−60.01	−55.05	0.6704 E-5

Appendix B. (Continued).

Sub-bottom depth (m)	Declination (°)	Inclination (°)	Intensity (G)
Hole 575B (Cont.)			
97.16	−176.90	−1.03	0.6099 E-5
97.46	178.33	−10.71	0.9730 E-5
97.76	179.56	−1.30	0.6344 E-5
98.06	86.70	5.50	0.4404 E-6
98.36	−125.74	−52.16	0.5685 E-5
98.96	173.29	39.86	0.8889 E-6
99.26	151.86	32.10	0.1766 E-5
99.86	−17.13	−22.42	0.1027 E-4
100.16	−86.85	−53.50	0.9060 E-6
100.46	−9.43	−7.56	0.1923 E-5
100.76	−40.98	−7.20	0.1272 E-4
101.06	2.43	−17.90	0.1723 E-5
101.36	−52.32	−40.93	0.8013 E-5
101.66	−109.80	−17.03	0.1783 E-5
101.96	−35.92	−3.36	0.1620 E-5
102.26	2.00	4.02	0.8173 E-6
102.56	−1.35	−1.32	0.2005 E-5
102.86	−6.37	−19.62	0.1964 E-5
103.46	−56.46	1.46	0.1908 E-5
103.76	−101.92	−3.87	0.1656 E-5
104.06	−72.82	−15.17	0.2156 E-5
104.36	−1.31	−14.98	0.6102 E-6
104.66	−2.15	−0.92	0.7449 E-6
104.96	−50.93	−13.78	0.1806 E-5
105.26	−4.52	−12.01	0.1153 E-5
105.56	−63.75	−30.20	0.1696 E-5
105.86	−2.15	−18.88	0.1801 E-5
106.16	−28.52	−20.47	0.4574 E-5
106.46	43.37	−11.14	0.8331 E-5
106.76	25.25	−14.07	0.4791 E-5
107.06	−53.15	−28.19	0.3274 E-5
107.36	−5.72	−18.47	0.9945 E-6
107.66	−9.07	6.60	0.1371 E-5
108.26	−17.97	−19.47	0.1213 E-4
108.86	−42.15	19.83	0.3178 E-4
109.46	−80.07	2.60	0.3019 E-4
109.76	−76.33	−18.74	0.2381 E-4
110.06	−57.28	13.37	0.6019 E-5
110.36	−91.20	−19.19	0.9835 E-5
110.66	−98.53	−10.65	0.6354 E-5
110.96	−45.36	−19.66	0.4839 E-5
111.26	−82.87	−24.12	0.4936 E-5
111.56	−92.97	−1.40	0.3689 E-4
111.86	67.74	49.61	0.2473 E-5
112.46	179.73	11.33	0.1053 E-4
112.76	37.84	8.25	0.2326 E-5
113.06	46.41	7.98	0.9392 E-5
113.36	69.82	12.65	0.2791 E-4
113.66	46.45	18.48	0.7660 E-5
113.96	71.69	−0.52	0.3150 E-5
114.42	92.58	−30.47	0.7197 E-5
114.66	124.66	−8.40	0.4473 E-5
114.96	159.35	34.72	0.1882 E-4
115.26	135.74	16.43	0.1159 E-4
115.56	−48.30	3.83	0.5576 E-4
115.86	−31.86	10.05	0.1060 E-4
116.16	−35.28	28.83	0.1309 E-4
116.46	−44.92	22.00	0.4554 E-5
116.76	−37.86	7.38	0.6037 E-5
117.06	139.31	−2.87	0.1220 E-4
117.36	150.60	7.96	0.1796 E-4
117.66	115.59	−11.01	0.1223 E-5
117.96	84.11	15.25	0.3027 E-5
118.26	−29.03	4.87	0.4357 E-4
118.56	−80.39	1.25	0.9431 E-4
118.86	−43.96	0.99	0.1959 E-4

PART VI: PALEOCEANOGRAPHY AND SYNTHESES

Reprinted from Mayer, L., Theyer, F., et al., 1985
Initial Reports of the Deep Sea Drilling Project, Volume LXXXV, Washington (U. S. Government Printing Office)

30. SYNTHESIS OF BIOSTRATIGRAPHY, CENTRAL EQUATORIAL PACIFIC, DEEP SEA DRILLING PROJECT LEG 85: REFINEMENT OF OLIGOCENE TO QUATERNARY BIOCHRONOLOGY[1]

John A. Barron, U.S. Geological Survey, Menlo Park
Catherine A. Nigrini, Scripps Institution of Oceanography
Annick Pujos, Université de Bordeaux
Tsunemasa Saito, Yamagata University
Fritz Theyer, Hawaii Institute of Geophysics
Ellen Thomas, Scripps Institution of Oceanography
and
Norbert Weinreich, Institut für Geophysik, Ruhr Universität Bochum[2]

ABSTRACT

Biostratigraphic studies using planktonic and benthic foraminifers, calcareous nannofossils, radiolarians, diatoms, and silicoflagellates are summarized for the four main sequences (Sites 572 to 575) collected during DSDP Leg 85 in the central equatorial Pacific. Upper Eocene through Quaternary reference sections were recovered at Sites 573 and 574, and middle Miocene through Quaternary and lower Miocene through Quaternary reference sections were cored at Sites 572 and 575, respectively. Detailed graphic correlation plots suggest that Site 573 may contain as many as nine short hiatuses. Site 572 in the fertile eastern equatorial Pacific is apparently free of hiatuses, and Sites 574 and 575 have hiatuses (two each) only in the compressed upper sections.

Few inconsistencies exist in the various microfossil stratigraphies. Diachronous species occurrences are identified, and age estimates for 66 late Eocene through Quaternary microfossil datums have been extrapolated from age-vs.-depth plots constructed from 63 datums with direct and/or indirect ties to paleomagnetic stratigraphy.

An addendum presents an alternative biostratigraphic time scale for the middle and late Miocene based on a correlation of paleomagnetic Anomaly 5 with paleomagnetic Chron 11.

INTRODUCTION

Upwelling associated with the equatorial current system renews the supply of nutrients to the surface waters along the equator in the central Pacific and creates one of the Earth's most fertile planktonic belts. Production rates of both biogenic carbonate (planktonic foraminifers and calcareous nannofossils) and silica (diatoms and radiolarians) are high in this equatorial belt, which has a present-day width of 3 to 4° and a maximum expression in the sediment slightly offset to the north of the equator. Siliceous microfossils (mostly diatoms) are dominant in sediment east of 120°W, whereas carbonate microfossils become increasingly more abundant to the west. Spreading and rotation of the ocean crust away from the East Pacific Rise has resulted in a northwestward displacement of this equatorial Pacific sediment bulge.

The central equatorial Pacific has received considerable attention for biostratigraphic and paleoceanographic studies in recent years (van Andel et al., 1975; Leinen, 1979; Savin et al., 1981; Keller and Barron, 1983). DSDP Site 77 has been thoroughly studied for planktonic foraminifers (Jenkins and Orr, 1972; Keller, 1980, 1981, 1983a), calcareous nannofossils (Bukry, 1972; Gartner, 1972; Lohmann and Carlson, 1981), radiolarians (Goll, 1972, 1979; Westberg and Riedel, 1978), and diatoms (Milow in Hays et al., 1972; Keller et al., 1982; Barron, 1981, 1983; Harwood, 1982). Site 77 has undoubtedly been the most important reference section for establishing microfossil datum sequences for the low-latitude Pacific and for correlating planktonic microfossil stratigraphies. Site 77 has also been well researched for benthic and planktonic foraminiferal isotopes (Haq et al., 1980; Savin et al., 1981; Keigwin and Keller, 1984).

A primary purpose of DSDP Leg 85 was to complete hydraulic piston coring in this high-productivity area of the central equatorial Pacific. Recovery of relatively undisturbed cores in sediment with moderate to high (>15 m/m.y.) accumulation rates would allow high-resolution stratigraphic and isotope studies to be extended back in time at least as far as the early Miocene. Such high-resolution studies are needed not only to refine the resolution of Cenozoic time; they are also crucial for understanding the mechanisms and sequencing of paleoceanographic and paleoclimatic changes (e.g., Keller and Barron, 1983; Vincent and Killingley, this volume).

Five sites were occupied during Leg 85 (Sites 571 to 575) (Fig. 1). Sites 571 and 572 lie near the eastern edge of the equatorial sediment bulge; Sites 573 to 575 form a south-to-north transect (0°N to 6°N) at about 133°W,

[1] Mayer, L., Theyer, F., et al., *Init. Repts. DSDP*, 85: Washington (U.S. Govt. Printing Office).

[2] Addresses: (Barron) U.S. Geological Survey, Menlo Park, CA 94025; (Nigrini, present address) 510 Papyrus Dr., La Habra Heights, CA 90631; (Pujos) Université de Bordeaux, 33405 Talence, France; (Saito) Yamagata University, Yamagata 990, Japan; (Theyer, present address) University of Southern California, Los Angeles, CA 90089; (Thomas, present address) Lamont-Doherty Geological Observatory, Columbia University, Palisades, NY 10964; (Weinreich) Institut für Geophysik, Ruhr-Universität Bochum, Bochum, Federal Republic of Germany.

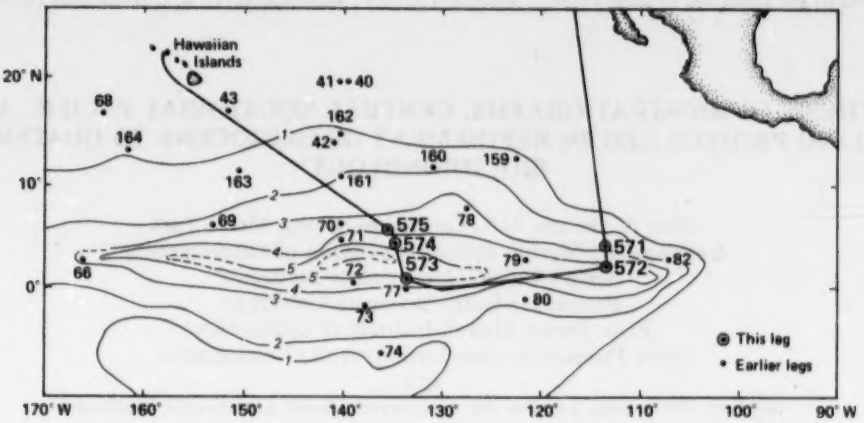

Figure 1. Cruise track and site locations of DSDP Leg 85 in relation to acoustic sediment thickness (contours in tenths of seconds of two-way traveltime) and previously drilled DSDP holes in the central equatorial Pacific.

near the center of the bulge. Seventeen holes, the majority of which were completed with hydraulic piston coring, were drilled at the five sites (Table 1).

BIOSTRATIGRAPHIC TIME SCALE

The biostratigraphic time scale adopted for Leg 85 (Fig. 2) incorporates the planktonic foraminiferal zones of Blow (1969) and Berggren (1969) (with some modification by Saito, this volume); the calcareous nannofossil zones of Bukry (1975), with notation after Okada and Bukry (1980); the radiolarian zones of Nigrini (1971) and Riedel and Sanfilippo (1978); and the diatom zones of Burckle (1972) and Barron (1983, in press, and this volume). The silicoflagellate zones of Bukry (1981, 1983) have also been included on the time scale on the basis of their correlation with other microfossil zones in Leg 85 material.

The paleomagnetic time scale utilized is that of Berggren, Kent, and Flynn (in press) and Berggren, Kent, and Van Couvering (in press), and the paleomagnetic chrons are recognized in the manner of LaBrecque et al. (1977) and Tauxe et al. (1983). See also the Addendum to this chapter.

Correlation of the Eocene and Oligocene zones with paleomagnetic stratigraphy follows Poore et al. (1983) and Berggren, Kent, and Flynn (in press), for the most part. Radiolarian zonal boundaries have been shifted somewhat, on the basis of Leg 85 results (Nigrini, this volume). Correlation of the CP17/CP18 calcareous nannofossil zone boundary with the upper part of the reversed event of paleomagnetic Chron C12 at about 33.3 Ma (Lowrie et al., 1982) is accepted in preference to correlation of that datum lower in Chron C12 at about 34.1 Ma (Berggren, Kent, and Flynn, in press), because it is more consistent with Leg 85 planktonic foraminiferal and radiolarian stratigraphy (see section on age-vs.-depth plots).

The Miocene correlations of biozones with paleomagnetic stratigraphy are after Barron et al. (in press), and include new direct paleomagnetic correlations for paleo-

Table 1. Summary of locations, coring records, and oldest sediments cored, DSDP Leg 85 holes.

Hole	Latitude	Longitude	Water depth[a] (m)	Sub-bottom depth range cored (m)	Number of cores	Total core recovered (m)	Oldest sediment cored
571	03°59.84′N	114°08.53′W	3962	0–7.11	1	7.11	Pleistocene
572	01°26.09′N	113°50.52′W	3893	0–18.7	2	9.25	Pleistocene
572A	01°26.09′N	113°50.52′W	3893	0–154	17	154.35	upper Miocene
572B	01°26.09′N	113°50.52′W	3893	154–169.4	4	19.95	upper Miocene
572C	01°26.09′N	113°50.52′W	3893	0–169.5	20	161.56	upper Miocene
572D	01°26.09′N	113°50.52′W	3893	151–489.0	34	258.87	middle Miocene
573	00°29.91′N	133°18.57′W	4301	0–158.6	19	159.4	upper Miocene
573A	00°29.91′N	133°18.57′W	4301	14.0–57.7	6	53.5	lower Pliocene
573B	00°29.91′N	133°18.57′W	4301	138.5–529.0	43	279.7	upper Eocene
574	04°12.52′N	133°19.81′W	4561	0–206.5	31	208.93	lower Miocene
574A	04°12.52′N	133°19.81′W	4561	6.0–186.2	23	180.74	lower Miocene
574B	04°12.52′N	133°19.81′W	4561	185.0–194.0	1	9.45	lower Miocene
574C	04°12.53′N	133°19.81′W	4561	194.5–532.5	37	197.35	upper Eocene
575	05°51.00′N	135°02.16′W	4536	0–98.6	11	99.35	lower Miocene
575A	05°51.00′N	135°02.16′W	4536	93.8–208.4	33	140.53	lower Miocene
575B	05°51.00′N	135°02.16′W	4536	3.3–119.0	14	118.68	lower Miocene
575C	05°51.00′N	135°02.16′W	4536	0–15.8	2	15.91	upper Miocene

[a] Water depth from sea level.

magnetic Chrons 16 and 17 in Hole 575A, utilizing the paleomagnetic data of Weinreich and Theyer (this volume). The Pliocene and Pleistocene time scale adopted results from paleomagnetic correlations of planktonic foraminifers (Saito et al., 1975; Berggren et al., 1980), calcareous nannofossils (Gartner, 1973; Backman and Shackleton, 1983), radiolarians (Theyer et al., 1978; Labracherie, this volume), and diatoms (Burckle, 1972, 1978).

The epoch boundaries adopted in the Leg 85 biostratigraphic time scale (Fig. 2) include those of Berggren, Kent, and Flynn (in press) for the Eocene/Oligocene, early Oligocene/late Oligocene, and Oligocene/Miocene boundaries; that of Ryan et al. (1974) for the early Miocene/middle Miocene boundary; those of Berggren (1984) for the middle Miocene/late Miocene, Miocene/Pliocene, and early Pliocene/late Pliocene boundaries; and that of Berggren et al. (1980) for the Pliocene/Pleistocene boundary.

It should be noted that this biostratigraphic time scale is updated from the time scale presented in the Introduction to this volume, although most differences are minor (see Addendum for larger changes).

SITE SUMMARIES

The records of coring, biostratigraphic zonation, and paleomagnetic stratigraphy at Sites 572 to 575 are summarized on Figures 3 to 7. Only one core (of uppermost Quaternary sediment) was recovered at Site 571, because that site was occupied primarily for heat-flow studies. The base of that core (Core 571-1) contains planktonic foraminifers of Zone N23, calcareous nannofossils of Subzone CN14a, radiolarians of the *Amphirhopalum ypsilon* Zone, and diatoms of the *Pseudoeunotia doliolus* Zone, and is approximately 500,000 to 650,000 yrs. old. The reader is referred to the calcareous nannofossil chapter of Pujos ("Nannofossils from Quaternary Deposits," this volume) and the radiolarian chapter of Labracherie (this volume) for detailed stratigraphic data from Core 571-1.

Site 572

Site 572 lies within the eastern equatorial Pacific, where the permanent thermocline is relatively shallow (>60 m) (Wyrtki, 1966) and diatoms dominate the sediment. A complete reference section apparently free of hiatuses was recovered from the lower middle Miocene (about 15 Ma) through the Quaternary at the site (Fig. 3). Hydraulic piston coring extended down to the uppermost Miocene (about 170 m sub-bottom), and was completed in four of the five holes (Holes 572, 572A, 572B, and 572C). Uppermost Quaternary sediment was present in the single core successfully recovered from Hole 572, so Hole 572 is not included on Figure 3. Rotary coring (Hole 572D) extended from the uppermost Miocene (151.0 m sub-bottom) to the lower middle Miocene (464.5 m sub-bottom), and was terminated 13 m above the sediment/basalt contact.

Dissolution of calcareous microfossils (especially planktonic foraminifers) is common to sporadic in the Miocene section at Site 572. A sharp downhole change from rich, well preserved planktonic foraminiferal assemblages to monotonous, moderately well preserved assemblages occurs at about 155 m sub-bottom (about 5.9 Ma). Pliocene and Quaternary planktonic foraminifers can be readily correlated with the paleomagnetically dated deep-sea sequences west of Site 572 (Hays et al., 1969; Saito et al., 1975), and coiling changes in *Pulleniatina* are also useful for biostratigraphy (Saito, this volume).

Site 572 lies a few miles south and west of Site 81 (Fig. 1). Although the paleontologists of Leg 9 (Hays et al., 1972) assigned the basal sediments of Site 81 to planktonic foraminiferal Zone N8, basal sediments of Site 572 (Sample 572-33,CC) contain sparse specimens of *Orbulina universa* and are assigned to Zone N9. Radiolarians (*Dorcadospyris alata* Zone) and diatoms (Subzone B of the *Cestodiscus peplum* Zone) are consistent with this Zone N9 assignment (Fig. 3).

The sequence of microfossil zones and subzones at Site 572 is in good agreement with the Leg 85 biostratigraphic time scale (Fig. 2), except for the CN9 calcareous nannofossil zones of Pujos ("Cenozoic Nannofossils," this volume) and Gartner and Chow (this volume). The CN8/CN9 boundary has been calibrated in numerous Pacific sections with lower Zone N17, upper *Didymocyrtis antepenultima* Zone, and Subzone A of the *Nitzschia porteri* Zone by Keller et al. (1982) and Barron et al. (in press). Gartner and Chow's placement of the CN8/CN9 boundary in Core 572D-8 agrees well with this correlation, whereas Pujos' assignment of the CN8/CN9 boundary to the base of Core 572D-2 coincides with the lowermost parts of the *Stichocorys peregrina* and *Thalassiosira convexa* zones, and is more than 2 m.y. younger (6.0 Ma vs. 8.3 Ma). Similarly, Gartner and Chow's placement of the CN9a/CN9b boundary in Core 572D-7 agrees well with the results of Keller et al. (1982) and Barron et al. (in press), who note that the CN9a/CN9b boundary (the first occurrence of the calcareous nannofossil *Amaurolithus primus*) almost coincides with the base of the *Nitzschia miocenica* Zone in the eastern equatorial Pacific (7.3 Ma). Pujos, on the other hand, places the CN9a/CN9b boundary substantially higher in Core 572A-17 (about 5.9 Ma).

Pujos' assignment of the CN9/CN10 boundary, to the base of Core 572A-13, approximates the N18/N19 boundary (5.2 Ma) and the Subzone B/Subzone C boundary of the *Thalassiosira convexa* Zone (5.1 Ma), a correlation noted elsewhere in the eastern equatorial Pacific by Keller et al. (1982). Gartner (1973) tied the last occurrence of *Discoaster quinqueramus*, the marker for the CN9/CN10 boundary, with the middle of paleomagnetic Chron 5 (about 5.5 Ma), but more recently Gartner et al. (1983) have argued for a correlation of this calcareous nannofossil zonal boundary with the Miocene/Pliocene boundary, or about 5.1 Ma. At Site 572, Gartner and Chow's placement of the CN9/CN10 boundary in Core 572A-11 falls well into the lower Pliocene, and is certainly too high.

The *Dorcadospyris alata/Diartus petterssoni* zonal boundary is somewhat older at Site 572 (Fig. 3), with respect to diatoms and planktonic foraminifers, than it is in the Leg 85 biostratigraphic time scale (Fig. 2) and at

Epochs
Quaternary
Pliocene
early
late
Miocene
early
middle
late
Plankton zones
Silicoflagellates (Bukry [1981, 1983])
Diatoms (Burckle [1972]; Barron [in press; this report])
Radiolarians (Nigrini [1971]; Riedel and Sanfilippo [1978])
Calcareous nannofossils (Bukry [1975]; Okada and Bukry [1980])
Foraminifers (Blow [1969]; Berggren [1969])
Magnetic polarity
Berggren et al. (in press)
Anomaly
Chron
Brun.
Matuyama
Gauss
Gilbert
Age (Ma)

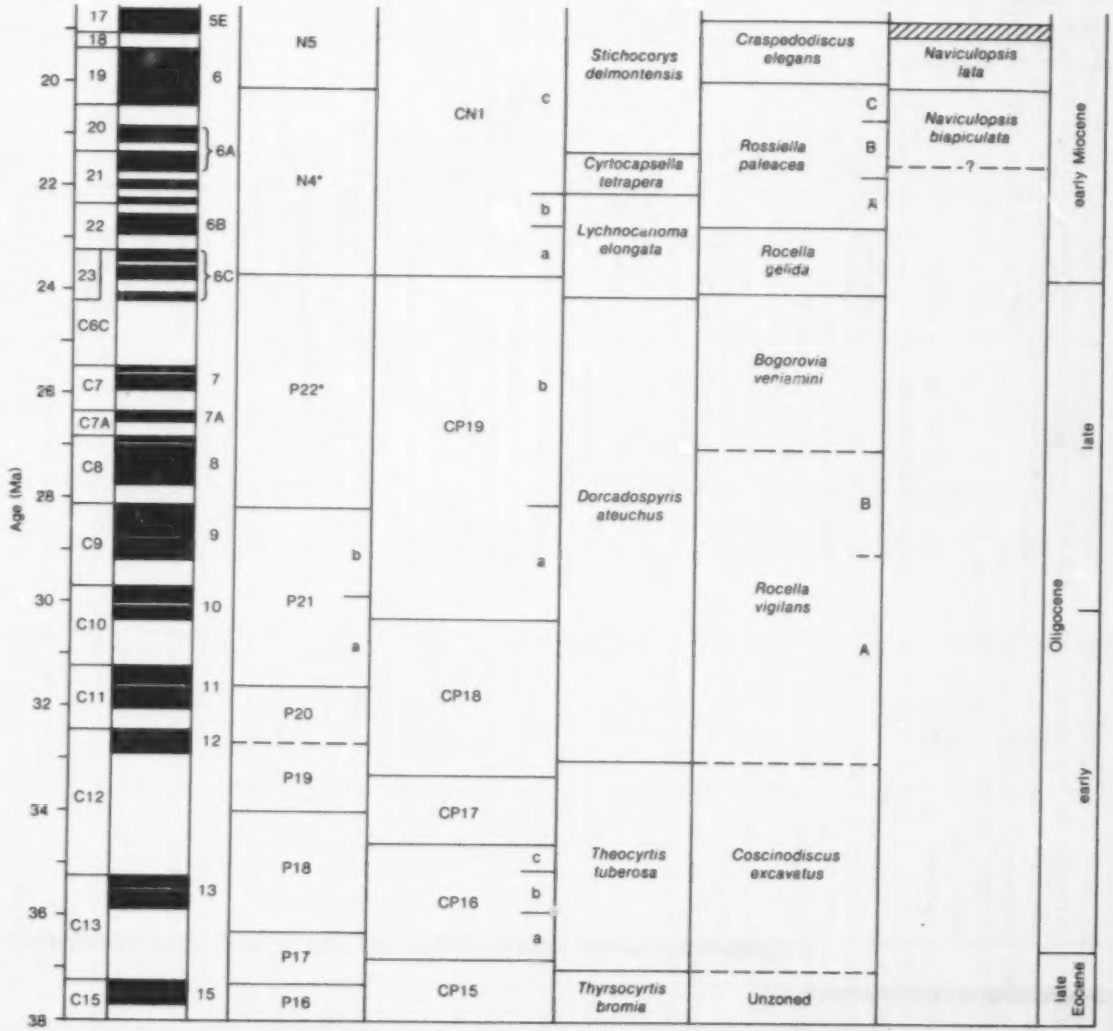

Figure 2. Biostratigraphic time scale adopted for Leg 85. Paleogene correlations mostly after Berggren, Kent, and Flynn (in press); Miocene correlations after Barron et al. (in press); and Pliocene–Pleistocene correlations synthesized from the results of Saito et al. (1975), Burckle (1972), Theyer et al. (1978), Berggren et al. (1980), and Backman and Shackleton (1983). Minor adjustments to correlations are based on Leg 85 results. Epoch boundaries follow Berggren (1984) and Berggren et al. (1980; in press), except for the early Miocene/middle Miocene boundary, which is after Ryan et al. (1974). Asterisk denotes planktonic foraminiferal zones with modified definitions (Saito, this volume). Silicoflagellate subzonal abbreviations: *Dd = Dictyocha delicata, Doo = D. ornata ornata, Da = D. angulata, Dp = D. pulchella, Dn = D. neonautica.*

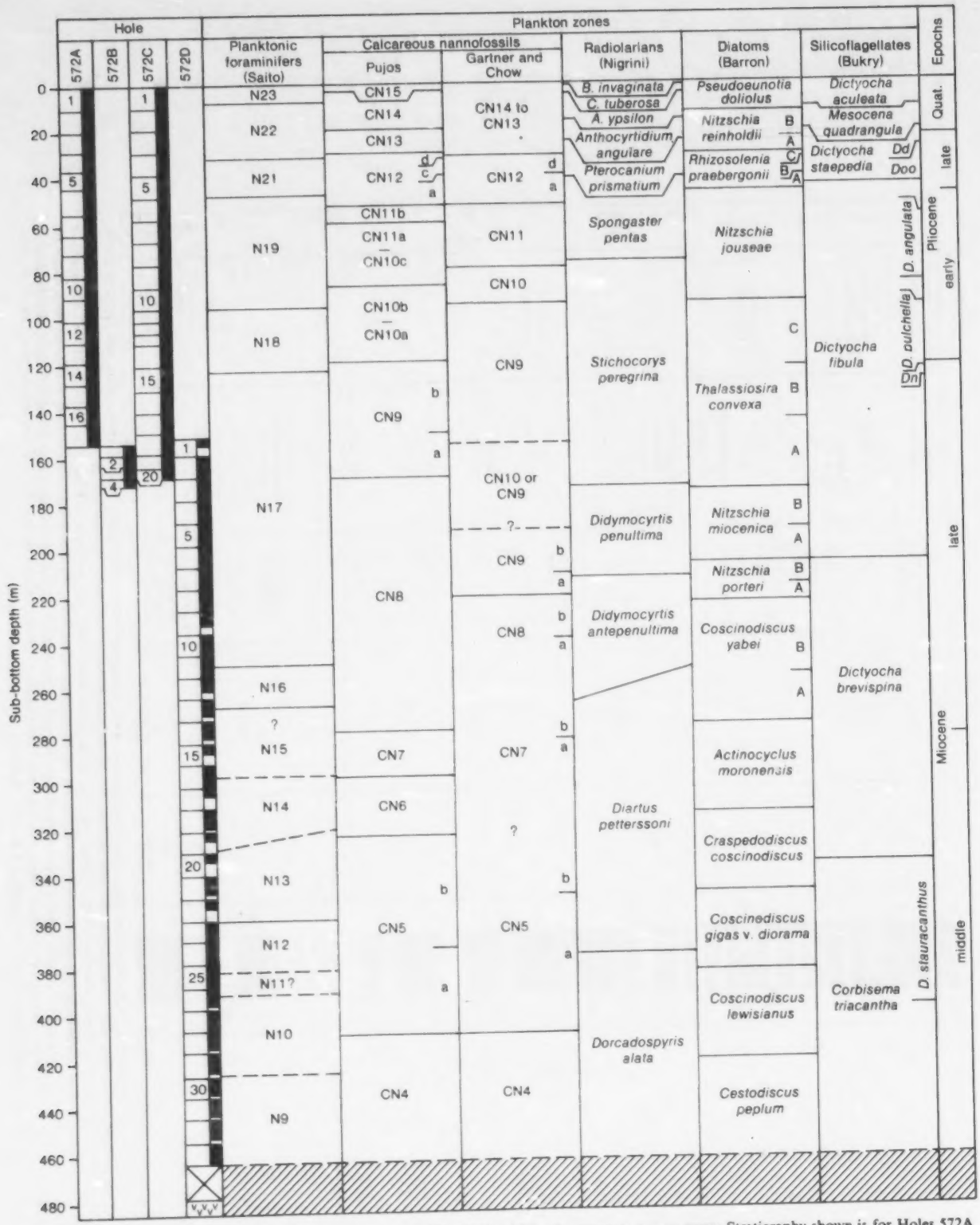

Figure 3. Coring record and biostratigraphic zonation at Site 572. Shaded intervals represent core recovery. Stratigraphy shown is for Holes 572A and 572D. Refer to Nigrini (this volume) and Barron (this volume) for correlation between duplicated holes.

both Site 574 and Site 575. In these latter cases, the *D. alata/D. petterssoni* zonal boundary approximates the N12/N13 and *Coscinodiscus gigas* var. *diorama/Craspedodiscus coscinodiscus* zonal boundaries. At Site 572, however, the *D. alata/D. petterssoni* zonal boundary falls in lower Zone N12 and lower *C. gigas* var. *diorama* Zone (Fig. 3); at Site 573 (Fig. 4), a correlation with the even older Zone N11 and *Coscinodiscus lewisianus* Zone is suggested.

It should also be noted that Nigrini's (this volume) placement of the *Amphirhopalum ypsilon/Collosphaera tuberosa* radiolarian zonal boundary in Core 572A-2 is about 6 m stratigraphically below Labracherie's (this volume) assignment in Core 572A-1.

Site 573

Site 573 was chosen near Site 77, which has been the location of the most extensively studied central equatorial Pacific deep-sea section in recent years. The objective at Site 573 was to obtain an HPC section for the upper part of the Site 77 section and to core the Eocene/Oligocene boundary. Site 573 is about 10 km (6 mi.) west of Site 77, over a sediment section about 50 m thicker than that at Site 77.

Upper Eocene through Quaternary sediment, typically containing well-preserved planktonic and benthic foraminifers, calcareous nannofossils, radiolarians, and diatoms, was recovered at Site 573 (Fig. 4). Virtually all of the sediment section is readily zonable by planktonic microfossils, although the thin upper Eocene section lacks both radiolarians and diatoms and part of the lower Miocene section is essentially barren of diatoms. In Hole 573, hydraulic piston coring extended down to 158.6 m sub-bottom, just above the middle Miocene/upper Miocene boundary. Rotary coring in Hole 573B was completed to 529.0 m sub-bottom, with the sediment/basalt contact encountered at 528.0 m sub-bottom in upper Eocene sediments assignable to Zones P16 and CP15.

The Eocene/Oligocene boundary lies within Core 573B-42 (at approximately 525 m sub-bottom), in a very dark brown metalliferous claystone unit (Subunit IIIB of site chapter) relatively poor in microfossils. The stratigraphically lowest radiolarians and diatoms at Site 573 occur in Sample 573-42-1, 0–1 cm, and are assignable to the Oligocene *Theocyrtis tuberosa* and *Coscinodiscus excavatus* zones, respectively. Pujos ("Cenozoic Nannofossils," this volume) places the CP15/CP16b boundary of calcareous nannofossils between Samples 573B-42-4, 58 cm and 573B-42-2, 50 cm. Planktonic foraminiferal assemblages correlated with Zone P16 occur in Sample 573B-42-4, 123–124 cm, whereas Saito (this volume) tentatively assigns Sample 573B-42-2, 5–8 cm to Oligocene Zone P18. The Eocene benthic foraminifers *Nuttallides truempyi* and *Alabamina dissonata* are present in Sample 573B-42-4, 144–147 cm, but poor preservation in the immediately overlying samples prevents accurate placement of their last-appearance datums. The sum of all the evidence suggests that a hiatus, or greatly compressed interval equivalent to Zone P17 (37.4 to 36.3 Ma), is present in Section 3 of Core 573B-42. A coeval hiatus at the Eocene/Oligocene boundary is present at Site 289 on the Ontong-Java Plateau in the western equatorial Pacific (Andrews et al., 1975), and is extensive in the Pacific Basin (Kennett et al., 1975).

In Hole 573, paleomagnetic stratigraphy was obtained down to the lower Gauss paleomagnetic Chron (Core 573-6); paleomagnetic stratigraphy extended down to the Cochiti event of the Gilbert Chron in Hole 573A (Weinreich and Theyer, this volume). Within the constraints of the sample intervals, correlations of the various microfossil zones with paleomagnetic stratigraphy are consistent with the Leg 85 time scale (Figs. 2, 4). The detailed studies of the Quaternary by Pujos ("Nannofossils from Quaternary Deposits," this volume, calcareous nannofossils) and Labracherie (this volume, radiolarians) show more precise calibration of microfossil events to paleomagnetic stratigraphy.

The sequence of planktonic microfossil zones (Fig. 4) encountered at Site 573 shows some inconsistencies when compared with the Leg 85 time scale (Fig. 2). The N5/N6 and N17/N18 zonal boundaries appear to be slightly older with respect to the other microfossil zones at Site 573. The N5/N6 boundary was correlated with paleomagnetic stratigraphy in Hole 575A, where an age of 18.1 Ma was implied, coincident with the lower part of the *Stichocorys wolffii* Zone of radiolarians. At Site 573, Zone N6 appears to be longer in duration, its base correlating with the middle of the *Stichocorys delmontensis* Zone. Correlation of the base of N6 in Hole 574C (Fig. 5) is also with the middle of the *S. delmontensis* Zone, so it is possible that the correlation of the N5/N6 boundary with the upper normal event of paleomagnetic Chron 17, inferred from Hole 575A, is too young. Berggren (1984) indirectly correlates the N5/N6 boundary with earliest paleomagnetic Chron 17 (about 19.0 Ma), a correlation supported by correlations with radiolarian stratigraphy at Sites 573 and 574.

In a similar manner, placement of the N17/N18 boundary in Core 573-11 is at odds with calcareous nannofossil and diatom stratigraphies, which suggest that the Miocene/Pliocene boundary should lie in Core 573-10 (Fig. 4).

There are also a number of inconsistencies between the calcareous nannofossil stratigraphies of Pujos and Gartner and Chow at Site 573 (Fig. 4). As at Site 572, the CN8/CN9 and CN9a/CN9b boundaries of Gartner and Chow are more consistent with the Leg 85 biostratigraphic time scale than are the CN8/CN9 and CN9a/CN9b boundaries of Pujos. It is worthwhile to note, however, that Pujos' placement of these boundaries is internally consistent with respect to the other microfossil zones at Sites 572 and 573 (Figs. 3, 4). Pujos' assignment of the CN7/CN8 boundary in Core 573B-4 is favored over Gartner and Chow's placement of that boundary in Core 573B-5, on the basis of the near coincidence of her CN7/CN8 boundary with the *Actinocyclus moronensis/Coscinodiscus yabei* zonal boundary of diatoms at Sites 572 (Fig. 3) and 574 (Fig. 5).

Differences in placement of the CN1/CN2 and CP18/CP19 zonal boundaries by Pujos and by Gartner and Chow will be discussed in a later section dealing with graphic correlation plots between the sites.

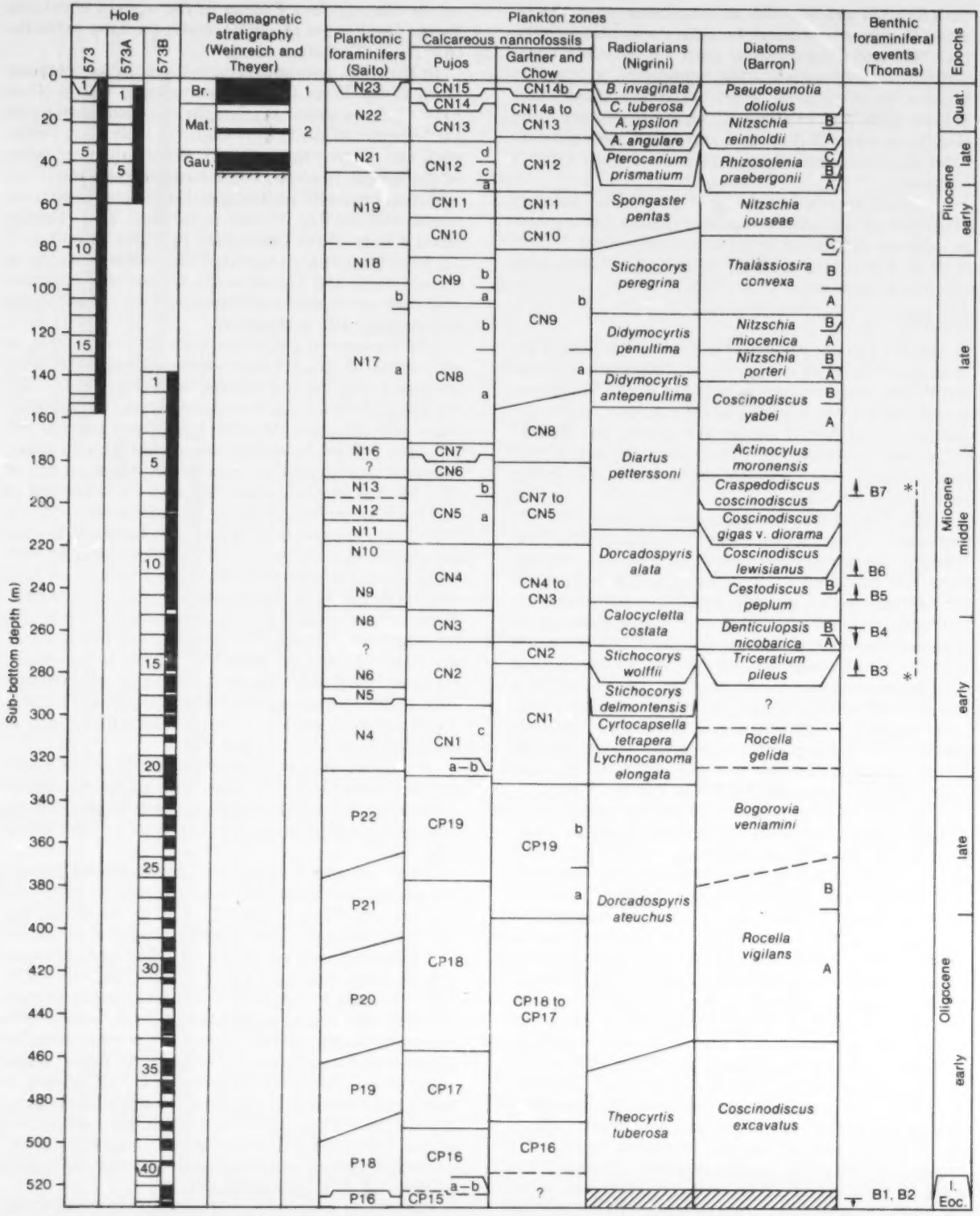

Figure 4. Coring record, biostratigraphic zonation, benthic foraminiferal events, and paleomagnetic stratigraphy at Site 573. Shaded intervals represent core recovery. Stratigraphy shown is for Holes 573 and 573B. See Nigrini (this volume), Barron (this volume), and Weinreich and Theyer (this volume) for correlation between duplicated holes. Benthic foraminiferal events are labeled on Table 6; vertical bar with asterisks represents time of maximum turnover in benthic foraminiferal assemblages. Paleomagnetic chrons are listed in left part of column, paleomagnetic anomaly numbers in right part of column.

As discussed earlier, the *Dorcadospyris alata/Diartus petterssoni* radiolarian zonal boundary seems anomalously old at Site 573 with respect to the other microfossil stratigraphies, but other radiolarian zonal boundaries appear to agree reasonably well with the Leg 85 biostratigraphic time scale.

Selected benthic foraminiferal datums which show the most consistency in correlations between Sites 573, 574, and 575 (Thomas, this volume) are numbered B1 through B7 on Figures 4 to 6. Events B1 and B2, the last appearances of *Alabamina dissonata* and *Nuttallides truempyi*, respectively, closely approximate the Eocene/Oligocene boundary, and have been discussed earlier. Events B3 through B7 include the first appearance of *Melonis barleeanus* (B3), the last appearance of *Cibicidoides laurisae* (B4), and the first appearances of *C. wuellerstorfi* (B5), *Francesita advena* (B6), and *Melonis pompilioides*. These events took place in the late early Miocene to middle Miocene interval (18 to 13 Ma) which shows the maximum turnover in benthic foraminiferal assemblages (Thomas, this volume).

Site 574

Site 574 is the second of the three-site latitudinal transect (Sites 573 to 575) along 133°W across the equatorial Pacific high-productivity belt. Because Site 574 lies at 4°N, north of the present-day high-biologic-productivity zone (Koblentz-Mishke et al., 1970), the Pliocene and Quaternary section is compressed relative to that at Site 573 (0°N) (Figs. 4, 5).

The hydraulic piston coring in Hole 574 reached 206.5 m sub-bottom (approximately 16.7 Ma) and was duplicated, for the most part, by the coring in Hole 574A. Rotary coring extended from 194.5 to 532.5 m sub-bottom in Hole 574C, reaching the sediment/basalt contact at 520.0 m, in upper Eocene sediments assigned to Zones P17 and CP15.

Throughout most of the section, siliceous microfossils occur in common to high abundances and show good preservation. The abundance of diatoms declines and diatom preservation becomes poorer downhole, in the upper Oligocene to upper part of the lower Oligocene, and again downhole in Cores 574C-33 and 574C-34, near the Eocene/Oligocene boundary. Core 574C-35, the core immediately overlying the basalt, is barren of both diatoms and radiolarians. Radiolarians are generally abundant and well preserved throughout the section at Site 574.

The abundance and preservation of planktonic foraminifers fluctuates at Site 574. Parts of the lowermost Oligocene, uppermost lower Miocene, and uppermost middle Miocene show severe dissolution of planktonic foraminifers, making zonation difficult. Calcareous nannofossils, on the other hand, are typically abundant to common throughout the section.

Site 574 appears to contain an uninterrupted sequence through the Eocene/Oligocene boundary. Planktonic foraminifers suggest that the P17/P18 boundary occurs between Samples 574C-35-1, 126–128 cm and 574C-34,CC; the last occurrence of *Hantkenina primitiva* may, however. have been influenced by dissolution. The CP15/CP16 calcareous nannofossil zonal boundary is placed in Core 574C-33 by Pujos, but between Cores 574C-35 and 574C-34 by Gartner and Chow (Fig. 5). The *Theocyrtis tuberosa/Thyrsocyrtis bromia* radiolarian zonal boundary appears to be in lower Core 574C-33, and the base of the lower Oligocene *Coscinodiscus excavatus* Zone of diatoms lies between Cores 574C-33 and 574C-34. The last occurrences of the Eocene benthic foraminifers *Alabamina dissonata* and *Nuttallides truempyi* (events B1 and B2, Fig. 5) are in lower Core 574C-33, in close agreement with the Eocene/Oligocene boundary (CP15/CP16) determined from calcareous nannofossils by Pujos and with the Eocene/Oligocene boundary determined from radiolarians and diatoms. These data are also supported by the presence of a major increase (0.9‰) in benthic foraminiferal ^{18}O in the upper part of Core 574C-33 (between 33-1, 113–115 cm and 33-2, 113–115 cm) (Miller and Thomas, this volume). Keigwin (1980) demonstrated that this shift occurs immediately above the extinction levels of *Hantkenina* spp. and *Globorotalia cerroazulensis cerroazulensis*, which mark the top of planktonic foraminiferal Zone P17.

Reworked calcareous nannofossils and diatoms are common in the uppermost part of the section (Cores 574-4 through 574-1), and reworked Oligocene planktonic foraminifers and calcareous nannofossils occur in several horizons within the lower middle Miocene at Site 574.

In general, there are few inconsistencies between the Site 574 microfossil stratigraphy (Fig. 5) and the Leg 85 biostratigraphic time scale (Fig. 2). As mentioned in the discussion of Site 573, planktonic foraminiferal Zone N6 is thicker (of longer duration) with respect to the other microfossil zones at Site 574 than it is at Site 575 (Fig. 6). Pujos' placement of the CP15/CP16, CP18/CP19, and CN9/CN10 calcareous nannofossil zonal boundaries is favored over Gartner and Chow's assignments, because they are more consistent with the Leg 85 biostratigraphic time scale. As at Sites 572 and 573 (Figs. 3, 4), however, Pujos' CN8/CN9 boundary is too high, and Gartner and Chow's CN8/CN9 boundary in Core 574-7 is favored.

The radiolarian and diatom stratigraphies show no major conflicts, although coincidence of the *Craspedodiscus elegans/Triceratium pileus* diatom zonal boundary with the CN1/CN2 and *Stichocorys delmontensis/S. wolffii* zonal boundaries at about 238 m sub-bottom (Core 574C-5) is at odds with the relationship at Site 575 (Fig. 6) and with the Leg 85 biostratigraphic time scale (Fig. 2). Barron (this volume) has suggested that a short hiatus, equivalent to hiatus NH1 of Keller and Barron (1983), is present at the *C. elegans/T. pileus* boundary at Site 574.

Comparison of the stratigraphic positions of the seven benthic foraminiferal datums, B1 through B7 (see discussion of Site 573), at Site 574 (Fig. 5) and Site 573 (Fig. 4) suggests that only one, the last occurrence of *Cibicidoides laurisae* (B4), is noticeably diachronous; it lies one calcareous nannofossil zone, one radiolarian zone, and one diatom zone lower at Site 574 than at Site 573. The interval of maximum turnover in the benthic fora-

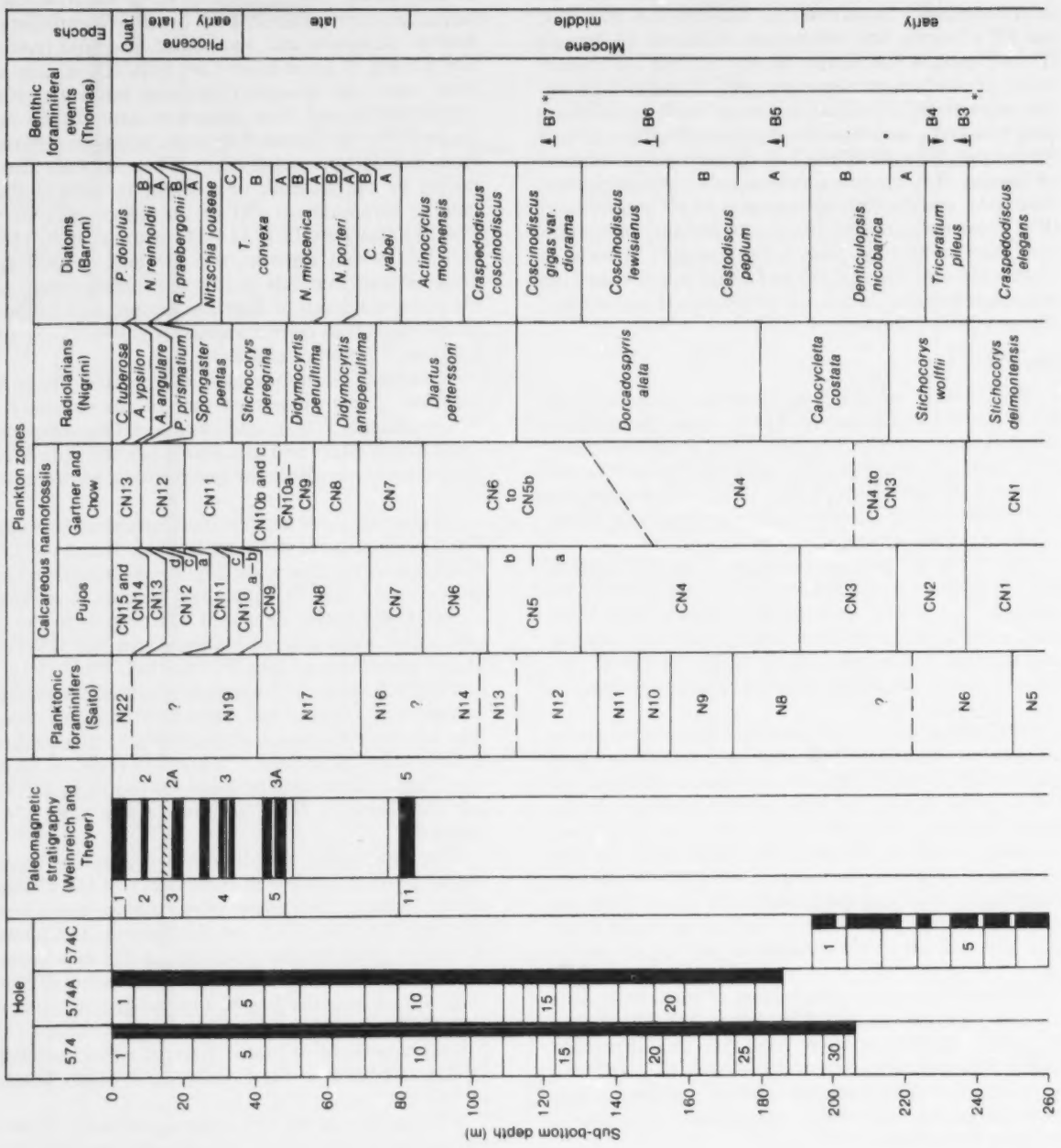
Epochs
Quat
Pliocene
early
late
late
Miocene
middle
early
Benthic foraminiferal events (Thomas)
Plankton zones
Diatoms (Barron)
Radiolarians (Nigrini)
Gartner and Chow
Calcareous nannofossils
Pujos
Planktonic foraminifers (Saito)
Paleomagnetic stratigraphy (Weinreich and Theyer)
Hole
574
574A
574C
P. doliolus
N. reinholdii
R. praebergonii
Nitzschia jouseae
T. convexa
N. miocenica
N. porteri
C. yabei
Actinocyclus moronensis
Craspedodiscus coscinodiscus
Coscinodiscus gigas var. diorama
Coscinodiscus lewisianus
Cestodiscus peplum
Denticulopsis nicobarica
Triceratium pileus
Craspedodiscus elegans
C. tuberosa
A. ypsilon
A. angulare
P. prismatium
Spongaster pentas
Stichocorys peregrina
Didymocyrtis penultima
Didymocyrtis antepenultima
Diartus petterssoni
Dorcadospyris alata
Calocycletta costata
Stichocorys wolffii
Stichocorys delmontensis
CN15 and CN14
CN13
CN12
CN11
CN10 a–b
CN9
CN8
CN7
CN6
CN5
CN4
CN3
CN2
CN1
CN13
CN12
CN11
CN10b and c
CN10a–CN9
CN8
CN7
CN6 to CN5b
CN4
CN4 to CN3
CN1
N22
N19
N17
N16
N14
N13
N12
N11
N10
N9
N8
N6
N5
B7
B6
B5
B4
B3
Sub-bottom depth (m)

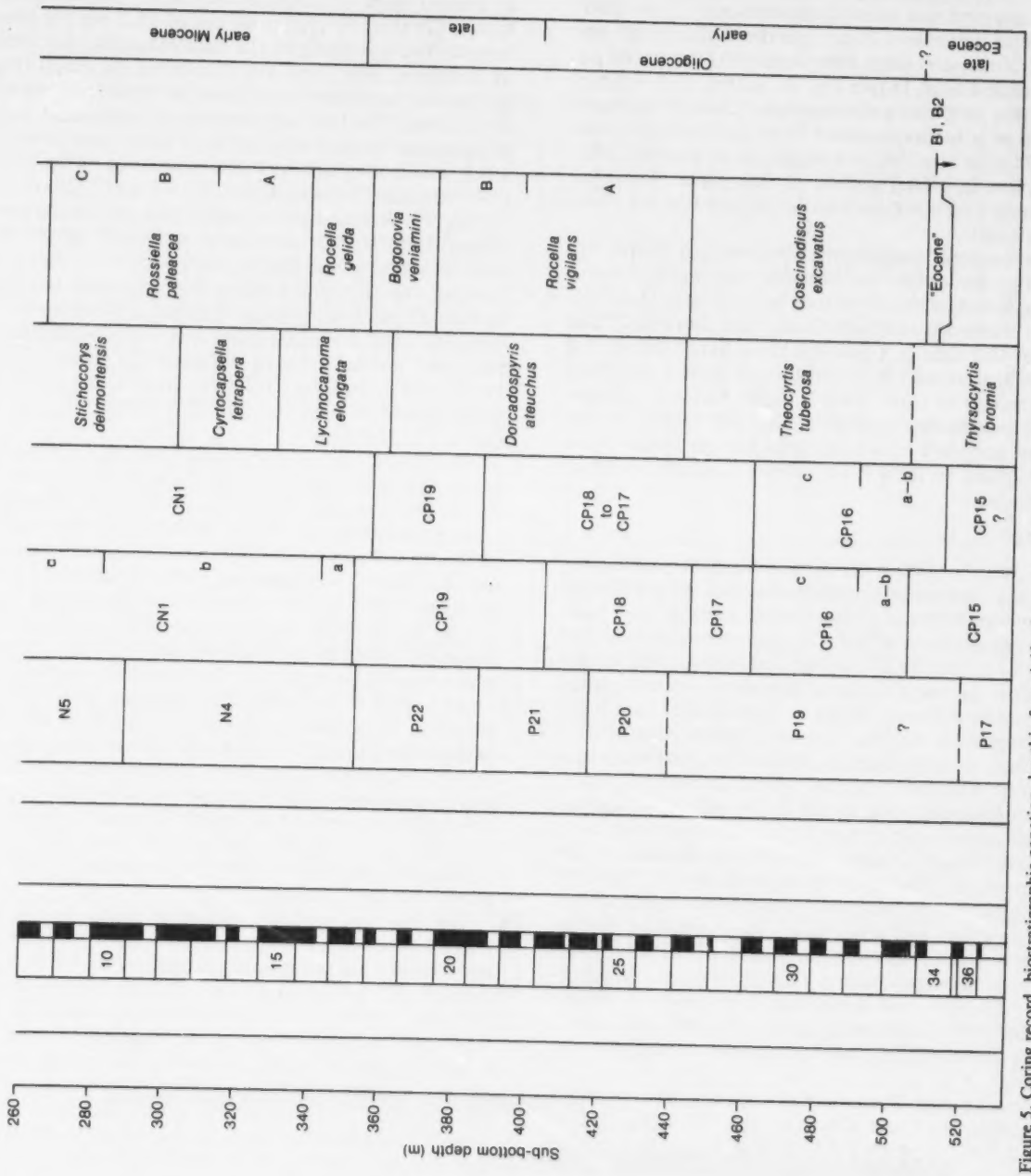

Figure 5. Coring record, biostratigraphic zonation, benthic foraminiferal events, and paleomagnetic stratigraphy at Site 574. Stratigraphy shown is for Holes 574 and 574C. See caption to Figure 4 for further explanation.

miniferal assemblage covered roughly the same period of time (18 to 13 Ma) at both Site 573 and Site 574.

Weinreich and Theyer (this volume) identify paleomagnetic events between the Olduvai Event and the base of Chron 5 at Site 575 (Fig. 5). They also record the top of Chron 9 at about 79 m sub-bottom (lower Core 574-9); however, this interval coincides with Zone CN7, the *Diartus petterssoni* Zone, and the *Actinocyclus moronensis* Zone, and more likely represents the top of paleomagnetic Chron 11 (see Fig. 2). Barron (this volume) argues that much of paleomagnetic Chron 9 has been removed at a hiatus at about 70 m sub-bottom (lower Core 574-8) at Site 574, as is suggested by graphic correlation plots in a later section of this paper. Weinreich and Theyer's (this volume) extrapolations did not allow for this hiatus.

Paleomagnetic stratigraphy (Weinreich and Theyer, this volume) indicates that the Jaramillo Event of the Matuyama paleomagnetic Chron may be missing in Hole 574. Pujos ("Nannofossils from Quaternary Deposits," this volume) also reports a possible short hiatus (about 1.0 to 0.6 Ma) at about 5 m sub-bottom, in upper Core 574-2. The lithology of Core 574-2 is highly variable throughout, with alternating intervals of very pale brown, brownish gray, and dark brown siliceous and carbonate oozes (site chapter), so there is no definite lithologic evidence for a hiatus.

Site 575

Site 575, the third of the three-site south-to-north transect in the central equatorial Pacific, was occupied to extend hydraulic piston coring further back in time from the record obtained at Site 574. The second objective at Site 575—to recover a complete and undisturbed section across the Eocene/Oligocene boundary—unfortunately could not be achieved, owing to lack of time. Four holes were completed with the hydraulic piston corer (HPC) at the site, with the deepest, Hole 575A, extending into lowermost Miocene sediment (about 22 Ma) (Fig. 6).

With few exceptions, all the major microfossil groups are well represented at Site 575, and most of the early Miocene through Quaternary biozonal boundaries can be recognized. The upper 30 m of the section, however, accumulated very slowly, and a combination of carbonate dissolution and reworking makes zonation of this section difficult (especially for planktonic foraminifers). A 1000-m-high seamount is located 10 km to the northeast of Site 575, and centimeter-thick sandy to pebbly turbidite layers, containing mostly foraminifers, basalt, and/or volcanic glass, are interbedded throughout the section.

Weinreich and Theyer's (this volume) paleomagnetic stratigraphy for Cores 575-1 through 575-4 (Fig. 7) and Cores 575A-1 through 575A-10 (Fig. 6) can be correlated with the microfossil stratigraphies for those cores, and the resultant correlations can be compared with published correlations between microfossil datum levels and paleomagnetic stratigraphy. Paleomagnetic stratigraphy was also obtained for Hole 575C and, in part, for Hole 575B, but will not be discussed here, because most microfossil studies were concentrated on material from Holes 575 and 575A. The chapters by Pujos ("Nannofossils from Quaternary Deposits," this volume, calcareous nannofossils) and Labracherie (this volume, radiolarians) discuss Quaternary correlations for Hole 575C.

Direct correlation of the CN1/CN2 and *Stichocorys delmontensis/S. wolffii* zonal boundaries with the lower normal event of Anomaly 5D (upper paleomagnetic Chron 17) (Fig. 6) implies an age of 18.2 Ma for these boundaries, according to the paleomagnetic time scale of Berggren, Kent, and Van Couvering (in press) (Fig. 2). Gartner and Chow's placement of CN1/CN2 boundary in Core 575A-10 is supported by an independent study of calcareous nannofossils by David Bukry (pers. comm., 1983), and is favored over Pujos' placement of the CN1/CN2 boundary between Cores 575A-8 and 575A-7.

The N5/N6 boundary correlates with the normal event within Anomaly 5D, and has an estimated age of 18.1 Ma. As stated in the discussions of Sites 575 and 574, however, the N5/N6 boundary may be placed too high in Hole 575A. The *Triceratium pileus/Denticulopsis nicobarica* zonal boundary correlates with the middle of the upper normal event of Anomaly 5D (upper Chron 17, 17.8 Ma), and the CN2/CN3 zonal boundary is almost coincident with the top of Anomaly 5D (top of Chron 17, 17.6 Ma).

The N6/N7 and *Naviculopsis ponticula/Corbisema triacantha* (silicoflagellate) zonal boundaries lie immediately above the top of Anomaly 5D, in the lowermost part of paleomagnetic Chron 16 (17.5 Ma). Correlation of the N6/N7 and CN2/CN3 zonal boundaries with the top of Chron 17 was suggested earlier (Ryan et al., 1974; Berggren, 1984), and is confirmed here for the first time.

The *Stichocorys wolffii/Calocycletta costata* zonal boundary is tied to lower Chron 16 (17.3 Ma), a correlation slightly younger than the correlation with Chron 17 by Theyer et al. (1978). The Subzone A/Subzone B boundary of the *Denticulopsis nicobarica* Zone also falls in the lower part of Chron 16, and has an estimated age of 17.0 Ma. Finally, the *Denticulopsis nicobarica/Cestodiscus peplum* zonal boundary is calibrated with the upper normal event of Anomaly 5C (middle Chron 16) (16.4 Ma), a correlation younger than that with Chron 17 suggested by Burckle (1978) but consistent with the extrapolations of Barron (1983).

For the most part, correlation of planktonic microfossil datum levels and zonal boundaries with Weinreich and Theyer's paleomagnetic stratigraphy for Cores 575-1 through 575-4 (Fig. 7) agrees well with published calibrations. Events tied to paleomagnetic Chron 12, the N13/N14 boundary (Ryan et al., 1974), the CN5/CN6 boundary (Barron et al., in press), and the last occurrence of the diatom *Craspedodiscus coscinodiscus* (= the top of the *C. coscinodiscus* Zone) (Barron et al., in press) all fall within Chron 12, according to Weinreich and Theyer. Likewise, events previously calibrated with paleomagnetic Chron 10 fall within the interval Weinreich and Theyer assign to Chron 10: the CN7/CN8 boundary (Ryan et al., 1974); the transition of the radiolarian *Diartus petterssoni* to *D. hughesi* (= top of the *D. petterssoni* Zone) (Johnson and Wick, 1982); and the last occurrence of the diatom *Actinocyclus moron-*

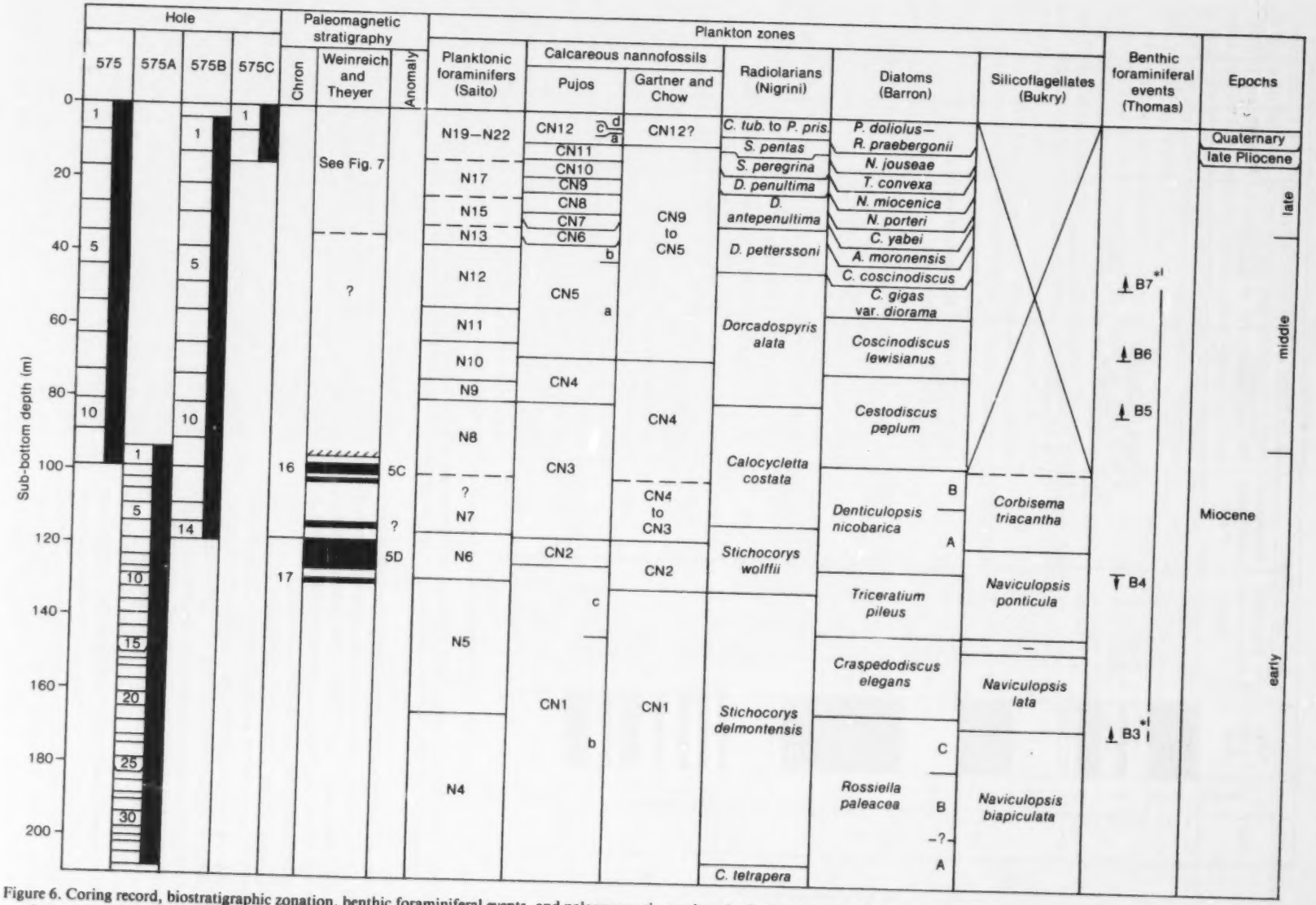

Figure 6. Coring record, biostratigraphic zonation, benthic foraminiferal events, and paleomagnetic stratigraphy for Site 575. (Detail of Cores 575-1 through 575-4 shown on Fig. 7.) Stratigraphy shown is for Holes 575 and 575A. See caption to Figure 4 for further explanation.

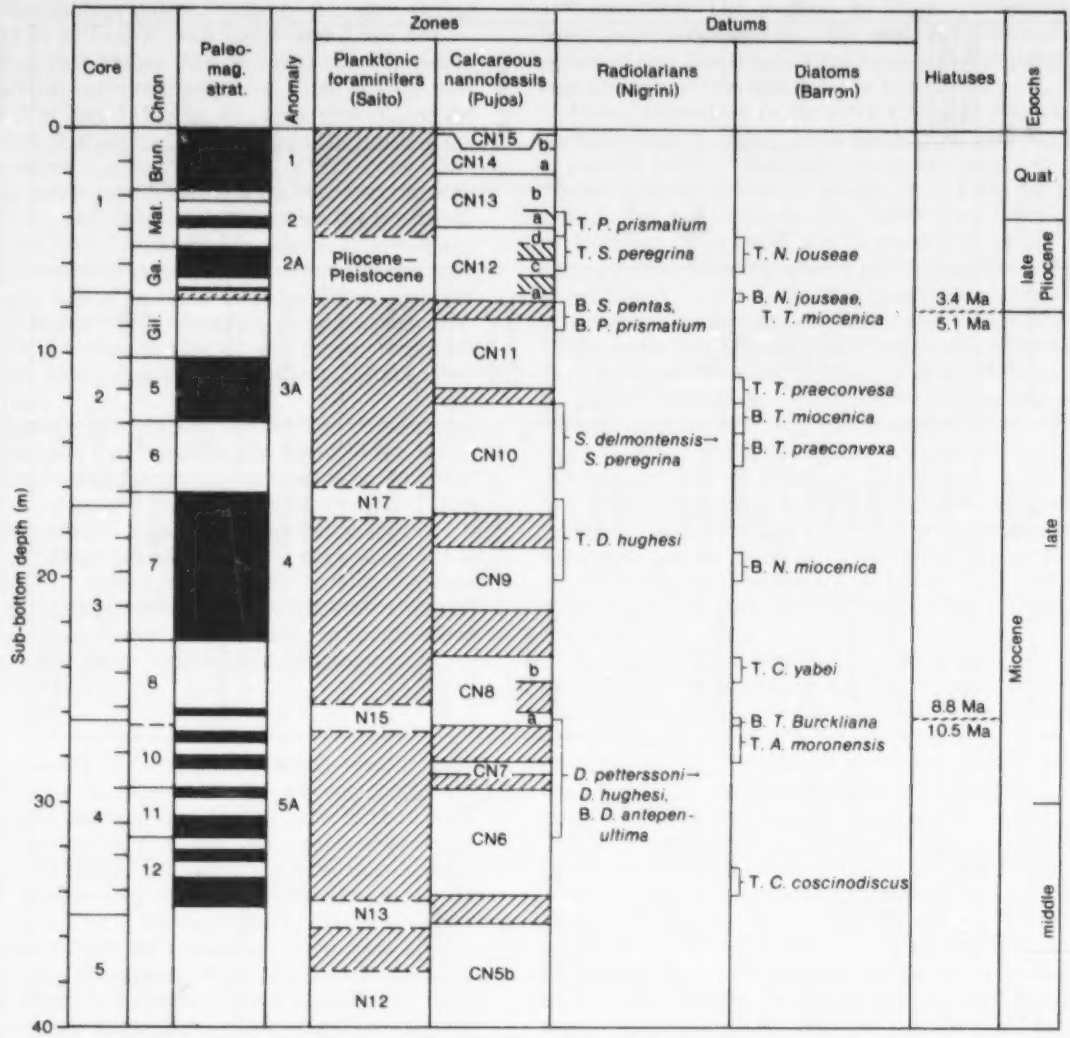

Figure 7. Paleomagnetic stratigraphy, calcareous plankton zones, and selected siliceous plankton datums for Hole 575, Cores 1 through 4. B = first occurrence (bottom); T = last occurrence (top). Shaded intervals have not been zoned.

ensis (= top of the *A. moronensis* Zone) (Burckle, 1978). A hiatus (NH5) which removes paleomagnetic Chron 9 is shown by Weinreich and Theyer (this volume) at the base of Core 575-3, and finds supporting evidence in the diatom stratigraphy of Barron (this volume).

Interestingly, Pujos' CN8/CN9 boundary at Site 575 correlates with uppermost paleomagnetic Chron 8 near the last occurrence of the diatom *Coscinodiscus yabei*. This calibration agrees with the Leg 85 biostratigraphic time scale (Fig. 2), and is considerably older than Pujos' placements of the CN8/CN9 boundary at Sites 572 to 574, in terms of both diatoms and radiolarians.

The last occurrence of *Diartus hughesi* (= top of the *Didymocyrtis antepenultima* Zone) and first occurrence of *Nitzschia miocenica* (= base of the *N. miocenica* Zone) have both been tied to paleomagnetic Chron 7 (Keller et al., 1982; Burckle, 1978), in agreement with Hole 575 paleomagnetic stratigraphy (Fig. 7), but the CN9/CN10 boundary should correlate with the top of Chron 5 (Gartner et al., 1983). Consequently, it is assumed that Pujos' CN9/CN10 boundary in Hole 575 is placed too low; Gartner and Chow (this volume) do not recognize the CN9/CN10 boundary in Hole 575.

Weinreich and Theyer's assignment of paleomagnetic Chron 6 is supported by the transition of the radiolarian *Stichocorys delmontensis* to *S. peregrina* (Theyer et al., 1978) and by the first occurrences of the diatoms *Thalassiosira praeconvexa* and *T. miocenica* (Burckle, 1978). The last occurrence of *T. praeconvexa* at about 12 m sub-bottom confirms paleomagnetic Chron 5, but the CN10/CN11 boundary should lie in the upper part of the Gilbert Chron (Backman and Shackleton, 1983).

The presence of a hiatus in the uppermost part of Core 575-2, which removes almost all of the Gilbert Chron (about 5.1 to 3.4 Ma), is supported by the near coincidence of lowermost Gilbert events, the last occurrence

of *Thalassiosira miocenica* (Burckle, 1978), and the first occurrence of *Pterocanium prismatium* (Theyer et al., 1978), with the base of the Gauss paleomagnetic Chron. The last occurrences of *Stichocorys peregrina* and *Nitzschia jouseae* have been tied to the upper Gauss by Theyer et al. (1978) and Burckle (1978), respectively, in agreement with the paleomagnetic stratigraphy of Weinreich and Theyer for Hole 575 (Fig. 7).

The various subzonal boundaries of calcareous nannofossil Zone CN12 recognized by Pujos at Site 575 (Fig. 7) can be compared with age estimates of Backman and Shackleton (1983) for the North Atlantic. Backman and Shackleton's (1983) ages for the CN12a/CN12b, CN12b/CN12c, and CN12c/CN12d boundaries are 2.65, 2.41, and 2.35 Ma, respectively. Pujos does not recognize Subzone CN12b, but her CN12a/CN12c boundary is middle Gauss, or approximately 3.1 to 2.8 Ma. Pujos' CN12c/CN12d boundary is near the top of the Gauss, and could be as young as Backman and Shackleton's (1983) 2.35 Ma.

Backman and Shackleton (1983) estimate the age of the CN12/CN13 boundary, the last occurrence of *Discoaster brouweri*, at 1.88 Ma, near the base of the Olduvai Event. Pujos's assignment of the CN12/CN13 boundary in Hole 575 lies very close to the base of Weinreich and Theyer's Olduvai Event (Fig. 7).

GRAPHIC CORRELATION PLOTS

To refine correlations between the individual sites and to evaluate the completeness of the stratigraphic sections, graphic correlation plots have been constructed for four stratigraphic intervals: the uppermost Eocene to lowermost Miocene of Sites 573 and 574 (Fig. 8); the lower Miocene of Sites 573, 574, and 575 (Fig. 9); the middle Miocene and most of the upper Miocene (to 6.2 Ma) of Sites 572, 573, and 574 (Fig. 10); and the uppermost Miocene through Quaternary of Sites 572 and 573 (Fig. 11). Graphic correlation plots allow comparison of the stratigraphic sequencing of the numerous datum levels identified for planktonic foraminifers (Saito, this volume), calcareous nannofossils (Pujos, both chapters, this volume; Gartner and Chow, this volume), radiolarians (Nigrini, this volume; Labracherie, this volume), diatoms (Barron, this volume; Baldauf, this volume), and benthic foraminifers (Thomas, this volume). Diachronous datum levels can be identified, and a best-fit correlation plot between sections can be produced (Shaw, 1964). In addition, other stratigraphic events—paleomagnetic, carbonate, isotopic, and lithologic—can be used on such plots to greatly refine correlations. Correlation of carbonate, isotope, and lithologic events is not attempted here, but carbonate and isotopic tuning of the record is addressed in the chapter by Pisias and Prell (this volume). Construction of graphic correlation plots is also a convenient way of relating the datum levels of different microfossil groups. Where individual datum levels of one microfossil group have been directly calibrated to paleomagnetic stratigraphy, indirect correlation of other datum levels with paleomagnetic stratigraphy is often possible.

Tables 2 to 6 list the radiolarian, diatom, calcareous nannofossil, planktonic foraminiferal, and benthic fora-

Table 2. Radiolarian datum levels used for correlations on Figures 3 to 13.

Event	Datum[a]	Age (Ma): Paleomagnetic correlation[b]	Age (Ma): Extrapolated (this chapter)[c]
R60	B. *Buccinosphaera invaginata*	0.65–0.72[d]	
R59	B. *Collosphaera tuberosa*	0.28[e]	
R58	T. *Axoprunum angelinum*	0.42[e]	
R57	T. *Amphispyris roggenthenі*	0.78[e]?	
R56	T. *Anthocyrtidium angulare*	1.05[e]	
R55	T. *Theocorythium vetulum*	1.20[e]	
R54	T. *Pterocanium prismatium*	1.6[e]	
R53	T. *Stichocorys peregrina*	2.4[f]	
R52	T. *Spongaster pentas*	3.4[f]	
R51	T. *Didymocyrtis penultima*	3.7[f]	
	B. *Spongaster tetras*	3.6[f]	
R50	T. *Spongaster berminghami*		4.2–4.3
R49	T. *Botryostrobus bramlettei*		4.6
R48	B. *Pterocanium prismatium*	4.8[f]	
R47	B. *Botryostrobus aquilonaris*		5.1
	T. *Siphostichartus corona*		5.1
R46	T. *Acrobotrys tritubus*	5.5[g], 5.0[f]	5.5
R45	T. *Calocycletta caepa*		5.6
R44	*Stichocorys delmontensis* → *S. peregrina*	6.2[f]	
R43	B. *Solenosphaera omnitubus*	7.3[g]	
R42	T. *Diartus hughesi*	7.9[g]	
R41	T. *Botryostrobus miralestensis*		8.8–8.9
	T. *Dictyocorne ontongensis*		8.8–8.9
R40	B. *Didymocyrtis penultima*	9.8[g]	
	T. *Diartus petterssoni*	10.4[g]	9.8–10.0
R39	B. *Diartus hughesi*	11.5[f]	10.4–11.2
R38	T. *Stichocorys wolffii*	10.4[g]	10.8
R37	T. *Cyrtocapsella japonica*	11.5[d]	11.4
R36	T. *Spirocyrtis subtilis*		11.5
R35	B. *Didymocyrtis antepenultima*	11.5[f]	
R34	T. *Cyrtocapsella cornuta*	12.5[g]	12.6–12.7
R33	T. *Lithopera renzae*		12.6–12.8
R32	T. *Dorcadospyris alata*	11.3[f], 12.8[d]	12.8–14.5
R31	T. *Giraffospyris toxaria*		12.9–13.0
R30	B. *Diartus petterssoni*	12.6[d]	12.8–13.3
R29	B. *Lithopera thornburgi*	>13.5[d]	13.6
R28	B. *Didymocyrtis laticonus*	13.8[f]	
R27	T. *Calocycletta costata*	14.8[g]	
	T. *Didymocyrtis tubaria*		14.7–14.8
R26	T. *Dorcadospyris dentata*	15.3[f]	
	T. *Didymocyrtis violina*		15.0–15.3
R25	T. *Dorcadospyris forcipatata*		15.2–15.3
	T. *Liriospyris stauropora*		15.2–15.3
R24	B. *Dorcadospyris alata*	15.5[f]	
R23	B. *Liriospyris parkerae*		16.1–16.4
R22	B. *Giraffospyris toxaria*	16.5[h]	
R21	B. *Calocycletta costata*	17.3[h]	
R20	B. *Stichocorys wolffii*	18.2[h]	
	T. *Dorcadospyris ateuchus*	18.2[h]	
R19	B. *Siphostichartus corona*	18.2[h]	18.2–19.8
R18	B. *Didymocyrtis tubaria*	20.3[g]	
	B. *Didymocyrtis violina*	20.2[f]	
R17	B. *Stichocorys delmontensis*	21.1[f]	20.3–20.5
R16	T. *Theocyrtis annosa*	21.3[f]	20.9
R15	B. *Calocycletta virginis*	21.5[f,*]	
R14	T. *Cyclampterium pegetrum*		21.9–22.1
R13	B. *Cyrtocapsella cornuta*	22.1[g]	
	B. *Cyrtocapsella tetrapera*	22.1[g]	
R12	B. *Carpocanopsis favosa*		22.4–22.6
R11	T. *Artophormis gracilis*	22.6[g]	
R10	B. *Lychnocanoma elongata*	24.1[f,*]	
R9	B. *Calocycletta robusta*	25.5[f,*]	
R8	B. *Dorcadospyris forcipata*		28.0–28.5
R7	T. *Lithocyclia angustata*		31.8–32.0
R6	B. *Theocyrtis annosa*		32.2–32.8
R5	T. *Lithocyclia crux*		32.1–33.6?
R4	B. *Dorcadospyris ateuchus*	33.0[i]	
	T. *Tristylospyris triceros*		32.8–33.5
	T. *Cyclampterium milowi*		32.8–33.5
R3	B. *Eucyrtidium diaphanes*		33.6–33.8
	T. *Theocyrtis tuberosa*		33.6–33.8
R2	B. *Lithocyclia angustata*		34.6
R1	lowermost *Theocyrtis tuberosa* Zone		36.4–36.6

Note: Asterisks identify reinterpreted paleomagnetic chron assignments.
[a] T. = top; B. = bottom.
[b] Absolute age estimates are from direct and indirect correlations with paleomagnetic stratigraphy. The paleomagnetic time scale of Berggren et al. (in press) is used; see Addendum and Table 8.
[c] Extrapolated age estimates are from Figures 12 and 13.
[d] Johnson and Wick (1982).
[e] Labracherie (this volume).
[f] Theyer et al. (1978).
[g] Barron et al. (in press).
[h] Leg 85 paleomagnetic calibration in Hole 575A.
[i] F. Theyer (unpubl. data).

Table 3. Diatom datum levels used for correlations on Figures 3 to 13.

Event		Datum[a]	Age (Ma) Paleomagnetic correlation[b]	Age (Ma) Extrapolated (this chapter)[c]
D43	T.	*Nitzschia reinholdii*	0.65[d]	0.65–0.70
D42	T.	*Rhizosolenia praebergonii* var. *robusta*	1.6[e]	
D41	B.	*Pseudoeunotia doliolus*	1.8[e]	1.8–2.0?
D40	T.	*Thalassiosira convexa*	2.2[e]	
D39	T.	*Nitzschia jouseae*	2.6[e]	
D38	B.	*Rhizosolenia praebergonii*	3.0[e]	
D37	B.	*Asterolampra elegans*	3.9[e]	
D36	T.	*Nitzschia cylindrica*	4.4[e]	
D35	B.	*Nitzschia jouseae*	4.6[e]	
D34	T.	*Thalassiosira miocenica*	5.1[e]	
D33	T.	*Asterolampra acutiloba*	5.35[e]	
D32	T.	*Nitzschia miocenica*	5.6[e]	
D31	T.	*Nitzschia miocenica* var. *elongata*	5.65[f]	
D30	T.	*Thalassiosira praeconvexa*	5.8[e]	
D29	B.	*Thalassiosira convexa*	6.2[e]	
D28	B.	*Thalassiosira praeconvexa*	6.3[e]	
D27	B.	*Nitzschia miocenica*	7.3[e]	
D26	T.	*Thalassiosira burckliana*	8.0[e]	
D25	T.	*Coscinodiscus vabei*	8.6[e]	
D24	B.	*Nitzschia fossilis*		9.8
D23	B.	*Thalassiosira burckliana*	9.0[e]	10.5–10.6
D22	T.	*Coscinodiscus vetustissimus* var. *javanica*	10.7[e]	
D21	B.	*Coscinodiscus vetustissimus* var. *javanica*	11.2[e]	
D20	T.	*Actinocyclus moronensis*	11.3[e]	
D19	T.	*Coscinodiscus tuberculatus*	12.0[g]	
D18	T.	*Craspedodiscus coscinodiscus*	12.2[h]	
D17	B.	*Hemidiscus cuneiformis*	12.6[e]	
D16	B.	*Coscinodiscus temperei* var. *delicata*	12.8[g]	
D15	T.	*Coscinodiscus lewisianus*	13.5[i]	
D14	T.	*Cestodiscus peplum*	14.2[e]	
D13	T.	*Annellus californicus*	15.0[e]	
D12	B.	*Cestodiscus peplum*	16.4[h]	
D11	T.	*Thalassiosira bukryi*	17.0[h]	
D10	B.	*Denticulopsis nicobarica*	17.8[h]	
D9	T.	*Craspedodiscus elegans*	18.7[i]	18.4–18.5
D8	T.	*Bogorovia veniamini*	19.9[j]	19.5–19.7
D7	T.	*Coscinodiscus oligocenicus*	20.6[k]	20.2
D6	T.	*Thalassiosira primalabiata*	21.7[k]	20.7–21.7
D5	B.	*Actinocyclus hajosiae*		21.0
D4	B.	*Rocella gelida*		23.8–24.0
D3	B	*Bogorovia veniamini*		26.4–27.3
D2	T.	*Cestodiscus mukhinae*		28.5–28.7
D1	T.	*Coscinodiscus excavatus*		33.0±

[a] T. = top; B. = bottom.
[b] Absolute age estimates are from direct and indirect correlations with paleomagnetic stratigraphy. The paleomagnetic time scale of Berggren et al. (in press) is used.
[c] Extrapolated age estimates are from Figures 12 and 13.
[d] Burckle (1972).
[e] Burckle (1978).
[f] L. H. Burckle (pers. comm., 1980).
[g] Burckle et al. (1982).
[h] Leg 85 paleomagnetic calibration in Hole 575A.
[i] Barron et al. (in press).

miniferal datum levels (or zonal boundaries) used in the graphic correlation plots. Published age estimates of these datum levels from direct and indirect calibrations with paleomagnetic stratigraphy are also included. The majority of datums used here are those of radiolarians and diatoms, because Nigrini, Labracherie, and Barron (all this volume) have provided tables giving the stratigraphic positions of numerous datums in the sections at Sites 572 to 575. Calcareous microfossil datums used for correlations are mostly zonal and subzonal boundaries, although Pujos ("Nannofossils from Quaternary Deposits," this volume) provides correlation of numerous Quaternary calcareous nannofossil datums at Sites 571 to 575.

Uppermost Eocene to Lowermost Miocene

Graphic correlation of the uppermost Eocene to lowermost Miocene sections at Sites 573 and 574 is shown on Figure 8. The correlation between the two sections is well constrained by 12 radiolarian, 4 diatom, 7 calcareous nannofossil, 5 planktonic foraminiferal, and 2 ben-

Table 4. Planktonic foraminiferal datum levels (and zonal boundaries) used for correlations on Figures 3 to 13.

Event		Datum[a]	Age (Ma) Paleomagnetic correlation[b]	Age (Ma) Extrapolated (this chapter)[c]
P14		N21/N22	1.9[d]	
P13	T.	*Sphaeroidinella seminulina*	3.05[d]	
P12		N18/N19	4.9[d]	4.6–4.8
P11		N16/N17	9.0[e]	9.8–10.7
P10		N11/N12	13.7[e]	13.6
P9		N10/N11	14.2[e]	14.0
P8		N8/N9	15.2[f]	
P7		N5/N6	18.1[g]	18.1–19.0
P6		N4/N5	20.1[e]	20.1–20.6
P5		P22/N4	23.7[f]	
P4		P21/P22	28.2[f]	
P3		P20/P21	31.6[f]	
P2		P19/P20	32.7[f]	
P1		P16/P17	36.3[f]	

[a] T. = top.
[b] Absolute age estimates are from direct and indirect correlations with paleomagnetic stratigraphy. The paleomagnetic time scale of Berggren et al. (in press) is used.
[c] Extrapolated age estimates are from Figures 12 and 13.
[d] Saito et al. (1975).
[e] Barron et al. (in press).
[f] Poore et al. (1983).
[g] Leg 85 paleomagnetic calibration in Hole 575A.

Table 5. Calcareous nannofossil datum levels (and zonal and subzonal boundaries) used for correlations on Figures 3 to 13.

Event		Datum[a]	Age (Ma) Paleomagnetic correlation[b]	Age (Ma) Extrapolated (this chapter)[c]
N20	T.	*Pseudoemiliana lacunosa*	0.47[d]	
N19		CN12/CN13	1.88[e]	
N18		CN11/CN12	3.56[e]	3.5
N17		CN9/CN10	5.5[f]	5.1–5.2
N16		CN8/CN9	8.3[g]	6.0 (Pujos)
N15		CN7/CN8	11.1[h]	
N14		CN6/CN7	12.0[i]	11.7–11.8
N13		CN5/CN6	12.3[i]	
N12		CN5a/CN5b	12.8[i]	
N11		CN4/CN5	14.1[i]	13.7–14.0
N10		CN3/CN4	15.7[i]	
N9		CN2/CN3	17.5[j]	
N8		CN1/CN2	18.2[j]	
N7		CN1a/CN1b	22.7[i]	
N6		CP19/CN1	23.7[k]	
N5		CP18/CP19	30.7[k]	
N4		CP17/CP18	33.3[l]	
N3		CP16/CP17	34.6[k]	
N2		CP16b/CP16c	35.0[k]	
N1		CP15/CP16	36.8[k]	

[a] T. = top.
[b] Absolute age estimates are from direct and indirect correlations with paleomagnetic stratigraphy. The paleomagnetic time scale of Berggren et al. (in press) is used.
[c] Extrapolated age estimates are from Figures 12 and 13.
[d] Berggren et al. (1980).
[e] Backman and Shackleton (1983).
[f] Gartner (1973).
[g] Haq et al. (1980).
[h] Leg 85 paleomagnetic calibration in Hole 575A.
[i] Barron et al. (in press).
[j] Ryan et al. (1974).
[k] Poore et al. (1983).
[l] Lowrie et al. (1982).

Table 6. Benthic foraminiferal datum levels used for Leg 85 correlations.

Event	Datum[a]	Age (Ma)	
		Paleomagnetic correlation[b]	Extrapolated (this chapter)[c]
B7	B. *Melonis pompilioides*		13.0–13.1
B6	B. *Francesita advena*		13.4–14.6
B5	B. *Cibicidoides wuellerstorfi*		14.7–15.4
B4	T. *Cibicidoides laurisae*		17.2–17.7
B3	B. *Melonis barleeanus*		18.8–19.8
B2	T. *Nuttallides truempyi*	About 36.5[c]	
B1	T. *Alabamina dissonata*		About 36.5

[a] B. = bottom; T. = top.
[b] Extrapolated age estimates are from Figures 12 and 13.
[c] Tjalsma and Lohmann (1983).

thic foraminiferal datum levels. Only the R5 datum level, the last occurrence of the radiolarian *Lithocyclia crux*, lies off the correlation line, although Pujos' N5 datum (the CP18/CP19 boundary) also appears off the line. The general relationship suggests that the Site 573 section accumulated at a rate typically about twice that of the Site 574 section throughout most of the Oligocene, except during two hiatuses and one compressed interval (possibly a hiatus) (Fig. 8). During the early Oligocene interval of calcareous nannofossil Zone CP16 (datums N1 to N3, or 36.8 to 34.6 Ma), accumulation rates at Sites 573 and 574 are approximately equal (Fig. 8).

The Eocene/Oligocene hiatus mentioned in the discussion of Site 573 is apparent at about 525 m sub-bottom at Site 573. This hiatus appears to cover at least the interval from the base of Zone P17 (37.3 Ma) to the top of Zone CP15 (36.8 Ma) (Table 7). An Oligocene/Miocene hiatus (hiatus PH) at nearby Site 77, mentioned by

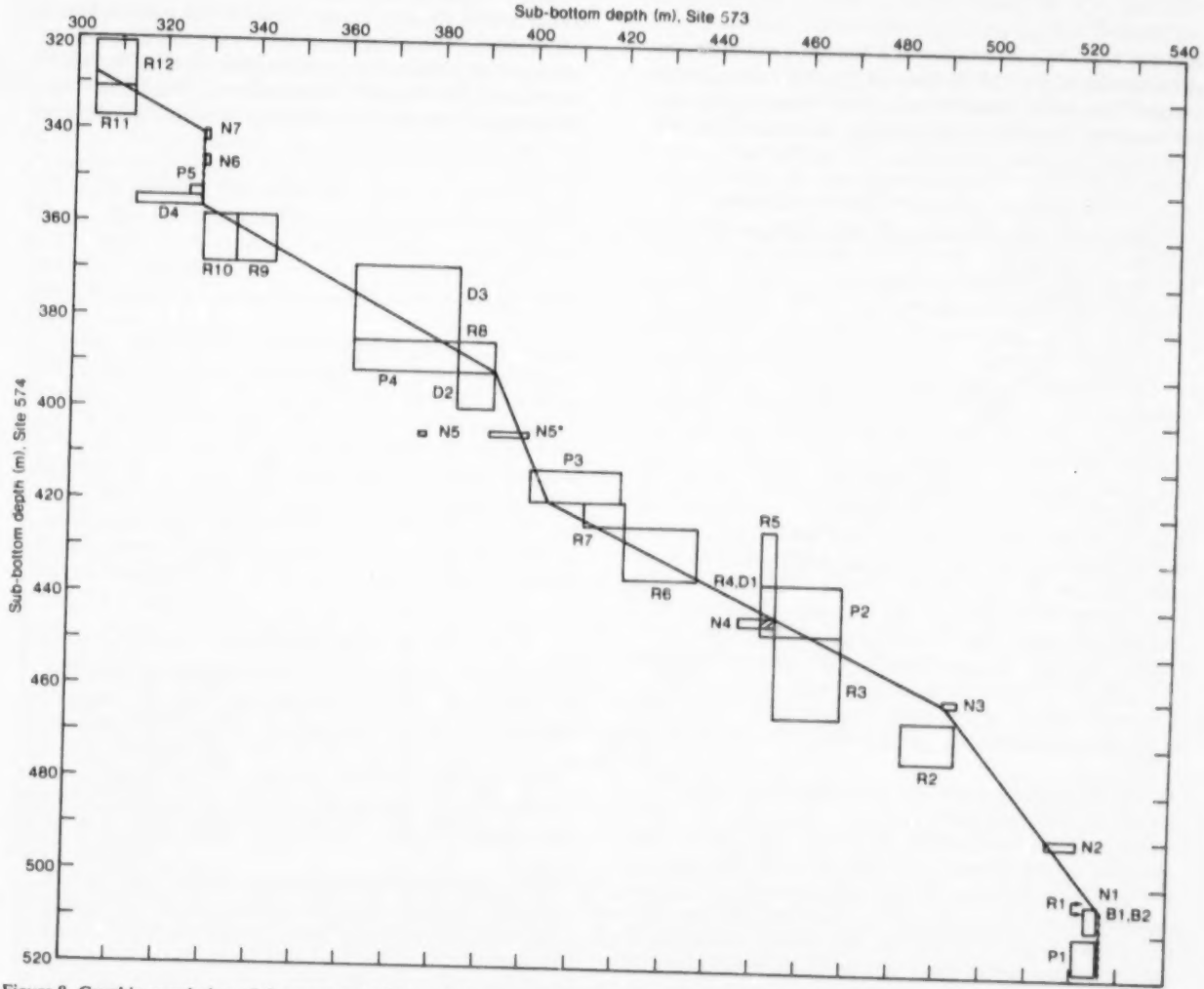

Figure 8. Graphic correlation of the uppermost Eocene to lowermost Miocene sections at Sites 573 and 574. Boxes constrain the stratigraphic positions of the microfossil datums used for the correlation—refer to Tables 2 to 6. Overlaps of boxes are shaded. Calcareous nannofossil datum levels used are those of Pujos (this volume), except for those marked with an asterisk, which are from Gartner and Chow (this volume).

Table 7. Summary of hiatuses and compressed intervals in Leg 85 sediment.

Site	Sub-bottom depth (m)	Age (Ma)	Hiatus (H) or compressed (C)	Lithologic change	Recorded elsewhere
573	76	4.6–5.1	H?	Yes	NH7[a]
573	158	9.8–10.5	H	Yes	NH5[a]
573	177	11.5–12.0	H	No	NH4[a]
573	187	12.3–12.7	H? or C	No	NH3?[a]
573	272	18.2–19.7	H	Yes[b]	NH1b[a]
573	290	20.5–21.5	H	Yes	NH1a[a]
573	328	22.7–24.0	H	No	PH[a]
573	392–404	28.7–32.0	C	No	[c]
573	525	36.8–37.3	H	Yes	[d]
574	5	0.6–1.0	H	Yes?	
574	70	9.8–11.1	H	Yes	NH5[a]
575	8	3.4–5.1	H	No	NH7[a,e]
575	26	8.8–10.5	H	No	NH5[a]

[a] Keller and Barron (1983).
[b] Downhole change in diatom preservation.
[c] Keller (1983a).
[d] Kennett et al. (1975).
[e] Osborn et al. (1983).

Hays et al. (1972) and Keller and Barron (1983), is present at about 328 m sub-bottom at Site 573. As noted by Pujos ("Cenozoic Nannofossils," this volume), this hiatus removes calcareous nannofossil Subzone CN1a. An estimated duration of 24.0 to 22.7 m.y. for this Oligocene/Miocene hiatus is suggested by the Leg 85 biostratigraphic time scale (Fig. 2, Table 7).

A compressed interval is present at Site 573 within planktonic foraminiferal Zone P21 (datums P3 to P4, 404 to 392 m sub-bottom). This compressed interval in Zone P21 (31.6 to 28.2 Ma) coincides with a widespread deep-sea hiatus (Keller, 1983a), major lowering of sea level (Vail and Hardenbol, 1979), and oxygen-isotope enrichment in benthic foraminiferal tests both at Site 77 (Keigwin and Keller, 1984) and at Site 574 (Miller and Thomas, this volume).

Lower Miocene

Graphic correlation plots for the lower Miocene sections at Sites 573, 574, and 575 are shown on Figure 9. The records at Sites 574 and 575 are quite similar, without any apparent hiatuses, whereas one major or two lesser hiatuses are predicted within the Site 573 section.

Most of the 23 datum levels correlated between Sites 574 and 575 lie on or very close to the plotted line of correlation. The exceptions are events D6 (the last occurrence of *Thalassiosira primalabiata*), P6 (the N4/N5 boundary), P7 (the N5/N6 boundary), and B3 (the first occurrence of *Melonis barleeanus*). Barron (this volume)

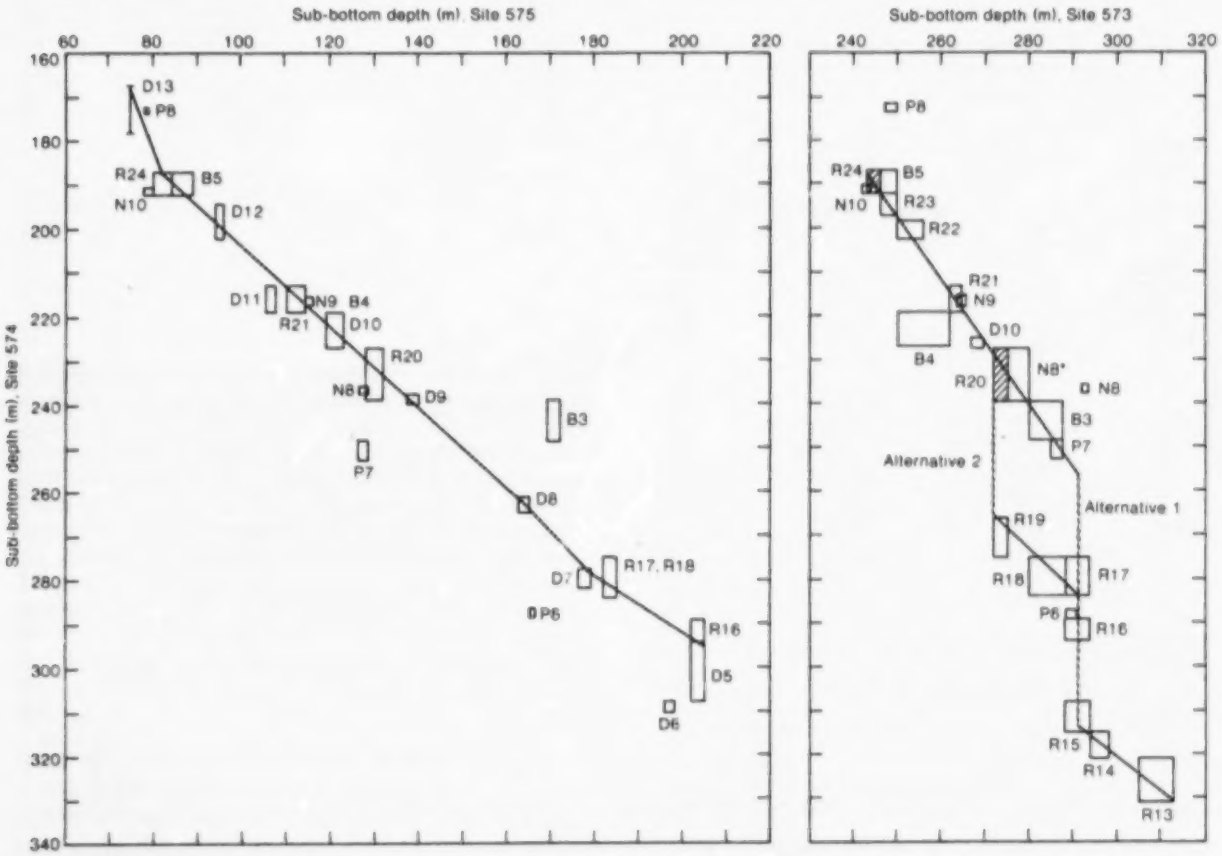

Figure 9. Graphic correlation of the lower Miocene sections at Sites 573, 574, and 575. See caption to Figure 8 for further explanation. The two alternatives for the Site 574–Site 573 correlation are discussed in the text.

noted that the last occurrence of *T. primalabiata* at Site 575 seemed diachronous with correlations at Sites 574 and 71, when compared with radiolarian stratigraphy. Discrepancies in site-to-site correlations of the N5/N6 boundary have been discussed earlier. The Leg 85 time scale (Fig. 2) suggests that the N4/N5 boundary (datum P6, 20.1 Ma) should lie stratigraphically higher at Site 574 if it is to be isochronous with correlations elsewhere. The correlation plot suggests about a 265-m sub-bottom depth (Core 574C-8) for an isochronous placement of the N4/N5 boundary at Site 574.

The two alternatives for correlation of the lower Miocene at Sites 573 and 574 (Fig. 9) both recognize a hiatus at about 290 m sub-bottom at Site 573. A sharp lithologic contact at 290.6 m sub-bottom (uppermost Core 573B-17), between brown ooze (Subunit IIC) above and white-gray chalk (Subunit IID) below, is consistent with this interpretation.

One of the alternatives extends the upper Site 573–Site 574 correlation line down through datums B3 and P7 and allows for one major hiatus (about 21.5 to 18.5 Ma by extrapolation). The second alternative ignores events B3 and P7 (which were shown to be diachronous in the Site 574–Site 575 correlation) in favor of radiolarian datums R18 (the first occurrences of *Didymocyrtis tubaria* and *D. violina*) and R19 (the first occurrence of *Siphostichartus corona*), and suggests a second hiatus at about 272 m sub-bottom, between Cores 573B-14 and 573B-15. Under the second alternative, the older hiatus would be from about 21.5 to 20.5 Ma and the younger hiatus would be from about 19.7 to 18.2 Ma. Barron (this volume) proposed a slightly younger hiatus within the middle of Core 573B-14.

Keller and Barron (1983) favor two such hiatuses (NH1a and NH1b) at nearby Site 77, but estimated ages for these hiatuses, 20.3 to 19.8 Ma (NH1a) and 19.0 to 17.8 Ma (NH1b) (ages adjusted by Barron et al., in press), differ somewhat for the age estimates at Site 573. No lithologic changes are noted between Cores 573B-14 and 573B-15, but the preservation of diatoms deteriorates dramatically downhole at that level at Site 573. At present, the second alternative, with its two hiatuses, is favored over the first alternative with its single hiatus (Table 7).

Middle Miocene to Uppermost Miocene

Graphic correlation plots of the middle Miocene to uppermost Miocene sections of Sites 572, 573, and 573 are shown on Figure 10. Comparison of the Site 572 and Site 573 records (right side of the figure) suggests three hiatuses in the Site 573 section, at approximately 187 m (upper Core 573B-6), 177 m (lowermost Core 573B-5), and 158 m (uppermost Core 573B-3) sub-bottom depths (Table 7).

Barron (this volume) argues for the uppermost of these hiatuses, and estimates its age from 10.5 to 9.8 Ma. Pujos ("Cenozoic Nannofossils," this volume) also postulates a hiatus at about this interval in the lower part of the calcareous nannofossil CN8 Zone. Barron (*this volume*) notes that this hiatus (NH5 of Keller and Barron, 1983) coincides with the top of a distinctive purple-banded unit in Section 1 of Core 573B-3. At Site 574, Barron (this volume) recognized a coeval hiatus in lowermost Core 574-8 (about 70 m sub-bottom), where a purple-banded unit was also present. Pujos ("Cenozoic Nannofossils," this volume) also supports a hiatus in Zone CN8 at Site 574. The Site 573–Site 574 plot (left side of Fig. 10) shows that a section present at Site 573 has been removed at a hiatus at 70 m sub-bottom at Site 574, implying that hiatus NH5 was of longer duration at Site 574 than at Site 573. The additional interval removed at Site 574 has an estimated age of 11.1 to 10.5 Ma (Table 7).

Barron (this volume) notes compression in the age-vs.-depth curve for Site 573 between 12.0 and 11.5 Ma, at about 174 to 176 m sub-bottom. At nearby Site 77, Barron (this volume) postulates a hiatus between 12.0 and 11.5 Ma, on the basis of the absence of a pronounced abundance peak in the diatom *Denticulopsis hustedtii*. Section equivalent to this middle hiatus at Site 572 (310 to 290 m sub-bottom) is characterized by very low percent carbonate values (site chapter), so that dissolution of carbonate at Site 573 may have been partly responsible for this hiatus. This middle hiatus correlates with widespread deep-sea hiatus NH4 of Keller and Barron (1983), which coincides with low values of percent carbonate throughout the equatorial Pacific (Barron and Keller, 1982). At this approximate interval, Mayer et al. (this volume) also note a sharp seismic boundary in sediments throughout the equatorial Pacific. The Site 573–Site 574 plot (left side of Fig. 10) has not been drawn to show this hiatus, although the vertical distribution of the D19, N14, R35, and R36 datums could be construed to be consistent with existence of this hiatus at 177 m sub-bottom at Site 573.

Evidence for the lowermost hiatus, which had an estimated duration of between 12.7 and 12.3 m.y., is less certain. Vertical distribution of the R33, R34, D17, N13, and D18 datums in both the Site 572–Site 573 plot and the Site 573–Site 574 plot support arguments for a hiatus at about 187 m sub-bottom at Site 573, although the hiatus is not plotted in the latter graph. No such hiatus at nearby Site 77 is suggested, however, by Keller (1980), Keller and Barron (1983), or Barron (this volume). Percent carbonate values within the equivalent interval (342 to 320 m sub-bottom) at Site 572 are typically high (site chapter). Hiatus NH3 of Keller and Barron (1983) (13.5 to 12.5 Ma) overlaps this lower hiatus only in part, and is typically older. No obvious lithologic changes are present in upper core 573B-6 at 187 m sub-bottom (site chapter)

During the middle Miocene, the section at Site 574 accumulated at a rate 1.5 to 1.2 times greater than the section at Site 573. During the late Miocene (after 10 Ma), however, the Site 573 section accumulated at a rate averaging 1.5 times the rate of accumulation at Site 574. This reversal in relative rates reflects the northwestward movement of Sites 574 and 573 through the equatorial belt of high biologic productivity (Weinreich *and Theyer, this volume*).

The relative rates of sediment accumulation during the late middle Miocene to latest Miocene are generally

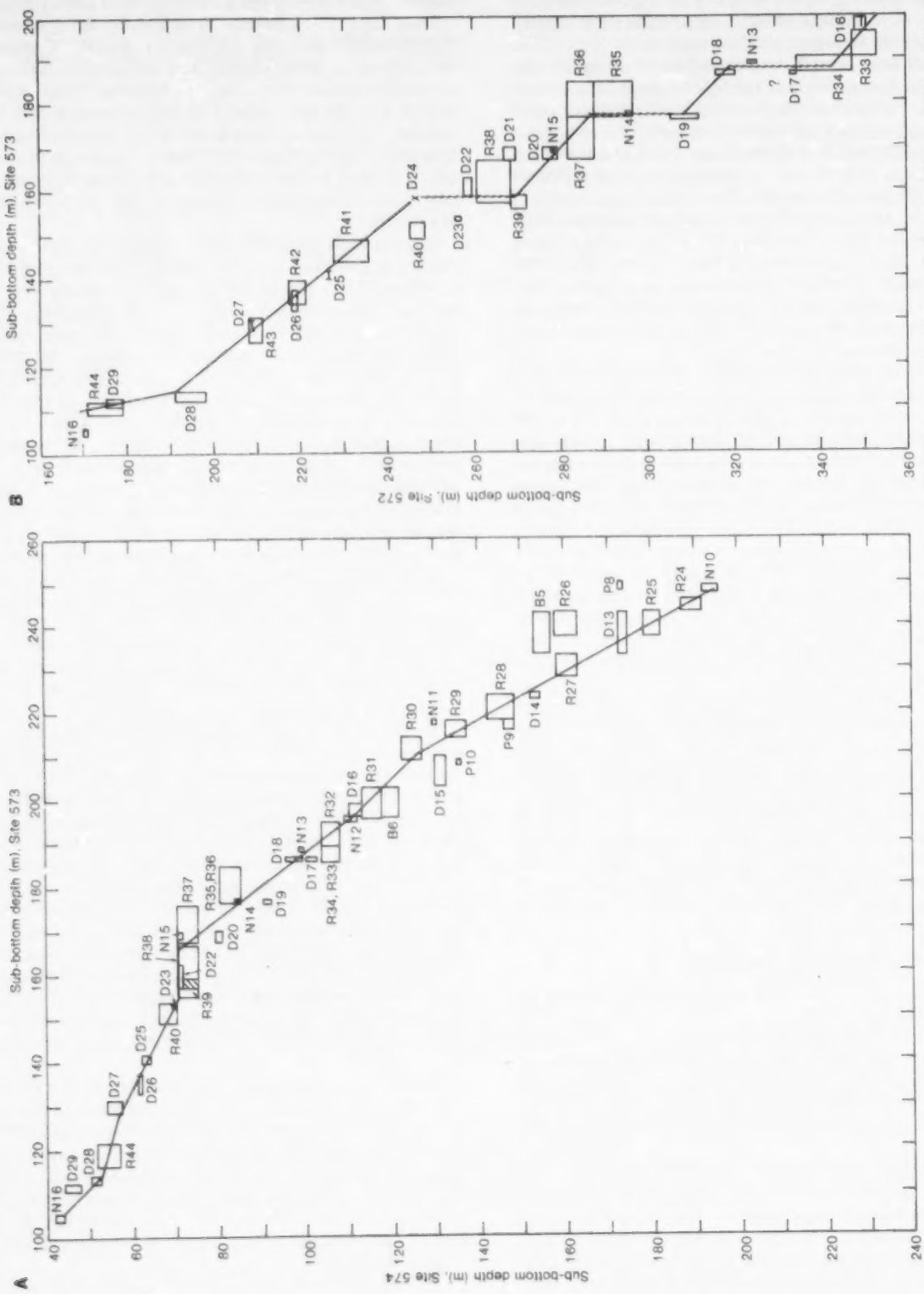

Figure 10. Graphic correlation of (A) the middle Miocene to uppermost Miocene sections at Sites 573 and 574 and (B) the upper middle Miocene to uppermost Miocene sections at Sites 572 and 573. See caption to Figure 8 for further explanation.

comparable between Sites 572 and 573, except during the three hiatus intervals at Site 573 (Fig. 10). After 6.3 Ma (datum D28), the accumulation rates at Site 572 appear to have been markedly higher than those at Site 573; this will be discussed in the following section on the uppermost Miocene through Quaternary graphic correlation plot.

As the plots are drawn, only datums P8 (the N8/N9 boundary), R26 (the last occurrences of the radiolarians *Dorcadospyris dentata* and *Didymocyrtis violina*), and B5 (the first occurrence of the benthic foraminifer *Cibicidoides wuellerstorfi*) lie appreciably off the correlation line between Sites 573 and 574. The N8/N9 boundary, however, was recognized by differing criteria (Saito, this volume) at Sites 573 and 574, namely, by the last occurrence of *Globigerinoides sicanus* at Site 573 and by the first occurrence of *Orbulina suturalis*, the zonal marker, at Site 574.

Uppermost Miocene through Quaternary

Figure 11 is a graphic correlation plot of the sections at Sites 572 and 573 for the uppermost Miocene through the Quaternary. More detailed correlations of Leg 85 Quaternary sections by calcareous nannofossils and radiolarians are provided in the chapters by Pujos "Nannofossils from Quaternary Deposits," this volume) and Labracherie (this volume), respectively.

The section at eastern Site 572 accumulated at rates approximately twice as great as those at Site 573 during the latest Miocene (datum D29, or 6.2 Ma, to datum N17, or 5.1 Ma). The lowermost Pliocene (about 5.1 to 4.6 Ma), however, is extremely compressed at Site 573, in that the interval between datums N17 (the CN9/CN10 boundary) and D35 (the first occurrence of *Nitzschia jouseae*) encompasses 25 m of section at Site 572 but only 6 m of section at Site 573. On the basis of diatom stratigraphy, Barron (this volume) and Baldauf (this volume) argue for a hiatus between 5.1 and 4.6 Ma (at the base of Core 573-9, about 76 m sub-bottom). They correlate this hiatus with widespread deep-sea hiatus NH7 of Keller and Barron (1983) (Table 7). As mentioned earlier, a more extensive hiatus at Site 575 has removed the section representing the interval between 5.1 and 3.4 Ma (Fig. 7, Table 7).

Above this compressed interval at Site 573, accumulation rates at Site 572 remained greater than rates at Site 573 by a ratio of about 1.7:1.0 between 4.6 and 3.6 Ma (datums D35 to R51). The uppermost parts of Sites 573 and 572, on the other hand, show nearly equivalent accumulation rates (compare also age-vs.-depth plots of Pujos, "Nannofossils from Quaternary Deposits," this volume, and Baldauf, this volume). The brief hiatus (about 2.2 to 1.8 Ma) predicted by diatoms at about 33 m sub-bottom at Site 572 (Core 572A-4) (Barron, this volume; Baldauf, this volume) is not apparent in Figure 11, so it is possible that between Sites 572 and 573 some diachrony exists between the ages of the last occurrence of *Thalassiosira convexa* (D40) and the first occurrence of *Pseudoeunotia doliolus* (D41).

Of the 37 latest Miocene through Quaternary datum levels correlated between Sites 572 and 573, all but three lie on the plotted correlation line (Fig. 11). Those three aberrant datums include the first occurrence of the radiolarian *Pterocanium prismatium* (R48) and the last occurrences of the diatoms *Asterolampra acutiloba* (D33) and *Thalassiosira miocenica* (D34). Nigrini (this volume) notes that *P. prismatium* is rare at the lower end of its range, so its first occurrence may actually be lower at Site 573 than what has been plotted on Figure 11. It is possible that the diatoms *A. acutiloba* and *T. miocenica* are reworked slightly upsection at Site 573.

AGE-VS.-DEPTH PLOTS

The graphic correlation plots (Figs. 8 to 11) show which of the Leg 85 sections are the most complete for any interval of time between the latest Eocene and the Quaternary. In addition, diachronous occurrences of datum levels have been noted and the sequencing of the various microfossil datum levels has been established.

On Figure 12, age-vs.-depth graphs for the middle Miocene through Quaternary of Site 572 and a composite section from Sites 573 and 574 have been constructed using the published age estimates for the various datum levels shown on Tables 2 to 6. A composite section consisting of the Quaternary through upper Miocene of Site 573 and the middle Miocene of Site 574 is plotted, because the younger section at Site 574 is compressed (Fig. 5) and the middle Miocene of Site 573 apparently contains two hiatuses (Fig. 10). Both Site 573 and Site 574 have a hiatus between about 10.5 and 9.8 Ma (NH 5) (Table 7).

The Site 572 plot shows high rates of sediment accumulation (about 50 m/m.y.) in the middle Miocene between 15.0 and 11.0 Ma and across the Miocene/Pliocene boundary between 6.3 and 3.8 Ma. Lower rates (about 16 m/m.y.) characterized most of the late Miocene (11.1 to 6.3 Ma) and the late Pliocene through Quaternary (3.8 to 0 Ma).

Middle Miocene accumulation rates at Site 574 were also relatively high, averaging 26 m/m.y. between 15.5 and 11.1 Ma. Rates during the late Miocene interval from 9.8 to 6.3 Ma were about 12 m/m.y. at Site 573. As at Site 572, accumulation rates returned to middle Miocene values (26 m/m.y.) across the Miocene/Pliocene boundary between 6.3 and 3.5 Ma. An exception is a compressed interval or hiatus between 5.1 and 4.6 Ma at Site 573. Late Pliocene through Quaternary accumulation rates at Site 573 were about 14 m/m.y., or nearly equal to accumulation rates at Site 572 (16 m/m.y.).

Of the datums plotted on Figure 12, only R30, the first occurrence of the radiolarian *Diartus petterssoni*, lies appreciably off the age-vs.-depth plot. The diachrony of this datum, which corresponds to the *Dorcadospyris alata/Diartus petterssoni* boundary, has been discussed earlier.

On Figure 13, age-vs.-depth plots for the lower Miocene of Site 575 and the lower Miocene to upper Eocene of Site 574 have been constructed. As mentioned earlier, the Paleogene section at Site 573 contains two hiatuses and one compressed interval (possibly a hiatus), so it was not plotted.

Between 37.0 and 35.0 Ma and between 34.6 and 30.7 Ma, accumulation rates at Site 574 were approxi-

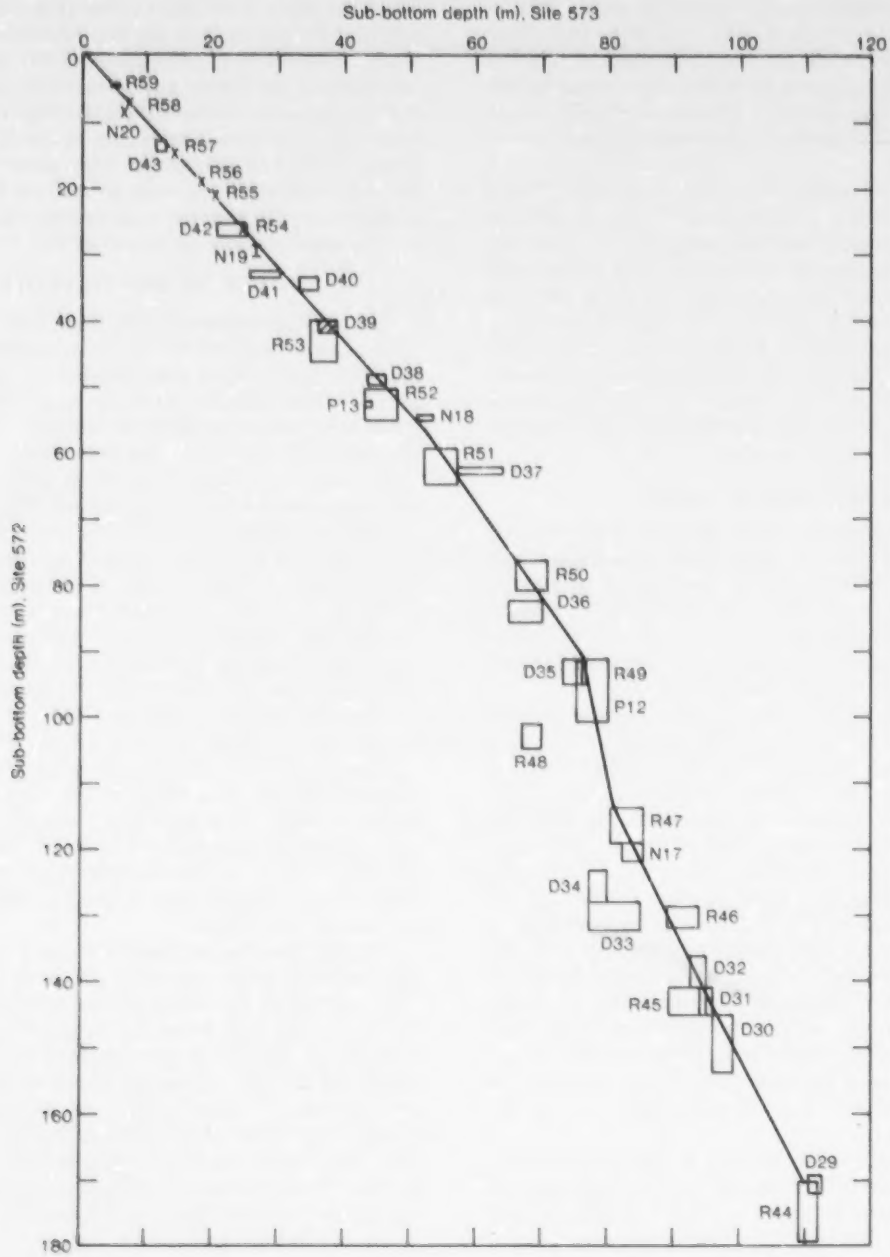

Figure 11. Graphic correlation of the uppermost Miocene through Quaternary sections at Sites 572 and 573. See caption to Figure 8 for further explanation.

mately 12 m/m.y. A brief interval from 35.1 to 34.6 Ma, however, corresponding to calcareous nannofossil Subzone CP16c, according to both Pujos and Gartner and Chow (Fig. 5), apparently accumulated at very high rates approaching 60 m/m.y. It is possible that these anomalously high accumulation rates are an artifact of the time scale, but both Berggren, Kent, and Flynn (in press) and Bukry (1975) independently estimate a duration of only 0.5 m.y. for Subzone CP16c. Further complicating the picture is the coincidence of relatively low percent carbonate values (60 to 80% vs. typical Oligocene values of 90%) (site chapters) with Subzone CP16c at both Site 573 and Site 574. No explanation can presently be given for these high accumulation rates, but it should be noted that Keigwin (1980), Keller (1983 a, b), and Keigwin and Keller (1984) report that benthic foraminiferal oxygen isotopes at Pacific Sites 77, 277, and 292 and Atlantic Site 563 show their highest positive early Oligocene values (cooling) in Subzone CP16c or its equivalent.

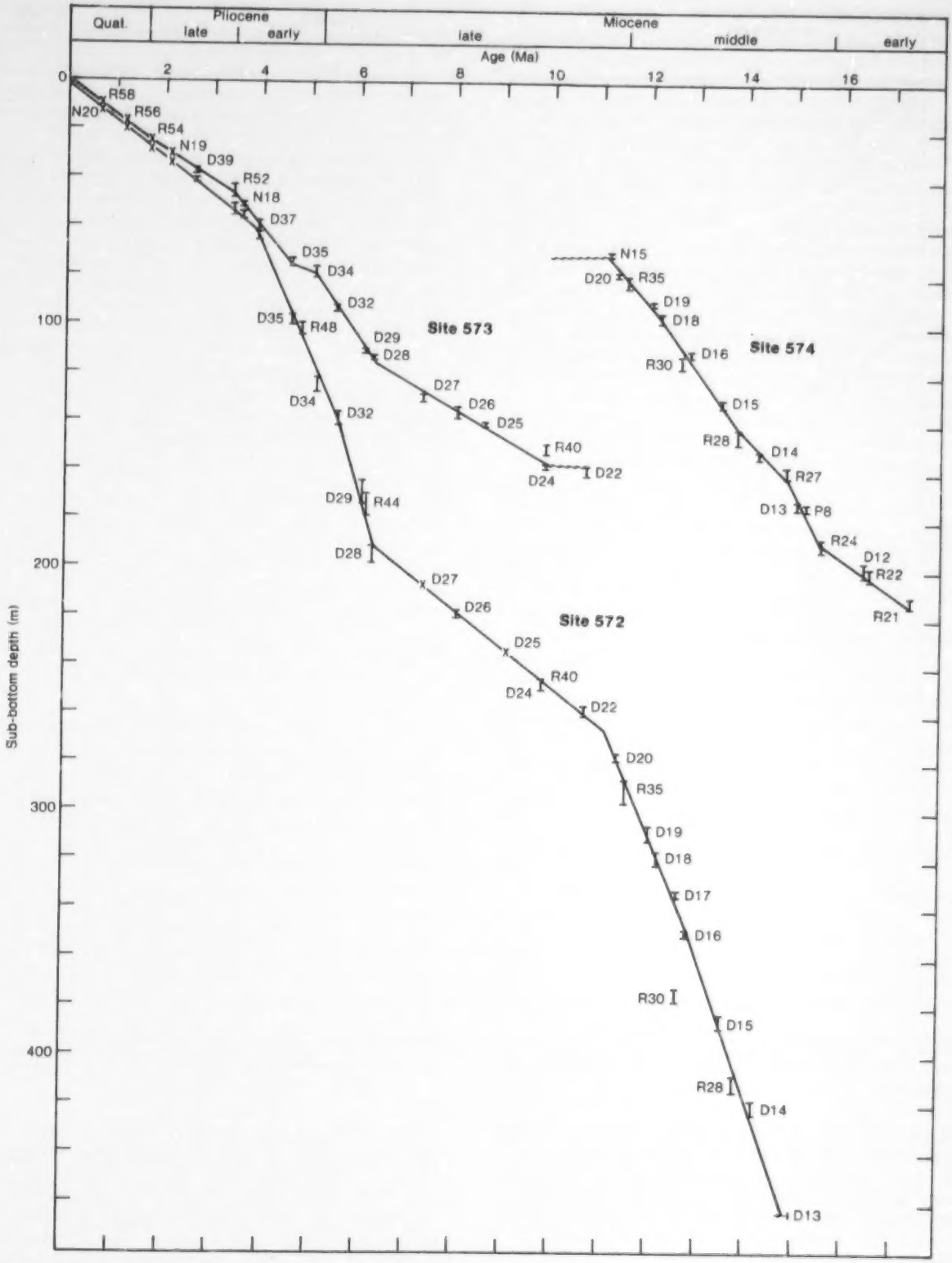

Figure 12. Age-vs.-depth plots for the Quaternary through middle Miocene at Site 572 and a composite section from Site 573 (Quaternary through late Miocene) and Site 574 (middle Miocene). Microfossil datums from Tables 2 to 5, for which absolute age estimates exist, have been used to construct the plots.

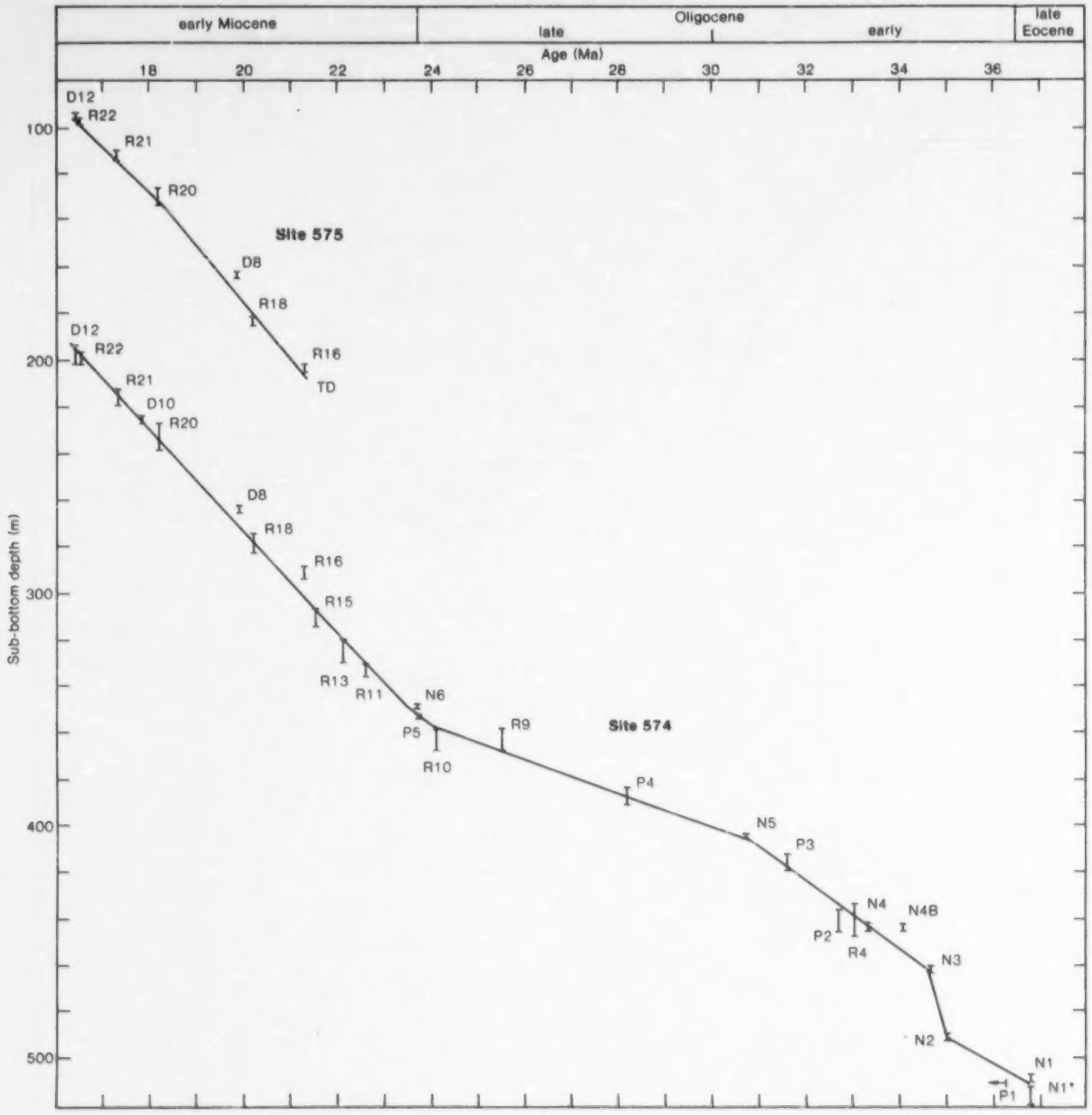

Figure 13. Age-vs.-depth plots for the early Miocene at Site 575 and the early Miocene to late Eocene at Site 574. Microfossil datums from Tables 2 to 5, for which absolute age estimates exist, have been used to construct the plots. N4B refers to the age correlation (34.1 Ma) by Berggren et al. (in press) for the CP17/CP18 calcareous nannofossil zonal boundary. Asterisk denotes calcareous nannofossil datums after Gartner and Chow (this volume).

Low accumulation rates of about 7 m/m.y. during the late Oligocene (30.7 to 24.0 Ma) are implied for Site 574. Early Miocene accumulation rates, on the other hand, increased to 20 to 25 m/m.y. at both Site 574 and Site 575 (Fig. 13).

Significance of Accumulation Rates

In the central equatorial Pacific, the present-day zone of high primary productivity extends from about 3–4°S to about 0–1°N, at 145° to 120°W, and from about 5°S to about 5°N, between 120° and 105°W (Koblentz-Mishke et al., 1970). Backtracking of the Leg 85 sites according to the model of van Andel et al. (1975) (see Theyer et al., this volume) can be used to suggest the interval of time during which the Leg 85 sites lay beneath waters of high biologic productivity (assuming no major change in the position of that productivity zone with respect to the equator). Such an exercise yields the following resi-

dence times for the Leg 85 sites within the equatorial Pacific high-productivity zone: Site 572, 0 to 15 Ma = entire record; Site 573, 0 to 10 Ma; Site 574, 12 to 25 Ma; and Site 575, 16 to 35 Ma.

To a large extent, comparison of the relative sediment accumulation rates in the graphic correlation plots (Figs. 8 to 11) and age-vs.-depth plots (Figs. 12, 13) reflects this model, in that the highest relative accumulation rates correspond to those intervals deposited beneath the high-productivity zone. Consequently, Site 574 had higher accumulation rates than Site 573 during the middle Miocene, whereas the opposite relationship was true during the late Miocene (Fig. 10). Accumulation rates at eastern Site 572, however, were typically always higher than rates at the western sites (Fig. 12), attesting to the higher primary productivity in the eastern equatorial Pacific (Koblentz-Mishke et al., 1970).

During the late Oligocene, Site 573 lay farther south of the equator (7 to 8°S) than Site 574 (3 to 4°S), yet accumulation rates at Site 573 were typically twice those at Site 574 (Fig. 8). This contradiction of the model may result from enhanced carbonate preservation at Site 573, since upper Oligocene percent carbonate values at Site 573 are on the average slightly higher than those at Site 574 (site chapters). The water depth at Site 574 was probably slightly greater than that at Site 573 during the late Oligocene, because the present-day water depths of Sites 574 and 573 are 4560 and 4300 m, respectively. During the earliest Oligocene (34.6 to 36.5 Ma, below datum N3), accumulation rates at Sites 573 and 574 were about equal (Fig. 8), indicating that the two sites experienced similar levels of productivity (see also Theyer et al., this volume).

Extrapolation of Ages for Datum Levels

If the age-vs.-depth plots (Figs. 12, 13) are considered accurate, then one can use them to extrapolate absolute age estimates for those datums which have not been calibrated directly to paleomagnetic stratigraphy. This exercise has been done in Tables 2 to 6 (right-hand column). The age ranges given for the individual datums reflect the constraints of their plotted values on the graphs. In making these determinations, uniform accumulation rates between those datums with published absolute ages are assumed unless hiatuses are predicted on the graphic correlation plots (Figs. 8 to 11). The extrapolated absolute ages differ in some cases from published age estimates (compare columns on Tables 2 to 6). These differences may reflect differences in taxonomic interpretations between workers, differences in the accuracy of the extrapolations, or true diachrony in species ranges.

SUMMARY

A major objective of DSDP Leg 85 was to recover relatively undisturbed hydraulic piston cores within the high-productivity zone of the central equatorial Pacific. Earlier drilling during Legs 5, 8, 9, and 16 produced rotary-drilled cores which have been of key importance in developing biochronologies for the Oligocene through Quaternary, and which have been a focus for low-latitude Pacific paleoceanographic studies (van Andel et al., 1975; Keller and Barron, 1983). Hydraulic piston coring in this area would allow the development of high-resolution bio-, magneto-, seismic-, carbonate, and stable-isotope stratigraphies, needed for determining the sequencing and mechanisms of paleoceanographic changes.

During Leg 85, hydraulic piston cores were recovered at five sites which form an east–west transect from 114°W (Sites 571, 572) to 133–135°W (Sites 573 to 575) and a south–north transect across the high-productivity zone from 0°N (Site 573) to 6°N (Site 575). At each of the four main sites (572 to 575), duplicate hydraulic piston cores were collected through the Quaternary and Pliocene and into successively older (deeper) levels of the Miocene: at Site 572, to 6.2 Ma; at Site 573, to 10 Ma; at Site 574, to 16.7 Ma; and at Site 575, to 22 Ma.

Paleomagnetic stratigraphy was obtained for the Quaternary through late Pliocene at Site 573, for the Quaternary to late Miocene at Site 574 , and for the Quaternary to late middle Miocene plus an interval within the late early Miocene (18.2 to 16.4 Ma) at Site 575. At Site 575, for the first time, many microfossil datums were calibrated directly to the interval from the upper part of paleomagnetic Chron 17 to the middle part of paleomagnetic Chron 16.

At eastern Site 572, a complete sequence apparently free of hiatuses was cored through the Quaternary to the lower middle Miocene (about 15 Ma). High sediment accumulation rates (about 50 m/m.y.) characterize the middle Miocene (15 to 11 Ma) and uppermost Miocene to lower Pliocene (6.3 to 3.8 Ma), and diatoms typically are the dominant microfossils.

At Site 573, about 10 km from Site 77, Quaternary to upper Eocene sediment was cored in three holes. Numerous short to medium-length hiatuses are present at Site 573, including hiatuses at the Eocene/Oligocene, Oligocene/Miocene, middle Miocene/upper Miocene, and (possibly) at the Miocene/Pliocene boundaries (Table 7). Most of these hiatuses have been earlier postulated to exist at nearby Site 77, but they are confirmed at Site 573 by graphic correlation plots with the other Leg 85 sections.

A complete sequence through the Eocene/Oligocene boundary was obtained at Site 574 (4°N), as was a thick reference section for the middle Miocene through Oligocene. An early late Miocene hiatus (11.1 to 9.8 Ma) (Table 7) is represented at the site, and the upper Miocene through Quaternary section is compressed relative to that at Site 573 (0°N).

At Site 575 (6°N), coring was terminated in the lower Miocene (about 22 Ma) owing to lack of ship time. Nevertheless, a thick lower Miocene section free of hiatuses was recovered at the site. Two hiatuses in the early late Miocene (10.5 to 9.8 Ma) and early Pliocene (5.1 to 3.4 Ma) are recorded in the relatively compressed upper section at Site 575 (Table 7).

Throughout the Leg 85 sequences, planktonic foraminiferal, calcareous nannofossil, radiolarian, and diatom stratigraphies are typically consistent with one another and with the Leg 85 biostratigraphic time scale. Most of the few discrepancies that exist can be explained by diachronous species ranges, reworking, or differences

in taxonomic concepts between workers. Graphic correlation plots between the sequences are especially helpful in identifying diachronous datums, and can also be used to check the isochrony of benthic foraminiferal datum levels.

Age-vs.-depth plots have been constructed using datums with published absolute age estimates, and ages of other datums have been extrapolated from the plots. In some cases the extrapolated age estimates differ from published age estimates, but usually they agree to within 100,000 to 200,000 yrs.

The biostratigraphic studies discussed in this chapter certainly can be refined by closer sampling intervals and by quantitative studies (see Pujos, and Baldauf, both this volume). Detailed carbonate and stable-isotope studies, such as those by Pisias and Prell (this volume) and Pisias and Shackleton (this volume), allow even greater refinement of time in the hydraulic piston cores. The sediment sequences recovered during Leg 85 are excellent for such high-resolution studies, and will undoubtedly provide a focal point for future paleoceanographic studies in the central equatorial Pacific.

ADDENDUM

Since 1974 it has widely been accepted that paleomagnetic Anomaly 5 correlates with paleomagnetic Chron 9 as recognized in the sediment (Berggren and Van Couvering, 1974; Theyer and Hammond, 1974; Ryan et al., 1974). As discussed by Theyer and Hammond (1974), Foster and Opdyke's (1970) correlation of Anomaly 5 with Chron 11 was rejected, because biostratigraphic and radiometric calibrations of the middle Miocene/upper Miocene boundary were in better agreement with an Anomaly 5–Chron 9 correlation. Berggren and Van Couvering (1974) and Ryan et al. (1974) all presented arguments, based on available radiometric evidence, that the middle/upper Miocene boundary must be older than the base of Anomaly 5 (about 10.2 to 10.4 Ma). At the same time, Berggren and Van Couvering (1974) and Ryan et al. (1974) all showed that middle Miocene microfossils ranged into lower paleomagnetic Chron 11 or higher, so it seemed impossible that Anomaly 5 could correlate with Chron 11.

Recently, however, W. A. Berggren (pers. comm., 1984; and Berggren, Kent, and Van Couvering, in press) has suggested that Anomaly 5 does indeed correlate with Chron 11 (as it has been recognized in the sediment), and that earlier radiometric calibrations of the middle/upper Miocene boundary are in error. Berggren cited paleomagnetic–biostratigraphic correlations at DSDP Site 519 in the South Atlantic by Poore et al. (1984) and Hsü et al. (1984). Site 519 was drilled on crust slightly older than Anomaly 5, and middle Miocene calcareous nannofossils (Zones CN6 and CN7) were recorded within a relatively long (10 m) normally polarized interval immediately above basement. Because correlations of CN6 and CN7 (= NN8 and NN9) calcareous nannofossils with paleomagnetic Chron 11 have been well established (Ryan et al., 1974; Berggren and Van Couvering, 1978; Keller et al., 1982; Barron et al., in press), it seems apparent that the normal interval containing CN6 and CN7 calcareous nannofossils at Site 519 correlates with both Anomaly 5 and Chron 11 (Hsü et al., 1984).

The Leg 85 biostratigraphic time scale (Fig. 2) incorporates an Anomaly 5–Chron 9 correlation, as do the various chapters of this volume. The purpose of this addendum is to present the alternative middle to late Miocene biostratigraphic time scale based on an Anomaly 5–Chron 11 correlation (compare Berggren, Kent, and Van Couvering, in press), so that readers favoring such a correlation can reassign absolute ages to middle and late Miocene intervals discussed in the Leg 85 chapters.

Figure 14 shows reassignment of paleomagnetic Chrons 7 through 14 to the polarity sequence between Anomalies 3A and 5B, based on an Anomaly 5–Chron 11 correlation. W. A. Berggren (pers. comm., 1984) feels that the correlation of the chrons above Chron 7 and below Chron 14 with the paleomagnetic time scale proposed by Ryan et al. (1974) and LaBrecque et al. (1977) (and adopted in the Leg 85 biostratigraphic time scale) does not require adjustment. The adopted correlation (Fig. 14) largely follows alternative "A" of Theyer and Hammond (1974). It could be argued that this older numbering system of chrons (Ryan et al., 1974; LaBrecque et al., 1977) should be abandoned in favor of a newer system proposed by Tauxe et al. (1983). Tauxe et al. (1983) label successive chrons, from the top of one numbered anomaly to the top of the next oldest numbered anomaly, with the same number as the included anomaly, and preface those numbers with a "C." Such a numbering system is also shown on Figure 14, and has been incorporated in the Paleogene part of Figure 2. Earlier published paleomagnetic correlations of microfossil datum levels refer, however, almost exclusively to the older system of numbering chrons, so much of the following discussion will utilize that system.

Correlation of the microfossil zones and subzones with the paleomagnetic chrons on Figure 14 differs little from the correlation shown on Figure 2, but the new anomaly–chron correlation results in changes in the estimated absolute ages of the microfossil zones and subzones (Figs. 2, 14). This correlation has been accomplished by reassigning absolute ages to the middle and late Miocene microfossil datum levels, which have been directly calibrated with paleomagnetic stratigraphy (Table 8) on the basis of the Anomaly 5–Chron 11 correlation model of Figure 14. Absolute ages of additional datum levels (and zonal boundaries) have been extrapolated from replotted age-vs.-depth curves for Sites 572 to 574 (Fig. 15) in the manner used to extrapolate absolute ages on Tables 2 to 6. Thus, the age of the middle Miocene/upper Miocene boundary changes from about 11.5 Ma to about 9.5 Ma when an Anomaly 5–Chron 11 correlation is adopted (Fig. 14).

It is immediately apparent that the new age-vs.-depth curves for Sites 572 to 574 (Fig. 15) differ considerably from those of Figure 12, in that no kink of low sediment accumulation rates occurs in the new plots between 11 and 6.2 Ma. As stated earlier, Sites 572 and 574 probably lay within the equatorial region of highest productivity during the entire late Miocene, and it is difficult to explain why sediment accumulation rates would have

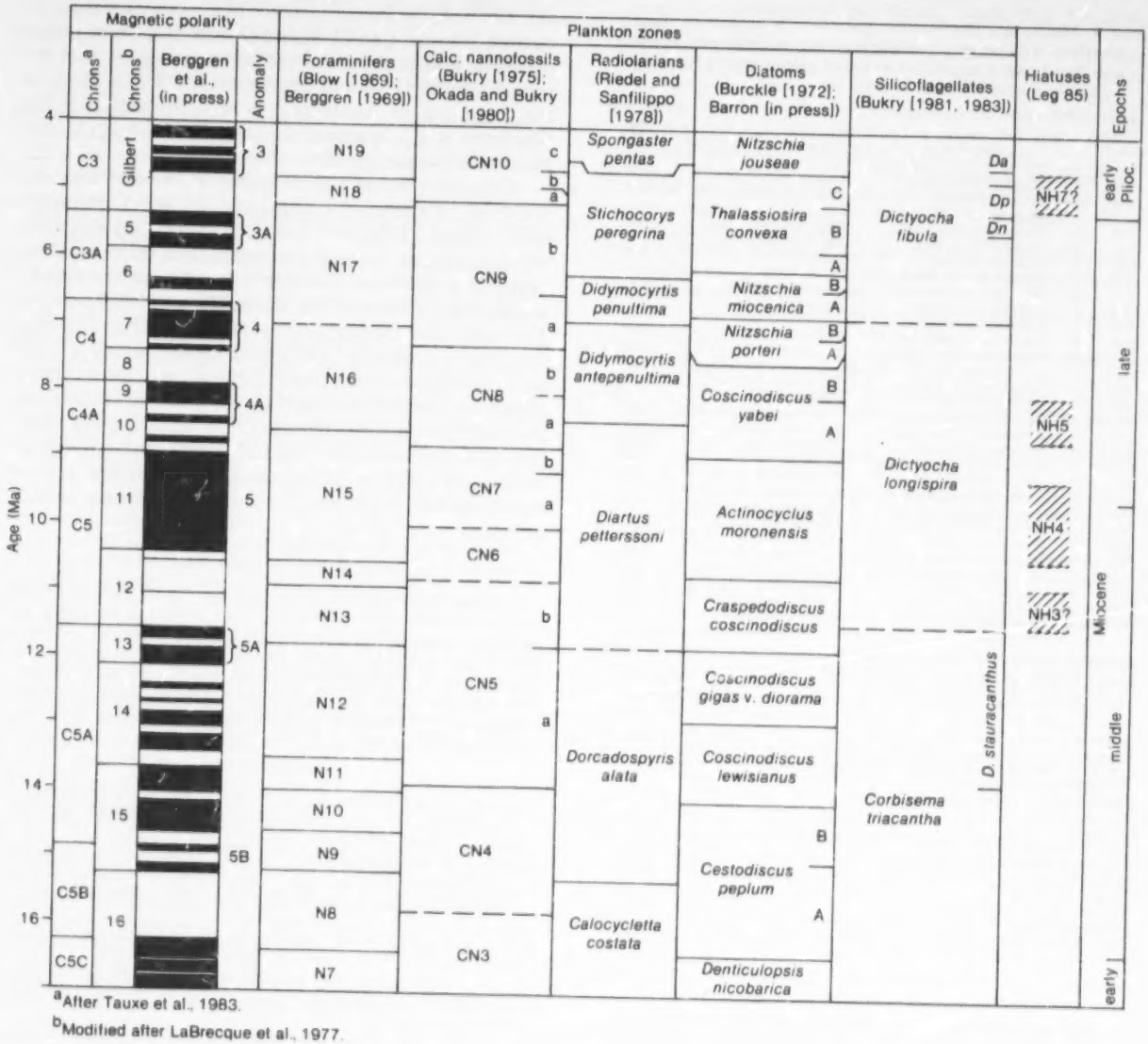

Figure 14. Alternative biostratigraphic time scale for the middle and late Miocene, based on a correlation of paleomagnetic Anomaly 5 with paleomagnetic Chron 11. See caption to Figure 2 for further explanation.

dropped sharply between 11 and 6.2 Ma. As the replotted curves of Figure 15 show no such drop in sediment accumulation rates between 11 and 6.2 Ma at Sites 572 and 574, but rather show relatively constant rates (about 25 to 30 m/m.y. at Site 572 and about 14 to 18 m/m.y. at Site 574), they both add support to the Anomaly 5–Chron 11 correlation of Figure 14.

It should also be noted that the ages and durations of hiatuses NH3, NH4, and NH5 are changed by an Anomaly 5–Chron 11 correlation (Figs. 14, 15). In Leg 85 sediment, hiatus NH3 ranges from 11.5 to 10.7 Ma, hiatus NH4 ranges from 10.4 to 9.2 Ma, and hiatus NH5 ranges from 8.6 to 7.9 Ma (8.8 to 7.9 Ma at Site 574) (Figs. 14, 15).

Extrapolations by Weinreich and Theyer (this volume) for Site 574 also reinforce an Anomaly 5–Chron 11 correlation. As stated earlier, Weinreich and Theyer (this volume) recognize the top of a long, normally polarized interval at about 79 m sub-bottom in lower Core 574-9, which they extrapolate to be the top of Anomaly 5 (about 8.9 Ma). Microfossils within this interval (CN7 calcareous nannofossils, *Diartus petterssoni* Zone radiolarians, and *Actinocyclus moronensis* Zone diatoms) suggest, however, a Chron 11 assignment (Figs. 2, 5). Correlation of Anomaly 5 ages (10.42 to 8.92 Ma) with Chron 11 would eliminate this apparent discrepancy.

Finally, a brief review of the literature reveals that radiometric and paleomagnetic calibrations of the last occurrence of the radiolarian *Cyrtocapsella japonica* at DSDP South Atlantic Sites 512 and 513 (50°S) (Ciesielski, 1983) also lend support for an Anomaly 5–Chron 11 correlation. Ciesielski (1983) shows that at Site 512

Table 8. Middle and late Miocene microfossil datum levels directly correlated with paleomagnetic stratigraphy and estimated absolute ages based on the correlation model of paleomagnetic Anomaly 5 with paleomagnetic Chron 11 (Fig. 14).

Event[a]	Datum[b]	Paleomagnetic correlation	Age (Ma)
D29	B. *Thalassiosira miocenica*	Uppermost Chron 6	6.1[c]
R44	*Stichocorys delmontensis* → *S. peregrina*	Uppermost Chron 6	6.2[d]
D28	B. *Thalassiosira praeconvexa*	Upper Chron 6	6.3[c]
Np	B. *Amaurolithus primus*	Rev. event, Chron 6	6.5[e]
D27	B. *Nitzschia miocenica*	Upper Chron 7	6.8[c]
D26	T. *Thalassiosira burckliana*	Middle Chron 7	7.0[c]
N17	B. *Discoaster quinqueramus*	Lowermost Chron 7	7.3[e]
D25	T. *Coscinodiscus plicatus*	Lowermost Chron 7	7.3[f]
R40	B. *Didymocyrtis penultima*	Uppermost Chron 9	7.9[d]
D23	B. *Thalassiosira burckliana*	Uppermost Chron 9	8.0[c]
Pa	B. *Neogloboquadrina acostaensis*	Middle Chron 10	8.6[g,h]
N15	T. *Discoaster hamatus*	Lower rev. event, Chron 10	8.8[h]
D20	T. *Actinocyclus moronensis*	Lowermost Chron 10	8.9[c]
R37	T. *Cyrtocapsella japonica*	Uppermost Chron 11	9.1[g,i]
Nc	B. *Catinaster calyculus*	Upper Chron 11 (Anom. 5)	9.2[j]
D19	T. *Coscinodiscus tuberculatus*	Lowermost Chron 11	10.4[k]
Pt	T. *Globorotalia siakensis*	Uppermost Chron 12?	10.6[g]
D18	T. *Craspedodiscus coscinodiscus*	Upper Chron 12	10.7[g]
Rt	T. *Cyrtocapsella tetrapera*	Lowermost Chron 12	11.4[f]
Rj	B. *Cyrtocapsella japonica*	Lower Chron 13	12.0[f]
D15	T. *Coscinodiscus lewisianus*	2nd normal above Chron 15	12.9[c]
R28	B. *Didymocyrtis laticonus*	Uppermost Chron 15	13.8[d]
D14	T. *Cestodiscus peplum*	Top rev. event, Chron 15	14.1[c]
Rc	T. *Calocycletta costata*	3rd normal, Chron 15	14.9[f]
D13	T. *Annellus californicus*	Lower rev. event, Chron 15	15.0[c]
D12	B. *Cestodiscus peplum*	Upper normal, Chron 16	16.4[f]
R22	B. *Giraffospyris taxaria*	Upper normal, Chron 16	16.5[f]
R21	B. *Calocycletta costata*	Lower Chron 16	17.3[f]

Note: All correlations made from original paleomagnetic stratigraphy with chrons labeled as in Figure 14. Note that changes from the results of Tables 2 to 4 occur in the intervals older than 6.4 Ma and younger than 13 Ma. Note also that the correlation by Poore et al. (1984) of the first occurrence of the calcareous nannofossil *Catinaster coalitus* with Chron 9 (adjusted to Chron 11, this report) is rejected because Percival (1984) does not record *C. coalitus* at Site 519.

[a] Diatom (D), radiolarian (R), calcareous nannofossil (N), and planktonic foraminiferal (P) datum levels labeled as in Tables 2 to 5. Additional datum levels not used in Tables 2 to 5 labeled with letters only.

[b] B. = bottom; T. = top.

[c] Burckle (1978).

[d] Theyer et al. (1978).

[e] Haq et al. (1980).

[f] Barron, unpublished data, Core RC-12-418.

[g] Ciesielski (1983).

[h] Ryan et al. (1974).

[i] Johnson and Wick (1982).

[j] Poore et al. (1984).

[k] Burckle et al. (1982).

[l] Paleomagnetic correlations, Hole 575A (this chapter).

the last occurrence of *C. japonica* is near the top of a normally polarized interval (at about 10 to 4 m sub-bottom), which is either the top of Chron 11 or the lower normal event of Chron 10, according to the presence of N15 planktonic foraminifers. Johnson and Wick (1982) directly calibrate the last occurrence of *C. japonica* with the top of Chron 11 in seven piston cores from the tropical Pacific. Because *C. japonica* is a tropical radiolarian, is unlikely that it ranges higher at Site 512 (50°S) than it does it the tropical Pacific. The same argument applies to N15 planktonic foraminifers. Consequently, correlation of the last occurrence of *C. japonica* with the upper part of Chron 11 at Site 512 is favored over correlation with lower Chron 10.

Ciesielski (1983) notes that R. D. Dallmeyer of the University of Georgia obtained a radiometric date of 8.7 + 0.2 Ma on a $^{40}Ar/^{39}Ar$ analysis of a volcanic ash from Site 513 (Sample 513A-10-7, 10–13 cm), which lies at about the same latitude (48°S) as Site 512. This ash lies immediately above the last occurrence of *C. japonica* in Section 1 of Core 513A-11 (Weaver, 1983; Ciesielski, 1983). If the last occurrence of *C. japonica* is isochronous between Leg 71 Sites 512 and 513, these paleomagnetic and radiometric calibrations suggest that the top of Chron 11 should approximate 8.8 Ma. Because the dated top of Anomaly 5 is approximately 8.9 Ma (Berggren et al., in press), an Anomaly 5–Chron 11 correlation is favored by these Leg 71 data.

Although there is a good argument for the Anomaly 5–Chron 11 correlation suggested by W. A. Berggren (pers. comm., 1984; and Berggren, Kent, and Van Couvering, in press), it seems premature (and impractical because of publication deadlines) to alter all the Leg 85 absolute-age estimates for the middle and late Miocene. The alternative biostratigraphic time scale (Fig. 14), ages for paleomagnetically calibrated middle and late Miocene microfossil datum levels (Table 8), and age-vs.-depth curves for Sites 572 to 574 (Fig. 15) presented in this addendum should serve the reader in adjusting the absolute ages derived from biostratigraphic and paleomagnetic correlations in the various Leg 85 chapters, should the Anomaly 5–Chron 11 correlation become widely accepted.

ACKNOWLEDGMENTS

Appreciation is due Fritz Theyer and Larry Mayer (the Co-Chiefs) and the entire crew for making Leg 85 a scientifically rewarding and enjoyable experience. This manuscript benefited from the reviews of David Bukry and Gerta Keller of the U.S. Geological Survey. David A. Johnson and W. A. Berggren of Woods Hole Oceanographic Institution were very helpful in explaining the basis for the alternative paleomagnetic correlations discussed in the Addendum. E.T.'s research was partially funded by NSF grant OCE 8310518.

REFERENCES

Andrews, J. E., Packman, G., et al., 1975. Site 289. *In* Andrews, J. E., Packman, G., et al., *Init. Repts. DSDP*, 30: Washington (U.S. Govt. Printing Office), 231–398.

Backman, J., and Shackleton, N. J., 1983. Quantitative biochronology of Pliocene and early Pleistocene calcareous nannofossils from the Atlantic, Indian and Pacific oceans. *Mar. Micropaleontol.*, 8: 141–170.

Barron, J. A., 1981. Middle Miocene diatom biostratigraphy of equatorial Pacific DSDP Hole 77B. *Geosci. J.*, 2:137–144.

———, 1983. Latest Oligocene through early middle Miocene diatom biostratigraphy of the eastern tropical Pacific. *Mar. Micropaleontol.*, 7:487–515.

———, in press. Miocene to Quaternary planktic diatom biostratigraphy. *In* Bolli, H. M., and Saunders, J. B. (Eds.), *Biostratigraphy by Marine Plankton:* Cambridge (Cambridge University Press).

Barron, J. A., and Keller, G., 1982. Widespread Miocene deep-sea hiatuses: coincidence with periods of global cooling. *Geology*, 10: 577–581.

Barron, J. A., Keller, G., and Dunn, D. A., in press. A multiple microfossil biochronology for the Miocene. *In* Kennett, J. P. (Ed), *The Miocene Ocean: Paleoceanography and Biogeography.* Mem. Geol. Soc. Am. 163.

Berggren, W. A., 1969. Paleogene biostratigraphy and planktonic Foraminifera of northern Europe. *In* Brönnimann, P., and Renz, H. H. (Eds.), *Proc. First Internat. Conf. Planktonic Microfossils:* Leiden (Brill), 121–160.

———, 1984. Correlation of Atlantic, Mediterranean, Indo-Pacific Neogene stratigraphics: geochronology and chronostratigraphy. *In* Ikebe, N., and Tsuchi, R. (Eds.), *IGCP Project 114: Internat. Workshop Pacific Neogene Biostratigraphy* (Osaka and Kobe, Japan, Nov. 24–29, 1981): Tokyo (Univ. Tokyo Press), pp. 93–110.

Berggren, W. A., Burckle, L. H., Cita, M. B., Cooke, H. B. S., Funnell, B. M., et al., 1980. Towards a Quaternary time scale. *Quat. Res.*, 13:277–302.

Berggren, W. A., Kent, D. V., and Flynn, J. J., in press. Paleogene geochronology and chronostratigraphy. *In* Snelling, N. J. (Ed.), *Geo-*

chronology and the Geologic Time Scale. Spec. Pap. Geol. Soc. London.

Berggren, W. A., Kent, D. V., and Van Couvering, J. A., in press. Neogene geochronology and chronostratigraphy. *In* Snelling, N. J. (Ed.), *Geochronology and the Geologic Time Scale*. Spec. Pap. Geol. Soc. London.

Berggren, W. A., and Van Couvering, J. A., 1974. The Late Neogene: biostratigraphy, geochronology, and paleoclimatology of the last 15 million years in marine and continental sequences. *Palaeogeogr. Palaeoeclimatol. Palaeoecol.*, 16(1-2):1-216.

———, 1978. Biochronology. *In* Glassner, G. V., and Hedberg, H. D. (Eds.), *Contributions to the Geologic Time Scale*. Stud. Geol. (Tulsa, Okla.), 6:39-55.

Blow, W. H., 1969. Late middle Eocene to Recent planktonic foraminiferal biostratigraphy. *In* Brönnimann, P., and Renz, H. H. (Eds.), *Proc. First Internat. Conf. Planktonic Microfossils:* Leiden (Brill), 199-422.

Bukry, D., 1972. Coccolith stratigraphy, Leg 9, DSDP. *In* Hays, J. D., et al., *Init. Repts. DSDP*, 9: Washington (U.S. Govt. Printing Office), 817-839.

———, 1975. Coccolith and silicoflagellate stratigraphy, northwestern Pacific, Deep Sea Drilling Project Leg 32. *In* Larson, R. L., Moberly, R., et al., *Init. Repts. DSDP*, 32: Washington (U.S. Govt. Printing Office), 677-701.

———, 1981. Synthesis of silicoflagellate stratigraphy for Maestrichtian to Quaternary marine sediment. *Spec. Publ. Soc. Econ. Paleontol. Mineral.*, 32:433-444.

———, 1983. Upper Cenozoic silicoflagellates from offshore Ecuador, Deep Sea Drilling Project Site 504. *In* Cann, J. R., Langseth, M. G., Honnorez, J., Von Herzen, R. P., White, S. M., et al., *Init. Repts. DSDP*, 69: Washington (U.S. Govt. Printing Office), 321-342.

Burckle, L. H., 1972. Late Cenozoic planktonic diatom zones from the eastern equatorial Pacific. *Nova Hedwigia*, 39:217-246.

———, 1978. Early Miocene to Pliocene diatom datum levels for the equatorial Pacific. *Proc. Second Working Group Meeting, Biostrat. Datum-Planes Pacific Neogene, IGCP Project 114* (Bandung, Indonesia, May 30-June 1, 1977). Spec. Publ. Geol. Res. Dev. Cent., 1:25-44.

Burckle, L. H., Keigwin, L. D., and Opdyke, N. D., 1982. Middle and late Miocene stable isotope stratigraphy: correlation to the paleomagnetic reversal record. *Micropaleontology*, 25(3):281-293.

Ciesielski, P. F., 1983. The Neogene and Quaternary diatom biostratigraphy of subantarctic sediments, Deep Sea Drilling Project Leg 71. *In* Ludwig, W. J., Krasheninnikov, V. A., et al., *Init. Repts. DSDP*, 71: Washington (U.S. Govt. Printing Office), 635-665.

Foster, J. H., and Opdyke, N. D., 1970. Upper Miocene to Recent magnetic stratigraphy in deep-sea sediments. *J. Geophys. Res.*, 75: 4464-4473.

Gartner, S., 1972. Coccolith age determinations, Leg 9, DSDP. *In* Hays, J. D., et al., *Init. Repts. DSDP*, 9: Washington (U.S. Govt. Printing Office), 833-840.

———, 1973. Absolute chronology of late Neogene calcareous nannofossil succession in the equatorial Pacific. *Geol. Soc. Am. Bull.*, 84:2021-2034.

Gartner, S., Chen, M. P., and Stanton, R. J., 1983. Late Neogene nannofossil biostratigraphy and paleoceanography of the northeastern Gulf of Mexico and adjacent areas. *Mar. Micropaleontol.*, 8:17-50.

Goll, R. M., 1972. Radiolaria. *In* Hays, J. D., et al., *Init. Repts. DSDP*, 9: Washington (U.S. Govt. Printing Office), 947-1058.

———, 1979. The Neogene evolution of *Zygocircus, Neosemantis*, and *Callimitra:* their bearing on nasselarian classification. *Micropaleontology*, 25(4):365-396.

Haq, B. U., Worsley, T. R., Burckle, L. M., Douglas, R. G., Keigwin, L. D., Jr., et al., 1980. Late Miocene marine carbon isotope shift and synchroneity of some phytoplanktonic biostratigraphic events. *Geology*, 8:427-431.

Harwood, D. M., 1982. Oligocene-Miocene diatom biostratigraphy from the equatorial to the Antarctic Pacific [Master's thesis]. Florida State University, Tallahassee.

Hays, J. D., Saito, T., Opdyke, N. D., and Burckle, L. H., 1969. Pliocene-Pleistocene sediments of the equatorial Pacific: their paleomagnetic, biostratigraphic and climatic record. *Geol. Soc. Am. Bull.*, 80:1481-1514.

Hays, J. D., and Shipboard Scientific Party, 1972. Site 77. *In* Hays, J. D., et al., *Init. Repts. DSDP*, 9: Washington (U.S. Govt. Printing Office), 43-208.

Hsü, K. J., LaBrecque, J. L., and Shipboard Scientific Party, 1984. Site 519. *In* Hsü, K. J., LaBrecque, J. L., et al., *Init. Repts. DSDP*, 73: Washington (U.S. Govt. Printing Office), 27-93.

Jenkins, D. G., and Orr, W. N., 1972. Planktonic foraminiferal biostratigraphy of the eastern equatorial Pacific—DSDP Leg 9. *In* Hays, J. D., et al., *Init. Repts. DSDP*, 9: Washington (U.S. Govt. Printing Office), 1059-1193.

Johnson, D. A., and Wick, B. J., 1982. Precision of correlation of radiolarian datum levels in the middle Miocene equatorial Pacific. *Micropaleontology*, 28(1):1-30.

Keigwin, L. D., Jr., 1980. Paleoceanographic change at the Eocene/Oligocene boundary. *Nature*, 287:722-725.

Keigwin, L. D., Jr., and Keller, G., 1984. Middle Oligocene cooling from equatorial Pacific DSDP Site 77B. *Geology*, 12(1):16-18.

Keller, G., 1980. Early to middle Miocene planktonic foraminifera datum levels of the equatorial and subtropical Pacific. *Micropaleontology*, 26:372-391.

———, 1981. Miocene biochronology and paleoceanography of the North Pacific. *Mar. Micropaleontol.*, 6:535-551.

———, 1983a. Biochronology and paleoclimate implications of middle Eocene to Oligocene planktic foraminiferal faunas. *Mar. Micropaleontol.*, 7:463-486.

———, 1983b. Paleoclimatic analysis of middle Eocene through Oligocene planktic foraminiferal faunas. *Palaeogeogr. Palaeoclimatol. Palaeoecol.*, 43:73-94.

Keller, G., and Barron, J. A., 1983. Paleoceanographic implications of Miocene deep-sea hiatuses. *Geol. Soc. Am. Bull.*, 94:590-613.

Keller, G., Barron, J. A., and Burckle, L. H., 1982. Paleomagnetic, stable isotope, carbonate, and microfossil stratigraphies in upper Miocene sediments in the North Pacific Ocean. *Mar. Micropaleontol.*, 7:327-357.

Kennett, J. P., Houtz, R. E., Andrews, P. B., et al., 1975. Cenozoic paleoceanography in the southwest Pacific Ocean, Antarctic glaciation, and the development of the circum-Antarctic current. *In* Kennett, J. P., Houtz, R. E., et al., *Init. Repts. DSDP*, 29: Washington (U.S. Govt. Printing Office), 1155-1169.

Koblentz-Mishke, O. J., Volkovinsky, V. V., and Kabanova, J. G., 1970. Plankton primary production of the world ocean. *In* Wooster, W. S. (Ed.), *Scientific Exploration of the South Pacific:* Washington (Natl. Acad. Sci.), pp. 183-193.

LaBrecque, J. L., Kent, D. V., and Cande, S. C., 1977. Revised magnetic polarity time scale for Late Cretaceous and Cenozoic time. *Geology*, 5:330-335.

Leinen, M. A., 1979. Biogenic silica accumulation in the central equatorial Pacific and its implications for Cenozoic paleoceanography. *Geol. Soc. Am. Bull.*, 90:801-803.

Lohmann, G. P., and Carlson, J. J., 1981. Oceanographic significance of Pacific late Miocene calcareous nannoplankton. *Mar. Micropaleontol.*, 6:553-579.

Lowrie, W., Alvarez, W., Napoleone, G., Perch-Nielsen, K., Premoli-Silva, I., et al., 1982. Paleogene magnetic stratigraphy in Umbrian pelagic carbonate rocks: the Contessa sections, Gubbio. *Geol. Soc. Am. Bull.*, 93:414-432.

Nigrini, C., 1971. Radiolarian zones in the Quaternary of the equatorial Pacific Ocean. *In* Funnell, B. M., and Riedel, W. R. (Eds.), *Micropaleontology of Oceans:* Cambridge (Cambridge University Press), pp. 443-461.

Okada, H., and Bukry, D., 1980. Supplementary modification and introduction of code numbers to the low-latitude coccolith biostratigraphic zonation (Bukry, 1973-1975). *Mar. Micropaleontol.*, 5: 321-325.

Osborn, N. I., Ciesielski, P. F., and Ledbetter, M. T., 1983. Disconformities and paleoceanography in the southeast Indian Ocean during the past 5.4 million years. *Geol. Soc. Am. Bull.*, 94:1345-1358.

Percival, S. F., Jr., 1984. Late Cretaceous to Pleistocene calcareous nannofossils from the South Atlantic, Deep Sea Drilling Project Leg 73. *In* Hsü, K. J., LaBrecque, J. L., et al., *Init. Repts. DSDP*, 73: Washington (U.S. Govt. Printing Office), 391-424.

Poore, R. Z., Tauxe, L., Percival, S. F., Jr., LaBrecque, J. L., Wright, R., et al., 1983. Late Cretaceous–Cenozoic magnetostratigraphic and biostratigraphic correlations of the South Atlantic Ocean: DSDP Leg 73. *Palaeogeogr. Palaeoclimatol. Palaeoecol.*, 42: 127–149.

_____, 1984. Late Cretaceous–Cenozoic magnetostratigraphic and biostratigraphic correlations for the South Atlantic Ocean, Deep Sea Drilling Project Leg 73. *In* Hsü, K. J., LaBrecque, J. L., et al., *Init. Repts. DSDP*, 73: Washington (U.S. Govt. Printing Office), 645–655.

Riedel, W. R., and Sanfilippo, A., 1978. Stratigraphy and evolution of tropical Cenozoic radiolarians. *Micropaleontology*, 24(1):61–96.

Ryan, W. B. F., Cita, M. B., Dreyfus-Rauson, M., Burckle, L. H., and Saito, T., 1974. A paleomagnetic assignment of Neogene stage boundaries and the development of isochronous datum planes between the Mediterranean, the Pacific, and Indian oceans in order to investigate the response of the world ocean to the Mediterranean "salinity crisis." *Riv. Ital. Paleontol. Strat.*, 80:631–688.

Saito, T., Burckle, L. H., and Hays, J. D., 1975. Late Miocene to Pleistocene biostratigraphy of equatorial Pacific sediments. *In* Saito, T., and Burckle, L. (Eds.), *Late Neogene Epoch Boundaries:* New York (Am. Mus. Nat. History), pp. 226–244.

Savin, S. M., Douglas, R. G., Keller, G., Killingley, J. S., Shaughnessy, L., et al., 1981. Miocene benthic foraminiferal isotope records: a synthesis. *Mar. Micropaleontol.*, 6:423–450.

Shaw, A. B., 1964. *Time in Stratigraphy:* New York (McGraw-Hill).

Tauxe, L., Tucker, P., Petersen, N. P., and LaBrecque, J. P., 1983. The magnetostratigraphy of Leg 73 sediments. *Palaeogeogr. Palaeoclimatol. Palaeoecol.*, 42:65–90.

Theyer, F., and Hammond, S. R., 1974. Paleomagnetic polarity sequence and radiolarian zones, Brunhes to Epoch 20. *Earth Planet. Sci. Lett.*, 22:307–319.

Theyer, F., Mato, C. Y., and Hammond, S. P., 1978. Paleomagnetic and geochronologic calibration of latest Oligocene to Pliocene radiolarian events, equatorial Pacific. *Mar. Micropaleontol.*, 3: 377–395.

Tjalsma, R. C., and Lohman, G. P., 1983. Paleocene–Eocene bathyal and abyssal benthic foraminifera from the Atlantic Ocean. *Micropaleontology Spec. Publ. 4.*

Vail, P. R., and Hardenbol, J., 1979. Sea level changes during the Tertiary. *Oceanus*, 22(3):71–80.

van Andel, T. H., Heath, G. R., and Moore, T. C., Jr., 1975. Cenozoic history and paleoceanography of the central equatorial Pacific Ocean. *Mem. Geol. Soc. Am.*, 143:1–134.

Weaver, F. M., 1983. Cenozoic radiolarians from the southwest Atlantic, Falkland Plateau region, Deep Sea Drilling Project Leg 71. *In* Ludwig, W. J., Krasheninnikov, V. A., et al., *Init. Repts. DSDP*, 71: Washington (U.S. Govt. Printing Office), 667–686.

Westberg, M. J., and Riedel, W. R., 1978. Accuracy of radiolarian correlations in the Pacific Miocene. *Micropaleontology*, 24:1–23.

Wyrtki, K., 1966. Oceanography of the eastern equatorial Pacific Ocean. *In* Barnes, H. (Ed.), *Ann. Rev. Oceanog. Mar. Biol.*, 4: 33–68.

Date of Initial Receipt: 1 February 1984
Date of Acceptance: 22 March 1984

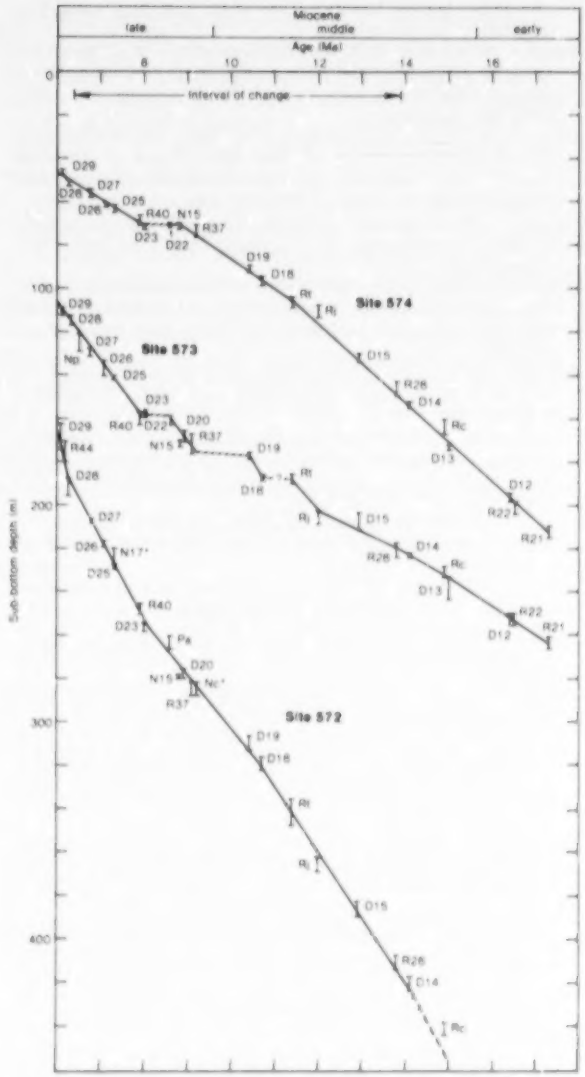

Figure 15. Age-vs.-depth plots for the middle and late Miocene at Sites 572, 573, and 574, based on a correlation of paleomagnetic Anomaly 5 with paleomagnetic Chron 11. See Table 8 for microfossil datum levels used to construct the plots. Asterisk denotes calcareous nannofossil datums after Gartner and Chow (this volume).

31. DIATOM PALEOCEANOGRAPHY AND PALEOCLIMATOLOGY OF THE CENTRAL AND EASTERN EQUATORIAL PACIFIC BETWEEN 18 AND 6.2 Ma[1]

John A. Barron, U.S. Geological Survey, Menlo Park[2]

ABSTRACT

Diatom assemblages in the central and eastern equatorial Pacific record the effects of polar cooling in the middle Miocene and across the middle/late Miocene boundary. Diatom evolutionary events (appearances and extinctions) were numerous between 14.5 and 13.5 Ma, presumably reflecting reorganization of equatorial surface-water masses in response to polar cooling. Increasing numbers of the cold-water diatom *Denticulopsis hustedtii* indicate cooling of equatorial Pacific surface waters during the middle Miocene, especially between 12 and 11.5 Ma. The onset of severe carbonate dissolution at 12 Ma marked the beginning of the late Neogene period of high-amplitude fluctuations of carbonate in the equatorial Pacific. Initiation or a substantial increase in the production of North Atlantic Deep Water (NADW) in the North Atlantic at 12 Ma is believed to have been a possible triggering event for these middle/late Miocene changes. Increased polar cooling at 11.3 Ma contributed to steepening of latitudinal thermal gradients by altering circulation patterns. Tropical surface waters became warmer, cold-water diatoms were excluded from the equatorial Pacific, and latitudinal provincialism was enhanced in all planktonic groups. Most of the modern-day features of equatorial Pacific surface-water circulation were probably present by 11 Ma.

INTRODUCTION

A primary purpose of DSDP Leg 85 was to collect a series of upper Eocene to Quaternary reference sections across the region of high productivity of the central equatorial Pacific Ocean. Cores previously collected from the area on DSDP Legs 5, 8, 9, and 16 have provided a wealth of paleoceanographic information (van Andel et al., 1975), but high-resolution biostratigraphic studies have been hindered by the disturbed nature of the rotary-drilled cores and by spotty recovery. Use of the hydraulic piston corer (HPC) on Leg 85 allowed recovery of relatively undisturbed cores in sediments with moderate to high (≥ 15 m/m.y.) sedimentation rates at five locations (Sites 571 to 575) across the central equatorial Pacific (Fig. 1).

Sites 571 and 572 lie along the western edge of the highly productive eastern equatorial Pacific, where sediments are dominated by diatoms and the regional thermocline is relatively shallow. Sediment accumulation rates were at least 1.7 times faster at Sites 571 and 572 than the rates at the more carbonate-rich western sites (Sites 573 to 575) (Barron, this volume). Only one uppermost Quaternary core was recovered at Site 571, but over 400 m of lower middle Miocene to Quaternary diatom-rich sediments were recovered at Site 572. HPC coring at Site 572 extended down to 172 m sub-bottom (about 6.1 Ma); rotary coring extended to the base of the hole.

Sites 573 to 575 form a south-to-north transect across the northward-migrating Oligocene to Holocene equator. Upper Eocene to Quaternary sections were recovered at Sites 573 and 574; HPC coring extended down to the lower upper Miocene and upper lower Miocene, respectively. All coring at Site 575 was done with the HPC, and the oldest sediments recovered are about 22 Ma old (Barron, this volume).

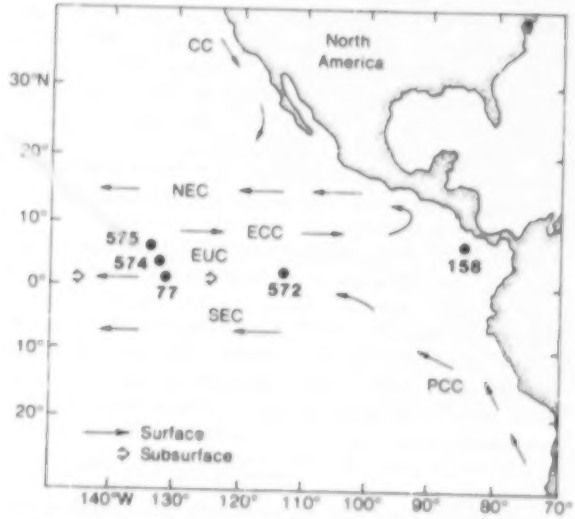

Figure 1. Locations of studied DSDP sites in the central and eastern equatorial Pacific. Surface currents: PCC = Peru-Chile Current, SEC = South Equatorial Current, ECC = Equatorial Countercurrent, NEC = North Equatorial Current, CC = California Current. Subsurface current: EUC = Equatorial Undercurrent. Currents after Wyrtki (1966).

The middle and late Miocene were times of maximum diatom abundance in the central equatorial Pacific (van Andel et al., 1975; Leinen, 1979). Major global cooling occurred in the middle Miocene (Shackleton and Kennett, 1975; Woodruff et al., 1981), and modern patterns of surface-water circulation were largely established (van Andel et al., 1975; Keller and Barron, 1983), although circulation of surface waters across the Central

[1] Mayer, L., Theyer, F., et al., *Init. Repts. DSDP*, 85: Washington (U.S. Govt. Printing Office).

[2] Address: U.S. Geological Survey, 345 Middlefield Rd., Menlo Park, CA 94025.

American Seaway did not cease until the Pliocene. Because diatoms are phytoplankton, they respond to conditions in the photic zone (temperature, salinity, nutrients), and, therefore, they should monitor fluctuations in surface water masses (Kanaya and Koizumi, 1966; Cooke-Poferl et al., 1975). With this in mind, stratigraphic intervals were selected for study between the upper lower Miocene (about 18 Ma) and the uppermost Miocene (6.2 Ma) across the central and eastern equatorial Pacific at DSDP Sites 77, 158, 572, 574, and 575. Planktonic diatoms were counted at sampling intervals representing, on average, 100,000 yrs. in the early and middle Miocene and 200,000 to 300,000 yrs. in the late Miocene. The greater sampling interval for the late Miocene reflects slower sedimentation rates. Results are presented in Barron (this volume), along with quantitative trends (paleogeography) across the central and eastern equatorial Pacific. The purpose of this chapter is to apply those quantitative data in a study of the oceanography and climatology of the interval from 18 to 6.2 Ma in the central and eastern equatorial Pacific.

MIDDLE MIOCENE COOLING

The +1.00‰ increase in benthic foraminiferal $\delta^{18}O$ that occurred throughout the ocean basins in the early middle Miocene (Shackleton and Kennett, 1975; Savin et al., 1975; Woodruff et al., 1981; Blanc and Duplessy, 1982) is the most distinctive feature of late Cenozoic oxygen-isotope curves. This increase has been interpreted as a response to polar cooling and growth of the Antarctic Ice Cap, although Matthews and Poore (1980) have questioned whether it represented the initiation of Antarctic glaciation.

Benthic and planktonic microfossil assemblages at both high and low latitudes underwent pronounced changes in response to global cooling in the middle Miocene (Keller and Barron, 1983, and references therein). Oligocene and lower Miocene benthic foraminifers in the western Pacific disappeared and were replaced by more characteristic Neogene assemblages at about 13.5 Ma, presumably reflecting the increasing amount of Antarctic Bottom Water (AABW) entering the deep Pacific (Woodruff and Douglas, 1981). The number of evolutionary events (first and last appearances) of planktonic microfossils was high during the middle part of the middle Miocene (14.5 to 13.5 Ma), in response to reorganization of surface and intermediate water masses. Planktonic foraminifers (Blow, 1969; Keller, 1981; Srinivasan and Kennett, 1981), radiolarians (Riedel and Sanfilippo, 1978; Goll, 1979), calcareous nannofossils (Martini, 1971; Bukry, 1978), silicoflagellates (Bukry, 1981a), and diatoms (Burckle, 1978; Barron, 1981a, b) all had numerous appearances and extinctions during that part of the middle Miocene.

The following list shows diatom evolutionary events for the late early Miocene to latest Miocene (18.0 to 5.1 Ma) of the equatorial Pacific, as compiled from Tables 1 and 3 of Barron (this volume) for 500,000-yr. intervals; all datum-level ages are rounded off to 100,000 yrs., and intervals shown are inclusive.

Age (Ma)	Number of appearances/extinctions
5.1-5.5	1/3
5.6-6.0	0/3
6.1-6.5	3/0
6.6-7.0	0/1
7.1-7.5	1/1
7.6-8.0	1/3
8.1-8.5	1/0
8.6-9.0	2/1
9.1-9.5	0/2
9.6-10.0	2/1
10.1-10.5	2/0
10.6-11.0	0/2
11.1-11.5	2/1
11.6-12.0	0/1
12.1-12.5	3/4
12.6-13.0	2/1
13.1-13.5	1/3
13.6-14.0	7/3
14.1-14.5	4/2
14.6-15.0	0
15.1-15.5	1/1
15.6-16.0	0/3
16.1-16.5	1/2
16.6-17.0	1/1
17.1-17.5	6/2
17.6-18.0	1/4

For the period studied, diatoms average 3.4 first appearances and 3.1 last appearances per million-year interval. Periods of maximum turnover occur between 17.5 and 17.1 Ma (6 appearances and 2 extinctions), 14.5 and 14.1 Ma (4 appearances and 2 extinctions), 14.0 and 13.6 Ma (7 appearances and 3 extinctions), and 12.5 and 12.1 Ma (3 appearances and 4 extinctions). The older (17.5 to 17.1 Ma) and younger (12.5 to 12.1 Ma) of these times of rapid turnover in diatom taxa precisely match periods of rapid change in planktonic foraminifers (Keller, 1981) and radiolarians (Goll, 1979) at DSDP Site 77. The middle periods (14.5 to 13.6 Ma) correspond to that part of the middle Miocene where the $\delta^{18}O$ of benthic foraminifers shows a +1.0‰ increase and all planktonic organisms have high numbers of evolutionary events (Ryan et al., 1974; Barron et al., in press).

PALEOTEMPERATURE CURVES

Denticulopsis nicobarica (17.8 to 13.6 Ma)

Figure 2 compares the abundance of *Denticulopsis nicobarica* at Sites 574 and 575 (Barron, this volume) with the benthic foraminiferal oxygen-isotope curves for Sites 289 (Woodruff et al., 1981) and 574 (Shackleton and Pisias, this volume). The Site 574 isotope curve is simplified from that of Shackleton and Pisias (this volume), in that only isotope values from the same depth intervals as those for which the abundance of *D. nicobarica* was determined are plotted. The overall trend of increasing *D. nicobarica* between 15.5 and 13.6 Ma is mirrored by a greater than +1.00‰ increase in $\delta^{18}O$ at Site 289. The rapid decline in *D. nicobarica* abundance beginning at 13.5 Ma, however, does not represent warming in the isotope curve, but rather corresponds to a time of rapid species turnover in diatoms (see preceding tabulation), and may have been caused by reorganiza-

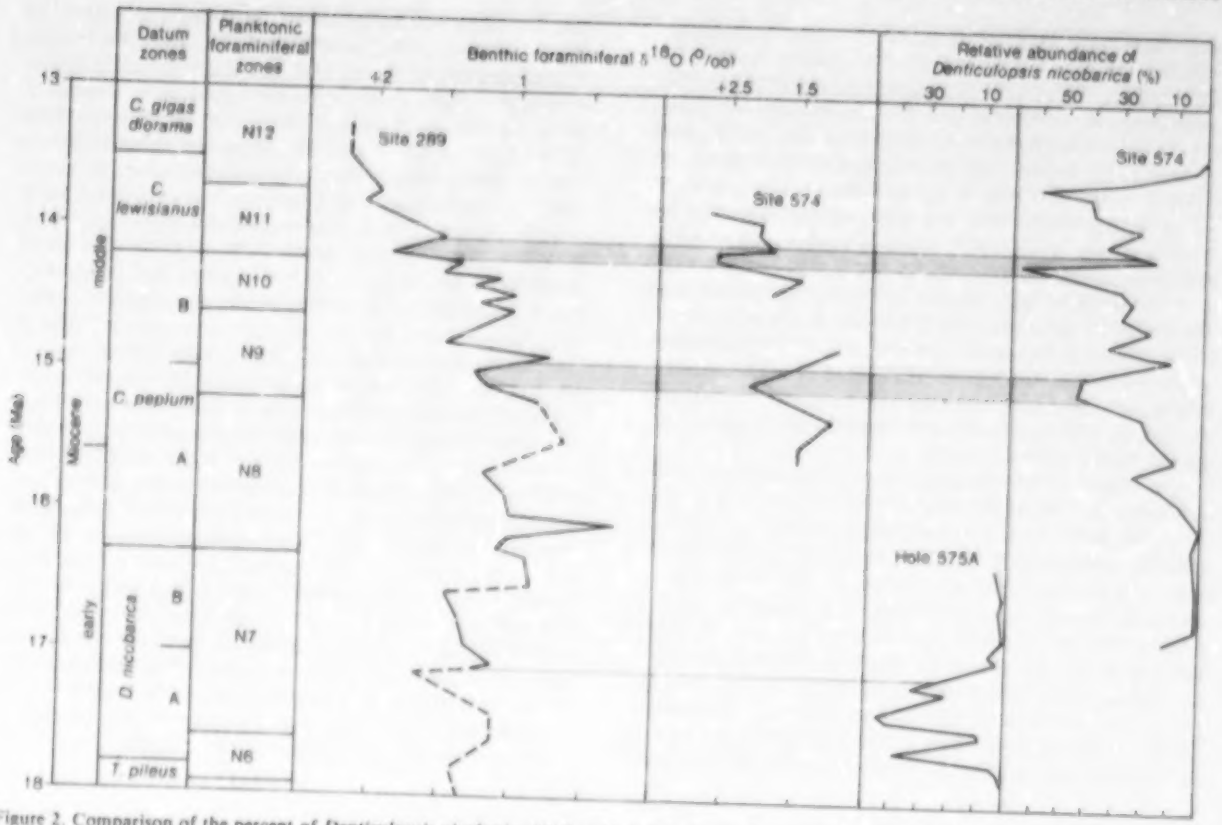

Figure 2. Comparison of the percent of *Denticulopsis nicobarica* (17.8 to 13.2 Ma) at central equatorial Pacific DSDP Sites 575 (Hole 575A) and 574 (Barron, this volume) with benthic foraminiferal oxygen-isotope curves for Sites 289 (Woodruff et al., 1981) and 574 (Shackleton and Pisias, this volume). The Site 575 isotope curve is constructed only from those points at the same sub-bottom depths as the Site 574 diatom samples. Shaded area emphasizes correlation between abundant *D. nicobarica* and more positive $\delta^{18}O$ (‰) values.

tion of equatorial Pacific water masses (Woodruff and Douglas, 1981). Individual spikes in the curves from 15.1 to 14.9, 14.2 to 14.1, and 13.6 Ma are strongly correlative. The increasing abundance of *D. nicobarica* between 17.6 and 17.1 Ma (Site 575) correlates closely with a cooling in the silicoflagellate paleotemperature curve Bukry (this volume), and is equivalent to the interval removed by hiatus NH1b at Site 573 (Barron, this volume). The relatively wide spacing of isotope values in the isotope curve below 16.5 Ma hinders effective comparison with the *D. nicobarica* curve. Lower oxygen-isotope values (+1.0‰) between 17 and 15 Ma, however, generally correspond to minimal values (10%) of *D. nicobarica*. In this interval of lower *D. nicobarica* values, the warm-water diatoms *Cestodiscus pulchellus* and *Synedra jouseana* are relatively common (Barron, this volume). It thus appears that the relative abundance of *D. nicobarica* between its first appearance at 17.8 Ma and its decline at 13.5 Ma in the central equatorial Pacific varies positively with polar cooling, as measured by oxygen isotopes.

Comparison of the *D. nicobarica* abundance curves for central equatorial Pacific Sites 574 and 77 with that for eastern equatorial Pacific Site 572 between 14.4 and 13.5 Ma (Barron, this volume) shows an eastern abundance preference of *D. nicobarica* of 10 to 20%. This would be expected if increases of *D. nicobarica* at Sites 77 and 574 represent expansion of *D. nicobarica* westward from the cooler eastern equatorial Pacific during times of polar cooling.

Thalassionema nitzschioides

Studies of the latest Quaternary by CLIMAP (1976) indicate that the central equatorial Pacific is an excellent place to investigate paleotemperature changes associated with expanded polar glaciation. During the last glacial maximum 18,000 yrs. ago, sea-surface temperatures in the central equatorial Pacific were as much as 6°C cooler than present-day August temperatures there; this represents a maximum cooling for the low-latitude ocean. Presumably, this cooling resulted from increased upwelling along the equatorial divergences caused by a more energetic circulation system (CLIMAP, 1976). Pedersen (1983) argues that a pronounced enrichment in the organic-carbon content of eastern equatorial Pacific sediments during the last glacial maximum suggests increased productivity rates and supports other evidence that global trade-wind speeds (and thus upwelling rates) increase significantly during glacial stages. Romine (1982) shows that during the last glacial maximum, radiolarian as-

semblages associated with the Peru–Chile Current expanded westward into the central equatorial Pacific. Cooke-Poferl et al. (1975) suggest that the diatoms *Thalassionema nitzschioides* and *T. nitzschioides* var. *parva* are associated with the Peru–Chile Current, and Burckle et al. (1982) argue that the increasing abundance of these diatoms in the early late Miocene at eastern equatorial Pacific DSDP Site 158 reflected an increasing influence of the Peru–Chile Current in the area. Barron (1982) used similar arguments, linking *T. nitzschioides* with subtropical and equatorial upwelling (Bukry and Foster, 1973; Sancetta, 1983; Barron and Keller, 1983), to suggest that increased abundance of *T. nitzschioides* at central equatorial Pacific DSDP Site 77 coincided with late middle Miocene and late Miocene periods of middle-latitude cooling identified by Barron and Keller (1983) for the northeastern Pacific.

On Figure 3, the percentage of *Thalassionema nitzschioides* at central equatorial Pacific DSDP Sites 572 and 574 (Barron, this volume) is plotted along with the benthic foraminiferal oxygen-isotope curves for DSDP Sites 289 (Woodruff et al., 1981), 158 (Keigwin, 1979), and 574 (Shackleton and Pisias, this volume), for the middle Miocene interval from 16.0 to 10.5 Ma. Correlations with isotope curves for the late Miocene were not attempted, because detailed sampling is lacking in both the diatom abundance and isotope curves. Conversion of the isotope curve for Site 289 to Ma follows Barron et al. (in press) and utilizes the same time scale as this chapter. Ages for the Site 158 curve are after Barron (this volume). The +1.00‰ increase in the Site 289 isotope curve between 14.5 and 13.5 Ma is immediately apparent, and roughly coincides with a general increase in *T. nitzschioides* abundance at both Site 574 (from about 10% to about 30%) and Site 572 (from about 15% to about 30%). In addition, the +0.5‰ increase in the Site 158 isotope curve at about 11.3 Ma corresponds to further increases in *T. nitzschioides* abundance at both Site 574 (from 25–35% to 45–55%) and Site 572 (from 30–40% to 60+ %). This latter increase is the one identified by Burckle et al. (1982) at Site 158. Point-for-point comparison between the various curves reveals that *T. nitzschioides* values are typically at least 10% greater at eastern Site 572 than at western Site 574 after 14.2 Ma. This is to be expected, since Site 572 lies within the cooler, more diatom-rich eastern equatorial Pacific and is closer to the northwest fringes of the Peru–Chile Current. Not only do the overall trends in the oxygen-isotope curve appear to correlate with the overall abundance trends of *T. nitzschioides*, but individual peaks in *T. nitzschioides* abundance appear to correlate with positive peaks in the oxygen-isotope curves. Admittedly, this correlation is tenuous because of the limits of correlation and the general high variability of both curves. Paired samples should be studied for isotopes and diatom abundance to establish such a relationship. The isotope curve plotted for Site 574 does, however, consist only of points measured on samples from the same depths as the dia-

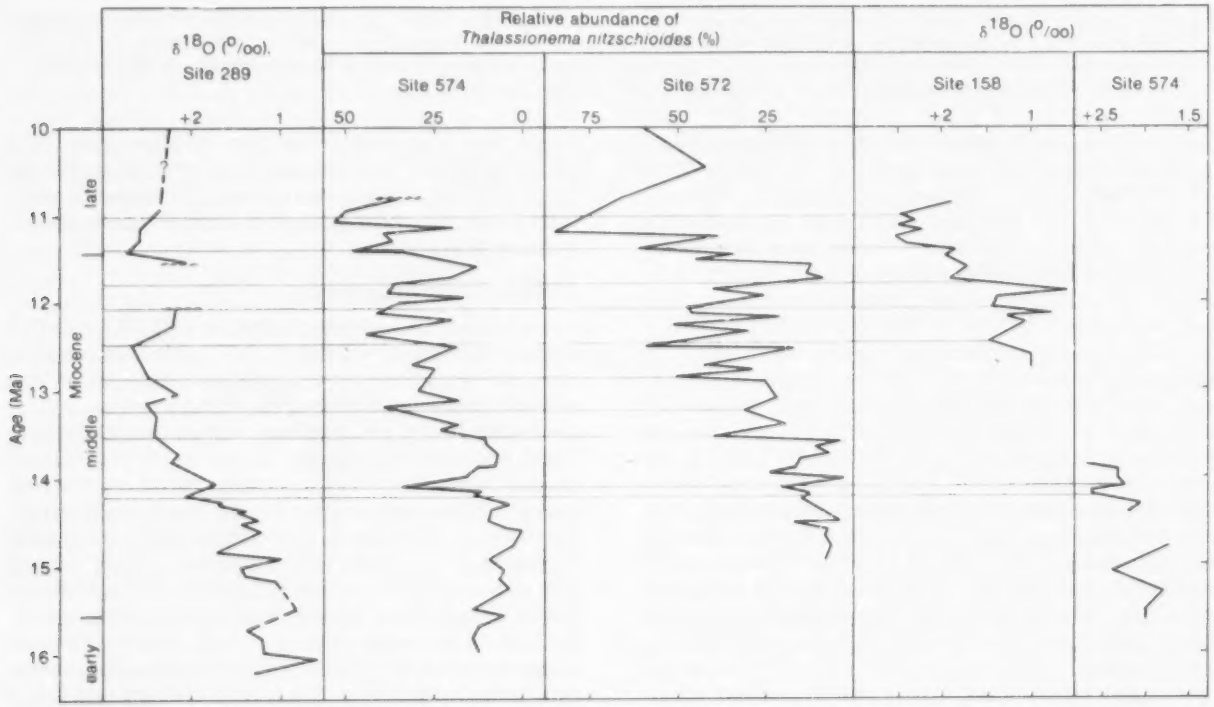

Figure 3. Comparison of the percent of *Thalassionema nitzschioides* at DSDP Sites 574 and 572 (Barron, this volume) with oxygen-isotope curves for Sites 289 (Woodruff et al., 1981), 158 (Keigwin, 1979), and 574 (Shackleton and Pisias, this volume) for the middle and earliest late Miocene. The Site 574 isotope curve is plotted only from those points that are at the same sub-bottom depth as the Site 574 diatom samples.

tom samples studied by Barron (this volume). Figure 2 supports the general hypothesis that polar cooling (as reflected by the benthic foraminiferal oxygen-isotope curves) results in a more energetic circulation system and increased upwelling along equatorial divergences in the eastern equatorial Pacific.

On Figure 4, the percent of *T. nitzschioides* at Sites 77 and 572 between 11.5 and 6.2 Ma is plotted and compared with Keller's (in press) late Miocene planktonic foraminiferal climatic curve for Site 289. The sampling interval at Site 574 for the late Miocene is large (typically 500,000 yrs.), so a Site 574 *T. nitzschioides* curve was not plotted.

For the late Miocene, Keller (in press) utilizes a ratio of surface-dwelling to intermediate-depth planktonic foraminifers as a measure of relative paleotemperature; higher numbers of intermediate-depth planktonic foraminifers indicate a shallower thermocline and cooling.

Cooling peaks in the *T. nitzschioides* curves at 10.0, 9.2, 8.8 to 8.7, 8.1 to 7.9 and about 7.1 Ma correlate with cooling peaks in Keller's (in press) planktonic foraminiferal curve. Between 11.5 and 11.0 Ma, the character of the curves differs, but the sampling interval at Site 289 is rather broad and may produce an anomalous curve.

In the middle-latitude northeastern Pacific, Barron and Keller (1983) compared the percentage of cold-water diatoms and planktonic foraminifers in three sections to identify 14 cold peaks and 12 warm peaks during the middle and late Miocene. Late Miocene cold events C8 (11.4 to 11.0 Ma), C9 (10.1 to 9.7 Ma), C10 (8.8 to 8.7 Ma), and C11 (8.2 to 7.9 Ma) (ages adjusted to the Leg 85 time scale as described in the Introduction, this volume) show good agreement with the late Miocene cool events identified by abundance peaks of *T. nitzschioides* and Keller's (in press) planktonic foraminiferal curve for Site 289 (Fig. 4). Cold event C12 (6.3 to 6.1 Ma) is not readily apparent in the tropical paleotemperature curves. According to the arguments presented by Barron (1982), cooling periods of the California Current should coincide with periods of increased equatorial upwelling (or intensification of the Peru–Chile Current). These arguments assume that the energy of the whole surface-

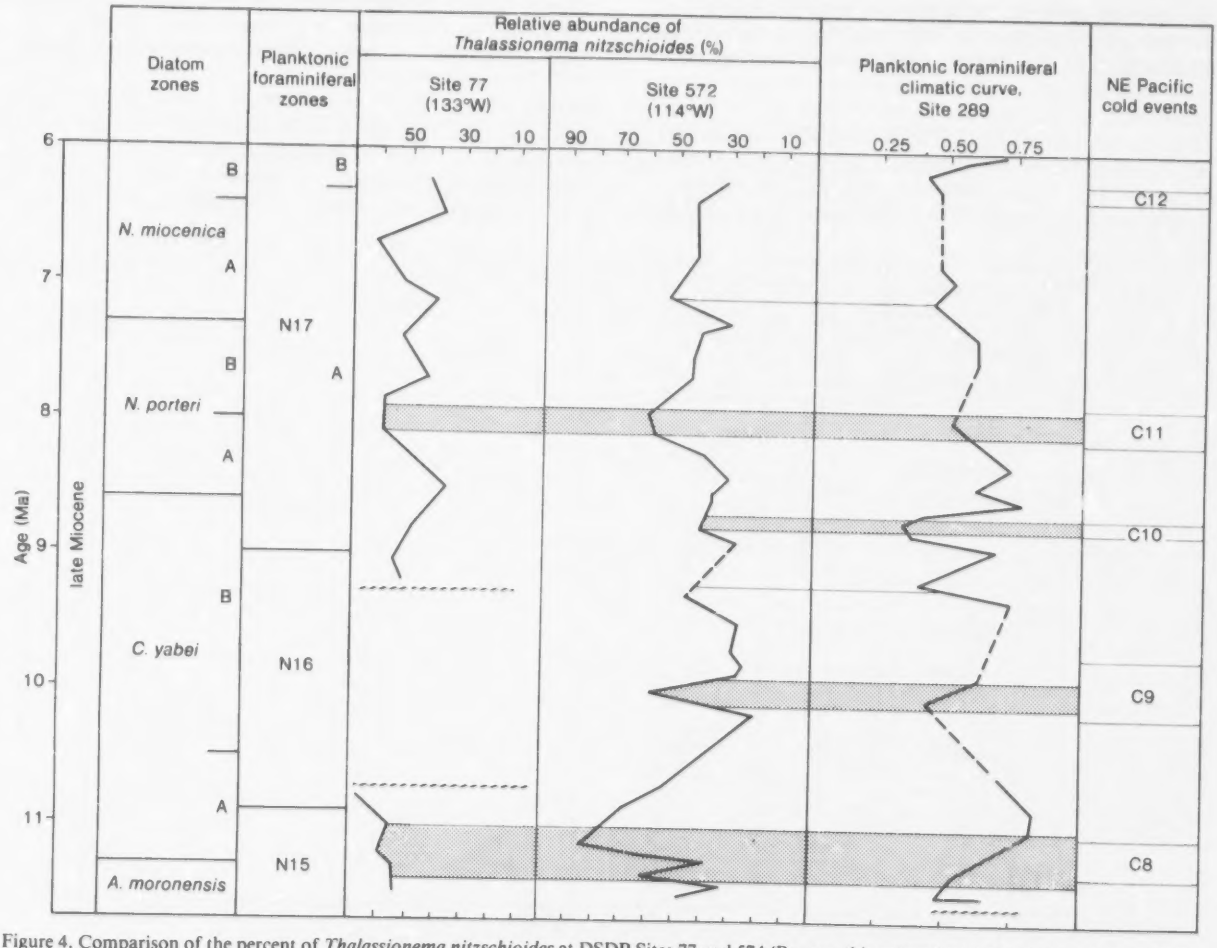

Figure 4. Comparison of the percent of *Thalassionema nitzschioides* at DSDP Sites 77 and 574 (Barron, this volume) with the planktonic foraminiferal climatic curve of Keller (in press) for Site 289 (see text) and the cold events of Barron and Keller (1983) (northeastern Pacific) for the late Miocene before 6 Ma (see text). Shaded areas show correlation between cold events, cooler values in the planktonic foraminiferal climatic curve, and increased abundance of *T. nitzschioides*.

water circulation system is enhanced during times of expanded polar glaciation.

Middle Miocene Pulses of Cold-Water Diatoms

Cold-water diatoms (*Denticulopsis hustedtii, D. praedimorpha, Actinocyclus ingens*, and *Coscinodiscus marginatus*) are common in the middle Miocene of the central and eastern equatorial Pacific (Fig. 5); by the 11-Ma level, however, they are essentially absent from low-latitude assemblages. Presence of these dominantly middle- to high-latitude diatoms at low latitudes suggests a relatively free exchange of surface water masses between middle and low latitudes. The rapid decline of *D. hustedtii* in the tropical Pacific between 11.5 and 11.3 Ma represents the onset of paleoceanographic isolation between middle- and low-latitude diatom assemblages that typifies the late Miocene (Burckle, 1978; Barron, 1981a). Presumably, conditions in the eastern equatorial Pacific changed at about 11.3 Ma so that dominantly cold-water diatoms could no longer live in the equatorial Pacific. It can be assumed, however, that below the 11.3-Ma level the percentage of cold-water diatoms in tropical middle Miocene assemblages is a measure of the strength of the eastern boundary currents that would carry these middle-latitude diatoms into the tropics. Consequently, peaks in the abundance of cold-water diatoms on Figure 5 should correspond to cooling of equatorial surface waters during the middle Miocene.

Keller (in press) showed that surface-dwelling planktonic foraminifers displayed a strong east–west provincialism in the equatorial Pacific during the early and middle Miocene. She grouped surface-dwelling foraminifers into eastern and western faunas, and argued that the ratio of eastern to western faunal abundance at a given equatorial site reflects surface-water paleotemperatures. The ratio of western fauna to total eastern and western fauna at western equatorial Pacific Site 289 was proposed by Keller (in press) as the basis of a paleotemperature curve for the early and middle Miocene of the western Pacific. She showed that individual cooling spikes (decreases in relative abundance of the western fauna) correlated with cooling peaks in the benthic foraminiferal isotope curve for Site 289.

Comparison of Keller's (in press) curve with the abundance curves for cold-water diatoms at Sites 572 and 574 (Fig. 5) reveals a relatively good correlation of cooling peaks between 16 and 13 Ma but poor correlation between 13 and 12 Ma. Keller's (in press) cooling peak at 15.5 Ma corresponds to the introduction of *Actinocyclus ingens* into the tropics from middle latitudes (Bar-

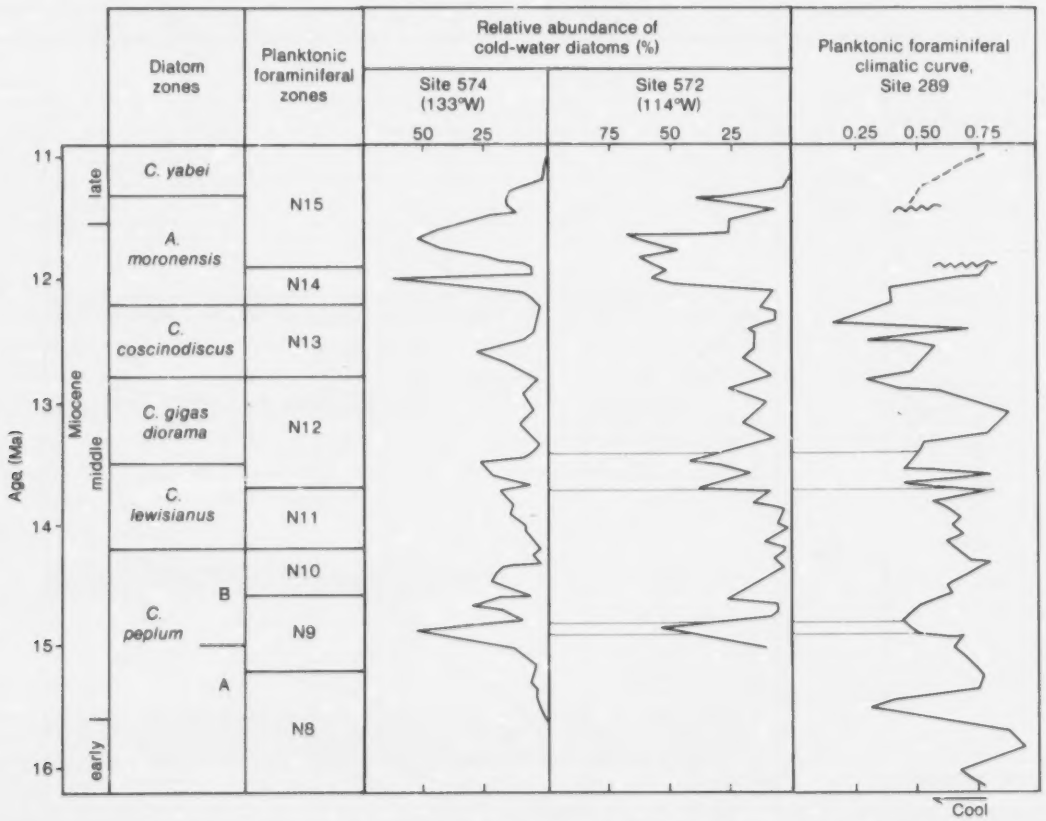

Figure 5. Comparison of the percent of cold-water diatoms (*Denticulopsis hustedtii, D. praedimorpha, Actinocyclus ingens*, and *Coscinodiscus marginatus*) in the middle Miocene of DSDP Sites 574 and 572 with the planktonic foraminiferal climatic curve of Keller (in press) at Site 289 (see text).

ron, this volume). Cooling from 14.9 to 14.8 Ma and from 13.7 to 13.4 Ma is also apparent in both types of curves. Cooling in the Site 289 curve at 12.8 and 12.4 Ma, however, is not apparent in the curves of percent cold-water diatoms, although Figure 3 (percent *Thalassionema nitzsehioides*) does indicate increased upwelling (or intensification of the Peru–Chile Current) at 12.8 and 12.5 Ma.

The large increase in the abundance of *Denticulopsis hustedtii* between 12 and 11.5 Ma (Fig. 6) corresponds to hiatus NH4 at Site 289, and coincides with generalized carbonate dissolution throughout the tropics in lower planktonic foraminiferal Zone N15 (Keller, 1981), so comparisons of the two types of curves between 12.0 and 11.5 Ma are not possible. All three paleotemperature curves of Figure 6, however, show warming between 11.5 and 11.0 Ma.

The dramatic increases in the abundance of *D. hustedtii* from 5–10% to 50–60% of the assemblage at 12.0 Ma at Sites 158, 572, and 574 correlates closely with a sharp drop in the percent carbonate at all three sites (Figs. 6, 7). Earlier increases of *D. hustedtii* in the middle Miocene also appear to coincide with carbonate lows at Sites 572 and 574 (Fig. 6). Coincidence of *D. hustedtii* abundance peaks with middle Miocene carbonate-dissolution troughs lends support to arguments that tie polar cooling (benthic foraminiferal oxygen-isotope enrichment) to carbonate dissolution (Dunn et al., 1981; Vincent, 1981). Pedersen (1983) showed that productivity was increased in the eastern equatorial Pacific during the last glacial maximum. Emerson and Bender (1981) argue that increased rain of organic carbon to the seafloor, such as would occur during periods of greater productivity, would result in higher CO_2 levels in bottom waters and would stimulate carbonate dissolution there. Berger and Vincent (1981) point out that periods of global cooling and sea-level regression should also release trapped organic carbon to the ocean system by erosion of transient nearshore carbon reservoirs. Consequently, Figures 6 and 7 support arguments—by Keller (1980), Dunn et al. (1981), Vincent (1981), and Barron and Keller (1982)—suggesting that late middle Miocene and late Miocene periods of carbonate dissolution in the Pacific coincided with periods of expanded Antarctic glaciation.

Denticulopsis hustedtii is a dominantly middle- to high-latitude diatom common in the middle and late Miocene of the North Pacific (Koizumi, 1973; Barron, 1980; Barron and Keller, 1983), North Atlantic (Baldauf, 1985), and Southern Ocean (Schrader, 1976; Weaver and Gombos, 1981; Ciesielski, 1983). It was most likely associated with cool, low-salinity water masses that are typical of those regions. Introduction of *D. hustedtii* into the tropical Pacific at 13.9 Ma (Burckle, 1978; Barron, this volume) corresponds to increased positive values of $\delta^{18}O$ in the benthic foraminiferal oxygen-isotope curves for Sites 289 (Woodruff et al., 1981) and 574 (Shackleton and Pisias, this volume), and also coincides with an increase in the abundance of *D. hustedtii* in the middle-latitude northeastern Pacific (Barron and Keller, 1983). Benthic foraminiferal oxygen-isotope enrichment of about +0.5‰ at 11.7 Ma at Site 158 slightly lags behind the increases in *D. hustedtii* abundance at 12.0 Ma (Fig. 7).

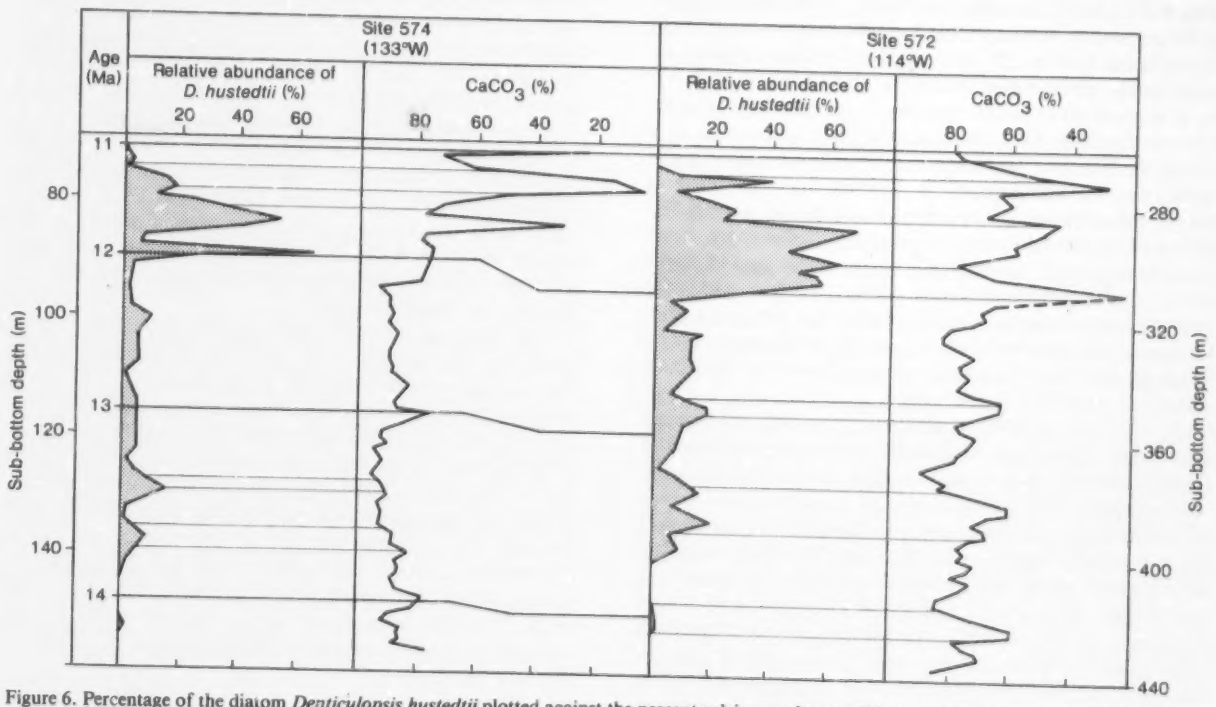

Figure 6. Percentage of the diatom *Denticulopsis hustedtii* plotted against the percent calcium carbonate (Pisias and Dunn, this volume) for DSDP Sites 574 and 572.

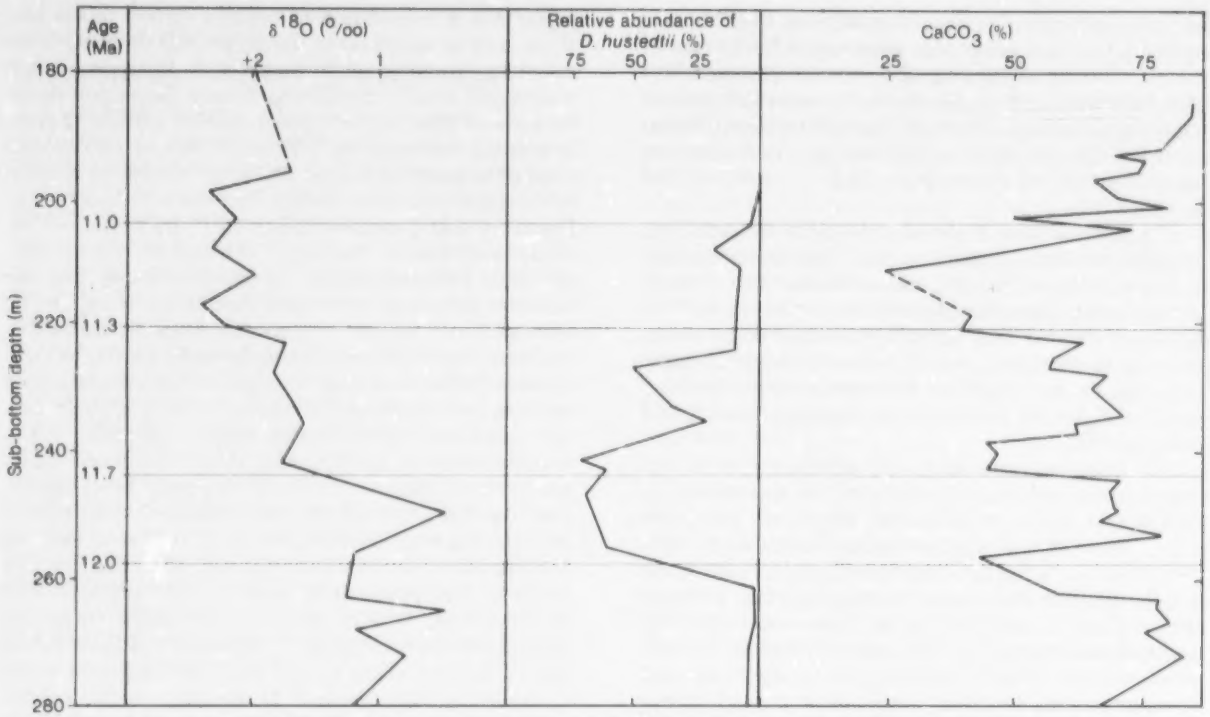

Figure 7. Comparison of the benthic foraminiferal oxygen-isotope record (Keigwin, 1979), the relative abundance of *Denticulopsis hustedtii* (Barron, this volume), and the percent calcium carbonate (Bode and Cronan, 1973) between 280 and 180 m sub-bottom depth at eastern equatorial Pacific Site 158. Ages from Barron (this volume).

Keigwin's (1979) sampling interval for isotopes, however, is large, and he notes problems with diagenesis at these lower levels at Site 158, so it is possible that oxygen-isotope values do increase briefly at the 12.0-Ma level.

A second increase of +0.5‰ in the Site 158 oxygen-isotope curve at 11.3 Ma interestingly corresponds to a sharp decline in the abundance of *D. hustedtii* in the equatorial Pacific (Figs. 6, 7). This decline was followed by the exclusion of *D. hustedtii* from the equatorial Pacific by 11.0 Ma (Barron, this volume). *D. hustedtii*, however, continued to thrive in the North Pacific and Southern Ocean (Barron and Keller, 1983; Ciesielski, 1983) for at least 2 m.y. after its exclusion from the tropics. Clearly, something happened in the eastern equatorial Pacific at about 11.3 Ma that ended the ability of *D. hustedtii* to live successfully in the tropics.

Savin et al. (1983) have shown, by oxygen-isotope studies on planktonic foraminifers from throughout the tropical Pacific, that polar cooling in the late Miocene was accompanied by warming of tropical surface waters. The calcareous nannofossil data of Lohmann and Carlson (1981) also suggest that a pronounced warming of tropical Pacific surface waters occurred at about 11 Ma. Keller (in press) notes that western equatorial Pacific surface-water assemblages of planktonic foraminifers (*Globigerinoides*) expanded into the eastern Pacific in the early late Miocene. Presumably, warming of tropical surface waters, coupled with high-latitude cooling at about 11 Ma, was responsible for the pronounced increases in provincialism—between middle- and low-latitude planktonic foraminifers (Ingle, 1973; Keller, 1981; Srinivasan and Kennett, 1981), calcareous nannofossils (Haq, 1980; Bukry, 1981b), silicoflagellates (Bukry, 1981a), and diatoms (Burckle, 1978; Keller and Barron, 1981)—that occurred in the early late Miocene.

Keller (in press) and Leinen (1979) both argue that the Equatorial Undercurrent intensified in the earliest late Miocene. Leinen (1979) reports that opal accumulation rates along the equator became markedly higher at the eastern end of the Pacific in the early late Miocene, presumably reflecting increased upwelling associated with the Equatorial Undercurrent.

Upwelling of nutrients in the present-day eastern equatorial Pacific results from surface divergences in the South Equatorial Current (Pak and Zaneveld, 1974) and vertical mixing associated with the Equatorial Undercurrent (Jones, 1973). Wyrtki (1966) stresses that the Equatorial Undercurrent drives the South Equatorial Current in the equatorial Pacific, both through diffusion of cool waters upward above the core of the undercurrent and through major input into the eastern end of the South Equatorial Current in the vicinity of the Galapagos Islands, where the undercurrent surfaces. Wyrtki (1966) states that the Peru–Chile Current alone is not strong enough to supply the relatively high velocities of the South Equatorial Current.

Leinen (1979) notes that present-day productivity in the equatorial Pacific is highest southwest of the Gala-

pagos Islands, where upwelling is intensified by surfacing of the Equatorial Undercurrent, and she argues that changes in the strength and amount of vertical mixing in the Equatorial Undercurrent could cause major changes in biologic productivity in the eastern equatorial Pacific.

Keller's (in press) argument that the Equatorial Undercurrent intensified in the earliest late Miocene hinges on the expansion at that time of intermediate-depth planktonic foraminifers (mostly *Globorotalia menardii*) at the expense of the surface-dwelling foraminifers, and on the breakdown of the east–west provincialism of surface-dwelling planktonic foraminifers that had typified the early and middle Miocene.

If the Equatorial Undercurrent was intensified at about 11.3 Ma, it may have raised surface-water salinities or altered other water-mass properties enough in the eastern equatorial Pacific to create an effective barrier to the dispersal of *D. hustedtii* and other middle-latitude diatoms into the tropics after 11 Ma. Warming of tropical Pacific surface waters may have also resulted if the equatorial countercurrents were also intensified. The increased abundance of *Thalassionema nitzschioides* from 11.3 to 11.0 Ma (Fig. 4), which occurred in the eastern equatorial Pacific immediately after the decline of *D. hustedtii*, may have reflected increased productivity associated with the Equatorial Undercurrent, as suggested by Leinen (1979), rather than intensification of the Peru–Chile Current, as suggested by Burckle et al. (1982).

INITIATION OF MIDDLE/LATE MIOCENE CHANGES

Blanc and Duplessy (1982) argue that North Atlantic Deep Water (NADW) was initiated in the latest middle Miocene *(Catinaster coalitus* Zone = [CN6] of calcareous nannofossils), owing to subsidence of the Scotland–Faroe–Iceland–Greenland Ridge. According to the Leg 85 time scale (Introduction, this volume), this event would have an approximate age of 12.0 Ma. Miller and Fairbanks (1983) believe, however, that NADW was initiated in the earliest Oligocene. Keller and Barron (1983) suggest that this event of 12 Ma represented a significant increase in the production of NADW rather than its initiation. In either case, increased production of NADW would have caused major changes in circulation and sedimentation in both the Atlantic and Pacific oceans. Keller and Barron (1983) show that siliceous sedimentation decreased at this time in the middle-latitude North Atlantic and increased in the North Pacific, presumably because expansion of NADW into the North Atlantic would have hindered the upward diffusion of silica-rich Antarctic Bottom Water (AABW) there and increased the amount of silica available elsewhere. Similarly, Isaacs (in press) notes a significant increase in opal accumulation rates in the Monterey Formation of California beginning about 11.5 Ma.

Increased production of NADW would increase the flow of warm, saline water into the Antarctic through upwelling of NADW at the Antarctic Divergence. Southward flow of warm, saline water into the modern Weddell Sea brings to the Antarctic moisture, which, in turn, is precipitated and maintains the Antarctic Ice Cap. Thus, initiation or increased NADW production at 12 Ma would have resulted in expansion of Antarctic glaciation, and would have led to increased production of AABW (Schnitker, 1980).

Increased production of AABW at 12 Ma is reflected by the widespread nature of hiatus NH4 (12 to 11 Ma) of Keller and Barron (1983) in the world ocean. This hiatus coincides with three pronounced carbonate lows during paleomagnetic Chron 11 and lower Chron 10 throughout the equatorial Pacific (Barron et al., in press; Vincent, 1981; Fig. 7 of this chapter), as was pointed out by Barron and Keller (1982). Indeed, the sediment record of the late Miocene is characterized by numerous widespread deep-sea hiatuses (Keller and Barron, 1983), pronounced intervals of carbonate dissolution alternating with intervals of higher carbonate values (Dunn et al., 1981), and benthic foraminiferal oxygen-isotope values that are enriched positively compared with those of the middle Miocene (Woodruff et al., 1981).

Two enrichment events, each recording about +0.5‰ in benthic foraminiferal oxygen isotopes at DSDP Site 158 (Keigwin, 1979), followed closely after the event of 12 Ma. The latter of these two events, at 11.3 Ma, may have resulted in intensification of the strength of the Equatorial Undercurrent and the evolution of a late Miocene circulation system characterized by isolation of middle- and low-latitude planktonic microfossil assemblages and steep latitudinal thermal gradients.

SUMMARY

Three different types of relative paleotemperature curves have been proposed to represent the equatorial Pacific between 18 and 6.2 Ma. From 18 to 13.5 Ma, the abundance curves of *Denticulopsis nicobarica* at central equatorial Pacific Sites 574 and 575 reflect the strength of surface-water circulation, with increasing numbers of *D. nicobarica* being displaced westward from the cooler eastern Pacific during times of polar cooling. At 13.5 Ma, *D. nicobarica* declines abruptly immediately before its extinction at 13.2 Ma. At about the same time, *Thalassionema nitzschioides*, presently associated with the Peru–Chile Current, becomes important (>15% of the assemblage) in the equatorial Pacific. During periods of polar cooling in the late middle and late Miocene, increases in the abundance of *T. nitzschioides* in the central equatorial Pacific resulted from increases in upwelling and/or intensification of the strength (or flow) of the Peru–Chile Current. Abundant cold-water diatoms in middle Miocene equatorial Pacific sediments suggest an open communication between middle- and low-latitude surface-water diatom assemblages. The abundance curves of cold-water diatoms at Sites 572 and 574 record equatorial surface-water cooling more extreme than that responsible for increases in *T. nitzschioides*. From 11.3 to 11.0 Ma, increased polar cooling was accompanied by a steepening of latitudinal thermal gradients that strengthened provinciality; tropical surface waters apparently became warmer, and cold-water diatoms were excluded from the tropics.

A possible sequence of events accounting for the marked changes in sedimentation and floral and faunal

distribution across the middle/late Miocene boundary can be summarized as follows. Subsidence of the Scotland–Faroe–Iceland–Greenland Ridge at 12.0 Ma allowed an increased volume of Norwegian Overflow water to mix with saline waters from the North Atlantic Drift, and significantly increased the production of NADW. This change enhanced differences in water-mass formation and circulation between the Atlantic and Pacific (Berger, 1970), and caused a decline in siliceous sedimentation in the middle-latitude North Atlantic and a corresponding increase in the Pacific (Keller and Barron, 1983). At the same time, introduction of relatively warm, saline NADW to the Antarctic increased precipitation in the Antarctic and caused expanded glaciation. Production of AABW was enhanced by increased ice in contact with the ocean, which resulted in carbonate dissolution and the widespread hiatus NH4 which characterizes the period between 12 and 11 Ma (Barron and Keller, 1982). The global circulation system was thus made more energetic and the eastern equatorial Pacific cooled, as reflected by pronounced increases in the abundance of the cool-water diatom *Denticulopsis hustedtii* between 12 and 11.5 Ma. The greater amounts of organic carbon that reached the seafloor—consequent either to increased upwelling and productivity or to erosion of transient nearshore carbon reservoirs, caused by sea-level regression—led to higher CO_2 levels in bottom water and increased carbonate dissolution. Further polar cooling at about 11.3 Ma caused a further acceleration of the global circulation system, greatly increasing the strength of the Equatorial Undercurrent. Tropical surface waters warmed, possibly because the equatorial countercurrents were also strengthened; high-latitude waters became cooler, and tropical surface-water planktonic assemblages became ecologically isolated from middle-latitude assemblages. Between 11.3 and 6.2 Ma, equatorial Pacific oceanographic conditions were more stable and less variable than during the late middle Miocene. Periods of middle-latitude cooling and intensification of eastern boundary currents appear to coincide with increased upwelling in the central equatorial Pacific.

ACKNOWLEDGMENTS

I thank the Leg 85 Co-Chiefs, Larry Mayer and Fritz Theyer, and the entire staff for making Leg 85 rewarding and successful. This manuscript was reviewed by Greta Keller, James V. Gardner, and Charles A. Repenning of the U.S. Geological Survey. Jack G. Baldauf, Dean A. Dunn, Lloyd Burckle and David Bukry provided helpful comments. Nick Pisias kindly supplied preliminary copies of carbonate and isotope data. Samples were made available for study by the National Science Foundation through the Deep Sea Drilling Project.

REFERENCES

Baldauf, J. G., 1985. Cenozoic diatom biostratigraphy and paleoceanography of the Rockall Plateau region, North Atlantic, Deep Sea Drilling Project Leg 81. *In* Roberts, D. G., Schnitker, D., et al., *Init. Repts. DSDP*, 81: Washington (U.S. Govt. Printing Office), 439–478.

Barron, J. A., 1980. Miocene to Quaternary diatom biostratigraphy of DSDP Leg 57, off northeast Japan. *In* Scientific Party, *Init. Repts. DSDP*, 56, 57, Pt. 2: Washington (U.S. Govt. Printing Office), 641–685.

_____, 1981a. Late Cenozoic diatom biostratigraphy and paleoceanography of the middle-latitude eastern North Pacific. *In* Yeats, R. S., Haq, B. U., et al., *Init. Repts. DSDP*, 63: Washington (U.S. Govt. Printing Office), 507–538.

_____, 1981b. Middle Miocene diatom biostratigraphy of DSDP Site 77B in the eastern equatorial Pacific. *Geosci. J.*, 2(2):137–144.

_____, 1982. Enhanced late Miocene upwelling in the middle- and low-latitude Pacific. *Geol. Soc. Am. Abstr. Progr.*, 14(17):439. (Abstract)

Barron, J. A., and Keller, G., 1982. Widespread Miocene deep-sea hiatuses: coincidence with periods of global cooling. *Geology*, 10: 577–581.

_____, 1983. Paleotemperature oscillations in the middle and late Miocene of the northeastern Pacific. *Micropaleontology*, 29(2): 150–181.

Barron, J. A., Keller, G., and Dunn, D. A., in press. A multiple microfossil biochronology for the Miocene. *In* Kennett, J. P. (Eds.), *The Miocene Ocean: Paleoceanography and Biogeography*. Mem. Geol. Soc. Am.

Berger, W. H., 1970. Biogenous deep-sea sediments: fractionation by deep-sea circulation. *Geol. Soc. Am. Bull.*, 81:1385–1402.

Berger, W. H., and Vincent, E., 1981. Chemostratigraphy and biostratigraphic correlations: exercises in systemic stratigraphy. *Proc. 26th Int. Geol. Congr., Geol. of Oceans Symp.* (Paris, July 7–17, 1980), Oceanol. Acta, No. SP, pp. 115–127.

Blanc, P. L., and Duplessy, J. C., 1982. The deep-water circulation during the Neogene and the impact of the Messinian salinity crisis. *Deep Sea Res.*, 29(12A):1391–1414.

Blow, W. H., 1969. Late middle Eocene to Recent planktonic foraminiferal biostratigraphy. *In* Brönniman, P., and Renz, H. H. (Eds.), *Proc. First Int. Conf. Planktonic Microfossils*: Leiden (E. J. Brill), pp. 199–421.

Bode, G. W., and Cronan, D. S., 1973. Carbon and carbonate analyses, Leg 16. *In* van Andel, T. H., Heath, G. R., et al., *Init. Repts. DSDP*, 16: Washington (U.S. Govt. Printing Office), 521–528.

Bukry, D., 1978. Biostratigraphy of Cenozoic marine sediment by calcareous nannofossils. *Micropaleontology*, 24:44–60.

_____, 1981a. Synthesis of silicoflagellate stratigraphy for Maestrichtian to Quaternary marine sediment. *Spec. Publ. Soc. Econ. Paleontol. Mineral.*, 32:433–444.

_____, 1981b. Cenozoic coccoliths from the Deep Sea Drilling Project. *Spec. Publ. Soc. Econ. Paleontol. Mineral.*, 32:335–353.

Bukry, D., and Foster, J. H., 1973. Silicoflagellate and diatom stratigraphy, Leg 16, Deep Sea Drilling Project. *In* van Andel, T. H., Heath, G. R., et al., *Init. Repts. DSDP*, 16: Washington (U.S. Govt. Printing Office), 815–871.

Burckle, L. H., 1978. Early Miocene to Pliocene diatom datum levels for the equatorial Pacific. *Proc. Second Working Group Meeting, Biostrat. Datum-Planes Pacific Neogene, IGCP Project 114* (Bandung, May 30–June 1, 1977). Spec Publ. Geol. Res. Dev. Ctr., Indonesia, 1:25–44.

Burckle, L. H., Keigwin, L. D., and Opdyke, N. D., 1982. Middle and late Miocene stable isotope stratigraphy: correlation to the paleomagnetic reversal record. *Micropaleontology*, 25(3):281–293.

Ciesielski, P. F., 1983. The Neogene and Quaternary diatom biostratigraphy of subantarctic sediments, Deep Sea Drilling Project Leg 71. *In* Ludwig, W. J., Krasheninnikov, V. A., et al., *Init. Repts. DSDP*, 71: Washington (U.S. Govt. Printing Office), 635–665.

CLIMAP, 1976. The surface of the Ice-Age earth. *Science*, 191: 1131–1144.

Cooke-Poferl, K., Burckle, L. H., and Riley, S., 1975. Diatom evidence bearing on late Pleistocene climatic changes in the equatorial Pacific. *Geol. Soc. Am. Abstr. Progr.*, 7:1038–1039.

Dunn, D. A., Moore, T. C., Jr., and Keigwin, L. D., Jr., 1981. Atlantic-type carbonate stratigraphy in the late Miocene Pacific. *Nature*, 291:225–227.

Emerson, S., and Bender, M., 1981. Carbon fluxes at the sediment-water interface of the deep-sea: calcium carbonate preservation. *Mar. Res.*, 39(1):139–161.

Goll, R. M., 1979. The Neogene evolution of *Zygocircus, Neosemantic,* and *Callimitra*: their bearing on nasselarian classification. *Micropaleontology*, 25(4):365–396.

Haq, B. U., 1980. Biogeographic history of Miocene calcareous nannoplankton and paleoceanography of the Atlantic Ocean. *Micropaleontology*, 26(4):414–443.

Ingle, J. C., Jr., 1973. Summary comments on Neogene biostratigraphy, physical stratigraphy, and paleo-oceanography in the marginal northeastern Pacific Ocean. *In* Klum, L. D., von Huene, R., et al., *Init. Repts. DSDP*, 18: Washington (U.S. Govt. Printing Office), 949–960.

Isaacs, C. M., in press. Hemipelagic deposits in a Miocene basin, California: toward a model of lithologic variation and sequence. *In* Stow, D. A. V., and Piper, D. J. W. (Eds.), *Fine-Grained Sediments: Deep-Water Processes and Environments*. Spec. Publ. Geol. Soc. London.

Jones, J. H., 1973. Vertical mixing in the Equatorial Undercurrent. *J. Phys. Oceanogr.*, 3(3):286–296.

Kanaya, T., and Koizumi, I., 1966. Interpretations of diatom thanatocoenoses from the North Pacific applied to a study of Core V20-130. *Tohoku Univ. Sci. Rept.*, Ser. 2, 37(2):89–130.

Keigwin, L. D., Jr., 1979. Late Cenozoic stable isotope stratigraphy and paleoceanography of DSDP sites from the east equatorial and central North Pacific. *Earth Planet. Sci. Lett.*, 45:361–382.

Keller, G., 1980. Middle to late Miocene planktonic foraminiferal datum levels and paleoceanography of the North and southeastern Pacific Ocean. *Mar. Micropaleontol.*, 5:249–281.

———, 1981. Miocene biochronology and paleoceanography of the North Pacific. *Mar. Micropaleontol.*, 6:535–551.

———, in press. Depth stratification of planktonic foraminifers in the Miocene ocean: paleoceanographic and paleoclimatic implications. Part II. *In* Kennett, J. P. (Ed.), *The Miocene Ocean: Paleoceanography and Biogeography*. Mem. Geol. Soc. Am.

Keller, G., and Barron, J. A., 1981. Integrated planktic foraminiferal and diatom biochronology for the northeast Pacific and the Monterey Formation. *In* Garrison R. E., et al. (Eds.), *The Monterey Formation and Related Siliceous Rocks of California*. Spec. Publ. Pacific Sec., Soc. Econ. Paleontol. Mineral., pp. 43–54.

———, 1983. Paleoceanographic implications of Miocene deep-sea hiatuses. *Geol. Soc. Am. Bull.*, 94:590–613.

Koizumi, I., 1973. The late Cenozoic diatoms of Sites 183–193, Leg 19. *In* Creager, J. S., Scholl, D. W., et al., *Init. Repts. DSDP*, 19: Washington (U.S. Govt. Printing Office), 805–855.

Leinen, M., 1979. Biogenic silica accumulation in the central equatorial Pacific and implications for Cenozoic paleoceanography. *Geol. Soc. Am. Bull.*, 90:1310–1376.

Lohmann, G. P., and Carlson, J. J., 1981. Oceanographic significance of Pacific late Miocene calcareous nannoplankton. *Mar. Micropaleontol.*, 6:553–579.

Martini, E., 1971. Standard Tertiary and Quaternary calcareous nannoplankton zonation. *In* Farinacci, A. (Ed.), *Proc. Second Planktonic Conf.*: Rome (Ed. Tecnoscienza), pp. 739–777.

Matthews, R. K., and Poore, R. Z., 1980. Tertiary ^{18}O record and glacioeustatic sea-level fluctuations. *Geology*, 8:501–504.

Miller, K., and Fairbanks, R. G., 1983. Abyssal circulation in the North Atlantic during the early to middle Miocene. *Geol. Soc. Am. Abstr. Progr.*, 15(4):645. (Abstract)

Pak, H., and Zaneveld, J. R. V., 1974. Equatorial front in the eastern Pacific Ocean. *J. Phys. Oceanogr.*, 4(4):570–578.

Pedersen, T. F., 1983. Increased productivity in the eastern equatorial Pacific during the last glacial maximum (19,000 to 14,000 yr. BP). *Geology*, 11:16–19.

Riedel, W. R., and Sanfilippo, A., 1978. Stratigraphy and evolution of tropical Cenozoic radiolarians. *Micropaleontology*, 24(1):61–96.

Romine, K., 1982. Late Quaternary history of atmospheric and oceanic circulation in the eastern equatorial Pacific. *Mar. Micropaleontol.*, 7(2):163–187.

Ryan, W. B. F., Cita, N. B., Rawson, M. D., Burckle, L. H., and Saito, T., 1974. A paleomagnetic assignment of Neogene stage boundaries and the development of isochronous datum planes between the Mediterranean, the Pacific, and Indian oceans in order to investigate the response of the world ocean to Mediterranean "salinity crisis." *Riv. Ital. Paleontol.*, 80:631–688.

Sancetta, C., 1983. Biostratigraphic and paleoceanographic events in the eastern equatorial Pacific: results of Deep Sea Drilling Project Leg 69. *In* Cann, J. R., Langseth, M. G., Honnorez, J., Von Herzen, R. P., White, S. M., et al., *Init. Repts. DSDP*, 69: Washington (U.S. Govt. Printing Office), 311–342.

Savin, S. M., Barrera, E., Bender, M., Hodell, D., Keller, G., et al., 1983. Three-dimensional temperature evolution of Miocene oceans, as inferred from foraminiferal oxygen isotopes. *Geol. Soc. Am. Abstr. Progr.*, 15(4):678. (Abstract)

Savin, S. M., Douglas, R. G., and Stehli, F. G., 1975. Tertiary marine paleotemperatures. *Geol. Soc. Am. Bull.*, 86:1499–1510.

Schnitker, D., 1980. North Atlantic oceanography as possible cause of Antarctic glaciation and eutrophocation. *Nature*, 284:615–616.

Schrader, H. J., 1976. Cenozoic planktonic diatom biostratigraphy of the southern Pacific Ocean. *In* Hollister, C. D., Craddock, C., et al., *Init. Repts. DSDP*, 35: Washington (U.S. Govt. Printing Office), 605–671.

Shackleton, N. J., and Kennett, J. P., 1975. Paleotemperature history of the Cenozoic and the initiation of Antarctic glaciation: oxygen and carbon isotope analysis in DSDP Sites 277, 279, and 281. *In* Kennett, J. P., Houtz, R. E., et al., *Init. Repts. DSDP*, 29: Washington (U.S. Govt. Printing Office), 743–755.

Srinivasan, M. S., and Kennett, J. P., 1981. Neogene planktonic foraminiferal biostratigraphy and evolution: equatorial to subantarctic South Pacific. *Mar. Micropaleontol.*, 6:499–533.

van Andel, T. H., Heath, G. R., and Moore, T. C., Jr., 1975. Cenozoic history and paleoceanography of the central equatorial Pacific Ocean. *Mem. Geol. Soc. Am.*, 143:1–134.

Vincent, E., 1981. Neogene carbonate stratigraphy of Hess Rise (central North Pacific) and paleoceanographic implications. *In* Thiede, J., Vallier, T. L., et al., *Init. Repts. DSDP*, 62: Washington (U.S. Govt. Printing Office), 571–606.

Weaver, F. M., and Gombos, A. M., Jr., 1981. Southern high-latitude diatom biostratigraphy. *Spec. Publ. Soc. Econ. Paleontol. Mineral.*, 32:445–470.

Woodruff, F., and Douglas, R. G., 1981. Response of deep sea benthic foraminifera to Miocene paleoclimatic events, DSDP Site 289. *Mar. Micropaleontol.*, 6:617–632.

Woodruff, F., Savin, S. M., and Douglas, R. G., 1981. Miocene stable isotope record: a detailed deep Pacific Ocean study and its paleoclimatic implications. *Science*, 212:665–668.

Wyrtki, K., 1966. Oceanography of the eastern equatorial Pacific Ocean. *In* Barnes, H. (Ed.), *Oceanography and Marine Biology, Ann. Rev.*: London (George Allen and Unwin Ltd.), 4:33–68.

Date of Initial Receipt: 14 October 1983
Date of Acceptance: 6 March 1984

32. SEISMIC MODELING AND PALEOCEANOGRAPHY AT DEEP SEA DRILLING PROJECT SITE 574[1]

Larry A. Mayer, Department of Oceanography, Dalhousie University, Halifax, Nova Scotia
Thomas H. Shipley, University of Texas Institute of Geophysics
Fritz Theyer, Hawaii Institute of Geophysics, University of Hawaii
Roy H. Wilkens, Department of Earth, Atmospheric and Planetary Sciences, Massachusetts Institute of Technology
and
Edward L. Winterer, Scripps Institution of Oceanography[2]

ABSTRACT

The analysis of high-resolution watergun seismic profiles collected in support of DSDP Leg 85 drilling reveals several major, regionally traceable reflectors that can be correlated over more than 360,000 km^2 in the central equatorial Pacific. Synthetic seismograms generated from shipboard physical property measurements (carefully corrected to *in situ* values) for DSDP Site 574 show excellent agreement with the field records; the agreement suggests that the traveltime-to-depth conversion is accurate and permits the precise (± 5 m) location of reflectors in the cored section. The reflectors can be dated (± 0.5 Ma) as follows: Orange, 21.5 to 22.5 Ma; Yellow, 20.5 to 21.5 Ma; Lavender, 16 to 17 Ma; Red, 13.5 to 14.5 Ma; Purple, 11 to 12 Ma; Brown, 7 to 8 Ma; and Green, 3 to 4 Ma. Similar analyses at the other Leg 85 sites result in identical ages. The reflectors are thus time surfaces; this chapter relates them to major paleoceanographic events and changes in the relative sea-level curve. The Orange and Yellow reflectors are associated with a marked increase in $\delta^{13}C$, a major change in planktonic foraminiferal assemblages, the development of the deep Circum-Antarctic Current, and the establishment of steep thermal gradients between tropical and polar regions. This reorganization of the oceanic circulation system was probably a response to the opening of the Drake Passage, and it resulted in changes in the chemistry of tropical Pacific waters that caused the induration (and thus impedance contrasts) associated with these reflectors.

The Lavender reflector is associated with a large carbonate minimum, the "Chron 16 carbon shift," a widespread hiatus (NH2), major eustatic sea-level fluctuations, and a significant increase in silica deposition in the Pacific. It is not associated with ^{18}O enrichment or climatic cooling. We conclude that this event represents an intensification in Antarctic Bottom Water (AABW) circulation and the partitioning of silica between the Atlantic and the Pacific, caused by the introduction of North Atlantic Deep Water (NADW) in response to paleobathymetric and tectonic events. The Red reflector is associated with a subdued carbonate minimum, a widespread hiatus (NH3), a sea-level drop, significant changes in microfossil assemblages, and a major increase in $\delta^{18}O$ that has been linked with the buildup of Antarctic ice. Detailed isotopic analyses reveal that this isotopic shift occurred within an interval of 30,000 yr. and precisely at the depth of the Red reflector.

The Purple reflector is associated with an extremely large carbonate minimum, a change in the style of carbonate deposition in the Pacific, a major lithologic boundary, a widespread hiatus (NH4), an increase in the provincialism between low and high latitudes in all planktonic microfossil assemblages, an apparent fall in eustatic sea level, an enrichment in $\delta^{18}O$, and a major North Atlantic reflector interpreted as representing an intensification of North Atlantic bottom-water circulation.

The Brown reflector is roughly associated with a small carbonate minimum, an enrichment in $\delta^{18}O$, the late Miocene $\delta^{13}C$ depletion, a drop in the relative sea-level curve, and major faunal changes.

The Green reflector is associated with a large carbonate minimum, an enrichment in $\delta^{18}O$, a major western North Atlantic erosional event, and a widespread eastern Atlantic seismic reflector. The bulk of evidence supports correlation with the onset of Northern Hemisphere glaciation, but detailed isotopic analyses indicate that this isotopic event may be linked to the establishment of colder bottom waters without major ice-sheet development.

Several types of reflectors have been identified. The reflectors in the older section result from diagenetic effects; the regionally correlatable reflectors are associated with global events. In the younger (post-18 Ma) section, local reflectors are characterized by velocity contrasts, whereas regional reflectors are associated with density contrasts caused by carbonate minima. Two modes of generation of carbonate minima (and thus of reflectors) spanning the equatorial Pacific are (1) the intensification of AABW without the concurrent intensification of NADW and so without fractionation of silica between the Atlantic and the Pacific; this mode results in the less extreme carbonate minima; and (2) the intensification of AABW in response to the intensification of NADW; this mode results in extreme carbonate minima and a correlation of equatorial Pacific reflectors with North Atlantic events.

INTRODUCTION

The fertile waters of the central equatorial Pacific have produced a thick section of biogenic sediment that is an extremely sensitive indicator of the interplay among tectonism, circulation, productivity, and diagenesis. Studies of equatorial Pacific piston cores (e.g., Arrhenius, 1952; Berger, 1973; CLIMAP, 1976; Hays et al., 1969;

[1] Mayer, L., Theyer, F., et al., *Init. Repts. DSDP*, 85: Washington (U.S. Govt. Printing Office). This work was supported by ONR contract N00014-82-K-0625 to L.M. and by the Natural Sciences and Engineering Council of Canada. F.T.'s research was supported by NSF grants OCE 81-17997 and OCE 85-04146. T.S. was supported by N00014-81-K-0728.

[2] Addresses: (Mayer) Dalhousie University, Halifax, Nova Scotia, Canada B3H 4J1; (Shipley) University of Texas, Institute of Geophysics, Austin, TX 78712; (Theyer, present address) Department of Geological Sciences, University of Southern California, University Park, Los Angeles, CA 90089; (Wilkens) Department of Earth, Atmospheric and Planetary Sciences, Massachusetts Institute of Technology, Cambridge, MA 02139; (Winterer) Scripps Institution of Oceanography, University of California at San Diego, La Jolla, CA 92093.

Luz, 1973; Shackleton and Opdyke, 1973, 1976) have resulted in a fairly detailed picture of the distribution of modern oceanographic parameters and the paleoceanography of the past 2 to 3 m.y. Deep-sea drilling in the region has produced an intriguing record of paleoceanographic change for the past 40 m.y. (e.g., Tracey, Sutton, et al., 1971; Hays et al., 1972, pp. 43–61; van Andel and Heath, 1973; Winterer, 1973; van Andel et al., 1975; Leinen, 1979; Kennett, in press), but truly detailed studies on this older material have been frustrated by incomplete coring and by core disturbance. Deep Sea Drilling Project Leg 85, however, using the hydraulic piston corer (HPC) in the upper, unconsolidated part of the section and rotary coring in the deeper parts of the section, returned to the central equatorial Pacific and collected nearly complete and relatively undisturbed sedimentary records of the past 40 m.y. (site chapters, this volume). The Leg 85 coring has provided a wealth of material that is ideal for studies of fine-scale biostratigraphy (Barron et al.; Bukry; Labracherie; Jarvis and Tocher; all this volume), paleomagnetism (Weinreich and Theyer, this volume), carbonates (Pisias and Prell, this volume), isotopes (Pisias and Shackleton; Miller and Thomas; Vincent and Killingley; all this volume), and physical properties (Wilkens and Handyside, this volume). In addition, the Leg 85 sites were the first surveyed for DSDP with the relatively new high-resolution watergun seismic source (Shipley and Winterer, this volume). The collection of detailed physical and stratigraphic data in conjunction with high-quality, digital, high-resolution seismic profiles presents a unique opportunity to investigate the origin of the seismic record in this region by using quantitative modeling techniques (synthetic seismograms) and to evaluate the potential of equatorial Pacific seismic stratigraphy as a paleoceanographic tool.

For most of the relatively short (60-yr.) history of seismic exploration, reflection profiling has had an invaluable but rather limited role in the exploration of the subsurface. Numerous constraints (e.g., resolution limitations due to narrow bandwidth and data degradation due to geometric or instrumental artifacts and small dynamic recording and display ranges) limited the role of the reflection profile to that of a structural or geometric tool. The profile yielded information on arrival time and dip (and therefore structural styles and faulting) but little more. Recently, however, with rapid advancement in the development of seismic sources and data acquisition and processing techniques, and with the pioneering work of Vail et al. (1977) and Brown and Fisher (1977), we have begun to extract detailed and direct stratigraphic information from the seismic record. With the derivation of stratigraphic information from the seismic record, we are approaching the true potential of reflection profiling—that is, the rapid and remote determination of the exact nature (lithologic parameters, sediment facies, depositional environment) of the subsurface material, and, from this, the determination of the geologic history of a region.

The success of the application of seismic stratigraphic concepts to petroleum exploration problems on land and in shallow water results, in part, from the numerous boreholes and large amount of high-quality seismic data available. The scientist working on deep-sea problems, however, is often faced with a few widely spaced DSDP holes and limited seismic data. Nonetheless, significant progress has been made in deep-sea seismic stratigraphy. This is particularly true for the western North Atlantic, where the analysis of a fair number of multichannel seismic (MCS) lines and numerous DSDP sites has resulted in an evolving stratigraphic framework (Sheridan et al., 1983; Shipley et al., 1978; Tucholke, 1979; Tucholke and Mountain, 1979). Shipley (1983) used seismic modeling and DSDP sites in this region in an attempt to reconcile discrepancies in well-hole seismic correlations. A careful study of the problem led him to conclude that the uncertainties associated with incomplete coring and core disturbance made the development of a single unique correlation between existing drill-hole and seismic data impossible, however.

In the central equatorial Pacific, unlike the western North Atlantic, no MCS data have been collected. Most of the data collected in this region have been analog, single-channel airgun data that can be analyzed only in terms of seismic character (e.g., transparent, opaque, or reverberant) and yield little direct stratigraphic information (Ewing et al., 1968; Houtz and Ludwig, 1979). Recently, Shipley et al. (1983), using digital airgun data, have demonstrated the potential of the application of seismic stratigraphic techniques to the deep-sea environment (Hess Rise); but detailed correlations of their data were impossible because of the very limited core recovery in the region. Despite these limitations, Winterer, Riedel, et al. (1971), Winterer et al. (1974), Schlanger and Douglas (1974), Berger et al. (1977), Berger and Mayer (1978), and others have suggested that the seismic record of equatorial Pacific sediments, which are biogenic in origin and sensitive to changes in the chemistry of the oceans, might hold important paleoceanographic information. Mayer (1979a), using 10-m–long piston cores and high-resolution 4-kHz seismic profiles, demonstrated that, for at least the upper 10 m of equatorial Pacific sediments, contrasts in acoustic impedance can be directly related to glacial/interglacial cycles. When these impedance contrasts were compared with the 4-kHz seismic record, however, it became clear that the closely spaced reflections visible in the seismic profile were not direct representations of the impedance contrasts in the sediment column but, rather, interference patterns resulting from complex interactions between closely spaced impedance boundaries and the seismic wavelet (Mayer, 1979b). Thus, even a 4-kHz profiling system with resolution of less than 1 m cannot resolve the discrete stratigraphic discontinuities that are ultimately responsible for seismic reflections. An understanding of the implications of this result is critical to the proper application of the principles of seismic stratigraphy to deep-sea sediments.

It is fundamental to the stratigraphic interpretation of seismic data that the seismic information be expressed in geologic terms. The accurate transformation of seismic data into geologic information requires an understanding of the limitations of the techniques involved, particularly, as just mentioned, the limitations in resolu-

tion due to the characteristics of the seismic wavelet. The principal mechanism by which we gain insight into the nature of this transformation is the synthetic seismogram. Varying degrees of complexity can be applied to the generation of synthetic seismograms, but in essence the technique models the interaction between a seismic wavelet and a given well-constrained geological model. If we have an accurate representation of the seismic source wavelet and an accurate and detailed picture of subsurface geologic variations, the synthetic seismogram should provide a record of their interactions and allow us to address the origin and geologic significance of the seismic reflections with some confidence.

In this chapter we use the detailed stratigraphic and physical property results of Leg 85 and the high-resolution seismic data collected during the Leg 85 site surveys to evaluate the potential of seismic stratigraphic work in the central equatorial Pacific. To do this, we briefly examine the nature of the seismic section in the region, discuss the approach to and results of seismic modeling at DSDP Site 574, and attempt to infer the paleoceanographic significance of the major regional seismic horizons.

THE SEISMIC REFLECTION DATA

Objectives and Criteria

The seismic reflection data presented here were collected aboard the *Thomas Washington* as part of a site-survey program in support of Leg 85 drilling (Shipley et al., this volume). The site surveys were undertaken to acquire high-resolution records of seafloor bathymetry and the subsurface seismic section. Pelagic carbonate sequences are usually highly reflective, and the reflectors show substantial lateral continuity. Signal-to-noise ratios are thus often not critical in this sediment type (Berger et al., 1977; Schlanger and Douglas, 1974; Winterer et al., 1974). These factors combine to make most conventional seismic data from these environments appear to be of high quality and to be related to the geology in a simple manner. As discussed earlier, however, Mayer (1979b) has demonstrated that in equatorial carbonates, downsection variations in acoustic properties occur more rapidly than conventional sound sources can resolve.

EQUIPMENT AND METHODS

With resolution, penetration, cost, and safety as criteria, we examined the sound sources available for underway geophysical studies. We identified the Seismic Systems 80-in.^{3} (1.3-l), 2000-psi (136-atm.) watergun as a good compromise between power and bandwidth. A far-field source signature for the gun at our usual towing depth of 3 m shows the short duration of the pulse, which translates to a fairly broad bandwidth (Figs. 1A, B). A prominent "precursor" (a long-duration, low-amplitude, early-arriving portion of this pulse) is the only significant aberration. We tried several band-limiting filters and deconvolution routines to remove this precursor. We were most successful using Digicon's DECONS program, which calculates a deconvolution filter so that the output is a minimum-phase pulse of bandwidth similar to that of the original data. This filter, when applied to the original source-signature pulse, substantially reduced the precursor as well as other ringing in the pulse (Fig. 1C). Since we only recorded source signatures at one site, the application of the filter to all the field data is suspect, even though we tried to keep the source, receiver, and towing arrangements as constant as possible throughout the cruise. Even so, the use of the minimum-phase filter at the other sites does appear to be equally effective.

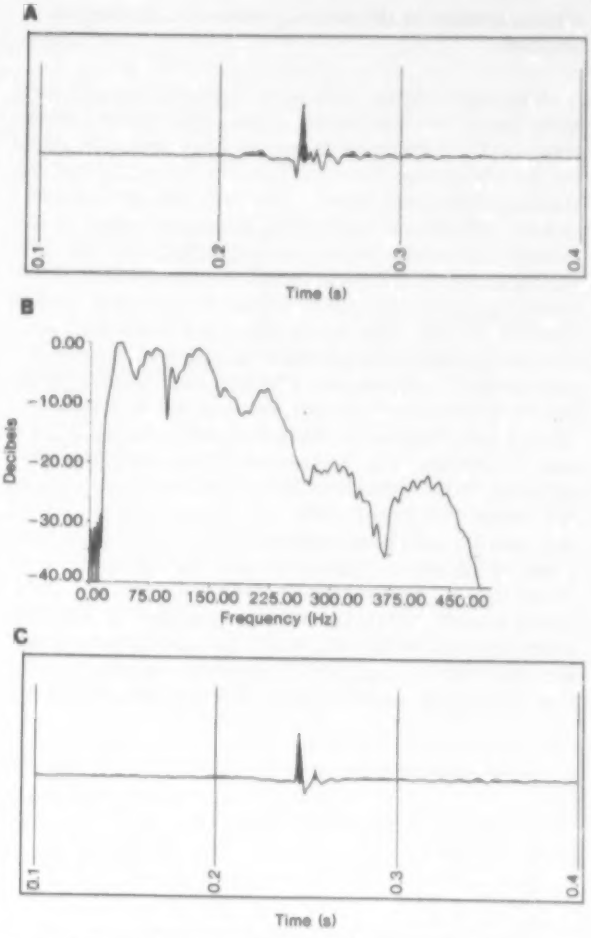

Figure 1. Source signatures for SIO 80-in.^{3} watergun. A. Raw source signature. B. Spectrum of raw source signature. C. Source signature with DECONS operator applied.

The streamer we used for the work south of the Clipperton Fracture Zone is a Teledyne streamer with acceleration-canceling hydrophones in a linear array. The streamer was driven with a preamplifier designed at the Scripps Institution of Oceanography. The streamer depth was monitored with a calibrated depth sensor at the head of the leader. The towing depth varied between 5 and 15 m but remained between 6 and 10 m most of the time.

The analog data were first bandpass filtered 13 Hz to 500 Hz with a low cut slope of 10 dB/oct. and a high cut slope of 50 db/oct. The data were then digitized at a 0.5-ms period with a binary gain ranging scheme that gives the system about 60 dB of dynamic range. A 12-bit number and gain bits were then passed to the computer, and the data and gain information were recombined and then written on tape in standard SEGY 32-bit integer format.

The data used in interpretations and presented in this chapter are mostly filtered 30 to 250 Hz or 30 to 400 Hz with various filter tapers and rolloff severity. The minimum-phase filter was applied to some sections. None of the data have been amplitude normalized, windowed, or corrected for spherical divergence. These data are true amplitude, in the sense that all recording gains have been removed. For some sections, the plot amplitude was raised to enhance the later arrivals, with overdriving affecting some of the earlier strong events. Plot amplitude is strictly the multiplication factor applied to each sample; it is in no way a time- or trace-varying gain.

Characteristics of the Seismic Section in the Region Studied

Although seismic data were collected on well over 8000 km of the site survey cruise, this report concentrates on the portion of the survey track that is bounded by the Clipperton Fracture Zone to the north and the Galapagos Fracture Zone to the south and forms a quadrilateral 600 km on a side (Fig. 2). In particular, we will discuss the seismic section in the vicinity of Site 574, which, except as otherwise noted, is characteristic of the seismic record in the region defined by this quadrilateral (Fig. 3). The profiles along this track were examined, and major, regionally traceable reflectors were identified and assigned color names. The reflectors labeled, in order of increasing traveltime (or age) are G (Green), B (Brown), P (Purple), R (Red), L (Lavender), Y (Yellow), and O (Orange) (Fig. 3). One other regionally traceable reflector, M (Magenta), which normally occurs between the Green and Brown reflectors, is not identifiable on this profile. All these reflectors are traceable for hundreds of kilometers both south and west of Site 574; all except the Purple and Yellow reflectors are traceable completely around the 600-km-per-side quadrilateral. The Lavender and Red reflectors, which are particularly prominent and easy to trace, are recognizable on lower-resolution airgun profiles for at least 1500 km west and 600 km

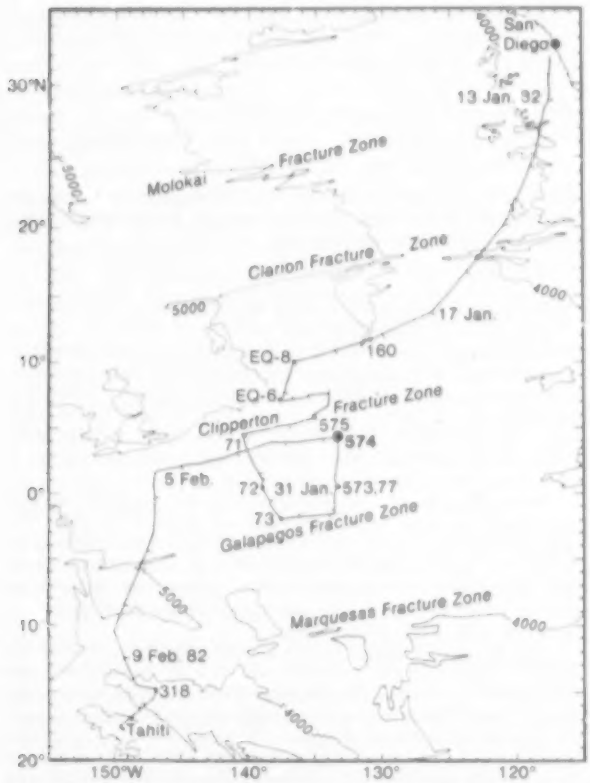

Figure 2. Ship track of the *Thomas Washington* for DSDP Leg 85 site surveys.

east of Site 574, within the great lens of equatorial biogenic sediments. These reflectors are clearly regional and can be identified over an area of at least 20° by 6°, or 1.6 million km^2.

The seismic section in the vicinity of Site 574 shows a number of features common to records elsewhere in the equatorial sediment lens.

1. The dominant "style" or geometry of the acoustic stratigraphy is simple pelagic drape. Most reflectors are remarkably parallel to their neighbors.

2. Erosional effects (Shipley et al., this volume, figs. 9, 10, 13, 14) are especially common in the younger (post–Green reflector) strata. Channels are most commonly associated with buried or exposed basement relief, and some channels take the form of partial or complete moats around hills. In some places, the effect of bottom currents is to inhibit sedimentation (bypassing) rather than to erode, and this effect is shown by the progressive convergence of reflectors; the convergence is in contrast to the clear angular truncation that characterizes the older reflectors where erosion has removed previously deposited sediments.

3. A ubiquitous feature of the profiles is the evidence of the progressive infilling and smoothing of original basement relief (Shipley et al., this volume, figs. 5, 6). The filling in of troughs occurs mostly in the early (pre-Red) stages of sedimentation: the acoustic reflectors between the Red and Green reflectors tend to be nearly parallel, except for thinning over buried hills.

4. Slopes between the hills and troughs, especially in the lower, pre-Red strata, commonly show mounds of acoustically chaotic sediments that we interpret as slide or slump masses (Shipley et al., this volume, figs. 5, 6, 10).

5. In terms of acoustic "character," that is, the relative transparency or spacing of the reflectors in various parts of the section, we see great variability in detail, but a few generalizations hold true:

A. The post-Red reflectors are generally fairly closely spaced and continuous compared with the pre-Red reflectors.

B. There is often a relatively transparent interval between the Red and Lavender reflectors.

C. Below the Lavender reflector and down to a level about 0.1 s above acoustic basement, the reflectors become progressively more faint and difficult to trace.

D. In the lowest 0.1 s above acoustic basement, the reflectors have progressively greater amplitude.

E. The top of acoustic basement is commonly difficult to pick unequivocally, in spite of the large impedance contrast at the sediment/basalt interface.

We turn now to the major, regionally traceable seismic horizons identified at Site 574; using the techniques of seismic modeling, we shall look at their origins and paleoceanographic significance.

SEISMIC MODELING

We have already discussed the importance of the synthetic seismogram in evaluating the geologic significance of seismic reflections. The two critical inputs into the synthetic seismogram are the seismic wavelet and the ge-

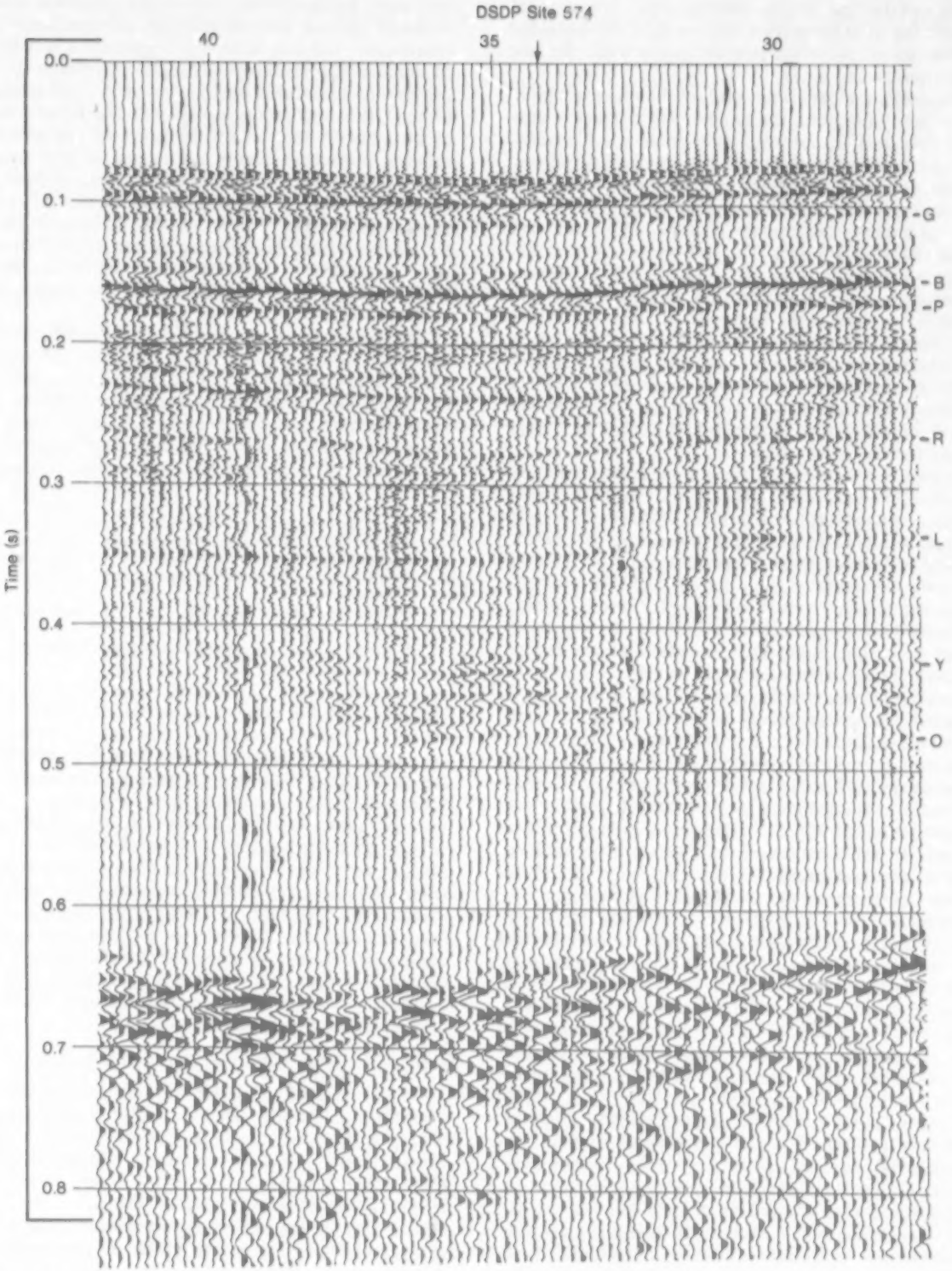

Figure 3. 80-in.^{3} watergun profile near DSDP Site 574.

ologic model. The seismic wavelet used to produce the results and the field sections presented here was obtained by applying a deconvolution filter to the field-measured far-field source signature (see discussion under Seismic Reflection Data; Fig. 1).

The geologic model is the result of the shipboard physical property program. On Leg 85, sonic velocity, saturated bulk density, porosity, water content, grain density, formation factor, thermal conductivity, and percent calcium carbonate were measured at least once per cored section (every 150 cm). The techniques and details of the physical property program are discussed by Wilkens and Handyside (this volume). The sections acquired at Site 574 provided the most reliable and continuous physical property results; measurements on the second HPC hole at the site replicated the values determined on the first HPC hole almost perfectly (see Wilkens and Handyside, this volume). Because of our confidence in the quality of the measurements and in our depth control on the samples, we merged all four holes at Site 574 to produce a single data set for each property. The resulting average sample interval is less than 1 m.

From the standpoint of seismic modeling, the most important physical properties are saturated bulk density and sonic velocity. It is the product of these two properties that results in acoustic impedance, and contrasts in acoustic impedance produce seismic reflections. The original data for saturated bulk density and sonic velocity versus depth are presented in Figure 4. Close inspection of Figure 4 reveals that saturated bulk density and velocity are not always measured at exactly the same depths. To calculate acoustic impedance, we chose to use the density data as the primary data set, and to each depth for which there was a density value we assigned the nearest velocity value. This procedure is easy to justify. First, almost all the velocity measurements were made within a few centimeters of the density measurements. Bioturbation mixes the sediment over an interval thicker than this (Berger and Heath, 1968; Berger and Killingley, 1982). Second, an examination of the downcore variation in both density and velocity reveals that for most of the section velocity does not vary significantly (less than 6% of its mean value), whereas density fluctuates by more than 25% of its mean value. Thus, most of the variation in acoustic impedance is due to the fluctuation in saturated bulk density, not velocity. The reasons for this relationship are examined in detail by Mayer (1979a, 1982).

Given a set of velocity of saturated bulk density values at the same depths below the seafloor, we now face one of the most critical and difficult steps in applying stratigraphic significance to seismic data—the transformation of sub-bottom depth information into traveltime information. All the downcore information whether biostratigraphic, magnetic, physical property, or isotopic is measured as a function of depth below the seafloor—a spatial-domain record. The seismic section, on the other hand, is a time-domain record. Therefore the correlation of seismic data with well hole data is dependent on the assumption that the conversion from traveltime to depth (or vice versa) is accurate. This assumption implies an exact knowledge of the *in situ* velocity versus depth function—a knowledge that is rarely available.

Sediment velocity information can be obtained in several ways. Refraction and wide-angle reflection experiments can provide interval velocities between major discontinuities, but they usually provide only a very limited number of solutions in the sediment column. In the presence of a borehole, logging and vertical seismic profiling (VSP) experiments can provide a detailed picture of the velocity-versus-depth structure of the sediment column, but unfortunately, no logging or VSP experiments were undertaken at the Leg 85 sites. A final approach is the detailed laboratory measurement of velocity on cored samples. This is customarily done on DSDP cruises, but before this information can be used for converting traveltime to depth, the laboratory measurements must be corrected to *in situ* values. This correction is neither straightforward nor trivial.

The magnitude of the problem can easily be seen in the following tabulation, which compares the average velocities at Site 574 computed from (1) uncorrected laboratory measurements, (2) averages of wide-angle reflection/refraction measurements made in equatorial carbonates, and (3) the ratio of basement depth (determined by drill string) to the best pick of basement traveltime.

Average velocity—laboratory measurements	1580 m/s
Average velocity—sonobuoy/refraction	1987 m/s[a]
Basement pick (0.60 s)/drill-string depth to basement	1747 m/s
Average final corrected velocities	1691 m/s

[a] From Johnson et al. (1978); Kroenke (1972); Winterer, Riedel, et al. (1971); Ewing et al. (1968).

It is clear from this tabulation that the laboratory values are 15 to 20% less than those more closely representing *in situ* conditions. Although there is some uncertainty in the actual pick of basement on the seismic section (Fig. 3, between 0.57 and 0.62 s), the use of laboratory velocity values in a point-by-point conversion of depth to traveltime would place basement at 0.641 s, well below a reasonable position. If we were interested only in accurately determining the average velocity in the sediment column, the division of the drill-string–determined basement depth by the best pick of traveltime to basement would suffice. We are concerned, however, with detailed correlation of the major reflections with the borehole results, so we must know the *in situ* velocity over small, discrete intervals.

Conversion from Laboratory to *in Situ* Values

When a sample is removed from a borehole and brought to laboratory conditions (1 atm. and approximately 25°C), it is subject to changes in several conditions that will affect the measured velocity. Hamilton (1965, 1976) discusses four factors that must be accounted for in order to correct laboratory measurements to *in situ* values: (1) the change in temperature; (2) the decrease in hydrostatic pressure; (3) the decrease in porosity caused by the removal of overburden; and (4) the decrease in rigidity (intergranular locking) that results from the removal of overburden. Of these factors, the decrease in porosity caused by the removal of overburden has the

READEX FICHE best copy available

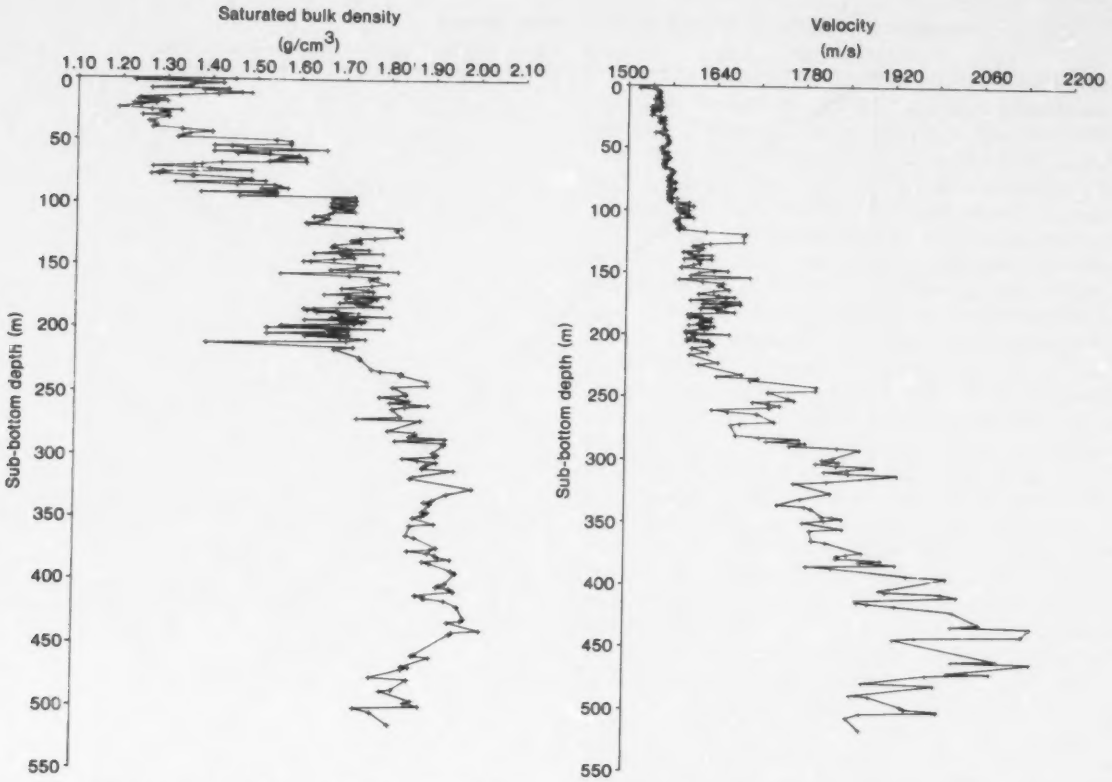

Figure 4. Laboratory-measured saturated bulk density and sonic velocity versus sub-bottom depth for DSDP Site 574.

most significant effect (Hamilton, 1976, 1979; Boyce, 1976).

Rebound-Corrected Porosity/Density

Using consolidation test data on carefully selected DSDP samples, Hamilton (1979) constructed a series of curves that predict the elastic rebound resulting from the removal of overburden pressure for each of the major deep-sea sediment types. Entering the Site 574 porosity and depth data into Hamilton's (1976) equation for deep-sea carbonates results in a rebound curve that predicts the need for an approximately 5.5% reduction in porosity for the deepest Site 574 samples (518 m sub-bottom, Fig. 5). Geally and Gerard (1970) and Shipley (1983) have found that logging-derived porosity values in deep-sea carbonates closely follow Hamilton's predicted curve to depths of 700 m, strongly supporting this correction procedure. Because of the well established linear relationship between saturated bulk density and porosity in deep-sea carbonates (Fig. 6), a rebound correction can easily be applied to the saturated bulk density values measured in the laboratory.

Rebound-Corrected Velocity

Substantial empirical data have permitted the establishment of curves predicting the effect of rebound on porosity, but very few data are available for the direct correction of velocity values. Laughton (1957) did directly measure the increase of velocity with increasing pressure on a carbonate sample, but this single data set is not sufficient to permit the derivation of general relationships. In the absence of direct measurements, we must determine the rebound-corrected velocity indirectly, from the rebound-corrected porosity. Seeking a similar correction, Boyce (1976) and Shipley (1983) plotted laboratory porosity against laboratory velocity and used a graphic offset to estimate *in situ* velocities. We have a much more continuous data set than either Boyce or Shipley, and given the clearly nonlinear relationship between laboratory porosity and velocity (Fig. 7), we chose to use a series of multiple linear regressions to attempt to establish a means of predicting velocity from porosity. We tested our prediction scheme by comparing the measured laboratory velocities against the velocities predicted by our regression equations, and we found that by dividing the sediment column into four discrete sections and using a third-order regression in each section we were able to duplicate the original laboratory velocity curve accurately (Fig. 8). The need to divide the sediment column into discrete sections and to establish individual correlations between porosity and velocity for each section suggests that different processes are at work in each depth zone, and that this sort of correlation may provide a way to examine these processes. For example, between 450 and 510 m, porosity increases but velocity does not decrease. This anomalous relationship probably indicates an increase in silica content and the onset of cementation. The ramifications of this finding will be

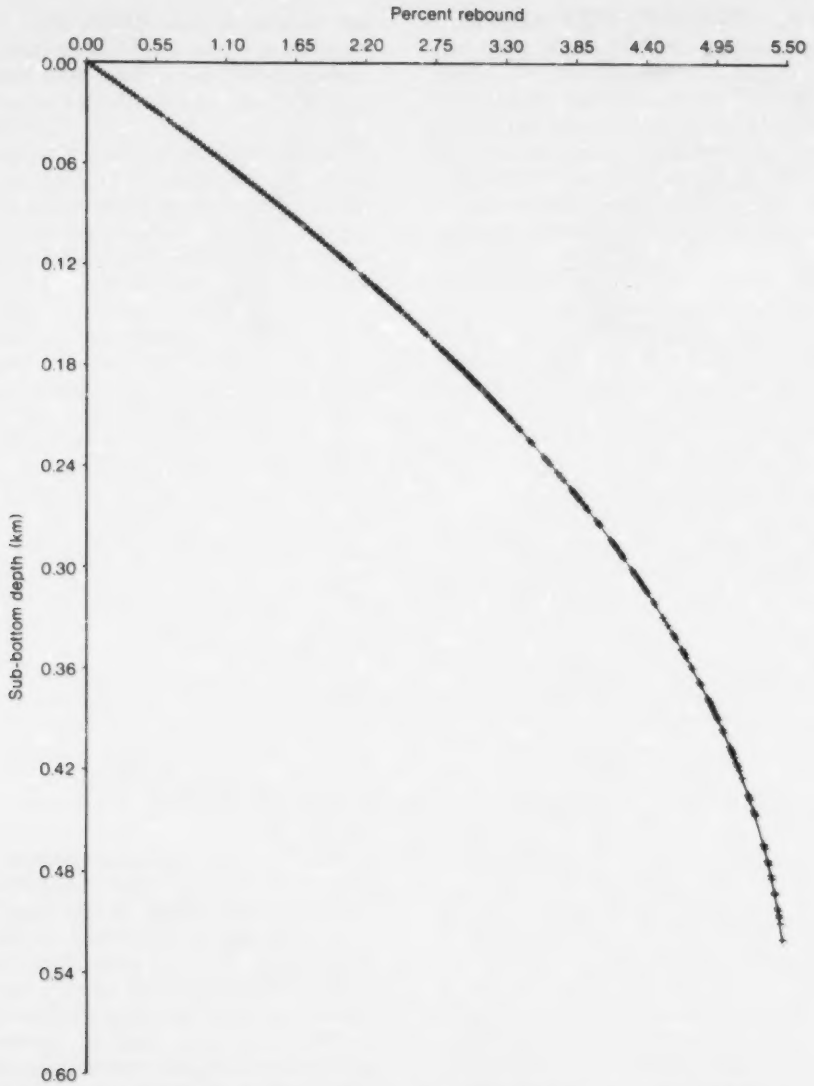

Figure 5. Calculated percent porosity rebound versus sub-bottom depth for DSDP Site 574.

discussed elsewhere. With a way to accurately predict laboratory velocity from laboratory porosity, we can use rebound-corrected porosities to calculate rebound-corrected velocities.

Corrections for Temperature and Pressure

To correct for the effects of temperature and hydrostatic pressure, profiles of *in situ* temperature and pressure must be established. To estimate hydrostatic pressure, we multiplied an assumed seawater density of 1.06 g/cm^3 by the depth below sea level. To estimate the temperature profile, we used the results of detailed heat-flow studies in the region (Crowe, 1981), which show an average heat flow of 1.76 cal/cm^2 s $\times$ 10^{-6} and an average conductivity of 2.08 cal/cm s °C $\times$ 10^{-3}. We established a temperature profile by using these values as initial points and using Hamilton's (1979) generalized curve for conductivity versus depth in deep-sea carbonates. Although temperature and pressure affect both the liquid and solid phases of the saturated sediment system, Boyce (1976), citing Hughes and Cross's (1951) experiments on wet and dry limestone, suggests that the variation in velocity of the solid end-member (calcite) is less than 1% for the pressure and temperature ranges that exist at Site 574. We therefore assumed that the *in situ* velocity of the solid end-member was the same as that measured in the laboratory. The variations in velocity with changes in the temperature and pressure of the liquid phase (seawater), on the other hand, are significant, but they are well documented (U.S. Naval Oceanographic Office, 1962; Wilson, 1960) and are easy to calculate. Given the rebound-corrected velocities and the velocity of the liquid and solid end-members at laboratory and *in situ* conditions, we then calculated the *in situ* velocity by using the

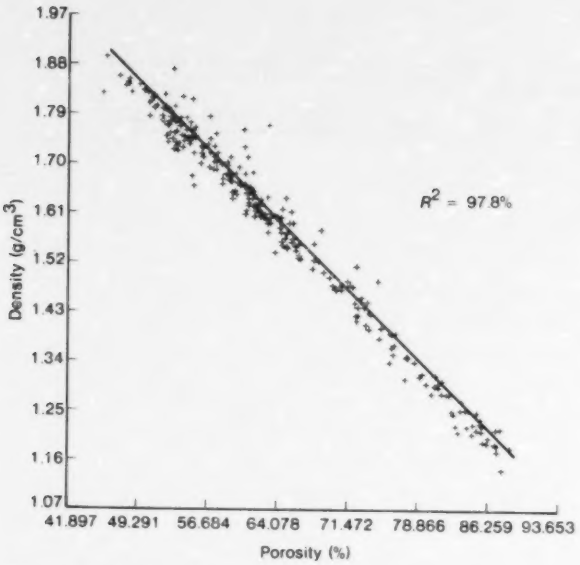

Figure 6. Regression of saturated bulk density against porosity for DSDP Site 574. R^2 = correlation coefficient.

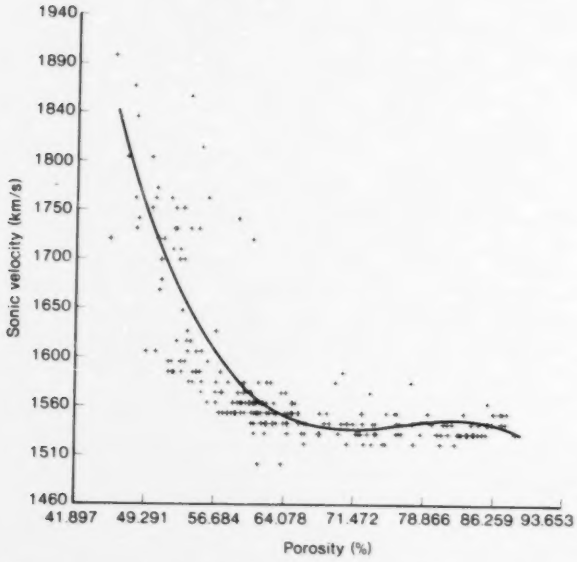

Figure 7. Regression of porosity against sonic velocity for DSDP Site 574. Solid curve is a third-order regression line.

technique of Boyce (1976; Fig. 9). The resulting velocities are corrected for all the factors discussed by Hamilton (1965, 1976) except the decrease in rigidity caused by the removal of overburden. The evidence available at present is insufficient to permit a correction for this factor to be derived empirically, so our *in situ* velocities are minimum values. Calculations made using these velocities, however, place basement at 0.611 s (Fig. 10), which is well within the uncertainty of the basement pick and which indicates that the unaccounted-for rigidity factor is probably of minor significance.

Calculation of Synthetic Seismograms

The corrected velocities and saturated bulk densities can then be used to calculate acoustic impedance (the product of velocity and density) as a function of traveltime (Fig. 10). The impedance curve shows numerous high-frequency fluctuations with several major offsets; the origin of the impedance fluctuations will be discussed in detail later. The parameter of key importance to seismic profiling is the reflection coefficient—the ratio of the amplitude of the reflected wave to that of the incident wave. For normal incidence (the situation with which we are concerned), the reflection coefficient can be expressed strictly in terms of the impedances of the media involved. After the impedance curve is interpolated and resampled (at a sample interval equivalent to that at which the source signature was sampled), a reflection-coefficient log (Fig. 11) can easily be computed. As is typical of deep-sea carbonates, the reflection-coefficient structure is extremely complicated and has much fine structure beyond the resolution of conventional profiling systems. This reflection-coefficient log is convolved with the selected source signatures (the field-measured source signatures with and without a deconvolution filter applied to them) to generate a synthetic seismogram (Fig. 12). The synthetic seismogram is then filtered with the same bandpass filter as that used for the field data, and it is displayed on a similar scale for comparison. The modeling algorithm used to generate these synthetic seismograms assumes that we are dealing with normally incident plane waves, that no energy is lost to attenuation, and that interbed multiples play no significant role. The validity of these assumptions will be tested by comparing the synthetic seismogram with the field record.

Synthetic seismograms were generated by using both the raw source signature and a deconvolved operator (Fig. 12). To increase the signal-to-noise ratio and reduce shot-to-shot variations, three trace mixes were also calculated. Comparison of the synthetic with the field data (Fig. 13) shows generally good agreement for the major reflectors. The major differences are in the shape and amplitude of the reflections (e.g., Purple, Brown, and Red appear as several positive amplitude peaks in the synthetic and as only a single peak in the field data). This is not very surprising in view of the extremely short wavelength variation in the reflection-coefficient log (Fig. 11) and the number of uncertainties associated with this sort of comparison. As discussed earlier, and as demonstrated by Mayer (1979b), much of the reflection profile (and the synthetic profile) in deep-sea carbonates is an interference composite; subtle changes in the source function can have significant effects on the type of interference (e.g., compare the Green reflector in the raw source-function synthetic with that in the deconvolved source-function synthetic). More important, the slightest change or inaccuracy in the determination of the reflection-coefficient log will have a similar effect, and the absence of the inclusion of internal multiples and attenuation certainly degrades the synthetic. Although we believe that the low reflection coefficients

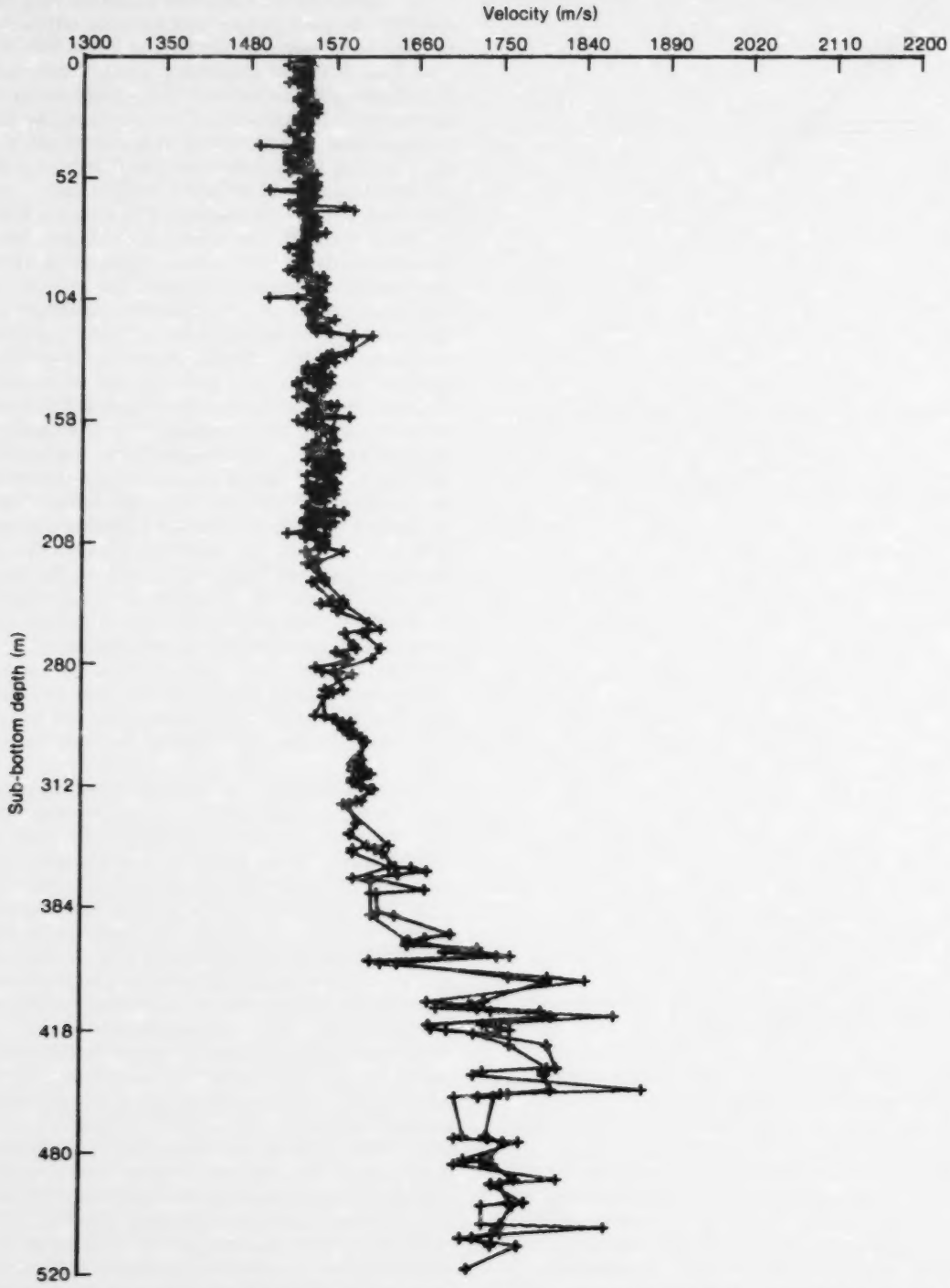

Figure 8. Predicted (from porosity) laboratory velocity versus sub-bottom depth and measured laboratory velocity versus sub-bottom depth, DSDP Site 574.

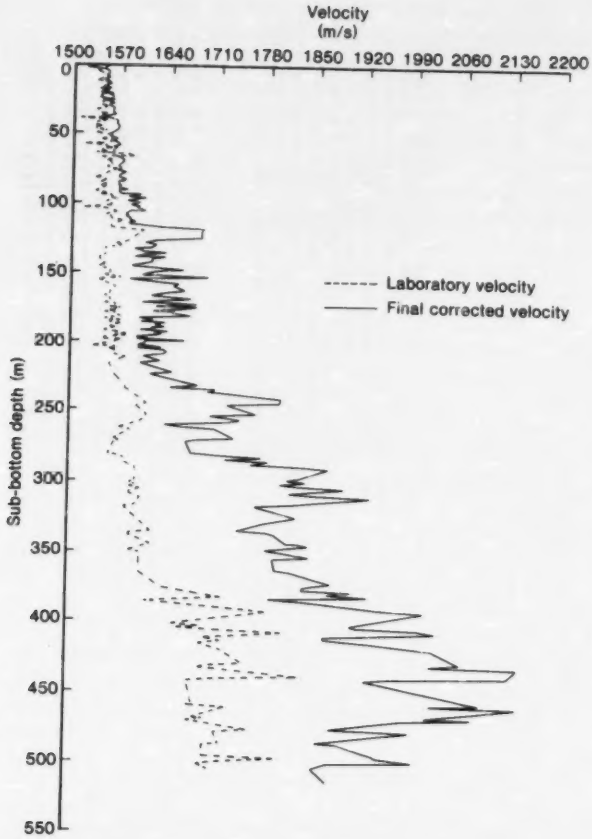

Figure 9. Laboratory velocity and final corrected velocity versus sub-bottom depth.

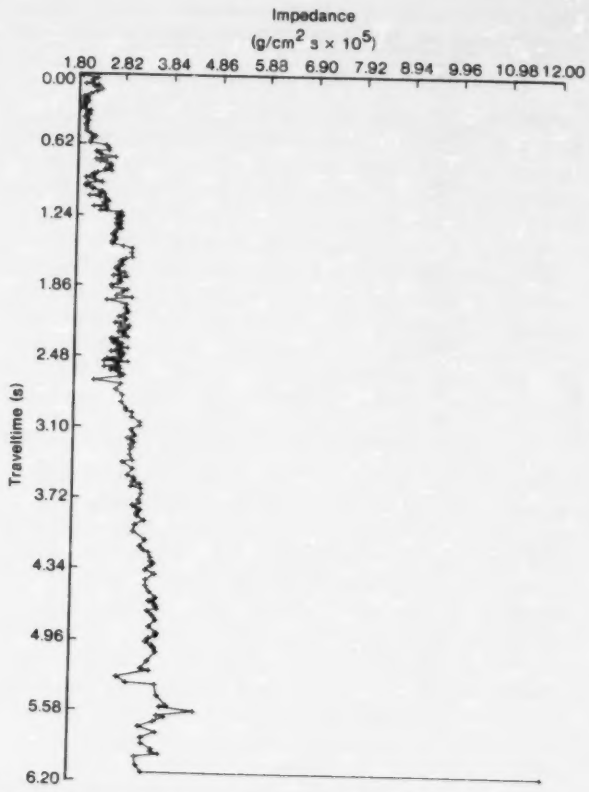

Figure 10. Impedance versus traveltime, DSDP Site 574.

calculated for this sediment (Fig. 11) will minimize any effect of internal multiples, a study of the role of attenuation and internal multiples in this particular sequence is currently under way.

Sources of Error

In addition to the errors associated with the conversion of traveltime to depth, numerous other factors add to the uncertainty of correlating the field seismic profile with the synthetic seismogram. First, the seismic profile does not precisely cross the drill site. The synthetic is placed near the closest point of approach on the profile where it best matches the field record. The lateral variability in the position of the major reflectors within the survey area is greater than any of the field record/synthetic mismatches of reflector positions, and thus the uncertainty of the location of the drill site with respect to the profile may contribute to any error. Second, the source signature was not monitored on every shot; rather, a representative signature is used for the synthetics. If the source signature when the profile across the drill site was collected differs from the representative signature, the synthetic will certainly differ from the field record. Finally, some error is probably associated with the inconsistent picking of horizons, because reflectors merge and separate as a function of sedimentation rate. Clearly, the synthetic is not a perfect match of the field record; all of the foregoing factors probably contribute to this imperfect matching. For the purpose of stratigraphic correlation, the traveltime to a given reflector, as picked from the field record, is used in the calculated velocity function to yield a depth-in-hole. This maximizes the potential stratigraphic miscorrelation for a given reflector but eliminates the possibility that the wrong reflector is being used. Despite these uncertainties, the major reflectors are clearly identifiable on the synthetic seismogram, and their positions are correlatable with the field record within about 0.01 s (approximately 8 m). This ability to correlate the synthetic with the field record suggests that we are not far off with our traveltime-to-depth conversion; and most important, it allows us to look at the measured downcore properties and determine precisely (within the limits of our resolution) where the reflectors occur.

ORIGIN OF REFLECTORS

Armed with an acceptable traveltime-to-depth conversion, we can now address the problem of the origin and geologic significance of the reflections. Our discussion is limited to the major traceable reflectors (those that have been assigned color names); the origin of the fine-scale reflection events will be addressed in future studies. Table 1 summarizes the traveltime picks of these

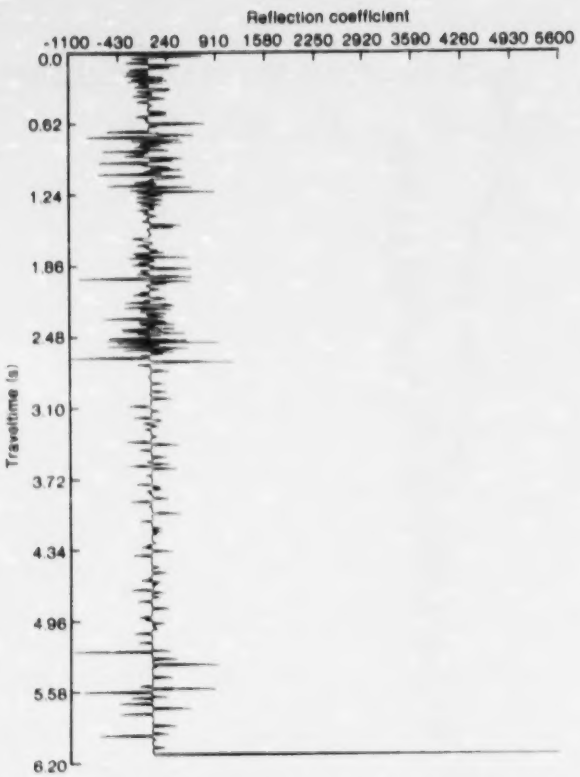

Figure 11. Reflection coefficient versus traveltime, DSDP Site 574.

reflectors from the field record and from the synthetic seismogram and reports the depths at which they occur as derived from our final corrected velocities.

The Site 574 impedance-versus-depth profile reveals that a significant shift or contrast in acoustic impedance is associated with each major reflector (Fig. 14). There are, however, numerous other large contrasts in impedance that are not associated with regionally correlatable reflectors (e.g., the impedance contrast at 121 m subbottom). To understand why some of these impedance contrasts result in regionally correlatable reflectors and others do not, we must take a closer look at the origin of the impedance contrasts. Impedance is the product of velocity and saturated bulk density. If we examine the relative contribution of each component by regressing velocity against impedance and density against impedance (Fig. 15), we see that there is an excellent correlation between density and impedance (Fig. 15A) but a poor linear correlation between velocity and impedance (Fig. 15B). The contrast can be explained by the relatively minor degree of fluctuation in sonic velocity (less than 6% of its mean value) and the significant degree of variation in saturated bulk density (more than 25% of its mean value). Thus, for the most part, the impedance curve is responding to fluctuations in saturated bulk density instead of velocity. To explain the changes in impedance, therefore, we need to understand the reasons for the changes in saturated bulk density.

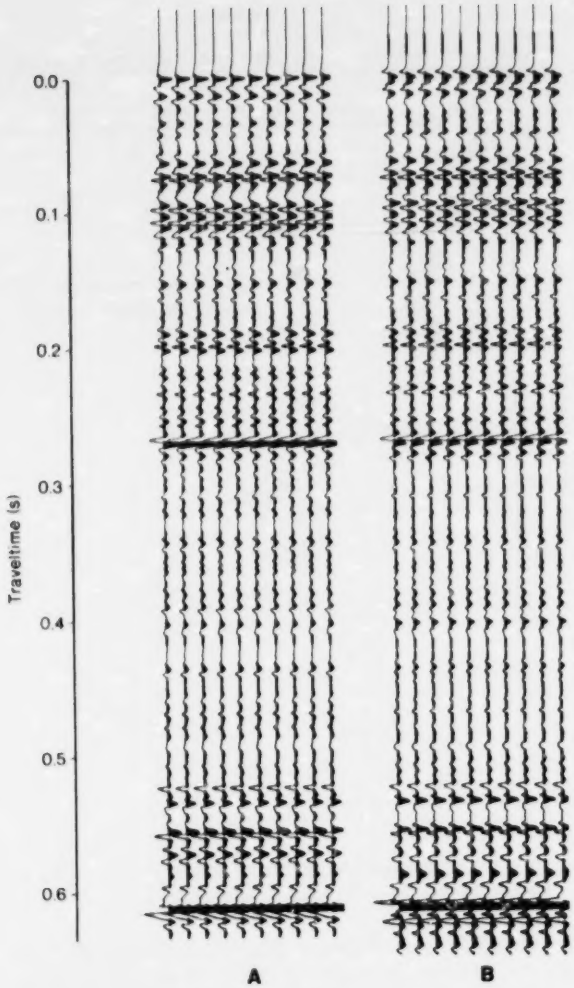

Figure 12. Calculated synthetic seismograms, DSDP Site 574. A. Deconvolved source signature. B. Raw source signature.

The dominant role of density in controlling the impedance curve (and thus the seismic profile) is evident when the positions of the major reflectors are marked on the density and velocity curves (Figs. 14B, C). All the major reflectors are associated with significant density contrasts, but only the deepest reflectors—Orange and Yellow—are associated with velocity contrasts. The cause of the density contrasts is clear when the carbonate curve (Fig. 14D) is compared with the density curve (Fig. 14C): a large change from high to extremely low carbonate values is associated with each of the major reflectors (except Yellow and Orange). In a detailed study of equatorial Pacific piston cores, Mayer (1979a) found a similar relationship and demonstrated that when the percentage of carbonate is low, the percentage of biogenic silica is very high, a composition that results in decreased saturated bulk density and thus decreased impedance. Thus, the Green, Brown, Purple, Red, and Lavender reflectors can be tied directly to major shifts in the carbonate con-

tent of the sediment. The two deeper reflectors (Yellow and Orange) are associated with minor carbonate shifts and pose a more difficult problem. The velocity curve (Fig. 14B), however, reveals that these reflectors are correlated with velocity changes; examination of the core descriptions reveals that the first occurrence of chalk is recorded at the depth of the Yellow reflector and that numerous small indurated layers are associated with the Orange reflector. Thus, these deeper reflectors appear to represent diagenetic changes. There are numerous other velocity events, occurrences of chalk, and associated reflectors deeper in the section, but these reflectors are not regionally correlatable. We believe that this phenomenon is explained by the concept of diagenetic potential, which was first introduced by Schlanger and Douglas (1974); that is, that the processes responsible for the smaller changes in carbonate content and sediment induration at the Yellow and Orange reflectors were regional in extent, whereas the processes responsible for the other velocity contrasts were more local. A prime example of this is the large velocity offset associated with the reflector, not regionally correlatable, located at 121 m subbottom. A density and impedance change is associated with this velocity contrast, but there is no change in percent carbonate. The core descriptions at this interval reveal a large increase in the abundance of sand-sized material (i.e., foraminifers), which results in increases in velocity, density, and impedance and suggests localized winnowing or redeposition.

AGE OF REFLECTORS

The association of the major reflectors with carbonate or diagenetic events suggests that the seismic record in this region may indeed contain important and retrievable paleoceanographic information. To evaluate the paleoceanographic significance of these reflectors, we used the Leg 85 biostratigraphic results (Barron et al., this volume) to assign ages to the reflectors (Table 2).

A detailed study of the stratigraphic resolution obtainable on Leg 85 cores (Pisias et al., this volume) indicates that resolution varies with sedimentation rate but that for the closest sampling interval used, it can be taken to be approximately 4 m (125,000 to 380,000 yr.). Because the resolution of our reflector correlations is less than this (± 5 m), we conservatively report the ages plus or minus 500,000 yr. A uniform time scale incorporating an Anomaly 5–Chron 9 correlation was used for all the Leg 85 analyses; but Barron et al. (this volume) propose an alternative middle to late Miocene time scale based on an Anomaly 5–Chron 11 correlation. This latter interpretation may prove to be more accurate, and we present alternative absolute ages based on this correlation in parentheses in Table 2. More detailed stratigraphic work may permit the further refinement of the absolute ages of the reflectors.

We have made similar analyses of Sites 573 and 575, and the ages of the regionally traceable reflectors are, within the limits of our resolution, identical to those determined for Site 574. Thus, the reflectors are essentially time surfaces; their association with carbonate or regional diagenetic events suggests that they are related to major changes in oceanographic parameters that operated over a large area and over a wide range of depths.

PALEOCEANOGRAPHIC SIGNIFICANCE

If, as we believe, the major traceable reflectors represent time surfaces associated with basinwide carbonate or diagenetic events, it becomes appropriate to attempt to identify these events and to assess their paleoceanographic significance. The speculations below are based on the identification (from Leg 85 results and previous studies) of significant changes in oceanographic parameters that took place at or near the same time as the seismic events. These correlations are general; the detailed biostratigraphic analyses necessary to establish precise relationships are beyond the scope of this study, but will, we hope, be the subject of future work.

Orange and Yellow (20.5 to 22.5 Ma)

The Miocene was a time of critical climatic transition, and as such it has been the subject of numerous paleoceanographic studies (e.g., Savin et al., 1981, and references therein). Little detailed work has been done on the early Miocene; we are less confident of our correlation between reflectors Y and O and paleoceanographic events than we are for the younger horizons, but it is still possible to identify paleoceanographic events that may have been responsible for these reflectors. Vincent and Killingley (this volume) have identified eight levels within the middle and lower Miocene at which there are significant changes in the isotopic and carbonate record at the Leg 85 sites. The deepest of these two levels (events A and B; Vincent and Killingley, this volume) correlate well with the positions of the Orange and Yellow reflectors. These levels are marked by an increase in $\delta^{13}C$ (1.0‰) for A, a decrease in $\delta^{13}C$ (0.2‰) for B, and an increase in the percent sand. In general, the interval between A and B is one of high $\delta^{13}C$ values. Small changes in percent carbonate are associated with these levels, although the changes are nowhere near as large as those associated with the younger reflectors. As discussed earlier, the Orange and Yellow reflectors differ significantly from the younger ones in that they are associated with significant changes in velocity. We infer from this that they are diagenetic in origin, an inference supported by the presence of chalk and indurated layers at these depths. The coincidence of regionally traceable reflectors of diagenetic origin with the regional isotopic events described by Vincent and Killingley suggests the occurrence of significant oceanographic changes. Keller (1981) describes a major reorganization of planktonic foraminifers, marking the evolution of the highly diverse Neogene fauna, that took place during the early Miocene. This reorganization is linked to the development of the deep Circum-Antarctic Current, which resulted from the opening of the Drake Passage by about 22.5 Ma (Kennett et al., 1975), and to the establishment of steep thermal gradients between polar and tropical regions (Kennett, 1977; Keller, 1981). Although we cannot, at this point, draw specific links between the lower Miocene reflectors and identifiable oceanographic events (other than the isotopic shifts), we can speculate that the reorganization of the

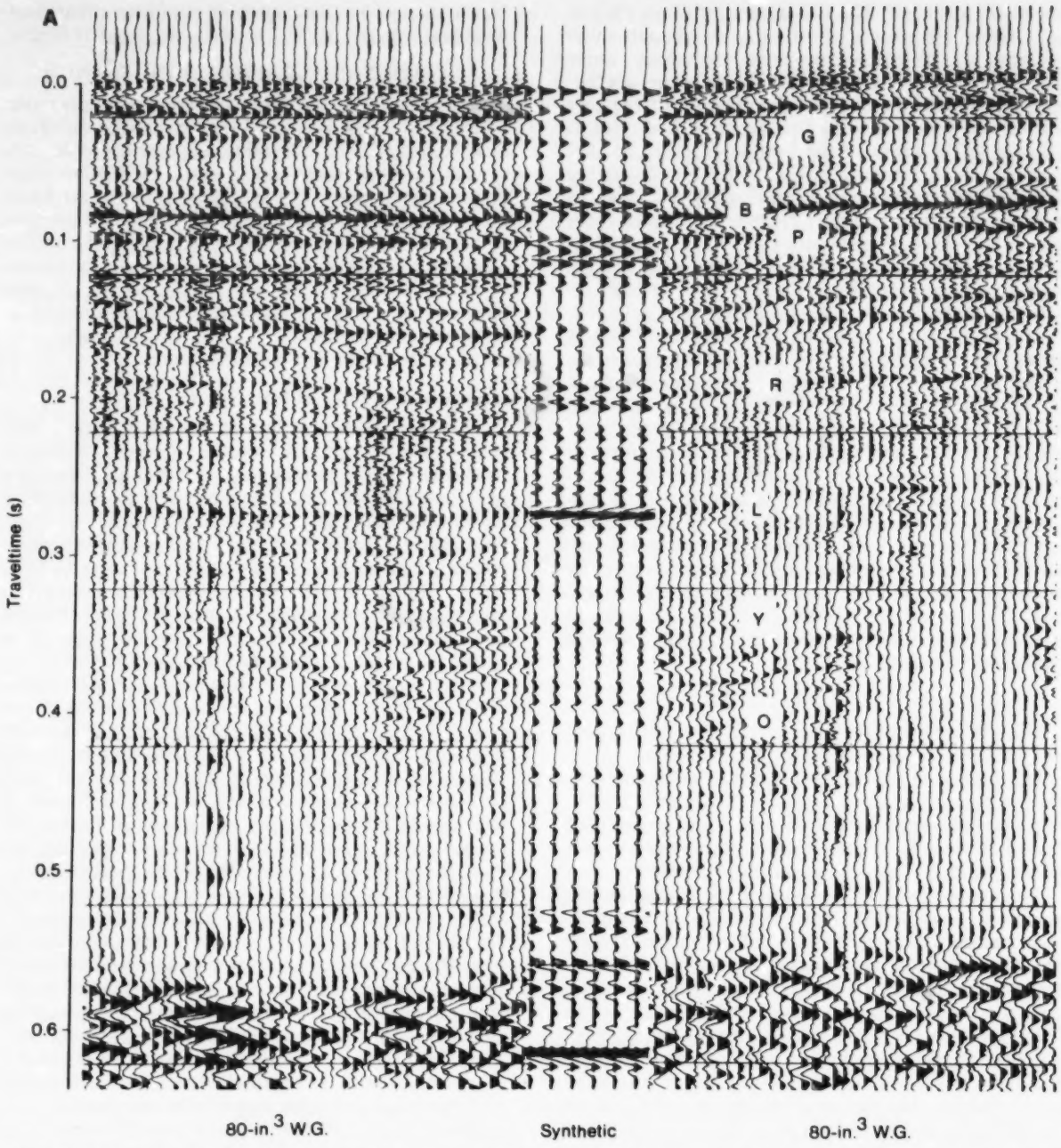

Figure 13. Comparisons of field data with synthetic seismograms. W.G. = field watergun record. A. Deconvolved source, no mix. B. Deconvolved source, 3-trace mix. C. Raw source, no mix. D. Raw source, 3-trace mix.

oceanic circulation system associated with the opening of Drake Passage resulted in changes in the chemistry of tropical Pacific waters that account for the isotopic shifts and the propensity of this material to indurate. The induration associated with this material accounts for the changes in velocity and saturated bulk density that result in the impedance contrasts responsible for the Orange and Yellow reflectors.

Lavender (16 to 17 Ma)

There is an unequivocal association of the Lavender reflector with a major, sharp, early Miocene decrease in carbonate content that occurs at approximately 213 m sub-bottom (Fig. 14). This carbonate minimum has been reported previously (event 16g of Dunn, 1982), and it is correlatable over much of the equatorial Pacific (Dunn,

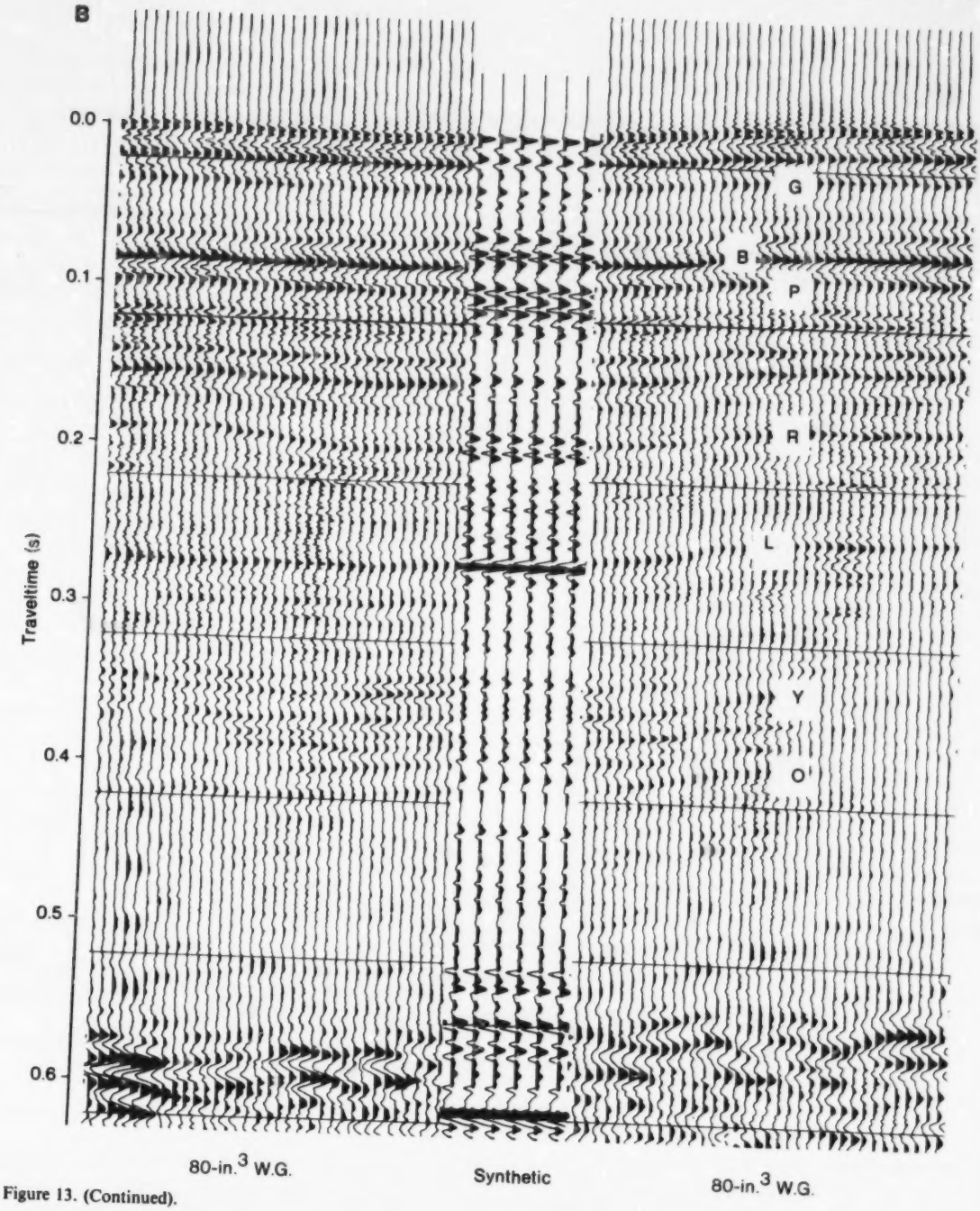

Figure 13. (Continued).

in press). Coincident with this carbonate minimum is the beginning of a marked enrichment (about 1‰) in $\delta^{13}C$—the level E event of Vincent and Killingley (this volume). This $\delta^{13}C$ enrichment has been identified in numerous Indian Ocean cores and labeled the "Chron 16 carbon shift" by Vincent et al. (1983). The beginning of this shift predates the cessation of an early Miocene warming trend (event F of Vincent and Killingley, this volume), as seen in the $\delta^{18}O$ signal (Savin et al., 1981), and it is attributed to the accumulation around the North Pacific margins of organic-carbon-rich sediments that preferentially extract ^{12}C from the ocean (Vincent et al., 1983). Also associated with this period is the occurrence of a widespread hiatus (NH2), which is interpreted as being the result of intensified bottom flow (Keller and Barron, 1983). Unlike the younger carbonate minima,

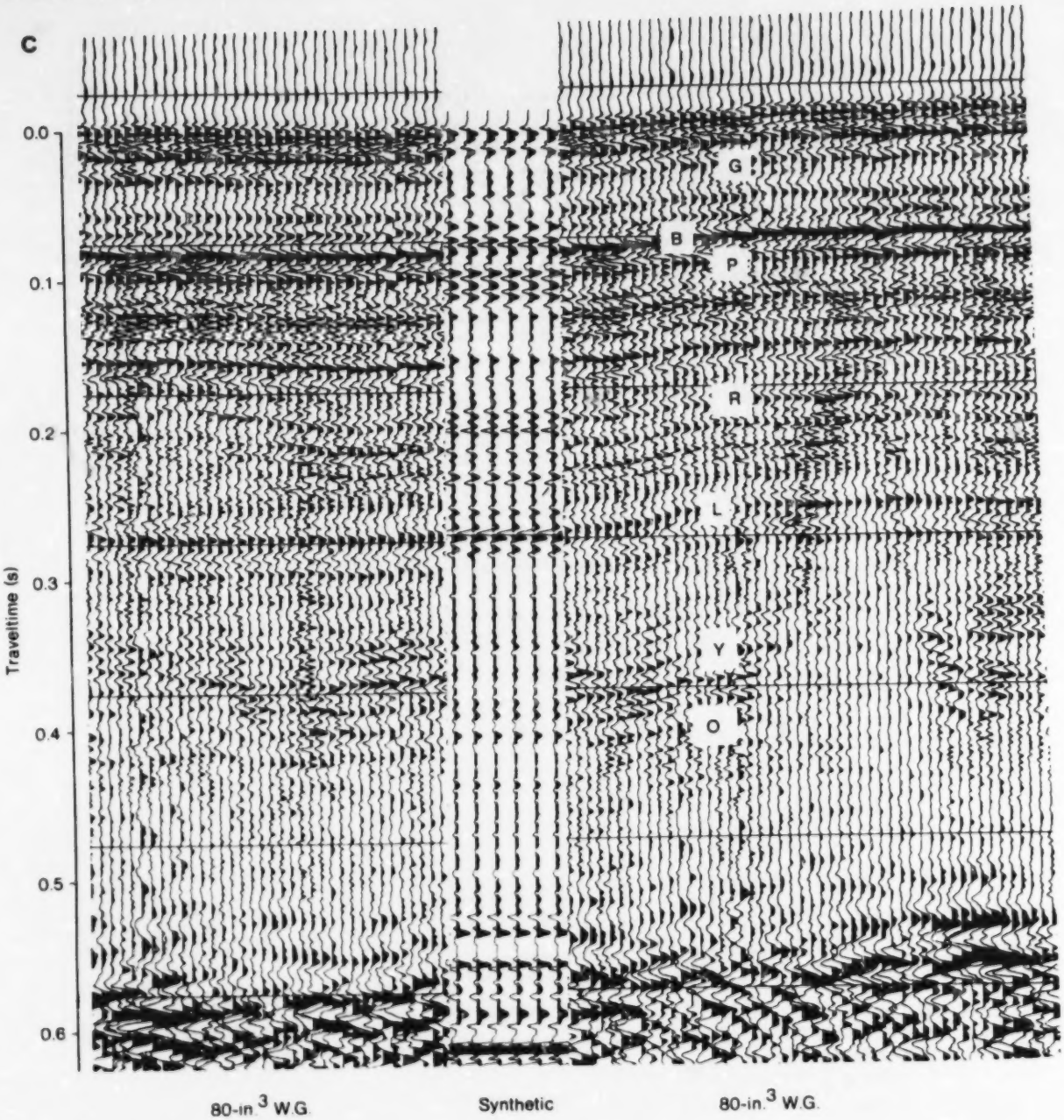

Figure 13. (Continued).

the "dissolution spike" associated with the Lavender reflector is not also associated with a $\delta^{18}O$ enrichment (in fact, bottom waters at this time were the warmest of the Miocene; Savin et al., 1981), so the Lavender reflector is the only post-18 Ma reflector that is not correlated with an apparent climatic deterioration. Also coincident with the timing of the Lavender reflector are the onset of significant siliceous-ooze deposition in the equatorial Pacific and North Pacific margins, a decline in the deposition of siliceous sediment in the North Atlantic (Keller and Barron, 1983), and a sharp rise and fall in eustatic sea level as determined by Vail and Hardenbol (1979).

The absence of climatic cooling, in association with a sharp decrease in carbonate content, tends to support the hypothesis of Keller and Barron (1983) that tectonic events (perhaps the closing of the Tethyan Seaway, uplift in Central America, and the sinking of the Iceland–Faroe Ridge), in concert with eustatic sea-level fluctuations, may ultimately have caused the changes in circulation patterns that resulted in the introduction or intensifica-

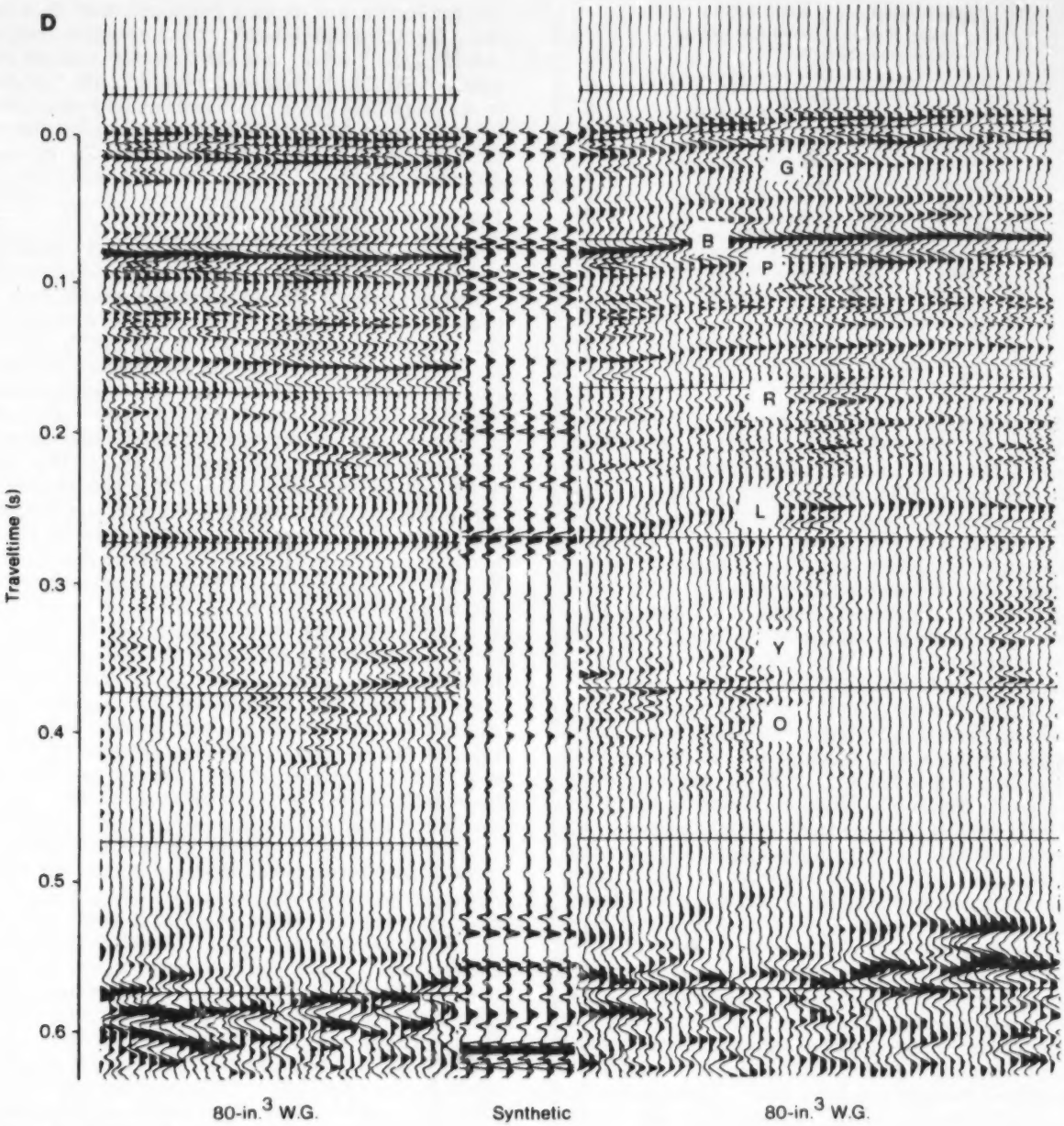

Figure 13. (Continued).

tion of Norwegian Overflow Water into the North Atlantic. This southward incursion of North Atlantic Deep Water decreased the amount of upwelling of Antarctic Bottom Water in the Atlantic and provided more of this silica-rich bottom water to the Pacific (Berger, 1970; Keller and Barron, 1983). The intensification of AABW circulation in the Pacific resulted in severe carbonate dissolution and thus the Lavender reflector. Increased upwelling of AABW in the equatorial Pacific and Pacific margins led to the rapid extraction of organic carbon from the ocean–atmosphere system and to the beginning of the "Monterey carbon excursion" of Vincent and Berger (in press), which may explain the onset of global cooling.

Red (13.5 to 14.5 Ma)

As with all of the pre–18 Ma reflectors, the impedance contrast associated with the Red reflector results from a carbonate minimum (Fig. 14). Once again, this carbonate minimum has been identified in other equatorial Pacific cores and shown to be regionally correlatable (event 15c of Dunn, in press). The timing of this

Table 1. Traveltime to major reflectors as picked from field record and synthetic seismogram, Site 574.

Reflector	Traveltime (s)		Depth in section[a] (m)
	Field record	Synthetic	
Green	0.03	0.031	24
Brown	0.08	0.075–0.08	58–62
Purple	0.098	0.093–0.103	72–80
Red	0.193	0.188–0.195	147–155
Lavender	0.267	0.268	213
Yellow	0.365	0.362–0.367	290–300
Orange	0.410	0.403	325–335
Basement	0.6025	0.611	520

[a] Depth in section is depth calculated using the field record traveltime and the calculated velocity-versus-depth function.

event is coincident with the occurrence of a widespread hiatus (NH3; Keller and Barron, 1983), a major change (drop in sea level?) in the coastal-onlap curve of Vail and Hardenbol (1979), and significant changes in planktonic and benthic foraminiferal assemblages (Keller, 1980; Woodruff et al., 1981) as well as diatom assemblages (Barron, this volume). Significant changes in benthic faunas at Site 574 are not clearly associated with the increase in $\delta^{18}O$, however (Thomas, this volume). More striking is the correspondence of this reflector with the very rapid increase in ^{18}O reported by Savin et al. (1975), Shackleton and Kennett (1975a and b), Savin et al. (1981), and Woodruff et al. (1981). This isotopic shift has been associated with high-latitude cooling and the buildup of ice on Antarctica, although Matthews and Poore (1980) argue for a drop in temperature of the deep waters rather than the substantial buildup in Antarctic ice.

An extremely detailed study (sample interval representing 3000 yr.) of the carbon, oxygen, and carbonate stratigraphy of the interval spanning the Red reflector was conducted by Pisias and Shackleton (this volume). They determined that the major $\delta^{18}O$ shift (approximately 1‰) representing this oceanic event occurred in the remarkably short interval of 30,000 yr. and is recorded precisely (within the limits of our resolution) at the depth of the Red reflector (155 m). Pisias and Shackleton (this volume) use the high degree of variability in the isotopic record before this middle Miocene event to hypothesize significant variations in ice volume, although they acknowledge that a radically different deep-water structure before 14.5 Ma could also explain the variability.

Thus, the increase in AABW associated with climatic degradation, and probably with the rapid buildup or increase in volume of Antarctic ice, resulted in increased carbonate dissolution and the Red reflector. It is interesting that the carbonate minimum associated with this major oceanic event is much less pronounced than that associated with the Lavender reflector (and the younger ones). We speculate that carbonate remains comparatively stable because no North Atlantic Deep Water event is associated with this time interval. When NADW becomes intensified, it forms a lid on AABW in the Atlantic (as with the Lavender, Purple, and Green reflectors—see discussion following); more, silica-rich AABW is put into the Pacific, and we see a fractionation of silica between the Atlantic and Pacific and an overall increase in upwelling, productivity, and silica deposition in the Pacific. AABW during these times is particularly corrosive to carbonate, and extreme carbonate minima result. The Lavender event, however, is the response to just the intensification of AABW, and it results in a less extreme carbonate minimum.

Purple (11 to 12 Ma or 8.5 to 9.5 Ma)

The Purple reflector is associated with the most extreme of the carbonate minima (from 80 to 2% $CaCO_3$), a mechanism clearly likely to generate an impedance contrast. More significantly, this event marks a change in the style of carbonate deposition in the Pacific. Before the Purple event, carbonate values are generally high, with small-amplitude fluctuations (except for occasional events like Lavender); after Purple, there are large, high-amplitude, high-frequency swings in carbonate content reminiscent of Pleistocene dissolution cycles. This shift in the style of carbonate deposition is also associated with a major sediment color change, and it marks a major lithologic boundary (cyclic siliceous calcareous ooze to calcareous ooze chalk—see Site 574 site chapter, this volume). As with the other carbonate minima, this event has been previously reported and correlated over a large area of the equatorial Pacific (mid-Epoch 10, Vincent, 1981). Associated with this event are a widespread hiatus (NH4, Keller and Barron, 1983), an increase in provincialism between low- and high-latitude planktonic microfossil assemblages (Barron, this volume; Bukry, this volume), and an apparent fall in eustatic sea level (Vail et al., 1977). Detailed isotopic analyses have not yet been performed on Leg 85 samples over this interval, but generalized equatorial Pacific isotope curves presented by Savin et al. (1981) and Woodruff et al. (1981) clearly show an enrichment (about 0.5‰) in $\delta^{18}O$ at this time. Approximately coincident with this interval is a major erosional event that can be identified in North Atlantic seismic profiles (Mountain and Tucholke, 1983; Tucholke and Laine, 1982), which is interpreted as resulting from an intensification of North Atlantic bottom-water circulation. This event directly predates the onset of major drift deposition in the western North Atlantic.

The resulting paleoceanographic scenario is therefore similar to that described for reflector Lavender. An intensification of NADW (and an associated global cooling) resulted in the southward spread of NADW, causing decreased deposition of silica in the Atlantic and increased deposition of siliceous material in the Pacific (Keller and Barron, 1983). Intensified, highly corrosive AABW in the Pacific results in the carbonate minimum and the Purple reflector. The climatic degradation results in the intensification of the Equatorial Undercurrent system and the establishment of the steep latitudinal thermal gradients that have characterized the Pacific since this time (Barron, this volume).

Brown (7 to 8 Ma or 6.5 to 7.5 Ma)

The Brown reflector is more difficult to correlate with paleoceanographic events than the others. The reflector

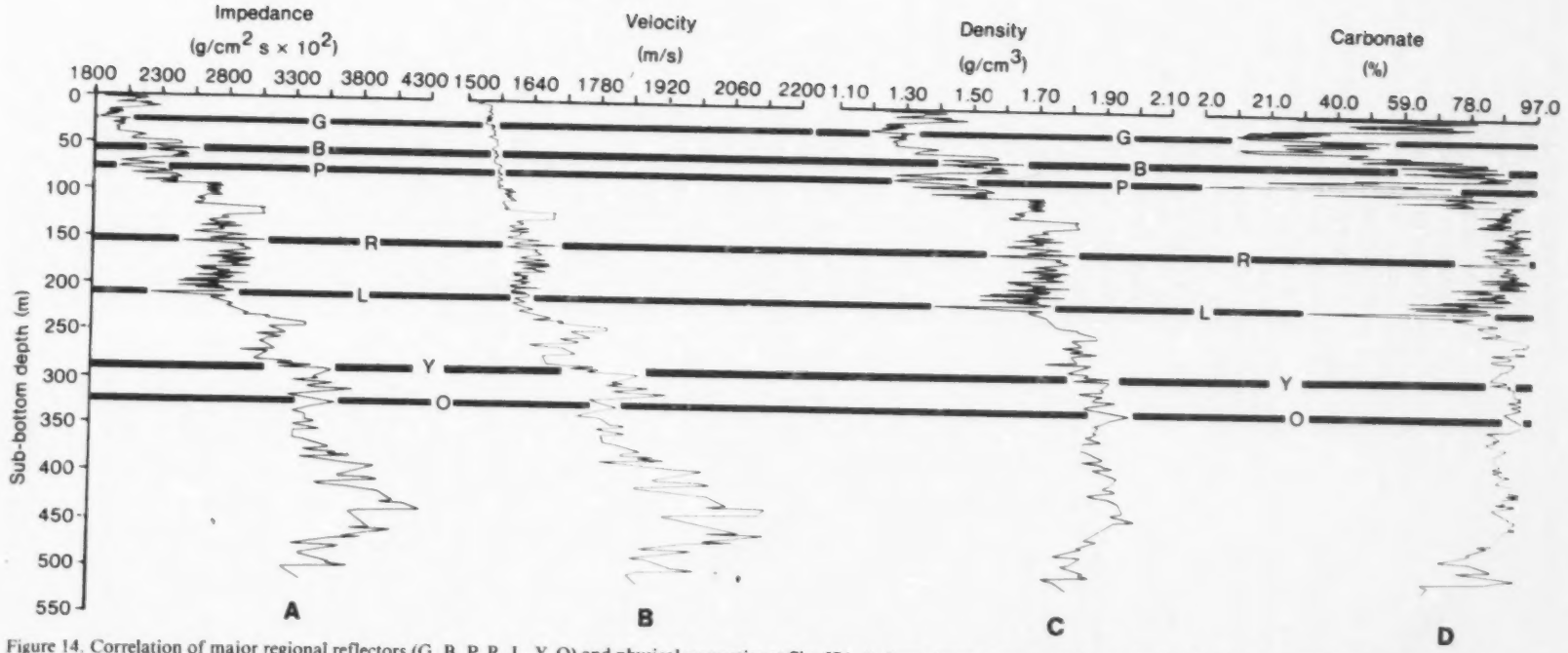

Figure 14. Correlation of major regional reflectors (G, B, P, R, L, Y, O) and physical properties at Site 574. A. Impedance versus sub-bottom depth, Site 574. B. Sonic velocity versus sub-bottom depth, Site 574. C. Saturated bulk density versus sub-bottom depth, Site 574. D. Percent carbonate versus sub-bottom depth, Site 574.

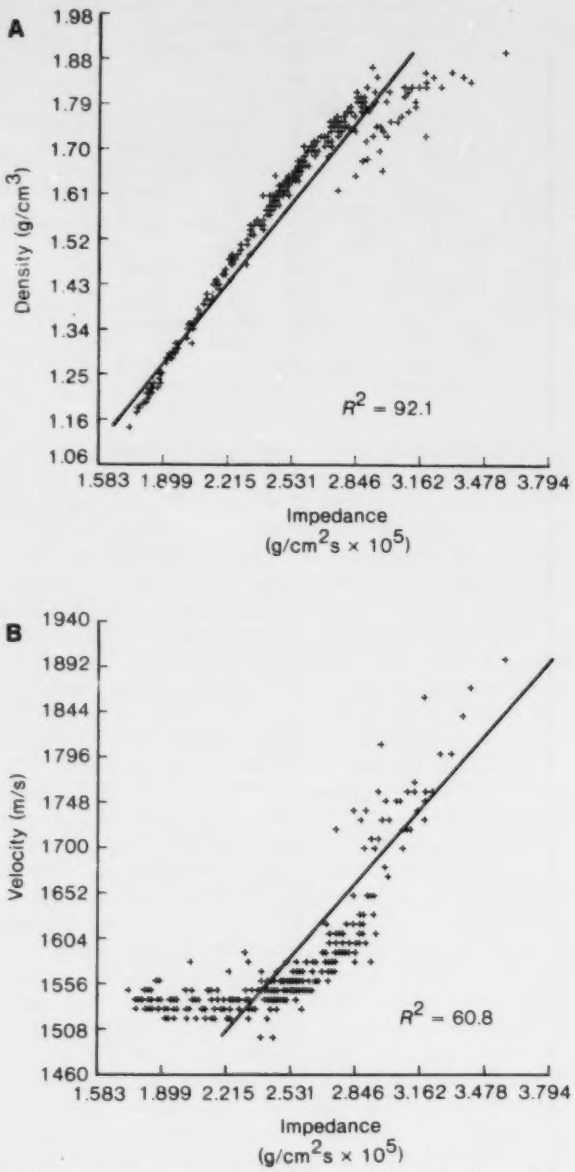

Figure 15. Correlation between density, velocity, and impedance. Solid line represents linear regression; R^2 = correlation coefficient. A. Regression of impedance against density, Site 574. B. Regression of impedance against velocity, Site 574.

does correlate with a small carbonate minimum, but this minimum is one of several in a region of generally high carbonate values (Fig. 14). These closely spaced carbonate fluctuations cause a complicated impedance structure that results in a complex reflector structure at this level on the synthetic seismogram (Fig. 13). It is just this sort of closely spaced structure that is most susceptible to interference effects, because small inaccuracies can result in miscorrelations.

In terms of paleoceanographic events, the Brown reflector is roughly coincident with a worldwide hiatus (NH6, Keller and Barron, 1983), the onset of a permanent $\delta^{13}C$ depletion (Keigwin, 1979; Vincent et al., 1980), a shoaling of the carbonate compensation depth (CCD) (van Andel et al., 1975), a major change in the relative sea-level curve (Vail et al., 1977), general climatic cooling (Woodruff et al., 1981), and a major faunal change in benthic foraminifers in the western Pacific (Woodruff and Douglas, 1981).

The constraints imposed by limited resolution are clearly evident when we look at the Brown reflector. The depth-in-hole chosen for the Brown reflector on the basis of the field record is a few meters below a major carbonate shift. Close examination of the field seismic record (Fig. 13) reveals another reflector several meters above the Brown reflector that varies appreciably in amplitude over even the small lateral distance represented by this section. Despite the amplitude variations in the field record, the synthetic seismogram shows this reflector as a significant event (0.061 ms; 44 to 48 m sub-bottom, Fig. 13). The major carbonate shift occurs at about the this same depth (Fig. 14). The carbonate shift is coincident with the regionally correlatable carbonate event (6e; Vincent, 1981), that is associated with the Epoch 6 carbon-isotopic depletion. A more detailed analysis of both the seismic section and the stratigraphic relationships will be necessary to resolve this problem.

Green (3 to 4 Ma)

The youngest of our regionally correlatable reflectors (Green) presents few of the problems associated with the Brown reflector, despite the severe attenuation of this part of the section and the difficulty of distinguishing the Green reflector from the Magenta reflector (dated at 5 to 5.5 Ma), which is visible at the other Leg 85 sites. The Green reflector is clearly associated with a large carbonate minimum that results in a relatively large impedance contrast and can be tied into existing carbonate stratigraphies (Prell, this volume). Associated with the timing of this Pacific carbonate event is the major North Atlantic erosional event, which was followed by the onset of substantial turbidite deposition (Tucholke and Laine, 1982), an apparent eustatic sea-level drop (Vail et al., 1977), and a ubiquitous eastern Atlantic seismic reflection (J. Mienert, pers. comm., 1984).

We are tempted also to correlate the Green reflector with the initiation of Northern Hemisphere glaciation, as determined by ice-rafted sediments (Berggren, 1972) and $\delta^{18}O$ trends (Shackleton and Kennett, 1975a; Shackleton and Opdyke, 1977; Keigwin, 1979). These studies report an enrichment in benthic $\delta^{18}O$ of approximately 0.4‰ at about 3.2 Ma and an association with the closing of the Isthmus of Panama. Prell (this volume), however, after looking at the detailed (5000-yr. sample interval) isotopic record from DSDP Site 572, argues that a steplike enrichment in $\delta^{18}O$ is not found in the benthic record at 3.2 Ma (although a broad increase is found in the planktonic record). He infers from these data that, although a short ice growth may have occurred at this time, no permanent addition of ice volume was initiated. Instead, he postulates the establishment of colder bottom waters at this time, perhaps with an Antarctic

Table 2. Sub-bottom depths, biostratigraphic zones, and ages for major reflectors at DSDP Site 574.

	Sub-bottom depth (m)	Foraminifers	Calcareous nannofossils	Radiolarians	Diatoms	Age (Ma)[a]
Green	24	N19	CN11	*Spongaster pentas*	*Nitzschia jouseae*	3–4
Brown	58–62	N17	CN8	*Didymocyrtis pentultiima/ Didymocyrtis antepenultima*	*Nitzschia porteri*	7–8 (6.5–7.5)
Purple	72–80	? (N16–N14)	CN7	*Diartus petterssoni*	*Asteromphalus moronensis*	11–12 (8.5–9.5)
Red	147–155	N10	CN4	*Dorcadospyris alata*	*Coscinodiscus lewisianus*	13.5–14.5
Lavender	213	? (N8–N6)	CN3	*Calocycletta costata*	*Denticula nicobarica*	16–17
Yellow	230–300	N4	CN1	*Stichocorys delmontensis/ Cyrtocapsella tetrapera*	*Rossiella paleacea*	20.5–21.5
Orange	325–335	N4	CN1	*Cyrtocapsella tetrapera/ Lynchnocanoma elongata*	*Rocella gelida*	21.5–22.5

[a] Ages are based on Leg 85 time scale (see Introduction, this volume). Ages in parentheses represent alternative time scale using an Anomaly 5–Chron 11 correlation (see Barron et al., this volume).

source (Prell, this volume). The seismic record cannot resolve this controversy; it can only indicate that a globally synchronous event (or series of events) took place that resulted in current-controlled sedimentation in the Atlantic and enhanced carbonate dissolution in the Pacific.

CONCLUSIONS

The combination of high-resolution seismic reflection profiles and continuous, nearly undisturbed cores produced by DSDP Leg 85 site surveys and drilling have presented us with a unique opportunity to examine the paleoceanographic significance of the seismic record. We have identified eight major, regionally traceable reflectors (labeled Orange, Yellow, Lavender, Red, Purple, Brown, Green, and Magenta) that can be traced around a 360,000-km^2 area of the central equatorial Pacific, bounded by the Clipperton and Galapagos fracture zones. The seismic section in this region is typical of that for pelagic carbonates; pelagic drape is the dominant geometry, but numerous erosional and slump features are also present. To examine the origin and paleoceanographic significance of the major, traceable reflectors, we have focused our study on DSDP Site 574, where seven of the eight reflectors are easy to identify and core recovery and core quality were excellent.

Essential to the geologic interpretation of the seismic record is the ability to transform the seismic information (a time-domain record) into a depth-domain record that can be directly compared with downhole stratigraphies. This transformation assumes accurate knowledge, not readily available, of the *in situ* velocity structure. We concentrated efforts on converting the laboratory-determined velocity and density values to *in situ* values and made corrections for porosity rebound and changes in temperature and pressure. These corrections are significant (8 to 10% for the deepest samples); without them, the correlation of the seismic record with borehole results would be impossible. Synthetic seismograms—generated by using the corrected physical property values and a field-measured source signature—showed excellent agreement with the field records, suggesting that our traveltime-to-depth conversion is accurate and allowing us to determine precisely where in the cored section the reflectors occur (within the limits of our resolution [± 5 m]).

The origins of the impedance contrasts responsible for the major traceable reflectors reveal that, for the most part, impedance contrasts are dominated by changes in saturated bulk density rather than velocity. All except the two oldest regionally traceable reflectors at Site 574 are associated with distinct density contrasts that correlate with carbonate minima. There are other strong reflectors in the section that are not regionally traceable. These reflectors, however, are not associated with carbonate minima, but correlate instead with velocity and grain-size contrasts. We interpret these reflectors as representing more local events, perhaps responses to localized winnowing and redeposition. Thus, in the younger part of the section, two distinct types of reflectors are present: those resulting from major, regionally traceable carbonate events, and those, caused by velocity contrasts, that are more local in their extent. In the deeper part of the section, most reflectors are associated with velocity contrasts and changes in induration. We conclude that the two regionally traceable reflectors in this part of the section result from basinwide events that caused more rapid induration of the sediment at these levels.

Comparison of the stratigraphic positions of the major regionally traceable reflectors with the Leg 85 time scale permits the assignment of ages (± 500,000 yr.) to each of the reflectors. These ages are as follows: Orange, 21.5 to 22.5 Ma; Yellow, 20.5 to 21.5 Ma; Lavender, 16 to 17 Ma; Red, 13.5 to 14.5 Ma; Purple, 11 to 12 Ma; Brown, 7 to 8 Ma; and Green, 3 to 4 Ma. Similar analyses at the other Leg 85 sites reveal that, within the limits of our resolution, the ages of these reflectors are identical at all sites. Thus, the reflectors are time surfaces (at least within our study area), and their association with carbonate or diagenetic events suggests that they are related to major changes in ocean chemistry that operated over a wide range of depths.

The Orange and Yellow reflectors are associated with a marked increase in $\delta^{13}C$, a major reorganization of planktonic foraminiferal assemblages, the development of the deep Circum-Antarctic Current, and the establish-

ment of steep thermal gradients between tropical and polar regions. This reorganization of the oceanic circulation system was probably a response to the opening of the Drake Passage, and it resulted in changes in the chemistry of tropical Pacific waters that caused the induration (and thus the impedance contrasts) associated with these reflectors.

The Lavender reflector is associated with a large carbonate minimum, the "Chron 16 carbon shift," a widespread hiatus (NH2), major eustatic sea-level fluctuations, and a significant increase in silica deposition in the Pacific. Unlike the other reflectors, Lavender is not associated with a $\delta^{18}O$ enrichment or climatic cooling. We conclude that this event represents intensification of AABW circulation and the partitioning of silica between the Atlantic and the Pacific, resulting from the introduction of NADW in response to tectonic events. Increased Pacific upwelling associated with intensified silica-rich AABW circulation may account for the beginning of the "Monterey carbon excursion" (Vincent and Berger, in press) and the onset of global cooling in the middle Miocene.

The Red reflector is associated with a subdued carbonate minimum, a widespread hiatus (NH3), a sea-level drop, significant changes in microfossil assemblages, and a major increase in $\delta^{18}O$ that has been linked with the buildup or increase in volume of Antarctic ice. Detailed isotopic analyses (Pisias and Shackleton, this volume) reveal that this isotopic shift occurred within an interval of 30,000 yr. and precisely at the depth of the Red reflector.

The Purple reflector is associated with an extremely large carbonate minimum, a change in the style of carbonate deposition in the Pacific, a major lithologic boundary, a widespread hiatus (NH4), an increase in the provincialism between low and high latitudes in all planktonic microfossil assemblages, an apparent fall in eustatic sea level, an enrichment in $\delta^{18}O$, and a major North Atlantic reflection interpreted as representing an intensification of North Atlantic bottom-water circulation. Once again we call upon the intensification of NADW, resulting in highly corrosive AABW, to account for the extreme carbonate dissolution in the Pacific and the Purple reflector.

The Brown reflector is associated with a small carbonate minimum, an enrichment in $\delta^{18}O$, the late Miocene $\delta^{13}C$ depletion, a drop in the relative sea-level curve, and faunal changes. A large carbonate minimum and a strong reflector that precisely correlate with the timing of the ^{13}C event are clearly seen on our synthetic seismograms a few meters above the Brown reflector. More detailed analyses of both the seismic section and stratigraphic relationships will be necessary to resolve this discrepancy.

The Green reflector is associated with a large carbonate minimum and with enrichment in $\delta^{18}O$, a major western North Atlantic erosional event, and a ubiquitous eastern Atlantic seismic reflector. The bulk of evidence supports a correlation with the onset of Northern Hemisphere glaciation, but detailed isotopic analyses (Prell, this volume) indicate that this event may be linked to the establishment of colder bottom waters without major ice-sheet development.

In beginning this study, we set out to evaluate the potential of high-resolution seismic stratigraphy as a paleoceanographic tool in the central equatorial Pacific. We have been surprised by the impressive correlations that have resulted. We have seen that there are several types of reflectors in the equatorial Pacific. In the older (lower Miocene) section, reflectors resulted from diagenetic effects, and the regional reflectors were caused by global events. In the younger section (postdating lower Miocene), local reflectors are characterized by velocity contrasts, whereas regional reflectors are associated with density contrasts resulting from carbonate minima and global oceanographic changes. We have identified two modes for the generation of equatorial Pacific–wide carbonate minima and subsequent reflectors. The first mode calls for the intensification of AABW without concurrent intensification of NADW and without subsequent partitioning of silica between the Atlantic and the Pacific. This mode results in less extensive carbonate minima (the Red reflector). The second mode involves the intensification of AABW in response to the intensification of NADW and the associated enrichment of silica in the Pacific. This mode results in extreme carbonate minima and a correlation of Pacific reflectors with North Atlantic events (Lavender, Purple, Brown[?], and Green). Each of these types (local or regional, NADW-associated or not) is identifiable strictly from close study of the interrelationships among the physical properties responsible for the reflectors.

More important, we have established that careful analysis of the seismic record can be a powerful paleoceanographic tool. The results of this study will now permit us to trace identifiable, dated, synchronous events over large regions of the central equatorial Pacific. As the resolution of our profiling systems and stratigraphic analyses improves, our ability to link seismic features to paleoceanographic events will also improve (e.g., the result of very detailed sampling that correlates the Red reflector with a 30,000-yr. event), and the sometimes vague correlations we have established will become more precise. The seismic record is, by nature, the response to sharp contrasts. It is therefore an ideal tool for evaluating the already established "climatic steps" (Berger, 1982) in the Earth's history, and it may, in the future, provide a mechanism for identifying paleoceanographic events as yet undiscovered.

REFERENCES

Arrhenius, G., 1952. Sediment cores from the East Pacific. *Rep. Swed. Deep Sea Exped. (1947–1948)*, 5:1–228.

Berger, W. H., 1970. Biogenous deep-sea sediments: fractionation by deep-sea circulation. *Geol. Soc. Am. Bull.*, 81:1385–1402.

_____, 1973. Cenozoic sedimentation in the eastern tropical Pacific. *Geol. Soc. Am. Bull.*, 84:1941–1954.

_____, 1982. Climate steps in ocean history—lessons from the Pleistocene. *In* Berger, W. H., Crowell, J. C., et al. (Eds.), *Climate in Earth History, Studies in Geophysics:* Washington (National Academy Press), pp. 43–53.

Berger, W. H., and Heath, G. R., 1968. Vertical mixing in pelagic sediments. *J. Mar. Res.*, 26(2):134–143.

Berger, W. H., Johnson, T. C., and Hamilton, E. L., 1977. Sedimentation on Ontong Java Plateau: observations on a classic "carbonate monitor." *In* Anderson, N. R., and Malahoff, A. (Eds.), *The Fate of Fossil Fuel CO_2 in the Oceans:* New York (Plenum Press), pp. 543–567.

Berger, W. H., and Killingley, J., 1982. Box cores from the equatorial Pacific: ^{14}C sedimentation rates and benthic mixing. *Mar. Geol.*, 45:93–126.

Berger, W. H., and Mayer, L. A., 1978. Deep sea carbonates: acoustic reflectors and lysocline fluctuations. *Geology*, 6:11–15.

Berggren, W. A., 1972. Late Pliocene–Pleistocene glaciation. *In* Laughton, A. S., Berggren, W. A., et al., *Init. Repts. DSDP*, 12: Washington (U.S. Govt. Printing Office), 953–963.

Boyce, R. E., 1976. Sound velocity–density parameters of sediment and rock from DSDP Drill Sites 315–318 on the Line Island Chain, Manihiki Plateau, and Tuamotu Ridge in the Pacific Ocean. *In* Schlanger, S. O., Jackson, E. D., et al., *Init. Repts. DSDP*, 33: Washington (U.S. Govt. Printing Office), 695–728.

Brown, L. F., and Fisher, W. L., 1977. Seismic stratigraphic interpretation of depositional systems: examples from Brazilian rift and pull-apart basins. *In* Payton, C. E. (Ed.), *Seismic Stratigraphy—Applications to Hydrocarbon Exploration.* Mem. Am. Assoc. Pet. Geol., 26:213–248.

CLIMAP, 1976. The surface of the Ice Age Earth. *Science*, 191: 1131–1137.

Crowe, J., 1981. Mechanisms of heat transport through the floor of the equatorial Pacific Ocean [Ph.D. dissert.]. Mass. Inst. Technol., Cambridge.

Dunn, D. A., 1982. Miocene sediments of the equatorial Pacific Ocean: carbonate stratigraphy and dissolution history [Ph. D. dissert]. Univ. Rhode Island, Narragansett.

_____, in press. Early to middle Miocene carbonate stratigraphy and correlations of Pacific DSDP sites. *In* Kennett, J. P. (Ed.), *The Miocene Ocean: Paleoceanography and Biogeography.* Mem. Geol. Soc. Am.

Ewing, J., Ewing, M., Aitken, T., and Ludwig, W. J., 1968. North Pacific sediment layers measured by seismic profiling. *In* Knopoff, L., Drake, C. L., and Hart, P.J. (Eds.), *The Crust and Upper Mantle of the Pacific Area.* Am. Geophys. Union Geophys. Monograph, 12:147–186.

Geally, E. L., and Gerard, R. D., 1970. *In situ* petrophysical measurements in the Caribbean. *In* Bader, R. G., Gerard, R. D., et al., *Init. Repts. DSDP*, 4: Washington (U.S. Govt. Printing Office), 267–294.

Hamilton, E. L., 1965. Sound speed and related physical properties of sediments from Experimental Mohole (Guadalupe Site). *Geophysics*, 30(2):257–261.

_____, 1976. Variations of density and porosity with depth in deep sea sediments. *J. Sediment. Petrol.*, 46(2):280–300.

_____, 1979. Sound velocity gradients in marine sediments. *J. Acoust. Soc. Am.*, 65(4):909–922.

Hays, J. D., Cook, Harry E., III, Jenkins, D. G., Cook, F. M., Fuller, J. T., et al., 1972. Site 77. *In* Hays, J. D., et al., *Init. Repts. DSDP*, 9: Washington (U.S. Govt. Printing Office), 43–208.

Hays, J. D., Saito, T., Opdyke, N. D., and Burckle, L. H., 1969. Pliocene–Pleistocene sediments of the Equatorial Pacific: their paleomagnetic, biostratigraphic, and climatic record. *Geol. Soc. Am. Bull.*, 80:1481–1514.

Houtz, R. E., and Ludwig, W. J., 1979. Distribution of reverberant subbottom layers in southwest Pacific Basin. *J. Geophys. Res.*, 84: 3497–3504.

Hughes, D. S., and Cross, J. H., 1951. Elastic wave velocity in rocks at high pressures and temperatures. *Geophysics*, 16:577.

Johnson, T. C., Hamilton, E. L., Bachman, R. T., and Berger, W. H., 1978. Sound velocities in calcareous oozes and chalks from sonobuoy data: Ontong Java Plateau, western equatorial Pacific. *J. Geophys. Res.*, 83:283–288.

Keigwin, L. D., Jr., 1979. Late Cenozoic stable isotope stratigraphy and paleoceanography from the east equatorial and north central Pacific Ocean. *Earth Planet. Sci. Lett.*, 45:361–382.

Keller, G., 1980. Middle to late Miocene planktonic foraminiferal datum levels and paleoceanography of the North and southeastern Pacific Ocean. *Mar. Micropaleontol.*, 5:249–281.

_____, 1981. Miocene biochronology and paleoceanography of the North Pacific. *Mar. Micropaleontol.*, 6:535–551.

Keller, G., and Barron, J. A., 1983. Paleoceanographic implications of Miocene deep-sea hiatuses. *Geol. Soc. Am. Bull.*, 94:590–613.

Kennett, J. P., 1977. Cenozoic evolution of Antarctic glaciation, the circum-Antarctic Ocean and their impact on global paleoceanography. *J. Geophys. Res.*, 82:3843–3859.

_____, in press. The Miocene ocean: paleoceanography and biogeography. *Mem. Geol. Soc. Am.*

Kennett, J. P., Houtz, R. E., Andrews, P. B., Edwards, A. R., Gostin, V. A., et al., 1975. Cenozoic paleoceanography in the southwest Pacific Ocean, Antarctic glaciation, and the development of the Circum-Antarctic Current. *In* Kennett, J. P., Houtz, R. E., et al., *Init. Repts. DSDP*, 29: Washington (U.S. Govt. Printing Office), 1155–1170.

Kroenke, L. W., 1972. Geology of the Ontong Java Plateau [Ph.D. dissert.]. Hawaii Inst. Geophys., Honolulu.

Laughton, A. S., 1957. Sound propagation in compacted ocean sediments. *Geophysics*, 22:223–260.

Leinen, M., 1979. Biogenic silica accumulation in the central equatorial Pacific and implications for Cenozoic paleoceanography. *Geol. Soc. Am. Bull.*, 90:1310–1376.

Luz, B., 1973. Stratigraphic and paleoclimate analysis of Pleistocene tropical southeast Pacific cores. *Quat. Res.*, 3(1):56–72.

Matthews, R. K., and Poore, R. Z., 1980. Tertiary ^{18}O record and glacioeustatic sea-level fluctuations. *Geology*, 8:501–504.

Mayer, L. A., 1979a. Deep sea carbonates: acoustic, physical, and stratigraphic properties. *J. Sediment. Petrol.*, 49(3):0819–0836.

_____, 1979b. The origin of fine scale acoustic stratigraphy in deep-sea carbonates. *J. Geophys. Res.*, 84(B11):6177–6184.

_____, 1982. Physical properties of sediment recovered on Deep Sea Drilling Project Leg 68 with the hydraulic piston corer. *In* Prell, W. L., Gardner, J. V., et al., *Init. Repts. DSDP*, 68: Washington (U.S. Govt. Printing Office), 365–382.

Mountain, G. S., and Tucholke, B. E., 1983. Abyssal sediment waves. *In* Bally, A. W. (Ed.), *Seismic Expressions of Structural Styles.* Stud. Geol. (Tulsa, Okla.) 15.

Savin, S. M., Douglas, R. G., Keller, G., Killingley, J., Shaughnessy, L., et al., 1981. Miocene benthic foraminiferal isotope records: a synthesis. *Mar. Micropaleontol.*, 6:423–450.

Savin, S. M., Douglas, R. G., and Stehli, F. G., 1975. Tertiary marine paleotemperatures. *Geol. Soc. Am. Bull.*, 86:1495–1510.

Schlanger, S. O., and Douglas, R. G., 1974. The pelagic ooze–chalk–limestone transition and its implications for marine stratigraphy. *In* Hsü, K. J., and Jenkyns, H. C. (Eds.), *Pelagic Sediments on Land and under the Sea.* Spec. Publ. Int. Assoc. Sedimentol., 1: 117–148.

Shackleton, N. J., and Kennett, J. P., 1975a. Late Cenozoic oxygen and carbon isotopic changes at DSDP Site 284: implications for glacial history of the Northern Hemisphere and Antarctic. *In* Kennett, J. P., Houtz, R. E., et al., *Init. Repts. DSDP*, 29: Washington (U.S. Govt. Printing Office), 801–807.

_____, 1975b. Paleotemperature history of the Cenozoic and the initiation of Antarctic glaciation: oxygen and carbon isotope analyses in DSDP Sites 277, 279, and 281. *In* Kennett, J. P., Houtz, R. E., et al., *Init. Repts. DSDP*, 29: Washington (U.S. Govt. Printing Office), 743–755.

Shackleton, N. J., and Opdyke, W. D., 1973. Oxygen isotope and paleomagnetic stratigraphy of equatorial Pacific Core V28-238: oxygen isotope temperatures and ice volume on 10^5 year and 10^6 year scale. *Quat. Res.*, 3:39–55.

_____, 1976. Oxygen isotope and paleomagnetic stratigraphy of Pacific Core V28-239: late Pliocene to latest Pleistocene. *Mem. Geol. Soc. Am.*, 145:449–464.

_____, 1977. Oxygen isotope and paleomagnetic evidence for early Northern Hemisphere glaciation. *Nature*, 270:216–219.

Sheridan, R. E., Bates, L. G., Shipley, T. H., and Crosby, J. T., 1983. Seismic stratigraphy in the Blake–Bahama Basin and the origin of Horizon D. *In* Sheridan, R. E., Gradstein, F. M., et al., *Init. Repts. DSDP*, 76: Washington (U.S. Govt. Printing Office), 667–683.

Shipley, T. H., 1983. Physical properties, synthetic seismograms, and seismic reflections: correlations at Deep Sea Drilling Project Site 534, Blake–Bahama Basin. *In* Sheridan, R. E., Gradstein, F. M.,

et al., *Init. Repts. DSDP*, 76: Washington (U.S. Govt. Printing Office), 653–666.

Shipley, T. H., Buffler, R. T., and Watkins, J. S., 1978. Seismic stratigraphy and geologic history of the Blake Plateau and adjacent western Atlantic continental margins. *Am. Assoc. Petrol. Geol.*, 62:792–812.

Shipley, T. H., Winterer, E. L., and Lonsdale, P. F., 1983. Seismic stratigraphic analysis in the pelagic environment: the central Hess Rise, northwest Pacific. *Mar. Geol.*, 51:47–62.

Tracey, J. I., Jr., Sutton, G. H., et al., 1971. *Init. Repts. DSDP*, 8: Washington (U.S. Govt. Printing Office).

Tucholke, B. E., 1979. Relationships between acoustic stratigraphy and lithostratigraphy in western N. Atlantic basin. *In* Tucholke, B. E., Vogt, P. R., et al., *Init. Repts. DSDP*, 43: Washington (U.S. Govt. Printing Office), 827–846.

Tucholke, B. E., and Laine, E. P., 1982. Neogene and Quaternary development of the lower continental rise off the central U.S. east coast. *In* Watkins, J. S., and Drake, C. L. (Eds.), *Studies in Continental Margin Geology.* Mem. Am. Assoc. Petrol. Geol., 34: 295–307.

Tucholke, B. E., and Mountain, G. S., 1979. Seismic stratigraphy, lithostratigraphy, and paleosedimentation patterns in the western North Atlantic. *Am. Geophys. Union, Maurice Ewing Ser.*, 3:58–86.

U.S. Naval Oceanographic Office, 1962. *Tables of Sound Speed in Seawater.* U.S. Navoceano Spec. Publ. 58.

Vail, P. R., and Hardenbol, J., 1979. Sea level changes during the Tertiary. *Oceanus*, 22(3):71–80.

Vail, P. R., Mitchum, R. M., Todd, R. G., Widmier, J. M., Thompson, S., et al., 1977. Seismic stratigraphy and global changes in sea level. *In* Payton, C. E. (Ed.), *Seismic Stratigraphy, Applications to Hydrocarbon Exploration.* Mem. Am. Assoc. Petrol. Geol., 26: 49–205.

van Andel, T. H., Heath, G. R., et al., 1973. *Init. Repts. DSDP*, 16: Washington (U.S. Govt. Printing Office).

van Andel, T. H., Heath, G. R., and Moore, T. C., 1975. Cenozoic tectonics, sedimentation, and paleoceanography of the central equatorial Pacific. *Mem. Geol. Soc. Am. 143.*

Vincent, E., 1981. Neogene carbonate stratigraphy of Hess Rise (central North Pacific), and paleoceanographic implications. *In* Thiede, J., Vallier, T. L., et al., *Init. Repts. DSDP*, 62: Washington (U.S. Govt. Printing Office), 571–606.

Vincent, E., and Berger, W. H., in press. Carbon dioxide and polar cooling in the Miocene: the Monterey Hypothesis. *In* Sundquist, E. T., and Broecker, W. (Eds.), *Chapman Conf. on Natural Variations in Carbon Dioxide and the Carbon Cycle.* Am. Geophys. Union Monogr. Ser.

Vincent, E., Killingley, J. S, and Berger, W. H., 1980. The Magnetic Epoch-6 carbon shift: a change in the ocean's $^{13}C/^{12}C$ ratio 6.2 million years ago. *Mar. Micropaleontol.*, 5:185–205.

_____, 1983. The Chron-16 carbon event in the Miocene Indian Ocean. *Geol. Soc. Am. Abstr. Prog.*, 15:712. (Abstract)

Wilson, W. D., 1960. Speed of sound in seawater as a function of temperature, pressure, and salinity. *J. Acoust. Soc. Am.*, 32(6): 641–644.

Winterer, E. L., 1973. Sedimentary facies and plate tectonics of the equatorial Pacific. *Am. Assoc. Petrol. Geol. Bull.*, 57:265–282.

Winterer, E. L., Lonsdale, R. F., Matthews, J. L., and Rosendahl, B. R., 1974. Structure and acoustic stratigraphy of the Manihiki Plateau. *Deep Sea Res.*, 21:793–814.

Winterer, E. L., Riedel, W. R., et al., 1971. *Init. Repts. DSDP*, 7: Washington (U.S. Govt. Printing Office).

Woodruff, F., and Douglas, R. G., 1981. Response of deep sea benthic foraminifera to Miocene paleoclimatic events, DSDP Site 289. *Mar. Micropaleontol.*, 6:617–632.

Woodruff, F., Savin, S. M., and Douglas, R. G., 1981. Miocene stable isotope record: a detailed deep Pacific Ocean study and its paleoclimatic implications. *Science*, 212:665–668.

Date of Initial Receipt: 10 October 1984
Date of Acceptance: 29 January 1985

33. THE EQUATORIAL PACIFIC HIGH-PRODUCTIVITY BELT: ELEMENTS FOR A SYNTHESIS OF DEEP SEA DRILLING PROJECT LEG 85 RESULTS[1]

F. Theyer, Department of Geological Sciences, University of Southern California
L. A. Mayer, Department of Oceanography, Dalhousie University, Halifax, Nova Scotia
J. A. Barron, U.S. Geological Survey, Menlo Park
and
E. Thomas, Scripps Institution of Oceanography, University of California, San Diego[2]

ABSTRACT

Leg 85 of the Deep Sea Drilling Project operated in the eastern central Pacific in the region of the equatorial high-productivity belt. We recovered uppermost Eocene to Quaternary reference sections amenable to fine-scale stratigraphic and paleoceanographic research, using primarily the hydraulic piston corer. Four sites (572 to 575) were drilled along an east–west (about 114 to 133°W) and north–south (about 0.5 to 6°N) transect across the equatorial belt.

At Site 572 an apparently complete lower middle Miocene to Quaternary sequence was recovered: the sediment sections are dominantly siliceous–calcareous oozes and chalks, and sediment accumulation rates were high (30 to 60 m/m.y.). Sediments at Sites 573 to 575 are similar and dominated by siliceous and calcareous oozes and chalks. Sediment accumulation rates at Site 573 were generally between 10 and 35 m/m.y. The upper Eocene to Quaternary sequence is punctuated by seven hiatuses. At Site 574 a nearly complete upper Eocene to Quaternary sequence was retrieved, including a continuous Eocene to Oligocene transition. At Site 575 a lower Miocene to Quaternary section was cored. The lower to middle Miocene section is characterized by high, constant carbonate contents and sediment accumulation rates of about 20 m/m.y.; the top of the recovered section contains two hiatuses and has accumulated at rates of less than 10 m/m.y.

Except for thin, basal metalliferous layers, compositional changes in Leg 85 sediments result from shifts in the relative abundances of the biogenic siliceous or calcareous components. Leg 85 sites subsided and migrated at about 0.3 cm/yr., from about 3000 m in the eastern Pacific, south of the equator, to deeper (4000 to 4600 m), more western locations at or north of the equator. The sedimentary sequences recorded regional changes in productivity (biogenic sedimentation), dissolution, and erosion associated with the equatorial belt, as well as global paleoceanographic events. The most striking regional trend is an east–west decreasing gradient in deposition of biogenic silica, prevailing from middle Miocene to Recent, which mirrors present-day surface-water productivity. A less pronounced middle Miocene to Recent latitudinal trend in deposition appears to be the result of enhanced carbonate solution to the north. The effects of deposition in the equatorial high-productivity belt have not changed since the early Miocene. Below the middle/upper Miocene boundary, the sediments have a relatively constant high carbonate content, whereas above, carbonate percentages are highly variable. The changeover level is generally marked by a hiatus and significant changes in physical, chemical, and magnetic properties of the sediments.

Results of Leg 85 contributed to advances in the four elements needed for an eventual paleoceanographic synthesis: (1) a high-resolution, multidisciplinary, and integrated datum-plane scheme and time scale, with an overall resolution of 0.13 to 0.38 m.y., was established; (2) a system of correlatable acoustic reflectors was delineated over vast distances, and these reflectors were calibrated against age and physical and chemical properties at Sites 574; (3) a fine-scale geochemical (stable isotope and $CaCO_3$) and micropaleontological climatic reconstruction was developed (discontinuously) from Oligocene to Pleistocene; and (4) broadly correlatable hiatuses (NH, PH), defined by previous work, were recognized at Sites 573 to 575.

The interval from 8 to 9 Ma serves to outline how integration of the foregoing elements could lead to a future synthesis. In the central basin of the equatorial Pacific, the interval from 8 to 9 Ma is marked by a hiatus (NH5) in siliceous clays. A correlative hiatus occurs in carbonate oozes of the equatorial region and in the northeastern Pacific rim, and may be correlated with the "Purple" equatorial Pacific reflector. The interval is characterized globally by a regression, by strong carbonate dissolution, and by isotopic and micropaleontological evidence of marked cooling. Further study of these paleoceanographic phenomena in a variety of depositional environments will lead to an understanding of their relationships and functioning.

INTRODUCTION

The central equatorial Pacific, and especially its eastern central high-productivity belt, is a region of fundamental importance to marine geology. Beginning with Murray and Renard (1891), many of the pioneering marine geological deep-sea investigations (i.e., Arrhenius, 1952; Bramlette, 1961; Riedel and Funnel, 1964; Peterson, 1966; Hays et al., 1969, 1972; Berger, 1973; Winterer, 1973) concentrated on this area, where four previous DSDP legs (5, 8, 9, 16) operated (Fig. 1). These previous efforts culminated in the marine geological and paleoceanographic synthesis of the equatorial Pacific by van Andel et al. (1975). Characterized by intensive activity and rapid advances, this initial phase of central Pacific research was instrumental in establishing global Tertiary tropical biostratigraphy and chronology, in shap-

[1] Mayer, L., Theyer, F., et al., *Init. Repts. DSDP*, 85: Washington (U.S. Govt. Printing Office).

[2] Addresses: (Theyer) Department of Geological Sciences, University of Southern California, University Park, Los Angeles, CA 90089; (Mayer) Dalhousie University, Halifax, Nova Scotia, Canada B3H 4J1; (Barron) U.S. Geological Survey, 345 Middlefield Rd., Menlo Park, CA 94025; (Thomas, present address) Lamont-Doherty Geological Observatory, Columbia University, Palisades, NY 10964.

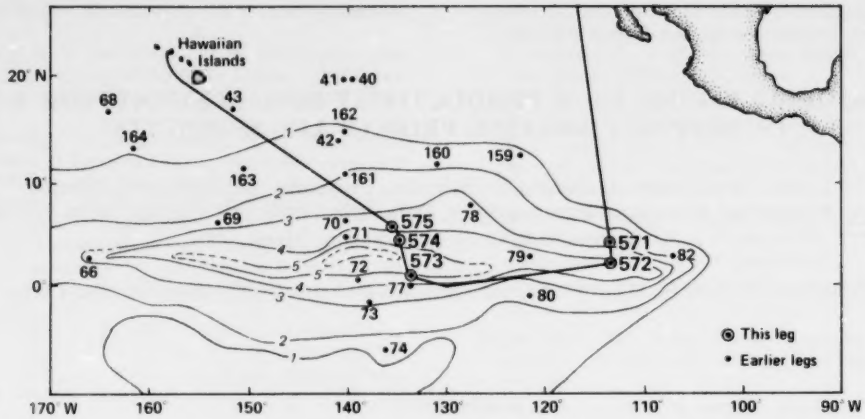

Figure 1. Cruise track and DSDP Leg 85 site locations in relation to acoustic sediment thickness (tenths of second, two-way traveltime) and previous DSDP operations (Legs 5, 8, 9, 16). Acoustic stratigraphy from Ewing et al. (1968).

ing our broad understanding of paleoceanography, and in developing tectonic reconstructions of the Pacific. Publication of the synthesis by van Andel et al. (1975) was followed by a leveling off in regional research activity. The *Glomar Challenger* did not return to the area until 1982, and paleoceanography began to focus primarily on elucidating the fine details of latest Tertiary and Quaternary records. This fine-scale work requires expanded sedimentary sequences amenable to high-resolution sampling. Such sequences were available only in relatively short (5- to 15-m) conventional piston cores; rotary-drilled sections from previous DSDP central Pacific legs were too disturbed in the upper, generally unconsolidated 100 to 300 m (which comprises much of the Neogene) to be useful for high-resolution research.

With the development of the hydraulic piston corer (HPC) by Storms and Serocki (Prell, Gardner, et al., 1982) came the ability for the *Glomar Challenger* to recover undisturbed cores from the upper part of the sedimentary record and thus to begin a high-resolution phase in studies of the central equatorial Pacific. DSDP Leg 85 was designed to recover undisturbed and continuous equatorial Pacific Tertiary and Quaternary reference sections, using a modified, variable-length HPC (VLHPC; see Introduction, this volume).

Five sites were chosen by the JOIDES Ocean Paleoenvironment Panel (Fig. 1). Two sites (571 and 572) are in the eastern Pacific, whereas three of the sites (573, 574, and 575) form a north–south line, along approximately 133°W, across the equatorial high-productivity zone. We piston cored each site twice to ensure complete recovery of the sedimentary sequences; then followed rotary drilling to basement (in the stiffer sediments below the reach of the HPC) at Sites 572 to 574. Basement is Miocene at Sites 571 and 572 (Site 572 repeats Site 81 of Leg 9; Hays et al., 1972) and uppermost Eocene at Sites 573 to 575 (Fig. 2).

Leg 85 was expected to expand significantly the scope of earlier equatorial Pacific studies by providing the sediments and data necessary to carry out fine-scale stratigraphic and paleoceanographic research. The detail and breadth of the results in the present volume show that this expectation was met. In this preliminary synthesis we present the salient results of work completed for this volume and discuss the scientific elements uncovered by Leg 85 that seem essential to an understanding of this region.

GEOLOGICAL AND OCEANOGRAPHIC SETTING

The interplay of three fundamental processes has shaped the depositional history of the central and eastern equatorial Pacific. These processes are the tectonism of the spreading seafloor, biological productivity in the overlying waters, and changes in oceanographic conditions, both on the surface and near the seafloor (van Andel et al., 1975).

The dominant tectonic feature of the region is the East Pacific Rise (Fig. 2), at which new crust is generated at rates of 8 to 20 cm/yr., and which delineates four major plates, the Pacific (on which all Leg 85 sites lie), North American, Cocos, and Nazca (Sclater et al., 1971; Anderson and Sclater, 1972; Herron, 1972). During the last 50 m.y., new Pacific crust has been continuously moving (and rotating) northwestward (Francheteau et al., 1970), spreading away from the East Pacific Rise and subsiding from an initial depth of about 3000 m (Sclater et al., 1971). This motion has two crucial results. First, it continuously alters the relationship between the equatorial high-productivity belt (surface waters) and its depositional expression on the seafloor (Fig. 1). And, second, the subsidence with age resulting from cooling of the young crust exposes solution-susceptible calcium carbonate to corrosive waters below or near the lysocline (Berger, 1973; Berger and Winterer, 1974).

Superimposed on this tectonic framework, biological productivity plays its role. The equatorial current system and its associated zones of upwelling create one of the Earth's most fertile planktonic belts along the equator, especially in the eastern Pacific (Austin, 1960; Defant, 1961; Reid, 1962; Lisitsin, 1970; Koblentz-Mishke et al., 1970). The sediments associated with this belt are

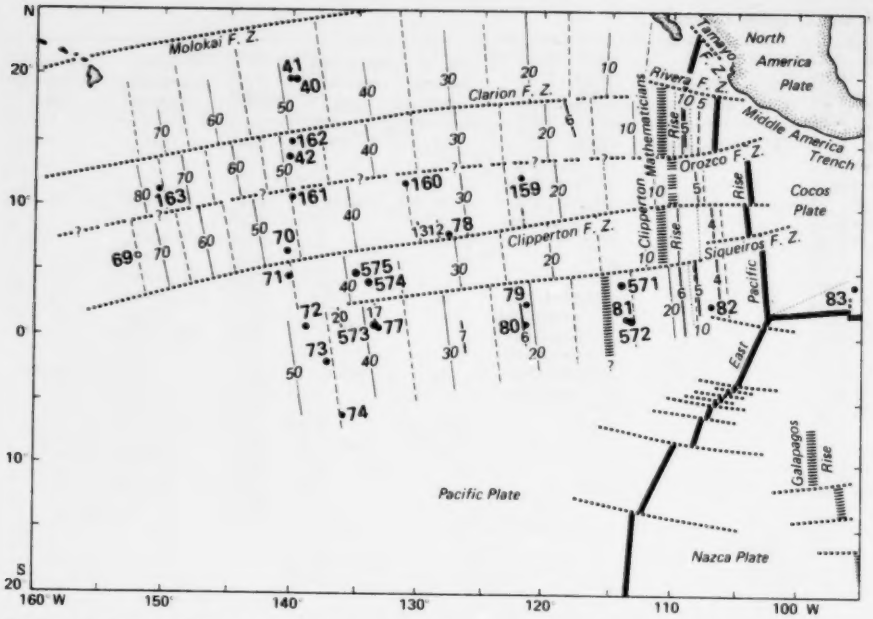

Figure 2. Tectonic setting of the eastern central equatorial Pacific. Numbered dots indicate DSDP drill sites; medium-sized numbers show extrapolated crustal ages (Ma); and small numbers refer to magnetic anomalies. Modified after van Andel et al. (1975).

dominated by carbonate and silica produced by planktonic foraminifers, calcareous nannofossils, diatoms, and radiolarians. Throughout most of the Cenozoic, the relationships between surface-water productivity and sediment accumulation have remained roughly constant, as indicated by the deposition of a more or less lens-shaped body of sediments (Ewing et al., 1968). On a smaller scale, however, this highly productive belt, and its sedimentary expression on the seafloor, is regionally and temporally variable in width (van Andel et al., 1975); today it is roughly 3 to 4° wide and has its maximum expression slightly offset to the north of the equator. This sedimentary bulge (Fig. 1) is dominated by calcareous sediments along its crest, and it is increasingly more siliceous toward its northern and southern flanks (Winterer, 1973).

The product of this simple tectonic-productivity model of the equatorial region is altered by changes in oceanographic conditions during geological history (van Andel et al., 1975). These temporal changes manifest themselves primarily through fluctuations in the position of dissolution surfaces. In addition, thermohaline currents may physically remove and mix sections of the depositional record. Indeed, numerous submarine outcrops of Tertiary sediments and widespread hiatuses in the equatorial Pacific testify to the effectiveness of bottom-water erosion throughout the Cenozoic (Riedel and Funnell, 1964; Moore, 1970; Johnson, 1972).

DRILLING RESULTS

Table 1 summarizes locations, operations, and other coring data, and Figures 1 and 2 show the locations of the sites in relation to previous DSDP operations, sediment cover, and basement ages in the region. Figures 3 and 4 summarize the coring operations and the general lithostratigraphy at the sites. The time scale used in this synthesis follows Berggren et al. (in press), in which magnetostratigraphic Chron 11 is correlated with Anomaly 5 (see Barron et al., this volume).

Site 572

Located at the eastern edge of the equatorial high-productivity zone (Fig. 1; Table 1), Site 572 is several kilometers west of Site 81 (DSDP Leg 9), where only the uppermost and lowermost few meters of the section were recovered. We completed four HPC holes (Fig. 3) and then rotary drilled to a depth of 485.5 m. Basement is at 479.5 m sub-bottom, and the last core of the site recovered 43 cm of basalt.

The sedimentary section consists of (Fig. 4) laminated and burrow-mottled siliceous–calcareous oozes and siliceous nannofossil oozes grading to siliceous nannofossil chalks. Cyclic variations in sediment color occur throughout the section and are used to divide the section into four subunits. These subdivisions are arbitrary; sediment color does not appear to be directly related to texture or microfossil composition. The subunits, however, can be recognized in all five holes, and they can be correlated with the "oceanic formations" defined (Hays et al., 1972) for Site 81. Throughout, and especially in the chalky section, burrows of Chondrites, Planolites, and Zoophycos occur. The lowermost samples of the recovered sequence show indications of hydrothermal activity. The entire section is characterized by cyclic alternations between intervals of high (80 to 90%) and low (45 to 65%) carbonate content.

Biostratigraphic data indicate that we recovered a continuous sequence (Fig. 4) from upper Pleistocene through

Table 1. Leg 85 coring summary.

Site	No. holes	Water depth (corrected m)	Operations	No. of received cores	Maximum penetration (m)	Hole[a]	Cored sub-bottom range (m)	Est. age of oldest seds. (Ma)	Nature of basement
571 (02°59.84′N, 114°08.53′W)	1	3962	HPC; heat flow/ pore meter	1	7.1	+571	0–7.1	—	—
572[b] (01°26.09′N, 113°50.52′W)	5	3893	Double HPC; rotary core	76	486.0	+572	0–19.0	14–15	Basalt
						+572A	0–154.0		
						+572B	154.0–172.1		
						+572C	0–169.5		
						572D	151.0–486.0		
573[c] (00°29.91′N, 133°18.57′W)	3	4301	Double HPC; rotary core; heat flow/ pore water	68	529.0	+573	0–158.6	38–39	Basalt
						+573A	0–53.2		
						573B	138.5–529.0		
574 (04°12.52′N, 133°19.81′W)	4	4561	Double HPC; rotary core	92	532.5	+574	0–206.5	38–39	Basalt
						+574A	0–180.2		
						574B	185.0–204.0		
						574C	194.5–532.5		
575 (05°51.00′N, 135°02.16′W)	4	4536	Double HPC	60	196.3	+575	0–98.6	22	—
						+575A	93.8–196.8		
						+575B	0–99.89		
						+575C	0–15.8		

[a] HPC holes are marked +
[b] Near Site 81 (Leg 9).
[c] Near Site 77 (Leg 9).

the lowest middle Miocene (about 15 Ma). Holocene and uppermost Pleistocene sediments were apparently lost in the coring process. All major microfossil groups are represented at Site 572. Siliceous microfossils occur in common to high abundances throughout the section, and calcareous microfossils are abundant and well preserved throughout the Pliocene and Pleistocene. A sharp break in carbonate preservation occurs at approximately 150 m sub-bottom (uppermost Miocene, about 6 Ma). From this level down to the lowermost part of the section (435 m, middle Miocene), calcareous microfossils are represented by species with particularly high dissolution indices (Berger and von Rad, 1972). Well preserved assemblages reappear in the three deepest core (436 to 464.5 m, middle Miocene, 14 to 15 Ma). Radiolarians are well preserved throughout the section, whereas diatoms show good preservation above 365 m sub-bottom and generally poor to moderate preservation below that level. High percentages of the diatoms *Thallassionema nitzschioides* and *Thalassiothrix longissima*, which are thought to indicate upwelling, dominate the intervals from 64 to 218 m and from 246 to 322 m.

Sediment accumulation rates at Site 572 have been variable, and, in some intervals, remarkably high (Fig. 5). The rate from about 12 to 15 Ma averaged approximately 32 m/m.y., whereas early Pliocene to latest Miocene (3.8 to 6.4 Ma) rates varied between 46 and 67 m/m.y. Between the 5- and 8-Ma levels, $CaCO_3$ percentages are relatively low (~70%), implying dilution of carbonate by biogenic silica during periods of high sedimentation rate. Comparison of carbonate and noncarbonate accumulation rates (Fig. 6) reveals that when accumulation rates shift from low to high, the carbonate accumulation rate increases by a factor of 3 while the noncarbonate (mainly biogenic silica) rate increases by a factor of 6.

Site 573

The southernmost of the north–south line of sites across the equatorial sediment bulge, Site 573 (Fig. 1, Table 1), was selected as a high-resolution duplicate of DSDP Site 77 (Hays et al., 1972). Whereas Site 77 was drilled on the flank of a basement ridge with 0.51 s of sediment cover, Site 573 is located over a basement trough covered by 0.62 s of acoustically well stratified sediment.

The oldest sediment recovered (Fig. 5) is uppermost Eocene limestone (Hole 573B, 528 m), separated by a baked sediment interface from basalt with glassy rinds (1 m recovered). Four lithostratigraphic units can be recognized, which correlated with the three oceanic formations established at Site 77 (Hays et al., 1972).

Planktonic foraminifers, calcareous nannofossils, radiolarians, and diatoms are, with exceptions, well represented in the sediments, allowing recognition of nearly all standard Eocene to Quaternary biozonal boundaries; but the Eocene/Oligocene boundary could not be located unequivocally. Biostratigraphic evidence points to the presence of seven hiatuses and two intervals of very slow sediment accumulation rates in the cored sequence (Barron et al., this volume; also Fig. 5). A prominent hiatus is bracketed by foraminiferal Zones P16 (uppermost Eocene) and P18 (basal Oligocene) and nannofossil Subzones CP15b (Eocene) and CP16b (Oligocene). This absence of foraminiferal Zone P17 may also be explained, however, by assuming that the metalliferous claystone between 520.5 and 528 m (Fig. 4) represents a greatly compressed depositional record of latest Eocene to earliest Oligocene time. Perhaps the metalliferous layer is the remnant of a normal biogenic ooze from which hydrothermal activity has removed all microfossils by solution. Three hiatuses follow in the topmost Oligocene and

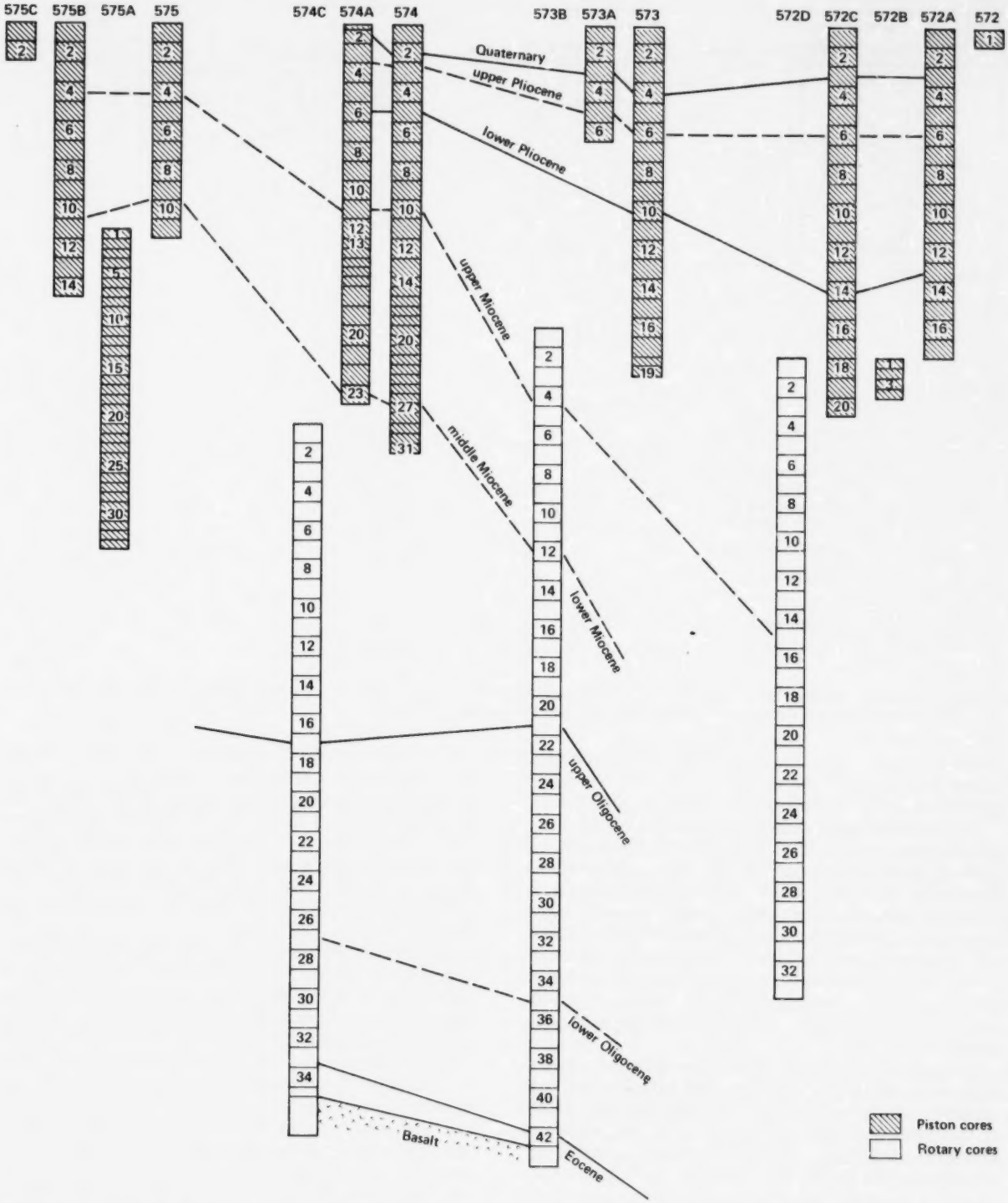

Figure 3. Holes cored and drilled during Leg 85. Hatching indicates VLHPC cores; others were rotary drilled. The cores generally measure 5 or 9 m in length.

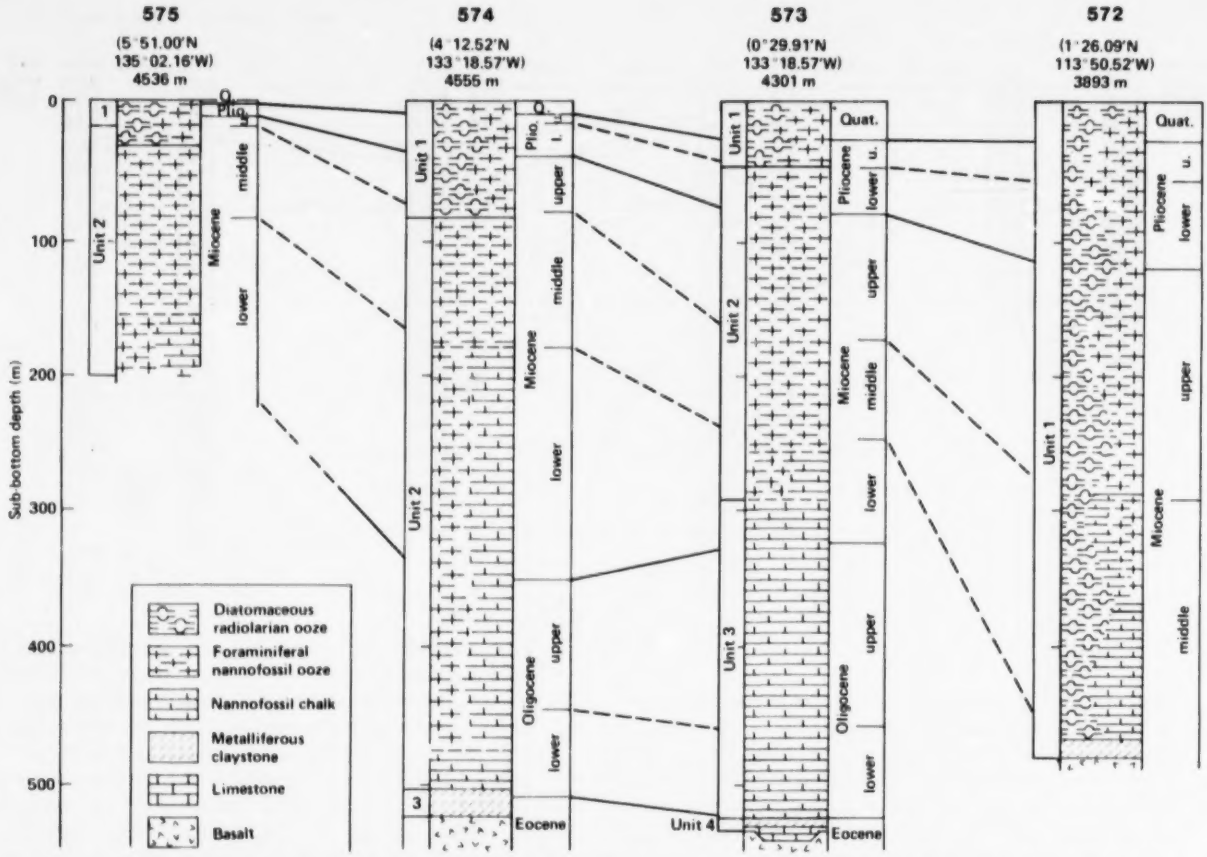

Figure 4. Generalized lithology and stratigraphy of Sites 572 through 575. Stratigraphic boundaries follow time scale based on foraminiferal, nannofossil, radiolarian, and diatom datum levels (see Barron et al., this volume).

lower Miocene, and three more occur in the middle and upper Miocene (Fig. 5). At nearby Site 77, correlative gaps were found in the record (Hays et al., 1972).

Sediment accumulation rates at Site 573 varied generally between 10 and 35 m/m.y. (Fig. 5). Two peaks exceeding 30 m/m.y. occurred between 5 and 6 Ma (latest Miocene) and from about 32 to 35 Ma (earliest Oligocene). In some instances, the changes in accumulation rate correlate with lithologic contrasts. Thus, the silica-rich sediments between about 160 and 200 m contain three hiatuses, and the brown sedimentary unit between 260 and 360 m is roughly equivalent to a time of slow accumulation and hiatus formation (Barron et al., this volume).

Compaction has a marked effect on estimates of sediment accumulation rate, as demonstrated by calculations of mass accumulation rate (Fig. 6). For example, the intervals from 4 to 8 Ma and from 30 to 33 Ma show similar rates of sediment accumulation, yet mass accumulation rates in the Oligocene chalks are significantly higher than in the Pliocene/Pleistocene sediments.

Site 574

Site 574 (Fig. 1; Table 1) is the second of a three-site north–south transect across the equatorial high-productivity zone. Its position (near the crest of the equatorial sediment bulge) was selected to provide a sediment record of the migration of this site across the equator and to permit recovery of the Eocene/Oligocene boundary. The section at Site 574 is divided, primarily on the basis of sediment composition (Fig. 4), into three lithologic units: (1) a cyclic siliceous–calcareous ooze unit, (2) a calcareous ooze/chalk unit, and (3) a metalliferous calcareous unit.

Stratigraphically important is the remarkably complete recovery, at this site, of the transition from the uppermost Eocene to the lowermost Oligocene. This transition occurs in the metalliferous unit (502.5 to 520.0 m) directly above basement (Fig. 4), the boundary's precise location varying with the microfossil zonations.

The major microfossil groups are generally well represented, providing a fairly complete uppermost Eocene to Quaternary section. Siliceous microfossils are abundant and well preserved in most of the section. Diatom abundance and preservation, however, decline in the upper Oligocene, the upper part of the lower Oligocene, and near the Eocene/Oligocene boundary. Planktonic foraminiferal abundances fluctuate, and this group provides good stratigraphic control only in the lower middle Miocene. Calcareous nannofossils are common to

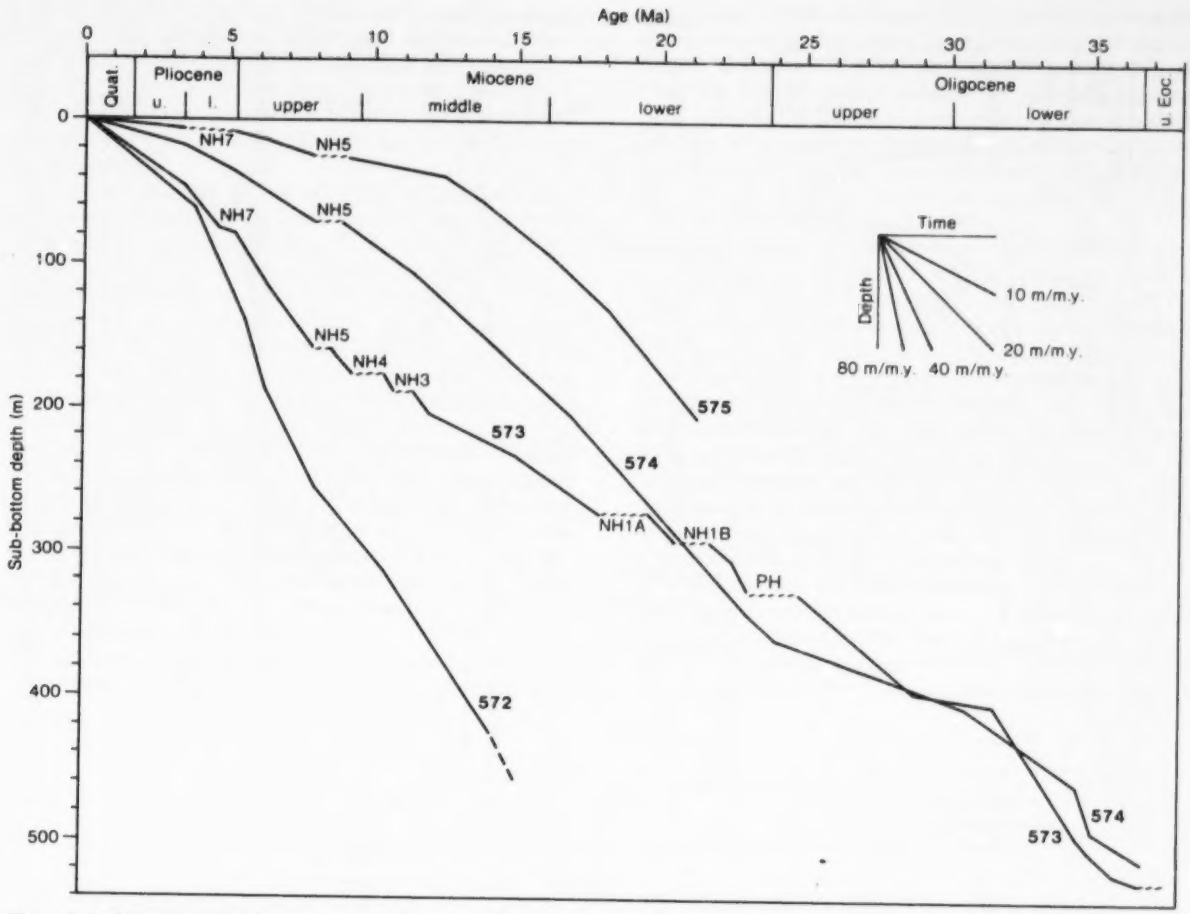

Figure 5. Sediment accumulation rates at Sites 572 through 575. Breaks denote hiatuses or extremely slow accumulation. The time scale follows Barron et al. (this volume), and NH numbers and PH are hiatuses after Barron and Keller (1982).

abundant throughout the section. Reworked Oligocene foraminifers and nannofossils occur in three zones of the middle Miocene.

Sediment accumulation rates at Site 574 are moderate. Oligocene rates average about 12 m/m.y., increasing to 20 m/m.y. in the lower to middle Miocene (Fig. 5). Above this level they decrease and remain low, and a hiatus occurs at 70 m sub-bottom (7.8 to 8.8 Ma). In contrast to Sites 572 and the upper section at Site 473, the sediment accumulation rate at Site 574 is strongly dominated by calcium carbonate: high mass accumulation rates occur during times of little biogenic silica deposition (Fig. 6).

Site 575

Site 575, just south of the Clipperton Fracture Zone (Table 1; Fig. 1), completes a three-site latitudinal transect along approximately 133°W, across the equatorial sedimentary "bulge." Time limitations prevented completion of drilling to basement, but the paleoenvironment and stratigraphic objectives were satisfied by four HPC holes (Fig. 3) that penetrated to 196.3 m sub-bottom and ended in lowermost Miocene (Fig. 4). A combined total of 374.47 m (the upper 120 m overlap) of sediments was recovered, mostly undisturbed.

The lower to middle Miocene part of the section records a highly productive environment dominated by equatorial sedimentation, whereas the upper part of the section testifies to the site's northward migration from under the equatorial belt system. Two lithologic units were identified, an upper Miocene to Quaternary calcareous cyclic unit (0 to 32.2 m sub-bottom) and a siliceous-calcareous ooze/chalk unit (32.3 to 196.2 m). The upper unit is characterized by cyclic alternations in carbonate content, whereas the lower unit has relatively constant, high (94%) carbonate values down to the lower Miocene, where mean carbonate percentages decrease slightly (86%). Subunits, based primarily on color, can be distinguished in both units. Centimeter-thick sandy to pebbly turbidites, composed primarily of allochthonous foraminifers and volcanic debris, are interbedded throughout the section. A large seamount 10 km northeast of the site, and rising 1000 m above the regional seafloor, is the most likely source of these turbidites.

All major microfossil groups occur throughout, although preservation of calcareous skeletons is poor to

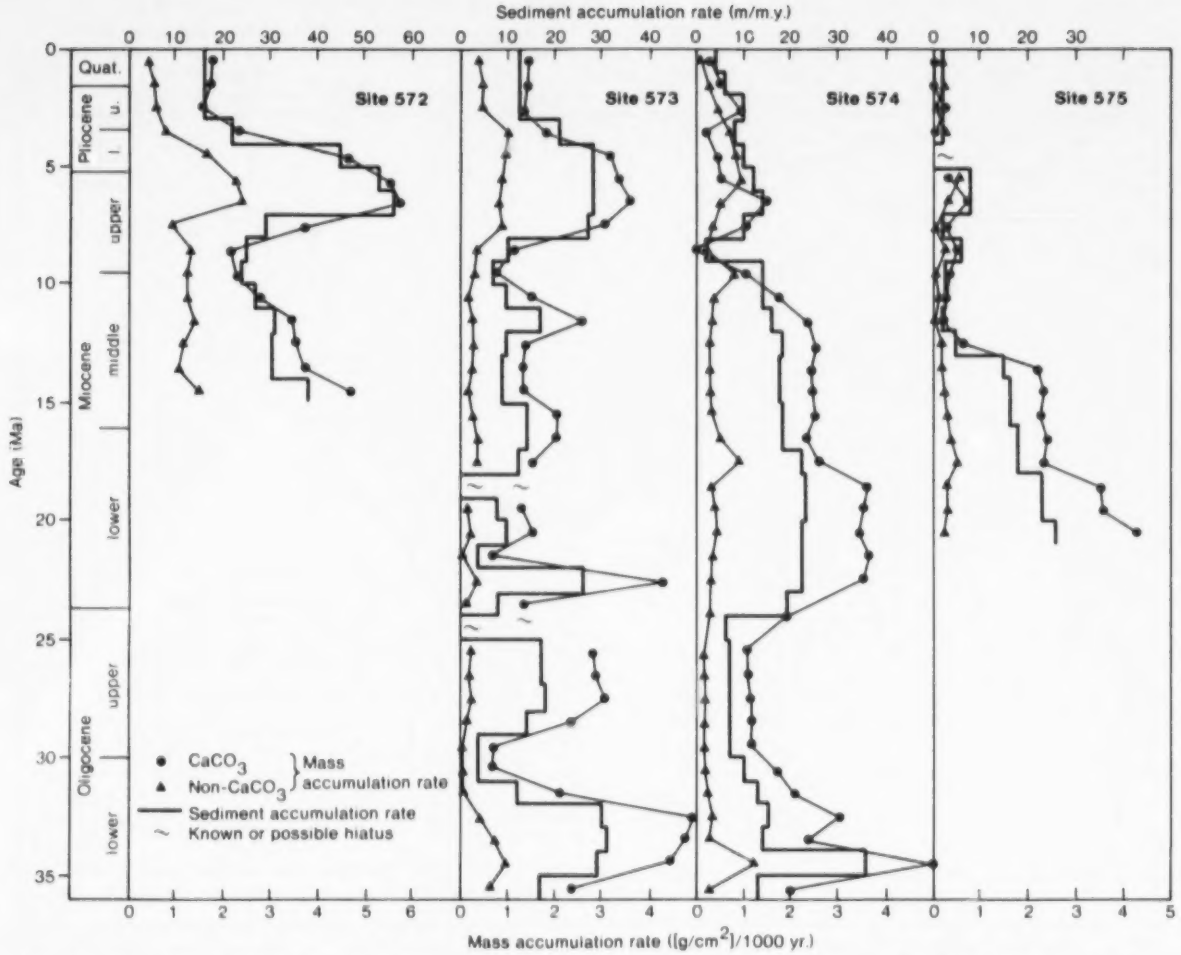

Figure 6. Sediment accumulation rates and carbonate and noncarbonate mass accumulation rates versus age for Sites 572 through 575.

almost nil in the topmost siliceous–calcareous cyclic unit. Calcareous dissolution is pervasive in the uppermost unit and is compounded by microfossil reworking and the extreme stratigraphic compression of the section, obscuring recognition of some biozonal boundaries. In contrast, the expanded character of the ooze/chalk unit and the excellent preservation of microfossils (except for a brief interval from 102 to 108 m sub-bottom, about 16.5 Ma) make it one of the most complete lower Neogene sequences available from the equatorial Pacific.

Sediment accumulation-rate fluctuations (Fig. 5) correlate with the lithostratigraphic subdivisions. Moderate rates of about 20 m/m.y. characterize the oozes of the lower unit; low rates typify the siliceous–calcareous unit, which is also marked by two hiatuses, one at 8 m (3.4 to 5.1 Ma) and one at 26 m (7.8 to 9.2 Ma) sub-bottom depth.

ELEMENTS FOR A SYNTHESIS

Overall Trends

The geographic distribution of the Leg 85 sites permits a longitudinal, latitudinal, and temporal evaluation of the major influences on equatorial pelagic deposition. Except for the relatively thin metalliferous layers of hydrothermal origin (Jarvis, this volume) at the base of each section (Fig. 4), the major compositional changes in the recovered sediments result from shifts in the relative abundances of the preserved biogenic siliceous or calcareous components.

The fundamental causes of these sedimentation shifts are obvious: all Leg 85 sites subsided and migrated from relatively shallow (about 3000-m) depths in the eastern Pacific, south of the equator, to deeper (4000- to 4600-m), more western locations at or north of the equator (Fig. 3). This northwesterly migration proceeded at about 0.3 cm/yr. (Weinreich and Theyer, this volume). During their migration and subsidence, the sites passed first under the equatorial high-productivity zone, where biogenic silica and carbonate sedimentation rates increased and the CCD (carbonate compensation depth) is depressed. While under this zone, fluctuations of the width of the equatorial high-productivity zone, and of latitudinal and longitudinal gradients in productivity (biogenic sedimentation), were imprinted on the sedimentary records. Then, continued subsidence and northwesterly migration of the sites

beyond the equatorial high-productivity zone led to increased carbonate dissolution in their sequences. Thus, this basic, tectonically driven system is complicated by imprints left in the record from temporal variations in productivity, dissolution, and erosion. These temporal changes may range from global paleoclimatic shifts to regional events.

The most striking overall characteristic of the region is a strong east-west depositional gradient, prevailing from middle Miocene to Recent (Fig. 7). At Site 572 (114°W), overall sedimentation and accumulation rates are highest (often more than 40 m/m.y.; Fig. 5), whereas, in comparison, at Site 573 (about 2100 km to the west), rates are clearly attenuated in sections older than 5 to 8 Ma (Fig. 5). Water depth and latitude influence the differences between Sites 572 and 573. More important, however, the carbonate and noncarbonate accumulation rates (Fig. 8), the foraminiferal dissolution index, and qualitative evaluation of diatom and benthic foraminiferal species distribution all support the idea that the strong east-west gradient is the sedimentary expression of a surface-water primary productivity trend similar to that observed today (Austin, 1960; Koblentz-Mishke et al., 1970). Indeed, the lithologic and stratigraphic variation from east to west may be primarily due to a strong east-to-west decrease in diatom productivity. Assuming that the noncarbonate component in this region is mainly biogenic silica, this increasing influence of silica productivity in the east is also shown by a comparison of the carbonate and noncarbonate accumulation rates (Fig. 6). Moreover, diatom species indicative of upwelling are abundant at times of increased noncarbonate accumulation. For Site 572, a plot of carbonate rate vs. noncarbonate rate shows a positive, linear relationship (Fig. 8). For Site 573, the data reveal a similar trend, but the noncarbonate component is less dominant.

The influence of the east-west productivity gradient is particularly noticeable when one compares sedimentation rates, mass accumulation rates (Figs. 5, 6, 8), carbonate content, and dissolution-index curves (Mayer et al., this volume; Saito, this volume) of Sites 572 and 573. At Site 573, the carbonate and noncarbonate accumulation rates and carbonate contents track nicely: high carbonate values are associated with high accumulation rates (productivity) and better preservation. At Site 572, however, the same relationship occurs only during periods of relatively lower accumulation rates; times of highest accumulation are associated with enhanced dissolution of $CaCO_3$ and decreased carbonate content. A possible explanation for these differences between the sites may depend on the magnitude of noncarbonate accumulation at each site. The highest noncarbonate rate at Site 573 is about 0.5 g/cm²/1000 yr., whereas the maximum value at Site 572 is almost three times that amount.

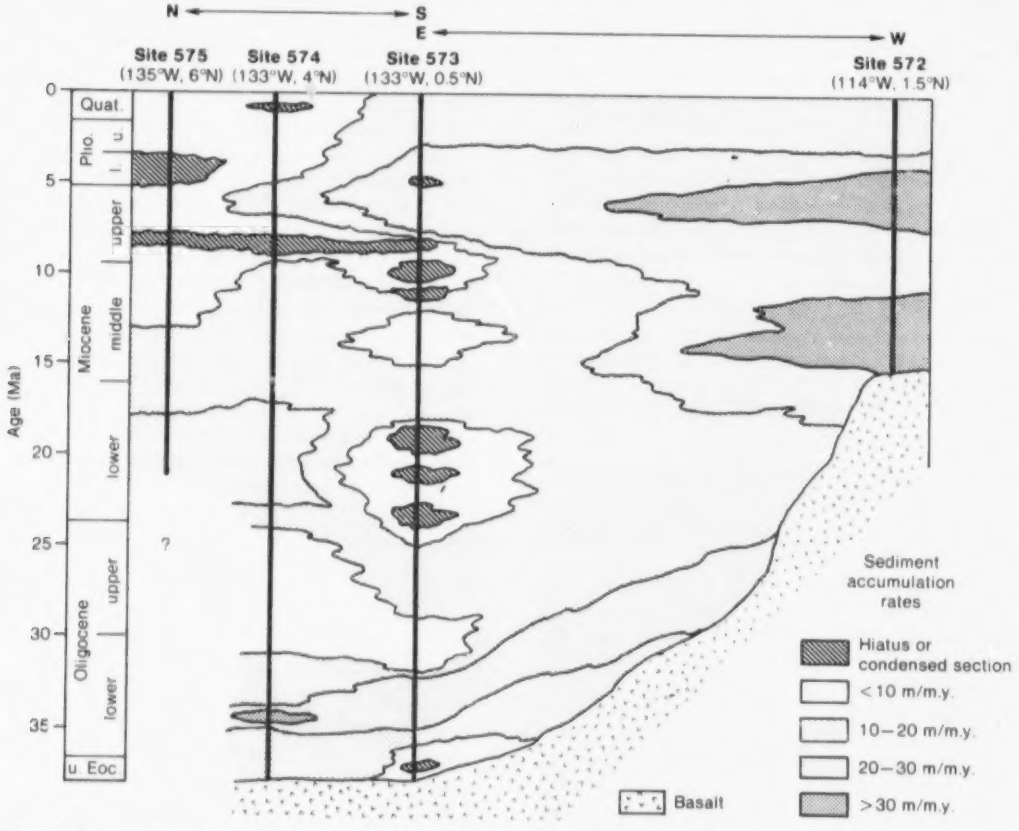

Figure 7. Schematic model of overall sedimentation trends (east-west, north-south) at Sites 572 to 575.

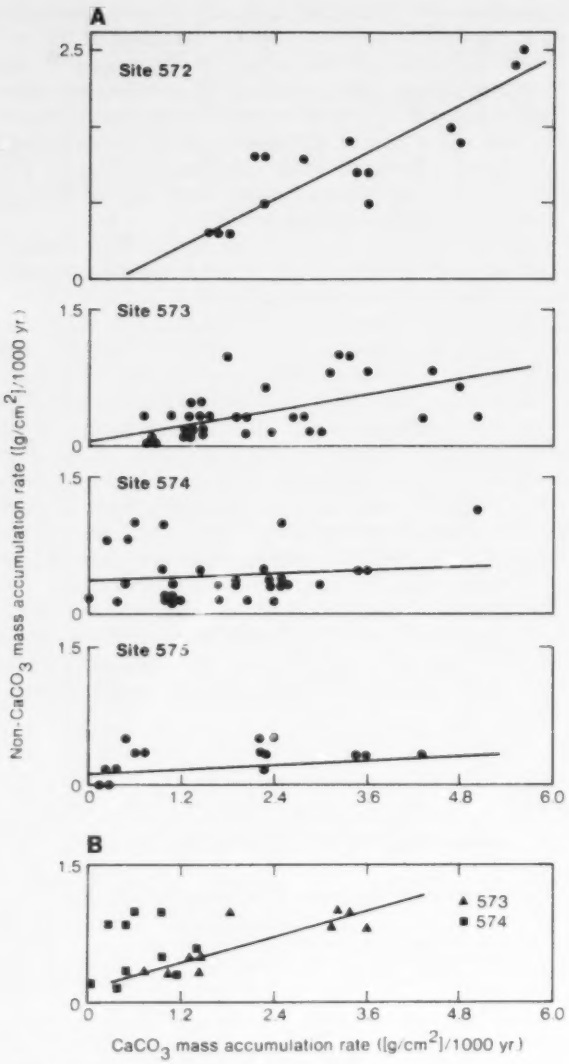

Figure 8. Correlation between carbonate and noncarbonate (presumed to be mostly biogenic silica) mass accumulation rates for Sites 572 through 575. A. Single-site comparison. B. Data for the last 10 m.y. from Sites 573 and 574, plotted together; regression line based on Site 573.

We suggest that when a certain noncarbonate accumulation-rate (productivity) threshold is reached, oxidation of the abundant organic matter produces steep dissolution gradients and enhanced dissolution.

A latitudinal trend in deposition is apparent between Site 573, 574, and 575 from about middle Miocene to Recent (Figs. 4 to 8), but it is less pronounced than the east-west gradient. This latitudinal trend of the last 15 m.y. appears to be predominantly the result of enhanced dissolution to the north. At Sites 574 and 575, we find a correlation of low sediment accumulation rates and low percent calcium carbonate. At Sites 572 and 573 (the equatorial belt sites), we find high sediment accumulation rates correlated with low percent $CaCO_3$, implying that $CaCO_3$ was removed from the northern sites while SiO_2 was added to equatorial sites. In the lower Miocene, however, the sense of the latitudinal trend is reversed: sediment accumulation rates at Sites 574 and 575 exceed those of Site 573 (Fig. 7). This temporal change in the latitudinal sense of the depositional trend, which occurs at about 15 Ma, may be the result of the passage of the sites beneath the equatorial high-productivity zone. Sites 574 and 575 were close to or at the equator between 15 and 20 Ma (Weinreich and Theyer, this volume), and Site 573 was at about 5°S. Then, at the beginning of the middle Miocene, Sites 574 and 575 moved away from the equator, causing a sequential decrease in sediment accumulation rates at both sites—first at Site 575 (at about 13 Ma) and then at Site 574 (at about 9 Ma). Thus, these data suggest that the effect of the high-productivity zone along the equator has not changed since the early Miocene: deposition at a particular site is clearly affected when that site is at the equator.

Oligocene was recovered only at Sites 573 and 574. At Sites 573 and 574, we recovered the most complete Oligocene carbonate records of the equatorial Pacific. Although few data are presently available, we can say that sediment accumulation rates at both sites were relatively low in the late Oligocene and high in the early Oligocene, and that greater overall variability characterized Site 573.

Finally, an impressive example of a temporal trend is the major shift in the nature of carbonate deposition which occurs near the time of the middle/upper Miocene boundary at Sites 573, 574, and 575. Not only is there a hiatus or very compressed interval at about 8 to 9 Ma at all sites, but sediments deposited after the middle Miocene generally have a highly variable carbonate content, whereas sediments predating late Miocene have a relatively constant high carbonate content (Fig. 4; see site chapters). Associated with this shift from carbonate–silica cycles to high-carbonate sediments are significant changes in the physical, chemical, and magnetic properties (see site chapters; Mayer et al.; Wilkens and Handyside; Weinreich and Theyer; all this volume).This shift from a carbonate to a carbonate–silica regime near the time of the middle/upper Miocene boundary may be linked to worldwide cooling and to the change of the major sink for silica from Atlantic to Pacific (Keller and Barron, 1983).

Central Pacific Paleoceanography

Paleoceanographic results of Leg 85 contributed to advances in four key areas: (1) A high-resolution, multidisciplinary, and integrated datum-plane correlation scheme and time scale for the central equatorial Pacific is now largely completed (Barron et al., in press; Barron et al., this volume; Berggren et al., in press; Keller et al., 1982; Pisias et al., stratigraphic resolution, this volume; Saito et al., 1975; Theyer et al., 1978). (2) A system of correlative acoustic reflectors (Embley and Johnson, 1980; Mayer, 1979a, b; Schlanger and Douglas, 1974; Shipley et al., this volume) is being delineated over vast distances in the biogenic Tertiary sediments of the region (Mayer et al., this volume). (3) Fine-scale, global to regional geochemical and micropaleontological climatic

reconstructions are beginning to emerge for the Tertiary (Barron, this volume; Bukry, this volume; Hays et al., 1969, 1972; Keller, 1983; Miller and Thomas, this volume; Pisias et al., isotope studies, Site 574, this volume; Prell, this volume; Shackleton and Opdyke, 1973; Thomas, this volume; Vincent and Killingley, this volume; Woodruff et al., 1981). (4) A recurring punctuation of the Tertiary deep-sea record by widely correlative hiatuses or drastic accumulation-rate reductions is finding ever-increasing documentation (Barron and Keller, 1982; Keller and Barron, 1983; Barron et al., this volume).

Although the "absolute" time scale may be the least absolute reference frame available to geologists, it is the first element of any synthesis. And, in terms of correlative power and resolution, we have made vast gains; to appreciate this, one need only compare the biostratigraphic synthesis of DSDP Leg 7 (Hays et al., 1972) with that of the present volume (Barron et al., this volume). Much of this increase in stratigraphic power is directly attributable to the recovery of continuous and barely disturbed HPC sections. Given that our typical sampling interval was 1.5 m, the practical limit of resolution for most of the Tertiary sections cored on Leg 85 is 0.13 to 0.38 m.y. (Barron et al., this volume; Pisias et al., stratigraphic resolution, this volume), and much higher resolution is obviously possible with closer sampling (e.g., Pisias et al., isotope studies, Site 574, this volume). Thus, our chronostratigraphic framework approaches resolutions that allow reliable detection and correlation, over large distances, of at least the major Tertiary oceanographic events that we presently know (Berger, 1982; Keller and Barron, 1983; Kennett, 1983; Loutit and Keigwin, 1982; Vail and Hardenbol, 1979). This level of chronostratigraphic resolution in compositionally different sequences is of fundamental importance; without it, attempts to trace and understand global—or even regional—events lasting 0.01 to 0.1 m.y. will, even though important, yield only generalized results (Keller and Barron, 1983; Vail et al., 1977). A single short event may appear as a hiatus in one sequence, as a cooling event in another, as a sea-level change in yet another, and may result in a distinct acoustic horizon elsewhere. Given possible local distortions of the sedimentary record, only precise cross-correlation would allow us to sort through such a plethora of depositional expression.

The second element of broad significance for a general synthesis of the central Pacific's paleoceanographic history may also be the most fascinating overall result of the drilling. A system of correlatable Tertiary seismic reflectors, spanning vast areas of the carbonate-bearing sediments of the central Pacific, was defined (Mayer et al., this volume). This seismic record of paleoceanographic events results from sedimentary contrasts left in the depositional record by the physical and chemical changes associated with the global events summarized in Table 2. Once each reflector is further understood and defined at several more drill sites, we could enter a phase of rapid and large-scale paleoceanographic assessment and mapping using remote sensing techniques. This possibility holds significant promise for the rapid advancement of this branch of geology.

The third component of an eventual regional paleoceanographic synthesis is a thorough understanding of the climatic and oceanographic cycles and changes that shaped the Tertiary central Pacific depositional record. This understanding is being rapidly achieved. Discrete and significant Tertiary isotopic and carbonate events (Table 2) are discussed in the contributions to this volume (upper Eocene to Oligocene isotopic record of benthic foraminifers [Miller and Thomas]; isotopic analyses of planktonic and benthic foraminifers in the lowermost Miocene to middle Miocene [Vincent and Killingley; Pisias et al.]; and studies of portions of the upper Miocene to Pleistocene geochemical record [Pisias and Prell; Prell]). These geochemical studies are complemented by an evaluation, using micropaleontological data, of oceanographic events ranging from the late Eocene to the Quaternary (Thomas; Barron; Bukry; Saito; Pujos; Labracherie). Despite the discontinuous nature of these studies, and the current uncertainties associated with parts of the "absolute" time scale (Barron et al., this volume), a sequence of regionally correlatable paleoceanographic events is slowly evolving from these multidisciplinary investigations (Table 2; also Mayer et al., this volume).

The final category of studies that will help in elucidating a unified paleoceanographic view of broader scale lies in the ever-widening recognition that the oceanic depositional record is punctuated by recurrent and correlatable hiatuses or drastic decreases of sedimentation rates (Johnson, 1972; van Andel et al., 1975; Moore et al., 1978; Barron and Keller, 1982; Keller and Barron, 1983). Although some oceanic hiatuses are local phenomena, many are likely to be synchronous depositional expressions of global paleoceanographic variations. The latter possibility is reflected in the temporal and spatial incidence and variations of hiatuses, both within and between major ocean basins (Moore et al., 1978; Keller and Barron, 1983). Even though deposition at the easternmost site of Leg 85 (Site 572) was under such highly productive waters that no hiatuses were detected (Barron et al., this volume), sections at Sites 573 to 575 contain prominent examples of these correlative hiatuses or compressed depositional records (Figs. 4 to 7), beginning with the time of the Eocene/Oligocene boundary. Most of these can be correlated (Fig. 5; also Barron et al., this volume) with the "NH" hiatus system developed by Barron and Keller (1982).

According to Moore et al. (1978), hiatuses result when the rate of sediment removal (by dissolution or bottom-current erosion) exceeds the rate of sediment supply (dominantly biological productivity in this region). Barron and Keller (1982) showed that the NH hiatuses occurred during times of polar cooling, except for NH2 (15 to 16 Ma). The authors inferred increased production of Antarctic Bottom Water during such episodes of polar cooling to be the active erosive/corrosive force responsible for the hiatuses. It is also possible for decreased biological productivity to cause hiatuses by reducing the rate of biogenic sediment supply relative to the rate of sediment removal. Although the Leg 85 sites allow an initial assessment of Tertiary productivity changes (discussed ear-

Table 2. Seismic reflectors of the eastern central equatorial Pacific, their age, sedimentary causes, and associated events.

Reflector	Age[a] (Ma)	Impedance[b]	Primary cause[b]	Geochemical events	Hiatus[c]	Paleoceanographic events[d]
Green	3–4	Large density contrast	Carbonate minimum	$\delta^{18}O$ enrichment[e]; $CaCO_3$ dissolution	—	N. Hemisphere glaciation; N. Atlantic erosion; closing of Panama Isthmus
Brown	6.5–7.5	Large density contrast	Carbonate minimum	Chron 6 $\delta^{13}C$ depletion	NH6	Climatic deterioration
Purple	8.5–9.5	Large density contrast	Extreme carbonate minimum	$\delta^{18}O$ enrichment[f]; mid-Chron 10 $CaCO_3$ dissolution[g]	NH5? NH4?	Major N. Atlantic erosion; increase of siliceous deposition in Pacific; major cooling; major drop in sea levels
Red	13.5–14.5	Large density, small velocity contrast	Carbonate minimum	15c $CaCO_3$ dissolution event[h]; 1‰ $\delta^{18}O$ enrichment[i,j]	NH3	Ice buildup in Antarctica; intensification of Antarctic Bottom Water
Lavender	16–17	Very large density, very small velocity contrast	Carbonate minimum	16g $CaCO_3$ dissolution event[k]; Chron 16 $\delta^{13}C$ shift[i]	NH2	Closing of Tethys; Norwegian sea spill; intensified Pacific upwelling
Yellow-Orange	20.5–22.5	Large velocity, small density contrast	Diagenesis	Interval of high $\delta^{13}C$ (Events A, B)[i]	PH?	Opening of Drake Passage; establishment of Circum-Antarctic Current and of steep N–S thermal gradients

[a] Barron et al. (this volume).
[b] Based on Site 574 (Mayer et al., this volume).
[c] Barron and Keller (1982); Keller and Barron (1983).
[d] Discussed in Mayer et al., (this volume).
[e] Prell (this volume).
[f] Savin et al. (1981).
[g] Vincent (1981).
[h] Dunn (in press).
[i] Vincent and Killingley (this volume).
[j] Pisias and Shackleton (this volume).
[k] Dunn (1982).

lier), a proper study of regional productivity changes with time, latitude, and longitude would require considerably more extensive HPC transects (east–west, north–south).

To conclude, we focus on the interval of about 8 to 9 Ma (on the Berggren et al. [in press] time scale; about 9 to 10 Ma on earlier scales) to outline a possible path toward a future paleoceanographic synthesis involving the four elements just iterated. The central basin of the central equatorial Pacific, which lies roughly 30 to 40° west of the Leg 85 drill sites, and thus well outside the high-productivity belt, is an area where accumulation of sediments during the Neogene has generally proceeded below the CCD. Sediment accumulation rates are therefore an order or more slower in this basin (Theyer and Hammond, 1974) than in the region of Leg 85 that lies to the east. The sediments of the central basin are composed primarily of clays, with varying percentages of biogenic silica. Current work on piston cores from the area (W. Dorn, dissertation research under F. T.) demonstrates that many of the NH events (Barron and Keller, 1982) are nevertheless developed there as well. More specifically, the middle to upper Miocene piston core M70-17 (Fig. 9) contains magnetostratigraphic, biostratigraphic, mineralogic, and textural evidence (in X-ray photographs) of a major hiatus that correlates with NH5 of Keller and Barron (1983). (Note that the time scale—that is, the correlation of marine magnetic anomalies with the "absolute" time scale of this particular late Miocene interval—is currently under discussion and revision [Barron et al., this volume; Berggren et al., in press]. The revision means that hiatuses NH4 and NH5, and associated paleoceanographic events, previously separated by about 1.5 m.y., are now separated in time by less than 1 m.y.) NH5 was first described (Barron and Keller, 1982) in sequences of the northeastern Pacific rim, in a depositional environment vastly different from that of Core M70-17.

At Sites 573 to 575, about 30° to the east of Core M70-17, and in a depositional environment above the CCD dominated by carbonate, there is also evidence for the presence of hiatus NH5 (Fig. 9; also Weinreich and Theyer, this volume; Barron et al., this volume). At Site 572, farther to the east (Fig. 1), and under a zone of extreme surficial productivity, this hiatus is not developed, but Bukry (this volume) records a strong nannofloral cooling event at 8 to 9 Ma at this site. This same stratigraphic interval corresponds (at Sites 572 to 575 and elsewhere; Table 2) also to a major drop in $CaCO_3$ percentages (site chapters, this volume). Mayer et al. (this volume) have shown that such a decrease in $CaCO_3$ causes an acoustic impedance change which appears as a strong reflector during seismic profiling (Table 2). Thus, pending resolution of current time-scale quandaries, it is likely that the "Purple" reflector of Mayer et al. (this volume), defined at Site 574, is the seismic expression of NH5 in the carbonate-rich equatorial Pacific (although it may also be correlatable with NH4). On a global scale, the interval between 8 and 9 Ma is generally accepted (Barron and Keller, 1982) to be marked by a dramatic drop in sea level (Vail and Hardenbol, 1979), and by a significant shift to heavier values, indicating cooling, in the oxygen-isotope curve derived from benthic foraminifers (Woodruff et al., 1981).

Evaluation of these diverse lines of evidence requires a more precise stratigraphic linking. Close examination may well reveal that several more or less independent events occurred during this interval. Nevertheless, there is now no doubt that globally drastic cooling, coupled with a strong regression, and significant drops in carbonate deposition, characterized this interval between 8

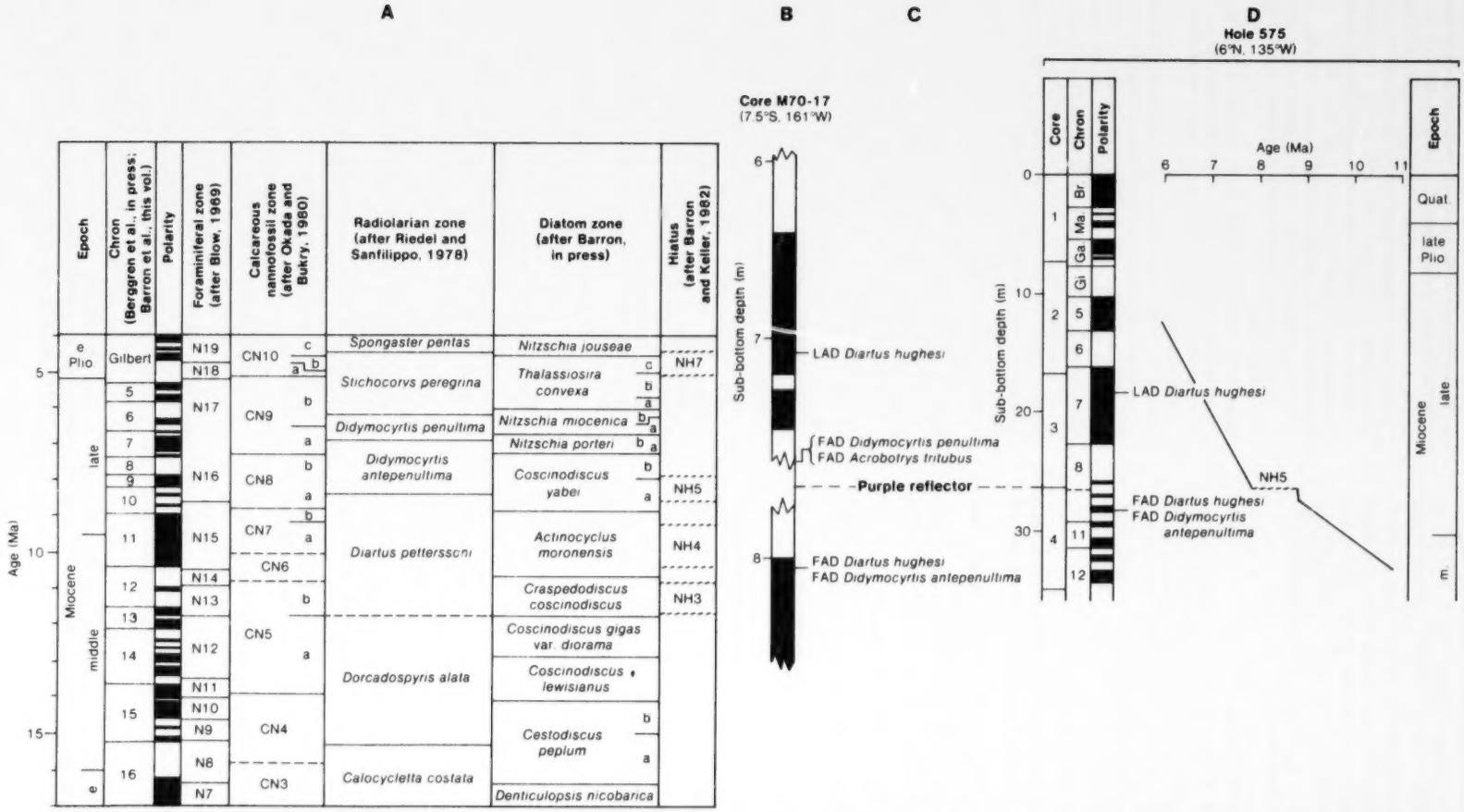

Figure 9. Correlation between (A) the hiatus stratigraphy of Barron and Keller (1982), (B) HIG Piston Core M70-17 from the Pacific's central basin, (C) the "Purple" reflector, and (D) DSDP Site 575 (Hole 575) in the east central equatorial Pacific. Magnetostratigraphic and radiolarian data of Hole 575 (D; Weinreich and Theyer, this volume; Barron et al., this volume) indicate a correlative hiatus. The presence of the hiatus at Site 575 is further supported by the planktonic foraminiferal (Saito, this volume) and diatom (not shown; Barron et al., this volume) stratigraphies. Although separated by more than 26° of longitude, and situated in different depositional environments, the hiatus at both locations spans the entire Chron 9 interval and correlates with NH5. The Purple reflector (C) of Mayer et al. (this volume) also appears to correlate with NH5.

and 9 Ma. What triggered them—and how these changes specifically interacted to cause hiatus NH5 (NH4?) in environments as dissimilar as the Pacific central basin clays, the high-productivity deposits of the Leg 85 area, and the northeast Pacific rim—is at this time still open to speculation. We must continue to study such paleoceanographic phenomena in a variety of depositional environments and within a precise stratigraphic framework to elucidate their functioning.

ACKNOWLEDGMENTS

Our special thanks go to R. G. Douglas, J. D. Hays, and the JOIDES OPP, who led the "battle" for this leg. F. Theyer's research was supported by NSF grants OCE81-17997 and OCE85-04146. L. A. Mayer's work was supported in part by ONR contract N00014-82-K-0625, and by the Natural Sciences and Engineering Council of Canada. E. Thomas's research was supported by NSF grant OCE83-10518.

REFERENCES

Anderson, R. N., and Sclater, J. G., 1972. Topography and evolution of the East Pacific Rise between 5°S and 20°N. *Earth Planet. Sci. Lett.*, 14:433–441.

Arrhenius, G. O., 1952. Sediment cores from the East Pacific. *Swedish Deep-Sea Exped. Rept. 1947–48*, 5(Pt. 3):189–201.

Austin, T. S., 1960. Oceanography of the east central equatorial Pacific as observed during Expedition Eastropic. *U.S. Fishery Bull.*, 168(60):257–282.

Barron, J. A., in press. Miocene to Quaternary planktic diatom biostratigraphy. *In* Bolli, H. M., and Saunders, J. B. (Eds.), *Biostratigraphy of Marine Plankton*: Cambridge (Cambridge University Press).

Barron, J. A., and Keller, G., 1982. Widespread Miocene deep-sea hiatuses: Coincidence with periods of global cooling. *Geology*, 10: 577–581.

Barron, J. A., Keller, G., and Dunn, D. A., in press. A multiple microfossil biochronology for the Miocene. *In* Kennett, J. P. (Ed), *Cenozoic Paleoceanography Synthesis (CENOP)*. Mem. Geol. Soc. Am.

Berger, W. H., 1973. Cenozoic sedimentation in the eastern tropical Pacific. *Geol. Soc. Am. Bull.*, 84:1941–1954.

_____, 1982. Climate steps in ocean history—lessons from the Pleistocene. *In* Berger, W. H., Crowell, J. C., et al. (Eds.), *Climate in Earth History, Studies in Geophysics*: Washington (National Academy Press), pp. 43–54.

Berger, W. H., and von Rad, U., 1972. Cretaceous and Cenozoic sediments from the Atlantic Ocean. *In* Hayes, D. E., Pimm, A. C., et al., *Init. Repts. DSDP*, 14: Washington (U.S. Govt. Printing Office), 787–954.

Berger, W., and Winterer, E. L., 1974. Plate stratigraphy and the fluctuating carbonate line. *In* Hsü, K. J., and Jenkins, H. C. (Eds.), *Pelagic Sediments on Land and Under the Sea*. Int. Assoc. Sedimentol. Spec. Publ., 1:11–48.

Berggren, W. A., Kent, D. V., and Van Couvering, J. A., in press. Neogene geochronology and chronostratigraphy. *In* Snelling, N. J. (Ed.), *Geochronology and the Geologic Time Scale*. Spec. Pap. Geol. Soc. London.

Blow, W. H., 1969. Late middle Eocene to Recent planktonic foraminiferal biostratigraphy. *First Int. Conf. Planktonic Microfossils* (Geneva, 1967), pp. 199–421.

Bramlette, M. N., 1961. Pelagic sediments. *In* Sears, M. (Ed.), *Oceanography*: Washington, D. C. (Am. Assoc. Adv. Sci.), pp. 345–366.

Defant, A., 1961. *Physical Oceanography* (Vol. 1): New York (Pergamon Press).

Dunn, D. A., 1982. Miocene sediments of the equatorial Pacific Ocean: Carbonate stratigraphy and dissolution history [Ph.D. thesis]. University of Rhode Island.

_____, in press. Early to middle Miocene carbonate stratigraphy and correlations of Pacific DSDP sites. *In* Kennett, J. P. (Ed.), *Cenozoic Paleoceanography Synthesis (CENOP)*. Mem. Geol. Soc. Am. 163.

Embley, R. W., and Johnson, D. A., 1980. Acoustic stratigraphy and biostratigraphy of Neogene carbonate horizons in the north equatorial Pacific. *J. Geophys. Res.*, 85:5423–5437.

Ewing, J., Ewing, M., Aitken, T., and Ludwig, W. J., 1968. North Pacific sediment layers measured by seismic profiling. *In* Knopoff, L., Drake, C. L., and Hart, P. J. (Eds.), *The Crust and Upper Mantle of the Pacific Area*. Am. Geophys. Union Geophysical Monograph no. 12, pp. 147–186.

Francheteau, J., Harrison, C. G. A., Schlater, J. G., and Richards, M. L., 1970. Magnetization of Pacific seamounts: A preliminary polar wander curve for the northeastern Pacific. *J. Geophys. Res.*, 75:2035–2061.

Hays, J. D., Saito, T., Opdyke, N. D., and Burckle, L. H., 1969. Pliocene–Pleistocene sediments of the equatorial Pacific: Their paleomagnetic, biostratigraphic and climatic record. *Geol. Soc. Am. Bull.*, 80:1481–1514.

Hays, J. D., et al., 1972. An interpretation of the geologic history of the eastern equatorial Pacific from the drilling results of the *Glomar Challenger*, Leg 9. *In* Hays, J. D., et al., *Init. Repts. DSDP*, 9: Washington (U.S. Govt. Printing Office), 909–931.

Herron, E. M., 1972. Sea floor spreading and the Cenozoic history of the east-central Pacific. *Geol. Soc. Am. Bull.* 83:1671–1692.

Johnson, D. A., 1972. Ocean-floor erosion in the equatorial Pacific. *Geol. Soc. Am. Bull.*, 83:3121–3144.

Keller, G., 1983. Paleoclimatic analyses of middle Eocene through Oligocene planktic foraminiferal faunas. *Palaeogeogr., Palaeoclimatol., Palaeoecol.*, 43:73–94.

Keller, G., and Barron, J. A., 1983. Paleoceanographic implication of Miocene deep sea hiatuses. *Geol. Soc. Am. Bull.*, 94:590–613.

Keller, G., Barron, J. A., and Burckle, L. H., 1982. Paleomagnetic, stable isotope, carbonate, and microfossil stratigraphies in upper Miocene sediments in the North Pacific Ocean. *Mar. Micropaleontol.*, 7:327–357.

Kennett, J. P., 1983. Paleo-oceanography—global ocean evolution. *Rev. Geophys. Space Phys.*, 21:1258–1274.

Koblentz-Mishke, O. J., Volkovinsky, V. V., and Kabanova, J. G., 1970. Plankton primary production of the world ocean. *In* Woosten, W. S. (Ed.), *Scientific Exploration of the South Pacific*: Washington (Nat. Acad. Sci.), pp. 183–193.

Lisitsin, A. P., 1970. Sedimentation and chemical considerations. *In* Wooster, W. S. (Ed.), *Scientific Exploration of the South Pacific*: Washington (Nat. Acad. Sci.), pp. 89–132.

Loutit, T., and Keigwin, L. R., Jr., 1982. Stable isotopic evidence for latest Miocene sea-level fall in the Mediterranean region. *Nature*, 300:163–166.

Mayer, L. A., 1979a. Deep-sea carbonates: Acoustic, physical and stratigraphic properties. *J. Sedimentol. Petrol.*, 49(3):819–836.

_____, 1979b. The origin of fine scale acoustic stratigraphy in deep-sea carbonates. *J. Geophys. Res.*, 84(B11):6177–6184.

Moore, T. C., Jr., 1970. Abyssal hills in the central equatorial Pacific: Sedimentation and stratigraphy. *Deep-Sea Res.*, 17:573–593.

Moore, T. C., Jr., van Andel, T. H., Sancetta, C., and Pisias, N., 1978. Cenozoic hiatuses in marine sediments. *Micropaleontology*, 24:113–138.

Murray, J., and Renard, A. F., 1891. Deep sea deposits: report of the scientific results of the HMS *Challenger*, 1873–1876: London (H.M.S.O.).

Okada, H., and Bukry, D., 1980. Supplementary modification and introduction of code numbers to the low-latitude coccolith biostratigraphic zonation (Bukry, 1973, 1975). *Mar. Micropaleontol.*, 5: 321–325.

Peterson, M. N. A., 1966. Calcite rates of dissolution in a vertical profile in the central Pacific. *Science*, 154:1342–1544.

Prell, W. L., Gardner, J. V., et al., 1982. *Init. Repts. DSDP*, 68: Washington (U.S. Govt. Printing Office).

Reid, J. L., 1962. On the circulation, phosphate-phosphorus content and zooplankton volumes in the upper part of the Pacific Ocean. *Limnol. Oceanogr.*, 7:287–306.

Riedel, W. R., and Funnell, B. M., 1964. Tertiary sediment cores and microfossils from the Pacific Ocean floor. *Q. J. Geol. Soc. London*, 120:305–368.

Riedel, W. R., and Sanfilippo, A., 1978. Stratigraphy and evolution of tropical Cenozoic radiolarians. *Micropaleontology*, 24(1):61–96.

Saito, T., Burckle, L. H., and Hays, J. D., 1975. Late Miocene to Pleistocene biostratigraphy of equatorial Pacific sediments. *In* Saito, T., and Burckle, L. (Eds.), *Late Neogene Epoch Boundaries*: New York (Am. Mus. Nat. History), pp. 226–244.

Savin, S. M., Douglas, R. G., Keller, G., Killingley, J. S., Shaughnessy, L., et al.,1981. Miocene benthic foraminiferal isotope records: A synthesis. *Mar. Micropaleontol.*, 6:423–450.

Schlanger, S. O., and Douglas, R. G., 1974. The pelagic ooze-chalk-limestone transition and its implications for marine stratigraphy. *In* Hsü, K. J., and Jenkyns, H. C. (Eds.), *Pelagic Sediments on Land and Under the Sea*. Int. Assoc. Sedimentol. Spec. Publ., 1: 117–148.

Sclater, J. G., Anderson, R. N., and Bell, M. L., 1971. Elevation of ridges and evolution of the central eastern Pacific. *J. Geophys. Res.*, 76:7888–7915.

Shackleton, N. J., and Opdyke, N. D., 1973. Oxygen isotope and paleomagnetic stratigraphy of equatorial Pacific core V28-238: Oxygen isotope temperatures and ice volume on 105-year and 106-year scale. *Quat. Res.*, 3:39–55.

Theyer, F., and Hammond, S. R., 1974. Paleomagnetic polarity sequence and radiolarian zones, Brunhes to Epoch 20. *Earth Planet. Sci. Lett.*, 22:307–319.

Theyer, F., Mato, C. Y., and Hammond, S. R., 1978. Paleomagnetic and geochronologic calibration of latest Oligocene to Pliocene radiolarian events, equatorial Pacific. *Mar. Micropaleontol.*, 3: 377–395.

Vail, P. R., and Hardenbol, J., 1979. Sea-level changes during the Tertiary. *Oceanus*, 22:71–79.

Vail, P. R., Mitchum, R. M., Jr., and Thompson, S., 1977. Global cycles of relative changes of sea level. *In* Payton, C. E. (Ed.), *Seismic Stratigraphy—Applications to Hydrocarbon Exploration*. Am. Assoc. Petrol. Geol. Mem., 26:63–81.

van Andel, T. H., Heath, G. R., and Moore, T. C., Jr., 1975. Cenozoic history and paleoceanography of the central equatorial Pacific Ocean. *Mem. Geol. Soc. Am.*, 143:1–134.

Vincent, E., 1981. Neogene carbonate stratigraphy of Hess Rise (central North Pacific) and paleoceanographic implications. *In* Thiede, J., Vallier, T. L., et al., *Init. Repts. DSDP*, 62: Washington (U.S. Govt. Printing Office), 571–606.

Winterer, E. L., 1973. Sedimentary facies and plate tectonics of the equatorial Pacific. *Am. Assoc. Pet. Geol. Bull.*, 57:265–282.

Woodruff, F., Savin, S. M., and Douglas, R. G., 1981. Miocene stable isotope record: A detailed deep Pacific Ocean study and its paleoclimatic implications. *Science*, 212:665–668.

Date of Initial Receipt: 4 October 1984
Date of Acceptance: 1 March 1985

APPENDIX. SEDIMENT PHYSICAL PROPERTIES, LEG 85[1]

WET DENSITY, GRAIN DENSITY, POROSITY, WATER CONTENT

HOLE	CORE	SECTION	DEPTH (METERS)	WET DENS. (GM/CC)	GRAIN DENS. (GM/CC)	POROSITY (%)	WATER CONT. (%)
572	1	1	1.08	1.26	2.23	79.4	63.2
572	1	2	2.44	1.37	2.13	67.1	48.8
572	1	3	3.69	1.41	2.19	65.2	46.1
572	1	4	5.21	1.27	1.74	64.2	50.7
572	1	5	6.85	1.42	2.33	68.1	47.9
572	1	6	7.50	1.43	2.46	70.8	49.6
572A	1	1	0.75	1.40	2.61	75.2	53.7
572A	1	2	2.24	1.27	2.30	79.3	62.4
572A	1	3	3.75	1.27	1.99	72.8	57.3
572A	1	4	5.24	1.31	1.99	69.2	53.0
572A	1	5	6.75	1.35	2.39	75.2	55.9
572A	1	6	8.25	1.39	2.25	68.9	49.7
572A	2	1	9.50	1.32	2.06	70.2	53.3
572A	2	2	11.00	1.28	1.77	63.2	49.2
572A	2	3	12.50	1.30	1.88	65.6	50.3
572A	2	4	14.00	1.31	1.90	65.3	49.7
572A	2	5	15.50	1.34	2.19	71.2	53.0
572A	2	6	17.79	1.28	1.91	69.3	54.2
572A	3	1	19.77	1.33	2.44	77.2	58.1
572A	3	2	21.25	1.29	2.32	77.6	60.0
572A	3	3	22.77	1.31	2.76	82.1	62.5
572A	3	4	24.27	1.37	2.63	77.5	56.6
572A	3	5	25.77	1.37	2.74	78.5	57.2
572A	3	6	27.24	1.38	2.69	77.3	55.9
572A	4	1	29.35	1.36	2.54	76.6	56.3
572A	4	4	33.96	1.35	2.60	78.3	58.2
572A	4	5	34.60	1.43	2.65	74.1	51.9
572A	5	1	37.08	1.33	2.38	76.2	57.3
572A	5	2	38.58	1.37	2.62	77.1	56.2
572A	5	3	40.08	1.40	2.26	68.3	48.8
572A	5	4	41.58	1.43	2.41	69.3	48.3
572A	5	5	43.08	1.43	2.52	71.9	50.4
572A	5	6	44.58	1.34	2.73	80.2	59.8
572A	6	2	48.16	1.36	2.49	75.9	55.9
572A	6	3	49.68	1.47	2.53	69.1	46.9
572A	6	4	51.18	1.45	2.68	73.2	50.4
572A	6	5	52.68	1.30	2.43	79.3	61.1
572A	6	6	54.18	1.37	2.51	75.6	55.3
572A	7	2	57.48	1.38	2.50	74.4	53.8
572A	7	3	58.98	1.31	2.62	80.7	61.5
572A	7	4	60.48	1.48	2.61	70.2	47.4
572A	7	5	61.98	1.47	2.38	66.3	45.2
572A	7	6	63.48	1.52	2.61	67.9	44.8
572A	8	1	64.88	1.51	2.56	67.6	44.8
572A	8	2	66.38	1.42	2.69	75.3	53.1
572A	8	4	69.38	1.22	1.97	77.5	63.6
572A	8	5	70.88	1.25	2.15	78.5	62.9
572A	9	1	73.06	1.45	2.61	72.0	49.7
572A	9	2	74.56	1.41	2.50	72.8	51.7
572A	9	3	76.06	1.39	2.81	78.5	56.6
572A	9	4	77.56	1.56	2.89	70.5	45.2
572A	9	5	79.07	1.61	2.82	66.6	41.5
572A	9	6	80.58	1.40	2.15	65.1	46.5
572A	10	2	84.06	1.48	2.66	70.9	47.8
572A	10	3	85.56	1.51	2.64	69.0	45.8
572A	10	4	87.09	1.58	2.79	67.8	43.0
572A	10	5	88.56	1.63	3.02	68.8	42.2
572A	11	1	92.17	1.36	2.30	72.6	53.6
572A	11	2	93.65	1.53	2.67	68.1	44.5
572A	11	3	95.16	1.44	2.56	71.8	49.9
572A	11	4	96.66	1.49	2.62	69.7	46.8
572A	11	5	98.16	1.35	2.15	69.5	51.4
572A	11	6	99.66	1.36	2.31	72.8	53.7
572A	12	1	101.46	1.45	2.67	73.0	50.4
572A	12	2	102.96	1.34	2.19	71.0	52.8
572A	12	3	104.46	1.37	2.36	73.0	53.4

[1] Mayer, L., Theyer, F., et al., *Init. Repts. DSDP*, 85: Washington (U.S. Govt. Printing Office).

HOLE	CORE	SECTION	DEPTH (METERS)	WET DENS. (GM/CC)	GRAIN DENS. (GM/CC)	POROSITY (%)	WATER CONT. (%)
572A	12	5	107.46	1.26	1.75	65.1	51.6
572A	12	5	107.46	1.40	2.39	71.3	51.1
572A	12	6	108.96	1.47	2.53	69.0	46.9
572A	13	1	110.64	1.26	2.22	78.5	62.2
572A	13	2	112.18	1.50	2.67	70.3	47.0
572A	13	3	113.66	1.45	2.71	73.7	50.9
572A	13	4	115.16	1.50	2.67	70.1	46.8
572A	13	5	116.68	1.42	2.45	70.7	49.6
572A	13	6	118.16	1.39	2.48	73.5	52.8
572A	14	1	119.86	1.43	2.43	70.1	49.1
572A	14	2	121.36	1.31	2.21	74.4	56.8
572A	14	3	122.86	1.44	2.40	68.5	47.6
572A	14	4	124.36	1.38	2.39	72.8	52.8
572A	14	5	125.86	1.44	2.42	68.9	47.8
572A	14	6	127.36	1.32	1.97	67.1	50.8
572A	15	1	129.06	1.55	2.53	63.8	41.0
572A	15	2	130.56	1.54	2.73	68.5	44.3
572A	15	3	132.06	1.27	1.81	65.8	51.6
572A	15	4	133.56	1.40	2.20	66.3	47.3
572A	15	5	135.06	1.35	2.38	74.4	55.0
572A	15	6	136.56	1.47	2.52	69.0	46.8
572A	16	2	139.36	1.68	3.41	71.6	42.5
572A	16	4	142.36	1.60	2.67	64.1	40.0
572A	16	5	143.88	1.61	2.82	66.6	41.4
572A	17	1	146.06	1.53	2.68	68.6	44.9
572A	17	2	147.58	1.49	2.59	69.2	46.4
572A	17	3	149.08	1.51	2.82	71.9	47.6
572A	17	4	150.58	1.44	2.37	67.8	47.0
572A	17	5	152.08	1.46	2.92	76.3	52.4
572B	1	2	156.26	1.41	2.37	70.3	50.0
572B	1	3	157.76	1.45	2.51	70.4	48.7
572B	2	1	160.08	1.47	2.66	71.9	49.0
572B	2	2	161.68	1.41	2.45	71.5	50.6
572B	2	3	163.48	1.34	2.17	70.9	53.0
572B	3	1	164.98	1.21	1.82	74.3	61.3
572B	3	2	166.48	1.33	2.19	72.0	54.0
572B	3	3	167.98	1.27	1.90	69.7	54.8
572B	4	1	169.58	1.36	2.23	70.9	52.2
572B	4	2	171.08	1.30	2.45	79.5	61.2
572C	1	1	0.78	1.34	2.74	80.7	60.4
572C	1	2	2.28	1.26	2.13	76.8	60.9
572C	1	3	3.78	1.48	2.94	75.4	51.0
572C	1	5	6.78	1.41	2.38	69.9	49.4
572C	1	6	8.28	1.48	2.88	74.2	50.0
572C	2	1	10.88	1.36	2.68	78.5	57.6
572C	2	2	12.38	1.50	2.83	72.8	48.6
572C	2	3	13.88	1.39	2.88	79.2	57.0
572C	2	4	15.38	1.41	3.43	83.1	58.9
572C	2	5	16.88	1.41	2.82	77.3	54.7
572C	2	6	18.38	1.45	3.14	78.9	54.3
572C	3	1	20.48	1.32	2.38	76.8	58.1
572C	3	2	21.98	1.34	2.86	81.7	61.0
572C	3	3	23.48	1.39	2.82	78.2	56.0
572C	3	4	24.98	1.36	2.81	79.9	58.5
572C	3	5	26.48	1.31	2.34	76.7	58.5
572C	3	6	27.98	1.36	2.83	80.2	58.8
572C	4	1	30.08	1.41	2.81	77.1	54.5
572C	4	2	31.58	1.35	2.43	75.8	56.3
572C	4	3	33.08	1.41	2.67	75.5	53.6
572C	4	4	34.58	1.38	2.67	77.4	56.2
572C	4	5	36.08	1.40	2.67	75.7	53.9
572C	4	6	37.58	1.26	2.19	78.4	62.4
572C	5	1	39.66	1.30	2.02	71.0	54.8
572C	5	2	41.20	1.26	1.82	67.8	53.7
572C	5	3	42.66	1.39	2.53	74.3	53.3
572C	5	4	44.16	1.30	2.16	74.0	56.8
572C	5	5	45.66	1.26	2.34	80.8	64.2
572C	5	6	46.99	1.20	1.88	77.1	64.1
572C	6	1	49.15	1.45	2.45	68.7	47.3
572C	6	2	50.74	1.44	2.68	74.0	51.5
572C	6	3	52.24	1.35	2.56	77.5	57.3
572C	6	4	53.76	1.33	2.15	71.3	53.6
572C	6	5	55.26	1.47	2.54	69.5	47.3
572C	6	6	56.76	1.29	2.53	80.8	62.5
572C	7	1	58.86	1.33	2.26	74.0	55.7
572C	7	2	60.36	1.33	2.23	72.9	54.7
572C	7	3	61.86	1.44	2.32	67.0	46.7
572C	7	4	63.36	1.43	2.35	68.3	47.9
572C	7	5	64.91	1.39	2.75	77.5	55.5
572C	7	6	66.36	1.43	2.26	66.0	46.2
572C	8	1	68.46	1.33	2.12	71.0	53.6
572C	8	2	69.96	1.48	2.64	70.8	47.9

HOLE	CORE	SECTION	DEPTH (METERS)	WET DENS. (GM/CC)	GRAIN DENS. (GM/CC)	POROSITY (%)	WATER CONT. (%)
572C	8	3	71.56	1.20	1.65	69.8	58.3
572C	8	4	72.98	1.33	2.30	74.3	55.7
572C	8	5	74.46	1.34	2.26	72.6	54.0
572C	8	6	75.98	1.25	1.82	69.8	56.0
572C	9	1	78.06	1.54	2.69	67.8	43.9
572C	9	2	79.58	1.40	2.34	70.3	50.3
572C	9	3	81.06	1.44	2.40	68.9	48.0
572C	9	4	82.56	1.39	2.27	69.4	50.0
572C	9	5	84.07	1.48	2.46	66.7	45.0
572C	9	6	85.57	1.36	2.04	65.6	48.3
572C	10	1	87.66	1.50	2.63	69.2	46.1
572C	10	2	89.16	1.41	2.23	66.5	47.1
572C	10	3	90.66	1.36	2.06	66.0	48.5
572C	10	4	92.16	1.34	2.17	70.7	52.7
572C	10	5	93.66	1.31	2.02	70.0	53.6
572C	10	6	95.16	1.41	2.29	68.4	48.6
572C	11	1	97.26	1.29	1.99	71.2	55.3
572C	11	2	98.76	1.30	2.08	71.8	55.0
572C	11	3	100.26	1.46	2.48	69.0	47.3
572C	12	1	102.26	1.26	1.92	72.1	57.3
572C	12	2	103.76	1.35	2.11	68.1	50.3
572C	12	3	105.28	1.40	2.34	70.3	50.2
572C	13	1	107.28	1.42	2.56	73.1	51.5
572C	13	2	108.78	1.36	2.38	74.2	54.7
572C	13	3	110.28	1.41	2.56	73.6	52.2
572C	14	1	112.26	1.51	2.66	69.3	45.9
572C	14	2	113.78	1.35	2.42	75.2	55.6
572C	14	3	115.28	1.41	2.39	70.8	50.3
572C	14	4	116.78	1.41	2.66	75.1	53.1
572C	14	5	118.28	1.50	2.67	70.4	47.1
572C	15	1	121.88	1.45	2.46	69.2	47.7
572C	15	2	123.38	1.46	2.56	70.7	48.6
572C	15	3	124.88	1.47	2.57	70.2	47.9
572C	15	4	126.38	1.54	2.66	67.7	44.1
572C	15	5	127.88	1.56	2.57	64.1	41.0
572C	15	6	129.38	1.56	2.69	66.7	42.7
572C	16	1	131.48	1.47	2.61	70.5	47.8
572C	16	3	134.48	1.46	2.49	69.2	47.4
572C	16	3	134.48	1.46	2.49	69.2	47.4
572C	16	4	135.98	1.58	2.63	64.8	41.1
572C	16	5	137.48	1.57	2.61	64.7	41.3
572C	16	6	138.98	1.58	2.73	66.7	42.4
572C	17	1	141.08	1.55	2.63	65.2	42.7
572C	17	2	142.58	1.59	2.67	64.6	40.6
572C	17	3	144.08	1.61	2.67	63.6	39.6
572C	17	4	145.58	1.48	2.64	70.5	47.6
572C	18	2	152.18	1.52	2.63	67.9	44.7
572C	18	3	153.68	1.50	2.64	69.8	46.6
572C	18	4	155.18	1.50	2.56	68.2	45.6
572C	18	5	156.68	1.39	2.31	69.7	50.0
572C	18	6	158.18	1.49	2.52	67.5	45.2
572C	20	1	165.28	1.35	2.43	75.4	55.8
572C	20	2	166.78	1.33	2.19	72.5	54.5
572C	20	3	168.28	1.39	2.41	72.0	51.6
573	1	1	0.78	1.43	2.66	74.2	51.9
573	2	1	2.76	1.33	2.59	79.1	59.4
573	2	2	4.26	1.38	2.69	77.3	55.9
573	2	3	5.76	1.42	2.72	75.5	53.2
573	2	4	7.26	1.53	2.78	70.4	46.1
573	2	5	8.76	1.44	2.68	73.6	51.0
573	2	6	10.26	1.50	2.66	69.6	46.2
573	3	1	12.26	1.57	2.74	67.0	42.6
573	3	2	13.76	1.49	2.73	71.7	48.1
573	3	3	15.26	1.41	2.61	74.7	53.0
573	3	4	16.76	1.53	2.67	68.5	44.9
573	3	5	18.26	1.22	2.10	80.2	65.9
573	3	6	19.76	1.45	2.59	71.5	49.2
573	4	1	22.04	1.28	2.53	81.8	64.0
573	4	2	23.33	1.44	2.51	70.6	49.0
573	4	3	24.76	1.48	2.61	70.2	47.4
573	4	4	26.26	1.53	2.78	69.9	45.5
573	4	5	27.76	1.33	2.47	77.4	58.1
573	4	6	29.27	1.36	2.74	79.5	58.7
573	5	1	31.26	1.47	2.80	74.1	50.5
573	5	2	32.76	1.31	2.32	76.2	58.0
573	5	3	34.26	1.52	2.65	68.2	44.8
573	5	4	35.76	1.34	2.51	77.7	58.1
573	5	5	37.26	1.49	2.67	70.4	47.2
573	5	6	38.76	1.56	2.73	67.4	43.1
573	6	1	40.56	1.40	2.54	74.4	53.3
573	6	2	41.56	1.43	2.82	76.3	53.3
573	6	3	43.06	1.32	2.43	77.8	59.0
573	6	4	44.56	1.36	2.59	77.3	56.9

HOLE	CORE	SECTION	DEPTH (METERS)	WET DENS. (GM/CC)	GRAIN DENS. (GM/CC)	POROSITY (%)	WATER CONT. (%)
573	6	5	46.06	1.32	2.40	76.8	58.0
573	6	6	47.56	1.44	2.84	76.2	53.1
573	7	2	50.26	1.39	3.03	80.8	58.2
573	7	3	51.76	1.29	2.29	77.4	59.9
573	7	4	53.26	1.26	2.59	83.8	66.7
573	7	5	54.76	1.24	2.44	83.2	66.9
573	7	6	56.26	1.47	2.70	72.3	49.2
573	8	1	57.76	1.39	2.52	74.0	53.1
573	8	2	59.26	1.32	2.78	82.1	62.3
573	8	3	60.76	1.46	2.78	74.1	50.7
573	8	4	62.26	1.36	2.67	78.7	58.0
573	8	5	63.76	1.50	2.50	66.8	44.6
573	8	6	65.26	1.39	2.51	73.8	52.9
573	9	1	67.46	1.49	2.54	68.3	45.9
573	9	2	68.96	1.37	2.61	64.2	40.8
573	9	3	70.46	1.52	2.68	69.2	45.6
573	9	4	71.96	1.36	2.64	66.0	42.3
573	9	5	73.46	1.61	2.69	64.0	39.8
573	9	6	74.96	1.57	2.64	65.2	41.5
573	10	1	76.96	1.47	2.62	70.7	48.0
573	10	2	78.46	1.40	2.58	74.5	53.1
573	10	3	79.96	1.44	2.55	71.3	49.4
573	10	4	81.46	1.53	2.64	67.9	44.5
573	10	5	82.96	1.49	2.62	70.1	47.2
573	10	6	84.46	1.35	2.53	77.2	57.3
573	11	1	86.46	1.43	2.47	70.5	49.1
573	11	2	87.96	1.41	2.55	73.7	52.4
573	11	3	89.46	1.67	2.98	66.3	39.8
573	11	4	90.96	1.61	2.59	61.6	38.3
573	11	5	92.46	1.62	2.64	62.2	38.5
573	11	6	93.96	1.65	2.66	60.6	36.7
573	12	1	95.96	1.60	2.71	63.0	40.6
573	12	2	97.46	1.80	2.74	54.0	30.0
573	12	3	98.96	1.60	2.70	65.0	40.8
573	12	4	100.46	1.57	2.74	67.3	42.9
573	12	5	101.96	1.53	2.64	67.7	44.3
573	12	6	103.46	1.55	2.66	67.1	43.4
573	13	1	105.16	1.53	2.56	65.7	42.8
573	13	2	106.26	1.51	2.65	68.9	45.5
573	13	3	107.76	1.47	2.64	71.2	48.4
573	13	4	109.26	1.52	2.71	69.5	45.7
573	13	5	110.76	1.54	2.68	67.8	44.0
573	13	6	112.26	1.60	2.63	63.4	39.7
573	14	1	113.36	1.65	2.69	61.3	37.1
573	14	2	114.86	1.63	2.72	63.3	38.8
573	14	3	116.36	1.64	2.69	62.4	38.1
573	14	4	117.86	1.57	2.57	63.5	40.3
573	14	5	119.36	1.64	2.66	61.7	37.7
573	14	6	120.86	1.62	2.67	63.1	39.1
573	15	1	122.86	1.53	2.63	67.2	43.9
573	15	2	124.36	1.52	2.51	65.8	43.4
573	15	3	125.86	1.55	2.66	66.7	42.9
573	15	4	127.36	1.61	2.68	63.7	39.6
573	15	5	128.86	1.55	2.64	66.6	43.0
573	15	6	130.36	1.66	2.74	62.0	37.3
573	16	1	132.06	1.61	2.63	62.5	38.8
573	16	2	133.56	1.65	2.68	61.3	37.2
573	16	3	135.06	1.50	2.60	68.7	45.8
573	16	4	136.56	1.56	2.62	65.6	42.2
573	16	5	138.06	1.51	2.60	68.1	45.1
573	16	6	139.56	1.49	2.60	69.3	46.5
573	17	1	140.86	1.51	2.44	64.7	42.9
573	17	1	140.86	1.51	2.52	66.5	44.1
573	17	2	142.36	1.54	2.52	64.7	42.1
573	17	3	143.86	1.63	2.61	61.2	37.7
573	17	5	146.86	1.60	2.59	62.2	38.9
573	17	6	148.36	1.49	2.43	65.6	44.0
573	18	1	149.76	1.59	2.67	65.0	41.0
573	18	2	151.26	1.69	2.70	59.4	35.2
573	18	3	152.77	1.34	2.23	72.4	54.1
573	19	1	154.76	1.56	2.71	67.5	43.3
573	19	2	156.26	1.54	2.60	66.3	43.1
573	19	3	157.76	1.34	2.23	72.2	53.8
573A	1	1	5.26	1.36	2.54	76.8	56.7
573A	1	2	6.76	1.42	2.72	75.8	53.5
573A	1	3	8.26	1.36	2.54	76.3	56.0
573A	1	4	9.76	1.48	2.69	71.6	48.5
573A	1	5	11.26	1.53	2.73	69.2	45.1
573A	1	6	12.76	1.54	2.77	69.5	45.2
573A	2	1	14.76	1.53	2.70	68.5	44.6
573A	2	2	16.26	1.53	2.74	69.4	45.3
573A	2	3	17.76	1.29	2.65	82.2	63.5
573A	2	4	19.26	1.48	2.27	61.8	41.7

HOLE	CORE	SECTION	DEPTH (METERS)	WET DENS. (GM/CC)	GRAIN DENS. (GM/CC)	POROSITY (%)	WATER CONT. (%)
573A	2	5	20.76	1.42	2.63	74.1	52.0
573A	3	1	22.86	1.53	2.71	69.3	45.4
573A	3	2	24.36	1.44	2.73	74.5	51.6
573A	3	3	25.86	1.42	2.69	75.2	53.0
573A	3	4	27.36	1.36	2.59	77.4	56.9
573A	3	5	28.86	1.32	2.59	79.8	60.4
573A	3	6	30.36	1.43	2.64	73.5	51.3
573A	4	1	32.06	1.41	2.66	75.4	53.6
573A	4	2	33.56	1.52	2.67	68.8	45.3
573A	4	3	35.06	1.42	2.68	74.8	52.6
573A	4	4	36.56	1.43	2.71	74.9	52.4
573A	4	5	38.06	1.48	2.80	73.2	49.4
573A	4	6	39.56	1.42	2.59	73.7	51.9
573A	5	1	40.66	1.41	2.61	74.4	52.8
573A	5	2	42.06	1.39	2.65	76.3	54.9
573A	5	3	43.56	1.34	2.69	79.7	59.3
573A	5	4	45.06	1.32	2.75	81.9	62.3
573A	5	5	46.56	1.45	2.78	74.9	51.8
573A	5	6	48.06	1.31	2.65	81.0	61.7
573A	6	1	49.96	1.36	2.57	77.2	56.9
573A	6	2	51.46	1.27	2.65	83.5	65.6
573A	6	3	52.96	1.31	2.82	83.2	63.7
573A	6	4	54.46	1.44	2.96	77.5	53.7
573A	6	5	55.96	1.43	2.77	75.8	53.0
573A	6	6	57.46	1.31	2.50	79.3	60.5
573B	1	1	139.26	1.54	2.63	67.0	43.5
573B	1	2	140.76	1.61	2.66	63.4	39.4
573B	1	3	142.26	1.66	2.71	61.5	37.1
573B	1	4	143.76	1.53	2.63	67.2	43.8
573B	1	5	145.26	1.71	2.70	58.3	34.2
573B	1	6	146.59	1.59	2.66	64.6	40.7
573B	2	1	148.76	1.53	2.65	67.6	44.1
573B	2	2	150.31	1.61	2.66	62.9	39.0
573B	2	3	151.61	1.53	2.58	66.7	43.7
573B	2	5	154.76	1.58	2.62	64.3	40.8
573B	2	5	155.24	1.55	2.61	66.0	42.7
573B	2	6	156.26	1.58	2.62	64.0	40.5
573B	3	1	158.26	1.59	2.64	69.3	46.1
573B	3	2	159.56	1.47	2.59	70.8	48.3
573B	3	3	161.26	1.49	2.60	69.1	46.3
573B	3	4	162.76	1.47	2.60	70.8	48.3
573B	3	5	164.26	1.47	2.50	68.5	46.5
573B	3	6	165.76	1.52	2.65	68.6	45.1
573B	4	1	167.76	1.51	2.67	69.1	45.6
573B	4	2	169.26	1.57	2.68	66.2	42.2
573B	4	3	170.76	1.51	2.64	68.7	45.5
573B	4	4	172.26	1.49	2.65	70.2	47.0
573B	4	5	173.76	1.53	2.70	68.7	44.8
573B	4	6	175.26	1.48	2.67	71.1	47.9
573B	5	2	178.76	1.62	2.71	64.1	39.7
573B	5	3	180.26	1.65	2.61	59.2	35.8
573B	5	4	181.76	1.65	2.51	56.8	34.5
573B	5	5	183.26	1.70	2.68	58.7	34.6
573B	5	6	184.76	1.70	2.70	59.1	34.8
573B	6	2	188.26	1.63	2.68	62.2	38.0
573B	6	3	189.76	1.69	2.70	59.3	35.1
573B	6	4	191.26	1.65	2.69	61.2	37.0
573B	6	5	192.76	1.67	2.73	61.2	36.7
573B	6	6	194.26	1.66	2.68	60.6	36.5
573B	7	1	195.71	1.69	2.68	58.7	34.7
573B	7	2	197.41	1.82	2.74	52.8	28.9
573B	7	3	199.26	1.73	2.69	56.5	32.6
573B	7	4	200.76	1.78	2.74	54.8	30.7
573B	7	5	202.26	1.75	2.62	53.4	30.4
573B	8	1	205.76	1.61	2.63	62.6	38.8
573B	8	2	207.26	1.65	2.60	59.6	36.2
573B	8	3	208.76	1.63	2.77	64.6	39.7
573B	8	4	210.26	1.65	2.59	58.9	35.6
573B	8	5	211.76	1.64	2.64	61.0	37.3
573B	8	6	213.26	1.66	2.59	58.5	35.2
573B	9	2	216.76	1.68	2.82	62.8	37.5
573B	9	2	216.76	1.66	2.94	66.0	39.8
573B	9	3	218.26	1.78	2.98	60.5	33.9
573B	9	4	219.76	1.77	3.04	62.2	35.1
573B	9	5	221.26	1.76	3.00	61.9	35.2
573B	9	6	222.76	1.73	2.84	60.1	34.7
573B	10	1	224.76	1.63	2.65	62.0	38.0
573B	10	2	226.36	1.74	2.79	58.7	33.7
573B	10	3	227.76	1.75	2.79	58.0	33.1
573B	10	4	229.26	1.77	2.86	58.3	32.9
573B	10	5	230.76	1.73	2.68	56.5	32.7
573B	10	6	232.26	1.58	2.62	63.8	40.3
573B	11	1	234.26	1.74	2.67	55.7	32.0

HOLE	CORE	SECTION	DEPTH (METERS)	WET DENS. (GM/CC)	GRAIN DENS. (GM/CC)	POROSITY (%)	WATER CONT. (%)
573B	11	2	235.76	1.79	2.70	53.2	29.6
573B	11	3	237.26	1.76	2.75	56.2	31.9
573B	11	4	238.76	1.71	2.65	57.0	33.3
573B	11	5	240.26	1.66	2.67	60.4	36.3
573B	11	6	241.76	1.71	2.62	56.2	32.9
573B	12	1	243.76	1.72	2.73	58.7	34.2
573B	12	2	245.26	1.63	2.62	61.4	37.8
573B	12	3	246.76	1.75	2.77	57.6	32.9
573B	12	4	248.21	1.67	2.86	63.8	38.1
573B	12	5	249.51	1.72	2.71	57.8	33.6
573B	13	1	253.26	1.67	2.68	60.0	35.9
573B	13	2	254.76	1.74	2.75	57.6	33.1
573B	13	3	256.26	1.72	2.76	59.3	34.5
573B	13	4	257.76	1.63	2.62	61.2	37.5
573B	13	5	259.26	1.67	2.64	59.3	35.5
573B	13	6	260.76	1.56	2.59	64.7	41.3
573B	14	1	262.76	1.68	2.68	59.6	35.5
573B	14	2	264.26	1.60	2.47	59.0	36.8
573B	14	3	265.76	1.65	2.66	61.0	37.0
573B	14	4	267.26	1.69	2.64	57.9	34.3
573B	14	5	268.76	1.68	2.60	57.6	34.3
573B	14	6	270.26	1.67	2.58	57.7	34.6
573B	15	1	272.26	1.70	2.59	55.8	32.8
573B	15	2	273.76	1.81	2.74	53.5	29.5
573B	15	2	273.76	1.80	2.81	55.8	31.0
573B	15	3	275.26	1.79	2.73	54.3	30.4
573B	15	5	278.26	1.83	2.74	52.6	28.8
573B	16	1	281.76	1.64	2.66	61.3	37.2
573B	16	2	283.26	1.75	2.71	56.4	32.3
573B	16	3	284.76	1.78	2.71	54.5	30.6
573B	16	4	286.26	1.78	2.71	54.2	30.4
573B	16	5	287.76	1.72	2.67	57.2	33.3
573B	17	1	291.26	1.85	2.80	53.0	28.7
573B	17	2	292.76	1.80	2.71	53.3	29.6
573B	17	3	294.26	1.80	2.65	51.3	28.5
573B	17	4	295.76	1.82	2.69	51.6	28.4
573B	17	5	297.26	1.80	2.74	54.0	30.0
573B	18	1	300.76	1.81	2.69	51.8	28.6
573B	18	2	302.26	1.84	2.69	50.2	27.2
573B	18	3	303.76	1.77	2.66	53.8	30.5
573B	19	1	310.26	1.76	2.71	55.4	31.4
573B	19	2	311.76	1.77	2.71	55.0	31.1
573B	20	1	319.79	1.89	3.08	57.0	30.1
573B	20	2	321.26	1.80	2.69	52.6	29.2
573B	20	3	322.66	1.83	2.70	51.4	28.1
573B	20	4	324.26	1.83	2.72	51.7	28.2
573B	20	5	325.76	1.80	2.70	52.7	29.2
573B	20	6	327.46	1.79	2.74	54.5	30.4
573B	21	1	329.51	1.75	2.70	56.2	32.2
573B	21	2	330.86	1.77	2.69	54.5	30.8
573B	21	3	332.39	1.80	2.70	53.3	29.7
573B	21	4	333.76	1.81	2.71	52.8	29.2
573B	22	1	338.71	1.76	2.67	54.3	30.8
573B	22	2	340.46	1.81	2.76	53.8	29.7
573B	22	3	341.86	1.78	2.67	53.1	29.8
573B	22	4	343.16	1.81	2.71	52.7	29.1
573B	23	1	348.41	1.83	2.72	51.5	28.1
573B	23	2	349.74	1.81	2.72	52.6	29.0
573B	23	3	351.61	1.81	2.69	52.2	28.9
573B	23	4	352.81	1.82	2.69	51.3	28.1
573B	24	1	357.53	1.85	2.73	51.0	27.6
573B	24	2	359.02	1.85	2.70	49.8	26.9
573B	24	3	360.67	1.81	2.70	52.6	29.1
573B	25	1	367.22	1.83	2.74	52.2	28.5
573B	26	2	378.40	1.80	2.68	52.8	29.4
573B	26	3	379.75	1.77	2.72	55.2	31.1
573B	26	4	381.20	1.80	2.75	54.3	30.1
573B	26	5	382.33	1.80	2.70	52.6	29.2
573B	27	1	386.09	1.84	2.72	51.5	28.1
573B	27	2	387.61	1.85	2.72	50.7	27.4
573B	27	3	388.94	1.83	2.71	51.5	28.2
573B	27	4	390.63	1.78	2.71	54.1	30.3
573B	28	1	395.71	1.82	2.72	52.3	28.7
573B	28	2	397.47	1.83	2.71	51.5	28.2
573B	28	3	398.61	1.83	2.71	51.2	27.9
573B	29	1	405.40	1.84	2.68	50.1	27.3
573B	29	2	407.11	1.80	2.71	53.0	29.3
573B	29	3	408.07	1.83	2.72	51.6	28.1
573B	29	4	409.91	1.80	2.70	52.7	29.2
573B	29	5	411.03	1.80	2.68	52.2	28.9
573B	30	1	414.97	1.80	2.71	53.3	29.6
573B	30	3	418.27	1.80	2.70	53.1	29.5
573B	30	4	418.93	1.79	2.70	53.3	29.8
573B	31	1	424.21	1.83	2.71	51.2	27.9

HOLE	CORE	SECTION	DEPTH (METERS)	WET DENS. (GM/CC)	GRAIN DENS. (GM/CC)	POROSITY (%)	WATER CONT. (%)
573B	32	1	434.17	1.86	2.72	50.1	26.9
573B	32	2	436.11	1.84	2.70	51.0	27.8
573B	33	5	449.13	1.83	2.76	53.2	29.1
573B	34	1	452.71	1.81	2.68	51.7	28.5
573B	35	1	462.16	1.68	2.59	57.0	33.9
573B	35	2	463.36	1.67	2.58	57.7	34.5
573B	35	3	465.21	1.69	2.59	56.6	33.5
573B	35	4	467.06	1.76	2.61	52.5	29.8
573B	35	5	468.31	1.77	2.64	52.8	29.7
573B	36	1	471.76	1.78	2.64	52.1	29.2
573B	36	2	473.74	1.81	2.66	51.6	28.6
573B	36	3	474.14	1.82	2.69	51.5	28.3
573B	37	1	481.04	1.78	2.67	53.0	29.7
573B	38	1	490.71	1.84	2.68	50.1	27.3
573B	38	2	492.79	1.68	2.49	54.0	32.1
573B	38	3	494.29	1.79	2.64	51.6	28.8
573B	39	1	499.76	1.79	2.59	50.5	28.2
573B	39	2	501.66	2.08	2.65	34.6	16.6
573B	39	3	503.26	1.83	2.45	42.7	23.3
573B	40	1	509.81	1.63	2.44	56.5	34.8
573B	42	1	520.94	1.81	2.68	51.7	28.5
573B	42	1	520.94	1.81	2.67	51.7	28.6
573B	42	2	523.31	1.62	3.06	70.0	43.3
573B	42	3	523.69	1.65	3.13	69.4	42.1
573B	42	4	526.43	1.97	2.75	44.5	22.6
574	1	1	0.65	1.41	2.54	73.2	51.7
574	1	2	2.26	1.18	2.70	89.3	75.7
574	1	3	3.75	1.38	2.57	75.5	54.6
574	2	1	5.26	1.31	2.69	81.5	62.0
574	2	2	6.76	1.30	2.71	82.2	63.0
574	2	3	8.47	1.22	2.44	84.8	69.5
574	2	4	9.76	1.34	2.63	79.3	59.2
574	2	5	11.26	1.42	2.59	73.2	51.4
574	2	6	12.76	1.37	2.62	77.1	56.2
574	3	2	16.26	1.19	2.45	86.8	73.0
574	3	3	17.76	1.24	2.47	83.4	67.1
574	3	4	19.26	1.25	2.66	85.0	67.9
574	3	5	20.76	1.17	2.45	87.9	74.9
574	3	6	22.26	1.19	2.54	87.8	73.8
574	4	1	24.26	1.14	2.22	88.4	77.5
574	4	2	25.76	1.22	2.52	85.8	70.6
574	4	3	27.26	1.23	2.69	86.2	69.9
574	4	4	28.76	1.25	2.49	83.2	66.6
574	4	5	30.26	1.19	2.42	86.4	72.5
574	4	6	31.76	1.25	2.58	84.1	67.3
574	5	2	35.11	1.21	2.41	85.3	70.7
574	5	3	36.76	1.22	2.36	83.6	68.4
574	5	4	38.26	1.22	2.85	88.3	72.6
574	5	5	39.76	1.21	2.56	86.3	71.2
574	5	6	41.26	1.28	2.48	81.0	63.3
574	6	1	43.26	1.35	2.62	78.5	58.3
574	6	2	44.76	1.29	2.58	81.4	62.9
574	6	3	46.26	1.28	2.63	82.9	64.8
574	6	4	47.76	1.27	2.69	84.2	66.5
574	6	5	49.26	1.49	2.98	75.3	50.6
574	6	6	50.76	1.53	2.68	68.6	44.9
574	7	1	52.76	1.52	2.70	69.1	45.3
574	7	2	54.26	1.39	2.68	76.8	55.2
574	7	3	55.76	1.42	2.57	73.0	51.3
574	7	4	57.26	1.61	2.71	64.5	40.1
574	7	5	58.76	1.35	2.62	78.4	58.1
574	7	6	60.26	1.40	2.65	75.7	54.0
574	8	1	61.76	1.54	2.63	66.7	43.2
574	8	2	63.26	1.50	2.66	69.6	46.3
574	8	3	64.76	1.49	2.66	70.2	47.0
574	8	4	66.26	1.47	2.63	71.0	48.2
574	8	5	67.76	1.37	2.58	76.8	56.3
574	8	6	69.26	1.32	2.59	80.1	60.8
574	9	1	71.26	1.21	2.30	83.9	69.3
574	9	2	72.76	1.34	2.44	76.6	57.2
574	9	3	74.26	1.43	2.68	74.5	52.1
574	9	4	75.76	1.23	2.64	86.2	70.3
574	9	5	77.26	1.22	2.76	87.8	72.3
574	9	6	78.76	1.30	2.53	80.5	62.0
574	10	1	80.76	1.43	2.68	74.6	52.3
574	10	2	82.26	1.46	2.74	73.6	50.5
574	10	3	83.76	1.25	2.64	84.7	67.7
574	10	4	85.26	1.48	2.75	72.7	49.2
574	10	5	86.76	1.49	2.76	72.1	48.4
574	10	6	88.26	1.45	2.74	74.2	51.2
574	11	1	90.26	1.48	2.74	72.4	48.9
574	11	2	91.76	1.48	2.69	71.5	48.2
574	11	3	93.26	1.48	2.68	71.5	48.3

HOLE	CORE	SECTION	DEPTH (METERS)	WET DENS. (GM/CC)	GRAIN DENS. (GM/CC)	POROSITY (%)	WATER CONT. (%)
574	11	4	94.76	1.66	2.71	61.3	36.9
574	11	5	96.26	1.61	2.70	64.0	39.7
574	11	6	97.76	1.66	2.72	61.6	37.1
574	12	1	99.36	1.61	2.72	64.7	40.3
574	12	2	100.86	1.66	2.73	61.9	37.3
574	12	3	102.36	1.60	2.68	63.9	39.8
574	12	4	103.86	1.65	2.72	62.0	37.5
574	12	5	105.36	1.64	2.68	62.0	37.8
574	12	6	106.86	1.66	2.70	61.2	36.8
574	13	1	108.86	1.59	2.77	66.4	41.6
574	13	2	110.36	1.57	2.64	65.5	41.8
574	13	3	111.86	1.60	2.70	64.9	40.6
574	13	4	113.36	1.59	2.67	65.0	41.0
574	13	5	114.86	1.58	2.59	63.7	40.4
574	13	6	116.36	1.55	2.59	65.2	42.0
574	14	1	118.36	1.67	2.67	59.6	35.6
574	14	2	119.86	1.76	2.71	55.4	31.4
574	14	3	121.36	1.75	2.69	55.6	31.7
574	15	3	126.36	1.76	2.72	55.7	31.6
574	15	4	127.86	1.70	2.72	59.4	35.0
574	16	1	128.36	1.67	2.69	60.5	36.3
574	16	2	129.86	1.64	2.71	62.2	37.8
574	16	3	131.36	1.67	2.69	60.5	36.3
574	17	1	133.36	1.61	2.58	61.3	38.1
574	17	2	134.86	1.60	2.65	63.5	39.7
574	17	3	136.36	1.63	2.70	62.8	38.5
574	18	1	138.36	1.62	2.64	62.4	38.6
574	18	2	139.86	1.56	2.61	65.1	41.8
574	18	3	141.36	1.63	2.63	61.6	37.9
574	19	2	144.86	1.61	2.63	62.9	39.2
574	19	3	146.36	1.53	2.62	67.0	43.6
574	20	2	149.86	1.67	2.66	59.7	35.7
574	20	3	151.36	1.65	2.72	62.1	37.6
574	21	1	153.26	1.59	2.65	64.0	40.1
574	21	2	154.76	1.75	2.70	56.0	32.0
574	21	3	156.26	1.48	2.63	70.6	47.7
574	22	1	158.26	1.64	2.66	61.6	37.6
574	22	2	159.76	1.70	2.70	58.8	34.6
574	22	3	161.26	1.68	2.68	59.4	35.3
574	23	2	164.76	1.72	2.73	58.3	33.9
574	23	3	166.26	1.68	2.72	60.2	35.7
574	24	1	168.26	1.62	2.66	62.8	38.9
574	24	2	169.76	1.68	2.68	59.7	35.6
574	24	3	171.26	1.66	2.62	58.8	35.3
574	25	1	173.26	1.58	2.65	65.1	41.3
574	25	2	174.76	1.72	2.70	57.5	33.4
574	25	3	176.26	1.63	2.66	62.3	38.3
574	26	1	178.26	1.68	2.67	59.2	35.2
574	26	2	179.76	1.61	2.65	63.0	39.0
574	26	3	181.26	1.65	2.64	60.2	36.4
574	27	1	182.96	1.71	2.69	58.2	34.1
574	27	2	184.46	1.53	2.60	66.9	43.7
574	27	3	185.96	1.60	2.64	63.2	39.4
574	28	1	187.96	1.65	2.68	61.3	37.2
574	28	2	189.46	1.63	2.65	62.2	38.3
574	28	3	190.96	1.72	2.86	61.5	35.9
574	29	1	192.96	1.64	2.77	63.6	38.8
574	29	2	194.46	1.66	2.71	61.2	36.8
574	29	3	195.96	1.65	2.73	62.2	37.6
574	30	2	199.46	1.62	2.78	65.2	40.2
574	30	3	200.96	1.71	2.73	59.3	34.8
574	31	1	202.96	1.62	2.82	66.2	41.0
574A	2	2	8.56	1.39	2.69	76.7	55.1
574A	2	4	11.56	1.45	2.65	72.9	50.3
574A	2	6	14.56	1.28	2.61	82.6	64.6
574A	3	2	17.76	1.18	2.53	87.9	74.1
574A	3	4	20.76	1.23	2.55	85.4	69.7
574A	4	2	26.16	1.28	2.57	82.1	64.1
574A	4	4	29.16	1.25	2.74	85.8	68.8
574A	7	2	54.16	1.35	2.53	77.0	56.9
574A	7	6	60.16	1.47	2.63	70.9	48.1
574A	8	2	63.66	1.55	2.68	66.9	43.0
574A	8	4	66.66	1.56	2.77	68.6	44.0
574A	8	6	69.66	1.30	2.63	81.7	63.0
574A	9	4	75.76	1.22	2.64	86.4	70.6
574A	9	5	77.26	1.20	2.54	87.0	72.5
574A	9	6	78.66	1.29	2.61	81.8	63.2
574A	10	2	82.16	1.41	2.57	74.1	52.7
574A	10	4	85.16	1.39	2.72	77.2	55.5
574A	10	6	88.16	1.51	2.62	68.4	45.3
574A	11	2	91.46	1.31	2.54	79.8	60.8
574A	11	4	94.46	1.40	2.56	74.4	53.2
574A	11	6	97.46	1.66	2.69	60.7	36.5

HOLE	CORE	SECTION	DEPTH (METERS)	WET DENS. (GM/CC)	GRAIN DENS. (GM/CC)	POROSITY (%)	WATER CONT. (%)
574A	12	4	103.96	1.61	2.65	62.7	38.9
574A	12	6	106.96	1.61	2.71	64.5	40.1
574A	13	2	110.46	1.57	2.68	66.3	42.4
574A	14	2	115.36	1.55	2.60	65.7	42.5
574A	17	2	130.06	1.66	2.71	61.6	37.2
574A	18	2	134.16	1.61	2.73	65.1	40.5
574A	18	4	137.16	1.68	2.69	59.5	35.3
574A	18	6	140.16	1.72	2.77	59.7	34.8
574A	19	2	143.65	1.65	2.69	61.6	37.3
574A	19	4	146.66	1.55	2.65	66.6	42.9
574A	19	6	149.66	1.71	2.68	58.0	34.0
574A	22	2	170.66	1.69	2.64	57.9	34.2
574A	22	4	173.66	1.63	2.65	61.7	37.8
574A	22	6	176.66	1.70	2.64	57.5	33.9
574A	23	1	178.66	1.65	2.63	60.3	36.7
574A	23	2	180.16	1.67	2.67	59.8	35.8
574A	23	5	184.66	1.55	2.61	65.7	42.3
574B	1	1	185.76	1.54	2.52	64.5	41.9
574B	1	2	187.26	1.56	2.65	66.3	42.5
574B	1	3	188.76	1.61	2.64	62.9	39.2
574B	1	4	190.26	1.61	2.65	62.9	39.0
574B	1	5	191.76	1.59	2.63	63.7	40.0
574B	1	6	193.26	1.53	2.61	67.2	44.0
574C	1	1	195.41	1.61	2.67	63.4	39.3
574C	1	2	196.76	1.64	2.72	63.0	38.5
574C	1	3	198.26	1.47	2.66	71.5	48.6
574C	1	4	199.76	1.44	2.68	73.9	51.4
574C	1	5	201.26	1.58	2.68	65.7	41.7
574C	2	1	204.71	1.59	2.74	66.0	41.4
574C	2	2	206.26	1.51	2.91	73.1	48.2
574C	2	3	207.76	1.61	2.61	62.3	38.8
574C	2	4	209.26	1.66	2.73	61.8	37.3
574C	2	5	210.76	1.62	2.65	62.4	38.5
574C	2	6	212.26	1.31	2.41	78.2	59.8
574C	3	2	215.76	1.63	2.71	63.0	38.7
574C	3	3	217.26	1.58	2.89	69.3	43.8
574C	4	1	223.76	1.65	2.68	61.5	37.3
574C	4	2	225.26	1.64	2.86	65.6	40.0
574C	5	1	233.26	1.67	2.64	58.8	35.1
574C	5	2	234.76	1.69	2.81	62.0	36.8
574C	5	3	236.26	1.74	2.73	57.3	33.0
574C	5	4	237.76	1.73	2.75	58.0	33.4
574C	6	1	242.66	1.80	2.70	53.1	29.5
574C	6	3	245.76	1.80	2.71	53.3	29.6
574C	6	4	247.26	1.72	2.66	56.6	32.9
574C	7	1	252.26	1.75	2.67	55.2	31.5
574C	7	2	253.76	1.75	2.66	54.8	31.3
574C	7	3	255.26	1.69	2.65	58.2	34.4
574C	7	4	256.76	1.73	2.69	56.8	32.8
574C	7	5	258.16	1.75	2.71	56.0	31.9
574C	7	6	259.76	1.71	2.65	56.8	33.1
574C	8	1	261.76	1.77	3.14	63.8	36.0
574C	8	2	263.26	1.73	2.89	61.2	35.3
574C	8	3	264.76	1.71	2.70	58.0	33.8
574C	9	1	271.26	1.73	2.69	56.6	32.7
574C	9	2	272.76	1.64	2.59	59.9	36.6
574C	9	3	274.03	1.76	2.96	61.1	34.6
574C	10	2	282.26	1.70	2.77	60.6	35.7
574C	10	3	283.76	1.76	2.81	58.1	33.1
574C	10	4	285.26	1.76	2.70	55.0	31.2
574C	10	5	286.78	1.75	2.76	57.5	32.9
574C	10	6	288.26	1.83	2.82	54.6	29.9
574C	11	1	290.26	1.72	2.63	55.8	32.4
574C	11	2	291.76	1.83	2.76	52.8	28.9
574C	11	3	293.26	1.83	2.71	51.6	28.3
574C	12	1	299.76	1.80	2.71	53.1	29.5
574C	12	2	301.26	1.81	2.75	53.8	29.8
574C	12	3	302.76	1.81	2.71	52.8	29.2
574C	12	4	304.26	1.74	2.61	54.2	31.2
574C	12	5	305.76	1.77	2.64	53.0	29.9
574C	12	6	307.26	1.81	2.66	51.1	28.2
574C	13	1	309.26	1.79	2.66	52.5	29.3
574C	13	2	310.76	1.78	2.69	53.8	30.3
574C	13	3	312.26	1.78	2.64	52.5	29.4
574C	13	4	313.76	1.85	2.70	50.1	27.1
574C	14	1	318.91	1.76	2.64	53.8	30.6
574C	14	2	320.35	1.75	2.70	56.0	32.0
574C	15	1	328.26	1.87	2.89	53.7	28.6
574C	15	4	332.76	1.82	2.85	55.7	30.6
574C	16	1	337.81	1.79	2.85	57.5	32.2
574C	16	2	339.26	1.78	2.74	55.4	31.2
574C	16	3	340.76	1.79	2.75	55.0	30.8

HOLE	CORE	SECTION	DEPTH (METERS)	WET DENS. (GM/CC)	GRAIN DENS. (GM/CC)	POROSITY (%)	WATER CONT. (%)
574C	17	1	347.01	1.78	2.70	54.5	30.7
574C	17	1	347.26	1.78	2.70	53.8	30.2
574C	17	2	348.76	1.78	2.67	53.3	29.9
574C	17	3	350.06	1.77	2.69	54.3	30.7
574C	17	4	351.76	1.75	2.70	55.8	31.9
574C	18	1	356.76	1.80	2.71	53.3	29.7
574C	18	2	358.26	1.74	2.67	55.4	31.8
574C	19	1	366.16	1.74	2.65	55.3	31.8
574C	19	2	367.71	1.75	2.66	54.5	31.1
574C	20	1	375.76	1.80	2.69	52.5	29.1
574C	20	2	377.36	1.79	2.69	53.4	29.9
574C	20	3	378.56	1.74	2.61	53.9	31.0
574C	20	4	380.26	1.78	2.70	54.0	30.3
574C	20	5	381.81	1.80	2.66	51.7	28.6
574C	20	6	383.31	1.80	2.70	52.7	29.2
574C	21	1	385.17	1.83	2.70	51.0	27.8
574C	21	2	386.86	1.77	2.74	56.0	31.6
574C	21	3	388.26	1.79	2.72	54.4	30.5
574C	22	1	394.16	1.84	2.69	50.6	27.5
574C	22	2	395.86	1.85	2.66	48.9	26.5
574C	23	1	404.45	1.82	2.69	51.4	28.2
574C	23	2	405.91	1.81	2.68	51.9	28.7
574C	23	3	407.16	1.80	2.66	51.7	28.6
574C	23	4	408.64	1.83	2.64	49.2	26.9
574C	23	5	410.72	1.85	2.64	48.6	26.4
574C	24	1	414.21	1.76	2.62	53.3	30.3
574C	24	2	415.85	1.77	2.65	53.2	30.0
574C	24	3	416.49	1.78	2.64	52.6	29.6
574C	24	4	418.28	1.82	2.68	51.3	28.2
574C	25	1	423.93	1.85	2.66	48.9	26.4
574C	26	1	432.67	1.86	2.66	48.0	25.8
574C	26	2	434.31	1.86	2.68	49.0	26.4
574C	26	3	435.72	1.83	2.55	46.2	25.2
574C	27	1	442.25	1.90	2.68	46.5	24.5
574C	27	2	443.71	1.84	2.69	50.6	27.5
574C	27	3	445.09	1.83	2.71	51.6	28.3
574C	29	1	461.82	1.75	2.60	52.9	30.2
574C	29	2	462.65	1.75	2.61	53.5	30.6
574C	29	3	464.21	1.79	2.61	51.1	28.6
574C	30	1	471.49	1.73	2.57	53.7	31.1
574C	30	2	472.13	1.74	2.58	53.0	30.5
574C	30	3	473.71	1.73	2.58	54.1	31.4
574C	31	1	480.21	1.66	2.49	55.8	33.6
574C	31	2	482.06	1.74	2.60	54.0	31.1
574C	32	1	490.11	1.70	2.61	56.5	33.2
574C	32	2	491.26	1.68	2.53	55.6	33.1
574C	33	1	499.16	1.74	2.64	54.7	31.4
574C	33	2	500.81	1.73	2.61	54.6	31.6
574C	33	4	503.46	1.76	2.65	54.0	30.7
574C	33	5	505.01	1.62	2.59	61.3	38.0
574C	34	1	508.44	1.65	2.62	59.8	36.3
574C	35	1	518.23	1.68	2.76	61.2	36.4
575	1	1	0.76	1.25	2.53	84.2	67.6
575	1	2	2.26	1.36	2.63	78.0	57.4
575	1	3	3.76	1.23	2.38	83.2	67.6
575	1	4	5.26	1.28	2.61	82.4	64.3
575	1	5	6.76	1.20	2.34	84.8	70.5
575	2	1	8.06	1.25	2.50	83.4	66.9
575	2	2	9.56	1.26	2.51	83.0	66.0
575	2	3	11.06	1.35	2.58	78.0	57.9
575	2	4	12.56	1.29	2.53	80.9	62.6
575	2	5	14.06	1.37	2.63	77.6	56.8
575	2	6	15.36	1.64	2.69	62.1	37.8
575	3	2	18.66	1.33	2.59	79.2	59.5
575	3	3	20.56	1.39	2.58	75.2	54.0
575	3	4	22.06	1.52	2.64	68.4	45.1
575	3	5	23.56	1.55	2.61	65.6	42.2
575	3	6	25.06	1.62	2.66	62.5	38.6
575	4	1	27.06	1.26	2.86	86.0	68.2
575	4	2	28.56	1.35	2.64	78.5	58.1
575	4	3	30.06	1.44	2.65	73.2	50.7
575	4	4	31.56	1.52	2.69	69.0	45.2
575	4	5	33.06	1.65	2.67	61.1	37.1
575	4	6	34.56	1.63	2.69	63.1	38.8
575	5	1	35.76	1.62	2.66	62.7	38.8
575	5	2	37.26	1.65	2.68	61.3	37.2
575	5	3	38.76	1.63	2.63	61.7	38.0
575	5	4	40.47	1.63	2.80	64.7	39.6
575	5	5	41.76	1.50	2.57	68.3	45.5
575	5	6	43.26	1.58	2.57	62.8	39.7
575	6	1	45.26	1.76	2.74	56.4	32.1
575	6	2	46.76	1.72	2.67	56.7	32.9
575	6	3	48.26	1.70	2.65	57.8	34.1

HOLE	CORE	SECTION	DEPTH (METERS)	WET DENS. (GM/CC)	GRAIN DENS. (GM/CC)	POROSITY (%)	WATER CONT. (%)
575	6	4	49.76	1.71	2.72	59.0	34.6
575	6	5	51.26	1.65	2.72	62.5	38.0
575	6	6	52.76	1.59	2.64	63.8	40.0
575	7	1	54.76	1.62	2.73	63.9	39.4
575	7	2	56.26	1.62	3.14	71.2	44.0
575	7	3	57.76	1.57	2.62	64.6	41.1
575	7	4	59.26	1.57	2.77	67.6	43.0
575	7	5	60.76	1.62	2.66	62.9	38.9
575	7	6	62.26	1.61	2.67	63.8	39.7
575	8	1	64.26	1.61	2.63	62.7	39.0
575	8	2	65.76	1.63	2.70	63.3	39.0
575	8	3	67.26	1.65	2.65	60.4	36.5
575	8	4	68.76	1.62	2.65	62.3	38.4
575	8	5	70.26	1.61	2.78	65.4	40.5
575	8	6	71.76	1.58	2.66	65.4	41.5
575	9	1	73.76	1.66	2.71	61.5	37.0
575	9	2	75.26	1.62	2.63	61.9	38.2
575	9	3	76.76	1.41	2.28	67.9	48.2
575	9	4	78.26	1.62	2.65	62.6	38.7
575	9	5	79.76	1.60	2.84	67.6	42.4
575	10	2	82.46	1.66	2.73	61.6	37.0
575	10	3	83.96	1.68	2.64	58.3	34.6
575	10	4	85.46	1.56	2.63	66.0	42.3
575	10	5	86.96	1.58	2.65	64.8	41.0
575	10	6	88.46	1.62	2.68	63.0	38.8
575	11	1	89.81	1.52	2.90	72.4	47.5
575	11	2	91.36	1.60	2.64	63.6	39.8
575	11	3	92.86	1.57	2.53	63.0	40.3
575	11	4	94.36	1.57	2.64	65.0	41.3
575	11	5	95.86	1.68	2.59	57.0	33.8
575	11	6	97.36	1.60	2.66	64.0	40.1
575A	1	1	94.56	1.61	2.73	64.7	40.1
575A	1	2	96.06	1.61	2.67	63.7	39.7
575A	1	3	97.56	1.53	2.60	66.8	43.7
575A	2	2	99.46	1.54	2.72	68.7	44.7
575A	2	3	100.96	1.43	2.63	73.6	51.4
575A	3	2	103.36	1.39	2.61	75.8	54.5
575A	3	3	104.86	1.46	2.63	71.8	49.3
575A	4	1	105.96	1.51	2.64	68.8	45.5
575A	4	2	107.46	1.59	2.65	64.3	40.4
575A	4	3	108.96	1.62	2.66	62.6	38.6
575A	5	2	111.26	1.66	2.71	61.5	37.1
575A	5	3	112.76	1.52	2.77	70.4	46.2
575A	6	1	114.86	1.55	2.73	68.2	44.1
575A	6	2	116.36	1.57	2.67	65.9	42.0
575A	6	3	117.86	1.60	2.66	64.1	40.1
575A	7	2	120.66	1.55	2.77	68.9	44.4
575A	7	3	122.16	1.61	2.65	63.3	39.4
575A	8	1	123.86	1.59	2.66	64.6	40.7
575A	8	2	125.36	1.55	2.72	68.1	43.9
575A	9	2	127.56	1.58	2.66	65.0	41.1
575A	10	2	129.56	1.71	2.77	59.7	34.9
575A	10	3	131.06	1.67	2.92	65.3	39.2
575A	11	2	132.86	1.64	2.65	61.1	37.2
575A	11	3	134.36	1.54	2.58	65.6	42.5
575A	12	2	137.36	1.69	2.65	58.0	34.2
575A	12	3	138.86	1.67	2.62	58.8	35.2
575A	13	2	141.06	1.69	2.64	58.3	34.6
575A	13	3	142.56	1.86	2.70	49.1	26.3
575A	14	2	144.16	1.72	2.71	58.2	33.9
575A	14	3	145.66	1.68	2.65	58.5	34.7
575A	15	2	146.96	1.73	2.77	59.0	34.2
575A	15	3	148.46	1.71	2.70	58.0	33.8
575A	16	2	150.26	1.73	2.74	58.1	33.7
575A	16	3	151.51	1.69	2.69	59.1	35.0
575A	17	2	152.26	1.71	2.70	58.6	34.4
575A	17	3	153.38	1.70	2.71	59.1	34.8
575A	18	2	154.76	1.67	2.63	58.7	35.1
575A	18	3	156.26	1.63	2.71	63.0	38.6
575A	19	2	159.06	1.69	2.69	59.0	34.8
575A	19	3	160.31	1.67	2.67	59.9	35.9
575A	20	2	163.06	1.69	2.71	59.7	35.4
575A	20	3	164.16	1.68	2.68	59.6	35.5
575A	21	1	165.46	1.66	2.79	63.0	37.9
575A	21	2	166.96	1.66	2.71	61.5	37.1
575A	21	3	168.46	1.75	2.71	56.3	32.2
575A	22	2	170.44	1.56	2.57	64.3	41.2
575A	22	3	171.86	1.74	2.77	58.5	33.7
575A	23	1	172.86	1.68	2.72	60.5	35.9
575A	23	2	174.36	1.70	2.69	58.7	34.6
575A	24	2	176.46	1.73	2.77	58.7	33.9
575A	24	3	177.96	1.67	2.68	60.1	36.0
575A	25	3	180.96	1.72	2.56	53.7	31.2

HOLE	CORE	SECTION	DEPTH (METERS)	WET DENS. (GM/CC)	GRAIN DENS. (GM/CC)	POROSITY (%)	WATER CONT. (%)
575A	26	2	182.36	1.69	2.81	61.8	36.5
575A	26	3	183.86	1.70	2.63	57.1	33.5
575A	28	2	189.46	1.94	2.76	46.4	23.9
575A	29	2	191.96	1.82	2.72	52.1	28.6
575A	29	3	193.16	1.80	2.77	54.6	30.3
575A	30	1	194.36	1.87	2.80	52.0	27.9
575A	30	2	195.86	1.68	2.71	60.0	35.7
575A	30	3	197.36	1.75	2.71	56.5	32.4
575A	31	2	199.66	1.77	2.63	53.1	30.1
575A	31	3	201.14	1.75	2.70	55.7	31.8
575A	32	2	203.56	1.77	2.67	54.1	30.6
575A	32	3	204.88	1.81	2.69	52.1	28.8
575A	33	2	206.56	1.74	2.65	55.3	31.8
575A	33	3	208.06	1.74	2.69	56.0	32.2
575B	1	1	4.06	1.43	2.66	74.3	52.1
575B	1	2	5.53	1.28	2.52	81.7	64.0
575B	1	3	7.06	1.32	2.63	80.4	60.9
575B	1	4	8.56	1.25	2.59	84.3	67.5
575B	1	5	10.06	1.20	2.33	85.0	70.9
575B	1	6	11.56	1.26	2.58	83.3	65.9
575B	2	1	12.76	1.23	2.45	84.5	69.0
575B	2	2	14.26	1.25	2.51	83.2	66.3
575B	2	3	15.73	1.41	2.67	75.4	53.5
575B	2	4	17.26	1.27	2.70	83.8	65.7
575B	2	5	18.76	1.36	2.51	76.3	56.2
575B	2	6	20.26	1.59	2.61	69.2	46.3
575B	3	1	21.76	1.59	2.61	63.7	40.2
575B	3	2	23.26	1.36	2.60	77.7	57.2
575B	3	3	24.76	1.52	2.57	66.8	43.9
575B	3	4	26.26	1.35	2.56	77.4	57.2
575B	3	5	27.76	1.47	2.56	69.6	47.2
575B	3	6	29.26	1.56	2.66	66.1	42.3
575B	4	2	31.76	1.59	2.73	66.1	41.7
575B	4	3	33.26	1.61	2.69	64.3	40.1
575B	4	4	34.76	1.34	2.64	79.3	59.1
575B	4	5	36.26	1.29	2.42	79.3	61.4
575B	4	6	37.76	1.25	2.65	85.2	68.3
575B	5	2	41.26	1.30	2.50	79.8	61.2
575B	5	3	42.76	1.34	2.50	77.5	58.0
575B	5	4	44.26	1.54	2.68	67.9	44.2
575B	5	5	45.76	1.66	2.73	61.9	37.3
575B	5	6	47.26	1.63	2.67	62.0	37.9
575B	6	2	50.26	1.66	2.70	61.2	36.8
575B	6	3	51.76	1.61	2.63	62.6	38.9
575B	6	4	53.26	1.57	2.67	66.1	42.2
575B	6	5	54.76	1.59	2.66	64.2	40.3
575B	7	2	57.66	1.78	2.65	53.0	29.8
575B	7	3	59.16	1.73	2.73	58.0	33.5
575B	7	4	60.66	1.74	2.70	56.6	32.6
575B	7	5	62.16	1.66	2.63	59.6	36.0
575B	7	6	63.66	1.69	2.69	59.1	35.0
575B	8	2	66.96	1.60	2.72	65.2	40.8
575B	8	3	68.46	1.51	2.78	71.5	47.4
575B	8	4	69.96	1.57	2.68	66.2	42.2
575B	8	5	71.46	1.65	2.77	63.3	38.4
575B	8	6	72.96	1.56	2.71	67.3	43.1
575B	9	2	76.06	1.55	2.66	67.1	43.4
575B	9	3	77.56	1.62	2.68	63.1	39.0
575B	9	4	79.06	1.68	2.71	60.2	35.8
575B	9	5	80.56	1.68	2.77	61.4	36.5
575B	10	2	83.66	1.62	2.76	64.8	40.0
575B	10	3	85.16	1.66	2.66	60.3	36.3
575B	10	4	86.66	1.44	3.00	77.9	54.0
575B	10	5	88.16	1.68	2.74	60.6	36.0
575B	10	6	89.66	1.69	2.84	62.5	37.0
575B	11	2	93.16	1.62	2.85	66.5	41.1
575B	11	3	94.66	1.71	2.80	60.6	35.5
575B	11	4	96.16	1.66	3.09	68.6	41.4
575B	11	5	97.66	1.71	2.74	59.3	34.7
575B	11	6	99.16	1.59	2.64	64.1	40.3
575B	12	2	101.86	1.73	2.84	60.5	35.1
575B	12	3	103.36	1.58	2.61	63.8	40.4
575B	12	4	104.86	1.53	2.54	65.4	42.7
575B	12	5	106.36	1.58	2.69	66.1	42.0
575B	13	2	111.46	1.50	2.71	70.5	46.9
575B	13	3	112.96	1.59	2.75	66.1	41.5
575B	14	2	116.36	1.63	2.68	62.8	38.7
575B	14	3	117.86	1.58	2.63	64.3	40.6

VELOCITY

HOLE	CORE	SECTION	DEPTH (METERS)	VELOCITY (KM/SEC)	HOLE	CORE	SECTION	DEPTH (METERS)	VELOCITY (KM/SEC)
572	1	1	1.08	1.51	572	1	4	5.20	1.53
572	1	2	2.43	1.50	572	1	5	6.85	1.55
572	1	3	3.67	1.53	572	1	6	8.24	1.51
572A	1	1	0.74	1.54	572A	9	6	80.55	1.53
572A	1	2	2.23	1.53	572A	10	2	84.07	1.53
572A	1	3	3.74	1.53	572A	10	3	85.57	1.54
572A	1	4	5.25	1.53	572A	10	5	88.55	1.52
572A	1	5	6.75	1.51	572A	10	6	90.05	1.53
572A	1	6	8.25	1.52	572A	11	1	92.16	1.53
572A	2	1	10.24	1.60	572A	11	2	93.65	1.53
572A	2	2	11.74	1.53	572A	11	3	95.15	1.52
572A	2	3	13.24	1.52	572A	11	4	96.65	1.53
572A	2	4	14.74	1.52	572A	11	5	98.15	1.53
572A	2	5	16.24	1.53	572A	11	6	99.65	1.54
572A	3	1	19.74	1.53	572A	12	1	101.45	1.53
572A	3	2	21.24	1.54	572A	12	2	102.95	1.53
572A	3	3	22.74	1.52	572A	12	3	104.45	1.51
572A	3	4	24.24	1.53	572A	12	4	105.95	1.53
572A	3	5	25.74	1.47	572A	12	5	107.45	1.53
572A	3	6	27.24	1.54	572A	12	6	108.95	1.53
572A	4	1	29.35	1.53	572A	13	1	110.65	1.54
572A	4	4	33.95	1.52	572A	13	2	112.15	1.52
572A	4	5	35.37	1.52	572A	13	3	113.65	1.54
572A	5	1	37.07	1.52	572A	13	4	115.15	1.54
572A	5	2	38.57	1.53	572A	13	5	116.65	1.54
572A	5	3	40.07	1.53	572A	13	6	118.15	1.54
572A	5	4	41.57	1.52	572A	14	1	119.85	1.53
572A	5	5	43.07	1.53	572A	14	2	121.35	1.56
572A	5	6	44.57	1.53	572A	14	3	122.85	1.54
572A	6	2	48.17	1.54	572A	14	4	124.35	1.54
572A	6	3	49.67	1.53	572A	14	5	125.85	1.53
572A	6	4	51.17	1.53	572A	14	6	127.35	1.53
572A	6	5	52.67	1.53	572A	15	1	129.05	1.53
572A	6	6	54.17	1.53	572A	15	2	130.55	1.53
572A	7	2	57.47	1.57	572A	15	3	132.05	1.55
572A	7	3	58.97	1.54	572A	15	4	133.55	1.54
572A	7	4	60.47	1.53	572A	15	5	135.05	1.56
572A	7	5	61.97	1.52	572A	15	6	136.35	1.55
572A	7	6	63.45	1.54	572A	16	2	139.35	1.51
572A	8	1	64.85	1.53	572A	16	3	140.85	1.52
572A	8	3	67.85	1.53	572A	16	5	143.85	1.53
572A	8	4	69.35	1.55	572A	17	1	146.05	1.54
572A	8	5	70.85	1.55	572A	17	2	147.55	1.54
572A	9	1	73.05	1.54	572A	17	3	149.05	1.53
572A	9	2	74.55	1.54	572A	17	4	150.55	1.52
572A	9	3	76.05	1.51	572A	17	5	152.05	1.53
572A	9	4	77.55	1.54	572A	17	6	153.55	1.53
572A	9	5	79.05	1.54					
572B	1	2	156.25	1.63	572B	3	1	164.95	1.55
572B	1	3	157.75	1.54	572B	3	2	166.45	1.54
572B	2	1	160.05	1.52	572B	3	3	167.95	1.57
572B	2	2	161.55	1.54	572B	4	1	169.55	1.54
572B	2	3	163.45	1.55	572B	4	2	171.05	1.57
572C	1	1	0.75	1.54	572C	5	6	47.15	1.54
572C	1	2	2.25	1.53	572C	6	1	49.14	1.53
572C	1	3	3.75	1.53	572C	6	2	50.75	1.53
572C	1	5	6.75	1.53	572C	6	3	52.25	1.53
572C	1	6	8.25	1.53	572C	6	4	53.75	1.60
572C	2	1	10.85	1.53	572C	6	5	55.25	1.53
572C	2	2	12.35	1.53	572C	6	6	56.75	1.53
572C	2	3	13.85	1.53	572C	7	1	58.85	1.52
572C	2	4	15.35	1.54	572C	7	2	60.35	1.53
572C	2	5	16.85	1.53	572C	7	3	61.85	1.53
572C	2	6	18.35	1.54	572C	7	4	63.35	1.53
572C	3	1	20.45	1.53	572C	7	5	64.90	1.52
572C	3	2	21.95	1.54	572C	7	6	66.35	1.52
572C	3	3	23.45	1.52	572C	8	1	68.45	1.52
572C	3	4	24.95	1.52	572C	8	2	69.95	1.52
572C	3	5	26.45	1.53	572C	8	3	71.55	1.53
572C	3	6	27.95	1.60	572C	8	4	72.97	1.52
572C	4	1	30.05	1.53	572C	8	5	74.45	1.53
572C	4	2	31.55	1.53	572C	8	6	75.97	1.53
572C	4	3	33.05	1.53	572C	9	1	78.05	1.53
572C	4	4	34.55	1.53	572C	9	2	79.57	1.51
572C	4	5	36.05	1.52	572C	9	3	81.05	1.53
572C	4	6	37.55	1.53	572C	9	4	82.55	1.52
572C	5	1	39.65	1.52	572C	9	5	84.06	1.52
572C	5	2	41.15	1.52	572C	9	6	85.55	1.53
572C	5	3	42.65	1.52	572C	10	1	87.65	1.53
572C	5	4	44.15	1.54	572C	10	2	89.15	1.52
572C	5	5	45.65	1.53	572C	10	3	90.65	1.53

HOLE	CORE	SECTION	DEPTH (METERS)	VELOCITY (KM/SEC)	HOLE	CORE	SECTION	DEPTH (METERS)	VELOCITY (KM/SEC)
572C	10	4	92.15	1.53	572C	15	5	127.85	1.55
572C	10	5	93.65	1.48	572C	15	6	129.35	1.55
572C	10	6	95.15	1.54	572C	16	1	131.45	1.54
572C	11	1	97.25	1.53	572C	16	2	132.95	1.53
572C	11	2	98.75	1.54	572C	16	3	134.45	1.54
572C	11	3	100.25	1.54	572C	16	4	135.95	1.55
572C	12	1	102.25	1.53	572C	16	5	137.45	1.55
572C	12	2	103.75	1.53	572C	16	6	138.95	1.55
572C	12	3	105.25	1.68	572C	17	1	141.05	1.54
572C	13	1	107.25	1.54	572C	17	2	142.55	1.55
572C	13	2	108.75	1.54	572C	17	3	144.05	1.55
572C	13	3	110.25	1.54	572C	17	4	145.55	1.56
572C	14	1	112.25	1.54	572C	18	2	152.15	1.53
572C	14	2	113.75	1.53	572C	18	3	153.65	1.54
572C	14	3	115.25	1.53	572C	18	4	155.15	1.55
572C	14	4	116.75	1.54	572C	18	5	156.65	1.54
572C	14	5	118.25	1.54	572C	18	6	158.15	1.55
572C	15	1	121.85	1.53	572C	20	1	165.25	1.55
572C	15	2	123.35	1.53	572C	20	2	166.75	1.56
572C	15	3	124.85	1.52	572C	20	3	168.25	1.56
572C	15	4	126.35	1.54					
573	2	2	4.25	1.51	573	10	4	81.45	1.52
573	2	3	5.75	1.54	573	10	5	82.95	1.53
573	2	4	7.25	1.51	573	10	6	84.45	1.51
573	2	5	8.75	1.48	573	11	2	87.95	1.51
573	2	6	10.25	1.51	573	11	3	89.45	1.54
573	3	1	12.25	1.54	573	11	4	90.95	1.54
573	3	2	13.75	1.53	573	11	5	92.45	1.54
573	3	3	15.25	1.53	573	11	6	93.95	1.54
573	3	4	16.75	1.54	573	12	1	95.95	1.54
573	3	5	18.25	1.53	573	12	2	97.45	1.60
573	3	6	19.75	1.52	573	12	3	98.95	1.54
573	4	1	22.05	1.52	573	12	4	100.45	1.54
573	4	2	23.55	1.53	573	12	5	101.95	1.53
573	4	3	25.05	1.53	573	12	6	103.45	1.53
573	4	4	26.55	1.54	573	13	2	106.25	1.53
573	4	5	28.05	1.52	573	13	3	107.75	1.52
573	4	6	29.55	1.52	573	13	4	109.25	1.55
573	5	1	31.55	1.51	573	13	5	110.75	1.60
573	5	2	33.05	1.52	573	13	6	112.25	1.54
573	5	3	34.25	1.53	573	14	1	113.35	1.56
573	5	4	35.75	1.51	573	14	2	114.85	1.55
573	5	5	37.25	1.52	573	14	3	116.35	1.56
573	5	6	38.75	1.53	573	14	4	117.85	1.55
573	6	1	40.05	1.53	573	14	5	119.35	1.57
573	6	2	41.55	1.53	573	14	6	120.85	1.55
573	6	3	43.05	1.53	573	15	1	122.85	1.54
573	6	4	44.55	1.53	573	15	2	124.35	1.54
573	6	5	46.05	1.53	573	15	3	125.85	1.53
573	6	6	47.55	1.53	573	15	4	127.35	1.49
573	7	2	50.25	1.53	573	15	5	128.85	1.55
573	7	3	51.75	1.54	573	15	6	130.35	1.56
573	7	4	53.25	1.54	573	16	1	132.05	1.54
573	7	5	54.75	1.54	573	16	2	133.55	1.55
573	7	6	56.25	1.53	573	16	3	135.05	1.54
573	8	1	57.75	1.53	573	16	4	136.55	1.55
573	8	2	59.25	1.53	573	16	5	138.05	1.54
573	8	3	60.75	1.53	573	16	6	139.55	1.54
573	8	4	62.25	1.53	573	17	1	140.85	1.52
573	8	5	63.75	1.53	573	17	2	142.35	1.53
573	8	6	65.25	1.53	573	17	3	143.85	1.48
573	9	1	67.45	1.52	573	17	4	145.35	1.53
573	9	2	68.95	1.52	573	17	5	146.85	1.53
573	9	3	70.45	1.52	573	17	6	148.35	1.48
573	9	4	71.95	1.53	573	18	1	149.75	1.53
573	9	5	73.45	1.54	573	18	2	151.25	1.59
573	9	6	74.95	1.54	573	18	3	152.75	1.53
573	10	1	76.95	1.53	573	19	1	154.75	1.53
573	10	2	78.45	1.52	573	19	2	156.25	1.51
573	10	3	79.95	1.52	573	19	3	158.10	1.52
573A	1	1	5.25	1.51	573A	3	6	30.35	1.54
573A	1	2	6.75	1.53	573A	4	2	33.55	1.54
573A	1	3	8.25	1.52	573A	4	4	36.55	1.53
573A	1	4	9.75	1.53	573A	4	6	39.55	1.54
573A	1	5	11.25	1.56	573A	5	2	42.05	1.53
573A	1	6	12.75	1.56	573A	5	4	45.05	1.48
573A	2	2	16.25	1.55	573A	5	6	48.05	1.54
573A	2	4	19.25	1.56	573A	6	2	51.45	1.54
573A	3	2	24.35	1.54	573A	6	4	54.45	1.54
573A	3	4	27.35	1.54					
573B	1	3	142.25	1.56	573B	1	4	143.75	1.56

HOLE	CORE	SECTION	DEPTH (METERS)	VELOCITY (KM/SEC)	HOLE	CORE	SECTION	DEPTH (METERS)	VELOCITY (KM/SEC)
573B	1	5	145.92	1.58	573B	17	4	295.75	1.58
573B	2	2	150.30	1.53	573B	18	2	302.25	1.59
573B	2	3	151.60	1.56	573B	18	3	303.75	1.56
573B	2	4	153.73	1.56	573B	19	2	311.85	1.60
573B	2	5	154.75	1.56	573B	20	1	319.76	1.63
573B	2	6	156.25	1.56	573B	20	2	321.25	1.68
573B	3	1	158.25	1.55	573B	20	3	322.65	1.65
573B	3	3	161.25	1.55	573B	20	5	325.75	1.66
573B	3	4	162.75	1.60	573B	20	6	327.43	1.63
573B	3	5	164.25	1.55	573B	21	1	329.50	1.67
573B	3	6	165.75	1.56	573B	21	2	330.85	1.63
573B	4	2	169.25	1.54	573B	21	3	332.38	1.66
573B	4	3	170.75	1.54	573B	22	1	338.70	1.66
573B	4	4	172.25	1.54	573B	22	2	340.45	1.66
573B	5	3	180.25	1.58	573B	22	4	343.20	1.69
573B	6	4	191.25	1.55	573B	23	1	348.40	1.67
573B	6	6	194.25	1.55	573B	24	1	357.52	1.61
573B	8	3	200.75	1.55	573B	24	2	359.00	1.65
573B	8	5	211.75	1.54	573B	24	3	360.66	1.63
573B	9	2	216.75	1.56	573B	25	1	367.21	1.66
573B	9	3	218.25	1.57	573B	26	2	378.39	1.61
573B	9	4	219.73	1.56	573B	26	4	381.19	1.63
573B	9	5	221.25	1.63	573B	26	5	382.32	1.62
573B	10	2	226.35	1.56	573B	27	1	386.08	1.67
573B	10	3	227.75	1.57	573B	27	2	387.60	1.66
573B	10	4	229.25	1.58	573B	27	3	388.93	1.67
573B	10	5	230.75	1.56	573B	27	4	390.62	1.65
573B	10	6	232.25	1.56	573B	28	1	395.70	1.65
573B	11	2	235.75	1.59	573B	28	2	397.46	1.66
573B	11	3	237.25	1.58	573B	28	3	398.60	1.61
573B	11	4	238.75	1.57	573B	29	1	405.39	1.59
573B	11	5	240.25	1.57	573B	29	2	407.10	1.61
573B	11	6	241.75	1.57	573B	29	3	408.06	1.65
573B	12	2	245.25	1.55	573B	29	4	409.90	1.61
573B	12	3	246.75	1.57	573B	29	5	411.02	1.61
573B	12	4	248.25	1.56	573B	30	1	414.96	1.60
573B	12	5	249.50	1.56	573B	30	3	418.26	1.63
573B	13	2	254.75	1.58	573B	30	4	418.92	1.64
573B	13	3	256.25	1.57	573B	31	1	424.20	1.62
573B	13	4	257.75	1.57	573B	32	1	434.16	1.62
573B	13	5	259.25	1.56	573B	32	2	436.10	1.67
573B	13	6	260.75	1.56	573B	34	1	452.70	1.64
573B	14	1	262.75	1.55	573B	35	1	462.15	1.65
573B	14	2	264.25	1.58	573B	35	2	463.35	1.64
573B	14	3	265.75	1.57	573B	35	3	465.20	1.64
573B	14	4	267.25	1.57	573B	35	4	467.05	1.71
573B	14	5	268.75	1.58	573B	36	1	471.75	1.69
573B	14	6	270.25	1.58	573B	37	1	481.03	1.63
573B	15	2	273.75	1.60	573B	38	1	490.70	1.69
573B	15	3	275.25	1.60	573B	38	2	492.15	1.86
573B	15	4	276.75	1.59	573B	38	2	492.78	1.68
573B	15	5	278.25	1.61	573B	39	1	499.75	1.78
573B	16	2	283.25	1.60	573B	39	3	503.25	1.77
573B	16	3	284.75	1.59	573B	42	1	520.93	1.87
573B	16	4	286.25	1.60	573B	42	2	523.30	1.63
573B	16	5	287.75	1.59	573B	42	3	523.68	1.55
573B	17	1	291.25	1.67	573B	42	4	526.42	1.70
573B	17	2	292.75	1.62	573B	42	4	526.42	1.74
573B	17	3	294.25	1.61					
574	1	1	0.66	1.55	574	5	6	41.25	1.53
574	1	2	2.25	1.53	574	6	1	43.25	1.52
574	1	3	3.75	1.53	574	6	2	44.75	1.53
574	2	1	5.25	1.53	574	6	3	46.25	1.53
574	2	2	6.75	1.53	574	6	4	47.75	1.53
574	2	3	8.46	1.54	574	6	5	49.25	1.53
574	2	4	9.75	1.53	574	6	6	50.75	1.55
574	2	5	11.25	1.53	574	7	1	52.75	1.55
574	2	6	12.75	1.54	574	7	2	54.25	1.56
574	3	2	16.25	1.54	574	7	3	55.75	1.55
574	3	3	17.75	1.53	574	7	4	57.25	1.51
574	3	4	19.25	1.54	574	7	5	58.75	1.55
574	3	5	20.75	1.55	574	7	6	60.25	1.56
574	3	6	22.25	1.55	574	8	1	61.75	1.54
574	4	1	24.25	1.56	574	8	2	63.25	1.54
574	4	2	25.75	1.54	574	8	3	64.75	1.59
574	4	3	27.25	1.53	574	8	4	66.25	1.59
574	4	4	28.75	1.54	574	8	5	67.75	1.54
574	4	5	30.25	1.54	574	8	6	69.25	1.55
574	4	6	31.75	1.53	574	9	1	71.25	1.56
574	5	2	35.10	1.54	574	9	2	72.75	1.55
574	5	3	36.75	1.53	574	9	3	74.25	1.54
574	5	4	38.25	1.54	574	9	4	75.75	1.56
574	5	5	39.75	1.54	574	9	5	77.25	1.56

HOLE	CORE	SECTION	DEPTH (METERS)	VELOCITY (KM/SEC)	HOLE	CORE	SECTION	DEPTH (METERS)	VELOCITY (KM/SEC)
574	9	6	78.75	1.54	574	18	3	141.35	1.54
574	10	1	80.75	1.54	574	19	2	144.85	1.54
574	10	2	82.25	1.53	574	19	3	146.35	1.54
574	10	3	83.75	1.55	574	20	2	149.85	1.55
574	10	4	85.25	1.53	574	20	3	151.35	1.55
574	10	5	86.75	1.54	574	21	1	153.25	1.55
574	10	6	88.25	1.54	574	21	2	154.75	1.57
574	11	1	90.25	1.53	574	21	3	156.25	1.54
574	11	2	91.75	1.53	574	22	1	158.25	1.55
574	11	3	93.25	1.54	574	22	2	159.75	1.56
574	11	4	94.75	1.56	574	22	3	161.25	1.56
574	11	5	96.25	1.56	574	23	2	164.75	1.55
574	11	6	97.75	1.55	574	23	3	166.25	1.55
574	12	1	99.35	1.55	574	24	1	168.25	1.54
574	12	2	100.85	1.56	574	24	2	169.75	1.55
574	12	3	102.35	1.55	574	24	3	171.25	1.55
574	12	4	103.85	1.51	574	25	1	173.25	1.54
574	12	5	105.35	1.56	574	25	2	174.75	1.56
574	12	6	106.85	1.56	574	25	3	176.25	1.56
574	13	1	108.85	1.54	574	26	1	178.25	1.56
574	13	2	110.35	1.55	574	26	2	179.75	1.53
574	13	3	111.85	1.55	574	26	3	181.25	1.57
574	13	4	113.35	1.57	574	27	1	182.95	1.58
574	13	5	114.85	1.57	574	27	2	184.45	1.54
574	13	6	116.35	1.56	574	27	3	185.95	1.56
574	14	1	118.35	1.55	574	28	1	187.95	1.57
574	14	2	119.85	1.59	574	28	3	190.95	1.57
574	16	1	128.35	1.58	574	29	1	192.95	1.54
574	16	2	129.85	1.56	574	29	2	194.45	1.57
574	16	3	131.35	1.57	574	29	3	195.95	1.57
574	17	1	133.35	1.54	574	30	2	199.45	1.54
574	17	2	134.85	1.55	574	30	3	200.95	1.56
574	17	3	136.35	1.54	574	31	2	204.45	1.52
574	18	1	138.35	1.54	574	31	3	205.95	1.56
574	18	2	139.85	1.54					
574A	2	2	8.55	1.54	574A	8	6	69.65	1.55
574A	2	4	11.55	1.54	574A	9	4	75.65	1.55
574A	2	6	14.55	1.54	574A	9	5	77.15	1.56
574A	3	2	17.75	1.54	574A	9	6	78.65	1.54
574A	3	4	20.75	1.55	574A	10	2	82.15	1.53
574A	4	2	26.15	1.54	574A	10	4	85.15	1.53
574A	4	4	29.15	1.53	574A	10	6	88.15	1.54
574A	4	6	32.15	1.53	574A	11	4	94.45	1.53
574A	5	2	35.35	1.54	574A	11	6	97.45	1.57
574A	5	4	38.35	1.50	574A	12	4	103.95	1.54
574A	5	6	41.35	1.53	574A	13	2	110.45	1.56
574A	6	2	44.65	1.53	574A	15	2	120.25	1.61
574A	6	4	47.65	1.54	574A	22	2	170.65	1.55
574A	6	6	50.65	1.54	574A	22	4	173.65	1.56
574A	7	2	54.15	1.53	574A	22	6	176.65	1.57
574A	7	4	57.15	1.54	574A	23	1	178.65	1.56
574A	7	6	60.15	1.54	574A	23	2	180.15	1.56
574A	8	2	63.65	1.53	574A	23	5	184.65	1.56
574A	8	4	66.65	1.53					
574B	1	1	185.75	1.57	574B	1	4	190.25	1.56
574B	1	2	187.25	1.55	574B	1	5	191.75	1.55
574B	1	3	188.75	1.56	574B	1	6	193.25	1.54
574C	1	1	195.40	1.58	574C	9	3	274.02	1.57
574C	1	2	196.75	1.58	574C	10	2	282.25	1.56
574C	1	3	198.25	1.55	574C	10	3	283.75	1.57
574C	1	4	199.75	1.57	574C	10	4	285.25	1.58
574C	1	5	201.25	1.57	574C	10	5	286.77	1.58
574C	2	1	204.70	1.56	574C	10	6	288.27	1.59
574C	2	2	206.25	1.56	574C	11	1	290.25	1.59
574C	2	3	207.75	1.57	574C	11	2	291.75	1.60
574C	2	4	209.25	1.57	574C	12	2	301.25	1.60
574C	2	5	210.75	1.57	574C	12	3	302.75	1.60
574C	2	6	212.25	1.59	574C	12	4	304.25	1.61
574C	3	3	217.25	1.56	574C	12	5	305.75	1.60
574C	4	1	223.75	1.56	574C	12	6	307.25	1.61
574C	4	2	225.25	1.56	574C	13	1	309.25	1.59
574C	5	1	233.25	1.58	574C	13	2	310.75	1.60
574C	5	2	234.75	1.58	574C	13	3	312.25	1.60
574C	6	3	245.75	1.62	574C	13	4	313.75	1.62
574C	6	4	247.25	1.61	574C	14	1	318.90	1.61
574C	7	2	253.75	1.63	574C	14	2	320.34	1.58
574C	7	5	258.25	1.61	574C	16	1	337.80	1.63
574C	8	2	263.25	1.58	574C	16	2	339.25	1.60
574C	8	3	264.75	1.59	574C	16	3	340.75	1.60
574C	9	1	271.25	1.57	574C	17	1	347.00	1.64
574C	9	2	272.75	1.58	574C	17	4	351.75	1.60

HOLE	CORE	SECTION	DEPTH (METERS)	VELOCITY (KM/SEC)	HOLE	CORE	SECTION	DEPTH (METERS)	VELOCITY (KM/SEC)
574C	17	5	353.25	1.61	574C	26	3	435.71	1.72
574C	18	2	358.25	1.61	574C	27	1	442.24	1.91
574C	19	2	367.50	1.62	574C	27	2	443.70	1.75
574C	20	3	378.55	1.66	574C	27	3	445.08	1.70
574C	21	1	385.16	1.77	574C	29	1	461.80	1.72
574C	21	3	388.25	1.62	574C	29	2	462.64	1.71
574C	22	1	394.15	1.81	574C	29	3	464.20	1.78
574C	22	2	395.85	1.85	574C	30	1	471.48	1.72
574C	23	1	404.44	1.67	574C	30	2	472.10	1.73
574C	23	2	405.90	1.73	574C	30	3	473.70	1.71
574C	23	3	407.15	1.69	574C	31	1	480.20	1.81
574C	23	4	408.63	1.74	574C	31	2	482.05	1.75
574C	23	5	410.71	1.88	574C	32	1	490.10	1.77
574C	24	1	414.20	1.73	574C	32	2	491.25	1.73
574C	24	2	415.84	1.75	574C	33	1	499.15	1.74
574C	24	3	416.48	1.76	574C	33	2	500.80	1.87
574C	24	4	418.27	1.73	574C	33	4	503.45	1.75
574C	25	1	423.02	1.76	574C	33	5	505.00	1.72
574C	26	1	432.66	1.80	574C	34	1	508.40	1.74
574C	26	2	434.30	1.74					
575	1	1	0.75	1.52	575	6	3	48.25	1.57
575	1	2	2.25	1.51	575	6	4	49.75	1.57
575	1	3	3.75	1.52	575	6	5	51.25	1.56
575	1	4	5.25	1.52	575	6	6	52.75	1.54
575	1	5	6.75	1.53	575	7	1	54.75	1.54
575	2	1	8.05	1.52	575	7	2	56.25	1.59
575	2	2	9.55	1.52	575	7	3	57.75	1.54
575	2	3	11.05	1.51	575	7	4	59.25	1.53
575	2	5	14.05	1.52	575	7	5	60.75	1.55
575	2	6	15.55	1.55	575	7	6	62.40	1.55
575	3	2	18.65	1.53	575	8	1	64.25	1.54
575	3	3	20.55	1.53	575	8	2	65.75	1.55
575	3	4	22.05	1.53	575	8	3	67.25	1.56
575	3	5	23.55	1.54	575	8	4	68.75	1.55
575	3	6	25.05	1.54	575	8	5	70.25	1.54
575	4	1	27.05	1.54	575	8	6	71.75	1.54
575	4	2	28.55	1.53	575	9	1	73.75	1.54
575	4	3	30.05	1.53	575	9	2	75.25	1.55
575	4	4	31.55	1.53	575	9	3	76.75	1.54
575	4	5	33.05	1.54	575	9	4	78.25	1.56
575	4	6	34.55	1.54	575	9	5	79.75	1.55
575	5	1	35.75	1.55	575	10	2	82.45	1.56
575	5	2	37.25	1.56	575	10	3	83.95	1.58
575	5	2	37.41	1.63	575	10	4	85.45	1.59
575	5	3	38.75	1.56	575	10	5	86.95	1.56
575	5	4	40.25	1.59	575	10	6	88.45	1.55
575	5	4	40.25	1.55	575	11	1	89.80	1.53
575	5	5	41.75	1.53	575	11	2	91.35	1.55
575	5	5	42.05	1.62	575	11	3	92.85	1.55
575	5	5	42.25	1.62	575	11	4	94.35	1.56
575	5	6	43.25	1.55	575	11	5	95.85	1.59
575	6	1	45.25	1.58	575	11	6	97.35	1.53
575	6	2	46.75	1.58					
575A	1	1	94.55	1.55	575A	14	3	145.65	1.58
575A	1	2	96.05	1.50	575A	15	2	146.95	1.57
575A	1	3	97.55	1.58	575A	15	3	148.45	1.52
575A	2	2	99.45	1.55	575A	16	2	150.25	1.57
575A	2	3	100.95	1.54	575A	16	3	151.50	1.58
575A	3	2	103.35	1.55	575A	17	2	152.25	1.61
575A	3	3	104.85	1.55	575A	17	3	153.37	1.56
575A	4	1	105.95	1.54	575A	18	2	154.75	1.57
575A	4	2	107.45	1.55	575A	18	3	156.25	1.56
575A	4	3	108.95	1.56	575A	19	2	159.05	1.58
575A	5	2	111.25	1.56	575A	19	3	160.30	1.57
575A	5	3	112.75	1.56	575A	20	2	163.05	1.57
575A	6	1	114.85	1.56	575A	20	3	164.15	1.57
575A	6	2	116.35	1.56	575A	21	1	165.45	1.56
575A	6	3	117.85	1.56	575A	21	2	166.95	1.58
575A	7	2	120.65	1.55	575A	21	3	168.45	1.61
575A	7	3	122.15	1.58	575A	22	2	170.43	1.69
575A	8	1	123.85	1.56	575A	22	3	171.85	1.57
575A	8	2	125.35	1.54	575A	23	1	172.85	1.56
575A	9	2	127.55	1.55	575A	23	2	174.35	1.58
575A	10	2	129.55	1.57	575A	24	2	176.45	1.56
575A	10	3	131.05	1.56	575A	24	3	177.95	1.58
575A	11	2	132.85	1.54	575A	25	3	180.95	1.60
575A	11	3	134.35	1.60	575A	26	2	182.35	1.55
575A	12	2	137.35	1.55	575A	26	3	183.85	1.57
575A	12	3	138.85	1.56	575A	27	2	187.15	1.60
575A	13	2	141.05	1.58	575A	28	2	189.45	1.69
575A	13	3	142.55	1.61	575A	29	3	193.15	1.61
575A	14	2	144.15	1.56	575A	30	1	194.35	1.63

HOLE	CORE	SECTION	DEPTH (METERS)	VELOCITY (KM/SEC)	HOLE	CORE	SECTION	DEPTH (METERS)	VELOCITY (KM/SEC)
575A	30	3	197.35	1.58	575A	32	3	204.87	1.63
575A	31	2	199.65	1.60	575A	33	2	206.57	1.58
575A	31	3	201.12	1.59	575A	33	3	208.05	1.59
575A	32	2	203.55	1.58					
575B	1	1	4.05	1.53	575B	6	5	54.75	1.54
575B	1	2	5.55	1.53	575B	7	2	57.65	1.58
575B	1	3	7.05	1.53	575B	7	3	59.15	1.57
575B	1	4	8.55	1.54	575B	7	4	60.65	1.58
575B	1	5	10.05	1.54	575B	7	5	62.15	1.56
575B	1	6	11.55	1.52	575B	7	6	63.65	1.56
575B	2	1	12.75	1.53	575B	8	2	66.95	1.55
575B	2	2	14.25	1.52	575B	8	3	68.45	1.53
575B	2	3	15.75	1.51	575B	8	4	69.95	1.53
575B	2	4	17.25	1.52	575B	8	5	71.45	1.54
575B	2	5	18.75	1.53	575B	8	6	72.95	1.54
575B	2	6	20.25	1.53	575B	9	2	76.05	1.53
575B	3	1	21.75	1.52	575B	9	3	77.55	1.55
575B	3	2	23.25	1.52	575B	9	4	79.05	1.55
575B	3	3	24.75	1.51	575B	9	5	80.55	1.56
575B	3	4	26.25	1.52	575B	10	2	83.65	1.54
575B	3	5	27.75	1.52	575B	10	3	85.15	1.57
575B	3	6	29.25	1.53	575B	10	4	86.65	1.53
575B	4	2	31.71	1.53	575B	10	5	88.15	1.56
575B	4	3	33.25	1.54	575B	10	6	89.65	1.55
575B	4	4	34.75	1.54	575B	11	2	93.15	1.53
575B	4	5	36.25	1.54	575B	11	3	94.65	1.55
575B	4	6	37.75	1.54	575B	11	4	96.15	1.55
575B	5	2	41.25	1.52	575B	11	5	97.65	1.58
575B	5	3	42.75	1.53	575B	11	6	99.15	1.55
575B	5	4	44.25	1.53	575B	12	2	101.85	1.57
575B	5	5	45.75	1.55	575B	13	2	111.45	1.54
575B	5	6	47.25	1.54	575B	13	3	112.95	1.54
575B	6	2	50.25	1.55	575B	14	2	116.35	1.57
575B	6	3	51.75	1.54	575B	14	3	117.85	1.54
575B	6	4	53.25	1.53					

THERMAL CONDUCTIVITY

HOLE	CORE	SECTION	DEPTH (METERS)	THERMAL COND. (MCAL/CM-C-SEC)	HOLE	CORE	SECTION	DEPTH (METERS)	THERMAL COND. (MCAL/CM-C-SEC)
572	1	2	2.44	2.90	572	1	5	6.85	3.20
572	1	3	3.69	3.04	572	1	6	8.25	2.76
572	1	4	5.22	2.64					
572A	1	1	0.75	2.64	572A	7	3	58.95	2.43
572A	1	2	2.25	2.38	572A	7	4	60.45	2.83
572A	1	3	3.75	2.53	572A	7	5	61.95	2.90
572A	1	4	5.25	2.64	572A	7	6	63.45	2.90
572A	1	5	6.75	2.43	572A	9	2	74.55	2.38
572A	1	6	8.25	2.76	572A	9	3	76.05	2.29
572A	2	1	10.25	2.90	572A	9	4	77.55	2.76
572A	2	2	11.75	2.90	572A	9	5	79.05	3.04
572A	2	3	13.25	2.64	572A	9	6	80.53	2.90
572A	2	4	14.75	2.76	572A	10	2	84.05	2.76
572A	2	5	16.25	2.64	572A	10	3	85.53	2.90
572A	2	6	17.75	2.64	572A	10	4	87.05	3.12
572A	3	1	19.75	2.34	572A	10	5	88.55	3.04
572A	3	2	21.25	2.29	572A	10	6	90.05	2.64
572A	3	3	22.75	2.25	572A	11	1	92.15	2.33
572A	3	5	24.09	2.53	572A	11	2	93.65	2.03
572A	3	6	25.75	2.53	572A	11	3	95.15	2.64
572A	4	1	29.35	2.53	572A	11	4	96.65	2.90
572A	4	2	30.85	2.70	572A	11	5	98.15	2.64
572A	4	4	33.85	2.43	572A	11	6	99.65	2.48
572A	4	5	35.35	2.64	572A	12	3	104.45	2.34
572A	5	2	38.57	2.34	572A	12	4	105.95	2.53
572A	5	3	40.03	2.76	572A	12	5	107.45	2.53
572A	5	4	41.55	2.34	572A	12	6	108.95	2.90
572A	5	5	43.05	3.12	572A	14	1	119.85	2.90
572A	5	6	44.55	2.25	572A	14	2	121.35	2.25
572A	6	2	48.15	2.64	572A	14	3	122.85	2.90
572A	6	3	49.65	2.97	572A	14	4	124.35	2.43
572A	6	4	51.15	2.76	572A	14	5	125.85	2.64
572A	6	5	52.65	2.25	572A	14	6	127.35	2.64
572A	6	6	54.15	2.48	572A	15	1	129.05	2.76
572A	7	2	57.45	2.64	572A	15	2	130.55	3.20

HOLE	CORE	SECTION	DEPTH (METERS)	THERMAL COND. (MCAL/CM-C-SEC)	HOLE	CORE	SECTION	DEPTH (METERS)	THERMAL COND. (MCAL/CM-C-SEC)
572A	15	3	132.05	2.64	572A	17	1	146.05	2.64
572A	15	4	133.55	2.53	572A	17	2	147.55	2.64
572A	15	5	135.05	2.53	572A	17	3	149.05	2.76
572A	15	6	136.35	2.53	572A	17	4	150.53	2.64
572A	16	2	139.35	2.90	572A	17	5	152.05	2.34
572A	16	3	140.85	3.20	572A	17	6	153.30	2.76
572B	2	1	160.05	2.53	572B	3	2	166.45	2.48
572B	2	2	161.55	2.70	572B	3	3	167.95	2.10
572B	2	3	163.05	2.21	572B	4	1	169.55	3.04
572B	3	1	164.95	2.29	572B	4	2	171.05	1.90
572C	1	1	0.75	2.43	572C	9	3	81.05	2.64
572C	1	2	2.25	2.64	572C	9	4	82.55	2.64
572C	1	3	3.75	2.70	572C	9	5	84.05	2.90
572C	1	4	5.25	2.25	572C	9	6	85.55	2.64
572C	1	5	6.75	3.04	572C	10	1	87.65	2.90
572C	1	6	8.25	2.70	572C	10	2	89.15	2.76
572C	2	1	10.85	2.43	572C	10	3	90.65	2.90
572C	2	2	12.35	2.90	572C	10	4	92.15	2.53
572C	2	3	13.85	2.43	572C	10	5	93.65	2.53
572C	2	4	15.35	2.34	572C	10	6	95.15	2.64
572C	2	5	16.85	2.64	572C	11	1	97.25	2.34
572C	2	6	18.35	2.43	572C	11	2	98.75	2.53
572C	3	1	20.45	3.04	572C	11	3	100.25	2.90
572C	3	2	21.95	1.90	572C	12	1	102.25	2.43
572C	3	3	23.45	2.53	572C	12	2	103.75	2.76
572C	3	4	24.95	2.25	572C	12	3	105.25	2.76
572C	3	5	26.45	2.34	572C	13	1	107.25	2.43
572C	3	6	27.95	2.34	572C	13	2	108.75	2.43
572C	4	1	30.05	2.64	572C	13	3	110.25	2.43
572C	4	2	31.55	2.43	572C	14	1	112.25	2.76
572C	4	3	33.05	2.53	572C	14	2	113.75	2.53
572C	4	4	34.55	2.34	572C	14	3	115.25	2.53
572C	4	5	36.05	3.04	572C	14	4	116.75	2.43
572C	4	6	37.55	2.25	572C	14	5	118.25	2.64
572C	5	1	39.65	2.53	572C	15	1	121.85	2.76
572C	5	2	41.15	2.53	572C	15	2	123.35	2.64
572C	5	3	42.65	2.64	572C	15	3	124.85	2.90
572C	5	4	44.15	2.53	572C	15	4	126.35	2.76
572C	5	5	45.65	2.17	572C	15	5	127.85	3.04
572C	5	6	47.15	2.25	572C	15	6	129.35	2.76
572C	6	1	49.25	2.90	572C	16	1	131.45	2.43
572C	6	2	50.75	2.53	572C	16	2	132.95	2.34
572C	6	3	52.25	2.34	572C	16	3	134.45	2.90
572C	6	4	53.75	2.43	572C	16	4	135.95	3.38
572C	6	5	55.25	2.64	572C	16	5	137.45	3.04
572C	6	6	56.75	2.10	572C	16	6	138.95	3.38
572C	7	1	58.85	2.34	572C	17	1	141.05	3.04
572C	7	2	60.35	2.64	572C	17	2	142.55	3.04
572C	7	3	61.85	2.90	572C	17	3	144.05	3.04
572C	7	4	63.35	2.64	572C	17	4	145.55	2.76
572C	7	5	64.85	2.64	572C	18	2	152.15	2.83
572C	7	6	66.35	2.76	572C	18	3	153.65	2.83
572C	8	1	68.45	2.90	572C	18	4	155.15	2.70
572C	8	2	69.95	2.76	572C	18	5	156.65	2.70
572C	8	3	71.45	2.53	572C	18	6	158.15	2.70
572C	8	4	72.95	2.64	572C	19	2	161.75	3.04
572C	8	5	74.45	2.64	572C	19	3	163.25	2.53
572C	8	6	75.95	2.43	572C	20	1	165.26	2.53
572C	9	1	78.05	3.04	572C	20	2	166.75	2.17
572C	9	2	79.55	2.76					
573	2	2	4.25	2.06	573	7	2	50.25	2.05
573	2	3	5.75	2.17	573	7	3	51.75	1.92
573	2	4	7.25	2.41	573	7	4	53.25	1.82
573	2	5	8.75	2.22	573	7	5	54.75	1.83
573	2	6	10.25	2.43	573	7	6	56.25	2.29
573	3	2	13.75	2.51	573	8	2	59.45	2.02
573	3	3	15.25	2.36	573	8	3	60.95	2.29
573	3	4	16.75	2.62	573	8	4	62.45	2.06
573	3	5	18.25	2.29	573	8	5	63.95	2.24
573	3	6	19.75	2.53	573	8	6	65.45	2.16
573	4	2	23.25	2.39	573	9	2	68.95	2.56
573	4	3	24.75	2.32	573	9	3	70.45	2.44
573	4	4	26.25	2.38	573	9	4	71.95	2.50
573	4	5	27.75	2.09	573	9	5	73.45	2.64
573	4	6	29.25	1.89	573	9	6	74.95	2.56
573	5	5	37.25	1.87	573	10	2	78.45	2.17
573	6	2	41.55	2.16	573	10	3	79.95	2.21
573	6	3	43.05	2.08	573	10	4	81.45	2.45
573	6	4	44.55	2.08	573	10	5	82.95	2.41
573	6	5	46.05	2.22	573	10	6	84.45	2.00
573	6	6	47.55	2.15	573	11	2	87.95	2.14

HOLE	CORE	SECTION	DEPTH (METERS)	THERMAL COND. (MCAL/CM-C-SEC)	HOLE	CORE	SECTION	DEPTH (METERS)	THERMAL COND. (MCAL/CM-C-SEC)
573	11	3	89.45	2.70	573	15	3	125.85	2.49
573	11	4	90.95	2.73	573	15	4	127.35	2.56
573	11	5	92.45	2.55	573	15	5	128.85	2.57
573	11	6	93.95	2.74	573	15	6	130.35	2.76
573	12	2	97.45	3.17	573	16	2	133.55	2.70
573	12	3	98.95	2.62	573	16	3	135.05	2.36
573	12	4	100.45	2.44	573	16	4	136.55	2.52
573	12	5	101.95	2.47	573	16	5	138.05	2.53
573	12	6	103.45	2.46	573	16	6	139.55	2.32
573	13	2	106.25	2.18	573	17	2	142.35	2.60
573	13	3	107.75	2.34	573	17	3	143.85	2.78
573	13	4	109.25	2.41	573	17	4	145.35	2.47
573	13	5	110.75	2.53	573	17	5	146.85	2.72
573	13	6	112.25	2.64	573	17	6	148.35	2.36
573	14	2	114.85	2.69	573	18	1	149.65	2.58
573	14	3	116.35	2.73	573	18	2	150.15	2.86
573	14	4	117.85	2.56	573	18	3	152.65	2.04
573	14	5	119.35	2.63	573	19	1	154.65	2.38
573	14	6	120.85	2.59	573	19	3	157.65	2.39
573	15	2	124.35	2.42					
573A	1	2	6.75	1.78	573A	4	3	35.05	2.21
573A	1	3	8.25	1.86	573A	4	4	36.55	2.03
573A	1	4	9.75	2.33	573A	4	5	38.05	2.31
573A	1	5	11.25	2.57	573A	4	6	39.55	2.35
573A	1	6	12.75	2.55	573A	5	2	42.05	2.05
573A	2	2	16.25	2.38	573A	5	3	43.55	1.99
573A	2	3	17.75	1.74	573A	5	4	45.05	1.92
573A	2	4	19.25	2.28	573A	5	5	46.55	2.28
573A	2	5	20.75	2.18	573A	5	6	48.05	1.93
573A	3	2	24.35	2.26	573A	6	2	51.45	2.00
573A	3	3	25.85	2.12	573A	6	3	52.95	1.93
573A	3	4	27.35	2.06	573A	6	4	54.45	2.15
573A	3	5	28.85	1.89	573A	6	5	55.95	2.18
573A	3	6	30.35	2.17	573A	6	6	57.45	1.98
573A	4	2	33.55	2.48					
573B	1	2	140.75	2.57	573B	11	3	237.45	3.21
573B	1	3	142.25	2.66	573B	11	4	238.95	3.00
573B	1	4	143.75	2.45	573B	11	5	240.45	2.70
573B	1	5	145.25	2.74	573B	11	6	241.95	2.89
573B	2	2	150.25	2.59	573B	12	2	245.25	2.63
573B	2	3	151.75	2.38	573B	12	3	246.75	2.95
573B	2	4	152.25	2.52	573B	12	4	248.25	2.70
573B	2	5	154.75	2.47	573B	12	5	249.75	2.90
573B	2	6	156.25	2.57	573B	13	2	254.95	2.73
573B	3	3	161.25	2.30	573B	13	3	256.45	2.72
573B	3	4	162.75	2.22	573B	13	4	257.95	2.64
573B	3	5	164.25	2.30	573B	13	5	259.45	2.77
573B	3	6	165.75	2.32	573B	13	6	260.95	2.32
573B	4	2	169.75	2.76	573B	14	2	264.25	2.72
573B	4	3	170.75	2.52	573B	14	3	265.75	2.63
573B	4	4	172.25	2.44	573B	14	4	267.25	2.89
573B	4	5	173.75	2.61	573B	14	5	268.75	2.87
573B	4	6	175.25	2.39	573B	14	6	270.25	2.76
573B	5	2	178.75	2.71	573B	15	2	273.75	2.65
573B	5	3	180.25	2.83	573B	15	3	275.25	2.48
573B	5	4	181.75	2.79	573B	15	4	276.75	2.65
573B	5	5	183.25	2.92	573B	15	5	278.25	2.66
573B	5	6	184.75	2.84	573B	16	2	283.25	3.12
573B	6	2	188.25	2.77	573B	16	3	284.75	3.10
573B	6	3	189.75	2.78	573B	16	4	286.25	3.14
573B	6	4	191.25	2.70	573B	16	5	287.75	2.93
573B	6	5	192.75	2.83	573B	17	2	292.75	3.33
573B	6	6	194.25	2.67	573B	17	3	294.25	3.28
573B	7	2	197.75	2.95	573B	17	4	295.75	3.22
573B	7	3	199.25	3.03	573B	17	5	297.25	3.25
573B	7	4	200.75	3.06	573B	18	1	300.75	3.21
573B	7	5	202.75	3.03	573B	18	2	302.25	3.36
573B	8	2	207.25	2.66	573B	18	3	303.75	3.00
573B	8	3	208.75	2.29	573B	19	1	310.25	3.12
573B	2	4	210.25	2.80	573B	19	2	311.75	3.32
573B	8	5	211.75	2.80	573B	20	2	321.25	3.59
573B	8	6	213.25	2.83	573B	20	3	322.75	3.24
573B	9	2	216.75	3.02	573B	20	4	324.25	3.39
573B	9	3	218.25	3.00	573B	20	5	325.75	3.74
573B	9	4	219.75	3.00	573B	20	6	327.25	3.56
573B	9	5	221.25	2.70	573B	21	1	329.75	3.24
573B	10	2	226.25	2.93	573B	21	2	330.75	2.93
573B	10	3	227.75	2.92	573B	21	3	332.25	3.07
573B	10	4	229.25	2.91	573B	21	4	333.75	3.10
573B	10	5	230.75	2.94	573B	22	1	338.75	3.07
573B	10	6	232.25	2.62	573B	22	2	340.25	3.40
573B	11	2	235.95	3.20	573B	22	3	341.75	3.32

HOLE	CORE	SECTION	DEPTH (METERS)	THERMAL COND. (MCAL/CM-C-SEC)	HOLE	CORE	SECTION	DEPTH (METERS)	THERMAL COND. (MCAL/CM-C-SEC)
573B	22	4	343.25	3.31	573B	33	2	444.75	3.46
573B	23	1	348.25	3.38	573B	33	3	446.25	3.52
573B	23	2	349.75	3.30	573B	33	4	447.75	3.30
573B	23	3	351.25	2.90	573B	33	5	449.25	3.37
573B	24	1	357.75	3.47	573B	36	1	471.75	3.08
573B	24	2	359.25	3.36	573B	36	2	473.25	3.07
573B	27	2	387.55	3.45	573B	36	3	474.75	3.12
573B	27	3	389.35	3.28	573B	37	1	481.25	3.22
573B	27	4	390.55	3.16	573B	38	1	490.75	3.50
573B	28	2	397.25	2.59	573B	38	2	492.20	2.56
573B	29	2	406.65	3.89	573B	38	2	492.58	2.73
573B	29	3	408.25	3.35	573B	38	3	493.75	2.59
573B	29	5	411.00	3.64					
574	1	1	0.75	2.07	574	15	3	126.35	2.92
574	1	2	2.24	1.68	574	17	1	133.35	2.71
574	2	2	6.75	1.85	574	17	1	133.55	2.64
574	2	3	8.25	1.74	574	17	2	134.85	2.68
574	2	4	9.75	2.01	574	17	2	135.05	2.65
574	2	5	11.25	2.17	574	17	3	136.35	2.38
574	2	6	12.75	1.96	574	18	1	138.35	2.61
574	3	2	16.25	1.73	574	18	2	139.85	2.63
574	3	3	17.75	1.81	574	18	2	140.05	2.60
574	3	4	19.25	1.74	574	18	3	141.35	2.69
574	3	5	20.75	1.66	574	18	3	141.55	2.73
574	3	6	22.25	1.70	574	19	1	143.35	2.80
574	4	2	25.75	1.75	574	19	1	143.55	2.77
574	4	3	27.25	1.75	574	19	2	144.85	2.70
574	4	4	28.75	1.81	574	19	2	145.05	2.73
574	4	5	30.25	1.70	574	19	3	146.35	2.34
574	4	6	31.75	1.80	574	20	1	148.35	1.76
574	5	2	35.25	1.78	574	20	2	149.85	2.91
574	5	3	36.75	1.75	574	20	2	150.05	2.92
574	5	4	38.25	1.68	574	20	3	151.35	2.75
574	5	5	39.75	1.72	574	20	3	151.55	2.85
574	5	6	41.25	1.87	574	21	1	153.25	2.60
574	6	2	44.75	1.93	574	21	2	154.75	2.99
574	6	3	46.25	1.91	574	21	2	154.95	2.84
574	6	4	47.75	1.82	574	21	3	156.25	2.22
574	6	5	49.25	2.25	574	21	3	156.45	2.66
574	6	6	50.75	2.38	574	22	1	158.25	2.77
574	7	2	54.25	2.04	574	22	1	158.45	2.82
574	7	5	58.75	2.01	574	22	2	159.75	2.91
574	7	6	60.25	2.01	574	22	2	*159.95	2.98
574	8	1	61.75	2.57	574	22	3	161.25	2.80
574	8	2	63.25	2.60	574	23	1	163.25	2.15
574	8	3	64.75	2.37	574	23	2	164.75	2.88
574	8	5	67.75	2.20	574	23	2	164.95	2.96
574	8	6	69.25	2.00	574	23	3	166.25	2.91
574	9	2	72.75	2.02	574	23	3	166.45	2.92
574	9	3	74.25	2.15	574	24	1	168.25	2.62
574	9	4	75.75	1.66	574	24	2	169.75	2.92
574	9	5	77.25	1.67	574	24	2	169.95	2.86
574	9	6	78.75	1.87	574	24	3	171.25	2.81
574	10	2	82.25	2.28	574	24	3	171.45	3.16
574	10	3	83.75	1.89	574	25	1	173.25	2.66
574	10	4	85.25	2.27	574	25	2	174.75	3.05
574	10	5	86.75	2.39	574	25	2	174.95	3.10
574	10	6	88.25	2.28	574	25	3	176.25	2.62
574	11	2	91.75	2.37	574	25	3	176.45	2.75
574	11	3	93.25	2.26	574	26	1	178.25	2.83
574	11	4	94.75	2.81	574	26	2	179.75	2.57
574	11	5	96.25	2.49	574	26	2	179.95	2.89
574	12	2	100.85	2.79	574	26	3	181.25	2.83
574	12	3	102.35	2.67	574	26	3	181.45	2.83
574	12	4	103.85	2.79	574	27	1	182.95	2.92
574	12	5	105.35	2.46	574	27	2	184.45	2.47
574	12	6	106.85	2.80	574	27	3	185.95	2.60
574	13	2	110.35	2.62	574	28	2	189.45	2.69
574	13	3	111.85	2.67	574	28	3	190.95	2.84
574	13	4	113.35	2.58	574	29	1	192.95	2.67
574	13	5	114.83	2.56	574	29	2	194.45	2.83
574	13	6	116.35	2.75	574	29	3	195.95	2.71
574	14	1	118.33	2.84	574	30	2	199.45	2.55
574	14	2	119.45	2.96	574	30	3	200.95	2.96
574	14	2	119.85	2.97	574	31	1	202.95	2.50
574	14	3	121.35	2.96	574	31	2	204.10	2.30
574	15	1	123.35	2.87	574	31	2	204.45	2.18
574	15	2	124.45	2.60	574	31	3	205.95	2.63
574	15	2	124.85	2.80					
574A	2	2	8.55	2.00	574A	2	5	13.05	2.09
574A	2	3	10.05	1.87	574A	2	6	14.55	1.89
574A	2	4	11.55	2.29	574A	3	1	16.25	1.96

APPENDIX

HOLE	CORE	SECTION	DEPTH (METERS)	THERMAL COND. (MCAL/CM-C-SEC)
574A	3	2	17.75	1.93
574A	3	3	19.25	1.85
574A	3	4	20.75	1.99
574A	3	5	22.25	1.92
574A	5	1	33.85	1.80
574A	5	2	35.35	1.67
574A	5	3	36.85	1.87
574A	5	4	38.35	2.26
574A	5	5	41.35	2.08
574A	6	2	44.65	1.82
574A	6	3	46.15	2.05
574A	6	4	47.65	2.58
574A	6	5	49.15	2.59
574A	6	6	50.65	2.54
574A	7	2	54.15	2.06
574A	7	3	55.65	2.17
574A	7	4	57.15	2.03
574A	7	5	58.65	2.46
574A	7	6	60.15	2.30
574A	8	2	63.65	2.47
574A	8	3	65.15	2.35
574A	8	4	66.65	2.43
574A	8	5	68.15	1.91
574A	8	6	69.65	2.04
574A	9	2	72.65	1.89
574A	9	3	74.15	1.92
574A	9	4	75.65	1.73
574A	9	5	77.15	1.71
574A	9	6	78.65	1.94
574A	10	2	82.15	2.18
574B	1	2	187.25	2.54
574B	1	3	188.75	2.77
574B	1	4	190.25	2.63
574C	1	2	196.75	2.66
574C	1	3	198.25	2.28
574C	1	4	199.75	2.13
574C	1	5	201.25	2.48
574C	2	2	206.25	2.31
574C	2	3	207.75	2.62
574C	2	4	209.25	2.60
574C	2	5	210.75	2.68
574C	2	6	212.25	1.89
574C	3	1	214.25	2.47
574C	3	2	215.75	2.61
574C	3	3	217.25	2.45
574C	4	1	223.75	2.65
574C	4	2	225.25	2.71
574C	5	2	234.75	2.76
574C	5	3	236.25	2.96
574C	5	4	237.75	2.81
574C	6	3	245.75	3.14
574C	6	4	247.25	2.81
574C	7	2	253.75	3.05
574C	7	3	255.25	2.67
574C	7	4	256.75	2.38
574C	8	1	261.75	2.91
574C	8	2	263.25	2.82
574C	8	3	264.40	2.86
574C	8	3	264.75	2.95
574C	9	1	271.25	3.00
574C	9	1	271.45	2.93
574C	9	2	272.75	2.78
574C	9	2	272.95	2.81
574C	9	3	274.00	2.90
574C	10	2	282.25	2.86
574C	10	3	283.75	2.92
574C	10	4	285.25	2.91
574C	10	5	286.73	3.06
574C	10	3	288.23	3.15
574C	11	1	290.25	3.15
574C	11	1	290.45	3.22
574C	11	2	291.75	3.28
574C	11	2	291.95	3.25
574C	11	3	293.25	3.44
574C	12	1	301.23	3.26
574C	12	2	302.75	3.16
574C	12	4	304.25	3.09
574C	12	5	305.75	3.07
574C	12	6	307.25	3.21
574C	13	2	310.75	3.21
574C	13	3	312.25	3.14
574C	13	4	313.75	3.24
574A	10	3	83.65	2.13
574A	10	4	85.15	2.11
574A	10	5	86.65	2.18
574A	10	6	88.15	2.48
574A	11	2	91.45	2.26
574A	11	3	92.95	2.20
574A	11	4	94.45	2.15
574A	11	5	95.95	2.78
574A	11	6	97.45	2.71
574A	12	2	100.95	2.66
574A	12	3	102.45	2.61
574A	12	4	103.95	2.57
574A	12	5	105.45	2.44
574A	13	1	106.95	2.85
574A	13	2	110.05	2.66
574A	13	2	110.45	2.49
574A	13	3	111.95	2.52
574A	15	1	118.75	2.98
574A	15	2	119.85	2.83
574A	15	2	120.25	3.09
574A	15	3	121.75	3.11
574A	22	2	170.65	2.81
574A	22	3	172.15	3.02
574A	22	4	173.65	2.74
574A	22	5	175.15	3.02
574A	22	6	176.65	2.86
574A	23	1	178.65	2.68
574A	23	2	180.15	2.77
574A	23	5	181.65	2.49
574B	1	5	191.75	2.64
574B	1	6	193.25	2.51
574C	14	1	318.75	3.10
574C	14	2	320.25	3.06
574C	15	2	329.75	3.13
574C	15	3	331.25	3.05
574C	15	4	332.75	3.02
574C	15	5	334.25	3.19
574C	15	6	335.75	2.58
574C	16	1	337.75	3.23
574C	16	2	338.85	3.00
574C	16	2	339.25	2.90
574C	16	3	340.75	3.09
574C	17	2	348.75	3.14
574C	17	3	350.25	3.22
574C	17	4	351.75	3.09
574C	17	5	353.25	3.01
574C	17	6	354.75	3.20
574C	18	1	356.75	3.06
574C	18	2	358.25	3.13
574C	19	1	366.25	2.90
574C	19	2	367.75	3.02
574C	20	2	377.25	3.21
574C	20	3	378.75	3.25
574C	20	4	380.25	3.10
574C	20	5	381.75	3.33
574C	20	6	383.80	3.35
574C	21	1	385.25	3.37
574C	21	2	386.75	3.18
574C	21	3	388.25	3.25
574C	21	4	389.75	3.13
574C	22	2	395.90	3.40
574C	22	2	396.25	3.16
574C	22	3	397.40	3.31
574C	22	3	397.75	3.28
574C	23	2	405.75	3.26
574C	23	3	407.25	3.32
574C	23	4	408.75	3.07
574C	23	5	410.25	3.46
574C	23	6	411.75	3.30
574C	24	1	413.75	2.87
574C	24	2	415.25	3.09
574C	24	3	416.75	3.23
574C	24	4	418.25	3.35
574C	25	1	423.25	3.27
574C	26	1	432.75	3.55
574C	26	2	434.25	3.17
574C	27	1	442.25	3.22
574C	27	2	443.75	3.45
574C	27	3	445.25	3.45

HOLE	CORE	SECTION	DEPTH (METERS)	THERMAL COND. (MCAL/CM-C-SEC)	HOLE	CORE	SECTION	DEPTH (METERS)	THERMAL COND. (MCAL/CM-C-SEC)
575	1	1	0.75	1.61	575	6	5	51.25	2.70
575	1	2	2.25	1.65	575	6	6	52.75	2.69
575	1	3	3.75	1.51	575	7	2	56.25	2.79
575	1	4	5.25	1.50	575	7	3	57.75	2.99
575	1	5	6.75	1.38	575	7	4	59.25	2.87
575	2	2	9.55	1.83	575	7	5	60.75	3.10
575	2	3	11.05	1.53	575	7	6	62.25	2.94
575	2	4	12.55	1.41	575	8	2	62.75	2.69
575	2	5	14.05	1.51	575	8	3	67.25	2.83
575	2	6	15.55	1.82	575	8	4	68.75	2.79
575	3	2	17.55	1.95	575	8	5	70.25	2.65
575	3	3	19.05	2.13	575	8	6	71.75	2.57
575	3	4	20.55	2.32	575	9	1	73.75	2.82
575	3	5	22.05	2.47	575	9	2	75.25	2.80
575	3	6	23.55	2.66	575	9	3	76.75	2.46
575	4	2	26.35	2.03	575	9	4	78.25	2.72
575	4	3	30.05	2.20	575	9	5	79.75	2.56
575	4	4	31.55	2.55	575	10	2	82.45	2.76
575	4	5	33.05	2.86	575	10	3	83.95	2.53
575	4	6	34.55	2.76	575	10	4	85.45	2.49
575	5	2	37.25	2.83	575	10	5	86.95	2.63
575	5	3	38.75	2.79	575	10	6	88 45	2.68
575	5	4	40.25	2.56	575	11	2	91.35	2.69
575	5	5	41.75	2.39	575	11	3	92.85	2.73
575	5	6	43.25	2.62	575	11	4	94.35	2.54
575	6	2	46.75	3.11	575	11	5	95.85	2.81
575	6	3	48.25	2.98	575	11	6	97.35	2.66
575	6	4	49.75	2.89					
575A	1	1	94.55	2.60	575A	15	2	146.95	2.74
575A	1	2	96.05	2.61	575A	15	3	148.45	2.88
575A	1	2	96.55	2.64	575A	16	2	150.25	2.96
575A	1	3	97.55	2.36	575A	16	3	151.75	2.95
575A	2	1	97.95	2.43	575A	17	2	152.25	2.82
575A	2	2	99.45	2.48	575A	17	3	153.50	2.80
575A	2	2	99.95	2.35	575A	18	2	154.75	2.85
575A	2	3	100.95	2.15	575A	18	3	156.25	2.66
575A	3	2	103.35	2.04	575A	19	2	159.05	2.89
575A	3	3	104.85	2.18	575A	19	3	160.55	2.86
575A	4	2	107.45	2.57	575A	20	2	162.80	2.97
575A	4	3	108.95	2.69	575A	20	2	163.05	2.84
575A	5	2	111.25	2.67	575A	20	2	163.40	2.69
575A	5	2	111.75	2.63	575A	20	3	164.30	2.89
575A	5	3	112.75	2.31	575A	21	2	166.95	2.87
575A	5	3	113.25	2.79	575A	21	3	168.45	3.12
575A	6	1	114.85	2.40	575A	22	2	170.35	2.71
575A	6	2	116.35	2.53	575A	22	3	171.85	2.96
575A	6	3	117.85	2.61	575A	23	1	172.85	3.30
575A	7	2	120.65	2.50	575A	23	2	174.35	3.67
575A	7	3	122.15	2.72	575A	24	2	176.45	3.82
575A	8	2	125.35	2.54	575A	24	3	177.95	3.49
575A	8	2	125.85	2.72	575A	25	2	179.45	2.97
575A	9	1	126.55	2.62	575A	25	3	180.95	3.03
575A	8	3	126.85	2.49	575A	26	2	182.35	2.88
575A	8	3	127.35	2.69	575A	26	3	183.85	2.92
575A	9	2	127.55	2.44	575A	27	2	187.15	3.13
575A	9	2	127.85	2.95	575A	28	1	187.95	2.88
575A	10	2	129.55	2.89	575A	29	2	191.95	3.10
575A	10	3	131.05	2.69	575A	29	3	193.15	3.01
575A	11	2	132.85	2.73	575A	30	2	195.85	2.86
575A	11	3	134.35	2.48	575A	30	3	197.35	2.97
575A	12	2	137.35	2.97	575A	31	2	199.65	3.06
575A	12	3	138.85	2.95	575A	31	3	201.15	3.05
575A	13	2	141.05	2.85	575A	32	2	203.55	3.03
575A	13	3	142.55	3.15	575A	32	3	205.05	3.32
575A	14	2	144.15	2.94	575A	33	2	206.55	3.07
575A	14	3	145.65	2.94	575A	33	3	208.05	3.06

FORMATION FACTOR

HOLE	CORE	SECTION	DEPTH (METERS)	FORMATION FACT. VERT.	HORIZ.	HOLE	CORE	SECTION	DEPTH (METERS)	FORMATION FACT. VERT.	HORIZ.
572	1	1	1.00	1.52	1.52	572	1	4	5.20	1.52	1.67
572	1	2	1.63	1.37	1.46	572	1	4	5.70	1.71	1.77
572	1	2	2.23	1.55	1.61	572	1	5	6.17	1.48	1.52
572	1	2	2.74	1.09	1.09	572	1	5	6.70	1.69	1.78
572	1	3	3.18	1.78	1.59	572	1	5	7.20	1.45	1.73
572	1	3	3.79	1.62	1.73	572	1	6	7.60	1.42	1.47
572	1	3	4.28	1.16	1.30	572	1	6	8.20	1.56	1.78
572	1	4	4.63	1.63	1.78	572	1	6	8.75	1.70	1.75
572A	1	1	0.05	1.61	1.70	572A	7	6	63.45	1.76	1.84
572A	1	1	0.60	1.71	1.73	572A	8	1	64.85	2.09	2.19
572A	1	1	1.17	1.39	1.59	572A	8	2	66.35	1.67	1.80
572A	1	2	1.60	1.23	1.13	572A	8	3	67.85	1.83	1.87
572A	1	2	2.12	1.31	1.38	572A	8	4	69.35	1.72	1.72
572A	1	2	2.70	1.32	1.46	572A	8	5	70.85	1.68	1.68
572A	1	3	3.07	1.35	1.48	572A	9	1	73.05	1.69	1.78
572A	1	3	3.74	1.35	1.47	572A	9	2	74.55	1.69	1.82
572A	1	3	4.26	1.41	1.63	572A	9	3	76.05	1.50	1.56
572A	1	4	4.58	1.27	1.52	572A	9	4	77.55	1.89	2.00
572A	1	4	5.20	1.54	1.70	572A	9	5	79.05	2.09	2.16
572A	1	4	5.80	1.39	1.52	572A	9	6	80.55	1.87	1.91
572A	1	5	6.07	1.48	1.62	572A	10	2	84.05	1.79	1.88
572A	1	5	6.68	1.61	1.57	572A	10	3	85.55	1.82	1.82
572A	1	5	7.27	1.54	1.51	572A	10	4	87.05	1.98	1.87
572A	1	6	7.57	1.58	1.75	572A	10	5	88.48	2.00	2.09
572A	1	6	8.17	1.45	1.55	572A	10	6	89.96	1.91	2.04
572A	1	6	8.77	1.54	1.70	572A	11	1	91.96	1.65	1.83
572A	2	1	9.57	1.33	1.50	572A	11	2	92.99	1.74	1.91
572A	2	1	10.17	1.50	1.67	572A	11	3	94.31	1.73	1.82
572A	2	1	10.77	1.62	1.25	572A	11	4	95.76	1.73	1.78
572A	2	2	11.07	1.77	1.83	572A	11	5	97.15	1.67	1.82
572A	2	2	11.70	1.53	1.55	572A	11	6	98.75	1.60	1.69
572A	2	2	12.20	1.64	1.70	572A	12	1	101.37	1.65	1.83
572A	2	3	12.57	1.45	1.60	572A	12	2	102.87	1.78	1.82
572A	2	3	13.27	1.27	1.27	572A	12	3	104.37	1.69	1.78
572A	2	3	13.77	1.50	1.53	572A	12	4	105.87	1.87	1.96
572A	2	4	14.07	1.53	1.64	572A	12	5	107.37	1.78	1.87
572A	2	4	14.70	1.62	1.19	572A	12	6	108.87	1.87	2.00
572A	2	4	15.20	1.19	1.34	572A	13	1	110.65	1.91	1.98
572A	2	5	15.57	1.45	1.56	572A	13	2	112.15	2.19	2.19
572A	2	5	16.20	1.45	1.53	572A	13	3	113.65	2.02	2.07
572A	2	5	16.71	1.32	1.55	572A	13	4	115.15	2.26	2.31
572A	2	6	17.78	1.54	1.71	572A	13	5	116.65	2.07	2.12
572A	3	1	19.76	1.55	1.70	572A	13	6	118.15	1.93	2.05
572A	3	2	21.25	1.57	1.67	572A	14	1	119.90	1.58	1.67
572A	3	3	22.75	1.45	1.50	572A	14	2	121.27	1.54	1.67
572A	3	4	24.25	1.66	1.76	572A	14	3	122.77	1.74	1.91
572A	3	5	25.58	1.57	1.70	572A	14	4	124.27	1.68	1.77
572A	3	6	27.25	2.70	2.88	572A	14	5	125.77	1.91	2.05
572A	4	1	29.35	1.52	1.68	572A	14	6	127.27	1.65	1.78
572A	4	4	33.95	1.51	1.56	572A	15	1	128.97	2.27	2.27
572A	4	5	35.35	1.72	1.77	572A	15	2	130.47	2.04	2.13
572A	5	1	37.05	1.52	1.63	572A	15	3	131.97	1.91	2.00
572A	5	2	38.55	1.48	1.61	572A	15	4	133.47	1.91	2.13
572A	5	3	40.05	1.63	1.75	572A	15	5	134.97	1.87	2.04
572A	5	4	41.55	1.89	2.00	572A	15	6	136.27	2.00	2.11
572A	5	5	43.05	1.91	2.00	572A	16	2	139.35	2.11	2.22
572A	5	6	44.55	1.41	1.52	572A	16	3	140.85	2.17	2.26
572A	6	2	48.15	1.53	1.42	572A	16	4	142.35	2.15	2.26
572A	6	3	49.65	1.67	1.80	572A	16	5	144.20	2.15	2.30
572A	6	4	51.15	1.61	1.74	572A	17	1	146.05	1.98	2.06
572A	6	5	52.65	1.38	1.38	572A	17	2	147.55	1.96	2.00
572A	6	6	54.15	1.43	1.51	572A	17	3	149.05	1.91	2.04
572A	7	2	57.45	1.73	1.82	572A	17	4	150.55	2.02	2.07
572A	7	3	58.95	1.56	1.60	572A	17	5	152.05	1.82	1.87
572A	7	4	60.45	1.89	1.96	572A	17	6	153.55	1.91	2.00
572A	7	5	61.95	1.91	2.00						
572B	1	2	156.13	2.04	2.09	572B	3	1	164.95	1.53	1.67
572B	1	3	157.67	1.84	1.88	572B	3	2	166.45	1.78	1.39
572B	2	1	160.05	1.84	1.87	572B	3	3	167.95	1.78	1.87
572B	2	2	161.65	1.87	1.89	572B	4	1	169.55	1.74	1.80
572B	2	3	163.45	1.73	1.87	572B	4	2	171.05	1.51	1.64
572C	1	1	0.73	1.53	1.60	572C	2	6	18.35	1.69	1.78
572C	1	2	2.23	1.67	1.76	572C	3	1	20.45	1.58	1.64
572C	1	3	3.73	1.71	1.84	572C	3	2	21.95	1.60	1.64
572C	1	5	6.73	1.84	2.09	572C	3	3	23.45	1.67	1.78
572C	1	6	8.23	1.84	1.89	572C	3	4	24.95	1.47	1.56
572C	2	1	10.65	1.51	1.58	572C	3	5	26.45	1.64	1.76
572C	2	2	12.35	1.82	1.87	572C	3	6	27.95	1.56	1.60
572C	2	3	13.85	1.58	1.67	572C	4	1	30.05	1.67	1.78
572C	2	4	15.33	1.56	1.64	572C	4	2	31.55	1.64	1.60
572C	2	5	16.85	1.78	1.82	572C	4	3	33.05	1.58	1.62

HOLE	CORE	SECTION	DEPTH (METERS)	FORMATION FACT. VERT.	HORIZ.	HOLE	CORE	SECTION	DEPTH (METERS)	FORMATION FACT. VERT.	HORIZ.
572C	4	4	34.55	1.58	1.62	572C	11	1	97.10	1.40	1.48
572C	4	5	36.05	1.78	1.82	572C	11	2	198.69	1.40	1.56
572C	4	6	37.55	1.42	1.56	572C	11	3	100.17	1.76	1.80
572C	5	1	39.47	1.60	1.73	572C	12	1	102.17	1.50	1.60
572C	5	2	40.67	1.56	1.56	572C	12	2	103.67	1.60	1.76
572C	5	3	42.47	1.64	1.73	572C	12	3	105.17	1.60	1.70
572C	5	4	43.97	1.42	1.56	572C	13	1	107.25	1.58	1.64
572C	5	5	45.47	1.38	1.64	572C	13	2	108.72	1.50	1.60
572C	5	6	46.97	1.38	1.33	572C	13	3	110.25	1.60	1.70
572C	6	1	49.10	1.78	1.78	572C	14	1	112.25	1.82	1.88
572C	6	2	50.60	1.64	1.69	572C	14	2	113.75	1.56	1.62
572C	6	3	52.17	1.47	1.56	572C	14	3	115.25	1.80	1.80
572C	6	4	53.67	1.64	1.73	572C	14	4	116.75	1.64	1.68
572C	6	5	55.17	1.64	1.78	572C	14	5	118.25	1.72	1.84
572C	6	6	56.67	1.64	1.56	572C	15	1	121.85	1.68	1.74
572C	7	1	58.67	1.42	1.47	572C	15	2	123.35	1.82	1.82
572C	7	2	60.17	1.56	1.64	572C	15	3	124.85	1.90	1.90
572C	7	3	61.67	1.78	1.91	572C	15	4	126.35	1.90	1.96
572C	7	4	63.17	1.64	1.82	572C	15	5	127.85	1.96	2.04
572C	7	5	64.67	1.69	1.82	572C	15	6	129.35	1.88	1.96
572C	7	6	66.17	1.87	1.91	572C	16	1	131.45	1.90	1.80
572C	8	1	68.27	1.60	1.78	572C	16	2	132.95	1.64	1.72
572C	8	2	69.77	1.78	1.89	572C	16	3	134.45	1.76	1.88
572C	8	3	71.27	1.60	1.64	572C	16	4	135.95	2.00	2.04
572C	8	4	72.87	1.53	1.73	572C	16	5	137.45	2.00	2.00
572C	8	5	74.19	1.64	1.78	572C	16	6	138.95	1.92	2.00
572C	8	6	75.77	1.51	1.64	572C	17	1	141.05	1.98	2.00
572C	9	1	77.87	1.87	2.04	572C	17	2	142.55	1.96	2.00
572C	9	2	79.47	1.73	1.82	572C	17	3	144.05	2.04	2.12
572C	9	3	80.97	1.82	1.96	572C	17	4	145.55	1.86	1.94
572C	9	4	82.47	1.78	1.91	572C	18	2	152.15	2.04	2.07
572C	9	5	83.97	1.73	1.91	572C	18	3	153.65	2.07	2.24
572C	9	6	85.47	1.69	1.87	572C	18	4	155.15	1.96	2.02
572C	10	1	87.57	2.09	2.13	572C	18	5	156.65	1.87	1.91
572C	10	2	89.07	2.09	2.00	572C	18	6	158.15	1.87	2.07
572C	10	3	90.57	1.73	1.87	572C	20	1	160.25	1.65	1.76
572C	10	4	92.07	1.69	1.82	572C	20	2	161.75	1.85	2.07
572C	10	5	93.57	1.56	1.68	572C	20	3	163.25	1.85	2.02
572C	10	6	95.07	1.60	1.68						
573	2	2	4.25	1.87	1.93	573	9	5	73.45	2.36	2.56
573	2	3	5.75	1.87	1.89	573	9	6	74.95	2.33	2.44
573	2	4	7.25	2.11	2.13	573	10	1	76.95	2.27	2.44
573	2	5	8.75	1.89	2.07	573	10	2	78.45	1.89	2.00
573	2	6	10.25	2.13	2.22	573	10	3	79.95	1.93	2.02
573	3	1	12.25	2.36	2.44	573	10	4	81.45	2.22	2.31
573	3	2	13.75	1.96	2.09	573	10	5	82.95	2.22	2.27
573	3	3	15.25	1.64	1.91	573	10	6	84.45	1.93	2.04
573	3	4	16.75	2.11	2.27	573	11	2	87.95	2.00	2.04
573	3	5	18.25	1.64	1.87	573	11	3	89.45	2.47	2.67
573	3	6	19.75	2.00	2.09	573	11	4	90.95	2.44	2.60
573	4	1	21.75	1.56	1.64	573	11	5	92.45	2.40	2.53
573	4	2	23.25	1.98	2.04	573	11	6	93.95	2.67	2.78
573	4	3	24.75	1.82	2.00	573	12	1	95.95	2.67	2.76
573	4	4	26.25	2.00	2.09	573	12	2	97.45	3.11	3.47
573	4	5	27.75	1.60	1.69	573	12	3	98.95	2.38	2.53
573	4	6	29.75	1.56	1.60	573	12	4	100.45	2.29	2.40
573	5	1	31.25	1.87	2.00	573	12	5	101.95	2.31	2.40
573	5	2	32.75	1.60	1.69	573	12	6	103.45	2.31	2.40
573	5	3	34.25	2.18	2.27	573	13	2	106.25	2.18	2.33
573	5	4	35.75	1.64	1.78	573	13	3	107.75	2.13	2.31
573	5	5	37.25	2.00	2.18	573	13	4	109.25	2.27	2.42
573	5	6	38.75	2.09	2.22	573	13	5	110.75	2.44	2.47
573	6	1	40.85	1.91	2.09	573	13	6	112.25	2.44	2.62
573	6	2	41.35	1.82	1.91	573	14	1	113.35	2.71	2.80
573	6	3	43.95	1.69	1.82	573	14	2	114.85	2.58	2.71
573	6	4	44.35	1.60	1.78	573	14	3	116.35	2.58	2.67
573	6	5	46.05	1.73	1.91	573	14	4	117.85	2.44	2.56
573	6	6	47.55	1.87	2.09	573	14	5	119.35	2.58	2.69
573	7	2	50.35	1.69	1.82	573	14	6	120.85	2.56	2.67
573	7	3	51.75	1.60	1.82	573	15	1	122.85	2.47	2.67
573	7	4	53.25	1.51	1.60	573	15	2	124.35	2.33	2.47
573	7	5	54.75	1.42	1.69	573	15	3	125.85	2.31	2.44
573	7	6	56.25	1.87	2.09	573	15	4	127.35	2.44	2.60
573	8	1	57.95	1.91	2.04	573	15	5	128.85	2.49	2.58
573	8	2	59.45	1.64	1.69	573	15	6	130.35	2.53	2.67
573	8	3	60.95	1.96	2.09	573	16	1	132.05	2.60	2.78
573	8	4	62.45	1.78	1.87	573	16	2	133.53	2.56	2.71
573	8	5	63.93	2.00	2.13	573	16	3	135.05	2.27	2.36
573	8	6	65.43	1.87	1.96	573	16	4	136.55	2.38	2.51
573	9	1	67.43	2.11	2.22	573	16	5	138.05	2.36	2.56
573	9	2	68.93	2.36	2.56	573	16	6	139.55	2.33	2.49
573	9	3	70.43	2.13	2.31	573	17	1	140.85	2.40	2.56
573	9	4	71.93	2.31	2.42	573	17	2	142.35	2.36	2.56

HOLE	CORE	SECTION	DEPTH (METERS)	FORMATION FACT. VERT.	HORIZ.	HOLE	CORE	SECTION	DEPTH (METERS)	FORMATION FACT. VERT.	HORIZ.
573	17	3	143.85	2.53	2.67	573	18	2	150.15	2.58	2.71
573	17	4	145.35	2.22	2.36	573	18	3	152.65	1.96	2.09
573	17	5	146.85	2.53	2.62	573	19	1	154.65	2.27	2.40
573	17	6	148.35	2.27	2.36	573	19	2	155.15	2.44	2.44
573	18	1	149.65	2.44	2.58	573	19	3	157.65	2.00	2.11
573A	1	1	5.25	1.91	2.00	573A	3	6	30.35	2.02	2.09
573A	1	2	6.75	1.82	2.00	573A	4	2	32.05	2.20	2.36
573A	1	3	8.25	1.69	1.89	573A	4	4	35.05	1.89	2.06
573A	1	4	9.75	2.09	2.22	573A	4	6	38.05	2.07	2.31
573A	1	5	11.25	2.22	2.31	573A	5	2	42.05	1.89	1.98
573A	1	6	12.75	2.22	2.33	573A	5	4	45.05	1.87	2.00
573A	2	2	16.25	2.33	2.49	573A	5	6	48.05	1.73	1.96
573A	2	4	19.25	2.31	2.36	573A	6	2	51.45	1.67	1.84
573A	3	2	24.35	2.00	2.18	573A	6	4	54.45	2.00	2.04
573A	3	4	27.35	1.67	1.89						
573B	1	3	142.25	2.58	2.67	573B	11	5	240.25	2.31	2.53
573B	1	4	143.75	2.42	2.53	573B	11	6	241.75	2.49	2.76
573B	1	5	145.95	2.78	2.89	573B	12	2	245.25	2.33	2.44
573B	2	2	150.30	2.56	2.73	573B	12	3	246.75	2.56	2.62
573B	2	3	151.60	2.27	2.44	573B	12	4	248.25	2.40	2.53
573B	2	4	152.73	2.40	2.51	573B	12	5	249.75	2.58	2.58
573B	2	5	154.75	2.44	2.53	573B	13	2	254.75	2.53	2.56
573B	2	6	156.25	2.42	2.56	573B	13	3	256.25	2.56	2.58
573B	3	1	158.35	2.31	2.42	573B	13	4	257.75	2.33	2.36
573B	3	3	161.25	2.22	2.38	573B	13	5	259.25	2.31	2.40
573B	3	4	162.75	2.13	2.33	573B	13	6	260.75	2.04	2.22
573B	3	5	164.25	2.20	2.31	573B	14	1	262.75	2.33	2.49
573B	3	6	165.75	2.24	2.44	573B	14	2	264.25	2.49	2.56
573B	4	2	169.25	2.47	2.53	573B	14	3	265.75	2.40	2.49
573B	4	3	170.75	2.22	2.38	573B	14	4	267.25	2.36	2.53
573B	4	4	172.25	2.22	2.11	573B	14	5	268.75	2.44	2.71
573B	5	3	180.25	2.58	2.78	573B	14	6	270.25	2.27	2.40
573B	6	4	191.25	2.58	2.73	573B	15	2	273.75	2.89	3.02
573B	6	6	194.25	2.58	2.76	573B	15	3	275.25	2.89	3.02
573B	7	2	197.40	3.33	3.22	573B	15	4	276.75	3.20	3.20
573B	8	3	208.75	2.76	2.67	573B	15	5	278.25	2.78	2.98
573B	8	5	211.75	2.60	2.71	573B	16	1	281.75	2.80	3.07
573B	9	2	216.75	2.31	2.44	573B	16	2	283.25	2.69	2.98
573B	9	3	218.25	2.27	2.47	573B	16	3	284.75	2.87	3.16
573B	9	4	219.75	2.58	2.98	573B	16	4	286.25	2.78	2.89
573B	9	5	221.25	2.53	2.67	573B	16	5	287.75	2.67	2.78
573B	9	6	222.75	2.58	2.71	573B	17	1	291.25	4.11	3.51
573B	10	2	226.25	2.53	2.76	573B	17	2	292.75	2.93	3.24
573B	10	3	227.75	2.58	2.80	573B	17	3	294.25	2.78	2.93
573B	10	4	229.25	2.71	2.84	573B	17	4	295.75	2.84	2.96
573B	10	5	230.75	2.49	2.62	573B	17	5	297.25	3.20	3.29
573B	10	6	232.25	2.58	2.67	573B	18	2	302.25	3.31	3.33
573B	11	2	235.75	2.58	2.93	573B	18	3	303.75	2.80	2.93
573B	11	3	237.25	2.62	2.84	573B	19	2	311.75	3.22	3.29
573B	11	4	238.75	2.53	2.67	573B	20	1	319.78	3.27	3.42
574	1	1	0.66	2.63	2.50	574	7	2	54.25	1.88	1.95
574	1	2	2.24	1.35	1.50	574	7	3	55.75	1.93	2.10
574	1	3	3.74	1.75	1.65	574	7	4	57.25	2.40	2.60
574	2	1	5.25	1.88	2.05	574	7	5	58.75	1.93	2.00
574	2	2	6.75	1.45	1.85	574	7	6	60.25	1.98	1.98
574	2	3	8.46	1.35	1.38	574	8	1	61.75	2.20	2.38
574	2	4	9.75	1.50	1.70	574	8	2	63.25	2.13	2.30
574	2	5	11.25	1.75	1.85	574	8	3	64.75	2.13	2.15
574	2	6	12.75	1.65	1.85	574	8	4	66.25	2.15	2.20
574	3	2	16.25	1.45	1.60	574	8	5	67.75	1.88	2.03
574	3	3	17.75	1.60	1.65	574	8	6	69.25	1.88	1.85
574	3	4	19.25	1.50	1.65	574	9	1	71.25	1.75	1.85
574	3	5	20.75	1.45	1.60	574	9	2	72.75	1.88	2.00
574	3	6	22.25	1.50	1.55	574	9	3	74.25	2.05	2.13
574	4	1	24.25	1.45	1.55	574	9	4	75.75	1.73	1.80
574	4	2	25.75	1.90	1.50	574	9	5	77.25	1.73	1.75
574	4	3	27.25	1.45	1.55	574	9	6	78.75	1.88	1.98
574	4	4	28.75	1.50	1.60	574	10	1	80.75	2.10	2.15
574	4	5	30.25	1.45	1.50	574	10	2	82.25	2.13	2.25
574	4	6	31.75	1.55	1.63	574	10	3	83.75	1.88	1.95
574	5	3	36.75	1.75	1.75	574	10	4	85.25	2.25	2.35
574	5	4	38.25	1.45	1.58	574	10	5	86.75	2.15	2.35
574	5	5	39.75	1.40	1.50	574	10	6	88.25	2.15	2.25
574	5	6	41.25	1.60	1.70	574	11	1	90.25	2.25	2.30
574	6	1	43.25	1.65	1.85	574	11	2	91.75	2.23	2.38
574	6	2	44.75	1.70	1.75	574	11	3	93.25	2.13	2.28
574	6	3	46.25	1.60	1.70	574	11	4	94.75	2.75	2.88
574	6	4	47.75	1.70	1.65	574	11	5	96.25	2.75	2.88
574	6	5	49.25	2.00	2.10	574	11	6	97.75	2.78	2.88
574	6	6	50.75	2.26	2.35	574	12	1	99.35	2.55	2.85
574	7	1	52.75	2.35	2.45	574	12	2	100.85	2.73	2.88

HOLE	CORE	SECTION	DEPTH (METERS)	FORMATION FACT. VERT.	HORIZ.	HOLE	CORE	SECTION	DEPTH (METERS)	FORMATION FACT. VERT.	HORIZ.
574	12	3	102.35	2.65	2.75	574	22	1	158.25	2.93	2.60
574	12	4	103.85	2.75	2.80	574	22	2	159.75	2.75	2.88
574	12	5	105.35	2.64	2.83	574	22	3	161.25	2.85	2.95
574	12	6	106.85	2.88	2.98	574	23	1	163.25	2.63	2.75
574	13	1	108.85	2.60	2.63	574	23	2	164.75	2.63	2.75
574	13	2	110.35	2.50	2.63	574	23	3	166.25	2.60	2.75
574	13	3	111.85	2.35	2.70	574	24	1	168.25	2.50	2.60
574	13	4	113.35	2.60	2.75	574	24	2	169.75	2.63	2.85
574	13	5	114.85	2.50	2.78	574	24	3	171.25	2.63	2.75
574	13	6	116.35	2.70	2.80	574	25	1	173.25	2.50	2.55
574	14	1	118.35	2.90	3.08	574	25	2	174.75	2.70	2.95
574	14	2	119.85	3.35	3.50	574	25	3	176.25	2.55	2.65
574	16	1	128.35	2.75	3.00	574	26	1	178.25	2.88	2.90
574	16	2	129.85	2.75	2.88	574	26	2	179.75	2.65	2.68
574	16	3	131.35	2.88	3.00	574	26	3	181.25	2.75	2.88
574	17	1	133.35	2.65	2.75	574	27	1	182.95	2.80	2.98
574	17	2	134.85	2.63	2.70	574	27	2	184.45	2.38	2.50
574	17	3	136.35	2.38	2.65	574	27	3	185.95	2.60	2.63
574	18	1	138.35	2.40	2.50	574	28	1	187.95	2.60	2.78
574	18	2	139.85	2.40	2.60	574	28	3	190.95	2.85	2.90
574	18	3	141.35	2.55	2.70	574	29	1	192.95	2.50	2.63
574	19	2	144.85	2.35	2.45	574	29	2	194.45	2.63	2.75
574	19	3	146.35	2.25	2.38	574	29	3	195.95	2.63	2.70
574	20	2	149.85	2.55	2.63	574	30	2	199.45	2.63	2.73
574	20	3	151.35	2.50	2.70	574	30	3	200.95	2.85	2.90
574	21	1	153.25	2.50	2.55	574	31	2	204.45	2.08	2.25
574	21	2	154.75	2.95	2.95	574	31	3	205.95	2.70	2.68
574	21	3	156.25	2.00	2.10						
574A	2	2	8.55	2.07	2.47	574A	9	5	77.15	1.60	1.73
574A	2	4	11.55	2.47	2.67	574A	9	6	78.65	1.60	1.73
574A	2	6	14.55	2.03	2.20	574A	10	2	82.15	1.83	2.00
574A	3	2	17.55	1.93	2.13	574A	10	4	85.15	1.73	2.47
574A	3	4	20.75	2.10	2.17	574A	10	6	88.15	2.13	2.13
574A	4	2	26.15	2.00	2.17	574A	11	4	94.45	1.83	1.93
574A	4	4	29.15	2.00	2.13	574A	11	6	97.45	2.50	2.67
574A	4	6	32.15	2.00	2.27	574A	12	4	103.95	2.33	2.40
574A	5	2	35.35	1.40	1.50	574A	12	6	106.95	2.20	2.33
574A	5	4	38.35	1.47	1.60	574A	13	2	110.45	2.17	2.27
574A	5	6	41.35	1.50	1.67	574A	15	2	120.25	3.00	3.33
574A	6	2	44.65	1.47	1.60	574A	17	2	130.05	2.50	2.67
574A	6	4	47.65	1.83	2.07	574A	18	2	134.15	2.47	2.67
574A	6	6	50.65	2.20	2.27	574A	18	4	137.15	2.50	2.83
574A	7	2	54.15	1.60	1.80	574A	18	6	140.15	2.50	2.83
574A	7	4	57.15	1.60	1.80	574A	22	2	170.65	2.40	2.60
574A	7	6	60.15	1.83	2.07	574A	22	4	173.65	2.17	2.33
574A	8	2	63.65	2.13	2.33	574A	22	6	176.65	2.47	2.53
574A	8	4	66.65	2.07	2.27	574A	23	1	178.65	2.33	3.20
574A	8	6	69.65	1.50	1.73	574A	23	2	180.15	2.33	2.40
574A	9	4	75.65	1.50	1.73	574A	23	5	184.65	2.13	2.27
574B	1	1	185.75	2.50	2.53	574B	1	4	190.25	2.33	2.67
574B	1	2	187.25	2.40	2.33	574B	1	5	191.75	2.27	2.53
574B	1	3	188.75	2.47	2.67	574B	1	6	193.25	2.13	2.33
574C	1	1	195.25	2.33	2.67	574C	9	1	271.25	2.73	3.40
574C	1	2	196.75	2.47	3.07	574C	9	2	272.75	2.47	2.83
574C	1	3	198.25	2.00	2.67	574C	9	3	274.02	2.40	2.50
574C	1	4	199.75	2.17	2.33	574C	10	2	282.25	2.00	2.40
574C	1	5	201.25	2.27	2.83	574C	10	3	283.75	2.67	2.97
574C	2	1	204.75	2.33	2.50	574C	10	4	285.25	2.67	2.87
574C	2	2	206.25	2.13	2.57	574C	10	5	286.62	2.60	2.67
574C	2	3	207.75	2.37	2.53	574C	10	6	288.25	2.60	2.87
574C	2	4	209.25	2.33	2.50	574C	11	1	290.20	3.00	3.17
574C	2	5	210.75	2.33	2.40	574C	11	2	291.75	3.07	3.50
574C	2	6	212.25	1.80	2.60	574C	12	2	301.25	3.35	3.00
574C	3	3	217.25	2.17	2.33	574C	12	3	302.75	2.83	3.33
574C	4	1	223.75	3.17	2.83	574C	12	4	304.25	2.80	3.17
574C	4	2	225.25	2.33	3.17	574C	12	5	305.75	2.87	3.13
574C	5	1	233.25	2.73	3.00	574C	12	6	307.25	3.20	3.60
574C	5	2	234.75	2.47	2.60	574C	13	1	309.25	3.13	3.13
574C	5	3	236.25	2.67	2.93	574C	13	2	310.75	2.83	3.17
574C	5	4	237.75	3.00	3.27	574C	13	3	312.25	2.73	3.33
574C	6	3	245.75	2.87	2.97	574C	13	4	313.75	3.00	3.27
574C	7	2	253.75	3.10	3.27	574C	14	1	319.09	2.73	3.47
574C	7	5	258.15	3.60	3.27	574C	14	2	320.25	2.67	3.13
574C	8	1	261.75	2.80	2.83	574C	16	1	337.20	2.83	3.00
574C	8	2	263.25	2.50	2.97	574C	16	2	339.25	2.83	3.00
574C	8	3	264.75	2.50	3.13	574C	16	3	340.75	2.93	3.00
575	1	1	0.75	1.83	2.50	575	1	5	6.75	1.53	2.00
575	1	2	2.25	1.83	1.83	575	2	1	8.05	1.67	1.67
575	1	3	3.75	1.50	1.67	575	2	2	9.55	1.57	1.67
575	1	4	5.25	1.67	2.00	575	2	3	11.05	1.83	1.83

HOLE	CORE	SECTION	DEPTH (METERS)	FORMATION FACT. VERT.	HORIZ.	HOLE	CORE	SECTION	DEPTH (METERS)	FORMATION FACT. VERT.	HORIZ.
575	2	5	14.05	0.67	1.73	575	8	1	64.25	2.33	2.50
575	2	6	15.55	2.53	2.53	575	8	2	65.75	2.50	2.67
575	3	2	17.15	1.60	1.73	575	8	3	67.25	2.33	2.80
575	3	3	19.05	1.80	1.87	575	8	4	68.75	2.50	2.67
575	3	4	20.55	2.00	2.13	575	8	5	70.25	2.33	2.40
575	3	5	22.05	2.17	2.27	575	8	6	71.75	2.27	2.40
575	3	6	23.55	2.27	2.47	575	9	1	73.75	2.40	2.67
575	4	1	27.05	1.53	1.60	575	9	2	75.25	2.40	2.50
575	4	2	28.55	1.60	1.67	575	9	3	76.75	2.33	2.17
575	4	3	30.05	1.60	1.50	575	9	4	78.25	2.33	2.67
575	4	4	31.55	1.93	2.00	575	9	5	79.75	2.20	2.67
575	4	5	33.05	2.40	2.83	575	10	2	82.45	2.13	2.50
575	4	6	34.55	2.40	2.60	575	10	3	83.95	2.67	2.80
575	6	1	45.25	3.20	3.27	575	10	4	85.45	2.47	2.47
575	6	2	46.75	3.17	3.27	575	10	5	86.95	2.27	2.33
575	6	3	48.25	2.93	3.13	575	10	6	88.45	2.33	2.80
575	6	4	49.75	3.00	3.13	575	11	1	89.74	1.87	2.07
575	6	5	51.25	2.67	2.80	575	11	2	91.35	2.17	2.33
575	6	6	52.75	2.50	2.67	575	11	3	92.85	2.33	2.67
575	7	3	57.75	2.17	2.50	575	11	4	94.35	2.20	2.33
575	7	4	59.25	2.30	2 47	575	11	5	95.85	2.47	2.83
575	7	5	60.75	2.33	2.50	575	11	6	97.35	2.37	2.50
575	7	6	62.40	2.27	2.43						
575A	21	1	165.45	1.91	1.96	575A	28	2	189.45	2.45	2.62
575A	21	2	166.95	1.89	1.93	575A	29	3	193.15	2.13	2.18
575A	22	2	170.45	1.84	1.96	575A	30	1	194.35	2.45	2.55
575A	22	3	171.85	2.07	2.07	575A	30	2	195.85	2.00	2.09
575A	23	1	172.85	1.91	1.95	575A	30	3	197.35	2.09	2.15
575A	23	2	174.35	1.96	2.09	575A	31	2	199.70	2.15	2.27
575A	24	2	176.45	2.02	2.09	575A	31	3	201.03	2.07	2.15
575A	24	3	177.95	2.09	2.15	575A	32	2	203.55	2.09	2.18
575A	25	3	180.95	1.98	2.15	575A	32	3	204.80	2.44	2.45
575A	26	2	182.35	1.98	2.04	575A	33	2	206.50	2.11	2.18
575A	26	3	183.85	2.09	2.15	575A	33	3	208.00	2.09	2.22
575A	27	2	187.15	2.09	2.11						
575B	1	1	4.00	1.60	1.71	575B	6	5	54.75	1.75	1.85
575B	1	3	7.00	1.27	1.36	575B	7	2	57.65	2.07	2.22
575B	1	4	8.55	1.24	1.31	575B	7	3	59.15	2.04	2.11
575B	1	5	10.05	1.24	1.27	575B	7	4	60.65	2.09	2.18
575B	1	6	11.50	1.24	1.31	575B	7	5	62.15	1.85	2.00
575B	2	1	12.70	1.36	1.53	575B	7	6	63.65	1.91	2.00
575B	2	2	14.25	1.36	1.42	575B	8	2	66.95	1.84	1.89
575B	2	3	15.75	1.45	1.53	575B	8	3	68.45	1.65	1.71
575B	2	4	17.25	1.27	1.35	575B	8	4	69.95	1.78	1.89
575B	2	5	18.75	1.36	1.49	575B	8	5	71.45	1.89	1.93
575B	2	6	20.25	1.60	1.69	575B	8	6	72.95	1.73	1.78
575B	3	1	21.75	1.73	1.85	575B	9	2	76.05	1.73	1.82
575B	3	2	23.25	1.36	1.42	575B	9	3	77.55	1.91	1.96
575B	3	3	24.75	1.60	1.75	575B	9	4	79.05	2.00	2.05
575B	3	4	26.25	1.38	1.49	575B	9	5	80.55	1.93	2.02
575B	3	5	27.75	1.53	1.64	575B	10	2	83.65	1.84	1.91
575B	3	6	29.05	1.67	1.78	575B	10	3	85.15	2.00	2.09
575B	4	2	31.75	1.75	1.93	575B	10	4	86.65	1.55	1.64
575B	4	3	33.25	1.73	1.89	575B	10	5	88.15	1.98	2.00
575B	4	4	34.75	1.31	1.42	575B	10	6	89.65	1.93	1.96
575B	4	5	36.25	1.27	1.36	575B	11	2	93.15	1.82	1.91
575B	4	6	37.75	1.24	1.27	575B	11	3	94.65	2.00	2.09
575B	5	2	41.25	1.36	1.42	575B	11	4	96.15	1.89	1.98
575B	5	3	42.75	1.42	1.53	575B	11	5	97.65	2.02	2.07
575B	5	4	44.25	1.65	1.73	575B	11	6	99.15	1.82	1.85
575B	5	5	45.75	1.82	1.93	575B	12	2	101.85	2.02	2.11
575B	5	6	47.25	1.85	1.93	575B	13	2	111.45	1.73	1.73
575B	6	2	50.25	1.82	2.04	575B	13	3	112.95	1.78	1.91
575B	6	3	51.75	1.82	1.93	575B	14	2	116.35	1.91	1.96
575B	6	4	53.25	1.73	1.82	575B	14	3	117.85	1.85	1.91

CARBONATE

HOLE	CORE	SECTION	DEPTH (METERS)	CARBONATE (%)	HOLE	CORE	SECTION	DEPTH (METERS)	CARBONATE (%)
572	1	1	0.02	73.0	572	1	2	2.31	91.0
572	1	1	0.21	73.0	572	1	3	3.01	85.0
572	1	1	0.41	69.0	572	1	3	3.81	84.0
572	1	1	0.61	61.0	572	1	4	4.51	81.0
572	1	1	0.81	74.0	572	1	4	5.31	83.0
572	1	1	1.00	84.0	572	1	5	6.01	85.0
572	1	1	1.21	84.0	572	1	5	6.81	89.0
572	1	1	1.41	83.0	572	1	6	7.51	78.0
572	1	2	1.51	82.0	572	1	6	8.31	82.0
572A	1	1	0.01	78.0	572A	7	5	62.01	86.0
572A	1	1	0.81	84.0	572A	7	6	62.71	77.0
572A	1	2	1.51	77.0	572A	7	6	63.51	89.0
572A	1	2	2.31	71.0	572A	8	1	64.10	88.0
572A	1	3	3.01	75.0	572A	8	1	64.90	90.0
572A	1	3	3.81	71.0	572A	8	2	65.60	88.0
572A	1	4	4.51	80.0	572A	8	2	66.40	76.0
572A	1	4	5.31	73.0	572A	8	3	67.10	80.0
572A	1	5	6.01	89.0	572A	8	3	67.90	81.0
572A	1	5	6.81	68.0	572A	8	4	68.60	68.0
572A	1	6	7.51	86.0	572A	8	4	69.40	61.0
572A	1	6	8.31	85.0	572A	8	5	70.10	75.0
572A	2	1	9.51	84.0	572A	8	5	70.90	47.0
572A	2	1	10.31	82.0	572A	8	6	71.60	58.0
572A	2	2	11.01	83.0	572A	9	1	72.31	72.0
572A	2	2	11.81	85.0	572A	9	1	73.10	76.0
572A	2	3	12.51	82.0	572A	9	2	73.81	77.0
572A	2	3	13.31	78.0	572A	9	2	74.60	72.0
572A	2	4	14.01	87.0	572A	9	3	75.31	60.0
572A	2	4	14.81	84.0	572A	9	3	76.10	70.0
572A	2	5	15.51	75.0	572A	9	4	77.60	83.0
572A	2	5	16.31	79.0	572A	9	5	78.31	74.0
572A	2	6	17.01	74.0	572A	9	5	79.10	79.0
572A	2	6	17.81	77.0	572A	9	6	79.81	80.0
572A	3	1	19.03	83.0	572A	9	6	80.60	85.0
572A	3	2	20.53	80.0	572A	10	2	83.31	81.0
572A	3	6	26.53	74.0	572A	10	2	84.12	80.0
572A	3	6	27.31	72.0	572A	10	3	84.81	81.0
572A	3	7	28.03	65.0	572A	10	3	85.62	88.0
572A	4	1	28.80	66.0	572A	10	4	86.31	77.0
572A	4	1	29.36	73.0	572A	10	4	87.12	82.0
572A	4	2	30.30	66.0	572A	10	5	87.81	88.0
572A	4	2	30.86	74.0	572A	10	5	88.62	85.0
572A	4	3	31.80	74.0	572A	10	6	89.31	81.0
572A	4	3	32.36	76.0	572A	10	6	90.12	84.0
572A	4	4	33.30	84.0	572A	10	7	90.81	70.0
572A	4	4	33.86	66.0	572A	11	1	91.41	86.0
572A	4	5	34.80	75.0	572A	11	1	92.21	75.0
572A	4	5	35.36	82.0	572A	11	2	92.91	72.0
572A	5	1	36.31	79.0	572A	11	2	93.71	89.0
572A	5	1	37.11	73.0	572A	11	3	94.41	72.0
572A	5	2	37.81	71.0	572A	11	3	95.21	75.0
572A	5	2	38.61	73.0	572A	11	4	95.91	83.0
572A	5	3	39.31	72.0	572A	11	4	96.71	84.0
572A	5	3	40.11	85.0	572A	11	5	97.41	74.0
572A	5	4	40.81	82.0	572A	11	5	98.21	70.0
572A	5	4	41.61	75.0	572A	11	6	98.91	53.0
572A	5	5	42.31	73.0	572A	11	6	99.71	64.0
572A	5	5	43.11	82.0	572A	11	7	100.41	80.0
572A	5	6	43.81	70.0	572A	12	1	100.71	57.0
572A	5	6	44.61	67.0	572A	12	1	101.51	69.0
572A	5	7	45.31	60.0	572A	12	2	102.21	70.0
572A	6	1	45.91	53.0	572A	12	2	103.01	67.0
572A	6	1	46.71	67.0	572A	12	3	103.71	71.0
572A	6	2	47.41	65.0	572A	12	3	104.51	69.0
572A	6	2	48.21	74.0	572A	12	4	105.21	71.0
572A	6	3	48.91	67.0	572A	12	4	106.01	69.0
572A	6	3	49.71	88.0	572A	12	5	106.71	74.0
572A	6	4	50.41	75.0	572A	12	5	107.51	65.0
572A	6	4	51.21	80.0	572A	12	6	108.21	63.0
572A	6	5	51.91	74.0	572A	12	6	109.01	74.0
572A	6	5	52.71	53.0	572A	13	1	109.91	74.0
572A	6	6	53.41	64.0	572A	13	1	110.71	55.0
572A	6	6	54.21	77.0	572A	13	2	111.41	76.0
572A	6	7	54.91	71.0	572A	13	2	112.21	73.0
572A	7	1	55.21	69.0	572A	13	3	112.91	72.0
572A	7	1	56.01	71.0	572A	13	3	113.71	71.0
572A	7	2	56.71	56.0	572A	13	4	114.41	83.0
572A	7	2	57.51	76.0	572A	13	4	115.21	76.0
572A	7	3	58.21	62.0	572A	13	5	115.91	74.0
572A	7	3	59.01	61.0	572A	13	5	116.71	73.0
572A	7	4	59.71	77.0	572A	13	6	117.41	79.0
572A	7	4	60.51	72.0	572A	13	6	118.21	60.0
572A	7	5	61.21	85.0	572A	13	7	118.91	75.0

HOLE	CORE	SECTION	DEPTH (METERS)	CARBONATE (%)	HOLE	CORE	SECTION	DEPTH (METERS)	CARBONATE (%)
572A	14	1	119.10	65.0	572A	16	1	137.90	77.0
572A	14	1	119.90	75.0	572A	16	2	138.60	71.0
572A	14	2	120.60	77.0	572A	16	2	139.40	76.0
572A	14	3	122.10	70.0	572A	16	3	140.10	87.0
572A	14	3	122.90	83.0	572A	16	3	140.90	89.0
572A	14	4	123.60	74.0	572A	16	4	141.60	84.0
572A	14	4	124.40	47.0	572A	16	4	142.40	83.0
572A	14	5	125.10	74.0	572A	16	5	143.10	75.0
572A	14	5	125.90	77.0	572A	16	5	143.90	82.0
572A	14	6	126.60	66.0	572A	16	6	144.60	90.0
572A	14	6	127.40	63.0	572A	17	1	145.31	78.0
572A	15	1	129.10	84.0	572A	17	1	146.10	76.0
572A	15	2	129.81	81.0	572A	17	2	146.81	81.0
572A	15	2	130.61	83.0	572A	17	2	147.60	75.0
572A	15	3	131.31	82.0	572A	17	3	148.31	69.0
572A	15	3	132.10	71.0	572A	17	3	149.10	71.0
572A	15	4	132.81	64.0	572A	17	4	149.81	68.0
572A	15	4	133.60	76.0	572A	17	4	150.60	73.0
572A	15	5	134.31	71.0	572A	17	5	151.31	64.0
572A	15	5	135.10	75.0	572A	17	5	152.10	63.0
572A	15	6	135.81	72.0	572A	17	6	152.81	77.0
572A	15	6	136.60	73.0					
572B	1	1	154.01	78.0	572B	2	4	163.81	69.0
572B	1	1	154.86	72.0	572B	3	1	164.21	52.0
572B	1	2	155.51	74.0	572B	3	1	165.01	41.0
572B	1	2	156.31	72.0	572B	3	2	165.71	63.0
572B	1	3	157.01	65.0	572B	3	2	166.51	59.0
572B	1	3	157.81	78.0	572B	3	3	167.21	67.0
572B	1	4	158.51	67.0	572B	3	3	168.01	57.0
572B	2	1	159.31	69.0	572B	4	1	168.81	62.0
572B	2	1	160.10	71.0	572B	4	1	169.60	70.0
572B	2	2	160.81	45.0	572B	4	2	170.31	63.0
572B	2	2	161.60	71.0	572B	4	2	171.10	40.0
572B	2	3	162.31	65.0	572B	4	3	171.81	58.0
572B	2	3	163.10	37.0					
572C	1	1	0.01	81.0	572C	2	4	14.95	84.0
572C	1	1	0.76	74.0	572C	2	4	15.46	70.0
572C	1	1	1.10	74.0	572C	2	4	15.94	76.0
572C	1	2	1.51	72.0	572C	2	5	16.45	77.0
572C	1	2	2.26	77.0	572C	2	5	16.96	83.0
572C	1	2	2.60	75.0	572C	2	5	17.44	75.0
572C	1	3	3.01	77.0	572C	2	6	17.95	77.0
572C	1	3	3.76	89.0	572C	2	6	18.46	77.0
572C	1	4	4.51	85.0	572C	2	6	18.94	78.0
572C	1	4	5.51	88.0	572C	2	7	19.45	86.0
572C	1	4	5.60	83.0	572C	3	1	20.05	84.0
572C	1	5	6.01	85.0	572C	3	1	20.56	74.0
572C	1	5	6.76	89.0	572C	3	1	21.04	77.0
572C	1	5	7.10	89.0	572C	3	2	21.59	77.0
572C	1	6	7.51	88.0	572C	3	2	22.09	73.0
572C	1	6	8.26	92.0	572C	3	2	22.59	68.0
572C	1	6	8.60	81.0	572C	3	3	23.09	70.0
572C	1	7	9.01	87.0	572C	3	3	23.59	72.0
572C	2	1	10.45	84.0	572C	3	3	24.09	70.0
572C	2	1	10.96	76.0	572C	3	4	25.59	80.0
572C	2	1	11.44	80.0	572C	3	5	26.09	74.0
572C	2	2	11.95	83.0	572C	3	5	26.59	74.0
572C	2	2	12.46	84.0	572C	3	5	27.09	82.0
572C	2	2	12.94	82.0	572C	3	6	27.59	83.0
572C	2	3	13.45	82.0	572C	3	6	28.09	79.0
572C	2	3	13.96	70.0	572C	3	7	29.09	68.0
572C	2	3	14.44	84.0					
573	1	1	0.77	85.0	573	5	1	31.26	79.0
573	2	1	2.76	62.0	573	5	2	32.76	69.0
573	2	2	4.26	74.0	573	5	3	34.26	88.0
573	2	3	5.76	75.0	573	5	4	35.76	66.0
573	2	4	7.26	81.0	573	5	5	37.26	81.0
573	2	5	8.76	78.0	573	5	6	38.76	88.0
573	2	6	10.26	85.0	573	6	1	40.56	73.0
573	3	1	12.26	88.0	573	6	2	41.56	76.0
573	3	2	13.76	82.0	573	6	3	43.06	65.0
573	3	3	15.26	76.0	573	6	4	44.56	68.0
573	3	4	16.76	86.0	573	6	5	46.06	69.0
573	3	5	18.26	52.0	573	6	6	47.56	74.0
573	3	6	19.76	82.0	573	7	2	50.26	63.0
573	4	1	22.04	58.0	573	7	3	51.76	60.0
573	4	2	23.33	81.0	573	7	4	53.26	42.0
573	4	3	24.76	83.0	573	7	5	54.76	40.0
573	4	4	26.26	84.0	573	7	6	56.26	76.0
573	4	5	27.76	65.0	573	8	1	57.76	69.0
573	4	6	29.27	63.0	573	8	2	59.26	52.0

HOLE	CORE	SECTION	DEPTH (METERS)	CARBONATE (%)	HOLE	CORE	SECTION	DEPTH (METERS)	CARBONATE (%)
573	8	3	60.76	75.0	573	13	5	110.76	77.0
573	8	4	62.26	61.0	573	13	6	112.26	81.0
573	8	5	63.76	79.0	573	14	1	113.36	85.0
573	8	6	65.26	70.0	573	14	2	114.86	84.0
573	9	1	67.46	76.0	573	14	3	116.36	89.0
573	9	2	68.96	81.0	573	14	4	117.86	83.0
573	9	3	70.46	78.0	573	14	5	119.36	84.0
573	9	4	71.96	81.0	573	14	6	120.86	87.0
573	9	5	73.46	83.0	573	15	1	122.86	77.0
573	9	6	74.96	82.0	573	15	2	124.36	77.0
573	10	1	76.96	71.0	573	15	3	125.86	77.0
573	10	2	78.46	67.0	573	15	4	127.36	82.0
573	10	3	79.96	74.0	573	15	5	128.86	79.0
573	10	4	81.46	81.0	573	15	6	130.36	86.0
573	10	5	82.96	79.0	573	16	1	132.06	83.0
573	10	6	84.46	56.0	573	16	2	133.56	85.0
573	11	1	86.46	73.0	573	16	3	135.06	73.0
573	11	2	87.96	67.0	573	16	4	136.56	81.0
573	11	3	89.46	82.0	573	16	5	138.06	76.0
573	11	4	90.96	85.0	573	16	6	139.56	66.0
573	11	5	92.46	85.0	573	17	1	140.86	78.0
573	11	6	93.96	88.0	573	17	2	142.36	79.0
573	12	1	95.96	84.0	573	17	3	143.86	84.0
573	12	2	97.46	88.0	573	17	4	145.36	76.0
573	12	3	98.96	83.0	573	17	5	146.86	84.0
573	12	4	100.46	78.0	573	17	6	148.36	77.0
573	12	5	101.96	81.0	573	18	1	149.76	79.0
573	12	6	103.46	78.0	573	18	2	151.26	86.0
573	13	1	105.16	74.0	573	18	3	152.77	53.0
573	13	2	106.26	78.0	573	19	1	154.76	74.0
573	13	3	107.76	73.0	573	19	2	156.26	75.0
573	13	4	109.26	74.0	573	19	3	157.76	55.0
573A	1	1	5.26	70.0	573A	4	2	33.56	82.0
573A	1	2	6.76	77.0	573A	4	3	35.06	74.0
573A	1	3	8.26	75.0	573A	4	4	36.56	70.0
573A	1	4	9.76	84.0	573A	4	5	38.06	75.0
573A	1	5	11.26	88.0	573A	4	6	39.56	73.0
573A	1	6	12.76	86.0	573A	5	1	40.66	74.0
573A	2	1	14.76	84.0	573A	5	2	42.06	73.0
573A	2	2	16.26	86.0	573A	5	3	43.56	62.0
573A	2	3	17.76	57.0	573A	5	4	45.06	56.0
573A	2	4	19.26	82.0	573A	5	5	46.56	76.0
573A	2	5	20.76	73.0	573A	5	6	48.06	53.0
573A	3	1	22.86	85.0	573A	6	1	49.96	72.0
573A	3	2	24.36	78.0	573A	6	2	51.46	44.0
573A	3	3	25.86	73.0	573A	6	3	52.96	57.0
573A	3	4	27.36	67.0	573A	6	4	54.46	69.0
573A	3	5	28.86	58.0	573A	6	5	55.96	70.0
573A	3	6	30.36	71.0	573A	6	6	57.46	53.0
573A	4	1	32.06	72.0					
573B	1	1	139.26	79.0	573B	6	5	192.76	86.0
573B	1	2	140.76	84.0	573B	6	6	194.26	88.0
573B	1	3	142.26	87.0	573B	7	1	195.71	90.0
573B	1	4	143.76	76.0	573B	7	2	197.41	93.0
573B	1	5	145.26	89.0	573B	7	3	199.26	92.0
573B	1	6	146.59	79.0	573B	7	4	200.76	93.0
573B	2	1	148.76	74.0	573B	7	5	202.26	94.0
573B	2	2	150.31	86.0	573B	8	1	205.76	82.0
573B	2	3	151.61	81.0	573B	8	2	207.26	88.0
573B	2	4	154.76	79.0	573B	8	3	208.76	81.0
573B	2	5	155.24	79.0	573B	8	4	210.26	84.0
573B	2	6	156.26	82.0	573B	8	5	211.76	84.0
573B	3	1	158.26	78.0	573B	8	6	213.26	86.0
573B	3	2	159.56	71.0	573B	9	2	216.76	85.0
573B	3	3	161.26	76.0	573B	9	2	216.76	79.0
573B	3	4	162.76	65.0	573B	9	3	218.26	88.0
573B	3	5	164.26	73.0	573B	9	4	219.76	84.0
573B	3	6	165.76	75.0	573B	9	5	221.26	88.0
573B	4	1	167.76	75.0	573B	9	6	222.76	87.0
573B	4	2	169.26	82.0	573B	10	1	224.76	81.0
573B	4	3	170.76	74.0	573B	10	2	226.36	88.0
573B	4	4	172.26	70.0	573B	10	3	227.76	86.0
573B	4	5	173.76	78.0	573B	10	4	229.26	94.0
573B	4	6	175.26	68.0	573B	10	5	230.76	90.0
573B	5	2	178.76	85.0	573B	10	6	232.26	77.0
573B	5	3	180.26	89.0	573B	11	1	234.26	91.0
573B	5	4	181.76	89.0	573B	11	2	235.76	91.0
573B	5	5	183.26	91.0	573B	11	3	237.26	97.0
573B	5	6	184.76	92.0	573B	11	4	238.76	88.0
573B	6	2	188.26	89.0	573B	12	1	243.76	89.0
573B	6	3	189.76	87.0	573B	12	2	245.26	73.0
573B	6	4	191.26	84.0	573B	12	3	246.76	88.0

HOLE	CORE	SECTION	DEPTH (METERS)	CARBONATE (%)	HOLE	CORE	SECTION	DEPTH (METERS)	CARBONATE (%)
573B	12	4	248.21	79.0	573B	23	3	351.61	92.0
573B	12	5	249.51	87.0	573B	23	4	352.81	96.0
573B	13	1	253.26	83.0	573B	24	1	357.53	98.0
573B	13	2	254.76	86.0	573B	24	2	359.02	93.0
573B	13	3	256.26	85.0	573B	24	3	360.67	89.0
573B	13	4	257.76	72.0	573B	25	1	367.22	92.0
573B	13	5	259.26	84.0	573B	26	2	378.49	92.0
573B	13	6	260.76	66.0	573B	26	3	379.73	97.0
573B	14	1	262.76	83.0	573B	26	4	381.20	96.0
573B	14	2	264.26	81.0	573B	26	5	382.33	92.0
573B	14	3	265.76	80.0	573B	27	1	386.09	91.0
573B	14	4	267.26	84.0	573B	27	2	387.61	98.0
573B	14	5	268.76	82.0	573B	27	3	388.94	92.0
573B	14	6	270.26	83.0	573B	27	4	390.63	95.0
573B	15	1	272.26	90.0	573B	28	1	395.71	95.0
573B	15	2	273.76	89.0	573B	28	2	397.47	97.0
573B	15	2	273.76	93.0	573B	28	3	398.61	91.0
573B	15	3	275.26	91.0	573B	29	1	405.19	96.0
573B	15	5	278.26	91.0	573B	29	2	407.11	99.0
573B	16	1	281.76	78.0	573B	29	3	408.07	93.0
573B	16	2	283.26	91.0	573B	29	4	409.91	92.0
573B	16	3	284.76	85.0	573B	29	5	411.03	81.0
573B	16	4	286.26	92.0	573B	30	1	414.97	89.0
573B	16	5	287.76	85.0	573B	30	3	418.27	96.0
573B	17	1	291.26	95.0	573B	30	4	418.93	93.0
573B	17	2	292.76	94.0	573B	31	1	424.21	91.0
573B	17	3	294.26	93.0	573B	32	1	434.19	92.0
573B	17	4	295.76	90.0	573B	32	2	436.11	94.0
573B	17	5	297.26	92.0	573B	33	5	449.15	93.0
573B	18	1	300.76	97.0	573B	34	1	452.71	93.0
573B	18	2	302.26	90.0	573B	35	1	462.16	81.0
573B	18	3	303.76	92.0	573B	35	2	463.36	77.0
573B	19	1	310.26	93.0	573B	35	3	465.21	79.0
573B	19	2	311.76	90.0	573B	35	4	467.06	87.0
573B	20	1	319.78	87.0	573B	35	5	468.31	91.0
573B	20	2	321.26	90.0	573B	36	1	471.76	90.0
573B	20	3	322.66	93.0	573B	36	2	473.74	95.0
573B	20	4	324.26	91.0	573B	36	3	474.14	84.0
573B	20	5	325.76	91.0	573B	37	1	481.04	88.0
573B	20	6	327.46	93.0	573B	38	1	490.71	93.0
573B	21	1	329.51	91.0	573B	38	2	492.79	61.0
573B	21	2	330.86	91.0	573B	38	3	494.29	76.0
573B	21	3	332.39	93.0	573B	39	1	499.76	87.0
573B	21	4	333.76	92.0	573B	39	3	503.26	93.0
573B	22	1	338.71	91.0	573B	40	1	509.81	65.0
573B	22	2	340.46	92.0	573B	42	1	520.94	92.0
573B	22	3	341.86	91.0	573B	42	1	521.81	97.0
573B	22	4	343.16	92.0	573B	42	2	522.19	2.0
573B	23	1	348.41	92.0	573B	42	3	524.93	3.0
573B	23	2	349.74	91.0	573B	42	4	525.44	88.0
574	1	1	0.65	84.0	574	7	3	55.76	74.0
574	1	2	2.26	28.0	574	7	4	57.26	88.0
574	1	3	3.75	80.0	574	7	5	58.76	59.0
574	2	1	5.26	65.0	574	7	6	60.26	67.0
574	2	2	6.76	59.0	574	8	1	61.76	85.0
574	2	3	8.47	43.0	574	8	2	63.26	83.0
574	2	4	9.76	67.0	574	8	3	64.76	84.0
574	2	5	11.26	79.0	574	8	4	66.26	81.0
574	2	6	12.76	72.0	574	8	5	67.76	66.0
574	3	2	16.26	21.0	574	8	6	69.26	52.0
574	3	3	17.76	38.0	574	9	1	71.26	24.0
574	3	4	19.26	35.0	574	9	2	72.76	63.0
574	3	5	20.76	13.0	574	9	3	74.26	73.0
574	3	6	22.26	11.0	574	9	4	75.76	15.0
574	4	1	24.26	15.0	574	9	5	77.26	4.0
574	4	2	25.76	35.0	574	9	6	78.76	48.0
574	4	3	27.26	55.0	574	10	1	80.76	73.0
574	4	4	28.76	48.0	574	10	2	82.26	79.0
574	4	5	30.26	24.0	574	10	3	83.76	33.0
574	4	6	31.76	49.0	574	10	4	85.26	79.0
574	5	2	35.11	31.0	574	10	5	86.76	80.0
574	5	3	36.76	36.0	574	10	6	88.26	76.0
574	5	4	38.26	13.0	574	11	1	90.26	77.0
574	5	5	39.76	19.0	574	11	2	91.76	78.0
574	5	6	41.26	45.0	574	11	3	93.26	79.0
574	6	1	43.26	61.0	574	11	4	94.76	94.0
574	6	2	44.76	54.0	574	11	5	96.26	90.0
574	6	3	46.26	53.0	574	11	6	97.76	90.0
574	6	4	47.76	47.0	574	12	1	99.36	89.0
574	6	5	49.26	80.0	574	12	2	100.86	90.0
574	6	6	50.76	83.0	574	12	3	102.36	87.0
574	7	1	52.76	86.0	574	12	4	103.86	89.0
574	7	2	54.26	70.0	574	12	5	105.36	90.0

HOLE	CORE	SECTION	DEPTH (METERS)	CARBONATE (%)	HOLE	CORE	SECTION	DEPTH (METERS)	CARBONATE (%)
574	12	6	106.86	90.0	574	22	1	158.26	87.0
574	13	1	108.86	90.0	574	22	2	159.76	90.0
574	13	2	110.36	87.0	574	22	3	161.26	90.0
574	13	3	111.86	88.0	574	23	2	164.76	91.0
574	13	4	113.36	86.0	574	23	3	166.26	92.0
574	13	5	114.86	90.0	574	24	1	168.26	88.0
574	13	6	116.36	88.0	574	24	2	169.76	90.0
574	14	1	118.36	96.0	574	24	3	171.26	90.0
574	14	2	119.86	91.0	574	25	1	173.26	81.0
574	14	3	121.36	92.0	574	25	2	174.76	95.0
574	15	3	126.36	96.0	574	25	3	176.26	82.0
574	15	4	127.86	93.0	574	26	1	178.26	89.0
574	16	1	128.36	92.0	574	26	2	179.76	87.0
574	16	2	129.86	89.0	574	26	3	181.26	87.0
574	16	3	131.36	93.0	574	27	1	182.96	95.0
574	17	1	133.36	92.0	574	27	2	184.46	73.0
574	17	2	134.86	93.0	574	27	3	185.96	85.0
574	17	3	136.36	88.0	574	28	1	187.96	89.0
574	18	1	138.36	89.0	574	28	2	189.46	87.0
574	18	2	139.86	82.0	574	28	3	190.96	89.0
574	18	3	141.36	90.0	574	29	1	192.96	86.0
574	19	2	144.86	93.0	574	29	2	194.46	90.0
574	19	3	146.36	82.0	574	29	3	195.96	91.0
574	20	2	149.86	92.0	574	30	2	199.46	81.0
574	20	3	151.36	86.0	574	30	3	200.96	89.0
574	21	1	153.26	86.0	574	31	1	202.96	78.0
574	21	2	154.76	95.0	574	31	2	204.46	61.0
574	21	3	156.26	75.0	574	31	3	205.96	84.0
574A	2	1	7.06	60.0	574A	12	3	102.46	88.0
574A	2	2	8.56	73.0	574A	12	4	103.96	87.0
574A	2	3	10.06	45.0	574A	12	5	105.46	80.0
574A	2	4	11.56	77.0	574A	12	6	106.96	86.0
574A	2	5	13.06	72.0	574A	12	7	107.85	86.0
574A	2	6	14.56	55.0	574A	13	1	108.93	89.0
574A	3	1	16.24	25.0	574A	13	2	110.46	85.0
574A	3	2	17.76	15.0	574A	13	3	111.93	84.0
574A	3	3	19.24	14.0	574A	13	4	112.80	83.0
574A	3	4	20.76	31.0	574A	14	1	113.85	90.0
574A	3	5	22.24	27.0	574A	14	2	115.36	81.0
574A	4	1	24.66	23.0	574A	14	3	116.85	80.0
574A	4	2	26.16	55.0	574A	14	4	117.69	89.0
574A	4	3	27.66	36.0	574A	16	1	123.56	89.0
574A	4	4	29.16	39.0	574A	16	2	125.06	91.0
574A	4	5	30.66	52.0	574A	16	3	126.56	91.0
574A	5	1	33.86	25.0	574A	17	1	128.56	85.0
574A	5	3	36.86	12.0	574A	17	2	130.06	90.0
574A	5	5	39.86	49.0	574A	17	3	131.56	88.0
574A	6	1	43.16	43.0	574A	18	1	132.66	89.0
574A	6	3	46.16	76.0	574A	18	2	134.16	90.0
574A	6	5	49.16	83.0	574A	18	3	135.66	90.0
574A	7	1	52.66	58.0	574A	18	4	137.16	94.0
574A	7	2	54.16	66.0	574A	18	5	138.66	86.0
574A	7	3	55.66	73.0	574A	18	6	140.16	94.0
574A	7	5	58.66	76.0	574A	18	7	141.16	88.0
574A	7	6	60.16	82.0	574A	19	1	142.16	86.0
574A	8	1	62.16	85.0	574A	19	2	143.66	96.0
574A	8	2	63.66	90.0	574A	19	3	145.16	87.0
574A	8	3	65.16	81.0	574A	19	4	146.66	84.0
574A	8	4	66.66	89.0	574A	19	5	148.16	84.0
574A	8	5	68.16	45.0	574A	19	6	149.66	93.0
574A	8	6	69.66	47.0	574A	19	7	150.66	91.0
574A	9	1	71.16	20.0	574A	20	1	151.66	85.0
574A	9	3	74.16	59.0	574A	20	3	154.66	88.0
574A	9	4	75.66	22.0	574A	20	5	157.66	79.0
574A	9	5	77.16	2.0	574A	20	7	160.16	91.0
574A	9	6	78.66	47.0	574A	21	1	160.66	89.0
574A	10	1	80.66	73.0	574A	21	3	163.66	88.0
574A	10	2	82.16	76.0	574A	21	5	166.66	87.0
574A	10	3	83.66	42.0	574A	22	1	169.16	93.0
574A	10	4	85.16	72.0	574A	22	2	170.66	92.0
574A	10	5	86.66	71.0	574A	22	3	172.16	92.0
574A	10	6	88.16	86.0	574A	22	4	173.66	90.0
574A	11	1	89.96	73.0	574A	22	5	175.16	90.0
574A	11	2	91.46	57.0	574A	22	6	176.66	96.0
574A	11	3	92.96	76.0	574A	23	1	178.66	87.0
574A	11	4	94.46	71.0	574A	23	2	180.16	93.0
574A	11	5	95.96	90.0	574A	23	3	181.66	88.0
574A	11	6	97.46	93.0	574A	23	4	183.16	88.0
574A	11	7	98.30	90.0	574A	23	5	184.66	83.0
574A	12	1	99.46	87.0	574A	23	6	186.16	82.0
574A	12	2	100.96	91.0					
574B	1	1	185.76	84.0	574B	1	2	187.26	77.0

HOLE	CORE	SECTION	DEPTH (METERS)	CARBONATE (%)	HOLE	CORE	SECTION	DEPTH (METERS)	CARBONATE (%)
574B	1	3	188.76	87.0	574B	1	5	191.76	81.0
574B	1	4	190.26	85.0	574B	1	6	193.26	75.0
574C	1	1	195.41	86.0	574C	16	1	337.81	91.0
574C	1	2	196.76	86.0	574C	16	2	339.26	84.0
574C	1	3	198.26	70.0	574C	16	3	340.76	86.0
574C	1	4	199.76	61.0	574C	17	1	347.01	88.0
574C	1	5	201.26	76.0	574C	17	1	347.26	86.0
574C	2	1	204.71	80.0	574C	17	2	348.76	87.0
574C	2	2	206.26	63.0	574C	17	3	350.06	86.0
574C	2	3	207.76	79.0	574C	17	4	351.76	84.0
574C	2	4	209.26	85.0	574C	18	1	356.76	88.0
574C	2	5	210.76	80.0	574C	18	2	358.26	90.0
574C	2	6	212.26	32.0	574C	19	1	366.16	86.0
574C	3	2	215.76	80.0	574C	19	2	367.71	86.0
574C	3	3	217.26	74.0	574C	20	1	375.76	88.0
574C	4	1	223.76	87.0	574C	20	2	377.36	88.0
574C	4	2	225.26	81.0	574C	20	3	378.56	86.0
574C	5	1	233.26	88.0	574C	20	4	380.26	89.0
574C	5	2	234.76	82.0	574C	20	5	381.81	86.0
574C	5	3	236.26	89.0	574C	20	6	383.31	88.0
574C	5	4	237.76	92.0	574C	21	1	385.17	88.0
574C	6	1	242.66	96.0	574C	21	2	386.86	91.0
574C	6	3	245.76	95.0	574C	21	3	388.26	89.0
574C	6	4	247.26	91.0	574C	22	1	394.16	87.0
574C	7	1	252.26	92.0	574C	22	2	395.86	91.0
574C	7	2	253.76	95.0	574C	23	1	404.45	91.0
574C	7	3	255.26	85.0	574C	23	2	405.91	94.0
574C	7	4	256.76	90.0	574C	23	3	407.16	90.0
574C	7	5	258.16	91.0	574C	23	4	408.64	94.0
574C	7	6	259.76	90.0	574C	23	5	410.72	89.0
574C	8	1	261.76	85.0	574C	24	1	414.21	89.0
574C	8	2	263.26	86.0	574C	24	2	415.85	90.0
574C	8	3	264.76	92.0	574C	24	3	416.49	87.0
574C	9	1	271.26	90.0	574C	24	4	418.28	93.0
574C	9	2	272.76	88.0	574C	25	1	423.03	86.0
574C	9	3	274.03	86.0	574C	26	1	432.67	91.0
574C	10	2	282.26	85.0	574C	26	2	434.31	91.0
574C	10	3	283.76	89.0	574C	26	3	435.72	93.0
574C	10	4	285.26	90.0	574C	27	1	442.25	91.0
574C	10	5	286.78	85.0	574C	27	2	443.71	93.0
574C	10	6	288.26	91.0	574C	27	3	445.09	90.0
574C	11	1	290.26	90.0	574C	29	1	461.82	86.0
574C	11	2	291.76	92.0	574C	29	2	462.65	82.0
574C	11	3	293.26	92.0	574C	29	3	464.21	85.0
574C	12	1	299.76	92.0	574C	30	1	471.49	79.0
574C	12	2	301.26	94.0	574C	30	2	472.13	80.0
574C	12	3	302.76	93.0	574C	30	3	473.71	79.0
574C	12	4	304.26	94.0	574C	31	1	480.21	71.0
574C	12	5	305.76	90.0	574C	31	2	482.06	80.0
574C	12	6	307.26	93.0	574C	32	1	490.11	86.0
574C	13	1	309.26	94.0	574C	32	2	491.26	76.0
574C	13	2	310.76	91.0	574C	33	1	499.16	93.0
574C	13	3	312.26	93.0	574C	33	2	500.81	88.0
574C	13	4	313.76	94.0	574C	33	4	503.46	84.0
574C	14	1	318.91	89.0	574C	33	5	505.01	66.0
574C	14	2	320.35	90.0	574C	34	1	508.44	68.0
574C	15	1	328.26	94.0	574C	35	1	518.23	66.0
574C	15	4	332.76	94.0					
575	1	1	0.76	41.0	575	5	3	38.76	85.0
575	1	2	2.26	65.0	575	5	4	40.47	87.0
575	1	3	3.76	34.0	575	5	5	41.76	78.0
575	1	4	5.26	52.0	575	5	6	43.26	77.0
575	1	5	6.76	14.0	575	6	1	45.26	92.0
575	2	1	8.06	28.0	575	6	2	46.76	91.0
575	2	2	9.56	38.0	575	6	3	48.26	90.0
575	2	3	11.06	56.0	575	6	4	49.76	93.0
575	2	4	12.56	40.0	575	6	5	51.26	89.0
575	2	5	14.06	85.0	575	6	6	52.76	85.0
575	2	6	15.56	90.0	575	7	1	54.76	88.0
575	3	2	18.66	47.0	575	7	2	56.26	99.0
575	3	3	20.56	64.0	575	7	3	57.76	85.0
575	3	4	22.06	77.0	575	7	4	59.26	83.0
575	3	5	23.56	80.0	575	7	5	60.76	90.0
575	3	6	25.06	86.0	575	7	6	62.26	89.0
575	4	1	27.06	10.0	575	8	1	64.26	89.0
575	4	2	28.56	56.0	575	8	2	65.76	92.0
575	4	3	30.06	70.0	575	8	3	67.26	93.0
575	4	4	31.56	81.0	575	8	4	68.76	91.0
575	4	5	33.06	92.0	575	8	5	70.26	88.0
575	4	6	34.56	91.0	575	8	6	71.76	85.0
575	5	1	35.76	88.0	575	9	1	73.76	90.0
575	5	2	37.26	89.0	575	9	2	75.26	87.0

HOLE	CORE	SECTION	DEPTH (METERS)	CARBONATE (%)	HOLE	CORE	SECTION	DEPTH (METERS)	CARBONATE (%)
575	9	3	76.76	73.0	575	10	6	88.46	88.0
575	9	4	78.26	91.0	575	11	1	89.81	74.0
575	9	5	79.76	81.0	575	11	2	91.36	86.0
575	10	2	82.46	90.0	575	11	3	92.86	84.0
575	10	3	83.96	87.0	575	11	4	94.36	90.0
575	10	4	85.46	93.0	575	11	5	95.86	91.0
575	10	5	86.96	86.0	575	11	6	97.36	86.0
575A	1	1	94.56	88.0	575a	17	2	152.26	93.0
575A	1	2	96.06	85.0	575A	17	3	153.38	92.0
575A	1	3	97.56	94.0	575A	18	2	154.76	92.0
575A	2	2	99.45	75.0	575A	18	3	156.26	90.0
575A	2	3	100.96	60.0	575A	19	2	159.06	92.0
575A	3	2	103.36	53.0	575A	19	3	160.31	92.0
575A	3	3	104.86	67.0	575A	20	2	163.06	93.0
575A	4	1	105.96	74.0	575A	20	3	164.16	92.0
575A	4	2	107.46	81.0	575A	21	1	165.46	91.0
575A	4	3	108.96	86.0	575A	21	2	166.96	85.0
575A	5	2	111.26	89.0	575A	21	3	168.46	93.0
575A	5	3	112.76	69.0	575A	22	2	170.44	94.0
575A	6	1	114.86	78.0	575A	22	3	171.86	92.0
575A	6	2	116.36	76.0	575A	23	1	172.86	92.0
575A	6	3	117.86	82.0	575A	23	2	174.36	94.0
575A	7	2	120.66	77.0	575A	24	2	176.46	91.0
575A	7	3	122.16	83.0	575A	24	3	177.96	96.0
575A	8	1	123.86	81.0	575A	25	3	180.96	99.0
575A	8	2	125.36	83.0	575A	26	2	182.36	93.0
575A	9	2	127.56	75.0	575A	26	3	183.86	94.0
575A	10	2	129.56	92.0	575A	27	3	188.66	95.0
575A	10	3	131.06	85.0	575A	28	2	189.46	96.0
575A	11	2	132.86	89.0	575A	29	2	191.96	94.0
575A	11	3	134.36	97.0	575A	29	3	193.16	96.0
575A	12	2	137.36	88.0	575A	30	1	194.36	95.0
575A	12	3	138.86	88.0	575A	30	2	195.86	89.0
575A	13	2	141.06	90.0	575A	30	3	197.36	94.0
575A	13	3	142.56	96.0	575A	31	2	199.66	94.0
575A	14	2	144.16	93.0	575A	31	3	201.14	98.0
575A	14	3	145.66	94.0	575A	32	2	203.56	94.0
575A	15	2	146.96	95.0	575A	32	3	204.88	97.0
575A	15	3	148.46	94.0	575A	33	2	206.56	91.0
575A	16	2	150.26	92.0	575A	33	3	208.06	91.0
575A	16	3	151.51	94.0					
575B	1	1	4.06	73.0	575B	7	2	57.66	
575B	1	2	5.53	48.0	575B	7	3	59.16	98.0
575B	1	3	7.06	59.0	575B	7	4	60.66	97.0
575B	1	4	8.56	36.0	575B	7	5	62.16	92.0
575B	1	5	10.06	3.0	575B	7	6	63.66	99.0
575B	1	6	11.56	42.0	575B	8	2	66.96	91.0
575B	2	1	12.76	26.0	575B	8	3	68.46	77.0
575B	2	2	14.26	32.0	575B	8	4	69.96	87.0
575B	2	3	15.73	67.0	575B	8	5	71.46	88.0
575B	2	4	17.26	35.0	575B	8	6	72.96	85.0
575B	2	5	18.76	65.0	575B	9	2	76.06	85.0
575B	2	6	20.26	80.0	575B	9	3	77.56	93.0
575B	3	1	21.76	89.0	575B	9	4	79.06	93.0
575B	3	2	23.26	54.0	575B	9	5	80.56	91.0
575B	3	3	24.76	81.0	575B	10	2	83.66	90.0
575B	3	4	26.26	54.0	575B	10	3	85.16	95.0
575B	3	5	27.76	73.0	575B	10	4	86.66	64.0
575B	3	6	29.26	86.0	575B	10	5	88.16	96.0
575B	4	2	31.76	85.0	575B	10	6	89.66	94.0
575B	4	3	33.26	87.0	575B	11	2	93.16	89.0
575B	4	4	34.76	49.0	575B	11	3	94.66	93.0
575B	4	5	36.26	41.0	575B	11	4	96.16	85.0
575B	4	6	37.76	15.0	575B	11	5	97.66	96.0
575B	5	2	41.26	52.0	575B	11	6	99.16	88.0
575B	5	3	42.76	58.0	575B	12	2	101.86	96.0
575B	5	4	44.26	87.0	575B	12	3	163.36	85.0
575B	5	5	45.76	96.0	575B	12	4	104.86	87.0
575B	5	6	47.26	96.0	575B	12	5	106.36	82.0
575B	6	2	50.26	96.0	575B	13	2	111.46	73.0
575B	6	3	51.76	92.0	575B	13	3	112.96	83.0
575B	6	4	53.26	88.0	575B	14	2	116.36	91.0
575B	6	5	54.76	94.0	575B	14	3	117.86	85.0

Drilling locations

Leg	Location	Sites
Phase 1 1968–1970		
1	North Atlantic	1–7
2	North Atlantic	8–12
3	South Atlantic	13–22
4	Central Atlantic	23–31
5	North Pacific	32–43
6	North Pacific	44–60
7	Central Pacific	61–67
8	Central Pacific	68–75
9	Central Pacific	76–84
Phase 2 1970–1972		
10	Gulf of Mexico	85–97
11	North Atlantic	98–108
Re-entry trials		109–110
12	North Atlantic	111–119
13	Mediterranean	120–134
14	Central Atlantic	135–144
15	Caribbean	146–154
16	Central Pacific	155–163
17	Central Pacific	164–171
18	North Pacific	172–182
19	North Pacific	183–193
20	North Pacific	194–202
21	Coral Sea	203–210
22	Indian Ocean	211–218
23	Arabian Sea	219–230
24	Indian Ocean	231–238
25	Indian Ocean	239–249
Phase 3 1972–1975		
26	Indian Ocean	250–258
27	Indian Ocean	259–263
28	Antarctic	264–274
29	Tasman Sea	275–284
30	South Pacific	285–289
31	North Pacific	290–302
32	North Pacific	303–313
33	North Pacific	314–318
34	South Pacific	319–321
35	South Pacific	322–325
36	South Atlantic	326–331
37	North Atlantic	332–335
38	Arctic	336–352
39	Atlantic	353–359
40	South Atlantic	360–365
41	South Atlantic	366–370
42A	Mediterranean	371–378
42B	Black Sea	379–381
43	North Atlantic	382–387
44	North Atlantic	388–392
44A	North Atlantic	393–394
IPOD I 1975–present		
45	North Atlantic	395–396
46	North Atlantic	396A–396B
47	North Atlantic	397–398
48	North Atlantic	399–406
49	North Atlantic	407–414
50	North Atlantic	415–416
51A	North Atlantic	417–417A
51B	North Atlantic	417B–417D
52	North Atlantic	417D–418A
53	North Atlantic	418A–418B
54	Central Pacific	419–429
55	North Pacific	430–433
56	North Pacific	434–437
57	North Pacific	438–441
58	North Pacific	442–446
59	North Pacific	447–451
60	North Pacific	452–461
61	Central Pacific	462
62	North Pacific	463–466
63	North Pacific	467–473
64	Gulf of California	474–481
65	Gulf of California	482–485
66	Central Pacific	486–493
67	Central Pacific	494–500
68	Central Pacific	502–503
69	Central Pacific	504–505, 501
70	Central Pacific	506–510, 504B
71	South Atlantic	511–514
72	South Atlantic	515–518
73	South Atlantic	519–524
74	South Atlantic	525–529
75	South Atlantic	530–532
76	North Atlantic	533–534
77	Caribbean	535–540
78	North Atlantic	541–543, 395A, B
79	North Atlantic	544–547
80	North Atlantic	548–551
81	North Atlantic	552–555
82	North Atlantic	556–564
83	Central Pacific	504B
84	Central Pacific	565–570
85	Central Pacific	571–575

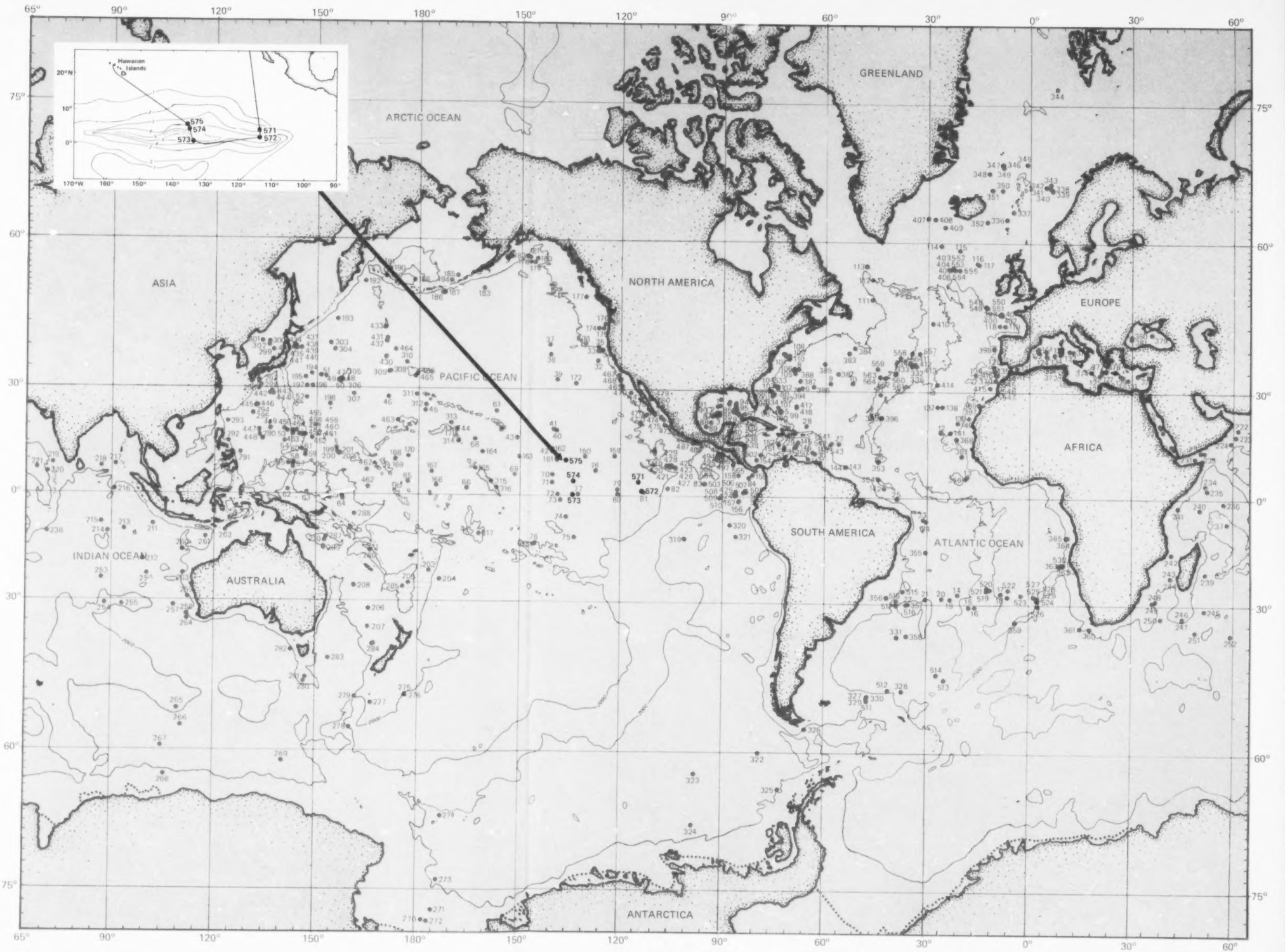

DEEP SEA DRILLING PROJECT

| Hole | Core-Section (interval in cm) | Sub-bottom depth (m) | Age (Ma) | Number of specimens | Number of species | Abditodentrix dilatata | Allomorphina gigas | Allomorphina regina | Allomorphina trigona | Allomorphinella conversa | Anomalinoides hyphalosus | Anomalinoides sp. | Angulogerina fornasa | Anomalina abiaensis s. spaulding | Anomalinoides acuta | Anomalinoides dorri s. stigmatus | Anomalinoides globulina | Anomalinoides umiatensis | Astacolus crepidula | Astacolus eroderma | Astacolus gutticostata | Astacolus pygmaea | Astrononion novozealandicum | Bigenerina nodosaria | Bolivina cubana | Bolivina decussata | Bolivina gracilenta | Bolivina pisciformis | Bolivina seminuda | Bolivina subadvena | Bolivina subexcavata | Bolivina tumidula | Bolivinopsis mexicana | Bolivinopsis robusta | Bolivinopsis subedentula | Buccella frigida | Buccella inusitata | Buccella japonica | Buccella macfarlani | Buccella mansfieldi | Buccella microxestos | Buccella peruviana | Buccella simplex | Buccella tasmanica | Buccella tenerrima | Buccella turbata | Bulimina aculeata | Bulimina costata | Bulimina elongata | Bulimina exilis | Bulimina mexicana | Bulimina rostrata | Bulimina semicostata | Bulimina striata | Bulimina subulata | Bulimina tenuata | Bulimina truncana | Bulimina vacca | Bulimina variabilis | Bulimina velascoensis | Buliminella curta | Buliminella elegantissima | Buliminella subfusiformis | Cancris auriculus | Cancris oblongus | Cancris sagra | Cassidulina carinata | Cassidulina crassa | Cassidulina laevigata | Cassidulina limbata | Cassidulina minuta | Cassidulina neocrassa | Cassidulina norcrossi | Cassidulina obtusa | Cassidulina parva | Cassidulina subglobosa | Cassidulina teretis | Cassidulina translucens | Cassidulina transversa | Cassidulina trigonica | Cassidulina weddellensis | Cassidulinoides bradyi | Cassidulinoides parkerianus | Chrysalogonium tetracuspis | Chrysalogonium tridentatum | Cibicidoides bradyi | Cibicidoides cicatricosus | Cibicidoides deliformis | Cibicidoides eocenicus | Cibicidoides havanensis | Cibicidoides hyphalus | Cibicidoides kullenbergi | Cibicidoides mundulus | Cibicidoides pachyderma | Cibicidoides perlucidus | Cibicidoides praemundanus | Cibicidoides robertsonianus | Cibicidoides rugosus | Cibicidoides wuellerstorfi | Cibicidoides wuellerstorfi s. l. | Cibicidoides wuellerstorfi s. l. C | Cyclammina cancellata | Cyclammina rotundata | Dentalina communis | Dentalina ittai | Dentalina mexi | Dentalina obliqua | Dentalina soluta | Dentalina spissa | Dentalina subtilis | Dentalina sublinearis | Dentalina tenuis | Dentalina vetusta | Dentalina wetherbyi | Dimorphina australis | Dimorphina tuberosa | Discorbis bertheloti | Discorbis bertis | Discorbis dimidiatus | Discorbis evolutus | Discorbis globularis | Discorbis mira | Discorbis orbicularis | Discorbis patagonicus | Discorbis peruvianus | Discorbis praeglobularis | Discorbis rosea | Discorbis subglobularis | Discorbis tenuimargo | Discorbis tuberculatus | Discorbis vilardeboanus | Discorbis wilsoni | Discorbis wuellerstorfi | Discorbis sp. | Ehrenbergina glabra | Ehrenbergina pacifica | Ehrenbergina trigona | Ehrenbergina variabilis | Ellipsoglandulina labrosa | Ellipsoglandulina sp. | Ellipsonodosaria glabra | Ellipsonodosaria sp. | Elphidium advenum | Elphidium cf. advenum | Elphidium aculeatum | Elphidium articulatum | Elphidium barleeanum | Elphidium bartletti | Elphidium batialis | Elphidium bentzi | Elphidium bimammatum | Elphidium birnageae | Elphidium cf. birnageae | Elphidium bonplandi | Elphidium cf. bonplandi | Elphidium cf. bonplandi s. l. | Elphidium cf. bonplandi s. l. A | Elphidium cf. bonplandi s. l. B | Elphidium cf. bonplandi s. l. C | Elphidium cf. bonplandi s. l. D | Elphidium cf. bonplandi s. l. E | Elphidium cf. bonplandi s. l. F | Elphidium cf. bonplandi s. l. G | Elphidium cf. bonplandi s. l. H | Elphidium cf. bonplandi s. l. I | Elphidium cf. bonplandi s. l. J | Elphidium cf. bonplandi s. l. K | Elphidium cf. bonplandi s. l. L | Elphidium cf. bonplandi s. l. M | Elphidium cf. bonplandi s. l. N | Elphidium cf. bonplandi s. l. O | Elphidium cf. bonplandi s. l. P | Elphidium cf. bonplandi s. l. Q | Elphidium cf. bonplandi s. l. R | Elphidium cf. bonplandi s. l. S | Elphidium cf. bonplandi s. l. T | Elphidium cf. bonplandi s. l. U | Elphidium cf. bonplandi s. l. V | Elphidium cf. bonplandi s. l. W | Elphidium cf. bonplandi s. l. X | Elphidium cf. bonplandi s. l. Y | Elphidium cf. bonplandi s. l. Z | Elphidium cf. bonplandi s. l. AA | Elphidium cf. bonplandi s. l. AB | Elphidium cf. bonplandi s. l. AC | Elphidium cf. bonplandi s. l. AD | Elphidium cf. bonplandi s. l. AE | Elphidium cf. bonplandi s. l. AF | Elphidium cf. bonplandi s. l. AG | Elphidium cf. bonplandi s. l. AH | Elphidium cf. bonplandi s. l. AI | Elphidium cf. bonplandi s. l. AJ | Elphidium cf. bonplandi s. l. AK | Elphidium cf. bonplandi s. l. AL | Elphidium cf. bonplandi s. l. AM | Elphidium cf. bonplandi s. l. AN | Elphidium cf. bonplandi s. l. AO | Elphidium cf. bonplandi s. l. AP | Elphidium cf. bonplandi s. l. AQ | Elphidium cf. bonplandi s. l. AR | Elphidium cf. bonplandi s. l. AS | Elphidium cf. bonplandi s. l. AT | Elphidium cf. bonplandi s. l. AU | Elphidium cf. bonplandi s. l. AV | Elphidium cf. bonplandi s. l. AW | Elphidium cf. bonplandi s. l. AX | Elphidium cf. bonplandi s. l. AY | Elphidium cf. bonplandi s. l. AZ | Elphidium cf. bonplandi s. l. BA | Elphidium cf. bonplandi s. l. BB | Elphidium cf. bonplandi s. l. BC | Elphidium cf. bonplandi s. l. BD | Elphidium cf. bonplandi s. l. BE | Elphidium cf. bonplandi s. l. BF | Elphidium cf. bonplandi s. l. BG | Elphidium cf. bonplandi s. l. BH | Elphidium cf. bonplandi s. l. BI | Elphidium cf. bonplandi s. l. BJ | Elphidium cf. bonplandi s. l. BK | Elphidium cf. bonplandi s. l. BL | Elphidium cf. bonplandi s. l. BM | Elphidium cf. bonplandi s. l. BN | Elphidium cf. bonplandi s. l. BO | Elphidium cf. bonplandi s. l. BP | Elphidium cf. bonplandi s. l. BQ | Elphidium cf. bonplandi s. l. BR | Elphidium cf. bonplandi s. l. BS | Elphidium cf. bonplandi s. l. BT | Elphidium cf. bonplandi s. l. BU | Elphidium cf. bonplandi s. l. BV | Elphidium cf. bonplandi s. l. BW | Elphidium cf. bonplandi s. l. BX | Elphidium cf. bonplandi s. l. BY | Elphidium cf. bonplandi s. l. BZ | Elphidium cf. bonplandi s. l. CA | Elphidium cf. bonplandi s. l. CB | Elphidium cf. bonplandi s. l. CC | Elphidium cf. bonplandi s. l. CD | Elphidium cf. bonplandi s. l. CE | Elphidium cf. bonplandi s. l. CF | Elphidium cf. bonplandi s. l. CG | Elphidium cf. bonplandi s. l. CH | Elphidium cf. bonplandi s. l. CI | Elphidium cf. bonplandi s. l. CJ | Elphidium cf. bonplandi s. l. CK | Elphidium cf. bonplandi s. l. CL | Elphidium cf. bonplandi s. l. CM | Elphidium cf. bonplandi s. l. CN | Elphidium cf. bonplandi s. l. CO | Elphidium cf. bonplandi s. l. CP | Elphidium cf. bonplandi s. l. CQ | Elphidium cf. bonplandi s. l. CR | Elphidium cf. bonplandi s. l. CS | Elphidium cf. bonplandi s. l. CT | Elphidium cf. bonplandi s. l. CU | Elphidium cf. bonplandi s. l. CV | Elphidium cf. bonplandi s. l. CW | Elphidium cf. bonplandi s. l. CX | Elphidium cf. bonplandi s. l. CY | Elphidium cf. bonplandi s. l. CZ | Elphidium cf. bonplandi s. l. DA | Elphidium cf. bonplandi s. l. DB | Elphidium cf. bonplandi s. l. DC | Elphidium cf. bonplandi s. l. DD | Elphidium cf. bonplandi s. l. DE | Elphidium cf. bonplandi s. l. DF | Elphidium cf. bonplandi s. l. DG | Elphidium cf. bonplandi s. l. DH | Elphidium cf. bonplandi s. l. DI | Elphidium cf. bonplandi s. l. DJ | Elphidium cf. bonplandi s. l. DK | Elphidium cf. bonplandi s. l. DL | Elphidium cf. bonplandi s. l. DM | Elphidium cf. bonplandi s. l. DN | Elphidium cf. bonplandi s. l. DO | Elphidium cf. bonplandi s. l. DP | Elphidium cf. bonplandi s. l. DQ | Elphidium cf. bonplandi s. l. DR | Elphidium cf. bonplandi s. l. DS | Elphidium cf. bonplandi s. l. DT | Elphidium cf. bonplandi s. l. DU | Elphidium cf. bonplandi s. l. DV | Elphidium cf. bonplandi s. l. DW | Elphidium cf. bonplandi s. l. DX | Elphidium cf. bonplandi s. l. DY | Elphidium cf. bonplandi s. l. DZ | Elphidium cf. bonplandi s. l. EA | Elphidium cf. bonplandi s. l. EB | Elphidium cf. bonplandi s. l. EC | Elphidium cf. bonplandi s. l. ED | Elphidium cf. bonplandi s. l. EE | Elphidium cf. bonplandi s. l. EF | Elphidium cf. bonplandi s. l. EG | Elphidium cf. bonplandi s. l. EH | Elphidium cf. bonplandi s. l. EI | Elphidium cf. bonplandi s. l. EJ | Elphidium cf. bonplandi s. l. EK | Elphidium cf. bonplandi s. l. EL | Elphidium cf. bonplandi s. l. EM | Elphidium cf. bonplandi s. l. EN | Elphidium cf. bonplandi s. l. EO | Elphidium cf. bonplandi s. l. EP | Elphidium cf. bonplandi s. l. EQ | Elphidium cf. bonplandi s. l. ER | Elphidium cf. bonplandi s. l. ES | Elphidium cf. bonplandi s. l. ET | Elphidium cf. bonplandi s. l. EU | Elphidium cf. bonplandi s. l. EV | Elphidium cf. bonplandi s. l. EW | Elphidium cf. bonplandi s. l. EX | Elphidium cf. bonplandi s. l. EY | Elphidium cf. bonplandi s. l. EZ | Elphidium cf. bonplandi s. l. FA | Elphidium cf. bonplandi s. l. FB | Elphidium cf. bonplandi s. l. FC | Elphidium cf. bonplandi s. l. FD | Elphidium cf. bonplandi s. l. FE | Elphidium cf. bonplandi s. l. FF | Elphidium cf. bonplandi s. l. FG | Elphidium cf. bonplandi s. l. FH | Elphidium cf. bonplandi s. l. FI | Elphidium cf. bonplandi s. l. FJ | Elphidium cf. bonplandi s. l. FK | Elphidium cf. bonplandi s. l. FL | Elphidium cf. bonplandi s. l. FM | Elphidium cf. bonplandi s. l. FN | Elphidium cf. bonplandi s. l. FO | Elphidium cf. bonplandi s. l. FP | Elphidium cf. bonplandi s. l. FQ | Elphidium cf. bonplandi s. l. FR | Elphidium cf. bonplandi s. l. FS | Elphidium cf. bonplandi s. l. FT | Elphidium cf. bonplandi s. l. FU | Elphidium cf. bonplandi s. l. FV | Elphidium cf. bonplandi s. l. FW | Elphidium cf. bonplandi s. l. FX | Elphidium cf. bonplandi s. l. FY | Elphidium cf. bonplandi s. l. FZ | Elphidium cf. bonplandi s. l. GA | Elphidium cf. bonplandi s. l. GB | Elphidium cf. bonplandi s. l. GC | Elphidium cf. bonplandi s. l. GD | Elphidium cf. bonplandi s. l. GE | Elphidium cf. bonplandi s. l. GF | Elphidium cf. bonplandi s. l. GG | Elphidium cf. bonplandi s. l. GH | Elphidium cf. bonplandi s. l. GI | Elphidium cf. bonplandi s. l. GJ | Elphidium cf. bonplandi s. l. GK | Elphidium cf. bonplandi s. l. GL | Elphidium cf. bonplandi s. l. GM | Elphidium cf. bonplandi s. l. GN | Elphidium cf. bonplandi s. l. GO | Elphidium cf. bonplandi s. l. GP | Elphidium cf. bonplandi s. l. GQ | Elphidium cf. bonplandi s. l. GR | Elphidium cf. bonplandi s. l. GS | Elphidium cf. bonplandi s. l. GT | Elphidium cf. bonplandi s. l. GU | Elphidium cf. bonplandi s. l. GV | Elphidium cf. bonplandi s. l. GW | Elphidium cf. bonplandi s. l. GX | Elphidium cf. bonplandi s. l. GY | Elphidium cf. bonplandi s. l. GZ | Elphidium cf. bonplandi s. l. HA | Elphidium cf. bonplandi s. l. HB | Elphidium cf. bonplandi s. l. HC | Elphidium cf. bonplandi s. l. HD | Elphidium cf. bonplandi s. l. HE | Elphidium cf. bonplandi s. l. HF | Elphidium cf. bonplandi s. l. HG | Elphidium cf. bonplandi s. l. HH | Elphidium cf. bonplandi s. l. HI | Elphidium cf. bonplandi s. l. HJ | Elphidium cf. bonplandi s. l. HK | Elphidium cf. bonplandi s. l. HL | Elphidium cf. bonplandi s. l. HM | Elphidium cf. bonplandi s. l. HN | Elphidium cf. bonplandi s. l. HO | Elphidium cf. bonplandi s. l. HP | Elphidium cf. bonplandi s. l. HQ | Elphidium cf. bonplandi s. l. HR | Elphidium cf. bonplandi s. l. HS | Elphidium cf. bonplandi s. l. HT | Elphidium cf. bonplandi s. l. HU | Elphidium cf. bonplandi s. l. HV | Elphidium cf. bonplandi s. l. HW | Elphidium cf. bonplandi s. l. HX | Elphidium cf. bonplandi s. l. HY | Elphidium cf. bonplandi s. l. HZ | Elphidium cf. bonplandi s. l. IA | Elphidium cf. bonplandi s. l. IB | Elphidium cf. bonplandi s. l. IC | Elphidium cf. bonplandi s. l. ID | Elphidium cf. bonplandi s. l. IE | Elphidium cf. bonplandi s. l. IF | Elphidium cf. bonplandi s. l. IG | Elphidium cf. bonplandi s. l. IH | Elphidium cf. bonplandi s. l. II | Elphidium cf. bonplandi s. l. IJ | Elphidium cf. bonplandi s. l. IK | Elphidium cf. bonplandi s. l. IL | Elphidium cf. bonplandi s. l. IM | Elphidium cf. bonplandi s. l. IN | Elphidium cf. bonplandi s. l. IO | Elphidium cf. bonplandi s. l. IP | Elphidium cf. bonplandi s. l. IQ | Elphidium cf. bonplandi s. l. IR | Elphidium cf. bonplandi s. l. IS | Elphidium cf. bonplandi s. l. IT | Elphidium cf. bonplandi s. l. IU | Elphidium cf. bonplandi s. l. IV | Elphidium cf. bonplandi s. l. IW | Elphidium cf. bonplandi s. l. IX | Elphidium cf. bonplandi s. l. IY | Elphidium cf. bonplandi s. l. IZ | Elphidium cf. bonplandi s. l. JA | Elphidium cf. bonplandi s. l. JB | Elphidium cf. bonplandi s. l. JC | Elphidium cf. bonplandi s. l. JD | Elphidium cf. bonplandi s. l. JE | Elphidium cf. bonplandi s. l. JF | Elphidium cf. bonplandi s. l. JG | Elphidium cf. bonplandi s. l. JH | Elphidium cf. bonplandi s. l. JI | Elphidium cf. bonplandi s. l. JJ | Elphidium cf. bonplandi s. l. JK | Elphidium cf. bonplandi s. l. JL | Elphidium cf. bonplandi s. l. JM | Elphidium cf. bonplandi s. l. JN | Elphidium cf. bonplandi s. l. JO | Elphidium cf. bonplandi s. l. JP | Elphidium cf. bonplandi s. l. JQ | Elphidium cf. bonplandi s. l. JR | Elphidium cf. bonplandi s. l. JS | Elphidium cf. bonplandi s. l. JT | Elphidium cf. bonplandi s. l. JU | Elphidium cf. bonplandi s. l. JV | Elphidium cf. bonplandi s. l. JW | Elphidium cf. bonplandi s. l. JX | Elphidium cf. bonplandi s. l. JY | Elphidium cf. bonplandi s. l. JZ | Elphidium cf. bonplandi s. l. KA | Elphidium cf. bonplandi s. l. KB | Elphidium cf. bonplandi s. l. KC | Elphidium cf. bonplandi s. l. KD | Elphidium cf. bonplandi s. l. KE | Elphidium cf. bonplandi s. l. KF | Elphidium cf. bonplandi s. l. KG | Elphidium cf. bonplandi s. l. KH | Elphidium cf. bonplandi s. l. KI | Elphidium cf. bonplandi s. l. KJ | Elphidium cf. bonplandi s. l. KK | Elphidium cf. bonplandi s. l. KL | Elphidium cf. bonplandi s. l. KM | Elphidium cf. bonplandi s. l. KN | Elphidium cf. bonplandi s. l. KO | Elphidium cf. bonplandi s. l. KP | Elphidium cf. bonplandi s. l. KQ | Elphidium cf. bonplandi s. l. KR | Elphidium cf. bonplandi s. l. KS | Elphidium cf. bonplandi s. l. KT | Elphidium cf. bonplandi s. l. KU | Elphidium cf. bonplandi s. l. KV | Elphidium cf. bonplandi s. l. KW | Elphidium cf. bonplandi s. l. KX | Elphidium cf. bonplandi s. l. KY | Elphidium cf. bonplandi s. l. KZ | Elphidium cf. bonplandi s. l. LA | Elphidium cf. bonplandi s. l. LB | Elphidium cf. bonplandi s. l. LC | Elphidium cf. bonplandi s. l. LD | Elphidium cf. bonplandi s. l. LE | Elphidium cf. bonplandi s. l. LF | Elphidium cf. bonplandi s. l. LG | Elphidium cf. bonplandi s. l. LH | Elphidium cf. bonplandi s. l. LI | Elphidium cf. bonplandi s. l. LJ | Elphidium cf. bonplandi s. l. LK | Elphidium cf. bonplandi s. l. LL | Elphidium cf. bonplandi s. l. LM | Elphidium cf. bonplandi s. l. LN | Elphidium cf. bonplandi s. l. LO | Elphidium cf. bonplandi s. l. LP | Elphidium cf. bonplandi s. l. LQ | Elphidium cf. bonplandi s. l. LR | Elphidium cf. bonplandi s. l. LS | Elphidium cf. bonplandi s. l. LT | Elphidium cf. bonplandi s. l. LU | Elphidium cf. bonplandi s. l. LV | Elphidium cf. bonplandi s. l. LW | Elphidium cf. bonplandi s. l. LX | Elphidium cf. bonplandi s. l. LY | Elphidium cf. bonplandi s. l. LZ | Elphidium cf. bonplandi s. l. MA | Elphidium cf. bonplandi s. l. MB | Elphidium cf. bonplandi s. l. MC | Elphidium cf. bonplandi s. l. MD | Elphidium cf. bonplandi s. l. ME | Elphidium cf. bonplandi s. l. MF | Elphidium cf. bonplandi s. l. MG | Elphidium cf. bonplandi s. l. MH | Elphidium cf. bonplandi s. l. MI | Elphidium cf. bonplandi s. l. MJ | Elphidium cf. bonplandi s. l. MK | Elphidium cf. bonplandi s. l. ML | Elphidium cf. bonplandi s. l. MM | Elphidium cf. bonplandi s. l. MN | Elphidium cf. bonplandi s. l. MO | Elphidium cf. bonplandi s. l. MP | Elphidium cf. bonplandi s. l. MQ | Elphidium cf. bonplandi s. l. MR | Elphidium cf. bonplandi s. l. MS | Elphidium cf. bonplandi s. l. MT | Elphidium cf. bonplandi s. l. MU | Elphidium cf. bonplandi s. l. MV | Elphidium cf. bonplandi s. l. MW | Elphidium cf. bonplandi s. l. MX | Elphidium cf. bonplandi s. l. MY | Elphidium cf. bonplandi s. l. MZ | Elphidium cf. bonplandi s. l. NA | Elphidium cf. bonplandi s. l. NB | Elphidium cf. bonplandi s. l. NC | Elphidium cf. bonplandi s. l. ND | Elphidium cf. bonplandi s. l. NE | Elphidium cf. bonplandi s. l. NF | Elphidium cf. bonplandi s. l. NG | Elphidium cf. bonplandi s. l. NH | Elphidium cf. bonplandi s. l. NI | Elphidium cf. bonplandi s. l. NJ | Elphidium cf. bonplandi s. l. NK | Elphidium cf. bonplandi s. l. NL | Elphidium cf. bonplandi s. l. NM | Elphidium cf. bonplandi s. l. NN | Elphidium cf. bonplandi s. l. NO | Elphidium cf. bonplandi s. l. NP | Elphidium cf. bonplandi s. l. NQ | Elphidium cf. bonplandi s. l. NR | Elphidium cf. bonplandi s. l. NS | Elphidium cf. bonplandi s. l. NT | Elphidium cf. bonplandi s. l. NU | Elphidium cf. bonplandi s. l. NV | Elphidium cf. bonplandi s. l. NW | Elphidium cf. bonplandi s. l. NX | Elphidium cf. bonplandi s. l. NY | Elphidium cf. bonplandi s. l. NZ | Elphidium cf. bonplandi s. l. OA | Elphidium cf. bonplandi s. l. OB | Elphidium cf. bonplandi s. l. OC | Elphidium cf. bonplandi s. l. OD | Elphidium cf. bonplandi s. l. OE | Elphidium cf. bonplandi s. l. OF | Elphidium cf. bonplandi s. l. OG | Elphidium cf. bonplandi s. l. OH | Elphidium cf. bonplandi s. l. OI | Elphidium cf. bonplandi s. l. OJ | Elphidium cf. bonplandi s. l. OK | Elphidium cf. bonplandi s. l. OL | Elphidium cf. bonplandi s. l. OM | Elphidium cf. bonplandi s. l. ON | Elphidium cf. bonplandi s. l. OO | Elphidium cf. bonplandi s. l. OP | Elphidium cf. bonplandi s. l. OQ | Elphidium cf. bonplandi s. l. OR | Elphidium cf. bonplandi s. l. OS | Elphidium cf. bonplandi s. l. OT | Elphidium cf. bonplandi s. l. OU | Elphidium cf. bonplandi s. l. OV | Elphidium cf. bonplandi s. l. OW | Elphidium cf. bonplandi s. l. OX | Elphidium cf. bonplandi s. l. OY | Elphidium cf. bonplandi s. l. OZ | Elphidium cf. bonplandi s. l. PA | Elphidium cf. bonplandi s. l. PB | Elphidium cf. bonplandi s. l. PC | Elphidium cf. bonplandi s. l. PD | Elphidium cf. bonplandi s. l. PE | Elphidium cf. bonplandi s. l. PF | Elphidium cf. bonplandi s. l. PG | Elphidium cf. bonplandi s. l. PH | Elphidium cf. bonplandi s. l. PI | Elphidium cf. bonplandi s. l. PJ | Elphidium cf. bonplandi s. l. PK | Elphidium cf. bonplandi s. l. PL | Elphidium cf. bonplandi s. l. PM | Elphidium cf. bonplandi s. l. PN | Elphidium cf. bonplandi s. l. PO | Elphidium cf. bonplandi s. l. PP | Elphidium cf. bonplandi s. l. PQ | Elphidium cf. bonplandi s. l. PR | Elphidium cf. bonplandi s. l. PS | Elphidium cf. bonplandi s. l. PT | Elphidium cf. bonplandi s. l. PU | Elphidium cf. bonplandi s. l. PV | Elphidium cf. bonplandi s. l. PW | Elphidium cf. bonplandi s. l. PX | Elphidium cf. bonplandi s. l. PY | Elphidium cf. bonplandi s. l. PZ | Elphidium cf. bonplandi s. l. QA | Elphidium cf. bonplandi s. l. QB | Elphidium cf. bonplandi s. l. QC | Elphidium cf. bonplandi s. l. QD | Elphidium cf. bonplandi s. l. QE | Elphidium cf. bonplandi s. l. QF | Elphidium cf. bonplandi s. l. QG | Elphidium cf. bonplandi s. l. QH | Elphidium cf. bonplandi s. l. QI | Elphidium cf. bonplandi s. l. QJ | Elphidium cf. bonplandi s. l. QK | Elphidium cf. bonplandi s. l. QL | Elphidium cf. bonplandi s. l. QM | Elphidium cf. bonplandi s. l. QN | Elphidium cf. bonplandi s. l. QO | Elphidium cf. bonplandi s. l. QP | Elphidium cf. bonplandi s. l. QQ | Elphidium cf. bonplandi s. l. QR | Elphidium cf. bonplandi s. l. QS | Elphidium cf. bonplandi s. l. QT | Elphidium cf. bonplandi s. l. QU | Elphidium cf. bonplandi s. l. QV | Elphidium cf. bonplandi s. l. QW | Elphidium cf. bonplandi s. l. QX | Elphidium cf. bonplandi s. l. QY | Elphidium cf. bonplandi s. l. QZ | Elphidium cf. bonplandi s. l. RA | Elphidium cf. bonplandi s. l. RB | Elphidium cf. bonplandi s. l. RC | Elphidium cf. bonplandi s. l. RD | Elphidium cf. bonplandi s. l. RE | Elphidium cf. bonplandi s. l. RF | Elphidium cf. bonplandi s. l. RG | Elphidium cf. bonplandi s. l. RH | Elphidium cf. bonplandi s. l. RI | Elphidium cf. bonplandi s. l. RJ | Elphidium cf. bonplandi s. l. RK | Elphidium cf. bonplandi s. l. RL | Elphidium cf. bonplandi s. l. RM | Elphidium cf. bonplandi s. l. RN | Elphidium cf. bonplandi s. l. RO | Elphidium cf. bonplandi s. l. RP | Elphidium cf. bonplandi s. l. RQ | Elphidium cf. bonplandi s. l. RR | Elphidium cf. bonplandi s. l. RS | Elphidium cf. bonplandi s. l. RT | Elphidium cf. bonplandi s. l. RU | Elphidium cf. bonplandi s. l. RV | Elphidium cf. bonplandi s. l. RW | Elphidium cf. bonplandi s. l. RX | Elphidium cf. bonplandi s. l. RY | Elphidium cf. bonplandi s. l. RZ | Elphidium cf. bonplandi s. l. SA | Elphidium cf. bonplandi s. l. SB | Elphidium cf. bonplandi s. l. SC | Elphidium cf. bonplandi s. l. SD | Elphidium cf. bonplandi s. l. SE | Elphidium cf. bonplandi s. l. SF | Elphidium cf. bonplandi s. l. SG | Elphidium cf. bonplandi s. l. SH | Elphidium cf. bonplandi s. l. SI | Elphidium cf. bonplandi s. l. SJ | Elphidium cf. bonplandi s. l. SK | Elphidium cf. bonplandi s. l. SL | Elphidium cf. bonplandi s. l. SM | Elphidium cf. bonplandi s. l. SN | Elphidium cf. bonplandi s. l. SO | Elphidium cf. bonplandi s. l. SP | Elphidium cf. bonplandi s. l. SQ | Elphidium cf. bonplandi s. l. SR | Elphidium cf. bonplandi s. l. SS | Elphidium cf. bonplandi s. l. ST | Elphidium cf. bonplandi s. l. SU | Elphidium cf. bonplandi s. l. SV | Elphidium cf. bonplandi s. l. SW | Elphidium cf. bonplandi s. l. SX | Elphidium cf. bonplandi s. l. SY | Elphidium cf. bonplandi s. l. SZ | Elphidium cf. bonplandi s. l. TA | Elphidium cf. bonplandi s. l. TB | Elphidium cf. bonplandi s. l. TC | Elphidium cf. bonplandi s. l. TD | Elphidium cf. bonplandi s. l. TE | Elphidium cf. bonplandi s. l. TF | Elphidium cf. bonplandi s. l. TG | Elphidium cf. bonplandi s. l. TH | Elphidium cf. bonplandi s. l. TI | Elphidium cf. bonplandi s. l. TJ | Elphidium cf. bonplandi s. l. TK | Elphidium cf. bonplandi s. l. TL | Elphidium cf. bonplandi s. l. TM | Elphidium cf. bonplandi s. l. TN | Elphidium cf. bonplandi s. l. TO | Elphidium cf. bonplandi s. l. TP | Elphidium cf. bonplandi s. l. TQ | Elphidium cf. bonplandi s. l. TR | Elphidium cf. bonplandi s. l. TS | Elphidium cf. bonplandi s. l. TT | Elphidium cf. bonplandi s. l. TU | Elphidium cf. bonplandi s. l. TV | Elphidium cf. bonplandi s. l. TW | Elphidium cf. bonplandi s. l. TX | Elphidium cf. bonplandi s. l. TY | Elphidium cf. bonplandi s. l. TZ | Elphidium cf. bonplandi s. l. UA | Elphidium cf. bonplandi s. l. UB | Elphidium cf. bonplandi s. l. UC | Elphidium cf. bonplandi s. l. UD | Elphidium cf. bonplandi s. l. UE | Elphidium cf. bonplandi s. l. UF | Elphidium cf. bonplandi s. l. UG | Elphidium cf. bonplandi s. l. UH | Elphidium cf. bonplandi s. l. UI | Elphidium cf. bonplandi s. l. UJ | Elphidium cf. bonplandi s. l. UK | Elphidium cf. bonplandi s. l. UL | Elphidium cf. bonplandi s. l. UM | Elphidium cf. bonplandi s. l. UN | Elphidium cf. bonplandi s. l. UO | Elphidium cf. bonplandi s. l. UP | Elphidium cf. bonplandi s. l. UQ | Elphidium cf. bonplandi s. l. UR | Elphidium cf. bonplandi s. l. US | Elphidium cf. bonplandi s. l. UT | Elphidium cf. bonplandi s. l. UU | Elphidium cf. bonplandi s. l. UV | Elphidium cf. bonplandi s. l. UW | Elphidium cf. bonplandi s. l. UX | Elphidium cf. bonplandi s. l. UY | Elphidium cf. bonplandi s. l. UZ | Elphidium cf. bonplandi s. l. VA | Elphidium cf. bonplandi s. l. VB | Elphidium cf. bonplandi s. l. VC | Elphidium cf. bonplandi s. l. VD | Elphidium cf. bonplandi s. l. VE | Elphidium cf. bonplandi s. l. VF | Elphidium cf. bonplandi s. l. VG | Elphidium cf. bonplandi s. l. VH | Elphidium cf. bonplandi s. l. VI | Elphidium cf. bonplandi s. l. VJ | Elphidium cf. bonplandi s. l. VK | Elphidium cf. bonplandi s. l. VL | Elphidium cf. bonplandi s. l. VM | Elphidium cf. bonplandi s. l. VN | Elphidium cf. bonplandi s. l. VO | Elphidium cf. bonplandi s. l. VP | Elphidium cf. bonplandi s. l. VQ | Elphidium cf. bonplandi s. l. VR | Elphidium cf. bonplandi s. l. VS | Elphidium cf. bonplandi s. l. VT | Elphidium cf. bonplandi s. l. VU | Elphidium cf. bonplandi s. l. VV | Elphidium cf. bonplandi s. l. VW | Elphidium cf. bonplandi s. l. VX | Elphidium cf. bonplandi s. l. VY | Elphidium cf. bonplandi s. l. VZ | Elphidium cf. bonplandi s. l. WA | Elphidium cf. bonplandi s. l. WB | Elphidium cf. bonplandi s. l. WC | Elphidium cf. bonplandi s. l. WD | Elphidium cf. bonplandi s. l. WE | Elphidium cf. bonplandi s. l. WF | Elphidium cf. bonplandi s. l. WG | Elphidium cf. bonplandi s. l. WH | Elphidium cf. bonplandi s. l. WI | Elphidium cf. bonplandi s. l. WJ | Elphidium cf. bonplandi s. l. WK | Elphidium cf. bonplandi s. l. WL | Elphidium cf. bonplandi s. l. WM | Elphidium cf. bonplandi s. l. WN | Elphidium cf. bonplandi s. l. WO | Elphidium cf. bonplandi s. l. WP | Elphidium cf. bonplandi s. l. WQ | Elphidium cf. bonplandi s. l. WR | Elphidium cf. bonplandi s. l. WS | Elphidium cf. bonplandi s. l. WT | Elphidium cf. bonplandi s. l. WU | Elphidium cf. bonplandi s. l. WV | Elphidium cf. bonplandi s. l. WW | Elphidium cf. bonplandi s. l. WX | Elphidium cf. bonplandi s. l. WY | Elphidium cf. bonplandi s. l. WZ | Elphidium cf. bonplandi s. l. XA | Elphidium cf. bonplandi s. l. XB | Elphidium cf. bonplandi s. l. XC | Elphidium cf. bonplandi s. l. XD | Elphidium cf. bonplandi s. l. XE | Elphidium cf. bonplandi s. l. XF | Elphidium cf. bonplandi s. l. XG | Elphidium cf. bonplandi s. l. XH | Elphidium cf. bonplandi s. l. XI | Elphidium cf. bonplandi s. l. XJ | Elphidium cf. bonplandi s. l. XK | Elphidium cf. bonplandi s. l. XL | Elphidium cf. bonplandi s. l. XM | Elphidium cf. bonplandi s. l. XN | Elphidium cf. bonplandi s. l. XO | Elphidium cf. bonplandi s. l. XP | Elphidium cf. bonplandi s. l. XQ | Elphidium cf. bonplandi s. l. XR | Elphidium cf. bonplandi s. l. XS | Elphidium cf. bonplandi s. l. XT | Elphidium cf. bonplandi s. l. XU | Elphidium cf. bonplandi s. l. XV | Elphidium cf. bonplandi s. l. XW | Elphidium cf. bonplandi s. l. XX | Elphidium cf. bonplandi s. l. XY | Elphidium cf. bonplandi s. l. XZ | Elphidium cf. bonplandi s. l. YA | Elphidium cf. bonplandi s. l. YB | Elphidium cf. bonplandi s. l. YC | Elphidium cf. bonplandi s. l. YD | Elphidium cf. bonplandi s. l. YE | Elphidium cf. bonplandi s. l. YF | Elphidium cf. bonplandi s. l. YG | Elphidium cf. bonplandi s. l. YH | Elphidium cf. bonplandi s. l. YI | Elphidium cf. bonplandi s. l. YJ | Elphidium cf. bonplandi s. l. YK | Elphidium cf. bonplandi s. l. YL | Elphidium cf. bonplandi s. l. YM | Elphidium cf. bonplandi s. l. YN | Elphidium cf. bonplandi s. l. YO | Elphidium cf. bonplandi s. l. YP | Elphidium cf. bonplandi s. l. YQ | Elphidium cf. bonplandi s. l. YR | Elphidium cf. bonplandi s. l. YS | Elphidium cf. bonplandi s. l. YT | Elphidium cf. bonplandi s. l. YU | Elphidium cf. bonplandi s. l. YV | Elphidium cf. bonplandi s. l. YW | Elphidium cf. bonplandi s. l. YX | Elphidium cf. bonplandi s. l. YY | Elphidium cf. bonplandi s. l. YZ | Elphidium cf. bonplandi s. l. ZA | Elphidium cf. bonplandi s. l. ZB | Elphidium cf. bonplandi s. l. ZC | Elphidium cf. bonplandi s. l. ZD | Elphidium cf. bonplandi s. l. ZE | Elphidium cf. bonplandi s. l. ZF | Elphidium cf. bonplandi s. l. ZG | Elphidium cf. bonplandi s. l. ZH | Elphidium cf. bonplandi s. l. ZI | Elphidium cf. bonplandi s. l. ZJ | Elphidium cf. bonplandi s. l. ZK | Elphidium cf. bonplandi s. l. ZL | Elphidium cf. bonplandi s. l. ZM | Elphidium cf. bonplandi s. l. ZN | Elphidium cf. bonplandi s. l. ZO | Elphidium cf. bonplandi s. l. ZP | Elphidium cf. bonplandi s. l. ZQ | Elphidium cf. bonplandi s. l. ZR | Elphidium cf. bonplandi s. l. ZS | Elphidium cf. bonplandi s. l. ZT | Elphidium cf. bonplandi s. l. ZU | Elphidium cf. bonplandi s. l. ZV | Elphidium cf. bonplandi s. l. ZW | Elphidium cf. bonplandi s. l. ZX | Elphidium cf. bonplandi s. l. ZY | Elphidium cf. bonplandi s. l. ZZ | Elphidium cf. bonplandi s. l. AAA | Elphidium cf. bonplandi s. l. AAB | Elphidium cf. bonplandi s. l. AAC

| Hole | Core-Section (interval in cm) | Sub-bottom depth (m) | Age (Ma) | Number of specimens | Number of species | *Ajanella frodoi* | *Algamia vivarinae* | *Bhutanina ornithia* | *Globigerina* sp. | *Globigerinella adamsi* | *Globigerinella calida* | *Globigerinella obesa* | *Globigerinella siphonifera* | *Globigerinella* aff. *regina* | *Globigerinita glutinata* | *Globigerinita* sp. | *Tenuitella iota* | *Tenuitella munda* | *Tenuitella* sp. | *Turborotalita quinqueloba* | *Acarinina bullbrooki* | *Acarinina collactea* | *Acarinina primitiva* | *Acarinina soldadoensis* | *Acarinina* sp. | *Morozovella aragonensis* | *Morozovella crater* | *Morozovella formosa* | *Morozovella lensiformis* | *Morozovella occlusa* | *Morozovella* sp. | *Subbotina angiporoides* | *Subbotina eocaena* | *Subbotina hagni* | *Subbotina linaperta* | *Subbotina* sp. | *Turborotalia cerroazulensis* | *Turborotalia frontosa* | *Turborotalia pomeroli* | *Turborotalia* sp. | *Catapsydrax dissimilis* | *Catapsydrax* sp. | *Dentoglobigerina altispira* | *Globoquadrina baroemoenensis* | *Globoquadrina dehiscens* | *Globoquadrina globosa* | *Globoquadrina* sp. | *Paragloborotalia mayeri* | *Paragloborotalia opima* | *Paragloborotalia pseudokugleri* | *Paragloborotalia siakensis* | *Paragloborotalia* sp. | *Globorotalia* sp. | *Globoturborotalita ampliapertura* | *Globoturborotalita connecta* | *Globoturborotalita euapertura* | *Globoturborotalita* sp. | *Orbulina suturalis* | *Orbulina universa* | *Praeorbulina glomerosa* | *Praeorbulina sicana* | *Praeorbulina* sp. | *Globigerinoides altiaperturus* | *Globigerinoides bollii* | *Globigerinoides diminutus* | *Globigerinoides obliquus* | *Globigerinoides* sp. | *Globigerinoides trilobus* | *Globigerinoides* spp. | *Sphaeroidinella dehiscens* | *Sphaeroidinella* sp. | *Sphaeroidinellopsis disjuncta* | *Sphaeroidinellopsis kochi* | *Sphaeroidinellopsis paenedehiscens* | *Sphaeroidinellopsis seminulina* | *Sphaeroidinellopsis* sp. | *Globigerina angulisuturalis* | *Globigerina ciperoensis* | *Globigerina eamesi* | *Globigerina euapertura* | *Globigerina gortanii* | *Globigerina labiacrassata* | *Globigerina* sp. | *Globigerina tapuriensis* | *Globigerina venezuelana* | *Globigerina woodi* | *Globigerina yeguaensis* | *Globigerina* spp. | *Globigerinella obesa* | *Globigerinella siphonifera* | *Globigerinella* spp. | *Globigerinita minuta* | *Globigerinita naparimaensis* | *Globigerinita uvula* | *Globigerinita* spp. | *Tenuitella angustiumbilicata* | *Tenuitella clemenciae* | *Tenuitella gemma* | *Tenuitella insolita* | *Tenuitella munda* | *Tenuitella parkerae* | *Tenuitella pseudoobesa* | *Tenuitella* spp. | *Chiloguembelina cubensis* | *Chiloguembelina midwayensis* | *Chiloguembelina* spp. | *Clavigerina jacksonensis* | *Clavigerina nuttalli* | *Clavigerina* spp. | *Dentoglobigerina galavisi* | *Dentoglobigerina venezuelana* | *Globigerina ampliapertura* | *Globigerina angiporoides* | *Globigerina anguliofficinalis* | *Globigerina bulloides* | *Globigerina cf. bulloides* | *Globigerina decoraperta* | *Globigerina druryi* | *Globigerina falconensis* | *Globigerina foliata* | *Globigerina fringa* | *Globigerina gortanii gortanii* | *Globigerina gortanii marginata* | *Globigerina gortanii* spp. | *Globigerina howchini* | *Globigerina juvenilis* | *Globigerina luterbacheri* | *Globigerina mexicana* | *Globigerina nepenthes* | *Globigerina nojimai* | *Globigerina ouachitaensis* | *Globigerina parabulloides* | *Globigerina praebulloides* | *Globigerina praedigitata* | *Globigerina quadrarcus* | *Globigerina quinqueloba* | *Globigerina rubescens* | *Globigerina* spp. | *Globigerinoides conglobatus* | *Globigerinoides extremus* | *Globigerinoides immaturus* | *Globigerinoides mitra* | *Globigerinoides obliquus extremus* | *Globigerinoides obliquus obliquus* | *Globigerinoides quadrilobatus* | *Globigerinoides ruber* | *Globigerinoides ruber pyramidalis* | *Globigerinoides ruber ruber* | *Globigerinoides sacculifer* | *Globigerinoides* spp. | *Globigerinoides subquadratus* | *Globigerinoides trilobus* | *Globigerinoides* spp. | *Orbulina bilobata* | *Orbulina suturalis* | *Orbulina universa* | *Praeorbulina circularis* | *Praeorbulina curva* | *Praeorbulina glomerosa curva* | *Praeorbulina glomerosa glomerosa* | *Praeorbulina glomerosa* spp. | *Praeorbulina sicana* | *Praeorbulina transitoria* | *Praeorbulina* sp

Volume 85: Chapter 17: Appendix A: (Continued).

| Hole | Core Section (interval in cm) | Sub-bottom depth (m) | Age (Ma) | Number of specimens | Number of species | *Pleurosigma* marginatum | *Pleurosigma* weyli | *Pleurosigma* bicuneiformis | *Pleurosigma* obtusum | *Pleurosigma* akidoides | *Pleurosigma* aestuarii | *Pleurosigma* elongatum | *Pleurosigma* borgei | *Pleurosigma* balticum | *Pleurosigma* balticoides | *Pleurosigma* normanii | *Pleurosigma* obscurum | *Pleurosigma* sp. | *Pseudoamphora* sp. | *Psammodictyon* sp. | *Psammodictyon* panduriforme | *Petrodictyon* gemmatum | *Petrodictyon* sp. | *Pinnularia* sp. | *Plagiogramma* staurophorum | *Plagiogramma* sp. | *Plagiotropis* sp. | *Plagiotropis* lepidoptera | *Plagiotropis* vanheurckii | *Plagiotropis* sp. | *Placoneis* sp. | *Placoneis* elginensis | *Placoneis* gastrum | *Placoneis* pacifica | *Placoneis* sp. | *Pinnularia* viridis | *Pinnularia* sp. | *Pinnularia* interrupta | *Pinnularia* sp. | *Pinnularia* sp. | *Pinnularia* sp.

9514

Volume 85: Chapter 22: Figure 6. Isotope stratigraphy and biostratigraphy at Sites 216 (tropical Indian Ocean), 575 (central equatorial Pacific), and 289 (west equatorial Pacific).

Site 216

Site 575

Site 289

Note: Isotope data at Site 216 are from Vincent et al. (in press), at Site 575 from this study (Tables 3 and 4, Holes 575A and 575B), and at Site 289 from Woodruff et al. (1981) and Savin et al. (1981, pp. 441 to 446). At Site 289 all data points within each 1-m increment are plotted at the same level; small dots refer to one data point and large dots to 2 to 5 data points. Biostratigraphy at Site 216 is from various authors as summarized in Vincent (1977). Biostratigraphy at Site 289 is from Srinivasan and Kennett (1981b) for foraminifers, Burky (1975) for calcareous nannofossils, and Holdsworth (1975) and G. Lombari (pers. comm., 1983) for radiolarians. Levels of correlations C to H are from Figure 5. The three sites are aligned on the initiation of the Chron 16 Carbon Shift (level E).

A *Globoquadrina venezuelana*
○ *Orbulina universa*
● *Orbulina suturalis*
◇ *Globigerinoides sacculifer*

× *Globoquadrina venezuelana* (Hole 575A)
+ *Globoquadrina venezuelana* (Hole 575B)
• *Orbulina universa* (Hole 575A)
○ *Orbulina universa* (Hole 575B)